Computational Intelligence and Neuroscience

Advanced Computational Intelligence for Smart Healthcare and Human Health Using Few-Shot Learning

Lead Guest Editor: Xin Ning
Guest Editors: Guangming Zhang and Xiao Bai

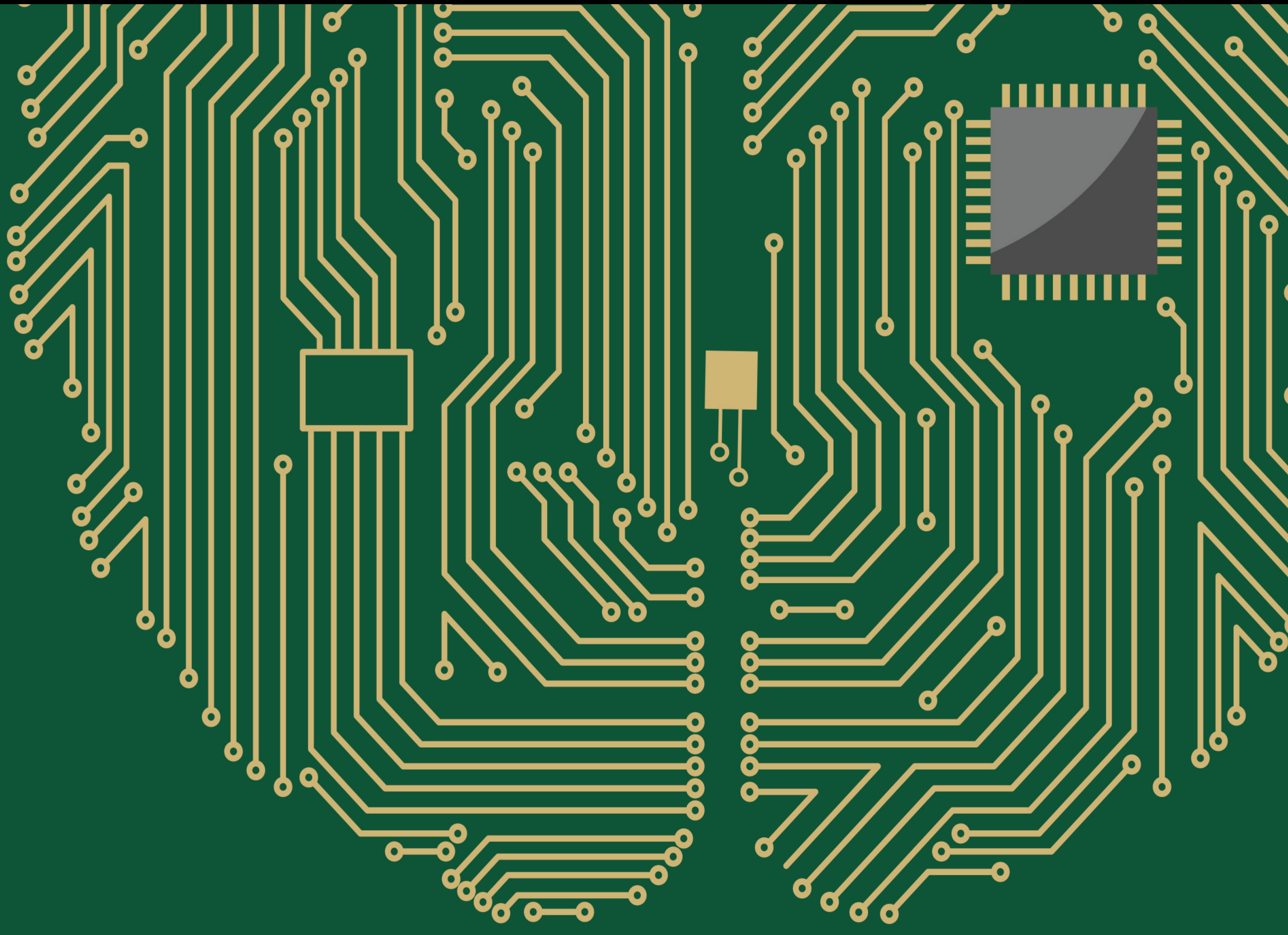

Advanced Computational Intelligence for Smart Healthcare and Human Health Using Few-Shot Learning

Advanced Computational Intelligence for Smart Healthcare and Human Health Using Few-Shot Learning

Lead Guest Editor: Xin Ning
Guest Editors: Guangming Zhang and Xiao Bai

Contents

Contents

Contents

Contents

Contents

Contents

Contents

Contents

Contents

Hindawi
Computational Intelligence and Neuroscience
Volume 2023, Article ID 9783816, 1 page
https://doi.org/10.1155/2023/9783816

Retraction

Retracted: Design of Teaching Quality Analysis and Management System for PE Courses Based on Data-Mining Algorithm

Computational Intelligence and Neuroscience

Received 26 September 2023; Accepted 26 September 2023; Published 27 September 2023

This article has been retracted by Hindawi following an investigation undertaken by the publisher [1]. This investigation has uncovered evidence of one or more of the following indicators of systematic manipulation of the publication process:

(1) Discrepancies in scope
(2) Discrepancies in the description of the research reported
(3) Discrepancies between the availability of data and the research described
(4) Inappropriate citations
(5) Incoherent, meaningless and/or irrelevant content included in the article
(6) Peer-review manipulation

The presence of these indicators undermines our confidence in the integrity of the article's content and we cannot, therefore, vouch for its reliability. Please note that this notice is intended solely to alert readers that the content of this article is unreliable. We have not investigated whether authors were aware of or involved in the systematic manipulation of the publication process.

Wiley and Hindawi regrets that the usual quality checks did not identify these issues before publication and have since put additional measures in place to safeguard research integrity.

We wish to credit our own Research Integrity and Research Publishing teams and anonymous and named external researchers and research integrity experts for contributing to this investigation.

The corresponding author, as the representative of all authors, has been given the opportunity to register their agreement or disagreement to this retraction. We have kept a record of any response received.

References

[1] S. Li and Y. Luo, "Design of Teaching Quality Analysis and Management System for PE Courses Based on Data-Mining Algorithm," *Computational Intelligence and Neuroscience*, vol. 2022, Article ID 6830375, 9 pages, 2022.

Hindawi
Computational Intelligence and Neuroscience
Volume 2023, Article ID 9767693, 1 page
https://doi.org/10.1155/2023/9767693

Retraction

Retracted: MOOC and Flipped Classroom Task-Based English Teaching Model for Colleges and Universities Using Data Mining and Few-Shot Learning Technology

Computational Intelligence and Neuroscience

Received 26 September 2023; Accepted 26 September 2023; Published 27 September 2023

This article has been retracted by Hindawi following an investigation undertaken by the publisher [1]. This investigation has uncovered evidence of one or more of the following indicators of systematic manipulation of the publication process:

(1) Discrepancies in scope
(2) Discrepancies in the description of the research reported
(3) Discrepancies between the availability of data and the research described
(4) Inappropriate citations
(5) Incoherent, meaningless and/or irrelevant content included in the article
(6) Peer-review manipulation

The presence of these indicators undermines our confidence in the integrity of the article's content and we cannot, therefore, vouch for its reliability. Please note that this notice is intended solely to alert readers that the content of this article is unreliable. We have not investigated whether authors were aware of or involved in the systematic manipulation of the publication process.

In addition, our investigation has also shown that one or more of the following human-subject reporting requirements has not been met in this article: ethical approval by an Institutional Review Board (IRB) committee or equivalent, patient/participant consent to participate, and/or agreement to publish patient/participant details (where relevant).

Wiley and Hindawi regrets that the usual quality checks did not identify these issues before publication and have since put additional measures in place to safeguard research integrity.

We wish to credit our own Research Integrity and Research Publishing teams and anonymous and named external researchers and research integrity experts for contributing to this investigation.

The corresponding author, as the representative of all authors, has been given the opportunity to register their agreement or disagreement to this retraction. We have kept a record of any response received.

References

[1] Y. Gong and J. Zhou, "MOOC and Flipped Classroom Task-Based English Teaching Model for Colleges and Universities Using Data Mining and Few-Shot Learning Technology," *Computational Intelligence and Neuroscience*, vol. 2022, Article ID 9770747, 11 pages, 2022.

Hindawi
Computational Intelligence and Neuroscience
Volume 2023, Article ID 9765386, 1 page
https://doi.org/10.1155/2023/9765386

Retraction

Retracted: Optimization of Vocal Singing Training Methods Using Intelligent Big Data Technology

Computational Intelligence and Neuroscience

Received 26 September 2023; Accepted 26 September 2023; Published 27 September 2023

This article has been retracted by Hindawi following an investigation undertaken by the publisher [1]. This investigation has uncovered evidence of one or more of the following indicators of systematic manipulation of the publication process:

(1) Discrepancies in scope
(2) Discrepancies in the description of the research reported
(3) Discrepancies between the availability of data and the research described
(4) Inappropriate citations
(5) Incoherent, meaningless and/or irrelevant content included in the article
(6) Peer-review manipulation

The presence of these indicators undermines our confidence in the integrity of the article's content and we cannot, therefore, vouch for its reliability. Please note that this notice is intended solely to alert readers that the content of this article is unreliable. We have not investigated whether authors were aware of or involved in the systematic manipulation of the publication process.

Wiley and Hindawi regrets that the usual quality checks did not identify these issues before publication and have since put additional measures in place to safeguard research integrity.

We wish to credit our own Research Integrity and Research Publishing teams and anonymous and named external researchers and research integrity experts for contributing to this investigation.

The corresponding author, as the representative of all authors, has been given the opportunity to register their agreement or disagreement to this retraction. We have kept a record of any response received.

References

[1] Y. Lin and K. Mao, "Optimization of Vocal Singing Training Methods Using Intelligent Big Data Technology," *Computational Intelligence and Neuroscience*, vol. 2022, Article ID 8589517, 9 pages, 2022.

Hindawi
Computational Intelligence and Neuroscience
Volume 2023, Article ID 9756573, 1 page
https://doi.org/10.1155/2023/9756573

Retraction

Retracted: Sports Video Athlete Detection Based on Associative Memory Neural Network

Computational Intelligence and Neuroscience

Received 26 September 2023; Accepted 26 September 2023; Published 27 September 2023

This article has been retracted by Hindawi following an investigation undertaken by the publisher [1]. This investigation has uncovered evidence of one or more of the following indicators of systematic manipulation of the publication process:

(1) Discrepancies in scope
(2) Discrepancies in the description of the research reported
(3) Discrepancies between the availability of data and the research described
(4) Inappropriate citations
(5) Incoherent, meaningless and/or irrelevant content included in the article
(6) Peer-review manipulation

The presence of these indicators undermines our confidence in the integrity of the article's content and we cannot, therefore, vouch for its reliability. Please note that this notice is intended solely to alert readers that the content of this article is unreliable. We have not investigated whether authors were aware of or involved in the systematic manipulation of the publication process.

Wiley and Hindawi regrets that the usual quality checks did not identify these issues before publication and have since put additional measures in place to safeguard research integrity.

We wish to credit our own Research Integrity and Research Publishing teams and anonymous and named external researchers and research integrity experts for contributing to this investigation.

The corresponding author, as the representative of all authors, has been given the opportunity to register their agreement or disagreement to this retraction. We have kept a record of any response received.

References

[1] J. Yang, "Sports Video Athlete Detection Based on Associative Memory Neural Network," *Computational Intelligence and Neuroscience*, vol. 2022, Article ID 6986831, 9 pages, 2022.

Hindawi
Computational Intelligence and Neuroscience
Volume 2023, Article ID 9839378, 1 page
https://doi.org/10.1155/2023/9839378

Retraction

Retracted: Application of Artificial Intelligence Computing in the Universal Design of Aging and Healthy Housing

Computational Intelligence and Neuroscience

Received 25 July 2023; Accepted 25 July 2023; Published 26 July 2023

This article has been retracted by Hindawi following an investigation undertaken by the publisher [1]. This investigation has uncovered evidence of one or more of the following indicators of systematic manipulation of the publication process:

(1) Discrepancies in scope
(2) Discrepancies in the description of the research reported
(3) Discrepancies between the availability of data and the research described
(4) Inappropriate citations
(5) Incoherent, meaningless and/or irrelevant content included in the article
(6) Peer-review manipulation

The presence of these indicators undermines our confidence in the integrity of the article's content and we cannot, therefore, vouch for its reliability. Please note that this notice is intended solely to alert readers that the content of this article is unreliable. We have not investigated whether authors were aware of or involved in the systematic manipulation of the publication process.

Wiley and Hindawi regrets that the usual quality checks did not identify these issues before publication and have since put additional measures in place to safeguard research integrity.

We wish to credit our own Research Integrity and Research Publishing teams and anonymous and named external researchers and research integrity experts for contributing to this investigation.

The corresponding author, as the representative of all authors, has been given the opportunity to register their agreement or disagreement to this retraction. We have kept a record of any response received.

References

[1] Q. Shu and H. Liu, “Application of Artificial Intelligence Computing in the Universal Design of Aging and Healthy Housing,” *Computational Intelligence and Neuroscience*, vol. 2022, Article ID 4576397, 7 pages, 2022.

Hindawi
Computational Intelligence and Neuroscience
Volume 2023, Article ID 9816273, 1 page
https://doi.org/10.1155/2023/9816273

Retraction

Retracted: The Management of Educational Talents in Vocational Colleges Based on Wireless Network in the Artificial Intelligence Era

Computational Intelligence and Neuroscience

Received 25 July 2023; Accepted 25 July 2023; Published 26 July 2023

This article has been retracted by Hindawi following an investigation undertaken by the publisher [1]. This investigation has uncovered evidence of one or more of the following indicators of systematic manipulation of the publication process:

(1) Discrepancies in scope
(2) Discrepancies in the description of the research reported
(3) Discrepancies between the availability of data and the research described
(4) Inappropriate citations
(5) Incoherent, meaningless and/or irrelevant content included in the article
(6) Peer-review manipulation

The presence of these indicators undermines our confidence in the integrity of the article's content and we cannot, therefore, vouch for its reliability. Please note that this notice is intended solely to alert readers that the content of this article is unreliable. We have not investigated whether authors were aware of or involved in the systematic manipulation of the publication process.

Wiley and Hindawi regrets that the usual quality checks did not identify these issues before publication and have since put additional measures in place to safeguard research integrity.

We wish to credit our own Research Integrity and Research Publishing teams and anonymous and named external researchers and research integrity experts for contributing to this investigation.

The corresponding author, as the representative of all authors, has been given the opportunity to register their agreement or disagreement to this retraction. We have kept a record of any response received.

References

[1] Y. Zhang and C. Wang, "The Management of Educational Talents in Vocational Colleges Based on Wireless Network in the Artificial Intelligence Era," *Computational Intelligence and Neuroscience*, vol. 2022, Article ID 2298139, 10 pages, 2022.

Hindawi
Computational Intelligence and Neuroscience
Volume 2023, Article ID 9816045, 1 page
https://doi.org/10.1155/2023/9816045

Retraction

Retracted: Evolutionary Analysis of Supply Chain Integration Strategy on Chinese Steel-Producing Firms considering Policy Risk Cost Factor

Computational Intelligence and Neuroscience

Received 25 July 2023; Accepted 25 July 2023; Published 26 July 2023

This article has been retracted by Hindawi following an investigation undertaken by the publisher [1]. This investigation has uncovered evidence of one or more of the following indicators of systematic manipulation of the publication process:

(1) Discrepancies in scope
(2) Discrepancies in the description of the research reported
(3) Discrepancies between the availability of data and the research described
(4) Inappropriate citations
(5) Incoherent, meaningless and/or irrelevant content included in the article
(6) Peer-review manipulation

The presence of these indicators undermines our confidence in the integrity of the article's content and we cannot, therefore, vouch for its reliability. Please note that this notice is intended solely to alert readers that the content of this article is unreliable. We have not investigated whether authors were aware of or involved in the systematic manipulation of the publication process.

Wiley and Hindawi regrets that the usual quality checks did not identify these issues before publication and have since put additional measures in place to safeguard research integrity.

We wish to credit our own Research Integrity and Research Publishing teams and anonymous and named external researchers and research integrity experts for contributing to this investigation.

The corresponding author, as the representative of all authors, has been given the opportunity to register their agreement or disagreement to this retraction. We have kept a record of any response received.

References

[1] L. Zhu, R. Zhou, X. Li, and J. Chen, "Evolutionary Analysis of Supply Chain Integration Strategy on Chinese Steel-Producing Firms considering Policy Risk Cost Factor," *Computational Intelligence and Neuroscience*, vol. 2022, Article ID 1136601, 11 pages, 2022.

Hindawi
Computational Intelligence and Neuroscience
Volume 2023, Article ID 9805282, 1 page
https://doi.org/10.1155/2023/9805282

Retraction

Retracted: Study of Trunk Morphological Imbalance and Rehabilitation Outcome of Adolescent Idiopathic Scoliosis with Intelligent Medicine

Computational Intelligence and Neuroscience

Received 25 July 2023; Accepted 25 July 2023; Published 26 July 2023

This article has been retracted by Hindawi following an investigation undertaken by the publisher [1]. This investigation has uncovered evidence of one or more of the following indicators of systematic manipulation of the publication process:

(1) Discrepancies in scope
(2) Discrepancies in the description of the research reported
(3) Discrepancies between the availability of data and the research described
(4) Inappropriate citations
(5) Incoherent, meaningless and/or irrelevant content included in the article
(6) Peer-review manipulation

The presence of these indicators undermines our confidence in the integrity of the article's content and we cannot, therefore, vouch for its reliability. Please note that this notice is intended solely to alert readers that the content of this article is unreliable. We have not investigated whether authors were aware of or involved in the systematic manipulation of the publication process.

In addition, our investigation has also shown that one or more of the following human-subject reporting requirements has not been met in this article: ethical approval by an Institutional Review Board (IRB) committee or equivalent, patient/participant consent to participate, and/or agreement to publish patient/participant details (where relevant).

Wiley and Hindawi regrets that the usual quality checks did not identify these issues before publication and have since put additional measures in place to safeguard research integrity.

We wish to credit our own Research Integrity and Research Publishing teams and anonymous and named external researchers and research integrity experts for contributing to this investigation.

The corresponding author, as the representative of all authors, has been given the opportunity to register their agreement or disagreement to this retraction. We have kept a record of any response received.

References

[1] Q. Zhao, Y. Huang, M. Wu et al., "Study of Trunk Morphological Imbalance and Rehabilitation Outcome of Adolescent Idiopathic Scoliosis with Intelligent Medicine," *Computational Intelligence and Neuroscience*, vol. 2022, Article ID 6775674, 8 pages, 2022.

Hindawi
Computational Intelligence and Neuroscience
Volume 2023, Article ID 9804502, 1 page
https://doi.org/10.1155/2023/9804502

Retraction

Retracted: Influencing Factors and Improvement Path of Synergistic Value Creation Efficiency of Emerging Enterprises

Computational Intelligence and Neuroscience

Received 25 July 2023; Accepted 25 July 2023; Published 26 July 2023

This article has been retracted by Hindawi following an investigation undertaken by the publisher [1]. This investigation has uncovered evidence of one or more of the following indicators of systematic manipulation of the publication process:

(1) Discrepancies in scope
(2) Discrepancies in the description of the research reported
(3) Discrepancies between the availability of data and the research described
(4) Inappropriate citations
(5) Incoherent, meaningless and/or irrelevant content included in the article
(6) Peer-review manipulation

The presence of these indicators undermines our confidence in the integrity of the article's content and we cannot, therefore, vouch for its reliability. Please note that this notice is intended solely to alert readers that the content of this article is unreliable. We have not investigated whether authors were aware of or involved in the systematic manipulation of the publication process.

Wiley and Hindawi regrets that the usual quality checks did not identify these issues before publication and have since put additional measures in place to safeguard research integrity.

We wish to credit our own Research Integrity and Research Publishing teams and anonymous and named external researchers and research integrity experts for contributing to this investigation.

The corresponding author, as the representative of all authors, has been given the opportunity to register their agreement or disagreement to this retraction. We have kept a record of any response received.

References

[1] M. Liu, G. Wang, and H. Huang, "Influencing Factors and Improvement Path of Synergistic Value Creation Efficiency of Emerging Enterprises," *Computational Intelligence and Neuroscience*, vol. 2022, Article ID 8075349, 10 pages, 2022.

Hindawi
Computational Intelligence and Neuroscience
Volume 2023, Article ID 9803532, 1 page
https://doi.org/10.1155/2023/9803532

Retraction

Retracted: Probabilistic Statistics-Based Endurance Life Prediction of Bridge Structures

Computational Intelligence and Neuroscience

Received 25 July 2023; Accepted 25 July 2023; Published 26 July 2023

This article has been retracted by Hindawi following an investigation undertaken by the publisher [1]. This investigation has uncovered evidence of one or more of the following indicators of systematic manipulation of the publication process:

(1) Discrepancies in scope
(2) Discrepancies in the description of the research reported
(3) Discrepancies between the availability of data and the research described
(4) Inappropriate citations
(5) Incoherent, meaningless and/or irrelevant content included in the article
(6) Peer-review manipulation

The presence of these indicators undermines our confidence in the integrity of the article's content and we cannot, therefore, vouch for its reliability. Please note that this notice is intended solely to alert readers that the content of this article is unreliable. We have not investigated whether authors were aware of or involved in the systematic manipulation of the publication process.

Wiley and Hindawi regrets that the usual quality checks did not identify these issues before publication and have since put additional measures in place to safeguard research integrity.

We wish to credit our own Research Integrity and Research Publishing teams and anonymous and named external researchers and research integrity experts for contributing to this investigation.

The corresponding author, as the representative of all authors, has been given the opportunity to register their agreement or disagreement to this retraction. We have kept a record of any response received.

References

[1] Y. Zhang, "Probabilistic Statistics-Based Endurance Life Prediction of Bridge Structures," *Computational Intelligence and Neuroscience*, vol. 2022, Article ID 8035028, 12 pages, 2022.

Hindawi
Computational Intelligence and Neuroscience
Volume 2023, Article ID 9791745, 1 page
https://doi.org/10.1155/2023/9791745

Retraction

Retracted: Image Recognition of Sports Athletes' High-Intensity Sports Injuries Based on Binocular Stereo Vision

Computational Intelligence and Neuroscience

Received 25 July 2023; Accepted 25 July 2023; Published 26 July 2023

This article has been retracted by Hindawi following an investigation undertaken by the publisher [1]. This investigation has uncovered evidence of one or more of the following indicators of systematic manipulation of the publication process:

(1) Discrepancies in scope
(2) Discrepancies in the description of the research reported
(3) Discrepancies between the availability of data and the research described
(4) Inappropriate citations
(5) Incoherent, meaningless and/or irrelevant content included in the article
(6) Peer-review manipulation

The presence of these indicators undermines our confidence in the integrity of the article's content and we cannot, therefore, vouch for its reliability. Please note that this notice is intended solely to alert readers that the content of this article is unreliable. We have not investigated whether authors were aware of or involved in the systematic manipulation of the publication process.

Wiley and Hindawi regrets that the usual quality checks did not identify these issues before publication and have since put additional measures in place to safeguard research integrity.

We wish to credit our own Research Integrity and Research Publishing teams and anonymous and named external researchers and research integrity experts for contributing to this investigation.

The corresponding author, as the representative of all authors, has been given the opportunity to register their agreement or disagreement to this retraction. We have kept a record of any response received.

References

[1] D. Chen, "Image Recognition of Sports Athletes' High-Intensity Sports Injuries Based on Binocular Stereo Vision," *Computational Intelligence and Neuroscience*, vol. 2022, Article ID 4322597, 10 pages, 2022.

Hindawi
Computational Intelligence and Neuroscience
Volume 2023, Article ID 9783759, 1 page
https://doi.org/10.1155/2023/9783759

Retraction

Retracted: An Entity Relationship Extraction Model Based on BERT-BLSTM-CRF for Food Safety Domain

Computational Intelligence and Neuroscience

Received 25 July 2023; Accepted 25 July 2023; Published 26 July 2023

This article has been retracted by Hindawi following an investigation undertaken by the publisher [1]. This investigation has uncovered evidence of one or more of the following indicators of systematic manipulation of the publication process:

(1) Discrepancies in scope
(2) Discrepancies in the description of the research reported
(3) Discrepancies between the availability of data and the research described
(4) Inappropriate citations
(5) Incoherent, meaningless and/or irrelevant content included in the article
(6) Peer-review manipulation

The presence of these indicators undermines our confidence in the integrity of the article's content and we cannot, therefore, vouch for its reliability. Please note that this notice is intended solely to alert readers that the content of this article is unreliable. We have not investigated whether authors were aware of or involved in the systematic manipulation of the publication process.

Wiley and Hindawi regrets that the usual quality checks did not identify these issues before publication and have since put additional measures in place to safeguard research integrity.

We wish to credit our own Research Integrity and Research Publishing teams and anonymous and named external researchers and research integrity experts for contributing to this investigation.

The corresponding author, as the representative of all authors, has been given the opportunity to register their agreement or disagreement to this retraction. We have kept a record of any response received.

References

[1] Q. Zhang, M. Li, W. Dong et al., "An Entity Relationship Extraction Model Based on BERT-BLSTM-CRF for Food Safety Domain," *Computational Intelligence and Neuroscience*, vol. 2022, Article ID 7773259, 13 pages, 2022.

Hindawi
Computational Intelligence and Neuroscience
Volume 2023, Article ID 9781472, 1 page
https://doi.org/10.1155/2023/9781472

Retraction

Retracted: Comprehensive Health Evaluation Model of Art Psychotherapy Using Genetic Algorithm

Computational Intelligence and Neuroscience

Received 25 July 2023; Accepted 25 July 2023; Published 26 July 2023

This article has been retracted by Hindawi following an investigation undertaken by the publisher [1]. This investigation has uncovered evidence of one or more of the following indicators of systematic manipulation of the publication process:

(1) Discrepancies in scope
(2) Discrepancies in the description of the research reported
(3) Discrepancies between the availability of data and the research described
(4) Inappropriate citations
(5) Incoherent, meaningless and/or irrelevant content included in the article
(6) Peer-review manipulation

The presence of these indicators undermines our confidence in the integrity of the article's content and we cannot, therefore, vouch for its reliability. Please note that this notice is intended solely to alert readers that the content of this article is unreliable. We have not investigated whether authors were aware of or involved in the systematic manipulation of the publication process.

Wiley and Hindawi regrets that the usual quality checks did not identify these issues before publication and have since put additional measures in place to safeguard research integrity.

We wish to credit our own Research Integrity and Research Publishing teams and anonymous and named external researchers and research integrity experts for contributing to this investigation.

The corresponding author, as the representative of all authors, has been given the opportunity to register their agreement or disagreement to this retraction. We have kept a record of any response received.

References

[1] F. Zhang and X. Liu, "Comprehensive Health Evaluation Model of Art Psychotherapy Using Genetic Algorithm," *Computational Intelligence and Neuroscience*, vol. 2022, Article ID 5718050, 11 pages, 2022.

Hindawi
Computational Intelligence and Neuroscience
Volume 2023, Article ID 9890364, 1 page
https://doi.org/10.1155/2023/9890364

Retraction

Retracted: A New Generation of ResNet Model Based on Artificial Intelligence and Few Data Driven and Its Construction in Image Recognition Model

Computational Intelligence and Neuroscience

Received 25 July 2023; Accepted 25 July 2023; Published 26 July 2023

This article has been retracted by Hindawi following an investigation undertaken by the publisher [1]. This investigation has uncovered evidence of one or more of the following indicators of systematic manipulation of the publication process:

(1) Discrepancies in scope
(2) Discrepancies in the description of the research reported
(3) Discrepancies between the availability of data and the research described
(4) Inappropriate citations
(5) Incoherent, meaningless and/or irrelevant content included in the article
(6) Peer-review manipulation

The presence of these indicators undermines our confidence in the integrity of the article's content and we cannot, therefore, vouch for its reliability. Please note that this notice is intended solely to alert readers that the content of this article is unreliable. We have not investigated whether authors were aware of or involved in the systematic manipulation of the publication process.

Wiley and Hindawi regrets that the usual quality checks did not identify these issues before publication and have since put additional measures in place to safeguard research integrity.

We wish to credit our own Research Integrity and Research Publishing teams and anonymous and named external researchers and research integrity experts for contributing to this investigation.

The corresponding author, as the representative of all authors, has been given the opportunity to register their agreement or disagreement to this retraction. We have kept a record of any response received.

References

[1] H. Wang, K. Li, and C. Xu, "A New Generation of ResNet Model Based on Artificial Intelligence and Few Data Driven and Its Construction in Image Recognition Model," *Computational Intelligence and Neuroscience*, vol. 2022, Article ID 5976155, 10 pages, 2022.

Hindawi
Computational Intelligence and Neuroscience
Volume 2023, Article ID 9872618, 1 page
https://doi.org/10.1155/2023/9872618

Retraction

Retracted: Blockchain-Based Information Supervision Model for Rice Supply Chains

Computational Intelligence and Neuroscience

Received 25 July 2023; Accepted 25 July 2023; Published 26 July 2023

This article has been retracted by Hindawi following an investigation undertaken by the publisher [1]. This investigation has uncovered evidence of one or more of the following indicators of systematic manipulation of the publication process:

(1) Discrepancies in scope
(2) Discrepancies in the description of the research reported
(3) Discrepancies between the availability of data and the research described
(4) Inappropriate citations
(5) Incoherent, meaningless and/or irrelevant content included in the article
(6) Peer-review manipulation

The presence of these indicators undermines our confidence in the integrity of the article's content and we cannot, therefore, vouch for its reliability. Please note that this notice is intended solely to alert readers that the content of this article is unreliable. We have not investigated whether authors were aware of or involved in the systematic manipulation of the publication process.

Wiley and Hindawi regrets that the usual quality checks did not identify these issues before publication and have since put additional measures in place to safeguard research integrity.

We wish to credit our own Research Integrity and Research Publishing teams and anonymous and named external researchers and research integrity experts for contributing to this investigation.

The corresponding author, as the representative of all authors, has been given the opportunity to register their agreement or disagreement to this retraction. We have kept a record of any response received.

References

[1] J. Wang, X. Zhang, J. Xu et al., "Blockchain-Based Information Supervision Model for Rice Supply Chains," *Computational Intelligence and Neuroscience*, vol. 2022, Article ID 2914571, 17 pages, 2022.

Hindawi
Computational Intelligence and Neuroscience
Volume 2023, Article ID 9871807, 1 page
https://doi.org/10.1155/2023/9871807

Retraction

Retracted: Study on the Global Stability for a Generalized SEIR Epidemic Model

Computational Intelligence and Neuroscience

Received 25 July 2023; Accepted 25 July 2023; Published 26 July 2023

This article has been retracted by Hindawi following an investigation undertaken by the publisher [1]. This investigation has uncovered evidence of one or more of the following indicators of systematic manipulation of the publication process:

(1) Discrepancies in scope
(2) Discrepancies in the description of the research reported
(3) Discrepancies between the availability of data and the research described
(4) Inappropriate citations
(5) Incoherent, meaningless and/or irrelevant content included in the article
(6) Peer-review manipulation

The presence of these indicators undermines our confidence in the integrity of the article's content and we cannot, therefore, vouch for its reliability. Please note that this notice is intended solely to alert readers that the content of this article is unreliable. We have not investigated whether authors were aware of or involved in the systematic manipulation of the publication process.

Wiley and Hindawi regrets that the usual quality checks did not identify these issues before publication and have since put additional measures in place to safeguard research integrity.

We wish to credit our own Research Integrity and Research Publishing teams and anonymous and named external researchers and research integrity experts for contributing to this investigation.

The corresponding author, as the representative of all authors, has been given the opportunity to register their agreement or disagreement to this retraction. We have kept a record of any response received.

References

[1] C. Xue, "Study on the Global Stability for a Generalized SEIR Epidemic Model," *Computational Intelligence and Neuroscience*, vol. 2022, Article ID 8215214, 6 pages, 2022.

Hindawi
Computational Intelligence and Neuroscience
Volume 2023, Article ID 9870280, 1 page
https://doi.org/10.1155/2023/9870280

Retraction

Retracted: Online and Offline Interaction Model of International Chinese Education Based on Few-Shot Learning

Computational Intelligence and Neuroscience

Received 25 July 2023; Accepted 25 July 2023; Published 26 July 2023

This article has been retracted by Hindawi following an investigation undertaken by the publisher [1]. This investigation has uncovered evidence of one or more of the following indicators of systematic manipulation of the publication process:

(1) Discrepancies in scope
(2) Discrepancies in the description of the research reported
(3) Discrepancies between the availability of data and the research described
(4) Inappropriate citations
(5) Incoherent, meaningless and/or irrelevant content included in the article
(6) Peer-review manipulation

The presence of these indicators undermines our confidence in the integrity of the article's content and we cannot, therefore, vouch for its reliability. Please note that this notice is intended solely to alert readers that the content of this article is unreliable. We have not investigated whether authors were aware of or involved in the systematic manipulation of the publication process.

Wiley and Hindawi regrets that the usual quality checks did not identify these issues before publication and have since put additional measures in place to safeguard research integrity.

We wish to credit our own Research Integrity and Research Publishing teams and anonymous and named external researchers and research integrity experts for contributing to this investigation.

The corresponding author, as the representative of all authors, has been given the opportunity to register their agreement or disagreement to this retraction. We have kept a record of any response received.

References

[1] F. Cao and J. Cai, "Online and Offline Interaction Model of International Chinese Education Based on Few-Shot Learning," *Computational Intelligence and Neuroscience*, vol. 2022, Article ID 8281670, 11 pages, 2022.

Hindawi
Computational Intelligence and Neuroscience
Volume 2023, Article ID 9865718, 1 page
https://doi.org/10.1155/2023/9865718

Retraction

Retracted: Personalized Teaching Strategy of University Ideology Course Based on Lagrange Neural Network and Big Data Technology

Computational Intelligence and Neuroscience

Received 25 July 2023; Accepted 25 July 2023; Published 26 July 2023

This article has been retracted by Hindawi following an investigation undertaken by the publisher [1]. This investigation has uncovered evidence of one or more of the following indicators of systematic manipulation of the publication process:

(1) Discrepancies in scope
(2) Discrepancies in the description of the research reported
(3) Discrepancies between the availability of data and the research described
(4) Inappropriate citations
(5) Incoherent, meaningless and/or irrelevant content included in the article
(6) Peer-review manipulation

The presence of these indicators undermines our confidence in the integrity of the article's content and we cannot, therefore, vouch for its reliability. Please note that this notice is intended solely to alert readers that the content of this article is unreliable. We have not investigated whether authors were aware of or involved in the systematic manipulation of the publication process.

Wiley and Hindawi regrets that the usual quality checks did not identify these issues before publication and have since put additional measures in place to safeguard research integrity.

We wish to credit our own Research Integrity and Research Publishing teams and anonymous and named external researchers and research integrity experts for contributing to this investigation.

The corresponding author, as the representative of all authors, has been given the opportunity to register their agreement or disagreement to this retraction. We have kept a record of any response received.

References

[1] J. Zuo, F. Zhou, and Y. Liang, "Personalized Teaching Strategy of University Ideology Course Based on Lagrange Neural Network and Big Data Technology," *Computational Intelligence and Neuroscience*, vol. 2022, Article ID 1251839, 8 pages, 2022.

Hindawi
Computational Intelligence and Neuroscience
Volume 2023, Article ID 9843760, 1 page
https://doi.org/10.1155/2023/9843760

Retraction

Retracted: Decision-Making Application of the Cloud-Fog Hybrid Model Based on the Improved Convolutional Neural Network in Financial Services in Smart Medical Care

Computational Intelligence and Neuroscience

Received 25 July 2023; Accepted 25 July 2023; Published 26 July 2023

This article has been retracted by Hindawi following an investigation undertaken by the publisher [1]. This investigation has uncovered evidence of one or more of the following indicators of systematic manipulation of the publication process:

(1) Discrepancies in scope
(2) Discrepancies in the description of the research reported
(3) Discrepancies between the availability of data and the research described
(4) Inappropriate citations
(5) Incoherent, meaningless and/or irrelevant content included in the article
(6) Peer-review manipulation

The presence of these indicators undermines our confidence in the integrity of the article's content and we cannot, therefore, vouch for its reliability. Please note that this notice is intended solely to alert readers that the content of this article is unreliable. We have not investigated whether authors were aware of or involved in the systematic manipulation of the publication process.

Wiley and Hindawi regrets that the usual quality checks did not identify these issues before publication and have since put additional measures in place to safeguard research integrity.

We wish to credit our own Research Integrity and Research Publishing teams and anonymous and named external researchers and research integrity experts for contributing to this investigation.

The corresponding author, as the representative of all authors, has been given the opportunity to register their agreement or disagreement to this retraction. We have kept a record of any response received.

References

[1] S. Lu, "Decision-Making Application of the Cloud-Fog Hybrid Model Based on the Improved Convolutional Neural Network in Financial Services in Smart Medical Care," *Computational Intelligence and Neuroscience*, vol. 2022, Article ID 5732379, 8 pages, 2022.

Hindawi
Computational Intelligence and Neuroscience
Volume 2023, Article ID 4208231, 26 pages
https://doi.org/10.1155/2023/4208231

Review Article

An Overview of Deep Learning Methods for Left Ventricle Segmentation

Muhammad Ali Shoaib[1,2] **Joon Huang Chuah**[1] **Raza Ali**[1,2] **Khairunnisa Hasikin**[3] **Azira Khalil**[4] **Yan Chai Hum**[5] **Yee Kai Tee**[5] **Samiappan Dhanalakshmi**[6] **and Khin Wee Lai**[1]

[1]*Department of Electrical Engineering, Faculty of Engineering, Universiti Malaya, Kuala Lumpur, Malaysia*
[2]*Faculty of Information and Communication Technology, BUITEMS, Quetta, Pakistan*
[3]*Department of Biomedical Engineering, Faculty of Engineering, Universiti Malaya, Kuala Lumpur, Malaysia*
[4]*Faculty of Science & Technology, Universiti Sains Islam Malaysia, Nilai 71800, Malaysia*
[5]*Department of Mechatronics and Biomedical Engineering, Lee Kong Chian Faculty of Engineering and Science, Universiti Tunku Abdul Rahman, Malaysia*
[6]*Department of Electronics and Communication Engineering, SRM Institute of Science and Technology, Kattankulathur, India*

Correspondence should be addressed to Azira Khalil; azira@usim.edu.my, Samiappan Dhanalakshmi; dhanalas@srmist.edu.in, and Khin Wee Lai; lai.khinwee@um.edu.my

Received 22 April 2022; Revised 25 October 2022; Accepted 24 November 2022; Published 30 January 2023

Academic Editor: Xin Ning

Cardiac health diseases are one of the key causes of death around the globe. The number of heart patients has considerably increased during the pandemic. Therefore, it is crucial to assess and analyze the medical and cardiac images. Deep learning architectures, specifically convolutional neural networks have profoundly become the primary choice for the assessment of cardiac medical images. The left ventricle is a vital part of the cardiovascular system where the boundary and size perform a significant role in the evaluation of cardiac function. Due to automatic segmentation and good promising results, the left ventricle segmentation using deep learning has attracted a lot of attention. This article presents a critical review of deep learning methods used for the left ventricle segmentation from frequently used imaging modalities including magnetic resonance images, ultrasound, and computer tomography. This study also demonstrates the details of the network architecture, software, and hardware used for training along with publicly available cardiac image datasets and self-prepared dataset details incorporated. The summary of the evaluation matrices with results used by different researchers is also presented in this study. Finally, all this information is summarized and comprehended in order to assist the readers to understand the motivation and methodology of various deep learning models, as well as exploring potential solutions to future challenges in LV segmentation.

1. Introduction

The capability of a machine to simulate and impersonate human intelligence processes is referred to as artificial intelligence. Machine learning is a subbranch of artificial intelligence which is based on the idea to enable machines or computers to perform without being specifically programmed. The machine can learn from data and focus on the use of the pattern and experience to improve the performance of the computer in making decisions on its own. In this way, the machine becomes capable of developing analytical models to adopt new situations autonomously.

Deep learning (DL) is a subfield of machine learning associated with a process inspired by the formation and function of the brain called an artificial neural network (ANN). DL is concerned with the interpretation of data based on the mechanism of the human brain by developing and simulating the algorithm worked on human brain analysis and learning. The training data are fed into the algorithm as input, and the successive layers of the DL algorithm analyse the original data to extract the features required for the targeted task. The training data is fed into the algorithm as input, and the successive layers of the DL algorithm analyse the original data to extract the features required for the targeted task. The entire process is free of human manipulation. One of the earliest practiced DL techniques is ANN with a deep network structure [1]. The multilayer perceptron models [2] have been proposed with the rapid progress in the research areas of computer vision (CV) and human brain neurons. This yields the development of other classical models such as back-propagation neural network models, convolutional neural network (CNN) models [3], bidirectional recurrent neural networks [4], transformers [5], long short-term memory (LSTM) [6], and deep belief network [7] models.

These research findings have significantly helped the expansion of DL architectures, flooring the way for its substantial level applications in numerous areas, especially in image processing. Image classification, image registration, object detection, and image segmentation were among the main tasks performed by the DL algorithms very efficiently.

These image processing methods were applied in various fields such as surveillance [8, 9], intelligent transportation system [10, 11], wireless communication [12, 13], web mining [14, 15], robotics [16, 17], civil [18], and the most important in medical image processing [19]. In medical, DL is used for the segmentation of various structures from the medical images [20], detection of different diseases [21–23], and also for image registration to have a better view of images [24].

The cardiac images are one of the medical images used for the assessment of patient health. Different cardiac images are used for the analysis of cardiac function. Assessment of cardiac function performs an essential part in medical cardiology for patient supervision, risk estimation, disease analysis, and therapy evaluation [25, 26]. For cardiac diagnosis, digital images are the basic tool used for the computation of subsequent clinical indices from the shape and structure of the heart. From the structure of the heart, the assessment of the left ventricle (LV), right ventricle (RV), and myocardium (MYO) are the main assessments. LV is one of the central issues and the attention of cardiac function study and disease diagnosis. Delineation of LV boundary is of great clinical importance for the study of heart parameters such as the ejection fraction (EF), stroke volume (SV), LV mass (LVM), end-systolic volume (ESV), and end-diastolic volume (EDV) [27].

Some studies have reviewed the segmentation of medical and cardiac images. However, to the best of the author's knowledge, those investigations did not investigate LV segmentation solely and explicitly. Keeping in mind the importance of LV, the primary focus of this research is to review only the segmentation of LV using DL models. This paper provides a comprehensive overview of different DL architectures used for the LV segmentation. This review has been carefully summarized to present the state-of-the-art DL algorithms focusing on the LV segmentation task. To find out the quality research in the area, the Web of Science database was used as a search engine. The keywords, "left ventricle", "segmentation, and "deep learning" were used to find out the related papers. The articles which primarily do not emphasize LV segmentation were excluded because the scope of this review included an analysis of LV based segmentation. The review has been conducted using resources published between 2018 and onwards until December 2021.

In this article first, we discussed the three different imaging modalities used for the LV assessment in Section 2. Section 3 presents the basics concepts related to DL and CNN. Different DL architectures used for the LV segmentation are reviewed in Section 4. The section is subdivided based on the different approaches used with DL such as preprocessing, deformable models, and clinical indices calculation. The discussion about the architecture, hardware, software, and datasets used for training, and evaluation matrices used to analyze the performance of models is presented in Section 5. The complete structure of the article is depicted in Figure 1.

2. Medical Images for LV Assessment

Different medical imaging modalities were used for the assessment of LV. These modalities include magnetic resonance images (MRI), echocardiography, computer tomography (CT) scan, myocardial perfusion imaging, multiple gated acquisition scanning, gated blood-pool SPECT, and fusion imaging. However, the most used imaging modalities in literature for LV segmentation are MRI, US, and CT scans. The detail of these images is presented in this section.

2.1. Magnetic Resonance Images. MR imaging is a widely used technique in the cardiac armamentarium. The official name is recognized as "cardiovascular magnetic resonance (CMR)," when the MRI is employed on the heart or cardiovascular system. Its diagnostic precision has preceded it to become the gold-standard for heart analysis [28].

MRI is suitable for the evaluation of heart chambers [29, 30], size, and blood flow through major vessels [31], heart valves [32], and pericardium [33]. In addition, for LV size and mass measurement, the MRI is considered a reference standard [34, 35]. Its adaptability is incomparable to other different imaging methods. It provides not only precise anatomic information but also gives functional information that helps in finding patients at risk. Three-dimensional geometric analysis of the LV by CMR provided more appropriate information about the shape of the LV than the traditional echocardiography with high fertility and low variability [36]. CMR has also been successful in observing LV hypertrophy in patients with apparently normal echocardiographic results [37].

Besides these outstanding outcomes, a few important limitations of CMR need to be remembered. It faces problems with costs, limited availability, and lack of portability. These constraints prevent the use of CMR normally. Compared with other imaging modalities, CMR inspections

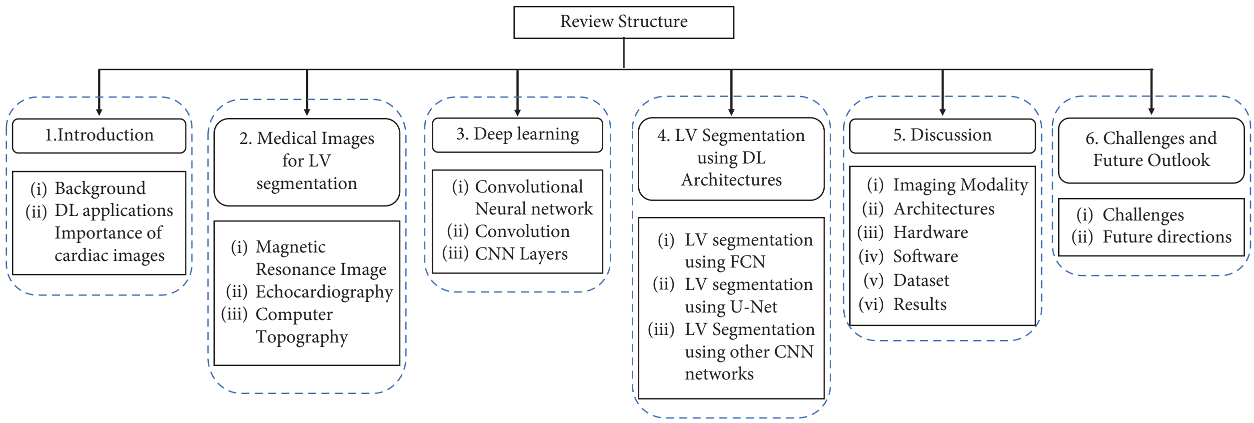

Figure 1: Article structure diagram.

are very costly and inadvisable for patients with metallic implants such as graft stents and cardiac pacemaker devices. Cardiac MRI may not be accessible immediately in all centers, and it can be a difficult instrument to work out in patients who require serial monitoring. Another condemnation of CMR is the period of examination to acquire LVM data. It also has some minor issues such as device incompatibilities and patient tolerance. Figure 2 shows LV segmentation in MRI images. The red area is LV segmented using a CNN. [38].

2.2. Echocardiography. Echocardiography used high-frequency ultrasound waves to produce anatomical images of the heart. That is why it is referred to as ultrasound (US) imaging. It is the largely used imaging modality for the examination of cardiovascular diseases [39]. Due to its easy accessibility, outstanding temporal resolution, real-time imaging, and noninvasive nature, the US is considered the basic imaging for measuring the LV function. US has become the primary preference for the analysis of LVM. A regular LVM calculation is an essential part of the US examination [40]. US imaging is also used in measuring the decrease in LVM after the treatment [41].

The most used US imaging is two-dimensional US (2DE) and three-dimensional US (3DE). An example of 2DE is shown in Figure 3 and the LV boundary is shown by the red line. Although M-mode US imaging is also in use, due to different limiting factors of M-mode such as it only identifies the function of the basal segment while 2D and 3D can perform the whole LV segmentation, the use of M-mode is very limited. Using the 2DE, LVM can directly be calculated. Similarly, by attaining the pyramidal image, we can look at the 3-dimensional image of the whole heart. The 3D imagining of heart anatomy can be obtained using 3DE and it has also overcome the limitation of 2D imagining. Therefore, 3DE has gained considerable importance over 2DE and M-mode in various patient populations [42]. Inadequately, 3DE is not commonly available and costly compared to 2D imagining. The other limitation of the US imaging is the speckle noise [43] and low contrast ratio [44], which limits its performance.

2.3. Computer Topography. A computed tomography (CT) scan of the heart provides a cross section of the structure of the heart. It characterizes the X-ray attenuation features of tissues being imaged [45, 46]. CT is a growing imaging method for the noninvasive computation of heart anatomy and function. LV size and mass estimation can be computed using the CT modality. CT is also found as a good alternative for the LV size and mass calculation for those patients who have contraindications to CMR [42]. The study in [47] compares CT and US and also finds that CT can be used as an alternative to the US.

Though CT has many advantages, a few constraints are not ignorable. CT cannot be employed as real-time intraprocedural assistance due to unavoidable ionization radiation exposure called a stochastic effect [48]. Repetitive regular use can raise the cancer risk. The increase in image quality results in a higher dose of radiation. The left part of Figure 4 is a CT scan of the heart and in the right part, the LV is highlighted. [49].

3. Deep Learning

DL can be defined as a machine learning algorithm that deals with neural networks. Neural networks with a deep structure or with more than 2 hidden layers are also referred as deep neural networks. A general architecture of DL is shown in Figure 4. DL is a representation learning (subtype of machine learning) with multiple levels of representation [50]. For the past several years, DL has been developed as a popular tool that attracts the attention of researchers from several fields. It helps to overcome the weaknesses of traditional methods and solve complex problems to achieve better results. The popularity of DL is doable due to large datasets, computational performance, training techniques (ReLu), and advanced networks (CNN). With the increase in databases, DL has exponentially achieved success both in commercial and academia. Not only the software base advancement help DL to achieve success, the latest hardware such as graphical processing units (GPU's) improved the ability of DL [51]. Deeper layers improve the system's experience by learning the features from data and making complex structures deeper and simple [52]. Therefore, it is a

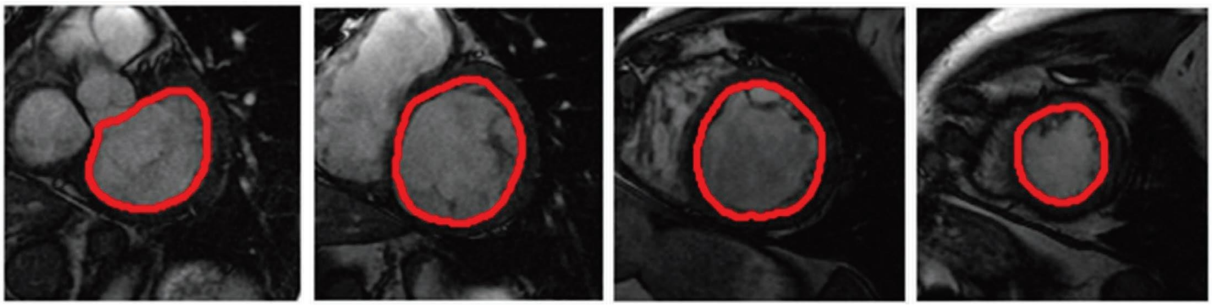

Figure 2: Four examples of LV boundary in CMR images.

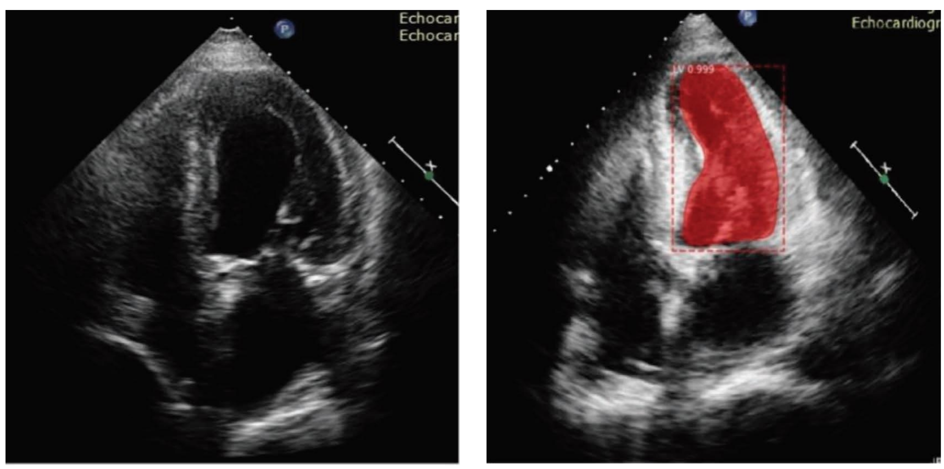

(a) (b)

Figure 3: US image (a) and its US image with LV boundary (b).

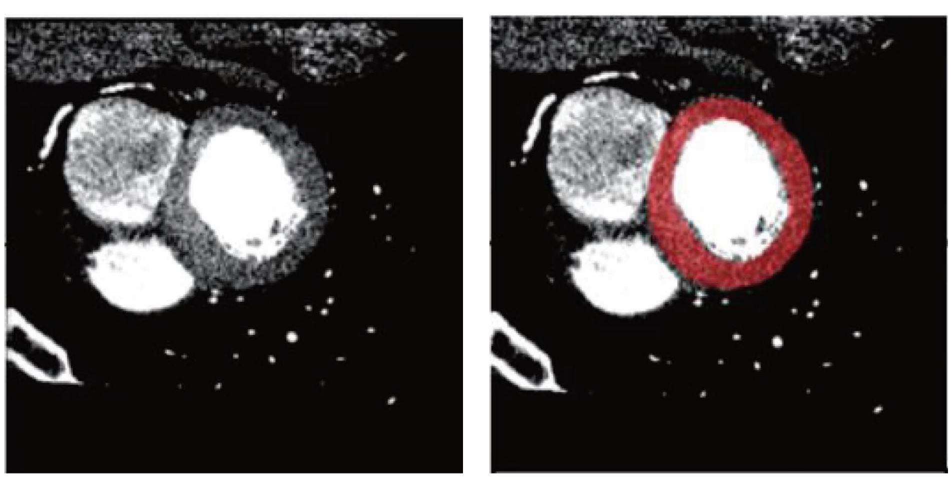

(a) (b)

Figure 4: CT scan of LV (a) and LV boundary (b).

novel discovery for solving problems in those areas which has high dimensional data. Inspired by brain function, deep neural networks are built from many hidden layers sandwiched between the input and output layers. The general architecture of a deep neural network is presented in Figure 5.

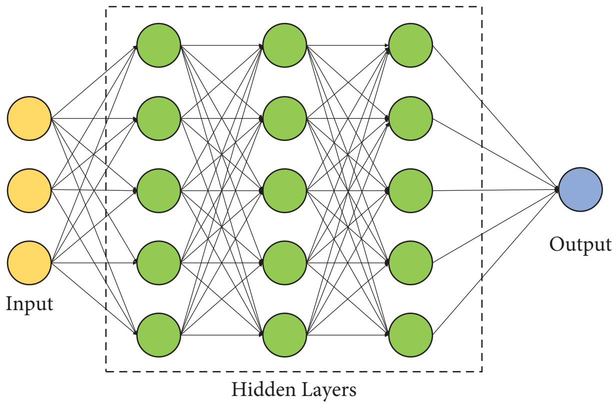

FIGURE 5: A general architecture of a deep neural network with three hidden layers.

3.1. Convolutional Neural Network. DL architectures are performing excellently in solving traditional artificial intelligence problems. The most established, progressive, and widely used is CNN. The following section discusses CNN, its variants, and its applications.

Among all the models of neural networks, CNN is the most dominant approach to solving problems of CV. The idea of CNN architecture was developed in the 1980s [53] but due to the lack of computational ability of hardware, high processing machines, and large storage devices to deal with big images, the idea did not flourish. The concept accelerated as the processing of machines increased in terms of computation and database to retrieve and store. Later in [54], CNNs were successfully applied in classification problems and performed brilliantly in CV applications. The gradient-based learning algorithm highly motivated CNN to produce optimized weights. CNN performed far better than other multi-layered perceptrons. The CNN weights are shared and are not needed to learn again for the same object at different locations. It recognizes visual patterns, directly from raw image pixels. This decreases the number of learnable parameters. CNN performance is impressive on 2D and 3D images. CNN model has minimized the preprocessing task and the back-propagation learning method improved the performance as it has provided a solution to deal with nonlinearity with the decrease in computation process due to a smaller number of weights. CNN has been producing better results in object recognition, behavior recognition, audio recognition, detection, recommendations localization, classification, and segmentation tasks.

3.1.1. Convolution. Convolution is a mathematical operation that involves the multiplication and addition (weighted average) of two functions. The first function (x) represents input data and the second function (w) represents kernel and together they produce the output, called feature maps. CNN is similar to neural networks that use weights and biases. It involves a convolutional layer in the neural network that applies to input data of an acceptable type. The CNN architecture is divided into two divisions: feature extractors and classifiers. Each convolution layer finds specific features from the input data using a shared weight called kernels, and with n number of kernels, the convolution layer determines n features. The input of each layer is the result of the previous layer. A simple CNN consists of a convolutional layer, pooling layer, rectifier unit, fully connected layer, and classifier. The convolutional layer is a building block of CNN. The input image convolves with the kernel (learnable filter). The kernel slides over the input image and the size of the kernel are somehow learned from the input image. Some parameters drive the size of output i.e., depth, stride, and padding. The CNN compresses the fully convolutional network by lessening the connections and sharing the weight of the edge.

Figure 6 shows a general CNN structure; the input image is convolved with kernels to extract the features. The result of convolution is then passed through the pooling layer (mostly Max pooling). The CNN extracts the features using these layers and finally a fully connected layer [55] gives the predicted output.

Convolution performs 3 main tasks: sparse interaction, parameter sharing, and equivariant representation.

(i) Sparse interaction: In a neural network, every output unit interacts with every input having separate parameters. These parameters help to determine the relationship or interaction between the input and output units. CNN uses kernels of different sizes which are smaller than input data in size. This reduces the number of learning parameters and the storage space and increases computation efficiency.

(ii) Parameter sharing: It uses the same parameter for more than one chunk. In convolution, each kernel value is used at every point of input other than boundary values. It helps CNN to use only one set instead of multiple parameters for every location. It reduces the storage requirement further.

(iii) Equivariance: It refers to the shift in the feature map by the same amount as the input shifts. Convolution does the same but not naturally [50].

3.1.2. CNN Layers. For the past few decades, CNN is performing intensely in CV (detection, recognition, tracking, estimation, processing, analysis, learning, restoration, and reconstruction) as the popular machine learning algorithm. The GPUs have also brought extra efficiency in their results. The boost CNN gain is through several factors such as a large labeled training dataset, rectifier linear unit, regularization (dropout), and augmentation. The strength of CNN is extracting discriminative features at different levels. The CNN architecture consists of a convolutional layer, a nonlinearity layer, and a polling layer followed by a fully connected layer.

(i) Input layer: This layer understands the input data. It gives the contents of input data and has no learnable parameters. So, this layer has nothing to do with learning.

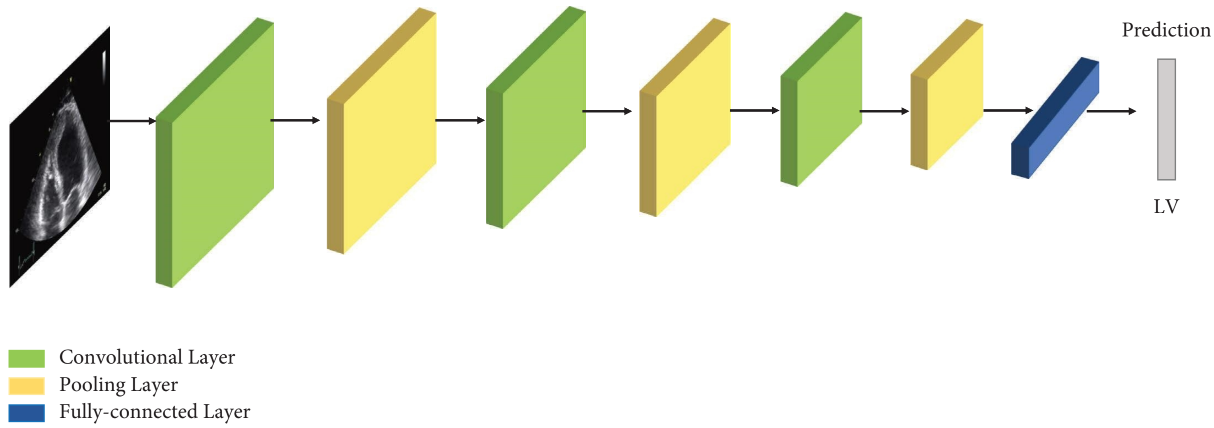

Figure 6: General structure of deep convolutional neural network.

(ii) Convolutional layer: Convolutional layer performs convolution operation which is the trademark of CNN architecture. This layer holds learnable parameters such as weights and biases. This layer contains filters or kernels, used to detect edges, shapes, and patterns of the given input image. Kernels are convolved with each input feature/image pixel to produce feature maps as an output. A dot product between each input and filter is performed, followed by summing each dot product output, and finally, a bias is added. Bias can be configured according to network requirements. The convolutional layer reduces the computational cost by reducing the input size:

$$Z_i^l = \sum_{J=1}^{K^{l-1}} W_{i,j}^l * Z_j^{l-1} + B^l. \quad (1)$$

The kernel computes the product of weight and input of kernel size. It also determines the desired features based on kernel weights. Equation (1) shows the operation of the convolutional layer, where Z_i^l and Z_i^{l-1} are the outputs of the current layer and previous layer, respectively, and $W_{i,j}^l$ and B^l represent filters and biases. Each neuron need not be connected to all other neurons in the preceding and following layer. The input is convolved with filters to produce an output where bias is added for nonzero value. The final output goes through a nonlinear activation function which activates the feature maps and forwarded the result to the next layer.

(iii) Pooling layer: The other name of this layer is the subsampling layer. This layer reduces the dimensions through downsampling operation. Average (uses the average value) and Max (uses the highest value) pooling are the two most used operations. The following subsampling function represents a pooling operation:

$$Z_i^l = Sub - Sampling\left(Z_j^{l-1}\right). \quad (2)$$

(iv) Nonlinearity layer: It applies the relevant nonlinear activation function. The most common functions are sigmoid, rectified linear unit (ReLU), hyperbolic function, and SoftMax:

$$a^l = f\left(Z^l\right). \quad (3)$$

(v) Dropout: This layer regularizes the CNN model, decreases computation, and increases the generalization. It randomly drops the units by assigning the zero weight to a set of units. This layer helps to avoid the overfitting problem.

Fully connected layer: This is a flattened layer with each neuron of the previous layer connected to each neuron of the current layer. Each neuron has a separate weight for each connection. This layer has the highest number of learnable parameters. The input data are linearly processed, passed through a nonlinearity, and then propagated to the next layer.

4. LV Segmentation Using DL Architectures

CNN has performed several CV tasks effectively and precisely, that is why it is a widely used DL technique for image segmentation, especially for medical images. In Section 4.1, several CNN architectures are reviewed which are used for the LV segmentation.

4.1. LV Segmentation Using Fully Convolutional Network. The fully convolutional network (FCN) [56] introduces the fully convolutional layers instead of fully connected layers. Therefore, FCN can handle the variable size of images and fewer parameters to be learned which also make the network faster. The FCN and its variants used for LV segmentation are explained below.

4.1.1. FCN with Pre/Postprocessing. A three-step (preprocessing, LV segmentation, and postprocessing) LV segmentation method is proposed in [57]. In the first phase, LV is localized using the over feat algorithm [58] to determine the region of interest (ROI) which is then fed to the next phase where the segmentation is performed using a temporal FCN (T-FCN) architecture. The CNN model is pretrained with GoogLeNet and fine-tuned using LV images. The T-FCN adds another hidden layer at the decoding path to restore the original size. The segmented LV boundary is further refined in the third phase by using one of the two algorithms: fully connected conditional random fields (CRFs) with Gaussian edge potentials [59] and semantic flow [60]. To train the network, the TWINS-UK database was used which consists of more than 12,000 images. The result showed that T-FCN with CRF performs better segmentation and achieved the dice similarity coefficient (DSC) value of 0.9815, average perpendicular distance (APD) of 6.2903, and conformity index of 0.9610. This work only focused on the LV segmentation.

One of the preprocessing methods is to crop the ROI first and then apply the segmentation to the selected ROI. This procedure for LV segmenting is presented in [61]. The clinical parameters such as LV volume (LVV), LVM, SV, and EF were also analyzed by estimating the size of LV from MRI images. The class imbalance challenge was tackled by first finding out the ROI using an FCN model. A new FCN model was applied to these ROI images for LV segmentation. Class entropy and radial distance were used as loss functions. The model is trained and tested using two datasets: the Automatic Cardiac Diagnosis Challenge (ACDC) 2017 publicly available dataset and a local dataset. The ACDC-2017 dataset consists of 150 patients' data, while the local dataset consists of almost 6000 images. The performance is evaluated using the DSC and Hausdorff distance (HD) for cross-entropy loss and radial distance loss. The model is analyzed for both datasets and achieves almost the same results, which yield that the model is generalized and applicable to any dataset. The proposed model attained better DSC and HD values than that of U-Net and ConvDeconv-Net. The DSC value for LV segmentation of the proposed model on the local dataset is 0.95 and ACDC dataset is 0.94. Similarly, the HD value is 9.31 and 11.21 for the local and ACDC dataset, respectively.

4.1.2. Improved FCN for Clinical Index Calculation. Chen Qin et al. [62] proposed a model that consists of two branches: the motion estimation branch and the segmentation branch. The unsupervised Siamese style recurrent spatial transformer network is utilized for motion estimation and FCN is used for the segmentation. Motion estimation is an unsupervised method that combined the motion estimation and segmentation layer which can also be referred to as a weakly supervised model. A total of 220 short-axis view subjects were obtained from a UK biobank study. The LV segmentation is assessed by separately segmenting the LV and also by combining the two models. The DSC value of 0.9217 is achieved for only segmentation, while 0.9348 is achieved for the combined model which depicts that the model performs better in combine mode.

Similarly, the LVV is calculated using MRI images in [63]. The volume of LV is a very important feature to evaluate the patient's cardiac health which requires LV segmentation. The method segments the LV for diastolic and systolic to calculate the volume of LV. The Sunnybrook dataset is used to train and test the model. Data augmentation is also applied by rotating the slice in different directions. The method used a local binary pattern in cascade to detect the ROI. Then, a CNN model is used to score the ROI and select the one with the maximum score. Finally, LV is segmented using hypercolumn FCN (HFCN) from the ROI. The HFCN features from different levels were concatenated to form a new layer, and segmentation was based on this new layer. The volume is calculated using both manual and HFCN. The variance estimation method is used to estimate the final prediction. This algorithm ranked fourth in the Second Annual Data Science Bowl competition organized by Kaggle. Although this algorithm performs very well in segmentation, still sometimes the model generated the irregular shape of LV as it does not use the prior knowledge of the 3D shape of LV.

The feasibility and accuracy of FCN to segment the scar tissues in LV were analyzed in [64]. The modified version of FCN, efficient neural network (ENet), is applied to cardiac images. The proposed network consists of 13 convolutional layers with a 3×3 kernel size and stride of 2, while a parametric rectified linear unit (PReLU) was used as an activation function. Cross-entropy was used as a loss function. The two protocols, protocol-1 and protocol-2, were used for the segmentation. In protocol-1, the ground-truth and original images were directly fed to the network for training and segmentation. Whereas, in protocol-2, the desired LV area was cropped before training the network. The images were cropped using Hough transform [65]. The dataset consists of 250 images of 30 patients which is further increased to 2000 images by applying the data augmentation technique. Protocol-1 and protocol-2 achieved the accuracy of 95.97% and 96.83%, the sensitivity of 97.31% and 87.89, the specificity of 68.77% and 88.07%, and the DSC value of 0.54 and 0.71, respectively. The result demonstrated that protocol-2 performs better than protocol-1, which depicts that cropping the ROI gives better results in segmentation.

4.1.3. Loss Functions and Optimization Algorithm. Until now, we have explained the FCN models and their performance based on preprocessing or by applying some changes in the model. Nevertheless, one very important parameter is the loss function. In [66], the updated model of FCN with different loss functions was analyzed. An iterative multipath FCN (IMFCN) segmentation model for LV, RV, and MYO from MRI images was proposed. To tackle the class imbalanced problem, searching for ROI was performed and images were cropped using the method proposed in [67]. The proposed model consists of an encoder, feature fusion, decoder, and deep supervision. Encoder part used s $[i]$ current slice, previous slice $s\ [i-1]$, adjacent slice $s\ [i+1]$, and already predicted segmentation $M\ [i]$ as input. These features are inserted into the encoder part to extract new features. The new features are fed to the feature fusion which consists of different convolution layers of different sizes. The output features from the fusion block are fed to the decoder block which has unsampled features. Finally, the deep supervision part performs the segmentation. The efficiency of the model is also compared using different loss functions. Batch-wise class reweighting mechanism and batch-wise weighted dice loss function were utilized for multiclass segmentation. The results of the proposed models were evaluated and compared with U-Net and LVRV-Net. To quantitatively evaluate the performance, three metrics: DSC, average symmetric surface distance (ASSD), and HD were employed. Batch-wise weighted dice loss function shows the best results among all loss functions. In this research, the most inaccuracies in segmentation have occurred in apical and basal slices. Additional processing mechanisms can lessen these errors.

The focal loss was analyzed with the four skip connections in the FCN model [68]. The model was referred to as the focal residual network (FR-net). RestNet50 was used as a backbone network. Cross-entropy loss was calculated across the predicted probability and labeling. Focal loss was applied to improve preliminary segmentation results. Sunnybrook dataset was used. DSC and APD were used to evaluate the performance. The model results were also compared with U-Net and FCN and other work based on the Sunnybrook dataset. The models attained the DSC value of 0.93 and APD of 1.41.

In addition to the loss function, the optimization algorithm is also a key feature of the CNN model. In [69], the performance of optimization factors was analyzed for the CNN model. Six different optimization algorithms, namely, stochastic gradient descent (SGD), nesterov accelerated gradient [70], RMSProp [71], Adam [72], AdaDelta [73], and AdaGrad [74] were implemented to train CNN model. A CNN model was proposed and trained separately using all six optimization factors. Sunnybrook dataset was used for training and testing. The best performance was obtained by the RMSProp optimization technique. The model achieved the DSC of 0.93, APD 2.13, and percentage of good contour (GC) 95.64 using RMSProp optimization.

4.1.4. Other FCN Techniques. One key limiting factor in DL is the amount of data. Training the FCN model using a large dataset for LV segmentation is studied in [75]. The FCN model is trained on the UK Biobank dataset. The images of 5,008 subjects (93,500 images) were used to train the model after data augmentation. The data were manually annotated by eight different experts. DSC, mean counter distance, and HD values of 0.94, 1.04, and 3.16 were achieved, respectively. The segmented LV is also used to measure the LV-EDV, LV-ESV, and LVM.

Another technique to enhance the model performance is to take advantage of the pretrained model. A pretrained VGG model (trained on ImageNet) was combined with FCN called FCN-all-at-once-VGG16 [49]. The model used skip connections to combine the hierarchical features from convolutional layers with different scales. Adam was used as an optimizer with an initial rate of 10^{-4}. A dataset of a total of 1100 subjects was used by splitting the dataset of 100 subjects into 50 training, 30 validations, and 20 tests images. The next 1000 cases (diastolic) are segmented using a trained model and compared by 1000 manually drawn by an expert technician. The manual drawing was performed using the in-house software (A-view Cardiac, Asan Medical Centre, Seoul, Korea). For quantitative analysis, sensitivity and specificity evaluation matrices were used. The method is limited when the number of pixels of background (i.e., image pixels other than the LV mask) is large. The model was evaluated using four performance indices, i.e., DSC, Jaccard similarity coefficient, mean surface distance (MSD), and HD.

FCN was also used with a graph matching algorithm. The motion estimation of LV from MRI images was studied in [38]. The method consists of four steps: (1) endocardial contours of the LV were predicted using a FCN, (2) features of points in short-axis cine MRI were extracted using an FCN feature descriptor, (3) the correspondence between contours of the LV myocardium was estimated by a novel graph matching algorithm, and (4) the correspondence between two LV contours and the LV motion field was estimated using the FCN feature descriptor into the graph matching algorithm. The Medical Image Computing and Computer-Assisted Intervention (MICCAI) 2009 challenge database and the 33 subject's database [53] were employed to evaluate the proposed method.

Consequently, FCN and its modifications show very decent results for LV segmentation. To enhance the performance different preprocessing and postprocessing techniques, loss functions, and data variability can be used. Figure 7 illustrates examples of segmented images generated by FCN models.

4.2. LV Segmentation Using U-Net. In medical images, the required area to be segmented consists of a small area of the entire image. The U-Net [76] has shown substantial results in the segmentation of medical images. This is possible due to the ability of U-Net to continuously suppress the background region in training and emphasis the required areas that need to be segmented. That is why the most used network for LV segmentation is U-Net and its modification models.

4.2.1. U-Net with Pre/Postprocessing. Studies applied the postprocessing or preprocessing with DL methods to yield good results. Guo et al. investigated the postprocessing effect on MRI images in [77]. Input Cardiac MRI is fed to U-Net and then labeling probabilities were generated. For the postprocessing Kernel cut, a segmentation technique was used. The output of U-Net is the input of continuous kernel cut which segments the desired part. LV, MYO, and RV were segmented using this approach. The result shows that, with less training data, reasonable segmentation results can be achieved.

The postprocessing on vivo diffusion tensor CMR was performed in [78]. A five-layer U-Net architecture is used to perform the LV segmentation followed by image registration. This helps to remove the bad images, and then, the final segmentation was applied. To increase the size of the dataset, data augmentation was used (translation and rotation).

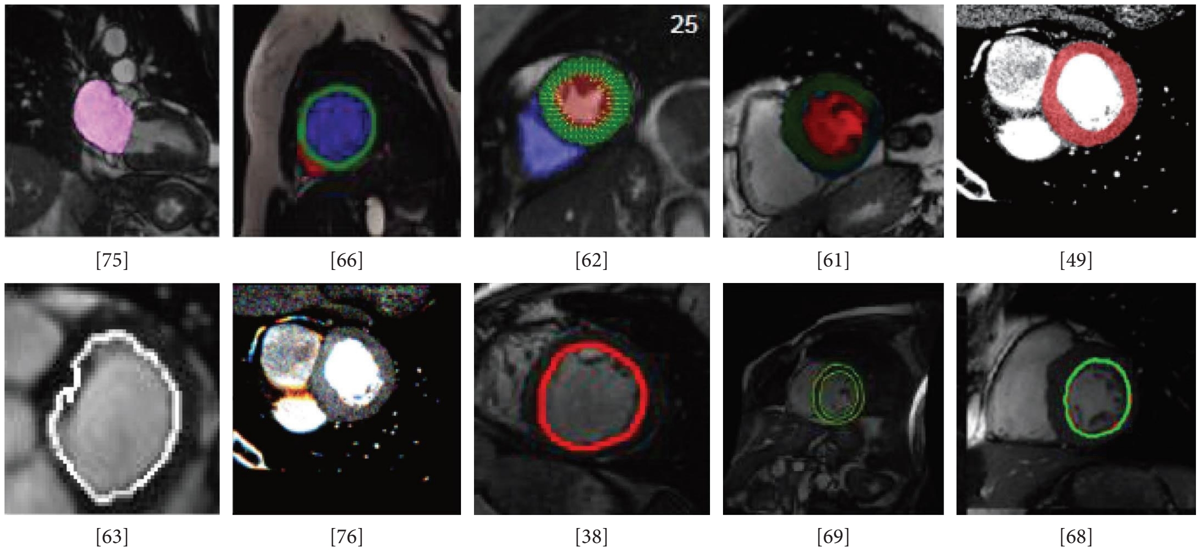

Figure 7: Sample of segmented images using FCN.

Batch normalization was used with U-Net to avoid overfitting. The model achieved a 0.93 median value of DSC.

The approach in [79] performs the preprocessing on the images by selecting the ROI by using the SinMod method. The ROI contains the desired part of the heart that is fed to the U-Net model for training. The curriculum learning (CL) strategy was utilized as a training strategy. The proposed methods were compared together with U-Net without CL, FCN (with and without CL), and hybrid gradient vector flow snake. The DSC, overlap, and mean average distance (MAD) were used as evaluation matrices.

In [80], the labeled images from the Kaggle database were used before training. The concept of transfer learning is utilized by pretraining the 3D U-Net model using Harvard data. The U-Net model was used to segment the LV, MYO, and RV. The DSC value achieved for LV segmentation was 0.87 without transfer learning and 0.95 using transfer learning.

The determination of ROI makes the segmentation task simple and accurate as the targets area is reduced to ROI instead of a complete image. This strategy was used in [81] and proposed for the three U-Net-based models. The proposed CNN architectures classify myocardial tissues and detect LV-ROI before LV quantification. For this experiment, the Sunnybrook cardiac dataset and the Cardiac Atlas Project (CAP) were used, which consists of 45 and 95 cases, respectively. Three new CNN architectures were proposed which are based on U-Net. The main purpose of the proposed models is to quantify the LV. Before LV quantification, LV-ROI detection and myocardial tissue classification were performed using the same U-Net architectures.

In the first proposed model, the encoding path comprises two 3×3 convolution operations, batch normalization, and residual learning. The 2×2 Max-pooling operation with stride 2 was performed after the residual learning [24]. The second and third proposed architecture is named as uInception and uXception. The network complexity was reduced in these networks. The SGD was used as an optimization factor and Jaccard distance as a loss function. The data augmentation was applied to increase the data size from 4,048 to 20,000. The segmentation accuracy was measured using the DSC and achieved 0.870, 0.869, and 0.868 for the proposed networks, respectively. Mean square errors of 0.0135, 0.0136, and 0.0138 were achieved while the mean absolute error was 0.0137, 0.0136, and 0.0138. Furthermore, EDV, ESV, SV, LVM, and EF were calculated as clinical indices.

4.2.2. U-Net with Deformable Model. The combination of DL and deformable models as postprocessing can be combined to segment the LV. Veni et al. trained the U-Net model for LV segmentation from the A4C chamber view of US [82]. The segmented output is further refined using the deformable model. Using this technique, high accuracy is achieved by training the model with a very fewer amount of data, i.e., 69 images. The DSC value of 0.86 ± 0.06 was achieved.

4.2.3. Improved U-Net for Clinical Index Calculation. Many studies focus on the calculation of various heart parameters such as EF, global longitudinal strain, or LVM, and for measurement of these parameters, LV segmentation is one of the primary tasks to be performed. A study was performed to validate that the DL methods can be used in real-time software that streams images directly from an ultrasound scanner [83]. A U-Net model was utilized for LV segmentation. The main goal was to calculate ventricular volume, EF, and mitral annular plane systolic excursion (MAPSE). All these parameters were based on the segmentation of LV. The accuracy of the model was evaluated by Bland–Altman analysis. The dataset of 75 patients was used and a value of $(-13.7 \pm 8.6)\%$ for EF and (-0.9 ± 4.6) mm for MAPSE was achieved for Bland–Altman. The results show that DL is a feasible solution for the real-time calculation of clinical indices used for cardio analysis.

Similarly, LV segmentation was also performed to measure the GLS. The work in [84] utilizes the standard U-Net architecture and performs the four tasks on US images: (i) classification of cardiac view, (ii) segmentation of LV from the cardiac view, (iii) estimates of the regional motion, and (iv) a fusion of measurement. The segmentation architecture comprises five levels of upsampling and downsampling. All levels consist of two convolution layers with filters ranging from 32 to 128. The 3×3 filter size, 2×2 Max pooling, and 2×2 equal stride were utilized. Dice was used as a loss function and Adam as an optimizer.

A method to achieve LV segmentation based on temporal area correlation was proposed in [85]. U-Net was used as a base CNN model, and then, the multitask module is utilized for epicardium and endocardium segmentations. The output of the multitask module was fed to recurrent neural network (RNN). The RNN performs the temporal area correlation optimization. The average DSC of 0.90 ± 0.05 and average HD of 7.6 ± 4.5 was achieved. The LVM and EF have also been calculated to cross-validate the results.

For the quantitative analysis of the LV, segmentation is performed before quantification of LV parameters (area and dimension) [86]. The segmentation provides the structural information of LV which is further used for quantification. Initially, U-Net architecture was used as a segmentation model. Furthermore, a Deep-CQ segmentation model was proposed for LV segmentation that comprises the proposed loss function. The binary classification of each pixel as LV or background was performed using the Gibbs distribution function [87]. The segmentation performance was evaluated using DSC matrices and achieved 0.893 ± 0.05 value for Deep-CQ models, while U-Net yields 0.897 ± 0.041. The main object of this research work is the quantification of LV, and the Deep-CQ model performed better than U-Net for quantification while U-Net performed better than the Deep-CQ model in segmentation.

Estimation of myocardial perfusion is an essential step to measure the blood flow through the heart muscle. The arterial input function (AIF) extraction is an important phase for calculating the myocardial perfusion. The AIF estimation is highly dependent on detecting the LV size accurately. The LV segmentation to measure the AIF was performed in [88]. A U-Net model based on RestNet was designed to segment the LV. RestNet consists of batch normalization, ReLU, and convolution layers. To estimate the output probability, sigmoid or SoftMax was used. The kernel size used was 3×3 with 1 stride and 1 padding in all convolution layers. A weighted sum of cross-entropy and IoU was used as a loss function. To find out the best hyperparameters, 45 training sessions were performed and the best hyperparameters were used for final training. The labeling of LV and RV was performed using an ad hoc algorithm and experts cross-check the labeling. The model was trained using two different sets of classes: (i) LV and background and (ii) LV, RV, and background. The model achieved DSC values of 0.87 ± 0.08 for three classes and 0.82 ± 0.22 for two classes. The performance of the model trained for three classes was better than two classes because the contextual information extracted from three classes improves the LV segmentation performance.

From an entire echo cine, automatic LV segmentation was performed in [89]. The US images and optical flow of US images were first fed to the temporal window. The optical flow was calculated by the Horn–Schunck algorithm. The output of US image and optical flow US images act as input to the two separate encoder parts of U-Net. The output of both the U-Nets was concatenated. In the third part of the model, the concatenated data were passed to the bidirectional LSTM. The U-Net decoder finally up-sampled and segmented the LV. The data of 563 patients were used with a training and testing ratio of 80 and 20, respectively. Dice was used as a loss function and Adam as an optimizer. Network performance was compared with U-Net and U-Net Bi-Conv LSTM using the DSC. The model U-Net optical Bi-Conv LSTM achieved the best DSC value of 0.936 and accuracy of 0.977.

4.2.4. Comparison of Different U-Net Models. The comparison of three well-known CNN architectures was performed by [90]. U-Net, wide U-Net, and U-Net++ were trained using the data of 94 patients. Data augmentation was used to increase the data size and to avoid the overfitting problem. The U-Net has 32, 64, 128, 256, and 512 feature maps, while the wide U-Net has 35, 70, 140, 280, and 560 feature maps. U-Net++ has an additional block of feature maps and skip connections. Exponential linear units (ELU) were used as an activation function in all layers except the last layer, where sigmoid was used. The model was trained using the original dataset and augmented dataset and the performance was assessed. The U-Net++ model performance was the best among the three models using an augmented dataset. The highest DSC value of 92.28 is obtained. Moreover, U-Net++ was less overfitted than U-Net and wide U-Net.

4.2.5. U-Net Performance Based on Dataset Properties. Although the comparison among different variants of U-Net was performed in [90], the training dataset and data variability also affect the performance of the network. The effect of training datasets from different variability on the performance of the CNN model was analyzed in [91]. U-Net architecture was used as a segmentation model and assigned the names CNN1, CNN2, and CNN3 based on the training dataset variability. Three different training sets were collected for this research experiment. CNN1 was trained using the data from single center and single vendors with 25,389 images. CNN2 was trained by the set consisting of images from multiple centers by the single vendor and 27,488 images, while multiple centers and multiple vendor data were used to train the CNN3 model with 41,593 images. The training images were preprocessed for normalizing the resolution, cropping the images to 256×256, and normalizing the signal intensity. APD was used as an evaluation metric. CNN3 had the largest number of training samples and the highest variability, and it has achieved the best performance on unseen heterogeneous testing data with the highest value of 1 mm for CNN3. While EDV, ESV, LVM, and EF were used as clinical indices.

Similar and detailed research to analyze the impact of the amount of data, quality of images, and influence of expert annotation on LV segmentation was executed in [92]. A US images dataset that is openly available was also introduced in this work. The dataset consists of an apical 4-chamber view of 500 patients and is called the Cardiac Acquisitions for Multistructure Ultrasound Segmentation (CAMUS) dataset. The authors compared the performance of different CNN models based on U-Net. The models used for LV segmentation were U-Net1, U-Net2, anatomically constrained neural network, stacked hourglasses, and U-Net++. All these architectures were based on encoder-decoder and the main difference among these architectures is the use of different layers and learning parameters. The U-Net2 yields the best segmentation results, and the performance was slightly better than U-Net1, but U-Net1 needs fewer parameters to learn, so the authors choose U-Net1 for further experiments. The model was trained to segment only LV and multistructure in which the model segments the LV endocardial (endo), LV epicardial (epi), and left atrium (LA). The model performance was consistent for both LV segmentation and LV segmentation in the context of LA.

The effect of image quality on training was also tested. Two different sets of images are given to the network for training. One set comprises only high-quality images while the other consists of high- and low-quality images. The output of both sets does not vary significantly. The author infers that the encoder-decoder-based techniques can cope with variability in image quality. The influence of the size of the training dataset on the performance was also tested. The U-Net1 model was trained by increasing the dataset from 50 patients to 400 patients. At each level, 50 more patients' data are added for network training. The results show that the performance of the model increases to 250 patients and slightly improved by increasing the training data further to 400. It is concluded that U-Net1 requires 250 patient data to attain a good promising result. The impact of expert annotation was evaluated by annotating the data by three different experts. The network was trained each time using the data of 50 patients labeled by every three different experts. The validation data were kept the same, and the model was tested by the remaining 400 patients' data. The network trained using the expert's data showed better results in testing. It is analyzed that the data contouring images are cardiologist dependent. Furthermore, the encoder-decoder network can learn a specific way of segmenting.

The labeling of large dataset problem was addressed in [93]. A model was proposed to generate the ground-truth images. Pseudoimages were generated using a graphical model such as the principal component analysis. The CycleGAN model was employed to generate the labeled images by using the pseudoimages and unlabeled original images. These labeled images were utilized to train a U-Net model. CAMUS dataset, EchoNet dataset, and synthetic dataset were used to train and test the model. The results show that the model trained using the synthetic data also performs very well.

4.2.6. Other Models Based on U-Net Architectures. Segmentation of LV, RV, and MYO from apical 2 chamber (A2C) view or apical 4-chamber (A4C) view has been implemented using DL methods [94]. In this work, neural network was tested to segment the LV, RV, and MYO from the apical long axis view (ALAX). In ALAX the main difference is the LV outflow tract (LVOT) which restricts the view. Four different approaches were used in this research. First, U-Net1 was trained from scratch and used to segment the ALAX. This model was referred as a baseline model in this work. Secondly, the baseline network was trained on A2C/A4C views, used as a transfer learning, and then trained for ALAX segmentation. Third, the baseline network was trained using A2C, A4C, and ALAX data. As ALAX data are less than A2C/A4C, so to compensate for this, ALAX data were repeated ten times in each epoch. In the fourth approach, the network was fed with US images and binary indicators. The purpose of the binary indicator is to inform the network about the input image whether it is ALAX or A2C/A4C. As the U-Net model has no dense layer, so an image is created from a binary indicator and fed to the network. The dataset of CAMUS challenge consisting of 500 patients was used for training, while for ALAX view, separate data of 106 patients were collected. The proposed multiview segmentation network achieved the best DSC value of 0.921.

To achieve the accurate and precise LV boundary and size, different studies modify the U-Net to elevate its performance. Gutierrez-Castilla et al. [95] improved the U-Net model by applying the changes in skip connections. The features' maps from each decoder layer were selected and upsampled according to the size of the final decoder output. After upsampling each decoder feature map, all feature maps were concatenated or added together. Using these dense skip connections, the decoder can flow directly to the final layer from each decoder layer. As no extra layers or filter is added, so this model does not add any extra parameters. For training, the model two datasets ACDC and Sunnybrook were used which consist of 150 and 45 patients' data, respectively. LV, RV, and MYO were segmented for diastolic and systolic. DSC and HD were used as evaluation matrices. As a clinical index, EF was also calculated by segmenting the LV for ED and ES. For ED, 0.968 and 4.855 (mm) values of DSC and HD were achieved, respectively. Likewise, DSC of 0.944 and HD of 6.254(mm) were attained for ES.

In the same way, a CNN model, named batch-normalization-U-Net (BNU-Net) was designed for LV segmentation from MRI images [96]. The proposed model was based on U-Net architecture, where the successive layers in the encoding path were followed by an ELU as an activation function and batch normalization was applied after convolutional filters. The BNU-Net has 4 layers in the contraction path and 7 layers in the expansion path. The 2×2 Max pooling was used after a pair of convolutional layers in the contraction path. The model was also trained using the

ReLU activation function and was found that the model gives better performance with the ELU activation function. The model was trained using the publicly available Sunnybrook dataset and the training data size was increased by applying the affine method for data augmentation. DSC and sensitivity matrices were used to compare the performance of BNU-Net with U-Net (with and without data augmentation). The BNU-Net performed better with data augmentation and gave a value of 0.93 for DSC and 0.97 for sensitivity.

Also, a novel U-Net-based method, CNN module, named the "OF feature aggregation network" (OF-Net) as integrated temporal information from cine MRI into LV segmentation [97]. The proposed model integrates the motion information with the U-Net model. Furthermore, two more CNN models were used to localize (ROI-Net) and then segment the LV (called attention module). The model is trained using a flying chair dataset and fine-tuned using the MRI datasets. Two different publicly available datasets, Statistical Atlases and Computational Modelling of the Heart (STACOM) and ACDC datasets, were used. Out of 100 subjects, 66 were used for training and 34 for testing. Total of 12,720 images for training and 6972 for testing (from the STACOM dataset). A DSC value of 94.8 ± 3.3 was achieved.

In [98], a graphical user interface is developed for LV segmentation from MRI images using PyQT libraries. Images were labeled manually, and the labeled LV images were fed to train the CNN model. A publicly available dataset and the internal dataset were used to train the model with 13,535 images and test the model with 4,148 images. The model achieved the DSC of 0.87 ± 0.02.

The sonographers also used the point-of-care ultrasound (POCUS), which is portable ultrasonography used for diagnosis. The feasibility of translating the POCUS echo images to the high-quality traditional echo images was studied in [99]. To improve the quality of POCUS data according to the level of cart-based US data, the mapping from POCUS images to cart-based US images was an obligatory task. To achieve this goal, the POCUS images were analyzed, compared, and mapped with the traditional US images. The dataset of 5000 POCUS images and 16000 US images was used for the mapping purpose. The anatomy of LV was extracted from POCUS (using A2C view) using the DL method and then mapped with high-quality US images. The images were classified as low quality (fair + medium) and high quality. This classification was performed based on the visibility of the anatomy of the desired region. Fully convolutional encoder-decoder networks based on U-Net architecture were utilized for the translation of images. The size of the input image was 128×128. The model comprises ten encodings and eight decoding convolutional layers. ReLU activation, batch normalization, and dropout with ratio = 0.2 were used. In the first layer, batch normalization was not employed. Max-pooling and transpose convolution layers with stride 2×2 were used in downsampling and expansive paths, respectively. The average DSC value obtained is 82.6 ± 12.3 and 88.3 ± 5.0 for low- and high-quality images, respectively. Similarly, 2.6 ± 2.7 and 1.9 ± 0.8 mm values of HD for low- and high-quality images.

Despite the several advantages of using the U-Net in medical images, it ignores the effects of features maps on different scales directly. To solve this problem, a pyramid network is combined with the dilated U-Net model and named as multifeature pyramid U-Net (MFP-UNet) [100]. In dilated U-Net model, two more downsampling layers were added to extract more dense details of an image. As the US images were usually low contrast images, the images were preprocessed to enhance the contrast of US images using Niblack's method for global thresholding. The model was trained using a self-collected dataset of 137 2D-US sequences which yields 1080 training images and 290 test images. Furthermore, the model was also trained using the publicly available CAMUS dataset. The proposed model did not only yield good segmentation results but also took less runtime. The model was compared with U-Net, dilated U-Net, and DeepLabv3. It takes about 1.2 sec for the classic U-Net, 1.33 sec for DeepLabv3, and 0.81 sec for MFP-UNet to segment a test image. DSC, HD, Jaccard distance, and mean absolute distance were used to compare the performance of the model.

Another concerning issue is, while computing the parameters, most of the DL models extract similar features at low levels. To avoid this problem, modification in the attenuation U-net model was proposed by introducing the attention gates mechanism [101]. This model focuses on the desired region of varying size and shape automatically. Furthermore, the class imbalance problem was addressed by introducing the Tversky loss. The model achieves 0.75, 0.87, and 0.92 for Jaccard index, sensitivity, and specificity, respectively.

One of the main problems which arise in DL architectures is gradient vanishing. The research [102] focuses on the gradient vanishing problem and proposed a model residual of residual (ROR) U-Net model. The encoding path of the proposed model is similar to ResNet-U-Net, but three shortcut levels are introduced in the ResNet-U-Net model. The First 3×3 convolutions and zero padding on the input image are applied. At the second level ResNet, the identity and convolutional blocks of ResNet are divided into three branches, while, at the third level, convolutional blocks and identity blocks are used. The proposed model was trained and tested using the Sunnybrook dataset and compared with U-Net and ResNet-Unet models. The 0.866, 0.926, 0.923, 0.120, and 0.945 of Jaccard index, DSC, precision, false positive rate (FPR), and recall are achieved by the model.

The study [103] used the unsupervised learning method to segment the LV, RV, and MYO. A U-Net model was trained using ACDC and tetralogy of fallot dataset (TOF) dataset on short-axis (SAX) view of MRI images. Then, using the transformation network, the model segment the LV, RV, and MYO from the SAX view. The model has never seen the SAX view of images before.

In [104], the localization and detection of the area containing LV and RV were performed by a network known as the Left Ventricle Localization NET (LVLNET). This model is a lightweight encoder-decoder such as CNN. This CNN model contains two 3×3 kernels, batch normalization, and Max pooling in each layer having four layers in total.

This localization model identifies the central part containing the LV and RV. The image is cropped and then pass to the next proposed CNN model called multigate dilated inception architecture (MGDIB). The MGDIB is based on U-Net architecture, but the kernel weights are expanded by the dilation factor and called a dilated convolution. The number of parameters does not increase using the dilated convolution. Two publicly available datasets, LV segmentation challenge (LVSC) + ACDC, were used. LVSC is used for the first part for localization while ACDC is for the segmentation of LV and RV. Different clinical measurements such as EDV, ESV, EF, and LVM are also calculated. DSC and HD values obtained were 0.900 and 0.910 for ED and ES, while HD values were 8.330 and 11.040 for ED and ES. Figure 8 depicts instances of segmented images by the U-Net model.

4.3. LV Segmentation Using Other CNN Networks. Several studies also used various CNN models other than FCN and U-Net. The detail of other CNN models utilized for LV segmentation is explained in this section.

4.3.1. CNN Models with Preprocessing. US imaging was also used for the heart analysis of children. For this analysis, the segmentation of LV and LA was performed on the paediatric US images [105]. Preprocessing was applied to the images before the training. The meaningless background was removed by resizing the images to 512×512. Furthermore, image augmentation was also used by rotating, random cropping, using salt and paper, and speckle noise with a probability of 0.01. To extract the spatial features, a spatial path module was designed. The spatial path is a convolutional network consisting of three layers with stride = 2, followed by batch normalization and ReLU activation function. It extracts a large amount of low-level spatial information. A submodule spatial attention was added to exploit the interspatial information and it focused on the "where" information part. The second parallel part of the network extracts the contexture information using five convolutional layers. RestNet50 was used as a backbone network. The submodule contextual attention was used at the end of this part to refine the extracted information and to know the "what" information part in an image is important. The context attention submodule focuses on "what" to look at, whereas the spatial attention submodule focuses on "where." The authors compare the results of each submodule and conclude that "where" is more important in LV segmentation rather than focusing on "what." In the last part, the features of both the parts are fed into another module called feature fusion module that generates the final refine features. A self-collected dataset of 127 4CH videos (100 for training and 27 for testing) was used. Images were extracted from the videos and 3654 images were used for training and 831 for testing. The segmentation results were evaluated step by step by adding each model, and finally, full Attention-guided Dual-path Network shows the best result. Additionally, well-known CNN architectures (FCN, U-Net, DeepLab, PSP Net, and BiSeNet) were also trained and results were compared with the proposed network. The DSC coefficient achieved a score of 0.951 and 0.914, in the LV and atrium segments, respectively.

4.3.2. Hybrid Segmentation Methods. Some researchers analyzed the performance of hybrid CNN models for LV segmentation. The morphological models, snake models, and active shape model (ASM) were combined with CNN models in different studies. A hybrid model using DL and morphological methods was employed in [106]. The ROI was detected using a CNN model; then, LV was segmented using a multiscope CNN model. Three different patches were used for training the network, i.e., 8×8, 16×16, and 24×24, covering different scopes. Finally, morphological filtering was used to refine the boundary segmented by CNN. The LUMC dataset was utilized for this work. The model achieved the DSC value of 0.71.

Another hybrid approach based on CNN and the double snake model was proposed to segment the LV from MRI images [107]. A SegNet architecture was used for the initial segmentation result. Then, ROI was plotted around the coarsely segmented region taking the center point of the segment object and rectangular ROI was formed using polar transform. Output from SegNet was fed to the snake models which perform the final segmentation of LV. For training, the model 45 subjects were used and accessed from the MICCAI challenge. The DSC value of 0.96 and 0.97 was achieved for endo and epi. EF and LVM were calculated as clinical indices. Additionally, regression and Bland–Altman analysis was also performed.

Similarly, the work in [108] combines the ASM and neural network to segment the LV. A diffusion filter was applied to the images as a preprocessing step before feeding the data to the model. This filter used eight neighboring edges to preserve the edge information along with noise removal. A CNN architecture, Faster-RCNN, was used to determine the position of LV, and ASM used this location to segment the LV. As the ASM needs the initial position of the object to determine the position, so the region proposal network (RPN) was used to propose the regions that might contain the LV. Then, Faster-RCNN located the LV in the proposed ROI. Both RPN and Faster-RCNN were fine-tuned with ImageNet. The dataset of 30 patients was used for this work. The DSC, MAD, and HD were used to evaluate the performance. Furthermore, the models were also compared with other models proposed in the literature. The proposed model yields a DSC value of 0.921, MAD 1.95, HD 6.29 mm, and Jaccard 0.86.

One more hybrid approach was proposed consisting of the CNN model and dynamic programming [109]. Initially, SegNet [110] with 17 stacked convolution layers was used for coarse segmentation which segments the boundaries of LV. The batch normalization, ReLU activation function, and four MaxPool layers were used after the first four convolution layers. Secondly, the segmented results from SegNet were refined for endocardial contour. In the last step, a dynamic programming model was used to calculate the epicardium and endocardium of the heart. The 900 subjects from Hubei hospitals were used for this study. Jaccard and DSC were

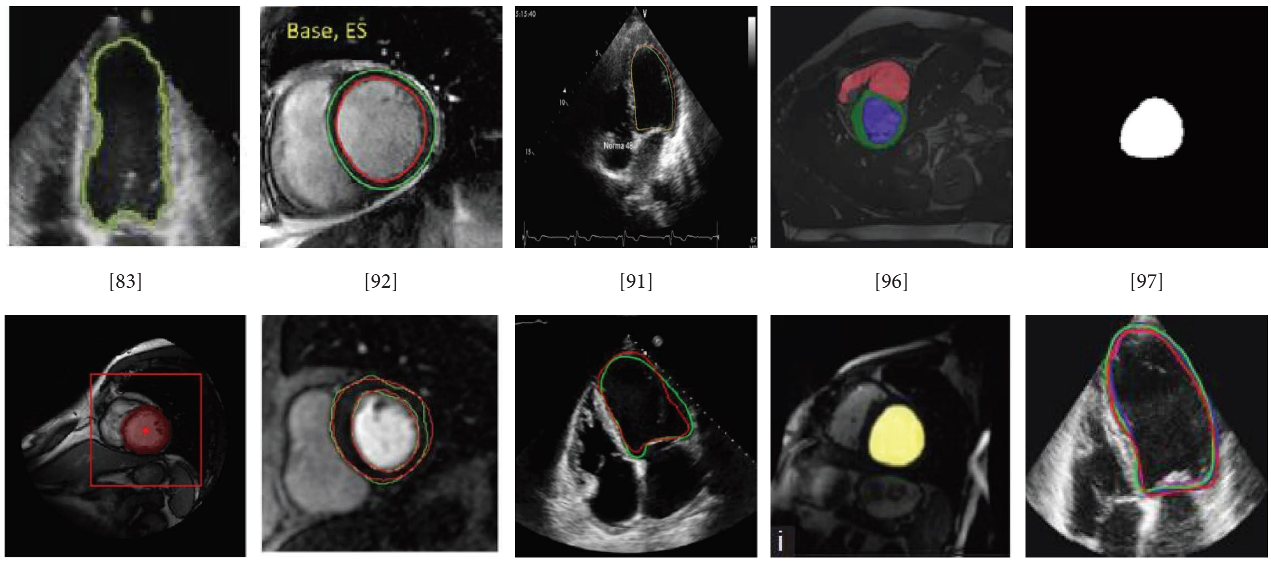

[83] [92] [91] [96] [97]

[82] [99] [101] [103] [90]

FIGURE 8: Sample of segmented images using U-Net.

used for the evaluation. The DSC of 0.90 (0.03) and 0.93 (0.02) were obtained for endo and epi, respectively. Similarly, 0.80 ± 0.06 and 0.76 ± 0.09 average value of Jaccard was obtained. The LV-EDV, LV-ESV, SV, EF, LVM in the diastolic phase, and LVM in the systolic phase were also measured. The Bland–Altman analysis was performed for the comparison of these clinical indices.

4.3.3. CNN + LSTM. A combination of encoder-decoder network and LSTM was used in [111] with Fire dilated and D-Fire dilated layers as a replacement for standard convolutional layers. The Fire dilated modules add an extra dilation rate in the kernel by inserting zeros between the consecutive values of the kernel and skip connections were applied to keep the temporal information of the image. Using the Fire dilated module, the network extracted more image information by adding extra parameters. Between the encoder and decoder, an LSTM module is added which is a special RNN structure. LSTM along with propagating the characteristics also captures the temporal dependencies between consecutive frames. Images were preprocessed by cropping the image based on ROI and resized to 80×80. A total of 2900 images from 145 subjects were used to evaluate the performance of the model and two experts manually labeled the images. DSC, Jaccard distance, accuracy, and positive predictive value (PPV) were used as evaluation metrics. The model achieved the DSC 0.960, Jaccard 0.903, accuracy 0.991, and PPV of 0.960 for LV. The proposed model was compared with simple Conv-Deconv, SegNet, FCN, and U-Net architectures.

A segmentation-based deep multitask regression learning model (Indices-JSQ) was proposed in [112]. The model is mainly divided into two parts. The first part is a segmentation network named Img2Contour and the second part is a multitask regression model (Contour2Indices). The segmentation model is based on deep convolutional encoder-decoder architecture with three convolution layers. The ReLU activation function along with Max-pooling was employed. Feature maps were generated by the use of the convolution layers with the kernel size of 5×5. This part segmented the LV and then passed the information to the next part of the model. The second part consists of RNN with LSTM. Three parallel CNN architectures were used that differ in kernel size and pool size. For the 1st CNN model, kernel size and pool size were 3×3 and 2×2, the 2nd model was 3×3 and 5×5, and the 3rd model have the same size of kernel and pool, i.e., 5×5. The dropout layer was used to avoid the overfitting problem. Information was passed to the LSTM which further quantifies the indices. A total of 2900 short-axis views of 145 subjects were used for training. DSC and mean absolute error (MAE) were used for the performance evaluation, and the performance is compared with other CNN models. Area, dimension, and wall thickness were also calculated as clinical indices. The proposed model automatically calculates these indices which is one of the major contributions of the model.

The tumor extraction using the convolutional LSTM network was performed in [113]. To prove the generalization of the proposed ST-ConvLSTM model, it was applied on 4D ultrasound for LV segmentation. The model was trained on the publicly available 3D + time ultrasound dataset challenge on Endocardial Three-dimensional Ultrasound Segmentation (CETUS) consisting of data from 15 patients. The proposed model achieved the DSC of 0.868 and 0.859 for ED and ES phases, respectively.

The classification and segmentation of LV from multiview (A2C, A3C, A4C) US images were implemented in [114]. Initially, pyramid dilated dense convolution (PDDConv) was used to extract multilevel and multiscale features. PDDConv network consists of batch normalization, ReLU, and dilated convolution. After extracting the features, hierarchical convolutional layers with LSTM recurrent units (hConvLSTM) were used for segmentation. The fully connected layers were used to perform the classification task using 3DCNN. Data of three different views, i.e., A2C, A3C, and A4C with 150 patients for each view yielding a total of 450 patients' data consisting of 13,500 frames, were utilized for training and testing. Furthermore, the model was trained and tested using the publicly available CAMUS dataset which has 1800 frames. To evaluate the performance of the models, MAD, DSC, and HD matrices were used. DSC of 0.92 for all A2C, A3C, and A4C views was obtained. The mean HD of 6.06 mm, 5.96 mm, and 6.06 and mean MAD of 2.80 mm, 2.77 mm, and 2.83 were achieved for A2C, A3C, and A4C views, respectively. The proposed model was compared with U-Net, ACNN, and U-Net++ and achieved better results. The EDV, ESV, and EF for the CAMUS dataset were also estimated using the segmented LV.

4.3.4. Alternative CNN Models. A DL model was proposed to segment the LV and calculate such as cavity area, MYO area, cavity dimension, and wall thickness [115]. The model is named cascaded segmentation and regression network (CSRNet) and has two parts: a CNN model that segments the LV and a regression model to quantify the LV metrics. The dense connected convolutional neural network (DenseNet) was employed to reduce the number of learning parameters. The network mainly consists of three dense and three transition blocks. It generates three different probability maps for background, MYO, and cavity. Output from the last layer was fed to the regression component and passes to a CNN model with three convolution layers and two fully connected layers. To train the network, 2900 images (145 subjects) were used. These images were parted into 2320 training and 580 for testing. Several preprocessing methods such as landmark labeling, rotation, ROI cropping, and resizing were also applied to the images. DSC is calculated and compared with U-Net. The performance of DenseNet was better and achieved 0.989, 0.886, and 0.959 for background, MYO, and cavity. Similarly, the number of parameters, training, and testing time of CSRNet were compared with U-Net and DenseNet. The CSRNet has 0.6 M learning parameters with 17.62 training time and 1.20 sec testing time in 100 epochs.

A good initialization is a key parameter that optimizes the CNN model quickly. In [116], an initialization method was designed for the DCNN model to segment LV using MRI images. The model was trained and tested using two initialization methods: random initialization and Gabor filter initialization. Gabor filters can provide an accurate description of most spatial characteristics of simple receptive fields. Furthermore, spectral and spatial domains were simultaneously optimized in these filters which minimized the number of features. The authors demonstrated that using Gabor filter initialization requires less amount of training data and less complexity due to lower parameters. The York Cardiac Segmentation database (5011 images) was used for training. The model achieved the DSC of 0.798 with random initialization and 0.80 with Gabor initialization, while if Gabor filtered was maintained, the value further increased to 0.803.

A dense V-Net model was proposed which is based on V-Net architecture [117]. Few dense layers were added to the original V-Net model to improve the performance. For training, 30 patients' data (86 frames and each frame containing 73 images) were collected and manually labeled by 3 experts. The improvement of the proposed model was shown by comparing it with U-Net, FCN, and V-Net. The proposed model achieved a DSC of 0.90.

A transformers-based [5] DL model was designed to handle the sequential data. Transformers were mainly used for natural language processing and in [118] it is used to learn the image parameters. In the first part, 3D LV volume was passed to the transformer net which consists of 3D Conv layers, batch normalization, ReLU, Max-pooling layers, and fully connected layers. These layers extracted the transform parameters from the LVV and were inserted into AtlasNet, a new shape generation framework. The Atlas network has several advantages such as improved precision and generalization capabilities, and the possibility to generate a shape of arbitrary resolution without memory issues. AtlasNet consists of deformable layers and generates the 3D LV shape using the parameters achieved from the transformer. DSC, MSD, and HD were used for evaluation and achieved 0.91 ± 0.027, 1.99 ± 0.64, and 8.92 ± 7.16 respectively.

The CNN models such as FCN and U-Net focused on single-frame image processing. While, in the study [119], a dense RNN was proposed to segment the LV from a four-chamber view of the MRI time sequence. RNN can deal with sequential information. In RNN, information from the previous cell was transmitted to the next LSTM cell, but the first cell does not get any previous information. The proposed model used the two RNN models. The first layer of the second RNN model, which performs the segmentation, receives the information from the first RNN model. In this experiment, data from 137 patients were used. The performance of the model was compared with state-of-the-art CNN models. The proposed model achieved the IoU of 92.13%. Few examples of the segmented LV by CNN models are depicted in Figure 9.

5. Discussion

The performance of DL methods depends on various parameters, and the time for the data processing is based on hardware. The details of the several modified models and proposed architectures are explained in Section 4. Here, in this section, some important data from the reviewed literature are presented. The section is divided into five sections and conveyed in a tabular form so that readers can have an overview of all important information related to hardware, software, imaging modality, database, architecture, and results.

5.1. Imaging Modality. For the analysis of cardiac diseases, different imaging modalities have been used such as the US, CT scan, and MRI. Due to its high resolution, MRI is the gold

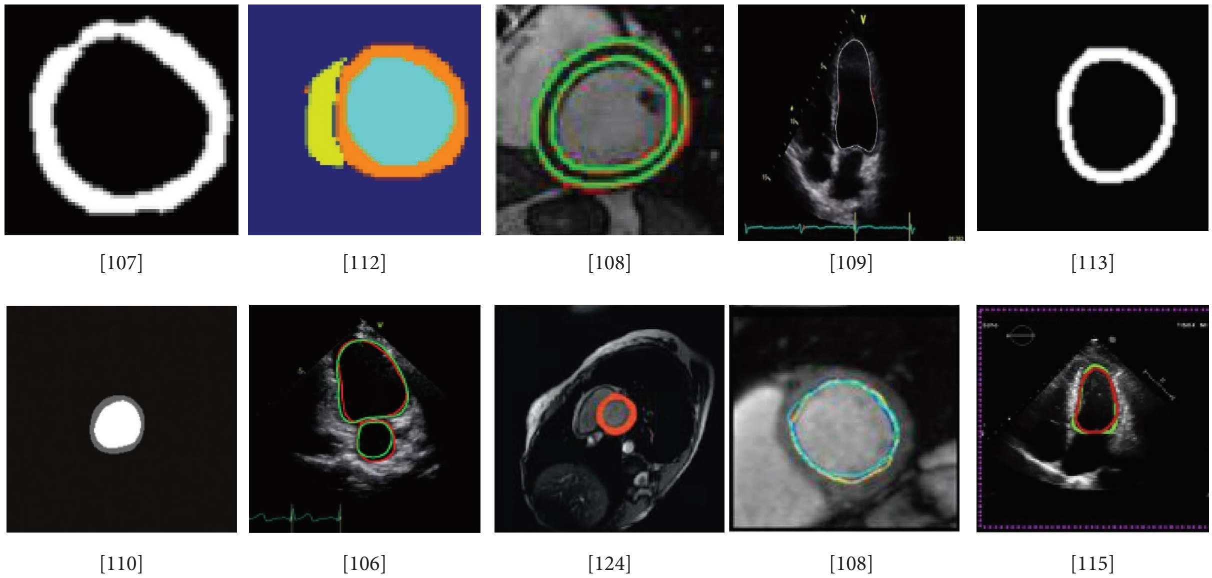

Figure 9: Sample of segmented images using other CNN models.

standard and is mostly used. On the contrary, US images are also highly recommended due to their ease of use and low cost. The third type of image used for the cardiac analysis is CT.

5.2. Architectures. Several CNN architectures are used by researchers for LV segmentation. The U-Net architecture is specifically designed for medical images; therefore, the use of U-Net and its variants are mostly used for the segmentation of LV. Besides U-Net architecture, FCN is the second most used network architecture for LV segmentation. Table 1 shows the CNN architectures used for LV segmentation.

5.3. Hardware. During the training process, the neural networks learn millions of weights. It may take several days to train such a huge number of weights on CPUs. The training time taken by the machine is one of the parameters to be focused on while implementing the models. Therefore, for the processing of DL models, hardware configuration plays an important role. A striking option for DL is a GPU. The use of GPUs makes the training and testing process fast, and results can be attained and compared in a short time. Hardware configurations used by authors for LV segmentation are listed in Table 2.

5.4. Software. An appropriate software framework is necessary to execute the complex DL architectures. Various frameworks have been used to implement the LV segmentation through DL architectures. These frameworks are generally used in Python programming. Python is an open-source programming language; furthermore, it supports a remarkable set of easy to utilize library functions for the execution of DL models; therefore, Python is widely used in DL-based applications. The software frameworks described in this section are primarily developed in Python language. The most general among them are TensorFlow, Theano, Keras, CAFFE, Torch, and Deeplearning4j. Few researchers have also used MATLAB as a programming language. Software used by researchers is enlisted in Table 3.

Table 1: Studies used different CNN models for LV segmentation.

Architecture	Study
FCN	[38, 49, 49, 57, 61–63, 66, 68, 69, 75]
U-Net	[77–86, 88–104, 120]
Other CNN models	[64, 105–109, 111–119, 121, 122]

5.5. Dataset. The performance of DL models is highly affected by the dataset. The number of images or number of patient data used to train and test the model is one of the key attributes of LV segmentation. Most researchers have used self-collected data, but, at the same time, several public datasets are also available. The details of the datasets are explained below and summarized in Table 4.

Data are from the 2009 Cardiac MR Left Ventricle Segmentation Challenge, often known as the Sunnybrook Cardiac Data. The data collection includes 45 cine-MRI images from a variety of different people and pathologies.

After registering on a website dedicated to the online evaluation, the ACDC database is made accessible to participants through two datasets. One dataset, referred to as the training dataset, contains 100 patients and manual references based on the study of one clinical expert. Second is a testing dataset consisting of fifty additional cases without manual annotations.

The MICCAI 2009 database contains 45 samples of short-axis cine MR images, 15 training cases, 15 test cases, and 15 online cases, which are randomly divided. The MICCAI 2018 challenge dataset comprises 145 participants'

Table 2: Details of hardware for LV segmentation.

Study	Hardware
[75]	Nvidia Tesla K80 GPU
[63]	CPU: Intel 4790k, GPU: NVIDIA TitanX
[66]	Intel Xeon(R) E5-2640 CPU @ 2.60 GHz, NVIDIA Tesla K40c GPU, 128 GB RAM
[38]	Intel (R) Core (TM) i7-6700 CPU @ 3.40 GHz with 4 cores and 32 GB RAM; the graphics processing unit used was an Nvidia GTX 1080Ti model with 11 GB RAM and 3584 CUDA cores
[69]	Intel (R) Xeon (R) processor ES-1650 at 3.50 GHz with 12 cores; Nvidia Quadro K4200 model with 4 GB of RAM and 1440CUDA cores
[82]	NVIDIA DIGITS DevBox
[83]	Intel i7-6700 CPU and an NVIDIA GeForce GTX 980M GPU
[84]	Nvidia GTX 1070 GPU
[85]	3.4 GHz Core i7 CPU, 64 GB RAM, Nvidia TiTan X (12 GB memories)
[91]	GeForce GTX 1080; Nvidia, Santa Clara, Calif
[90]	Nvidia GTX 1080Ti
[95]	Titan Xp GPU donation from NVIDIA Corporation
[96]	NVIDIA GeForce Titan X Pascal GPU
[81]	NVidia GTX 1080 Ti (12 GB)
[120]	Nvidia 11 GM RAM
[98]	8 GB GPU (NVIDIA GeForce GTX 1080).
[92]	Nvidia Tesla M60 GPUs (8 G RAM).
[100]	12 GB of RAM, a GPU-based graphic card with 2496 CUDA cores (Tesla K80), and an Intel Xeon CPU.
[77]	(Intel(R) CPU i7-7770K, 4.2 GHz, 16G RAM) with an NVIDIA GPU (GeForce, GTX TITAN X, NVIDIA Corp., Santa Clara, CA, USA)
[78]	Two Intel Xeon 8 core CPUs, 12 GB of RAM, and an NVIDIA Quadro P6000 GPU
[88]	Four NVIDIA GTX 2080Ti GPU cards, each with 11 GB RAM
[101]	3 Nvidia GTX 1080 Ti GPU
[80]	NVIDIA Titan GPU
[104]	NVIDIA GeForce GTX 1080 Ti GPU
[111]	Intel Core i5-7400 CPU. The graphics card is an NVIDIA GeForce GTX 1060
[115]	GeForce GTX 1080 ti GPU
[107]	Pentium dual-core 2.60 GHz hardware
[108]	CPU of AMD Phenom II X6 1055T Processor 2.8 GHz, 8G RAM, and VGA card of NVIDIA GeForce GTX 960 (CUDA v6.5)
[64]	GeForce GTX 1050 (4 GB GDDR5 dedicated) on an Intel Core i7-7700HQ (2.8 GHz, 6 MB cache, 4 cores) computer with 16 GB DDR4-2400 SDRAM
[105]	GTX 1080Ti graphic processor
[121]	GTX 1080Ti graphic processor
[117]	GTX 1080Ti graphic processor
[118]	NVIDIA Titan X GPU on Dell T7920 (GPU is Core I7, and memory size is 24 GB)
[113]	DELL TOWER 7910 workstation with 2.40 GHz Xeon E5-2620 v3 CPU, 32 GB RAM, and an Nvidia TITAN X Pascal GPU of 12 GB of memory
[114]	Two Intel Xeon 2.10 GHz CPU and four 12 GB Nvidia Titan XP GPU
[122]	GTX 1080Ti
[119]	NVIDIA Tesla P100

Table 3: Detail of software used for LV segmentation.

Study	Software
[57]	TensorFlow
[75]	TensorFlow
[63]	Not reported
[66]	Keras
[38]	MATLAB R2015b
[69]	Café
[82]	Keras
[83]	TensorFlow
[84]	TensorFlow
[85]	Café
[91]	TensorFlow
[81]	Keras

Table 3: Continued.

Study	Software
[120]	MATLAB 2019a
[98]	TensorFlow
[92]	Python/Keras
[100]	TensorFlow r1.12 and Keras 2.2.4.
[86]	Keras
[77]	MATLAB 2013a
[99]	Python with Keras-TensorFlow
[78]	TensorFlow/Ubuntu 18.04
[88]	Pytorch/Ubuntu18.04
[101]	Keras
[102]	Keras
[80]	MATLAB R2020
[89]	Keras
[106]	TensorFlow
[111]	Keras
[115]	TensorFlow
[107]	MATLAB
[108]	MATLAB *R* 2016b
[64]	TensorFlow
[105]	TensorFlow
[121]	TensorFlow
[116]	MatConvNet, an open-source library in MATLAB
[117]	TensorFlow
[118]	Pytorch
[113]	TensorFlow
[114]	TensorFlow
[122]	Anaconda 5.0.1 (python 3.5), TensorFlow, and Tensorlayer environment
[119]	PyCharm

Table 4: The detail of datasets used for LV segmentation.

Study	Dataset
[63, 68, 69, 81, 95, 96, 102],	Sunnybrook
[57]	TWINS-UK
[61, 66, 77, 95, 97, 103, 104, 120],	ACDC
[38, 61, 66, 85, 86, 107, 121],	MICCAI
[92, 94, 100, 114]	CAMUS
[101, 104]	LVSC
[97, 101]	STACOM
[77]	(UKBB)
[81]	Cardiac Atlas
[113]	CETUS
[103]	TOF
[62]	Own dataset (220 subjects)
[75]	Own dataset (5008 subjects and 93,500 images)
[61]	Own dataset
[49]	Own dataset 1100 subjects
[49]	Own dataset 1100 subjects
[82]	Own dataset (69 images)
[83]	Own dataset (500 patients)
[84]	Own dataset (250 patients)
[91]	Own dataset (596 subjects)
[90]	Own dataset (94 cases)
[98]	York + own dataset (17,683 images)
[100]	Own dataset (1080 + 290) +
[99]	Own dataset (5000 Pocus + 16000 cart base)
[78]	Own dataset: 492 scans
[88]	Own dataset 25,027 scans ($N = 12{,}984$ patients)

Table 4: Continued.

Study	Dataset
[79]	Own dataset 23 sequences (670 images)
[93]	Four different datasets
[80]	Kaggle, 484 examinations
[89]	Own dataset 563 patients
[106]	143 postinfarction patients, LUMC
[111]	Own dataset (2900 2D short-axis cine MR images of 145 subjects)
[115]	Own dataset (2900 2D short-axis cine MR images of 145 subjects)
[108]	Own dataset
[64]	Own dataset (30 scans and 2000 images)
[112]	Own dataset (2900 short-axis cardiac MR images of 145 subjects)
[109]	Own dataset (900 cases)
[105]	Own dataset (127 videos)
[116]	York cardiac segmentation database
[117]	Own dataset (30 patients)
[118]	Own dataset (50 scans)
[122]	Cap a total of 2490 images from 83 subjects
[119]	Own dataset 137 patients

processed CMR sequences. The ages of the individuals range from 16 to 97, with an average of 58.9 years.

The CAMUS dataset includes clinical exams performed on 500 patients at the University Hospital of St. Etienne (France). The LVSC dataset is accessible to the general public as part of the 2011 STACOM short-axis cine MRI semi-automatic LV myocardial segmentation challenge. This dataset is comprised of 200 individuals with myocardial infarction and coronary artery disease.

The short-axis steady-state free precession cine MRI from the Cardiac Atlas Project database is used to make up the STACOM dataset. In total, 100 individuals with post-myocardial infarction and coronary artery disease are included in the dataset. Every image contains a ground truth annotation.

The TWINS-UK is a volunteer register consisting of more than 12,000 twins. One thousand four hundred and sixty eight consecutive female volunteers (mean age 62 9 years) were recruited for this investigation. Each dataset had 12 to 14 short-axis cine that were continuous and evenly spaced from the atrioventricular (AV) ring to the apex, covering both ventricles.

The UKBB dataset is comprised mostly of a large number of healthy volunteers. By stacking a series of 2D cine images, 3D images of the LV and RV were created. LV, MYO, and RV were manually segmented in the ES and ED phases by 8 observers under the direction of 3 lead investigators, and hundred subjects were chosen.

The Cardiac Atlas Project offers CMR for 95 individuals with coronary artery disease and mild-to-moderate left ventricular dysfunction from prospective, multicenter, and randomised clinical studies. Sufficient slices along the short axis were collected to cover the whole heart in SAX. Also included in these acquisitions was the manual segmentation of the myocardium. The CETUS dataset came from 15 patients. Each patient had 13–46 3D volumetric imaging sequences, and each sequence had two manually segmented volumes at the end-diastole (ED) and end-systole (ES) phases. Figure 10 is an illustration of original and labeled image taken from four distinct datasets.

5.6. Results. The segmentation performance of models is evaluated using well-known evaluation matrices such as DSC, HD, and Jaccard distance, although some authors also used other matrices for accuracy, sensitivity, etc.

The DSC [123] is overlap based and calculated using equation (1). In the equation, S_{GT} represents the ground-truth image that represents the original LV size and boundary. S_{Seg} is the segmented mask by the model. To calculate the DSC, the intersection region of two masks is divided by the total region of both masks. The range of DSC is 0 and 1, where 0 represents no similarity or overlap and 1 represents exact overlap:

$$DSC = \frac{2\left|S_{GT} \cap S_{Seg}\right|}{\left|S_{GT}\right| + \left|S_{Seg}\right|}. \tag{4}$$

The HD [124] is a spatial distance-based index to measure the "closeness" of two sets of points. The HD between two-point sets A and B is defined by equation (2).

$$d_H(A, B) = \max(h(A, B), h(B, A)), \tag{5}$$

where $h\ (A,\ B)$ is direct Hausdorff distance, and it can be calculated by equation (3).

$$h(A, B) = \max_{a\epsilon A} \min_{b\epsilon B} \|a - b\|, \tag{6}$$

where $\|a - b\|$ is any norm value, e.g., Euclidean distance.

The Jaccard distance [123] can be calculated using the formula presented in equation (4).

$$J = \frac{|X \cap Y|}{|X\, U\, Y|}, \tag{7}$$

where X and Y are the ground-truth and segmented output images, respectively.

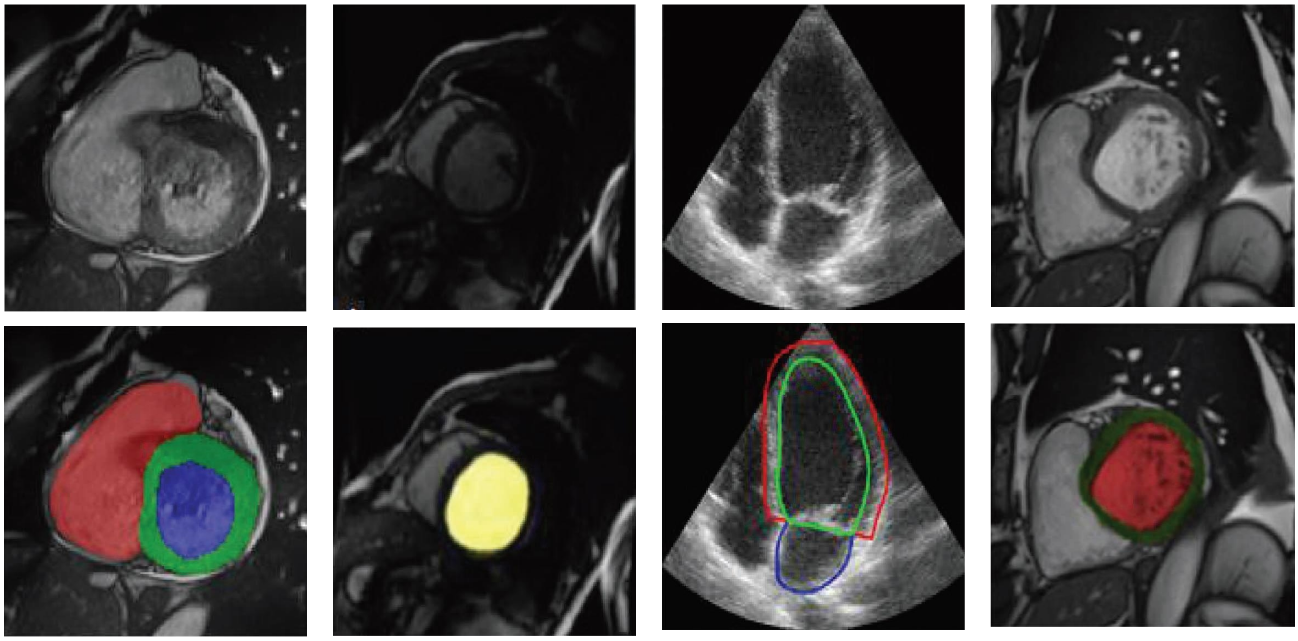

Figure 10: Example of the original image (top) and ground truth (bottom) of (a) ACDC, (b) Sunnybrook, (c) CAMUS, and (d) MICCAI datasets.

Similarly, the precision, specificity, and IoU can be computed with the use of equations (5)–(7), respectively:

$$\begin{aligned}\text{Accuracy} &= \frac{TP+TN}{TP+TN+FP+FN},\\ \text{Specificity} &= \frac{TP}{TP+FP},\\ \text{IoU} &= \frac{\text{overlapping area}}{\text{combined area}}.\end{aligned} \tag{8}$$

The assessment matrices and theoretical values attained by researchers are shown in Table 5.

6. Challenges and Future Outlook

The article shows that DL approaches have equally performed or outperformed the previous state-of-the-art LV segmentation techniques. DL algorithms are expected to completely replace the current LV segmentation techniques. Given this, it is reasonable to consider whether DL techniques can be directly applied to real-world applications to reduce medical practitioners' workload. However, there are still challenges to make the existing DL methods viable for real-time applications.

In medical images and, particularly, cardiac images, acquiring the annotated images is the most prevalent challenge. As this article demonstrates, most of the research employed supervised learning, which necessitates the usage of a significant number of annotated images. To properly label, the LV needs both specialised knowledge and a significant investment of time. As a result, the datasets of the annotated LV are quite limited in comparison to other publicly available datasets in other fields, such as natural images.

Moreover, the performance of DL on data that differs from the training dataset is another challenge. Even though the trained DL model is tested on unseen data, the training and testing data are received from the same source, such as the same sort of scanner. The model does not provide the anticipated outcome if new types of data, e.g., from multiple scanners or different disease patients, are used to test the model. A few studies have utilized training data for LV segmentation from different sources and scanners to train the model to get over this problem.

Also, the DL performance is highly dependent on the quality of the training images. Many imaging modalities such as CT and US are of low quality due to many factors such as speckle noise and poor contrast ratio. To produce high-quality images, many researchers use some sort of data preprocessing.

Therefore, further studies are required to investigate the methods to improve the image quality. Therefore, the efficiency of the DL model and the accuracy of LV segmentation may be significantly boosted by improving the image quality. There is a significant demand for a DL-based system that has the ability to improve image quality in an efficient and effective manner while simultaneously reducing noise. Therefore, the LV segmentation will be considerably more accurate when the segmentation and enhancing methods are combined.

In addition, the integration of LV segmentation algorithms with additional patient data, such as patient history, age, and demographics, is an important area of the article

Table 5: The details of results achieved for LV segmentation.

Study	Results
[57]	DSC (0.981 ± 0.025), APD (6.290 ± 8.381) mm, and conformity index (0.961 ± 0.0551)
[62]	DSC (0.934 ± 0.041)
[75]	DSC (0.94 ± 0.04), HD (3.16 ± 0.98), and MCD (0.35)
[63]	Volume estimation
[66]	DSC (0.963 ± 0.026) and (0.932 ± 0.075) and HD (5.58 ± 3.75) and (6.92 ± 4.69) for ED and ES, respectively
[61]	DSC (0.93 and 0.94) and HD (9.52 and 6.71) with cross-entropy loss and radial distance, respectively
[49]	DSC (0.883 ± 0.062), JD (0.795 ± 0.07), HD (13.4 ± 12.2) mm, MSD (1.0 ± 2.4) accuracy (0.883), sensitivity (0.921), and specificity (0.997)
[38]	APD (1.71)
[69]	DSC (0.93 ± 0.02) and (0.92 ± 0.01), APD (2.23 ± 0.31) and (2.13 ± 0.28) mm, and good contour (94.19 ± 7.38) and (95.64 ± 7.11) for endo and epi
[68]	DSC (0.93 ± 0.03) and APD (1.41 ± 0.24)
[49]	DSC (88.3 ± 6.2), Jaccard (79.5 ± 7.0), MSD (1.0 ± 2.4) mm, and HD (13.4 ± 12.2) mm
[82]	DSC (0.86 ± 0.06)
[83]	A bland-altman analysis mean difference of -13.7% and a standard deviation of 8.6% for EF
[84]	DSC (0.87 ± 0.03)
[85]	DSC (0.90 ± 0.05) and (0.81 ± 0.005) and HD (7.6 ± 4.5) and (0.91 ± 0.018) for endo and epi, respectively
[91]	Accuracy (0.93 ± .006) and (0.94 ± 0.005) for endo and epi
[90]	DSC (0.923 ± 0 : 03) and (0 : 924 ± 0 : 04) for ALAX and A2C/A4C
[95]	DSC (0.968) and (0.944) and HD (4.855) and (6.245) mm for ED and ES, respectively
[96]	DSC (0.93 ± 0.03) and sensitivity (0.97)
[81]	DSC (0.87 ± 0.0053), (0.869 ± 0.0051), and (0.868 ± 0.0047), MSE (0.0135 ± 0.0006), (0.0136 ± 0.0008), and (0.0138 ± 0.0007), and MAE (0.0137 ± 0.0006), (0.0138 ± 0.0008), and (0.0140 ± 0.0007) for U-net-BN-RL, uInception, and uXception, respectively
[120]	DSC (0.919) and IOU (0.860)
[97]	DSC (94.8 ± 3.3)
[98]	DSC (0.87 ± 0.02)
[92]	DSC (0.95 ± .023) and (0.95 ± 0.039), HD (5.3 ± 3.6) and (5.5 ± 3.8) mm, MSD (1.6 ± 1.3) and (1.6 ± 1.6) for ED and ES, respectively
[100]	DSC (0.94 ± 0.12), HD (1.62 ± .05), JD (0.98 ± .01), and MSD (1.32 ± .53)
[86]	DSC (0.893)
[77]	DSC (0.921), HD (3.9 mm), and ASSD (1.43 mm)
[99]	DSC (82.6 ± 12.3) and (88.3 ± 5.0) for low- and high-quality images, respectively
[78]	DSC (0.94)
[88]	DSC (0.87 ± 0.08) (3CS) and (0.82 ± 0.22) (2CS)
[101]	Jaccard (0.75), sensitivity (0.87), and specificity (0.92)
[102]	DSC (0.926), Jaccard (0.866), precision (0.87), FPR (0.120), and recall (0.945)
[103]	DSC (0.93 ± 0.04)
[79]	DSC (0.917), MAD (1.66 pixels), and overlap (85.57%)
[93]	
[80]	DSC (0.87 and 0.95) with and without transfer learning
[104]	DSC (0.900 and 0.901) and HD (8.330 and 11.040) for ED and ES
[94]	DSC (0.921)
[89]	DSC (93.6) and accuracy (97.7)
[106]	DSC (0.71 ± 0.09)
[111]	DSC (0.960 ± 0.008), JD (0.903 ± 0.026), accuracy (0.991 ± 0.005), and PPV (0.960 ± 0.040)
[115]	DSC (0.959) and HD (3.557),
[107]	DSC (0.97 and 0.96) for endo and epi
[108]	DSC (0.921 ± 1.87), JD (0.86 ± 0.007), and HD (6.29 ± 2.01 mm)
[64]	DSC (0.712 ± 0.031), sensitivity (0.881 ± 0.17), accuracy (0.968 ± 0.032), and specificity (0.978 ± 0.029)
[112]	DSC (0.87 ± 0.06)
[109]	DSC (0.90 ± 0.03) and (0.93 ± 0.02) and JD (0.80 ± 0.06) and (0.76 ± 0.09) for endo and epi
[105]	DSC (0.951 ± 0.031), accuracy (0.987 ± 0.007), precision (0.960 ± 0.050), specificity (0.996 ± 0.006), and sensitivity (0.950 ± 0.050)
[121]	DSC (0.803 ± 0.204), JD (0.706 ± 0.214), sensitivity (0.859 ± 0.2), specificity (0.998 ± 0.002) PPV (0.771 ± 0.206), and NPV (0.999 ± 0.001)
[116]	DSC (0.803), pixel accuracy (0.973), specificity (0.984), sensitivity (0.841), and mean accuracy (0.903)
[117]	DSC (0.9 ± 0.12)
[118]	DSC (0.91 ± 0.027), HD (8.92 ± 7.16), and MSD (1.99 ± 0.64)
[113]	DSC (0.868 ± 0.021) and (0.859 ± 0.016) for ES and ED, respectively
[114]	DSC (0.92 ± 0.04), HD (6.06 ± 2.11), (5.96 ± 2.07), and (6.06 ± 2.04) mm, MSD (2.80 ± 1.02), (2.77 ± 1.05), and (2.83 ± 1.04) mm for A2C, A3C, and A4C, respectively
[122]	Localization accuracy (6.45 ± 4.53 mm)
[119]	IoU (92.13%)

that might further improve the performance of clinical decision making and assist physicians in calculating clinical indices.

As discussed above, one of the main challenges is the availability of large datasets, and there is abundant new research aimed at levitating the limited dataset size problem, and some LV datasets are publicly available. There is a pressing need for architectures and algorithms that have been purposed and built for the segmentation of medical images and, therefore, LVs, and that can also perform admirably when applied to limited datasets.

7. Conclusion

In this article, a comprehensive review of the literature focused on the analysis of cardiac images using DL for LV segmentation is presented. In the field of image processing CNN, a subbranch of DL has shown very promising results for different types of identification including classification, object detection, and segmentation. CNN is also seen as a futuristic approach specifically in image processing. The application of CNN in medical images is extensive. Therefore, this work details and summarizes the uses of CNN for LV segmentation. The most common imaging modalities (MRI, US, and CT scan) were briefly introduced in the article. The basics of CNN architectures were also discussed to have a better understanding of these models. Among the different CNN models, FCN, U-Net, and modified model two are mostly used for LV segmentation. This work also gives a detailed discussion of hardware, software, and dataset used for LV segmentation. The different evaluation matrices used for the performance analysis of the models were also discussed. A comparative summary was tabulated to ease the comparison for the readers. This work lays a foundation for the readers for an instinctive understanding of DL methods used for LV segmentation specifically for medical and cardiac images.

Data Availability

All the data used to support the findings of the study are included within the article as references.

Conflicts of Interest

The authors declare that they have no conflicts of interest.

Acknowledgments

This work was supported by the Fundamental Research Grant Scheme (FRGS), Ministry of Higher Education Malaysia, and University Malaya under the project no. FRGS/1/2019/TK04/UM/01/2.

References

[1] J. Dayhoff and J. DeLeo, “Artificial Neural Networks,” *Cancer*, vol. 91, 2021.

[2] Y. Chen and F. Bastani, “Optimal initialization for multilayer perceptrons,” *IEEE International Conference on Systems, Man and Cybernetics*, vol. 8, pp. 370–372, 1990.

[3] P. Simard, L. Bottou, P. Haffner, and Y. LeCun, “Boxlets: a fast convolution algorithm for signal processing and neural networks,” in *Proceedings of the Advances in Neural Information Processing Systems*, vol. 11, Denver, CO, USA, November 1999.

[4] M. Schuster and K. K. Paliwal, “Bidirectional recurrent neural networks,” *IEEE Transactions on Signal Processing*, vol. 45, no. 11, pp. 2673–2681, 1997.

[5] M. Jaderberg, K. Simonyan, A. Zisserman, and K. Koray, “Spatial transformer networks,” in *Proceedings of the Advances in Neural Information Processing Systems*, vol. 28, San Francisco. CA. USA, 2015.

[6] S. Hochreiter and J. Schmidhuber, “Long short-term memory,” *Neural Computation*, vol. 9, no. 8, pp. 1735–1780, 1997.

[7] G. E. Hinton, S. Osindero, and Y.-W. Teh, “A fast learning algorithm for deep belief nets,” *Neural Computation*, vol. 18, no. 7, pp. 1527–1554, 2006.

[8] C. Peng, W. Bu, J. Xiao, K. c. Wong, and M. Yang, “An improved neural network cascade for face detection in large scene surveillance,” *Applied Sciences*, vol. 8, no. 11, p. 2222, 2018.

[9] R. Kute, V. Vyas, and A. Anuse, “Transfer Learning for Face Recognition Using Fingerprint Biometrics,” *J. King Saud Univ. - Eng. Sci.*, 2021.

[10] F. C. Soon, H. Y. Khaw, J. H. Chuah, and J. Kanesan, “PCANet-based convolutional neural network architecture for a vehicle model recognition system,” *IEEE Transactions on Intelligent Transportation Systems*, vol. 20, no. 2, pp. 749–759, Feb. 2019.

[11] X. Wang, W. Zhang, X. Wu, L. Xiao, Y. Qian, and Z. Fang, “Real-time vehicle type classification with deep convolutional neural networks,” *Journal of Real-Time Image Processing*, vol. 16, no. 1, pp. 5–14, Feb. 2019.

[12] M. Rohmatillah, H. Suyono, R. Rahmadwati, and S. Hadi Pramono, “Implementation of deep learning in spatial multiplexing MIMO communication,” *Indonesian Journal of Electrical Engineering and Computer Science*, vol. 12, no. 2, p. 699, Nov. 2018.

[13] E. Al Hadhrami, M. Al Mufti, B. Taha, and N. Werghi, “Ground moving radar targets classification based on spectrogram images using convolutional neural networks,” in *Proceedings of the 2018 19th International Radar Symposium (IRS)*, pp. 1–9, Bonn, Germany, Jun. 2018.

[14] J. Young, L. Kunze, V. Basile, E. Cabrio, N. Hawes, and B. Caputo, “Semantic web-mining and deep vision for lifelong object discovery,” in *Proceedings of the 2017 IEEE International Conference on Robotics and Automation (ICRA)*, pp. 2774–2779, Singapore, May 2017.

[15] Q. Guo and M. Zhang, “Implement web learning environment based on data mining,” *Knowledge-Based Systems*, vol. 22, no. 6, pp. 439–442, Aug. 2009.

[16] H. A. Pierson and M. S. Gashler, “Deep learning in robotics: a review of recent research,” *Advanced Robotics*, vol. 31, no. 16, pp. 821–835, Aug. 2017.

[17] R. Miyajima, “Deep learning triggers a new era in industrial robotics,” *IEEE MultiMedia*, vol. 24, no. 4, pp. 91–96, Oct. 2017.

[18] R. Ali, J. H. Chuah, M. S. A. Talip, N. Mokhtar, and M. A. Shoaib, “Crack segmentation network using additive

attention gate—csn-II," *Engineering Applications of Artificial Intelligence*, vol. 114, Article ID 105130, 2022.

[19] C. Chen, J. H. Chuah, R. Ali, and Y. Wang, "Retinal vessel segmentation using deep learning: a review," *IEEE Access*, vol. 9, Article ID 111985, 2021.

[20] L. K. Meng, A. Khalil, M. H. Ahmad Nizar et al., "Carpal bone segmentation using fully convolutional neural network," *Current Medical Imaging Formerly Current Medical Imaging Reviews*, vol. 15, no. 10, pp. 983–989, Nov. 2019.

[21] J. Islam and Y. Zhang, "A Novel Deep Learning Based Multi-Class Classification Method for Alzheimer's Disease Detection Using Brain MRI Data," *Lecture Notes in Computer Science*, pp. 213–222, Springer, New York, NY, USA, 2017.

[22] M. Hanif, A. Nizar, A. Khalil, C. K. Chan, N. P. Utama, and K. W. Lai, "Pilot Study on Machine Learning for Aortic Valve Detection in Echocardiography Images," *Journal of Medical Imaging and Health Informatics*, vol. 8, pp. 1–6, 2018.

[23] M. H. A. Nizar, C. K. Chan, A. Khalil, A. K. M. Yusof, and K. W. Lai, "Real-time detection of aortic valve in echocardiography using convolutional neural networks," *Current Medical Imaging Formerly Current Medical Imaging Reviews*, vol. 16, no. 5, pp. 584–591, 2020.

[24] G. Haskins, U. Kruger, and P. Yan, "Deep learning in medical image registration: a survey," *Machine Vision and Applications*, vol. 31, no. 1–2, p. 8, Feb. 2020.

[25] H. D. White, R. M. Norris, M. A. Brown, P. W. Brandt, R. M. Whitlock, and C. J. Wild, "Left ventricular end-systolic volume as the major determinant of survival after recovery from myocardial infarction," *Circulation*, vol. 76, no. 1, pp. 44–51, Jul. 1987.

[26] R. M. Norris, H. D. White, D. B. Cross, C. J. Wild, and R. M. L. Whitlock, "Prognosis after recovery from myocardial infarction: the relative importance of cardiac dilatation and coronary stenoses," *European Heart Journal*, vol. 13, no. 12, pp. 1611–1618, 1992.

[27] A. F. Frangi, W. J. Niessen, and M. A. Viergever, "Three-dimensional modeling for functional analysis of cardiac images, a review," *IEEE Transactions on Medical Imaging*, vol. 20, no. 1, pp. 2–5, 2001.

[28] Y. M. Liew, R. A. McLaughlin, B. T. Chan et al., "Motion corrected LV quantification based on 3D modelling for improved functional assessment in cardiac MRI," *Physics in Medicine and Biology*, vol. 60, no. 7, pp. 2715–2733, 2015.

[29] C. Mekkaoui, T. G. Reese, M. P. Jackowski et al., "Diffusion tractography of the entire left ventricle by using free-breathing accelerated simultaneous multisection imaging," *Radiology*, vol. 282, no. 3, pp. 850–856, 2017.

[30] S. Weingärtner, M. Akcakaya, S. Roujol et al., "Free-breathing combined three-dimensional phase sensitive late gadolinium enhancement and T 1 mapping for myocardial tissue characterization," *Magnetic Resonance in Medicine*, vol. 74, no. 4, pp. 1032–1041, 2015.

[31] M. Bustamante, S. Petersson, J. Eriksson et al., "Atlas-based analysis of 4D flow CMR: automated vessel segmentation and flow quantification," *Journal of Cardiovascular Magnetic Resonance*, vol. 17, no. 1, p. 87, 2015.

[32] A. W. Dowsey, J. Keegan, M. Lerotic, S. Thom, D. Firmin, and G.-Z. Yang, "Motion-Compensated MR Valve Imaging with COMB Tag Tracking and Super-resolution Enhancement," *Med Image Anal*, vol. 11, pp. 364–371, 2006.

[33] X. Zhuang, K. S. Rhode, R. S. Razavi, D. J. Hawkes, and S. Ourselin, "A registration-based propagation framework for automatic whole heart segmentation of cardiac MRI," *IEEE Transactions on Medical Imaging*, vol. 29, no. 9, pp. 1612–1625, 2010.

[34] K. Gul, A. S. Celebi, F. Kacmaz et al., "Tissue Doppler imaging must be performed to detect early left ventricular dysfunction in patients with type 1 diabetes mellitus," *European Journal of Echocardiography*, vol. 10, no. 7, pp. 841–846, Oct. 2009.

[35] J. C. Lyne and D. J. Pennell, "Cardiovascular magnetic resonance in the quantitative assessment of left ventricular mass, volumes and contractile function," *Coronary Artery Disease*, vol. 16, no. 6, pp. 337–343, Sep. 2005.

[36] M. Moriuchi, S. Saito, Y. Kasamaki, K. Komaki, K. Kanmatsuse, and K. Hayasaka, "Three-dimensional analysis of left ventricular geometry using magnetic resonance imaging: feasibility and comparison with echocardiographic analysis," *Journal of Cardiology*, vol. 42, no. 6, pp. 249–260, 2003.

[37] F. Bogazzi, M. Lombardi, E. Strata et al., "High prevalence of cardiac hypertophy without detectable signs of fibrosis in patients with untreated active acromegaly: an in vivo study using magnetic resonance imaging," *Clinical Endocrinology*, vol. 68, no. 3, pp. 361–368, Mar. 2008.

[38] J. Wu, Z. Gan, W. Guo, X. Yang, and A. Lin, "A fully convolutional network feature descriptor: application to left ventricle motion estimation based on graph matching in short-axis MRI," *Neurocomputing*, vol. 392, pp. 196–208, 2020.

[39] A. Khalil, A. Faisal, S.-C. Ng, Y. M. Liew, and K. W. Lai, "Multimodality registration of two-dimensional echocardiography and cardiac CT for mitral valve diagnosis and surgical planning," *Journal of Medical Imaging*, vol. 4, no. 3, p. 1, 2017.

[40] N. B. Schiller, P. M. Shah, M. Crawford et al., "Recommendations for quantitation of the left ventricle by two-dimensional echocardiography," *Journal of the American Society of Echocardiography*, vol. 2, no. 5, pp. 358–367, Sep. 1989.

[41] B. Dahlöf, R. Devereux, U. de Faire et al., "The losartan intervention for endpoint reduction (LIFE) in hypertension study: rationale, design, and methods. The LIFE study group," *American Journal of Hypertension*, vol. 10, no. 7, pp. 705–713, 1997.

[42] J. S. Gottdiener, J. Bednarz, R. Devereux et al., "American Society of Echocardiography recommendations for use of echocardiography in clinical trialsA report from the american society of echocardiography's guidelines and standards committee and the task force on echocardiography in clinical trials," *Journal of the American Society of Echocardiography*, vol. 17, no. 10, pp. 1086–1119, 2004.

[43] M. A. Shoaib, M. B. Hossain, Y. C. Hum, J. H. Chuah, M. I. Mohd Salim, and K. W. Lai, "Speckle noise diffusion in knee articular cartilage ultrasound images," *Current Medical Imaging Formerly Current Medical Imaging Reviews*, vol. 16, no. 6, pp. 739–751, 2020.

[44] M. B. Hossain, B. Pingguan-Murphy, Y. Chai Hum, and K. Wee Lai, "Contrast Enhancement of Ultrasound Image of Knee Joint Cartilage by Using Multipurpose Beta Optimized Recursive Bi-histogram Equalization Method," in *Proceedings of the 3rd IIAE International Conference on Intelligent Systems and Image Processing 2015*, pp. 37–43, Fukuoka, Japan, 2016.

[45] M. Mahesh and D. D. Cody, "Physics of cardiac imaging with multiple-row detector CT," *RadioGraphics*, vol. 27, no. 5, pp. 1495–1509, 2007.

[46] A. Khalil, S. C. Ng, Y. M. Liew, and K. W. Lai, "An overview on image registration techniques for cardiac diagnosis and treatment," *Cardiology Research and Practice*, vol. 2018, pp. 1–15, 2018.

[47] P. Stolzmann, H. Scheffel, P. T. Trindade et al., "Left ventricular and left atrial dimensions and volumes," *Investigative Radiology*, vol. 43, no. 5, pp. 284–289, May 2008.

[48] A. S. Celebi, H. Yalcin, and F. Yalcin, "Current cardiac imaging techniques for detection of left ventricular mass," *Cardiovascular Ultrasound*, vol. 8, no. 1, pp. 19–11, 2010.

[49] H. J. Koo, J. G. Lee, J. Y. Ko et al., "Automated segmentation of left ventricular myocardium on cardiac computed tomography using deep learning," *Korean Journal of Radiology*, vol. 21, no. 6, p. 660, 2020.

[50] J. Heaton, "Ian goodfellow, yoshua bengio, and aaron courville: deep learning," *Genetic Programming and Evolvable Machines*, vol. 19, no. 1–2, pp. 305–307, Jun. 2018.

[51] A. C. Ian Goodfellow and Y. Bengio, *Deep Learning*, Aaron Courville - Google Books, Quebec, Canada, 2016.

[52] A. G. Josh Patterson, *Deep Learning: A Practitioner's Approach*, O'Reilly Media, Inc, Sebastopol, CA, USA, 2017.

[53] K. Fukushima, "Neocognitron: a hierarchical neural network capable of visual pattern recognition," *Neural Networks*, vol. 1, no. 2, pp. 119–130, Jan. 1988.

[54] Y. LeCun, L. Boser, B. Denker, and J. S. Howard, "Handwritten Digit Recognition with a Back-Propagation Network," *Advances in neural information processing systems*, Morgan Kaufmann Publishers Inc, San Francisco, CA, USA, 1989.

[55] I. Arel, D. C. Rose, and T. P. Karnowski, "Deep machine learning - a new frontier in artificial intelligence research [research frontier]," *IEEE Computational Intelligence Magazine*, vol. 5, no. 4, pp. 13–18, 2010.

[56] E. Shelhamer, J. Long, and T. Darrell, "Fully convolutional networks for semantic segmentation," *IEEE Transactions on Pattern Analysis and Machine Intelligence*, vol. 39, no. 4, pp. 640–651, 2017.

[57] N. Savioli, M. S. Vieira, P. Lamata, and G. Montana, "Automated segmentation on the entire cardiac cycle using a deep learning work - flow," in *Proceedings of the 2018 Fifth International Conference on Social Networks Analysis, Management and Security (SNAMS)*, pp. 153–158, Valencia, Spain, Oct. 2018.

[58] P. Sermanet, D. Eigen, X. Zhang, M. Mathieu, R. Fergus, and Y. LeCun, "OverFeat: integrated recognition, localization and detection using convolutional networks," 2014, https://arxiv.org/abs/1312.6229.

[59] P. Krähenbühl and V. Koltun, "Efficient Inference in Fully Connected CRFs with Gaussian Edge Potentials," 2012, http://arxiv.org/abs/1210.5644.

[60] L. Sevilla-Lara, D. Sun, V. Jampani, and M. J. Black, "Optical flow with semantic segmentation and localized layers," in *Proceedings of the 2016 IEEE Conference on Computer Vision and Pattern Recognition (CVPR)*, pp. 3889–3898, Las Vegas, NV, USA, Jun. 2016.

[61] H. Abdeltawab, F. Khalifa, F. Taher et al., "A deep learning-based approach for automatic segmentation and quantification of the left ventricle from cardiac cine MR images," *Computerized Medical Imaging and Graphics*, vol. 81, Article ID 101717, 2020.

[62] C. Qin, B. Wenjia, S. Jo et al., "Joint learning of motion estimation and segmentation for cardiac MR image sequences," in *Lecture Notes in Computer Science*, pp. 472–480, Springer, New York, NY, USA, 2018.

[63] F. Liao, X. Chen, X. Hu, and S. Song, "Estimation of the volume of the left ventricle from MRI images using deep neural networks," *IEEE Transactions on Cybernetics*, vol. 49, no. 2, pp. 495–504, Feb. 2019.

[64] S. Moccia, R. Banali, C. Martini et al., "Development and testing of a deep learning-based strategy for scar segmentation on CMR-LGE images," *Magnetic Resonance Materials in Physics, Biology and Medicine*, vol. 32, no. 2, pp. 187–195, Apr. 2019.

[65] A. S. Hassanein, S. Mohammad, M. Sameer, and M. E. Ragab, "A Survey on Hough Transform, Theory, Techniques and Applications," 2015, http://arxiv.org/abs/1502.02160.

[66] Z. Ma, X. Wu, X. Wang et al., "An iterative multi-path fully convolutional neural network for automatic cardiac segmentation in cine MR images," *Medical Physics*, vol. 46, no. 12, pp. 5652–5665, 2019.

[67] Q. Zheng, H. Delingette, N. Duchateau, and N. Ayache, "3-D consistent and robust segmentation of cardiac images by deep learning with spatial propagation," *IEEE Transactions on Medical Imaging*, vol. 37, no. 9, pp. 2137–2148, 2018.

[68] M. Chen, L. Fang, and H. Liu, "Fr-Net: Focal loss constrained deep residual networks for segmentation of cardiac MRI," in *Proceedings of the 2019 IEEE 16th International Symposium on Biomedical Imaging (ISBI 2019)*, pp. 764–767, Washington, DC, USA, Apr. 2019.

[69] L. V. Romaguera, F. P. Romero, C. F. Fernandes Costa Filho, and M. G. Fernandes Costa, "Myocardial segmentation in cardiac magnetic resonance images using fully convolutional neural networks," *Biomedical Signal Processing and Control*, vol. 44, pp. 48–57, 2018.

[70] Y. Nesterov, "A method for solving the convex programming problem with convergence rate $O(1/k2)$," *Proc. USSR Acad. Sci*, vol. 269, pp. 543–547, 1983.

[71] T. Tieleman and G. Hinton, "Rmsprop: divide the gradient by a running average of its recent magnitude," *COURSERA Neural Networks Mach. Learn*, 2012.

[72] D. P. Kingma and J. Ba, "Adam: a method for stochastic optimization," 2014, https://arxiv.org/abs/1412.6980.

[73] M. D. Zeiler, "Adadelta: an adaptive learning rate method," 2012, https://arxiv.org/abs/1212.5701.

[74] J. C. Duchi, E. Hazan, and Y. Singer, "Adaptive Subgradient Methods for Online Learning and Stochastic Optimization," *The Journal of Machine Learning Research*, vol. 12, 2011.

[75] W. Bai, M. Sinclair, G. Tarroni et al., "Automated cardiovascular magnetic resonance image analysis with fully convolutional networks," *Journal of Cardiovascular Magnetic Resonance*, vol. 20, no. 1, p. 65, Dec. 2018.

[76] O. Ronneberger, P. Fischer, and T. Brox, *U-Net: Convolutional Networks for Biomedical Image Segmentation*, Springer Cham, New York, NY, USA, 2015.

[77] F. Guo, M. Ng, M. Goubran et al., "Improving cardiac MRI convolutional neural network segmentation on small training datasets and dataset shift: a continuous kernel cut approach," *Medical Image Analysis*, vol. 61, Article ID 101636, 2020.

[78] P. F. Ferreira, R. R. Martin, A. D. Scott et al., "Automating in vivo cardiac diffusion tensor postprocessing with deep learning–based segmentation," *Magnetic Resonance in Medicine*, vol. 84, no. 5, pp. 2801–2814, 2020.

[79] X. Zou, Q. Wang, and T. Luo, "A novel approach for left ventricle segmentation in tagged MRI," *Computers & Electrical Engineering*, vol. 95, Article ID 107416, 2021.

[80] T. Wech, M. J. Ankenbrand, T. A. Bley, and J. F. Heidenreich, "A data-driven semantic segmentation model for direct

cardiac functional analysis based on undersampled radial MR cine series," *Magnetic Resonance in Medicine*, vol. 87, no. 2, pp. 972–983, Feb. 2022.

[81] A. H. Curiale, F. D. Colavecchia, and G. Mato, "Automatic quantification of the LV function and mass: a deep learning approach for cardiovascular MRI," *Computer Methods and Programs in Biomedicine*, vol. 169, pp. 37–50, 2019.

[82] G. Veni, M. Moradi, H. Bulu, G. Narayan, and T. Syeda-Mahmood, "Echocardiography segmentation based on a shape-guided deformable model driven by a fully convolutional network prior," in *Proceedings of the 2018 IEEE 15th International Symposium on Biomedical Imaging (ISBI 2018)*, pp. 898–902, Washington, DC, USA, Apr. 2018.

[83] E. Smistad, A. Ostvik, I. M. Salte, S. Leclerc, O. Bernard, and L. Lovstakken, "Fully automatic real-time ejection fraction and MAPSE measurements in 2D echocardiography using deep neural networks," in *Proceedings of the 2018 IEEE International Ultrasonics Symposium (IUS)*, vol. 2018, pp. 1–4, Kobe, Japan, Oct. 2018.

[84] A. Østvik, E. Smistad, T. Espeland, E. A. R. Berg, and L. Lovstakken, "Automatic myocardial strain imaging in echocardiography using deep learning," in *Lecture Notes in Computer Science*, pp. 309–316, Springer Cham, New York, NY, USA, 2018.

[85] G. Luo, K. Wang, S. Cao, Q. Li, and H. Zhang, "A temporal area variation regularized deep learning network for left ventricle segmentation on cardiac magnetic resonance," *Computers in Cardiology*, vol. 2018, pp. 1–4, 2018.

[86] R. Chen, C. Xu, Z. Dong, Y. Liu, and X. Du, "DeepCQ: deep multi-task conditional quantification network for estimation of left ventricle parameters," *Computer Methods and Programs in Biomedicine*, vol. 184, Article ID 105288, 2020.

[87] M. Kesseböhmer and B. O. Stratmann, "Hölder-differentiability of Gibbs distribution functions," *Mathematical Proceedings of the Cambridge Philosophical Society*, vol. 147, no. 2, pp. 489–503, 2009.

[88] H. Xue, E. Tseng, K. D. Knott et al., "Automated detection of left ventricle in arterial input function images for inline perfusion mapping using deep learning: a study of 15, 000 patients," *Magnetic Resonance in Medicine*, vol. 84, no. 5, pp. 2788–2800, 2020.

[89] M. H. Jafari, G. Hany, L. Zhibin et al., "A unified framework integrating recurrent fully-convolutional networks and optical flow for segmentation of the left ventricle in echocardiography data," in *Lecture Notes in Computer Science*, pp. 29–37, Springer International Publishing, New York, NY, USA, 2018.

[90] V. Zyuzin and T. Chumarnaya, "Comparison of Unet architectures for segmentation of the left ventricle endocardial border on two-dimensional ultrasound images," in *Proceedings of the 2019 Ural Symposium on Biomedical Engineering, Radioelectronics and Information Technology (USBEREIT)*, pp. 110–113, Yekaterinburg, Russia, Apr. 2019.

[91] Q. Tao, W. Yan, Y. Wang et al., "Deep learning–based method for fully automatic quantification of left ventricle function from cine MR images: a multivendor, multicenter study," *Radiology*, vol. 290, no. 1, pp. 81–88, Jan. 2019.

[92] S. Leclerc, E. Smistad, J. Pedrosa et al., "Deep learning for segmentation using an open large-scale dataset in 2D echocardiography," *IEEE Transactions on Medical Imaging*, vol. 38, no. 9, pp. 2198–2210, 2019.

[93] A. Gilbert, M. Marciniak, C. Rodero, P. Lamata, E. Samset, and K. McLeod, "Generating synthetic labeled data from existing anatomical models: an example with echocardiography segmentation," *IEEE Transactions on Medical Imaging*, vol. 40, no. 10, pp. 2783–2794, 2021.

[94] E. Smistad, I. M. Salte, A. Ostvik, S. Leclerc, O. Bernard, and L. Lovstakken, "Segmentation of apical long axis, four- and two-chamber views using deep neural networks," in *Proceedings of the 2019 IEEE International Ultrasonics Symposium (IUS)*, pp. 8–11, Glasgow, UK, Oct. 2019.

[95] N. Gutierrez-Castilla, R. S. da Torres, A. X. Falcão et al., "Long-range decoder skip connections: exploiting multi-context information for cardiac image segmentation," in *Proceedings of the 2019 32nd SIBGRAPI Conference on Graphics, Patterns and Images (SIBGRAPI)*, pp. 60–67, Rio de Janeiro, Brazil, Oct. 2019.

[96] W. Chu, G. Molina, N. V. Navkar et al., "BNU-net: a novel deep learning approach for LV MRI analysis in short-Axis MRI," in *Proceedings of the 2019 IEEE 19th International Conference on Bioinformatics and Bioengineering (BIBE)*, pp. 731–736, Athens, Greece, Oct. 2019.

[97] W. Yan, Y. Wang, R. J. van der Geest, and Q. Tao, "Cine MRI analysis by deep learning of optical flow: adding the temporal dimension," *Computers in Biology and Medicine*, vol. 111, Article ID 103356, 2019.

[98] Y.-C. Kim, K. R. Kim, K. Choi, M. Kim, Y. Chung, and Y. H. Choe, "EVCMR: a tool for the quantitative evaluation and visualization of cardiac MRI data," *Computers in Biology and Medicine*, vol. 111, Article ID 103334, 2019.

[99] M. H. Jafari, H. Girgis, N. Van Woudenberg et al., "Cardiac point-of-care to cart-based ultrasound translation using constrained CycleGAN," *International Journal of Computer Assisted Radiology and Surgery*, vol. 15, no. 5, pp. 877–886, May 2020.

[100] S. Moradi, M. G. Oghli, A. Alizadehasl et al., "MFP-Unet: a novel deep learning based approach for left ventricle segmentation in echocardiography," *Physica Medica*, vol. 67, pp. 58–69, Nov. 2019.

[101] H. Cui, C. Yuwen, L. Jiang, Y. Xia, and Y. Zhang, "Multiscale attention guided U-Net architecture for cardiac segmentation in short-axis MRI images," *Computer Methods and Programs in Biomedicine*, vol. 206, Article ID 106142, 2021.

[102] S. Shojaedini, M. Zarvani, S. Saberi, and R. Azmi, "Residual learning: a new paradigm to improve deep learning-based segmentation of the left ventricle in magnetic resonance imaging cardiac images," *J. Med. Signals Sens*, vol. 11, no. 3, pp. 159–168, 2021.

[103] S. Koehler, T. Hussain, Z. Blair et al., "Unsupervised domain adaptation from axial to short-Axis multi-slice cardiac MR images by incorporating pretrained task networks," *IEEE Transactions on Medical Imaging*, vol. 40, no. 10, pp. 2939–2953, 2021.

[104] D. Abdelrauof, M. Essam, and M. Elattar, "Light-weight localization and scale-independent multi-gate UNET segmentation of left and right ventricles in MRI images," *Cardiovascular Engineering and Technology*, vol. 13, no. 3, pp. 393–406, 2021.

[105] Y. Hu, B. Xia, M. Mao et al., "AIDAN: an attention-guided dual-path network for pediatric echocardiography segmentation," *IEEE Access*, vol. 8, Article ID 29176, 2020.

[106] X. Li, Y. Wang, W. Yan, R. J. Van der Geest, Z. Li, and Q. Tao, "A multi-scope convolutional neural network for automatic left ventricle segmentation from magnetic resonance images: deep-learning at multiple scopes," in *Proceedings of the 2018 11th International Congress on Image and Signal Processing, BioMedical Engineering and Informatics (CISP-BMEI)*, pp. 1–5, Beijing, China, Oct. 2018.

[107] Y. Lan and R. Jin, "Automatic segmentation of the left ventricle from cardiac MRI using deep learning and double snake model," *IEEE Access*, vol. 7, Article ID 128641, 2019.

[108] W.-Y. Hsu, "Automatic left ventricle recognition, segmentation and tracking in cardiac ultrasound image sequences," *IEEE Access*, vol. 7, Article ID 140524, 2019.

[109] H. Hu, N. Pan, J. Wang, T. Yin, and R. Ye, "Automatic segmentation of left ventricle from cardiac MRI via deep learning and region constrained dynamic programming," *Neurocomputing*, vol. 347, pp. 139–148, 2019.

[110] V. Badrinarayanan, A. Kendall, and R. Cipolla, "SegNet: a deep convolutional encoder-decoder architecture for image segmentation," *IEEE Transactions on Pattern Analysis and Machine Intelligence*, vol. 39, no. 12, pp. 2481–2495, 2017.

[111] X. Du, S. Yin, R. Tang, Y. Zhang, and S. Li, "Cardiac-DeepIED: automatic pixel-level deep segmentation for cardiac Bi-ventricle using improved end-to-end encoder-decoder network," *IEEE Journal of Translational Engineering in Health and Medicine*, vol. 7, pp. 1–10, 2019.

[112] X. Du, R. Tang, S. Yin, Y. Zhang, and S. Li, "Direct segmentation-based full quantification for left ventricle via deep multi-task regression learning network," *IEEE Journal of Biomedical and Health Informatics*, vol. 23, no. 3, pp. 942–948, May 2019.

[113] L. Zhang, L. Lu, X. Wang et al., "Spatio-temporal convolutional LSTMs for tumor growth prediction by learning 4D longitudinal patient data," *IEEE Transactions on Medical Imaging*, vol. 39, no. 4, pp. 1114–1126, 2020.

[114] M. Li, C. Wang, H. Zhang, and G. Yang, "MV-RAN: multiview recurrent aggregation network for echocardiographic sequences segmentation and full cardiac cycle analysis," *Computers in Biology and Medicine*, vol. 120, Article ID 103728, 2020.

[115] W. Wang, Y. Wang, Y. Wu, T. Lin, S. Li, and B. Chen, "Quantification of full left ventricular metrics via deep regression learning with contour-guidance," *IEEE Access*, vol. 7, Article ID 47918, 2019.

[116] S. Molaei and M. E. Shiri Ahmad Abadi, "Maintaining filter structure: a Gabor-based convolutional neural network for image analysis," *Applied Soft Computing*, vol. 88, Article ID 105960, 2020.

[117] W. Qin, Y. Wu, S. Li et al., "Automated segmentation of the left ventricle from MR cine imaging based on deep learning architecture," *Biomed. Phys. Eng. Express*, vol. 6, no. 2, Article ID 025009, 2020.

[118] S. Dong, G. Luo, C. Tam et al., "Deep Atlas network for efficient 3D left ventricle segmentation on echocardiography," *Medical Image Analysis*, vol. 61, Article ID 101638, 2020.

[119] Y. Wang and W. Zhang, "A dense RNN for sequential four-chamber view left ventricle wall segmentation and cardiac state estimation," *Frontiers in Bioengineering and Biotechnology*, vol. 9, Article ID 696227, 2021.

[120] F. Yang, Y. Zhang, P. Lei et al., "A deep learning segmentation approach in free-breathing real-time cardiac magnetic resonance imaging," *BioMed Research International*, vol. 2019, Article ID 5636423, 12 pages, 2019.

[121] Z. Wang, L. Xie, and J. Qi, "Dynamic pixel-wise weighting-based fully convolutional neural networks for left ventricle segmentation in short-axis MRI," *Magnetic Resonance Imaging*, vol. 66, pp. 131–140, 2019.

[122] X. Wang, S. Zhai, and Y. Niu, "Left ventricle landmark localization and identification in cardiac MRI by deep metric learning-assisted CNN regression," *Neurocomputing*, vol. 399, pp. 153–170, 2020.

[123] T. Eelbode, J. Bertels, M. Berman et al., "Optimization for medical image segmentation: theory and practice when evaluating with dice score or jaccard index," *IEEE Transactions on Medical Imaging*, vol. 39, no. 11, pp. 3679–3690, 2020.

[124] D. Karimi and S. E. Salcudean, "Reducing the Hausdorff distance in medical image segmentation with convolutional neural networks," *IEEE Transactions on Medical Imaging*, vol. 39, no. 2, pp. 499–513, 2020.

Hindawi
Computational Intelligence and Neuroscience
Volume 2023, Article ID 9843760, 1 page
https://doi.org/10.1155/2023/9843760

Retraction

Retracted: Decision-Making Application of the Cloud-Fog Hybrid Model Based on the Improved Convolutional Neural Network in Financial Services in Smart Medical Care

Computational Intelligence and Neuroscience

Received 25 July 2023; Accepted 25 July 2023; Published 26 July 2023

This article has been retracted by Hindawi following an investigation undertaken by the publisher [1]. This investigation has uncovered evidence of one or more of the following indicators of systematic manipulation of the publication process:

(1) Discrepancies in scope
(2) Discrepancies in the description of the research reported
(3) Discrepancies between the availability of data and the research described
(4) Inappropriate citations
(5) Incoherent, meaningless and/or irrelevant content included in the article
(6) Peer-review manipulation

The presence of these indicators undermines our confidence in the integrity of the article's content and we cannot, therefore, vouch for its reliability. Please note that this notice is intended solely to alert readers that the content of this article is unreliable. We have not investigated whether authors were aware of or involved in the systematic manipulation of the publication process.

Wiley and Hindawi regrets that the usual quality checks did not identify these issues before publication and have since put additional measures in place to safeguard research integrity.

We wish to credit our own Research Integrity and Research Publishing teams and anonymous and named external researchers and research integrity experts for contributing to this investigation.

The corresponding author, as the representative of all authors, has been given the opportunity to register their agreement or disagreement to this retraction. We have kept a record of any response received.

References

[1] S. Lu, "Decision-Making Application of the Cloud-Fog Hybrid Model Based on the Improved Convolutional Neural Network in Financial Services in Smart Medical Care," *Computational Intelligence and Neuroscience*, vol. 2022, Article ID 5732379, 8 pages, 2022.

Hindawi
Computational Intelligence and Neuroscience
Volume 2022, Article ID 5732379, 8 pages
https://doi.org/10.1155/2022/5732379

Hindawi

Research Article

Decision-Making Application of the Cloud-Fog Hybrid Model Based on the Improved Convolutional Neural Network in Financial Services in Smart Medical Care

Shan Lu

University of International Business and Economics, Beijing 100050, China

Correspondence should be addressed to Shan Lu; 2016151651070@stu.scu.edu.cn

Received 20 June 2022; Revised 2 July 2022; Accepted 14 July 2022; Published 9 August 2022

Academic Editor: Xin Ning

In order to alleviate the "difficulty in seeing a doctor" for the masses, continuously optimize the service process, and explore new financial service processes for admission and discharge, this study proposes a cloud-fog hybrid model UCNN-BN based on an improved convolutional neural network and applies it to financial services in smart medical care. Decision-making applications: this research improves and designs the UCNN network based on AlexNet and introduces small convolution layers to form convolution groups, making the network more adjustable. The network structure is simpler and more flexible, and it is easy to adjust the algorithm. The number of parameters is small, and it can be directly superimposed without having to add new network hidden layers. The experimental results show that the recognition rate of the UCNN network on the FER2013 and CK+ datasets is higher than that of other recognition methods, and the recognition rates on the FER2013 and CK+ datasets are 98% and 68.01%, due to other methods. This shows that the improved convolutional neural network used in this study for financial services in smart medical care has certain applicability, and small convolution kernels help to extract more subtle features, so as to identify more accurately.

1. Introduction

In the 1990s, two scholars, Michael Hammer and Jame Champy, put forward the theory of "business process reengineering" [1]. The core of which is to use advanced information technology and modern management methods to reengineer business processes to improve service quality and efficiency. Business goals [2]: the First Affiliated Hospital of Wenzhou Medical University applies the concept of "smart medical care" to the reconstruction of the financial service process of admission and discharge. With the help of information technology, a new model of financial service for admission and discharge is constructed, and the financial procedures for admission and discharge are directly handled by the nursing staff in the ward. Through the new model, the financial procedures for admission and discharge have been optimized, the waiting time of patients in line has been shortened, hospital costs have been reduced, and patient satisfaction has been significantly improved [3]. Smart healthcare consists of three parts, namely, the smart hospital system, the regional health system, and the family health system. The smart hospital system consists of a digital hospital and an improved application. The regional health system consists of a regional health platform and a public health system. The home health system is the health protection closest to the citizens, including those who cannot be sent to the hospital for mobility problems.The home medical system is suitable for chronic diseases, remote care of elderly and young patients, health monitoring of mentally retarded, disabled, infectious diseases and other special groups, and video medical treatment for patients. Its intelligent medication system can automatically prompt medication time, contraindications, remaining medication, etc.The financial part of this study belongs to the family health system.

Computing technology is already a very mature technology in today's computer market, and cloud computing service products produced by using cloud computing also play an important role in today's markets in various fields.

There are many large, medium, and small enterprises in various fields using cloud computing products. Cloud computing can provide enterprises with functions such as information storage, management, and maintenance [4] and can also simplify the investment of enterprises in building networks, software, and systems. Human resources and the number of customers using cloud computing technology products are increasing, and it has been expanding from enterprise customers to individual users. Also, because of the increasing market demand, more and more information technology companies are moving their research centers to cloud computing technology research and product development. Major domestic and foreign information companies, including communication companies, are making efforts in this regard. Some researchers [5, 6] described the application of fog computing in IoT systems and its application characteristics; Pang et al. [5] placed computing at the edge of the cloud computing network to improve the availability and scalability of the system architecture and reduce transmission load and cloud processing burden. Rabinovich et al. [7] and Vaquero and Rodero-Merino [8] studied key technologies such as sensor network, peer-to-peer network, network virtualization in cloud-fog hybrid computing, and the main challenges faced by cloud-fog fusion. Zao et al. [9] studied the multilayer cloud and fog computing infrastructure and linked data network and its possible future intelligent environment in terms of the wearable user interface. Zhu et al. [10] studied the data access and interaction mechanism of edge network edge devices in fog computing. Giordano et al. [11] studied the layered distributed architecture of fog computing and its resource advantages in large-scale distributed computing based on the big data interference problem brought by the Internet of Things. Cloud computing is becoming an important force for change, but due to the proliferation of access devices and limited network bandwidth, the combination of fog computing or cloud-fog computing may bring about real computing changes.

A convolutional neural network is a method that can automatically extract object features, and feature extraction and feature classification are a simultaneous process (Ying et al.). AlexNet is one of the classic convolutional neural networks. AlexNet is deeper than LeNet in terms of network depth. It uses the combined structure of the convolutional layer and pooling layer to obtain features of graphic images. This research mainly explores the decision-making application of the cloud-fog hybrid model based on the improved convolutional neural network in financial services in smart medical care, so as to optimize the financial procedures for admission and discharge through the new model and shorten the patients' wait in line, reduce hospital costs, and improve patient satisfaction.

2. Model Introduction

2.1. AlexNet Network. As a commonly used convolutional neural network for deep learning [12, 13], AlexNet is improved based on the classic network LeNet, and on this basis, it can obtain more deep image features by extending the depth of the network. AlexNet is deeper than LeNet in terms of network depth and uses the combined structure of the convolution layer and pooling layer to obtain the features of graphic images [14]. At the same time, AlexNet also uses dropout regularization to suppress overfitting and uses the ReLU function instead. The sigmoid function is used as the activation function of the convolutional neural network, and the results prove that the ReLU function performs better in the deep convolutional neural network and also solves the problem of gradient dispersion and gradient disappearance caused by the sigmoid function (A et al., 2021), and the ReLU function has a faster learning speed. AlexNet has a total of 8 layers of network structure. The first 5 convolutional layers include 1 11×11 convolutional layer, 1 5×5 convolutional layer, and 3 3×3 convolutional layers, with 2 maxpool and 3 FC layers.

2.2. BN Normalization Algorithm. The role of the BN (batch normalization) layer is to prevent the gradient from dispersing and disappearing [15] so that a larger learning rate can be set when training the network, which significantly improves the training speed of the network model so that the model training does not rely too much on parameter initialization. To some extent, it reduces the dropout layer in the convolutional neural network [16]. So, its importance is the same as other structural layers in the network, and it is also an important structural part of the convolutional neural network. In general, the design of convolutional neural networks is more inclined to place the BN layer after the convolutional layer and the fully connected layer; of course, it can also be placed before the activation function [17]. The principle is that when each layer of the network is input, another normalization layer is inserted, that is, a normalization process is performed first, and then the next layer is entered, and it is a learnable one with parameters (γ, β) of the network layer. Assuming the input is n-dimensional, the normalization formula is as follows:

$$X = \left(x^{(1)} \cdots x^{(n)}\right). \tag{1}$$

Normalize each dimension, then

$$x = \frac{x^{(1)} - E\left[x^{(k)}\right]}{\sqrt{Var\left[x^{(k)}\right]}}. \tag{2}$$

If you just use the above normalization formula to normalize the output of a certain layer of the network and then send it to the next layer, this will affect the features learned by the output data of the previous layer, so the transformation and reconstruction method is introduced. The idea is to introduce the learnable parameters γ and β, and the formula is as follows:

$$\begin{aligned} y^{(k)} &= \gamma^{(k)}\widehat{x}^{(k)} + \beta^{(k)}, \\ \gamma^{(k)} &= \sqrt{Var\left[x^{(k)}\right]}, \\ \beta^{(k)} &= E\left[x^{(k)}\right]. \end{aligned} \tag{3}$$

It can be seen from the above formula that by reconstructing the parameters γ and β and learning these two parameters, the original features learned by a certain layer in the convolutional neural network can be recovered. However, in the actual test, the following formula is still used:

$$\hat{x} = \frac{x - E[x]}{\sqrt{Var[x] + \varepsilon}}. \tag{4}$$

2.3. Cloud Model. Since the concept of cloud computing appeared in 2006, the two IT technologies of computing and network have been continuously integrated and then coexisted with each other, which has effectively promoted the development of the information society [18]. In these IoT scenarios, a more secure, faster, and more stable computing mode is required, and at the same time, computing needs to have better mobility support [19]. The above requirements cannot be met for cloud computing with high latency, low security, and reliability. Therefore, the concept of fog computing emerges as the times require.

Fog computing was proposed by Cisco in 2011. It deploys a large number of micro-fog node data centers with limited computing and storage capacity between the cloud and the object to disperse the computing pressure of the cloud center and reduce the amount of data transmitted to the remote network [20]. Due to the limited computing power of fog computing itself, it cannot replace cloud computing, but expands and supplements it. The integrated use of these two technologies not only retains the powerful computing and storage advantages of the cloud layer but also expands the scope of network computing. At the near-user end, that is, the network edge, network computing has lower latency and higher location awareness [21]. The benefits brought by fog computing have made a huge impact in the IT industry. In 2015, IT industry leaders such as Cisco, Dell, and Intel jointly established the OpenFog Consortium to promote the rapid development of cloud-fog hybrid computing. Today, more than fifty institutions from North America, Asia, and Europe have joined the Open Fog Alliance [22]. In 2018, the National Institute of Standards and Technology restandardized the definition of fog computing on the basis of Cisco's years of fog computing research: fog computing is a combination of smart devices and traditional cloud data centers. A horizontal computing model combines physical and virtual resources. With the standardization of fog computing-related concepts, the technical architecture of cloud-fog hybrid computing has become increasingly mature [23].

2.3.1. Cloud Computing Center Layer. In the cloud-fog hybrid computing model, the traditional cloud computing center is retained. The cloud computing center uses a large number of virtual resources and provides extremely strong computing power and storage capacity with the help of task scheduling, load balancing, and parallel computing technologies to meet the processing of complex computing tasks. In the Internet of Things scenario, the cloud computing center is suitable for intelligent analysis and learning of large data volume information and storage of historical data, which is a supplement to the computing capability of the fog layer.

2.3.2. Network Layer. The network layer includes the access network layer and the core network layer. The access network layer mainly connects end-user equipment and fog layer node equipment through network equipment, which includes both wired and wireless networks. The core network connects the cloud computing center and the fog layer computing nodes through the wired network.

2.3.3. Fog Computing Layer. The introduction of the fog computing layer is the core of cloud-fog hybrid computing, which requires certain business processing and data computing capabilities. At the same time, the fog computing layer also needs to be able to cooperate with the cloud layer to carry out reasonable network control and resource scheduling to complete more complex computing and storage tasks. In addition, the scale of computing nodes in the fog computing layer may also become huge due to business requirements, and the hardware and software costs of a single computing node are relatively low. In order to meet the above functional requirements, in terms of hardware, the fog computing layer can be composed of general-purpose servers, white-label switches, routers, and other devices. In terms of software, in addition to the software system responsible for business computing and processing, it is also necessary to introduce software defined network (SDN) technology responsible for network traffic control and forwarding, and network functions virtualization (NFV) responsible for providing virtual network functions. Table 1 shows the main software and hardware resources required for the general fog computing layer.

Building fog computing nodes is an important part of fog computing layer construction. The Central Office Rearchitected as a Datacenter (CORD), DC transformation of network computer room, project promoted by the Open Network Alliance (ONF) basically meets the requirements of fog-layer computing nodes. The CORD platform integrates SDN, NFV, and other technologies and provides the possibility of fog-layer computing, traffic control, and network services with the help of hardware resources such as general-purpose servers and white-brand switches. If business services are added to it, it will become a suitable fog layer-compute node.

2.3.4. End User Layer. In the era of the Internet of Things, there are more and more types of devices in the end-user layer, including smartphones, computers, smart wearable devices, and various sensors. In order to realize the vision of the Internet of Everything, these intelligent terminal devices are connected together through wired or wireless networks, thus creating the necessity for the development of cloud-fog hybrid computing. In cloud-fog hybrid

Table 1: Comparison of classification accuracy on FER2013 and CK+ datasets during model improvement.

Ways to improve	Precision	
	Dataset of FER2013	Dataset of CK+
Introduce 4 convolution groups	67.80	96.55
Introduce 3 convolution groups	68.55	97.51

computing, the intelligent terminal device is the initiator of the task, and the task is forwarded to the corresponding fog computing node after being scheduled by the network device in the access network. After the task is processed by the fog layer and cloud layer, the processing result will be sent back to the terminal device through the network.

3. Network Improvements

3.1. Improvement Method. In this section, the UCNN network is designed on the basis of AlexNet, and the convolution group structure is introduced into the AlexNet network, that is, the convolution group convset of the small convolution kernel. The advantage of this structure design is that it is convenient to adjust the algorithm, and the convolution group can be directly added [24]. In this convolution group, there is a 1×1 convolutional layer at the beginning and the end, which can be connected with convolutional layers of any scale. A 3×3 convolution kernel and a 5×5 convolution kernel are used in the middle. The structure is shown in Figure 1.

A convolutional neural network is mainly composed of the input layer, convolution layer, activation layer, pooling layer, and fully connected layer. The network model in this paper introduces more than 3 of the above convolution groups to replace the 11×11 large convolution kernels in the AlexNet network. Each convolution group introduces 4 3×3 convolution layers and 2 max-pooling layers and then adds a batch normalization layer (BN layer), which can speed up the convergence of the model.The convolutional layers are supplemented with 0 to prevent edge pixels from being omitted when the convolution kernel performs convolution calculations. Using dropout regularization, all neurons are discarded according to the probability of 0.3, which simplifies the entire network model, suppresses overfitting, and further improves the classification ability of the model [25].

Dropout regularization can effectively suppress the phenomenon of overfitting. The main idea is that a part of the neurons in each layer of the network is randomly discarded, and the probability of random discarding is set according to the training situation of the model. This paper has carried out many experiments, starting from the probability of 30%, 40%, and 50%. The experimental results show that the random discarding of neurons with a probability of 0.3 is the best. Therefore, this paper sets the dropout regularization parameter to 30%, which simplifies the network structure while suppressing overfitting.

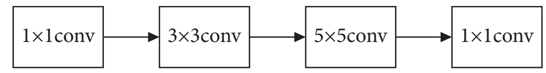

Figure 1: Structure of convolution group convset.

In this paper, the main idea of improving the AlexNet network structure is to replace the 11×11 large convolution kernel with a convolution group of small convolution kernels to extract more subtle features in smart medical financial services, and other convolution layer parameters are set the same. In the overall network structure improvement, convolution groups with small convolution kernels have been introduced 4 times. The two improved methods are given in Table 1. Figures 2 and 3 are the experimental results of the recognition accuracy of the two design methods on the FER2013 and CK+ datasets, respectively.

The results of the cubic and quaternary convolution groups are studied. From Figures 2 and 3, it can be found that the cubic convolution group has higher accuracy than the quaternary convolution group, and the accuracy rate of the quaternary convolution group is higher. In FER2013 and CK+, the two datasets used in this experiment are always slightly lower than the cubic convolution group. In the following fitting, the cubic convolution group is selected.

3.2. UCNN Network Structure. Compared with the classification accuracy, the effect of introducing 3 convolution groups is better, so this paper finally adopts the introduction of 3 convolution groups as the final network model, named UCNN (Unit CNN) network. Figure 4 shows the whole improved network model diagram.

4. Simulation Results and Analysis

This section first introduces the dataset used and then performs data enhancement on the dataset. The improved network model in this paper is used to train and test the expression dataset and compared with a variety of newer expression recognition methods; the comparison results show that the improved network model is more effective. The experimental environment of this paper is a Windows system, the deep learning model is Pytorch, the CPU is Intel i59600kf, and the GPU is NVIDIA GTX1080ti.

4.1. Dataset Processing

4.1.1. FER2013 Dataset. The FER2013 dataset is a commonly used identification research dataset, which itself has been divided into a training set, validation set, and test set. Among them, there are 28,709 training sets, 3,589 validation sets, and 3,589 test sets.

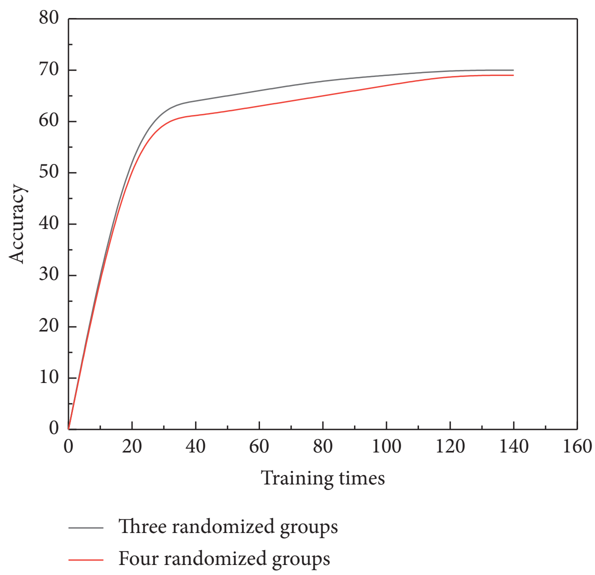

Figure 2: Comparison of two networks on FER2013 dataset.

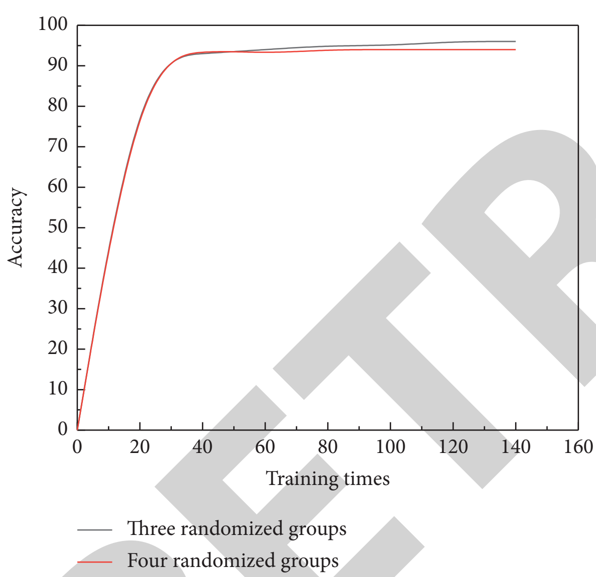

Figure 3: Comparison of two networks on CK+ dataset.

4.1.2. CK+ Dataset. The CK+ dataset was released in 2010. It is a dataset with a larger amount of data obtained by expanding the dataset on the CK dataset. In this paper, 30% of the dataset is divided into the test set, and 70% is divided into the training set.

4.2. Data Augmentation. Convolutional neural networks are often supported by a large number of parameters. Some large neural networks, such as GoogleNet, even have millions of network parameters. To make these huge network parameters work properly, a large amount of data is required. Train the network for a long time. However, the reality is that there is not that much data to work with. Therefore, data augmentation plays a great role in network training. It can expand the amount of data, improve the generalization

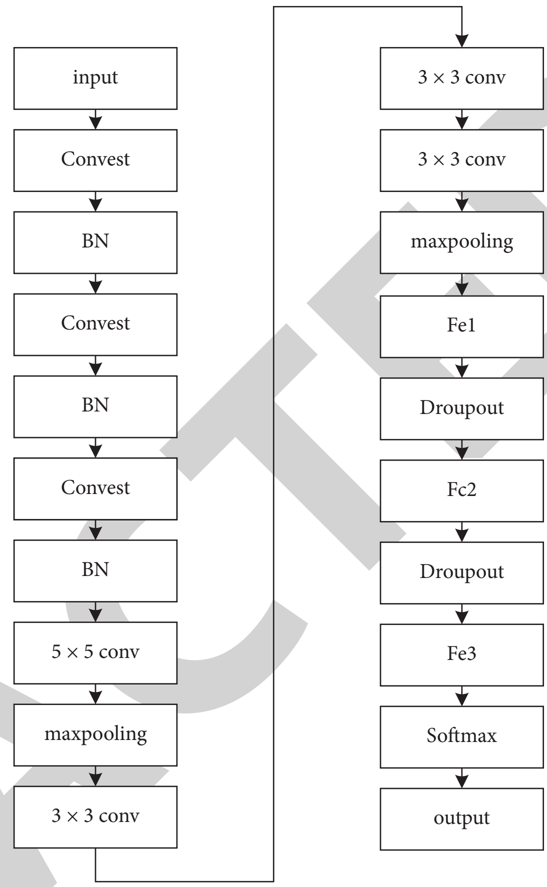

Figure 4: UCNN network structure.

ability of the model, and improve the robustness of the model. The data augmentation method used in this paper is random sampling.

4.3. Improved Analysis. This paper improves the original AlexNet, introduces three convolution groups with small convolution kernels to replace the 11×11 convolution kernels in the original AlexNet, constructs a new network UCNN, and uses the UCNN network on the FER2013 dataset and CK+ dataset, respectively. Train and test: the dataset has been expanded, and the CK+ dataset has been expanded to 2000, of which 70% are used as training sets and 30% are used as test sets. The FER dataset is not expanded, because the amount of data in the original dataset itself is relatively large.

Figures 5 and 6 show the training accuracy and test accuracy of the improved network UCNN on the CK+ dataset and the FER2013 dataset. It can be seen that the UCNN network performs well on the two datasets, where the dotted line represents the training accuracy. The solid line represents the test accuracy, which reached the recognition rate of 98% and 68.01% respectively, and there is no obvious overfitting phenomenon, indicating that the network in this paper has a relatively good generalization ability.

On the FER2013 and CK+ datasets, other network models are used for testing, and compared with the UCNN network, the results are shown in Figures 7 and 8.

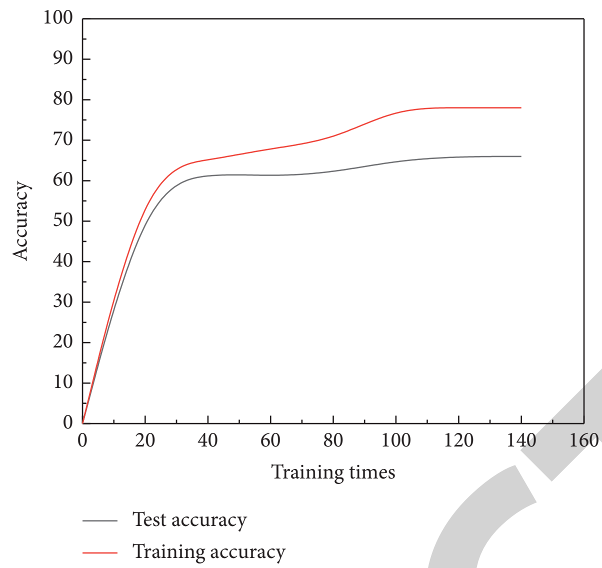

Figure 5: Training and test performance of the UCNN network on FER2013 dataset.

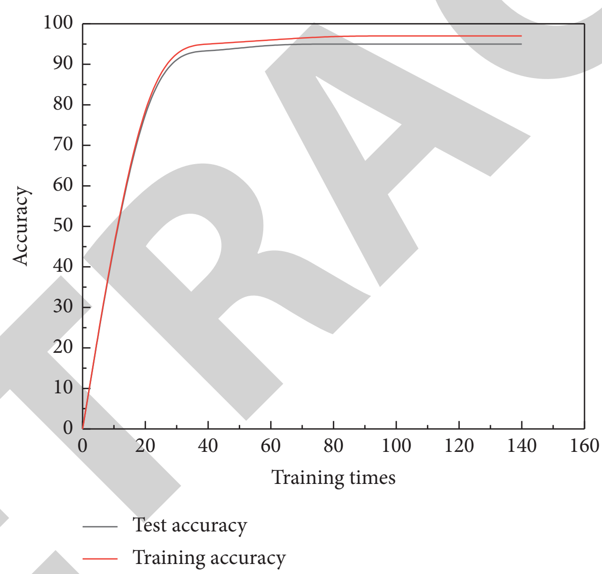

Figure 6: Training and test performance of the UCNN network on CK+ dataset.

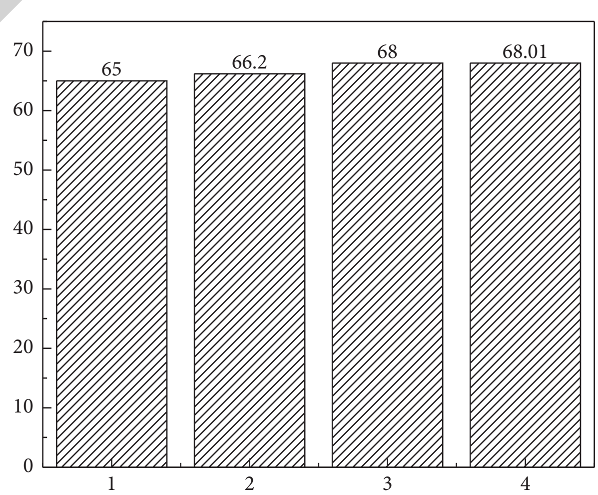

Figure 7: Comparison of training and test performance of recognition rate between this method and other methods on FER2013 dataset.

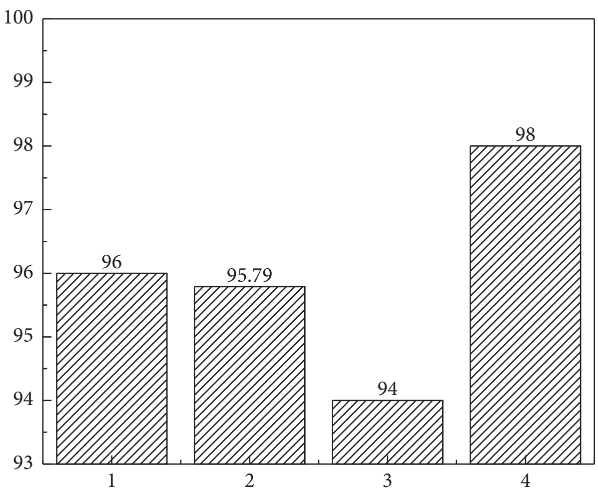

Figure 8: Comparison of recognition rate between this method and other methods on CK+ dataset.

Reference [26], reference [27], and reference [28] all conducted experiments on the FER2013 dataset, and reference [29], reference [30] and reference [31] all conducted experiments on the CK+ dataset. As can be seen from the chart, the method in this paper performs the best on both datasets.

5. Conclusion

The information system compiled according to the internal control requirements objectively enforces and regulates the operation behavior of operators, eliminates arbitrary and subjective factors, and is an important means to reduce the risk of errors and fraud. Aiming at the low utilization rate of small and medium-sized convolutional neural networks in smart medical financial systems, this study designs the UCNN network, which uses the convolution group of small convolution kernels to replace the 11×11 large convolution kernels in the AlexNet network. Small convolution kernels help to extract more subtle features of the original data, thereby improving the recognition rate. A BN batch normalization layer is added after each convolution group to prevent the gradient from disappearing and improve the training speed of the network. In order to reduce the network parameters, a fully connected layer in the original structure is removed, and dropout regularization is added behind the remaining two fully connected layers to further prevent overfitting. During the training process, the dataset was enhanced to solve the problem of insufficient data. The research results are as follows: (1) the improved network UCNN based on AlexNet designed in this paper has a simpler structure, fewer parameters, faster model convergence speed, and higher recognition rate compared with the current newer methods; FER2013 and CK+ datasets achieved recognition rates of 98% and 68.01%, respectively; (2) compared with the quadruple convolution group, the cubic convolution group has higher accuracy, and the accuracy of the cubic convolution group is higher than that of the quaternary convolution group by 67.80% and 96.55%; (3) data enhancement significantly expands the data volume, improves the generalization ability of the model, and improves the robustness of the model [32].

Data Availability

The dataset used to support the findings of this study is available from the corresponding author upon request.

Conflicts of Interest

The authors declare that they have no conflicts of interest.

References

[1] Multhammer and Michael, "Michael Multhammer: lessings Rettungen". Geschichte und Genese eines Denkstils," *Journal for the History of Modern Theology*, vol. 22, no. 1, pp. 101–106, 2015.

[2] M. Imhoff, S. Kuhls, U. Gather, and R. Fried, "Smart alarms from medical devices in the OR and ICU," *Best Practice & Research Clinical Anaesthesiology*, vol. 23, no. 1, pp. 39–50, 2009.

[3] B. R. Soller, M. Ca Brera, S. M. Smith, and J. P. Sutton, "Smart medical systems with application to nutrition and fitness in space," *Nutrition*, vol. 18, no. 10, pp. 930–936, 2002.

[4] M. Hil De Brandt, *Profiling and the Identity of the European Citizen*, Springer Netherlands, Cham, 2008.

[5] M. Di, R. H. Deng, H. H. Pang, and J. Zhou, dx, Authenticating query results from untrusted servers," vol. 11, 2005.

[6] A. Foga and A. G. Fett-Neto, "Role of auxin and its modulators in the adventitious rooting of Eucalyptus species differing in recalcitrance," *Plant Growth Regulation*, vol. 45, no. 1, pp. 1–10, 2005.

[7] C. Canali, M. Rabinovich, and X. Zhen, *Utility Computing for Internet Applications*, Springer, US, 2005.

[8] L. M. Vaquero and L. Rodero-Merino, "Finding your way in the fog: towards a comprehensive definition of fog computing," *Computer communication review*, vol. 44, no. 5, pp. 27–32, 2014.

[9] S. Stirenko, Y. Gordienko, T. Shemsedinov et al., "User-driven Intelligent Interface on the Basis of Multimodal Augmented Reality and Brain-Computer Interaction for People with Functional Disabilities," 2017, https://arxiv.org/abs/1704.05915.

[10] J. Zhu, X. Huang, and Y. Yang, "Myeloid-derived suppressor cells regulate natural killer cell response to adenovirus-mediated gene transfer," *Journal of Virology*, vol. 22, 2012.

[11] S. Giordano, I. Stojmenovic, and L. Blazevic, "Position Based Routing Algorithms for Ad Hoc Networks: A Taxonomy," *network theory & applications*, Springer, Cham, .

[12] M. Z. Alom, T. M. Taha, C. Yakopcic, S. Westberg, and V. K. Asari, "The History Began from AlexNet: A Comprehensive Survey on Deep Learning Approaches," 2018, https://arxiv.org/abs/1803.01164.

[13] Y. Yang, Z. Zhao, H. Cho-Jui, and D. James, "100-epoch ImageNet Training with AlexNet in 24 Minutes," *Journal of Jinggangshan University*, vol. 13, 2016.

[14] W. Cai, B. Zhai, Y. Liu, R. Liu, and X. Ning, "Quadratic polynomial guided fuzzy C-means and dual attention mechanism for medical image segmentation," *Displays*, vol. 70, Article ID 102106, 2021.

Hindawi
Computational Intelligence and Neuroscience
Volume 2023, Article ID 9871807, 1 page
https://doi.org/10.1155/2023/9871807

Retraction

Retracted: Study on the Global Stability for a Generalized SEIR Epidemic Model

Computational Intelligence and Neuroscience

Received 25 July 2023; Accepted 25 July 2023; Published 26 July 2023

This article has been retracted by Hindawi following an investigation undertaken by the publisher [1]. This investigation has uncovered evidence of one or more of the following indicators of systematic manipulation of the publication process:

(1) Discrepancies in scope
(2) Discrepancies in the description of the research reported
(3) Discrepancies between the availability of data and the research described
(4) Inappropriate citations
(5) Incoherent, meaningless and/or irrelevant content included in the article
(6) Peer-review manipulation

The presence of these indicators undermines our confidence in the integrity of the article's content and we cannot, therefore, vouch for its reliability. Please note that this notice is intended solely to alert readers that the content of this article is unreliable. We have not investigated whether authors were aware of or involved in the systematic manipulation of the publication process.

Wiley and Hindawi regrets that the usual quality checks did not identify these issues before publication and have since put additional measures in place to safeguard research integrity.

We wish to credit our own Research Integrity and Research Publishing teams and anonymous and named external researchers and research integrity experts for contributing to this investigation.

The corresponding author, as the representative of all authors, has been given the opportunity to register their agreement or disagreement to this retraction. We have kept a record of any response received.

References

[1] C. Xue, "Study on the Global Stability for a Generalized SEIR Epidemic Model," *Computational Intelligence and Neuroscience*, vol. 2022, Article ID 8215214, 6 pages, 2022.

Hindawi
Computational Intelligence and Neuroscience
Volume 2022, Article ID 8215214, 6 pages
https://doi.org/10.1155/2022/8215214

Research Article

Study on the Global Stability for a Generalized SEIR Epidemic Model

Chunrong Xue

School of Mathematics and Statistics, Weinan Normal University, Weinan, Shaanxi 714000, China

Correspondence should be addressed to Chunrong Xue; xuechunrong@wnu.edu.cn

Received 12 May 2022; Revised 15 June 2022; Accepted 24 June 2022; Published 8 August 2022

Academic Editor: Xin Ning

In the current study, a generalized SEIR epidemic model is studied. The generalized fractional-order SEIR model (susceptible-infected-recovered (SIR) epidemic) model differentiated the population into susceptible population, exposure population, infected population, and rehabilitation population and has fundamental mentoring importance for the forecast of the probable outburst of infectious ailments. The fundamental duplicated quantity R_0 is inferred. When $R_0 < 1$, the disease-free equilibrium (DFE) is particular and tending towards stability. When $R_0 > 1$, the endemic equilibrium is sole. In addition, certain circumstances are set up to make sure the local progressive stability of disease-free and endemic equilibrium. Considering the influence of the individual behavior, a broader SEIR epidemic model is raised, which classified the population into susceptible, exposure, infected, and rehabilitation. What is more, the basic reproduction number, that regulates whether the infection will die out or not, is obtained by the spectral radius of the next-generation matrix; moreover, the global stability of DFE and endemic equilibrium are analyzed by a geometry method.

1. Introduction

Nowadays, some infectious diseases are still aimed at large populations [1, 2]. They are regarded as the potential causes of death, particularly in numerous developing countries [3, 4]. As a result of this, mathematical modeling in epidemiology plays a more and more important role in public health research [5, 6]. This academic subject facilitates interpreting the studies in epidemiological phenomena and catch the distinctive elements that could result in a serious epidemic or even to a hazardous pandemic in the world [7, 8]. The established susceptible-infected-recovered (SIR) epidemic model was firstly described by Kermackin 1991 [9].The infection latency often needs a long-time range [7] In the meantime, an incubated individual is still latent but hasn't contagious [10]. Consequently, another type of exposed individuals might be supplemented to SIR and the novel epidemic model SEIR was introduced by Ricardo [11]. This SEIR model with treatment and offeredcertain adequate conditions to certify the local stability of equilibrium points. Additionally, epidemiological studies have exposed that mutation leads to more and more unaffected viruses offering the emergence of numerous new damaging epidemics or even new hazardous pandemics [12]. The laws of disease spreading should be urgently investigated because of infectious diseases bring disaster to human health and might provide a theoretical basis for the infection prevention and control [13]. Due to infectious disease existing certain latency before its breaking out, the SEIR epidemic model was researched in a latent period. As described in the study [14], Zhang, Li, and Ma et al. analyzed an SEIR epidemic model with the immigration of different compartments and adequate contact rates and proved the overall stability of the system by variable transformation. In addition, Meng, Chen, and Song introduced the delayed SEIR epidemic model with perpendicular propagation and pulsed vaccination [15].They considered the infection-free periodic solution, which was globally attractive under some appropriate conditions; furthermore, time delay, pulse vaccination and vertical transmission brought obvious efforts to the dynamics of the model. The previous research [16] contained random agitations into SIR and SEIR epidemic models with saturated incidence and set that the solution under some conditions had ergodic property by utilizing the stochastic Lyapunov function. Li and Chen discussed an age structured SEIR epidemic model with vertically and horizontally transformation. They established the threshold of endemic existence and showed threshold parameters usually computable in [17]. Chen et al. [18] investigated an SEIR epidemic Model with a non-monotone incidence, then obtained the global stability. It's worth repeating: the morbidity provides further data about the disease broadcast. Therefore, the overall incidence characteristic has as aim of denoting a big collection of infection incidence rate. Meng group, Michael Y. Li, and Ke Wang in [19] considered an SEIR epidemic model for the dynamic transmit of communicable disease that propagate in population by connecting to hosts and analyzed a geometric method to global stability. A great deal of processes of mutation was detected in a large number of communicable diseases. Due to this reason, the multi-strain SEIR epidemic model is a critical tool for investigating a number of communicable diseases that comprise a lengthy incubation period and also diverse infection strains. The correlation of learning multi-strain models is finding out the diverse situations allowing all operating strains to coexist. The global dynamics of the SEIR model is the focus of numerous explorations by studying bilinear or nonlinear incidence. In the current study, a comprehensive SEIR epidemic model is studied, and the threshold is obtained. By the method of geometric approach, global stability of disease-free equilibrium (DFE) and endemic equilibrium are analyzed; furthermore, the infection will die away if $R_0 < 1$, or become endemic if $R_0 > 1$.

2. Preliminaries and Model Derivation

The incidence provides further evidence about the spread of the disease [20] Therefore, the goal of the general incidence rate function is to characterize the incidence rate of a large group of infections. Consequently, the aim of this study is to summarize the earlier models by thinking over a SEIR model with general prevalence rate. Therefore, this current study would be carried out on the subsequent comprehensive SEIR epidemic model:

$$\begin{cases} \dfrac{dS}{dt} = A - f(S, I) - dS, \\[2ex] \dfrac{dE}{dt} = f(S, I) - \varepsilon E - dE, \\[2ex] \dfrac{dI}{dt} = \varepsilon E - \delta I - dI, \\[2ex] \dfrac{dR}{dt} = \delta I - dR, \end{cases} \tag{1}$$

where (S)is the numbers of susceptible population; (E)is the numbers of each latent individual's class;(I) denotes the amount of communicable population;(R) is the amount of deleted population; With regard to the issues coping with population dynamics, all the variables might be positive. We would suppose firstly that all the model indicators are positive. The paraments A is positive constant, which represents the birth rate of the population. The paraments d is positive invariable too, which represents the death rate of the population. The non-negative constant ε describes the transfer rates from exposed to infected, and the non-negative constant δ describes the transmission rates from infection to recovery. The function f (S, I) represents the ratio of new infection and is expected to be sufficiently smooth to ensure the existence and uniqueness of solution to the system (1) with non-negative initial situations. By the functional framework of basic theory of differential equations, we verify that there is a particular local solution to the issues. To verify the positive results, we would demonstrate that any settlement beginning from positive orthant. To meet biological sense, the function f (S, I) is assumed to fulfill the conditions as below for all S ≥ 0, I ≥ 0:

(a) $f(0,0) = f(S,0) = f(0,I) = 0$,
(b) $f(S,I) > 0$ for $S > 0$, $I > 0$,
(c) $\partial f(S,I)/\partial S \geq 0$, $(\partial f(S,I)/\partial I) > 0$,
(d) $I(\partial f(S,I)/\partial I) \geq f(S,I)$,
(e) $I(\partial f(S,I)/\partial I) - E(\partial f(S,I)/\partial S) - f(S,I) > 0$.

The total population $N = S + E + I + R$ satisfies $N' = A - dN$ may vary in time. It is easy to see the population scale N converges to (A/d) without disease, thus we study system (1) in the following feasible region:

$$D = \left\{(S, E, I, R) \in R_+^4 \colon S + E + I + R \leq \frac{A}{\mathrm{d}}\right\}. \tag{2}$$

Which is a positive invariant set in R_+^4, represents the border and inner of D by ∂D and D° respectively.

The condition (a) ensures the existence of unique DFE $P_0(A/\mathrm{d}, 0, 0, 0) \in \partial D$ for system (1). Setting the right-hand sides of the last three equation to zero, and the sum of the first two equation to zero, it is easy to obtain a particular endemic equilibrium $P^*(S^*, E^*, I^*, R^*)$, where,

$$\begin{aligned} S^* &= \frac{A\varepsilon - (\mathrm{d}+\varepsilon)(\mathrm{d}+\delta)I^*}{\mathrm{d}\varepsilon}, \\ E^* &= \frac{\mathrm{d}+\delta}{\varepsilon}I^*, \\ R^* &= \frac{\delta}{\mathrm{d}}I^* \end{aligned} \tag{3}$$

Simultaneously obtained

$$\begin{aligned} f(S^*, I^*) &= \frac{(\mathrm{d}+\varepsilon)(\mathrm{d}+\delta)}{\varepsilon}I^*, \\ \frac{\partial f}{\partial I}(S^*, I^*) &= \frac{(\mathrm{d}+\varepsilon)(\mathrm{d}+\delta)}{\varepsilon}. \end{aligned} \tag{4}$$

3. The Basic Reproduction Number

In this section, the basic reproduction number R_0 is studied. R_0 is clarified as the spectral radius of next-generation matrix in [7], i.e.

In this section we study the fundamental reproduction number R_0, R_0 is expressed as the spectral radius of next-generation matrix in [7], i. e. $R_0 = \rho(FV^{-1})$. In system (1), only E and I is directly related to epidemic. There followed the way of van den driessche and Watmough, that is

$$\begin{pmatrix} \frac{dE}{dt} \\ \\ \frac{dI}{dt} \end{pmatrix} = \begin{pmatrix} f(S,I) \\ \\ 0 \end{pmatrix} - \begin{pmatrix} (d+\varepsilon)E \\ \\ -\varepsilon E + (d+\delta)I \end{pmatrix},$$

$$F = \begin{pmatrix} 0 & \frac{\partial f}{\partial I}\left(\frac{A}{d},0\right) \\ \\ 0 & 0 \end{pmatrix}, \tag{5}$$

$$V = \begin{pmatrix} d+\varepsilon & 0 \\ \\ -\varepsilon & d+\delta \end{pmatrix},$$

then $V^{-1} = (1/(d+\varepsilon)(d+\delta))\begin{pmatrix} d+\delta & 0 \\ \varepsilon & d+\varepsilon \end{pmatrix}$

The next-generation matrix is

$$FV^{-1} = \frac{1}{(d+\varepsilon)(d+\delta)} \begin{pmatrix} \varepsilon \frac{\partial f}{\partial I}\left(\frac{A}{d},0\right) & (d+\varepsilon)\frac{\partial f}{\partial I}\left(\frac{A}{d},0\right) \\ \\ 0 & 0 \end{pmatrix}. \tag{6}$$

Hence the fundamental reproduction number as,

$$R_0 = \frac{\varepsilon}{(d+\varepsilon)(d+\delta)} \frac{\partial f}{\partial I}\left(\frac{A}{d},0\right). \tag{7}$$

4. Global Stabilities of Disease-free Equilibrium (DFE)

The disease-free equilibrium (DFE) is characterized by the demising of the infecting, and the sickness could not attack the individuals. The DFE first nonzero component is determined by the infant natality and mortality of the predisposed population and does not rely on the morbidity functional indicators. The infection disappeared, the susceptibility gets their greatest numerical, and the rest of variables eliminate. In this paragraph, concentration might be concentrated to the statistical stability of this DFE. In fact, we could suppose the stability of DFE when the fundamental reproduction quantity is less than the unified value. This makes us to seek for the proper model indicators to inspect statistically the steadiness of the original stable status.

By the framework of van den Driessche and Watmough [21], we immediately obtained the following local asymptotical stability of DFE:

Theorem 1. *Allow R_0 be defined in (7), the unique DFE of system (1) is local asymptotical stability provided that $R_0 < 1$ and unsteady provided that $R_0 > 1$.*

To explore the global stability of DFE, the following result explained in [22]is needed:

Lemma 1. *Take into account a model expressed in a form*

$$\begin{cases} \frac{dX_1}{dt} = F(X_1, X_2), \\ \\ \frac{dX_2}{dt} = G(X_1, X_2), G(X_1, 0) = 0, \end{cases} \tag{8}$$

where $X_1 \in R^m$ represents the amount of population without infection and $X_2 \in R^m$ represents the sum of infected population containing potential, infectious, etc; $X_0 = (X_1^*, 0)$ indicates the DFE of system (8).

Also suppose the conditions (H1) and (H2) as following:

(H1) For $dX_1/dt = F(X_1, 0)$, X_1^* is global asymptotical stability.

(H2) $G(X_1, X_2) = AX_2 - \widehat{G}(X_1, X_2)$, $\widehat{G}(X_1, X_2) \geq 0$ for $(X_1, X_2) \in \Omega$, the Jacobian matrix $A = (\partial G/\partial X_2)(X_1^*, 0)$ is an M-matrix and Ω is the feasible region.

Then the DFE $X_0 = (X_1^*, 0)$ is global asymptotical stability if $R_0 < 1$.

Theorem 2. *The DFE of system (1) is global asymptotical stability if $R_0 < 1$.*

Proof. In system (1), permit $X_1 = (S, R)^T$,$X_2 = (E, I)^T$, the uninfected model is

$$\begin{pmatrix} \frac{dS}{dt} \\ \\ \frac{dR}{dt} \end{pmatrix} = F(X_1, X_2) = \begin{pmatrix} A - f(S,I) - dS \\ \\ \delta I - dR \end{pmatrix}, \tag{9}$$

the infected model is

$$\begin{pmatrix} \frac{dE}{dt} \\ \\ \frac{dI}{dt} \end{pmatrix} = G(X_1, X_2) = \begin{pmatrix} f(S,I) - (d+\varepsilon)E \\ \\ \varepsilon E - (d+\delta)I \end{pmatrix}. \tag{10}$$

and $G(X_1, 0) = 0$.

Next requireto verify the conditions (H1) and (H2).

When $X_2 = 0$, i.e. $E = I = 0$, the model (9) is

$$\begin{pmatrix} \frac{dS}{dt} \\ \\ \frac{dR}{dt} \end{pmatrix} = \begin{pmatrix} A - dS \\ \\ -dR \end{pmatrix}. \tag{11}$$

And the solution of system (11) is $S(t) = A/d - (S(0) - (A/d))e^{-dt}, R(t) = R(0)e^{-dt}$.

It is easy to see $S(t) \longrightarrow A/d, R(t) \longrightarrow 0$, as $t \longrightarrow +\infty$. Hence $X_1^*(A/d, 0)$ is global asymptotical stability. The condition (H1) is verified.

$$G(X_1, X_2) = \frac{\partial G}{\partial X_2}(X_1^*, 0)X_2 - \widehat{G}(X_1, X_2)$$

$$= \begin{pmatrix} -(\mathrm{d}+\varepsilon) & \dfrac{\partial f}{\partial I}\left(\dfrac{A}{\mathrm{d}}, 0\right) \\ \varepsilon & -(\mathrm{d}+\delta) \end{pmatrix} \begin{pmatrix} E \\ I \end{pmatrix} - \begin{pmatrix} I\dfrac{\partial f}{\partial I}\left(\dfrac{A}{\mathrm{d}}, 0\right) - f(S, I) \\ 0 \end{pmatrix}, \tag{12}$$

obviously $A = (\partial G/\partial X_2)(X_1^*, 0)$ is an M-matrix. According to assumption (d) we obtain $\widehat{G}(X_1, X_2) \geq 0$. The condition (H2) is verified.

According to Lemma 1, The DFE $P_0(A/\mathrm{d}, 0, 0, 0)$ of system (1) is global asymptotical stability if $R_0 < 1$. □

5. Global stabilities of endemic equilibrium

Theorem 3. *There exists a unique positive endemic equilibrium for system (1) if $R_0 > 1$, and no positive endemic equilibrium if $R_0 < 1$.*

Let $F(I) = f(S^*, I)/I = f(A\varepsilon - (d+\varepsilon)(d+\delta), I/d\varepsilon, I)/I$, $y = (d+\varepsilon)(d+\delta)/\varepsilon$. Let y=F(I)

$$f\left(\frac{A\varepsilon - (\mathrm{d}+\varepsilon)(\mathrm{d}+\delta)I}{\mathrm{d}\varepsilon}, I\right) = \frac{(\mathrm{d}+\varepsilon)(\mathrm{d}+\delta)}{\varepsilon}. \tag{13}$$

It is clearly to see $F(I) = 0$ at $I = (A\varepsilon/(\mathrm{d}+\varepsilon)(\mathrm{d}+\delta))$, then

$$F(I) < \frac{(\mathrm{d}+\varepsilon)(\mathrm{d}+\delta)}{\varepsilon}. \tag{14}$$

with the help of inequality (d)

$$\lim_{I\longrightarrow 0^+} F(I) = \lim_{I\longrightarrow 0^+} \frac{f(A/\mathrm{d}, 0)}{I} = \frac{\partial f}{\partial I}\left(\frac{A}{\mathrm{d}}, 0\right) > \frac{(\mathrm{d}+\varepsilon)(\mathrm{d}+\delta)}{\varepsilon}. \tag{15}$$

The equation y =F(I) has unique solution if and only if $\partial f/\partial I(A/\mathrm{d}, 0) > ((\mathrm{d}+\varepsilon)(\mathrm{d}+\delta)/\varepsilon)$, then $\varepsilon\partial f/\partial I(A/\mathrm{d}, 0)/(\mathrm{d}+\varepsilon)(\mathrm{d}+\delta) > 1$, namely $R_0 > 1$.

Clearly $R_0 > 1$, there is a unique positive endemic equilibrium for system (1), and no positive endemic equilibrium for $R_0 < 1$.

Theorem 4. *The unique positive endemic equilibrium of system (1) is local asymptotical stability provided that $R_0 > 1$.*

Proof To study the local asymptotical stability, the equivalent system of (1) is researched

$$\begin{cases} \dfrac{dS}{dt} = A - f(S, I) - dS \\ \dfrac{dE}{dt} = f(S, I) - (d+\varepsilon)E \\ \dfrac{dI}{dt} = \varepsilon E - (d+\delta)I. \end{cases} \tag{16}$$

The Jacobian matrix of system (16) is

$$J = \begin{pmatrix} -\dfrac{\partial f}{\partial S}(S, I) - d & 0 & -\dfrac{\partial f}{\partial I}(S, I) \\ \dfrac{\partial f}{\partial S}(S, I) & -(d+\varepsilon) & \dfrac{\partial f}{\partial I}(S, I) \\ 0 & \varepsilon & -(d+\delta) \end{pmatrix}, \tag{17}$$

and the characteristic equation at $P^*(S^*, E^*, I^*, R^*)$ is

$$\mathrm{Det}\,(\lambda E - J) = \lambda^3 + a_1\lambda^2 + a_2\lambda + a_3 = 0, \tag{18}$$

where $a_1 = 3\,d + \varepsilon + \delta + (\partial f/\partial S)(S^*, I^*) > 0$, $a_2 = (\partial f/\partial S(S^*, I^*) + d)(2\,d + \varepsilon + \delta) > 0$,

$$a_3 = \varepsilon\frac{\partial f}{\partial I}(S^*, I^*)\frac{\partial f}{\partial S}(S^*, I^*) > 0. \tag{19}$$

In order to prove all roots, have negative real parts, using (4) and obtain $a_1 > d + \varepsilon$, $a_2 > \partial f/\partial S(S^*, I^*)(d+\delta)$, $a_3 = (d+\varepsilon)(d+\delta)\partial f/\partial S(S^*, I^*)$, therefore $a_1a_2 - a_3 > 0$.

According to Routh-Hurwitz theory the unique positive endemic equilibrium of system (1) is local asymptotical stability provided that $R_0 > 1$.

Theorem 5. *The unique positive endemic equilibrium of system (1) is global asymptotical stability provided that $R_0 > 1$.*

Proof In line with Theorem 1 the unique DFE of system (1) is unstable provided that $R_0 > 1$, and $P_0(A/\mathrm{d}, 0, 0, 0) \in \partial D$, then system (1) is uniform persistence [23], i.e. $\exists c > 0$, $\lim_{t\longrightarrow\infty} \inf\{S(t), E(t), I(t)\} > c$. Uniform persistence implies the presence of compact subsets $K \subset D$. It is easy to see system (1) satisfies the conditions in [24].

Next, we only need to prove the Bendixson criterion $q < 0$.

The Jacobian matrix of system (16) is (17), and the associated second compound matrix is,

$$J^{[2]} = \begin{pmatrix} -\dfrac{\partial f}{\partial S}(S, I) - (2\,d+\varepsilon) & \dfrac{\partial f}{\partial I}(S, I) & \dfrac{\partial f}{\partial I}(S, I) \\ \varepsilon & -\dfrac{\partial f}{\partial S}(S, I) - (2\,d+\delta) & 0 \\ 0 & \dfrac{\partial f}{\partial S}(S, I) & -(2\,d+\varepsilon+\delta) \end{pmatrix}. \tag{20}$$

Let the matrix function $P(S, E, I) = \mathrm{diag}(1, E/I, E/I)$, then

$P_fP^{-1} = \mathrm{diag}(0, (E'/E) - (I'/I), (E'/E) - (I'/I))$, matrix $B = P_fP^{-1} + PJ^{[2]}P^{-1}$ can be written in the form

$B = \begin{pmatrix} B_{11} & B_{12} \\ B_{21} & B_{22} \end{pmatrix}$ where $B_{11} = -(2\ d + \varepsilon) - \partial f/\partial S(S, I), B_{12} = [\partial f/\partial I(S, I)I/E, \partial f/\partial I(S, I)I/E], B_{21} = [\varepsilon(E/I), 0]^T$,

$$B_{22} = \begin{pmatrix} \frac{E'}{E} - \frac{I'}{I} - (2\ d + \delta) - \frac{\partial f}{\partial S}(S, I)0 \\ \\ \frac{\partial f}{\partial S}(S, I)\frac{E'}{E} - \frac{I'}{I} - (2\ d + \varepsilon + \delta) \end{pmatrix}. \tag{21}$$

We define a norm $\|(u, v, w)\| = \max\{|u|, |v + w|\}$ for any vector (u, v, w) in R^3, and $\mu(B)$ denote the Lozinskil measure with respect to this norm. Using the valuation method in [25] we have $\mu(B) \leq \sup(g_1, g_2)$, with $g_1 = \mu_1(B_{11}) + |B_{12}|$, $g_2 = |B_{21}| + \mu_1(B_{22})$. $|B_{12}|$, $|B_{21}|$ are the matrix norm about l_1 vector norm, μ_1 is Lozinskil measure about l_1 norm. For example, $|A| = \max_{1\leq k\leq n} \sum_{i=1}^{n} |a_{ik}|, \mu_1(A) = \max_{1\leq k\leq n}(a_{kk} + \sum_{i=1, i\neq k}^{n} |a_{ik}|)$ for any matrix $A = (a_{ij})_{n\times n}$, then

$$\begin{aligned} \mu_1(B_{11}) &= -(2d + \varepsilon) - \frac{\partial f}{\partial S}(S, I), |B_{12}| = \frac{\partial f}{\partial I}(S, I)\frac{I}{E}, |B_{21}| = \varepsilon\frac{E}{I}, \\ \mu_1(B_{22}) &= \frac{E'}{E} - \frac{I'}{I} - (2d + \delta). \end{aligned} \tag{22}$$

Hence

$$\begin{aligned} g_1 &= -(2\ d + \varepsilon) - \frac{\partial f}{\partial S}(S, I) + \frac{\partial f}{\partial I}(S, I)\frac{I}{E}, \\ g_2 &= \varepsilon\frac{E}{I} + \frac{E'}{E} - \frac{I'}{I} - (2\ d + \delta). \end{aligned} \tag{23}$$

From system (16), we obtain $I'/I = \varepsilon(E/I) - (d + \delta)$ and $-(d + \varepsilon) = (E'/E) - (f(S, I)/E)$, then $g_2 = E'/E - d$ and $g_1 = ((E'/E) - (f(S, I)/E) - d - (\partial f/\partial S)(S, I) + (\partial f/\partial I)(S, I)(I/E))$, by assumption (e), $g_1 = ((E'/E) - d - (\partial f/\partial S)(S, I) < (E'/E) - d)$, then $\mu(B) \leq \sup(g_1, g_2) = (E'/E) - d$.

Since system (1) is uniform persistence, there is $\xi > 0, T > 0$ so that when $t > T$, $E(t) > \xi, I(t) > \xi$ for all $(S(0), E(0), I(0)) \in K$, we have $1/t \ln(E(t)/E(0)) < \mathrm{d}/2$, then $1/t \int_0^t \mu(B)\mathrm{d}s \leq (1/t)\ln E(t)/E(0) - d < -(\mathrm{d}/2)$, namely

$q = \lim_{t\to\infty} \sup \sup_{x_0\in K} 1/t \int_0^t \mu(s, x_0)\mathrm{d}s < -(\mathrm{d}/2) < 0$, thus, the associated second compound matrix is local asymptotical stability, verified the proof.

6. Discussion and conclusion

It is well described that the spreading of a contagious illness implicates disease-related elements including infectious mediator, route of broadcast, latent period, infectious stage, susceptivity, and resistance [26]. Infectious disease model defining a spread mediators in an enclosed population and containing susceptible (S), infectives (I), and recovers (R) were introduced by Kermack in 1927. According to the Kermack model, diverse epidemic models have been advanced in current periods, such as SIR, SIS, SEIR models [27]. Functional form of the incidence rate plays a critical role in of epidemic model. Several previous studies highlight that the route of disease transmission might have a nonlinear incidence ratio [28]. To explore the effect of the non-linearity, Korobeinikov take into account diversified models with the incidence and set up Lyapunov functions that make them to create global properties for SEIR model. Thereafter, Korobeinikov proven global properties for multiple epidemic models with incidence of a more commonformula [29].

In the current study, we have explored the global stability of the generalized SEIR model with quantitative overview of the complex analysis and certain qualitative characteristics of the SEIR model have been discussed. This model included some compartments, namely the susceptible, exposing individuals, infecting individuals, and the removal individuals. We have created the existence, positivity and boundedness of settlement which ensure the well-formedness of the SEIR model. To validate our distinctive results theoretically, numerical simulation is carried out. It is measured that the model with extensive association capabilities contains many typical correlation features, which could better understand the equilibrium stability. The long-term forecast desires to amend the model properly based on the alteration of strategic and medical aspects. We might talk about this in the future work.

Data Availability

The datasets used and analyzed during the current study are available from the corresponding author on reasonable request.

Conflicts of Interest

All authors declare that they have no competing interests.

References

[1] G. L. Glassock, C. E. Grueber, K. Belov, and C. J. Hogg, "Reducing the extinction risk of populations threatened by infectious diseases," *Diversity*, vol. 13, no. 2, p. 63, 2021.

[2] W. Cota, D. Soriano-Paños, A. Arenas, S. C. Ferreira, and J. Gómez-Gardeñes, "Infectious disease dynamics in metapopulations with heterogeneous transmission and recurrent mobility," *New Journal of Physics*, vol. 23, no. 7, Article ID 073019, 2021.

[3] M. P. Kieny, J. A. Rottingen, J. Farrar, WHO R&D Blueprint Team, and R&D Blueprint Scientific Advisory Group, *The Need for Global R&D Coordination for Infectious Diseases with Epidemic Potential*, Lancet, vol. 388, no. (10043), pp. 460-461, London, England, 2021.

[4] G. S. Gonsalves, A. D. Paltiel, T. Thornhill et al., "The dynamics of infectious diseases associated with Injection Drug Use in Lawrence and lowell, Massachusetts," *Open Forum Infectious Diseases*, 2021.

[5] H. J. Shimozako, J. Wu, and E. Massad, "Mathematical modelling for Zoonotic Visceral Leishmaniasis dynamics: a new analysis considering updated parameters and notified human Brazilian data," *Infectious Disease Modelling*, vol. 2, no. 2, pp. 143–160, 2017.

[6] F. Baldassi, F. D'Amico, M. Carestia et al., "Testing the Accuracy Ratio of the Spatio-Temporal Epidemiological Modeler

Hindawi
Computational Intelligence and Neuroscience
Volume 2023, Article ID 9781472, 1 page
https://doi.org/10.1155/2023/9781472

Retraction

Retracted: Comprehensive Health Evaluation Model of Art Psychotherapy Using Genetic Algorithm

Computational Intelligence and Neuroscience

Received 25 July 2023; Accepted 25 July 2023; Published 26 July 2023

This article has been retracted by Hindawi following an investigation undertaken by the publisher [1]. This investigation has uncovered evidence of one or more of the following indicators of systematic manipulation of the publication process:

(1) Discrepancies in scope
(2) Discrepancies in the description of the research reported
(3) Discrepancies between the availability of data and the research described
(4) Inappropriate citations
(5) Incoherent, meaningless and/or irrelevant content included in the article
(6) Peer-review manipulation

The presence of these indicators undermines our confidence in the integrity of the article's content and we cannot, therefore, vouch for its reliability. Please note that this notice is intended solely to alert readers that the content of this article is unreliable. We have not investigated whether authors were aware of or involved in the systematic manipulation of the publication process.

Wiley and Hindawi regrets that the usual quality checks did not identify these issues before publication and have since put additional measures in place to safeguard research integrity.

We wish to credit our own Research Integrity and Research Publishing teams and anonymous and named external researchers and research integrity experts for contributing to this investigation.

The corresponding author, as the representative of all authors, has been given the opportunity to register their agreement or disagreement to this retraction. We have kept a record of any response received.

References

[1] F. Zhang and X. Liu, "Comprehensive Health Evaluation Model of Art Psychotherapy Using Genetic Algorithm," *Computational Intelligence and Neuroscience*, vol. 2022, Article ID 5718050, 11 pages, 2022.

Hindawi
Computational Intelligence and Neuroscience
Volume 2022, Article ID 5718050, 11 pages
https://doi.org/10.1155/2022/5718050

Research Article

Comprehensive Health Evaluation Model of Art Psychotherapy Using Genetic Algorithm

Fupeng Zhang[1,2] and Xia Liu[2]

[1]*Luliang University, Luliang 033001, China*
[2]*Jeonju University, Jeonju-si 55068, Republic of Korea*

Correspondence should be addressed to Xia Liu; yaya7285@163.com

Received 14 May 2022; Accepted 28 June 2022; Published 2 August 2022

Academic Editor: Xin Ning

In order to explore the real effect of art mental health therapy, this paper proposes a feature selection algorithm based on genetic algorithm. The algorithm takes college students as the research object and discusses the effect of psychotherapy on college students through painting art therapy. The results showed that there were extremely significant differences in EPQ extraversion factors among the people treated with the educational intervention of art psychology course ($P < 0.01$), and there was no significant change in other factors ($P > 0.05$). There was no significant change in total depression score and depression index ($P > 0.05$). There were significant differences in social avoidance factors and social anxiety ($P < 0.05$), and there were relatively significant differences in the total score of sadness ($P < 0.01$). It is concluded that the use of artistic elements can effectively help people express themselves and express their psychological emotions, which has a certain effect in mental health treatment.

1. Introduction

Before the formation of language and words, early human beings mainly used graphics and painting to record events in life and through graphics to reflect emotions and ideas of colossus. Therefore, the artistic expression in the form of graphics and painting is the innate instinct of human beings. The key point of artistic therapy is to effectively integrate different forms of art types into psychotherapy and, at the same time, use artistic media such as painting, music, and dance to promote the growth of people's mind and cure people's psychological problems in a supportive environment. Therefore, art psychotherapy is also a process of discovering and expressing oneself with the help of art forms derived from the depths of emotion. And in the process of self-psychotherapy using art forms, people usually do not pay too much attention to the beauty of visual art, the grammatical arrangement of words, and the harmony and fluency of songs. They just use art to release, express and relax, and obtain insight by studying symbolic and metaphorical information to achieve the effect of psychotherapy, as shown in Figure 1.

2. Literature Review

Modern psychotherapy with speech as the medium has a good effect in correcting irrational cognition and thinking, but it is powerless in dealing with psychological problems with emotional distress as the main symptoms, such as emotional disorder and traumatic experience. In brain science, emotion and art (painting, music, etc.) are controlled by the right hemisphere at the same time. Therefore, even speech therapists with rich clinical experience do not despise the excellent effect of painting in dealing with emotional distress. A large number of studies abroad have proved the artistic way of using the right hemisphere to deal with emotional disorder [1].

Children with family and development problems were treated with spontaneous painting creation method. It was found that painting therapy can alleviate the pressure from family and society, express anxiety, and strengthen the self-concept of visitors [2]. Individual and group painting therapy was carried out for children with learning disabilities. It was found that, in the treatment, children and peers

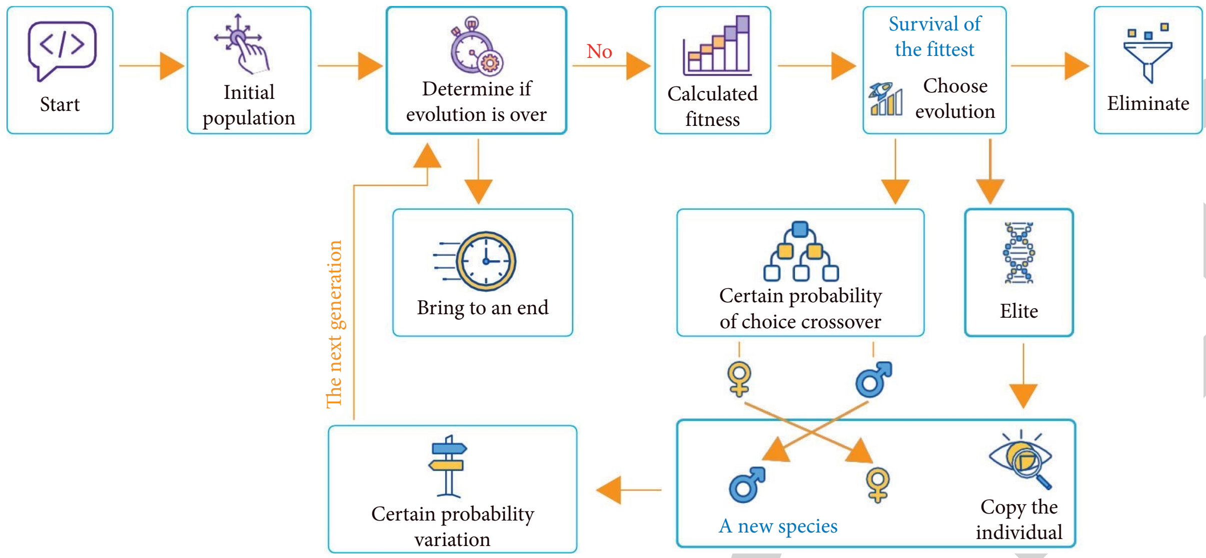

Figure 1: Comprehensive evaluation model of artistic psychotherapy health based on genetic algorithm.

promoted the development of social skills through interpersonal interaction and finally improved individual self-esteem. Babin applied painting psychotherapy to 3 women with anorexia and 3 women with obesity. The results showed that the self-concept of 5 women was significantly improved [3]. It is found that painting intervention can promote homeless women to improve their sense of self-esteem and self-awareness. The research of some scholars has found a physiological basis for painting to promote the improvement of self-esteem. He found that fluctuations in the amount of neurotransmitter serotonin in the brain can affect the quality of movement and the level of self-esteem. The high content of serotonin is related to self-affirmation and movement control, and the low content is easy to lead to anger and impulsive behavior. Human life depends on movement, and effective and elegant movement produces a sense of satisfaction. The training provided by art happens to produce such skill movements. The display of these movements leads to positive feedback among people, thus strengthening self-esteem [4].

Since the 1940s, psychologists have also developed a variety of painting projection techniques for psychotherapy and testing, but basically painting projection techniques can be divided into three categories: free painting, painting with specified content, and painting techniques in between. The first is free painting technology. The stimulation given is only paper and pen, giving the visitor the greatest freedom to express the inner world he is most eager to express. However, analysts need extensive knowledge background and rich analysis experience, which makes it difficult to quantify and ensure reliability and validity. The second category is the painting technology that specifies the content. Fang Shuren painting test is the most comprehensive and widely used typical representative. It gives standard guidelines and has certain provisions on content, tools, and location, which is more conducive to the popularization of experience and application in experimental research. The last one is between the two. It gives a certain stimulation, but it does not regulate what content to paint at the same time. In addition, the final analysis of this technology is not for the painting content of the subjects, but for the nature of the changes made by the subjects on the given stimulus [5].

Domestic painting psychotherapy has also achieved some applied research results in the treatment and diagnosis of mental disorders, special groups such as intellectual disabilities, crisis intervention and psychological education, and group psychological counseling and treatment [6].

In the study of a case of children's depression, painting image was used to regulate children's depression, and the effect was remarkable. This paper discusses the application of painting therapy in middle school students with emotional disorders and uses the room tree person test method to treat 6 middle school students who come to psychological counseling. It is found that the use of painting therapy can better understand the causes of middle school students' emotional conflict and has played a good effect in the process of psychological counseling. The study tried to use painting projection technology, free association, and positive imagination in a psychological counseling case of depression to fully present the patient's past experience, internal image, and unconsciousness and communicate the patient's consciousness and unconsciousness. The results show the patient's inner growth and development, and the performance has been changed and transformed in real life. Through the experimental treatment of college students' depressive symptoms through painting aesthetic treatment activities, the results show that the design can significantly improve the level of college students' depressive symptoms, promote the college students with depressive symptoms, and significantly improve the overall mental health level of the subjects. Its effect is mainly reflected in the significant improvement of four factors: somatization, interpersonal sensitivity, psychosis, and paranoia [7].

A team explored the effect of group painting art therapy on the rehabilitation of physiological, psychological, and social functions of schizophrenic patients. The results show that group painting art intervention can alleviate the mental symptoms of schizophrenic patients and promote the improvement of patients' self-concept and quality of life. The application of painting therapy in interpersonal group counseling is an effective method for college students with development crisis, personality problems, and international communication problems. Through group counseling, the self-acceptance of members can be improved, the sense of self-harmony can be enhanced, and the level of self-esteem can be improved to varying degrees. Group counseling promotes the personality growth of members as a whole and improves their mental health level. Collective painting therapy starts from the two points of collectivity and painting to easily create a treatment environment and guide most people. Patients talked about its novelty and being easy to understand after treatment. As an auxiliary form of psychotherapy, painting therapy has its uniqueness [8].

3. Unsupervised Feature Selection Algorithm Based on Genetic Algorithm

3.1. Feature Selection Algorithm. Feature selection, at first, is a technology in the classification problem. The purpose is to find out which features have a great influence on the label, minimize the influence of irrelevant features in the classifier training process, and avoid overfitting and high time complexity. From the definition, the process of feature engineering is mainly composed of the following aspects, as shown in Figure 2.

Feature selection algorithms often use some evaluation criteria to measure the candidate subsets. The evaluation criteria are divided into two categories according to whether they are related to the subsequent machine learning model. One kind of evaluation criteria is independent of the learning model and evaluates the feature selection as an independent process. This feature selection algorithm is called filter algorithm. This feature selection process is shown in Figure 3 below.

The other is called wrapper algorithm. In this algorithm, the evaluation criterion is the performance of the subsequent machine learning model. In this process of machine learning, feature selection is a part of the establishment of machine learning model [9]. For each candidate feature subset, the model needs to be retrained. The specific process is shown in Figure 4.

In the field of practical application, when the feature dimension is high and there are many redundant features, these two hybrid strategies are often used for feature selection. Firstly, the independent evaluation criterion algorithm is used to preliminarily evaluate the features and quickly eliminate most irrelevant features. Then, the encapsulated feature selection is carried out for the remaining few features to obtain the feature subset with the best neutral energy for the subsequent machine learning model [10].

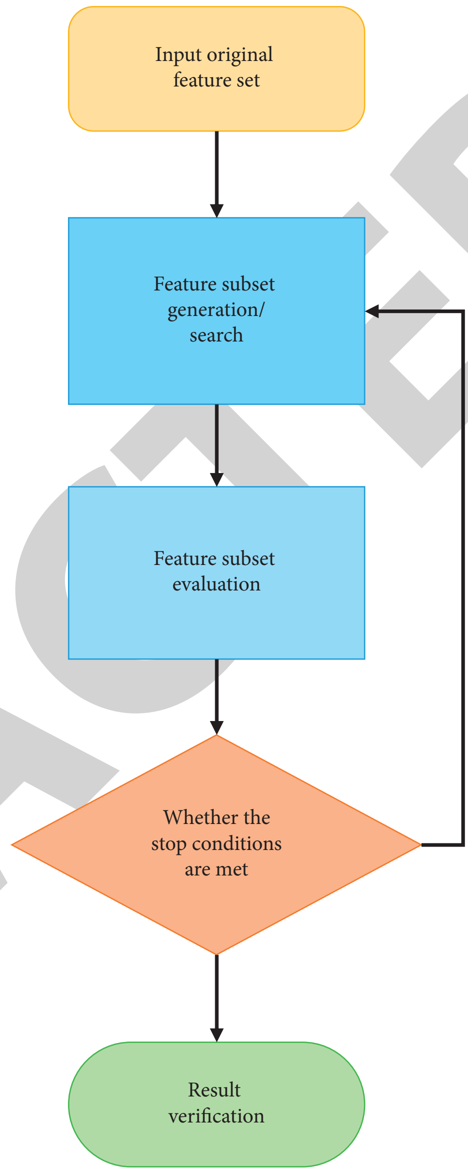

Figure 2: Feature selection process.

3.2. Genetic Algorithm

3.2.1. Conceptual Process. The core idea of the algorithm is to characterize the iterative process of the solution of the optimization problem by the heredity of genes in the population. Among them, the population represents the set of all feasible solutions, and each individual gene in the population represents a feasible solution. By artificially setting a natural environment (fitness function, or evaluation function), the way of survival of the fittest in nature is simulated. Filter the individuals in the population that are not suitable for the natural environment and inherit the individual genes suitable for the environment. Through the characteristics of gene crossover and variation in the genetic process, the offspring population can not only retain the characteristics of good solutions in the previous generation population, but also retain the possibility of producing better solutions

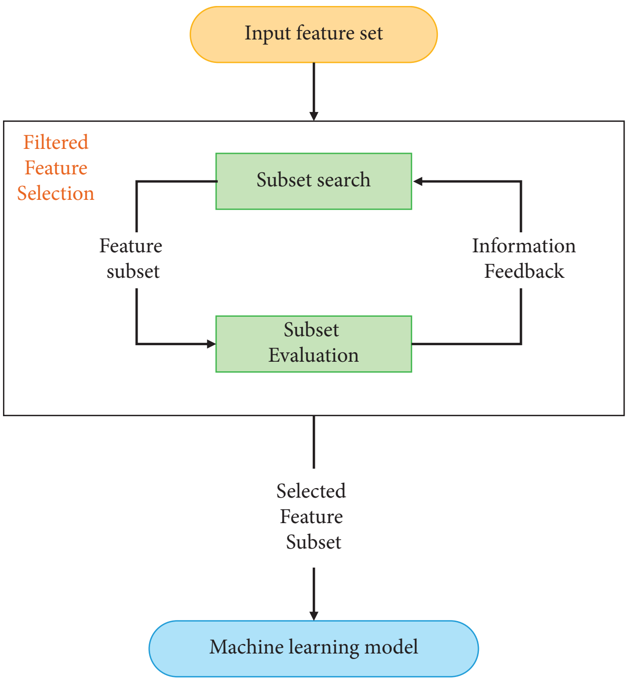

Figure 3: Filter feature selection process.

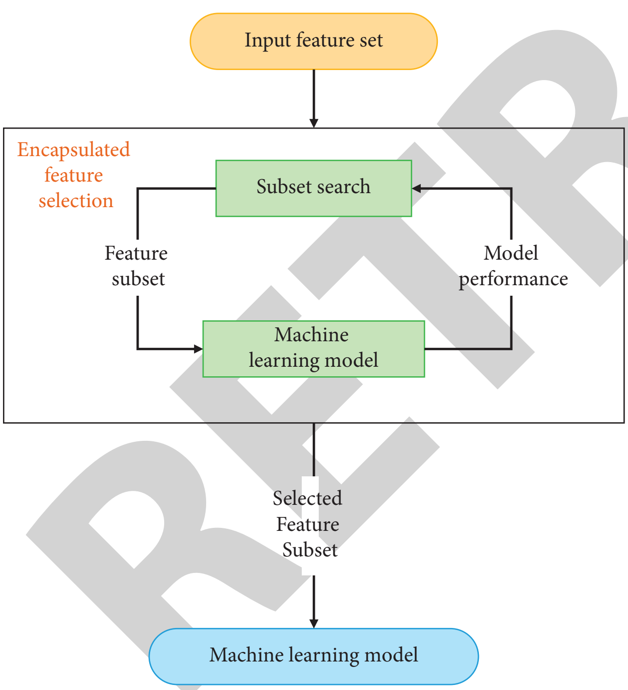

Figure 4: Wrapper feature selection process.

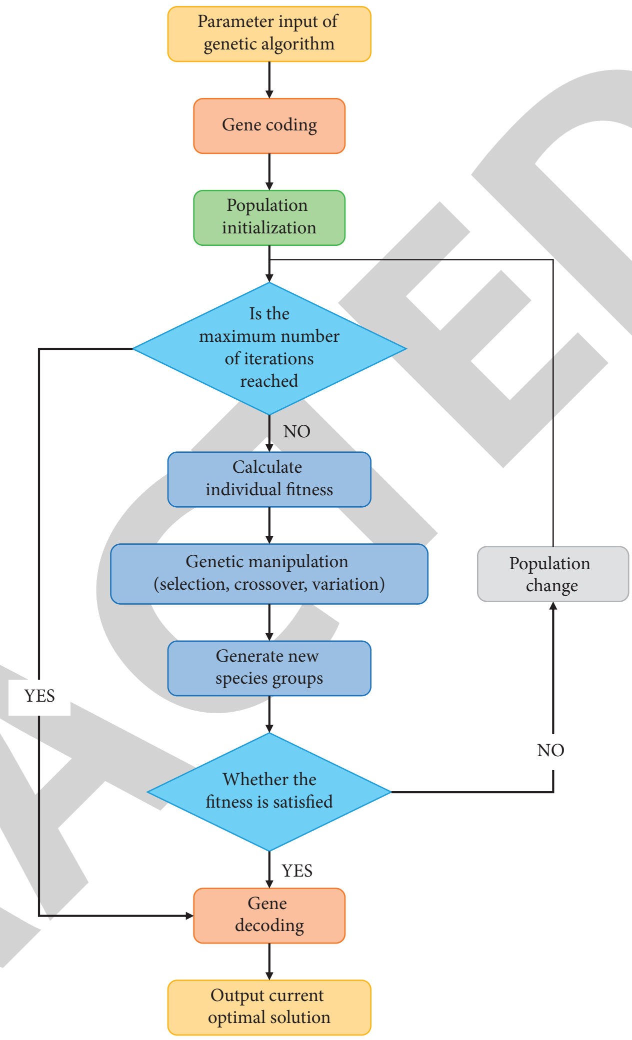

Figure 5: Principle of genetic algorithm.

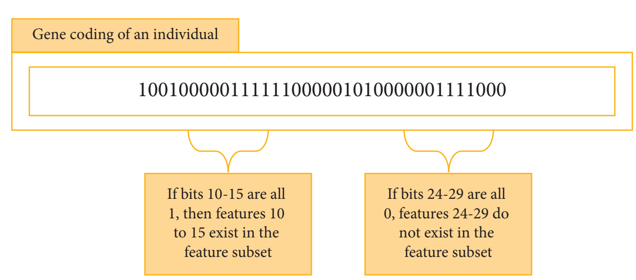

Figure 6: Coding of a gene.

[11]. The flow of genetic algorithm is shown in Figure 5 below.

In the feature selection problem, as shown in Figure 6, for a data set with feature number n, a binary gene sequence with length n is usually used to represent a feasible solution. In each gene, 0 indicates that the feature is not in the individual, and 1 indicates that the feature exists in the individual. Each coding sequence represents an individual [12].

3.2.2. Definition of Population Genetic Mode. Roulette selection algorithm: roulette selection algorithm comes from roulette gambling. The main principle is that, on the roulette surface, regions with different angles have different probability of being selected; that is, the larger the proportion, the easier it is to be selected. In the feature selection algorithm, the higher the fitness, the easier it is to be selected. In a population with N individuals, for individual x_i, given its fitness $f(x_i)$, the probability of individual selection is carried out according to the following algorithm:

(1) Use formula (1) below to calculate the individual fitness ratio, which is similar to the ratio of different areas on the roulette.

$$p(x_i) = \frac{f(x_i)}{\sum_{j=1}^{N} f(x_i)}. \tag{1}$$

(2) Calculate the cumulative fitness distribution from x_1 to x_N, similar to the probability distribution function, as shown in formula (2) below:

$$q_i = \sum_{j=1}^{i} p(x_i). \tag{2}$$

(3) Take random number as shown in formula (3):

$$r \in (0, 1). \tag{3}$$

If the following formula is satisfied, it is shown in formula (4):

$$q_{i-1} < r q_i > r, i > 1. \tag{4}$$

Then select individual x_i; otherwise select individual x_1. It can be seen that, in the roulette algorithm, the third step is more likely to select individuals with high fitness.

Random traversal sampling algorithm: this algorithm is similar to roulette selection algorithm. The first two steps are also to calculate the individual fitness proportion and fitness distribution. However, in the third step, random traversal sampling adopts the concept of equidistant sampling. Assuming that the number of individuals in the population is N and the number of individuals to be selected is d, the selection sequence is as shown in formula (5):

$$\{r_1, r_2, \ldots, r_d\}, \tag{5}$$

where r_1 is the random number between $(0, 1/d)$; it is shown in formula (6):

$$r_j = r_{j-1} + \frac{1}{d}. \tag{6}$$

Tournament selection method: different from the first two, the tournament selection method does not need to calculate the probability distribution function but selects individuals by simulating the way similar to the group competition, which is mainly divided into three steps:

(1) Determine the scale of each competition; for example, select 30% of the individuals in the original population to compete.

(2) Select the champion (with the highest fitness) among the individuals who meet the number by random sampling.

(3) Repeat steps 1 and 2 until a sufficient number of individuals are selected.

Crossover refers to the process of hybridization of parent individuals to produce offspring, which is divided into single point hybridization and multipoint hybridization, as shown in Figure 7.

3.3. Clustering Algorithm

3.3.1. Algorithm Process. Clustering technology, also known as cluster analysis, is a technology to analyze the data according to the correlation between the data itself in the absence of prior knowledge. Therefore, clustering is an important part of unsupervised learning, and it is also widely used in pattern recognition, machine learning, and other fields [13].

In cluster analysis, there are two cases—a single data belongs to and only belongs to one category or may belong to multiple categories, corresponding to hard clustering and fuzzy clustering, respectively. In the hard clustering model, the clustering results are shown in formula (7):

$$U = \begin{bmatrix} u_{11} & u_{12} & \ldots & u_{1n} \\ u_{21} & u_{22} & \ldots & u_{2n} \\ \ldots & \ldots & \ldots & \ldots \\ u_{k1} & u_{k2} & \ldots & u_{kn} \end{bmatrix}, \tag{7}$$

where U is the $k \times n$ matrix, where k is the number of clusters, n is the number of samples, and u_{ij} indicates whether sample i belongs to cluster j, which satisfies the following formula, as shown in formula (8):

$$u_{ij} \in \{0, 1\}, 1 \le j \le k, 1 \le i \le n. \tag{8}$$

In hard clustering, sample i either belongs to cluster j or does not belong to cluster j, and there is no value between 0 and 1. In fuzzy clustering, the formula should be modified as shown in formula (9):

$$u_{ij} \in [0, 1], 1 \le j \le k, 1 \le i \le n. \tag{9}$$

In the two different clustering methods, u_{ij} is also constrained by formulas (10) and (11):

$$\sum_{j=1}^{k} u_{ij} = 1, 1 \le i \le n, \tag{10}$$

$$\sum_{i=1}^{n} u_{ij} > 0, 1 \le j \le k. \tag{11}$$

In fuzzy clustering, the sum of distribution probability of samples in all clusters is 0. Formula (11) imposes a basic constraint on the cluster capacity; that is, any existing cluster has at least one sample that belongs or has a probability of belonging to it; otherwise the cluster does not exist [14].

3.3.2. Algorithm Evaluation Index. The following is a brief introduction to these evaluation indicators: CA: judge whether all samples in the cluster are classified into appropriate clusters by giving a label, and evaluate the clustering effect by statistical accuracy. The calculation is shown in formula (12):

$$CA = \sum_{i=1}^{K} \frac{\max(C_i|L_i)}{|\Omega|}. \tag{12}$$

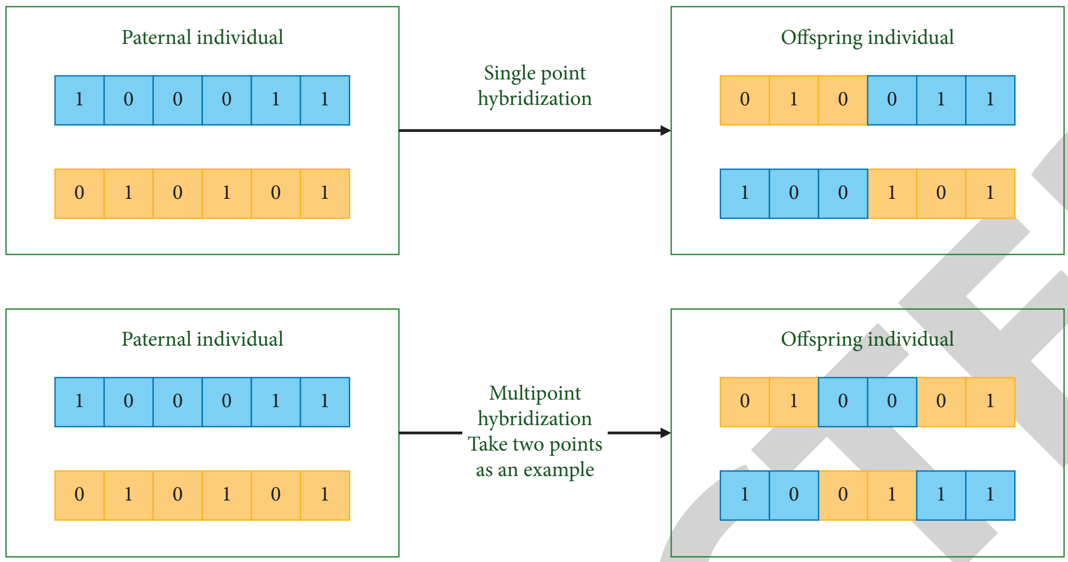

FIGURE 7: Two hybridization methods.

RI and ARI: given the sample label, all point pairs can form four indicators, the same label but belonging to different clusters, the same label and the same cluster, the same cluster of different labels, and different clusters of different labels, as shown in Table 1.

TABLE 1: Corresponding table of cluster labels.

	Homocluster	Different clusters	Total
Same label	a	b	a + b
Different labels	c	d	c + d
Total	a + c	b + d	a + b + c + d

Then the RAND coefficient is calculated with formula (13):

$$RI = \frac{a+d}{a+b+c+d}. \tag{13}$$

In the case of random, the ARI value is close to 0. With the improvement of clustering index, the ARI value is closer to 1. Its calculation method is shown in formula (14):

$$\mathrm{ARI} = \frac{RI - E[RI]}{\max(RI) - E[RI]}. \tag{14}$$

The value range of ARI becomes [−1, 1]. The larger the value, the closer the clustering effect to the real data distribution.

NMI: mutual information (MI) is a concept in information theory, which is mainly used to evaluate the correlation between the distribution of two random variables. There are two random variables X, Y, $p(x)$ is the edge distribution of x, $p(y)$ is the edge distribution of y, and $p(x, y)$ is its joint distribution; then MI is calculated as formula (15):

$$MI(X,Y) = \sum_x \sum_y p(x,y) \log \frac{p(x,y)}{p(x)p(y)}. \tag{15}$$

Standardized mutual information (NMI) is also called normalized mutual information; that is, standardize the value of mutual information to between [0, 1] through the standardization method, as shown in formula (16):

$$\mathrm{NMI}(X,Y) = 2\frac{MI(X,Y)}{H(X)+H(Y)}, \tag{16}$$

where $H(\cdot)$ represents the information entropy of random variables, and the calculation is shown in formula (17):

$$H(X) = \sum_{k \in S} p(x) \log_2 p(x). \tag{17}$$

Through the above formula, the mutual information between two random variables is normalized to [0, 1]. At the same time, NMI can also correct the bias of MI for more variables.

CP and SP: compactness CP refers to the average distance from each point in the cluster to the cluster center; that is, the smaller the CP value, indicating that the closer the distance within the cluster in the clustering model, the smaller the CP value in theory, the better. The tightness calculation can be calculated by formulas (18) and (19).

$$CP = \sum_{i=1}^{k} CP_i, \tag{18}$$

$$CP_i = \left(\frac{1}{|C_i|} \sum_{k \in C_i} d^p(x, c_i) \right)^{(1/p)}. \tag{19}$$

DBI index: due to the limitations of CP and SP, it is easy to fall into the local optimal solution when using CP or SP alone to evaluate the clustering model, while DBI balances the two and defines the performance of the clustering model on its basis. The calculation method can be determined by formula (20):

$$\mathrm{DBI} = \frac{1}{k}\sum_{i=1}^{k}\max_{j\neq i}\left(\frac{CP_i + CP_j}{\left\|c_i - c_j\right\|_2}\right). \tag{20}$$

Here is the DBI index description of Euclidean distance. From the definition of DBI, we can see that it takes into account the benefits of CP and SP for the quality evaluation of clustering model. The smaller the DBI value in application, the better.

4. Research on Comprehensive Health Evaluation of Art Psychotherapy

4.1. Research Assumptions. The purpose of this study is to compare the experimental effects through quantitative analysis. In the research, mainly guided by the viewpoint of "post-modern experiential art creation," the intervention group and control group were designed, and the pretest was conducted for group A and group B to ensure the equality of grouping. SPAT group psychological counseling was carried out. After the intervention, the experimental effects of the following aspects were analyzed and compared to explore its internal mechanism [15].

According to the above specific research purposes, the overall research assumptions of the intervention results in the second part of the study are as follows:

Experimental preconditions: equal histochemical design Pre A = Pre B.

Expected results of the experiment: paired samples of pretest and posttest in the same group: *t*-test: Post A > Pre A.

Analysis of variance of posttest comparison of differences between different groups: Post A > Post B.

The specific meanings of the general assumptions are described as follows:

Hypothesis a: compared with before and after intervention group A, spat group counseling (intervention group A) has significant differences in six aspects: self-harmony, depression, Eysenck personality type, social avoidance and anxiety, life orientation, optimism, and trait coping style [16].

Hypothesis AB: compared with control group B, spat group counseling has significant differences in six aspects: self-harmony, depression, Eysenck personality type, social avoidance and anxiety, life orientation, optimism, and trait coping style [17].

4.2. Implementation Process. The research object of this study is college students. Due to the particularity of the course, after consultation and discussion with relevant teachers and departments before the course, it is possible to implement a unique teaching form of comprehensive painting therapy in a college students' mental health course. The educational intervention of spat curriculum in this study was undertaken by an associate professor of psychology and one of the authors of this paper. The professor has 20 years of teaching experience in psychology. The author is a graduate student majoring in psychology and obtained the qualification certificate of national second-class psychological consultant and secondary vocational teacher. The author is responsible for preparing all the art media required for the course before class. In addition to reading a large number of relevant literature before the course, the interveners also discussed the spat course education plan in detail to ensure the quality of course education [18].

The course site is a fixed large classroom to meet the needs of activities in the course. The selection of specific art media, evaluation tools, and data processing are basically the same as the group counseling part of the second research. It should be noted that the love attitude scale (LAS) used in this study has good structural validity through confirmatory factor analysis. There are 22 items in 6 subscales, and the reliability of each subscale is between 0.706 and 0.818. The concept of love composed of six love styles: romance, game, companion, reality, possession, and dedication also exists among college students in mainland China. The view of love is a multidimensional psychological value. The initially formed love attitude scale can be used as a tool to evaluate the tendency of college students' view of love [19].

Comprehensive painting art therapy is committed to the unified and coordinated development of students' cognition, emotion, behavior, and personality as a whole. Therefore, different art experience activities such as painting are designed from different levels, and the curriculum education implementation plan is finally determined in combination with the basic teaching content of mental health curriculum [20]. The number of students in this course is 116, collectively known as the intervention group. There are ten courses, one hour and 30 minutes each time. See Table 2 for the specific contents of the curriculum education program.

Comprehensive painting art therapy is committed to the unified and coordinated development of the three levels of cognition, emotion, behavior, and personality of group members. Therefore, different painting and other art experience activities are designed from different levels. At the same time, the group counseling activity plan of this study is finally determined by referring to the existing painting art treatment group plans at home and abroad and under the guidance of professionals [21]. SPAT group psychological counseling activities were carried out for 9 times, once a week, about 2 hours each time. The control group did not intervene. See Table 3 for the specific contents of the activity plan.

The measurement part of the questionnaire is the reevaluation of the psychological scale. Fill in the self-compiled feedback form of group counseling effect, and then give full feedback and discussion between the instructor and members. Finally, the team farewell activity is called "big reunion." The purpose is to bid farewell to the group in a

Table 2: Implementation plan of SPAT mental health course.

Course time	Course unit topics	Course implementation process and method	Remarks: art media
1 March 1, 2010	Purpose of family formation: to understand the course form, eliminate the strangeness among members, understand each other, and form a small family Establish reasonable coping styles before, after, or after falling in love	(1) Course introduction: introduce the course content, form, and teaching methods (2) The first test of psychological scale is the pretest (3) Warm-up activities: use the Gestalt grouping method to group according to age, zodiac, and exchange personality characteristics with each other (4) Group grouping "simulated family": divided into 10 small families, with more than 11 people in each group. Each group selects two principal and deputy parents to be responsible for management and gives a sentence of "who is (she)," and finally shares it (5) Situational drama activities: the performance of "the development process of love emotion" in situational drama, that is, acquaintance, development, conflict, redevelopment, and decision, who is most able to think about their own pursuit and ideas, emotional needs, and how to actively guide	A4 sketch paper, Hb pencil, eraser, etc. Zhi, glue, scissors, self-brought pictures, and photos related to love, etc.
9 May 10, 2010	Emotional integration purpose: to integrate friendship, family affection, and love emotion from the level of knowing and doing	(1) Introduction to the course: the explanation of love sentiment, that is, sense of reason, aesthetics, and morality (2) Emotional test and case discussion and explanation (3) Painting and story analysis: "future life—a better tomorrow" nine-division painting and story sharing, according to the operation steps of the nine-division integration painting method (4) Viewing of audiovisual materials: emotion and marital emotion	24 color watercolor pens, oil painting stick, color pencil, A4 sketch paper, Hb pencil, eraser, etc.
10 May 17, 2010	The purpose of personality integration: members share deeply, integrate the curriculum harvest, and integrate into personality	(1) Course introduction: course summary (2) Personal painting: "a growing tree of life" and sharing (3) Group painting: "emotional garden," small family as a group, using large rice paper (4) Explore the future career blueprint, discuss, and share (5) After the second test of the psychological scale, the students bid farewell to each other	Watercolor pen, oil painting stick, watercolor pigment, rice paper, A4 sketch paper, pencil, eraser, etc.

warm, sweet, and cohesive situation, go to life, and leave a beautiful and unforgettable memory.

4.3. Research Results and Discussion

4.3.1. Comparison of Pretest Results of Psychological Measurement between SPAT Group Psychological Counseling Intervention Group and Control Group. Before spat group counseling, the intervention group and the control group were measured with the professional psychological scale. The analysis of variance showed that there was no significant difference between the intervention group and the control group in these aspects. The specific test results on different scales are shown in Table 4.

4.3.2. The Influence of Educational Intervention of SPAT Course on the Types of Love Attitude. In order to investigate whether there are statistically significant changes in students' love attitude before and after the educational intervention of spat course, the *t*-test of paired samples of "pretest and posttest" is carried out. The results are shown in Table 5.

Table 3: SPAT group psychological counseling program.

Activity name	Activity objectives	Process and method	Art media
(1) A new family 2010.03.04	(1) Clarify the objectives of the group and the formation of the group (2) Be familiar with team members and art media (3) Build trust and warm group atmosphere	(1) Introduction and discussion on the content and form of group activities (20 minutes) (2) Psychological scale measurement and signing informed consent (20 minutes) (3) Warm-up activities—social measurement and body bumper car (20 minutes) (4) Set up three small families to discuss and display "family name," "family number," "family song," and "family dance" (25 minutes) (5) Nine-cell emotional painting (20 minutes) (6) End sharing (15 minutes)	Watercolor pen, color pencil, oil painting stick, color small cardboard; psychological scale and informed consent
(2) Who am I 2010.03.11	(1) Emphasize group commitment and enhance group motivation (2) Improve self-awareness	(1) Group dynamic reconstruction (15 minutes) (2) Self-portrait painting (30 minutes) (3) Music image painting (30 minutes)	2B pencil, eraser, A4 sketch paper: oil paint, rice paper, brush, platter;

Table 4: Results of pretest ANOVA of psychological scale in intervention group and control group.

Scale and its factor name	Group	N	Mean	SD	Variance homogeneity test			Analysis of variance results
					Levene statistics	Sig. (P value)	F value	P
Disharmony factors of SCCS self and experience	Intervention group A	15	41.470	6.543				
	Control group B	15	46.070	10.879	2.430	0.130	1.802	0.190
SCCS self-spirit	Intervention group A	15	21.730	3.918				

Table 5: T-test results before and after spat curriculum education intervention love attitude scale.

Paired comparison of pretest and posttest differences			T-test results	
Scale and factor name	Mean	SD	T value	P
Romantic love	0.257	2.557	1.030	0.305
Game love	−0.124	3.021	−0.420	0.675
Companion love	0.705	3.079	2.346	0.021*
Possessive love	−0.114	2.569	−0.456	0.650
Realistic love	−0.105	2.382	−0.451	0.653
Give love	−0.057	2.541	−0.230	0.818

$^{*}P < 0.05$, $^{**}P < 0.01$.

It can be found from the data in the table that, before and after the experiment, there is a significant difference in the peer love factor in the pretest and posttest results of the intervention group ($P < 0.05$), and there is no significant difference in other factors. There was no significant difference in other factors. This shows that spat curriculum intervention can enhance the tendency of "peer love" and has a positive effect on improving the types of love attitudes of college students. The ternary theory of love holds that love should have three core points: intimacy, passion, and commitment. "Peer love" is the love for intimate partners formed by the combination of intimacy and commitment. This kind of love is characterized by mutual respect and trust between the two sides. What people experience is more a sense of trust and dependence on each other. This type of love will be concentrated in a long and happy marriage. Although the passion is gone, common ideals, common interests, common values, tolerance, and habits can better maintain good feelings. Therefore, more guidance should be given to college students.

4.3.3. Influence of Educational Intervention of SPAT Course on Eysenck's Personality Type Characteristics. In order to investigate whether there are statistically significant changes in the factors of students' Eysenck personality type before and after the educational intervention of SPAT course, the t-test of paired samples of "pretest-posttest" is carried out. The results are shown in Table 6.

It can be found from the data in the table that, before and after the experiment, there is an extremely significant difference in EPQ extraversion factor in the pretest and posttest results of the intervention group ($P < 0.01$), and there is no significant difference in other factors. This shows that spat curriculum intervention can significantly improve the extraversion of college students' personality types. The reason may be that the curriculum education improves the openness of members, stimulates their internal spontaneity and initiative, and is willing to show more characteristics such as good communication, enthusiasm, and impulse. Fang

Table 6: Results of t-test before and after the short EPQ scale of educational intervention in SPAT course.

Paired comparison of pretest and posttest differences			T-test results	
Scale and factor name	Mean	SD	T value	P
EPQ psychoticism factor	−0.123	1.357	−0.935	0.352
EPQ extraversion factor	−0.686	2.105	−3.339	0.001**
EPQ neuroticism factor	−0.019	2.780	−0.070	0.944
EPQ masking factor	0.076	1.895	0.412	0.681

*stands for $P < 0.05$, $^{**}P < 0.01$.

Table 7: T-test results before and after LOT-R of educational intervention in SPAT course.

Paired comparison of pretest and posttest differences			T-test results	
Scale and factor name	Mean	SD	T value	P
Total score of LOT-R life orientation scale	−0.029	3.712	−0.079	0.937

$^{*}P < 0.05$, $^{**}P < 0.01$.

Table 8: T-test results before and after TCSQ of educational intervention in spat course.

Paired comparison of pretest and posttest differences			T-test results	
Scale and factor name	Mean	SD	T value	P
TCSQ negative coping style factor	−0.038	5.932	−0.066	0.948
TCSQ positive coping style factor	−0.419	6.978	−0.615	0.540

$^{*}P < 0.05$, $^{**}P < 0.01$).

Shuren depicted in the curriculum intervention is a specific image and a psychological "self-sufficiency," resulting in no significant change before and after the educational intervention LOT-R. The comparison results before and after the educational intervention LOT-R are shown in Table 7.

4.3.4. The Influence of Educational Intervention in SPAT Curriculum on Trait Coping Style. In order to investigate whether there are statistically significant changes in students' trait coping styles before and after the educational intervention of spat course, a paired sample t-test of "pretest and posttest" was carried out. The results are shown in Table 8.

It can be found from the data in the table that there is no significant difference between the pretest and posttest results of the intervention group in the negative and positive factors of trait coping style before and after the experiment. The reason may be that the students participating in the curriculum intervention do not have coping style problems, and there is no significant change before and after.

5. Conclusion

From the overall results of this study, compared with the control group, spat group psychological counseling significantly enhances college students' self-flexibility, improves the degree of self-harmony, reduces college students' social avoidance tendency, improves college students' extraversion of personality types, has a more positive effect on reducing personality concealment, and can improve college students' optimistic attitude. The positive coping style factor increased, and the scores of other depressive tendencies, neuroticism factors, negative coping styles, and social anxiety factors decreased, which is in line with the initial assumption of this study. The specific research conclusions are as follows:

In the rehearsal group discussion, there was a difference in personal transformation between this group (sampan) and other groups before and after the experiment ($P < 0.05$). There was no significant difference in group B before and after the experiment ($P > 0.05$). After the experiment, there was a significant difference in individual stereotype types between the affected group and the control group ($P < 0.05$), and there was no statistical difference between the other groups ($P > 0.05$).

In the group discussion of art design improvement, there was a significant difference in EPQ concealment ($P < 0.01$) and a significant difference in EPQ extroversion factor ($P < 0.05$) before and after the experiment, but there was no significant difference in the control panel. After the experiment, the difference in EPQ extroversion between the control group and the control group was statistically significant ($P < 0.05$).

In the group discussion of art deco, there was a significant difference between the groups of avoidance before and after the experiment ($P < 0.05$), and there was no significant difference with other groups. After the experiment, there was a significant difference in the total stress score between the control group and the control group ($P < 0.05$).

In the art deco group discussion, the LOT-R life orientation total score listed in the group was significantly different before and after the experiment ($P < 0.05$), but there was no significant difference in the control group. After the experiment, there was a statistically significant difference in the total score of life direction between the affected group and the control group ($P < 0.01$).

In the group discussion of decorative art design, the adverse effects of TCSQ on the intervention process were significantly different in each group before and after the experiment ($P < 0.05$), but there was no significant difference in the control group. After the experiment, there was no significant difference between the intervention group and the control group in both adverse and positive performance.

With all the benefits of this study, the spat data reported effects on improving college students' romantic behaviors, increasing college students' extroversion, reducing underlying behaviors more effectively, and lowering student relationships and stress. Other factors did not change significantly, but scores increased on positive thinking for good solution quality and positive behavior and increased on other stressors, mental disorders, neurotic factors, and poor resolution, consistent with the original theory. The main points of the special research are as follows:

In the research on the effect of layered art, the point-to-point interaction before and after the experiment was

Hindawi
Computational Intelligence and Neuroscience
Volume 2022, Article ID 3762431, 10 pages
https://doi.org/10.1155/2022/3762431

Research Article

Data Analysis of Educational Evaluation Using K-Means Clustering Method

Rui Liu

Science Teaching Department, Zhengzhou Preschool Education College, Zhengzhou 450000, China

Correspondence should be addressed to Rui Liu; 1351160205@xzyz.edu.cn

Received 2 April 2022; Revised 29 April 2022; Accepted 30 April 2022; Published 31 July 2022

Academic Editor: Xin Ning

It is thought to be an effective technique to handle the problem of educational data explosion and lack of information by identifying potential relationships between data and directing decision-makers through the extraction, transformation, analysis, and modeling of educational data. Based on this, this research constructs a data analysis model for education evaluation using the K-means clustering technique in DM. The weight of each index of students' comprehensive quality is calculated using AHP, and the value of the weight is used to determine whether the index is the important feature of analysis system mining. Improved sampling technology is used to deal with the representation of large-scale data sets; a sample partition clustering technique is proposed as a general framework. The best accuracy of this method, according to experimental data, is 95.6 percent, which is 12.1 percent greater than Mi cluster algorithm and 6.8 percent higher than DRCluster algorithm. The K-means clustering analysis technology is used to analyze students' comprehensive evaluation data in this paper, with the goal of determining the regularity of data implication, accurately diagnosing learning problems, and providing the foundation for developing effective student management strategies.

1. Introduction

With the implementation of teaching reform, enrollment continues to rise, and a large number of children face significant obstacles in terms of school construction, teaching management, and teacher management [1]. Schools have amassed a considerable amount of complex student data, such as student status information, accomplishment information, specialty information, and moral information [2]. It has been challenging to adapt the old management mode to the large student population and data management. How to properly utilize and analyze massive raw data and turn it into useable knowledge and value has become an important topic of common concern at home and abroad to tackle the difficult problems in educational data processing [3]. The introduction of information management technology to tackle data problems produced by the influx of students in the field of education has played a major role in the construction of schools [4], thanks to the rapid development of Internet technology. It is vital to acquire the necessary data for evaluating education. Researchers gradually find that the collection channels are restricted and that there are a lot of unstructured data when they collect data. It takes a long time to store meaningful data, and it is far more difficult to acquire timely information feedback [5]. Faced with these growing issues, a variety of educational applications and platforms to assist teachers in collecting and analyzing data arose and are now extensively used [6]. The rise of information technology has aided educational research by allowing for the collecting, storage, analysis, and decision-making of data and allowing for the timely collection of student studies. Simultaneously, it gives data support for teachers to properly and timely analyze students' development and change their own teaching style [7]. The introduction of information technology may not only remove a lot of repetitive manpower and increase staff efficiency, but it can also play an essential role in the collaborative administration of schools due to its fast information transmission mechanism.

DM (data mining) is also called knowledge discovery in database. DM is the process of discovering hidden, regular, and unknown but potentially useful and understandable information and knowledge from a large number of incomplete, noisy, fuzzy, and random practical application data. Cluster analysis is an important and active research field in DM [8]. As an unsupervised learning method, clustering is essentially a density estimation problem. The data to be clustered are not labeled with its category in advance and can be generated by a mixed model. Its main idea is to divide data into several classes or clusters to maximize the similarity of data objects within clusters and minimize the similarity of data objects between clusters [9]. The clustering algorithm can be selected by the data type of field attributes in the database and the characteristics of objects operated by clustering. Common clustering algorithms include partition-based clustering algorithm, hierarchical clustering algorithm, density-based method, grid-based method, model-based method, and constraint-based method. At present, large-scale data sets frequently emerge in the field of education, which poses new challenges to data analysis and research. In the face of large-scale data, traditional analysis algorithms are no longer as "handy" as small- and medium-sized data, but there are many problems such as difficult processing, long processing time, difficult parameter determination, low efficiency, and low clustering quality. Moreover, the collection content of evaluation data is single, and the analysis method lacks a certain depth. For the current situation of education data analysis, this paper introduces K-means clustering algorithm to analyze the education evaluation data. The innovations of this paper are as follows:

(i) From the perspective of cognitive learning theory, this paper aimed to address the current educational data's long processing time, uncertain parameters, and low clustering quality; the collection content of evaluation data is single, and the analysis method lacks certain depth and many other issues. To analyze the education evaluation data, the K-means clustering algorithm is introduced. The proposed approach is suitable for large-scale DM, according to a series of experiments. For relevant researchers, this has some reference and guiding relevance.

(ii) In this paper, the data are cleaned, integrated, and transformed into data storage format, and the input data fulfilling the K-means algorithm are created, with the goal of solving problems such as data duplication, missing data, and inconsistent storage kinds. We may also uncover commonalities between students using the K-means technique to cluster and analyze their comprehensive evaluation results. Students are categorized based on their commonality, allowing student managers to provide tailored education management for various types of students.

2. Related Work

In these years of rapid DM growth, various disciplines' research topics are continually presented, including data retrieval technology, artificial intelligence, neural networks, virtual reality technology, and associated basic mathematical theories. Simultaneously, DM's applicability in the realm of education is expanding. DM has been used by a number of academics to analyze educational data in recent years.

Kelly et al. proposed a fast relaxed clustering algorithm based on graph theory. The asymptotic time complexity of this algorithm is linearly related to the data capacity when applied to larger-scale datasets [10]. Charles et al. proposed an efficient K-means clustering algorithm, which uses precomputed distances between points and dormant clusters to reduce the amount of distance computation, greatly reducing the running time and space used [11]. Rosenkranz et al. believe that the current educational data statistical analysis platforms and tools have been promoted and applied in school teaching, but there are still many problems in how to effectively analyze and use these data [12]. Scott and others believe that in the process of education, educational evaluation data occupy a large proportion, and it clearly shows the actual learning situation of students, which plays an important guiding role in teachers' teaching. Therefore, from the perspective of teachers, it uses the "Jike Big Data" system to optimize the use of educational evaluation data [13]. Hopper et al. studied the related problems of teaching optimization based on the analysis of educational evaluation data. It proposes to use educational evaluation data to determine the learning starting point of learners, design quantifiable learning goals, select learning content suitable for learners, and accurately evaluate teaching quality, and conduct personalized learning analysis and feedback in a timely manner [14]. Wolbring et al. pointed out that the collection and analysis of educational evaluation data are not only a reflection of students' learning achievements but also a reflection of teachers' teaching effect [15]. Goldberg et al. used the ideological and moral quality, intellectual education quality, physical and mental quality, and development ability quality indicators to evaluate and subdivided the indicators into multiple secondary indicators. The evaluation adopts evolutionary algorithm, fuzzy comprehensive evaluation, multivariate statistical analysis method, etc., to obtain effective weights, and the data items are summed according to the weights to obtain the quantitative score evaluation value [16]. Kang et al. selected some data from a large-scale data set, used these data to construct an adjacency matrix, and obtained eigenvectors by eigendecomposition of the adjacency matrix, and finally used Nyström to approximate the eigensolution of the original matrix [17]. Aiming at the main methods of DM, Hou et al. studied the ideas and applications of related algorithms, analyzed the advantages and disadvantages of existing methods and compared them. Based on this, a data analysis method based on the optimal decision tree algorithm is proposed [18]. Lavelle et al. analyzed and designed an evaluation database based on the functional requirements of the school education and teaching situation evaluation system. It can realize functions such as maintenance of basic information, statistics, and query of evaluation data [19]. Wang et al. proposed a new fuzzy clustering algorithm based on genetic algorithm, which realized the clustering analysis of characteristic data with mixed attributes. By introducing the genetic algorithm into the algorithm, the global optimal solution can be obtained quickly and effectively, and it does not depend on prototype initialization at all [20].

Based on these studies, this paper proposes an educational evaluation data analysis method based on K-means clustering algorithm to solve the problems of difficult processing, long processing time, and difficult parameter determination. In this paper, firstly, the cluster analysis method in DM technology is applied to establish a model to quantitatively analyze the indicators and their values of objects, and then, a new comprehensive evaluation method for students combining quantitative analysis with qualitative analysis is proposed. Then, AHP is used to calculate the weight of each index of students' comprehensive quality and judge whether the index is the key attribute of analysis system mining according to the value of the weight. Finally, the improved sampling technique is used to deal with the representation of large-scale data sets. A general framework of sampling partition clustering algorithm is proposed. The validity of the framework is verified by implementing K-means and k-medoids algorithms. It is proven that this method is practical and feasible.

3. Methodology

3.1. DM-Related Technology. With the gradual development of educational big data, artificial intelligence, learning analysis, and intelligent network learning platform, learners' whole-process learning data can be recorded. At the same time, with the rapid development of DM, artificial intelligence, and other technologies, these educational data can be automatically and deeply analyzed and processed, and learners can be personalized analyzed and diagnosed. The core function of DM technology is to discover potential rules from large-scale data. DM (data mining) is a specialized technology for mining extraordinary knowledge from large-scale data. It is a process of mining useful information from incomplete, massive, noisy, fuzzy, and random data that people do not know in advance. DM is a process of discovering potentially useful information or knowledge in reality. This process is essential for discovering knowledge in the database, in which knowledge discovery is a process of converting raw data into effective information that can be used for analysis. DM is a process of selecting, exploring, and modeling a large amount of data to discover unknown rules and relationships in advance. The purpose of DM is to get clear and useful results for the owner of education database. The DM process generally consists of business object determination, data preparation, DM, and result analysis.

Cluster analysis in DM is an active and challenging research field. In recent decades, its importance and cross characteristics with other research directions have been widely recognized by people. It plays a very important role in identifying the internal structure of data and has become one of the important research contents of DM, machine learning, and pattern recognition. The differences between groups are obvious, and the data in the same group are as similar as possible. Data clustering divides physical or abstract objects into several groups. Within each group, there is high similarity between objects, but low similarity between groups. It is the same as and different from classification. The same thing is that the data source is divided into several parts. The difference is that it is a kind of unsupervised learning, and it does not know the final grouping number and grouping standard. As a classical clustering algorithm, K-means mainly realizes different classifications of data sets through an iterative process. This algorithm has the advantages of simplicity and strong scalability. In DM field, the typical requirements for clustering mainly include the following aspects: ① scalability, ② ability to handle attributes of different data types, ③ any shape cluster can be found, ④ insensitive to the entered record order, ⑤ high dimension, ⑥ minimization of domain knowledge for determining input parameters, ⑦ ability to effectively deal with noise and abnormal data, and ⑧ availability and interpretability. In DM stage, the task or goal of mining is determined, and the mining method is selected, to implement DM operation and obtain useful patterns. The specific DM application requirements are determined, the goal of mining is cleared, and the effect that can be achieved after the system is completed. The application field background is analyzed, and the problem objective is determined. The background knowledge of related fields is understood, the needs of users are made clear, and data are collected to solve problems, and services are provided for the follow-up work. Traditional data analysis is a kind of verification analysis. It is a kind of user-driven data analysis, focusing on describing the facts that have happened in the past. DM is to mine information and discover knowledge without hypothesis. The obtained information has three characteristics: effective, unknown in advance, and practical. It is to predict the future situation and explain the factual reasons of the past. To obtain potentially effective information to meet the needs of users, it is required to fully mine the surface information, remove redundant data, and visually display key data to users. Prediction and description are the two goals of DM. Prediction refers to the use of some information fields and variables in the database to predict the hidden useful information, and description refers to the description of data as an understandable pattern. There are two aspects to consider when choosing an algorithm: first, according to the different characteristics of different data, the algorithm is selected related to it to mine; second, according to the needs of users or the actual operation of the system. This stage is the core and difficulty of knowledge discovery process.

3.2. Big Data of Education and Educational Evaluation. This paper holds that educational big data refer to the data collection generated in the whole process of educational activities and collected according to educational needs, which is used for educational development and can create great potential value. Big data for education are a subset of big data, and it is a collection of data generated throughout the educational process and collected based on educational needs, which is utilized for educational improvement and has a lot of potential value. Schools have purchased or adapted educational administration systems to better handle

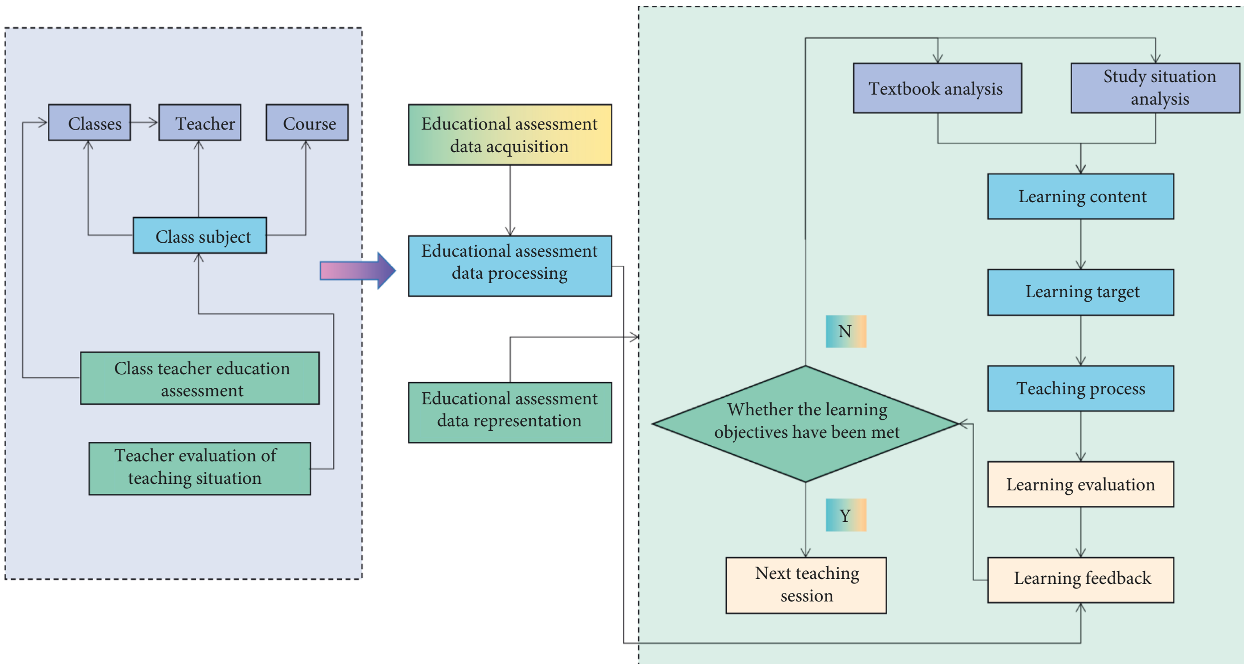

Figure 1: Teaching optimization method based on educational evaluation data.

students' information as the student population has grown. The system's principal purpose is to keep track of pertinent information about pupils' academic achievement, for example, students' test scores and grade points, information about their curriculum, examination schedules, attendance, and information regarding rewards and discipline violations, among other things. All of this is educational big data. Different classification standards exist for big education data, depending on the perspective. Teaching data, management data, scientific research data, and service data can all be found in the data sources. According to the degree of organization, it can be separated into structured data, semi-structured data, and unstructured data. It can be separated into process data and result data at the collection stage. Process data are information gathered during the teaching process that is difficult to quantify directly. Quantifiable data are referred to as result data.

A huge education database is built to collect massive student data, including students' test scores, social activities, class attendance, and hobbies. Relying on tens of millions of data collected by the database can help students in various universities to do data analysis, help them find out the reasons why they cannot improve their grades, and help them adjust their learning styles or change their lifestyles in time to avoid dropping out of school. The data collected in each evaluation are defined as educational evaluation data in this paper, and the data types are mainly data generated in the learning process including the knowledge points, questions, difficulty, discrimination, learners' right and wrong situation, grades, and ranking. At present, the application value of educational evaluation data is mainly reflected in six aspects, namely, promoting more scientific teaching management, promoting the innovation and reform of teaching mode, promoting the realization of personalized learning, promoting the reconstruction of educational evaluation system, promoting the successful transformation of scientific research paradigm, and promoting the humanization of educational service. Educational evaluation refers to the process of scientifically measuring and judging various educational activities, educational processes, and educational results using certain technologies and methods under the guidance of certain educational values and according to established educational goals. At present, the research in the field of basic education has just started, and the data analysis platform of education evaluation has not been able to provide accurate education decisions for teachers and personalized teaching services for students. Therefore, the research on educational big data needs to be strengthened. Figure 1 is a teaching optimization method based on educational evaluation data.

Education evaluation data are the data fact obtained for the education effect or the development of students in all aspects, and education evaluation is the process of value judgment based on these data. Student evaluation data are one of the subsets of educational big data that educators are most familiar with. Its sources are abundant, including formative evaluation, unit test, midterm and final test, and large-scale regional test. There are various types of data, including test scores and teacher evaluation. When confronted with diverse and customized student groups, fixed, homogenous, and dogmatic educational and administrative systems have revealed numerous flaws. To reform educational techniques and management modes, we should begin with the dominant position of students and provide tailored instruction based on their qualities. In school education, evaluation data are regarded as the most important indicator of educational and teaching improvement. These data are mainly test scores gathered through measurement, and

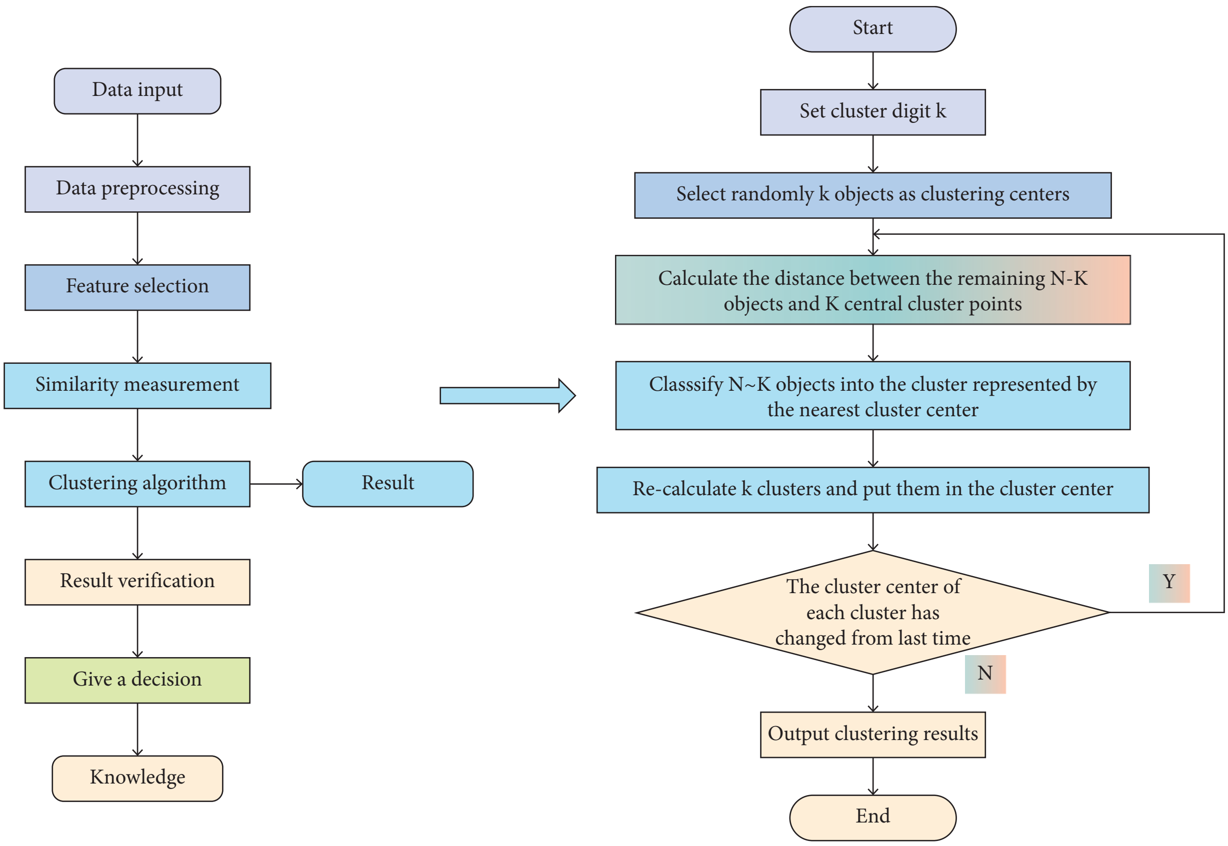

FIGURE 2: General flow of K-means clustering algorithm.

careful collection, categorization, sorting, statistics, and analysis can turn them into very valuable big data in education. Teachers are the leaders of pupils in the sphere of education. The more they know about students, the better they can choose the most appropriate learning content in class, set the most precise learning objectives, conduct objective learning evaluations and provide timely learning feedback, provide students with personalized guidance, and help them develop their abilities to their full potential. The use of educational evaluation data analysis software or tools in the teaching process, as well as the routine collecting and analysis of these data, is critical to maximizing the value of evaluation data. Teachers can stay on top of changes in their students' knowledge, help them modify their learning speed, and continually enhance and optimize the instructional design process.

3.3. Educational Evaluation Data Analysis Based on K-Means Algorithm. Data integration, data selection, and data preprocessing are the three sub-steps of data preparation. Data integration unifies data from numerous files or databases, cleans it, and resolves semantic ambiguity. The goal of data selection is to figure out what the operation object of the discovery task is, which is the target data, which is a collection of data taken from the original database to meet the demands of users. The goal of data preparation is to convert raw data into a format that can be analyzed. Data preprocessing entails combining data from several sources, eliminating duplicate data values and noisy data, and screening out data sets and feature qualities that are not relevant to present DM activities. K-Means uses the rule algorithm to compute the distance between data items and then iteratively calculates the grouping situation of the obtained data objects until the center does not move, resulting in K clustering outcomes. The general algorithm flow is shown in Figure 2.

After the DM stage, the obtained result patterns are usually redundant or do not meet the user's requirements, so it is necessary to delete, filter, or return to the previous stage according to certain standards and reselect data and methods to obtain meaningful patterns and knowledge. In the course of the task, different data sources and different formats of the collected data are also different, so different data should be integrated and cleaned and processed. The general process of clustering includes feature selection, similarity measurement, clustering algorithm, result verification, and decision-making. K-Means algorithm is simple and efficient. However, there is no clear standard definition for the clustering number k and the selection of the center point of the algorithm, and most of them are given randomly, which will easily cause great influence on the algorithm results. Therefore, a selection method to solve the initial value k is used. Given a set of n data points:

$$X = \{x_1, x_2, x_3, \ldots, x_n\}. \tag{1}$$

The algorithm is to find a partition of X, $P_k = \{C_1, C_2, C_3, \ldots, C_k\}$, which minimizes the value of the objective function J.

$$J = \sum_{i=1}^{k} \sum_{x_j \in C_i} \left| x_j - o_i \right|^2, \tag{2}$$

where o_i represents the center point of class C_i. The Euclidean distance between two p-dimensional data points x_i and x_j is set, as in formula:

$$\begin{aligned} x_i &= \left(x_{i1}, x_{i2}, x_{i3}, \ldots, x_{ip}\right), \\ x_j &= \left(x_{j1}, x_{j2}, x_{j3}, \ldots, x_{jp}\right), \\ d\left(x_i, x_j\right) &= \sqrt{\left(x_{i1} - x_{j1}\right)^2 + \left(x_{i2} - x_{j2}\right)^2 + \ldots + \left(x_{ip} - x_{jp}\right)^2}. \end{aligned} \tag{3}$$

The average distance of all samples is determined as follows:

$$\text{Meandist}(S) = \frac{2}{n(n-1)} \times \sum_{i \neq j, i, j=1}^{n} d\left(x_i, x_j\right). \tag{4}$$

The square error criterion function for determining the objective function is as follows:

$$\sigma_i = \sqrt{\frac{\sum_{i=1}^{n_i} \left(x_i - c_i\right)^2}{C_i - 1}}. \tag{5}$$

In the formula, c_i is the centroid point of the same category of data. The c_i calculation formula is defined as follows:

$$c_i = \frac{1}{\left|C_i\right|} \sum_{x_i \in T_i} x_j. \tag{6}$$

In the formula, $|C_i|$ is the number of C_i-like data objects; c_i represents the ith cluster center.

Data cleaning is the process of cleaning problematic data. Its task is to clean the data that do not meet the requirements, usually deleting or modifying, but not simply modifying. Data that do not meet the requirements are redundant, missing, and wrong data. Data cleaning mainly includes standardization of format, removal of abnormal data and duplicate data, and correction of error data. It is necessary to clear some duplicate data in the test data management system and obtain data of other dimensions from other systems to supplement the whole database. The purpose of data cleaning is to ensure the accuracy and validity of data, to ensure good mining efficiency in the process of mining. At the same time, data cleaning is the foundation to complete the whole mining work. Given data input as information, features are extracted to represent the whole data set, so that redundant information can be reduced as much as possible. Then, according to the similarity between data points, a specific clustering algorithm is applied to the data set, and the cost function usually determined by the similarity of data points is reduced to the minimum. When the algorithm converges, it will return the output cluster. Clustering is very complicated. Different clustering analysis is applied to the same data, and the results are completely different, and the definition of clustering is usually relative. There are different clustering methods for the same group of objects, and different clustering of the same data probably corresponds to different applications.

Based on the minimum distance principle, we classify the data points x in the remaining datasets into the current cluster, namely,

$$c = \arg\min\left(\left|x - \mu_j\right|^2\right), \tag{7}$$

where μ_j is the centroid of class C_j and c is the class assigned to the data. Once new data have been assigned a class label, the cluster centroids are updated iteratively until all data points have been processed:

$$\mu_j = \frac{\mu_j m_j + x}{m_j + 1}, m_j = m_j + 1. \tag{8}$$

The data in the assessment system can be separated into two groups: one that can be represented using mathematical language and another that can be stated using words. The language's data can be examined and sorted, and DM technology's decision tree, correlation analysis, and cluster analysis methods can be used to create a model to quantify the analysis object. Because of the irregularity of data acquired from various sources, data conversion is required to develop a process suitable for DM. The quality of K-means clustering is insecure when dealing with huge data sets. As a result, this study introduces a sampling strategy to make the partition clustering algorithm acceptable for large-scale data sets. The simplest way is to choose numerous partitions at random from the original large-scale data collection. Each partition employs a clustering technique, with clustering results that are both reliable and capable of representing the entire data set. Input data are information saved on various digital media in various formats, such as an electronic report or a data relation table. These data might be kept in centralized databases or distributed site systems.

4. Result Analysis and Discussion

This study investigates the impact of data analysis on education evaluation using the K-means algorithm, as well as conducting teaching trials. The similarities between students are discovered through clustering analysis of students' comprehensive evaluation scores using the K-means technique. Students are categorized based on their commonality, allowing student managers to provide tailored education management for various types of students. The evaluation findings and learners' understanding levels are assessed before and after deployment, and the learning effect provided by this model is tracked. During the experiment, learners were interviewed and given questionnaires to gain feedback and suggestions for optimizing and refining the model, which was then iteratively improved to measure its overall performance. Finally, a feedback questionnaire is created to assess the model's use feedback across several

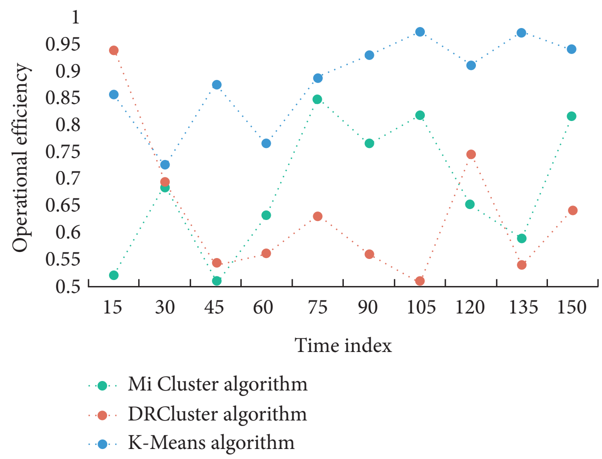

Figure 3: Running efficiency of different algorithms.

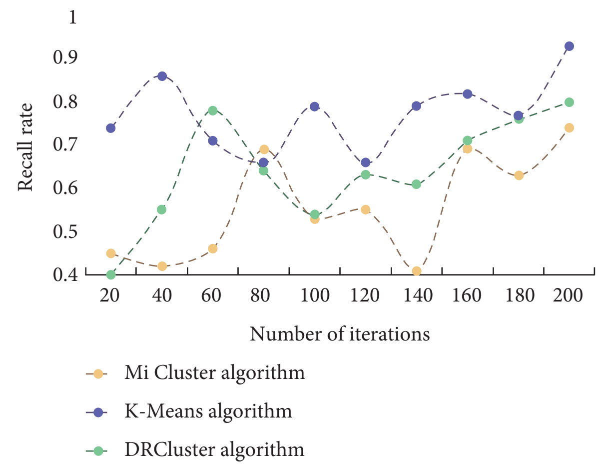

Figure 4: Recall of different algorithms.

dimensions. To begin, this section compares and contrasts the efficiency and effect of the DRCluster and Mi cluster algorithms with this algorithm, as well as analyzes and evaluates their biological importance. The running efficiency of different algorithms is shown in Figure 3. The accuracy of different algorithms is shown in Figure 4.

It can be seen that the running efficiency of this algorithm is high, and the running efficiency of DRCluster algorithm and Mi cluster algorithm is lower than that of this algorithm. In terms of recall rate, this method also has certain advantages, and the recall rate of this method is better than the other two algorithms. This conclusion also verifies the superior performance of this algorithm. To further evaluate the mining effectiveness of the algorithm, different algorithms are used for biclustering mining of six data sets, and the number of biclusters they can find is compared. Table 1 shows the number of double clusters that the three algorithms can mine in six data sets.

It can be seen from the table that the Mi cluster algorithm can find the least number of double clusters, which is mainly related to the differential support defined by the algorithm. However, the algorithm in this paper adopts effective support degree, transformation into differential weight graph, effective pruning strategy, and so on, which makes the number of mining biclusters the largest. A significant amount of experimental data are analyzed in this section. The software Office Visio was used to create the expert knowledge structure map and the student knowledge structure map. The Questionnaire website was used to gather and evaluate student feedback questionnaires, which were then analyzed using SPSS. The educational administration employees should compile the basic data needed for the evaluation and keep track of pertinent information such as the classes participating in the evaluation, the class teachers, the class subjects, and the teachers prior to the evaluation. Second, a system is set for students to rate their teachers and classmates. Finally, the evaluation is questioned by leaders and teachers. The analysis and application of educational evaluation data will examine every student's homework, test, and examination, transforming diagnostic evaluation into process evaluation and allowing teachers to grasp students' learning progress and place in time and reflect and adjust their teaching accordingly. Figures 5 and 6 depict the outcomes of clustering data sets using the DRCluster algorithm, Mi cluster algorithm, and this algorithm mode, respectively.

The test results reveal that the suggested method has a high level of accuracy, with an error rate of less than 2% over time. In these three modes, the K-means clustering algorithm suggested in this paper is valid. Routine exercises and examination evaluation tasks are carried out by students. Explicit data are the result of statistically studied evaluation data, such as score ranking, true or false situations, and answer time. Qualitative outcomes that require more examination, such as knowledge structure and comprehension level, are referred to as implicit data. The thorough evaluation score sheet includes factors such as ideological quality, cultural and athletic activity innovation, and academic accomplishment. All scores are in percentages, with a minimum scoring unit of 1 and no order of magnitude difference. The existing data dimension table is separated into three categories, and the values are taken according to the supplied weight coefficient, to compare with the current measurement and quantification result data. Students' evaluation data collection uses marking instrument and extreme class big data platform, and teachers use extreme class big data platform to arrange knowledge unit test papers, print them into papers, and distribute them to students. The test paper scanner is used to collect students' evaluation data, and the students' evaluation data are stored in the polar class big data platform. The evaluation data are analyzed, and the achievement of learning goal A of a class after the implementation of targeted education management is analyzed as shown in Table 2.

It can be seen that the total success rate of the class is 92.14%. The overall average score rate of the class is higher than that of the grade, which indicates that the class has a good grasp. Using K-means algorithm, DRCluster algorithm, and Mi cluster algorithm, the comprehensive evaluation scores of students are clustered and analyzed, respectively, and then, the changes in students' test scores after implementing targeted education management for different types of students are shown in Figure 7.

Table 1: Comparison of algorithm effectiveness.

Data set	Number of genes	Number of samples	Mi cluster algorithm/ number of biclusters	DRCluster algorithm/number of double clusters	Number of algorithms/ biclusters in this paper
Yeast	21498	297	30	139	254
Lymphoma	11024	209	37	131	167
Breast	3014	184	42	126	326
Live	4125	99	51	154	312
Lung	54926	82	15	142	106
Path_ metabolic	801	73	9	136	89

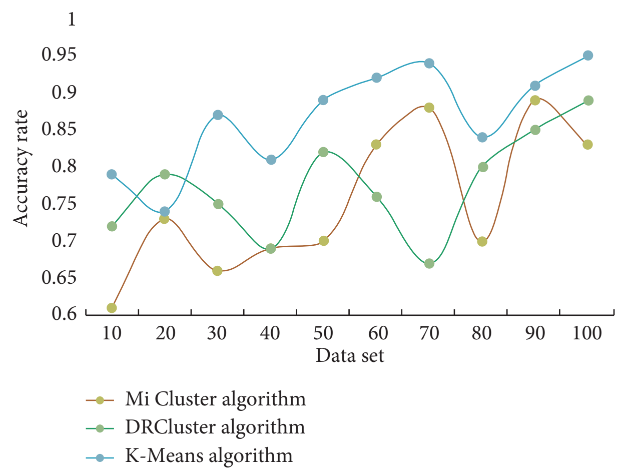

Figure 5: Accurate recognition rate.

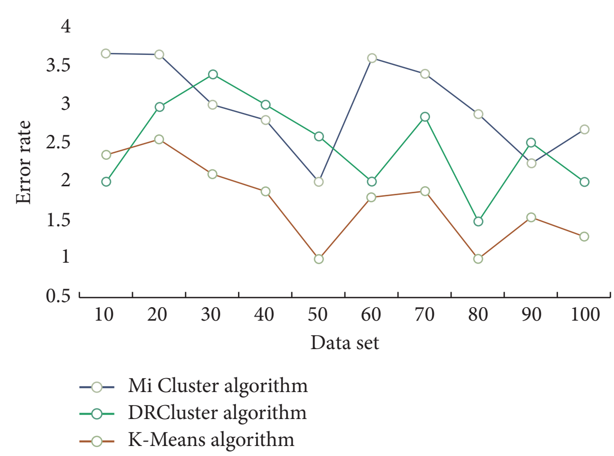

Figure 6: False recognition rate.

Table 2: Analysis of the achievement of students' learning objective A.

Student number	Students should meet the standards	Actual score rate of students	Determine whether students meet the standard	Class should meet the standard (%)	Actual score rate of class (%)	Actual grade score rate (%)	Probability of reaching the standard (%)
1	72%	80%	Yes				
2	75%	90%	Yes				
3	88%	100%	Yes				
4	90%	95%	Yes	80.57	92.75	88.69	92.14
5	93%	100%	Yes				
6	96%	100%	Yes				
...	...	...	...				

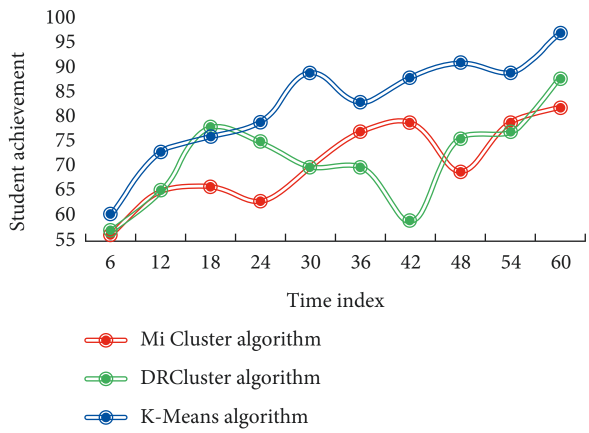

Figure 7: Changes in student achievement.

From the data analysis in Figure 7, it can be seen that after the analysis and targeted teaching management with this method, the students' scores show an obvious upward trend. Its influence on the improvement of students' grades is far greater than the other two methods. This result shows that this method is effective and feasible.

5. Conclusions

E-learning institutions contain a lot of useful information. Many educators are grappling with how to accurately uncover the important knowledge concealed in school evaluation data in the midst of such a massive amount of data. This work creates an educational evaluation data analysis model based on the K-means clustering method from the perspective of cognitive learning theory, based on existing research and application of educational evaluation data analysis at home and abroad. The model generates corresponding categorization rules based on a large number of students' educational assessment data; the main factors that can affect students' overall quality are determined based on the study of these rules. In addition, the K-means clustering algorithm is used to statistically assess the indicators and their values of the objects, resulting in the proposal of a new comprehensive student evaluation technique that combines quantitative and qualitative analysis. Experiments demonstrate that this method can achieve a maximum accuracy of 95.6 percent, which is 12.1 percent higher than Mi cluster and 6.8 percent higher than DRCluster. This method efficiently solves the drawbacks that traditional algorithms have, such as low processing per unit time, high processing times when dealing with big amounts of data, and difficulty in attaining the desired results. It has some practical and theoretical value in the field of data analysis, as well as some reference value for other academics. Despite the fact that this study accomplished certain research outcomes, numerous influencing factors and controls were not taken into account in the design process due to time constraints and a lack of understanding. The analysis technique will be improved in the future to improve the educational evaluation data analysis model. [21].

Data Availability

The data used to support the findings of this study are included within the article.

Conflicts of Interest

The author does not have any possible conflicts of interest.

References

[1] M. A. Jan, *Application of Big Data, Blockchain, and Internet of Things for Education Informatization*, Springer Nature, 2021.

[2] W. A. Hall, "Consumerism and consumer complexity: implications for university teaching and teaching evaluation," *Nurse Education Today*, vol. 33, no. 7, pp. 720–723, 2013.

[3] T. J. Weston, C. N. Hayward, and S. L. Laursen, "When seeing is believing: generalizability and decision studies for observational data in evaluation and research on teaching," *American Journal of Evaluation*, vol. 42, no. 3, pp. 377–398, 2021.

[4] A. Antoci, I. Brunetti, P. Sacco, and M. Sodini, "Student evaluation of teaching, social influence dynamics, and teachers' choices: an evolutionary model," *Journal of Evolutionary Economics*, vol. 31, pp. 1–24, 2020.

[5] T. Sánchez, R. Gilar-Corbi, J. L. Castejón, J. Vidal, and J. Leon, "Students' evaluation of teaching and their academic achievement in a higher education institution of Ecuador," *Frontiers in Psychology*, vol. 11, 2020.

[6] M. D. Johnson, A. Narayanan, and W. J. Sawaya, "Effects of course and instructor characteristics on student evaluation of teaching across a college of engineering," *Journal of Engineering Education*, vol. 102, no. 2, pp. 289–318, 2013.

[7] K. Prochazkova, P. Novotny, M. Hancarova, D. Prchalova, and Z Sedlacek, "Teaching a difficult topic using a problem-based concept resembling a computer game: development and evaluation of an e-learning application for medical molecular genetics," *BMC Medical Education*, vol. 19, no. 1, p. 390, 2019.

[8] C. Bergin, S. A. Wind, S. Grajeda, and C. L. Tsai, "Teacher evaluation: are principals' classroom observations accurate at the conclusion of training?" *Studies In Educational Evaluation*, vol. 55, pp. 19–26, 2017.

[9] E. Litke, M. Boston, and T. A. Walkowiak, "Affordances and constraints of mathematics-specific observation frameworks and general elements of teaching quality," *Studies In Educational Evaluation*, vol. 68, no. 1, Article ID 100956, 2021.

[10] M. Kelly, D. Bennett, and P. Mcdonald, "Evaluation of clinical teaching in general practice using the Maastricht Clinical Teaching Questionnaire," *Medical Teacher*, vol. 34, no. 12, p. 1089, 2012.

[11] E. G. Charles, "The teaching model and evaluation of teaching performance," *The Journal of Higher Education*, vol. 40, no. 8, pp. 636–642, 2016.

[12] S. K. Rosenkranz, S. Wang, and W. Hu, "Motivating medical students to do research: a mixed methods study using Self-Determination Theory," *BMC Medical Education*, vol. 15, no. 1, p. 95, 2015.

[13] K. M. Scott, L. Baur, and J. Barrett, "Evidence-based principles for using technology-enhanced learning in the continuing professional development of health professionals," *Journal of Continuing Education in the Health Professions*, vol. 37, no. 1, pp. 61–66, 2017.

[14] M. K. Hopper, "Assessment and comparison of student engagement in a variety of physiology courses," *Advances in Physiology Education*, vol. 40, no. 1, pp. 70–78, 2016.
[15] T. Wolbring and E. Treischl, "Selection bias in students' evaluation of teaching," *Research in Higher Education*, vol. 57, no. 1, pp. 51–71, 2016.
[16] D. E. Goldberg and M. Somerville, "The making of*A whole new engineer*: four unexpected lessons for engineering educators and education researchers," *Journal of Engineering Education*, vol. 104, no. 1, pp. 2–6, 2015.
[17] M. J. Kang and R. K. S. Ngissah, "Self-reported confidence and perceived training needs of surgical interns at a regional hospital in Ghana: a questionnaire survey," *BMC Medical Education*, vol. 20, no. 1, p. 386, 2020.
[18] Y. W. Hou, L. Che-Wei, and M. G. Gunzenhauser, "Student evaluation of teaching as a disciplinary mechanism: a foucauldian analysis," *The Review of Higher Education*, vol. 40, no. 3, pp. 325–352, 2017.
[19] J. M. LaVelle, "Book review: building evaluation capacity: activities for teaching and training," *American Journal of Evaluation*, vol. 39, no. 4, pp. 612–615, 2018.
[20] W. Wang, "Evaluation principles' influence of critical thinking foreign language teaching on German literature classroom learning motivation," *Revista de Cercetare şi Intervenţie Socială*, vol. 73, pp. 81–94, 2021.
[21] F. Sendra-Portero, O. E. Torales-Chaparro, M. J. Ruiz-Gómez, and M Martinez-Morillo, "A pilot study to evaluate the use of virtual lectures for undergraduate radiology teaching," *European Journal of Radiology*, vol. 82, no. 5, pp. 888–893, 2013.

Hindawi
Computational Intelligence and Neuroscience
Volume 2022, Article ID 4482669, 10 pages
https://doi.org/10.1155/2022/4482669

Research Article

Interactive Mode of Visual Communication Based on Information Visualization Theory

Xiaoke He

Jiangxi Modern Polytechnic College, Nanchang 330095, China

Correspondence should be addressed to Xiaoke He; 2018050500063@jlxy.nju.edu.cn

Received 19 April 2022; Revised 7 May 2022; Accepted 9 May 2022; Published 31 July 2022

Academic Editor: Xin Ning

In the modern environment, visual communication design has become a comprehensive subject that combines technology and art. The development of various technologies has promoted the emergence of new design art forms, and at the same time, it has also promoted the change of design concepts and thinking modes. Visual representation, as a representation practice to express the meaning of information in the form of visual symbols, is a method and means to realize information visualization. Based on visual interface design, this article takes interactivity and user experience as innovation points and digs into the design process of interactive information visualization to achieve the purpose of information transmission. By analyzing the cognitive tasks of users in each stage of visual thinking activities in visual terminals, this article proposes to optimize the interactive design of visual communication from the key points of attention, consciousness, and memory. In order to verify the feasibility of the interactive mode of visual communication based on information visualization theory, this article has carried out several comparative experiments with different models. Experimental results show that this algorithm has a faster convergence speed and a greater generalization ability, the accuracy of the algorithm reaches 96.03%, and the highest evaluation of user satisfaction is 95.93%. The interactive mode of visual communication in this article can provide means and reference value for the development direction of visual communication design.

1. Introduction

Computer science was the first field to use visualization. It entails transforming a substance into a medium that can be seen with the eyes, that is, the object can be seen and understood through the eyes of the audience [1]. Its goal is to improve the audience's information knowledge and comprehension. In the field of computer graphics, information visualization is a significant accomplishment. Information visualization has long been thought of as a method and tool for helping people understand and analyze large amounts of data. The data age is currently in full swing, and humans are confronted with not only "anything is possible," but also unprecedented challenges [2]. Visualization technology has been pushed from the laboratory to a broad terminal market as information visualization has gradually branched out from scientific visualization. The research will focus on the analysis of information experience and the availability of information services against the backdrop of the information age. Information visualization is a new subject field that combines multidisciplinary theories and methods from a variety of disciplines, including communication, psychology, statistics, and design [3]. Information visualization typically focuses on assisting expert users in performing complex data exploration and analysis tasks as efficiently and effectively as possible, thanks to its historical roots in scientific reasoning, computer graphics, and algorithm optimization. This advanced data visualization technique is frequently regarded as a scientific tool [4]. At the moment, simply improving visualization quality through advanced technical means is insufficient to meet users' information needs. In order to improve information visualization more comprehensively, it is necessary to fully comprehend users' cognitive processes from perceptual experience to rational thinking.

The research object of information visualization can be divided into three aspects as an interdisciplinary field: data, visualization technology, and visualization performance [5]. People in the information age not only passively accept information, but also actively produce and disseminate it, resulting in a shift in their visual concepts. Image and symbolic information provide obvious visual pleasure to the audience, which provides a good audience foundation for the design and communication of visual communication [6]. Humans organize various visual elements such as words, images, colors, and other elements to achieve the dissemination of public information through visual communication design. It is a type of design that uses visuals to communicate. Visual communication is the process by which the designer transforms ideas and concepts into visual symbols, whereas visual communication is the process by which the receiver transforms ideas and concepts into visual symbols. Visual communication design is a type of design that communicates through visual symbols. The sender of information is the designer, and the receiver of information is the object of communication [7]. An urgent problem is how to make visualization technology better serve information users through a visual communication scheme, make information users understand and process information more easily, and improve the interactive effect of visual communication [8]. Visual representation design of information refers to a designer's visual representation design of information based on the subject of information visualization, using visual communication design knowledge, in order to make the audience easily obtain effective information in the era of big data and achieve maximum dissemination of information. Based on the information visualization theory, this article makes an in-depth study on the interactive mode of visual communication, and its innovations are as follows:

(1) Based on the existing theoretical basis of information visualization and visual communication, this article studies the relationship among information visualization, visual representation, and visual communication design and analyzes the communication mechanism of visual representation of information visualization. In the application innovation of dynamic visual innovation and multisensory interactive experience in visual communication design, some typical cases under new technologies are used for research, trying to explore new ideas and methods through case analysis.

(2) Based on the existing research results, this article puts forward new views, discusses the visual cognitive representation of information visualization, and broadens the research field of information visualization. According to the existing mode of thinking, combined with our own practice, a systematic design method of visual communication of information visualization is constructed. The effectiveness of this method is verified by experiments, and the superiority of dynamic visual communication in information dissemination is analyzed. In the future, visual communication design in other fields can provide a reference basis.

This article's research content and structure are as follows: Section 1 introduces the article's research context, significance, and organizational structure. Section 2 is primarily a summary and review of relevant domestic and international literature. It also introduces the research and innovation methods used in this article, which are based on these related literatures. Section 3 focuses on information visualization theory and related issues of visual communication interaction mode as well as the interactive information visualization design process. Section 4 details on the experimental analysis. The actual test is carried out in this section, and the test results are obtained, based on the relevant data. The algorithm's performance is evaluated in comparison to the experimental results of other methods. Section 5 concludes the study. This section primarily summarizes the research's main points and findings, summarizes the research conclusions, and suggests future research directions.

2. Related Works

Information visual design is a unique discipline that cuts across many industries and is a design category with a wide range of applications. Nowadays, relevant researchers in the field of information visualization have their own unique knowledge and understanding from their respective perspectives as well as a level of depth. Simultaneously, as the vocabulary of media grew, many design firms and avant-garde designers began to experiment with digital multimedia to express creativity and convey information. Visual communication design, as part of the creative field, is attracting increasing attention from all walks of life, playing an increasingly important role in people's lives, and defining the function of information transmission.

Papasarantou et al. examined the often-overlooked appeal of visual appeal in information visualization and discussed the broader role of emphasizing visual communication design principles in the design process [9]. Vera believed that improving the efficiency of visual thinking in processing information and reducing the cognitive load in this process can allow more cognitive costs to be allocated to later abstract understanding and decision-making. Therefore, they conducted research on finding ways to optimize the design of information visualization by understanding the characteristics of visual thinking activities [10]. In order to further understand and engage in scientific information visualization and visual communication design methods, Wu et al. proposed a mutual learning strategy of art and practice [11]. Combined with the development characteristics of information visualization under the background of experience economy, Li and Liu et al. explored solutions to improve the quality of visualization services from the perspective of information users and provided useful suggestions for the research of information visualization in visual communication design and visual effect evaluation [12]. Kosara and Mackinlay used a large number of cases to conduct an in-depth exploration of the practical innovation of visual communication design, thus confirming the two main visual expressions of visual language in new media—one is dynamic and the other is multisensory humanization of interaction [13]. Winstel pointed out that the visual communication design under information technology should not only stay in the traditional design under the influence of technology, but should focus on the "new communication" and "new language" of visual design, and new forms of expression and specific applications in new media are studied in-depth [14]. Compared with other disciplines, visual communication design occupies a pivotal position in information design by Pfeffer. The communication of visual graphics vocabulary is the key to information design and the most basic requirement of visual information construction. On this basis, with the expansion of the application field of information design, its design concept affects business planning, cultural construction, and audience visual interaction experience [15]. Reif et al. obtained the commonality and individuality of digital visual communication design and print design through the comparative analysis of digital visual communication design; and then combined with examples to analyze the immaterial, interactive, and multidimensional language characteristics and dynamics of digital visual communication design, multimedia, and interactive communication characteristics [16]. Haustein et al. took visual communication as the main body of their research and explored the communication mechanism of visual representation of information visualization and the corresponding design method of visual communication of information visualization [17]. Estrada et al. believed that the current design forms for information dissemination only pay too much attention to design symbols, ignoring the psychological needs of the audience and the process of information dissemination, resulting in the inability to maximize the dissemination of information [18]. Han and Deng focused on new media and visual communication design and analyzed the occurrence of new media and its characteristics of the times. At the same time, the connotation and development process of visual communication design are explained in simple terms, and it is concluded that the change of media technology is the main reason for the evolution of visual communication design [19].

In this article, some viewpoints and ideas are put forward based on previous studies on visual communication. On the basis of visual interface design, and taking interactivity and user experience as innovation points, the design process of interactive information visualization is deeply explored. Combining theory with practice, this article explores a systematic design method of visual representation of information visualization. According to the application of design thinking and design methods, the simulation experiment is carried out, and all kinds of boring data information are presented through visual symbols, which eliminates the obstacles between the public and all kinds of information and improves the effectiveness of visual communication interaction.

3. Methodology

3.1. Information Visualization Theory and Visual Communication Design. Information is defined as meaningful data that can express the objective facts that the data describe. The data that have been organized and sorted have relevance and have become information, but it remains data for those who are not experts in this field and cannot comprehend the meaning expressed by these data. Information visualization is the use of effective visual expression to assist users in reading, identifying, and interpreting data subjectively in order to provide them with access to critical data. More personalized and customized information visualization works have been published through the Internet platform since the arrival of the experience economy, which not only benefits users' information quality but also poses new challenges to information visualization design. The visualization product should be able to reach the brain via human vision, hearing, touch, and even other senses, and instantly understand a large amount of data [20]. Information visualization emphasizes people's receptivity while also incorporating psychology, visual design, human-computer interaction, business methods, and other disciplines. The symbolic design in the practice of visual representation is the reason why the visual view of information can convey information to the public. The ability of the audience to interpret the meaning of symbols provided by designers determines the effectiveness of information communication. Information communication is ineffective if the audience does not understand the meaning of the symbols.

Information visualization has been adopted by many media and educational, government, and corporate organizations due to its understandable visual form and inherent ability to present complex data. When users contact the information visualization platform, one of the most common cognitive activities is visual thinking. Visual thinking, in contrast to other abstract thinking activities, is based on perceptual experience and can complete a variety of cognitive tasks. The disseminator, receiver, information, and carrier are all involved in the visual representation of information, which is a two-way interaction between coding and decoding in information dissemination. At the same time, the information visualization view is a type of construction, with the representation being the representation that is dependent on the construction, and the construction being the construction that requires representation, all of which combine to form the information visualization view's meaningful communication. Information can be visualized while being read to alleviate the pressure of a "information explosion" caused by a large amount of data. When creating information graphs, the accuracy of information visualization is critical. Before beginning the design, it is necessary to have a solid foundation of theory, science, and technology, and the resulting infographic must be completely accurate. When designing infographics, this is where designers can easily make mistakes. In comparison to large data sets generated by scientific calculations and engineering surveys, information visualization resources are nonphysical and abstract, with no obvious spatial characteristics. The information visualization process and system structure are shown in Figure 1.

With the gradual expansion of the scope of modern design, digital technology and network technology have penetrated into all fields of visual communication design, and the influence and participation of multimedia technology on art and design are getting deeper and deeper, which makes visual communication design step onto a brand-new stage. Information design and graphic design serve different purposes: the former is concerned with "effective information transmission," while the latter is concerned with "exquisite artistic expression." The visual effect is more innovative and unique because the image generation technology for information visualization is not complicated, and its expression methods are diverse. Individuals, businesses, and even countries can be clients of information visualization. These forms are important, but the service content is what matters most. Information visualization covers a wide range of disciplines and application fields as an important method in information design. It can be used to solve specific professional problems. The faster and more agile the visual thinking can respond to the input visual information, the more accurate and reasonable the visual communication of information is. Information visualization examines the data visualization presentation results, extracts the hidden value from the data, and assists in making sound decisions. Because this type of decision is not invariable in a constantly updated data environment, information visualization is a continuous process that allows users to discover potential problems and improve the final decision in stages over time. In the visual communication design of information visualization, color serves as a classification and emphasis tool. Color distinguishes primary and secondary relationships and categories. In visual perception, color is the most intuitive, and information can be obtained without using logic.

Computer science research [21, 22] in information visualization mainly focuses on solving users' functional requirements. This technical research can reduce the impact of other problems such as aesthetics or user experience [23]. Visual communication design always takes the audience's acceptance of visual information through their own aesthetic judgment as the ultimate goal, and visual communication design always pursues and yearns for a rational interaction with the audience, thus turning the communication of visual information into effective communication with people. Interaction is a convenient way for users to operate content and its attributes. Interaction is a technology that can easily explain products and make the audience feel relaxed when reading information. The two-way interactive communication mode of visual information makes the new media visual communication design pay more and more attention to the audience's necessity and "participation" in the design. On the contrary, more and more people are looking forward to bringing their ideas and wishes into the design, which promotes the formation of interactive design. As information visualization design is a very wide range of disciplines, in the process of visualization, the application of visual communication design has a transformational impact on the ways and means of attaching importance to teaching and carrying out information visualization research. Graphic symbols account for the largest proportion in information view, which is the soul of visual representation of information. Graphic symbols include pictures, theme graphics, attached icons, charts, and characters. This article analyzes and summarizes the classification of graphics, the effectiveness of attached icons, the model construction of charts, and different types of characters. The more and faster cognitive tasks are accomplished by visual thinking, the more cognitive costs can be allocated to abstract thinking activities, thus improving the efficiency of people's deep understanding of information and making decisions.

3.2. Interactive Design of Visual Communication Based on Information Visualization. Graphic symbols are image materials generated by various graphic software, and their visual representation differs from that of words and languages. Graphics, which are the main visual representation symbol in information visualization design, can be copied in large quantities using various methods. Because the main graphic symbol is so closely linked to the information visualization theme, it can be said that the main graphic symbol is the information theme's mapping. Visual communication design in the modern world is interactive design with people that emphasizes the audience's active cognition in the process of receiving information and selectively accepts visual information based on their own aesthetic demands and wishes. The more experience and knowledge an information user has with information acquisition and understanding, the faster and more accurately he can extract the information content he needs from the visual interface and the more effectively he can dig out the connotation and relationship of information and find solutions to problems. Tagged words are concise, clear, and easy-to-understand that appear in the view as expressive keywords. The introduction or explanation of a specific piece of information or a group of related pieces of information is included in descriptive text. The orderly arrangement of some data and information in the information view, which makes the information more intuitive and reduces the audience's visual pressure, is known as organized text. A basic visual model is chosen to express it is "representation." This step essentially determines the nascent form of the visualization effect, and it is necessary to consider the appropriate representation method based on the data dimensions, such as a list, tree structure, or other methods. The goal of "decoration" is to make information expression simple and clear while also being rich in connotation, practical, and beautiful. To create a logical structure, the information hierarchy must first be divided. After grouping and classifying the data, graphic design is used to convey information of various dimensions, such as category, attribute, degree, orientation, etc., and data of all types and dimensions are sorted according to the information needs of users to highlight the most pressing issues. Figure 2 depicts an interactive

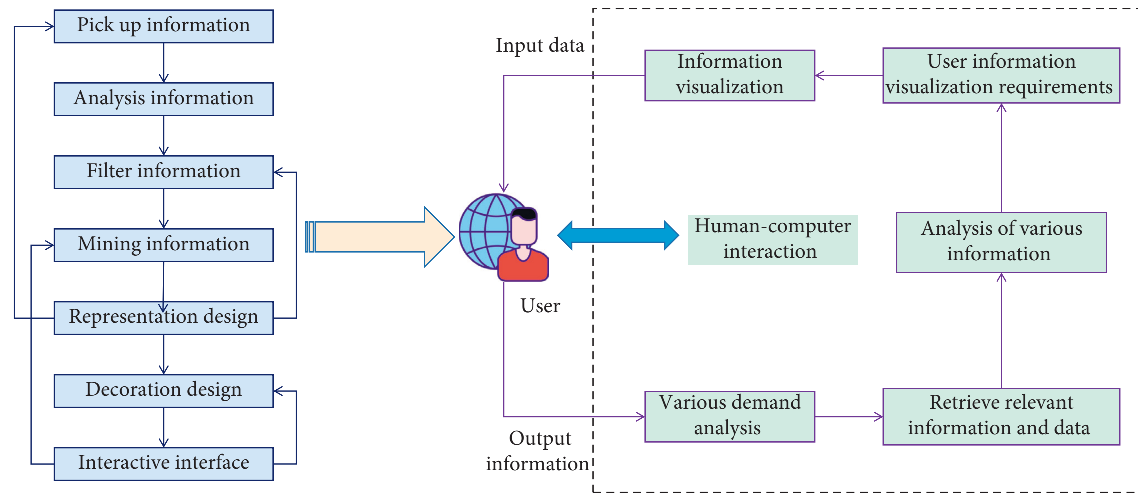

FIGURE 1: Information visualization process and system structure diagram.

design diagram of visual communication based on information visualization.

Abstract graphic symbols are completely out of the natural form, and it is impossible to extract a specific image from them, so it is necessary for viewers to create graphics with their imagination. Figurative figure is a form that is close to the viewer's daily life and the objective facts. It can reproduce the features of things and is direct, vivid, clear, and easy to identify. Dynamic visual symbols can attract more attention from the audience, which also makes the new media visual communication design not only need to pay attention to the expression form of plane visual elements, but also consider its animation effect in the picture. The difference of visual information determines its "pop-up effect." The better the pop-up effect, the easier it is to pay attention to screening. Therefore, the target information can be "popped up" from the background or nontarget information by changing the visual features such as color, size, position, and shape. Data mining or statistical methods are used to analyze the data format or put the data in a mathematical environment. Its purpose is to find some rules in a pile of chaotic data, so as to provide organized raw materials for subsequent data representation. Visual representation is the method and way to realize information visualization. It refers to the multi-method of "visualization" for information representation, so that the represented information can be "visualized," and finally the information can be optimized, so as to promote the public's acceptance and understanding of information, maximize the information dissemination, and innovate the information dissemination process.

If the coordinate of the root node is (X_0, Y_0), the selected radius is r; the number of direct child nodes is count. Then the formula for calculating the coordinate (X_i, Y_i) of the ith child node is as follows:

$$X_i = X_0 + r^* \cos\left(\frac{2p^* i}{\text{count}}\right), \tag{1}$$

$$Y_i = Y_0 + r^* \sin\left(\frac{2\pi^* i}{\text{count}}\right). \tag{2}$$

If the coordinate of A is (X_0, Y_0), and the included angle of A on its concentric circle is initAngle, the formula for calculating the coordinate (X_i, Y_i) of the ith child node in the next layer of A is as follows:

$$\begin{aligned} \text{initAngle} &= \arctan\left(\frac{Y_0}{X_0}\right), \\ X_i &= X_0 + r^* \cos\left(\text{initAngle} + 2p + \frac{i}{\text{count}}\right), \\ Y_i &= Y_0 + r^* \sin\left(\text{initAngle} + 2\pi + \frac{i}{\text{count}}\right). \end{aligned} \tag{3}$$

It is possible to improve the quality of the user experience by creating a favourable situation. Information visualization design can incorporate materials related to users' knowledge base, life experience, and personal details. The arrow is the most widely used directional symbol in the visual representation design of information visualization, and it has various meanings in various contexts. Computers perform the majority of the design work. The user's status shifts from passive to active in the interactive stage, from acceptance to discovery and consideration. The ability to control and explore data through interface interaction allows them to truly combine computer and human intelligence. The visible part of the user's interface is called the man-machine interface. Communication and operation with the system require a man-machine interface. Under new media technology, it is the most unique design language in visual

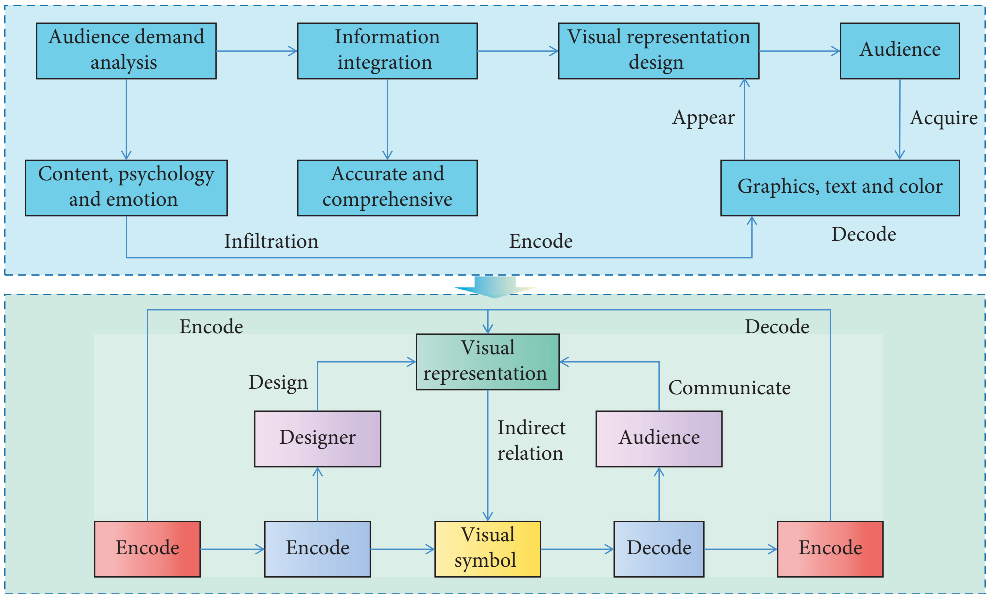

FIGURE 2: Interactive design of visual communication based on information visualization.

communication design, and the interactivity of visual communication design has been fully demonstrated in a variety of design practices. Expert users can understand and analyze data at a deeper level thanks to interaction. For obtaining implicit data knowledge, an interface is required. The introduction of a comprehensive digital network has created unprecedented opportunities for interaction and the collection of a wide range of data, including text, image, and sound. Information users are surprised and their knowledge and experience are challenged as expressive methods of information visualization evolve. As a result, appropriately adding guidance or comments in the visual interface will help users understand information better. Aside from formal symbols, the design should also conform to the audience's visual experience, place the core information content in the center, and guide the reading sequence with flow symbols like arrows to improve reading efficiency.

Class perception is used to measure the perceptual strength of the color and spatial distribution of each class. For any point p in class c^m, the perception degree V_p of this point is calculated by the following formula:

$$V_p = w_p S_p, \tag{4}$$

where w_p refers to the weight of point p in class c^m, and the weight is determined by the neighbor points of point p. S_p refers to the significant value of p. This value is obtained by formula (2). S_p expresses the color difference between point p and its surrounding neighbors.

$$\begin{gathered} S_p = \Delta\varepsilon\left(C_p, \frac{1}{N_p} \sum_{q \in N_p} C_q\right), \\ \Delta\varepsilon(x, y) = \sqrt{\left(\Delta L^{*2}\right) + \left(\Delta a^{*2}\right) + \left(\Delta b^{*2}\right)}, \end{gathered} \tag{5}$$

where

$$\begin{aligned} \Delta L^* &= L_x^* - L_y^*, \\ \Delta a^* &= r_x \cos\theta_x - r_y \cos\theta_y, \\ \Delta b^* &= r_x \sin\theta_x - r_y \sin\theta_y. \end{aligned} \tag{6}$$

Assuming that X is divided into C classes, and each x_i corresponds to a class label $I(x_i)$, then the data of class c are expressed as

$$\{X_1^c, X_2^c, \ldots, X_n^c\}, \tag{7}$$

where n is the number of data in the c class, $c \in \{1, 2, \ldots, C\}$. The data of different classes are divided as much as possible, and the objective function is as follows:

$$\max tr \frac{P^T S_b P}{P^T S_w P}, \tag{8}$$

where S_b and S_w represent the class spacing dispersion and the intra-class distance dispersion, respectively, and the specific definitions are as follows:

$$S_b = \sum_{C=1}^{C} n_c (u_c - u)(u_c - u)^T,$$
$$S_w = \sum_{C=1}^{C} \sum_{i}^{n} (x_i^c - u_c)(x_i^c - u_c)^T, \quad (9)$$

where $u_c = \sum x_i^c / n_c$ is the mean value of the cth data; u is the mean value of all data, the center point of all data.

The purpose of data analysis is to concentrate, extract, and refine a large amount of hidden information of data to find the inherent laws of the research objects, so that people can understand, judge, and make corresponding decisions and actions faster and better. On the one hand, information visualization should try to call the familiar visual features of users to construct the visual effect of information; and on the other hand, frequent visual thinking training can enrich information users' experience and knowledge stored in their brains and make visual thinking activities more efficient. In information visualization, it is not to look for symbols with specific meanings to represent, but to consider the whole information view, combine information content and context, and adopt the "proper principle" to represent with visual symbols. The modern environment provides a space for innovation and breakthrough in the design thinking and concept of visual communication design. We can make visual creation according to this selective way of reading information, so that the audience can fully participate in the whole design process, thus obtaining a more humanized visual experience.

4. Result Analysis and Discussion

With the progress of society, the carrier of visual information dissemination is constantly changing with the development of technology, which all affects the expression of visual information such as graphics, characters, colors, etc. in visual communication design, and also affects the change of thinking mode of design creation. In the practice of visual representation of information visualization, the construction of information model refers to the selection of appropriate organization arrangement. Visual representation design of information is a process of rational and perceptual thinking. Rational information model construction plays an important supporting role in visual representation design of information visualization. Human-computer interaction plays an important role in information visualization, and a large amount of data can only be perceived through human-computer interaction. Man-machine interaction transmits information naturally and efficiently, and allows users to get a good understanding. Good interactive mode and simple user interface can help people get relevant information quickly. Figure 3 shows the convergence of the three algorithms as the number of iterations increases.

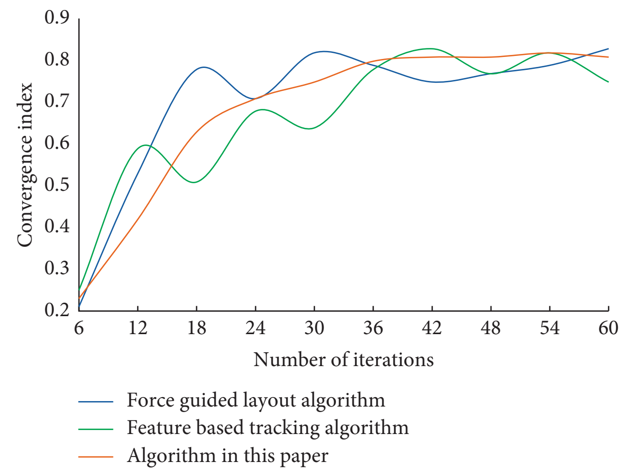

FIGURE 3: Convergence of algorithm.

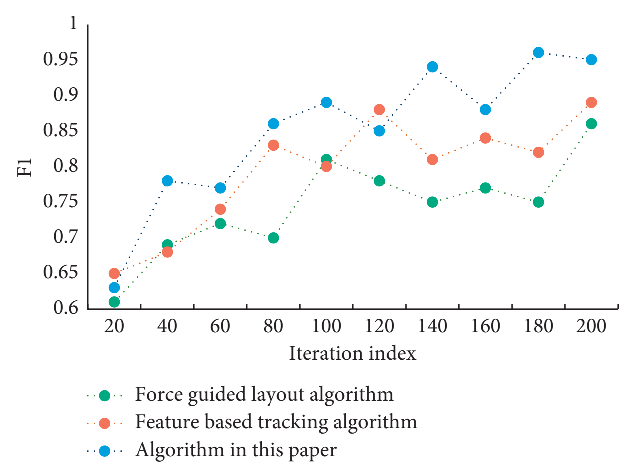

FIGURE 4: Experimental results of F1 value of algorithm.

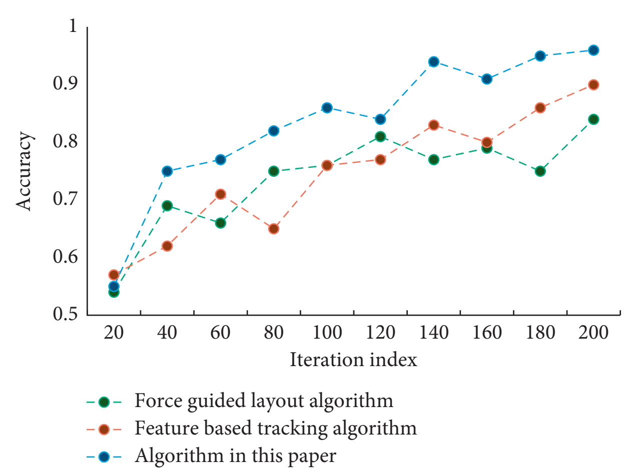

FIGURE 5: Experimental results of algorithm accuracy.

It can be seen that the algorithm in this article gradually converges with the increase of iteration times. This is due to the difference of objective functions of different methods. The four elements of visual design, such as text, graphics, color, and layout, are the foundation of information design, and the accurate application of them will help the accurate expression of information design. Timeliness is the main feature of dynamic visual design. From graphic design to dynamic design, the form of font design changes from a

Table 1: Experimental results of each index.

Algorithm	Average absolute error	Recall rate	Accuracy rate
Grid layout algorithm	0.373	0.874	0.798
Force-guided layout algorithm	0.469	0.806	0.806
Climbing algorithm	0.327	0.769	0.884
Color optimization algorithm	0.389	0.9050.5	0.914
Feature-based tracking algorithm	0.205	0.914	0.908
Algorithm in this article	0.097	0.958	0.948

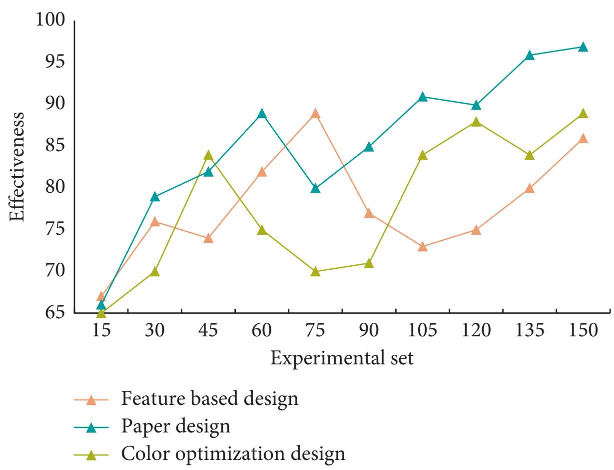

Figure 6: Comparison of the effectiveness of visual communication interaction design.

Table 2: Survey results of audience demand satisfaction of visual information communication design.

Index	Score (1–10)				
	1~2 (%)	3~4 (%)	5~6 (%)	7~8 (%)	9~10 (%)
Functionality	18.64	21.36	29.78	52.24	37.48
Cognition	17.02	20.35	49.31	46.57	42.35
Interactivity	19.93	23.64	24.57	34.32	76.61
Comprehensiveness	5.89	8.97	14.63	18.54	78.32
Accuracy	10.15	16.79	19.03	25.24	81.69
Interesting	23.69	19.63	24.35	59.37	43.57
Artistry	9.87	28.73	77.32	40.51	27.65
Novelty	17.98	37.46	20.56	18.69	19.54
Emotional expression	18.54	12.89	16.67	42.05	56.14
Color	15.57	27.99	48.51	19.79	20.06

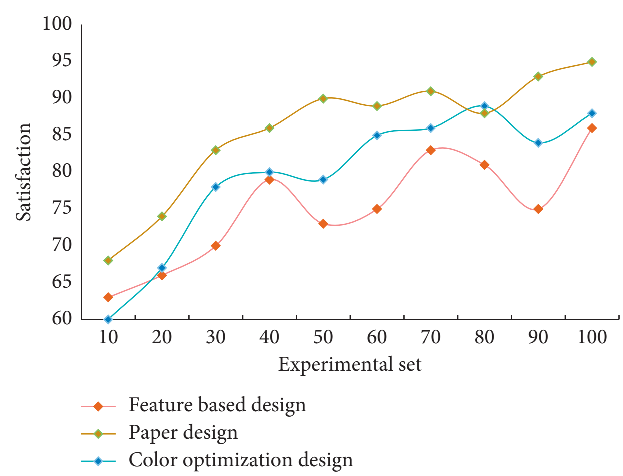

Figure 7: User satisfaction results.

static entity to a digital virtual scene based on the concepts of time and space. Visual information from the physical world is detected visually, and then the target information is screened by visual attention mechanism, and it is decided which information needs to be processed by consciousness and which can be directly reflected. Consciousness will further process the input information, eventually forming empirical knowledge and storing it in memory for later advanced rational cognition. In order to verify the performance of this algorithm, we selected F1 value and precision as two indexes for many experiments. The experimental results of F1 value are shown in Figure 4, and the precision results are shown in Figure 5.

Systematic design method includes two processes: analysis and synthesis. Analysis precedes synthesis, and existing data information is improved after analysis to achieve new synthesis. For graphic information integration design, it is required to link the analysis and integration methods, start with the whole system, analyze and extract effective data information, and synthesize it into information visualization presentation form. In dynamic design, the development of digital technology and information technology makes it possible for the spatial attribute of characters. Time and space are two inseparable concepts in the movement. In the transformation of space, we can constantly experience the visual experience brought by movement and feel the flow of time, so as to better receive information. The interactive infographic is programmed by software such as Flash or Dreamweaver, integrates the data that have been converted into graphic language, and presents it in the form of aesthetics according to scientific data. Its presentation form is not only a moving picture, but also viewers can interact with short films on the media with their own concerns, which is more flexible than video infographics. In this chapter, several experiments are carried out to verify the feasibility and practicability of this algorithm. The experimental results of different indexes of the algorithm are shown in Table 1.

Parametric design is a term used in the design world to describe the process of establishing a specific relationship. Other elements change when one changes. Because of its various meanings and postures, each font has a unique emotional effect. Fonts are valuable due to their diverse personalities. As a result, understanding the expression of words for the transmission of information is critical in visual communication design. Consciousness will focus on dealing with new and different information, learning and adapting as a result, and the information processed by consciousness will be stored in memory as a new source of knowledge. As a result, based on visual objectives, information visualization should provide a reasonable explanation or cognitive clues to some strange and novel information, and then assist consciousness in better completing cognitive tasks. Figure 6 depicts the effectiveness assessment of visual communication interaction design.

From the data in Figure 6, it can be seen that this design is effective and practical, which can enhance the perception of visual trajectory. Long-term memory, like a permanent box, holds a large amount of information and can extract activation information at any time. This requires a series of structures in the design process to conform to cognitive thinking and human cognitive behavior, so that the design activities can be carried out according to evidence and in the right direction. The survey results of audience demand satisfaction of visual information communication design are shown in Table 2.

The “dynamic design” in interface design has been paid more and more attention by visual design practitioners. The unique dynamic design can express the distinctive personality of the software and create fascinating effects. At the same time, it can also appease users through the use experience, so that the audience can get a relaxed and pleasant feeling when reading information, thus truly achieving humanization. Figure 7 shows the survey results of user satisfaction with different design methods.

From the survey results of user satisfaction, it can be seen that users are more satisfied with this design method. This chapter carries out a lot of experiments and analyzes and summarizes the superiority of visual communication design in information transmission. Through research, it is found that the accuracy of this algorithm is 96.03%, and the highest evaluation of user satisfaction is 95.93%. This algorithm has faster convergence speed and greater generalization ability.

5. Conclusion

In the field of information visualization, visual communication design is becoming more and more involved. It is an essential component of the development of data visualization. Information visualization will develop in a more personalized and customized direction in the future, with the arrival of experience economy and the rapid development of Internet applications, and the presentation form of information visualization will not be limited to two-dimensional plane, but will pay more attention to integration with interactive experience. Through the power of images, information visualization brings dull data to life, allowing readers to grasp information quickly and leave a lasting impression. Relevant personnel should concentrate on the visualization form and mode of interaction when dealing with information visualization design. With the help of psychology and communication knowledge, this article examines the kernel of information visualization and visual representation. The audience “decodes” information through visual symbols to obtain information, according to this study. Simultaneously, it is proposed that by expounding on the concept of information visualization and analyzing the cognitive tasks and characteristics of each stage of visual communication, information users can be effectively assisted to acquire and understand information better by lowering the cost of information users in the visual thinking stage and improving their visual thinking response efficiency. Many tests show that the algorithm has a faster convergence speed and a greater ability to generalize. This algorithm has a 96.3% accuracy rating and a 95.93% user satisfaction rating. This research has certain reference value. However, due to the limitation of knowledge level and research time, there are still some problems in this article. This article is only a preliminary study of information expression, and there are still a lot of research on the details of expression and visual elements. The research of visual information interaction mode has sustainable attention and exploration significance in the future academic research and production practice and should be deeply discussed and studied.

Data Availability

The data used to support the findings of this study are available from the author upon request.

Conflicts of Interest

The author does not have any possible conflicts of interest.

References

[1] S. Faisal, A. Blandford, and H. W. Potts, “Making sense of personal health information: challenges for information visualization,” *Health Informatics Journal*, vol. 19, no. 3, pp. 198–217, 2013.

[2] M. Conner and M. Browne, “Navigating the informationscape: information visualization and student search,” *Reference Services Review*, vol. 41, no. 1, pp. 91–112, 2013.

[3] Z. Xu, K. K. R. Choo, A. Dehghantanha, R. Parizi, M. Hammoudeh et al., *Cyber Security Intelligence and Analytics*, Springer, Berlin, Germany, 2019.

[4] K. Zhang and X. S. Zheng, “Special issue on visual information communication – theory and practice,” *Information Sciences*, vol. 330, pp. 424–426, 2015.

[5] J. Bian and Y. Ji, “Research on the Teaching of Visual Communication Design Based on Digital Technology,” *Wireless Communications and Mobile Computing*, vol. 2021, Article ID 8304861, 10 pages, 2021.

[6] J. Zhang, J. Sun, J. Wang, and X.-G. Yue, “Visual object tracking based on residual network and cascaded correlation filters,” *Journal of Ambient Intelligence and Humanized Computing*, vol. 12, no. 8, pp. 8427–8440, 2021.

[7] T. Pham, J. Jones, R. Metoyer, and F. Colwell, "Toward exploratory analysis of diversity unified across fields of study: an information visualization approach," *Environmental Earth Sciences*, vol. 72, no. 10, pp. 3803–3825, 2014.
[8] L. Min, G. Ke, G. Zhai, P. Le Callet, and W. Zhang, "Perceptual reduced-reference visual quality assessment for contrast alteration," *IEEE Transactions on Broadcasting*, vol. 63, no. 1, pp. 71–81, 2017.
[9] C. Papasarantou, G. Kalaouzis, and V. Bourdakis, "Info-data Constructions: from data to spatialized info visualization," *Automation in Construction*, vol. 33, no. 4, pp. 95–103, 2013.
[10] A. Vera, "Applying interaction design process to the creation of the OASIS user interface," *Endocrine Journal*, vol. 62, no. 2, pp. 153–160, 2014.
[11] I.-C. Wu and S.-H. Hsieh, "A framework for facilitating multidimensional information integration, management and visualization in engineering projects," *Automation in Construction*, vol. 23, no. 5, pp. 71–86, 2012.
[12] Y. Li and C. Liu, "Information resource, interface, and tasks as user interaction components for digital library evaluation," *Information Processing & Management*, vol. 56, no. 3, pp. 704–720, 2019.
[13] R. Kosara and J. Mackinlay, "Storytelling: the next step for visualization," *Computer*, vol. 46, no. 5, pp. 44–50, 2013.
[14] B. Winstel, "Interface design: an introduction to visual communication in UI design," *Technical Communication*, vol. 63, no. 2, pp. 160-161, 2016.
[15] J. Pfeffer, "Fundamentals of visualizing communication networks," *China Communications*, vol. 10, no. 3, pp. 82–90, 2013.
[16] D. M. Reif, M. Sypa, E. F. Lock et al., "ToxPi GUI: an interactive visualization tool for transparent integration of data from diverse sources of evidence," *Bioinformatics*, vol. 29, no. 3, pp. 402-403, 2013.
[17] S. Haustein, R. Dr Cassidy, Dr Su, V. Uren, and A. S. Dadzie, "Public science communication on Twitter: a visual analytic approach," *Aslib Journal of Information Management*, vol. 67, no. 3, pp. 337–355, 2015.
[18] F. C. Rodríguez Estrada and L. S. Davis, "Improving visual communication of science through the incorporation of graphic design theories and practices into science communication," *Science Communication*, vol. 37, no. 1, pp. 140–148, 2014.
[19] G. M. Han and X. Q. Deng, "Application OF media art visual communication concept IN multi-scale control," *Open House International*, vol. 41, no. 3, pp. 113–117, 2016.
[20] N. A. Costa, E. Holder, and S. N. Mackinnon, "Implementing human centred design in the context of a graphical user interface redesign for ship manoeuvring," *International Journal of Human-Computer Studies*, vol. 100, pp. 55–65, 2017.
[21] Z. Wang, Z. Huang, Y. Xu, Y. Zhang, X. Li, and W. Cai, "Image noise level estimation by employing chi-square distribution," in *Proceedings of the 2021 IEEE 21st international conference on communication technology (ICCT)*, pp. 1158–1161, IEEE, Tianjin, China, October 2021.
[22] W. Cai, Y. Song, H. Duan, Z. Xia, and Z. Wei, "Multi-feature fusion-guided multiscale bidirectional attention networks for logistics pallet segmentation," *Computer Modelling in Engineering and Sciences*, vol. 131, no. 3, pp. 1539–1555, 2022.
[23] Z. Xu, K. K. Raymond Choo, D. Ali, R. Parizi, and M. Hammoudeh, "Cyber Security Intelligence and Analytics," in *Proceedings of the International Conference on Cyber Security Intelligence and Analytics*, pp. 3–8, Haikou, China, February 2020.

Hindawi
Computational Intelligence and Neuroscience
Volume 2022, Article ID 6710631, 10 pages
https://doi.org/10.1155/2022/6710631

Research Article

Application of Personal Information Privacy Protection Based on Machine Learning Algorithm

Fang Lang [1] and Yunfei Zhong [2]

[1] *Law School of Weifang University, Weifang 261061, China*
[2] *Shandong Weifang Tobacco Co Ltd., Weifang 261061, China*

Correspondence should be addressed to Fang Lang; 20110605@wfu.edu.cn

Received 25 April 2022; Revised 3 June 2022; Accepted 4 June 2022; Published 31 July 2022

Academic Editor: Xin Ning

Based on a machine learning algorithm, this paper deeply explores the privacy protection of personal information. In this paper, the definition of the machine learning algorithm is put forward, the design idea of privacy protection in joint machine learning platform is studied, and the architecture model and model parameter updating strategy of joint machine learning under privacy protection are designed. To protect the privacy of personal information, this paper also proposes a data homomorphic verification mechanism to prevent the global parameters from being tampered with by malicious cloud servers. In order to verify the performance of the models constructed in this paper, the comparative experiments of different models are carried out. The experimental results show that this algorithm has a fast convergence speed, and the average error rate decreases by 4.17% compared with the traditional algorithm. Moreover, the accuracy of this algorithm reaches 95.37%, which is about 8.76% higher than the previous algorithm. This model is applied to the field of personal information privacy protection, which can provide a safe and reliable environment for personal information privacy and effectively protect the privacy of data owners. And, means and reference value is provided for the development direction of privacy protection.

1. Introduction

The amount of data generated by all walks of life is exploding as we enter the information age, thanks to the development of information technology such as the Internet; with the enhancement and aggravation of online data behavior, the protection of personal information and privacy is particularly prominent in the contemporary era [1]. As a result, the purposeful collection, investigation, utilization, transmission, disclosure, and sale of personal information via the Internet has reached an unprecedented level. Although easy-to-obtain personal data have become a staple of academia and industry, the process of data collection, publication, processing, and storage will be aided by a slew of third-party service providers, expanding the number of possible data sources [2]. Personal data collection, expansion, mining, and use for more precise business marketing activities have gradually become a new focus of business development for traditional businesses, Internet businesses, data-related businesses, and so on. With business's continued growth and prosperity, it also brings with it potential conflicts of interest and hidden risks for various individuals [3]. In addition, due to the prevalence of online fraud, user privacy breaches do occur from time to time. Personal privacy protection has become one of the problems brought on by the information society in the network environment. Despite the fact that the definition of privacy is complex and varied, personal information plays an important role in privacy [4]. The abuse and control of information is a major concern in today's world of privacy. People are gradually becoming more aware of personal privacy as big data-related technologies advance. As a result, countries' focus in formulating laws and regulations on privacy protection has shifted to how to properly protect privacy without impeding network development.

The content of privacy right is extensive, including the information secret of a natural person's personal life, the peace of his personal life, and even his own decision on private life. Therefore, from the content, the right to privacy can be said to be a collection of rights [5]. Personal information may be infringed in the commercial data behavior of Internet enterprises, that is, personal information risk; that is, personal information may be harmed as an Internet user. In the traditional differential privacy model, data from different sources are concentrated in the central server, and then the data are treated with privacy protection, and the central server publishes the inquiry information satisfying the differential privacy [6]. However, in the process of data collection, third-party service providers are often uncontrollable, which easily leads to privacy leakage [7]. The characteristics of diverse data sources, fragmented information, and personalized and differentiated privacy requirements lead to the risk of privacy leakage when multi-party data are merged. At the same time, the separation of data ownership and storage rights, multi-source, high-dimensional, and dynamic characteristics aggravate the risk of privacy leakage in the process of data sharing and pose new challenges to privacy protection technology. Personal information, as an original part of "privacy," has become a prominent contemporary problem in the background of the increasingly prosperous enterprise data behavior [8]. At the same time, data privacy has become the core issue of machine learning, especially when using some sensitive data in cloud computing, the cloud is not completely trustworthy. Therefore, privacy protection and machine learning algorithms must be designed for the cloud. Machine learning provides a potentially powerful framework for automated perception and reasoning. However, a good machine learning framework still needs a large number of data sets to fully realize its potential of perception and reasoning. In this paper, a personal information privacy protection model based on a machine learning algorithm is constructed, and its innovations are as follows:

① This paper studies the structure design and working mechanism of distributed machine learning system under privacy protection and analyzes the design strategy of privacy protection in a distributed machine learning system. Aiming at the privacy protection of personal information, this paper designs a data homomorphic verification mechanism to prevent the global parameters from being tampered by malicious cloud servers.

② This paper investigates vector addition, number multiplication, linear transformation, and weighted inner product homomorphism operations using vector homomorphism encryption; this allows the vector homomorphic encryption scheme to meet the basic operations in machine learning. A local differential privacy data stream protection protocol is proposed that can provide data stream privacy while also ensuring high data availability and requiring less storage and computing power.

This paper mainly explores the privacy protection of personal information, which is divided into five sections. The specific research framework is as follows:

Section 1 is the introduction. This part introduces the research background, significance, and methods of this paper and gives the innovation and organizational structure of this paper. Section 2 is a summary and research of related literature at home and abroad and introduces the research methods of this paper. Section 3 mainly constructs the privacy protection model of personal information based on a machine learning algorithm. Among them, Section 3.1 analyzes the concept connotation of privacy protection and machine learning and summarizes the related basic theories. Section 3.2 focuses on the construction method and implementation of the personal information privacy protection model. Section 4 is the experimental analysis. In this part, many experiments are carried out, and the experimental results of other models are compared to analyze the performance of the models. Section 5 is the conclusion and prospect. This part mainly reviews the main contents and results of this research, summarizes the research conclusions, and points out the direction of further research.

2. Related Work

The arrival of the information age has brought about changes in all aspects of our lives, and profound business changes have taken place in the global society. With the rapid growth of intelligent terminal devices, massive data are generated anytime and anywhere. These data have profound value, and all kinds of enterprises and institutions begin to collect personal data on a large scale and analyze and mine the collected data. While enjoying the convenience brought by information technology, information security and privacy have become the focus of people's attention. Therefore, many researchers have made relevant explorations on data search and personal information privacy protection technology.

Ocansey et al. [9] proposed a fully dynamic fully homomorphic encryption scheme that no longer limits the number of allowable parties [9]. Wang et al. [10] propose an outsourced secure multi-party computation framework. The scheme uses two noncollusion cloud servers, one for storage and computing, and the other contains the master private key that can decrypt user data and realizes computing outsourcing by constructing a secure protocol [10]. Wang et al. [11] proposed a security outsourcing detection system, the system classification is completed by the support vector machine algorithm, and privacy protection is achieved by designing a secure multiparty protocol [11]. Yin et al. [12] focused on data outsourcing services on the basis of analyzing the risks of privacy leakage in the stages of data release, storage, and search and combined with the multiparty requirements for data privacy protection granularity, data availability, timeliness, and other dimensions at different stages. Research on key technologies of data privacy protection under the mode [12]. Reza et al. [13] took the hybrid cloud as the data bearing platform, proposed a data segmentation technology based on the k-anonymity criterion, and designed a complete set of data anonymity segmentation scheme to solve the balance of data privacy protection and availability when the set-valued data is released [13]. Wei et al. [14] believe that attackers can obtain data privacy by filtering random noise. Furthermore, random perturbations may expose the privacy of outliers when attackers have access to external information, i.e., published data about individuals may contain quasi-identifier properties that may be linked to public databases to reidentify individual records [14]. Liu and Zhou [15] proposed a privacy protection scheme based on differential privacy, and its protection of data privacy has nothing to do with the background knowledge mastered by the attacker. This scheme ensures that statistical queries on the target dataset and on datasets that differ by only one record are identical in results [15]. Ke et al. [16] proposed the use of differential privacy computing to achieve privacy-preserving mining of joint datasets [16]. Barni et al. [17] proposed a distributed algorithm, which assumes that the same record has a unique global identifier in a vertically divided data environment, and all parties involved in data fusion only have data with partial attributes; the original information is hidden in the communication process, and the privacy protection of the data fusion process is realized by constructing a complete anonymity table to determine whether the anonymity threshold is met [17]. Hu et al. [18] proposed an algorithm for users to learn game equilibrium. The classifier built by this algorithm enables each user to strike a balance between the accuracy of the classification task and data privacy [18]. Xie et al. [19] proposed an abstract model to support databases with any number of public and private variables and formulated application-independent privacy protection granularity and utility metrics, where privacy protection granularity was quantified by ambiguity, and data utility was measured by Fidelity to quantify [19].

Based on research on privacy protection of personal information in related literature studies, this paper proposes a new research approach and method. Using the machine learning architecture model, this paper creates the overall architecture of the joint machine learning platform, as well as the key structure of the central server. A fast synchronous random gradient descent method is designed for a heterogeneous multiclient situation to ensure fast training and convergence of the model, as well as to improve the generalization ability of the existing model. The traditional disturbance mechanism is used to protect the key attribute data, with noise satisfying the definition of local differential privacy added to the model's local update. As a result, the aggregation operation can be used to initialize the global model parameters, resulting in fewer model training communication rounds. Experiments show that the model is stable and reliable, as well as that it performs as expected.

3. Methodology

3.1. Privacy Protection and Machine Learning. As a contributor of individual knowledge and content, participate in knowledge creation and sharing in the information age. At the same time, with the help of the Internet, individuals can realize some or all activities or projections in reality and conduct business transactions, self-construction, social interaction, information acquisition, and other actions. At present, the collection, expansion, mining, and use of personal information for more accurate business marketing activities has gradually become a new focus of business development for traditional enterprises, Internet companies, data-related enterprises, and so on [20]. With the continuous development and prosperity of business, it also brings potential conflicts of interests and risks of different individuals. Internet privacy refers to the right that a natural person enjoys on the Internet that his personal affairs are not publicly publicized, his private life is not disturbed, and his personal information related to online activities is protected from being illegally collected, known, utilized, and disclosed by others. In the information age, massive data have brought obvious privacy security problems in the practical application of machine learning. Users' personal highly sensitive data are collected and kept in commercial companies indefinitely. Users can neither delete these data nor restrict the use of them by commercial companies. Considering the privacy and security of data, many data holders are reluctant to share their data sets, so they can not directly use the joint data sets of participants for machine learning [21]. As an important component of the original concept of privacy, personal information will face more prominent and severe challenges in the information age and networking. The new emphasis of network privacy in the era lies in the problem of "privacy digitalization" brought by network society. This is the core issue of "privacy" in the information age.

In the information age, the right of network privacy should include the following aspects: ① the control of personal information. ② The right to be free from interference when individuals conduct online behavior. ③ The obligee's knowledge of the use and collection of personal information on the Internet by others, and his request to withdraw from deletion, etc. In the network society, the mass production of personal information and the precipitation of structured and unstructured data make it possible to use data to analyze consumer behavior and preferences and increasingly move towards accurate consumer description and database marketing. The more accurate you understand the marketing audience, the more you can achieve the marketing management goal of low cost and high return. With the development of cloud computing technology, it has gradually become a trend for enterprises to go to the cloud [22]. Personal information such as users' personal photos, home address, contact information, etc., may be permanently stored in the company server of the cloud service provider, which is beyond the control of the owner. The violations of users' privacy rights involved in the management of network resources mainly include improper use of network users' personal information, privacy of personal activities, traces of personal networks, and infringement of personal cyberspace. The collected person of personal information has the right to ask the collector to take necessary and reasonable measures to protect the security of his personal data. First of all, you can ask the website to take certain technical measures and policies to keep the collected data; secondly, their personal data shall not be transmitted or disclosed to any third party; finally, within the network service group, we should also pay attention to the disclosure of relevant information. On the user side, the user's cognition, attitude, and behavior of personal information risks when participating in interaction are the basic elements to be included in the interaction model to protect the user's personal privacy information. On the enterprise side, the appropriateness of its data behavior and the integrity of its protection are feasible and effective guarantees for the protection of personal privacy information. The data mining model of personal privacy protection is shown in Figure 1.

The data provider has shifted from service organizations to individuals as a result of the rapid adoption of personal smart devices, and traditional privacy protection methods are no longer adequate for the protection of personal privacy data. To achieve effective personal information protection, we must first clarify the most basic data behavior and provide the most practical reference from the enterprise behavior and regulation level. To solve the problem of personal data protection in particular, we must first address the problem [23]. The method of data encryption encrypts data while also completing complex calculations with the help of secure multi-party protocols, as the name implies. The difficult assumption of encryption algorithm and protocol construction underpins security. In academia and industry, the privacy difference is the most common method for protecting data privacy and the evaluation standard for privacy schemes. This model assumes that the adversary has sufficient background knowledge and that the addition or deletion of any record has no impact on the query's final result. Differential privacy protection technology is a well-defined privacy protection model that can withstand all attacks based on assumptions about background knowledge. Its main principle is to achieve privacy protection by adding random noise to distort the original data while maintaining the original data's statistical characteristics. Differential privacy mainly distorts data by adding noise to protect privacy. Privacy difference is independent of the background knowledge of the adversary, and it can provide a stronger privacy protection ability than the traditional anonymous protection mechanism. However, the differential privacy protection technology is difficult to be applied to the application scenarios where multiple data owners do not collude.

The server aggregates the user's personal disturbance reports from the client and decodes them to obtain valuable statistical information, while local privacy sets the privacy protection mechanism directly at the client. To avoid the privacy leakage of the untrusted third-party server, this process does not need to collect the client's real original data information, and it can be applied to a variety of complex collection scenarios. Although differential privacy protection technology improves privacy protection to some extent, noise introduces changes in the original data distribution, reducing the accuracy of results and data availability. Differential privacy technology can be used to store databases, effectively resolving the local storage privacy security problem [24]. Differential privacy, on the other hand, resolves the local storage privacy leakage problem. Secure multiparty computing is based on the assumption that multiple service users who do not trust each other exchange data information via secure multiparty protocols, allowing each service user to perform distributed machine learning tasks based on their own data. Federated learning, as a distributed machine learning framework, aims to train a high-quality centralized model while keeping local training data distributed on clients and allowing multiple users to train the same learning tasks at the same time. Each user downloads the global model, calculates the local model's update using the local data set, and uploads the update to the central server at the end of each training round. To calculate a new global model, the central server combines the local updates from clients.

3.2. Construction of Privacy Protection Model Based on Machine Learning. Machine learning is a branch of artificial intelligence. Machine learning is a scientific study of algorithms and statistical models used by computer systems to gradually improve the performance of specific tasks. The machine learning algorithm is a mathematical model based on the so-called "training data set." It can complete forecasting or decision-making problems without the guidance of a specific program. Most of the traditional machine learning training algorithms are only suitable for single machine learning. Therefore, machine learning in the distributed environment needs the corresponding distributed machine learning platform to complete. Machine learning algorithms are closely related to computational statistics. Machine learning problems can often be attributed to an optimization problem. The theory of optimization provides a theory and method for machine learning. In machine learning security, the adversary model is often used to describe the strength of an adversary. Distributed machine learning has three advantages: ① using data distributed in different nodes to train the model together increases the accuracy of the model. ② Storage units distributed in different nodes are used to store data, which increases the data set capacity for model training. ③ The computing units distributed in different nodes are used for training, which enhances the computing ability of the system itself. Machine learning is widely used in data mining, computer vision, e-mail filtering, detection of credit card fraud, and medical diagnosis and analysis. While machine learning is widely used in various fields, it also brings many threats to security and privacy. Generally speaking, learning in machine learning can be divided into three categories: supervised learning, unsupervised learning, and reinforcement learning. In supervised learning, the machine learning algorithm is based on a set of data sets with standard input and output. Supervise the use of data of known labels or classes. In unsupervised learning, the algorithm establishes a mathematical model of a set of data, which only contains the input but not the expected output. Reinforcement learning is based on the maximization of some scalar reward goals, based on data and some future rewards. However, this type of learning is limited to dealing with a small number of key parameters. The general process of personal information processing is shown in Figure 2.

Vector homomorphic encryption is a homomorphic encryption scheme for vector encryption. In machine

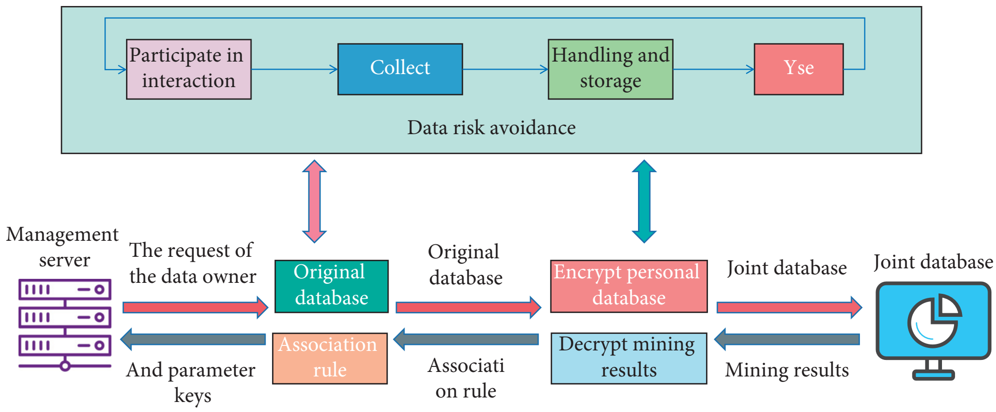

Figure 1: Data mining model of personal privacy protection.

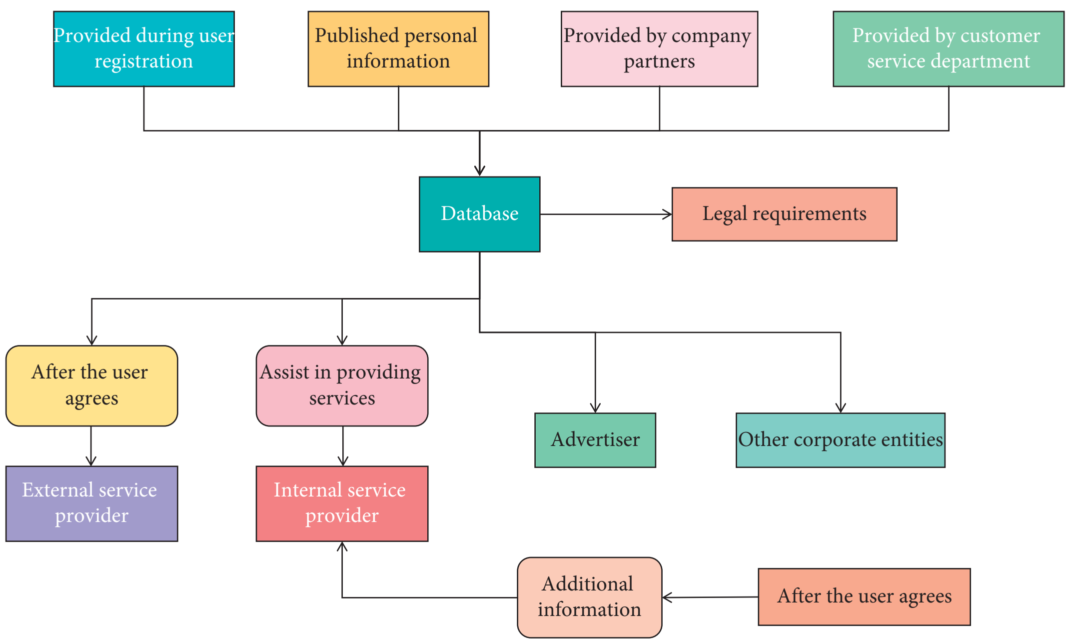

Figure 2: Flow chart of personal information processing.

learning, there are many operations for vectors. Therefore, a vector homomorphic encryption scheme is very important for machine learning. Homomorphic encryption technology is a kind of public key encryption system, which encrypts the original data to protect the privacy of data. Homomorphic encryption has its natural advantages, which makes it one of the candidates for privacy protection solutions in the era of big data. Its main advantage is that it can make the third-party complete homomorphic operation of data without decryption. The security of a homomorphic encryption algorithm is based on the difficulty assumption of the algorithm, which can provide a good security guarantee. Homomorphic encryption can encrypt both local data and model parameters. Using homomorphic encryption to support ciphertext calculation can solve the problem of machine learning by combining multiple participants' data sets and provide a data security guarantee for machine learning in a big data environment. The algorithm framework is divided into two parts: initialization and classification. Initialization includes the following steps: data preparation and data uploading; Classification includes the following steps: query matrix generation, secure similarity calculation, and secure multiparty calculation to obtain results. The homomorphic properties of subtraction and scalar multiplication of the algorithm are shown in the following formulas:

$$\begin{aligned}
&((c_1 - \ldots - c_n) - 2l_1 Z_1)\bmod p_3 \\
&= s^d (r_1 p_2 + km_1 + l_1 e_1) - \ldots - (r_n p_2 + km_n + l_n e_n) \\
&- (2r' p_2 + 2l_1 e_1)\bmod p_3 \\
&\triangleq s^d (r p_2 + k(m_1 - \ldots - m_n) - \varepsilon p_1)\bmod p_3 \\
&(N \times C_T)\bmod p_3 = \left(N \times s^d (r p_2 + kT)\bmod p_3\right) \\
&\triangleq s^d (r p_2 + kNT)\bmod p_3,
\end{aligned} \tag{1}$$

where N is a positive integer; $Z_1 = Enc_K^{e_1}(0)$ is a publicly available value generated by the first data owner.

The correctness of decryption is guaranteed by the following formula:

$$x = \left|\frac{S_c}{w}\right|_q = \left|\frac{S(M_x + e)}{w}\right|_q = \left|x + \frac{S_e}{w}\right|_q. \quad (2)$$

To recover plaintext x from ciphertext c and key S, the condition $|S_e/w| < (1/2)$ needs to be satisfied. Because there is the following formula:

$$\sum_{i=1}^{m} |S| e_i < \frac{w}{2}. \quad (3)$$

Going a step further e is

$$|e| < \frac{w}{2m|S|}. \quad (4)$$

The following formula can be obtained:

$$S_c = wx + e. \quad (5)$$

Before clients share local parameters, the parameters are processed by a privacy-protecting and verifiable mechanism, and the processed data is shared with the cloud server, obfuscating each client's local gradient and making it difficult for the cloud to extract any useful information from the collected gradient. Furthermore, a verifiable mechanism ensures the accuracy of transmission results, allowing for the effective detection of false results produced by malicious clouds. Due to the introduction of noise, the support vector machine algorithm scheme based on differential privacy protection alters the distribution of original data, lowering the accuracy, and usability of the results. Individual user data will never leave the device if local differential privacy is used. The proposed protocol strengthens data stream privacy protection, reduces attackers' options for destroying privacy and collects useful statistical data. The central idea of this paper is to query data sets in batches. Because the homomorphic encryption scheme supports homomorphic linear transformation operation, all query vectors can be placed in the same linear transformation matrix to achieve the purpose of the simultaneous query. In order to adapt to the distributed characteristics of the system, the system adopts the distributed selection random gradient descent method to update the model parameters. The core of the distributed random gradient descent method is the distributed and cooperative deep learning protocol.

If $pk_{l,i} = pk_{l,j}, sk_{l,i} = sk_{l,j}$, then $i = j$. At this time, the ciphertext polynomial kernel function of the data object m_i and the support vector g_j can be expressed as follows:

$$\begin{aligned} p_{j,i} &= K\left(SV_j, C_i\right) \\ &= \left(s_{j,i} + c(1)\right)^u \\ &= \left(\sum_{z=1}^{d}\left(c_{jz}^{*} \otimes c_{iz}\right) + c(1)\right)^u. \end{aligned} \quad (6)$$

Evaluate all ciphertexts $c_{ij}\,(j = 1, 2, 3, \ldots, l_i)$ of the i th data owner as follows:

$$\begin{aligned} c_i &= Eva\left(c_{i1}, \ldots, c_{il_i}\right) \\ &= \sum_{j=1}^{l_i} Enc_K^{e_i}\left(m_{ij}\right) \underline{\Delta}\, s^d \left(r_i p_2 + km_i + l_i e_i\right) \bmod p_3. \end{aligned} \quad (7)$$

Evaluating the ciphertext $c_i\,(i = 1, 2, 3, \ldots, n)$. for all n data owners is

$$\begin{aligned} c &= Eva\left(c_i, \ldots, c_n\right) \\ &= \sum_{i=1}^{n} s^d \left(r_i p_2 + km_i + l_i e_i\right) \underline{\Delta}\, s^d \left(r p_2 + km + \varepsilon p_1\right); \varepsilon \in Z. \end{aligned} \quad (8)$$

The correlation error is used as a measure of an average calculation error, while MAPE is used as a measure of frequency estimation error. The absolute value of the predicted value minus the actual value divided by the actual value is the correlation error. The following is the definition of the relevant error:

$$\text{Related error} = \left|\frac{y_i - x_i}{x_i}\right| \times 100\%. \quad (9)$$

The absolute value of the difference between the estimated and real frequencies is known as MAPE. Divide the absolute value by the real frequency, then add these numbers together and divide by the data range's length. The following is the MAPE definition:

$$\text{MAPE} = \frac{\sum_{i=1}^{|D|}\left|(y_i - x_i)/x_i\right|}{|D|} \times 100\%. \quad (10)$$

The ciphertext of personal data is of no use to individuals and needs to be kept confidential to other data owners. Therefore, the decryption algorithm of the ciphertext of personal data is abandoned in the design. In this paper, the algorithm classifies the test data set by calculating the similarity between the test data set and the training data set. The test data set selects the most similar k data from the training data set, and these k data confirm the label of the test data by voting mechanism. Privacy difference realizes privacy protection by adding noise to the survey results, and the added amount of noise not only protects users' privacy but also keeps data availability, so sensitivity becomes the key parameter of noise control. In local differential privacy, the concept of sensitivity is based on any two pieces of data. The mining sharing method similar to secret sharing in the algorithm is to prevent the fall and conspiracy attacks. The sharing method ensures that different data owners have different personal keys. Therefore, only when the databases of all the data owners participating in the mining are spliced into a joint database can the ciphertext mining results be decrypted correctly.

4. Result Analysis and Discussion

The privacy stream is released in real time using sliding window technology in this paper. It lowers computing and storage costs while also lowering privacy budget

Table 1: Anti-attack performance of different security schemes.

Serial number	Attack type	Secure data aggregation scheme	Secure data mining scheme on vertically partitioned database	Mining scheme on horizontal partitioned database	The security data mining scheme in this paper
1	Ciphertext-only attack	Can defend	Can defend	Can defend	Can defend
2	Known plaintext attack	Can defend	Unprotectable	Unprotectable	Can defend
3	Select plaintext attack	Can defend	Unprotectable	Unprotectable	Can defend
4	Selected ciphertext attack	Unprotectable	Unprotectable	Unprotectable	Unprotectable
5	Unauthorized mining attack	Can defend	Unprotectable	Unprotectable	Can defend
6	Forgiveness attack	Can defend	Unprotectable	Unprotectable	Can defend
7	Unauthorized decryption attack	Unprotectable	Unprotectable	Can defend	Can defend
8	Owner fall	Unprotectable	Unprotectable	Unprotectable	Unprotectable

consumption when compared to traditional privacy protection methods. The proposed protocol adaptively determines the window length of the stable subdata stream, detects significant movement, opens a new window in time, and captures the trend and distribution of the data stream to further reduce storage space and better allocate the privacy budget. This section examines the antiattack performance of this scheme as well as several comparison schemes in order to verify the security of this method. The performance of these schemes against attacks is detailed in Table 1.

It can be seen that this scheme can defend against more types of attacks and has higher security. In the distributed selection random gradient descent method, a small number of local model parameters are selected to update in each iteration, and this selection process is completely random. The distributed random selection gradient descent method assumes that there are two or more participants, who are independent of each other and participate in the training in parallel. After each round of local training, participants share the gradients of the calculated parameters, and each participant completely controls which gradients to share and how often to share them. To verify the impact of privacy budget on usability in real data sets, different algorithms are used to conduct experiments on real data sets. Figure 3 shows the impact of the privacy budget on evenly distributed data sets. Figure 4 shows the impact of the privacy budget on real data sets.

Experiments show that under different privacy budgets, the usability of this algorithm is higher than that of the other two algorithms, which proves that this algorithm is also feasible in practical application. The data encryption stage is a constant complexity operation. After the encrypted data is processed, the future expenses mainly come from the data query users. As for secure multiparty calculation, the steps to obtain the results are clear and simple, so the efficiency is very high. In the comparative evaluation stage, this paper does not consider the two stages of data preparation and secure multiparty calculation to obtain the results. Different schemes are applied to personal information privacy protection, and their security performance is compared. The results are shown in Figure 5.

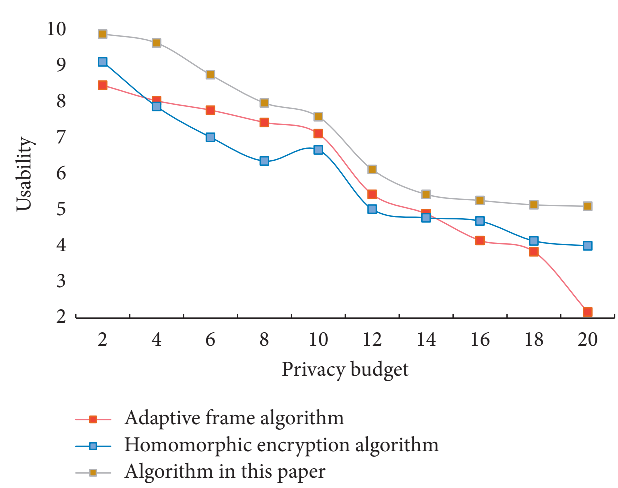

Figure 3: The influence of privacy budget on evenly distributed data sets.

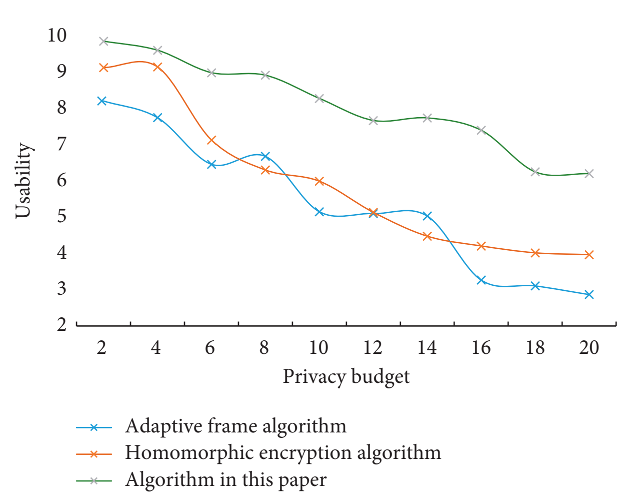

Figure 4: The impact of privacy budget on real data sets.

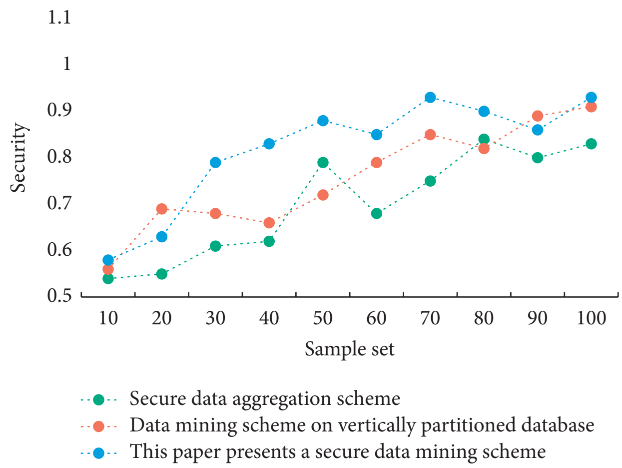

Figure 5: Security comparison of different schemes.

The method in this paper is safe and has some practical application value, according to the data in Figure 5. Significant movement in the data stream indicates the occurrence of a new event or trend. The newly observed tuples can be added to the current window to form a stable subdata stream if they maintain the current window's stability. A new window should be opened if new trends in the data stream emerge. Table 2 compares the results of various algorithms in terms of performance.

It can be seen that the performance of this algorithm is generally better than other comparison algorithms. Many participants in the system participate in the training on the same combined data set to complete machine learning and ensure that no local information of the participants is leaked to the central server during this process. Figure 6 is the simulation diagram of the secure distance calculation protocol.

From the data analysis, it can be seen that the decision-making process of the scheme classification in this paper is completely outsourced, and the data belonging to the master only needs to undertake the encryption in the initial stage and the decryption in the result acquisition stage. Comparing the adaptive framework algorithm and homomorphic encryption algorithm with the algorithm in this paper, the accuracy of different algorithms is shown in Figure 7.

It can be seen that the accuracy of this algorithm is higher than that of the adaptive frame algorithm and homomorphic encryption algorithm, and it has a certain superior performance. The experimental results show that the proposed protocol has high practicability, which is applicable to both numerical attributes and classified attributes and can keep its practicability under different distributions and data stream sizes. This algorithm has a fast convergence speed, and the average error rate decreases by 4.17% compared with the traditional algorithm. Moreover, the accuracy of this algorithm reaches 95.37%, which is about 8.76% higher than the previous algorithm. The scheme proposed in this paper has obvious advantages. At the same time, it realizes multidata ownership setting, complete outsourcing calculation, and zero communication consumption. At the same time, it supports the inner product kernel function and polynomial kernel function classification. This scheme can not only protect the privacy of the stream, but also ensure high practicability, and the overhead of storage and computing power is small.

Table 2: Performance comparison results of different algorithms.

Algorithm	Average error	Recall rate	Accuracy rate
Distributed privacy protection algorithm	0.548	0.874	0.862
Adaptive frame algorithm	0.496	0.887	0.894
Homomorphic encryption algorithm	0.217	0.926	0.918
K-means clustering algorithm	0.301	0.894	0.901
Algorithm in this paper	0.131	0.963	0.954

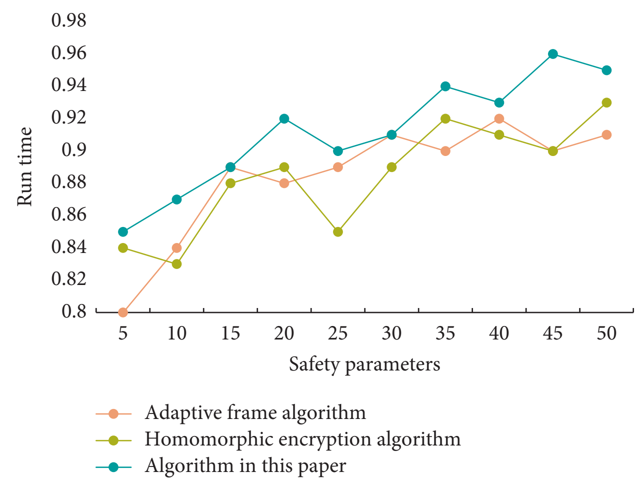

Figure 6: Simulation diagram of safety distance calculation protocol.

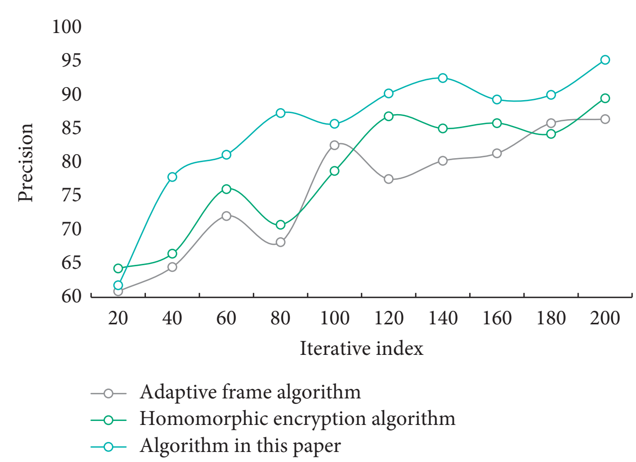

Figure 7: Accuracy comparison of different algorithms.

5. Conclusions

In view of the threats to personal information privacy, we need to further explore the defense technologies against poisoning attacks, confrontation attacks, and other attacks, improve the robustness of the model, and study the defense means against stronger attacks. In this paper, aiming at the existing privacy protection of personal information, combined with the research status at home and abroad, the machine learning platform and homomorphic encryption scheme are studied, respectively. By observing the characteristics of big data and the new publishing mode, this paper analyzes the potential risks of privacy leakage caused by data association analysis. Then, the privacy protection criterion matching its characteristics is studied, and the user's demand for data privacy protection and data availability is understood, and a privacy protection model based on machine learning is constructed. A privacy protection mechanism based on elliptic curve and homomorphic encryption is designed to cover the local gradient of each client, which makes it difficult for malicious adversaries and semitrusted cloud to reason the original information of the data set. The proposed privacy protection mechanism keeps the high prediction accuracy of the training model and balances the security and efficiency well. In this paper, based on vector homomorphic encryption, the similarity measure of vectors under ciphertext is designed. It has the advantages of low interaction cost, safety, and high efficiency. In order to verify the performance of the algorithm, a lot of experiments are carried out. The experimental results show that this algorithm has a fast convergence speed, and the average error rate decreases by 4.17% compared with the traditional algorithm. Moreover, the accuracy of this algorithm reaches 95.37%, which is about 8.76% higher than the previous algorithm. Although this paper has achieved some research results, there are still some shortcomings and places to be improved in the research process. For example, the low efficiency of the data fusion operation of local model parameter group ciphertext will be improved in the followup work.

Data Availability

The data used to support the findings of this study are included within the article.

Conflicts of Interest

The authors declare that they have no conflicts of interest.

References

[1] Z. Liu, "Personal information risks and key technologies of data privacy protection in big data era," *Revista de la Facultad de Ingenieria*, vol. 32, no. 14, pp. 790–794, 2017.

[2] M. Niimi, F. Masutani, and H. Noda, "Protection of privacy in JPEG files using reversible information hiding," *The Journal of the Institute of Image Electronics Engineers of Japan*, vol. 43, no. 1, pp. 21–27, 2014.

[3] S. Yu, P. Mueller, and J. Qian, "Security and Privacy in Digital Economy," in *Proceedings of the First International Conference SPDE 2020*, vol. 1268, Quzhou China, November 1 2020.

[4] Y. Nakashima, T. Ikeno, and N. Babaguchi, "Evaluating protection capability for visual privacy information," *IEEE Security & Privacy*, vol. 14, no. 1, pp. 55–61, 2016.

[5] K. Zhang, K. Yang, X. Liang, Z. Su, X. Shen, and H. H. Luo, "Security and privacy for mobile healthcare networks: from a quality of protection perspective," *IEEE Wireless Communications*, vol. 22, no. 4, pp. 104–112, 2015.

[6] J. Wang, F. Wang, Z. Cao, F. Lin, and J. Wu, "Sink location privacy protection under direction attack in wireless sensor networks," *Wireless Networks*, vol. 23, no. 2, pp. 1–13, 2017.

[7] F. Kai, J. Wei, L. Hui, and Y. Yang, "Lightweight RFID protocol for medical privacy protection in IoT," *IEEE Transactions on Industrial Informatics*, vol. 14, no. 4, pp. 1656–1665, 2018.

[8] N. Ruchaud and J. L. Dugelay, "JPEG-based scalable privacy protection and image data utility preservation," *IET Signal Processing*, vol. 12, no. 7, pp. 881–887, 2018.

[9] S. K. Ocansey, W. Ametepe, X. W. Li, and C. Wang, "Dynamic searchable encryption with privacy protection for cloud computing," *International Journal of Communication Systems*, vol. 31, no. 1, pp. e3403.1–e3403.8, 2018.

[10] N. Wang, J. Fu, J. Zeng, and B. K. Bhargava, "Source-location Privacy Full protection in Wireless Sensor networks," *Information ences*, vol. 444, pp. 105–121, 2018.

[11] J. Wang, R. Zhu, S. Liu, and Z. Cai, "Node location privacy protection based on differentially private grids in industrial wireless sensor networks," *Sensors*, vol. 18, no. 2, p. 410, 2018.

[12] C. Yin, J. Xi, and R. Sun, "Location privacy protection based on ImprovedK-value method in augmented reality on mobile devices," *Mobile Information Systems*, vol. 2017, no. 12, pp. 1–7, 2017.

[13] K. J. Reza, M. Z. Islam, and V. Estivill-Castro, "Privacy protection of online social network users, against attribute inference attacks, through the use of a set of exhaustive rules," *Neural Computing & Applications*, vol. 33, no. 19, pp. 12397–12427, 2021.

[14] W. Wei, S. Liu, W. Li, and D. Du, "Fractal intelligent privacy protection in online social network using attribute-based encryption schemes," *IEEE Transactions on Computational Social Systems*, vol. 5, no. 3, pp. 736–747, 2018.

[15] J. Liu and S. Zhou, "Application research of data mining technology in personal privacy protection and material data analysis," *Integrated Ferroelectrics*, vol. 216, no. 1, pp. 29–42, 2021.

[16] C. Ke, R. Wang, F. Xiao, and Z. Huang, "Requirement-oriented privacy protection analysis architecture in cloud computing," *Journal of Communications*, vol. 10, no. 1, pp. 55–63, 2015.

[17] M. Barni, G. Droandi, and R. Lazzeretti, "Privacy protection in biometric-based recognition systems: a marriage between cryptography and signal processing," *IEEE Signal Processing Magazine*, vol. 32, no. 5, pp. 66–76, 2015.

[18] Z. Hu, J. Yang, and J. Zhang, "Trajectory privacy protection method based on the time interval divided," *Computers & Security*, vol. 77, no. 8, pp. 488–499, 2018.

[19] P. S. Xie, T. X. Fu, and H. J. Fan, "An algorithm of the privacy security protection based on location service in the Internet of vehicles[J]," *International Journal on Network Security*, vol. 21, no. 4, pp. 556–565, 2019.

[20] J. Chen, H. Ma, D. Zhao, and D. S. L. Wei, "Participant density-independent location privacy protection for data aggregation in mobile crowd-sensing," *Wireless Personal Communications*, vol. 98, no. 1, pp. 699–723, 2018.

[21] Z. Qi, W. Haoxin, and H. Jing, "Application and design of mobile intelligent terminal security protection system based on Android platform," *Acta Technica CSAV (Ceskoslovensk Akademie Ved)*, vol. 62, no. 2, pp. 849–857, 2017.

[22] G. Kalogridis, M. Sooriyabandara, Z. Fan, and M. A. Mustafa, "Toward unified security and privacy protection for smart meter networks," *IEEE Systems Journal*, vol. 8, no. 2, pp. 641–654, 2014.

[23] Y. Guo, X. Fang, Z. Dong, and H. Mi, "Research on multi-sensor information fusion and intelligent optimization algorithm and related topics of mobile robots," *EURASIP Journal on Applied Signal Processing*, vol. 2021, no. 1, p. 111, 2021.

[24] H. Zhu, C. Huang, and H. Li, "Information diffusion model based on privacy setting in online social networking services," *The Computer Journal*, vol. 58, no. 4, pp. 536–548, 2015.

Hindawi
Computational Intelligence and Neuroscience
Volume 2023, Article ID 9791745, 1 page
https://doi.org/10.1155/2023/9791745

Retraction

Retracted: Image Recognition of Sports Athletes' High-Intensity Sports Injuries Based on Binocular Stereo Vision

Computational Intelligence and Neuroscience

Received 25 July 2023; Accepted 25 July 2023; Published 26 July 2023

This article has been retracted by Hindawi following an investigation undertaken by the publisher [1]. This investigation has uncovered evidence of one or more of the following indicators of systematic manipulation of the publication process:

(1) Discrepancies in scope
(2) Discrepancies in the description of the research reported
(3) Discrepancies between the availability of data and the research described
(4) Inappropriate citations
(5) Incoherent, meaningless and/or irrelevant content included in the article
(6) Peer-review manipulation

The presence of these indicators undermines our confidence in the integrity of the article's content and we cannot, therefore, vouch for its reliability. Please note that this notice is intended solely to alert readers that the content of this article is unreliable. We have not investigated whether authors were aware of or involved in the systematic manipulation of the publication process.

Wiley and Hindawi regrets that the usual quality checks did not identify these issues before publication and have since put additional measures in place to safeguard research integrity.

We wish to credit our own Research Integrity and Research Publishing teams and anonymous and named external researchers and research integrity experts for contributing to this investigation.

The corresponding author, as the representative of all authors, has been given the opportunity to register their agreement or disagreement to this retraction. We have kept a record of any response received.

References

[1] D. Chen, "Image Recognition of Sports Athletes' High-Intensity Sports Injuries Based on Binocular Stereo Vision," *Computational Intelligence and Neuroscience*, vol. 2022, Article ID 4322597, 10 pages, 2022.

Hindawi
Computational Intelligence and Neuroscience
Volume 2022, Article ID 4322597, 10 pages
https://doi.org/10.1155/2022/4322597

Research Article

Image Recognition of Sports Athletes' High-Intensity Sports Injuries Based on Binocular Stereo Vision

Dongdong Chen

Xinyang Normal University, Xinyang 464000, China

Correspondence should be addressed to Dongdong Chen; 14521223@xzyz.edu.cn

Received 27 May 2022; Revised 10 June 2022; Accepted 11 June 2022; Published 31 July 2022

Academic Editor: Xin Ning

Sports athletes are prone to certain injuries during high-intensity exercise training. In the process of treating an injury, images of the injury site need to be collected and identified. However, the traditional recognition method cannot effectively extract the features of the image. At the same time, it ignores the optimization of the damage image recognition results, resulting in low recognition accuracy and poor efficiency. Binocular stereo vision technology can quickly and accurately detect moving objects. Therefore, in order to more accurately identify high-intensity sports injury images, this study takes the high-intensity sports injury images as the basic research object. Several processes of image processing based on binocular stereo vision are analyzed, and the vulnerable parts of the body in high-intensity sports are also studied. Finally, the method in this study is verified. The experimental results show that the method proposed in this study reduces the average error rate by 0.19% compared with the traditional recognition method. It can effectively identify and detect injury images, thereby improving the accuracy and stability of sports injury image identification. The identification time is also shortened accordingly, which has certain practicability and feasibility. In addition, the binocular camera used in this study has high accuracy, and the obtained images of sports injuries are of good quality, which lays a foundation for image detection and recognition.

1. Introduction

Athletes who participate in high-intensity and technically difficult sports are more likely to sustain injuries during exercise, such as cervical spine and lumbar spine injuries. Binocular stereo vision closely resembles how the human eye processes images. It is a very dependable and simple algorithm that has proven its worth in a variety of fields. As a result, this study proposes a binocular stereo vision-based recognition method for high-intensity sports injury images, which is critical for the repair and treatment of injured athletes' parts.

Timely detection and identification of injury sites in athletes can more accurately diagnose the type and severity of injuries. Some scholars have conducted some studies on the identification of sports injuries. Prabhu et al. discovered that diffusion tensor imaging, magnetic resonance spectroscopy, and fMRI can detect changes in encephalopathy. The pathological examinations he performed documented progressive neuronal degeneration of the tau protein. It was found that prevention, early diagnosis, and appropriate treatment are the recommended methods for the treatment of these diseases [1]. Zhu et al. used a research method based on big data technology and CNN-based computer vision technology and theoretical analysis related to sports mechanics and image recognition. His research provided technical support for injury risk prediction in athletes [2]. Wang research purpose is to find how to intelligently process images of soccer games based on computer intelligence techniques. First of all, he identified and processed the dynamic images of sports and collected static and dynamic images of football. The experimental results showed that the systematic error of the auxiliary identification technology based on the Internet of things is 0.63. So, his proposed algorithm and the obtained experimental results effectively demonstrate the reliability of using intelligent image recognition techniques for soccer sports image recognition [3]. Based on the characteristics of athletes, Ma et al. developed and designed a C/S mode athlete training process monitoring system, using GPS to obtain real-time position information of athletes. In order to reveal the changing laws of various indicators of athletes under training, he followed a series of physical conditions of the athletes, such as the characteristics of physical functions, training programs and arrangements, the status of brain functions, routine physiological and biochemical indicators, and basic conditions of injuries [4]. The above researchers have combined the treatment and prediction of sports injuries with intelligent technology, which has played a certain role in promoting the recovery of athletes, but they did not put it into practice and lacked reliability.

Binocular stereo vision technology is a high-speed, high-precision noncontact measurement method. For this technology, many scholars have conducted research. Lin et al. aimed to develop a 3D image reconstruction method based on laser line scanning (LLS) technology to establish a binocular stereo vision system for preliminary research on obstacle detection technology for autonomous underwater vehicles (AUVs). Therefore, the results of the stereo vision system evaluation demonstrate the reliability and performance of the tank [5]. Based on the binocular stereo vision measurement principle and wireless sensing theory, Li and Zhang studied the measurement and analysis method of the athlete's movement displacement parameters. He developed a noncontact displacement measurement system. The experimental results showed that the integrated displacement measurement system designed in this study has high precision and good stability [6]. Lin et al. discussed one of the foundations of 3D reconstruction methods in binocular stereo vision, that is, feature matching. He studied the operation principles, feature matching algorithms of binocular stereo vision system, and 3D reconstruction system. Based on these studies, he proposed a set of more feasible algorithms to improve the effect of 3D reconstruction [7]. Sun et al. established a perspective projection model of any section of the elbow. Based on this model, he proposed a method to locate the precise projected position of the on-axis point on the image plane and reconstruct the 3D coordinates of the on-axis point using binocular stereo vision. He measured three bends of different diameters. Compared with the classical method, this method effectively reduced the reconstruction error [8]. The abovementioned scholars used this technology to analyze their research objects and proved the reliability and stability of this technology, but they did not conduct experiments on its application and lacked data support.

After a series of experimental analysis, it can be concluded that the error of the method in this study for the coordinate positioning of the damage image is less than 0.5 mm, and the error rate is less than 2%. This shows that the method in this study can locate the damage target more accurately. The recognition rate of the method in this study is significantly higher than that of other methods, and the lowest is more than 60%, which proves the operability of the method. In addition, the method proposed in this study consumes the shortest time when the number of recognized images is different, and the lowest is 0.5 seconds. This also shows that the recognition rate of this method is the highest, and it has great advantages over other methods. As the number of experiments increases, the error rates of different methods show different trends. The error rate of the method proposed in this study is much lower than other methods, with an average of about 0.06%, and that of other methods is about 0.25%. This shows that the method proposed in this study can reduce the error to a relatively low level when recognizing sports-impaired images.

2. Binocular Stereo Vision, High-Intensity Sports Injury, and Image Recognition

2.1. Binocular Stereo Vision. There are many ways that humans get information, and 70 percent of it comes from what people see. Therefore, vision has played an extremely important role in the process of people observing the world and understanding the world. Studies have shown that when people see things with the left eye and see things with the right eye, their perception of distance and spatial perception of objects will become different. The reason for this phenomenon is that the positions of the two eyes of human beings are different, which makes the things and images seen by the left eye and the right eye different. However, when the left and right eyes look at things at the same time, the neural tissue of the brain will fuse the received image information to form a sense of space for the object. This formation process is called binocular stereo vision. It is generally called BSV, that is, binocular stereo vision. Binocular stereo vision is an important part of computer vision [9–11].

The theoretical basis of binocular stereo vision technology is parallax theory (as long as the parallax angle and the baseline length are known, the distance between the target and the observer can be calculated). The main purpose of this technology is to restore and reconstruct the depth information and three-dimensional geometric coordinates of pixels, the purpose of which is mainly achieved by acquiring images. The "image" here is based on the simultaneous acquisition of the left and right perspectives, so it has certain passivity. With this technology, the real three-dimensional world can be quickly restored, providing the user with a description of the location of the target during the navigation process. Binocular stereo vision technology is more comprehensive, and it contains a variety of subject knowledge, such as optics, physics, and computer science. The most difficult and critical component of binocular stereo vision technology is the process of camera position calibration and feature matching. The model structure based on binocular stereo vision is extremely simple, and the operation efficiency is also very high, so its application prospect is very broad. In particular, this model is widely used in the automated production of factories. The human eye is capable of perceiving three-dimensional objects in three dimensions, and binocular stereo vision systems mimic this criterion. The simulation process is based on the principle of triangulation. This system uses imaging equipment and a computer to perform a series of processing on images. The system is generally divided into four functional modules, as shown in Figure 1.

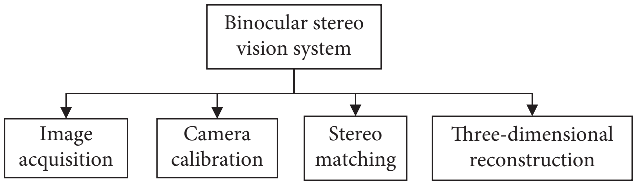

Figure 1: Functional modules of the binocular stereo vision system.

Next, the binocular stereo vision system will be introduced in detail. It consists of three components, namely a binocular camera, a frame grabber, and a computer. First, as the name implies, the binocular camera has two cameras, which also allows it to collect two images of the detected object from different positions. Second, the image acquisition card is connected to the camera and the computer, and the specific process is as follows: first, the binocular camera collects the image signal. Then, the acquisition card converts the collected signal into a digital signal and then transmits the digital signal to the computer. The computer saves it to the hard disk. Third, the computer mainly completes a series of tasks through algorithms, including image preprocessing and segmentation, feature extraction, and stereo matching, to calculate the three-dimensional geometric information of the detected graphics and reconstruct the three-dimensional scene. The basic principle of binocular stereo vision is shown in Figure 2.

The image processing process of binocular stereo vision will be introduced in detail as follows:

(1) *Image Preprocessing* [12, 13]. The camera can capture the image of the detected object, and then, the capture card transmits the image captured by the camera to the computer. In this process, it is easy to be subject to various interferences, which leads to the degradation of image quality and brings certain difficulties to subsequent image recognition. Therefore, image preprocessing becomes a necessity. The main purpose of image preprocessing is to remove the interference factors in the transmission process and enhance the pixels of the detected object in the image. If this task is done well, it will be more conducive to feature extraction and stereo matching of detected objects. In addition, this process can operate in both spatial (the two-dimensional plane where the image plane is located) and frequency (the spatial frequency of the gray value of the image pixel changing with the position) domains simultaneously, so it can also effectively reduce noise.

(2) *Selection of Color Space*. When processing more complex images, people usually select the part they are interested in and extract the feature information of this part. This process is called image processing. The basic flow of general image processing and recognition is shown in Figure 3. The result frame of image recognition based on binocular stereo vision is shown in Figure 4. For image information of different difficulties, it is necessary to select an appropriate color model, so as to facilitate its analysis, and also help computer equipment to quickly identify the characteristic information of the image. There are many general color models. Among them, hue, saturation, and intensity (HSI), luminance a and b (Lab), cyan, magenta, and yellow (CMY), red, green, and blue (RGB) are relatively common, which have different characteristics.

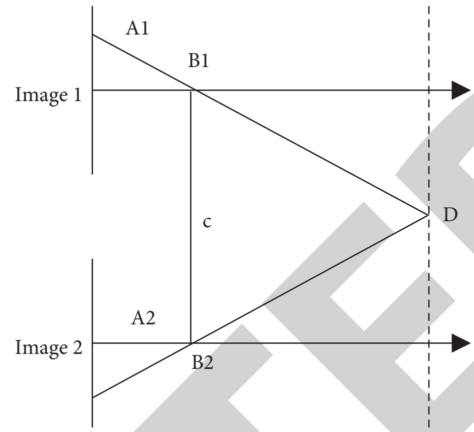

Figure 2: Basic principle of binocular stereo vision.

(3) *Image Segmentation*. Image segmentation [14, 15] refers to dividing the basic information of an image into several parts according to different characteristics. These parts are called image elements. The advantage of doing this is that it is conducive to fast matching of features. Each image element has its own characteristics, so they are also very easy to identify and distinguish. The advantage of image segmentation is that it can greatly reduce the workload of computers and administrators, thereby further improving the recognition efficiency of computers [16]. In general, there are various methods and classification criteria for image segmentation, mainly because the basis of segmentation is different. Among them, there are mainly three segmentation methods based on gray threshold, region growth, and edge detection. Among them, the first method is further divided into the maximum value method, the average method, and the weighted average method, as shown in Table 1.

(4) *Extraction of Image Features*. What this process needs to do is to compare the different features of the two images, so that the coordinates of the same point in the three-dimensional space in the two different images can be obtained. The features of images can be divided into local features (points, lines, surfaces) and global features (polygons, images) according to different classification [17] criteria, which can also be divided into color, texture, shape, spatial relationship features, etc. Different features use different algorithms.

(5) *Stereo Matching Process*. Stereo relative refers to two images taken by two cameras in a binocular camera

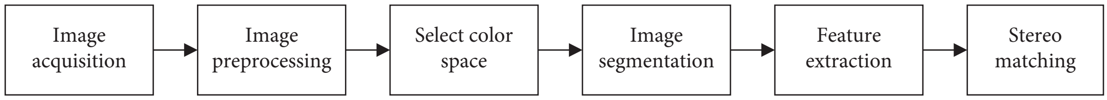

Figure 3: Basic flow chart of image recognition.

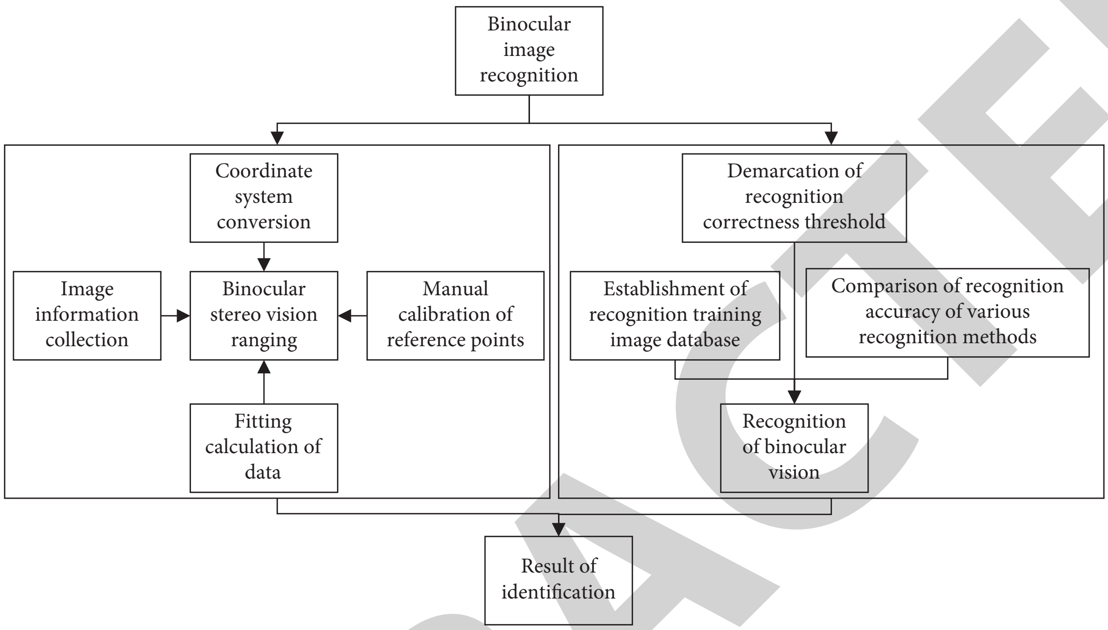

Figure 4: Structural framework of image recognition based on binocular stereo vision.

Table 1: Commonly used segmentation methods.

Segmentation method	Operation	Effect
Segmentation method based on gray threshold	Grayscale processing	Reduce redundant information
Segmentation method based on region growth	Split by pixel	Complete image extraction
Segmentation method based on edge detection	Split according to contour	Image segmentation

of the same object. The purpose of stereo matching is to discover and find the coordinates and relationships of the corresponding points in the two images, which is also the focus of 3D reconstruction. Stereo matching is also known as disparity estimation, or binocular depth estimation. Two algorithms are available for this process, that is, local descriptions based on invariants and statistical learning methods. This process is unique and reproducible, with some physical meaning.

2.2. High-Intensity Sports Injuries. High-intensity exercise training can greatly enhance the function of the human body, so that the maximum oxygen uptake of the organism can be improved, and myocardial functions such as heart rate, speed, and endurance can be improved [18]. The main characteristics of high-intensity exercise training are shown in Table 2. Under normal circumstances, the main contents of high-intensity exercise training include running and leapfrog, as shown in Table 3.

Sports injuries are clinically manifested as pain, swelling, etc., at the injury site of different severities. High exercise intensity is more likely to lead to muscle damage. As the name suggests, sports injuries refer to various injuries suffered by athletes during sports training [19]. Sports injuries are closely related to a series of factors, such as the intensity of sports, the type of sports, training environment, and sports auxiliary equipment. The specific classification of sports injuries is shown in Table 4.

Table 2: Basic parameter information of high-intensity exercise training.

Items	Remarks
Environment	Aerobic environment
Maximum load intensity	75%–80%
Heart rate	About 140 times/min
Oxygen supply method	Intermittent load method

In real life, injuries to athletes are unavoidable because most high-intensity sports involve relatively intense confrontation. With the passage of time, the injury develops concealment and long-term characteristics, causing permanent damage to the athlete's body. Abrasions, sprains, strains, and joint injuries are all common types of injuries

Table 3: Basic content of high-intensity exercise training.

Serial numbers	Contents	Exercise intensity
1	800 m jogging	6 min to complete
2	5 times × 5 m turn back to run	3 groups, rest 2 min between groups
3	50 m run	5 groups, rest 1 min between groups
4	Leapfrog	3 groups, each group 20 times, rest 3 min between groups
5	Squat	
6	Relax and stretch	5 min

Table 4: Basic classification of sports injuries.

Division angle	Classification	Remarks
Damage property	Chronic injury	Heavy local body load
	Acute injury	Muscle strain
Damaged tissue structure	Skin, muscle, joint, and nerve injury	
Damage degree	Mild injury	No effect on normal training or competition
	Moderate injury	Affect normal training or competition for over 1 day
	Severe injury	Need hospitalization

Table 5: Causes of sports injuries and their prevention strategies.

Reason	Specific description	Preventive measure
Psychological quality	Focus on tactical skills	Psychological counselling and mental health education Psychological supervision
	Less training	Soothe and regulate emotions Raise awareness of prevention
Physical quality	High physical consumption	Strengthen physical fitness and strength training Develop training programs
	High demand for strength	Improve basic physical fitness Standardize and correct tactical actions
Objective reasons	Improper infrastructure maintenance	Strict requirements and specifications Check the equipment regularly
	Clothing discomfort	Meet reasonable requirements Check and prevent damage

[20]. Abrasions are common in sports with more physical contact. Scratches can occur as a result of falls caused by low friction on the ground or excessive slippage, or as a result of collisions or scratched fingernails as a result of physical contact between athletes. Second, some high-intensity sports have an excessive range of motion, resulting in injuries to the athletes' soft tissues and ligaments, particularly in the ankle, knee, and waist joints. Third, one of the most common causes of injury is athletes' lack of warm-up and preparation. If the preparation is insufficient, the muscles, including the thighs, calves, shoulders, and backs, will not stretch. Fourth, if a joint injury, such as the metacarpophalangeal joints, ankle joints, or knee joints, persists, it is likely to become an old injury. Joint injuries are difficult to treat and can lead to complications.

According to the above analysis, the reasons for the injury can be summed up in three points, namely psychological reasons, physical quality, and objective factors. There are also some preventive measures and strategies for these three points, as shown in Table 5.

2.3. Image Recognition and Processing of High-Intensity Sports Injuries. To identify the injury image, the main cause of sports injury must first be determined. The formula for calculating the injury rate of each sport in high-intensity training is as follows:

$$\Delta\Delta\Delta\mathcal{E}_{\mathcal{B}}(\mathcal{Y}) = \frac{\sum_{i=1}^{\Delta}\mathcal{C}_{\Delta\Delta\Delta}(\Delta_{\Delta\Delta})}{\mathcal{L}\times\beta_{\Delta}}. \quad (1)$$

In formula (1), β_{Δ} refers to the parts of the body that are easily damaged during high-intensity training; $\mathcal{L}$ refers to the maximum heart rate before high-intensity exercise; and $\Delta_{\Delta\Delta}$ refers to the severity of the injury. $\mathcal{C}_{\Delta\Delta\Delta}$ refers to different sports, and Δ refers to the number of vulnerable parts.

All factors that contribute to an athlete injury are as follows:

$$\mathcal{S} = \frac{\mathcal{E}_{\Delta}(\mathcal{Y})\cdot\mathcal{R}'}{\Delta\times\mathcal{Y}_{\ell\Delta\Delta}\cdot\Delta_{\Delta}}\cdot\mathcal{B}_{\ell\Delta\Delta}. \quad (2)$$

In formula (2), $\mathscr{B}_{\ell\Delta\Delta}$ refers to the various causes of damage; $\mathscr{Y}_{\ell\Delta\Delta}$ refers to the probability of various damage types; and $\mathscr{E}_{\Delta}(\mathscr{Y})$ refers to the law of damage.

The relationship between high-intensity exercise training intensity and injury is as follows:

$$\mathscr{K}_{\alpha} = \frac{\Delta\Delta\Delta\mathscr{G}_{\mathscr{B}}(\mathscr{Y})}{\mathscr{S} \times \mathscr{B}_{\ell\Delta\Delta}} \Delta\mathscr{S}_0. \tag{3}$$

In formula (3), $\mathscr{S}_0$ refers to the probability of injury to various joint parts of sports players.

The relationship between sport and injury severity is as follows:

$$\mathscr{P}_{(\Delta)} = \frac{\Delta_{\Delta} \cdot \Delta_{\Delta}\phi(\Delta_{\Delta})}{\beta_{\Delta}} \times \frac{\mathscr{L}(\Delta, \Delta_{\Delta})}{\Delta_{\Delta\Delta}} + \Delta. \tag{4}$$

In formula (4), Δ_{Δ} refers to the injury site; ϕ refers to the general pattern of the injury; and Δ_{Δ} refers to the duration of the sportsman's exercise. Δ refers to the important part of the injury. $\mathscr{L}(\Delta, \Delta_{\Delta})$ refers to the proportion of the number of people injured in each sport.

The statistical formula of the injured parts that sports athletes are prone to produce in the process of high-intensity sports training is as follows:

$$\mathscr{X}_{\Delta}^{\mathscr{M}} = \frac{[\Delta_{\ell}(\Delta_{\Delta}) \cdot \Delta_{\Delta}(\Delta_{\Delta})]}{\mathscr{R}_{\mathscr{J}\Delta\Delta\Delta\Delta} \cdot \mathscr{R}_{\Delta\Delta\Delta}} \cdot \frac{\phi}{\mathscr{P}_{(\Delta)}}. \tag{5}$$

In formula (5), Δ refers to the cumulative number of injuries in sports athletes. $\Delta_{\ell}(\Delta_{\Delta})$ refers to the type of cause that causes the injury, and $\Delta_{\Delta}(\Delta_{\Delta})$ refers to the ratio of various causes of injury. $\mathscr{R}_{\mathscr{S}\Delta\Delta\Delta\Delta}$ refers to the joints that are susceptible to injury, and $\mathscr{R}_{\Delta\Delta\Delta}$ refers to the joints with the highest proportion.

The main factors of sports athlete injury are as follows:

$$\mathscr{E}(\mathscr{A}) = \mathscr{X}_{\Delta} \frac{\mathscr{A}\mathscr{P}_{(\Delta)}}{\mathscr{Q}_{\Delta\Delta}} \times \mathscr{Y}. \tag{6}$$

In formula (6), $\mathscr{Y}$ refers to the detection of high-intensity exercise training intensity.

The basic law of the formation of the main factors is as follows:

$$\mathscr{N}_{\omega} = \frac{\Delta(\mathscr{B})\Delta\gamma}{\beta \times \omega \cdot \alpha}. \tag{7}$$

Here, γ refers to the maximum speed and endurance of the athlete, and β refers to the characteristics of the injury. ω refers to the probability of an injury occurring, and α refers to the severity of the injury.

The main factors of the injury are classified, the formula of which is as follows:

$$\Delta\Delta\mathscr{Y}_{\Delta} = \Delta_{\Delta}\Delta_{\Delta} \cdot \frac{\Delta\Delta - \Delta_{\Delta\ell}}{(\Delta(\gamma) * \chi)} \cdot \alpha\mathscr{N}_{\varphi}. \tag{8}$$

In formula (8), $\Delta(\gamma)$ refers to the variability of injuries among sports players, and α refers to the type and severity of injuries. $\Delta_{\Delta}\Delta_{\Delta}$ refers to the injury probability of each part; $\Delta_{\Delta\ell}$ refers to the probability of injury caused by strains and sprains; and χ refers to the training volume of athletes.

Then, the sports injuries and their causes are classified and counted. The formula is as follows:

$$\mathscr{U}_{\Delta\Delta}(\Delta + 1) = \frac{\mathscr{V}\mathscr{U}_{\Delta\Delta} + \mathscr{B}_{\Delta}\Delta_{\Delta\Delta}(\Delta) - \mathscr{Y}_{\Delta\Delta}(\Delta)}{\mathscr{Y}_{\Delta\Delta}(\Delta) + \sqsupset \cdot \Delta_{\Delta}} \Delta\Delta_{\mathscr{Y}_{\Delta}}. \tag{9}$$

In formula (9), $\sqsupset$ refers to training phases with different intensities; Δ_{Δ} refers to training time; and $\mathscr{U}_{\Delta\Delta}$ refers to the speed of the athlete. $\mathscr{Y}_{\Delta\Delta}$ refers to the endurance time of athletes; $\mathscr{B}_{\Delta}$ refers to the weight of the cause of injury; and $\Delta_{\Delta\Delta}$ refers to the injury rate caused by the characteristics of different sports. (Δ) refers to the training level of the athlete.

The relationship between the training history process and the probability of sports injury is expressed as follows:

$$\mathscr{G} = \frac{\theta}{\Delta_{\Delta}\Delta \cdot \delta} \mathscr{P} * \mathscr{U}_{\Delta\Delta}(\Delta + 1). \tag{10}$$

In formula (10), θ refers to the historical process of an athlete's injury; Δ_{Δ} refers to the injury samples collected; and $\mathscr{P}$ refers to the basic situation and data information of the athlete.

After analyzing the cause of the injury, the grayscale conversion operation on the image of sports injury can be performed. If the motion-impaired image is colored, its pixels are represented by three bytes, which correspond to the brightness generated by the three components of R, G, and B. The formula for grayscale conversion is as follows:

$$\mathscr{G}\Delta\Delta\Delta(\Delta, \Delta) = \mathscr{S}(\Delta, \Delta) + \mathscr{F}(\Delta, \Delta) + \mathscr{A}(\Delta, \Delta). \tag{11}$$

The converted grayscale image is represented by a 24-bit image, which can effectively improve the recognition efficiency of high-intensity sports injury images. To further improve the recognition effect of sports injury images, it is necessary to extract the basic contour of the injury site. According to the characteristics of the damage image itself, the curve fitting method (substituting the existing data into a mathematical expression through mathematical methods) is used to obtain the final damage contour.

To make the model of the damaged contour reach a state where the active contour converges on the edge of the damaged part, the contour energy is calculated. Its formula is as follows:

$$\mathscr{F}(\mathscr{B}) = [\beta\mathscr{F}_{\Delta\Delta}(\mathscr{B}) + \alpha\mathscr{F}_{\Delta\Delta}(\mathscr{B})]\mathscr{G}\Delta\Delta\Delta(\Delta, \Delta). \tag{12}$$

Here, $\mathscr{F}(\mathscr{B})$ refers to the energy value of the broken contour, and $\mathscr{F}_{\Delta\Delta}(\mathscr{B})$ refers to the internal energy value of the active contour. $\mathscr{F}_{\Delta\Delta}(\mathscr{B})$ refers to the external energy value of the active contour. β and α refer to the weight coefficient.

The image is divided to get the center of the target contour. The formula is as follows:

$$\overline{\Delta} = \frac{1}{\Delta} \sum_{\Delta=1}^{\Delta} \Delta_{\Delta}, \tag{13}$$

$$\overline{\Delta} = \frac{1}{\Delta} \sum_{\Delta=1}^{\Delta} \Delta_{\Delta}. \tag{14}$$

After the basic contour of the damage is extracted, the transformation analysis method is used to initially identify the damage site. The digital matrix is constructed according to the obtained number and information of the pixel points of the damaged position. To improve the recognition accuracy, the length pattern with the feature vector of sixty-four is selected. The mean of the image population vector is as follows:

$$\lambda = \frac{1}{\Delta}\sum_{\Delta=1}^{\Delta}\Delta_{\Delta}\cdot\mathscr{F}(\mathscr{B}). \tag{15}$$

In formula (15), Δ refers to the number of sports injury images.

Next, a matrix $\mathscr{B}$ is set and the eigenvectors of the covariance matrix are calculated. The formula is as follows:

$$\Delta_{\Delta} = \mathscr{B}\frac{1}{\sqrt{\mu_{\Delta}}}\mathscr{Y}\cdot\Delta_{\Delta}\cdot\lambda. \tag{16}$$

Here, Δ_{Δ} refers to the eigenvector values of the matrix and μ_{Δ} refers to the nonzero eigenvalues of the matrix. Δ_{Δ} refers to the vector corresponding to the nonzero eigenvalues.

All training samples and image samples are projected into eigenspace $\mathscr{T}$, and the projection coefficient is calculated. The formula is as follows:

$$\Delta_{\Delta} = \mathscr{T}^{\mathscr{S}}\cdot\Delta_{\Delta}. \tag{17}$$

Next, the Euclidean distance is used to calculate the minimum distance, which is the initial recognition result of the image sample. The calculation formula is as follows:

$$\Delta(\Delta,\Delta) = \left[\sum_{\Delta=1}^{\Delta}\left(\Delta_{\Delta}-\Delta_{\Delta}\right)^{2}\right]^{1/2}. \tag{18}$$

Here, $\Delta(\Delta,\Delta)$ refers to the Euclidean distance (the straight-line distance between two points in Euclidean space) between image samples and training samples, and Δ refers to the number of training samples.

Next, the binocular stereo vision algorithm is used to further identify it, and the area of the damaged part is calculated. Then, the function of the position target of the camera can be expressed as follows:

$$\mathscr{K}_{\Delta} = \sum_{\Delta=1}^{\Delta}\mathscr{U}_{\Delta} - \Delta_{\Delta}^{2}\cdot\Delta(\Delta,\Delta). \tag{19}$$

Here, $\mathscr{U}_{\Delta}$ refers to the pixel cluster center, and Δ refers to the number of pixel cluster centers of the camera. Δ_{Δ} refers to the clustered object, and the minimum value of $\mathscr{K}_{\Delta}$ is the best clustering point, that is, $\Delta\Delta\Delta_{\mathscr{K}_{\Delta}}$.

Combined with the above analysis, the relative area of the damage image can be calculated, namely as follows:

$$\mathscr{A}\Delta\Delta\Delta_{\ell\Delta\Delta\Delta\Delta} = \left(\frac{\mathscr{V}'}{\mathscr{C}'}\right)\cdot\left(\frac{\mathscr{G}'}{C'}\right). \tag{20}$$

Here, $\mathscr{V}^{*}$ refers to the number of long pixels in the lesion image; $\mathscr{G}^{*}$ refers to the number of wide pixels in the lesion image; and $\mathscr{C}^{*}$ refers to the resolution of the image.

After segmenting the image, the absolute area of the damaged image is as follows:

$$\mathscr{A}\Delta\Delta\Delta_{\Delta} = \frac{\mathscr{Q}}{\mathscr{Q}'}\cdot\mathscr{A}\Delta\Delta\Delta_{\Delta\Delta\Delta\Delta\ell}\cdot\Delta\Delta\Delta_{\mathscr{K}_{\Delta}}. \tag{21}$$

Here, $\mathscr{A}\Delta\Delta\Delta_{\Delta}$ refers to the pixel area of the damaged part; $\mathscr{Q}$ refers to the total number of pixels in the damaged part; and $\mathscr{Q}^{*}$ refers to the total number of image pixels.

3. Comparison of Recognition Effects of Different Damage Detection Methods

To identify images of sports injuries, it is first necessary to locate the injury target. Next, some samples of sports injury images are selected, and then, three-dimensional reconstruction is performed on the coordinates in the samples, to perform the localization test of the method proposed in this study. The result obtained is shown in Figure 5.

According to Figure 5, it can be known that the error between the method in this study and the actual value is less than 0.5 mm, and the error rate is less than 2%. This shows that the method in this study can locate the damage target more accurately. Next, to verify the overall performance of high-intensity sports injury image recognition based on binocular stereo vision proposed in this study, one hundred athletes are selected, whose specific conditions are shown in Table 6.

Then, the instrument of the binocular stereo vision system is used to collect the data of the injured part of the subject. It is compared with other injury detection methods, to verify the recognition efficiency and time-consuming of the method in this study. Other damage detection methods include linear discrimination, ultrasound image features, and improved spectral clustering. For the convenience of expression, these methods are abbreviated as linear discriminant (LD), UIF, and ISC, respectively. Figure 6 shows the recognition rate results of different methods of damage detection.

It is obvious from the experimental data in Figure 6 that the recognition rate of the first two methods is an inverted U-shaped curve, and the recognition rate is relatively low as a whole. The recognition rate of the third method fluctuates greatly and is extremely unstable, so it is not very feasible. The recognition rate of the method in this study is significantly higher than other methods, and the lowest is more than 60%, which proves the operability of the method. In fact, the number of images to be recognized also has a certain impact on the recognition rate. Therefore, the selection of the detection method is adjusted, and the improved spectral clustering is replaced by the wavelet coefficient Hu; that is, the LD, UIF, WCHU, and the method in this study are compared. The results are shown in Figure 7.

According to the data in Figure 7, it can be seen that the method proposed in this study consumes the shortest time when the number of recognized images is different, with a minimum of 0.5 seconds. This also shows that the recognition rate of this method is the highest, and it has great advantages over other methods. Next, different times of

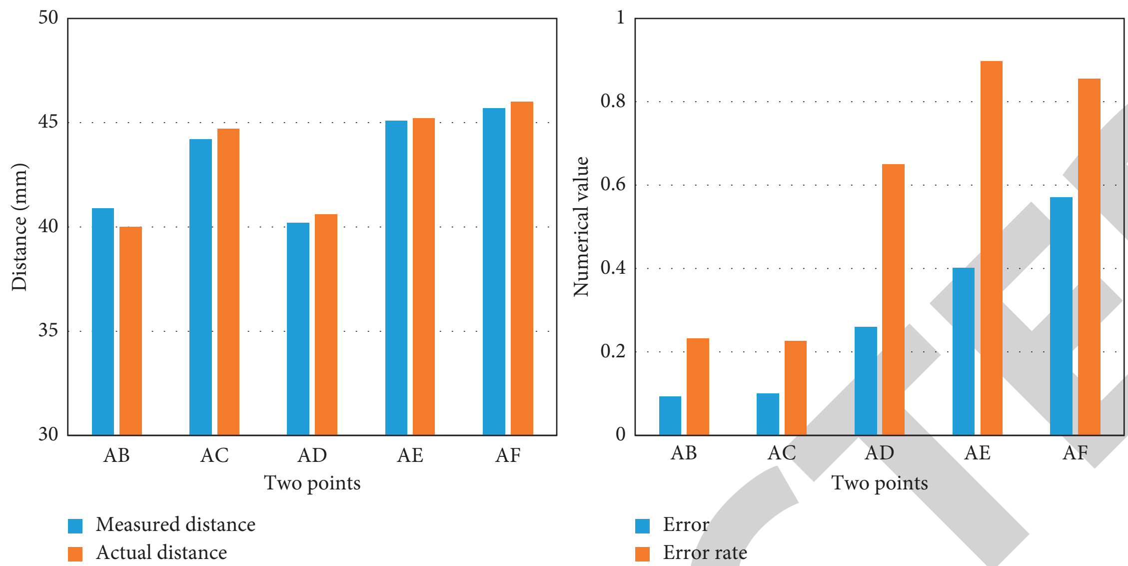

FIGURE 5: Comparison of 3D reconstruction coordinates and actual targets.

TABLE 6: Details of the experimental subjects.

Items	Remarks
Male/person	55
Female/person	45
Height range (cm)	162–183
Weight range (kg)	44–75
Training program	Weightlifting, long-distance running, long jump, high jump, basketball, football, table tennis

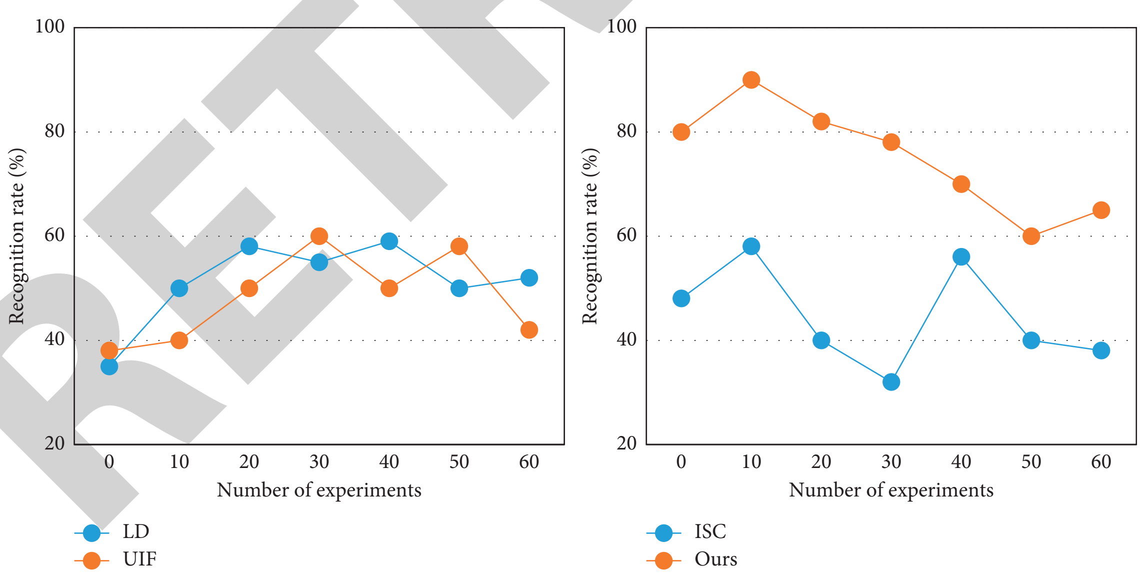

FIGURE 6: Comparison of recognition rates of different damage detection methods.

experiments are carried out, and the recognition error rates of these methods are compared. The comparison results are shown in Figure 8.

According to the data in Figure 8, it can be seen that with the increase in the number of experiments, the error rates of different methods show different development trends. The error rate of the method proposed in this study is much lower than other methods, about 0.06% on average, and about 0.25% for other methods, which shows that the method proposed in this study can reduce the error to a

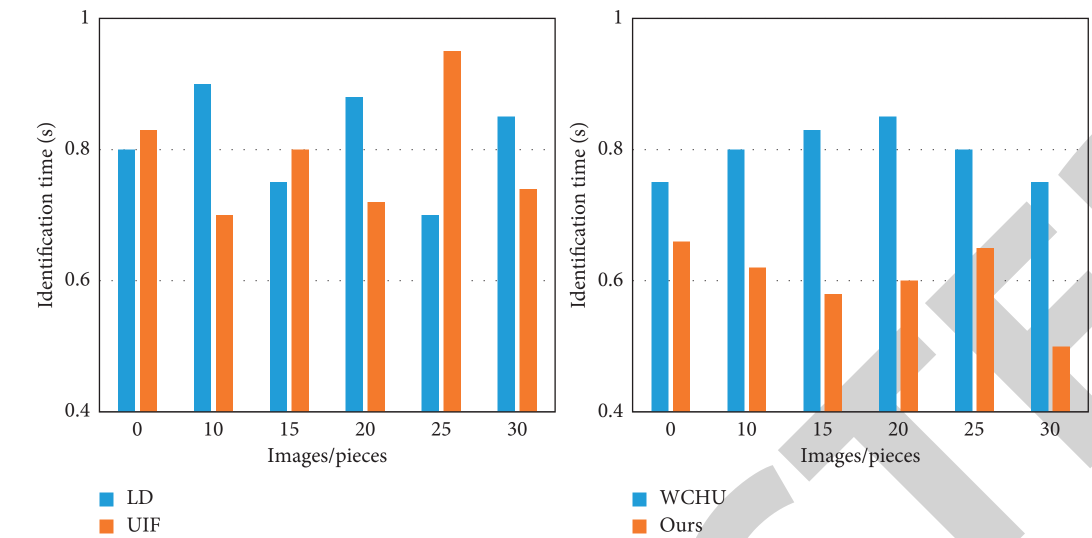

FIGURE 7: Time-consuming comparison of identification of different damage detection methods.

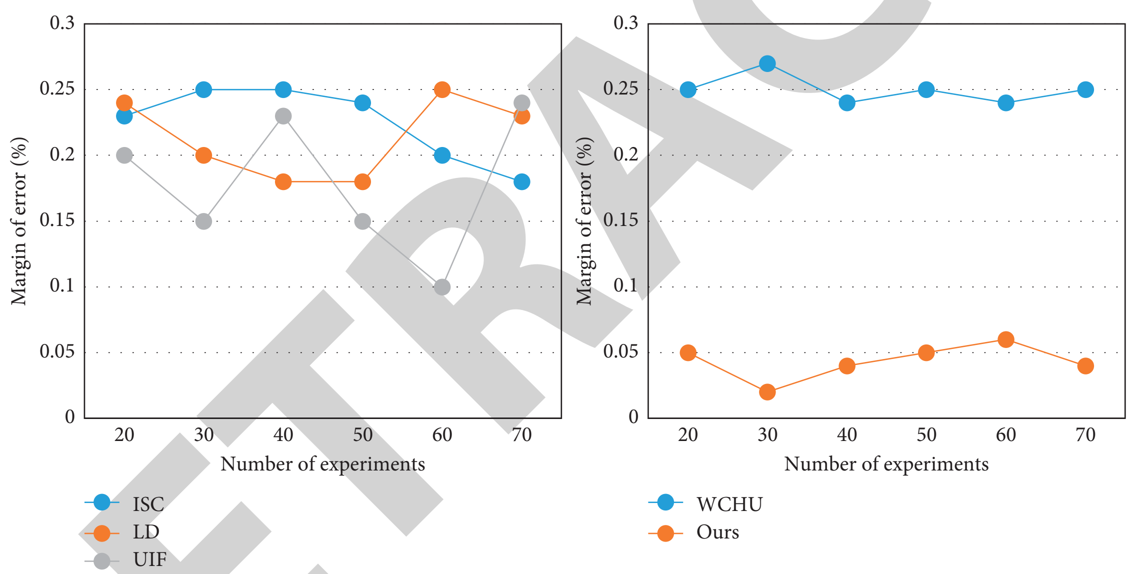

FIGURE 8: Comparison of error rates of different damage detection methods.

relatively low level when recognizing images of sports injuries.

4. Conclusions

High-intensity sports injuries can take a variety of forms. The longer a training period lasts, the more likely an athlete's body part will sustain repeated injuries. As a result, current research is focusing on how to reduce sports-related injuries by identifying injury images. There have always been issues with low recognition precision and frequent occurrences of errors in the process of recognizing damage images. This study proposes a binocular stereo vision-based method for high-intensity sports injury image recognition, and the damaged images are processed, including contour extraction of damaged parts and pixel calculation. The experimental analysis demonstrates the method's reliability and applicability, which is embodied in high recognition accuracy, short recognition time, and high recognition performance. However, there are some drawbacks to the method proposed in this study. The recognition accuracy and speed of the method in this study need to be improved for images of damaged parts with less obvious edge features. In the future, more research into this area will be conducted.

Data Availability

The data used to support the findings of this study are available from the author upon request.

Conflicts of Interest

The author declares no conflicts of interest.

Hindawi
Computational Intelligence and Neuroscience
Volume 2022, Article ID 6901184, 9 pages
https://doi.org/10.1155/2022/6901184

Research Article

Application of Intelligent Taste Analysis Based on Random Forest Algorithm in Food Quality Inspection

Xinghua Zhang,[1] Yongjie Sun,[2] and Yongxin Sun[3]

[1]*Changchun Sci-Tech University, Changchun 130600, JiLin, China*
[2]*College of Life Science, Changchun Sci-Tech University, Changchun 130600, JiLin, China*
[3]*College of Physics and Electronic Information, Baicheng Normal University, Baicheng 137000, Jilin, China*

Correspondence should be addressed to Yongxin Sun; sunyongxin@bcnu.edu.cn

Received 11 May 2022; Revised 14 June 2022; Accepted 8 July 2022; Published 30 July 2022

Academic Editor: Xin Ning

Food safety is a major concern that has an impact on the national economy and people's lives. The food industry has grown in quality and innovation in tandem with the rapid development of the economy and society. The emergence of new food technologies, as well as changes in dietary habits, has increased public concern about food safety. With the emergence of various counterfeit and substandard products, food quality and safety testing have become even more important. Traditional testing methods rely on sensory analysis and physical and chemical analysis. This approach is subjective and poorly adapted to the general public. It requires a high level of technical operation and is difficult to carry out on a large scale. To address this situation, this paper proposes an intelligent approach to food safety quality testing. The core idea is, first, to use sensors to collect data on the various components of the sample to be tested. Second, the random forest (RF) model used in this paper is trained. Third, the trained model is used to classify and identify the test samples. Based on the classification results, a conclusion is drawn as to whether the food product is a variant or a counterfeit. The advantage of this study is that the training model used is a weighted RF algorithm based on mutual information. The correlation between any two decision trees is calculated using mutual information, and for the more correlated decision trees, only the one with the highest evaluation accuracy is retained to form a new RF, and the evaluation accuracy is converted into voting weights, resulting in an RF model with less redundancy and higher evaluation accuracy. The experimental results show that the method used in this paper can successfully identify spoiled or counterfeit products and has good practicality.

1. Introduction

Food safety usually means that the items people consume are nontoxic; that is, they do not cause any harm to the body after consumption, and they provide the body with the nutrients it needs [1, 2]. Food safety is not just something that the producer needs to be aware of since there are multiple components involved in the process of food from production to consumption. Food safety is a matter that is jointly guaranteed in many fields. Eating is one of the most important things for human beings. Therefore, food safety and security are of the utmost importance. With the development of technology, many unscrupulous businessmen use high technology to make some poor-quality food products for sale to earn high profits. The packaging of these foods often looks attractive, and the food looks fresh and tasty. In order to achieve the purpose of attracting customers, unscrupulous businessmen will use some ingredients that are toxic and harmful to the human body. And consumers often focus only on the packaging or indication of the food and lack of food safety awareness. Consumers should therefore increase their awareness and knowledge of food safety, develop a healthy and scientific view of consumption, and actively participate in the regulation of food safety to ensure food safety and health. The protection of food safety is the legal responsibility of all food producers and operators, governments at all levels, and relevant regulatory agencies. Regulation should be continuously strengthened to promote a steady improvement in the internal management capacity of producers and operators by enhancing constraints from society. At the same time, the whole community must take an interest in and maintain food safety and support the work of the government. At present, many consumers have little awareness of the importance of safety management in food businesses, knowledge of consumer culture is still lacking, and the basis for social development of food safety is still not strong. When we are in food safety and find illegal problems, we should take positive action and take the initiative to report them to the regulatory authorities, rather than just complaining and grumbling, not to mention creating false information out of thin air, which will only interfere with normal regulatory work and bring about consumer panic, with the ultimate victim being the consumer.

Food quality and safety are very important, and the government is also the introduction of relevant policies to protect the quality of food. The current policy is mainly from the following aspects. The first is to strengthen the quality control of food sources and strict food into the market trading system. Food safety must start at the source, from planting, breeding, production and processing, wholesale and retail, and consumer four links to carry out a full range of supervision. The use of computers and other modern technical means is to establish a series of systems such as commodity labeling and quality tracing. The second is to establish an industry self-regulatory mechanism to ensure food safety. The credit self-regulation of food production and operation enterprises is particularly important to ensure food safety. Therefore, it is necessary to accelerate the construction of a food safety credit system and establish industry credit standards for food distribution enterprises. We should strengthen the legal system construction and integrity education for operators and urge enterprises to improve their awareness of integrity, quality, and legal operation. The third is the establishment of food safety standards and inspection and testing systems. Product and health standards are established comprehensively related to food safety, and a food safety standards system is built. At the same time, the food safety testing system is improved to ensure that the hygienic quality of food listed for sale meets the requirements of health standards. Fourth, a traceability system that can be traced back to the source is established. Food safety is a complex process that must consider all stages of the food chain, from farm to fork.

The government has given a series of safeguards from the production of food to its final consumption in people's mouths. The most important part of the whole safeguarding process is the occasional inspection of food quality. Traditionally, food quality checks have relied on manual inspection by quality inspectors, which is both energy and time consuming and inefficient. As a result, in recent years, smarter methods of food quality inspection have emerged one after another. The core idea is to identify the quality of food by recognizing the taste of the food. Reference [3] proposed an improved K-means algorithm for detecting spoiled food. The core idea of the study is to segment the pictures of food products in order to determine the degree of spoilage. Reference [4] uses deep learning algorithms based on computer vision techniques to detect and analyze the quality of complex food products. Reference [5] devised a relationship between food quality and preservation conditions based on Fourier's law of conduction. Reference [6] proposed a quality inspection technique for frozen foods. The core technique used in this study was Raman spectroscopy. Reference [7] introduced blockchain technology for the storage and preservation of food products, thus guaranteeing food quality and safety. Reference [8] summarizes a variety of deep learning techniques applied to the inspection of food quality such as fruits, vegetables, and meat. Reference [9] uses image processing techniques applied to the detection of egg quality. The study combines hyperspectral imaging, multivariate analysis, and image processing to identify the freshness of eggs as well as the breakage of eggs. Experimental results showed that this aspect was able to achieve a detection rate of over 97%. For quality detection of palletized packaged food, reference [10] used a deep neural network based on a principal component analysis network. Experiments were conducted using support vector machines (SVM) [11] as well as K-nearest neighbours (KNN) [12] for experimental comparison, which showed that the study has advantages not only in terms of detection accuracy but also speed. From the above studies, it can be seen that for food quality inspection, more and more scholars are introducing intelligent algorithms such as machine learning algorithms [13–15] and deep learning [16–18] algorithms. The use of intelligent technologies has indeed improved the efficiency and accuracy of food quality inspection and saved human and material resources. In this paper, RF algorithm is introduced for food quality inspection based on taste analysis. Experiments on vinegar demonstrate the effectiveness of the method in this paper.

2. Relevant Knowledge

2.1. Taste Analysis Methods. It is well known that the taste signals received by the human brain are produced by taste receptor cells in the mouth (mainly the tongue). These taste receptor cells interact with specific chemicals in food. Different types of taste cells are sensitive to specific flavour substances. This property enables humans as well as animals to recognize different tastes. Early artificial taste systems used generic sensors or methods to recognize the physicochemical properties of food. For example, for salty tastes, they can be measured using conductive agents, and for sour tastes, their pH can be measured directly to characterize the acidity. The most primitive calibrations were obtained using a comparison of the human evaluation of salty and sour flavours and the quantitative values detected by the sensors. AsHumans have vague descriptions of taste, e.g. "a little sour", "very sour." The machine, on the other hand, obtains precise measured values. This method therefore only yields results that are not uniform. Later research, towards multisensor multicomponent analytical chemistry methods, which rely on specific chemical sensors, is difficult to implement and difficult to generalize.

On the other hand, there is ongoing research into the underlying perceptual mechanisms of the taste nerve. It has been found that taste cells are not actually sensitive to only one chemical substance but respond to a variety of substances. At the same time, when different taste nerve cells perceive a stimulus at the same time, they transmit their respective signals to the center, which ultimately decides what type of taste stimulus to receive. A diagram of this process is shown in Figure 1. This mechanistic understanding is the cornerstone of modern taste sensing and analysis, resulting in the approach of cross-response sensor arrays. That is, a small number of types of sensors, through a mechanism similar to that of a neural network, are ultimately able to identify a larger number of types of taste stimuli. The number of stimulus types is an order of magnitude greater than the number of sensor types. Importantly, this approach draws on bionic ideas and breaks through the constraints of strongly selective taste sensors.

The traction in this mechanistic understanding has led to a move away from reliance on specific taste sensors for taste sensing. Tests have been carried out using less selective sets of sensors, which are analyzed by chemical analysis methods as well as by pattern recognition methods. This approach allowed pattern recognition to be used naturally in taste recognition scenarios. This was followed by the development of artificial taste sensing. And nowadays, the conceptual definition of taste sensors and electronic tongues and the mathematical processing methods used have gradually become clearer. With the development of materials, computers, and physical-chemical testing techniques, more sensors are available, and the accuracy and range of tests have advanced dramatically. A schematic representation of modern methods of artificial taste analysis is shown in Figure 2.

2.2. Application of Taste Analysis Methods. With the rapid development of electronic tongues and taste sensors, the recognition of types of taste is no longer limited to the recognition of simple basic characteristics such as sweet, sour, bitter, spicy, and salty. Application scenarios now include flavour and quality recognition, such as flavour recognition of alcohol and beverages, determination of the quality of liquid and solid foods, and can even be used to distinguish minor differences between different manufacturers' brands of the same type of food. More work has been carried out on the artificial taste analysis of liquid beverages than on the taste analysis of solid foods. A large body of literature deals with, for example, fruit juices, alcoholic beverages, and liquid flavourings. Reference [19] used multiple sensors to capture the composition of red wine in order to correctly differentiate the taste of red wine. Pattern recognition techniques were also used to perform operations such as preprocessing and classification of the collected data from the red wines. The experimental results show that the method used in this literature can successfully identify red wines as well as nonred wines. Reference [20] used a highly cross-selective sensor to capture the composition of red wines and combine it with principal component analysis and clustering algorithms to model and identify changes in the taste of red wines during storage. Reference [21] used an electronic tongue to capture the concentration of bisulphite in wine and trained a prediction model using the PLS method. The results showed that the method was effective in predicting the bisulphite concentration. PLS combined with linear discriminant analysis (LDA) was used in reference [22] to determine the taste of yellow wine (a Chinese rice wine). The data were used to analyze the taste characteristics of yellow wine from various regions.

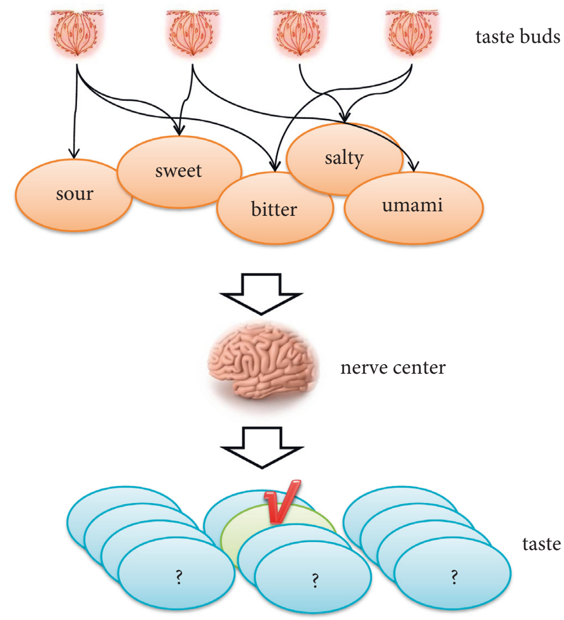

Figure 1: Nerve center determines taste stimuli.

3. Improved RF-Based Food Quality Detection Algorithm

3.1. Traditional RF. In the 1980s, Breiman et al. developed the classification tree algorithm, which was much less computationally intensive than repeatedly dichotomizing data for classification or regression. Breiman combined the classification trees into an RF in 2001 by randomly generating many classification trees and then aggregating the classification tree results. RF improves prediction accuracy without requiring significantly more computing power. RF is considered one of the best current algorithms because they are insensitive to multicollinearity. RF can deal with noisy and unbalanced data very well, which is one of the important reasons why the algorithm can be widely used.

RF selects n samples from the N training samples, which are typically much smaller than N, and repeats the process C times to generate C decision trees. When splitting each node of the decision tree, d attributes are chosen at random from all D attributes, and the best attribute from the d attributes is chosen as the splitting attribute. The CART algorithm is commonly used to select the splitting attributes. The Gini index can determine the splitting attributes in this algorithm. The Gini value of V is calculated by (1). Assuming that the proportion of the i-th category in the current sample set V is s_i, where $S_i = 1$ and k denotes the total number of categories.

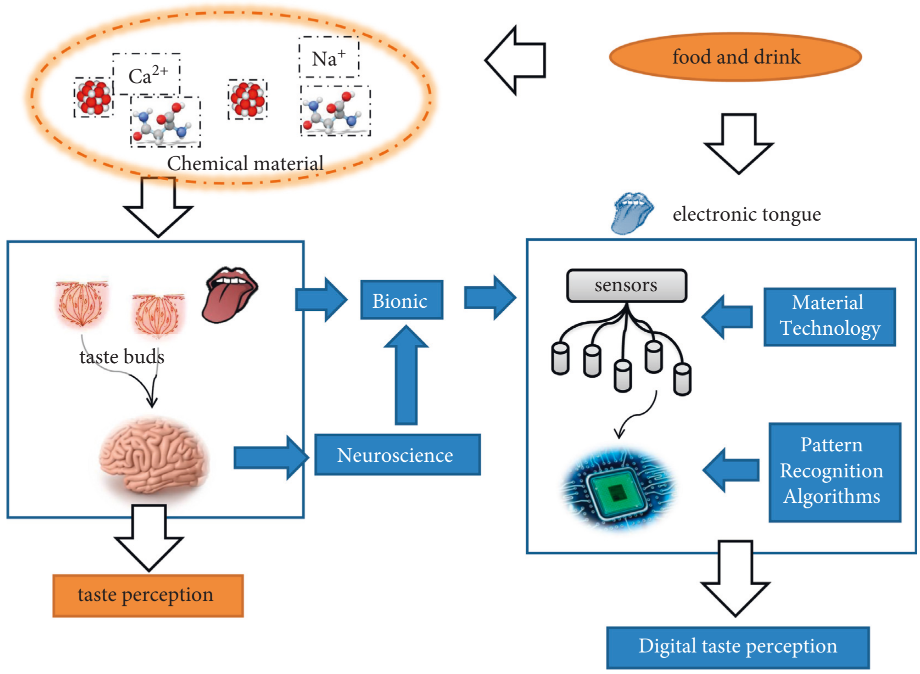

Figure 2: Artificial taste analysis.

$$\mathrm{Gini}(V) = 1 - \sum_{i=1}^{|k|} s_i^2. \quad (1)$$

The Gini value is taken to be between 0 and 1. The test attribute β is used to dichotomize the random variable V into two categories V_1 and V_2, and then, the Gini index for attribute a is calculated as follows:

$$\mathrm{Gini}(V,\beta) = \frac{|V_1|}{|V|}\mathrm{Gini}(V_1) + \frac{|V_2|}{|V|}\mathrm{Gini}(V_2). \quad (2)$$

Assuming that the set of candidate attributes is $(B = \beta_1, \beta_2, \ldots, \beta_d)$, then the attribute that minimizes the Gini index after division is selected as the optimal divided attribute.

$$\beta^* = \arg\min(\mathrm{Gini\_index}(V,\beta)). \quad (3)$$

3.2. Improving RF. Traditional RF generates decision trees with high similarity, rendering the trained model obsolete. Furthermore, in the voting process, all decision trees are given the same weight by default, ignoring any differences in performance between different decision trees. To address these issues, this paper proposes IRF that incorporates mutual information and a weighting strategy to optimize the RF. The correlation between any two decision trees is calculated using mutual information, and only the one with the highest evaluation accuracy is retained for the more correlated decision trees, forming a new RF and converting the evaluation accuracy into voting weights to obtain a RF model with less redundancy and higher evaluation accuracy.

Mutual information is used to measure the interdependence between two variables. For two sets of given random variables X_1 and X_2, their mutual information is expressed as

$$\begin{aligned} MI(X_1, X_2) &= L(X_1) \sum_{x_1 \in X_1} \sum_{x_2 \in X_2} p(x_1, x_2) \log \frac{p(x_1, x_2)}{p(x_1)p(x_2)}, \\ &= L(X_1) + L(X_{21}) - L(X_1, X_2), \end{aligned} \quad (4)$$

where $p(x_1, x_2)$ is the joint probability distribution of X_1, X_2, $p(x_1)$ and $p(x_2)$ are the marginal probability distributions of X_1, X_2, respectively, and $L(X_1)$ is the information entropy of X_1, which is calculated as

$$L(X_1) = -\sum_{x_1 \in X_1} p(x_1) \log p(x_1), \quad (5)$$

where $p(x_1)$ denotes the probability of event x occurring; $L(X_2)$ is the information entropy of X_2, and $L(X_1, X_2)$ is the joint entropy, which is calculated as

$$L(X_1, X_2) = -\sum_{x_1 \in X_1} \sum_{x_2 \in X_2} p(x_1, x_2) \log p(x_1, x_2). \quad (6)$$

For a decision tree l_i $(i = 1, 2, \ldots, C)$ in a RF, $MI(l_i, l_c)$ $(c \neq i)$ represents the mutual information of the decision tree l_i and l_c. In this paper, $MI(l_i, l_c)$ $(c \neq i)$ is used to calculate the correlation between decision trees l_i and l_c. The formula is

$$MI(l_i, l_c) = MI(z_i, z_c), \quad (7)$$

where z_i $(i = 1,2, \ldots, C)$ is the i-th decision tree's output state. The greater the value of $MI(l_i, l_c)$, the greater the correlation between the two decision trees, and the greater the degree of information overlap. A group of decision trees with mutual information values greater than a threshold ε will be combined by calculating the mutual information of any two decision trees. $MI(l_i, z)$ represents the mutual information between the decision tree l_i and the actual label z, that is, the correlation between the decision tree l_i's output evaluation result and the actual evaluation result. The equation is

$$MI(l_i, z) = MI(z_i, z). \tag{8}$$

The larger the value of $MI(l_i, z)$, the higher the evaluation accuracy of the decision tree l_i. Finally, the decision trees with less correlation and higher accuracy are formed into an IRF. The steps of IRF implementation are as follows:

(1) Step 1: get the training set $X = \{(x_1, y_1), (x_1, y_1), \ldots, (x_N, y_N)\}$, validation set $X' = \{(x_1, y_1), (x_1, y_1), \ldots, (x_L, y_L)\}$, x_i is the sample, and y_i is label.

(2) Step 2: draw n samples from X by bootstrap sampling and repeat T times to obtain T training sets.

(3) Step 3: for each internal node of the decision tree, d attributes are randomly selected from the sample D attributes, and the best splitting attribute among the d attributes is chosen as the test attribute of the node.

(4) Step 4: generate T completely random decision trees to form a RF $R = \{l_1, l_2, \ldots, l_t\}$.

(5) Step 5: input the validation set X′ into R to get the result.

(6) Step 6: based on the results, the correlation between each decision tree and the rest of the decision trees is calculated in turn. All the decision trees with $MI(l_i, l_c)\,(i \neq c)$ greater than the threshold ε are combined into one decision tree group. If the correlation between h, and all other decision trees is less than or equal to the threshold ε, then the decision trees are grouped separately.

(7) Step 7: repeat step 6 for the out-group decision trees in order until all decision trees are grouped.

(8) Step 8: obtain the decision tree with the highest accuracy in each group based on the accuracy $MI(l_i, z)$.

(9) Step 9: form a new RF from the obtained decision trees $R' = \{l_1', l_2', \ldots, l_t'\}$.

When evaluating the input sample data, the traditional RF has the same voting weight for each decision tree, which ignores the influence of the evaluation accuracy of different decision trees on the final result and reduces the evaluation accuracy of the RF as a whole. In order to increase the number of decision trees with high evaluation accuracy and reduce the influence of decision trees with low evaluation accuracy on the final evaluation results, this paper proposes a weighted voting method to convert the evaluation accuracy into the voting weights of decision trees. After the traditional RF is streamlined, the evaluation accuracy matrix A of decision trees in the IRF is

$$A = \begin{bmatrix} a_{11} & a_{11} & \cdots & a_{11} \\ a_{21} & a_{22} & \ddots & a_{2c} \\ \vdots & \vdots & \ddots & \vdots \\ a_{G1} & a_{G2} & \cdots & a_{GC} \end{bmatrix}, \tag{9}$$

where a_{gc} denotes the evaluation accuracy of the c-th decision tree for the g-th running state, where $c = 1,2, \ldots, C$, $g = 1,2, \ldots, G$, G is the number of classes of evaluation results, and C is the number of improved decision trees which obtained by substituting the validation set X' into IRF and calculating the correctness of the output of each decision tree for each class.

Based on the evaluation accuracy matrix, the weight matrix Q is defined as

$$Q = \begin{bmatrix} q_{11} & q_{11} & \cdots & q_{11} \\ q_{21} & q_{22} & \ddots & q_{2c} \\ \vdots & \vdots & \ddots & \vdots \\ q_{G1} & q_{G2} & \cdots & q_{GC} \end{bmatrix}, \tag{10}$$

where Q_{gc} is the weight of the p th tree for the g-th running state, which is calculated as

$$q_{gc} = a_{gc}. \tag{11}$$

The specific flow of the IRF is shown in Figure 3.

4. Experimental Analysis

4.1. Experimental Background. In recent years, there has been an increase in the number of counterfeit and shoddy products. These products often have identical outer packaging, but the quality of the product varies. This paper uses a taste-based food quality detection method. To verify the effectiveness of the method, data from different brands of vinegar are collected and analyzed, and the brands of the respective products are identified. If the results obtained by the RF algorithm for a product captured do not belong to an existing product class, this indicates that there is a problem with the quality of the product. Based on this idea, a Chinese food product vinegar was experimentally analyzed in the experimental part. The evaluation metrics used during the experiments to quantify the effectiveness of the classification models used in this paper are shown in Table 1.

Since the sample size collected during the experiment was not very large, a 5-fold cross-validation method was used to ensure the validity of the experiment, and 60% of the sample overview was selected as the training sample and 40% of the sample as the test sample. The comparison algorithms used were all classical classification algorithms, mainly SVM [23], RF (RF) [24], radial basis function neural network (RBFNN) [25], and Naive Bayes (NB) [26].

4.2. Vinegar Quality Inspection Experiment. The taste of different types of table vinegar is different because the raw materials and processes used to make them are different. Edible vinegar is an acidic condiment that is often used when people cook ingredients. Protein, fat, carbohydrates, ash, water, energy, riboflavin, sodium, potassium, calcium, magnesium, iron, manganese, zinc, copper, phosphorus, and selenium are the main components of table vinegar. Leucine, isoleucine, lysine, methionine, cystine, phenylalanine, tyrosine, threonine, tryptophan, arginine, histidine, alanine, valine, glycine, proline, glutamic acid, serine, and aspartic

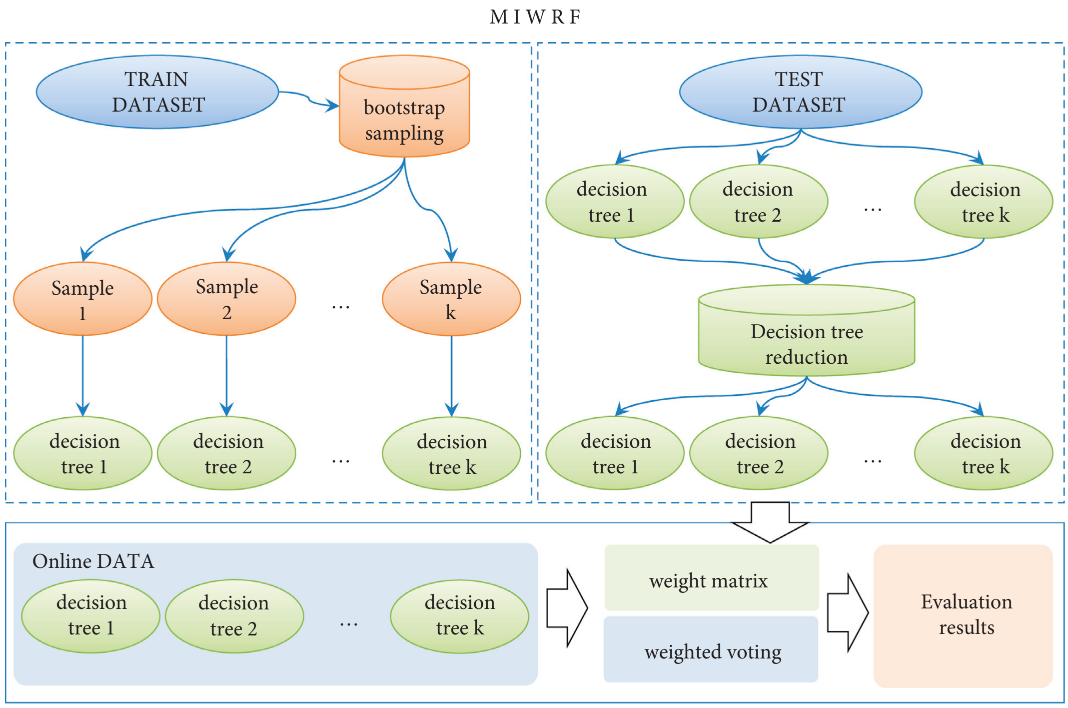

Figure 3: IRF flow chart.

Table 1: Introduction to evaluation indicators.

Name	Expressions
Accuracy	Accuracy = (Number of correctly classified samples/total number of samples)
Precision	Precision = (true sample number/true sample number + false positives number)
Recall	Recall = (true sample number/true sample number + false negatives number)
$F1$ score	$F1 = 2^{*}\text{Precision} * \text{Recall}/\text{Precision} + \text{Recall}$

Table 2: Quantitative indicators for table vinegar.

Index\Type	Vinegar 1	Vinegar 2	Vinegar 3	Vinegar 4	Vinegar 5
$I1$ (%)	3.86 ± 0.57	7.55 ± 0.73	14.51 ± 0.28	14.64 ± 0.63	7.17 ± 0.81
$I2$ (%)	4.82 ± 0.62	6.46 ± 1.03	5.45 ± 0.53	5.35 ± 0.55	4.65 ± 1.02
$I3$ (%)	0.94 ± 0.38	1.28 ± 0.84	1.82 ± 0.44	1.79 ± 0.84	1.42 ± 0.87
$I4$ (%)	0.80 ± 0.92	1.17 ± 091	2.66 ± 0.38	2.74 ± 0.97	1.54 ± 0.53
$I5$	2.53 ± 0.86	2.49 ± 0.40	3.32 ± 0.64	3.54 ± 0.63	3.38 ± 0.62

acid are all found in it. In this paper, a total of five types of edible vinegar were selected: white vinegar, rice vinegar, aged vinegar, balsamic vinegar, and sugar vinegar. The quantitative indexes of each edible vinegar are shown in Table 2. $I1$, $I2$, $I3$, $I4$, and $I5$ represent total soluble sugar, total acid, salt, sugar-acid ratio, and pH, respectively. The sugar-acid ratio was determined by averaging total sugar and total acid.

Principal component analysis was conducted on the five component indicators of the above five types of vinegar, and the principal component score plots are shown in Figures 4 and 5. The variance contribution of the first principal component was 56.28 percent, the variance contribution of the second principal component was 25.93 percent, and the cumulative variance contribution of the first and second principal components was 83.54 percent, explaining the majority of the variance. Therefore, the first 2 principal components can only represent 82.21% of the information contained in the original 5 physical and chemical indicators. In addition, the five types of samples could not be well separated on the first principal component score axis, only white vinegar and sugar vinegar could be distinguished from the other types of vinegar, and there was great dispersion between the different brands of rice vinegar, while aged vinegar and balsamic vinegar were seriously confused with each other, which indicated that aged vinegar and balsamic vinegar had some similarity, while white vinegar and sugar vinegar were very different from the other types and showed specificity, and the samples of rice vinegar were more different from each other. It is difficult to group them together because of the relatively large differences between the samples of rice vinegar. This indicates that the first principal

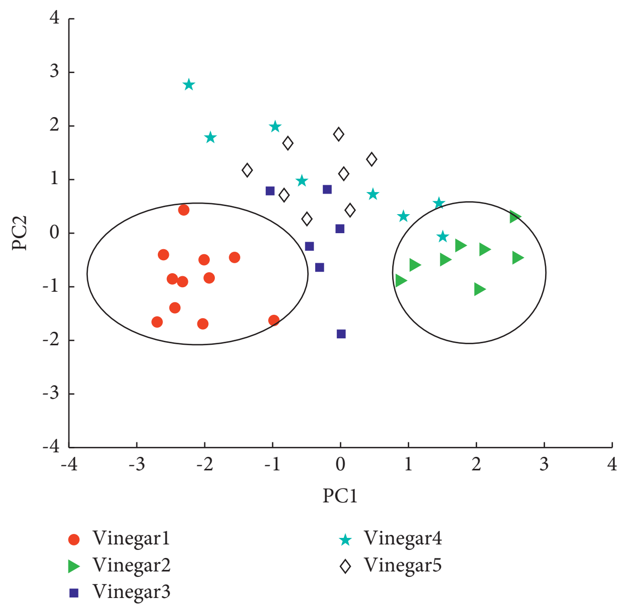

FIGURE 4: Schematic diagram of principal component analysis of component indicators.

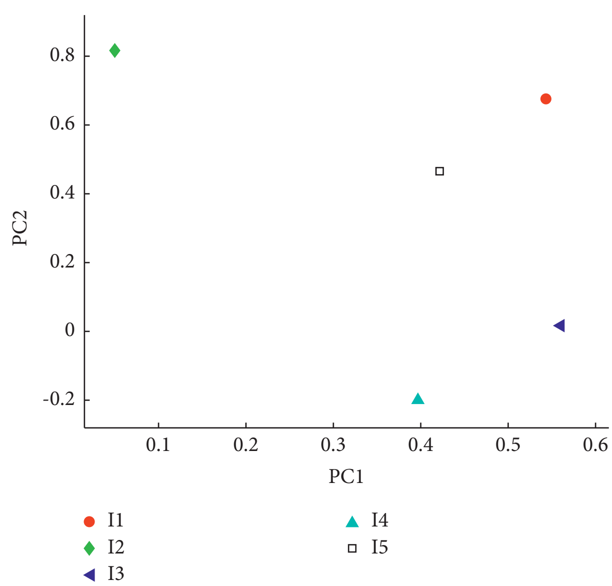

FIGURE 5: Factor loading diagram.

component obtained from the physicochemical indicators can be interpreted as the sugar content (sweetness) and that the first principal component is positively correlated with the sugar content. Furthermore, the distribution from left to right is roughly in the ascending order of the sugar-acid ratio, indicating that the first principal component can also be interpreted as the sugar-acid ratio and that the first principal component is positively related to the sugar-acid ratio. On the second principal component score axis, the five types of samples are also differentiated, and intuitively, the five types are distributed on the second principal component score axis from bottom to top in an ascending order of total acidity, which indicates that the second principal component

TABLE 3: Classification results of different models for vinegar.

Model\Index	Accuracy	Precision	Recall	*F*1
SVM	71.49%	67.35%	78.10%	72.33%
RBFNN	75.87%	67.99%	76.25%	71.88%
NB	78.83%	70.89%	71.92%	71.40%
RF	90.53%	81.93%	74.03%	77.78%
IRF	100%	99.83%	96.47%	98.12%

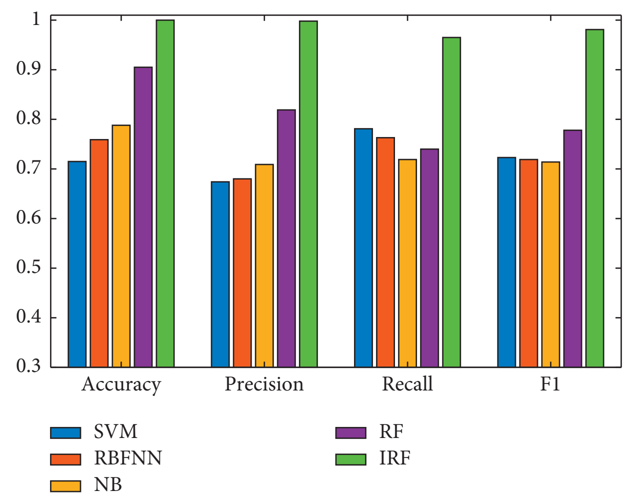

FIGURE 6: Comparison of classification results of different models.

obtained from the physicochemical indicators can be interpreted as acidity (sourness) and that the second principal component is positively correlated with acidity. In general, the results of the principal component analysis obtained from the physicochemical indicators were mainly related to the brix and acidity characteristics of vinegar, which is not unrelated to the fact that vinegar is an acidic condiment. However, these five physicochemical indicators alone are not sufficient to distinguish the different types of vinegar.

Sixty samples were taken from each category of edible vinegar. The total number of samples was 300. Eight indicators were collected for each type of edible vinegar. These 8 indicators were collected by 8 sensors. The size of the samples was $300 * 8$. Since there were 5 types of edible vinegar in total, the number of categories was 5. The results of the experiment are shown in Table 3 and Figure 6.

In terms of recognition accuracy, the IRF method used in this paper improves 0.40, 0.32, 0.27, and 0.10 compared to other SVM, RBFNN, NB, and RF. The improvement ratios fully demonstrate the superiority of this method. In terms of accuracy, the IRF method improves 0.48, 0.47, 0.41, and 0.22 over SVM, RBFNN, NB, and RF, respectively. The high *F*1 scores indicate that the model used in this paper has a good recognition rate for both positive and negative samples. The value range of the four indicators used in this paper is between 0 and 1. The larger the value, the better the performance of the model. The experimental results show that the IRF algorithm has the largest value on the four indicators and is far ahead of other comparison models. The experimental results verify the effectiveness of the IRF algorithm in the detection of edible vinegar quality.

5. Conclusion

There have been numerous issues with food quality and safety in recent years. Although the government has introduced relevant policies, it has not been able to eliminate all kinds of counterfeit and shoddy products. On the other hand, many food products are prone to deterioration during storage. If people do not detect these food products in time, they can be harmful to their health. This paper proposes the use of an improved RF algorithm to improve the speed and accuracy of food quality detection. The algorithm uses mutual information to calculate the correlation of any two decision trees, and for the more correlated decision trees, only the decision tree with the highest evaluation accuracy is retained, thus forming a new RF, converting the evaluation accuracy into voting weights, and finally obtaining an RF model with less redundancy and higher evaluation accuracy. The experimental results show that the method used in this paper can successfully identify spoiled or counterfeit products. However, although the algorithm in this paper is more intelligent than traditional food detection methods, there are some problems. One is that the model used does not achieve the desired results for high-dimensional data. Second, it is unknown how well the food testing method proposed in this paper can detect the quality of other food products, as the core ingredients of different food products are different. The determination of the core components has a great impact on the final identification effect. For the above two problems, this paper will be followed by an in-depth study.

Data Availability

The labeled data set used to support the findings of this study is available from the corresponding author upon request.

Disclosure

Xinghua Zhang and Yongjie Sun are the same work, and they share the same article.

Conflicts of Interest

The authors declare that they have no conflicts of interest.

Acknowledgments

This work was supported by the Changchun Sci-Tech University and Baicheng Normal University.

References

[1] N. Casado, S. Morante-Zarcero, and I. Sierra, "The concerning food safety issue of pyrrolizidine alkaloids: an overview," *Trends in Food Science & Technology*, vol. 120, pp. 123–139, 2022.

[2] M. O. Caglayan, S. Sahin, and Z Ustundag, "Detection strategies of zearalenone for food safety: a review," *Critical Reviews in Analytical Chemistry*, vol. 52, no. 2, pp. 294–313, 2022.

[3] L. Goel, S. Raman, S. S. Dora et al., "Hybrid computational intelligence algorithms and their applications to detect food quality," *Artificial Intelligence Review*, vol. 53, no. 2, pp. 1415–1440, 2020.

[4] Y. Liu, H. Pu, and D. W. Sun, "Efficient extraction of deep image features using convolutional neural network (CNN) for applications in detecting and analysing complex food matrices," *Trends in Food Science & Technology*, vol. 113, pp. 193–204, 2021.

[5] P. S. Mkwae, S. A. Ogundipe, M. Jozela, N. Revaprasadu, and S. S. Nkosi, "The heat rate kinetics on the liquefied hydrocarbon gases sensing and food quality control detecting strategy," *Materials Chemistry and Physics*, vol. 277, Article ID 125550, 2022.

[6] W. Zhang, J. Ma, and D. W. Sun, "Raman spectroscopic techniques for detecting structure and quality of frozen foods: principles and applications," *Critical Reviews in Food Science and Nutrition*, vol. 61, no. 16, pp. 2623–2639, 2021.

[7] M. Creydt and M. Fischer, "Blockchain and more - algorithm driven food traceability," *Food Control*, vol. 105, pp. 45–51, 2019.

[8] L. Zhou, C. Zhang, F. Liu, Z. Qiu, and Y. He, "Application of deep learning in food: a review," *Comprehensive Reviews in Food Science and Food Safety*, vol. 18, no. 6, pp. 1793–1811, 2019.

[9] K. Yao, J. Sun, C. Chen et al., "Non-destructive detection of egg qualities based on hyperspectral imaging," *Journal of Food Engineering*, vol. 325, Article ID 111024, 2022.

[10] M. Benouis, L. D. Medus, M. Saban, G. Łabiak, and A. Rosado-Muñoz, "Food tray sealing fault detection using hyperspectral imaging and PCANet," *IFAC-PapersOnLine*, vol. 53, no. 2, pp. 7845–7850, 2020.

[11] O. Bader, D. Haddad, A. Y. Kallel, T. Hassine, N. E. B. Amara, and O. Kanoun, "Identification of communication cables based on scattering parameters and a support vector machine algorithm," *IEEE Sensors Letters*, vol. 5, no. 7, pp. 1–4, 2021.

[12] B. Sowmia and G. Suseendran, "Anomaly detection in business process event using KNN algorithm," *Lecture Notes in Networks and Systems*, vol. 248, pp. 189–199, 2021.

[13] S. Shrivastava, R. Singh, C. Jain, and S. Kaushal, "A research on fake news detection using machine learning algorithm," *Smart Innovation, Systems and Technologies*, vol. 235, pp. 273–287, 2022.

[14] G. Manjula, G. Govinda Rajulu, R. Anand, and J. T. Thirukrishna, "Implementation of smart parking application using IoT and machine learning algorithms," *Lecture Notes on Data Engineering and Communications Technologies*, vol. 75, pp. 247–257, 2022.

[15] R. G. Siqueira, G. V. Veloso, E. I. Fernandes-Filho, M. . R. Francelino, C. E. G. R. Schaefer, and G. R. Corrêa, "Evaluation of machine learning algorithms to classify and map landforms in Antarctica," *Earth Surface Processes and Landforms*, vol. 47, no. 2, pp. 367–382, 2022.

[16] T. H. H. Aldhyani and H. Alkahtani, "Attacks to automatous vehicles: a deep learning algorithm for cybersecurity," *Sensors*, vol. 22, no. 1, p. 360, 2022.

[17] D. Baskakov and D. G. Arseniev, "On the computational complexity of deep learning algorithms," *Smart Innovation, Systems and Technologies*, vol. 220, pp. 343–356, 2021.

[18] M. İnce, "Automatic and intelligent content visualization system based on deep learning and genetic algorithm," *Neural Computing & Applications*, vol. 34, no. 3, pp. 2473–2493, 2022.

[19] A. Legin, A. Rudnitskaya, Y. Vlasov, C. Di Natale, E. Mazzone, and A D'Amico, "Application of electronic tongue for quantitative analysis of mineral water and wine," *Electroanalysis*, vol. 11, pp. 814–820, 1999.

[20] V. Parra, A. A. Arrieta, J. A. Fernandez-Escudero, M. Iniguez, J. A. Saja, and M. L Rodriguez-Mendez, "Monitoring of the ageing of red wines in oak barrels by means of an hybrid electronic tongue," *Analytica Chimica Acta*, vol. 563, no. 1-2, pp. 229–237, 2006.

[21] M. Gutiérrez, A. Llobera, A. Ipatov et al., "Application of an e-tongue to the analysis ofmonovarietal and blends of white wines," *Sensors*, vol. 11, no. 5, pp. 4840–4857, 2011.

[22] H. Yu, J. Zhao, F. Li, H. Tian, and X Ma, "Characterization of Chinese rice wine taste attributes using liquid chromatographic analysis, sensory evaluation, and an electronic tongue," *Journal of Chromatography B*, vol. 997, no. 1, pp. 129–135, 2015.

[23] N. Narkhede, S. Mathur, and A. A. Bhaskar, "Automatic classification of music genre using SVM," *Lecture Notes on Data Engineering and Communications Technologies*, vol. 75, pp. 439–449, 2022.

[24] B. Hamdaoui, A. Elmaghbub, and S. Mejri, "Deep neural network feature designs for RF data-driven wireless device classification," *IEEE Network*, vol. 35, no. 3, pp. 191–197, 2021.

[25] G. M. Rajathi, "Optimized radial basis neural network for classification of breast cancer images," *Current Medical Imaging Formerly Current Medical Imaging Reviews*, vol. 17, no. 1, pp. 97–108, 2021.

[26] E. Hato, "Impact of feature selection for data classification using naive Bayes classifier," *Journal of Physics: Conference Series*, vol. 1879, no. 2, Article ID 022088, 2021.

Hindawi
Computational Intelligence and Neuroscience
Volume 2022, Article ID 5716698, 11 pages
https://doi.org/10.1155/2022/5716698

Research Article

Application of SDN Network Traffic Prediction Based on Speech Recognition in Educational Information Optimization Platform

Susheng Zheng and Shengxue Yang

Jiangxi University of Technology, Nanchang 330098, China

Correspondence should be addressed to Shengxue Yang; ysx@jxut.edu.cn

Received 25 May 2022; Revised 23 June 2022; Accepted 24 June 2022; Published 22 July 2022

Academic Editor: Xin Ning

This paper constructs a SDN network traffic prediction model based on speech recognition and applies it to the educational information optimization platform. By analyzing the influencing factors of SDN network equipment, communication links, and network traffic, this paper constructs the initial index set of SDN network traffic situation. In the data plane of SDN, the queue management algorithm is used to control the flow. On this basis, an IRS mechanism is proposed based on the advantages of SDN centralized control and the difference of transmission performance requirements between large and small streams. For the transmission of large traffic, IRS adopts greedy routing and multipath routing based on the remaining bandwidth to make the traffic evenly distributed in the network, and IRS adds the scheduling strategy based on IP addressing to avoid packet disorder. Simulation results show that the effectiveness of this algorithm can reach 95.67% at the highest, and the MSE convergence is 0.0021 at the lowest. At the same time, this method completes the quantitative evaluation of SDN network traffic situation, effectively solves the problem that SDN traffic situation labels cannot be determined, and opens a new vision of global state observation for SDN network management. This research can provide some technical support for the educational information optimization platform.

1. Introduction

In the knowledge economy era, education directly transforms into the mechanism for resource formation and allocation as well as the capacity to possess and distribute capital. An unstoppable trend of networked development of global information resources has been brought about by the quick development of information technology [1]. The main resource in modern society is information. It will be challenging to maximize economic and social benefits if resource development and use are not brought into the economic operating system. With the assistance of the development of deep NN (neural network) technology [2–4] in the new century, speech recognition technology has achieved ground-breaking successes. Speech recognition's primary function is to translate the data present in a speech signal into the corresponding text data. The ultimate objective is not to translate speech into words. Making machines understand humans is the aim of speech recognition. Future research may focus more on how to integrate semantic understanding with speech recognition. The four main components of the speech recognition framework are the decoder, language model, acoustic model, and feature extraction and processing module of the speech signal. Information technology professionals are currently considering how to better apply speech recognition technology to the field of education and teaching due to the technology's rapid development. The phonetic teaching approach is straightforward and effective in the educational setting. As a result, research into the use of phonetic recognition in the educational setting has gained importance and drawn a lot of attention from scientists. Economic and social benefits are very likely to result from it. With the general advancement of artificial intelligence, speech recognition technology will inevitably become more sophisticated. To advance the deep integration of information technology and education and teaching, speech recognition technology will be extensively applied to all facets of teaching and learning in the future. Studying the use of SDN network traffic prediction based on speech recognition in the educational information optimization platform is therefore important from both a theoretical and practical standpoint.

The importance of traffic control engineering as a mechanism for enhancing network performance has grown as a result of the diversified development of network applications, the expansion of services available over networks, and the constant rise in bandwidth demand. In addition, the unit integration mechanism used by traditional network management is unable to accurately describe the network traffic situation, and network resources have subpar global performance capabilities [5]. The question of how to increase network throughput, decrease network delay, and implement flexible scheduling to solve the traffic optimization problem of the data center network has become urgent due to the increase in traffic volume, the number of application deployments, and the increased requirements for service quality. OpenFlow, an SDN technology that has recently emerged, has created a new opportunity to address this issue [6]. A new network architecture called SDN divides network control and forwarding tasks. It can make network administration easier and increase the network's programmability and flexibility. SDN networks are continuously being developed on the foundation of traditional networks, and they have the potential to significantly increase network resource utilization [7]. SDN is a concept rather than a specific technology that refers to designing network architecture with the separation of forwarding and control. It plans the relationships and interfaces between each level of the network's hierarchy. Uneven traffic distribution in the data center network is one of the factors contributing to network congestion, which can be minimized by using a routing strategy that distributes traffic evenly among several accessible paths [8]. Currently, most multipath routing strategies use static hashing or shunting to divide data streams among different paths, which is easily problematic and can result in issues like large stream conflicts or packet disorder. This paper suggests a speech recognition-based SDN network traffic prediction model based on this and applies it to the platform for optimizing educational information. The innovation of this paper is as follows:

(1) This paper summarizes the application of speech recognition technology in the optimization of educational information resources. By analyzing the influencing factors of SDN network equipment, communication links, and network traffic, the initial index set of SDN network traffic situation is constructed. In the data plane of SDN, this paper uses queue management algorithm to perform flow control. The same set of parameters is used to implement the same management strategy for different data stream packets, and the influence of packet arrival and departure in buffer area on queue length is also considered. Experiments show that the network parameters calculated according to this model can meet all kinds of network requirements.

(2) In this paper, the data acquisition module in the SDN controller is designed, and the SDN network platform is built, which realizes the data acquisition and storage of traffic situation indicators. Aiming at the problems of packet disorder, this paper proposes an IRS mechanism based on the advantages of SDN centralized control and the characteristics of different performance requirements of large and small streams. For large streams, IRS uses greedy routing and multipath routing based on remaining bandwidth to make the traffic evenly distributed in the network, and IRS adds a scheduling strategy based on IP addressing to avoid packet disorder.

This paper will be broken up into five sections in accordance with the needs of the research. Each section contains the following primary work and organizational structure. Introduction is the first section. This section explains the background of the research, the research's subject matter, its originality, and its organizational design. The second section provides an overview of the state of research both domestically and internationally before moving on to discuss the research's main points and ideas. The third section is divided into two sections. The optimization of educational information and network traffic forecast are related topics that are covered in Section 3.1. Using speech recognition, Section 3.2 creates a model for SDN network traffic prediction. The model that was built in this paper is repeatedly simulated in Section 4, and the outcomes are examined. Summary and prospects are covered in the fifth section. It mainly elaborates on the research findings from this paper and anticipates the challenges ahead as well as the work that will come after.

2. Related Work

Shu et al. explored the working method of speech recognition technology and its teaching application, and emphatically introduced several main forms of speech recognition technology in the field of education and teaching. The current problems of speech recognition technology and the feasible way for future development to mature are discussed [9]. Ji et al. combined rough set analysis, DL (deep learning), and other methods to evaluate and predict the SDN network traffic situation [10]. The experimental results show that the model has high prediction accuracy. Chan et al. proposed an optimization algorithm based on color grouping for the data layer [11]. The model classifies different kinds of data streams, marked with different colors. Jha et al. proposed a new SDN network traffic situation assessment method [12]. This method uses the AK-means clustering method to determine the decision-making attributes of the traffic situation factor matrix and constructs a rough set analysis information system for situation information reduction and attributes importance to calculation and finally generates an unsupervised traffic situation assessment model. Konstanteli et al. conducted an in-depth analysis of network traffic control methods and proposed an algorithm-based traffic control model [13]. It points out the deficiencies in the flow control of the network from the control layer and the data layer. Liu et al. designed a multitenant-oriented network resource allocation and management platform based on SDN [14]. The platform provides its own view interface for different tenant networks and implements tenant resource allocation and traffic isolation. Based on the SDN network structure, Fabrizio et al. proposed the main functional modules of the SDN network traffic situation assessment and prediction system, including the data collection module and the situation assessment and prediction system module, and introduced the functions and implementation methods of each module in detail [15]. Chun et al. proposed a new model of SDN traffic control, which is based on the multicommodity flow algorithm and queue management algorithm to control SDN network traffic more finely [16]. Qi et al. proposed a maximum entropy network traffic prediction and controller predeployment model based on hidden Markov optimization [17]. The model classifies SDN traffic according to the type of protocol, uses the captured historical data flow, uses the maximum entropy algorithm to predict the distribution of future data flow, generates the predeployment scheme of various controllers in the control plane, and joins the hidden Markov chain which optimizes the timeliness of the forecast plan. Compared with the SVR model, this model has higher prediction accuracy, and the generated predeployment scheme can adapt to the dynamic changes in the complex SDN environment.

This paper builds an SDN network traffic prediction model based on speech recognition and applies it to the educational information optimization platform using research from related literature. This paper builds the initial index set of SDN network traffic situation by examining the influencing factors of SDN network hardware, communication links, and network traffic. This paper suggests an IRS mechanism based on the benefits of SDN centralized control and the characteristics of various performance requirements of large and small streams in order to address the issues of packet disorder. In order to evenly distribute traffic across the network for large streams, IRS employs greedy routing and multipath routing based on available bandwidth. Additionally, IRS incorporates a scheduling strategy based on IP addressing to prevent packet disorder. In this paper, flow control is implemented in the SDN data plane using a queue management algorithm. Studies reveal that the network parameters computed using this model can satisfy a variety of network needs.

3. Methodology

3.1. Application of Speech Recognition Technology in Optimization of Educational Information Resources. The ultimate goal of the application of modern information technology in education is to improve the educational efficiency. The utilization rate of educational resources has been improved, and the number of people enjoying educational information resources has increased geometrically. Education is essentially the process of information transmission [18]. The extensive, continuous, and in-depth influence of modern information technology on education has created a brand-new educational form-information education. At present, in the field of information research, the optimal allocation and efficient development of educational information resources is one of the frontiers and hotspots, and it is of great practical significance to implement it in the subject practice of educational scientific research. Educational information resources under modern information technology refer to the collection of useful information that is selected, organized, and ordered by human beings and is suitable for learners to effectively develop among themselves. With modern information technology, educational resources all over the world can be connected into an information ocean for the majority of educational users to share [19]. The educational information environment includes four elements: people, educational information resources, educational information technology, and educational information norms. These four elements and their many factors constitute a sustainable and dynamic educational information environment system. The effective use of educational information can help students to effectively reconstruct their knowledge structure, strengthen their self-learning and self-management, and at the same time help teachers and administrators to conduct in-depth research in teaching management. The content of modern information resources is very rich, among which network education resources are the most important part of modern education information resources. It has many types, including educational websites, e-books, electronic journals, virtual libraries, virtual software libraries, news groups, and electronic encyclopedias. Computer network technology is increasingly infiltrating into people's daily life, and digital survival has become a brand-new way of life. While people enjoy the surprises brought by the information society, they also expose their poor adaptability to the information society. This is manifested in students and teachers who generally lack the knowledge and experience of information retrieval, identification and integration, and the concept of online security is also very indifferent, and they do not know how to consciously abide by the norms of online behavior. Speech recognition technology is a technology that converts speech signals into corresponding commands so that computers can understand them. With the rapid development of speech recognition technology, the application scenarios of speech recognition have become more extensive, and it has different tasks and functions in various fields, resulting in different design schemes for different application scenarios, but the speech recognition systems all have the same overall structure.

The process of simulating human information exchange by using a computer mainly goes through the following processes: (1) natural language generation, (2) speech synthesis, (3) speech recognition, and (4) natural language understanding. The main task of speech recognition is to identify the information contained in the speech signal into the corresponding text information. The three main components of speech recognition are feature extraction, pattern matching, and reference pattern library. Although phonetics has been around for a while, it has not been widely used because of the difficulty of the corresponding model base and phonetic knowledge. The process of fairly classifying, organizing, managing, and processing the gathered complex information is known as information architecture. Its primary

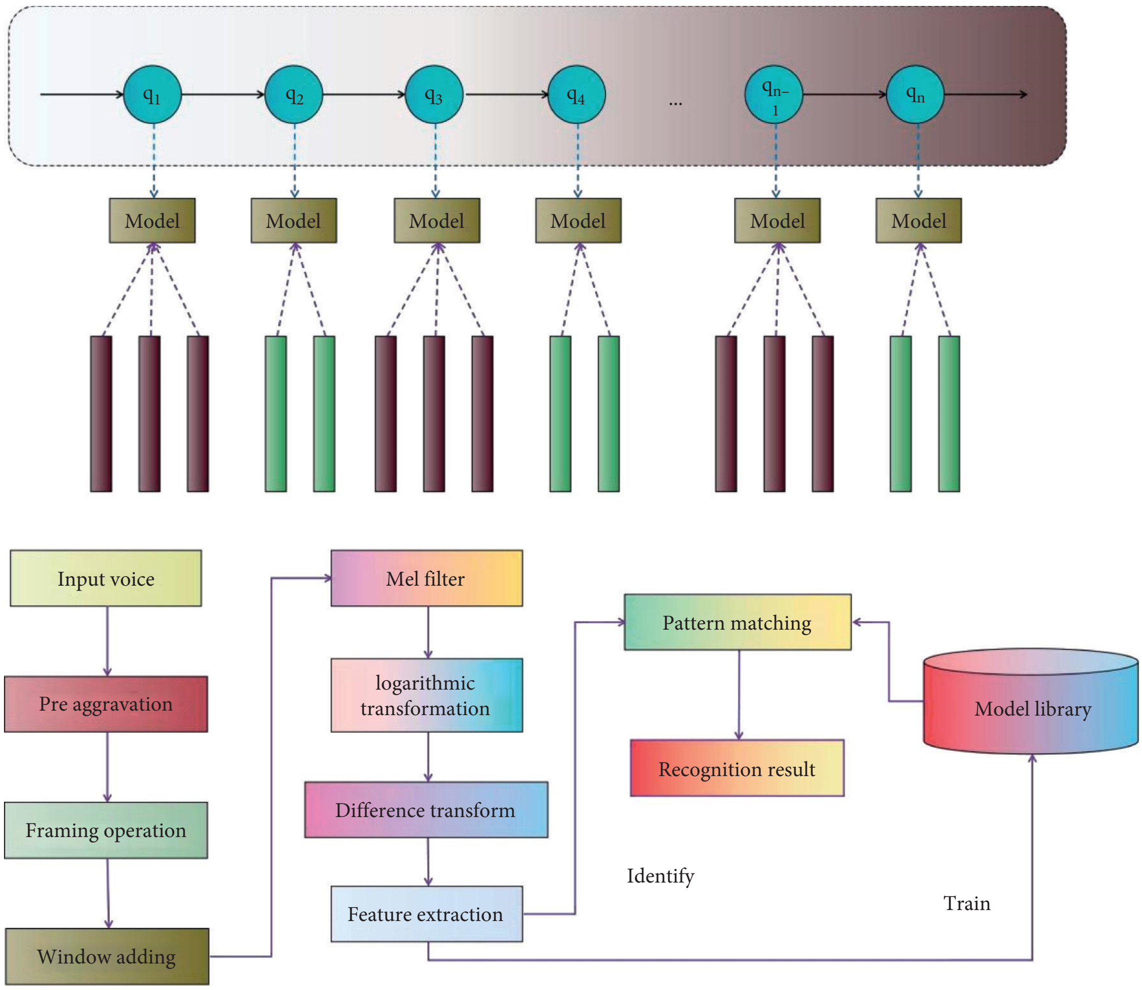

FIGURE 1: Framework and process of the speech recognition system.

responsibility is to combine the components of information expression, determine its course, and edit the expression's content in order to create a cognitive link between users and the data. Academic and industrial researchers are enthusiastic about DL theory due to its superior modeling capability for complex data. The performance of models based on DL has also significantly improved in many real-world application fields, particularly in speech recognition [20]. The computer will automatically produce the recognition results following preprocessing, feature extraction, training, pattern matching, and other units. From this procedure, it is clear that speech recognition is essentially a pattern recognition system and that the effectiveness and precision of recognition depend on the quality of the speech template and algorithm. Network media's ability to disseminate information quickly and with a wide range of influence is improved by the network's rapid growth and update frequency. Because educational information resources are highly time-sensitive, it is important to gather, process, and use educational information as soon as possible. The framework and process of speech recognition system are shown in Figure 1.

Although teaching itself is a systematic process with a clear goal, producers and consumers of educational information frequently do not interact directly, and many producers frequently produce educational information in accordance with their own intentions. Speech recognition technology has undergone significant technological changes recently due to the growth of the DL field, and the acoustic model has gradually shifted from the conventional Gaussian mixture model to the NN model [21]. The NN model significantly boosts the speech recognition system's recognition performance, enhancing its ability to support human daily life and industrial production. People are accustomed to understanding information in the context of their interpersonal relationships, and they selectively gather, arrange, and assess the information's relevance in light of their own needs. The degree to which information resources are accepted by learners and how well they are accepted by them largely depend on how well the information resources correspond to the learners' own concepts and knowledge bases. The speech recognition industry currently uses a lot of NN-based speech systems. Neurons, the training algorithm, and the network structure make up the majority of NN. Speech recognition suffers greatly from noise and interference, which lowers the rate of recognition. Due to the issues of comprehensive teaching content, rich and diverse speech expressions, and relatively small speech data sets in the educational scene, applying speech recognition to the educational scene is still a difficult research project. The high recognition rate is currently stuck at the "near-field speech recognition" stage and is unable to advance to the stage of "far-field speech recognition," which is the mode of natural man-machine interaction. The proliferation of inaccurate information and the challenge of finding high-quality resources are issues that we must simultaneously address despite the fact that education technology expands the learning environment for students. The environment for educational information needs to be optimized. A complete speech recognition system usually consists of three parts: (1) the speech front-end processing part responsible for processing speech signals, (2) the language model and acoustic model, which are trained by text corpus and voice data set, and (3) speech recognition, that is, pattern matching.

3.2. Construction of the SDN Network Traffic Prediction Model Based on Speech Recognition. Traditional network has been restricted in function expansion and network configuration. In order to make network management more convenient, SDN network has begun to appear in public view. SDN is a new network architecture that separates network control and forwarding functions, which can simplify network management and improve network programmability and flexibility. SDN can maximize the utilization of network resources, restrain the unlimited expansion of network infrastructure, and shield the complexity of the underlying network for the upper users. It simplifies the configuration and management of the network and promotes the innovation and development of the network. SDN network is continuously developed on the basis of traditional network, and the utilization rate of network resources can be greatly improved through SDN network. The latest development of SDN network and switching technology can make the network protocol stack abstract from the physical topology level to the flow level for business control. SDN carries the idea of designing network architecture for forwarding and control, rather than a specific technology. It plans the hierarchical structure of the network and the relationships and interfaces among all levels. With the popularization and development of this concept, different participants have further enriched its content, and they have different understandings of it from different angles. Network traffic will change with time and space. In the time dimension, the network traffic will change with different time periods of the day, for example, the traffic in the daytime is higher than that in the night. In addition, the network traffic may change dramatically in a very short time. SDN network is characterized by hierarchical design of data forwarding and network control. The SDN controller is interconnected with each switch, and control information is uploaded and sent through OpenFlow protocol. SDN network is divided into three layers: application layer, control layer, and data layer. It includes commercial applications used by users in the application layer through which network services can be provided to end users. The control layer consists of one or a group of controllers and connects the data forwarding layer with the application layer through an interface. The control layer has mastered the core, can obtain the global topology of the whole network, and design strategies to control the transmission path of the data layer. The data forwarding layer is composed of switches, hosts, and other underlying network devices, which is the realization of the data plane. The data layer does not have the function of selecting the forwarding path but can only transmit information according to the forwarding path provided by the control layer. The network structure of SDN is shown in Figure 2.

SDN network breaks through the limitation that the service interfaces of traditional network hardware devices cannot be configured and adjusted uniformly and in real time. Its advantages are mainly reflected in two aspects: (1) SDN separates the control plane and the data plane of the current network; the data plane is simply forwarded by the actual network equipment, and the control plane is controlled by a logically centralized controller. This simplifies the implementation and optimization of the strategy and the configuration of the network. (3) SDN improves the programmability of the network system by providing developers with powerful and extensible programming interfaces. Network flow is a dynamic variable that is constantly changing from a fine-grained perspective, but it is comparatively stable over time. If the load balancing model only takes into account this change based on the current time point, without taking into account the change trend of the future data flow, it may result in low cost performance controller migration. However, this migration cannot guarantee the overall improvement of the network performance in a specific amount of time, as it only supports the current burst network data flow, which may increase the overall network delay. Additionally, the load flow may exceed the network capacity when the SDN network uses the optimized routing configuration, particularly when the network experiences burst flow. In order to prevent this kind of congestion, which is the main goal of traffic control, we must allocate suitable transmission resources for data traffic in accordance with its transmission requirements and restrict some traffic flows from entering the network at the bottleneck links. Hedera, a dynamic traffic scheduling strategy that can sense the traffic size, is a representative scheme for addressing the issue of network congestion brought on by heavy traffic collision in an SDN-based data center network. Hedera's strategy is to use centralized scheduling for large flows with long durations and small quantities and default ECMP routing for small flows. To determine the flow rate and size of the large flow in this routing scheme, the edge switch using OpenFlow technology first counts the data of the flow generated by the source.

From the perspective of communication theory, obtaining the best decoded word sequence in speech recognition needs to be transformed into a pattern recognition problem. The core idea of solving the word sequence with the highest probability is to adopt the maximum posterior probability discrimination, and its calculation formula is as follows:

$$\widehat{W} = \underset{W}{\operatorname{argmax}}\, P(W|X). \tag{1}$$

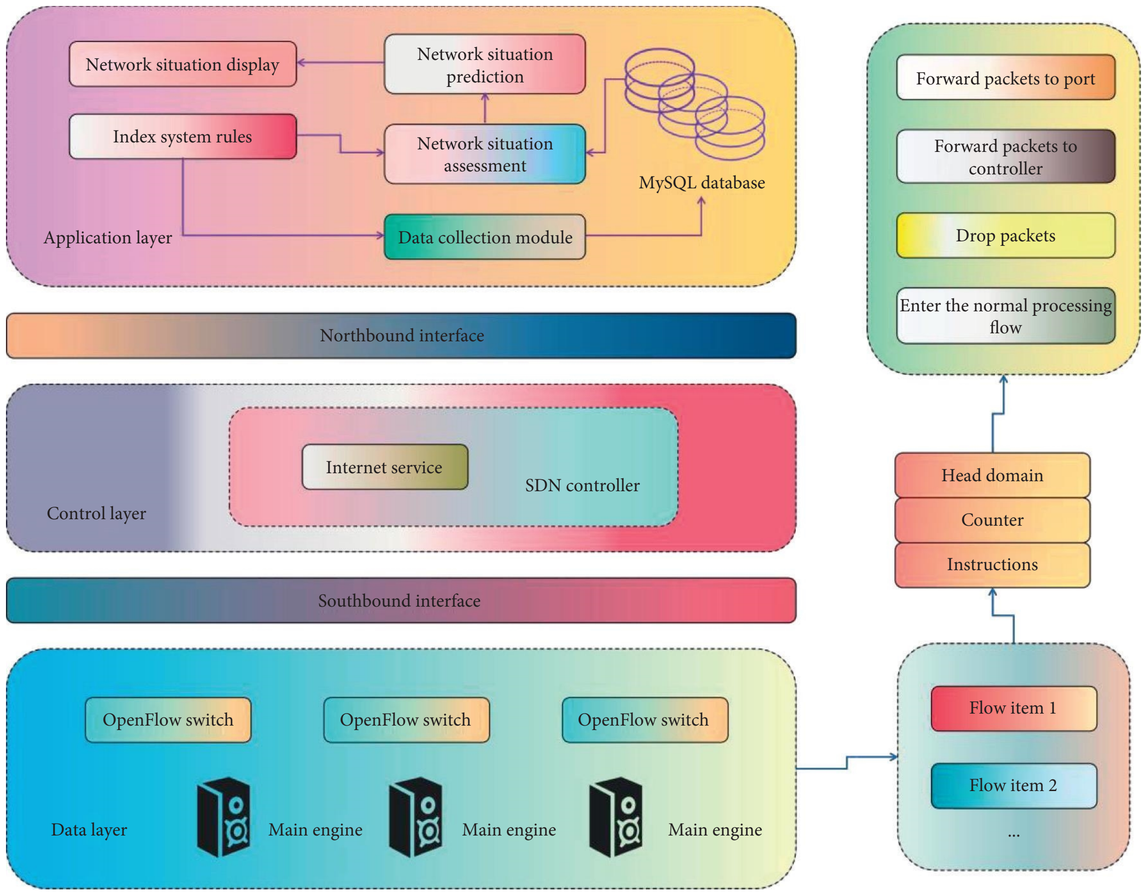

FIGURE 2: SDN network structure.

In the speech recognition problem, $P(W|X)$ is difficult to calculate directly, and it can be converted into the following formula by using the Bayesian formula:

$$\begin{aligned}\widehat{W} &= \underset{W}{\operatorname{argmax}} \frac{P(X|W)P(W)}{P(X)} \\ &= \underset{W}{\operatorname{argmax}} P(X|W)P(W),\end{aligned} \tag{2}$$

where $P(X)$ represents the prior probability of the feature vector, which is a constant for all word sequences, so it can be discarded. $P(X|W)$ represents the probability of using a given word sequence to generate the corresponding acoustic feature vector, which is modeled and calculated by the acoustic model. $P(W)$ is the prior probability of the word sequence, which can be modeled and calculated by the language model. After framing the speech signal, it is necessary to continue windowing the speech signal to deal with the nonstationary characteristics of the speech signal. The most commonly used window adding methods are the rectangular window and Hamming window. The definition of rectangular window function is shown in the following formula:

$$w(x) = \begin{cases} 1, & 0 \le n \le N-1, \\ 0 & \text{other}. \end{cases} \tag{3}$$

Define the currently available bandwidth $c(p)$ for path p:

$$c(p) = \min_{e \in p} c(e). \tag{4}$$

In the formula, $c(e) = x(e) - u(e)$, which is the remaining bandwidth of link e. Define the vulnerability of path p as $\alpha(p)$:

$$\alpha(p) = \max_{e \in p} \alpha(e). \tag{5}$$

In the formula, $\alpha(e)$ is the number of paths in different $p_1 s$ passed on the link e:

$$\alpha(e) = \sum_{l=1}^{L} \delta_l(e). \tag{6}$$

Among them,

$$\delta_1(e) = \begin{cases} 1, & \text{if } p \in p_1^k,\ e \in p, \\ 0, & \text{else}. \end{cases} \tag{7}$$

Network bandwidth utilization refers to the average of the ratio of link load to link bandwidth of all links in the recent period. The calculation formula of network bandwidth utilization is

$$\text{Link\_utirate}(t) = \frac{\sum_{l=1}^{L}\left(\text{portBytes\_}Rx_l(t) * 100\%/\text{bandwidth}_l\right)}{L},\quad L = 1,2,3,\ldots,L. \tag{8}$$

Among them, bandwidth_l refers to the bandwidth of the lth link, that is, the maximum number of bits that can theoretically be transmitted by the physical channel per unit time. $\text{portBytes\_}Rx_l$ represents the number of bits transmitted by the sender of the lth link. The link transmission delay refers to the maximum value of the communication delay from the sending port to the receiving port of all links. The calculation formula is

$$\text{Link\_delay} = \max_i\{p\text{topDelay}(i)\}. \tag{9}$$

Among them, the network delay can be calculated by the maximum transmission delay of the link, that is, the maximum time interval $p\text{topDelay} = T_2 - T_1$ between the time T_1 of the transmission data packet leaving the source point and the time T_2 arriving at the destination in the network; $p$topDelay represents the end-to-end delay. Network throughput refers to the total number of bytes passing through the switch port connected to the host in unit time without packet loss. It can be calculated by the total number of bytes imported and exported, namely,

$$\text{Net\_throughput} = \frac{(\text{dataBytes\_inNum} + \text{dataBytes\_outNum})}{T}. \tag{10}$$

Among them, T represents the sampling interval; dataBytes_inNum represents the number of incoming bytes connected to the host; and dataBytes_outNum represents the number of exported bytes connected to the host.

In this paper, the machine learning algorithm is used to compare the actual data stream with the predicted data stream, and if the deviation is greater than the set threshold, the deployment scheme is regenerated. Otherwise, the old scheme is still adopted. During the running of the scheme, the controller does not migrate any more to reduce the impact of migration on network performance. In an SDN network, all network resources are pooled together, and the controller distributes path and bandwidth resources evenly among the network's data streams. The data streams processed by the switch will be stored in the buffer area for transmission, and its only responsibility is to forward the data streams in accordance with the controller's defined policies. The network topology discovery module's network topology information and the network monitoring module's link remaining bandwidth information are used by the large flow routing calculation module in the SDN controller to determine the convergence layer link pair of the large flow's source and destination using the greedy algorithm. In this paper, the situation is assessed using a model based on rough sets and clustering [22], which can improve decision tables and assess the current network traffic situation in accordance with the decision rules derived from rough set analysis theory. The historical situation value and current situation value in the SDN network operation process are finally obtained by investigating the calculation method of situation index weight based on attribute importance, allowing for an intuitive and unmistakable understanding of the global network view and network operation trend through the situation value.

Table 1: Parameter setting of the simulation experiment.

Serial number	Parameter	Set up
1	Link bandwidth	10 Mbps
2	Link delay	3ms
3	Sending node	S1, S2
4	Receiving node	D1, D2
5	Minimum threshold	50
6	Maximum threshold	100
7	Maximum packet loss probability	0.2
8	Weight	0.03

4. Result Analysis and Discussion

Through Hurst index calculation of the SDN network traffic situation value, the sequence H value is 0.88, which indicates that the situation value sequence has strong self-similarity and long correlation. In order to verify the effectiveness of SDN network traffic prediction model based on speech recognition, this paper designs several simulation experiments on the MATLAB simulation platform. The platform can automatically configure network controllers, switches, etc., and execute protocols. In the simulation experiment, the controller with visual boundary is installed as the control layer of the network. Based on Python programming language, network switches and terminals can be easily configured on Floodlight. At the same time, in this chapter, a large number of comparative experiments are made between the prediction model in this paper and other different prediction models including the convergence of training iteration of traffic situation, the relative error of situation value prediction, the influence of super parameters of the model, and the generalization ability of different data sources. The simulation parameters are shown in Table 1.

When a large number of data flows pass through SDN network, network congestion will occur. On this basis, this chapter simulates and analyzes the pet control algorithm based on queue management. Because the network flow is complex and changeable, and many artificial subjective predictions are difficult to be verified, constructing the probability matrix through objective historical data to obtain the probability matrix under the condition of maximum entropy as the prediction result at that time can maximize the accuracy of the prediction. During the experiment, the training sample group is input to train the prediction model, and the maximum number of iterations is set to 2000. The change of training MSE (mean square error) in the network training iterative process is shown in Figure 3.

It can be seen that the MSE is decreasing from the initial 0.08 or so, and it reaches convergence after 600 iterations, and the MSE at convergence is 0.0021. This shows that with the increase of iteration times, the weight update can

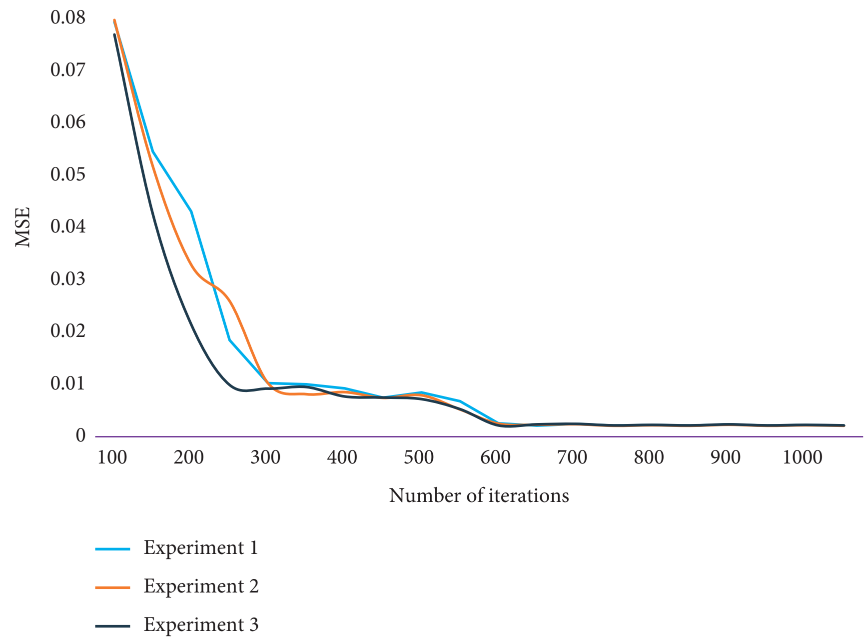

Figure 3: Changes of training MSE in the iterative process of network training.

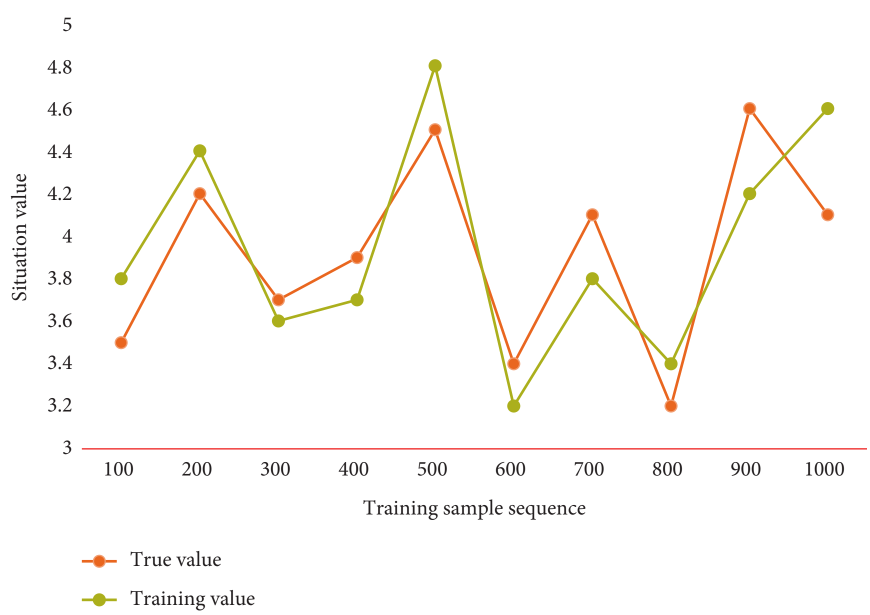

Figure 4: Effect of network training.

converge in the process of gradient descent, and the convergence speed is faster.

First, the parameters are compared and analyzed. Then the maximum and minimum threshold values are changed, and the performance parameters of each packet are further analyzed. Under the condition that the buffer size is constant, this chapter changes the minimum threshold of queue length. The network training effect is shown in Figure 4.

For this paper, the main factors that affect traffic prediction are the number, time, and protocol type of packets. Therefore, the model takes packet size, packet protocol name, and time as eigenvalues and generates the network flow data matrix by sorting the data. The trained network model is used to predict 20 groups of untrained samples. The prediction effect is shown in Figure 5.

It can be seen from Figure 5 that the prediction model can achieve good prediction results for any group of traffic situation samples to be predicted, and the relative error of prediction is basically controlled within 15%. In this paper, network throughput, average flow completion time, the remaining bandwidth jitter in Pod and remaining bandwidth jitter in the core layer are selected as performance evaluation indexes. Among them, the average stream completion time refers to the average time taken to complete

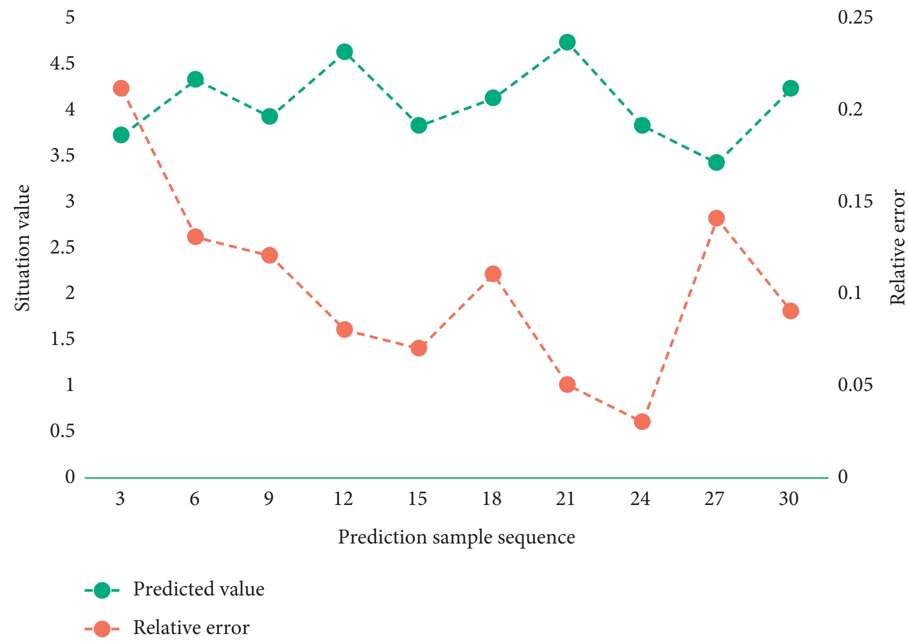

Figure 5: Prediction effect of the model.

Table 2: Test results of each index.

Index	IRS	ECMP
Network throughput	1058	957
Average flow completion time	48	53
Remaining bandwidth jitter of Pod link	26	30
Core layer link remaining bandwidth jitter	20	24

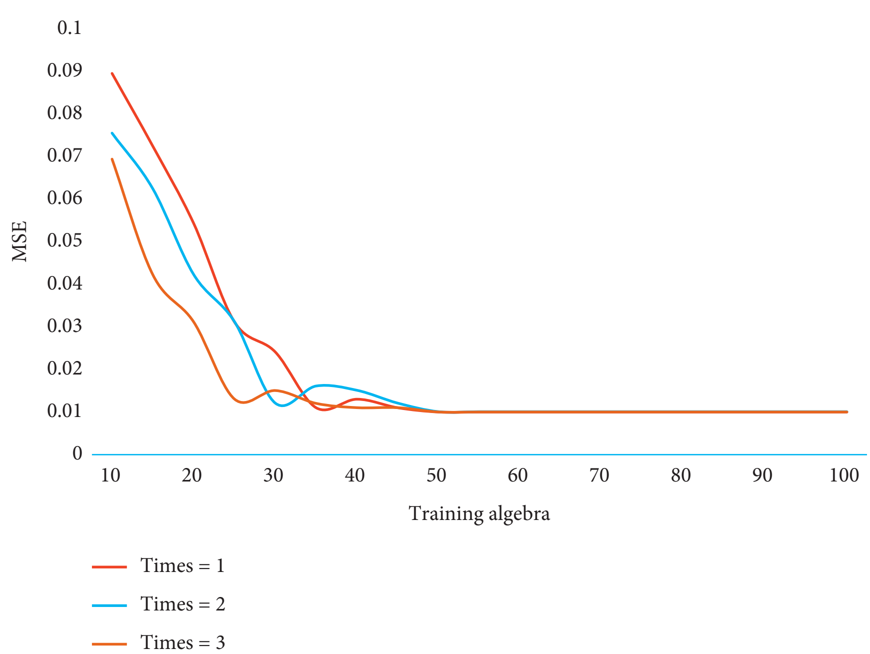

Figure 6: Comparison of the iterative convergence effect.

all 100 MB data block transmissions, and the smaller the time, the better the performance. Network throughput refers to the amount of data transmitted and successfully accepted through the network per unit time in the network. The larger the data, the better the performance. The jitter of the remaining bandwidth in the Pod and the jitter of the remaining bandwidth in the core layer refer to the standard deviation of the remaining bandwidth of each link in the Pod

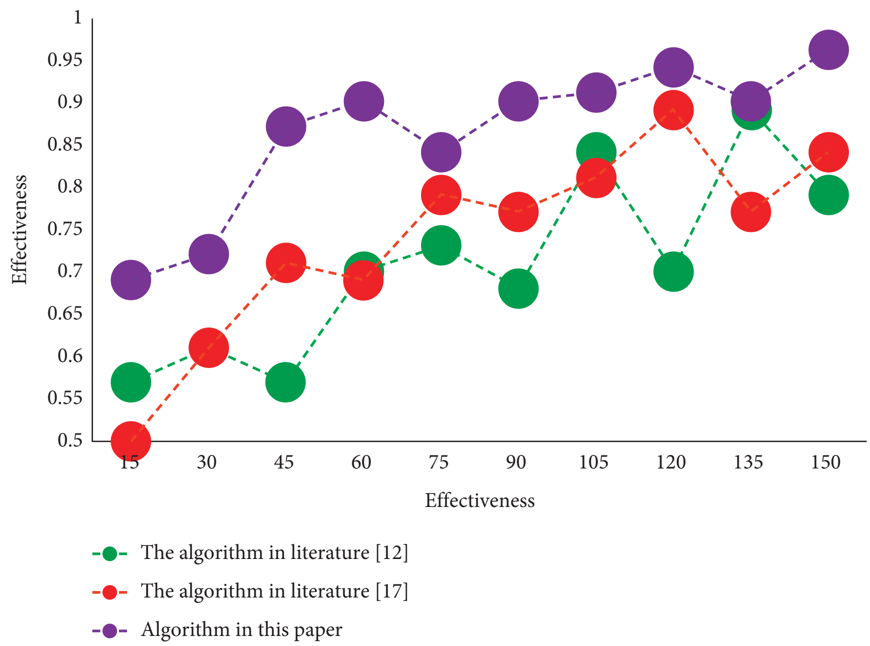

Figure 7: Effectiveness test results of the algorithm.

and the core layer, respectively. The smaller the jitter, the better the equalization performance. Table 2 shows the test results of each index.

On the whole, the traffic balancing effect of IRS is better than that of ECMP, which is mainly because IRS uses the dynamic routing method based on the remaining link bandwidth in convergence layer of the network, and large flows are always routed to low-load paths. Moreover, IRS uses the shunting method to route large flows in the core layer, which further balances the load in the network. Because the model uses random initial weights to initialize the network, different initial weights may have different effects on the network iterative convergence. In this paper, the results of three experiments are compared. Times means times, and the values are 1, 2, and 3. The iterative convergence effect is shown in Figure 6.

From the comparison results of curve slopes, it can be seen that the convergence speed of this model is faster than that of the other two models in the three experiments. At the same time, the initial MSE of this model is obviously better than the other two models. It shows that the algorithm in this paper can effectively improve the convergence speed of network model, and the training effect is better. The SDN controller only selects the forwarding path for the new flow injected into the network according to the usage of the remaining flow table of the switches on the feasible path in the current tenant network. The effectiveness test results of the algorithm are shown in Figure 7.

In order to verify the effectiveness of SDN network traffic prediction model based on speech recognition, this chapter designs several simulation experiments on the MATLAB simulation platform. Experimental results show that the effectiveness of this algorithm can reach 95.67% at the highest, and the MSE convergence is 0.0021 at the lowest. The results show that this model has faster iterative convergence speed, better training effect, and higher prediction accuracy.

5. Conclusions

The development of voice technology will further help education and teaching, improve teaching efficiency and teaching effect, and promote the overall development of artificial intelligence technology. Based on the research of related literature, this paper constructs a SDN network traffic prediction model based on speech recognition and applies it to the educational information optimization platform. In this paper, the data acquisition module in the SDN controller is designed, and the SDN network platform is built, which realizes the data acquisition and storage of traffic situation indicators. Aiming at the problems of packet disorder, this paper proposes an IRS mechanism based on the advantages of SDN centralized control and the characteristics of different performance requirements of large and small streams. For large streams, IRS uses greedy routing and multipath routing based on remaining bandwidth to make the traffic evenly distributed in the network, and IRS adds a scheduling strategy based on IP addressing to avoid packet disorder. Simulation results show that the effectiveness of this algorithm can reach 95.67% at the highest, and the MSE convergence is 0.0021 at the lowest. The algorithm can effectively realize the relative priority of each packet queue without reducing the utilization of network resources and can smoothly upgrade and downgrade the priority. On the whole, this model has faster iterative convergence speed, better training effect, and higher prediction accuracy. This research can provide some technical support for the educational information optimization platform. Although this paper has achieved some research results, the research is still shallow, and there are still many places that need to be improved and supplemented. In the future research, we should find a unified solution in different algorithms so that the performance of packet delay and system throughput is better and the utilization of network resources is maximized.

Data Availability

The data used to support the findings of this study are available from the corresponding author upon request.

Conflicts of Interest

The authors do not have any possible conflicts of interest.

Acknowledgments

This research was supported by the 2018 Social Science Planning Project of Jiang Xi Province under Grant 18JY40 (An Instructional Resources Allocation Strategy for Private University Based on The Analysis of Teaching Process Big Data—Tack Jiang Xi University of Technology for example).

References

[1] M. Atiquzzaman, N. Yen, and Z. Xu, *Big Data Analytics for Cyber-Physical System in Smart City: BDCPS 2019*, pp. 28-29, Springer Nature, Shenyang, China, 2020.

[2] E. Q. Wu, P. Xiong, Z. R. Tang, G. J. Li, A. Song, and L. M. Zhu, "Detecting dynamic behavior of brain fatigue through 3-d-CNN-LSTM," *IEEE Transactions on Systems, Man, and Cybernetics: Systems*, vol. 52, no. 1, pp. 90–100, 2022.

[3] J. Kong, C. Yang, Y. Xiao, S. Lin, K. Ma, and Q. Zhu, "A Graph-Related High-Order Neural Network Architecture via Feature Aggregation Enhancement for Identification Application of Diseases and Pests," *Computational Intelligence and Neuroscience*, vol. 2022, Article ID 4391491, 16 pages, 2022.

[4] J. Zhang, J. Sun, J. Wang, and X. G. Yue, "Visual object tracking based on residual network and cascaded correlation filters," *Journal of Ambient Intelligence and Humanized Computing*, vol. 12, no. 8, pp. 8427–8440, 2021.

[5] W. Chen, Q. Duan, G. Wei, Y. Aizhong, D. Zhenhua, and M. Chiyuan, "An evaluation of adaptive surrogate modeling based optimization with two benchmark problems," *Environmental Modelling & Software*, vol. 60, no. 10, pp. 167–179, 2014.

[6] M. Liyanage, A. B. Abro, M. Ylianttila, and A. Gurtov, "Opportunities and challenges of software-defined mobile networks in network security," *IEEE Security & Privacy*, vol. 14, no. 4, pp. 34–44, 2016.

[7] X. Xu, S. Wang, and Y. Li, "Identification and predication of network attack patterns in software-defined networking," *Peer-to-Peer Networking and Applications*, vol. 12, no. 2, pp. 337–347, 2019.

[8] L. Huo, D. Jiang, S. Qi, and L Miao, "A blockchain-based security traffic measurement approach to software defined networking," *Mobile Networks and Applications*, vol. 26, no. 2, pp. 586–596, 2021.

[9] Z. Shu, J. Wan, J. Lin et al., "Traffic engineering in software-defined networking: m," *IEEE Access*, vol. 4, pp. 3246–3256, 2016.

[10] Y. Ji, J. Zhang, Y. Zhao et al., "All optical switching networks with energy-efficient technologies from components level to network level," *IEEE Journal on Selected Areas in Communications*, vol. 32, no. 8, pp. 1600–1614, 2014.

[11] C. W. Chan, N. Bambos, and J. P. Singh, "Network-assisted mobile computing with optimal uplink query processing," *IEEE Transactions on Mobile Computing*, vol. 12, no. 6, pp. 1065–1078, 2013.

[12] M. K. Jha and B. Datta, "Linked simulation-optimization based dedicated monitoring network design for unknown pollutant source identification using dynamic time warping distance," *Water Resources Management*, vol. 28, no. 12, pp. 4161–4182, 2014.

[13] K. Konstanteli, T. Cucinotta, K. Psychas, and T. Varvarigou, "Elastic admission control for federated cloud services," *IEEE Transactions on Cloud Computing*, vol. 2, no. 3, pp. 348–361, 2014.

[14] T. Liu, Z. Gao, and H. Guan, "Educational information system optimization for artificial intelligence teaching strategies," *Complexity*, vol. 2021, no. 3, pp. 1–13, Article ID 5588650, 2021.

[15] B. Fabrizio and B. Héctor-Cebolla, "Previous school results and social background: compensation and imperfect information in educational transitions," *European Sociological Review*, vol. 30, no. 2, pp. 207–217, 2014.

[16] Y. J. Chun, D. I. Kim, and S. W. Kim, "Optimization of network coded MIMO transmission in multiple-access relay network," *IEEE Transactions on Wireless Communications*, vol. 12, no. 5, pp. 2436–2444, 2013.

[17] S. Qi, D. Jiang, and L. Huo, "A prediction approach to end-to-end traffic in space information networks," *Mobile Networks and Applications*, vol. 26, no. 2, pp. 726–735, 2021.

[18] M. Li, "The application of computer speech recognition technology in oral English teaching," in *Proceedings of the 2021 4th International Conference on Information Systems and Computer Aided Education*, pp. 1271–1274, Dalian, China, September 2021.

[19] X. Ma, Z. Dai, Z. He, J. Ma, Y. Wang, and Y. Wang, "Learning traffic as images: a deep convolutional neural network for large-scale transportation network speed prediction," *Sensors*, vol. 17, no. 4, p. 818, 2017.

[20] F. Tang, B. Mao, Z. M. Fadlullah, and N Kato, "On a novel deep-learning-based intelligent partially overlapping channel assignment in SDN-IoT," *IEEE Communications Magazine*, vol. 56, no. 9, pp. 80–86, 2018.

[21] W. Cai, M. Gao, Y. Jiang et al., "Hierarchical domain adaptation projective dictionary pair learning model for EEG classification in IoMT systems," *IEEE Transactions on Computational Social Systems*, 1–9, 2022, in Press.

[22] J. Chen, C. Du, Y. Zhang, P. Han, and W. Wei, "A clustering-based coverage path planning method for autonomous heterogeneous UAVs," *IEEE Transactions on Intelligent Transportation Systems*, vol. 1, pp. 1–11, 2021.

Hindawi
Computational Intelligence and Neuroscience
Volume 2022, Article ID 4109170, 11 pages
https://doi.org/10.1155/2022/4109170

Research Article

Deconstruction and Realization of Sports Entity Simulation Based on Fish Swarm Algorithm

Kai Wu

School of Public Teaching and Practice, Wuhan Technical College of Communications, Wuhan 430065, Hubei, China

Correspondence should be addressed to Kai Wu; wukai@whtcc.edu.cn

Received 23 May 2022; Revised 22 June 2022; Accepted 23 June 2022; Published 22 July 2022

Academic Editor: Xin Ning

Due to the limitation of sports movement, the current simulation technology of sports entities is prone to deficiencies in capturing dynamic motion figures and is prone to lack of accuracy. It is also affected by external noise and brightness. To solve these problems, this paper proposes a sports entity simulation based on the fish swarm algorithm and compares the figure effectiveness, figure segmentation, core point, and noise reduction effect of the two in the shooting figure. Through the comparison, it is found that the figure is more appropriate to the real moving figure, the motion capture is more accurate, and the number of core points is related to the accuracy of motion capture. The more core points, the more accurate the motion capture, and the noise reduction effect is also increased by 20.3%, which reduces the impact of brightness on the motion simulation. The difference in the effect of the traditional simulation technology (particle swarm algorithm) and the entity simulation based on the fish swarm algorithm was also compared. The combination with the artificial fish swarm algorithm is to simulate the moving entity and learn from some reference data. By comparing the data between the two after the experiment, it is concluded that the fish swarm algorithm is more effective in the simulation of sports entities.

1. Introduction

The physical simulation of sports is recorded by sensors, and then the movement information in the space is transmitted to the processing center of the computer and processed by computer to get the basic three-dimensional human body model. On this basis, the human body frame is drawn to realize the physical simulation of sports. At present, the main technologies used to capture sports movements include optical capture, mechanical capture, and electroacoustic capture. Mechanical and electroacoustic capture methods are limited by sports and have a relatively broad acquisition range. However, the accuracy of motion capture is not enough. The advantage of the optical capture method is that it will not be blurred, but the number of captured points is not enough to meet the requirements of moving entities, and the collection location is affected by the brightness, and the equipment itself is also easily affected. It is easy to cause the external light data to interfere with the motion data, resulting in confusion in the analysis of the equipment during operation, and it is more complicated to deal with. Although electroacoustic capture has low operating costs, the capture accuracy is not enough. In this regard, motion capture technology is not satisfactory. In this paper, the simulation calculation of moving entities based on fish swarm algorithm is introduced.

In this paper, based on the fish swarm algorithm, the sports motion detection system is compared. By simulating the irregular images under human body dynamics, through the corresponding tools, under the condition that the background is not set, the influencing factors existing in sports are removed, background, shadows, brightness, noise, and so forth, and the main moving points of the human body under sports are extracted and simulated, which is of great significance to the improvement of simulation technology.

In this paper, a physical simulation of sports based on fish swarm algorithm is proposed. By comparing the figure effectiveness, figure segmentation, core point, and noise reduction effect of the two in the shooting figure, it is found that the figure is more appropriate to the real moving figure, the motion capture is more accurate, and the noise reduction effect is also increased by 20.3%. By comparing the data between the two after the experiment, it is concluded that the fish swarm algorithm is more effective in the simulation of sports entities.

2. Related Work

With the gradual acceleration of urbanization, people's quality of life has gradually improved. Every household has begun to prepare a car as a means of transportation, and the problem of urban traffic has gradually become more and more serious, and it is easy to cause congestion. The urban green wave traffic control system is one of the effective means to solve the problem of urban traffic congestion and reduce vehicle delays. In response to the problem of green waves, Ma C investigated the causes of congestion in the city through the fish swarm algorithm and found that the irregular movement of the crowd, the irregular parking of vehicles, and people's traffic awareness are the main reasons for the impact [1]. The progress of industrialization has brought about changes in weather, increasingly serious smog pollution, and a significant decline in air quality. Zhu X proposed a haze prediction method based on multifractal dimension (MFD) and coevolutionary discrete artificial fish swarm algorithm (CDAFSA). Using CDAFSA, MFD, and extreme learning machine (ELM), the algorithm population is initialized through good point set theory; the swarming, chasing, and foraging behaviors are improved by introducing the swimming speed of artificial fish; the algorithm is discretized; and competition and cooperative operation are introduced. Second, the haze dataset is reduced by CDAFSA and MFD; finally, a haze prediction model is established by using ELM. The experimental results show that the proposed prediction method is superior to the traditional method and has high stability and credibility [2]. The accurate prediction of wind power in wind farms is of great significance to the economic operation of wind farms and the safe operation of power grids. The randomness and volatility of wind in wind farms make wind power forecasting more difficult. Based on the characteristics of wind in wind farms, combined with relevant meteorological data such as wind speed, temperature, and humidity in wind farms, Zhai built the ultimate learning machine model (ELM) for wind energy forecasting and established an artificial fish swarm algorithm (AFSA) for rapid optimization. The constructed model is trained and predicted by the actual meteorological data and wind data of the wind farm. The results show that this method has higher predictive ability than the wind power prediction model of particle swarm [3]. The fish swarm algorithm is not only used in green waves, air quality surveys, and wind farms but also gradually used in sports.

Simulation technology, which is essential to virtual reality, has been extensively applied in the study of physical education. This ground-breaking programme has had a profound effect on conventional teaching methods and ways of thinking, and it has created enormous opportunities for the advancement of physical education. Yili examined the use of simulation technology and stimulus-response theory in the field of physical education with a focus on the drawbacks of the conventional physical education teaching method. This served as the foundation for the invention of the teaching method for physical education. The findings demonstrate that auxiliary teaching can enhance students' theoretical and practical understanding of physical education, enhance their academic performance and learning enthusiasm, and serve as a useful benchmark for physical education teaching innovation [4]. The active safety capabilities of cars have evolved into a crucial criterion for assessing their quality as the automotive industry continues to grow. The antilock braking system is an important tool to increase the active safety of the vehicle and prevent the wheels from locking. It does this by adjusting the torque to ensure that the vehicle slips at the ideal rate. It can still turn even when braking hard, cutting down on braking distance and time to lessen tyre wear. Song conducted research on an antilock braking system based on simulation technology on the basis of examining the pertinent principles. A simulation model for the antilock braking system in cars has been developed. It simulates the simulation model. According to the findings, antilock braking systems on vehicles perform better than conventional braking systems at maintaining slip rate, braking distance, and braking time [5]. During the wiring process of complex mechatronic products, the spatial pose and shape of the flexible wiring harness are prone to change. As a result, the sampling information of the wiring harness is inaccurate during the wiring process, which seriously affects the wiring efficiency. Wang proposed a physical property modeling and deformation simulation method of flexible cable harness based on the exact Cosserat model. The physical property model of the wiring harness based on the exact Cosserat model was established, and then the dynamic balance formula of the flexible wiring harness was constructed [6]. Simulation technology is an emerging technology in the field of system modeling and simulation research in recent years, and it has always been the focus of research. According to the simulation technology requirements of battlefield command decision-making, equipment task planning, and equipment maintenance support, the outstanding problems of existing simulation technology are summarized. That is, the domain model is stable and has no self-evolution ability. Ge put forward the concept of equipment parallel simulation technology and pointed out its characteristics. It systematically introduces its theoretical origin and research status of related technologies and discusses the main modeling technologies such as online perception of equipment degradation status and establishment of equipment degradation [7]. Simulation technology has been widely used now and is a milestone technology for the country to enter into rapid development.

3. Simulation System Description and Key

3.1. Simulation System. The simulation system must go through a standard motion figure processing stage before capturing, simulate the dynamic figure data in the computer body, and maintain the background's original state. Additionally, noise interference may get in the way of capturing.

The image cannot be captured directly as the background because the brightness in the capture space is also subject to slight variations, which will influence the capture [8]. The flow figure of system processing is shown in Figure 1.

Because the light intensity needs to be processed, it is necessary to extract new data from the background image and replace the previous background image. The replacement condition requires that the previous background image be relatively stable, and there is not much numerical deviation. When replacing, it cannot be said to be a complete replacement but only covers the previous information with part of the information and uses the difference algorithm between the sports image and the replaced background image to obtain the required background image. Through color processing, the image color is converted to the original gray. Then, the image data is differentiated through the threshold algorithm, and differential processing can identify differences in the background and quickly fill in the blanks. The differentiated data is used to complete the empty space in the replacement in a dynamic mathematical way, and a relatively complete three-dimensional map of sports points is obtained. 3D map is the basis of human motion contour and the most basic step of simulation technology. By extracting the edge points of the three-dimensional image [9], it will not be completely closed under normal conditions. By connecting the edge points, the key points of human body movement can be obtained, and the direction or position of other movements can be obtained instantly. The motion data outline will also coincide with the connected line segments. Through the obtained key points, the outline of human motion can be realized by drawing and 3D construction through simulation technology.

3.2. *Influence Points of the Realization System*

3.2.1. Background Extraction. There are many algorithms for background extraction. For example, there are interframe difference method, background difference method, ViBe algorithm, ViBe + algorithm, and so on. In this paper, the traditional fish swarm algorithm and the improved artificial fish swarm algorithm are used. Before extracting the background, the captured image points need to be sorted in a certain order. It is concluded that the sorted image is different from the previous background image and becomes cluttered. In ascending order from small to large, the pixel of the first image is the minimum value in the image. Similarly, the pixel value of the last image is the maximum value. Assuming that all image pixels are L, the noise interference is placed next to the background image, and the pixels arranged in the middle are used as the background, which can also prevent the pixels from being too large or small, resulting in the confusion of the entire image. The value of L in the system is selected as 9, and then the fifth figure is the background image. For the value of L, its size also has certain requirements. If it is too large, it will easily lead to too much calculation and affect the result. If it is too small, it cannot handle noise. Background extraction is the first shot of motion capture, but it cannot be captured as soon as it is turned on. Because of direct capture, the figures returned by the system are inconsistent, or there is a delay, or there are other cases where the pixels are not clear. This needs to be prepared in advance before capturing. When the figure reaches 25 frames, it will gradually stabilize. When the system is running, the previous frames can basically be abandoned directly, and the figures are the main ones, which are stabilized images. The frame rate is also a point to consider, because VC++ is used in this article as an auxiliary tool, the camera is the main sensing instrument, and the control instrument is a computer. Because, during image processing [10, 11], for image capture, the computer processing time is assumed to be t, if the T value is very large, the processing time of each photo is too long, which is not considered in this article, and does not meet the actual operation purpose. If the value of T is small, assuming that it is 0.01 s, it means that the computer needs to process hundreds of figures per second. But, for sports, the magnitude of the change is only a few microseconds, and the images in the vicinity of a few microseconds are similar, and there is not much difference. The general camera frame rate is 20–120 Hz. If the value of t is smaller, more images will be processed, and the situation of half-image will easily appear when the computer processes it. Get either the image of the upper half frame or the image of the lower half frame, or even there may be no figure. In order to ensure validity and accuracy, the processing frequency of the computer must be less than the capture frequency of the camera.

3.2.2. Human Motion Detection. There are three methods currently used for detection, the difference detection method [12], the background difference method, and the optical flow method [13]. The difference method is used in this paper. For the difference method, the background image and the previous frame image are determined through the calculation of the difference image, but it cannot be directly used in the background image because the image has color difference [14]. There are many influencing factors in the image, the color difference of the image, the scene of brightness, the number of recorded frames, and so forth, which cannot be directly used as the data information of the movement. The pixels are mainly formed in three ways, and the relationship between them is

$$\text{Gray} = 0.3R + 0.6G + 0.1B. \quad (1)$$

In the above formula, R, G, and B are the main paths of pixels. The color of the background is converted into the original gray through color, and the image data is differentiated through the threshold algorithm. Finally, the irrelevant points in the image are eliminated by the erosion algorithm. After adjusting and shrinking the image, the adjusted image is calculated, connected, and filled to supplement the empty points [15].

3.3. *Motion Profile and Straight Line Fitting.* First, the data points of the obtained foreground image are connected by line segments. Because the obtained image is a binary image,

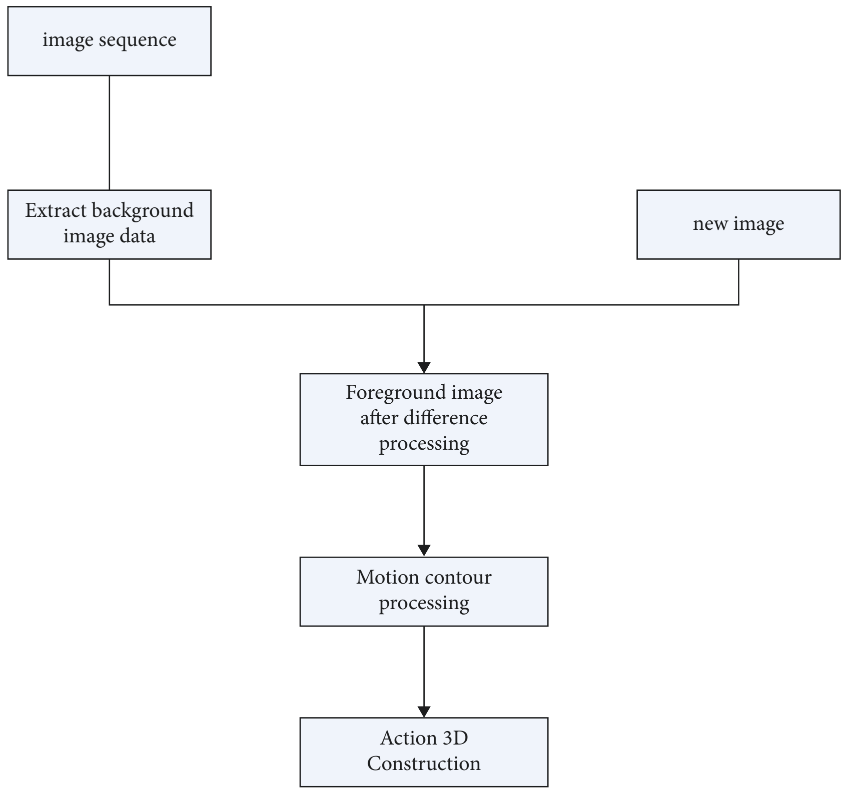

Figure 1: Flowchart of the simulation system.

the edge points need to be eliminated by tools. Connecting the points whose edges conform to the outline, the pixels slowly form a spatial figure, and these points are saved in ascending order to remove the useless line segments that are spent separately. Finally, the multisegmented lines are formed into the core, and the core is found to realize the fitting. The obtained image data is arranged and combined in space through pixels to form a mathematical problem, which is also conducive to finding the position of pixels. Drawing through spatial coordinate points, in order from small to large, the order of connections is very important for image formation. If the order of connections is wrong, it may not be possible to form the outline of the human body, and you need to start from the first step. Because the contour line segments of the image are not necessarily all closed, there will be some redundant points to form connecting line segments. These useless line segments need to be removed, which can prevent subsequent processing [16]. The traditional simulation technology to realize the influence points of the system is not perfect, and the artificial fish swarm algorithm is introduced to improve the imperfect points.

3.4. Artificial Fish Swarm Algorithm. Chinese researchers proposed an intelligent calculation technique called the artificial fish swarm algorithm. The algorithm uses the various locations of the artificial fish as potential answers and the amount of food the fish can detect as the importance of the response. By simulating fish swimming, foraging, gathering, and tail-chasing, the best solution can be found. Figure 2 [17] depicts the various states that fish schools could be in. In this study, cloud theory is applied, cloud learning and cloud variation factors are incorporated into a single artificial fish, and a cloud-based artificial fish swarm algorithm is proposed to address potential issues with artificial fish calculation [18].

In traditional fish swarm algorithm, assuming that the number of fish schools is S, the number of experiments is C, the fish school detection distance is D, the step size is L, θ is the proportion of fish in the artificial pond, and the interval between each fish is X, the food visibility of the artificial fish pond is

$$Q = f(x). \tag{2}$$

In the above formula, Q is the value of the correlation function. For the four behaviors of the fish school, the expressions of tail-chasing, foraging, gathering, and swimming are as follows.

As regards rear chasing behavior, when the status of artificial fish breeding is W_i, find the most suitable W_j within the detection distance [19], and the proportion of fish in the artificial pool is less than θ, and move W_i to W_j by one step. According to the following formula, if not executed, foraging behavior will be performed.

$$W_i = W_i + L \times \text{rand} \times \frac{W_j - W_i}{\left\| W_j - W_i \right\|}. \tag{3}$$

Considering foraging behavior, when the state of artificial breeding is W_i, the most suitable new state is W_j within

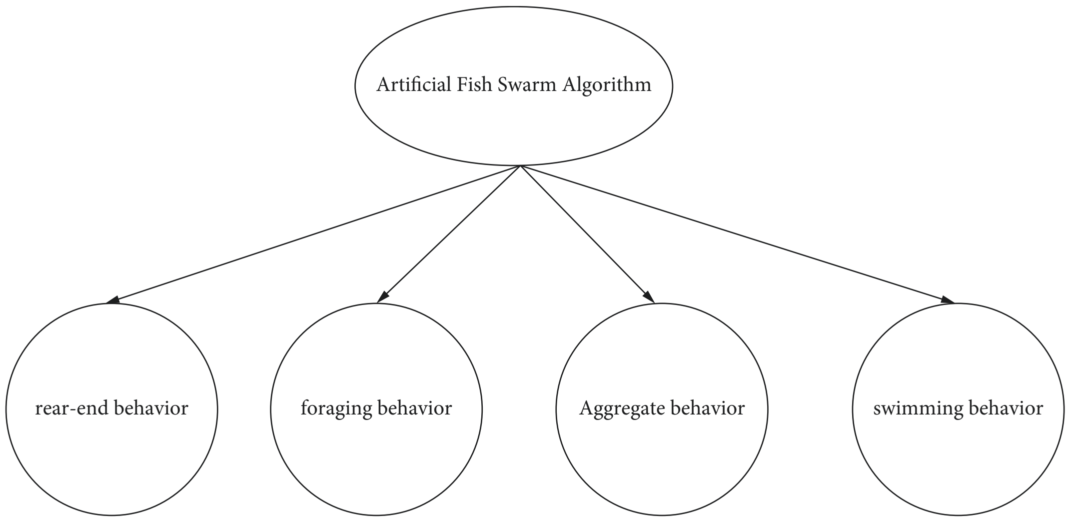

Figure 2: Fish presence status.

the detection distance. If suitable W_j is found, the artificial fish will move to W_j; if no suitable W_j is found, then W_i will continue to find the most suitable W_j and move towards W_j; after C times, if no suitable W_j is found, the following formula is performed:

$$\begin{aligned} W_j &= W_x + (2\text{rand}() - 1) \times D, \\ W_x &= W_x \times (1 + (2\text{rand}() - 1)) \times L). \end{aligned} \tag{4}$$

For aggregation behavior, when the status of artificial fish breeding is W_i, find the most suitable W_c within the detection distance, and the proportion of fish in the artificial pool is less than θ, move W_i to W_c by one step, and gradually form aggregation. If aggregation is not achieved, foraging behavior will be performed [20].

$$W_i = W_i + L \times \text{rand} \times \frac{W_c - W_i}{\left\| W_c - W_i \right\|}. \tag{5}$$

For swimming behavior, when the state of artificial breeding fish is W_i, and it swims freely within the detection distance, this behavior can be regarded as foraging behavior or free swimming behavior.

From the four modes of fish swarms, the tail-chasing behavior indicates that there is an intersection of answers in the process of finding a solution, the foraging behavior is on the way to find the optimal solution, and the aggregation behavior is that the answer to the optimal solution is very close, and swimming behavior indicates no solution. It can be understood that the traditional artificial fish swarm algorithm strengthens the aggregation of fish swarms but reduces the role of individual fish in the swarm. The free swimming of the fish will lead to a larger range of results in the subsequent algorithm, which in turn affects the foraging behavior of the fish [21]. When seeking the optimal solution, it enters a local circle, which is not perfect enough. Therefore, in this paper, the fish swarm algorithm of cloud theory is combined, and the two are modeled, which is also called Zhengtaiyun. Introduce cloud learning factors and cloud variation factors to improve algorithm learning ability in self-learning algorithms. The improved algorithm will be obtained, by comparing the behavior of the fish before with the individual fish, which can greatly improve the degree of learning identification, reduce the free swimming behavior of fish, enhance the aggregation of the optimal solution, and make it possible to search for the optimal solution more quickly [22]. The density here is the function corresponding to the best solution in the largest fish group. When finding the smallest solution, it can be obtained by the inverse of the maximum value. Assuming that the current position of the artificial fish is (x_i, y_i) and the density value is (F_x, F_y), there can be

$$\begin{aligned} R_x &= \frac{F_x}{F_x + F_y} \times x_i + \frac{F_x}{F_x + F_y} \times y_i, \\ R_n &= \frac{D}{L_1}, \\ H_e &= \frac{R_n}{L_2}. \end{aligned} \tag{6}$$

The cloud variation factor is the transformation of a single fish individual into an individual under the new model under the condition of Zhengtai cloud. Let the current position of the artificial fish be x_i and the density of a single artificial fish be F_x, which can be expressed as

$$\begin{aligned} R_x &= x_i, \\ R_n &= \frac{D}{L_3}, \\ H_e &= \frac{R_n}{L_4}. \end{aligned} \tag{7}$$

The random distribution certainty of random fish swarms can be achieved through Zhengtaiyun, which is denoted by G in the text. This is a vague concept that has a certain relationship with probability. In the improved artificial fish swarm algorithm, the distance of fish with high density is small, so as to obtain a suitable specified value, the range of G needs to be dynamically processed by the objective function, and there are two processing methods [23].

Randomness X-condition cloud generator method is expressed as follows:

$$R_x = F_{\max}\text{: } R_n = \frac{F_{\max} - F_{\min}}{L_5}\text{: } H_e = \frac{R_n}{L_6},$$
$$R'_n = \operatorname{randn}\left(R_n, H_e\right)\text{: } G = e^{\left(F' - R_x\right)/-2R'_n\left(F' - R_x\right)/R'_n}. \tag{8}$$

In the X-condition cloud generator, three special values are assigned, which are R_x, R_n, and H_e, and the influence value drop(x_0, G_i) is formed.

Deterministic linear function method is expressed as follows:

$$G = G_{\max} - \frac{F_{\max} - F'}{F_{\max} + F_{\min}}\left(G_{\max} - G_{\min}\right). \tag{9}$$

In the above formula, $F_{\max}$ is the maximum fish school fitness, $F_{\min}$ is the minimum fish school fitness value, $G_{\max}$ is the maximum fish school density due to external influence, and $G_{\min}$ is the minimum fish school density. In general, $G_{\max}$ is within (0.93–1), $G_{\max}$ is selected as 0.96, and $G_{\min}$ is selected as 0.19, which is also a conventional value. It can be seen from the above that the fitness value of the individual fish is inversely proportional to the search range. The larger the value, the smaller the range. When the fitness is the largest, $G = 1$. After the processing operation is carried out, it is brought into (7), and the result is unfavorable for population diversity. When G is 0.95, according to R_n, the value of L_5 is less than 4, which is 3.7. In the normal range, the result of L6 is 5–15, and the value of L6 is 10. Although R_n and H_e play a key role in the model, when multiple calculations are performed, replacement iterations will be performed to replace the previous data, so this has little effect on the values in the following text.

3.5. Segmentation of Sports Images Based on Fish Swarm Algorithm. The pixels of the image are arranged in order from low to high, and the image formed by the pixels needs to be segmented to obtain the core points. Then separate the multiple images of the movement, and segment them from the background image. When the color difference between the background image and the required image is obvious, when the computer processes as high values on both sides, this is the best separation period. If the computer processing is not at the highest level, no image segmentation is required. In this paper, threshold image segmentation is used. In this paper, threshold image segmentation is used. Through the thresholds U and $U \in (0\ ,\ L-1)$, the figure can be divided into two parts, and the background and positioning are B and W, respectively. Assuming that P is the probability of the original gray in Figure 2, $P_t = \sum_{i=0}^{t} p_i$, and then the entropy function is

$$H(t) = H_B + H_W,$$
$$H_B = -\sum_{i=0}^{t}\frac{p_t}{P_t}\ln\frac{p_t}{P_t},$$
$$H_W = -\sum_{i=t+1}^{L-1}\frac{p_t}{P_t}\ln\frac{p_t}{1-P_t}. \tag{10}$$

When $H(t)$ is the maximum value, t^* is the optimal solution. When there are K thresholds in the thresholded image, which is t^K, the entropy function can be calculated to obtain the maximum value; then there are

$$H\left(t_1, t_2, \ldots t_k\right) = -\sum_{i=0}^{t_1}\frac{p_i}{P_{t_0}}\ln\frac{p_i}{P_{t_0}} - \sum_{i=t_1+1}^{t_2}\frac{p_i}{P_{t_1}}\ln\frac{p_i}{P_{t_1}}$$
$$-\cdots\sum_{i=t_k+1}^{L-1}\frac{p_i}{P_{t_k}}\ln\frac{p_i}{P_{t_k}}. \tag{11}$$

The same as above, when $H(t_1, t_2, \ldots t_k)$ is the largest, $t_1^* t_2^* \ldots t_k^*$ is the best solution obtained.

The threshold image segmentation in the artificial fish school is calculated by the maximum value of the entropy value function of the artificial fish school in the original gray image. The threshold value map optimization process of the artificial fish school is shown in Figure 3.

(1) Fish swarm initialization. Suppose that the number of fish schools is S, the number of experiments is C, the fish school detection distance is D, the step size is L, and θ is the proportion of fish schools in the artificial pool.
(2) Calculate the fitness of each fish in the fish group by calculating the entropy function, and arrange the fitness values in order, from small to large; and change the information value at any time, and keep abreast of the dynamic maximum $F_{\max}$ and minimum $F_{\min}$ adaptive value.
(3) Randomly perceive the surrounding of the nth artificial fish, find the optimal artificial fish, and judge whether there is a rear-end relationship between the two. If not, go directly to the next step. If there is, follow the rear-end execution.
(4) Perform processing W_n on a single artificial fish; if the n value is lower than 0.62 k, perform cloud mutation processing on the fish, and if it is greater than 0.62 k, perform a cloud learning phase.
(5) Replace the maximum and minimum fitness values and update them on the dynamic board at any time.
(6) After processing all the individual fish, go to the next step. If not, continue to repeat the previous steps.
(7) Compare the number of updates with the set number of experiments. If the number of updates is greater than the set number, the algorithm terminates; otherwise, the second step is performed. Continue to find the fitness of the fish.

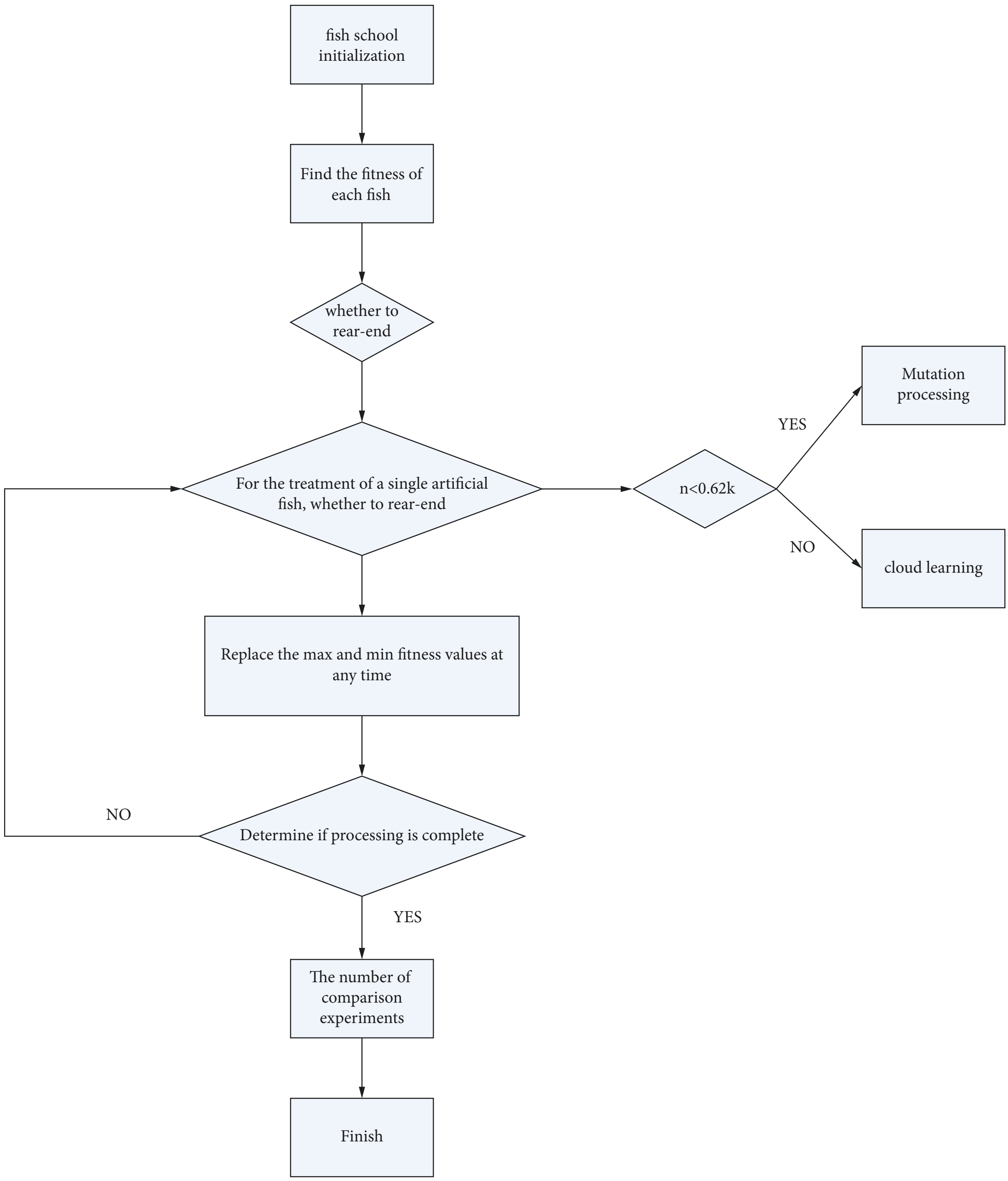

Figure 3: Flowchart of threshold map optimization for artificial fish swarms.

4. Simulation Experiments

In order to verify the effectiveness of the method, the paper uses different emphases as the experimental objects and compares the artificial fish swarm algorithm with particle swarm and genetic algorithm. The traditional motion simulation uses the particle swarm computing method. The experimental equipment and materials were the following: computer with Windows 10, Intel 10, Core(TM) i8-3632QM CPU, and 8G running memory, and the translation tool was Matlab (R2017b). Through many experiments, the effectiveness of the image entity simulation image under human motion, the segmentation of the image processing, the number of core points, and the noise reduction effect are compared. The experimental data are as follows.

Table 1: Initial parameter table.

Evolutionary algorithms	Parameter settings				
CT-AFSA	$S = 22$	$C = 100$	$D = 12$	$L = 10$	$\theta = 0.75$
Related data 1	$S = 22$	$C = 100$	W (min) = 0.38	W (max) = 0.92	Expansion factor
Related data 2	$S = 22$	$C = 100$	Code length = 10	Crossover probability = 0.65	Mutation probability = 0.1

Figure 4: Captured image comparison.

Figure 5: Apple image segmentation comparison.

The two algorithms to be compared need to be compared through a threshold before calculation. In order to ensure consistency, the threshold is uniformly set to 3 in this paper. The reference data obtained in the literature are obtained after experiments and have practical significance. The data sheet is shown in Table 1.

4.1. Captured Moving Images. In the first step, an image of human motion needs to be taken, because the original color hierarchy of the background image and the foreground image is easier to distinguish, so the image is used as a contrast image. The comparison of the captured images is shown in Figure 4.

The comparison in Figure 4 shows that the particle swarm algorithm has no way to clear the background and target of the shooting, and there is chromatic aberration, and the background processing is simple. The fish swarm algorithm can see obvious foreground, background, and color, and, in Figure 4, the distinction of brightness is also more obvious.

4.2. Monotone Background Image. As shown in Figure 5, the apple image of 512×384 is selected because the background is relatively monotonous, and the foreground and background are easier to separate when pixels are separated. From the comparison of the figures, it can be seen that the particle swarm algorithm does not distinguish the background and the foreground clearly, and it is basically impossible to see it. However, the image after the fish swarm algorithm can save the original image information, and, for

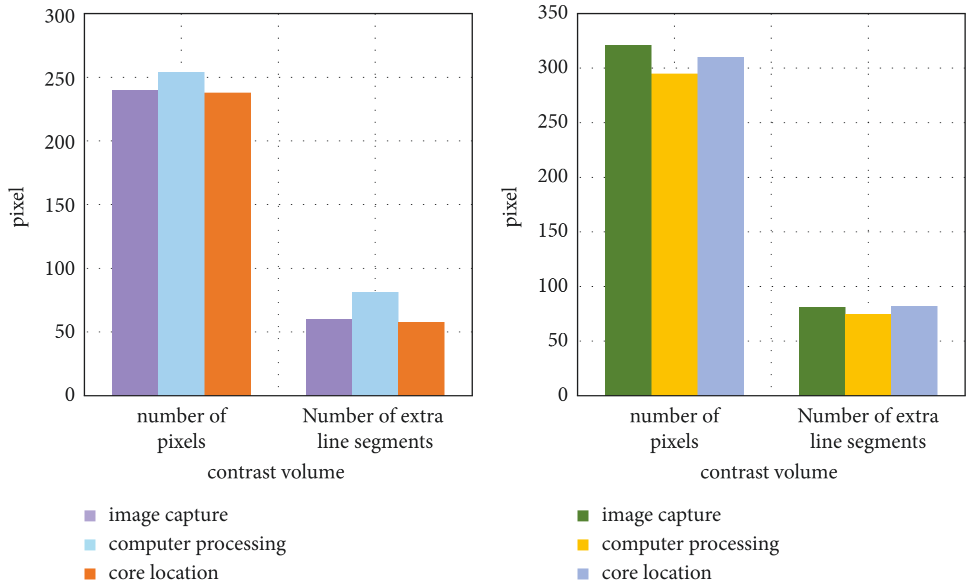

Figure 6: Core point comparison of pixel points.

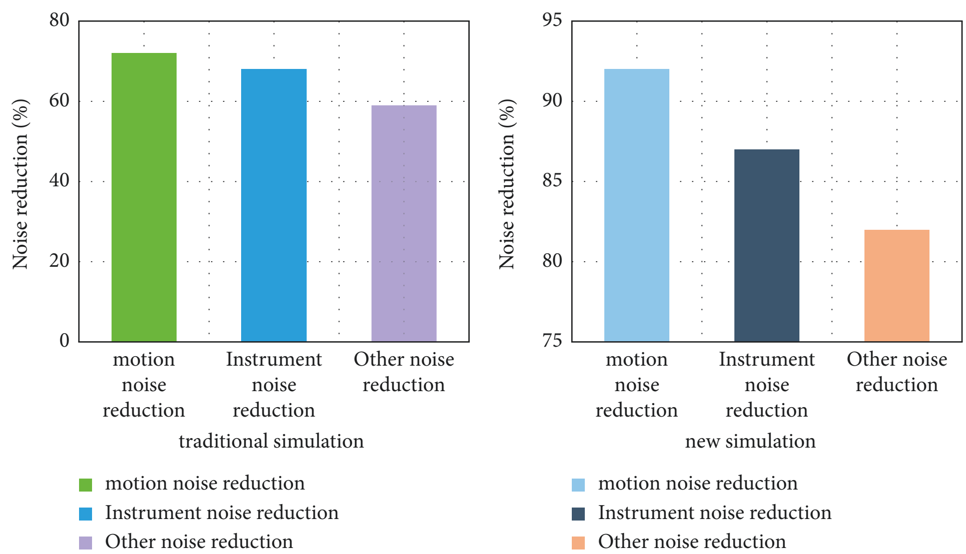

Figure 7: Comparison of traditional simulation and new noise reduction.

the information expression of the foreground edge, the particle swarm algorithm is not easy to distinguish between the foreground and the background, which is not conducive to the expression of the internal and edge information of the image.

For the physical simulation of human motion, the arrangement of the pixel points is arranged according to certain rules. However, in the physical simulation of traditional sports, there will be redundant line segments, the core points of the pixel points are judged by the number of line segment connections, and the number of core points is judged by the data of the two physical simulations, as shown in Figure 6.

Through comparison, it is found that the pixel core point of the traditional entity simulation is lower than that based on the fish swarm algorithm, and it is increased by about 35% on the traditional basis. The image obtained in this way is also more vivid, and there is no rough room. The core point reflects the key position of sports. The more core points, the more accurate the capture of sports.

When capturing moving images, it is necessary to remove the external sound and then better input into the system for information processing. After processing by the computer, ensure the stability of the computer, because the information with sound is entered into the system will have an impact on the simulation model. The noise reduction comparison between the two is shown in Figure 6. The simulation paper based on the fish swarm algorithm becomes a new type of simulation, as shown in Figure 7.

By comparing the noise reduction effect between the two, it is found that the simulation calculation based on the fish swarm algorithm is 20.3% higher compared to the traditional simulation. At the same time of simulation, it also restores the real motion, well preserves the integrity of the information input to the computer, and also has a good effect on noise reduction of other effects and has obvious optimization in traditional simulation technology.

5. Conclusions

In this paper, the physical simulation of traditional sports is compared through sports based on fish swarm algorithm. Through the shortcomings of traditional simulation, the moving entity simulation technology of fish swarm algorithm is introduced. By comparing the effectiveness of the simulated image under human motion, the segmentation of the image processing, the number of core points for the 3D model, and the noise reduction of the two in computer processing, the results found that the physical simulation based on the fish swarm algorithm is more restored on the image, and the captured figures are more segmentable, and the more core points, the more accurate the 3D model, and the noise reduction effect is also improved by 20.3%. The inadequacy of this paper is that the physical simulation is not verified by other algorithms, and only the fish swarm algorithm is verified in the physical simulation. The data referenced in this article also has a certain year, and there may be some errors in the experimental data. With the gradual development of current science and technology, the simulation technology for moving entities will become more mature, and more and more suitable algorithms will be used in entity simulation. The obtained data will also be more accurate, and the influence of external factors on the simulation entity can be excluded. This paper studies the physical simulation of sports, which has certain reference significance for the physical simulation technology.

Data Availability

The data used to support the findings of this study are available from the author upon request.

Conflicts of Interest

The author does not have any possible conflicts of interest.

References

[1] C. Ma and R. He, "Green wave traffic control system optimization based on adaptive genetic-artificial fish swarm algorithm," *Neural Computing & Applications*, vol. 31, no. 7, pp. 2073–2083, 2019.

[2] X. Zhu, Z. Ni, and M. Cheng, "Haze prediction method based on multi-fractal dimension and co-evolution discrete artificial fish swarm algorithm," *Systems Engineering-Theory & Practice*, vol. 37, no. 4, pp. 999–1010, 2017.

[3] X. Zhai and L. Ma, "Medium and long-term wind power prediction based on artificial fish swarm algorithm combined with extreme learning machine," *International Core Journal of Engineering*, vol. 5, no. 10, pp. 265–272, 2019.

[4] S. Yili, "Research on the application of computer simulation technology in the field of physical education," *Agro Food Industry Hi-Tech*, vol. 28, no. 1, pp. 1617–1620, 2017.

[5] L. T. Song and J. J. Chen, "Research on automotive anti-lock braking system based on simulation technology," *Agro Food Industry Hi-Tech*, vol. 28, no. 1, pp. 917–921, 2017.

[6] F. Wang, W. Liao, and G. Yu, "Physical characteristics modeling and deformation simulation technology for flexible cable harness based on exact Cosserat model," *Jisuanji Fuzhu Sheji Yu Tuxingxue Xuebao/Journal of Computer-Aided Design and Computer Graphics*, vol. 29, no. 7, pp. 1343–1355, 2017.

[7] C. Ge, Y. Zhu, and Y. Di, "Basic theoretical issues of equipment parallel simulation technology," *Xi Tong Gong Cheng Yu Dian Zi Ji Shu/Systems Engineering and Electronics*, vol. 39, no. 5, pp. 1169–1177, 2017.

[8] Z. Huang, Y. Zhang, Q. Li et al., "Joint analysis and weighted synthesis sparsity priors for simultaneous denoising and destriping optical remote sensing images," *IEEE Transactions on Geoscience and Remote Sensing*, vol. 58, no. 10, pp. 6958–6982, 2020.

[9] E. Q. Wu, P. Xiong, Z. R. Tang, G. J. Li, A. Song, and L. M. Zhu, "Detecting dynamic behavior of brain fatigue through 3-d-CNN-LSTM," *IEEE Transactions on Systems, Man, and Cybernetics: Systems*, vol. 52, no. 1, pp. 90–100, 2022.

[10] J. Zhang, W. Feng, T. Yuan, J. Wang, and A. K. Sangaiah, "SCSTCF: spatial-channel selection and temporal regularized correlation filters for visual tracking," *Applied Soft Computing*, vol. 118, Article ID 108485, 2022.

[11] Z. Huang, Y. Zhang, Q. Li et al., "Unidirectional variation and deep CNN denoiser priors for simultaneously destriping and denoising optical remote sensing images," *International Journal of Remote Sensing*, vol. 40, no. 15, pp. 5737–5748, 2019.

[12] E. Q. Wu, D. Hu, P. Y. Deng et al., "Nonparametric bayesian prior inducing deep network for automatic detection of cognitive status," *IEEE Transactions on Cybernetics*, vol. 51, no. 11, pp. 5483–5496, 2021.

[13] H. H. Tung, "Embracing renovation and innovation during the pandemic: application of virtual simulation technology in nurse practitioner education," *Hu li za zhi The journal of nursing*, vol. 68, no. 5, pp. 7–12, 2021.

[14] A. P. Cockerill and U. Satish, "Real-world implications of high-performance competencies and strategic management simulation technology," *Journal of Applied Social Psychology*, vol. 51, no. 12, pp. 1145–1150, 2021.

[15] T. Ryosuke, H. Nobuyuki, I. Tomoyuki et al., "Analysis of Wetting and Coalescing Behavior of Minute Ink Droplets by MPS Simulation," *Nihon Gazo Gakkaishi*, vol. 55, no. 2, pp. 176–183, 2016.

[16] C. Liu, L. Liu, and C. Liu, "Analysis of wind resistance of high-rise building structures based on computational fluid dynamics simulation technology," *International Journal of Heat and Technology*, vol. 36, no. 1, pp. 376–380, 2018.

[17] P. Hou, Y. Ning, and Y. Song, "Retraction Note: an auxiliary training system for swimming in coastal areas based on remote sensing images and virtual simulation technology," *Arabian Journal of Geosciences*, vol. 14, no. 24, p. 2817, 2021.

[18] I. N. Raptanova, N. V. Streneva, O. V. Strizhkova, and N. V. FomichenkoYankina, "Bachelors' independent work: stages of organization through the application of simulation technology," *Humanities & Social Sciences Reviews*, vol. 8, no. 2, pp. 296–304, 2020.

[19] L. You, H. Jiang, J. Hu et al., "GPU-Accelerated Faster Mean Shift with Euclidean Distance Metrics," 2021, https://arxiv.org/abs/2112.13891.
[20] H. Wang and R. Wen, "Ground-motion simulation for the MW6.1 Ludian earthquake on 3 August 2014 using the stochastic finite-fault method," *Earthquake Science*, vol. 32, no. 3-4, pp. 101–114, 2019.
[21] Y. Xiang, S. Tahmid, and P. Owens, "Single task optimization-based planar box delivery motion simulation and experimental validation," *Journal of Mechanisms and Robotics*, vol. 13, no. 2, pp. 1–18, 2021.
[22] S. H. An, J. B. Kyung, S. G. Kyung, H. Song, and H. Cho, "Analysis of intensity attenuation characteristics using physics-based earthquake ground-motion simulation with site effect in the southern Korean peninsula," *Journal of the Korean Earth Science Society*, vol. 41, no. 3, pp. 238–247, 2020.
[23] H. Choi, "Strong ground motion simulation at seismic stations of metropolises in South Korea by scenario earthquake on the causative fault of the 2016 gyeongju earthquake," *Journal of the Earthquake Engineering Society of Korea*, vol. 24, no. 2, pp. 59–65, 2020.

Hindawi
Computational Intelligence and Neuroscience
Volume 2022, Article ID 3410153, 6 pages
https://doi.org/10.1155/2022/3410153

Research Article

Application of Improved VMD-LSTM Model in Sports Artificial Intelligence

Tiancong Zhang[1] and Caihua Fu [2]

[1]*School of Physical Education, Sanya University, Sanya 572000, China*
[2]*School of Management, Sanya University, Sanya 572000, China*

Correspondence should be addressed to Caihua Fu; caihuafu@sanyau.edu.cn

Received 19 June 2022; Accepted 29 June 2022; Published 14 July 2022

Academic Editor: Xin Ning

In recent years, with the rapid development of a new generation of artificial intelligence technology, how to deeply apply artificial intelligence technology to physical education and break through the limitations of time-space scenarios and knowledge transfer methods in traditional models has become a key issue in intelligent physical education in the era of artificial intelligence. In order to realize the online monitoring of wearable devices with artificial intelligence in sports and overcome the problem of low recognition accuracy of electrocardiogram, blood oxygen, and respiratory signals in many cases, this paper proposes a combination of variational modal decomposition based on the maximum envelope kurtosis method. Long-short-term neural network (VMD-LSTM) monitoring method for wearable sports equipment. Through experimental analysis and verification, the current signal of the VMD model shows a trend of fluctuating from large to stable and then to large with motion, while the training accuracy of LSTM after the 150th iteration is 94.09%, which shows that the coupling model VMD LSTM can better predict the direction of sports artificial intelligence. In addition, although the training time of the BP neural network is shorter than that of the LSTM model, there is a large gap between the recognition effect and the LSTM, and there are also large differences between different neural network structures. This shows that the VMD-LSTM model has broad application prospects in such models.

1. Introduction

Artificial intelligence (Artificial Intelligence, referred to as "AI") is a discipline that studies how to make machines do things that humans need intelligence to accomplish [1]. Artificial intelligence has experienced the early game, expert system, and other algorithmic models and has developed to the current research direction of machine learning and deep learning [2]. Artificial intelligence is essentially a branch of computer science. With the rapid iterative update of computer technology, it shows stronger intelligence and practicability and is generally accepted by the public. My country's artificial intelligence started late, and there is still a certain gap compared with developed countries such as the United States. Physical education is one of the important contents of the implementation of comprehensive quality education in my country, and it has a basic supporting role in improving the national physique and improving the quality of life [3]. In recent years, the rapid development of a new generation of artificial intelligence technology has had a significant impact on the content, mode, method, and system of traditional physical education [4]. How to deeply apply artificial intelligence technology to physical education and break through the limitations of time-space scenarios and knowledge transfer methods in traditional models has become a key issue in intelligent physical education in the era of artificial intelligence.

In recent years, sports artificial intelligence research, the main subject is computer science, and the algorithm empirical research of basic theory is preferred [5]. It mainly involves the use of neural network-based machine learning-related algorithms, involving sports performance prediction [6], human action recognition and evaluation [7], technical and tactical decision support, sports injury assessment, etc.

[8, 9], [10] As the most important research direction in the field of artificial intelligence in recent years, deep learning (Deep Learning) is a kind of intelligent learning algorithm based on deep neural network and representation level, so as to obtain humanlike analytical learning ability, thus promoting the progress of artificial intelligence related technologies [11, 12]. Among them, the human posture recognition technology in deep learning is a technology that can accurately describe the posture and behavior by sensing the structural parameters of human limbs through sensing signals, images, and other data [13]. Detection of human skeleton joints is the core problem of pose recognition [14]. Since 2012, the rapid development of deep learning technology has promoted the continuous improvement of the detection effect of human skeleton joints [15].

Aiming at the lack of error correction design in the traditional Long and Short-term Memory Network (LSTM) structure [16], a sports artificial intelligence based on Variational Modal Decomposition (VMD) was proposed. Intelligent models [17, 18]. Combining the new ideas of "artificial intelligence" with the needs of sports provides a beneficial guarantee for meeting the needs of scientific training. Based on the VMD-LSTM model and the design and use of portable equipment, this paper constructs a sports monitoring service system, which combines a new method of artificial intelligence to analyze the real-time parameters of the sports process. By establishing this service model, the physical activity of athletes can be monitored.

2. Principles and Methods

2.1. Metamorphic Mode Decomposition. Variational mode decomposition is an adaptive signal processing method proposed in 2014. By iteratively searching for the optimal solution of the variational mode, the modal function and center frequency are continuously updated to obtain several modes with a certain bandwidth function [19]. Variational modal decomposition is an improvement of the EMD algorithm, which has the advantage of better avoiding modal aliasing and end-point effects [20]. Metamorphic Mode Decomposition.

Variational mode decomposition decomposes wearable sports equipment into several eigenmode functions (IMFs) with center frequencies on the premise that each decomposed eigenmode function has a limited bandwidth, by constructing and solving a variational problem to find each eigenmode function and its center frequency [21]. The VMD method decomposes the signal into predefined K eigenmode components IMF, where the IMF is redefined as an AM-FM signal.

$$u_k(t) = A_k(t)\cos(\phi_k(t)). \tag{1}$$

The accuracy of the decomposition result of the VMD algorithm depends on the number of modes K and the value of the penalty factor. If the value of K is too large, it will cause excessive signal decomposition, so that a component determined by the center frequency will be scattered in different eigenmode components; while the value of K is too small, it will cause modal aliasing, that is, different centers. The frequency signal components are in the same eigenmode component after being decomposed by VMD, resulting in components that have no practical significance. Both of these cases can lead to inaccurate results of the decomposition. The value of α will affect the frequency bandwidth of each modal obtained after the signal is decomposed by the variational modal decomposition algorithm, the degree of modal aliasing and the speed of the algorithm. If the value of the penalty factor α is too small, the bandwidth of each frequency is too large, and similar frequencies are mistaken for the large bandwidth part of the same center frequency so that they are decomposed into the same component, and the problem of modal aliasing occurs. When the value is too large, part of the bandwidth is reduced, which may cause the signal to be overresolved and spurious components appear. Therefore, the selection of appropriate parameter values is crucial to the accuracy of the PPG signal decomposition results [22].

2.2. LSTM Model. Long Short-Term Memory (LSTM) is a temporal recurrent neural network [2]. The outstanding contribution of this network lies in the use of the self-loop design, and the weight of the self-loop can also be updated in each loop iteration, thus cleverly avoiding the gradient dispersion problem that occurs when the recurrent neural network model updates the weights [23].

Each hidden node of the LSTM network model contains a storage unit, and the entrance of the storage unit is controlled by some logic units. These control units are generally called "gates." At the entrance of each hidden unit, there are three gates, namely, input gate, output gate, and forget gate [24]. The input gate is used to selectively save the input data, the output gate is used to determine when to output the value, and the forget gate is used to determine when the value should be memorized or forgotten [25]. Hidden nodes are shown in Figure 1. In the whole model, the parameters of the input gate, output gate, and forget gate in each hidden node are learned during the training process [26]. The calculation formulas for the three gates are as follows:

$$\begin{aligned}
\mathbf{i_t} &= \boldsymbol{\sigma}(\mathbf{W_{xi}x_t} + \mathbf{W_{hi}h_{t-1}} + \mathbf{b_i}),\\
\mathbf{o_t} &= \boldsymbol{\sigma}(\mathbf{W_{xo}x_t} + \mathbf{W_{ho}h_{t-1}} + \mathbf{b_o}),\\
\mathbf{f_t} &= \boldsymbol{\sigma}(\mathbf{W_{xf}x_t} + \mathbf{W_{hf}h_{t-1}} + \mathbf{b_f}),\\
\mathbf{c_t} &= \mathbf{f_t c_{t-1}} + \mathbf{i_t}\,\mathbf{tanh}(\mathbf{W_{xc}x_t} + \mathbf{W_{hc}h_{t-1}} + \mathbf{b_c}),\\
\mathbf{h_t} &= \mathbf{o_t}\,\mathbf{tanh}(\mathbf{c_t}).
\end{aligned} \tag{2}$$

3. Experimental Procedure and Result Analysis

3.1. Feature Extraction Using VMD Method. The maximum envelope kurtosis method is used to determine the optimal decomposition level K of the VMD, randomly extract several groups of current signals from the first group, and use the maximum envelope kurtosis method for analysis. By observing the variation trend of the local maximum envelope

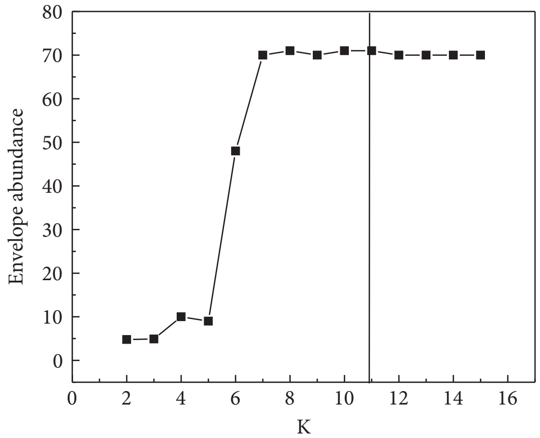

Figure 1: Variation Trend of maximum envelope kurtosis.

kurtosis in Figure 1, it can be found that the envelope kurtosis is the largest when $K = 11$.

So take $K = 11$ VMD for current signal processing. It can be seen from the decomposed current signal that IMF1, IMF2, and IMF3 are low-frequency signals, the frequency components are relatively single, and the main frequency components of the current signal are concentrated in the low-frequency current signal. Therefore, the features of the first three IMFs can be directly extracted to represent the movement and detect changes in parameters. There are interference signals such as noise in the high-frequency signal of the current signal, and after calculation, the signal-to-noise ratio in the high-frequency signal is less than 0, which is dominated by noise, and the soft threshold denoising method needs to be used for denoising. The original signal can be regarded as the sum of the decomposed IMFs, so the high-frequency signal can be simplified as follows:

$$\mathrm{IMF}_h = \sum_{i=4}^{11} \mathrm{IMF}_i \, i = 4, 5, \ldots, 15. \tag{3}$$

It can be seen from the calculation that the amplitude of the curve of the denoised signal is smaller than that of the high-frequency signal, which means that some noise is removed and the characteristics of the tool wear signal are preserved. The signal-to-noise ratio of the high-frequency signal before denoising is 6.581 dB, and the signal-to-noise ratio after denoising is improved to 2.024 dB.

Since it is difficult to find the relationship between the signal and sports parameters by directly observing the signal, the original signal is processed to extract features that are related to the body motion parameters. This paper extracts 7-dimensional time domain features, including mean, root mean square, peak value, standard deviation, variance, and kurtosis factor, margin factor; 2-dimensional frequency domain feature, including barycentric frequency and frequency energy value, extracting the mean, root mean square, and peak value of 3 low-frequency IMFs, and one high-frequency IMF, a total of 21 dimension features. Since the classification of sports parameters under multiple working conditions in this paper needs to consider the influence of parameters such as heart rate on the current signal, the three sports parameters are also classified as features, with a total of 24-dimensional features. The model training speed will be slowed down due to too many feature dimensions, and there may be features that are not related to motion parameters in these features. In this paper, the SelectKBest class in the feature-selection of the Python library is combined with the mutual information method to filter the features, and the 6-dimensional features plus 3 cutting parameters are selected from the 21-dimensional feature parameters as the model input.

3.2. Validation of Model Recognition Effect. A total of 921 groups of experimental data were collected in this experiment, and the number of experimental data in each group. Taking the first group as an example, the current signal is divided into three stages, the initial stage of exercise, the middle stage of exercise, and the later stage of exercise. The variation trend of the current signal eigenvalues with motion is shown in Figure 2.

It can be observed from Figure 2 that in the initial stage, the current signal fluctuates greatly, because the body movement state is good, and the body function parameters have not yet adapted to the body. In the normal stage, the current change is relatively gentle, and in the severe stage, it rises sharply, which is caused by the sudden strengthening of the exercise state after the exercise adaptation.

3.3. Normalization. Since there are few initial and late samples in each group of experiments, normal samples occupy the vast majority, and unbalanced samples will affect the final classification effect. Therefore, the SMOTE algorithm is used to oversample the interval with fewer samples. This method is used in minority samples. New sample points are generated on the Euclidean distance [27]. After dividing the 4 groups of experimental data into 3 intervals, the training set and the test set are divided according to the ratio of 3:1. For the multiclassification model, the output label corresponding to each state needs to be coded. In this paper, the One-Hot coding method is used. The data set composed of features after optimization needs to be normalized before classification, and the normalization formula is

$$x = \frac{x - x_{\min}}{x_{\max} - x_{\min}}. \tag{4}$$

As a variant of Recurrent Neural Network (RNN), LSTM can better avoid the problem of gradient disappearance and can effectively deal with the long-term dependency problem [1]. Due to the small number of samples collected, this paper designs a model with only a single LSTM layer, the number of LSTM neural units is set to 30, the batch size is set to 32, the cross entropy is selected as the loss function, and the Adam optimization algorithm is used to optimize the model parameters [28], and the structure of the LSTM model is shown in Table 1.

Figure 3 shows the accuracy and loss curve of the LSTM model training process. It can be observed from the figure

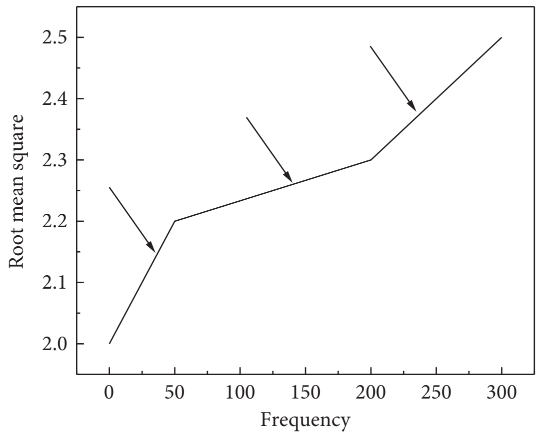

Figure 2: Trend chart.

Table 1: Inspection and test results of external wall damage.

LSTM model structure	Neurons of each layer quantity	Incentive at all levels function	Input of each layer dimension<
Input layer	Feature dimension	—	(None, 1)
LSTM layer	30	Sigmoid	(None, 30)
Full connection layer	8	ReLu	(None, 8)
Output layer	3	Softmax	(None, 3)

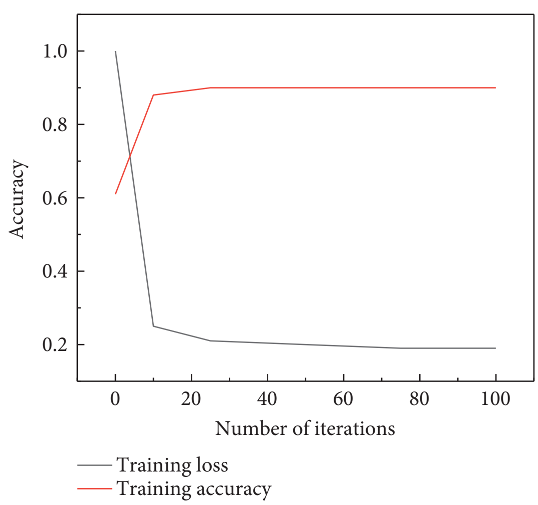

Figure 3: Model accuracy training and loss curve.

that the training accuracy value and loss tend to converge after the 150th iteration, and the training accuracy during the training process reaches 94.09%. The classification accuracy rate on the test set reached 92.44%. The loss rate is another way of expressing the accuracy. The loss rate in Figure 3 is stable at about 10% after multiple iterations, which indicates that the model selected in this study has good accuracy and strong applicability. It can be concluded that the model has high recognition accuracy and strong generalization ability, which can meet the recognition requirements of actual motion state parameters. The selected features can better characterize the change of motion state, which is similar to the research results of some scholars [29].

In order to verify the superiority of the model in this paper for the recognition of motion states under multiple working conditions, this paper uses empirical mode decomposition (EMD) and ensemble empirical mode decomposition to construct different feature vectors for the same sample set [28] and uses the LSTM model for Classification [30], the final result is far from the method in this paper, and the accuracy is not high. And, this paper compares the LSTM model with the traditional machine learning method Support Vector Machine (SVM) and BP neural network, in which the kernel function parameter σ and penalty factor C of SVM use particle swarm optimization algorithm to find the best parameters, respectively, are 11.580 and 12.926. The BP neural network adopts the structure of $30 \times 8 \times 3$, and the number of iterations is 500 times. In order to avoid experimental chance, each model was tested 5 times to take the average of the accuracy of the test set. Table 2 shows the test results of the model.

It can be seen from the table that the training time of SVM is longer than that of LSTM, and the accuracy of the test set is lower than that of LSTM. The data samples in this paper are changed from 921 to 1851 groups after sample synthesis. Efficiency is lower. Although the training time of the BP neural network is shorter than that of the LSTM model, there is a big gap between the recognition effect and LSTM, and there are also big differences between different neural network structures, which is similar to the research results of some scholars [31].

4. Model Predictions

In the research on the physical health of different groups of people, intelligent wearable devices based on machine learning and deep learning algorithms can identify, monitor, and analyze the muscular endurance and physical activity status of people with different physical fitness, including children, adolescents, and adults. Proposing exercise methods suitable for individuals with different physical conditions can promote the formation of healthy living habits.

In the monitoring test, there are many factors that affect the effect of sports wearable devices, including respiratory rate, heart rate, and real-time measurement of hemoglobin. The measurement of respiratory rate is affected by detection time and exercise intensity. Therefore, to obtain accurate respiratory frequency measurement, it is necessary to remove the influence of clutter on the respiratory measurement results. The least mean square can solve the respiratory frequency well, so the system decides to use the least mean square respiratory signal filtering algorithm as the main technology of this module. If all the influencing factors are considered, the experiment becomes very complicated and requires a huge cost. Therefore, the simplified variables in this paper are the fluctuation of electrocardiogram, respiratory signal, and monitoring of blood oxygen concentration.

Table 2: Model test results.

Classification model	Test set average classification accuracy (%)	Optimal classification of test set accuracy (%)	Train time (S)
LSTM	93.78	94.02	83.35
PSO-SVM	90.43	91.67	89.49
BP neural network	88.59	89.21	39.86

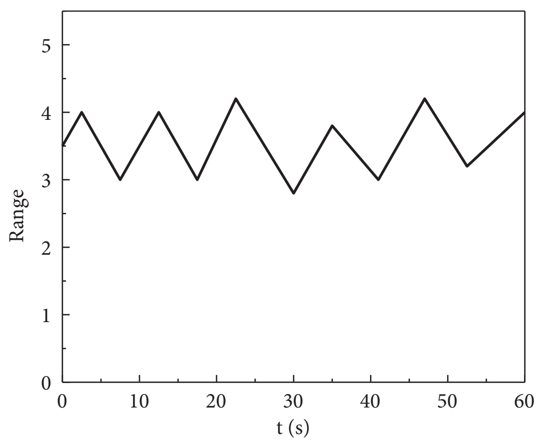

Figure 4: Respiratory signal after filtering respiratory signal using least mean square.

The electrocardiogram is an electrical activity process that reflects the excitement of the heart. It has important medical reference significance and reflects the activity process of the human body's electrocardiogram. It has considerable medical and sports measurement importance. In the ECG monitoring part, the system uses textile electrodes as the main material, because when the material contacts the skin, an equivalent capacitance C1 will be generated, which can achieve signal impedance matching and improve the sensitivity and accuracy of signal detection. The single-lead ECG measurement module made of textile electrodes is placed at two points on the surface of the human body. By measuring the potential difference between the two points, the signal can be transmitted to the analog ECG signal conversion interface through the wire, as shown in Figure 4.

The respiratory signal spectrum after filtering processing has regular breathing fluctuation as a whole, and the fluctuation is stable. The maximum amplitude of the fluctuation is 1.5 V, which occurs between 21 and 29 seconds. Within seconds, it can be seen that the monitored exercise participant's breathing is stable, the exercise training intensity is reasonable, and there is no need to adjust the amount of exercise. The least mean square can solve the respiratory frequency well, so the system decides to use the least mean square respiratory signal filtering algorithm as the main technology of this module. The least-mean-square respiratory signal filtering algorithm consists of five operating modules, firstly measuring n times of inhalation signal x, then measuring n times of exhalation signal e, and then adding the two different signals to calculate the sum signal frequency value, then the three-axis acceleration and the breathing signal are input into the digital filter together, and the breathing signal processed by the digital filter is then output for correlation detection. In square algorithm operation, the operation result will be input into the digital filter again, so as to reciprocate until the error is wirelessly reduced and the error is corrected continuously, so as to obtain the accurate respiratory data measurement signal. Capture, the process of data capture is the real-time measurement of human body functions such as heart rate and hemoglobin by wearable devices, so the monitor of the wearable device becomes the key device for this step.

5. Conclusion

Based on the perspective of the era of intelligence, on the basis of traditional sports and with the help of deep learning technology in the field of artificial intelligence, this research proposes an intelligent evaluation algorithm for sports wearable devices. Sports smart wearable system. In order to realize the online monitoring of wearable devices with artificial intelligence in sports and overcome the problem of low recognition accuracy of electrocardiogram, blood oxygen, and respiratory signals in many cases, this paper proposes a combination of variational modal decomposition based on the maximum envelope kurtosis method. Long-short-term neural network (VMD-LSTM) monitoring method for wearable sports equipment. Through experimental analysis and verification, the following conclusions are drawn: (1) in the early stage of the exercise, the current signal fluctuates greatly, and the current changes relatively gently in the normal stage, and then rises sharply in the severe stage; (2) after the 150th iteration, the training accuracy value, and the loss tends to converge, in which the training accuracy reached 94.09% during the training process, and the classification accuracy of the model on the test set reached 92.44%; (3) the training time of SVM is longer than that of LSTM, and the testing time is longer than that of LSTM. The accuracy rate of the set is lower than that of LSTM, and the efficiency of using SVM is relatively low; (4) although the training time of the BP neural network is shorter than that of the LSTM model, the recognition effect has a large gap with LSTM, and there are also differences between different neural network structures.[32], [33].

Data Availability

The data used to support the study are included in the paper.

Conflicts of Interest

The authors declared that there is no conflict of interest.

References

[1] A. Ligeza, "Artificial intelligence: a modern approach," *Applied Mechanics and Materials*, vol. 263, no. 2, pp. 2829–2833, 2009.

[2] T. H. Wen, M. Gasic, N. Mrksic, P. H. Su, D. Vandyke, and S. Young, "Semantically conditioned LSTM-based natural language generation for spoken dialogue systems," in *Proceedings of the 2015 Conference on Empirical Methods in Natural Language Processing*, arXiv, 2015.

[3] Z. Jin, D. He, Y. Chen, C. Liu, and S. Shan, "Research on fault diagnosis method of train rolling bearing based on variational modal decomposition and bat algorithm-support vector machine," *Journal of Physics: Conference Series*, vol. 1820, no. 1, Article ID 012170, 2021.

[4] F. Chollet, "Xception: deep learning with depthwise separable convolutions," in *Proceedings of the 2017 IEEE Conference on Computer Vision and Pattern Recognition (CVPR)*, 2017.

[5] L. Ying, Z. Qian Nan, W. Fu Ping et al., "Adaptive weights learning in CNN feature fusion for crime scene investigation image classification," *Connection Science*, vol. 33, no. 3, pp. 719–734, 2021.

[6] X. Liu and H. Wang, "Research on the training strategy of aerobic physical education talents under the background of artificial intelligence era," *Applied Bionics and Biomechanics*, vol. 2022, pp. 1–7, 2022.

[7] J. Liu, A. Shahroudy, D. Xu, A. C. Kot, and G. Wang, "Skeleton-Based Action Recognition Using Spatio-Temporal LSTM Network with Trust Gates," *IEEE Transactions on Pattern Analysis & Machine Intelligence*, vol. 40, no. 99, pp. 3007–3021, 2017.

[8] J. Pavitt, D. Braines, and R. Tomsett, *Cognitive Analysis in Sports: Supporting Match Analysis and Scouting through Artificial Intelligence*, 2021.

[9] X. Wang, G. Sui, J. Xiang, G. Wang, Z. Huo, and Z. Huang, "Multi-domain extreme learning machine for bearing failure detection based on variational modal decomposition and approximate cyclic correntropy," *IEEE Access*, vol. 8, pp. 197711–197729, 2020.

[10] X. M. Yang, C. X. Qu, T. H. Yi, H. N. Li, and H. Liu, "Modal analysis of a bridge during high-speed train passages by enhanced variational mode decomposition," *International Journal of Structural Stability and Dynamics*, vol. 20, no. 13, Article ID 2041002, 2020.

[11] X. Chen, "Research on the application of artificial intelligence technology in the field of sports refereeing," *Journal of Physics: Conference Series*, vol. 1952, no. 4, Article ID 042048, 2021.

[12] A. Zhu, Q. Wu, R. Cui et al., "Exploring a rich spatial-temporal dependent relational model for skeleton-based action recognition by bidirectional LSTM-CNN," *Neurocomputing*, vol. 414, no. 5, pp. 90–100, 2020.

[13] N. J. Nilsson, "Artificial intelligence: a modern approach," *Applied Mechanics and Materials*, vol. 263, no. 5, pp. 2829–2833, 2003.

[14] T. Liu, D. Wilczynska, M. Lipowski, and Z. Zhao, "Optimization of a sports activity development model using artificial intelligence under new curriculum reform," *International Journal of Environmental Research and Public Health*, vol. 18, no. 17, p. 9049, 2021.

[15] H. Zhao, S. Guo, and D. Gao, "Fault feature extraction of bearing faults based on singular value decomposition and variational modal decomposition," *Journal of Vibration and Shock*, vol. 118, no. 1–2, pp. 477–502, 2016.

[16] J. Yang, L. Tang, and X. W. Li, "Research on face recognition sports intelligence training platform based on artificial intelligence," *The International Journal on Artificial Intelligence Tools*, vol. 30, no. 06n08, 2021.

[17] M. Zhou, T. Hu, K. Bian et al., "Short-term electric load forecasting based on variational mode decomposition and grey wolf optimization," *Energies*, vol. 14, no. 16, p. 4890, 2021.

[18] W. Shan, "Digital streaming media distribution and transmission process optimisation based on adaptive recurrent neural network," *Connection Science*, vol. 34, no. 1, pp. 1169–1180, 2022.

[19] A. Lapham and R. M. Bartlett, "The use of artificial intelligence in the analysis of sports performance: a review of applications in human gait analysis and future directions for sports biomechanics," *Journal of Sports Sciences*, vol. 13, no. 3, pp. 229–237, 1995.

[20] J. Liu, A. Shahroudy, X. Dong, and W. Gang, "Spatio-temporal LSTM with trust gates for 3D human action recognition," *European Conference on Computer Vision (ECCV)*, pp. 816–833, 2016.

[21] H. Li, G. Zhu, L. Zhang, J. Song, and P. Shen, "Graph-temporal LSTM networks for skeleton-based action recognition," *Pattern Recognition and Computer Vision*, vol. 34, no. 1, pp. 990–1004, 2020.

[22] Z. Yu, S. Li, L. N. U. Sun, L. Liu, and W. Haining, "Multi-distribution noise quantisation: an extreme compression scheme for transformer according to parameter distribution," *Connection Science*, 2022.

[23] S. Yi, X. Wang, and X. Tang, "Deep learning face representation by joint identification-verification," *Advances in Neural Information Processing Systems*, vol. 27, 2014.

[24] B. Alipanahi, A. Delong, M. T. Weirauch, and B. J. Frey, "Predicting the sequence specificities of DNA- and RNA-binding proteins by deep learning," *Nature Biotechnology*, vol. 33, no. 8, pp. 831–838, 2015.

[25] G. Wang, M. Li, W. Guo, K. Cengiz, and R. Tomar, "Research on recognition method of sports injury parts based on artificial intelligence enabled 3D image simulation analysis," *International Journal of System Assurance Engineering and Management*, vol. 1, pp. 1–11, 2021.

[26] J. Miao, Z. Wang, X. Ning, N. Xiao, W. Cai, and R. Liu, "Practical and secure multifactor authentication protocol for autonomous vehicles in 5G. Software: practice and Experience," *Journal of Network and Computer Applications*, vol. 131, no. 1, 2022.

[27] F. Rossi, P. V. Beek, T. Walsh, and I. Booksx, *Handbook of Constraint Programming: Foundations of Artificial Intelligence*, Elsevier Science Inc, Amsterdam, Netherlands, 2006.

[28] J. Xu, "A Novel Method of Bolt Detection Based on Variational Modal Decomposition," *Transactions of Nanjing University of Aeronautics and Astronautics*, vol. 36, no. 4, pp. 628–634, 2017.

[29] W. Cai, B. Zhai, Y. Liu, R. Liu, and X. Ning, "Quadratic polynomial guided fuzzy C-means and dual attention mechanism for medical image segmentation," *Displays*, vol. 70, Article ID 102106, 2021.

[30] A. Zhang, Z. A. Zhang, B. A. Bai, N. B. Ning, and A. Zhou, "Uncertainty Estimation for Stereo Matching Based on Evidential Deep Learning," *Pattern Recognition*, vol. 124, 2021.

[31] R. Q. Charles, H. Su, M. Kaichun, and L. J. Guibas, "PointNet: deep learning on point sets for 3D classification and segmentation," in *Proceedings of the 2017 IEEE Conference on Computer Vision and Pattern Recognition (CVPR)*, July2017.

[32] Geert, T. Litjens, Kooi, Babak, Ehteshami, and Adiyoso, "A Survey on Deep Learning in Medical Image Analysis," *Medical Image Analysis*, vol. 42, pp. 60–88, 2017.

[33] Z. Huang, X. Wei, and Y. Kai, "Bidirectional LSTM-CRF models for sequence tagging," *Computer Science*, vol. 47, 2015.

Hindawi
Computational Intelligence and Neuroscience
Volume 2022, Article ID 1765550, 7 pages
https://doi.org/10.1155/2022/1765550

Research Article

The Application of Knowledge Distillation toward Fine-Grained Segmentation for Three-Vessel View of Fetal Heart Ultrasound Images

Qiwen Cai,[1] Ran Chen,[2] Lu Li,[3] Chao Huang,[4] Haisu Pang,[5] Yuanshi Tian,[2] Min Di,[2] Mingxuan Zhang,[2] Mingming Ma,[2] Dexing Kong,[1] and Bowen Zhao[2]

[1]*School of Mathematical Sciences, Zhejiang University, Hangzhou, China*
[2]*Sir Run Run Shaw Hospital, Zhejiang University School of Medicine, Hangzhou, China*
[3]*College of Pharmaceutical Sciences, Zhejiang University, Hangzhou, China*
[4]*Ningbo First Hospital, Ningbo, China*
[5]*The First Affiliated Hospital, Zhejiang University School of Medicine, Hangzhou, China*

Correspondence should be addressed to Bowen Zhao; zbwcjp@zju.edu.cn

Received 29 March 2022; Revised 29 May 2022; Accepted 30 June 2022; Published 14 July 2022

Academic Editor: Guangming Zhang

Objectives. Measuring anatomical parameters in fetal heart ultrasound images is crucial for the diagnosis of congenital heart disease (CHD), which is highly dependent on the clinical experience of the sonographer. To address this challenge, we propose an automated segmentation method using the channel-wise knowledge distillation technique. *Methods*. We design a teacher-student architecture to conduct channel-wise knowledge distillation. ROI-based cropped images and full-size images are used for the teacher and student models, respectively. It allows the student model to have both the fine-grained segmentation capability inherited from the teacher model and the ability to handle full-size test images. A total of 1,300 fetal heart ultrasound images of three-vessel view were collected and annotated by experienced doctors for training, validation, and testing. *Results*. We use three evaluation protocols to quantitatively evaluate the segmentation accuracy: Intersection over Union (IoU), Pixel Accuracy (PA), and Dice coefficient (Dice). We achieved better results than related methods on all evaluation metrics. In comparison with DeepLabv3+, the proposed method gets more accurate segmentation boundaries and has performance gains of 1.8% on mean IoU (66.8% to 68.6%), 2.2% on mean PA (79.2% to 81.4%), and 1.2% on mean Dice (80.1% to 81.3%). *Conclusions*. Our segmentation method could identify the anatomical structure in three-vessel view of fetal heart ultrasound images. Both quantitative and visual analyses show that the proposed method significantly outperforms the related methods in terms of segmentation results.

1. Introduction

It is reported that the annual birth rate of congenital heart disease (CHD) in children is 0.8–1% [1, 2], and the incidence rate has ranked first among all birth defects. At present, fetal echocardiography is an important medical imaging technology and most used for prenatal detection and diagnosis of CHD. Well-trained and experienced doctors can make a reliable diagnosis of 80–90% CHD by fetal echocardiography, while the diagnostic accuracy of doctors who lack experience in fetal echocardiography operation and diagnosis is significantly decreased [3, 4].

The three-vessel and trachea (3VT) view is one of the fetal echocardiography views, which was introduced by Yagel et al. [5] as a complementary cardiac view to easily assess the aortic arch anomalies. Gireadă et al. [6] performed a retrospective study on 1,596 unselected pregnant patients presenting at 11–37 weeks of gestation for a routine anomaly scan and analyzed the performance of the four-chamber (4C) view and 3VT view in detecting CHD. The results demonstrated 4C view detected 47.8% of all CHD, going up to 71.7% by adding grayscale 3VT view. The 3VT view is deemed desirable if technically feasible by both International Society of Ultrasound in Obstetrics and Gynecology (ISUOG) and American Institute of Ultrasound in Medicine (AIUM) screening guidelines [7, 8], especially due to its utility in detecting outflow tract anomalies [9–11].

Automatic image segmentation can guide operators to standardize and serialize the display and analysis of fetal echocardiography data. Semantic segmentation has been extensively studied for natural images and is expected to be applied to medical images to assist in diagnosis. However, unlike natural images, medical images are often more difficult to acquire and annotate, which results in a small amount of annotated data. In addition, the special imaging modality (e.g., ultrasound) of medical images produces images of low quality with noises and blurred boundaries. These factors often lead to unsatisfactory segmentation of images. For the segmentation of three-vessel view of fetal heart ultrasound images, we collected a total of 1,300 annotated images, which is completely incomparable to large natural image segmentation datasets.

Recently, machine learning methods have widely used in fetal image processing or ultrasound image processing, such as quality assessment [12–14], detection, and segmentation [15–17]. In the field of vessel image processing, physical models or properties are sometimes introduced to simulate realistic environment to obtain higher evaluation accuracy [18–20].

In this paper, we propose to utilize the channel-wise knowledge distillation [21, 22] technique toward fine-grained segmentation of three vessels in the 3VT view of fetal heart ultrasound images. Particularly, we first train a teacher model whose training data is precisely cropped to a region of three vessels. Such a teacher model enables fine-grained segmentation because it focuses only on the target region. However, such a model cannot be directly applied to the test data because we are not able to crop the test image to the target region before prediction. To this end, we train the student model by distilling the knowledge of the pretrained teacher model using full-size training data. This allows the student model to have both the fine-grained segmentation capability of the teacher model and the ability to handle full-size test images. Experiments show that the proposed method outperforms the most widely used existing methods by a significant margin.

2. Methods

2.1. Channel-Wise Knowledge Distillation. Knowledge distillation was originally designed for model compression: a compact student model is trained to perform better under the supervision of a large teacher model [23–25]. A subsequent study [26] has also shown that a student model with the same configuration as the teacher model can even exceed the performance of the teacher model. In this work, we employ the channel-wise knowledge distillation method, as it was shown to be more effective than the pixel-wise knowledge distillation that simply aligns point-wise classification scores per pixel [27, 28].

Channel-wise knowledge distillation was first introduced by Zhou et al. [21]. Its basic idea is to convert the feature map on each channel to a probability map and then align the channel-wise probabilities of the teacher model and the student model. The corresponding channel-wise distillation loss $\mathscr{L}_{CD}(\cdot,\cdot)$ is defined in the form of a KL divergence:

$$\mathscr{L}_{KD}\left(y^T, y^S\right) = \frac{\tau^2}{C}\sum_{c=1}^{C}\sum_{i=1}^{W\cdot H}\phi\left(y_{c,i}^T\right)\cdot\log\left[\frac{\phi\left(y_{c,i}^T\right)}{\phi\left(y_{c,i}^S\right)}\right], \tag{1}$$

where T and S denote the teacher and student models, $y^{(\cdot)}$ denotes the predicted logits of size $H \times W \times C$; i indexes the spatial location of pixels, where W and H are the width and height of the predicted logits; $c = 1, 2, .., C$ indexes the channel, where C is the number of classes including the background; τ is a hyperparameter called distillation temperature; $\phi(\cdot)$ is a channel-wise softmax function which converts the logits on each channel into a soft probability distribution, defined as

$$\phi\left(y_{c,i}\right) = \frac{\exp\left(y_{c,i}/\tau\right)}{\sum_{i=1}^{W\cdot H}\exp\left(y_{c,i}/\tau\right)}. \tag{2}$$

2.2. Our Method. In this paper, we use a model of the DeepLabv3+ [29] architecture with channel-wise knowledge distillation to segment three vessels in 2D fetal heart ultrasound images.

DeepLabv3+ is an encoder-decoder network designed for segmentation tasks. A modified aligned Xception model is used as the encoder, while the Atrous Spatial Pyramid Pooling (ASPP) layer is used as the decoder as the default setting of DeepLabv3+.

As shown in Figure 1, the teacher and student networks use the same architecture. According to the groundtruth label masks, we crop the region of interest (ROI, i.e., the region of three vessels) from full-size images to train the teacher model. Meanwhile, we record the coordinates of cropped regions to restore them to the corresponding spatial location in the full-size image afterwards. After training teacher network with cropped inputs, its logits output is used to distill knowledge on channels for student model training. This allows the student model to have the same ability to segment the ROI as the teacher model. For the training of the student model, we use full-size images as input and align the logits of the teacher model to the full-size ones as additional knowledge. The loss of our network is made up of three components:

$$L = \alpha\cdot\mathscr{L}_{CE}\left(y_{gt}, y_{\text{pred}}\right) + \beta\cdot\mathscr{L}_{\text{Dice}}\left(y_{gt}, y_{\text{pred}}\right) + \gamma\cdot\mathscr{L}_{KD}\left(y^T, y^S\right). \tag{3}$$

Here, $\mathscr{L}_{CE}(\cdot,\cdot)$ and $\mathscr{L}_{\text{Dice}}(\cdot,\cdot)$ denote cross-entropy loss and dice loss, respectively, y_{gt} is the groundtruth label mask, and y_{pred} is the predicted probability map showing the probability that each pixel being categorized in each class. $\mathscr{L}_{KD}(\cdot,\cdot)$ is defined in Section 2.1. Note that for the teacher network, γ is set to 0, since no knowledge distillation is used.

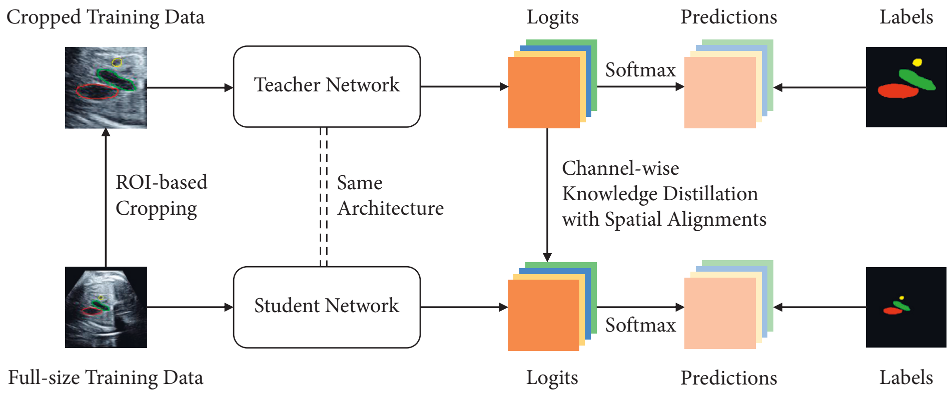

Figure 1: Overview of the proposed channel-wise knowledge distillation method.

2.3. Materials. 1300 pregnant women who underwent fetal echocardiography examination in Sir Run Run Shaw Hospital from 2016 to 2021 were randomly recruited. The gestational age was 20 to 40 weeks. The inclusion criteria were as follows: (1) normal fetus without heart or noncardiac malformations, especially there has no abnormality in the nine standard fetal echocardiography views posted by ISUOG; (2) low risks of chromosome abnormalities were confirmed by early NT and maternal serological examination, or amniocentesis and umbilical cord blood puncture; (3) gestational weeks estimated by ultrasound were consistent with those calculated by menopause history (difference <2 weeks); and (4) the mothers who had no diabetes, hypertension, or pregnancy complications. All pregnant women were informed the purpose of this study and agreed that their fetal heart ultrasound related data should be used for scientific research, and consents should be signed.

Philips IE33 (Philips Medical Systems, Bothell, WA, USA) color ultrasound diagnostic instrument was used, with S5-1 2D imaging probe and a frequency of 1~6 MHz. Firstly, the fetal echocardiography mode was used to comprehensively evaluate the structure and function of the fetal heart, clearly displaying the standard three-vessel view images and storing the original data. Pregnant women are requested to hold their breath or reduce the range of breathing as much as possible during the whole collection process.

Seven experienced doctors annotated and reviewed the collected fetal heart ultrasound images. They annotated the pulmonary artery (PA), aorta (AO), and superior vena cava (SVC) regions on each image as the groundtruth. The resolution of the original image is 1024×768. All images are simply center-cropped and resized to 512×512 as full-size training data in the student network. The ROI-based cropped images described in Section 2.2 are generated by padding the annotated three-vessel region with 50 pixels per edge and resizing them to a square region of size 512×512. We selected 1040, 130, and 130 images in all experiments for training, validation, and testing, respectively.

Figure 2 shows two examples of the fetal heart ultrasound images, as well as their corresponding full-size labeled images and ROI-based cropped images.

2.4. Training. The proposed method is implemented on an NVIDIA RTX 3090 GPU using the Keras and TensorFlow frameworks and trained using the Adam optimizer. We train the network through two stages:

(1) During the first stage, the initial learning rate is 0.0005 and the parameters are initialized by pretraining on the PASCAL VOC 2012 [30] dataset. All parameters of the Xception backbone are frozen. We set $\alpha = 1$, $\beta = 1$, and $\gamma = 0$. Since the main purpose of this stage is to speed up the training, we do not use the channel-wise knowledge distillation here. The batch size is set to 8.

(2) During the second stage, the initial learning rate is 0.00005 and all layers are trainable. We set $\alpha = 1$, $\beta = 1$ for both teacher and student models, while the hyperparameters of the channel-wise knowledge distillation are $\gamma = 3$ and $\tau = 4$ and are used only in the student model. In equation (1), $C = 4$ as we have 4 classes including the background, PA, AO, and SVC. The batch size is set to 2, since backpropagation to the backbone layers requires a larger amount of GPU memory.

In both stages, we set the decayed learning rate as $lr = lr_{\text{init}} \cdot 0.92^{\text{iterations}-1}$ and train for 50 epochs with an early stopping setting when the validation loss stops decreasing.

The following random data augmentation methods are used in the training: scale transformation, displacement, flip, rotation, and color jittering.

3. Results

To evaluate the performance of the proposed method, we compare with the most used existing methods, including U-Net [31] and the original DeepLabv3+. U-Net is a classical network and is widely used in medical image segmentation. The original DeepLabv3+ is also adopted as our teacher network; we train it on full-size images for performance comparison. For ablation study, we train the models for comparison by using a combination of cross-entropy loss and dice loss without the knowledge distillation.

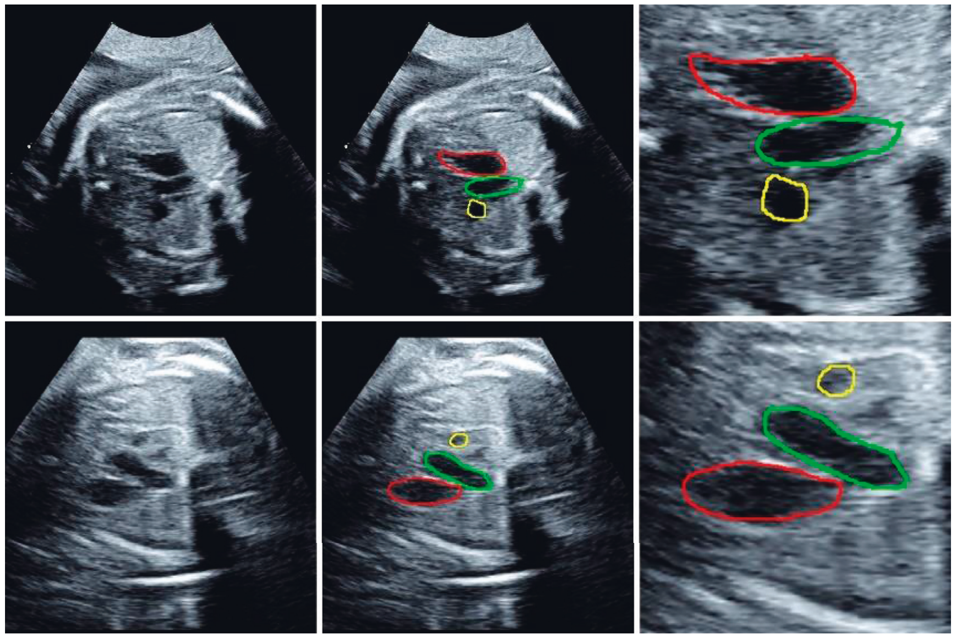

Figure 2: The 1st column shows original 3VT view of fetal heart ultrasound images. The 2nd column shows full-size labelled images, the red region is pulmonary artery (PA), the green region is aorta (AO), and the yellow region is superior vena cava (SVC). The 3rd column shows ROI-based cropped images, which are cropped from full-size images.

To quantitatively evaluate the segmentation accuracy, we use three evaluation protocols: Intersection over Union (IoU), Pixel Accuracy (PA), and Dice coefficient (Dice).

IoU:

$$\mathrm{IoU} = \frac{|S_a \cap S_b|}{|S_a \bigcup S_b|} \times 100\%. \quad (4)$$

PA:

$$PA = \frac{|S_a \cap S_b|}{|S_a|} \times 100\%. \quad (5)$$

Dice:

$$\mathrm{Dice} = \frac{2 \cdot |S_a \cap S_b|}{|S_a| + |S_b|} \times 100\%. \quad (6)$$

Here, S_a is the predicted segmentation result of the network and S_b is the groundtruth.

Table 1 shows the performance of our method. We present the IoU, PA, and Dice for each class evaluated on the test data. The mean value over three vessels' segmentation accuracies is shown in the bottom row. The mean IoU, PA, and Dice of the proposed method are 68.6%, 81.4%, and 81.3%, respectively.

Table 2 shows the comparison of three methods. The displayed measurements are the average of the three vessels' segmentation accuracies from all test data. It is evident that the proposed method performs better than the other methods.

To intuitively demonstrate the effectiveness of our results, we plot segmentation contours of the listed methods in Figure 3.

Table 1: Performance of the proposed method.

	IoU (%)	PA (%)	Dice (%)
Pulmonary artery (PA)	71.2	83.5	83.2
Aorta (AO)	69.7	82.8	82.1
Superior vena cava (SVC)	64.9	77.8	78.7
Mean	68.6	81.4	81.3

The segmentation accuracies of three vessels and their mean values are shown.

Table 2: Performance comparison to existing methods.

	IoU (%)	PA (%)	Dice (%)
U-Net	62.4	77.5	76.9
DeepLabv3+	66.8	79.2	80.1
Ours	**68.6**	**81.4**	**81.3**

The mean segmentation accuracy of three vessels over all test data is shown.

Specifically, we observed that when using existing segmentation methods, the SVC vessel is sometimes undetected or incorrectly segmented due to its small size. In addition, since the three vessels occupy only a small portion of the image, the existing methods only produce rough and incorrectly segmented boundaries.

4. Discussion

The incidence of birth defects in China is about 5.6% and the number of new birth defects is about 900,000 every year [1]. Amongst them, there are about 250,000 cases of birth defects that can be observed clinically at birth. Birth defects are the main causes of early abortion, stillbirth, perinatal death, infant death, and congenital disability, which not

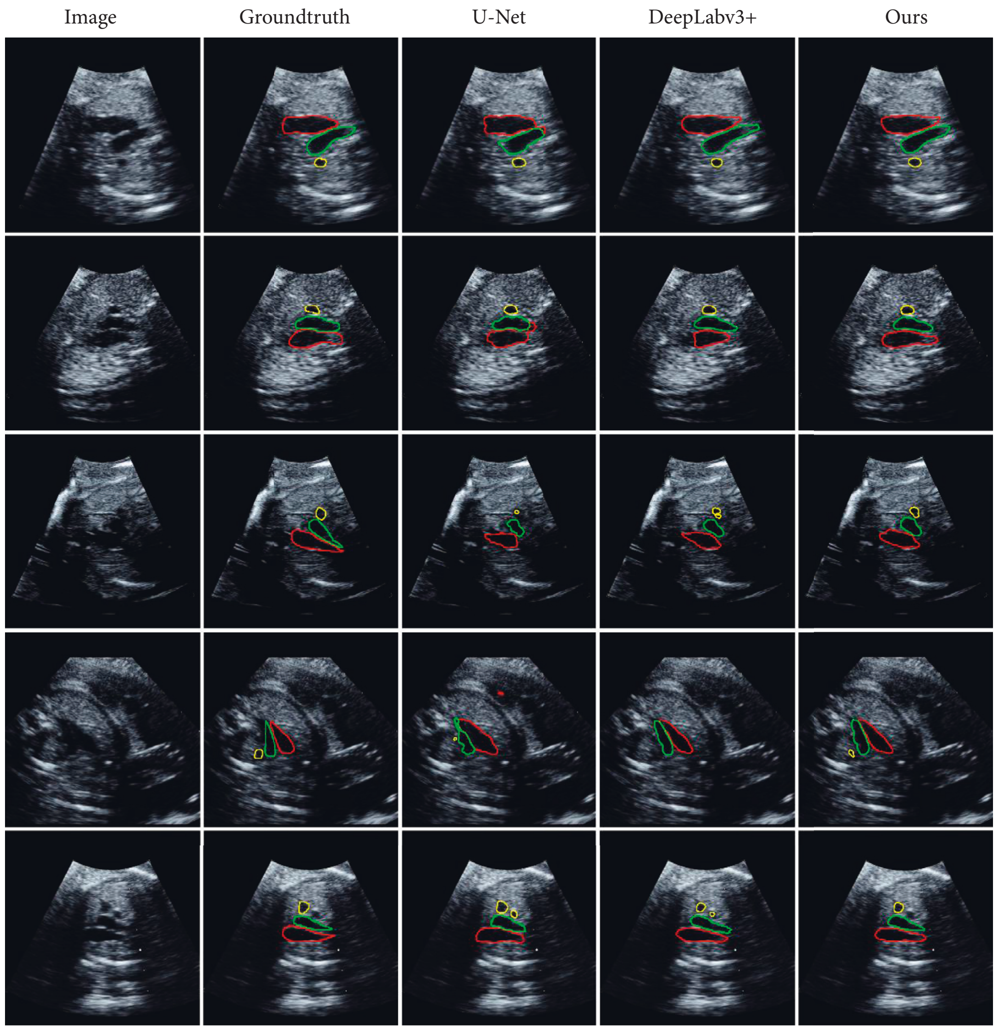

Figure 3: Segmentation results of different methods. The original 3VT view of fetal heart ultrasound images are shown in the first column and the groundtruth are shown in the second column. The segmentation results of U-Net, DeepLabv3+ and our proposed method are shown in the last three columns, respectively.

only seriously harm the survival and quality of life of children but also affect the happiness and harmony of families. It will also lead to potential life loss and increasing social and economic burden. Accurate prenatal diagnosis can significantly improve the perioperative treatment effect of CHD and the success rate of operation and reduce neonatal mortality.

Many studies have shown that improving the ability of routine obstetricians to recognize CHD is the most important issue to improve the successful rate of CHD prenatal diagnosis. However, doctors who complete obstetrical ultrasound diagnoses in their daily medical work are always lacking the diagnostic basis and evaluation experience of complex CHD, and it is difficult to obtain all basic views needed for CHD diagnosis [32–35], including four-chamber cardiac view, left and right ventricular outflow tract view, and three-vessel view, so it is difficult to make reliable display and diagnosis of CHD. As a result, CHD has become the most easily missed structural abnormality in prenatal routine ultrasound examination.

As we know, the 4C view is the most commonly used and easily obtained basic view in fetal heart examination. The acquisition rate at 16–40 weeks is around 95–99.5%, but four-chamber abnormalities only account for 48–63% of congenital cardiovascular malformations. A variety of fetal congenital cardiovascular malformations do not show abnormal shape of the four-chamber heart, including tetralogy of fallot, persistent truncus arteriosus, aortic valve stenosis, pulmonary valve stenosis, transposition of great arteries, and double outlet of ventricle. The extended basic views include three-vessel view, three-vessel trachea view, aortic arch view, pulmonary artery-ductus arteriosus arch view, and vein-atrium connection view. The detection rate of congenital cardiovascular malformation can be increased from 48–63% to 83–86%. Amongst which, the number, internal diameter, course, vascular arrangement, and abnormal blood flow direction of the major vessels can be clearly observed in the three-vessel and three-vessel trachea view, which plays an important role in the screening of fetal cardiac macrovascular malformations. Therefore, it is clinically important to collect and identify the three vessels, and the automatic segmentation algorithm could help doctors to easily operate and accurately diagnose CHD.

Automated segmentation of fetal heart ultrasound images is a challenging task due to low signal-to-noise ratio, low contrast, and blurred boundaries. Collecting and accurately annotating the data is also a difficult task. We believe that the performance of the proposed model can be further improved by using a larger and more standard dataset. Nonetheless, we achieved better results than DeepLabv3+ on all evaluation metrics, with performance gains of 1.8% on mean IoU (66.8% to 68.6%), 2.2% on mean PA (79.2% to 81.4%), and 1.2% on mean Dice (80.1% to 81.3%).

5. Conclusion

In summary, we propose a fully automated segmentation method for fine-grained segmentation of three vessels in the 3VT view of fetal heart ultrasound images using a channel-wise knowledge distillation technique. We design a teacher-student architecture to distill channel-wise knowledge from ROI-based cropped images to full-size images. The logits output of the teacher model empowers the student model with fine-grained segmentation capability. In this way, we obtain more accurate segmentation boundaries. Both quantitative and visual analyses show that the proposed method significantly outperforms other methods in terms of segmentation results of the three vessels in the 3VT view of fetal heart ultrasound images.

Data Availability

The image data used to support the findings of this study have not been made available due to information that could compromise the privacy of research participants.

Conflicts of Interest

The authors declare that they have no conflicts of interest.

Acknowledgments

This research was funded by Major Program of the National Natural Science Foundation of China (Grant no. 12090025) and the Natural Science Foundation of Zhejiang Province, China (Grant no. LGF22H180008).

References

[1] C. Li, "Report on the prevention and treatment of birth defects in China," *Ministry of Health PRC*, vol. 3, no. 37, 2012.

[2] S. C. Mitchell, S. B. Korones, and H. W. Berendes, "Congenital heart disease in 56,109 births incidence and natural history," *Circulation*, vol. 43, no. 3, pp. 323–332, 1971.

[3] U. Gembruch and A. Geipel, "Indications for fetal echocardiography: screening in low-and high-risk populations," *Fetal cardiology*, vol. 96, 2003.

[4] D. Paladini, "Expert consensus of fetal heart ultrasonography standardization," *Chinese Journal of Ultrasound Imaging*, vol. 20, no. 10, pp. 904–909, 2011.

[5] S. Yagel, R. Arbel, E. Y. Anteby, D. Raveh, and R. Achiron, "The three vessels and trachea view (3VT) in fetal cardiac scanning," *Ultrasound in Obstetrics and Gynecology*, vol. 20, no. 4, pp. 340–345, 2002.

[6] R. Gireadă, D. Socolov, E. Mihălceanu et al., "The additional role of the 3-vessels and trachea view in screening for congenital heart disease," *Medicina*, vol. 58, no. 2, p. 262, 2022 Feb 10.

[7] J. Carvalho, L. D. Allan, R. Chaoui et al., "ISUOG Practice Guidelines (updated): sonographic screening examination of the fetal heart," *Ultrasound in Obstetrics and Gynecology*, vol. 41, no. 3, pp. 348–359, 2013.

[8] J. Pellerito, B. Bromley, S. Allison et al., "AIUM-ACR-ACOG-SMFM-SRU practice parameter for the performance of standard diagnostic obstetric ultrasound examinations," *Journal of Ultrasound in Medicine*, vol. 37, no. 11, pp. E13–E24, 2018.

[9] M. Pasternok, A. Nocun, A. Knafel et al., ""Y sign" at the level of the 3-vessel and trachea view: an effective fetal marker of aortic dextroposition anomalies in the first trimester," *Journal of Ultrasound in Medicine*, vol. 37, no. 8, pp. 1869–1880, 2018.

[10] A. Palatnik, W. A. Grobman, L. S. Cohen, J. S. Dungan, and N. L. Gotteiner, "Role of the 3-vessel and trachea view in antenatal detection of Tetralogy of Fallot," *Journal of Ultrasound in Medicine*, vol. 35, no. 8, pp. 1799–1809, 2016.

[11] H. Edwards and R. Hamilton, "Single centre audit of early impact of inclusion of the three vessel and trachea view in obstetric screening," *Ultrasound*, vol. 26, no. 2, pp. 93–100, 2018.

[12] C. P. Bridge, C. Ioannou, and J. A. Noble, "Automated annotation and quantitative description of ultrasound videos of the fetal heart," *Medical Image Analysis*, vol. 36, pp. 147–161, 2017.

[13] J. Dong, S. Liu, Y. Liao et al., "A generic quality control framework for fetal ultrasound cardiac four-chamber planes," *IEEE journal of biomedical and health informatics*, vol. 24, no. 4, pp. 931–942, 2020.

[14] Z. Lin, S. Li, D. Ni et al., "Multi-task learning for quality assessment of fetal head ultrasound images," *Medical Image Analysis*, vol. 58, Article ID 101548, 2019.

[15] X. Li, Y. Hong, D. Kong, and X. Zhang, "Automatic segmentation of levator hiatus from ultrasound images using U-net with dense connections," *Physics in Medicine and Biology*, vol. 64, no. 7, Article ID 075015, 2019.

[16] S. Dong, G. Luo, C. Tam et al., "Deep atlas network for efficient 3D left ventricle segmentation on echocardiography," *Medical Image Analysis*, vol. 61, Article ID 101638, 2020.

[17] L. Wang, L. Zhang, M. Zhu, X. Qi, and Z. Yi, "Automatic diagnosis for thyroid nodules in ultrasound images by deep neural networks," *Medical Image Analysis*, vol. 61, Article ID 101665, 2020.

[18] Z. Gao, J. Chung, M. Abdelrazek et al., "Privileged modality distillation for vessel border detection in intracoronary imaging," *IEEE Transactions on Medical Imaging*, vol. 39, no. 5, pp. 1524–1534, 2020.

[19] Z. Gao, X. Wang, S. Sun et al., "Learning physical properties in complex visual scenes: an intelligent machine for perceiving blood flow dynamics from static CT angiography imaging," *Neural Networks*, vol. 123, pp. 82–93, 2020.

[20] Z. Gao, H. Xiong, X. Liu et al., "Robust estimation of carotid artery wall motion using the elasticity-based state-space approach," *Medical Image Analysis*, vol. 37, pp. 1–21, 2017.

[21] Z. Zhou, C. Zhuge, X. Guan, and W. Liu, "Channel Distillation: Channel-Wise Attention for Knowledge Distillation," 2020, https://arxiv.org/abs/2006.01683.
[22] C. Shu, Y. Liu, J. Gao, Z. Yan, and C. Shen, "channel-wise knowledge distillation for dense prediction," in *Proceedings of the IEEE/CVF International Conference on Computer Vision*, pp. 5311–5320, Seoul Korea, June 2021.
[23] G. Hinton, O. Vinyals, and J. Dean, "Distilling the Knowledge in a Neural Network," 2015, https://arxiv.org/abs/1503.02531.
[24] S. Zagoruyko and N. Komodakis, "Paying more attention to attention: improving the performance of convolutional neural networks via attention transfer," 2016, https://arxiv.org/abs/1612.03928.
[25] F. Tung and G. Mori, "Similarity-preserving knowledge distillation," in *Proceedings of the IEEE/CVF International Conference on Computer Vision*, pp. 1365–1374, Las Vegas, June 2019.
[26] T. Furlanello, Z. Lipton, M. Tschannen, L. Itti, and A. Anandkumar, "Born again neural networks," *International Conference on Machine Learning*, PMLR, vol. 3, , pp. 1607–1616, 2018.
[27] J. Hu, L. Shen, and G. Sun, "Squeeze-and-excitation networks," in *Proceedings of the IEEE Conference on Computer Vision and Pattern Recognition*, pp. 7132–7141, Las Vegas, June 2018.
[28] Y. Wang, W. Huang, F. Sun, T. Xu, Y. Rong, and J. Huang, "Deep multimodal fusion by channel exchanging," *Advances in Neural Information Processing Systems*, vol. 33, 2020.
[29] L. C. Chen, Y. Zhu, G. Papandreou, F. Schroff, and H. Adam, "Encoder-decoder with atrous separable convolution for semantic image segmentation," in *Proceedings of the European conference on computer vision (ECCV)*, pp. 801–818, Seoul Korea, June 2018.
[30] M. Everingham, L. Van Gool, C. Williams, J. Winn, and A. Zisserman, "The Pascal visual object classes challenge 2012 results," *Pattern Anal. Stat. Model. Comput. Learn*, vol. 5, 2012.
[31] O. Ronneberger, P. Fischer, and T. Brox, "U-net: convolutional networks for biomedical image segmentation," in *Proceedings of the International Conference on Medical Image Computing and Computer-Assisted Intervention*, pp. 234–241, Springer, Cham, 2015 Octomber 5.
[32] J. Rychik, N. Ayres, B. Cuneo et al., "American Society of Echocardiography guidelines and standards for performance of the fetal echocardiogram," *Journal of the American Society of Echocardiography*, vol. 17, no. 7, pp. 803–810, 2004.
[33] "Cardiac screening examination of the fetus: guidelines for performing the "basic" and "extended basic" cardiac scan," *Ultrasound in obstetrics & gynecology the official journal of the International Society of Ultrasound in Obstetrics and Gynecology*, vol. 27, no. 1, pp. 107–113, 2006.
[34] W. Lee, L. Allan, J. S. Carvalho et al., "ISUOG consensus statement: what constitutes a fetal echocardiogram?" *Ultrasound in Obstetrics and Gynecology*, vol. 32, no. 2, pp. 239–242, 2008.
[35] F. E. Force, "American college of obstetricians and gynecologists, society for maternal-fetal medicine. AIUM practice guideline for the performance of fetal echocardiography," *Journal of Ultrasound in Medicine: Official Journal of the American Institute of Ultrasound in Medicine*, vol. 30, no. 1, pp. 127–136, 2011.

Hindawi
Computational Intelligence and Neuroscience
Volume 2022, Article ID 7608937, 10 pages
https://doi.org/10.1155/2022/7608937

Research Article

Analyzing the Effectiveness of Finance in Supply Chain in Solving the Financing Difficulties of SMEs Based on Grey Theory Model

Guofeng Piao [1] **and Biyan Xiao** [2]

[1] *School of Economics and Management, Yan'an University, Yan'an 716000, China*
[2] *School of Economics and Management, Weifang University of Science and Technology, Weifang 262700, China*

Correspondence should be addressed to Guofeng Piao; piaogf922@yau.edu.cn

Received 15 May 2022; Revised 8 June 2022; Accepted 9 June 2022; Published 14 July 2022

Academic Editor: Xin Ning

Small and medium-sized enterprises (SMEs) play an indispensable role in China's national economic system, and they can play a critical role in promoting economic growth and full employment. The main reason for the disruption and impediment to the development of SME clusters is that the enterprises in the clusters are experiencing a "capital shortage," as a result of the double contradiction between the clusters' financial benefits and the difficulties in financing. Grey theory is a relatively new concept in the field of information processing. It proposes theories and methods for processing and analyzing incomplete information systems using mathematical methods. This study uses finance in supply chain as a new research perspective to investigate the effectiveness of finance in supply chain in resolving SMEs' financing problems using the Grey theory model, with the goal of resolving SMEs' financing problems. When comparing the results of the Grey theory model and the regression analysis model, the relative error of the Grey theory model is on average 12.2% lower than that of the regression analysis model, indicating that the Grey theory model greatly improves accuracy. As a result, using the Grey theory model to solve supply chain financing and SMEs' difficulties can share risks, share credit, reduce transaction costs, weaken information asymmetry, and achieve mutual benefits and a win-win situation. It is expected to promote the development of the finance in supply chain model, mobilise enterprise enthusiasm for using finance in supply chain, improve finance in supply chain operational efficiency, and promote finance in supply chain development.

1. Introduction

At present, financing for SMEs is one of the major concerns of the whole society, and "supply chain financing" is a hot topic in the banking industry [1]. At present, with the improvement of capital market access standards, it is difficult for many enterprises to raise funds by issuing stocks or bonds, and in this case, the main way for enterprises to obtain sufficient funds is from banks [2]. Although the state has introduced support and incentive policies for SMEs, the effective implementation of the policies has a certain time lag effect and the effects that take time to appear [3]. In the development of SMEs, there are many problems, and the most important of which is the financing problem [4]. Domestic and foreign industrial competition is becoming increasingly fierce, and the development of SMEs is increasingly constrained by factors such as resource scarcity, energy shortage, and environmental damage [5]. The deep-rooted contradictions in the development of SMEs are becoming increasingly prominent, and the survival of SMEs is facing enormous pressure and challenges [6].

Finance in the supply chain is an important tool for SMEs to overcome their financial difficulties [7]. Corporate mergers and acquisitions are increasingly being used by companies to expand their business scale and change their development direction because of their multifaceted impact [8]. The practice and development of domestic commercial banks' supply chain finance have provided a good solution to the SMEs' financing problem [9]. This business model has broken the constraints of traditional financing and greatly expanded the credit market for SMEs, which has been recognised and imitated by an increasing number of commercial banks [10]. Although the state has eased SMEs' access to the market, it has not provided more preferential policies to help them grow [11]. In this case, establishing a special mechanism to create a new financing model to meet the financial needs of SMEs through collaboration among multiple participants or stakeholders in the credit market would be a more effective approach [12].

Grey theory [13] uses the similarity of the various factors affecting the system to determine the degree of relevance of various factors. The development of the system can be quantified by analyzing and comparing various factors to determine the most important factors in the system's and things' development [14]. Small businesses are constrained by their own capital in the continuous production process, making it difficult to organise the optimal production scale in accordance with market demand and maximise profits [15]. As a result, the preliminary work of planning the company's M&A financing, the basis of financing decision, will directly affect the ultimate success or failure of the company's M&A. Correct judgement of the macrorisks of financing and comprehensive risk analysis of the available financing methods is the preliminary work of planning the company's M&A financing, which will directly affect the ultimate success or failure of the company's M&A. According to Grey theory, the prediction of a system with both known and unknown or uncertain information is the prediction of a time-related Grey process changing in a particular direction.

The innovative points of this study are as follows:

(1) It is of great practical significance to assess whether finance in supply chain can promote the development of SME clusters. The study provides a theoretical basis for it by establishing a mathematical model.

(2) Focusing on the unique advantages of finance in supply chain financing model to solve the financing difficulties of SMEs, it directly reflects the specific effectiveness of finance in supply chain in the actual operation process and the inherent advantages of risk control.

(3) Combining the characteristics and coupling relationship between finance in supply chain and SME clusters, a new "$1+N$" pooled invoice financing method of finance in supply chain is proposed. It is innovative to connect SME cluster financing with finance in supply chain to improve financing efficiency.

This study's research framework is divided into five sections, which are organised as follows: the first section of this study introduces the research background and significance before moving on to the main work. The second part introduces the work done in supply chain finance to solve SMEs' financing issues, as well as the Grey theory model. The method of establishing the Grey theory model and the development model of finance in supply chain is sorted out in the third section, so that readers of this study can have a better understanding of the concept of analyzing finance in supply chain based on the Grey theory model to solve the financing of SMEs. The thesis' core section describes the use of the Grey theory model to analyze small business financing problems from two perspectives: serial Grey correlation analysis and sliding Grey correlation analysis. The thesis concludes with a summary of the entire work.

2. Related Work

2.1. Financial Supply Chain Financing for SMEs. With the deepening of reform and opening up, China's economy has developed rapidly and SMEs have also started to develop rapidly, becoming an indispensable and important part of China's economic system. Despite their increasingly prominent role in promoting the stable development of the national economy, fostering scientific and technological innovation, and providing a platform for employment, the number of SMEs is also increasing. However, their growth environment is not ideal, and the problem of having financial difficulties is particularly prominent. The rise of finance in supply chain has made it possible for this idea to become a reality.

Kouvelis et al. pointed out that in the UK financial system, SMEs still face financial difficulties in raising the necessary long-term capital. With the outstanding contribution of SMEs in expanding employment, solving the imbalance of regional economic development, and ensuring sustainable and stable economic growth, SMEs have become an important driving force of China's market economy [16]. According to Gaea, SME clusters create a good "green" environment for the development of finance in supply chain, and finance in supply chain provides a guarantee for the realization of the financial strategy of SME clusters [17]. Abbasi et al. proposed the net income theory, the net operating income theory, and the intermediate tradition theory as the initial theory of capital structure [18]. Luca et al. argue that various types of SMEs within an industrial cluster form an integrated supply, production, and marketing supply chain through a clear division of labor and mutual cooperation. The objective conditions are created due to the frequent capital transactions between the participants [19]. Sun et al. argued that SMEs inevitably encounter financial difficulties due to factors such as low credit levels, lack of collateral, and inadequate small and medium-sized guarantee institutions [20].

Finance in supply chain is a new financing model that has taken the world by storm in recent years. It unites core enterprises and upstream and downstream enterprises to provide flexible financing methods and effectively alleviate the financial difficulties of SMEs. Rather than assessing the production and operation status and credit risk of individual enterprises in isolation, finance in supply chain studies the financing needs of SMEs from the perspective of the whole industry chain, taking into account the core enterprises and upstream and downstream enterprises. It also considers logistics, capital flow, and information flow to achieve efficient connection.

2.2. Grey Theory Model. It is difficult to obtain a more complete and accurate understanding of complex systems due to the limitations of people's level of understanding, their ability to obtain information, and the existence of interactive interference between different types of information. The main characteristics of SMEs are small size, flexibility, and vitality, but they face difficulties in the development process in terms of capital, talents, and information. How to effectively extract, filter, and process information has attracted widespread attention and great importance, so Grey theory is a new discipline that has emerged.

Yao and Zhu introduced the concept of buffer operator and proposed a new method to attenuate serial shock perturbations and improve the prediction accuracy [21]. Zhou classified the expected returns of assets into two categories: risk-free returns and risky returns. The risk-free return is the risk-free rate in the capital market, and the higher the risky return is relative to the overall market risk, the higher the risk-return ratio needs to be achieved [22]. He uses function transformations to normalize the raw data and further improve the smoothness of the raw data stream. Also, theory and examples show that this mathematical transformation method is highly advantageous for improving the smoothing of the series [23]. Liu treats real security returns as the result of changes in many factors in the economy and assigns corresponding weights to each variable, assigning higher weights to factors with greater influence and less influential factors to those with greater influence [24]. Ning used the buffer operator forecasting principle to make short-term forecasts of Chinese energy consumption using a second-order weakening operator acting on the original series [25].

Under the effect of financial disincentives, there will be a "capital gap" in SME financing, resulting in an imbalance between supply and demand for capital. In the absence of supply chain support, enterprises in the group are likely to produce homogeneous and indistinguishable products, leading to fierce competition among enterprises. Based on the Grey theory model, through the coordination and integration of capital flow, logistics, and information flow, the smooth operation can be effectively ensured.

3. Based on the Grey Theory Model, The Idea of Finance in Supply Chain to Solve the Financing Problem of SMEs Is Analyzed

3.1. Establishment of Grey Theory Model. In cybernetics, things can usually be represented visually in different colors depending on the amount of information and whether the information is clear or not [26]. For a thing, if its information is informative and clear, then it can be said to be white [27]. If a thing has very little information and the information is vague, then it is black. What is in the middle is called Grey [28]. When considering a Grey theory model, sometimes the occurrence of certain events can lead to certain fluctuations in the returns of the event window. Therefore, the impact of events on the return must be fully considered in the Grey theory model, and the return forecasting method is shown in Figure 1.

First, to bring our Grey portfolio-based investment model closer to the real market, we refer to semiabsolute diversification risk in measuring risk. The process of model modeling involves using the original data series as solutions of the differential equation and modeling the approximate differential equation for those series that can approximately satisfy the conditions of the differential model. Assume that $S = S(i)$ represents the consumer or investor surplus of a financial product and $\Pi = \pi(i)$ represents the profit of a financial firm, both of which are functions of financial market prices. Then, the political production function is as follows:

$$M = M(S, \pi). \tag{1}$$

A necessary condition for the formation of SME clusters is the degree of association between enterprises. The characteristics, status, and role of each enterprise in the cluster, as well as the cooperative relationship between related enterprises, determine the network structure of the cluster [29]. Since many SMEs have an inadequate management system, the company's management system is not well developed and the disclosed operational information is not very complete. In this case, an information asymmetry is created [30]. Therefore, by borrowing from core enterprises and funding the actual transactions with them with supply chain financial services, we can effectively help SMEs to obtain the required loans at a lower cost and alleviate the problem of insufficient capital liquidity. In particular, when it is difficult to determine the optimal structure through visualization, comparative methods and quantitative analysis are used to determine the nuances of different structures in order to achieve the differentiation of structural strengths and weaknesses. Currently, in the actual operation of Chinese banks, together with the adoption of the receivables financing commitment method, the flowchart of the receivables financing model is shown in Figure 2.

The second is to mainly consider the case where the investor's expected return is uncertain; that is, the return on investment is represented by a Grey number. Since the expected return on assets of investors may fluctuate within a certain interval, the interval Grey number is used to represent the return on assets. In practical applications, when shock perturbations have a distorting effect on the original data stream, the buffer operator can be given priority to act on the original data stream to attenuate the perturbation distortion. The residual is the difference between the actual value and the simulated value, and the residual test actually tests the degree of deviation of the simulated value from the actual value. Let the original and simulated data be

$$\begin{aligned} x^{(0)} &= \left\{x^{(0)}(1), x^{(0)}(2), x^{(0)}(3), \ldots, x^{(0)}(n)\right\}, \\ \hat{x}^{(0)} &= \left\{\hat{x}^{(0)}(1), \hat{x}^{(0)}(2), \hat{x}^{(0)}(3), \ldots, \hat{x}^{(0)}(n)\right\}. \end{aligned} \tag{2}$$

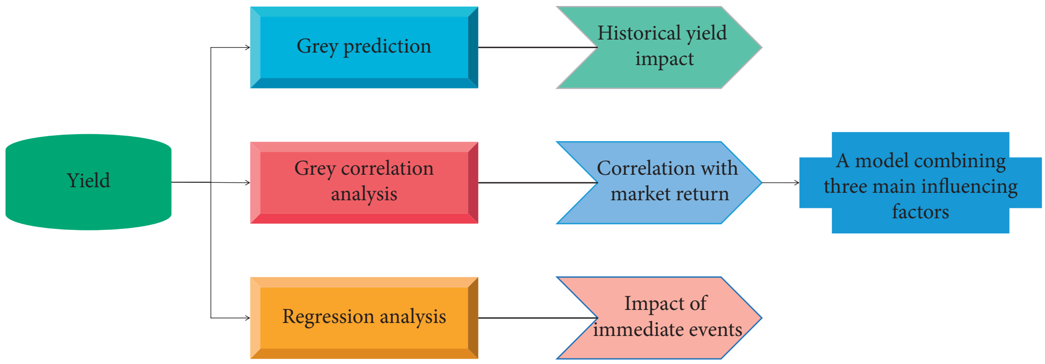

Figure 1: Forecast method of yield.

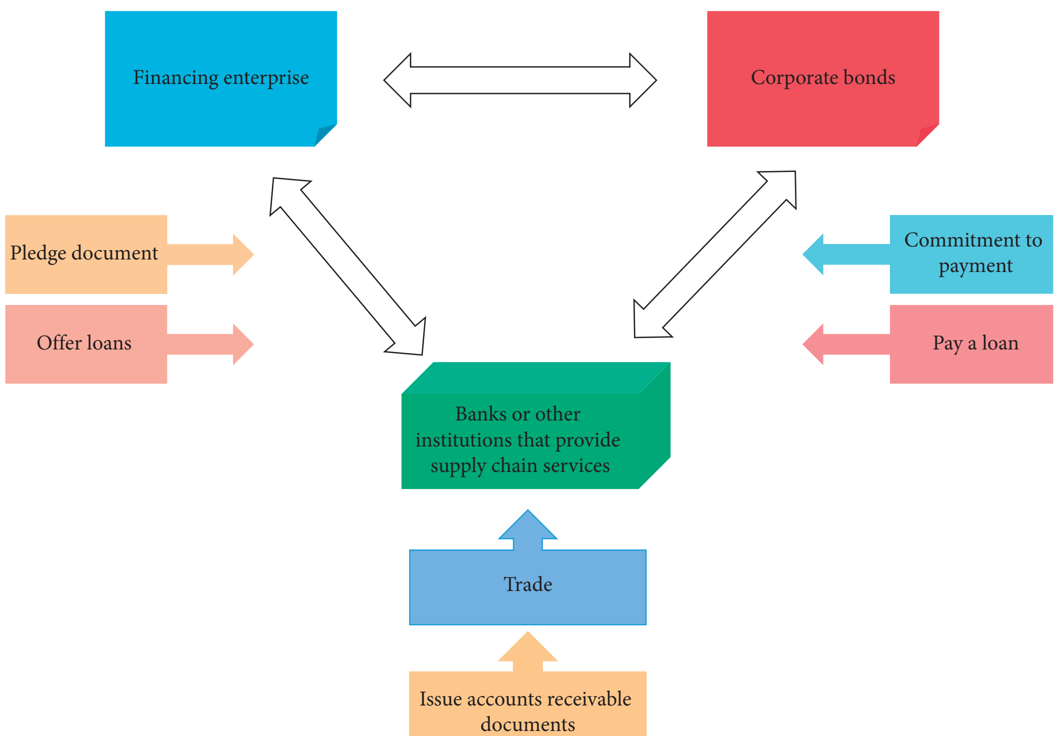

Figure 2: Flowchart of accounts receivable financing mode.

The residual sequence is as follows:

$$\begin{aligned} E &= (e(1), e(2), \ldots, e(n)) \\ &= X(0) - \widehat{X}(0). \end{aligned} \tag{3}$$

Among them

$$e(i) = x^{(0)}(i) - \widehat{x}^{(0)}(i), \quad (i = 1, 2, \ldots, n). \tag{4}$$

The cluster is a gathering place of many highly related industries, with clear division of labor and close connection, forming a "sub-network" of the supply chain. For the non-negative discrete series, the current theory describes the model by approximating the exponential form of the first-order differential equation to the exponential form of the first-order differential equation. The first stage is the primary stage, in which bank credit is introduced in the supply chain business cooperation to improve the business credit and stability of the whole supply chain. It also encourages upstream and downstream SMEs to establish long-term and stable strategic cooperation with leading enterprises to improve the operational efficiency and competitiveness of the whole supply chain. Let $X(0) = (x^{(0)}(1), x^{(0)}(2), \ldots, x^{(0)}(n))$ be the sequence of system behavioral characteristics, and the observed data sequence of system behavioral characteristics is as follows:

$$\begin{aligned} X(x(1), x(2), \ldots, x(n)) &= \big(x^{(0)}(1) + \varepsilon_1, x^{(0)}(2) \\ &\quad + \varepsilon_2, \ldots, x^{(0)}(n) + \varepsilon_n\big) \\ &= x^{(0)} + \varepsilon. \end{aligned} \tag{5}$$

Finally, the risk of the model is represented by a Grey number on top of the expected ROI, so that only one Grey number is needed for the whole model. The SMEs in the cluster have their own supply chains, distributed in various nodes. Due to the complexity of their internal relationships, the supply chains of SMEs can be single or multiple chains, cooperating and competing with each other. Grey theory defines the temporal measure of the sequence based on the open set topology and then defines the information density, the Grey derivative, and the Grey differential equation. In the finance in supply chain model, financial institutions such as banks no longer focus on individual financial companies, but on the risk of the entire supply chain and its transactions.

3.2. Supply Chain Financial Development Mode-"1 + N" Financing Service Mode. In the production and operation processes of SMEs, due to the time lag effect between the purchase of raw materials requiring prepayment, the sale of enterprise inventory products, and the recovery of sales payments, the enterprises have high capital flow requirements, and capital shortages occur from time to time. The development mode of finance in supply chain has innovated credit technology by providing overall service to the supply chain, integrating logistics, and information flow and closed operation, which has improved the efficiency of financial services, eased information asymmetry, and reduced transaction costs, and provided new ideas and ways to solve the financing problems of SMEs. According to the financing stage, the establishment of a more stage-specific financing risk evaluation index system provides a system guarantee for the evaluation and control of multistage financing risk, and the flowchart of comprehensive evaluation of financing risk is shown in Figure 3.

To begin with, due to a lack of short-term funds, downstream purchasers (financing companies) prefinance by confirming business on the assumption that the supply chain's presales company will buy back, relieving the pressure on downstream companies' procurement funds. Risk-averse investors are more concerned about investment risk and prefer to invest in a portfolio with a lower risk. Low risk, of course, entails a low reward. This financing model takes into account the cluster and supply chain as a whole, not only to solve individual company financing issues but also to provide financial support to individual company's upstream and downstream customers. Let the stochastic process $\{X_n, n \in T\}$, whose parameter set T is a discrete set in time, that is, $T = \{0, 1, 2, \ldots\}$, and whose state space consisting of the entire set of possible values of the corresponding X_n is a discrete set of states $I = \{i_1, i_2, i_3, \ldots\}$. If any integer $n \in T$ and any $i_0, i_1, i_2, \ldots, i_{n+1} \in T$, then the conditional probabilities satisfy the following equation:

$$\begin{aligned} P\{X_{n+1} = i_{n+1} | X_0 = i_0, X_1 = i_1, \ldots, X_n = i_n\} \\ = P\{X_{n+1} = i_{n+1} | X_n = i_n\}, \end{aligned} \tag{6}$$

$$\sum_{j=1}^{\infty} P_{i,j}(m, m+n) = 1, \quad i = 1, 2, \ldots, n. \tag{7}$$

Throughout the loan financing process, the principal is the debtor of the receivables and acts as a guarantor for the upstream company, providing collateral to the bank. Once the borrower defaults on the loan, the principal firm must take over the responsibility of repaying the loan. Starting from the framework of the multivariate Markov model, it is assumed that the financial position of the firm at the time of i, t and its financial position at the time of $t + 1$ satisfy the following recursive relationship:

$$x_{t+1}^{(i)} = \sum_{j=1}^{N} \lambda_{i,j} P^{(i,j)} x_t^{(j)}, \quad i = 1, 2, \ldots, N. \tag{8}$$

Here, $x_{t+1}^{(i)}$ is the probability vector of financial status.

Second, considering the conversion of existing inventory goods or operational raw materials into collateral that banks are willing to accept is a new idea for SMEs to recover bank loans. According to the evaluation criteria of indicators determined by the banking system, the evaluation indicators are graded based on the collected data and expert evaluations, so as to obtain the sample whitening number matrix for general risk assessment of supply chain financing. For the original data series with a high growth rate in the first half of the data series and small growth rate in the second half, the actual simulation error is smaller after modeling, and the construction operator attenuates or weakens the effect of the data distortion phenomenon caused by the shock perturbation shock. $X = (x(1), x(2), \ldots, x(n))$ is the data series of system behavior characteristics, and the data series of X after the effect of the operator D is noted as follows:

$$XD = (x(1)d, x(2)d, \ldots, x(n)d). \tag{9}$$

At the same time, the financial support provided by the bank can enhance the cohesion among the companies in the cluster and make transactions more convenient. However, when choosing Greyscale generation, attention needs to be paid to choosing the appropriate Greyscale generation operation based on known data characteristics and paying attention to choosing Greyscale generation with less error.

Finally, during the sales stage, SMEs can use large parent company accounts receivables as collateral to obtain funds from banks and other financial institutions. A linear whitening weighting function is constructed based on the actual situation of supply chain financing to classify its risk into three equal low risks: low risk, average risk, and high risk. Due to the fact that the core company is a market leader with a high credit rating and good operating condition, the default risk will be reduced. The receivables generated during the subject's participation in the transaction are not invoiced, so this model is essentially indirect financing. The bank will take on the entire supply chain, including

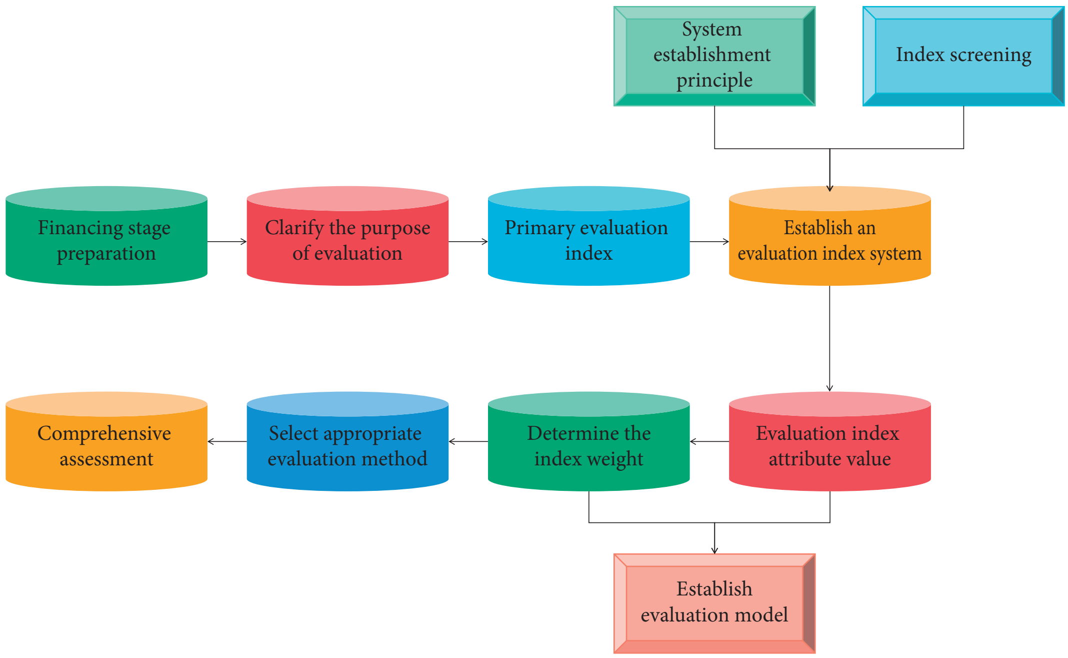

Figure 3: Flowchart of comprehensive evaluation of financing risk.

manufacturers, suppliers, and vendors, as a part of supply chain financing. This combined transaction operation eliminates many unnecessary losses and improves the fund setting. Inventory financing, also known as supply chain finance, enables SMEs to convert movable assets that banks are hesitant to accept into asset collateral via core business collateral, logistics, and storage supervision.

4. Application of Grey Theory Model in Analysis of Financing Problems of Small Enterprises

4.1. Sequence Grey Correlation Analysis. Grey theory provides a method for collecting and processing known information about systems and things in order to explore their corresponding patterns of development and change. The correlation test is a geometric test that examines the similarity between the model value curve and the actual value curve used for modeling.

The average relative error and the predicted value are obtained by comparing the corresponding time functions after the action of the no-buffer operator and the action of the buffer operator, calculating the simulated predicted value and comparing it with the actual value, which are shown in Figures 4 and 5, respectively.

First, the method of characterizing the geometry or the dynamics of how things develop between sequences in terms of the degree of velocity difference is called absolute correlation. The degree of speed difference here is also known mathematically as the first-order slope difference. For banks, most of them choose to increase the input cost when lending to SMEs in order to reduce the risk problem, thus improving the information collection and supervision of SMEs. The predicted values of the model for 2021 after the first-order weakening of each buffer operator are listed in Table 1.

In general, the closer the geometry and the closer the trend of change, the greater the degree of correlation. The step test is a point-by-point test, the correlation test is a test of the approximation of the model to the specified function, and the posterior difference test is a test of the stochastic properties of the step distribution. The test uses the relative error size test method, which is an intuitive comparative and point-by-point arithmetic test. The predicted data are compared with the actual data to see if the relative error meets the actual requirements.

Second, all the Greyscale information described by the sequences can be used to highlight the “white part” and weaken the “black part” to highlight the regularity between the sequences, which establishes the optimal solution model of the whitening equation. The whitening portfolio model is a multiobjective planning problem. Therefore, the multiobjective planning model of the first whitening equation, the second whitening equation, and any whitening equation is transformed into a single-objective planning model. The supply chain financing is designed by a certain operation model so that the business income of the trust company automatically returns to a specific credit-granting bank account, which in turn repays the loan or is repaid as collateral to reduce the credit risk of the bank. A method of whitening the Grey process in the generation process has the effect of attenuating or weakening the randomness of the original data stream and plays an extremely important role in the Grey modeling process. Interval values are necessary for the theory of interval Grey number prediction, and it is necessary to provide not only the possibility of converting fuzzy numbers into interval values but also the corresponding

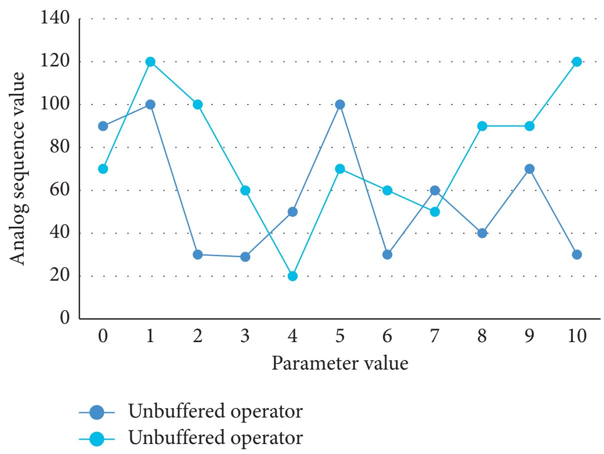

Figure 4: Simulation sequence diagram with or without buffer operator.

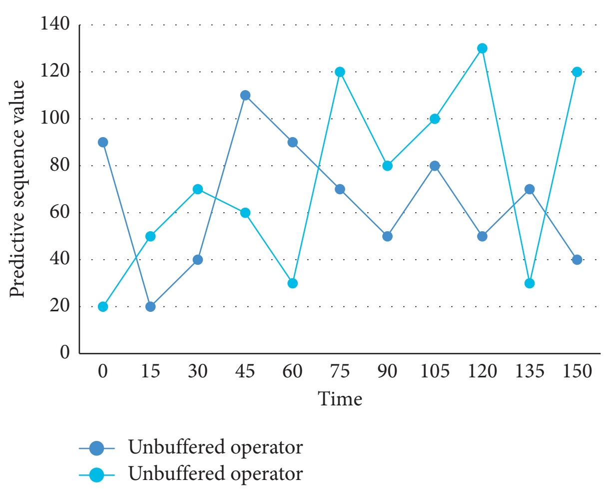

Figure 5: Prediction sequence diagram with or without buffer operator.

Table 1: Predicted values of each buffer operator after first-order weakening.

Sequence	Average relative error	Estimated value (10,000 people)
X	2.89	122
XD_1	4.82	371
XD_2	6.77	658

conversion methods and algorithms. When the development coefficients take different values, the accuracy curves of the Grey theory model, the original GM model, and the improved GM model are shown in Figure 6.

Finally, the Grey series is transformed into the underlying data reflecting the essential intrinsic characteristics, that is, achieving the so-called dimensionlessness, for comparison between pairs. The risk acceptance coefficients are determined according to the different risk acceptance levels of different investors, solving the single-objective planning problem of the whitened portfolio model, and finally determining the optimal solution of the model.

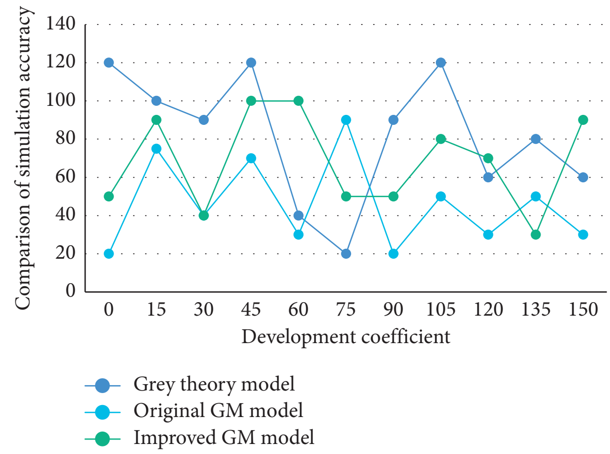

Figure 6: Comparison of simulation accuracy of three types of models with different development coefficients.

Cumulative generation is the accumulation of data between each series at each moment to get a new data series. Finance in supply chain integrates information, capital, logistics, and other resources, which is a scientific, personalized, and targeted financial service process. It takes the illiquid assets and the future cash flow generated by the assets in the supply chain operation link and certainty as the source of repayment and enhances the coordination of the supply chain to reduce its operation cost. From the calculation of the correlation coefficient, we can get the correlation coefficient values of the comparison series, that is, the model value series and the reference series, that is, the actual value series, which have many results at each point, and the information is too sparse to facilitate comparison. The correlation coefficient is embedded in a value, which is the sequence space before the accumulation of Greyscale correlation, called the original sequence space, and the sequence space formed after the accumulation of new data is called the generated sequence space.

4.2. Sliding Grey Relational Analysis. One of the most important indicators of national economic development is gross national product or GDP, which can reflect whether a country's economy is in the development stage or the recession stage. Due to the characteristics of Grey correlation, it makes up for the shortcomings of some mathematical and statistical methods, which are equally applicable to the sample size and whether the sample is regular or not, and the calculation is small and very convenient. At the development coefficient of 0.5 and 1, the multistep prediction accuracy of the Grey theory model is compared in the experiment, and the experimental results are shown in Figure 7.

First, things that have some factors in common with existing things are searched for and asynchronous comparisons are made between the factors. Therefore, the concept of sliding Grey correlation is proposed to project the trend by comparing the series of different time periods (looking for analogies). In practical applications, the Grey character of portfolio investment uncertainties, the variance of risk, and expected return of portfolio investment ranges from light numbers in the classical

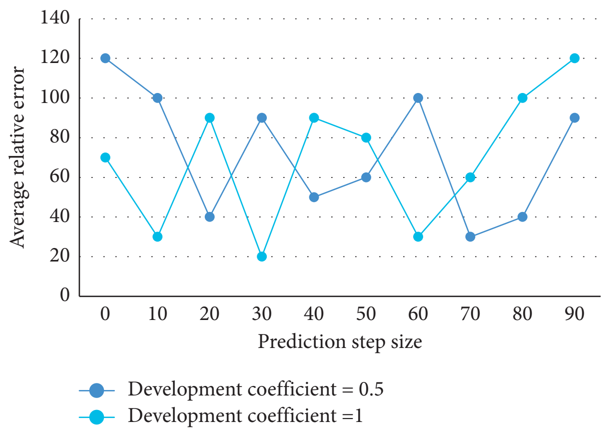

Figure 7: Comparison of multistep prediction accuracy of grey theory models with different development coefficients.

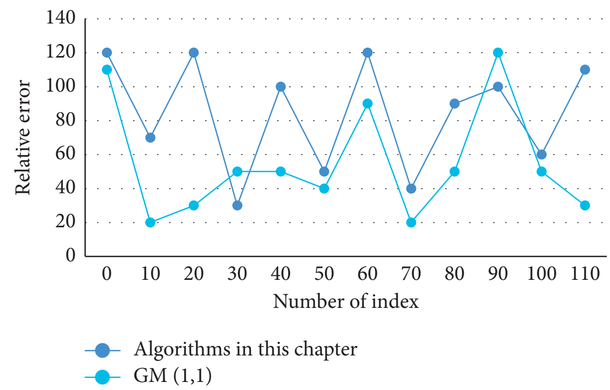

Figure 8: Comparison of simulation residuals between the GM (1, 1) model and the proposed model.

model to interval Grey numbers are considered, as the model is closer to the real situation. The higher the smoothness of the data stream, the higher the accuracy of the established model, and vice versa, the accuracy of the model is difficult to achieve satisfactory results. Therefore, the effective evaluation coefficients of each criterion in the criteria set need to be given to increase the stability of voting and the scientificity of evaluation to obtain a more accurate ranking of the importance of members. The unbiased GM (1, 1) model eliminates the exponential bias inherent in the traditional GM (1, 1) model and the distortion of the data series when the original data series is perturbed by shocks in the traditional GM (1, 1) model. The main reason is that the unbiased model avoids jumping from the difference equation to the differential equation when modeling the GM (1, 1) model. A comparison of the simulated residuals of the GM (1, 1) model and the proposed model in this study is shown in Figure 8.

Second, the amount of the slider on the left represents the time series' advancement, while the amount of the slider on the right represents the time series' lag. Because interval Grey numbers were introduced, any set of interval Grey number whitening values in the model corresponds to a possible scenario, and the results are unreliable and could be good or bad. In general, cumulative generations can give data a degree of regularity, and if that is not enough, the number of cumulative generations can be increased. Although the requirements for meeting multiple sets of criteria are more stringent, the affiliation metric quantified values combining group consensus and individual understanding can be more accurately reflected among multiple sets of criteria, and the discriminative ability will improve. We choose the Grey theory model for forecasting and the regression analysis model for forecasting three stocks of the same type, assuming no events will affect the stock price during the forecast period. The relative errors are compared in Table 2.

Comparing the results of the Grey theory model and the regression analysis model, we can see that the relative error of the Grey theory model is on average 12.2% lower than that of the regression analysis model, which greatly improves the measurement accuracy.

Table 2: Error comparison of different methods.

Stock		Stock 1	Stock 2	Stock 3
Grey theory model	Estimated value	0.152	0.162	0.186
	Relative error	15.4%	12.9%	11.6%
Regression analysis model	Estimated value	0.231	0.243	0.267
	Relative error	1.56%	1.29%	0.98%

Finally, overruns and lags are unique time-series properties that are only used as reference indicators during the correlation investigation process and do not represent good overruns or lags. The processed generative series are used to create a Grey generative model, which is then compared to the GM (1, 1) model created directly from the original data. The simulated prediction series can be obtained after recovering the model. To understand the decision risk, it is necessary to find the best and worst solutions for linear interval planning problems, as well as provide decision-makers with a range of effective solutions under certain conditions. Although some generative models have high prediction accuracy for Greyscale generated series, after recovering the original series, the prediction accuracy may be low, so the type of Greyscale generation used has an impact on the prediction accuracy. As a result, the dominance measure must take into account all of these factors in order to construct a reasonable set of evaluation criteria, and it is also necessary to consider the overall impact of different criteria sets on the evaluation problem and change the content of the criteria sets as needed to suit different evaluation criteria.

5. Conclusions

In the increasingly competitive modern market economy, the competition among enterprises is changing into the competition among supply chains. The development of finance in supply chain has brought hope to solve the financing problems of many SMEs in China. Finance in supply chain has fully integrated financial resources and realized model innovation, and the service scope has been extended to SMEs. The difficulty of SME financing is a classic issue with complex historical and objective reasons, while finance in supply chain is a newly emerged financing model in recent years, and it is the entry point of this study to crack the old problem with a new model, which is also the main purpose of this research. This study takes the financing of SME clusters as the research object and makes comprehensive use of theoretical knowledge such as the Grey theory model and finance in supply chain to conduct an in-depth study on the current situation of SME cluster financing. Using the Grey theory model to analyze the finance in supply chain has the unique advantage in solving the financial difficulties of SMEs. Introducing the Grey theory model can effectively weaken the information asymmetry between banks and SMEs and increase the possibility of banks to provide credit to SMEs. The Grey theory model can not only make a reasonable and accurate assessment of the overall risk situation of finance in supply chain but also predict the future development trend of the supply chain by comparing the risk levels of various indicators.

Data Availability

The data used to support the findings of this study are included within the article.

Conflicts of Interest

The authors declare that they have no conflicts of interest.

Acknowledgments

This study was supported by a doctoral research project of Yan'an University (YAU202203083).

References

[1] L. Xiaoyi, "Analysis of SME financing model from the perspective of supply chain finance," *International Core Journal of Engineering*, vol. 6, no. 4, pp. 115–117, 2020.

[2] E. Kusrini, M. Rifai, and S. Miranda, "Performance measurement using supply chain operation reference (SCOR) model: a case study in a small-medium enterprise (SME) in Indonesia," *IOP Conference Series: Materials Science and Engineering*, vol. 697, no. 1, Article ID 012014, 2019.

[3] C. Carnovale, D. S. Rogers, and S. Yeniyurt, "Broadening the perspective of supply chain finance: the performance impacts of network power and cohesion," *Journal of Purchasing and Supply Management*, vol. 25, no. 2, pp. 134–145, 2019.

[4] L. G. Zanon, F. Marcelloni, M. C. Gerolamo, and L. C. Ribeiro Carpinetti, "Exploring the relations between supply chain performance and organizational culture: a fuzzy grey group decision model," *International Journal of Production Economics*, vol. 233, no. 14, Article ID 108023, 2021.

[5] P. Y. Brunet, V. Babich, and T. Aouam, "Supply chain finance: overview and future directions," *Foundations and Trends® in Technology Information and Operations Management*, vol. 10, no. 3-4, pp. 237–252, 2017.

[6] Y. Su and B. Zhong, "Supply chain finance decision analysis with a partial credit guarantee contract," *Journal of Applied Mathematics and Physics*, vol. 5, no. 6, pp. 1355–1369, 2017.

[7] B. Sang, "Application of genetic algorithm and BP neural network in supply chain finance under information sharing," *Journal of Computational and Applied Mathematics*, vol. 384, Article ID 113170, 2021.

[8] T. Krinjari, "Dynamic portfolio optimization based on grey relational analysis approach," *Expert Systems with Applications*, vol. 147, Article ID 113207, 2020.

[9] X. Xu, X. Chen, J. Fu, Steve Brown, Yu Gong, and Yifan Xu, "Supply chain finance: a systematic literature review and bibliometric analysis," *International Journal of Production Economics*, vol. 204, 2018.

[10] F. Emtehani, N. Nahavandi, and F. M. Rafiei, "A joint inventory–finance model for coordinating a capital-constrained supply chain with financing limitations," *Financial innovation*, vol. 7, no. 1, p. 39, 2021.

[11] J. Chen, T. Cai, W. He, L. Chen, G. Zhao, W. Zou, and L. Guo, "A blockchain-driven supply chain finance application for auto retail industry," *Entropy*, vol. 22, no. 1, p. 95, 2020.

[12] T. L. Zhang, J. J. Li, and X. Jiang, "Analysis of supply chain finance based on blockchain," *Procedia Computer Science*, vol. 187, no. 2, pp. 1–6, 2021.

[13] J. Martin, "Suppliers' participation in supply chain finance practices: predictors and outcomes," *International Journal of Integrated Supply Management*, vol. 11, p. 193, 2017.

[14] L. Y. Meng and C. Du, "Zheshang bank's "blockchain + supply chain finance" accounts receivable financing model of research," *E3S Web of Conferences*, vol. 275, Article ID 01074, 2021.

[15] M. Zhang, J. Zhang, and R. Ma, "Quantifying credit risk of supply chain finance: a Chinese automobile supply chain perspective," *IEEE Access*, no. 99, 1 page, 2019.

[16] P. Kouvelis, L. Dong, and D. Turcic, "Advances in supply chain finance and FinTech innovations overview," *Foundations and Trends® in Technology Information and Operations Management*, vol. 14, no. 1–2, pp. 1–4, 2020.

[17] R. Gaea, "Supply chain finance," *Bankarstvo*, vol. 49, no. 4, pp. 100–111, 2020.

[18] W. A. Abbasi, Z. Wang, and A. Alsakarneh, "Overcoming SMEs financing and supply chain obstacles by introducing supply chain finance," *International Journal of Business and Management*, vol. 13, no. 6, 2018.

[19] Luca, Mattia, and Gelsomino, "An optimisation strategy for concurrent Supply Chain Finance schemes - ScienceDirect," *Journal of Purchasing and Supply Management*, vol. 25, no. 2, pp. 185–196, 2019.

[20] N. Sun, L. I. Li, and L. I. Li, "Does geographic distance have a significant impact on enterprise financing costs?" *Journal of Geographical Sciences*, vol. 29, no. 12, pp. 1965–1980, 2019.

[21] X. Yao and Zhu, "Research on Comparison of Enterprise Financing Efficiency under Layered Background," *Academic circle*, vol. 10, no. 10, p. 10, 2017.

[22] S. Zhou, "Research on promotion of industry development by using financing at enterprise groups—case studies and enlightenment to CNPC," *Finance and Finance*, vol. 3, no. 003, pp. 26–32, 2018.

[23] R. He, "The study on the problem of the relationship between the "heterogeneity" of the neighbor enterprise and the financing efficiency of SMEs in China —empirical data from China industrial enterprises database," *Open Journal of Applied ences*, vol. 07, no. 4, pp. 171–183, 2017.

[24] J. Liu, "Research on the prevention and control of supply chain financial risks from the perspective of enterprise financing," *Financial Marketing*, vol. 6, no. 1, p. 49, 2021.

[25] X. Ning, "Financing decisions analysis of E-commerce supply chain finance for fresh agricultural products in China," *Journal of Financial Research*, vol. 5, no. 2, p. 5, 2021.
[26] S. F. Lehenchuk, N. V. Valinkevych, and I. M. Vyhivska, "The significant principles of development of accounting support for innovative enterprise financing," *International Journal of Advanced Science and Technology*, vol. 56, pp. 2282–2289, 2020.
[27] S. Zhao and N. Lv, "Pgpermaking enterprise financing and the mechanism of financial risk transmission based on cluster model," *Paper Asia*, vol. 35, no. 2, pp. 40–44, 2019.
[28] O. Kaya and O. Masetti, "Small- and medium-sized enterprise financing and securitization: firm-level evidence from the euro area," *Economic Inquiry*, vol. 57, no. 1, pp. 391–409, 2019.
[29] P. Pluskota, "Challenges faced by the regional financial institutions engaged in enterprise financing," *European Journal of Service Management*, vol. 28, pp. 339–349, 2018.
[30] J. Martin and E. Hofmann, "Involving financial service providers in supply chain finance practices," *Journal of Applied Accounting Research*, vol. 18, no. 1, pp. 42–62, 2017.

Hindawi
Computational Intelligence and Neuroscience
Volume 2022, Article ID 8204999, 5 pages
https://doi.org/10.1155/2022/8204999

Research Article

Advocacy for the Development of Teacher Leadership in the Context of ECC Reforms in China

Xiaoyan Shen

School of ECE, Shanghai Normal University Tianhua College, Shanghai, China

Correspondence should be addressed to Xiaoyan Shen; sxy2094@sthu.edu.cn

Received 12 April 2022; Revised 12 June 2022; Accepted 13 June 2022; Published 14 July 2022

Academic Editor: Xin Ning

China's development is inseparable from the reform of education, so ECE is very important in the development of Chinese society. Based on this reason, this paper introduces the three reform waves of communist Chinese society under the influence of western culture. Because the professional level of kindergarten teachers does not match the concepts and requirements of the three preschool curriculum reforms in Chinese society, this paper analyzes the solutions based on this problem and holds that the leadership of kindergarten teachers should be vigorously developed.

1. Introduction

China has long recognized the important role of ECE in children's development [1]. Under the mutual influence of Chinese local culture and western culture, China's ECE has experienced many landmark changes. This paper introduces the changes of Chinese social culture under the influence of Chinese traditional local culture and western culture under communism. There have been three reforms of preschool education. For more than a century, China's educational practice has been influenced by Chinese traditional culture and Soviet thoughts, and it is also hoped to learn from advanced western educational ideas and methods and actively explore educational practices suitable for China. Although the third comprehensive reform of ECE has made great progress and had a wide impact on society, there are still many problems. One of the outstanding problems is that the quality of kindergarten teachers does not match the idea and demand of education reform. Some experts point out that teachers play an important role in the new curriculum reform. Focusing on the development of teachers' leadership is the most reliable solution under the mutual influence of Chinese native culture and western culture.

2. The Current Situation of ECE and Care in China

Preschool education refers to the education of children from 0 to 6 years of age. In recent years, the age range of children enrolled in kindergartens in some provinces has also begun to expand, meaning that children aged 2-3 can also enter the kindergarten [3].

In China's education system, ECE belongs to basic education, but not to nine-year compulsory education (six years of primary school and three years of middle school), which will get more education budget from the government. In all the stages of basic teaching, the budget for ECE is the least. For example, ECE has received only 1.3-1.4% of the national education budget in the last 17 years in China [4].

With the Third Plenary Session of the Eleventh Central Committee in 1978, China began to implement the policy of internal reform and opening to the outside world. Under the influence of the reform and opening-up policy, all walks of life in China have undergone earth-shaking changes, including preschool education, and the reform results of preschool education are the most remarkable [5]. As a result, there has been noticeable and dramatic improvements in ECE. However, there were still many challenges and difficulties to be solved by Chinese early education professionals [6]. One of the prominent issues was that the professional development level of most early childhood educators cannot meet the requirements of the reform. In response to this phenomenon, this paper attempted to propose the advocacy from the social and historical aspect of ECC reforms and the influence of the hybrid of three cultures on the reform.

3. A Social and Historical Aspect of ECC Reforms in China

In the past decades, under the interaction between Chinese local culture and foreign culture, especially western culture, a series of tremendous changes have taken place in ECE in China. In China, ECE is a full-time program of primary education for children. Generally speaking, the need to verify the quality of ECE starts with examining the characteristics of the curriculum, which is the key core of education [7].

In the development of ECE in China, the early childhood curriculum (ECC) reform mainly went through three stages, which were, respectively, affected by the social development and cultural characteristics at that time. The three stages of ECC reform, along with the historical process of major social changes of different origins, took place in 1920s to 1940s, 1950s to 1960s, and 1980s to the present, respectively [8].

3.1. The ECC Reform from 1920s to 1940s. The formal development of ECE in China began in the early 20th century. In 1903, China's first kindergarten was established in Wuhan (Zhu & Zhang, 2008), which copied the Japanese education model from the content and methods to the toys and facilities [9]. At that time, the influence of western missionaries was very extensive, and China's ECE also received its influence.

The May 4th New Culture Movement broke out in 1919, created conditions for the spread of various western educational thoughts in China, and had a profound influence on the reform of modern education in China, among which the ideological influence of John Dewey was particularly obvious [10]. In addition, the famous western scholars of ECE at that time, such as German Froebel and Italian Montessori, and their ECC models also became the object of imitation and learning for Chinese teachers [11].

However, local Chinese educators such as Chen Heqin, Tao Xingzhi, and Zhang Xuemen also had insight into the disadvantages brought about by copying foreign countries in ECE, which did not adapt to the social and cultural conditions in China at that time, and put forward the idea of starting with ECC reform to make ECC scientific and localized [12]. A curriculum called "unit integrated curriculum" was implemented in Nanjing in 1923, which initiated the first ECC reform (1920s–1940s) in China. In theory, it confirmed the subjectivity of children in the curriculum, and the curriculum should include all activities of children in kindergarten.

3.2. Full Acceptance of Soviet Theory (1950s–1960s). After the founding of the People's Republic of China in 1949, under the background of comprehensive learning from the Soviet Union, ECC also fully accepted the theory and practical experience of the Soviet Union. In the 1950s, China began the second ECC reform. Although the Chinese ECC no longer used the word "curriculum," it actually reflected a narrow understanding of the curriculum at that time, that is, the curriculum was regarded as a subject, and children were educated through the teaching of various subjects in kindergartens [13]. The Chinese Ministry of Education had completely rejected the previous practice, requiring kindergartens to systematically teach young children through "homework," emphasizing the leading role of teachers, and attaching importance to the learning of knowledge and skills for young children.

From 1966 to 1976, the "Cultural Revolution" occurred in China, which made China's education suffer a catastrophe, and ECE was no exception. That period was known as the dark period of ECE in China [14].

3.3. Progress for the Third ECC Reform (1980s to the Present). After the ten-year Cultural Revolution from 1966 to 1976, Chinese leader Deng Xiaoping put forward the famous reform and opening-up policy [15]. This reform has changed China's traditional education concept and made China's ECE go out of the dark period and turn into the golden period of ECE. After about 30 years of efforts, China's ECE reform has made great achievements [16].

Since the 1980s, Chinese early childhood educators have launched a large-scale ECC reform movement with ECC reform as a breakthrough point. Various foreign child development and education theories, such as Montessori, Dewey, Bronfenbrenner, Bruner, and especially Piaget's ideas, began to spread widely, and the thoughts of modern educators in China, especially those of Chen Heqin, were emphasized again, which provided theoretical background for the ECE reform since the 1980s [11]. Since then, the influence of the Soviet Educational theory on ECE in China has gradually weakened.

The third ECC reform started from the spontaneous experiment of China's kindergartens and played a great role in promoting it. In 1989, China's education authorities issued the Kindergarten Work Regulations (trial version). Since then, ECC reform has been transformed into a "top-down" reform led and promoted by the national administrative power [17]. In order to further deepen this reform, in 2001, the Ministry of Education issued the Supplementary Guidelines for Kindergarten Education Practice (trial version). These reforms and policies are aimed at the previously long-existing teacher-centered curriculum system, which has shifted to emphasizing the development of children and taking plays as basic activities [18]. The Supplementary Guidelines issued in 2001 reflected the core concept of ECC reform to provide integrated, situational, and life-oriented experience for children. Taking the five fields of "health, language, society, science, and art" as examples, the curriculum objectives, contents, and requirements as well as guiding points were elaborated [19].

Furthermore, during this reform period, some well-known western curriculum models such as Project Approach in the United States, Reggio Emilia Practice in Italy, and Montessori curriculum mode in Italy were widely known by Chinese ECE scholars and gradually localized in some kindergartens [20]. In addition, Chinese early education experts have also developed local curriculum based on China's national conditions and social needs, such as the theme-based integrated curriculum led by Zhu Jiaxiong [21], and the Anji Play Approach developed by Cheng Xueqin [22].

The reform in this stage is still going on, and its scale, length of time, and amount of resources are unmatched by previous ECC reforms. However, with the development of society and the passage of time, people began to evaluate this reform from multiple perspectives and put forward many problems at the conceptual and practical levels [23].

4. A Mixture of Three Cultures in China

China's ECC reform in these three stages happened to be accompanied by great social changes, and all of them were influenced by foreign cultures without exception. Unfortunately, the introduced curriculum did not necessarily meet the needs of Chinese children nor did ECE teachers in China have the expertise to handle it. This also reflects the need to pay enough attention to cultural compatibility in the ECC reform in China [24]. That is to say, the mixture of three cultures: Chinese native culture, Soviet Union (communist) culture, and western culture, has an indelible impact on China's social changes, including different aspects of ECC reform [25].

As is known to all, Chinese native culture originated from Confucianism, which had exerted a far-reaching and comprehensive influence on the Chinese people. The impact on education lied in the emphasis on repetition and memorization of individuals rather than encouraging and fostering creativity and flexibility. In the ECC reform, although Chinese teachers accepted the curriculum or pedagogies of foreign culture, they still adopted traditional teaching methods in practice because of the long-term influence of deep-rooted Confucianism [26].

The influence of Soviet culture is mainly reflected in China's second-stage ECC reform, which was generally stable and smooth. Traditional Chinese culture and communist culture were compatible to a certain extent because both value centralized management, planning systems, learning outcomes, clear goals, and teachers' guidance.

As a representative of western culture, the United States put forward a famous open door policy. Under the influence of this policy, the advantages of other cultures also had an impact on the third reform of China's preschool education. Although many ECE practitioners in China imitate the western education methods and try to change the traditional teaching methods from adult-centered to child-centered, they find that there are still many shortcomings to be improved in the process of teaching practice, and these problems cannot be solved in a short time [27].

The influence of these three cultures on ECE is not immutable, but developed dynamically, and each one had an impact on different aspects of ECC. Sometimes two cultures could produce a combined influence, for example, the commonality of Chinese native culture and communist culture strengthened the authority of teachers, and sometimes the influence of two cultures would offset each other to a certain extent, for instance, collectivism in Chinese native culture was the exact opposite of the cultivation of individuality in western culture.

5. One Noticeable Issue in ECC Reform: EC Teachers' Professional Level Did Not Match the Requirement

As mentioned above, EC teachers in China have been fully affected by the ECC reform. They have recognized the importance of learning child-centered educational theories and also have tried to change the traditional education system centered on knowledge transfer and skill acquisition, but it was still difficult to get rid of the old curriculum mode and traditional teaching methods in practice [28]. Early educators want to achieve results in the reform of ECE, so they can learn about the children's experiences, interests, and wants of the objects of education before teaching practice, which is very significant for the improvement of teaching effect [22]. With the advancement of the third phase of ECC reform, many methods and practices in the field of early education have been implemented, but few have achieved success, especially in developing regions of China. New cognition may not necessarily have an impact on traditional teaching methods.

In the exploration of preschool teaching reform, many preschool teachers are not clear about the main purpose of teaching, and the meaning of teaching is rather vague, especially in the complicated and changeable teaching environment at that time [29]. With the development of preschool education reform, preschool education requires higher and higher professional level of preschool teachers. However, the current problem is that the professional level of preschool teachers cannot meet the requirements of preschool education reform, which is the most important problem to be solved in preschool education reform and the key to the success of the reform.

The ultimate goal of the reform is to make both teachers' teaching and students' learning meaningful. As the first contact with children, teachers have the most say in the practicality and effectiveness of the curriculum. Therefore, in the development and implementation of a new curriculum, teachers should also have certain decision-making power, which requires them to achieve more professional levels [30]. The Chinese government is launching actions to promote EC teachers' professional development. One of its views is that EC teachers should participate in school-based research and reflect their own classroom behavior and be able to strike a certain balance between their preset learning tasks and activities of interest to children.

The main problems in the third reform of ECE in Chinese society are that the professional level of early childhood teachers cannot meet the requirements of the latest early childhood teaching level and the number of early childhood teachers is insufficient. To make the teaching reform successful, we must put forward concrete and effective solutions to these two problems. In order to solve these two main problems, the Chinese government has set up three levels of training programs for preschool teachers, namely, the national level, the provincial level, and the municipal level [31]. The kindergarten teachers who receive training have different teaching levels and regions, so different types of training programs should be set up according to different kindergarten teachers' needs. However, at present, most preschool teaching and training programs are not aware of this problem but blindly study the western preschool teacher training courses. As the training courses for preschool teachers are not targeted, the training effect for preschool teachers is not very satisfactory at present. Therefore, there is still a certain gap between the overall professional level of preschool teachers and the professional level required by preschool education reform. The third preschool education reform in China has not achieved obvious results [32].

6. Developing Teacher Leadership as a New Direction for the ECC Reform

At present, as the connection between countries in the world is increasing, if you want to gain an advantage in the competition in this era of globalization, you must make teaching develop with the times. So, countries all over the world have started their own educational reforms. Southeast Asian countries have borrowed the teaching mode of distributed leadership from the ECE reform in western developed countries. It can be seen that teacher leadership is very similar to distributed leadership, which is another form of distributed leadership.

Relevant scholars have found in the exploration of ECE reform that teacher leadership plays a crucial role in the quality of teaching and the success of teaching effect. Although teacher leadership is a decisive factor for the success of teaching, there is no unified explanation for the definition of teacher leadership in the field of early childhood teaching reform. The term "agent" means "a person or group responsible for leading change at the school level." Relevant scholars involved in the reform of ECE think that teachers who are "agents" can be divided into two different leadership roles in performing administrative and teaching duties, namely, formal leadership role and informal leadership role. Teachers' role in schools has been expanded, and they participate in school-related affairs, including curriculum development, staff training, school improvement, personnel affairs, school management, and decision making, instead of being confined to classroom teaching.

Ho Tikly (2012) found that in the process of preschool education reform, preschool teachers who have been receiving professional training have realized their leading role in the education process. However, under the influence of this out-and-out educational reform and innovation and different cultures, at present, the professional level of most preschool teachers still cannot reach the level required by preschool education reform, so there is still a long way to go for the success of preschool education reform in China. This paper holds that promoting the development of teachers' leadership can make preschool teachers change from passive recipients to initiators of preschool education reform, which will achieve more effective results in solving the above problems.

7. Conclusion

Under the guidance of the reform and opening-up policy, the Chinese government has learned from the west, making various fields develop towards diversification. Through the combination of the three ECE reforms and the latest ECE reform and development goals proposed by the Chinese government, the development of preschool teachers' leadership can enable them to have more opportunities to participate in the decision making of teaching reform and thus have more active decision-making power, which has a very significant effect on mobilizing the enthusiasm of preschool teachers. This may be a feasible method for improving the professional level of teachers under the specific cultural soil and era background.

Data Availability

The data used to support the findings of this study are available from the corresponding author upon request.

Conflicts of Interest

The author declares that there are no conflicts of interest.

References

[1] Y. Wang, "Teachers' curriculum leadership and promotion strategies under the background of curriculum reform," *Journal of Shaanxi Preschool Teachers College*, vol. 29, no. 4, p. 3, 2013.

[2] C. Zheng and Y. Jiang, "The development status and influencing factors of empowerment and empowerment of kindergarten teachers," *Research in Preschool Education*, no. 1, p. 12, 2019.

[3] Q. Zhang, "Research on the teaching reform of "Music" course in preschool education majors in higher normal schools under the background of "National Examination" for teacher qualification certificate," *University: Teaching Education*, 2021.

[4] C. Zou, L. Wang, and C. Chen, "Research on the professional growth path of preschool teachers under the background of deepening reform and standardization of preschool education," *Education Observation*, vol. 8, no. 22, p. 3, 2019.

[5] H. Zhou, "Actions and research on improving kindergarten curriculum leadership in shanghai," *Early Childhood Education: Education and Teaching*, no. 7, pp. 54–57, 2013.

[6] M. Fleer and B. Van Oers, Eds., *International Handbook of Early Childhood Education*, Springer, Berlin, Germany, 2017.

[7] R. Jiao and Z. Zhang, "Inheritance and change: kindergarten improvement in the new era," *Educational Research*, vol. 39, no. 4, p. 1, 2018.

[8] Y. Wen and C. S. Zhang, "An analysis of the problems and causes of preschool teachers' professional development in my country under the background of kindergarten-based curriculum," *Research in Preschool Education*, no. 4, p. 3, 2008.
[9] Y. Yao, "The reform and development of teacher education in my country in the 21st century," *Journal of Chengdu University of Traditional Chinese Medicine: Education Science Edition*, vol. 7, no. 2, p. 3, 2005.
[10] Z. Xiang, W. Ma, and J. Cao, "The influence of occupational burnout on the leadership of kindergarten principals and the mediating effect of social support," *China Health Education*, vol. 37, no. 11, p. 4, 2021.
[11] X. Xu, "Teacher development evaluation in the background of curriculum reform," *Chinese Journal of Education*, no. 5, pp. 83–85, 2009.
[12] S. F. Jiang, "The enlightenment of Reggio educational concepts on the role of preschool teachers in my country," *Educational Research*, vol. 3, no. 5, 2020.
[13] G. Wang, "Social responsibility of the reform and development of teacher education in contemporary China," *Jiangsu Higher Education*, no. 04, pp. 90-91, 2014.
[14] X. Yang and J. Yin, "A brief analysis of the factors affecting the professional development of preschool teachers in the development of this curriculum," *Research in Preschool Education*, 2005.
[15] Y. Sun, "Research on the development of teachers' abilities in the Open University from the perspective of lifelong education—taking the practical exploration of Tianjin Radio and Television University as an example," *Vocational Education Forum*, no. 3, p. 4, 2018.
[16] Y. Hu and Q. Hu, "The development, achievements and problems of preschool teacher education in my country in the 40 years of reform and opening up," *Teacher Education Research*, vol. 30, no. 6, p. 9, 2018.
[17] The Secretariat of the Teacher Education Expert Committee, "Suggestions on the development strategy and reform measures of teacher education in my country - minutes of the inaugural meeting and the first plenary meeting of the national teacher education expert committee," *Teacher Education Research*, vol. 16, no. 3, p. 5, 2004.
[18] K. Zheng, "Research on the development path of teacher education under the background of the reform of the national teacher qualification examination," *Journal of the National Academy of Education Administration*, no. 8, p. 6, 2017.
[19] L. Sun and Z. Fang, "Comparison and reflection on the three editions of "development suitability practice" in American early education," *Comparative Education Research*, no. 5, p. 7, 2014.
[20] J. Gan, "Review of the national seminar on education reform of preschool teachers," *Research in Preschool Education*, no. 6, p. 1, 2005.
[21] Y. Chen and L. Sen, "From teaching management to teaching leadership: the natural choice to promote the professional development of kindergarten teachers," *Research in Preschool Education*, no. 6, p. 5, 2008.
[22] H. Hu and S. Chen, "The connotation, implementation characteristics and enlightenment of EYPS training for British preschool teachers," *Foreign Primary and Secondary Education*, no. 1, p. 6, 2014.
[23] H. Zhang and X. Wang, "The implication, framework and promotion of cultural leadership of kindergarten principals," *Guangxi Social Sciences*, no. 7, p. 4, 2017.
[24] J. Yan, J. Wang, and J. Cai, "The current situation and improvement strategies of information-based leadership of kindergarten principals," *Research in Preschool Education*, no. 10, p. 9, 2015.
[25] Q. Li, H. Xu, and W. He, "The competency model and performance characteristics of middle-level managers in kindergartens," *Research in Preschool Education*, no. 9, p. 10, 2016.
[26] None, "The Ministry of education issued the "opinions on the implementation of the national primary and secondary school teachers' information technology application ability improvement Project 2.0"," *Educational Development Research*, vol. 39, no. 7, p. 1, 2019.
[27] X. Xu, "Teacher Development Evaluation in the Background of Curriculum Reform," *Chinese Journal of Education*, 2009.
[28] J. Wang and J. Yan, "A case-based analysis of the information leadership of kindergarten principals," *Educational Research and Experiment*, no. 3, p. 6, 2018.
[29] J. Zhang, "From appealing to grand theories to taking root in specific backgrounds: reflections on the professional development of kindergarten teachers [J]," *Research in Preschool Education*, no. 7, p. 3, 2008.
[30] J Zhaolin, "Early childhood teacher education reform from the perspective of postmodernism: paths and strategies," *Teacher Education Research*, vol. 29, no. 6, p. 8, 2017.
[31] N. Lu and L. Wang, "Teacher professionalism and teacher responsibility under the background of educational reform," *Teacher Education Research*, vol. 25, no. 1, p. 5, 2013.
[32] W. Liu and L Qian, "Thoughts on teacher cultural reconstruction under the background of teacher education reform," *Global Education Prospects*, no. 8, p. 5, 2009.

Hindawi
Computational Intelligence and Neuroscience
Volume 2022, Article ID 7331210, 9 pages
https://doi.org/10.1155/2022/7331210

Research Article

Matching Model of Dance Movements and Music Rhythm Features Using Human Posture Estimation

Dandan Jiang

Yangtze University, Jingzhou 434020, China

Correspondence should be addressed to Dandan Jiang; m18627233113@163.com

Received 27 March 2022; Revised 27 April 2022; Accepted 28 April 2022; Published 13 July 2022

Academic Editor: Xin Ning

The essential issue in music understanding and dance synthesis research is how to improve the degree of matching between dance motions and music rhythm elements. The matching model of dance movements and music rhythm features is created in this study based on human posture estimation research to tackle the problems that existing matching methods are prone to rapid changes in movements and cannot keep the original movement features. The rhythm properties of movement and music data are first analyzed, and then the degree of matching between movement and music pieces is measured using a dynamic time warping technique. A constraint-based dynamic planning approach is also used to synthesize the dance action sequence that best matches the supplied music. Experiments reveal that this model has a matching accuracy of 95.1 percent, which is higher than the two comparative models' matching accuracy of 5.2 percent and 7.6 percent, respectively. The matching score of this paper is high, reaching around 94 percent, according to the user research results. The method suggested in this work has apparent advantages in that it may efficiently help users in the arrangement of desired dance moves or backing music, and it can be applied in the field of actual choreography and scoring.

1. Introduction

Music, as we all know, has the power to inspire people and to express themselves in various ways. "Rhythm" [1] is the element of music that has absolute appeal to individuals. The duration of music and the intensity of timbre make up rhythm [2]. The length relationship between the action and the time value in the process of completing the dance action is referred to as dance rhythm. Long, short, strong, and weak, and their relationships create dance movements' regularity through alternation, repetition, change, and contrast [3]. You may communicate the rhythm, melody, mode, and emotion of music through dance. Human beings' evolved artistic expression is dance with music. When listening to music, many people may unconsciously dance [4]. Professional dancers will carefully control their dancing with the music based on their previous expertise, in order to more accurately represent the feelings expressed in the song. The emotions portrayed by music in dance might be playful and attractive, gorgeous and elegant, joyous and vibrant, or vigorous and unrestrained, all of which have specific dancing qualities. At the same time, the dancer's mastery of "rhythm" is reflected in his or her sense of rhythm. The dancers' perception and presentation of dance are directly affected by the rhythm. Professional dancers will tightly manage their dancing during a stage performance according to the melody, pace, and intensity of the music, in order to more accurately portray musical feelings through dance. Professional choreographers frequently create tight rules for the synchronization of dance and music. Choreography is a difficult and talented job that requires this type of dance design effort.

Although a skilled dancer can match music and dance movements manually, it takes a lot of time. And compared with the editor of solo dance, everyone's posture in group dance is different, and the editing work will be more complicated. Therefore, it is of practical value to make the computer match the characteristics of dance movements and music rhythm, and its intelligence and automation are of certain practical value to dance arrangement. Action and music are time-series signals of two different perceptual channels. In order to properly evaluate the matching degree between them, it is necessary to establish a reasonable matching model between dance action and music rhythm. Human pose estimation is the basis of many tasks in the computer vision field [5–7]. It involves many disciplines, such as pattern recognition, image processing, computer vision, and artificial intelligence. It can be used in human-computer interaction, motion analysis, motion recognition, and other fields [8, 9]. At present, in the field of human posture estimation, convolutional neural network, as a representative algorithm of deep learning, has the ability of representation learning. Compared with traditional computer vision technology and expert system, it has better performance in target detection and recognition, natural language processing, and other fields. Therefore, this paper applies convolutional neural network to human posture estimation and constructs a matching model between dance movements and music rhythm features based on human posture estimation. Its innovations are as follows:

(1) Based on the motion capture data, this paper constructs a motion database to store the rhythm and intensity characteristics of each motion segment. And in order to synthesize the dance action sequence that best matches the input music, a constraint-based dynamic planning process is introduced. Thereby, improving the matching degree of music and dance features and the smoothness of the resulting action sequence.

(2) The pyramid pool layer is utilized at the end of the feature extraction module to consider the features of multilayer convolution more thoroughly. The attention network based on time dimension features is added after the pooling layer, the relevance weight is added to the features in the video frame, and the weight of the features is updated through iteration of the attention mechanism. Simultaneously, the upgraded 3D network is trained on the input data using various combinations of diverse data, and the best input data format is chosen by assessing the trial outcomes of various groups. Experiments suggest that this strategy can significantly increase the network's accuracy.

2. Related Work

In modern music, the matching of dance movements and musical rhythm features has been widely used in choreography and score, and the practical value of all aspects and the complexity of technology have become a problem worthy of further study. Many scholars have studied the feature analysis and feature matching of dance and music. The research contents and emphases are also different.

Romina et al. first extracted musical features such as rhythm, beat position, and dynamic features, and then controlled the actions of character animations according to predefined feature mapping criteria. This method can realize the synchronization of music and dance movements, but due to the limitation of mapping criteria, the generated dance movements are relatively monotonous, and cannot reflect the intrinsic connection between music and dance [10]. Nabila et al. took the different movement rhythms and bouncing techniques of dance as the research objects, and took the students of a dance art school as the experimental objects; from the various processing methods of the action rhythm, they showed different bouncing techniques, showing different dances or dance styles, and the matching relationship between dance and music was studied [11]. Vincent et al. used machine learning to construct the mapping relationship between movements and music from a database of samples and proposed a method to create dance movements based on the emotion and content of the music [12]. Jola et al. took the rhythm pattern of the movement as the main feature of the movement and combined the speed curves of the hands, feet, and center of gravity of the body when analyzing the rhythm of traditional dance [13]. Yu et al. proposed a rhythmic feature-based action-music matching model. However, the model ignores other features than rhythm, and the generated dance movements need to be improved in terms of globality and coordination [14]. Zhang et al. propose a rhythm analysis method. In this method, the extreme point of joint angular velocity is taken as the candidate point of the segmentation rhythm, and then it is refitted into the action characteristic curve according to the distribution of the candidate points [15]. In terms of music feature analysis, Xue et al. comprehensively analyzed the rhythm of music with features such as note onset, chord change, and drum pattern and used information such as music playback speed and tempo as the main music features [16]. In order to synthesize dance movements, Zhu et al. first analyzed the music and extracted the music beats, and then, based on the original movement database, they used the movement generation method to generate new movement data. The method for music and dance synthesis is based on the beat of the music, ignoring other musical features [17]. Burnett et al. believe that dance is an orderly organization of basic movements according to a certain theme. And by setting several basic movements and scheduling rules to generate music-independent dance sequences, and then editing the dance appropriately when it matches the music [18]. Govindan et al. proposed a method to synthesize music and dance synchronously according to the rhythm and intensity characteristics of movements and music. The main idea is that musical rhythm is strongly correlated with action rhythm, and the musical intensity that represents musical mode is also strongly correlated to the action intensity that represents action strength [19]. Mir et al. proposed a genetic algorithm to match rhythms. The genetic algorithm modifies the movements based on the generated movements to improve dance diversity. This method searches for candidate actions by constructing action graphs in advance, which improves the search efficiency of the choreography system. However, this method only utilizes rhythm matching and does not fully exploit other relevant features of actions and music [20].

This paper makes an in-depth study of related literature, summarizes the shortcomings and advantages, and constructs a matching model of dance movements and music rhythm features based on human posture estimation. Firstly, the underlying features of music and action are extracted, and some feature pairs are excluded by correlation analysis. Then, genetic algorithm is used to optimize and select the corresponding relationship between matching accuracy and operation speed. At the same time, in order to obtain the mapping relationship between movements and music, we train the sample data and get the evaluation function of the matching degree between dance and music. Based on the rhythm and intensity, the feature matching analysis of music segments and action segments is carried out, and according to the rhythm matching, the most matched action segments are screened out for each music segment. Then, connectivity analysis is carried out on adjacent action segments, and a plurality of result action sequences are obtained according to the connectivity, and then the most matched action sequence is obtained according to intensity matching. Finally, the experimental comparison with other different models shows that the performance of this model is better. This method is feasible and practical.

3. Methodology

3.1. Analysis and Extraction of Rhythm Characteristics of Dance and Music. It is a common feature of rhythm, dance, and music. First, select a set of optimal motion and music features, which should be able to reveal the features of motion and music data most effectively, thus facilitating the analysis of the relationship between music and motion. In order to fully tap the local correlation between music and dance and improve the richness of generated dance, this paper does not match the input music directly with the actions in the action database. Instead, the target audio is segmented first, and then feature matching is performed for each music segment and action segment. Therefore, the music needs to be segmented. The average length of the movements and music pieces used in this paper is about 2 seconds. Cutting the data into action segments can not only fully mine the features in finer granularity but also greatly facilitate the reuse of action data.

Assuming that the overall music sequence is denoted as M, after the music is segmented, m music segments are obtained, and denoted as

$$\begin{aligned} &M_1, M_2, \ldots, M_m, \\ &M = [M_1, M_2, \ldots, M_m]. \end{aligned} \tag{1}$$

The extraction of music features is all based on music segments, and the music segments $M_i\,(1 \le i \le m)$ mentioned later all refer to the music segments in the music sequence M. The music features extracted by the music fragment M_i are recorded as

$$\text{Music}\,Feature(f) = \begin{bmatrix} F_R^{\text{Music}}(f) \\ F_I^{\text{Music}}(f) \end{bmatrix} \quad f \in M_i. \tag{2}$$

Among them, f is the frame number of the music segment M_i, and F_R^{Music} and F_I^{Music} are the rhythm and intensity features of the music segment, respectively.

For the vast majority of music segments, the quarter-note position of a music bar is often the starting point of all kinds of notes, and it is also the stress of the music, so the quarter-note position often coincides with the beat position of the notes. Music spectrum analysis provides the basis for music segmentation, music rhythm extraction, and music intensity extraction. Since the feature matching of music and action is based on the common features of music and action, namely rhythm and intensity, it is necessary to extract the rhythm and intensity features of music. In this paper, we adopt the following eight basic audio features: amplitude envelope, spectrum, cepstrum, spectrum histogram, periodicity histogram, fluency pattern, root-mean-square energy, and low-energy rate. The original music signal is a waveform signal in the time domain, but in order to extract richer information of music, such as rhythm and intensity, it is necessary to transform the music signal from the time domain to frequency domain and then analyze it. In order to ensure the stability of music rhythm and match with the internal structure of action bars, this paper only selects 4/4 beats of music pieces, and the music sequence is divided into music nodes according to bars. The map and workflow of this model are shown in Figure 1.

The mannequin used in this paper is a skeleton structure of human body, and the skeleton is composed of joint points that make up the human body. Human joints include head, hip, shoulder, chest, upper limbs, and lower limbs. These joint points constitute the human skeleton model according to the hierarchical relationship, with the hip as the root node, and other joint points are represented by rotation and displacement relative to their parent nodes. The orientation change of the rotation sub-joint point relative to the joint point is defined, and the displacement represents the spatial distance between the joint point and the sub-node. Each of the correlation coefficients may be the clue of the mapping relationship between action and music. However, considering all the coefficients at the same time will bring a very heavy amount of calculation. And some coefficient components will bring noise to the correlation between mining action and music. Therefore, this paper adopts the optimal feature selection algorithm to extract a representative feature subset, which should effectively represent the relationship between action-music and reduce unnecessary noise. Since the feature matching of music and action is based on the common features of music and action and rhythm and intensity, it is necessary to extract the rhythm and intensity features of action. In order to fully mine features in finer granularity and facilitate the reuse of action data, actions are segmented. The action mode is the same as the music segmentation mode above.

The action speed m_velocity of the joint point refers to the displacement of the joint point of the human body in unit time, and its calculation method is as follows:

$$m\_velocity = \frac{f_i(j+1) - f_i(j)}{\Delta t}, \tag{3}$$

wherein, $f_i(j)$ represents the position of the joint point i at the jth frame; $f_i(j+1) - f_i(j)$ represents the position change of the joint point i at the frame j; Δt is the time length

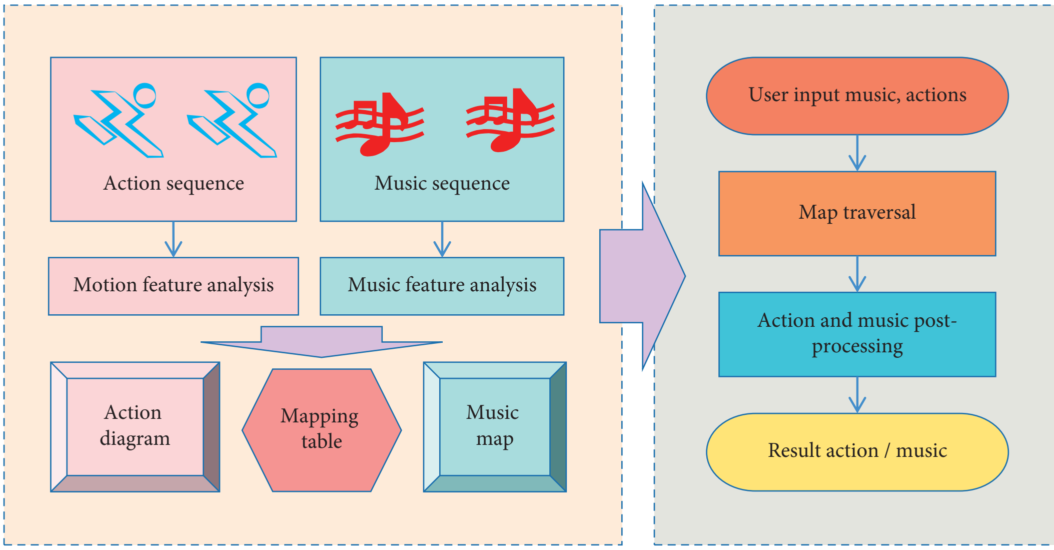

Figure 1: Workflow of the model in this paper.

of the jth frame. The formula for calculating the acceleration of the action is as follows:

$$m\_acceleration = \frac{v_i(j+1) - v_i(j)}{\Delta t}. \tag{4}$$

Among them, $v_i(j)$ represents the velocity of the joint point i at the jth frame. The formula for calculating the action distance is as follows:

$$\begin{aligned} C_i &= \frac{1}{N}\left(\sum_{j=1}^{N} f_i(j)\right), \\ m\_\text{span} &= \sum_{i=2}^{n}\sum_{j=1}^{N}\left|f_i(j) - C_i\right|. \end{aligned} \tag{5}$$

Among them, C_i is the center position of all positions of the ith joint point of the human body in the action clip, N represents the number of frames in the action clip, and n represents the number of joint points used in the human body model.

Because every joint point of an action segment can construct a cosine curve, in order to fully express the characteristics of the whole action, it is necessary to compound the curves of specific joint points that users are interested in, and the compound curve obtained by weighted average of each curve is the whole action curve. Static features are used to describe the pose characteristics of human characters. The static features extracted in this paper include motion spacing, motion density, arm shape, foot footprint, and balance. Traditional rhythm extraction methods that only aim at certain types of dance movements have great limitations. Because the feature extraction of the motion data is preprocessed and stored in the motion database, it can be extracted manually by its suitable rhythm extraction algorithm according to the dance style.

3.2. Construction of the Match Model between Motion and Music Features. Human pose estimation can be simply regarded as the combination of feature extraction [21] and classifier recognition. From preprocessing to feature selection, human motion information is extracted from the underlying data, and then classified by classifier to complete motion recognition. The process of human body motion recognition is the process of acquiring high-level motion information through the underlying data, thus learning the motion characteristics and finally realizing the motion classification. When estimating the human posture, the input data are the video frame sequence, so we need to consider not only the spatial representation of actions but also the sequence of atomic actions in the video frame sequence. There are three types of motion feature extraction based on nondeep learning algorithm: low-level features, middle-level, and high-level features and silhouettes. Low-level features usually refer to spatio-temporal interest points and dense optical flow. And middle-level features, mainly long-term tracking track or semantic representation. The premise of recognizing human movements by silhouette features is to assume that human movements are regarded as a continuous process of body posture. The learning process is extracted from a series of silhouettes, and then the traditional classifier is used to identify human movements. According to different application requirements, some researchers use single-view data, but the results are often vague. Especially in the method based on target silhouette, the system falls into local minima because multiple poses correspond to the same silhouette. Moreover, the traditional 2D convolution network cannot deal with the sequence of atomic actions when dealing with motion recognition in video, which has great limitations. This problem can be solved in 3D convolution network.

Assuming that the neuron has three input values: x_1, x_2, x_3, and the output is as follows:

$$h_{W,b}(x) = f\left(\sum_{i=1}^{3} W_i x_i + b\right), \tag{6}$$

where W_i and b are the neuron parameters at the input and $f(\cdot)$ is the activation function. Sigmoid function

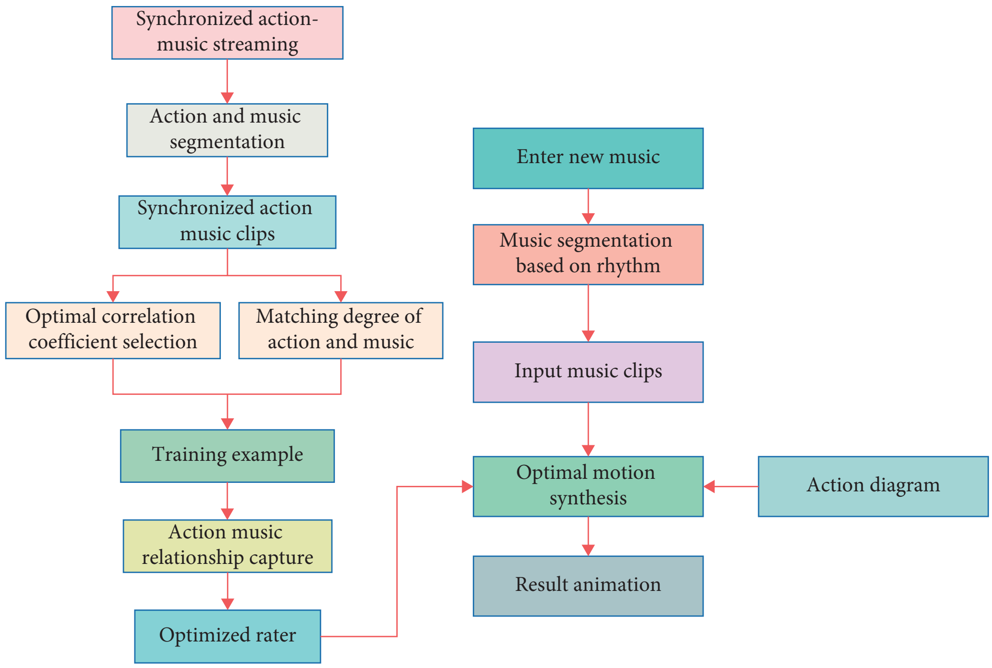

Figure 2: Algorithm flow.

$$\sigma(x) = \frac{1}{1 + \exp(-x)}. \tag{7}$$

Hyperbolic tangent tanh function

$$\tanh(x) = \frac{e^{x} - e^{-x}}{e^{x} + e^{-x}}. \tag{8}$$

The rhythm of the dance is synchronized with the music. Dancers always step on the rhythm points of the music when dancing, similar to clapping and beating, which can be roughly regarded as the coincidence of the stop action and rhythm points of the dancers. For each action and music segment combination, we extract 40 music features and 455 action features. Through correlation analysis, a correlation coefficient can be obtained, which together form a correlation coefficient matrix. Theoretically, the rate of change of eigenvalues can better reflect the development and change of things than the eigenvalues themselves. For a given well-matched action and music piece, the greater the change of the action part, the worse the matching degree with the original music piece. Feature matching is mainly based on rhythm and intensity matching. However, in order to ensure that the action segments can finally be connected into a coherent and natural dance action, it is necessary to analyze the connectability between every two adjacent action segments whose rhythm matches each music segment. In this chapter, the connectability analysis controls the current action and the previous action. When the adjacent action is the same action, the action distance between them is set to infinity, so that when the adjacent action is the same action, the two actions cannot be connected. The algorithm flow is shown in Figure 2.

In order to obtain positive training samples, all matching action-music piece combinations can be selected as positive training samples. We randomly chose a clip from all captured action footage and coupled it with a music clip to collect examples of negative training. The algorithm is used to determine the combination's matching score for each action-music piece combination. We can discover the best matching K music nodes for each action segment by comparing the scores, and these matching results will then be placed in an action-music mapping table. Similarly, a tag is provided for rhythm matching of dance action database with strong rhythm for music.

Let $\{v_{i1}, v_{i2}, \ldots, v_{iK}\}$ and $\{v_{j1}, v_{j2}, \ldots, v_{jK}\}$ be the set of K music nodes that best match u_i and u_j obtained from the map, respectively. Then, the music edges corresponding to u_i and u_j are the directed edges v_{im0} and v_{jn0} with the smallest distance in the music graph in

$$\begin{aligned} v_{im0} &\in \{v_{i1}, v_{i2}, \ldots, v_{iK}\}, \\ v_{jn0} &\in \{v_{j1}, v_{j2}, \ldots, v_{jK}\}. \end{aligned} \tag{9}$$

Therefore, the music nodes v_{im0} and v_{jn0} can be used as the background music corresponding to the action nodes u_i and u_j, respectively. The corresponding dance moves are calculated in the same way. The matching error of the action and the music is estimated as follows:

$$L(A_j, M_j) \triangleq 1 - \exp\left(-\text{Dist}_m\left(M_i, M_j\right)\right). \tag{10}$$

In this paper, we choose a specific correlation coefficient for each dance. The termination condition of feature coefficient selection is that when six new correlation coefficients are allowed to be selected into this subset, the accuracy should be increased by at least 4%. Start with an empty feature subset and add new features to the set until the termination condition is not met. The size setting of threshold is a measure of cohesion and connectivity. If the threshold setting is small, the adjacent actions are very similar, and the cohesion is very coherent, but the connectible action sequences will decrease accordingly. Anyway, if the threshold setting is large, the adjacent actions will be connected without being very similar, resulting in poor connection, but the connectible action sequence will increase accordingly. In addition, threshold setting has different requirements for different action types. Music-action correspondence is a set of music-action feature pairs, which is used for the matching calculation of music and dance. The music features and action features that make up the feature pair are in one-to-one correspondence and have high correlation characteristics.

In order to extract connectible actions based on connectivity, this section proposes a graph-based depth-first traversal algorithm for extracting connectible actions. Each action segment is regarded as a node, and a directed edge is established according to whether adjacent segments are connected or not. If adjacent segments are connectible, a directed edge is established; On the other hand, if the adjacent segments are not connectible, there is no directed edge in the adjacent segments. According to the best matching path of the sequence of motion and music feature points given by this algorithm, the motion (music) segment can be deformed to map the motion (music) feature points to the corresponding music (motion) feature points, thus further improving the matching degree between the motion and music segments.

4. Result Analysis and Discussion

The algorithm proposed in this paper is tested on multiple sequences, including synthetic and real data. The configuration of the experimental platform is Intel Pentium D2.80 GHz CPU, 16 GB memory, and uses QT4.2 and MatLab development environment. Dance sequences were acquired at a frame rate of 30 fps using a motion analysis optical motion capture device. The size of the voxels in the experiment is set to $18 \times 18 \times 18$. The dance movements used are recorded as movement data in BVH format. The data have 65 degrees of freedom, which contain 24 joint points, each joint point has about 2 degrees of freedom. The actions are recorded to the file at a frame rate of 35 frames per second. The accompanying background music is all single-channel music with a sampling frequency of 45 kHz. The sampling rate of the motion data is 35 Hz. The music in WAV audio format is extracted from the video file by the software Adobe Premiere, and the parts without sound at the beginning and end of the video are manually removed. In the experiment, an action graph containing 1069 nodes is constructed, and each node corresponds to an action segment. The total node length is about 726 seconds. The comparison results of the corresponding relationship accuracy of the underlying features and the corresponding relationship accuracy of the high-level statistical features are shown in Table 1.

From the experimental data in Table 1, it can be seen that, compared with the high-level statistical features, using the low-level features to construct the music-action correspondence can get higher accuracy. While the accuracy of

Table 1: Comparison of the accuracy of the corresponding relationship between low-level features and high-level statistical features.

Music number	Low-level feature correspondence accuracy	High-level statistical feature correspondence accuracy		
		SHI	KIM	SMS
1	77.6	67.2	70.9	69.8
2	75.4	60.3	67.5	71.4
3	76.3	64.7	65.9	72.3
4	74.5	71.3	70.5	69.4
5	76.8	68.4	69.7	62.8

the correspondence of high-level statistical feature is relatively low. In order to test the rationality of matching the characteristics of music rhythm and intensity with those of dance movements, several experiments were designed. In order to evaluate the effectiveness of the method proposed in this paper, the F1 index, which can comprehensively reflect the performance of the algorithm is selected to experiment the algorithm in this paper and compare different algorithms, and the result shown in Figure 3.

In practical application, the action map and music map in the action-music map are mostly composed of the same kind of dance, so the matching quality of the result animation created by the system when the action map and music map are constructed by the same kind of dance is evaluated. Every time it is necessary to determine an action segment from the candidate action set, the action segment with the best coherence is the first. Then randomly choose one of them as the action segment of the matching music. All initial postures are chosen from the live dance of motion capture. From the existing music-action database, based on the music similarity and the input music, the music-action data with corresponding matching are obtained, and the path of its action data is extracted as the reference path. When the action map part and music map part of the action-music map are composed of different dance types, the difference of style between the action bar and the music bar may lead to the change of algorithm performance. This paper also evaluates the matching quality for this situation. The accuracy of matching dance movements with music rhythm features by different methods is shown in Figure 4.

The matching action sequences can be counted, and if a certain number of values are reached, the traversal can be terminated. Because every time an adjacent point is visited, the adjacent point with the best rhythm is preferentially visited, so the action sequence obtained in priority matches the rhythm of the input music signal better. This paper puts forward the definition of fluency function and uses quantitative data to objectively analyze the connection between dance movements and music matching. The cohesion of dance movements using different matching methods is shown in Figure 5.

It can be seen that the dance movement cohesion of this matching method is obviously higher than that of the other two methods. Table 2 shows the time performance evaluation in this chapter. In this test, the time performance

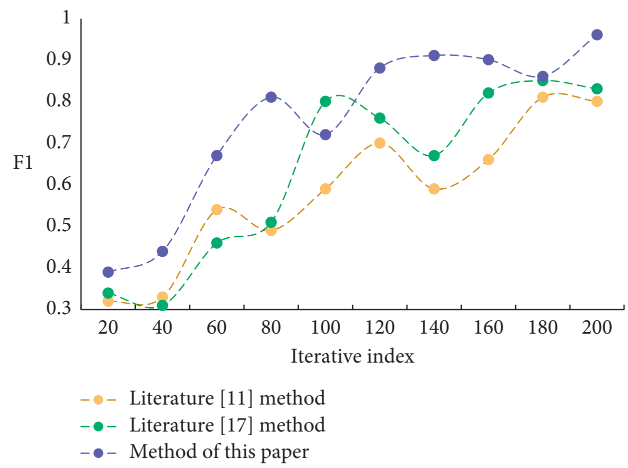

FIGURE 3: F1 value comparison.

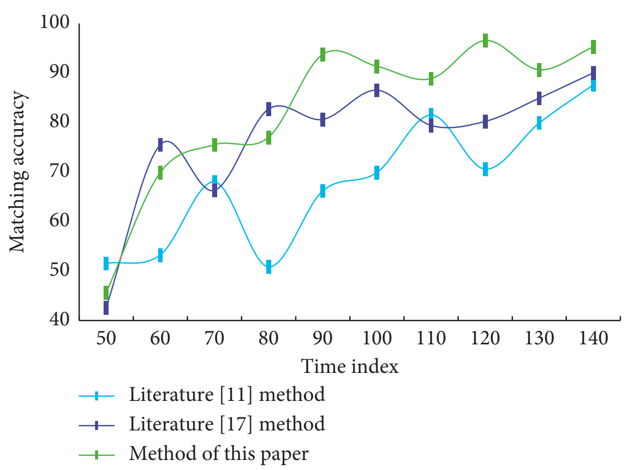

FIGURE 4: Matching accuracy of different methods.

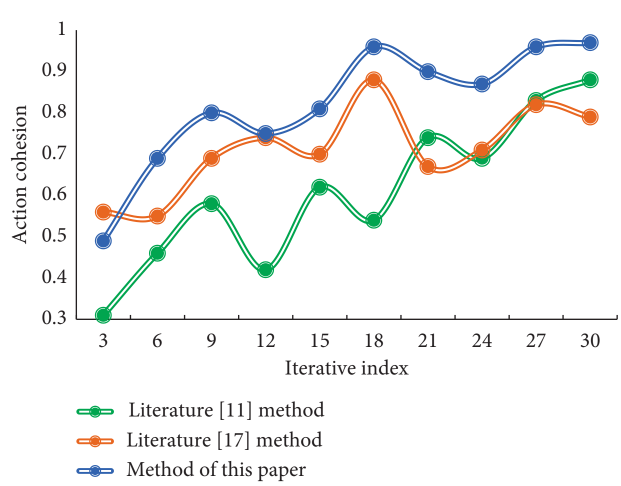

FIGURE 5: Dance movement cohesion results of different matching methods.

differences of the method in reference [11] and the method in reference [17] are compared.

In the methods of literature [11] and literature [17], it is important to traverse the music or action graph for each action or music segment to locate the best matching music node. We simply need to query the map for the best matched node in our function. As a result, our method's search speed is substantially faster than the other two techniques. 150 students were asked to complete a user experience research in order to objectively evaluate and test the model's performance. A user ability test was conducted prior to the experiment to guarantee that the participants could actually identify whether the action matched the music. Experimenters who did not have a strong musical background or who had difficulty appropriately perceiving the movement-music connection were removed. The user research study drew a total of 100 participants. Figure 6 depicts the pleasure of these 100 students with various model matching results.

In order to give more credibility to the evaluation results, we will compare the degree of difference between human and machine ratings. The results of automatic scoring by the algorithm are shown in Figure 7.

From the comprehensive analysis of the data in the two figures, it can be seen that the result of manual scoring is very similar to that of algorithm scoring. This also verifies the reliability of the score and draws the conclusion that the dance movements of this paper match the rhythm features of music to a high degree. According to the experiments in this chapter, the matching accuracy of this model is as high as 95.1%, which is higher than 5.2% and 7.6% of the two comparative models, respectively. This model effectively improves the efficiency and accuracy of the choreography and score system. And the matching score of this paper is high, reaching about 94%. It can be used in the field of actual choreography and score.

Table 2: Time efficiency comparison of choreography and soundtrack of different systems.

Choreographer					Soundtrack				
Serial number	Number of feature points	Literature [11] method	Literature [17] method	Method of this paper	Serial number	Number of feature points	Literature [11] method	Literature [17] method	Method of this paper
1	30	44.69	43.14	16.24	5	25	30.98	31.46	13.27
2	32	46.59	45.87	17.58	6	20	25.87	24.96	11.54
3	35	50.16	50.34	19.24	7	23	28.49	27.68	12.63
4	37	53.19	52.87	21.16	8	19	20.39	21.58	10.01

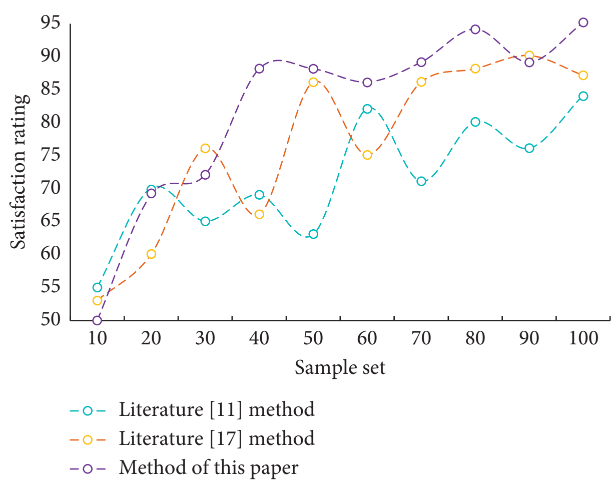

Figure 6: Satisfaction comparison of matching results of different models.

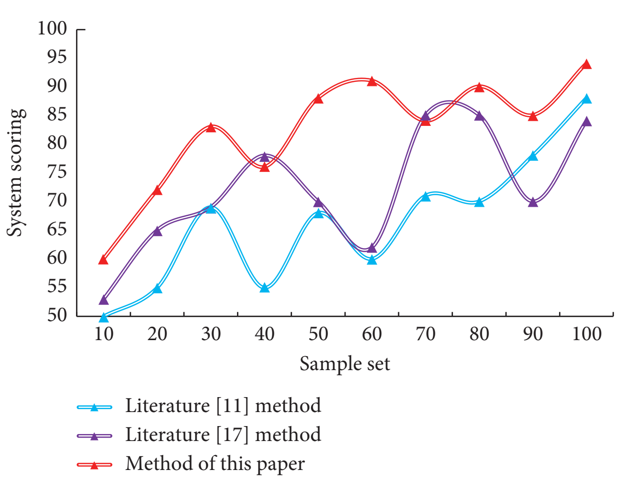

Figure 7: The result of the automatic scoring of the algorithm.

5. Conclusions

This is the law according to which rhythmic sequence and movements develop. Based on the estimation of human posture, this paper constructs a feature matching model of dance movements and music rhythm, which solves the problem of matching movements and music well. Firstly, based on the synchronization number of rhythm points of music and dance movements in time, the paper carries out rhythm matching. And in order to ensure the cohesion of adjacent action segments, the connectability analysis of adjacent action segments is made based on the action distance. At the same time, in order to generate the optimal dance action sequence, a dynamic planning process based on constraints is introduced. This process takes into account both the matching degree between actions and music and the coherence degree between actions in the result. The experimental results show that the matching score of this paper is high, reaching about 94%. And the matching accuracy of this model is as high as 95.1%, which is higher than 5.2% and 7.6% of the two comparative models, respectively. From the database point of view, this model effectively improves the efficiency and accuracy of the choreography and score system. The integration of movement and music has always been a difficult problem, which needs to be improved and dealt with at a deeper level. Although some research achievements have been made in this paper, the score algorithm of this paper has not considered enough the harmony of the transition between music pieces, and this content will be studied in depth in the next step.

Data Availability

The data used to support the findings of this study are available from the corresponding author upon request.

Conflicts of Interest

The author declares no conflicts of interest.

References

[1] X. Zhai, "Dance movement recognition based on feature expression and attribute mining," *Complexity*, vol. 2021, no. 21, pp. 1–12, 2021.

[2] A. Jalal, I. Akhtar, K. Kim, P. E. Human, and E. Sustainable, "Classification via pseudo-2D stick model and K-ary tree hashing," *Sustainability*, vol. 2020, p. 12, 2020.

[3] Z. Gao, P. Wang, H. Wang, M. Xu, and W. Li, "A review of dynamic maps for 3D human motion recognition using ConvNets and its improvement," *Neural Processing Letters*, vol. 52, no. 2, pp. 1501–1515, 2020.

[4] S. Z. Gurbuz and M. G. Amin, "Radar-based human-motion recognition with deep learning: promising applications for indoor monitoring," *IEEE Signal Processing Magazine*, vol. 36, no. 4, pp. 16–28, 2019.

[5] J Zhou, D Zhang, and W Zhang, "Underwater image enhancement method via multi-feature prior fusion," *Applied Intelligence*, vol. 2022, pp. 1–23, 2022.

[6] W. Cai, M. Gao, R. Liu, and J. Mao, “MIFAD-net: multi-layer interactive feature fusion network with angular distance loss for face emotion recognition,” *Frontiers in Psychology*, vol. 12, Article ID 762795, 2021.
[7] J. Zhou, Y. Wang, and W. Zhang, “Underwater image restoration via information distribution and light scattering prior,” *Computers & Electrical Engineering*, vol. 100, Article ID 107908, 2022.
[8] D. Yao, Z. Zhi-li, Z. Xiao-feng et al., “Deep hybrid: multi-graph neural network collaboration for hyperspectral image classification,” *Defence Technology*, vol. 2022, 2022.
[9] W. Cai and Z. Wei, “Remote sensing image classification based on a cross-attention mechanism and graph convolution,” *IEEE Geoscience and Remote Sensing Letters*, vol. 19, pp. 1–5, 2022.
[10] T. Romina and G. M. T. Maurilio, “Overcoming depression with dance movement therapy: a case report,” *Psychiatria Danubina*, vol. 30, pp. 515–520, 2018.
[11] M. Nabila, A. I. Mohammed, and B. J. Yousra, “Gait-based human age classification using a silhouette model,” *IET Biometrics*, vol. 7, no. 2, pp. 116–124, 2018.
[12] H. Vincent, D. Davood, B. Vahid, and K. Dana, “Lower body kinematics estimation from wearable sensors for walking and running: a deep learning approach - ScienceDirect,” *Gait & Posture*, vol. 83, pp. 185–193, 2021.
[13] C. Jola, F. E. Pollick, and M. H. Grosbras, “Arousal decrease inSleeping beauty: audiences’ neurophysiological correlates to watching a narrative dance performance of two-and-a-half hours,” *Dance Research*, vol. 29, pp. 378–403, 2011.
[14] W. Yu, L. Jiao, S. Wang, R. Bie, Y. Chen, and D. Liu, “Sports motion recognition using MCMR features based on interclass symbolic distance,” *International Journal of Distributed Sensor Networks*, vol. 2016, no. 3, pp. 1–15, 2016.
[15] D. Zhang, “Intelligent recognition of dance training movements based on machine learning and embedded system,” *Journal of Intelligent and Fuzzy Systems*, vol. 2021, no. 1, pp. 1–13, 2021.
[16] Y. Xue, X. Ji, D. Zhou, J. Li, and Z. Ju, “SEMG-based human in-hand motion recognition using nonlinear time series analysis and random forest,” *IEEE Access*, vol. 7, pp. 176448–176457, 2019.
[17] M. Zhu and Q. Huang, “Research on 3D human motion analysis and action recognition method,” *Revista de la Facultad de Ingenieria*, vol. 32, no. 5, pp. 552–560, 2017.
[18] J Burnett, “Why Stromae matters: dance music as a master class for the social issues of our time,” *French Review*, vol. 91, no. 1, pp. 79–92, 2017.
[19] R. Govindan, V. H. Saran, and S. P. Harsha, “Subjective discomfort analysis of human body in semi-supine posture caused by vertical sinusoidal vibration,” *Ergonomics*, vol. 64, no. 2, pp. 1–26, 2020.
[20] A. M. Mir, M. H. Yousaf, and H. Dawood, “Criminal action recognition using spatiotemporal human motion acceleration descriptor,” *Journal of Electronic Imaging*, vol. 27, no. 6, p. 1, 2018.
[21] X. Jin, J. Zhang, J. Kong, T. Su, and Y. Bai, “A reversible automatic selection normalization (RASN) deep network for predicting in the smart agriculture system,” *Agronomy*, vol. 12, no. 3, p. 591, 2022.

Hindawi
Computational Intelligence and Neuroscience
Volume 2022, Article ID 2024686, 10 pages
https://doi.org/10.1155/2022/2024686

Research Article

Optimization Algorithm of Urban Rail Transit Network Route Planning Using Deep Learning Technology

Yaqi Ma

School of Transportation, Soochow University, Suzhou 215131, China

Correspondence should be addressed to Yaqi Ma; 201772494@yangtzeu.edu.cn

Received 15 May 2022; Revised 9 June 2022; Accepted 10 June 2022; Published 13 July 2022

Academic Editor: Xin Ning

Under the present background, optimizing the existing urban rail transit network is the focus of urban rail transit construction at present. Based on DL, this paper constructs the optimization algorithm of urban rail transit network route planning. According to the current urban layout and urban planning, build a suitable rail transit network line form; according to the function, the types of urban rail transit stations are divided, and the optimization of urban rail transit network lines is realized. In addition, according to the K short path algorithm, this paper calculates the effective path between any stations of rail transit and, according to the model, allocates the passenger flow to each path. Experimental results show that the accuracy of real-time traffic flow prediction by this algorithm can reach 94.98%, which is about 9% higher than other methods. This algorithm can effectively optimize the route planning of urban rail transit network. This verifies the effectiveness of the route planning optimization algorithm proposed in this paper. Using the algorithm in this paper for line planning can get good real time, rationality, and optimality.

1. Introduction

One of the most serious issues that has plagued cities all over the world, particularly large and medium-sized cities, is traffic congestion. In recent years, the scale of Chinese cities has grown, the urbanization process has accelerated, and urban economic development has progressed rapidly. The number and distance of people's trips have increased as the city has grown and their living standards have improved, and traffic flow has increased significantly [1]. The rationality of urban traffic network layout, the scientificity of line facility configuration, and the effectiveness of network line services are all factors in urban rail transit planning [2]. It is critical to the city's overall development, functional layout, land use, and urban form evolution. Transportation, as an important infrastructure for promoting the exchange of materials and information within urban agglomerations, is critical in providing channels for city internal development and interconnection [3]. Fast transportation has the potential to amplify the power of urban development and connect cities. Network route planning is a subset of overall urban planning that uses the overall urban planning as a guide and, at the same time, has some impact on the overall urban planning due to the characteristics of urban rail transit [4]. It is a comprehensive, long-term, and guiding macro planning that involves many specialties such as urban planning, traffic engineering, rail transit engineering, architectural engineering, and social economy. Furthermore, urban rail transit requires a significant financial investment and a lengthy construction period, all of which have a significant impact on the city's social and economic development, as well as land development and utilization. To do a good job on such a large system project, we need to do overall planning and reasonable arrangements, as well as scientific and reasonable rail transit planning, to lay a good foundation and set the stage for the follow-up work.

Due to the slow construction of rail transit and the lack of practical verification and summary, there have been some problems such as too simple planning content, strong planning color, and poor implementability. At the same time, due to the uncertain factors in the process of urban development, the early planning of some cities can no longer meet the needs of current urban development. Therefore, it is necessary to optimize the urban rail transit network and improve its performance and transportation service capacity. The concept of deep learning (DL) [5, 6] originates from the research of ANN (artificial neural network) [7] and is a new research direction of machine learning [8–10]. ANN is a mathematical model that imitates biological NN (neural network) for distributed parallel information processing [8]. In ANN, neurons connect and interact with each other to form NN. There are different ways of linking neurons in different NN types. The obtained deep network structure of DL contains a large number of neurons, which has more levels and depths than the simple NN structure, so it is intended to study more abstract data representations. The "learning" of DL mainly focuses on the abstract representation of data and finds the essential relationship between variables by constantly mining the internal structure of data. A good data representation can keep the information useful to the learning task, and at the same time, it can eliminate the influence of the change of factors unrelated to the learning task in the input data on the learning performance. DL has the advantages of high model accuracy and simple feature extraction, and it has excellent applications in speech recognition, natural language processing, image recognition, and other fields. In this paper, DL algorithm is applied to the optimization of urban rail transit network route planning, and its innovations are as follows:

(1) Based on the idea that urban rail transit plays a key role in urban traffic, this paper studies the line planning theory of urban rail transit network; based on the analysis of existing practice and research results at home and abroad, and combining theory with practice, this paper puts forward solutions to several common problems in the route planning of urban rail transit network. Based on this, DL theory is used to study the optimization of urban rail transit network, which provides some reference for the optimization of urban rail transit network.

(2) The disequilibrium coefficient of passenger flow distribution in the section is calculated. This paper analyzes the influencing factors of cross section passenger flow from the aspects of network line conditions, land use, passenger factors, and environmental conditions. Based on the calculated cross section passenger flow data, several cyclic DL prediction models with time series as input are established and the parameters are optimized. The verification results show that the algorithm has high prediction accuracy and high running efficiency and meets the requirements of accuracy and timeliness. It provides a brand-new perspective for the route planning algorithm of urban rail transit network.

The main structure of this article is as follows: the first chapter is the introduction. This chapter mainly expounds the research object, background, purpose, and significance of the paper, and summarizes the research methods and the structure of the paper. The second chapter introduces the related research literature of urban rail transit network route planning at home and abroad, and further leads to the research work and research methods of this paper. The third chapter is divided into two parts. Section 3.1 compares and analyzes the development status of rail transit and introduces the related contents of DL. Section 3.2 mainly discusses the optimization algorithm of urban rail transit network route planning based on DL. The fourth chapter is the experimental part. In this chapter, the optimization algorithm of urban rail transit network planning based on DL proposed in this paper is tested and compared with other algorithms. The performance of this algorithm is comprehensively analyzed from the experimental results. The fifth chapter is the summary and outlook. Firstly, it reviews and summarizes the research content of this paper, points out the deficiency and improvement space of the research content, and looks forward to the follow-up research.

2. Related Work

The construction of urban rail system is the basic facilities of a city. It is also a systematic project with large investment and long construction period. At the same time, urban rail transit, as an important part of urban public transport, has a very important impact on urban social economy and land development. Therefore, according to the future development of the city, how to plan a reasonable rail transit network line form, scale, and surrounding land development form has attracted more and more attention from government departments, research institutions, experts, and scholars.

Wang et al. calculated the line density of the rail transit network based on the population density of a city, judged the rationality of the construction scale of its network lines, classified the urban space and the layout of the rail transit network lines, and analyzed the corresponding relationship between the two [11]. Shang et al. studied the vulnerability of urban rail transit systems and the optimization of network resilience [12]. Based on the analysis of the reasonable scale of network lines and its influencing factors, Li et al. took the traffic demand and the service level of network lines as the main influencing factors of the reasonable scale of urban rail transit and carried out a reasonable scale calculation [13]. Ding et al. constructed the probability distribution function of subway passenger flow and analyzed a certain urban rail transit system as an example, showing that the station passenger flow is closely related to the development degree of the surrounding land, industry, commerce, and residence [14]. Xin et al. took the algebraic connectivity as the objective function and the construction cost as the constraint condition, established an optimization model of the urban rail transit network invulnerability, and used the improved particle swarm optimization algorithm to solve the model [15]. Based on the directed connection graph of factors affecting the scale of network lines, Hu et al. obtained the hierarchical structure of factors affecting network lines by establishing an accessibility matrix; the matrix is based on the hierarchical division of influencing factors, and the hierarchical structure of each influencing factor is obtained [16]. Li et al. believed that the overall urban passenger demand is jointly undertaken by the road traffic passenger system and the rail transit passenger system; based on this supply-demand balance principle, a reasonable scale of network lines was calculated [17]. Through in-depth research on the demand relationship of rail transit, Nie et al. came to the conclusion that rail transit demand is concentrated in urban passenger flow corridors [18]. Ding et al. took urban rail transit network construction as the research object and established an urban rail transit network optimization model [19]. The model takes the rationality and accessibility of rail transit lines as constraints and selects the minimum total travel time, the minimum total line length, and the minimum total number of transfers to establish a multiobjective function. Wang et al. believed that urban rail transit planning can be divided into three interrelated problems [20]. The first category is to study the design of rail transit network; the second category is to analyze and forecast rail transit demand; the third category is to evaluate and decide on urban transportation planning. Jeongwoo et al. studied the robustness optimization problem of urban rail transit network under uncertain demand [21]. The research proposes the concept of robustness of rail transit network under uncertain demand and establishes predictable and unpredictable models of uncertain demand.

This paper proposes an optimization algorithm for urban rail transit network route planning based on DL, and analyzes and discusses the design and implementation of the algorithm in detail, based on a thorough review of previous literature. The passenger flow is allocated to each train on each line based on the passengers' arrival and departure times, the cross section passenger flow in the statistical period is calculated, and the stability of its time series is examined in this paper. The historical data information of the corresponding date type is selected as the network's training data for different forecast periods, and the trained LSTM (long short-term memory neural network) model is used to make short-term forecasts of cross section passenger flow, with the forecasting accuracy calculated by each error index to test the model's validity. Experiments show that this algorithm is more feasible and effective than other algorithms, and that it can produce better predictions.

3. Methodology

3.1. DL and Urban Rail Transit Network Route Planning. The concept of DL comes from the study of ANN, and it is a new research direction of machine learning. ANN evolved from biological NN, and a neuron is a nerve cell. Artificial neuron is the most basic unit to process information by using NN. Theoretically, the more parameters a model has, the higher its complexity and capacity, and correspondingly it can complete more complex learning tasks. However, in general, complex models often fall into low training efficiency and are easily over-fitted, so it is difficult to be favored by researchers. Compared with the traditional NN or machine learning, DL is a relatively novel research method and research direction. The advantages of DL are high model accuracy and simple feature extraction [22]. Practice has proved that it has good effects in computer vision, natural language processing, and future trend prediction. In this paper, the DL theory is applied to urban rail transit network route planning, and an optimization algorithm of urban rail transit network route planning based on DL is proposed. The DL model increases the number of nonlinear hidden layers and transforms the original signal layer by layer to obtain new abstract features for subsequent learning tasks. DL, as a major breakthrough in realizing machine learning and accelerating human beings to the era of artificial intelligence, is based on the research in the field of NN. The obtained deep network structure of DL contains a large number of neurons, which has more levels and depths than the simple NN structure, so it is intended to study more abstract data representations. DL is also a multilevel and multistep learning process. In order to better simulate the neuron structure of human brain, more hidden layers are added, and the learned knowledge is transferred layer by layer to achieve the purpose of information stratification and systematic learning. The basic model framework of DL includes convolutional NN, stacked automatic coder, recursive NN, and deep belief network. The NN model is shown in Figure 1.

The urban population has exploded in recent years, and a large number of migrant workers have flooded into cities. Urban traffic faces severe situations and challenges due to frequent exchanges of people and materials. Road congestion, chaotic traffic order, frequent traffic accidents, and traffic environmental pollution are all serious issues in many cities. Because of its large capacity and high speed, rail transit has gradually become the development focus of transportation infrastructure in large cities in this environment. It has been instrumental in resolving traffic congestion in cities and promoting the efficient use of urban land. To fully exploit the leading role of urban rail transit in economic development, it is critical to optimize the existing urban rail transit network and build new lines in the modern environment [23]. Urban rail transit, which includes subways, light rail, monorails, trams, new traffic, and high-speed maglev trains, is referred to as rapid rail transit. Large transportation capacity, high speed, safety, reliability, and punctuality are all common characteristics. It has the ability to travel on wheels and rails on the ground, in the air, and underground. Because of these characteristics, urban rail transit has obvious advantages as a mode of urban transportation. It is especially advanced compared to other modes of public transportation when it comes to resolving traffic congestion in large and medium-sized cities, such as heavy passenger traffic during peak hours. With the rapid development of rail transit and the continuous expansion of rail network lines in recent years, urban rail transit network operation has become a new trend. Because the urban rail transit system serves as a mode of transportation, its transportation service function must be considered. At the same time, it has the nature of a network, and optimizing it solely from one perspective is not comprehensive. The basic types of rail transit usually include subway system, light rail system, suburban railway, monorail system, new transport system, tram, and automatic passenger rapid transit system.

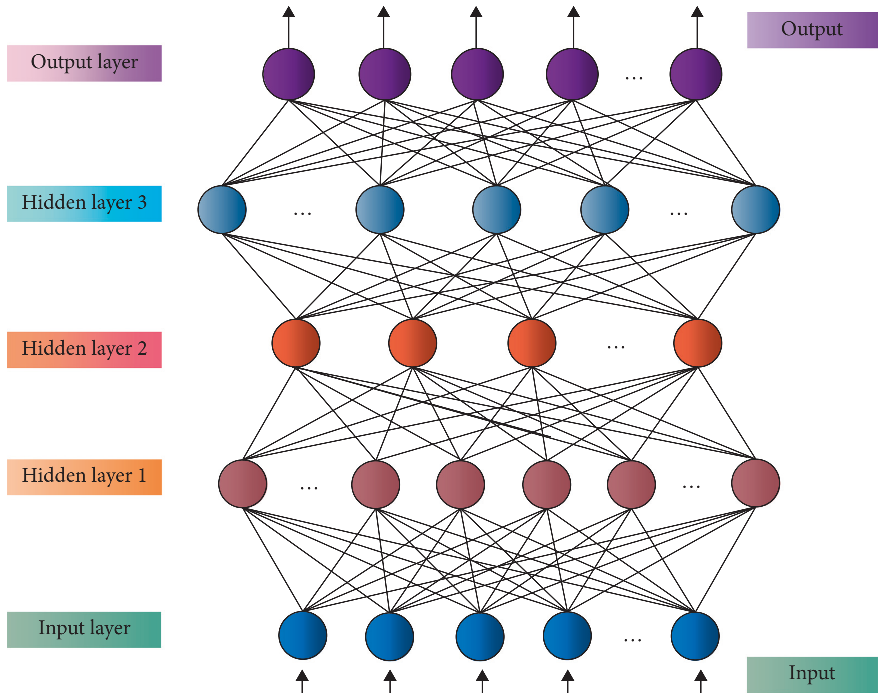

Figure 1: NN model.

In order to reasonably select the form of rail transit system under different objectives, the basic types of urban rail transit can be classified according to different standards.

The main objectives of urban rail transit planning include ① solving the contradiction between traffic demand and supply, ② achieving the goal of urban planning, and ③ meeting the needs of sustainable development. Rail transit can guide the development of urban structure, and its principle is to greatly improve the traffic supply and guide the high-intensity utilization of surrounding land. Urban rail transit with large capacity, high speed, and independent dedicated track has already met the conditions as the backbone transportation mode of public transportation system in big cities. The backbone system is to undertake a large proportion of urban passenger transport turnover [24]. It is generally difficult for a single rail transit line to meet this backbone requirement; this is mainly because of the limitations of its attracting range of passenger flow and route direction. Therefore, rail transit must form a network to play a key role. The research of network planning involves many specialties such as urban planning, traffic engineering, rail transit engineering, architectural engineering, and social economy. It is a comprehensive, long-term, and guiding macro planning. It emphasizes the unity of stability and flexibility. Stability is to plan that the overall layout of network lines should be stable in space, central city, and time; flexibility is the extension condition of planning. Under the condition of constantly changing urban conditions, there should be room for flexible changes in the outer urban areas in space and in the long term in time. In the planning of urban rail transit, the principles of functionality, rationality, economy, and sustainable development must be followed. There are actually three ways of urban rail transit lines: elevated, ground, and underground. They all have their advantages and disadvantages. In addition, the determination of standards such as curve and slope also needs to consider the specific conditions of the line. An important part of the route planning is the station planning and site selection, which needs to consider the station attraction, station form, station spacing, cost, and other aspects. The location of depot is also an important part of route planning. It requires the approach to the trunk line as much as possible and the necessary land conditions. Urban rail transit has a huge investment and a long construction period, which has a great influence on the social and economic development of the city, land development and utilization, etc. However, due to the uncertain factors in the process of urban development, the early planning of some cities can no longer meet the needs of current urban development. Therefore, it is necessary to optimize the urban rail transit network and improve its performance and transportation service capacity.

3.2. Optimization Algorithm of Urban Rail Transit Network Route Planning. Through DL-related content, this chapter focuses on the optimization algorithm for urban rail transit network route planning. The neuron model is the most fundamental unit in NN. According to the training data set, the NN learning process adjusts the connection weight between neurons as well as the threshold or bias of each functional neuron. NN can fit any nonlinear system, even if it only has one hidden layer. As a result, only one hidden layer is typically employed. After comparing and analyzing the fitting results of multiple hidden layers and a single hidden layer, it was discovered that the fitting results are not significantly different, so the reasonable scale of urban rail transit was calculated and analyzed using NN with three layers, including one hidden layer. However, as the prediction time step is increased, the influence of the previous time node on the current time node diminishes, and when information from a distant time node is needed in the model, the network model is unable to effectively reflect this connection; the learning ability is greatly weakened, the gradient disappears, and the model's prediction effect deteriorates. Therefore, LSTM is introduced in this paper. The LSTM structure and algorithm flowchart are shown in Figure 2.

In this paper, the SpaceL method is used to construct the urban rail transit network model. In the model, the nodes represent the urban rail transit stations and the connecting edges represent the interval routes. Transformation of rail transit network diagram into mathematical model is as follows:

$$G = (V, E). \tag{1}$$

Among them, V represents the set of nodes. If the rail transit includes n stations, there are

$$\begin{aligned} |V| &= \mathrm{nV} \\ &= (v_1, v_2, v_3, \ldots, v_n). \end{aligned} \tag{2}$$

E represents the set of edges. If the rail transit includes m section routes, there are

$$\begin{aligned} |E| &= \mathrm{mE} \\ &= (e_1, e_2, e_3, \ldots, e_m). \end{aligned} \tag{3}$$

In a subway network, a passenger travel path consists of stations and segments, and the base travel time for a path is equal to the inbound time, ride time, outbound time, and if transfers are involved, plus the sum of the transfer times. Let C_w^k denote the total time spent by most passengers traveling on the k th route between the traffic trip volume pair W, then

$$C_k^w = J_o + \sum_{i,j} T_{i,j}\delta_{ij,k}^w + \sum_i e_i^{l,m}\phi_{i,lm}^{w,k} + K_d, \tag{4}$$

where J_o represents the inbound time spent by passengers at the starting station on the route and K_d represents the exit time spent by passengers at the end station on the route. $\delta_{ij,k}^w$ and $\phi_{i,lm}^{w,k}$ are the relationship between the unit interval $[i, j]$, the transfer station i, and the traffic travel volume in the subway network to the path k between W.

Based on the idea of importance contribution matrix, this paper combines the structural holes and centrality features of the network to identify key sites. The K-kernel importance is used to describe the role of nodes in the network information dissemination, and the structural hole importance index and K-kernel importance index of adjacent nodes are used as the importance contribution values to reflect the local importance.

In the hidden layer of the LSTM model, the complexity of the hidden layer is increased due to the addition of three gate structures. Three different gate structures interact inside the hidden layer in a very specific way. The first structure is simpler and is often referred to as the forget gate. The input of the gate structure is the output of the hidden layer of the previous time node and the input of the hidden layer of the current node. The activation function of the gate structure is σ, and the output result is $f^{(t)}$, which is sent to the upper part to interact with the $C^{(t)}$ of the previous hidden layer. The forget gate structure can be expressed by the following formula:

$$C_k^w = J_o + \sum_{i,j} T_{i,j}\delta_{ij,k}^w + \sum_i e_i^{l,m}\phi_{i,lm}^{w,k} + K_d. \tag{5}$$

Among them, σ represents the activation function of the forget gate structure, which is the sigmoid function. W_f, U_f, and b_f represent the weight parameters and biases in the forget gate structure, respectively. The middle structure is called the input gate, and the input gate structure can be expressed as

$$\begin{aligned} i^{(t)} &= \sigma\left(W_i * h^{(t-1)} + U_i * x^{(t)} + b_i\right), \\ \widetilde{C^{(t)}} &= \tanh\left(W_c * h^{(t-1)} + U_c * x^{(t)} + b_c\right), \end{aligned} \tag{6}$$

where σ represents the activation function of the first part of the input gate. W_i, U_i, W_c, U_c, b_i, and b_c represent the weight parameters and biases of the corresponding parts, respectively. The last gate is called the output gate. The output gate structure can be expressed as

$$\begin{aligned} o^{(t)} &= \sigma\left(W_o * h^{(t-1)} + U_o * x^{(t)} + b_o\right), \\ h^{(t)} &= o^{(t)} * \tanh\left(C^{(t)}\right), \end{aligned} \tag{7}$$

where σ represents the activation function of the first part of the output gate. W_o, U_o, and b_o represent the weight parameters and bias of the output gate, respectively. The normalization formula of the indicator data is as follows:

$$y = \left(y_{\max} - y_{\min}\right) * \frac{\left(x - x_{\min}\right)}{\left(x_{\max} - x_{\min}\right)} + y_{\min}. \tag{8}$$

Among them, $y_{\min} = -1$ and $y_{\max} = 1$.

In this paper, a method for processing input real-number data using Gaussian distribution characteristics is presented, allowing the newly constructed deep belief network to process the experimental data effectively. Because each impact index has a different physical meaning and no uniform dimensional unit, it is difficult to get a satisfactory answer directly using the impact index as an input quantity, which will slow the network's convergence. This study applies dimensional processing to the data in order to make the indexes comparable. In general, due to the large range of collected data, it is generally required that the value of input data be between [−1, 1] in order to improve training speed and effectively avoid the saturation area of the sigmoid function. The DL feature extraction process can ignore the complex coupling relationship between urban rail transit vehicle equipment systems and the complex functional relationship between feature vectors, mine the data's internal structure, and find the essential relationship between variables. Robustness refers to the system's ability to provide alternate routes in the event of accidents or targeted attacks, and it is one of the key indicators used to assess the rail transit system's quality. The system's robustness is conducive to improving the urban rail transit system's reliability, service quality, and resilience, allowing it to fully exploit rail transit's

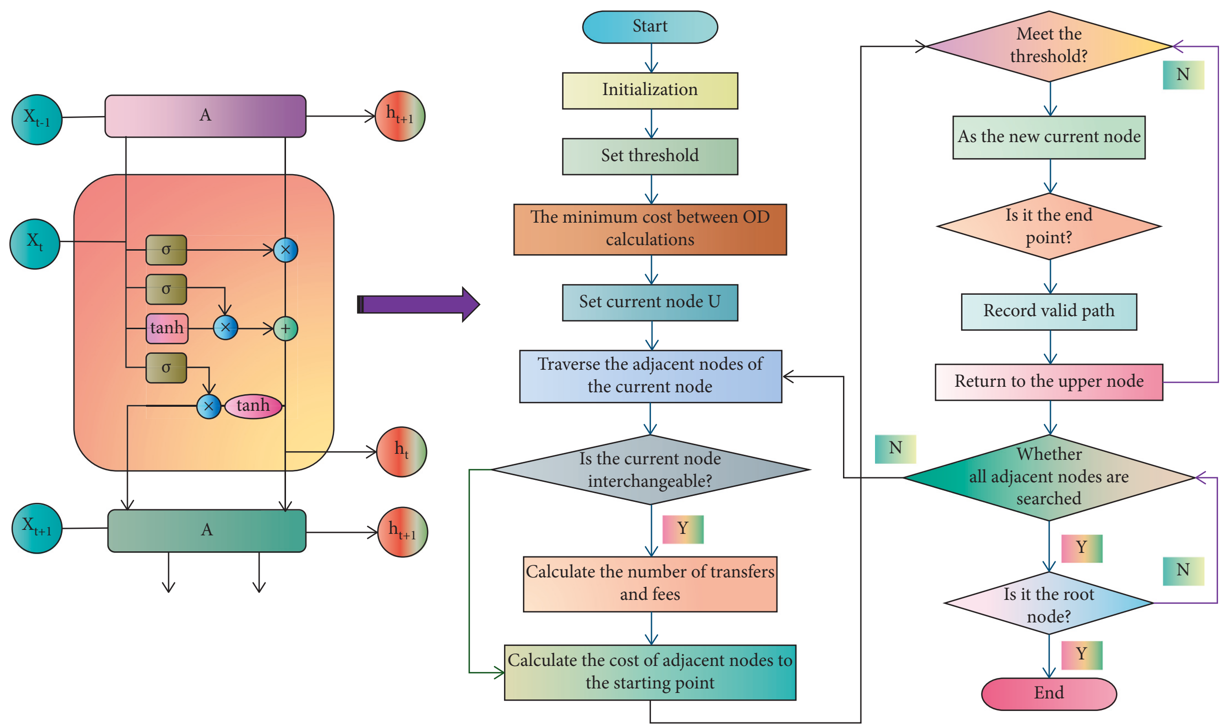

FIGURE 2: LSTM structure and algorithm flowchart.

obvious advantages. The LSTM model goes through the same training and optimization process as the NN model. To iteratively update all parameters in the model, it also uses a time-based back propagation algorithm and the gradient descent method. All of the parameters are based on partial derivatives of the loss function, which is the most important point. The network is trained and tested in a circular fashion in this paper, with the reasonable error range as the final error range. Finally, all of the remaining cities serve as training samples and models, with the trained models being used to research urban rail transit network route planning.

4. Result Analysis and Discussion

The model training platform is Windows 10, equipped with Intel 8-core CPU; memory is 32G. Python is chosen as the main programming language. TensorFlow framework in Keras not only has good usability and practicability, but also has flexibility and high efficiency, fast training speed, and flexible parameter change. It can provide corresponding operation support on multiple platforms. Therefore, this paper chooses TensorFlow in Keras as the back-end framework of DL model. After analysis and screening, 40 cities with developed urban rail transit were selected for analysis and research, and finally 12 representative cities were selected as samples for experiment. Then, the model parameters and targets are selected to be digitized. In order to get more accurate results and reasonable error range, 2 cities are selected as test samples from 12 cities, and the remaining cities are used as training samples. Run the program and record the error. Figure 3 shows the training results of the model.

In this study, the results obtained for the established predictive model are numerical data. Therefore, this chapter selects the representative MSE (mean squared error), RMSE (root mean square error), and MAE (mean absolute error) three indicators to test the algorithm, respectively. The calculation formulas of the three indicators are as follows:

$$\begin{aligned} \text{MSE} &= \frac{1}{n}\sum_{k=1}^{n}\left(y_k - y_k'\right)^2, \\ \text{RMSE} &= \sqrt{\frac{1}{n}\sum_{k=1}^{n}\left(\left|y_k - y_k'\right|\right)^2}, \\ \text{MAE} &= \frac{1}{n}\sum_{k=1}^{n}\left|y_k - y_k'\right|. \end{aligned} \tag{9}$$

Among them, n represents the number of predicted samples, y_k is the actual value, and y_k' is the model output value. The prediction accuracy evaluation methods of the three models are suitable for DL models. By comparing the evaluation indexes among different models, we can roughly understand the performance of the models. These three indexes are used to test different algorithms, and the results are shown in Table 1.

It can be seen from the data in the table that the errors of the optimization algorithm of urban rail transit network route planning in this paper are smaller than those of the comparison algorithm, and their values are at a low level. This shows the accuracy and reliability of this algorithm. Figure 4 shows the recall results of different

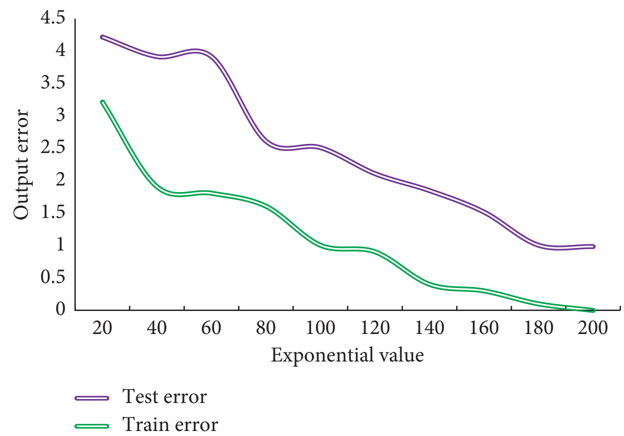

Figure 3: The training results of the model in this paper.

Table 1: Index test results of different algorithms.

Algorithm	MSE	RMSE	MAE
Multiscale path planning algorithm	0.157	0.437	0.658
Cyclic neural network optimization algorithm	0.096	0.396	0.437
Algorithm in this paper	0.049	0.215	0.426

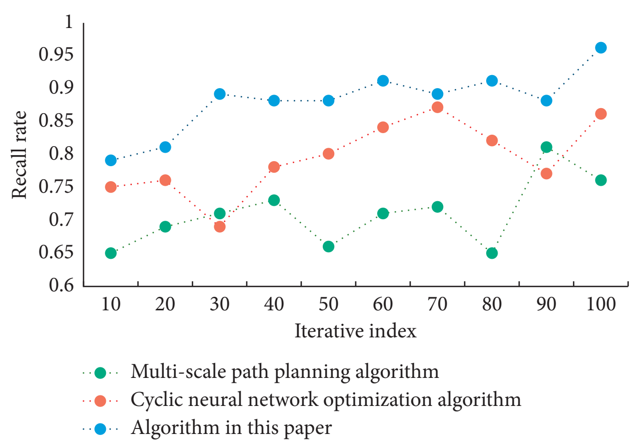

Figure 4: Recall results of different algorithms.

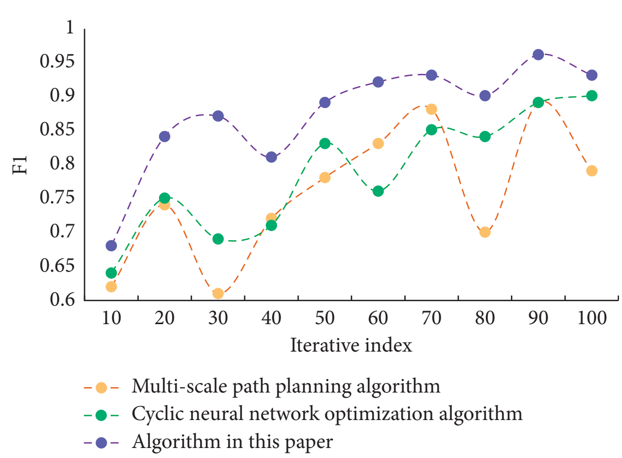

Figure 5: F1 value results of different algorithms.

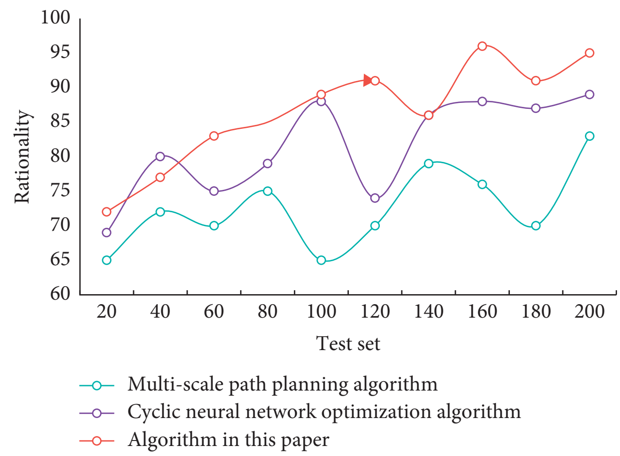

FIGURE 6: Comparison of rationality of planning with different methods.

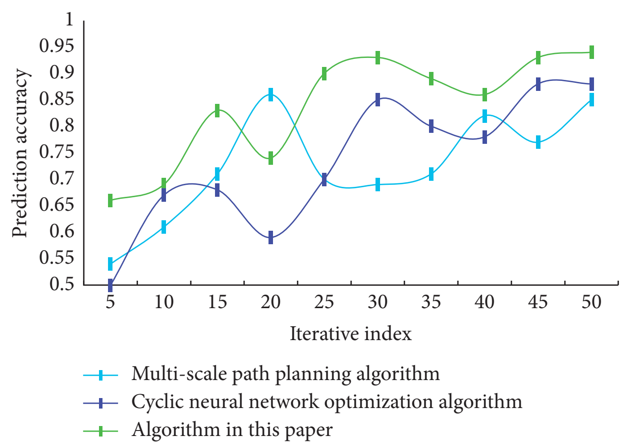

FIGURE 7: Accuracy of traffic flow prediction of different algorithms.

TABLE 2: Execution time of different algorithms.

Group	Starting point	Target point	Multiscale path planning algorithm	Cyclic neural network optimization algorithm	Algorithm in this paper
1	396	3678	894	136	81
2	579	3541	1103	94	46
3	863	2796	1039	87	51
4	827	3024	1004	98	58
5	978	4169	936	86	29

algorithms. Figure 5 shows the F1 values of different algorithms.

The existing saturation of rail transit of each sample is taken as the output target value of NN, and the training sample and the inspection sample should be representative. Through training and learning, the network adapts to the nonlinear mapping relationship between the input sample and the target value, and then it is used for simulation calculation. Test the rationality of using different algorithms for urban rail transit network route planning. The rationality comparison is shown in Figure 6.

The prediction results of several DL models are compared one by one according to the same evaluation index, among which the traditional time series prediction method and autoregressive summation average model are added to achieve the effect of horizontal comparison. The traffic flow prediction accuracy of different algorithms is shown in Figure 7.

According to the data in Figure 7, the accuracy rate of real-time traffic flow prediction by this algorithm can reach 94.98%, which is about 9% higher than other methods. The prediction results and accuracy prove the rationality and effectiveness of the proposed prediction method. This paper simulates the actual traffic conditions. Table 2 shows the comparison results of execution time of different algorithms.

It can be seen that under the same conditions, the execution time of the route planning optimization algorithm in this paper is short. This shows that the algorithm in this paper has higher efficiency and better performance.

Experiments in this chapter show that the accuracy rate of real-time traffic flow prediction by this algorithm can reach 94.98%, which is about 9% higher than other methods. This verifies the real time, rationality, and optimality of the proposed algorithm, which can reduce the management cost and obtain a higher input-output ratio. The algorithm proposed in this paper can achieve good results in the route planning of urban rail transit network.

5. Conclusions

Congestion is a major issue in today's major cities, and there are numerous solutions available. Construction of fast, large-capacity, safe, and environmentally friendly urban rail transit has almost become the default option for all major cities looking to alleviate traffic congestion. As a result, systematically analyzing and studying the functional positioning of urban rail transit network lines in the urban agglomeration regional rail transit system, integrating the regional rail transit system, and comprehensively planning and optimizing the network line layout in conjunction with the urban spatial structure and personnel travel characteristics are critical. It can effectively promote the formation of a regional high-speed comprehensive transportation system, ease people's travel, reduce traffic congestion, and lay a solid foundation for good urban traffic development. This paper proposes an optimization algorithm based on DL to address the low rationality and optimality of traditional urban rail transit network route planning. This paper describes the algorithm's design and implementation. The accuracy of this algorithm in predicting real-time traffic flow can reach 94.98 percent, which is about 9% higher than other methods, according to experimental results. This validates the proposed algorithm's real time, rationality, and optimality, lowering management costs and increasing the input-output ratio. The content of the urban rail transit mode is complex, involving a wide range of variables and numerous influencing factors. Despite the fact that this paper has made some progress in the theory and practice of urban rail transit network route planning, due to a lack of knowledge and time, there are still some issues that need to be addressed. We will expand the sample data set while appropriately deepening the model's depth, and we will determine the parameters in the model by distinguishing the samples during the week and at the weekend in the follow-up study in order to make the prediction model more applicable.

Data Availability

The data used to support the findings of this study are available from the corresponding author upon request.

Conflicts of Interest

The author declares that there are no conflicts of interest.

Acknowledgments

This study was supported without any funding.

References

[1] L. Zhang, H. Wen, J. Lu, D. Lei, and S. Li, "Comparing the time-varying topology-based dynamics between large-scale bus transit and urban rail transit networks from a mesoscopic perspective," *Nonlinear Dynamics*, vol. 106, no. 1, pp. 657–680, 2021.

[2] H. Lv, Y. Zhang, K. Huang, X. Yu, and J. Wu, "An energy-efficient timetable optimization approach in a Bi-DirectionUrban rail transit line: a mixed-integer linear programming model," *Energies*, vol. 12, no. 14, p. 2686, 2019.

[3] E. Hassannayebi, S. H. Zegordi, and M. Yaghini, "Train timetabling in urban rail transit line using Lagrangian relaxation approach," *Applied Mathematical Modelling*, vol. 40, no. 23-24, pp. 9892–9913, 2016.

[4] X. Zhu, R. Zhang, W. Dai, Z. Zhang, and J. Li, "Performance and safety assessment of ATO systems in urban rail transit systems in China," *Journal of Transportation Engineering*, vol. 139, no. 7, pp. 728–737, 2013.

[5] J. Zhang, J. Sun, J. Wang, and X. Yue, "Visual object tracking based on residual network and cascaded correlation filters," *Journal of Ambient Intelligence and Humanized Computing*, vol. 12, no. 8, pp. 8427–8440, 2021.

[6] Q. Liu, L. Cheng, A. L. Jia, and C. Liu, "Deep reinforcement learning for communication flow control in wireless mesh networks," *IEEE Network*, vol. 35, no. 2, pp. 112–119, 2021.

[7] Y. Ding, Z. Zhang, X. Zhao et al., "Multi-feature Fusion: Graph Neural Network and CNN Combining for Hyperspectral Image Classification," *Neurocomputing*, vol. 501, pp. 246–257, 2022.

[8] L. You, H. Jiang, J. Hu, C. Chang, L. Chen, X. Cui, and M. Zhao, "GPU-Accelerated Faster Mean Shift with Euclidean Distance metrics," 2021, https://arxiv.org/abs/2112.13891.

[9] Z. Huang, Y. Zhang, Q. Li et al., "Joint analysis and weighted synthesis sparsity priors for simultaneous denoising and destriping optical remote sensing images," *IEEE Transactions on Geoscience and Remote Sensing*, vol. 58, no. 10, pp. 6958–6982, 2020.

[10] W. Cai, "Hierarchical domain adaptation projective dictionary pair learning model for EEG classification in IoMT systems," *IEEE Transactions on Computational Social Systems*, pp. 1–9, 2022.

[11] Q. Wang and L. Deng, "Integrated optimization method of operational subsidy with fare for urban rail transit," *Computers & Industrial Engineering*, vol. 127, no. 1, pp. 1153–1163, 2018.

[12] P. Shang, Y. Yao, L. Yang, L. Meng, and P. Mo, "Integrated model for timetabling and circulation planning on an urban rail transit line: a coupled network-based flow formulation," *Networks and Spatial Economics*, vol. 21, no. 3, pp. 1–34, 2021.

[13] Z. Ming, "Continuous-behavior and discrete-time combined control for linear induction motor-based urban rail transit," *IEEE Transactions on Magnetics*, vol. 52, no. 7, pp. 1–4, 2016.

[14] X. Ding, S. Zhang, Z. Liu, H. Hu, X. Xu, and W. Xu, "The analysis and calculation method of urban rail transit carrying capacity based on express-slow mode," *Mathematical Problems in Engineering*, vol. 2016, pp. 1–9, Article ID 6820394, 2016.

[15] Y. Xin, A. Chen, B. Ning, and T. Tang, "Measuring route diversity for urban rail transit networks: a case study of the

beijing metro network," *IEEE Transactions on Intelligent Transportation Systems*, vol. 18, no. 2, pp. 259–268, 2017.
[16] X. Hu, X. Li, and Y. Huang, "Urban rail transit risk evaluation with incomplete information," *Procedia Engineering*, vol. 137, pp. 467–477, 2016.
[17] D. W. Li and N. D. Yi, "Real-time forecast of passenger crowd index on urban rail transit station platform based on test data of internet of things," *Journal of the China Railway Society*, vol. 36, no. 3, pp. 9–13, 2014.
[18] X. L. Nie and Q. C. Wei, "Research on the location of emergency rescue stations for urban rail transit based on the PSO," *Journal of Railway Engineering Society*, vol. 32, no. 7, pp. 100–105, 2015.
[19] X. Ding, X. Yang, H. Hu, and Z. Liu, "The safety management of urban rail transit based on operation fault log," *Safety Science*, vol. 94, pp. 10–16, 2017.
[20] Y. Wang, Z. Liao, T. Tang, and B. Ning, "Train scheduling and circulation planning in urban rail transit lines," *Control Engineering Practice*, vol. 61, no. 4, pp. 112–123, 2017.
[21] L. Jeongwoo, B. Marlon, H. Douglas, and H. Nixon, "Changes in service and associated ridership impacts near a new light rail transit line," *Sustainability*, vol. 9, no. 10, p. 1827, 2017.
[22] J. Kong, C. Yang, Y. Xiao, S. Lin, and K. Ma, "A graph-related high-order neural network architecture via feature aggregation enhancement for identification application of diseases and pests," *Computational Intelligence and Neuroscience*, vol. 2022, Article ID 4391491, 2022.
[23] Z. Jiang, J. Gu, W. Fan, W. Liu, B. Zhu, and Q. Zhu, "Q-learning approach to coordinated optimization of passenger inflow control with train skip-stopping on a urban rail transit line," *Computers & Industrial Engineering*, vol. 127, no. 1, pp. 1131–1142, 2018.
[24] L. U. Gongyuan, M. A. Si, W. Kun, and D. N, "Integer programming model of passenger flow assignment for congested urban rail lines," *Xinan Jiaotong Daxue Xuebao/Journal of Southwest Jiaotong University*, vol. 52, no. 2, pp. 319–325, 2017.

Hindawi
Computational Intelligence and Neuroscience
Volume 2022, Article ID 2452291, 10 pages
https://doi.org/10.1155/2022/2452291

Review Article

Face Mask-Wearing Detection Model Based on Loss Function and Attention Mechanism

Zhong Wang, Wu Sun, Qiang Zhu, and Peibei Shi

School of Computer Science and Technology, Hefei Normal University, Hefei 230601, China

Correspondence should be addressed to Qiang Zhu; qiangzhu@hfnu.edu.cn

Received 18 May 2022; Accepted 15 June 2022; Published 12 July 2022

Academic Editor: Xin Ning

Face mask-wearing detection is of great significance for safety protection during the epidemic. Aiming at the problem of low detection accuracy due to the problems of occlusion, complex illumination, and density in mask-wearing detection, this paper proposes a neural network model based on the loss function and attention mechanism for mask-wearing detection in complex environments. Based on YOLOv5s, we first introduce an attention mechanism in the feature fusion process to improve feature utilization, study the effect of different attention mechanisms (CBAM, SE, and CA) on improving deep network models, and then explore the influence of different bounding box loss functions (GIoU, CIoU, and DIoU) on mask-wearing recognition. CIoU is used as the frame regression loss function to improve the positioning accuracy. By collecting 7,958 mask-wearing images and a large number of images of people without masks as a dataset and using YOLOv5s as the benchmark model, the mAP of the model proposed in the paper reached 90.96% on the validation set, which is significantly better than the traditional deep learning method. Mask-wearing detection is carried out in a real environment, and the experimental results of the proposed method can meet the daily detection requirements.

1. Introduction

The spread of COVID-19 endangers public safety, and its known transmission routes mainly include droplet transmission and close contact. Therefore, wearing masks has become the main means of preventing the spread of the virus [1, 2]. The traditional methods of inspecting mask-wearing are mostly manual inspections, which not only consume manpower and material resources and are inefficient but also cause certain difficulties in personnel management, which is more likely to cause crowds to gather and increase the risk of virus spread.

Mask-wearing detection technology is one of the key prevention means supervised by epidemic prevention departments, and the stability and robustness of mask detection algorithms are particularly important. Mask-wearing detection is developed based on face detection and target classification. Compared with simple face detection, mask-wearing detection needs to address many problems, such as different lighting, side faces, occlusion, and density. However, solving these problems and improving mask-wearing detection accuracy are of great significance [3, 4].

With the development of deep learning technology, mask-wearing detection technology based on deep learning has been widely used [5, 6]. However, due to the influence of a complex environment, the existing algorithms have the problems of low accuracy and slow detection speed, which cannot achieve real-time detection. To this end, based on the YOLOv5 model, this paper introduces an attention mechanism to selectively enhance the fused features, highlight important features, reduce the impact of redundant features, and use the CIoU loss function as a new bounding regression loss function to make the regression of the target model more documented and the positioning more accurate. The main contributions of the paper are as follows:

(1) Study the effect of different attention mechanisms (CBAM, SE, and CA) on improving the deep network model.

(2) Explore the impact of different bounding box loss functions (GIoU, CIoU, and DIoU) on mask-wearing recognition.

The rest of the content is arranged as follows: Section 2 introduces the work related to mask-wearing detection. Section 3 focuses on describing the framework and implementation details of the mask-wearing detection model. Section 4 verifies the performance of the proposed method through experimental tests and finally gives a summary and outlook.

2. Related Works

Mask-wearing detection is an object detection task that determines the location and category of each object in the image. Mask-wearing detection methods based on deep learning are divided into two categories. One is a two-stage target detection model based on region extraction, such as RCNN (regions convolutional neural networks) [7], Fast R-CNN [8], Faster R- CNN [9], R-FCN [10], Cascade R-CNN [11], and DeRPN [12], which divide the target detection into two steps: feature extraction and feature classification. The other is to obtain the classification results directly based on the regression method, which can realize real-time detection in terms of detection speed, but it is slightly insufficient in detection accuracy, such as SSD (single shot multibox detector) [13], YOLO (you only look once) [14, 15] series, RetinaNet [16], and RefineDet [17]. Recently, researchers have proposed various mask-wearing detection technologies based on the above methods. Fan and Jiang [18] proposed a high-performance single-stage mask-wearing detector named RetinaFaceMask, which includes a new dataset, a contextual attention module, and transfer learning. Jignesh Chowdary et al. [19] proposed a transfer learning model to automatically detect mask-wearing, which was performed by fine-tuning the pretrained InceptionV3 model. Rahman et al. [20] proposed a system to limit the growth of COVID-19 by using deep learning models and cameras to discover people who are not wearing masks in urban networks. Loey et al. [21] proposed a hybrid model based on deep learning and classical machine learning, including two parts: the first part uses ResNet50 for feature extraction, and the second part uses SVM and ensemble algorithms for classification. Ren and Liu [22] designed a YOLOv3-based convolutional neural network named Face_mask Net.

Attention mechanisms have achieved great success in various computer vision tasks [23]. The purpose of introducing an attention mechanism is to select key information from many redundant pieces of information to submit the detection ability of the network. Attention-based models include four stages in the field of computer vision: combining deep neural networks with attention mechanisms, representative methods include RAM [24]; in explicit prediction of discriminative input features, representative methods include STN [24, 25] and DCN [26]; to implicitly and adaptively predict potential key features, representative methods are SENet [27], CBAM [28], and CA [29]; attention methods are related to the self-attention mechanism, and the representative methods are nonlocal [30] and ViT [31]. Attention mechanisms are also divided into channel attention, spatial attention, temporal attention, branch attention, and multiple class mixing methods.

Bounding box regression is a mainstream technique in object detection that uses a rectangular bounding box to predict the location of the target object in the image, aiming to refine the predicted bounding box location. Bounding box regression adopts the overlapping area between the predicted bounding box and the ground-truth bounding box as the loss function, which is called the IoU-based loss function. Deep learning optimization suffers when the predicted and ground-truth bounding boxes do not intersect. GIoU [32] is an improvement on IoU. While maintaining the advantages of IoU, it also addresses other non-overlapping regions, reflecting the degree of overlap between the two to a certain extent. DIoU [33] considers the overlapping area and the center point distance. When the target frame wraps the prediction frame, it directly measures the distance between the two frames, so the convergence is faster. Based on DIoU, CIoU uses the aspect ratio of the prediction box and the target box as an impact factor. Alpha-IoU [34] can significantly outperform existing IoU-based losses and is more robust to small datasets and noise. Aiming at the problem of dense targets in mask recognition, Zhang et al. [35] proposed to learn the IoU-Aware classification score and design a new loss function named Varfocal Loss to propose a new bounding box feature representation method for prediction and boundary refinement. At the same time, real-time mask-wearing detection [36, 37] and transfer learning methods [38–40] have been widely studied. For example, Mahmoud et al. [36] proposed a real-time feature extraction module based on deep convolutional neural network. Xu [37] proposed a lightweight YOLOv5 model and used alpha-CIoU as the loss function. Mercaldo and Santone [38] proposed a transfer learning method that uses the MobileNetV2 model to identify illegal mask-wearing behaviors in videos. Su et al. [39] proposed a mask-wearing recognition method that integrates transfer learning and Efcient-Yolov3, using EfcientNet as the backbone network and CIoU as the loss function.

3. Methodology

3.1. Improved YOLOv5. YOLOv5 is a representative of a single-stage detection model, which has the advantages of fast speed and high accuracy. Compared with YOLOv4, the model has fewer parameters, simple operation, and easier transplantation to the mobile terminal. It was proposed by Ultralytics in May, 2020. There are four network models, namely, YOLOv5s, YOLOv5m, YOLOv5l, and YOLOv5x. Among them, YOLOv5s has the smallest network depth and feature map width, and the other three models are continuously deepened and widened based on YOLOv5s.

Based on YOLOv5s, this paper adds the CBAM attention mechanism in the feature fusion process to improve feature utilization and uses CIoU as the bounding loss function to improve the positioning accuracy. The model structure is shown in Figure 1. The improved model is the same as the traditional YOLOv5s, including four parts: input, backbone, neck, and prediction:

(1) The input includes an adaptive anchor box and an adaptive image scaling.

(2) The backbone includes the focus module and the CSP module. The slicing operation in the focus module reduces the number of computations and improves the speed while realizing downsampling. The CSP module is beneficial for improving the network learning ability and reducing the memory cost. Two structures, CSP1 and CSP2, are designed in YOLOv5s. The CSP1 structure and the CSP2 structure are applied to the backbone and neck networks, respectively, to further speed up the inference speed of the network model.

(3) The core of the neck adopts FPN and PAN structures. The FPN and PAN structures realize the fusion and complementation of high-level features and low-level features. FPN is top-down and uses upsampling process to transfer and fuse the new type to obtain the predicted feature map. The PAN adopts a bottom-up feature pyramid. In this paper, CBAM is introduced into FPN, and the fused feature map is sent to CBAM to reduce the influence of redundant features after fusion.

(4) The prediction includes the bounding box loss function and nonmaximum suppression (NMS). In this paper, CIoU is used as the loss function to locate the target box more accurately. In the target detection prediction result processing stage, the optimal target frame is obtained by using the weighted NMS operation for screening numerous target frames.

3.2. Attention Mechanism. The convolutional block attention module (CBAM) is a lightweight convolutional attention module that combines channel and spatial attention mechanism modules. CBAM includes two submodules, the channel attention module (CAM) and the partial attention module (SAM), which perform channel and spatial attention, respectively. This not only saves parameters and computing power but also ensures that it can be integrated into the existing network architecture as a plug-and-play module. CAM is an adjustment to the structure of the SE module. Based on the SE module, a global maximum pooling operation is added to the CAM. CAM compresses the feature map into a one-dimensional vector in the spatial dimension, uses global average pooling and global maximum pooling to aggregate the feature information of the spatial map, and performs an element-by-element sum operation on the results by sharing the fully connected layer. The structure setting of the double pooling operation can make the extracted high-level features richer and provide more detailed information. SAM performs the concatenating operation on the result of the CAM operation based on the channel and performs single-channel dimensionality reduction through convolution. Similar to CAM, SAM adopts a double pooling operation. CBAM is similar to the SE module. The module structure mostly uses a 1×1 convolution to operate and completes the information extraction of the feature map through the entire channel dimension of the SAM, as shown in Figure 2.

Since the CBAM model adds a global maximum pooling operation to the CAM, it can make up for the information lost by the global average pooling to a certain extent. In addition, the generated 2D spatial attention map is encoded using a convolutional layer with a kernel size of 7, and a larger kernel is good for preserving important spatial regions. The YOLOv5s network with CBAM added can not only classify and identify the target more accurately but also locate the target more accurately.

3.3. Complete-IoU. The loss function of the target detection task consists of two parts: classification loss and bounding box regression loss. The most commonly used bounding box regression loss is IoU and its improved algorithm. The full name of the IoU algorithm is the intersection and union ratio, which is obtained by calculating the ratio of the intersection and union of the predicted box and ground-truth box, that is, $\mathrm{IoU}(A,B) = (A \cap B)/(A \cap B)$, where A is the predicted box and B is the ground-truth box. IoU can be used as the distance; then, $\mathrm{Loss}_{\mathrm{IoU}} = 1 - \mathrm{IoU}$. The advantage of IoU is that it can reflect the detection effect between the predicted box and the ground-truth box. IoU has two disadvantages: when the prediction bounding box and the ground-truth bounding box do not intersect and $\mathrm{IoU}(A,B) = 0$, the distance between A and B cannot be reflected. At this time, the loss function is not steerable and IoU loss cannot optimize the situation where the two bounding boxes do not intersect. Assuming that the sizes of the prediction bounding box and the ground-truth bounding box are determined, as long as the intersection value of the two boxes is determined and their IoU values are the same, the IoU value cannot reflect how the two boxes intersect. To this end, the paper adopts the CIoU loss function, and its formula is as follows:

$$\begin{aligned}
\mathrm{IoU} &= \mathrm{IoU} - \left(\frac{p^2\left(b, b^{gt}\right)}{c^2} + \alpha v\right),\\
\mathrm{Loss} &= 1 - \mathrm{IoU} + \left(\frac{p^2\left(b, b^{gt}\right)}{c^2} + \alpha v\right),\\
v &= \frac{4}{\pi^2}\left(\arctan\frac{w^{gt}}{\pi^{gt}} - \arctan\frac{w^2}{h}\right),\\
\alpha &= \frac{v}{(1 - \mathrm{IoU}) + v},
\end{aligned} \tag{1}$$

where b and b^{gt} represent the center points of prediction box B and ground-truth box B^{gt}, respectively, c represents the square of the diagonal length of the minimum bounding box C, p represents the calculation of the Euclidean distance between the two center points, α is the weight parameter, and v is used to measure the similarity of the aspect ratio. In addition, it can be seen that the CIoU loss function not only

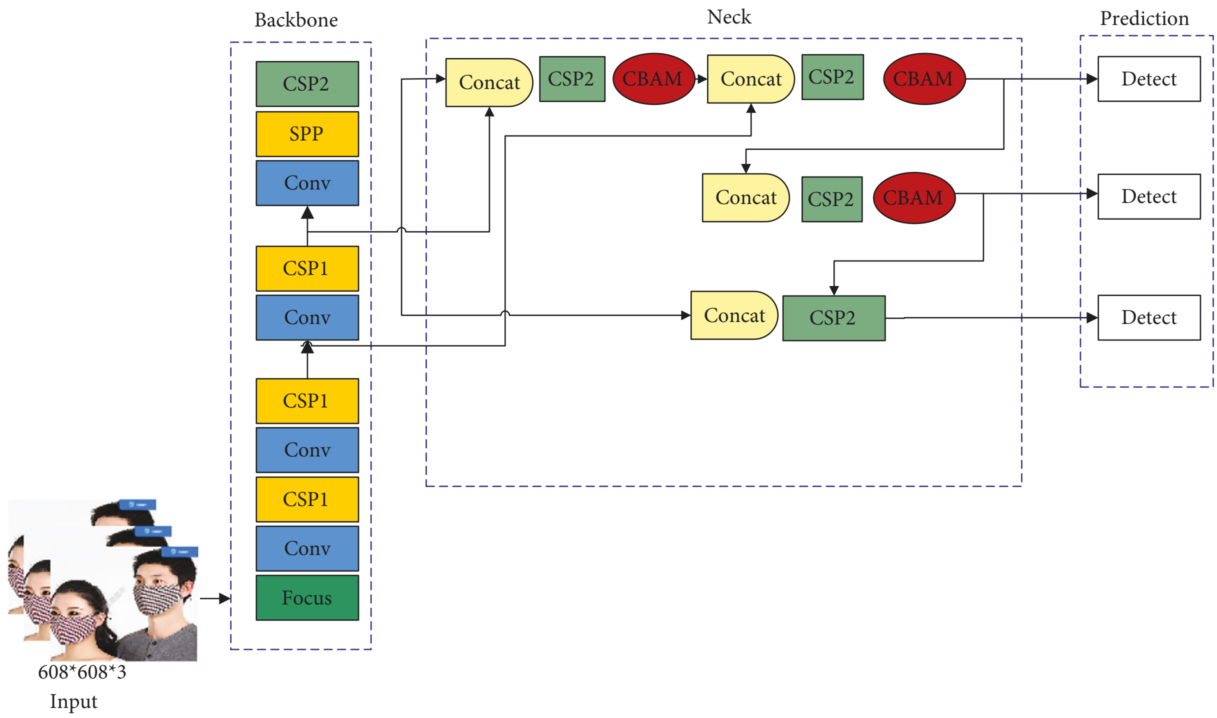

Figure 1: The proposed model network structure.

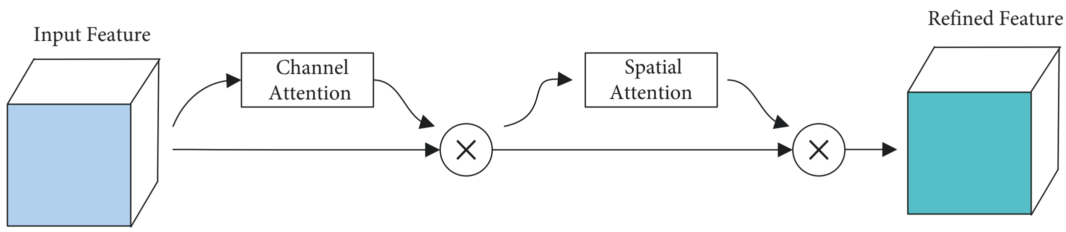

Figure 2: Convolutional block attention module.

considers the overlapping area of the predicted frame and the real frame but also considers the distance between the center points and the aspect ratio of the two. Therefore, in the mask-wearing detection environment, the performance is better than other loss functions.

4. Experimental Results

4.1. Experimental Data and Environment. The paper collects 7,958 pictures of people wearing masks and not wearing masks in the network and real scenes as a dataset, including 7,158 training sets and 800 test sets. The ratio of the training set and test set is 9 : 1, and 0 and 1 are used to label the two categories. The sample images are shown in Figure 3.

The experimental environment of this paper was completed on the Ubuntu18.04 operating system. The GPU model is an NVIDIA GeForce RTX3060 12G, and the software environment is CUDA11 and PyTorch 1.7.

4.2. Evaluation Standard. In this paper, the precision rate, recall rate, average precision (AP), and mean average precision (mAP@0.5) are used as model accuracy evaluation indicators, where AP represents the area under the PR curve and mAP@0.5 represents the average precision (AP) of all categories when IoU is set to 0.5. The specific formula is as follows:

$$\begin{aligned} \text{precision} &= \frac{\text{TP}}{(\text{TP}+\text{FP})}, \\ \text{recall} &= \frac{\text{TP}}{(\text{TP}+\text{FN})}, \\ \text{AP} &= \int_0^1 PdR, \\ \text{mAP} &= \frac{\sum_{i=1}^{N} AP_i}{N}, \end{aligned} \tag{2}$$

where TP is the number of correctly classified bounding boxes that are predicted and the bounding box coordinates that are correct, FN is the number of all unpredicted bounding boxes, and FP is the number of predicted bounding boxes that are misclassified or whose bounding box coordinates that are not up to the standard.

Figure 3: Sample images from the dataset.

4.3. Experimental Results. In the training phase of the YOLOv5s model, the initial parameter batchSize is set to 8 and 8 images are randomly selected for training each time. The epoch is set to 450 rounds, and the rect is true. By setting the same parameters, different loss functions are used to train the network. When the model is trained to 300 epochs, the model begins to converge. After 450 epochs, each model takes the optimal result.

4.3.1. Comparison of Attention Mechanisms. To verify the performance of the CBAM, this paper uses SE, CBAM, and CA to conduct comparative experiments. Among them, SE attention is channel attention, to solve the loss problem caused by the different weights occupied by different channels of the feature map in the process of neural network feature extraction. CBAM attention is additional spatial attention based on SE attention. The feature of CA is that the channel attention is divided into two different directions, horizontal and vertical, so that the information of the position and spatial direction of the input feature image can be fused, which can make the model more accurately locate the detection target.

By adding three attention mechanisms of SE, CBAM, and CA to different positions of the YOLOv5 network model (such as backbone network and neck network), the paper found that the performance of the same attention in different positions is different. Table 1 presents the optimal results of different attention mechanisms, where CA is the worst and CBAM performs the best, which can improve mAP by 0.52% compared to the normal model without increasing the network complexity. Figure 4 shows the comparison experiment curves based on the CBAM and the traditional network. It can be seen in the figure that adding the CBAM has a certain improvement effect.

4.3.2. Comparison of Loss Functions. To verify the detection performance of the CIoU loss function, the paper uses IoU, GIoU, DIoU, alpha-IoU [34], and Varifocal [35] for comparative experiments. Among them, alpha-IoU (aIoU for short) is a unified exponentiation of existing losses based on IoU for accurate bbox regression and object detection. In this paper, the alpha-IoU is improved based on CIoU and the alpha is set to 2 and 3 for experimental comparison. When alpha = 1, it corresponds to the original CIoU loss function. Varifocal is a new loss function for training dense object detectors.

Table 1: The performance of different attention mechanisms.

Model	Precision (%)	Recall (%)	mAP@0.5 (%)
YOLOv5s + SE	95.00	84.03	89.70
YOLOv5s + CBAM	94.78	85.56	90.95
YOLOv5s + CA	95.15	76.91	82.51

Table 2 presents the detection results of different loss functions. As can be seen from Table 2, CIoU is better than DIoU, GIoU, and aIoU and slightly lower than Varifocal. Figure 5 represents the precision, recall, and mAP curves for different algorithms. When alpha = 3, the recall curve of aIoU-3 has obvious advantages. In addition, Figure 6 shows the detection result pictures based on Varifocal and CIoU. Although Varifocal achieves slightly better mAP, there will be obvious false positives in the case of the side face. Overall, the CIoU loss function is better.

To further verify the effectiveness of the method proposed in the paper, Table 3 also gives the traditional two-stage algorithm Faster R-CNN and the one-stage algorithm YOLOv3 as comparative experiments and uses mAP, precision, and recall to evaluate and compare each mainstream algorithm. Table 3 shows that the comprehensive performance of the network model proposed in the paper is the best; its mAP is 1.18% higher than that of Faster R-CNN and 4.85% higher than that of the YOLOv3 network model structure. After adding the CBAM to the backbone network, the performance of the network model is further improved and the final mAP reaches 90.96%.

Pictures of people wearing masks and pictures of people without masks in real scenes are collected, and the YOLOv5s + CIoU and YOLOv5s + CIoU + CBAM network models are used to evaluate the collected pictures. The

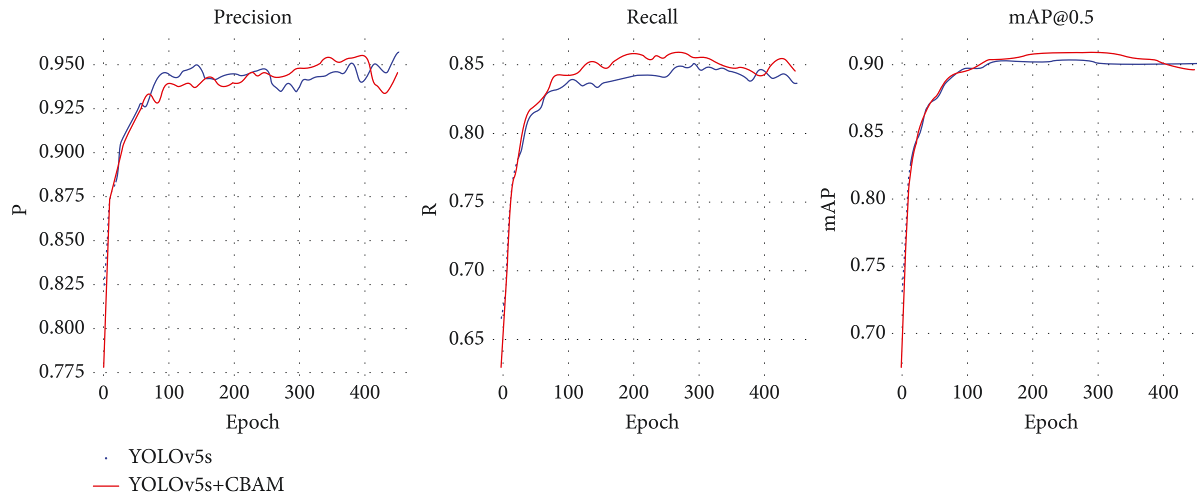

Figure 4: Performance detection curves of different attention mechanisms.

Table 2: The performance of different loss functions.

Loss function	Precision (%)	Recall (%)	mAP@0.5 (%)
IoU	93.99	84.15	89.68
GIoU	93.87	85.24	90.17
DIoU	94.57	83.51	90.21
aIoU-2	95.13	85.06	89.87
aIoU-3	95.05	90.78	89.01
Varifocal	96.20	86.23	90.78
CIoU	93.69	84.90	90.43

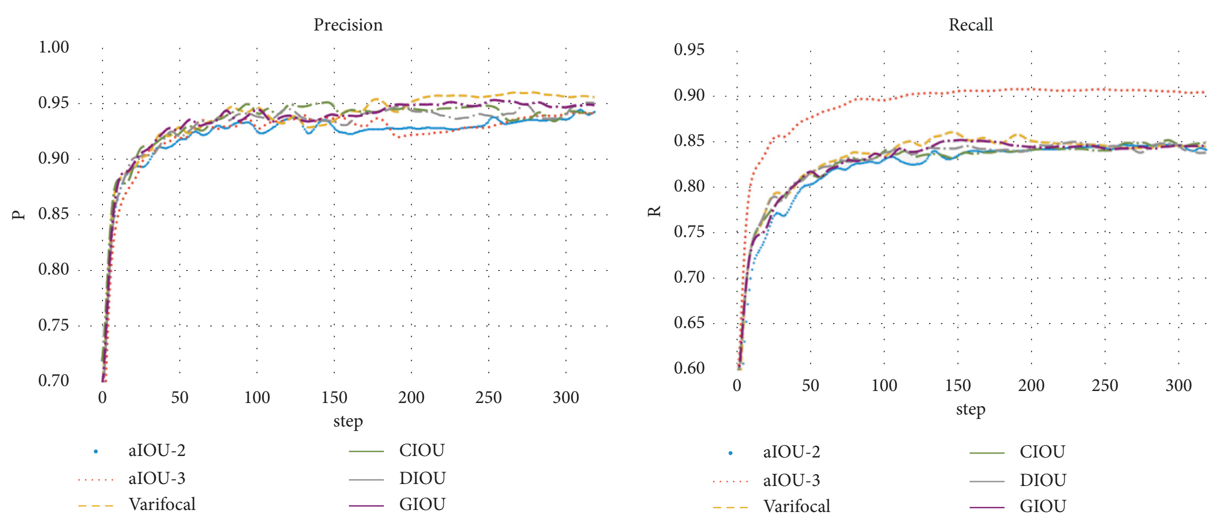

(a) (b)

Figure 5: Continued.

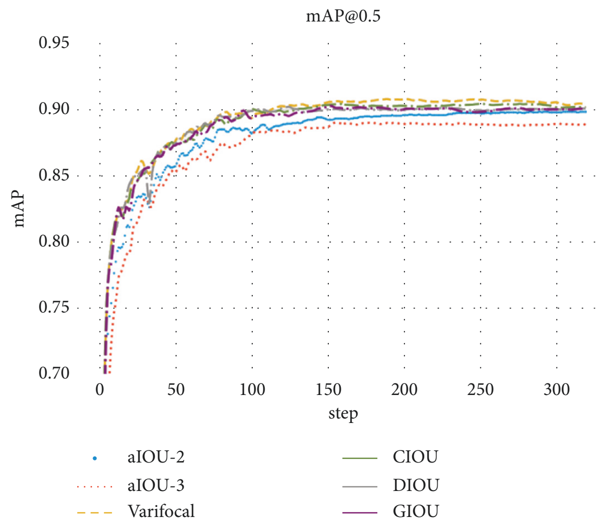

(c)

Figure 5: Performance curves of different loss functions. (a) Precision. (b) Recall. (c) mAP@0.5.

(a) (b)

Figure 6: Detection results with different loss function. (a) Varifocal. (b) CIoU.

Table 3: The performance of different models.

Model	Precision (%)	Recall (%)	mAP@0.5 (%)
YOLOv3	95.73	78.01	86.11
Faster R-CNN	72.99	90.51	89.78
YOLOv5s + CIoU	93.69	84.90	90.43
YOLOv5s + CBAM + CIoU	94.68	85.63	90.96

detection results in the real environment are shown in Figure 7. As can be seen from the figure, the two face targets on the left are occluded. The above picture does not use the CBAM attention mechanism, resulting in missed detection, while the following picture can be applied to face detection under occlusion. From the above experimental results, YOLOv5s has occlusion and missed detection in the real environment. In contrast, the model proposed in this paper performs relatively well, especially for small target detection, which can achieve relatively accurate detection, but there is still missing detection in the shadow area. With the addition of the CBAM, the performance of the network model can be enhanced, corresponding with the expected experimental results.

(a)

(b)

Figure 7: Detection results with the proposed model. (a) YOLOv5s + CIoU and (b) YOLOv5s + CBAM + CIoU.

5. Conclusion

Aiming at the occlusion and density problems of mask-wearing detection, this paper proposes a mask-wearing detection model based on an attention mechanism and loss function and carries out experimental tests based on different attention mechanisms and loss functions. Taking YOLOv5s as the basic framework, the experimental results show that the CBAM is significantly better than the other two attention mechanisms. Experimental tests on different loss functions show that the CIoU loss function is slightly better than the other three loss functions. The experimental results tested in the real environment show that the proposed model is robust to small targets and occlusion. Future work will further study the new network model to improve the accuracy of mask detection.

Data Availability

The data used to support the findings of this study are included within the article.

Conflicts of Interest

The authors declare that there are no conflicts of interest regarding the publication of this paper.

Acknowledgments

This research was funded by the National Natural Science Foundation of China (No. 61976198), Natural Science Research Key Project for Colleges and University of Anhui Province (No. KJ2019A0726), High-Level Scientific

Research Foundation for the Introduction of Talent of Hefei Normal University (No. 2020RCJJ44), the University-Industry Collaborative Education Program (No. 202102373013), and the Scientific Research Project by Enterprises of Hefei Normal University (HXXM2022007).

References

[1] C. W. Yang, T. H. Phung, H. H. Shuai, and W. H. Cheng, “Mask or non-mask? robust face mask detector via triplet-consistency representation learning,” *ACM Transactions on Multimedia Computing, Communications, and Applications*, vol. 18, no. 1s, pp. 1–20, 2022.

[2] B. Wang, Y. Zhao, and C. L. P. Chen, “Hybrid transfer learning and broad learning system for wearing mask detection in the covid-19 era,” *IEEE Transactions on Instrumentation and Measurement*, vol. 70, pp. 1–12, 2021.

[3] H. Goyal, K. Sidana, C. Singh, A. Jain, and S. Jindal, “A real time face mask detection system using convolutional neural network,” *Multimedia Tools and Applications*, vol. 81, pp. 1–17, 2022.

[4] J. Zhang, F. Han, and Y. Chun, “A novel detection framework about conditions of wearing face mask for helping control the spread of covid-19,” *IEEE Access*, vol. 9, pp. 42975–42984, 2021.

[5] A. Kumar, A. Kalia, A. Sharma, and M. Kaushal, “A hybrid tiny YOLO v4-SPP module based improved face mask detection vision system,” *Journal of Ambient Intelligence and Humanized Computing*, pp. 1–14, 2021.

[6] Z. Zhao, K. Hao, X. Ma et al., “SAI-YOLO: a lightweight network for real-time detection of driver mask-wearing specification on resource-constrained devices,” *Computational Intelligence and Neuroscience*, vol. 2021, Article ID 4529107, 15 pages, 2021.

[7] R. Girshick, J. Donahue, and T. Darrell, “Rich feature hierarchies for accurate object detection and semantic segmentation,” in *Proceedings of the IEEE Conference on Computer Vision and Pattern Recognition*, pp. 580–587, Columbus, OH, USA, June 2014.

[8] R. Girshick, “Fast R-CNN,” in *Proceedings of the IEEE international conference on computer vision*, pp. 1440–1448, Santiago, CI, USA, December 2015.

[9] S. Ren, K. He, and R. Girshick, “FasterR. Cnn: towards real-time object detection with region proposal networks,” in *Proceedings of the Advances in Neural Information Processing Systems*, pp. 91–99, Grenada, Spain, June 2015.

[10] J. Dai, Y. Li, and K. He, “R-fcn: object detection via region-based fully convolutional networks,” in *Proceedings of the-Advances in Neural Information Processing Systems*, New York, NY, USA, December 2016.

[11] Z. Cai, N. Vasconcelos, and R.-C. N. N. Cascade, “Delving into high quality object detection,” in *Proceedings of the IEEE Conference on Computer Vision and Pattern Recognition*, pp. 6154–6162, Salt Lake City, UT, USA, June 2018.

[12] L. Xie, Y. Liu, L. Jin, and Z. Xie, “DeRPN: taking a further step toward more general object detection,” in *Proceedings of the AAAI Conference on Artificial Intelligence*, pp. 9046–9053, Honolulu, HI, USA, February 2019.

[13] W. Liu, D. Anguelov, D. Erhan et al., “Ssd: Single Shot Multibox detector,” in *Proceedings of the European Conference on Computer Vision*, pp. 21–37, Munich, Germany, October 2016.

[14] J. Redmon, S. Divvala, R. Girshick, and A. Farhadi, “You only look once: unified, real-time object detection,” in *Proceedings of the IEEE Conference on Computer Vision and Pattern Recognition*, pp. 779–788, Las Vegas, NV, USA, June 2016.

[15] J. Redmon and A. Farhadi, “YOLO9000 better faster stronger,” in *Proceedings of the IEEE conference on computer vision and pattern recognition*, pp. 7263–7271, Vegas, NV, USA, June 2016.

[16] T. Y. Lin, P. Goyal, R. Girshick, K. He, and P. Dollár, “Focal loss for dense object detection,” in *Proceedings of the IEEE International Conference On Computer Vision*, vol. 42, pp. 2980–2988, Chongqing, China, July 2020.

[17] S. Zhang, L. Wen, and X. Bian, “Single-shot refinement neural network for object detection,” in *Proceedings of the IEEE Conference on Computer Vision and Pattern Recognition*, pp. 4203–4212, Lake City, UT, USA, June 2018.

[18] X. Fan and M. Jiang, “A single stage face mask detector for assisting control of the COVID-19 pandemic,” *IEEE*, in *Proceedings of the 2021 IEEE international conference on systems, man, and cybernetics (SMC)*, pp. 832–837, Melbourne, Australia, October 2021.

[19] G. Jignesh Chowdary, N. S. Punn, S. K. Sonbhadra, and S. Agarwal, “Face mask detection using transfer learning of inceptionv3,” in *Proceedings of the International Conference on Big Data Analytics*, pp. 81–90, Ahmedabad, India, December 2020.

[20] M. M. Rahman, M. M. H. Manik, M. M. Islam, S. Mahmud, and J. H. Kim, “An Automated System to Limit COVID-19 Using Facial Mask Detection in Smart City network,” in *Proceedings of the 2020 IEEE International IOT, Electronics and Mechatronics Conference (IEMTRONICS)*, IEEE, Vancouver, Canada, September 2020.

[21] M. Loey, G. Manogaran, M. H. N. Taha, and N. E. M. Khalifa, “A hybrid deep transfer learning model with machine learning methods for face mask detection in the era of the COVID-19 pandemic,” *Measurement*, vol. 167, Article ID 108288, 2021.

[22] X. Ren and X. Liu, “Mask wearing detection based on YOLOv3[C]//Journal of physics: conference series,” *IOP Publishing*, vol. 1678, no. 1, Article ID 012089, 2020.

[23] M. H. Guo, T. X. Xu, J. J. Liu et al., “Attention mechanisms in computer vision: a survey,” *Computational Visual Media*, vol. 8, no. 3, pp. 331–368, 2022.

[24] V. Mnih, N. Heess, and A. Graves, “Recurrent models of visual attention,” in *Proceedings of the Advances in Neural Information Processing Systems*, pp. 2204–2212, New York, NY, USA, December 2014.

[25] M. Jaderberg, K. Simonyan, and A. Zisserman, “Spatial transformer networks,” in *Proceedings of the Advances in Neural Information Processing Systems*, pp. 2017–2025, New York, NY, USA, December 2015.

[26] X. Zhu, H. Hu, S. Lin, and J. Dai, “Deformable convnets v2: more deformable, better results,” in *Proceedings of the IEEE/CVF Conference on Computer Vision and Pattern Recognition*, Beach, CA, USA, June 2019.

[27] J. Hu, L. Shen, S. Albanie et al., “Squeeze-and-Excitation networks,” *IEEE Transactions on Pattern Analysis and Machine Intelligence*, vol. 42, no. 8, pp. 2011–2023.

[28] S. Woo, J. Park, J. Y. Lee, and I. S Kweon, “Cbam: Convolutional Block Attention module,” *European Conference on Computer Vision (ECCV)*, pp. 3–19, 2018.

[29] Q. Hou, D. Zhou, and J. Feng, “Coordinate attention for efficient mobile network design,” in *Proceedings of the IEEE/CVF Conference on Computer Vision and Pattern Recognition*, pp. 13713–13722, Nashville, TN, USA, June 2021.

[30] X. Wang, R. Girshick, A. Gupta, and K. He, “Non-local Neural networks,” in *Proceedings of the IEEE Conference on Computer*

Vision and Pattern Recognition, pp. 7794–7803, Lake City, UT, USA, June 2018.

[31] A. Dosovitskiy, L. Beyer, A. Kolesnikov et al., “An image is worth 16x16 words: transformers for image recognition at scale,” in *Proceedings of the International conference on learning representations*, pp. 1–21, Vienna, Austria, May 2021.

[32] H. Rezatofighi, N. Tsoi, and J. Y. Gwak, “Generalized Intersection over union: A Metric and a Loss for Bounding Box regression,” in *Proceedings of the IEEE/CVF Conference on Computer Vision and Pattern Recognition*, Beach, CA, USA, June 2019.

[33] Z. Zheng, P. Wang, and W. Liu, “Distance-IoU loss: faster and better learning for bounding box regression,” in *Proceedings of the AAAI Conference on Artificial Intelligence*, vol. 34, no. 7, pp. 12993–13000, April 2020.

[34] J. He, S. Erfani, X. Ma, J. Bailey, Y. Chi, and X. S. Hua, “Alpha-IoU: a family of power intersection over union losses for bounding box regression,” *Advances in Neural Information Processing Systems*pp. 1–13, Montreal, Canada, 2021.

[35] H. Zhang, Y. Wang, F. Dayoub, and N. Sunderhauf, “Varifocalnet: an iou-aware dense object detector,” in *Proceedings of the IEEE/CVF Conference on Computer Vision and Pattern Recognition*, Ashville, TN, USA, June 2021.

[36] H. A. H. Mahmoud, N. S. Alghamdi, and A. H. Alharbi, “Real time feature extraction deep-CNN for mask detection,” *Intelligent Automation and Soft Computing*, vol. 31, pp. 1423–1434, 2022.

[37] S. Xu, “An improved lightweight yolov5 model based on attention mechanism for face mask detection,” 2022, https://arxiv.org/abs/2203.16506.

[38] F. Mercaldo and A. Santone, “Transfer learning for mobile real-time face mask detection and localization,” *Journal of the American Medical Informatics Association*, vol. 28, no. 7, pp. 1548–1554, 2021.

[39] X. Su, M. Gao, J. Ren, Y. Li, M. Dong, and X. Liu, “Face mask detection and classification via deep transfer learning,” *Multimedia Tools and Applications*, vol. 81, no. 3, pp. 4475–4494, 2022.

[40] M. F. S. Sabir, I. Mehmood, W. A. Alsaggaf et al., “An automated real-time face mask detection system using transfer learning with faster-rcnn in the era of the covid-19 pandemic,” *Computers, Materials & Continua*, vol. 71, pp. 4151–4166, 2022.

Hindawi
Computational Intelligence and Neuroscience
Volume 2023, Article ID 9765386, 1 page
https://doi.org/10.1155/2023/9765386

Retraction

Retracted: Optimization of Vocal Singing Training Methods Using Intelligent Big Data Technology

Computational Intelligence and Neuroscience

Received 26 September 2023; Accepted 26 September 2023; Published 27 September 2023

This article has been retracted by Hindawi following an investigation undertaken by the publisher [1]. This investigation has uncovered evidence of one or more of the following indicators of systematic manipulation of the publication process:

(1) Discrepancies in scope
(2) Discrepancies in the description of the research reported
(3) Discrepancies between the availability of data and the research described
(4) Inappropriate citations
(5) Incoherent, meaningless and/or irrelevant content included in the article
(6) Peer-review manipulation

The presence of these indicators undermines our confidence in the integrity of the article's content and we cannot, therefore, vouch for its reliability. Please note that this notice is intended solely to alert readers that the content of this article is unreliable. We have not investigated whether authors were aware of or involved in the systematic manipulation of the publication process.

Wiley and Hindawi regrets that the usual quality checks did not identify these issues before publication and have since put additional measures in place to safeguard research integrity.

We wish to credit our own Research Integrity and Research Publishing teams and anonymous and named external researchers and research integrity experts for contributing to this investigation.

The corresponding author, as the representative of all authors, has been given the opportunity to register their agreement or disagreement to this retraction. We have kept a record of any response received.

References

[1] Y. Lin and K. Mao, "Optimization of Vocal Singing Training Methods Using Intelligent Big Data Technology," *Computational Intelligence and Neuroscience*, vol. 2022, Article ID 8589517, 9 pages, 2022.

Hindawi
Computational Intelligence and Neuroscience
Volume 2022, Article ID 8589517, 9 pages
https://doi.org/10.1155/2022/8589517

Research Article

Optimization of Vocal Singing Training Methods Using Intelligent Big Data Technology

Yong Lin[1] and Kang Mao[2]

[1]*Conservatory of Music, Jeonbuk National University, Jeonju 561756, Republic of Korea*
[2]*Conservatory of Music, Huaiyin Normal University, Jiangsu 223300, China*

Correspondence should be addressed to Kang Mao; 18403215@masu.edu.cn

Received 5 May 2022; Revised 4 June 2022; Accepted 6 June 2022; Published 9 July 2022

Academic Editor: Xin Ning

The development of art education and information technology has led to the importance of computer technology and multimedia technology in the development of students' independent inquiry and research skills. In the context of "Internet+," new modes of teaching phonics have emerged, reconfiguring the spatial and temporal relationship of phonics education. The use of Internet resources is not only a simple collection and sharing of educational resources, but also a new way of teaching voice, which has the magic charm of becoming one of the resources for the majority of voice enthusiasts. However, in practice, there are very few assistive software suitable for music classroom teaching. It is important to research and implement teaching aids suitable for music classroom teaching. Based on intelligent big data technology to optimize the phonetic training methods, the teaching methods are more specific, scientific, and diverse, and improve the self-learning ability and learning interest of Chinese phonetic learners. The experimental results show that the weight of the phonetic teaching optimization process is 0.154 higher than the weight before processing, which is expressed as the value of the control reliability fuzzy quantifier in this test. In other words, the reliability is "absolutely reliable." Therefore, this study is expected to promote the modernization and scientific process of Chinese vocal education and propose a new way of thinking for Chinese vocal education.

1. Introduction

With the rapid development of the economy, music education in the Internet era is gradually developing in the direction of intelligence and networking [1]. Being in the new media environment is like being in a "university without walls." New media has brought great convenience and development to modern education [2]. The biggest difference between vocal education and other education is that the vocal teaching method is relatively abstract with the focus on performance, and it is an art form that resonates directly with the subject matter [3], which can be concretized, visualized, and informed if intelligent big data technology is applied to the vocal teaching method [4]. A set of basic information management, student music assignment management, music practice management, online classroom management, and information notification management is built by making full use of web technology and combining the characteristics of music majors [5]. The integrated educational platform of student big data platform can develop students' potential more effectively, promote students to acquire learning skills, and improve learning efficiency [6].

Computer technology is increasingly infiltrating the field of education [7], thanks to its advantages of speed, efficiency, convenience, and wide connectivity. The development of society is dependent on "Internet+," which allows us to innovate boldly [8]. It has enabled closer integration between industries for the benefit of society, increased people's convenience, and accelerated China's economic development [9]. Existing teaching methods have a number of flaws, including single teaching methods, a lack of teaching resources, and dull content, all of which are undergoing qualitative changes as computers are introduced [10]. In the future development of education and teaching, digitalization and informatization will become an unavoidable trend [11]. Vocal music is a highly technical and practical professional field [12]. It is both a science and an art. Learning by relying solely on theoretical knowledge and book materials is extremely difficult [13]. Correct vocal conditions, long and continuous hard training, and the singer's skills are all important factors in the vocal and singing process of vocal singing.

The use of intelligent big data technology to optimize vocal songs is undeniably of practical significance when traditional vocal music education is combined with information technology. In the traditional teaching process, live vocal music teaching solves the problems of uneven teacher distribution, timely teacher-student interaction during the teaching process, and passive student feedback after class [14, 15]. The following are the paper's unique features. (1) Using intelligent big data technology, an in-depth study and research on the teaching mode of vocal singing training are conducted, highlighting the benefits and drawbacks of the teaching mode and teaching form of vocal singing training. It also gives more room for future training methods to be improved. (2) This paper can analyze all of the students in a group specified by the teacher, such as several classes or a specific college, using a rule-based expert system, so that this system can better serve for teaching. (3) The purpose of this paper is to provide a systematic and comprehensive discussion and summary of vocal music teaching in the new media environment, including its uncertainty reasoning and optimization process.

2. Related Work

2.1. Vocal Music Training Method. In recent years, with the education goal of cultivating well-rounded and high-quality talents in the new era of China, music teaching, as an important part of quality education, has received the attention and love of many students. Whether for the love of the profession or for future employment, the number of students choosing music majors is increasing year by year, so colleges and universities have also taken this opportunity to expand their professional enrollment. With the help of the Internet platform and advantageous resources, a variety of innovative models such as massive open online courses, cell phone APPs, and WeChat have also emerged in vocal music teaching, which has laid a certain foundation for the development and research of vocal music teaching.

Medeiros et al. introduced the concept of e-learning support systems, the idea of which has been used until today. Under the influence of this idea, many similar e-learning service systems have been developed by foreign educational institutions and software manufacturers in the past two decades [16]. E-Learning support systems were proposed by Baker and Cohen et al., and their ideas have been used until today. Under the influence of this idea, many similar e-learning service systems have been developed by foreign educational institutions and software manufacturers one after another. The basic design model is to fully utilize computer multimedia technology to deliver knowledge to learners through video and audio [17]. Xiong et al. argue that the creation and development of the online classroom are based on the Internet. This Internet breaks the limitations of the traditional time and space processes, allowing learners to leave home and no longer be restricted by geography and time [18]. Li proposed three centers that represent "progressive education" in the traditional educational center of Herbart: the center of the teacher, the center of the classroom, the center of systematic book knowledge, the center of the child, the center of activities, and the center of personal direct marketing [19]. Chi argues that the emergence of online classrooms means that the walls of traditional campuses will be broken down and the traditional function of sharing quality educational resources will become inevitable [20].

After the informationization of music teaching resources, with the help of computer technology and the Internet, teaching resources are rapidly spread in the network, which will make it more convenient for students to obtain music teaching resources and knowledge, and learning will no longer be affected by geography and time.

2.2. Intelligent Big Data Technology. With the increasing number of students in colleges and universities, the teacher-student ratio has increased substantially compared to the past. In the limited teaching time, teachers pay more attention to the teaching of vocal expertise and some singing skills, making vocal teaching more theoretical. Big data technology is an emerging edge discipline developed on the basis of the interpenetration of computer science, cybernetics, information theory, neurophysiology, psychology, philosophy, linguistics, and other disciplines.

Yang proposed the Online Education Platform System, a representative online education platform that actively uses e-books and textbooks and has more than 100 million registered users [21]. Rosenzweig et al. describe the "Internet + education" model and propose that the "Internet + education" model should evolve into the "Internet education" model [22]. Simones and Lima concluded that although online voice teaching has many advantages over traditional voice teaching, it does not replace traditional voice in terms of the specificity of vocal music. Voice instruction is a teaching method. Sun pointed out that the education industry is facing the challenges of the "Internet+" era and the responsibility system of education informatization construction, and it is necessary to establish a "big database" in colleges and universities [23]. Sun pointed out that the education industry is facing the challenges of the "Internet+" era and the accountability of education informatization construction, and it is necessary to establish a "big database" for team analysis in universities [24]. "The concept of educational system proposed by Sturtevant can provide tools that allow even nontechnical general teachers to easily create online courses and secure websites for courses, homepages, student management, and learning process tracking functions" [25].

Therefore, through intelligent big data technology, learners can complete real-time playback of online learning resources within limited bandwidth without having to completely download courseware and learning materials. Learners can independently select a certain segment of learning content, and learning is more actionable and convenient.

3. Optimization of Vocal Singing Training Method Based on Intelligent Big Data Technology

3.1. Big Data Technology Optimizes Vocal Training and Establishes Expert System. The combination of big data technology and music has existed for quite a long time, the development of digital sound processing and software programs for music has made great progress, and the combination of big data technology and music education has produced numerous research results [26]. Vocal teaching can be divided into two parts: vocal practice and song singing, and vocal practice is the basis of song singing, so it is very important to practice vocal practice [27]. With the help of multimedia and the development of emotional robots and deep learning, the efficiency of learning and practicing is greatly improved and a good training cycle will be formed, as shown in Figure 1.

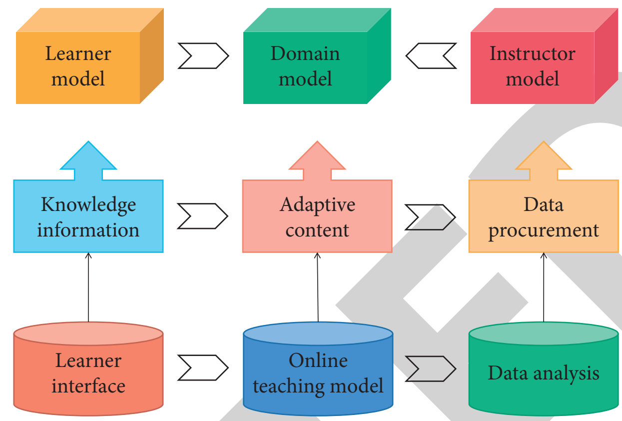

Figure 1: Interactive learning loop diagram.

To begin with, the teacher's explanation of vocal exercises in the traditional vocal teaching mode is very abstract. Only the student's own understanding and comprehension can cause him or her to feel it. Students can intuitively feel the application and changes of the diaphragm, throat, mouth, tongue, teeth, and other organs and grasp their rules by showing 3D animations of concepts such as "breathing" and "resonance" in the process of introducing modern information technology into vocal teaching. The content of vocal teaching for acting training is usually chosen by the teacher, who uses models to sing and explain the work, so catering to the acceptance of all students will inevitably be difficult. The best student in the current class is the teacher, because he or she is the one who knows the most. The following formula calculates the difference between the current average student level and the corresponding teacher level for each subject:

$$\text{Difference} - \text{Mean}_{j,}i = r_i\left(X_{j,k\text{best},i} - \text{TF} \times M_{j,i}\right). \tag{1}$$

$X_{j,k\text{best},i}$ is teacher's level in subject j.
r_i is random number from 0 to 1.
TF is teaching factor.
TF is randomly determined as 2 or 3 by the following formula:

$$\text{TF} = \text{round}\left[2 + \text{rand}(0, 1)\right]. \tag{2}$$

Therefore, to build an expert system, the development process follows the same steps and principles of software engineering as any other large software development process. The development toward emotional robotics and deep learning [28] with the help of multimedia significantly increases the efficiency of learning and practice. The process of the student phase is to adjust the learning by analyzing the differences between the two students. The stage process is shown in the following equation:

$$X'_{j,P_i} = \begin{cases} X'_{j,P_i} + r_i\left(X'_{j,P_i} - X'_{j,Q_i}\right), & f\left(X'_{j,P_i}\right) < f\left(X'_{j,Q_i}\right), \\ X'_{j,P_i} + r_i\left(X'_{j,Q_i} - X'_{j,P_i}\right), & f\left(X'_{j,Q_i}\right) < f\left(X'_{j,P_i}\right). \end{cases} \tag{3}$$

Therefore, the learning phase is modified in conjunction with realistic situations to enhance population diversity and improve the development of algorithms. The modalities are as follows:

$$X_{\text{new}i} = X_i + \text{Rand}\left(T_k - T_i\right). \tag{4}$$

k is k iteration.
X_i is individual.
Rand is random digit.

The instruction is divided into beginner, intermediate, and advanced levels, and students with vocal fundamentals can choose intermediate and advanced levels for their studies [29]. A detailed investigation and careful analysis of user requirements are performed, followed by the development of a unified design specification by designers, domain experts, and knowledge engineers based on the application problem to be solved, specifying the design goals, including the type and scope of the problem itself, and the people involved in the development process. That is, the value of TF decreases linearly as the iterations proceed. The improved teaching factor TF is as follows:

$$\text{TF} = \text{TF}_{\max} - \left(\frac{\text{TF}_{\max} - \text{TF}_{\min}}{\text{iter}_{\max}}\right)\text{iter} \tag{5}$$

$\text{TF}_{\max}, \text{TF}_{\min}$ are maximum and minimum values of teaching factors.
$\text{iter}_{\max}$ is maximum iterative algebra.
iter is current iterative algebra.

As a general performing arts discipline, the online vocal classroom is divided into a learner management module, a course education module, and a learning activity module. The online collaborative learning process based on the cloud course platform integrating social media is shown in Figure 2.

Second, by incorporating modern information technology into vocal learning, students can create their own vocal accompaniment using fun software, making their vocal practice more rich and interesting, and by creating their own accompaniment, they can strengthen their inadequate practice and comprehensively improve their vocal level. Under current technical conditions, consult a variety of domestic and international materials to collect, summarize, and organize domain knowledge, select appropriate knowledge acquisition methods, such as manual knowledge acquisition, semi-automatic knowledge acquisition, and

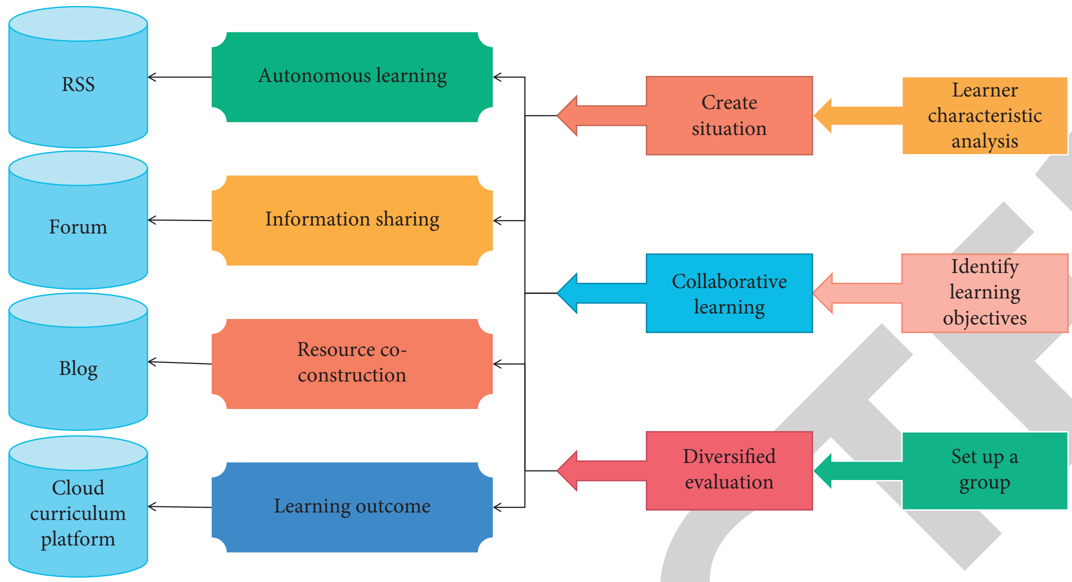

Figure 2: Design of teaching activities based on network collaborative learning.

automatic knowledge acquisition, and then conceptualize them.

Finally, modern information technology can effectively assist students in recording knowledge points and appropriate practice methods in the classroom, allowing them to practice correctly outside of class time and increasing learning continuity. To align with the characteristics of the problem to be solved, knowledge engineers must collect and reorganize formal knowledge, including the separation of knowledge and fact bases, knowledge representation, implementation of reasoning mechanisms, and human-computer interaction. Based on a thorough understanding of information users' needs, organize digital and web-based information and provide retrieval and relevant links. The most cutting-edge knowledge is delivered to those who need it most, ensuring that information resources are widely disseminated and resources are shared quickly and efficiently. Teachers can share their production results and exchange teaching methods and means via the campus network, which not only improves the quality of teaching but also creates opportunities for new "blood" to enter the teaching circle.

3.2. Optimizing Vocal Music Singing with Intelligent Big Data Technology. In traditional vocal music teaching, heuristic teaching mode is often used, which only abstractly introduces the feelings of daily life into vocal singing and allows students to imagine and comprehend the emotions and singing techniques of the songs by themselves [30]. Moreover, with the adoption of digital technology, there is no need to purchase expensive music equipment or to perform routine maintenance tasks. Educators only need basic computer operation skills and basic music knowledge to perform the most basic teaching tasks. The flowchart of the sight-singing and ear training is shown in Figure 3.

First, students can experience the songs directly through multimedia. Music learners access the learning portfolio by logging into the client, which is generally a learning platform, and then present the learning results to the teacher through human-computer interaction. For example, the traditional teaching model of "Morning in Miaoling" with flowery singing is just imagining the text.

Through the means of information technology, the content of the song can be produced, and the birds in the picture can jump to the rhythm. Students can not only hear the song, but also see the song directly and understand their emotions so they can sing with more enthusiasm. The users of the music teaching system include teachers, students, and system administrators. User information management is the basis of system management, including maintenance, query, and statistics of user information. During the teaching phase, individual students are updated by

$$X_{\text{new}} = X_{\text{old}} + \text{Difference} - \text{Mean}_i. \tag{6}$$

X_{old} is individual before update.
X_{new} is updated individual.

Secondly, through the application of modern information technology, students can use DV to film their singing process, then watch it afterward to find out the deficiencies, and then correct and improve their singing. The core algorithm model of the interactive music intelligence system uses big data technology algorithm. User queries are done by entering user keywords or combining multiple conditions, for any point x on the interval $[a, b]$; let its reverse point be x^*, the general reverse point be $\overline{x}$, the probability function of any point on the interval to the optimal solution be $P(\cdot)$, and the distance function be $d(\cdot)$, then the following conclusion holds

$$P(d(\overline{x})) < d(x) > \frac{1}{2}. \tag{7}$$

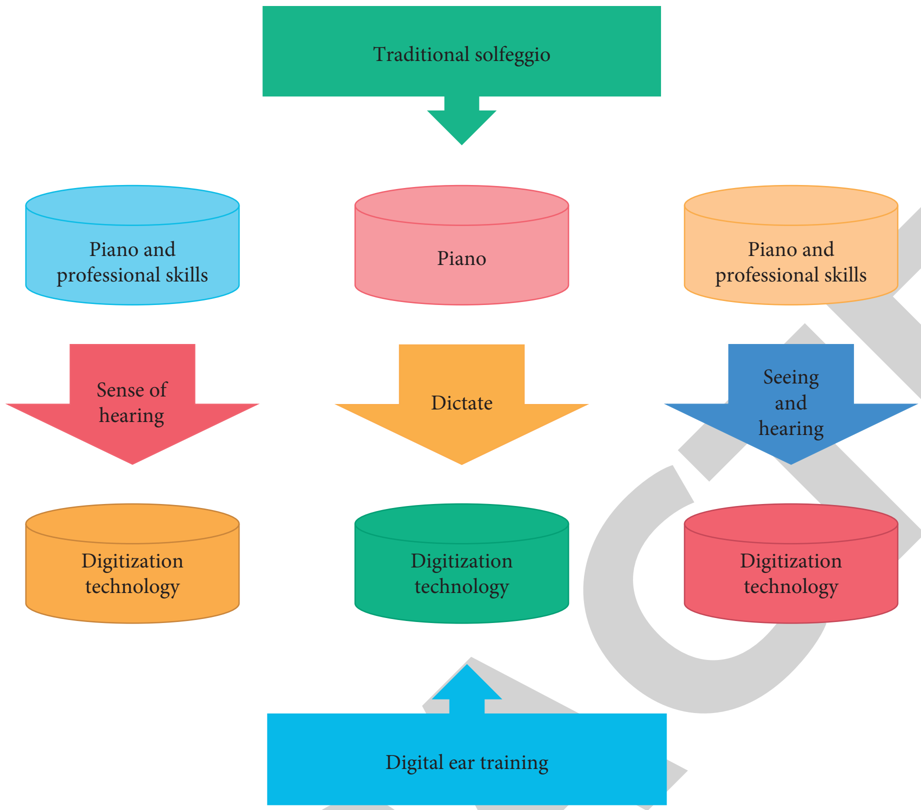

FIGURE 3: Flowchart of solfeggio.

When the teacher sings the training, they can choose from a number of templates for students with different voice conditions or different singing problems, explaining the key points and difficulties of the class in a variety of ways. The students watching the training can then choose their own optimal solution among these solutions to apply and improve the effectiveness of the lesson. Suppose that in the k th iteration, for some individual student $X_i = (x_1, x_2, \ldots, x_D)$, such that M_k is the average score of all students and T_k is the teacher, then

$$M_k = \frac{1}{NP}\left(\sum_{i=1}^{NP} X_{i,1}, \sum_{i=1}^{NP} X_{i,2}, \ldots, \sum_{i=1}^{NP} X_{i,D}\right),$$
$$T_k = \min\{f(X_i) \mid i = 1, 2, \ldots, NP\}. \tag{8}$$

Finally, we can teach remotely by means of the Internet, which not only saves teaching costs, but also teaches vocal music to a wider range of students. In order to improve the evaluation of the course itself, the review of the singing training evaluation should be conducted by experts, including educational experts, technologists, psychologists, and vocal teaching experts, in addition to the source network. A matrix of size $\max - \text{iter} \times D$ and a vector of $1 \times \max - \text{iter}$ are to be created to store the optimal individual and the optimal fitness values in each generation, respectively. The final space complexity is obtained as

$$S(D) = O((\max - iter + 2 \times NP) \times D). \tag{9}$$

That is, the basic maintenance of user information includes user name, user number, user address, etc. This basic information is the basis of the system, and the details of users can be viewed at any time throughout the system. The maintenance of user information includes add, modify, and delete operations. When a new user needs to be included in the charge, the user administrator needs to enter the user's details. This is a teaching method that uses Internet technology to solve the space limitation by teaching online instantly. When D takes a large enough value, the effect of lower powers on the time complexity is small and can be neglected, then the time complexity of the basic TLBO can be obtained from the above analysis as

$$T(D) = O(\max - \text{iter} \times 2 \times NP \times D). \tag{10}$$

D is dimension.

$\max - \text{iter}$ is iterations.

NP is population size.

The premise of this teaching method is to establish a voice or video chat room through the Internet, and then inform and advertise the chat room ID and the arrangement of video vocal teaching, so that people can learn and communicate online at the agreed time. By inheriting the UserControl class, developers can develop various controls according to their needs, and after creation, they can also be compiled into DLL files for other WPF programs to use.

4. Application and Analysis of Big Data Technology in the Optimization of Vocal Singing Training

4.1. Uncertainty Reasoning Analysis. In the actual development process of expert systems, the problem solving of expert systems is generally not as rigorous and accurate as that of mathematics and physics and other disciplines. Therefore, the knowledge of domain experts and the information we have to deal with are often uncertain and inaccurate.

First, uncertainty and ignorance are distinguished by introducing a trust function, which satisfies the axiom that is weaker than the probability function. Thus, the probability function is a subset of the trust factor. We specify the travel path and remove the average error and low-pass filter or low-precision approximation of the encoded trajectory curve to extract the smooth path curve. The results are shown in Figure 4.

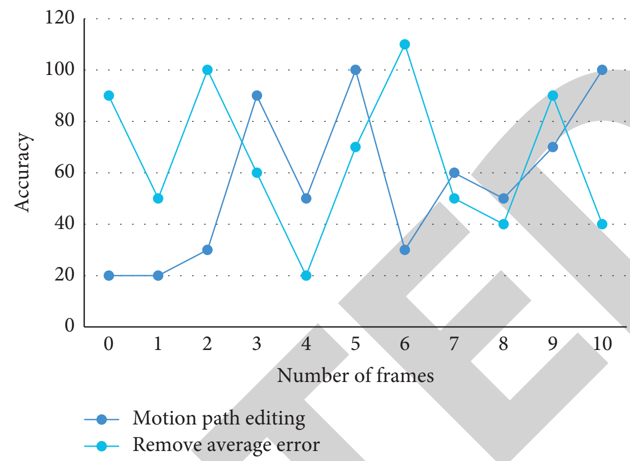

Figure 4: Results of editing motion path and removing average error.

In the control mode of vocal performance or training, students' live participation is added to achieve the basic interaction between computer and music training and performer-human-computer interaction. Through digital technology and multimedia means, animated effects of chest breathing, abdominal breathing, and combined chest and abdominal breathing are created to show the muscle groups in each movement in the working section. It gives the learner an immersive feeling from which he can see why chest and abdominal breathing are not suitable for singing. The multimedia depicts the fuzzy rule count. By learning samples, we try to make the least number of rules to learn and the most important. As the core of digital technology, the computer can be controlled by the teacher. For example, the vocal teacher can control the playing time of the computer music through the pedal, so that the feedback can be used to adjust the teaching at any time, so that the students are really the main focus, using "digital technology" for students and teaching. For the convenience of teachers, some fuzzy quantifiers and quantitative expressions were chosen to represent the confidence level, as shown in Table 1, taking into account the experience of experts in the field.

Table 1: Numerical representation of confidence fuzzy quantifiers.

Fuzzy quantifier	Absolutely credible	Strong credibility	Weak credibility	Untrustworthy
Numerical value	1	0.557	0.429	0.186

Second, possibility theory represents uncertainty in terms of likelihood, which is calculated by introducing an affiliation function. Cubase 5 software, developed by Steinberg, was used for the analysis and study. This software not only performs the necessary recording and production functions, but also allows editing the recordings. Another device in this software is a spectrum analyzer, which allows detailed analysis of the singer's spectrum and derives patterns. When targeting a series of larger data, the first m of the music data are used as initial training, which leads to the construction of an RBF model of students learning music knowledge, which is continuously evaluated through the designed software platform until a perfect model is finally constructed. Allowing the possibilities of interaction in computer music to be deeper, making this interaction more organic and giving the computer more room to play, for example, allowing the computer to "hear" the singer's real-time vocals or voice while deciding on its own what to feed back. A comparison was made between the performance of the vocal teaching system and the use of computer memory. Figures 5 and 6 compare the CPU and memory usage of the system before and after loading.

Finally, the adequacy and necessity measures are defined as probability ratios, and domain experts are only required to provide probability ratios rather than precise probability estimates. Professional software, on the other hand, can split the singer's voice and accompaniment into two tracks. Following the performance, the tutor can provide a detailed breakdown of what went wrong and improve interactive teaching. The algorithm concept is incorporated into the platform's design, and the algorithm is fully demonstrated while writing the code and implemented in the platform's functions to effectively match the interactive learning mode. By judging the accuracy of the singer's pitch, tone quality, volume, timbre, and vocal language during the singing or vocalization process, the computer determines what, what, how, and how to improve the feedback information. Learners can edit a set of orchestral or band accompaniment tapes to become familiar with the role of each instrument and the combination of accompaniment and voice once they are familiar with the song.

4.2. Analysis on the Process of Vocal Music Teaching Optimization. For vocal music teaching, there are certain differences from other teaching. Only very short classroom teaching necessarily requires a strong instantaneous memory, and for some students with weak memories, classroom teaching time becomes insufficient. Such a network means

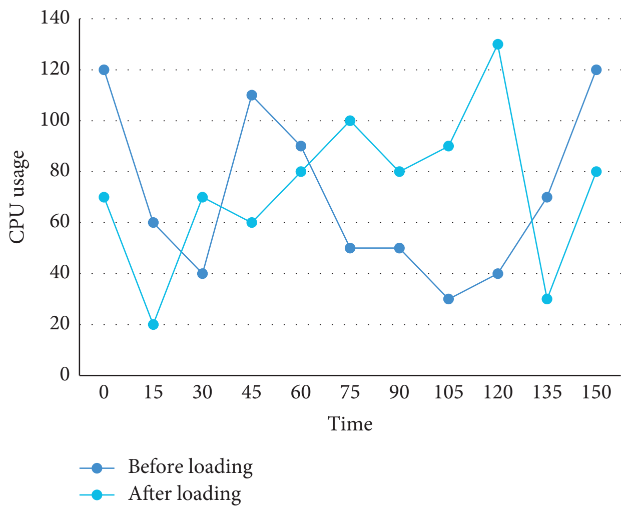

Figure 5: CPU usage comparison.

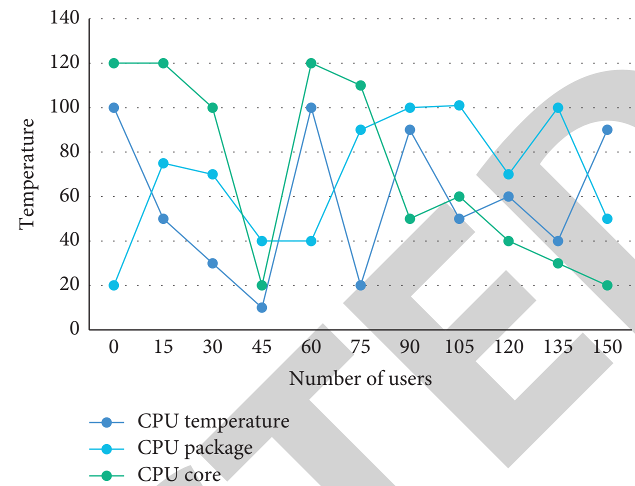

Figure 7: Curve changes after the number of users increases.

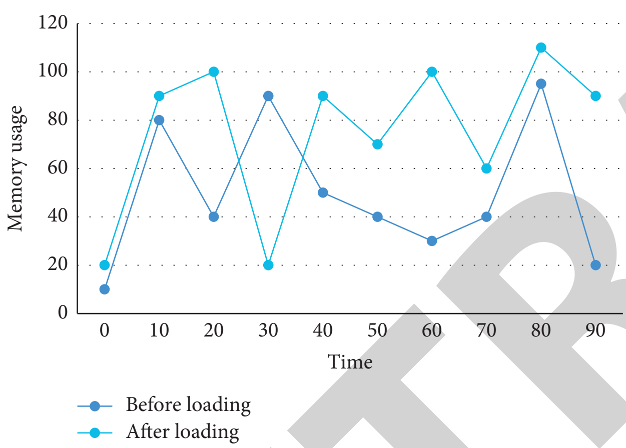

Figure 6: Comparison of memory usage.

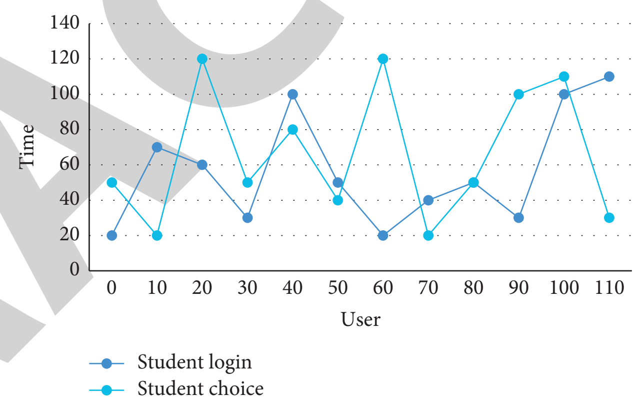

Figure 8: Curve of response time.

can solve the spatial constraint of the heterogeneous location of vocal learners and vocal teachers, and also allow learners to independently choose their favorite or interested teachers or teaching resources. Therefore, the optimization process of vocal music teaching is as follows.

First, teachers organize exams according to their respective teaching contents, teaching objectives, students' levels and usual exams, log into the system, add exams, select exam topics, receive exam papers, and take exams. The database links between the expert application system and other systems are relatively poor, resource sharing is not fully reflected, unified management is not convenient, and mutual access between users is restricted. All these factors limit the information exchange between expert systems. Therefore, with more and more users of the vocal teaching system, some computer-related hardware indicators such as CPU temperature, CPU package, CPU core difference, and other variables are shown in Figure 7.

However, through intelligent big data technology devices, such as MP4, MD, and some other classical teaching can do "eternal." On the one hand, after the class, students can listen to what the teacher teaches. On the other hand, teachers can listen to students' classroom recordings to find out some problems of students and develop some targeted measures to solve these problems in the next teaching activities.

Secondly, students choose an exercise mode to practice, and after the diagnostic exercises are completed, the system will analyze the students' exercises according to the exercises. Figure 8 shows accurately the average response time when different users access the music education information system.

MIDI and ZIPI are the main protocols used in devices to accomplish computer music technology interaction. Therefore, to make a qualitative change in the traditional expert system, the application system of the expert system must first of all have a strong network interconnection function. To achieve network interconnection between expert systems, it is necessary to solve the technical problems of the following kinds of interfaces: the interface between the system and various relational databases, multimedia information processing interfaces, full-text database interfaces, etc. It is a new protocol standard for data exchange between digital musical instruments proposed to overcome many

Table 2: Comparison of weight vectors before and after optimization of vocal music teaching.

Weight vector	μ_1	μ_2	μ_3	μ_4
Preweighting	0.556	0.257	0.461	0.672
After weighting	0.672	0.443	0.572	0.875
Differential value	0.116	0.186	0.111	0.203

shortcomings such as slow transmission rate and one-way transmission of MIDI. Its transmission rate is nine times that of MIDI, and there is no maximum bandwidth limit in order to adapt to the rapid development of computer technology. In addition, the network media has a huge amount of information, rich information content, and shorter information metabolism cycle, which can enable people to grasp the latest vocal theory knowledge in time and meet their learning needs. The credibility vector is the credibility of the rules in the knowledge base, and the weight vector is the weight vector given by experts. The comparison results of the weight vectors before and after the vocal music teaching optimization process are shown in Table 2.

According to the comparison of the ‘s weight vectors before and after the optimal treatment of vocal music, the weight of the optimal treatment of vocal music increased by 0.154 compared to that before the treatment. Therefore, in this test, the value of the fuzzy term of relative credibility was used; i.e., the credibility was “absolute credibility.”

Finally, a basic evaluation was given after each exercise to encourage students to practice on their own and to pique their interest in learning. This can be done without a tutor at home, at school, anywhere, and at any time. All that is required is that you record the entire process of the tutor’s singing using digital multimedia technology, and then record yourself singing and compare the two using the software to see where you went too far in terms of amplitude. The focus on the humanistic aspects of computer music, particularly the interaction of curriculum, vocal training, vocal performance, or lesson production with computer characteristics, can help to establish new computer music aesthetic principles. After all, music intelligence systems are closely linked to teachers, students, and teaching resources, so the corresponding services are slightly different.

5. Conclusions

Informationization has already pervaded people’s lives, and the information-based classroom will pervade future college classrooms and the general public’s learning life. To further improve the shortcomings of traditional vocal teaching methods, existing vocal teaching methods should be combined with digital vocal teaching methods. If multimedia and the Internet are solely used for informational purposes, they will inevitably be phased out over time. Modern information technology, in combination with multimedia and online education, has the potential to significantly improve the quality and efficiency of vocal education, as well as promote vocal singing. Its technical advantages can provide voice learners with a new method of learning vocal art, which has a broad application space and application prospects in the field of vocal education, by optimizing voice training methods based on intelligent big data technology. It completes the basic evaluation of the knowledge points learned by college music teachers and realizes the comprehensive evaluation of a single lesson using a combination of generative and framing knowledge expressions and uncertain reasoning techniques. Vocal music education should not only keep up with the evolution of the information society, but also provide a variety of information services to information users and continue to innovate. The advancement of modern information technology is the general trend, and vocal music must keep up with the times and develop and progress more comprehensively. The combination of big data technology and vocal music education has not only accelerated the diversification of music education, but also improved traditional vocal music education.

Data Availability

The data used to support the findings of this study are available from the corresponding author upon request.

Conflicts of Interest

The authors do not have any possible conflicts of interest.

References

[1] S. Muzaffarova and B. Khurshid, “Modern training methods in vocal education[j],” *Culture and Arts of Central Asia*, vol. 9, no. 1, p. 15, 2019.

[2] W. Fu, S. Liu, and J. Dai, *E-Learning, E-Education, and Online Training*, Springer International Publishing, New York City, NY, USA, 2021.

[3] X. Wang, “Design of vocal music teaching system platform for music majors based on artificial intelligence,” *Wireless Communications and Mobile Computing*, vol. 2022, Article ID 5503834, 11 pages, 2022.

[4] M. M. Tanik, “Big data optimization: recent developments and challenges.[J],” *Computing Reviews*, vol. 58, no. 3, pp. 166–168, 2017.

[5] N. Chen and G. Wen, “Music composition feasibility using a quality classification model based on artificial intelligence[J],” *Aggression and Violent Behavior*, vol. 1, no. 1, Article ID 101632, 2021.

[6] M. Zhou and T. Gong, “Optimization of multimedia computer-aided interaction system of vocal music teaching based on voice recognition,” *Computer-Aided Design and Applications*, vol. 8, pp. 113–122, 2020.

[7] W. Zhang, A. Shankar, and A. Antonidoss, “Modern art education and teaching based on artificial intelligence[J],” *Journal of Interconnection Networks*, vol. 3, Article ID 2141005, 2021.

[8] C. Xu, “A big-data oriented recommendation method based on multi-objective optimization,” *Knowledge-Based Systems*, vol. 177, no. 1, pp. 11–21, 2019.

[9] G. Su, “Analysis of optimisation method for online education data mining based on big data assessment technology,” *International Journal of Continuing Engineering Education and Lifelong Learning*, vol. 29, no. 4, pp. 321–335, 2019.

Hindawi
Computational Intelligence and Neuroscience
Volume 2022, Article ID 2205936, 9 pages
https://doi.org/10.1155/2022/2205936

Research Article

A Novel Piano Arrangement Timbre Intelligent Recognition System Using Multilabel Classification Technology and KNN Algorithm

Yuan Lu [1] and Chiawei Chu [2]

[1]*Academy of Music, Yuxi Normal University, Yuxi 653100, China*
[2]*Faculty of Data Science, City University of Macau, Macau 999078, China*

Correspondence should be addressed to Chiawei Chu; cwchu@cityu.mo

Received 4 May 2022; Revised 4 June 2022; Accepted 7 June 2022; Published 9 July 2022

Academic Editor: Xin Ning

In this paper, melody and harmony are regarded as the task of machine learning, and a piano arranger timbre recognition system based on AI (Artificial Intelligence) is constructed by training a series of samples. The short-time Fourier transform spectrum analysis method is used to extract the piano timbre characteristic matrix, and the electronic synthesis of timbre recognition is improved by extracting the envelope function. Using the traditional multilabel classification method and KNN (K-nearest neighbor) algorithm, a combined algorithm of these two algorithms is proposed. The experimental results show that the detection rate increases from 61.3% to 70.2% after using the combined classification algorithm. The correct rate also increased from 40.3% to 48.9%, and the detection rate increased to 74.6% when the K value was set to 6. The experimental results show that, compared with the traditional classification algorithm, this algorithm has a certain improvement in recognition rate. Using this system to recognize the timbre of piano arrangement has a high recognition accuracy, which is worthy of further popularization and application.

1. Introduction

The art of music is vast and profound; for a true pianist or piano educator, touching the tip of the iceberg of piano music works is insufficient; they must also broaden their horizons to include all aspects of music art. It is obvious that you can hear the sounds of various instruments when playing the digital recording of the piano concerto. People may not be able to correctly identify the names of some instruments, but they should be able to recognize their general categories, such as stringed or wind instruments. The loss of information such as bells, melodies, and ringtones will have a significant impact on the accuracy of music recovery results, resulting in low recovery efficiency. The development of contemporary electronic music has been aided by the rise of AI (Artificial Intelligence) technology [1], and the technology's application fields are constantly expanding. The use of AI technology to solve problems like timbre recognition and feature extraction in music arrangers has gotten a lot of attention.

The exploration and research in the field of music have developed rapidly with the progress of computer science. Nowadays, the digital music creation mode has completely changed the traditional music industry and greatly improved the quality and production efficiency of music works. Patil and Elhilali recognized music as a series of music fragments, analyzed their music styles, and then established a statistical model in the existing music database to predict the style classification of other music [2]. Aucouturier and Pachet defined the emotional attribute value as an emotional plane and proposed a fusion algorithm, considering that a piece of music may have multiple emotions with interval changes [3]. Kailash et al. introduced the recognition principle of machine auditory system and applied the heuristic processing method to the sound signal, which can preliminarily understand the sound signal [4]. Chen and Guo put forward a timbre model based on piano pronunciation waveform, which uses the spectrum characteristics and amplitude envelope characteristics of timbre to construct piano timbre model [5]. Wu et al. introduced a timbre model based on trapezoidal wave. The model is divided into two parts: vibration submodel and inclusion submodel. Time, asymmetry, trapezoidal degree, and three angles are defined as timbre parameters for timbre synthesis [6]. A series of research works have been made on multipart piano music, and a machine hearing system has been developed, which can recognize multipart piano music. In the research process of machine hearing, the frequency spectrum analysis of musical instrument timbre signal has always been a research hotspot, which requires the selection of frequency spectrum feature extraction technology. Different technical application fields and analysis results are different.

The AI-based piano arranger timbre recognition system separates harmonic signals at the edge of music, transmits timbre, analyzes timbre signal continuity, and implements the system design, but the system's performance is poor. It is demonstrated that timbre is a type of sound feature that includes frequency spectrum and time based on psychological judgments of music timbre, analysis of physical characteristics of sound, and research of machine learning methods. To fully comprehend the true meaning of timbre, it is necessary to fully comprehend the number and significance of characteristic parameters that affect timbre. As a result, to design a piano arrangement timbre recognition system based on AI, this paper uses the Fourier analysis method. The use of computer technology in the field of music, as well as the use of computer technology in the field of music, will provide mankind with new musical experiences.

The innovation of this paper is summarized as follows:

(1) In this paper, taking piano music signal recognition and synthesis as an example, the characteristics of piano music signals are recognized and analyzed by mathematical methods, and the extracted characteristics of piano music signals are digitized to realize piano timbre recognition and simulation.

(2) Using the multilabel classification method [7, 8] and KNN algorithm, a combined algorithm of these two algorithms, namely, ML_KNN classification algorithm, is proposed. The experimental results show that the recognition rate of the classification algorithm based on ML_KNN is higher than that based on multilabel decision tree.

The following is a list of the sections of this article: The first section discusses the research's background and significance before moving on to the paper's main work. The second section focuses on the related timbre recognition techniques used in piano arrangements. The third section outlines the research's specific methods and methods of implementation. The superiority and feasibility of this research model are confirmed in the fourth section. The summary of the full text is found in the fifth section.

2. Related Work

2.1. Timbre Feature Recognition Method. Musical instrument timbre recognition is an important research trend of machine hearing. However, from the academic point of view of machine hearing, the difficulty of musical instrument timbre recognition is roughly equal to that of speech recognition. However, scholars who study musical instrument recognition need to be proficient in both music and computer, so the research population is small, and the progress of musical instrument timbre recognition is slower than that of speech recognition, with few achievements and few references.

Mitrovic et al. adopted KNN (K-nearest neighbor) method and Gaussian mixture model to realize automatic classification of musical instrument features. The experimental results show that the highest recognition rate of 14 musical instruments is 90% [9]. Peretz et al. extracted a series of musical sound features that can be perceived by human auditory system from the musical sounds of 27 musical instruments and applied these features to the classification of musical instruments. Finally, the recognition rate of musical instrument perception difference reached 71%, and the system developed by them had good stability in dealing with reverberation and noise syllables [10]. The music composition system developed by Han et al. allows people without music skills to intervene in its composition system to create music, and the generated melody can reach 16 bars in length [11].

Xing et al. pointed out that when using genetic algorithm to solve melody harmony, we will encounter the problem of harmony search space in irrelevant local optimal area [12]. Omar et al. put forward a graph [13] of arranging very interesting harmony for a given melody based on the training data. This graph model may be better than the hidden Markov model in obtaining the root sound movement showing global correlation. Wang et al. think that the timbre space of musical instruments includes five dimensions, and besides the characteristic dimensions of time domain and frequency domain, it also includes the dimension of time-frequency combination [14].

2.2. Research Status of Multilabel Classification. A natural scene can contain multiple target objects. For example, the scene can be described with multiple class labels. They usually use multiple labels to train samples to solve problems. However, this method is not suitable for music database, because each instrument can play different notes, and some of them can express different timbres by using different playing skills.

Xiang et al. discussed the emotion classification in music clips, which involved six kinds of emotion classification labels and a small number of timbre feature values. Emotion is a higher level of information, which can be further obtained from pitch, volume, rhythm, and timbre [15]. Mancia and Janssen used the trained neural network to recognize and classify 166 groups of music samples and achieved good classification results [16]. Cerri et al. proposed a pitch-independent instrument recognition system [17]. Further extracting features including basic frequency, spectrum, time domain, and modulation and solving their respective multivariate normal distributions, the recognition rate of the final instrument family reaches 90%, and the recognition rate of a single instrument reaches 80%. Sering et al. proposed several methods for high-order statistical modeling of musical sound signals and evaluated them in the environment of multimedia sound retrieval [18]. Ju et al. made it possible to separate two or more musical instruments by using single channel speech separation method through Gaussian modeling [19].

The multilabel emotion classification method based on dictionary is to extract the emotion keywords from the text on the basis of emotion dictionary database, so as to classify the text. Yong et al. designed a chat system based on text and embedded conversation messenger emotion estimation. This system is based on an emotional content evaluation module that evaluates text chat messages, extracts related emotions from the text through keywords, and then evaluates the text emotions through syntactic features, speech synthesis, and related emotional gestures [20]. Yan et al. put forward an interdisciplinary approach to study the structure of emotion and society, analyzed the influence of society on cognition and emotional interaction, examined how emotions are stimulated and expressed in society, and studied how society affects the processing and regulation of emotions [21].

3. Methodology

3.1. Piano Arrangement Timbre Recognition

3.1.1. Piano Spectrum Analysis. Timbre is the basis of identifying musical instruments, and it is the characteristic information that distinguishes musical instruments from other musical instruments. The sound of an instrument consists of fundamental tone and overtone. It is the tone with the lowest pitch frequency, and those that are not pitch are collectively called overtones. The human auditory system can tell which musical instrument the sound comes from, because the high-frequency harmonic components of musical instruments are different, and the harmonic proportions of different musical instruments are also different. The definition of timbre is too subjective to lead to automatic classification of music. Therefore, the main work of this paper is to parameterize the timbre features in detail for automatic recognition and classification.

Piano arrangers must play the parts of multiple people at the same time, which necessitates exceptional performance skills. The piano arranger represents the combination of conductor and orchestra, and the orchestra is made up of multipart staff. It is necessary to use both hands to play the condensed version of the previous parts. The band's concert editing is moderately difficult and plays a major and minor role in the overall work; the reduction of band accompaniment is relatively simple. Because the accompaniment part usually does not have a lot of "scenes," it is usually only used to fill in the gaps in the solo and highlight the band's characteristics.

Even if the strength, position, and striking method are all the same for piano strings, the volume is not always the same. Through simple music training, humans can tell the difference between musical instrument timbres. Humans can quickly distinguish piano tones from the sounds of a variety of musical instruments as well as background noise. To achieve musical instrument timbre recognition by listening machine, we must first understand the mathematical principle of sound waves and then determine the differences between musical instrument timbres in mathematical expression and then use these differences to quickly identify and distinguish musical instrument timbres. The projection function is used to represent the low-dimensional features of the spectrum after the rank reduction:

$$y_t = \left[r_t, \tilde{x}_t^T v_1, \tilde{x}_t^T v_2, \ldots, \tilde{x}_t^T v_k\right], \tag{1}$$

where $r_t, \tilde{x}_t^T, v_1, \ldots, v_k$ is calculated by the spectrum basis function.

The resonance frequency of different instrument resonators is different, and the shape of resonance peak in frequency spectrum is also different. Not only is resonance peak the decisive factor of sound quality, but also it reflects the physical characteristics of the resonant cavity. Cepstrum coefficient is a method to express resonance peak.

The cepstrum coefficient containing the signal quantity $y(n)$ is defined as F, and F represents discrete Fourier transform.

$$c(n) = F^{-1}\{\log |F\{y(n)\}\}. \tag{2}$$

The analysis of MFCC (Mel frequency cepstrum coefficient) is based on human auditory mechanism; that is, the spectrum of speech is analyzed according to the results of human auditory experiments, in the hope of obtaining good speech characteristics [17]. The delineation of the frequency domain of human subjective perception is not linear, and there is the following formula:

$$F_{mel} = 1125 \log \left(1 + \frac{f}{700}\right)_V, \tag{3}$$

where F_{mel} is the perceived frequency in Mel; f is the actual frequency in Hz.

The process of extracting MFCC features includes the following steps:

(1) Input the audio signal to be processed.

(2) Select the window length N to preemphasize, frame, and window the input audio signal.

(3) The processed audio segments of each frame are subjected to FFT (fast Fourier transform) to obtain the corresponding frequency spectrum.

(4) Mel cepstrum is obtained according to formula (3).

(5) Take the logarithm of Mel frequency cepstrum and do inverse Fourier transform (get Mel frequency cepstrum coefficient MFCC), and the 2nd–13th coefficients after discrete cosine transform are MFCC coefficients.

The lowest frequency of the piano is 28.5 Hz, so it can be seen that all the sound bands of the piano remain in the Fourier transform analysis area. Based on the auditory nervous system, human ears can fully perceive the music spectrum and feel the timbre of piano, so the choice of spectrum structure analysis is actually a simulation of human auditory nervous system. Based on Matlab software, according to the principle of Fourier transform, the FFT function program is written, and the spectrum analysis diagram of single tone is obtained. It shows that there are multiple octave overtones and octave vibrations in the piano, and the uniqueness of the piano and the rich characteristics of piano timbre are expounded.

3.1.2. Extraction of Timbre Matrix. Strings are the piano's basic sound source. The player presses the keys to cause the hammer to strike the strings, causing the strings to vibrate and producing the original sound, which then causes the resonance system to resonate. Some researchers discovered that some functional waveforms resemble those found on the piano. Sinc, Gaussian, and Cauchy functions are examples of specific functions that can be selected. The frequency domain waveform of piano tones can also be approximated using these specific functions, according to the researchers. Choose a suitable piano accompaniment type metastructure from the existing library, and configure the piano accompaniment spectrum for the new melody using the modes of melody segments, the root of chords, and various permutation functions provided in the selected piano accompaniment type metastructure.

In order to improve the high-frequency resolution of music signal and analyze the whole spectrum of the whole frequency band, a processing method is proposed, which usually uses a first-order digital filter for preemphasis before signal extraction. The transfer function of this filter is expressed as

$$H(z) = 1 - \alpha z^{-1}. \tag{4}$$

In the above formula, α is the preemphasis factor, which is generally taken as a decimal close to 1. In this paper, it is taken as 0.95. Preemphasis process transforms the signal as follows:

$$x(n) = x(n+1) - \alpha x(n). \tag{5}$$

The data obtained from the above formula is the preemphasized data, where $x(n)$ is the original audio signal.

In the calculation of short-time autocorrelation function detection method, multiple multiplications lead to a large amount of calculation, while the average amplitude difference method with long and short time uses a simpler difference form, which avoids multiple multiplications and achieves a performance similar to autocorrelation function.

The short-time average amplitude difference function $F_n(k)$ of the audio signal $s(m)$ is defined as follows:

$$F_n(k) = \sum_{m=0}^{N-k-1} \left| S_n(m+k) - S_n(m) \right|. \tag{6}$$

In the above formula, N represents the window length added by the audio signal $s(m)$; $S_n(m)$ is defined as follows:

$$S_n(m) = s(m) w(n-m). \tag{7}$$

The process of estimating pitch frequency by short-time average amplitude difference function detection method includes the five following steps:

(1) Input the audio signal to be processed.

(2) The input audio signal is preprocessed by windowing, framing, and endpoint detection, so that the audio signal of each frame becomes a short-term stable signal.

(3) Calculate the short-term average amplitude difference function of each frame signal, and get the valley value of the pitch period position.

(4) The obtained valley value estimates the pitch period and calculates the inverse of the pitch period to obtain the pitch frequency.

Because the weighted Cauchy function waveform is close to the piano waveform and can describe the fundamental frequency and frequency doubling analysis, and the simulation effect is similar to the actual timbre, the fifth frequency doubling method is selected to simulate and extract the piano timbre. Assume that the discrete Fourier transform of the discrete event signal $x(m)$, namely, $X(i\lambda)$, can be expressed as

$$X_j(i\lambda) = T_j(i\lambda) * P_j(i\lambda),$$
$$T_j(i\lambda) = \begin{cases} B_j \dfrac{b_j}{b_j^2 + \left(\lambda - \lambda_j\right)^2}, & \lambda_j - b_j \le \lambda \le \lambda_j + b_j, \\ B_j \dfrac{2}{\left|\lambda - \lambda_j\right|}, & \text{Other.} \end{cases} \tag{8}$$

In the above formula, λ_j represents the fundamental frequency or frequency multiplication of j sound; B_j represents amplitude; b_j stands for adjusting the waveform width around λ_j; P_j stands for sine and cosine function, which accurately simulates playing timbre, intensity, and pitch to realize computer performance.

The basic idea of KNN (K-Nearest Neighbor) is as follows: according to the traditional vector space model, the text content is formalized as a weighted feature vector in the feature space. For a test text, calculate its similarity with each text in the training sample set, find out K most similar texts, and judge the category of the test text according to the weighted distance. According to the feature words, a test text vector is formed. Calculate the text similarity between the test text and each text in the training set, and the calculation formula is

$$\mathrm{Sim}\left(d_i, d_j\right) = \frac{\sum_{k=1}^{M} W_{ik} \times W_{jk}}{\sqrt{\sum_{k=1}^{M} W_{ik}^2} \sqrt{\sum_{k=1}^{M} W_{jk}^2}}, \tag{9}$$

where d_i is the feature vector of the test text and dj is the center vector of class j; M is the dimension of the feature vector; W_k is the k-th dimension of the vector.

In the k neighbors of the test text, calculate the weight of each class in turn, and the calculation formula is as follows:

$$P\left(X, C_j\right) = \begin{cases} 1, & \sum\limits_{d_i \in KNN} \mathrm{Sim}\left(x, d_i\right) y\left(d_i, C_j\right) - b \geq 0, \\ 0, & \text{Other}, \end{cases} \tag{10}$$

where x is the feature vector of the test text; $Sim\,(x, d_i)$ is the similarity calculation formula; b is the threshold, which needs to be optimized; and the value of $y\,(d_i, C_j)$ is 1 or 0. If d_i belongs to C_j, the function value is 1; otherwise, it is 0.

In this chapter, KNN algorithm is improved. By introducing multilabel classification, an extended KNN algorithm, namely, ML_KNN (multilabel k-nearest neighbor) classification algorithm, is proposed to further improve the efficiency of classification matching. ML_KNN algorithm is the realization of this paper based on ML_KNN classification. The algorithm is as follows:

(1) Divide the audio file of chord music into divided frames with index window of 1 s.

(2) 12 MPEG eigenvalues and 72 new time domain eigenvalues are extracted.

(3) N tags with the highest confidence are selected as candidate tags for the current frame, and other tags with low confidence are discarded.

(4) After all the individual frames in the index window are classified, the average confidence of each candidate instrument tag is calculated, and if the average confidence is greater than the optimal threshold parameter, the candidate tag is retained. Otherwise, it will be discarded.

To sum up, the flow chart of piano arrangement timbre recognition is shown in Figure 1.

Using self-developed amplitude feature extraction code, the relationship between amplitude and time of sine wave, piano, flute, and guitar music is analyzed, and the envelope function of different instruments is determined to be different. With a good envelope function, we can simulate the sound intensity and amplitude characteristics of wind instruments and stringed instruments and even the subtle differences between percussion instruments and plucked instruments.

3.2. System Implementation. The sound library generation module, which includes the piano arrangement sound recognition system, is the system's core module. This module generates the piano sound library in the audio system using the audio synthesis model and recognizes the timbre of the piano arrangement using the audio data provided by the sound acquisition module and the timbre parameters provided by the man-machine interaction module. Different timbre parameters can be used to generate different piano timbres. A computer-based sound library generation module is used to realize the piano arrangement timbre recognition system in the application experiment for this document's sound library generation. The system is modular in design and has a high degree of versatility, with modules such as audio file reading and writing, audio information analysis, timbre parameter acquisition, and timbre and simulation performance. The general architecture of piano arrangement pitch recognition system is shown in Figure 2.

In piano simulation function module, piano can play different types of music and opera scores, which is widely used and can act as a band, so piano is the best choice for playing musical instruments. Piano timbre editing function module can record timbre editing in various ways in detail; in particular, the music timbre editing with wide range is difficult, but timbre editing is very critical. The acquisition module edits and acquires the timbre parameters through the man-machine interface. The timbre synthesis module is used for synthesizing timbre files, supporting batch synthesis of various timbres, and displaying the synthesis progress in real time. The simulation performance module is used to assess the simulation performance of timbre or music.

The unique piano timbre obtained from the recording is determined by the vibration equation of the strings, and the amplitude energy changes from strong to weak, so it cannot be processed twice. On the other hand, the monophonic amplitude of electronic synthetic piano is stable, and the loudness does not change. In the postprocessing, envelope function can be added to control the change of amplitude, so as to reproduce the difference between hitting strength and delaying pedal and make music more emotional. Here, the pitch variable in the metastructure of the piano accompaniment sound mode can be determined. If some notes in the metastructure are imitated, their pitch is related to the pitch of the original melody being imitated.

4. Experiment and Results

We can build a data prediction model by machine learning algorithm and automatically identify the emotional features of music by computer. From the dataset of 400 pieces of music, we selected the feature data of 300 pieces of music as the training set (80% of the data as the training set and 20% as the test set) and the feature data of the other 100 pieces of music as the test set. When using ML_KNN, the training set is cross-validated, so as to obtain the optimal values of the parameters in the model. Finally, we tested the model, and the specific results of model comparison are shown in Figures 3 and 4.

The average correlation coefficient (CC) for the test set is 45.36 percent. The test set's MSE (mean squared error) is 0.038. It can be seen that the ML_KNN algorithm performs better in terms of musical emotional cognition. However, recognition rates for three emotions, Modest, Dream, and Graceful, are all very low in the test set, indicating that more research is needed. Correlation is a general method that is independent of the stream because it is done in the audio domain. This eliminates the tedious task of parsing the text's outline. This function can clearly reflect the intensity change

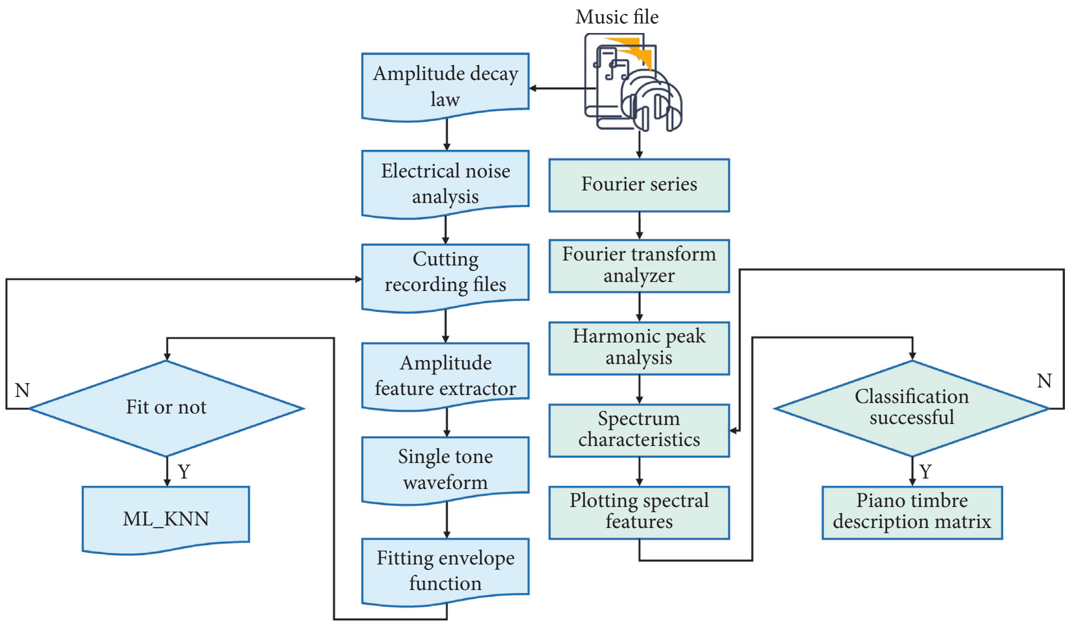

Figure 1: Flow chart of piano arrangement timbre recognition.

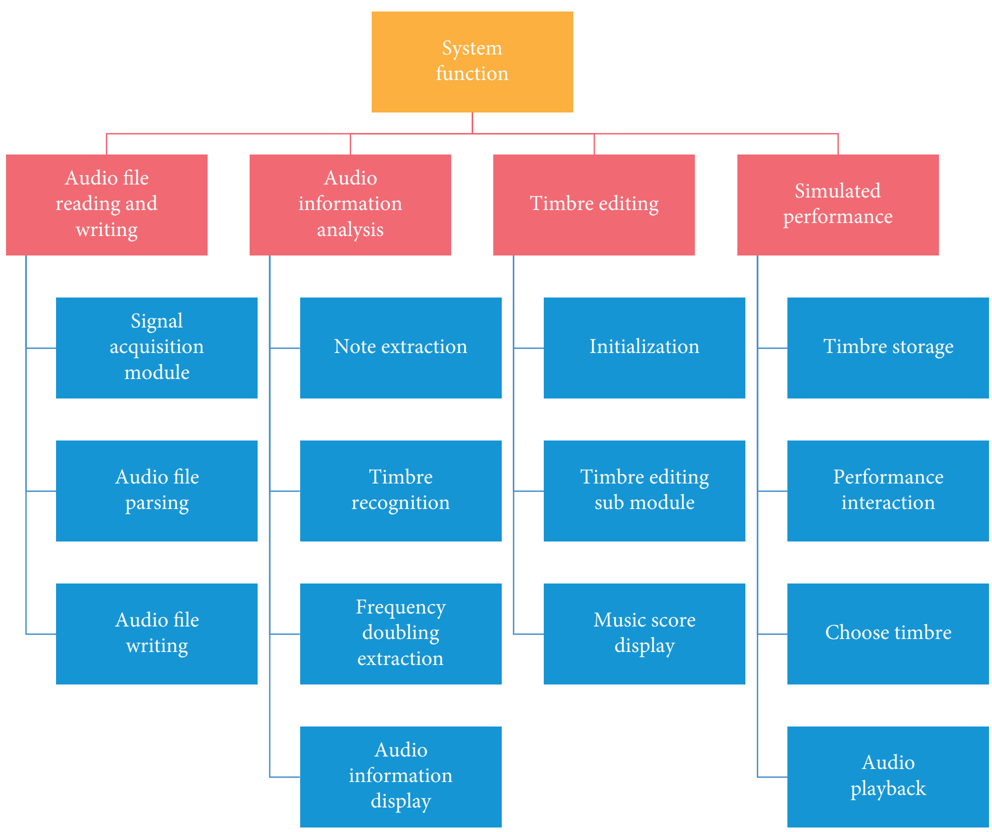

Figure 2: Overall architecture of piano arrangement timbre recognition system.

of sound at different times during the arrangement process. It is possible to ensure that the pitch synthesis process of a piano arrangement is essentially consistent with the changing trend of tone using the envelope function extraction. This function is performed while removing some unwanted noise. This method can be used in practice indefinitely. If the processing is done in a professional lab with a well-configured computer cluster, it can achieve extremely high efficiency while saving time and money.

The frequency composition and proportion of synthetic timbre and real timbre are different (the proportion of harmonic amplitude coefficient is also different), so the two

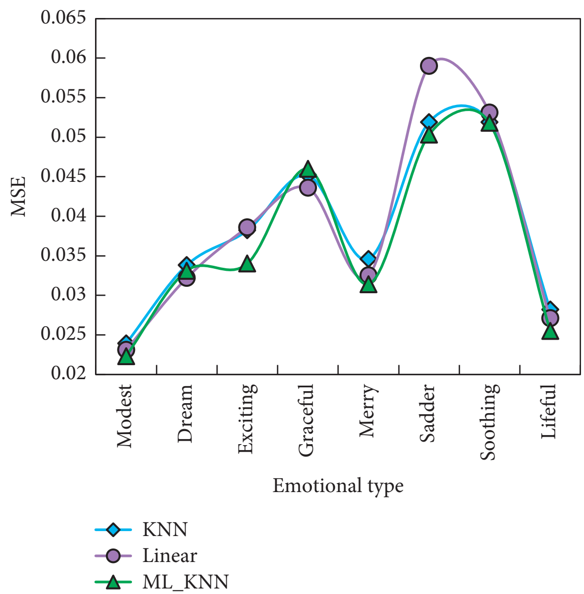

Figure 3: MSE test results of music emotion cognitive model.

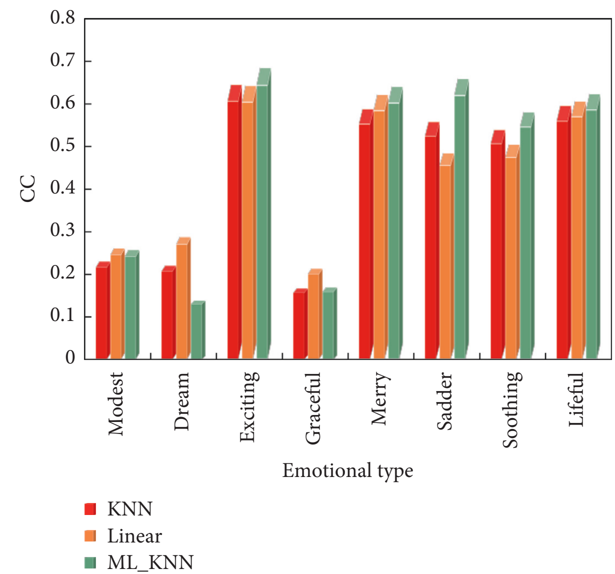

Figure 4: CC test results of music emotion cognitive model.

timbres are different in theory, which is proved by listening timbre. Compared with the positions surrounded by squares in Figure 4, although the synthesized timbre is very smooth in time domain, there are many burrs in frequency domain, and the timbre shows great noise. Therefore, their frequency domain characteristics are quite different. The single-tone datasets of musical instruments are classified, and the timbre expression spectrum is compared and analyzed based on the harmony structure proposed in this paper, so as to find the characteristics that can best reflect the timbre of musical instruments. Split the mono dataset of the instrument into five different datasets. The classification results based on different timbre features in different musical instrument monophonic datasets are shown in Table 1 and Figure 5. In the experiment, KNN is used as the classifier, the training set is 4/5 of the experimental data, and the test set is 1/5 of the experimental data.

It can be seen that the recognition rate of dataset 1 is generally high, because the timbre features of dataset 1 are all within a certain range, and the recognition of a single instrument is to find the specific corresponding point within this range. Regardless of the type of function set on which MFCC is based, the timbre expression spectrum of this paper performs well. According to the timbre expression spectrum function, the recognition rate of dataset 1 reaches 91.5%. According to MFCC function, the recognition rate of dataset 2 is 95.2%, that of dataset 3 is 78.4%, that of dataset 4 is 94.1%, and that of dataset 5 is 92.6%, which is the best result.

Extracting the same combination features of timbre and based on four supervised pattern recognition algorithms, KNN, Naive Bayes, Decision Tree, and ML_KNN, the classification and recognition experiments of single tones of musical instruments are carried out, respectively. The results are shown in Table 2 and Figure 6.

As can be seen, ML_KNN has the highest recognition rate across all datasets, so ML_KNN is chosen as the classifier for musical instrument classification and recognition in this paper. In addition, KNN is second only to ML_KNN in terms of classification and recognition of musical instruments. The performance of a detuned mode oscillator is better than that of a critical mode oscillator in various networks, which can be attributed to the clamping phenomenon mentioned earlier. The process of hijacking between local oscillator groups in the network to better track the time can be thought of as the rhythm change of a piece of music. The oscillator will show similar frequencies in the local area where strong resonance occurs. Average field networks have higher evaluation indices than other networks, but they also have a higher standard deviation. This demonstrates that the results of each round in the cross-validation process vary widely.

We conclude from our timbre analysis that all frequency components in the frequency domain interact to form a rich piano timbre and that synthesis of piano timbre cannot rely solely on overtone frequency components. The ratio of the vibration frequencies of the two pitches that make up the intervals determines the harmony of intervals, which is a characteristic that reflects the basic properties of intervals. Concordant intervals sound good and blend together, whereas dissonant intervals sound rougher and do not blend together. The Fourier transform algorithm is used to calculate the frequency, amplitude, and phase of various sine wave signals by accumulation [18]. Different playing skills of many musical instruments can produce different timbres. MFCC is extracted from these single-frame musical instrument sounds by describing the standard equation. The frame size is 130 ms, and the overlapping size of two adjacent frames is 80 ms, which reduces the information loss caused by window function. The hop count of the frame is 45 ms. The classifier is trained on these feature databases. Figure 7 shows the comparison results of ring estimation based on multilabel classifier.

It can be concluded that, after introducing ML_KNN classification algorithm, the label Decision Tree classification

Table 1: Single-tone classification results of musical instruments based on different timbre features.

Dataset number	Frequency domain characteristics	Time domain characteristics	MFCC	Timbre expression spectrum
1	43.2	62.1	87.4	91.5
2	25.6	37.4	95.2	90.2
3	22.1	52.1	78.4	75.6
4	40.6	49.3	94.1	88.5
5	23.9	47.7	92.6	91.6

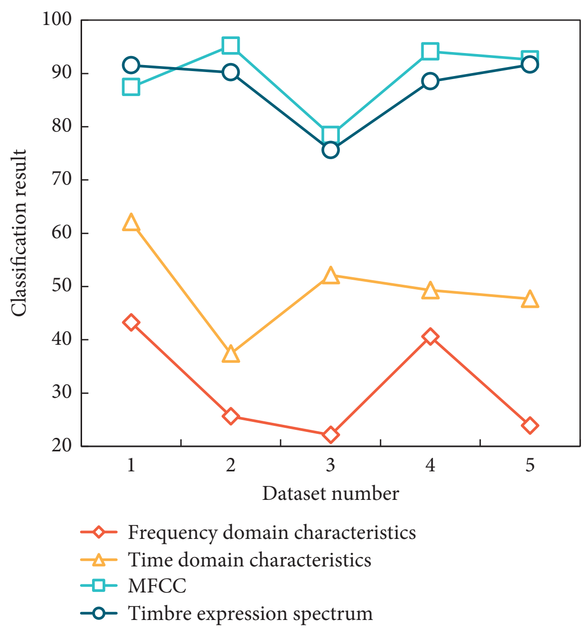

Figure 5: Single-tone classification results of musical instruments.

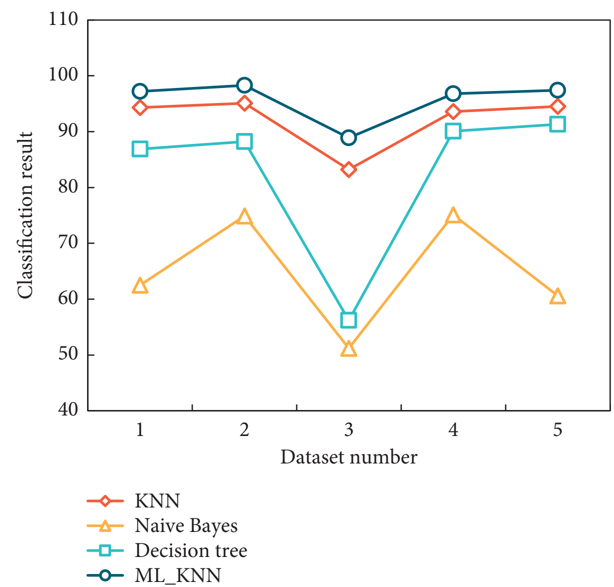

Figure 6: Classification and recognition results of musical instrument tones.

Table 2: Classification and recognition results of musical instrument tones based on different classifiers.

Dataset number	KNN	Naive Bayes	Decision Tree	ML_KNN
1	94.3	62.5	86.9	97.2
2	95.1	74.9	88.2	98.3
3	83.2	51.2	56.2	88.9
4	93.6	75.1	90.1	96.8
5	94.5	60.6	91.3	97.4

algorithm with more prediction effects is obviously improved. After using ML_KNN classification algorithm, the detection rate is increased from 61.3% to 70.2%. The correct rate also increased from 40.3% to 48.9%. When the k value was set to 6, the detection rate increased to 74.6%, but the correct rate decreased to 41.2%. The conclusion of this experiment is that ML_KNN classification algorithm has better recognition effect than Decision Tree classification algorithm.

In the process of learning and studying music scores, pianists will naturally find a lot of music knowledge to supplement, such as musical instrument materials, pronunciation principles, staff of various transposed musical instruments, orchestration methods, and performance methods. To shorten the spectrum of vocal music, we need to know the pronunciation methods. No matter what note it is, the same attenuation rate is used, but, through the judgment

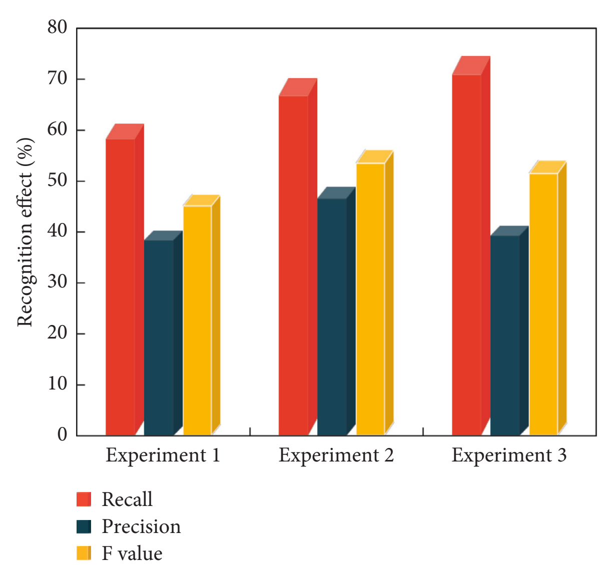

Figure 7: Comparison results of timbre estimation of multilabel classifiers.

of human ears, it can be found that the noise is reduced but not eliminated, so the music played is not very effective, and it is not musical with fluctuations. The combination of piano timbre characteristic matrix and sound intensity envelope curve can effectively distinguish the timbre differences of different songs, that is, identify the timbre of piano arrangement.

5. Conclusions

To sum up, this paper designs an AI-based piano arranger timbre recognition system based on Fourier analysis. Through short-time Fourier frequency shift spectrum analysis, the ringing characteristic matrix can be extracted. Get a tone shift envelope curve. The piano timbre can be clearly identified by the timbre characteristic matrix and transposition envelope curve. ML_KNN classification algorithm is applied to timbre recognition of chord music. The experimental results show that ML_KNN classification algorithm can improve the accuracy of chord music timbre recognition. After using ML_KNN classification algorithm, the detection rate increased from 61.3% to 70.2%. The correct rate also increased from 40.3% to 48.9%, and the detection rate increased to 74.6% when the k value was set to 6. The experimental results show that the timbre recognition system designed in this paper can synthesize clear piano music and has good timbre recognition performance, which is worthy of wide application.

Data Availability

The data used to support the findings of this study are available from the corresponding author upon request.

Conflicts of Interest

The authors do not have any possible conflicts of interest.

References

[1] J. Zhang, J. Sun, J. Wang, Z. Li, and Xi Chen, "An object tracking framework with recapture based on correlation filters and Siamese networks," *Computers & Electrical Engineering*, vol. 98, Article ID 107730, 2022.

[2] K. Patil and M. Elhilali, "A biomimetic multi-resolution spectrotemporal model for musical timbre recognition," *Journal of the Acoustical Society of America*, vol. 127, no. 3, p. 1951, 2010.

[3] J. J. Aucouturier and F. Pachet, "The influence of polyphony on the dynamical modelling of musical timbre," *Pattern Recognition Letters*, vol. 28, no. 5, pp. 654–661, 2007.

[4] Kailash, D. Patil, S. Shamma, and M. Elhilali, "Music in our ears: the biological bases of musical timbre perception," *PLoS Computational Biology*, vol. 8, no. 11, Article ID 1002759, 2012.

[5] D. Chen and X. Guo, "Application of multiacoustic data in feature extraction of anemometer," *Complexity*, vol. 2021, Article ID 7955909, 10 pages, 2021.

[6] J. Wu, E. Vincent, S. A. Raczynski, T. Nishimoto, N. Ono, and S. Sagayama, "Polyphonic pitch estimation and instrument identification by joint modeling of sustained and attack sounds," *IEEE Journal of Selected Topics in Signal Processing*, vol. 5, no. 6, pp. 1124–1132, 2011.

[7] Y. Ding, Z. Zhang, X. Zhao et al., "Multi-feature fusion: graph neural network and CNN combining for hyperspectral image classification," *Neurocomputing*, vol. 501, 2022.

[8] W. Wei and Z. Wei, "Remote sensing image classification based on a cross-attention mechanism and graph convolution," *IEEE Geoscience and Remote Sensing Letters*, vol. 19, pp. 1–5, Article ID 8002005, 2022.

[9] D. Mitrovic, M. Zeppelzauer, and H. Eidenberger, "Analysis of the data quality of audio descriptions of environmental sounds," *Journal of Digital Information Management*, vol. 5, no. 5, pp. 1228–1237, 2007.

[10] I. Peretz, N. Gosselin, P. Belin, R. J. Zatorre, J. Plailly, and Tillmann, "Music lexical networks: the cortical organization of music recognition," *Annals of the New York Academy of Sciences*, vol. 1169, pp. 256–265, 2010.

[11] D. Han, Y. Kong, J. Han, and G. Wang, "A survey of music emotion recognition," *Frontiers of Computer Science*, vol. 16, no. 6, pp. 1–11, 2022.

[12] L. Xing, K. Nie, N. Imennov, J. H. Won, L. Atlas, and J. Rubinstein, "Speech and music recognition with acoustic simulations of a harmonic single sideband encoding strategy for cochlear implants," *Journal of the Acoustical Society of America*, vol. 129, no. 4, p. 2656, 2011.

[13] R. Omar, S. Henley, J. W. Bartlett et al., "The structural neuroanatomy of music emotion recognition: evidence from frontotemporal lobar degeneration," *NeuroImage*, vol. 56, no. 3, pp. 1814–1821, 2011.

[14] J. C. Wang, Y. S. Lee, Y. H. Chin, Y. R. Chen, and W.-C. Hsieh, "Hierarchical dirichlet process mixture model for music emotion recognition," *IEEE Transactions on Affective Computing*, vol. 6, no. 3, pp. 261–271, 2015.

[15] C. Xiang, S. G. Zhao, X. Xuan, and K. C. Chou, "IATC-mHyb: a hybrid multi-label classifier for predicting the classification of anatomical therapeutic chemicals," *Oncotarget*, vol. 8, no. 35, pp. 58494–58503, 2017.

[16] E. L. Mencía and F. Janssen, "Learning rules for multi-label classification: a stacking and a separate-and-conquer approach," *Machine Learning*, vol. 105, no. 1, pp. 1–50, 2016.

[17] R. Cerri, R. C. Barros, A. C. PLF De Carvalho, and Y. Jin, "Reduction strategies for hierarchical multi-label classification in protein function prediction," *BMC Bioinformatics*, vol. 17, no. 1, pp. 373–386, 2016.

[18] K. Sering, P. Milin, and R. H. Baayen, "Language comprehension as a multi-label classification problem," *Statistica Neerlandica*, vol. 72, no. 3, pp. 339–353, 2018.

[19] J. Ju, M. Zhang, and L. Xiao, "Robust label compression for multi-label classification," *Knowledge-Based Systems*, vol. 107, no. 1, pp. 32–42, 2016.

[20] Z. Yong, D. W. Gong, X. Y. Sun, and Y. N. Guo, "A PSO-based multi-objective multi-label feature selection method in classification," *Entific Reports*, vol. 7, no. 1, p. 376, 2017.

[21] Y. Yan, W. Ying, W. C. Gao, B. W. Zhang, C. Yang, and X. C. Yin, "LSTM2: multi-label ranking for document classification," *Neural Processing Letters*, vol. 47, no. 7, pp. 1–22, 2017.

Hindawi
Computational Intelligence and Neuroscience
Volume 2022, Article ID 2689949, 13 pages
https://doi.org/10.1155/2022/2689949

Research Article

E-Sports Training System Based on Intelligent Gesture Recognition

Hui Li, Yao Lu, and Hongqiao Yan

School of Sport Communication and Information Technology, Shandong Sport University, Jinan 250000, China

Correspondence should be addressed to Hongqiao Yan; yanhongqiao@sdpei.edu.cn

Received 18 May 2022; Accepted 14 June 2022; Published 9 July 2022

Academic Editor: Xin Ning

In order to improve the effect of e-sports training, this paper combines the intelligent gesture recognition technology to construct an e-sports training system and judges the training effect of players through the recognition of players' gestures. Moreover, this paper studies the commonly used feature extraction algorithms and proposes an improved SLC-Harris feature extraction algorithm, and the feasibility of this algorithm is verified by the experimental results on the EUROC data set. In addition, this paper uses the KLT optical flow algorithm to track the extracted feature points and calculates the pure visual pose through epipolar geometry, triangulation, and PnP algorithms. The experimental research results show that the electronic economic training system based on intelligent gesture recognition proposed in this paper has certain effects.

1. Introduction

The reason why e-sports can become a sports competition is that it is closely related to the progress of society, the development of science and technology, and the spiritual and cultural needs of the people. Although there are countless people who enjoy this high-tech intellectual sports event, in fact, public opinion instills the harmful opinion of e-sports in people intentionally or unintentionally. Some media reported extensively that some students were addicted to games and could not extricate themselves, wasting their youth and studies, which made e-sports become "electronic heroin" that everyone shouted. The huge pressure of public opinion makes e-sports face severe survival pressure, and it is difficult for enterprises to enter this market justifiably. Moreover, athletes can only be called "players," and their treatment cannot be compared with that of ordinary athletes. At the same time, the majority of fans can only engage in e-sports secretly. In addition, in the face of huge pressure from public opinion, it is difficult for the government to guide and supervise confidently, and sometimes, it has to prohibit escrow. The ban on television broadcasting of e-sports competitions can be described as a huge obstacle to the normal development of the current social discrimination against the e-sports sports industry.

Generally speaking, the development of e-sports is not yet mature, and the development of e-sports is still in its infancy [1], which is manifested in many aspects: the public recognition is not enough, there are few related large-scale events, there is no professional-scale operation, there is less research in this area, and so on [2]. Especially on college campuses, although students have more time for self-discipline than before, the school does not pay enough attention to e-sports, and there is no relatively formal organization and management of participants, which has led to many human resources problems waste [3].

In order to cater to the trend of e-sports development, vigorously develop e-sports business, improve the overall level of e-sports, and enable e-sports activities to develop well in colleges and universities, the current primary task is to deepen the characteristics of students participating in e-sports activities [4]. Among them, the analysis and research on the current situation, development trend, and participation significance of e-sports in colleges and universities are particularly important in order to discover the problems existing in the development of campus e-sports and put forward reasonable suggestions for the development [5].

As emerging sports, e-sports are mainly participated by the younger generation, which has the characteristics of younger and younger age. E-sports can exercise people's thinking ability, psychological pressure resistance, unity and cooperation, hand-eye coordination, and so on. It can also make the younger generation have the awareness of abiding by the rules in the process of participating in e-sports [6]; trained participants have a fair and open, never admit defeat, pursue a stronger competitive spirit, and have a positive impact on the lives of participants. Many colleges and universities have successively opened related majors in e-sports. Although e-sports is popular in the world, the related research and guiding theories on how to cultivate e-sports talents are rare [7].

Different scholars have different views on the attributes and characteristics of e-sports. Literature [8] proposed that "e-sports include three basic characteristics: one is electronics, the other is competitive sports, and the third is a confrontation between people. At the same time, e-sports sports are divided into virtualized e-sports sports and fictionalized sports." Literature [9] pointed out that "the most fundamental characteristics of video games that distinguish them from other artificial games are: virtual environment, absence of the body and artificial intelligence," emphasizing the main position of electronic communication technology in e-sports. Scholar Yang Fang believes that "e-sports should return to the essence of games, and games to competitive sports are based on the evolution trend of play-game-competitive sports" and based on the development process of traditional competitive sports, puts forward a plan for the development of e-sports. Jia Peng and Yao Jiaxin believe that e-sports has great characteristics: the diversity of functional structure requirements, the full expansion of self-awareness, the complexity of sports information pattern recognition, the agility of information processing efficiency, and the accuracy of intuitive thinking and decision-making. Sex analyzes and clarifies the various attributes of e-sports from many aspects [10].

The discussion on the attributes of e-sports is still going on. Based on the current research, it can be determined that the two essential attributes of e-sports are electronic interaction and confrontational competition. Without electronic interaction, it becomes traditional competitive sports; it becomes a video game, so the two are interdependent and indispensable. With the development of electronic interaction technology, various forms of e-sports have emerged [11].

Event services are mainly engaged in e-sports referees, coaches, club operation and management, game commentary, data and tactical analysis, and so on. Practitioners need to have data analysis capabilities, management capabilities, and commentary capabilities. The production and broadcast of the event include content production and external dissemination, mainly involving the design of live content and promotion plans, venue layout, equipment debugging, video data collection, postprocessing, background data analysis, and so on. The practitioners should have journalism, communication, broadcasting, TV technology, and other related professional abilities [12].

Since the e-sports industry is an emerging industry, most employees are not from e-sports majors and have not received a complete and systematic e-sports theoretical education, but nearly 90% of the employees believe that the e-sports industry needs prejob training [13]. Judging from the current situation of the development of the entire industry, it is undoubtedly the most attractive option to work for game manufacturers, but it is difficult for game manufacturers to absorb more human resources without major business adjustments. Therefore, the need to train practitioners in support organizations around e-sports events becomes more obvious [14]. For example, training content production capabilities (reporters, screenwriters, copywriters, and anchors) requires a professional background in journalism and communication; training event support capabilities (coaches, data analysts, nutritionists, and brokers) requires sports and information technology. Professional background: training public relations, marketing capabilities (products, business, brand marketing, and media), requires a professional background in marketing and management [15].

E-sports self-media is still a media, and you must have the ability to report news, or you can dig deep into a vertical field, such as specializing in video commentary of games, specializing in game clearance strategies, specializing in sharing game skills, and so on. After all, hot spots can bring traffic. WeMedia is a personalized media with social attributes; it communicates with users; and it has its own distinct character orientation [16]. To be a self-media, you should also have strong analytical skills and be able to interpret a topic or special event from a unique or professional perspective. Current e-sports professional ability training pathways.

1.1. Current E-Sports Professional Ability Training Pathways. Most training institutions in society position themselves as training professional players but basically lack training resources. Training institutions do not have coaches, data analysts, or club managers, and it is difficult for the trained people to find a suitable position in the e-sports circle. Rather than cultivating professional skills, it is better to make money from e-sports hot spots. Money has no intention or inability to contribute to the development of the e-sports industry [17].

At present, the main e-sports talents are cultivated by e-sports companies and e-sports clubs. The club mainly trains professional players, coaches, and data analysts in order to achieve better results in the league. Game companies train referees, game developers, commentators, and other related talents to ensure the healthy development of the e-sports industry [18]. An analysis of the revenue structure of the e-sports industry can help us see the e-sports industry more transparently. The truly profitable institutions are still game manufacturers, which continuously create market value through development and operation. In the context of the continuous development and popularization of the video game industry, competition has become a starting point for expanding influence and creating new commercial value. The comprehensive development of competitive value is inseparable from the promotion of surrounding formats, and new jobs such as video, live broadcast, and commentary emerge in an endless stream [19].

This paper combines the intelligent gesture recognition technology to construct an e-sports training system and uses the player's gesture recognition to judge the player's training effect to improve the e-sports training effect.

2. Intelligent Gesture Recognition

2.1. Gesture Intelligent Positioning. The structural framework of the gesture autonomous localization algorithm is shown in Figure 1.

Monocular visual-inertial odometry uses a pure camera in the front end for motion estimation. The algorithm firstly extracts the features of the image information collected by the camera, then uses the optical flow method to track the feature points, and finally uses PnP (Perspective-n-Point) to perform motion estimation on the tracked feature points. Then, the algorithm eliminates the mismatched point pairs through random sampling consistency (RANSAC) and uses nonlinear optimization to optimize the pose. The front-end process is shown in Figure 2.

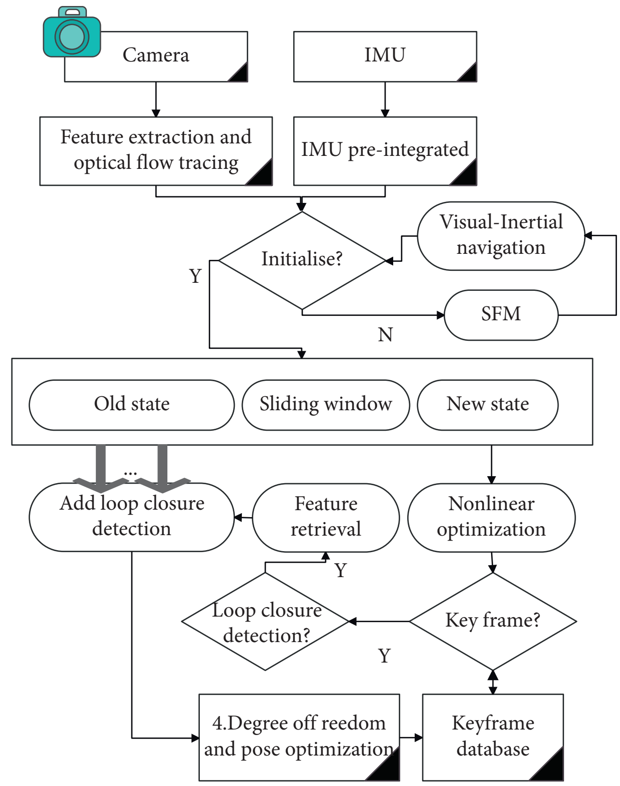

Figure 1: Gesture positioning algorithm structural framework.

2.2. SLC-Harris Feature Extraction. The feature is the digital expression of the object in the image, and the image can be quantitatively analyzed by extracting the feature. Commonly used feature extraction methods mainly include SIFT algorithm, SURF algorithm, and ORB algorithm.

The traditional Harris algorithm calculates the angular responsivity as shown below. It is mainly based on the weighted summation of the squared and multiplied gradients of all pixels in the window.

$$R = |C| - k \times (\text{trace}(C))^2. \tag{1}$$

Among them, there are

$$|C| = \lambda_1 \times \lambda_2, \tag{2}$$

$$\text{trace}(C) = \lambda_1 + \lambda_2. \tag{3}$$

In formula (1), k is a constant ranging from 0.04 to 0.06, and both λ_1 and λ_2 in formula (2) represent eigenvalues.

For a grayscale image, the value of any point (x, y) in the integral image ii (x, y) refers to the sum of all grayscale values from the upper left corner of the image to the area where this point is located, as shown in Figure 3.

The calculation formula of pixels in the rectangular window is as follows:

$$ii(x, y) = \sum_{x' \le x, y' \le y} I(x', y'). \tag{4}$$

The most complex calculation in the Harris algorithm is the calculation of diagonal responsivity. The original calculation method causes the calculation overlap between each pixel in the integration window, resulting in high computational complexity. For this, the gradient values in g_x^2, g_y^2 and $g_x g_y$ are used to integrate the image to speed up the calculation of the angular responsivity. The calculation formula is as follows:

$$\begin{aligned} ii_{xx}(x, y) &= \sum_{x' \le x, y' \le y} g_x^2(x', y'), \\ ii_{yy}(x, y) &= \sum_{x' \le x, y' \le y} g_y^2(x', y'), \\ ii_{xy}(x, y) &= \sum_{x' \le x, y' \le y} g_x(x', y') g_y(x', y'). \end{aligned} \tag{5}$$

Efficient nonmaximum suppression (E-NMS) is used to efficiently extract unique feature locations for each corner region, and the region thresholds are compared using image patches instead of pixels. The principle is shown in Figure 4.

2.3. KLT Optical Flow Tracking. After the key points are extracted, the optical flow method is used to calculate the minimum photometric error by establishing an error model. This method does not need to calculate descriptors or feature point matching, which will greatly save the amount of calculation.

The basic idea of LK optical flow is to assume that the optical flow in the local neighborhood of a pixel is invariant, and based on this assumption, construct a least-squares problem about the optical flow of the neighborhood pixels.

First, it is assumed that the light intensity of the pixel in each frame of the image is constant. According to this, for the pixel located at (x, y) at time t, moving to $(x + dx, y + dy)$ at time $t + dt$, there are

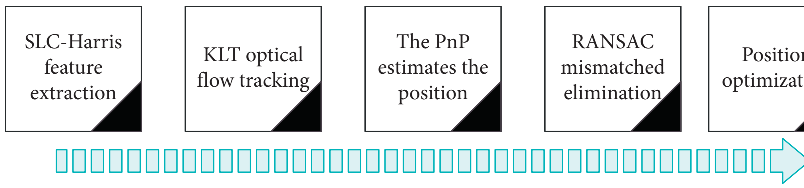

FIGURE 2: Front-end flowchart.

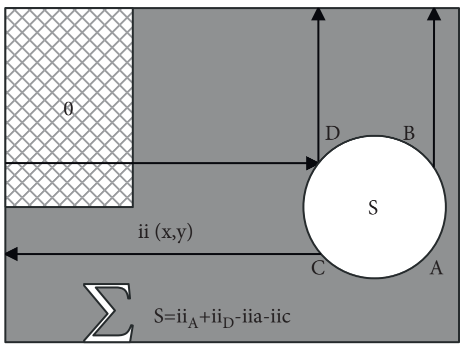

FIGURE 3: Rectangular window pixel calculation.

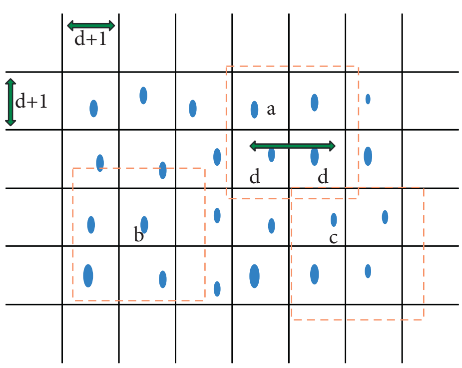

FIGURE 4: Efficient nonmaximum suppression.

$$I(x, y, t) = I(x + dx\ , y + dy\ , t + dt). \tag{6}$$

Then, according to another basic assumption of LK optical flow, the displacement of pixels in adjacent images is small; the Taylor expansion of formula (6) is

$$I(x + dx\ , y + dy\ , t + dt) \approx I(x, y, t) + \frac{\partial I}{\partial x}dx + \frac{\partial I}{\partial y}dy + \frac{\partial I}{\partial t}dt. \tag{7}$$

Combining the above formulas and dividing by dt into both sides of the formula, we get:

$$\frac{\partial I}{\partial x}\frac{\mathrm{d}x}{\mathrm{d}t} + \frac{\partial I}{\partial y}\frac{\mathrm{d}y}{\mathrm{d}t} = -\frac{\partial I}{\partial t}, \tag{8}$$

where $\mathrm{d}x/\mathrm{d}t$ represents the motion speed of the pixel on the x-axis, $\mathrm{d}y/\mathrm{d}t$ represents the motion speed of the pixel on the y-axis, and the two speeds are recorded as u and v, respectively. At the same time, $\partial I/\partial x$ represents the gradient value of the image in the x-axis direction at the pixel point; $\partial I/\partial y$ represents the gradient value in the y-axis direction at the pixel point; and $\partial I/\partial t$ represents the derivative value of the image in the t direction, which are denoted as I_x, I_y, and I_t, respectively. Therefore, formula (8) can be written in matrix form as follows:

$$\begin{bmatrix} I_x & I_y \end{bmatrix}\begin{bmatrix} u \\ v \end{bmatrix} = -I_t. \tag{9}$$

Finally, according to the third basic assumption of the LK optical flow method, adjacent pixels in the same image plane have similar motion; a $w \times w$ size window is defined. According to the same motion of all pixels in the window, w^2 formulas can be listed; the overdetermined formulas can be constructed; and the motion parameters of the center point can be obtained by the least square method. Accordingly, its formula can be expressed as follows:

$$\begin{pmatrix} \sum I_x I_x & \sum I_x I_y \\ \sum I_x I_y & \sum I_y I_y \end{pmatrix}\begin{pmatrix} u \\ v \end{pmatrix} = -\begin{pmatrix} \sum I_x I_t \\ \sum I_y I_t \end{pmatrix}. \tag{10}$$

Each image frame is downsampled by pyramid layering, and multilevel pyramids are established.

$$\begin{aligned} I^L(x, y) = {} & \frac{1}{4}I^{L-1}(2x, 2y) + \frac{1}{8}\begin{pmatrix} I^{L-1}(2x-1, 2y) + I^{L-1}(2x+1, 2y) \\ +I^{L-1}(2x, 2y-1) + I^{L-1}(2x, 2y+1) \end{pmatrix} \\ & + \frac{1}{16}\begin{pmatrix} I^{L-1}(2x+1, 2y+1) + I^{L-1}(2x+1, 2y+1)+ \\ I^{L-1}(2x+1, 2y+1) + I^{L-1}(2x+1, 2y+1) \end{pmatrix}, \end{aligned} \tag{11}$$

where L represents the Lth layer image.

The algorithm calculates the value of the bottom layer from top to bottom according to the Gaussian pyramid and calculates the pixel value near the edge of the image based on the following formulas:

$$\begin{aligned} I^{L-1}(-1, y) &\approx I^{L-1}(-1, y), \\ I^{L-1}(x, -1) &\approx I^{L-1}(x, 0), \\ I^{L-1}\left(n_x^{L-1}, y\right) &\approx I^{L-1}\left(n_x^{L-1} - 1, y\right), \\ I^{L-1}\left(x, n_y^{L-1}\right) &\approx I^{L-1}\left(x, n_y^{L-1} - 1\right), \\ I^{L-1}\left(n_x^{L-1}, n_y^{L-1}\right) &\approx I^{L-1}\left(n_x^{L-1} - 1, n_y^{L-1} - 1\right). \end{aligned} \tag{12}$$

The camera motion pose is estimated using SFM in the vision front end. For a monocular camera, the camera pose can be estimated by the geometric relationship between two points in different locations in real space and their projected points on their respective imaging planes. As shown in Figure 5, P is any point in the three-dimensional space, and its coordinates are $[X, Y, Z]^T$; O_1 and O_2 are the optical centers of the two camera positions. p_1 and p_2 are the projection points of point P on the imaging plane I_1 and the imaging plane I_2, respectively. According to the pixel positions of the two matched point pairs p_1 and p_2, the essential matrix E and the fundamental matrix F can be obtained.

According to the camera imaging model, we assume that K is the camera internal parameter matrix, and R and t represent the rotation matrix and translation vector from plane I_1 to plane I_2, and the following formula can be obtained:

$$s_1 p_1 = KP, s_2 p_2 = K(RP + t). \tag{13}$$

Homogeneous coordinate transformation and normalization between 2D and 3D, we can get

$$x_1 = K^{-1} p_1, x_2 = K^{-1} p_2, \tag{14}$$

where x_1 and x_2 represent the coordinates of pixels p_1 and p_2 in the normalized plane, respectively. The algorithm combines formuls (13) and (14) and multiplies by $x_2^T t^\wedge$ to obtain the essential matrix E and the fundamental matrix F, which can be sorted out as follows:

$$\begin{aligned} p_2^T K^{-T} t^\wedge R K^{-1} p_1 = 0, \\ E = t^\wedge R, F = K^{-T} E K^{-1}, \end{aligned} \tag{15}$$

where $t^\wedge$ represents the antisymmetric matrix.

When there are more than eight sets of point pairs such as p_1 and p_2, the eight-point method can be used to construct a linear formula system for the simplified formula, and then the unique solution of R and t can be obtained.

$$x_2^T E x_1 = p_2^T F p_1 = 0. \tag{16}$$

When the monocular camera recovers the pose through the epipolar geometric relationship, the obtained translation is the normalized value, which has no practical significance.

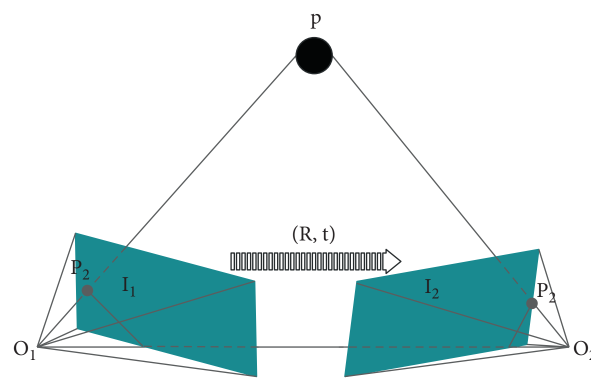

Figure 5: Epipolar geometric constraints.

In order to obtain the depth information on feature points, triangulation needs to be introduced. We assume that s_1 and s_2 represent the depth of the two feature points; we can get

$$s_2 x_2 = s_1 R x_1 + t. \tag{17}$$

The feature point depth values $x_2^\wedge$ and $x_1\wedge$ can be obtained by left-multiplying formula (17) by s_1 or s_2, respectively, as follows:

$$\begin{aligned} s_1 x_2^\wedge R x_1 + x_2^\wedge t = 0, \\ s_2 x_1^\wedge R x_2 - x_1^\wedge t = 0. \end{aligned} \tag{18}$$

When the positions of multiple points in space are known, the camera pose can be estimated by the PnP algorithm. Common PnP algorithms include P3P, DLT, and BA optimization. Among them, the P3P algorithm is the most common method. The algorithm needs to know at least three points and their projection points on the camera imaging plane. Then, the camera pose can be estimated by solving the relationship between point pairs according to the similar triangle principle and the cosine theorem. A schematic diagram of the P3P relationship is shown in Figure 6.

The coordinate system convention is as follows: the world coordinate system is represented by $(\cdot)^w$, and $(\cdot)^b$ and $(\cdot)^c$ represent the IMU coordinate system and the camera coordinate system, respectively. The relationship between the coordinate systems is shown in Figure 7. $(.)^v$ represents the visual reference frame in the sliding window, which is independent of the IMU measurement and can represent any frame in the visual structure. $(.)_b^w$ represents the transformation from the IMU coordinate system to the world coordinate system; b_k represents the IMU frame of the kth image; $(\cdot)_c^v$ represents the transformation from the camera coordinate system to the visual reference system; and c_k represents the camera frame of the kth image. $\widehat{(\cdot)}$ represents the measured value and parameter estimation value of the sensor; $\overline{(\cdot)}$ represents the latest scale parameter of the sliding window; and the rotation can be represented by the rotation matrix $\mathbf{R}$ and the quaternion $\mathbf{q}$. $\mathbf{g}^w = [0, 0, g]^T$ represents the gravity vector in the world coordinate system, and g^v represents the gravity vector in the visual reference coordinate system.

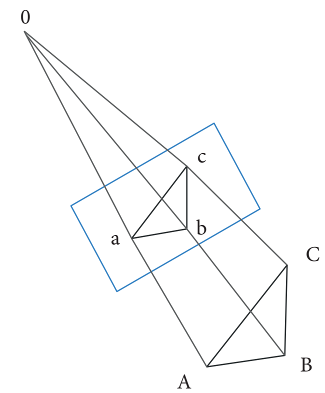

Figure 6: Schematic diagram of P3P relationship.

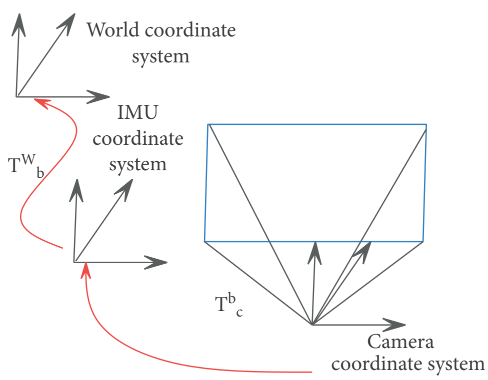

Figure 7: Coordinate conversion relationship.

2.4. IMU Preintegration. The sampling frequency of the camera used in this paper is 20 Hz, and the sampling frequency of the IMU is 200 Hz. It can be seen that the frequency of the IMU is much higher than that of the image. In order to avoid the repeated integration phenomenon caused by the frequency change of the visual frame optimization state caused by the high sampling rate of the IMU, a pre-integration technique is used for all IMU sampling data between two image key frames. Furthermore, inertial measurements between adjacent image key frames are aggregated into a relative motion constraint through a pre-integration technique. The principle of preintegration is shown in Figure 8.

In Figure 8, from top to bottom are the time scale line, the number of image frames generated, the number of image key frames generated, the number of IMU samples, and the IMU preintegration value.

The measurement error of the system is mainly affected by bias random walk b and white noise η, and other errors such as the Markov process are ignored. Then, the measurement model of the accelerometer and gyroscope in the IMU can be expressed by the following formula:

$$\hat{\omega}^b = \omega^b(t) + b_\omega + \eta_\omega \frac{1}{2},$$
$$\hat{a}^b = q_b^{w^T}\left(a^w - \mathbf{g}^w\right) + b_a + \eta_a, \tag{19}$$

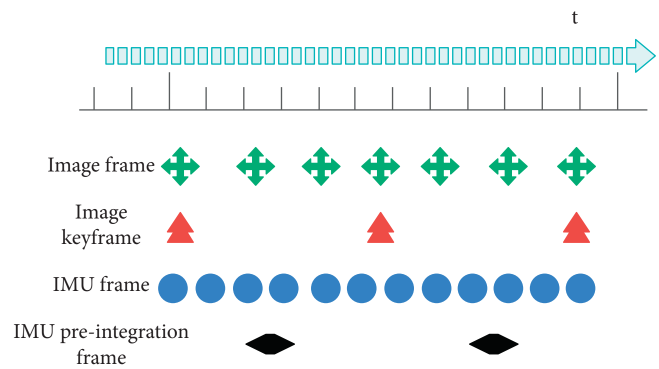

Figure 8: Principle of preintegration.

where $\hat{\omega}^b, \hat{a}^b(t), \omega^b(t)$, and $a^w(t)$ represent the measured value and real value of angular velocity and acceleration, respectively; $b_\omega, b_a, \eta_\omega$, and η_a represent the random walk noise and measurement white noise of angular velocity and acceleration, respectively; and $q_b^{w^T}$ is the rotation matrix transformed from the world coordinate system to the IMU coordinate system.

White noise obeys a Gaussian distribution, that is, $\eta_a \sim N(0, \sigma_a^2), \eta_\omega \sim N(0, \sigma_\omega^2)$. The derivative of random walk noise also obeys the Gaussian distribution, that is, $\eta_{b_a} \sim N(0, \sigma_{b_a}^2), \eta_{b_\omega} \sim N(0, \sigma_{b_\omega}^2)$.

The differential kinematic formulas for P, V, Q (representing the position, velocity, and rotation expressed in quaternions, respectively) versus time can be written as follows:

$$\dot{p}_{b_t}^w = v_t^w,$$
$$\dot{v}_t^w = a_t^w,$$
$$\dot{q}_{b_t}^w = q_{b_t}^w \otimes \begin{bmatrix} 0 \\ \frac{1}{2}\omega^{b_t} \end{bmatrix}, \tag{20}$$

where $\otimes$ represents quaternion multiplication.

Through the above derivative relationship, the position, velocity, and rotation at time $k+1$ can be obtained from the position, velocity, and rotation at time k and by integrating the measured values of the IMU over time Δt_k. The continuous integration formula for PVQ is as follows:

$$p_{b_{k+1}}^w = p_{b_k}^w + v_{b_k}^w \Delta t_k + \iint_{t\in[k,k+1]} \left[R_t^w\left(\hat{a}_t - b_{a_t}\right) - g^w\right] dt^2,$$
$$v_{b_{k+1}}^w = v_{b_k}^w + \int_{t\in[k,k+1]} \left[R_t^w\left(\hat{a}_t - b_{a_t}\right) - g^w\right] dt,$$
$$q_{b_{k+1}}^w = q_{b_k}^w \otimes \int_{t\in[k,k+1]1/2} \Omega\left(\hat{\omega}_t - b_{w_t}\right) q_t^{b_k} dt, \tag{21}$$

where $\hat{a}_t$ and $\hat{\omega}_t$ represent the acceleration and angular velocity measured in the IMU coordinate system, respectively. Δt_k represents the time difference from the kth frame to the $k+1$ frame. R_t^w represents the rotation matrix from the world coordinate system to the IMU coordinate system. Because the measured $\hat{a}_t$ and $\hat{\omega}_t$ belong to the IMU coordinate system, in order to transform the IMU measured value to the world coordinate system, the rotation matrix needs to be left-multiplied. $\Omega(\omega)$ means quaternion right multiplication; ω_x means antisymmetric matrix in quaternion multiplication (ω means the imaginary part value of quaternion). We assume that the quaternion is $q = [\,x \;\; y \;\; z \;\; s\,] = [\,\omega \;\; s\,]$; then we have

$$\begin{aligned}\Omega(\omega) &= \begin{bmatrix} -\omega_\times & \omega \\ -\omega^T & 0 \end{bmatrix},\\ \omega_\times &= \begin{bmatrix} 0 & \omega_z & \omega_y \\ \omega_z & 0 & -\omega_x \\ -\omega_y & \omega_x & 0 \end{bmatrix}.\end{aligned} \tag{22}$$

By observing the continuous integral formula of PVQ, it can be seen that the current state is recursively obtained from the state of the previous time, and the estimated value is constantly changing. This will cause the IMU measurements to be repropagated, causing the velocity and rotation to be reintegrated after each nonlinear optimization iteration, resulting in a higher computational cost. Therefore, the optimization variables are separated from the IMU preintegration terms of the two key frames, and the rotation matrix $R_w^{b_k}$ of the world coordinate system to the IMU coordinate system can be obtained by simultaneously left-multiplying the left and right sides of the continuous integration formula of PVQ:

$$\begin{aligned}R_w^{b_k} p_{b_{k+1}}^w &= R_w^{b_k}\left(p_{b_k}^w + v_{b_k}^w \Delta t_k - \frac{1}{2} g^w \Delta t_k^2\right) + \alpha_{b_{k+1}}^{b_k},\\ R_w^{b_k} v_{b_{k+1}}^w &= R_w^{b_k}\left(v_{b_k}^w - g^w\right) + \beta_{b_{k+1}}^{b_k},\\ q_w^{b_k} \otimes q_{b_{k+1}}^w &= \gamma_{b_{k+1}}^{b_k}.\end{aligned} \tag{23}$$

The image frames b_k and b_{k+1} of two consecutive moments are given, and the linear acceleration and angular velocity are preintegrated in the local coordinate system b_k to obtain

$$\begin{aligned}\alpha_{b_{k+1}}^{b_k} &= \int\int_{t\in[k,k+1]} R_t^{b_k}\left(\hat{a}_t - b_{a_t}\right) \mathrm{d}t^2,\\ \beta_{b_{k+1}}^{b_k} &= \int_{t\in[k,k+1]} \left[R_t^{b_k}\left(\hat{a}_t - b_{a_t}\right)\right] \mathrm{d}t,\\ \gamma_{b_{k+1}}^{b_k} &= \int_{t\in[k,k+1]2} (1/2)\Omega\left(\hat{\omega}_t - b_{\omega_t}\right)\gamma_t^{b_k} \mathrm{d}t,\end{aligned} \tag{24}$$

where $\alpha_{b_{k+1}}^{b_k}, \beta_{b_{k+1}}^{b_k}, \gamma_{b_{k+1}}^{b_k}$ represent the relative pose, velocity, and rotation constraints, respectively, and are also the relative motion of b_{k+1} to b_k. It can be seen that they are only related to $\hat{a}_t$ and $\hat{\omega}_t$ in b_k and b_{k+1}, and they have nothing to do with the initial position and velocity of coordinate system b_k.

Therefore, the preintegration formula is rediscussed, in terms of $\alpha_{b_{k+1}}^{b_k}$; it is related to $\hat{a}_t$ and $\hat{\omega}_t$ of the IMU; and $\hat{a}_t$ and $\hat{\omega}_t$ are also variables that need to be optimized. When the bias change is small, $\alpha_{b_{k+1}}^{b_k}, \beta_{b_{k+1}}^{b_k}, \gamma_{b_{k+1}}^{b_k}$ are adjusted according to their first-order approximations to the bias.

$$\begin{aligned}\alpha_{b_{k+1}}^{b_k} &\approx \hat{\alpha}_{b_{k+1}}^{b_k} + J_{b_a}^{\alpha}\delta b_a + J_{b_\omega}^{\alpha}\delta b_\omega,\\ \beta_{b_{k+1}}^{b_k} &\approx \hat{\beta}_{b_{k+1}}^{b_k} + J_{b_a}^{\beta}\delta b_a + J_{b_\omega}^{\beta}\delta b_\omega,\\ \gamma_{b_{k+1}}^{b_k} &\approx \gamma_{b_{k+1}}^{b_k} \otimes \begin{bmatrix} 0 \\ \\ \dfrac{1}{2}J_{b_a}^{\gamma}\delta b_\omega \end{bmatrix},\end{aligned} \tag{25}$$

where $J_{b_a}^{\alpha}$ and $J_{b_\omega}^{\alpha}$ are the block matrices in $J_{b_{k+1}}^{\alpha}$ and $J_{b_a}^{\beta}$ and $J_{b_\omega}^{\beta}$ are the block matrices in $J_{b_{k+1}}^{\beta}$.

There are errors in the integral values of the IMU at different times, and the errors at time t are mainly related to the measured values of $\alpha_t^{b_k}, \beta_t^{b_k}, \theta_t^{b_k}, b_{a_t}$, and b_{ω_t} at time t. The following definition is given to represent the error vector:

$$\delta z_t^{b_k} = \begin{bmatrix} \delta\alpha_t^{b_k} \\ \delta\beta_t^{b_k} \\ \delta\theta_t^{b_k} \\ \delta b_{a_t} \\ \delta b_{\omega_t} \end{bmatrix}. \tag{26}$$

The derivation is based on the derivative of the error term kinetic formula. First, two concepts are introduced: true and nominal, where true represents the real measurement value containing noise and nominal represents the theoretical value without noise, and δ represents the measurement error; there are

$$\begin{aligned}\delta\dot{\alpha} &= \dot{\alpha}_{\text{true}} - \dot{\alpha}_{\text{nominal}},\\ \delta\dot{\beta} &= \dot{\beta}_{\text{true}} - \dot{\beta}_{\text{nominal}}.\end{aligned} \tag{27}$$

Among them, there are:

$$\begin{aligned}\dot{\beta}_{\text{true}} &= R_t^{b_k}\left[\hat{a}_t - \eta_a - b_{a_t} - \delta b_{a_t} - \left[\hat{a}_t - b_{a_t\times}\delta\theta\right],\right.\\ \dot{\beta}_{\text{nominal}} &= R_t^{b_k}\left(\hat{a}_t - b_{a_t}\right).\end{aligned} \tag{28}$$

Combining the above formulas, we can obtain

$$\delta\dot{\beta} = -R_t^{b_k}\hat{a}_t - b_{a_t\times}\delta\theta - R_t^{b_k}\delta b_{a_t} - R_t^{b_k}\eta_a. \tag{29}$$

The derivation of $\delta\dot{\theta}$ is as follows, and according to the formula in the literature, it can be known that

$$q_{\text{true}} = q_{\text{nominal}} \otimes \delta q. \tag{30}$$

In this paper, according to the noise model and bias, we can get

$$\delta\dot{\theta} \approx -\hat{\omega}_t - b_{\omega_t\times}\delta\theta - \eta_\omega - \delta b_{\omega_t}. \tag{31}$$

In summary, the derivative of the IMU measurement error term at time t can be as follows:

$$\begin{bmatrix} \delta\dot{\alpha}_t^{b_k} \\ \delta\dot{\beta}_t^{b_k} \\ \delta\dot{\theta}_t^{b_k} \\ \delta\dot{b}_{a_t} \\ \delta\dot{b}_{\omega_t} \end{bmatrix} = \begin{bmatrix} 0 & I & 0 & 0 & 0 \\ 0 & 0 & -R_t^{b_k}\widehat{a}_t - b_{a_t\times} & -R_t^{b_k} & 0 \\ 0 & 0 & -\widehat{\omega}_t - b_{\omega_t\times} & 0 & -I \\ 0 & 0 & 0 & 0 & 0 \\ 0 & 0 & 0 & 0 & 0 \end{bmatrix} \begin{bmatrix} \delta\alpha_t^{b_k} \\ \delta\beta_t^{b_k} \\ \delta\theta_t^{b_k} \\ \delta b_{a_t} \\ \delta b_{\omega_t} \end{bmatrix} + c \begin{bmatrix} \eta_a \\ \eta_\omega \\ \eta_{b_a} \\ \eta_{b_\omega} \end{bmatrix}. \tag{32}$$

We set $F_t = \begin{bmatrix} 0 & I & 0 & 0 & 0 \\ 0 & 0 & -R_t^{b_k}\widehat{a}_t - b_{a_t\times} & -R_t^{b_k} & 0 \\ 0 & 0 & -\widehat{\omega}_t - b_{\omega_t\times} & 0 & -I \\ 0 & 0 & 0 & 0 & 0 \\ 0 & 0 & 0 & 0 & 0 \end{bmatrix}, G_t = \begin{bmatrix} 0 & 0 & 0 & 0 \\ -R_t^{b_k} & 0 & 0 & 0 \\ 0 & I & 0 & 0 \\ 0 & 0 & I & 0 \\ 0 & 0 & 0 & I \end{bmatrix}$. The above formula can be simplified to

$$\delta\dot{z}_t^{b_k} = F_t \delta z_t^{b_k} + G_t n_t. \tag{33}$$

According to the definition of the derivative, the prediction formula of the mean is as follows:

$$\begin{aligned} \delta\dot{z}_t^{b_k} &= \lim_{\delta_t \longrightarrow 0} \frac{\delta z_{t+\delta t}^{b_k} - \delta z_t^{b_k}}{\delta_t}, \\ \delta z_{t+\delta_t}^{b_k} &= (1 + F_t\delta_t)\delta z_t^{b_k} + (G_t\delta_t)n_t. \end{aligned} \tag{34}$$

According to the error value at the current moment, the mean and covariance at the next moment can be predicted. The prediction formula for covariance is as follows:

$$P_{t+\delta t}^{b_k} = (1 + F_t\delta_t)P_t^{b_k}(1 + F_t)^T + (G_t\delta_t)Q(G_t\delta_t)^T, \tag{35}$$

where $P_t^{b_k}$ represents the initial value of the iteration and its value is zero and Q represents the diagonal covariance matrix of the noise term as follows:

According to formula (35), the iterative formula of the error term Jacobian can be obtained as follows:

$$J_{t+\delta t} = (1 + F_t)J_t, \tag{36}$$

where the iterative initial value of the Jacobian matrix J_t is I.

2.5. Sliding Window Initialization. When the camera extrinsic parameter matrix $(\overline{p}_{b_k}^{v}, \overline{p}_{c_k}^{v})$ is known, the pose obtained by the initialization of the monocular camera is transformed from the visual coordinate system to the IMU coordinate system to obtain the following formula:

$$\begin{aligned} q_{b_k}^{v} &= q_{c_k}^{v} \otimes q_b^{v}, \\ s\overline{p}_{b_k}^{v} + q_{c_k}^{v} p_b^{c} &= s\overline{p}_{c_k}^{v}, \end{aligned} \tag{37}$$

where s is the translation factor obtained by visual initialization, which has no real information.

The pure visual initialization method lacks absolute scale information. Therefore, the value estimated by the visual SFM is aligned with the IMU after preintegration to estimate the true scale. Visual-inertial alignment initialization is mainly to solve the following problems, including the initialization of gyroscope bias, the initialization of velocity, gravitational acceleration, and scale.

The first is to initialize the gyroscope. The gyroscope bias can be obtained from two consecutive key frames with known orientations, considering two consecutive frames b_k and b_{k+1} in the sliding window, and q_{bk}^{v} and $q_{b_{k+1}}^{v}$ represent the rotations obtained from the pure visual sliding window optimization, respectively. Linearize the IMU preintegration term for the gyroscope bias and minimize the following function:

$$\min_{\delta b_w} \sum_{k \in \mathscr{B}} \left\| q_{b_{k+1}}^{v-1} \otimes q_{b_k}^{v} \otimes \gamma_{b_{k+1}}^{b_k} \right\|^2. \tag{38}$$

Among them, there are:

$$\gamma_{b_{k+1}}^{b_k} \approx \widehat{\gamma}_{b_{k+1}}^{b_k} \otimes \begin{bmatrix} J_{b_w}^{\gamma} & 1 \\ & \delta b_w \end{bmatrix}. \tag{39}$$

In formula (42), $\mathscr{B}$ represents all the frames in the window, and the product of the two quaternions indicates that the camera rotates from the kth frame to the $k+1$th frame, and the gyroscope rotates from the $k+1$th frame to the kth frame, and the optimized objective function is

$$q_{b_{k+1}}^{v-1} \otimes q_{b_k}^{v} \otimes \gamma_{b_{k+1}}^{b_k} = \begin{bmatrix} 1 \\ 0 \end{bmatrix}. \tag{40}$$

The algorithm takes $\widehat{\gamma}$ into the formula and multiplies the inverse moment ordering of the relative constraints obtained from the preintegration to the left on both sides of formula (40) and obtains by Cholesky decomposition (multiplying the transpose of $J_{b_w}^{\gamma}$ on both sides of the formula):

$$J_{b_w}^{\gamma T} J_{b_w}^{\gamma} \delta b_w = 2J_{b_w}^{\gamma T} 2\left(\widehat{\gamma}_{b_{k+1}}^{b_k-1} \otimes q_{b_k}^{v} \otimes q_{b_{k+1}}^{v-1}\right)_{vec}. \tag{41}$$

In this way, the initial calibration value of the gyroscope bias b_w can be estimated, and then the IMU preintegration terms $\widehat{\alpha}_{b_{k+1}}^{b_k}, \widehat{\beta}_{b_{k+1}}^{b_k}, \widehat{\gamma}_{b_{k+1}}^{b_k}$ are corrected with the new gyroscope bias.

The second is the initialization of velocity, gravitational acceleration, and scale. The initialized state vector is as follows:

$$\chi_I = \left[v_{b_0}^{v}, v_{b_1}^{v}, \ldots v_{b_n}^{v}, \mathbf{g}^{v}, s\right], \tag{42}$$

where the state vector $v_{b_k}^{v}$ represents the speed of the visual coordinate system of the kth frame image, $\mathbf{g}^{v}$ represents the gravity vector in the visual coordinate system, and s is the estimated scale parameter. To sum up, the dimension of χ_I is $3(n+1)+3+1$. The constraint relationship between the scale parameter and the speed of the visual SFM is as follows:

$$\widehat{z}_{b_{k+1}}^{b_k} = \begin{bmatrix} \widehat{\alpha}_{b_{k+1}}^{b_k} \\ \\ \widehat{\beta}_{b_{k+1}}^{b_k} \end{bmatrix} = \mathbf{H}_{b_{k+1}}^{b_k}\chi_I + \mathbf{n}_{b_{k+1}}^{b_k} \approx ,$$

$$\begin{bmatrix} -q_v^{b_k}\Delta t_k & 0 & \frac{1}{2}q_v^{b_k}\Delta t^2 & q_v^{b_k}\left(\overline{p}_{b_{k+1}}^v - \overline{p}_{b_k}^v\right) \\ \\ -q_v^{b_k} & q_v^{b_k} & q_v^{b_k}\Delta t_k & 0 \end{bmatrix} \begin{bmatrix} v_{b_k}^v \\ v_{v_{k+1}}^{g^v} \\ g^v \end{bmatrix}, \tag{43}$$

where $q_{b_k}^V, q_{b_k}^V, q_{b_k}^V$ are all obtained from visual SFM. $q_V^{b_k}$ and $q_{b_k}^V$ are mutually inverse matrices. The following linear least squares problem is constructed to complete the initialization of velocity, gravitational acceleration, and scale:

$$\min_{\chi_I} \sum_{k\in\mathcal{B}} \left\| \widehat{z}_{b_{k+1}}^{b_k} - \mathbf{H}_{b_{k+1}}^{b_k}\chi_I \right\|^2. \tag{44}$$

2.6. Monocular Visual Inertial Coupling Nonlinear Optimization. When coupling the visual constraint value and the IMU constraint value, the data of the inertial sensor should be introduced first, and the constraint value of the IMU on the state should be added to the optimized state vector. Then, nonlinear optimization is performed within a sliding window, and all state vectors of the sliding window are as follows:

$$\begin{aligned} \chi &= \left[\mathbf{x}_0, \mathbf{x}_1, \ldots \mathbf{x}_n, \mathbf{x}_c^b, \lambda_0, \lambda_1, \ldots \lambda_m\right], \\ \mathbf{x}_k &= \left[\mathbf{p}_{b_k}^w, \mathbf{v}_{b_k}^w, \mathbf{q}_{b_k}^w, \mathbf{b}_a, \mathbf{b}_g\right], k\epsilon[0,n], \\ \mathbf{x}_c^b &= \left[\mathbf{p}_c^b, \mathbf{q}_c^b\right], \end{aligned} \tag{45}$$

where $\mathbf{x}_k$ represents the state of the IMU when the kth image is captured. There are $n+1$ states in the sliding window, and each state contains the position, velocity, and rotation in the world coordinate system, and the IMU offsets in the IMU coordinate system. λ_m represents the inverse depth information of the mth 3D point, and $\mathbf{x}_c^b$ represents the external parameter from the camera to the IMU. The objective function is

$$\begin{aligned} \min_\chi \Bigg\{ &\left\| r_p - \mathbf{H}_p\chi \right\|^2 + \sum_{k\in\mathcal{B}} \left\| r_{\mathcal{B}}\left(\widehat{\mathbf{z}}_{b_{k+1}}^{b_k}, \chi\right) \right\|_{\mathbf{P}_{b_{k+1}}^{b_k}}^2 \\ &+ \sum_{(l,j)\acute{o}C} \rho\left(\left\| r_C\left(\widehat{z}_l^{c_j}\right) \right\|_{\mathbf{P}_l}^2 c_j \right) \Bigg\}, \end{aligned} \tag{46}$$

where $\mathbf{H}_p$ is the Huber norm, which is defined as follows:

$$\rho(s) = \begin{cases} 1, s \geq 1, \\ 2\sqrt{s} - 1, s < 1. \end{cases} \tag{47}$$

In formula (52), $\|\cdot\|_P$ represents the Mahalanobis distance weighted by the covariance matrix $\mathbf{P}$, and $\{r_p, \mathbf{H}_p\}$, $r_B(\widehat{z}_{b_{k+1}}^{b_k}, X)$, and $r_C(\widehat{z}_l^c, X)$ represent the marginalized prior information, the IMU measurement residual, and the visual reprojection error, respectively. $\mathcal{B}$ is the set of all IMU measurement frames, and $\mathcal{C}$ is the set of visual features in the sliding window.

According to the Gauss–Newton method, the incremental method can be used to calculate the minimum value of the Gaussian objective function, as follows:

$$\begin{aligned} &\min_{\delta X} \left\| r_{\mathcal{B}}\left(\widehat{\mathbf{z}}_{b_{k+1}}^{b_k}, \chi + \Delta X\right) \right\|_{\mathbf{P}_{b_{k+1}}^{b_k}}^2 \\ &= \min_{\delta X} \left\| r_{\mathcal{B}}\left(\widehat{\mathbf{z}}_{b_{k+1}}^{b_k}, \chi\right) + J_{b_{k+1}}^{b_k}\Delta X \right\|_{\mathbf{P}_{b_{k+1}}^{b_k}}^2, \end{aligned} \tag{48}$$

where $J_{b_{k+1}}^{b_k}$ is the Jacobian matrix of the error term $r_{\mathcal{B}}$ with respect to all state vectors χ.

The algorithm differentiates the above formula from ΔX and then sets its derivative to 0, and the formula for the increment ΔX can be calculated as follows:

$$J_{b_{k+1}}^{b_k T} P_{b_{k+1}}^{b_k -1} J_{b_{k+1}}^{b_k} \Delta X = -J_{b_{k+1}}^{b_k T} P_{b_{k+1}}^{b_k -1} J_{b_{k+1}}^{b_k} r_{\mathcal{B}}. \tag{49}$$

The overall incremental equation of the objective function is as follows:

$$\begin{aligned} &\left(\mathbf{H}_p + \sum J_{b_{k+1}}^{b_k T} P_{b_{k+1}}^{b_k -1} J_{b_{k+1}}^{b_k} + \sum J_l^{c_j^T} P_l^{c_j -1} J_l^{c_j}\right)\Delta X \\ &= b_p + \sum J_{b_{k+1}}^{b_k T} P_{b_{k+1}}^{b_k -1} r_{\mathcal{B}} + \sum J_l^{C_j^T} P_l^{C_j^{-1}} r_C, \end{aligned} \tag{50}$$

where $P_{b_{k+1}}^{b_k}$ represents the covariance of the IMU preintegrated noise term and $P_l^{C_j}$ represents the visually observed noise covariance. When the noise covariance $P_{b_{k+1}}^{b_k}$ of the IMU is larger, the inverse of $P_{b_{k+1}}^{b_k}$, that is, its information matrix is smaller, which means that the IMU observations are not as reliable as the visual observations. Formula (50) can be simplified to

$$\left(\Lambda_p + \Lambda_B + \Lambda_C\right)\Delta X = b_p + b_B + b_C, \tag{51}$$

where Λ_p, Λ_B, and Λ_C represent the Hessian matrix. Using the perturbation method to calculate, we can get

$$\begin{aligned} J &= \frac{\partial r}{\partial X} \\ &= \lim_{\delta X \longrightarrow 0} \frac{r(X \oplus \delta X) - r(X)}{\delta X}, \end{aligned} \tag{52}$$

where δX represents the small disturbance of the state vector instead of the incremental ΔX, $\oplus$ represents the disturbance of the state vector.

The continuous preintegration formula is derived in the IMU preintegration, and the IMU residuals are as follows:

$$r_{\mathscr{B}}\left(\widehat{z}_{b_{k+1}}^{b_k}, \chi\right) = \begin{bmatrix} \delta\alpha_{b_{k+1}}^{b_k} \\ \delta\beta_{b_{k+1}}^{b_k} \\ \delta\theta_{b_{k+1}}^{b_k} \\ \delta b_a \\ \delta b_g \end{bmatrix} = \begin{bmatrix} R_w^{b_k}\left(p_{b_{k+1}}^w - p_{b_k}^w - v_{b_k}^w \Delta t_k + \frac{1}{2} g^w \Delta t_k^2\right) - \alpha_{b_{k+1}}^{b_k} \\ R_w^{b_k}\left(v_{b_{k+1}}^w \Delta t_k - v_{b_k}^w \Delta t_k + g^w \Delta t_k\right) - \beta_{b_{k+1}}^{b_k} \\ 2\left[\gamma_{b_{k+1}}^{b_k} \otimes q_{b_k}^w \otimes q_{b_{k+1}}^w\right]_{xyz} \\ b_{a_{b_{k+1}}} - b_{a_{b_k}} \\ b_{\omega_{b_{k+1}}} - b_{\omega_{b_k}} \end{bmatrix}. \tag{53}$$

According to the above formula, it can be seen that the optimization variables of the IMU residual mainly include the position, rotation, speed, and inertia bias at the i and j times:

$$\begin{gathered} \left[p_{b_k}^w, q_{b_k}^w\right], \left[v_{b_k}^w, b_{a_k}, b_{\omega_k}\right], \\ \left[p_{b_{k+1}}^w, q_{b_{k+1}}^w\right], \left[v_{b_{k+1}}^w, b_{a_{k+1}}, b_{\omega_{k+1}}\right]. \end{gathered} \tag{54}$$

To calculate the Jacobian matrix, perturbation is added to each optimization variable to obtain

$$\begin{gathered} \left[\delta p_{b_k}^w, \delta\theta_{b_k}^w\right], \left[\delta v_{b_k}^w, \delta b_{a_k}, \delta b_{\omega_k}\right], \\ \left[\delta p_{b_{k+1}}^w, \delta\theta_{b_{k+1}}^w\right], \left[\delta v_{b_{k+1}}^w, \delta b_{a_{k+1}}, \delta b_{\omega_{k+1}}\right]. \end{gathered} \tag{55}$$

Taking the partial derivatives for the above disturbance variables, respectively, we can get

$$\begin{aligned} J[0]^{15\times 7} &= \left[\frac{\partial r_B}{\delta p_{b_k}^w}, \frac{\partial r_B}{\delta\theta_{b_k}^w}\right], \\ J[1]^{15\times 7} &= \left[\frac{\partial r_B}{\delta v_{b_k}^w}, \frac{\partial r_B}{\delta b_{a_k}}, \frac{\partial r_B}{\delta b_{\omega_k}}\right], \\ J[2]^{15\times 7} &= \left[\frac{\partial r_B}{\delta p_{b_{k+1}}^w}, \frac{\partial r_B}{\delta\theta_{b_{k+1}}^w}\right], \\ J[3]^{15\times 7} &= \left[\frac{\partial r_B}{\delta v_{b_{k+1}}^W}, \frac{\partial r_B}{\delta b_{a_{k+1}}}, \frac{\partial r_B}{\delta b_{\omega_{k+1}}}\right]. \end{aligned} \tag{56}$$

The visual residual is a reprojection error, which represents the difference between the estimated value and the observed value of the feature point in the normalized camera coordinate system. The small receiver camera used in this paper belongs to the fisheye camera model and belongs to the fisheye with a large viewing angle, so its projection on the unit sphere needs to be considered, as shown in Figure 9.

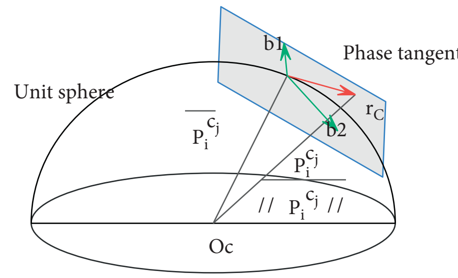

Figure 9: Unit spherical projection model.

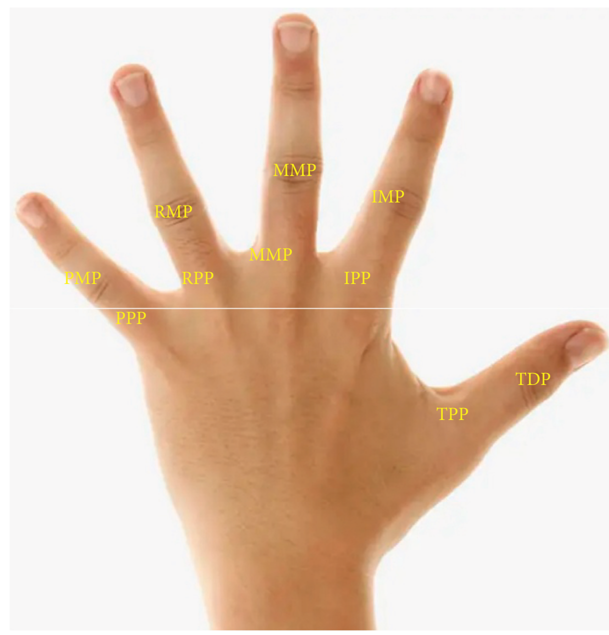

Figure 10: Demarcation boundaries of hand movements.

Through the unit spherical projection model illustrated in the figure above, the value of the visual residual is decomposed into two directions. The final visual residual model looks like this:

$$\begin{aligned} r_c\left(\widehat{z}_l^{c_j}, \chi\right) &= \left[b_1, b_2\right]^T \cdot \left(\widehat{p}_l^{c_j} - \frac{p_l^{c_j}}{\left\|p_l^{c_j}\right\|}\right), \\ \widehat{p}_l^{c_j} &= \pi_c^{-1}\left(\begin{bmatrix} \widehat{u}_l^{c_j} \\ \widehat{v}_l^{c_j} \end{bmatrix}\right), \\ p_l^{c_j} &= R_c^b\left\{R_w^{b_j}\left[R_{b_i}^w\left(R_c^b \frac{1}{\lambda_l} \overline{P}_l^{c_i} + p_c^b\right) + p_{b_i}^w - p_{b_j}^w\right] - p_c^b\right\}, \end{aligned} \tag{57}$$

where $\widehat{\overline{p}}_l^{c_j}$ and $p_l^{c_j}$ represent the estimated and observed coordinates of the landmark point 1 in the j-th frame image under the normalized camera coordinate system,

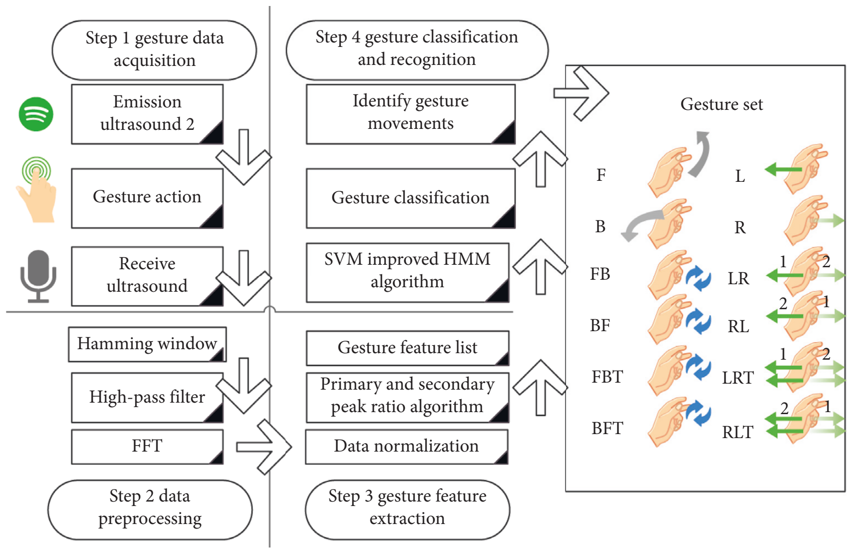

Figure 11: Overall system framework.

Table 1: Gesture recognition effect of the system.

Number	Gesture recognition	Number	Gesture recognition	Number	Gesture recognition
1	86.095	13	87.363	25	86.633
2	88.782	14	89.124	26	90.414
3	90.695	15	90.055	27	86.697
4	86.325	16	89.968	28	86.916
5	86.705	17	88.482	29	89.003
6	89.557	18	91.278	30	88.446
7	86.623	19	89.215	31	89.911
8	91.281	20	86.272	32	90.202
9	88.050	21	91.253	33	89.507
10	87.621	22	86.770	34	88.130
11	88.498	23	86.843	35	91.326
12	86.304	24	90.614	36	86.846

Table 2: The application effect of the method proposed in this paper in the e-sports training system.

Number	Training effect	Number	Training effect	Number	Training effect
1	82.685	13	82.234	25	79.365
2	80.315	14	78.537	26	81.356
3	79.700	15	81.913	27	78.790
4	78.179	16	82.938	28	79.700
5	82.942	17	78.167	29	78.194
6	80.821	18	78.250	30	78.253
7	81.176	19	81.512	31	80.133
8	78.183	20	80.076	32	82.668
9	82.636	21	81.925	33	83.747
10	81.613	22	82.857	34	82.354
11	80.514	23	82.951	35	78.416
12	80.913	24	79.066	36	83.128

respectively. The optimization variables of the visual residual are as follows:

$$\left[p_{b_i}^{w}, q_{b_i}^{w}\right], \left[p_{b_j}^{w}, q_{b_j}^{w}\right], \left[p_c^{b}, q_c^{b}\right], \lambda_l, \tag{58}$$

where λ_l represents the inverse depth value when the landmark point 1 is first observed by the j-th image. The inverse depth is used as the optimization variable because the inverse depth satisfies the Gaussian distribution, and it can reduce the parameter variables in the actual optimization process. According to the above formula, by adding disturbance to each optimization variable, the following Jacobian is obtained:

$$J[0]^{3\times 7} = \left[\frac{\partial r_C}{\partial p_{b_i}^{w}}, \frac{\partial r_C}{\partial q_{b_i}^{w}}\right],$$

$$J[1]^{3\times 7} = \left[\frac{\partial r_C}{\partial p_{b_j}^{w}}, \frac{\partial r_C}{\partial q_{b_j}^{w}}\right], \tag{59}$$

$$J[2]^{3\times 7} = \left[\frac{\partial r_C}{\partial p_{c}^{b}}, \frac{\partial r_C}{\partial q_{c}^{b}}\right],$$

$$J[3]^{3\times 1} = \frac{\partial r_C}{\partial \lambda_l}. \tag{60}$$

3. E-Sports Training System Based on Intelligent Gesture Recognition

This paper combines the finger joints and the sensor in the data glove to demarcate the movement of the finger joints. This paper mainly considers the distal phalanx of the thumb (TDP) and the proximal joint proximal phalanx of the thumb (TPP) of the thumb as shown in Figure 10 and the changes in the intermediate joints middle phalanges (MP) and proximal phalanges (PP) of the remaining four fingers.

This paper combines the algorithm part of the second part to construct the e-sports training system, and the overall framework of the system is shown in Figure 11.

The simulation of the system proposed in this paper is carried out through the MATLAB platform, and the gesture recognition effect of the system and the application effect in the e-sports training system are evaluated, and the obtained results are shown in Tables 1 and 2.

It can be seen from the above research that the electronic economic training system based on intelligent gesture recognition proposed in this paper has certain effects.

4. Conclusion

As emerging sports, e-sports are mainly participated by the younger generation, which has the characteristics of younger and younger age. E-sports can exercise people's thinking ability, psychological pressure resistance, unity and cooperation, hand-eye coordination, and so on. Moreover, in the process of participating in e-sports, it can also make the younger generation have the awareness of abiding by the rules, cultivate the participants to have a fair and open, never admit defeat, pursue a stronger competitive spirit, and have a positive impact on the participants' lives. This paper combines the intelligent gesture recognition technology and the construction of the performance e-sports training system and judges the training effect of the players through the player gesture recognition. The research shows that the electronic economic training system based on intelligent gesture recognition proposed in this paper has certain effects.

Data Availability

The labeled data set used to support the findings of this study is available from the corresponding author upon request.

Conflicts of Interest

The authors declare that there are no conflicts of interest.

Acknowledgments

This study was sponsored by Shandong Sport University.

References

[1] D. J. D. Q. Martins, L. C. L. Moraes, and W. M. Júnior, "COVID-19 impacts on school sports events: an alternative through E-sports," *Managing Sport and Leisure*, vol. 27, no. 1-2, pp. 45–49, 2022.

[2] M. Yasumoto and T. Teraoka, "Physical e-Sports in VAIR Field system," in *SIGGRAPH Asia 2019 XR*, pp. 31–33, ACM, New York, NY, U.S.A, 2019.

[3] U. Hussain, B. Yu, G. B. Cunningham, and G. Bennett, ""I can be who I Am when I play tekken 7": E-sports women participants from the islamic republic of Pakistan," *Games and Culture*, vol. 16, no. 8, pp. 978–1000, 2021.

[4] B. B. Romanenko, C. C. Pyatisotska, B. C. Ashanin, and A. M. Yefremenko, "Analysis of sensorimotor abilities and nervous system properties of players of different e-sports disciplines.Scientific journal of the National Pedagogical University named after MP Drahomanov. Series 15," *Scientific and pedagogical problems of physical culture (physical culture and sports)*, vol. 11, no. 143, pp. 125–131, 2021.

[5] W. Lu, G. Xu, X. Gong, and Q. Chen, "On the interdisciplinary education among undergraduate students majoring in E-sports," in *Proceedings of the 2021 International Conference on Culture-oriented Science & Technology (ICCST)*, pp. 63–66, IEEE, Beijing, China, November 2021.

[6] M. Jasny, "Doping in e-sports. An empirical exploration and search for sociological interpretations," *Acta Universitatis Lodziensis. Folia Sociologica*, vol. 26, no. 75, pp. 85–99, 2020.

[7] S. Akkaya, B. S. Gezer, and M. Kapidere, "A multi-directional assessment related to E-sports as A new game experience field and socialising tool," *Atatürk Üniversitesi Sosyal Bilimler Enstitüsü Dergisi*, vol. 25, no. 3, pp. 968–988, 2021.

[8] Д. Чалык, "E-sports broadcasts as a new format in journalism," *Al-Farabi kazakh national university*, vol. 52, no. 2, pp. 202–209, 2019.

[9] R. Ardianto, T. Rivanie, Y. Alkhalifi, F. S. Nugraha, and W. Gata, "Sentiment analysis on E-sports for education curriculum using naive Bayes and support vector machine," *Jurnal Ilmu Komputer dan Informasi*, vol. 13, no. 2, pp. 109–122, 2020.

[10] S. Kwag, W. J. Lee, and Y. D. Ko, "Optimal seat allocation strategy for e-sports gaming center," *International Transactions in Operational Research*, vol. 29, no. 2, pp. 783–804, 2022.

[11] M. Marelić, D. Vukušić, and D. Vukušić, "E-sports: definition and social implications," *Exercise and Quality of Life*, vol. 11, no. 2, pp. 47–54, 2019.

[12] A. Çeti̇n and M. Coşkuner, "A conceptual overview of E-sports tourism as a new trend in the tourism industry," *Turk Turizm Arastirmalari Dergisi*, vol. 3, no. 1, pp. 28–34, 2021.

[13] R. F. Marta, A. A. Prasetya, B. Laurensia, S. Stevani, and K. L. Syarnubi, "Imbalance identity in E-sports news intersectionality on covid-19 pandemic situation," *Jurnal ASPIKOM*, vol. 5, no. 2, p. 206, 2020.
[14] D. H. Shin, J. S. Kim, and C. W. Kim, "A Study on subtitle synchronization calibration to enhance hearing-impaired persons' viewing convenience of e-sports contents or game streamer contents," *Journal of Korea Game Society*, vol. 19, no. 1, pp. 73–83, 2019.
[15] J. Hwang, "Cheating in E-sports: a proposal to regulate the growing problem of E-doping," *Northwestern University Law Review*, vol. 116, no. 5, pp. 1283–1318, 2022.
[16] A. Ersin, H. C. Tezeren, N. O. Pekyavas et al., "The relationship between reaction time and gaming time in e-sports players," *Kinesiology*, vol. 54, no. 1, pp. 36–42, 2022.
[17] J. Hou, X. Yang, and E. Panek, "How about playing games as a career? The evolution of E-sports in the eyes of mainstream media and public relations," *International Journal of Sport Communication*, vol. 13, no. 1, pp. 1–21, 2020.
[18] C. Tjokrodinata, C. R. A. Bangun, F. Dinansyah, and A. R. Farmita, "Gamers with different ability and the role of EAI (E-Sports ability Indonesia)," *Jurnal Interaksi: Jurnal Ilmu Komunikasi*, vol. 6, no. 1, pp. 52–66, 2022.
[19] B. Göktaş, "Level of awareness of e-sports concept and its effect on image of sports clubs in Turkey," *Uluslararası Toplumsal Bilimler Dergisi*, vol. 3, no. 1, pp. 68–85, 2019.

Hindawi
Computational Intelligence and Neuroscience
Volume 2022, Article ID 5133543, 21 pages
https://doi.org/10.1155/2022/5133543

Research Article

PDNet: Improved YOLOv5 Nondeformable Disease Detection Network for Asphalt Pavement

Zhen Yang,[1] **Lin Li**,[1,2] **and Wenting Luo**[2]

[1]*College of Transportation and Civil Engineering, Fujian Agriculture and Forestry University, Fuzhou, Fujian 350108, China*
[2]*College of Transportation Engineering, Nanjing Tech University, Nanjing, Jiangsu 211816, China*

Correspondence should be addressed to Lin Li; 18805915371@163.com

Received 12 May 2022; Revised 4 June 2022; Accepted 6 June 2022; Published 7 July 2022

Academic Editor: Xin Ning

In the daily inspection task of the expressway, accuracy and speed are the two most important indexes to reflect the detection efficiency of nondeformation diseases of asphalt pavement. To achieve model compression, accelerated detection, and accurate identification under multiscale conditions, a lightweight algorithm (PDNet) based on improved YOLOv5 is proposed. The algorithm is improved based on the network structure of YOLOv5, and the improved network structure is called YOLO-W. Firstly, a novel cross-layer weighted cascade aggregation network (W-PAN) is proposed to replace the original YOLOv5 network. Secondly, more economical GhostC3 and ShuffleConv modules are designed to replace C3 and Conv modules in the original network model. In terms of parameter setting, CIoU is selected as the loss function of the model, and the K-Means ++ algorithm is used for anchor box clustering. Before the model training, the confrontation generation network (GAN) and Poisson migration fusion algorithm (Poisson) are used for data enhancement and the negative sample training (NST) method is used to improve the robustness of the model. Finally, Softer-NMS is used to remove the prediction box in the prediction stage. Seven common asphalt pavement disease data sets (FAFU-PD) are constructed at the same time. Compared with the original YOLOv5 algorithm, PDNet improves the scores of FAFU-PD data sets on F1-score by 10 percentage points and FPS by 77.5%.

1. Introduction

Asphalt pavements on expressways are damaged by natural disasters, such as prolonged exposure to sunlight, rain erosion, and natural weathering. And the durability of asphalt pavement will also be reduced due to factors such as pavement materials, traffic flow, construction quality, and postmaintenance levels. If these damaged roads cannot be discovered and maintained in time, the service life of the expressway will be shortened, which may induce traffic accidents [1].

At present, the detection of highway asphalt pavement diseases is mainly based on manual methods. This method has some disadvantages. For example, the detection takes a long time and requires more manpower and material resources, and the detection will cause congestion on the highway, and the safety of the detection personnel is difficult to be guaranteed. At the same time, some human factors interfere with the test results. With the continuous increase of highway mileage, manual detection methods are difficult to meet the detection requirements of large-scale highways and cannot meet the needs of highway development [2].

To further improve the service life of highways and use an accurate and efficient detection method to replace the traditional manual detection method, some researchers have conducted research on the automatic detection of pavement diseases based on visual technology, which includes image processing, machine learning, and deep learning. Image processing research includes threshold segmentation, edge detection, and regional growth. The threshold segmentation method is mainly to set the appropriate pixel threshold in the image and separate the disease from the background by using the pixel difference between the crack and the surrounding background. The edge detection method mainly realizes the edge detection through various edge detection operators. These edge detection operators include Sobel operator [3], Prewitt operator [4], and Canny operator [5]. The region growing method mainly displays the specific information inside the disease through pixel integration.

Compared with the traditional manual detection method, the image processing method has been greatly improved, but this method is easily disturbed by external factors such as road background and sunlight, the types of road diseases are complex and diverse, and the image processing method is difficult to detect various types of complex diseases [6].

In recent years, machine learning and deep learning have developed rapidly, especially in industrial applications. It has become possible to use machine learning or deep learning to build a model for pavement disease detection. Machine learning methods mainly include wavelet transform, support vector machine, and random forest methods. Among the deep learning methods, convolutional neural networks (CNNs) have made great progress in semantic segmentation and target detection tasks. From the current development status of the target detection field, the target detection methods based on deep learning are mainly divided into one-stage method and two-stage method. The two-stage method mainly includes R-CNN [7], fast-RCNN [8], and faster-RCNN [9]. The advantages of these algorithms are high recognition accuracy, but they also have the disadvantage of slow speed, so it is not suitable for engineering applications. To solve this shortcoming of the two-stage method, the researchers proposed the algorithm framework of the one-stage method. The representative works include SSD [10], YOLO series, and anchor-based RetinaNet [11], Adaptive Sample Selection (ATSS) [12], Fully Convolutional One-Stage Object Detection (FCOS) [13], and Anchor-Free Based RepPoints [14].

At present, whether it is based on traditional image processing methods or methods based on machine learning and deep learning, there are still some problems in the detection of asphalt pavement diseases: (1) based on traditional image processing methods, in terms of recognition speed, the effect is poor, and it is difficult to deal with complex engineering tasks. (2) The cost of network training and prediction using machine learning and deep learning methods is too high, and the use of feature extraction will make the network lose real-time performance and cannot meet industrial needs. (3) The engineering application scenarios are complex, and there are various types of diseases, and it is difficult to guarantee the accuracy and recall rate of disease identification. Figures 1(a) and 1(b) are schematic diagrams of the redundancy of the target frame; Figures 1(c) and 1(d) show that the model incorrectly identifies negative samples as positive samples; Figures 1(e) and 1(f) show a schematic diagram of inaccurate prediction of anchor boxes; Figures 1(g) and 1(h) show the situation that the model does not extract disease features in place. (4) There is a lack of large data sets for various types of diseases.

To meet the real-time performance and improve the accuracy and recall rate of target recognition, this study proposes a real-time, lightweight, and higher-precision target detection algorithm (PDNet) based on YOLOv5. In Section 2, this article mainly introduces the domestic and foreign research status of nondeformation disease detection of asphalt pavement, and Section 3 introduces the research methods used in this article. Section 3.1 introduces the overall architecture of the YOLO-W network proposed in this article; Section 3.2 introduces the cross-layer weighted cascade aggregation network (W-PAN); Section 3.3 introduces the improved GhostC3 module; Section 3.4 introduces the improved ShuffleConv module; Section 3.5 is mainly about the settings of network model parameters, including loss function and anchor frame settings, respectively; Section 3.6 introduces a data set of seven diseases including transverse cracks, longitudinal cracks, and repair strips collected from one province and four cities (FAFU-PD); Section 3.7 introduces a negative sample algorithm (NST) for the problem of model misidentification, which can effectively improve the recognition accuracy of the model; Section 3.8 uses an adversarial generative network (GAN) to generate a larger number of samples; Section 3.9 uses the Poisson transfer fusion algorithm, which is transplanted based on GAN to generate disease-free pictures to generate new disease samples; Section 3.10 introduces the Softer-NMS algorithm. It solves the problem that there are many false detections of diseases in dense scenes and the positioning of the prediction frame with high default confidence of NMS is not very accurate. Section 4 is the experimental part, Section 4.1 introduces the data and experimental environment used in this experiment, and Section 4.2 is the ablation experiment for each method proposed in Section 3. Section 5 analyzes the methods proposed in this article and describes the advantages of each method. Section 6 summarizes this article.

The main contributions of this article are as follows:

(1) It proposes an improved target detection network YOLO-W. First, to prevent the loss of shallow target features, a cross-layer cascaded weighted fusion structure is added to the PANet structure to transfer detailed information to the deep network, and a cross-layer weighted cascaded path aggregation network (W-PAN) is proposed to obtain richer semantic information, deepen the depth of the pyramid, correspondingly increase the detection layer of the head part, and perform detection at four scales, so that the laying interval of anchor boxes is more reasonable; finally, it reduces the feature loss caused by the upsampling process, which improves the upsampling method.

(2) Lightweight network: the GhostC3 module is used to replace the original C3 module, and the ShuffleConv module is used to replace part of the Conv module, which alleviates the problem of computational occupancy in the process of feature channel fusion and enhances the expressiveness of features.

(3) uses the K-Means ++ algorithm to redesign the size of the prior box and match it to the corresponding feature layer.

(4) The negative sample training method (NSTM) is adopted to improve the detection accuracy without

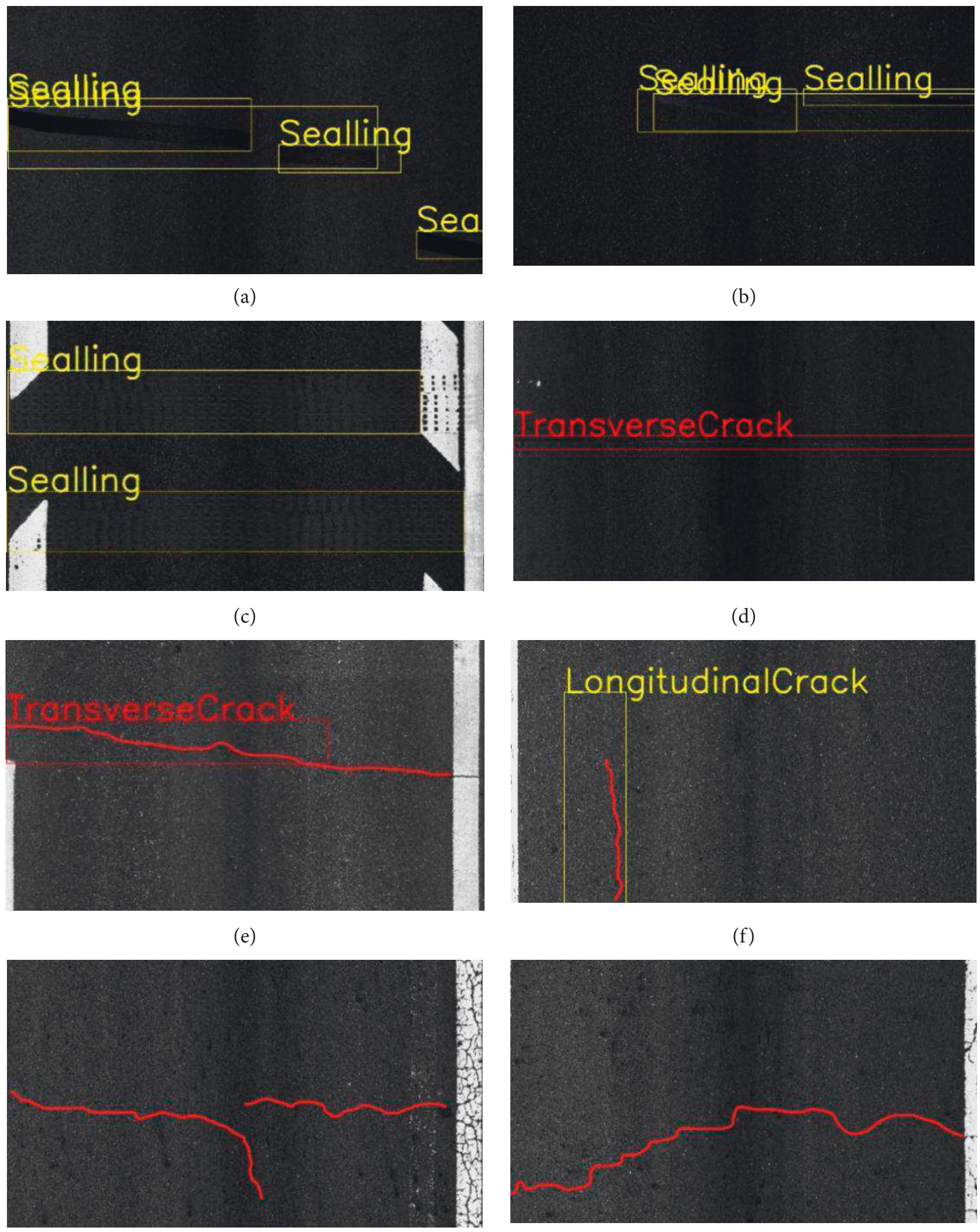

(a) (b) (c) (d) (e) (f) (g) (h)

Figure 1: Misrecognition or inaccurate recognition of deep learning models in engineering application scenarios: (a, b) target detection frame redundancy, (c, d) background is misidentified, (e, f) the target frame recognition is inaccurate, and (g, h) the disease characteristics are not obvious, and the detection is missed.

reducing the detection speed and reduce the false detection rate.

(5) uses an adversarial generative network (GAN) to generate diseases with a small number of samples.

(6) uses the Poisson transfer fusion algorithm to transfer the color of the sample generation disease to make it better match the sample and add the generated sample to the training set and the validation set.

(7) constructs 7000 data sets (FAFU-PD) including one province, four cities, and seven diseases.

2. Related Studies

2.1. Pavement Damage Detection Method Based on Image Processing and Machine Learning. In the early days, most of the pavement disease detection methods based on image processing [15–17] were based on threshold segmentation, because, in images with cracks and other diseases, the pixel values of cracks and diseases are darker than the surrounding background, and threshold segmentation is used. The contours of diseases such as cracks can be well extracted. Early researchers proposed crack detection algorithms based

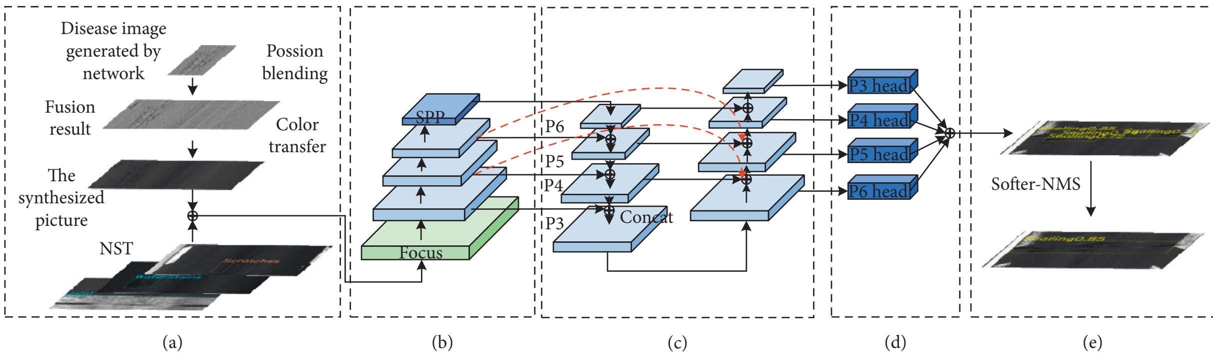

FIGURE 2: PDNet overall network framework. (a) Preprocessing side, (b) backbones, (c) necks, (d) heads, and (e) nondeformation disease detection of asphalt pavement.

on threshold segmentation from different perspectives. Oliveira and Correia [18] proposed a new framework for automatic crack detection and classification. This framework preprocesses the generated images using morphological filters to reduce pixel intensity variations. Then, dynamic thresholding was applied to identify dark pixels in the image, and a second dynamic threshold was applied to the resulting matrix of entropy blocks, which was used as a basis for identifying image blocks containing cracked pixels. Ayenu-Prah and Attoh-Okine used BEMD and Sobel edge operators for pavement crack detection. Multiple images were filtered by BEMD to remove noise, and the residual image was analyzed by Sobel edge operator [19]. Yan et al. introduced morphology into crack detection of high-grade highway pavement and proposed a new image processing method. This method reconstructs the median filter algorithm to enhance the pavement grayscale image and combines the morphological gradient operator and the morphological closure operator to extract crack edges and fill crack gaps [20]. Wei et al. proposed a pavement crack detection algorithm based on Beamlet transform [21]. Wavelet transform is also one of the common methods for pavement crack detection [22–24]. However, the above methods are very susceptible to noise interference, and it is difficult to obtain accurate detection results. Nguyen et al. proposed a new method that considers both brightness and connectivity in the segmentation step for crack detection in road surface images. Features computed along each free path can detect cracks in any form and any direction [25]. Amhaz et al. proposed a new algorithm for automatic crack detection from 2D road surface images. This algorithm, which relies on the localization of the smallest path in each image, has been intensively validated on synthetic and real images, and it provides very stable and accurate results in a variety of situations in a completely unsupervised manner [26]. Ai et al. proposed a new method to automatically detect pixel-level pavement cracks using multiscale neighborhood information and pixel intensities. Using the pixel intensity information, a probabilistic generative model (PGM) based method was developed to calculate the crack presence probability for each pixel [27]. Shi et al. introduced random structure forests to generate high-performance crack detectors that can identify arbitrarily complex cracks [28]. However, these traditional methods rely heavily on postprocessing and require a large amount of computation, which is not conducive to engineering applications.

2.2. Pavement Damage Detection Method Based on Deep Learning. In recent years, the application of deep learning methods in the field of target detection has become more and more extensive, including the identification of nondeformable diseases of asphalt pavement. Neural networks such as CNN and R-CNN have played an important role in the field of target detection. Cha et al. proposed a vision-based approach that uses a deep architecture of convolutional neural networks (CNNs) to detect cracks without computing defect features. Since CNN can learn image features automatically, the proposed method can extract features without IPT conjugation [29]. Zhang et al. used CNN convolutional neural network for image preclassification [30]. Yang et al. implemented a novel deep learning technique called a fully convolutional network (FCN) to solve the pixel-level crack identification problem [31]. Chen and Jahanshahi proposed a deep learning framework based on convolutional neural network (CNN) and a naive Bayesian data fusion scheme called NB-CNN for analyzing a single video frame for crack detection and proposed a new data fusion scheme is proposed to aggregate information to improve the overall performance and robustness of the system [32]. Park et al. proposed a CNN-based deep learning model, patch-CNN, which consists of segmentation and classification modules for crack detection [33]. Zou et al. proposed an end-to-end trainable deep convolutional neural network (DeepCrack) for automatic crack detection by learning high-level features represented by cracks [34]. These deep learning-based methods can improve the accuracy of disease identification to a certain extent, but they cannot achieve both recognition speed and accuracy and lose speed while improving the accuracy of disease identification.

3. Methodology

Figure 2 shows the overall network structure of the algorithm (PDNet) shown in this article. In the preprocessing stage, a generative adversarial network (GAN) is used to generate a small number of disease types, and then the Poisson color transfer algorithm is used to generate the generated diseases. The image is fused with the background to obtain new disease samples. Secondly, all negative samples that are prone to misidentification are labeled (NST). After processing, all training and validation sets are sent to the training network (YOLO-W). At the prediction end, the Softer-NMS algorithm is used to remove redundant boxes to obtain the final recognition result.

3.1. The Overall Architecture of the YOLO-W Network. YOLO-W is a high-performance target detection network based on YOLOv5. It adopts a cross-layer weighted cascaded path aggregation network (W-PAN) to improve the accuracy of model recognition and lightweight modules GhostC3 and ShuffleConv to reduce the complexity of the network. The network structure of YOLO-W is shown in Table 1. The changes in the backbone and neck parts of YOLO-W compared with the original YOLOv5 network model are shown in Figures 3 and 4.

Among them, "from" represents the output layer corresponding to this layer module, and "−1" represents the previous layer. "Add" represents the cross-layer weighted addition module in W-PAN, and "GhostC3" and "ShuffleConv" represent the GhostC3 module and ShuffleConv module used in YOLO-W, respectively.

3.2. Cross-Layer Weighted Cascade Aggregation Network (W-PAN). The shallow network of deep learning focuses on detailed information, such as edge features. Based on obtaining simple features, it can help the network return to the target boundary more accurately; the deep network focuses on extracting high-level semantic information and can extract more complex features, which can help the network detect the target accurately. The FPN structure uses shallow features to distinguish simple objects and deep features to distinguish complex objects, aiming to obtain more robust detection results. The FPN structure of YOLOv5 is based on PAN, which creates a bottom-up path enhancement, accelerates the flow of underlying information, and can well integrate semantic information at all levels. To further enhance the model's attention to shallow semantics, fully integrate the semantic information extracted by each layer of the FPN, and enhance the network's ability of returning to the target boundary, this study improves the FPN of YOLOv5, called W-PAN, and the specific improvement points are as follows:

(1) Add cross-layer weighted connections between input and output nodes of the same size [35]. The cross-layer cascade structure can effectively integrate the shallow details, edges, contours, and other information into the deep network and can fuse the shallow details of the target with almost no increase in the amount of calculation so that the network can be more sensitive to the target boundary. The regression is more accurate, and the intersection ratio

Table 1: YOLO-W algorithm architecture diagram.

Number	From	Parameters	Module
0	−1	3520	Focus
1	−1	10756	ShuffleConv
2	−1	10016	GhostC3
3	−1	40868	ShuffleConv
4	−1	41840	GhostC3
5	−1	159460	ShuffleConv
6	−1	173304	GhostC3
7	−1	466468	ShuffleConv
8	−1	325016	GhostC3
9	−1	925028	ShuffleConv
10	−1	656896	SPP
11	−1	575112	GhostC3
12	−1	103872	ShuffleConv
13	−1	0	Upsample
14	[−1, 8]	0	Concat
15	−1	466512	GhostC3
16	−1	52864	ShuffleConv
17	−1	0	Upsample
18	[−1, 6]	0	Concat
19	−1	208608	GhostC3
20	−1	18240	ShuffleConv
21	−1	0	Upsample
22	[−1, 4]	0	Concat
23	−1	53104	GhostC3
24	−1	75584	ShuffleConv
25	[−1, 20]	0	Concat
26	[−1, 6]	36482	Add
27	−1	143072	GhostC3
28	−1	298624	ShuffleConv
29	[−1, 6]	0	Concat
30	[−1, 8]	105730	Add
31	−1	368208	GhostC3
32	−1	669120	ShuffleConv
33	[−1, 12]	0	Concat
34	−1	695744	GhostC3
35	[23, 27, 31, 34]	96300	Detect

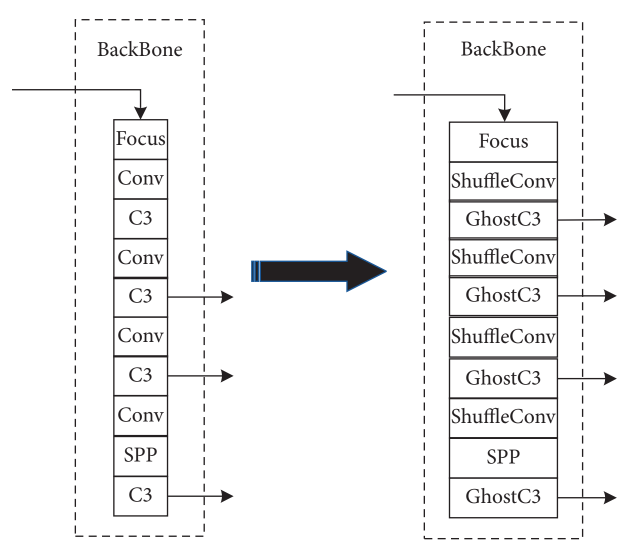

Figure 3: The improved backbone module.

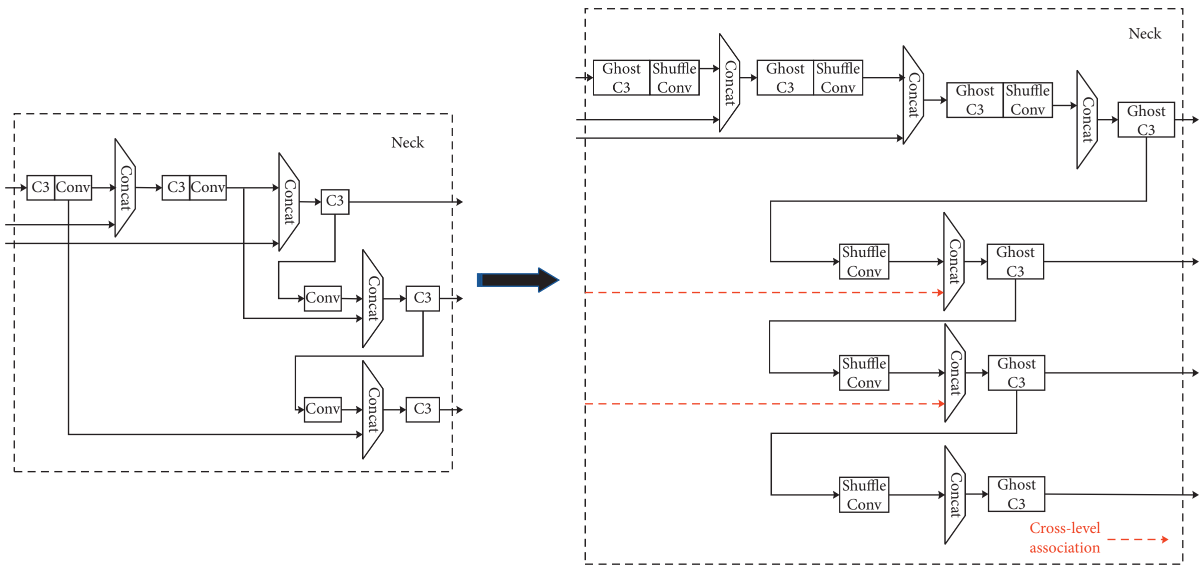

FIGURE 4: The improved neck module.

between the predicted frame and the real frame is effectively improved. At the same time, considering that the integration of shallow features will have a certain impact on deep semantic information when using cross-level concatenation, a learnable method is adopted for fusion. The two fusion methods used in this study are given as follows: in the process of feature fusion, since the information flow of the top and bottom nodes is fast and the number of convolutions experienced is small, the loss of detailed information is not much. There is complexity of the small model, so the concat operation is directly used to perform feature fusion by channel. The process is shown in Figure 5. F represents the feature map, w represents the width of the feature map, h represents the height of the feature map, and c represents the number of channels of the feature map.

For nodes in other layers, the concat operation is used for feature fusion on adjacent paths, and the weighted add operation with learnable weights is used for feature fusion on nonadjacent paths. The add operation can not only reduce the amount of calculation but also reduce the amount of invalid shallow information. Fusion calculation is shown in the following formula:

$$\mathrm{OUT} = \sum_i \frac{\mu_i \cdot x_i}{\varepsilon + \sum_j \mu_j}, \tag{1}$$

where x_i represents each feature map to be fused; ? is the weight coefficient of the feature map, which can be updated through learning. The initial weight coefficient is set to 1, indicating that the two layers of feature maps are fused equally; ε is a very small number ($\leq 10^{-3}$) which can effectively prevent numerical instability. Normalizing the weights between 0 and 1 increases the speed of training while preventing unstable training. According to formula (1), the feature fusion method for an intermediate layer is shown in Figure 6.

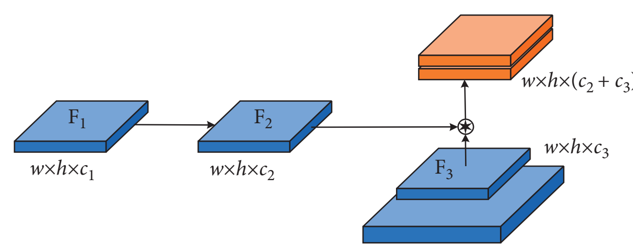

FIGURE 5: Schematic diagram of general feature fusion.

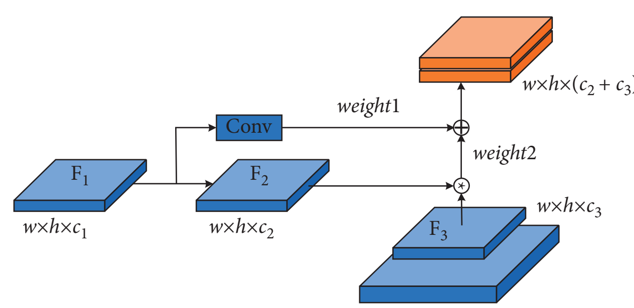

FIGURE 6: Schematic diagram of the cross-layer connection.

In Figures 5 and 6, given the input feature map $F_1 \in \mathbb{R}^{w\times h\times c_1}$ of a certain layer, the top-down path corresponds to the layer's feature map $F_2 \in \mathbb{R}^{w\times h\times c_2}$, and the bottom-up path corresponds to the layer's feature map $F_3 \in \mathbb{R}^{w\times h\times c_3}$, " $*$ " indicates the concat operation, "+" indicates the add operation, and weight1 and weight2 are the weight values of the feature map fusion on the two paths, respectively. It can be seen from the two figures that the feature fusion of the top and bottom output nodes adopts the concat operation, while the feature fusion of the

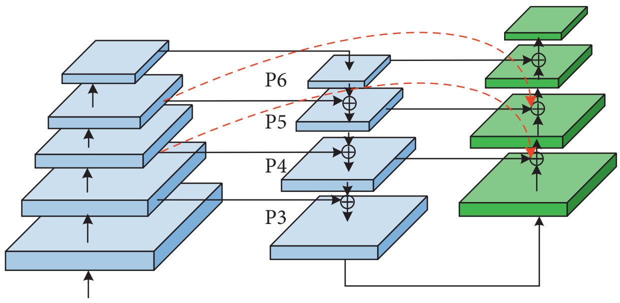

Figure 7: FPN structure used in this article (W-FPN).

middle layer nodes first undergoes the concat operation and then performs weighted add with the channel-aligned input layer operation. The final feature map obtained at the output node is a composite feature map containing details, edges, and high-level semantic information. For ease of understanding, taking the middle layer P4 as an example, the calculation of the output on each path is shown in the following formulas:

Table 2: Comparison of YOLOv5s effects before and after deepening the pyramid.

Module	Parameters	GFLOPs	F1-score (%)
PAN	7114785	16.5	81.34
W-PAN-Deep	12395500	16.7	84.39

$$P4^{td} = \mathrm{Concat}\left(P4^{in}, \mathrm{Resize}\left(Conv\left(P5^{in}\right)\right)\right), \tag{2}$$

$$P4^{out} = \frac{\mu_1 \cdot \mathrm{Concat}\left(P4^{td}, \mathrm{Resize}\left(Conv\left(P3^{out}\right)\right)\right) + \mu_2 \cdot P3^{out}}{\varepsilon + \mu_1 + \mu_2}, \tag{3}$$

where Pk^{in} represents the input of the kth layer, Pk^{td} represents the output of the kth layer intermediate node in the top-down path, and Pk^{out} represents the output of the kth layer output node in the bottom-up path.

(2) Increase the depth of the feature pyramid upwards. The high-level perception field of FPN is large, and the semantic information contained is more advanced, which can increase the learning ability of the network and further improve the detection accuracy. The FPN of YOLOv5 is 3 layers. Based on improvement 1, this study deepens it to 4 layers, which can make full use of the proposed cross-layer cascade structure. In addition, to match the depth of FPN, this study adds the detection layers of the detect part, named tiny, small, medium, and large, respectively, performs target detection on the feature maps output by P3, P4, P5, and P6 in turn, and increases the detection. The laying interval of anchor boxes after the layer becomes more reasonable, and the stability of training and the convergence speed and accuracy of the model will be effectively improved. Based on the improvement points 1 and 2, the simplified version of the FPN structure used in this article is shown in Figure 7.

The red dotted line in Figure 7 is the cross-layer cascading. It can be seen from the figure that the cross-layer weighted fusion is only used for the two middle layers P4 and P5. For the top layer P6 and the bottom layer P3, there is no much loss due to information flow. Considering the operating efficiency of the model, this study directly splices the two feature maps by channel. To objectively give the impact of deepening the pyramid on the network, Table 2 shows the comparison of the effect of YOLOv5s before and after deepening the pyramid, where W-PAN-Deep represents the PAN module after deepening the pyramid.

The comparison of the effect of YOLOv5s before and after deepening the pyramid shows that, after deepening the pyramid, although the F1-score of the model has been greatly improved, the large increase in the number of parameters makes loading the network need more video memory, which not only increases the hardware requirements for model training but also affects the speed at which the model runs. To solve such a problem, this study introduces the Ghost series of modules to lighten the network, to a certain extent, to make up for the negative impact of the increased network complexity after deepening the pyramid.

(3) Improve the YOLOv5 upsampling method. YOLOv5 uses the nearest neighbor interpolation method for upsampling. This method uses a single reference point pixel value for estimation. Although the speed is fast and the overhead is small, the upsampling process will cause serious feature loss and reduce the detection accuracy of small targets. The bilinear interpolation method uses four points to estimate the interpolation, and the obtained feature map is more delicate and the loss of details is less. Therefore, this study changed the upsampling method to the bilinear interpolation method, and the complexity of the two is only a constant level gap, relatively to the improvement in accuracy; the computational overhead is acceptable. Table 3 shows the experimental accuracy comparison of YOLOv5s using PAN structure and two W-PAN structures; W-PAN

Table 3: Comparison of the effects of W-PAN-Deep and PAN under YOLOv5s.

Module	F1-score (%)
PAN	81.34
W-PAN-Deep	84.39
W-PAN	85.77

indicates that the FPN structure proposed in this study is completely used.

It can be seen from the table that the F1-score index of using W-PAN is improved by 5.16% compared with that of PAN and the F1-score index of W-PAN-Deep, which deepens the pyramid, is improved by 1.6%, which proves that the cross-level cascade structure can further improve the regression accuracy of the network to the boundary. In general, the W-PAN structure makes the fusion of semantic information at all levels of the network more reasonable and sufficient. The introduction of W-PAN has greatly improved the accuracy of the network, especially the accuracy of high intersection and is higher than the required accuracy, which proves that the network from The W-PAN structure incorporates more effective feature information, which can better return the bounding box of the target and fit the industrial target detection task of high cross-comparison.

3.3. Improved GhostBottleneckCSP. GhostNet proposes an innovative module Ghost, which generates more feature maps with fewer parameters and computations [36]. The implementation of Ghost is divided into 2 parts, one is ordinary convolution, and the other is a linear operation with fewer parameters and computations. First, a part of the feature map is obtained through limited ordinary convolution, and then the obtained feature map is linearly operated to generate more feature maps, and finally the two sets of feature maps are spliced in the specified dimension. The operating principle of Ghost is shown in Figure 8.

The operation of the ordinary convolution layer is shown in

$$Y = X * f + b. \tag{4}$$

The Ghost module containing block contains a small number of convolutions, a population identity map, and $m \times (s-1)$ linear operations. First, generate a small number of feature maps through general convolution; then perform cheap linear operations on the feature maps obtained in the first step to generate Ghost feature maps. Finally, the two sets of feature maps are spliced by channel to generate enough feature maps to match the given number of output channels.

For an input $X \in \mathbb{R}^{W\times H\times C}$, the output $Y \in \mathbb{R}^{W'\times H'\times n}$ of a general convolution can be denoted by $Y = X \cdot f + b$, the $f \in \mathbb{R}^{k\times k\times C\times n}$ represents $C\times n$ convolution operations with a kernel size of $k\times k$, and b represents the bias term. W and H represent the width and height of the input feature map, respectively. W' and H' represent the width and height of the output feature map, respectively. C refers to the number of input channels. The FLOPs of a general convolution can be denoted by $W'\cdot H'\cdot n\cdot k\cdot k\cdot C$. Ghost convolution adopts the step-by-step strategy, and the calculation method is shown in

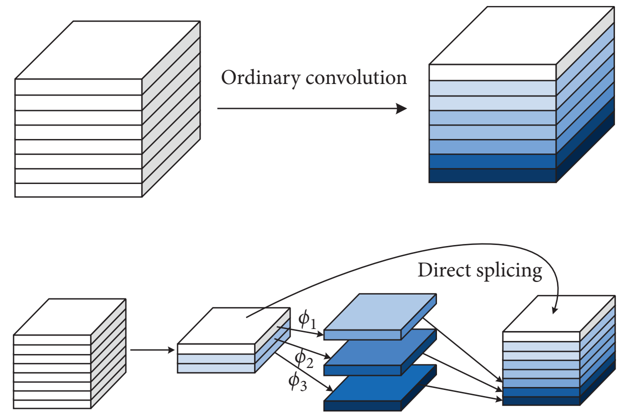

Figure 8: Comparison of Ghost convolution and general convolution.

$$Y' = X \cdot f', \tag{5}$$

$$Y_{ij} = \Phi_{ij}\cdot Y_i', i \in [1, m], \quad j \in [1, s]. \tag{6}$$

In a small number of convolution results, $Y \in \mathbb{R}^{W'\times H'\times m}$ represent the m feature maps ($m \ll n$) generated by the general convolution $f' \in \mathbb{R}^{k\times k\times C\times m}$ on the input X; then the m feature maps are linearly operated one by one, and each feature map generates s feature maps, and a total of $n = m\times s$ feature maps are generated. Feature map Φ_{ij} represents the ith linear operation on the jth feature map Y_i' generated in the first step of convolution; $\Phi_{i,s}$ represents a direct feature identity map. To ensure the efficiency and practicability of CPU or GPU, set the size of the convolution kernel of each linear operation to be $d\times d$; then the speed ratio of general convolution and Ghost convolution can be calculated by

$$\begin{aligned}
RATE_s &= \frac{W'\cdot H'\cdot n\cdot k\cdot k\cdot C}{W'\cdot H'\cdot m\cdot k\cdot k\cdot C + W'\cdot H'\cdot (n-m)\cdot d\cdot d\cdot C}\\
&= \frac{W'\cdot H'\cdot n\cdot k\cdot k\cdot C}{W'\cdot H'\cdot (n/s)\cdot k\cdot k\cdot C + W'\cdot H'\cdot (s-1)\cdot (n/s)\cdot d\cdot d\cdot}\\
&= \frac{k\cdot k\cdot C}{(1/s)\cdot k\cdot k\cdot C + ((s-1)/s)\cdot d\cdot d}\\
&\approx \frac{s\cdot C}{s + C - 1}\\
&\approx s.
\end{aligned} \tag{7}$$

Here, $k\times k$ and $d\times d$ have the same size, and $s \ll C$. From the simplification results, the calculation amount of general convolution is roughly s times that of Ghost convolution. Similarly, the number of parameters can be calculated as s times. Ghost convolution is a lighter and faster module. Based on this, this study designs GhostBottleneck

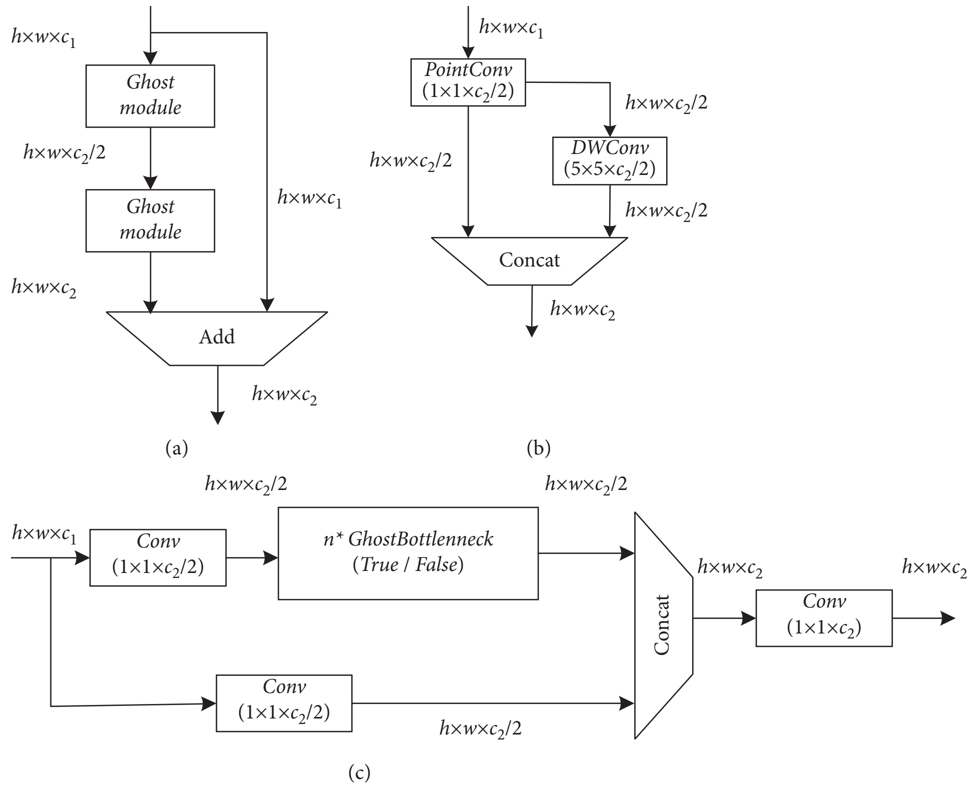

Figure 9: (a) Ghost module, (b) GhostBottleneck, and (c) GhostBottleneckCSP.

and GhostBottleneckCSP modules based on the Ghost module. The specific structure is shown in Figure 9.

C_1 and C_2 in Figure 9 refer to the number of channels of input and output characteristic graphs, respectively. In this article, the 1×1 ordinary convolution shown in Figure 9(a) is used to reduce the number of channels to 1/2 of the number of output channels, and then a depthwise convolution with a size of 5×5 is performed according to the obtained feature map. Finally, the two sets of features are spliced together. The first Ghost module in Figure 9(b) first reduces the number of output channels to 1/2 of the number of target output channels, and then the second Ghost module restores the number of channels to the number of target output channels and transmits the number of channels together with the residual. The incoming input feature maps are added point by point for feature fusion. As shown in Figure 9(c), use GhostBottleneck to replace all bottleneck modules in YOLOv5 and form a new GhostBottleneckCSP with the C3 module. The original bottleneck consists of 1×1 and 3×3 standard convolutions. The new structure replaces the original bottleneck. There are more 3×3 standard convolutions in the model, which reduces the amount of computation and compresses the model.

3.4. ShuffleConv. Most of the current excellent lightweight networks use group convolution or deep separable convolution to reduce the amount of computation generated by convolution operations. However, to achieve feature fusion between channels, the 1×1 convolution used in these

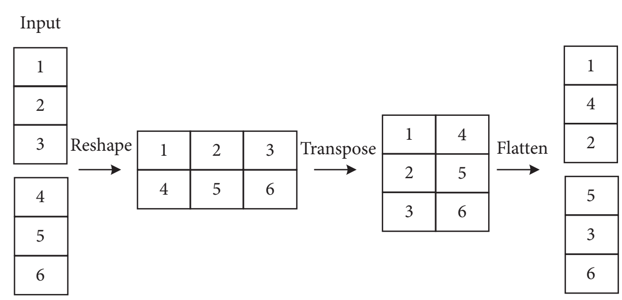

Figure 10: Experimental process of mixed washing in channels.

networks takes up more computation throughout the process. To alleviate this problem, ShuffleNet [37] proposed the concept of channel mixing. After group convolution, the use of channel blending can realize the flow of information between groups and enhance the expression ability of features in a more economical way. Channel mixing can be achieved by conventional tensor operations, as shown in Figure 10.

The number in Figure 10 is the number of the input channels. The channel is extended to two dimensions using the reshape operation, and the extended two dimensions are replaced by transpose. Through this operation, the information between the group convolution channels can be fused without increasing the amount of computation. Finally, the flatten operation restores the two dimensions to the original initial dimension and completes the channel washing. Based on the above principle, it can be considered that a point-by-point convolution can be replaced by a 1×1 group convolution and a channel mixing operation combination. Compared with the standard convolution, the parameter number and calculation amount of the group convolution are greatly reduced, and the group convolution has a similar regular effect, which can reduce the probability of overfitting. For these advantages, this article improves the ordinary convolution operation in 6 Conv modules of 3×3 and 2 Conv modules of 1×1 in YOLOv5. The original ordinary convolution is replaced by group convolution and channel mixing module, which can theoretically realize further compression of the model.

3.5. Parameter Setting

3.5.1. Loss Function. In the prediction of YOLOv5, Generalized IoU (GIoU) [38] is used as the loss function of BBox, and weighted nonmaximum suppression (NMS) is used. The loss function is shown in

$$L_{GIoU} = 1 - IoU + \frac{C - \left(B \cup B^{gt}\right)}{C}, \quad (8)$$

$$IoU = \frac{A \cap B}{A \cup B}. \quad (9)$$

However, when the prediction box is in the ground-truth box and the size of the prediction box is the same, the relative position of the prediction box and the ground-truth box cannot be distinguished.

Therefore, this article uses Complete IoU (CIoU) [39] to replace GIoU. Based on considering GIoU loss, CIoU loss considers the consistency of BBox overlapping area, center distance, and BBox aspect ratio. It can better predict the target. The definition of the loss function of GIoU is shown in

$$R_{CIoU} = \frac{\rho^2\left(b, b^{gt}\right)}{c^2} + \alpha\nu, \quad (10)$$

$$\nu = \frac{4}{\pi^2}\left(\arctan\frac{w^{gt}}{h^{gt}} - \arctan\frac{w}{h}\right)^2, \quad (11)$$

$$L_{CIoU} = 1 - IoU + R_{CIoU}, \quad (12)$$

where $\rho^2\,(b, b^{gt})$ represents the Euclidean distance between the prediction box and the target box and c^2 represents the diagonal distance of the minimum enclosing rectangle. w^{gt}/h^{gt} and w/h represent the width-to-height ratios of the target box and the prediction box, respectively. The trade-off parameter is defined as α, which is a parameter greater than 0. The definition of trade-off parameters is shown in

$$\alpha = \frac{\nu}{(1 - IoU) + \nu}. \quad (13)$$

3.5.2. K-Means ++ Clustering Anchor Frame. YOLOv5 conducts K-Means clustering on the COCO data set of general target detection and obtains the initial prior anchor frame. However, there are many types of targets in the

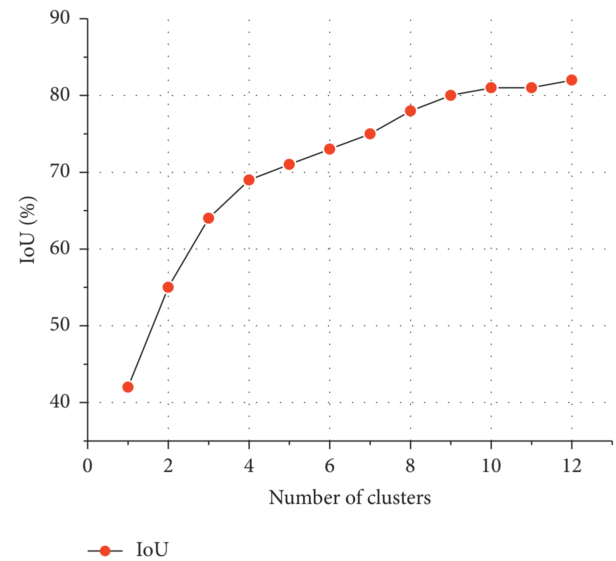

Figure 11: Number of centers of different clusters and average intersection-sum ratio.

COCO data set, which can reach more than 80 categories, and the types of pavement diseases in this article are 6 categories, which cannot meet the needs of actual disease detection. Therefore, it is necessary to redesign the size of the prior anchor frame. In this article, the K-Means ++ clustering algorithm is used to cluster the annotated target boundary anchor frames in the disease data many times, and different numbers and sizes of prior frames are generated as much as possible to increase the matching degree between the prior box and the actual target box, to further improve the detection accuracy. In the clustering process, the average intersection corresponding to the number of centers of different clusters is shown in Figure 11.

It can be seen from Figure 11 that when the number of prior frames is from 0 to 9, IoU shows a rapid upward trend, but when the number of prior frames is from 9 to 12, the growth rate of IoU slows down. In order to balance the detection accuracy and rate, nine prior anchor frames are finally selected, and the sizes of the anchor frames after clustering are, respectively, [54.2 99.2], [32.7 634.1], [604.1 354.2], [194.9 300.1], [251.2 95.9], [39.4 258.0], [47.1 427.7], [239.2 611.0], and [574.1 109.9]. The clustering center effect is shown in Figure 12.

3.6. FAFU-PD Data Set. Training a deep learning model with high accuracy and strong generalization ability needs to rely on large-scale and high-quality data sets, but many specific problems do not have a rich variety of public data sets, so it is particularly important to obtain high-definition pavement disease images. At present, the existing pavement disease data sets are collected by cameras installed in the cab or on the roof. In the actual highway inspection task, the image data collected in this way cannot well determine the pile number of the collection sites. There are two sources of road disease image data in this article: one is the road disease data provided by Fujian Highway Datong Detection Co., Ltd.,

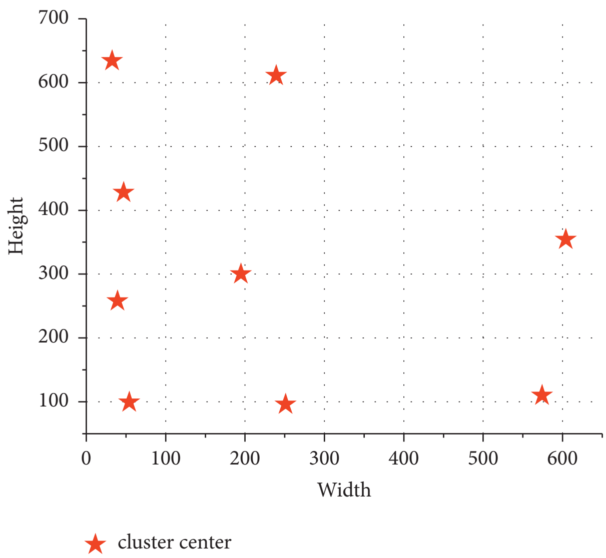

Figure 12: Cluster center effect diagram.

Figure 13: DHDV multifunctional detection vehicle.

and the other is the road disease data collected by the Digital Highway Data Vehicle (DHDV). As shown in Figure 13, the DHDV multifunction detection vehicle is jointly developed by Oklahoma State University, Arkansas University, and WAYLINK Company. The detection vehicle can collect road data at the speed of 100 km/h, and the acquisition range can cover a 4 m lane width. The accuracy of surface texture data collected in the vertical direction can reach 0.3 mm, and the accuracy of data in the longitudinal direction can reach 1 mm. The PaveVision3D sensor equipped on DHDV carries the latest imaging technology, which can obtain 2D and 3D laser imaging data from the road through two separate left and right sensors. Customized optical filters and high-power line laser projection systems enable DHDV to maintain consistency in image quality both during the day and night. DHDV collected part of the two-dimensional laser asphalt pavement nondeformation disease images as shown in Figure 14.

3.7. NST Algorithm. When detecting targets according to the characteristics of the object, the objects with similar characteristics are often classified as a class. Asphalt pavement disease is the target that we need to detect. In the actual detection process, it often conflicts with some other background targets. For example, the detection of crack diseases is often affected by the induction coil under the road, the lane scratch, and the pavement spray. The disease detection of patch type is often affected by pavement construction expansion joints, road markings, and indicator arrows. When the disease of patch type is detected, it is often affected by water stain, oil stain, and rutting. Particularly, when continuous water stain and oil stain occur on the pavement, the probability of false detection will be greatly improved. Figure 15 shows the partial misdetection of the model.

To solve the hidden dangers brought by negative samples to road inspection, this article proposes a new negative sample training method. When training and labeling the target object, it is used as data for a series of backgrounds such as induction coils, water stains, and oil stains. The centralized negative sample labels, that is, the negative samples such as induction coils, water stains, and oil stains, are labeled. During the training process of the data set, the model will simultaneously label the positive samples (horizontal seam, vertical seam, patch, patch, etc.) and negative sample labels (induction coils, water and oil stains, etc.) for detection, and these negative sample labels can be excluded from the final detection results.

The advantages of this negative sample training method can be analyzed from the theory of information entropy. Information entropy is often used as a quantitative index of the information content of a system, which can be further used as the objective of system equation optimization or the criterion of parameter selection. The definition of information entropy is shown in

$$H(X) = -\sum_{i=1}^{n} p_i \log p_i, \tag{14}$$

where p_i represents the probability that the *ith* symbol appears in the information source. H stands for information entropy.

After applying the NST method, positive sample (disease) tags and negative sample (background) tags may appear in the XML file generated by the detection. According to the principle of YOLOv5 and formula (14), the information entropy of the data set with and without negative sample labels can be obtained. From the principle of the neural network, it can be known that when the size of the image sent to the detection is different, it will affect the final recognition effect. We found that when the size of the image is 896, the number of false detections is converted into probability, before and after adding negative samples. The information entropy is 0.07405 and 0.07809, respectively; obviously, the gain is increased by 5.17%.

The negative samples and their labels of the NST method are shown in Figure 16.

3.8. Generative Adversarial Network Data Augmentation Algorithms. A generative adversarial network (GAN) is a game model based on adversarial generation proposed by

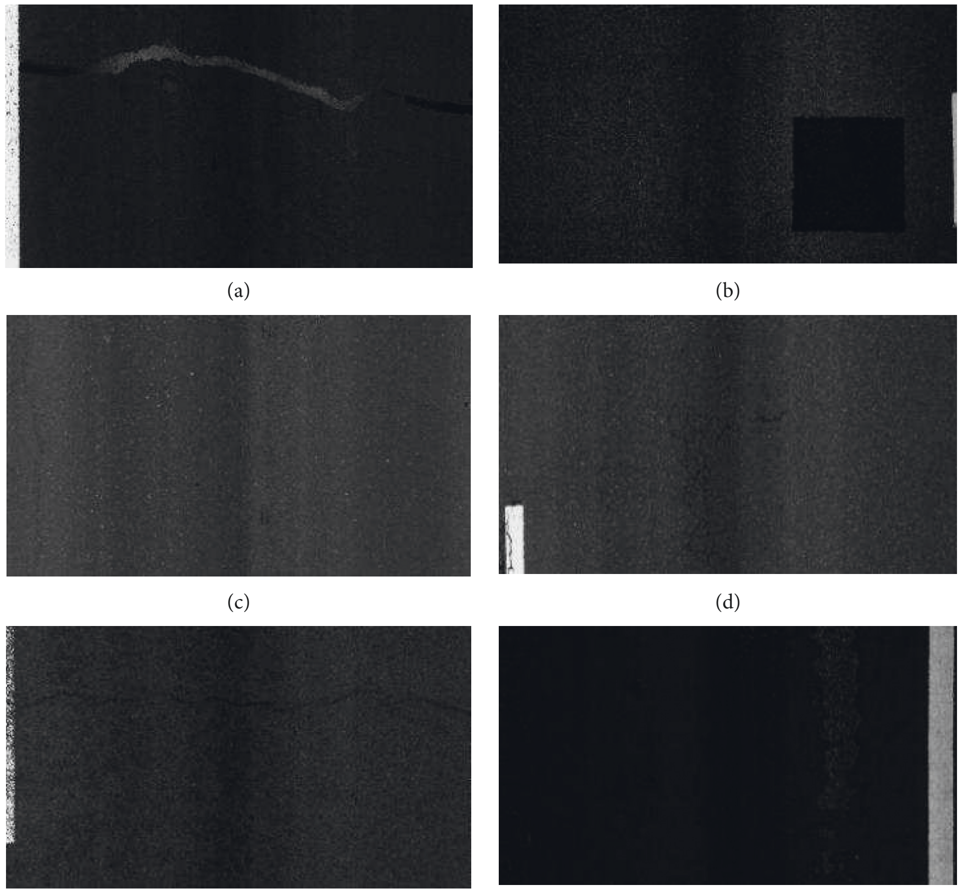

(a) (b) (c) (d) (e) (f)

Figure 14: Two-dimensional laser asphalt pavement nondeformation disease image. (a) Repair-strip, (b) patch, (c) longitudinal crack, (d) crack, (e) transverse crack, and (f) loose.

Creswell et al. [40]. The GAN framework includes a generator network (G) and discriminator network (D). G and D confront each other through their respective strategies and reuse each other's strategies to adjust their strategies in time [41].

In our collected highway asphalt pavement disease data, the number of cracks, loose, and other diseases is small. To reduce the impact of unbalanced data types, we choose the GAN data enhancement algorithm to expand the amount of data on cracks, loose, and other diseases.

The basic framework of the GAN network used in this article is shown in Figure 17. The noise is fused into the original image to generate data. The generated data are input to G and the feature information of the pit is extracted. The fitting data are generated to deceive D, and D is used to identify the authenticity of the output data and feedback to the generated network to train the model.

Ratliff et al. [42] proposed Wasserstein distance to replace JS divergence (Jensen-Shannon divergence, JS), that is, Wasserstein generated adversarial network (WGAN) to improve the mode collapse problem of GAN. WGAN still has the problem of gradient explosion and gradient disappearance caused by gradient clipping. Therefore, Hsu et al. [43] proposed WGAN-GP with gradient penalty term. In this study, WGAN-GP with better data generation performance was used to generate pit data. The G and D of WGAN-GP were set to five layers of convolutional neural networks, and the number of layers was 1~5. G is composed of transposed convolution (ConvTrans2d), batch norm (BN), and ReLu and Tanh activation functions. D is composed of convolution (Conv2d), instance norm (IN), and LeakyRelu activation functions. The detailed parameter settings of the network are shown in Table 4. In the table, K (kernel size, K) represents the size of the convolution kernel, N_out (number of out, N_out) represents the number of convolution kernels, and S (stride, S) represents the step size.

3.9. Poisson Migration Fusion Algorithm. In this study, the groove image generated by WGAN-GP is inserted into the disease-free road image to generate new training data. Firstly, the Poisson algorithm is used to output the fused image [44], and then the synthesized image is output by the color migration algorithm [45]. When integrating the image, the image should be integrated as real as possible. When synthesizing the image, the natural effect of the original data set should be maintained. Therefore, the color migration is added based on the Poisson fusion, which is called the

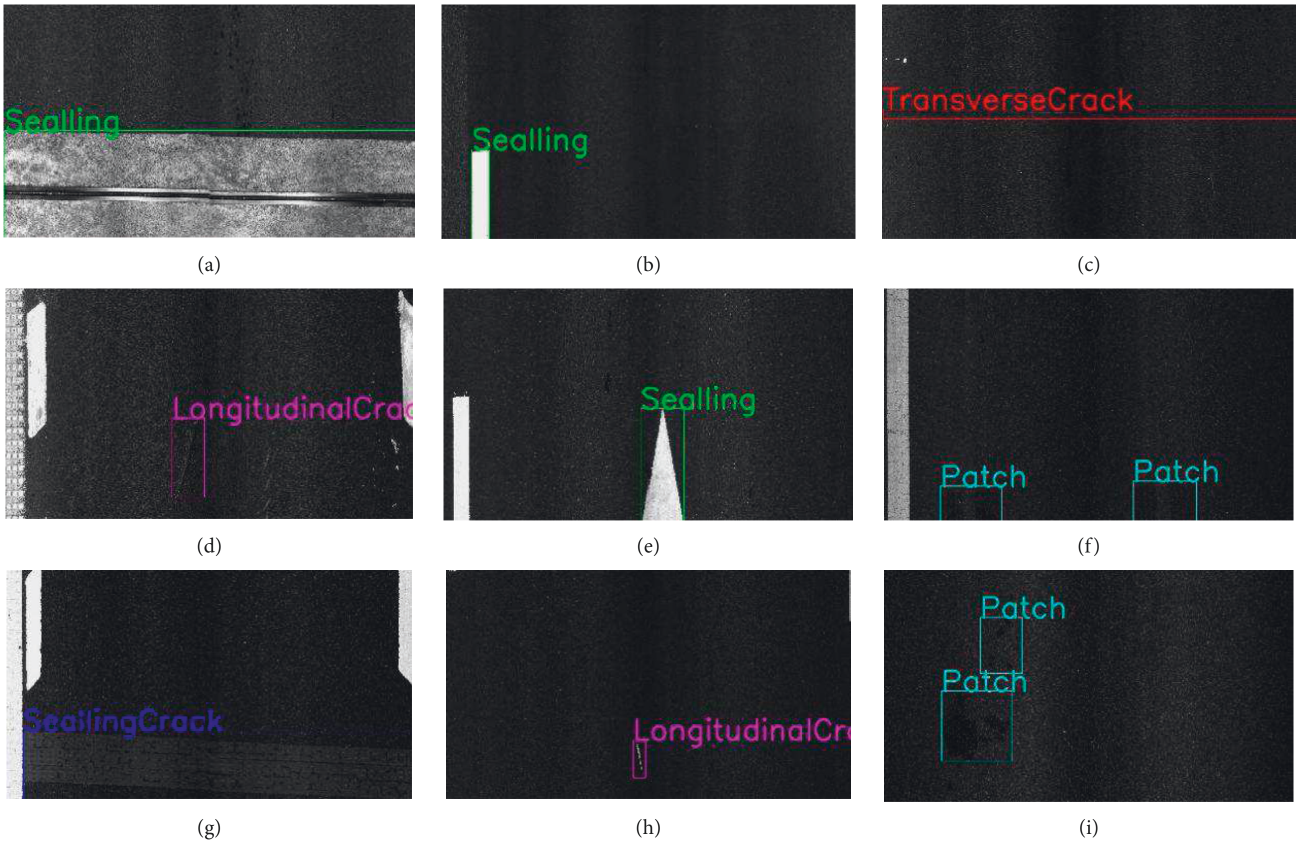

Figure 15: Misdetection. (a) Misidentification of joints as a patch, (b) misidentification of lane markings as a patch, (c) misidentification of induction coils as transverse cracks, (d) misidentification of pavement scratches as longitudinal cracks, (e) misidentification of lane indicator arrows as patch, (f) misidentification of rut imprints as a patch, (g) misidentification of deceleration belts as patch, (h) misidentification of pavement splits as longitudinal cracks, and (i) misidentification of water stains as a patch.

Poisson migration fusion. As an image fusion method, the Poisson algorithm can better integrate the source image into the target image. In this study, the reference code of Poisson fusion implementation is shown in the literature. The color transfer algorithm can ensure that the target image and the reference image have the same pixel mean and variance in the color space. In this study, the color transfer implementation code is shown in the literature. In the Poisson algorithm, the pixel value of the unknown region is calculated by the Poisson equation, and the calculation method is shown in

$$\left\{\begin{array}{l} \min\limits_{f} \iint_{\omega} |\nabla f - v|^2 \\ f|\partial_{\omega} = f^{*}|\partial_{\omega}. \end{array}\right\}. \tag{15}$$

Type: ω for the target image; ∇ is a gradient operator; v is the gradient region in the image; f is the unknown function of the target image; f^{*} is the known function of the source image; ∂_{ω} is the boundary between the source image and the target image.

In the color transfer algorithm, the best matching pixel of the target image is found according to the color component of the reference image. The calculation method is shown in

$$T_{i,j} = \left|d_i - d_j\right| + \left|\sigma_i - \sigma_j\right| + \left|f_i - f_j\right|, \tag{16}$$

where i and j are pixels of two images, respectively; d_i and d_j are the distance between pixels and clustering points; σ_i and σ_j are spatial dynamic selection coefficients of images; f_i and f_j are the average brightness of two images. The schematic diagram of the Poisson migration fusion algorithm is shown in Figure 18.

3.10. Softer-NMS. Softer-NMS for final result processing nonmaximum suppression (NMS) is mainly used for postprocessing of target detection model output based on deep learning, to remove redundant detection boxes and obtain correct detection results. But through the analysis we can find that NMS has the following defects:

(a) There are more missed detections in dense scenarios: when there is partial overlap between two targets nearer, there is a greater likelihood of missed detections for targets with less confidence.

(b) The NMS default box with higher confidence scores is more accurate, and this condition is not always valid because classification and regression tasks are not directly related. High confidence border boxes are not always more reliable than low confidence border boxes.

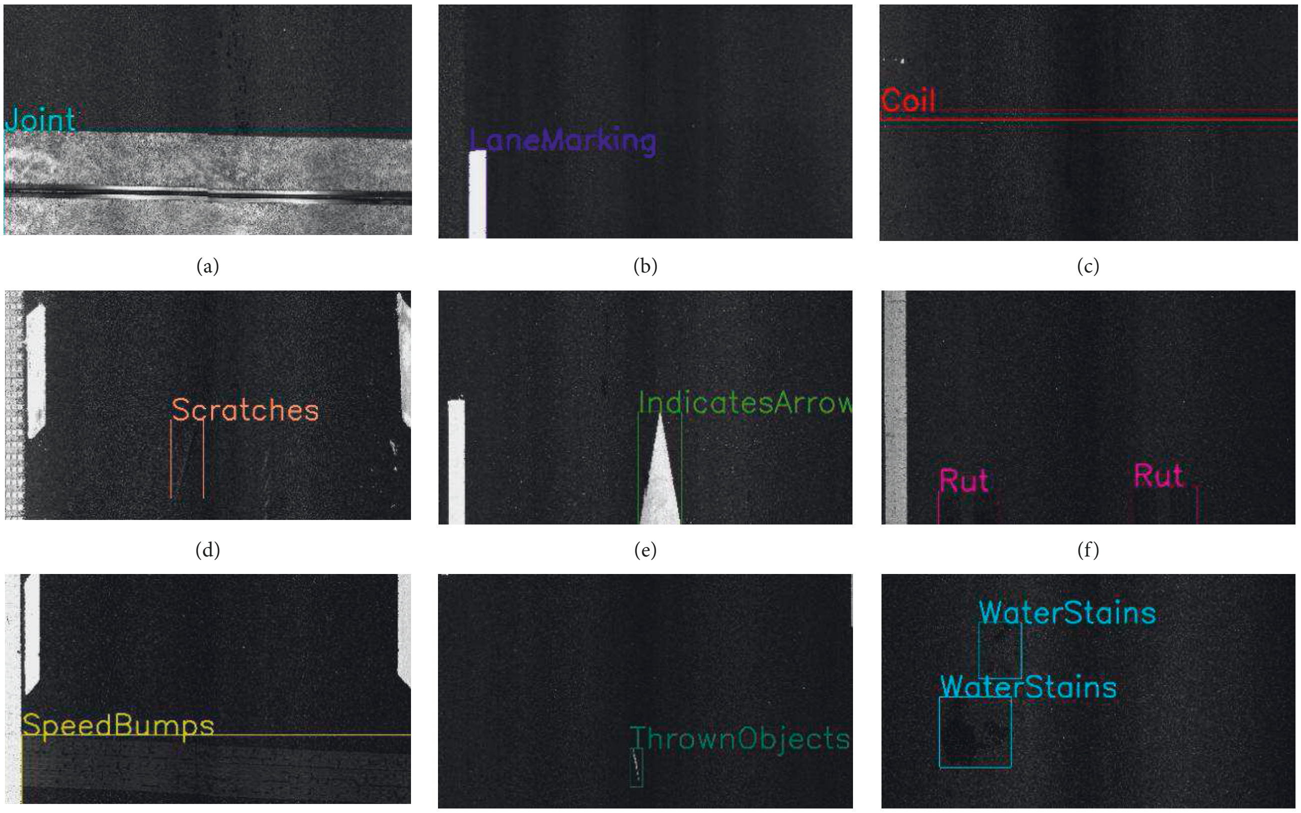

(a) (b) (c) (d) (e) (f) (g) (h) (i)

Figure 16: Negative sample labels. (a) Expansion joints (joint), (b) road markings (laneMarking), (c) induction coils (coil), (d) lane scratches (scratches), (e) lane indication arrows (indicatesArrow), (f) rut, (g) speedBumps, (h) thrownObjects, and (i) waterStains.

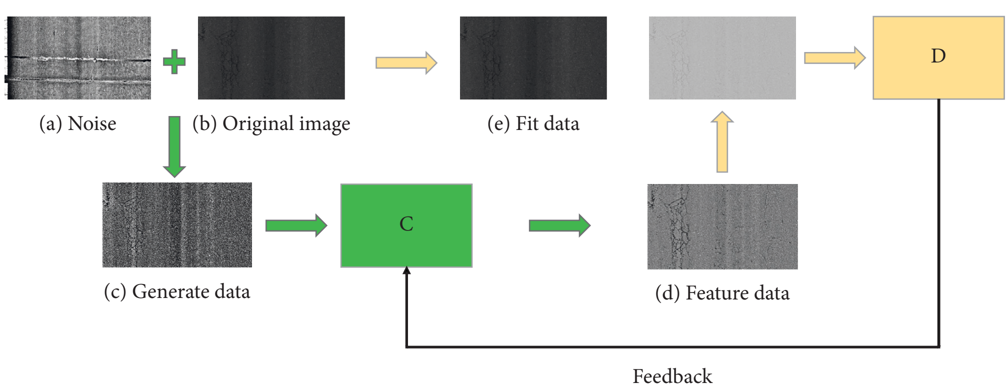

Figure 17: Generating the basic framework of an adversarial network (GAN).

(c) The labeling of ground truth may not be reliable.

Aiming at the first problem of NMS, Soft-NMS designs the degree function of confidence score decline according to the size of IoU and has achieved certain results. But for the other two problems the classification confidence score is not strongly correlated with the IoU of the box, so a new method is needed to measure the location confidence of the box. Based on this, Softer-NMS puts forward two ideas, respectively, to build the confidence of IoU to model how much grasp that the current frame and GT are coincident; a method is proposed to combine multiple frames according

Table 4: WGAN-GP network detailed parameter table.

Layers	Net	Parameters
G1	ConvTrans2d + BN + ReLu	K: 4, N_out : 512, S: 1
G2	ConvTrans2d + BN + ReLu	K: 3, N_out : 256, S: 2
G3	ConvTrans2d + BN + ReLu	K: 3, N_out : 128, S: 3
G4	ConvTrans2d + BN + ReLu	K: 4, N_out : 64, S: 4
G5	ConvTrans2d + Tanh	K: 6, N_out : 64, S: 4
D1	Conv2d + IN + LeakyReLu	K: 6,N_out : 64,S: 4
D2	Conv2d + IN + LeakyReLu	K: 4, N_out : 64, S: 4
D3	Conv2d + IN + LeakyReLu	K: 3, N_out : 128, S: 3
D4	Conv2d + IN + LeakyReLu	K: 3, N_out : 256, S: 2
D5	Conv2d	K: 4, N_out : 512, S 1

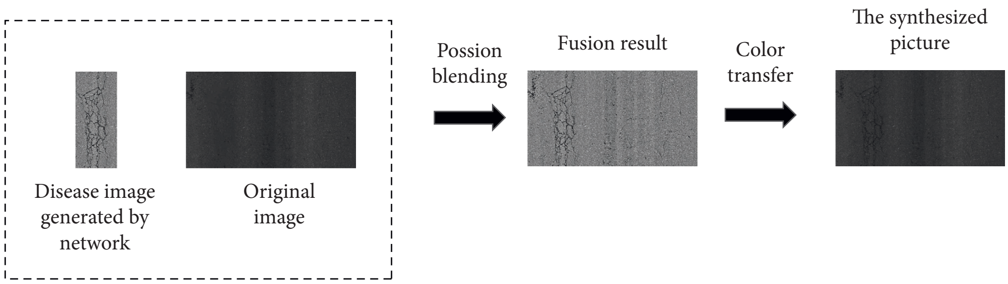

Figure 18: Schema of Poisson migration fusion algorithm.

Table 5: Experimental operational environment.

Category	Entry	Version
Hardware configuration	System	Windows 10
Software configuration	Graphics card CPU	GeForce RTX 3080 Intel(R) core(TM) i7-6700 CPU
	Python version	3.8
	Deep learning framework	PyTorch
	CUDA	10.0

to the IoU confidence to optimize the final generated frame. For IoU confidence, Softer-NMS uses Gaussian functions to model the prediction box. The calculation method is shown in

$$P_\theta(x) = \frac{1}{2\pi\sigma^2} e^{-(x-x_e)^2/2\sigma^2}. \tag{17}$$

Using delta distribution to model GT frame, the calculation method is shown in

$$P_D(x) = \delta\left(x - x_g\right). \tag{18}$$

In formulas (17) and (18), $P_\theta(x)$ represents the Gaussian probability distribution of the predicted bounding box, $P_D(x)$ represents the delta probability distribution of the predicted bounding box, x represents the value of the actual bounding box, σ represents the standard deviation, x_e represents the prediction box after offset, and the output x_g represents the GT box.

Softer-NMS method can effectively avoid missed detection in complex asphalt pavement disease processing scenarios, to improve the recall rate and meet the needs of engineering tasks.

4. Experiments

4.1. Data and Experimental Environment. The experiment in this article requires good hardware configuration and GPU acceleration. The running environment of the experiment is shown in Table 5. The data set used in this article is from the subgrade and pavement safety detection platform of the Digital Fujian Intelligent Transportation Technology Internet of Things Laboratory of Fujian Agriculture and Forestry University and Fujian Expressway Datong Detection Company. This data set selects 7,000 training set images and 1750 test set images, respectively. To increase the robustness of the training model, the data set adds background images that do not contain diseases and adds background labels such as road markings, indicator arrows, and bridge joints. All label categories are shown in Table 6.

4.2. Ablation Experiment

4.2.1. Evaluating Indicator. The automatic identification of highway asphalt pavement diseases belongs to the category of target detection. At present, the commonly used indexes to evaluate the training performance and robustness of the model are precision (P), recall (R), and mean average precision (mAP).

The target detection and evaluation index is applied to the test of highway asphalt pavement diseases, and two kinds of results images can be obtained, including images with diseases and images without diseases. True-positive (TP), false-positive (FP), true-negative (TN), and false-negative (FN) are important indicators to describe the accuracy of the model. The specific formulas of the above metrics are shown in

$$\text{Precision} = \frac{\text{TP}}{\text{TP} + \text{FP}} = \frac{\text{TP}}{\text{all detections}}, \tag{19}$$

$$\text{Recall} = \frac{\text{TP}}{\text{TP} + \text{FN}} = \frac{\text{TP}}{\text{all ground truths}}, \tag{20}$$

$$\text{AP} = \int_0^1 P\,\mathrm{d}R, \tag{21}$$

$$\text{mAP} = \frac{\sum_{i=1}^{N} \text{AP}_i}{N}. \tag{22}$$

TP, FP, and FN refer to correct check box, wrong check box, and missing check box, respectively. AP value is the area of the P-R curve, and N represents the total number of detection categories; this article is 10. mAP @ 0.5 refers to the average AP of all categories when IoU is set to 0.5. mAP @ 0.5 :

Table 6: All label categories in the data set.

Disease	Label	Nondisease	Label
Transverse crack	TransverseCrack	Deck expansion joint	Joint
Longitudinal crack	LongitudinalCrack	Road marking	LaneMarking
Alligator crack	AlligatorCrack	Induction coil	Coil
Repair-strips	Sealing	Scratch	Scratches
Repair block	Patch	Guide finger	IndicatesArrow
Loose	Loose	Rut	Rut
Repair seam	SealingCrack	Deceleration strip	SpeedBumps
		Sprinkler	ThrownObjects
		Water stain	WaterStains

0.95 refers to the average mAP on different IoU thresholds. The IoU value ranges from 0.5 to 0.95, and the step length is 0.05. The average detection processing time includes network self-inference time and NMS processing time.

F1-score is a measure of classification problems. Some machine learning competitions for multiclassification problems often use F1-score as the final evaluation method. It is the harmonic average of precision rate and recall rate, with a maximum of 1 and a minimum of 0. Based on this, this article selects F1-score as the final model evaluation criteria. The calculation method of the F1-score is shown in

$$F_1 = 2 \times \frac{\text{precision} \times \text{recall}}{\text{precision} + \text{recall}}. \tag{23}$$

4.2.2. Selection of Detection Image Size. In the process of image recognition, the larger the size of the image, the higher the clarity, the higher the recognition accuracy, and the slower the speed. The image with a small size is exactly the opposite. Therefore, how to balance the relationship between speed and accuracy is a very critical factor for us to select the image size. The variation trend of F1-score and FPS with the size of the detected image is shown in Figure 19. The black curve in the figure represents the change of the F1-score with the size of the detected image. The red curve represents the change of FPS with image size. It can be seen from the figure that the F1-score increases rapidly with the increase in image size. When the detection size exceeds 896, the curve becomes smooth. At the same time, the detection speed decreases with the increase of detection size. Considering this comprehensively, 896 is selected as the size of image detection, and 1024 is selected as the reference standard.

4.2.3. Network Structure Ablation Experiment. In this section, the performance change caused by the change in network structure is gradually verified by ablation experiments. Four experiments are conducted for the target detection model of YOLOv5. Four networks, YOLOv5, YOLOv5-WPAN, YOLOv5-WPAN-Ghost, and YOLOv5-WPAN-Ghost-Shuffle (YOLO-W), are trained, respectively, in the four experiments. The network name can correspond to the structure described above one by one. Figure 20 shows the precision curve of the four networks when the input image size is 896, and Figure 21 shows the recall curve of the four networks when the input image size is 896. The

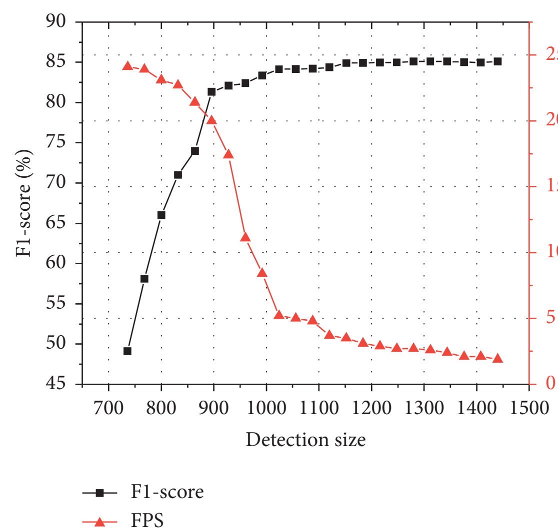

Figure 19: F1-score and FPS versus image size.

brightness of the curve increases in turn, respectively, representing YOLOv5, YOLOv5-W-PAN, YOLOv5-WPAN-Ghost, and YOLOv5-WPAN-Ghost-Shuffle (YOLO-W). In Figure 20, the accuracy of YOLOv5-WPAN-Ghost-Shuffle has an obvious loss, and the fluctuation is more intense. Fortunately, in the late training period, the difference between the accuracy of the model and YOLOv5 is lower than that in the early stage. The cause of fluctuations found during later debugging is related to batch-size settings.

As can be seen from Table 7, when the image size is 896, the calculation amount and parameters of the YOLOv5 network model with W-PAN structure are increased by 1.2% and 27.9%, respectively, and the F1-score is increased by 5.2%. After adding GhostBottleneck, the computation and parameters of the model are reduced to 53.3% and 65.3% of the original YOLOv5 network, respectively. The F1-score is increased by 7.5%, the model size is reduced by 37.8%, and the speed is increased by 5.9% with GPU.

After the standard convolution is replaced by ShuffleConv, the number of model parameters and the amount of calculation are further reduced to 29.5% and 29.3%, the F1-score is increased by 0.6%, and the model size is reduced by 29.9%. The result that the speed is not improved in the case of GPU is also expected. On the GPU platform with sufficient computing power, although the group convolution reduces the amount of computation and parameters, due to

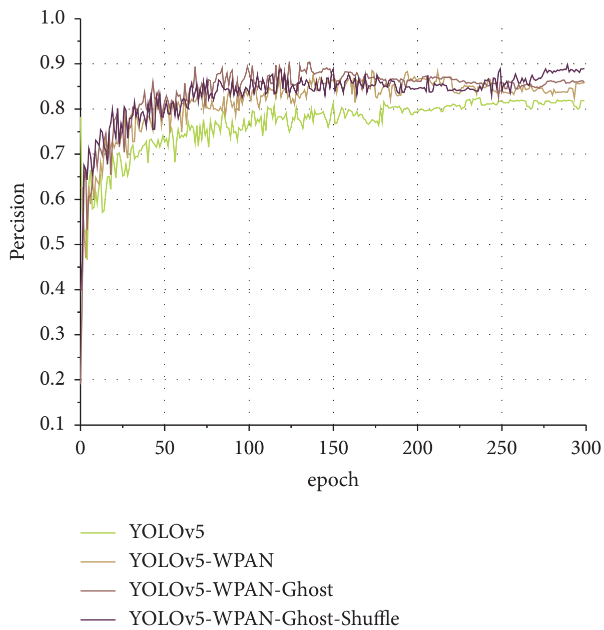

Figure 20: Schematic diagram of the precision change curve.

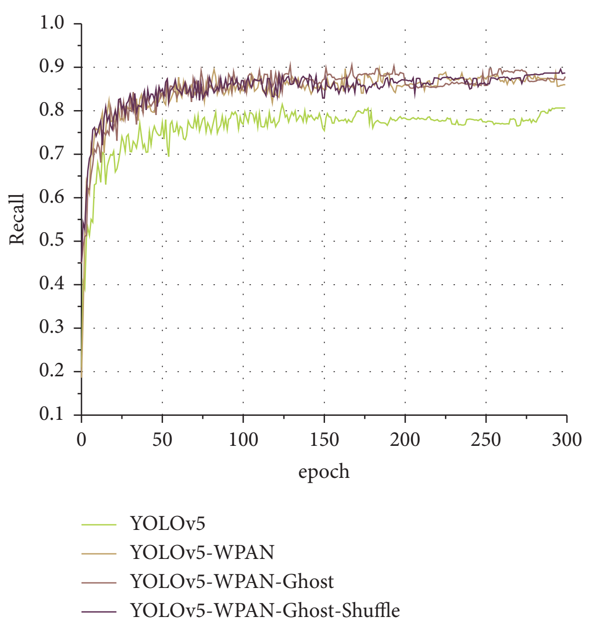

Figure 21: Recall change curve diagram.

the limitation of memory exchange speed, the bottleneck of ShuffleConv is not the computational strength, so this module has little effect on the GPU environment. In addition, YOLOv5-WPAN-Ghost-Shuffle improves F1-score compared with YOLOv5-WPAN-Ghost, which proves the regularization effect of group convolution to some extent.

To further verify the efficiency of the proposed modules and networks, it is compared with similar lightweight networks YOLOv3-tiny and YOLOv4-tiny. It can be seen from Table 7 that the proposed network model has absolute advantages over YOLOv3-tiny and YOLOv4-tiny. The model size was only 59.0% and 44.7% of the above models, but the F1-score exceeded YOLOv3-tiny and YOLOv4-tiny by 13.6% and 10.6%. Therefore, the proposed model is reasonable and economical in engineering applications.

Secondly, by adding YOLOv3-tiny-Ghost-Shuffle, YOLOv3-tiny, YOLOv4-tiny-Ghost-Shuffle, and YOLOv4-tiny into two groups of comparative experiments, the optimization versatility of GhostBottleneck and ShuffleConv modules on other networks is proved. Compared with YOLOv3-tiny, YOLOv3-tiny-Ghost-Shuffle reduces the computation and parameter by 81.4% and 92.8%, respectively. The model size was compressed by 91.6% and the F1-score was increased by 1.4%. Compared with YOLOv4-tiny, YOLOv4-tiny-Ghost-Shuffle reduced the calculation amount and the number of parameters by 58.5% and 64.4%, respectively, reduced the model size by 58.5%, and increased the F1-score by 1.2%.

4.2.4. GAN Ablation Experiment. In this section, we verify the performance change of the network model caused by the confrontational generation network (GAN) through ablation experiments. Three experiments are carried out for the YOLOv5 network model. The three experiments train YOLOv5, YOLOv5 + GAN + Poisson, and YOLO-W + GAN + Poisson networks, respectively. The experimental results are shown in Table 8. Taking the input image size of 896 as an example, YOLOv5 + GAN + Poisson is 2.54% higher than YOLOv5 in F1-score, and YOLO-W + GAN + Poisson is 9.13% higher than YOLOv5. Experiments show that the performance of the model can be effectively improved by adding a small number of diseases generated by the confrontation generation network (GAN) in the data set.

4.2.5. NST Ablation Experiment. In this section, the data sets with and without nondisease labels are used for training, and the performance of each model in the NST ablation experiment is shown in Table 9. Taking the input image size of 896 as an example, YOLOv5+NST is 3.55% higher than YOLOv5 in F1-score, YOLOv5+GAN +Poisson+NST is 2.32% higher than YOLOv5+GAN+Poisson, and YOLO-W+GAN+-Poisson+NST is 2% higher than YOLO-W+GAN+Poisson. Experiments show that the NST algorithm can effectively improve the performance of the model.

5. Analysis

To further verify the efficiency of the PDNet network architecture proposed in this article, the MMDetection tool is used to compare it with other classical networks on the FAFU-PD data set (including negative samples and generating disease data). These classical networks include a single-stage target detection network and a two-stage target detection network. The comparison results of different network performances are shown in Table 10.

The results show that this article improves the detection accuracy and speed of nondeformation diseases of asphalt pavement by improving the model network architecture

Table 7: Performance comparison of models in network structure ablation experiment.

Size	Model	Parameters	GFLOPS	Speed-GPU	Weight	F1-score (%)
896	YOLOv5	7114785	16.5	1.7	14.2	81.34
	YOLOv5-WPAN	9874167	16.7	1.9	15.6	85.77
	YOLOv5-WPAN-Ghost	3419817	7.8	1.6	9.7	87.97
	YOLOv5-WPAN-Ghost-Shuffle	2419191	5.5	1.6	6.8	88.49
	YOLOv3-tiny	8669002	12.9	1.7	16.6	76.44
	YOLOv3-tiny-Ghost-Shuffle	620344	2.4	2.3	1.4	77.56
	YOLOv4-tiny	6399178	21.8	1.9	12.3	79.13
	YOLOv4-tiny-Ghost-Shuffle	2278010	8.4	1.9	5.1	80.11
1024	YOLOv5	9347865	16.7	1.6	17.8	84.13
	YOLOv5-WPAN	11934134	16.9	1.8	19.1	86.14
	YOLOv5-WPAN-Ghost	4321786	8.4	1.8	7.4	88.03
	YOLOv5-WPAN-Ghost-Shuffle	3376145	6.3	1.2	5.4	89.32
	YOLOv3-tiny	9478945	13.1	1.5	18.7	77.44
	YOLOv3-tiny-Ghost-Shuffle	6945879	3.7	2.1	2.9	79.56
	YOLOv4-tiny	7456849	22.3	1.7	6.8	80.99
	YOLOv4-tiny-Ghost-Shuffle	3415684	10.4	1.7	7.5	81.46

Table 8: Performance comparison of GAN ablation models.

Size	Model	F1-score (%)
896	YOLOv5	81.34
	YOLOv5 + GAN + Poisson	83.46
	YOLO-W + GAN + Poisson	89.51
1024	YOLOv5	84.13
	YOLOv5 + GAN + Poisson	84.55
	YOLO-W + GAN + Poisson	90.74

Table 9: Performance comparison of NST ablation models.

Detection size	Model	Training set classes	F1-score (%)
896	YOLOv5	Disease	81.34
	YOLOv5 + NST	Disease + nondisease	84.33
	YOLOv5 + GAN + Poisson	Disease	83.46
	YOLOv5 + GAN + Poisson + NST	Disease + nondisease	85.44
	YOLO-W + GAN + Poisson	Disease	89.51
	YOLO-W + GAN + Poisson + NST	Disease + nondisease	91.34
1024	YOLOv5	Disease	84.13
	YOLOv5 + NST	Disease + nondisease	84.33
	YOLOv5 + GAN + Poisson	Disease	84.55
	YOLOv5 + GAN + Poisson + NST	Disease + nondisease	86.74
	YOLO-W + GAN + Poisson	Disease	90.74
	YOLO-W + GAN + Poisson + NST	Disease + nondisease	92.38

design, parameter setting, and preprocessing algorithm. Combining our model with different processing techniques and using this as a comparison, our PDNet is essentially a YOLOv5-based nondeformable disease detection algorithm for asphalt pavements with additions such as Generative Adversarial Networks (GAN), Poisson transfer fusion algorithm, and negative sample algorithm (NST). The performance of the model is inseparable from the technology it adds. In the following, we will analyze the advantages of various processing techniques and how they work.

The W-PAN structure makes the fusion of semantic information at al levels of the network more reasonable and sufficient. The introduction of W-PAN has greatly improved the accuracy of the network, especially the accuracy of high-intersection which is higher than required. However, during its introduction also the parameter amount and calculation amount of the model are increased.

The addition of the Ghost module and Shuffle module reduces the computational complexity and parameter volume of the model and compresses the model.

Adversarial generative network (GAN) and Poisson transfer fusion algorithm generate disease types with a small number of samples, which solves the imbalance of training samples to a certain extent and improves the performance of the model without reducing the speed of the model.

The NST algorithm also improves the score without reducing the speed, because in the nondisease samples we

Table 10: Performance comparison table of different network models.

Methods	Backbone	F1-score (%)
Two-stage		
Faster R-CNN	Resnext101	75.14
Cascade R-CNN	Resnext101	75.17
Libra R-CNN	Resnext101	76.33
Grid R-CNN	Resnext101	76.22
Mask R-CNN	Resnext101	76.22
Dynamic R-CNN	Resnet50	76.23
One-stage		
FCOS	Resnext101	76.13
FreeAnchor	Resnext101	76.13
RepPoints	Resnext101	76.12
PAA	Resnext101	76.32
ATSS	Resnet101	75.11
FoveaBox	Resnet101	74.36
FSAF	Resnext101	76.12
VFNet	Resnext101	76.11
SSD512	Vgg16	75.33
RetinaNet	Resnext101	76.46
YOLOv3	CSPdarknet	76.47
YOLOv4	CSPdarknet	79.33
YOLOv5s	CSPdarknet	81.34
Ours	Ours	91.34

Table 11: Performance parameters of each model in the actual test section.

Model	896		1024	
	Speed (FPS)	F1-score (%)	Speed (FPS)	F1-score (%)
YOLOv5	20.0	81.34	5.2	84.13
YOLO-W	33.5	88.49	16.0	89.32
YOLO-W + GAN + Poisson	35.5	89.51	16.1	90.74
YOLO-W + GAN + Poisson + NST(PDNet)	35.5	91.34	16.7	92.38

increase the information entropy and increase the amount of useful information for disease detection.

In addition, the performance of the model is also affected by some parameter settings. For some parameters, some minor adjustments may cause the performance of the model to oscillate, such as the setting of the anchor box, the size of the detection image, and the number of detection layers.

Table 11 visually shows some performance differences of different types of models in the actual road test. From the YOLOv5 model to PDNet, the F1-score with detection sizes of 896 and 1024 is increased by 10.0% and 8.25% respectively; the speed of the model is increased by 15.5% FPS and 11.5 FPS to meet the needs of industrial applications.

6. Conclusion

In this study, based on the YOLOv5 target detection model, a real-time and high robustness detection network-PDNet for nondeformable diseases of asphalt pavement was realized. It realized the rapid and accurate detection of nondeformable diseases of asphalt pavement in the actual road detection process. When the image detection size was 896, the F1-score of 91.34 and the speed of 35.5 FPS were obtained on the Jetson nanoplatform. This algorithm will provide data support for the realization of highway daily maintenance. At the same time, the proposed W-PAN, GAN, Poisson, NST, and other technologies provide a reference for the specific application of artificial neural network optimization methods in edge computing equipment.

Data Availability

The data used to support the findings of this study are included within the article.

Conflicts of Interest

The authors declare that there are no conflicts of interest regarding the publication of this article.

Acknowledgments

The research was supported and funded by the National Key Research and Development Program of China (Grant no. 2021YFB3202901), Major Project of Industry-University Cooperation Science and Technology in Universities in Fujian Province (Grant no. 2020H6009), and the State Key Laboratory of Rail Traffic Control and Safety (Contract no. RCS2020K004), Beijing Jiaotong University.

References

[1] J. Huang, W. Liu, and X. Sun, "A pavement crack detection method combining 2D with 3D information based on dempster-shafer theory," *Computer-Aided Civil and Infrastructure Engineering*, vol. 29, no. 4, pp. 299–313, 2014.

[2] G. X. Hu, B. L. Hu, Z. Yang, L. Huang, and P. Li, "Pavement crack detection method based on deep learning models," *Wireless Communications and Mobile Computing*, vol. 2021, Article ID 5573590, 13 pages, 2021.

[3] J. Y. Zhang, C. Yan, and X. X. Huang, "Edge detection of images based on improved Sobel operator and genetic algorithms," in *Proceedings of the 2009 International Conference on Image Analysis and Signal Processing*, pp. 31–35, IEEE, Linhai, China, April 2009.

[4] S. Balochian and H. Baloochian, "Edge detection on noisy images using Prewitt operator and fractional order differentiation," *Multimedia Tools and Applications*, vol. 81, no. 7, pp. 9759–9770, 2022.

[5] E. S. Li, S. L. Zhu, B. S. Zhu, Y. Zhao, and L. H. Song, "An adaptive edge-detection method based on the canny operator," in *Proceedings of the 2009 International Conference on Environmental Science and Information Application Technology*, pp. 465–469, IEEE, Wuhan, China, July 2009.

[6] Y. Zhang, Q. Li, X. Zhao, and M. Tan, "TB-Net: a three-stream boundary-aware network for fine-grained pavement disease segmentation," in *Proceedings of the IEEE/CVF Winter Conference on Applications of Computer Vision*, pp. 3655–3664, IEEE, Snowmass Village, USA, March 2021.

[7] R. Girshick, J. Donahue, T. Darrell, and J. Malik, "Rich feature hierarchies for accurate object detection and semantic segmentation tech report (v5)," in *Proceedings of the IEEE Conference on Computer Vision and Pattern Recognition*, pp. 580–587, IEEE, Columbus, USA, June 2014.

[8] M. Li, H. Ge, and H. Wang, "IMG-centernet: an optimized algorithm based on CenterNet for pedestrian detection," in *Proceedings of the 2022 IEEE 6th Information Technology and Mechatronics Engineering Conference (ITOEC)*, pp. 203–208, IEEE, Chongqing, China, March 2022.

[9] S. Ren, K. He, R. Girshick, J. Sun, and R.-C. N. N. Faster, "Faster R-CNN: towards real-time object detection with region proposal networks," *IEEE Transactions on Pattern Analysis and Machine Intelligence*, vol. 39, no. 6, pp. 1137–1149, 2017.

[10] W. Liu, D. Anguelov, D. Erhan et al., "SSD: single shot multibox detector," in *Proceedings of the European Conference on Computer Vision*, pp. 21–37, Springer, Cham, September 2016.

[11] T. Y. Lin, P. Goyal, R. Girshick, K. He, and P. Dollar, "Focal loss for dense object detection," in *Proceedings of the IEEE International Conference on Computer Vision*, pp. 2980–2988, IEEE, Venice, Italy, October 2017.

[12] S. Zhang, C. Chi, Y. Yao, Z. Lei, and S. Z. Li, "Bridging the gap between anchor-based and anchor-free detection via adaptive training sample selection," in *Proceedings of the IEEE/CVF Conference on Computer Vision and Pattern Recognition*, pp. 9759–9768, IEEE, Washington, USA, June 2020.

[13] Z. Tian, C. Shen, H. Chen, and T. He, "FCOS: fully convolutional one-stage object detection," in *Proceedings of the IEEE/CVF International Conference on Computer Vision*, pp. 9627–9636, IEEE, Seoul, Korea, October 2019.

[14] Z. Yang, S. Liu, H. Hu, L. Wang, and S. J. I. Lin, "RepPoints: point set representation for object detection," in *Proceedings of the IEEE/CVF International Conference on Computer Vision*, pp. 9657–9666, IEEE, Seoul, Korea, October 2019.

[15] W. Huang and Z. Ning, "A novel road crack detection and identification method using digital image processing techniques," in *Proceedings of the 2012 7th International Conference on Computing and Convergence Technology (ICCCT)*, pp. 397–400, IEEE, Seoul, Korea, December 2012.

[16] L. Wang and Z. Zhang, "Automatic detection of wind turbine blade surface cracks based on UAV-taken images," *IEEE Transactions on Industrial Electronics*, vol. 64, no. 9, pp. 7293–7303, 2017.

[17] L. Peng, W. Chao, S. Li, and B. Feng, "Research on crack detection method of airport runway based on twice-threshold segmentation," in *Proceedings of the 2015 Fifth International Conference on Instrumentation and Measurement, Computer, Communication and Control (IMCCC)*, pp. 1716–1720, IEEE, Qinhuangdao, China, September 2015.

[18] H. Oliveira and P. L. Correia, "CrackIT-an image processing toolbox for crack detection and characterization," in *Proceedings of the 2014 IEEE International Conference on Image Processing (ICIP)*, pp. 798–802, IEEE, Paris, France, October 2014.

[19] A. Ayenu-Prah and N. Attoh-Okine, "Evaluating Pavement cracks with bidimensional empirical mode decomposition," *EURASIP Journal on Applied Signal Processing*, vol. 1, 2008.

[20] M. Yan, S. Bo, K. Xu, and Y. He, "Pavement crack detection and analysis for high-grade highway," in *Proceedings of the 2007 8th International Conference on Electronic Measurement and Instruments*, pp. 548–552, IEEE, Xi'an, China, 2007.

[21] N. Wei, X. M. Zhao, X. Y. Dou, H. X. Song, and T. Wang, "Beamlet transform based pavement image crack detection," in *Proceedings of the 2010 International Conference on Intelligent Computation Technology and Automation*, pp. 881–883, IEEE, Changsha, China, May 2010.

[22] J. Zhou, P. S. Huang, and F. P. Chiang, "Wavelet-based pavement distress detection and evaluation," *Optical Engineering*, vol. 45, no. 2, p. 027007, 2006.

[23] P. Subirats, J. Dumoulin, V. Legeay, and D. Barba, "Automation of pavement surface crack detection using the continuous wavelet transform," in *Proceedings of the 2006 International Conference on Image Processing*, pp. 3037–3040, IEEE, Atlanta, USA, October 2006.

[24] Z. Lin and X. Zhao, "Geometrical flow-guided fast beamlet transform for crack detection," *IET Image Processing*, vol. 12, no. 3, pp. 382–388, 2018.

[25] T. S. Nguyen, S. Bégot, F. Duculty, and M. Avila, "Free-form anisotropy: a new method for crack detection on pavement surface images," in *Proceedings of the 2011 18th IEEE International Conference on Image Processing*, pp. 1069–1072, IEEE, Brussels, Belgium, September 2011.

[26] R. Amhaz, S. Chambon, J. Idier, and V. Baltazart, "Automatic crack detection on two-dimensional pavement images: an algorithm based on minimal path selection," *IEEE Transactions on Intelligent Transportation Systems*, vol. 17, no. 10, pp. 2718–2729, 2016.

[27] D. Ai, G. Jiang, L. Siew Kei, and C. Li, "Automatic pixel-level pavement crack detection using information of multi-scale neighborhoods," *IEEE Access*, vol. 6, pp. 24452–24463, 2018.

[28] Y. Shi, L. Cui, Z. Qi, F. Meng, and Z. Chen, "Automatic road crack detection using random structured forests," *IEEE Transactions on Intelligent Transportation Systems*, vol. 17, no. 12, pp. 3434–3445, 2016.

[29] Y.-J. Cha, W. Choi, and O. Büyüköztürk, "Deep learning-based crack damage detection using convolutional neural

networks," *Computer-Aided Civil and Infrastructure Engineering*, vol. 32, no. 5, pp. 361–378, 2017.

[30] K. Zhang, H. D. Cheng, and B. Y. Zhang, "Unified approach to pavement crack and sealed crack detection using preclassification based on transfer learning," *Journal of Computing in Civil Engineering*, vol. 32, no. 2, 2018.

[31] X. Yang, H. Li, Y. Yu, X. Luo, T. Huang, and X. Yang, "Automatic pixel-level crack detection and measurement using fully convolutional network," *Computer-Aided Civil and Infrastructure Engineering*, vol. 33, no. 12, pp. 1090–1109, 2018.

[32] F.-C. Chen and M. R. Jahanshahi, "NB-CNN: deep learning-based crack detection using convolutional neural network and naïve bayes data fusion," *IEEE Transactions on Industrial Electronics*, vol. 65, no. 5, pp. 4392–4400, 2018.

[33] S. Park, S. Bang, H. Kim, and H. Kim, "Patch-based crack detection in black box images using convolutional neural networks," *Journal of Computing in Civil Engineering*, vol. 33, no. 3, 2019.

[34] Q. Zou, Z. Zhang, Q. Li, X. Qi, Q. Wang, and S. Wang, "DeepCrack: learning hierarchical convolutional features for crack detection," *IEEE Transactions on Image Processing*, vol. 28, no. 3, pp. 1498–1512, 2019.

[35] M. Tan, R. Pang, and Q. V. Le, "EfficientDet: scalable and efficient object detection," in *Proceedings of the IEEE/CVF Conference on Computer Vision and Pattern Recognition*, pp. 10781–10790, IEEE, Eattle, USA, June 2020.

[36] K. Han, Y. Wang, Q. Tian, J. Guo, and C. Xu, "GhostNet: more features from cheap operations," in *Proceedings of the IEEE/CVF Conference on Computer Vision and Pattern Recognition*, pp. 1580–1589, IEEE, Seattle, USA, June 2020.

[37] X. Zhang, X. Zhou, M. Lin, and J. Sun, "ShuffleNet: an extremely efficient convolutional neural network for mobile devices," in *Proceedings of the IEEE Conference on Computer Vision and Pattern Recognition*, pp. 6848–6856, IEEE, Salt Lake City, USA, June 2018.

[38] H. Rezatofighi, N. Tsoi, J. Gwak, A. Sadeghian, and S. Savarese, "Generalized Intersection over union: a metric and a loss for bounding box regression," in *Proceedings of the IEEE/CVF Conference on Computer Vision and Pattern Recognition*, pp. 658–666, IEEE, Long Beach, USA, June 2019.

[39] Z. Zheng, P. Wang, W. Liu, J. Li, R. Ye, and D. Ren, "Distance-IoU loss: faster and better learning for bounding box regression," *Proceedings of the AAAI Conference on Artificial Intelligence*, vol. 34, no. 07, pp. 12993–13000, 2020.

[40] A. Creswell, T. White, V. Dumoulin, K. Arulkumaran, B. Sengupta, and A. A. Bharath, "Generative adversarial networks: an overview," *IEEE Signal Processing Magazine*, vol. 35, no. 1, pp. 53–65, 2018.

[41] M. Arjovsky, S. Chintala, and L. Bottou, "Wasserstein GAN," in *Advances In Neural Information Processing Systems, NeurIPS, Montréal*, Canada, December 2018.

[42] L. J. Ratliff, S. A. Burden, and S. S. Sastry, "Characterization and computation of local Nash equilibria in continuous games," in *Proceedings of the 2013 51st Annual Allerton Conference on Communication, Control, and Computing (Allerton)*, pp. 917–924, IEEE, Monticello, USA, October 2013.

[43] C. C. Hsu, H. T. Hwang, Y. C. Wu, Y. Tsao, and H. M. Wang, "Voice conversion from unaligned corpora using variational autoencoding wasserstein generative adversarial networks," in *Proceedings of the Computation and Language*, June 2017.

[44] F. Luleci, F. N. Catbas, and O. Avci, "Generative adversarial networks for labeled data creation for structural monitoring and damage detection," in *Proceedings of the Machine Learning, Computer Science*, New York, USA, Decmber 2021.

[45] E. Reinhard, M. Adhikhmin, B. Gooch, and P. Shirley, "Color transfer between images," *IEEE Computer Graphics and Applications*, vol. 21, no. 4, pp. 34–41, 2001.

Hindawi
Computational Intelligence and Neuroscience
Volume 2022, Article ID 6679237, 11 pages
https://doi.org/10.1155/2022/6679237

Research Article

Marketing Archive Management of Drama Intangible Cultural Heritage Based on Particle Swarm Algorithm

Cenxi Li[1] and Boya Liu[2]

[1]*Sichuan Conservatory of Music, Chengdu 610000, China*
[2]*Chongqing Normal University, Chongqing 401331, China*

Correspondence should be addressed to Boya Liu; 20132044@cqnu.edu.cn

Received 27 May 2022; Revised 9 June 2022; Accepted 10 June 2022; Published 7 July 2022

Academic Editor: Xin Ning

Each Chinese region has its own ancient opera, which is a treasure of folk culture and a living fossil for studying the historical origins of a local culture. It has significant academic value and historical significance at the national and local levels, whether from the perspective of promoting and disseminating national culture or from the perspective of protecting the world's intangible cultural heritage. Based on this practical significance, this paper conducts a study using the particle swarm algorithm to manage the marketing archives of drama intangible cultural heritage. The article employs the PSO algorithm to test the particle swarm optimization algorithm's convergence and conditions. The effectiveness of the algorithm is analysed in the Sphere function, Rosenbrock function, Griewanks function, and Rastrigin noncont function, and then the algorithm is compared, including the calculation speed comparison between the algorithm in this paper and the three optimal fitness functions. The experimental results show that the PSO algorithm has the highest four items in the statistics of the Schwefel function experimental results. About 45.0379 is the best value and 70.5878 is the maximum precision. The optimal average value is 6.1524, while the average value is 56.15245. In comparison to the QPSO and PSO algorithms, the algorithm in this paper has a faster convergence speed and better search accuracy. The topic of the intersection of the disciplines of drama, intangible cultural heritage marketing, and archive management using the particle swarm algorithm is well-developed.

1. Introduction

Intangible cultural heritage is the precious cultural wealth of mankind. It is the embodiment and memory of national cultural traditions. It can promote the inheritance of traditional culture and the protection of cultural diversity. Nowadays, more and more people organically combine the protection of intangible cultural heritage with tourism development, attracting the emerging elements of intangible cultural heritage into tourism activities, which has become an important way for intangible cultural heritage to meet the needs and development of modern society. Various forms of folk performances, including folk activities and performing arts, are constantly being updated and gradually integrated into this cultural heritage with great potential for development. As intangible cultural heritage, its scope has a definition, including poetry, mythology, etc. However, it is not limited to this category. In addition, there are many kinds of folk performing arts, such as epics and stories. Even rituals passed down from generation to generation by ordinary people and practices related to traditional folk knowledge and cultural sites are included. For example, the electronic file information management module includes four business modules of file maintenance, review, query, and statistics.

In recent years, China is committed to the protection of intangible cultural heritage, and many experts and scholars have carried out research on this aspect. Hammou I considered that intangible heritage is increasingly featured in the planning of several agencies that aim to raise awareness among countries about safeguarding their cultural diversity and to help them develop programmes so as to protect and preserve this type of heritage. However, there was a lack of information when he solved this problem [1]. Zhang and Lee explored the dialectical relationship between authenticity and alienation in intangible cultural heritage (ICH) tourism research based on assessing the role of cultural values in Chinese tourism. His research has certain implications for tourism marketing, aiming to understand the authenticity of the supply side of intangible cultural heritage tourism. However, his research data is not processed by mixed methods, and there may be data errors [2]. Zhang et al. proposed a tourist-based authenticity model to address this problem, where the authenticity of heritage sporting events contains both "cool" and "hot" factors. Using Naadam as an example, the model examined these factors and their impact on tourist satisfaction and loyalty. About 700 questionnaires were distributed in six locations from eastern to western Inner Mongolia, China. His research showed that there are two separate factors for coldness and heatness. Both factors of cold authenticity directly affect thermal authenticity and satisfaction [3]. Veghe explored the links between cultural heritage, marketing and local community sustainability based on secondary data on engagement, perceived importance, access and stewardship. He argued that despite the increasing recognition and expansion of capitalization, the use of tangible and intangible cultural heritage as assets that may benefit local communities remains limited. However, his research did not involve the different geographical conditions at home and abroad, and has geographical limitations [4]. Although the research content is sufficient, the research on intangible cultural heritage is still limited by geographical and human resources, which makes people in the era of big data and algorithms cannot help considering: Is it possible to manage the intangible cultural heritage archives using the ideas of the intersection of disciplines?

Particle swarm optimization is a hot research topic recently, and people have tried to use this algorithm to study many aspects. Jain et al. reviewed the research progress of particle swarm optimization algorithm (PSO) from 1995 to 2017. He discussed the progress, improvement, and application of particle swarm optimization algorithm. He divided PSOs into nine categories according to different aspects. However, his research did not hybridize PSO technology with other evolutionary technologies, which did not have theoretical breadth [5]. Tang and Guan took time delay as an additional parameter and gave parameter estimates for chaotic systems with time delays. The parameter estimation problem is transformed into an optimization problem, which finds an optimal parameter combination, that is, minimizes the objective function [6]. Chen proposed a multiple attribute decision-making (MADM) method based on interval-valued intuitionistic fuzzy-weighted geometric mean (IIFWGA) operator, interval-valued intuitionistic fuzzy-valued precision function (IVIFV), and particle swarm optimization (PSO) techniques. Among them, the attribute weight and the evaluation value of the alternatives relative to the attribute are denoted by IVIFV. But his research did not generate optimal weights for attributes, which has limitations [7]. Gong Y J first developed a new framework to organically combine PSO with another "learning" optimization technique, leading to the generalized paradigm of "PSO learning". He also proposed a new *L-PSO algorithm, called genetic learning PSO (GL-PSO), using genetic evolution techniques to generate promising samples for particle swarm optimization (PSO) algorithms. But his study did not perform mechanical parallel stacking [8]. In the research of these scholars, it is inevitable to encounter the limitations of particle swarm optimization. The algorithm is very easy to "premature," and the population diversity is lacking in the late iteration, which makes it easy to fall into the local optimum situation. This is very unfavorable for the analysis of the problem.

Since its inception, the PSO algorithm has attracted the attention of many researchers due to its few parameters, simple operation, and easy implementation. In a very short period of time, a large number of research findings have emerged. Due to some flaws in the PSO algorithm, relevant scholars have made a number of enhancements, which are primarily focused on the following three aspects: (1) improvements to the PSO algorithm, such as inertia factor and parameter selection; (2) integrating PSO with other optimization algorithms to improve; and (3) optimising the PSO algorithm's network topology. The PSO algorithm has been improved in recent years. Adding the weight w, for example, can achieve the goal of balancing particle local search and overall search ability, which can improve the PSO algorithm's performance. Another example is the dynamic inertia weight change strategy, which uses two attractor and repulsion processes to optimise particle evolution and speed up the algorithm's convergence. It accelerates population convergence and effectively prevents particles from settling in local best-fit solutions. The goal of the article is to improve the algorithm's shortcomings and apply it to the creation of drama intangible cultural heritage archives.

2. Particle Swarm Optimization and Intangible Cultural Heritage Deconstruction Methods

2.1. Swarm Intelligence Overview. In recent years, team intelligence has received extensive attention in many fields [9, 10]. In nature, although many biological individuals are simple and without intelligence, the behavior of groups is often very complex [11]. This natural phenomenon has aroused great interest of biologists and computer scientists at home and abroad [12]. In recent years, with the rise of biomimicry and research, scientists have begun to study social organisms, such as ants, schools of fish, and flocks of birds, so as to solve practical problems, and swarm intelligence algorithms were born. The swarm intelligence algorithm is a stochastic optimization algorithm that solves practical problems by simulating the intelligent characteristics of certain swarm behaviors in nature [13]. The main characteristics of swarm intelligence include the followings: 1. simplicity; 2. distribution; 3. robustness; 4. wide applicability. Adaptability means that the algorithm proposed in this paper can not only solve the problem of numerical optimization, but also solve the problem of the distribution of discrete variables. It can be a single set of data or a combination of many discrete variables. The initial flowchart is shown in Figure 1:

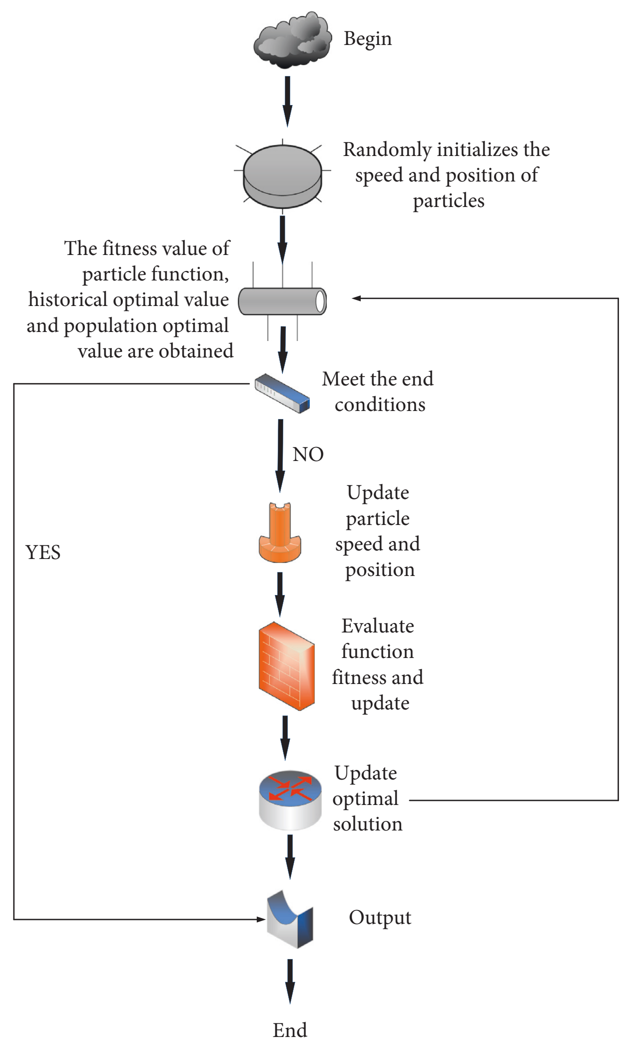

Figure 1: Initial PSO flowchart.

2.2. Explanation of Correlation between the Coordinated Development of Intangible Cultural Heritage and Ecotourism. Since the end of the last century, China's intangible cultural heritage has been dying. The main reasons include two aspects: (1) Many traditional intangible cultural heritage heirs are getting old, and young people are reluctant to learn, resulting in the inheritance of intangible cultural heritage culture. (2) With economic construction and development, many intangible cultural heritage sites have been demolished, resulting in fewer places for cultural heritage. Different from nature tourism, ecotourism is characterized in that it has certain functions of ecological environment education and protection of local characteristic culture [14], which can help tourists and local communities to establish awareness of natural and humanistic environmental protection. It makes tourists have a certain sense of responsibility for the environment and reduce the adverse impact on the environment of ecotourism areas [15], making tourists consciously maintain the stable state of the ecosystem and local culture. The employees of the scenic spot need to take the sustainable development of the scenic spot as the working principle, strengthen the awareness and habits of saving and protection in their work, and infect tourists with practical actions [16], as well as use the cultural heritage of intangible cultural heritage to attract tourists. Intangible culture is closely related and inseparable from traditional Confucianism in the inheritance of thousands of years. It can be said that intangible cultural heritage is a carrier of Confucianism.

Coordination refers to the phenomenon in which two (or more) systems or system factors influence each other through different interactions [17]. This is a benign relationship between multiple systems or elements. "Development" refers to the process in which the system itself or system elements change from small to large, from simple to complex, from low to high, and from disorder to order [18]. "Coordinated development" seems to be based on a virtuous circle, in which the system or system factors develop from low to high, from simple to complex, and from disorder to order. It emphasizes the comprehensive integrated development of multiple systems or systemic factors under the constraints and regulations of "coordination," seeking global optimization, structural optimization, and joint development based on overall improvement [19]. The degree of coordinated development includes the system or element coordination system (that is, collaborative planning) and the level of development of both [20].

Initiative refers to the principle that the initiative stipulates that collectors of intangible cultural heritage archives must have or cultivate a high sense of responsibility to improve their own enthusiasm and initiative, and have a spirit of loyalty.

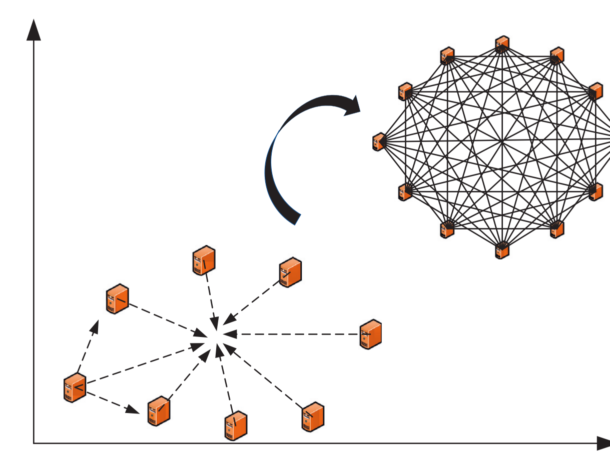

Figure 2: PSO algorithm principle and ER network structure diagram.

2.3. Particle Swarm Optimization Algorithm. Particle swarm optimization is a random search algorithm. Its evolution equation is a discrete dynamic system equation. By analyzing the state change of the dynamic system, the necessary and sufficient conditions for the algorithm to converge are determined, which provides a theoretical basis for the

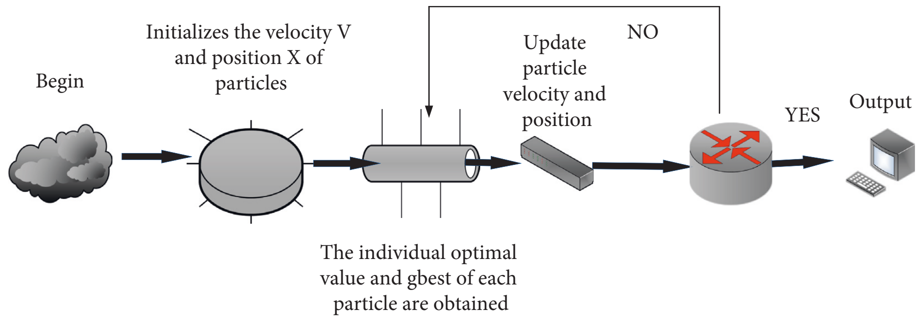

Figure 3: Running process of the standard particle swarm algorithm.

improvement of the algorithm. The PSO optimization algorithm was originally inspired by the life patterns of flocks of birds and fish. In nature, in the process of foraging, birds sometimes need to forage in groups. Sometimes they also need to forage in groups. In each search, there is always a bird with a strong ability to detect the location of the food, so it will transmit information between the flocks and then guide the flock to the food source. The principle of the PSO algorithm and the structure of the ER network are shown in Figure 2:

Information fusion is an information processing process that automatically analyzes and integrates multisource information through certain rules to achieve prediction, reasoning, and decision-making tasks. Through the above research, the operation process of the standard particle swarm algorithm can be given, as shown in Figure 3.

In order to verify the convergence and conditions of the particle swarm optimization algorithm, the evolution equation of the standard particle swarm optimization algorithm is used for analysis, as shown in the following formulas:

$$V_{\mathrm{id}}(t+1) = \omega V_{\mathrm{id}}(t) + c_1 r_1 \left(\mathrm{pbest}_{\mathrm{id}} - x_{\mathrm{id}}(t)\right) + c_2 r_2 \left(\mathrm{gbest}_d - x_{\mathrm{id}}(t)\right), \quad (1)$$

$$x_{\mathrm{id}}(t+1) = x_{\mathrm{id}}(t) + v_{\mathrm{id}}(t+1). \quad (2)$$

First, the d in the evolution equation is removed, and the particle swarm optimization problem is formulated as a one-dimensional optimization problem, namely as formulas (3) and (4):

$$V_i(t+1) = \omega V_i(t) + c_1 r_1 \left(\mathrm{pbest}_i - x_i(t)\right) + c_2 r_2 \left(\mathrm{gbest} - x_i(t)\right), \quad (3)$$

$$x_i(t+1) = x_i(t) + v_i(t+1). \quad (4)$$

In the form of a matrix vector, formula (5) can be obtained as follows:

$$\begin{bmatrix} V_i(t+1) \\ x_i(t+1) \end{bmatrix} = P \begin{bmatrix} V_i(t) \\ x_i(t) \end{bmatrix} + Q \begin{bmatrix} p_i \\ p_s \end{bmatrix}. \quad (5)$$

Among them, there is formula (6) as follows:

$$P = \begin{bmatrix} \omega & -\omega \\ \omega & 1-\phi \end{bmatrix}, \quad Q = \begin{bmatrix} \phi_1 & \phi_2 \\ \phi_1 & \phi_2 \end{bmatrix}. \quad (6)$$

Formula (5) is a discrete-time linear system of equations. Therefore, a sufficient and necessary condition for the algorithm to converge is that the modulus of the eigenvalues of P is less than 1 as follows:

$$f(\lambda) = \lambda E - P = \begin{bmatrix} \lambda - \omega & -\omega \\ \omega & \lambda - (1-\phi) \end{bmatrix}. \quad (7)$$

It can be simplified as follows:

$$\lambda^2 + (\varphi - 1 - \omega)\lambda - \omega = 0. \quad (8)$$

The eigenvalues of P can be obtained as follows:

$$\lambda = \frac{\varphi - 1 - \omega \pm (\varphi - 1 - \omega)^2}{2} = 0. \quad (9)$$

For the convenience of discussion, if the modulus of the eigenvalue is less than 1, formula (10) can be obtained as follows:

$$-2 < \omega + 1 - \phi + (\varphi - 1 - \omega)^2 - 4\omega < 2. \quad (10)$$

In order to test the effectiveness of the algorithm, several functions are selected for comparison.

(1) Sphere function

$$f(x) = \sum_{i=1}^{n} x_i^2. \quad (11)$$

(2) Rosenbrock function

$$f(x) = \sum_{i=1}^{n-1}\left(100\left(x_i^2 - x_{i+1}^2\right)^2 + \left(x_i - 1\right)^2\right). \quad (12)$$

(3) Griewanks function

$$f(x) = \sum_{i=1}^{n} \frac{x_i^2}{4000} - \cos\frac{x_i}{i} + 1. \quad (13)$$

(4) Rastrigin_noncont function

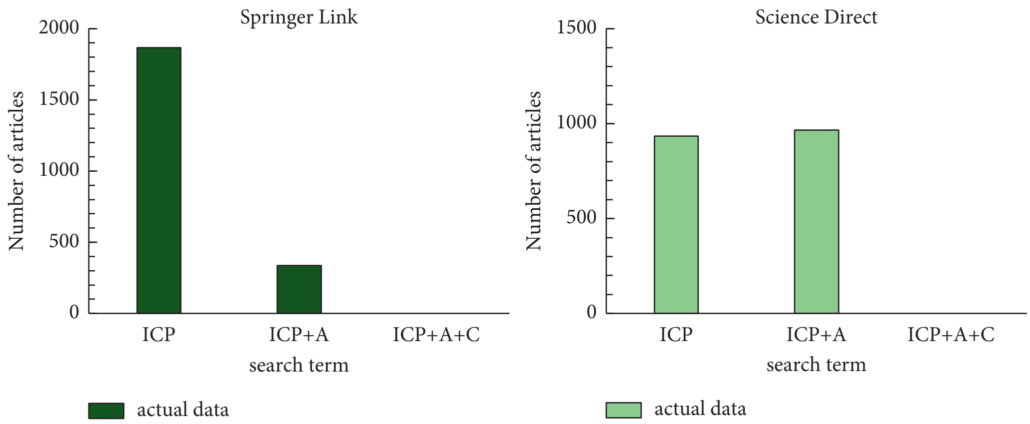

Figure 4: Springer link and science direct literature search results.

$$f(x) = \sum_{i=1}^{n} \left(z_i^2 - 10 \cos(2\pi z_1) + 10 \right),$$
$$z_1 = \begin{cases} x_1 & x_1 < 1/2, \\ \text{round}(2x_i), & x_1 \geq 1/2 \\ 2, & \end{cases} \tag{14}$$

In order to change such limitations, generalized transition distributions and acceptance criteria can be used, which can greatly reduce the problem of lack of diversity. In summary, the speed update formula proposed in this paper is as follows:

$$\begin{aligned} V_{\text{id}}(t+1) = {} & \omega V_{\text{id}}(t) + c_1 r_1 \left(\text{Pbest}_{\text{id}} - x_{\text{id}}(t) \right) \\ & + c_2 r_2 0.7 \times \left(p_b - X_{\text{id}}(t) \right) 0.2 \times \left(p_m - x_{\text{id}}(t) \right) \\ & + 0.1 \times \left(p_w - x_{\text{id}}(t) \right), \end{aligned} \tag{15}$$

$$x_{\text{id}}(t+1) = x_{\text{id}}(t) + V_{\text{id}}(t+1). \tag{16}$$

3. Experiment on the Archives' Management System of Drama Intangible Cultural Heritage

3.1. Data of Intangible Cultural Heritage Archives. At present, the full-text electronic journals provided by Springer link include a total of 439 academic journals. The journals published by Science Direct are recognized as high-quality academic journals in the world, such as the well-known Science journals. Most of them are core journals and are included in many famous secondary literature databases in the world. A data survey was carried out on the research results of foreign cultural heritage archives. ICP stands for "intangible cultural heitage protection." $\text{ICP} + A$ means "intangible cultural heitage protection + archives," and $\text{ICP} + A + \text{C}$ represents "intangible cultural heitage protection + archives + classification." The result is shown in Figure 4.

As can be seen from Figure 4, there are more documents on intangible cultural heritage archives in Springer Link, but there are no documents on intangible cultural heritage protection + archives + classification in the two libraries.

The CNKI journal database was used to search the full-text database of master and doctoral dissertations in China. The results are shown in Table 1.

3.2. Distribution Characteristics of Drama Intangible Cultural Heritage in a Province. When studying the distribution of intangible cultural heritage in a province, statistics were made on the regional distribution of national and provincial intangible cultural heritage in the province, which are expressed from A to U according to the ranking of prefecture-level cities in the province, as shown in Figure 5.

It can be seen from Figure 5 that the total amount of intangible cultural heritage in the province is relatively large, but the regional distribution is uneven. There is a positive correlation between the number of national intangible cultural heritage and the regional distribution.

Since the culture of the province is the cultural basis for the survival of traditional drama, the intangible cultural heritage of the province mainly focuses on drama. From 2015 to 2021, the development of tourism to the province due to intangible cultural heritage such as drama is shown in Figure 6.

As can be seen from Figure 6, the province's year-on-year growth rate of intangible cultural heritage tourism revenue has changed from 27.4% to 29.8%, and the proportion of its contribution to the country's tourism has also increased from 9.38% in 2015 to 10.88% in 2021. It shows that the protection of intangible cultural heritage can promote the development of tourism in this area.

A survey was conducted on tourists and ordinary citizens on the intangible cultural heritage of drama. The results are shown in Figure 7.

For plays unique to the province, 17 had seen some, 146 had heard of it but had not seen it, and 19 had not heard of it. It shows that the popularity of the drama is average. About 94% of people have not seen it, while only 6% of people have seen it. Therefore, the drama should be brought into the life of the masses, so that more people have the opportunity to enjoy the drama.

Table 1: Results of domestic literature search.

	File management	Archives protection	Intangible cultural heritage + archives protection	Intangible cultural heritage + archives classification
Journal full text	6	21	88	167
Master's thesis	4	2	6	13
Doctoral dissertation	0	0	1	0

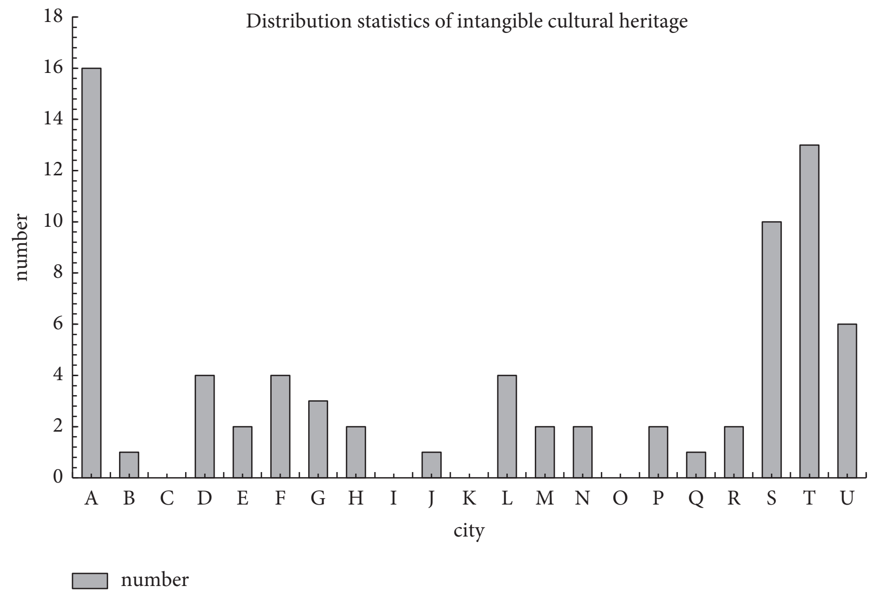

Figure 5: Statistics on the distribution of national intangible cultural heritage in the province.

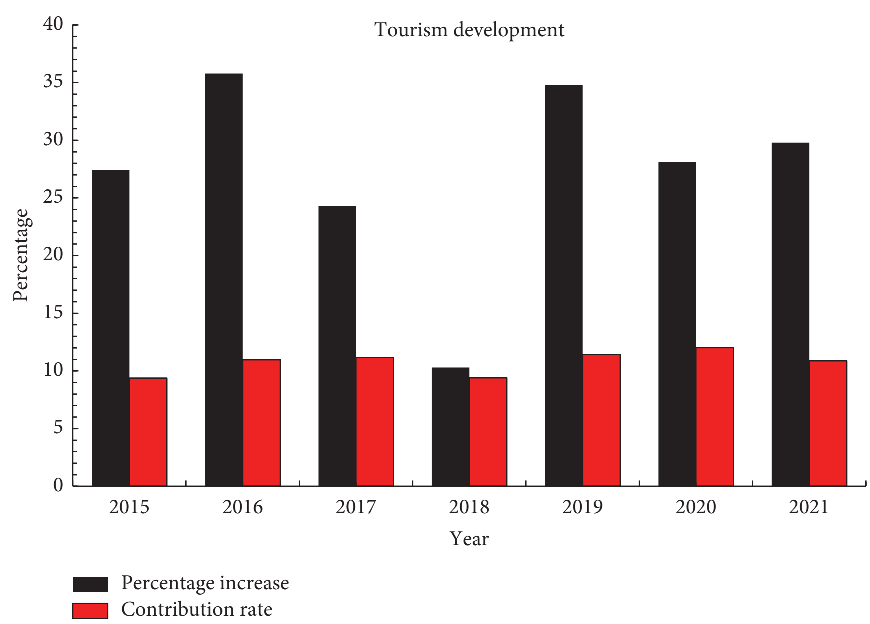

Figure 6: Map of tourism development in the province.

3.3. Simulation Test Results of the Intangible Cultural Heritage Archives' Management System. In order to show the performance of different algorithms more intuitively, PSO, DRWS-PSO, and ST-PSO were compared and the three algorithms were run independently for 50 times. The maximum, minimum, average, and average time for each algorithm were derived, as shown in Table 2.

According to Table 2, it can be seen that for the four functions used for testing, the improved ST-PSO algorithm takes less time, which is more efficient than the traditional

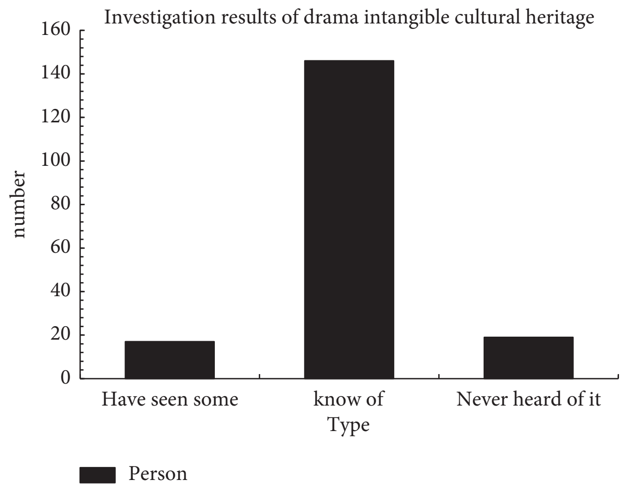

Figure 7: Results of the investigation on the intangible cultural heritage of drama.

Table 2: Function test results.

Test function	Algorithm	Max	Min	Average	Average time
$F1$	PSO	18.6564	21.1245	43.0168	0.98
	DRSW-PSO	17.1547	14.6653	20.1518	0.99
	ST-PSO	16.4155	12.1544	13.2201	0.88
	PSO	14.1524	11.1545	10.1576	1.15
$F2$	DRSW-PSO	24.4587	21.2545	22.1547	1.04
	ST-PSO	34.4154	29.2584	32.4557	1.00
	PSO	18.9694	8.7015	8.4852	1.29
$F3$	DRSW-PSO	19.6673	4.8814	4.3343	1.21
	ST-PSO	18.8685	1.0015	1.1205	1.05
	PSO	615.5458	598.5245	606.2218	1.13
$F4$	DRSW-PSO	374.2545	361.5245	368.7541	1.33
	ST-PSO	330.1545	298.5247	311.2435	0.85

PSO and DRSW-PSO. In addition, since the ST-PSO algorithm refers to the scale-free network as the domain structure of particles, the experimental results confirm that its algorithm performance is significantly better than that of PSO and DRSW-PSO.

The best solution and worst value of each algorithm and the average and standard deviation of the optimal fitness function are listed below.

Rosenbrock functions are generally nonconvex functions for testing optimal algorithms, which is also called the banana function. The statistics of the experimental results of the Rosenbrock function are shown in Table 3.

In the experimental results of Rosenbrock function, the optimal value of the PSO algorithm is the highest. The worst value is the lowest. The optimal fitness is moderate, which are 44.7568, 237.248, and 26.4578, respectively.

The statistics of the experimental results of the Griewank function are shown in Table 4.

Table 3: Statistics of experimental results of the Rosenbrock function.

	Best	Worst	Average	Stdev
PSO	44.7568	237.2487	62.4154	26.4578
DRSW-PSO	44.5247	111.4154	48.4558	9.3457
ST-PSO	32.1547	148.1545	56.4789	36.5847

Table 4: Statistics of experimental results of Griewank function.

	Best	Worst	Average	Stdev
PSO	0.0916	4.9451	1.3215	1.0145
DRSW-PSO	0.0223	-1.1147	0.2558	0.1685
ST-PSO	0.0578	0.4935	0.1998	0.05457

Table 5: Statistics of experimental results of Schwefel function.

	Best	Worst	Average	Stdev
PSO	45.0379	70.5878	56.15245	6.1524
DRSW-PSO	16.2457	39.2458	24.2415	4.2459
ST-PSO	23.2458	39.2456	30.5487	4.1558

In the statistics of the experimental results of the Griewank function, the average value of the PSO algorithm is the highest, and the optimal fitness is extremely high. The results are 1.3215 and 1.0145, respectively.

The statistics of the experimental results of the Schwefel function are shown in Table 5.

In the statistics of the experimental results of the Schwefel function, the four items of the PSO algorithm are the highest. The optimal value is 45.0379. The maximum accuracy is 70.5878. The average value is 56.15245, and the optimal average value is 6.1524. Therefore, in general, APSO algorithm has faster convergence speed and better search accuracy than QPSO algorithm and PSO algorithm.

In order to test the scheduling performance of the improved particle swarm algorithm, the following compares the completion time of the Chebyshev dynamic chaotic perturbation particle swarm optimization algorithm with adaptive inertia weight and traditional particle swarm optimization algorithm, round-robin scheduling algorithm (RR), and Max-Min algorithm. When the tasks are 20 and 50, the comparison results are shown in Figure 8.

Compared with the traditional particle swarm optimization algorithm, the traditional chaotic perturbation particle swarm optimization algorithm, and the chaotic perturbation particle swarm optimization algorithm, the improved particle swarm optimization algorithm converges faster in the repeated initial stage. However, in the later stage of algorithm repetition, the improved algorithm has better convergence effect, which is more stable. It has a shorter total completion time, which obviously meets the needs of users.

In order to expand the task volume, the algorithms are compared when the tasks are 200 and 500. The comparison results are shown in Figure 9.

It can be seen from Figure 9 that the Chebyshev chaos perturbation particle swarm optimization (Chevbyshev-FAPSO) with adaptive inertia weight has better scheduling

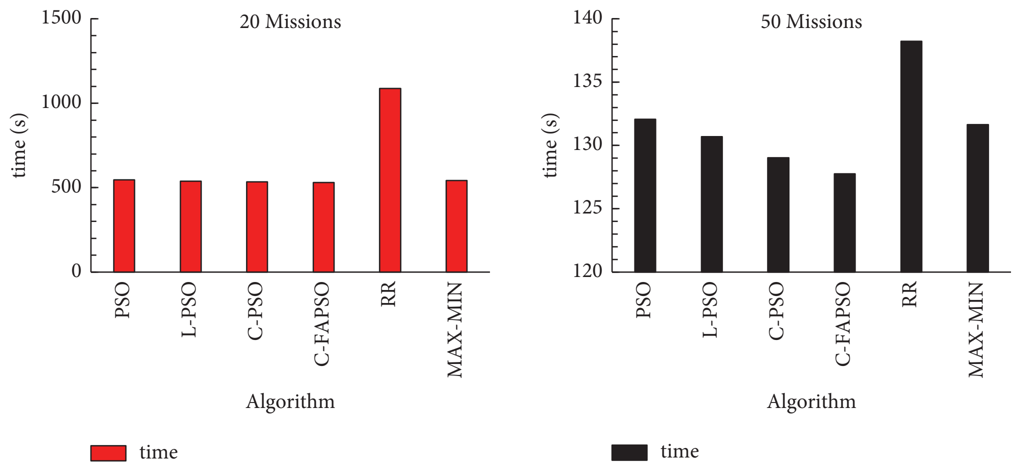

Figure 8: Time spent when there are 20 and 50 tasks.

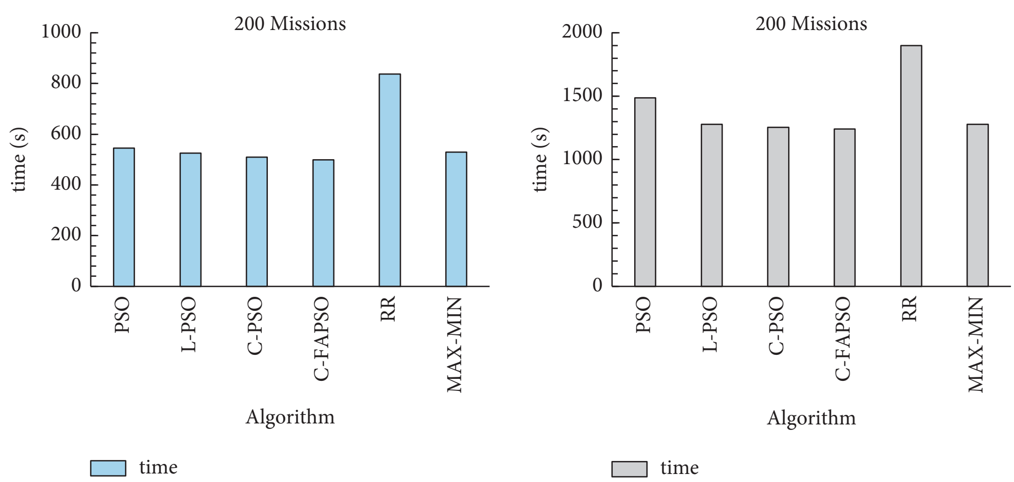

Figure 9: Time spent when there are 200 and 500 tasks.

results, and the improved particle swarm optimization takes the shortest time to complete the same tasks.

4. Particle Swarm Algorithm and File Management

4.1. Agent Modeling and Chaos Mapping. Agent often refers to a person who has the ability to recognize and practice in the objective world. For machines, it is an intelligent body with autonomous perception, judgment, reasoning, and decision-making. From the perspective of knowledge, the Agent is defined as an agent who has experience knowledge and can use knowledge to solve problems. The characteristics of Agent determine that the system it builds is nondeterministic, because the autonomy of Agent will make the system also have autonomy. Such a system is difficult to accurately predict, evaluate, and make decisions. Similarly, the behavior and state of the Agent system are random in design, and it is difficult to determine. Although the behavior of each Agent can be standardized, the system will only show the randomness of the state when it is running. Therefore, the unpredictability of the behavior of the traditional Agent model is a problem that needs to be solved.

Although the Agent method has inherent defects, it is necessary to expand and enhance the interactive semantic representation ability of Agent. The cyber-physical system (CPS) can provide this function to make up for the defect of the Agent system. CPS includes system engineering such as environment perception, embedded computing, network communication, and network control, so that the Agent system has the functions of autonomous perception, communication interaction, judgment, reasoning and decision-making, remote cooperation, and autonomy. Such a CPS-Agent system can accurately predict, evaluate, and make decisions based on the perception of itself, the environment and other agents, which can also solve the real-time dynamic randomness problem of the system.

Chaos covers almost every branch of the natural and social sciences. It has its own unique characteristics. The phenomenon of chaos seems to be random, but it has its inherent delicate structure, instead of intricate and disorganized chaos, which is a variable that fluctuates in the interval [0, 1]. In recent decades, gratifying results have been achieved in the study of chaos theory. Approximation methods and numerical integration methods of nonlinear differential equations have enabled people to fully and thoroughly understand, understand and apply the chaos.

The chaotic variable is ergodic, that is, it can search every state of the space without repetition. The randomness of a chaotic variable means that the turbid variable is as cluttered as a random variable. Chaotic variable is very sensitive to the initial conditions, and a small change in the initial value will cause a huge change in the later movement, which may lead to a large discrepancy. Due to these characteristics, the turbidity-based search technology is more advantageous.

4.2. File Management. In recent years, network management and automated document management have quietly become research directions in related fields. Meanwhile, good progress has been made in management level and innovation in theory and practice. For example, developed countries in Europe and the United States, Australia, and other advanced regions have integrated the research methods of network information document management into the national development planning process, and management tools have also changed. That is, they have their own management plans for the company in the country, from loose management to complex unified centralized management. These changes fully demonstrate that network information management has become an inevitable trend in the development of document management. The development of these documents also affects the management of our country.

Because in the original database table, it is often necessary to input file information, and the file information statistics need to generate monthly loan information. Therefore, multiple queries are required to statistic file information. Eventually monthly files are created and stored in statistic view. In countries such as Europe and the United States, it has been proposed to manage documents and documents through a network management framework. At the same time, it will also combine e-government for effective document and archive management. More than 90% of important official documents will no longer be stored on printed materials and computers. In other words, the information management of network file records has become an effective means of government management. Australia also put forward the strategic idea of network file management, aiming to transform traditional management into a more effective network management tool.

4.3. RFID Technology. With the rapid development of electronic technology, electronic file management system came into being. It not only improves the efficiency of work, but also backs up the original paper archives to ensure the safety of the archives. However, electronic files are not suitable for storing all data, and large enterprises and companies have a large number of files, so it is impossible to completely convert all files into electronic storage in a short period of time. Therefore, the management method of physical archives is still irreplaceable. It is very urgent to develop a set of archives management system that can meet the current needs.

RFID (Radio Frequency Identification) technology is a new technology that was born at the end of the last century and has developed rapidly in recent years, which is one of the key technologies of the Internet of Things. RFID technology uses radio-frequency antennas to communicate to achieve the purpose of exchanging data and identifying targets, and integrates signal transmission, automatic identification, radar, and other technologies. It has the characteristics of strong storage capacity, high security, and outstanding antipollution ability, and has been maturely used in various fields of society. RFID systems can be classified according to energy supply mode, operating frequency, and working mode.

China's RFID technology started relatively late, with a lack of core technology, especially in RFID UHF is still in its infancy. In addition, China's RFID technology standards are not unified. The products produced by various manufacturers are quite different, and they are not compatible with each other, which greatly limits the development of RFID technology. But in recent years, China's RFID technology has also made great progress. Among them, the automatic identification system of railway vehicle number (ATIS) is the earliest system using RFID technology in China. Using ATIS can accurately collect the running status data of locomotives and vehicles, such as vehicle number, vehicle number, status, location, and departure time, and can track vehicle movements in real time. At present, China has issued a total of 1.4 billion second-generation ID cards, realizing the large-scale application of RFID technology, and it has also been widely used in mobile payment, public transportation, commodity tracking and anticounterfeiting, and medical and health fields.

4.4. Backup and Storage of Intangible Cultural Heritage Archives. Sudden and highly destructive events such as fires, earthquakes, and environmental hazards often seriously threaten the security of archives and affect the order of archives work. The daily management of intangible cultural heritage archives includes the formulation of emergency plans. Through drills and training, the staff's emergency rescue ability can be improved in multiple ways. When emergencies occur, emergency protection techniques can be widely used and effective rescue work can be carried out in time, which can not only prevent the slow response, insufficient rescue, and ineffective response caused by insufficient preparation, but also reduce or even avoid the damage of intangible cultural heritage archives. These emergency measures cannot guarantee that the precious intangible cultural heritage will be avoided from the danger of extinction, so the backup and preservation of the intangible cultural heritage archives should also be implemented. The backup storage of intangible cultural heritage archives mainly includes the implementation of off-site backup storage, and heterogeneous backup storage. The off-site backup strategy of archives refers to making real-time available safe copies of intangible cultural heritage archives in another place. Off-site backup storage can minimize the losses caused by unexpected events, but the disadvantage is that the capital demand is too large. Therefore, off-site backup storage is mainly aimed at particularly important intangible cultural heritage files, for example, microforms of precious paper intangible cultural heritage files, files of traditional skills that are on the verge of being lost, etc.

In addition to off-site backup files, intangible cultural heritage files should also implement heterogeneous backup of intangible cultural heritage files. Heterogeneous backup is to realize the backup of different file forms, and use materials of different textures to store the intangible cultural heritage information, for example, the use of optical discs, magnetic disks, or other materials of different textures for backup, in order to achieve the purpose of backup. Compared with the disadvantage of large demand for storage funds for off-site backup, the cost of heterogeneous backup is low and the difficulty of storage is small. After the heterogeneous backup, the intangible cultural heritage archives have multiple copies, which is helpful for the long-term preservation of the intangible cultural heritage archives.

In addition, there is a cloud backup of intangible cultural heritage files. Cloud backup has the advantages of high storage capacity, high utilization rate, high security performance, and low cost. Cloud backup is mainly suitable for intangible cultural heritage electronic files with high frequency of use and large access volume. It can not only ensure the security of archive data, but also realize automatic management and backup for users of intangible cultural heritage archives, which can be fully used in the utilization of intangible cultural heritage archives.

5. Conclusions

The treasure of human society is intangible cultural heritage. It carries a nation's history and culture, as well as the nation's cohesion and centrifugal force, which is vital. Intangible cultural heritage has become increasingly marginalised in modern society as our country's economy has developed rapidly. When the feedback algorithm interacts with a human, the process becomes more complicated, and the accuracy of the feedback algorithm is severely limited. The optimization of particle swarm optimization is critical in order to achieve breakthroughs in both retrieval efficiency and accuracy. The topic of using algorithms to manage the archives of the intangible cultural heritage of drama is relatively new at a time when ideas about the intersection of disciplines are gaining traction. It has been tried by a small number of people, and research on it is scarce. The particle swarm algorithm and file management are examined from this practical perspective in this article. Backup storage, intangible cultural heritage file management, RFID, and other contents are among the features introduced. The particle swarm algorithm has been integrated into the marketing archives management of drama intangible cultural heritage, and the research has been completed to a high standard. When the task volume is 20, 50, or 200, 500, the article compares adaptive inertia weight algorithms, and the experimental results are excellent. For future research and development of this academic hotspot, researchers can try to generalise more intangible cultural heritage archives. The protection of intangible cultural heritage can also be done by individuals.

Data Availability

The data used to support the findings of this study are available from the corresponding author upon request.

Conflicts of Interest

The authors do not have any possible conflicts of interest.

References

[1] I. Hammou, S. Aboudou, and Y. Makloul, "Social media and intangible cultural heritage for digital marketing communication: case of marrakech crafts," *Marketing and Management of Innovations*, vol. 7, no. 1, pp. 121–127, 2020.
[2] Y. Zhang and T. J. Lee, "Alienation and authenticity in intangible cultural heritage tourism production," *International Journal of Tourism Research*, vol. 1, no. 9, pp. 77–89, 2021.
[3] T. Zhang, H. Wen, and X. Li, "A tourist-based model of authenticity of heritage sporting events: the case of naadam," *Sustainability*, vol. 11, no. 1, pp. 99–121, 2018.
[4] C. Veghe, "Cultural heritage: the forgotten resource for marketing and sustainable development of the local communities," *European Journal of Sustainable Development*, vol. 8, no. 3, p. 41, 2019.
[5] N. K. Jain, U. Nangia, and J. Jain, "Economic load dispatch using adaptive social acceleration constant based particle swarm optimization," *Journal of the Institution of Engineers: Serie Bibliographique*, vol. 99, no. 5, pp. 431–439, 2018.
[6] Y. Tang and X. Guan, "Parameter estimation for time-delay chaotic system by particle swarm optimization," *Chaos, Solitons & Fractals*, vol. 40, no. 3, pp. 1391–1398, 2009.
[7] S. M. Chen and Z. C. Huang, "Multiattribute decision making based on interval-valued intuitionistic fuzzy values and particle swarm optimization techniques," *Information Sciences*, vol. 397-398, no. 1, pp. 206–218, 2017.
[8] Y. J. Gong, J. J. Li, Y. Zhou et al., "Genetic learning particle swarm optimization," *IEEE Transactions on Cybernetics*, vol. 46, no. 10, pp. 2277–2290, 2016.
[9] M. Zhao, A. Jha, Q. Liu et al., "Faster Mean-shift: GPU-accelerated clustering for cosine embedding-based cell segmentation and tracking," *Medical Image Analysis*, vol. 71, Article ID 102048, 2021.
[10] J. Zhang, J. Sun, J. Wang, Z. Li, and X. Chen, "An object tracking framework with recapture based on correlation filters and Siamese networks," *Computers & Electrical Engineering*, vol. 98, Article ID 107730, 2022.
[11] Y. Zhang, K. Xia, Y. Jiang et al., "Multi-modality Fusion & Inductive Knowledge Transfer Underlying Non-sparse Multi-Kernel Learning and Distribution adaption," *IEEE/ACM Transactions on Computational Biology and Bioinformatics*, 2022.
[12] K. F. Tehrani, Y. Zhang, P. Shen, and P. Kner, "Adaptive optics stochastic optical reconstruction microscopy (AO-STORM) by particle swarm optimization," *Biomedical Optics Express*, vol. 8, no. 11, p. 5087, 2017.

[13] Y. Hong, B. Choi, G. Oh, K. Lee, and Y. Kim, "Nonlinear conflict resolution and flow management using particle swarm optimization," *IEEE Transactions on Intelligent Transportation Systems*, vol. 18, no. 12, pp. 3378–3387, 2017.
[14] S. Sarathambekai and K. Umamaheswari, "Task scheduling in distributed systems using heap intelligent discrete particle swarm optimization," *Computational Intelligence*, vol. 33, no. 4, pp. 737–770, 2017.
[15] L. Peng, D. Xu, and Z. Zhou, "Stochastic optimal operation of microgrid based on chaotic binary particle swarm optimization," *IEEE Transactions on Smart Grid*, vol. 7, no. 1, pp. 66–73, 2017.
[16] Y. Li, X. Bai, L. Jiao, and Y. Xue, "Partitioned-cooperative quantum-behaved particle swarm optimization based on multilevel thresholding applied to medical image segmentation," *Applied Soft Computing*, vol. 56, pp. 345–356, 2017.
[17] J. J. Kim and J. J. Lee, "Trajectory optimization with particle swarm optimization for manipulator motion planning," *IEEE Transactions on Industrial Informatics*, vol. 11, no. 3, pp. 620–631, 2015.
[18] R. E. Gamil, "Storytelling as a tool for safeguarding and marketing the intangibl cultural heritage (ich): the case of nubia city, Egypt," *Tourism Research Institute*, vol. 18, no. 7, pp. 410–467, 2017.
[19] Q. Qiu, T. Zheng, and Z. Xiang, "Visiting intangible cultural heritage tourism sites: from value cognition to attitude and intention," *Sustainability*, vol. 12, no. 6, pp. 412–501, 2019.
[20] B. Merrilees, D. Miller, G. L. Ge, and C. C. C. Tam, "Asian city brand meaning: a Hong Kong perspective," *Journal of Brand Management*, vol. 25, no. 1, pp. 14–26, 2018.

Hindawi
Computational Intelligence and Neuroscience
Volume 2022, Article ID 8591303, 13 pages
https://doi.org/10.1155/2022/8591303

Research Article

An Evaluation Model of English Normal Students' Informatization Teaching Ability Based on Technical Pedagogical Content Knowledge and Few-Shot Learning

Honghong Zeng and Ronghua Tan

Yuzhang Normal University, Nanchang 330103, China

Correspondence should be addressed to Honghong Zeng; 6180206054@stu.jiangnan.edu.cn

Received 5 April 2022; Revised 26 April 2022; Accepted 27 April 2022; Published 5 July 2022

Academic Editor: Xin Ning

Information-based instruction is the most important and recently altered sort of instruction. Numerous changes in educational techniques have emerged from the ongoing growth of science and technology. Teachers must also grasp and enhance their capacity to educate with information on a regular basis. The goal of this research is to look at how to use the TPACK model and computational intelligence to build and explain a model for evaluating English normal students' informatization teaching skills. To measure information-based teaching competence, this research recommends using the Technical Pedagogical Content Knowledge model and Few-Shot Learning technology. As a result, this paper covers the principles and related algorithms of both, as well as constructing and assessing the case design and analysis of the information-based teaching ability evaluation model. According to the experimental data, the average CK of normal students' subject material knowledge is 3.522, which is the highest among the seven dimensions. The subject content is well-understood by ordinary students. When compared with teaching abilities, the competence level is low, and the performance of the integration of technology and teaching content needs to be improved.

1. Introduction

The rapid advancement of information technology has altered the way we work, learn, and play, and this is true in education as well. Education faces significant hurdles in today's quickly evolving digital culture. To raise the level of teacher education, a scientific and effective evaluation plan for teachers' information teaching competence is required. The TPACK framework is a knowledge system that combines technology into topic teaching in the classroom. Teachers actively select appropriate technical tools based on the actual teaching situation. It is the process of bringing individual topic expertise to teaching practice, with a focus on the importance of incorporating technology into the classroom.

It examines concerns linked to the cultivation of ordinary students' information teaching capacity using the TPACK model. This can provide a specific theory for nurturing ordinary students' information teaching ability, as well as a deeper understanding of teachers' information teaching ability from the theoretical standpoint of TPACK. TPACK opens up a new study field for the effective integration of information technology and curriculum, as well as theoretical direction for teachers on how to teach in a technological context more effectively. It is a novel idea to improve teacher professional development, and it is the knowledge base for teachers to effectively carry out instruction when the technology of the information age has invaded education.

The innovation of this paper is (1) through the combination of the TPACK model and information teaching, this paper introduces the theory and related methods of TPACK and computational intelligence in detail, as well as artificial neural network and genetic algorithm. (2) Based on a comprehensive review of the importance of information technology teaching ability, this paper proposes an index system for evaluating teachers' information technology teaching skills. And this paper uses the TPACK theoretical model to determine the structural relationship between the index system and teaching ability. Through weight calculation, it is concluded that the teaching ability level of normal students is relatively high, but the ability related to technology is relatively low, and the ability to integrate technology and subject content is not strong.

2. Related Work

With the development of information technology and the continuous advancement of educational informatization, TPACK has become an important standard for measuring teachers' teaching ability in the information age. The main purpose of Gomez-Trigueros I M is to evaluate the realization of spatial and digital competence through the intervention of the TPACK teaching model in the classrooms of primary school teachers at the University of Alicante. However, he did not take into account the influence of other factors [1]. Salas-Rueda RA analyzed the impact of the TPACK model in the design of predicate logic instructional units, taking into account the use of Raptor software, YouTube videos, and the social network Facebook. However, the number of samples in his experiments is small [2]. Almenara J C aimed to assess knowledge based on the TPACK (Technical, Pedagogical, and Content Knowledge) model and he used quantitative, descriptive, and relational methods. The conclusions he drew underscore the need for a kind of teacher training that is based not only on the technical aspects but also on the pedagogical and content aspects in an integrated approach. However, his views are not supported by a large amount of objective evidence [3]. D Mourlam used a mixed methods approach to attempt to describe teacher development experiences based on TPACK and adult learning theories directed by teacher developers. The findings suggest that teachers find the ongoing nature of the development experience valuable and value the support of teacher developers in achieving their goals. The survey results also showed an increase in TPACK for both teachers and teacher education candidates participating in the program. However, his experiments are one-sided [4]. Miguel-Revilla D analyzed the practical utility of the TPACK model and the effectiveness of a pedagogical intervention for social studies secondary education prospective teachers in a university setting over a two-year period. Finally, his experimental results can lead to the conclusion that the pedagogical and conceptual orientation of the teaching program has shown positive effects, demonstrating that the effectiveness of an integrated approach that can adapt to the specificities and challenges of social studies education. However, he ignored the interference of realistic factors [5]. Eutsler L explored how the use of TPACK's pedagogical knowledge structure and steps to release responsibility framework can help senior teachers design instruction to read and write using the iPad. His analysis revealed that teacher-controlled teaching methods attract the attention of experienced teachers to lesson plans. The pedagogical approach "teacher as facilitator" increases user confidence and exploration. Problem-based teaching methods help target individualized students. However, his analysis is not universal [6]. Stefani S aimed to describe the use of a Problem-Based Learning (PBL) model based on Theology, Teaching and Content Knowledge (TPACK) to improve the integrated topic learning process in V SDN 07 Pandam Gadang. The findings suggest that a Problem-Based Learning (PBL) model based on Technology, Pedagogical, and Content Knowledge (TPACK) can improve the integrated topic learning process in the elementary classroom. However, his model is not very feasible [7]. Starting from a theoretical framework, Bustamante C described the development of joint displays in mixed methods research case studies. However, the method he describes is somewhat monolithic [8].

3. TPACK and Computational Intelligence Methods

3.1. TPACK

3.1.1. Connotation of TPACK. TPACK is a new concept emerging in the process of teacher specialization, and it is a comprehensive science and technology of knowledge teaching. It was originally called PACK but was changed to TPACK for ease of memory and pronunciation. TPACK provides a new way of thinking. Once it is proposed, it has attracted great attention of educational scientists at home and abroad. TPACK is a new requirement for teachers' computer skills.

If teachers can effectively integrate technology into their professional knowledge structure in a modern educational environment and complete teaching efficiently, it will also become an important criterion for measuring teachers' teaching ability in the information age.

3.1.2. TPACK Structure. The use of instructional technology in educational contexts has become synonymous with technology integration. To help measure and guide teachers' use of educational technology, a variety of educational technology models and frameworks have been established. Many educational technology specialists believe that topic knowledge has an impact on how technology is used in the classroom. There are substantial contrasts, for example, between technology in science curriculum, successful curriculum integration, and effective technology and curriculum integration in social sciences. A new theory integrating pedagogical knowledge, subject knowledge, and technical knowledge (PK, CK, and TK) is shown in Figure 1.

This theoretical framework is called Technical Educational Content Knowledge (TPCK or TPACK) and expands its definition on the basis of the PCK knowledge structure, adding an element of technical support. The structural framework of TPACK consists of seven components, namely, TK, CK, PK, TPK, PCK, TCK, and TPACK.

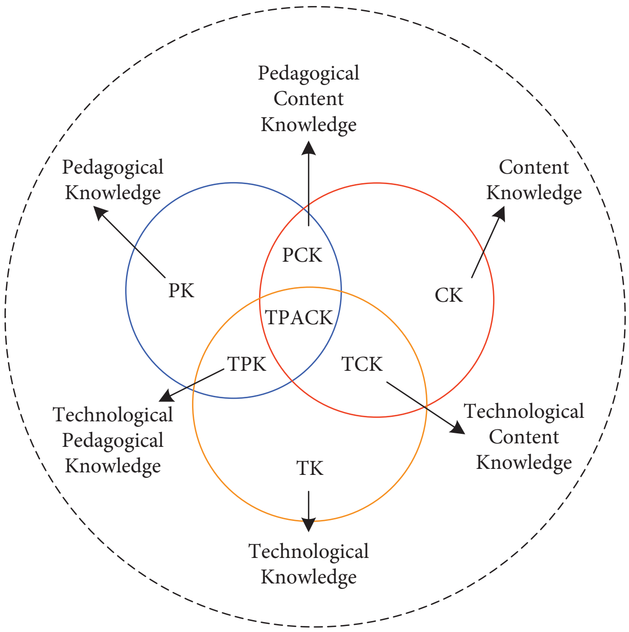

Figure 1: TPACK framework.

(1) *TK (Technological Knowledge).* Technical knowledge such as the use of blogs and various mobile devices, computers, projectors, and laboratory equipment is used in teaching. Office software such as PPT and word in teaching design is the necessary technical knowledge for teachers.

(2) *PK (Pedagogical Knowledge).* It is general pedagogical knowledge. General teaching strategies include teaching of theorems, concepts, definitions, and arrangement of teaching links such as the design of lesson plans. It is the basic teaching method that teachers must master.

(3) *CK (Content Knowledge).*It is subject knowledge required to be taught to students in various disciplines, such as laws, definitions, concepts, and formula theorems in science teaching. Students mastering these subject knowledge is the main goal of teaching but also the knowledge background that teachers must have.

(4) *TCK (Technological Content Knowledge).* It is disciplinary knowledge that integrates technology. Technical knowledge is used to help present a particular subject knowledge, but this composite knowledge is independent of pedagogical knowledge. For example, in the teaching of functions in mathematics courses, using technology to show the changing trend of functions can be considered as TCK.

(5) *TPK (Technological Pedagogical Knowledge).* It is pedagogical knowledge that integrates technology. The process of using technology to help teaching in the teaching of various disciplines is a combination of technology and pedagogical knowledge. This integrated pedagogical knowledge is not so much specific to the teaching of a specific subject as it is applicable to all subject pedagogical knowledge. The classroom discussion teaching is used in the Internet environment, that is, the learning environment supported by the computer (CSCL teaching environment).

(6) *PCK (Pedagogical Content Knowledge).* It is subject teaching method knowledge. This knowledge is intended to enable students to experience a complete teaching experience so that they can understand and master the knowledge of the subject.

(7) *TPACK (Technological Pedagogical Content Knowledge).* There is a debate on the definition of TPACK. One is that TPACK is an extension of PCK; that is, the element of technology is added to Schulman's PCK theory. The other is that it is a cross combination of three basic elements (TK, CK, and PK), TPACK is to strengthen students in learning a certain subject, such as using Google Earth in geography teaching to help students explore and learn El Niño phenomenon. It is a fusion of technology and pedagogical knowledge of subject knowledge, designed to allow students to experience a certain learning process and better understand the content that needs to be mastered.

3.2. Computational Intelligence Technology. Computational intelligence methods [9, 10] are inspired by biological evolutionary mechanisms and some natural phenomena, and many new solutions to complex optimization problems are widely used in various fields of problems, concerns, and applications due to their high optimization performance and less requirement for specific information. Computational intelligence methods include neural network [11, 12], fuzzy control, genetic algorithm, immune computing, and swarm intelligence.

3.2.1. Artificial Neural Network. The artificial neural network [13, 14] is based on the physiological research results of brain tissue, simulates some mechanisms and mechanisms of the brain, starts from the basic functions of neurons, and gradually forms a network from simple to complex. Its organization simulates the interaction of biological nervous systems with real-world objects. It simulates parallel processing on a large scale, has strong robustness and fault tolerance, and has strong self-learning ability. The first one is about the most basic and primitive model in the neuron synapse model: the binary threshold unit (Binarythresholdunit), the famous M-P model, as shown in Figure 2.

In Figure 2, θ represents the threshold when neurons are excited, and the M-P model reflects the structural and functional characteristics of biological neurons to a certain extent. Its mathematical description is as follows:

$$\begin{cases} \sum_{i=1}^{a} E_i - \theta \geq 0, & \text{and} \sum_{j=0}^{b} I_i = 0, Y = 1, \\ \text{other}, & \text{Y} = 0. \end{cases} \tag{1}$$

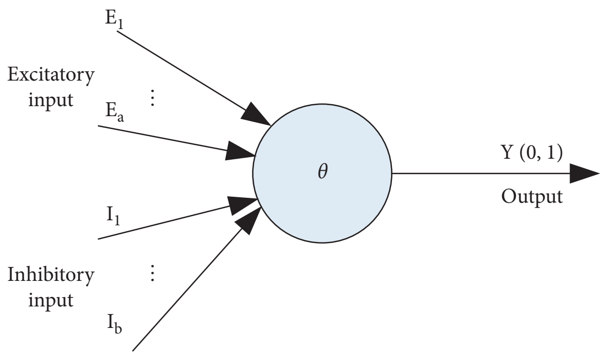

Figure 2: M-P model.

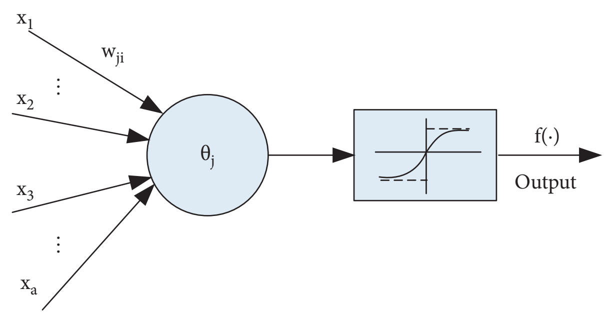

Figure 3: Neuron structure model.

With proper setting of neuron thresholds and combination weights, the model can approximate any binary function and can complete any finite logical function. The basic idea is that when two neurons are excited or inhibited at the same time, the connection strength between them increases. It is mathematically expressed as follows:

$$\begin{cases} \sum_{k=1}^{a} x_i^{(k)} x_j^{(k)}, & i \neq j, \\ 0, & i = j. \end{cases} \tag{2}$$

The meaning of this learning rule is that the adjustment of the connection weight is proportional to the product of the activity states of the two neurons, and the connection weight is symmetric. The connection weight of a neuron to itself is zero, which is still used in various neural network models.

A typical single artificial neuron model is shown in Figure 3.

The neuron input-output relationship is as follows:

$$\begin{aligned} y_j &= f\left(\sum_{i=1}^{a} w_{ji} x_i - \theta_j\right) \\ &= f\left(\sum_{a=1}^{a} w_{ji} x_i\right), \\ \mathrm{inx}_0 &= \theta_j, \\ w_0 &= -1. \end{aligned} \tag{3}$$

In the formula, the threshold is θ_j, the link weight coefficient is w_{ji}, and f(·) is the output transformation function, also known as the excitation function and the transfer function.

The more commonly used transfer functions are as follows:

(1) *Symbol Function*. As shown in Figure 4(a),

$$y = f(\varphi) = \begin{cases} 1, & \varphi \geq 0, \\ 0, & \varphi < 0. \end{cases} \tag{4}$$

(2) *Piecewise Linear Function*. As shown in Figure 4(b),

$$y = f(\varphi) = \begin{cases} 1, & \varphi \geq \alpha, \\ \vartheta, & 0 \leq \varphi < \alpha, \\ 0, & \varphi < 0. \end{cases} \tag{5}$$

(3) *Sigmoid Function*. As shown in Figure 4(c),

$$f(\varphi) = \frac{1}{1 + e^{-\varphi}}. \tag{6}$$

(4) *Hyperbolic Tangent Function*. As shown in Figure 4(d),

$$f(\varphi) = \frac{1 - e^{-\varphi}}{1 + e^{-\varphi}}. \tag{7}$$

Commonly used neural network learning algorithms are as follows:

(1) Error Correction Learning. $y_k(t)$ is the actual output of neuron k at time t when $x_k(t)$ is input, and $y_{k\,d}(t)$ is the expected output, and then the error signal is as follows:

$$e_k(t) = y_{k\,d}(t) - y_k(t). \tag{8}$$

The ultimate goal of error correction learning is to minimize a specific objective function $e_k(t)$, so that the actual output of each output unit on the network approximates the expected output in a statistical sense. The most commonly used objective functions are as follows:

$$\lambda(t) = \frac{1}{2} \sum_k e_k^2(t). \tag{9}$$

Calculate the minimum value of λ(t) for the weight w as follows:

$$\Delta w_{kj} = \sigma e_k(t) x_j(t). \tag{10}$$

In the formula, the learning step size is σ.

(2) Hebb Learning. "When neurons at both ends of a synapse are activated (activated and inhibited) at the same time, the strength of the connection should be strengthened, otherwise it should be weakened" is a summary of Hebb's learning rule. The mathematical expression is as follows:

$$\Delta w_{kj}(t) = F\big(y_k(t), x_j(t)\big). \tag{11}$$

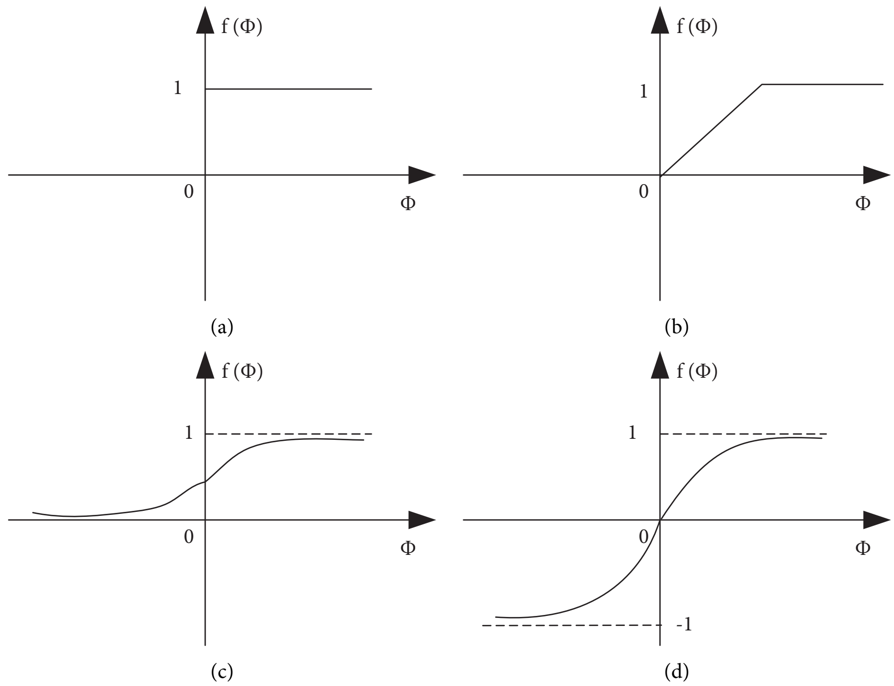

Figure 4: Neuron state transition function.

Among them, the states of neurons at both ends of w_{kj} are $y_k(t)$ and $x_k(t)$, and the most common cases are as follows:

$$\Delta w_{kj} = \sigma y_k(t) x_j(t). \tag{12}$$

Since Δw_{kj} is proportional to the correlation between $y_k(t)$ and $x_j(t)$, it is sometimes called the correlation learning rule.

(3) Competitive Learning. In the competitive learning process, each network output unit competes with each other and finally only one strongest unit is activated, as shown in Figure 5. The most common case is inhibitory lateral phase connections between output neurons. So, in the initial output unit, if one unit is stronger, it will win and overwhelm the others, and in the end, only this stronger unit will be active.

The most commonly used competitive learning rules can be written as follows:

$$\Delta w_{kj} = \begin{cases} \sigma\left(x_i - w_{ji}\right), & \text{Ifneuron}\, j\,\text{competestowin}, \\ 0, & \text{Ifneuron}\, j\,\text{failstocompete}. \end{cases} \tag{13}$$

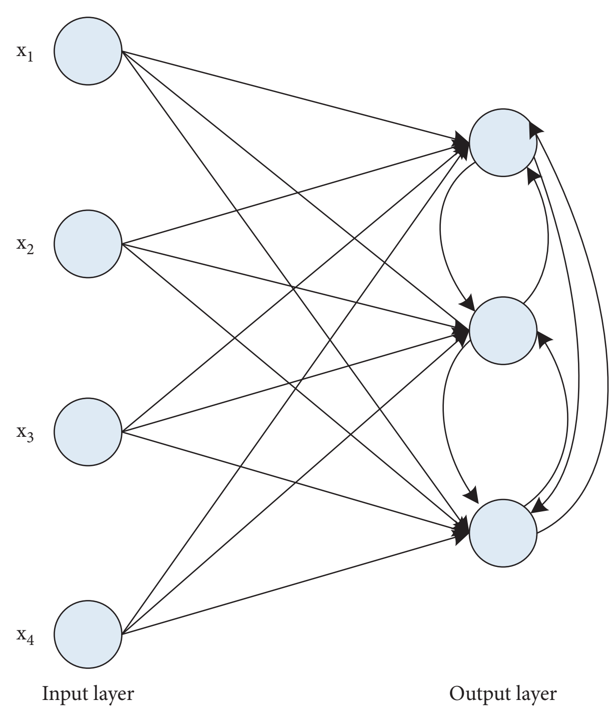

Figure 5: Competitive learning network with lateral inhibitory connections.

3.2.2. Genetic Algorithm. Genetic algorithm is an optimization method that simulates natural selection and genetic mechanisms, simulating the phenomena of reproduction, hybridization, and mutation in natural selection and natural genetic processes. When solving a problem using a genetic algorithm, each possible solution to the problem is encoded as a "chromosome," that is, an individual and thousands of individuals form a group (all possible solutions). At the beginning of a genetic algorithm, some individuals (i.e., initial solutions) are always randomly generated. Each individual is evaluated against a predetermined objective function, which gives a fitness value. Based on this fitness value, it selects individuals to replicate in the next generation. The selection operation embodies the principle of "survival of the fittest," where "good" individuals are selected for replication and "bad" individuals are eliminated. Then, the selected individuals are recombined through crossover and mutation operators to generate a new generation. Because this group of new individuals inherits some excellent characters of the previous generation, their performance is better than that of the previous generation, which gradually evolves towards a better solution. Therefore, the genetic algorithm can be regarded as a process of gradual evolution of a group composed of feasible solutions. The basic process of the genetic algorithm is shown in Figure 6.

The execution process of the genetic algorithm contains many random operations, so it is necessary to analyze its mathematical mechanism. A schema is a collection of strings that take the same characters at certain positions. Extract the following symbols as follows:

P: a certain mode

f_i: fitness of the i-th string (solution)

$\overline{f}(t)$: the average fitness of the t-th generation population

$\overline{f}(P,t)$: the average fitness of pattern P in the t-th generation population

$n_i(P,t+1)$: the expected value of the number of offspring produced by the solution i of the P mode of the t generation in the $t+1$ generation

$n(P,t)$: the number of solutions belonging to pattern P in the t-th generation

$\varphi(P)$: the definition distance of P

$O(P)$: the order of P

Consider first the outcome of the selection. In the standard genetic algorithm, the selection criteria are based on the principle of proportionality; therefore, through the action of the ith selector, the expected value of the number of people who will continue to exist in the next generation is $n(f_i/\sum f)$ and then

$$\overline{f}(P,t)=\frac{1}{n(P,t)}\sum f_i. \tag{14}$$

Then,

$$n(P,t+1)=n(P,t)\cdot\overline{f}\,\frac{(P,t)}{f(t)}. \tag{15}$$

The formula shows that the role of the selection operator will increase (decrease) the ability of a pattern that is above (below) average in its applicability across generations, improving quality.

This plan can obviously be maintained in the next generation if there is no intersection or if the intersection point is beyond the character positions specified on the left and right ends of Figure 6. Therefore, the probability R_s that the P mode will continue to exist in the next generation should satisfy

$$R_s\geq 1-R_c\cdot\frac{\varphi(P)}{(L-1)}. \tag{16}$$

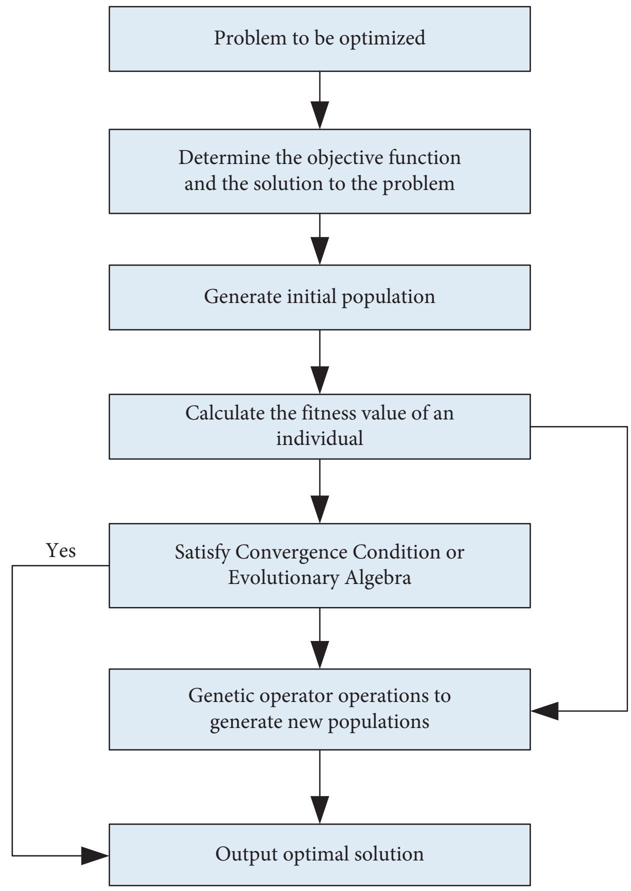

Figure 6: Basic flow chart of the simple genetic algorithm.

Taking into account the effects of selection and crossover, there are

$$n(P,t+1)\geq n(P,t)\cdot\overline{f}(P,t)\cdot\left[1-R_c\cdot\frac{\varphi(P)}{(L-1)/\overline{f}(t)}\right. \tag{17}$$

Finally, because R_m represents the probability of the mutation operator acting, the constant probability is $1-R_m$.

$$\left(1-R_m\right)^{O(P)}\approx 1-R_m\cdot O(P). \tag{18}$$

The probability of unreserved is about $O(P)\cdot R_m$. Therefore, considering the functions of selection, crossover, and mutation operators, we end up with

$$n(P,t+1)\geq n(P,t)\cdot\overline{f}(P,t)\cdot\frac{\left[1-R_c\cdot\varphi(P)/L-1\cdot R_m\right]}{\overline{f}(t)}. \tag{19}$$

This result is the so-called model theorem. If only the influence of the selection operator is considered, the amount of solution contained in the standard solution increases or decreases with the passage of generations, which is related to the average suitability of the standard solution. Specifically, if $\overline{f}(P,t)=f(t)(1+c)$, $c>0$ is a constant and then

$$n(P,t)=n(P,t-1)(1+c)=n(P,O)(1+c)^t. \tag{20}$$

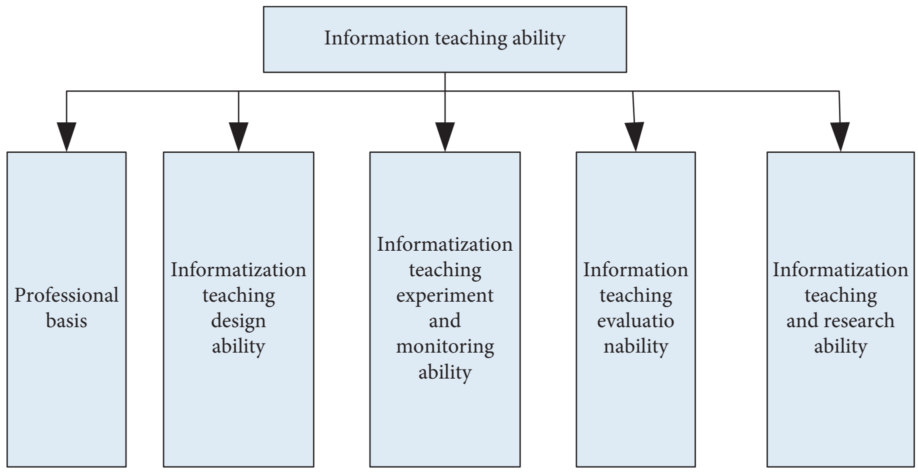

Figure 7: Theoretical framework of the first-level index of informatization teaching ability.

That is, functions with high average fitness grow exponentially in their ability to compete with other functions. However, high average conditions alone are not enough to guarantee high growth rates. When considering other impacts in detail, the definition of an operating model that requires good quality should be smaller in length and shorter in scope. High average suitability modes, low resolutions, and low order distances enable exponential growth in the number of solutions contained in generation after generation of group transmissions, which is the essence of the model theorem [15].

3.3. Information-Based Teaching Ability. "Competence" is the subjective condition that people need to solve problems, complete specific tasks, and be competent. Informatization teaching ability refers to the ability of teachers to rationalize and optimize the teaching process under the condition of providing sufficient information to use information technology and information resources. It is a reflection of the comprehensive quality of teachers combining various technologies and resources to carry out practical teaching. It is a composite of various abilities that teachers have in the integration of information technology and curriculum, and it points to the level of teaching practice, the application of technology, and the ability to integrate [16, 17].

In this study, the training object of information-based teaching ability is normal students. In view of the fact that normal students are in the survival stage of teachers' professional development, they mainly focus on whether they can stand on the podium and how to complete a class but do not really pay attention to students. In addition, the main task of normal students is to learn the theoretical knowledge related to the professional development of teachers and to imitate the theoretical knowledge learned into practice; in this process, there are fewer opportunities to actually contact students. During the four-year study process, the normal students in most normal colleges and universities in China are limited by various conditions, and the contact time with students ranges from 2 to 4 months.

The research on information-based teaching ability emerges along with the research on teachers' ability, which is the product of the information age. Awareness of technology integration, subject teaching methods, and knowledge are important ways to improve teachers' information teaching ability and teaching ability. Teachers' computer skills are the ability to implement TPACK. In other words, teachers' informatization teaching ability is their ability to integrate technology, classroom pedagogy, and subject content knowledge. Figure 7 shows the content related to the first-level indicators of information-based teaching ability.

Informatization teaching ability and educational technology ability are included, and the relationship between information literacy and information technology ability is a cross relationship, with the same part and different parts [18]. The relationship between the four is shown in Figure 8.

4. Experiment and Analysis on the Evaluation Model of Normal Students' Informatization Teaching Ability

4.1. Investigation and Analysis of TPACK Level of English Normal Students. The scale is a common tool for measuring the level of TPACK. In order to ensure the scientificity and validity of the scale, the accuracy of the data, and the objectivity of the results, the questionnaire was tested in this study. The test subjects were English normal students from normal universities, a total of 100 people, and 100 questionnaires were distributed, all of which were valid questionnaires.

The questionnaire is divided into two parts, one part is the TPACK level survey scale for normal students and the other part includes 7 basic information questions and 2 open-ended questions. In order to test the scientificity and accuracy of the questionnaire design, the author uses SPSS19 software to test the reliability and validity of the scale, so as to make the questionnaire more reasonable and effective. Reliability refers to the stability, reliability, and consistency of the results presented by the measurement tools. The higher the reliability is, the more stable and reliable the

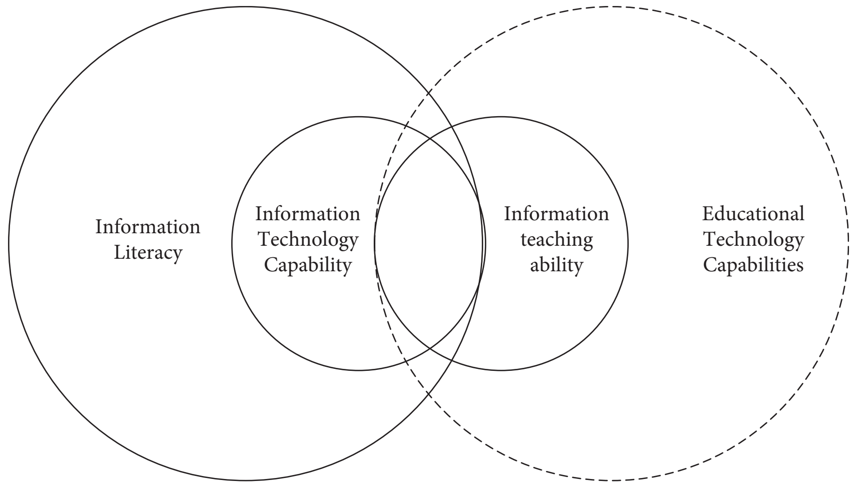

Figure 8: The relationship between information teaching ability and related concepts.

Table 1: Questionnaire reliability analysis table.

Dimension	Number of items	Cronbach's alpha coefficient	Cronbach's alpha coefficients based on standardized terms
PK	7	0.89	0.89
CK	4	0.81	0.81
TK	8	0.81	0.81
TPK	6	0.88	0.88
PCK	5	0.72	0.72
TCK	4	0.81	0.82
TPACK	6	0.88	0.88
Overall	40	0.95	0.95

Table 2: KMO and Bartlett sphericity test.

Kaiser–Meyer–Olkin measure of sampling adequacy		0.819
	Sig.	0.000
Bartlett's sphericity test	Approximate chi-square	1633.041
	df	526

measurement results are. If the a coefficient of the questionnaire is between [0.7, 0.8], it means that the reliability of the questionnaire is high, and the a coefficient between [0.8~0.9) means that the reliability of the questionnaire is very high. A coefficient above 0.9 indicates that the reliability of the entire questionnaire is very high.

The internal consistency of each part of the TPACK scale was tested by Cronbach's alpha using SPSS19 software, and the results are shown in Table 1.

It can be seen from the reliability analysis of the questionnaire in Table 1 that, in each dimension of the scale, except for the PCK dimension, the reliability of the remaining dimensions is above 0.8. It can be seen that the internal consistency of the scale is relatively satisfactory, and the overall reliability is high, which can be used for research.

Validity testing usually includes two parts, content validity and construct validity, which are tested after many discussions and revisions. Therefore, it ensures the scientific nature of the questionnaire content validity test to a certain extent. In the structural validity test of the scale, factor analysis is usually used to verify it according to the KMO decision criteria. The value of KMO is between 0 and 1. The larger the KMO value, the more common factors among the variables in the questionnaire and the more suitable for factor analysis. When the KMO is less than 0.5, it means that it is not suitable for factor analysis, and when the KMO is greater than 0.8, it means that the quantity is expressed to a good degree [19].

The construct validity of the TPACK scale was tested using SPSS19 software, and the results are shown in Tables 2 and 3.

It can be seen from the reliability analysis of the questionnaire in Table 2 that the KMO values of each category of the scale are all above 0.70. The overall KMO was 0.819, which was greater than 0.8 in the Kaiser decision criterion, the chi-square value of Bartlett's sphericity test was 1633.041, the degree of freedom P was 528, and the Sig. was 0.000, reaching a significant level ($P < 0.05$). Based on the data analysis [20], the scale has common factors in the overall correlation table. According to its construct validity analysis, the correlation factors among different dimensions of the questionnaire and the correlation between dimensions, the coefficients reached a significant level, indicating that the scale has high construct validity. Overall, the TPACK

Table 3: Questionnaire construct validity analysis.

Dimension	PK	CK	TK	TPK	PCK	TCK	TPACK	Overall
PK	1							
CK	0.615**	1						
TK	0.396**	0.614**	1					
TPK	0.574**	0.659**	0.598**	1				
PCK	0.666**	0.580**	0.463**	0.608**	1			
TCK	0.409**	0.573**	0.530**	0.676**	0.608**	1		
TPACK	0.678	0.539**	0.534**	0.789**	0.677**	0.721**	1	
Overall	0.720**	0.768**	0.732**	0.880**	0.824**	0.821**	0.884**	1

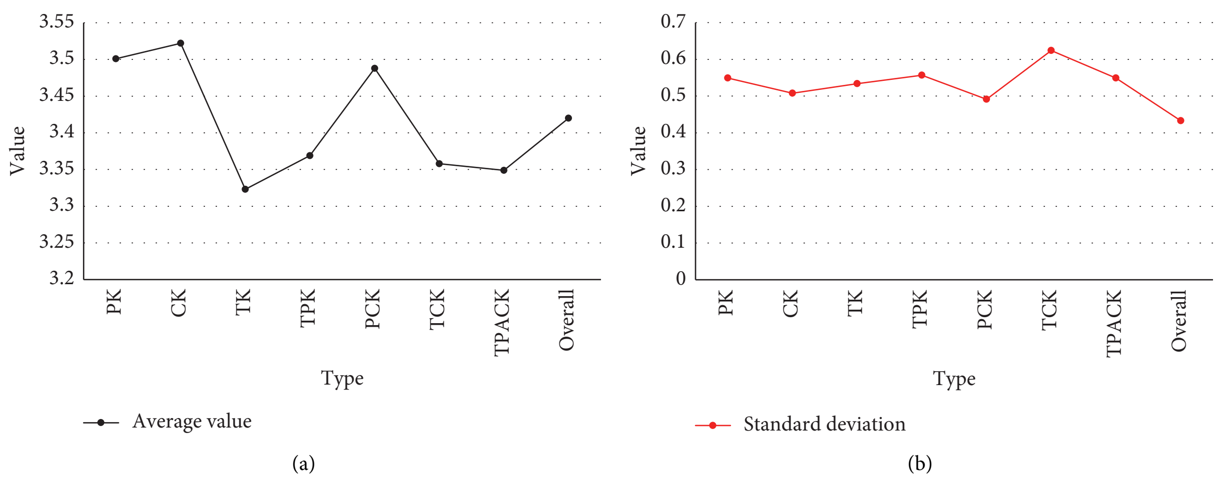

Figure 9: Descriptive analysis of each dimension of TPACK.

Normal Student Research Scale has high reliability and validity.

In order to investigate the overall level of TPACK of normal students, English normal students from normal universities were selected as the research objects. In order to reflect the overall situation of TPACK, this paper selects a total of 100 normal students in different stages from freshman to junior year and distributes 100 questionnaires, all of which are valid questionnaires. In order to understand the overall level of TPACK of normal students, this paper uses SPSS19 software to analyze the mean and standard deviation of the survey results by dimension, as shown in Figure 9.

It can be seen from Figure 9 that the average value of each TPACK dimension of normal students is $M = 3.420$, which is between "average" and "good," which is a medium level. Second, there are differences between the dimensions of TPACK for normal students. The seven dimensions present different levels, and they are sorted to obtain TK < TPACK < TCK < TPK < PCK < PK < CK. The highest among the seven dimensions is knowledge of course content, with an average CK of 3.522, indicating that normal students have higher knowledge of subject content than other dimensions. The average values of the three dimensions of PCK's subject pedagogy knowledge, PK's pedagogical knowledge, and CK's subject content knowledge are also higher. It shows that normal students have high self-confidence in subject content knowledge and pedagogical knowledge.

4.2. Scenario Application Ability of Informatization Teaching. According to the research results of the TPACK structure model and the specific meaning of the indicators for evaluating information teaching ability, Figure 10 shows the structure model of the evaluation index of normal students' informatization teaching ability.

In terms of the quantitative relationship between the evaluation indicators of informatization teaching ability, the path coefficients in the model are $\rho 1 \sim \rho 6$. They represent the influence weights of the three second-level indicators of the basic ability of informatization teaching on the three second-level indicators of the integration and application ability of informatization teaching. Among them, $\rho 1$ and $\rho 2$ are the influence weights of technology-related capabilities on the ability to integrate technology and teaching and the ability to integrate technology and subject content, respectively. $\rho 3$ and $\rho 4$ are the influence weights of teaching-related ability on integration of technology and teaching ability and subject teaching ability, respectively. $\rho 5$ and $\rho 6$ are the influence weights of subject-related ability on subject teaching ability and ability to integrate technology and subject content, respectively. The path coefficients $\rho 7 \sim \rho 9$, respectively, represent the influence weights of the three secondary indicators of the integrated application ability of informatization teaching on the situational application ability of informatization teaching. Among them, $\rho 7$ is the influence weight of integrating technology and teaching ability on the subject teaching ability integrating technology. $\rho 8$ is the influence

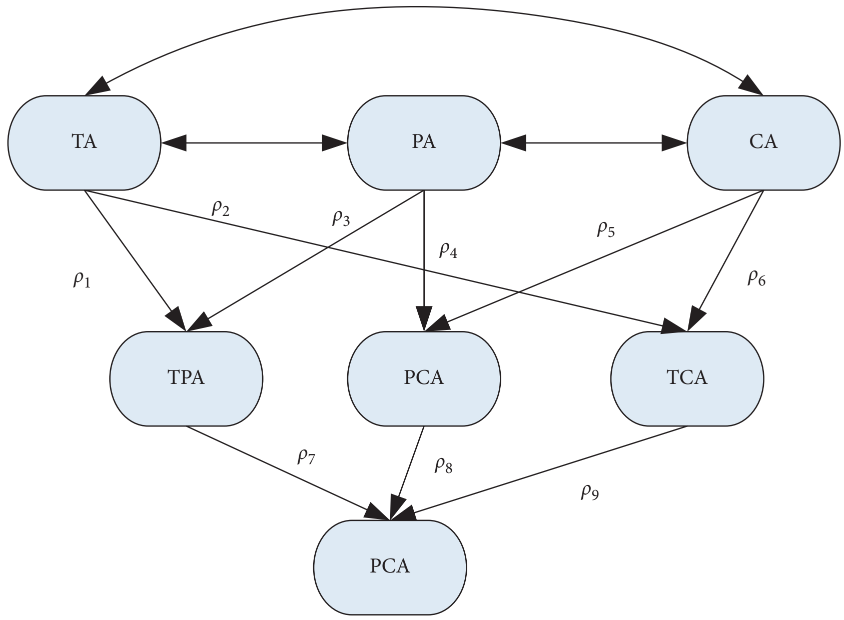

Figure 10: The structure model of the evaluation index of information teaching ability.

Table 4: Weights of evaluation indicators of information-based teaching ability.

First-level indicator	Index weight	Secondary indicators	Index weight
Basic ability of informatization teaching	$\rho_{TA} + \rho_{PA} + \rho_{CA}/\rho_{\mathrm{SUM}}$	TA PA CA	$\rho_{TA} = \rho_1 \times \rho_7 + \rho_2 \times \rho_9$ $\rho_{PA} = \rho_3 \times \rho_7 + \rho_4 \times \rho_8$ $\rho_{CA} = \rho_5 \times \rho_8 + \rho_6 \times \rho_9$
Informatization teaching integration application ability	$\rho_{TCA} + \rho_{PCA} + \rho_{TCA}/\rho_{\mathrm{SUM}}$	TPA PCA TCA	$\rho_{TPA} = \rho_7$ $\rho_{PCA} = \rho_8$ $\rho_{TCA} = \rho_9$
Informatization teaching situation application ability	$\rho_{\mathrm{TPCA}}/\rho_{\mathrm{SUM}}$	TPACK	$\rho_{\mathrm{TPCA}}/\rho_{\mathrm{SUM}} = 1.00$

weight of subject teaching ability on subject teaching ability integrating technology. $\rho 9$ is the influence weight of integrating technology and subject content ability on the subject teaching ability integrating technology.

Regarding the calculation of the weight, the ability to apply the IT teaching status has the most important influence on the teacher's informatization teaching ability. The weight of the secondary indicator integrated technology subject teaching ability is defined in 1.00. The weight should be calculated according to the index influence path coefficient reflected in the teaching ability rating index structure model. Based on this information, the influence path coefficient of this paper on the subject teaching ability of integrated technology is shown in Table 4.

4.3. Evaluation Model of Informatization Teaching Ability. In order to verify the validity of the teacher's structured information evaluation model and calculate the weight evaluation of each index, this study carried out an empirical research on the evaluation of information-based teaching ability. The seven subindicators should be measured proportionally, and the measurement data should be modeled through a path analysis model to determine the weight of each indicator. The empirical research results show that the actual measurement data are in good agreement with the structural model of the evaluation index of information teaching ability. This also shows that the model can more accurately evaluate the informatization teaching ability of normal students. According to the weight model of indicators at all levels, among the three first-level indicators, the ability to apply educational information context is crucial. The ability to integrate and apply information teaching is secondary, and the basic skills of informatics teaching are the least important. Among all secondary indicators, the target teaching ability index of integrated technology has the largest weight, the integrated technology and teaching ability index has the second weight, and the ability index related to subject teaching has the lowest weight. Figures 11 and 12 are the descriptive statistical analysis results of each index level and the overall level of informatization teaching ability.

After completing the three-year teacher training course, the general level of information teaching ability of normal students is relatively high. Among the three first-level indicators, the ability to implement the state of informatization teaching is the highest, the completion and application index of computer teaching is at the middle level, and the basic skills index of computer teaching [21] is at the middle level.

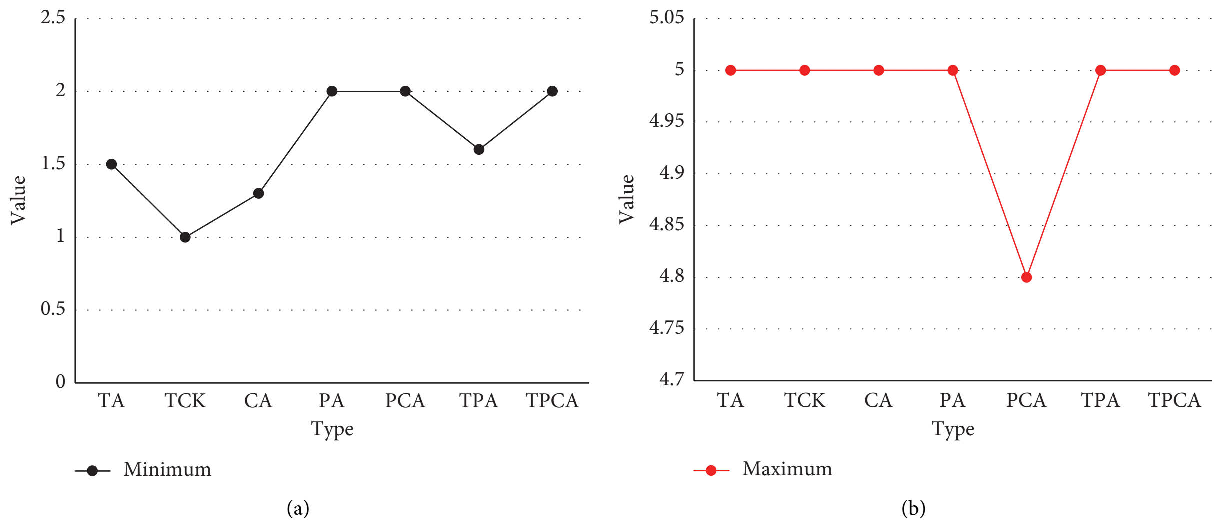

Figure 11: The minimum value and maximum value of the evaluation index of information teaching ability.

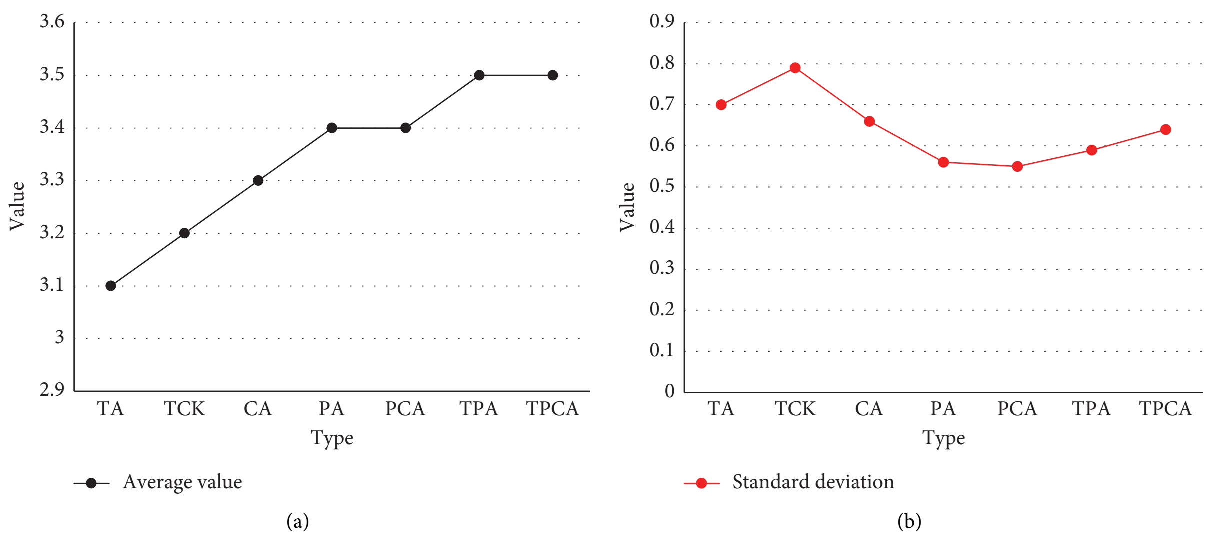

Figure 12: Mean and standard deviation of the evaluation indicators of information-based teaching ability.

Among the seven secondary evaluation indicators, the skill index related to technology is the lowest, and the skill index of teaching objects related to technology is the highest [22]. Among the three secondary indicators of ability to complete and implement computer-based instruction, the level of ability to integrate technology and subject content was lower than the other two indicators. Among the three secondary indexes of basic computer teaching ability, the level of technology-related ability indexes is lower than the other two indexes.

To sum up, normal students have high information teaching ability, which to a certain extent reflects that general education has achieved remarkable results in cultivating teachers' information teaching ability. The measurement results show that normal students have high teaching ability and can well integrate technology, teaching methods, and content to form good teaching decisions. Compared with teaching ability, normal students have relatively low technology-related abilities, and their ability to integrate technology and disciplinary content is poor. In the future, the proportion of courses related to technology integration in different subject courses should be increased to promote the comprehensive development of normal students' information teaching ability, thereby improving the level of educational development.

5. Discussion

First of all, through the study of relevant knowledge points of literature works, this paper initially masters the relevant basic knowledge and analyzes how to conduct research on the evaluation of the information-based teaching ability of medical-oriented English normal students based on the TPACK model and computational intelligence. This paper expounds TPACK and informatization teaching ability, focuses on the method of computational intelligence, and analyzes the evaluation of informatization teaching ability based on TPACK and computational intelligence through experiments. And this paper constructs the evaluation model of information teaching ability. This paper also focuses on artificial neural network and genetic algorithm, and artificial neural network is an artificial neural network created according to the physiological structure and information processing process of the brain, imitating human intelligence. The genetic algorithm is more suitable for large scale, large population, complex environment, and unclear problem structure [23, 24].

Through experimental analysis, this paper shows that normal students have high informatization information teaching ability and teaching ability and can well integrate technology, teaching methods, and content to form good teaching decisions. Compared with teaching ability, normal students have lower skill levels and lower performance in integrating technology and teaching content.

6. Conclusion

Computer science is an inevitable trend of future development, and computer science teaching is an important part of future education development. The final foothold of the evaluation index system of teachers' informatization teaching ability is still practice. This research also hopes to update the teaching concept ideologically and improve teachers' understanding of the development of information-based teaching. Teachers should actively use multimedia technology to assist teaching, optimize the teaching process, fundamentally change the traditional teaching structure and teaching methods, and achieve the goal of quality education in the new era. Although the traditional exam-oriented education is strong, the development of science and technology is rapid. With the popularization of computer teaching methods, teachers' computer teaching ability has been continuously improved. With the implementation of the quality education policy, the overall quality of national education will surely rise to a higher level.

Data Availability

The data used to support the findings of this study are available from the corresponding author upon request.

Conflicts of Interest

The authors declare that they have no conflicts of interest.

Acknowledgments

This study was funded by Project of Humanities and Social Sciences Research in Jiangxi Universities and Department of Education Jiangxi Province under Grant No. JY17252.

References

[1] I. M. Gomez-Trigueros, "The geospace competences with the tpack model and outdoor educationautor," *European Journal of Geography*, vol. 10, no. 3, pp. 33–45, 2019.

[2] R. A. Salas-Rueda, "Use of the TPACK model as an innovation tool for the teaching-learning process on mathematics," *Perspectiva Educacional*, vol. 57, no. 2, pp. 3–26, 2018.

[3] J. C. Almenara, R. Roig-Vila, and S. Mengual-Andrés, "Technological, pedagogical, and content knowledge of future teachers according to the TPACK model," *Digital Education Review*, vol. 23, no. 32, pp. 73–84, 2017.

[4] D. Mourlam, "Preparing for infusion: emergence of a model for faculty TPACK development," *Journal of Technology and Teacher Education*, vol. 35, no. 3, pp. 301–325, 2017.

[5] D. Miguel-Revilla, J. M. Martínez-Ferreira, and M. Sánchez-Agustí, "Assessing the digital competence of educators in social studies: an analysis in initial teacher training using the TPACK-21 model," *Australasian Journal of Educational Technology*, vol. 36, no. 2, pp. 1–12, 2020.

[6] L. Eutsler, "TPACK's pedagogy and the gradual release of responsibility model coalesce: integrating technology into literacy teacher preparation," *Journal of Research on Technology in Education*, vol. 12, no. 1, pp. 1–18, 2021.

[7] S. Stefani, N. Elva, and C. Sumiati, "Peningkatan proses pembelajaran tematik terpadu dengan menggunakan model problem based learning (PBL) berbasis TPACK di Kelas V SDN 07 Pandam gadang," *Jurnal Pendidikan Tambusai*, vol. 5, no. 2, pp. 3255–3260, 2021.

[8] C. Bustamante, "TPACK and teachers of Spanish: development of a theory-based joint display in a mixed methods research case study," *Journal of Mixed Methods Research*, vol. 13, no. 2, pp. 163–178, 2019.

[9] Y. Zhang, K. Xia, Y. Jiang et al., "Multi-modality Fusion & Inductive Knowledge Transfer Underlying Non-sparse Multi-Kernel Learning and Distribution Adaption," *IEEE/ACM Transactions on Computational Biology and Bioinformatics*, 2022.

[10] J. Chen, C. Du, Y. Zhang, P. Han, and W. Wei, "A clustering-based coverage path planning method for autonomous heterogeneous UAVs," *IEEE Transactions on Intelligent Transportation Systems*, pp. 1–11, 2021.

[11] W. Cai and Z. Wei, "Remote sensing image classification based on a cross-attention mechanism and graph convolution," *IEEE Geoscience and Remote Sensing Letters*, vol. 19, pp. 1–5, Article ID 8002005, 2022.

[12] Y. Wang, T. Wang, X. Zhou et al., "TransEffiDet: Aircraft Detection and Classification in Aerial Images Based on EfficientDet and Transformer," *Computational Intelligence and Neuroscience*, vol. 202210 pages, Article ID 2262549, 2022.

[13] J. Zhou, Y. Wang, and W. Zhang, "Underwater image restoration via information distribution and light scattering prior," *Computers & Electrical Engineering*, vol. 100, Article ID 107908, 2022.

[14] Y. Ding, X. Zhao, Z. Zhang, Y. Nengjun, and Z. Ying, "Semi-supervised locality preserving dense graph neural network with ARMA filters and context-aware learning for hyperspectral image classification," *IEEE Transactions on Geoscience and Remote Sensing*, vol. 60, 2021.

[15] K. E. Brinkley-Etzkorn, "Learning to teach online: measuring the influence of faculty development training on teaching effectiveness through a TPACK lens," *The Internet and Higher Education*, vol. 38, no. JUL, pp. 28–35, 2018.

[16] M. Risti, "Model digitalnog nastavnog okruenja za strani jezik struke," *Inovacije U Nastavi*, vol. 32, no. 2, pp. 106–121, 2019.
[17] L. Irmita and S. Atun, "The influence of Technological Pedagogical and Content Knowledge (TPACK) approach on science literacy and social skills[J]," *Journal of Turkish Science Education*, vol. 15, no. 3, pp. 27–40, 2018.
[18] J. M. Marbán and E. J. Sintema, "Pre-service teachers' TPACK and attitudes toward integration of ICT in mathematics teaching[J]," *International Journal for Technology in Mathematics Education*, vol. 28, no. 1, pp. 37–46, 2021.
[19] H. Yulisman, A. Widodo, R. Riandi, and C. I. E Nurina, "The contribution OF content, pedagogy, and technology ON the formation OF science teachers' TPACK ability," *EDUSAINS*, vol. 11, no. 2, pp. 173–185, 2020.
[20] C. Huang, Y. W. Chan, and N. Yen, Eds., *Data Processing Techniques and Applications for Cyber-Physical Systems (DPTA 2019)*, Springer, New York , NY, USA, 2020.
[21] M. H. Shu, K. C. Chung, and J. C. Huang, "Computer teaching reform in colleges and universities under the background of informatization," in *Proceedings of the International Conference on Applications and Techniques in Cyber Security and Intelligence*, pp. 1731–1735, Springer, Cham, Switzerland, July 2019.
[22] Z. Arifin, M. Nurtanto, A. Priatna, N. Kholifah, and M Fawaid, "Technology andragogy work content knowledge model as a new framework in vocational education: revised technology pedagogy content knowledge model," *TEM Journal*, vol. 9, no. 2, pp. 786–791, 2020.
[23] R. Scherer, J. Ton De Ur, and F. Siddiq, "On the quest for validity: testing the factor structure and measurement invariance of the technology-dimensions in the Technological, Pedagogical, and Content Knowledge (TPACK) model," *Computers & Education*, vol. 112, no. sep, pp. 1–17, 2017.
[24] J. Carpendale, S. Delaney, and E. Rochette, "Modeling meaningful chemistry teacher education online: reflections from chemistry preservice teacher educators in Australia," *Journal of Chemical Education*, vol. 97, no. 9, pp. 2534–2543, 2020.

Hindawi
Computational Intelligence and Neuroscience
Volume 2022, Article ID 7646000, 11 pages
https://doi.org/10.1155/2022/7646000

Research Article

Music Individualization Recommendation System Based on Big Data Analysis

Pengfei Sun

The School of Arts, Yangtze University, Jingzhou 434023, China

Correspondence should be addressed to Pengfei Sun; 1507044230@st.nuc.edu.cn

Received 20 March 2022; Revised 8 May 2022; Accepted 11 May 2022; Published 5 July 2022

Academic Editor: Xin Ning

This study discovers a certain complementary relationship between different algorithms after conducting a comprehensive and in-depth analysis of proposal algorithms. This study proposes a big data music individualization proposal method based on big data analysis, which integrates user behaviour, behaviour context, user information, and music work information, based on traditional music proposal methods; improves the collaborative filtering proposal algorithm based on user behaviour; and calculates the semantic similarity between lyrics, as well as the song co-occurrence similarity based on the user's music download history. Because the lyrics represent the thoughts and feelings that the song wishes to convey to the listeners, the proposal module is completed, and the music proposal system is realized, by combining the two different similar information, using the improved algorithm and the Hadoop distributed framework. The music similarity and label similarity are combined to alleviate the problem of cold start and data sparseness, and a mixed similarity calculation formula is proposed to calculate the similarity between music. The accuracy similarity of the big data music proposal model proposed in this study is improved by about 20% through experimental comparison when compared with the collaborative filtering model and the hybrid model. It reflects the efficiency, scalability, and stability of the music proposal system as well as the ability to meet users' individual music needs.

1. Introduction

With the development of network technology, the music recommendation system has also developed rapidly, and online music platforms have become the first choice for people to listen to music. However, the music recommendation system also faces some problems, such as data storage confusion, low computational efficiency, cold start, and data sparsity caused by the large scale of data [1]. Aiming at the above problems, this study designs and implements a music recommendation system. Firstly, two channels of offline data transmission and real-time data transmission are designed to collect and transmit data. A music data warehouse is built to process and store the data in layers. Then the data are preprocessed to facilitate the calculation of the recommendation model [2]. Secondly, based on the improved algorithm, combined with the Hadoop distributed framework, the proposal module is completed, and the music proposal system is realized. Finally, after the functional test and nonfunctional test, it reflects the efficiency, scalability, and stability of the music recommendation system, which can meet the individualization music needs of users.

The core algorithm of the personalized music recommendation system developed in this article is the semantic-enhanced big data technology. Experiments show that when recommending unpopular music, the big data recommendation algorithm proposed in this article is more effective than pure content-based and collaboration-based recommendation methods. In order to meet the needs of the current huge user group to recommend massive music, the current mainstream big data distributed computing platform is used in the development of this system. Through a comprehensive and in-depth analysis of the two types of recommendation algorithms, it is found that there is a certain complementary relationship between the two types of algorithms. Therefore, this study proposes a semantic-enhanced big data technology [3] that combines content-based recommendation algorithms and collaborative filtering recommendation algorithms. The algorithm first analyzes the semantic information implied in the lyrics and calculates the semantic similarity between song lyrics, and then calculates the co-occurrence similarity of songs based on the user's music download history. Because the lyrics represent the thoughts and feelings that a song wants to convey to the listeners, this recommendation algorithm can improve the shortcomings of big data technology by combining these two different similar information [4]. The research object of this study is lyric songs. In the following, music and song refer to a song with lyrics.

Through the mapping relationship between interest degree and time, the algorithm introduces the influence of time decay factor when calculating the item rating matrix through historical behaviour, so as to obtain a more accurate recommendation result [5]. In the face of the cold start problem, a hybrid recommendation mode based on tags and collaborative filtering is adopted. When the system is first deployed and the number of users and rating items is less than a certain threshold, the songs are matched by the initial preference tag when the user registers, whereas when the number of users is sufficient, the improved collaborative filtering algorithm is used for music recommendation. The user's operations are monitored and recorded in real time, and the user's personalized recommendation list will be updated accordingly. The system should be developed by investigating the needs of users, referring to the current excellent music recommendation system, designing each functional module of the system, developing a good user interface, and aiming to design an accurate and easy-to-use system of personalized music recommendation [6].

The innovation of this study are as follows: the proposal algorithm combined with user behaviour analysis realizes the proposal according to a series of user behaviour records. The model, according to the complexity and diversity of user interests, learns the influence of different attributes on user interests.

The rest of the article is organized as follows: Section 2 introduces related big data technology concepts. Section 3 applies big data technology to the individualization music model. Section 4 applies big data technology [7] to the individualization music model. Based on the proposed big data proposal model, collaborative filtering model, and hybrid model, the section makes recommendations. Section 5 summarizes the entire article.

2. Related Works

Common recommendation methods have a number of flaws, including the inability to improve recommendation effects, migrate with changes in users' hobbies, mine users' potential hobbies, and make accurate recommendations based on users' hobbies. However, with the rapid development of big data and artificial intelligence [7, 8], traditional recommendation methods can now be improved. To meet users' daily needs, we can combine the benefits and drawbacks of traditional recommendation methods with new elements, as well as learn from each other. As a result of the new circumstance, the music recommendation system should also keep up with the pace of change. It is critical at this time to design and implement a comprehensive music recommendation system that is both accurate and easy to use. It is critical to create a music recommendation system that provides a better user experience.

Wang et al. implemented a user-based collaborative filtering algorithm on the cloud computing platform Hadoop, which solved the scalability problem of the collaborative filtering algorithm [9]. Yuqiao et al. used a collaborative filtering proposal algorithm to use user preference data to predict products that new users may like [10]. Hu et al. introduced matrix factorization techniques applied in recommendation systems and analyzed the impact of each matrix factorization technique on recommendation systems [11]. Tong et al. studied a hybrid proposal algorithm based on collaborative filtering and used the dimensionality reduction method of singular value decomposition to find the most similar items and users in item clusters and user clusters, which effectively improved collaboration [12]. Zhang et al. proposed a collaborative filtering proposal algorithm based on the social network. Based on the traditional matrix factorization model, the user preferences of social networks were integrated to obtain a trust feature matrix, which reduced the impact of data sparsity [13]. Liang et al. proposed a new deep learning model to utilize image content for content proposal in social networks. W. Cai et al. [7] applied the k-means clustering algorithm to a traditional content-based proposal and proposed a new proposal algorithm [14]. Chen et al. proposed the field of music proposal. The previous collaborative proposal can no longer meet the requirements of the audience. The essence of music proposal has become the proposal of listening experience. The article describes the solutions to the current music proposal problem in academia and industry: playlist generation, contextual proposal, and music production proposal [15]. Huang et al. proposed research on the robustness of recommender systems, including classifying the types of proposal model attacks, computing the impact of research attacks, and recommending replacement plans [16]. Jiang et al. reviewed and summarized the principles and challenges of recommender systems used in online music and looked forward to some future techniques that might be used to improve music proposal results [17]. Zhang et al. believed that traditional proposal systems try to help users find related items, but this is not enough. Proposals need to give more appropriate results based on the time and location of the user at that time, that is, considering the scene recommended [18]. Bauer and Schedl first extracted acoustic features from the audio inquiries and used the content-based collaborative filtering proposal method to complete music proposal. Domestic scholars' research on music individualization proposal has also formed a series of scientific research results [19]. Su et al. used spectrogram analysis to obtain the characteristic data matrix of musical works and calculated the similarity between stored music and query data to achieve Top-N proposal [20]. Zhang et al. studied the multi-domain recommender systems, because traditional recommender systems only consider items in the same field, while cross-field recommender systems support operations on items in different fields, making the recommender system more accurate [21]. Feng used the method of bibliographical analysis to complete the proposal algorithm from different perspectives by using differential strategies and analyzed various descriptions of music-related documents to obtain its regularity to complete the proposal [22].

In this era of excess data, there are various connections between data, and it is obviously unrealistic to rely on humans to distinguish. However, with the rise of big data technology, various tools for data processing have made it possible for us to discover the internal connection of data. This is a significant breakthrough by mining potential connections between data and serving recommender systems. Data can be analyzed from multiple perspectives, such as user behaviour context, scene atmosphere, time perception, etc., to improve the accuracy of the proposal system from multiple perspectives.

3. Concepts Related to Individualization Proposal Technology Based on Big Data Analysis Technology

Data acquisition is the basic premise of processing. With the rapid development of the Internet, Internet of Things, and cloud computing, they have become important channels for obtaining data. Especially with the rapid development of smart mobile terminals, a large amount of data is generated every day, among which mobile phones and mobile terminals are representative.

The main functions of data integration are data extraction, cleaning, and storage. The data collected during the data acquisition stage are typically large in scale and diverse in nature. Data extraction's main goal is to convert complex data types into unified or easy-to-understand data structures. The amount of data collected is usually large, but the amount of valid data is not. Many of the data may be of little or no use in specific application scenarios, and even more data may contain incorrect information. Data cleaning ensures data quality, while data storage serves as a platform for data processing. The core of the processing process and the process of extracting useful information from big data is data analysis. The only way to get useful information is to use the right method. After the user's historical data, such as search terms, have been used, it is saved in the database and never used again. Big data typically contain some basic data, and valuable information can be mined by expanding these data. Parts of the data have less value than the overall value, so different data sets are reorganized for analysis to achieve a relatively high total value. Sometimes useful information can be found in error data, such as spell-checking during searches. The Internet can be used to obtain very public data, and the majority of them are obtained by advanced enterprises and research institutions both at home and abroad. These open data can be used by researchers to conduct research and create more value. The user is presented with the processed results during data interpretation. In contrast to data analysis, which requires professional knowledge, the results of data processing are displayed to ordinary users who do not necessarily understand the technology of data analysis. As a result, how to clearly display the results to ordinary users is a critical issue, which is usually accomplished through the use of graphics, charts, or tabular methods.

As shown in Figure 1, user 1 purchases three items A, B, and D, and user 3 purchases items B and D. By analyzing the purchase behaviour of users, it can be found that the similarity between user 1 and user 3 is relatively high. Among them, user 1 has purchased item A, so it can be inferred that user 3 is very inclined to purchase item A, so it is recommended to user 3.

The concept of big data technology has been deeply influenced at the interaction level. This chapter will combine the theory of interaction to expound the interaction in music. Audience research has become an increasingly important part of social media research. When the real interpersonal communication is more and more carried out in the virtual network, the social activities between people will also change more or less, which are shown in Figure 2.

The algorithm is divided into three steps: the first is item representation, in which we must extract the item's content features to represent the item; the second is song recommendation, in which we can use the song's tags as well as the singer's tag and other features; and the third is item recommendation, in which we must extract the item's content features to represent the item. We can use the user's historical behaviour to describe the user's item feature preference for feature learning. This type of preference can be expressed in music recommendations based on the user's song behaviour data. Finally, a recommendation sequence is generated, and through similarity comparison, a set of items with the highest similarity is generated for the user. Data on the user's online behaviour are collected and stored. User online behaviour refers to a user's new behaviour, such as listening to new songs, dancing to new songs, collecting albums, saving the data in the appropriate database, and classifying the information in the database. Users can sort their preferences, and they can check their listening records at any time. When a user contacts the system and registers as a new user, the user can display the music he likes and hide the music he does not like based on his personal preferences, and the user can change the information set by himself at any time. The music recommendation system can recommend songs that the user is interested in and prevent songs that the user does not like from appearing in his music playlist based on the user's music preference information.

4. Design of Music Proposal Model Based on Big Data Analysis

4.1. User Preferences Similarity Calculation Based on Big Data Analysis. The similarity formula is used at the heart of massive data technology to calculate project similarity, and

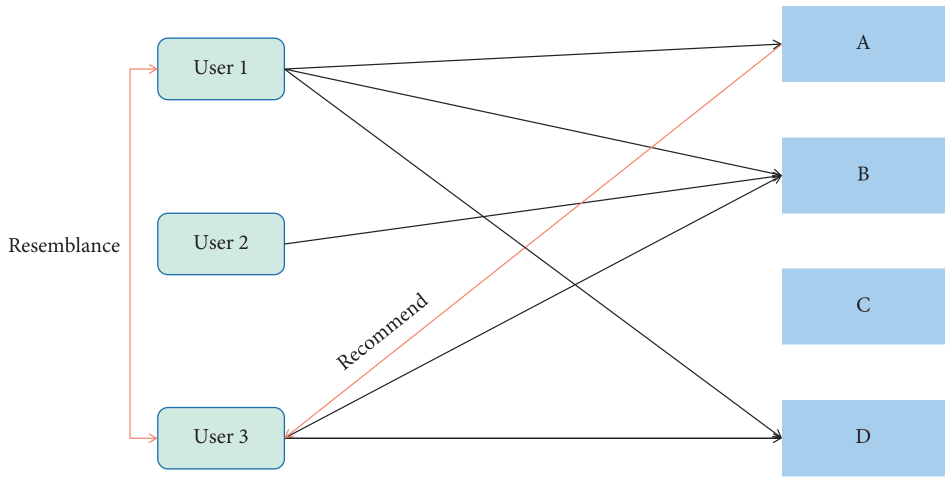

Figure 1: Proposal process based on big data technology.

the similarity that can be selected for different projects is also different. Massive data technology, in comparison to collaborative filtering and mixed model algorithms, can learn the influence weights of different attributes and the interaction between attributes on user interests. Big data technology, for example, can learn not only the impact of a single attribute on user interest, but also the impact of any combination of attributes. Using the example of user age, gender, and time, big data technology can determine the impact of these three attributes alone on user interest as well as the impact of any two or even three attributes combined on user interest. This is classic modelling. Algorithms are incapable of accomplishing this. This study takes into account the impact of modelling and the amount of computation, but only considers the impact of a single attribute and any two attributes on user interest.

The user information is represented as $X(x) = \{x1, x2, \ldots, xz, y\}$ after processing, where y is the user's preference value for the item expressed by this behaviour, and xi is the value of the i feature of the user's current behaviour. The method of big data technology is to use user data to pass learning to obtain a prediction function $f(x)$. It represents different interest models of users, and the calculation formula is as follows:

$$f(X) = w_0 + \sum_{i=1}^{n} w_i x_i + \sum_{i=1}^{n} \sum_{j=i+1}^{n} v_{ij} x_i x_j, \tag{1}$$

where w_0 is the global parameter deviation, x_i is the value of the i attribute of the user's current behaviour, the meaning of the $w_i x_i$ part is the contribution of the attribute x_i to the user's interest, and $v_{ij} w_i x_j$ represents the effect of the attributes x_i and x_j on the user's interest.

The data set is to learn the function $f(x)$ by using big data technology on the data in the data set. The purpose of the test set is to test the learning effect of the function $f(x)$. The following formula defines the loss function L of the big data technology:

$$L = \sum_{i=1}^{N} \operatorname{loss}(f(X), Y) = \sum_{i=1}^{N} (\hat{y}(x_i) - y_i)^2. \tag{2}$$

In the pursuit of minimizing the loss function, it is necessary to prevent the occurrence of overfitting. The regularization term in this article introduces the parameter vector formula (3), which is the calculation of the optimization problem of big data technology.

$$L = \arg\min \sum_{i=1}^{N} (\hat{y}(x_i) - y_i)^2. \tag{3}$$

The above formula represents all the model parameters of big data technology, that is, the specific influence weights of attributes on user interests. There are two related functions $g(x)$ and $h(x)$ for any parameter of $f(x)$, as shown in the following formula:

$$\hat{y}(x) = g(x) + h(x). \tag{4}$$

When $w_0 = 0$,

$$\hat{y}(X) = \sum_{i=1}^{n} w_i x_i + \sum_{i=1}^{n-1} \sum_{j=i+1}^{n} \left(v_i^T v_j\right) x_i x_j + w_0. \tag{5}$$

When $w_0 = 1, 2, \ldots, n$, as shown in (5),

$$\hat{y}(x) = w_0 + \sum_{i=1}^{n} w_i x_i + \sum_{i=1}^{n-1} \sum_{j=i+1}^{n} \left(\sum v_{ls} v_{js}\right) x_i x_j. \tag{6}$$

Only one parameter is optimized in each calculation process, and the iterations are performed round by round. Music can usually have a variety of tag information, which can be analyzed and described from different dimensions. The more tags, the better the representation of items. Each piece of music has a different label, and the more common labels between two pieces of music, the more similar they are. The calculation formula for defining the similarity of labels is as follows:

$$\mathrm{sim}_{tah(u,v)} = \frac{I_u \cap I_v}{I_u \cup I_v}. \tag{7}$$

The tag-based proposal algorithm can still recommend music in the absence of user ratings and alleviate the problem of cold start to a certain extent. Although the tag-

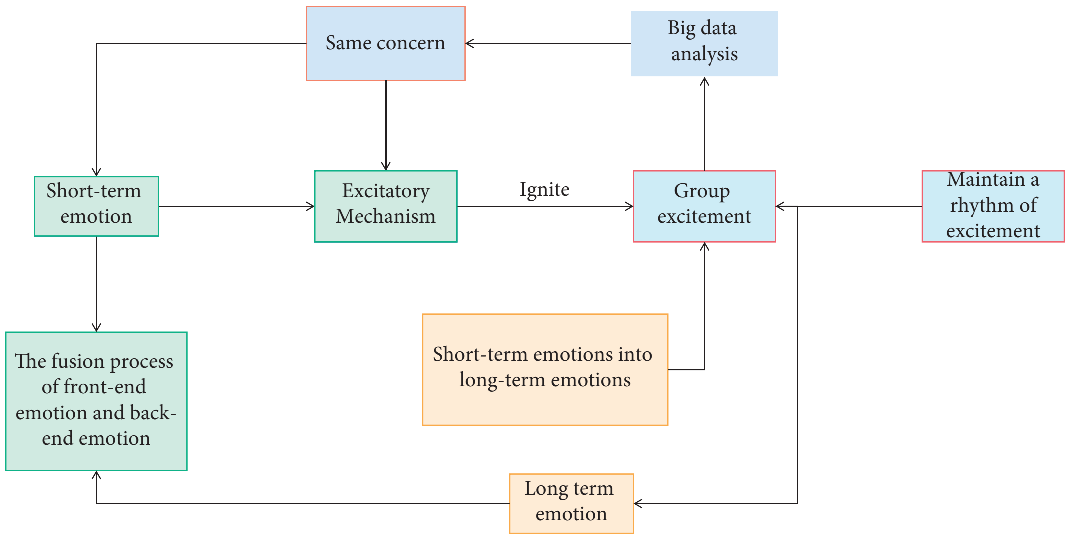

FIGURE 2: The interactive ritual chain linked to emotion in music.

based proposal algorithm does not require the user's score record, only the tag of the music itself is needed. Combining the tag-based proposal algorithm with other proposal algorithms can improve the proposal effect.

4.2. Music Score Clustering Algorithm. Each user has his own scale when scoring the music. For a very favorite item, conservative-type users rate lower than positive-type users. From a mathematical point of view, different users have different mean and variance of ratings. Therefore, in order to have a unified standard for user preferences, it is necessary to normalize user ratings. In the method based on the clustering algorithm, the principle is to subtract the average of the user's score from the user's score on the music, which is shown in the following formula:

$$h(r_{ui}) = r_{ui} - \overline{r}_u. \tag{8}$$

Bringing formula (8) into formula (9), we can get the predicted user u score for the new music i as

$$r_{ui} = \overline{r}_u + \frac{\sum_{v\in N_i(u)} w_{uv}\left(r_{vi} - \overline{r}_v\right)}{\sum_{v\in N_i(u)} \left|w_{uv}\right| \sum} \tag{9}$$

The special feature of big data technology is that normalization takes into account the variance of user ratings. For user-based methods, the definitions are shown in the following expression:

$$h(r_{ui}) = \frac{r_{ui} - \overline{r}_u}{\sigma_u}. \tag{10}$$

Bringing this formula into formula (9), the user's rating of the new music can be predicted, which is shown in the following formula:

$$\widehat{r}_{ui} = \overline{r}_u + \sigma_i \frac{\sum_{j\in N_i(i)} \left(w_{ij}\left(r_{vj} - \overline{r}_j\right)/\sigma_j\right)}{\sum_{j\in N_i(u)} \left|w_{uv}\right|}. \tag{11}$$

4.3. Individualization Proposal Model Based on Big Data Technology. The main component of the recommendation module is the recommendation model, which is the heart of the recommendation system. As a result, the user experience is directly related to a good recommendation model. After analyzing and summarizing a variety of common recommendation models, it was discovered that each model has distinct advantages and disadvantages in terms of generating an accurate user recommendation list. This system uses a hybrid recommendation system that relies heavily on the use of tags and collaborative filtering. When the number of users or the number of user-rated items is insufficient, a tag-based recommendation model is used. This is primarily used to address the collaborative filtering recommendation problem—problem with cold start. The improved collaborative filtering algorithm is enabled when the number of users and user rating items is sufficient. Time considerations are introduced into traditional collaborative filtering because users' interests may change over time. Figure 3 depicts the recommendation process for accurate recommendations.

The core idea behind the big data-based recommendation algorithm is to use audio features to describe a piece of audio data, and then use those features to calculate similarity with other audios. It analyses the feature information of the tracks, traverses the music database, and recommends tracks based on a user's listening time, number of clicks, collection, and download behaviour. The music recommendation system's data content primarily consists of user data, music data, and user-system interaction behaviour data. Basic information about the user is contained in user data. Music data contain various details about music and can be used to extract interesting features, making it an important data source for recommender systems. The user's interaction with music is included in user behaviour data, and the recommendation system can be used to mine the user's potential information. The purpose of data processing technology is to clean, process, and transform the system's data so that the algorithm layer can obtain clean and effective data, thereby

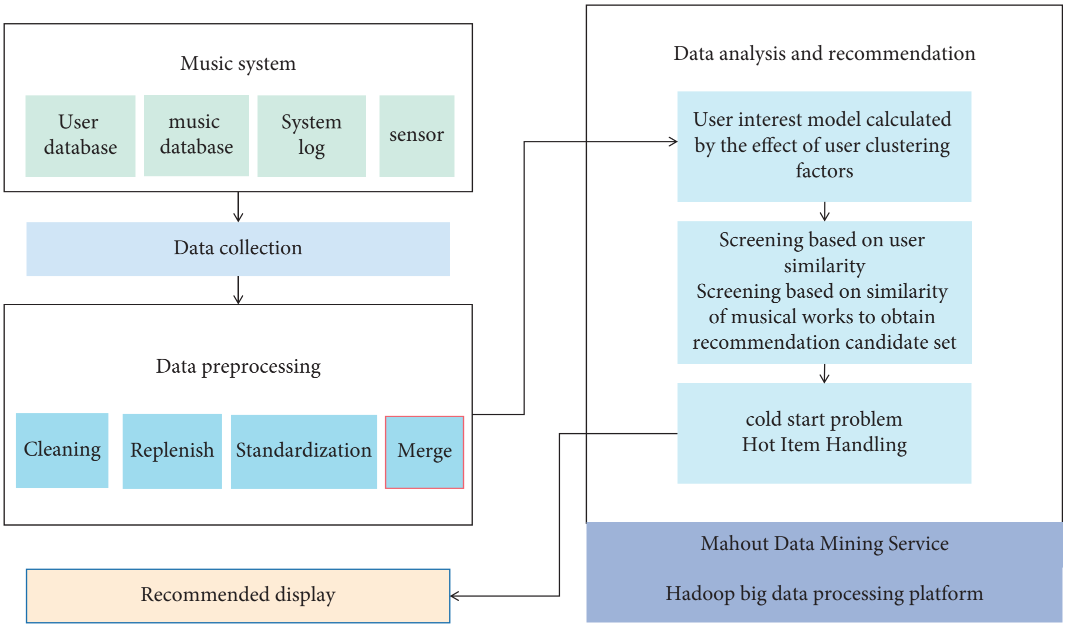

FIGURE 3: Big data music individualization proposal process.

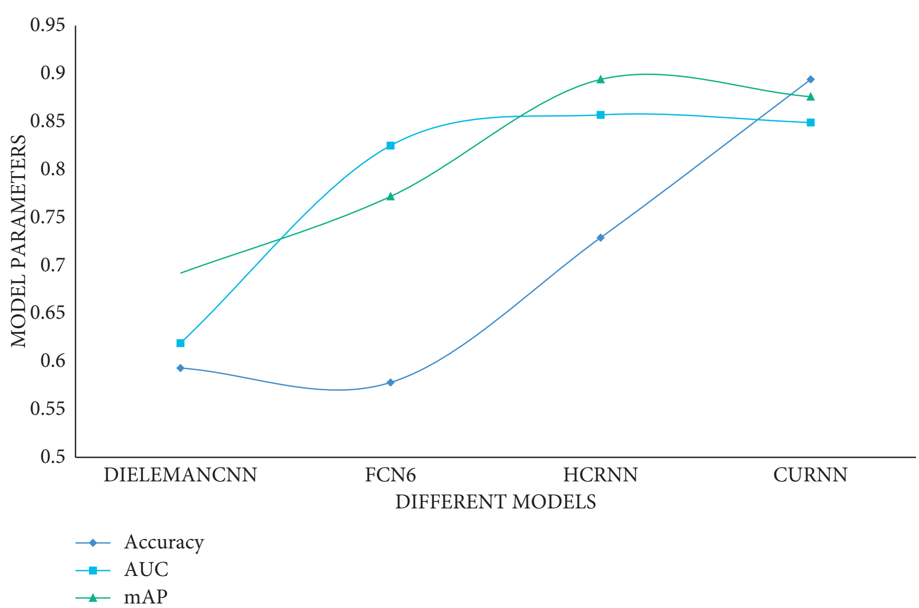

FIGURE 4: Comparison of different model experiments.

improving the recommendation system's performance. The validity of the behaviour data directly affects whether the recommendation result can meet the user's needs because the user's historical behaviour information reflects the user's preferences at different times. The background log information will record each user's behaviour, such as clicking on music, commenting on music, and sharing music, and the stored content format will be in the form of a dictionary. Finally, a data format that is beneficial to the calculation of the recommendation algorithm can be obtained after systematic processing. The information gathered will be processed. Missing data, data noise, and data duplication may occur during the data collection and transmission process, affecting subsequent model training and resulting in low model robustness. As a result, the information must be processed. There may be many data attributes when analyzing and processing data, but some are irrelevant and some are relevant, so it is necessary to select the most relevant features for processing to improve the model's robustness. The accuracy of a recommendation is insufficient. The diversity of recommendation results is critical with the growing number of Internet services and changing user needs. If users listen to ancient songs for a long time, for example, our recommendation list should include some variety based on personalization and precision, such as sad songs that are not very similar to ancient styles. The recommendation is

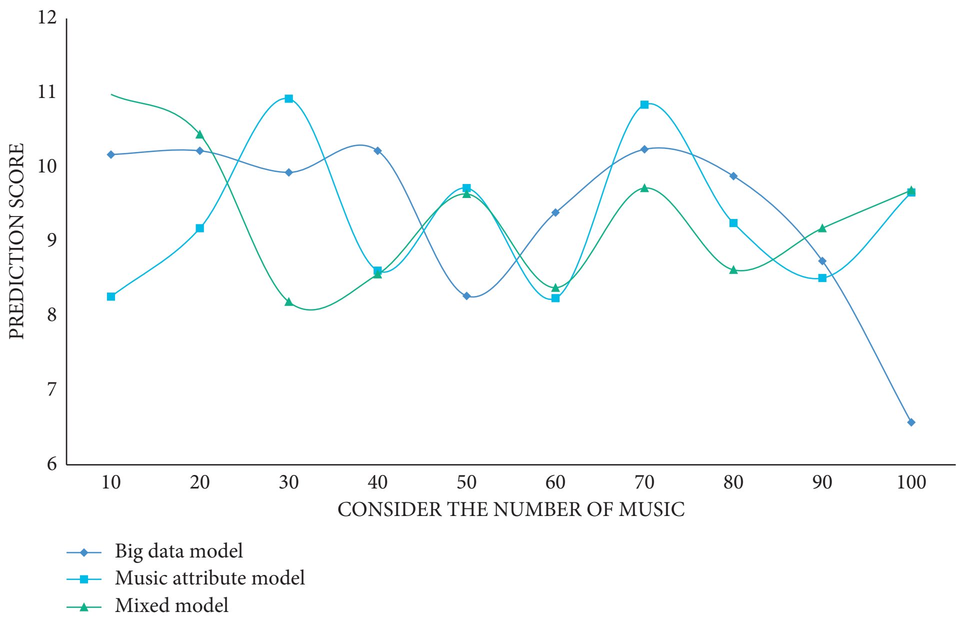

Figure 5: Comparison experiment of L value of different models.

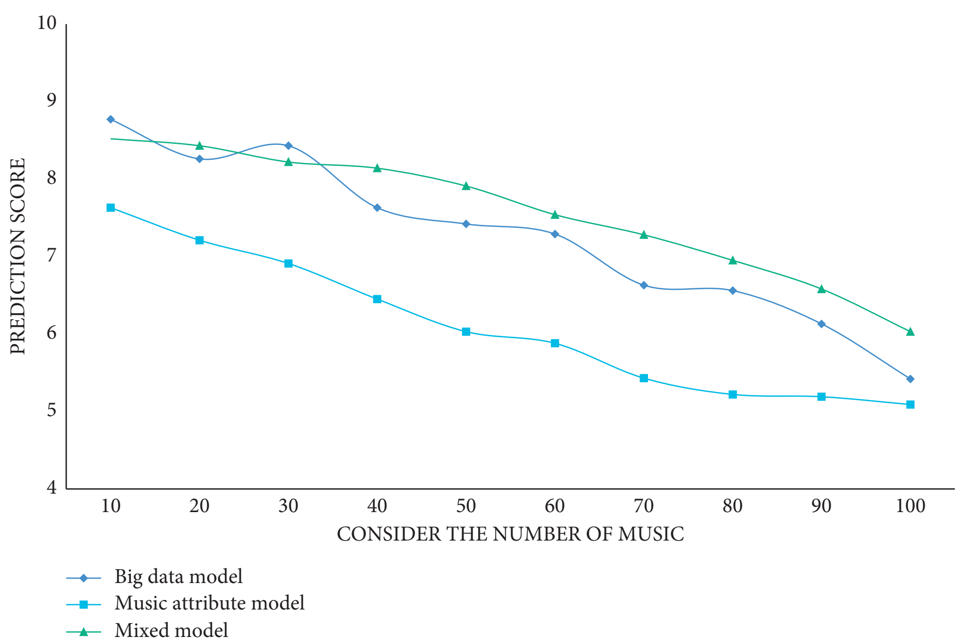

Figure 6: Comparison experiment of R value of different models.

successful if the user clicks. The recommendation results differ depending on each user's unique historical behaviour data. The system can update the recommendation in real time based on short-term data and long-term data, allowing the user to experience the system's personalization. The recommender system learns from the user's past behaviour and improves its personalization and accuracy over time.

The higher the big data recommendation model's evaluation value, the more interested in music the user is; the big data recommendation model is generated into the nearest neighbour set, which is the user's big data recommendation model set that is similar to the user's interest. Two user big data recommendation models are regarded as two vectors in the vector space using the method of vector space similarity calculation, and the similarity between them is measured by calculating the cosine value of the angle between the two vectors in the big data recommendation model. Finally, the big data recommendation model's recommendation set is generated. The user's evaluation value of the song is predicted based on the similarity between neighbour users and the user as well as the neighbour users' evaluation value of the song. Then, using the big data recommendation model, the first few songs with the highest ratings are measured, and the recommendation results are

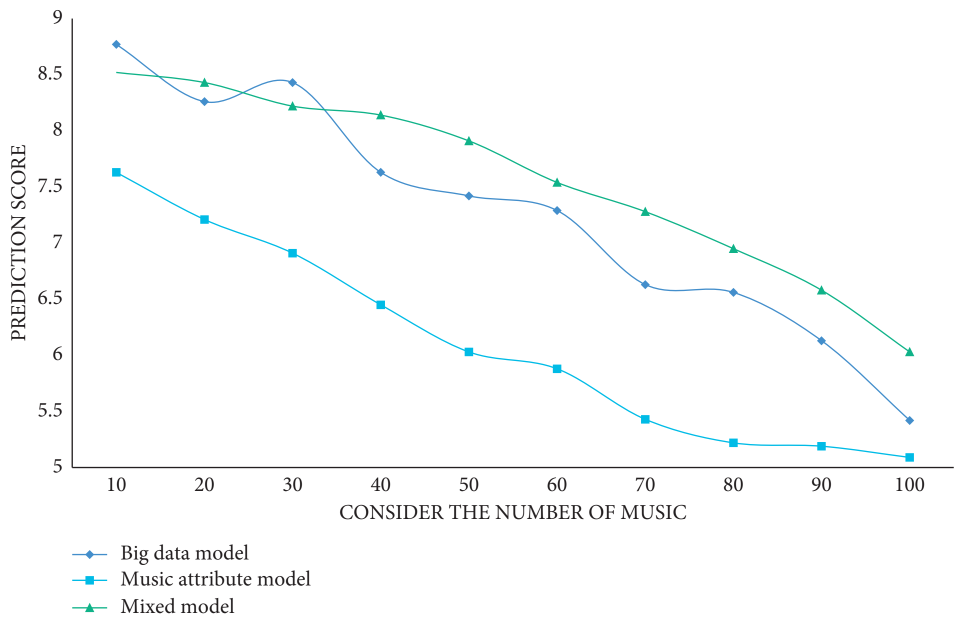

Figure 7: Comparison experiment of G values of different models.

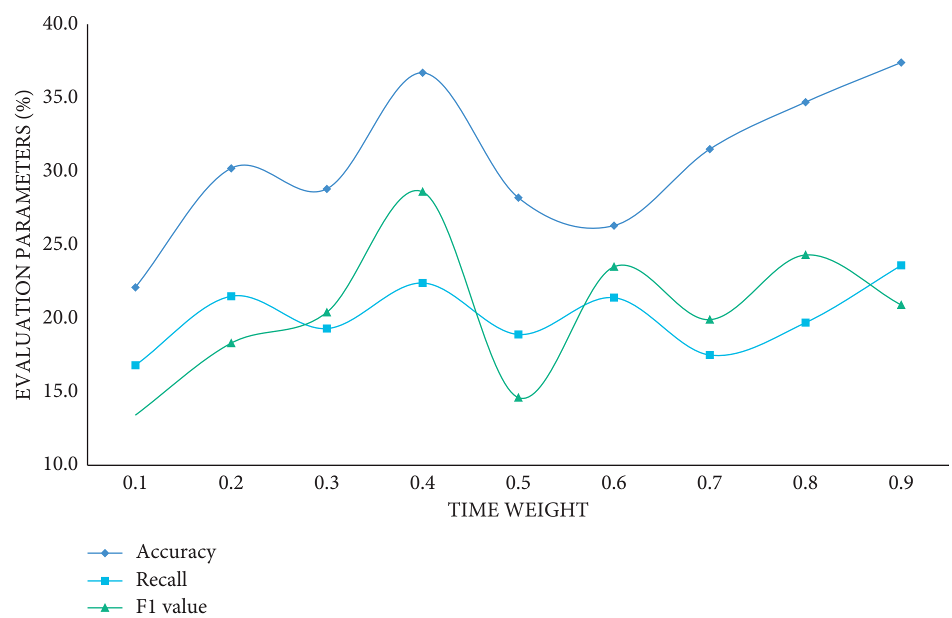

Figure 8: Improved big data proposal model.

fed to the model's first few users. To begin, their features are extracted to generate the user interest model of the big data recommendation model based on the music resources downloaded, searched, and rated within a certain period of time according to the big data recommendation model, and then different big data recommendation models are generated from the ringtone resources in the ringtone library. The content recommendation set is made up of music and user interest models with similar attribute values; second, the big data recommendation model predicts the user's predicted score for some songs and finds the nearest neighbour based on the users with similar interests. The big data recommendation model's recommendation set is recommended; third, the content recommendation set in the recommendation set and the music sorted by the nearest neighbour big data recommendation model are scored according to the weight, and the big data recommendation model with the highest score is chosen as the final recommendation item to be recommended to the user.

5. Experiments on Proposal Models Based on Big Data

The individualization music proposal model of big data technology proposed in this study introduces the GRU network after the XCNN network, which has long-term

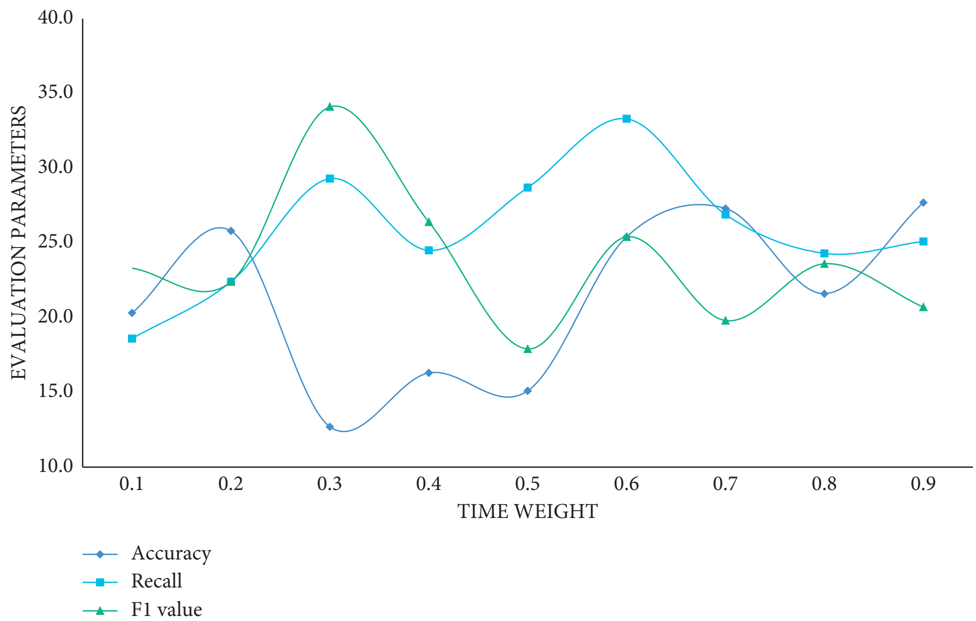

Figure 9: Improved collaborative filtering proposal model.

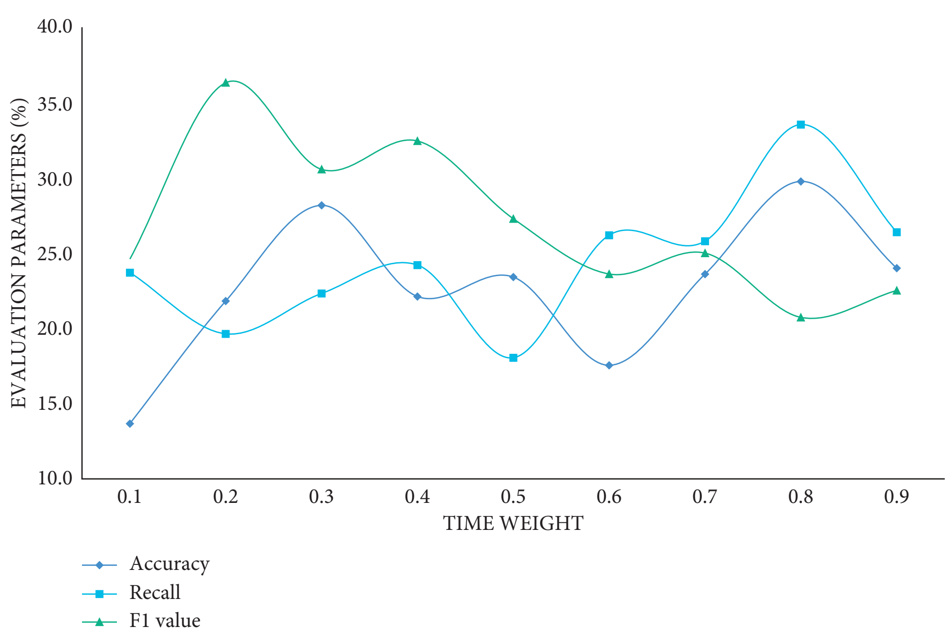

Figure 10: Improved hybrid proposal model.

memory ability and can extract the feature relationship between pre- and post-sequence images. In order to verify the music classification effect of the CURNN model in this study, the experimental results are compared with music classification methods such as HCRNN, FCN6, and DielemanCNN, and the accuracy, AUC, and mean average accuracy mAP of each method are calculated. The results are shown in Figure 4.

It can be seen from the experimental data that CURNN has higher accuracy, AUC, and mean average accuracy rate mAP than the other three models due to the addition of a big data proposal model. The closer the accuracy, AUC, and mAP values are to 1, the better the classification effect is, so the classification effect of the model CURNN proposed in this study is much higher than that of DielemanCNN and FCN6 that only use their own data. Compared with the HCRNN model that also uses the RNN network, CURNN is still ahead. For the three music proposal models proposed in this article, the user's score is predicted on the collection of songs; the predicted scores of 10 to 100 songs are randomly selected; and the L, R, and G values are calculated. The experimental results are shown in Figures 5–7.

As the number of predicted scores increases, the parameter scores decrease continuously. According to the experimental results, the prediction scores of the prediction results of the big data proposal model are higher than those of the other two models, and it has a better proposal effect. The user's behaviour is temporal, so time weights should be introduced into the user prediction scoring formula. Different time weights have different effects, thus affecting the final proposal result. This study sets the time weight value of 0.1 to 0.9 for comparative experiments. In this section, the experimental results will be displayed and analyzed, and the evaluation indicators will be precision rate, recall rate, and $F1$ score. The specific experimental results are shown in Figures 8–10.

The relationship between the time weight coefficient, precision rate, recall rate, and $F1$ is neither positive nor negative, as can be seen. Precision, recall, and $F1$ scores increase steadily as the time weight increases, and when the time weight reaches 0.4, the three indicators' scores tend to be flat. To summarize, the proposed big data music proposal model is about 20% more accurate than the collaborative filtering model and the hybrid model when the time weight is 0.4. And the big data-based proposal algorithm is clearly superior to the single similarity proposal algorithm.

6. Conclusions

Traditional proposal methods frequently limit themselves to user behaviour data while ignoring background data and other issues. This study investigates a data collection method that combines system logs, system databases, network interfaces, and sensors; collects data from multiple sources; and prepares a complete data set for individualization proposals, in conjunction with the big data collection method. Following the completion of data collection, this study uses the appropriate standardization processing methods to perform data standardization work in the preprocessing according to the various types of data collected. We start with two aspects in the proposal candidate set screening stage. On the one hand, it seeks out similar users' favorite music, and on the other, it uses clustering to find music that is similar to the user's favorite music. Starting with two aspects, it ensures that the candidate set is personalized, as well as fully covering the user's interests and improving the quality of the final proposal results. Massive music works and users cause a slew of issues for recommender systems. This study solves the problem of cold start and hot item processing by increasing proposal probability and decreasing item weight, which not only improves the coverage of the proposal system but also ensures the accuracy of the proposal, thus alleviating these issues. The ability of the system to process data is also important in the big data environment. Using the Hadoop big data processing framework, this study improves the system's processing ability. To begin, the recommender system's functional and nonfunctional requirements are analyzed, and various designs required for system implementation are completed. A working environment is created in which a music individualization proposal system can be implemented. Finally, testing is used to confirm the system's feasibility and effectiveness. To mine user preferences and complete the recommendation process, this study primarily uses user data, music work data, user behaviour data, and behaviour context data. However, there is a lot of data that can be added to the recommendation process calculation. Tag data are typically used by users to mark their feelings and experiences with musical works, allowing tags to link users to musical works. These data should be the focus of future research.

Data Availability

The data used to support the findings of this study are available from the corresponding author upon request.

Conflicts of Interest

The author declares that there are no conflicts of interest.

References

[1] S. Dieleman, A. van den Oord, and K. Simonyan, "The challenge of realistic music generation: modelling raw audio at scale," *Advances in Neural Information Processing Systems*, vol. 31, 2018.

[2] Z. Huang, Y. Liu, C. Zhan, C. Lin, W. Cai, and Y. Chen, "A novel group recommendation model with two-stage deep learning [J]," *IEEE Transactions on Systems, Man, and Cybernetics: Systems*, vol. 5, 2021.

[3] X.-B. Jin, W.-T. Gong, J.-L. Kong, Y.-T. Bai, and T.-L. Su, "A variational bayesian deep network with data self-screening layer for massive time-series data forecasting," *Entropy*, vol. 24, no. 3, p. 335, 2022.

[4] P. Wang, Z. Wang, and Q. Ma, "Research on the association of mobile social network users privacy information based on big data analysis," *Journal of Information Hiding and Privacy Protection*, vol. 1, no. 1, pp. 35–42, 2019.

[5] M. Asenova and C. Chrysoulas, "Personalized micro-service recommendation system for online news," *Procedia Computer Science*, vol. 160, pp. 610–615, 2019.

[6] X. M. Liu, F. U. Xiao-Hui, and S. Wang, "Research on the influence of perceived value of individualization proposal system on user acceptance—based on the adjustment of psychological capital," *Technology and Innovation Management*, vol. 8, 2017.

[7] W. Cai, Y. Song, and Z. Wei, "Multimodal data guided spatial feature fusion and grouping strategy for E-commerce commodity demand forecasting," *Mobile Information Systems*, vol. 2021, Article ID 5568208, 2021.

[8] J. Chen, C. Du, Y. Zhang, P. Han, and W. Wei, "A clustering-based coverage path planning method for autonomous heterogeneous UAVs," *IEEE Transactions on Intelligent Transportation Systems*, vol. 2021, Article ID 3066240, 11 pages, 2021.

[9] L. Wang, H. Xu, and Y. Cao, "Research and implementation of precision marketing system based on big data analysis[J]," *IOP Conference Series: Materials Science and Engineering*, vol. 394, 2018.

[10] Y. Yuqiao, Z. Weiping, L. Fangdan, and Z. Hongli, "Personalized information recommendation simulation system based on compound recommendation algorithm--A research tool to study the push effect of algorithm," *IOP Conference Series: Materials Science and Engineering*, vol. 740, no. 1, Article ID 012167, 2020.

[11] X. Hu, Y. Wang, Q. B. Chen, Q. Liu, and X. Fan, "Research on personalized learning based on collaborative filtering

method," *Journal of Physics: Conference Series*, vol. 1757, no. 1, Article ID 012050, 2021.

[12] H. Tong, C. Zhang, and J. Hu, "Design and research of mobile learning recommendation system based on deep learning perspective," *Journal of Physics: Conference Series*, vol. 1915, no. 2, Article ID 022065, 2021.

[13] J. Zhang, J. Zhao, and Z. Jiang, "Research on collaborative filtering proposal algorithm based on spark optimization," *Journal of Changchun University of Science and Technology (Natural Science Edition)*, vol. 8, 2018.

[14] H. Liang, D. Zeng, Y. Yu, Y. Yu, and K. Oyama, "Individualization music proposal with triplet network," 2019, https://arxiv.org/abs/1908.03738.

[15] W. Chen, G. Yin, G. Zhao, and C. Penna, "Communications in Computer and Information Science] Big Data Technology and Applications," *Individualization Proposal System on Hadoop and HBase*, vol. 590, pp. 34–45, 2016.

[16] X. Huang, S. Guo, Y. Zhang, P. Zhang, and S. Xu, "Automatic recommendation method of network data based on big data technology," *Journal of Physics: Conference Series*, vol. 1550, no. 3, Article ID 032120, 2020.

[17] S. Jiang, Y. Zhang, and H. Xu, "Personalized recommendation method of E-commerce based on fusion technology of smart ontology and big data mining," *IOP Conference Series: Materials Science and Engineering*, vol. 750, no. 1, Article ID 012134, 2020.

[18] L.-k. Zhang, S.-q. Sun, B.-x. Xing, R.-m. Luo, and K.-j. Zhang, "Using psychophysiological measures to recognize personal music emotional experience," *Frontiers of Information Technology & Electronic Engineering*, vol. 20, no. 7, pp. 964–974, 2019.

[19] C. Bauer and M. Schedl, "Global and country-specific mainstreaminess measures: definitions, analysis, and usage for improving personalized music recommendation systems," *PLoS One*, vol. 14, no. 6, Article ID e0217389, 2019.

[20] J. H. Su, C. Y. Chin, Y. W. Liao, H. C. Yang, V. S. Tseng, and S. Y. Hsieh, "A individualization music recommender system using user contents, music contents and preference ratings [J]," *Vietnam Journal of Computer Science*, vol. 7, no. 1, 2019.

[21] J. Zhang, X. Zeng, K. Liu, H. Yan, and M. Dong, "Jeans knowledge base development based on sensory evaluation technology for customers' personalized recommendation," *International Journal of Clothing Science & Technology*, vol. 30, no. 1, pp. 101–111, 2018.

[22] N. Feng, "Call for papers: multimedia big data analytics in technology enhanced learning house advertisement[J]," *IEEE Multimedia*, vol. 23, no. 1, p. c3, 2016.

Hindawi
Computational Intelligence and Neuroscience
Volume 2022, Article ID 3965416, 12 pages
https://doi.org/10.1155/2022/3965416

Research Article

Application of New Sensor Technology and Few-Shot Learning in Education Based on IoT Era

Jianwen Feng

Dean's Office, Hanshan Normal University, Chaozhou 521041, Guangdong, China

Correspondence should be addressed to Jianwen Feng; fengjw@hstc.edu.cn

Received 24 March 2022; Revised 11 May 2022; Accepted 12 May 2022; Published 4 July 2022

Academic Editor: Xin Ning

In recent years, with the rapid development of emerging Internet of Things technology and short-range wireless communication technology, smart healthcare monitoring network technology has become a research hotspot. It provides convenience for people and enhances the development of people's own healthcare awareness. This paper aims to study how to make its application in the field of smart healthcare education more applicable through the use of related technologies in the Internet of Things era and few-shot learning. For this reason, this paper proposes to optimize and improve the new sensor technology and the algorithm of few-shot learning, and to adjust some parameters as a whole. At the same time, related experiments and analysis are designed for the improved algorithm to study and understand its performance. The experimental results in this paper show that the improved algorithm improves its application effect by 36.9% and is relatively more applicable than the unimproved algorithm.

1. Introduction

Intelligent medical care is a new medical service sharing system that combines computer technology, communication network technology, and modern medical technology. Smart healthcare is designed to serve as a link between patients and hospital specialists, allowing patients to seek advice from specialists in distant hospitals at any time and from any location, and to receive effective treatment and healthcare, as well as other medical services, based on recommendations. It achieves "zero distance" consultation between specific medical costs and time, and patients and hospital experts and medical personnel, and improves medical resource efficiency and distribution rationality.

Intelligent medical monitoring can continuously send human physiological parameter information to a medical monitoring center in a remote hospital for analysis and diagnosis by experts or medical personnel using medical sensors and communication networks. As a result, hospital experts and medical personnel can quickly obtain the patient's testing results, record historical data, and describe reasonable and correct diagnoses and treatment options. In the hospital's database center, the function of long-term tracking of the patient's physical condition can also be realized. The demand for remote medical monitoring is increasing, and the market prospect is broad, thanks to the rise of network applications of medical supplies and the gradual improvement of people's own health awareness.

The novelty of this paper is that it adjusts the classification of the algorithm and other related parameters based on research and understanding of new sensor technology in the emerging Internet of Things era, combined with algorithm optimization for few-shot learning. It makes the improved algorithm's application effect in the actual field of education more applicable, and it can play its role more effectively.

2. Related Work

With the rapid development of Internet-related technologies, people have a wide range of applications for decorrelation. As one of the main extensions of the Internet of Things technology, sensor technology has never been interrupted. Mokhtari et al. proposed a new body recognition sensor that can effectively distinguish multiple residents in a home environment to detect their height as a unique biometric. The sensor includes three sensing/communication modules: a pyroelectric infrared (PIR) occupancy, an ultrasonic array, and a Bluetooth Low Energy (BLE) communication module. The PIR occupancy module is used to detect the moving direction, while the ultrasonic array module is used to detect the height of the moving residents [1]. Shimada proposes that, with the application of magnetic fields and magnetically responsive fluids such as magnetic composite fluids (MCFs) as fillers, the effect of electrolytic polymerization on NR-latex such as plastic-type polymer solutions is enhanced. The current new MCF rubber vulcanization method is efficient enough to be widely used in tactile sensors in robotics and engineering applications [2]. Miao et al. believe that new sensor technologies such as near-infrared spectroscopy, chemical imaging, electronic nose, and electronic tongue play an important role in the quality evaluation of traditional Chinese medicine and have prospects and opportunities for future research [3]. Ebrahimi and Mardani propose a new, simple, and inexpensive sensor to detect multipoint contact of a typical robotic wheel. The new sensor enables wheeled robots to scan surfaces and find stability margins during real-time motion without the need for cameras or laser sensors. In addition, it enhances the real-time solution capability of dynamic equations [4]. Chaiendoo et al. proposed a selective colorimetric method for the detection of formaldehyde (FA) based on polymethacrylic acid-(PMAA-) templated silver nanoclusters (AgNCs). In the presence of AgNCs (AgNCs@Tollens), chemical dosimeters are easily fabricated by forming Tollens reagents. Compared with other aldehyde-containing compounds, the proposed method exhibits excellent selectivity for FA [5]. Kuchlyan et al. proposed that Mercury ions pose a great threat to humans due to their high toxicity in living systems. Therefore, its detection at the nanometer level is of current interest. Rhodamine derivatives are one of the rarest examples of Hg2+ fluorescent chemosensors, in which the phthalic acid moiety showing antibacterial activity is responsible for specific binding [6]. Wu and Yan believe that adaptive immune cells are usually not equipped with pattern recognition receptors. In immunity, they revealed an “innate-like” cytosolic DNA sensing mechanism of KU complexes in senescent CD4+ T cells, which exacerbates senescence-related autoimmunity [7]. The new sensor-based wearable technology proposed by Monje et al. is gradually revolutionizing PD care by objectively measuring these manifestations and improving PD diagnosis and treatment monitoring. However, their use in clinical practice remains limited, probably due to the lack of external validation and standards for their continued use at home [8]. The abovementioned articles are very comprehensive for the introduction of related new sensors, and the structure of the sensor and its specific design principles are clearly expressed. However, there is no experimental verification for the application of the sensor in related fields, and there is a lack of research on the reliability of the sensor.

3. Application Method of Few-Shot Learning in Smart Health

3.1. Smart Healthcare System. The smart healthcare system [9] is to monitor the basic parameters of the human body’s important physiological parameters such as human body temperature, pulse, and blood pressure. These parameters can reflect a basic health condition of the human body, so the system chooses to monitor the parameters of the human body’s body temperature, pulse, blood pressure, and blood oxygen. The most important part of the system is to transmit the collected data. Data transmission is generally divided into two forms: wired transmission and wireless transmission. The cost of wired transmission is high, the wiring is cumbersome, and the scalability is not very good. When new equipment is added, rewiring may be required, and the disturbed lines may cause psychological pressure on the ward [10]. The wireless transmission method is relatively simple in terms of placement, because it does not require cables, so the cost is relatively low, and the adaptability and scalability are good. It does not require rewiring, and because there are no complicated wires, the instrument is easy to carry and move. This system is designed to be able to monitor their own health at home, requiring the instrument to be portable, simple to operate, simple and easy to install, and easy to expand [11]. According to the above comparison of wired transmission and wireless transmission, the wireless transmission mode is selected. It replaces the cables used in the traditional monitoring system, which not only facilitates the movement of the ward but also reduces the trouble and psychological pressure caused by the disturbed wires.

The system is mainly composed of three parts: parameter acquisition and transmission system, client monitoring software system, database management system. The parameter acquisition and transmission system is composed of parameter acquisition sensors, Zigbee acquisition nodes, and coordinators, which are responsible for acquiring the health parameters of the monitored person, such as pulse, blood pressure, body temperature, and other parameter data [12]. Each acquisition node transmits the collected data to the coordinator through the wireless network, and the coordinator processes the data and sends it to the PC serial port through RS232. The client monitoring software system displays and stores the data received by the serial port. At the same time, the client also has the functions of video consultation and health parameter historical data and abnormal data query, which constitute the diagnosis and treatment subsystem. The client also provides doctor data and electronic medical records, which constitute the data query subsystem. The database management system mainly stores and performs simple data processing, deletion, addition, and query of user information and parameter data [13]. The block diagram of the system structure is shown in Figure 1.

3.1.1. Selection of Wireless Transmission Methods. In recent years, with the rapid development of technology and network, especially the rapid development of the Internet industry, the popularity of portable electronic products such as

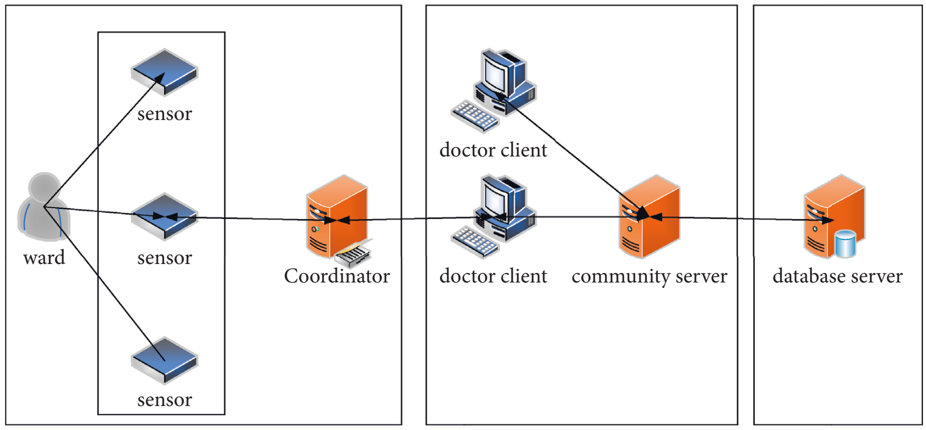

Figure 1: System structure block diagram.

mobile phones and laptop computers has been quite high. People's requirements for network communication are gradually increasing, and wired communication can no longer meet people's mobile needs. They hope to obtain mobile, convenient, and short-distance wireless networks to provide services for these mobile electronic products [14]. The current more common centralized short-range wireless communication technology is shown in Figure 2.

Figure 2: Common centralized short-distance communication methods.

3.1.2. Selection of Network Topology. At present, Zigbee mainly supports star, tree, and mesh network topologies, which constitute three network structures of star network, tree network, and mesh network [15]. The schematic diagram of the star network topology is shown in Figure 3.

The star network belongs to the slave-master-slave structure, and each wireless network node realizes the network connection through the coordinator. Communication between nodes can only be done through the coordinator. There is no direct communication between nodes, only through the coordinator, which belongs to the point-to-point communication mode [16]. When an FFD is activated, it will automatically form a network and become the main coordinator of the entire Zigbee network. Only one master coordinator is allowed in each Zigbee star network structure, which means that each star network is independent. The uniqueness of the network is ensured by selecting a PAN identifier. After selecting the PAN identifier, the master coordinator will allow the FFD or RFD to join the network. In addition, when multiple wireless nodes transmit data messages to the coordinator at the same time, it is easy to cause network congestion, resulting in data loss or transmission failure. However, it is still widely used due to its advantages of simple structure, flexible layout, and convenient management. The star network structure is suitable for occasions with a small range and few terminal devices [17]. The tree network topology is different. The schematic diagram of the tree network topology is shown in Figure 4.

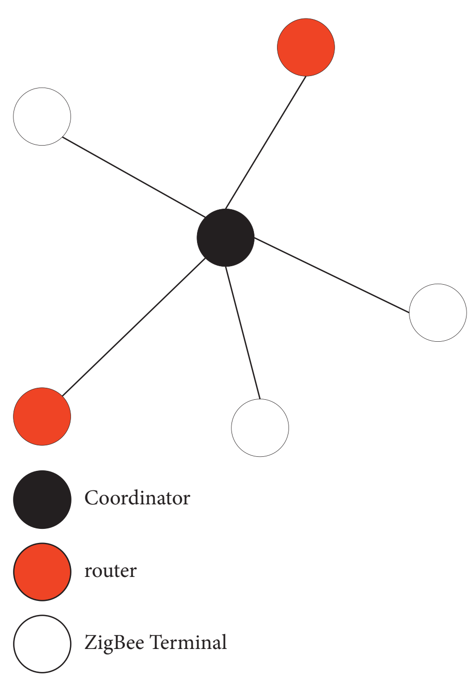

Figure 3: Star network topology.

In a tree-shaped network topology, the communication between nodes can only be carried out along the path of the tree; that is, each node can only communicate with its parent and child nodes. If two nodes have the same parent node, the data will be transmitted from one node to the parent node during data transmission, and then from the parent node to

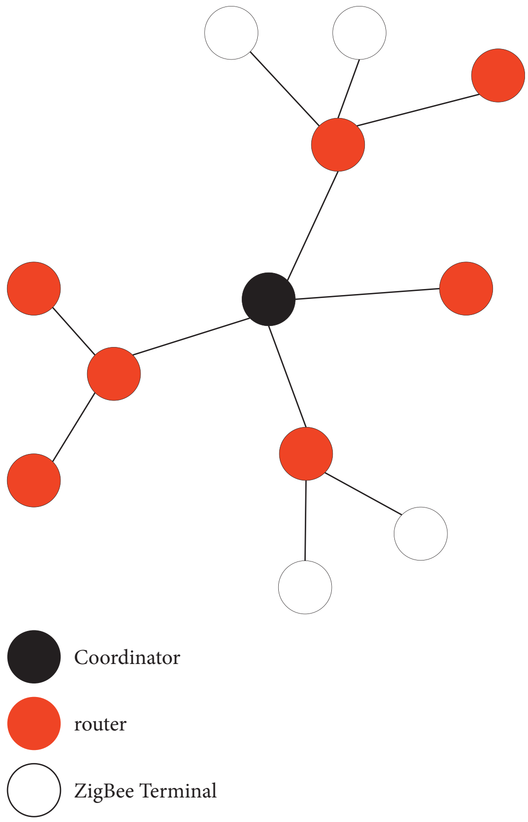

Figure 4: Tree network.

another node [18]. If two nodes have different parents, the information will be passed up the tree path. When it is passed to the nearest ancestor node, it finds the parent node of the target node along the path and then continues to pass down to the final target node.

A mesh network is more flexible than a tree network. Similar to the tree network structure, it also includes a coordinator, multiple routers, and multiple terminal nodes, but the connection method is different [19]. The schematic diagram of the mesh network topology is shown in Figure 5.

Most of the nodes in the mesh structure are FFDs with complete functional characteristics. Each FFD node can communicate directly; it can not only send and receive information but also automatically forward the information to other nodes in the network. FFD has the function of rerouting. When a node in the network fails, the nearby nodes will automatically replace the faulty node and continue to transmit information according to the principle of optimal path. The "multihop" mechanism is adopted when the mesh network transmits data, which greatly increases the reliability of the system, increases the security in the process of data transmission, and reduces the delay of data transmission. The mesh network structure is relatively complex, has self-organization and self-healing ability, and can adapt to extremely complex environments [20]. It is suitable for a wide range of applications with complex environments.

3.2. Few-Shot Improved Algorithm. Since the introduction of linear discriminant analysis, a lot of supervised learning has been developed in the past few decades to improve the few-shot problem. Representative ones include subspace selection based on geometric mean, local sensitive discriminant analysis, and edge analysis [21]. GMSS uses the general mean definition to replace the arithmetic mean in LDA, so it can get more robust results than LDA. LSDA and MFA are classical manifold learning algorithms, and both have their own solutions to the SSS problem. The PAF framework can better sort out the essential differences of this kind of manifold learning. Although the local geometric information preservation and how to extract discriminative information are fully discussed in current algorithms, the hyperparameter selection problem that exists in most manifold supervised dimensionality reduction is rarely addressed.

Based on the findings, this paper proposes a new essential manifold estimation method based on the RPDA algorithm and ensemble learning that preserves the ensemble manifold's ordering information. This method investigates the problem of supervised learning from two perspectives. To begin, the objective function is optimized on the block based on the RPDA algorithm; that is, the preservation of the ordering information of the same samples is emphasized on the local block formed by the sample, in order to achieve the goal of obtaining the sample's original distribution information, while maximizing sample edge distance between classes in order to retain discriminative information. Second, a new objective function with essential manifold estimation is defined based on the previous step, and the essential manifold of the data is approximated by finding the optimal linear combination of registration matrices, avoiding the hyperparameter selection problem in the traditional manifold supervised learning algorithm.

The ranking information of the samples within the class is available for classification. Inspired by the LE algorithm, we define the intraclass ordering information on a local block as

$$R(y_i) = \sum_{j=1}^{k_1} \left\| y_i - y_{i^j} \right\|^2 (w_i)_j. \tag{1}$$

Here the weight factor $(w_i)_j$ is defined as

$$(w_i)_j = \begin{cases} \exp\left(\dfrac{-\left\|x_i - x_{i^j}\right\|^2}{t}\right), & \text{if } x_{i^j} \in N_{k_1}(x_i); \\ 0, & \text{otherwise.} \end{cases} \tag{2}$$

According to the PAF framework, we can deduce the formula as follows:

$$\begin{aligned} R(y_i) &= tr\left\{ \begin{bmatrix} (y_i - y_{i^1})^T \\ \vdots \\ (y_i - y_{i^j})^T \end{bmatrix} \operatorname{diag}(w_i) \left[y_i - y_{i^1}, \ldots, y_i - y_{i^j} \right] \right\}, \\ &= tr\left(Y_{R(i)} L_{R(i)} Y_{R(i)}^T \right). \end{aligned} \tag{3}$$

Here,

$$L_{R(i)} = \begin{bmatrix} -e_{k_1}^T \\ I_{k_1} \end{bmatrix} \operatorname{diag}(w_i) \left[-e_{k_1} \quad I_{k_1} \right]. \tag{4}$$

For popular supervised learning, discriminative information plays a crucial role. As far as the EMRP algorithm is concerned, we consider the purpose of extracting discriminative information by maximizing the distance sum of y_i and its k_2 interclass samples, namely,

$$D(y_i) = \sum_{p=1}^{k_2} \left\| y_i - y_{i_p} \right\|^2 (v_i)_j. \tag{5}$$

The definition of the weight factor $(v_i)_j$ here considers the factor of removing the interclass ranking information, namely,

$$(v_i)_j = \begin{cases} 1, & \text{if } x_{ij} \in N_{k_1}(x_i); \\ 0, & \text{otherwisel.} \end{cases} \tag{6}$$

Under the framework of PAF, we can further derive (5):

$$\begin{aligned} D(y_i) &= tr\left\{ \begin{bmatrix} \left(y_i - y_{i_1}\right)^T \\ \vdots \\ \left(y_i - y_{i_p}\right)^T \end{bmatrix} \operatorname{diag}(v_i) \left[y_i - y_{i_1}, \ldots, y_i - y_{i_p} \right] \right\}, \\ &= tr\left(Y_{D(i)} L_{D(i)} Y_{D(i)}^T\right). \end{aligned} \tag{7}$$

Here,

$$L_{D(i)} = \begin{bmatrix} -e_{k_2}^T \\ I_{k_2} \end{bmatrix} \operatorname{diag}(v_i) \left[-e_{k_2} \quad I_{k_2} \right]. \tag{8}$$

Therefore, we can get the optimization objective function on the local block:

$$\arg\min_{y_i} \left(\sum_{j=1}^{k_1} \left\| y_i - y_{ij} \right\|^2 (w_i)_j - \gamma \sum_{p=1}^{k_2} \left\| y_i - y_{i_p} \right\|^2 (v_i)_j \right). \tag{9}$$

Here, $\gamma \in [0,1]$ is the balance parameter used to synthesize the contributions of intraclass samples and interclass samples on the local patch. By defining an indexed collection,

$$F_i = \left\{ i, i^1, i^2, \ldots, i^{k_1}, i_1, i_2, \ldots, i_{k_2} \right\}. \tag{10}$$

And we derive (9):

$$\begin{aligned} &\arg\min_{y_i} \sum_{j=1}^{k_1} \left\| y_i - y_{i_j} \right\|^2 (w_i)_j - \gamma \sum_{p=1}^{k_2} \left\| y_i - y_{i_j} \right\|^2 (v_i)_j, \\ &= \arg\min_{y_i} tr\left\{ Y_i \begin{bmatrix} -e_{k_1+k_2}^T \\ I_{k_1+k_2} \end{bmatrix} \operatorname{diag}(w_i) \left[-e_{k_1+k_2} \quad I_{k_1+k_2} \right] Y_i^T \right\}. \end{aligned} \tag{11}$$

Here, $tr(\ )$ is the matrix trace operator:

$$e_{k_1+k_2} = [1, \ldots, 1]^T \in R^{k_1+k_2}. \tag{12}$$

According to the PAF framework, we further define the registration matrix:

$$L_i = \begin{bmatrix} -e_{k_1+k_2}^T \\ I_{k_1+k_2} \end{bmatrix} \operatorname{diag}(w_i) \left[-e_{k_1+k_2} \quad I_{k_1+k_2} \right]. \tag{13}$$

Formula (11) can be simplified to

$$\arg\min_{Y_i} tr\left(Y_i L_i Y_i^T\right). \tag{14}$$

We define the selection matrix:

$$(S_i)_{pq} = \begin{cases} 1, & \text{If } p = F_i\{q\}; \\ 0, & \text{else.} \end{cases} \tag{15}$$

Here,

$$\text{where } S_i \in R^{N \times (k_1+k_2+1)}. \tag{16}$$

Subsequently, we can unify all local blocks on a consistent coordinate system. The specific operation method is as follows: first, coordinate Y_i comes from the global coordinate system, and its coordinate expression can be given by the following formula:

$$Y = U^T X = \left[y_1, y_2, \ldots y_N \right] \in R^{d \times N}. \tag{17}$$

That is,

$$Y_i = Y S_i. \tag{18}$$

Therefore, the optimization objective function 14 on the local block can be written as

$$\arg\min_{Y} tr\left(Y S_i L_i S_i^T Y^T\right). \tag{19}$$

Secondly, by accumulating the optimization objective function 19 defined on the local block formed by N samples, we can obtain the global registration objective function, which has the following form:

$$\begin{aligned} &\arg\min_{Y} \sum_{i=1}^{N} tr\left(Y S_i L_i S_i^T Y^T\right), \\ &= \arg\min_{Y} tr\left(Y L Y^T\right). \end{aligned} \tag{20}$$

However, different hyperparameters correspond to manifolds with different geometric information, which will seriously affect the final recognition accuracy. Therefore, an automatic manifold estimation method is valuable for solving this problem.

3.3. Wireless Sensor Networks. WSN is a network application system composed of multiple intelligent nodes centrally arranged in a monitoring area, and a multihop self-organized network system formed by wireless communication. It is widely used in facility security, environmental monitoring, industrial applications, traffic control, etc. Therefore, WSN

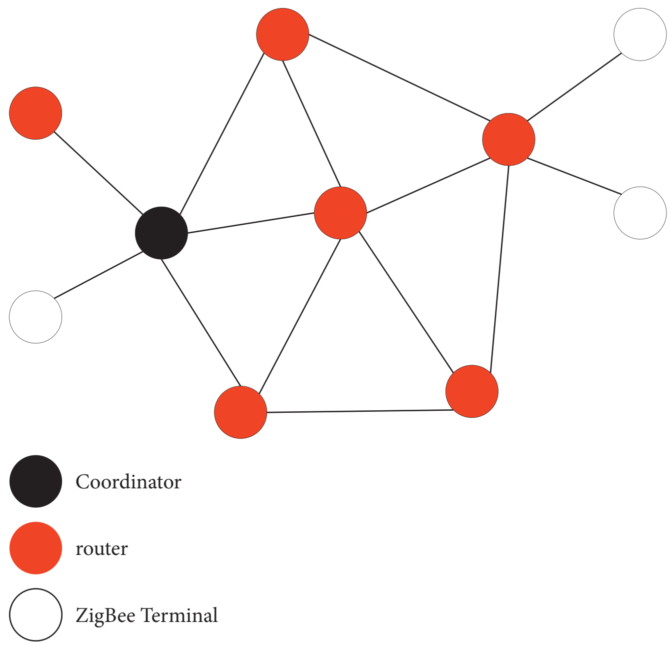

FIGURE 5: Network structure.

can be said to combine the world of logical information with the world of objective physics, changing the interaction between humans and nature. The wireless sensor network structure is shown in Figure 6.

A sensor network system usually includes sensor nodes, sink nodes, and management nodes. A large number of sensor nodes are randomly deployed in the detection area to form a network in a self-organizing manner. It transmits the detected data to the sink node through multihop relay and finally reaches the management node through the Internet or satellite. The measured data is sent to the sink node and finally reaches the management node through the Internet or satellite. The user configures and manages the sensor network through the management node, publishes detection tasks, and collects detection data.

4. Algorithm Module Implementation Experiment

4.1. Heart Sound Signal Recognition Experiment

Production Mechanism. The vibrations of the heart valves and great vessels under the impact of blood flow pass through the cardiothoracic conduction system to the chest wall to form heart sounds that can be received by a stethoscope. The wavelet transform method is used for denoising, and then the envelope algorithm is used to extract the peaks. It defines the feature vector and then uses the multiclass support vector machine decision tree (SVM-DT) for pattern recognition to distinguish the type of signal; in order to measure the predictive performance of the classifier for unknown samples, it needs to be tested, and the number in the test set is increased to 50, and $p = 2$ is also set. The test results are shown in Table 1.

It can be seen from the above table that the algorithm has good prediction ability for unknown samples while maintaining high training accuracy. Through this method, we have established a correct and relatively complete heart sound recognition algorithm, which can reduce the uncertainty of signal recognition and identify the type of signal accurately and effectively.

4.2. Breath Sound Signal Recognition Experiment. There are usually two types of breath sounds: normal breath sounds and additional sounds. The breath sound energy of normal and bronchitis patients are mainly concentrated in the inspiratory phase and less in the expiratory phase; the opposite was true in asthmatic patients. Therefore, we need to study the expiratory phase and the inspiratory phase separately, so that the characteristics of the breath sound signal are more obvious.

Input the sample feature vector group of unknown breath sound type after feature extraction to the learned network, and the output is the classification result as shown in Table 2.

4.3. Pulse Signal Recognition Experiment. Firstly, the most primitive sampling sequence is used to discretize the pulse signal, and the signal is decomposed twice by the wavelet transform of the discrete sequence; thresholding and secondary reconstruction of the high-frequency coefficients of the signal to obtain the signal after noise removal; normalizing the denoised signal, extracting the signal envelope, and then defining the eigenvectors; finally using the cluster analysis method for pattern recognition.

The pulse data obtained by the final screening were analyzed by using the classical statistical dynamic K-means

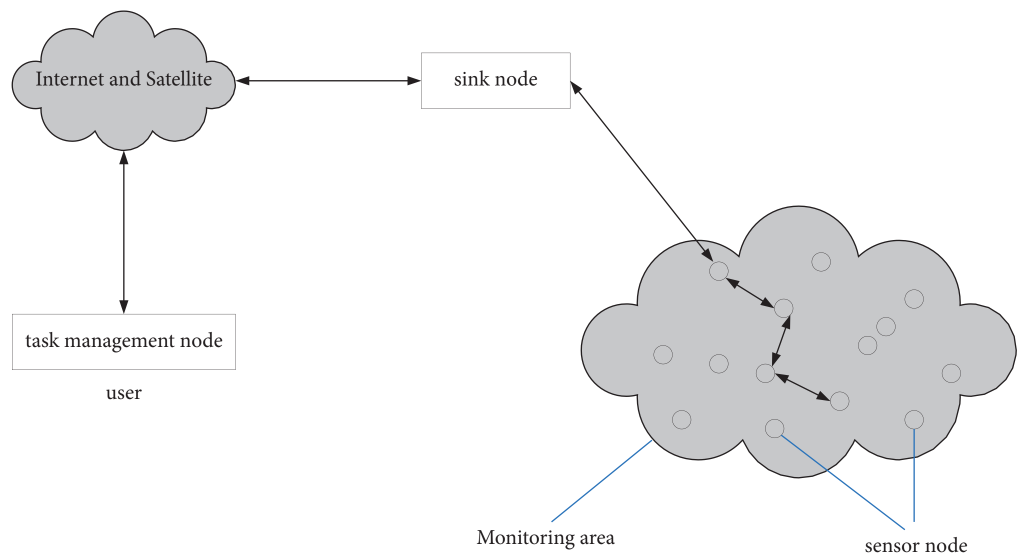

Figure 6: Wireless sensor network architecture.

Table 1: Calculation results of the classifier during testing.

Heart sound type	Training set		Test set	
	Number of misclassified samples	Accurate %	Number of misclassified samples	Accurate %
X	0	100	0	100
Y	2	95.2	1	96.7%
Z	1	96.4	0	100
Total	3	97.4	1	96.5%

Table 2: Classification results.

Type	Number of test samples	Normal	Asthma	Tracheitis	Recognition rate	Average value
Normal	25	23	1	1	92%	
Asthma	25	0	22	3	88%	92%
Tracheitis	25	1	0	24	96%	
Total	75	24	23	28		

Table 3: Class centers.

Cluster center	Vascular compliance coefficient	Peripheral resistance coefficient	Aortic valve function coefficient	Cardiac ejection function	Heart rate
First kind	1.61	1.4	0.07	4.6	0.5
Second kind	1.4	1.25	0.05	4.3	0.8
Third kind	1.22	1.01	0.03	3.8	1.2

cluster analysis function. When $K = 3$, the class centers of the cluster analysis results are shown in Table 3.

Passing N groups of test samples through the test of the training network, the error we get has reached the expected result. This algorithm has a concise idea and fast clustering speed. However, there are still some problems, such as the inappropriate selection of initial agglomeration points, which has a great influence on the clustering results and still needs to be improved.

4.4. Fusion Algorithm Experiment. Through the above algorithms, we identify and classify the signals collected by each sensor. In this section, we can obtain the final probability distribution value by calculating each classification result of each sensor and the correlation coefficient in each sensor. *Fusion Idea*. The probability distribution value of each sensor target type obtained by the weighted average method (or template method) is fused through the DS evidence theory, which can reduce the uncertainty of the signal and obtain the user's physical condition more accurately, as shown in Table 4.

After getting the probability distribution values corresponding to the sensors, we need to fuse these probability distribution values. When the intersection proposition is an empty set, the decision result can be obtained through evidence fusion. The fusion process is shown in Table 5.

Table 4: Probability assignment values.

	O_1	O_2	O_3	O_4
m_1	0.321	0.1928	0.0913	0.3949
m_2	0.4101	0.234	0.2465	0.1094
m_3	0.51	0.1143	0.0056	0.3701

Table 5: Fusion process.

$m_1(u) = 0.3949$	$m(o_1) = 0.1619$	$m(o_2)$ 0.0924	$m(o_3)$ 0.0973	$m(u)$ 0.0432
$m_1(o_3)$ 0.0913	$m(\phi)$ 0.0374	$m(\phi)$ 0.0021	$m(o_3)$ 0.0225	$m(o_3)$ 0.01
$m_1(o_2)$ 0.1928	$m(\phi)$ 0.0791	$m(o_2)$ 0.0451	$m(\phi)$ 0.0475	$m(o_2)$ 0.021
$m_1(o_1)$ 0.321	$m(o_1)$ 0.1316	$m(\phi)$ 0.0751	$m(\phi)$ 0.0791	$m(o_1)$ 0.0351
	$m_2(o_1)$ 0.4101	$m_2(o_1)$ 0.2340	$m_2(o_3)$ 0.2465	$m_2(u)$ 0.1094

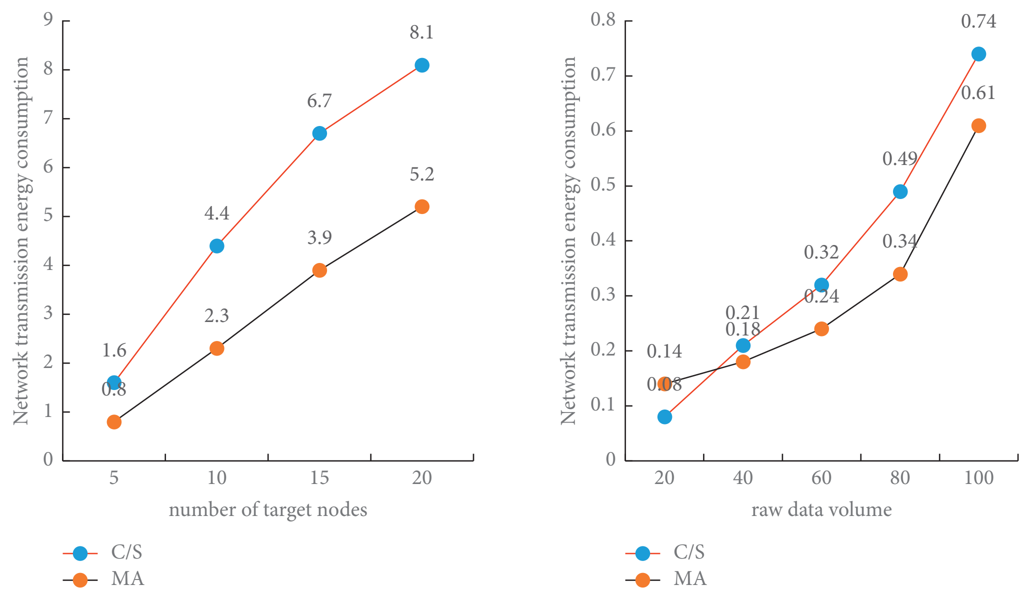

Figure 7: The relationship between the number of target nodes and the amount of raw data, transmission energy consumption, and network energy consumption.

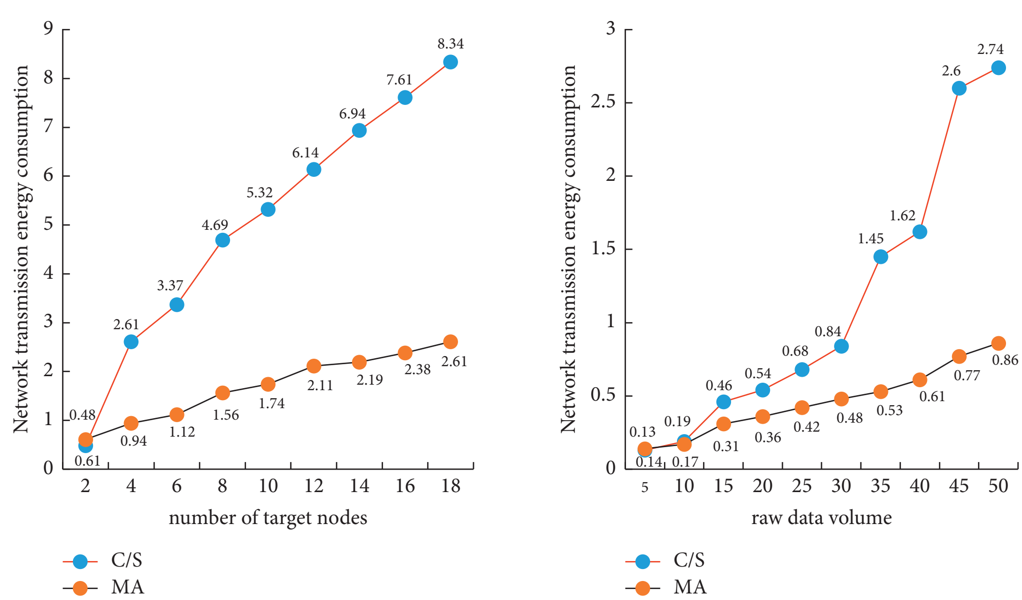

Figure 8: Simulation results between the target node and the original data volume and transmission energy consumption.

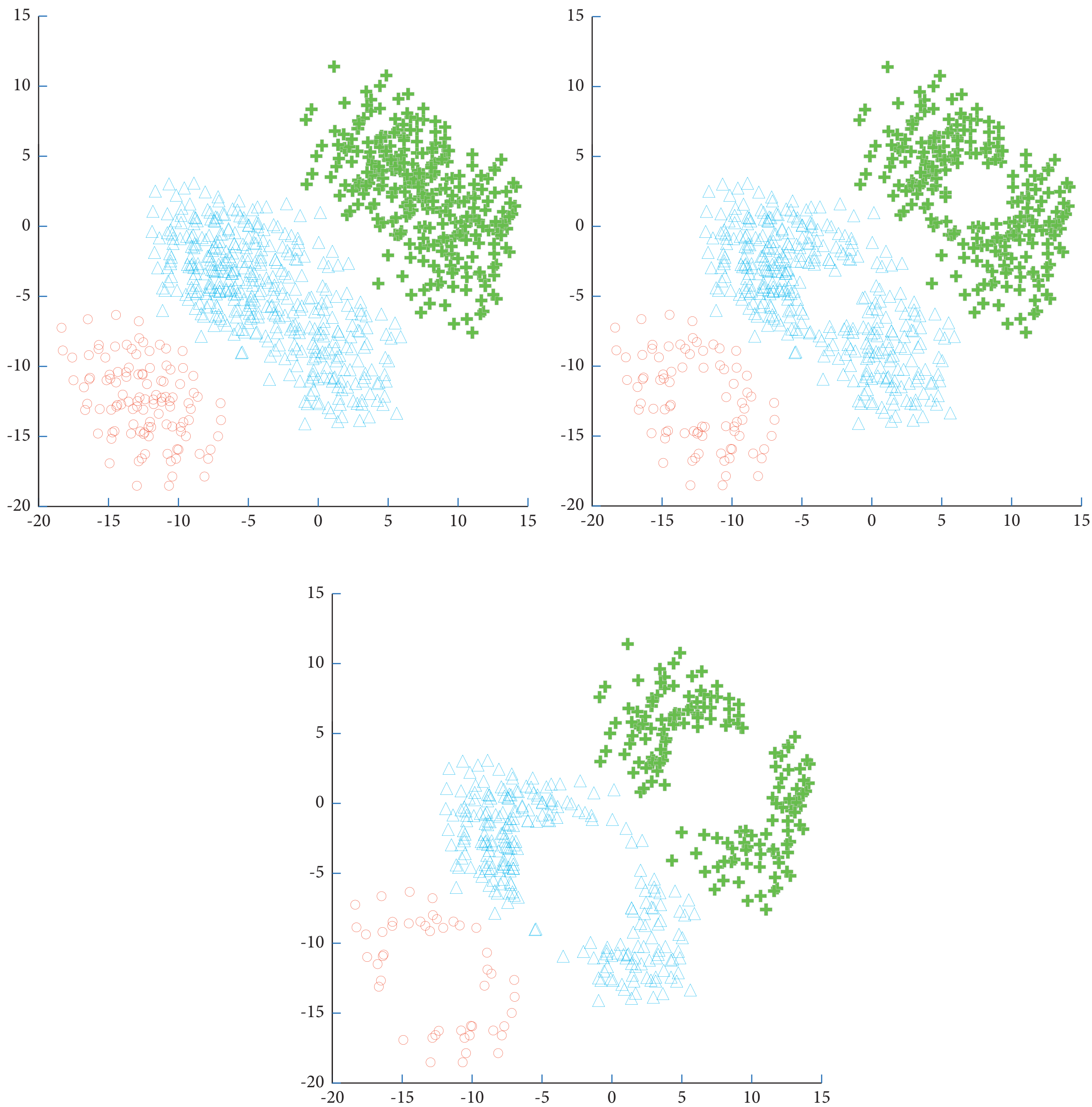

Figure 9: The subset of data selected by the SE algorithm during the iterative process.

It can be seen from the above experimental data that the fusion algorithm can significantly reduce the uncertainty and obtain a more accurate physical condition of the patient.

5. Multisensor Model Analysis

5.1. Model Analysis. This section will quantitatively analyze the difference between mobile agent-based wireless sensor network applications and traditional Client/Server model sensor network applications, focusing on the data transmission model and network energy consumption.

The modules that consume energy in the sensor node include sensor module, processor module and communication module. Since most of the energy consumption of sensor nodes is in the wireless communication module, the energy consumption of the wireless communication module is approximately 30 times the total energy consumption of the sensor module and the processor module. Therefore, the energy consumption of the sensor module and the processor module can be ignored in the energy analysis of the sensor node, and only the energy consumption of the communication module can be considered. In the Client/Server mode and the mobile agent mode, respectively, Figure 7 shows the comparison of the number of target nodes and network energy consumption, as well as the comparison of the original data volume and

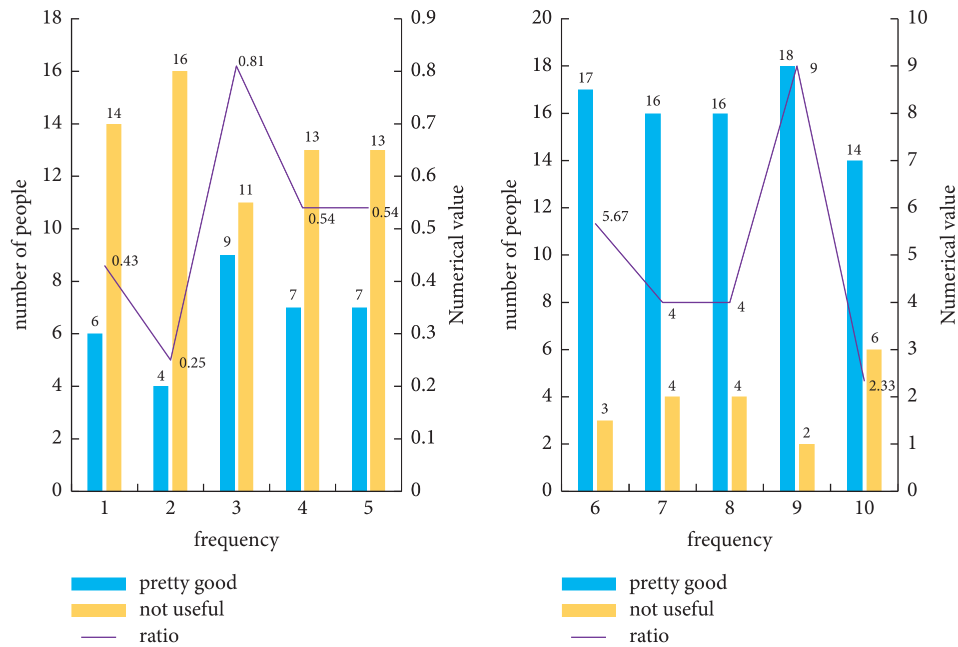

Figure 10: Effect evaluation of few-shot learning algorithm before and after improvement.

network energy consumption. The number of target nodes in the network has little effect on the energy consumption of the sensor network using the mobile agent mode, as can be seen on the left side of the figure; however, when the number of target nodes is small, the mobile agent mode may consume more energy. The right side of the figure shows that the mobile agent mode saves more energy than the traditional Client/Server mode as the amount of raw network data grows; however, when the amount of raw data grows small, the mobile proxy mode consumes more energy.

At the same time, OMNet is used to simulate the relationship between energy consumption in Client/Server mode and mobile agent mode. Suppose there are 600 nodes irregularly distributed in an area of 300 meters × 300 meters, and the code length of the mobile agent itself is 50 bytes. *kr* is related to the original data volume, the default value is 2 bytes, and the default original data volume of the node is 10 bytes. The specific results are shown in Figure 8: the left side of Figure 8 is the change diagram of network energy consumption during the process of increasing the number of target nodes from 2 to 18.

It can be seen from Figure 8 that the network energy consumption of Client/Server mode and mobile agent mode increases with the increase of the number of target nodes, but the mobile agent mode consumes less energy. Moreover, the growth rate of energy consumption in Client/Server mode is higher than that in mobile agent mode, which is consistent with the above theoretical analysis. The right side of Figure 8 is a simulation diagram of data transmission volume and network energy consumption. The right side of Figure 8 shows that as the amount of raw data increases, the energy consumption of both modes increases. With the increase of the amount of raw data, the energy consumption based on the Client/Server mode increases significantly and exceeds that of the proxy mode, which is also consistent with the above theoretical analysis. When the length of the original data itself is very small compared to the length of the mobile agent code, the Client/Server model has less energy consumption.

5.2. Parameter Analysis. In this experiment, a set of two-dimensional datasets is artificially generated, which consists of 1500 instances and contains 3 categories. The dataset shown in Figure 9 shows the instance selection results of the SE algorithm under different reduction rate conditions, which is helpful to observe the SE algorithm process.

In order to further understand the influence of parameters on the performance (accuracy and speed) of SE algorithm, this experiment conducted an in-depth analysis of SE on artificial datasets and Newsgroup datasets.

The SVM classification surface is obviously shifted because a large number of support vectors are accidently deleted. When dealing with multiclassification problems, this type of geometric algorithm must be transformed into multiple binary classification problems for processing: positive classes are considered positive, while negative classes are considered negative. As a result, edge instances in the positive class must be identified with the help of the negative class. It will be very difficult to identify edge instances if the distribution of negative classes surrounds the distribution of positive classes. Furthermore, CNN and KMSVM only retain a small portion of the support vectors, whereas NNSVM only eliminates a few samples that overlap each other.

5.3. Application Effect Analysis. In order to better understand the effect of the improved few-shot learning algorithm on the promotion of the new sensor technology in the current Internet of Things era before and after the improvement, this paper designs 10 different experiments, numbered 1–10. The first five experiments are to improve the application effect of the previous algorithm on the new sensor technology on smart healthcare, and the last five experiments are the application effect of the improved algorithm on the new sensor technology on smart healthcare. To ensure that the five experiments are the same except for the sample learning algorithm, other irrelevant variables are the same, and other irrelevant variables are controlled. Statistical experimental data are shown in Figure 10.

From Figure 10 above, we can see that the ratios of good and bad applications considered before the improvement are 0.43, 0.25, 0.81, 0.54, and 0.54, respectively, and the overall ratio is low; after the improvement, the ratios of good and bad applications were considered to be 5.67, 4, 4, 9, and 2.33. The overall ratio is much higher than that before the improvement, and the effect is increased by 36.9%, which can be better applied to the field of smart healthcare education.

6. Conclusions

This paper mainly uses the new wireless sensor technology and few-shot learning in the Internet of Things era to explore its application in the field of education. First of all, this paper proposes to improve the algorithm of few-shot learning. By redefining the classification method of the algorithm, the algorithm is optimized. At the same time, it designs relevant experiments to adjust some parameters and conducts data analysis and comparison in the analysis part. From the conclusions of the analysis part, it is not difficult to see that the optimized algorithm has been greatly improved in performance and practical application effect and can be better applied to the application of new sensors in the field of education.

Data Availability

The data used to support the findings of this study are available from the corresponding author upon request.

Conflicts of Interest

The author does not have any possible conflicts of interest.

References

[1] G. Mokhtari, Q. Zhang, G. Nourbakhsh, and S. M. Ball, "BLUESOUND: a new resident identification sensor-using ultrasound array and BLE technology for smart home platform," *IEEE Sensors Journal*, vol. 17, no. 5, pp. 1503–1512, 2017.

[2] K. Shimada, "Development of new sensor and sensing technique by electrolytic polymerization with utilizing a magnetic field and MCF rubber on robotics," *Journal of the Japan Society of Applied Electromagnetics and Mechanics*, vol. 25, no. 1, pp. 28–35, 2017.

[3] X. Miao, Q. Cui, H. Wu, Y. Qiao, Y. Zheng, and Z. Wu, "New sensor technologies in quality evaluation of Chinese materia medica:2010–2015," *Acta Pharmaceutica Sinica B*, vol. 02, no. 7, pp. 31–39, 2017.

[4] S. Ebrahimi and A. Mardani, "A new resistive belt sensor for multipoint contact detection of robotic wheels," *Iranian Journal of Science and Technology, Transactions of Mechanical Engineering*, vol. 43, no. S1, pp. 399–414, 2019.

[5] K. Chaiendoo, S. Sooksin, S. Kulchat, and V. T. W. Promarak, "'A new formaldehyde sensor from silver nanoclusters modified Tollens' reagent," *Food Chemistry*, vol. 255, no. JUL.30, pp. 41–48, 2018.

[6] J. Kuchlyan, S. Basak, D. Dutta, and A. K. D. N. Das, "A new rhodamine derived fluorescent sensor: detection of Hg 2+ at cellular level," *Chemical Physics Letters*, vol. 673, no. Complete, pp. 84–88, 2017.

[7] J. Wu and N. Yan, "A "KU" new sensor f'or cytosolic DNA in T cells," *Immunity*, vol. 54, no. 4, pp. 603–605, 2021.

[8] M. H. Monje, G. Foffani, J. Obeso, and Á. Sánchez-Ferro, "'New sensor and wearable technologies to aid in the diagnosis and treatment monitoring of Parkinson's disease," *Annual Review of Biomedical Engineering*, vol. 21, no. 1, pp. 111–143, 2019.

[9] W. Cai, M. Gao, Y. Jiang et al., "Hierarchical domain adaptation projective dictionary pair learning model for EEG classification in IoMT systems," *IEEE Transactions on Computational Social Systems*, pp. 1–9, 2022.

[10] A. Gauthier, M. Pruvost, O. Gamache, and A. Colin, "A new pressure sensor array for normal stress measurement in complex fluids," *Journal of Rheology*, vol. 65, no. 4, pp. 583–594, 2021.

[11] K. M. Thaler, R. Niessner, and C. Haisch, "Laboratory and field studies on a new sensor for dissolved N2O," *Analytical and Bioanalytical Chemistry*, vol. 409, no. 20, pp. 1–9, 2017.

[12] R. Rickenbach and D. N. Horwitz, "POF-BASED rotary and linear position sensor enables new medical and industrial applications," *POF newsletter*, vol. 28, no. 6, pp. 7–14, 2018.

[13] Q. Zheng, Q. Weng, and K. Wang, "Developing a new cross-sensor calibration model for DMSP-OLS and Suomi-NPP VIIRS night-light imageries," *ISPRS Journal of Photogrammetry and Remote Sensing*, vol. 153, no. JUL, pp. 36–47, 2019.

[14] G. Pierucci, C. Balocco, and M. De Lucia, "Development of a new heat flux sensor for building applications," *International Journal of Heat and Technology*, vol. 38, no. 4, pp. 794–800, 2020.

[15] M. Lezgy-Nazargah, S. Saeidi-Aminabadi, and M. A. Yousefzadeh, "Design and fabrication of a new fiber-cement-piezoelectric composite sensor for measurement of inner stress in concrete structures," *Archives of Civil and Mechanical Engineering*, vol. 19, no. 2, pp. 405–416, 2019.

[16] Q. Liu, L. Cheng, A. L. Jia, and C. Liu, "Deep reinforcement learning for communication flow control in wireless mesh networks," *IEEE Network*, vol. 35, no. 2, pp. 112–119, 2021.

[17] A. Pathirana, C. K. G. Piyadasa, and A. D. Rajapakse, "Development and modelling of a new type of sensor for detecting current transients for power system protection," *International Journal of Electrical Power & Energy Systems*, vol. 101, no. OCT, pp. 243–254, 2018.

[18] S. Zhang and H. Yang, "New soft-sensor modeling method based on improved shuffled frog leaping algorithm," *Journal of Nanjing University of Science and Technology*, vol. 41, no. 2, pp. 173–180, 2017.

[19] Q. Lin, Z. Zhu, J. Chen, and D. H. Liu, "A new piezomagnetic film force sensor model for static and dynamic stress measurements," *Journal of Magnetism and Magnetic Materials*, vol. 466, no. NOV, pp. 106–111, 2018.
[20] S. Nagata, H. Sawamoto, T. Sakamaki, and T. Morikawa, "Development of new BM sensor system without radiation," *Japan Tappi Journal*, vol. 72, no. 4, pp. 368–372, 2018.
[21] W. Dong, G. Lin, H. Wang, and W. Lu, "New dp sensor with good reversible t ability in aqueous solution and solid film," *ACS Applied Materials & Interfaces*, vol. 9, no. 13, pp. 11918–11923, 2017.

Hindawi
Computational Intelligence and Neuroscience
Volume 2022, Article ID 9900219, 10 pages
https://doi.org/10.1155/2022/9900219

Research Article

Analysis of the Rare Earth Mineral Resources Reserve System and Model Construction Based on Regional Development

Dafang Shi and Shouting Zhang

China University of Geosciences (Beijing), Beijing 100191, China

Correspondence should be addressed to Dafang Shi; 3001170126@cugb.edu.cn

Received 11 April 2022; Revised 15 May 2022; Accepted 16 May 2022; Published 4 July 2022

Academic Editor: Xin Ning

China is a large rare earth country that has pushed for related rare earth research, development, and application in the global development and progress of rare earths. The rare earth resource reserve strategy must be implemented by China due to the situation of rare earth resources at home and abroad, national security, and the need to strengthen the right to speak in the international market. This article builds the rare earth mineral resources reserve system and model from the perspective of regional development and uses the improved SURF algorithm to solve the problems of inaccurate mine location, mine location deviation, dislocation, overlap, and other issues, resulting in more accurate mineral resources reserve management data. The results show that the maximum relative error between the parallel profile method and the traditional method is 2.6%, which meets the requirement for mineral reserve calculation accuracy and can be used to calculate reserves. China's peak ionic rare earth output will be 46,797.06 tonnes in 2024, and then, it will decline at a 4% annual rate thereafter. This demonstrates how a graded reserve and orderly promotion can improve the workflow and efficiency of the rare earth mineral resources reserve.

1. Introduction

China has the world's richest proven rare earth reserves, and the variety, quality, output, and export of rare earths frequently rank first in the world [1, 2], making it critical to the global rare earth supply. China is a large rare earth country that has pushed for related rare earth research, development, and use in the global development and progress of rare earths. However, environmental damage, backward technology, low technological content of products, excessive export, low price, indiscriminate mining and excavation, and other serious issues plague China's development and utilization of rare earth resources.

Modeling of reserves: A steady supply of resources is critical whether it is for national economic security or national defence security. To begin with, a country's economic development is heavily reliant on resources, particularly strategic resources, and the economy's long-term viability cannot be separated from a reliable supply of resources. In modern industry [3], high-tech, and national defence technology, rare earth is an essential strategic mineral resource. Pan et al. believed that there have been many studies on the catalytic and surface performance of alkali metal, alkaline earth metal, and other metal oxides, but rare earth oxides have received relatively little attention [4]. Krishnamurthy presented and explained the geochemical characteristics, classification, and distribution of rare earth elements in sedimentary rocks [5]. Xiao investigated the effect of rare earth elements on the compressive ductility of ferromagnetic shape memory alloys and found that rare Earth elements can significantly improve the material's compressive ductility [6]. According to Ilyas et al., the output of foreign rare earths will increase significantly due to the restart of rare earth projects in countries other than China and the expansion of related rare earth enterprises [7]. Rare earth is a crucial component of modern weapons and equipment. To ensure national sovereignty and protect against foreign invasion, rare earth must be preserved. As a result, we can only ensure domestic demand for a sustainable supply of rare earth and national defence security by reserving rare earth and other strategic resources and increasing the degree of protection of rare earth resources.

The research on the optimal allocation of rare earth resources is conducive to solving the problems existing in the development and utilization of rare earth resources, improving the economic and social benefits of rare earth resources development, contributing to the healthy and sustainable development of rare earth industry, and having important practical significance for the optimization of regional development economic layout structure and the implementation of national rare earth strategy [8]. At the same time, the research on this topic also has reference significance for the research of other important mineral resources optimal allocation.

The main innovations of this article are as follows:

(1) The reserve system of rare earth mineral resources oriented to regional development has been constructed, and the quantitative evaluation standards of some indexes have been established, which not only helps to improve the scientificity and accuracy of index evaluation but also provides a reference for the research of other resources' optimal allocation.

(2) Aiming at the characteristics of a large matching area and high precision of mine spatial location, the SURF algorithm is improved in the order of feature point extraction, pixel optimization in the feature extraction stage, and image segmentation in the feature extraction process.

(3) The clustering results of geochemical sampling points by K-means have a corresponding relationship with the stratigraphic lithology distribution in the corresponding sampling areas, and clustering can achieve good geological results. Graded reserve and sequential advance can clarify the workflow and improve the work efficiency of rare earth mineral resources reserve.

The section structure of this study is as follows: Section 1 introduces the research background and significance and then introduces the main work of this article. Section 2 mainly introduces the related research status of rare earth mineral resources. Section 3 puts forward the specific methods and implementation of this research. Section 4 verifies the superiority and feasibility of this research model. Section 5 is the summary and prospect of the full text.

2. Related Work

2.1. Research on Rare Earth Resources. Rare earth is of great strategic value. With its abundant rare earth resources and cheap production cost, China has achieved the first output, the first application, and the first export in the world rare earth resources. Nassani et al. pointed out that the current supply cost of rare earths is too low, and the supply of rare earths far exceeds the demand, which is an important reason for the low price of rare earths [9]. Li and Peng pointed out that there are some problems in China's rare earth industry, such as waste of resources, environmental pollution, unreasonable product structure, lagging development of end products, and imperfect quota management. They put forward some measures to promote the development of China's rare earth industry, such as strengthening the source control of rare earth, strengthening the research of rare earth application theory, and perfecting quota management [10].

Raharjo et al. think that the government should strengthen the management and protection of rare earth resources, actively guide enterprises to develop into high-end application industries, and increase the economic added value of industries, so as to promote the sustainable development of rare earth industry and improve its competitiveness in the international market [11]. Gromov et al. focused on the storage and exploitation status of rare earth resources. On the basis of the research on the whole rare earth resources, they found that there were some problems in the rare earth industry, such as serious resource waste, severe environmental pollution, and chaotic industry supervision, and put forward some measures to improve the utilization efficiency of rare earth resources and turn the advantages of rare earth resources into economic advantages [12]. Diether et al. thought that the upstream and downstream enterprises of rare earth industry are all self-interested, and the main bodies in the industry chain are in their own way, and there is no sufficient information communication between them, ignoring the government's policy guidance, which leads to the low comprehensive performance of the rare earth industry chain [13]. Zhai et al. studied the important role of rare earth in iron and steel production and pointed out that rare earth elements can improve the shape and distribution of inclusions, refine grains, and then significantly improve the impact toughness, tensile strength, and oxidation resistance of products [14].

2.2. Research on Optimal Allocation of Resources. Optimal allocation of resources is the core topic of economic research, which can be summarized as static allocation and dynamic allocation of resources in terms of methodology. Norregaard et al. studied the optimal utilization of exhaustible resources by a mathematical model and pointed out that if the social value of nonrenewable resources is to be maximized, the price growth rate of the resources should be equal to the discount rate [15]. Chen et al. have made a long-term and in-depth study on the optimal depletion path and capital accumulation of nonrenewable resources [16]. Fu et al. thought that the mining industry is facing many severe sustainability challenges and studied and constructed the indicator system framework of sustainable development of the mining industry, which includes economic, environmental, social, and comprehensive indicators [17]. Liu et al. deeply studied the physical and chemical properties of rare earth elements and discussed the related applications of rare earth elements in catalytic materials, permanent magnet materials, hydrogen storage materials, luminescent materials, and agriculture [18].

Wang et al. systematically summarized the utilization status and broad prospects of rare earth elements in tricolor fluorescent lamps, electroluminescent materials, and fluorescent materials for medical devices. At the same time, they also pointed out that there was still a big gap between the application level of rare earth elements in China and some foreign countries [19]. Shibuya et al. elaborated the process and polishing mechanism of polishing powder, focused on the application fields of polishing powder, and looked forward to the future application of products [20]. Liu et al. thought that the total amount of nonrenewable mineral resources in the crust is a fixed value, but the economically recoverable reserves change dynamically with time. Liu et al. discussed how to use the market mechanism to optimize the allocation of mineral resources under the market economy [21].

3. Research Method

3.1. Rare Earth Mineral Resources Reserve System. The crust is rich in rare earth elements, but they are scattered. As a result, although rare earth elements have vast absolute reserves, there are currently few rare earth minerals that can be used in industrial production, and they are also unevenly distributed around the globe. Whether it is Japan, the European Union, or other major rare earth consumer countries, or the United States, Russia, India, Australia, and other major rare earth producers and consumers, they have recognized the strategic position and importance of rare earth mines, formulated relevant laws and regulations, established a rare earth resource strategy that is appropriate for their own economic development, and made arrangements and arrangements for the production and consumption of rare earths. Many countries' practises in this area have significant reference significance for China's rare earth development and are worthy of in-depth study and enlightenment by relevant Chinese departments and experts in order to improve China's rare earth resource strategy.

Because a large portion of the areas where rare earth resources are reserved are rare earth mining provinces, these areas with rare earth industry as the pillar and local rare earth resources as the main source of fiscal revenue, once the reserve of rare earth resources is implemented, it will reduce the income from resource development in rare earth resources reserve areas, causing local economic backwardness. As a result, it is important to understand how central interests and local interests can be reconciled, taking into account the stark contradiction between rare earth resources and mineral reserves and local development, and ensuring that local economic interests are not jeopardized and social development is stable, which is also a major impediment to China's implementation of strategic rare earth resource reserves.

The research results of optimal allocation and protection zoning of rare earth resources serve the practice of mineral resources planning, which determines the practicability of the research method. It is the working principle of this study to adopt the principle research method that the optimal allocation of empirical rare earth resources should strictly implement the access conditions of technology and environmental protection. China is rich in rare earth resources, and there are great differences in rare earth ore reserves, types, grades, and industrial basic conditions for regional development in different regions. These differences determine the differences in the initial conditions for developing rare earth resources and developing economy in different regions. The analysis and research of these differences can make a scientific evaluation of the resource elements for developing different regions.

The development and utilization of rare earth resources, as well as their optimal allocation and other activities, must be carried out not only in accordance with the characteristics of the resources, the level of regional industrial development, and other factors but also in accordance with a number of constraints. The resource development and utilization constraint index is a negative factor. The greater the impact on resource development, utilization, and allocation, the stronger the constraint. The smooth development of rare earth resources is directly linked to the degree of water security and water cost. The cost of land use in the early stages of resource development, which primarily affects mining areas that have not yet begun construction or large-scale expansion, is known as land resource constraint. The cost of developing rare earth resources or destroying other resources is known as other resource constraints. The cost constraint becomes more severe as the cost rises. The index hierarchy of the evaluation index system is shown in Figure 1.

The geographic location, geometric shape, and reserve information of mineral resources are the key points of mineral resources management [4]. Three-dimensional geological models established by mining software are mainly divided into three categories: exploration engineering database, geological entity model, and reserve block model. Then, based on the standards, the coordination of modeling and design of geological survey and mining is realized, and a unified process and standardized model data are formed. Through the execution management of geological survey production, the sequential and real-time geological survey data can be realized so as to realize the three-dimensional dynamic management of mineral resources reserves. The construction framework is shown in Figure 2.

The digital standard provides the foundation for managing rare earth mineral resources digitally. Mine geological survey digital standards include technological standards, production and operation standards, data standards, and geological survey knowledge base, which involve geological modeling and model updating, reserves estimation and statistics, and actual measurement modeling and statistics. The fine management of the entire process of mineral resources by mines and mining groups can be realized, and the dynamic integrated management of geological exploration reserves, production reserve, mineral production consumption, and resource reserve can be realized by systematically guiding the planning management of mine geological exploration and mining production.

The digitized and informationized technological process of geology, survey, and mining underpins the collaborative platform for geological survey and mining. It can streamline and standardize 3D digital modeling and design by allowing real-time data sharing and collaborative operation on the same platform and environment. Change the traditional technical mode, lowering labour intensity and production costs while increasing technician productivity and quality.

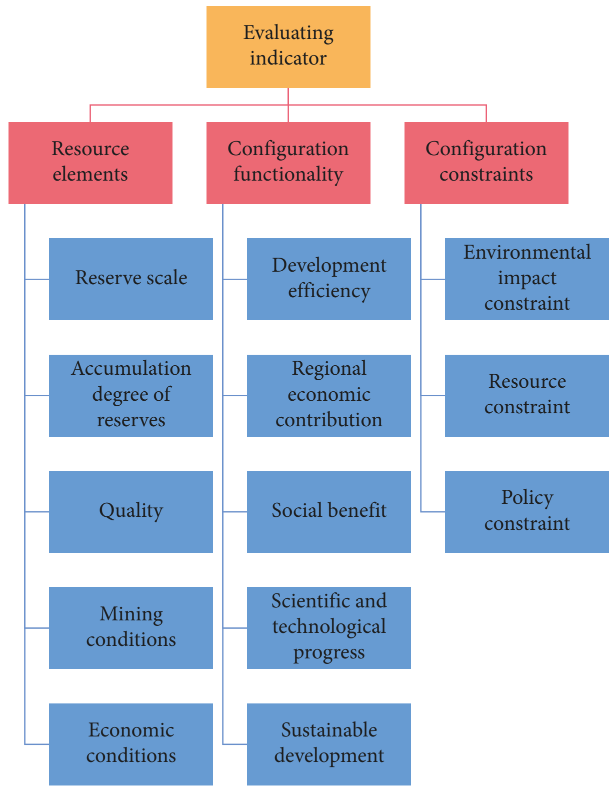

Figure 1: Index hierarchy chart of the evaluation index system.

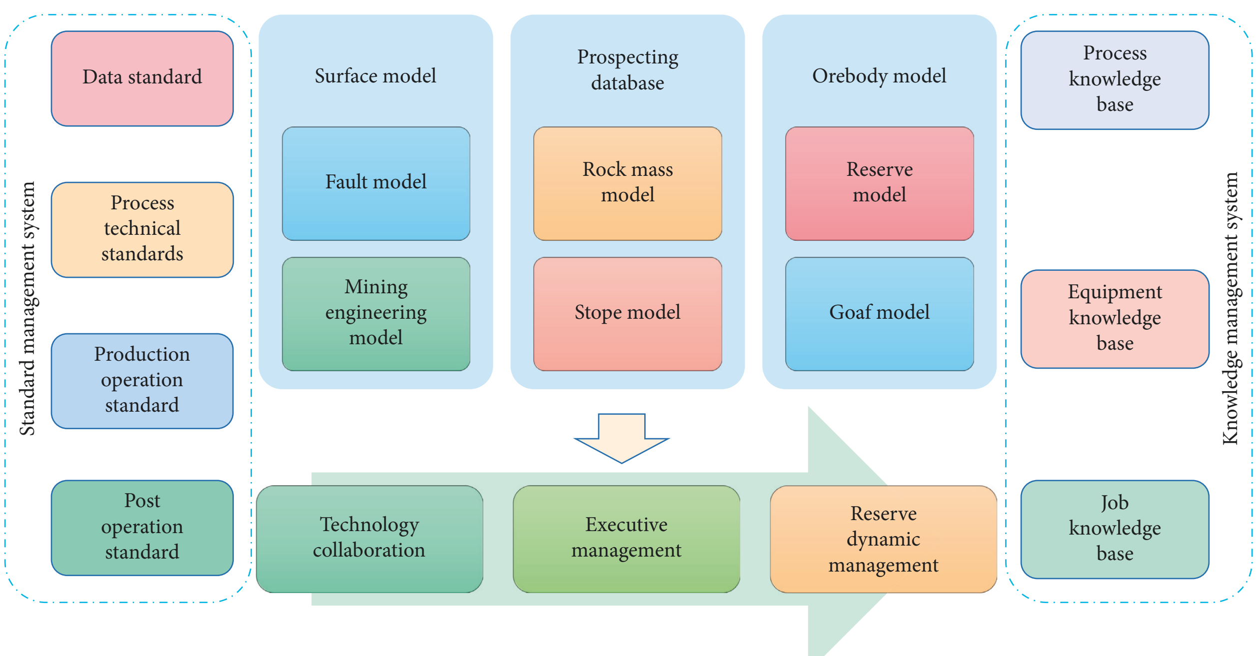

Figure 2: Construction framework of dynamic management of rare earth reserves.

3.2. Classification of Reserve Levels. There are basically two forms of mineral resources reserves in the world: mineral products reserves and mineral resources strategic base reserves. Comparatively speaking, the reserve cost of mineral resources strategic base is low, and the reserve is safe. The disadvantage is that it takes a long period to use, and it has a weak ability to reflect short-term supply interruption and price changes. The reserve cost of mineral products is high and the operation and management are complicated, but its advantage is that it can be put into the market quickly to ensure timely supply.

Mineral resources are strategic base reserves, the object of reserves is the areas that contain or may contain important strategic minerals, and in fact, the reserves are proved reserves or unexplored resources. The operation of other metal mineral resources reserves and the management of mineral resources can also refer to the practice of oil to establish product reserves. It should be noted that it is necessary to select the reserve of mineral resources strategic base, raw material type or product type reserve, or both in combination with specific minerals.

A strategic reserve is the reserve of mineral land to prevent the shortage of resources caused by unexpected events or uncertain factors and ensure the sustainable supply of the mineral resources in China. In order to improve the reliability of T value, the average value of historical survey data of several discovered resource sites is used to express it.

$$T = t_{\text{generalsurvey}} + t_{\text{siftthrough}} + t_{\text{explore}}. \tag{1}$$

Then the reserve scale model of strategic reserve can be established as shown in the following formula:

$$R_1 = \sum_{i=1}^{n} \frac{C_i^1}{\alpha}, \tag{2}$$

where R_1 is the scale of strategic reserve; C_i^1 is the domestic consumption in i year after the reserve starts; α is the comprehensive utilization rate of resources, which is the product of mining recovery rate and mineral processing recovery rate.

Advantage reserve is to prevent the worldwide resource shortage caused by unexpected events or uncertain factors and to ensure the sustainability of the advantage of mineral resources in advantage strategy. It must be emphasized that the reserve can meet the consumption of this mineral in foreign T time, which is not the same as having to meet foreign demand but only as a strategic bargaining chip of the country when resources are in short supply. Therefore, the scale model of the advantageous reserve can be established, as shown in the following formula:

$$R_2 = \sum_{i=1}^{n} \frac{C_i^2}{\alpha}, \tag{3}$$

where R_2 is the advantageous reserve scale; C_i^2 is the consumption of this mineral product in the world except China in i year after the reserve starts; α is the comprehensive utilization rate of resources.

When calculating the volume of ore bodies in blocks, a reasonable calculation formula should be selected according to the geometric shape and relative area ratio of ore bodies in two adjacent sections, and there are usually the following situations.

When the shapes of two adjacent sections are similar and the relative area difference between them is less than 40%, the block volume is calculated by the trapezoidal formula:

$$V = \frac{1}{2} l (S_1 + S_2). \tag{4}$$

When the shapes of two adjacent sections are similar, but the relative difference of their areas is greater than or equal to 40%, the section cone formula is used to calculate the block volume:

$$V = \frac{1}{3} l (S_1 + S_2 + \sqrt{S_1 S_2}). \tag{5}$$

In the above formulas, V is the ore body volume of the block, m^3; l is the distance between two sections, m; $S_1 S_2$ is the area of the ore body on the block in two adjacent sections, m^2.

The ore reserves of ore blocks are equal to the volume of ore blocks multiplied by the average weight of ore, which is calculated by the following formula:

$$Q = VD, \tag{6}$$

where Q is the ore reserve of ore block, t; V is the ore body volume of ore block, m^3; D is the average ore weight of the ore block, and t/m^3. D is replaced with the arithmetic average of the weights of two sections.

3.3. Establishment of the Mathematical Model of Reserve Scale. Rare earth resource reserves cannot be sustained without significant reserve fund investment. The reserve fund is a hybrid of a national reserve fund and a private reserve fund, comprising both the government-backed reserve fund and a large number of privately raised funds. Despite the fact that the gap between China's economic development and that of developed countries around the world is gradually closing, the conditions for rare earth resource reserves are currently met. The author believes that adopting independent legislation for rare earth resource reserves is more appropriate and that China's reserve legislation system will continue to improve as the reserve system is implemented and the economy develops.

SURF (Speeded-Up Robust Features) is a "high robustness" and "high stability" local image feature point detection and matching algorithm, which has few requirements and conditions for image matching. SURF algorithm has been widely used in military reconnaissance, traffic management, face recognition, target detection and tracking, image matching, and many other fields [10].

Assuming a point $p(i, j)$ of an image $f(x, y)$, on the scale σ, the Hessian matrix $H(x, \sigma)$ of this image is defined as follows:

$$H(x, \sigma) = \begin{bmatrix} L_{XX}(X, \sigma) & L_{XY}(X, \sigma) \\ L_{XY}(X, \sigma) & L_{YY}(X, \sigma) \end{bmatrix}. \tag{7}$$

Among them, L_{XX} is the convolution of the second derivative of the Gaussian template and image $f(x, y)$ at point $p(i, j)$. When the local value of the Hessian determinant is the largest, we think that the value we seek is the feature point of the image, and its L_{XX}, L_{YY} is the same.

When SURF calculates the feature point information of the image, a 3D template is used. According to the preset Hessian matrix threshold H, when $h > H$, the points that are larger than the response values of 26 adjacent points are selected as the interest points [12]. Finally, the position of the feature points is accurately determined by interpolation. Figure 3 shows the interpolation diagram.

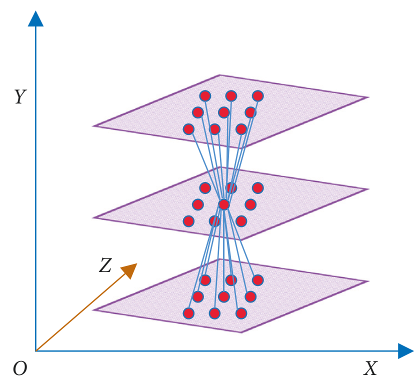

Figure 3: Construct scale space map.

However, the traditional SURF algorithm still has its shortcomings, especially when the algorithm calculates the main direction of feature vectors, it has certain limitations. For example, some images have higher exposure, while others have lower exposure. Therefore, in view of the characteristics and shortcomings of the traditional SURF algorithm in the geoscience field, this article optimizes and improves the matching of mine DEM (digital elevation model).

In this matching work, the edge of the image is protected by using the advantages of the bilateral filter. At the same time, the filter filters out a large amount of image noise, which avoids the result of matching failure caused by multisource and multitemporal imaging methods. The following is the mathematical expression of the bilateral filtering method:

$$H_{BL}(I_x) = \frac{1}{W_X} \sum_{y \in s} G\sigma_d(\|x-y\|) G\sigma_\gamma(I_x - I_y) I_y. \quad (8)$$

Among them,

$$W_X = \sum_{y \in s} G\sigma_d(\|x-y\|) G\sigma_\gamma(I_x - I_y). \quad (9)$$

K-means is a commonly used partition-based clustering method [22], which is used to group samples according to the similarity between sample attribute values. *K*-means is regarded as an unsupervised classification method. The basic idea is to divide the data set into K classes, and the samples in each class are very similar, but the samples in different classes are very different.

In each iteration of the algorithm, each sample is assigned to the class represented by the nearest centroid. The distance is expressed by the square of Euclidean distance, so the distance from sample i to centroid j is as follows:

$$d_{ij} = \|X_i - C_j\|^2 = \sum_{q=1}^{Q} (X_{qi} - C_{qi})^2, \quad (10)$$

where X_i is the vector composed of attribute values of sample i, C_j is the centroid vector of class j, Q is the number of attributes, X_{qi} is the q attribute value of the i th sample, and C_{qi} is the q attribute value of the centroid of class j.

For each sample, calculate its distance from each centroid. The record is assigned to the class whose centroid is closest to the record. In this process, a sample may be transferred from one class to another.

Taking geochemical sampling points as data objects, geochemical elements of sampling points as attributes, and element analysis results as attribute values, K-means is used for clustering analysis. Get the category characteristics of each sample and the average value and standard deviation of each category. The purpose of cluster analysis is to study the distribution characteristics and laws of regional geochemical elements and find meaningful resource targets.

When $K = 7$, the correlation analysis is carried out on the data of one area, and the correlation coefficients among 25 groups of element samples are obtained. After $r < 0.3$, the elements are connected with each other, and no research is done. Generate the correlation analysis linear graph, as shown in Figure 4.

There is a certain gap in the correlation results due to the difference in the five correlation data of k as 7,8,9,10, and 11. We take the correlation analysis results that have the same majority; that is, La is related to Pr, Nd is related to Pm, Eu is related to Gd, Tb, and Er is related to Y.

4. Result Analysis

Taking a rare earth mine as an example, this article introduces how to use the parallel section method to estimate resource reserves in DIMINE software. DIMINE software can calculate the mine reserves and then calculate the mine metal quantity according to the average grade of each block. In this article, the calculation data of four blocks are selected and calculated by the traditional reserve estimation method and the parallel section method, respectively. The calculation results are given in Table 1. The calculation results of the two methods are analyzed and compared, and the comparison results are given in Table 2.

The results of the calculations show that the maximum relative error between the parallel section method and the traditional method is 2.6 percent, which meets the requirements for mineral reserve calculation accuracy and can be used to calculate reserves. This demonstrates that the parallel section method can be used to estimate mine reserves. This method improves not only the working efficiency of reserves estimation but also the visual analysis degree of reserves estimation to some extent.

Based on the output data of ionic rare earths, we choose the annual data with a good linear relationship and use the linear trial and error method to calculate and predict the future output of mixed rare earths. The forecast results show that the peak output of ionic rare earths in China will appear in 2024, with a peak output of 46,797.06 tons, and then it will decrease at an average annual rate of 4% (Figure 5).

Rare earth is the general name of a group of elements, including La, Ce, Pr, and Nd, which mostly occur in the form of rare earth oxides. Due to the differences in the electronic layer structure and physical and chemical properties of each element atom, the application fields of different elements are also different. From the forecast results, the oxides of each element show different growth trends and peak output (Figure 6).

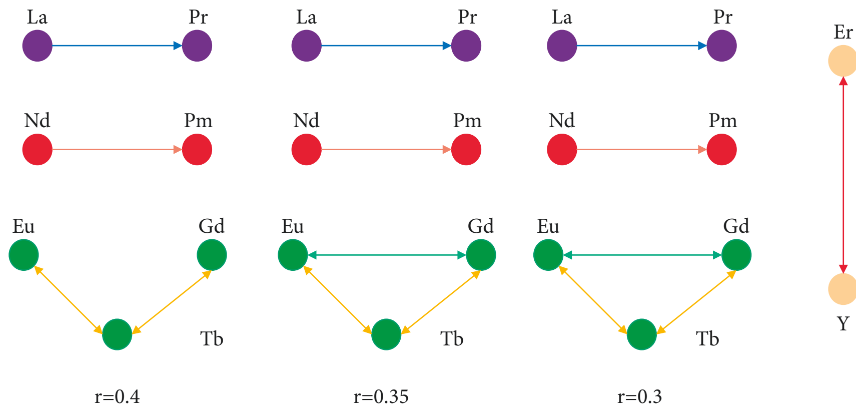

Figure 4: Data correlation analysis linear graph.

Table 1: Block reserves calculation.

Method	Block name	Segment volume (m^3)	Volumetric weight of ore (tm^{-3})	Mineral resources (t)	Block grade (%)	Rare earth quantity (t)
Traditional method	A1-21	8736.21	2.88	2213.71	0.55	141.21
	A2-22	5886.01	2.88	1628.93	0.63	102.37
	A3-23	996.27	2.88	2849.72	0.87	22.17
	A4-24	7896.62	2.88	2214.66	0.66	140.61
Parallel section method	A1-21	8512.71	2.88	2336.89	0.56	142.47
	A2-22	6003.87	2.88	19632.25	0.81	147.25
	A3-23	1022.41	2.88	2886.91	0.89	116.85
	A4-24	8201.93	2.88	20124.76	0.64	66.89

Table 2: Comparative analysis of block reserves calculation.

Block	Traditional method	Parallel section method	Contrast (%)
A1-21	8736.21	8512.71	2.6
A2-22	5886.01	6003.87	2
A3-23	996.27	1022.41	2.6
A4-24	7896.62	8201.93	3.9

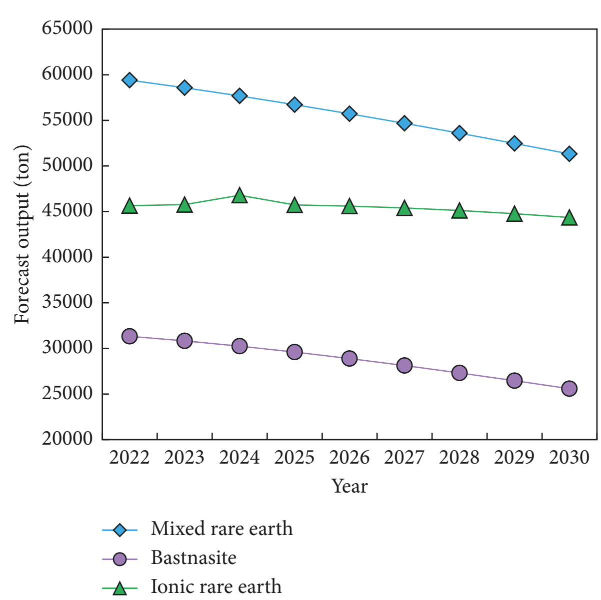

Figure 5: Prediction of rare earth ore yield.

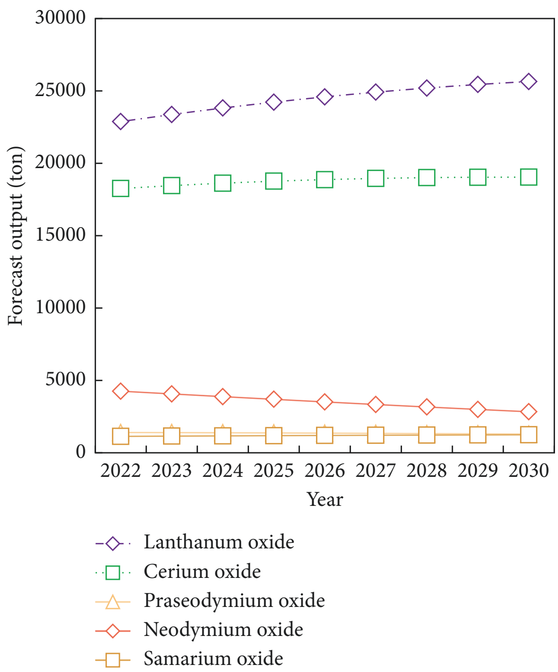

Figure 6: Output prediction of each element oxide.

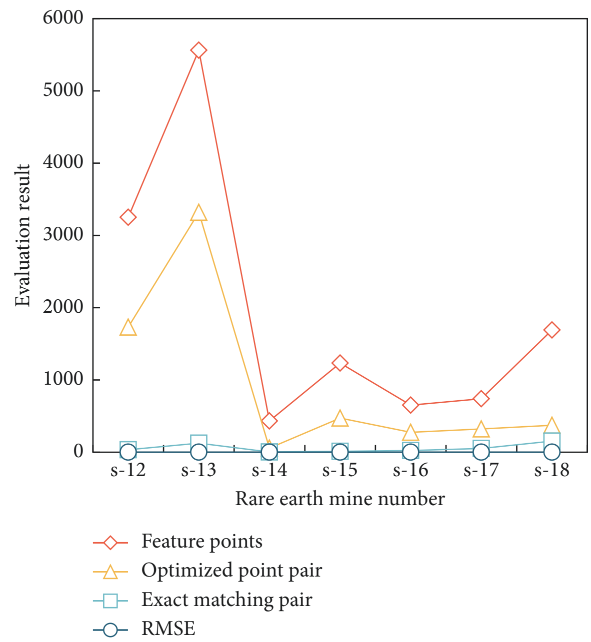

Figure 7: Verification result of the mine positioning effect.

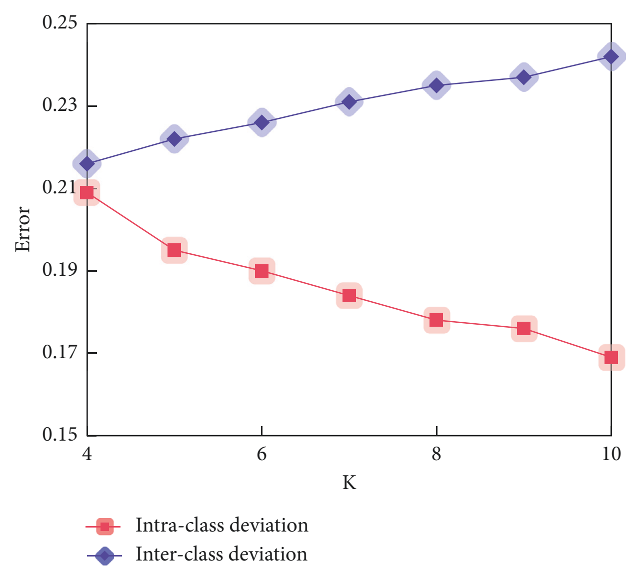

Figure 8: Class deviation comparison.

Mixed rare earth and bastnaesite output has reached or will soon reach a peak, owing to the fact that the minerals containing light rare earth are primarily mixed rare earth and bastnaesite, whereas ionic rare earth output is steadily increasing. It is because only ion adsorption minerals and xenotime contain heavy rare earths, and they are mostly concentrated in southern China. As a result, the world's heavy rare earths (such as terbium, erbium, dysprosium, and yttrium) are primarily supplied by ion adsorption rare earth mines in southern China, and this pattern cannot be significantly improved in a short period of time, and China retains its monopoly advantage.

In order to verify the practicability of the SURF algorithm in mine spatial location determination, this article designed a verification test to verify the robustness of the algorithm. We used several rare earth mines as experimental objects and carried out matching experiments from different angles. The verification results of the mine positioning effect are shown in Figure 7.

As can be seen from Figure 7, only one of the seven different types of mines selected from the database under different geological conditions failed to identify their spatial positions, and the other six mines could identify the feature points to be matched with high accuracy. We began to study when k took 3, and the research value below 3 was not significant. The value of K determines how many sampling points (data objects) we classify. The purpose of choosing different K values is to analyze the stability and reliability of clustering results. The quality report generated by $K = 4 \sim 10$ is shown in Figures 8–10.

The red background area in the class similarity report indicates that the similarities between classes are very close, the yellow background area indicates that the similarities between classes are not far or near, and the green background area indicates that the similarities between classes are far. The clustering segmentation is considered strict when most or all of the background colours are green, and the clustering effect is excellent because there is sufficient separation between classes. The absence of a red background indicates that the clustering result is satisfactory. When K is greater than 10, although the intraclass deviation is small, the interclass deviation is large. However, the red and yellow background increased, while the green background decreased. It shows that the clustering effect begins to decline. Therefore, in this topic, we only study the K-means clustering analysis with K from 4 to 9. The clustering effect is better according to the summary of the quality report generated by clustering. It

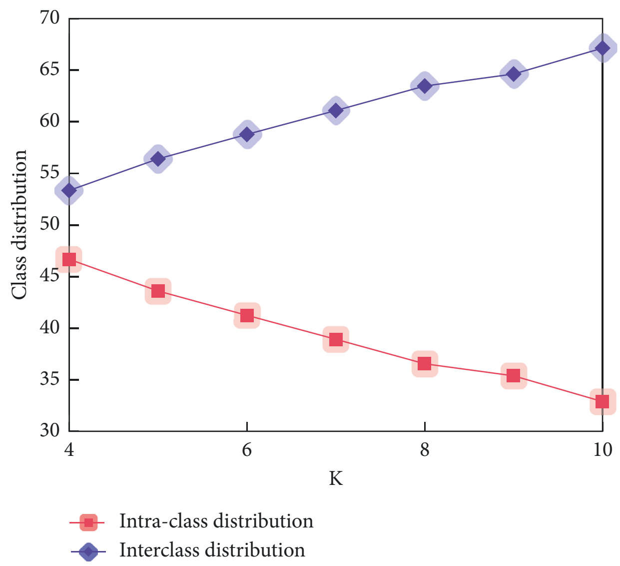

Figure 9: Class distribution comparison.

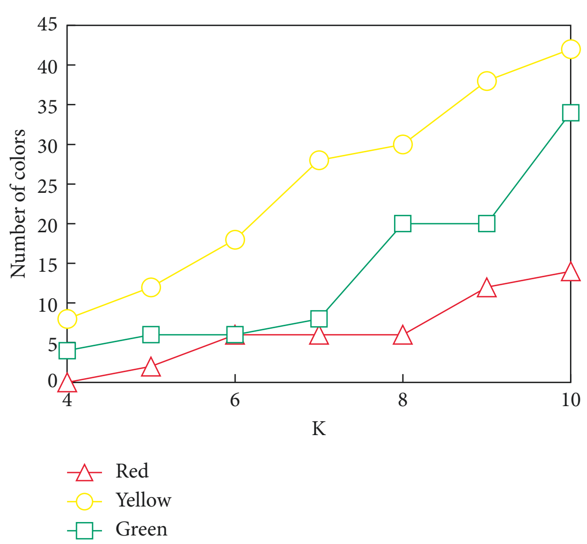

Figure 10: Class similarity comparison.

conforms to the basic idea of clustering: make the similarity of samples within the class as large as possible and the similarity of samples between classes as small as possible.

5. Conclusion

Due to their unique physical and chemical properties, rare earths are widely used in national economic development, national defence, and military construction. This article analyzes the current situation and existing problems of rare earth resources development and utilization in China and constructs a rare earth mineral resources reserve system based on research on the construction of rare earth mineral resources reserve system and model based on regional development. The reserves of rare earth mineral resources are divided into different levels of mineral reserves, including strategic reserves, dominant reserves, and controlled reserves, according to different levels of strategic objectives, and corresponding mathematical models of reserves scale are established for strategic reserves and dominant reserves. The maximum relative error between the parallel profile method and the traditional method is 2.6 percent, which meets the precision requirement of mineral reserve calculations and can be used to calculate reserves. China's peak ionic rare earth output will be 46,797.06 tonnes in 2024, and then, it will decline at a 4% annual rate thereafter. The stratigraphic lithology distribution in the corresponding sampling areas has a corresponding relationship with the K-means clustering results of geochemical sampling points. Clustering has the potential to improve geological effect and geochemical exploration efficiency.

Data Availability

The data used to support the findings of this study are available from the corresponding author upon request.

Conflicts of Interest

The authors declare that they have no conflicts of interest.

References

[1] Y. Takaya, K. Yasukawa, T. Kawasaki et al., "The tremendous potential of deep-sea mud as a source of rare-earth elements," *Scientific Reports*, vol. 8, no. 1, p. 5763, 2018.

[2] C. Marien, A. H. Dijkstra, and C. Wilkins, "The hydrothermal alteration of carbonatite in the Fen Complex, Norway: mineralogy, geochemistry, and implications for rare-earth element resource formation," *Mineralogical Magazine*, vol. 82, no. S1, pp. S115–S131, 2018.

[3] J. Miao, Z. Wang, X. Ning, C. Weiwei, and L. Ruimin, "Practical and secure multifactor authentication protocol for autonomous vehicles in 5G[J]," *Software: Practice and Experience*, 2022.

[4] J. Pan, C. Zhou, M. Tang et al., "Study on the modes of occurrence of rare earth elements in coal fly ash by statistics and a sequential chemical extraction procedure," *Fuel*, vol. 237, no. FEB.1, pp. 555–565, 2019.

[5] P. Krishnamurthy, "Rare metal (RM) and rare earth element (REE) resources: world scenario with special reference to India," *Journal of the Geological Society of India*, vol. 95, no. 5, pp. 465–474, 2020.

[6] R. Xiao, "Geological and tectonic evolution characteristics of polymetallic metallogenic belt," *Arabian Journal of Geosciences*, vol. 13, no. 18, p. 902, 2020.

[7] S. Ilyas, H. Kim, and R. R. Srivastava, "Hydrometallurgical recycling of rare earth metal-cerium from bio-processed residual waste of exhausted automobile catalysts," *Journal of Occupational Medicine*, vol. 73, no. 1, pp. 19–26, 2021.

[8] V. G. Khomich, K. Nemeth, and N. G. Boriskina, "Indicators of geodynamic control of the formation of mineral resources along a convergent plate margin: sakhalin-South Kuril areas, Russia[J]," *International Journal of Earth Sciences*, vol. 109, no. 8, pp. 1–14, 2020.

[9] A. A. Nassani, A. M. Aldakhil, and K. Zaman, "Ecological footprints jeopardy for mineral resource extraction: efficient use of energy, financial development and insurance services to conserve natural resources," *Resources Policy*, vol. 74, no. 1, Article ID 102271, 2021.

[10] S. U. Li and S. Peng, "Metallogenic correlations for the Fe-Nb-ree mineralization in the west mine of the bayan obo deposit, inner Mongolia, China[J]," *Acta Geologica Sinica*, vol. 92, no. 02, pp. 614–626, 2018.
[11] J. Raharjo, M. Damisih, M. Masmui et al., "Effect of the rare earth oxide impurities on the physical and thermal properties of Ce0.9Gd0.1O0.195 (GDC) composite electrolyte IT-SOFC," *Materials Science Forum*, vol. 929, pp. 116–120, 2018.
[12] E. V. Gromov, V. V. Biryukov, and A. M. Zotov, "Solving problems in ore mining and processing using information technologies," *Journal of Mining Science*, vol. 54, no. 6, pp. 995–1003, 2018.
[13] D. Diether, C. Maichle-Mössmer, and R. Anwander, "Implications of indenyl substitution for the structural chemistry of rare-earth metal (Half-)Sandwich complexes and performance in living isoprene polymerization," *Organometallics*, vol. 38, no. 15, pp. 3007–3017, 2019.
[14] D. Zhai, Y. Shui, K. Feng, and Y. Zhang, "Effects of rare-earth oxides on the microstructure and properties of Fe-based friction materials synthesized by in situ carbothermic reaction from vanadium-bearing titanomagnetite concentrates," *RSC Advances*, vol. 9, no. 36, pp. 20687–20697, 2019.
[15] R. D. Norregaard, H. Kaarsholm, L. Bach, and S. Christian, "Bioaccumulation of rare earth elements in juvenile arctic char (*Salvelinus alpinus*) under field experimental conditions [J]," *The Science of the Total Environment*, vol. 688, no. Oct.20, pp. 529–535, 2019.
[16] X. Chen, F. Guo, Q. Chen, X. Liu, and Z. Zhao, "Leaching tungsten and rare earth elements from scheelite through H2SO4-H3PO4 mixed acid decomposition," *Minerals Engineering*, vol. 156, no. 10, Article ID 106526, 2020.
[17] W. Fu, X. Li, Y. Feng et al., "Chemical weathering of S-type granite and formation of Rare Earth Element (REE)-rich regolith in South China: critical control of lithology," *Chemical Geology*, vol. 520, pp. 33–51, 2019.
[18] W. Liu, Y. Chen, R. Liao, J. Zhao, H. Yang, and F. Wang, "Authentication of the geographical origin of Guizhou green tea using stable isotope and mineral element signatures combined with chemometric analysis," *Food Control*, vol. 125, Article ID 107954, 2021.
[19] Y. Wang, Y. Guo, Q. Zeng, and L. Guo, "Petrogenesis and tectonic setting of the Shiduolong skarn Pb-Zn deposit in the East Kunlun Orogenic Belt: constraints from whole-rock geochemical, zircon U-Pb and Hf isotope analyses," *Geological Journal*, vol. 53, no. 3, pp. 1022–1038, 2018.
[20] T. Shibuya, M. Sumino, S. Kagami, T. Manako, and A. Shibuya, "Porosity optimization of rare-earth oxide emitters for thermophotovoltaics," *Applied Physics Letters*, vol. 113, no. 24, Article ID 243903, 2018.
[21] W. Liu, Z. Zhang, J. Ji, and L. Yixuan, "Rare-earth chalcogenides: a large family of triangular lattice spin liquid candidates[J]," *Chinese Physics Letters*, vol. 35, no. 11, pp. 84–99, 2018.
[22] T. Liu, D. L. Ying, Y. Z. Zhou, and Q. L. Zeng, "Application of random initial cluster center K-means algorithm to native kaolin classification," in *Proceedings of the 2012 Fourth International Conference on Computational and Information Sciences*, pp. 278–281, IEEE, Chongqing China, August 2012.

Hindawi
Computational Intelligence and Neuroscience
Volume 2022, Article ID 9363023, 13 pages
https://doi.org/10.1155/2022/9363023

Research Article

Construction and Model Realization of Financial Intelligence System Based on Multisource Information Feature Mining

Jing Li

School of Henan Institute of Economics and Trade, Zhengzhou 450000, Henan, China

Correspondence should be addressed to Jing Li; lijing@henetc.edu.cn

Received 18 April 2022; Revised 7 May 2022; Accepted 9 May 2022; Published 4 July 2022

Academic Editor: Xin Ning

Multisource information mining systems and related business intelligence technology are currently a hot topic of research. However, the current commercial applications and applications are not ideal in terms of application. Because there is still much work to be done before decision support, it is best to transition to them only financially. This paper examines the multisource part of the information used in mining and introduces research hotspots in the fields of accounting informatization, the development status of intelligent financial analysis software, the research and application status of data warehouse, data mining, and decision support systems. This paper examines the specific composition and content of a financial information system using information mining to lay a solid foundation. Financial intelligent analysis, financial intelligent monitoring, financial intelligent decision-making, and financial intelligent early warning are the four parts of the financial intelligent system. It then examined the structure and processing of the financial intelligence system and proposed a financial intelligence system operation strategy. Financial intelligence low-risk integrated implementation strategies and ideal financial intelligence models, according to the current state of research and practical applications. According to the findings, the overall discrimination accuracy of the financial information system based on mining multisource information features is up to 95%, which is 42% higher than the traditional model. The development and use of financial information benefit from the realization and exploration of the financial intelligence system model.

1. Introduction

Industrialization, processization, and decision-making are the three stages of the development of an information system. Financial records can neither fully reflect the work level and needs of modern network technology and enterprise records nor they fully cover their important content, due to the rapid development of network information technology. Communication will consider not only the use of information technology but also its financial impact on the company. It differs from traditional records and computer people who are only interested in technology or dealing with a specific machine component. A financial decision support system (FDSS) is a computer-assisted decision-making process that assists industry –decision makers in obtaining relevant data. Small-scale processing and financial management models, for example, have a relatively poor financial status in terms of economic management. Intelligent financial systems are popularizing China's accounting information system at the same time. The system's benefit is that it can display and provide information about business efficiency. ERP business management software also has a business intelligence application. From a difficult decision to a scientific one, the decision-making process has evolved. Financial information, sales information, purchasing information, and production information are all covered by business intelligence, which brings financial business information to the world of financial software. Financial information includes the ability to identify short-term solutions to complex problems, the ability to test the impact of various strategies, the ability to test new ideas and insights, good management skills, low costs, and the ability to make objective and important decisions. The audit and execution of financial information will become the focus of financial statement auditing and execution under the guidance of this system.

As an important branch of data analysis in the computer field, machine learning mainly analyzes data, mines potential laws, and uses laws to predict unknown samples, that is, to discover and count useful information, knowledge, and even wisdom from data. As an interdisciplinary field, machine learning mainly includes ensemble learning, semi-supervised learning, transfer learning, and rule learning. Among them, rule learning, as a research method of knowledge discovery in the field of machine learning, mines hidden patterns or rules with practical significance from data. For classification problems, rule learning is often used to make judgments about the class labels of unknown samples. Classification-oriented rule learning methods have been widely used in various practical application fields. For example, in the structural information prediction of biological proteins, the function of protein structure can be predicted by using rule learning. In judging the type of mechanical failure, it is possible to determine what kind of failure the machine has by learning the rules. This paper uses the method of multisource information mining features to design and implement the construction of financial function system.

First, research the inevitable development process required to support future computing, financial intelligence, with specific and long-term goals in mind, such as creating a platform for account computing and business intelligence, as well as ample space for follow-up. Second, it is through the promotion and implementation of intelligent financial analysis systems, such as cabin management, electronic reporting, and clear tables, which is exactly what is required for statistics and is also a key factor for accountants that education will gradually transform. Third, from the standpoint of businesses, research ideas guide the employment transformation of financial practitioners while also using computers to collaborate, so that financial practitioners can lead financial practitioners into the information age.

2. Related Work

In the construction and realization of the financial intelligence system, many experts at home and abroad have done the research. Zhang W believed that the intelligent financial system can improve the utilization rate of data, improve the work efficiency of financial personnel, and increase the security of financial processing services. The system can help managers make important financial decisions, financial budgets, etc. [1]. *D* Aikman et al. provided a framework for assessing the accumulation of vulnerabilities in the financial system. They collected 46 indicators of financial and balance sheet health, covering valuation pressures, nonfinancial borrowing, and measures of financial sector health [2]. Prochniak M et al.'s study aimed to analyze the impact of the development and stabilization of the financial sector on economic growth based on quantitative methods that yield robust results. It is tested that the relationship between the development of the financial sector and economic growth is nonlinear [3]. Polzin F et al. believed that diversification makes financial systems more resilient. Furthermore, the transition to a more sustainable energy system presents diverse financial investment needs [4].

However, the traditional financial system construction is not perfect, and there are many shortcomings, so in the experiment, the paper uses the method of multisource information feature mining to construct the functional financial system. Han *Z* et al. proposed a method to identify key assembly structures in assembly models from the perspective of assembly topology and multisource properties. The assembly model is based on complex network representation, and a two-level evaluation model is proposed to evaluate the importance of assembly parts [5]. *X* Gao et al. believed that the Dempster–Shafer theory has inestimable value in dealing with uncertainties in the field of multisource information fusion, but how to fuse highly conflicting information is still an open question [6]. Wu B et al.'s research proposed a multisource information fusion method combining cloud model, support vector machine, and evidence-based reasoning. In the data processing stage, various information sources are trained through different models to analyze financial value at risk [7]. Wu Y et al. believed that the multisource information fusion model consists of three heterogeneous meta-learning machines, namely, neural network, support vector machine, and random forest, and the final metaspectrum can be obtained by executing the final decision method [8]. However, the above data have not been recognized by the public because the experimental process is not rigorous enough.

3. Multisource Data Mining Source Ensemble Learning Method

In reality, many application fields [9, 10] are faced with multisource data sources, and the structure information of data sources is inconsistent; that is, data sources are divided into two categories: labeled data sources and unlabeled data sources. Therefore, it is difficult to traditionally integrate multiple data sources directly into a single data source for learning. Based on this, the research makes full use of the label information of the labeled data source and the internal structure information of the unlabeled data source, proposes two label propagation methods to make the unlabeled data source have class labels, and then constructs an ensemble learning method of multiple data sources. The experimental results showed that compared with the two traditional classification algorithms [11], the multiheterogeneous data source ensemble learning method based on label propagation has higher classification accuracy, better robustness, and stronger scalability. In addition, when the number of unlabeled data sources is large, the local consistent label propagation method is better than the global consistent label propagation method.

Multisource data source ensemble learning is essentially a multiclassifier system in which subclassifiers are trained by local data sources. Figure 1 shows the integrated learning framework of multisource data sources. The main ideas are given as multiple data sources; based on label propagation to

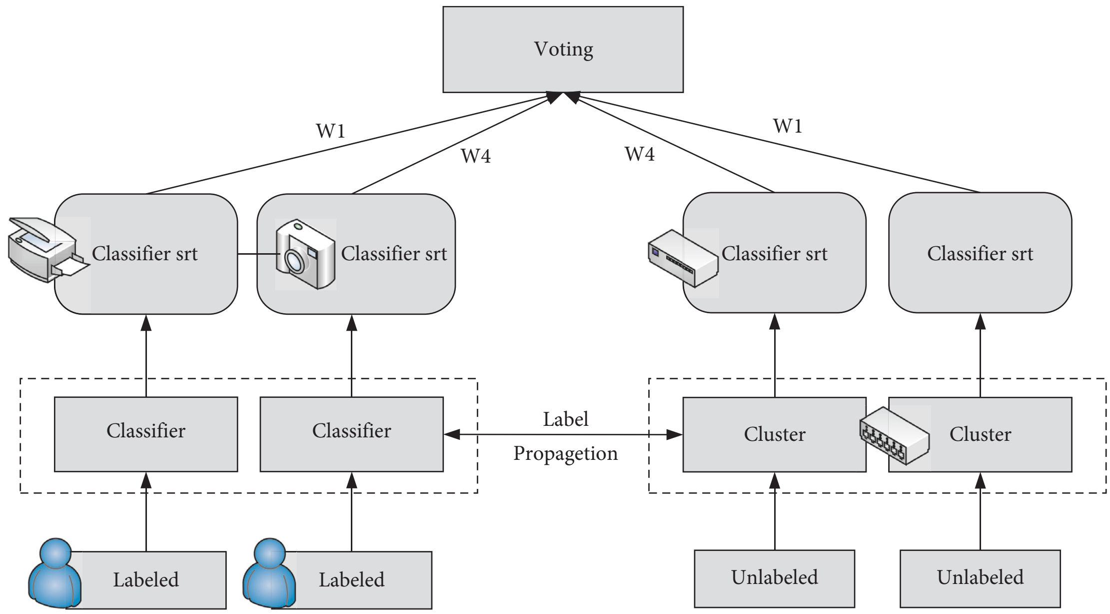

Figure 1: An ensemble learning framework for multisource data sources.

make unlabeled data sources have labels, a base classifier is obtained by training each local data source, and the result pair distribution of the multibase classifier is fused, which tests the classification results of samples in different data sources as the final prediction results. Based on the ensemble learning framework for obtaining multisource data sources, the following will introduce the two label propagation methods of global consistency and local consistency in detail and point out that these two label propagation methods are mutually replaceable.

The research provides a multisource information system composed of multiple data sources. First, the sampling range is computed at each local data source to obtain a set of local decision rules [12]. Second, the rules are constrained by certain local decision-making standards; local decision-making standards that do not meet the minimum coverage are removed, and selection is made according to the minimum coverage. Third, the votes for each rule are counted in all local decision documents, and some rules for candidate decision voting include the global coverage and global average coverage of candidate decision rules [13]. Finally, the decision rules that do not meet the world average are excluded from the decision-making rules set by the high-voted candidates, and all the decision-making rules that get high votes are combined. The specific algorithm flow is shown in Figure 2.

3.1. Using Weights to Synthesize Decision Rules. Given a multisource decision information system, neighborhood granulation is used to extract decision rules from each local data source, and these decision rules are, respectively, forwarded to the corresponding knowledge base. Meanwhile, the decision rules in the knowledge base are called local decision rules. Finally, all local decision rules are synthesized to solve the global decision rules [14]. In order to synthesize global decision rules from multiple knowledge bases, the weight of each data source is obtained by learning, and the weight is used to infer the neighborhood size of each global decision rule. Figure 3 presents the framework of a multisource decision rule synthesis model [15]. The traditional multidata source learning algorithm concentrates the data from all data sources into a unified data source for processing, which will lead to problems such as large data volume, data privacy leakage, and high transmission cost. Compared with traditional methods, the method using the weight synthesis model can effectively avoid these problems, thus providing a new feasible technique for multi-information source knowledge discovery [16].

3.2. Integration Model. Different data sources can provide descriptive information from different perspectives of the sample set, so the integrated learning model can be built directly on the multisource information system. To build an ensemble model on multiple heterogeneous data sources, on the basis of label propagation through global consistency or local consistency, all data sources describing the training sample set have class labels [17]. Among them, Figure 4 shows the label propagation algorithm based on global consensus.

3.3. Dataset and Its Statistics. This study introduces two real-world datasets used to evaluate recommendation performance, including their preprocessing and simple statistics on the datasets. Then, the evaluation metrics and evaluation protocol of recommendation performance are given. It is evaluated on two datasets: Epinions and Ciao [18]. Users can rate items, trust relationships can be established between users, and users can express their opinions on products and write review texts. First, it needs to eliminate stop words, and then, select the first $L = 8000$ words by word frequency as

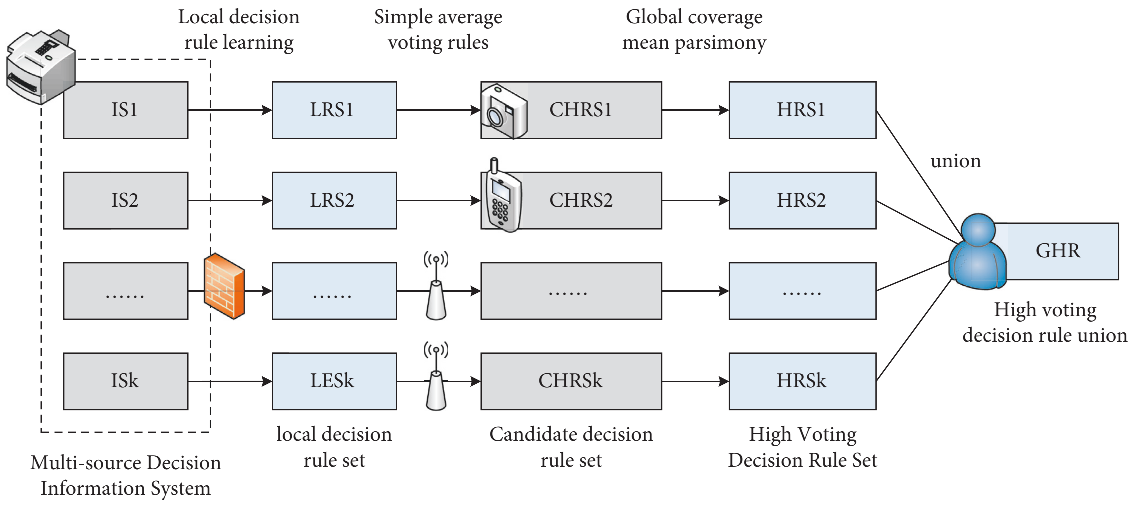

Figure 2: The mining process of high-voting decision rules in multisource information systems.

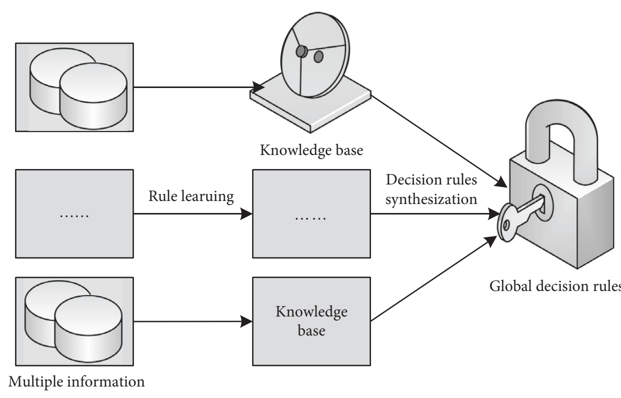

Figure 3: Decision rule synthesis model in multisource information system.

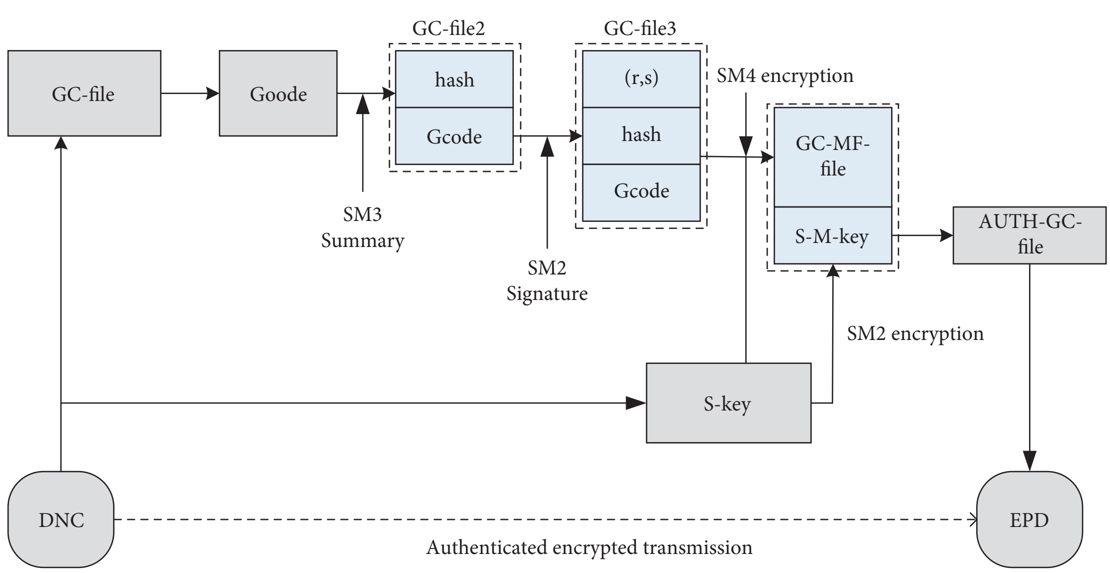

Figure 4: ELMG algorithm framework.

vocabulary. To reduce noise and errors, it keeps only users who clicked on at least 4 items and deletes those users with only 1 or 2 points [19]. The item index in the rating matrix corresponds to the document index of the document matrix in the review repository, that is, combining all user reviews of an item into the total reviews of an item [20]. The final statistics are shown in Table 1.

It can be found that the scores on both datasets are very sparse, and the average length of documents on the Epinions dataset is very short. The average number of comment words contained in each item on the Ciao dataset is 42 times that of Epinions, and Ciao's social relationship density is 12 times that of Epinions. Therefore, the additional data sources are included in the Ciao dataset; information reviews and social information are richer and of higher quality, and they can be expected to have a greater impact on the final recommendation performance. This observation is consistent with previously obtained quantitative assessments. A more compact use of scoring information and social information, that is, capturing social influence with a neighbor graph structure through trust values, can improve the RMSE prediction performance on both datasets. For example, compared to the LOCABAL model, the eSMF model has a relative RMSE performance improvement of 1.18%, 0.89%, and 0.72% when the Epinions training set accounts for 20%, 50%, and 70%, respectively, as shown in Figure 5.

3.4. Evaluating the Multisource Information Fusion Model. Mean: this method uses the mean of the scores in the entire training set to predict, which is the term μ in the formula. This method is the best constant prediction under the RMSE metric [21]:

$$\widehat{R}_{u,i} = \mu + b_u + b_i + P_u^T Q_i. \tag{1}$$

In this method, PMF decomposes the scoring matrix to learn user and item feature vectors, as shown in the formula. It is a representative method of hidden factor collaborative filtering, which only utilizes the scoring data source:

$$\min_{P,Q} \sum_{Ru,i\neq 0} \left(R_{u,i} - \widehat{R}_{u,i}\right)^2 + \lambda\left(\|P\|_F^2 + \|Q\|_F^2\right). \tag{2}$$

The LOCABAL method is based on matrix factorization, exploiting both social local and global context, as shown in Equations 3–6. It is a representative method of the social matrix decomposition method, which only utilizes the scoring data source and social information:

$$\min_{P,Q,H} \sum_{Ru,i=0} \left(R_{u,i} - \widehat{R}_{u,i}\right), \tag{3}$$

$$\lambda_{rel} \sum_{T_{u,u\neq 0}} \left(S_{u,v} - P_u^T H P_v\right)^2 + \lambda_{\text{norm}} \Omega(\Theta). \tag{4}$$

HFT hidden topics are learned from reviews, as shown in the formula. It is a representative method of the topic matrix factorization method, which only utilizes the scoring data source and comment text information. The RMSE comparison results are shown in Table 2.

$$\min_{P,Q,\Phi} \sum_{Ru,i\neq 0} \left(R_{u,i} - \widehat{R}_{u,i}\right)^2, \tag{5}$$

$$\lambda_{rev} \sum_{d-1}^{N} \sum_{n\in Nd} \left(\log \theta_{zd,n} + \log \varphi_{zd,n,wd,n}\right). \tag{6}$$

The data have shown that eliminating all auxiliary data sources MR3/content/social from the fusion model MR3 results in a 7.99% decrease in the overall relative RMSE, and the study wanted to know how the additional data sources helped the MR3 model improve its predictive performance. The problem can be examined from the richness of review data and social information. Figure 6 shows the prediction performance of MR3 and its S components.

For the first time, this paper proposes the MR3 fusion model, which can use multiple recommendation data sources at the same time. Unlike other fusion models, both components used are tried and true techniques. Simultaneously, an efficient extended social recommendation model, eSMR, is obtained, and the efficiency of the two proposed models has been verified on two large-scale datasets, indicating that recommendation performance can be improved further by using the neighbor graph structure and adding additional data sources. We will discuss how to extend the fusion model MR3, which mines implicit feedback information from scoring data sources, in order to delve deeper into the limited recommendation data sources. The fusion model and the extended fusion model both mine implicit feedback, and their model parameter learning processes are similar. Figure 7 shows the multisource information mining performance prediction.

3.5. Evaluation and Selection Methods of Information Source Quality. Multi-information sources refer to providing description information from multiple perspectives for the same sample set. First of all, it is pointed out that importance and redundancy are two important factors for evaluating the quality of information sources. Among them, the degree of importance represents the contribution of one information source to the classification, and the degree of redundancy represents the degree of overlap of the available information in different information sources. Second, a metric is devised using mutual-neighborhood information to assess quality and select information sources with the highest importance and least redundancy. Experimental results show that the metric is useful for finding a range of task-relevant information sources and outperforms many commonly used methods. Given a random variable, the entropy of A is defined as follows:

$$H(A) = -\sum_{i=1}^{n} p(a_i)\log(a_i), \tag{7}$$

$$H(A,B) = -\sum_{i=1}^{n}\sum_{j=1}^{m} p\left(a_i,b_j\right)\log\, p\left(a_i,b_j\right), \tag{8}$$

Table 1: Dataset statistics.

Statistics	Epinions	Ciao	Notes
User number	49454	7340	56794
Number of items	74154	22472	96626
Ratings/comments	790940	183947	974914
Social relationship	434680	112942	547622
Word count	2246837	288740000	31120837
Scoring density	0.00022	0.0011	N/A
Social density	0.00018	0.0021	N/A
Average number of words per item	30.3	1284.9	N/A
Average number of relationships per user	8.78	15.38	N/A

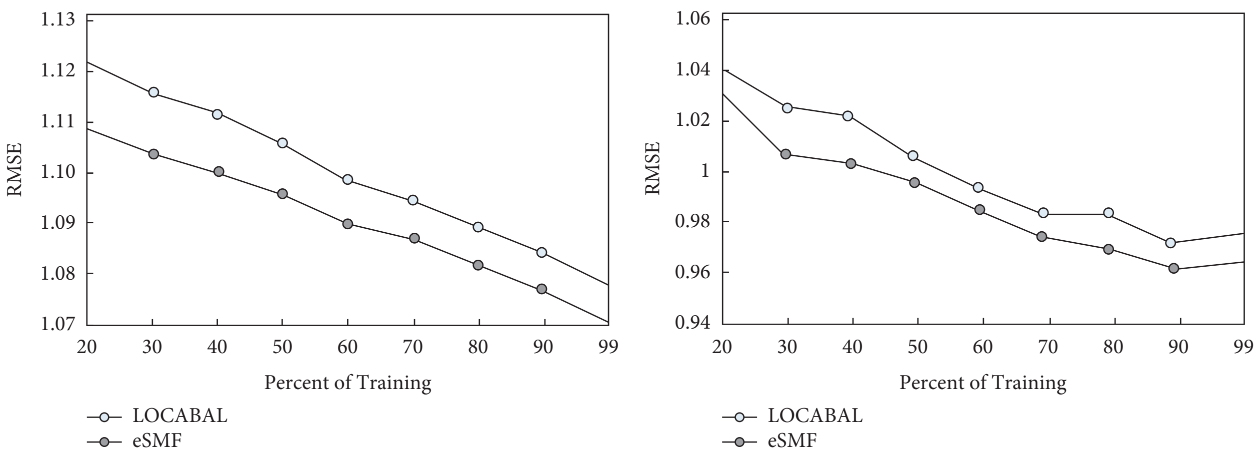

Figure 5: Comparison of the eSMF model with a standard social matrix decomposition model LOCABAL.

Table 2: RMSE comparison of fusion model MR3 and different methods.

Datasets	Training (%)	Methods				
		Mean	PMF	HFT	LOCABAL	MR3
Epinions	20	1.2265	1.2001	1.1857	1.1222	1.1051
	50	1.2239	1.1604	1.1323	1.1055	1.0809
	80	1.2225	1.1502	1.0960	1.0892	1.0648
	90	1.2187	1.1484	1.0867	1.0840	1.0634
Ciao	20	1.1095	1.0877	1.0439	1.0287	1.0142
	50	1.0964	1.0536	1.0379	0.9930	0.9740
	80	1.0899	1.0418	0.9958	0.9709	0.9521
	90	1.0841	1.0391	0.9644	0.9587	0.9451
Average						

$$H(A|B) = H(A,B) - H(B) = -\sum_{i=1}^{n}\sum_{i=1}^{m} p\left(a_i,b_j\right)\log\, p\left(a_i \mid b_j\right). \tag{9}$$

Given A and B, the mutual information between A and B is

$$MI(A;B) = -\sum_{i=1}^{n}\sum_{j=1}^{m} p\left(a_i,b_j\right)\log\frac{p\left(a_i \mid b_j\right)}{p\left(b_j\right)}. \tag{10}$$

To describe the numerical or discrete feature set F, the neighborhood of sample x on f is defined as f(x), so the uncertainty of the example in this field is defined as follows:

$$NH_{xi}^{\delta} = -\log\frac{\left\|\delta_f\left(x_i\right)\right\|}{n}, \tag{11}$$

$$NH^{\delta}(f) = -\frac{1}{n}\sum_{i=1}^{n}\log\frac{\left\|\delta_f\left(x_i\right)\right\|}{n}. \tag{12}$$

Suppose r and f are two self-feature sets. The conditional neighborhood entropy of r with respect to f can be defined as follows:

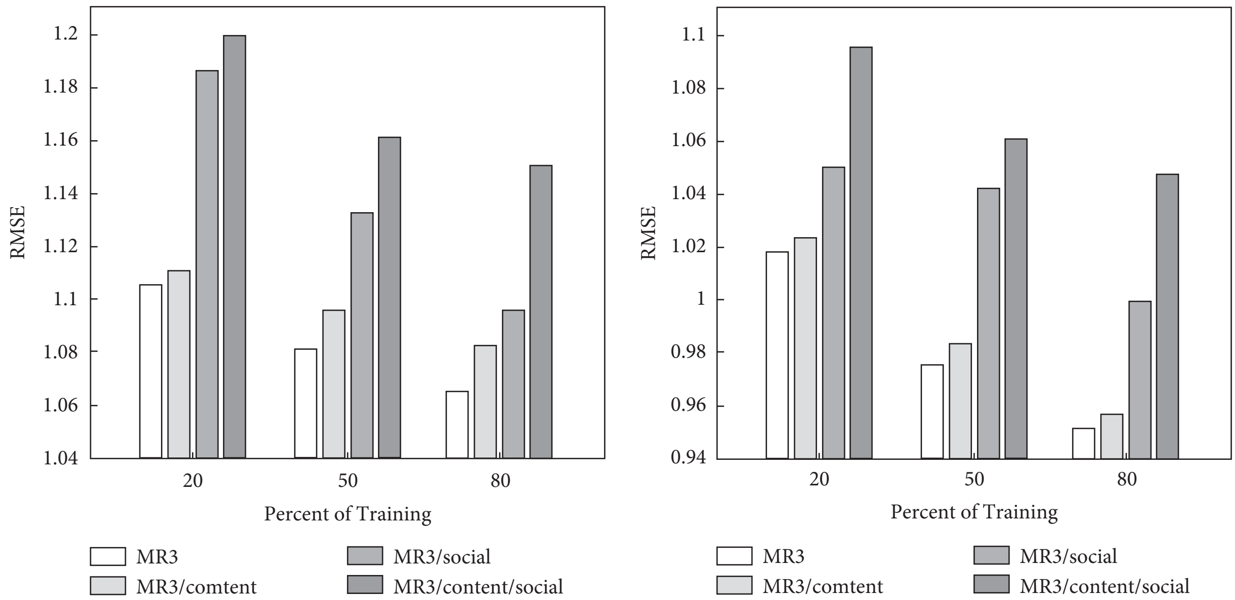

Figure 6: Prediction performance of fusion model MR3 and its S components.

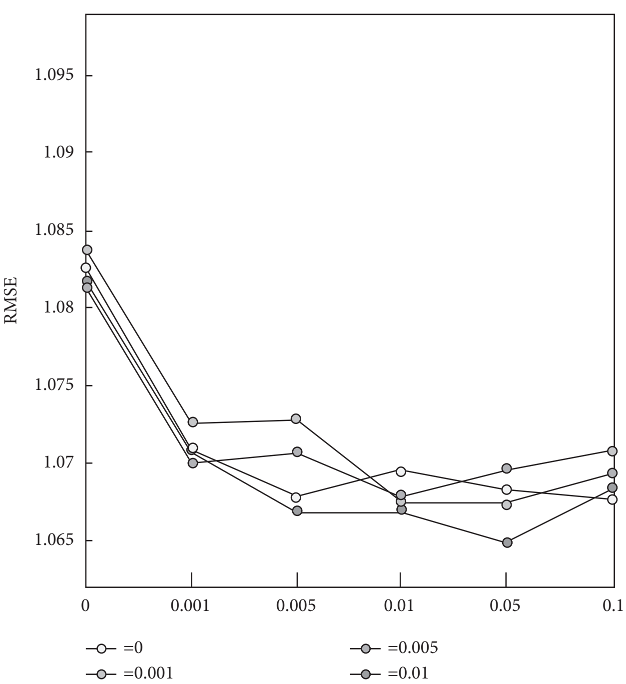

Figure 7: Prediction performance of fusion model MR3.

$$NH^{\delta}(r,f) = -\frac{1}{n}\sum_{i=1}^{n}\log\frac{\left\|\delta_{f\cup r}(x_i)\right\|}{n}, \tag{13}$$

$$NH^{\delta}(r,c) = -\frac{1}{n}\sum_{i=1}^{n}\log\frac{\left\|\delta_{r\cup c}(x_i)\right\|}{n}, \tag{14}$$

$$NH^{\delta}(r\mid f) = -\frac{1}{n}\sum_{i=1}^{n}\log\frac{\left\|\delta_{r\cup f}(x_i)\right\|}{\left\|\delta_{f}(x_i)\right\|}, \tag{15}$$

$$NMI^{\delta}(r;f) = -\frac{1}{n}\sum_{i=1}^{n}\log\frac{\left\|\delta_{r}(x_i)\right\|\bullet\left\|\delta_{f}(x_i)\right\|}{n\left\|\delta_{r\cup f}(x_i)\right\|}. \tag{16}$$

In the process of information source selection in a multisource environment, a set of information sources with the greatest contribution to the classification is selected first. Usually, the selection process of information sources is based on the magnitude of importance. Therefore, the formula for selecting according to the importance of the information source is

$$SU(f_1;f_2) = 2\left[\frac{MI(f_1;f_2)}{H(f_1)+H(f_2)}\right], \tag{17}$$

$$NSU^{\delta}(f_1;f_2) = 2\left[\frac{NMI^{\delta}(f_1;f_2)}{H^{\delta}(f_1)+H^{\delta}(f_2)}\right], \tag{18}$$

$$TSU^{\delta}(F;c) = \frac{nNSU^{\delta}_{cf}}{\sqrt{n+n(n-1)NSU^{\delta}_{ff}}}, \tag{19}$$

$$\max\ D(S,c),\ D = \frac{1}{|S|}\sum_{si,\notin S} TSU^{\delta}(s_i;c). \tag{20}$$

In addition, ten-fold cross-validation method and ensemble learning based on majority voting are used to verify the classification ability of the proposed algorithm; that is, for each dataset, one hundred information sources are generated ten times, and ensemble learning is performed based on multiple information sources each time to obtain classification accuracy. Then, the average of the ten running results is used as the final classification accuracy. In addition, the threshold of the neighborhood is set to 0.01 and the class label of each information source is consistent with the class label of the original dataset, as shown in Table 3.

Table 3: Descriptive information for the dataset [22].

Datasets	Samples	Features	Classes
COLON	62	2000	2
SRBCT	63	2308	4
TOX-171	171	5748	4
PIE10P	210	2420	10
AR10P	130	2400	10
YALE	165	1024	15

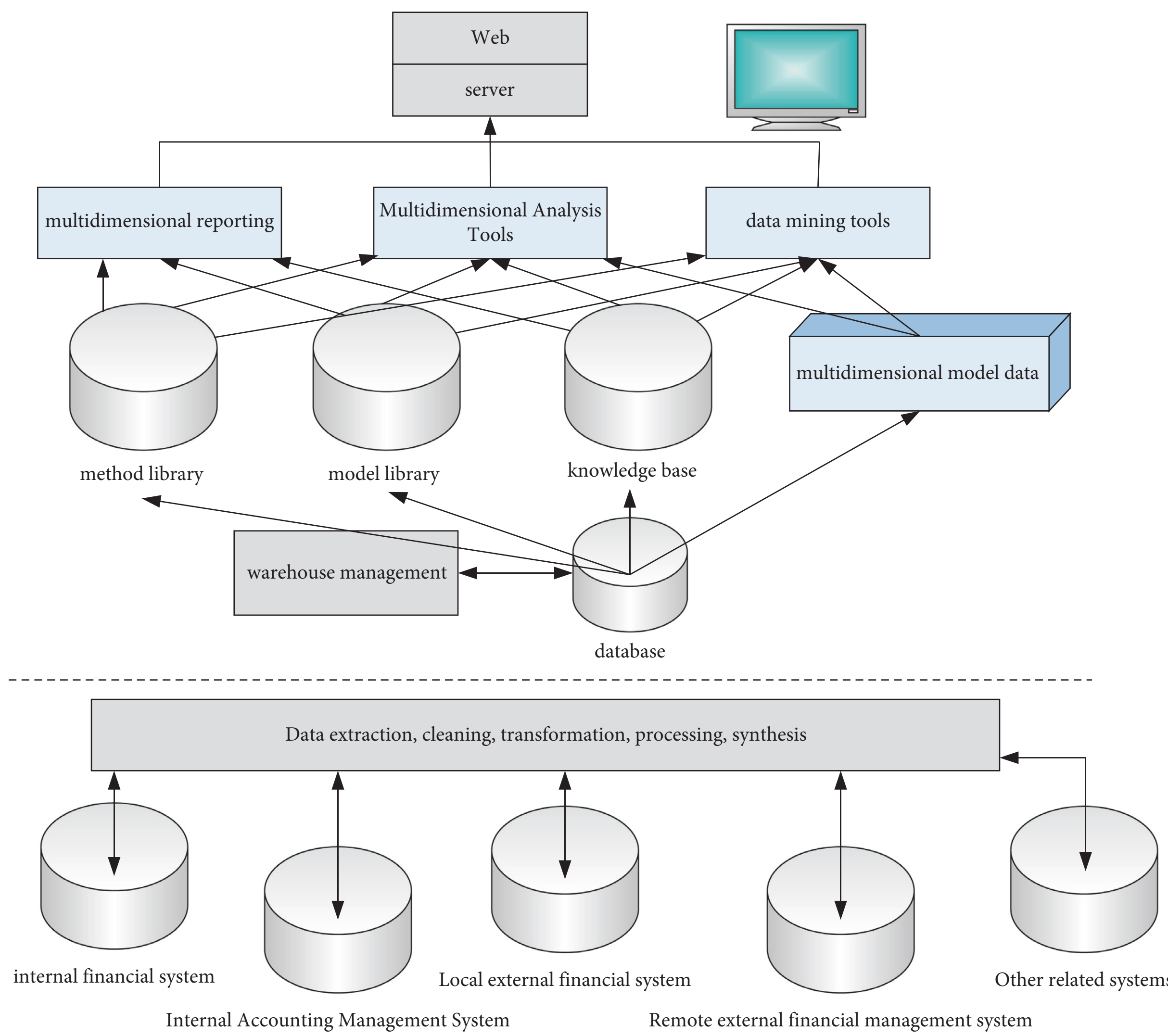

Figure 8: Financial intelligence system.

4. Financial Intelligence System Architecture and Implementation Strategy

The overall architecture of the financial intelligence system is divided into three layers, the data acquisition layer, the data organization storage organization layer, and the data analysis display layer, as shown in Figure 8.

Data are extracted from the original business processing system by the data acquisition layer. Internal financial system, internal accounting management system, local external financial system, remote external financial system, and so on are all included. The financial data are loaded into the data warehouse, and the material data are prepared for the construction of the next analysis model, thanks to data extraction, cleaning, conversion processing, and comprehensive improvement. The data organization and storage layer, which includes the data warehouse, is a platform for organizing and storing data retrieved from the data source after ETL. ETL tools are used to extract, clean, update, process, and synthesize source data to create a comprehensive statistical element library. The data layer of each granularity is an enterprise-level global data repository established according to the needs of subject analysis, and it includes detailed level, light integration level, medium level, and high level integration. Because the data warehouse is different from a traditional database, its management is also different. The data warehouse serves as the foundation for the method base, model base, knowledge base, and multidimensional analysis model base. The method library provides data mining and data analysis method guidance. Concrete models are available in the model library. The knowledge base converts data and information into knowledge by processing the results of data mining and data analysis. The purpose of the multidimensional analysis model library is to keep a hierarchical analysis model of commonly used dimensions and to answer complex analysis questions quickly. Multidimensional reporting, multidimensional analysis, and data mining tools, as well as interactive imaging and data drilling technology, are used in the data analysis display layer. All tasks such as reporting, analysis, and charting can be done quickly and easily in a relaxed environment, enhancing the data volume and providing truly informative data.

4.1. Advantages of Low-Risk Financial Intelligence Implementation Strategies. ERP is a "top-level project," and the financial intelligence mainly used for decision support for senior managers is data engineering. The support of senior managers is directly related to the success or failure of implementation. The traditional financial intelligence implementation strategy has long battle lines, and the establishment of data warehouses is difficult. The main reason is that data warehouses are subject-oriented, and managers have an insufficient understanding of requirements. In addition, today's social environment changes very fast, so the themes often change, which makes it very difficult to implement and extend the front line, and a lot of resources are invested but no effect can be seen. If the data cannot see the effect, it will not support the implementation of the project, and the lack of data to support the project will make it more difficult to implement and even directly lead to the failure of the project implementation. The adoption of low-risk financial intelligence strategies can allow managers to see the visual display and analysis of data for decision support through some simplified processes from time to time and constantly communicate with managers to understand their needs in the process. Through the continuous promotion of the low-risk implementation strategy, the managers' understanding of the entire system has been continuously improved, and the requirements put forward on this basis are more targeted and reasonable. In this way, the confidence in the implementation of financial intelligence will be enhanced, the support of data will be obtained, and the probability of successful project implementation will be greatly improved.

In the implementation of the financial intelligence system, the business personnel should be the protagonists compared with the technical personnel. The business personnel should make detailed analysis on the macro demands put forward by the decision makers, and the technical personnel should provide the platform and technical support for the business personnel. In the low-risk financial intelligence implementation strategy, through simple training of business personnel, they can turn data into information, visualize and interactively display it, improve business insight, and discover knowledge from information. Table 4 is the data structure of the voucher and detailed table.

4.2. Low-Risk Financial Intelligence Implementation Strategy Practice. From the above analysis, it can be seen that using ExcelCrystal and EasyTable tools, we can realize data warehouse, data mining, OLAP, interactive data, visualization data analysis, and other functions. From the perspective of business personnel, these two programs do not require programming or coding. After self-study or simple training, they can create excellent interactive visualizations according to their own business. Excel is a common data analysis software used by any enterprise. As long as you have a little understanding of the business, it is a boon for those who simplify the business. The training bit can master the skills of data mining and analysis. Therefore, at this stage, management decisions can be fully supported by implementing a low-risk financial intelligence strategy. Here is an example of data drilling in a sales report, showing how to achieve low-risk financial intelligence through the combination of Excel and Crystal Xcelsius. Sales data are generally the basis for the analysis and evaluation of business performance, but sales data are generally very large, with many dimensions, and there are many levels under each dimension. Faced with a large amount of complex data, in the past, when managers needed data, they needed to filter and summarize these large amounts of data to obtain the required data of the corresponding dimensions and levels. However, when the demand changes and other information is needed, these large and complex data must be filtered and summarized to obtain data of other dimensions and levels. These tasks will be repeated every time the requirements change, and different reports will be provided. The timeliness and accuracy of the reports are very low, which seriously affects the decision-making. And EXCEL's pivot table summarizes all the data into a pivot table and then sets multiple page fields such as year, region, product category, price, and channel to realize the multidimensional display of data, as shown in Table 5.

Due to the flexibility of the pivot table, each field can be dragged and placed at the desired position, and many data can be constructed into multidimensional tables to display all the data, and then filter out the required data. It can be seen that the more page fields are set, the more data can be stored. Not only page fields but also row fields and column fields can be added to increase the dimension of data. And it is also very flexible in the processing of time, which can be aggregated by month, quarter, year, and even by hour, minute, and second. In this way, when the management requirements change, the required data can be found by

Table 4: Data for the voucher schedule.

Serial number	Field name	Illustrate	Type	Length
1	I-id	Unique ID when entering	Int	4
2	I period	0 refers to the initial transaction detailed account, 21 refers to the preliminary bank account to be checked, 20 refers to the balance before adjustment of the bank account, and 1 refers to the voucher and details	Tinyint	1
3	Csign		Varchar	8
4	I signseq	According to the assignment by the system, it can be null at the beginning of the period	Int	4
5	Ino-id	The voucher number is assigned by the system and can be null at the beginning of the period	Smalint	2
6	Inid	Assigned by the system, it is 1 at the beginning of the period	Smalint	2
7	Dbill-date	Amendments to a limited range of dates available	Datetime	8
8	Idoc		Smalint	2
9	Cbill		Varchar	20
10	Ccheck		Varchar	20
11	Cbook		Tinyint	20
12	IBook		Varchar	1
13	Ccashier		Varchar	20
14	Iflag		Tinyint	1
15	Ctex1		Varchar	10
16	Ctex2		Varchar	10
17	Cdigest		Varchar	60
18	Ccode		Varchar	15
19	Cexch-name		Varchar	8

Table 5: Pivot table analysis model for sales data.

Year	Date	Children's products	Clothing	Food	Sporting goods	Artwork	Bike
2019	Season 1		68		336	805	685
	Season 2	63	5372	1166		1969	1204
	Season 3	182	2825	2734	341	1752	1294
	Season 4		8232	2215		855	1533
2020	Season 1	194		304	375	1134	
	Season 2		3458	1192	229	800	1285
	Season 3	203	6756	2680	961	1350	1670
	Season 4	103					
2021	Season 1		5555			940	2824
	Season 2	255	4076	3100	279		
	Season 3		7945		551	2192	2557
	Season 4	235					

simply dragging and dropping, and the information needed for decision-making can be obtained quickly and accurately. In addition, a chart analysis model with analysis and graphic display functions can also be drawn, as shown in Figure 9.

Product sales revenue is the key monitoring of enterprises. In this model, the line chart on the right can easily monitor the actual sales and planned sales amount of each product each month and the forecasted sales for future months based on that. The difference between actual and planned is visualized by the scale on the left. The scale at the bottom left shows the sales contribution of each product in the form of a pointer. In the upper right bar area, you can monitor the cumulative actual sales, planned cumulative sales, and corresponding variances for each product. Figure 10 is a comparison of financial system performance between traditional financial statistics and multisource information feature mining.

5. Discussion

In this model, there are not only two variables of sales volume and adjustment volume but also intuitive understanding of the value of income. The model uses a structure diagram to illustrate the relationship between several factors that affect profitability. For example, by setting the variable cost sliders, change the different factors that affect changes in value, total cost, and final revenue. The revenue growth model uses a transition line with advance notice. If the profit is positive, the growth line will appear green, and if the profit is negative, the loss line will appear red, creating a red flag and attracting the attention of decision makers. In the transaction progress process, there is an initial alert table that visually determines the gap between current transaction volume and downtime and provides a way to adjust the gap. Also, for

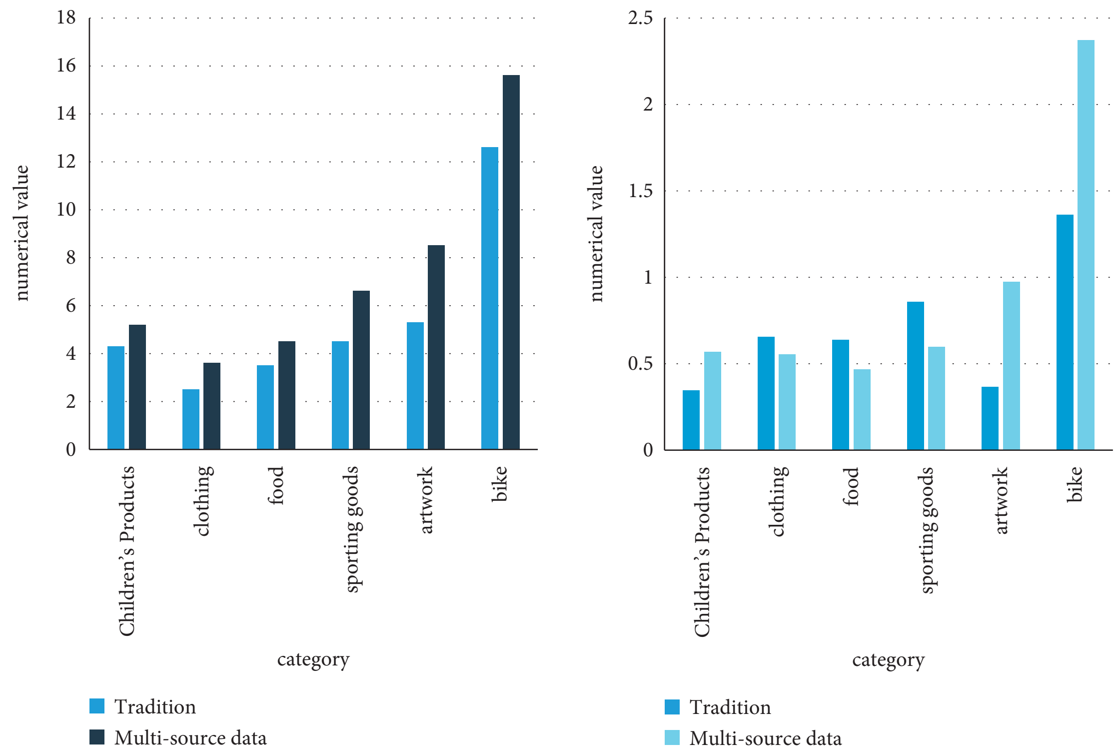

Figure 9: Graphical presentation model of sales data.

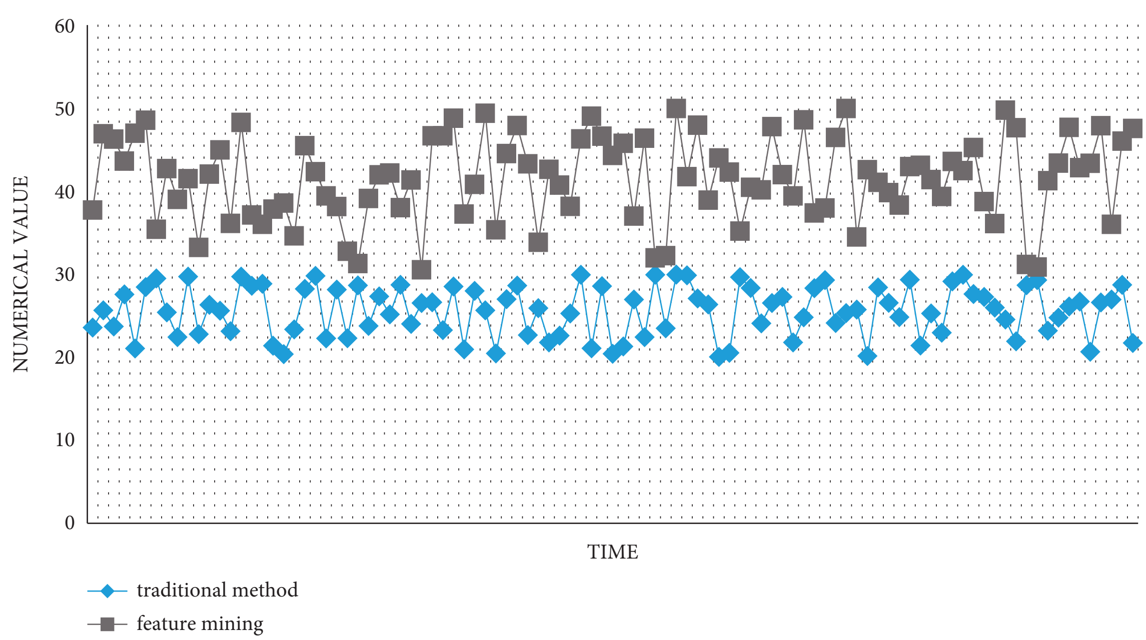

Figure 10: Product sales revenue monitoring.

breakeven, you can change unit prices, fixed or variable prices, change breakeven sales, etc.

Furthermore, the model includes an operational risk dashboard that allows decision makers to see the impact of various factors on profits in their current state. When the selected factors move in an unfavorable direction in the current state, operational risk is defined as the percentage impact on profits. To select the influencing factors, click the "factor selection" button and then choose the single most important influencing factor. Check "unit price" to see the impact of unit price changes on profit; if the sales volume is unstable, check "sales" to see the impact of sales volume changes on profit, etc., that is, single factor analysis. It can also be chosen multiple important factors, such as unstable product prices and unstable raw material supply prices; simply check "unit price" and "material" to see how these two factors interact to affect profits, which is known as multifactor analysis. The business subinsurance is displayed as a dashboard, and an early warning system is used to visually see the impact of the selected factors on profit in the current state. There are also scheme buttons in this model for saving, loading, and deleting schemes, allowing users to save their results after adjusting all of the variables, as well as view and delete them after loading.

6. Conclusion

Financial data are primarily used for business management decision-making, and Chinese SMEs are limited in their use and promotion of financial data due to a variety of factors including capital and technology. Financial intelligence solutions that are both cost-effective and simple to use are in high demand. On the basis of research on some of the financial intelligence products currently used by large domestic enterprises, this paper examines the basic theories of business intelligence and financial intelligence, as well as the construction of financial intelligence in small- and medium-sized enterprises. The following are the main aspects of this paper's research findings: propose a low-risk enterprise financial intelligence strategy and locate the enterprise financial information system model construction. This is the conclusion reached after examining existing technical abilities and previous knowledge, as well as the characteristics of EXCEL and Xcelsius. An example of financial intelligence analysis, an example of financial intelligence monitoring, an example of financial intelligence decision-making, and an example of financial intelligence early warning are all established on the basis of the actual combat financial system. These examples enable businesses to assess the feasibility of the proposed financial intelligence application scheme. The use of multisource information feature mining and VBA technology in EXCEL in the technical realization is the most notable feature of this paper's research results. Their use among Chinese financial personnel is rapidly spreading due to their outstanding performance. Because the design and construction of a financial intelligence system is a very complex project, only a few parts that are closely related to the research of this topic are included in this paper, as well as some issues that have not been discussed, due to time, materials, and the author's own ability. This paper only provides a broad classification of financial intelligence systems and attempts to implement some common models. It is also necessary to conduct extensive research on the specific models of each component, which is a continuous improvement process. In the realization of financial intelligence, this paper mainly not only considers adopting low-risk financial intelligence implementation strategies but also needs to do in-depth research on ideal and comprehensive implementation strategies. This research focuses on financial intelligence, but after the research and application of financial intelligence are fully mature, it is necessary to study the transition to business intelligence and even decision support on this basis.

Data Availability

The data used to support the findings of this study are available from the author upon request.

Conflicts of Interest

The author declares that there are no conflicts of interest.

Acknowledgments

This study was supported by the Soft Science Project Of Henan Provincial Department of Science and Technology (Research on the construction of local government debt management system under public health emergencies, project no. 212400410565).

References

[1] W. Zhang, R.-S. Chen, Y. C. Chen, S. Y. Lu, N. Xiong, and C. M. Chen, "An effective digital system for intelligent financial environments," *IEEE Access*, vol. 7, no. 99, pp. 155965–155976, 2019.

[2] D. Aikman, M. Kiley, S. J. Lee, M. G. Palumbo, and M. Warusawitharana, "Mapping heat in the U.S. financial system," *Journal of Banking & Finance*, vol. 81, pp. 36–64, 2017.

[3] M. Prochniak and K. Wasiak, "The impact of the financial system on economic growth in the context of the global crisis: empirical evidence for the EU and OECD countries," *Empirica*, vol. 44, no. 2, pp. 295–337, 2017.

[4] F. Polzin, M. Sanders, and F. Täube, "A diverse and resilient financial system for investments in the energy transition," *Current Opinion in Environmental Sustainability*, vol. 28, no. OCT, pp. 24–32, 2017.

[5] Z. Han, R. Mo, Z. Chang, L. Hao, and W. Niu, "Key assembly structure identification in complex mechanical assembly based on multi-source information," *Assembly Automation*, vol. 37, no. 2, pp. 208–218, 2017.

[6] X. Gao and F. Xiao, "A generalized χ^2 divergence for multisource information fusion and its application in fault diagnosis," *International Journal of Intelligent Systems*, vol. 37, no. 1, pp. 5–29, 2022.

[7] B. Wu, W. Qiu, W. Huang, G. Y. Meng, and J. Huang, "A multi-source information fusion evaluation method for the tunneling collapse disaster based on the artificial intelligence deformation prediction," *Arabian Journal for Science and Engineering*, vol. 47, no. 4, pp. 5053–5071, 2022.

[8] Y. Wu, X. Li, and Z. Cao, "Effective DOA estimation under low signal-to-noise ratio based on multi-source information meta fusion[J]," *Journal of Beijing Institute of Technology (Social Sciences Edition)*, vol. 30, no. 4, pp. 377–396, 2021.

[9] J. Chen, C. Du, Y. Zhang, P. Han, and W. Wei, "A clustering-based coverage path planning method for autonomous heterogeneous UAVs," *IEEE Transactions on Intelligent Transportation Systems*, pp. 1–11, 2021.

[10] W. Cai, Y. Song, and Z. Wei, "Multimodal Data Guided Spatial Feature Fusion and Grouping Strategy for E-Commerce Commodity Demand Forecasting," *Mobile Information Systems*, pp. 1–14, 2021.

[11] Y. Ding, X. Zhao, Z. Zhang, W. Cai, N. Yang, and Y. Zhan, "Semi-supervised locality preserving dense graph neural network with ARMA filters and context-aware learning for

hyperspectral image classification," *IEEE Transactions on Geoscience and Remote Sensing*, 2021.

[12] J. D. Brown and J. S. Earle, "Finance and growth at the firm level: evidence from SBA loans," *The Journal of Finance*, vol. 72, no. 3, pp. 1039–1080, 2017.

[13] C. Dang, Z. Li, and C. Yang, "Measuring firm size in empirical corporate finance," *Journal of Banking & Finance*, vol. 86, pp. 159–176, 2018.

[14] J. de Haan and J.-E. Sturm, "Finance and income inequality: a review and new evidence," *European Journal of Political Economy*, vol. 50, pp. 171–195, 2017.

[15] J. H. Block, M. G. Colombo, D. J. Cumming, and S. Vismara, "New players in entrepreneurial finance and why they are there," *Small Business Economics*, vol. 50, no. 2, pp. 1–12, 2018.

[16] D. J. Higham, X. Mao, and L. Sapruch, "Convergence, non-negativity and stability of a new milstein scheme with applications to finance," *Discrete and Continuous Dynamical Systems - Series B*, vol. 18, no. 8, pp. 2083–2100, 2017.

[17] J. B. Heaton, N. Polson, and J. H. Witte, "'Rejoinder to 'Deep learning for finance: deep portfolios'," *Applied Stochastic Models in Business and Industry*, vol. 33, no. 1, pp. 19–21, 2017.

[18] M. K. Linnenluecke, X. Chen, X. Ling, T. Smith, and Y. Zhu, "Research in finance: a review of influential publications and a research agenda," *Pacific-Basin Finance Journal*, vol. 43, no. jun, pp. 188–199, 2017.

[19] A. Ferrando and C. Preuss, "What finance for what investment? Survey-based evidence for European companies," *Economia Politica*, vol. 35, no. 3, pp. 1015–1053, 2018.

[20] A. Lusardi and O. S. Mitchell, "How ordinary consumers make complex economic decisions: financial literacy and retirement readiness," *Quarterly Journal of Forestry*, vol. 7, no. 3, pp. 1750008.1–1750008.31, 2017.

[21] B. Li, T. Li, W. Zhang, and Z. L. Liu, "Multisource information risk evaluation technology of mine water inrush based on vwm: a case study of weng'an coal mine," *Geofluids*, vol. 2021, no. 4, pp. 1–12, 2021.

[22] Y. Lin, X. Hu, and X. Wu, "Quality of information-based source assessment and selection," *Neurocomputing*, vol. 133, pp. 95–102, 2014.

Hindawi
Computational Intelligence and Neuroscience
Volume 2022, Article ID 1817990, 9 pages
https://doi.org/10.1155/2022/1817990

Research Article

Optimization Model of Mathematics Instructional Mode Based on Deep Learning Algorithm

Rui Liu

Science Teaching Department, Zhengzhou Preschool Education College, Zhengzhou 450000, China

Correspondence should be addressed to Rui Liu; 1351160205@xzyz.edu.cn

Received 2 May 2022; Revised 4 June 2022; Accepted 6 June 2022; Published 4 July 2022

Academic Editor: Xin Ning

This paper proposes corresponding teaching methods and instructional modes based on predecessors' research on mathematics instructional mode and the current state of mathematics teaching. In addition, this paper constructs a teaching evaluation model based on DL algorithm based on an in-depth study of DL-related theories in order to accurately and scientifically analyze the problems that exist in mathematics teaching. This paper constructs an instructional quality evaluation index system based on rationality and fairness, and uses the BPNN evaluation model to train and study a set of instructional quality data. Finally, the experimental results show that this system has a high level of stability, with a 96.37 percent stability rate and a 95.42 percent evaluation accuracy rate. The results of this paper's evaluation of the mathematical instructional quality model are objective and reasonable. It can accurately assess instructional quality while also assessing problems in the teaching process based on the instructional quality scores and making reasonable recommendations for teaching improvement based on the weak links in the teaching process. It has the potential to provide a workable system for assessing instructional quality.

1. Introduction

The modernization of education necessitates the improvement of instructional quality [1]. Many teachers use the boring lecturing classroom mode in the traditional mathematics classroom, resulting in a serious and boring classroom atmosphere. Students are effectively shackled as a result of this, and their ability to learn in class suffers as a result. We can optimize the mathematics instructional mode to change the above teaching phenomenon. Mathematics instructional mode optimization can effectively deepen students' understanding of mathematics. Teachers should constantly optimize the mathematical model based on students' learning situations and cognitive characteristics in order for students to comprehend and master the theoretical knowledge and content of mathematics from multiple angles and dimensions during actual teaching. The new curriculum reform emphasizes establishing students' dominance in classroom instruction. This necessitates teachers completely altering the traditional model and establishing a new teacher-student relationship. In general, the optimization of a mathematical model entails the following components: language category optimization, language syntax optimization, and language logic optimization. The optimization of classroom instructional mode and the construction of effective mathematics classrooms are of great teaching and practical importance in today's environment.

The scientificity, rationality, and timeliness of instructional quality evaluation play a key role in the optimization of instructional mode. However, the limitations of the traditional instructional quality evaluation method itself make it controversial. Therefore, it is of practical significance to establish a scientific and reasonable instructional quality evaluation model to evaluate mathematics instructional quality. Deep learning (DL) [2–4] is an extension of the research field of machine learning [5–7] and an effective way to realize artificial intelligence. Due to the rapid development of DL, NN (neural network) [2, 8] in DL has also been well developed, and its effect has been well verified in many network models. NN is a complex calculation method to simulate the neuron and neuron connection structure of human brain. NN technology is mainly based on the workflow of human nerves and uses human nerves to process related contents for calculation. BPNN (back-propagation neural network) is a three-layer feedforward hierarchical network composed of input layer, hidden layer, and output layer. Its learning process consists of two processes: forward propagation of information and backward propagation of errors. BPNN has the advantages of strong generalization and fault tolerance, but it also has some shortcomings. Genetic algorithm is an algorithm that refers to and simulates biological genetic mechanism and natural selection. Its basic idea is to simulate the evolution process of population. After three genetic operations, selection, crossover, and mutation, the population is constantly updated, and the excellent degree of the population is constantly enhanced, approaching the global optimal solution. Aiming at the shortcomings of BPNN, genetic algorithm can be used to improve it. This paper mainly studies the optimization model of mathematics instructional mode based on DL algorithm, and its innovation lies in: (1) this paper improves the existing evaluation index system and constructs a new instructional quality evaluation index system based on rationality and fairness. To train and study the instructional quality data, the BPNN evaluation model is used. After demonstration, the instructional quality evaluation index system in this paper is scientific, objective, and reasonable. (2) This paper improves the problem that extracting principal components from the correlation coefficient matrix of indexes cannot reflect the difference information of the variation degree of each index by introducing the basic principle of principal component analysis. Because BPNN is highly dependent on its initial weights and thresholds, a genetic algorithm is used to optimize BPNN's initial weights and thresholds in order to improve the prediction accuracy and convergence speed of instructional quality evaluation results. The experiment shows that this system can be used as a benchmark for evaluating instructional quality and making decisions.

2. Related Work

Based on the content of the instructional quality evaluation index system, Sergis et al. constructed a convolutional neural network instructional quality evaluation model based on the convolutional neural network learning expert instructional quality evaluation samples [9]. Maulana et al. mainly considered different disciplines and majors, set up different evaluation index projects, and established different evaluation index systems. And we use the powerful functions of the MATLAB toolbox to establish a BP neural network, train the network, test the network, and finally analyze the experimental results [10]. Choi and Kim et al. pointed out that under the current background, more and more emphasis is placed on strengthening the interaction between teachers and students, and the main form of interaction is the "dialogue" in the classroom. And we summarize the effective instructional mode of mathematics around "dialogue" [11, 12]. Starting from a brief analysis of the optimization of classroom instructional mode, Petraki E analyzed the main points of constructing an effective mathematics classroom after expounding the problems existing in today's mathematics classroom [13]. Onozawa M uses a deep learning algorithm to design an instructional quality evaluation system, which intelligently evaluates the instructional quality and puts forward rationalization suggestions [14]. Aiming at the problems existing in the quality evaluation of NC bilingual teaching courses, Liu et al. tried to use the analytic hierarchy process to carry out exploratory analysis, thus providing a scientific case basis for the evaluation of bilingual course instructional quality [15]. Northrup et al. believed that improving the pertinence of homework is one of the core contents of constructing an effective mathematics classroom. While intensifying in-class training in mathematics and improving the effectiveness of feedback correction, we must pay attention to the efficiency of mathematics after-school homework training [16, 17]. Ottmar et al. expounded the design idea and implementation method of neural network for instructional quality evaluation, introduced and analyzed the traditional instructional quality evaluation method, and trained and tested the designed neural network for instructional quality evaluation [18].

This paper proposes corresponding teaching methods and instructional modes based on predecessors' research on mathematics instructional mode and the current state of mathematics teaching. Furthermore, this paper constructs a teaching evaluation model based on DL algorithm based on an in-depth study of DL-related theories. The optimization of the mathematics instructional mode is carried out based on the evaluation of the teaching evaluation model. In this paper, a rich basic dataset of teaching evaluation has been formed through the evaluation of teaching experts, teachers' peers, and students. The normalization formula is used to process the input samples. Furthermore, because BPNN is so reliant on its initial weights and thresholds, this paper employs a genetic algorithm to optimize BPNN's initial weights and thresholds and reduce the time it takes for BPNN to find the weights and thresholds that satisfy the training termination conditions, in order to improve NN's instructional quality evaluation results' prediction accuracy and convergence speed.

3. Methodology

3.1. Optimizing Classroom Instructional Mode and Constructing Efficient Mathematics Classroom. Math textbooks for each stage are also designed according to students' knowledge base, cognitive level, and thinking ability, as there are high expectations for mathematics students' thinking ability. However, many teachers adopt the tedious lecture-based classroom mode during the actual teaching process, resulting in a serious and monotonous classroom environment [19]. We can improve the mathematics instructional mode to change the above-mentioned teaching phenomenon. Students' understanding of mathematics can be effectively deepened by optimizing mathematics instructional mode [20]. The term "dialogue" is used in class to describe how teachers and students communicate. The amount of "dialogue" and its effect on the classroom atmosphere and instructional quality are both directly determined by the amount of "dialogue." An effective dialogue instructional mode can help students break free from the constraints of their thinking, causing them to think and express more actively, and thus promoting the development of independent thinking abilities. Because mathematical models are all expressed in mathematical languages, they must be transformed using different mathematical languages. In order to successfully transform mathematical languages, students must master a variety of mathematical languages, including geometric language, algebraic language, and symbolic language. Therefore, in mathematics teaching, teachers should pay attention to the training of students' mutual conversion between different languages when changing "numbers" into "shapes" through the equivalent exchange of mathematical model languages. Besides, the guiding ideology of optimizing classroom instructional mode also includes the corresponding concept of "efficient classroom." The main contents of this concept include teaching preparation, teaching process, training and testing, after-class counseling, teaching evaluation, and other aspects of different courses. Therefore, on this basis, the optimization of classroom instructional mode can be better applied.

First of all, in order to realize the correct and efficient conversion between mathematical languages, teachers must help students establish a correct mathematical language structure. Usually, mathematical models are based on mathematical concepts, which are connected by verbs. The main reasons for their complexity are the order relationship, hierarchical relationship, and logical relationship in the structure of mathematical models. Therefore, in order to correctly grasp the mathematical model, it is necessary to correctly sort out the structural relationship between mathematical concepts to ensure the correct transformation of mathematical model. Furthermore, teachers must teach students how to ask questions in class; that is, the questions posed must be of sufficient inquiry value, conform to classroom teaching content, and have a clear purpose. Students will have a better understanding of the meaning of asking questions as a result of the increased teaching time, and they will be able to grasp the points that are appropriate for asking questions more accurately and master effective questioning methods, resulting in a better awareness of questions. This not only is beneficial for creating a productive classroom but also allows students to improve their mathematical inquiry learning abilities. At the same time, the most important thing is to cultivate students' interest in mathematics. Students' interest in mathematics learning is influenced not only by the number of mathematical concepts and formulas taught in class by mathematics teachers but also by the number of classic questions explained and analyzed in exercise classes, as well as other factors. Mathematics teachers must not only have good mathematics knowledge, teaching skills, and teaching process to improve students' interest in mathematics learning; they must also have better mathematics teaching methods, mathematics teaching emotions, mathematics teaching attitudes, and mathematics teaching values.

Teachers should master the effective teaching method of question situation and avoid the traditional acceptance method of asking questions. We should not only attach importance to the results but also to the whole process of students' participation in classroom interaction. The effective construction of mathematics classroom needs the effective support of corresponding points. This is mainly reflected in the effective preparation before class, the reasonable improvement of classroom teaching efficiency, the emphasis on promoting students' cooperative learning, and the pertinence of homework after class. In classroom teaching, teachers can realize the simplification of mathematical problems by flexibly changing mathematical thinking patterns. Through the rational application of the above strategies, students can successfully realize the transformation between mathematical models. This method can get better results in the application of trigonometric function, geometry, and complex number knowledge. In the process of inquiry learning, teachers do not instill knowledge stiffly, but let students actively participate in knowledge exploration, and naturally digest and absorb knowledge in the process of exploration. Therefore, it can promote the effective improvement of mathematics classroom instructional quality and cultivate students' interest in mathematics invisibly. At the same time, the effective cooperative learning among students can play a very good role in promoting the creation and optimization of teaching links. The exploration of effective mathematics instructional mode cannot be separated from the joint efforts of students and teachers. Finally, in order to promote the continuous improvement of classroom instructional quality, teachers should also organize students to carry out classroom teaching and evaluation of learning situation, so as to better find problems and put forward improvement measures. For some good places, it is necessary to keep them.

3.2. Application of DL Algorithm in Instructional Quality Evaluation. It is an extension of the research field of machine learning and an effective way to realize artificial intelligence [21]. As a new technology, DL has opened up a new way for pattern recognition [22], nonlinear classification [23], artificial intelligence, and other research with its basic characteristics such as nonlinear mapping, learning classification, and real-time optimization. It involves biology, electronics, computer, mathematics, physics, and other disciplines, and has a wide application prospect. Due to the rapid development of DL, NN in the field of DL has also been well developed, and its effect has been well verified in many network models. NN is a complex calculation method to simulate the neuron and neuron connection structure of human brain. NN technology is mainly based on the workflow of human nerves and uses human nerves to process related contents for calculation. Because of the parallelism of NN, it is very effective for solving combinatorial optimization problems. From the point of view of automatic control, NN can be regarded as a high-dimensional nonlinear dynamic system. Neurons are the processing units in this system. This system has many inputs and many outputs, and we regard its input-output relationship as a mapping from input to output. Therefore, it is reasonable to apply NN to the design of instructional quality model. The three-layer BPNN model is shown in Figure 1.

BPNN is an iterative algorithm consisting of two processes: forward propagation of input vector and backward propagation of error. The algorithm is divided into two stages: ① forward propagation of input vector. ② Back-propagation of error. BPNN has the following advantages: ① BPNN is suitable for solving problems with complex internal mechanisms. ② It can process information in parallel. ③ It can abstract the relevant laws from the samples. ④ It has a strong self-learning function. ⑤ For the input samples in BPNN, there may be errors with large errors. But BPNN still has some limitations. For example, it is easy to fall into the local optimum, the recognition accuracy is easily affected, there is no fixed basis for setting network parameters, there is a tendency to forget the old samples when learning new ones during training, and the generalization ability is poor. Based on DL algorithm, this paper constructs an instructional quality evaluation model. For an instructional quality evaluation system, it can be regarded as a mapping from input to output. NN's self-learning ability, that is, the plasticity of mapping, enables it to simulate the required mapping relationship through training, thus replacing domain experts to automatically evaluate the evaluation object.

3.3. Construction of the Teaching Evaluation Model Based on DL. Instructional quality evaluation system is an evaluation of teachers' phased teaching effect, which provides favorable analysis basis for mastering teachers' teaching ability and improving instructional quality. When evaluating the instructional quality, we should adhere to an objective, fair, and rational attitude. We should not speculate subjectively or mix personal feelings, and we should be ideological, scientific, and feasible. The establishment of a reasonable model of teacher's teaching evaluation system can not only enable teachers to revise and improve the teaching plan according to the teaching effect in time but also help the school to understand the implementation of teachers' teaching tasks and make macro-control. More importantly, a perfect evaluation system is of great significance to the establishment of a teaching evaluation model for teachers in colleges and universities. The instructional quality evaluation system based on DL algorithm is designed based on B/S mode. The advantages of designing the instructional quality evaluation system based on B/S mode are as follows: it is convenient for different types of users to operate, the online evaluation can be completed in a short time, and the system maintenance is convenient. Client, application unit, and database are three important components of the system. According to the experience of this article, we try to use an implicit layer first. The DL-based instructional quality evaluation model and algorithm flow are shown in Figure 2.

The samples used in data analysis frequently contain a large number of variables, and adding more variables increases the complexity of the analysis problem. The information contained in these principal components should be required to be independent of one another in order for them to not overlap. The main goal of principal component analysis (PCA) is to reduce the dimensions of variables and simplify problems by retaining the most important information from the original variables, making it easier to understand the main contradictions when studying complex problems. The function of DL is to learn the inherent law and representation level of sample data. The BPNN model in the DL algorithm is used to evaluate instructional quality when designing the instructional quality evaluation system. The evaluation method is a nonlinear problem because there are many uncertain and complex factors in the evaluation process. BPNN has demonstrated its unique advantages in solving such problems by having a strong adaptive learning ability that can approximate any function. The steps of BPNN learning rules are as follows: the output of the i neuron in the hidden layer is as follows:

$$a1_i = f1\left(\sum_{j=1}^{r} wl_{ij}p_j + b1_i\right), \quad i = 1, 2, 3, \ldots, s1. \tag{1}$$

The output of the kth neuron in the output layer is as follows:

$$a2_k = f2\left(\sum_{i=1}^{s1} w2_{ki}a1_i + b2_i\right), \quad k = 1, 2, 3, \ldots, s2. \tag{2}$$

We define the error function as follows:

$$E(W, B) = \frac{1}{2}\sum_{k=1}^{s2}\left(t_k - a2_k\right)^2. \tag{3}$$

We assume that the evaluation indicators of the evaluation system are N, the result grades are M, and the classification of the total indicators is divided into L categories; the evaluation scores of each indicator can be used as the input of the scoring comprehensive network, which is expressed as follows:

$$X = \left[x_{11} < x_{1j} < x_{1m} < x_{i1} < x_{ij} < x_{im} < x_{n1} < x_{nj} < x_{nm}\right]^T. \tag{4}$$

The rating coefficient of the evaluation result is taken as the output of the scoring comprehensive network, which is expressed as follows:

$$K = \left[k_1 k_2 < k_j < k_m\right]^T. \tag{5}$$

The importance coefficient of each index is connected by the synaptic weight matrix, which is expressed as follows:

$$W = \left[W_1 W_2 < W_j < W_m\right]^T. \tag{6}$$

In this paper, roulette is adopted. First, the fitness value of a certain generation of individuals, namely, BPNN weight and threshold, is calculated. Then, we calculate the proportion of the fitness value in the total fitness value, that is, the probability of the individual being selected in the

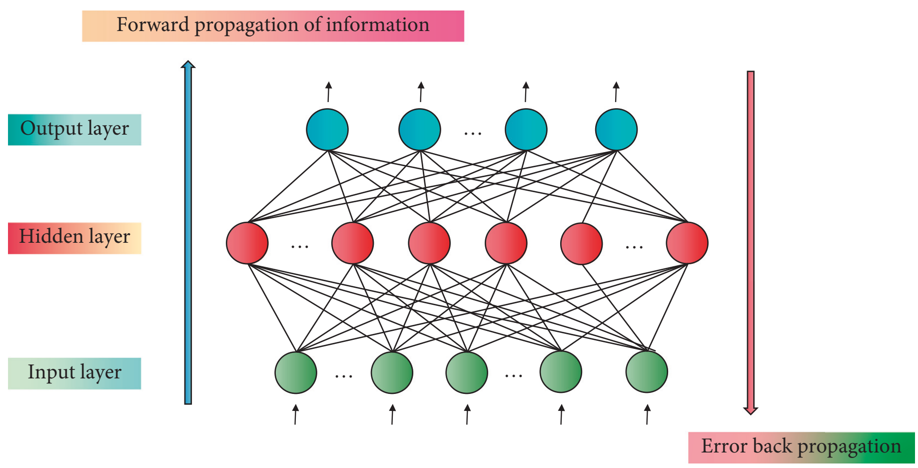

FIGURE 1: Three-layer BPNN model.

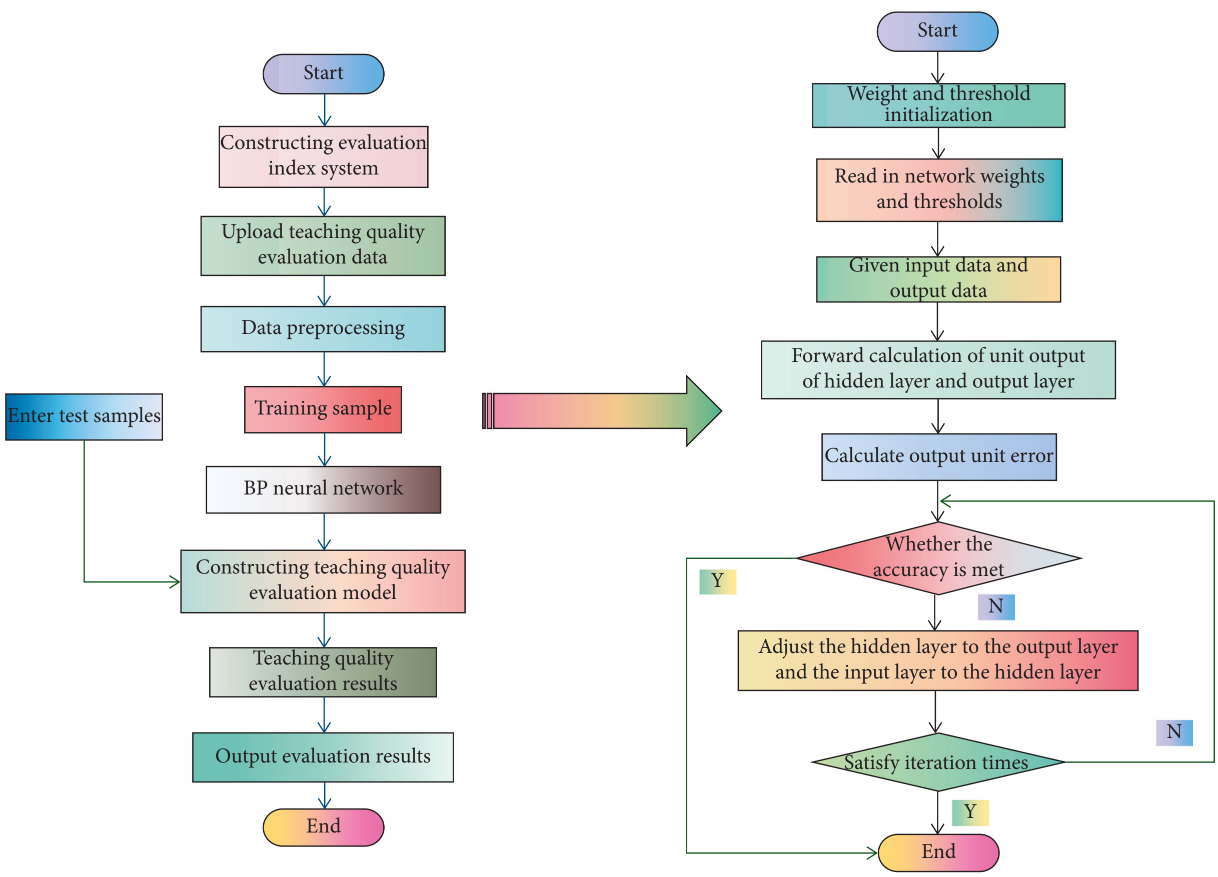

FIGURE 2: DL-based instructional quality evaluation model and algorithm flow.

selection process. The calculation of the selection probability is shown in the following formula:

$$z(a_j) = \frac{f(a_j)}{\sum_{j=1}^{d} f(a_j)}. \quad (7)$$

Among them, a_j represents an individual in the group, $z(a_j)$ is the probability that a_j is selected, $f(a_j)$ is the fitness value of individual a_j, and d is the population size. After calculating the probability of each individual being selected, it is necessary to determine whether the selected individual can continue to be inherited to the next generation of individuals according to the size of the cumulative probability. The calculation formula is as shown below.

$$q(a_k) = \sum_{j=1}^{k} z(a_j). \quad (8)$$

Among them, $q(a_k)$ is the cumulative probability of individual a_k, and then, a new population of the next generation is obtained through genetic manipulation, the fitness value is judged, and the above steps are repeated until the population is stable. The action function of each neuron is taken as a linear function:

$$F(S_j) = S_j. \tag{9}$$

The output of the node at this point is as follows:

$$K_j = S_j = W_j^T X. \tag{10}$$

In this paper, the average method is used for dimensionless processing, which can extract more original information with less principal components, thus reducing the workload and making the solution to the problem more perfect, more accurate, and more comprehensive. Valuable data such as instructional quality evaluation index data, evaluation subject, and object data are stored in the database. The evaluation is divided into two aspects: index scoring and grading and classification. Therefore, two networks can be used for processing, and one network can store and memorize the importance coefficients of each index and synthesize the scores, which is called comprehensive network. The other one classifies the index scores linearly or nonlinearly, so as to obtain the final evaluation result of the total index, which is called classification network. In the process of evaluating the instructional quality, certain principles should be followed. Evaluation principle plays a key role in ensuring the validity and reliability of evaluation results, and is the basic requirement of evaluation work. The evaluation index system of instructional quality designed in this paper follows the following basic principles: ① the principle of comprehensiveness, ② principle of directionality. ③ scientific principle, ④ principle of measurability, ⑤ principle of encouragement and improvement, ⑥ principle of objectivity, ⑦ principle of subjectivity, and ⑧ principle of consistency. In this paper, the teaching process, teaching environment, teaching teachers, and instructional quality monitoring are the first-level indicators of the instructional quality evaluation index system. There are several secondary indicators under the primary indicators. The evaluation index system of instructional quality constructed in this paper is shown in Table 1.

After the establishment of the evaluation index system, it is more scientific to set the corresponding weights of the index system. In the process of setting weights, we can first establish the weights set by experts' evaluation indicators and build a BPNN model learning network through the powerful function of MATLAB toolbox according to the weights of experts' indicators. Then, we input the weights set by experts and adjust the weights of indicators set by experts through network training according to the functions of BPNN model. The final error is minimized, and the weight is relatively more reasonable. The user management unit of the system is divided into two aspects: system login and security management. Different types of users log in to the instructional quality evaluation system according to different unit entrances, and users perform operations in their respective permission pages. Considering the security of user information, users are divided into five types: teaching supervisor, audit administrator, administrator, teacher, and student.

4. Result Analysis and Discussion

The instructional quality evaluation system designed based on DL algorithm in this paper contains a large amount of data, so there are certain requirements for the running hardware and software environment. In order to ensure the efficient operation of the system, the test environment in this paper is set as follows: the CPU is 2.4 GHz, the memory size is 8 GB, the computer hard disk is 1 T, and the system is Windows. In this paper, the number of nodes in the input layer, hidden layer, and output layer is $16 \times 4 \times 1$, respectively; the learning rate is 0.8; and the function of each node adopts the Sigmoid function. After testing, the convergence curve of the algorithm is obtained as shown in Figure 3.

The commonly used mean square error and accuracy rate are selected as the indexes to test the performance of this algorithm. These two indexes are used in different algorithms for testing and comparison. The mean square error of different algorithms is shown in Figure 4. The accuracy of different algorithms is shown in Figure 5.

The results show that this algorithm can not only speed up the convergence of the network but also improve the evaluation accuracy of the model. Its performance is better than that of the comparison model. Taking ten math classes in the second grade of a school as examples, the quality of math teaching was evaluated, respectively. The evaluation results of mathematics instructional quality are shown in Table 2.

The above statistics of mathematics instructional quality evaluation in different classes show that this system can identify the highest score, lowest score, and average score of instructional quality evaluation in different classes. It provides different types of data for comprehensive analysis of mathematics instructional quality. Figure 6 shows the stability test results of different systems.

It can be seen from Figure 6 that the stability of this system is high. Moreover, the analysis and suggestion function of the instructional quality evaluation system designed in this paper reflects the degree of intelligence of the system, shares the workload of manually evaluating teachers' teaching effect, and improves the operational efficiency of instructional quality evaluation. Through training, quantifiable classification criteria or experts' experience information that is not easy to quantify is stored in the nonlinear network, and the instructional quality evaluation NN is measured with new experimental data. Comparison between different system evaluation results and expert evaluation results is shown in Figure 7.

It can be seen from Figure 7 that, compared with other systems, the evaluation network constructed in this paper can give results consistent with expert evaluation. This shows that this method has certain accuracy and reliability. The experimental results show that the stability of this system is high, reaching 96.37%, and the evaluation accuracy rate can

Table 1: Instructional quality evaluation index system.

	Primary index	Secondary index	Index sequence
Instructional quality evaluation index	Teaching process	Degree of interaction	X1
		Assess rationality	X2
		Organizational science	X3
		Cultivation of innovative ability	X4
		Cultivation of practical ability	X5
		Cultivating students' interest	X6
		Students' final grades	X7
	Teaching teachers	Scientific teaching	X8
		Teaching attitude	X9
		Teaching ability	X10
		Teach students in accordance with their aptitude	X11
	Teaching environment	Supporting facilities	X12
		Practice frequency	X13
	Instructional quality monitoring	Teacher self-evaluation	X14
		Student evaluation	X15
		Teachers' mutual evaluation	X16
		Leadership evaluation	X17
		Teaching supervision	X18

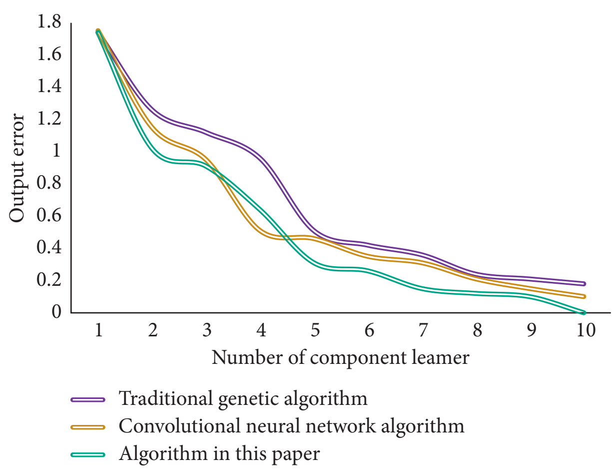

Figure 3: Convergence curve of the algorithm.

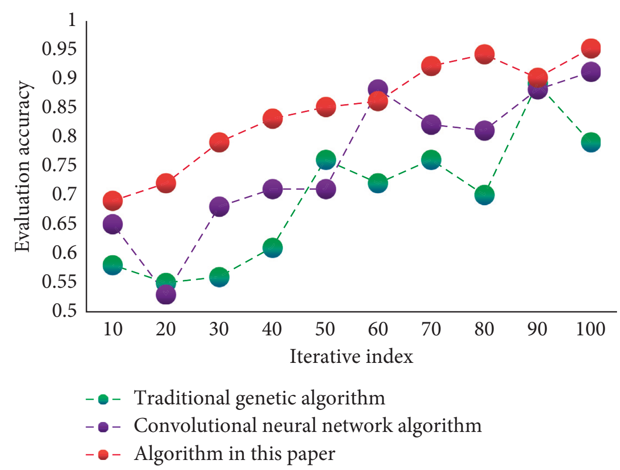

Figure 5: Comparison of accuracy of different algorithms.

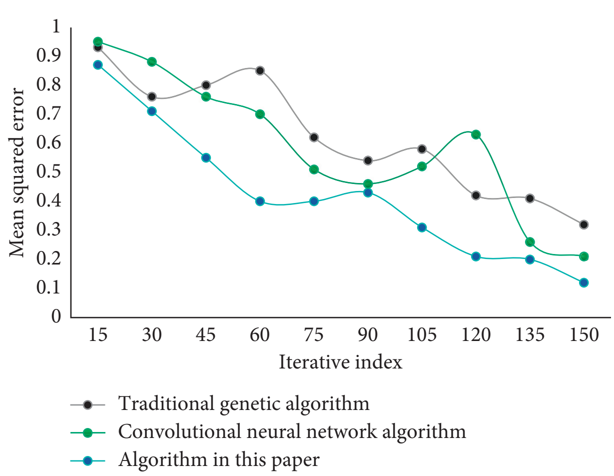

Figure 4: Comparison of mean square error of different algorithms.

Table 2: Evaluation results of mathematics instructional quality of ten classes.

Classes	Lowest score	Highest score	Average score
1	89.6	92.7	91.2
2	91.5	94.5	93.1
3	88.3	92.6	90.5
4	92.1	95.8	94.2
5	89.3	94.5	92.5
6	88.9	93.1	90.8
7	89.6	93.5	91.7
8	84.7	89.8	86.6
9	86.1	90.5	88.2
10	89.4	92.7	90.9

reach 95.42%. This system has certain reliability. Compared with the general instructional quality evaluation system, the instructional quality evaluation system based on DL

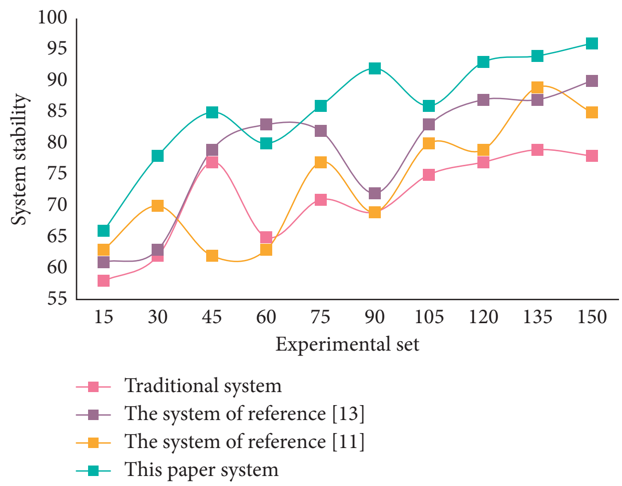

Figure 6: System stability test results.

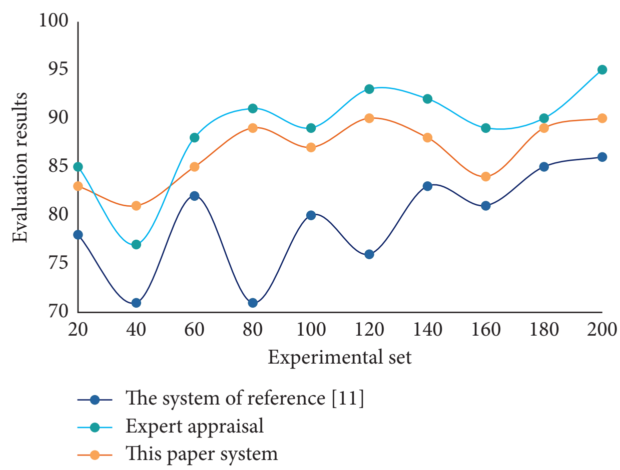

Figure 7: Comparison between different system evaluation results and expert evaluation results.

algorithm has the advantage of being able to analyze the existing problems in teaching and put forward suggestions for improving instructional quality.

5. Conclusions

With the continuous improvement of teaching levels and the rapid development of classroom instructional mode, the optimization of mathematics classroom instructional mode has become increasingly important in the process of instructional mode innovation. Mathematical instructional mode optimization has a distinct value and function. Teachers must update their teaching concepts, adopt various teaching strategies to promote the development of students' mathematical thinking, and develop students' thinking flexibility and creativity through the training of various mathematical exercises in order to continually optimize mathematics instructional mode and construct more efficient classroom teaching. Simultaneously, mathematics teachers should have a thorough understanding of how to optimize classroom teaching content in order to effectively improve the overall level of mathematics teaching through practice. The current state of mathematics instructional mode is examined in this paper, as well as the implementation strategy for mathematics classroom teaching optimization. Furthermore, the instructional quality evaluation system is based on the DL algorithm. This paper's system has a high level of intelligence. It can accurately assess instructional quality while also assessing problems in the teaching process based on the instructional quality scores and making reasonable suggestions for teaching improvement based on the weak links in the teaching process. The experimental results show that the system's stability is high, with a 96.37 percent stability rate and a 95.42 percent evaluation accuracy rate. This system has a high level of reliability and practical utility, and it can be used to develop a feasible scheme for evaluating instructional quality. The analysis and suggestion function of the instructional quality evaluation system proposed in this paper reflects the system's intelligence, reduces the workload of manually evaluating teachers' teaching effectiveness, and improves the operational efficiency of instructional quality evaluation. However, due to my limited knowledge and time, there are still some flaws in this paper's instructional quality evaluation system. The next step will be to discuss how to improve the system's efficiency without sacrificing accuracy.

Data Availability

The data used to support the findings of this study are available from the author upon request.

Conflicts of Interest

The author does not have any possible conflicts of interest.

References

[1] L. Yang, "Fuzzy cluster correlation mapping for online evaluation of teaching efficacy towards IoT study," *Cognitive Systems Research*, vol. 52, no. 12, pp. 365–370, 2018.

[2] J. Kong, C. Yang, Y. Xiao, and Q. Zhu, "A graph-related high-order neural network architecture via feature aggregation enhancement for identification application of diseases and pests[J]," *Computational Intelligence and Neuroscience*, vol. 2022, Article ID 4391491, 16 pages, 2022.

[3] L. Lili, "A mobile terminal-based college English teaching evaluation method," *Mathematical Problems in Engineering*, vol. 2022, Article ID 4566802, 9 pages, 2022.

[4] Z. Huang, Y. Liu, C. Zhan, and Y. Chen, "A novel group recommendation model with two-stage deep learning," *IEEE Transactions on Systems, Man, and Cybernetics: Systems*, In Press, 2021.

[5] M. Gao and J. Mao, "A novel active rehabilitation model for stroke patients using electroencephalography signals and deep learning technology," *Frontiers in Neuroscience*, vol. 1459, 2021.

[6] M. Zhao, A. Jha, Q. Liu et al., "Faster Mean-shift: GPU-accelerated clustering for cosine embedding-based cell segmentation and tracking," *Medical Image Analysis*, vol. 71, Article ID 102048, 2021.

[7] W. Gao, Y. Jiang, X. Gu, X. Ning, P. Qian, and T. Ni, "Hierarchical domain adaptation projective dictionary pair learning model for EEG classification in IoMT systems," *IEEE Transactions on Computational Social Systems*, vol. 1, pp. 1–9, 2022.

[8] Y. Ding, Z. Zhang, X. Zhao, and W. W. Cai, "Multi-feature fusion: graph neural network and CNN combining for hyperspectral image classification[J]," *Neurocomputing*, vol. 501, 2022.

[9] S. Sergis, D. G. Sampson, M. J. Rodriguez-Triana, and T. Jong, "Using educational data from teaching and learning to inform teachers' reflective educational design in inquiry-based STEM education[J]," *Computers in Human Behavior*, vol. 92, no. 3, pp. 724–738, 2017.

[10] R. Maulana, M. Helms-Lorenz, and V. van de Grift, "Pupils' perceptions of teaching behaviour: evaluation of an instrument and importance for academic motivation in Indonesian secondary education," *International Journal of Educational Research*, vol. 69, pp. 98–112, 2015.

[11] B. K. Choi and J. W. Kim, "The influence of student and course characteristics on monotonic response patterns in student evaluation of teaching in South Korea," *Asia Pacific Education Review*, vol. 15, no. 3, pp. 483–492, 2014.

[12] G. A. Boysen, "Uses and misuses of student evaluations of teaching," *Teaching of Psychology*, vol. 42, no. 2, pp. 109–118, 2015.

[13] E. Petraki, "Teaching oral requests: an evaluation of five English as a second language coursebooks[J]," *Pragmatics*, vol. 23, no. 3, pp. 499–517, 2013.

[14] M. Onozawa, "Critique of individualized teaching and evaluation: focused on small group learning with achievement levels and performance based evaluation (research project report 2)," *Journal of Educational Research*, vol. 11, pp. 155–164, 2014.

[15] Y. Liu, L. Han, J. Jiang, and X. Su, "The application and teaching evaluation of Japanese films and TV series corpus in JFL classroom," *The Electronic Library*, vol. 36, no. 4, pp. 721–732, 2018.

[16] A. Northrup, E. Berro, C. Spang, and M. Brown, "Teaching poverty: evaluation of two simulated poverty teaching interventions with undergraduate nursing students," *Journal of Nursing Education*, vol. 59, no. 2, pp. 83–87, 2020.

[17] W. A. Hall, "Consumerism and consumer complexity: implications for university teaching and teaching evaluation," *Nurse Education Today*, vol. 33, no. 7, pp. 720–723, 2013.

[18] E. R. Ottmar, S. E. Rimm-Kaufman, R. A. Larsen, and R. Q. Berry, "Mathematical knowledge for teaching, standards-based mathematics teaching practices, and student achievement in the context of the responsive classroom Approach," *American Educational Research Journal*, vol. 52, no. 4, pp. 787–821, 2015.

[19] K. Bhandari, "Teaching evaluation practices: an early career practitioner's reflections," *Journal of Hospitality, Leisure, Sports and Tourism Education*, vol. 20, pp. 27–31, 2017.

[20] J. B. Christman, C. B. Ebby, and K. Edmunds, "Data use practices for improved mathematics teaching and learning: the importance of productive dissonance and recurring feedback cycles," *Teachers College Record: The Voice of Scholarship in Education*, vol. 118, no. 11, pp. 1–32, 2016.

[21] J. Chen, C. Du, Y. Zhang, P. Wei, and W. Wei, "A clustering-based coverage path planning method for autonomous heterogeneous UAVs," *IEEE Transactions on Intelligent Transportation Systems*, vol. 208, pp. 1–11, 2021.

[22] Z. Huang and A. Pan, "Non-local weighted regularization for optical flow estimation," *Optik*, vol. 208, Article ID 164069, 2020.

[23] M. Gao, R. Liu, and J. Mao, "Noise robustness low-rank learning algorithm for electroencephalogram signal classification," *Frontiers in Neuroscience*, vol. 15, 2021.

Hindawi
Computational Intelligence and Neuroscience
Volume 2022, Article ID 6836524, 9 pages
https://doi.org/10.1155/2022/6836524

Research Article

Design of Drug Sales Forecasting Model Using Particle Swarm Optimization Neural Networks Model

Chenggong Yu

Zhejiang Pharmaceutical University, Ningbo 315000, China

Correspondence should be addressed to Chenggong Yu; 1441240335@xs.hnit.edu.cn

Received 25 April 2022; Revised 4 June 2022; Accepted 6 June 2022; Published 4 July 2022

Academic Editor: Xin Ning

The establishment of enterprise target inventory is directly related to the forecast of drug sales volume. Accurate sales forecasting can help businesses not only set accurate target inventory but also avoid inventory backlogs and shortages. In this paper, NN technology is used to forecast sales and is optimized using the PSO algorithm, resulting in the creation of a drug sale forecast model. The model optimizes the weights and thresholds of NN using the improved PSO optimization algorithm and predicts the periodic components based on time correlation characteristics, effectively describing the trend growth and seasonal fluctuations of sales forecast data. Furthermore, the model in this paper has been creatively improved according to the needs of practical application, which has improved the shortcomings of traditional NN, such as long training time, slow convergence speed, and ease to fall into local minima, to improve performance and quality, and has received positive results in application. The experimental results show that this model has a prediction accuracy of 96.14 percent, which is 12.78 percent higher than the traditional BP model. The optimized model can be used to forecast drug sales in a practical and feasible way.

1. Introduction

With the intensification of market competition, users of information systems are no longer satisfied with the fact that computers are only used for daily affairs, and they urgently need information that supports the decision-making process [1]. At the same time, in today's market, the market environment that enterprises face is so complicated and changeable as understanding the course, carrying out work actively and effectively, and making decisions are problems that an enterprise must solve [2]. The sales link, which connects suppliers, sellers, and consumers, is an important link in enterprise planning. The most important part of the sales process is sales forecasting, and most commodity circulation industries' supply chains have inventory and sales problems due to a lack of appropriate sales forecasting methods. The sales forecast is modeled using a set of highly complicated nonlinear systems that are manually defined [3]. One of the most important aspects of a company's sales plan, as we all know, is sales forecasting. It is inseparable from the planning of the future development direction, regardless of how large the company is or how complicated the sales staff is. However, because the future sales situation will inevitably and to a large extent influence the development direction, the sales forecast is almost an important pending event for enterprise managers and decision-makers related to the survival of enterprises. At present, many enterprises are still using traditional sales forecasting methods. Although the traditional sales forecasting method is widely used and the effect is good, it is difficult to deal with the complicated nonlinear relationship and various complicated influencing factors. Therefore, we need a new method [4]. Based on this, this paper will forecast and analyze the historical sales data of the sales department of the pharmaceutical group through PSONN (particle swarm optimization neural network) and provide some references for decision-makers in purchasing, selling, and storing drugs.

With the development of computer science, more and more researchers began to explore the use of artificial intelligence forecasting methods for medium and long-term load forecasting. At present, the most commonly used forecasting methods mainly include time series analysis, linear regression, nonlinear regression, grey forecasting, input-output forecasting, Markov forecasting, and ANN (Artificial neural network) [5–7] forecasting. Among several commonly used forecasting methods, the ANN forecasting method has attracted much attention in recent years. BPNN (backpropagation neural network) is a kind of commonly used ANN, which is used to train multilayer forward NN (neural network). BPNN contains the best part of NN theory, with a simple structure and strong plasticity. It adopts a Sigmoid type transfer function, and its learning mode is a multilayer feedforward network with minimum mean square error. There have been a lot of research studies on NN prediction [8, 9], but simply using NN to predict can no longer meet the real-time needs, and in the increasingly complex environment, more and more methods are needed to improve NN research. In this paper, the learning theory of PSOBPNN (particle swarm optimization backpropagation neural network) is used to establish an algorithm to predict the drug sales in the next year, and an optimization method is proposed for drug production, thus forming an effective drug production decision model. The innovations of this paper are as follows:

① This paper analyzes the difficulties in forecasting the sales volume of multivariety drugs in enterprises, the difficulties in the application of existing forecasting methods, and the advantages of the model in dealing with the problems and difficulties. To solve these problems, a BPNN learning algorithm is put forward. On this basis, PSOBPNN is used to forecast the sales data.

② In this paper, the PSO optimization algorithm is used to globally search the weights and thresholds of BPNN, and the optimized BPNN is used to establish a prediction model to predict the drug sales index. This model improves the shortcomings of traditional NN, such as long training time, slow convergence speed, ease to fall into a local minimum, and makes it have superior performance quality, and it has received good results in application.

2. Related Work

Prediction analysis is the process of speculating and predicting unknown future events based on known past and present events, as well as providing qualitative and quantitative descriptions of some uncertain factors and unknown events that may occur during the course of the predicted events. In general, an enterprise's sales forecast is the process of using past sales volume, sales amount, profit, and other indicators in the system to calculate future demand indicators using an algorithm mining model. Currently, a large number of academics are researching enterprise sales forecasting. The related literature of sales forecasting theory at home and abroad is discussed in this chapter, as are the benefits and drawbacks of various methods, as well as the research methods and ideas of this paper.

Arinaminpathy et al. proposed a method to build a data warehouse based on historical drug sales data and established a drug sales forecast model [10]. The improved NN by Yucesan et al. made self-calibration with reference to the prediction of synchronous time series and used a genetic algorithm to achieve self-optimization through calibration, simplifying the network structure [11]. Lian et al. took the preliminary prediction results as the input of the improved BPNN, then trained and predicted on this basis, and constructed a combined prediction model based on the improved BPNN [12]. Aiming at the characteristics of a company's drug sales, inventory, and the main problems in the sales process, Duan et al. proposed a hierarchical clustering model for multivariety drug sales forecast to predict the company's drug sales [13]. Russo et al. proposed a combinatorial optimization grey ANN model for seasonal load forecasting. The trend is predicted with a grey model; the seasonality is predicted with NN; finally, the optimal combination is carried out [14]. Aiming at some of the problems of BPNN, Curtis et al. added a momentum term to improve learning efficiency and avoid local minima [15]. Shibata et al. proposed a model for time series forecasting based on the discounted least-squares idea, and the discount is reflected in the constructed error function [16]. The discounted least squares error function biases the NN learning towards more recent observations and contemporaneous observations, while also taking into account long-term trends in the time series. Urquhart proposed an improved extreme learning machine algorithm combining batch processing and successive iterations and applied it in medium and long-term forecasting [17]. This method can improve the recognition performance of ANN in extension ability by continuously updating the training sample set. Ali and Pinar proposed two prediction models based on information fusion: one is a fusion model based on the weighted average of multiple models; the other is a fusion model that uses the advantages of various algorithms to complement each other [18]. Hassani et al. proposed an improved sales forecasting algorithm based on NN [19]. Stormi et al. studied the research on sales forecasting of the model combining NN, genetic algorithm, and PSO (particle swarm optimization) algorithm in intelligent algorithms [20].

Based on the previous research results on drug sales forecast, this paper puts forward a new research perspective and method. Because NN can approximate a nonlinear function with arbitrary precision, it can well establish the functional mapping relationship between sales volume and its various influencing factors. In this paper, using PSONN, a prediction model is constructed. A drug sales forecasting algorithm based on chaotic PSONN is proposed to improve the PSO algorithm. Inert particles tend to appear in the later stage of optimization and converge to the local optimal point prematurely. The simulation results show that the prediction effect of this model is better than that of the traditional NN model. The model and research method established in this paper are practical and effective, which not only simplifies the network structure and improves the convergence speed but also improves the prediction accuracy.

3. Methodology

3.1. NN Algorithm and Sales Forecast. ANN processor has the natural characteristics of storing and applying empirical knowledge, which is similar to that of the human brain. ANN is mainly trained by two learning algorithms, namely, the guided learning algorithm and nonguided learning algorithm. Among them, the representative BPNN is a multilayer feedforward network with hidden layers, which is a kind of error back propagation [21]. BPNN is a very effective intelligent forecasting method. Generally, BPNN is a multilayer feedforward NN, and its transfer function usually adopts the Sigmoid function. This algorithm consists of the forward transmission of information and the backward propagation of error. Its basic principle is to constantly revise the weights and thresholds of nodes at all levels in the network until the output of the network reaches the target output value, and it has good generalization ability. BPNN uses the error between the output response of the network to the learning signal and the expectation as the tutor signal and adjusts the network connection strength. Through repeated adjustments, the error is minimized, thus completing the learning process.

The learning process of BPNN is divided into two stages: ① input the known learning samples and calculate the output of each neuron backward from the first layer of the network through the set network structure and the weights and thresholds of the previous iteration; ② modify the weights and thresholds, calculate the influence of each weight and threshold on the total error from the last layer forward, and modify the weights and thresholds accordingly. Each neuron of NN can calculate and process independently according to the received information and then transmit the output results to other neurons for parallel processing. In the training process, as long as the input patterns are provided to NN, NN can automatically adapt to the connection weights, so that similar features can group the input patterns together. The sales forecast is an important part of the enterprise decision support system. The sales forecast is to take the purchase and sale of commodities in the market as the main object, to foresee and speculate on the changes in various purchase and sale activities, prices, and competitive conditions of commodities, and to take advantage of the situation and results. For the current sales industry, it is very important to forecast the sales of commodities [22], but the difficult problem is how to forecast the sales quickly and efficiently, but it is not easy. Traditional sales forecasting methods are mainly divided into qualitative sales forecasting methods and quantitative sales forecasting methods. In recent years, the quantitative sales forecasting method is widely used because of its objectivity and high interpretability [23]. In fact, the sales forecast of products can be regarded as a process of searching for "knowledge." It is mainly a process of fitting the forecast model and outputting the forecast results of sales through visual software based on the data information of related commodity sales in the past and converting the original and superficial information into the relevant "knowledge" we want. Since sales forecast is to forecast the future data demand by using the characteristics of historical data, it is an effective method to divide the data into historical data and future data at different time points and then to forecast the future data by exploring the characteristics of historical data. The conventional method has some limitations in nonlinear prediction. Recently, ANN has attracted people's attention. At present, many scholars use ANN to build sales forecast models. However, the traditional BPNN has some shortcomings, so it needs to be improved. The process of using PSOBPNN in this paper is shown in Figure 1.

The network parameters and size are related to the properties of NN used for prediction. The number of neurons, the number of hidden layers, and the connection mode are all part of the network structure. The training process for a given structure consists of adjusting the parameters to obtain an approximate basic relation. The root mean square error is used to define the error, and the training process can be thought of as an optimization problem. PSO is a population-based optimization method in which the population is referred to as a particle swarm and the individual is referred to as a particle. Its basic concept is based on the simulation of seabird predation behavior, such as that of seagulls. PSO outperforms traditional random methods in terms of simplicity, ease of implementation, global optimization ability, and computing speed [24]. The position of the particle in the basic PSO algorithm represents the potential solution of the optimized problem in the search space. The optimized function determines the fitness value of each particle, and each particle has a speed that determines its flying direction and distance. Particles search the solution space by following the current best particle. Each particle state is a possible solution to the optimization problem and a fitness value determined by the objective function to be optimized in the algorithm's search space. PSO has a number of advantages, including ease of implementation, a small number of parameters to adjust, quick convergence, and low computational requirements. It has been widely used and has been proven to be an effective method for solving many global optimization problems.

3.2. Construction of Drug Sales Forecast Model of PSONN. Sales forecasting is a highly complex nonlinear system, and the modeling of sales forecasting needs the guidance of many theories, including mathematical statistics theory, artificial intelligence theory, economic theory, and nonlinear dynamics theory. In this section, PSONN is used to build a drug sales forecasting model. In this method, the weights and thresholds of BPNN are trained by PSO, the hidden rules can be automatically extracted from massive data by NN, and the advantages of global search and fast convergence of PSO are integrated to predict the economic indicators. The process of drug sales forecast based on PSONN is shown in Figure 2.

All of the weights of connections between neurons are encoded as real vectors, which are used to represent individuals in the population. The original steps of the algorithm are used to generate groups of these vectors at random and iterate them. The mean square deviation of all NN-generated

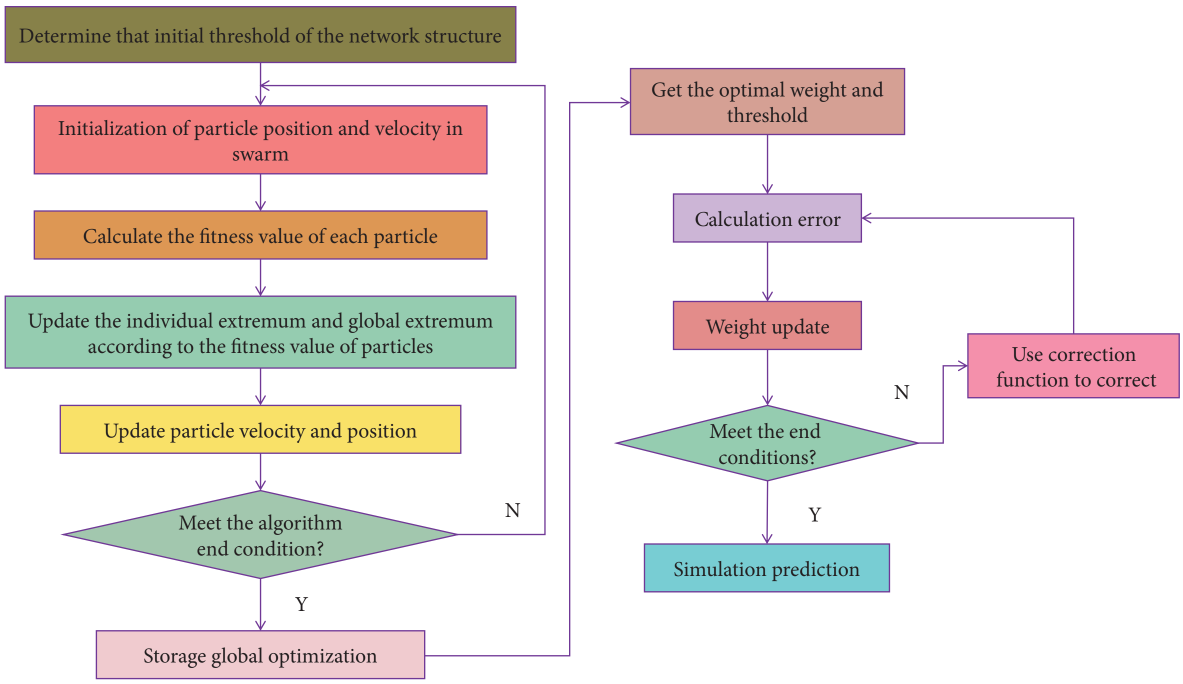

Figure 1: Flow chart of BPNN.

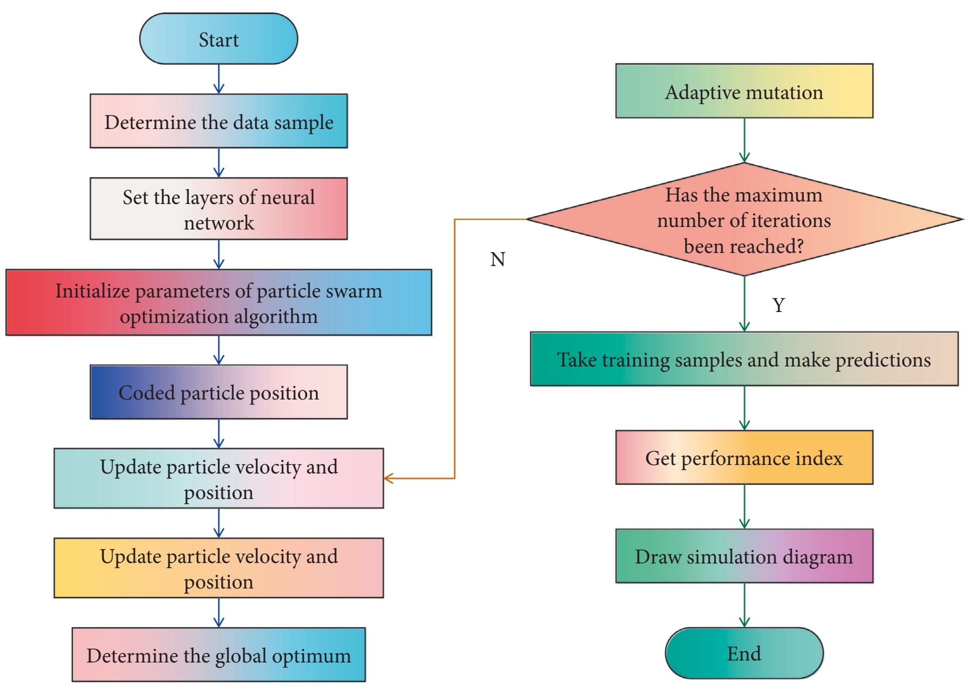

Figure 2: Flow chart of drug sales forecast based on PSONN.

samples is calculated after the newly generated individual vectors in the iteration are reduced to NN weights. The training process is stopped if it is less than the system-specified error; otherwise, it is continued until the maximum number of iterations is reached. The error information is returned according to the original route during the backward propagation process, and the weights and thresholds of NN are corrected according to the learning rules. The forward propagation process is then performed, and the two processes are repeated until the actual training output of all training samples falls within a certain error range when compared to the expected output.

The emphasis of BPNN is network error and weight adjustment. When the network output is not equal to the expected output, there is an output error E, which is defined as follows:

$$E = \frac{1}{2}(d-o)^2 = \frac{1}{2}\sum_{k=1}^{l}(d_k - o_k)^2. \quad (1)$$

Expand the above error definition to the hidden layer as follows:

$$\begin{aligned} E &= \frac{1}{2}\sum_{k=1}^{l}\left[d_k - f(\mathrm{net}_k)\right]^2 \\ &= \frac{1}{2}\sum_{k=1}^{l}\left[d_k - f\left(\sum_{j=0}^{m} w_{jk} y_i\right)\right]^2. \end{aligned} \quad (2)$$

Expand further to the input layer as follows:

$$\begin{aligned} E &= \frac{1}{2}\sum_{k=1}^{l}\left[d_k - f\left(\sum_{j=0}^{m} w_{jk} y_i\right)\right]^2 \\ &= \frac{1}{2}\sum_{k=1}^{l}\left\{d_k - f\left[\sum_{j=0}^{m} w_{jk} f\left(\sum_{i=0}^{n} v_{ij} x_i\right)\right]^2\right\}. \end{aligned} \quad (3)$$

It can be seen from the above formula that the network input error is a function of the weights w_{jk} and v_{ij} of each layer, so the weights can change the error E.

In this paper, we first consider setting up only one hidden layer. When the number of hidden nodes in a hidden layer is too large to improve the network performance, we only consider adding another hidden layer. We determine the predetermined error requirements, the maximum allowed iteration steps, the search range, the maximum speed, and the number of particles according to the network scale. In order to avoid the phenomenon of weight oscillation and slow convergence in the learning process, it is necessary to consider the influence of the previous weight change on the current weight change and add the momentum factor.

Given the original data sequence with variable $x^{(0)}$,

$$x^{(0)} = \left[x^{(0)}(1), x^{(0)}(2), \ldots, x^{(0)}(n)\right]. \quad (4)$$

Generate a first-order cumulative generation sequence as follows:

$$x^{(1)} = \left[x^{(1)}(1), x^{(1)}(2), \ldots, x^{(1)}(n)\right]. \quad (5)$$

Among them,

$$x^{(1)}(k) = \sum_{i=1}^{k} x^{(0)}(i). \quad (6)$$

Since the sequence $x^{(1)}(k)$ has an exponential growth law and the solution of the first-order differential equation is exactly the solution of the exponential growth form, it can be considered that the $x^{(1)}$ sequence satisfies

$$\frac{\mathrm{d}x^{(1)}}{\mathrm{d}t} + ax^{(1)} = u. \quad (7)$$

In the formula, α and u are parameters and u is called the control term. The solution to this differential equation is

$$x^{(1)}(k+1) = \left[x^{(0)}(1) - \frac{\widehat{u}}{\widehat{\alpha}}\right]e^{-\widehat{\alpha}k} + \frac{\widehat{u}}{\widehat{\alpha}}, \quad (8)$$

where $\widehat{\alpha}$ and $\widehat{u}$ are approximate solutions of equation (7).

When learning BPNN, the initial value of its weight is very important. If the initial value is too large or too small, it will affect the learning speed, which is a complicated process of parameter system optimization. In this paper, the weights are coded by real numbers, the initial weights are set to random numbers, each particle represents the initial distribution of weights of NN, and the maximum speed limit of particles is set. We set the number of neurons in the input layer, hidden layer, and output layer of the NN. The connection weights w_{ij} and w_j to be optimized, the scaling factor a_j, and the translation factor b_j are taken as the position vector of each particle, which is

$$\mathrm{present}(m) = \left[w_{ij}, w_j, a_j, b_j\right]. \quad (9)$$

Among them, m is the number of particle swarms. We calculate the initial fitness value as follows:

$$F = \sum_{i=1}^{n}\left|y_i - h_i\right|. \quad (10)$$

We update the record that each particle has searched for the best position so far and the global search for the best position. The fitness function is the absolute sum of the prediction errors of the NN. n is the total number of network output nodes, y_i is the predicted output of the i th node, and DD is the expected output of the h_i th node. In this section, PSO is introduced, and by using its good algorithm convergence, the problem can converge to the global optimal solution or suboptimal solution with high probability, which solves the local convergence problem of BPNN itself. At the same time, the weights and thresholds of BPNN can be optimized, and the accuracy of BPNN in economic index prediction can be improved.

4. Result Analysis and Discussion

This section will introduce the data testing scheme and design process of the PSONN prediction model in detail. It will also test the model through actual data sets and compare it with other commonly used and similar models. The experimental results are discussed and analyzed. In this paper, Matlab software is used for simulation and prediction. Firstly, we design the structure and parameters of the network. The parameters to be determined in this paper are the number of nodes in the input layer and output layer of the network, the number of hidden layers, the number of nodes in hidden layers, the initial weights, etc. We set the number of nodes in the middle layer to 25, the hidden layer of the model to 30, and the weight learning rate to 0.2. The number of neurons in the input layer is 10, and the number of neurons in the output layer is 1. When the number of hidden neurons is 16, the model has the best prediction effect. We initialize the parameters of the PSO algorithm, with iteration times of 200 and a population number of 30. We take the sales data of a pharmaceutical company in 2019 as the original test data. The data are classified into training sample data and test data. Three terms of "sales time," "commodity number," and "sales quantity" are extracted from the test data, and the original sales details data are preliminarily screened and then summarized. The results are shown in Table 1.

In this paper, the original data are normalized, that is, the input and output data are uniformly limited to [0, 1] or [−1,1] by a certain linear transformation. The normalization process makes the drug sequences with different units and dimensions mapped into the [0,1] interval, which eliminates the influence of different dimensions on the input data and speeds up the training speed of NN and its related algorithms. The PSONN model is tested by using the preprocessed drug sales series. A simple mutation operator is added to reinitialize the particles with a certain probability, and the optimization is carried out by cyclic iteration until the maximum number of iterations is reached, and the optimal individual fitness value is recorded. The variation process of the optimal individual fitness value in the optimization process based on the adjusted inertia weight PSONN is shown in Figure 3.

From Figure 3, it can be seen that the PSO algorithm has a strong optimization ability, and the optimization of the algorithm is faster at the initial stage of iteration. Through the construction and testing of the model proposed in this paper, the AdaBoost-BP model and AdaBoost-ELM model, the prediction accuracy of each drug, the average accuracy of all drugs, and the total running time of the three models are obtained. Figure 4 shows the comparison of prediction accuracy of different models. Figure 5 shows the running time comparison of different models.

As can be seen from Figure 4, the sales forecasting accuracy of this model is higher than that of the other two models, and it is at a high level. The prediction accuracy of this model can reach 96.14%, which is about 12.78% higher than that of the traditional BP model. From the analysis of Figure 5, it can be seen that the running time of this model is short and its efficiency is high. Therefore, the sales forecasting method based on PSONN proposed in this paper has certain superior performance and has certain reliability and practicability.

The connection weights and thresholds are fixed in the prediction knowledge base. At this time, the whole NN is a time series prediction model, and the performance of the model is tested by test samples. The prediction error defined in this paper is the difference between the predicted value and the actual value. Figure 6 shows the error comparison of different models.

It can be seen that, on the whole, the error rate of this model is at a low level, indicating that the accuracy of this method is high. Table 2 shows the specific situation of the corresponding predicted performance indicators.

It can be seen from the data in the table that the overall trend between the predicted value and the actual value is consistent, which indicates that it is feasible to forecast the drug sales based on PSONN. The simulation diagram of drug sales forecast based on PSONN and traditional BPNN is shown in Figure 7.

Table 1: Summary of original sales details data.

Sales time	Commodity number	Sales volumes
2019-01	23769	758
2019-02	13875	544
2019-03	36974	721
2019-04	25897	473
2019-05	23521	130
2019-06	13267	167
2019-07	53679	871
2019-08	89732	165
2019-09	13078	746
2019-10	75890	752
2019-11	18970	546
2019-12	57698	655

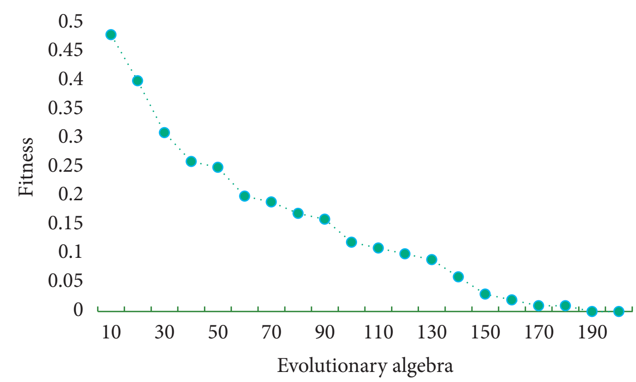

Figure 3: PSO process of adjusting inertia weight.

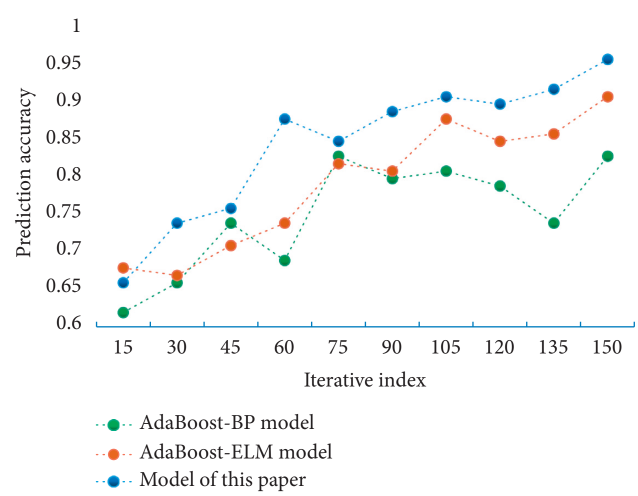

Figure 4: Comparison of prediction accuracy of different models.

It can be seen from the prediction chart that the predicted value based on PSONN is closer to the actual value, and its prediction effect is better than that of traditional BPNN. It shows that the improved algorithm is better than the traditional prediction model. A large number of experimental results in this chapter show that the NN sales forecasting model optimized by PSO can achieve 96.14% forecasting accuracy, which is about 12.78% higher than the

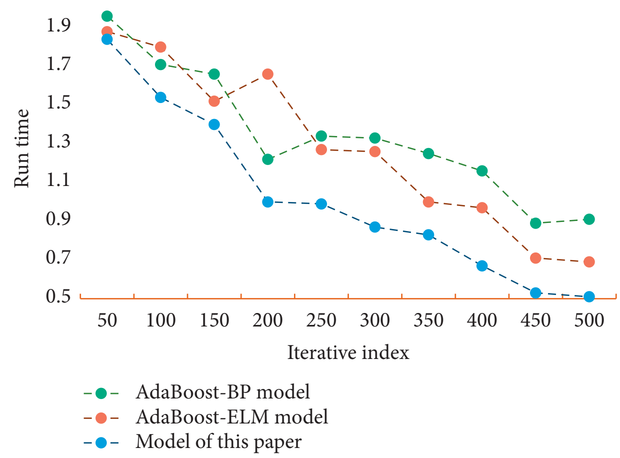

Figure 5: Comparison of running time of different models.

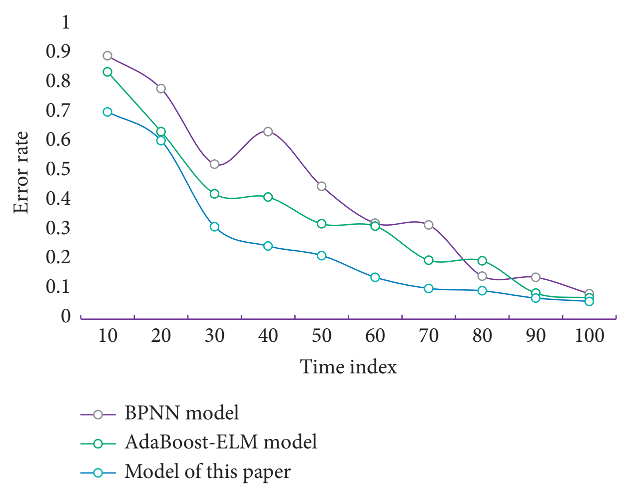

Figure 6: Error comparison of different models.

Table 2: Comparison of evaluation indexes of different methods.

Method	Mean square error	Mean absolute error	Average absolute percentage error	Mean square percentage error
Traditional BPNN	18.692	3.217	0.0814	0.0169
AdaBoost-ELM	13.417	2.136	0.0689	0.0132
Support vector machine	14.685	2.987	0.0897	0.0187
PSONN in this paper	12.374	2.054	0.0657	0.0124

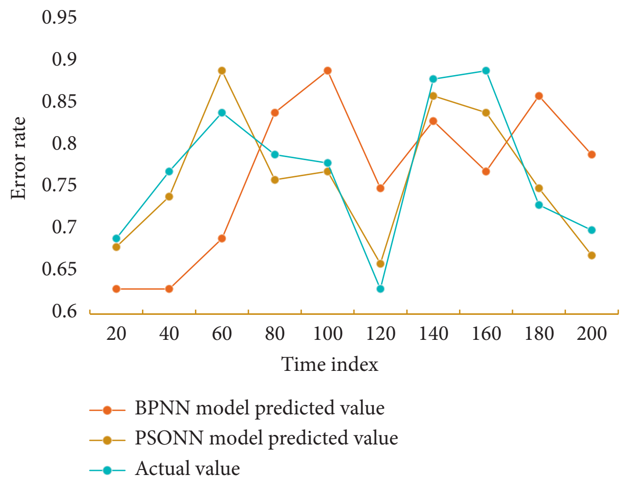

Figure 7: Simulation diagram of the drug sales forecast.

traditional BP model. Using PSO instead of the traditional training method of gradient descent of NN improves the dilemma that NN easily falls into the minimum value, improves the convergence speed, and makes the model have a certain superior performance.

5. Conclusions

The sales link, which connects suppliers, sellers, and consumers, is an important link in enterprise management. The most important part of the sales process is sales forecasting, and most commodity circulation industries' supply chains have inventory and sales problems due to a lack of appropriate sales forecasting methods. ANN has some advantages in dealing with nonlinear problems because it can cluster and learn from a large amount of historical data and then find some rules of behavior changes. As a result, the BPNN model is chosen as the basic forecasting model for drug sales forecasting, as it is the most widely used among the NN models. PSO is used to overcome the drawbacks of traditional NN, such as long training times, slow convergence speeds, and the ease with which it falls into local minima, resulting in improved performance. Experiments show that the PSO-optimized NN sales forecasting model can achieve a forecasting accuracy of 96.14 percent, which is about 12.78 percent higher than the traditional BP model. This model addresses traditional NN's flaws, such as long training times, slow convergence speeds, and a proclivity to fall into local minima, among others, and improves performance quality, yielding positive results in practice. The research shows that the forecasting method presented in this paper has a better forecasting effect on drug sales forecasting and that using the optimized model presented in this paper to forecast drug sales is practical and feasible. It is a good starting point for creating a prediction model for other problems. Although this model's prediction accuracy and run time have clearly improved, it still has some limitations. PSONN and particle swarm improvement have randomness, which makes prediction stability poor. In addition, the model comparison does not include the testing of some algorithms related to sales forecasting in this paper. I hope that the optimization algorithm will be further investigated in future work and research and that the algorithm's stability will be improved, resulting in a more perfect and reasonable model.

Data Availability

The data used to support the findings of this study are available from the corresponding author upon request.

Conflicts of Interest

The author declares that there are no conflicts of interest.

Acknowledgments

This study was supported by the 2020 Zhejiang Philosophy and Social Science Planning Project (20NDJC221YB): Research on Collaborative Governance Path of High-Quality Development of Drugs in Zhejiang Province under Big Data Strategy.

References

[1] Y. Zhang, "Application of improved BP neural network based on e-commerce supply chain network data in the forecast of aquatic product export volume," *Cognitive Systems Research*, vol. 57, no. 10, pp. 228–235, 2019.

[2] X. Yu, Z. Qi, and Y. Zhao, "Support vector regression for newspaper/magazine sales forecasting," *Procedia Computer Science*, vol. 17, pp. 1055–1062, 2013.

[3] L. C. Kung and Y. J. Chen, "Impact of reseller's and sales agent's forecasting accuracy in a multilayer supply chain," *Naval Research Logistics*, vol. 61, no. 3, pp. 207–222, 2014.

[4] Y. Liu, Y. Hu, W. Cai, J. Zhan, and L. Liujun, "DCCAM-MRNet: mixed residual connection network with dilated convolution and coordinate attention mechanism for tomato disease identification," *Computational Intelligence and Neuroscience*, vol. 2022, Article ID 4848425, 15 pages, 2022.

[5] J. Zhang, J. Sun, J. Wang, and X.-G. Yue, "Visual object tracking based on residual network and cascaded correlation filters," *Journal of Ambient Intelligence and Humanized Computing*, vol. 12, no. 8, pp. 8427–8440, 2021.

[6] G. Xie, L. Huang, H. Bin, and C. Apostolidis, "Sustainable entrepreneurship in rural E-commerce: identifying entrepreneurs in practitioners by using deep neural networks approach," *Frontiers in Environmental Science*, vol. 10, p. 370, 2022.

[7] Y. Ding, Z. Zhang, X. Zhao, N. Yang, and W. W. Cai, "Multi-feature fusion: graph neural network and CNN combining for hyperspectral image classification," in *Neurocomputing*, vol. 501, press, 2022.

[8] X. B. Jin, W. T. Gong, J. L. Kong, Y. T. Bai, and T. L. Su, "PFVAE: a planar flow-based variational auto-encoder prediction model for time series data," *Mathematics*, vol. 10, no. 4, p. 610, 2022.

[9] X. Jin, J. Zhang, J. Kong, Y. Su, and T. Bai, "A reversible automatic selection normalization (RASN) deep network for predicting in the smart agriculture system," *Agronomy*, vol. 12, no. 3, p. 591, 2022.

[10] N. Arinaminpathy, D. Batra, S. Khaparde et al., "The number of privately treated tuberculosis cases in India: an estimation

from drug sales data," *The Lancet Infectious Diseases*, vol. 16, no. 11, pp. 1255–1260, 2016.
[11] M. Yucesan, M. Gül, and E. CelikGul, "Performance comparison between ARIMAX, ANN and ARIMAX-ANN hybridization in sales forecasting for furniture industry," *Drvna Industrija*, vol. 69, no. 4, pp. 357–370, 2018.
[12] H. Lian, B. Liu, and P. Li, "A fuel sales forecast method based on variational Bayesian structural time series," *Journal of High Speed Networks*, vol. 27, no. 1, pp. 1–22, 2021.
[13] Z. Duan, B. Gutierrez, and L. Wang, "Forecasting plug-in electric vehicle sales and the diurnal recharging load curve," *IEEE Transactions on Smart Grid*, vol. 5, no. 1, pp. 527–535, 2014.
[14] A. Russo, P. G. Lind, and F. Raische, "Neural network forecast of daily pollution concentration using optimal meteorological data at synoptic and local scales," *Atmospheric Pollution Research*, vol. 6, no. 3, pp. 540–549, 2015.
[15] A. Curtis, R. J. Lundholm, and S. E. Mcvay, "Forecasting sales: a model and some evidence from the retail industry," *Contemporary Accounting Research*, vol. 31, no. 2, pp. 581–608, 2014.
[16] S. Shibata, R. Uemura, and T. Suzuki, "Evaluating the effectiveness of repricing for market expansion in the Japanese drug pricing system," *Therapeutic Innovation & Regulatory Science*, vol. 50, no. 6, pp. 751–758, 2016.
[17] L. Urquhart, "Top companies and drugs by sales in 2021," *Nature Reviews Drug Discovery*, vol. 21, no. 4, p. 251, 2022.
[18] O. G. Ali and E. Pinar, "Multi-period-ahead forecasting with residual extrapolation and information sharing—utilizing a multitude of retail series," *International Journal of Forecasting*, vol. 32, no. 2, pp. 502–517, 2016.
[19] H. Hassani, Z. Ghodsi, R. Gupta, and M. Segnon, "Forecasting home sales in the four census regions and the aggregate US economy using singular spectrum analysis," *Working Papers*, vol. 49, no. 1, pp. 1–15, 2014.
[20] K. Stormi, T. Laine, P. Suomala, and T. Elomaa, "Forecasting sales in industrial services," *Journal of Service Management*, vol. 29, no. 2, pp. 277–300, 2018.
[21] C. O. Yeru, J. Choy, and L. Cheong, "Demand forecasting using a growth model and negative binomial regression framework," *RSC Advances*, vol. 4, no. 3, p. 1163, 2013.
[22] W. Cai, Y. Song, and Z. Wei, "Multimodal data guided spatial feature fusion and grouping strategy for E-commerce commodity demand forecasting," *Mobile Information Systems*, vol. 2021, 2021.
[23] D. Yang and A. N. Zhang, "Impact of information sharing and forecast combination on fast-moving-consumer-goods demand forecast accuracy," *Information*, vol. 10, no. 8, p. 260, 2019.
[24] M. Zhao, A. Jha, Q. Liu et al., "Faster Mean-shift: GPU-accelerated clustering for cosine embedding-based cell segmentation and tracking," *Medical Image Analysis*, vol. 71, Article ID 102048, 2021.

Hindawi
Computational Intelligence and Neuroscience
Volume 2022, Article ID 4703975, 10 pages
https://doi.org/10.1155/2022/4703975

Research Article

Higher Education Management and Student Achievement Assessment Method Based on Clustering Algorithm

Zhihui Wang

Huanghe S&T University, Zhengzhou 450005, China

Correspondence should be addressed to Zhihui Wang; 201772476@yangtzeu.edu.cn

Received 23 April 2022; Revised 17 May 2022; Accepted 18 May 2022; Published 4 July 2022

Academic Editor: Xin Ning

Monitoring and guiding instructional management require student performance evaluation. Traditional evaluation and analysis methods based on absolute scores, on the other hand, have certain flaws and are unable to fully reflect the information contained in student performance, thus limiting the impact of student performance evaluation on teaching and learning management. Data mining is regarded as the backbone technology for future information processing, and it introduces a new concept to the way humans use data. Schools must analyse and evaluate the performance of students in the same grade level and secondary school in a timely and staged manner. Clustering is a type of data mining that uses similarity rules to classify sample data into groups with a high degree of similarity. To address the difficulties caused by the wide variation in course difficulty in student performance evaluation, a method based on the *K*-means clustering algorithm is proposed. The *K*-means algorithm and the improved K-means algorithm with student information are investigated. The test results showed that the *K*-means clustering algorithm, the improved algorithm in this paper, and the fast global mean clustering algorithm all cluster the same randomly generated data set with noisy points, but the clustering time of the algorithm in this paper is only 0.04, which has obvious advantages. As a result, the clustering algorithm-based higher education management and student performance evaluation mechanism provides some insights for future research on student learning patterns. It is hoped that instructional administrators will gain a better understanding of students' learning characteristics so that they can better guide their teaching.

1. Introduction

Humans have greatly improved their ability to collect, process, organise, and produce information using information technology as the world moves toward an information society [1]. This has resulted in the creation of tens of thousands of databases of various types, all of which play an important role in scientific research, technology development, production management, market expansion, business operations, government offices, and other areas [2, 3]. Schools now have a variety of systems and databases that collect a large amount of data on the student achievement. Staff can only obtain a small amount of information through simple statistics of Excel tools due to a lack of relevant mining knowledge and technology, and the information hidden in these large amounts of data cannot be applied [4]. The globalised information reserve is expanding, and the amount of information available to people is expanding as well [5]. However, people's thirst for knowledge grows as they learn how to quickly find the information they need from such a vast amount of data [6].

However, there are some issues with evaluating teaching quality in universities in general. Traditional teaching quality evaluation methods have a number of flaws, and the results obtained are not scientific or accurate enough [7]. Various systems and databases are used by universities to collect large amounts of data [8]. Through a series of scientific and systematic evaluations, the primary goal of evaluation is to encourage universities to optimise their own resources, improve efficiency, improve academic research and talent training quality, and realise the social functions of universities [9]. Higher education management is a critical aspect of higher education operations, as it is linked to the quality and efficiency of the institution [10]. Data structure can be classified without prior classification using the cluster analysis method, revealing the inherent differences and connections of objective things [11]. Massive data analysis can provide useful guidelines for business management, project development, Internet finance, and efficient scientific research, allowing data resources to be fully utilised [12].

There are several clustering methods available, the most basic of which is partitioned clustering [13, 14]. Partitioned clustering tries to divide a data set into disjoint subsets in order to find the best clustering criteria. Researchers have divided clustering analysis into four categories to address these specific practical issues: partition-based methods, hierarchical methods, density-based methods, and grid-based methods [15]. Clustering algorithms are an important step in the modernization of education, which promotes the cultivation of innovative talents and improves the quality of all people. It completes the digital network automation of educational teaching management, campus life management, and other activities, encourages the growth of the educational information industry and the effective use of educational big data, and gradually develops an innovative educational management model that adapts to the needs of social informatization. Among them, the K-means algorithm is a traditional clustering algorithm based on division that performs clustering through continuous iteration. When the algorithm reaches the end condition, the iterative process is completed and the clustering results are output. The following are the paper's unique features. (1) In this study, data mining technology [16] is used to analyse students' academic performance data using fuzzy clustering, and "teaching" and "learning" are organically combined. (2) We can identify a number of undesirable phenomena in teaching activities, judge whether the teaching methods are reasonable, consider whether existing teaching theories can support classroom teaching, and assist in the development of teaching theories by evaluating classroom teaching quality. (3) Analyzing higher education management and student performance evaluation mechanisms using clustering algorithms. Data mining techniques can be used to describe and classify data, predict future behaviors and trends, and solve the time-consuming problem of traditional data analysis.

2. Related Work

2.1. Higher Education Management and Student Achievement Evaluation. Exams and teaching are inextricably linked in school education, and exam results are crucial in determining how well the students learn. Colleges and universities frequently use the average or total score as the grade standard when evaluating the general qualifications of students. This evaluation method is simple and easy to use in real-world teaching feedback, but it ignores the singularity and one-sidedness of the evaluation results caused by the test paper difficulty. As a result, we should investigate the current state of academic achievement evaluation in China's secondary schools, use data mining technology to investigate models and methods suitable for secondary school academic achievement analysis and comprehensive evaluation, and infuse new thinking into secondary school education quality comprehensive evaluation reform.

Omar's academic achievement evaluation should pay special attention to the process evaluation, which is a dynamic evaluation. It should not only be the evaluation of learning achievement, but should include learning attitude, behavior, and habit in the evaluation system. Li et al. judged from three aspects of evaluation view, evaluation method, and evaluation process, and proposed the evaluation model of two-way evaluation subject, comprehensive evaluation method, and multi-way evaluation perspective [17]. Goh et al.'s school uses test scores to evaluate students in a single way, which causes valuable data resources of wasting. It is recommended to use better models and software to analyse the scores [18]. Omolewa et al. analysed evaluation activities in terms of pedagogical elements and constructed a new evaluation model in terms of objectives, form, and content [19]. Wiechetek and Pastuszak argue that the evaluation of students' academic performance should tend to be diversified, focusing not only on their creativity, but also on their behavioral habits and values [20].

Through the comprehensive evaluation of students' academic performance, we can identify the gaps between students and classes, and then recognize the differences between the level of discipline teachers' teaching and classroom management of classroom teachers, so as to guide the next stage of discipline teaching and classroom management more effectively. In addition, through the analysis and comparison of various types of students' performance, corresponding improvement suggestions are given, which provide a theoretical basis for students' performance evaluation, personalized development and teachers' differentiated teaching.

2.2. Clustering Algorithm. Evaluation is an important tool for assessing and monitoring educational quality, as well as guiding teachers' teaching practices and encouraging students to pursue learning. Traditional performance analysis methods, on the other hand, are unable to objectively and accurately reflect the relative distribution of students' performance and the classification of their learning situation. It can only perform statistical analysis on the scores and knowledge points on candidates' test papers, and it cannot mine and analyse large amounts of data from the remote examination system well. If we are to make full use of the vast amount of data accumulated in the past and dig them out, we must first understand the characteristics of students' learning. We can analyse these academic performance data in depth as school administrators, classroom teachers, and subject teachers, discarding the "criticism" brought on by traditional performance ranking and exploring the data's value in providing powerful support for the implementation of the education strategy of "teaching according to students' abilities"

Davenport constructed a variable precision rough set model based on relational algorithms and performed a preliminary analysis of student performance [21]. Anoopkumar and Rahman et al. proposed a nonparametric clustering method for categorical attribute data, which became the K-modes-CGC algorithm, similar to the traditional K-means algorithm for

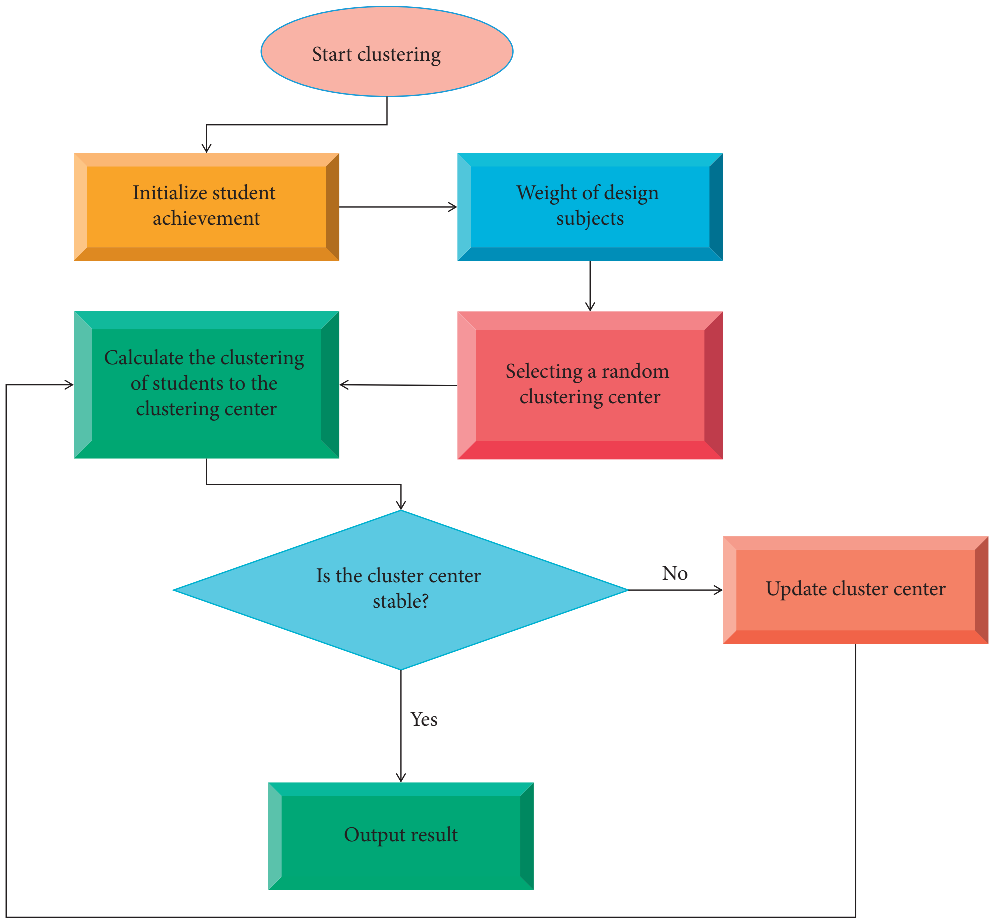

Figure 1: K-means algorithm studies the process of students' achievement.

numerical data [22]. Mayureshwar et al. used data mining techniques for distance learning in educational systems. In a distance personalized learning system, resources can be allocated for the individual learning needs of the students [23]. The Weka tool built by Belan Velasco et al. integrates various data mining algorithms into an interactive interface, which includes a variety of data preprocessing, categorization, degradation, regression, clustering, correlation rules, and optimization [24].

The process of teaching informatization has produced a vast volume of educational data, and these valid records are a reliable support for us to carry out the next stage of data mining. Clustering to several classes or clusters of data objects enables high similarity among objects in the identical clusters, but with significant differences among objects in various clusters. Through aggregation, one can identify dense and sparse regions, and discover global distribution patterns and interesting relationships among data attributes.

3. Thoughts on Higher Education Management and Student Achievement Evaluation Based on Clustering Algorithm

3.1. Performance Evaluation Scheme Based on Clustering Algorithm. Student performance evaluation is a kind of educational evaluation, a key link and important element of teaching and instructional management, and the most important source of information for teaching quality evaluation. Clustering analysis, as an exploratory analysis method, is widely used in pattern recognition [25, 26], computer vision [27, 28], data mining, and other fields. Its purpose is to divide a physical or abstract set of objects into several subsets based on the principle of similarity, and analyse the intrinsic connections, patterns, and characteristics of data objects within each subset. The sum of data corresponding to each clustering element is calculated by dividing the data of each element by the sum of data of this element, i.e.,

$$x'_{ij} = \frac{x_{ij}}{\sum_{i=1}^{m} x_{ij}}, \ (i = 1, 2, \ldots, m; \ j = 1, 2, \ldots, n). \tag{1}$$

Scientific evaluation of students' learning performance can help teachers and parents to grasp students' learning, and teachers and parents can make corresponding adjustments to the teaching and supervision of students' learning based on the evaluation results. The flowchart of studying student performance with K-means algorithm is shown in Figure 1.

The first step is data collection. In order to ensure the completeness and accuracy of the data, the original data sources must be well selected and organised. The original data source is input and with the participation of experts, it is decided which attribute features to use to describe the nature

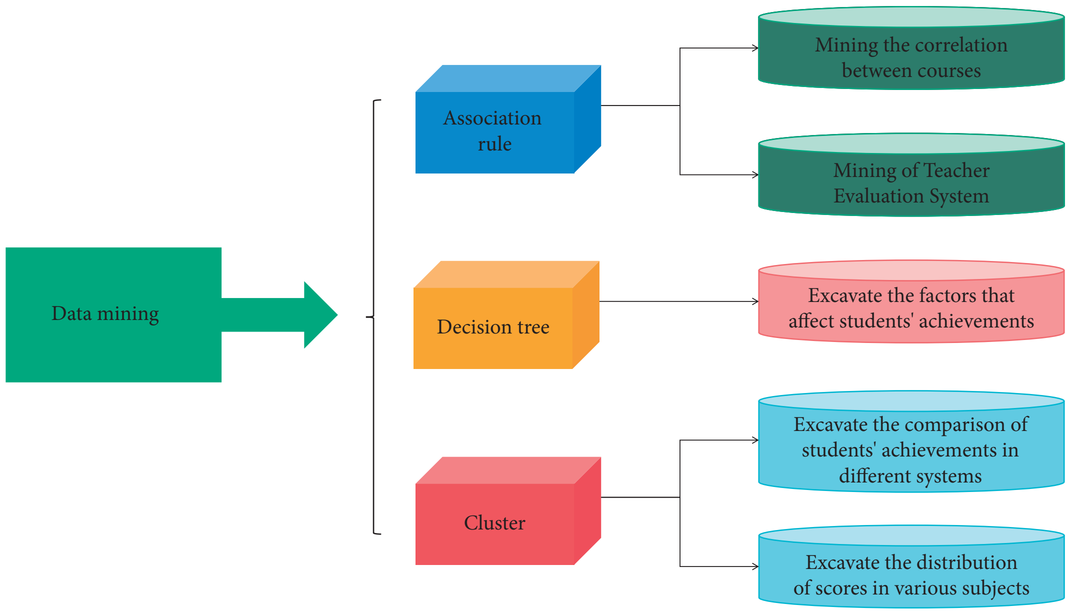

Figure 2: Data mining process.

and structure of the data source. Feature extraction outputs a matrix where each row represents a sample and each column represents a feature index variable. The new data obtained by this normalization has a maximum value of 1 for each element and all other values are less than 2. Therefore, the normalization is poor, i.e.,

$$x_{ij} = \frac{x_{ij} - \min(x_{ij})}{\max(x_{ij}) - \min(x_{ij})}, \; (i = 1, 2, \ldots, m; \; j = 1, 2, \ldots, n). \tag{2}$$

The representative data among them are extracted, and these extracted data are what are normally called sample data in data-related work [29]. Each data object is considered as a point in the d dimensional space, and then a certain distance is used to represent the similarity between the data objects. Data objects that are closer are similar in nature, while data objects that are farther away are very different. This is a phase of great workload and time. The data mining process is shown in Figure 2.

Next is data preprocessing, through the four steps of data review, data cleaning, data conversion, and data verification, the data is preprocessed to resolve data conflicts and data inconsistencies, and finally form student reports. The most commonly used clustering standard function, the error sum of squares, is applicable to all sample distributions with dense samples and small differences in sample size:

$$J_c = \sum_{j=1}^{c} \sum_{k=1}^{n_j} \left\| x_k - m_j \right\|_2. \tag{3}$$

The quality of data mining results will be adversely affected if the data input to the database has anomalous data, irrelevant fields, or even conflicting fields, improper data coding methods, and other anomalies [30, 31]. The sample matrix extracted in the first step is input to the clustering, and the individual sample is imagined as a point in the feature variable. The mean squared deviation is generally used as the standard measure function and is defined as follows:

$$E = \sum_{i=1}^{k} \sum_{p e C_i} \left| p - m_i \right|_2. \tag{4}$$

Since there are many indexes in the raw data, each index may have different dimensions and orders of magnitude. If the calculation is done directly using the raw data, it is likely that a large number of indexes will directly affect the clustering results. By definition, those data that are not suitable for training and learning are extracted from the sample data and excluded from the system. It should be noted that these data that need to be cleaned up generally refer to incomplete data. To accommodate the introduction of fuzzy partitioning [32, 33], the affiliation matrix allows the elements to have values between 0 and 1. However, using the normalization rules, the sum of the affiliations of the data set is always equal to 1:

$$\sum_{i=1}^{c} u_{ij} = 1, \forall j = 1, \ldots, n. \tag{5}$$

Finally, after performing the clustering algorithm to determine the mining task, the K-means clustering algorithm is written in matlab to implement the processing of the student achievement analysis. If the form of data used for mining does not match the characteristics of mining and they are necessary, in the face of this situation, what needs to be done is data conversion, conversion of display formats or coding formats, etc. After obtaining the clustering spectrum map in the second step, the expert can select the appropriate threshold value according to the particular applied situation. The data requires "sorting" and "filtering" to prevent

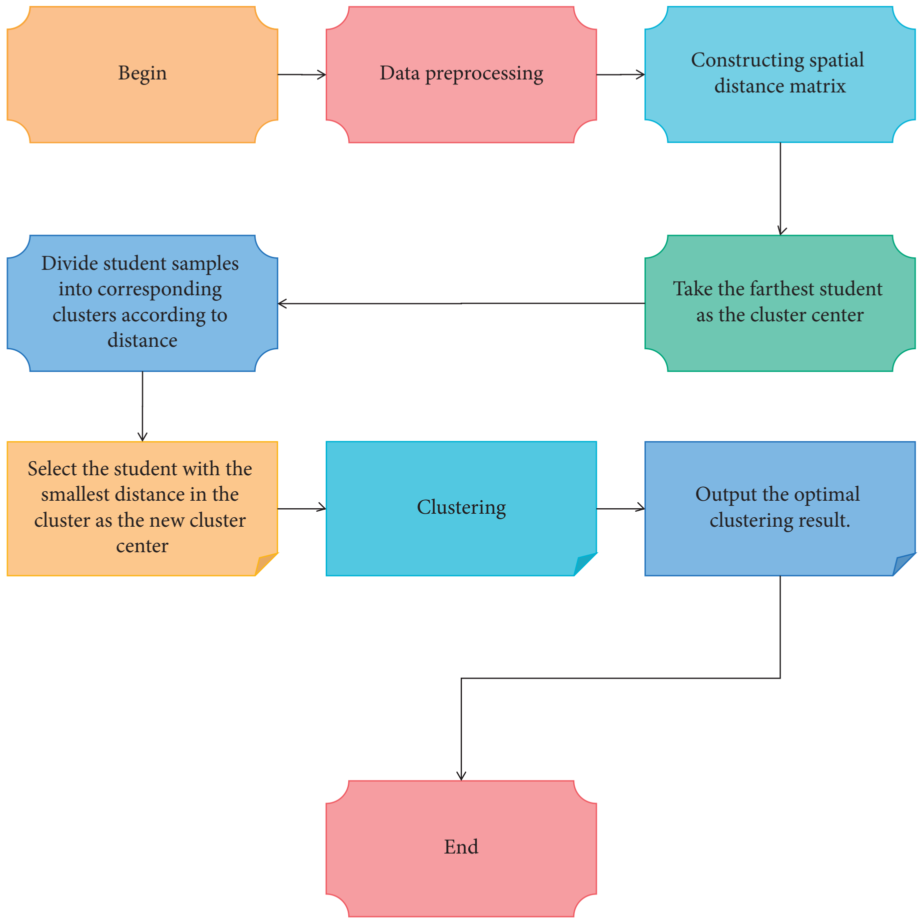

Figure 3: Clustering process of higher education management.

anomalies in the input data, which can enhance the effectiveness of data mining and the accuracy of mining results. When two vectors are similar in direction, the cosine of the angle is larger, and vice versa, it is smaller. When two vectors are parallel, the cosine of the angle is 1, and when the vectors are orthogonal, the cosine of the angle is 0.

3.2. Higher Education Management Method Based on Clustering Algorithm. As far as the school is concerned, the school needs data mining technology so that it can see the differences with other universities and enhance its competitiveness. It also needs a detailed and comprehensive understanding of its students' characteristics to improve their academic performance and practical skills, which in turn improves its teaching quality. The whole clustering higher education management process is divided into three parts: data preprocessing, multiple clustering result comparison, and optimal clustering result output, as shown in Figure 3.

First, you can tap into students' learning patterns, divide them into different groups, designate reasonable learning plans based on guidance, understand the characteristics of students in the groups, and strive for effective learning strategies. In the evaluation of student achievement, each class is an achievement group. Different classes divide each achievement group accordingly, corresponding to the central scores given to the different achievement groups. These center scores are one of the reference criteria for the classification of student achievement. We call the distance between two class centers the inter-class distance. If C_i is the clustered sample, define the class centers of C_i as follows:

$$\overline{x_i} = \frac{1}{n_i} \sum_{x \subset C_i} x, \tag{6}$$

n_i is the number of points in the ith cluster.

In practical problem analysis, different fuzzy similarity matrix construction methods may lead to different clustering results. It is necessary to decide the best fuzzy similarity matrix construction method based on the comparison results of the nature of the problem.

Next are class management, developing lesson plans, prescheduling, group class selection, managing scheduling, managing student attendance, and open control of teaching services. The total objective of evaluating teachers' teaching is divided into different secondary objectives, such as teaching attitude and teaching ability. Each secondary objective is then decomposed into several influencing factors, thus forming a hierarchical structure model. Standardized data can be processed by the following methods:

$$r_{ij} = \left\{ \begin{matrix} 1, & i = 1 \\ \frac{1}{m}\sum_{k=1}^{m} x_{ik} \cdot x_{jk}, & i \neq j \end{matrix} \right\} M = \max\left(\sum_{k=1}^{m} x_{ik}, x_{jk}\right). \tag{7}$$

The mined information is provided to teaching decision makers to adjust teaching strategies, further guide teaching efforts and improve student performance. Use the distance formula to calculate the distance between data objects; then select the k data objects with the first and last connection and the largest distance product from the distance matrix as the initial clustering centroid set. The distances between other data in the data set and the k centroids are also calculated, and the data are classified into the classes to which the nearest data belong by comparative filtering. When the absolute value of the data is compared with the specified threshold, the soft threshold noise is removed because the part less than or equal to the threshold is zero, and the part greater than or equal to the threshold is the difference from the specified threshold. The formula is as follows:

$$\omega\lambda = \begin{cases} [\mathrm{sign}(\omega)](|\omega| - \lambda), & |\lambda| \geq \lambda, \\ 0, & |\omega| < \lambda, \end{cases} \tag{8}$$

Then, exploratory factor analysis was used to explore the dimensions of each index system level and the loadings of each factor, remove unreasonable entries, determine the formal scale, and examine the correlation coefficients between the factors of the scale. Called X of the whole c fuzzy division space. If it contains degenerate division, then it is called degenerate c fuzzy division space. Let

$$V = i\frac{\sum_{j=1}^{n}\left(u_{ij}\right)^{m} x_j}{\sum_{j=1}^{n}\left(u_{ij}\right)^{m}}. \tag{9}$$

Finally, maintain the basic data needed to manage the academic affairs system, such as faculty information, major setting information, classroom information, teacher information, and textbook information. But if the result of mining is not what mining wants or the knowledge obtained is not meaningful, then it is necessary to go back to the previous stage in the process of data mining. In iterative optimization, the similarity metric can be changed and a new criterion function can be selected if necessary. Therefore, before selecting a new criterion function, the data needs to be preprocessed and transformed to be suitable for mining. Assume a certain mixed data $X(k)$, consisting of m dimensional observed signal vectors.

$$\mathrm{x}(k) = \left[x_1(k), x_2(k), \ldots, x_m(k)\right]^T. \tag{10}$$

Based on the distance between each cluster's mean and the remaining objects, the most similar cluster is assigned. Following that, each cluster's data matrix is computed. The data matrix is often referred to as a modal matrix because its rows and columns have different meanings, whereas the dissimilarity matrix's rows and columns represent the same entities, so it is referred to as a unimodal matrix. Self-reflexivity, symmetry, and transferability must be satisfied to determine whether a fuzzy relation satisfies the equivalence relation. The relation matrix is self-reflexive when all elements of the main diagonal are 1. The symmetry of a relation matrix can be demonstrated by showing it to be a symmetric matrix. Adjust the data set after calculating the centroid values of the new symmetric matrix. We consider that we have obtained the final data clustering result if the clustering centers between the new and old classes do not change or remain within a small range.

4. Analysis of the Clustering Algorithm in the Higher Education Management and Student Performance Evaluation Mechanism

4.1. Analysis of K-Means Clustering Algorithm. The K-means clustering algorithm is used to deal with data clustering problems. Due to its simplicity and early introduction, the algorithm has a wide impact in scientific and industrial applications. The K-Means algorithm allows us to understand the learning situation of a course by analyzing the students' comprehensive examination results. According to the characteristics of this course, combined with the students' own existence, it is possible to make a reasonable and scientific evaluation of the students' learning effectiveness, providing some guidance for teaching activities, and the final results will inspire the teachers' teaching methods. After clustering students' performance using the global central clustering algorithm, the results of $k = 2, 4, 6$ clustering were compared with CH indicators, and the relationship between the indicator values and the number of clusters is shown in Figure 4.

Firstly, k objects are arbitrarily selected from n data objects as the initial clustering centers. If the data is given in the form of a data matrix, the data matrix can be converted into a phase difference matrix. A new cluster center is calculated for each assigned cluster, and then the data assignment process continues. After several iterations, if the cluster centers no longer change, it means that all data objects are assigned to their clusters and the clustering criterion function converges; otherwise, the iterative process continues until convergence. Students are divided into two categories, excellent and deviant, and the number of clusters should be close to the number of clustering variables used. In this experiment, $k = 6$ was chosen. Several students' academic performance was randomly selected as the initial clustering centers through initial center of data analysis. The clustering results of the first class of students and the second class of students are shown in Figure 5.

Select an actual object that represents the cluster. Then, based on the similarity, each remaining object is clustered into the cluster where the most similar object is located. Based on the initial clustering of the set, the sample with the smallest distance and in the class is selected as the cluster center to generate a temporary set of cluster centers. A comparison of the distances between the scores of the students in the first category and the students in the second category to each cluster center is shown in Figure 6.

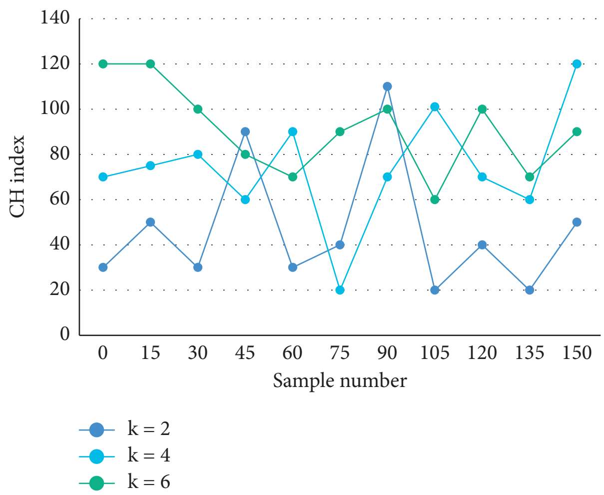

Figure 4: CH indicators of different k values.

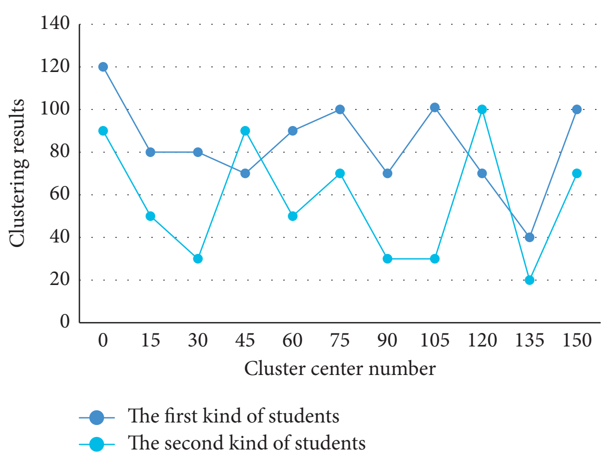

Figure 5: Comparison of clustering results between the first type of students and the second type of students.

Based on different classification patterns, the behavior of other data can be predicted. Obviously, the larger the value of interclass distance and criterion function, the better the separation of the various types of clustering results and therefore the higher the quality of clustering. Which distance calculation formula is used to measure the similarity between data objects needs to be chosen from the actual situation.

Next, the distance of each object to the center of each cluster is calculated and the object is assigned to the nearest cluster. Usually, clustering algorithms use the separation in characteristic space as a measurement to determine the similarity between the two samples. Suppose there is a data set containing n objects, and the data set is divided into k clusters by a division-based clustering method. With each sample as the center of the sphere and d as the radius, the number of samples that fall on the sphere is called the density of that point and is sorted by density. A batch of coalescing points is selected at first according to a certain method, and then the samples are allowed to coalesce to the

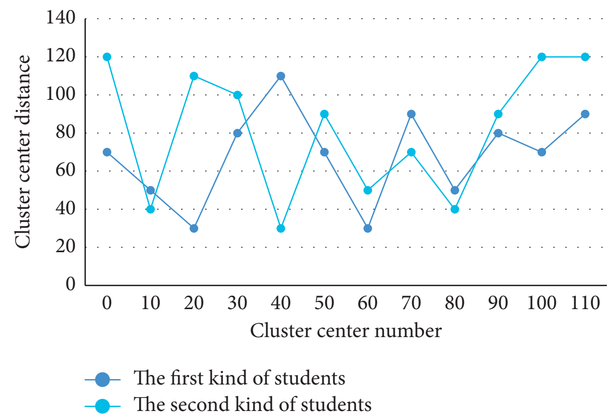

Figure 6: Comparison of the distance between the scores of the first class students and the second class students to each cluster center.

nearest coalescing point so that the points coalesce into classes to obtain the initial classification. There are many data preprocessing techniques that can be used to remove noise, and for those null values, we can also use some data normalization methods that can make the clustering algorithm more accurate. Then, according to the nearest distance principle, the unreasonable classification is corrected until the classification is reasonable, thus forming the final classification result.

Finally, the centers of the K clusters are recalculated after all objects have been specified. The method is implemented based on the principle of minimizing the sum of the differences between the corresponding reference points of all objects. Each sample is divided into corresponding clusters according to the minimum distance, and the iterative process of clustering centers is repeated until the clustering error sum-of-squares function converges and the clustering is completed. A characteristic of this algorithm is to adjust the distribution of all data points in each iteration, and then recalculate the clustering centers into the next iteration. If the positions of all data points are unchanged in a certain iteration and the corresponding clustering centers are unchanged, it indicates that the clustering criterion function has converged and the algorithm is finished.

4.2. Analysis of Improved K-Means Algorithm. Educational data mining takes a very vital function in the process of school education, and the huge and complex educational data brings difficulties to our work. How to utilise education data better for data mining and provide better support analysis for college decision making is another major problem we face. The traditional K-means algorithm can only be used when the mean value of the class is determined; the algorithm requires the user to give k in advance; this algorithm is not suitable for discovering clusters with non-convex shapes or clusters with large size differences. The improved K-means algorithm introduces a new measure of dissimilarity to deal with the classified objects. Instead, a simple matching pattern of phase dissimilarity measures is used and corrected using a frequency-based approach during clustering to minimize the value of

Table 1: Results of clustering.

	Good	Medium	Poor
Teaching ability	27.36	19.56	9.49
Teaching method	45.22	39.54	18.40
Content of courses	44.28	17.67	10.65
Teaching attitude	39.52	29.55	18.76
Number of samples	43	57	50
Percentage	29%	38%	33%

the clustering cost function. We collected 150 samples and conducted an experimental study of the data in these samples using the *K*-Means clustering algorithm. The number of clustering process was $k = 2$ and the results after clustering analysis are shown in Table 1.

First, we find a random representative object for each cluster, and determine the k clusters of n data objects. At present, academic examinations for secondary school students contain many subjects, and the results are basically presented in the form of "scores". The scores of each subject can be the same or different, usually 150 or 100 points. According to the distance axiom, four conditions of the distance axiom should be satisfied when defining the distance measure: self-similarity, minimum value, symmetry, and triangle inequality. If the distance between the attribute values calculated from the data samples is less than the set threshold, we consider these sample data as the same cluster and grouped into one category, otherwise, they are considered as different categories.

Secondly, if the quality of the obtained clusters can be improved by replacing a cluster representative, then the old cluster objects can be replaced by new ones and other objects will belong to each corresponding cluster according to their distances from these cluster representatives. Students have a well-defined interval for their exam results, with a minimum score of 0 and a maximum score of full. Each subject is measured in terms of scores within this range, and there are no cases of abnormally high or low data. The comparison of clustering time and sum of squared clustering errors using *K*-means clustering algorithm, fast global mean clustering algorithm, and the improved algorithm in this paper is shown in Table 2.

The *K*-means clustering algorithm, the fast global mean clustering algorithm, and the improved algorithm in this paper have the same clustering effect on randomly generated data sets with noisy points, but the clustering time of this algorithm is only 0.04, which has obvious advantages.

On the basis of the sample similarity measure, it is also necessary to determine the criterion function for evaluating the quality of the clustering results, so that the samples that really belong to the same class are aggregated into a type of subset and the samples of different classes are separated. The objects in the same cluster should be as close as possible, and the objects in different clusters should be "far away". After clustering, the similarity between data in the same cluster, i.e., the same class of data, is extremely high, while the similarity between data in different clusters is very low, i.e., the data in the clusters are very different. In order to show the superiority of *K*-means algorithm in time, the graphs of

Table 2: Comparison of clustering results of randomly generated data.

	E ($\times 10^3$)	T (s)
K-means clustering algorithm	0.567	1.23
Fast global mean clustering algorithm	0.674	0.12
Improved *K*-means clustering algorithm	0.749	0.04

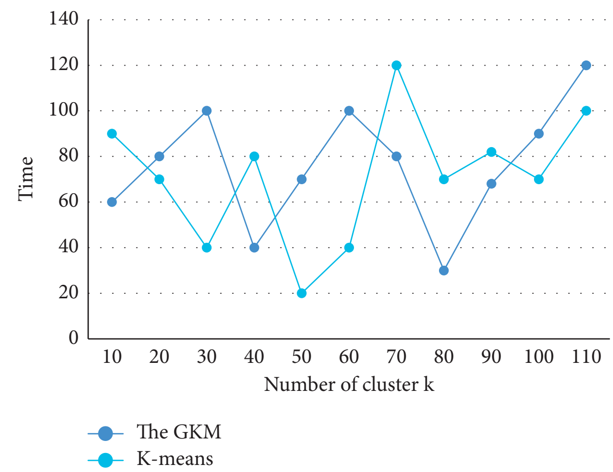

Figure 7: Running time of two algorithms on Iris data set with different number of categories.

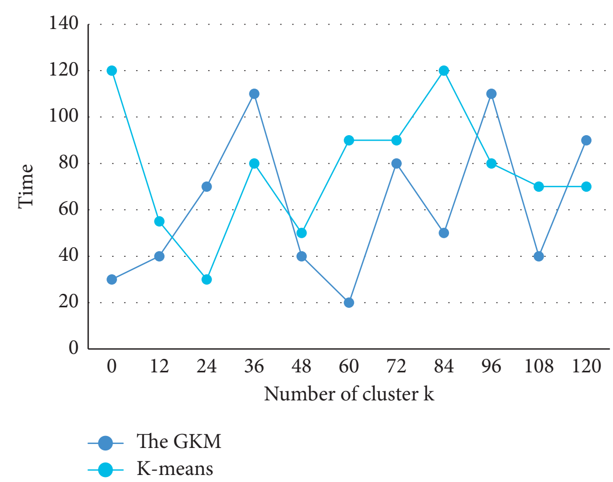

Figure 8: Running time of two algorithms when different categories are taken on Segmentation data set.

the GKM and *K*-means algorithm running time with increasing number of clusters on two sets of data are given in Figure 7 and 8.

Finally, the clustering quality is assessed using a cost function based on the distance between each object and its clustering representative, with the change in distance variance accumulated by replacing unsuitable representatives, which is the clustering criterion function's output. The mean of the data becomes a constant 0, the standard deviation is a constant 1, and the coefficient of variation does not exist after the translation standard deviation transformation, indicating that the data resolution is completely assimilated. The clustering criterion function can also be used to assess the clustering results' quality. The clustering process should be repeated if the clustering quality does not meet the requirements. Instead of considering the entire data set, a representative sample of the data is chosen, and then the centroids are chosen from the sample.

5. Conclusions

The rapid development of the Internet has provided excellent technical support for the growth of online education, allowing it to overcome the time and space constraints of the existing school education system and the teacher-led education model. Clustering is an unsupervised learning algorithm that can cluster data sets without using predefined classification rules, allowing it to mine hidden information in data and create relevant data models. In the trend of education informatization, the application of data mining technology to data analysis in the teaching field will undoubtedly have a very broad perspective. Academic performance evaluation is an important component of the comprehensive evaluation reform of education quality. The use of a clustering algorithm in student performance analysis compensates for the lack of traditional evaluation methods by comparing student performance differences horizontally. Clustering analysis has evolved into a tool that can be used not only for data processing but also for data analysis when combined with other algorithms. As a result, this paper proposes a mechanistic analysis of higher education management and student performance evaluation based on clustering algorithm to assess the quality of college classroom teaching from two perspectives: students' learning effects and teachers' teaching work, with the K-Means algorithm as the primary method. The theory and application of clustering are highlighted based on a summary of data mining theory. This research presents a set of scientific and reasonable management capability evaluation index systems for universities, which serves as a strong foundation for relevant departments to conduct university administration capability evaluations in the future and, as a result, contributes significantly to raising the standard of university administration.

Data Availability

The data used to support the findings of this study are available from the author upon request.

Conflicts of Interest

The author does not have any possible conflicts of interest.

References

[1] V. Sugumaran, Z. Xu, P. Shankar, and H. Zhou, Eds., *Application of Intelligent Systems in Multi-Modal Information Analytics*, vol. 929, Springer, Shenyang, China.

[2] Z. G. Wei, X. F. Cheng, and J. H. Liu, "A finite element model of roll-over protective structures for wheel loader frame[C]// Applied Mechanics and Materials," *Trans Tech Publications Ltd*, vol. 138, pp. 737–742, 2012.

[3] R. Dong, Z.-g. Wei, C. Liu, and J. Kan, "A novel loop closure detection method using line features," *IEEE Access*, vol. 7, pp. 111245–111256, 2019.

[4] R. Dash and B. B. Misra, "Performance analysis of clustering techniques over microarray data: a case study," *Physica A: Statistical Mechanics and Its Applications*, vol. 493, pp. 162–176, 2018.

[5] Patibandla and N. Veeranjaneyulu, "Performance analysis of partition and evolutionary clustering methods on various cluster validation criteria," *Arabian Journal for Science and Engineering*, vol. 43, no. 8, pp. 4379–4390, 2018.

[6] B. P Kalpesh and D. M Adhyaru, "Performance analysis of fuzzy subtractive clustering based MRAC[J]," *International Journal of Applied Engineering Research*, vol. 13, no. 3, pp. 6766–6770, 2018.

[7] A. S. Nagesh, C. Satyamurty, and C. V. S. Satyamurty, "Application of clustering algorithm for analysis of student academic performance," *International Journal of Computer Science and Engineering*, vol. 6, no. 1, pp. 381–384, 2018.

[8] K. Govindasamy and T. Velmurugan, "Analysis of student academic performance using clustering techniques[J]," *International Journal of Pure and Applied Mathematics*, vol. 119, no. 15, pp. 309–322, 2018.

[9] C. Martinez-Perez, C. Alvarez-Peregrina, C. Villa-Collar, and M. Á. Sánchez-Tena, "Current state and future trends: a citation network analysis of the academic performance field," *International Journal of Environmental Research and Public Health*, vol. 17, no. 15, p. 5352, 2020.

[10] C.-C. Chen, X. Fu, and C.-Y. Chang, "A terms mining and clustering technique for surveying network and content analysis of academic groups exploration," *Cluster Computing*, vol. 20, no. 1, pp. 43–52, 2017.

[11] A. M. Adewale, A. O. Bamidele, and U. O. Lateef, "Predictive modelling and analysis of academic performance of secondary school students: artificial Neural Network approach[J]," *International Journal of Science and Technology Education Research*, vol. 9, no. 1, p. 1, 2018.

[12] W. Cai, Y. Song, and Z. Wei, "Multimodal data guided spatial feature fusion and grouping strategy for E-commerce commodity demand forecasting," *Mobile Information Systems*, vol. 2021, Article ID 5568208, 2021.

[13] J. Chen, C. Du, Y. Zhang, P. Han, and W. Wei, "A clustering-based coverage path planning method for autonomous heterogeneous UAVs," *IEEE Transactions on Intelligent Transportation Systems*, vol. 1, pp. 1–11, 2021.

[14] Y. Gu, T. Ni, and Y. Jiang, "Deep possibilistic-means clustering algorithm on medical datasets," *Computational and Mathematical Methods in Medicine*, vol. 2022, Article ID 3469979, 2022.

[15] Y. L. Goh, Y. H. Goh, C. C. Yip, C H Ting, R. L. L Bin, and K, P Chen, "Students' academic performance analysis by K-means clustering for investigating students' health conditions within clusters[J]," *Annals of Tropical Medicine and Public Health*, vol. 23, no. 13, 2020.

[16] X.-B. Jin, W.-T. Gong, J.-L. Kong, Y.-T. Bai, and T.-L. Su, "A variational bayesian deep network with data self-screening layer for massive time-series data forecasting," *Entropy*, vol. 24, no. 3, p. 335, 2022.

[17] X. Y. Li, Y. Zhang, H. Cheng, F Zhou, and B Yin, "An unsupervised ensemble clustering approach for the analysis of student behavioral patterns[J]," *IEEE Access*, vol. 9, no. 99, p. 1, 2021.

[18] Y. L. Goh, Y. H. Goh, C.-C. Yip, C. H. Ting, fnm Raymond Ling Leh Bin, and K. P. Chen, "'Prediction of students' academic performance by K-means clustering," *Science Proceedings Series*, vol. 2, no. 1, pp. 1–6, 2020.

[19] O. Tinuke Omolewa, A. Taye Oladele, A. Adekanmi Adeyinka, and O. Roseline Oluwaseun, "'Prediction of student's academic performance using k-means clustering and multiple linear regressions," *Journal of Engineering and Applied Sciences*, vol. 14, no. 22, pp. 8254–8260, 2019.

[20] Ł. Wiechetek and Z. Pastuszak, "Academic social networks metrics: an effective indicator for university performance?" *Scientometrics*, vol. 127, no. 3, pp. 1381–1401, 2022.

[21] V. H Davenport, "Improved analysis of complete-linkage clustering[J]," *Computing Reviews*, vol. 59, no. 11, pp. 619-620, 2018.

[22] M. Anoopkumar and A. Rahman, "Bound model of clustering and classification (BMCC) for proficient performance prediction of didactical outcomes of students[J]," *International Journal of Advanced Computer Science and Applications*, vol. 9, no. 11, pp. 236–246, 2018.

[23] B. D. Mayureshwar, K. K. Eldose, R. Sridharan, and K. R. Kumar, "Markov analysis of academic performance of students in higher education: a case study of an engineering institution," *International Journal of Services and Operations Management*, vol. 1, no. 1, p. 1, 2020.

[24] A. I Beltrán-Velasco, M. Donoso-González, and J Clemente-Suárez, "Analysis of perceptual, psychological, and behavioral factors that affect the academic performance of education university students[J]," *Physiology & Behavior*, vol. 238, no. 3, Article ID 113497, 2021.

[25] J. Zhang, W. Feng, T. Yuan, J. Wang, and A. Kumar Sangaiah, "SCSTCF: spatial-channel selection and temporal regularized correlation filters for visual tracking," *Applied Soft Computing*, vol. 118, Article ID 108485, 2022.

[26] Y. Ding, X. Zhao, Z. Zhang, W. Cai, and N. Yang, "Graph sample and aggregate-attention network for hyperspectral image classification," *IEEE Geoscience and Remote Sensing Letters*, vol. 19, pp. 1–5, Article ID 5504205, 2022.

[27] J. Zhang, J. Sun, J. Wang, Z. Li, and Xi Chen, "An object tracking framework with recapture based on correlation filters and Siamese networks," *Computers & Electrical Engineering*, vol. 98, Article ID 107730, 2022.

[28] Y. Wang, Y. Chen, and R. Liu, "Aircraft image recognition network based on hybrid attention mechanism," *Computational Intelligence and Neuroscience*, vol. 2022, Article ID 4189500, 2022.

[29] K. H. Memon and D. H. Lee, "Generalised fuzzy c-means clustering algorithm with local information[J]," *Fuzzy Sets and Systems*, vol. 11, no. 1, pp. 1–12, 2018.

[30] J Jiang, D. Hao, Y. Chen, P Milan, and L Keqin, "GDPC: gravitation-based density peaks clustering algorithm[J]," *Physica A: Statistical Mechanics and its Applications*, vol. 502, pp. 345–355, 2018.

[31] W. Lu, "Research on student achievement evaluation and management mechanism based on support vector machine," in *Proceedings of the 2021 4th International Conference on Information Systems and Computer Aided Education*, pp. 2462–2466, ICISCAE 2021, Dalian China, September 2021.

[32] Y. Jiang, X. Gu, D. Wu et al., "A novel negative-transfer-resistant fuzzy clustering model with a shared cross-domain transfer latent space and its application to brain CT image segmentation," *IEEE/ACM Transactions on Computational Biology and Bioinformatics*, vol. 18, no. 1, pp. 40–52, 2021.

[33] Y. Jiang, Y. Zhang, C. Lin, and D. Wu, "EEG-based driver drowsiness estimation using an online multi-view and transfer TSK fuzzy system," *IEEE Transactions on Intelligent Transportation Systems*, vol. 22, no. 3, pp. 1752–1764, 2021.

Hindawi
Computational Intelligence and Neuroscience
Volume 2022, Article ID 4709146, 11 pages
https://doi.org/10.1155/2022/4709146

Research Article

Student Education Management Strategy Based on Artificial Intelligence Information Model under the Support of 5G Wireless Network

Yushu Guan

Fine Arts College, Shenyang University, Shenyang 110044, China

Correspondence should be addressed to Yushu Guan; 20120972@stumail.hbu.edu.cn

Received 23 April 2022; Revised 17 May 2022; Accepted 18 May 2022; Published 1 July 2022

Academic Editor: Xin Ning

With the popularity of the Internet and the advancement of information technology, more and more people are accepting the teaching and sharing of knowledge through the digitalization of information. The widespread adoption of 5G technology has pushed online learning even further into the mainstream. However, because online teaching does not have the drawback of being intuitive like classroom teaching, teachers' assessments of students' learning situations are less accurate. As a result, how to effectively evaluate students' academic performance in the context of 5G wireless network technology is a pressing issue that must be investigated. By processing these heterogeneous large-scale learning records and integrating multiple perspectives to analyze this learning record information to identify students' learning behaviors, this study proposes an integrated analysis algorithm based on artificial intelligence information technology. The possible learning outcomes of students are predicted based on their current learning situation, so teachers can provide auxiliary teaching strategies to students who may have learning difficulties based on the predicted information. The method proposed in this article uses information technology to predict students' grades, and the analysis shows that the method is very effective. In this article, different grades of classification methods are used to analyze and predict the whole students. All grade classification methods are effective in describing decision rules. No matter what grades classification method is used, the error rate of students' grades distribution is predicted to be below 40%.

1. Introduction

5G networks have significant advantages over traditional 3G and 4G communication networks, including high information transmission efficiency and relatively fast speeds. It is organically combined with big data, the Internet of Things, and other technologies, greatly promoting business needs and business model innovation in a variety of fields and providing strong support for society's intelligent development. Artificial intelligence is formed when computer technology and communication technology are combined in this way. Massive amounts of data are generated every second in the big data environment [1]. Artificial intelligence can greatly improve the speed and quality of data processing and be used to process large amounts of complex data, increasing data security. Artificial intelligence, when used extensively, not only improves the information processing capability of computer systems but also promotes their evolution toward intelligence and automation. Furthermore, it can completely ensure the system's stability. Massive amounts of data are generated every second in the big data environment. Artificial intelligence can greatly improve the speed and quality of data processing and be used to process large amounts of complex data to improve data security [2]. With the development of artificial intelligence and the arrival of the 5G communication era, in order to realize the effective management of massive network information, advanced artificial intelligence technology can be adopted, many scientific and reasonable solutions can be compiled, and an expert knowledge sharing system can be established to gradually improve the data analysis and processing effect. On the other hand, experts in the field of theory should effectively strengthen scientific research, summarize theoretical results, and fully reflect the advantages of artificial intelligence.

Based on artificial intelligence information technology, this article proposes an algorithm for predicting students' academic performance. The decision tree's input and output variables are determined by the algorithm using the student learning behavior factor data table [3]. Then, all samples are randomly divided into three datasets, which are used for training, testing, and validation, and the characteristics of students' learning behavior are analyzed accordingly, resulting in an algorithmic basis for predicting students' grades. Find the decision-making rules between students' various learning behavior attributes and learning outcomes for each course in the fifth and sixth semesters and explain the results. This study uses the same course in different semesters as the object of verification, and the data from the fifth, sixth, and seventh semesters as training data and test data, respectively, to verify the discovered decision rule. The training error rate and the test error rate are used as verification indicators to try to find the best prediction time point using different time units and to try to find the best grade classification method using various grade classification methods. The artificial intelligence-based decision tree for predicting students' academic performance analyses and discusses the students' learning situation and provides specific educational guidance based on the data analysis results [4].

This study examines the relationship between course attributes and decision rules under different courses, the relationship between different time points and decision rules under different time units, and the relationship between different grade classification methods and decision rules by processing these heterogeneous large-scale learning records, the relationship between each time point within the time unit and the high and low score prediction effect, the relationship between different grade classification methods and the high and low score prediction effect, and so on. Students' current learning circumstances predict their potential learning effect [5].

This article's chapter structure is as follows: this article extracts data from learning records, uses artificial intelligence technology to classify and analyze the data, and then provides teachers with information on the relationship between students' learning behavior and learning effectiveness, as well as the degree of correlation between the two. Teachers can predict various learning situations that may exist in current and future students based on their past learning behavior and provide learning assistance or adjust teaching strategies in real time.

The following are the article's unique features: the first chapter introduces related research on artificial intelligence information technology and teaching strategies; the second chapter examines current educational management needs in light of current educational development; the third chapter is based on artificial intelligence information technology. The fourth chapter uses intelligent information technology to quantitatively analyze the results and summarize the rules, and the fifth chapter is a summary of the entire text.

2. Related Work

The international empirical analysis of student achievement prediction has also developed from the original manual statistics to the joint statistics of artificial intelligence and information technology.

Combined with the current situation of information technology teaching in junior high schools, Kaptein MC built a junior high school information technology teaching model with the concept of flipped classroom teaching and proposes to improve learners' interest in information technology through independent learning or cooperative exploration among learners and cultivate students' ability in the learning process. In terms of research on learning motivation, creativity, and initiative [6], Zhou H tried to revise and perfect the new model in teaching practice through three rounds of action research. Through questionnaire survey and SOLO taxonomy, the impact of this model on the deep learning and learning ability of primary school students was analyzed [7]. After in-depth research, Luo X built a grade prediction model. By using this model, the characteristics of students can be predicted, and then the low-achieving students can be analyzed in a targeted manner [8]. Huang X collected students' learning information through questionnaires, studies students' learning behavior and then converted students' tacit knowledge into explicit information through the Apriori algorithm and cluster analysis, and this explicit information can be used as follow-up services so as to improve students' learning satisfaction [9]. Kirichenko A V et al. used a combination of a self-organizing competitive neural network (SOM) and BP neural network to establish a student achievement prediction model [10]. After intensive research, Cui L proposed a system that can predict student grades based on multiagent learning (MAFDS) behavior [11]. Jie H used two data mining methods, genetic algorithm and decision tree, to establish a model to find out the potential relationship between factors in student behavior data and use a decision tree for preliminary classification [12]. Zhang Z used three methods: support vector machine, logistic regression, and decision tree C5.0 to construct a low learning achievement risk classification model, and they used a 10-fold cross-validation method to verify the model and found that the method with the best prediction effect was support vector machine [13]]. Ting-Ting LU used a variety of data mining methods to integrate expert opinions and then used genetic algorithms to find the best combination solution to create an optimal integrated student achievement prediction model. The best prediction method is a neural network [14]. Liu Y's research found that the classification and prediction of students' grades is an important problem, and the commonly used classification methods often include the logistic regression model and Bayesian algorithm. Chen Y used the decision tree in data mining technology to classify the data mining application of predicting students' grades. The results show that the expected evaluation effect can be achieved by using the decision tree [16]. Zhang X pointed out that the use of support vector machines has achieved good prediction results in terms of student achievement, and studies have shown that the application of support vector machines in feature selection and prediction has achieved high classification accuracy [17].

In literature, it is generally emphasized that the application of innovation theory is used to reform teaching methods, but there are no articles that specifically propose methods and strategies for various management work in colleges and universities, such as teaching management, student management, campus culture construction, and enrollment work. Through the research on the application of data mining in student achievement prediction, it can be found that at present, most of the research on student achievement prediction is focused on students' examination results, but there is no research on how to effectively predict students' academic achievements under the new teaching method such as online education, and an in-depth study on the correlation between academic achievements and learning courses, learning time and learning patterns.

3. Education Management Needs Analysis

Most of the talents cultivated by higher education will become leaders and leaders of all walks of life and can be regarded as high-end talents in all walks of life. For this type of talent, in the actual leadership work, they need to put aside traditional and conservative old views and old ideas, so they need a more innovative spirit. As a cutting edge of the education industry, higher education should pay more attention to the cultivation of innovation ability and apply the innovation concept to daily education management. Since the concept of artificial intelligence information technology was put forward, more and more people began to realize the importance of innovation, and more and more people began to put it into practice [18]. Nowadays, the trend of educational development is no longer to align with scores, no longer to train high flyers of top universities, and no longer to blindly ask students how many scores they get in TOEFL and IELTS but to pay more attention to students' personal ability while valuing scores. Students with high test scores, low abilities, and a lack of innovative ability are already unpopular, and in today's information age, they will be questioned and eliminated. They are energetic, persistent, focused, imaginative, and adventurous; they have a strong ability to learn and explore themselves; they have broad and solid knowledge, a high professional level, good moral cultivation, and the ability to cooperate or coexist with others. True innovative talents with the aforementioned characteristics will become the most in-demand talents in today's society and Muhui's mainstay. Artificial intelligence information technology, on the surface, refers to making improvements to original educational concepts, educational methods, and educational methods in order to make them more current and effective. In essence, artificial intelligence information technology is used to break through the ingenious vertebrae of previous educational development through educational innovation, making education more grounded and in line with the needs of the times, rather than simply activating the classroom atmosphere and enriching the content of textbooks. In the new situation, education reform is focusing on improving students' innovative awareness and ability [19, 20].

Constructivist learning theory believes that learning is the process of students actively constructing internal mental representations in the process of interacting with the learning environment. Knowledge is not obtained through the teacher's teaching and transmission but is obtained by students in a certain situation, with the help of other means, using necessary learning materials and learning resources, and by means of meaning construction. Constructivism puts forward the viewpoint of situational cognition, emphasizes the situational nature of learning, knowledge, and wisdom and believes that knowledge cannot exist abstractly without being separated from the activity situation, and learning should be combined with situational social practice activities. These need to be arranged in a hierarchy from low level to high level, as shown in Figure 1.

The four needs at the bottom of the hierarchy are classified as missing needs, which are essential for individual survival and must be met to some extent [21]. When all of the missing needs are met, the individual will pursue the above three high-level needs, which are classified as growth needs and can improve the quality of the individual's life. According to Maslow's hierarchy of needs theory, everyone has a need for understanding, respect, and self-realization, and everyone has a desire and need to communicate. Even the most withdrawn, independent person, or the so-called poor students in the eyes of some teachers, hope to receive understanding, care, and assistance in their hearts. Students can benefit from rich learning resources, convenient interaction methods, and a humanized situation design in the information technology teaching environment, which can meet their communication, respect, knowledge, and aesthetic needs. Once these needs are met, students will have a positive attitude toward themselves and gain positive emotional experiences like satisfaction, happiness, and pride, which will aid in developing advanced social emotions like reason, beauty, and morality so that the students have a positive mental attitude [22].

4. Quantitative Evaluation of Teaching Based on Artificial Intelligence Information Technology

The ultimate goal of this article is to improve the level of school teaching management, make teaching management more convenient and fast in the future, digitize teaching evaluation information, and allow users of teaching evaluation to access the system from any location and time on the campus network without being limited by time and space. The purpose of reviewing the information you need is diversified, which can meet the current practical needs of various evaluation purposes. At the same time, focusing on the fundamental purpose of promoting the development of teachers, the main functions of the teaching management unit are transferred to the collection, processing, and transformation of digitalization, the realization of technical means, and the transformation of service methods [23].

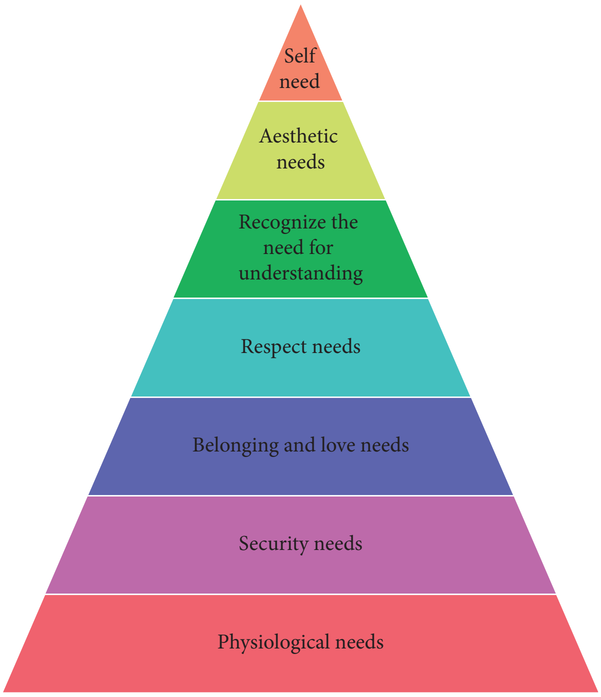

Figure 1: Need hierarchy theory diagram.

After an in-depth analysis of the problems, when the factors contained in the problems are divided into different levels, such as target level, criterion level, index level, scheme level, and measure level, the subordinate relationship of hierarchical structural factors of the levels is explained in the form of the block diagram. When a certain level contains many factors, the level can be further divided into several levels. Since it is quite difficult to directly use the definition to calculate the eigenroot and eigenvector of the matrix, after the paired comparison matrix is constructed, the sum-product method or the square root method can be used to approximate the maximum eigenroot and corresponding weight vector of the constructed paired comparison matrix. Using the sum-product method to calculate, the formula is shown in as follows:

$$a_{ij} = \frac{a_{ij}}{\sum_{k=1}^{n} a_{kj}} \, (i = 1, 2, \ldots, n). \tag{1}$$

For the judgment matrix normalized by column, sum it by row as shown in the following:

$$\overline{\omega}_i = \sum_{j=1}^{n} \overline{a}_{ij}. \tag{2}$$

Normalize the vector $\overline{\omega} = [\overline{\omega}_1, \overline{\omega}_2, \ldots, \overline{\omega}_n]^T$ as shown in the following:

$$\omega_i = \frac{\overline{\omega}_i}{\sum_{i=1}^{n} \overline{\omega}_i}. \tag{3}$$

In the actual evaluation, the evaluation experts can only roughly estimate the value of the element a_{ij} in the pairwise comparison matrix, which often leads to inconsistent logic errors. In this article, the difference between $\lambda_{\max}$ and n is used to test the consistency. First, calculate the maximum eigenvalue such as the following equation:

$$\lambda_{\max} = \sum_{i=1}^{n} \frac{(A\omega)_i}{n\omega_i}. \tag{4}$$

Calculate the consistency index as shown in the following equations:

$$CI = \frac{\lambda_{\max} - n}{n - 1}, \tag{5}$$

$$CR = \frac{CI}{RI}. \tag{6}$$

When $CR < 0.1$, the inconsistency scale of task A is within the allowable range. Otherwise, the evaluation expert needs to reestimate and adjust the value of the element a_{ij} in the pairwise comparison array until the consistency requirements are met. The average consistency principle is shown in Table 1.

After obtaining the relative weights between the indicators of the same layer, the absolute weights of the indicators at all levels can be calculated from the top to the bottom. Overall consistency is considered acceptable when $CR < 0.1$. Otherwise, it is necessary to adjust this paired comparison matrix until the consistency test of the total ranking of the hierarchy meets the requirements. In summary, the process of calculating the absolute weight can be obtained as shown in Figure 2.

Since the indicators have different unit dimensions, the indicators must be standardized, and all indicators are converted into indicators without units. There are positive indicators, reverse indicators, and moderate indicators in the indicator system, and the advantages and disadvantages of the indicators are not clear. Therefore, the method of fuzzy quantization, that is, fuzzy membership function, is used to carry out dimensionless processing of each indicator [24].

For the positive index, the semirising trapezoidal fuzzy membership function is used to quantify, and the processing of the positive index is shown in the following:

$$x_{ij} = \frac{x_{ij} - x_{\min}}{x_{\max} - x_{\min}}. \tag{7}$$

For the reverse index, the semidrop trapezoidal fuzzy membership function is used to quantify, and the reverse index processing is shown in the following:

$$x_{ij} = \frac{x_{\max} - x_{ij}}{x_{\max} - x_{\min}}. \tag{8}$$

For the moderate index, the semisublimation descending trapezoidal fuzzy membership function is used to quantify the moderate index processing, as shown in the following:

$$x_{ij} = \begin{cases} \dfrac{x_{ij} - x_{\min}}{x_{half} - x_{\min}}, & x_{ij} > x_{half}, \\ 1, x_{ij} = x_{half}, & \\ \dfrac{x_{ij} - x_{\min}}{x_{\max} - x_{half}}, & x_{ij} < x_{half}. \end{cases} \tag{9}$$

Table 1: Average consistency index.

N	1	2	3	4	5	6	6	7	8	9	11
RI	0.00	0.02	0.056	0.91	1.11	1.23	1.32	1.44	1.48	1.52	1.54

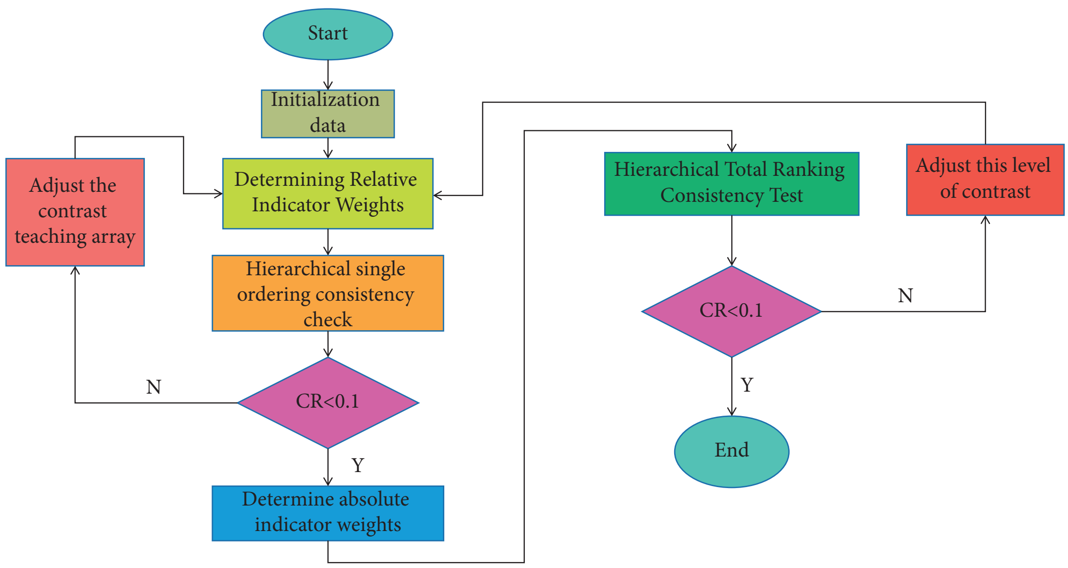

Figure 2: Flowchart of weight indicator.

The decision-making rules generated by artificial intelligence information technology analysis are for each course, and most of the analyzed data are historical data of the entire semester. For teachers, these decision-making rules are not directly helpful to the courses being taught, and they are based on the data of the whole semester. Whether these decision-making rules can be applied to the same courses in different semesters is indeed necessary to verify the accuracy of these decision-making rules in predicting the courses.

5. Data Analysis

5.1. Test Score Indicators. The median is the value of a point in the center to represent the central tendency of a set of data. The median is suitable not only for data with skewed distribution, irregular distribution, large difference between variable values, and unbounded at one or both ends but also for data with symmetrical distribution or unclear distribution. The arithmetic square root value of each variable value from the square of the mean deviation, also known as the square root of deviation from the mean. As an overall parameter, it is usually represented by a symbol, and the formula is shown as follows:

$$\sigma = \sqrt{\frac{\sum (X-u)^2}{N}}. \tag{10}$$

Evaluate the overall difficulty and discrimination of the test paper, and conduct difficulty analysis and discrimination analysis for each question. Through analysis, we can better understand the degree of difficulty and distinction of the test paper and evaluate the quality of the test paper as a whole. Evaluate the option ratio distribution of multiple-choice questions and design questions more scientifically. The test paper evaluation model validation process is shown in Figure 3.

Since the records of the log files are too scattered, they have no substantial meaning and help for teachers or students. Therefore, it is necessary to combine the basic data files of students and the data of the course database of the relationship between course information and students. After preprocessing and after the data are sorted and processed, a learning record database describing the learning behavior of each student in each course can be further established, which can be used as a reference for quickly querying the real-time learning status of students in each course in the future.

5.2. Data Analysis of Student Achievement Prediction. Analyzing the decision-making rules that link students' learning behaviors and learning outcomes in each course can help teachers and teaching assistants understand what learning behaviors students exhibit in this course and how they may affect academic performance. They can also observe the attribute value changes of related learning behaviors in subsequent lessons and provide assistance ahead of time. However, it is understandable to analyze these learning behaviors using only data from the entire semester; however, these decision rules can only describe students' learning behavior during the previous entire semester of the course, not at different time points, because the real learning behavior is not predictable. We can predict the possible learning effects of students based on their current learning

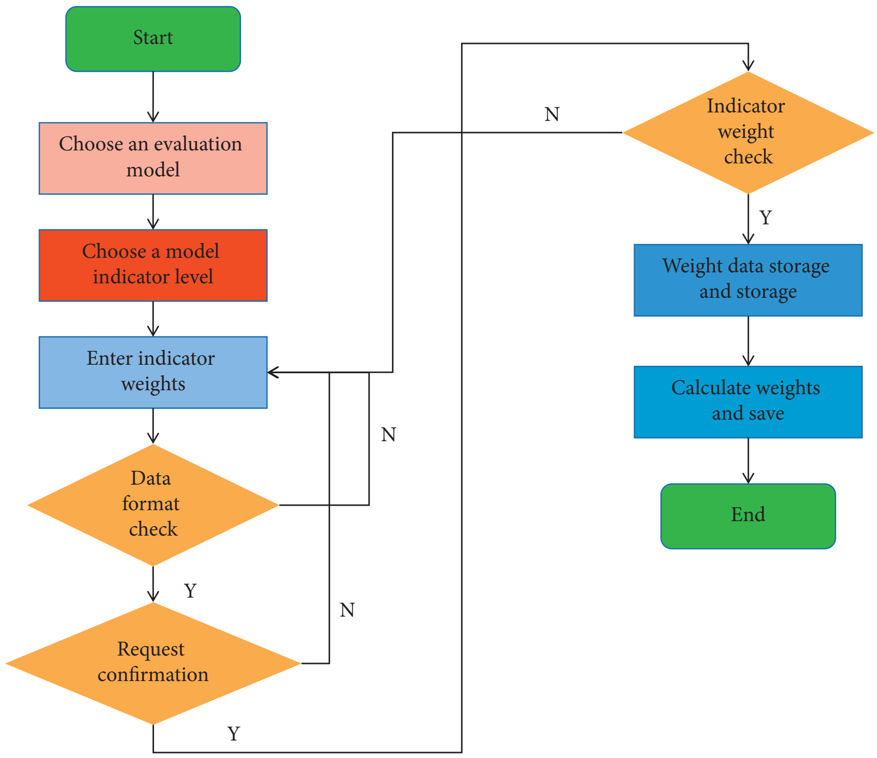

Figure 3: The flowchart of test paper evaluation model verification.

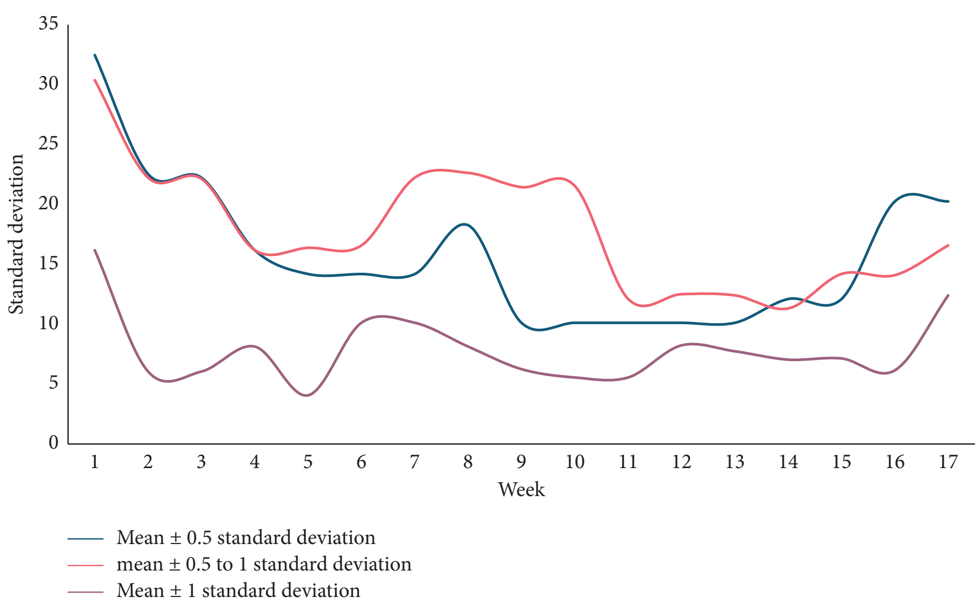

Figure 4: The standard deviation of the training error rate at each time point with 7 days as the time unit.

situation and give the purpose of auxiliary teaching in advance by observing these learning behaviors. This study uses the training error rate and the prediction error rate as comparison indicators for various analyses when validating the decision rules in order to verify the relationship between each time point and the decision rules. The goal of tracking the training error rate is to avoid having a high training error rate. The prediction error rate refers to the error rate of the decision rules trained in the sixth semester as the test data in the seventh semester. It can be used to ensure that decision rules are applied consistently across semesters. As a result, the focus of this section will be on observing the relationship between each time unit and the prediction error rate. It is primarily based on the cumulative amount of learning behavior attribute values at various time points; that is, the cumulative value of each frequency is calculated from the start of the school day to each time point, and by observing the relationship between changes in the cumulative amount

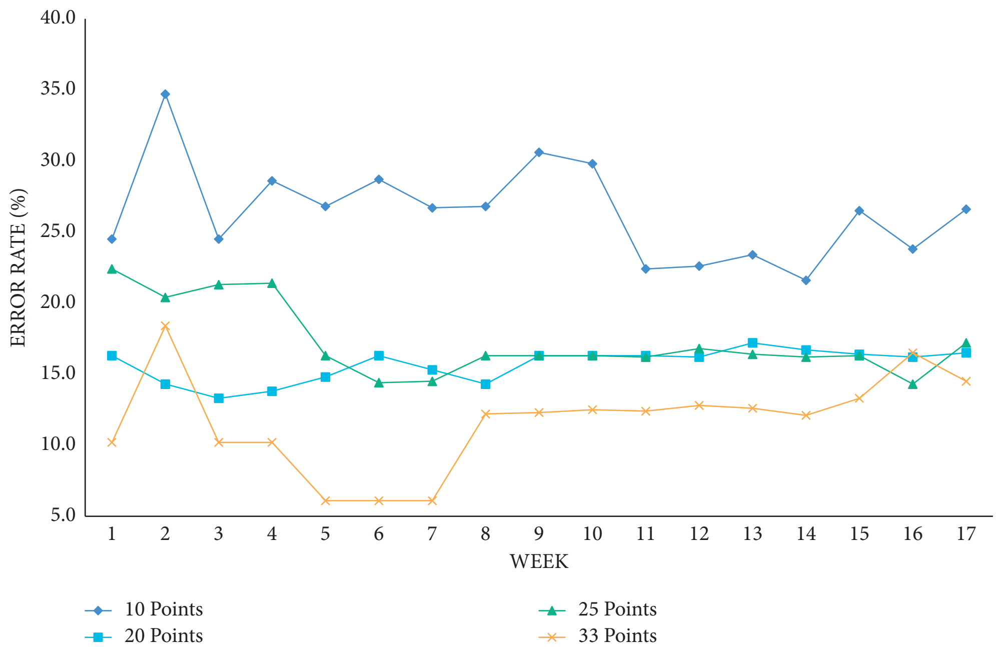

Figure 5: Training error rate at each time point with 7 days as the time unit.

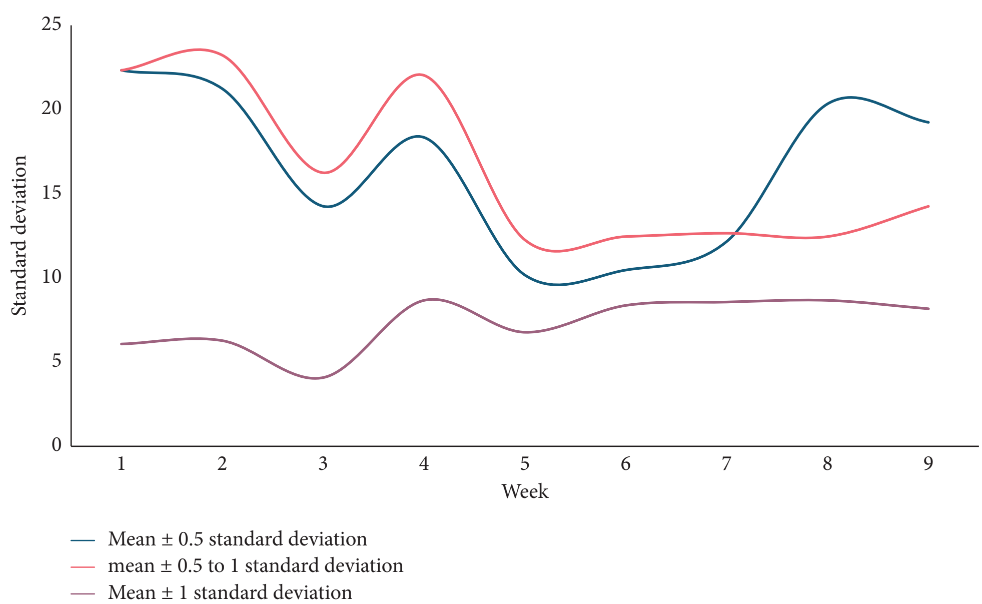

Figure 6: The standard deviation of the training error rate at each time point with fourteen days as the time unit.

of learning behavior variables at various times and the learning effect, to provide future decision tree analysis, by observing the relationship between attributes and the learning effect. The cut-off points for grades in this article are 10 points, 20 points, 25 points, and 33 points, and the time variables used in most previous studies are used as the observation dimensions of learning type analysis. In other words, whether the attributes in the decision rules are the same at all time points and whether it is possible to predict ahead of time which students will fall into the low-scoring group and have poor learning outcomes before the semester ends and provide remedial teaching or a related teaching strategy. Students' final semester grades in the course are used to assess learning outcomes.

This article first observes the changes and trends of the training error rate and prediction error rate at various time points under different time units such as seven days, fourteen days, and twenty-eight days. Finally, a conclusion is drawn by comparing the prediction effects of different time units. The training error rate at each time point with seven days as the time unit is shown in Figures 4 and 5.

Taking seven days as a time unit, the training error rate of various performance classification methods can be below 30%, and the average error rate of the mean ± 1 standard

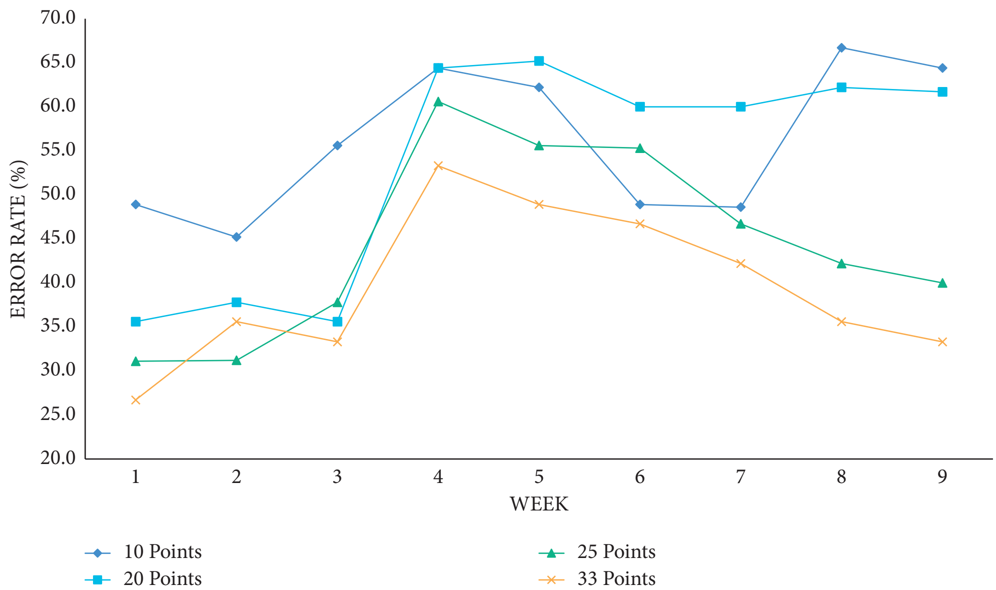

Figure 7: The training error rate at each time point with fourteen days as the time unit.

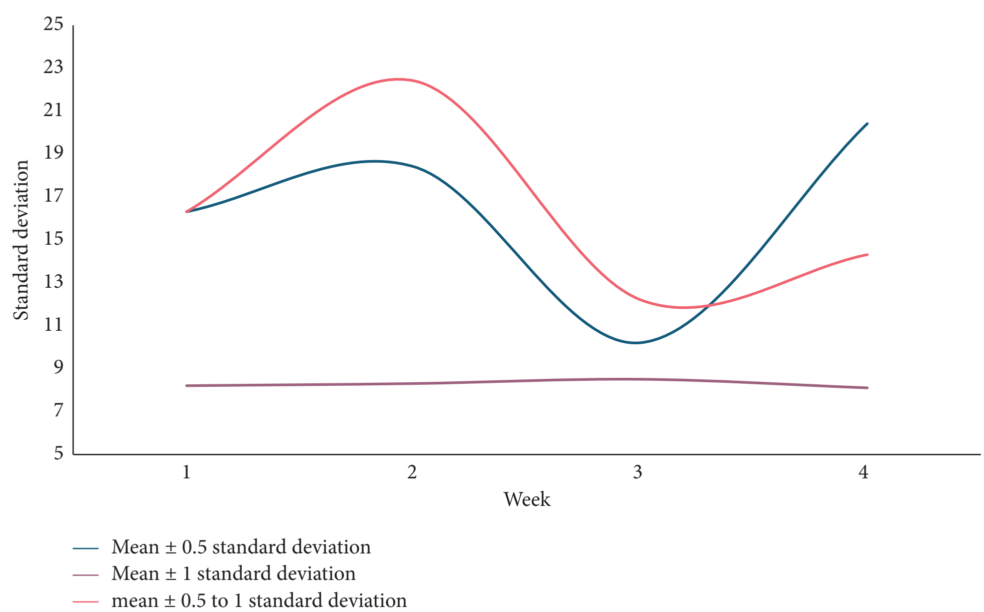

Figure 8: The standard deviation of the training error rate at each time point with twenty-eight days as the time unit.

deviation can be trained in the eighth to ninth weeks. The performance is lower if it falls below 15%, and each classification method can reduce the error rate over time and drop below 20% in the score range of 20, 25, and 33 points.

The training error rate at each time point with 14 days as the time unit is shown in Figures 6 and 7.

Figure 7 shows the prediction error rate at each time point under the time unit of fourteen days. Taking 14 days as the time unit, the prediction and practice error rates of various performance classification methods can be below 50%, and the average performance of the error rate with the mean ± 1 standard deviation is lower and the mean ± 1 standard deviation can drop to the error rate below 35% in weeks seven to eight. Among them, if compared with Figure 7, it can be seen that the two methods of mean ± 0.5 to 1 standard deviation and 20 points are the two methods, the prediction effect in the time unit of 14 days has become less obvious, so it is concluded. Therefore, as the time period increases, the effect of reducing the error rate will become less obvious, and the two are inversely proportional.

The training error rate at each time point with twenty-eight days as the time unit is shown in Figure 8 and Figure 9.

Figure 9 shows the training error rate at each time point under the time unit of twenty-eight days. Taking twenty-eight days as the time unit, the mean ± 1 standard deviation, and the difference between the mean ± 0.5 and 1 standard

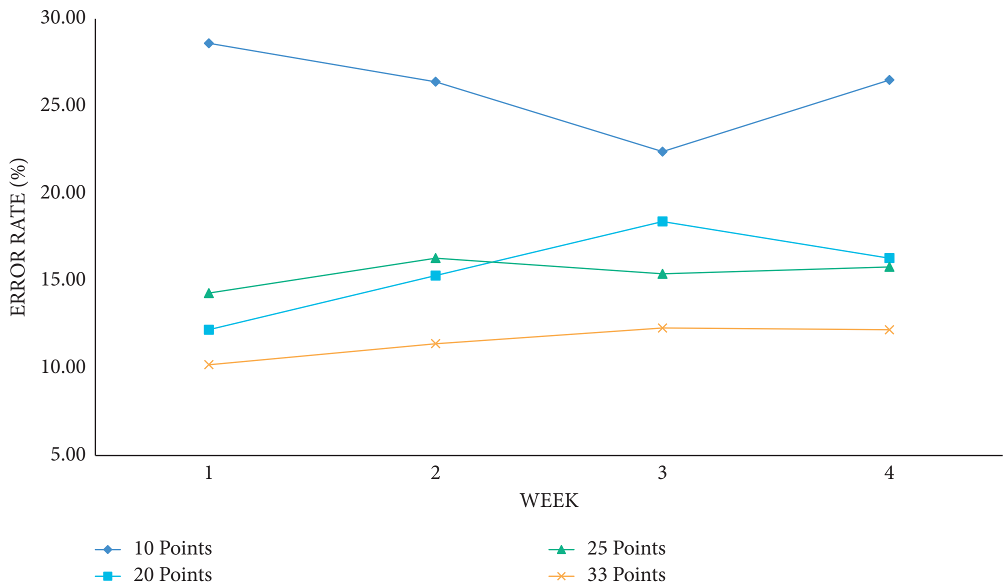

Figure 9: The training error rate at each time point with twenty-eight days as the time unit.

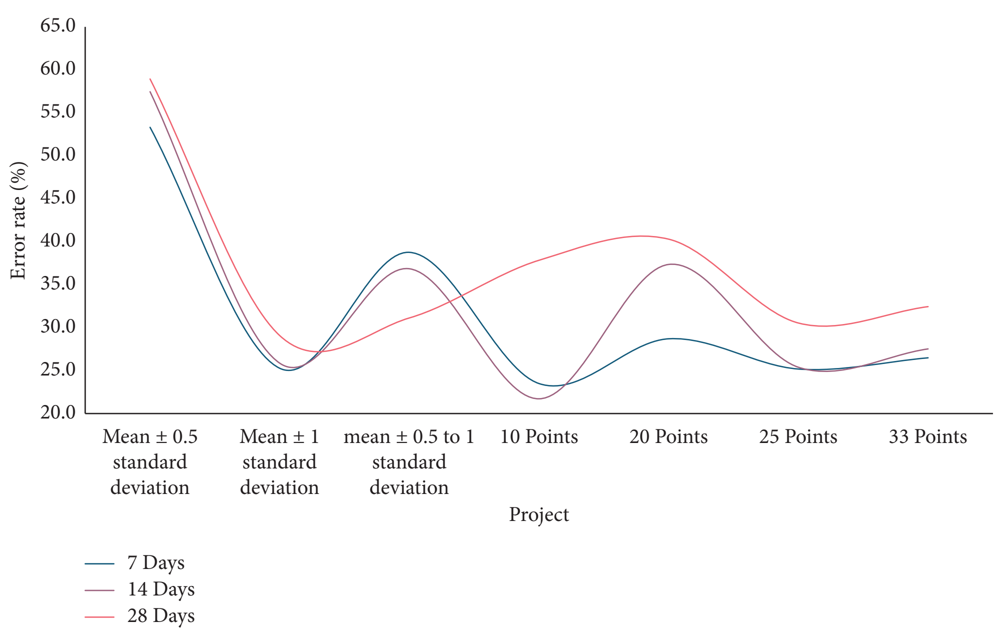

Figure 10: Prediction error rate at each time point in different time units.

deviation, the average performance for error rates is low, all below 40%. As mentioned earlier, the relationship between the accumulation over time and the decrease in error rate becomes less and less obvious, and the way of representing the time forecast in months is not ideal.

5.3. Prediction Error Rate Analysis of Different Grade Classification Methods. The decision-making rules of learning behavior and learning effect of various time units and different grades can be predicted for all students taking the course under different time units, but these decision-making rules are used regardless of the type of grades used. The accuracy of predicting a student's overall learning behavior and learning effect is not very good. Each time point under different time units will be used as the analysis point of observation and prediction in this subsection. The average training error rate in different time units for each time point: the prediction error rate at each time point under different time units is shown in Figure 10.

From Figure 10, an interesting phenomenon is found for the prediction error rates of high-segmentation groups at various time points in different time units; that is, from the perspective of seven days as a time unit, each classification method is the error rate at the beginning. The lowest is the lowest and then gradually increases. The effect of prediction in different time units is not very different. However, different classification methods of grades have a strong relationship with the effect of prediction for high-scoring groups. In this article, different grade classification methods are used to analyze and predict the whole students. All grade classification methods are effective in describing decision rules. No matter what grades classification method is used, the error rate of students' grades distribution is predicted to be below 40%. Other predictions are good, and it can be seen that in terms of average predictions, the results analyzed in this study can indeed effectively predict the distribution of academic performance.

To summarize, the longer the time unit, the less obvious the effect of lowering the error rate. High-scoring students' learning behavior, on the other hand, is more difficult to predict. The error rate starts out low and gradually rises. The effect of various grade classification methods on the prediction will then be examined. Whether it is seven days or seven months, the prediction effect is the same. Most grade classification methods can be significantly reduced after the eighth week, whether in terms of time units of 14 days or 28 days. This has more meaning for teachers because it means that the students' learning status and learning behavior can be observed in real time during the semester using the method used in this study, and which students may fall into the low-scoring group can be predicted in advance using the method used in this study. Students with low learning effectiveness are identified so that teachers or teaching assistants can provide immediate assistance in order to achieve targeted programme teaching.

6. Conclusions

The goal of this study is to develop an integrated analysis algorithm that will provide teachers with decision-making rules as auxiliary information for teaching, allowing them to instantly understand students' learning status during class and provide different teaching or assistance to students with different learning behaviors. It can help teachers and teaching assistants understand what kind of learning behavior students perform in the course, which may lead to a final academic performance of a high or low score, and can observe the attribute value changes of related learning behaviors when the same course is offered again, using intelligent information technology to analyze the decision-making rules between students' learning behavior and learning effectiveness in each course. This study uses the same course in different semesters as the verification object, and the data from two semesters as training and test data, respectively, and the training and test error rates in decision tree analysis as verification indicators to try to pass different levels of verification. It also tries out different grade classification methods to see which one is the best; the analysis objects are divided into three categories: overall students, high-scoring students, and low-scoring students. And in this way, you can examine the learning habits of various students and draw some useful conclusions. Learning records are analyzed through the time dimension using the classification analysis method in data mining, and individual course decision-making rules are generated to give teachers a better understanding of the possible relationship between students' learning behaviors and learning outcomes. This article presents a comprehensive analysis algorithm based on intelligent information technology, and the decision rules generated can predict students' learning behavior to a degree. Teachers and experts who can verify and provide feedback on these decision rules will help them become more widely used teaching aids. It can be used in conjunction with CAI to provide teachers with more information about relevant learning records.

Data Availability

The data used to support the findings of this study are available from the corresponding author upon request.

Conflicts of Interest

The author does not have any possible conflicts of interest.

References

[1] Z. Xu, K. K. R. Choo, A. Dehghantanha, R. Parizi, and M. Hammoudeh, Eds., *Cyber Security Intelligence and Analytics*, vol. 928, Springer, Salmon Tower Building New York, 2019.

[2] M. A. Alomari and M. O. Jabr, "The effect of the use of an educational software based on the strategy of artificial intelligence on students' achievement and their attitudes towards it," *Management Science Letters*, vol. 10, pp. 2951–2960, 2020.

[3] L. CuI, "A preliminary study on the management strategy of university personnel files based on artificial intelligence technology," *Journal of Electronic Research and Application*, vol. 5, no. 2, pp. 1–4, 2021.

[4] Z. Zhou, K. Yu, and S. O. Economics, "Research on the teaching reform of college students' mental health education under the strategy of "new economy and management"," *Journal of Heihe University*, vol. 23, no. 2, pp. 55–63, 2019.

[5] W. Tan, "Research on the online interactive mode of "one village, one university student" program course: from an OBE perspective," *OALib*, vol. 08, no. 9, pp. 1–13, 2021.

[6] M. C. Kaptein, P. Markopoulos, B. D. Ruyter, and E. Aarts, "Two acts of social intelligence," *AI & Society*, vol. 28, no. 12, pp. 339–348, 2011.

[7] H. Zhou, J. Lu, Y. Huang, and Y. Chen, "Research on key technology of classroom teaching evaluation based on artificial intelligence," *Journal of Physics: Conference Series*, vol. 1757, no. 1, Article ID 012014, 2021.

[8] X. Luo and L. Xie, "Research on Artificial Intelligence-Based Sharing Education in the Era of Internet+," in *Proceedings of the 2018 International Conference on Intelligent Transportation, Big Data & Smart City (ICITBS)*, pp. 335–338, Xiamen, China, 25-26 January 2018.

[9] X. Huang, J. Zhao, J. Fu, and X. Zhang, "Effectiveness of ideological and political education reform in universities based on data mining artificial intelligence technology," *Journal of Intelligent and Fuzzy Systems*, vol. 40, no. 2, pp. 1–12, 2020.

[10] A. V. Kirichenko, A. V. Reznichenko, and Z. I. A. Ranepa, "The methodology of applying the akmeologikal approach to education in a digital economy based on artificial

intelligence," *Scholarly Journal Of Psychology And Behavioral Sciences*, vol. 3, 2020.

[11] L. Cui, "A preliminary study on the management strategy of university personnel files based on artificial intelligence technology," *Journal of Electronic Research and Application*, vol. 5, no. 2, pp. 1–4, 2021.

[12] H. Jie and J. Library, "Research on the application of artificial intelligence technology in information retrieval of public library," *Electronics Test*, vol. 15, no. 22, pp. 59–69, 2018.

[13] Y. S. Zhang, Y. X. Xu, W. L. Fan, and Z. Y. Zhang, "Relationship between residual feed intake and production traits in a population of F_2 d," *The Journal of Poultry Science*, vol. 56, no. 1, pp. 27–31, 2019.

[14] L. U. Ting-Ting, "Research on overseas student management strategy in higher vocational colleges: taking changzhou college of information technology as an example," *Journal of Changzhou Vocational College of Information Technology*, vol. 22, no. 3, pp. 14–35, 2012.

[15] Y. Liu and T. University, "Research on strategy of university archives management under artificial intelligence environment," *Office Informatization*, vol. 14, no. 5, pp. 91–102, 2019.

[16] Y. Chen and Y. Chen, "Research on the application and influence of artificial intelligence technology," *Journal of Physics: Conference Series*, vol. 1952, no. 4, Article ID 042007, 2021.

[17] X. Zhang and L. Chen, "College English smart classroom teaching model based on artificial intelligence technology in mobile information systems," *Mobile Information Systems*, vol. 2021, no. 2, Article ID 5644604, 12 pages, 2021.

[18] Q. H. Jin, "Research on the possibility and development trend of artificial intelligence technology applied to music education," *Journal of Hubei Correspondence University*, vol. 14, no. 22, pp. 67–80, 2018.

[19] M. Kordaki, T. Daradoumis, D. Fragidakis, and M. Grigoriadou, "Adapting the collaborative strategy 'students team Achievement divisions' in an information technology work place," *Intelligent Adaptation and Personalization Techniques in Computer-Supported Collaborative Learning*, vol. 408, pp. 131–153, 2012.

[20] Y. Hu, Q. Q. Li, and S. W. Hsu, "Interactive visual computer vision analysis based on artificial intelligence technology in intelligent education," *Neural Computing & Applications*, vol. 20, pp. 1–19, 2021.

[21] Y. Zhang, "Research on precision teaching in artificial intelligence education model based on precision interactive behavior analysis of teaching," *Adult Education*, vol. 17, no. 3, pp. 26–36, 2019.

[22] Y. J. Liu and H. U. Rong, "Research on the information security situational awareness system based on big data and artificial intelligence technology," *Management & Technology of SME*, vol. 2, no. 10, pp. 47–53, 2019.

[23] N. Yang and Y. Wang, "Study on education resource search engine based on artificial intelligence technology[J]," *Journal of Jilin Institute of Architecture & Civil Engineering*, vol. 31, no. 19, pp. 58–64, 2012.

[24] X. Lv and M. Li, "Application and research of the intelligent management system based on Internet of Things technology in the era of big data," *Mobile Information Systems*, vol. 2021, no. 16, Article ID 6515792, 1-6 pages, 2021.

Hindawi
Computational Intelligence and Neuroscience
Volume 2022, Article ID 2307149, 10 pages
https://doi.org/10.1155/2022/2307149

Research Article

Prediction Algorithm of Uncertain Fund Demand for Regional Economics Using GM Model and Few-Shot Learning

Baoqian Wang

School of Economics and Finance, Zhanjiang University of Science and Technology, Zhanjiang 524094, China

Correspondence should be addressed to Baoqian Wang; 20148844@stu.sicau.edu.cn

Received 24 May 2022; Revised 9 June 2022; Accepted 10 June 2022; Published 1 July 2022

Academic Editor: Xin Ning

The forecast of capital demand has the characteristics of uncertainty. There are known and unknown information about the capital demand for regional economic development. In fact, there are also some in between, that is, uncertain. Consumption is the ultimate goal of production and a key link in realizing a virtuous circle of economic development. This paper uses the GM (1, 1) model to compare the predicted value of the test area with the actual value in 5 years, and the loudness is as high as 90%. Under the guidance of the profit model, the regional economic capital demand has a decisive influence on the regional economic development. The predictive analysis model of capital needs is conducive to fully mobilizing the impact of infrastructure construction of all parties and is an important factor affecting economic development. The mathematical model proposed in this paper is helpful for deepening the research on the management of regional economic development and enriching the theoretical system of regional economic development.

1. Introduction

At present, grey system modeling methods are mainly used for grey prediction and decision-making, and have achieved good results. The construction of grey model, through the action of grey generation or sequence operator, weakens randomness, taps potential laws, and realizes a new leap in establishing continuous dynamic differential equations using discrete data sequences through the exchange of grey difference equations and grey differential equations. The grey prediction of the sequence formed by the system behavior characteristic index value is called sequence prediction [1, 2]. In the GM (1, 1) model, GM (1, 1) represents a first-order, one-variable differential equation prediction model, which is a first-order single-sequence linear dynamic model, which is mainly used for time series prediction. For the sequence of system behavior characteristic indicators, through different combinations and trade-offs, multiple derived sequences are formed, and a prediction model is established for it.

It is difficult to distinguish the quantitative relationship between factors and the primary and the secondary relationship between systems among many factors in the objective world due to lack of data, incomplete information, and uncertainty. The goal of grey correlation analysis is to figure out how closely factors in a system are related. The abovementioned freight volume and cargo turnover can both represent capital demand, but which one is more representative? A type of social and economic activity that leads to demand is capital demand. The correlation analysis with the two indicators, expressed in terms of income elasticity value, can determine which indicator is more representative [3, 4]. The main issues arise during the transition from one mode of regional economic development to another. These issues are most visible in the following areas: regional energy consumption is excessive, and the growth mode is extensive, which makes it difficult to adjust and optimize the industrial structure; in the process of rapid regional economic growth, environmental protection issues have not been prioritized, resulting in serious pollution; for a long time, the region's primary sources of income were investment and export. Consumption has been insufficient for a long time, and the development of investment and consumption is uncoordinated; the industrial structure is unreasonable, traditional industries remain dominant, the proportion of high-tech industries is low, there are issues of weak agricultural foundations, low industrial quality, and lagging development of service industries: urban and rural; the industrial structure is unreasonable, traditional industries remain dominant, the proportion of high-tech industries is low; there are problems of weak agricultural foundations, low industrial quality, and lagging development of unbalanced regional development, widening income gaps between residents; low investment in scientific and technological talents, education, and research and development, affecting labour quality improvement; insufficient independent innovation ability, serious lack of independent brands; overseas enterprises' investment difficulties, and so on [5].

The innovation of this paper is to combine the grey system theory method with the classical consumption demand theory and econometric method, conduct a comprehensive analysis of regional consumption demand and regional economic development capital demand, combine the income elasticity value and forecast income elasticity value, and make a comparison; it is concluded that the degree of acquaintance between the predicted value and the actual value is as high as 90%. The structure of this paper is as follows. Section 1 studies and summarizes the related research on regional economic development theory and grey system model. Section 2 briefly introduces the concept of grey system model and establishes a mathematical model based on grey system model. Section 3 puts forward the relationship between regional residents' income and regional economic development, introduces a certain region's consumption expenditure as a sample, and conducts model statistics. Section 4 predicts and compares sample values based on GM (1, 1) model. Section 5 summarizes the full text.

2. Related Work

With the development of human society, especially the development of industrial revolution and information technology, human's understanding of the connotation of infrastructure has experienced a process of continuous development of levels and scope. In the mid-19th century, Hong et al. put forward the idea of social indirect capital on the basis of summarizing earlier economists' arguments, pointing out that social indirect capital includes all those foundations such as electricity, transportation, or communication industry [6]. Nowak et al. based on uncertainty and rational expectations, put forward the theory of excessive sensitivity, and the theoretical framework of consumption under uncertainty has been initially established [7]. Liu et al. introduced uncertainty into consumption theory for the first time and proposed a random walk model to analyze the influence of uncertainty factors on consumption [8]. Zu et al. put forward a hypothesis theory, which holds that there are two different types of consumers in the economy who choose consumption in each period according to the life cycle hypothesis and decide consumption behavior according to current income [9]. Man and Chen simulated and verified the buffer stock model through the backward method and found that there is a very significant linear relationship between income uncertainty, persistent income, and wealth goals. Consumption structure is also an important aspect that reflects the level of residents' consumption demand [10]. René et al. believe that infrastructure includes two categories: one is core infrastructure, mainly referring to transportation and electricity, whose role is to increase the productivity of physical capital and land, and the other is human infrastructure, including healthcare and education [11]. Ma et al. put forward the idea of social indirect capital on the basis of summarizing the early economists' discussions, pointing out that social indirect capital includes all those basic industries such as electricity, transportation, or communication [12].

It is further pointed out that social indirect capital is divided into broad and narrow senses, and it is believed that in its broad sense, it includes everything from law, order and education, public health to transportation and communication, power, water supply, and agricultural indirect capital such as irrigation and drainage systems. Public service [13]: regarding the development scale of infrastructure, it mainly focuses on the relationship between total public capital expenditure and total output, the relationship between physical stock of infrastructure and total output, infrastructure, and sectoral output, and the difference between infrastructure and regional economic growth. Research: the general conclusion is that there is an obvious elastic coefficient between the total expenditure of infrastructure and the total output [14]. The "priority development theory" advocated by Chen et al. believes that in order to rapidly change the face of economic backwardness, a region must concentrate its energy, invest a large amount of money at one time, and give priority to the development of infrastructure [15]. Zeng and Luo used ELES and AIDS models to compare and analyze the consumption demand of regional residents [16]. Ho et al. studied the evolution mechanism, characteristics, and laws of regional residents' consumption behavior from multiple perspectives, and made an empirical analysis on the influencing factors of regional residents' consumption behavior by combining the western neoclassical consumption theory with the actual situation in China [17]]. Liu et al. proposed an extended linear expenditure system model that further considers income distribution, and preliminarily constructed a more explanatory rural residents' consumption demand function according to the actual situation of the region. The function theory research has injected new blood [18].

The research results of the above scholars have important reference and reference significance for promoting the theory of capital demand for regional economic development, based on the above literature. However, most consumer demand theory research uses more mature economic theories of the grey system model to conduct exploratory and confirmatory analysis of the actual situation in the region; however, due to data availability and authenticity limitations and some scholars' lack of data processing methods, the results are frequently unsatisfactory, resulting in weak convincing. Furthermore, related researchers share a common research perspective on regional economic consumption demand. Majority of academic research focuses on the structure of economic development capital demand, but there is a lack of in-depth and detailed research on consumption rate and the factors that influence consumption demand. At the same time, some scholars have glaring flaws in their sample data selection or analysis methods.

3. Concept and Model Establishment of Grey System

The data model established by using grey theory is not the original data sequence, but the data model generated by a series of processing. The GM (n, m) model is the basic model of the grey forecasting method, where n is the order of the differential equation, and m is the number of variables. The GM (1, 1) model is a grey model with a differential equation order of 1 and a variable unit digit of 1. It is the simplest grey prediction model.

The modeling steps of the GM (1, 1) prediction model are as follows:

Suppose the original data sequence is (1):

$$X^{(0)} = \left(x^{(0)}(1), x^{(0)}(2), \ldots, x^{(0)}(n)\right). \tag{1}$$

Due to the low regularity and large fluctuation of the original data, it will adversely affect the prediction results [19, 20]. Therefore, in the grey prediction, the data is usually processed by the cumulative generation, and the cumulative generation sequence is (2):

$$X^{(1)} = \left(x^{(1)}(1), x^{(1)}(2), \ldots, x^{(1)}(n)\right), \tag{2}$$

Where, $X^{(1)}(k) = \sum_{i=1}^{k} x^{(0)}(i)$, $k = 1, 2, \ldots, n$ is the number of original data.

Define the data sequence on the basis of the data sequence generated after the accumulation $Z^{(1)}$ as $X^{(1)}$. The next-to-neighbor mean generation sequence is

$$Z^{(1)} = \left(z^{(1)}(2), z^{(1)}(3), \ldots, z^{(1)}(n)\right), \tag{3}$$

where $z^{(1)} = 1/2\left(x^{(1)}(k) + x^{(1)}(k-1)\right), k = 2, 3, \ldots, n$ is the number of original data.

Then, define the basic form of GM (1, 1) as (4):

$$x^{(0)}(k) + az^{(1)}(k) = b. \tag{4}$$

The parameters in formula (4) are:a represents the coefficient of development, the parameter b represents the grey action.

Use the least squares estimation method to find (5)

$$[a, b]^T = \left(B^T B\right)^{-1} B^T Y. \tag{5}$$

Perform whitening (6):

$$\frac{dx^{(1)}}{dt} + ax^{(1)} = b. \tag{6}$$

Get the time response sequence (7):

$$\widehat{x}(k+1) = \left(x^0(1) - \frac{b}{a}\right)e^{-ak} + \frac{b}{a}, k = 1, 2 \ldots. \tag{7}$$

Although the GM (1, 1) model has made great improvements in prediction accuracy and data requirements than other prediction models, it is easy to cause errors when the original data rules are weak and there are abnormal or missing data. Therefore, this paper establishes an improved grey forecasting model.

Assuming the regional economic development fund demand as a system factor, the data sequence of relevant factors is (8):

$$X_i = \left(x_i(1), x_i(2), \ldots, x_i(n)\right) \quad, i = 1, 2, \ldots. \tag{8}$$

Finally, according to the system factors, the evaluation value of the correlation coefficient is obtained, that is, the required correlation degree (9):

$$r_{0i} = \frac{1}{n}\sum_{k=1}^{n} r_{0i}(k), \quad i = 1, 2, 3, \ldots. \tag{9}$$

The value of r_{0i} is between 0 and 1, and the larger the value, the higher the correlation between the modification factor and the feature sequence.

4. Construction of Forecasting System of Fund Demand for Regional Economic Development

4.1. Analysis on the Composition of Investment and Financing Mechanism of Regional Economic Infrastructure. The essence of the investment and financing mechanism for regional economic infrastructure projects is to promote competition through the reform of the investment and financing system, and to realize that the market-oriented investment and financing mechanism plays a fundamental role in the allocation of various resources for regional economic infrastructure projects [21].

This paper believes that the construction of a market-oriented investment and financing mechanism system for regional economic infrastructure projects should include three mechanisms: investment and financing external restraint mechanism, investment and financing subject interest coordination mechanism, and investment and financing operation mechanism, based on the logical structure of investment and financing operation of regional economic infrastructure projects. The external investment and financing mechanism is the external environment constraint mechanism for the operation of regional economic infrastructure investment and financing projects, and it is the existence condition and foundation of the regional economic infrastructure investment and financing mechanism. Policy mechanisms, institutional guarantee mechanisms, and payment mechanisms are all included. The investment and financing subjects' interest coordination mechanism is a game and is a coordination mechanism for the behavioral constraints of investment and financing subjects of regional economic infrastructure projects, as well as their own interests. In the process of investing in and financing regional economic infrastructure projects, the investment and financing operation mechanism is the financing demand, investment, and financing channel and method selection, and operation procedure mechanism. External mechanisms for investment in and financing of regional economic infrastructure projects, as well as a mechanism to coordinate the interests of investment and financing entities and an investment and financing operation mechanism, are required [22]. The investment and financing mechanism is shown in Figure 1.

4.2. The Relationship between Economic Development and Consumer Demand. The demand for funds for economic development is reflected not only in terms of quantity but also in terms of consumption structure. The absolute quantity of various consumer goods reflected in a certain form of measurement (physical form or value form, this paper uses value form) is referred to as consumption quantity; the proportion of various consumer goods in total consumption is referred to as consumption structure. The entire process of changes in the level of consumption demand is accompanied by changes in consumption quantity and structure. They are two aspects of consumption demand that are complementary to each other. The upgrading of the consumption structure often leads to the increase in consumption quantity, and the increase in consumption quantity in turn promotes the upgrading of the consumption structure, so that the level of consumption demand develops in a fast and positive direction. The general rule governing the evolution of residents' consumption structures is that when income levels are low, people's consumption expenditures go toward food, clothing, and other necessities. The proportion of consumption expenditures dedicated to development and enjoyment will skyrocket [23].

General principles of economics state that economic activity is the most efficient only when the private rate of return on an investment is close to or equal to the social rate of return. Therefore, the efficient economic development of regional consumer demand projects should also follow such a rule and strive to make various investment entities obtain their reasonable expected returns when investing in regional consumer demand. In the practice of economic development of regional consumer demand projects, the source of funds can include both domestic capital and international capital. The main bodies of domestic capital include governments, enterprises, financial institutions, residents, and non-profit institutions, while international capital includes governments, financial institutions, enterprises, and individuals of various countries. As the main body of economic development, the government focuses more on obtaining social benefits from the construction of regional consumer demand, while other economic development bodies are relatively more willing to obtain economic benefits. The combination of the two constitutes the total expected return of investment. When the actual income from the completion of the regional consumer demand project is close to the total expected income of each investment entity, it is a feasible investment behavior in theory. Financing portfolio structure, resulting in various financing models, is shown in Figure 2.

As shown in Figure 2, the size of the economic contribution (benefit) of the consumer demand infrastructure project is reflected in the degree of satisfaction that its output products bring to consumers. The monetary performance of this degree of satisfaction is the consumer, that is, including all stakeholders. Willingness to pay: under the condition of market economy, the willingness to pay price is the shadow price of the product, and the willingness to pay of consumers for the output of the project is the contribution of the project to the economy. Consumer willingness to pay can be further divided into two parts: actual consumer payment and consumer surplus. Consumer surplus is the balance of the currency that consumers are willing to pay more than the currency actually paid when purchasing a certain commodity.

Consumption demand refers to the various types of consumption materials consumed by residents in the process of consumption under certain social and economic conditions, which can be divided into two types: physical form and value form. Among them, the physical form is the most basic and primitive form of various types of consumption materials consumed in the consumption process represented by the physical quantity; and the value form is represented by currency in the consumption process and the types of consumption data, which are embodied in various living consumption expenditures in real economic life. By analyzing the value of various types of consumption data consumed by regional residents, the development level and changing trend of regional residents' consumption demand at different time periods are revealed. The consumption demand of various types of consumer goods of regional residents analyzed in this paper is expressed in the form of value.

4.3. Statistical Data Selection of Regional Residents' Consumption Demand. Since it is not easy to distinguish developmental and enjoyment expenditures, this article will facilitate the forecasting and calculation of regional economic development capital needs in the future. Referring to the consumption expenditure statistics of a certain place, the living consumption expenditures of residents in the modified area are divided into food, clothing, housing, household equipment, transportation and communication, and culture, education and entertainment, healthcare, and other goods and services. The specific statistics are shown in Tables 1 and 2.

5. Consumption Demand Forecast Based on GM (1, 1)

5.1. Model Parameter Estimates and Errors. From Table 1, it can be seen that the housing expenditure data in the eighth year is abnormal, which is not increased but decreased compared with the previous data. This abnormal data should be excluded when using the GM (1, 1) model for simulation. Taking the horizontal data in Table 1 as the original time series data, a GM (1, 1) model is established, respectively,

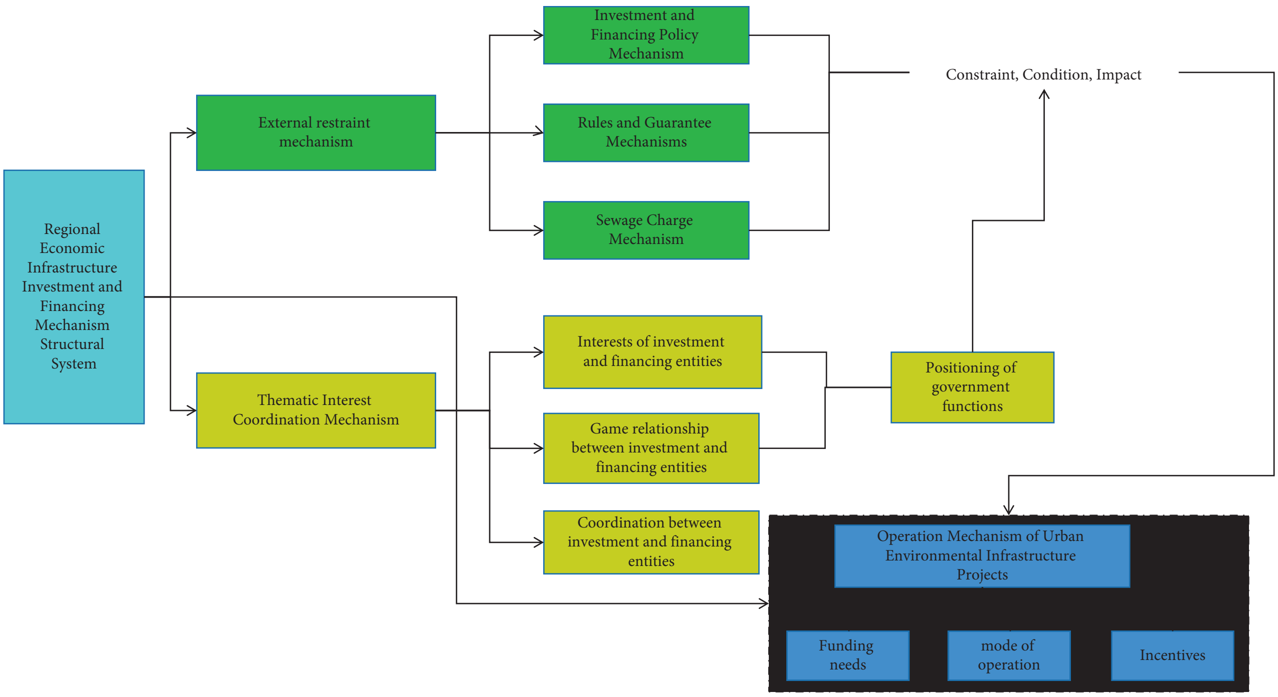

FIGURE 1: The structural system of regional economic infrastructure investment and financing mechanism.

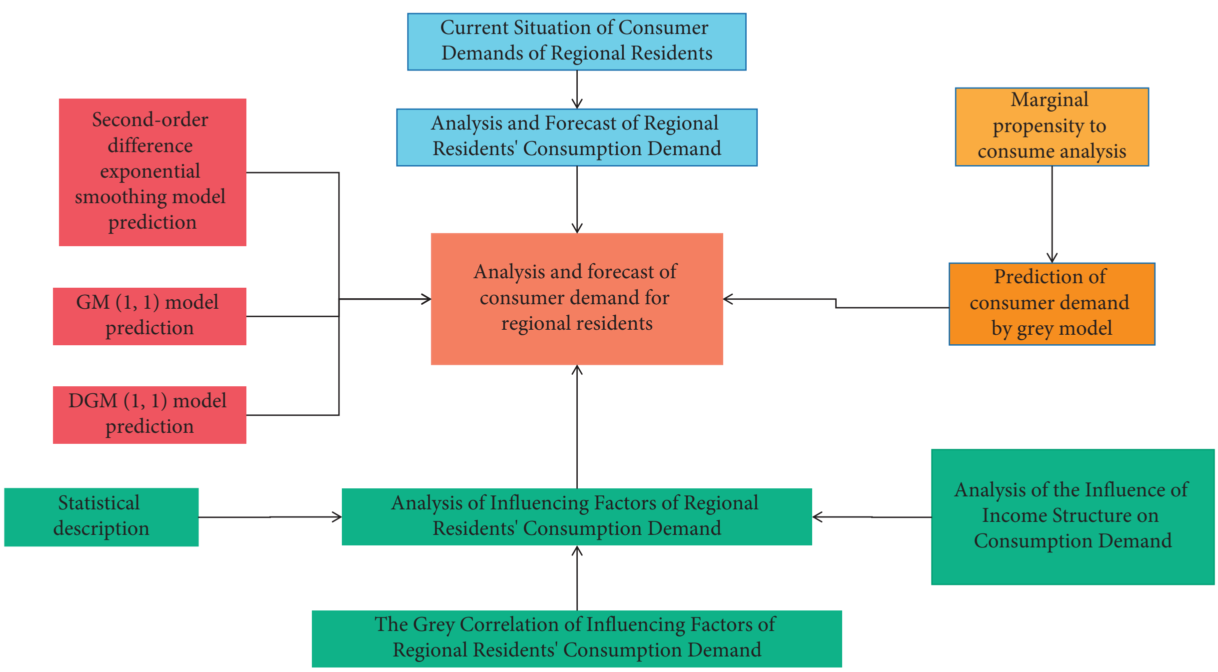

FIGURE 2: Investment and financing mechanism model of regional consumption demand and economic development.

and the average relative error of parameters a and b can be obtained as shown in Table 3 and Figure 3.

It can be seen from Figure 3 that the absolute value of the development coefficient a is less than 0.3, so GM (1, 1) can be used for medium- and long-term forecasting. The correlation degree and error are shown in Table 4 and Figure 4.

It can be seen from Figure 4 that the average relative error of other items except traffic communication is less than 5%, so the fitting accuracy is high. The average relative error of traffic communication is larger, reaching 7.245%, but it is within the acceptable range.

5.2. Model Based Parameter Estimation. The data required by the grey system model are the per capita net income of regional households, the total expenditure of living consumption, and the expenditure of its various components. From the data in Tables 1 and 3, the parameters b in Figure 3

Table 1: Average per capita net income and living consumption expenditure of residents in a certain region in 8 years (unit: yuan).

Project/year	1	2	3	4	5	6	7	8
Net income per capita ($A1$)	2236	2553	2871	3261	3852	4454	4807	5524
Living consumption expenditure ($A2$)	1509	1664	1892	2229	2676	3044	3388	3682
Food ($A3$)	727	808	859	911	1017	1166	1220	1371
Clothing ($A4$)	96	108	132	160	190	210	226	262
Residence ($A5$)	238	269	318	444	616	713	876	765
Household equipment supplies ($A6$)	63	64	83	105	136	170	204	254
Communications ($A7$)	100	121	160	221	269	291	310	401
Culture, education and entertainment ($A8$)	161	168	178	199	212	214	234	250
Healthcare ($A9$)	91	95	123	141	173	215	243	288
Other goods and services ($A10$)	33	31	39	49	62	66	76	90

Table 2: Composition of per capita living consumption expenditure of residents in a certain region in 8 years (unit: %).

Project/year	1	2	3	4	5	6	7	8
Living consumption expenditure ($A2$)	100	100	100	100	100	100	100	100
Food ($A3$)	48.18	48.56	45.4	40.87	38	38.3	36.01	37.24
Clothing ($A4$)	6.36	6.49	6.98	7.18	7.1	6.9	6.67	7.12
Residence ($A5$)	15.77	16.17	16.81	19.92	23.02	23.42	25.86	20.78
Household equipment supplies ($A6$)	4.18	3.85	4.39	4.71	5.08	5.58	6.02	6.9
Communications ($A7$)	6.63	7.27	8.46	9.91	10.05	9.56	9.15	10.89
Culture, education and entertainment ($A8$)	10.67	10.1	9.41	8.93	7.92	7.03	6.91	6.79
Healthcare ($A9$)	6.03	5.71	6.5	6.33	6.46	7.06	7.17	7.82
Other goods and services ($A10$)	2.19	1.86	2.06	2.15	2.35	2.14	2.21	2.47

Table 3: Average error parameters of parameters a and b.

Project	A	B
Net income per capita ($A1$)	0.6623	0.1284
Living consumption expenditure ($A2$)	0.1497	0.1312
Food ($A3$)	0.9232	0.0919
Clothing ($A4$)	0.1986	0.1336
Residence ($A5$)	0.3151	0.2328
Household equipment supplies ($A6$)	0.3792	0.2201
Communications ($A7$)	0.8973	0.1674
Culture, education and entertainment ($A8$)	0.6736	0.0639
Healthcare ($A9$)	0.4828	0.1759

Table 4: Average relative error (unit: %).

Project	r	Error
Net income per capita ($A1$)	2.235	2.657
Living consumption expenditure ($A2$)	2.184	1.654
Food ($A3$)	1.336	3.291
Clothing ($A4$)	1.842	2.941
Residence ($A5$)	3.842	4.325
Household equipment supplies ($A6$)	2.648	3.626
Communications ($A7$)	5.231	7.245
Culture, education and entertainment ($A8$)	3.482	1.228
Healthcare ($A9$)	1.254	3.327

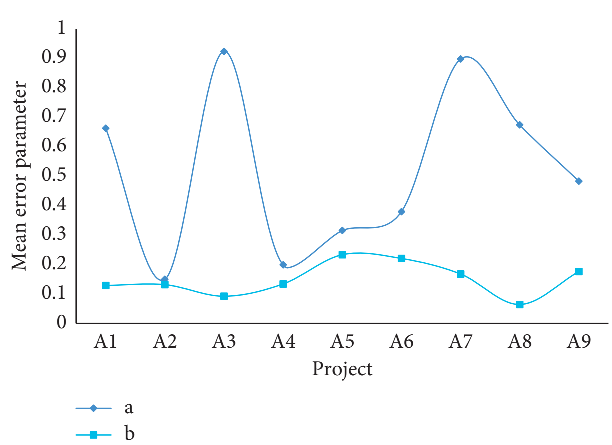

Figure 3: Error parameters of parameters a and b.

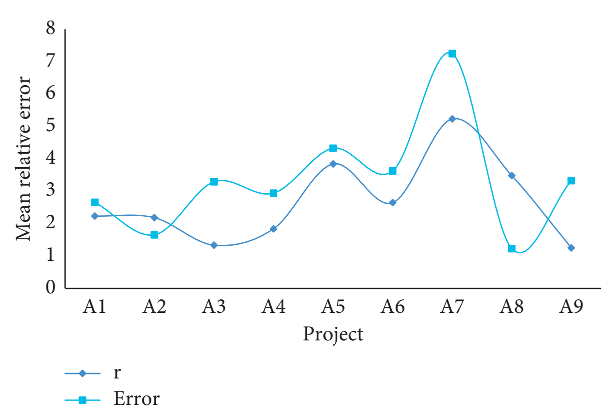

Figure 4: Average error parameters.

Table 5: Estimated values of the parameters of the living consumption expenditure of regional residents.

Project	1–8 years sample period		9–13 forecast period	
Net income per capita (*A*1)	*b*1	*r*	*b*2	*r*
Living consumption expenditure (*A*2)	65	0.6970	122	0.7068
Food (*A*3)	299	0.1924	511	0.1563
Clothing (*A*4)	13	0.0505	17	0.0507
Residence (*A*5)	212	0.2007	1504	0.4103
Household equipment supplies (*A*6)	85	0.0594	360	0.1059
Communications (*A*7)	89	0.0875	202	0.1059
Culture, education and entertainment (*A*8)	103	0.0268	153	0.0181
Healthcare (*A*9)	56	0.0616	185	0.0836

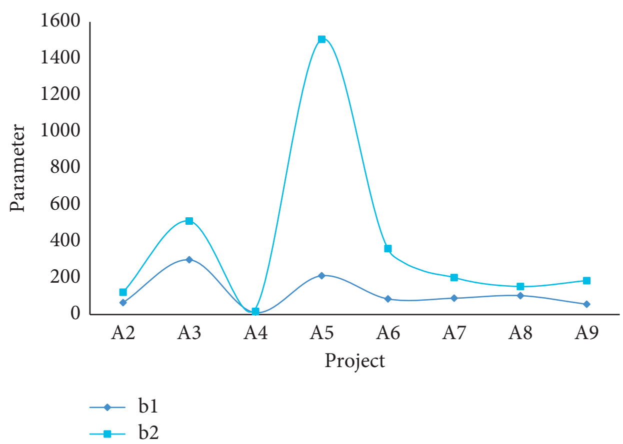

Figure 5: Comparison of parameter *b* samples and predictions.

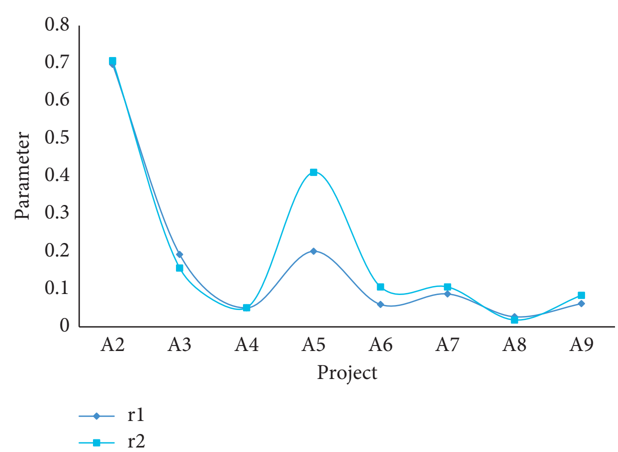

Figure 6: Comparison of parameter *r* samples and predictions.

are estimated by the least squares method in the mathematical model established above. The results are shown in Table 5, Figures 5 and 6.

It can be seen from the table that with the continuous improvement of income level, the consumption desire of regional residents has increased significantly. The marginal propensity to consume of regional residents' total living consumption expenditure increased from 0.6970 in the sample period to 0.7068 in the forecast period. This shows that regional residents will use 70.68% of the new net income for consumption; that is to say, for every RMB 1 increase in disposable income, regional residents will spend RMB 0.7068 for consumption. And the new net income is mainly used for food and housing consumption, which will help to improve the diet and living standards of regional households. It can also be seen from the table that the marginal propensity to consume of regional residents has grown the fastest, from 0.2007 in the sample period to 0.4103 in the forecast period, more than doubling. This shows that with the improvement of living standards, regional residents have a strong demand for the improvement of living conditions after the basic satisfaction of food and clothing. Followed by household equipment supplies and services, which increased from 0.0594 to 0.1059, an increase of 78.28%. This shows that the residents of the region are paying more attention to the improvement of basic living needs such as clothing, food, and housing, and at the same time, they are also pursuing more development-oriented and enjoyment-oriented consumption. Because durable household equipment such as washing machines, refrigerators, air conditioners, shower water heaters, mobile phones and color TVs, video cameras, home computers, and medium- and high-end musical instruments not only bring more enjoyment in life to the residents of the vast area, but also its own development has a great role in promoting. Therefore, the government should correctly guide the consumption of durable consumer goods by regional residents, continue to strengthen policies to strengthen and benefit farmers such as "home appliances to the countryside," and strive to improve the overall quality of regional residents while promoting domestic demand. In addition, the marginal propensity to consume for transportation, communication and healthcare also increased by varying degrees. Transportation and communication increased from 0.0875 to 0.1059, an increase of 21.03%; healthcare increased from 0.0616 to 0.0836, an increase of 35.71%. This shows that the regional residents' consumption demand for these two items has also increased. More travel, exchanges, and attention to physical health will enable them to develop their spirit and body well, and contribute to the construction of a new socialist region and lay the foundation for cultivating more new types of residents. However, the marginal propensity to consume of food and cultural, educational, and recreational goods and services has decreased by varying degrees. Food decreased from 0.1924 to 0.1563, a decrease of 18.76%; cultural, educational, and recreational goods and services decreased from 0.0268 to 0.0181, a

Table 6: Income elasticity of regional residents.

Project		A2	A3	A4	A5	A6	A7	A8	A9
Sample period	1	1.0328	0.5917	1.1762	1.8856	2.1082	1.9565	0.3722	1.5136
	2	1.0694	0.6079	1.1938	1.9048	2.3695	1.8462	0.4073	1.6554
	3	1.0577	0.6431	1.0984	1.8120	2.0547	1.1571	0.4323	1.4378
	4	1.0197	0.6887	1.0293	1.4740	1.8448	1.2911	0.4392	1.4247
	5	1.0033	0.7287	1.0238	1.2550	1.6824	1.2530	0.4870	1.3716
	6	1.0199	0.7349	1.0711	1.2537	1.5563	1.3393	0.5578	1.2761
	7	0.9889	0.7581	1.0741	1.1013	1.3997	1.3568	0.5504	1.2186
	8	1.0457	0.7752	1.0647	1.4492	1.2918	1.2054	0.5922	1.1815
Forecast period	9	1.0277	0.6615	1.0552	2.2983	2.1000	1.4209	0.4291	1.5193
	10	1.0248	0.6863	1.0476	2.0691	1.9174	1.3657	0.4570	1.4479
	11	1.0220	0.7118	1.0437	1.8613	1.7476	1.3140	0.4886	1.3824
	12	1.0193	0.7381	1.0375	1.6770	1.5962	1.2634	0.5211	1.3180
	13	1.0163	0.7655	1.0316	1.5100	1.4572	1.2159	0.5562	1.2570

decrease of 32.46%. The downward trend in the marginal propensity to consume food items is expected. Because, at this stage, the food needs of regional residents have been basically met and will be gradually increased. Therefore, with the basic satisfaction of regional residents' food consumption needs, their desire for food consumption needs will decrease. This is consistent with the Law of Diminishing Marginal Utility stage 3 and is basically consistent with the current situation in the region. The marginal propensity to consume of cultural, educational, and recreational goods services is the lowest in both the sample period and the forecast period, and continues to decline. It can be seen that the current consumption of cultural, educational, and recreational articles and services by regional residents is still at a very low level and has a downward trend, which may be closely related to the consumption habits of regional residents who focus on food consumption and less on spiritual consumption.

5.3. Regional Economic Development and Income Elasticity Analysis. When the income changes by 1% and the price remains unchanged, the percentage of change in consumption demand is an important indicator of the capital demand for regional economic development. w_k is the income elasticity of item k consumer goods demand, as shown in (10) .

$$w_k = \frac{dV_k}{dY}\frac{Y}{V_k} = \frac{\beta_k Y}{V_k}. \tag{10}$$

From the data in the table below and according to formula (10), the income elasticity of various consumption demands of regional residents in each year of the sample period and the forecast period can be calculated as shown in Table 6, Figures 7 and 8.

The income elasticity of regional residents' total consumption demand during the sample period and the forecast period is greater than 1, with the exception of the seventh year, indicating that regional residents' overall consumption demand is growing faster than their income. The income elasticity of consumer demand for clothing, residence, household equipment supplies and services, transportation

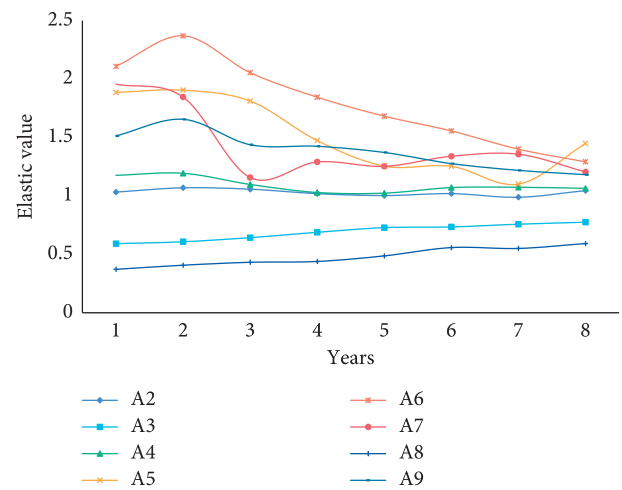

Figure 7: Income elasticity of regional residents during the sample period.

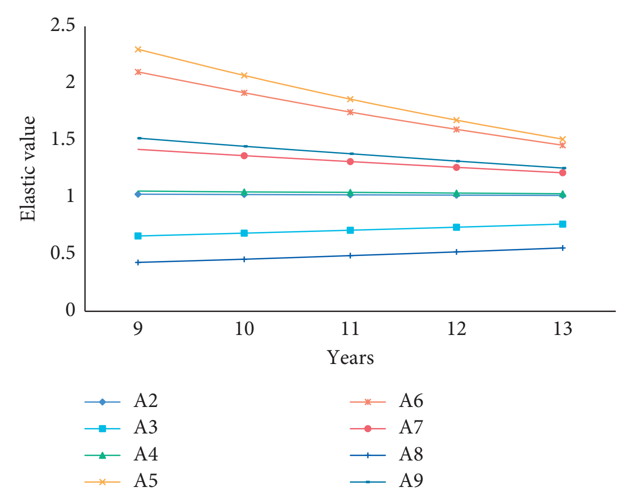

Figure 8: Income elasticity of regional residents during the forecast period.

and communication, and medical care is significantly greater than 1, indicating that regional residents' consumption demand for these types of goods and services is significantly

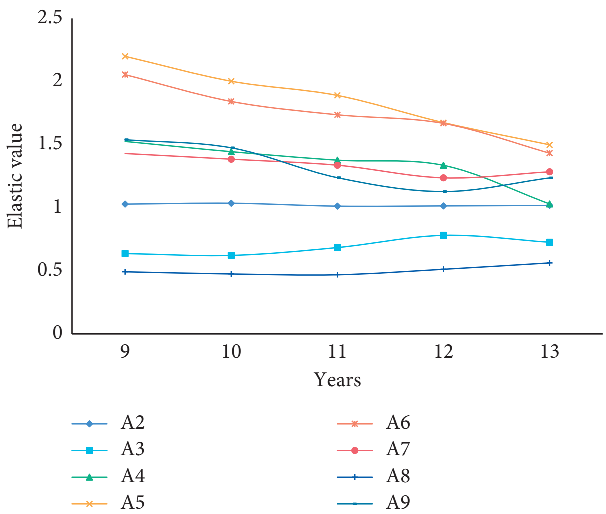

Figure 9: Income elasticity of residents in the sample area from 9 to 13 years.

higher than their income growth rate; the two items of household equipment, supplies, and services are significantly higher than the other items, indicating that regional residents' consumption demand for these types of goods and services is significantly higher than their income growth rate; and the two items of household equipment, supplies, and services are significantly higher. As a result, first, in the coming years, such consumer goods will become a powerful lever for leveraging consumer demand, contributing more to economic development. Second, the income elasticity of consumer demand for food and cultural, educational, and recreational goods and services are all less than 1, indicating that these two consumption demands are growing at a slower rate than residents' income; in particular, the income elasticity of consumer demand for cultural, educational, and recreational goods and services is much lower than 1. It demonstrates that regional residents' demand for such consumption is currently growing at a much slower rate than their income.

Based on this, we select the statistics of residents' consumption income and expenditure in the modified region from 9 to 13 years and compare it with the predicted elasticity value as shown in Figure 9.

No matter in the sample period or the forecast period, the income elasticity of consumer demand for each item whose income elasticity of consumption demand is greater than 1 shows a downward trend; at the same time, the income elasticity of consumption demand is less than 1 for food, cultural, educational, and recreational goods and services. However, the income elasticity of consumer demand shows a clear upward trend; thus, the total income elasticity of consumer demand tends to converge toward 1. The similarity between the predicted income elasticity value and the actual elastic growth value is 90%. With the development of the regional economy and the improvement of the living standards of the regional residents, the growth rate of capital demand will keep pace with the income growth.

This paper uses the grey relative correlation analysis method to analyze several main influencing factors that affect regional residents' economic development demand, based on the grey system model theory and the more representative economic development demand theory. The actual elasticity growth value is 90% similar to the predicted income elasticity value. Because it is difficult to find reasonable quantitative indicators for individual factors and data for some indicators is scarce, this paper analyses influencing factors such as regional residents' per capita net income, regional residents' economic development price index, urbanization rate, and per capita GDP. The findings show that each factor has a different impact on regional residents' economic development spending. Because per capita net income is the most important factor influencing economic development, this paper also examines the income structure of regional residents and the impact of various sources of income on economic development requirements. The findings show that net income from family businesses has the greatest impact on regional residents' economic development needs, followed by wage income, and property and transfer income. When regional residents' overall income growth is slow or difficult, improving the income structure can help to promote economic development.

6. Conclusions

Since some statistical data are difficult to obtain, this paper uses time series data instead of panel data when selecting sample points. Therefore, this study cannot reflect the economic development needs and development trends of regional residents of different income levels. In further research, we can consider selecting relevant panel data of regional residents at different income levels. For example, regional residents can be divided into low-income groups, middle-low-income groups, middle-income groups, middle-high-income groups, and high-income groups according to their income levels. Each of the five income levels are analyzed, and the economic development needs of different income levels of regional residents are specifically analyzed, and efforts are made to study the needs and future development trends of regional residents at different levels for different types of economic development in more detail.

Data Availability

The data used to support the findings of this study are available from the author upon request.

Conflicts of Interest

The author does not have any possible conflicts of interest.

References

[1] A. Bezuglov and G. Comert, "Short-term freeway traffic parameter prediction: application of grey system theory models," *Expert Systems with Applications*, vol. 62, pp. 284–292, 2016.

[2] W. Cai, Y. Song, and Z. Wei, "Multimodal data guided spatial feature fusion and grouping strategy for E-commerce commodity demand forecasting," *Mobile Information Systems*, vol. 2021, pp. 1–11, Article ID 5568208, 2021.

[3] F. Ye, C. Jie, Y. Li, and J. Kang, "Decision-making algorithm for multisensor fusion based on grey relation and DS evidence theory," *Journal of Sensors*, vol. 2016, Article ID 3954573, 11 pages, 2016.

[4] Z. Yuan, L. Wu, Z. Yuan, and H. Li, "Shape optimization of welded plate heat exchangers based on grey correlation theory," *Applied Thermal Engineering*, vol. 123, pp. 761–769, 2017.

[5] A. Dejamkhooy, A. Dastfan, and A. Ahmadyfard, "Modeling and forecasting nonstationary voltage fluctuation based on grey system theory," *IEEE Transactions on Power Delivery*, vol. 32, no. 3, pp. 1212–1219, 2017.

[6] X. Hong, Z. Lin, W. Zhang, L. Zhu, and S. Lan, "Construction of a comprehensive soundscape evaluation system in forest parks based on grey statistical theory," *Landscape Research: English Edition*, vol. 8, no. 6, pp. 25–28, 2016.

[7] M. Nowak, A. Rabczun, and P. Łopatka, "Impact of electrification on african development-analysis with using grey systems theory," *Energies*, vol. 14, no. 16, p. 5181, 2021.

[8] S. Liu, Q. Hu, P. Li, J. Zhao, M. Liu, and Z. Zhu, "Speckle suppression based on weighted nuclear norm minimization and grey theory," *IEEE Transactions on Geoscience and Remote Sensing*, vol. 57, no. 5, pp. 1–9, 2018.

[9] X. Zu, C. Yang, H. Wang, and Y Wang, "An EGR performance evaluation and decision-making approach based on grey theory and grey entropy analysis," *PLoS One*, vol. 13, no. 1, Article ID e0191626, 2018.

[10] D. Man and H. Chen, "59Tablet form optimization design based on grey theory and particle swarm optimization," *Journal of Investigative Medicine*, vol. 64, p. A21, 2016.

[11] S. H. René, U. Becker, and H. Manz, "Grey systems theory time series prediction applied to road traffic safety in Germany," *IFAC-PapersOnLine*, vol. 49, no. 3, pp. 231–236, 2016.

[12] X. Ma, M. Xie, and J. Suykens, "A novel neural grey system model with Bayesian regularization and its applications," *Neurocomputing*, vol. 456, no. 7553, pp. 61–75, 2021.

[13] M. Xin, A. Ww, Z. C. Bo, W. Yong, and W. Xingxin, "The conformable fractional grey system model," *ISA Transactions*, vol. 96, pp. 255–271, 2020.

[14] Z. Wang, Y.-S. Hwang, and Y. K. Choi, "Predicting Chinese tourism demand to South Korea using grey system model," *Journal of Social Sciences*, vol. 25, no. 3, pp. 219–234, 2018.

[15] L. Chen, Z. Liu, and N. Ma, "Time-delayed polynomial grey system model with the fractional order accumulation," *Mathematical Problems in Engineering*, vol. 2018, Article ID 3640625, 7 pages, 2018.

[16] B. Zeng and C. Luo, "Forecasting the total energy consumption in China using a new-structure grey system model," *Grey Systems: Theory and Application*, vol. 7, no. 2, pp. 194–217, 2017.

[17] I. L. Ho, S. C. Shih, and C. P. Tsai, "Decision model based on grey system theory and rough sets," *International Journal of Kansei Information*, vol. 9, no. 2, pp. 43–53, 2018.

[18] L. Liu, Q. Wang, J. Wang, and M. Liu, "A rolling grey model optimized by particle swarm optimization in economic prediction," *Computational Intelligence*, vol. 32, no. 3, pp. 391–419, 2016.

[19] L. Huang, G. Xie, W. Zhao, Y. Gu, and Y. Huang, "Regional logistics demand forecasting: a BP neural network approach," *Complex & Intelligent Systems*, vol. 1, pp. 1–16, 2021.

[20] Z. Shi, Y. Bai, X. Jin, X. Wang, T. Su, and J. Kong, "Deep prediction model based on dual decomposition with entropy and frequency statistics for nonstationary time series," *Entropy*, vol. 24, no. 3, p. 360, 2022.

[21] M. Kabir, S. Ahmad, M. Iqbal, Z. N. Khan Swati, Z. Liu, and D.-J. Yu, "Improving prediction of extracellular matrix proteins using evolutionary information via a grey system model and asymmetric under-sampling technique," *Chemometrics and Intelligent Laboratory Systems*, vol. 174, pp. 22–32, 2018.

[22] C. Lv, J. Wang, and F. Zhang, "Forest fire spread model based on the grey system theory," *The Journal of Supercomputing*, vol. 76, no. 5, pp. 3602–3614, 2018.

[23] H. Wang, X. Dong, Q. Li, and Z. Ren, "Confidence assessment and interval prediction for multi-input model via grey system theory," *Grey Systems: Theory and Application*, vol. 8, no. 1, pp. 69–83, 2018.

Hindawi
Computational Intelligence and Neuroscience
Volume 2022, Article ID 1233057, 10 pages
https://doi.org/10.1155/2022/1233057

Research Article

A Recommendation Model for College English Digital Teaching Resources Using Collaborative Filtering and Few-Shot Learning Technology

Juan Li

Baotou Medical College, Inner Mongolia University of Science and Technology, Baotou 014040, China

Correspondence should be addressed to Juan Li; 102003081@btmc.edu.cn

Received 24 April 2022; Revised 18 May 2022; Accepted 21 May 2022; Published 1 July 2022

Academic Editor: Xin Ning

This study designs and implements a digital English instructional resource management recommendation system based on collaborative filtering technology based on CF research and the construction of digital English instructional resources. This study designs the system with *B*/*S* structure combined with hierarchical design architecture, plans the overall design goal, architecture design, compilation structure, and key technologies, and designs and implements the system's core modules on the basis of fully analysing the functional and nonfunctional requirements of personalized educational resource recommendation system. Furthermore, the traditional CF has been improved to address scalability, data sparseness, and user cold start in the recommendation process. The evaluation results show that this algorithm has a recall rate of 96.37% and a system resource recommendation accuracy rate of 95.31%, both of which are higher than the traditional method's 6.37%. This algorithm can overcome the drawbacks of traditional algorithms, improve recommendation accuracy, and efficiently provide high-quality English teaching resources. Educators and students will be more likely to find high-quality digital English instructional resources if they use the instructional resource system proposed in this study.

1. Introduction

The use and development of digital technology have ushered in a technological revolution in the world of education. It has an impact on education, resulting in significant changes in educational and learning methods [1]. The result of the digitalization of teaching media is digital instructional resources. In the field of online education, particularly in the teaching environment, digital instructional resources have become indispensable. The information, digitalization, and networking era have posed a challenge to traditional college English instruction. The need for college English teaching reform is critical in order to adapt to the new situation and requirements [2]. The goal of digitalizing English knowledge is to divide it into manageable chunks, allowing students to customise, acquire, and organise the platform as they see fit. It is an English decomposition and matrix assembly process that assists students in establishing English logic and thinking as well as internalising English into habits by effectively connecting and bearing various knowledge such as society, life, major, and workplace [3]. People gradually realize that digital and multimedia network technology can be organically integrated with education and teaching. Digital technology provides technical support for delivering a variety of required scenarios that can vividly show phenomena and processes that are difficult to express in traditional teaching modes, as well as vividly express abstract content and guide learners to intuitively feel abstract language concepts [4]. In today's Internet age, the degree of educational informatization, the digitization of instructional resources, and the efficacy of their application have gradually become an important symbol for evaluating a country's or region's educational modernization process. With the advent of the Education 4.0 era, the creation and use of digital resources in English teaching will become more common [5]. Building and perfecting a digital college English instructional resource database can help college English teachers better accomplish their goals and develop English professionals who are well rounded in listening, speaking, reading, writing, and translation.

The acquisition range of college English instructional resources has greatly expanded in the information environment. It can now be extended to all of the world's instructional resources, not just those in schools and China. The abundance of instructional resources also encourages teaching mode innovation. The term "instructional resource bank" refers to a resource bank that can meet teaching requirements, has rich and diverse teaching content that adheres to specific requirements and norms, and is convenient for professors to impart knowledge and recipients to learn more effectively [6]. Digitalization of instructional resources in the information environment is easier to integrate than books, newspapers, and other written materials, which is beneficial to the role of resource allocation. Driven by reform power and teaching demand, all universities have set up their own instructional resource banks and network electronic resources to varying degrees after practice and development [7]. However, nowadays, the creation of digital resources frequently follows a centralised and unified management model, in which each university creates its own resource bank. As a result, each digital instructional resource bank and resource management system are relatively self-contained, and their resources are essentially closed off from one another, resulting in information barriers and islands [8]. The current research focus is on how to solve the problem of information isolation and personalized resource recommendation. Personalized recommendation services are now widely used in a variety of industries. Collaborative filtering technology is currently the most studied and widely used recommendation system, as well as a personalized recommendation system with high recommendation efficiency. Many mixed recommendation methods use collaborative filtering technology, according to research and analysis of the current personalized recommendation literature. In the recommendation process, CF (collaborative filtering) algorithm does not need to extract the content features of items and can make cross-domain recommendations, resulting in a high level of personalization and automation. This study focuses on the creation and implementation of CF-based digital English instructional resources. The following are some of its innovations:

① Based on the project characteristics of digital English instructional resources, this study designs a specific instructional resource recommendation process. When searching for the nearest neighbor of the target user, considering the relationship among users, resources, and resource attributes, the method of combining the similarity of rating with the similarity of preference of resource attributes is adopted, making full use of effective information to mine out more similar users, improving the recommendation quality of the system and solving the problem of data sparsity.

② According to the principle, advantages, and disadvantages of collaborative filtering recommendation algorithm in personalized recommendation technology, combined with learners' learning behavior characteristics, this study constructs a digital English instructional resource management recommendation model. In the construction of user model, the system extracts the features of users' personalized resource access to form an individual user model and clusters users with similar interests to form a group user model. Finally, an integrated user interest vector is formed to construct an integrated user model. This system provides a good solution for a personalized recommendation of digital English instructional resources.

This study is divided into five sections based on the research requirements: the first section is the introduction. This section explains the research's content, significance, methods, and definitions of related concepts and provides a quick overview of the study's structure. The second section is the literature review. This section summarises relevant literature from both domestic and international sources, as well as the study's research ideas and methods. The third section is methodology. This section explains the concept, types, and characteristics of English educational resources; this study examines the current state of English educational resource construction; a recommendation system for managing English instructional resources based on CF is developed, along with the implementation process. The fourth section conducts an experiment with the model developed in this study, analysing its performance and practical application impact. The fifth section is a summary and outlook. This section begins by summarising the research work of this study, explaining the findings, and then looking ahead to future research work and prospects.

2. Related Work

Network teaching relies heavily on the creation of digital instructional resources. Each website has formed a certain scale of instructional resources as a result of the establishment of various websites of instructional resources. However, how to find interesting information from a large number of instructional resources quickly and effectively remains a problem. Personalized recommendation services have a bright future in the information age, and they offer a fresh perspective on the instructional resource system. More platforms are introducing recommendation systems to provide personalized services to users, and many scholars and experts have devoted themselves to recommendation system research, with excellent results.

Li designed a flexible, reliable, high-performance personalized recommendation system architecture that can store and process petabytes of data and make real-time recommendations [9]. Osipov et al. proposed an intelligent online learning recommender system that can self-evolve while achieving self-adaptation to learners and an open network environment [10]. The information resources existing in the system are not fixed, and the learning resources on the network can be integrated into the system according to the interaction between users and the system. Kambanaros et al. analysed the user's browsing behavior and preference information by sampling and then presented the generated instructional resource recommendation list to the user, effectively realizing the sharing and recommendation of resources [11]. Davis studied the application of collaborative filtering technology in the personalized recommendation system of scientific literature and proposed two methods of collaborative recommendation [12]. One is a collaborative recommendation algorithm based on ontology concepts and user interests, and the other is a collaborative recommendation algorithm based on weighted association rules. Hafner pointed out that the existing network instructional resource system has not really applied the personalized recommendation technology and is only in the research stage. With the continuous enrichment of instructional resources, the need to realize personalized recommendation service of network instructional resource system is more and more urgent [13]. Shi and Yang proposed a method for real-time recommendation of current and subsequent learning materials based on learner interests and progress [14]. The method is implemented through three links: data and processing, mining neighbor learners, and recommendation of learning materials. Gee et al. proposed an online automatic recommendation system based on a hybrid filtering recommendation technique. The system combines content-based filtering and collaborative filtering to make recommendations based on the user's recent navigation history [15]. Yuan builds a user interest model by combining explicit tracking and implicit tracking of users [16]. Nielsen and Hoban applied web mining, association rule mining, and decision tree techniques to recommender systems to recommend suitable resources to users [17]. Arnaiz-González et al. studied the personalized resource recommendation service in the basic education resource network and proposed a personalized resource recommendation service model [18]. Aiming at the contradiction between the current ubiquitous mass instructional resources and the personalized needs of users, Barry proposed to introduce personalized recommendation technology into the network instructional resource system [19]. The system fully pays attention to the individual differences of learners and provides users with personalized services according to the learners' learning background and interests. For the sparsity problem of rating data, Cazden proposed that the dimensionality of item space can be reduced by using the singular value decomposition technique, thereby improving the sparsity of user rating data [20].

This study examines CF and related literature in the field of instructional resource construction, as well as personalized recommendation technology. A recommendation system for English instructional resource management based on CF is designed based on the foregoing. The algorithm chooses the user with the greatest distance as the initial clustering centre, divides users with similar resource attribute preferences into the same cluster through offline clustering, and searches the nearest neighbors in several clusters close to the target user, reducing the time and space cost of neighbor query. The flexible data processing ability of Spark and Hadoop technologies is realized in this study, and the discipline classification tree is constructed to form a better organisational resource model and user model of tagged data sources. The cold start problem is solved and the algorithm's accuracy is improved by using a hybrid recommendation algorithm based on content and collaborative filtering. The experiment demonstrates that the research presented in this study can aid in the creation and sharing of digital instructional resource databases and improve learners' learning efficiency.

3. Methodology

3.1. Digital English Instructional Resources. Digital instructional resources refer to all kinds of materials or systems that are processed digitally, support the effective operation of teaching, realize the teaching purpose, and can run on the computer or network environment [21]. It can reduce the macroworld, enlarge the microworld, turn the abstract into the concrete, turn the virtual into reality, and put history, future, and present into operation at the same time. It can fully arouse students' positive thinking in all senses. It can enable students to find and share digital knowledge and information resources through independent or creative ways, realize multilevel communication, evaluation, and exchange, and stimulate students' interest in learning. The design of digital instructional resources has two contents, one is the organisational design of instructional resources and the other is the description information design of instructional resources. In order to make the best use of digital English instructional resources, digital English instructional resources must be designed concisely, easy to understand, and operate. Some fashion elements can be added to the resource library to attract students. At the same time, it is necessary to fully consider the description of the resources themselves, that is, the design of descriptive information of instructional resources. Generally, it should include overall description, history and current situation description, metadata description, teaching characteristics description, ownership description, generic information description, and quality information description [22]. The particularity of digital English instructional resources lies in the following aspects: ① dealing with digitalization and realizing the quantification and standardization of information. ② Network transmission, clear information support points and links, and establishing an information chain. ③ Intelligent retrieval to meet the demand of customised information acquisition. ④ Multimedia presentation and realizing multilayer simultaneous stimulation such as audiovisual and speaking. ⑤ Hyperlinking of organisation, which realizes platform-type hyperlink of various information and resources and completes the knowledge structure. The digital college English instructional resource management model is shown in Figure 1.

The depth and breadth of college English textbooks and courseware are currently lacking [23]. Many teachers discover that the format of courseware solidifies over time. As a

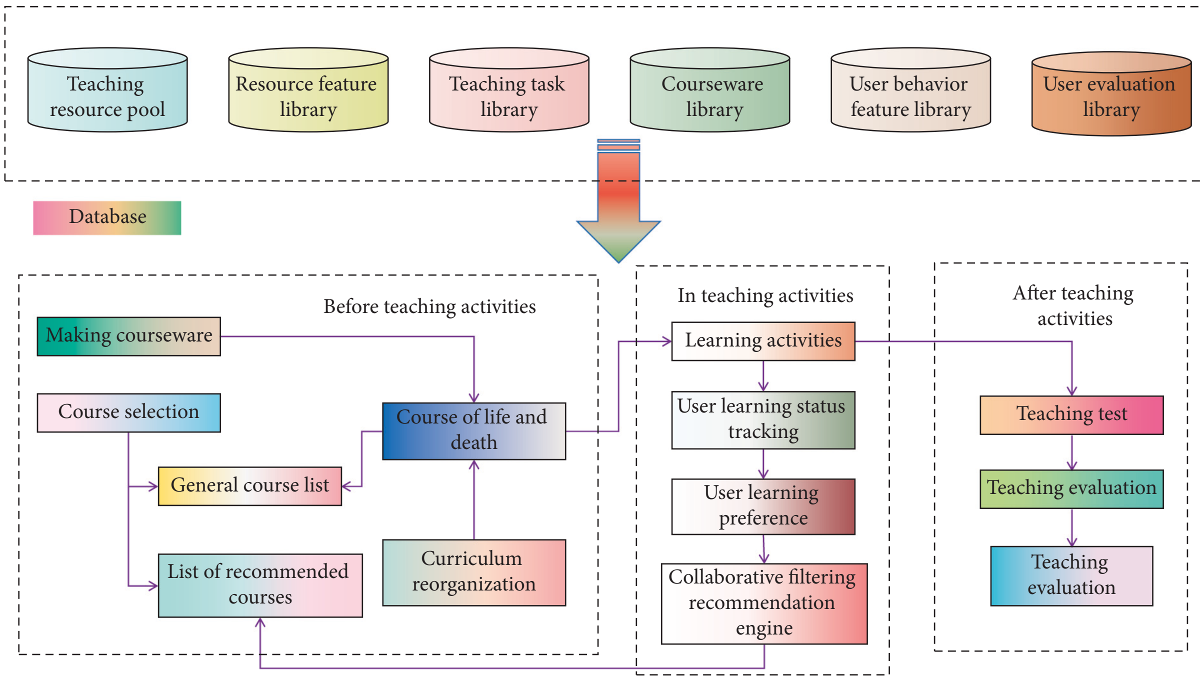

Figure 1: Digital college English instructional resource management model.

result, the digital English instructional resource database must use the existing or under-construction campus network to provide teachers with access to instructional resources and to aid in the teaching of students' English listening, speaking, reading, writing, and translation skills. Multimedia materials, teaching software, a network platform, and an integrated teaching system are just a few of the digital English instructional resources available. These digital resources can be organised by classifying knowledge points, teaching emphasis or difficulty, or knowledge and skill. It is important to note that the goal of digitalizing English knowledge is to divide it into manageable chunks so that students can customise, acquire, and organise the platform as they see fit. It is an English matrix assembly and linear decomposition process. It can assist students in developing English logic and thinking, as well as internalising English into habits, by effectively connecting and bearing various types of knowledge, such as society, life, major, and workplace. Learning resources in the network differ from traditional books and teaching materials due to the digitalization of learning objects. Traditional instructional resources are blocked and rigid due to the lack of digital media technology, making information sharing and transmission difficult. Learning objects that have been digitalized can help with the effective transmission of learning materials and resource sharing [24]. Digital instructional resources provide vivid and intuitive learning materials for students; through a large number of repeated information input, listening and speaking training becomes easy, thereby arousing the enthusiasm of students' classroom participation and promoting classroom interaction. It overcomes the passive situation of students in traditional classroom teaching and provides an effective guarantee for improving students' listening and speaking abilities. In the functional application of digital English instructional resources, teachers and students are more dependent on retrieval function and interactive function.

3.2. CF. This section mainly introduces the recommendation system and common collaborative filtering recommendation technology in detail. In the traditional system platform, the user browsing platform can only passively receive the information provided by the platform. Because of the different needs of each user, it cannot serve every user. With the development of educational informatization, the number of instructional resources on the Internet is also increasing [25]. Information technology has become increasingly difficult to help users find the resources they need. The personalized recommendation technology changes the system from a passive information provider to providing users with interesting information, which is more targeted than the traditional way. A personalized recommendation system can free users from massive information and greatly save the time and cost of finding commodities. At present, personalized service has become a new research hotspot in intelligent information processing and network technology. Personalized recommendation technology can analyse and predict users' behavior by collecting and analysing users' information, so as to better provide users with their corresponding services and achieve the purpose of personalized service. From the overall hierarchical structure, the recommendation system is mainly composed of three modules: ① *Input Function Module.* Its main function is to collect and update data and do some preprocessing work to improve data quality. ② *Recommendation Algorithm Module.* It is the core and part of the recommendation system, through which users will get the final recommendation result. ③ *Output*

Function Module. The results obtained by the recommendation algorithm module are displayed to users through this module.

The personalized recommendation algorithm is at the heart of the system, and it plays a critical role in recommendation quality. When selecting a personalized recommendation algorithm, it is necessary to weigh the benefits and drawbacks of various recommendation algorithms in light of the application field's unique characteristics in order to select the most appropriate recommendation algorithm for this application. A good recommendation algorithm can improve the performance of a recommendation service, find the information users require quickly and accurately, and increase resource utilisation and website service quality. User statistics-based recommendation, content-based recommendation, and collaborative filtering recommendation are the three types of personalized recommendation technology currently available. Users should be able to express their needs easily, and personalized recommendation systems should actively recommend resources to them. The system can adapt to changing user requirements over time. The advantage of a recommendation based on user statistics is that it does not rely on user behavior information, so there is no cold start problem. It can be used internally in a variety of fields because it is not dependent on the resource's information. In the field of information retrieval, content-based recommendation is proposed. Content-based recommendation is a recommendation method that was previously used with personalized recommendation technology. Content-based recommendations are based on the assumption that items that are similar in content to information items that the user was interested in previously will remain interesting to the user in the future. The basic idea behind content-based recommendation is to assess users' behaviors and needs based on the content they have access to. User interest files are used to describe each user's interests; a feature vector is created by extracting the features of each resource's information content; the recommendation system recommends resources based on similarity. This recommendation mechanism is more accurate than the statistical recommendation method of users because it can model the user's preference resources well.

The principle of collaborative filtering recommendation is to find the correlation between resources or between users according to their preferences for items or resources and then make recommendations based on these correlations. Collaborative filtering recommendation is mainly divided into user-based recommendation and project-based recommendation. The basic idea of collaborative filtering is very intuitive. In daily life, people often make some choices such as shopping, reading, and music according to the recommendations of friends and relatives. Collaborative filtering technology is to apply this idea to information recommendation and recommend a certain user based on other users' evaluation of certain information. Generally speaking, collaborative filtering needs to solve two problems: ① how to determine the user groups with similar interests and ② how to predict the resources or items that users are interested in. There are three basic starting points: ① users can be classified according to their interests, ② the user's rating information on the project includes the user's interest information, and ③ users' ratings of unevaluated items are similar to those of similar users. The structure of English instructional resource management recommendation system based on improved CF is shown in Figure 2.

Users must make an explicit subjective evaluation of the resources on the web page in order to score their preferences for resources. Implicit behavior, on the other hand, does not require users to make subjective judgments, and some website actions are recorded. We can combine display tracking with implicit tracking to better grasp the user's interest, using display tracking to obtain the static user's interest and implicit tracking to obtain the dynamic user's interest. The collaborative filtering recommendation algorithm makes recommendations to target users based on their closest neighbors' preferences. When determining the target users' nearest neighbors, it calculates the similarity between the target users and other users in the user group and then chooses the K users with the greatest similarity to form the target users' nearest neighbors. The collaborative filtering recommendation algorithm is based on the assumption that people have similar behaviors and will make similar decisions. The user's choice contains information about the user's interests. The algorithm calculates the similarity between users by analysing which items' users evaluate, generate the user set with the most similar interest to the current users, predict the current users' rating on the items by using the item ratings in this user set, and finally obtain the recommendation list and make recommendations. When CF recommends users, the main process is divided into three parts: constructing a scoring matrix, finding the nearest neighbors, and generating recommendations.

3.3. CF-Based Recommendation System for English Instructional Resources Management. The overall goal of the English instructional resource management recommendation system in this study is to realize the digital instructional resources that can be used by teachers and students in multicampus conveniently under the environment that conforms to the overall planning and design of the construction unit. The core of personalized network instructional resource system is recommendation module, which determines the performance of personalized network instructional resource system to a great extent. The key of recommendation module is to choose an appropriate personalized recommendation algorithm, which can effectively integrate with application fields, reduce possible problems, improve recommendation quality, and reduce the complexity of the system. The traditional recommendation of instructional resources focuses on the main body, while ignoring the interrelation between instructional resources. Aiming at the problems existing in CF and instructional resource recommendation, this study comprehensively considers the relationship between resources and the characteristic behavior information of users themselves to improve the algorithm. First, the learner's behavior and information are digitally modeled to form a model. Then,

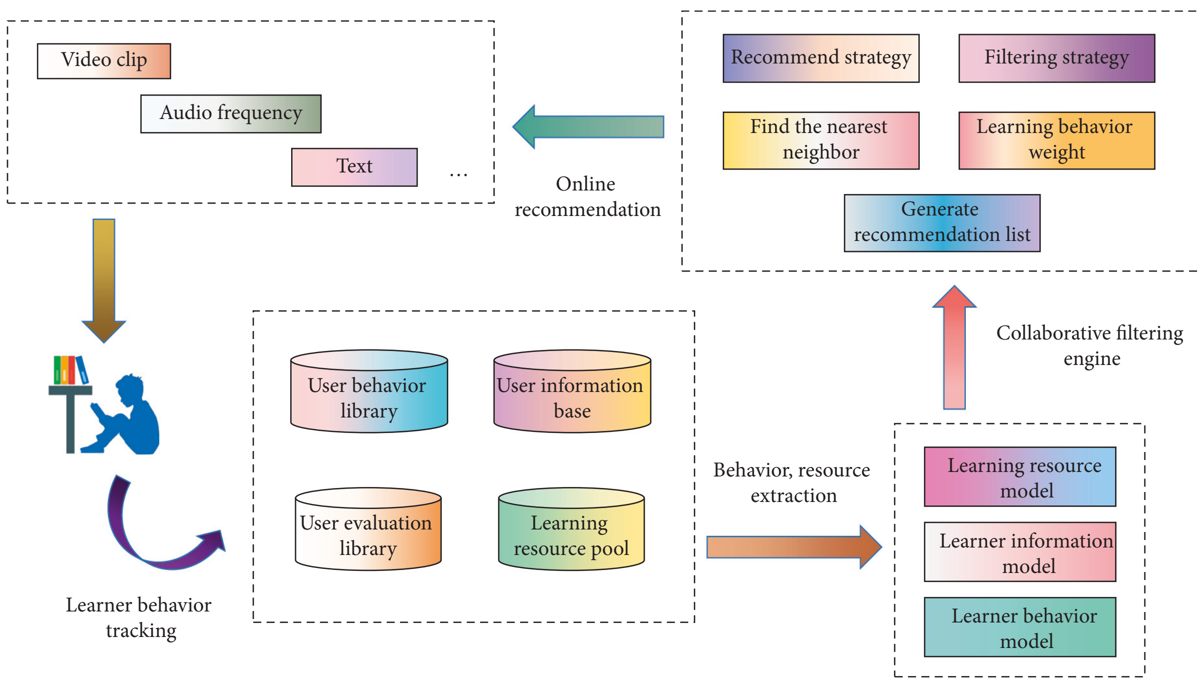

FIGURE 2: Improved structure of English instructional resource management recommendation system based on CF.

according to the current system situation, the filter strategy is selected, and the learner's behavior influencing factors are added to form the nearest neighbor set. Finally, online recommendation of learners in various media will be conducted, and the interaction between learners and the system will have an impact on the whole recommendation system, thus forming an organic whole repeatedly. In order to solve the cold start problem in recommendation system, that is, how new users recommend personalized resources to users without any interest preferences and associated friends, this study adopts content-based recommendation algorithm to solve this problem. In a recommendation system based on collaborative filtering technology, the input data can usually be expressed as a user-item evaluation matrix R with $m * n$, as follows:

$$R(m,n) = \begin{bmatrix} R_{1,1} & R_{1,2} & \dots & R_{1,n} \\ R_{2,1} & R_{2,2} & \dots & R_{2,n} \\ R_{3,1} & R_{3,2} & \dots & R_{3,n} \\ R_{m,1} & R_{m,2} & \dots & R_{m,n} \end{bmatrix}. \tag{1}$$

Among them, the rows represent users, with a total of m and the columns represent items, with a total of n. The value of R_{ij} represents the evaluation value of the item j by the user i, which is generally obtained by the user displaying the submission interest evaluation level. For two users i and j, the resource sets scored by the two users are as follows:

$$\begin{aligned} I_u &= \{i_c \mid i_c \in I \wedge r_{uc} \neq 0\}, \\ I_v &= \{i_c \mid i_c \in I \wedge r_{vc} \neq 0\}. \end{aligned} \tag{2}$$

The weight function can be expressed as follows:

$$f(u,v) = \frac{|I_u \cap I_v|^2}{|I_u| \times |I_v|}. \tag{3}$$

At the same time, the Pearson correlation coefficient modified by the weight function is shown in the following formula:

$$\mathrm{Sim}_p(u,v) = \frac{|I_u \cap I_v|^2}{|I_u| \times |I_v|} \frac{\sum_{i\in I_{UV}} (R_{ui} - \overline{R}_u)(R_{vi} - \overline{R}_v)}{\sqrt{\sum_{i\in I_{UV}} (R_{ui} - \overline{R}_u)^2} \sqrt{\sum_{i\in I_{UV}} (R_{vi} - \overline{R}_v)^2}}. \tag{4}$$

In the calculation of similarity, users' preferences for user resources can be used as a vector to calculate the similarity between users. The similarity is judged according to the distance between two vectors. The smaller the distance, the greater the similarity between them. Traditional CFs generally only recommend users according to the scoring matrix, but in the instructional resource system, the user scoring data are less than the resource scale, so the overall scoring data are sparse. Aiming at this problem, this study considers the attribute characteristics of resources. When a user generally gives a high rating to the resources with certain attributes, it can be considered that the user prefers such attributes. By comprehensively measuring user similarity through scoring similarity and resource attribute preference similarity, we can mine users' potential points of interest, increase data density, and alleviate data sparsity. By constructing a discipline classification tree as the basic structure of instructional resources classification and user tag data, the system labels users by using the professional direction selection and interest topics when users register or log in for the first time, and the skimming data come from the classification tree. User model updating is to improve the original model according to the explicit or implicit feedback from users. In this way, the model can be well matched with the latest preferences of users, thus improving the accuracy and recommendation quality of the model. The system information database is the data source of the whole digital collaborative system. In this model, we collect and record learners' learning behaviors and mine learners' learning behavior trajectories to establish learners' behavior models.

Items i and j can be viewed as vectors of two n dimensions. The similarity of two items is estimated by calculating the spatial angle of these two vectors. For the scoring matrix of $m * n$, the similarity calculation formula of item i and item j is as follows:

$$\mathrm{Sim}(i, j) = \cos(\vec{i}, \vec{j}) = \frac{\vec{i} \cdot \vec{j}}{|\vec{i}| \cdot |\vec{j}|}. \tag{5}$$

Among them, $\cdot$ represents the vector inner product. The predicted score of the target user u to the item j is as follows:

$$P_{u,j} = \frac{\sum_{j=1}^{k} \mathrm{Sim}(i, j) \times R_{u,j}}{\sum_{j=1}^{k} \mathrm{Sim}(i, j)}. \tag{6}$$

Among them, k represents the resource set most similar to item i in the nearest neighbor table, and $R_{u,j}$ represents the evaluation that user u has made on item j and the predicted evaluation value obtained by the content-based algorithm. Mainly combined with cross validation to achieve, the formula is as follows:

$$\mathrm{MAE} = \frac{\sum_{g^{\text{test}} \subset G^{\text{test}}} \left| g^{\text{test}}(\text{prediction}) - g^{\text{test}}(\text{authentic}) \right|}{\left| G^{\text{test}} \right|}. \tag{7}$$

Among them, $g^{\text{test}}(\text{authentic})$ is the real score, $g^{\text{test}}(\text{prediction})$ is the predicted score, and G^{test} is the entire set of user scores to be predicted. The system uses recall and precision to evaluate the performance of its personalized recommendation. The formula is as follows:

$$\text{Recall ratio} = \frac{\text{Recommended number of related resources}}{\text{Total number of related resources}} \times 100\%,$$
$$\text{Precision ratio} = \frac{\text{Recommended number of related resources}}{\text{Number of recommended resources}} \times 100\%. \tag{8}$$

The user-item scoring matrix is used in this study to express users' preferences for items, and it is used to implement collaborative filtering recommendation technology. Its advantage is that it is suitable for the representation and establishment of a specific group user model due to group users' interest bias. All users can benefit from the system's recommendation function, which allows both logged-in and non-logged-in users to recommend personalized results and non-logged-in users to capture their interests based on real-time page operations. Learners will rate their satisfaction with a course after completing it, and the data will be saved in the user evaluation database. The accuracy of collaborative filtering recommendations is affected by the detail of the user evaluation database. Users with similar resources have a high degree of similarity in this study. Users in the system are clustered based on scoring information and resource attribute information, and clustering technology is applied to collaborative filtering recommendation. Users who have similar resource attribute preferences are grouped together. Finding the nearest neighbor in several clusters near the target user reduces the space-time cost of neighbor search, alleviates some scalability and real-time issues, and improves recommendation efficiency and quality. The personalized network instructional resource system actively provides recommendation resources to users based on their registration information and behavior characteristics after the introduction of personalized recommendation technology, transforming users from passive browsers to active learners.

4. Result Analysis and Discussion

The comparison experiment of the model and algorithm, as well as the analysis of the results, is the main focus of this chapter. This study designs an evaluation experiment for the model and algorithm to quantitatively obtain the recommendation index of the recommendation model after the English instructional resource management recommendation system has been implemented. This will allow us to gain a better understanding of the recommendation model's benefits and drawbacks, as well as serve as a guide for optimising the model's parameters and further optimisation. The system has 100 users registered, and a database of 100 users' personality traits has been created. The instructional resource database has a scale of 200 and 50 interest groups. The top ten English instructional resources with the most similarity are chosen and made available to the appropriate users. The experiment data come from the user operation log in this system, which is used to train the homepage recommendation module. The system will call each module to calculate the recommendation degree of this instructional resource to the user and then save the recommendation degree and the user scoring characteristic value into the database, when the user browses the detailed page of instructional resources and scores the instructional resources. Table 1 lists the experimental setup.

The function of the instructional resource retrieval module is to receive users' retrieval requests. First, users express their query requirements as keywords or search expressions and input them into the system through the user interface. After the system receives the user's search words or search expressions, the traditional database management system will find out all qualified instructional resources from the instructional resource database according to the matching of the query fields, and form the search results. In the experiment, the sparse level of the data set is also considered, which is defined as the percentage of items in the user-item scoring matrix that are not scored. Figure 3 shows the subjective rating results of users on recommended resources of different recommendation systems.

Table 1: Experimental environment settings.

Category	Setup
Processor	Dikaryon
Internal storage	512
Hard disc	80 GB
Operating system	Windows
Development platform	MyEclipse
Program	Java
Database system	MySQL

It can be seen that the recommended results of English learning resources in this system are more in line with users' needs and preferences, so its score is higher. In addition, the evaluation algorithm, as a standard to measure the recommendation effect of recommendation system, plays a very important role. Therefore, the selection of evaluation algorithms and the characteristics of different evaluation algorithms need to be taken into account, so as to comprehensively evaluate the recommendation effect of a recommendation system. At the same time, it can compare with other recommendation systems comprehensively and get a comprehensive understanding of the recommendation effect of the recommendation system. Figure 4 shows the comparison of different algorithms when selecting different sparsity.

As can be seen from Figure 4, the improved CF is more accurate than other algorithms because it adds the user behavior weight calculation when the sparsity is small. In this experiment, the average absolute error and recall rate, which are the most widely used and intuitive statistical accuracy measurement methods, are used as evaluation criteria. During the experiment, the data set is divided into a training set and testing set. The algorithm works in the training set and predicts the items in the testing set through the data in the training set. The comparison algorithm used in this study is the classic user CF and project CF. The average absolute error results of different algorithms are shown in Figure 5. The recall results of different algorithms are shown in Figure 6.

The smaller the absolute error value, the higher the recommendation quality. The higher the recall rate of the algorithm, the better the performance of the algorithm. From the comparison results of the average absolute error and recall rate of the evaluation algorithm, it shows that the recommendation algorithm in this study is more accurate than the project CF and the user CF in recommending instructional resources. Table 2 lists the experimental results of filtering evaluation indexes.

Using the collected data set, under the condition of the same training set and testing set, the recommendation accuracy of different models is compared, and the nearest neighbor size is adjusted to make it produce the best effect in the recommendation process as much as possible. The recommended accuracy results of different models are shown in Figure 7.

The results show that the recommendation accuracy of this model is high. The average filtering accuracy of this system is slightly higher than that of the control

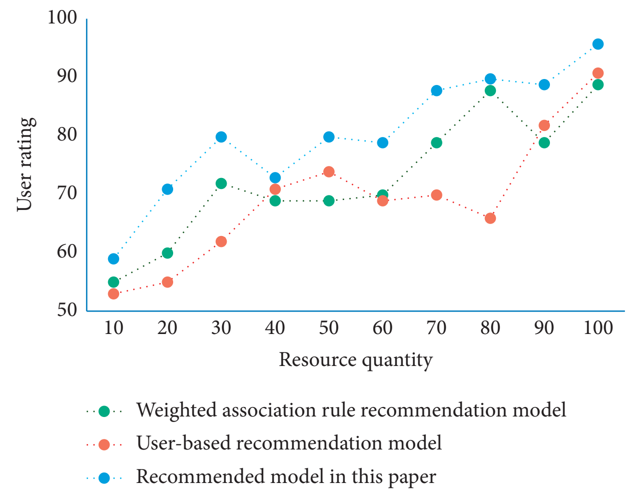

Figure 3: Comparison of users' subjective ratings.

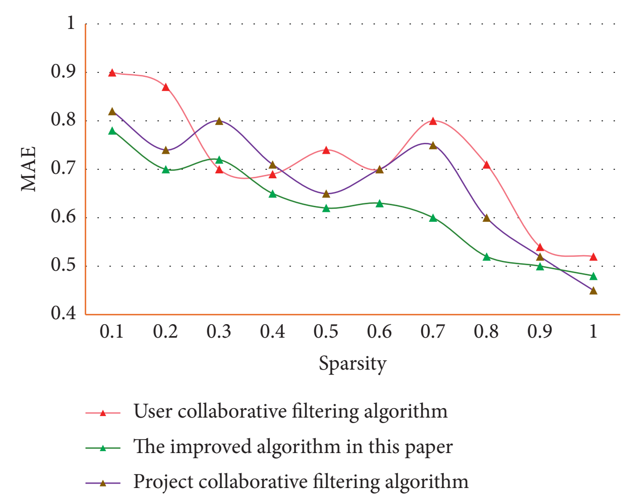

Figure 4: Comparison of algorithm results when selecting different sparsity.

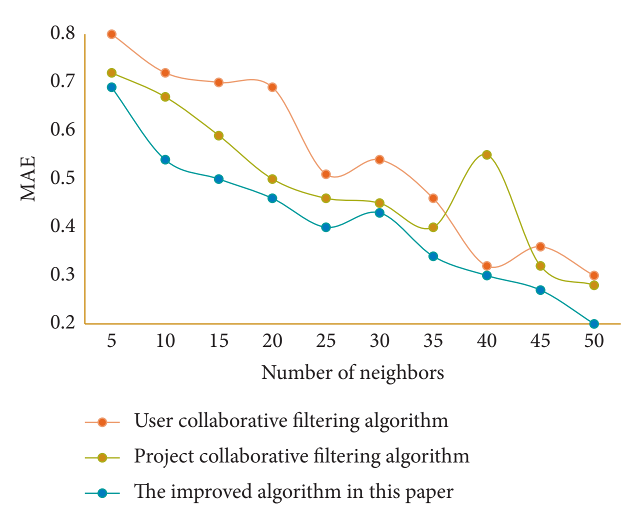

Figure 5: Average absolute error results of different algorithms.

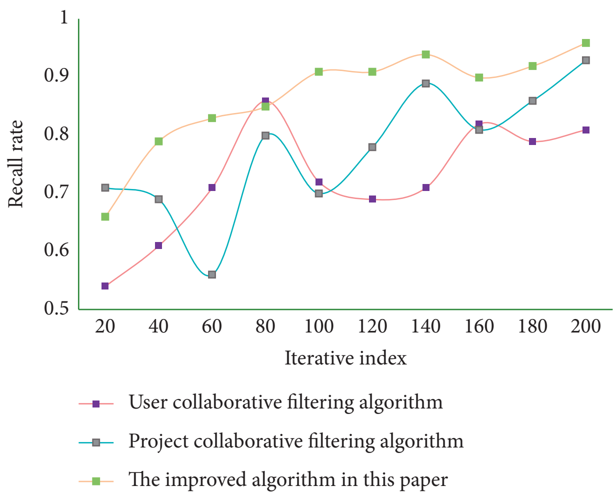

Figure 6: The recall results of different algorithms.

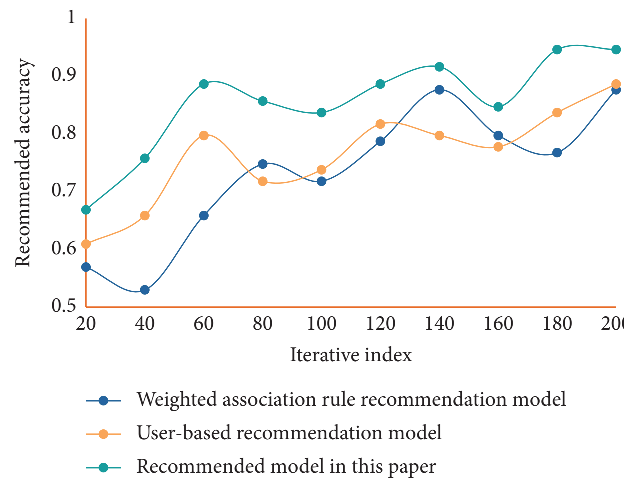

Figure 7: Recommended accuracy results of different models.

Table 2: Experimental results of evaluation index.

Model	Average precision rate (%)	Average recall rate (%)
Weighted association rule recommendation model	89.34	91.42
User-based recommendation model	84.12	86.37
Content-based recommendation model	82.36	85.24
Recommended model proposed in this study	95.36	96.17

experimental system. The main reason is that the former filters instructional resources according to the personalized characteristics of users, and the results are more targeted. Therefore, the model designed in this study, which has the learning function of users' personality characteristics and comprehensive filtering function, can effectively improve the recall and precision of personalized retrieval and personalized recommendation in English instructional resource service. Through the analysis of various experimental data, it can be seen that the English instructional resource management recommendation system constructed in this study is stable. The algorithm's recall rate can reach 96.37%, and the recommendation accuracy rate is as high as 95.31%, which is higher than the traditional method's 6.37%. The English instructional resource management recommendation system constructed in this study has good performance in all aspects and effectively improves the satisfaction of resource users. It can effectively provide high-quality resources for English teaching and can better satisfy users' experiences.

5. Conclusions

This study examines the use of personalized recommendation systems and digital English instructional resources, as well as the principle, recommendation process, and classification of collaborative filtering recommendation algorithms. This study has conducted extensive research on the topics of sparsity, cold start, and scalability of collaborative filtering recommendation algorithms, as well as proposed solutions. A CF-based English instructional resource management recommendation system is designed and implemented as a result of this. This study describes in detail the key technologies used in the system, presents the overall framework and functions of the digital English instructional resource system, and designs and implements a personalized recommendation module in the instructional resource system based on the learning habits and instructional resources of users. The system's advancement allows for better sharing and reuse of digital resources, as well as the discovery of instructional resources that learners may be interested in. The system's usability, ease of use, stability, and high real-time performance are demonstrated through the running test and performance analysis, and the system's convenient capacity expansion for many times in the future is also demonstrated. According to the research, this algorithm has a recall rate of 96.37% and a recommendation accuracy rate of 95.31%, which is higher than the traditional method's 6.37%. The English instructional resource management recommendation system developed in this study performs well in all areas and effectively increases resource users' satisfaction. It has the potential to effectively provide high-quality resources for English teaching while also improving user satisfaction. However, because the digital

English instructional resource system is a complex learning platform with time and technology constraints, there are still some issues in the system's research and development that need to be addressed. The balance between the real-time performance of the recommendation system and recommendation quality is the focus of the following work. Additional research into the characteristics of educational resources is necessary to expand the user interest model and instructional resource model.

Data Availability

The data used to support the findings of this study are available from the corresponding author upon request.

Conflicts of Interest

The author declares that there are no conflicts of interest.

References

[1] B. V. Tucker, M. C. Kelley, and C. Redmon, "A place to share teaching resources: speech and language resource bank," *Journal of the Acoustical Society of America*, vol. 149, no. 4, p. A147, 2021.

[2] X. Yang, "Research on integration method of AI teaching resources based on learning behavior data analysis," *International Journal of Continuing Engineering Education and Life Long Learning*, vol. 30, no. 1, p. 1, 2020.

[3] S. Huang, "Design and development of educational robot teaching resources using artificial intelligence technology," *International Journal of Emerging Technologies in Learning (iJET)*, vol. 16, no. 05, p. 116, 2021.

[4] S. Yanhong, "Design of digital network shared learning platform based on SCORM standard," *International Journal of Emerging Technologies in Learning (iJET)*, vol. 13, no. 07, p. 214, 2018.

[5] I. Moodie and H.-J. Nam, "English language teaching research in South Korea: a review of recent studies (2009-2014)," *Language Teaching*, vol. 49, no. 1, pp. 63–98, 2016.

[6] A. Waters, "Managing innovation in English language education: a research agenda," *Language Teaching*, vol. 47, no. 1, pp. 92–110, 2014.

[7] Y. Yi Lo and E. S. Chung Lo, "A meta-analysis of the effectiveness of English-medium education in Hong Kong," *Review of Educational Research*, vol. 84, no. 1, pp. 47–73, 2014.

[8] E. J. Erling, "Innovation and change in English language education," *ELT Journal*, vol. 69, no. 2, pp. 217–219, 2015.

[9] W. Li, "Application of cloud computing in informatization of physical education teaching resources[J]," *Revista de la Facultad de Ingenieria*, vol. 32, no. 11, pp. 626–631, 2017.

[10] I. V. Osipov, A. Y. Prasikova, and A. A. Volinsky, "Participant behavior and content of the online foreign languages learning and teaching platform," *Computers in Human Behavior*, vol. 50, no. 9, pp. 476–488, 2015.

[11] M. Kambanaros, C. N. Giannikas, and E. Theodorou, "English foreign language teachers' awareness of childhood language impairment[J]," *Clinical Linguistics and Phonetics*, vol. 35, no. 3, pp. 1–17, 2020.

[12] J. M. Davis, "Toward a capacity framework for useful student learning outcomes assessment in college foreign language programs," *The Modern Language Journal*, vol. 100, no. 1, pp. 377–399, 2016.

[13] C. A. Hafner, "Remix culture and English language teaching: the expression of learner voice in digital multimodal compositions," *Tesol Quarterly*, vol. 49, no. 3, pp. 486–509, 2015.

[14] Y. Shi and X. Yang, "A personalized matching system for management teaching resources based on collaborative filtering algorithm," *International Journal of Emerging Technologies in Learning (iJET)*, vol. 15, no. 13, p. 207, 2020.

[15] K. L. Gee, T. B. Neilsen, and S. D. Sommerfeldt, "Resources for teaching near-field acoustical holography in advanced acoustics courses," *Journal of the Acoustical Society of America*, vol. 135, no. 4, p. 2159, 2014.

[16] Q. Yuan, "Network education recommendation and teaching resource sharing based on improved neural network," *Journal of Intelligent and Fuzzy Systems*, vol. 39, no. 4, pp. 5511–5520, 2020.

[17] W. Nielsen and G. Hoban, "Designing a digital teaching resource to explain phases of the moon: a case study of preservice elementary teachers making a slowmation[J]," *Journal of Research in Science Teaching*, vol. 52, no. 9, pp. 1207–1233, 2015.

[18] Á. Arnaiz-González, J.-F. Díez-Pastor, I. Ramos-Pérez, and C. García-Osorio, "Seshat - a web-based educational resource for teaching the most common algorithms of lexical analysis," *Computer Applications in Engineering Education*, vol. 26, no. 6, pp. 2255–2265, 2018.

[19] W. J. Barry, "Perception and production of English vowels by German learners: instrumental-phonetic support in language teaching," *Phonetica*, vol. 46, no. 4, pp. 155–168, 1989.

[20] C. B. Cazden, "Primary school English-language education in Asia: from policy to practice," *Asia Pacific Journal of Education*, vol. 35, no. 1, pp. 144–147, 2015.

[21] Q. Liu, L. Cheng, A. L. Jia, and C. Liu, "Deep reinforcement learning for communication flow control in wireless mesh networks," *IEEE Network*, vol. 35, no. 2, pp. 112–119, 2021.

[22] Y.-T. Liu and A. G. Todd, "Dual-modality input in repeated reading for foreign language learners with different learning styles," *Foreign Language Annals*, vol. 47, no. 4, pp. 684–706, 2014.

[23] T. Strømme and A. Furberg, "Exploring teacher intervention in the intersection of digital resources, peer collaboration, and instructional design[J]," *Science Education*, vol. 99, no. 5, p. 837, 2015.

[24] I. P. Martin, "English language teaching in the Philippines," *World Englishes*, vol. 33, no. 4, pp. 472–485, 2014.

[25] N. C. Sifakis, "ELF awareness in English language teaching: principles and processes[J]," *Applied Linguistics*, no. 2, p. 2, 2017.

Hindawi
Computational Intelligence and Neuroscience
Volume 2022, Article ID 3342031, 11 pages
https://doi.org/10.1155/2022/3342031

Research Article

Neural Network-Based Routing Energy-Saving Algorithm for Wireless Sensor Networks

Lili Pang, Jiaye Xie, and Qiqing Xu

Industrial Center, Nanjing Institute of Technology, Nanjing 211167, China

Correspondence should be addressed to Lili Pang; panglili@njit.edu.cn

Received 27 May 2022; Revised 10 June 2022; Accepted 11 June 2022; Published 1 July 2022

Academic Editor: Xin Ning

With the evolvement, standards have changed, mobile Internet technology has also been upgraded, and it has also driven the development of smart objects mobile. With the continuous development of smart objects mobile, the bottleneck of small node size and low battery energy storage has not been solved in the end, which makes the research of wireless sensor network energy-saving technology become the focus, and the improvement of routing technology is an effective way to improve energy-saving technology. From the data transmission energy consumption of smart objects mobile, the routing algorithm of smart objects mobile is discussed and analyzed and the classical representative LEACH is the object of in-depth research. Routing algorithms can easily and reliably process network data and make the network work well and are widely used in highly secure military systems and smaller commercial networks. Aiming at these deficiencies, a corresponding improved algorithm is proposed, and it is tested through simulation and specific experiments to verify the correctness and the system's reliability. The SMPSO-BP algorithm converges when the number of iterations is about 600, which is earlier than the LEACH algorithm and the improved LEACH algorithm, so the SMPSO-BP algorithm is due to the other two algorithms. In the wireless sensor network routing energy consumption experiment, in addition, the SMPSO-BP algorithm uses less energy than the other two methods. Therefore, the energy-saving algorithm under the neural network data fusion mechanism is still feasible.

1. Introduction

The smart objects mobile is the main path of data transmission in the Internet of Things, along with the advancement of Internet, which is the main support for data transmission, and it is also the function that consumes the most energy in the wireless sensor network, which directly affects the overall performance of the entire network. As a new generation of communication technology integrating embedded computing, sensor, network, and wireless communication, wireless sensor network has been widely used in various fields. With information science's rapid growth, wireless sensors with the ability to obtain information from multiple technologies have been applied in various fields of intelligent data monitoring and are favored by various fields because of their low cost and multifunctionality.

The wireless sensor routing energy-saving algorithm aims at delaying the network service life under the premise that the node energy is exhausted and can undertake the network protection function. With the vigorous development of information technology, data transmission has become an indispensable part. The network routing is the carrier of data transmission, in order to improve the efficiency of data transmission and reduce energy consumption during the transmission process. According to the LEACH algorithm, the shortcomings of energy saving in wireless sensors are analyzed, and the redundancy of the original data collection by the sensor nodes is solved to boost downlink costs and decrease wireless carbon emissions using CNNs data space technology.

The combination of neural network and wireless sensor network is used to realize the data fusion in the network. First, the LEACH algorithm is a classic hierarchical routing algorithm used to stabilize the data transmission of wireless sensors, and then an improved LEACH algorithm is introduced on the basis of stable data transmission, and the improved LEACH algorithm is used to find the best path in the data transmission process. Finally, using the powerful platform complex utilization only fits the standards of co-operative sensing processes that are performed, improves the data transmission intelligence level of wireless sensors, reduces energy consumption, and prolongs service life.

2. Related Work

Wireless sensors have become one of the research hotspots because of their flexibility and high-precision monitoring capabilities. Dey et al. designed a home version of a wireless ECG monitoring system using Zigbee technology to monitor people's health at home, and the real-time monitoring system records, measures, and monitors ECG activity while maintaining consumer comfort [1]. Jamhour et al. proposed a new SDWSN control plane based on the Constrained Application Protocol to provide comprehensive specifications for the control plane, including the communication infrastructure, control plane protocols, and basic network functions in the controller [2]. Aarti and Anuj discovered the optimum path to transfer packet data from node to receiver, which includes communications systems, core router interfaces, and basic network activities in the computer. Aarti and Anuj considered the wide range of applications and delicate environments inside which WSNs are used, wherein transmission is as crucial as fuel economy, whereas the best route focused simulated annealing, simulated annealing, and efficient heuristic XGBoost have just been offered to increase delivery ratio [3]. These studies can analyze the relevant conditions of wireless sensors, but the research on sensor life and energy consumption needs to be improved.

With the increase of the number of distributed sensor nodes, researches on energy saving and consumption reduction of wireless sensors appear one after another. Song et al. used the Wasser procedure to execute data mining technique and conversation amongst sink nodes, guaranteeing that each node operates as a member node with quite an additional option, allowing the cable network nodes to spend energy more equitably [4]. Bhola et al. proposed LEACH, a modular technology that changes IoT devices with sensor nodes (CH), which analyzes and organizes data before sending it to the destination node to identify the best path [5]. In order to provide interesting solutions to problems related to agricultural resource optimization, decision support, and land monitoring, Khriji et al. proposed a localization-based RSSI algorithm to determine node locations and developed a low energy adaptive clustering approach adaptive neurofuzzy inference to minimize energy usage across all sink node [6]. In order to realize the efficient and optimal transmission of renewable energy power generation in the energy router, Guo et al. proposed a minimum loss routing algorithm based on the matchmaking tradeoff competition mechanism for the optimal selection of the existing ER transmission path [7]. Liu et al. proposed a Chaos Elite Eco-Evolutionary Algorithm (CENEA) for low-power clustering in EMWSNs for environmental monitoring. Results have shown that CENEA balances node energy and improves node energy usage efficiency, improves accuracy, and minimizes computation time [8]. The research on these energy-saving algorithms is instructive to a certain extent, but in some cases, the demonstration is not sufficient or accurate enough and can be further improved.

3. Energy-Saving Algorithm for Wireless Sensor Network Routing

3.1. LEACH Algorithm. The Scheme (LEACH) is a minimal flexible grouping routing mechanism that was the first to be published in sensor nodes [9]. The protocol is executed cyclically in units of rounds. Other ordinary nodes select the cluster head closest to themselves and join it to complete the establishment of the cluster; entering the stable data communication stage, the ordinary node transmits the collected data to the cluster head of the cluster where it belongs. After receiving the data, the cluster head completes the fusion operation and finally sends it directly to the sink node [10]. After a round of execution, waiting for a period of time, the network enters the next round of work cycle. The LEACH cluster routing algorithm mainly has two stages: the cluster establishment stage and the stable operation stage. The group building cycle primarily focuses on cluster setup, while the good performance of the proposed level mostly focuses on transmission, as shown in Figure 1. As one of the most classical routing algorithms, LEACH algorithm has some shortcomings, but its proposed hierarchical structure and round-robin mechanism have great reference value.

The LEACH algorithm is a hierarchical routing algorithm, and it is also the most classic one in hierarchical routing. Hierarchical routing algorithms have become a hot research direction of routing algorithms due to their high scalability, high energy utilization, and easy data fusion. The LEACH algorithm solves the stress problem by evenly dispersing the entire platform's electricity cost with each including to [11]. Hierarchical routing is shown in Figure 1. The algorithm randomly selects the cluster head and splits the cluster in a random cycle. This method of selecting cluster heads counterbalances the consumption of energy of nodes and improves the longevity of the network to some extent [12]. Energy saving, network lifetime, data fusion, and scalability are compared across three different topologies, as shown in Table 1.

As shown in Table 1, the Layered Routing algorithm outperforms the other two on all counts [13]. The sensor nodes perform real-time monitoring, information acquisition, and information processing functions on the monitoring object. The collected data is transmitted back to rendezvous junction, which processes the digital information and sends it to the user through the network, thus achieving the purpose of environmental monitoring, target tracking, and data collection [14]. Sensor nodes, sink nodes, and task management nodes form a wireless sensor network system. The traditional wireless sensor network structure is shown in Figure 2.

The routing computing capability of the node also needs to depend on the computing unit. The wireless communication module is composed of the network, MAC, and transceiver and mainly realizes the data communication

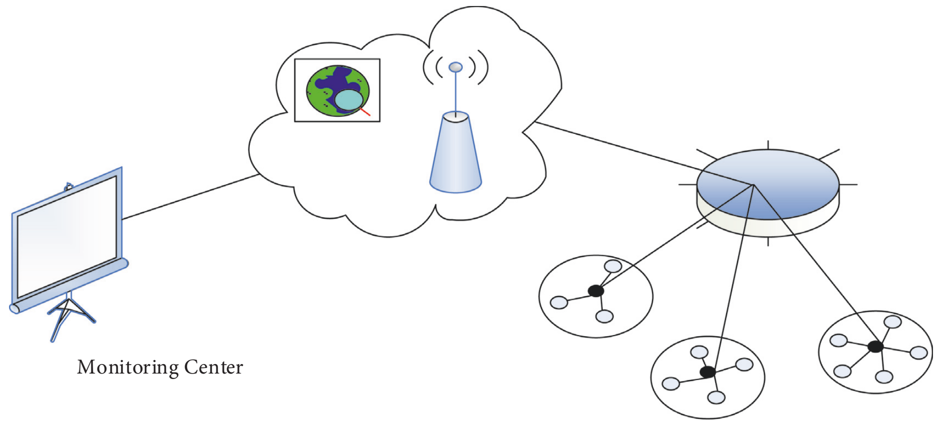

Figure 1: Hierarchical routing.

Table 1: Routing classification comparison.

Algorithm	SPIN	GAF	LEACH
Topology	Flat	Location	Level
Energy saving	Have	Have	Generally
Network life	Long	Long	Long
Data fusion	Have	None	Have
Extensibility	Generally	It is good	It is good

function: the power supply module supplies energy for the entire sensor node [15].

As can be seen from Figure 3, the power module is the most important module, and all other modules need the support of the power module. However, most power modules use batteries for energy supply, and the energy is limited, so an effective routing mechanism needs to be designed to lessen the power expenditure of the web and extend the lifespan of the web [5].

The advantages of trunking over flat roaming solutions in saving energy are reflected in the following points: the cluster member nodes simply send the data to the club leaders of the clusters after sensing such traffic. The upper layer backbone network consisting of club leader completes the long distance transmission of data to the sink nodes. The communications modalities can be turned off by the member nodes for the majority of the transmission time [16]. This working mode not only ensures the data communication in the entire network, but also greatly reduces the communication volume in the web and less power hungry. The nodes that constitute the wireless sensor network are usually deployed randomly, and closer to the point where the data gathered by the knots may be relatively resemblance. Meanwhile, the cluster topology is well expandable and applies to massive linear wireless transceiver systems. No matter what type of routing protocol is used, the purpose is to minimize the effort of energy overhead for data transmission and to extend the longevity of the system [17]. The running "round" of the LEACH algorithm is shown in Figure 4.

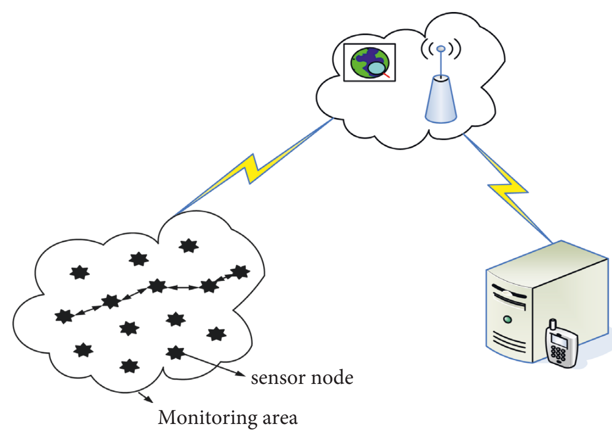

Figure 2: Wireless sensor network architecture.

In the initialization phase of wireless sensor network data transmission, each node generates a random value of [0, 1], and the node compares the random value generated by itself with the threshold. If the randomly selected value is less in value than the quota, which will be picked for container leaders. The formula is as follows:

$$T(i) = \begin{cases} \dfrac{z}{1 - z \times (r \times \operatorname{mod}(1/z))}, & i \in G, \\ 0, \quad \text{else.} \end{cases} \tag{1}$$

In WSN, the functions of sensor nodes are mainly to perceive, process, and transmit data. Since the power expenditure for performing data feeds is quite different from that of other functions, the energy consumption analysis of WSN only considers the communication power generation. The communication energy consumption of wireless sensor network increases with the increase of distance, so the data transmission route has a great influence on the energy consumption of the sensor. Correlation between communication distance Y meters and the energy consumption X bit generated by the generated data is expressed as the following formula:

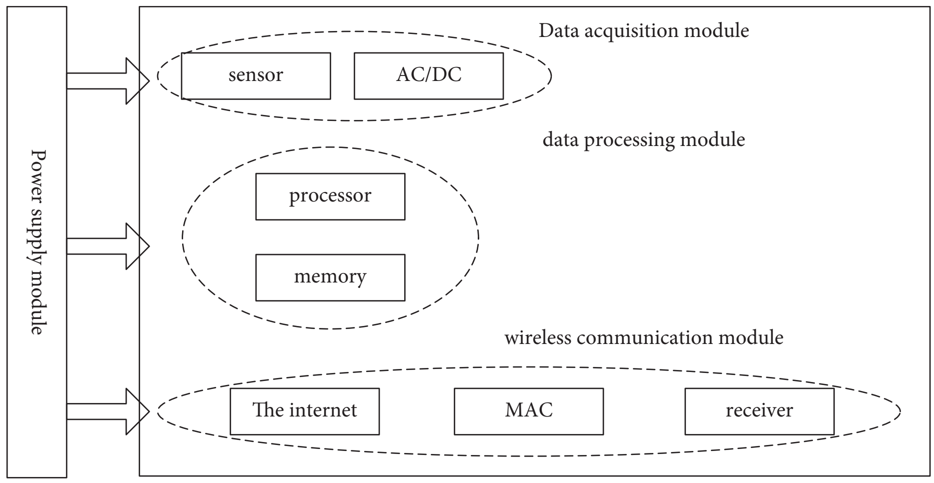

Figure 3: Sensor node block diagram.

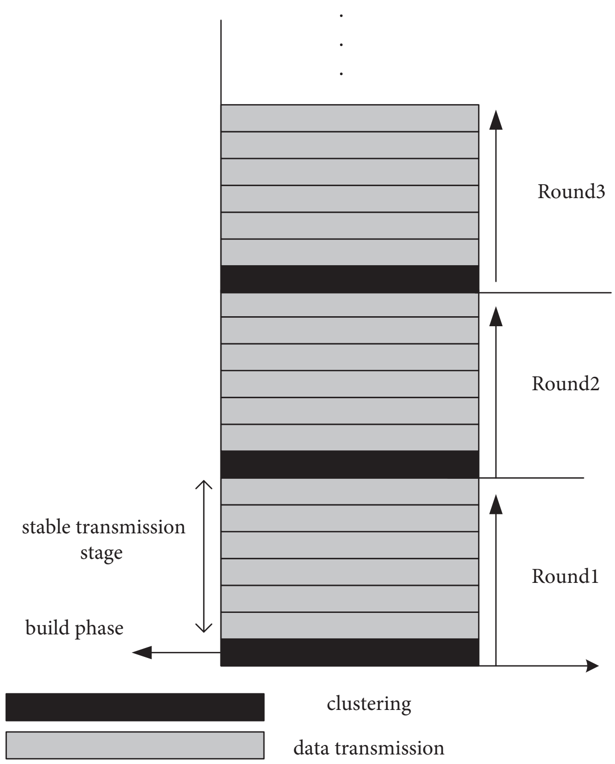

Figure 4: LEACH algorithm run cycle diagram.

$$Q_{ch}(X,Y)=\begin{cases} XQ_{\text{elec}}+X\varepsilon_{fs}Y^2, & Y\le D_{\text{threshold}},\\ XQ_{\text{elec}}+X\varepsilon_{ch}Y^4, & Y> D_{\text{threshold}},\end{cases} \tag{2}$$

$$y_{\text{threshold}}=\sqrt{\frac{\varepsilon_{fs}}{\varepsilon_{ch}}}, \tag{3}$$

$$Q_{RX}(X)=XQ_{\text{elec}}, \tag{4}$$

$$Q_{AG}(X)=XQ_{Ya}. \tag{5}$$

Here, Q_{Ya} represents the circuit loss energy of fusing unit-bit data [18]. Therefore, the transmission route has a great influence on the power generation speed of the sensor web, and it is very important for the wireless sensor network to design an efficient route to reduce the power expenditure of the web [19].

3.2. Improved LEACH Algorithm. The improved LEACH algorithm introduces the concept of temporary tuft leader head and final tuft leader in the first round of tuft head election. All temporary tuft leader located within the same cluster radius competes for the ultimate tuft leader, avoiding the phenomenon of multiple tuft leader within a tuft radius, and uniformizing the distribution of tuft leader [20]. Compared with the LEACH algorithm, the improved algorithm calculates the optimal number of cluster heads based on the energy characteristics of the base station, so that the cluster heads are distributed relatively uniformly in the node area. The energy threshold is judged during the rotation between the cluster heads within the cluster, and the energy consumption is effectively reduced through multihop transmission between the cluster heads to the base station.

Assuming that each node cluster is a circle with the tuft leader as the center, according to the network model of the algorithm, if the area of the node distribution area is m^2, the sum of knots is N, and the proportion of cluster heads is p, then there are N_p nodes in the network. If the clusters are to cover the entire node distribution area, the coverage radius of each cluster needs to be satisfied. R is also the shortest distance between cluster head nodes [21].

$$T=\frac{P}{\sqrt{Qn\pi}}, \tag{6}$$

$$Q_{ab}=Qn. \tag{7}$$

On average, there are (Q/Q_{ab}) nodes in each cluster in the network, including $Q/Q_{ab}-1$ cluster head and q member nodes [22]. The receiving node receives data, fuses data, and sends data. Let $N_{to\ \sin\ k}$ be the distance from the tuft leader to the flume knot, and then power expenditure of the tuft leader is

$$W_{ab} = k\left(\frac{Q}{Q_{ab}} - 1\right)W_{elec} + k\frac{Q}{Q_{ab}}W_{DA} + kW_{elec} + k\varepsilon_{mp}d^4_{tosink}. \tag{8}$$

During a single cluster in each round, the member knots in a single climate only need to transmit water to the leader of the climate. If Y_{totoch} is the distance from the member node to the leader of the climate, the power expenditure of the member node is

$$W_{cm} = kW_{elec} + k\varepsilon_{fs}Y^2_{\text{totoch}}. \tag{9}$$

It is assumed that the coverage area of each cluster is a swarm leader focused on a swarm with a root size of approximately of $R/\sqrt{Q_{ab}\pi}$. If the distribution density of nodes that are part of a fleet of node is $\partial(x, y)$, the expectation of the square of the distance from any member node in the circular cluster to the center of the circle is

$$W\left[Y^2_{\text{toch}}\right] = \iint\left(x^2 + y^2\right)\partial(x + y)YxYy, \tag{10}$$

$$W\left[Y^2_{\text{toch}}\right] = \iint r^2\partial(r, \theta)YrY\theta, \tag{11}$$

$$W\left[Y^2_{\text{toch}}\right] = \partial\int_0^{2\pi}\int_0^{\left(R/\sqrt{Q_{ch}\pi}\right)} r^3YrY\theta, \tag{12}$$

$$W\left[Y^2_{\text{toch}}\right] = \partial\frac{R^4}{2Q^2_{ch}\pi}. \tag{13}$$

If the nodes are evenly distributed throughout the network area, then

$$\partial = \frac{1}{\left(R^2/Q_{ch}\right)}, \tag{14}$$

$$W\left[Y^2_{\text{toch}}\right] = \frac{R^2}{2Q_{ch}\pi}, \tag{15}$$

$$W_{cm} = kW_{\text{elec}} + k\varepsilon_{fs}\frac{R^2}{2\pi Q_{ch}}. \tag{16}$$

Then, the power expenditure of a single cluster in each round is

$$W_{\text{cluster}} = W_{ch} + \left(\frac{Q}{Q_{ch}} - 1\right)W_{ch} \approx W_{ch} + \frac{Q}{Q_{ch}}kW_{cm}. \tag{17}$$

Then, the energy consumption of the whole network in each round is

$$W_{wsn} = Q_{ch}W_{\text{cluster}} = Q_{ch}\left(W_{ch} + \frac{Q}{Q_{ch}}W_{cm}\right), \tag{18}$$

$$W_{wsn} = k\left(2QW_{\text{elec}} + QW_{DA} + Q_{ch}\varepsilon_{mp}Y^4_{to\ \sin\ k} + \frac{\varepsilon_{fs}}{2\pi}\frac{QR^2}{Q_{ch}}\right). \tag{19}$$

In order to find out what value Q_{ch} takes, W_{wsn} is the smallest; let W_{wsn} take the first derivative of Q_{ch}, and let $(YW_{wsn}/YQ_{ch}) = 0$, and it can be obtained that

$$\varepsilon_{mp}Y^4_{to\ \sin\ k} = \frac{\varepsilon_{fs}}{2\pi}\frac{QR^2}{Q_{ch}}. \tag{20}$$

Then, the best amount of tuft leaders in terms of the number of tuft tips can be solved for

$$Q_{ch} = \frac{Q}{Y^2_{to\ \sin\ k}}\sqrt{\frac{Q\varepsilon_{fs}}{2\pi\varepsilon_{mp}}}. \tag{21}$$

It can be seen from the formula that the optimal number of tuft tips Q_{ch} is only related to parameters ε_{fs} and ε_{mp}, the size of the node distribution area R, the total number of nodes Q, and the distance $Y_{to\ \sin\ k}$ from the tuft tip to the sink node. The cluster heads generated by the LEACH random method cannot guarantee their uniform distribution. The information collected by these cluster heads has large redundancy, and the transmission of redundant data is a waste of the limited energy of nodes. Therefore, in the network initialization stage, the ideal quantity of pack leader in the web can be figured out according to the following formula parameters, and an appropriate number of cluster heads can be selected in the first round of cluster head election. In the cluster routing mechanism, the data collected by the member nodes are collected and merged by the cluster head before being forwarded, which reduces the data redundancy and reduces the traffic.

3.3. SMPSO-BP Data Fusion Algorithm. A neural web (NN), also known as an armed artificial network (ANN), is a process that simulates the thinking of the human brain through extensive interconnections. With the powerful error resilience and the ability of adaptive self-learning, self-organization, and self-adaptation, neural networks model sophisticated affine line mappings and can meet the processing demands of data fusion technology, which is especially suitable for sensor networks. Wireless sensor networks need to solve the problems of limited network energy supply, data transmission quality and network data transmission security in the process of mass data transmission, the ability of utilizing the system's signal manipulation function and auto-reasoning capabilities of neural net. Data fusion is realized, and the development of wireless sensor network application field is also promoted, so the emergence of artificial neural network data fusion technology is inevitable.

The basic idea of data fusion is to correlate and analyze the sensing data from multiple sensor nodes, filter invalid information, and extract feature information and combine it into a data packet of the same size with high accuracy. The reduction of data traffic means the reduction of the amount of data sent or received by sensor nodes, which can effectively extend the network life cycle. The total of packets are received at the sink node satisfactorily. Sink node is used as the basis for measuring the data traffic in the network. The comparison of this data can not only reflect the role of data fusion in wireless sensor network routing, but also reflect the difference in data volume control.

Neural network has the ability of parallel processing, distributed storage, and self-learning for a large amount of data, especially suitable for the stage where data needs to be processed at the same time and can solve the problem of inaccurate information processing. The main idea of the SMPSO algorithm is to mutate some particles whose fitness is too low in the early stage. The way is to update the position of the particle to be the average value of the position of the particle with the highest fitness value, thereby reducing the diversity of the population. Then, the particle calculation formula in the SMPSO algorithm is used to update each particle, and the optimal particle obtained after training is the optimal parameter output. Among them, the fitness value function $f(x)$ is the mean square error generated in the sample training, as shown in the following formula:

$$k(x) = \frac{1}{1 + (1/2n) \sum_{b=1}^{n} \left(y_b - t_b\right)}. \tag{22}$$

The standard deviation of the output sequence of the hidden layer node i is calculated according to the formula given below, and the correlation between the ith neuron node and the jth neuron node in the hidden layer is calculated.

$$f_t^2 = \sum_{b=1}^{n} \left(V_{ib} - \overline{V}_i\right)^2, \tag{23}$$

$$C_{ij} = \frac{\sum_{b=1}^{n} \left(V_{ib} V_{jb} - n\overline{V}_j \overline{V}_i\right)}{f_i f_j}. \tag{24}$$

Here, V_{ib} is the outcome value of the ith node of the hidden layer for sample p, and $\overline{V}_i$ is the average value of V_{ib}. If $C_{ij} > h_1, f_i > h_2, f_j > h_2$; delete neuron j and modify the connection weight w_{ei} and threshold θ_e of any neuron e in the next layer, as shown in the following formula:

$$w_{ei} = w_{ei} + aw_{ei}, \tag{25}$$

$$\theta_e = \theta_e + b\theta_e. \tag{26}$$

The wireless sensor network has limited energy, and the communication energy consumption is the main energy consumption of the network. The routing algorithm determines the stability of the entire network. The data fusion model based on BP neural web includes a BP web optimization algorithm based on optimized PSO, namely, the design of the SMPSO-BP algorithm, and it is used to implement the data merge course of the nodes in the wireless sensor web cluster.

4. Routing Test of Wireless Sensor Network Based on Neural Network

4.1. Test Parameter Settings. Before testing the relevant functions of the wireless sensor on the relevant algorithm, the preparation work should be done first, and the relevant parameters should be set:

(1) The sensor node does not move, and it will enter the state of death when its energy is exhausted.

(2) In the entire wireless sensor network, there is only one sink node, that is, the sink node, and this node has unlimited energy and computing power and does not need to consider energy supply and node death.

(3) Sensor nodes have unique IDs and can communicate with each other.

(4) The energy depletion model for text wireless transmission uses the WSN channel energy depletion model, and the node distance is set as the experimental approximate value of 90 m. The sensor knots are strategically located in the measurement area and have the same transmission range. The specific parameters are shown in Table 2.

4.2. Node Test Comparison of Related Algorithms. The convergence rate, which can be expressed by the average best fitness and the average number of iterations, is used to demonstrate the effect of the SMPSO-BP algorithm's search performance. The average number of iterations will be 100, based on previous experience and experimental testing conditions. Figure 5 shows the SMPSO-BP calculations for verification with the LEACH calculations and the improved LEACH calculations under the experimental parameter settings. We get the verification of the SMPSO-BP algorithm's convergence simulation results when the number of sensor nodes is 600, 700, and 800, respectively. The curve of the SMPSO-BP algorithm first reaches the level, as shown in the graph above, when the number of knots is 800, indicating that the individual particle swarm obtains the best fitness value first. The scenario with 700 points comes next, followed by the scenario with 600 points. As a result, the SMPSO-BP algorithm proposed in the paper can be applied not only to small-scale nets, but also to massive systems, with a relatively fast aggregation speed.

It is seen from Figure 5 that, by increasing the frequency of repeated generations, the fitness value is constantly approaching the optimal fitness value, and finally the average fitness value is close to 1, which is stable, and the curve converges. This shows that it is practicable to integrate and combine neural neck networks with SMPSO-BP algo for data fusion in radio signal systems. Further, the SMPSO-BP algorithm can arrive at the sweet fitness value much earlier compared to the improved LEACH method; that is, the optimal reading value of the BP neural network can be obtained faster. It can also be seen from the figure that the curve of the original LEACH algorithm without optimization is the slowest, which shows that the LEACH algorithm does have the problem of slow convergence. The other two algorithms with intelligent optimization have a significantly higher curve convergence rate than the LEACH algorithm. And the improved LEACH algorithm converges when the number of evolution iterations is about 700, while the SMPSO-BP algorithm converges, and when the total number of iterations is about 600, this suggests that the

Table 2: Experimental parameter value settings.

Parameter	Parameter value
The number of sensor nodes	1000
Node initial energy	0.8 J
Perceived data interval	0.5 s
Data transmission energy consumption	50 nJ/bit
Receive data energy consumption	35 nJ/bit

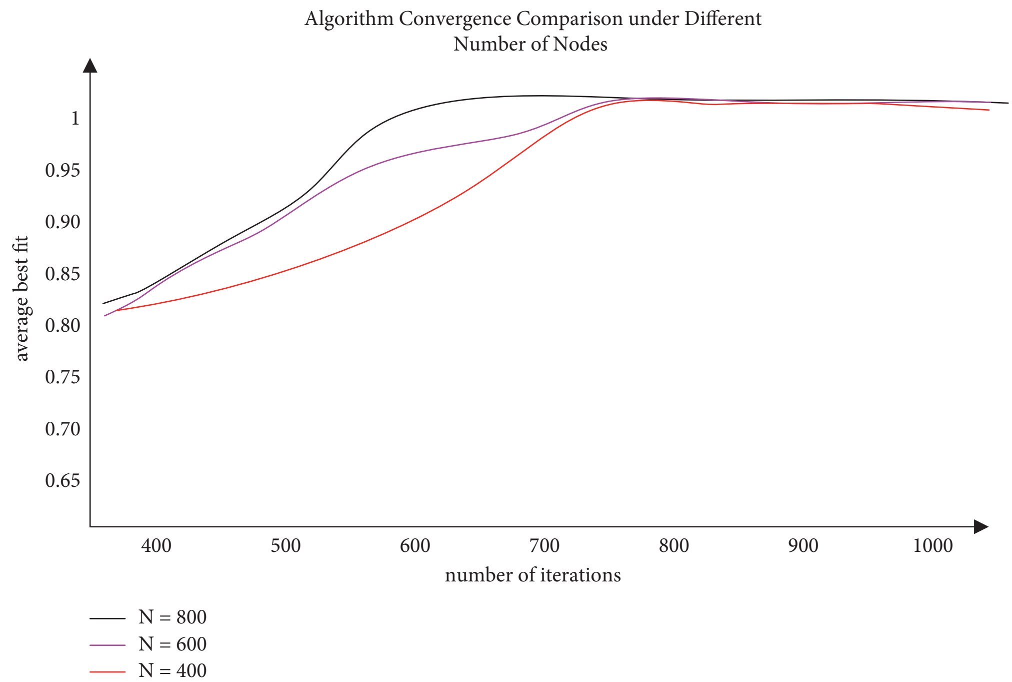

Figure 5: Convergence speed of different algorithms at the same number of nodes and different number of nodes.

speed of convergence of the SMPSO-BP algorithm is indeed faster than that of the improved LEACH algorithm.

The SMPSO-BP algorithm obtained from the experimental analysis is due to the other two algorithms, but at the expense of simulation time. Through 60 independent simulation experiments, the average operation time of SMPSO-BP algorithm, LEACH algorithm, and improved LEACH algorithm is obtained. The results are shown in Table 3.

Compared with the GABP algorithm, the BP network optimization algorithm requires longer operation time, and the BP algorithm without any optimization measures requires the shortest operation time. Although the SMPOS-BP algorithm achieves the optimization of the BP network at the expense of extending the operation time, from the results in the above table, the extended time is relatively within an acceptable range. Therefore, in general, for the application of data fusion in wireless sensor networks, the SMPSO-BP algorithm has shown good performance in terms of efficiency and accuracy.

The survival rate of sensor nodes is crucial to the normal operation of wireless sensor networks. Once a node enters a state of death due to energy exhaustion or other failures, the node cannot perform the task of sensing and collecting data.

Table 3: Comparison of operation time of different algorithms.

Algorithm	Operation time/s
LEACH algorithm	4.13
Improved LEACH algorithm	3.89
SMPSO-BP	3.55

Therefore, after the network has been running for a period of time, the comparison and analysis of the number of surviving nodes are an important part of examining the performance of the improved data fusion algorithm. The SMPSO-BP algorithm, the LEACH algorithm, and the improved LEACH algorithm are simulated and compared, and the results are shown in Figure 6.

The curve of the LEACH protocol is greater than the previous version in the early stages of network operation than in the other two cases, as shown in Figure 6. This is due to the fact that the data fusion mechanism is not constrained, so it is sent directly to the socket head point node. The node survival rate drops dramatically as the number of data transmissions grows too large. When the data fusion mechanism is implemented in a network where the SMPSO-BP operator performs the SMPSO-BP approach to

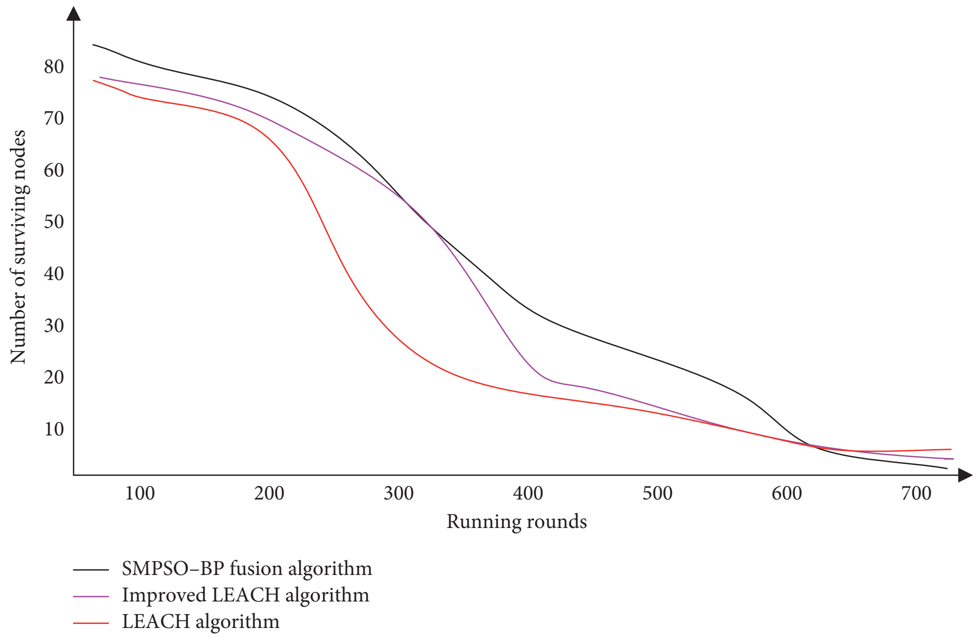

(a)

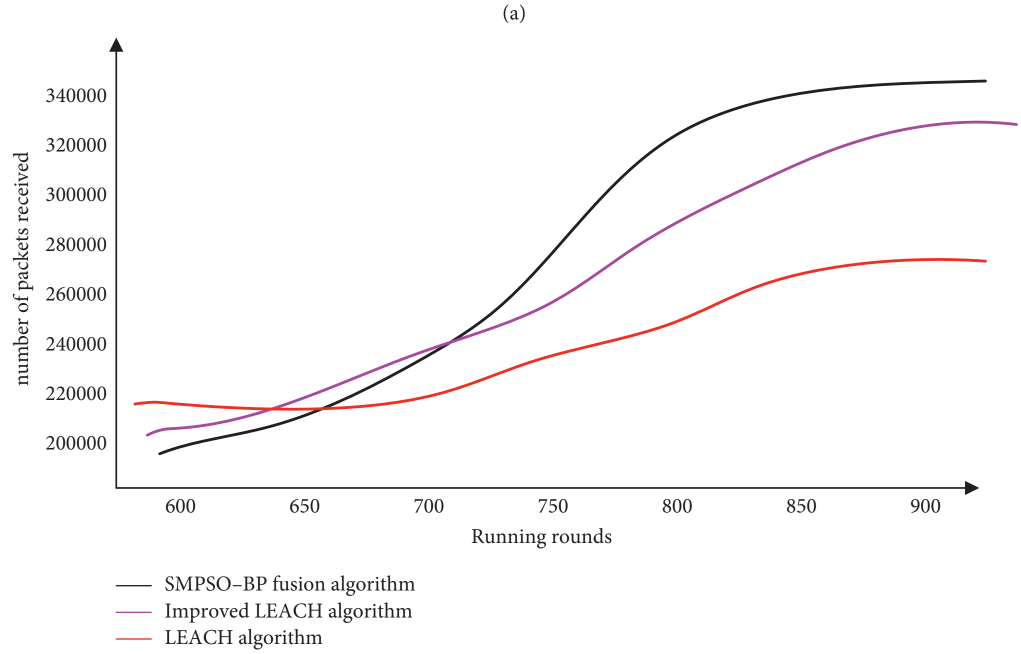

(b)

Figure 6: Survival number of network nodes with different algorithms. (a) Comparison of the number of surviving nodes in the network. (b) Comparison of the amount of data received by the node.

processing, the processed data is sent to the repository junction nodes in a stable manner as the amount of transmitted data grows. Because the amount of redundant data is reduced, and the nodes' energy consumption is low, environmental monitoring and data transmission can still be carried out normally, especially at a later stage. The fact that the number of packets received by the water sink nodes increased even after the death of a large number of sensor nodes shows that data fusion can reduce data traffic in the network effectively. During this time, the optimized LEACH protocol also played a supporting role, helping achieve the goal of extending the network's working time.

4.3. Comparison of Energy Consumption in the Network. In order to understand and solve the problem of energy consumption of routing nodes in wireless sensor networks, this paper uses SMPSO-BP algorithm, LEACH algorithm, and improved LEACH algorithm to calculate the change of the remaining energy of the whole network in the base

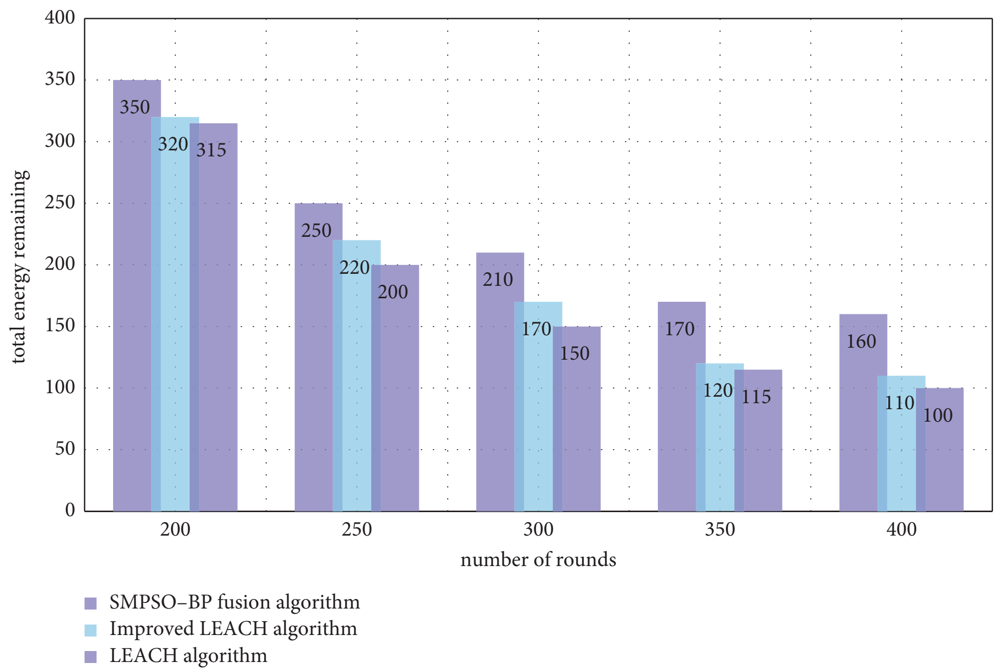

(a)

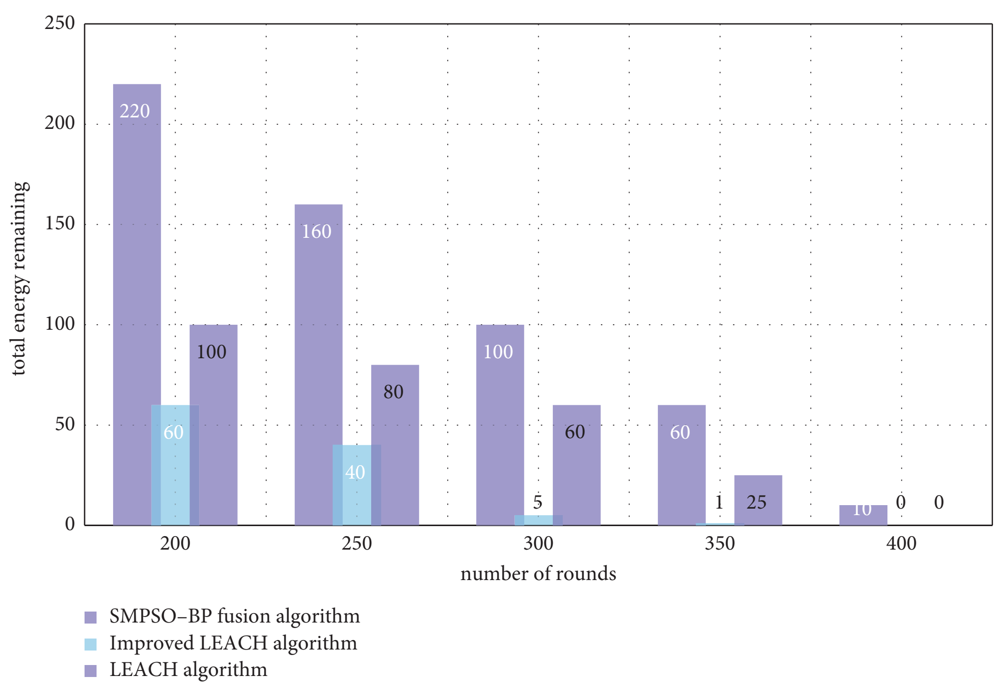

(b)

Figure 7: (a) The remaining energy of the whole network of the base station in the node area. (b) The remaining energy of the entire network of the base station outside the node area.

station node area and outside the area with time, to understand the energy consumption of the wireless sensor network routing nodes by the neural network of the data fusion technology.

Figure 7 shows the remaining energy of the whole network when the base station is in the node area, and the remaining energy of the whole network for the three protocols in the initial state is the same. The vertical axis in Figure 7 represents the total energy remaining in the network, and the horizontal axis represents the number of rounds performed. The steep energy curves of the LEACH algorithm and the improved LEACH algorithm indicate that the energy consumption per round is more, while the corresponding SMPSO-BP algorithm protocol energy curve is the flattest, indicating that the energy consumption per round is smaller than the other two. As the round increases, the nodes far from the base station in LEACH begin to die, resulting in a reduction in the number of nodes and a reduction in energy consumption. In this experiment, the SMPSO-BP algorithm, the LEACH algorithm, and the improved LEACH algorithm are simulated and compared, and the overall energy consumption of the network is analyzed. The results are shown in Figure 7.

The node death time in the improved LEACH algorithm is later than that in the LEACH algorithm. The SMPSO-BP algorithm does not need to select a new cluster head every round. The clustering is uniform, the position and residual energy of the candidate nodes are considered when the cluster head is rotated within the cluster, and the cluster head communicates with the base station in multiple hops. These measures make the SMPSO-BP algorithm consume less energy in a single round. The residual energy of the whole network is higher than that of the LEACH algorithm and the improved LEACH algorithm. Regarding the remaining energy of the entire network when the base station is outside the node area, due to the increase in the communication distance, the energy consumed by the three protocols in each round increases. The improved LEACH algorithm has the greatest impact because all nodes need to send messages to the base station. In the SMPSO-BP algorithm, the cluster head uses multihop to transmit data to the base station, reducing the loss caused by the long-distance communication.

5. Conclusion

The emergence of neural network data fusion technology can better and more comprehensively simulate the cognitive ability of the sensor node ad hoc network. Its application will greatly improve the intelligence level of sensor network applications, reduce node energy consumption, and effectively prolong the lifetime of sensor networks. Three kinds of routing nodes are analyzed by the convergence speed of node data and the survival rate of nodes when data transmission is increased, and the SMPSO-BP algorithm supported by neural network is compared with other algorithms. The convergence of the SMPSO-BP algorithm and the number of surviving nodes during the operation of the wireless sensor network are all due to the other two algorithms, and it can avoid falling into the local optimum. And the cluster head election process is more reasonable, which can achieve energy balance to a certain extent. The data fusion mechanism of the SMPSO-BP algorithm does reduce the amount of data transmission during the operation of the wireless sensor network, reduce the energy consumption of nodes, and achieve the purpose of extending the network life cycle. It is believed that the energy consumption of wireless sensor network routing nodes can be better reduced based on the neural network data fusion mechanism algorithm. Wireless communication is realized through the automatic data exchange of sensors, which improves the efficiency of data transmission, provides convenience for people's daily life, and has a positive impact.

Data Availability

The data used to support the findings of this study are available from the corresponding author upon request.

Conflicts of Interest

The authors declare no conflicts of interest.

References

[1] N. Dey, A. S. Ashour, and F. Shi, "Developing residential wireless sensor networks for ECG healthcare monitoring," *IEEE Transactions on Consumer Electronics*, vol. 63, no. 4, pp. 442–449, 2018.

[2] E. Jamhour, M. C. Penna, and M. L. F. Miguel, "A CoAP based control plane for software defined wireless sensor networks," *Journal of Communications and Networks*, vol. 19, no. 6, pp. 555–562, 2018.

[3] J. Aarti and P. Anuj, "Ant colony optimization and excess energy calculations based fast converging energy efficient routing algorithm for WSNs," *Wireless Personal Communications*, vol. 109, no. 4, pp. 2305–2328, 2019.

[4] W. Song, H. Chen, Q. Zhang, B. Zhang, H. Wang, and H. Xu, "On-chip embedded debugging system based on leach algorithm parameter on detection of wireless sensor networks," *Mathematical Problems in Engineering*, vol. 2020, no. 93, Article ID 7249674, 2020.

[5] J. Bhola, S. Soni, and G. K. Cheema, "Genetic algorithm based optimized leach protocol for energy efficient wireless sensor networks," *Journal of Ambient Intelligence and Humanized Computing*, vol. 11, no. 3, pp. 1281–1288, 2020.

[6] S. Khriji, D. E. Houssaini, I. Kammoun, K. Besbes, and O. Kanoun, "Energy-efficient routing algorithm based on localization and clustering techniques for agricultural applications," *IEEE Aerospace and Electronic Systems Magazine*, vol. 34, no. 3, pp. 56–66, 2019.

[7] H. Guo, F. Wang, and L. Zhang, "Matchmaking tradeoff based minimum loss routing algorithm in energy internet," *Dianli Xitong Zidonghua/Automation of Electric Power Systems*, vol. 42, no. 14, pp. 172–179, 2018.

[8] B. Liu, R. Yang, M. Xu, and J. Zhou, "A chaotic elite niche evolutionary algorithm for low-power clustering in environment monitoring wireless sensor networks," *Journal of Sensors*, vol. 2021, no. 3, 12 pages, Article ID 5558643, 2021.

[9] B. Subba, S. Biswas, and S. Karmakar, "A game theory based multi layered intrusion detection framework for wireless sensor networks," *International Journal of Wireless Information Networks*, vol. 25, no. 4, pp. 1–23, 2018.

[10] B. Cao, J. Zhao, P. Yang, Z. Lv, X. Liu, and G. Min, "3-D multiobjective deployment of an industrial wireless sensor network for maritime applications utilizing a distributed parallel algorithm," *IEEE Transactions on Industrial Informatics*, vol. 14, no. 12, pp. 5487–5495, 2018.

[11] B. M. Khan, R. Bilal, and R. Young, "Fuzzy-TOPSIS based Cluster Head selection in mobile wireless sensor networks," *Journal of Electrical Systems and Information Technology*, vol. 5, no. 3, pp. 928–943, 2018.

[12] P. S. Lorenz, G. Staples, S. Stacey, and A. Abdusy, "New path centrality based on operator calculus approach for wireless sensor network deployment," *IEEE Transactions on Emerging Topics in Computing*, vol. 7, no. 1, pp. 162–173, 2019.

[13] S. Jabbar, M. Ahmad, K. R. Malik, S. Khalid, J. Chaudhry, and O. Aldabbas, "Designing an energy-aware mechanism for lifetime improvement of wireless sensor networks: a comprehensive study," *Mobile Networks and Applications*, vol. 23, no. 3, pp. 1–14, 2018.

[14] J. Wang, X. Zhang, J. Xu et al., "Blockchain-based information supervision model for rice supply chains," *Computational Intelligence and Neuroscience*, vol. 2022, Article ID 2914571, 17 pages, 2022.

[15] K. Mounika, C. Rambabu, and V. V. K. D. V. Prasad, "Improving the network life time of wireless sensor network using MAODV protocol with LEACH algorithm," *International Journal Of Computer Sciences And Engineering*, vol. 6, no. 6, pp. 534–538, 2018.

[16] G. Nigam and C. Dabas, "Improved energy efficient leach in wireless sensor networks," *Journal of Theoretical and Applied Information Technology*, vol. 97, no. 4, pp. 1218–1230, 2019.

[17] W. Wang and G. Tong, "Multi-path unequal clustering protocol based on ant colony algorithm in wireless sensor networks," *IET Networks*, vol. 9, no. 2, pp. 56–63, 2020.

[18] L. You, H. Jiang, J. Hu et al., "GPU-Accelerated Faster Mean Shift with Euclidean Distance metrics," 2021, https://arxiv.org/abs/2112.13891.

[19] G. Xiang, Z. Boyao, and G. Xinyan, "Routing algorithm based on energy optimization in wireless sensor networks," *IPPTA: Quarterly Journal of Indian Pulp and Paper Technical-A*, vol. 30, no. 6, pp. 207–212, 2018.

[20] J. Huo, X. Deng, and H. M. M. Al-Neshmi, "Design and improvement of routing protocol for field observation instrument networking based on LEACH protocol," *Journal of Electrical and Computer Engineering*, vol. 2020, no. 20, 19 pages, Article ID 8059353, 2020.

[21] J. Chen, C. Du, Y. Zhang, P. Han, and W. Wei, "A clustering-based coverage path planning method for autonomous heterogeneous UAVs," *IEEE Transactions on Intelligent Transportation Systems*, vol. 1, pp. 1–11, 2021.

[22] S. P. Singh and S. C. Sharma, "An improved cluster-based routing algorithm for energy optimisation in wireless sensor networks," *International Journal of Wireless and Mobile Computing*, vol. 14, no. 1, pp. 82–89, 2018.

Hindawi
Computational Intelligence and Neuroscience
Volume 2022, Article ID 2636877, 9 pages
https://doi.org/10.1155/2022/2636877

Research Article

Simulation Training Auxiliary Model Based on Neural Network and Virtual Reality Technology

Wei Liu

Guangzhou Panyu Polytechnic, Guangzhou 511400, China

Correspondence should be addressed to Wei Liu; liuwei@gzpyp.edu.cn

Received 23 April 2022; Revised 23 May 2022; Accepted 25 May 2022; Published 1 July 2022

Academic Editor: Xin Ning

Training simulators have been gradually evolving in the direction of software, virtualization, networking, and multiplatform in recent years, with the continuous development of hardware and software technologies, particularly the maturity of VR (Virtual Reality) related technologies. The network intrusion program allows remote hackers to take control of the system, posing a serious threat to the network and computer security. As a result, this paper proposes a VR-based ID (intrusion detection) simulation training system. This paper proposes an ID model based on CNN (Convolutional Neural Networks) and LSTM to address these issues (Long Short-term Memory Networks). This model oversamples data from unbalanced data sets, reducing the difference in category data and thus improving the ID model's performance and existing detection methods to compensate for the flaw. 3DSMAX technology is used to simulate the process visualization scene, as well as some key equipment models and signal transmission simulations, during the system design and implementation process. The experimental results show that CNN LSTM outperforms BP, and the overall evaluation index $F1$ has significantly improved, particularly the $F1$ index of D4. CNN LSTM outperforms GA (genetic algorithm) by 12.75 percent and BP by 14.07 percent. The system essentially accomplishes the anticipated simulation training goal, and the simulation training effect is impressive.

1. Introduction

As a means of information transmission and communication, virtual reality technology can intuitively and realistically provide students with visual information such as the structure, size, working principle, and assembly process of equipment, allowing them to observe the team in a virtual environment. The working process and direct operation of each component help students understand and perceive tasks more effectively. Virtual reality is a new technology. Its goal is to make the information system as user-friendly as possible, to improve the direct interaction between users and data, and to make human-computer interaction more convenient and humanized [1]. The simulation training system based on VR technology has low cost, high versatility, easy upgrade, and easy maintenance, among other features, and is particularly well suited to the primary training of students' operation skills.

Network security technology has become a key technology of computer networks. ID (intrusion detection) is considered the second security door behind the firewall. It can monitor the network without affecting the network performance, provide real-time protection against internal attacks, external attacks, and improper operations, and greatly improve network security [2]. An efficient ID system can provide security for the computer system, network system, and even the whole information system and prevent huge economic losses. Wang et al. have studied and implemented a real-time ID system model, which is based on the profile of user behavior characteristics and uses statistical methods to describe the behavior of system subjects relative to system objects [3]. Riyaz and Ganapathy adopted a recursive network and combined it with traditional expert system for ID [4]. Esmeir and Markovitch proposed an anomaly detection algorithm based on a one-dimensional self-organizing feature mapping network [5]. Alkadi et al.

introduced information retrieval technology into ID. However, some algorithms are not practical, such as expert methods [6], and some algorithms are still in the experimental research stage, such as immunological methods and neural networks.

By examining the current state of information security, we can see that traditional security technology is unable to fully guarantee network security, and the existing ID system has numerous flaws. As a result, the development of identification technology must meet higher requirements in order to protect network security. The system may be attacked, according to the current security situation. If the system is attacked, further losses can be avoided if the attack is detected as quickly as possible, even in real time. In this regard, identity verification is critical for establishing a security system capable of compensating for the shortcomings of traditional security measures. This document develops an ID simulation training system using VR technology based on the ID process and the use of 3DSMAX software. Simultaneously, it can effectively solve students' learning and training problems, improve the efficiency of students' knowledge absorption, master skills, and improve the effectiveness of education and training. This paper contains the following innovations:

(1) In this paper, a simulation training system is established, and the virtual training scene is constructed and optimized by 3D modeling and 3DSMAX rendering software. Finally, the interactive settings of die-cutting, paper, and die-cutting actions are made by VR software, and the training interaction of virtual ID is realized.

(2) This paper presents an ID detection model based on a neural network. This model can extract the local features of data in the network by using CNN's deep feature learning [7, 8], which can improve the accuracy of ID and reduce the false alarm rate.

This paper has the following organizational structure: The first chapter discusses the research's background and significance before moving on to the paper's main work. The second chapter focuses on the technologies that are needed to implement the simulation training system. The research's concrete methods and implementation are presented in the third chapter. The superiority and feasibility of this research model are confirmed in the fourth chapter. The summary of the full text appears in the fifth chapter.

2. Related Work

2.1. ID System Research. After analyzing the characteristics of the traffic flowing through the network, ID can analyze the user's behavior to see if it is malicious, which is an active tracking behavior. From here on, ID has entered the development stage of network detection.

Fan et al. adopted a multilevel hierarchical ID method based on GA (genetic algorithm) to solve the problems of a single-level ID system [9]. Ghosh et al. proposed a method of constructing an ID system with a decision tree, which can identify unknown attacks in the network [10]. Alotaibi and Alotaibi proposed an abnormal traffic detection method based on a deep neural network, which can identify the normal or abnormal connections in the network, and the detection effect is good [11]. Kumar et al. proposed a deep neural network ID system based on context LSTM (Long Short-term Memory Networks) [12]. Firstly, the original data is obtained by social media on the internet, from which the push-level bots are detected, and then the context features are extracted and detected by LSTM. However, this method is only suitable for the detection of specific bots.

Kim et al. used a standard BP network to train and recognize the formed user behavior feature vectors [13]. Choobdar et al. used two different statistical analysis detection techniques to detect the abnormal behavior of the system [14]. Tian et al. used comprehensive traffic monitoring to find anomalies, combined with geographic information to show the location of intrusion events and applied the corresponding relationship between intrusion and vulnerability to give the risk analysis results between intrusion threats and asset vulnerability so as to effectively manage security events and timely handle and respond [15]. Rezaei and Liu applied the immune principle to the field of distributed ID [16].

2.2. VR Technology Research. In recent years, with the continuous development of computer hardware and software, new technology has developed rapidly-VR. It is an ideal man-machine interface between VR computers and users. VR system has three important characteristics: immersion, interactivity, and imagination. VR technology has a wide range of potential applications, such as national defense, architectural design, industrial design, training, medical treatment, and other fields.

With the help of specially designed sensors, users can interact with 3D images and manipulate virtual objects so that users can perceive the virtual environment equivalent to the real world [17]. Xue et al. further simplified it into a computer program that can present a simulated world [18]. It can be defined as a highly interactive three-dimensional digital media environment. Users can intuitively experience the simulated environment and get multisensory feedback such as hearing, touch, and vision. Wang and Zhu think that good spatial audio not only makes users deeply immersed in a virtual environment but also is an important channel for users to obtain environmental information [19]. Yong proposed an optical mapping near-eye 3D display method for wearable devices, the core of which is to adjust the eyes to the same distance as a binocular stereo vision to relieve eye fatigue and discomfort [20]. Compared with previous methods, this monitor has outstanding advantages in adaptability, dynamic range of images, and refresh rate.

It is a somatosensory interaction technology to interact with the virtual environment in a noncontact way through physical natural behaviors such as actions, sounds, or expressions. Foreign scholars generally believe that somatosensory interaction technology is a key component of VR and plays an important role in VR training. Yang et al. put forward a soft motion sensing device for measuring lower limb joint motion, which can effectively improve the shortcomings of the prior art in mobility and wear resistance [21]. Xia and Qi proved that distributed VR system can build a 3D collaboration environment for distributed users to interact with each other and complete various collaboration tasks [22]. Distributed VR system conforms to the new demands of the times, promotes communication and collaboration among users, and their application potential needs to be explored more. Bai et al. are committed to improving the user experience of VR devices, suggesting that a multiuser VR environment and wireless connection should be considered in future VR devices [23].

3. Methodology

3.1. ID Model Design. The algorithm used by the ID system has a direct impact on detection efficiency and accuracy. Pattern matching is now one of the most widely used detection methods and mechanisms in the field of identification. The next step in this concept is to define the pattern of existing problems. Then look for event data that corresponds to the pattern. Anomaly detection and production ID systems frequently employ statistics. Statistics is a relatively mature ID method that allows the ID system to learn the subjects' daily behavior and identify those activities that statistically differ from normal activities as abnormal. Because of the immune system's unique capabilities, an ID system based on immunological methods offers numerous benefits, including diversity, fault tolerance, distribution, dynamics, self-management, and adaptability.

The neural network has the ability of self-adaptation, self-organization, and self-learning. It can deal with some problems with complex environmental information and unknown background knowledge, which makes the samples have big defects and deficiencies [2]. From the perspective of pattern recognition, an ID system can use a neural network to extract pattern features from user behavior and then create profiles of user behavior features. In a word, the introduction of the neural network into the ID system can solve the dynamic characteristics of user behavior and the difficulty of accurate detection caused by incomplete and uncertain search data. The attack behavior in the network is not completed at a single point in time but will be sent continuously over a period of time. By analyzing the correlation performance of the time series before and after the network data, the intrusion behavior can be best detected. In this paper, an ID model combining CNN (Progressive Neural Network) and LSTM (Long Short-term Memory Networks) is proposed, and the loss function is optimized to improve the ID accuracy and reduce the false alarm rate. The ID is shown in Figure 1.

In this model, CNN is first used to extract depth local features in order to effectively extract sample data, and then LSTM is used to learn and extract correlation features between continuous data in both positive and negative directions. Finally, the softmax layer is used for classification, and the Focal Loss function is used to optimize the model. The model takes into account the temporal and spatial correlation of intrusion data and can extract unknown features and internal dependencies between data, lowering false alarm rates and improving detection effectiveness.

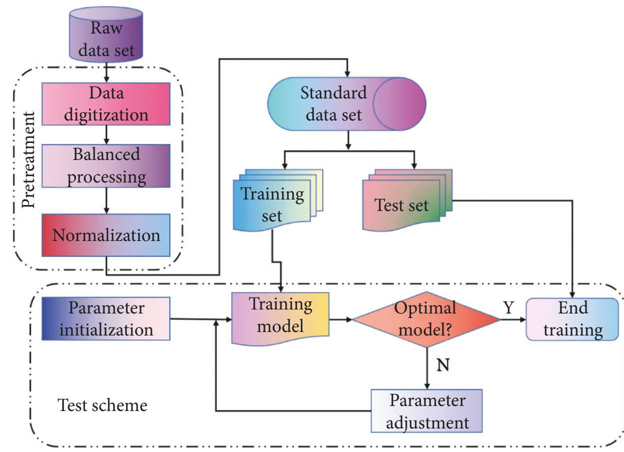

Figure 1: ID structure.

The role of the ID model based on deep learning is to divide the emerging abnormal data traffic into a group of known attack types according to their function or behavior. In the actual detection process, it is often necessary to preprocess the samples, including digitization, normalization, data equalization, and other operations, so as to make the data conform to the input format of the detection algorithm.

Select to keep the useful information in the memory cell, discard the unnecessary information, and normalize the value by activating the function. The specific calculation formula is shown as follows:

$$f_t = \sigma\left(W_f \cdot [h_{t-1}, x_t] + b_f\right). \tag{1}$$

σ is the sigmoid function. At $t-1$ time, the output vector of the hidden layer is expressed as $h(t-1)$, at t time, the input vector is expressed as x_t, and in f state, the weight matrix of x_t is expressed as W_f, and b_f is offset.

In the ID model designed in this paper, there is only one full connection layer, and the upper layer information is integrated and transmitted to LSTM. The output calculation formula of neurons in the whole layer is shown in the following:

$$y_j^l = \sum_i w_{ij}^l * x_i^{l-1} + b_j^l, \tag{2}$$

where w_{ij}^l represents the connection weight; x_i^{l-1} is the i th eigenvalue of the eigenvector in layer $l-1$; b_j^l represents the offset value; y_j^l is the calculated output of the j-th neuron in layer l.

Input the sample vector into the X competition layer, calculate the Euclidean distance between the sample point and the subcategory, and find the most suitable subcategory to belong to the following:

$$d(X, W_c) = \min\{d(X, W_i)\} \quad i = 1, 2, \ldots, R, \tag{3}$$

where W_c represents the initial weight of the network, $d(X, W_c)$ represents the distance between the i th input sample and the subcategory, and W_i represents the subcategory after winning the competition.

x_{ij} is set as training data, which contains data elements with large variation. The goal is to make the variation between elements less than 1. First calculate the average of all elements in X:

$$p_0 = \frac{1}{m*n}\sum_{i=1}^{n}\sum_{j=1}^{n} x_{ij}. \tag{4}$$

Among them, $i = 1, 2, \ldots, m$; $j = 1, 2, \ldots, n$.

Then, through a mapping function, the numerical values are mapped to each subinterval to be quantified so as to achieve the goal of normalization. The normalization method used here is linear normalization, and the expression is as shown in the following formula:

$$y = \frac{x - \text{Min Value}}{\text{Max Value} - \text{Min Value}}, \tag{5}$$

where x, y is the value before and after conversion, and Max Value, Min Value is the maximum and minimum value of the sample.

If the output is close to [0, 1], it is assumed that an intrusion has occurred, and the control center should be notified and appropriate measures taken. If the intrusion is new, the neural network should be investigated, retrained, the weights corrected, and the network's performance improved. Distributed object technology, software agent technology, and mobile code technology are all combined in mobile agent technology. It is a brand new computing technique for dealing with complex, dynamic, and distributed intelligent applications. The concept of distributed computing has been greatly expanded by the addition of intelligent functions and mobile creativity. Artificial intelligence combined with distributed computing is likely to become a key component of intelligent distributed computing. Figure 2 is the flow chart of mobile agent task analysis.

The scheduling manager is the core component of the mobile agent service environment. Assign all kinds of services required for normal mobile agent operation to the corresponding submodules, including setting the mobile agent execution environment, starting services, etc. In addition, it is also responsible for coordinating the cooperation among submodules to ensure their normal operation. Static agent mainly completes the interaction between agent scheduling manager and front-end agent.

3.2. Scene Modeling. One of the keys to building a high-fidelity virtual scene is to use 3D modeling technology and modeling software to present a scene almost identical to the real environment on the computer. Realistic virtual ID model is the basis of designing a virtual die-cutting training system as a visual, interactive, and realistic simulation training scene of die-cutting equipment. Virtual identity recognition is an important core part of the virtual simulation training system. Because these devices require high precision, this paper uses Solidworks to build parametric

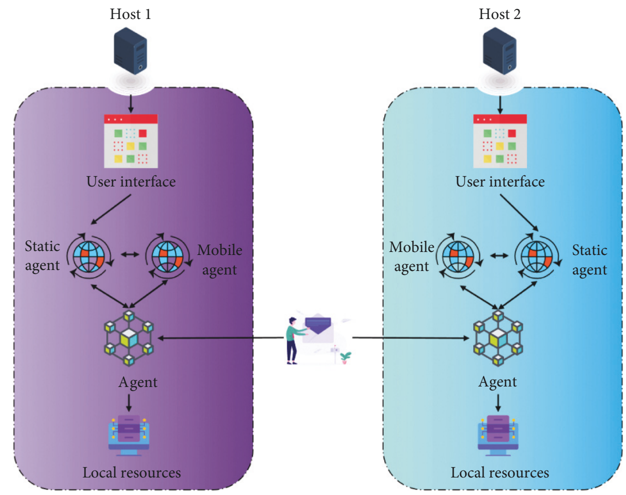

FIGURE 2: Flow chart of mobile agent task solving.

models of these devices and then imports them into 3DsMax for rendering, which can not only ensure the model precision but also ensure the fidelity.

Unique training is done by plane animation. An image is an original hand-drawn painting, and Photoshop is used to perform the effects of the image, such as color correction, motion processing, and stereo effects. The transition and continuity of actions are completed through key frames to ensure the accuracy and consistency of actions. It should be noted that when modeling in 3D Studio Max, the material must use standard material or multisubobject material and use the default scanline renderer. All the sizes of the maps are set according to the pixel of 2 to the n power, so as to reduce the memory overhead and improve the fluency of the software.

For a surface S, suppose we need to paste texture lines on the surface. First, we need to find out the relationship between space A and B. Let the radius of the surface S be R, and the chord height PF $= h$ be OP $= R - h$; Make AB $= x$, so we can get the following relationship:

$$\frac{R}{R+x} = \frac{R-h}{R}. \tag{6}$$

After simplification, you get the following:

$$x = \frac{hR}{h-R}. \tag{7}$$

There are

$$(s - x^*)^2 + (t - y^*)^2 + z^* = \left(\frac{hR}{h-R}\right)^2. \tag{8}$$

Then the $B(x^*, y^*, z^*)$ on the curved surface corresponds to the $A(s, t)$ on the texture pattern one by one, and similarly, other surfaces on the curved surface also have this corresponding relationship.

So you can get the following:

$$\sin\theta = \frac{|AB|}{|A^* B^*|} = \frac{am + bn + cp}{\sqrt{(x_1^* - x_2^*)^2 (y_1^* - y_2^*)^2 (z_1^* - z_2^*)^2}}. \tag{9}$$

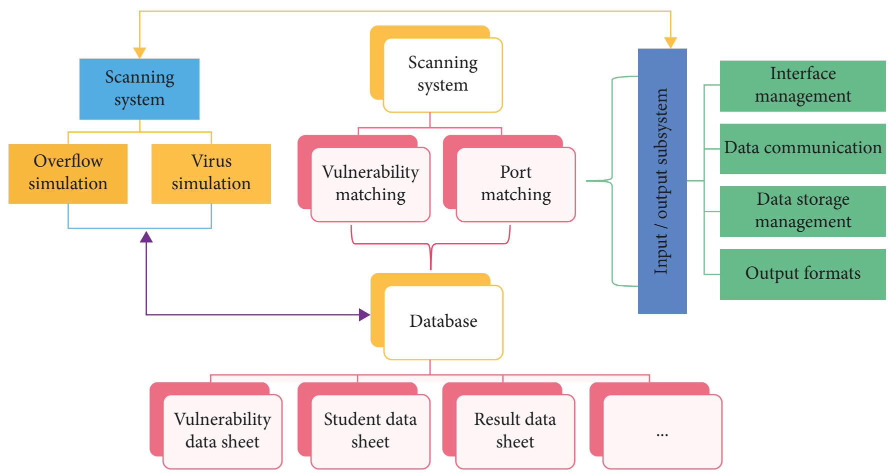

Figure 3: System structure.

After the above transformation, the texture space coordinate (x, y) and the concave-convex model mapping area coordinate (x^*, y^*, z^*) can form a one-to-one correspondence relationship so as to better realize concave-convex model mapping.

The color and properties of materials should be as close to real objects as possible to improve the fidelity of virtual scenes. Material Editor and Material/Map Browser tools are included in 3ds Max. You can choose different types of shading for objects, use different material components, and enhance materials with maps to make them look more realistic in light and environment in the Material Editor. To achieve the desired effect, we simply need to set and adjust the parameters of the particle system according to the characteristics of special effects during the development process. The time it takes to write and develop code can be cut in half while achieving special effects, and good results have been obtained [12].

3.3. Realization of Interactive Effect of Virtual Scene. As an important part of the network attack and defense training system, ID simulation training system mainly includes four main subsystems, as shown in Figure 3. The subsystem uses the database SQLServer database (the database name is net_fight) to store data. As the data storage center of the whole education and training system, the input subsystem is the general part of the whole education and training system and undertakes various input and output functions.

In this virtual simulation training system, there are many virtual scenes that need to interact with each other in order to realize the real representation of identity. Paper feeding includes two parts: paper feeding and paper discharging after die-cutting. Paper movement is set interactively with the path node, and the path node can move or rotate its parent node. In its property box, you can enter the moving position and direction of the paper at each time point to make the paper move along a certain path. Use the place node to complete the previous movement. When the start button is pressed, the template immediately rises. A user-defined function node can be described using a Script node. You must define a field list, event input and output, and what to do with these operations in this function node. The student users enter the Train system and begin attack training after the teacher has been set up. The student's attack is successful if the attack condition matches successfully; if the condition fails, the student immediately enters the temporary result and starts over. The attack subsystem's network intrusion function simulation module also sends interface information to the input-output subsystem, which saves the final information in the result data table.

Attack sequence table attack_state table stores information about students' attacks and Source_IP field indicates the IP address of the attacker. Server setup simulation includes verification code setting, password setting, server name setting, online prompt setting of the destination host and sending to mailbox, etc. When "student_state" = "1," the target IP is online; when "student_server" = "1," the target host has an intrusion server installed on the network.

4. Experiment and Results

In the experiment, 100,216 randomly selected and preprocessed data blocks are used as training sets for model training, and 4,227 randomly selected data blocks are used as test sets for performance testing. After numerical processing in data preprocessing, the single record in the set is finally changed from the original 40-dimensional feature vector to the 120-dimensional binary feature vector. Therefore, the model input in this document is a numerical array with a fixed size of $1 * 120$. In this paper, the loss function parameter $\alpha = 0.2, \gamma = 3$, which has been verified by the existing experiments, has been used for many experiments. Recall rate and false alarm rate are used as performance evaluation criteria. Experimental results are shown in Table 1.

The experimental results in the above table are displayed visually by charts, as shown in Figures 4 and 5.

According to the analysis of Figure 4, the recall rate first rises and then falls with the increase of the convolution kernel, and the difference is obvious. When the convolution kernel size is 5 and the number of hidden layer ganglia is 30,

Table 1: Influence of the number of hidden layer nodes on performance.

Convolution kernel size	Number of hidden layer nodes	Precision (%)	False alarm rate (%)
1	10	93.31	2.17
1	30	94.15	2.26
1	60	93.36	2.54
5	10	93.01	2.24
5	30	94.41	2.01
5	60	93.96	2.21
8	10	93.02	2.23
8	30	92.28	2.63
8	60	94.65	2.51
13	10	94.55	2.66
13	30	93.38	2.71
13	60	92.16	2.89

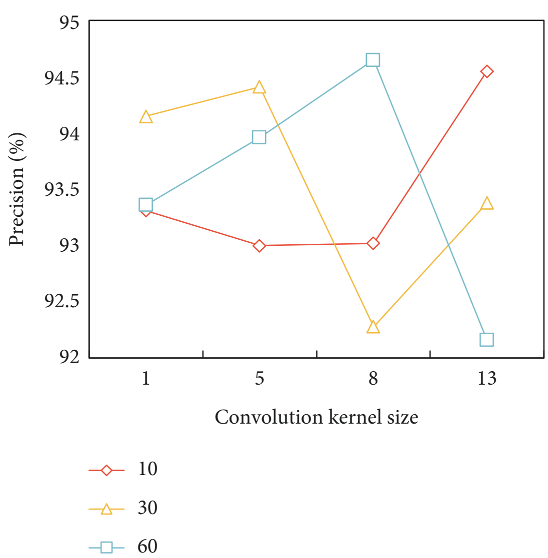

Figure 4: Influence of convolution kernel size and number of hidden layer nodes on recall.

the recall rate reaches the maximum value. According to the false alarm rate in Figure 5, when the convolution kernel size is 5 and the number of hidden layer nodes is 30, the false alarm rate is the lowest, and the larger the convolution kernel, the greater the error. Considering these two results, the optimal combination scheme is selected. In this paper, the size of the convolution kernel is set to 5, and the number of ganglion points in the hidden layer is set to 30.

In this paper, the experimental results of *F*1 overall evaluation indexes of three models on five data types are also given to verify the classification effect of the models on a few classes. The results are shown in Figure 6.

It can be seen that CNN_LSTM has more advantages than BP, and the overall evaluation index *F*1 has improved a lot. The *F*1 index of D_4 CNN_LSTM is 12.75% higher than GA and 14.07% higher than BP. The results verify the effectiveness of the data processed by oversampling method and the model trained by the Focal Loss function on unbalanced data sets.

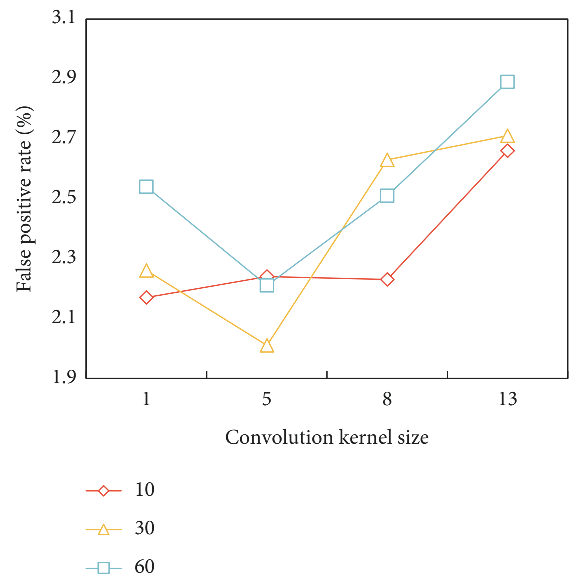

Figure 5: Influence of convolution kernel size and numb of hidden layer node on false alarm rate.

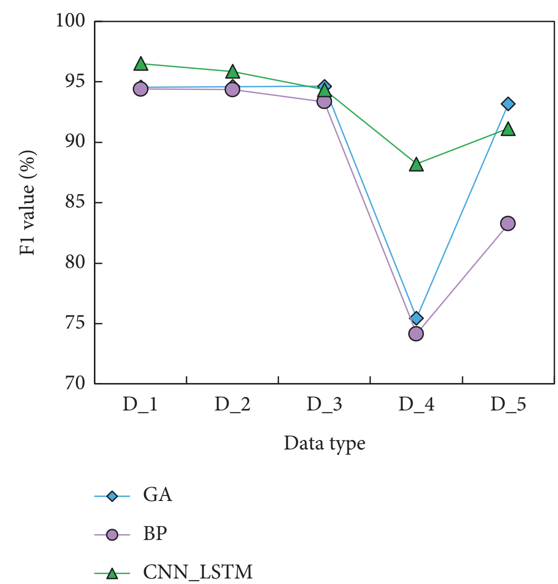

Figure 6: The *F*1 values of three types of detection for different categories.

The false positive and false negative rates have a direct impact on whether the system can be used in real-world situations. Although the neural model ID system can detect new types of intrusions that were previously unknown, it cannot completely eliminate the problem of false positives and false negatives. Establish the object's abnormal activity pattern, and by observing the proximity between current activity and the abnormal activity pattern, detect the same type of intrusion behaviour. The neural network is used for reverse learning when the rule system detects the intrusion, and the neural network ID is used at other times. When an intrusion occurs, the double detection system can reduce false alarms.

Table 2: Experimental results with different thresholds.

Threshold value	False alarm rate	False alarm rate
0.2	0.0061	0.22
0.4	0.0073	0.26
0.6	0.0082	0.12
0.8	0.021	0.086

The training data is input into CNN_LSTM for training, and the actual output simout is compared with the expected output simt, and the detection result of the whole neural network is obtained. Make $\theta_1 = \theta_2$, then take different values, and test with CNN_LSTM, which has been trained before. The experimental results are shown in Table 2:

It can be seen from the above table that the higher the threshold, the higher the false alarm rate and the lower the false alarm rate, while the lower the threshold, the lower the false alarm rate and the higher the false alarm rate, which is a contradictory relationship. If the false alarm rate is low, the false alarm rate will increase. If the false alarm rate is low, the false alarm rate will increase. Therefore, users can set appropriate thresholds according to their own needs so that the ID system can achieve the best detection performance.

Learning network intrusion takes place in virtual machines, and it consists of two parts: learning the statistical characteristics of normal users during operation and learning intrusion. When the system is in place, ordinary users' operation learning is completed, and many existing research results can be used as a reference. The virtual machine adapts the running parameters, extracts statistical data from the data packet conversion expert database, adjusts the input, and performs network learning based on the situation, determining if the learning is complete in light of the convergence situation and updating the neural network detection model. Following the completion of the neural network's learning and training, the pattern discrimination work is converted into a numerical operation that can be executed at high speed on a computer, resulting in an efficient parallel nonlinear dynamic processing system that can meet real-time processing requirements. The false alarm should theoretically be a subset of two independent systems for dual-system operation, which can greatly reduce the false alarm rate. New intrusion rules can be obtained through log analysis, and rule detection rules can be added to the rule detection system to make it more perfect.

The efficiency of the pattern matching algorithm is determined by three factors: text length, pattern length, and alphabet size. Because no pattern matching algorithm is optimal under all conditions, the purpose of the experiment is to test the performance of each algorithm when the above factors are modified. Figure 7 shows the execution time comparison of the three algorithms.

It can be seen from Figure 7 that the execution speed of CNN_LSTM is slightly faster than that of reference [18] algorithm and reference [20] algorithm. When the protected system is very important and the system manager needs to constantly correct the rules, it is necessary to collect the information of intruders, constantly improve and optimize the system, and transfer intruders to dedicated servers. The

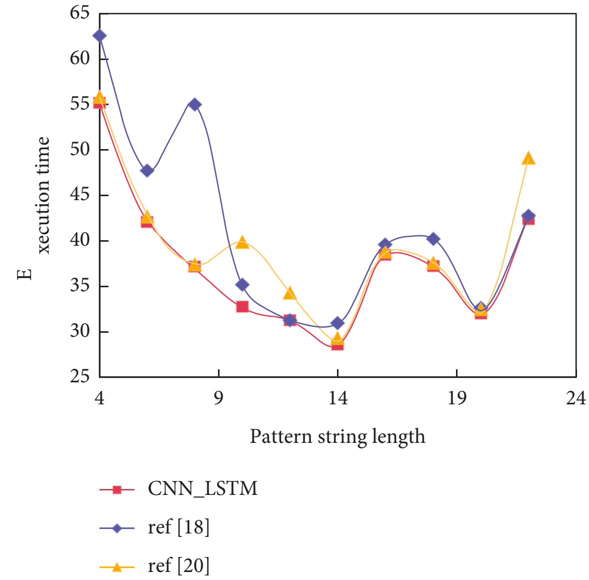

Figure 7: Comparison of the execution time of three algorithms.

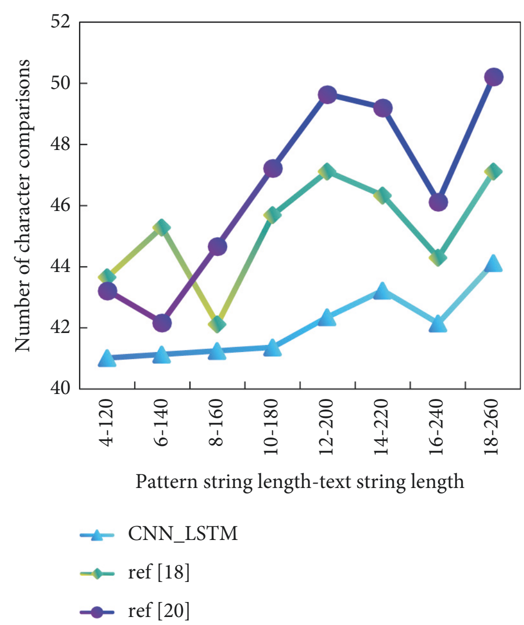

Figure 8: Total character comparison times of various algorithms.

most common alarm and notification method provided by the ID system is the screen alarm. When the ID system is installed, this alarm information will appear on the ID system console or other user-configured systems. They only process local data and only return the results to the control center, so there is no delay caused by network transmission, and the bandwidth occupied by original data transmission can be saved. Another advantage of processing data on each node is that it can be processed in parallel, which will improve the detection speed.

It can be found from Figure 8 that the total number of character comparisons of CNN_LSTM is always less than that of reference [18] algorithm and reference [20] algorithm, no matter how the pattern string length and text string length change.

This advantage becomes more apparent as the pattern string length increases. Because the length of a pattern string in an ID system is usually between 20 and 30, the CNN LSTM algorithm has some utility in an ID system. Finally, when compared to the first two algorithms, the CNN LSTM algorithm has a shorter execution time. As a result, each algorithm corresponds to a specific number of simple operations, and the more times an algorithm is executed, the longer the execution time. As a result, the number of simple operations included in an algorithm is commonly referred to as the algorithm's time complexity, which is used to assess the algorithm's runtime or computational performance. We must set up a neural network module for unknown intrusion behavior to judge whether it is an attack behavior through repeated training of unknown behavior. The data from the data processing module cannot be sent directly to the neural network for identification; instead, it must be preprocessed to obtain data that meets the requirements. Then, the next time the system is used, the uncertain "behaviour" judged in the first job is updated to the known attack information, and the alarm module is directly used to give an alarm, eliminating the need to enter the neural network and greatly improving the ID system's efficiency and practicability.

5. Conclusions

In this paper, VR technology is applied to ID simulation training, and an ID simulation training system is designed and implemented using the 3DSMAX software development platform. Through the combination of virtual and real simulation, the problem is that network intrusion software has special functions and powerful remote control functions, and it is difficult to achieve good simulation results while ensuring network security is overcome. File management, registration, etc., and safely complete functions such as table management, video monitoring, screen control, etc. In this paper, a detection method combining CNN and LSTM is proposed. Softmax is used for classification, and the Focal Loss function is used on the Softmax layer to optimize the model. This method comprehensively considers the temporal and spatial correlation of intrusion data and can extract unknown features and internal dependencies between data, improve the ID accuracy, and reduce the false alarm rate. The experimental results show that CNN_LSTM has more advantages than BP, and the overall evaluation rate $F1$ has been greatly improved. The $F1$ rate of D_4 CNN_LSTM is 12.75% higher than GA and 14.07% higher than BP. The results verify the effectiveness of the data processed by oversampling method and the model trained by the Focal Loss function on unbalanced data sets.

Data Availability

The data used to support the findings of this study are available from the author upon request.

Conflicts of Interest

The author does not have any possible conflicts of interest.

Acknowledgments

This study was supported by Guangdong Provincial Educational Science Planning Project (Higher Education Special Project): Exploration and Practice of Full-Time Teaching Mode and Resource Construction Based on "VR + Cloud Platform" in Post-Epidemic Period (No. 2021GXJK617).

References

[1] W. Wang, Y. Sheng, J. Wang et al., "HAST-IDS: learning hierarchical spatial-temporal features using deep neural networks to improve intrusion detection," *IEEE Access*, vol. 6, no. 99, pp. 1792–1806, 2018.

[2] H. Meng, T. Lei, M. Li, K. Li, N. Xiong, and L. Wang, "Advances in Natural Computation," *Fuzzy Systems and Knowledge Discovery*, vol. 1348, Springer Nature, 2021.

[3] Z. Wang, W. Liang, D. Yan et al., "An efficient network intrusion detection approach based on deep learning," *Wireless Networks*, vol. 5, no. 5, pp. 1–14, 2021.

[4] B. Riyaz and S. Ganapathy, "A deep learning approach for effective intrusion detection in wireless networks using CNN," *Soft Computing*, vol. 24, no. 22, pp. 17265–17278, 2020.

[5] S. Esmeir and S. Markovitch, "Anytime induction of low-cost, low-error classifiers: a sampling-based approach," *Journal of Artificial Intelligence Research*, vol. 33, no. 3, pp. 1–31, 2008.

[6] O. Alkadi, N. Moustafa, B. Turnbull, and K. Raymond, "A deep blockchain framework-enabled collaborative intrusion detection for protecting IoT and Cloud networks," *IEEE Internet of Things Journal*, vol. 8, no. 12, p. 1, 2020.

[7] Z. Huang, Y. Liu, C. Zhan, C. Lin, W. Cai, and W. Chen, "A novel group recommendation model with two-stage deep learning," *IEEE Transactions on Systems, Man, and Cybernetics: Systems*, vol. 1, pp. 1–12, 2021, In Press.

[8] D. Yao, Z. Zhi-li, Z. Xiao-feng et al., "Deep hybrid: multi-graph neural network collaboration for hyperspectral image classification," *Defence Technology*, vol. 23, 2022, In Press.

[9] Z. Fan, C. Li, Y. Chen et al., "Automatic crack detection on road pavements using encoder-decoder architecture," *Materials*, vol. 13, no. 13, p. 2960, 2020.

[10] A. Ghosh, Y. M. Gottlieb, A. Naidu et al., "Managing high volume data for network attack detection using real-time flow filtering," *China Communications*, vol. 10, no. 3, pp. 56–66, 2013.

[11] B. Alotaibi and M. Alotaibi, "A stacked deep learning approach for IoT cyber attack detection," *Journal of Sensors*, vol. 2020, no. 2, pp. 1–10, 2020.

[12] P. Kumar, A. A. Kumar, C. Sahayakingsly, and A. Udayakumar, "Analysis of intrusion detection in cyber attacks using DEEP learning neural networks," *Peer-to-Peer Networking and Applications*, vol. 14, no. 4, pp. 2565–2584, 2020.

[13] S. H. Kim, S. C. Lim, and D. Y. Kim, "Intelligent intrusion detection system featuring a virtual fence, active intruder detection, classification, tracking, and action recognition," *Annals of Nuclear Energy*, vol. 112, pp. 845–855, 2018.

[14] P. Choobdar, M. Naderan, and M. Naderan, "Detection and multi-class classification of intrusion in software defined networks using stacked auto-encoders and CICIDS2017

dataset," *Wireless Personal Communications*, vol. 123, no. 1, pp. 437–471, 2021.
[15] R. Tian, H. Shi, B. Guo, and L. Zhu, "Multi-scale object detection for high-speed railway clearance intrusion," *Applied Intelligence*, vol. 52, no. 4, pp. 3511–3526, 2021.
[16] S. Rezaei and X. Liu, "Deep learning for encrypted traffic classification: an overview," *IEEE Communications Magazine*, vol. 57, no. 5, pp. 76–81, 2019.
[17] D. Wu, "The realization of 3D building modelling and decoration design system based on virtual reality," *Boletin Tecnico/Technical Bulletin*, vol. 55, no. 18, pp. 452–457, 2017.
[18] X. Sun, H. Liu, G. Wu, and Y. Zhou, "Training effectiveness evaluation of helicopter emergency relief based on virtual simulation," *Chinese Journal of Aeronautics*, vol. 31, no. 151, pp. 2000–2012, 2018.
[19] J. Wang and L. Zhu, "Three-dimensional kinematics simulation of robot fighting platform in virtual environment," *Journal of Beijing Institute of Technology (Social Sciences Edition)*, vol. 02, pp. 43–47, 2010.
[20] P. Yong, "Novel relay protection and automation training system based on digital-physical hybrid simulating technology," *Electrical Engineering*, vol. 14, no. 07, pp. 68–73, 2013.
[21] Y. Yang, D. Wang, X. Ke, W. Changsheng, and D. Ziye, "Research and realization of operator training simulating system for the three gorges hydropower station," *Energy Procedia*, vol. 13, pp. 9015–9021, 2011.
[22] L. X. Liu and Y. Q. Zhuang, "Research on tactical communication simulation training federation development," *Key Engineering Materials*, vol. 439-440, no. 1, pp. 475–480, 2010.
[23] J. Bai, G. Zhang, and L. Wang, "Uncertainty analysis of the EMC simulation based on the non-intrusive galerkin method," *Applied Computational Electromagnetics Society Journal*, vol. 34, no. 8, pp. 1128–1133, 2019.

Hindawi
Computational Intelligence and Neuroscience
Volume 2022, Article ID 7345547, 10 pages
https://doi.org/10.1155/2022/7345547

Research Article

Innovative Mode of Human Resource Management of University Teachers Based on Intelligent Big Data Analysis

Yuhong Bai

Guangzhou Huali College, Guangzhou, Guangdong 511325, China

Correspondence should be addressed to Yuhong Bai; baiyuhong@hualixy.edu.cn

Received 28 April 2022; Revised 19 May 2022; Accepted 20 May 2022; Published 1 July 2022

Academic Editor: Xin Ning

In the era of knowledge economy, the competition between countries and enterprises is increasingly manifested in the competition of talents and education system. In this article, aiming at the drawbacks of the traditional HRM model of university teachers, we design and construct a management innovation model and decision-making model based on intelligent big data analysis. This article introduces DM technology. It also introduces the related knowledge of DM and the analysis and design process of HRM decision system. In this system, DM technology is used to analyze and process the existing data, predict the future situation, and provide auxiliary support for decision-making. Through simulation, the decision-making accuracy of this model can reach 95.68%, which is about 10.02% higher than other systems. It has certain practicability and reliability. This article makes a useful attempt for the application of DM technology in HRM. The research in this article is expected to play an important decision-making reference and service support for HRM of university teachers and further promote the development of HRM innovation of university teachers.

1. Introduction

In the modern environment, the demand for knowledge and intellectual capital in society is stronger than in any previous era, which leads to the aggravation of talent shortage. In some ways, economic growth mainly depends on the quality of labor force. Therefore, human resources are increasingly becoming strategic resources for economic and social development [1]. The competition between countries and enterprises is increasingly manifested as the competition of talents and the competition of educational system. As the quality of teaching in institution of higher learning directly determines the level of knowledge and personal quality of talents, the society has paid more attention to the management of college teachers who train senior talents [2]. However, the traditional management mode is increasingly showing many drawbacks. For example, the ideas of managers and managed people lag behind; the management mode is relatively closed and rigid; operating mechanisms such as competition mechanism, incentive mechanism, interest mechanism, responsibility mechanism, and flow mechanism are not well introduced into the management of teachers; the overall quality of teachers needs to be further improved; and teachers' resources have not been effectively allocated and developed. College teachers are the direct undertaker of college production activities and the main body and core of college human resources. The quantity, quality, and structure of teachers' resources directly determine the educational quality and school-running efficiency of institution of higher learning and then affect the national human resources and the level of economic and social development [3]. The purpose of human resource management of teachers in institution of higher learning is to mobilize the enthusiasm and creativity of every faculty member to the maximum extent and make more contributions to the school. Under the background of economic globalization, in order to realize the scientific task of human resource management in institution of higher learning, we must actively and effectively reform and innovate the human resource management of college teachers.

Relevant personnel should elevate HRM (human resource management) to the forefront of school development strategy; create a harmonious system for seeking, selecting, cultivating, knowing, loving, and employing talents; and establish a new HRM mode for modern university teachers [4]. This is critical in order to fully mobilize teachers' enthusiasm for teaching, scientific research, and work; effectively improve the quality and efficiency of school education; and promote the healthy development of higher education institutions. Various industries have accumulated a large amount of data in recent years as a result of the advancement of information technology. People's requirements for data processing technology are constantly improving due to the increasing importance of data in daily decision-making. In terms of university teacher human resource management, using intelligent big data to analyze all types of university human resource data has some practical implications for its management. We should clearly define the problems in HRM that need to be solved and recognize that DM (data mining) [5, 6] is an important step. Although the final outcome of excavation is unpredictable, the problems to be investigated should be. The requirements of DM in institutions of higher learning will continue to rise as the human management system develops [7]. As a result, improving university teachers' application research of DM technology in HRM is conducive to improving the further understanding of the theory of the HRM system in universities and promoting the improvement in the HRM system's application level. This article develops an innovative mode and decision-making model for university teachers' human resource management using intelligent big data. The following are some of its innovations: (1) This article systematically consults the theoretical and practical materials about human resource management at home and abroad, analyzes the characteristics and significance of human resource management of university teachers, and establishes the theoretical basis for research. Guided by the modern HRM theory, this article systematically analyzes the HRM situation in institution of higher learning by using DM technology "intelligently" and "automatically," so that a large amount of data information can be effectively utilized. (2) Based on the comparative analysis of the HRM modes of Chinese and foreign university teachers, this article constructs the innovative mode and decision-making model of university teachers' HRM. The research shows that the decision-making accuracy of this model can reach 95.68%, which is about 10.02% higher than other systems. And on the basis of studying relevant models, this article finds valuable knowledge.

2. Related Works

The development of society requires a sufficient number of high-level human resources, and a strong country also urgently needs the growth of outstanding talents from all walks of life. Under this premise, the construction of teaching staff in institution of higher learning has been promoted to a high position, and the requirements for teachers are quite different from those before. At present, many scholars have explored the HRM of university teachers.

Ke analyzed and discussed the existing practical problems in the development and management of human resources for college teachers and put forward corresponding strategies for the development and management of human resources for college teachers [8]. Zhao et al. pointed out that HRM of college teachers is a systematic project. It not only needs to optimize the internal elements of the system as a whole, but also needs to strengthen the construction of external related systems to jointly improve the level and efficiency of management [9]. Zhou et al. outlined the application conditions of DM technology in HRM in institution of higher learning, the application of DM technology in HRM in institution of higher learning, and the scope of application of DM technology in HRM in institution of higher learning [1]. Shu outlined the meaning of human resources and HRM and analyzed the current situation of human resources and management of teachers in institution of higher learning [11]. Kessler et al. conducted a comparative analysis of the HRM models of Chinese and foreign college teachers and obtained reference and inspiration from them [12]. Haneda and I put forward a series of forward-looking and pragmatic countermeasures and solutions for strengthening the incentive mechanism of human resource development and management of college teachers [13]. Its purpose is to strengthen the management of human resources of college teachers, so as to improve the overall level of the development and management of human resources of college teachers. Sadiq et al. pointed out that due to the improvement in teachers' subject status, the special group of teachers is more suitable for people-oriented management because of their knowledge-based human resources [14]. Cerne et al., based on the relevant theories of harmonious management, put forward the idea of constructing the harmonious management model of human resources for college teachers and pointed out its operation mechanism [15]. Dhar studied the rationality and fairness of salary distribution and its impact on employees; he believes that employees not only care about the absolute amount of their own compensation, but also care about the relationship between their own pay and other' pay [16]. Sandra and Rothenberg established a dynamic programming model based on the big data background to realize the dynamic planning of enterprise human resources and proposed the initial priority table of the intelligent scheduling algorithm [17].

The related literatures are thoroughly examined in this article. Then, DM technology is used to solve the problems of talent type division and performance appraisal system in human resource management in institutions of higher learning, starting with the theory of big data analysis and combining it with the theory of human resource management in institutions of higher learning. This article proposes an innovative mode and decision-making model for managing university teachers' human resources using intelligent big data. This model employs DM technology to analyze and process existing data and forecast future outcomes and provide decision-making support. This study has a lot of practical implications for the practice of intelligent decision-making in university teacher human resource management.

3. Methodology

3.1. HRM System for College Teachers. Human resources refer to the sum total of people with intellectual and physical labor ability who can promote the development of the whole society and economy within a certain range, and it is a group that can exert creative labor on the basis of labor resources [18]. It can also be said that within a certain range, it is the ability of working-age people who have been directly invested in construction and who have not yet invested in construction. Modern management science generally believes that running institution of higher learning well requires four resources: human resources, economic resources, material resources, and information resources. Among these four resources, human resources are the most important. It is the most active factor in production activities and the most important resource among all resources, which is called the first resource by economists. The macro concept of human resources is divided and measured by countries or regions. In the micro sense, the concept is divided and measured by departments, enterprises, and institutions. The most basic aspects of manpower include physical strength and intelligence. Human resource is a special and important resource for social production. Compared with other resources, this kind of resource has its own unique and distinct personality characteristics, including the times, initiative, sociality, creativity with great potential, etc. Compared with other resources, the particularity of human resources lies in the fact that it can only be developed and utilized through an effective incentive mechanism and brings visible economic value to the organization. The increasing income of human resources and its increasing economic role are not only the result of improving the quality of human resources, but also the self-enrichment characteristics of human resources. HRM refers to the use of modern scientific methods to train and allocate human resources reasonably, and at the same time to guide people's thoughts, psychology, and behaviors properly. The HRM system of college teachers constructed in this article is shown in Figure 1.

Human resources in higher education institutions cover a wide range of skills, including the total labor ability of teaching staff engaged in teaching, scientific research, management, and logistics services. The main body is that teachers demonstrate the significant social value that their teaching and educational activities, as well as scientific research and innovation activities, generate [19]. Teachers' human resource management system in higher education institutions considers all human resource management subsystems as a management engineering system. The HRM system for university teachers is built through group management. First and foremost, we must define the overall organizational goals, use these goals as the foundation for college teacher human resource management, and then create a human resource plan. Teachers' human resources refer to the sum of their knowledge, skills, attitudes, experiences, and creative ideas from the perspective of human resources. When compared to the human resources of other organizations, university teachers' human resources are unique. For example: (1) high educational level, (2) pursuing autonomy, (3) unique values, (4) strong desire to learn, and (5) strong willingness to flow. Teachers are the most precious human resources in institution of higher learning, but they are also the difficulties and emphases of human resources development in institution of higher learning. College teachers, in comparison to other human resources, have high subjective initiative, sense of accomplishment, and self-realization needs. The work is distinguished by its creativity and mobility, as well as the difficulty in monitoring and measuring the labor process. As a result, adopting a humanized and democratic management mode for teacher management is even more critical. At this stage, it is necessary to analyze the characteristics of university teachers' special human resource groups, as well as the existing problems with university teachers' human resource management, and to invent a new mode of university teachers' human resource management. The overall evaluation of university teachers' human resource management system is not only the foundation for implementing the talent rejuvenation strategy, but it is also a necessary precondition for improving the quality of university teachers' human resources and HRM efficiency. As a result, in today's environment, research on university teachers' innovative human resource management has both theoretical and practical implications. DM can identify talent patterns and rules within an organization, and thus the talent model. Simultaneously, studying DM methods, extracting valuable information, determining a reasonable human resource structure in accordance with the development goals of institutions of higher learning, and determining talent introduction and training goals are all critical.

3.2. Application of DM Technology. Various industries have accumulated a large amount of data in recent years as a result of the development of information technology, while the database system only provides data management and simple processing functions [20]. People require a method for assisting with these complex data, locating valuable information or knowledge to aid decision-making, and reducing workload. In this case, the DM technology was proposed. DM is the process of extracting hidden information and knowledge from a large number of incomplete, noisy, fuzzy, and random practical application data that people do not know about ahead of time but could be useful. We can automatically acquire useful knowledge from fault data accumulated by human users and expand the knowledge base using DM technology. This knowledge is objective and avoids the generation of accurate knowledge because it is based on the fault data that have occurred. The problem of automatic knowledge acquisition can be solved by combining DM technology and an expert system. One of the main tasks of DM is clustering [21]. Clustering is the process of dividing data objects into subsets so that each subset is a cluster, and the objects in the cluster are similar to each other but the cluster is not similar to the objects in the cluster, that is, the cluster has the maximum similarity within the cluster but the cluster has the least similarity between clusters. The clustering model divides data into different groups which is based on the

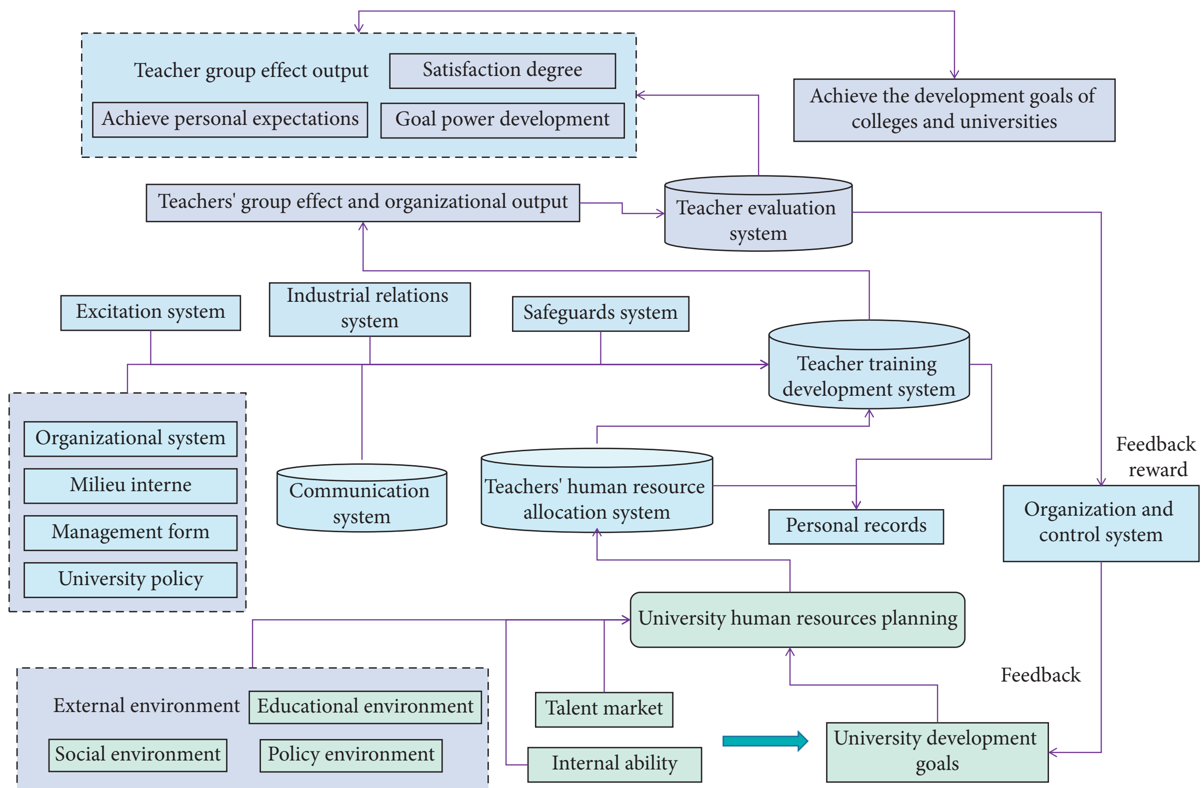

Figure 1: University teachers' human resource management system.

relationship between data content and data. Clustering patterns are highly random and arbitrarily distributed [22]. Association analysis uncovers two types of relationships: frequent itemsets and association rules. The frequent itemsets refer to a group of attributes that frequently appear together at the same time, whereas the association rules imply that the two attributes may have a strong relationship. Students' data are analyzed using DM technology, and a mathematical model is created using a clustering algorithm. The students are then analyzed using the correlation analysis algorithm, and an overall correlation analysis model of students is created. The DM architecture is shown in Figure 2.

To apply DM to this model, the following steps should be followed: (1) Determining the objects and targets of mining and finding out the problems clearly, (2) collecting the data, (3) carrying out the data conversion process, (4) classification and mining of data, (5) analyzing the results of classification rules, and (6) applying knowledge. The mining process is divided into two basic stages: initialization and iteration. The initial data structure is set in the initialization stage, and the decision tree is generated in the iterative process. Data cleaning of data warehouse is similar to data cleaning of DM. If the data have been cleaned when it is imported into data warehouse, it is probably unnecessary to clean it again when doing DM, and all data inconsistencies have been solved. Data extraction is the process of extracting data from the data source database of application system to the target database. Data extraction methods mainly include total extraction and incremental extraction. There are two factors to consider when choosing a mining algorithm. First, data with different properties should use algorithms related to their characteristics, and second, the user's requirements for the discovery results. If the discovered knowledge cannot meet the user's requirements, the whole discovery process needs to be returned to the discovery stage, and data should be re-selected, new data transformation methods should be adopted, new DM parameter values should be set, or even another mining algorithm should be changed. In addition, selecting and analyzing data may be the most important part of DM, even more important than algorithm selection. The reason is that DM is usually not driven by assumptions, but by data. DM can receive data and discover new associations, instead of selecting and testing variables in advance, so DM should obtain as clean data as possible and perform data profiling before trying any models. According to the requirements of DM, we should check the spelling and errors of the extracted data, check and fill the gaps in the data records, and convert the data types, which is called preprocessing.

3.3. Innovative Model of Teacher HRM Based on Big Data Analysis. With the enhancement of informatization in institution of higher learning, institution of higher learning now have a relatively complete information management system, and the basic data of human resource management are sufficient, which can select, preprocess, and convert human resources data and make data preparation for DM. Considering the structure of specific human resources, this article chooses the decision tree of classified knowledge discovery as the DM method. A decision tree is a tree

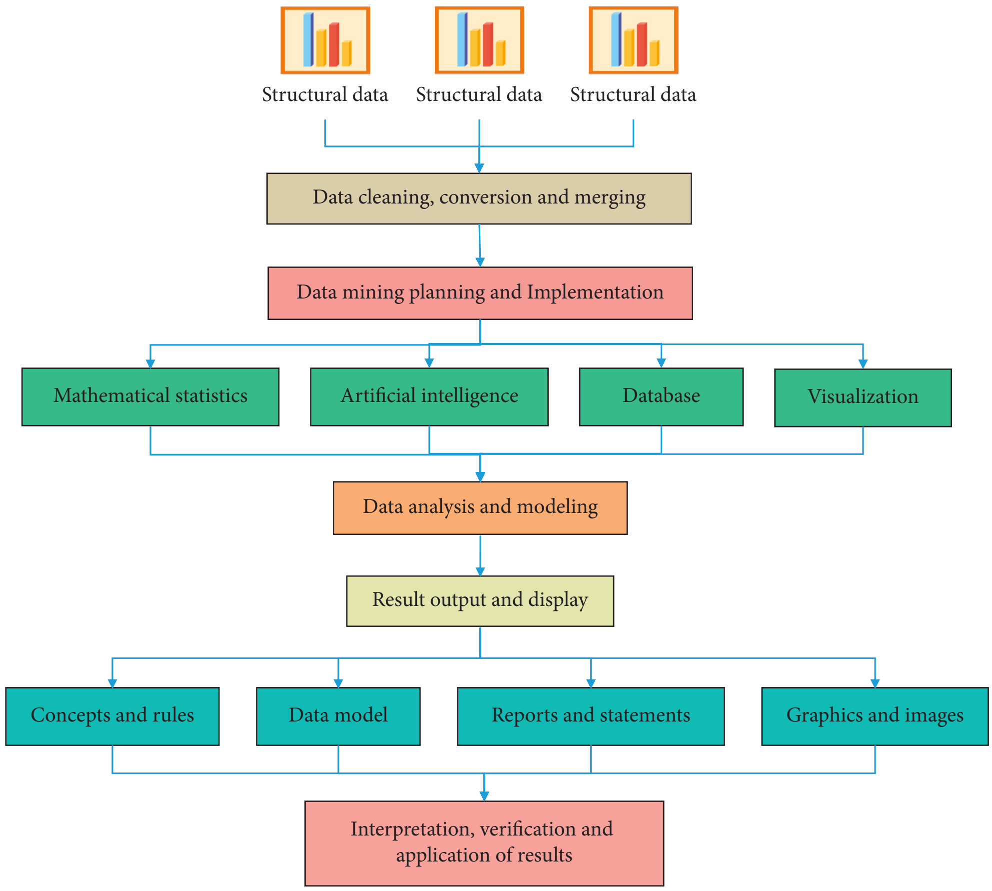

Figure 2: DM architecture.

structure similar to a flowchart, in which each internal node of the tree represents a test of an attribute, its branches represent each result of the test, and each leaf node of the tree represents a category. The top node of the tree is the root node. First, the data source is selected and the database is established. In order to prevent the repetition of data and the inconsistency of calling data, the data source is discretized before calling data, and the specific data are converted into unique letters or numbers. The quality of research data, in preparation for further analysis. And determine the type of mining operation to be performed. Data cleaning refers to the process of finding and correcting identifiable errors in data files, including checking data consistency, dealing with invalid values and missing values, etc. Generally, the principle of data cleaning is the process of reducing the database to eliminate duplicate attributes and converting the format into an acceptable standard format. Establishing a correspondence table between source data and processed data is equivalent to establishing a mapping relationship between them, which ensures that the change of one data will not affect the other, thus realizing the independence of source data and programs.

Assuming that the dataset S contains a set of s data samples, the category attribute can take m different values, corresponding to m different categories, namely:

$$C_i, i \in \{1, 2, 3, \ldots, m\}. \tag{1}$$

Assuming s_i is the number of samples in class C_i, the amount of information required to classify a given data object is

$$I(s_1, s_2, \ldots, s_m) = -\sum_{i=1}^{m} p_i \log(p_i), \tag{2}$$

where p_i is the probability that any data object belongs to category C_i, which can be calculated by s_i/s. The function of log is based on 2, because in information theory, information is encoded in bits.

Let an attribute A take v different $\{a_1, a_2, \ldots, a_v\}$. The set can be divided into v subsets using the attribute A, namely

$$\{S_1, S_2, \ldots, S_v\}, \tag{3}$$

where S_j contains the data samples whose public attribute value of S set is a_j. If the attribute is selected as the test attribute A, let s_{ij} be the number of samples of the attribute C_i category in the subset S_j. Then the information entropy required to divide the current sample set using attribute A can be calculated as follows:

$$E(A) = \sum_{j=1}^{v} \frac{s_{1j} + s_{2j} + \ldots + s_{mj}}{s} I\left(s_{ij}, \ldots, s_{mj}\right), \tag{4}$$

where $s_{1j} + s_{2j} + \ldots + s_{mj}/s$ is taken as the weight of the ith subset. It is divided by the sum of the sample data of attribute A taking a_j in all subsets by the total number of samples in the S set. The smaller the $E(A)$ calculation result, the better the result of its subset division. Assuming that there are n samples in the sample set, n data can be obtained for a certain indicator k of the samples, namely

$$h'_{1k}, h'_{2k}, \ldots, h'_{nk}, \tag{5}$$

where h'_{nk} represents the data obtained by the ith sample for the kth index. Their average is calculated as

$$h^{'}_{\overline{k}} = \frac{\left(h'_{1k}, h'_{2k}, \ldots, h'_{nk}\right)}{n} = \frac{\Sigma h'_{ik}}{n}, \quad k = 1, 2, \ldots, m. \tag{6}$$

The standard deviation of these raw data is as follows:

$$S_k = \sqrt{\frac{\sum_{i=1}^{n}\left(h'_{ik} - h'_{\overline{k}}\right)}{n}}. \tag{7}$$

The normalized value of each data is obtained by the following formula:

$$h''_{ik} = \left|\frac{h'_{ik} - h'_{k}}{S_k}\right|. \tag{8}$$

If the extreme value standardization formula of the obtained standardized data h''_{ik} is not within the closed interval of $[0, 1]$, the following extreme value standardization formula is used:

$$h_{ik} = \frac{h''_{ik} - h''_{\min k}}{h''_{\max k} - h''_{\min k}}, \tag{9}$$

where $h''_{\max k}$ and $h''_{\min k}$ represent the maximum and minimum values in $h''_{1k}, h''_{2k}, \ldots, h''_{nk}$, respectively.

DM technology can extract human resources data from a variety of databases containing information about the working conditions of the organization's employees as well as find connections and patterns among them, objectively reflecting the organization's talent pool. The most frequent set among the generated frequent sets is found and an algorithm is used to determine whether the data have any implicit relationships. Users or machines must evaluate the patterns discovered during the DM stage. Any redundant or irrelevant patterns are removed and returned to the previous stage if the mode cannot meet the user's needs. Re-selecting data, implementing new data transformation methods, adjusting parameter values, and so on are examples of such tasks. In DM, data preparation is a critical step in the knowledge discovery process, accounting for more than half of the workload. It is necessary to preprocess data, especially when DM is performed on data that contain noise, incompleteness, or even inconsistency, in order to improve the quality of DM and, ultimately, the quality of pattern knowledge acquired by DM. This article examines the human resources system's staff information database as well as the staff assessment results database. It has a relational database format, which sorts information attributes that are thought to be closely related to assessment results into data tables and deletes information attributes that are not. In order to figure out a few key variables for the DM process, the qualitative index attributes are calculated. The primary task of the implementation of the HRM plan of university teachers is to equip the organization with personnel and change the internal environment according to the requirements of the organization and then to establish the post responsibilities of all staff in each internal department. Therefore, this article establishes the following subsystems: (1) organization system, (2) incentive system, (3) communication system, (4) management relationship system and guarantee system, and (5) evaluation system. According to this HRM system, all subsystem plans and actions complement each other.

When the state is determined in the human resource scheduling of university teachers, the state transition equation can be used to show the law of this state deduction:

$$x_{p+1} = B_p\left(x_p, w_p\left(x_p\right)\right), p = 1, 2, \ldots n. \tag{10}$$

From the above equation, it is possible to further deduce the indexes that help define the whole stage process and all the back subprocesses. The formula of the index is:

$$Q_{kn}\left(x_p, w_p, \ldots, x_{n+1}\right), p = 1, 2 \ldots n. \tag{11}$$

According to the state transition equation and the formula of the indicator function, in the actual scheduling of human resources, the decision set x_p can be determined by the characteristics of the state variable x_p and the decision variable $W_n(x_n)$ itself, and then substituted into the state transition of equation (10). Suppose a real-time computing task requests R, then the sequence is

$$R = \left(e_i^{\text{born}}, e_i^{\text{wait}}, e_i^{\text{dead}}, y_i\right), \tag{12}$$

where i represents the real-time task number waiting to be executed, e_i^{born} represents the generation time of the real-time task, and e_i^{wait} represents the maximum waiting time when the task is queued for execution. This value is determined by the number of institution of higher learning, business volume, etc. Whereas e_i^{dead} stands for task deadline and y_i stands for the initial priority of the task. The smaller the value, the higher the initial priority of the task. When the current time is assumed to be s, then the relative deadline a_i of the real-time task satisfies:

$$a_i = e_i^{\text{dead}} - s. \tag{13}$$

From this, it can be calculated that the relative deadline a_i of a real-time task will gradually decrease over time, which means that its task priority will increase with time.

The association rule generation module's main task is to extract strong association rules from frequently occurring sets with the least amount of support and confidence. Because the association rules to be mined are strong association rules, and because the rules are generated by frequent itemsets, each rule meets the minimum support degree automatically, so generating association rules for frequent itemsets only requires meeting the confidence level. The decision tree induction algorithm calculates each attribute's information gain and chooses the attribute with the highest information gain as the test attribute of a given set, resulting in the branch nodes. The corresponding attributes are marked on the generated nodes, and corresponding branches of the decision tree are generated based on different values of this attribute, with each branch representing a partitioned sample subset. The generated selection tree can be used to define a rule set. A rule set is made up of a number of rules, each of which corresponds to a different path in the selection tree, which represents a link chevalier. The abstract preprocessing, frequent set mining, algorithm execution, and association rule generation processes are all intuitively displayed on the page in this article via FLASH animation. When that user enters the degree of trust and the degree of support, the text expression that corresponds to the generated strong regular formula is displayed, making it easy for the user to understand and analyze the relationship between the attribute fields.

4. Result Analysis and Discussion

This article studies the application of intelligent big data analysis in college teachers' human resource management, mainly using DM to solve problems in human resource management and innovating college teachers' human resource model and decision-making model. In this article, HRM is quoted from the market concept, and the management function of the HRM department in institution of higher learning is given by the internal faculty of institution of higher learning. In order to verify the feasibility of the innovative model and decision-making model of human resource management of university teachers designed and constructed in this article, this chapter conducts simulation experiments to test the performance of the model in all aspects. First, the feature selection of the five-fold cross data of the model in this article is carried out, and the experimental results are shown in Table 1.

Table 1: Feature subset selected by quintuple cross data.

Dataset	Feature subset
Train1	4, 6, 8, 9, 11, 13, 15, 21, 26, 28
Train2	5, 6, 8, 9, 11, 13, 15, 18, 26, 28
Train3	4, 5, 6, 8, 9, 11, 13, 15, 26, 28
Train4	4, 6, 8, 9, 11, 13, 15, 16, 19, 26, 28
Train5	4, 5, 6, 8, 9, 11, 13, 15, 26, 28

First of all, the data should be selected, all the internal and external data information related to the HRM issues is searched, the data suitable for DM applications are selected, then the data are preprocessed, and, finally, the data are converted into an analysis model. This analysis model is built for mining algorithm. The purpose of using decision tree to classify teachers' resources is to dig out potential turnover among teachers in the management office. Then, some measures should be taken to retain some potential important teachers, so as to reduce the losses of institution of higher learning and form a stable group of teachers. To verify the performance of this algorithm, three indexes, namely recall rate, average absolute error, and F1 value, are selected for testing, and the obtained result is compared with different algorithms. The result of the recall rate is shown in Figure 3. The mean square error comparison results are shown in Figure 4. The comparison results of F1 values are shown in Figure 5.

As can be seen from the data in Figure 3, the recall rate of this algorithm has certain advantages in comparison of the recall rates of different algorithms. Its recall rate is better. As can be seen from the data in Figure 4, with the increase of iteration index, the error of each algorithm becomes smaller and smaller. However, the error of this algorithm decreases faster and its error value is lower. From the data in Figure 5, it can be seen that the F1 value of this method is always at a high level in the comparison of F1 values of different algorithms. Generally speaking, the performance of this algorithm is better. It has certain accuracy and reliability.

In order to make the algorithm in this article more in line with the needs of human resource management of university teachers in the current era, we should give full consideration to innovating the scheduling decision algorithm of the platform and summarize the advantages and disadvantages of the algorithms that have been put into application before. Comparing the running time of different algorithms, the results are shown in Figure 6.

It can be seen that compared with the traditional algorithm, the decision algorithm proposed in this article can effectively shorten the time required to fuse and calculate the stage task data. Its operation performance and fusion effect are superior. Performance appraisal is an important task of HRM in institution of higher learning. Other work of HRM needs to be completed based on the results of performance appraisal. Therefore, the use of quantitative analysis methods to evaluate the performance appraisal system is of great significance for the effective implementation of performance appraisal. This article analyzes from two aspects: the correlation analysis between the assessment index variables, and the correlation analysis between the original index variables and the assessment index variables. Table 2 shows the teacher metrics chosen in this article.

In order to verify the feasibility of the innovative model and decision-making model of teacher human resource management constructed in this article, we make an experimental analysis of the decision-making accuracy of this model. The results obtained are compared with other models. The decision accuracy of different models is shown in Figure 7.

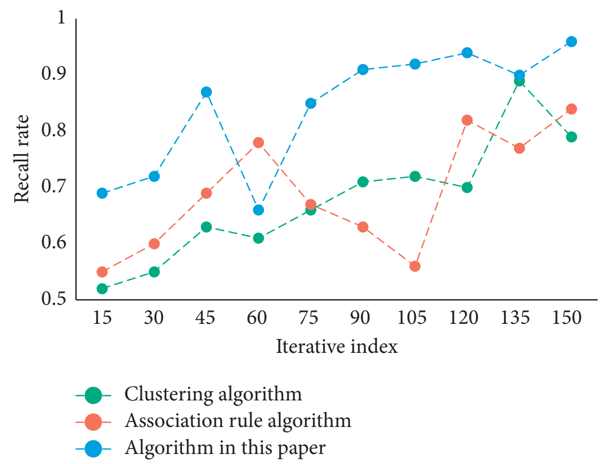

Figure 3: Recall results of different algorithms.

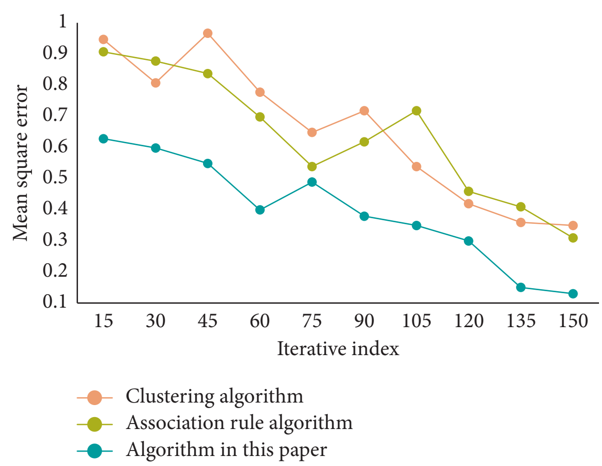

Figure 4: Comparison of mean square error of different algorithms.

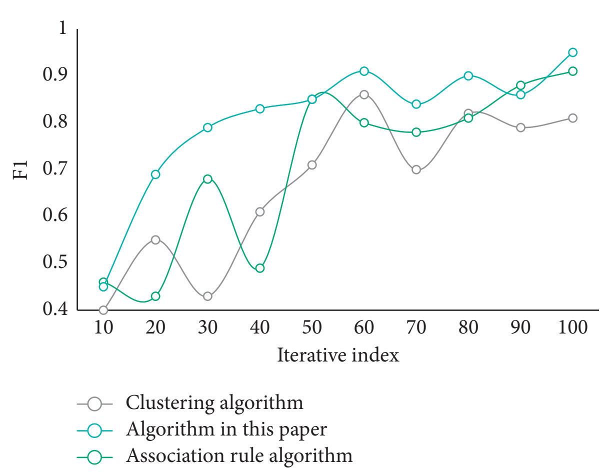

Figure 5: Comparison of F1 results of different algorithms.

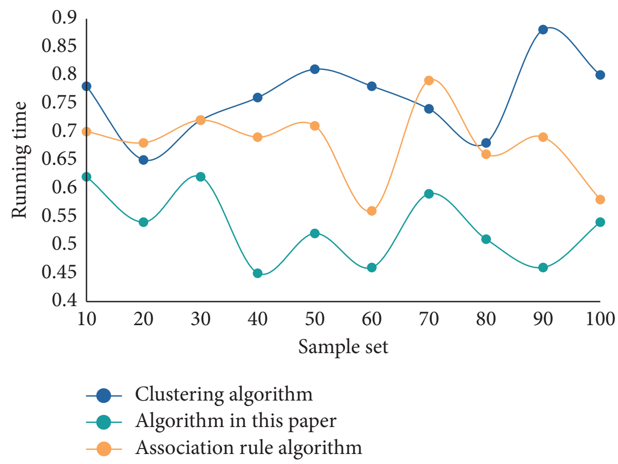

Figure 6: Time-consuming running of different algorithms.

Table 2: Selected teacher indicators.

Program	Knowledge level	Teaching skills	Teaching quality	Teaching effect
Teacher 1	4	3	3	3
Teacher 2	2	3.5	5	2
Teacher 3	3	3	5	4
Teacher 4	5	4	4	4
Teacher 5	4	4	3	3
Teacher 6	6	3	3	3
Teacher 7	5	3.5	2	2
Teacher 8	4	2	3	2
Teacher 9	5	2.5	4	3
Teacher 10	3	4	5	4

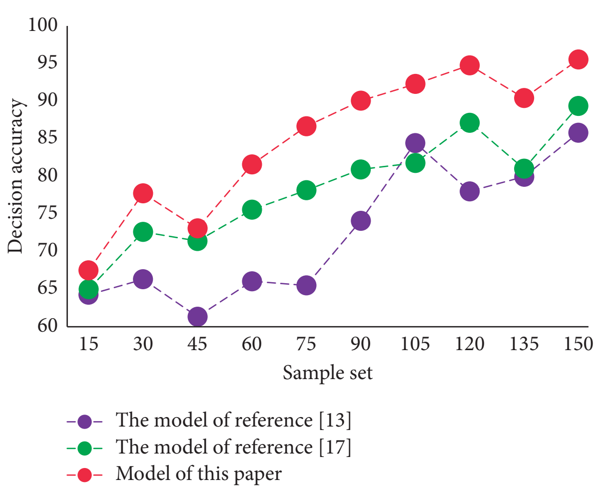

Figure 7: Decision accuracy results of different models.

According to the data analysis in the figure, compared with the other two decision-making models, the decision-making accuracy of the teacher HRM decision-making model in this article is the highest. It has certain decision-making effectiveness and accuracy. In this chapter, several simulation experiments were conducted to verify the performance of the innovative model and decision-making model of university teachers' human resource management based on intelligent big data. Experimental results show that the accuracy of the system can reach 95.68%, which is about 10.02% higher than other systems. From the test results, this system performs well, is feasible, and has excellent systematic performance.

5. Conclusions

Human resources, in comparison to other economic resources, have a distinct purpose, subjective initiative, and unique creativity. Traditional human resource management modes and information acquisition methods limit the development of human resource management in higher education institutions. In light of the growing drawbacks of traditional HRM, this article investigates various issues in HRM in higher education institutions using intelligent big data analysis technology and related HRM and DM theories. This article develops and implements an innovative mode and decision-making model for university teachers' human resource management. This system employs DM technology to analyze and process existing data and forecast future events and provide decision-making support. The outcome of the experiment is in line with the hypothesis. This model has a decision-making accuracy of 95.68%, which is 10.02% higher than other systems. This system can significantly reduce the workload of intelligent scheduling of university teachers' human resources based on big data analysis as well as the time it takes to fuse and calculate stage task data. It is feasible and practicable in some ways. This research has yielded some results, but due to my limited knowledge and research time, there are still some areas that could be improved. The model structure will be improved in future work, as will the model performance, and a quantitative analysis scheme will be proposed to solve the HRM problems of university teachers.

Data Availability

The data used to support the findings of this study are available from the author upon request.

Conflicts of Interest

The author does not have any possible conflicts of interest.

References

[1] H. De Cieri, K. Sanders, and C. Lin, "International and comparative human resource management: an Asia-Pacific perspective," *Asia Pacific Journal of Human Resources*, vol. 60, no. 1, pp. 116–145, 2022.

[2] T. Matsuzaki, H. Shigeno, Y. Ueki, and M. Tsuji, "Innovation upgrading of local small and medium-sized enterprises and regional innovation policy: an empirical study[J]," *Industrial Marketing Management*, vol. 94, pp. 128–136, 2021.

[3] J. Shen, J. Benson, and B. Huang, "High-performance work systems and teachers' work performance: the mediating role of quality of working life," *Human Resource Management*, vol. 53, no. 5, pp. 817–833, 2014.

[4] M. Biag, A. Srivastava, M. Landau, and E. Rodriguez, "Teachers' perceptions of full- and part-time nurses at school," *The Journal of School Nursing*, vol. 31, no. 3, pp. 183–195, 2015.

[5] X.-B. Jin, W.-Z. Zheng, J.-L. Kong et al., "Deep-learning temporal predictor via bidirectional self-attentive encoder-decoder framework for IOT-based environmental sensing in intelligent greenhouse," *Agriculture*, vol. 11, no. 8, p. 802, 2021.

[6] X.-B. Jin, W.-T. Gong, J.-L. Kong, Y.-T. Bai, and T.-L. Su, "PFVAE: a planar flow-based variational auto-encoder prediction model for time series data," *Mathematics*, vol. 10, no. 4, p. 610, 2022.

[7] H. Ma, "Enterprise human resource management based on big data mining technology of internet of things," *Journal of Intelligent and Fuzzy Systems*, vol. 1, no. 1, pp. 1–7, 2021.

[8] Y. Ke, "Exploration and development of public service of human resources and social security based on big data[J]," *Boletin Tecnico/Technical Bulletin*, vol. 55, no. 16, pp. 615–621, 2017.

[9] X. Zhao, D. Wang, and P. Zhu, "Analysis of the reform and mode innovation of human resource management in big data era[J]," *Revista de la Facultad de Ingenieria*, vol. 32, no. 12, pp. 219–225, 2017.

[10] Y. Zhou, X. Fan, and J. Son, "How and when matter: exploring the interaction effects of high-performance work systems, employee participation, and human capital on organizational innovation," *Human Resource Management*, vol. 58, no. 3, pp. 253–268, 2019.

[11] W. Shu, "88.Big-data-based model of human resource cost evaluation system of E-commerce[J]," *Revista de la Facultad de Ingenieria*, vol. 32, no. 15, pp. 495–499, 2017.

[12] I. Kessler, P. Heron, and K. Spilsbury, "Human resource management innovation in health care: the institutionalisation of new support roles," *Human Resource Management Journal*, vol. 27, no. 2, pp. 228–245, 2017.

[13] S. Haneda and K. Ito, "Organizational and human resource management and innovation: which management practices are linked to product and/or process innovation?[J]," *Research Policy*, vol. 47, no. 1, pp. 194–208, 2017.

[14] F. Sadiq, T. Hussain, and A. Naseem, "Managers' disruptive innovation activities: the construct, measurement and validity," *Management Decision*, vol. 59, no. 2, pp. 153–174, 2020.

[15] M. Černe, S. Batistič, and R. Kenda, "HR systems, attachment styles with leaders, and the creativity-innovation nexus," *Human Resource Management Review*, vol. 28, no. 3, pp. 271–288, 2018.

[16] R. L. Dhar, "The effects of high performance human resource practices on service innovative behaviour," *International Journal of Hospitality Management*, vol. 51, pp. 67–75, 2015.

[17] Sandra Rothenberg, Clyde Eiríkur Hull, and Zhi Tang, "The impact of human resource management on corporate social performance strengths and concerns[J]," *Business & Society*, vol. 56, no. 3, pp. 391–418, 2017.

[18] H. Florén, J. Rundquist, R. S. Schuler, T. Bondarouk, and H. Ruël, "HRM and innovation: themes, contingencies and directions for future research," *European Journal of International Management*, vol. 8, no. 5, pp. 570–577, 2014.

[19] F. Jorgensen and K. Becker, "The role of HRM in facilitating team ambidexterity[J]," *Human Resource Management Journal*, vol. 27, no. 2, pp. 264–280, 2017.

[20] H. O. Joseluis, "The changing environment: implications for human resource management[J]," *International Journal of Manpower*, vol. 34, no. 8, pp. 833–838, 2013.

[21] J. Chen, C. Du, Y. Zhang, P. Han, and W. Wei, "A clustering-based coverage path planning method for autonomous heterogeneous UAVs," *IEEE Transactions on Intelligent Transportation Systems*, pp. 1–11, 2021.

[22] P. Runhaar, "How can schools and teachers benefit from human resources management? Conceptualising HRM from content and process perspectives," *Educational Management Administration & Leadership*, vol. 45, no. 4, pp. 639–656, 2016.

Hindawi
Computational Intelligence and Neuroscience
Volume 2022, Article ID 7108029, 9 pages
https://doi.org/10.1155/2022/7108029

Research Article

The Adoption Factors of Mobile Games in the Wireless Environment

Bo Li

Business School, Central South University, Changsha 410083, China

Correspondence should be addressed to Bo Li; 151601008@csu.edu.cn

Received 14 May 2022; Revised 8 June 2022; Accepted 9 June 2022; Published 1 July 2022

Academic Editor: Xin Ning

The factors that influence how people play mobile games have been studied from a variety of perspectives in the wireless broadband environment. The original data in the background of the game, such as user operation records, consumption records, and social behavior records, are converted into user attributes, user tags are generated, and data sets are constructed in this study, which primarily uses data mining technology to study user behavior and form user portraits. By incorporating the similarity of players' subspace interests into the CFR (collaborative filtering recommendation) algorithm, a personalized game recommendation model, as well as the relationship management level of mobile game players, is created. The final fusion model's ROC-AUC value is 0.921, which has a percentile enhancement effect, according to the results. The findings show that using a personalized game recommendation model can help to improve the scalability of the CFR algorithm and the impact of data scarcity on the quality of mobile games recommended by players.

1. Introduction

People are increasingly using mobile devices as smartphones become more affordable and mobile data networks improve. Mobile games are a popular leisure activity due to their convenience, portability, and low cost. In the domestic game market, the rate of growth of game users has slowed, and users are showing signs of saturation. The cost of acquiring traffic for game companies is continuing to rise against the backdrop of wireless broadband, but the resulting increase in revenue is unlikely to be proportional. The popularity of smartphones, combined with the ongoing enrichment of mobile game content, has greatly increased users' interest in and experience with mobile games. Mobile games will become a high-growth business sector of the mobile Internet in the future. Measuring and evaluating the quality of the user experience are critical. Displaying abstract user experience in a user-friendly manner can directly reflect the benefits and drawbacks of products, which is useful for product improvement.

With the development of wireless broadband, the scale of mobile Internet is constantly expanding, and the users of mobile game industry are growing rapidly. Ma et al. proposed that the experience economy is being separated from the service economy to provide users with unique experiences. Experience transcends service because it realizes users' self-realization and is free [1]. Brand et al. put forward three quantification methods, namely behavior-centered quantification method, experience-centered quantification method, and task-centered quantification method [2]. Narudin et al. put forward that user experience is the user's experience of brand information, functionality, information availability, and content [3]. Yamamoto proposed that the user experience should include the environment used, the user's perception, and expectation [4]. Jeon et al. expounded the development status of mobile games [5], analyzed the characteristics of mobile games, such as portability, diversified game modes, and rich social interaction, and looked forward to the future development of mobile games. The loss of users can be divided into two situations: one is the lost users, who completely stop trading with the enterprise; the other is potential churn users, who tend to churn but are not completely cut off from the enterprise, but their purchase frequency has decreased, and they will go to their competitors to buy similar products or services.

Mobile games combine the benefits of mobile Internet with game entertainment. This study examines users' willingness to play mobile games and the factors that influence their willingness to play mobile games from the user's perspective using empirical research. A general model of mobile game users' willingness to use is constructed through literature reading and summarization, in combination with the technology acceptance model, opinion leader theory, and related theories, and combined with innovation and communication. Not only will this allow mobile game manufacturers and other content providers to improve their products on a continuous basis, but it will also encourage game operators, game platforms, and other service providers in the game industry chain to do so. More importantly, they have improved the game industry's service level and promoted the industry's development and progress. Innovations in research are as follows: (1) the factors influencing the variables are further explored, and a general model of mobile game users' willingness to use is established, by combining innovative variables such as endogenous value, perceived compatibility, and perceived ease of use. (2) This study divides the item set into several subspaces based on fuzzy clustering based on player behavior situation, considers the proportion of players' common game scores in each scoring scale, and introduces the similarity of players' interest differences in subspaces to improve the calculation of player similarity.

The organizational structure of this study is as follows: the first section introduces the research background and significance and then introduces the main work of this study. The second section mainly introduces the related technologies of user behavior analysis. The third section puts forward the specific methods and implementation of this research. The fourth section verifies the superiority and feasibility of this research model. The fifth section is the summary of the full text.

2. Related Work

2.1. Research on Mobile Games. The mobile game industry began to develop rapidly, and the number of users increased exponentially. Many mobile game manufacturers have emerged, and mobile games are gradually showing their charm. The entertainment, convenience, and universality of mobile games are more in line with the tastes of fashion people. There are three main reasons behind the rapid development of mobile games [6]: first, the rapid development of wireless broadband and hardware technology [7] has provided a good technical guarantee for the upgrading of mobile games, which has strongly stimulated the market demand; secondly, with the development of economy, the pressure of life is increasing, and the lifetime is becoming more and more fragmented. Mobile games can better fill the fragmented time and bring people psychological relaxation. Third, compared with traditional PC games, mobile games have the advantages of high investment, high return rate, short capital return cycle, and more attractive investment.

Fu et al.'s research shows that the cultural industry, as an important part of China's national economy, has made great progress in the past 40 years of reform and opening-up, with its overall scale greatly expanded, high growth rate, strong stages, and large increase of market players [8]. Duarte et al.'s research also shows that with the help of wireless broadband, a large number of new cultural industries, represented by the electronic economy, have begun to grow and develop, putting forward new requirements for national supervision and policy-making [9]. Liu et al. focused on the deep-seated reasons behind the intellectual property fever of mobile games and discussed the formation law and derivative ability of high-quality intellectual property [10]. Bell pointed out that emotional experience captures the psychology of consumers and makes them deeply impressed by the new products they come into contact with and dominate their own behavior [11]. Li and Bhanu put forward the first game evaluation method, referring to the usability evaluation method and the practical experience of game development companies, and divided the game design into three dimensions: game interface, game mechanism, and gameplay [12]. Takano et al. proposed that the game design is based on the user's interactive experience and the game should include immersion, pleasure, operability, and repeated playability [13]. Yang et al. applied immersion theory to the study of intention to use, and it proved to be effective. With the deepening of research, new theories will be introduced continuously, but the research has never been separated from users [14].

2.2. Research on User Behavior Analysis. User preference can be simply understood as the degree, to which a user prefers one thing to another. It is a subjective psychological tendency of users and belongs to the category of psychology. This research has penetrated into the fields of economics and computer science. Li et al. pointed out that user preferences can be simply summarized into two categories: individual preferences and situational preferences. The user's preference model is quantitatively constructed by assigning a certain value to each candidate by using the function [15]. Ye et al. use ontology knowledge to build a complex user preference model based on user text description information [16]. Nowadays, the widely used personalized service system uses the statistical learning method to model user preferences.

For games with a large number of users and complex data attributes, especially online games, data extraction, and utilization are very important. It is a set of behaviors derived from users' psychology. Only through the user's psychology, we can better predict the content of the game mechanism to meet the internal needs and desires, so as to create a successful game. Zhang et al. used a clustering algorithm to segment customers and a genetic algorithm to optimize variables, so as to build a customer lifetime value segmentation model [17]. Sarker et al. respectively selected customer segmentation variables and adjusted variable weights through group decision-making and analytic hierarchy process and then used clustering technology to segment customers of a rubber product manufacturer [18]. Teng and Khong first reduced the dimension of variables, then subdivided four kinds of customers by clustering method, and analyzed the customer characteristics of different subdivided types by the DT (decision tree) method [19]. Zhang et al. used the Bayesian method to calculate the category preference of situational users, and based on context awareness, adopted CFR (collaborative filtering recommendation) algorithm to recommend personalized information to users [20].

3. Methodology

3.1. Research on Mobile Game Users' Preference. Mobile games are mainly provided by mobile devices such as smartphones and tablets. In mobile games, there is no cost to produce virtual goods, so the more virtual goods players buy, the more profits operators will make [3]. In this study, the perceived usefulness of mobile games is defined as the degree, to which users can enhance the game experience by purchasing virtual goods and other consumer behaviors. The quality of service experience is influenced by many factors, such as personal background, environment, and product itself. Different people will have different judgments on the same product. The quantitative evaluation of user experience can better evaluate the service quality of products, and the evaluation results can also be used to improve products.

Game factors include system quality, service quality, game design, and brand image. The quality of the game system represents the stability, usability, and other factors of the game system, which is the key factor to ensure the normal experience of users when using the game. Service quality can guarantee users' use and ensure users feel comfortable and happy in the process of game experience; the performance of skill and effort games depends on the player's physical and mental state and subjective will at that time, while luck itself is the biggest uncertainty in theory, which may or may not have a certain probability. However, in game design, events are often regarded as a set with a specific probability, and the most interesting thing is the difficulty of the task. Mobile games are entertainment value-added services with the purpose of entertainment. People's increasing work, life pressure, and "fragmentation" time increase the demand for entertainment and leisure, so this study puts forward the variable of perceived entertainment.

User preferences do not remain constant over time; they evolve and change. The preferences of users will emerge, develop, and fade over time. It has qualities of immediacy, randomness, and spontaneity, is easily influenced by the user's situation, is elicited by the attraction of the characteristics of things themselves, and is a type of instantaneous feeling. People are gradually realizing that the quality of personalized service is dependent not only on algorithmic development and improvement but also on the quality of user preference models, which has become a research hotspot and direction. The reasonable acquisition and analysis of user data are the main focus of the user demand analysis of mobile games based on problem situations. The personas are modeled using the interview content, and typical users with common characteristics are created, such as goals and behavioral characteristics. The scenario scripts are created according to modeling roles, so as to easily extract and analyze user requirements. The specific process is shown in Figure 1.

If the m-dimensional data set is X, the cluster is divided into k clusters $w_1, \ldots, w_k$, and their centroids are $c_1, \ldots, c_k$; then,

$$c_i = \frac{1}{n} \sum_{x \in w_i} x. \tag{1}$$

Among them, the number of data points in cluster w_i is denoted as i and the number of objects in data set X is denoted as n.

In the above iteration process, the square error criterion is adopted to judge whether the iteration is finished or not, as shown in the following formula:

$$E = \sum_{i}^{k} \sum_{p \in c_i} \left| p - c_i \right|^2, \tag{2}$$

where p is a point in space, representing a given object.

This study simply divides user preferences into positive preferences and negative preferences. At this point, the problem of user preference extraction can be simply understood as a common binary classification problem in machine learning. The SVM (support vector machine) algorithm has a good classification effect when the number of samples is small. Based on the kernel function technique, it can handle nonlinear separable problems well, has strong generalization ability, and can handle high-dimensional data well. XGBoost, like DT, draws on the idea of boosting algorithm. The former has made some improvements on the latter algorithm, and its performance is better. The overall principle of the algorithm is shown in Figure 2.

SVM, RF (random forest), DT, and XGBoost are selected as the basic user preference extraction models. Based on the parameter optimization of single-model user preference extraction methods, the stacking integrated learning framework is used to model the extraction of individual user preferences fusion. The weights of single-model user preference extraction models are obtained through the training of logistic regression method, and the final user preference extraction method is obtained according to the combination of weights.

Logistic regression is a classification model [18], which is expressed by conditional probability $P(Y|X)$ and formalized as a parameterized logistic distribution. The value of random variable X is a real number; that is, the user preference characteristics extracted from each single model, and the value of random variable Y is 1 or 0, that is, the positive and negative preferences of users.

Binomial logistic regression is the following conditional probability distribution:

$$P(Y = 1|X) = \frac{\exp(w \cdot x + b)}{1 + \exp(w \cdot x + b)}, \tag{3}$$

$$P(Y = 0|X) = \frac{1}{1 + \exp(w \cdot x + b)}. \tag{4}$$

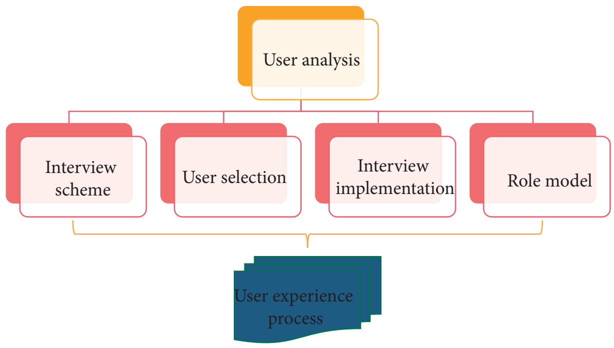

Figure 1: User experience process of mobile game.

By comparing the two conditional probabilities of users' positive and negative preferences, it classifies users' preferences into the one with higher probability. It can be obtained from the above two formulas:

$$\log \frac{P(Y=1\mid X)}{1-P(Y=1|X)} = w\cdot x + b. \tag{5}$$

That is to say, in the logistic regression model, the logarithmic probability of positive preference of output $Y=1$ users is a linear function of input x. The closer the obtained linear function value is to positive infinity, the closer its probability value is to linear function value, the closer it is to negative infinity, and the closer it is to zero.

We set the probability of user loss leave = T as p and the probability of nonloss as q, and then the probability of user loss is α times higher than that of nonloss under different behaviors, which is OR in logistic regression:

$$\log\text{it}(p) = \log(o\,dd\,s) = \log\left(\frac{p}{q}\right). \tag{6}$$

The log here is equivalent to ln at the base of e. Logistic regression is actually an ordinary regression process using logical functions, so

$$\log\text{it}(p) = \log(o\,dd\,s) = \log\left(\frac{p}{q}\right) = a + bX, \tag{7}$$

X is a variable, b is a coefficient, and p is the probability of Class = true, which means the coefficient of logistic regression is defined in terms of log ($odds$)interm of $\log(o\ dd\ s)$ [14].

3.2. Construction of Personalized Recommendation Model for Mobile Games. The utility derived from the perceived quality and expected performance of mobile game services is known as quality. The ability to play games on the go is a key feature of mobile game services. It means that users can play mobile games at any time and have complete control over the amount of time they spend playing [4]. Many gamers use video games as a time-consuming stress reliever. This means that the convenience of mobile games as a form of entertainment that is not constrained by time or space has a significant impact on player usage. The difficulty and complexity of users will increase as each link in the process becomes more complex. As a result, in order to measure the perception of global users, this study combines many practical features of the mobile game business in its analysis of perception and usability.

Quality of the system, information, service, game content design, brand image, and other factors all have an impact on game users' participation behavior. Satisfaction is a user's assessment of a product or service's ability to meet their own needs, and it has a positive impact on consumers' purchase intent. Opinion leaders are now inextricably linked to mobile game online marketing. The choices of friends around them will be influenced by the opinions of a group of leaders who are willing to try and spread new games. We can find the influence of opinion leaders in the field of games and the radiation of people through the investigation. In the investigation of this study, enabling factors are expanded into social driving factors according to individual wishes and purposes, such as the promotion of games and a series of marketing strategies adopted by operators. For mobile value-added services, enabling factors are an important means to transform potential users into actual users. Rich data insights can bring higher dimensional data features. When the amount of data is large enough, even if a relatively simple algorithm is selected, better performance can be obtained. In addition, entertainment is the main purpose for users to use mobile games. The greater the entertainment of mobile games, the easier it is to achieve its purpose. Therefore, this study believes that perceived entertainment affects perceived usefulness. The research model of this work is put forward, as shown in Figure 3.

Because these behavioral context attributes of mobile gamers have a certain correlation, this study uses the transitive closure grouping method based on fuzzy equivalence relation to group players. In this study, the ratio of the difference between the number of clusters before and after and the difference between the two clustering thresholds is used as an index to evaluate the clustering quality. The index for evaluating the clustering quality is shown in the following formula:

$$\Delta\delta_i = \frac{K_i - K_{i+1}}{\lambda_i - \lambda_{i+1}}, \tag{8}$$

K_i represents the number of clusters for the ith time and λ_i is the clustering threshold for the ith time. When the threshold value of the jth clustering is the maximum value of all clusters and the ratio is the minimum value of all clusters, as shown in the following formula, λ_j is the best threshold value:

$$\begin{cases} \lambda_j &= \max(\lambda_i) \\ \Delta\delta_j &= \min(\delta_i). \end{cases} \tag{9}$$

This work thinks that the evaluation of the surprise degree of recommendation system should be based on the similarity with users' long-term preferences and the quality of the game itself. As time goes by, preferences are gradually forgotten, and users tend to get a higher degree of surprise. Surprise evaluation of the recommendation results of the whole recommendation system can be expressed as follows:

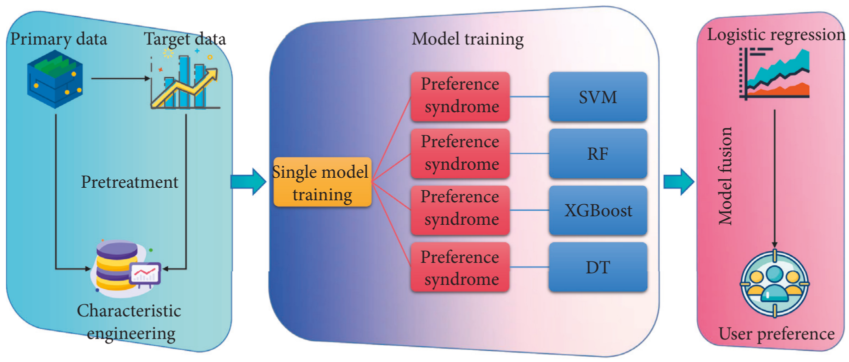

Figure 2: Principle block diagram of the user preference extraction algorithm based on multimodel fusion.

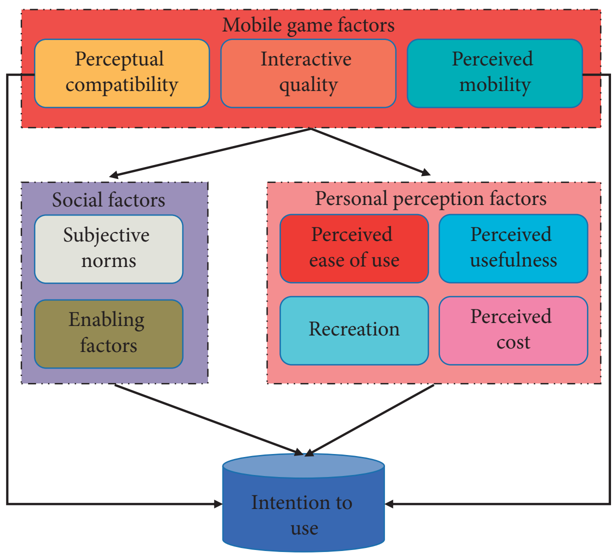

Figure 3: Model of influencing factors of mobile game use intention.

$$S_{\text{top}-K} = \frac{1}{K}\sum_{k=1}^{K} S_{i,K}, \tag{10}$$

where K represents the length of the whole recommendation list.

The main process of personalized game recommendation for mobile gamers is as follows:

(1) Audit the sample, select the sample player that meets the requirements, eliminate the users with missing or abnormal attribute values, and finally determine the sample users.

(2) Calculate the player's interest and fill it into the scoring matrix.

(3) The behavior and situational factors of mobile gamers are eliminated, and the original data format is clustered by transitive closure based on fuzzy equivalence relation.

(4) In these subspaces, the player game score matrix of the category of the target player is generated. Then, through the improved subspace player similarity calculation formula, the similarity between the target player and all players in the same class is obtained.

(5) Get the final player's predicted score value for the unrated game, and recommend the top N games with the highest score to the target player.

The personalized game recommendation process is shown in Figure 4.

4. Experiment and Results

The mobile game user acceptance model studied in this study has six variables, namely, convenience, ease of use, perceived pleasure, social needs, attitude, and willingness to use. Through the relevant statistical analysis of each model variable, the test results of mobile gamers' acceptance model of combined samples are obtained, as listed in Table 1.

H1–H5, respectively, indicate that convenience has a positive impact on the attitude of using mobile games; ease-of-use has a positive impact on the attitude of using mobile games; perceived fun has a positive impact on the attitude of using mobile games; social needs have a positive impact on the willingness to use mobile games.

As can be seen from Table 1, the P value of convenience reaches a significant level of 0.001, and the path coefficient is 0.263, indicating that convenience has a significant positive impact on the attitude of mobile gamers. When players choose mobile games, the convenience of mobile games improves their attitude towards mobile games. The P value of social demand reached a significant level of 0.05, and the path coefficient was 0.136, indicating that social demand can have a significant positive impact on mobile gamers' willingness to use. When players choose mobile games, mobile games that meet their social needs will increase their willingness to use mobile games. In the test results, ease of use has a significant negative impact on players' attitudes, but the coefficient is relatively small and the degree of impact is not high.

In this study, SPSS statistical software is used to analyze 180 sample data and 25 categories of mobile game user experience. For KMO and Bartlett tests, the value of KMO test is 0.933, indicating that it is very suitable for factor analysis, while the significance of Bartlett test is 0.000,

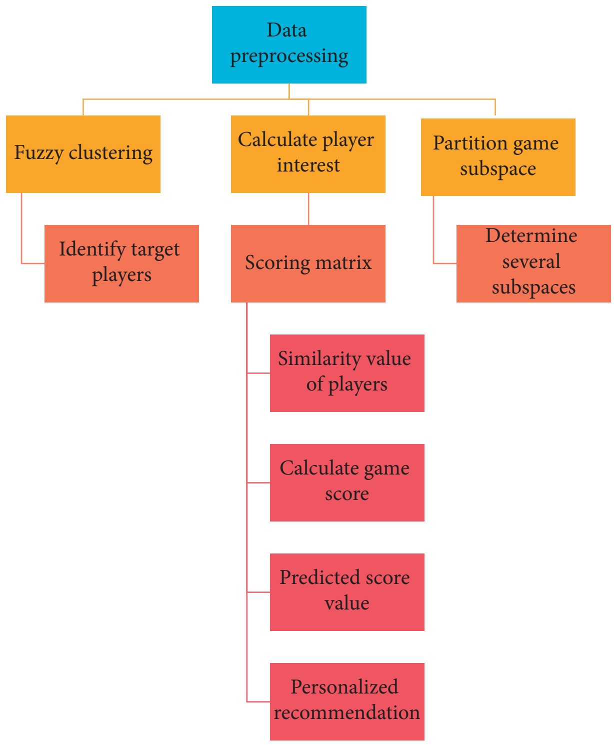

Figure 4: Personalized recommendation process of mobile games.

Table 1: Hypothesis test result.

Hypothesis	Standardized path coefficient	Test result
H1	0.263	Support
H2	−0.096	Refuse
H3	0.913	Support
H4	0.245	Support
H5	0.136	Support

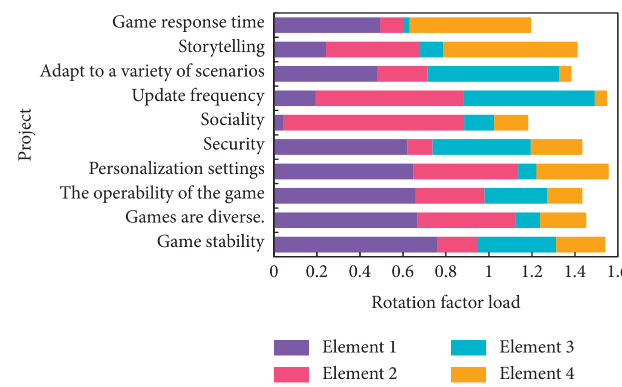

Figure 5: Rotating component matrix.

which has reached a significant level, indicating that the data come from a normal distribution and can be further analyzed. The result of rotating the component array is shown in Figure 5.

It can be seen that the effect of extracting the main factors is that the characteristic value of the first factor is particularly high, which contributes more to the interpretation of the original variables, and the factors that tend to be flat can be eliminated. Among the above assumptions, this study assumes that perceived compatibility, perceived mobility, subjective norms, enabling factors, perceived usefulness, perceived ease of use, and perceived entertainment have a positive impact on intention to use, while perceived cost has a negative impact on intention to use. The relevant analysis results are listed in Table 2.

Perceived compatibility, perceived mobility, subjective norms, causes, perceived usefulness, perceived ease of use, perceived entertainment, and perceived cost are all significantly positively correlated with the intention to use. The original hypothesis is accepted because it is negatively related to the clear intention of use. When making predictions, most students will generate a continuous truth value or probability value for the test sample and compare it to a given threshold. It is considered a positive example if the value exceeds the threshold; it is considered a negative example if the value falls below the threshold. Generally, the generalization performance of the classifier is measured by the area under the ROC (receiver operating characteristic) curve, namely, AUC (area under the curve). In this study, ROC-AUC is used as a standard to evaluate the experimental performance, as shown in Figure 6.

Among them, the user preference extraction results of SVM, RF, XGBoost, and DT in the ROC-AUC evaluation index are 0.501, 0.663, 0.724, and 0.799, respectively. After the stacked models are fused, the ROC-AUC value of the final fused model is 0.921, which has a percentile enhancement effect. In order to further explain the calculation formula of surprise score and its specific meaning and explore the influence of game quality and game similarity and user preference on the surprise score of recommendation system, the following two cases will be discussed. There are 4 games and 5 users in the item rating array, and the default values are filled with hyphens. In order to express the data more intuitively, we plot the data on a line chart, as shown in Figure 7.

It can be seen from Figure 7 that game 1 and game 2 have been scored by user 5, and these scores represent the user's long-term preference information, while game 3 and game 4 have not been scored by user 5. We can not only get the user's preference information but also get the preference similarity information by looking at the trend of the graph. If the line charts of two games have roughly the same trend, then they are similar. That is, the average score of game 4 is higher than that of game 3, which means that the quality of game 4 is higher than that of game 3. This is because when the 3rd and 4th games are the same as the long-term distance of the user 5, game 4 has a higher quality. This case illustrates the importance of game quality in surprise calculation.

To solve the problem that players are "different" due to data sparseness and alleviate the influence of data sparseness on recommendation quality, an improved subspace player similarity calculation method is proposed, which introduces the interest of players in subspace. The improved player similarity calculation method is compared with the traditional method in two different data sparseness. In terms of setting experimental parameters, the balance weight in the

Table 2: Correlation statistics.

Variable	Intention to use	Sig.
Perceptual compatibility	0.566	0.000
Perceptual mobility	0.347	0.000
Subjective norm	0.511	0.000
Contributing factors	0.286	0.000
Perceived ease of use	0.589	0.000
Perceptual entertainment	0.663	0.000
Perceived cost	−0.184	0.001

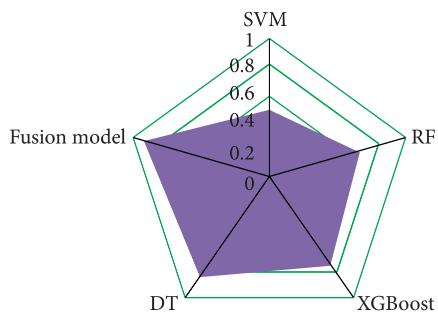

Figure 6: Model performance comparison.

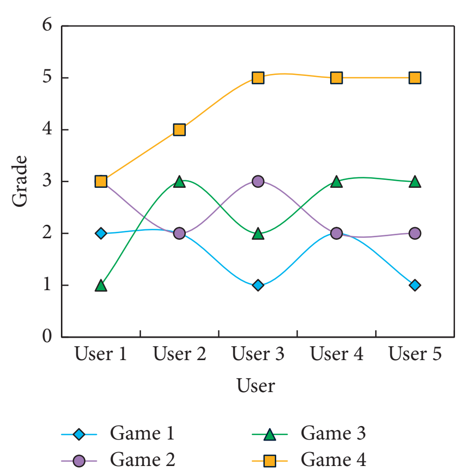

Figure 7: An analysis case of the influence of shadow quality on surprise.

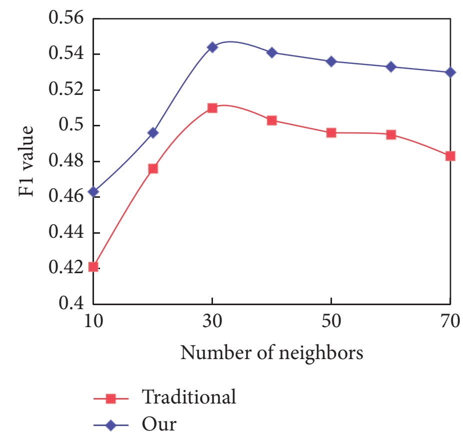

Figure 8: Performance comparison of two methods for calculating player similarity in an 80% training set.

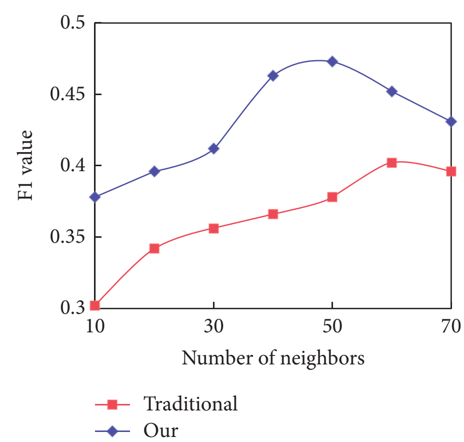

Figure 9: Performance comparison of two methods for calculating player similarity in a 20% training set.

new method of calculating player similarity is 0.8, and the weight of each subspace is equal. The number of adjacent players is selected from 10 to 70, and the recommended number of games is 15. The experimental results are shown in Figures 8 and 9, respectively.

The new method combining the interest differences in player subspace is slightly better than the traditional method in the 80% training set. With the scarcity of data, the difference of F1 index level between the two methods is increasing. Under the training set of 20%, the level difference of F1 indicators produced by the two methods is more obvious. Therefore, a new method of calculating players' similarity by introducing interest differences into subspace can improve the influence of sparse data on CFR quality to some extent by overcoming the problem of "similarity mismatch."

Through empirical research, it is found that the variable that has the greatest influence on the willingness to use mobile games is the perceived entertainment of games, and entertainment is the highest value attraction point for users to choose to use mobile games. Perceived compatibility, interactivity, and perceived mobility significantly affect the intention of perceived entertainment use. Mobile games should fully consider the different needs of segmented users and design game content according to the entertainment habits and value demands of segmented customer groups. With the accelerated pace of life, people's entertainment time is becoming more and more fragmented, and the demand for light mobile games is increasing. Therefore, game development can balance the two values of entertainment and lightweight and carry out the effective content design.

In the innovation and dissemination of mobile games, light gamers (casual gamers) have less recommendation, less communication, low self-confidence, and their game choices are easily influenced by others, and social channels are easy to reach. Excellent players have rich game experiences, and their game preferences are more consistent in different types of games. Perceived usability and perceived compatibility have limited influence on the reasons why mobile gamers use games, and they are variables that have no significant influence. It shows that the measurement of the above influencing factors is not applicable to mobile games, and mobile game manufacturers need to make other attempts and think about mode planning and promotion.

From the conclusion of the study, it can be found that for mobile game consumers in most areas, whether the game can bring fun or not is the main factor that everyone pays attention to, so it still needs a lot of investment in the future game design. Specifically, mobile games can establish a game community belonging to players in various ways and guide and encourage players to strengthen communication in the community by means of information dissemination, personal status display, and game sharing, so as to gather players with the same preferences. The player's recognition and dependence on the game are enhanced, and the player's sense of identity and participation are enhanced through self-display. At the same time, taking some skillful and complicated operations as the internal design of game level upgrading can not only meet the general users' game experience needs but also produce natural player level differentiation in the game and meet the users' achievement needs.

5. Conclusions

In the wireless broadband environment, this research divides the game factors into three main factors: game design, path dependence, and comparative advantage. Using scenario-based theoretical sampling method to conduct interviews, create task models, and scenario scripts, users' needs are analyzed, and preliminary analysis materials are collected. In the process of applying CFR, it is necessary to flexibly adjust the appropriate similarity weight according to the scarcity of data, so as to achieve the best recommendation quality of the algorithm. Experiments show that the new method of calculating the similarity of subspace players can improve the robustness of the algorithm in the case of sparse data, thus improving the impact of sparse data on the performance of the algorithm. In the future, there will be a large number of small models in the game operation, which are more likely to directly become a part of the game, bringing a better game experience to the end users and a long-term beneficial impact on the future development of the game field.

Data Availability

The data used to support the findings of this study are available from the corresponding author upon request.

Conflicts of Interest

The author declares that there are no conflicts of interest.

Acknowledgments

This study was supported without any funding.

References

[1] Q. Ma, G. Lin, Y. F. Liu, and J. Huang, "Economic analysis of crowdsourced wireless community networks," *IEEE Transactions on Mobile Computing*, vol. 16, no. 7, pp. 1856–1869, 2016.

[2] L Brand, A Beltran, R Buday et al., "Training vegetable parenting practices through a mobile game: iterative qualitative alpha test," *Journal of Medical Internet Research*, vol. 3, no. 2, 6 pages, 2015.

[3] F. A. Narudin, A. Feizollah, N. B. Anuar, and A. Gani, "Evaluation of machine learning classifiers for mobile malware detection," *Soft Computing*, vol. 20, no. 1, pp. 343–357, 2016.

[4] K. Yamamoto, "A comprehensive survey of potential game approaches to wireless networks," *IEICE - Transactions on Communications*, vol. 98, no. 9, pp. 1804–1823, 2015.

[5] H. Jeon, H. J. Ahn, and G. J. Yu, "What makes people react to the posts on the brand pages of mobile social network games?" *Online Information Review*, vol. 40, no. 3, pp. 435–448, 2016.

[6] T. E. Pronk, P. H. Wiersma, A. V. Weerden, and F. Schieving, "A game theoretic analysis of research data sharing," *PeerJ*, vol. 3, no. 3, p. 1242, 2015.

[7] M. Zhao, A. Jha, Q. Liu et al., "Faster Mean-shift: GPU-accelerated clustering for cosine embedding-based cell segmentation and tracking," *Medical Image Analysis*, vol. 71, Article ID 102048, 2021.

[8] L. Fu, D. Liu, Y. He, G. Cui, H. Liang, and W. Wang, "Co-operation strategies by cournot game for partner selection and power control in S-umts," *Bioinformatics*, vol. 30, no. 7, pp. 1045-1046, 2014.

[9] P. Duarte, Z. M. Fadlullah, A. V. Vasilakos, and N. Kato, "On the partially overlapped channel assignment on wireless mesh network backbone: a game theoretic approach," *IEEE Journal on Selected Areas in Communications*, vol. 30, no. 1, pp. 119–127, 2011.

[10] D. Liu, H. Li, and W. Ding, "Neural-network-based zero-sum game for discrete-time nonlinear systems via iterative adaptive dynamic programming algorithm," *Neurocomputing*, vol. 110, no. 13, pp. 92–100, 2013.

[11] M. G. H. Bell, "Measuring network reliability: a game theoretic approach," *Journal of Advanced Transportation*, vol. 33, no. 2, pp. 135–146, 2010.

[12] Y. Li and B. Bhanu, "Utility-based camera assignment in a video network: a game theoretic framework," *IEEE Sensors Journal*, vol. 11, no. 3, pp. 676–687, 2011.

[13] M. Takano, K. Wada, and I. Fukuda, "Reciprocal altruism-based cooperation in a social network game," *New Generation Computing*, vol. 34, no. 3, pp. 257–272, 2016.

[14] Y. Yang, B. Liu, Y. Shi, and Y. Liu, "Design and simulation of the cooperation incentive mechanism in ad hoc network based on evolutionary game," *ICIC Express Letters*, vol. 9, no. 10, pp. 2827–2834, 2015.

[15] C. Li, J. Liu, and S. Ouyang, "Large-scale user behavior characterization of online video service in cellular network," *IEEE Access*, vol. 4, pp. 3675–3687, 2017.

[16] Y. Ye, H. Sheng, and H. Shi, "Research on mobile internet user behavior preference based on support vector machine," *International Journal of Smart Home*, vol. 10, no. 6, pp. 247–260, 2016.

[17] J. Zhang, T. Wu, and Z. Fan, "Research on precision marketing model of tourism industry based on user's mobile behavior trajectory," *Mobile Information Systems*, vol. 2019, no. 4, Article ID 6560848, 2019.

[18] I. H. Sarker, A. Colman, M. A. Kabir, and J. Han, "Individualized time-series segmentation for mining mobile phone user behavior," *The Computer Journal*, vol. 61, no. 3, pp. 349–368, 2018.

[19] S. Teng and K. W. Khong, "Examining actual consumer usage of E-wallet: a case study of big data analytics," *Computers in Human Behavior*, vol. 121, no. 1, Article ID 106778, 2021.

[20] H. Zhang, M. Wang, L. Yang, and H. Zhu, "A novel user behavior analysis and prediction algorithm based on mobile social environment," *Wireless Networks*, vol. 25, no. 2, pp. 791–803, 2019.

Hindawi
Computational Intelligence and Neuroscience
Volume 2023, Article ID 9865718, 1 page
https://doi.org/10.1155/2023/9865718

Retraction

Retracted: Personalized Teaching Strategy of University Ideology Course Based on Lagrange Neural Network and Big Data Technology

Computational Intelligence and Neuroscience

Received 25 July 2023; Accepted 25 July 2023; Published 26 July 2023

This article has been retracted by Hindawi following an investigation undertaken by the publisher [1]. This investigation has uncovered evidence of one or more of the following indicators of systematic manipulation of the publication process:

(1) Discrepancies in scope
(2) Discrepancies in the description of the research reported
(3) Discrepancies between the availability of data and the research described
(4) Inappropriate citations
(5) Incoherent, meaningless and/or irrelevant content included in the article
(6) Peer-review manipulation

The presence of these indicators undermines our confidence in the integrity of the article's content and we cannot, therefore, vouch for its reliability. Please note that this notice is intended solely to alert readers that the content of this article is unreliable. We have not investigated whether authors were aware of or involved in the systematic manipulation of the publication process.

Wiley and Hindawi regrets that the usual quality checks did not identify these issues before publication and have since put additional measures in place to safeguard research integrity.

We wish to credit our own Research Integrity and Research Publishing teams and anonymous and named external researchers and research integrity experts for contributing to this investigation.

The corresponding author, as the representative of all authors, has been given the opportunity to register their agreement or disagreement to this retraction. We have kept a record of any response received.

References

[1] J. Zuo, F. Zhou, and Y. Liang, "Personalized Teaching Strategy of University Ideology Course Based on Lagrange Neural Network and Big Data Technology," *Computational Intelligence and Neuroscience*, vol. 2022, Article ID 1251839, 8 pages, 2022.

Hindawi
Computational Intelligence and Neuroscience
Volume 2022, Article ID 1251839, 8 pages
https://doi.org/10.1155/2022/1251839

Research Article

Personalized Teaching Strategy of University Ideology Course Based on Lagrange Neural Network and Big Data Technology

Jiqian Zuo,[1] Fang Zhou,[2] and Yajuan Liang[1]

[1]*College of Humanities and Marxism, Hebei Oriental University, Langfang 065001, China*
[2]*College of Artificial Intelligence, Hebei Oriental University, Langfang 065001, China*

Correspondence should be addressed to Yajuan Liang; 201772464@yangtzeu.edu.cn

Received 21 April 2022; Revised 7 May 2022; Accepted 9 May 2022; Published 30 June 2022

Academic Editor: Xin Ning

Individualized instruction is a type of educational principle. On the one hand, it necessitates the creation of individualized teaching resources, courses, and methods. Students, on the other hand, require a high level of autonomy and the ability to make personalized plans based on their own cognitive characteristics and needs. The big data (BD) era opens up new possibilities for IE (ideological education) work in universities, but it also poses some challenges. IE development will be greatly aided by recognizing opportunities to meet challenges and optimizing and integrating PL (political lesson) resources. The LNN (Lagrange neural network) model has been established. The simulation results show that the LNN network can converge to the optimal solution quickly and effectively and then reconstruct sparse signals. Individualized college PL instruction using LNN and BD technology helps students communicate more effectively and improves the pertinence, immediacy, and positivity of IE.

1. Introduction

Massive data provide great value for people. Contemporary young students can be said to grow up together with the Internet [1, 2], so contemporary youth can be described as real participants and pioneers. The corresponding BD (big data) [3–5] era also has a profound impact on the education of universities. BD has brought profound changes to all fields. Faced with the great transformation power of BD, ideological teachers' way of thinking is bound to change, actively adapt to the requirements of the BD era, keep up with the times to the greatest extent, and make rational use of its advantages and characteristics to improve teaching effect.

Many large-capacity data sets are obtained from many large-scale data sets through intelligent statistical measures [6], and BD capacity exceeds traditional data storage capacity. Large capacity, fast processing speed, high total value, and diverse data types are all characteristics of BD [7]. The research on PL (political lesson) teaching mode innovation is also slightly involved, but the research results on BD's influence on college PL practice teaching are almost blank [8, 9]. As a result, when developing university PL personalization with a BD background, we must fully grasp BD's development opportunity, fully comprehend and grasp the theoretical hotspots and academic frontiers of college students' IE (ideological education) personalization by BD, and perfectly connect academic research results with actual teaching [10]. Universities' ideological staffs should focus on overcoming the dilemma of BD personalized teaching in the BD era, actively creating a variety of personalized teaching conditions.

The construction of teaching systems in research universities has given the teaching quality standard a new meaning and orientation. We should not only reflect the teaching quality standards of research universities in the index system of teaching evaluation but also reflect the teaching ideas of research education through the corresponding evaluation models, methods, and operating mechanisms when assessing classroom teaching quality. Finding new ways to do things has become a top priority. This paper examines the challenges faced by ideological network teaching resources and proposes optimization and integration methods to improve the teaching effect of ideological network teaching, based on the connotation and characteristics of BD.

2. Related Work

Literature [11] pointed out that the development of freshmen's online teaching should give priority to solving the problems of standardization and process, improving the platform of online education and teaching, and realizing the guarantee of infrastructure. Literature [12, 13] points out that with the popularization of online education and teaching in all parts of the country, many problems faced by online education and teaching are gradually exposed. Literature [14, 15] optimizes the current teaching mode by the BD method, provides teachers with information about students' learning behaviors and learning ways, and helps teachers understand the areas that students are good at and interested in. Literature [16] makes a preliminary study on personalized teaching and makes a superficial analysis of the influence of teachers' personalities and other factors on cultivating students from the perspective of establishing personalized consciousness and concept. Literature [17] studies the development process of personalized teaching from the perspective of teachers and puts forward that personalized teaching means that teachers fully integrate their own knowledge, experience, personality, and other factors with teaching activities to form a kind of teaching with unique style, stability, and personal characteristics of teachers. Literature [18] analyzes the personalized teaching mode by using the role theory and points out the premise guarantee and countermeasures of personalized teaching in combination with the opportunities and challenges faced by personalized teaching, so as to promote the teaching reform. Literature [19] holds that a personalized teaching classroom should be characterized by selectivity, daily life, and democracy, in which selectivity is the basic feature of personalized teaching, returning to students' life world is the essence of personalized teaching, and democracy is the premise and guarantee of personalized teaching.

In literature [20], a single-layer feedback neural network based on projection operation is proposed to solve the nonsmooth optimization problem with different objective functions. Literature [21, 22] puts forward a new type of neural network to solve general nonlinear programming problems. Literature [23] proposed a new type of neural network, LNN (Lagrange neural network), to solve nonlinear programming problems. Literature [24] studies the stability and convergence time of LNN in solving optimization problems. However, the objective functions of the optimization problems they solve are only smooth functions, so it is necessary to extend the application and research of this kind of neural network to nonsmooth optimization problems.

To summarize, online learning is attracting an increasing number of students due to its time and space flexibility as well as significant cost savings. With the rise of fragmented learning, customized and personalized online teaching based on BD has become the online teaching platform's development trend, providing a large number of potential users for BD in the development of online teaching, and the combination of BD and online teaching also has promising practices and research prospects.

3. Research Method

3.1. Personalized Instructional Design Based on BD. Personalized teaching is becoming a hot topic in China's educational circles as they try to reform the curriculum and change teaching methods. Because students differ in cognitive ability, cognitive level, and personality, educators should integrate students' personalities and teaching activities, put people first, begin teaching with students' needs, respect students' personalities, and use personalized teaching. Personalized teaching is a type of teaching idea that has three meanings: first, personalized teaching emphasizes the diversification of teaching, and teaching materials, teaching resources, teaching forms, and teaching methods should be rich and colorful; second, personalized teaching is learner-centered, values learners' subjectivity, respects students' individual differences, and meets students' diverse needs; and third, personalized teaching is learner-centered, attaches importance to learners' subjectivity, respects students' individual differences, and meets students' diverse needs.

The data of a learner's entire learning process can be recorded using BD technology. Knowledge points are assigned to every topic and data collected in tests, assignments, and exams. Encourage students to study more effectively and improve the quality of their learning. Various text and video resources can also be pushed to learners to help them internalize and absorb knowledge points. Students' learning motivation and interest are stimulated, and students' innovative, problem-solving, and practical abilities are developed. The implementation process is shown in Figure 1.

Through digital analysis to build a data model and use this resource to get students' psychological feelings during this period. For students who behave abnormally, find the source of the problem through data analysis and guide the wrong ideas in time.

At the same time, abundant IE resources and various forms of IE models provide students with a comprehensive platform for learning, which can satisfy students' personality styles and learning initiatives. Therefore, study in an online classroom or use WeChat to brainstorm and learn. In short, college PL teachers should comply with the development requirements of the BD era, further use BD to find favorable resources and information to master the IE initiative, and enrich and adjust teaching content with dynamic data. Before entering the course, connect and arrange the learning contents according to the key points and subkey points; at the same time, arrange your own learning time, which time period to learn what content, and when to conduct self-evaluation; and constantly revise your personal plan in combination with teachers' teaching.

On the one hand, independent assessment has no bearing on the teaching process. Only in an environment where teaching quality is highly valued and pursued can the evaluation result information be considered an integral part of school decision-making, and it is this information that the school administrators use. On the other hand, schools' value choice in using teaching evaluation results should be based

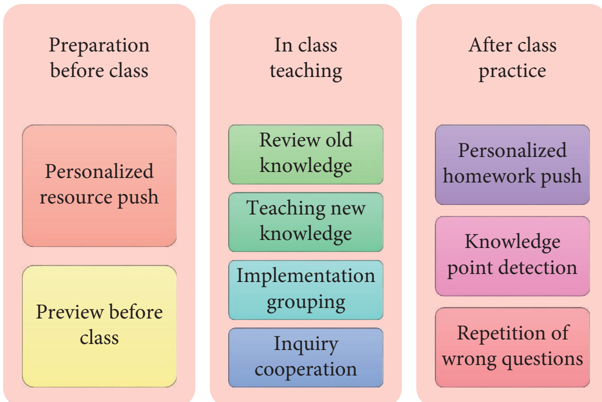

FIGURE 1: Implementation flow chart.

on improving teachers' teaching ability, promoting teachers' development, then promoting students' development, fully mobilizing teachers' enthusiasm, and stimulating teachers' potential so that both teachers and students can benefit from teaching evaluation and so that teaching evaluation can be widely recognized and continuously promote the improvement of both teachers and students.

The penalty coefficient of LNN is variable, and the neural network can still converge to the optimal solution of the optimization problem without calculating the initial value of the penalty term in advance. A neural network model of differential inclusion is established to solve the optimization problem. The similarity calculation formula of the two nodes is

$$\mathrm{sim}(U,U') = \sum_{i=1}^{n} w_j \cdot \mathrm{sim}P(U,U')_i, \tag{1}$$

where $\mathrm{sim}P_i(U,U')$ represents the similarity between node U and CN U' and w_j represents the weight value of this attribute in the i-th attribute.

$MAXL$ represents the length of the longest path in the tree and $P(a_1,a_2)$ represents the distance between nodes. Therefore, the similarity calculation formula is:

$$\mathrm{sim}_{cp} = (cp_1,cp_2) = \frac{MAXL - |p(cp_1,cp_2)|}{MAXL}. \tag{2}$$

Teachers can assign different difficulty problems to students at different levels in class, which meets the individualized needs of students at each level, increases teaching efficiency, and truly realizes individualized teaching. Teachers can also gather students with problems in the same knowledge point based on the correct or incorrect situation of knowledge points and provide targeted explanations and training to help students improve and progress quickly. To help students master the content related to knowledge points, focus on synchronous or asynchronous explanations of common problems. Students can have individualized communication for personality issues. The explanation methods for students vary according to different knowledge points, which can promote the development of students' personalities and allow questions to be solved and answered at any time.

Personalized teaching based on BD can collect all of the students' data automatically; manage all types of learning materials digitally, such as students' homework, pictures, grades, and teachers' comments; track and record students' learning behaviors with BD technology; provide adaptive learning feedback; and provide students with personalized learning guidance. It is more convenient for students to think and reflect, objectively promote students' progress, and make students more active in self-evaluation by collecting and managing their entire process data.

3.2. Probe into the Personalized Teaching Path of University PL Based on LNN. Introducing the thinking mode of planning into college IE teaching based on BD is to break through the fixed thinking mode, with new eyes, new viewpoints, and new methods, from the establishment of the thinking mode of college IE planning to the implementation of the plan and the realization of the target requirements. Under the influence of BD, the way of IE in traditional mode has undergone great changes.

One is to accurately judge the resources of ideological network teaching, that is, the selected teaching resources can be authentic, effective, and reliable enough. The second is to find the best resources from massive IE resources, so as to ensure the best teaching effect. Of course, on the basis of the principle of scientific construction, should reach a certain degree of adaptability, specifically, the selected materials can adapt to students' physical and mental characteristics and knowledge structure characteristics. This work should also pay attention to two points: one is to choose the teaching resources that fit the students' actual network, and the other is to seriously explore the students' concerns and interests and find out the places where students have insufficient knowledge to enhance the pertinence of the teaching process.

The goal of this paper is to design a neural network so that its equilibrium point can meet the optimal conditions. In order to explain the neural network model, firstly, a Lagrangian-like function is defined as follows:

$$L(x,\lambda) = f(x) + \lambda H(x). \tag{3}$$

in which Lagrange multiplier $\lambda > 0$.

$$H(x) = \begin{cases} 0, & x \in S, \\ \sum\limits_{j\in I^{+}(x)} h_j(x), & x \notin S. \end{cases} \tag{4}$$

Find the $L_1(x,\lambda)$-square x-guide number of the Lagrange function:

$$\nabla_x L(x,\lambda) = \partial f(x) + \lambda^T \nabla h(x). \tag{5}$$

According to the gradient descent, the following neural network can be constructed:

$$\left.\begin{aligned}\frac{\mathrm{d}x}{\mathrm{d}t} &= -\nabla_x E = -\nabla_x f(x) - \lambda A - \mu A^T (Ax - b)\\ \frac{\mathrm{d}\lambda}{\mathrm{d}t} &= \nabla_\lambda E = Ax - b\end{aligned}\right\}. \tag{6}$$

Because the operator $\|\cdot\|_0$ is not differentiable, the function $f(x_i) \approx x_i^2/x_i^2 + \sigma$ is considered to approximate $\|x\|_0$. The smaller σ is, the more accurate the approximation effect is, that is:

$$\|x\|_0 \approx f(x) = \sum_{i=1}^{n} f(x_i) = \sum_{i=1}^{n} \frac{x_i^2}{x_i^2 + \sigma}. \tag{7}$$

Differentiated assessment is possible thanks to the teaching cloud platform's ability to personalize curriculum assessment strategies for different classes. Most students who major in art or sports, for example, are outgoing and good communicators, but they dislike reading. College PL teachers can focus on content material learning and knowledge consolidation exercises and strive to help students lay a strong theoretical foundation and develop a practical learning attitude, depending on their characteristics. Create more personalized practice plans and improve the methods and forms of practice. Personalized practice schemes can effectively stimulate students' interest in learning, arouse participation in practical activities, and improve their overall creative ability in the relatively relaxed, happy, and free practice process.

Evaluate and judge the similarity between the given user portrait model and the user portrait model in the user portrait database. The user's current learning user portrait is called the main learning user portrait. The user portrait similarity calculation obtains the user portrait similarity by constructing a decision tree and performing node operation. Taking the user attribute elements as an example, the user portrait model tree is constructed, as shown in Figure 2.

Teachers' personalized teaching system is used to watch the completion and accuracy of students' preview self-test questions. Because each test question has different knowledge points, the students' mastery degree is analyzed to understand the overall preview of students. According to the real-time updated ranking of students' preview scores, this paper analyzes the changes in students' grades and the wrong questions of each student, so as to teach students in accordance with their aptitude in the process of teaching.

Cloud engine in BD infrastructure module realizes the management of distributed Hadoop nodes through task scheduling function. Considering that other modules in the system, such as database management module of user portrait, also need to manage the database by task scheduling, asynchronous task transfer is adopted, which also ensures the rapid development and debugging of submodules as shown in Figure 3.

The script is developed in python, which mainly includes two parts, task and task fragment. The task is initialized in the management server by reading the policy file, and the task script and shell script are packaged according to the corresponding configuration in the policy file. After the packaging is completed, it is sent to the proxy service module of the Hadoop node through socket. The proxy service module decompresses the task and shell script, executes the task fragment script, calls the corresponding shell script, completes the task scheduling, and returns the execution result to the cloud engine.

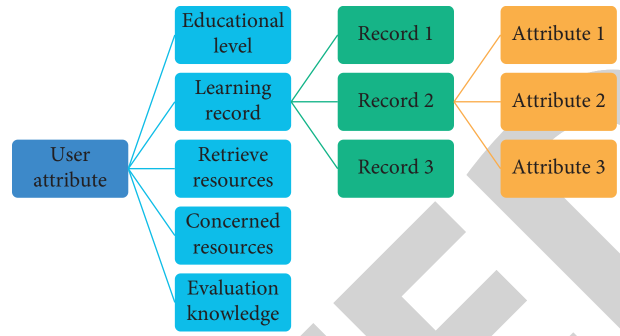

Figure 2: Schematic diagram of user attribute tree.

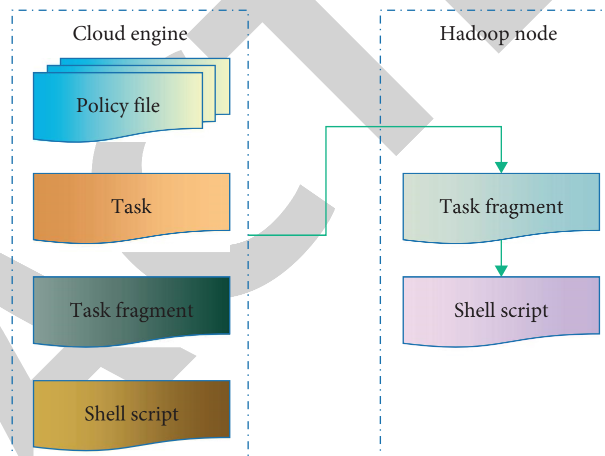

Figure 3: Working mechanism of task submodule.

Individualized teaching creates a democratic and harmonious atmosphere for teachers and students and allows students to have their own thoughts and answers, thus fully expressing their individuality. Personalized teaching is personalized in curriculum, teacher's teaching, and students' learning. Mind mapping also reflects personalization. Deal with the problem according to the way you handle the information, which obviously has a strong personal color. When thinking or solving problems and combine multidimensional information into a dynamic structure diagram, what is completed is a personalized mind map.

4. Results Analysis and Discussion

Under BD background, IE personalized teaching needs the comprehensive strength of teachers and technical teams. Specifically, the construction of a personalized teaching team can improve BD development literacy through the optimization and potential stimulation of the internal staff of the teaching team and strengthen the screening and optimization of massive teaching data. It can focus on future development education and fully absorb data professionals from all aspects to strengthen personalized teaching. This innovative personalized teaching method can gradually transform the traditional IE work from the extensive passive response mode to the active intervention and active guidance mode and create a new personalized teaching mode of college IE.

Using MATLAB to generate sparse signal x of order k, without losing generality, the positions of these k nonzero elements are randomly generated and meet the uniform distribution of $[1, n]$, and the sizes of the corresponding nonzero elements are randomly generated and meet the uniform distribution among [1, 100]. The generation of random signals is shown in Figure 4.

Students' intuitive and comprehensive qualitative evaluation of teachers and courses is referred to as aspect evaluation. The individual evaluation reflects the quantitative requirements for teaching based on subject characteristics or course nature. Teachers' personal styles and preferences, as well as the school's current reform focus, are reflected in the selective evaluation. Subjective evaluation captures characteristics of teaching quality that aren't captured by standardized indicators. Teachers can also use a specific knowledge point or piece of content as a theme for each group to investigate and promote. Teachers can allow students to create their own personalized mind map during the evaluation stage, which includes not only the relationships between knowledge points but also their own learning methods and cognitive strategies. Students can use this map to learn about their learning situation and provide timely feedback, making it easier for them to identify and correct their own flaws, humanize the evaluation, and make the cognitive and thinking processes operable.

Virtual practice teaching alleviates the difficulties of traditional practice teaching, such as students' lack of subjectivity, limited teaching time and space, shortage of teaching resources, and so on; highlights students' dominant position; expands the field of teaching virtual space; and enriches teaching resources. In the course system construction of personalized teaching, the setting of emotion and belief courses cannot be ignored. A complete personalized teaching course system should be the integration of three courses. Therefore, on the basis of the main courses, emotion and belief courses should be properly arranged, and at the same time, emotion courses should be refined into the specific teaching of the first two courses. Teachers can link the first two courses with the third related part in teaching; for example, they are often combined with corresponding emotions in the teaching of psychology, and the beliefs and thoughts of historical figures are linked with them in the teaching of anthropology so that the three courses are harmonious and unified.

In order to test the relationship between the observation times m and the correct reconstruction probability under different sparsity, take different sparsity $k = [10, 15, 20, 25]$ and perform 1,000 random experiments on each group of (k, m, n).

It can be seen from Figure 5 that for different sparsity k, when the number of observation points m is greater than or equal to 110, the probability that LNN method can correctly recover sparse signals is extremely high.

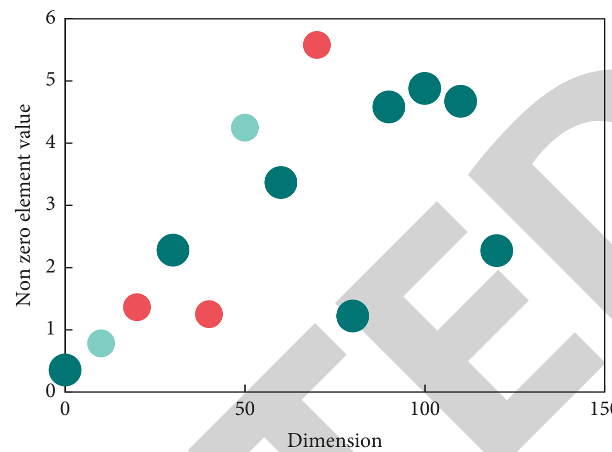

Figure 4: Discrete sparse signal.

The integration of BD and teaching is conducive to strengthening the supervision and management of college students' ideological fields. Through the digital analysis of students' ideological status, to control the operating mechanism of ideological education in colleges and universities, introduce new thinking ways and teaching methods, integrate the working resources of college IE, give full play to the advantages of digital technology, and cultivate the ability of college ideological educators to use data. Enhance the scientificity and modernity of college IE.

BD should be introduced into practice teaching, and more space for students to choose independently should be reserved in the PL teaching practice theme design. This can effectively stimulate students' initiative of independent innovation in the process of stimulating students' personal development potential. In the BD development environment, it can provide differentiated teaching ideas for college PL teaching and realize individualized education development. In personalized education, pay attention to actively listening to students' opinions and suggestions, praising students' personal strengths, which can safeguard students' personal dignity and interest.

As can be seen from Figure 6, for $m = [10, 15, 20, 25]$ with different observation points, when the sparsity k is less than or equal to 20, the LNN method has a very high probability of correctly recovering sparse signals.

Provide training, expert guidance, and technical support for teachers to help them improve their teaching level. Establish a website for the purpose of "serving teachers' teaching" to provide teachers with places for learning and communication. Organize a series of discussion lectures and classroom observations to help young teachers learn from other teachers' advanced teaching experiences and form their own teaching style and characteristics. Hire experienced old teachers as teaching consultants, listen to young teachers' classes regularly, and give guidance. Carry out a series of educational technology training to improve teachers' ability to master modern technologies such as multimedia.

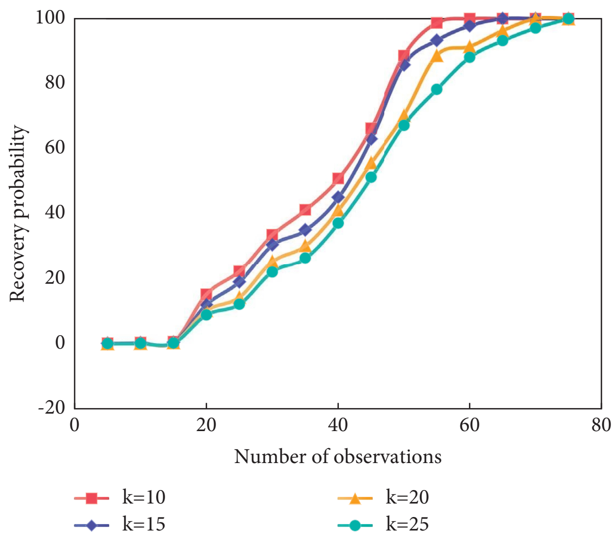

FIGURE 5: The relationship between the measured number m and the probability of successful recovery.

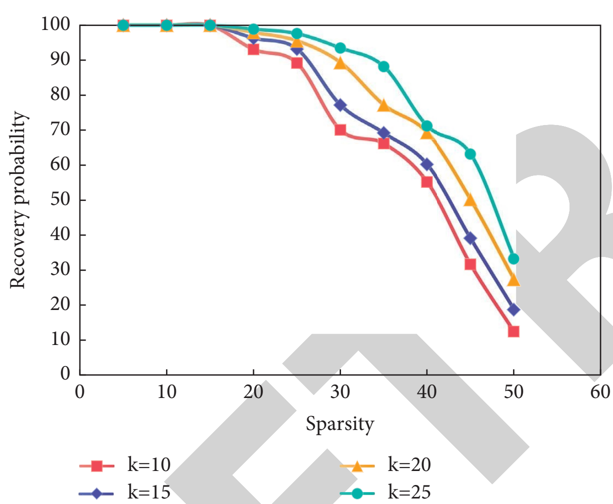

FIGURE 6: Relationship between sparsity k and probability of successful recovery.

The visualization of a mind map can help students understand the solutions and methods adopted by teachers and classmates when solving the same problem. At the same time, continuous reflection and regulation can promote the formation and transfer of their own cognitive strategies and cultivate their metacognitive ability. The explicit way of mind map opens tacit knowledge, realizes information exchange, connects more information to expand the breadth and depth of thinking, inadvertently exercises thinking, and lays the foundation for the emergence of new inspiration and the stimulation of creativity, thus promoting the innovation and perfection of knowledge.

Use MATLAB software programming to simulate the behavior of the neural network. Figure 7 shows the trajectory diagram of x_1, x_2. Figure 8 shows the trajectories in these four points x_1. Therefore, this is consistent with the minimum point set in problem analysis.

Learning objectives have a specific order, and they do not exist in parallel. Similarly, knowledge points follow a logical order: before learning a specific knowledge point, you must first learn its lower knowledge points, which serves as a necessary prelude to learning the upper knowledge points and improving the upper knowledge points. Students will be pushed to master the basic knowledge points, then the writing knowledge points of chemical equations, and finally the knowledge points related to the simple calculation of chemical equations. Students will master knowledge content ranging from easy to difficult, and personalized learning will be realized. There are two types of personalized teaching resources: static and dynamic. Words, pictures, animations, courseware, and material conditions are examples of static resources, whereas dynamic resources refer to dynamic information and active human resources. The construction of static resources is currently mostly in the stage of low-level repeated construction in the resource creation process, and the lack of individuality cannot meet the needs of students. Furthermore, it frequently overlooks the discovery of dynamic resources hidden in teaching activities, such as creativity and intellectual resources. However, mind maps can assist in the resolution of these issues.

It can be seen from Figure 9 that the initial point $(x_1 = 1, x_2 = 0.5)$ inside the feasible region finally converges to the minimum point. It can be seen from Figure 10 that the initial point $(x_1 = 0, x_2 = 5)$ outside the feasible region enters the feasible region after a period of operation and finally converges to the minimum point $(x_1 = 0, x_2 = 2)$.

In order to facilitate code maintenance and subsequent expansion of functions, Python and Shell scripts that can explain execution are selected. When running on the system line, the code can be modified. The task dispatching room executes in sequence through queues, and the cloud engine executes corresponding tasks according to the priority of the queues. So the elements that make up the user portrait must be able to be automatically identified by the computer, or the user can provide explicit information about the elements of the user portrait. When building a user portrait model, the finer the entity elements that make up the model, the more accurate the description of the model is. However, in the actual application process, many and fine user portrait elements will be dull. Therefore, the scope and accuracy of the user portrait model must meet the actual needs.

The platform will continuously collect user information and apply it to the current user portrait and constantly improve the user's portrait features through the current user portrait's use of data, so as to realize the continuous enrichment and perfection of data and portrait and ensure that the model has good adaptability. According to the difference of data dimensions, starting from multidimensions, the data is finally aggregated into a cluster set with the least differentiation in a certain dimension. There are often great differences between different clusters, so cluster analysis has become a commonly used data processing method in the field of machine learning.

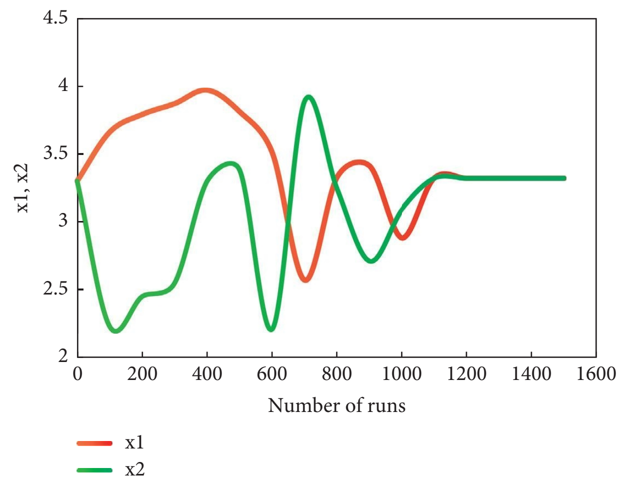

FIGURE 7: x_1, x_2 trajectory.

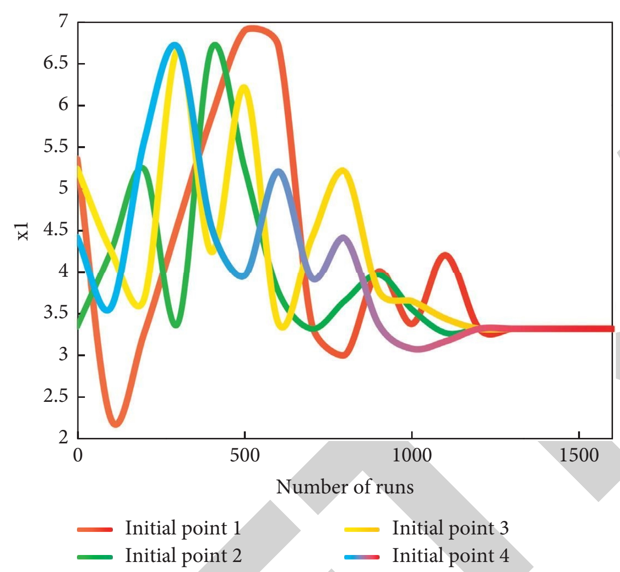

FIGURE 8: Trajectory of any four initial points x_1.

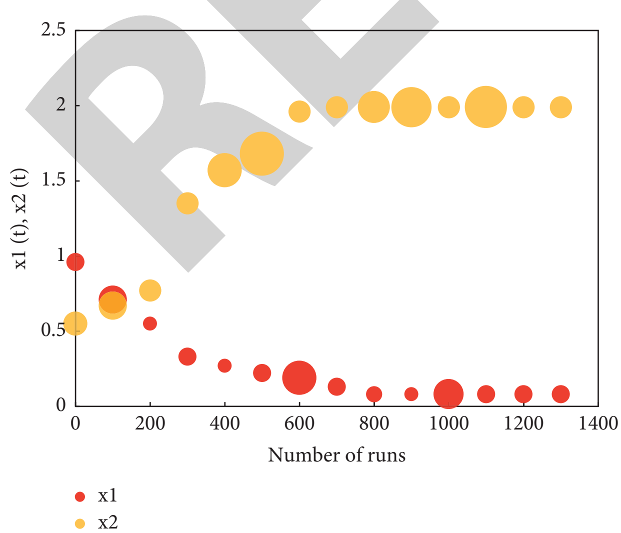

FIGURE 9: Trajectory of state vector $x(t)$ with an initial point in the feasible region.

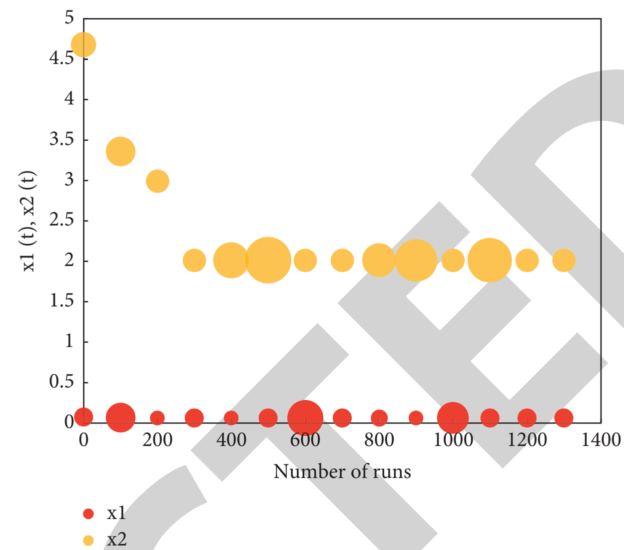

FIGURE 10: Trajectory of state vector $x(t)$ of an initial point outside the feasible region.

5. Conclusion

Students have more autonomy with personalized instruction. They will not get the corresponding effect if they are too free, so educators, particularly front-line teachers, must grasp and control it properly. Furthermore, no idea or tool can be flawless. We can make them work by constantly exploring and tapping their useful value. When incorporating the LNN development concept into university PL personalized teaching, it is important to keep in mind that students' personalized development differs. Encourage students to actively change their learning styles, pique their curiosity about learning, and develop their practical skills and creative spirit. Establish and improve the incentive and restraint mechanisms in the classroom, as well as stimulate teachers' awareness of the need to continually improve teaching and their level of expertise. The outcome of classroom evaluation is useful for postappointment teaching, professional and technical postappointment, and various awards.

Data Availability

The data used to support the findings of this study are available from the corresponding author upon request.

Conflicts of Interest

The authors do not have any possible conflicts of interest.

References

[1] W. Wang and D. Chen, "Analysis on the innovation path of ideological and political theory courses in colleges and universities in the big data era," *Ideological Education Research*, vol. 7, no. 7, 5 pages, 2017.

[2] Q. Lu and C. Li, "Synergy: the coupling development of big data and ideological and political theory courses in colleges

Hindawi
Computational Intelligence and Neuroscience
Volume 2022, Article ID 3682261, 11 pages
https://doi.org/10.1155/2022/3682261

Research Article

3D Digital Model of Folk Dance Based on Few-Shot Learning and Gesture Recognition

Ning Zhang

Shandong University of Arts, Jinan 250000, China

Correspondence should be addressed to Ning Zhang; 20155060@qlnu.edu.cn

Received 5 April 2022; Revised 27 May 2022; Accepted 30 May 2022; Published 30 June 2022

Academic Editor: Xin Ning

Folk dance is a very unique local culture in China, and dances in different regions have different characteristics. With the development of 3D digital technology and human gesture recognition technology, how to apply it in folk dance is a question worth thinking about. So, this paper recognizes and collects dance movements through human body detection and tracking technology in human gesture recognition technology. Then, this paper writes the data into the AAM model for 3D digital modeling and retains the information by integrating the manifold ordering. Finally, this paper designs a folk dance learning method combined with the Few-Shot learning method. This paper also designs a data set test experiment, an algorithm data set comparison experiment, and a target matching algorithm comparison experiment to optimize the learning method designed in this paper. The final results show that the Few-Shot learning method based on gesture recognition 3D digital modeling of folk dances designed in this paper reduces the learning time by 17% compared with the traditional folk dance learning methods. And the Few-Shot learning method designed in this paper improves the dance action score by 14% compared with the traditional learning method.

1. Introduction

Dance is an art with soul. It not only brings beautiful enjoyment to people, but also inherits rich and profound cultural connotations and is a cultural carrier. China is a multiethnic country, ethnic dance is prosperous, and the art of each ethnic group has a long history of development, and all have distinctive dance art culture. Ethnic folk dance is an important artistic carrier in the long history of China since ancient times, and it inherits and develops the cultural origin and artistic orientation of various ethnic groups.

The research on human action cognition, from simple to complex, can be summarized into three levels: mobile vision, action vision, and action vision according to the content of the action. At present, there are two main problems in studying the action vision of video people. One is that, during the recognition process, most of the action frame information in the video will be repeated, or the correlation with action recognition will be very low, the calculation will become complicated, and it will also affect the action. Second, in the process of feature selection and understanding, the main methods include fusing representational and pose-based features. However, the costumes of the stage background and dance moves can be changed, so in many cases, the motion information of the human body cannot be accurately and completely represented in the fusion of the expression information, and the static state of the human body is ignored according to the characteristics of the posture. The Few-Shot learning method based on gesture recognition 3D digital modeling of ethnic dance designed in this paper has great significance for students majoring in ethnic dance, which can allow students to learn ethnic dance very effectively.

The innovation of this paper is as follows: through the method of human body detection and tracking technology in the human body gesture recognition technology, this paper recognizes and collects the movements and human body postures of folk dances. Then, the AAM model is used for 3D digital modeling. In this paper, the information of manifold ordering is integrated and retained. Then, through the analysis, this paper designs a folk dance Few-Shot learning method. In order to optimize the Few-Shot learning method of 3D digital modeling of folk dance based on gesture recognition, this paper also designs a data set test experiment, an algorithm data set comparison experiment, and a target matching algorithm comparison experiment.

2. Related Work

Cell line screening has created extensive datasets for learning predictive markers of drug response, but these models are not easily translated to the clinic due to their diverse backgrounds and limited data. Ma J applies a recently developed technique, few-shot machine learning, to train a general neural network model in cell lines that can be adapted to new environments using few additional samples. His main research is based on medical aspects although it combines small sample methods, but it has little relevance in gesture recognition technology. Spectral prediction using deep learning [1, 2] has attracted a lot of attention in recent years. While existing deep learning methods have shown significant improvements in prediction accuracy, there is still considerable room for improvement, currently limited by differences in debris types or instrument settings. Lu Z presented an algorithmic framework to process acceleration and surface electromyography (SEMG) signals for gesture recognition. It includes a novel segmentation scheme, a score-based sensor fusion scheme, and two new features. The framework uses a Bayesian linear classifier and an improved dynamic time warping algorithm [3]. Human gesture recognition plays an important role in many human interaction applications, such as cell phones, health monitoring systems, and human-assisted robots. Electromyography (EMG) is one of the most common and intuitive methods for detecting gestures based on muscle activity. However, EMGs are often overly sensitive to environmental disturbances such as electrical noise, electromagnetic signals, and humidity. Jung P G proposed a new method for muscle activity recognition based on air pressure sensor and air bag. It detects muscle activity by measuring changes in air pressure in air sacs that contact the muscle of interest [4]. Numerous folk dance videos are uploaded online or added to Bollywood movies as situational songs. Classification of folk dance videos is critical for dance education, preservation of cultural heritage, and better customer-oriented service by music companies. Bhatt M proposed a folk dance classification framework. The framework extracts the audio signal from the video, extracts a 125-second segment from the beginning, and further divides it into a set of small segments. It computes Mel-Frequency Cepstral Coefficients (MFCC) and Linear Predictive Coding (LPC) coefficients to generate high-dimensional feature vectors. He uses Principal Component Analysis (PCA) to reduce dimensionality and uses a scale conjugate gradient neural network to classify segments [5]. Maintaining the quality of 3D data in the potentially long chain from digital scan to 3D model deployment is critical for the increasing number of advanced geometric design processes in the mesh domain, including digital fabrication. Centin M proposes an extremely general solution. It handles all previously described problems in a user-friendly way. And it is based on the original multiforward propulsion triangulation technique guided by implicit surfaces and based on the priority mechanism, which greatly reduces the frontal interference [6]. The three-dimensional (3D) revolution promises to transform archaeological practice. Among the techniques that aid in the proliferation of 3D data, photogrammetry facilitates fast and inexpensive digitization of complex subjects in field and laboratory settings. Magnani M discusses how the technique adapts and extends existing document and data visualization routines, while evaluating the opportunities it offers to solve archaeological problems and problems in innovative ways [7]. To sum up, most of the literature is about Few-Shot learning and pose recognition. Although it involves folk dance, the focus is not on the creation of its 3D digital model. So, the next focus of this paper is to combine Few-Shot learning and gesture recognition to perform 3D digital modeling of traditional folk dance.

3. Few-Shot Learning Method for 3D Digital Modeling of Folk Dance Based on Gesture Recognition Technology

3.1. Human Pose Recognition

3.1.1. Principle of Depth Map Acquisition. Since the release of Kinect [8, 9], depth cameras have received more and more attention. Depth cameras currently in the market can be divided into the following three categories according to technology: structured light-based cameras (SL), time-of-flight cameras (ToF), and stereo vision-based cameras (Stereovision).

3.1.2. Structured Light. The depth acquisition method based on structured light [10] is an active stereo vision technique. A series of known patterns are projected onto the object in turn and deformed according to the object's geometry, viewing the object from different directions. Depth information is extracted by analyzing the distortion of the observed patterns (e.g., differences from original mode), as detailed in Figure 1.

3.1.3. Flight Time. The acquisition method based on the time of flight [11] is to continuously send light pulses of different phases to the object and then use the sensor to receive the light reflected by the object to calculate the round-trip time (i.e., phase difference). A pulse of light is used to obtain the distance between the device and the object. As shown in Figure 2, the red line represents the infrared light wave transmitted to the object, and the infrared component reflected by the sensor is detected.

3.2. Human Detection and Tracking Technology. From photo and video streams, human detection techniques [12] extract people. Traditional detection technology [13, 14] and statistical principle detection technology are commonly used in human body detection technology. Human detection techniques based on statistics can be divided into two stages:

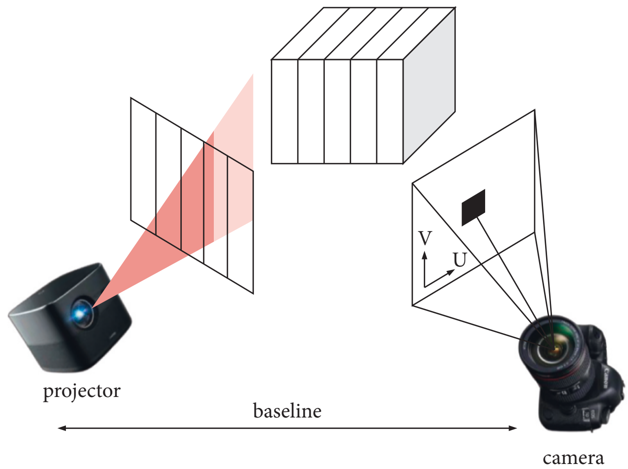

Figure 1: Principle of structured light collection.

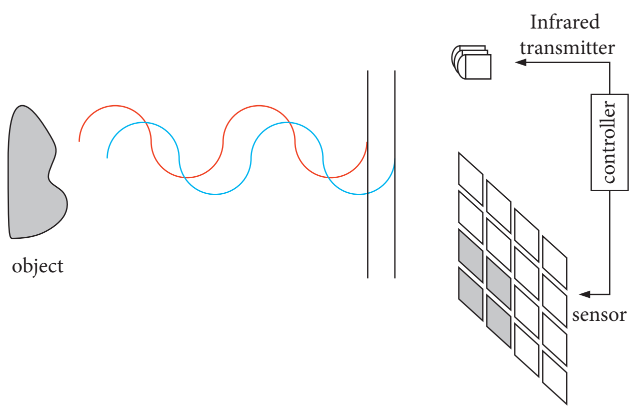

Figure 2: The principle of time-of-flight acquisition.

training and detection. Multiple detected and noise samples are collected during the training phase, positive and negative feature vectors are created, and features are created based on training and classification. The video frames to be detected are scanned one by one in the detection phase. At the corresponding position, a feature is formed, and then the person's target is determined.

So far, the human body detection technology needs to realize the detection of moving objects first, and the optical flow method and the adjacent frame difference method are general. Humans and non-humans are then classified based on the foreground, that is, the ratios and shapes of parts of the human body, or by analyzing the color of human skin against the characteristics of the image. This traditional detection method is not effective for the interference of complex external environment and external objects and is also easily affected by the noise of the underlying image features.

3.3. Moving Human Target Detection. Detecting moving objects is viewed as a spatial domain partition of video objects. Specifically, this refers to the detection and separation of regions of people moving independently in the video sequence for each frame. The most common ways of distinguishing are as follows.

Frame Difference Method [15]: the frame difference method is one of the commonly used moving object detection and segmentation methods. The basic idea is to use strong correlations between adjacent frames of an animation sequence in order to detect changes. The algorithm is characterized by high speed and high real-time performance, and changes in light have little effect on the algorithm. However, the segmentation accuracy of moving objects is not guaranteed, and large holes can be simply generated.

Background difference method [16]: the background difference method uses the difference between the current image and the background image to detect moving regions. This method is typically used for background static or slowly changing and provides the most complete characteristic data. However, due to the sensitivity to the interference of irrelevant objects in the scene, many scholars have focused on the research of background update algorithms.

Optical flow method [17]: the optical flow method is an approximate estimation of the plane projection of the two-dimensional image of the three-dimensional motion of the actual sports field scene, lens, target, etc. Its characteristic is that it can deal with the motion of the background more appropriately, but it is sensitive to noise and the calculation is very complicated.

3.4. Action Sequence Segmentation. The initial action recognition was only to recognize human movement through the computer, and later, it developed into simple actions including some simple actions, such as walking, running, and jumping. Each video frame sequence contains multiple types of actions, and each type of action contains multiple simple actions. Each simple movement consists of multiple human poses. The consistency and smoothness of various actions are due to the convergence of transition actions. In the case of dance moves, a complete dance performance includes multiple movement groups. Each action group consists of multiple simple actions, such as clips and steps, and simple actions consist of multiple basic poses such as raising hands and kicking feet. Therefore, the purpose of video frame sequence segmentation is to segment human action sequences into small actions. This will keep action sequences as short as possible but contain enough action information to identify the type of action. It is difficult to precisely find the dividing point if the human action is continuous and smooth. This is the main reason why the segmentation of video action sequences is not ideal, and only by extracting key frames for action sequence segmentation cannot achieve the shortest possible data to contain the most human action information. In fact, in most cases of video action recognition research work, we choose to manually process video, such as using manual segmentation to obtain the action sequence of the main data, or planning the action to be collected when collecting data. A whole video is divided into multiple small videos according to simple actions and recorded separately, and then the action sequences formed by all video frames are used for video action recognition].

3.5. 3D Digital Modeling

3.5.1. Motion Capture. People look forward to capturing human movements in the most intuitive and natural way. That is, the human body can move freely, and the camera can capture and record motion information just like the human eye. This is what the motion capture system based on computer vision system pursues, and its typical processing process is shown in Figure 3.

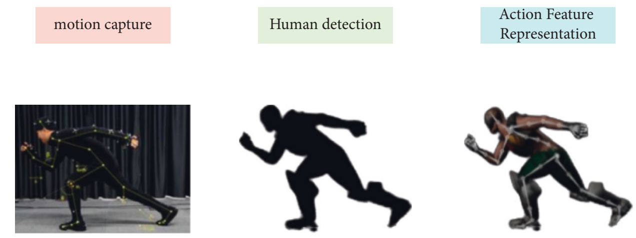

Figure 3: Motion capture system.

3.5.2. Overview of the AAM Model. Active appearance model is a feature point localization method widely used in pattern recognition and computer vision. In the process of establishing the AAM model, the global shape and texture information are fully considered, and the final AAM model can be obtained by modeling the shape and texture respectively, and by instantiating the model. In the process of image matching, the reverse composite method is adopted, which has achieved very good results in real-time and accuracy.

The establishment of AAM model is mainly divided into shape modeling, texture modeling, and the appearance model generated by combining these two models. The instantiation of the model is to map the appearance model to the corresponding shape instance through affine transformation.

The shape model of AAM refers to the ASM model. ASM is a model based on point distribution. It only trains the shape model and lacks the texture model, so the location of the feature points of the face is not accurate. The AAM model can solve this problem very well.

The general modeling object of the AAM model is a nonrigid object, such as a human face, and the main purpose is to describe the object through model parameters (feature points). Then, it can use this description to complete other tasks, such as image alignment, target location, tracking [18, 19], and recognition [20].

Because the active shape model ASM model only counts the shape model, we need to build a texture model that uses the grayscale information of the face to model, which is actually the grayscale value of the pixel. The number of pixels in the shape needs to be transformed to be consistent, and the method used is piecewise linear affine transformation. As shown in Figure 4, it is a piecewise linear affine transformation.

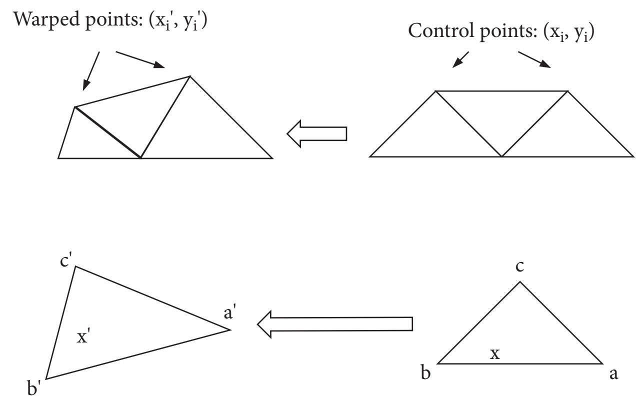

Figure 4: Piecewise affine transformation.

The calculation method of piecewise linear affine transformation [21] is shown in Figure 5:

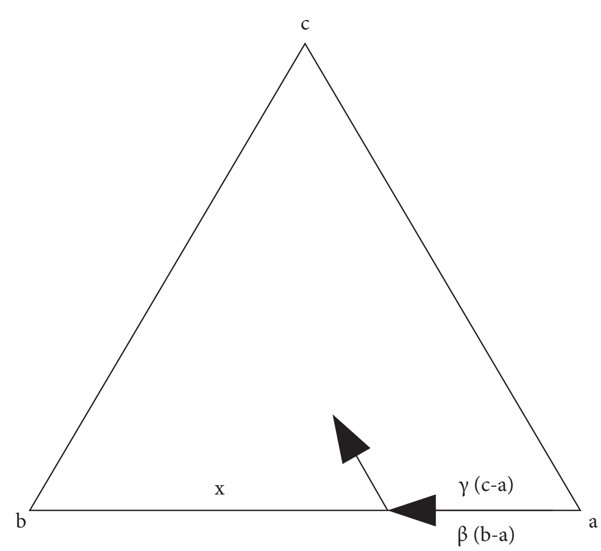

Figure 5: Calculation process of piecewise linear affine transformation.

3.5.3. Real-Time Control Technology of 3D Human Model. Controlling the human body model has always been an important direction of virtual reality research. Considering from different aspects to control the virtual human body model, the main methods are as follows: key frame control method, motion capture method, and dynamic method.

The key technology is to study the earliest method of controlling mannequins. The concept of keyframes started with the process of manga animation. In the process of making animation, the superior animator first made the main animation of the comic, which is the so-called key frame, and then the general staff completed the design and realization of the frame in the middle. After that, with the development of computer technology, the generation of the intermediate frame is gradually completed by computer. In animation, the parameters that affect the image of the screen are the parameters that affect the keyframes later.

Due to the particularity of human motion, the best way to use the human body model to express the human motion is to start directly from the motion of the human body. By using the sensor to directly capture the information of each position of the human body, use the parameters obtained by the sensor to reproduce the movement of the human body. Since the parameters obtained in this way are very real human state numbers, it is easy to restore the movement of the human body. However, motion capture technology also has many problems that restrict it to solve all practical applications.

The methods of kinematics are divided into forward kinematics and inverse kinematics. The joints of the virtual human can achieve effective movement through the forward kinematics method and the inverse kinematics method. In cis-kinematics, end-effectors (hands, feet, etc.) are used as a function of time. The position of the end effector is independent of the force or moment causing the action and is resolved by a fixed reference frame. Converting positions and velocities from joint space to Cartesian coordinates is a well-established method. The first application of cis-kinematics was a parametric keyframe animation, where the motion of the joint body was driven by interpolating the major joint angles into the cis-kinematics of the hands and feet. Advanced animators with years of experience can produce very realistic motions by means of cis-kinematics. But it is difficult for ordinary animators to produce realistic motion by setting individual keyframes in combination.

3.6. Integrated Manifold Ordering Information Retention. A new manifold supervised dimensionality reduction algorithm is proposed, that is, Integrated Manifold Ordering Information Preservation (EMRP). First, in order to solve the phenomenon of measurement concentration, we need to retain the ranking information of the samples within the class, and in order to extract the discriminative information, we need to maximize the edge distance of the samples between classes. To better understand the difference between method and other manifold supervision methods, this section adopts the PAF framework to construct EMRP.

For a certain recognition problem, K samples can be expressed by a matrix composed of fixed-length features:

$$A = [a_1, a_2, \ldots, a_K] \in R^{D\times K}. \tag{1}$$

The class of each D-dimensional feature vector $a_i \in R^D$ is labeled as

$$Z = [z_1, z_2, \ldots z_K] \in C^K. \tag{2}$$

The purpose of manifold supervised dimensionality reduction learning is to find the projection matrix $U \in R^{D\times d}$ to project the original sample A from the high-dimensional space to the low-dimensional subspace R^d, so as to obtain a concise expression:

$$B = U^S A = [b_1,, b_2, \ldots b_K] \in R^{d\times K}. \tag{3}$$

Here, $d < D$.

Under the PAF framework, we define an arbitrary sample a_i, its intraclass neighbor samples $a_{i_1}, \ldots, a_{i_{n_1}}$ and n_2 interclass neighbor samples $a_{i_1}, \ldots, a_{i_{n_2}}$ as a local block:

$$A_i = \left[a_{i_1}, a_{i_2}, \ldots, a_{i_{n_1}}, a_{i_1}, \ldots, a_{i_{n_2}}\right] \in R^{D\times\left(k_1+k_2+1\right)}. \tag{4}$$

EMRP finds the corresponding low-dimensional expression as

$$B_i = \left[b_{i_1}, b_{i_2}, \ldots, b_{i_{n_1}}, b_{i_1}, \ldots, b_{i_{n_2}}\right] \in R^{D\times\left(k_1+k_2+1\right)}. \tag{5}$$

The optimization goals on the block include the following:

(1) Retain the sorting and retention information between samples within a class;

(2) Maximize the discriminative information of between-class samples.

3.6.1. Retention of Sorting Information. The ranking information of the samples within the class is available for classification. Inspired by the LE algorithm, we define the intraclass ordering information on a local block as

$$R(b_i) = \sum_{j=1}^{n_1} b_i - b_{ij}^2 \left(w_i\right)_j. \tag{6}$$

Here, the weight factor (w_i) is defined as

$$(w_i)_j = \begin{cases} xp\left(-\dfrac{a_i - a_{ij}^2}{s}\right), & e \text{ if } a_{ij} \in K_{n_1}(a_i); \\ 0 & \text{otherwise} \end{cases}. \tag{7}$$

According to the PAF framework, we can deduce (6) as follows:

$$R(b_i) = \operatorname{tr}\left(B_{R(i)} L_{R(i)} B_{R(i)}^S\right). \tag{8}$$

Here,

$$L_{R(i)} = \begin{bmatrix} -e_{n_1}^S \\ I_{n_1} \end{bmatrix} \operatorname{diag}(w_i)\left[-e_{n_1} \ \ I_{n_1}\right],$$
$$e_{n_1} = \left[\overbrace{1, \ldots, 1}^{n_1}\right]^S, I_{n_1} = \operatorname{diag}\left[\overbrace{1, \ldots, 1}^{n_1}\right], B_{R(i)} = \left[b_i, b_{i_1}, \ldots, b_{i_{n_1}}\right]. \tag{9}$$

3.6.2. Maximize Identification Information. For popular supervised learning, discriminative information plays a crucial role. As far as the EMRP algorithm is concerned, we consider that the purpose of extracting discriminative information is achieved by maximizing the distance sum of the samples between b_i and n_2 classes, namely,

$$D(b_i) = \sum_{p=1}^{n_2} b_i - b_{i_p}^2 \left(v_i\right)_j. \tag{10}$$

The definition of the weight factor (v_i) here considers the factor of removing the ranking information between classes, namely,

$$(v_i)_j = \begin{cases} 1, & \text{if } a_{ij} \in K_{n_1}(a_i); \\ 0 & \text{otherwise} \end{cases}. \tag{11}$$

Under the framework of PAF, we can further derive (10) as

$$D(b_i) = \operatorname{tr}\left(B_{D(i)} L_{D(i)} B_{D(i)}^S\right). \tag{12}$$

Here,

$$\begin{aligned} L_{D(i)} &= \begin{bmatrix} -e_{n_2}^S \\ I_{n_2} \end{bmatrix} \operatorname{diag}(v_i)\left[-e_{n_2}\ \ I_{n_2}\right], \\ e_{n_2} &= [\overbrace{1, \ldots, 1}^{n_2}]^S, I_{n_2} = \operatorname{diag}[\overbrace{1, \ldots, 1}^{n_2}], B_{D(i)} = \left[b_i, b_{i_1}, \ldots, b_{i_{n_2}}\right]. \end{aligned} \tag{13}$$

Therefore, we can get the optimization objective function on the local block:

$$\arg\min\left(\sum_{j=1}^{n_1} b_i - b_{ij}{}^2 (w_i)_j - \gamma \sum_{p=1}^{n_2} b_i - b_{i_p}{}^2 (v_i)_j\right). \tag{14}$$

However, different hyperparameters (such as n_1 in (6) and n_2 in (10)) correspond to manifold with different geometric information, which can seriously affect the final recognition accuracy. In EMPR algorithm, the hyperparameters s, n_1, and n_2 that affect the objective function are difficult to choose optimal settings. Therefore, an automatic manifold estimation method is valuable for solving this problem.

3.7. Folk Dance. China is a multiethnic country. Every nation has a distinct national culture. Ethnic folk dance originates from life labor and is a dance that people dance to entertain themselves. People express their life through dance and show their unique national charm. The types of Chinese folk dances are shown in Figure 6.

With the changes of the times, ethnic folk dance has gradually evolved into a dance form with its own national characteristics and advancing with the times in the new era on the premise of retaining its original characteristics. It has also gradually expanded from a self-entertainment model to a professional and large-scale system. It is a dance course processed and refined by professional dancers. It is a dance work that expresses ideas in combination with life. The stage sublimation of the national folk dance drama flourished.

Folk dance is the art form of a people who have lived in a specific geographical location for a long time and have developed unique folk customs, religious beliefs, and agricultural civilization. It gradually developed a unique aesthetic taste when combined with the unique natural environment. Ethnic dance can be described as an important cultural carrier that can pass down ancient Chinese folk culture and serves as an external manifestation of national cohesion. Because each ethnic group has its own unique history, rich cultural connotation, and independent national aesthetic habits, each ethnic group has its own dance art language. Folk dance, as a result, has a distinct national character, a limited regional character, and a high level of "self-entertainment."

Ethnic dance has a long history and is created by workers of all ethnic groups in the context of long-term production practices and life changes. They use innovative dance techniques to convey national history, religious beliefs, life lessons, and even myths and stories. With so many cultural contents, the folk dance is destined to have historical and cultural value, as it is the spiritual wealth left by the forefathers. We can better inherit folk dance by learning it, and we can bring out the functions of cultural inheritance, cultural accumulation, cultural exchange, and cultural innovation of folk dance by learning it.

4. Algorithm Data Set Comparison Test Experiment

4.1. Dataset Test Experiment. Some images are randomly taken from a subset of the source data and test set LFW, it may be difficult to distinguish where they come from, and the image distributions of the source and target domains are similar. Table 1 shows experimental results on a subset of the test set LFW dataset.

It can be observed that the model learned in this paper in the source domain is directly tested in the target domain without transfer learning. The results are unsatisfactory, using the cosine and LRA methods to measure the similarity between faces with the lowest results of 82.01% and 85.23%, respectively.

The image distributions of the source and target domains are quite different. Considering the variation of expression, illumination, and occlusion, restricted parameter learning method RPL shows its superiority in the FERET dataset.

Two 2048-dimensional representative feature vectors are concatenated to a 4096-dimensional feature vector without principal component analysis (PCA) dimensionality reduction for face recognition. The similarity between features is then measured with the LRA method. The results of the RPL method in this paper on the two databases and the comparison results of other methods and other recent works are shown in Table 2.

All in all, using the restricted parameter learning (RPL) deep transfer learning method, the learning space of parameters in the target domain is constrained. By adjusting the source domain knowledge of the scarce target domain samples, overfitting and parameter structure damage can be prevented, and ideal results can be obtained in the same and different distributions. Unlike other state-of-the-art techniques, method can adjust knowledge from the source domain to the target domain offline; that is, it does not require training on both source and target data simultaneously. Therefore, the RPL method in this paper can be easily applied to many scenarios. The results validate the effectiveness of RPL, which uses very deep convolutional networks fine-tuned with sample knowledge in the target domain.

4.2. Algorithm Dataset Comparison Experiment. Figure 7 shows the best average recognition rate of the test set for the six algorithms under different training samples on the

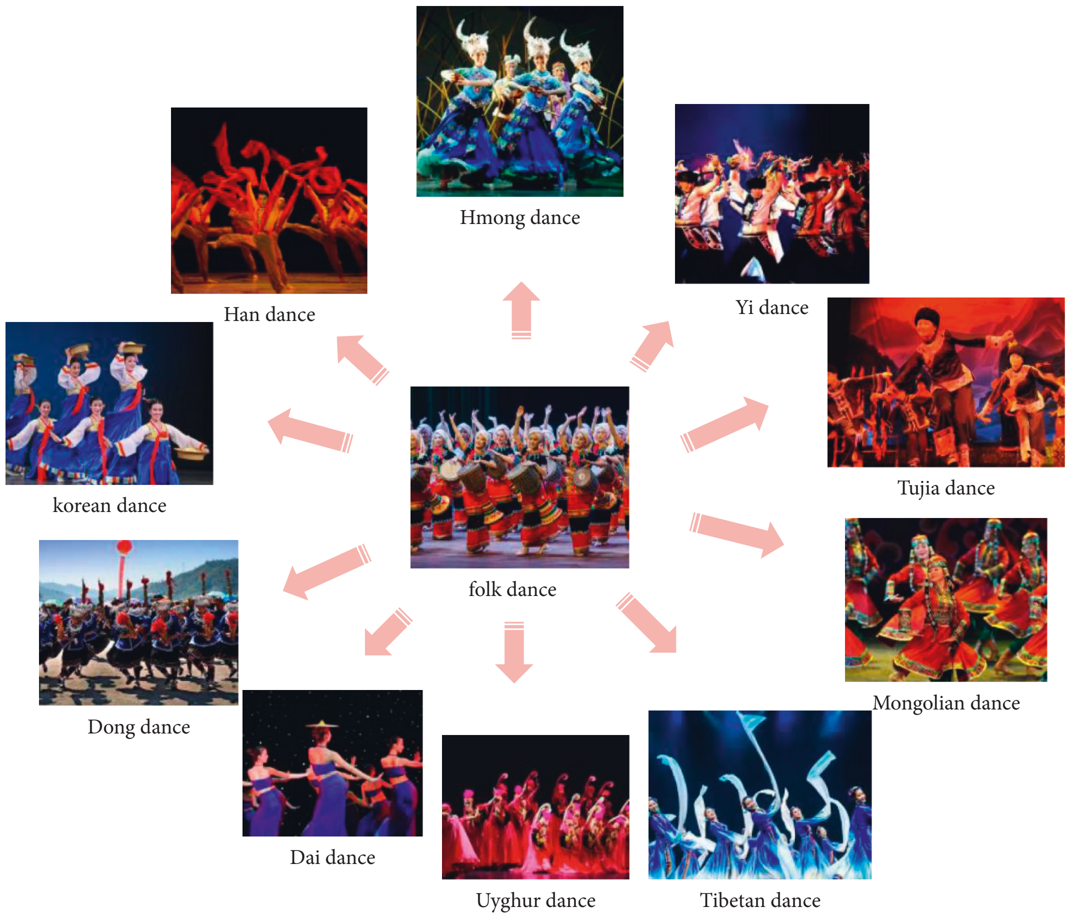

Figure 6: Types of Chinese folk dances.

Table 1: Test results on LFW dataset.

methods	ACC (%)	Methods	ACC (%)
Ws + cos	82.01	Ws + LRA	85.23
Pure + cos	84.52	Pure + L RA	87.87
RPL (L1) + cos	85.98	RPL (L1) + L/RA	88.91
RPL (L2) + cos	88.70	RPL (L2) + LRA	89.33

Table 2: Results of multiregion feature fusion.

Feret	fb	fc	dup1	dup2	Ave
G-LQP	99.9	100	93.2	91	96.03
LGBP-LGXP	99	99	94	93	96.25
sPOM + POD	99.7	100	94.9	94	97.15
GOM	99.9	100	95.7	93.1	97.18
PCANet2	99.58	100	95.43	94.02	97.26

NMHA-TP dataset (including two cases of $p = 20$ and $p = 30$).

It can be seen that, compared with several other algorithms, the EMPR algorithm can obtain the best classification performance on the NMHA-TP dataset.

Figure 8 shows the best average recognition rate of the six algorithms in the test set under different training samples on the NMHA-WP dataset (including two cases of $p = 20$ and $p = 30$).

It can be seen that, compared with several other algorithms, the EMPR algorithm can obtain the best classification performance on the NMHA-WP dataset.

Table 3 presents the best average recognition rates and corresponding dimensions of the six algorithms on the NMHA-TP-WP dataset.

It can be seen that, compared with several other algorithms, the EMPR algorithm can obtain the best classification performance on the NMHA-TP-WP dataset.

In addition, Table 4 shows the comparison results of the six algorithms and the RPDA algorithm on the SCUTNAA dataset. It can be seen that the EMRP algorithm has a certain advantage in the recognition rate compared with the RPDA algorithm. In addition, the experimental results of EMRP-81 and EMRP-9 show that more candidate matrices are helpful for the learning of the essential manifold.

The main conclusions of the EMRP-related experiments can be summarized as follows:

(1) Algorithms such as EMRP, RPDA, LSDA, and MFA are suitable for human action recognition based on acceleration sensor due to the intuitive consideration of the geometric information on the local block. The EMRP and RPDA algorithms perform better because of considering the balance between the ranking information of the intraclass neighbor samples and the neighbor ranking information of the interclass samples.

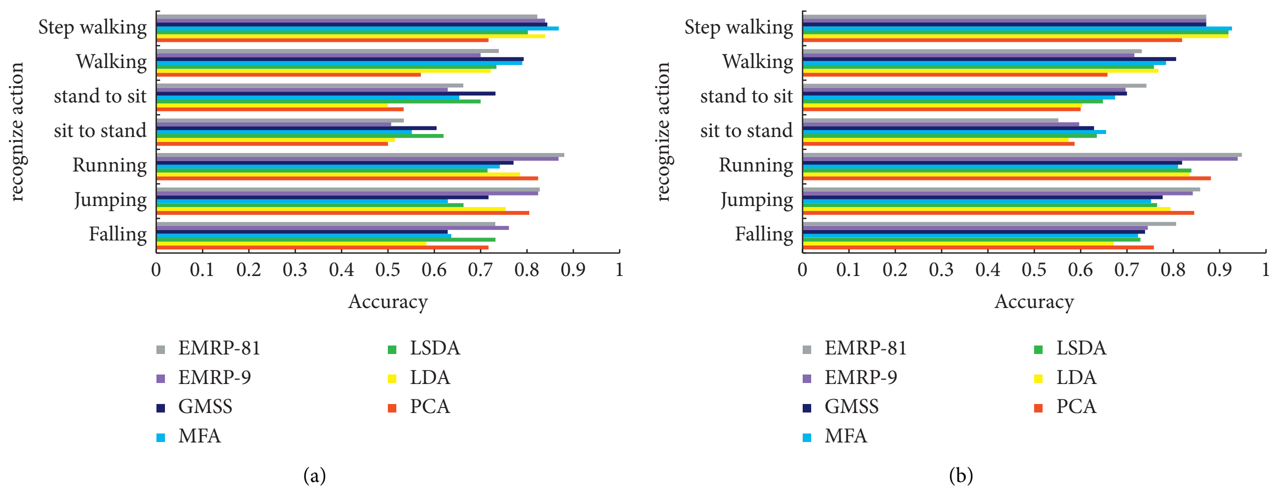

Figure 7: Best Average Recognition Rate of 6 Algorithms on NMHA-TP Dataset (a) $p = 20$ (b) $p = 30$.

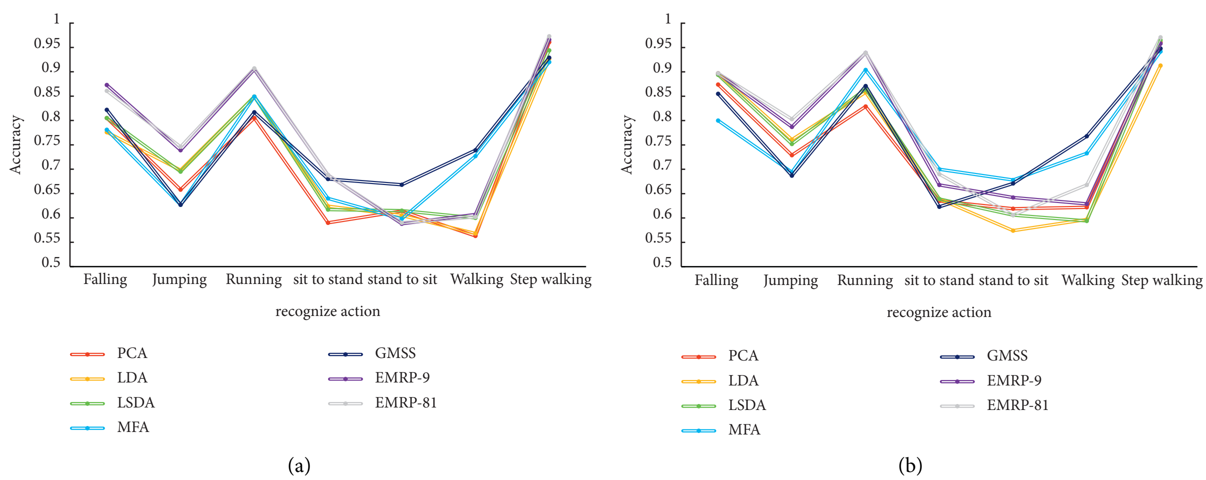

Figure 8: The best average recognition rate of the six algorithms on the NMHA-WP dataset (a) $p = 20$ (b) $p = 30$.

Table 3: The best average recognition rate of the six algorithms on the NMHA-TP-WP dataset.

algorithm	PCA	LDA	L SDA	MFA	GMSS	EMRP-9	EMRP-81
Falling	0.770	0.706	0.771	0.671	0.692	0.739	0.785
Jumping	0.849	0.860	0.850	0.795	0.821	0.910	0.911
Running	0.901	0.876	0.868	0.898	0.898	0.953	0.955
Sit to stand	0.588	0.584	0.558	0.611	0.485	0.606	0.585
Stand to sit	0.619	0.608	0.658	0.671	0.440	0.702	0.695
Walking	0.682	0.663	0.706	0.763	0.768	0.768	0.792
Step walking	0.859	0.882	0.965	0.932	0.950	0.924	0.937

(2) In the human action recognition test based on the acceleration sensor of mobile phone, EMRP-81 significantly improves the recognition accuracy and obtains the best average recognition rate. All of these demonstrate the robustness and effectiveness of the EMRP algorithm in the human action classification task. This also proves that the EMRP-based algorithm can learn a linear combination of candidate registration matrices to obtain better system performance.

4.3. Comparison Experiment of Target Matching Algorithms. The VOT dataset and six representative image sequences from the TempleColor128 dataset are used to evaluate the algorithm in this paper. The Juice image sequence is specifically included. The target has a slight spatial transformation, while the background has a small spatial transformation. The background in this data changes dramatically, the target is scaled and rotated, and there is also similar target interference. There are severe illumination changes in this data, as well as deformation in the target itself, in the motorcycle image sequence. The target in this data has scale, illumination, and certain morphological transformations, as seen in a helicopter image sequence. The shape of the target changes, the background changes slightly,

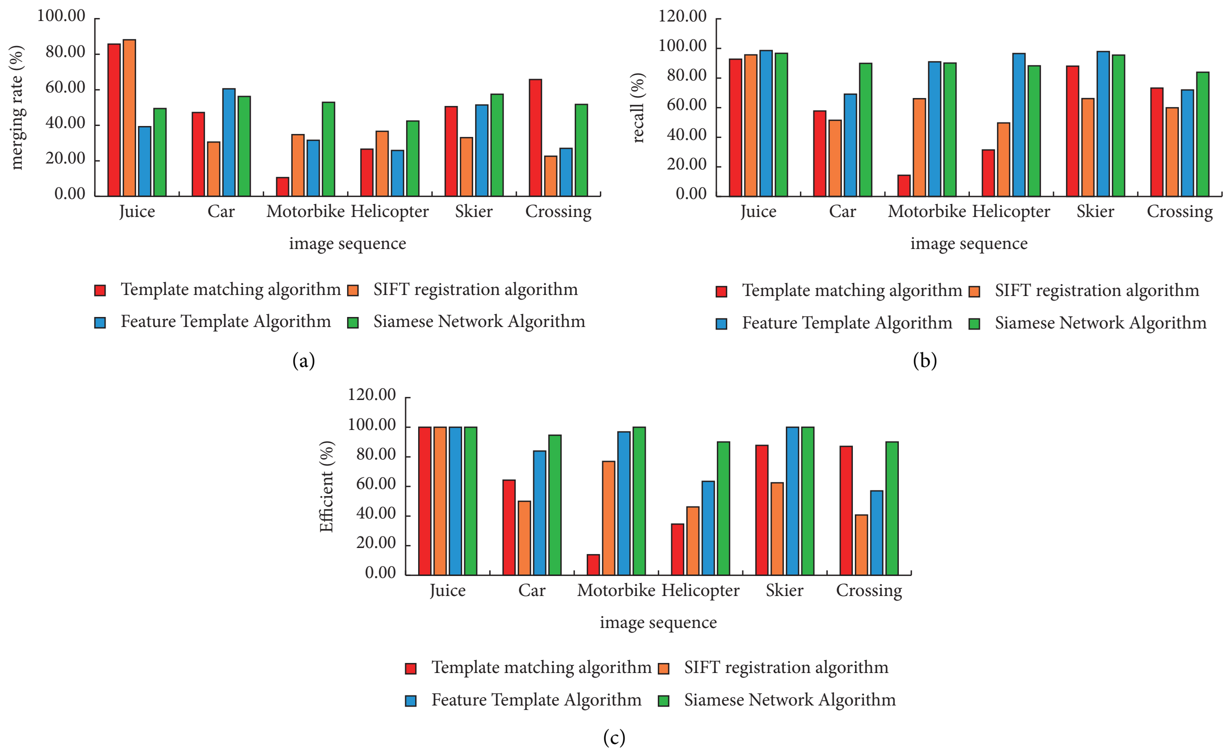

Figure 9: Comparison of experimental results of target matching algorithms. (a) Cross-comparison experimental results. (b) Recall experiment results. (c) Effectiveness experimental results.

and there is partial occlusion in this data from a skier image sequence. In this data, there are similar targets, the target has large deformation and scale transformation, and the background also has transformation. After manually culling the images whose targets were completely occluded and difficult to identify in the image sequence, about 10 images were selected as training data, and other images were used as test data in the experiment. The intersection ratio, recall, and efficiency of the four algorithms on six groups of image sequences are shown in Figure 9.

According to the experimental data, it can be seen that the traditional algorithm only has good results in some scenarios, while the method based on machine learning can take into account most scenarios.

The grayscale template matching based on the correlation coefficient has a good effect on simple scenes such as Juice image sequences and also has a good effect on scenes with simple backgrounds and small target deformation, such as Skier and Crossing image sequences. However, the target matching performance of these scenes depends on the influence of template selection, which is not very stable. Only when the template is selected properly, there is a better matching effect. The overall performance is not very stable.

The algorithm based on SIFT registration has better performance in simple scenes such as Juice image sequences, but when the target is deformed, or the imaging quality is poor, the matching effect is obviously degraded. The overall performance is poor.

The algorithm based on feature template also performs well in simple scenes, but when the scene is complex, the performance deteriorates, and the algorithm's intersection and union are relatively low, and the matching accuracy is poor. And the overall performance is poor.

5. Comparative Analysis of Few-Shot Learning for 3D Digital Modeling of Folk Dance Based on Gesture Recognition

The algorithm data set is analyzed through experiments, and finally the Few-Shot learning method for 3D digital modeling of folk dance based on gesture recognition designed in this paper is optimized. In order to verify how this Few-Shot method is different from traditional learning methods for folk dance learning, this paper designs a set of comparative experiments. In this paper, 20 students majoring in folk dance are divided into two groups. One group uses the Few-Shot learning method designed in this paper based on the three-dimensional digital modeling of folk dance based on gesture recognition. The other group used traditional folk dance learning methods and then judged their learning efficiency based on the learning time and movement scores of the two groups of students. The experimental data is shown in Figure 10.

As can be seen from Figure 10, the time for students majoring in ethnic dance to learn the Few-Shot learning method based on gesture recognition 3D digital modeling of ethnic dance designed in this paper is only 8.93 minutes for the same dance. The time used in the traditional folk dance learning method is 10.77 minutes. Compared with the traditional learning method, the Few-Shot learning method

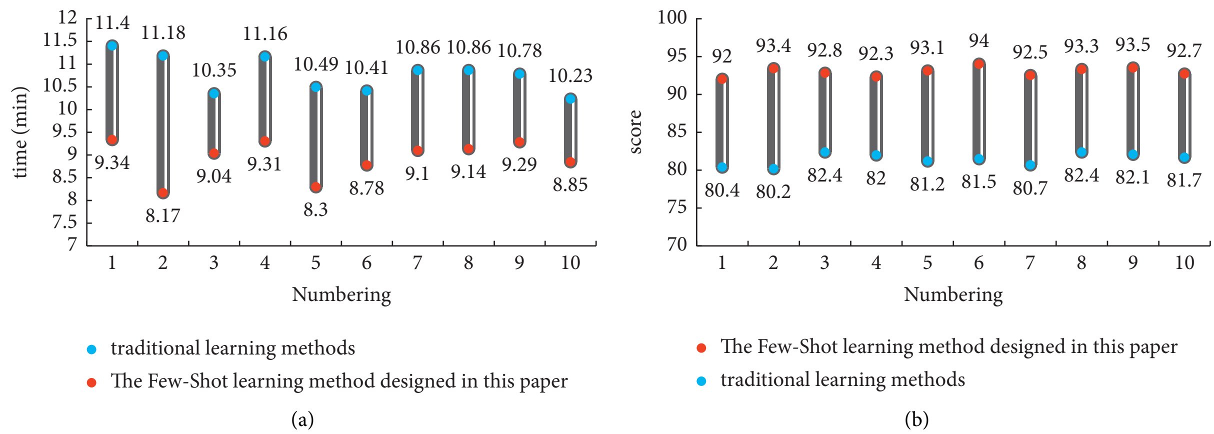

FIGURE 10: Comparison of learning efficiency between the few-shot learning method designed in this paper and the traditional learning method. (a) Study time comparison. (b) Action score comparison.

TABLE 4: Comparison of RPDA algorithm and 6 algorithms on SCUT NAA dataset.

number Of training samples					$P = 20$			
Algorithm	PCA	LDA	LSDA	MFA	GMSS	RPDA	EMRP-9	EMRP-81
Average accuracy	0.732	0.736	0.751	0.755	0.767	0.773	0.778	0.780
Dimensionality reduction	(30)	(8)	(7)	(9)	(5)	(27)	(27)	(28)

based on gesture recognition 3D digital modeling of folk dance designed in this paper reduces the learning time by 17%. And the dance action score of the Few-Shot learning method designed in this paper reaches 92.96 points, while the traditional learning method is only 81.46 points. It can be seen that the Few-Shot learning method designed in this paper is 14% higher than the traditional learning method. To sum up, the Few-Shot learning method based on gesture recognition and three-dimensional digital modeling of ethnic dance designed in this paper can effectively improve the learning efficiency of ethnic dance students majoring in ethnic dance.

6. Conclusion

This paper mainly studies the 3D digital model of folk dance based on Few-Shot learning and gesture recognition. Therefore, this paper combines the human body detection and tracking technology of human body posture recognition technology to collect the movement posture and human body posture data of folk dance. Then, this paper uses the AAM model to perform 3D digital modeling of the collected action poses. Then, this paper retains by integrating the manifold ordering information and finally designs a folk dance learning method combined with the Few-Shot learning method. This paper also designs a data set test experiment and an algorithm data set comparison experiment to optimize the algorithm test and data set design. Then, this paper carries out the final optimization according to the experimental results of the target matching algorithm comparison experiment. This paper designs a Few-Shot learning method for 3D digital modeling of folk dance based on gesture recognition. This method can scientifically and effectively improve the learning efficiency and performance of students majoring in ethnic dance.

Data Availability

The data used to support the findings of this study are available from the corresponding author upon request.

Conflicts of Interest

The author does not have any possible conflicts of interest.

References

[1] X. Jin, J. Zhang, J. Kong, T. Su, and Y. Bai, “A reversible automatic selection normalization (RASN) deep network for predicting in the smart agriculture system,” *Agronomy*, vol. 12, no. 3, p. 591, 2022.

[2] Z. Huang, Y. Liu, C. Zhan, M. Lin, W. Cai, and Y. Chen, “A novel group recommendation model with two-stage deep learning,” *IEEE Transactions on Systems, Man, and Cybernetics: Systems*, pp. 1–12, 2021.

[3] Z. Lu, X. Chen, Q. Li, X. Zhang, and P. Zhou, “A hand gesture recognition framework and wearable gesture-based interaction prototype for mobile devices,” *IEEE Transactions on Human-Machine Systems*, vol. 44, no. 2, pp. 293–299, 2014.

[4] P. G. Jung, G. Lim, S. Kim, and K. Kong, “A wearable gesture recognition device for detecting muscular activities based on air-pressure sensors,” *IEEE Transactions on Industrial Informatics*, vol. 11, no. 2, pp. 485–494, 2017.

[5] M. Bhatt and T. Patalia, “Neural network based Indian folk dance song classification using MFCC and LPC,” *International Journal of Intelligent Engineering and Systems*, vol. 10, no. 3, pp. 173–183, 2017.

[6] M. Centin and A. Signoroni, "Advancing mesh completion for digital modeling and manufacturing," *Computer Aided Geometric Design*, vol. 62, no. MAY, pp. 73–90, 2018.
[7] M. Magnani, M. Douglass, W. Schroder, J. Reeves, and D. R. Braun, "The digital revolution to come: photogrammetry in archaeological practice," *American Antiquity*, vol. 85, no. 4, pp. 1–24, 2020.
[8] A. Joncheere, "Kalbeliya dance from Rajasthan: invented gypsy form or traditional snake charmers' folk dance?" *Dance Research Journal*, vol. 49, no. 1, pp. 37–54, 2017.
[9] L. N. Wang, L. J. Zhao, L. Yu et al., "[Digital modeling and analysis of the applicability of backward rotation method in lumbar kyphoplasty with unilateral puncture]," *Zhongguo gu shang = China journal of orthopaedics and traumatology*, vol. 32, no. 6, pp. 524–530, 2019.
[10] L. A. Mejia and H. D. Arango, "Primary generators: the influence of digital modeling environments in the creative design process," *International Journal of Virtual and Augmented Reality*, vol. 3, no. 2, pp. 11–22, 2019.
[11] R. Kaluri and P. Ch, "An enhanced framework for sign gesture recognition using hidden markov model and adaptive histogram technique," *International Journal of Intelligent Engineering and Systems*, vol. 10, no. 3, pp. 11–19, 2017.
[12] M. Gao, W. Cai, and R. Liu, "AGTH-Net: attention-based graph convolution-guided third-order hourglass network for sports video classification," *Journal of Healthcare Engineering*, vol. 2021, pp. 1–10, 2021.
[13] J. Kong, H. Wang, C. Yang, X. Jin, M. Zuo, and X Zhang, "A spatial feature-enhanced attention neural network with high-order pooling representation for application in pest and disease recognition," *Agriculture*, vol. 12, no. 4, p. 500, 2022.
[14] M. Zhao, A. Jha, Q. Liu et al., "Faster Mean-shift: GPU-accelerated clustering for cosine embedding-based cell segmentation and tracking," *Medical Image Analysis*, vol. 71, Article ID 102048, 2021.
[15] G. Szcs and M. Németh, "Double-view matching network for few-shot learning to classify covid-19 in X-ray images," *Infocommunications Journal*, vol. 13, no. 1, pp. 26–34, 2021.
[16] I. L. Beilin, "The development of digital modeling in the theory of regional economics based on data on industrial petrochemical types of activity," *Russian Journal of Industrial Economics*, vol. 13, no. 1, pp. 35–47, 2020.
[17] S. Frommel, M. Gaiani, and S. Garagnani, "3-D Digital Modeling and Giuliano da Sangallo's Designs for Santa Maria delle Carceri in Prato," *Journal of the Society of Architectural Historians*, vol. 80, no. 1, pp. 30–47, 2021.
[18] J. Zhang, W. Feng, T. Yuan, J. Wang, and A. K. Sangaiah, "SCSTCF: spatial-channel selection and temporal regularized correlation filters for visual tracking," *Applied Soft Computing*, vol. 118, Article ID 108485, 2022.
[19] J. Zhang, J. Sun, J. Wang, and X.-G. Yue, "Visual object tracking based on residual network and cascaded correlation filters," *Journal of Ambient Intelligence and Humanized Computing*, vol. 12, no. 8, pp. 8427–8440, 2021.
[20] Y. Wang, Y. Chen, and R. Liu, "Aircraft Image Recognition Network Based on Hybrid Attention Mechanism," *Computational Intelligence and Neuroscience*, Article ID 4189500, 2022.
[21] G. Sawadwuthikul, T. Tothong, T. Lodkaew et al., "Visual goal human-robot communication framework with few-shot learning: a case study in robot waiter system," *IEEE Transactions on Industrial Informatics*, vol. 18, no. 3, pp. 1883–1891, 2022.

Hindawi
Computational Intelligence and Neuroscience
Volume 2022, Article ID 4740234, 9 pages
https://doi.org/10.1155/2022/4740234

Research Article

Aesthetic Characteristics of Dance Based on Few-Shot Learning and Neural Networks

Dixin Qu

Shandong University (Weihai), Weihai 264200, China

Correspondence should be addressed to Dixin Qu; 201269800019@sdu.edu.cn

Received 5 May 2022; Revised 7 June 2022; Accepted 8 June 2022; Published 29 June 2022

Academic Editor: Xin Ning

Dance is constantly discovering truth, goodness, and beauty in human social life, spreading truth, goodness, and beauty, and fully expressing the artistic pursuit of dance beauty. It shapes different dance images, expresses the aesthetic consciousness and feelings of dance, and resonates with the audience to meet their aesthetic needs through various forms of movement. Because the RBF neural network model is good at approximating functions, many researchers have begun to use the RBNN approximation model for engineering design. Due to the limited dance data available for research, this paper uses radial basis function neural network model to study the aesthetic characteristics of dance in the context of few-shot learning. When the time index reaches 50, the average ratio of the L-MBP algorithm is 33.4 percent, 32.5 percent for the RBNN algorithm, and 46.3 percent for this method. As can be seen, this method has the highest ratio of the three algorithms, giving it a distinct advantage in terms of dance aesthetics. As a result, this paper establishes a neural network model, trains and simulates the network model, studies and analyzes the influence of changes in influencing factors on the aesthetic characteristics of dance, and provides a new idea for the prediction of the aesthetic characteristics of dance and a reference for optimizing the design of the aesthetic system of dance using the prediction ability of radial basis function neural networks.

1. Introduction

Dance existed as a form of culture long before it was considered aesthetically pleasing. The evolution of cultural dance to aesthetic dance has become a historical necessity as time passes, productivity improves, and class emerges. The emergence of dance with aesthetic significance not only makes dance an art in the strict sense but also gradually forms a dance art discipline, and then produces a new discipline—dance aesthetics. Dance art incisively and vividly seeks out truth, goodness, and beauty in human social life; spreads truth, goodness, and beauty; and embodies the artistic pursuit of dance beauty. It shapes various dance images, expresses the aesthetic consciousness and aesthetic emotion of dance through various action forms, resonates with the audience, and meets their aesthetic needs through various action forms [1]. Don't you know that when you dance with beautiful eyes, a slim waist, and graceful hands and feet, your beautiful posture of expressing feelings and ideas is like flowing sculptures, shocking, and fascinating enough to arouse the viewer's resonance and reverie? Is n't this a one-of-a-kind dance language? The artistic effect of "silence is better than sound at this time" can often be obtained by the visual beauty of the image without saying anything. Dance, in contrast to Chinese national folk dance, transcends cultural boundaries. The inheritance and promotion of Chinese traditional culture, Chinese national temperament, and Chinese classical spirit are primarily reflected in its aesthetic characteristics. Dance beauty is a pleasurable psychological state in which people use their vision, hearing, and other senses to perceive, comprehend, and taste the dance image and spiritual needs. Only those with the ability to appreciate things can generate "aesthetic feelings" in the realm of sound. Aesthetics must also have a certain amount of imagination. Dance, in addition to vertical absorption, horizontally absorbs some characteristics of other art forms, and dance itself is constantly changing and developing, resulting in new developments in the dance inheritance, but it never changes, and the inheritance of Chinese national temperament and dance spirit is always the main vein of dance [2]. The more the life experience is, particularly life experience related to specific works, the more conducive to art appreciation one has. As far as dance appreciation is concerned, the appreciator should also know something about the characteristics, types, styles, and different styles of dance art, which is conducive to the in-depth feeling and comprehension of dance works. Being able to correctly discover, recognize, and evaluate beauty is the basic aesthetic ability to learn dance art. Therefore, in dance teaching, the study of dance aesthetic characteristics is closely related to improving students' aesthetic ability.

Because the RBF neural network model [3] is good at approximating functions, many researchers have begun to use the RBNN approximation model for engineering design. The radial basis function neural network is a feedforward neural network with only one hidden layer that can realize the hidden layer's nonlinear mapping and the output layer's linear mapping. The action function of the radial basis function neural network's hidden layer node generates a local response to the input signal. The hidden layer node produces a large output when the input signal is close to the basis function's central range. According to the RBF neural network model, the RBF neural network's training algorithm is investigated, and the K-means clustering algorithm is used to determine the hidden layer node center, hidden layer node width, and output weight of the network, as well as the network model framework [4]. The impact of the number of hidden layer nodes and distribution coefficient on the accuracy of the RBF neural network model is investigated using an empirical formula and a comparative test method, and the two parameters are finally determined to complete the RBF neural network model's establishment.

The dance focuses on "quietness," "harmony" is the most important, the coordination between breathing and body is emphasized, the harmony and unity between every detail is emphasized, and a kind of harmony and coordination is emphasized in the dance movements. This kind of adduction and harmony of dance comes from the Chinese character, characteristics of "harmony is the most important thing" and "the beauty of neutralization," and it is a highlight of the Chinese nation's aesthetic psychology. Its round, curved, twisted, and inclined posture and circular track of movements can well reflect the Chinese philosophical spirit of repeated cycles and constant renewal [5]. Therefore, with the help of the prediction ability of radial basis function neural network, this paper establishes a neural network model, trains and simulates the network model, studies and analyzes the influence of the changes of influencing factors on the aesthetic characteristics of dance, and provides a new idea for the prediction of the aesthetic characteristics of dance and a reference for optimizing the design of the aesthetic system of dance. Under the radial basis function neural network model, the aesthetic characteristics of dance are mainly embodied in original ecology, where original ecology is relative to performance and folk, and folk is relative to the former court [6]. Folk of dance refers to the folk customs and nationality reflected from dance movements and dance images, and the nationality of dance refers to the common national style, temperament, and spirit reflected from dance movements and dance images. Folk is the foundation of nationality, and nationality is folk. The innovations in this paper are as follows:

(1) This paper constructs the model diagram of radial basis function neural network. RBF neural network model reflects the nonlinear evolution relationship of the overall structure through repeated learning of sample data, so as to predict the unknown data. Therefore, the training sample data are very important for the fitting accuracy and generalization ability of neural network.

(2) The aesthetic characteristics of dance are tested and analyzed. When the time index reaches 50, the average proportion of L-MBP algorithm is 33.4%, the average proportion of RBNN algorithm is 32.5%, and the average proportion of this method is 46.3%. It can be seen that the proportion of this method in the three algorithms is the highest, so it plays a greater advantage in the aesthetic characteristics of dance.

The overall structure of this paper consists of five parts. The first section introduces the background and significance of dance aesthetic characteristics, and then introduces the main work of this paper. The second section mainly introduces the research status of dance aesthetic characteristics at home and abroad. The third section introduces the radial basis function neural network model. The fourth section introduces the aesthetic characteristics of dance and the analysis of the experimental part. The fifth chapter is the summary of the full text.

2. Research Status of Aesthetic Characteristics of Dance at Home and Abroad

So put forward that when people's inner feelings reach the point where language and words cannot express them, they cannot help dancing and expressing their inner feelings. This kind of progressive emotional expression from low to high just reflects that dance, as a "silent art," has surpassed such vocal languages as poetry and music, and has become the highest level of emotional expression, reflecting the strong lyrical aesthetic characteristics of dance art [7]. Habron and Merwe put forward that dance images are mainly figures, animal and plant images, or morphological objects created by dancers through their movements. Image is an important aesthetic feature of dance [8]. Christmas in dance teaching, capturing vivid dance images, is the premise and foundation of dance learning [9]. K. Skjoldager-Nielsen and D. Skjoldager-Nielsen put forward that this dance feature is also the inheritance of ancient Chinese dance. In ancient Chinese dance, people like to get close to the Earth or the site, and the dancers are mainly focused on gaining momentum. Generally, they rarely raise their feet, but move their feet slowly along the intended geometric figure, which is in favor of the ever-changing movements of arms and hands [10]. Lustig and Tan put forward that in dance teaching, it is important for students to understand and master the aesthetic characteristics and types of dance lyricism to improve their aesthetic ability [11]. Anderson put forward that accumulating rich life experience and artistic practice experience, going deep into the folk to carry out art gathering activities, being good at discovering and digging beauty from life, and absorbing rich nutrition from the "root" of dance art are important methods to capture dance images and enhance aesthetic ability, so as to better serve the shaping of dance images [12]. A. Wang and C. Wang proposed that many original ecological folk dances are formed within the same nation due to different branches, geographical distribution, economic status, and cultural development. These seemingly different original ecological folk dances have the nationality of the same nation and reflect the same aesthetic psychology and aesthetic habits [13]. Schuh proposed that the shape of dance occupies space and the melody of music occupies time. The audience's appreciation of dance must first be accepted through vision. Visibility has become a feature of dance aesthetics [14]. Jürgens puts forward that the aesthetic characteristics of ethnic minority dance are mainly embodied in performance, nationality, and folk. Both academic folk dance and ethnic minority dance have the characteristics of performance, nationality, and folk. Their dance movements are derived from the dance movements of original folk dance, which have been processed, refined, integrated, and transcended [15]. Adewale proposed that the aesthetic feature of dance is lyricism. Dance is good at lyricism and bad at narration. Only when poetry, song, and music are not enough to express feelings can we "dance with hands and dance with feet" [16].

Based on the above analysis, this paper puts forward a radial basis function neural network model to study the aesthetic characteristics of dance and then uses the improved optimal stop training method to control the training of these two parameters so that the established prediction model can obtain better generalization ability. Under the radial basis function neural network model, human body movements can only be developed into dance language with dance artistic attributes after people's artistic processing and creation in accordance with the regularity and purpose of dance aesthetic features, and can only become a tool for shaping dance images and a means of expressing dance so that the beauty of dance works can be planed and embodied on this basis. The dance features in the aesthetic features of dance reflect the psychological characteristics of outward development, the belief in God, and the commonness of Western traditional culture. Of course, this psychological feature of outward development is inseparable from the geographical environment in the west. Under the aesthetic characteristics of dance of radial basis function neural network model, the enthusiastic and unrestrained mental state of the actors and the rhythm of their feet with a sense of the times make the audience feel the pulse and rhythm of modern life psychologically, and bring people's thoughts to a brand-new realm, so as to arouse people's inner pursuit of beauty and inspire people's strong love for life, work, and study. The expression in the radial neural network model is the soul of form through facial expressions and body expressions. As the saying goes, "superb" means this. Therefore, in the performance, students should follow the principle of "taking the shape with the spirit," "expressing the spirit with the shape," and "having both the form and the spirit," as well as the artistic law of "taking the lead with the spirit before the body moves, and arriving with the spirit when the shape fails."

3. Radial Basis Function Neural Network Model

3.1. Principle and Algorithm of Radial Basis Function Neural Network. Radial basis function neural network is a feedforward neural network based on interpolation algorithm, which can approximate any nonlinear function with any accuracy [17]. Compared with BP network, the excitation function of RBF neural network is radial symmetric function, which only responds to the input signal locally, so it avoids the problem of long training time and easy to fall into local minimum of BP network. RBF neural network model reflects the nonlinear evolution relationship of the overall structure through repeated learning of sample data, so as to predict the unknown data. Therefore, the training sample data are very important for the fitting accuracy and generalization ability of neural network. When selecting sample data, we pay attention to the following three points:

① The sample data should be widely distributed, covering the whole structure of the problem and fully reflecting the potential law.

② The sample data should be distributed evenly to avoid the phenomenon of too dense local data.

③ Remove the impossible data, so as to prevent it from generating data noise and affecting the convergence of the network.

In the work of multilayer perceptron neural network, the function coincidence is imminent, which is defined by the nested function set of the weighted sum of input and threshold value, and the weight matrix is calculated through recursive iteration, and the output is calculated. Different from other feedforward neural networks such as MLP, the working principle of RBF neural network function fitting is to map the input directly to the high-dimensional space, and then carry out a single linear weighting and output in the output layer, so that the supervision and training time of weights are greatly reduced [18, 19]. In radial basis function neural network, the number of nodes in the input layer is consistent with the input dimension of the learning sample, while the number of nodes in the output layer is consistent with the output dimension of the actual problem. Therefore, once the learning sample is determined, the number of nodes in the input layer and the number of nodes in the output layer are determined at the same time [20]. The input layer node only transmits the input signal to the hidden layer. After the nonlinear transformation of the hidden layer node, the output is generated by the linear function of the output layer node. The neural network model consists of three layers, and its structure is shown in Figure 1.

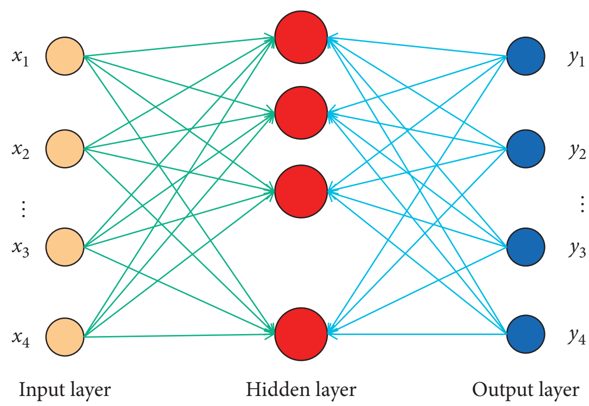

FIGURE 1: Radial basis function neural network model.

The first layer is the input layer, which consists of signal source nodes. The number of input nodes is the dimension of the input sample. Assuming that there are N input samples, each input sample is a I dimension column vector, that is, $X = (x_1, x_2, \ldots, x_1)^T$, and each element of the sample column vector is the node of the input layer. The second layer is the hidden layer, and the number of neurons in the hidden layer varies with the application to be solved. The activation function of each hidden node adopts radial basis function. Radial basis function is a kind of non-negative nonlinear function, which is symmetrical about the center point and attenuates radially, and it has local response function. The third layer is the output layer, which responds to the output of the hidden layer. Assuming that the number of nodes in the output layer is K, this layer maps the hidden layer space to the output layer. Because of the special properties of radial basis function, it has the selective response ability to input variables, which makes RBF network to have the local tuning ability. We take the hidden layer action function as Gaussian function, and the hidden layer output is

$$R_i(x) = \exp\left(-\frac{\|X - C_i\|^2}{2\sigma_i^2}\right), i = 1, 2, \ldots, h, \tag{1}$$

where h is the number of neurons in the hidden layer; $X = (X_1, X_2, \ldots, X_k)$ is the k dimensional input vector; C_i and σ_i are the center vector and width of the ith radial basis function in the hidden layer; $\|\circ\|$ is the 2 norm, representing the Euler distance between X and C_i; and $R_i(X)$ is the output of the i radial basis function. The output of the whole RBF neural network is

$$y_j = \sum_{i=1}^{h} w_{ji} R_j(X), j = 1, 2, \ldots, c_i = 1, 2, \ldots h, \tag{2}$$

where y_j is the output of j neuron in the output layer, and w_{ji} is the connection weight between i neuron in the hidden layer and j neuron in the output layer.

Let MN be the number of hidden nodes, CN be the number of original clusters of samples, and β be the redundancy coefficient of hidden nodes. Its value can be determined according to the network learning situation, and it is generally acceptable as $0 < \beta < 0.5$. The number of hidden nodes of radial neural network can be determined by formula.

$$MN = CN + \beta \circ CN. \tag{3}$$

In order to speed up the training of RBF neural network, it is necessary to initialize the center and width of hidden layer RBF appropriately. The center of hidden layer neurons is intuitively taken as the class mean value. The selection of width takes into account the dispersion of samples within the class and the distance between classes. If the dispersion of samples within the class is large or the distance between classes is large, the width of radial basis function shall be larger; otherwise, it shall be smaller, and its value shall be determined according to the formula.

$$\sigma_i = d_{dj} - d_j^{\text{inner}} = m_i n\left\|C_i - C_j\right\| - \sqrt{\frac{1}{\left|Y_i\right| \sum_{x\in Y}\left\|X - C_i\right\|_i^2}}, \tag{4}$$

where d_{ij} is the distance between class center C_i and C_j, m is the number of classes, d_j^{inner} is the dispersion degree within classes, X is the sample point within class Y_i, and $|Y_i|$ is the total number of samples in class Y_i.

The basic idea of this algorithm is that the response of hidden layer nodes in radial basis function neural network to input depends on the distance between the input vector and the center of hidden layer nodes. The smaller the distance between the input vector and the center, the greater the response of hidden layer nodes. Therefore, the process of determining the hidden layer nodes is the process of clustering the input samples according to the distance between samples. The input vectors with small distance from each other belong to the same category, and the clustering center is the center of the hidden layer nodes. Different network structures and weight training algorithms lead to different characteristics and application functions of the network. At the early stage of neural network development, the network structure was simple, with only input layer and output layer, and its application was single. The emergence of multilayer neural networks [21–23] is the inevitable result of the development of neural networks [24]. Besides the input layer and the output layer, the middle layer of the multilayer neural network is called the hidden layer, which can be one or more layers. The radial basis neural network is composed of radial base layer and linear output layer, and the first layer is radial base layer, which is composed of radial basis neurons. The second layer is a linear output layer composed of linear neurons. The structure diagram of radial neural network model is shown in Figure 2.

In Figure 2, R is the dimension of the input vector, S^1 is the number of neurons in the radial base layer, S^2 is the number of neurons in the linear output layer, and $\mathrm{IW}_{1,1}$ represents the $\mathrm{IW}_{1,1}$ row element of the weight matrix i. $\|\mathrm{dist}\|$ is the Euclidean distance between the input vector P and the weight matrix $\mathrm{IW}_{1,1}$, so the output vector consists of S_1 elements, which are the distance between the input vector P and the vector $\mathrm{IW}_{1,1}$ composed of the row vectors of the input weight matrix.

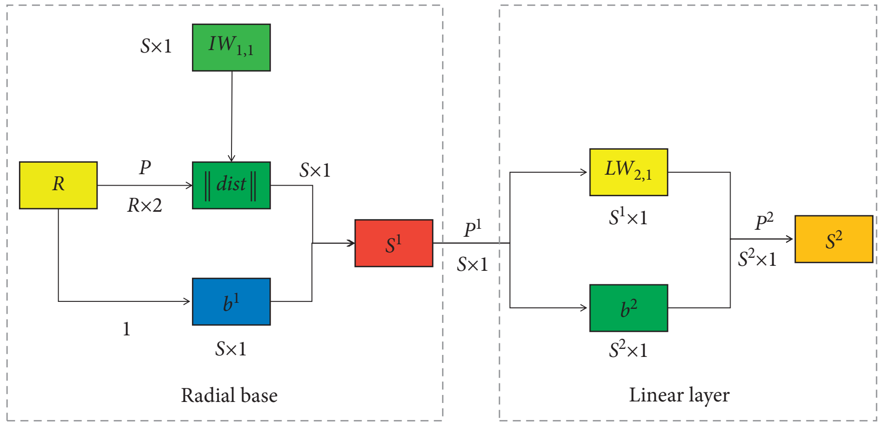

Figure 2: Structure diagram of radial basis function neural network.

The expression of radial neuron transfer function is shown in formula.

$$a = \text{radbas}\,(n) = \exp\left(-n^2\right). \tag{5}$$

The input n of the transfer function is the product of the weighted input $\|w - P\|$ and the offset b, w is the weight vector of the radial basis function neuron, and p is the input vector. The distribution coefficient SPREAD of radial basis function is defined as $0.8326/b$, so the output a of radial basis function neurons can be expressed as follows:

$$a = \text{radbas}\left\{0.8326 \times \frac{w - p}{\text{SPREAD}}\right\}. \tag{6}$$

When $\|w - p\|$ is equal to SPREAD, n is 0.8326, and the output a of neurons is exactly 0.5. When $\|w - p\|$ is greater than SPREAD, neurons will produce less than 0.5 output; when $\|w - p\|$ is less than SPREAD, neurons will produce an output higher than 0.5. The above is the mathematical significance of radial basis function distribution coefficient.

In order to facilitate processing, we use root mean square error (RMSE) to describe the average level of Q cross-validation errors

$$\text{RMSE} = \sqrt{\frac{1}{Q}\sum_{\text{i}=1}^{Q} cve_i^2}. \tag{7}$$

To sum up, when the training sample is given, the root mean square error (RMSE) is actually a function with the distribution coefficient SPREAD as the independent variable.

v_i represents the i element of vector v, and M_i represents the i row of matrix M; then, there is the following relationship:

$$n_i^1 = \left\|\left(\text{IW}_i^{1,1}\right)^T - p\right\| b_i^1;\, i = 1, \ldots, S^1, \tag{8}$$

$$a_i^1 = \text{rabdas}\left(n_i^1\right);\, i = 1, \ldots, S^1, \tag{9}$$

$$y_i = a_i^2 = \text{IW}_i^{2,1};\, a^1 + b_i^2;\, i = 1, \ldots, S^2. \tag{10}$$

It can be seen from the above formula that for a given input vector p, the output vector FF of RBF neural network can be completely determined according to $\text{IW}^{1,1}$, b^1, $\text{LW}^{2,1}$, b^2, and y.

The RBF neural network maps the input to the high-dimensional space by calculating the functional of the distance function between the input and the point in the hidden layer; that is, it completes the mapping by activating the function. The activation function is the basis function, which is radially symmetrical about a central point of the dimensional space. The activation degree of the input at the hidden layer neuron has a strong correlation with its distance from the middle, so this hidden layer node has "local characteristics."

3.2. Characteristics of Dance Beauty. Dance art is a comprehensive art that includes lyricism, movement, and image. To better understand dance, we must not only improve our aesthetic ability in dance but also our aesthetic ability in related arts. This will allow us to better appreciate the formal beauty of dance. Dance's history reveals that it coexists with human history and keeps pace with human social development, which is why it is so popular. As a result, its purpose is socially significant. Many countries now include dance in their school curricula. Dance classes have been offered in some university elective courses, which are very popular with young students, despite China's late start. It demonstrates that people's perceptions of dance's social function have been greatly enhanced. Nowadays, high speed and efficiency are valued in modern civilized life. The information society and the electronic world are icons of the industrial era, and they have had a significant influence on the original dance form. People prefer strong, powerful, heroic, and confident dancing when this psychological factor is in control. They perform a series of complex dance steps in a short amount of time, including rapid and colorful rotation, and rapid twisting. At the same time, people's aesthetic feelings about dance works are inextricably linked to the beauty of dance; however, people's subjective feelings must be grounded in the objectively existing beauty of dance, which must possess the basic characteristics of originality, craftsmanship, and comprehensiveness. This kind of originality is the result of a lot of sweat and hard work, and it is attained through a lot of hard study and exploration, even after a lot of failures. All of this reflects a spiritual beauty, and it is admirable. The created dance image can give people an aesthetic feeling, and this unique skill is beyond the reach of ordinary people.

In a dance work, first of all, it should have aesthetic characteristics such as originality, skill, and comprehensiveness, so as to give people a feeling of dance beauty, be loved by people, and be called excellent dance works. "Form and spirit, spirit and rhyme" is to analyze the aesthetic characteristics of dance movements through the research category of dance aesthetics, and it shows that the improvement of dance aesthetic ability plays an important role in teaching. Dance expresses thoughts through the moving human body, and the human body movements are linked by emotional logic. Like poetry and music, it has the structural method of literary thoughts. The structure of the article is words, words, sentences, paragraphs, and chapters, and the structure of dance is dancing, dancing, dancing, dancing, and dancing. Although in the long history, poetry, music, and dance have gradually taken an independent development path, and their respective artistic characteristics have been relatively highlighted, their internal relationship, that is, comprehensiveness, has never been interrupted or independent, and they have always maintained a state of "you and me" or "you and me." For dance, this phenomenon is more obvious and prominent.

As the external form of dance beauty, after having the artistic attribute of dance, the dance image must also go through the comprehensive development of dance aesthetic creation, that is, the integration of dance, music, poetry, and other different arts, so as to better understand the aesthetic attribute of dance, and finally complete the aesthetic of dance. Dance is embodied by a unique rhythm of "force." The movement of dance is the movement of "Qi." It is the rhythm of "force" of human body's "Qi" sensing the "Qi" of the universe. All dances should use the internal "Qi" to show the external "force." With the help of the research on the aesthetic characteristics of dance, this paper demonstrates the important role of dance aesthetic ability in dance teaching, which can provide some enlightenment to the theory and practice of dance teaching. There is a lack of exploration and innovation in artistic conception and artistic expression; that is, there is no originality; instead, the old routine is adopted in a light and familiar manner or in a conventional manner, and the performance is the theme and content that we have seen and understood for a long time. There will be no new ideas for people, and bringing beauty to people is impossible. As a result, dance must possess unique aesthetic characteristics. Dance serves as a vehicle for moral and emotional education. Real, kind, and beautiful feelings, wishes, and ideals of choreographers and dancers are reflected in the pleasing dance image. It has a subtle positive effect, cultivating people's temperament, evoking noble sentiment, inspiring emotion, inspiring fighting spirit, and so on. Because dance is a form of art in which human body movements are the primary means of expression, it is unavoidable that the means of expression of dance become more artistry as the scope of dance performance subjects and the depth of the theme content expands. The colorful life content and rich characters' inner world can only be fully displayed through a high level of artistry. These characteristics are often integrated and penetrated into each other in an excellent dance work, but they are sometimes hidden and sometimes prominent. However, a close examination reveals that these qualities are present in excellent works as well and that they are interdependent or inseparable.

4. Simulation and Results

4.1. Determination of the Number of Hidden Layer Nodes. In order to establish an ideal dance aesthetic feature model, the commonly used method of gradually increasing the number of hidden layer nodes is adopted to adjust the neural network, and 30, 70, and 120 hidden layer nodes are selected for experiments, respectively, and then, the mean square error between each output variable and the real value is calculated. Tables 1–3 show the mean variance of the output values of the three networks.

From Tables 1 to 3, it can be seen that the fitting accuracy of training data is higher and higher with the increase in hidden layer nodes. When the number of hidden layer nodes is the same as the number of training samples, the fitting error of the network to the training set reaches 0. But at this time, the prediction accuracy of the three dance aesthetic feature test sets is not high. However, because the proportion of dance aesthetic feature training samples in the total data is not large, and its absolute accuracy is not low, the interval of the number of hidden layer nodes can be preliminarily determined.

Table 1: Mean square error of 30 hidden layer nodes.

30	Test 1	Test 2	Test 3	Train
L	4.0276	4.3147	6.582	2.9947
A	5.051	4.4913	5.4983	3.2176
B	5.6398	5.7176	7.8707	3.3521

Table 2: Mean square error of 70 hidden layer nodes.

70	Test 1	Test 2	Test 3	Train
L	2.6595	1.9798	2.5888	0.5702
A	3.0583	2.7625	3.1556	0.97
B	3.5221	2.9441	4.1052	1.0325

Table 3: Mean square error of 120 hidden layer nodes.

120	Test 1	Test 2	Test 3	Train
L	0.9653	1.0663	1.225	0.1925
A	1.2467	1.1262	1.3702	0.2345
B	1.3062	1.3823	1.5531	0.2244

4.2. Analysis of Aesthetic Characteristics of Dance. In this experiment, L-MBP algorithm, RBNN algorithm, and this method are used to compare the aesthetic characteristics of dance, and the calculation results of RBNN approximate model are attached in Figure 3. The initial weights of FNN are randomly generated, and the set initial weights directly affect the final training results. The experimental results are shown in Figure 3.

As can be seen from Figure 3, when the conditions other than the initial weight under the aesthetic characteristics of dance are the same, the values of FNN approximate model based on L-MBP algorithm vary greatly; by contrast, when the training sample of dance aesthetic characteristics is given, the quality of RBNN approximate model is only related to the value of distribution coefficient. Once the value of spread is determined, the RBNN approximate model and its values will be completely determined. The RBF neural network model predicts the aesthetic characteristics of dance; that is, the principal component score coefficient is used to calculate the principal component value, and the data of dance aesthetic characteristics are normalized; finally, L-MBP algorithm, RBNN algorithm, and this method are used to establish the RBF neural network of dance aesthetic features in the mapping relationship, which constitutes the proportion of PCA-RBF network. The experimental results are shown in Figure 4.

As can be seen from Figure 4, when the time index reaches 50, the average proportion of L-MBP algorithm is 33.4%, RBNN algorithm is 32.5%, and the average proportion of this method is 46.3%. It can be seen that this method accounts for the highest proportion of the three algorithms, so it plays a greater advantage in the aesthetic characteristics of dance. In order to verify the advantages of radial basis function neural network over other networks, this paper constructs PCA-BP network and uses machine learning, decision tree algorithm, and this method to repredict the aesthetic characteristics of dance. Similarly, 2~20 groups of data are used as training samples, and 22~26 groups of data are used to evaluate and test the model. The test simulation results of soft sensor model are shown in Figure 5.

As can be seen from Figure 5, when the time index reaches 60, the average ratio of machine learning algorithm is 44.3%, that of decision tree algorithm is 49.5%, and that of this method is 57.8%. Similarly, the change of this method in the training of dance aesthetic feature errors among the three algorithms is the highest, which proves the feasibility and accuracy of this method. In the experiment, we use the proposed EDIW-PSO algorithm, LDIW-PSO algorithm, NDIW-PSO algorithm, and GLBESTIW-PSO algorithm to optimize the RBF neural network, train the training samples, and obtain the fitness function curves of the four optimization algorithms. When the fitness function reaches the

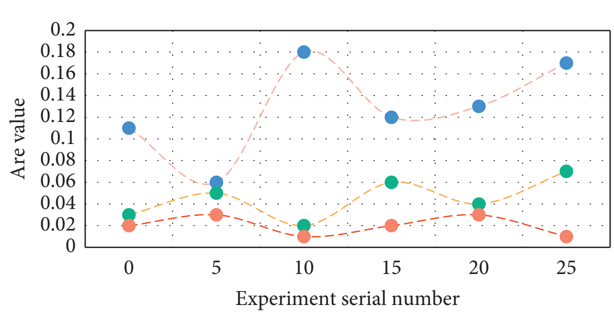

Figure 3: Comparison results of approximate models of dance aesthetic characteristics.

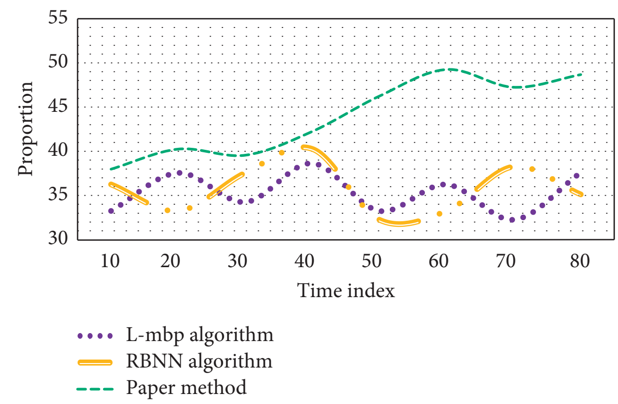

Figure 4: Error curves of dance aesthetic characteristics under different algorithms.

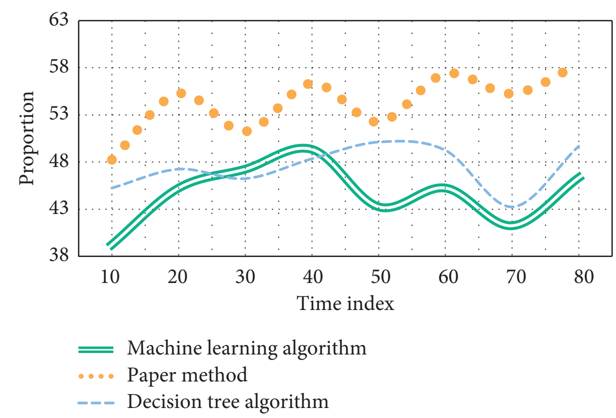

Figure 5: Training curve of dance aesthetic characteristic error under different algorithms.

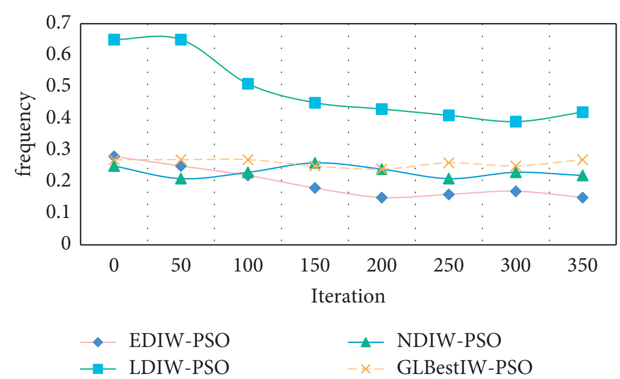

Figure 6: Fitness function curve.

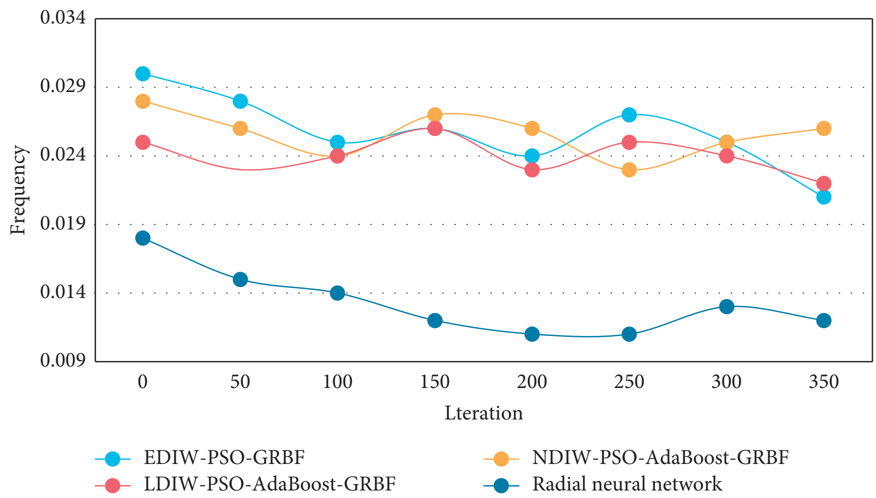

Figure 7: Fitness change of dance aesthetic characteristics of four models fitting two-dimensional nonlinear function.

minimum value, the optimal parameter value of neural network obtained by algorithm optimization is shown in the table. The fitness function curves of the four optimization algorithms are shown in Figure 6.

As can be seen from Figure 6, among the four methods, the PSO algorithm, which is an exponential declining inertia weight strategy, has a faster convergence rate, the smallest fitness function value, and the smallest training error of the neural network. The formal beauty of dance art is relatively independent, and formal beauty is one of the common forms of common beauty, which is most likely to cause a common sense of beauty, and the popularity of dance works is also likely to cause people's common sense of beauty. Because of the existence of common aesthetic feeling, good works can transcend national and national boundaries and reflect people's common interests, life ideals, and psychological needs. In this experiment, the changes of dance aesthetic feature fitness function fitting two-dimensional nonlinear function of four models are compared experimentally. EDIW-PSO-GRBF model, NDIW-PSO-ADABOOST GRBF model, LDIW-PSO-ADABOOST GRBF model, and radial basis function neural network model in this paper are used for experiments, respectively. The experimental results are shown in Figure 7.

As can be seen from Figure 7, the radial basis function neural network model in this paper has the fastest convergence speed, and the global optimal solution searched is better than the other four models, with smaller training error. The subjectivity embodied in aesthetic judgment created aesthetic comprehension's subjectivity. Aesthetic comprehension's subjectivity, as a form of rationality, is based on objectivity, but at the same time, it is latent and fuzzy.

5. Conclusions

The purpose of the rhythm of movements in dance works is to investigate the rhythm of dance by drawing inspiration from natural phenomena such as river, lake, and sea fluctuations, as well as the flashing of stars in the universe and the swaying of weeping willows by the lake. As a result, we must be adept at recognizing and learning the beauty and inner spirit of rhythm. Based on the RBF neural network model, this paper investigates the aesthetic characteristics of dance. When the time index reaches 50, the average proportion of L-MBP algorithm is 33.4 percent, 32.5 percent for RBNN algorithm, and 46.3 percent for this method. As can be seen, this method has the highest proportion in the three algorithms, so it has a greater advantage in the aesthetic characteristics of dance. The more difficult it will be, the higher the RBF neural network model's skill in dance performance. This is not something that ordinary people can do, which just goes to show how unique dance is in terms of innovation and creativity. With the ever-changing nature of life, dance art will change, develop, and improve, and will play a role in the construction of both material and spiritual civilizations. The simulation of surgery in the radial basis function neural network model can make people happy. On the contrary, the form of simulation content is changing and even deepening with the advancement of society and human civilization. The mode of production, lifestyle, and ideology is changing, much like China's transition from an agricultural to an industrial society, and the dance form and content of the aesthetic characteristics of dance are bound to change as well.

Data Availability

The data used to support the findings of this study are available from the author upon request.

Conflicts of Interest

The author does not have any possible conflicts of interest.

References

[1] D. W. Zaidel, "Culture and art: importance of art practice, not aesthetics, to early human culture," *Progress in Brain Research*, vol. 237, pp. 25–40, 2018.

[2] J. F. Christensen, C. J. Cela-Conde, and A. Gomila, "Not all about sex: neural and biobehavioral functions of human dance," *Annals of the New York Academy of Sciences*, vol. 1400, no. 1, pp. 8–32, 2017.
[3] R. Dong, Z. g Wei, C. Liu, and J Kan, "A novel loop closure detection method using line features," *IEEE Access*, vol. 7, pp. 111245–111256, 2019.
[4] F. Guo and Q. Huang, "Signal recognition based on APSO-RBF neural network to assist athlete's competitive ability evaluation," *Computational Intelligence and Neuroscience*, vol. 2021, p. 1, Article ID 4850020, 2021.
[5] H. Blades, *Dance and the Philosophy of Action: A Framework for the Aesthetics of Dance by Graham Mcfee. 2018*, pp. 109–111, Dance Books, Binsted, UK, 2020.
[6] N. Zervou, "Emerging frameworks for engaging precarity and "otherness" in Greek contemporary dance performances," *Theatre Survey*, vol. 51, no. 1, pp. 20–31, 2019.
[7] H. H. So, "You see the story was not quite as you were told: maleficent Dance Disney and Cynicism as the Choreo-philosophical Critique of Neoliberal Precarity[J]," *Dance Research*, vol. 35, no. 1, pp. 3–48, 2017.
[8] J. Habron and L. v. d. Merwe, "A conceptual study of spirituality in selected writings of émile Jaques-Dalcroze," *International Journal of Music Education*, vol. 35, no. 2, pp. 175–188, 2017.
[9] A. Christmas, "When ballet became French: modern ballet and the cultural politics of France, 1909–1939. By ilyana karthas," *Journal of Social History*, vol. 50, no. 3, pp. 581–583, 2017.
[10] K. Skjoldager-Nielsen and D. Skjoldager-Nielsen, "Para-Anthropo(s)cene aesthetics between despair and beauty," *Nordic theatre studies*, vol. 32, no. 1, pp. 44–65, 2020.
[11] E. Lustig and I. Tan, "All about that bass: audio filters on basslines determine groove and liking in electronic dance music," *Psychology of Music*, vol. 48, no. 6, pp. 861–875, 2020.
[12] B. Anderson, "Overcoming and denial: disability and modern dance in the United States," *Dance Research Journal*, vol. 52, no. 3, pp. 58–75, 2020.
[13] A. Wang and C. Wang, "Research on the application of sport dance in colleges and universities in the healthy development of sports," *Revista Brasileira de Medicina do Esporte*, vol. 27, no. 5, pp. 464–467, 2021.
[14] A. Schuh, "Having a personal (performance) practice: dance artists' everyday work, support, and form," *Dance Research Journal*, vol. 51, no. 01, pp. 79–94, 2019.
[15] A. S. Jürgens, "The pathology of joker's dance: the origins of arthur fleck's body aesthetics in todd phillips's 2019 *joker* film," *Dance Chronicle*, vol. 43, no. 3, pp. 321–337, 2020.
[16] Adewole, "Louise meintjes with photographs by T. J. Lemon, Dust of the Zulu: ngoma Aesthetics after apartheid," *Dance Research*, vol. 37, no. 1, pp. 116-117, 2019.
[17] K. Vedel, "Migratory choreography and spaces of resistance," *Dance Research Journal*, vol. 52, no. 1, pp. 58–70, 2020.
[18] M. Templeton, "Walking with the self: zab maboungou's interventions against eurocentrism through contemporary african dance," *Dance Research Journal*, vol. 49, no. 2, pp. 44–61, 2017.
[19] J. Mollenhauer, "A changing focus: the evolution of Irish step dancing competitions in Australia," *Dance Research Journal*, vol. 51, no. 2, pp. 68–85, 2019.
[20] G. K. B. Commodification and Emancipation, "The tango encounter," *Dance Research*, vol. 35, no. 1, pp. 49–60, 2017.
[21] W. Cai and Z. Wei, "Remote sensing image classification based on a cross-attention mechanism and graph convolution," *IEEE Geoscience and Remote Sensing Letters*, vol. 19, pp. 1–5, 2022, Art no. 8002005.
[22] J. Kong, H. Wang, C. Yang, X. Jin, M. Zuo, and X Zhang, "A spatial feature-enhanced attention neural network with high-order pooling representation for application in pest and disease recognition," *Agriculture*, vol. 12, no. 4, p. 500, 2022.
[23] Y. Ding, Z. Zhang, X. Zhao et al., "Multi-feature Fusion: Graph Neural Network and CNN Combining for Hyperspectral Image Classification," *Neurocomputing*, 2022.
[24] A. Pyg, A. Sct, A. Wpc, and C. P. Lim, "Adaptive rough radial basis function neural network with prototype outlier removal [J]," *Information Sciences*, vol. 505, pp. 127–143, 2019.

Hindawi
Computational Intelligence and Neuroscience
Volume 2022, Article ID 4526128, 10 pages
https://doi.org/10.1155/2022/4526128

Research Article

Construction of Digital Teaching Resources of British and American Literature Using Few-Shot Learning and Cloud Computing

Hui Zhang[1] and Fang Zuo[2]

[1]*School of Foreign Languages, Sichuan Technology and Business University, Meishan 620000, China*
[2]*Foreign Language School of Chengdu University of Traditional Chinese Medicine, Chengdu 611137, China*

Correspondence should be addressed to Fang Zuo; zuofang@cdutcm.edu.cn

Received 27 March 2022; Revised 27 April 2022; Accepted 28 April 2022; Published 26 June 2022

Academic Editor: Xin Ning

British and American literature is a compulsory course for English majors in Chinese colleges and universities. It plays an important role in cultivating students' aesthetic consciousness and moral cultivation, improving students' humanistic quality and cultural taste, and shaping students' complete personalities. With the rapid development of cloud technology and mobile Internet technology, mobile learning based on mobile devices will become an important direction of mobile Internet technology applications. Based on cloud computing, this paper studies the construction of digital teaching resources of the British and American literature. Through the experiment on the learning simplicity of literature courses for English majors, it is found that during the learning period of 40 people, the average proportion of the most difficult is 16.3%, the average proportion of the second difficult is 35.2%, and the average proportion of the easier is 18.5%. Compared with the next difficulty, the proportion of difficulty is the highest, followed by the easy and finally the most difficult. As one of the core technologies of cloud computing, data split storage technology adopts measures such as isomorphism and interchangeability of computing nodes, redundant storage, and multicopy fault tolerance to ensure the high security and reliability of user data and users do not have to worry about data loss and virus invasion. As a new generation of technical means, cloud computing can realize the unified management and scheduling of distributed and heterogeneous resources and provide a new development direction for promoting the coconstruction and sharing of the British and American literature digital teaching platforms in higher vocational colleges and truly realizing national learning and lifelong learning.

1. Introduction

British and American literature, as a required course for Chinese English majors in their third year, serves a critical function in broadening students' cultural horizons and cultivating high quality. It is critical in developing students' aesthetic consciousness and moral development, as well as strengthening their humanistic quality and cultural taste and forming their entire personality [1, 2]. The authorized curriculum of the postgraduate entrance test for English majors includes British and American literature. In recent years, this course's information has been included in the CET8 test content [3]. There are a variety of causes for the marginalization of British and American literature at colleges and universities, but there are two major reasons. It is a result of the contemporary mercantilist social climate. Some colleges and universities continue to add practical and effective Applied English courses such as business English, economic and trade English, financial English, legal English, and computer English when teachers are strictly prohibited in order to reduce the number of class hours of English and American literature courses as much as possible [4, 5]. Students dig deeper into and investigate the contents of literary works, fully integrating the collected information into their English knowledge system. They enhance their English level in addition to enhancing their literary literacy [6].

Mobile learning based on mobile devices will become an important path for mobile Internet technology applications with the rapid growth of cloud technology and mobile Internet technology. Based on the cloud platform, the mobile digital resource platform mines related learning needs and habits using cloud computing technology's storage space and data analysis capabilities [7, 8], allowing students and teachers to access the network resource cloud service platform and obtain resources at any time and from any location. The process of data processing is relocated from personal computers or servers to computer clusters on the Internet, which is dubbed "cloud" [9], using the high-speed transmission capabilities of cloud computing on the Internet. Cloud computing has accelerated the evolution of information technology and IT application mode, fundamentally altered working and business modes in the traditional mode, and increased resource utilization and computing speed, simplifying software, business processes, and access services. Cloud computing provides computation, services, software, and other services to a large number of users at the same time, and maintaining data security is the foundation for gaining consumers' trust. Data sharing storage technology, as one of the core technologies of cloud computing, employs features [10, 11] such as isomorphic and interchangeable computing nodes, redundant storage, multicopy fault tolerance, and other features to ensure that user data are secure and reliable, and users do not have to worry about data loss or virus intrusion [12, 13]. The core objective of cloud computing is to share the processing and storage resources of each node in the cloud, to deliver to end-users, and to take the required computer resources as its main role. Cloud computing will inevitably find its way into more and more digital teaching tools for British and American literature [14, 15]. In the cloud computing mode, by building a common cloud platform for digital teaching resources of British and American literature, the links within schools, between schools, and between schools and enterprises can be closer, and educational information resources can be effectively integrated and shared. With this platform, schools and enterprises can also effectively save human and material resources, realize resource complementarity, and promote two-way cooperation. As a new generation of technical means, cloud computing can realize the unified management and scheduling of distributed and heterogeneous resources so as to provide a new development direction for promoting the coconstruction and sharing of British and American literature digital teaching platforms in higher vocational colleges and truly realizing national learning and lifelong learning.

This article studies and innovates the above problems from the following aspects:

(1) A cloud server model of English and American literature digital teaching resources based on cloud computing is proposed. The digital teaching resource base based on cloud computing also reduces the difficulty of operation, and users can easily use the resource base without mastering complicated software operations. Digital resources store information in data centers to meet the needs of students and teachers; memory management is used to organize and manage data from cloud service end to mobile client application end; the management layer realizes the interaction between security control and memory management through the cloud management platform.

(2) A digital teaching resource construction system of British and American literature based on cloud computing is constructed. Through the digital teaching resources construction system of British and American literature, a resource information database and a resource catalogue database are established to manage resources and provide support for the rapid retrieval of resources. Because resources need to be shared with different databases, it is necessary to establish common technical standards and build database platforms according to the same specifications to prevent data incompatibility.

The article is divided into five parts, and the organizational structure is as follows: Section 1 introduces the research background and present situation of digital teaching resources of British and American literature and puts forward and summarizes the main tasks of this paper. Section 2 introduces the related work of digital teaching resources of British and American literature at home and abroad. Section 3 introduces the algorithms and models of cloud computing. Section 4 introduces the realization of the digital teaching resources of British and American literature and compares the performance of the system through experiments. Section 5 is the full-text summary.

2. Related Work

2.1. Research Status at Home and Abroad. Zhang L et al. put forward that there are many problems in the teaching materials of British and American literature. First, most of the teaching materials are of single style and not readable, which is difficult to attract students' interest; second, the replacement speed of teaching materials is too slow. Many teaching materials are old in content and viewpoint, which can not meet the students' desire to know the latest things; third, the textbook pays too much attention to the indoctrination of knowledge and lacks enlightenment, ignoring the cultivation of students' intelligence and ability [16]. Li proposed that the purpose of literature course is to cultivate students' ability to read, appreciate, and understand the original works of English literature, master the basic knowledge and methods of literary criticism, improve students' basic language skills and humanistic quality through reading and analyzing British and American literary works, and enhance students' understanding of western literature and culture [17]. Yi proposed that the construction of a digital teaching platform of British and American literature can integrate the existing human resources and academic resources, use the huge text, video, and audio information to increase students' knowledge, cultivate students' correct learning methods, and improve learning efficiency. In turn, it can enable students to join the classroom teaching links and the construction of a digital teaching platform, highlight their subjectivity and exercise their reading ability, scientific research ability, and expression ability [18]. Shan proposed that in view of the problems existing in the current British and American literature course, I think it is necessary to make use of the current rich network resources and use modern teaching methods to improve the teaching effect of the British and American literature course, so as to play its due role in higher education and get rid of its marginalization [19]. Ma and Bo proposed to improve students' basic language skills and humanistic quality and enhance students' understanding of western literature and culture by reading and analyzing British and American literary works [20]. Campbell put forward that it is necessary for teachers to optimize and reform the existing teaching mode of British and American literature, make full use of modern educational technology and network multimedia, update teaching contents, improve teaching efficiency, and cultivate students to master effective learning methods [21]. Al-Zoube et al. pointed out that some teachers of English and American literature courses started to use multimedia in the teaching process, but many of them just showed the contents of textbooks in the form of courseware. This kind of "textbook moving" courseware did not give full play to the advantages of multimedia, so it was not attractive [22]. Hwang and Li put forward the compiling characteristics of foreign English and American literature textbooks, analyzed the shortcomings in domestic textbooks, and put forward corresponding reform suggestions [23]. Yang pointed out that the contents of most English and American literature textbooks are relatively outdated, but the use of network resources can make up for this deficiency. Teachers can collect, download, and sort out some resources to meet students' needs from the Internet and selectively integrate the latest contents and research results of British and American literature into the lecture notes in time [24]. Li pointed out that literary appreciation ability, cross-cultural ability, and critical thinking ability are essential basic abilities for foreign language majors. Whether students have these abilities depends largely on the quality of teaching materials used in literature courses and the teaching effect on teachers and students [25].

2.2. Research Status of Digital Teaching Resources of the British and American Literature Based on Cloud Computing. This article analyzes the construction of digital teaching resources of British and American literature under cloud computing, the opportunities, and challenges faced by British and American literature teaching in Chinese universities and discusses how to reform the teaching mode and improve the teaching efficiency under cloud computing. Building and sharing a British and American literature teaching resource library using cloud computing technology is critical for China's talent development so that high-quality educational resources may be popularized and more students can benefit from them. It is difficult for pupils to understand abstract concepts solely through linguistic interpretation during the educational process. Cloud computing technology can help concretize abstract ideas and simplify complex situations, allowing you to achieve twice the outcome with half the effort. The use of cloud computing technology, on the other hand, offers teachers with a new digital teaching resource teaching system of British and American literature, which encourages teachers to challenge traditional teaching notions and promote constant innovation in all parts of education. Improving their English language skills is also conducive to creating a literary learning atmosphere integrating knowledge and interest, stimulating their interest in learning, and cultivating their autonomous learning habits. Therefore, the teaching of British and American literature can fully reflect its humanistic knowledge and improve its teaching quality.

3. Algorithm and Model of Cloud Computing

Cloud computing is a network made up of a large number of computers that can offer consumers the necessary computer services. This supercomputing mode reflects the future development trend of computer applications and is the newest development achievement of distributed computing, parallel computing, and grid computing in the field of computer science. "Computing" refers to a "computing resource pool" in cloud computing, while "cloud" refers to multiple networks that provide resource services. Cloud computing service providers are in charge of virtualized device management and operation, as well as dynamic resource deployment, real-time scheduling, and autonomous recycling, among other things. Virtualization technology is used to make cloud computing a reality. In general, the computer element runs on a real basis, but in virtualization technology, the computing element runs on a virtual basis. Cloud computing resources are always developing dynamically, and different computer terminals can add different types of information to the cloud for other users to download and share. End consumers do not need to understand how the cloud works, let alone have expert knowledge, and everything is as simple as connecting to the Internet.

Cloud services can govern and administer a vast number of educational information resources with the use of cloud computing. Any learner requires only a cloud-connected computer or a mobile terminal device that operates on a 3G or WiFi network. In any place and at any time, they can get the learning resources and services he needs from the cloud resource library in real time. They can also use cloud resources to debate a specific problem with teachers and specialists, making virtual network learning a reality. The operating difficulties are also reduced by the digital instructional resource library based on cloud computing. The resource library is simple to use and does not need users to grasp sophisticated software processes. The user interface is welcoming, and the experience is very humanized, which can help to boost the learning effect significantly. The following are the basic components of the mobile digital cloud server: The data center's information is stored in digital resources, which are used to suit the demands of students and teachers. From the cloud service to the mobile consumer application, memory management is used to organize and manage data. Through the cloud management platform, the management processing layer accomplishes the connection between security control and memory management. The cloud server model of digital teaching resources of British and American literature is shown in Figure 1.

Allocate virtual machines to each application according to the resource vector $R = (R_1, \ldots, R_j, \ldots, R_c)$ allocated to each application output by the application monitoring program module so as to minimize the total allocation cost. In other words, the purpose of this module is to assign the virtual machine of each application that minimizes the objective function as follows:

$$C = \min\left(\sum_{i=1}^{m} \cos t \cdot N_i\right), \tag{1}$$

where m is the number of applications, $\cos t$ is the operation cost vector of virtual machines, each item corresponds to the allocation cost of each type of virtual machine, N_i is the virtual machine vector allocated to application i and $N_i = (n_{i1}, \ldots, n_{ij}, \ldots, n_{ic})$, n_{ij} is the number of j-type virtual machines allocated to application i, and $\cos t \cdot N_i$ represents the cost of allocating virtual machine vector N_i to application i.

According to the assumption in this article, the number of each type of virtual machines in the data center is limited; that is, there is an upper threshold. The threshold vector of each type of virtual machine is defined as $N^{\max} = (n_1^{\max}, \ldots, n_j^{\max}, \ldots, n_c^{\max})$ and has the following relationship:

$$\sum_{i=1}^{m} n_{ij} \le N_j^{\max}, \quad 1 \le j \le c. \tag{2}$$

The number of resources allocated to each application should meet the resource requirements determined by the application monitoring module, namely,

$$\begin{aligned} &\sum_{j=1}^{c} n_{ij} \cdot V_j^{CPU} \ge R_i^{CPU}, \quad 1 \le i \le m, \\ &\sum_{j=1}^{c} n_{ij} \cdot V_j^{\text{memory}} \ge R_i^{\text{menory}}, \quad 1 \le i \le m, \\ &\sum_{j=1}^{c} n_{ij} \cdot V_j^{\text{network}} \ge R_i^{\text{network}}, \quad 1 \le i \le m. \end{aligned} \tag{3}$$

At the same time, the total resources of all virtual machines deployed on physical machines cannot exceed the total resources of all physical machines, so there is the following relationship:

$$\begin{aligned} &\sum_{i=1}^{m}\sum_{j=1}^{c} n_{ij} \cdot V_j^{CPU} \le \sum_{j=1}^{n} p_j^{CPU}, \\ &\sum_{i=1}^{m}\sum_{j=1}^{c} n_{ij} \cdot V_j^{\text{memory}} \le \sum_{j=1}^{n} p_j^{\text{memory}}, \\ &\sum_{i=1}^{m}\sum_{j=1}^{c} n_{ij} \cdot V_j^{\text{network}} \le \sum_{j=1}^{n} p_j^{\text{network}}. \end{aligned} \tag{4}$$

By solving the above model with the constraint method, we can get the virtual machine allocation vector with the lowest total cost, and each virtual machine allocation vector corresponds to the virtual machine allocation situation of each application, that is, what kind of virtual machines are allocated and the number of virtual machines allocated.

Therefore, a teaching resource model with the best energy consumption of heterogeneous servers can be established:

$$\text{minimize} \sum_{i \in P}\left(H_i \cdot E_i^{\text{dynamic}} + E_i^{\text{static}}\right), \tag{5}$$

where E_i is the energy consumption of physical server p_i. It can be concluded that the constraints on energy consumption are

$$E_i^{\text{static}} + H_i \cdot E_i^{\text{dynamic}} \le E_i^{\text{Max}} \, (1 \le i \le n). \tag{6}$$

Among them, E_i^{Max} is the maximum energy consumption that physical server p_i can bear; that is, the actual energy consumption of the physical server p_i must be less than or equal to E_i^{Max}.

Cloud computing provides resources, services, and platforms for users. It can provide users with safe, convenient, and efficient services as needed at any time, anywhere, and anyway. It has the characteristics of superscale, safety and reliability, on-demand service, and strong versatility. Cloud computing is a service-centered networked computing resource sharing pool. The main body of its architecture includes the application layer, platform layer, infrastructure layer, and virtualization layer, which provide software as a service, platform as a service, and infrastructure as a service, respectively. On-demand access through service support. In addition, the client and management together constitute the architecture of cloud computing. The architecture of cloud computing is shown in Figure 2.

The architecture of cloud computing is mainly divided into six layers:

① Application layer

In the application layer, services are provided through software applications, which interact with the client through web service and other technologies to realize the corresponding functions.

② Platform layer

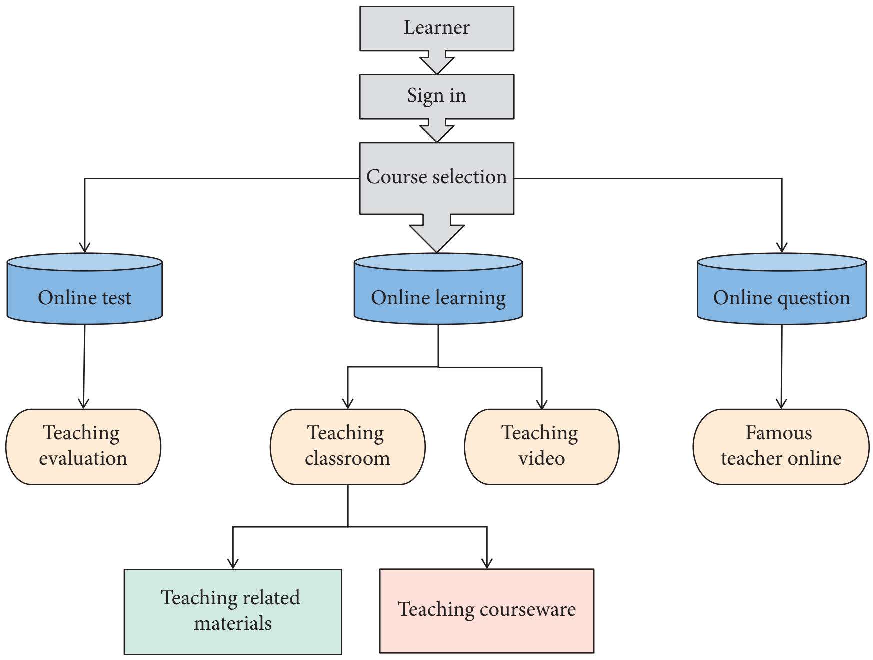

FIGURE 1: Cloud service model of British and American literature digital teaching resources.

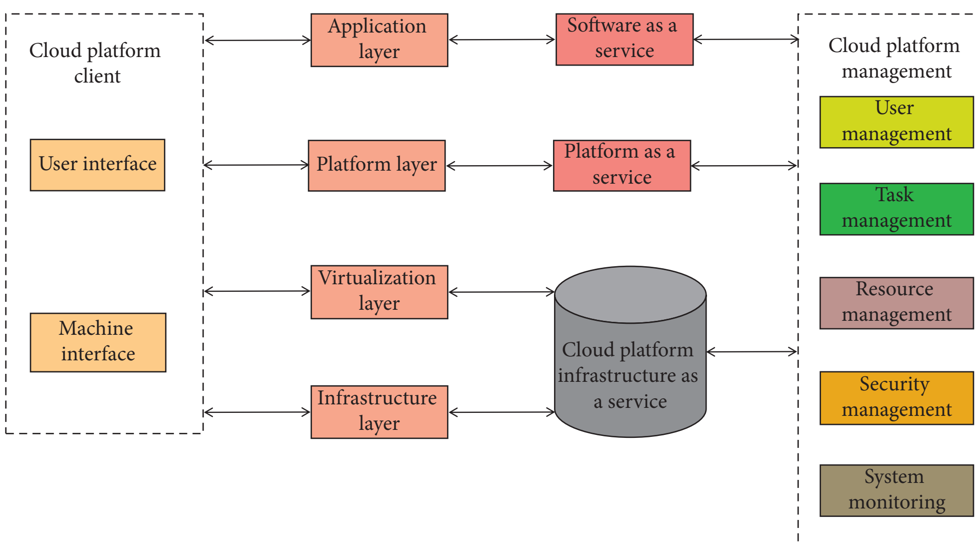

FIGURE 2: Architecture of cloud computing.

Based on the virtualization layer, the platform layer plays an important role in connecting the preceding and the following. It is responsible for responding to the requests sent by the application layer, using distributed technology to process massive data in parallel, dynamically allocating various resources of the virtualization layer according to the requests, and providing platform services is a key step to improving efficiency.

③ Virtualization layer

The virtualization layer is based on the infrastructure layer, which virtualizes the resources provided by the infrastructure layer. It can also be understood as the "multitenant" of the infrastructure layer, which makes efficient and rational use of the resources provided by the infrastructure according to the processing needs sent by the platform layer.

④ Infrastructure layer

The infrastructure layer provides the necessary resources for the virtualization layer, including software resources, network resources, and hardware resources. This layer can expand and optimize management based on the database.

⑤ Client

The client is used for human-computer interaction, including user interface and machine interface.

⑥ Management

The management manages the as a service at all levels. Through good user management technology, users can quickly log in under safe conditions and facilitate the unified management of accounts by administrators. Resource management is the overall allocation of all resources.

Cloud computing is to centralize computers in different parts of the country and realize collaborative work through the network. Users can get the services they need only through the network. In this way, there is no need to add a lot of computer hardware equipment and install various software programs for certain needs, which directly saves a lot of costs. Cloud computing users will have their own resource requirements. In order to make the resources requested by users run, it is necessary to allocate the specific resources requested by users to them. Typical cloud computing resource provision strategies include the strategy based on lease theory and dynamic multilevel resource pool, the strategy based on economics college, the strategy based on general optimization algorithm, and the optimal strategy based on random integer programming.

4. The Construction and Realization of Digital Teaching Resources of the British and American Literature

4.1. Teaching Resource Construction System under Cloud Computing. After the learner is authenticated and authorized, the cloud platform analyzes the learning contents of the digital teaching resources of British and American literature according to the learner's historical track and displays them in a list, thanks to the cloud platform's data analysis and processing capability. It may learn at any time and from any location, which is incredibly handy for students and teachers and boosts their efficiency. Many large network companies have now developed a number of relevant processes and standards to ensure customer data security, provided various solutions for schools based on their needs, built a cloud platform that meets the needs of schools, and created a private "public resource cloud" for schools to better serve their teachers and students. You may also specify multiple levels of permissions to link with external units to create a "hybrid cloud" that allows you to share resources. The operating system and computer hardware are targeted for virtualization in the instructional resource creation system platform. Application virtualization includes simulation, simulation, and interpretation technology. Resource virtualization focuses on specific system resources such as network resources, storage, and memory; resource virtualization focuses on specific system resources such as network resources, storage, and memory. Virtualization technology optimizes resource use and eliminates resource waste. Both software and hardware are capable of performing well. Computers solve real problems at a far faster rate. Light resources, accessible resource deployment, diversified resource channels, ubiquitous resource acquisition, and speedy resource browsing should be characteristics of the cloud-based digital teaching resources development system for British and American literature. On the basis of knowledge deconstruction, lightweight development of teaching resources is carried out to fulfill the needs of fragmented learning, MOOC teaching, and flipped classroom. The particle size of resources not only follows the instructional principles but also helps with network transmission. We should take full advantage of the resource pool's openness and boost its interactivity when building a cloud-based system of digital teaching tools for British and American literature. Despite the fact that the cloud stores a wide range of educational and teaching resources, users may quickly access them and set up storage, editing, calling, querying, and downloading. It is the primary driving factor behind the English and American literature digital teaching resource creation system. The construction will lack scale if the application scope is too narrow; the promotion will be worthless if the application is ineffective.

The building and application of digital teaching resources must be led by the construction and improvement of British and American literary resources, which should begin with the construction and improvement of British and American literature resources and formulate a professional curriculum system based on the professional talent training plan, which includes professional core courses, professional support courses, and expansion courses. Professional core courses are those that reflect professional core competencies, while professional support courses are those that provide support and basic support to the core courses. The efficient management of digital teaching resources in the resource cloud for British and American literature plays a critical role in increasing user experience and promotion effect. Rapid resource retrieval, fair resource scheduling, resource approved access, and so on are all aspects of management. The resource information database and resource directory database are established through the digital teaching resource construction system of British and American literature to manage resources and give support for speedy resource retrieval. Because separate databases must share resources, consistent technological standards must be established and a database platform built to the same specifications to avoid data incompatibility. Because the digital teaching resource construction system based on cloud computing for British and American literature is still in its early stages of development and research, the technology is not fully mature, and various standards are not fully unified. It is critical to establish corresponding technical specifications.

4.2. Experimental Results and Analysis. In this experiment, the students' interest and liking for digital teaching resource databases were investigated, and the interest and liking of secondary vocational school students for digital teaching resource database were basically the same. The degree of students' interest in the resource pool is shown in Table 1. The degree of students' liking for the resource pool is shown in Table 2.

Table 1: Questionnaire on students' interest in the resource database.

Degree	Very interested	Be interested	Commonly	Uninterested
Number of people	425	204	56	34
Proportion	58.8%	28.3%	7.8%	4.7%

Table 2: Questionnaire on students' preference for resource database.

Degree	Like it very much	Like	Commonly	Dislike
Number of people	397	222	67	33
Proportion	55.2%	30.7%	9.3%	4.6%

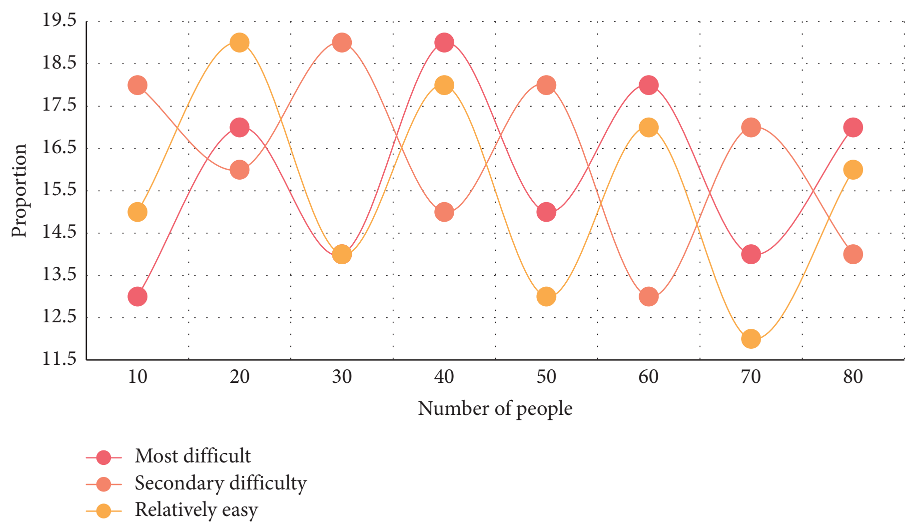

Figure 3: Learning effects of public English courses at different levels of difficulty.

From Tables 1 to 2, it can be seen that 58.8% and 55.2% of students are very interested in and like the resource bank, 28.3% and 30.7% are interested and like, 7.8% and 9.3% are generally interested and like, and 4.7% and 4.6% are not interested and dislike, respectively. In terms of content construction, we should comply with the characteristics and teaching methods of secondary vocational schools, update the content in time, and keep pace with teaching, and students can find the content they want in time to truly serve teachers' teaching and students' learning. The resource bank is mainly for teaching. In the design and construction, we should widely solicit the opinions of students and teachers, especially the direct and in-depth participation of front-line teachers. In addition to the systematic design of the content in line with the characteristics of secondary vocational teaching, it also needs to be designed in terms of management to facilitate teachers' teaching management and teacher-student interaction on the resource database platform.

In this experiment, the first three aspects of students' simplicity in learning English and American literature courses are analyzed. Two experiments were conducted to compare the most difficult and the second most difficult, respectively, and the total time spent by students studying the course after class was compared. The experimental results are shown in Figures 3 and 4.

From Figures 3 to 4, it can be seen that the three learning points of traditional language, cultural background, and text content have different difficult relationships in students' activities of learning English and American literature. According to the experiment of English major students' ease of learning literature courses, it is found that during the period of 40 students, the average proportion of the most difficult is 16.3%, the average proportion of the next difficult is 35.2%, and the average proportion of the easier is 18.5%. Compared with the next difficult one, the proportion of the difficulty in learning is the highest, followed by the easier one, and finally the most difficult one. Most students have greater difficulties than language barriers in understanding the content of literary works and related knowledge reflected by them. Only a small number of students' language barriers exceed the cognitive barriers of text content and related knowledge.

In this experiment, during the classroom teaching, after the teacher has finished explaining the works preliminarily, the students are divided into several groups, each with 4–6 people, to discuss a certain problem in the preview tips, respectively. According to the order in which these teaching

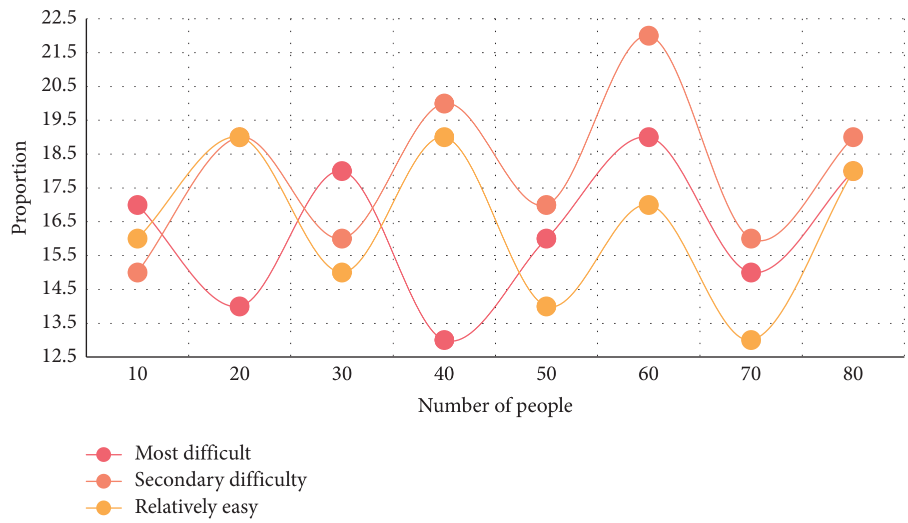

Figure 4: Learning effects of professional English courses at different levels of difficulty.

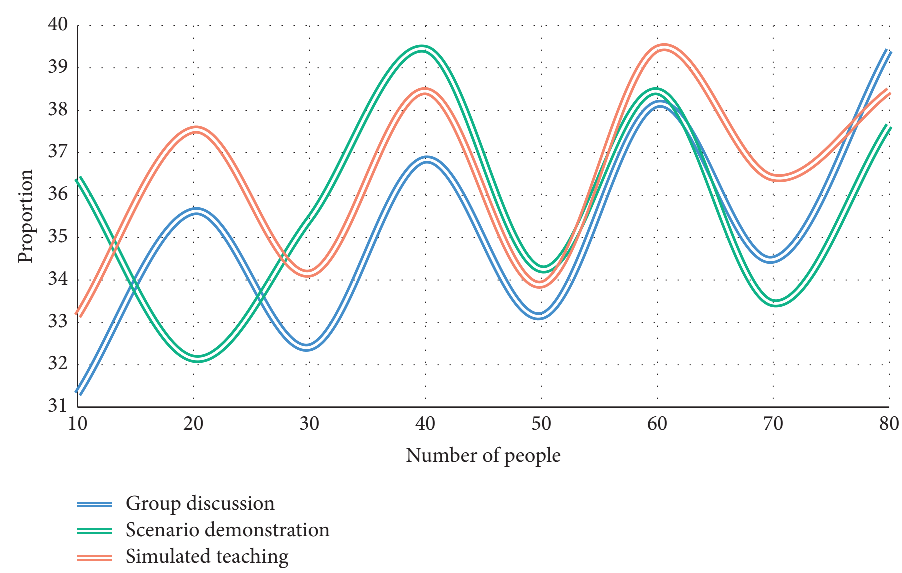

Figure 5: English majors' satisfaction with the reception response teaching model on 10% training samples.

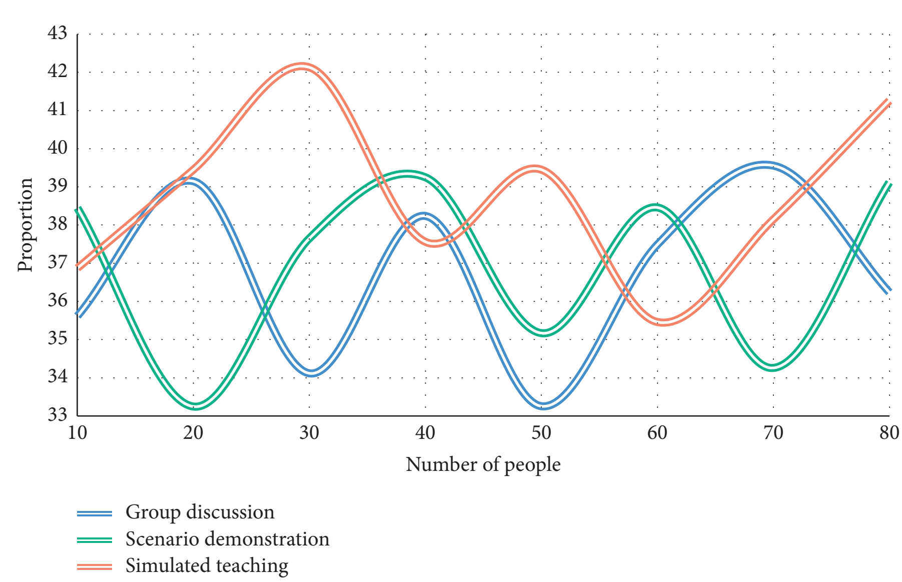

Figure 6: English majors' satisfaction with the reception response teaching model on 20% training samples.

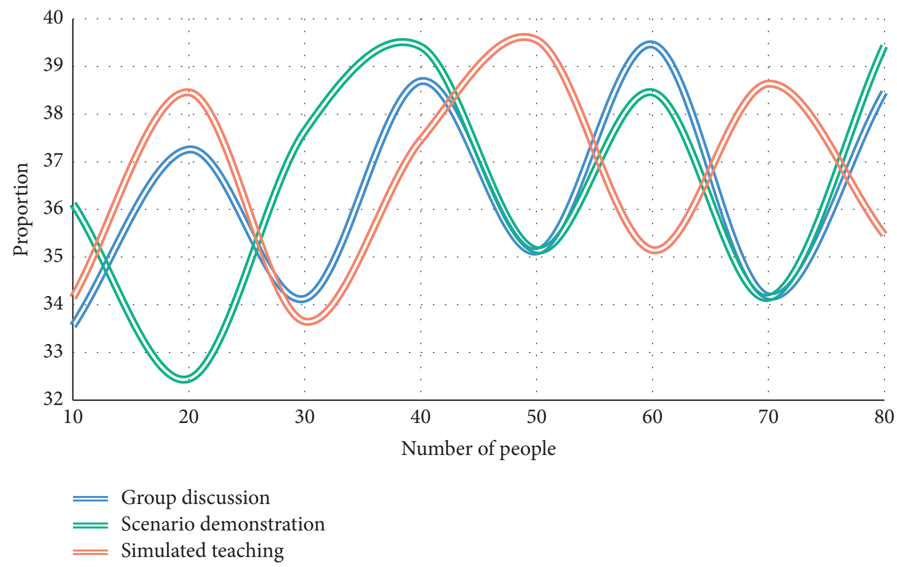

Figure 7: English majors' satisfaction with the reception response teaching model on 30% training samples.

AIDS appear in the teaching process, the order is as follows: (1) discuss in groups; (2) scenario demonstration; (3) simulation teaching. Group discussion aims to improve the efficiency of preview before class by training students' ability to collect effective information and communicate. Once again, we conducted three experiments to compare English majors' preferences for the response teaching mode. The experimental results are shown in Figures 5, 6, and 7.

As can be seen from Figures 5 to 7, for each single teaching auxiliary means of group discussion, scenario demonstration, and simulated teaching, when the number of students is 50, the average satisfaction rates of group discussion, scenario demonstration, and simulated teaching are 34.6%, 34.9%, and 37.6%, respectively. The results of this experiment reflect that the students affirmed the three teaching aids adopted under the guidance of reception response theory. The improvement of students' learning quality and learning interest shows the effectiveness of the above auxiliary teaching means: that is, to strengthen students' understanding of literary texts and promote the exchange and communication between learning subjects so as to obtain a better literary teaching effect.

5. Conclusions

It is of great significance for China's talent training to build and share the British and American literature teaching resource library through cloud computing technology so that high-quality educational resources can be popularized and more students can enjoy high-quality educational resources. The development and utilization of digital teaching resources of British and American literature based on cloud computing is not only conducive to creating a multimode humanistic teaching environment in which multiple meaningful symbols work together, enhancing the intuition and vividness of teaching, mobilizing students' multiple senses to participate in language information perception, and effectively improving English language skills but also conducive to creating a literary learning atmosphere in which knowledge and interest are combined and stimulating students' interest in learning, Cultivate students' autonomous learning habits, improve literary literacy, fully realize the teaching objectives of British and American literature, and reflect the teaching knowledge of British and American literature. Through the experiment on the difficulty and ease of learning literature courses for English majors, it is found that among the 40 students, the average proportion of the most difficult is 16.3%, the average proportion of the second difficult is 35.2%, and the average proportion of the easier is 18.5%. Compared with the next difficulty, the proportion of learning difficulty is the highest, followed by the easier, and finally the most difficult. Various materials provided by the cloud computing British and American literature teaching platform improve students' literary appreciation ability and critical judgment ability, enhance students' scientific research ability, expression ability, and innovation ability and improve students' comprehensive quality.

Data Availability

The data used to support the findings of this study are available from the corresponding author upon request.

Conflicts of Interest

The authors declare no conflicts of interest.

Acknowledgments

This study was supported by the 2020 Ideological Education Team "Intensive Reading Course Teaching Team for English Major" (Project no. KCSZSFJXTD09).

References

[1] T. Reeder, "The imperial nation: citizens and subjects in the British, French, Spanish, and American empires," *Journal of American History*, vol. 107, no. 3, pp. 727-728, 2020.

[2] Z. Huang, Y. Liu, C. Zhan, W. C. Lin, and Y. Chen, "A novel group recommendation model with two-stage deep learning [J]," *IEEE Transactions on Systems, Man, and Cybernetics: Systems*, vol. 1, 2021.

[3] C. Klein, *Cold war friendships: korea, vietnam, and asian American literature*p. 310, Oxford University Press, New York, 2016.

[4] E. Butcher, "British children's literature and the first world war: representations since 1914, by david budgen," *English Historical Review*, vol. 135, no. 574, pp. 721–723, 2020.

[5] V. Morkeviius, *Pursuing Moral Warfare: Ethics in American, British, and Israeli Counterinsurgency. By Marcus Schulzke*, p. 256p, Georgetown University Press, Washington, DC, 2019.

[6] F. M. Dagnino, Y. A. Dimitriadis, and F. Pozzi, "Exploring teachers' needs and the existing barriers to the adoption of Learning Design methods and tools: a literature survey," *British Journal of Educational Technology*, vol. 49, pp. 998–1013, 2018.

[7] J. Zhou, D. Liu, X. Xie, and W. Zhang, "Underwater image restoration by red channel compensation and underwater median dark channel prior[J]," *Applied Optics*, vol. 61, no. 10, pp. 2915–2922, 2022.

[8] J. Zhou, T. Yang, W. Chu, and W. Zhang, "Underwater image restoration via backscatter pixel prior and color compensation [J]," *Engineering Applications of Artificial Intelligence*, vol. 111, Article ID 104785, 2022.

[9] J. Chen, C. Du, Y. Zhang, P. Han, and W. Wei, "A Clustering-Based Coverage Path Planning Method for Autonomous Heterogeneous UAVs," *IEEE Transactions on Intelligent Transportation Systems*, vol. 2, 2021.

[10] Y. Hu, J. Zhan, G. Zhou et al., "Fast forest Fire Smoke Detection Using MVMNet," *Knowledge-Based Systems*, vol. 241, Article ID 108219, 2022.

[11] Y. Wang, T. Wang, X. Zhou et al., "TransEffiDet: aircraft detection and classification in aerial images based on EfficientDet and transformer[J]," *Computational Intelligence and Neuroscience*, vol. 2022, Article ID 2262549, 2022.

[12] M. B. D. Shomali and M. A. Gomaa, *The non-national in contemporary American literature: ethnic women writers and problematic belongings, American literature readings in the twenty-first century*p. 207, Palgrave Macmillan, Raleigh, N.C, 2016.

[13] S. Wizner, D. Biber, and P. Baker, "American and British English: divided by a common language?:[J]," *International Journal of Corpus Linguistics*, vol. 24, no. 4, pp. 536–540, 2017.

[14] T. Cheng and M. Deng, "Research on introduction to famous works and cultivation of humanistic quality in the teaching of British and American literature based on network information," *Journal of Physics: Conference Series*, vol. 1744, Article ID 032240, 2021.

[15] N. Matar, "Cornel zwierlein. Imperial unknowns: the French and British in the mediterranean, 1650–1750.[J]," *The American Historical Review*, vol. 123, no. 2, pp. 635-636, 2018.

[16] L. Zhang, M. Liu, Z. Shi, and X. Ma, "Research on virtual basic laboratory and experimental teaching resources platform based on cloud computing[J]," *LECTURE NOTES IN ELECTRICAL ENGINEERING*, vol. 271, no. 2, pp. 549–554, 2014.

[17] W. Li, "Application of cloud computing in informatization of physical education teaching resources[J]," *Revista de la Facultad de Ingenieria*, vol. 32, no. 11, pp. 626–631, 2017.

[18] G. Yi, "Study on new mode of higher education information based on cloud computing[J]," *Lecture Notes in Electrical Engineering*, vol. 226, pp. 157–165, 2013.

[19] C. Shan, "Improvement design of teaching management system based on cloud computing in colleges and universities [J]," *Boletin Tecnico/Technical Bulletin*, vol. 55, no. 19, pp. 642–650, 2017.

[20] K. Ma and Y. Bo, "Experiences in teaching virtualisation with private cloud platform[J]," *International Journal of Continuing Engineering Education and Lifelong Learning*, vol. 25, no. 3, pp. 301–314, 2015.

[21] S. Campbell, "Teaching cloud computing[J]," *Computer*, vol. 49, no. 9, pp. 91–93, 2016.

[22] M. Al-Zoube, S. A. El-Seoud, and M. F. Wyne, "Cloud computing based E-learning system[J]," *International Journal of Distance Education Technologies*, vol. 8, no. 2, pp. 58–71, 2010.

[23] K. Hwang and D. Li, "Trusted cloud computing with secure resources and data coloring[J]," *IEEE Internet Computing*, vol. 14, no. 5, pp. 14–22, 2010.

[24] J. Yang, "Researches on cloud computing-based design of online mathematics teaching system for colleges and universities[J]," *Revista de la Facultad de Ingenieria*, vol. 32, no. 11, pp. 882–888, 2017.

[25] Q. Li, "Research on the application design and development of multimedia database cloud platform in educational resource management[J]," *Revista de la Facultad de Ingenieria*, vol. 32, no. 2, pp. 778–787, 2017.

Hindawi
Computational Intelligence and Neuroscience
Volume 2022, Article ID 3905998, 9 pages
https://doi.org/10.1155/2022/3905998

Research Article

Breast Tumor Ultrasound Image Segmentation Method Based on Improved Residual U-Net Network

Tianyu Zhao [1] **and Hang Dai** [2]

[1] *Medical Technology Department, Qiqihar Medical University, Qiqihar, Heilongjiang 161006, China*
[2] *Foreign Language Department, Qiqihar Medical University, Qiqihar, Heilongjiang 161006, China*

Correspondence should be addressed to Hang Dai; yolander@qmu.edu.cn

Received 25 April 2022; Revised 19 May 2022; Accepted 31 May 2022; Published 25 June 2022

Academic Editor: Xin Ning

In order to achieve efficient and accurate breast tumor recognition and diagnosis, this paper proposes a breast tumor ultrasound image segmentation method based on U-Net framework, combined with residual block and attention mechanism. In this method, the residual block is introduced into U-Net network for improvement to avoid the degradation of model performance caused by the gradient disappearance and reduce the training difficulty of deep network. At the same time, considering the features of spatial and channel attention, a fusion attention mechanism is proposed to be introduced into the image analysis model to improve the ability to obtain the feature information of ultrasound images and realize the accurate recognition and extraction of breast tumors. The experimental results show that the Dice index value of the proposed method can reach 0.921, which shows excellent image segmentation performance.

1. Introduction

As a malignant disease with high mortality, breast cancer has seriously threatened the physical and mental health and life safety of women worldwide [1, 2]. According to the American Cancer Society, in 2017, 255180 new cases of breast cancer and 41070 deaths of breast cancer were reported in the United States. In China, there are about 66 thousand female breast cancer deaths each year, accounting for 7.82% of the total number of deaths from female malignant tumors. After breast cancer cells proliferate, free diffusion can occur. Breast cancer forms a tumor metastasis site through local invasion, intravascular infiltration, circulatory system, and/or lymphatic system transmission [3–5]. Clinically, the process of multiple organ disease caused by metastasis is one of the important factors leading to high mortality of breast cancer. The prognosis of patients with metastatic breast cancer usually is not good, and the average 5-year survival rate is only 27%. In the formation of clinically detectable cancer cell metastasis, often the patient's condition has developed into advanced tumor [6]. Thus, early detection, early diagnosis, and early treatment of breast cancer are of great significance.

With the development and application of computer technology, researchers choose to continuously train the tumor ultrasound image dataset to learn with the help of deep learning network and independently extract the information features in the dataset, so as to realize noninvasive tumor medical auxiliary judgment [7]. However, it should also be noted that, due to the deep structure of the depth network model, the gradient is easy to disappear when training the dataset to learn, which makes it difficult for the image segmentation network model to realize accurate and effective tumor region recognition.

In this study, U-Net network and attention mechanism module are combined to construct breast tumor ultrasound image segmentation model, improve image recognition accuracy, and provide auxiliary reference for medical staff. The contributions of the proposed method lie in the following:

(1) The residual block is used to optimize and improve the U-Net network, and the residual mapping is

obtained by convoluting the input features through the convolution layer, which can effectively solve the gradient disappearance problem of the deep network.

(2) The hybrid attention mechanism module is added to the image segmentation model to optimize the training and learning process of the image segmentation model, enhance the information feature acquisition ability of the model, and support the accurate and efficient recognition of the image segmentation model.

The remaining chapters are arranged as follows. The second chapter introduces the relevant work in this field. The third chapter introduces the breast tumor ultrasound image segmentation method based on improved residual U-Net network. In Chapter 4, experiments are designed to verify the performance of the proposed model. The fifth chapter is the conclusion.

2. Related Researches

Image segmentation is a technology to extract the region of interest in the image according to the pixel features (gray, texture, etc.). For breast ultrasound images, the region of interest is the breast nodule. It is necessary to extract the diseased nodule from the normal tissue region to provide input data for the next classification operation. At present, the main algorithms proposed by domestic and foreign scholars in the research of ultrasound image segmentation are threshold and edge method, region method, graph theory and clustering method, energy functional method, and neural network method [8].

Traditional image segmentation algorithms, such as threshold method, edge method, and region method, do not easily obtain ideal segmentation results directly. General researchers will make a lot of improvements and integration on the above algorithms. Liu et al. [9] proposed a framework for fully automatic segmentation of breast ultrasound image lesion area, which used Otsu-based adaptive thresholding (OBAT) method and morphological filtering method to locate the region of interest (ROI) and initialize the nodule contour [9]. Jiang et al. [10] used AdaBoost + Haar framework to locate a set of potential lesion locations in breast ultrasound images [10]. However, if only these methods are used in the above references, when the gray difference of the image to be segmented is small, there is large overlap within the gray value range, or the noise is serious, the accuracy of lesion area segmentation will be greatly reduced, especially when there is fat area near the breast nodule or the contrast is low, which will seriously affect the segmentation effect. Therefore, after initializing the nodule contour, Liu et al. [9] achieved accurate segmentation of breast nodules by improving the Chan-Vese model. Jiang et al. [10] further screened the detected lesion area set by using Support Vector Machine (SVM) on the basis of the original framework and refined and segmented the lesion area by Random Walk algorithm.

In recent years, ultrasound image segmentation algorithm based on neural network has been proposed continuously. For example, Li et al. [11] used encoder-decoder structure to segment amniotic fluid and fetal tissue in fetal ultrasound image effectively [11]. Zhang et al. [12] segmented the lesion area of lymph node ultrasound image from coarse to fine by improving Fully Convolutional Networks (FCN) [12]. Wu et al. [13] used Convolutional Neural Networks (CNN) to find the ROI in the fetal abdomen in the ultrasound image and evaluated the image quality by judging the clarity of description of the key structures of gastric vesicle and umbilical vein through another CNN, so as to screen high-quality ultrasound images for the measurement of fetal Abdominal Circumference (AC) [13]. Ma et al. [14] and Ma et al. [15] randomly cut the thyroid ultrasound image into multiple overlapping subgraphs, took the pixel ratio of normal tissue to lesion area as the classification label of each subgraph, trained the Deep Convolutional Neural Networks (DCNN), and finally used the trained DCNN for subgraph-level classification to realize the lesion area segmentation of thyroid ultrasound image. Among them, some scholars have achieved good research results in the field of breast ultrasound image nodule segmentation. Wang and Jiao [16] proposed an improved Simplified Pulse Coupled Neural Network (SPCNN) combined with fuzzy mutual information, which took the maximum fuzzy mutual information as the optimal decision criterion to obtain the result of whether each pixel belongs to the nodule area, and carried out morphological processing on the binary image after pixel classification to extract the breast lesion area [16]. Cao et al. [17] conducted multiscale transformation of breast ultrasound dataset and input it into the current mainstream target detection framework (including Fast R–CNN, Faster R–CNN, YOLO, and SSD) and backbone network (ZF-Net, VGG-16) [17]. The results show that SSD300 is more suitable for breast ultrasound lesion extraction. Although the deep learning method has made good achievements in the field of natural image processing, due to the characteristics of ultrasound imaging, breast ultrasound images have defects such as low resolution, low contrast, and a large amount of speckle noise and artifacts, and due to data sensitivity, there is a lack of large public breast ultrasound dataset. For the above reasons, the dataset-driven deep learning technology is disturbed in breast ultrasound image processing [18].

Vakanski et al. [19] integrated visual saliency into the U-Net segmentation model, drove the model to give priority to the highly significant spatial region features in the image, and obtained good experimental results on a small sample dataset composed of 510 breast ultrasound images [19]. Zhang et al. [20] proposed to optimize the convolution network AlexNet network with full connection structure to obtain the information features of the image, so as to complete the ultrasound image analysis of breast mass [20]. Ilesanmi et al. [21] optimized the processing of breast ultrasound images based on cascaded convolution network to realize image information recognition and segmentation [21]. Tang et al. [22] introduced the Transform Modal Ensemble Learning module into the nonlocal network of feature pyramid to construct the breast ultrasound image-aided diagnosis model and realize autonomous image analysis [22]. Fang et al. [23] constructed a full convolution network model M-Net to realize breast abnormal image analysis. The above methods still have limitations [23]. Due to deep network structure, the gradient of image segmentation model may disappear when recognizing images, resulting in the decline of image segmentation accuracy. At the same time, due to the large noise interference in the ultrasound image, there is independent phase interference when the depth model obtains the image features, resulting in the further decline of segmentation accuracy. This paper proposes a recognition method for breast tumor ultrasound images, improves the U-Net network, and integrates it with the hybrid attention mechanism network, which overcomes the problems of the current depth network model.

3. The Proposed Image Segmentation Method

The overall framework of the proposed model is shown in Figure 1. The model takes U-Net as the backbone network structure and includes three parts: encoder module, hybrid attention module, and decoder module. In each level of the codec in Figure 1, the characteristic tensor passes through a residual block and a multiscale convolution block in turn. First, the image is subjected to residual multiscale convolution and downsampling encoding. At the same time, the feature map output at each level is copied to the decoder at the corresponding level through the attention module, and then the feature map obtained by downsampling is concatenate and upsampled. Finally, the breast tumor ultrasound image segmentation is realized through the loss function [24, 25]. In this method, the features extracted by the shallow encoder are connected to the corresponding level of the decoder through the attention module, which can give higher weight to the edge details in those shallow features and suppress the useless information or noise in the shallow features to a certain extent while retaining the edge information.

3.1. Residual Block. In order to extract more detailed information from the image and alleviate the problem of undersegmentation in low contrast areas and weak edges, residual blocks are introduced into U-Net to replace the traditional convolution layer. The use of residual blocks can solve the problem of gradient disappearance with the deepening of network layers. The calculation formula of residual block foundation is

$$u = c\left(v, w_h\right) + v, \tag{1}$$

where v and u are, respectively, the input and output of the network, w_h is the parameter of h-th layer, and $c\left(v, w_h\right)$ is the residual mapping. Using residual block learning to fit a residual map $u - v$ is easier than directly learning to fit an approximate identity map u. The residual block solves the problem of gradient disappearance in deep network. The partial derivative of formula (1) is

$$\frac{\partial u}{\partial v} = 1 + \frac{\partial c\left(v, w_h\right)}{\partial v}. \tag{2}$$

Since the gradient of formula (2) is always greater than 1, the gradient will not disappear with the deepening of the number of network layers. In general, the feature dimension of $c\left(v, w_h\right)$ is different from that of v, so linear transformation parameter w is introduced to complete dimension matching. The calculation formula is

$$u = c\left(v, w_h\right) + w_v. \tag{3}$$

The network structure of the residual block is shown in Figure 2. The input features are convoluted through two-standard 6×6 convolution layers to obtain the residual mapping, then the feature dimension matching is completed through the 1×1 convolution layer, and finally the feature fusion is completed through the Add operation. This module avoids the degradation of model performance caused by the disappearance of gradient, reduces the training difficulty of deep network, and only increases the 1×1 convolution layer, which will not increase the computational complexity of the model. At the same time, the module shortens the distance between the front and back layers, effectively improves the learning ability of features, and helps to extract more detailed information, which reduces the interference of low contrast between cells and background to the model to a certain extent.

3.2. Attention Module. Although the spatial attention can find the relationship between features and task objectives from a global perspective and strengthen the attention to the target task, the spatial attention ignores the information in the channel and treats the feature map in each channel equally. Based on the attention of the channel, the global context information is extracted through the global maximum pooling and average pooling. As a guide, the correlation of the global information is judged from the perspective of channel correlation, and then the global features with high correlation are selected [26]. However, the attention of the channel is to pool the information in the channel globally, which ignores the local information in each channel. Combining the above two kinds of attention, a Spatial Channel Attention Block (SCAB) is proposed to allocate the weights of channel and spatial attention. The specific implementation process is shown in Figure 3.

As can be seen from the figure, the output d can be obtained by the following formula:

$$d = \mathrm{Cat}\left[e_s, e_c\right], \tag{4}$$

where e_s is the feature with spatial attention and e_c is the feature with channel attention.

SCAB combines channel attention and spatial attention to obtain a comprehensive attention information. It not only analyzes the relationship between each pixel and the task target but also distinguishes the correlation between each channel and the task. Specifically, by inputting the input features $b \in R(G \times P \times Q)$ into the spatial attention block and the channel attention block, respectively, the output of the spatial attention block e_s and the output of the channel attention block e_c can be obtained. e_s and e_c are combined to get the final output $d \in R(G \times P \times Q)$.

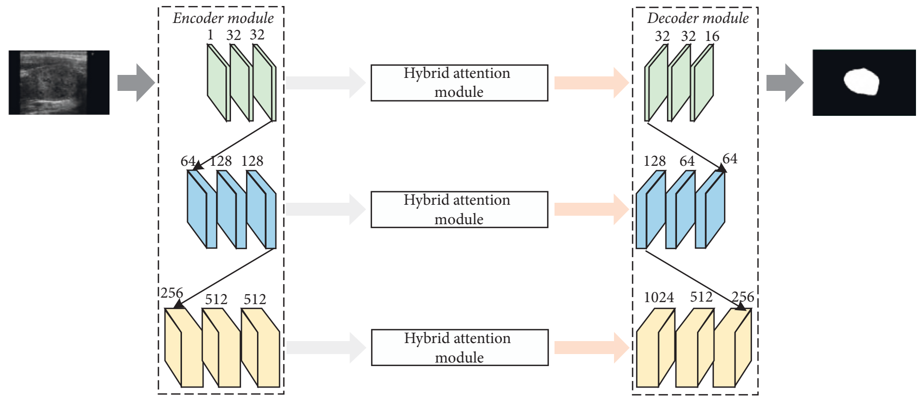

FIGURE 1: Image segmentation model based on improved residual U-Net network.

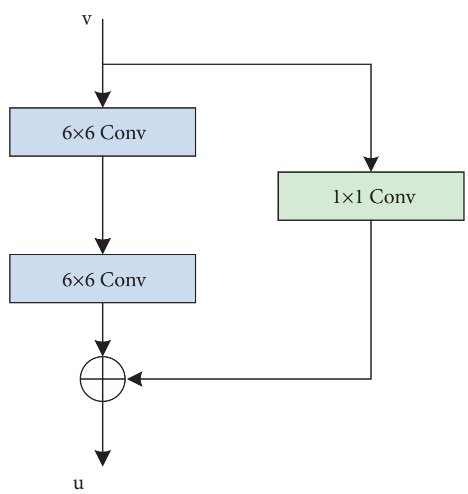

FIGURE 2: U-Net residual block structure.

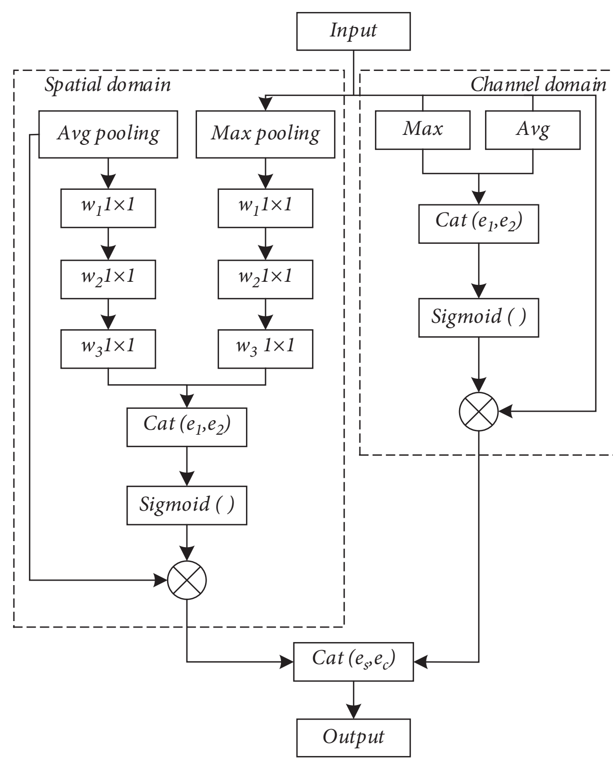

FIGURE 3: Space and channel attention module.

The structure of feature extraction block in U-Net is two 2×2 convolutions to extract the input features. The feature learning is carried out by fusing the input with the output in the way of skip connection. This method has the following advantages: (1) it simplifies the learning process and enhances the propagation of gradient. Due to the inclusion of residual structural identity, the backpropagation can be carried out effectively. (2) This design can break the asymmetry of the network. If only a small number of hidden units in each layer of the network change their activation value for different inputs, and most hidden units respond the same way to different inputs, the problem of network degradation will occur. (3) The generalization ability of the network is enhanced. Residual SCAB (RSCAB) is a new feature extraction module combined with attention mechanism and residual structure.

The specific implementation of RSCAB is as follows:

$$d_{\text{att}} = \text{SCAB}(\alpha\, d + \beta), \tag{5}$$

$$b = \alpha \text{Cat}\left[d_{\text{att}}, d\right] + \beta, \tag{6}$$

where the function of 1×1 convolution is to raise the input dimension. d_{att} is the feature map obtained by raising dimension and SCAB, and b is obtained by feature extraction again after feature fusion of d_{att} and d.

By embedding the attention transmitted by the residual connection, the module enables the network to obtain the location of the task target in the feature extraction stage. It has the following advantages:

(1) The shallow attention features are transferred to the deep by residual connection, which can pay more attention to the feature learning of the task target area.

(2) In this way, the interaction between layers can be closer, so as to facilitate the calculation of feature information.

(3) It enhances the information and gradient transmission between networks and facilitates the training of deeper networks.

3.3. Loss Function. In the classical U-Net model training, the output result of Softmax is used to calculate the cross entropy, which is regarded as the optimization function of the whole network. In medical image segmentation, there are usually only two classifications: lesions and background. At this time, the loss function is Binary Cross Entropy (BCE), and its formula is

$$\text{loss}_{\text{BCE}} = -\frac{1}{N}\left[t_j \sum_{j=1} p_j + \left(1 - t_j\right) \sum_{j=1} \left(1 - p_j\right)\right], \tag{7}$$

where N is the total number of pixels of the input image, t_j is the truth label of the j-th pixel, $t_j \in [0, 1]$ is the probability that the corresponding pixel is predicted as the foreground, 0 represents the background, and 1 represents the mass. When the number of foreground pixels is far less than the number of background pixels, that is, the number of $t_j = 0$ is far greater than the number of $t_j = 1$, the component $t_j = 0$ in the optimization process will dominate, making the model seriously biased towards the background.

There is a serious imbalance between foreground and background pixels in the dataset. Using the binary classification cross entropy loss function alone may mislead the optimization direction of the model and finally can only predict the meaningless background area with a larger area.

Dice similarity coefficient is a set similarity measurement function, which is usually used to calculate the similarity of two types of pixel samples, with a value range of [0, 1]. When the number difference between the two types of samples is huge, $\text{loss}_{\text{DICE}}$ can alleviate the problem of sample imbalance to a certain extent. $\text{loss}_{\text{DICE}}$ is defined as

$$\text{loss}_{\text{DICE}} = 1 - \frac{2\sum_j p_j t_j + \gamma}{\sum_j p_j^2 + \sum_j t_j^2 + \gamma}, \tag{8}$$

where γ is a constant added to maintain numerical stability and prevent denominator from changing to 0. In breast image segmentation, due to the extreme imbalance between tumor pixels and background pixels, using Dice loss function alone will make the whole optimization process unstable and reduce the reliability of the index. Therefore, in the training process, two loss functions are used to constrain the network training, and a weighted composite loss function loss_{NEW} is proposed, which is defined as follows:

$$\text{loss}_{\text{NEW}} = \tau \text{loss}_{\text{BCE}} + \text{loss}_{\text{DICE}}, \tag{9}$$

where τ is a constant weight to control the balance of optimization strength between cross entropy loss and Dice loss. After testing different τ values, it is found that better segmentation effect can be achieved at $\tau = 1.5 \times 10^{-3}$.

3.4. Network Training. Deep learning network training aims at minimizing the loss function and iteratively updating the weight parameters of the model. It consists of two parts: weight initialization and updating algorithm.

3.4.1. Weight Initialization. The weight initialization method in deep learning network model is very important, which affects the convergence performance and convergence speed of network model training. With the deepening of layers of neural network, the optimization method based on gradient descent is prone to gradient explosion and gradient disappearance, and a good weight initialization method can alleviate this problem.

The ReLU function is used as the activation function. The specific operation is to initialize the weight parameters of the convolution kernel using a Gaussian distribution with a mean value of 0 and a standard deviation of $\sqrt{2/\delta}$, where $\delta = k_r^2 z_{r-1}$, in which k_r refers to the size of the convolution kernel of r convolution layer and z_{r-1} represents the number of convolution kernels in the $r - 1$ layer.

3.4.2. Weight Update Method. The training of neural network is a process of finding the optimal value, and this process is actually a process of iteratively updating the weights. The optimization algorithm contains different weight updating methods. The optimization algorithm used in this paper is Adam algorithm. Adam algorithm is a stochastic optimization method of adaptive momentum, which iteratively updates the training parameters by combining the first-order moment and second-order moment information of the gradient. The specific update calculation is as follows:

$$y_t \leftarrow \nabla_\theta x_t\left(\theta_{t-1}\right), \tag{10}$$

$$o_t \leftarrow \varphi_1 \cdot o_{t-1} + \left(1 - \varphi_1\right) \cdot y_t, \tag{11}$$

$$z_t \leftarrow \varphi_2 \cdot z_{t-1} + \left(1 - \varphi_2\right) \cdot y_t^2. \tag{12}$$

$$\widehat{o}_t \leftarrow \frac{o_t}{\varphi_1}, \tag{13}$$

$$\widehat{z}_t \leftarrow \frac{z_t}{\varphi_2}, \tag{14}$$

$$\theta_t \leftarrow \theta_{t-1} - \frac{\varepsilon \cdot \widehat{o}_t}{\left(\sqrt{\widehat{z}_t + \sigma}\right)}, \tag{15}$$

where t is the number of iterations, $x(\theta)$ refers to the loss function, θ is the training parameter, that is, the weight or bias, y_t is the gradient calculated by the derivation of the loss function from the training parameter, φ_1 is the first-order moment attenuation coefficient, φ_2 is the second-order moment attenuation coefficient, ε is the learning rate, o_t is the first-order moment of the gradient y_t, z_t is the second-order moment of the gradient y_t, $\widehat{o}_t$ and $\widehat{z}_t$ are the deviation correction of o_t and z_t, and σ is a positive number to prevent the denominator from being zero.

The value of each parameter is as follows: $\varphi_1 = 0.95$, $\varphi_2 = 1.00$, $\varepsilon = 0.00015$, and $\sigma = 1.5 \times 10^{-8}$. Adam algorithm combines the characteristics of momentum method and RMSprop method to jump out of the local optimal solution as much as possible and accelerate the convergence speed of the network.

4. Experiment and Analysis

The computer hardware configuration of the experimental simulation is Intel Core i5-10400 and Nvidia GeForce RTX 3080Ti. The network model is trained and tested using the Keras open-source library with TensorFlow as the backend.

4.1. Experimental Dataset and Preprocessing. The experimental dataset is the Wisconsin Diagnostic Breast Cancer (WDBC) dataset. Breast ultrasound image has three inherent characteristics, including high noise, low contrast, and nonuniformity. Therefore, the segmentation of breast ultrasound image is still a challenging task. At the same time, a series of preprocessing operations are needed to process this kind of image.

4.1.1. Cutting of Region of Interest. For breast ultrasound image segmentation task, the region of interest is breast tumor. In the original breast ultrasound image, the proportion of tumor area is often small. In order to improve the efficiency of subsequent superpixel generation, the region of interest of the original image is cut. In the original breast ultrasound image, the operator determines two diagonal points and then draws a rectangular box. The box needs to meet two requirements: (1) the rectangular box contains breast tumors and (2) the area of the tumor accounts for about 30% of the area of the rectangular box. The region of interest is cut from the original Image, which greatly reduces the interference of irrelevant regions and improves the efficiency of the algorithm.

4.1.2. Image Denoising. Breast ultrasound image is full of noise, and the main noise is speckle noise, which needs denoising. In this paper, bilateral filter is used. The ultrasound image is denoised by bilateral filter. The filtering process integrates the gray similarity and spatial information between pixels, which can not only preserve the tumor edge but also reduce the noise.

4.1.3. Contrast Enhancement. In addition to high noise, breast ultrasound images also have the characteristics of low contrast. Specifically, the gray values of breast tumor area and some adjacent normal tissue areas are close, and the difference is small. It is easy to mistake this part of normal tissue area for tumor area. Therefore, it is necessary to enhance the contrast and the method of gray histogram equalization is adopted. The mathematical description of the specific transformation of histogram equalization is as follows:

$$e_j = U\left(v_j\right) = \sum_{i=1}^{j} G\left(v_i\right) = \sum_{i=1}^{j} \frac{c_i}{c}, \quad j = 1, 2, \ldots, J, \tag{16}$$

where the number of pixels of the input image is c, J represents the gray level, $G(v_i), i = 1, 2, \ldots, J$ represents the gray histogram of the region of interest, c_i is the number of pixels with gray level i, v_i is the gray value of the image before processing, and e_j is the gray value after equalization. The flow of image preprocessing is shown in Figure 4.

4.2. Evaluation Index. In addition to the loss function mentioned above, the ultrasound image segmentation reference indices with universality, objectivity, and quantifiability are still selected to evaluate the above algorithm, specifically including Dice, Intersection over Union (IoU), Hausdorff Distance (HD), and Mean Absolute Deviation (MAD). Dice is a regional error evaluation method. The pixels of the segmented region and the actual lesion area are calculated in a certain way. The higher the value, the better the segmentation effect. The principle of IoU is similar to the previous index, which refers to the overlap rate between the segmented area and ROI. In the ideal state, the ratio is 1; that is, the two completely overlap. Hausdorff Distance (HD) measures the maximum distance between the boundary generated by segmentation and the true subset of the actual lesion area. The lower the value, the smaller the boundary error. Mean Absolute Deviation (MAD) reflects the average dispersion between the real lesion area and the segmented area pixels. The lower the value, the more accurate the segmentation. The calculation formulas are shown in (17)–(20).

$$\text{Dice} = \frac{2|R \cap G|}{(|R| + |G|)}, \tag{17}$$

where R is the segmentation result area and G is the real lesion area.

$$\text{IoU} = \frac{|R \cap G|}{|R \cup G|}, \tag{18}$$

$$\text{HD} = \max\left\{\max_{x \in R}\{d(x, G)\}, \max_{y \in G}\{d(y, R)\}\right\}, \tag{19}$$

where $d(x, C) = \max_{y \in G}\{\|x - y\|\}$, $C = R \text{ or } G$.

$$\text{MAD} = \frac{1}{2}\left(\sum_{x \in R} \frac{d(x, G)}{N_R} + \sum_{y \in G} \frac{d(y, R)}{N_G}\right), \tag{20}$$

where N_R is the total number of pixels in the segmentation result area and N_G is the total number of pixels in the real lesion area.

4.3. Ultrasound Image Segmentation Model Analysis. In order to prove the feasibility of the proposed model, first, the performance of the segmentation model is evaluated. Figure 5 shows the change of Dice value curve on the validation set when the proposed network uses different loss functions in the training process, including loss function $\text{loss}_{\text{DICE}}$, loss function loss_{BCE}, and composite weighted loss function loss_{NEW} proposed in this experiment.

It can be seen from Figure 5 that when using the composite weighted loss function loss_{NEW} for training, the Dice value curve rises steadily, and the segmentation accuracy can reach more than 0.95 on the validation set in the

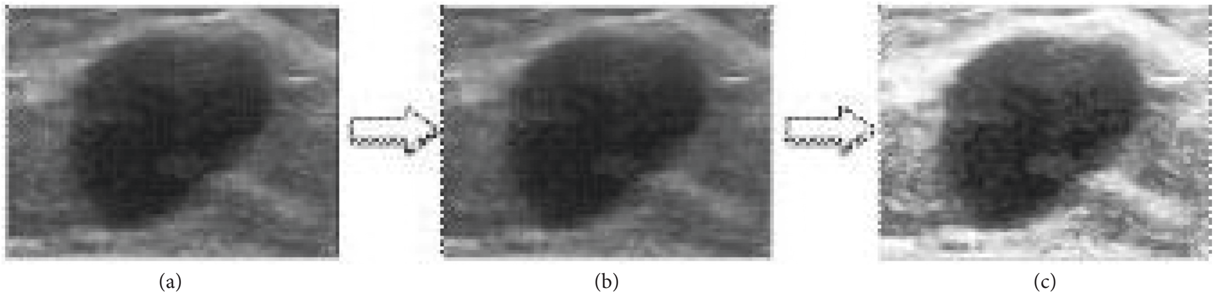

Figure 4: Process of image preprocessing. (a) Captured image. (b) Denoised image. (c) Enhanced image.

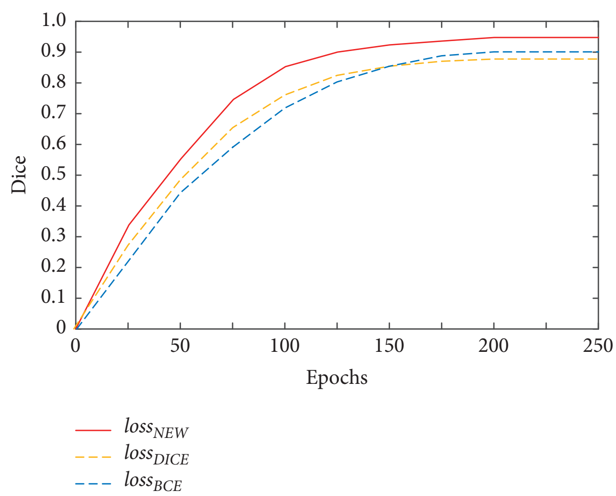

Figure 5: Changes of Dice value under different loss functions.

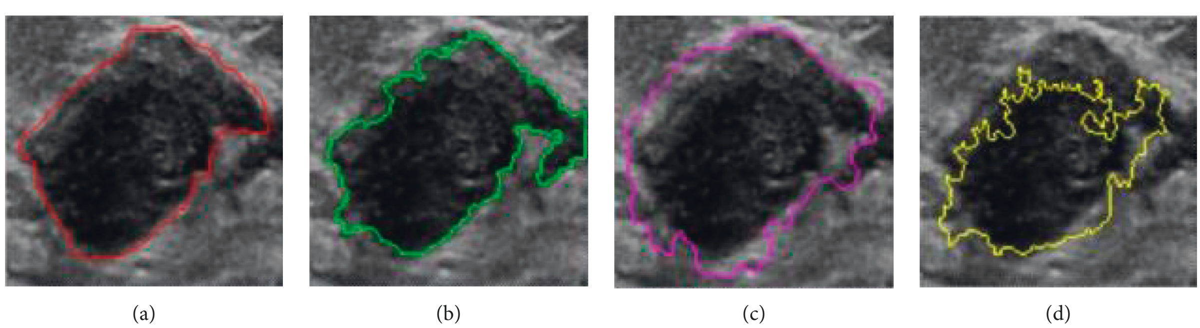

Figure 6: Image segmentation results under different methods. (a) Manual label. (b) Proposed model. (c) Reference [20]. (d) Reference [23].

later stage of training, while the other two loss functions enter the training bottleneck after reaching more than 0.85, and the Dice values do not break through 0.9 in the end.

Using [20, 23] as comparison methods, the experimental datasets are analyzed in the same environment. As shown in Figure 6, different colors represent the segmentation contour obtained by different methods. Among them, (a) is the image with the contour manually labeled by the doctor, (b) is the result of the segmentation model proposed in this paper, (c) is the segmentation result of the method in [20], and (d) is the segmentation result of the method in [23].

According to the qualitative experimental results shown in Figure 6, the segmentation performance of the segmentation model proposed in this paper is better than the comparison algorithms. Although there are still some defects in the extracted edge, compared with the other two methods, it is the closest to the manually labeled edge and has better visual effect. Methods of [20, 23] produce a certain degree of undersegmentation, the edge obtained by [23] is also rough, and [20] produces obvious oversegmentation. The reason is that the comparison method cannot obtain the data features in the sample set well and ignores some local features in the image. The segmentation model proposed in this paper adds the fusion attention mechanism module to the model, which can realize the global data feature extraction and analysis and help to realize the accurate image segmentation combined

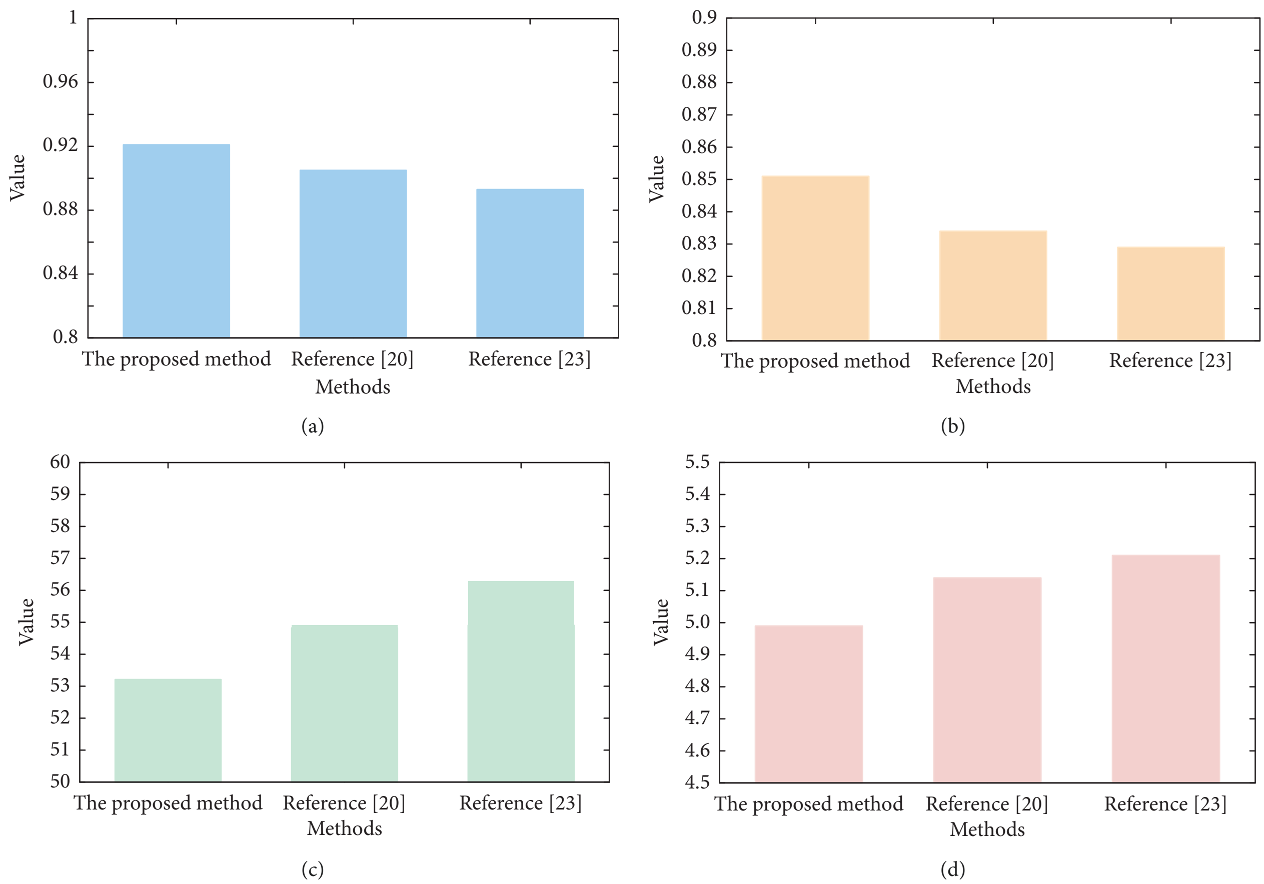

Figure 7: Comparison of segmentation results of different methods. (a) Dice index. (b) IoU index. (c) HD index. (d) MAD index.

with context-related information. In addition, due to the improvement and optimization of the loss function, it can also make the model perform calculation and analysis in the direction of global optimization, so as to avoid the interference of noise on the recognition results.

Further quantitative analysis is carried out. Figure 7 shows the comparison of quantitative segmentation results of different methods.

It can also be seen from Figure 7 that, for the analysis of ultrasound images of complex breast tumors, the segmentation errors of the comparison methods are large, and the accuracy of the proposed model is higher than those of other comparison methods. The Dice value of the proposed method is 0.921, which is 0.016 and 0.028 higher than those in [20, 23]. In terms of nodule edge segmentation accuracy, the HD index of the proposed model is 3.08 lower than that in [23]. IoU is 0.851 and MAD is 4.99, which are better than the evaluation indices in [20, 23]. This shows that the proposed model can effectively improve the accuracy of ultrasound image region segmentation.

5. Conclusion

A breast tumor ultrasound image segmentation method based on improved residual U-Net network is proposed. The U-Net network model is improved by introducing residual block optimization to avoid the disappearance of gradient caused by too deep network structure. Furthermore, the hybrid attention mechanism network is introduced into the ultrasound image segmentation model to obtain the global information features of the sample dataset and effectively improve the image analysis performance of the analysis model. The experimental results show that the proposed method can realize the analysis and processing of actual complex breast tumor ultrasound images and provide reliable medical diagnosis assistance for medical staff.

This paper mainly studies the shape feature constraints of breast nodules, but the situation of breast ultrasound images is complex and changeable. In real life, there are other types of difficult samples based on texture characteristics such as artifact and calcification. How to automatically mine these different types of difficult samples becomes the next research work.

Data Availability

The data used to support the findings of this study are included within the article.

Conflicts of Interest

The authors declare that there are no conflicts of interest regarding the publication of this paper.

Acknowledgments

This work was supported by the General Foundation of Qiqihar Academy of Medical Sciences in 2021, "Research on Ultrasonic Image Segmentation of Breast Tumor Based on Improved Particle Swarm Optimization Algorithm" (Project no. QMSI2021M-06).

References

[1] Y. J. Sun, Z. Y. Qu, and Y. H. Li, "Research on breast tumor target detection based on improved mask R-CNN," *Acta Optica Sinica*, vol. 41, no. 2, pp. 97–105, 2021.

[2] C. Kaushal, K. Kaushal, and A. Singla, "Firefly optimization based segmentation technique to analyze medical images of breast cancer," *International Journal of Computer Mathematics*, vol. 98, no. 7, pp. 1293–1308, 2020.

[3] V. J. Kriti and R. Agarwal, "Assessment of despeckle filtering algorithms for segmentation of breast tumours from ultrasound images," *Biocybernetics and Biomedical Engineering*, vol. 39, no. 1, pp. 100–121, 2019.

[4] W. X. Liao, P. He, J. Hao et al., "Automatic identification of breast ultrasound image based on supervised block-based region segmentation algorithm and features combination migration deep learning model," *IEEE Journal of Biomedical and Health Informatics*, vol. 24, no. 4, pp. 984–993, 2020.

[5] X. Wang, Y. Guo, Y. Wang, and J. Yu, "Automatic breast tumor detection in ABVS images based on convolutional neural network and superpixel patterns," *Neural Computing & Applications*, vol. 31, no. 4, pp. 1069–1081, 2019.

[6] A. Tashk, T. Hopp, and N. V. Ruiter, "An innovative practical automatic segmentation of ultrasound computer tomography images acquired from USCT system," *Iranian Journal of Science & Technology Transactions of Electrical Engineering*, vol. 43, no. 2, pp. 167–180, 2019.

[7] K. Wang, S. J. Liang, S. Zhong, Q. Feng, Z. Ning, and Y. Zhang, "Breast ultrasound image segmentation: a coarse-to-fine fusion convolutional neural network," *Medical Physics*, vol. 48, no. 8, pp. 4262–4278, 2021.

[8] Z. Y. Ning, S. Z. Zhong, Q. J. Feng, W. Chen, and Y. Zhang, "SMU-net: saliency-guided morphology-aware U-net for breast lesion segmentation in ultrasound image," *IEEE Transactions on Medical Imaging*, vol. 41, no. 2, pp. 476–490, 2022.

[9] L. Liu, K. Li, W. Qin et al., "Automated breast tumor detection and segmentation with a novel computational framework of whole ultrasound images," *Medical, & Biological Engineering & Computing*, vol. 56, no. 2, pp. 183–199, 2018.

[10] P. Jiang, J. Peng, G. Zhang, E. Cheng, V. Megalooikonomou, and H. Ling, "Learning-based Automatic Breast Tumor Detection and Segmentation in Ultrasound images," in *Proceedings of the 2012 9th IEEE International Symposium on Biomedical Imaging (ISBI)*, pp. 1587–1590, Barcelona, Spain, May2012.

[11] Y. Li, R. Xu, J. Ohya, and H. Iwata, "Automatic fetal body and amniotic fluid segmentation from fetal ultrasound images by encoder-decoder network with inner layers," in *Proceedings of 2017 39th Annual International Conference of the IEEE Engineering in Medicine and Biology Society*, pp. 1485–1488, Seogwipo, South Korea, July2017.

[12] Y. Zhang, M. T. C. Ying, L. Yang, A. T. Ahuja, and D. Z. Chen, "Coarse-to-fine stacked fully convolutional nets for lymph node segmentation in ultrasound images," in *Proceedings of 2016 IEEE International Conference on Bioinformatics and Biomedicine*, pp. 443–448, Shenzhen, China, December2016.

[13] L. Wu, J. Z. Cheng, S. Li, B. Lei, T. Wang, and D. Ni, "FUIQA: fetal ultrasound image quality assessment with deep convolutional networks," *IEEE Transactions on Cybernetics*, vol. 47, no. 5, pp. 1336–1349, 2017.

[14] J. Ma, F. Wu, T. Jiang, Q. Zhao, and D. Kong, "Ultrasound image-based thyroid nodule automatic segmentation using convolutional neural networks," *International Journal of Computer Assisted Radiology and Surgery*, vol. 12, pp. 1895–1910, 2017.

[15] J. Ma, F. Wu, T. Jiang, J. Zhu, and D. Kong, "Cascade convolutional neural networks for automatic detection of thyroid nodules in ultrasound images," *Medical Physics*, vol. 44, no. 5, pp. 1678–1691, 2017.

[16] Y. Wang and J. Jiao, "Detection of regions of interest from breast tumor ultrasound images using improved PCNN," *Optics and Precision Engineering*, vol. 19, no. 6, pp. 1398–1405, 2011.

[17] Z. Cao, L. Duan, G. Yang et al., "Breast Tumor Detection in Ultrasound Images Using Deep Learning," in *Proceedings of the International Workshop on, Patch-Based Techniques in Medical Imaging*, pp. 121–128, Quebec City, Canada, Augest 2017.

[18] H. Greenspan, B. Van Ginneken, and R. M. Summers, "Guest editorial deep learning in medical imaging: overview and future promise of an exciting new technique," *IEEE Transactions on Medical Imaging*, vol. 35, no. 5, pp. 1153–1159, 2016.

[19] A. Vakanski, M. Xian, and P. Freer, "Attention enriched deep learning model for breast tumor segmentation in ultrasound images," *Ultrasound in Medicine and Biology*, vol. 46, no. 10, pp. 2819–2833, 2020.

[20] Y. Zhang, Y. Liu, H. Cheng, Z. Li, and C. Liu, "Fully multi-target segmentation for breast ultrasound image based on fully convolutional network," *Medical, & Biological Engineering & Computing*, vol. 58, no. 1, pp. 2049–2061, 2020.

[21] A. E. Ilesanmi, U. Chaumrattanakul, and S. S. Makhanov, "A method for segmentation of tumors in breast ultrasound images using the variant enhanced deep learning," *Biocybernetics and Biomedical Engineering*, vol. 41, no. 2, pp. 802–818, 2021.

[22] P. Tang, X. Yan, Y. Nan, S. Xiang, and Q. Liang, "Feature pyramid non-local network with Transform modal Ensemble learning for breast tumor segmentation in ultrasound images," *IEEE Transactions on Ultrasonics, Ferroelectrics, and Frequency Control*, vol. 68, no. 12, pp. 3549–3559, 2021.

[23] Z. Fang, M. Y. Qiao, Y. Guo et al., "Combining a fully convolutional network and an active contour model for automatic 2D breast tumor segmentation from ultrasound images," *Journal of Medical Imaging and Health Informatics*, vol. 9, no. 7, pp. 1510–1515, 2019.

[24] J. Y. Li, L. L. Cheng, T. J. Xia, H. Ni, and J. Li, "Multi-scale fusion U-net for the segmentation of breast lesions," *IEEE Access*, vol. 9, no. 1, pp. 137125–137139, 2021.

[25] S. Hussain, X. M. Xi, I. Ullah et al., "Contextual level-set method for breast tumor segmentation," *IEEE Access*, vol. 8, no. 1, pp. 189343–189353, 2020.

[26] H. Lee, J. Park, and J. Y. Hwang, "Channel attention module with multiscale grid average pooling for breast cancer segmentation in an ultrasound image," *IEEE Transactions on Ultrasonics, Ferroelectrics, and Frequency Control*, vol. 67, no. 7, pp. 1344–1353, 2020.

Hindawi
Computational Intelligence and Neuroscience
Volume 2023, Article ID 9816045, 1 page
https://doi.org/10.1155/2023/9816045

Retraction

Retracted: Evolutionary Analysis of Supply Chain Integration Strategy on Chinese Steel-Producing Firms considering Policy Risk Cost Factor

Computational Intelligence and Neuroscience

Received 25 July 2023; Accepted 25 July 2023; Published 26 July 2023

This article has been retracted by Hindawi following an investigation undertaken by the publisher [1]. This investigation has uncovered evidence of one or more of the following indicators of systematic manipulation of the publication process:

(1) Discrepancies in scope
(2) Discrepancies in the description of the research reported
(3) Discrepancies between the availability of data and the research described
(4) Inappropriate citations
(5) Incoherent, meaningless and/or irrelevant content included in the article
(6) Peer-review manipulation

The presence of these indicators undermines our confidence in the integrity of the article's content and we cannot, therefore, vouch for its reliability. Please note that this notice is intended solely to alert readers that the content of this article is unreliable. We have not investigated whether authors were aware of or involved in the systematic manipulation of the publication process.

Wiley and Hindawi regrets that the usual quality checks did not identify these issues before publication and have since put additional measures in place to safeguard research integrity.

We wish to credit our own Research Integrity and Research Publishing teams and anonymous and named external researchers and research integrity experts for contributing to this investigation.

The corresponding author, as the representative of all authors, has been given the opportunity to register their agreement or disagreement to this retraction. We have kept a record of any response received.

References

[1] L. Zhu, R. Zhou, X. Li, and J. Chen, "Evolutionary Analysis of Supply Chain Integration Strategy on Chinese Steel-Producing Firms considering Policy Risk Cost Factor," *Computational Intelligence and Neuroscience*, vol. 2022, Article ID 1136601, 11 pages, 2022.

Hindawi
Computational Intelligence and Neuroscience
Volume 2022, Article ID 1136601, 11 pages
https://doi.org/10.1155/2022/1136601

Research Article

Evolutionary Analysis of Supply Chain Integration Strategy on Chinese Steel-Producing Firms considering Policy Risk Cost Factor

Lequn Zhu[1] **Ran Zhou**[1] **Xiaojun Li**[1] **and Jie Chen**[2]

[1]*Tianjin Research Institute for Water Transport Engineering, M.O.T., Tianjin, China*
[2]*Department of Management, Shenzhen Polytechnic, Shenzhen, China*

Correspondence should be addressed to Jie Chen; chenjie@szpt.edu.cn

Received 26 May 2022; Accepted 11 June 2022; Published 25 June 2022

Academic Editor: Xin Ning

Despite a number of adverse factors, China's steel industry has maintained a rapid growth trend. China continues to consume two-thirds of the world's iron ore, the majority of which is imported. In this context, Chinese steel companies have begun to consider integrating their supply chains to increase efficiency and lower costs. However, the increasingly volatile international environment makes this an extremely risky proposition. As a result, the issue of how Chinese steel producers should participate in global supply chain integration has emerged as a critical research question that requires investigation. In this paper, we examine the supply chain integration problem using a typical China–Australia steel trade as an example. Specifically, we discuss in detail whether relevant firms should continue to promote supply chain integration in the Chinese–Australian steel industry, as well as the decision boundary of influence, using evolutionary game theory and policy risk cost factors. The empirical analysis demonstrates that policy risk has a range of effects on different types of steel firms. Even when international tensions are considered, smaller steel companies may retain a greater willingness to integrate their supply chains. Overall, the above findings can provide necessary decision support for enterprises to formulate supply chain management strategies.

1. Introduction

Iron ore is one of the main raw materials of the steel industry. The bulk of Chinese iron ore reserves is of a poor grade, technically difficult to exploit, and located far from the major steel-producing centers on the eastern seaboard [1] (pp. 1084–1094). With the rapid development of the domestic steel industry, Chinese iron ore reserves and their exploitation cannot meet the large demand. Australia has long been China's primary iron ore supplier [2] (pp. 95–106). Despite the impact of the COVID-19 pandemic in 2019 and the deterioration of China–Australia relations, the two countries' iron ore trade has remained relatively stable. In 2020, China imported 712.986 million tons of iron ore from Australia (see Figure 1), accounting for 60.93 percent of total Chinese iron ore imports. It demonstrates that Australia remains a vital and irreplaceable source of high-quality iron ore for China.

Of course, the impact of political factors on the China–Australia iron ore trade cannot be underestimated. With the development of an intense rivalry between the two countries, both governments have imposed a number of explicit and implicit restrictions on iron ore trade and business cooperation in related areas. The Chinese government, for example, has restricted the offloading of iron ore ships from Australia and is actively developing or seeking alternative sources of Australian iron ore in Southeast Asia. The Australian government also announced plans to cancel mining rights already acquired by some Chinese companies in April 2021. Once implemented, the aforementioned measures will undoubtedly result in massive financial losses for the affected companies.

Although political factors have had a significant negative impact on the two countries' iron ore trade, both governments are well aware of the economic fundamentals: the iron

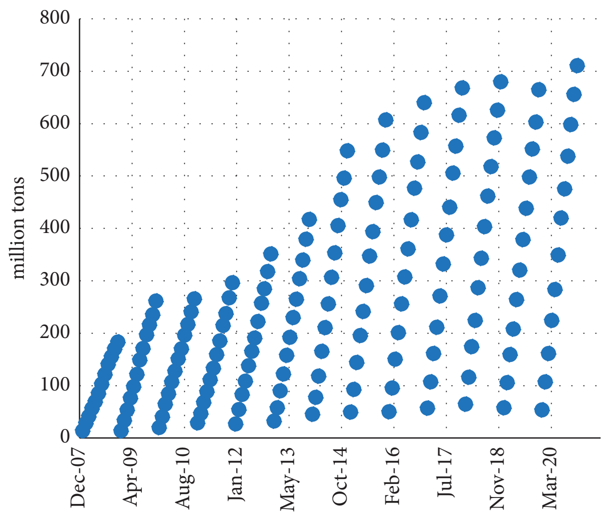

Figure 1: Comparison of cumulative annual data of Australian iron ore imports, 2006–2020.

ore trade between Australia and China cannot be artificially halted [3] (pp. 331–339). On the one hand, the China–Australia iron ore trade is critical to Australia's economic development, and a complete shutdown of the China–Australia iron ore trade would severely impair Australia's economic growth. On the other hand, China would have difficulty obtaining such a large supply of high-quality iron ore from other global suppliers. Additionally, Chinese companies have already invested significant capital in Australia. Numerous projects have been secured or put into operation, and the industrial integration of related resources is progressing steadily. As a result, we believe that with the adjustment of the new U.S. administration's anti-China sanctions policy, the intensity of trade frictions between China and Australia is likely to decrease, resulting in the recovery of the China–Australia iron ore trade.

In the aforementioned complex international political and economic environment, how Chinese steel producers should participate in the Chinese–Australian steel industry's supply chain integration (SCI) has become an important issue worth investigating. SCI takes many forms in practice, including the purchase of mining rights, direct investment in ore exploration or smelting, and so forth. Although SCI can help steel producers lower their operating costs and improve their competitiveness, it can also make them more vulnerable to changes in the trade environment and policies, exposing them to more operational risks. As a result, the decision makers in Chinese steel producers and the Chinese government must respond two questions in the face of an increasingly complex economic and trade environment, which are as follows: is it necessary for steel producers to continue to promote SCI? What effect will trade restrictions on iron ore have on Chinese steel producers' SCI? Based on evolutionary game theory, we will discuss these research questions in depth in this paper.

Overall, the contributions of this paper are broadly twofold. Firstly, for the first time, we consider the impact of political factors on related trade activities in the discussion of iron ore trade. Secondly, we use an evolutionary game model to provide decision recommendations of practical value for Chinese steel firms' decisions.

The remainder of this paper is divided into the following sections: Section 2 examines the relevant literature and identifies the research gap this paper attempts to fill. The model is introduced in Section 4, where we also analyze the evolutionary game and the case study we later conduct in Section 5. Section 3 introduces the evolutionary game framework of this paper, introducing the relevant hypotheses and the game mechanism. Section 4 introduces the model, where we also analyze the evolutionary game, and Section 5 introduces the case study we conduct. Finally, Section 6 contains the paper's conclusion and policy recommendations.

2. Literature Review

Over the years, scholars' focus on SCI practices has shifted significantly [4] (pp. 353–361) [5] (pp. 42–55). The majority of these studies agree on the fundamental premise that implementing SCI effectively throughout the supply chain is vital to modern businesses' capacity to maintain a competitive edge [6] (pp. 24–41).

Robinson believes that a paradigm shift is taking place in which value is sought and delivered through integrative efficiency rather than operational efficiency [7] (pp. 89–106). Effective SCI is crucial for some firms to minimize supply chain expenses and achieve a competitive edge [8] (pp. 119–134). Establishing strategic partnerships or alliances with suppliers increases the interaction between businesses and suppliers, enhancing the supply chain's performance [9] (pp. 58–71). SCI appears to be a primary method for Chinese steel makers to address their iron ore supply chain difficulties. For example, Baosteel Group, the second largest steel-producing company in China and the fourth largest steel-producing company in the world, established Baosteel Resources as a wholly owned subsidiary that is mainly engaged in mineral resource investment, trade, and logistics services and claimed that its 2009 investment in Aquila Resources would strengthen Baosteel's control over resources and lower purchasing costs.

Although most researchers accept that SCI can contribute to increasing supply network performance, it is notable that only a few studies have focused on the conditions of implementing SCI because SCI is not applicable in all cases. Mouritsen et al. demonstrate that similar levels of implementation of SCI practices do not always result in comparable improvements [10] (pp. 686–695). O'Leary-Kelly and Flores, as well as Wong et al., emphasize the urgent need to understand the conditions that maximize performance improvements [11] (pp. 221–240) [12] (pp. 604–615). Smith et al. note that trade costs along domestic and international supply chains in Asian economies can be significantly reduced by improving the logistics performance in each mode of transport involved in various logistics and supply chain transactions [13].

If steel-producing firms choose SCI, they must bear a considerable investment cost and substantial financial pressure. Although Chinese steel-producing firms can obtain assistance from the Chinese state-owned banking system, which can provide steel-producing firms loan finance on concessionary terms for investment in iron ore projects overseas, applying this strategy entails high risk and capital costs. Therefore, it is essential to investigate the conditions under which SCI can be more beneficial for Chinese steel-producing firms. As a result, it is critical to investigate the circumstances under which SCI can be more beneficial to Chinese steel producers.

Numerous scholars have already conducted research on the implementation conditions of SCI. According to Beresford et al., the optimal mode of transport for iron ore is a combination of sea and rail [14] (pp. 32–42). The global supply chain for iron ore is complex and involves multiple, diverse stakeholders, including foreign iron ore suppliers, foreign port authorities, shipping companies, domestic port authorities, and domestic logistics service providers. This makes it extremely difficult to directly assess SCI implementation conditions. However, the steel production market is typically monopolistic, which allows for the possibility of analyzing the implementation of SCI in this market. For instance, a monopolistic steel manufacturer can have a significant impact on another firm's decision to adopt SCI by adjusting the price of its products.

This study builds on this foundation by employing an evolutionary game approach to analyze the decision-making behavior of participants in the steel-producing market. From a managerial perspective, this paper emphasizes the critical nature of comprehending the conditions that enable SCI to be highly effective, as well as the impact of government relationships on the revenue of the companies involved and their willingness to integrate the supply chain.

3. Game Model

3.1. Problem Description and Setting. As the systematic establishment of SCI is not easily accomplished in a short period of time [5] (pp. 42–55), we can regard SCI as a long-term process. Additionally, while implementing SCI may result in increased productivity, it may also amplify the impact of political risk factors on a company's manufacturing activities. Because SCI connects steel producers to iron ore suppliers, the more integrated a supply chain, the greater the political risk the businesses face. We established the steel and iron ore supply markets as follows based on the foregoing facts.

Assume there are two distinct types of firms in the market (designated firm A and firm B), and they differ substantially in terms of not only profitability but also in SCI costs [15] (pp. 235–253). For each type of firm, two pure strategies are assumed: SCI or no SCI, and to simplify the problem, SCI is defined as the acquisition of mineral resource exploration rights, resource extraction facilities, and transportation investments. Additionally, we assume that the two types of firms are in an incomplete information game relationship, which means that they both have limited cognition and lack access to all necessary information when making SCI decisions. As a result, they cannot make perfectly rational decisions and must instead revise their decision strategies based on incomplete information, gradually improving their position in the game through adaptive learning in the process of continuous improvement. Furthermore, we postulate that the outcomes of the SCI decisions made by two distinct types of firms can affect one another.

The cost of SCI is assumed to consist of two components [16] (pp. 281–294). One is the fixed cost incurred as a result of chain integration, which includes investment in resource exploration, excavation, and transportation. The other is the loss incurred as a result of investment not being recovered (or the project being unable to proceed) because of political factors when Chinese firms invest their fixed assets overseas. In the following, we will utilize the fixed asset investment loss ratio to quantify the cost increase caused by political considerations. For instance, if we assume that the relationship between the Chinese and Australian governments deteriorates significantly and Chinese firms' licenses to develop mineral resources in Australia are completely terminated, then the associated loss ratio of investment is 100 percent, and this coefficient is treated as an exogenous variable in subsequent discussions.

In summary, we assume that the firms A and B face limited cognitive and information access difficulties, are not completely rational, and have asymmetric strategy choices and benefits. As a result, the problem is an asymmetric evolutionary game with imperfect information. As firms A and B must determine whether to integrate their supply chains in this game, there are four possible outcomes, as illustrated in Figure 2. We use the vectors (π_A^1, π_B^1), (π_A^2, π_B^2), (π_A^3, π_B^3), and (π_A^4, π_B^4) to denote the payoff of each game participant in different situations. For instance, in the first case, π_A^1 symbolizes the payment to firm A (where firms A and B implement integration strategies). The payouts of firms A and B are calculated in Table 1 for a variety of game outcomes.

3.2. Evolutionary Game Model. We investigate the behavior of firms A and B described above in this paper using an evolutionary game framework. The fundamental premise of this framework is to represent the two distinct types of firms as two distinct biological groups, dubbed group A and group B [17] (pp. 32–38). Individuals in the two groups mimic and refine their own strategies based on the available local information, and therefore, they learn to optimize their returns adaptively in a multistage (denoted as t) dynamic game process. Finally, the two groups' game results are evaluated in terms of the proportion of people who choose distinct decision options in the game equilibrium.

According to this framework, we use the terms x and x' for group A to denote individuals who use integrated versus nonintegrated strategies and $s_t(x)$ and $s_t(x')$ to denote the proportion of individuals who use strategies x and x′ in group A at stage t, respectively. For group B, we define similar variables, y and y' to denote individuals who use integrated versus nonintegrated strategies, and $s_t(y)$ and $s_t(y')$ to denote the proportion of individuals who use

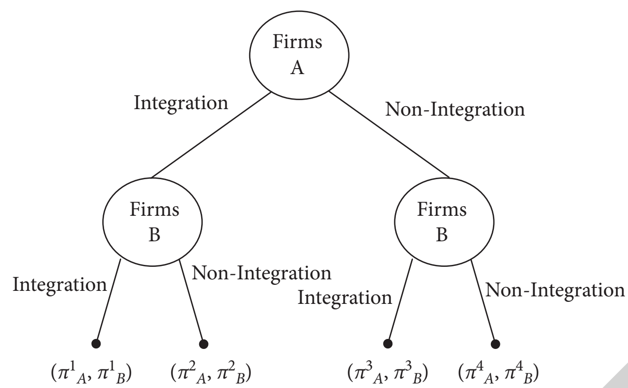

Figure 2: The four situations of the game.

Table 1: The payoff under different situations.

Firms A	Firms B	
	Integration	Nonintegration
Integration	$(P_A + S_A - C_A - R_A,\ P_B + S_B - C_B - R_B)$	$(P_A + S_A - C_A - R_A + E_A,\ P_B - L_B)$
Nonintegration	$(P_A - L_A,\ P_B + S_B - C_B - R_B + E_B)$	$(P_A,\ P_B)$

where P_A, P_B are the original profits of group A and group B under the nonintegration strategy. S_A, S_B are the supply chain cost savings of group A and group B under the integration strategy. C_A, C_B are the costs of supply chain integration of group A and group B. R_A, R_B are the SCI costs of risk $R_A = \alpha C_A$, $R_B = \alpha C_B$, where α is the investment loss ratio. E_A, E_B are the extra earnings of group A and group B. L_A, L_B are the extra losses of group A and group B.

strategies y and y' in group B at stage t, respectively. Based on the above settings, we can then define the expected payoff functions for strategies x and x', denoted as $u_t(x)$ and $u_t(x')$, respectively, as shown in (1) and (2). The average expected payoff $\overline{u_t^b}$ for group A is shown in (3).

$$u_t(x) = s_t(y)\pi_A^1 + s_t(y')\pi_A^2, \tag{1}$$

$$u_t(x') = s_t(y)\pi_A^3 + s_t(y')\pi_A^4, \tag{2}$$

$$\overline{u_t^b} = s_t(x)u_t(x) + s_t(x')u_t(x'). \tag{3}$$

Based on the fundamental concept of Taylor and Jonker's replication dynamic (RD) model [18, 19], we can then derive the RD equations for firm A and firm B to choose an integration strategy, as illustrated in (4) and (5) They will be used in the next sections to conduct an analysis of the evolutionary game's stable strategy.

$$\dot{s}_x = s(x)[1 - s(x)][S_A - C_A + E_A + s(y)(L_A - E_A), \tag{4}$$

$$\dot{s}_y = s(y)[1 - s(y)][S_B - C_B + E_B + s(y)(L_B - E_B). \tag{5}$$

4. ESS Analysis

4.1. Parameter Discussion. An evolutionary stable strategy (ESS) is one that is formed when all individuals in a finite-information repeated game adjust their strategies continuously until they reach equilibrium. An ESS can be either static or changing in a cyclical fashion. We can discuss ESS with the help of RD equations [20, 21].

4.1.1. Analysis for Firm A. Based on the RD equation of firm A, let $f(y) = a_1 s(y) + b_1$, $a_1 = L_A - E_A$, and $b_1 = S_A - C_A + E_A$. Then, (4) can be replaced by $\dot{s}_x = s(x)[1 - s(x)]f(y)$, $s(x) \in (0, 1)$.

If $a_1 = 0$, then the value of $f(y)$ depends on the value of b_1. If $b_1 > 0$, then $\dot{s}_x > 0$, and if $b_1 < 0$ then $\dot{s}_x < 0$.

If $a_1 \neq 0$, as $s(x) \in [0, 1]$, the value of $f(y)$ depends on the value of $-b_1/a_1$. Hence, the value of $-b_1/a_1$ needs to be discussed under different conditions.

(1) When $-b_1/a_1 \leq 0$, if $a_1 > 0$, then $\dot{s}_x > 0$; if $a_1 < 0$, then $\dot{s}_x < 0$.

(2) When $0 < -b_1/a_1 < 1$, if $a_1 > 0$ and $-b_1/a_1 < s(y) \leq 1$, then $\dot{s}_x > 0$, if $a_1 > 0$ and $0 \leq s(y) < -b_1/a_1$, then $\dot{s}_x < 0$, if $a_1 < 0$ and $0 \leq s(y) < -b_1/a_1$, then $\dot{s}_x > 0$, if $a_1 < 0$, and $-b_1/a_1 < s(y) \leq 1$, then $\dot{s}_x < 0$, and if $s(y) = -b_1/a_1$, then $\dot{s}_x = 0$.

(3) When $-b_1/a_1 \geq 1$, if $a_1 > 0$, then $\dot{s}_x < 0$; if $a_1 < 0$, then $\dot{s}_x > 0$.

Through the above discussion, we can conclude that if $-b_1/a_1 \leq 0$ or $-b_1/a_1 \geq 1$, the value of $\dot{s}_x$ is not affected by the value of $s(y)$, which means that, under this condition, firm A's decision is not affected by the choice of firm B. Otherwise, if $0 < -b_1/a_1 < 1$, firm A's decision is affected by the choice of firm B.

4.1.2. Analysis for Firm B. Based on the RD equation of firm B, let $g(x) = a_2 s(x) + b_2$, $a_2 = L_B - E_B$, and $b_2 = S_B - C_B + E_B$; then, $\dot{s}_y = s(y)[1 - s(y)]g(x)$. Similarly, we can conclude that if $-b_2/a_2 \leq 0$ or $-b_2/a_2 \geq 1$, the value of $\dot{s}_y$ is not affected by the value of $s(x)$, which means that firm B's decision is not affected by the choice of firm A under this condition.

Table 2: Game situations under different parameter values.

Classification	Situation	Parameter values of firm A	Parameter values of firm B
Unrelated	Firms A and B are independent of each other	$a_1 = 0$ or $-b_1/a_1 \le 0$ or $-b_1/a_1 \ge 1$	$a_2 = 0$ or $-b_2/a_2 \le 0$ or $-b_2/a_2 \ge 1$
One-way influence	Firm B is affected by firm A	$a_1 = 0$ or $-b_1/a_1 \le 0$ or $-b_1/a_1 \ge 1$	$0 < -b_2/a_2 < 1$
	Firm A is affected by firm B	$0 < -b_1/a_1 < 1$	$a_2 = 0$ or $-b_2/a_2 \le 0$ or $-b_2/a_2 \ge 1$
Mutual influence	Firms A and B interact with each other	$0 < -b_1/a_1 < 1$	$0 < -b_2/a_2 < 1$

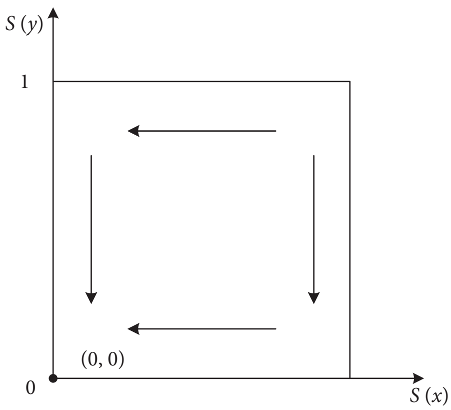

Figure 3: The evolutionary process in the unrelated situation.

Table 3: ESS in the unrelated situation.

Classification	Parameter value of firm A	ESS	Parameter value of firm B	ESS
Unrelated	$-b_1/a_1 \le 0$ and $a_1 < 0$	0	$-b_2/a_2 \le 0$ and $a_2 < 0$	0
	$-b_1/a_1 \le 0$ and $a_1 > 0$	1	$-b_2/a_2 \le 0$ and $a_2 > 0$	1
	$-b_1/a_1 \ge 1$ and $a_1 < 0$	1	$-b_2/a_2 \ge 1$ and $a_2 < 0$	1
	$-b_1/a_1 \ge 1$ and $a_1 > 0$	0	$-b_2/a_2 \ge 1$ and $a_2 > 0$	0

However, if $0 < -b_2/a_2 < 1$, firm B's decision will depend on the action of firm A. Different situations under different parameter values are shown in Table 2.

According to the results of the preceding analysis (as shown in Table 2), there are three basic game relationships: unrelated, one-way influence, and mutual influence. Each of these three scenarios will be discussed further below.

4.2. RD Process Analysis for the Unrelated Situation. In such states, the decisions of firms A and B do not affect each other. For example, if $-b_1/a_1 \le 0$, $a_1 < 0$, $-b_2/a_2 \ge 1$, and $a_2 > 0$, then $\dot{s_x} < 0$ and $\dot{s_y} < 0$. At this stage, as illustrated in Figure 3, the average probability that firms A and B will choose an integration approach diminishes, resulting in an ESS of (nonintegration, nonintegration). Similarly, we can derive more ESSs for this condition, as detailed in Table 3.

4.3. RD Process Analysis under One-Way Influence. This situation can be further classified into two categories based on the variations in the game's dominant player: (1) the one-way influence game in which firm A exerts influence over firm B and (2) the one-way influence game in which firm B exerts influence over firm A. For example, if $s(y) \in [0, -b_1/a_1)$, $-b_1/a_1 \in (0,1)$, $a_1 > 0$, $-b_2/a_2 \le 0$, and $a_2 > 0$, then $\dot{s_y} > 0$; if $s(y) \in [-b_1/a_1, 1)$, $-b_1/a_1 \in (0,1)$, $a_1 > 0$, $-b_2/a_2 \le 0$ and $a_2 > 0$, then $\dot{s_x} > 0$. The RD process is shown in Figure 4.

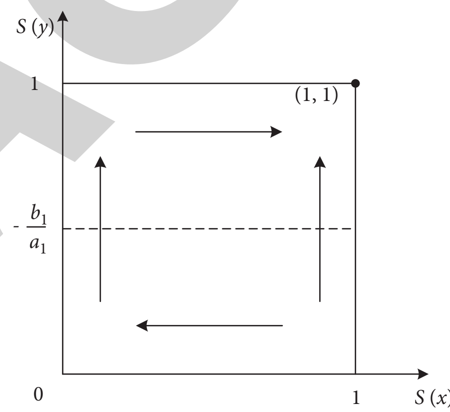

Figure 4: The evolutionary process of one-way influence.

The preceding results imply that if firm B's initial likelihood of integrating is within $[0, -b_1/a_1)$, firm B is more likely to select the integration strategy. When this likelihood reaches the interval $[-b_1/a_1, 1)$, firm B's decision begins to impact firm A, favoring the integration option. This step is repeated until the strategy's final ESS for both is established (integration, integration). Additional ESS results in this state are listed in Table 4.

4.4. RD Process Analysis in the Mutual Affect Situation. When $-b_1/a_1 \in (0,1)$ and $-b_2/a_2 \in (0,1)$, the decisions of firms A and B mutually affect each other.

When $a_1 a_2 > 0$, if $s(y) \in [0, -b_1/a_1)$, $-b_1/a_1 \in (0,1)$, $a_1 < 0$, $-b_2/a_2 \in (0,1)$ and $a_2 < 0$, then $\dot{s_x} > 0$; if $s(y) \in [-b_1/a_1, 1)$, $-b_1/a_1 \in (0,1)$, $a_1 < 0$, $-b_2/a_2 \in (0,1)$ and $a_2 < 0$, then $\dot{s_x} < 0$; if $s(x) \in [0, -b_2/a_2)$, $-b_1/a_1 \in (0,1)$, $a_1 < 0$, $-b_2/a_2 \in (0,1)$ and $a_2 < 0$, then $\dot{s_y} > 0$; and if $s(x) \in [-b_2/a_2, 1)$, $-b_1/a_1 \in (0,1)$, $a_1 < 0$, $-b_2/a_2 \in (0,1)$ and $a_2 < 0$, then $\dot{s_y} < 0$. The RD process for the preceding situation is depicted in Figure 5, and the figure contains four sections, A–D. If $(s(x), s(y))$ is located in region A, then ESS is (nonintegration, integration), which means that firm A pursues a nonintegration strategy, whereas firm B pursues an integration strategy. If $(s(x), s(y))$ is located in region C, then ESS is (nonintegration, integration). If $(s(x), s(y))$ is

Table 4: ESS in the situation that only one party is affected.

Classification	Parameter value of firm A	Parameter value of firm B	ESS
Firm B influences firm A	$0 < -b_1/a_1 < 1$ and $a_1 > 0$	$-b_2/a_2 \le 0$ and $a_2 < 0$	(0, 0)
		$-b_2/a_2 \le 0$ and $a_2 > 0$	(1, 1)
		$-b_2/a_2 \ge 1$ and $a_2 < 0$	(1, 1)
		$-b_2/a_2 \ge 1$ and $a_2 > 0$	(0, 0)
	$0 < -b_1/a_1 < 1$ and $a_1 < 0$	$-b_2/a_2 \le 0$ and $a_2 < 0$	(1, 0)
		$-b_2/a_2 \le 0$ and $a_2 > 0$	(0, 1)
		$-b_2/a_2 \ge 1$ and $a_2 < 0$	(0, 1)
		$-b_2/a_2 \ge 1$ and $a_2 > 0$	(1, 0)
Firm A influences firm B	$-b_1/a_1 \le 0$ and $a_1 < 0$	$0< -b_2/a_2 < 1$ and $a_2 > 0$	(0, 0)
	$-b_1/a_1 \le 0$ and $a_1 > 0$		(1, 1)
	$-b_1/a_1 \ge 1$ and $a_1 < 0$		(1, 1)
	$-b_1/a_1 \ge 1$ and $a_1 > 0$		(0, 0)
	$-b_1/a_1 \le 0$ and $a_1 < 0$	$0< -b_2/a_2 < 1$ and $a_2 < 0$	(1, 0)
	$-b_1/a_1 \le 0$ and $a_1 > 0$		(0, 1)
	$-b_1/a_1 \ge 1$ and $a_1 < 0$		(0, 1)
	$-b_1/a_1 \ge 1$ and $a_1 > 0$		(1, 0)

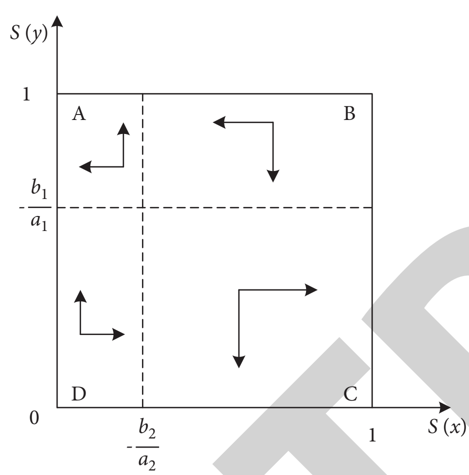

Figure 5: The evolutionary process of mutual effect under $a_1 a_2 > 0$.

located in region B or D, then ESS is (integration, nonintegration) or (nonintegration, integration). When $0 < -b_1/a_1 < 1$, $a_1 > 0$ and $0 < -b_2/a_2 < 1$, $a_2 > 0$, see Table 5 for the relevant results.

When $a_1 a_2 < 0$, if $s(y) \in [-b_1/a_1, 1)$, $-b_1/a_1 \in (0,1)$, $a_1 > 0$, $-b_2/a_2 \in (0,1)$ and $a_2 < 0$, then $\dot{s_x} > 0$; if $s(y) \in [0, -b_1/a_1)$, $-b_1/a_1 \in (0,1)$, $a_1 > 0$, $-b_2/a_2 \in (0,1)$ and $a_2 < 0$, then $\dot{s_x} < 0$; if $s(x) \in [0, -b_2/a_2)$, $-b_1/a_1 \in (0,1)$, $a_1 > 0$, $-b_2/a_2 \in (0,1)$ and $a_2 < 0$, then $\dot{s_y} > 0$; and if $s(x) \in [-b_2/a_2, 1)$, $-b_1/a_1 \in (0,1)$, $a_1 > 0$, $-b_2/a_2 \in (0,1)$, and $a_2 < 0$, then $\dot{s_y} < 0$. The RD process is shown in Figure 6. Finally, there is only one stable state in which each side will adapt to the mixed strategy and the ESS is $(-b_2/a_2, -b_1/a_1)$. Similarly, when $-b_1/a_1 \in (0,1)$, $a_1 < 0$ and $-b_2/a_2 \in (0,1)$, $a_2 > 0$, we obtain the results shown in Table 5.

5. Case Study

5.1. Background. The iron ore trade value between Australia and China is growing rapidly. According to the latest data from the China Iron and Steel Association (CISA), the volume of Chinese iron ore imports from Australia in 2020 was 713 million tons (accounting for 60.9% of the year's total). Western Australia is the main producer of iron ore in Australia, accounting for 99% of Australia's iron ore production. Western Australia had 836 Mt of iron ore sales in 2019–2020, which were mostly exported to China (83 percent). The main origin in Western Australia is the Pilbara Region (accounting for 97%), as shown in Figure 7.

According to the data from the Government of Western Australia Department of Mines and Petroleum, there are approximately 17 principal iron ore producers in Western Australia. Among them, three companies, Rio Tinto, BHP Billiton, and Fortescue Metals Group, account for more than 90% of production. These companies have built their own export supply chains, including rail lines and port facilities, as shown in Table 6.

Thus far, through joint-venture packages, which include Chinese firms taking minority equity stakes and offering long-term contracts for new iron ore exports, many Chinese steel-producing firms have taken measures to integrate their supply chains, as shown in Table 7.

5.2. Numerical Examples. We designed different scenarios based on data collected from Chinese steel-producing companies and iron-ore suppliers in Australia to analyze the best options for Chinese steel-producing firms. We observe two primary patterns used in SCI: the joint-venture pattern (which includes long-term contracts) and the self-support pattern. Figures 8 and 9 depict two integrated supply chain patterns. As a result, we created two cases, one to represent each integration pattern.

As firms with different market scales have different cost structures, we need to consider the influence that market scale has on decision-making. We choose Baosteel Group and Benxi Steel as targets, which are Chinese steel-producing firms but do not have same level of production. According to the data from the World Steel Association, their crude steel production for the period 2017–2020 is listed in Table 8. We chose their net profits in 2011 as original profits, which were

Table 5: ESS under mutual influence.

Situations	Parameter of firm A	Parameter of firm B	ESS
Mutual influence	$0 < -b_1/a_1 < 1$ and $a_1 < 0$	$0 < -b_2/a_2 < 1$ and $a_2 < 0$	(0, 1) or (1, 0)
	$0 < -b_1/a_1 < 1$ and $a_1 > 0$	$0 < -b_2/a_2 < 1$ and $a_2 > 0$	(0, 0) or (1, 1)
	$0 < -b_1/a_1 < 1$ and $a_1 > 0$	$0 < -b_2/a_2 < 1$ and $a_2 < 0$	$(-b_2/a_2, -b_1/a_1)$
	$0 < -b_1/a_1 < 1$ and $a_1 < 0$	$0 < -b_2/a_2 < 1$ and $a_2 > 0$	$(-b_2/a_2, -b_1/a_1)$

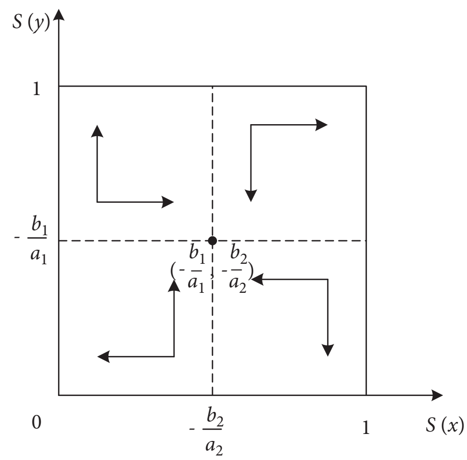

Figure 6: The evolutionary process of mutual effect under $a_1a_2 < 0$.

US\$ 2.895 billion and US\$542 million. Therefore, their unit profits in 2011 were US\$ 66.8/ton and US\$ 32.8/ton. Hence, $P_A = 66.8$ and $P_B = 32.8$. Following that, we will consider two scenarios. In scenario 1, we assume that both players can only use the "joint-venture pattern" to integrate their supply chains. We suppose in scenario 2 that they can only follow the "self-support pattern."

5.2.1. Scenario 1. In scenario 1, we consider the joint-venture pattern. Under this condition, Chinese steel-producing firms obtain cheaper iron ore by taking minority equity stakes and offering long-term contracts for new iron ore exports. As most Chinese steel-producing companies are in the process of integration projects, it is difficult to calculate supply chain cost savings from the whole raw material cost. Therefore, we obtain data on supply chain cost savings from iron ore producers in Australia, which provided the cost savings from integrating their export supply chains in their annual reports. Take, for example, the case of FMG, which committed to expansion in November 2010. We chose its cost data after expansion. As in the previous discussion, we believe that the supply chain cost saving consists of the saving of rail costs, port costs, and shipping costs. By decreasing the average cost, we can obtain $S_A = 3.6$, $S_B = 3.6$. Table 9.

To determine the cost of SCI in this model, we choose two real cases. One is Baosteel Group's investment in Aquila in 2009. In this case, Baosteel Group invested as much as US\$285.6 million in Aquila to obtain a 50% share of one 30 Mtpa project. The other case is Shougang investment in Balmoral in 2008. The specific data are shown in the table below. Assuming that the costs are shared equally from 2011 to 2014, we can obtain $C_A = 1.65$ and $C_B = 1.04$.

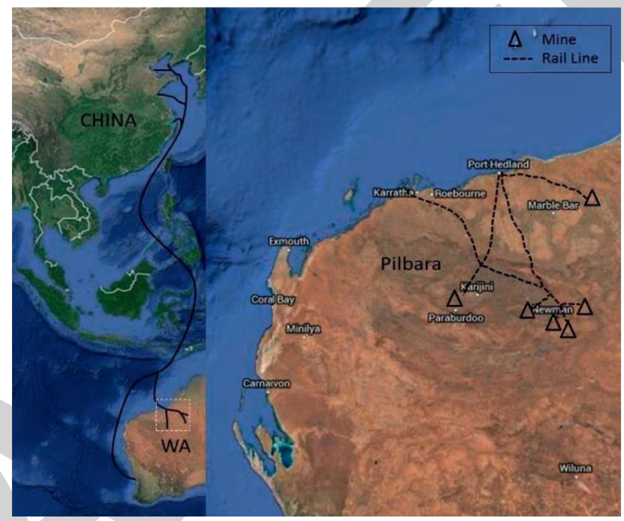

Figure 7: Iron ore transport routes between Australia and China.

Table 6: Iron ore export supply chain of the main producers.

Iron ore producer	Rail (km)	Port facility
Rio Tinto	1600	4 ports with 11 berths (Dampier port)
BHP	1000	8 berths (port Hedland)
FMG	620	4 berths and 1 under construction (port Hedland)

Table 7: Investment of Chinese steel-producing firms.

Firm	Project	Value (A\$ millions)	Size (Mtpa) and associated LTCs (% of output)
Ansteel	Karara JV	530	Plan 10 (100%)
Shougang	Balmoral south	58	Plan 12 (100%)
Shagang	Grange	NA	2.5 (100%)
Baosteel	Aquila	286	Plan 30 (50%)

As the steel-producing market is oligopolistic, we assume that company A with a larger market share will gain 10% excess profits if only it implements the SCI strategy. Otherwise, it will face a 20% excess loss. The same situation for company B (smaller market share) is 20% excess profits and 10% excess loss. Therefore, we can obtain $E_A = 6.68$, $L_A = 13.36$, $E_B = 6.56$, and $L_B = 3.28$. By applying MATLAB, we obtain the ESS (integration, integration) after deriving hundreds of initial solutions, as shown in Figure 10.

It means that in the short term, firms A and B will choose the joint-venture pattern for SCI. We perform a sensitivity analysis on the proportional coefficient of fixed asset

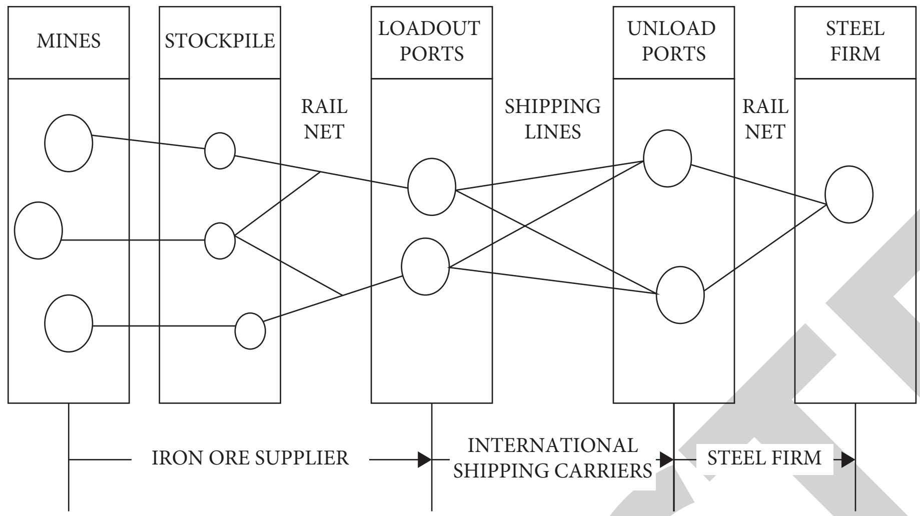

Figure 8: Joint-venture mode.

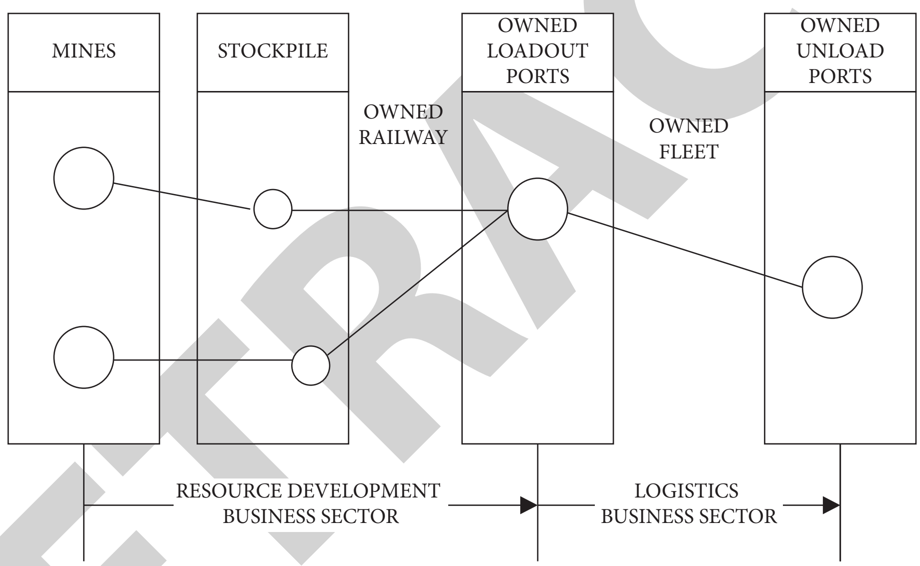

Figure 9: Self-support model.

Table 8: Crude steel production, 2017–2020.

Tonnage (million tonnes)	2017	2018	2019	2020
Baosteel group	46.17	47.10	46.88	45.62
Benxi steel	15.49	15.47	15.83	16.63

Table 9: FMG supply chain cost after expansion.

Supply chain costs U.S.$ m	After 1 year	After 2 years	After 3 years	After 4 years
Rail costs	128	139	182	238
Port costs	97	125	181	252
Shipping cost	509	672	769	1210
Ore shipped	40.9	57.5	75.9	118.4
Average cost U.S.$/wmt	17.95	16.28	14.91	14.35

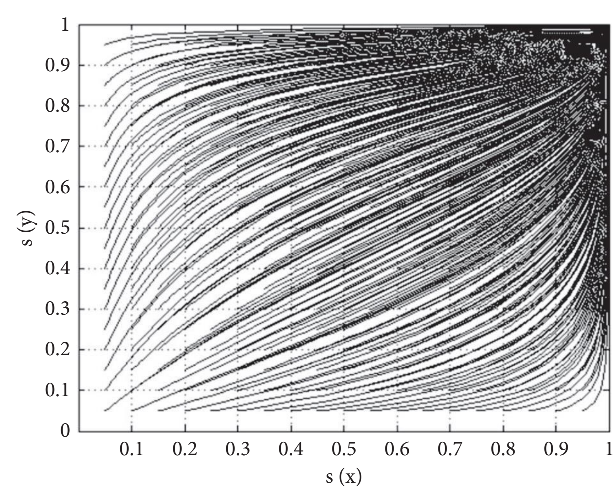

Figure 10: The simulation result of Scenario 1.

Table 10: Total delivered cost of FMG.

Supply chain costs	2011	2012	2013	2014
Total delivered cost US$/wmt	67	69	62	52

investment loss P. The calculation shows that the ESS is (integration, integration) for any P. It indicates that the decisions of firms A and B are not affected by the coefficient P in the short term if they are integrated using the joint-venture pattern.

5.2.2. Scenario 2. In Scenario 2, we consider the self-support model. The data on original profits are the same. Hence, $P_A = 66.8$ and $P_B = 32.8$. We also obtain data on supply chain cost savings from the case of FMG. The total delivered cost of FMG was significantly lower in 2014 than in 2011, as shown in Table 10, because of its expansion in the supply chain. However, as a result of their small size and comparatively high costs, it is unlikely that most of these projects will be cost-competitive with the Big-3 incumbents. Therefore, we assume that $S_A = 13.5$ ($15 * 90\%$) and $S_B = 12$ ($15 * 80\%$).

We choose BHP exploration projects as the data source. These projects included the Jimblebar Mine Expansion project and Orebody 24 mine project. The Jimblebar Mine expansion project costed U.S.$3.6 billion and achieved a capacity of 35 Mtpa. The Orebody 24 mine project costed U.S.$0.7 billion and achieved a capacity of 17 Mtpa after one year of construction. Both projects were approved in 2011 and lasted 4 years. Then, we can obtain $C_A = 24.28$ and $C_B = 16.12$. Similar to Scenario 1, $E_A = 6.68$, $L_A = 13.36$, $E_B = 6.56$, and $L_B = 3.28$. By applying MATLAB, we obtain the ESS (0.74, 0.61) after conducting hundreds of initial solutions, as shown in Figure 11.

Additionally, we conduct a sensitivity analysis for P in the following section. We make P take values between 0 and 1 and perform the calculations, obtaining the following results.

When $0 \leq p \leq 0.106$, the dynamic evolutionary process will reach an equilibrium state characterized by mixed strategies. As illustrated in Figure 12, the ESS equilibrium state moves to the upper left as the value of p increases, indicating that the probability of firm A (with a large market share) choosing an integration strategy continues to decrease, while the probability of firm B choosing an integration strategy increases. Note that because the investment loss ratio coefficient P can be interpreted as the probability of experiencing policy risk, the results of this calculation indicate that the probability of choosing an integration strategy for firm a with its dominant market share decreases significantly as the probability of experiencing policy risk increases.

When $0.106 < p \leq 0.151$, $-b1/a1 \geq 1$, and $0 < -b2/a2 < 1$. It means that in this case, the strategy evolution process of firm A is not influenced by the decision of firm B, while the strategy evolution process of firm B is influenced by firm A. In this case, the ESS is (nonintegration, integration), i.e., firm A chooses not to integrate, and firm B chooses to

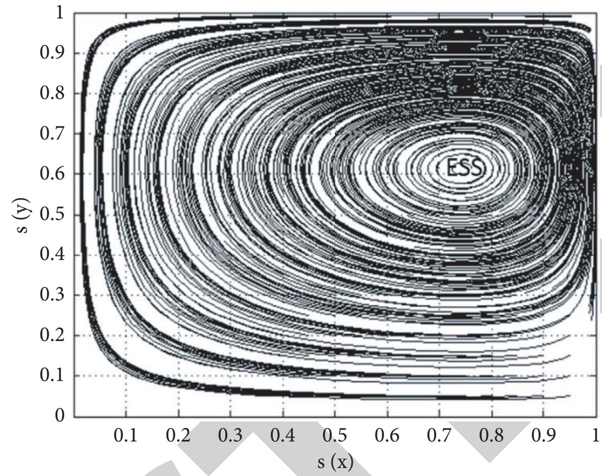

Figure 11: The simulation result of Scenario 2.

integrate. It indicates that as the probability of policy risk expands further, firm A's decision will change from preferring integration to nonintegration, while firm B still prefers to choose integration.

When $p > 0.151$, $-b_1/a_1 \geq 1$, and $-b_2/a_2 \leq 0$. Here, the strategy evolution processes of firms A and B are independent. At this stage, the ESS is (nonintegration, nonintegration). This finding implies that when risk reaches a particular level, both types of firms choose to pursue a nonintegration strategy. This outcome is entirely consistent with our expectations.

5.3. Discussion. The findings of the preceding study are congruent with the reality of the situation. Actual economic and trade data indicate that the relationship between China and Australia has a substantial impact on investment activity between the two countries. Because of ongoing tensions between the two nations, Chinese investment in Australia fell to its lowest level in nearly six years in 2020, as shown in Figure 13, by 61% year-on-year to $783 million from $2.08 billion the previous year. There were only 20 Chinese investment projects in Australia throughout 2019, far fewer than the 111 in 2016. From the standpoint of steel SCI, the model described in this article provides a quantitative explanation for this phenomenon.

In Scenario 1, the value of each parameter accords with the situation "unrelated," which means that firms A and B will make decisions based on their own situations, without considering the competitor's strategy. In this case, both of them will gain profits if they apply an SCI strategy. Additionally, we can see that, regardless of the value of p, neither side of the game can affect the other's decisions in Scenario 1, and the ESS is (integration, integration). It is primarily because both parties to the game employ the short-term joint venture pattern for SCI, which is an "asset-light pattern" with low investment and risk, and thus the integration decision effectively mitigates political concerns.

Unlike in Scenario 1, we assume that both players adopt the self-support pattern for SCI in Scenario 2. Because this

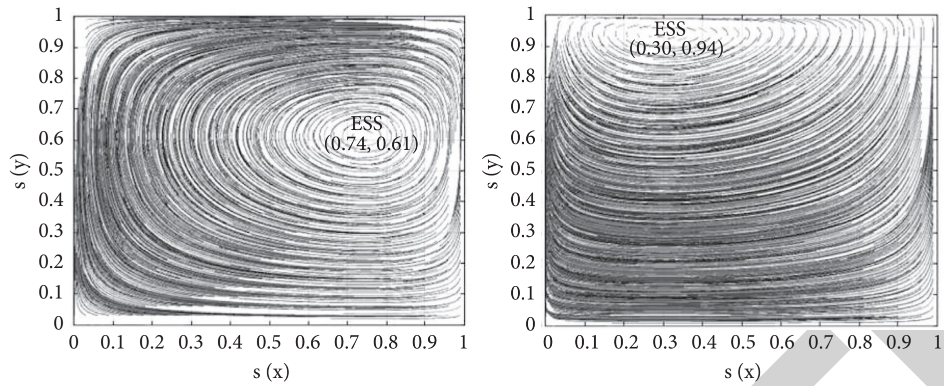

Figure 12: The comparison of simulation results under $p = 0$ & $p = 0.09$.

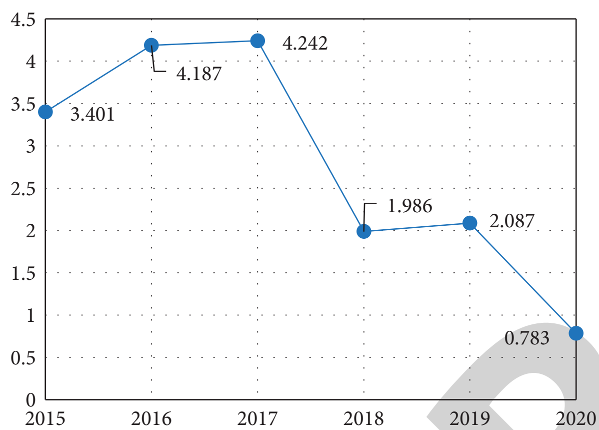

Figure 13: China's investment in Australia 2015–2020 ($ billion).

model requires significant investment and is essentially a fixed asset investment, it can be considered an "asset-heavy pattern." While SCI based on the self-support pattern can significantly reduce operating costs and increase efficiency, there is a significant investment risk associated with it. If the countries' relationship deteriorates, it will result in a series of irreversible and significant losses for the firms.

Note that the political risk factor has varying effects on firms in various market positions under the self-support pattern. Specifically, as risk (p) increases, the probability that firm A will choose the integration strategy decreases continuously until $p = 0.106$, at which point firm A becomes unwilling to choose the integration strategy, however, firm B always prefers the integration strategy when p is less than 0.106. At $p = 0.151$, the response of firm B changes. It demonstrates that even when p is less than 0.151, firm B is willing to accept the risk posed by policy factors. When p exceeds 0.151, firm B is also forced to abandon its integration strategy because of the high policy risk.

6. Summary and Conclusions

In this paper, we developed an evolutionary game model to analyze the decision-making of an SCI strategy for steel-producing firms. Considering the characteristics of an oligopolistic market, we formulated the supply chain decision-making problem as an asymmetric RD model and then proposed an RD process analysis to obtain every ESS result under different parameter situations. In addition, two scenarios were designed to demonstrate that such problems can be formulated and solved well by an evolutionary game model. Importantly, this paper adds to the literature by empirically testing the SCI strategy indirectly. Furthermore, it also allows for the generalization of special cases of oligopolistic market equilibrium problems and provides a detailed case study of Chinese steel-producing firms' iron ore supply chain.

In conclusion, there are some limitations of the research in this paper that suggest that future studies can be extended in several directions. Firstly, the complexity of participators' behavior in this oligopolistic market has been simplified in this evolutionary game model. Future studies can consider the cost structure of steel-producing firms and introduce a pricing model to analyze the extra profits and losses that each firm may face. Secondly, collecting data from steel-producing firms' supply chains could be more appropriate for evaluating the cost savings of the total supply network. Therefore, future research should replicate and integrate our study using numerical data from iron ore-producing firms. Obviously, it would also be worthwhile for further theoretical developments and empirical applications.

Data Availability

No data were used to support this study.

Conflicts of Interest

The authors declare that they have no conflicts of interest.

Acknowledgments

This work was supported by Project of Educational Commission of Guangdong Province of China (Grant no. 2021WTSCX222) and Key project of Shenzhen Polytechnic (Grant no. 6022310001S).

References

[1] M. Yellishetty, P. G. Ranjith, and A. Tharumarajah, "Iron ore and steel production trends and material flows in the world: is this really sustainable?" *Resources, Conservation and Recycling*, vol. 54, no. 12, pp. 1084–1094, 2010.

Hindawi
Computational Intelligence and Neuroscience
Volume 2023, Article ID 9816273, 1 page
https://doi.org/10.1155/2023/9816273

Retraction

Retracted: The Management of Educational Talents in Vocational Colleges Based on Wireless Network in the Artificial Intelligence Era

Computational Intelligence and Neuroscience

Received 25 July 2023; Accepted 25 July 2023; Published 26 July 2023

This article has been retracted by Hindawi following an investigation undertaken by the publisher [1]. This investigation has uncovered evidence of one or more of the following indicators of systematic manipulation of the publication process:

(1) Discrepancies in scope
(2) Discrepancies in the description of the research reported
(3) Discrepancies between the availability of data and the research described
(4) Inappropriate citations
(5) Incoherent, meaningless and/or irrelevant content included in the article
(6) Peer-review manipulation

The presence of these indicators undermines our confidence in the integrity of the article's content and we cannot, therefore, vouch for its reliability. Please note that this notice is intended solely to alert readers that the content of this article is unreliable. We have not investigated whether authors were aware of or involved in the systematic manipulation of the publication process.

Wiley and Hindawi regrets that the usual quality checks did not identify these issues before publication and have since put additional measures in place to safeguard research integrity.

We wish to credit our own Research Integrity and Research Publishing teams and anonymous and named external researchers and research integrity experts for contributing to this investigation.

The corresponding author, as the representative of all authors, has been given the opportunity to register their agreement or disagreement to this retraction. We have kept a record of any response received.

References

[1] Y. Zhang and C. Wang, "The Management of Educational Talents in Vocational Colleges Based on Wireless Network in the Artificial Intelligence Era," *Computational Intelligence and Neuroscience*, vol. 2022, Article ID 2298139, 10 pages, 2022.

Hindawi
Computational Intelligence and Neuroscience
Volume 2022, Article ID 2298139, 10 pages
https://doi.org/10.1155/2022/2298139

Research Article

The Management of Educational Talents in Vocational Colleges Based on Wireless Network in the Artificial Intelligence Era

Yang Zhang[1] and Ce Wang[2]

[1]*College of Modern Service, Harbin Vocational College of Science and Technology, Harbin 150300, China*
[2]*College of General Education, Heilongjiang Polytechnic, Harbin 150080, China*

Correspondence should be addressed to Ce Wang; wangce7899@163.com

Received 23 April 2022; Revised 16 May 2022; Accepted 17 May 2022; Published 24 June 2022

Academic Editor: Xin Ning

Faced with the AI (artificial intelligence) era, it is both theoretically and practically important to examine the challenges and opportunities that vocational college education in China faces, as well as to actively explore how vocational college education can overcome the challenges and achieve a realistic path. This paper proposes and implements a wireless network-based vocational college talent management system. The main personnel management system primarily completes business operations related to daily personnel file management, while the data mining subsystem mines talent data using the DT (decision tree) classification algorithm to aid talent selection. At the same time, a new topology optimization algorithm based on the principle of minimum rigidity graph is proposed for talent management system wireless network optimization. The maximum-minimum balance criterion and the user-by-user optimization mechanism are designed to obtain the optimal relay selection and subchannel allocation strategy, ensuring the system's reliability and fairness. The optimized algorithm has a user security satisfaction of 0.93 in the range of 250 m, which is higher than other algorithms. It demonstrates that this algorithm's communication link is short, and it has good network connectivity and structural stability.

1. Introduction

The essence of the reform of vocational talents training education mode is to change the types of talents to meet the needs of different types of talents in different periods and societies. Talent training mode mainly includes training objectives, training norms, training methods, and finally what kind of people to train. In recent years, Internet giants have devoted themselves to the research and development of driverless technology, constantly exploring and innovating, realizing the integration of AI (artificial intelligence) [1] and traditional automobile technology, which has triggered people's endless reverie of future intelligence. From the perspective of the AI era, people gradually realize that innovative engineering and technical talents are more in line with the needs of this social and industrial transformation.

Only by deeply studying the basic theory of vocational college education can we formulate scientific policies and guidelines to guide the development of vocational college education. As the standard and requirement of training talents in schools at all levels, the goal of training talents is of great significance to the whole education and the development of specific majors in specific schools. Stukalina pointed out that the typical application of AI in education mainly includes intelligent tutors assisting individualized teaching and learning [2]. Ginsburg et al. studied AI as a course and pointed out that it is of great significance to carry out AI education courses in vocational colleges [3]. Leńko-Szymańska suggested that AI should also play a role in motor skill learning [4]. He pointed out that many learning tasks need to be completed through repeated movements, such as learning to write, draw, play musical instruments, practice motor skills, dance, and use sign language. Derosa et al. believe that "standardized work" is easily replaced by AI, while creative work and those with "emotional color and artistic creation" are difficult to replace, resulting in the phenomenon of "intermediate skills being squeezed" [5]. Filho et al. think that we should improve the combination of production and learning, combine "decentralized teaching" to innovate the classroom, and construct an effective interdisciplinary compound model [6].

AI is essentially a technological revolution. When artificial intelligence (AI) continues to profoundly influence and change human production and life, vocational college education, as one of the factors of production, will inevitably be forced to actively consider how to deal with AI's arrival [7, 8]. Although AI is not human intelligence, technology products that contain AI act as a "carrier" for human intelligence, allowing them to think like humans and even surpassing human intelligence. This paper discusses the causes of some problems that exist in the innovation and development of engineering and technical talents in reality and offers suggestions for cultivating innovative talents, based on the fact that a new generation AI technology has entered the application stage. The following two aspects of this paper's innovation: (1) this paper constructs a vocational college education talent management system with a wireless network by studying the application of DT technology in talent management and using wireless network technology, with the goal of assisting enterprises in making talent management decisions and (2) the topology optimization algorithm is used to design and optimize the system database objects during the development process. It increases the readability of system design documents and provides a solid foundation for the system's implementation.

2. Related Work

2.1. Talent Management Research. With the continuous development of science and technology, mankind has gradually entered the era of the knowledge economy. In the era of the knowledge economy, it means that the development and renewal of knowledge become more and more valuable. As an important factor of production in people's lives, it has been widely accepted by people. The goal of talent cultivation plays a very important role in the whole vocational college education system. It is not only the starting point of practical education activities but also the standard to evaluate the success of a school. Judging from the orientation of talent training objectives, talent training objectives can be divided into national, higher vocational, and professional training objectives.

Zheng et al., from the perspective of AI's development's demand for social talents and its impact on the employment of vocational college graduates, discussed how vocational colleges should innovate the talent training mode to promote the talent training of vocational college education to adapt to the new market demand as soon as possible [9]. Sun et al. defined the training goal of higher vocational talents as training knowledge-based skilled talents, who have both a high level of professional theoretical knowledge and a high level of operational skills [10]. Chen analyzed the factors influencing the change of talent training objectives from five aspects, namely [11], the change of social and economic development mode, the transformation and upgrading of industry and the changes and requirements of market demand, the basic law of higher vocational colleges' education, the value pursuit of higher vocational colleges' education, and the change of social talent view. Dong et al. put forward the strategies to improve the training objectives of educational talents in higher vocational colleges under the reform of the education supply side: strengthening specialty construction, strengthening the integration of production and education and school-enterprise integration and reforming the school-running mode [12]. Yang said that if education cannot make the workforce acquire new skills in time, the mismatch between the skills required by new technologies and those provided by the workforce will hinder the transformation [13]. Wei and others think that both teaching and practice should be devoted to innovation [14]. Jian believes that compound talents should be cultivated in the AI era [15].

2.2. Research on Wireless Network Optimization. Wireless network optimization is a series of processes to obtain relatively stable network coverage, capacity, and quality through certain economic investment so as to obtain better performance. For wireless sensor networks with limited power, topology optimization can reduce power consumption, prolong the life cycle of the network, improve the stability of communication link structure, and make the network better used in a complex environment.

Sagduyu et al. proposed a four-level clustering algorithm, which considered the problem of residual energy between nodes, built a hierarchical link structure, and improved the network load balance [16]. However, when more clusters are generated, the node degree of the head node will increase rapidly, which will affect the connectivity of the sensor. Xiao et al. proposed a robust control algorithm, which introduced the node scheduling adjustment factor and quantified the network node degree, sought the value rule of the node degree, obtained the optimal node degree of the network, and improved the balance of the network structure [17]. A method of network positioning based on stiffness matrix characteristics of the rigid graph is proposed. In the positioning process, the selection of positioning points and the construction of the network improve the eigenvalue of the stiffness matrix of the generated network, which improves the stability of the network structure on the premise of ensuring network connectivity. However, the influence of link weights on network lifetime is not considered in the algorithm.

Zhang et al. proposed a joint power tying and subchannel allocation algorithm, which can improve the capacity of the Femtocell network and protect the communication service quality of macrocell users [18]. Wang et al. have done relevant research on soft frequency reuse technology in home base station network [19]. This technology has improved the degree of reuse. Based on Wang's noncooperative game theory, the energy efficiency of a mobile communication network is maximized by appropriate power control strategies [20]. Singh et al. proposed a noncooperative game power control algorithm to optimize the network energy efficiency. In order to reduce the complexity, the author adopted distributed solution, which effectively reduced the algorithm complexity while improving the network energy efficiency [21]. Daniel et al. put forward an energy-saving subchannel allocation strategy, but this strategy does not consider the interference to neighboring cells and is not suitable for multicell scenarios, which has certain limitations [22]. Kakadia et al. put forward a medium-sized node selection strategy based on the principle of minimum outage probability, which improves the total capacity of the system and reduces the outage probability by selecting the relay with the minimum outage probability from end to end for forwarding service [23].

3. Methodology

3.1. Design of Educational Talent Management System in Vocational Colleges Based on Wireless Network. Workers in the AI era will most likely be product designers, producers, or sellers. Workers will learn how to not only understand technology but also how to maintain and debug products, as well as how to communicate with various customers to meet their needs. Many traditional industries are disappearing in the AI era, with the rapid development of science and technology, as well as the continuous application of industrial robots, while many new industries emerge. To adapt to changes in industry structure, vocational colleges should actively adjust their career scenes in response to changes in market talent supply and demand. The traditional management system falls short of meeting the modern talent management business needs. The new system, which is based on the old system, absorbs new user requirements and can meet those requirements in the workplace. As a result, the system's feasibility is strong, and it is critical to improve user satisfaction and employee productivity.

The requirement to adapt to the transformation of business forms in the AI era is to discover new technologies with creativity. Engineering and technical professionals with advanced technologies and a knack for technological innovation are unquestionably in demand. Only engineers with such abilities will be able to stand out in a sea of technological change and gain the first opportunity for personal growth. New tools, new applications, new methods, and so on will continue to emerge as new technologies inspire and support them. Engineers must make efforts in all aspects, whether in the chemical and pharmaceutical industry or in the construction and processing industry. Only in this manner can technical capability and business level meet real-world requirements. The SaaS (software-as-a-service) model is a new software application model that is gradually emerging against the backdrop of the continued maturation of application software and the in-depth development of Internet technology.

The SaaS model has the following advantages:

(1) Each unit does not need to be equipped with special professional technicians to maintain the system. At the same time, access to the latest technology applications to meet changing needs;

(2) There is no need for each unit to build its own management platform, and there is no need to consider issues such as cost depreciation and subsequent platform upgrade, which can effectively alleviate the pressure of insufficient funds.

In a word, building a talent management system using SaaS model can greatly reduce the burden of building and maintaining infrastructure and applications in each unit. All units can rely on the unified management platform of provinces, cities, and counties to use management software conveniently, without a large amount of hardware and software investment.

According to the concept of the SaaS model, the author initially constructed a talent management platform, and its architecture is shown in Figure 1:

The framework layer is responsible for data transmission and monitoring of the application service layer and the application integration layer, including security services, application monitoring, data backup, network control, operation management, and so on. It is the basic running environment of SaaS. The model provides application services provided by many software vendors, which ensures the high reliability, high security, and high scalability of the whole system. According to the needs for talent training in the AI era, the main modules of the designed system include talent information continuous maintenance module, business declaration module, declaration confirmation and audit module, talent and employee file management module, SMS sending and receiving module, system background management module, and so on. The system module structure is shown in Figure 2.

Compiling talent information maintenance is one of them, and it consists of two submodules: talent information registration and talent information editing. Professional title declaration and talent development special fund declaration are two submodules of the business declaration module. Two small modules are included in the application and audit module: professional title application and special fund for talent development application and audit. Six small modules make up the talent and personnel file management module: talent file transfer application, transfer application approval, file information record, transfer application file, transfer application approval, and file transfer.

DT (decision tree) module will automatically complete the whole data extraction process, and users can use the provided parameters to adjust DT so that the prediction results are more ideal. These parameters include confidence pruning and whether to merge discrete attributes. Pruning confidence determines the severity of the pruning operation and is the most important parameter. If the user makes a prediction according to the rule set when making a prediction, in the prediction module, the rule set is read from the rule file, and then its prediction data is read. In the process of prediction, a test case may predict different classification results according to different rules, and these results may contradict each other.

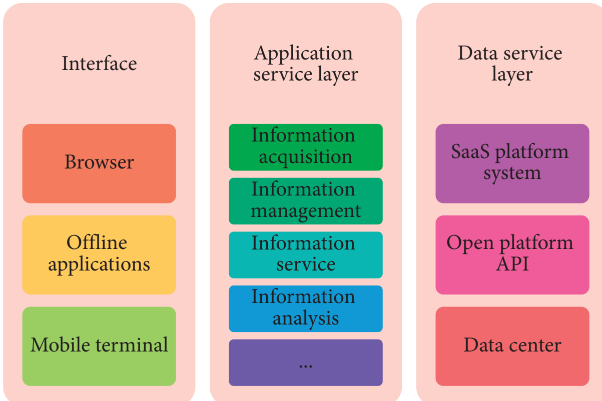

Figure 1: Talent management platform.

Considering the strong independence of this module, in order to reduce duplication of work, the system is changed to a web system, the codes of the DT generation module and prediction module are packaged in a DLL file independently, and the mining part is completed by calling dynamic link library system. In the stage of system design, DT module code design is the key and difficult point. As an independent subsystem of the talent management system, the data mining subsystem is mainly used by business decision-makers to support business talent management decisions. It includes three parts: the decision of outstanding talents, the decision of employee loyalty, and the decision of employee employment. Its structure is shown in Figure 3.

The model mainly selects the specific attributes according to the related contents of the talent index system established by the human resource management model. The indexes that reflect talent include education index, professional title index, age index, and industry index, and their credibility is proved by statistical methods.

According to business analysis, the conceptual database schema's common entity model structure, multivalued attributes, and entity relationships are transformed into a relational schema, which is then standardized. Every nonprimary attribute is functionally dependent on the relational schema code; the relationship ensures that each attribute's value range is a simple and indivisible data element. During the development process, staff not only can use out-of-the-box programme functions to operate the process but also can create many flexible processing links in the programme, and some functions and operation modules can be added, modified, and manually modified. This creates a good flexible space for system users, transforming the rigid programme into a living programme, and allowing them to experience the system's flexibility and humanized design ideas.

3.2. Wireless Network Optimization of Talent Management System. The era of AI is the era of machine revolution, and human-machine interaction is becoming more widespread. Many production processes necessitate the involvement of AI teams. Faced with the development situation in which start-up companies require a large number of AI talents, the talents trained by vocational colleges' original talent training objectives can no longer fully meet the new labor market demands. As a result, talent training objectives must be reset, and a new talent training plan must be developed, with the goal of meeting the new labor market demand for talents in the AI era and balancing the supply and demand of talents at the training end. All database access tasks are built in the database access class to improve the efficiency of project development and the speed of system execution. As a result, the database's public class is created and saved in the public class folder. The database control class can be called from the global module. A global file is configured in addition to the public class for accessing the database, in which the user name and password for accessing the database are stored in ciphertext form. This design method is adaptable and has a high rate of code reuse.

This paper presents a topology control algorithm for wireless sensor networks based on the optimization of algebraic stiffness characteristics of a minimum rigid body graph. The algorithm comprehensively considers the weight of communication links in the generated topological link graph and the rigidity of the generated rigid graph, which not only ensures the short communication links but also helps prolong the life cycle of the network, making the generated communication link graph more efficient and more stable in structure. The attenuation factor model is mainly used to predict the propagation loss in buildings and can deal with the influence of building types and the changes caused by obstacles. The model is flexible, and the standard deviation between the expected results and the measured values is small, while the deviation from the logarithmic distance model is much smaller. The attenuation model is

$$\overline{L}(d) = \overline{L}(d_0) + 10\gamma_{SE}\log_{10}\left(\frac{d}{d_0}\right) + ad + FAF, \tag{1}$$

where d_0 represents the standard reference distance, taking the empirical value of 1 m; d represents the distance between the signal transmitter and the signal receiver; a represents the channel attenuation index, in dB/m, and the typical apartment and office environment value is 0.2 m; γ_{SE} indicates the index value of the same building floor test. In different types of coverage areas, the value of γ_{SE} is different.

In the indoor environment, the attenuation factor model can be selected as the indoor wireless propagation model, and its expression is:

$$PL(d)[dB] = PL(d_0) + 10n\lg\left(\frac{d}{d_0}\right) + FAF. \tag{2}$$

The two-way relay transmission of the system is divided into two stages: multiple access stage (the first time slot) and transmission stage (the second time slot). In the multiaccess stage, all users send information to the relay station at the same time. In the transmission phase, the relay node amplifies the received information and sends it to the receiver. The two-way relay security network system model is shown in Figure 4.

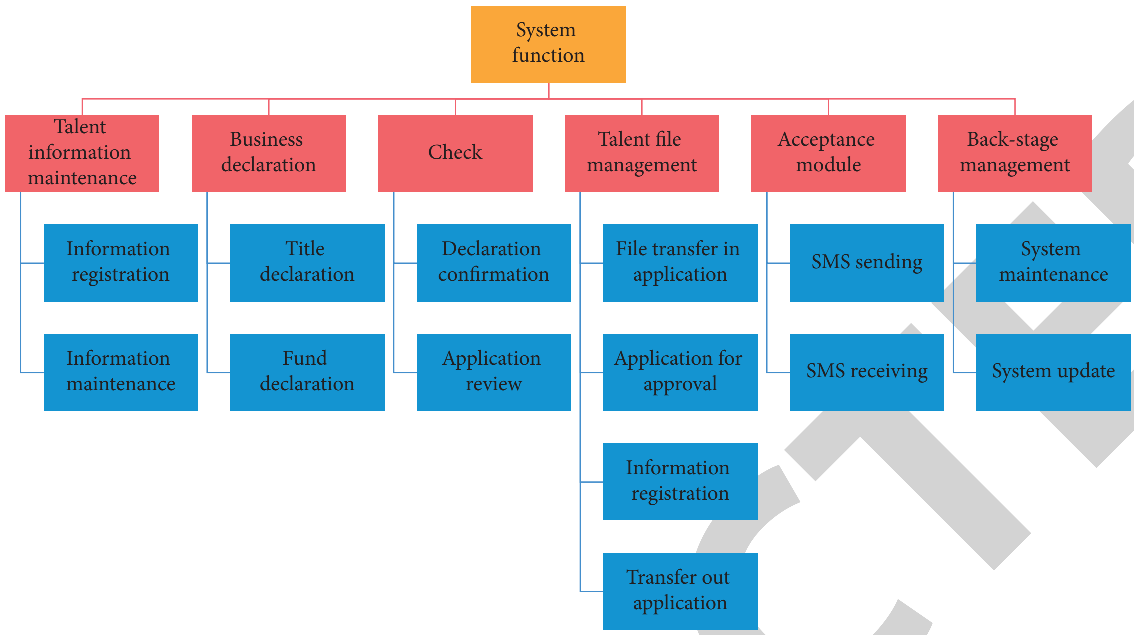

Figure 2: System function module structure.

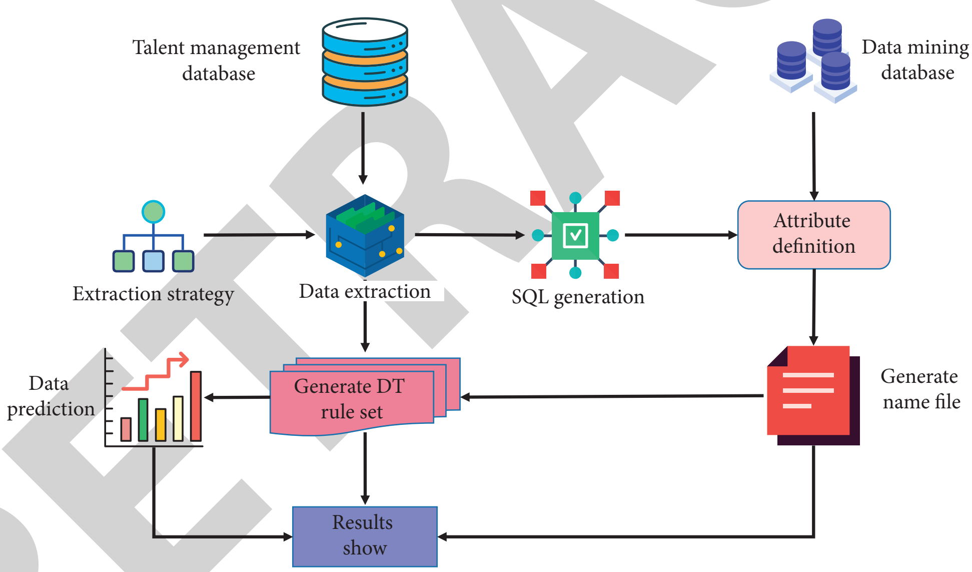

Figure 3: Overall structure diagram of data mining system.

Assume that each user group k is composed of A_k, B_k, and the bandwidth of each subchannel is B, and it is divided into N subchannels. Assume that in the multiple access stage, the user A_k, B_k occupies the subchannel i, and the signal received by the relay node is

$$Y^i_{EN} = \sqrt{p^i_{A_k} g^i_{A_k,RN}} X^i_{A_k} + \sqrt{p^i_{B_k} g^i_{B_k,RN}} X^i_{B_k} + Z^i_{RN}, \tag{3}$$

where $X^i_{A_k}, X^i_{B_k}$ are the transmission signal of A_k, B_k on subchannel i, $p^i_{A_k}, p^i_{B_k}$ are the emission power of A_k, B_k, $g^i_{A_k,RN}, g^i_{B_k,RN}$, respectively, represents the channel gain from A_k, B_k to relay station R on subchannel i, and Z^i_{RN} is that the average value of relay node RN on subchannel i is 0.

In the broadcast stage, the signals received by A_k, B_k and eavesdropper E on subchannel j are

$$\begin{aligned} Y^j_{A_{k,j}} &= \xi \sqrt{p^j_{RN}} h^j_{A_k} Y^i_{RN} + Z^j_{A_k}, \\ Y^j_{B_{k,j}} &= \xi \sqrt{p^j_{RN}} h^j_{B_k} Y^i_{RN} + Z^j_{B_k}, \\ Y^j_{E_j} &= \xi \sqrt{p^j_{RN}} h^j_{E} Y^i_{RN} + Z^j_{E}, \end{aligned} \tag{4}$$

where $j \in \{1, 2, \cdots, N\}$ is the subchannel occupied by the relay node in the broadcast stage; ξ is the forwarding amplification factor of the relay node; $h^j_{A_k}, h^j_{B_k}, h^j_E$ are the channel gain of relay node RN to A_k, B_k, E on subchannel j, respectively; p^j_{RN} is the transmitting power of the relay

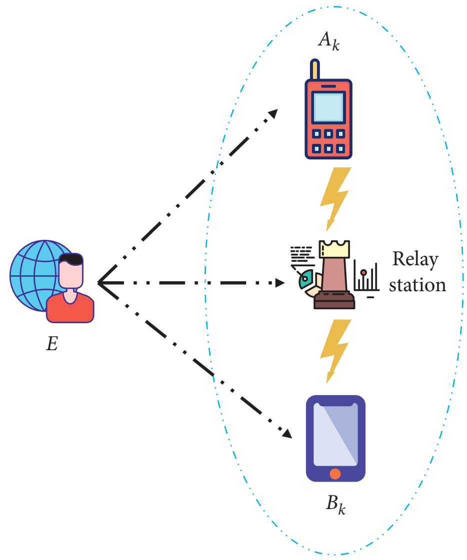

Figure 4: Two-way relay security network system.

node on the subchannel j in the broadcast stage; and $Z^j_{A_k}, Z^j_{B_k}, Z^j_E$ are the white Gaussian noise of A_k, B_k, E on subchannel j, respectively.

Each vertex in the minimum rigid graph has at least two adjacent edges [17], so the minimum rigid graph has less communication complexity and stronger robustness. Especially, the singular value of the stiffness matrix provides a method to measure the algebraic properties of the network [18]. Define the stiffness matrix of edges in the network as follows:

$$X_{(G,P)} = \overline{M}_{(G,P)}\overline{M}^T_{(G,P)} \in R^{|\varepsilon|\times|\varepsilon|}. \quad (5)$$

Among them, rigid graphs with larger determinant eigenvalue have better algebraic stiffness characteristics. Good stiffness characteristics can ensure that the network coverage positioning has a small error, thus improving the stability of the network.

Under the condition that the graph is the minimum stiffness graph, the trace value of the stiffness matrix can be maximized. This process can be transformed into an optimization problem:

$$\begin{aligned} &\underset{\varepsilon}{\text{maximize}}\ \text{trace}\left(\overline{M}_{G,P}\overline{M}^T_{G,P}\right),\\ &\text{subject to}\ \text{rank}\left(\overline{M}_{G,P}\right) = 2n - 3. \end{aligned} \quad (6)$$

This optimization problem can be solved by a classical greedy algorithm.

The coverage areas of base stations are not exactly the same. Therefore, a weight coefficient is introduced to correct it. This weight coefficient is determined by the ratio of user density to base station capacity. If the ratio is larger, the coverage radius will be smaller. On the contrary, it should be larger. Switching decision formula is

$$Mn + Ocn - Hys > Ms + Ocs + off, \quad (7)$$

where Mn represents the measurement result of the neighboring cell, Ocn represents the specific offset of the neighboring cell, Ms represents the measurement result of the serving cell, Ocs represents the specific offset of the serving cell, Hys represents the delay of the event, and off is the offset value of the event [21].

4. Experiment and Results

4.1. System Test Analysis. System performance testing is an important task in the testing task. When designing performance test cases, this system adopts the method of continuous iterative improvement, that is, the iterative process of testing, improvement, and retest. At the same time, when testing the performance of the system, it is not entirely based on test cases, but the test plan is adjusted in time according to the actual situation to meet the needs of the test system. Independent business performance test is actually the concurrent performance test of a business of the core business module, which can be understood as a unit performance test. Composite business performance testing is the concurrent performance testing of multiple services from one or more modules. The stress test scenario of concurrent user access is shown in Figure 5.

It can be seen from Figure 5 that when the number of users is less than 800, the response time of the system increases steadily with a slope. When the number of users is close to 1,000, the system drops obviously, and the drop is very serious, and a red line warning appears. Therefore, when less than 800 users access the system, the system performance may be in a stable state. If there are more than 1,000 users, there is a problem with the system performance. Try to keep it below 800. For the test of the improved system, the users who participated in the test of the existing management system before are still invited. The relevant data of six users who completed the usability task are shown in Table 1.

After completing the task, each user needs to fill out the scale. The number 1 stands for "very different," and 5 stands for "very much agree." The scores of the six user scales calculated are shown in Table 2.

The test results show that the improved user satisfaction is 62.23, and the user satisfaction has been improved to some extent. When users view a page, they do not need to think or spend a little time thinking to understand what the content on the page means and how to act. There is still a lot of attribute information in the real talent data, which can be gradually added in future applications. Keeping the attributes that have a great influence on outstanding talents' achievements and removing the attributes that have little influence will make the model more scientific and complete, and the prediction results will be more accurate.

Therefore, curriculum development must be based on a complete workflow, in-depth analysis of the workflow, and flawless integration of the entire production industry. Courses from various disciplines, occupations, and degrees should all be taken into account when creating a curriculum structure. Basic professional knowledge, interdisciplinary knowledge, professional ability, comprehensive application ability, and comprehensive ability should all be

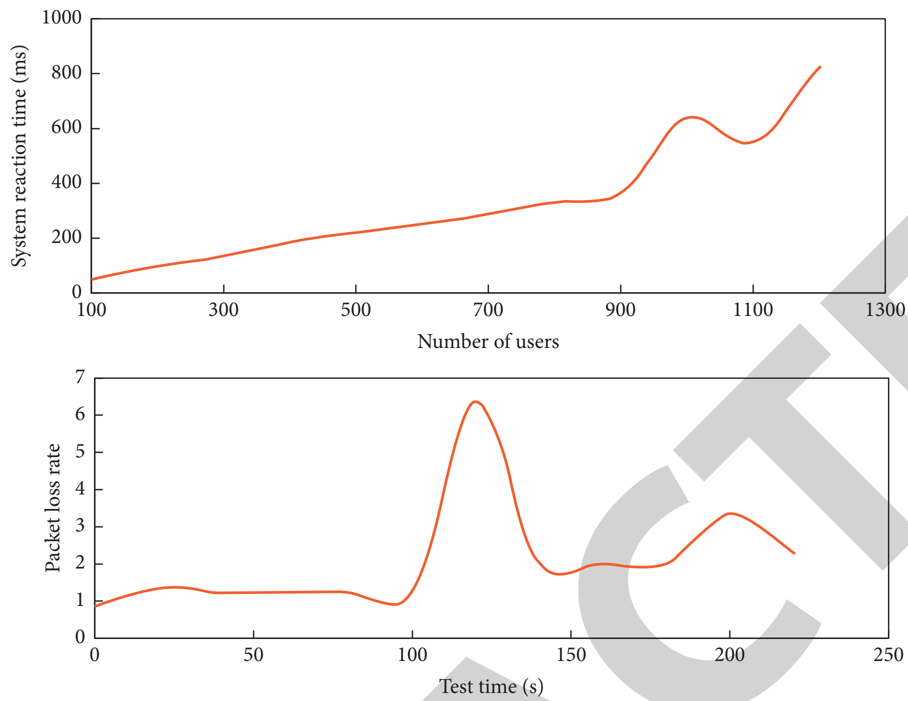

Figure 5: User concurrent access test.

Table 1: Completion rate and average time of tasks.

Task 1			Task 2		
Complete the task	After being prompted, the task is completed	Average completion time	Complete the task	After being prompted, the task is completed	Average completion time
100%	0	15 s	88.3%	9.6%	20 s

covered in the curriculum. The human society in the AI era is a complex multiparty coordination system, with real-world and virtual-world governance coexisting. This necessitates a re-examination of stakeholder relationships and a re-definition of governance scope in vocational college education. Continuous innovation and progress are required to strengthen the synergy of various stakeholders and to realize the Pareto optimal governance mechanism of vocational college education, such as restraint, encouragement, and guarantee.

Therefore, the professional training system in the AI era should no longer be limited to providing procedural training content for the workforce, such as computer science, data analysis, and so on, but should provide people-to-people training, machine training, and communication skills training between people and the world; provide training to deal with sudden problems; and provide training in critical cognition and thinking and cognition. The provision of these training contents will surely pave the way for the smooth transition of the labor force to the AI era.

4.2. Analysis of Wireless Network Optimization Algorithm. In order to verify the accuracy of the algorithm, this section uses MATLAB software to conduct simulation experiments to verify the effectiveness of the algorithm. The algorithm in this document is compared with other different algorithms, and the number of user groups is 18. In all simulations, the flat fading channel gain can be modeled by a unit random variable, which follows the average exponential distribution, and the path loss index is set to 3.

Table 2: User scale score.

User	Score
1	55
2	63
3	71
4	66
5	62.1
6	56.3

Figure 6 counts the traces of the stiffness matrix of the topological graph generated from the algorithm of reference [18] based on the topology of the least rigid graph and the least rigid graph constructed by the algorithm in this paper.

It can be seen from Figure 6 that in the same environment, the minimum rigid graph constructed by the algorithm in this paper has a large trace, which indicates that the minimum rigid graph generated by the algorithm has a good algebraic performance of stiffness, which is conducive to enhancing the stability of the network.

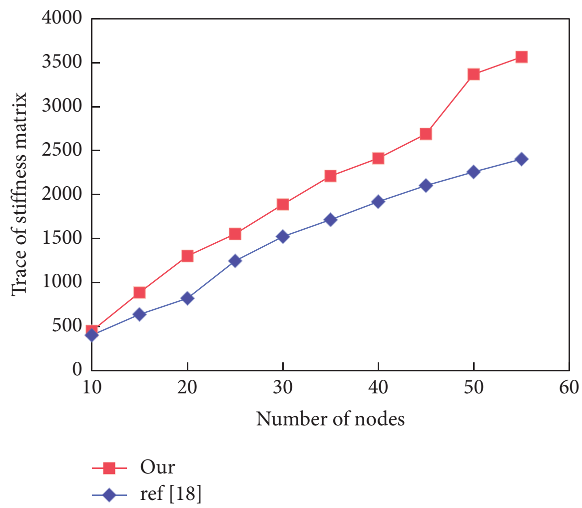

Figure 6: Trace of the stiffness matrix.

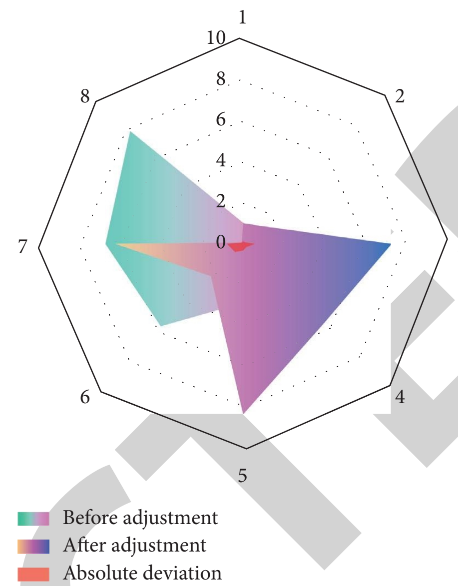

Figure 7: Relationship between the absolute deviation of different stations and deviation of handover success rate.

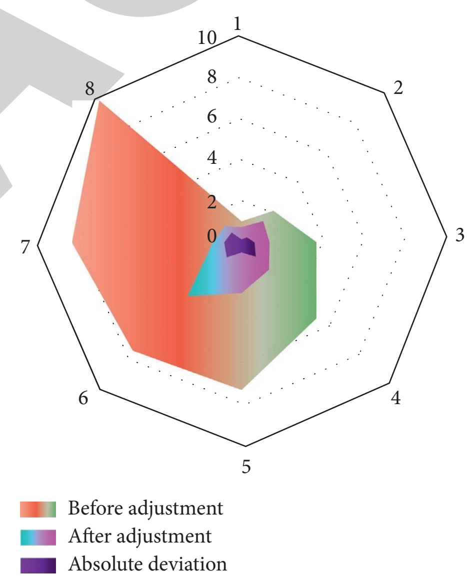

Figure 8: The relationship between the absolute deviation of different stations and the deviation of dropped call rate.

Drop call rate is an important indicator in mobile communication, which refers to the probability of unexpected interruption of communication in the process of mobile communication. Drop call rate reflects the communication quality of mobile networks to some extent. To illustrate the problem here, eight communities are selected from five sites. These five selected sites are macrosites, which are scattered and basically scattered in the whole cluster area. Then compare the relationship between your deviation and network indicators to guide optimization and replacement. The deviation here includes the absolute error between the physical site and the logical site and its replacement error. Figures 7 and 8 show the relationship between the adjusted wireless network index and polygon deviation.

According to the experimental data, it can be seen that the overlapping coverage deviation is obvious. When the absolute deviation is greater than 2, the network index fluctuates obviously, and the overall trend is upward, which increases with the increase of deviation. In the process of constructing the minimum stiffness graph, the edges are sorted in ascending order at first, and then the edge with the largest trace of the stiffness matrix is selected to join the stiffness matrix, that is, the communication link weight of the edge is further reduced while ensuring the algebraic performance of network stiffness. In the simulation, it is assumed that there is a relay node, an illegal E, and multiple legitimate users on the network. Users are randomly distributed in a circle with a radius of 50 meters centered on the relay node (all users are within the coverage of the relay node). Here, it is assumed that the distance between E and the relay node varies between 100 and 400 meters, and the total transmission power of the relay is set to 1,000 mW as shown in Figure 9.

It can be seen that when E is far away from the relay node, the average satisfaction of the user group shows an upward trend. When E is far away from the relay node, the signal-to-noise ratio it receives decreases, and the more and less communication information E can steal, the higher the security satisfaction of users will be. When E leaves the relay node within 250 meters, the average security satisfaction of all user groups increases rapidly. It is also found that within the range of 250 m, the user security satisfaction of the optimized algorithm in this paper is 0.93, and the user security satisfaction of the proposed optimized algorithm is higher than that of other algorithms. As E is far away from the relay node, this gap will become smaller and smaller.

5. Conclusions

The rise of AI has created a new demand for talent, requiring vocational colleges to adjust and reshape talent development goals in response to changing industry

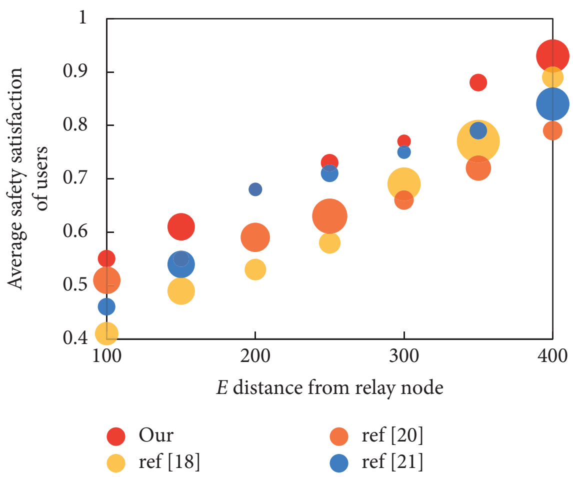

Figure 9: The relationship between the distance from E relay and users' safety satisfaction.

structures. As a result, establishing an educational talent training system in vocational colleges that incorporates AI technology can help mitigate the impact of AI on vocational college employees. The project developed a design scheme for a vocational college education talent management system based on a wireless network after conducting extensive field research to meet the needs of enterprise talent management in the AI era. The system essentially performs the expected system design function, and it has undergone a series of system tests. The results of the tests show that the system is functional and robust. The talent management system's wireless network optimization results show that within a range of 250 m, the optimized algorithm in this paper's user security satisfaction is 0.93, and the satisfaction of the optimized algorithm proposed by user security is higher than that of other algorithms. It demonstrates that the algorithm has good algebraic connectivity and stiffness properties.

Data Availability

The data used to support the findings of this study are available from the corresponding author upon request.

Conflicts of Interest

The authors declare that they have any possible conflicts of interest.

References

[1] Z. Huang, Y. Liu, C. Zhan, C. Lin, W. Cai, and Y. Chen, "A novel group recommendation model with two-stage deep learning," *IEEE Transactions on Systems, Man, and Cybernetics: Systems*, 2021.

[2] Y. Stukalina, "The management of integrated educational environment resources: the factors to be considered," *European Journal of Education*, vol. 45, no. 2, pp. 345–361, 2010.

[3] S. Ginsburg, C. van der Vleuten, K. W. Eva, and L. Lingard, "Hedging to save face: a linguistic analysis of written comments on in-training evaluation reports," *Advances in Health Sciences Education*, vol. 21, no. 1, pp. 175–188, 2015.

[4] A. Leńko-Szymańska, "Is this enough? A qualitative evaluation of the effectiveness of a teacher-training course on the use of corpora in language education," *ReCALL*, vol. 26, no. 2, pp. 260–278, 2014.

[5] N. M. Derosa, W. W. Fisher, and M. W. Steege, "An evaluation of time in establishing operation on the effectiveness of functional communication training," *Journal of Applied Behavior Analysis*, vol. 48, no. 1, pp. 115–130, 2014.

[6] S. B. Santos Filho and K. V. Souza, "Metodologia para articular processos de formação-intervenção-avaliação na educação profissional em enfermagem," *Ciência & Saúde Coletiva*, vol. 25, no. 1, pp. 79–88, 2020.

[7] J. Chen, C. Du, Y. Zhang, P. Han, and W. Wei, "A clustering-based coverage path planning method for autonomous heterogeneous UAVs," *IEEE Transactions on Intelligent Transportation Systems*, vol. 12, pp. 1–11, 2021.

[8] J. Zhang, W. Feng, T. Yuan, J. Wang, and A. K. Sangaiah, "SCSTCF: spatial-channel selection and temporal regularized correlation filters for visual tracking," *Applied Soft Computing*, vol. 118, 108485 pages, 2022.

[9] K.-n. Zheng, S.-m. Sun, and H. Yu, "College teaching quality evaluation based on system dynamics model," *MATEC Web of Conferences*, vol. 61, 04027 pages, 2016.

[10] M.-h. Sun, Y.-g. Li, and B. He, "Study on a quality evaluation method for college English classroom teaching," *Future Internet*, vol. 9, no. 3, p. 41, 2017.

[11] Y. Chen, "College English teaching quality evaluation system based on information fusion and optimized RBF neural network decision algorithm," *Journal of Sensors*, vol. 2021, no. 5, pp. 1–9, Article ID 6178569, 2021.

[12] Q. W. Dong, S. M. Wang, F. J. Han, and R. D. Zhang, "Innovative research and practice of teachers' teaching quality evaluation under the guidance of 'innovation and entrepreneurship'," *Procedia Computer Science*, vol. 154, pp. 770–776, 2019.

[13] X. Yang, "Research on the teaching quality evaluation of law course in colleges based on the AHP model," *Revista de la Facultad de Ingenieria*, vol. 32, no. 14, pp. 713–717, 2017.

[14] W. Liu, S. Zhao, and X. Li, "The practice of advanced mathematics teaching quality evaluation system," *Proceedings of the 2012 International Conference on Cybernetics and Informatics*, vol. 163, pp. 1501–1506, 2014.

[15] Q. Jian, "Multimedia teaching quality evaluation system in colleges based on genetic algorithm and social computing approach," *IEEE Access*, vol. 7, pp. 183790–183799, 2019.

[16] Y. E. Sagduyu, Y. Shi, A. Fanous, and J. H. Li, "Wireless network inference and optimization: algorithm design and implementation," *IEEE Transactions on Mobile Computing*, vol. 16, no. 1, pp. 257–267, 2017.

[17] F. Xiao, X. Xie, Z. Li, and Q. A. L. Deng, "Wireless network optimization via physical layer information for smart cities," *IEEE Network*, vol. 32, no. 4, pp. 88–93, 2018.

[18] P. Zhang, X. Ding, J. Xu, and J. L. Wang, "Successive interference cancellation based throughput optimization for multi-hop wireless rechargeable sensor networks," *Sensors*, vol. 20, no. 2, p. 327, 2020.

[19] R. Wang, G. He, X. Wu, F. Wang, and Y. Hu, "Multicast optimization and node fast location search method for wireless sensor networks based on ant colony algorithm," *Journal of Digital Information Management*, vol. 15, no. 6, pp. 303–311, 2017.

Hindawi
Computational Intelligence and Neuroscience
Volume 2022, Article ID 9602740, 10 pages
https://doi.org/10.1155/2022/9602740

Research Article

Application of Recurrent Neural Network Algorithm in Intelligent Detection of Clinical Ultrasound Images of Human Lungs

Yanjie Jia

Affiliated Hospital of Chifeng College, Chifeng 024000, Inner Mongolia, China

Correspondence should be addressed to Yanjie Jia; baixuhui1010@163.com

Received 7 April 2022; Revised 21 May 2022; Accepted 26 May 2022; Published 24 June 2022

Academic Editor: Xin Ning

Lung ultrasound has great application value in the differential diagnosis of pulmonary exudative lesions. It has good sensitivity and specificity for the diagnosis of various pulmonary diseases in neonates and children. It is believed that it can replace chest CT examination. It is routinely used for the diagnosis of pulmonary diseases in emergency critical care medicine. However, the interpretation of the impact of ultrasound on the human lungs relies heavily on experienced physicians, which greatly restricts the interpretation efficiency of the impact of ultrasound. In order to improve the efficiency of monitoring and interpretation of the impact of ultrasound, this paper proposes an intelligent detection algorithm for human lung clinical ultrasound images based on recurrent neural network. Transfer learning is used to replace the fully connected layer of the VGG16 model and improve the loss function, so that the same the Euclidean distance between category images can be reduced, and the Euclidean distance between different categories of images can be increased, enhancing the resolution of the entire model, thereby achieving better image feature extraction results. The experimental results show that the algorithm proposed in this paper can surpass the doctor's level in the identification of various lung diseases.

1. Introduction

The lungs are the main air-bearing organs of the body. Due to the physical characteristics of ultrasound itself, when the propagation path encounters gas, total reflection will occur, resulting in ultrasound not being able to capture the image of the normal lung tissue. In recent years, with the continuous development of ultrasound technology, ultrasound diagnosis of lung diseases has become an important means to check and monitor the treatment effect in the world, realizing the visualization of lung pathophysiology, known as the visual "stethoscope" [1].

With Lichtenstein's discovery of the value of pulmonary ultrasound, the establishment of perfect operating and scoring rules, and the formation of the imaging theory and procedure of LUS, LUS has become a simple and reliable means of diagnosing pulmonary diseases in recent years. The International Consortium of Lung Ultrasound has issued an international consensus on the diagnosis of lung diseases by ultrasound [2]. It is believed that lung ultrasound can not only accurately diagnose many lung diseases but also has higher accuracy and sensitivity than chest X-ray in the diagnosis of pneumothorax, pulmonary solids, and pleural effusion.

The determination of the type of lung disease relies mainly on the physician's subjective diagnosis of the patient's lung images. The accuracy of the diagnosis of lung diseases depends on the physician's personal condition and is highly subjective [3]. Moreover, the orientation of certain lung lesions varies from person to person, and the lung structure varies greatly from person to person. Therefore, it is also easy to create factors that may produce errors in this regard, thus failing to meet the requirements of precision medicine [4]. On the other hand, not all regions have good medical resources and medical conditions, and the medical conditions enjoyed by patients in different regions may be very different [5]. Computer-aided medical image recognition and diagnosis is able to overcome these difficulties and solve the current problems. Computer-aided medical image recognition and diagnosis aims to improve the accuracy of diagnosis by quickly and accurately detecting lesions.

This paper studies the theory of optimization on the one hand, will be conducive to the algorithm, On the other hand, it is beneficial to promote the efficiency of pulmonary ultrasound detection and has certain theoretical and application significance.

2. State of the Art

When it comes to image recognition, it is inseparable from the convolutional neural network of deep learning. Convolution neural network is a kind of feedforward neural network with convolution computation and depth structure. It is one of the representatives of the depth learning algorithm. It goes beyond the traditional learning tools and methods. Convolutional neural network, which is called neural network, plays a central role in the field of medical image recognition and image recognition. We have to mention the original convolutional neural network LeNet.

The proposal of LeNet marked the birth of CNN, and the 7-layer LeNet contains the basic modules of deep learning. The simple network is capable of automatic recognition of handwritten recognition numbers and automatic verification of CAPTCHA. AlexNet, designed by Hinton and his student Alex Krizhevsky, was the winner of the ILSVRC competition. Several technical breakthroughs and applications of new technologies were achieved in the AlexNet network. It is these techniques that take convolutional neural networks to new heights [6].

The innovations used in AlexNet include the following: (1) The use of the Relu activation function instead of the original Sigmoid activation function. When the number of layers of the neural network increases to a certain depth, if the Sigmoid activation function is used, the gradient will disappear and the whole network will converge too slowly, or there will be a gradient dispersion problem, using the Relu function is a good solution to this problem [7]. (2) The Dropout function is used during training, through which the parameters of some neurons can be randomly ignored, i.e., the activity of some neurons is suppressed, and this measure can also avoid overfitting of the model [8]. (3) Applying overlapping pooling layers to the convolutional neural network can not only significantly improve the computational speed compared with the previous average pooling layers but also—to a certain extent—reduce the overfitting of the model [9]. The overfitting of the model can be reduced to a certain extent. (4) The dataset expansion technique is used. (5) CUDA acceleration is used to reduce the computation time so that the number of layers of the neural network can be deepened to improve the overall model recognition accuracy. (6) The concept of LRU was introduced for the first time, adding LRU layer to CNN, the role of which is to filter the neurons in the network model layer, making the value of neurons with larger responses larger and the value of neurons with smaller responses smaller, which can well suggest the robustness and generalization ability of the model.

Since then, convolutional neural networks have developed rapidly and VGG series networks have emerged. The network structure of VGG16 is shown in Table 1. The advantage of VGG series is that the structure of the whole neural network is very simple, which can improve the calculation speed. Secondly, VGG series through the test of its own data, verified by deepening the depth of the neural network, improves the network identification performance, and can improve the accuracy of identification. Table 1 describes from top to bottom the number of neurons in VGG16 neural network layer, the arrangement of convolutional layer and pooling layer, and the size of the input and output image feature matrix of each neural network layer.

The core neural network representative of GoogLeNet is the Inception network, which is designed as a net-within-a-net structure, giving the model the ability to choose itself, with multiple choices for each layer, and the model automatically adjusts to choose the layer with higher recognition accuracy for training recognition. By adding 1×1 convolutional kernel layer, the whole Inception network can be designed to be deeper and the width can be expanded and adjusted, and the overall effect can reach 2–3 times of the original performance. The error rate of recognizing the top5 classified images was only 6.67%.

The biggest innovation highlight of Inception Net is the design of Module module. Module brings improvement not only in the overall model performance but also reduces the number of image data parameters. It provides the ability of the model to cross channels, improves the information transfer and expression ability of the network, and provides the model with more choices of linear transformation types. On the other hand, it is a regularization method that is first proposed and applied in the model for the whole network, which speeds up the convergence and improves the overall classification and recognition accuracy of the model [10]. The data are normalized in the implementation process to limit the range to $N(0, 1)$. The ResNets (residual networks) that emerged afterwards extend the depth of the network to several hundred layers by a special computational approach. This method is based on the idea of Highway Network, which opens up a "high speed channel" in the process of network propagation and is computed in an optimal fitting way [11].

Based on previous algorithm studies, the advantages of convolutional neural network in image recognition can be seen. Compared with other neural networks, the network has better fitting degree and higher accuracy rate of image recognition, so it can be better applied in intelligent detection of human lung clinical ultrasound images.

By combing the previous development context, we can see that the optimization of the past is a dark mass of optimization in the input layer. In order to take advantage of deep learning to interpret ultrasound images of lungs, we proposed a neural network algorithm based on VGG16, whose basic structure is shown in Figure 1. We replace the output layer of THE VGG16 neural network with the ultrasound image of the lung as the initial input, so as to improve the accuracy of the neural network results, and use

Table 1: VGG16 structure.

ConvNet configuration					
A 11 weight layers	A-LRN 11 weight layers	B 13 weight layers	C 16 weight layers	D 16 weight layers	E 19 weight layers
Input (224 × 224 RGB image)					
conv3-64	conv3-64 LRN	conv3-64 conv3-64	conv3-64 conv3-64	conv3-64 conv3-64	conv3-64 conv3-64
Maxpool					
conv3-128	conv3-128	conv3-128 conv3-128	conv3-128 conv3-128	conv3-128 conv3-128	conv3-128 conv3-128
Maxpool					
conv3-256 conv3-256	conv3-256 conv3-256	conv3-256 conv3-256	conv3-256 conv3-256 conv1-256	conv3-256 conv3-256 conv3-256	conv3-256 conv3-256 conv3-256 conv3-256
Maxpool					
conv3-512 conv3-512	conv3-512 conv3-512	conv3-512 conv3-512	conv3-512 conv3-512 conv1-512	conv3-512 conv3-512 conv3-512	conv3-512 conv3-512 conv3-512 conv3-512
Maxpool					
conv3-512 conv3-512	conv3-512 conv3-512	conv3-512 conv3-512	conv3-512 conv3-512 conv1-512	conv3-512 conv3-512 conv3-512	conv3-512 conv3-512 conv3-512 conv3-512
Maxpool					
FC-4096 FC-4096 FC-1000 Soft-max					

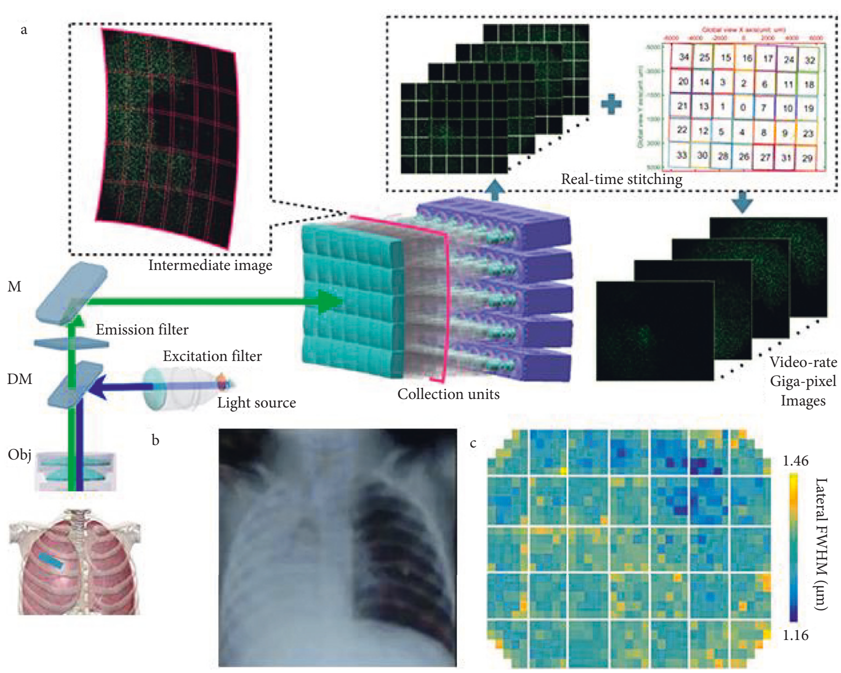

Figure 1: Algorithm structure diagram.

the transfer learning method to make the VGG16 neural network more suitable for lung ultrasound interpretation.

3. Methodology

3.1. Data Set. It is difficult to obtain medical images of lungs, and there are no datasets of lung medical images of the order of 10 million or millions at present. This is also a problem at present, and the solution is to expand the image dataset.

In order to ensure the integrity of the image data, ensure the scientific nature and authenticity of the experiment. The external library PIL in Python was used to realize the extension of lung medical image, and the image recognition and classification effects such as image rotation, mirror image, brightness adjustment, chroma adjustment, and random cropping were compared. Finally, image rotation and mirror were selected as the extension method of lung medical image dataset [12]. Because the whole model structure is divided into five branches, it is selected to use the original image to generate three image rotation directions, and then generate a mirror of a total of five pictures, that is to say, one original image will be extended to five, input different branches as the input images, the dataset expansion result is shown in Figure 2.

The purpose of dataset enhancement is mainly to perform some transformations on the input image data and train a model with better robustness, so that it can cope with various transformations and be more applicable to real scenes. For example, when taking pictures in life, the angle, brightness, stretching, etc., of the pictures obtained may be different due to different shooting locations or different cameramen, whether or not the different images can be recognized as the same structure. Again performing dataset enhancement is to train the model to be able to achieve excellent recognition accuracy with so many transformations [13]. AlexNet does a good job of dataset augmentation and eventually achieves good results.

There are many ways to enhance image datasets: one common method is to apply a bevel attribute to the image, and another is to add a shrink and expand factor.

The interface to the dataset enhancement algorithm is integrated in the Python external library Keras, which can be easily invoked by setting the corresponding parameters [14].

3.2. Recurrent Neural Network. Recursive neural network is an artificial neural network with tree-like hierarchical structure and the network nodes recurse the input information according to their connection order, which is one of the deep learning algorithms. Recursive neural networks can be trained using supervised and unsupervised learning theories. In supervised learning, recursive neural network uses back propagation algorithm to update weight parameters, and the calculation process can be similar to the back propagation algorithm over time of recurrent neural network. Unsupervised learning recursive neural networks are used for representational learning of structural information and the most common form of organization is recursive self-encoder.

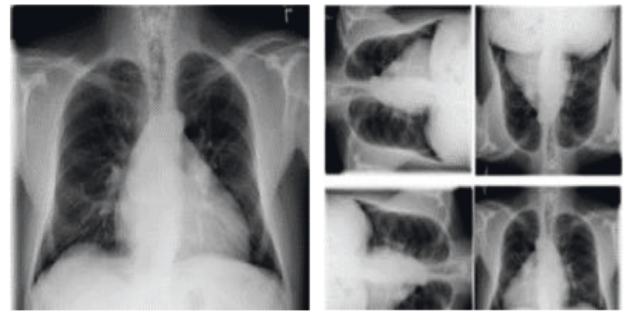

Figure 2: Lung image dataset expansion.

For a recurrent neural network, it is a network where the current output is related to the previous output as well. This means that the network remembers the last output result and then uses it in the calculation of this output, which makes the nodes between the intermediate layers transform from a connectionless one to a connected one, and the input given by the intermediate layers has both the output of the input layer and the output of the intermediate layer at the last moment.

Where X represents the input vector, U represents the weight matrix from the input to the intermediate layer, similarly W represents the weight matrix from the state to the intermediate layer, S is the state value of the node in the intermediate layer, V represents the weight matrix from the loop layer to the output layer, and Y represents the output. The value of state S is not only output to the output layer but also calculated by multiplying W and then used as input for the next calculation [15]. Figure 3 shows the expansion diagram of the recurrent neural network expanded along time in Figure 4.

Where the network input at time t is X_t, St denotes the value of the intermediate layer, and the output is Y_t. It is clear that the value of S_t depends not only on X_t but also on $S_t - 1$ as well. They can be expressed in equations as shown in (1) and (2), where g and f denote the activation functions.

$$Y_t = g(V_t S_t), \tag{1}$$

$$S_t = f(UX_i + W_t S_{t-1}). \tag{2}$$

Compared with other neural networks, the structure of recursive neural network can well introduce the concept of time into the neural network, which can make the input data at the previous moment directly affect the data calculation at that moment. St state can remember the information at the previous moment. Thus, it is beneficial for real-time image recognition. Therefore, this paper chose recursive neural network for pulmonary clinical image ultrasound detection. In practice, however, with the increase of depth of the model, the recursive neural network cannot handle well data dependency for a long time, so you can understand, the so-called back-propagation gradient disappeared and gradient caused by explosion problem, so this article think should optimize the recursive neural network so as to solve the data dependency problem for a long time. To solve these

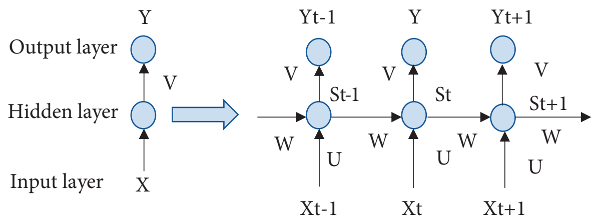

Figure 3: Structural diagram of recurrent neural network expansion.

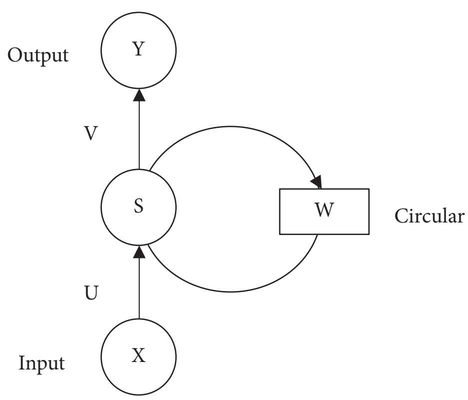

Figure 4: Recursive neural network structure.

problems, an improved recursive neural network, LSTM, is proposed.

LSTM adds three gate selection units in the recursive neural network, which solves the problems of gradient disappearance and gradient explosion of ordinary RNN (existing neural network), and forms an independent transmission mechanism for memory data and result data, so that information can be transmitted across regions. Overcomes the problem that standard RNN does not handle data dependency well over time. Deals with long time dependencies on data. Therefore, LSTM is one of the most popular recursive neural networks and has been widely used in several fields of artificial intelligence [16].

Figure 5 shows the structure of LSTM network, which has four network layers that make it different from the normal RNN network, LSTM stores the information selectively, while the normal RNN stores the information whether it is useful or not. The gates are sigmoid and tanh functions, and the process is implemented by multiplying the neural layers of the sigmoid or tanh functions with each point to make it possible [17]. The gates in this network are the forgetting gate and the input and output gates, respectively.

Where ⊗ denotes the dot product, f denotes the activation function, $C_t - 1$ denotes the cell state at the previous time step, $h_t - 1$ denotes the output value at the previous time step, ct is the cell state at this moment, and ht denotes the output value at this moment.

(1) forget gate is a judgment of what information is discarded by the cell state, and this judgment is done

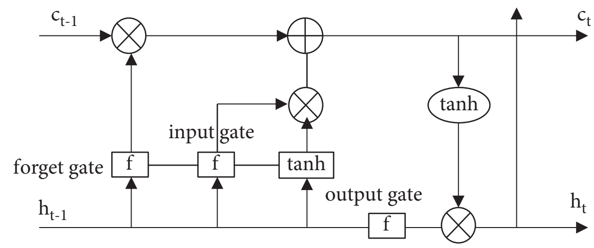

Figure 5: Structure of LSTM network.

by the sigmoid function, expressed as shown in the following equation:

$$f_t = \sigma\left(W_f\left[h_{t-1}, x_t\right] + b_f\right), \tag{3}$$

where $ht - 1$ denotes the last—moment output value, x_t denotes the input value at this moment, Wf denotes the weight matrix of this gate, b_t denotes the bias of this gate, and σ denotes the activation function.

(2) The input gate (input gatc) determines what information is stored in the cell state. First, the input gate is called a sigmoid layer, and second, a vector is created by calling the tanh layer as a new marquee value that can be added to the intermediate layer states [18]. Finally, the two parts are merged to create an update to the hidden layer state, which can replace the old memory information forgotten, then represented as shown in equations (4) and (5):

$$i_t = \sigma\left(W_i\left[h_{t-1}, x_t\right] + b_i\right), \tag{4}$$

$$\tilde{c}_t = \tanh\left(W_c\left[h_{t-1}, x_t\right] + b_c\right), \tag{5}$$

In this case, if we know the memories to be forgotten and those to be added, we can update the old cell state $c_t - 1$ to the new cell state ct. After that, the old m-server state will be multiplied by FT, which will determine the information to be forgotten, and then multiplied by the sum of the input gate of the current memory c_t [19]. After this series of operations, the new memory information will be derived, which is expressed as shown in the following equation (6):

$$c_t = f_t * c_{t-1} + i_t * \tilde{c}_t. \tag{6}$$

(3) The output gate is the information that needs to be decided for the output. Although the output is based on the cell state, it will be a post-selection value. This output gate needs to go through three steps to get the output information [20]. First, the output gate needs to go through a sigmoid layer, second, a partial selective output is performed for different parts of the cell state, and finally, the obtained cell state is fed into the tahn activation function so that it is multiplied with the sigmoid activation function to obtain a value that needs to be output, which is represented as shown in (7) and (8):

$$o_t = \sigma(W_o[h_{t-1}, x_t] + b_o), \tag{7}$$

$$h_t = o_t * \tanh(c_t), \tag{8}$$

where b_o denotes the output bias, W_o denotes the number of weights of the output, h_t denotes the output value of the cell state, and ot denotes the value of the output gate.

4. Result Analysis and Discussión

4.1. Principle of VGG16 Extraction of Image Features. Before introducing VGG16, it is necessary to introduce the general convolutional neural network computational rules and the important parts of it. The more important components of the convolutional neural network are the convolutional layer, the pooling layer, and the activation function, and the computational method is the BP back propagation algorithm.

The convolutional layer plays a crucial role in the whole neural network layer, which is equivalent to a filter, and consists of convolutional kernels, the number and size of which are set by the designer of the network, generally 3×3, 5×5, 7×7, 11×11. According to the set size of the convolution kernel, a weighted average calculation is performed on the corresponding size area of the input image. Depending on the step size, the size of the convolution kernel, and the setting of the convolution algorithm, the convolution process will extract different numbers of image features, and the final output matrix is the output of the convolution kernel on the image. The final convolution value is obtained by multiplying the convolution kernel parameters with the image pixel values in the matrix, and then the length of each convolution kernel move is determined by the convolution kernel step setting. After the convolution, kernel shift calculation will reduce the size of the whole image feature matrix, as seen in Figure 6.

The pooling layer is used to reduce the number of features extracted by the convolutional layer, i.e., to reduce the size of the feature matrix, thus reducing the system resources and time consumed during the model computation, and is also useful in preventing overfitting. This process can also be called “downsampling.” There are two main pooling layers: the maximum pooling layer, which extracts the largest value in the pooling matrix as the output, and the average pooling layer, which extracts the average value of the parameters in the pooling matrix as the output.

The activation function is set in each layer of the network, and each layer has input and output data. The input data are the parameter value transferred from the upper layer after the calculation, and the output value obtained after the calculation of the specific function is used as the input value for the lower layer of the network. The specific function in the middle refers to the activation function. There are many different types of activation functions. In order to make the values calculated by the activation function more nonlinear, the following activation functions are commonly used.

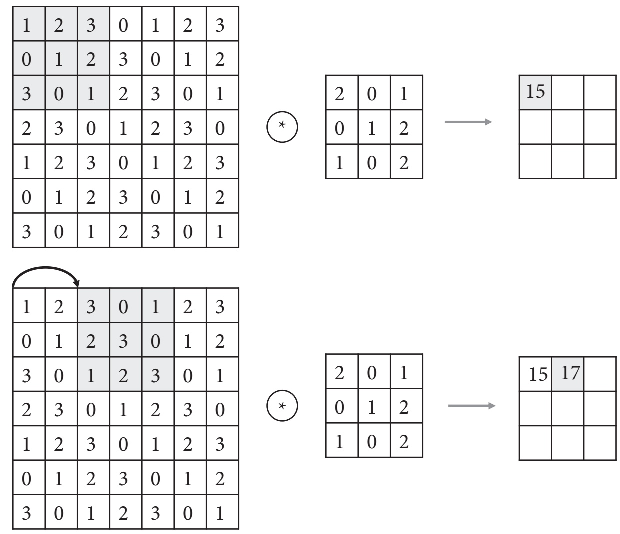

Figure 6: Convolution kernel to extract image features.

After the network reaches the last layer, the difference between the predicted result and the real result is calculated according to the corresponding loss function, according to which the BP back propagation algorithm goes forward to adjust the parameter values of the whole network model, so that the model can obtain better recognition and classification results.

The structure of the VGG16 model contains 13 convolutional layers, 3 fully connected layers, and 5 pooling layers. After training, the complete model is able to extract features from images.

4.2. Single-Branch Model Structure. In this paper, gradient advancing tree in traditional machine learning model is selected as the classification model of lung image recognition. The gradient advancing tree model is suitable for the classification and recognition scenes with small datasets. However, the traditional machine learning model requires manual extraction of image features on the one hand, and the upper limit of classification and recognition accuracy on the other hand is not very high. In order to solve these problems, the method commonly adopted abroad is to modify the classical model a lot, until it is applicable to the size of the corresponding dataset; using this method will cause a great loss of the ability of the VGG16 model to extract image features. Therefore, in the research method of this paper, we first use migration to adjust the parameters of the VGG16 model. Migration research is a machine learning method, which starts from a model in the development task. The model used in the development process is task B. The migration research method in this paper can improve the efficiency of model development. In this paper, the loss function of VGG16 is improved, the clustering effect is increased, and the ability of the whole model to extract image features is improved. Then, the function of the first half of the model is to extract the features of lung medical images, and then input the extracted features into the gradient enhanced tree model for recognition and classification.

In this paper, we modify the fully connected layer of the original VGG16 model by using the idea of migration learning, removing the fully connected layer, and replacing the fully connected layer with a fully connected network of our own design, and modifying the corresponding activation function and dropout parameters. The second and third layers are set to 256 neurons, respectively, reducing the number of neurons in each layer so that the training of the whole model can match the number of images in the training set and avoid the effect of overfitting the model. The loss function of the original classical model is innovatively improved to include clustering effect, so that the feature distance between images of the same category is reduced, while the feature distance between images of different categories is increased, thus improving the recognition and classification ability of the model. The image features extracted by the neural network are input to the gradient boost tree model for recognition and classification.

The first step of training the single-branch model is to obtain the lung medical image dataset and image preprocessing, after which the fully connected layer of VGG16 is replaced and the parameters are fine-tuned using migration learning, with the conflict of needing to extract image features manually. On the other hand, the single-branch model has certain advantages in terms of computational speed and computational efficiency because only one branch of training computation is required. However, the disadvantage of single-branch model is that the accuracy of recognition and classification may fluctuate greatly due to different scenes or different image datasets, which causes the stability and robustness of the model to be low and thus cannot be applied to the training recognition and classification of different scenes and different datasets; so we consider designing multiple-branch model structure and combining the recognition results of each branch through corresponding algorithms to finally complete the image. The model structure of multiple branches is considered, and the recognition results of each branch are combined by the corresponding algorithm to complete the classification of images.

4.3. Migration Learning of VGG16. The purpose of migration learning is to preserve the ability of VGG16 to extract features from images. Because of the small number of image datasets, the training cannot be done from scratch based on the original model, but rather fine-tuning the parameters for certain layers.

VGG16 consists of 13 convolutional layers, 5 pooling layers, and 3 fully connected layers. The changes in image size and number of channels per layer in the original and modified model structures are shown in Figure 6. The number of neurons in each of the three replacement layers is set to 4096, 256, and 256, respectively. The activation function uses the Relu function, which is called to splice the first 15 layers of the classical model with the fully connected layers designed by itself, and the parameters of the training layers can be adjusted so that the whole model is involved in the training, but only the parameters of the fully connected layers designed by itself are adjusted.

The first 15 layers of the VGG16 model have not been changed, but only the last three fully connected layers have been changed. The number of neurons in the fully connected layer is reduced and the corresponding activation function and dropout parameters are changed, the regularization coefficients are changed, and the training is performed using medical images of lungs. The training process only adjusts the three-layer model designed by ourselves, which can be set by the trainable parameter in the layer external library to avoid the participation of the first half of the VGG16 model in the training.

4.4. Model Accuracy and Robustness Verification and Analysis. The main objective of this research method is to solve the following problems: firstly, the VGG16 model is improved and fine-tuned by transfer learning to resolve the contradiction between the complex VGG16 model and insufficient lung images; secondly, the loss function in the VGG16 model is improved to include the judgment of inter-class similarity of lung images to make the model have the effect of clustering; after that, the VGG16 extracted image. Finally, the above model is used as a whole to combine multiple branches into a strong classifier by weighted voting or majority voting method to enhance the accuracy, precision, and recall of model recognition and improve the recognition ability and robustness of the model.

The data used in this study are from the publicly available ChestX-ray14 dataset, which is provided by https://www.kaggle.com/nih-chest-xrays/data. Images of five diseases (Atelectasis, Emphysema, Infiltration, Nodule, and Pneumonia) from the ChestX-ray14 dataset were selected. Some of the images in the dataset are shown in Figure 6. After that, the original images were rotated by 90°, 180°, and 270° and mirrored to obtain 4 patch images, thus expanding each 1 original image to 5. The number of images is then expanded by using data enhancement methods including image scaling, beveling, and panning. All images are converted to a uniform format and size and randomly divided into a training set and a test set (ratio 8 : 2). The recognition accuracy of the training set and the comparison results of the loss during training are shown in Figure 7.

From the accuracy graph, we can see that CheXNet starts to improve from 78%, while the model designed in this paper starts to improve from 65%, indicating that the dataset trained by CheXNet before is very similar to the lung images, while the initial dataset of the VGG16 model used in this paper is mostly images from daily life, which is different from the medical images.So the recognition accuracy of the model at the beginning will be improved. However, as the number of training iterations increases and the recognition accuracy of the model remains stable, the model designed in this paper clearly outperforms the recognition accuracy of CheXNet, and this conclusion can also be confirmed in the comparison of the loss results during training.

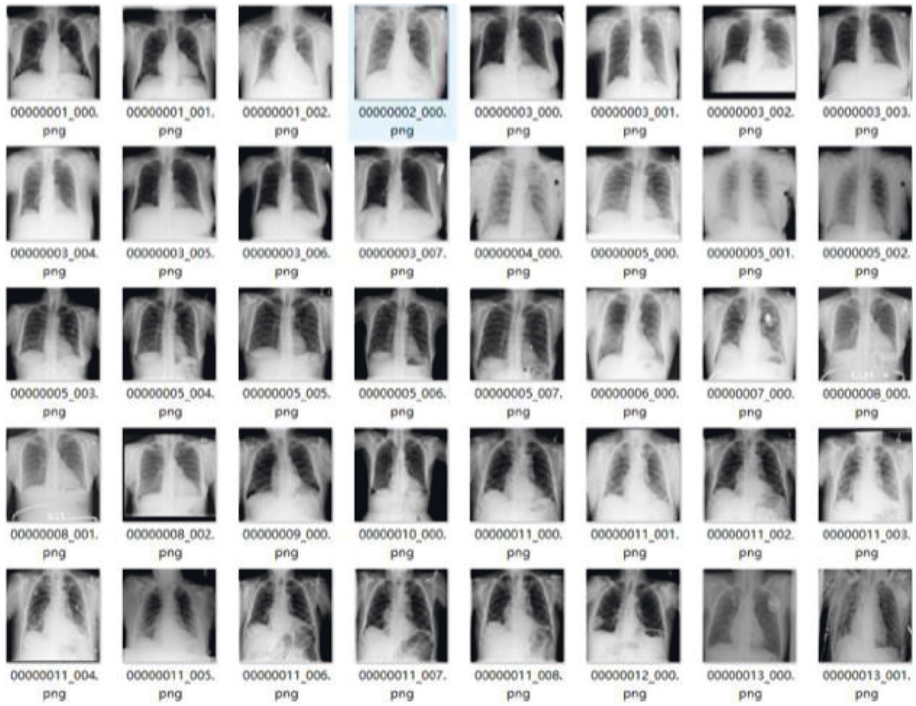

Figure 7: Partial dataset images.

In the comparison graph of model recognition accuracy, my_acc represents the recognition accuracy of the model designed in this paper, and standard_acc represents the recognition accuracy of CheXNet; in the comparison graph of loss during training, my_loss represents the change of loss during the iteration of the model designed in this paper, and standard_loss represents the change of loss during the iteration of the CheXNet model. my_loss represents the change of loss in the iterative process of the design model, and standard_loss represents the change of loss in the iterative process of the CheXNet model. In the comparison graph of recognition accuracy, when the recognition accuracy curve is close to smooth, the recognition accuracy of this design model is significantly better than that of CheXNet model; in the comparison graph of loss calculated during iteration, when the loss curve is close to smooth, the loss value calculated during iteration of this design model is lower than that calculated during iteration of CheXNet. The loss value calculated in the iterative process of the model designed in this paper is lower than that calculated in the iterative process of CheXNet when the loss curve is close to smooth. The loss here refers to the loss result value calculated by the loss function in each iteration of the model training process. By observing the loss value change graph, we can also analyze the advantages and disadvantages of different models in terms of recognition accuracy.

After the trained model is obtained, the recognition accuracy of the model is verified using the test set images obtained during image preprocessing, and the final accuracy verification conclusion is obtained by comparing the recognition accuracy of different models for the test set lung images, i.e., the model-assisted lung image disease classification accuracy.

Using the trained model for classification recognition on the test set, the test results are shown in Figure 8. In the comparison graph of recognition accuracy results, the CheXNet model and the model designed in this paper are tested and compared, and it is obvious that the model recognition accuracy is better or worse.

The blue curve in the figure shows the accuracy of the model designed in this paper in recognizing the test set data, and the red curve shows the accuracy of the CheXNet model in recognizing the test set images. It is obvious from the images that the model designed in this paper has better prediction effect than the current advanced CheXNet model.

In this paper, the different lung disease recognition accuracies were extracted separately and compared with the previous models. In this paper, the data from the original literature was selected and a row was added to include the data of the accuracy of the single lung disease recognized by the model designed in this paper for comparison with the previous models, as shown in Table 2. From the table, we can see the recognition accuracy of different models for each of the five lung images to be classified individually, which can also verify the advantages of the model designed in this paper in terms of recognition accuracy.

The robustness of the model designed in this paper was verified by comparing the accuracy and recall of the model designed in this paper with the CheXNet model and the F-values calculated by radiologists for image classification of

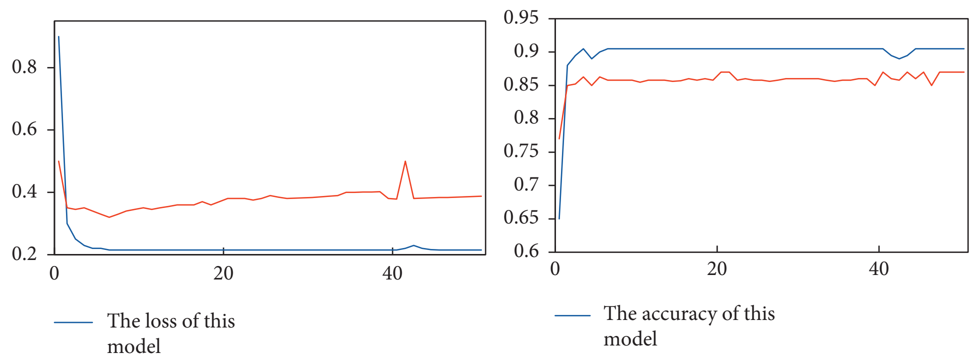

Figure 8: Comparison of training results.

Table 2: Comparison of accuracy rates of different models for lung diseases.

Disease type	Models			
	Wang et al., (2017)	Yao et al., (2017)	CheXNet models	Text model
Pulmonary atelectasis	0.716	0.772	0.8094	0.8243
Pulmonary emphysema	0.815	0.829	0.9371	0.9537
Pulmonary infiltration	0.609	0.695	0.7345	0.8211
Tuberculosis	0.671	0.717	0.7802	0.7981
Pneumonia	0.633	0.713	0.7680	0.7813

Table 3: Model robustness comparison.

Models	Standard		
	Accuracy rate	Recall rate	F-value
Physician average	0.330	0.442	0.378
CheXNet average	0.387	0.481	0.428
The model in this paper averages	0.415	0.496	0.452

five lung diseases, and the comparison results are shown in Table 3. It can be seen that the model in this paper has higher recognition accuracy.

5. Conclusion

In recent years, with the continuous development of ultrasound technology, ultrasound diagnosis of lung diseases has become an important means to check and monitor the treatment effect in the world, realizing the visualization of lung pathophysiology, known as the visual "stethoscope." In order to improve the recognition efficiency of lung ultrasound images, this paper proposed a lung image classification recognition method combining convolutional neural network VGG16 and gradient enhanced tree model. In order to improve the efficiency of model optimization, transfer learning is used to replace, train, and fine-tune the full connection layer of the VGG16 model. The original loss function is improved, and a new loss function is proposed, which reduces the Euclidean distance between the same category images and increases the Euclidean distance between different categories images, so as to enhance the recognition ability of the whole model and achieve better image feature extraction. Finally, multiple branches are designed and the classification results of these branches are combined by majority voting algorithm or weighted voting algorithm to obtain the detection results of lung images. It can be seen from the results that compared with the algorithm before optimization, the algorithm model designed in this paper has higher precision and accuracy.

Data Availability

The labeled dataset used to support the findings of this study is available from the corresponding author upon request.

Conflicts of Interest

The author declares that there are no conflicts of interest.

Acknowledgments

This work was supported by the Affiliated Hospital of Chifeng College.

References

[1] M. Qiu, H. Li, S. Meng, Q. Li, Z. Zhou, and J. Wang, "Detection of early-stage lung cancer by exhaled volatile organic compounds using a high-pressure photon ionization time-of-flight mass spectrometry," *Journal of Clinical Oncology*, vol. 38, no. 15_suppl, 2020.

[2] A. Jame, "Reduced lung cancer mortality with lowdose computed tomographic screening[J]," *Community Oncology*, vol. 36, no. 5, pp. 395–409, 2011.

[3] A. Snoeckx, P. Reyntiens, D. Desbuquoit, M. J. Spinhoven, P. E. V. Schill, and J. P. V. Meerbeeck, "Evaluation of the solitary pulmonary nodule: size matters, but do not ignore the power of morphology," *Insights Into Imaging*, vol. 24, no. 6, pp. 341–411, 2018.

[4] Q. Zhou, Y. Fan, Y. Wang, Y. Qiao, G. Wang, and Y. Huang, "China national guideline of classification, diagnosis and treatment for lung nodules (2016 version)," *Zhongguo fei ai za zhi Chinese journal of lung cancer*, vol. 19, no. 12, pp. 793–801, 1999.

[5] M. V. Davis, "The solitary pulmonary nodule," *Chest*, vol. 123, no. 1, pp. 34–49, 1957.

[6] W. Cao, R. Wu, G. Cao, and Z. He, "A comprehensive review of computer-aided diagnosis of pulmonary nodules based on computed tomography scans," *IEEE Access*, vol. 99, no. 11, p. 1, 2020.

[7] S. G. A. Iii and W. F. Sensakovic, "Automated lung segmentation for thoracic CT impact on computer-aided diagnosis," *Academic Radiology*, vol. 11, no. 9, pp. 1011–1021, 2004.

[8] I. Sluimer, A. Schilham, M. Prokop, and B. van Ginneken, "Computer analysis of computed tomography scans of the lung: a survey," *IEEE Trans.med.imaging*, vol. 25, no. 4, pp. 385–405, 2006.

[9] G. Li, W. Zhou, W. Chen, F. Sun, and F. Gong, "Study on the detection of pulmonary nodules in CT images based on deep learning," *IEEE Access*, vol. 99, no. 6, p. 1, 2020.

[10] R. Manickavasagam and S. Selvan, "Automatic detection and classification of lung nodules in CT image using optimized neuro fuzzy classifier with cuckoo search algorithm," *Journal of Medical Systems*, vol. 43, no. 3, pp. 231–237, 2019.

[11] F. Liao, M. Liang, Z. Li, and X. Hu, "Evaluate the malignancy of pulmonary nodules using the 3D deep leaky noisy-or network," *IEEE Transactions on Neural Networks and Learning Systems*, vol. 32, no. 7, pp. 176–182, 2017.

[12] S. Ziyad, V. Radha, and V. Thavavel, "Performance evaluation of contrast enhancement techniques in computed tomography of lung images," in *Proceedings of the IEEE 5th International Conference for Convergence in Technology*, pp. 67–82, Bombay, India, March 2019.

[13] W. Shen, M. Zhou, F. Yang et al., "Multi-crop Convolutional Neural Networks for lung nodule malignancy suspiciousness classification," *Pattern Recognition*, vol. 61, no. 61, pp. 663–673, 2017.

[14] A. K. Dhara, S. Mukhopadhyay, A. Dutta, M. Garg, and N. Khandelwal, "A combination of shape and texture features for classification of pulmonary nodules in lung CT images," *Journal of Digital Imaging*, vol. 29, no. 4, pp. 466–475, 2016.

[15] W. Shen, M. Zhou, F. Yang, C. Yang, and J. Tian, "Multi-scale convolutional neural networks for lung nodule classification," in *Proceedings of the International Conference on Information Processing in Medical Imaging*, pp. 123–132, 2015.

[16] F. Han, H. Wang, G. Zhang et al., "Texture feature analysis for computer-aided diagnosis on pulmonary nodules," *Journal of Digital Imaging*, vol. 28, no. 1, pp. 99–115, 2015.

[17] G. Wei, H. Cao, H. Ma, S. Qi, W. Qian, and Z. Ma, "Content-based image retrieval for lung nodule classification using texture features and learned distance metric," *Journal of Medical Systems*, vol. 42, no. 1, 2018.

[18] G. Wei, H. Ma, W. Qian et al., "Lung nodule classification using local kernel regression models with out-of-sample extension," *Biomedical Signal Processing and Control*, vol. 40, no. 2, pp. 1–9, 2018.

[19] M. Sergeeva, I. Ryabchikov, M. Glaznev, and N. Gusarova, "Classification of pulmonary nodules on computed tomography scans. Evaluation of the effectiveness of application of textural features extracted using wavelet transform of image," in *Proceedings of the 18th Conference of Open Innovations Association and Seminar on Information Security and Protection of Information Technology (FRUCT-ISPIT)*, St. Petersburg, Russia, April 2016.

[20] R. Gao, Y. Huo, S. Ban et al., "Distanced LSTM: time-distanced gates in long short-term memory models for lung cancer detection," in *Proceedings of the International Conference on Medical Image Computing and Computer-Assisted Intervention*, pp. 172–182, Shenzhen, China, October 2019.

Hindawi
Computational Intelligence and Neuroscience
Volume 2022, Article ID 2501693, 9 pages
https://doi.org/10.1155/2022/2501693

Research Article

Multi-Feature Intelligent Oral English Error Correction Based on Few-Shot Learning Technology

Fengxiang Zhang[1] and Jieli Sun[2]

[1]*College of Foreign Languages, Hebei University of Economics and Business, Shijiazhuang, Hebei 050061, China*
[2]*School of Information Technology, Hebei University of Economics and Business, Shijiazhuang, Hebei 050061, China*

Correspondence should be addressed to Jieli Sun; sunjieli@heuet.edu.cn

Received 20 March 2022; Revised 28 April 2022; Accepted 29 April 2022; Published 23 June 2022

Academic Editor: Xin Ning

The computer-aided language teaching system is maturing thanks to the advancement of few-shot learning technologies. In order to support teachers and increase students' learning efficiency, more computer-aided language teaching systems are being used in teaching and examinations. This study focuses on a multifeature fusion-based evaluation method for oral English learning, completely evaluating specific grammar, and assisting oral learners in improving their oral pronunciation skills. This study proposes an improved method based on HMM a posteriori probability scoring, in which the only standard reference model is no longer used as the basis for scoring and error determination, and instead, the average level of standard pronunciation in the entire corpus is introduced as another judgment basis, based on a preliminary study of speech recognition technology, scoring methods, and relevant theoretical knowledge of information feedback. This strategy can reduce the score limitation caused by standard pronunciation personal differences, lower the system's misjudgment rate in detecting pronunciation errors, and improve the usefulness of error correction information. An expert opinion database has been created based on the most prevalent forms of spoken pronunciation problems, which can successfully assist learners improve their spoken English level by combining the database's corrected information. Finally, this study proposes an artificial scoring system for spoken English that performs activities such as identification, scoring, error judgment, and correction opinion feedback, among others. Finally, it has been demonstrated through trials and tests that adding the average pronunciation level to the system improves the system's scoring performance and has a certain effect on increasing users' oral pronunciation level.

1. Introduction

In recent years, one of the hottest study topics in the domains of computer and education has been computer-assisted instruction systems. It has begun to gradually replace teachers to correct, particularly in large-scale language exams, which has become a significant change in the educational field. This type of technology is known as a computer-assisted language learning system [1]. Stress in English is a very essential prosody trait that affects rhythm and intonation, as well as having crucial grammatical and semantic implications. Mastering the stress rhythm correctly plays a crucial role in spoken English expression for language learners [2]. The oral English test now relies primarily on manual marking, which means that scoring is heavily impacted by the raters' psychological and physiological states, and objectivity and fairness of the scoring results cannot be guaranteed [3]. In the sphere of education, English is a critical topic. It will be extremely beneficial to boost students' enthusiasm in studying English, correct students' English pronunciation, evaluate students' academic achievement, and direct students' learning if artificial intelligence is combined with college English skill training [4]. The speech evaluation system is evolving in tandem with the advancement of voice recognition technology. It mostly uses a computer to assess people's pronunciation [5]. For example, the spoken Mandarin test system currently in use can not only score accurately, but it can also considerably enhance efficiency and save personnel [6]. Computer-assisted language learning has progressively begun to suit the diverse needs of language learners, thanks to the rapid development of speech recognition technology and other multimedia technologies. As a result, many researchers have been interested in a pronunciation evaluation system based on speech recognition technology.

Economic globalization has resulted in more regular exchanges between countries around the world today. The fact that English is an Esperanto has also sparked a lot of interest in learning English. People from non-native nations are increasingly keen to enhance their English abilities; in addition to understanding the necessary vocabulary and grammar, improving oral expression ability is also critical. As a result, in non-native countries, the methods of English education and learning have become a hot topic of discussion and research [7]. Oral English training is a crucial component of English instruction. It is difficult for teachers to provide one-on-one oral English instruction due to the large number of students in traditional classroom teaching. After class and examination, oral test questions have become an important link for students to assess their spoken English proficiency [8]. Fortunately, advances in voice processing technologies have made learning English easier and faster. In the realm of voice signal processing, the use of speech technology in language acquisition has become a major trend [9]. It is necessary to develop a system that can assist teachers in intelligently correcting subjective questions in language teaching in order to save time for teachers, save human and material resources for schools, and complete the correction requirements more accurately in order to save time for teachers, save human and material resources for schools, and complete the correction requirements more accurately [10]. Oral Q&A questions can be scored in two ways: from the perspective of pronunciation, and from the perspective of text. Acoustic variables like as pronunciation, frequency, and rhythm are typically used in pure speech scoring [11].

There are two factors to evaluating the level of spoken English in the CALL system based on speech technology. The core method entails identifying phoneme and word faults in learners' spoken language and providing appropriate feedback and solutions. Prosody judgment in spoken language is another factor to consider. For English learners, the latter is more challenging than the former [12]. It is now possible to obtain multidimensional automatic scoring for the open-ended oral language inquiry investigated in this research [13] because to advancements in speech recognition and artificial intelligence technology. This work will combine these mature new technologies with conventional automatic scoring-related technologies, with the goal of using text data after voice recognition as the research object and employing the multifeature fusion method to create a multifeature intelligent correction model. Make intelligent corrections from a variety of perspectives. Artificial intelligence can be used to grade oral expression questions, which appear to have no particular criteria and rely on teachers' subjective judgments. This is important for college English skill training guidance and correction [14]. The examinee's voice is used to do text recognition, with similarity and syntactic features taken from the text and phonetic features extracted from the speech. The automatic correction technology for closed-type oral exam questions cannot be directly transferred to open-type oral test questions due to the distinct principles of correction technology [15]. Because the traditional closed-type question type relies on known text to score speech, while open-type questions have nonunique responses, new text-independent technology is needed to overcome the challenge of open-type oral exam scoring [16]. Speech recognition technology has provided a solution for automatic scoring of large-scale Chinese-English oral translations. The automatic scoring approach not only ensures the correctness of Chinese-English oral translation scoring results, but it also considerably improves scoring efficiency and saves a lot of human, material, and financial resources.

2. Related Work

Document [17] examines the automatic correction of spoken language using an automatic composition correction system, and claims that it is possible to correct spoken language using speech recognition technology and a composition correction system. However, the spoken language correction approach suggested in this study has limits, and its scoring dimension is limited, therefore it does not allow for the evaluation of the pronunciation itself. Literature [18] pointed out that in the research of early stress recognition, the recognition system usually extracts some traditional phonetic features, such as sound length, energy, fundamental frequency, etc., and establishes a phonetic model by training linear discriminant function to recognize stressed syllables. Literature [19] puts forward that the functions of intelligent tutor system include building learning environment, communicating with students' emotions, and learning with students. Although the design of intelligent tutor system is called "intelligent" tutor system for evaluating students, it is not smart enough, and it still manages student information and arranges courses according to established rules, which canno't really replace tutors, and has certain limitations. Literature [20] lists the challenges faced by the modeling of simulated human scoring from the process and result levels, and points out that it is impossible to model the evaluation process comprehensively in the field of speech features and speech recognition at present. Literature [21] puts forward that under the dual influence of the abnormal needs of oral English learning and the development requirements of human computer interaction, the pronunciation evaluation system based on language lab recognition technology came into being. It fully integrates the two technologies of CALL and speech recognition to become a more intelligent English learning system, providing learners with opportunities for human computer interaction, and giving a lot of information feedback, completely changing the traditional English learning mode from "teacher teaching" to "student self-learning."

Literature [22] proposes that in the network environment, the automatic marking system plays a great role in the role orientation of teachers and students, because for non-English majors, their initiative in learning English is not high, and English learning is also very difficult for them. Literature [23] uses deep neural network to improve the robustness of the algorithm and retain the high discrimination of the algorithm, and obtains good experimental results. Although this algorithm is applied to reading questions, we can see that the application prospect of deep learning in oral automatic correction is very good. The combination of deep learning and automatic correction is an important direction for the development of automatic correction system in the future. Through the research on the application of automatic speech recognition system to non-native speech training, literature [24] pointed out that if appropriate methods are used and false pronunciation detection is added, the evaluation system can provide the same evaluation results as human experts. In terms of pronunciation quality evaluation, many studies at home and abroad have proposed various scoring algorithms, and the scoring performance produced by these algorithms has gradually approached the expert scoring level. However, in the research and implementation of pronunciation error detection and feedback information, many systems simply compare the phoneme recognition results with the phoneme correlation results of standard speech. Document [11] the automatic correction system is actually an upgrade of the intelligent tutor system. The intelligent tutor system guides students according to certain rules, and the automatic correction system also scores students' compositions according to the preset scoring rules. Automatic marking system is actually a combination of traditional intelligent tutor system and modern new technology.

3. Methodology

3.1. Multifeature English Spoken Scoring Algorithm. As one of the specific applications of computer-assisted language learning, the overall performance of spoken English scoring system largely depends on speech recognition technology. Multifeature fusion evaluation algorithm includes the evaluation algorithm of a single feature and the algorithm of fusing the evaluation results of multiple features. Because of the instability of the existing automatic speech recognition system, we can evaluate spoken English from this aspect. Multifeature comprehensive evaluation method should have at least the following characteristics: (1) scalability, that is, which features are selected and how many features are selected will not have great influence on the system, and it is easy to add or reduce features. (2) It has nothing to do with the evaluation algorithm of a single feature, that is, changing the evaluation algorithm of a single feature has no effect on the system when the evaluation result form of a single feature does not change. Speech signal analysis is the premise and foundation of speech signal processing. Only by analyzing the parameters that can represent the essential characteristics of speech signals can we use these parameters to process speech communication, speech synthesis, and speech recognition efficiently. And the quality of speech signal processing directly affects the effect of speech recognition. In the early speech recognition system, the isolated word recognition algorithm is the foundation, and its basic principle is to use template matching method for recognition. The fractal dimension characteristics of stressed syllables obtained by the polymorphic method are shown in Figure 1.

The following aspects are included in feature extraction: (1) energy features. The stationary process processing method and theory are incorporated into the short-term processing of speech signals, considerably simplifying speech signal analysis. (2) Characteristics of duration. The length of each syllable of a multisyllable English word is extracted and compared. Accents are defined as longer syllables. (3) The fundamental features of frequency. Fundamental tone detection is an important technology in speech processing that is frequently utilized in speech recognition, and fundamental frequency is one of the most important prosody parameters in the speech signal. (4) Prediction in linear form. Under the linear prediction technique, the LPC coefficient is a short-term measure of the speech signal. It is the foundation of speech processing and has been used in voice recognition, synthesis, coding, and other applications. The HMM-based scoring method requires pretraining a large number of acoustic models or reference models as a scoring standard, as well as combining the recognition and scoring mechanisms to determine the difference in phoneme pronunciation between the speech to be tested and the standard model and assigning a score. The scoring process based on HMM is shown in Figure 2.

In this method, the number of features can be increased or reduced as long as the weight a I is changed, which meets the first requirement of multifeature comprehensive evaluation method; changing the evaluation result form of a feature, as long as the corresponding quantitative method is changed, does not affect the whole algorithm, so it meets the second requirement of multifeature comprehensive evaluation method. In conclusion, this algorithm has strong scalability and independent of the evaluation model of single feature, and is suitable for comprehensive evaluation of spoken English. The similarity Manhattan distance formula is as follows:

$$D(A,B) = \sum_{k=1}^{n} |a_k - b_k|. \tag{1}$$

The formula for calculating the Dice coefficient is

$$D(A,B) = \frac{2 \cdot comm(A,B)}{leng(A) + leng(B)}. \tag{2}$$

Conditional probability mean of individual phonemes:

$$P = \frac{1}{n} \sum_{m=1}^{n} P(a_m \mid b_m). \tag{3}$$

The loss function is of the form

$$L(g_b, \hat{g}_b) = \left(g_b^{\gamma} - \hat{g}_b^{\gamma}\right)^2. \tag{4}$$

The multiscale shape distribution area is obtained as

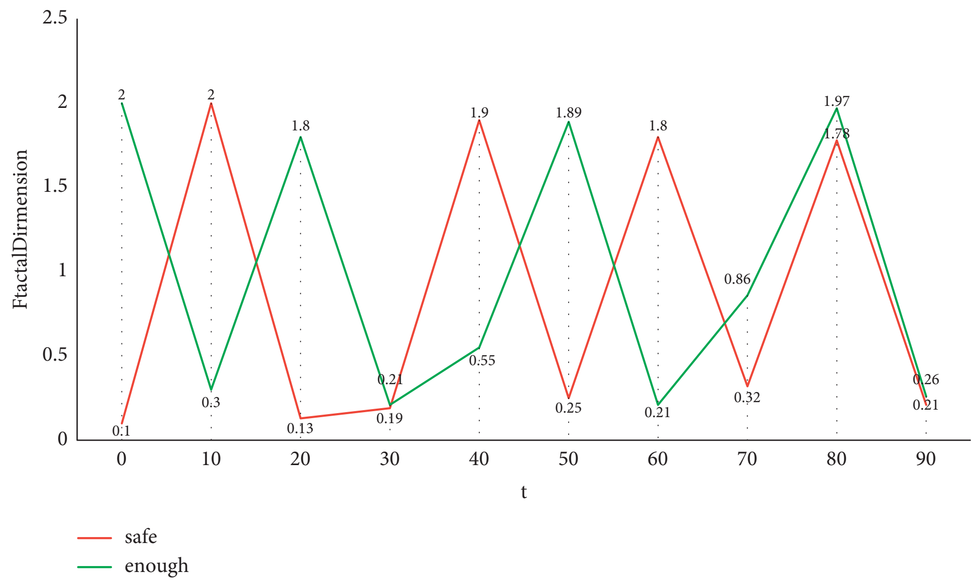

Figure 1: Fractal dimension characteristics of stressed syllables obtained by polymorphic coverage method.

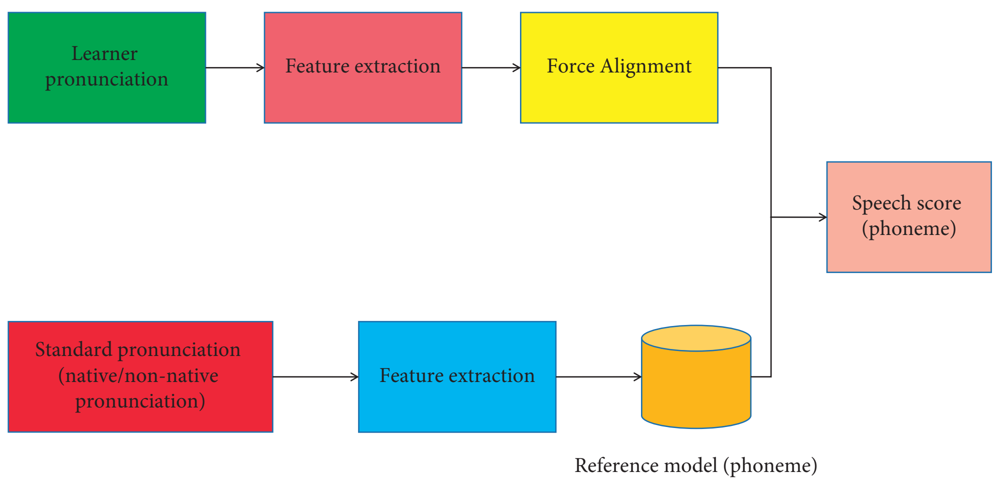

Figure 2: Scoring process based on HMM.

$$AB^{(\varepsilon)} = \text{area}\,(F \oplus \varepsilon B). \tag{5}$$

Linear rectification function of the formula is

$$f\,(x) = \max\,(0, x). \tag{6}$$

The log a posteriori probability scoring method based on HMM can not only better reflect the similarity between learners' pronunciation and standard pronunciation, but also reflect learners' pronunciation characteristics from pronunciation units such as phonemes and syllables, and has high stability. Therefore, this scoring method is widely used in relevant recognition systems or learning systems.

3.2. Design of Multifeature Intelligent Scoring Model. The whole scoring system includes three parts: speech recognition, feature extraction, and linear regression. The similarity features and syntactic features in feature extraction are extracted from the text after speech recognition, and the similarity features need to be compared with the reference answers. Automatic scoring of oral translation is mainly from two perspectives. One is to directly process the speech of oral translation and score oral translation directly; another point of view is to first convert the speech of oral translation into text, and indirectly score oral translation through text processing. The design purpose of the model does not focus on how to effectively recognize learners' speech, but how to improve the accuracy of system evaluation, reduce the misjudgment rate of pronunciation error detection, and whether the scoring accuracy of the system is improved when the average pronunciation scoring level is adopted under the same acoustic model. In the multifeature fusion evaluation system, the system only needs to recognize the input once, then evaluate the recognition results of multiple features respectively, and use the evaluation results of multiple features to give the final evaluation results. The multifeature intelligent scoring model is shown in Figure 3.

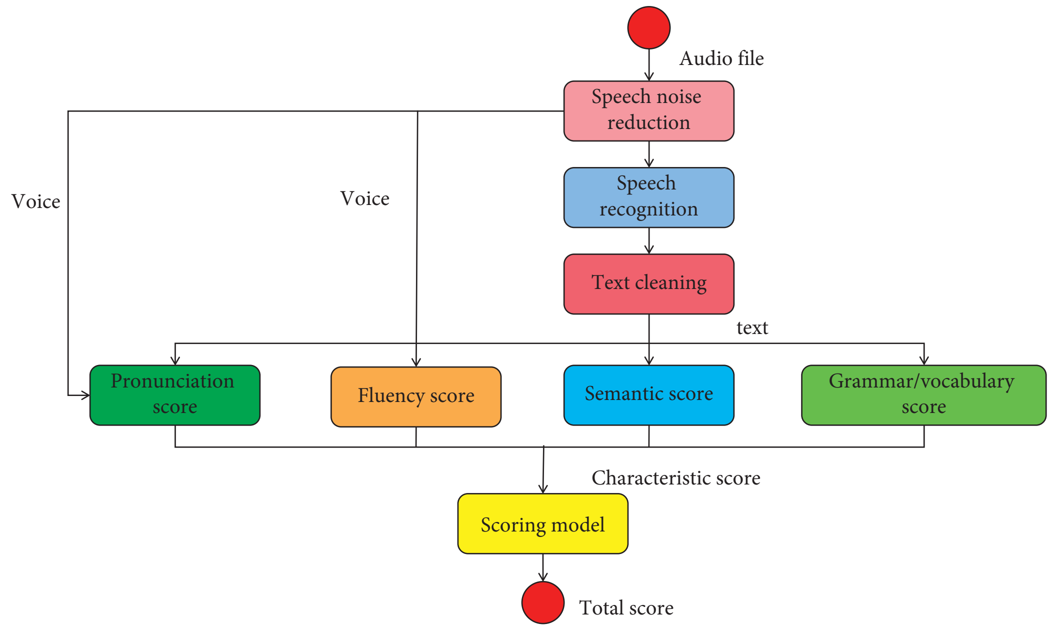

FIGURE 3: Multifeature intelligent scoring model.

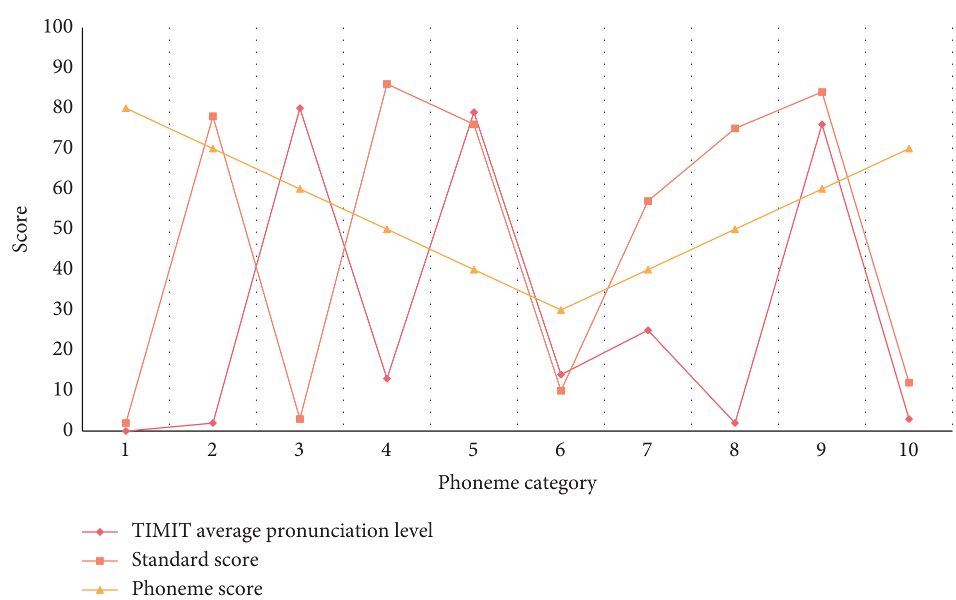

FIGURE 4: Comparison between score results and average pronunciation level.

Multifeature fusion evaluation system includes four parts: speech recognition, grammar expansion, single feature evaluation, and result processing. In order to make our feature extraction work smoothly and improve the accuracy, we also designed three data processing modules in the scoring model: (1) speech noise reduction module, (2) speech recognition module, and (3) text cleaning module. The training data is input into the neural network, and then the neural network is used for continuous training to train an intelligent scoring model. Then the test data is input into the intelligent scoring model to obtain the preliminary results of intelligent scoring, and the results are compared with the teacher's scores. Then, the model is feedback optimized, the model is improved, and finally the intelligent scoring model is determined. According to the statistical threshold of the corresponding phoneme, it is determined whether the learner's pronunciation is wrong, and the comparison between the score result and the average pronunciation level is shown in Figure 4.

Each extended new word's phonetic symbols are paired with the acoustic model and added to the system's lexicon. In this approach, the system can determine whether the oral practitioner pronounces the erroneous sound if the recognition result of the input speech is the expanded new word. When creating the system, the major design objectives should always be the system score, error

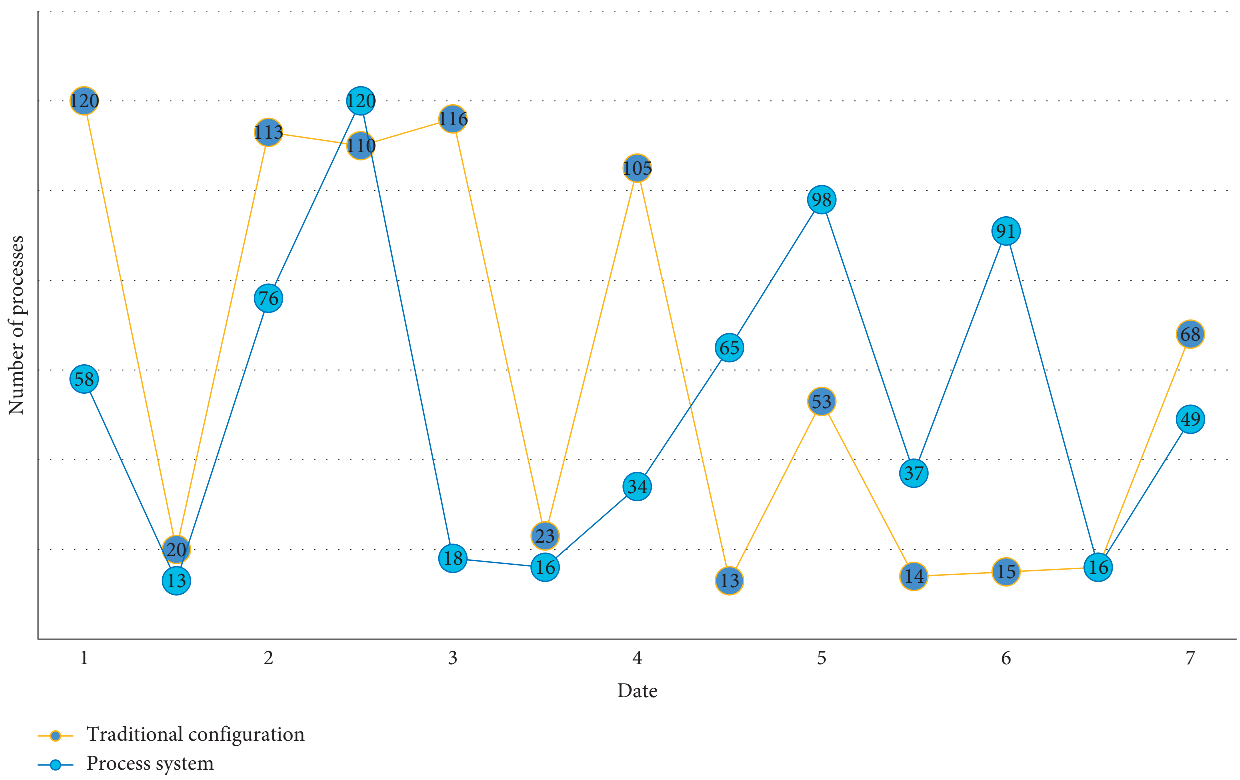

Figure 5: Comparison of the number of process runs.

prompt, and correction feedback. Simultaneously, we should consider the friendliness of the interactive interface between the system and users, as well as learning mode innovation, as additional objectives, in order to avoid reducing learning interest or efficiency due to boring learning forms or content, and to improve the system's operability. The statistical data of the operation process of the traditional configuration method and process system within one week are randomly intercepted, as shown in Figure 5.

First, feature extraction is performed on the dataset, and then these feature data together with the data labels are input into the neural network for supervised learning. After a period of learning and training, a classification model is finally generated, and we can use this model to extract features from the new spoken audio, and then input the features for scoring. The whole scoring process of the system is carried out from two aspects. On the one hand, the system itself needs to extract features and creates models for the selected standard corpus. At the same time, in order to eliminate the wrong scoring caused by the differences between standard pronunciation speakers, it also processes the standard pronunciation correspondingly, and selects the average of all phonemes as another reference factor to judge whether learners pronounce incorrectly or not. On the other hand, when learners input speech, the system will extract the features of their pronunciation through the speech recognizer, divide the feature values into phoneme-level scoring units, remove noises and noises, compare them with the standard reference model after forced alignment, and use the scoring algorithm in Chapter 3 to get the corresponding phoneme scores, thus completing the preliminary scoring of the system.

4. Result Analysis and Discussion

4.1. System Implementation. At first, the system will record the voice input by the user. After the user input is completed, the user input will be recognized by voice, and the result of the recognition will be expanded by grammar. Then, the linking and confusing sounds will be evaluated separately. Finally, the evaluation results of the two will be synthesized and the comprehensive evaluation results will be given. Automatic scoring performance is measured by correlation coefficient. The larger the correlation coefficient, the more consistent the scoring trend of experts on samples. The interface layout of English automatic scoring system is mainly divided into two parts. One is the selection and input of learners' pronunciation content, and the other is the feedback display of the system to users' pronunciation. Therefore, the realization of other main functions of the system, including speech recognition, is also realized in two parts. A linear criterion is used to distinguish the two categories optimally. The optimization criterion always increases the distance between classes and reduces the distance between classes. Most of the discriminant information can be obtained from the transferred feature space. The result processing part first quantifies the evaluation results of a single feature, and then synthesizes the quantized results to obtain the evaluation results of multifeature fusion. Finally, this chapter gives the realization method of the system. Users can choose the courses and exercises they want to learn. The

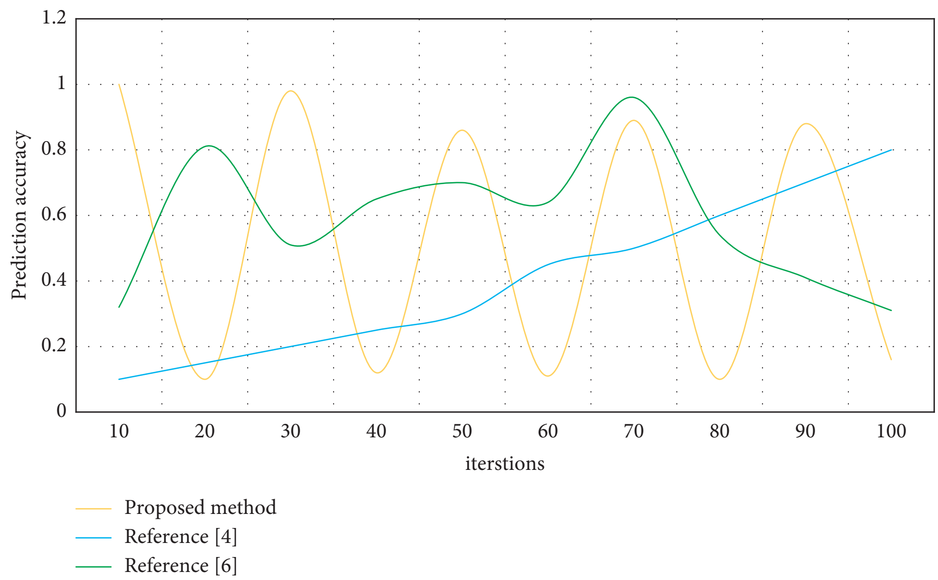

Figure 6: Comparison of detection performance.

system gives a comprehensive evaluation of the user's pronunciation, and marks the specific situation of the user's pronunciation and the areas that need improvement with special colors. Realize the pronunciation error detection of spoken English, test the detection performance, and get the results as shown in Figure 6.

Before comparing the scores, we must first segment the candidates' voice. Because the examinee has frustrations, repetitions, and other phenomena in oral expression, we are unable to 100% correspond the text and audio after speech recognition in the time dimension. Therefore, we need to segment the audio and try to align the pronunciation audio of standard words with the examinee's voice in the time series. If the user's pronunciation is not accurate enough, the system will refuse to evaluate and ask the user to learn again. After recording, learners can input their own pronunciation into the system, play back their previous pronunciation by using the user play function key, and get the score of previous pronunciation and corresponding correction opinions by using the scoring function key. Of course, if you cannot understand the problems of your pronunciation through scores and correction opinions, you can also compare the differences between your pronunciation and standard pronunciation to improve your pronunciation. You can only use standard playback. The whole process of system scoring mainly includes feature extraction, forced alignment, HMM-based posterior probability score calculation, mispronunciation judgment, correction feedback, and other processes. According to the needs of the system, the corresponding technical links are modified to realize the final scoring process. Learners can choose to play the standard pronunciation, and at the same time hear the pronunciation of the standard pronunciation, they can also see the score of the standard pronunciation in the right area of the scoring box, so that they can more intuitively see the differences between their own pronunciation and the standard pronunciation. At the same time, the expert opinion database will determine the final correction opinions according to learners' scores, standard pronunciation scores, and average pronunciation level of standard pronunciation.

4.2. Result Analysis. After using the average level as a reference, the judgment threshold has changed correspondingly, and the accuracy rate of wrong judgment of the system has been improved, which leads to the improvement of the accuracy rate and the reliability of feedback information. Figure 7 shows the results of comparing the accuracy of error capture of several approaches of spoken English pronunciation.

Because the learner's voice is first compared with the standard voice, the average level will be used for comparison when there is a large gap, so as to ensure that the learner's voice is infinitely close to the standard voice in terms of pronunciation level without pronunciation error and misjudgment, which also meets the design requirements of similar systems. The free English composition automatic correction online service based on corpus and cloud computing can instantly generate the scores, comments, and content analysis results of students' compositions by calculating the distance between students' compositions and standard corpora, which can provide multidimensional scoring results. Artificial intelligence can play the teaching role of constructivism, because artificial intelligence can analyze data in a short time, so it can find teaching resources that are conducive to learners' characteristics and in line with learners' cognitive style. Artificial intelligence can store and analyze a large amount of learner characteristic data. Through the analysis of learners' learning style and cognitive level, teachers can understand learners' advantages and disadvantages, make teachers timely and accurately adjust teaching strategies and teaching methods, and make learners more acceptable. Therefore, artificial intelligence can better guide teaching practice.

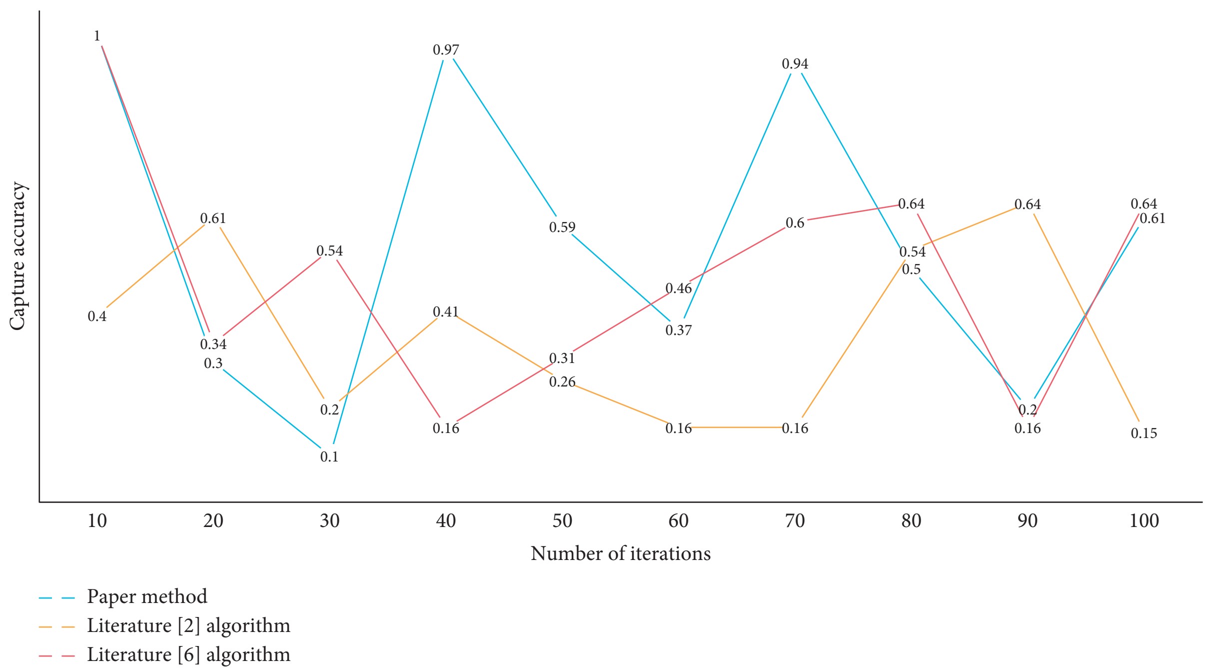

Figure 7: Comparison of capture accuracy.

After the system adopts an average pronunciation level based on standard speech as the error judgment standard, the accuracy of error detection has been improved to a certain extent. It is worth noting that since the system adopts the corpus of foreign pronunciation, it is possible to deviate from the normal value only from the score given to learners by the system, but when the same acoustic model is used as the system score. The verification of error detection accuracy is not affected, because the average pronunciation level used here is based on standard pronunciation as the source data. It is assumed that when the Chinese pronunciation corpus is used as the standard pronunciation for scoring and error judgment, the score is closer to the learners' real level, but the error and misjudgment caused by individual differences in standard pronunciation is still inevitable. Based on the multifeature fusion evaluation algorithm, the training and testing results show that the performance of the algorithm is good and the algorithm shows good stability under different weights. The automatic scoring system of spoken English is realized, with emphasis on the recording function, scoring process, and the realization process of expert correction feedback. The experimental data are analyzed by two error judgment methods: standard pronunciation score and average pronunciation level, and adding average pronunciation level to judge. The experiment shows that the method proposed in this study can effectively reduce the misjudgment rate, and the running performance of the system itself is stable, which basically meets the practical application standards of this kind of system.

5. Conclusion

The salient points of this study are: first, try to take speech recognition text as the research object to score the oral test; secondly, the similarity feature is improved, and a keyword coverage based on editing distance is proposed, and these two features are better than those obtained by traditional methods; thirdly, multiangle feature extraction and multifeature fusion in linear regression system. Fourth, select features and delete redundant features. Although the accuracy rate of speech recognition has been claimed to be over 95% in official documents, in the actual process, due to the test environment, the influence of students around and the noise nearby, the output result of speech recognition will be affected. The speech features are extracted by direct analysis of speech signals, the similarity features and syntactic features are extracted by analysis of the text after the speech signals are converted, and the automatic scoring system is obtained by using multiple regression analysis model. The corresponding evaluation algorithm is established, and features are added into the multifeature fusion evaluation system. Comprehensive evaluation system of spoken English, which integrates a large number of features, will be the future development direction. At present, the automatic scoring technology of open spoken questions is deeply studied and compared. Through feature fusion, Rank Net neural network maps the complex nonlinear relationship among features, and establishes the recognition model of stressed syllables in words and stressed sentences, which can accurately recognize stressed syllables in words and stressed sentences. This study summarizes the valuable experience of predecessors' work, innovatively applies and improves the key technologies, integrates and improves the latest technical schemes at present, puts forward and realizes a new open oral correction model, innovates the method of voice feature extraction, and improves the dimension of open oral scoring.

Data Availability

The data used to support the findings of this study are available from the corresponding author upon request.

Conflicts of Interest

The authors do not have any possible conflicts of interest.

References

[1] Y. Hai, "Computer-aided teaching mode of oral English intelligent learning based on speech recognition and network assistance," *Journal of Intelligent and Fuzzy Systems*, vol. 39, no. 4, pp. 5749–5760, 2020.
[2] R. Duan, Y. Wang, and H. Qin, "Artificial intelligence speech recognition model for correcting spoken English teaching," *Journal of Intelligent and Fuzzy Systems*, vol. 40, no. 1, pp. 1–12, 2020.
[3] D. Herbert and B. H. Kang, "Intelligent conversation system using multiple classification ripple down rules and conversational context," *Expert Systems with Applications*, vol. 112, no. DEC, pp. 342–352, 2018.
[4] S. Lee, H. Noh, J. Lee, K. Lee, and G. G. Lee, "Foreign language tutoring in oral conversations using spoken dialog systems," *IEICE - Transactions on Info and Systems*, vol. 95, no. 5, pp. 1216–1228, 2017.
[5] S. Sun, J. Han, and Z. Chen, "Open defecation and squat toilets, an overlooked risk of fecal transmission of COVID-19 and other pathogens in developing communities," *Environmental Chemistry Letters*, vol. 19, no. 2, pp. 787–795, 2020.
[6] P. Giampieri, "Spoken language features (and anomalies) in films for ESL classes," *Language Learning in Higher Education*, vol. 8, no. 2, pp. 399–425, 2018.
[7] R. Silhavy, P. Silhavy, and Z. Prokopova, "Cybernetics approaches in intelligent systems," *Advances in Intelligent Systems and Computing*, vol. 661, pp. 111–122, 2018.
[8] R. Zhao and H.-K. Lee, "Intelligent navigation for multiple mobile robots with dynamic obstacles," *Journal of Institute of Control, Robotics and Systems*, vol. 23, no. 9, pp. 711–717, 2017.
[9] Q. Cao and H. Hao, "Optimization of intelligent English pronunciation training system based on android platform," *Complexity*, vol. 2021, no. 4, Article ID 5537101, 11 pages, 2021.
[10] M. Hu, J. Peng, W. Zhang, J. Hu, L. Qi, and H. Zhang, "An intent recognition model supporting the spoken expression mixed with Chinese and English," *Journal of Intelligent and Fuzzy Systems*, vol. 40, no. 5, pp. 10261–10272, 2021.
[11] H. Zhang, "Research on spoken English analysis model based on transfer learning and machine learning algorithms," *Journal of Intelligent and Fuzzy Systems*, vol. 38, no. 99, pp. 1–11, 2020.
[12] M. Koklu and Y. S. Taspinar, "Identification of the English accent spoken in different countries by the k-nearest neighbor method," *International Journal of Intelligent Systems and Applications in Engineering*, vol. 8, no. 4, pp. 191–194, 2020.
[13] G. Leu, H. K. Singh, and S. Elsayed, "Intelligent and evolutionary systems," *Proceedings in Adaptation, Learning and Optimization*, vol. 8, pp. 183–194, 2017.
[14] R. Reppen, N. Ide, and K. Suderman, "The American national corpus," *Journal of English Linguistics*, vol. 32, no. 2, pp. 105–113, 2016.
[15] A. LEeMann, M.-J. Kolly, R. Purves, D. Britain, and E. Glaser, "Crowdsourcing language change with smartphone applications," *PLoS One*, vol. 11, no. 1, Article ID e0143060, 2016.
[16] Z. S. Sehyr and K. Emmorey, "The effects of multiple linguistic variables on picture naming in American Sign Language," *Behavior Research Methods*, pp. 1–20, 2021.
[17] H. Mukherjee, A. Dhar, S. M. Obaidullah, K. C. Santosh, S. Phadikar, and K. Roy, "Linear predictive coefficients-based feature to identify top-7 spoken language," *International Journal of Pattern Recognition and Artificial Intelligence*, vol. 34, no. 1, 2019.
[18] T. Yamaguchi, "Lexicogrammatical features in Japanese English: a study of five speakers," *Research in Language*, vol. 16, no. 3, pp. 341–355, 2018.
[19] D. Tizón-Couto, "Exploring the Left Dislocation construction by means of multiple linear regression:Complexity and orality of Modern English left-dislocated NPs," *Belgian Journal of Linguistics*, vol. 31, no. 1, pp. 299–325, 2017.
[20] H. S. Das and P. Roy, "A deep dive into deep learning techniques for solving spoken language identification problems," *Intelligent Speech Signal Processing*, vol. 5, pp. 81–100, 2019.
[21] H.-J. Song, J. Go, S.-B. Park, S.-Y. Park, and K. Y. Kim, "A just-in-time keyword extraction from meeting transcripts using temporal and participant information," *Journal of Intelligent Information Systems*, vol. 48, no. 1, pp. 117–140, 2017.
[22] S. Weigelt, T. Hey, and V. Steurer, "Detection of control structures in spoken utterances," *International Journal of Semantic Computing*, vol. 12, no. 03, pp. 335–360, 2018.
[23] A. Zadeh, R. Zellers, E. Pincus, and L.-P. Morency, "Multimodal sentiment intensity analysis in videos: facial gestures and verbal messages," *IEEE Intelligent Systems*, vol. 31, no. 6, pp. 82–88, 2016.
[24] K. K. Leung, C. Redmon, Y. Wang, A. Jongman, and J. Sereno, "Cross-linguistic perception of clearly spoken English tense and lax vowels based on auditory, visual, and auditory-visual information," *Journal of the Acoustical Society of America*, vol. 140, no. 4, p. 3335, 2016.

Hindawi
Computational Intelligence and Neuroscience
Volume 2022, Article ID 8046713, 11 pages
https://doi.org/10.1155/2022/8046713

Research Article

Analysis of Graphic Perception Education for Young Children Based on Fuzzy Clustering Analysis

Jie Gui [1,2] and Joohyun Suh [2]

[1] *Jiangsu Vocational College of Electronics and Information, Huaian, Jiangsu 223003, China*
[2] *Department of Family Welfare, Sangmyung University, Jongno-gu, Seoul 03016, Republic of Korea*

Correspondence should be addressed to Jie Gui; 150816@jsei.edu.cn

Received 23 April 2022; Revised 16 May 2022; Accepted 17 May 2022; Published 21 June 2022

Academic Editor: Xin Ning

Geometric ability includes elements of identification, conceptualization, combination, drawing, and reasoning, and graphic perception is an important part of it. Kindergarten science education includes geometry instruction. Children are guided to perceive the relationship between shapes and figures through direct perception, first-hand experience, and practical operation through concentrated educational activities, and form image-concrete thinking over time, enhancing their perception and experience of the relationship between shapes in the objective world, and accumulating certain mathematical perceptual experience. Clustering is a branch of unsupervised pattern recognition that is very useful. Fuzzy clustering, which establishes the uncertainty description of samples to categories and can objectively reflect the real world, has become the mainstream of cluster analysis research. The graphics perception education of children is investigated using fuzzy clustering analysis. The main topic of this paper is how to apply children's graphics to the design of children's educational institutions and open up new creative perspectives for the design of children's educational institutions. The method of graphic perception education: perception education for preschool children is proposed based on the multichannel characteristics of preschool children's aesthetic perception and with reference to the theory of perception. The experimental results show that the improved algorithm reduces segmentation time by 171.48 s when compared to the traditional FCM algorithm for both noisy and high-quality images and that it is significantly faster than the FCM algorithm in terms of segmentation speed. As a result, the model construction of a set of children's graphic perception education for the cognitive characteristics of the age group children can provide corresponding references and references for related topic research.

1. Introduction

The abstraction and generalization of shape are known as geometry. In the process of human understanding of nature, it appeared as a symbolic system before language and words [1]. Children's geometry education is an important part of their mathematics education, and the living of geometry education encourages children's perception and experience of graphical relationships in the objective world, allowing them to accumulate perceptual experience in mathematics [2]. The ability to recognize and combine plane figures is reflected in two main areas in early childhood [3]. Learning graphics properly aids children in developing a correct understanding of life and the world around them, as well as their curiosity, curiosity, and interest in geometry and mathematics [4]. It also aids in the development of children's thinking abilities and qualities, which will aid in their future mathematics learning in elementary school [5]. Living conditions are improving, and parents are becoming more aware of the importance of having their children educated in graphics, indicating that children's art education is entering a new era [6].

People communicate with the outside world through their senses. Children, in comparison to adults, rely on their senses to gather information about the world around them [7]. People always try to find features that can describe a new object or phenomenon in order to compare it to known objects or phenomena to see if they are similar according to some fixed criteria and rules in order to recognize it or understand it [8]. Only certain parts or regions of an image are of interest in the study and application of images, and these parts are referred to as the target or foreground, whereas other parts are referred to as the background and generally correspond to specific and unique regions of the image [9, 10]. Perceptual design and graphic design are being studied together in order to integrate perceptual design and children's art educational spaces. The main goal is to bring children closer to the art education space, reflect the educational function of the environment, mobilize children's perceptions through their visual, tactile, olfactory, and auditory senses, and promote children's enthusiasm for knowledge exploration [11].

Geometric thinking skills, which include elements of identification, conceptualization, combination, drawing, judgment, reasoning, and presentation, are an important part of geometric abilities [12]. The targets in an image must be separated and extracted before they can be identified and analyzed. It is possible to further measure the targets and use the images on this basis. Cluster analysis [13] in kindergartens for geometric educational activities helps children perceive geometric features through seeing, touching, thinking, guessing, and trying and deepens and consolidates their knowledge of geometric figures [14]. Color images, on the other hand, have unquestionably assumed a dominant position in the new century, thanks to technological advancements and lower hardware costs. Color images play an important role in people's daily lives and technological applications because of their visual properties and rich color information. Young children learn inexhaustibly and can achieve great success in their future learning if they are equipped with the ability to transfer and construct knowledge. The following are the paper's unique features.

(1) Applying perceptual design to graphics, children's educational space embodies space can promote children's art education through children's sense of hearing, touch, smell, and vision to promote children's learning process.

(2) To find the inner connection between fuzzy cluster analysis and children's geometric graphic education activities, and to dig, filter, and refine the mathematical elements in the resources that are suitable for children's geometric graphic education activities.

(3) To address the shortcomings that the fuzzy C-mean clustering image segmentation [15] algorithm does not consider the different degrees of the contribution of each dimensional feature to the clustering and easily falls into local optimum, an improved fuzzy clustering algorithm based on kernel function is proposed.

This paper's research framework is divided into five major sections, which are listed below. The first section of this paper introduces the research background and significance before moving on to the paper's main work. The second section covers graphic perception training for young children as well as work on fuzzy clustering analysis. The third section of the paper introduces the conceptual direction of graphic perception education as well as the steps for implementing perceptual strategies in graphic education so that readers can gain a better understanding of the concepts of graphic perception education for young children using fuzzy cluster analysis. The thesis's fourth section concludes the description of fuzzy clustering analysis' application in early childhood graphic perception education by looking at two aspects: the analysis of fuzzy C-mean clustering image segmentation algorithm and the analysis of improved kernel function-based fuzzy clustering algorithm. The final section of the paper is a summary of the entire project.

2. Related Work

2.1. Children's Graphic Perception Education. Geometry is an important part of a child's development and is one of the fundamental components of their mathematics education. Geometry education activities in kindergarten refer to the geometry education activities that teachers plan and implement purposefully, planned, organized, and systematically within the time constraints of normal kindergarten teaching activities, in accordance with the rules of children's physical and mental development, as well as the characteristics of mathematical cognitive development. Through the transformation and application of geometric figures, as well as the use of symmetrical features to analyze mathematical situations, children can analyze the characteristics and properties of two- and three-dimensional geometric figures ad use visual and spatial reasoning, as well as geometric models, to solve problems.

The applications proposed by Tai and Ledai require teachers to arrange and organize the content in a way that integrates with other artistic activities such as music, dance, and literature, as well as with children's life experiences, in a way that helps children to generate "common experiences" and "complementary experiences" [16]. Li et al. proposed the five developmental levels for children, which became the most influential theory for the geometry curriculum in the United States and has been refined in subsequent developmental studies [17]. Feng and Chen argued that art appreciation works should be appreciated in a sequence from abstract to concrete and then from abstract to concrete. Works with strong emotional expression are the primary consideration in selecting works [18]. Rajkumar et al.'s developmental levels of graphic perception education describe the process of children's geometric thinking and the characteristics of children's geometric thinking at each stage, not just how much geometric knowledge children have mastered [19]. Shakeri et al. argue that preschool children's preferences for color and expressive style of artworks reflect their preference for aesthetic features [20].

Exploring the characteristics and patterns of children's graphic perception not only helps teachers to better understand the importance of teaching children's geometry but also helps them to grasp the characteristics and patterns of children's graphic perception and to gain a concrete and in-depth understanding of the developmental process of children's geometric thinking skills.

2.2. Fuzzy Cluster Analysis. In recent years, domestic research on children's graphic perception abilities has begun to emerge, primarily from the perspective of child psychology. Further research in the areas of fuzzy cluster analysis and multicultural perspectives is required. Children learning mathematical knowledge is only the surface manifestation of development in mathematics education; the key is to encourage the development of children's thinking structures through the learning process. The basis of target representation is image segmentation based on fuzzy cluster analysis, which has a significant impact on feature metrics. Image segmentation and goal representation, segmentation-based feature extraction, and parameter measurement, on the other hand, reduce the original image to a more compact form, allowing for higher-level image analysis and comprehension.

Goyal et al. proposed clustering algorithms for image segmentation because the subjective nature of human vision makes images more suitable for fuzzy processing [21]. Pham et al. used fuzzy entropy to analyze the homogeneity of images to obtain initial major homogeneous regions and then grouped pixels with similar colors in these regions to prevent oversegmentation [22]. Berikov proposed that fuzzy should be used in image segmentation processing. Also, the absence of patches in training sample images requires unsupervised analysis, and fuzzy clustering satisfies both requirements, thus becoming a powerful research and analysis tool in image processing [23]. Mlr et al. proposed a combination of the histogram and fuzzy C-mean clustering. This method obtains all possible uniform regions in a color image by histogram thresholding and then improves the tightness of the regions by fuzzy C-mean clustering [24]. Jia and Zhang used an automatic histogram analysis method to obtain the peaks and troughs of the histogram by automatic histogram analysis, then performed fuzzy clustering according to the determined number of clusters, and then used the distance between adjacent troughs in the histogram The mean value between adjacent troughs in the histogram is used as the initial clustering center.

Unsupervised classification, also known as cluster analysis, is the process of distinguishing and classifying things according to certain requirements and rules. In this process, there is no a priori knowledge about the classification [25], only the similarity between things as a criterion for class classification. Through education in recognizing geometric figures, combining and dividing geometric figures, and drawing geometric figures, children can get an initial understanding of the characteristics of shapes, learn to spell and draw them creatively, stimulate their interest in learning mathematics, and develop their ability to think about concrete images.

3. Thoughts on Education of Children's Graphic Perception Based on Fuzzy Cluster Analysis

3.1. Conception Direction of Graphic Education. Perception is an active process based on the relationship between a person and the outside world. From the day of birth, a person can spontaneously acquire knowledge about the inner self and the outer environment through the different senses of the body [26]. The education of graphic perception needs to be diffused and recorded, taking the text closest to the design focus to further deepen it. By splitting and reorganizing the various visual elements, the information and ideas that are wanted to be conveyed are translated into concrete graphics and then clearly communicated to the viewer [27]. For the given number of categories c, fuzzy weighted division matrix U, and weighted coefficient matrix W, the fuzzy division entropy of the sample set X is defined as

$$H(U;c) = -\frac{1}{N}\sum_{k=1}^{n}\sum_{i=1}^{c} w_k u_{ik} \ln(u_{ik}). \tag{1}$$

The activities were adjusted according to the specific practice, and educational activities were suggested to promote the cognitive development of children in mathematics. The specific flow of the study is shown in Figure 1.

First, depicting reality is a depiction and replication of what exists in reality, a reproduction of the real thing. Also, parents say that the teaching environment is most likely to make a first impression. Teachers select appropriate domestic and international paintings based on the age, preferences, and appreciation of children and the "principle of difference" in their aesthetic psychology. Therefore, the composite index value is not equal to the simple sum of the indicators but a weighted summation relationship, namely,

$$S = \sum_{i=1}^{n} w_i f_i(I_i), \quad i = 1, 2, \ldots, n, \tag{2}$$

where $f_i(I_i)$ is some measure of I_i, and w_i is the weight value of each index.

The integration of cluster analysis into geometry educational activities can make geometry vivid and visual, stimulate children's interest, bring them sensory stimulation from many aspects, and mobilize children's multiple senses to participate in activities [28]. For a given number of categories c, fuzzy weighted division matrix U, and weighted coefficient matrix W, the modified division fuzziness of the sample set X is defined as

$$\mathrm{MPF}(U;c) = \frac{PF(U;c)}{H(U;c)}. \tag{3}$$

Feature extraction [29] is the generation of useful new features from the original features through some transformations, whereas feature selection is the selection of features that help to distinguish different objects from a set of candidate features. Perception is the knowledge of various other elements of things and a complete, three-dimensional, and multidimensional overall grasp of the shape, color, space, light, tension, and texture of things [30]. Children's senses are generated through their senses as a process of representation of different stimuli of the external environment and a reflection of the individual characteristics of things. The designed activity program places children at the center of the activity, incorporates perceptual education into the teaching process, and encourages children to participate

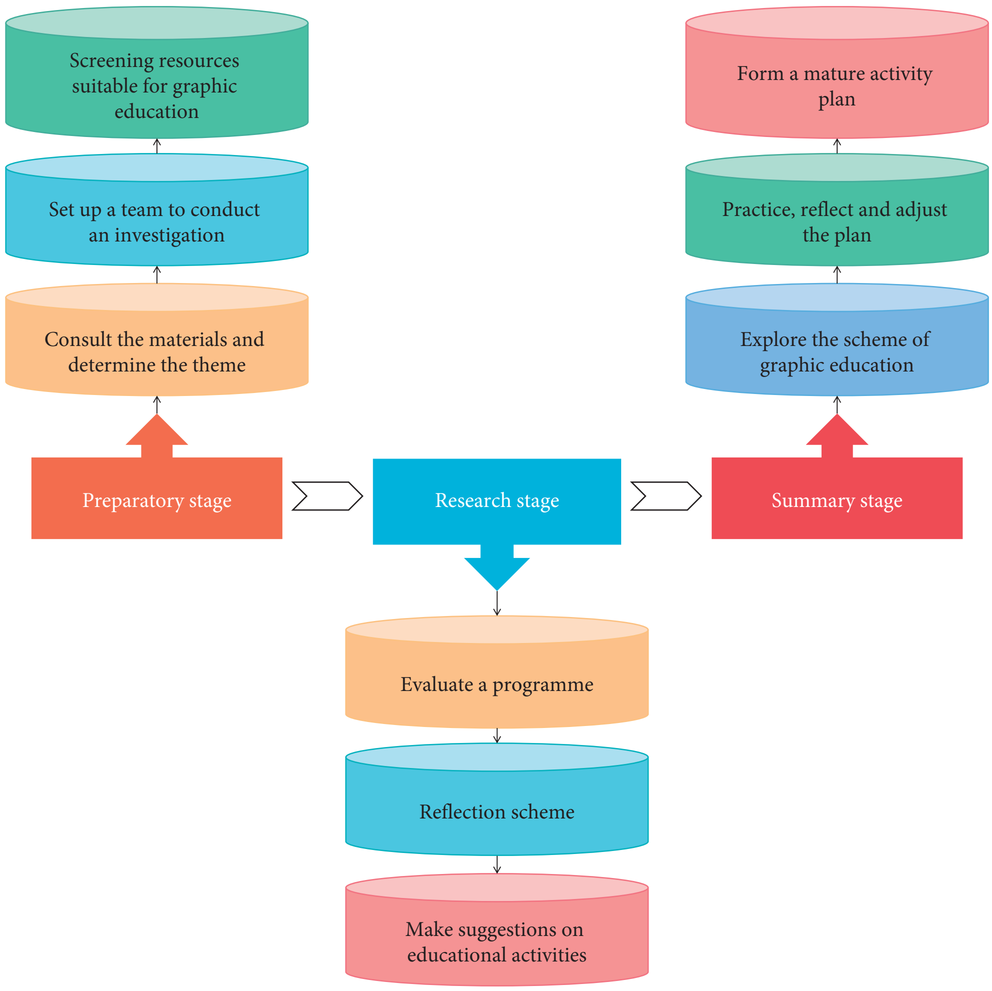

FIGURE 1: Research flow chart of kindergarten profit graph education activities.

in teaching activities in a fun way. The flowchart of teaching activities of geometric figures using kindergarten perceptual education is shown in Figure 2.

Secondly, artistic abstraction refers to the abstract expression of things; it is a kind of art form which is detached from the natural appearance. Generally speaking, artistic abstraction expresses subjective attitude through color and shape. The teacher needs to analyze the formal elements, spatial characteristics, and colors of the painting in a comprehensive, in-depth, and detailed manner in order to identify the forms that fit the definition of the "perception" strategy. This step is usually combined with the selection of the appropriate similarity measure and the establishment of a criterion function, followed by the grouping of samples according to whether they are similar to each other or not. For any sequence that iterates and eventually converges, the speed of convergence increases significantly and the number of iterations decreases significantly when the initial value of the iteration is close to the final convergence result. Children can understand the characteristics of graphs through experience, which is a favorable condition for teaching graphs. Also, this feature can explain the types of errors children make: similar graphs, similar objects, and confusing names. A higher affiliation is surrounded by a lower affiliation of the same category. Based on this understanding, a new objective function can be introduced:

$$J_m(U,V) = \sum_{k=1}^{n}\sum_{i=1}^{C}\left(u_{ik}\right)^m\left(d_{ik}\right)^2 + \frac{\beta}{N_R}\sum_{k=1}^{n}\sum_{i=1}^{C}\left(u_{ik}\right)^m\sum_{j\in Nk}\left(1-u_{ij}\right)^m. \tag{4}$$

Finally, spatial constructions were mostly made by stacking geometric shapes, and spatial constructions were made by matching the shapes and colors of geometric shapes. Compared to circles, squares, and triangles, circles accounted for the majority of children's scribbles, with a few concentrated in squares or triangles. Given a dataset, each clustering algorithm can generate a division regardless of the presence or absence of a clustering structure. Moreover, different methods usually produce different clustering results. Even for the same clustering algorithm, differences in parameters or the order of input samples may affect the final result. The urban kindergarten teacher did not teach the children geometry during this time, so the difference caused by the time factor is negligible.

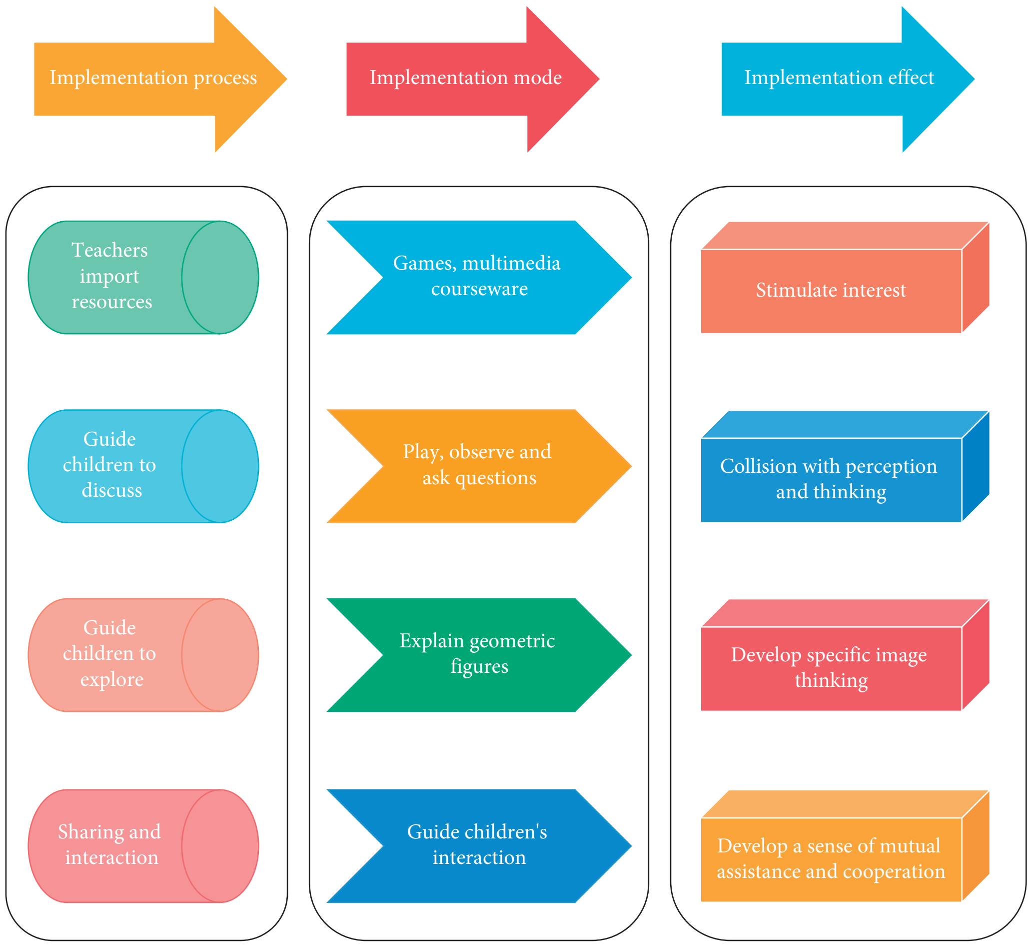

FIGURE 2: Flow chart of geometric figure teaching activities in kindergarten by using perceptual education.

3.2. Steps of Applying Perception Strategies in Graphic Education. When incorporating perceptual education in kindergarten geometry education activities, it is important to pay attention to the program design and the flow of activities according to the laws of kindergarten education and teaching activities and children's development. Children show disappointment in front of works with which they are very familiar, but they are indifferent when something completely unfamiliar is put in front of them. Only those things that are different from what they are familiar with, but can be seen to have some connection to them, are the ones that really appeal to them. The clustering method is to obtain homogeneous regions by manipulating the pixel features of images, while region growth is to divide regions by combining pixel features of the image domain and spatial information. The color image segmentation process in this paper is schematically shown in Figure 3.

First of all, choose paintings with strong musical expression. Geometry education activities applied to cluster analysis in kindergarten take the familiar living resources of young children as the carrier and the process of playing games as the main form of educational activities, so that children can increase their perception of geometric figures in the process of fun and education. Many masters of painting, both ancient and modern, have created numerous classic works, but not all of them are suitable for art appreciation activities using perceptual strategies. Because the unit used in each feature is incomparable, its size can represent the characteristics of the sample in that feature. Based on the principle of feature balance, that is, the contribution of each feature to the classification is essentially equally important, let the balance coefficient be r_j, which is calculated as follows:

$$r_j = \frac{\max\left\{\sum_{i=1}^{c} p_{il}, l = 1, 2, \ldots, s\right\}}{\sum_{i=1}^{c} p_{il}}, \quad j = 1, 2, \ldots, s. \tag{5}$$

The whole technique optimizes the points that may be pixels in the whole edge of the image, taking into account the overall variation of the large area, so as to obtain the most suitable set of edge points. The image is segmented using the standard FCM algorithm to obtain the best division matrix U and the objective function value J_{FCM}, and then the following function values corresponding to this division matrix U are calculated:

$$J_{\mathrm{add}} = \frac{1}{N_R} \sum_{k=1}^{n} \sum_{i=1}^{c} u_{ik}^{m} \sum_{j \in N_k} \left(1 - u_{ij}\right)^{m}. \tag{6}$$

Then use the following equation to calculate the coefficient β:

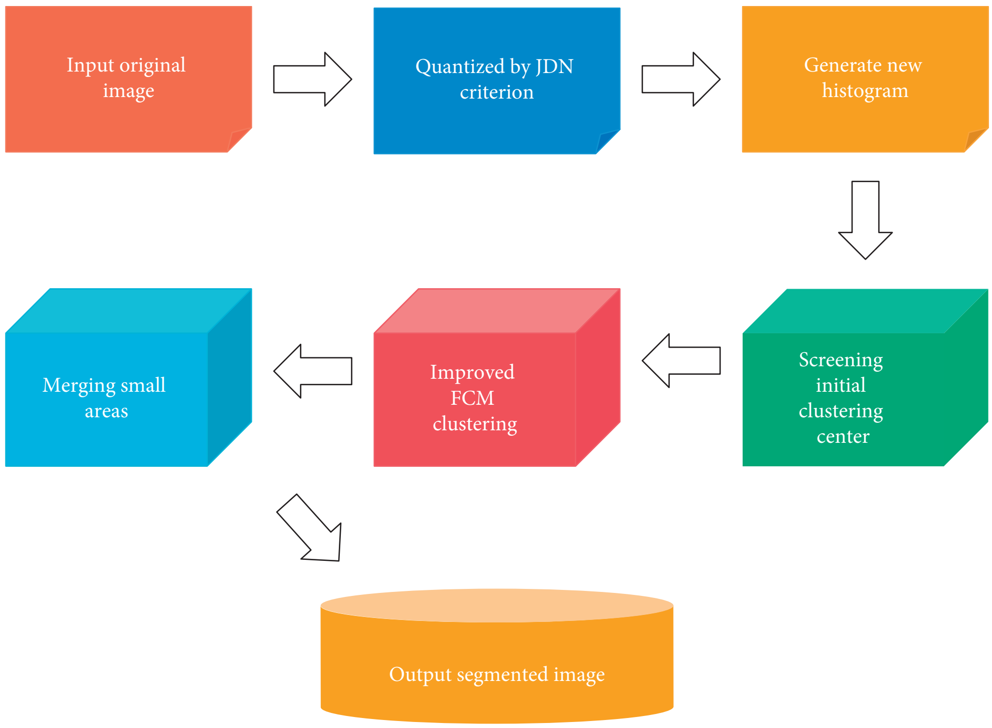

FIGURE 3: Schematic diagram of color image segmentation process.

$$\beta = \frac{J_{\mathrm{FCM}}}{J_{\mathrm{add}}}. \tag{7}$$

Children can master eight shapes in terms of difficulty. From easy to difficult, the order is circle, square, triangle, rectangle, semicircle, trapezoid, rhombus, and parallelogram. In the splitting phase, the homogeneity criterion is used to divide image regions into many homogeneous regions, and in the merging phase, adjacent similar regions are merged into one region. The instability of children's pattern recognition and the inattention to children's exams can affect the development of children's pattern recognition ability. As we know from the role of standard deviation in mathematical statistics, standard deviation describes the degree of concentration and dispersion of data. So the degree of class separation can be measured by the standard deviation of the clustering prototype, which is calculated as follows:

$$d_{ij} = \sqrt{\sum_{i=1}^{c} \left(p_{ij} - \overline{p_j}\right)^2}, \quad j = 1, 2, \ldots, s. \tag{8}$$

Second, timely and appropriate display of paintings is the second step in implementing the perception strategy. Based on the laws of children's physical and mental development, children are provided with objects, pictures, videos, etc. It is easy to use the surrounding life resources for visual observation and direct manipulation in educational activities and can be explained concisely in a language that children can understand to promote their correct perception of geometric figures. However, there is a mixture of nonestablishment and establishment in children's doodle investigations on a piece of paper, so it cannot be concluded that they are completely ignorant, but only that the degree of understanding of the investigation varies at this moment. Fuzzy clustering segmentation generally fails to effectively use the information of the spatial relationship between image pixels, which easily leads to discontinuity in the segmented region. In another segmentation, the number of categories may be incorrect, and there is often the possibility of oversegmentation. Let $X = \{x_1, x_2, \ldots, x_n\}$ be a collection of sample data mapped from the input pattern space R^s to the feature space R^p by a nonlinear transformation $\varphi(\bullet)$. The objective function for partitioning the data set into classes is

$$J_m = \sum_{i=1}^{c} \sum_{j=1}^{n} u_{ij}^m \left\| \varphi\left(x_j\right) - \varphi\left(v_i\right) \right\|^2. \tag{9}$$

Therefore, multiple clustering centers are selected as seed regions. Using these seeds as starting points, different strategies and methods are used to classify the neighboring pixels around them that satisfy their feature conditions. Generally, after the clustering is completed, the segmentation results need to be processed by some merging classes so that the final segmented regions are meaningful. Let K be the kernel function defined on the dataset, which is defined by an implicit mapping:

$$K(x, y) = \langle \varphi(x), \varphi(y) \rangle, \varphi\colon X \longrightarrow F. \tag{10}$$

Finally, mobilizing children's sensory systems such as hearing, smell, taste, and touch to improve the appreciation of drawing is the third step in implementing the perception

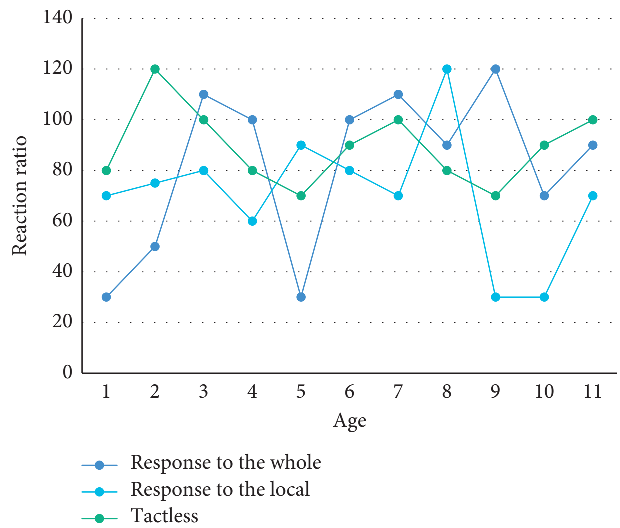

Figure 4: Ratio of responses of subjects of different age groups to global and local characteristics under the condition of free attention.

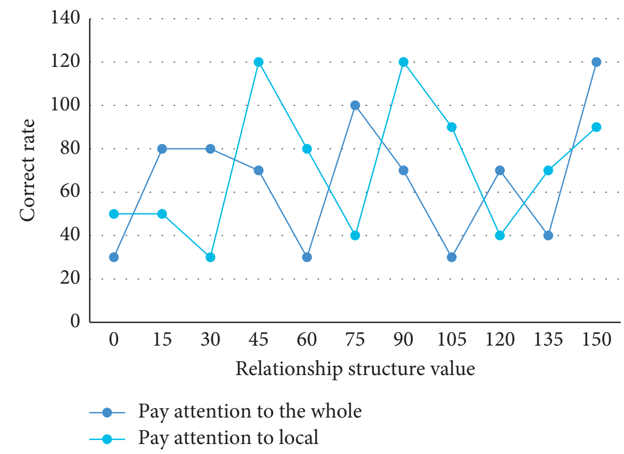

Figure 5: 5-year-old subjects' attention to the whole is influenced by the structural relationship.

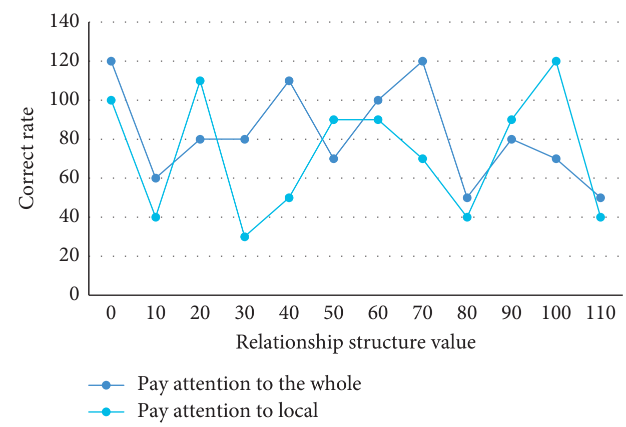

Figure 6: The 10-year-old group was influenced by the structural relationship when paying attention to the whole.

strategy. Children are fully guided to develop a strong interest in participating in geometric educational activities by creating contexts, providing manipulative materials, and designing games, with a focus on stimulating their interest in observation, thinking, and manipulation, making the process of educational activities vivid and interesting, and enhancing their desire to explore geometric shapes. The original histogram is recalculated using the JND color model with the minimum visible difference in human vision, and the three-dimensional axes of the original image histogram are sampled without affecting human vision to obtain new histogram pixel values, whether children's planar geometric figure recognition and combination abilities are positively or negatively correlated. Regardless of which research is conducted, the findings should ultimately guide practice, and the findings should assist kindergarten teachers in better understanding the characteristics and trends of young children's graphic perception.

4. Application Analysis of Fuzzy Cluster Analysis in Children's Graphic Perception Education

4.1. Analysis of Image Segmentation Algorithm Based on Fuzzy C-Means Clustering. The FCM algorithm is used for image segmentation by fuzzy clustering pixels with consistent attributes in an image and then calibrating the pixels in each class. In most cases, the given dataset consists of several samples. Each sample is multidimensional, and each dimension corresponds to a feature or attribute value. No matter how the objective function is defined in the FCM algorithm, there is a corresponding clustering prototype corresponding to it, so the convergence speed and even the clustering effect necessarily depend on the initial division. Since child subjects cannot respond as quickly as adult instructions, the response rates of subjects of different age groups to global and local features in the free attention condition are shown in Figure 4.

First, the pixels of the images are used as sample points of the data set, and the features of the pixels are the features of the grayscale images; i.e., the grayscale images are used as sample points. The test of children's planar geometry combination ability includes two parts. The characteristic of the combined audiovisual animation is that the animation content is a reproduction of the painting content, which gives life to the painting and makes the frozen moment flow. Since only the grayscale information of pixels is used in the grayscale threshold segmentation, the grayscale histogram can be used for clustering instead of the pixels of the image. However, because the statistical information of the original statistical histogram is scattered, the direction of the histogram curve may not be very clear and the peaks and valleys cannot be well selected for image segmentation. Therefore, the original histogram must be smoothed before it can be used in the subsequent segmentation center selection process. A further significance test was conducted to examine the difference between responses focusing on the whole and those focusing on the local. Setting up experiments in which

5- versus 10-year-old subjects were influenced by structural relations when paying attention to the whole, the experimental results are shown in Figure 5.

Second, the image is segmented using the difference between the background and the object as shown in Figure 6, taking a complete circle and dividing it into two semicircles, three obtuse sectors, and four right-angled sectors. To prepare for perceptual drawing, creatively recreate situations based on the teacher's picture composition using manipulable material materials, similar structural forms, and emotions. The number of samples in the grayscale domain is a fixed value independent of image size and equal to the number of grayscales in grayscale images once the grayscale of the image is known. If the image to be segmented has a clear difference between the background and the segmented object, i.e., if the histogram has a clear threshold that can segment the image into several separate parts, this method allows for quick and simple segmentation.

Finally, the pixel values of one or more image dimensions are counted to produce a histogram of pixel statistics for the image's dimensions. The histogram will show distinct peaks in homogeneous regions in an image with similar colors. The number of samples for clustering will be greatly reduced, the complexity of the computational matrix will be reduced, and the efficiency of the general-purpose algorithm for image segmentation will be increased if the pixels of an image are clustered with grayscale histograms instead. Geometry is vibrant, and so should the educational activities that accompany it. It is critical to fully explore children's interest in geometry and to allow them to enjoy geometry educational exploration activities through games. The juxtaposition of reality and imagination characterizes the combination of art appreciation and physical objects, with the same image highlighting the painting's unique color matching, form, and other artistic aesthetics. Set a color merging range after determining the central pixel values of several clusters. The color distance between all pixels in the image and these central pixels should then be calculated. The colors are merged if they are within the range; otherwise, they are identified as new cluster centers, and so on, until all pixels have been processed.

4.2. Analysis of Improved Fuzzy Clustering Algorithm Based on Kernel Function. Classical clustering algorithms directly use Euclidean distance as a similarity measure, and close samples in the sample space are clustered together. However, the commonly used edge operators are wide edges, so the obtained edges must be refined to ensure accurate color values are obtained. Therefore, the improved kernel function-based fuzzy clustering algorithm can map the samples in the input sample space to a high-dimensional feature space in which the nonlinear learning problem may become a linear learning problem. In this study, the mean scores and standard deviations of basic plane geometry figure recognition of 200 children in three age groups of elementary, middle, and large classes were statistically analyzed, as shown in Table 1.

Table 1: Average score and standard deviation of basic plane geometry recognition of children of all ages.

	Reception class	Middle class	Big class
Triangle average	3.24	5.98	10.54
Triangle standard deviation	0.45	1.65	2.77
Circular average	2.78	4.26	7.84
Circular standard deviation	0.27	1.27	1.85
Rectangle average	1.73	3.76	5.98
Rectangle standard deviation	0.17	0.94	1.26

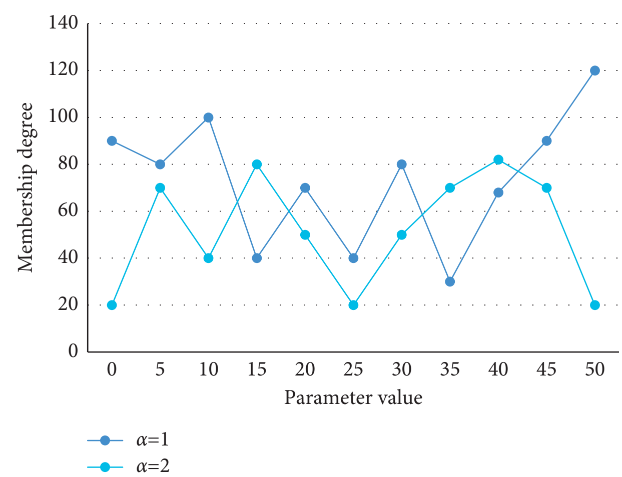

Figure 7: The membership histogram of each sample belonging to the first class when the α value takes some representative values.

The clustering process is guided by making the affiliation values of the labeled samples as close as possible to the labeled affiliation values, provided that the structure of the dataset is discovered in the unsupervised part of the previous section. The histogram of the affiliation of each sample belonging to class 1 when the α value is taken as some representative value is shown in Figure 7.

First, an image is viewed as a continuum of closely connected, interrelated pixels. Its individual features are part of the global features, affecting the values and features of other pixels on the edges, not in isolation. The cluster center values and affiliation of each sample to each cluster center value are corrected through iterative operations of the fuzzy classification matrix and the cluster center matrix to finally find the categorical features contained in the sample data set, thus classifying each sample into the category with the greatest affiliation. Children's understanding of geometric figures is significantly higher than their ability to name them correctly, and children's representations of figures are influenced by verbal expressions, which reveal inconsistencies between perception and expression. Subjects should be more accurate when paying attention to the whole than to the part, and the response to the whole should not vary with structural relations, whereas the part's response to contradictory structural relations should be worse than unrelated structural relations or even worse than consistent structural relations, and the response rate to the whole should be higher during free attention. The objective function is divided into two parts, similar to the improved kernel function-based fuzzy clustering algorithm FCM algorithm, but the latter part only contains labeled samples. The variation of the affiliation values of different supervised samples with increasing values of α is plotted in Figure 8.

Second, the color difference of each region to be segmented is small, but the difference between regions is large. From the concept of classification, the distance between classes is the smallest and the distance between classes is the largest. There is a positive transfer between children's perception of plane geometry and their perception of geometry. So the whole computational process is a process of iteratively modifying the clustering centers and classification matrix, which can converge from any given initial point along an iterative subsequence to the local minima or saddle points of its objective function. The inclusion of childlike graphics in the design of children's educational institutions helps children to acquire cognition, which in turn helps them to better understand their external environment. This proves that children can notice the front-back position and shading relationships of objects through visual perception and also want to represent them through drawing. Therefore, the difference between the gray value of the gray image and the gray value of the seed point is used as a criterion, and the rule for the end of growth is that all pixels grow completely and the distance between classes is greater than a certain threshold. In the improved algorithm, if both 2-DHs are from the original image, their binary groups will be distributed on the diagonal of the plane, so the segmentation of the improved algorithm is consistent with that of the standard FCM algorithm. The performance comparison of the two segmentation algorithms is shown in Table 2.

In summary, the segmentation time of the improved algorithm is significantly reduced by 171.48 s compared to the traditional FCM algorithm, whether it is used to segment noisy images or images with better quality, and thus significantly outperforms the FCM algorithm in terms of segmentation speed.

Finally, m sample instances are randomly selected from the training set. The correlation between each feature of each sample and the class is obtained by the difference between the selected samples and the two nearest neighbors belonging to the same class and different classes, and then the average value is taken as the weight of each feature. Children's perception of plane geometry and geometry goes through a process of pairing–identifying–naming from perceiving the external features of geometry to being able to name it. In order to get the best clustering results, the Lagrange multiplier method is used to obtain the affiliation function and the clustering prototype update formula, so as to obtain the alternatively optimized image segmentation results. The image is segmented into disjoint blocks, and then, the features of the blocks are judged to be consistent, and if they are consistent, they are merged, otherwise, the inconsistent blocks are segmented into blocks as parent blocks and judged again, and the process is repeated until all the features within the blocks are consistent, as well as the features between the blocks are different.

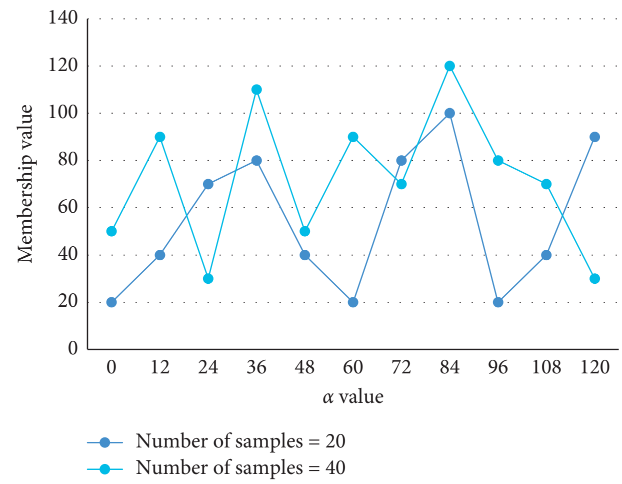

Figure 8: Changes in membership values of different supervised samples with the increase of α value.

Table 2: Comparison of segmentation results of Lena image polluted by the noise by two algorithms.

Algorithm	FCM	Improved algorithm
Split time (s)	189.26	17.78
Cluster center	24, 88, 137, 176	24, 90, 138, 177

5. Conclusions

Children's artworks reflect their perceptions of the outside world and express their inner feelings and thoughts. Art plays an essential role in preschool education as a fundamental subject. The ability of children to combine plane geometry is primarily at the fragmented combination and image stages, with some children at the precombination and shape combination stages. Preschoolers are in the early stages of self-awareness and understanding of the world, and their sense organs are rapidly developing. The development trend in children's thinking about the recognition of plane geometric figures is from visual to analytical, from focusing on the overall visual image to considering the figure's characteristics and concrete image thinking. Image segmentation is the problem of classifying the pixels of an image, and fuzzy theory has been found to have a good ability to describe image uncertainties. Graphics can help preschool children develop their visual system perceptual abilities by influencing their ability to perceive basic shapes, spatial relationships, colors, and visual memory. This research aims to improve children's perceptions of geometric figures, develop their unique figurative thinking, pique their interest in educational graphic perception activities, investigate the methods and paths of using fuzzy clustering analysis to develop educational geometric figure activities in kindergartens, and expand the ideas of developing garden-based curriculum resources in kindergarten science. As a result, the child-centered analysis of young children's graphic perception education proposed in this paper can combine the characteristics of preschool children's perceptual development and fuzzy cluster analysis to help graphic education implementers design a more popular curriculum for children and successfully carry out graphic perception teaching activities.

Data Availability

The data used to support the findings of this study are available from the corresponding author upon request.

Conflicts of Interest

The authors do not have any possible conflicts of interest.

References

[1] S. Liu, *Advanced Hybrid Information Processing*, G. Yang, Ed., Springer International Publishing, New York, NY, USA, 2021.
[2] T. Sapounidis, S. Demetriadis, P. M. Papadopoulos, and D. Stamovlasis, "Tangible and graphical programming with experienced children: a mixed methods analysis," *International Journal of Child-Computer Interaction*, vol. 19, pp. 67–78, 2019.
[3] H. Assal, A. Imran, and S. Chiasson, "An exploration of graphical password authentication for children," *International Journal of Child-Computer Interaction*, vol. 18, pp. 37–46, 2018.
[4] V. Vaknin-Nusbaum and E. Nevo, "What can children learn from exposure to visual-graphical representations?" *Thinking Skills and Creativity*, vol. 40, no. 3, Article ID 100830, 2021.
[5] C. Hartley, A. Trainer, and M. L. Allen, "Investigating the relationship between language and picture understanding in children with autism spectrum disorder," *Autism*, vol. 23, no. 1, pp. 187–198, 2017.
[6] M. Kalogiannakis, G. M. Nirgianaki, and S. Papadakis, "Teaching magnetism to preschool children: the effectiveness of picture story reading," *Early Childhood Education Journal*, vol. 2, no. 2, pp. 1–12, 2017.
[7] N. A. Kapikiran and A. Gündoğan, "Assessment for children's values: picture-based value survey for children adaptation study," *International Journal of Educational Research Review*, vol. 3, no. 2, pp. 9–21, 2018.
[8] P. Liu and S. Hansok, "Children's picture book is a powerful method of cultural communication of Zhuang folk tales," *Literature & Art Studies: English Version*, vol. 11, no. 7, p. 8, 2021.
[9] Z. Wang, Z. Huang, Y. Xu et al., "Image noise level estimation by employing chi-square distribution," in *Proceedings of the 2021 IEEE 21st International Conference on Communication Technology (ICCT)*, pp. 1158–1161, Tianjin, China, October 2021.
[10] Y. Ding, X. Zhao, Z. Zhang, W. Cai, N. Yang, and Y. Zhan, "Semi-supervised locality preserving dense graph neural network with ARMA filters and context-aware learning for hyperspectral image classification," *IEEE Transactions on Geoscience and Remote Sensing*, vol. 5, 2021.
[11] D. Liu, "Research on the application of children's picture book in English teaching of the junior class in primary school," *File*, vol. 7, no. 7, p. 50, 2017.
[12] M. C. Hidalgo Rodríguez, S. Blancas Alvarez, D. Navarro Mateu, and C. A. Valdivieso, "Picture book as a tool for encouraging inclusive values among children: picture book typologies and teaching activities using these publications," *The International Journal of Visual Design*, vol. 12, no. 2, pp. 17–34, 2018.
[13] J. Chen, C. Du, Y. Zhang, P. Han, and W. Wei, "A clustering-based coverage path planning method for autonomous heterogeneous UAVs," *IEEE Transactions on Intelligent Transportation Systems*, vol. 1, pp. 1–11, 2021.
[14] S. Kucharczyk and H. Hanna, "Balancing teacher power and children's rights: rethinking the use of picturebooks in multicultural primary schools in England," *Human Rights Education Review*, vol. 3, no. 1, pp. 49–68, 2020.
[15] W. Cai, B. Zhai, Y. Liu, R. Liu, and X. Ning, "Quadratic polynomial guided fuzzy C-means and dual attention mechanism for medical image segmentation," *Displays*, vol. 70, Article ID 102106, 2021.
[16] V. Tai and N. Ledai, "A new fuzzy time series model based on cluster Analysis problem," *International Journal of Fuzzy Systems*, vol. 21, no. 3, pp. 852–864, 2019.
[17] G. Li, L. Tian, Y. Guo, Y. Li, M. Sun, and H. Zou, "Cut-off values of neonatal lysosomal storage disease-related enzymes detected by tandem mass spectrometry," *Zhejiang da xue xue bao. Yi xue ban = Journal of Zhejiang University. Medical Sciences*, vol. 50, no. 7, pp. 1–5, 2021.
[18] S. Feng and C. L. P. Chen, "Performance analysis of fuzzy BLS using different cluster methods for classification," *Science China Information Sciences*, vol. 64, no. 4, Article ID 149205, 2021.
[19] K. V. Rajkumar, A. Yesubabu, and K. Subrahmanyam, "Fuzzy clustering and fuzzy c-means partition cluster analysis and validation studies on a subset of citescore dataset," *International Journal of Electrical and Computer Engineering*, vol. 9, no. 4, p. 2760, 2019.
[20] M. Shakeri, M. H. Dezfoulian, H. Khotanlou, A. H. Barati, and Y. Masoumi, "Image contrast enhancement using fuzzy clustering with adaptive cluster parameter and sub-histogram equalization," *Digital Signal Processing*, vol. 62, pp. 224–237, 2017.
[21] S. Goyal, S. Kumar, M. A. Zaveri, and A. K. Shukla, "Fuzzy similarity measure based spectral clustering framework for noisy image segmentation," *International Journal of Uncertainty, Fuzziness and Knowledge-Based Systems*, vol. 25, no. 04, pp. 649–673, 2017.
[22] N. V. Pham, L. T. Pham, T. D. Nguyen, and L. T. Ngo, "A new cluster tendency assessment method for fuzzy co-clustering in hyperspectral image analysis," *Neurocomputing*, vol. 307, no. 13, pp. 213–226, 2018.
[23] V. B. Berikov, "A probabilistic model of fuzzy clustering ensemble," *Pattern Recognition and Image Analysis*, vol. 28, no. 1, pp. 1–10, 2018.
[24] A. Mlr, B. K. Shaffer, C. B. Amini, and N. L. J. Spittler, "Advanced, interactive, image-based education: technology and pedagogy," *Current Problems in Diagnostic Radiology*, vol. 49, no. 2, pp. 74–81, 2020.
[25] Y. Wang, T. Wang, X. Zhou et al., "TransEffiDet: aircraft detection and classification in aerial images based on EfficientDet and transformer," *Computational Intelligence and Neuroscience*, vol. 2022, 2022.
[26] H. N. Mai, K. E. Lee, J. H. Ha, and D. H. Lee, "Effects of image and education on the precision of the measurement method for evaluating prosthesis misfit," *The Journal of Prosthetic Dentistry*, vol. 5, Article ID S0022391317304249, 2017.
[27] Y. Shen and W. Pedrycz, "Collaborative fuzzy clustering algorithm: some refinements," *International Journal of*

Approximate Reasoning, vol. 8, Article ID S0888613X17300701, 2017.
[28] X.-h. Wang, L.-s. Wu, H.-w. Chen, and H.-l. Shi, "Region segmentation of point cloud data based on improved particle swarm optimization fuzzy clustering," *Optics and Precision Engineering*, vol. 25, no. 4, pp. 1095–1105, 2017.
[29] J. Kong, H. Wang, C. Yang, X. Jin, M. Zuo, and X. Zhang, "A spatial feature-enhanced attention neural network with high-order pooling representation for application in pest and disease recognition," *Agriculture*, vol. 12, no. 4, p. 500, 2022.
[30] Z. Hu, Y. V. Bodyanskiy, Y. V. Bodyanskiy, O. K. Tyshchenko, and V. O. Samitova, "Fuzzy clustering data given in the ordinal scale," *International Journal of Intelligent Systems and Applications*, vol. 9, no. 1, pp. 67–74, 2017.

Hindawi
Computational Intelligence and Neuroscience
Volume 2022, Article ID 9684535, 10 pages
https://doi.org/10.1155/2022/9684535

Research Article

Biomechanical Analysis of Different Footwork Foot Movements in Table Tennis

Xinrong Li

School of Physical Education, Inner Mongolia University, Hohhot 010021, Inner Mongolia, China

Correspondence should be addressed to Xinrong Li; 20163077@ayit.edu.cn

Received 26 April 2022; Revised 25 May 2022; Accepted 2 June 2022; Published 21 June 2022

Academic Editor: Xin Ning

In order to solve the problem of athletes with lower limb movement injuries in table tennis footwork, with the increasing risk of sports, the incidence of acute injury also increased. The increase in athletic training, on the one hand, improves the skill level of the athlete; on the other hand, it increases the chances of more chronic injuries. Through the investigation of the injury site of 143 table tennis players, the researchers found that the lower limb injury accounted for 32% of the total injuries and the upper limb injury rate accounted for 33.14% of the trunk, accounting for 34.29%. The injury sites are mostly concentrated in the lumbar region, followed by the shoulders and knees. Through epidemiological research on the injuries of outstanding table tennis players, the survey results show that the probability of lower extremity injuries ranks in the top three, and most of them are acute sprains and chronic strain injuries. By applying the principles of sports biomechanics, a biomechanical analysis of the asynchronous foot movement in table tennis is proposed; from three aspects of kinematics, dynamics, and plantar pressure, it is found that the injury of table tennis is closely related to technical play connect. The risk of sports injury is inevitable in a sense, due to the long-term local overload, which causes the strain of the sports system. In order to avoid or reduce the occurrence of such sports injuries, coaches should standardize the technical movements of the players and arrange the exercise load reasonably according to the characteristics of the sports.

1. Introduction

Footwork refers to the movement method of footwork adopted by table tennis players in order to select the appropriate hitting position. Table tennis sports include technique and footwork, both of which are closely related and are indispensable. In training, especially in the early stage of youth enlightenment and basic training, due to the poor mobility of athletes, the main energy of coaches is often focused on cultivating correct techniques, while footwork training is often neglected. The result of this "hands first, footwork later" training results in athletes with good handwork and poor footwork. This affects the progress and improvement of children's sports technology level. Table tennis is a moderate-intensity sport, mainly aerobic metabolism, supplemented by anaerobic metabolism, seen as a healthy form of exercise; it has been accepted by more and more people in leisure and entertainment activities. The three elements of table tennis today are the following: The movement should be fast, the swing power should be strong, and the ball speed should be high. In order to meet the demand for physical fitness in multiround competitive competitions, this requires athletes to increase exercise load and improve motor units in their usual training. Moreover, in the physical training, the focus is on the strategic idea of "focusing on special physical training," effectively giving play to the physical fitness of athletes and making reasonable use of special endurance to improve competition performance. Scholars have found that, in the multiball practice of table tennis, the dynamic balance ability of the body will decline with the extension of training time, which will affect the performance level of players, and, compared with male table tennis players, female players will have an earlier decline in balance ability. Regarding the study of table tennis footwork, relevant scholars from various countries have actively integrated the advantages of various disciplines to analyze their in-depth mechanism. Athletes of different skill levels were selected to carry out systematic comparative research to reveal the internal laws and external connections of footwork itself. Using the improved letter notation method, the touchdown sequence of various footwork was analyzed from the perspective of footwork sequence, and the relationship between footwork, technique, and landing point was found. Sports biomechanics has become a powerful method for research in this field, modeling foot skeletal muscles based on software such as V3D, CAD, and finite element, and researchers can use a variety of measurement methods to obtain more detailed data on the foot and use computers for processing and analysis. The author aims to apply the principles of exercise biomechanics, from the three aspects of kinematics, dynamics, and plantar pressure, in addition to an in-depth study of the three footsteps in table tennis: the biomechanical laws of foot movement in stride, parallel step, and cross step; the following main conclusions are drawn: Forehand stride and forehand side-by-side strike have similar movement forms of the foot after the force foot hits the ground. There are similarities in the movement of the foot after the backhand step; the backhand side step and the backhand cross step hit the ball with the force foot on the ground. Among the three footwork movements, the movement form of the foot is similar when the pedal is extended off the ground when hitting the ball. Among the three footwork movements, the peak force of the vertical reaction force on the ground and the load rate of the force when the athlete completes the cross step are the largest; moreover, the flexion and extension range of the stepping joint of the force-generating foot and the change range of the heel angle are the largest; therefore, the frequent use of cross gait by athletes may increase the risk of foot fatigue injury. In the three kinds of footwork movements, when the peak force of the vertical reaction force of the ground on the hitting foot appears, the foot is in the flipping motion before and after the maximum valgus angle occurs; coupled with the maximum dorsiflexion state of stepping on the joint at this time, the probability of joint movement injury is increased. During the typical footwork of table tennis, the main bearing area of the plantar pressure of both feet is concentrated in the forefoot area, and the force in the midfoot area is not obvious. The peak value of plantar pressure in the rear area of the foot when hitting the ball was the largest, followed by the parallel gait, and the stride gait was the smallest. The middle area of the forefoot is a relatively stable main force area of the forefoot area, and the magnitude of the peak plantar pressure on the lateral area of the forefoot and the medial area of the forefoot is related to the action form of the gait, as shown in Figure 1.

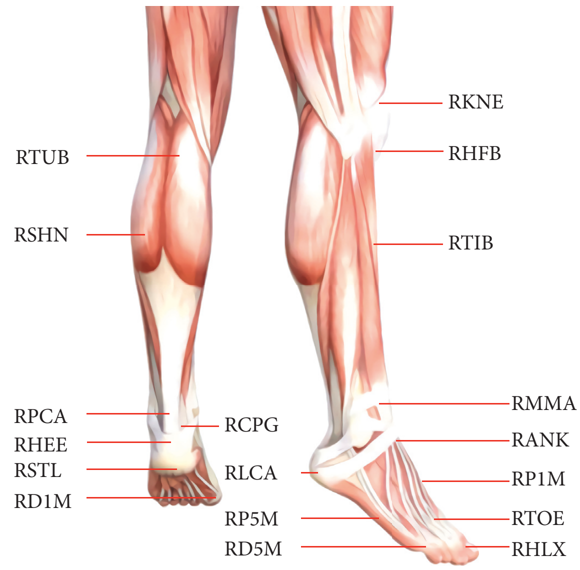

Figure 1: Biomechanical analysis of asynchronous foot movement in table tennis. The middle area of the forefoot is a relatively stable main force area of the forefoot area, and the magnitude of the peak plantar pressure on the lateral area of the forefoot and the medial area of the forefoot is related to the action form of the gait.

2. Literature Review

Since the beginning of the 21st century, Cf, A. et al. said that, with the fusion of various play styles, the sport of table tennis continues to develop in a fast and ferocious direction, requiring players to have outstanding expertise and comprehensive technology, be proactive, and be the first to get started [1]. In particular, the ITTF proposed three new rules in 2000: The sphere is changed from 38 mm to 40 mm; the 21-point system is changed to an 11-point system; the two-point rotation method and unobstructed serving are implemented in the serving rules. These rules place higher demands on table tennis players in various aspects. Shao et al. feel that as the competition becomes more and more confrontational and the ball turns more and more, the technical requirements for the movement range and direction of the athlete are also more refined, so that the athlete's footwork has become the decisive factor in the game [2]. Former Japanese world champion Nobuhiko Hasegawa had a famous quote: “Footwork is the life of table tennis.” It can be seen that table tennis footwork plays a vital role in the completion of the entire hitting action and the rationality, as well as effectiveness and scientificity of the completion of the action. Ardiyanto et al. felt that, in the study of table tennis footwork, the methods and theories of biomechanics provided a scientific means and basis for it [3]. The research scope of biomechanics includes the whole human body, and the research of foot biomechanics is an important part of it. The rise of foot biomechanical research is the result of several factors. Davide et al. said that, first, from a clinical point of view, with the continuous improvement of diabetes treatment methods, it has become possible to prolong the life of patients as much as possible, but, at the same time, the incidence of diabetic complications of diabetic foot is also increasing, medical workers are eager to know the causes of pathological phenomena such as diabetic foot, and biomechanics has begun to enter this field of research [4]. Second, in the work of Hong and Chao, from the perspective of the market, with the rapid development of competitive sports, the scientific scope of competitive sports has become more and more extensive, and the impact of sports shoes on sports has also received increasing attention; people have higher and higher requirements for the injury prevention ability and functional performance of special sports shoes, and it is particularly important to study the biomechanical characteristics of the foot in different special sports [5]. Finally, from a technical point of view, electronic measurement technology and computer technology provide a possibility for the study of foot biomechanics. Researchers can use a variety of measurement techniques to obtain plantar pressure and ground reaction force, process them with computers, and use CAD systems and professional finite element analysis software to model and analyze the foot. Bańkosz and Stefaniak said that “footwork is the soul of table tennis” and accurately summarized the importance of footwork movement in table tennis [6]. Footwork is an important part of table tennis batting and the beginning of each action, and the source of strength comes from the feet and legs. Wu et al. felt that when table tennis players take the initiative to attack the ball, in order to improve the quality of the shot, the movement of the upper limbs alone is not enough [7]. In other words, superb ball skills depend on precise footwork movement, and agile hitting awareness is achieved by flexible, fast, and stable footwork. Sports biomechanics is a common method used in table tennis footwork research; Li et al. felt that, using the theory of exercise biomechanics, in order to explore the biomechanical differences of the dominant foot between professional athletes and beginners in table tennis parallel gait and cross gait, the results and conclusions can improve the in-depth understanding of table tennis footwork for coaches and athletes and then promote the scientific development of table tennis footwork. Previous studies have mainly focused on the three-dimensional motion of human large joints, while the biomechanical characteristics of small foot joints in table tennis footwork have not yet been revealed [8]. Until the Oxford Foot Model (OFM) was discovered, the skeletal muscle model of the small joints of the foot was widely used. Tang et al. said that the Oxford Foot Model is improved on the basis of the traditional Plug-in-Gait model. This model provides more details of the foot and is a reliable multistage study of foot movement [9]. The research of this model mostly focuses on the motion analysis of the forefoot, hindfoot, and great toe, the three-dimensional motion of the forefoot relative to the hindfoot, and the hindfoot relative to the tibia, and the motion of the big toe on the sagittal plane is more detailed. In the analysis of a large number of movement patterns, the model can be widely used in foot analysis in sports and clinical medicine. Therefore, Tabrizi et al. think that using the Oxford Foot Model to study the foot biomechanical characteristics of table tennis footwork can find more movement patterns between the small joints of the foot and help us deeply understand its movement mechanism, which will be a brand new attempt [10].

3. Research Method

Based on the modeling and analysis of human kinematics, the author proposes a new marker point setting scheme and a gait motion measurement system composition scheme; research will be conducted on key techniques for gait motion measurement using established protocols, that is, to study how to obtain lower limb geometric parameters and gait kinematic parameters from gait measurement data. In the traditional gait motion measurement method, the position of the joint center (or axis) is calculated according to the coordinate position of a series of anatomical key points, combined with the manually measured geometric dimensions of the lower limbs. The positions of these anatomical key points are represented by physical measurement identification points on the skin surface or designated points (or virtual identification points) in the calibration process. Therefore, the accuracy of anatomical key point positioning in traditional measurement methods will directly affect the identification of joint positions; as a result, the accuracy and repeatability of gait motion measurement are affected, and the manual positioning process of anatomical key points is also a key factor affecting the pretest preparation time. Firstly, the fitting algorithm of joint position and model geometric parameters is established by analyzing the motion constraint relationship of lower limbs; then, the extraction algorithm of gait motion parameters is established by sampling inverse kinematics analysis method. For the implementation of this algorithm, algorithms and technical support are provided for marker point setting schemes and measurement methods, so that gait measurement does not depend on manual positioning of anatomical key points. Finally, through experiments and analysis of the experimental results, the feasibility of the gait measurement system and related algorithms proposed by the author is discussed [11]. When processing and analyzing the sampled data, it is often necessary to calculate the average posture of the lower limb movements, for example, attitude calculation of measuring rigid body under standard standing posture and attitude filtering. In the space three-dimensional coordinate system, the attitude description of the rigid body can take many forms, such as the direction cosine matrix, the finite rotation quaternion coordinate, the Euler quaternion coordinate, the Euler angle coordinate, and the Cardan angle coordinate. The general algorithm for the weighted average of vectors or matrices is shown in the following formula [12, 13]:

$$A = \frac{\sum_{i=1}^{n} w_i A_i}{\sum_{i=1}^{n} w_i}. \quad (1)$$

The Lifemod interface software of Python language is used to convert Motion’s 6 pieces of data and 2 pieces of kinematics data obtained from analysis and generate Slf files that Lifemod can recognize. The height, weight, and other information of the subjects were input, and the 19-link human model was established through Lifemod’s own human morphology database. The posture adjustment after data is given. The collected kinematic data is given to the model, and then, through posture adjustment and balance analysis, the floor pad model is established, and the contact between the human body model and the floor pad is established. The contact force between the human body model and the floor pad model, the force and moment of each link of the human body model, and the kinematic index of each link were simulated for 1 s to obtain 1000 pieces of data, which was the same as the acquisition frequency of the force table [14]. Formula (1) of inertia for strength training is shown below:

$$j\theta + k\theta = T(t), \tag{2}$$

where A is the weighted average matrix of matrix Ai ($i = 1, 2, \ldots, n$) and Wi is the weight of Ai. However, if the mean value calculation of the direction cosine matrix also adopts the above method, then the resulting matrix will no longer satisfy the constraints of the directional cosine matrix. Euler quaternion coordinates, Euler angle coordinates, and Cardan angle coordinates cannot use a simple weighted average to calculate the average attitude; this is mainly because these pose coordinates are essentially rotation vectors rather than ordinary vectors. Among the attitude coordinates, Euler quaternion is widely used because of its small calculation amount, nonsingularity, and full attitude work. Wahba proposed constructing the cost function to solve the Euler quaternion mean value problem in the 1960s; based on this idea, many researchers have proposed various algorithms. Among them, Markley et al. directly used the direction cosine matrix as the object to solve the weighted mean quaternion method, because the singular value decomposition of the matrix is not involved, making the algorithm relatively simple and widely used. The Euler quaternion n is a four-dimensional vector as shown in the following formula:

$$\underline{\Lambda = \left(\lambda_0, \underline{\lambda}^T\right)^T = \left(\lambda_0, \lambda_1, \lambda 2, \lambda_3\right)^T,} \tag{3}$$

where λ is the vector part and λ_0 is the scalar part. Since the Euler quaternion is essentially a rotation vector and its four variables are not independent, it must satisfy the normalization constraint as shown in the following formula:

$$\underline{\Lambda}^T\,\underline{\Lambda} = \|\underline{\Lambda}\|^2 = \lambda_0^2 + \lambda_1^2 + \lambda_2^2 + \lambda_3^2 = 1. \tag{4}$$

The direction cosine matrix corresponding to the Euler quaternion $\underline{\Lambda}$ is shown in the following formula:

$$\underline{A}(\underline{\Lambda}) = \left(2\lambda_0^2 - 1\right)\underline{I}_3 + \underline{\lambda}\,\overset{T}{\underline{\lambda}} + 2\lambda_0\underline{\tilde{\lambda}}, \tag{5}$$

In order to calculate the average Euler quaternion, construct the pose matrix cost function as shown in the following formula:

$$\overline{\underline{\Lambda}} = \arg\min \sum_i w_i \left\|\underline{A}(\underline{\Lambda}_i)\right\|_F^2. \tag{6}$$

From the definition of the Frobenius norm and the orthogonality of the directional cosine matrix, the following formula can be obtained:

$$\left\|\underline{A}(\underline{\Lambda}) - \underline{A}(\underline{\Lambda}_i)\right\|_F^2 = 6 - 2tr\left[\underline{A}(\underline{\Lambda}_i)\right]. \tag{7}$$

The time series of foot position coordinates and posture coordinates is the motion curve of the foot, and the position coordinates can be represented by the position coordinates of the stepping joints; the posture coordinates are represented by the direction cosine matrix of the foot conjoined base $e4$ with respect to the reference base or other posture coordinates. Corresponding to each sampling point, the changes in the position and posture of the foot in the pelvic conjoined base $e1$ are calculated; the following focuses on the motion curve of the foot in the overall base. For any sampling point, the direction cosine matrix $A04$ of the foot conjoined base $e4$ with respect to the overall base $e0$ is obtained. The position vector of the stepping joint in the overall base dream can be expressed as in the following formula:

$$r_{\text{ankle}} = r_{4b} - d. \tag{8}$$

Due to the influence of the model error, the actual lower limb joints are not truly pivoted, making it difficult to obtain accurate and consistent results for the fitting of the position of the joint rotation center (or rotation axis). For example, the movement pattern of the knee joint is not a simple flexion and extension movement; rather, it is a complex multi-DOF mode that combines flexion, roll, slide, lateral shift, and axial rotation. The flexion and extension movements do not revolve around the same center of rotation but generate multiple instantaneous centers of rotation according to the movement process. During the process of extending and flexing the knee joint, if the instantaneous center of rotation of each movement is continuously marked, the form one on the femoral bone, +*J*"-shaped trajectory, taking the lateral femoral skeleton as a reference, analyzing the electronic *X*-ray films at 9 different positions of the knee joint of 5 volunteers, and measuring the straight-line distance from the joint measurement axis to the lateral skeleton at each position, the measurement results are as follows: With flexion 40" as the center, the distance from the joint measurement axis to the lateral femoral skeleton gradually increases; the greater the flexion angle, the farther away from the lateral femoral skeleton, and the joint measurement axis in the entire range of motion is the same as that on the outer skeleton. The intraclass correlation coefficient (ICC) is often used to evaluate the reliability of a single measurement parameter, but it is not suitable for the repeatability evaluation of the entire curve or waveform; the evaluation index of the repeatability of the gait motion curve is called the adjusted coefficient of multiple correlation (CMC) or the adjusted coefficient of multiple determination (CMD). This method has been used by many researchers in related research. The CMC method is used to analyze the repetition reliability of joint motion parameters as shown in the following formula:

$$R_{wt}^2 = 1 - \frac{\sum_{i=1}^{M}\sum_{j=1}^{N}\sum_{t=1}^{T}\left(Y_{ijt} - \overline{Y}_{it}\right)^2 / MT(N-1)}{\sum_{i=1}^{M}\sum_{j=1}^{N}\sum_{t=1}^{T}\left(Y_{ijt} - \overline{Y}_{i}\right)^2 / MT(N-1)}. \tag{9}$$

The value of the curve is obtained by the *J*th test (trial) in the *i*th experiment in Y_{ijt} at the sampling point t; T is the total number of adopted points contained in the curve; N is the total number of trials for each subject in each experiment; in this experiment, $N = 3$; M is the total number of experiments (tests) for each subject, and $M = 4$ in this experiment; Y_{it} and Y_i are shown in the two following formulas:

$$Y_{it} = \frac{1}{N}\sum_{j=1}^{N} Y_{ijt}, \tag{10}$$

$$Y_i = \frac{1}{NT}\sum_{j=1}^{N}\sum_{t=1}^{T} Y_{ijt}. \tag{11}$$

The algorithm studied by the author is the key technology of the gait measurement system, which overcomes the limitations of the traditional gait measurement system. The realization of this technology makes the marking point layout of the gait measurement system independent of the manual positioning of anatomical key points, and the length of the lower limbs does not need manual measurement, so that the measurement method with fewer marking points can be realized, thus simplifying the measurement process, and, at the same time, it is helpful to reduce the influence of human error caused by the arrangement of marker points and improve the reliability of repeated measurement between experiments.

4. Experiments and Analysis

The stride method includes a forehand step and a backhand step. The experimental subjects all shoot with the right hand, move the right foot to the right for a forehand stride, and move the left foot to the left to perform a stride action during a backhand stride. Among them, the stride foot is the main moving foot that constitutes the stride gait, and it is also the main force-generating foot to complete the batting action, and, according to the research needs, the left foot (i.e., the supporting foot) in the forehand step is called the moving auxiliary foot, and the right foot (i.e., the stepping foot) is called the hitting force foot. The right foot in the backhand step is called the moving auxiliary foot, and the left foot is called the hitting force foot. Figure 2 shows the average-time curve of the flexion and extension angle, heel key angle, and toe extension angle during the forehand stride action of all subjects. As can be seen from Figure 2, when the subjects performed the forehand stride action, when the ball hit the ground, the foot basically did not turnover. However, after landing, the center of gravity of the body shifts to the foot where the ball is used, and the force on the foot increases and turns into a valgus state; when the calcaneal angle decreases and reaches the minimum value, that is, the maximum valgus angle, the stomping, flexion, and extension angle increases, and the restless joint performs hesitant movement. After the heel angle reaches the maximum valgus angle, it begins to increase; when the first peak force occurs, the foot is doing varus movement, the stomping joint is in the dorsiflexion movement, the toe extension angle decreases rapidly, and the foot that hits the ball with force enters the center of gravity adjustment stage of full-foot support.

The first stress stage is over, and the batting force foot enters the second stress stage. With the active push and extension of the hitting force foot, the force on the foot increases, the Achilles tendon angle begins to decrease, the

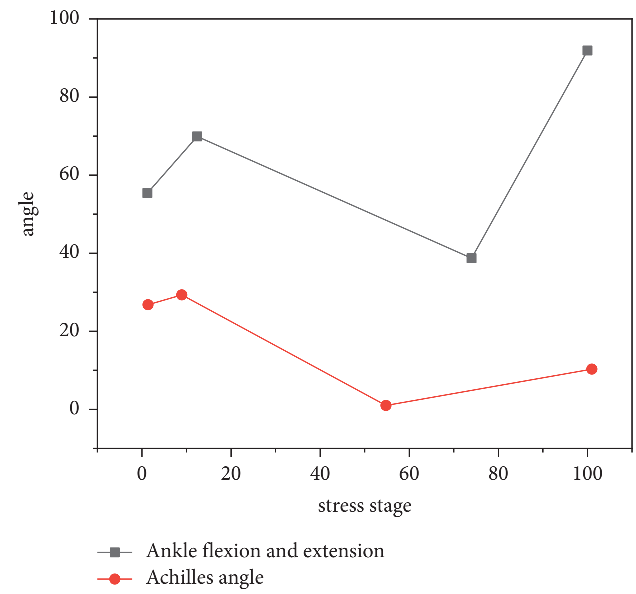

Figure 2: The average-time curve of each angle of the forehand stride strike. The right foot in the backhand step is called the moving auxiliary foot, and the left foot is called the hitting force foot.

foot performs valgus movement, and the restless joint continues to do dorsiflexion movement; when the foot reaches the maximum eversion of the second force stage and the manic joint reaches the maximum dorsiflexion angle, the second peak force appears. After hitting the ball, the force foot starts to push and extend off the ground, the stomping flexion and extension angle increases, and the restless joints do active flexion movement, and the maximum flexion angle is reached at the moment of lifting off the ground. In the stage of kicking off the ground, the toes and the toe joints land on the ground, and the heel is lifted; the toes begin to make the maximum toe extension movement around the toe extension joint, the calcaneal angle increases with the increase of the extension angle of the toe, and the foot performs a varus motion, which changes from the everted state to the initial state at the time of landing [15]. In the kinematic analysis of backhand stride action, all subjects performed backhand stride action when subjects performed backhand stride action, the force on the foot increased after hitting the ball with the force of the foot on the ground, and the foot turns into a valgus state and reaches the maximum valgus angle; at the same time, the stomping flexion and extension angle decreases. The manic joints do dorsiflexion movement; in the landing stage, the heel and toe joints land on the ground, and when the toes are off the ground, the toes begin to make the maximal toe extension movement around the toe joint; the toe extension angle increases first and then decreases before the toe hits the ground. When the first peak force appeared, the foot was in varus state and continued to do varus motion, and the pedal joint reached the maximum dorsiflexion angle. At this time, the extension angle of the toe decreases, and the hitting force foot enters the adjustment stage of the center of gravity supported by the full sole of the foot. Step on the joint to adjust the extension and flexion of a small angle, begin to do the valgus movement, and the toe extension angle enters the plateau phase of change. After the hitting force foot enters the second force stage, the force on the foot increases, the foot continues to do valgus movement, and the restless joint is adjusted in the form of dorsiflexion; when the second peak force occurs, the pedal joint reaches the maximum dorsiflexion angle of the second force stage, and the foot is in a valgus movement. After hitting the ball, the force foot starts to push and extend off the ground, the stomping flexion and extension angle increases, and the restless joints do active flexion and flexion, and the maximum kick angle at the moment of leaving the ground is reached. The toes begin to make the maximum toe extension movement around the toe joint, the extension angle of the toe increases, and the foot performs varus movement at the same time, from the eversion state to the initial varus state at the time of landing. It can be seen from the analysis of the plantar pressure of the stride gait that the main bearing area of the plantar pressure of both feet in the support stage is the forefoot area, and the pressure peak in the forefoot area is. The percentage reaches around 50% [16]. The stress on the midfoot area is not significant, the peak pressure is only about 30% of the body weight, and the peak pressure only accounts for about 15–18% of the total of the three areas. The peak pressure on the back of the foot during the support phase exceeds half of the body weight, but it is not as pronounced as that on the front of the foot. The step-step method is mostly used in the fast-break game near the table, counterattacking the ball from a large angle in the forehand position; when the subject moves to the forehand position with the forehand stride, in order to meet the near billiards, the body's center of gravity moves toward the near table; at this time, the force on the forefoot area is increased relative to the rear area, so the force on the forefoot area is the most obvious relative to each area during the forehand step; the same is true for the force on the sole of the backhand stride [17]. Comparing the mobile auxiliary foot with the batting force foot, there was no significant difference in the force in the midfoot area between the two, and the force in the forefoot area was greater when hitting the ball; the force of the auxiliary foot in the rear area of the foot is greater than that of the ball-hitting force [18, 19]. Because the batting force foot also undertakes the task of actively pushing and extending the force to participate in the batting action and returning to the original position, at this time, the forefoot area, which is the main force-bearing area of the kicking and stretching action, bears more pressure. However, the mobile auxiliary foot is in a state of full-foot support most of the time during the entire forehand step, and the force is relatively scattered; therefore, the difference between the force of the forefoot area and the rear area of the mobile auxiliary foot is small. Through the comparative analysis of the support time of the subjects' hitting power foot, it is found that the stride footwork action has more support time than the parallel footwork; this is because the movement speed and rhythm of the parallel footwork are faster than those of the stride footwork, and the ball-strengthening foot transitions to the active kick off the ground faster in the support phase. After the cross footwork action hits the ball with the force foot on the ground, wait until the mobile auxiliary foot moves the landing support and adjusts the body posture to the direction facing the initial position and then starts to actively push off the ground; therefore, the cross gait method is more complicated, and the support time of the hitting force foot is significantly longer than those of the stride gait method and the parallel gait method, and the difference is significant as shown in Figure 3.

As can be seen, the maximum load rate of the vertical reaction force on the ground after the strike force foot hits the ground in the cross-gait action is significantly larger than those of the stride gait and the parallel gait, and the difference is significant. This is because the first peak force after hitting the ball in the cross footwork is the largest among the three footwork movements, and its appearance time is also the earliest; the hitting force foot should reach the maximum first peak force in the shortest time as shown in Figure 4.

It can be seen that, among the three steps, after the cross footwork hits the ball with the power foot on the ground, the first peak force of the vertical reaction force from the ground is significantly larger than those of the other two footwork types. Due to the cross footwork, the batting force foot is in the single support stage for a period of time after landing, and the body weight is concentrated on the batting force foot, coupled with a large range of rapid movement, resulting in a high landing influenced by factors such as speed; as a result, in the action of the cross footwork, the first peak force of the hitting force foot in the first force stage is significantly greater than those of the other two footwork types. In the process of kicking off the ground after completing the hitting action, the distance back to the initial position of the cross footwork action is farther than those of the other two footwork types; compared with the other two types of footwork, the time left for the adjustment of the cross footwork between the two strokes is less, and the second peak force experienced is the largest [20], as shown in Figure 5.

The change range of the foot angle reflects the movement range of the subject's hitting force during the support force stage; with greater movement range of each link of the foot, especially in the state of continuous force, the risk of sports injuries increases accordingly. Athletes have the greatest flexion and extension of the restless joints during the cross-step process. The previous research on the change law of the angle of flexion and extension in the support stage of the hitting force has shown the maximum changes in the flexion and extension angles of the three footwork movements; they all appeared in the final stage of kicking and extending off the ground, reflecting the significant role of the kicking and flexing movement of stepping on the joint in the process of kicking and extending off the ground. In the action of cross footwork, the kicking foot is in the stage of kicking and extending off the ground, it is necessary to overcome greater resistance than the other two footsteps to return to a farther initial position, and the flexion movement of stepping on the joint is more important, and the range of motion is greater [21]. Therefore, the change range $\Delta\alpha$ of the angle of flexion and extension in the support stage of the impacting foot in the cross-footwork action is larger than those of the other

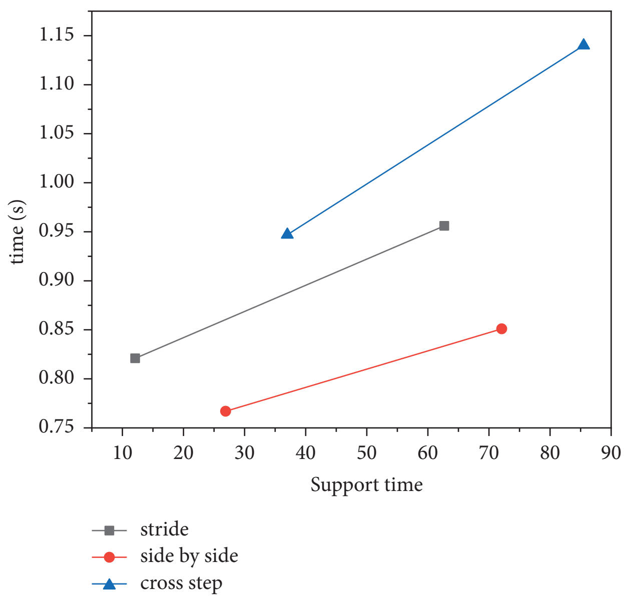

Figure 3: Comparison of the average support time at Farley corners. After the cross-footwork action hits the ball with the force foot on the ground.

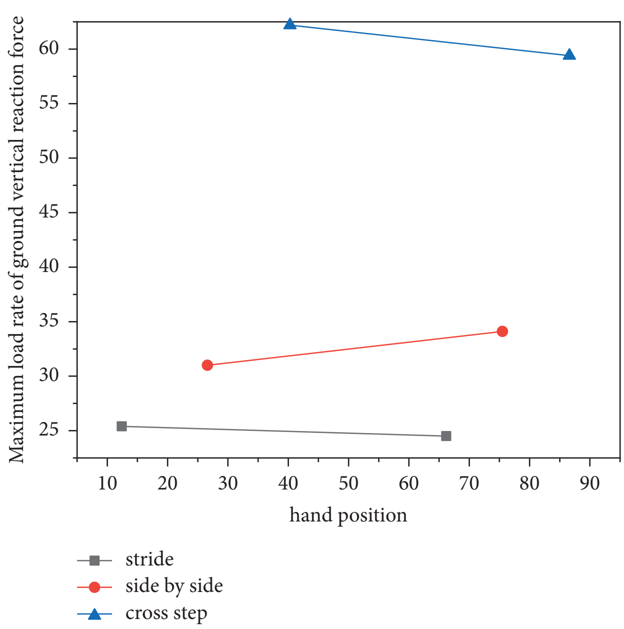

Figure 4: Comparison of the average value of the maximum load rate of the vertical reaction force on the ground of the hitting force. The difference is significant.

two footwork types, and the difference is significant. There was no significant difference in the change range $\Delta\gamma$ of the toe extension angle of the hitting foot when the subjects performed the three footwork movements, and the uniformity of the three footwork movements is not large, indicating that the toe extension movement of the hitting force foot in the process of supporting the force is not affected by the asynchronous movement, and the toe extension angle only changed within a small angle range, and there was no obvious movement of the toe extension. The heel angle is an

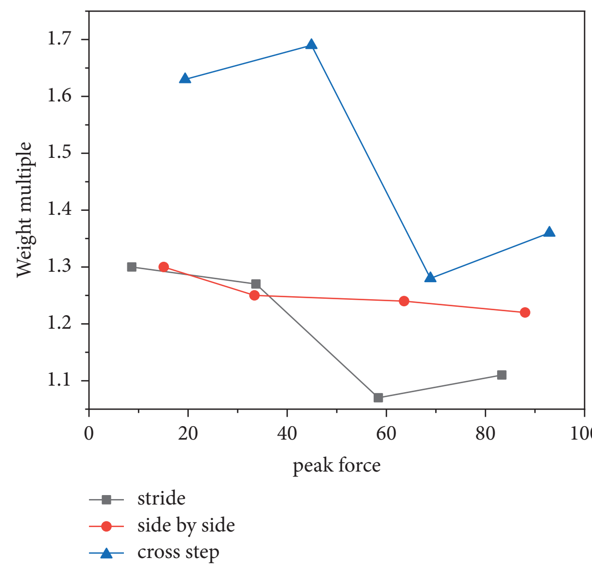

Figure 5: Comparison of the average value of the first peak force and the average value of the second peak force of the mana foot for three footwork strokes. Comparison with the other two types of footwork.

important index to reflect the flipping of the foot during exercise, and the magnitude of its variation $\Delta\beta$ is also an important reference index to evaluate the probability of sports injuries. As can be seen from Figure 6, the change amplitude $\Delta\beta$ of heel angle in the cross-gait action is significantly larger than those of the step-step and parallel gait, and the difference is significant. This may be because the cross footwork strikes the force foot away from the incoming ball, and the relative position of the strike force foot at the time of landing is beyond the body in the incoming ball direction, coupled with factors such as the faster initial speed before landing after a long moving distance; the results are shown in Figure 6.

From the previous results, it can be found that when the subjects perform the three footwork movements, there is a large change in the key angle in the support stage of the hitting force foot; most occur in the valgus movement of the first stress stage and the varus movement of the second stress stage. Comparing the kinetic data, it can be found that the maximum valgus angle of the heel angle mostly occurs near the time when the first peak force occurs in the first stress stage, which means that the foot is subjected to a large vertical force when the foot is in the valgus state, and the impact of the reaction force will increase the probability of foot sports injury [22, 23]. The maximum varus angle of the heel angle mostly occurs at the moment of kicking off the ground, with the appearance of the maximum extension angle of the restless joint; at this time, the hitting force foot is about to leave the ground, and the force is very small. As can be seen, the maximum varus/valgus angles of the power foot in the cross-footing action were larger than those in the other two footwork types, and the difference was significant. The results of the previous study also showed that, during the process of the subjects' performing, the three footwork movements and the peak force of the hitting force foot in the

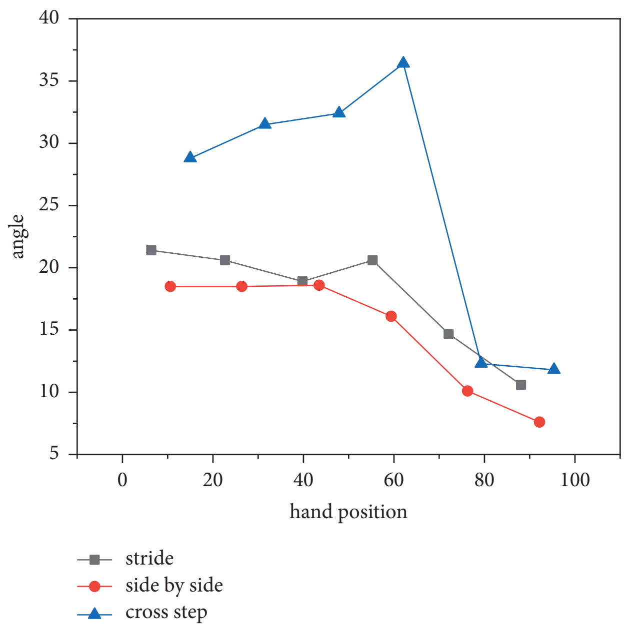

Figure 6: Comparison of the average value of the variation amplitude of the foot angles of the three gait styles, coupled with factors such as the faster initial speed before landing after a long moving distance.

support stage occur during the maximum dorsiflexion angle of the manic joint and the rapid turnover of the foot. In order to prevent sprains from stepping on joints, limit the force acting on the anterior ligament of the talus during stomping, the design of the shoe must strive to limit the varus and valgus forces acting on the restless joint, and this external twisting force is maximized during flexion. In addition, since the stomp joint has a certain degree of lateral flexibility when the stomp joint is flexed, this reduces its own stability; therefore, in order to provide support for sports shoes to resist the varus force that frequently causes sprains, sports shoes must provide stability to counteract the rotation of the pedal joints, especially in the flexion state. Based on the experimental results, the smaller joint range of motion of professional table tennis players when they complete the parallel footwork proves that professional athletes have better foot control and technical stereotypes [24]. For professional athletes, a larger internal rotation of the rear foot at the end of the lead can help the players to complete the gait better, and, with the larger abduction of the forefoot, it is beneficial to maintain the stability of the body's center of gravity. In addition, using V3D technology and high-speed cameras, we found that, during Phase I footwork movement, professional table tennis players are used to landing on the rear foot area, while beginners use the front corner area. This also explains why, during this process, the peak pressure of professional athletes occurs in three areas of the medial and lateral hindfoot and the lateral forefoot; for beginners, peak pressure occurs in three different areas: the big toe, the medial forefoot, and the middle. At the same time, this finding can illustrate that professional athletes can better distribute the body's center of gravity on the entire sole plane, providing a more stable swing foundation for the next stage [25, 26]. At the end of the lead-in period, professional athletes showed less hindfoot varus and forefoot valgus and greater extension of the big toe, which was beneficial to better maintain the balance of the center of gravity and adjust the posture for the rapid transition to be prepared to the next stage. From the results of the study, it was found that professional athletes have a more stable body weight transfer ability in the parallel gait. Professional athletes showed significantly greater dorsiflexion in the forefoot, relative to the hindfoot and relative to the tibial angle of the hindfoot than beginners. According to the systolic relaxation theory, the elastic potential energy previously stored in tendon extension can increase the concentric contraction of the muscle, which means that the professional table tennis player's greater dorsiflexion during the full lead phase can store more energy for the swing phase. The limitations of the author's study are manifested in the following aspects: First, the author's study lacked a gender-specific comparison of parallel gait and cross gait due to limitations in recruiting subjects [27]. Another potential limitation is that there are large differences in training years, although all professional table tennis players have the same level of skill level and are from the same university table tennis team, but this may limit the validity of the experiment to some extent [28]. In addition, beginners have different degrees of differences in their learning ability; this may affect the effectiveness of gait learning. Second, only the differences in the biomechanics of the dominant leg were compared. In fact, the nondominant leg also plays an important role in maintaining body stability during the swing phase. Finally, this experiment is to simulate the footwork movement process in actual combat, not in real competitive competitions. Considering a series of uncontrollable factors (athlete psychology, unfixed table tennis balls, etc.) will affect the results of the experiment.

5. Conclusion

Research shows the following: Compared to beginners, professional athletes spend less time performing side-step and cross-step footwork and show a smaller range of motion and faster angular velocity. This verifies that professional athletes have better ability to use foot drive and body balance in footwork movement techniques. At the end of the lead-up period, professional athletes in the gait show less forefoot valgus and hindfoot varus and greater flexion of the big toe, and the cross gait shows a smaller forefoot flexion and abduction angle, which is conducive to maintaining the stability of the body's center of gravity. For professional athletes, larger peak pressures and relative loads were found in the lateral forefoot and medial-lateral hindfoot regions in these two table tennis footwork styles. The results and analysis of this study are beneficial to provide more valuable theoretical reference for coaches and beginners in the process of footwork training and in the use of parallel and cross gait, how to use foot movement to improve the quality of technical movements and how to maintain body stability, and there are lessons to be learned. The author reveals in detail the kinematics and dynamics of the foot in the three footwork movements of table tennis, which provides data and theoretical basis for improving the effect of footwork movements and preventing foot injury in table tennis players. The movement forms of the foot after the forehand stride and the forehand parallel strike are similar. There are similarities in the movement of the foot after the backhand step, the backhand side step, and the backhand cross step hit the ball. In the three footwork movements, the motion forms of the feet when the pedals are extended and lifted off the ground are similar. The cross footwork is the longest, the stride footwork is the second, and the footwork is the shortest. In the cross-footwork method, the ball-strengthening foot is in the middle of the support stage, and the body posture and the center of gravity adjustment stage appear to be obviously unstressed or less stressed. Among the three footwork movements, the peak force of the vertical reaction force on the ground and the load rate of the force when the athlete completes the cross step are the largest; moreover, the flexion and extension range and calcaneal angle of the force-generating foot have the largest changes; therefore, the frequent use of cross gait by athletes may increase the probability of foot fatigue injury. In the three kinds of footwork movements, when the peak force of the vertical reaction force of the ground on the hitting foot appears, the foot is in a flipping motion before and after the maximum valgus angle occurs, coupled with the maximum dorsiflexion state of the stepping joint at this time, and the probability of injury of the stepping joint is increased. The main bearing area of the plantar pressure of the feet in the three gait movements is concentrated in the forefoot area, and the force in the midfoot area is not obvious. The peak value of plantar pressure in the rear area of the foot when hitting the ball was the largest, followed by the parallel gait, and the stride gait was the smallest. The middle area of the forefoot is the relatively stable main force area of the forefoot area, the peak size of the plantar pressure on the lateral area of the forefoot and the medial area of the forefoot is related to the action form of the footwork, the main force-bearing area of the forefoot area. The peak force of the ground reaction force received by the power foot in the buffering stage and the kicking stage of the three footwork movements is relatively large; therefore, special sports shoes for table tennis should have appropriate shock absorption and buffering functions, in order to relieve the load of frequent impact force on the feet of table tennis players during the game. The peak force of the three footwork movements hitting the power foot in the support stage appears in the maximum dorsiflexion angle of the restless joint and the rapid turnover of the foot. Therefore, special sports shoes for table tennis need to provide good stability support for the stepping joint to resist the foot in the support stage, especially in the state of stepping and bending, and the frequent torsional external force will reduce the probability of foot sports injury. Table tennis footwork action is the active and rapid exertion of the power foot in the stage of kicking off the ground; special sports shoes for table tennis are required to have good energy return performance, providing better conditions for table tennis players to move quickly.

Data Availability

The data used to support the findings of this study are available from the author upon request.

Conflicts of Interest

The author declares no conflicts of interest.

Acknowledgments

This work was supported by Philosophy and Social Science Research Project of Inner Mongolia Autonomous Region (project no. ZSZX21190).

References

[1] A. Cf, A. Tm, A. Yp, A. Pr, B. Pta, and A. Cs, “Physiology, biomechanics and injuries in table tennis: a systematic review,” *Science & Sports*, vol. 36, no. 2, pp. 95–104, 2021.

[2] S. Shao, C. Yu, Y. Song et al., “Mechanical character of lower limb for table tennis cross step maneuver,” *International Journal of Sports Science & Coaching*, vol. 15, no. 4, pp. 552–561, 2020.

[3] M. A. Ardiyanto, M. F. Hidayatullah, and S. S. Sabarini, “The effect of imagery training and concentration on forehand serve accuracy of the junior table tennis athletes,” *Budapest International Research and Critics in Linguistics and Education (BirLE) Journal*, vol. 4, no. 1, pp. 500–509, 2021.

[4] L. Davide, M. Fuchs, Z. Đokic, L. Malagoli, and G. Munivrana, “Comparasion between european elite senior and junior female table tennis players: rally length and serve-receive game,” *TIMS. Acta*, vol. 15, no. 1, pp. 5–15, 2021.

[5] S.-T. Hong and S.-L. Cho, “Application of a psychological skills training for a college table-tennis athlete’s recovery from injury: a single subject study,” *Journal of the Korean society for Wellness*, vol. 16, no. 1, pp. 231–237, 2021.

[6] Z. Bańkosz and T. Stefaniak, “Elbow joint position and hand pressure force sense under conditions of quick reaction in table tennis players,” *Kinesiology*, vol. 53, no. 1, pp. 95–103, 2021.

[7] E. Wu, M. Piekenbrock, T. Nakumura, and H. Koike, “Spinpong - virtual reality table tennis skill acquisition using visual, haptic and temporal cues,” *IEEE Transactions on Visualization and Computer Graphics*, no. 99, p. 1, 2021.

[8] L. Li, F. Ren, and J. S. Baker, “The biomechanics of shoulder movement with implications for shoulder injury in table tennis: a minireview,” *Applied Bionics and Biomechanics*, vol. 2021, no. 2, pp. 1–6, 2021.

[9] M.-Y. Tang, C.-M. Yang, and H. J. L. Jwo, “Expert perceptual behavior under the spatiotemporal visual constraints in table tennis,” *The Asian Journal of Kinesiology*, vol. 23, no. 3, pp. 3–10, 2021.

[10] S. S. Tabrizi, S. Pashazadeh, and V. Javani, “A deep learning approach for table tennis forehand stroke evaluation system using an imu sensor,” *Computational Intelligence and Neuroscience*, vol. 2021, no. 9, pp. 1–15, 2021.

[11] H. Zhao and F. Hao, “Target tracking algorithm for table tennis using machine vision,” *Journal of Healthcare Engineering*, vol. 2021, no. 1, pp. 1–7, 2021.

[12] J. Zhang, “Automatic detection method of technical and tactical indicators for table tennis based on trajectory prediction using compensation fuzzy neural network,”

Computational Intelligence and Neuroscience, vol. 2021, no. 1, pp. 1–12, 2021.

[13] L. Yang, H. Zhang, X. Zhu, and X. Sheng, "Ball Motion Control in the Table Tennis Robot System Using Time-Series Deep Reinforcement Learning," *IEEE Access*, vol. 9, no. 99, p. 1, 2021.

[14] X. Zhou, "Explanation and verification of the rules of attack in table tennis tactics," *BMC Sports Science, Medicine and Rehabilitation*, vol. 14, no. 1, pp. 1–8, 2022.

[15] A. Cf, A. Tm, A. Yp, A. Pr, B. Pta, and A. Cs, "Physiology, biomechanics and injuries in table tennis: a systematic review," *Science & Sports*, vol. 36, no. 2, pp. 95–104, 2021.

[16] Z. Bańkosz and S. Winiarski, "Using wearable inertial sensors to estimate kinematic parameters and variability in the table tennis topspin forehand stroke," *Applied Bionics and Biomechanics*, vol. 2020, no. 1-2, pp. 1–10, 2020.

[17] M. Lenartowicz and A. Ciok, "Foreign players in polish table tennis clubs: differences between sports cultures and coaches' perception of the impact of foreign players on polish table tennis," *Acta Universitatis Lodziensis Folia Sociologica*, no. 75, pp. 15–32, 2020.

[18] Z. Bańkosz and S. Winiarski, "Parameters of topspin forehand in table tennis and their inter-and intra-individual variability," *Journal of Sports Science and Medicine*, vol. 19, no. 1, pp. 138–148, 2020.

[19] A. Nabil, H. Hegazy, M. Abdelsalam, M. Hussien, and A. Atia, "Usability study of a comprehensive table tennis ar-based training system with the focus on players' strokes," *Journal of Ubiquitous Systems and Pervasive Networks*, vol. 13, no. 1, pp. 1–09, 2020.

[20] O. Kazemi, A. Letafatkar, and P. H. Marchetti, "Effect of stretching protocols on glenohumeral-joint muscle activation in elite table tennis players," *International Journal of Sports Physiology and Performance*, vol. 1, no. 1, pp. 1–7, 2020.

[21] A. Conchin, M. A. Ferrara, and J. F. Kaux, "Stress fracture of the distal femoral growth plate in a young belgian table tennis champion," *Revue Medicale de Liege*, vol. 75, no. 7-8, pp. 497–500, 2020.

[22] O. J. Kim, R. K. Kim, and H. S. Jeon, "A relationship among participation motive, leisure satisfaction, and sports continuity of table tennis coterie members," *Korean Journal of Sports Science*, vol. 29, no. 2, pp. 213–226, 2020.

[23] O. J. Choi, "Impact of the scoring system by stage on competition performance for national male table tennis player by country," *Korean Journal of Sports Science*, vol. 29, no. 5, pp. 1241–1249, 2020.

[24] A. Etn, "Examination of the table tennis players' general self-efficacy perceptions and sources of sports motivation," *Ankara Üniversitesi Beden Eğitimi ve Spor Yüksekokulu SPORMETRE Beden Eğitimi ve Spor Bilimleri Dergisi*, vol. 18, no. 3, pp. 52–61, 2020.

[25] S. Shao, C. Yu, Y. Song et al., "Mechanical character of lower limb for table tennis cross step maneuver," *International Journal of Sports Science & Coaching*, vol. 15, no. 4, pp. 552–561, 2020.

[26] C. H. Chi, "Analysis and research on the diagnosis of techniques, tactics and psychology in table tennis," *Study on China Physical Science*, vol. 2, no. 3, pp. 117–132, 2020.

[27] K. Lee, "The narrative inquiry of table tennis players' adapting experience to the professional team," *Korean Journal of Sport Psychology*, vol. 31, no. 3, pp. 45–65, 2020.

[28] C. H. Chi, "Research and analysis on the diagnosis of techniques, tactics of table tennis (ii)," *Study on China Physical Science*, vol. 2, no. 4, pp. 185–198, 2020.

Hindawi
Computational Intelligence and Neuroscience
Volume 2022, Article ID 3492175, 12 pages
https://doi.org/10.1155/2022/3492175

Research Article

The Navigation of Mobile Robot in the Indoor Dynamic Unknown Environment Based on Decision Tree Algorithm

Yupei Yan,[1] Weimin Ma ,[1] Yangmin Li,[2] Sengfat Wong,[3] Ping He,[4] Shaoping Zhu,[1] and Xuemei Yin[1]

[1]*Department of Artificial Intelligence, Zhuhai City Polytechnic College, Zhuhai 519090, China*
[2]*Department of Industrial and Systems Engineering, HongKong Polytechnic University, HongKong 999077, Hong Kong*
[3]*Faculty of Science and Technology, University of Macau, Macau 999078, Macau*
[4]*School of Intelligent System Science and Engineering, Jinan University, Zhuhai 519072, China*

Correspondence should be addressed to Weimin Ma; yb47409@connect.um.edu.mo

Received 16 March 2022; Revised 4 April 2022; Accepted 5 April 2022; Published 20 June 2022

Academic Editor: Xin Ning

This study proposes an optimized algorithm for the navigation of the mobile robot in the indoor and dynamic unknown environment based on the decision tree algorithm. Firstly, the error of the yaw value outputted from IMU sensor fusion module is analyzed in the indoor environment; then, the adaptive FAST SLAM is proposed to optimize the yaw value from the odometer; in the next, a decision tree algorithm is applied which predicts the correct moving direction of the mobile robot through the outputted yaw value from the IMU sensor fusion module and adaptive FAST SLAM of the odometer data in the indoor and dynamic environment; the following is the navigation algorithm proposed for the mobile robot in the dynamic and unknown environment; finally, a real mobile robot is designed to verify the proposed algorithm.The final result shows the proposed algorithms are valid and effective.

1. Introduction

There is a wide and extensive application of the mobile robot in many fields; it can fulfill the repeated, heavy, accurate, and complex work in many special environments; the navigation is important for the mobile robot because it is the basic function for the other actions of the mobile robot; it should move freely to the destination without colliding with the obstacles, just like people need to avoid colliding with the other people on the road. There are many navigation algorithms proposed which can be applied in many fields to fulfill the different requirement for human, so the optimization of the navigation is necessary to make the mobile robot moving more intelligently and effectively to the destination [1–3].

Different from the outside static known environment, if the mobile robot is running in the indoor dynamic unknown environment, more conflicts and limitations will be considered; the following is a comparison between them.

The first difference is the location and orientation function; the self-driving car is taken for example; all the cars are running in the outside environment where the GPS sensor can receive the satellite signals properly, so GPS can show the accurate position of the car on the roads, but if the car is running in the indoor environment where the satellite signal is weak or shielded, the GPS function will be unavailable and the corresponding GPS positioning function will be limited. It can only search few or no satellites and it cannot get the accurate position. The IMU sensors have the same problem, so the mobile robot cannot get its location and orientation through the IMU sensors in the indoor environment [4, 5].

The second difference is all environments are known for self-driving car because the map of all roads is provided for the car, but sometimes the mobile robot needs to work in the unknown environment where no map is provided, such as the environment of 24-hour lobby filled with moving people where it is not easy to build the map with SLAM technology [6]; otherwise, the mobile robot may need to fulfilling burrow adventure tasks where it is a totally unknown environment, so the mobile robot cannot locate its position on the map if it is running in an unknown environment.

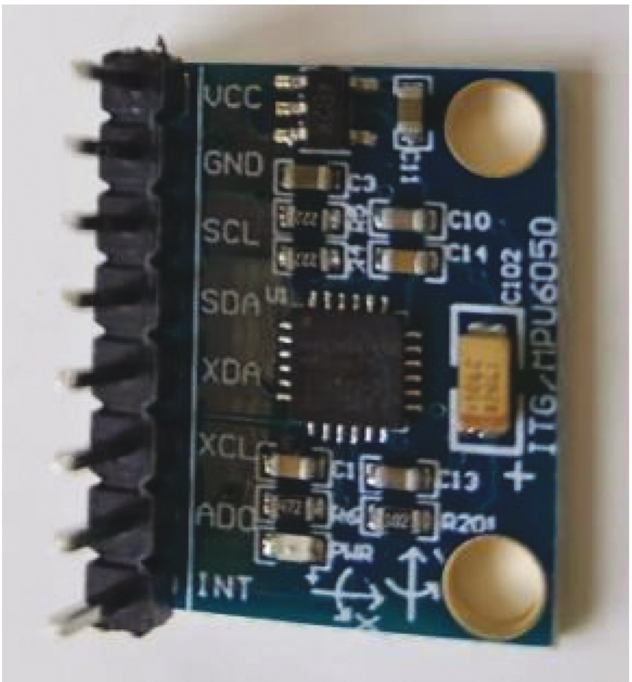

Figure 1: Gyroscope.

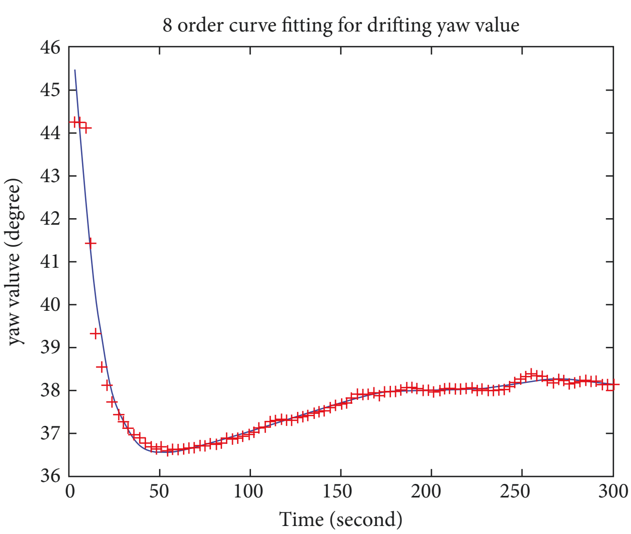

Figure 2: The 8-order curve fitting for the drifting yaw value.

The third difference is that sometimes mobile robot cannot be located in the dynamic environment; the home service mobile robot is taken for example; although it can build the map for the environment inside the house with SLAM, but people may move the position of the home appliance sometimes, so the mobile robot will recognize the wrong position through feature point matching whose data come from the laser sensor or the camera [7].

Based on the above comparisons, as well as considering the limited CPU and battery power for the mobile robot, the navigation algorithm in the indoor dynamic unknown environment should be improved.

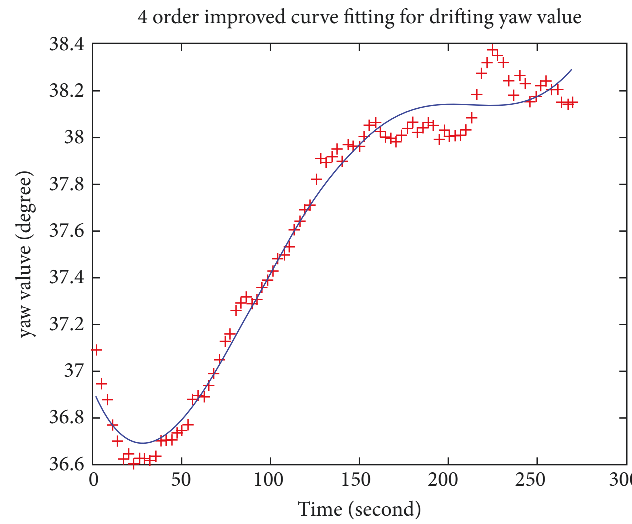

Figure 3: The 4-order improved curve fitting for the drifting yaw value.

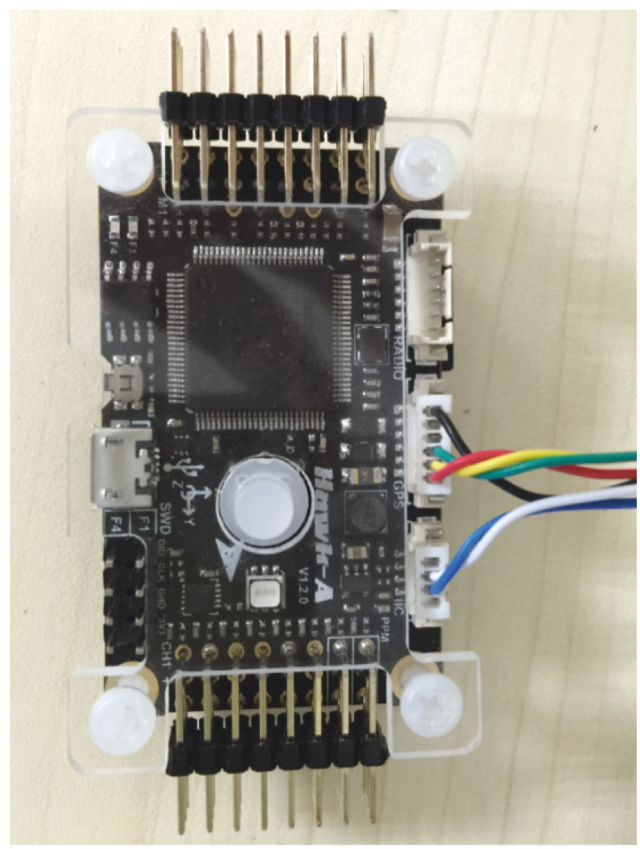

Figure 4: IMU sensor fusion module with GPS, gyroscope, electronic compass, magnetometer, and accelerometer.

2. Decision Tree Algorithm for the Yaw Value from IMU Sensor Fusion Module and Odometer

2.1. Yaw Value from IMU Sensor Fusion Module in the Indoor Environment. In the navigation process of the mobile robot,

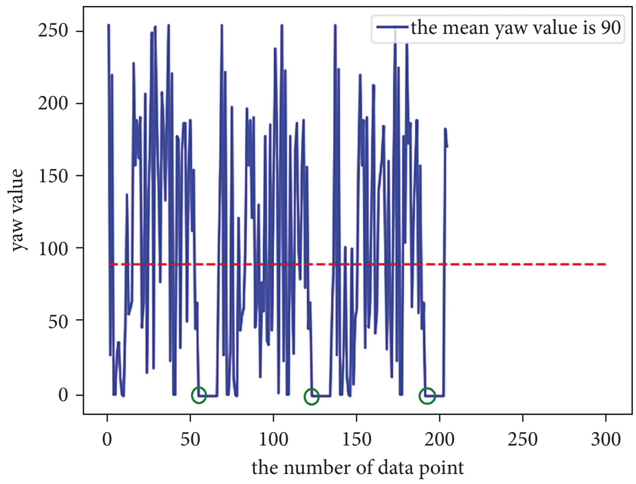

Figure 5: The output yaw value from multi-IMU sensor fusion module.

it is necessary to get the accurate current orientation of the mobile robot in every second, which can be obtained from gyroscope shown in Figure 1.

The output data of the gyroscope will be unavailable in the indoor environment; for example, when the mobile robot stops rotating and keeps static in the indoor environment, after the PID processing for gyroscope, the yaw value is collected and marked with the red cross as shown in Figure 2. It is obvious that the yaw value is still drifting and gradually maintains stability after 300 seconds (5 minutes); the blue line in Figure 2 shows the curve fitting for the yaw value during 300 seconds; the 1–7-order curve fitting is not perfect, but the 8 order can fit the curve more accurately as shown in Figure 2; the fitting function is

$$\begin{aligned} y = {} & 0.00000000000003 \times x^8 - 0.000000000000086 \times x^7 \\ & + 0.000000000049473 \times x^6 \\ & - 0.000000015493482 \times x^5 + 0.000002873185886 \times x^4 \\ & + 0.021422402741956 \times x^2 - 0.761774606869785 \times x \\ & + 47.571395698231385. \end{aligned} \tag{1}$$

Formula (1) is too complex and contains lots of double float data calculations which will consume lots of CPU resources and battery power, from the observation of Figure 2, that the data often drift dramatically in the first 30 seconds, which makes the curve complex and brings in lots of high-order term; if the data in the first 30 seconds can be deleted, it will simplify the curve fitting and polynomial formulas, compared with the other groups test data of yaw value; it is summarized that the yaw value will always drop 10%–20% in the first 30 seconds; the yaw value data at 30th second are often 80–90% of the initial yaw value, so it is often 85% of the initial yaw value for average.

Figure 3 shows the fourth-order improved curve fitting for drifting yaw value, and the yaw data in the first 30 seconds are deleted; the fitting formula is

$$\begin{aligned} y = {} & 0.000000003 \times x^4 - 0.000002660 \times x^3 + 0.000647 \times x^2 \\ & - 0.0514723 \times x + Y_i \times 0.85. \end{aligned} \tag{2}$$

It is clear that the 4-order curve fitting is more simple; if x has an assigned value as 270, the stable yaw value can be computed according to formula (2), but it is still not accurate because the yaw value comes from only one gyroscope in the indoor environment; if the cost of the device for the mobile robot is not considered, the multisensor fusion algorithm for GPS, gyroscope, electronic compass, magnetometer, and accelerometer is better than data processing for only one gyroscope as Figure 4 shows.

The multi-IMU sensor fusion module can be purchased on the market, which has downloaded the software of multi-IMU sensor fusion algorithm inside, so the output data of this module are more accurate [8]; when the mobile robot is rotating in the indoor environment and stops suddenly, the output yaw value is shown in Figure 5.

Figure 5 shows that the output yaw value is periodical which can be marked with green circle at the bottom of Figure 5; the baud rate is 115200; there are 90 data points in a period, and the output format is Byte, so the period is $10 * 90/115200 = 0.0078125$ second; in one period, the data still drift dramatically; it is needed to compute the mean yaw value in one period, which is 90 degree in Figure 5.

If the test is repeated for 10 times, when every time the mobile robot rotates and stops at a same direction, an object is placed to verify it is the same direction for 10 times' test, the result of 10 times test is shown in Figure 6.

From Figure 6, for the same direction in the indoor environment, the yaw value from one multi-IMU sensor fusion module is different every time and the range of value is between 87 to 94 in 10 times' test, so the yaw value from IMU sensors is not accurate in the indoor environment.

2.2. Odometer Data from the Processing of Adaptive FAST SLAM Algorithm. There is another method to obtain the yaw value, and the odometer can compute the yaw value [9]; generally, the reduction ratio of the gear motor is 1 : 50; the output pulses from the optical-electricity encoder is 500 when a DC motor rotate a circle; when gear motor connects to DC motor, the output pulse is 25000 when the wheel

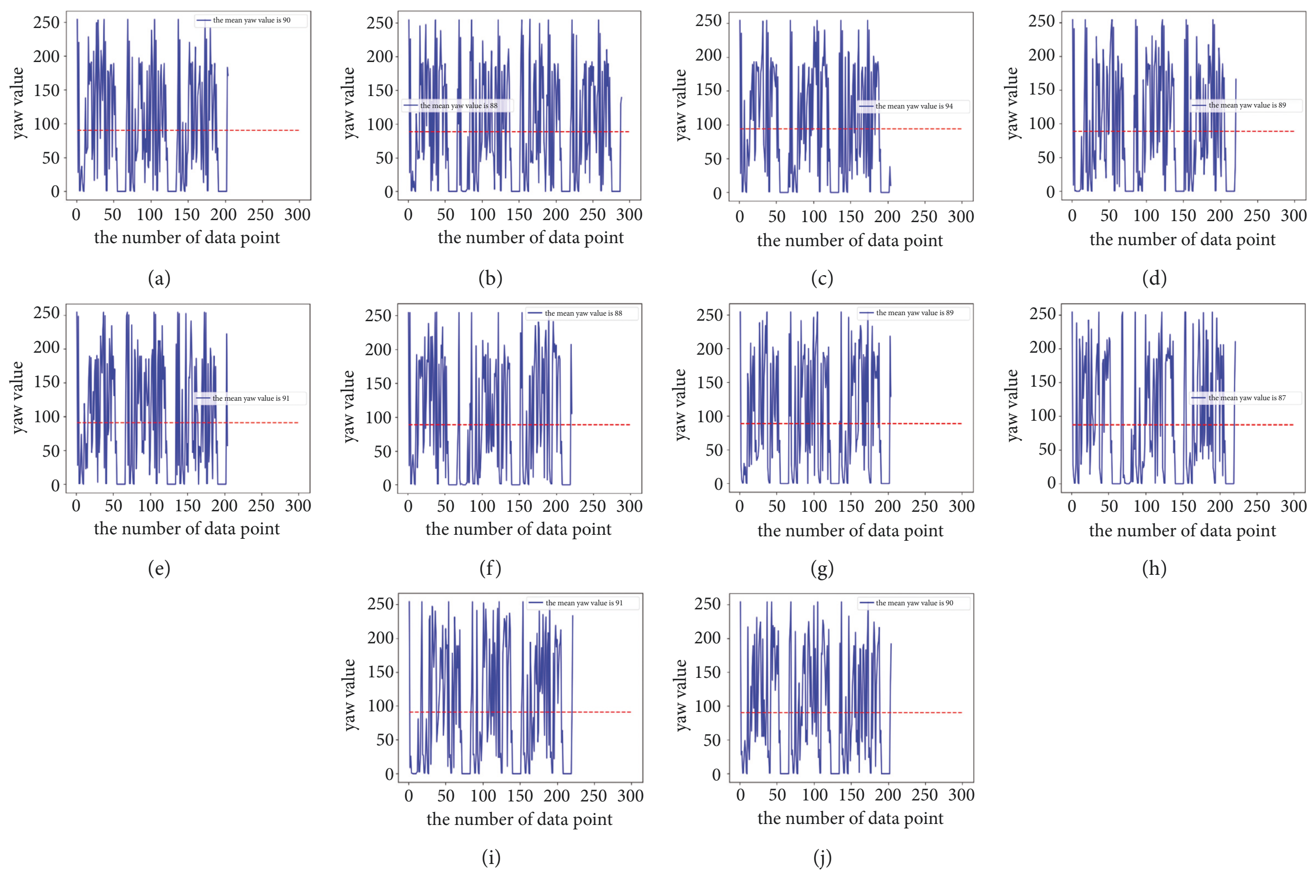

Figure 6: The 10 times' test of the output yaw value from multi-IMU sensor fusion module.

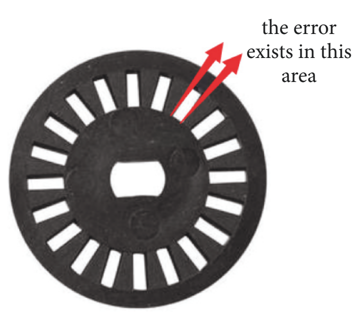

Figure 7: The error exists in each gap of grid of the optical-electricity encoder.

rotates in a circle; although the yaw value can reach a high accuracy when there is 25 KHz pulse outputted, there is still some error exists as shown in Figure 7.

The error is about 360/25000 = 0.0144 degree for a grid of optical-electricity encoder; when the mobile robot moves for a long time, the error will be accumulated to a large value; at the same time, ground friction is another source of error, especially when the mobile robot collides with a heavy obstacle and the wheel is slipping in the dynamic environment; in this status, the optical-electricity encoder is still computing, but the yaw value does not change; usually, the sensor error and observation error all can be accumulated, which is accumulated error. Because the true yaw value can

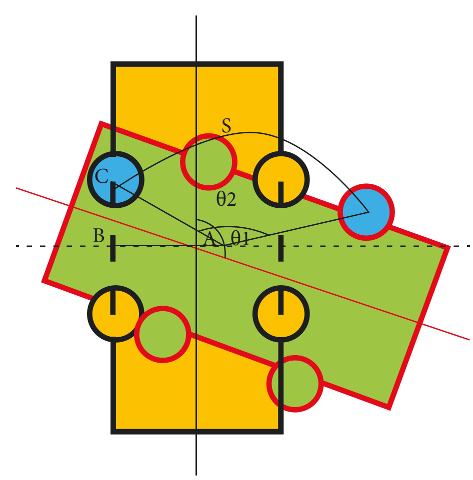

Figure 8: The yaw value of the mobile robot from the odometer.

be measured from round circle ruler in the indoor environment, so the accumulated error can be computed.

If the accumulated error is $v(k)$, the diameter of wheel is D, and the pulse from optical-electricity encoder is P, through analyzing the status of the mobile robot in Figures 8 and 9, the systematic observation model can be obtained from

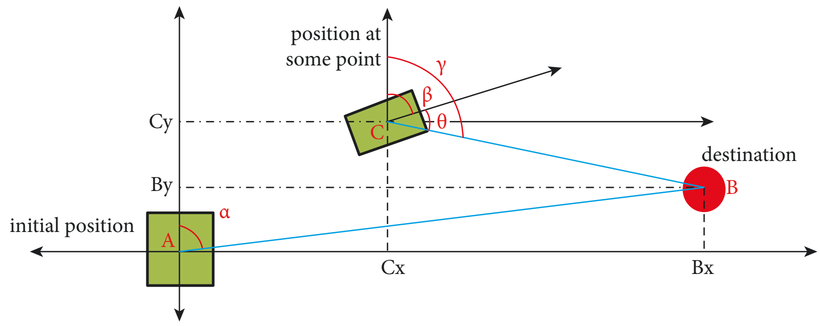

Figure 9: The simulation of the mobile robot moves in the indoor environment.

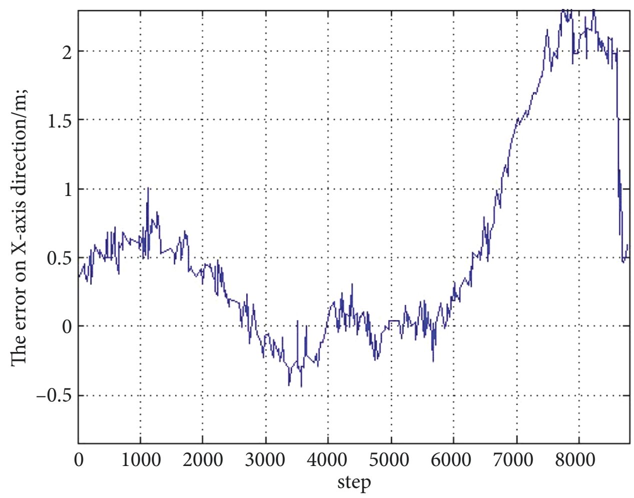

Figure 10: The error of EKF algorithm for the yaw value.

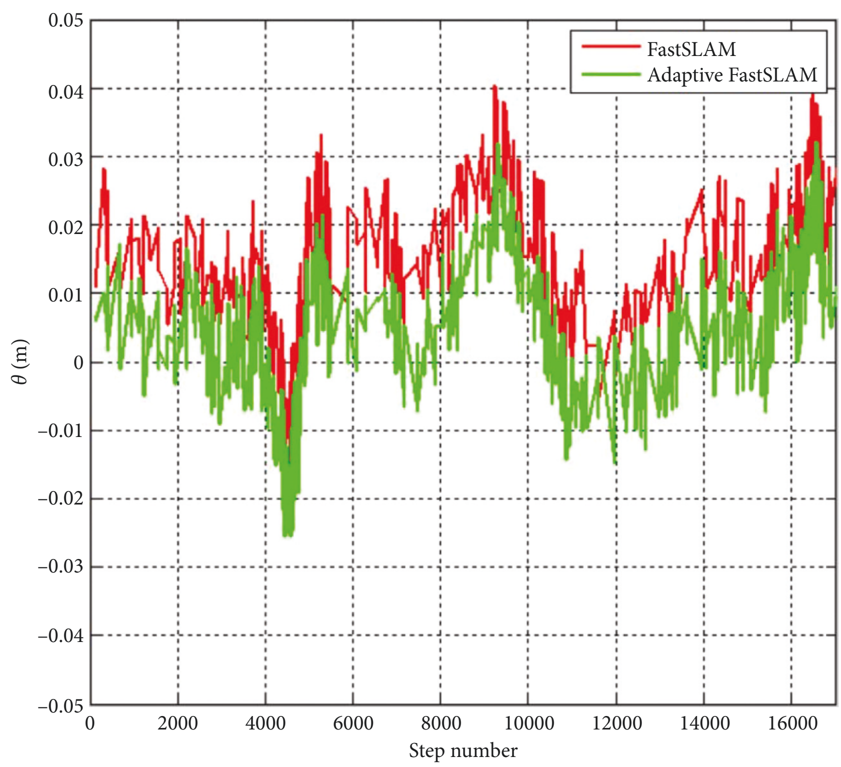

Figure 11: The comparison of yaw value error between Fast SLAM and Adaptive Fast SLAM.

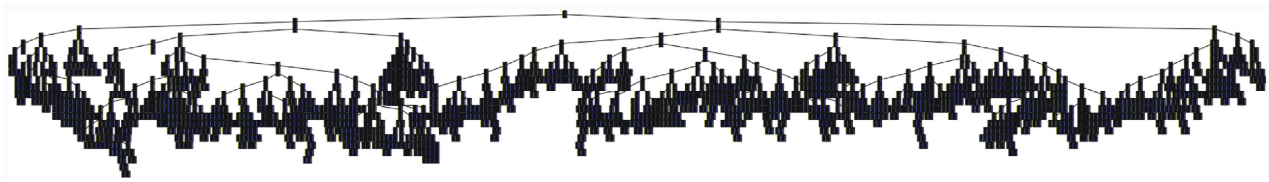

Figure 12: The 360 classifications of the decision tree.

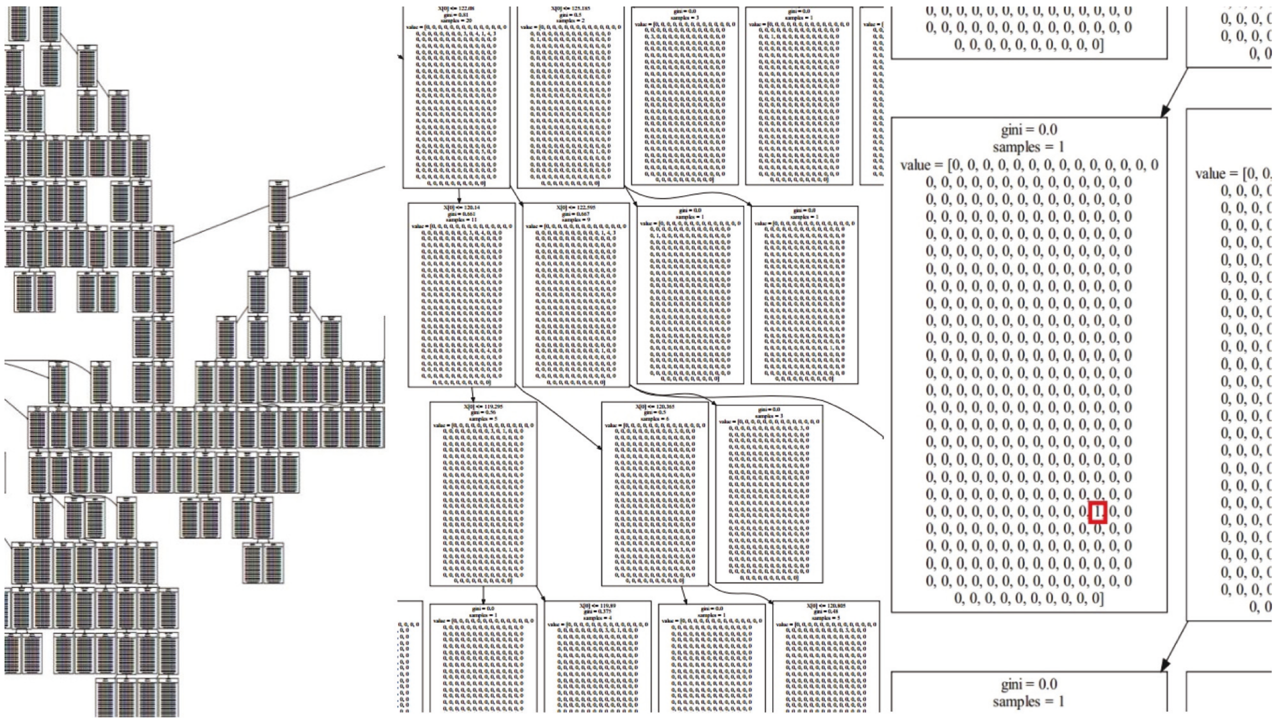

Figure 13: The detailed information of the decision tree.

$$Z(k) = \begin{bmatrix} \dfrac{r(k)}{\phi(k)} \end{bmatrix} + v(k) = \begin{bmatrix} \dfrac{BC}{\gamma - \beta} \end{bmatrix} + v(k) = \begin{bmatrix} \dfrac{\left((Bx - Cx)^2 + (By - Cy)^2\right)^{1/2}}{\tan^{-1}\left(\left(C_y - B_y\right)/\left(C_x - B_x\right)\right) + \pi/2 -} \\ \sum_{i=0}^{k} D \times P \times t_i / F \times \sqrt{AB^2 + BC^2} \end{bmatrix} + v(k). \quad (3)$$

The state estimation of the mobile robot is analyzed to get the method to eliminate the accumulated error; the purpose is to obtain the maximum probability of the state of the mobile robot:

$$\hat{x} = \arg \max_{x} p(x|v, y). \quad (4)$$

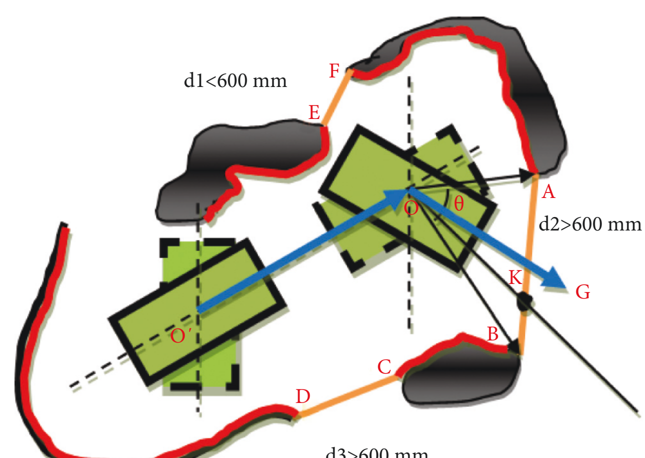

Figure 14: The movement of the mobile robot in the dynamic unknown environment.

Formula (4) can be decomposed by Bayes formulas, so the probability of pose under the condition of obtaining sensor value and observation value can be decomposed as the following formula:

Table 1: The relationship between angle of destination and turning direction.

The angle of destination compared the current orientation	Turning direction
If stop_forward = 0 and angle of destination is between 340° ~ 20°	Forward
If stop_forward > 0 and angle of destination is between 340° ~ 20°	Right
If angle of destination is between 20° ~ "160°"	Right
If stop_forward = 0 and angle of destination is between 160° ~ 200°	Backward
If stop_forward > 0 and angle of destination is between 160° ~ 200°	Right
If angle of destination is between 200° ~ "340°"	Left

$$\hat{x} = \arg \max_{x} \prod_{k=0}^{K} p(y_k|x_k) \cdot \left(p(x_0|\check{x}_0) \prod_{k=0}^{K} p(x_k|x_{k-1}, v_k) \right). \tag{5}$$

Usually, the distribution of the probability of the input value and observed value obeys Gauss distribution; in order to simplify the expression and computation, the maximum likelihood estimation is computed; for example, prior probability before the observation in each step can be expressed as the following:

$$\ln p(x_k|x_{k-1}, v_k) = -\frac{1}{2}(x_k - A_{k-1}x_{k-1} - v_k)^T Q_k^{-1}(x_k - A_{k-1}x_{k-1} - v_k) - \frac{1}{2}\ln\left((2\pi)^M \det Q_k\right)^T, \tag{6}$$

where Q_k is the noise in the moving process and A_{k-1} is the transfer matrix at time k-1 because the first part of the formula (6) is relative to the states x, which can be expressed as

$$J_{(v,k)}(x) = -\frac{1}{2}(x_k - A_{k-1}x_{k-1} - v_k)^T Q_k^{-1}(x_k - A_{k-1}x_{k-1} - v_k), \tag{7}$$

where $J_{(v,k)}(x)$ stands for the error from the real value to the estimated value, so it is necessary to get the minimum value of $J_{(v,k)}(x)$ as follows:

$$\frac{\partial J_{(v,k)}(x)}{\partial x^T} = 0, \tag{8}$$

where it means that when $J_{(v,k)}(x)$ get the minimum value, x can get the suitable estimated value whose probability is the maximum value; in this way, the EKF function can be deduced.

From Figure 10, it is obvious that, after the processing of EKF algorithm, the error of the yaw value is still large. EKF algorithm only considers the linear system; for the assessment of the nonlinear system, EKF algorithm will not be effective because it ignores Taylor's high-order term, which makes the big error of the status assessment. Because the particle filter algorithm has no limit for the system noise, it is taken as the good solution for the nonlinear Gaussian system [10–12].

However, as the number of particles increases, the computational complexity will also increase. In addition, due to the sequential importance sampling particle filter, the samples with bigger weight are chosen for many times, resulting in a decline in the diversity of the particle collection of samples, and thus, there will be sample depletion problems [13–15].

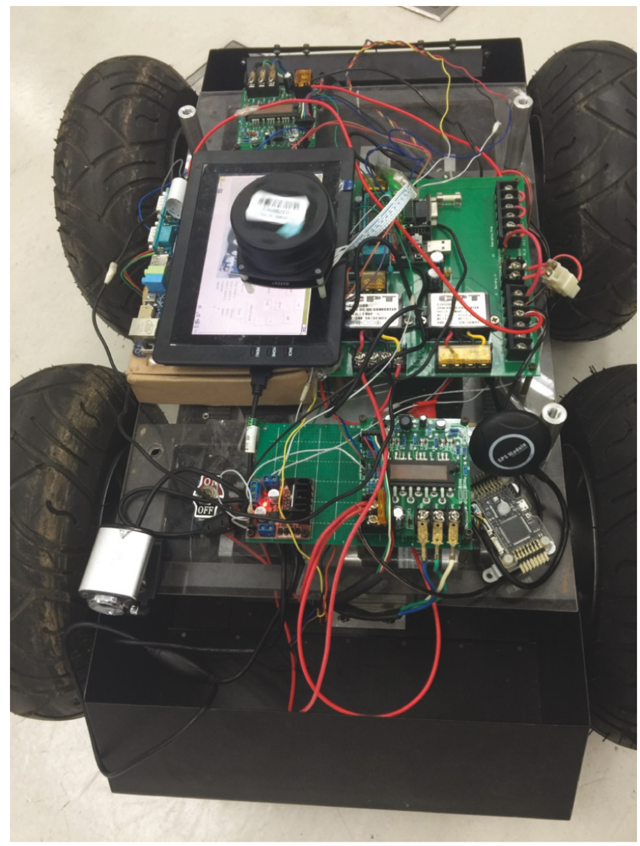

Figure 15: The designed mobile robot.

Fast SLAM is the universal SLAM technology, which can run the particle filter with few particles; similarly, low-dimensional KF is used to filter the surrounding features with known absolute position and consistency. Adaptive resampling algorithm can improve Fast SLAM algorithm; it sets the threshold number of resampling particles as 0.6 times of particles, which can take effective resampling operation by real time, computing effective particle number and particle degradation degree, to deal with the problem "sample degeneration" and "sample impoverishment" which is result in the frequent resampling [16].

The test between Fast SLAM and adaptive Fast SLAM is conducted on the mobile robot; in Figure 11, it is shown that when the mobile robot moves for a longer time, the yaw value error in adaptive FAST SLAM is much lower than it in FAST SLAM, so the yaw value which comes from odometer will be more accurate if they are processed by adaptive FAST SLAM [17].

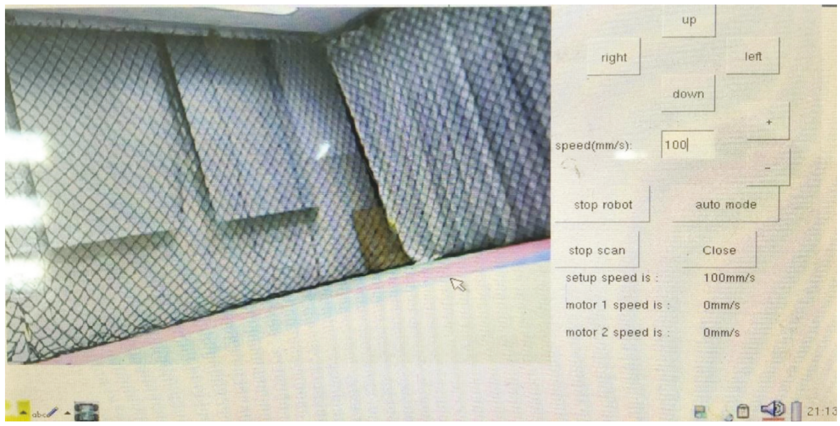

Figure 16: The LCD and touchscreen with camera video display in the embedded Linux system.

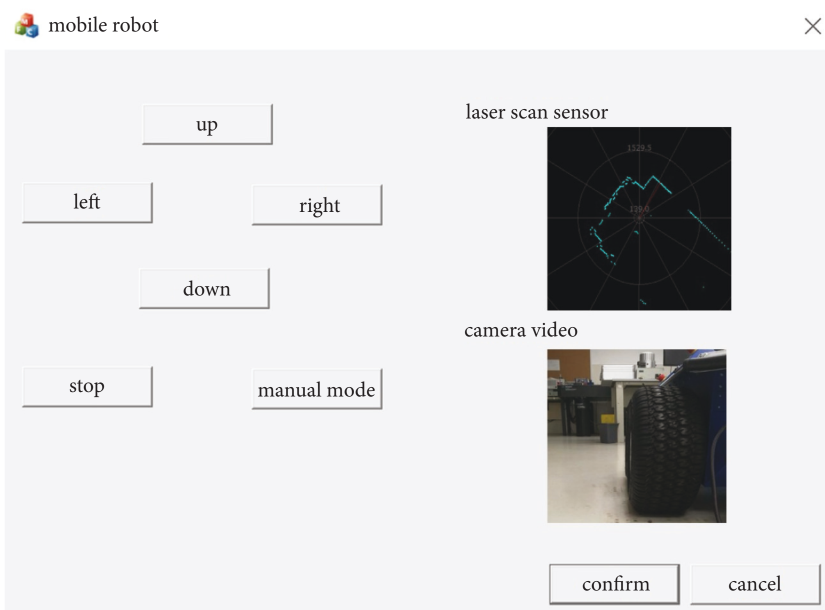

Figure 17: The software on the PC.

2.3. Decision Tree Algorithm. Lots of the data are obtained from the IMU sensor fusion module and the odometer every second, which can be analyzed through machine learning algorithms; considering the limited CPU and battery power of the mobile robot, the complex machine learning algorithms are not suitable for running on the mobile robot. For example, SVM algorithm can convert the data from low dimension to high dimension to classify the data into categories, but it will consume lots of hardware resource and take long time [18], so decision tree algorithm is suitable to run on the mobile robot to predict the yaw value every second because it runs fast and save CPU computation compared with the other machine learning algorithms.

Usually, decision tree algorithm can be used on the classification, but not prediction [19]; if the yaw value can be divided into 360 classifications, every classification stands for one degree; then, the classification can be converted into prediction.

The true yaw value can be measured by the round ruler, and there are only two attributes data, one is yaw value comes from the IMU sensor module and the other is the yaw value which comes from the odometer which is processed by adaptive FAST SLAM. The large number data can be divided into training set, test set, and validation set, with the K fold cross-validation method; then, the data can be trained to get a decision tree model [20]. It should be noted that the data should contain the yaw value when the mobile robot is in some special status, such as the wheel of the mobile robot slips when mobile robot collides with a heavy obstacle in the dynamic environment, or the mobile robot in the dense cluster of buildings where the Earth magnetic field is very weak and the outputted data from IMU sensor fusion module are vibrating dramatically; in this way, the overfitting ability of the model will be intensified.

In Figure 12, the yaw value can be classified into 360 classifications through the processing of decision tree algorithm, and each classification stands for the predicted yaw value in each second for the mobile robot; if Figure 12 is zoomed larger, some details can be visualized as shown in Figure 13.

In Figure 13, the each classification is distributed on the end point of the tree, the value in each end point is a matrix that contains 360 integers, in which one is 1 and others are 0, the position of integer 1 in the matrix stands for the corresponding yaw value. The outputted accuracy of the yaw value from the decision tree can reach 99%; it is very near the true yaw value which is measured by the round ruler, which provides a method to predict the true yaw value of the mobile robot in the indoor environment.

After the accurate yaw value is obtained in the indoor dynamic environment, the following is to judge the next step movement when mobile robot is in the dynamic unknown environment, as shown in Figure 14; the black object in Figure 14 is the dynamic moving object; the red line is the scanned environment from the laser scanning sensor. If the length of the mobile robot is 600 mm, it will go from the gap between moving objects whose length is larger than 600 mm while whose orientation is most near the angle of the destination. The distance and angle of the obstacles can be obtained from the laser scanning sensor, the location of the mobile robot can be computed from the odometer through adaptive FAST SLAM algorithm, and the orientation of the mobile robot can be computed through the decision tree algorithm. If there is an object appearing in the “320°” ~“40°” of the mobile robot, the mobile robot will stop move forward and start rotate left or right to move bypass the object; in this situation, the bit stop_forware is 1, else it is 0; based on the above analysis, the next step movement can be judged according to Table 1.

According to the above analysis, the mobile robot can move to the destination without colliding with moving obstacles in the indoor dynamic unknown environment.

3. Experiment

A mobile robot is designed by us; the CPU is S5PV210 CPU with ARM structure and OS is embedded Linux system, which is shown in Figure 15. On each side of the mobile robot, the belt connects 2 wheels that are driven by the DC motor and 1 : 50 reduction ratio gear motor, so the mobile robot can bear heavy object on it.

For hardware of the mobile robot, the first is the main board with “S5PV210” CPU and various connectors, which connecting the following IMU sensor fusion module, USB camera, LCD display, and touch screen operation, Serial port to Bluetooth module, USB to wifi module, and laser scan sensor. The second is the MCU board; it can send the speed of the motors to the serial port of mainboard and can receive the motor control command from the mainboard through the designed protocol. Because the Linux system is not the real-time operating system, the ARM board cannot read the high frequent pulse accurately, so the MCU board takes the task to read the 25 KHz motor speed pulse. The third part is the power board with SCM6716 chipset to supply the large current and power, and the peak current can reach 1.8 A, which is assurance that the mobile robot can carry the heavy objects.

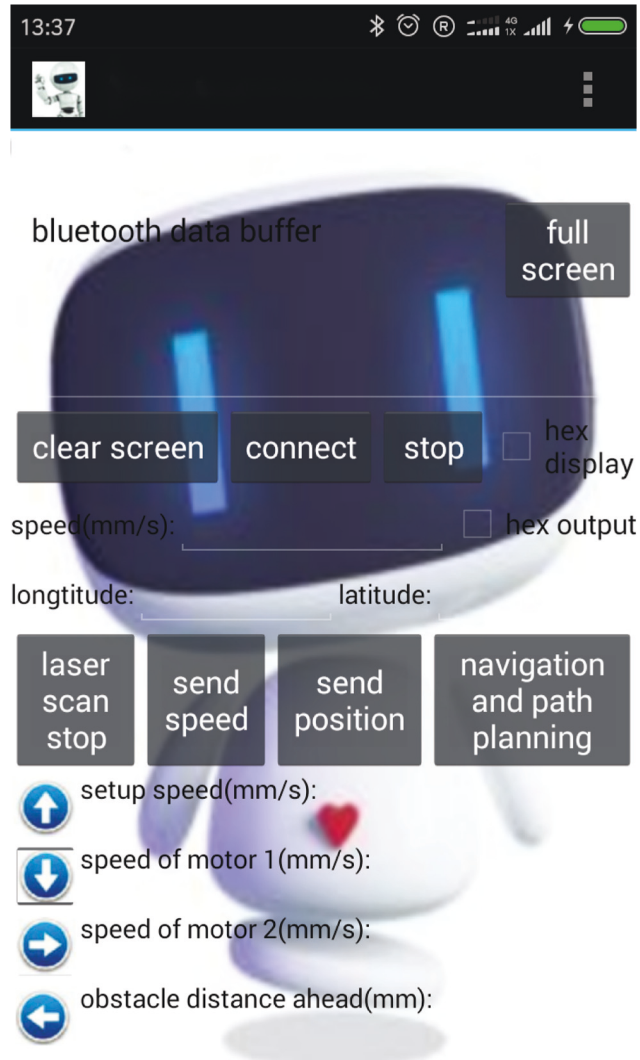

Figure 18: Android APP.

Various widgets on the LCD is designed with the embedded QT in the embedded Linux system, which is shown in Figure 16; through the signal and slot principle of QT, it can fulfill the LCD and touch screen functions. The software on the PC is designed to control the mobile robot and also to show the camera video and laser scanning environment, as shown in Figure 17. The Android APP is designed to communicate with the mainboard with Bluetooth protocol, which can send the value and command of the mobile robot to the Serial-Bluetooth module on the mainboard, as shown in Figure 18. The mjpeg-streamer is a universal tool for the remote monitoring in the B/S structure through the TCP/IP protocol, which can run on the mobile robot in the embedded Linux system; the camera video can be shown on Firefox browser in the Windows system with mjpeg-streamer as shown in Figure 19.

The map of the laboratory environment is not stored in the mobile robot; in order to test the navigation algorithm in the real world environment, the mobile robot is running in our laboratory environment which is the indoor dynamic

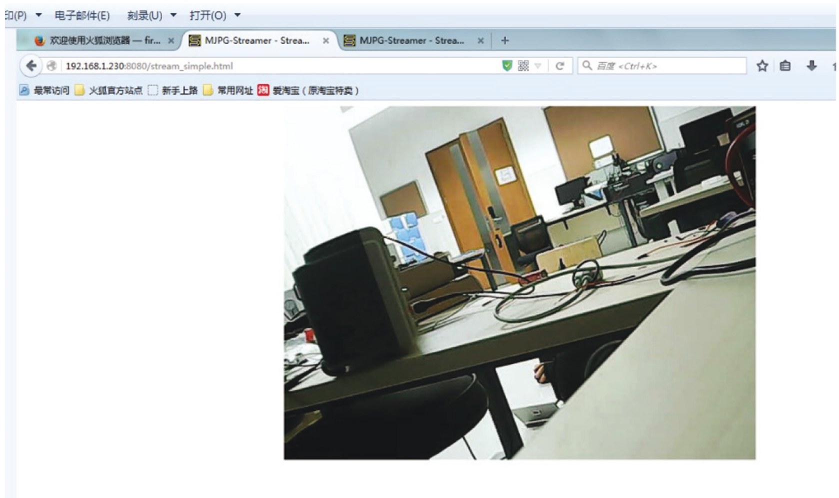

Figure 19: Remote monitoring on Firefox browser.

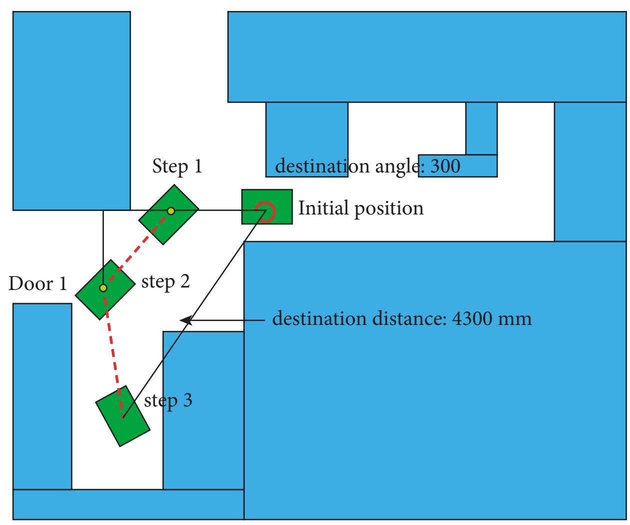

Figure 20: Navigation test of the mobile robot in the laboratory environment.

Figure 21: The navigation test on the designed mobile robot in the laboratory environment.

unknown environment just as shown in Figures 20 and 21; compared with initial position, the angle of destination is 300° and the distance of destination is 4300 mm which can be inputted in the Android APP; the orientation of the mobile robot can be computed according to the decision tree algorithm; the turning direction is judged according to Table 1 in every second; the angle of destination and distance is calculated and updated again in every second; finally, it can move to the destination without colliding with the obstacles on the path.

4. Conclusion

The testing result shows the proposed navigation algorithm is effective and real time responding in the indoor dynamic unknown environment. Compared with other algorithms, the mobile robot can obtain the accurate orientation through the decision tree algorithm in the indoor environment; it can obtain its location through the odometer data which are processed by adaptive FAST SLAM algorithm in the dynamic and unknown environment; it can scan the distance and angle of moving obstacles through the outputted data from the laser scanning sensor, which provide the data to judge the next step movement as shown in Table 1 in the dynamic and unknown environment.

There are some challenges in the navigation algorithm and realization of the mobile robot; one challenge is how to obtain the accurate orientation of the mobile robot in the indoor environment; through the decision tree algorithm, the predicted yaw value is much accurate especially when there is serious slipping of the wheels. The other challenge is that how to make the synchronization of the two threads; there is always errors when reading the outputted data from IMU sensor fusion module; finally, the problem detected that another thread is processing this data while this thread is reading this data; after adding the mutex lock on two threads, the none synchronous problem of two threads is solved and the reading and processing of the data from IMU sensor fusion module becomes normal.

The advantage of the proposed navigation algorithm is that it can be applied in the indoor dynamic unknown environment where there is the working environment for the home service robot; especially, this algorithm can save lots of CPU computation and battery power for the mobile robot which runs on the embedded platform. The next step work is to design and apply the deep learning algorithm on the mobile robot, which can recognize the human face and the appearance of home appliances, making the home service robot more stable and intelligent.

Data Availability

The data used to support the findings of this study are available from the corresponding author upon request.

Conflicts of Interest

The authors declare that they have no conflicts of interest.

Acknowledgments

Featured Innovation Project of Guangdong Province in 2018 (2018GKTSCX056). Key Project of Guangdong Provincial Department of Education in 2019 (2019GZDXM014). The research project of Zhuhai City Polytechnic College in 2021 (KY2021Y01Z). Project of Ministry of Education of Higher Education in 2020 (2020ITA03008).

References

[1] R. Cui, Y. Li, and W. Yan, "Mutual information-based multi-AUV path planning for scalar field sampling using multidimensional RRT," *IEEE Transactions on Systems, Man, and Cybernetics: Systems*, vol. 46, no. 7, pp. 993–1004, 2016.

[2] Y. Wang, P He, P. Shi, and H. Zhang, "Fault detection for systems with model uncertainty and disturbance via coprime factorization and gap metric," *IEEE Transactions on Cybernetics*, vol. 2, no. 8, pp. 1–11, 2021.

[3] P. He, "Consensus of uncertain parabolic PDE agents via adaptive unit-vector control scheme," *IET Control Theory & Applications*, vol. 12, no. 18, pp. 2488–2494, 2018.

[4] Y. Li and Y. Liu, "Real-time tip-over prevention and path following control for redundant nonholonomic mobile modular manipulators via fuzzy and neural-fuzzy approaches," *Journal of Dynamic Systems, Measurement, and Control*, vol. 128, no. 4, pp. 753–764, 2006.

[5] Y. P. Yan and S. F. Wong, "A Navigation Algorithm of the Mobile Robot in the Indoor and Dynamic Environment Based on the PF-SLAM Algorithm," *Cluster Computing*, vol. 22, pp. 1–12.

[6] Y. P. Yan and Y. M. Li, "Mobile robot autonomous path planning based on fuzzy logic and filter smoothing in dynamic environment," in *Proceedings of the 12th World Congress on Intelligent Control and Automation*, pp. 1479–1484, Guilin, China, June 2016.

[7] P. He, Y. Li, and J. H. Park, "Noise tolerance leader-following of high-order nonlinear dynamical multi-agent systems with switching topology and communication delay," *Journal of the Franklin Institute*, vol. 353, no. 1, pp. 108–143, 2016.

[8] Y. G. Yue and P. He, "A comprehensive survey on the reliability of mobile wireless sensor networks: taxonomy, challenges, and future directions," *Information Fusion*, vol. 44, pp. 188–204, 2018.

[9] Y. M. Li and Y. Liu, "Fuzzy logic self-motion planning and robust adaptive control for tip-over avoidance of redundant mobile modular manipulators," in *Proceedings of the IEEE/ASME International Conference on Advanced Intelligent Mechatronics(AIM)*, pp. 1281–1286, Monterey, CA, U.S.A, July 2005.

[10] S. Zhu and L. Xia, "Human action recognition based on fusion features extraction of adaptive background subtraction and optical flow model," *Mathematical Problems in Engineering*, vol. 2015, pp. 1–11, Article ID 387464, 2015.

[11] Y. P. Yan and Y. M. Li, "Autonomous path planning and navigation of a mobile robot with multi-sensors based on fuzzy logic in dynamic environment," *International Journal of Intelligent Systems and Applications in Robotics*, vol. 7, no. 1, pp. 1–14, 2016.

[12] K. Zhao and Y. M. Li, "Path Planning in Large-Scale Indoor Environment Using RRT," in *Proceedings of the 32nd Chinese Control Conference (CCC)*, pp. 5993–5998, Xian, China, July 2013.

[13] T. Ohki, K. Nagatani, and K. Yoshida, "Local path planner for mobile robot in dynamic environment based on distance time transform method," *Advanced Robotics*, vol. 26, no. 14, pp. 1623–1647, 2012.

[14] E. Keshavarz and E. Khorram, "A fuzzy shortest path with the highest reliability," *Journal of Computational and Applied Mathematics*, vol. 230, no. 1, pp. 204–212, 2009.

[15] S. Zhu and L. Xia, "Pain expression recognition based on pLSA model," *The Scientific World Journal*, vol. 2014, pp. 1–8, Article ID 736106, 2014.

[16] Y. P. Yan and S. F. Wong, "A Navigation Algorithm for the Mobile Robot in the Indoor and Dynamic Environment Based on the Image Recognition Algorithm," *The Hong Kong Institution of Engineers*, vol. 2, no. 1, pp. 1–12, 2018.

[17] X. N Shen, Y. Guo, and W. L. Hu, "Mobile robot path planning based on multi-objective evolutionary programming," in *Proceedings of the 6th World Congress on Intelligent Control and Automation*, pp. 3114–3118, Dalian, China, June 2006.

[18] X. H. Liu and S. F. Wong, "Mechanism using taguchi-based differential evolution algorithm to optimize the bicycle industry in China," *Industrial Engineering & Management Systems*, vol. 17, no. 1, pp. 72–81, 2018.

[19] S. Zhu, "Automatic recognition of facial expression based on computer vision," *International Journal On Smart Sensing And Intelligent Systems*, vol. 8, no. 3, pp. 1464–1483, 2015.

[20] X. Chen and Y. Li, "Smooth path planning of a mobile robot using stochastic particle swarm optimization," in *Proceedings of the 2006 International Conference on Mechatronics and Automation*, pp. 1722–1727, Luoyang, China, June 2006.

Hindawi
Computational Intelligence and Neuroscience
Volume 2022, Article ID 5181899, 8 pages
https://doi.org/10.1155/2022/5181899

Research Article

Music Emotion Classification Method Based on Deep Learning and Improved Attention Mechanism

Xiaoguang Jia

School of Music, Baotou Teacheis' College, Inner Mongolia University of Science and Technology, Baotou, Inner Mongolia 014030, China

Correspondence should be addressed to Xiaoguang Jia; jiaxiaoguang@jou.edu.cn

Received 24 April 2022; Revised 20 May 2022; Accepted 3 June 2022; Published 20 June 2022

Academic Editor: Xin Ning

Since the existing music emotion classification researches focus on the single-modal analysis of audio or lyrics, the correlation among models are neglected, which lead to partial information loss. Therefore, a music emotion classification method based on deep learning and improved attention mechanism is proposed. First, the music lyrics features are extracted by Term Frequency-Inverse Document Frequency (TF-IDF) and Word2vec method, and the term frequency weight vector and word vector are obtained. Then, by using the feature extraction ability of Convolutional Neural Network (CNN) and the ability of Long Short-Term Memory (LSTM) network to process the serialized data, and integrating the matching attention mechanism, an emotion analysis model based on CNN-LSTM is constructed. Finally, the output results of the deep neural network and CNN-LSTM model are fused, and the emotion types are obtained by Softmax classifier. The experimental analysis based on the selected data sets shows that the average classification accuracy of the proposed method is 0.848, which is better than the other comparison methods, and the classification efficiency has been greatly improved.

1. Introduction

Due to the complexity of music duration and composition, the emotional features extracted from music show the characteristics of large quantity, multiple dimensions, and difficult to analyze [1]. The results of music emotion classification can be well applied to music recommendation function to reduce the disadvantages of collaborative filtering recommendation [2, 3]. At the same time, music can artistically express the emotional information contained therein, and listeners can also obtain emotional tendency through music audio and lyrics information [4]. Music emotion analysis can be well applied to the music recommendation function. Major online music applications have launched the music recommendation function to recommend suitable music and improve the user experience by analyzing the listening habits of different users [5, 6]. However, most of the applications recommend popular songs but ignore personalized works, which is difficult to meet the needs of listeners under different emotions. Therefore, the research on emotional classification of songs has a good application prospect [7].

Before the emergence of intelligent algorithms, the way of establishing classification labels mainly depended on manual work, and the songs with different music styles were established into corresponding song lists [8]. However, such methods are not only inefficient, but also have high requirements for manual experience, and the classification accuracy is also uneven [9, 10]. On the basis of manual classification, the traditional classification methods are gradually mature, which mainly include methods such as logistic regression, naive Bayes, random forest, and support vector machine [11]. For example, Rao Veeranki et al. [12] analyzed and compared the performances of four traditional methods in the process of music emotion classification: logical regression, naive Bayes, random forest, and support vector machine, and took the parameters such as mean, variance, kurtosis, and skewness as analysis indicators, which effectively improved the efficiency of music emotion classification [12]. However, the targeted feature extraction in mixed audio needs to be improved. Kumar and Vardhan [13] made full use of other emotional features according to the rule-based emotion classification algorithm, and obtained better classification accuracy by adding more words to the dictionary [13]. However, the granularity segmentation of music needs to be further improved. Tiple and Patwardhan [14] proposed a new emotion classification system through link preprocessing, feature extraction, and classification steps [14]. The proposed Spiking Neural Network (SNN) classifier based on gradient descent was used to process frames and extract the time, spectrum, and energy features related to music. Combined with the optimal weight value to reduce the training error, the gradient descent method was optimized. Chen and Li [15] proposed a multi-modal ensemble learning method based on stacking [15]. This method was different from the feature-level and decision-level fusion methods. However, this classification method is inefficient in the environment facing a large number of new music creation, and cannot flexibly meet the needs of category expansion in the later stage [16].

Nowadays, classification algorithms based on machine learning methods and deep neural network learning have carried out extensive research in the fields of audio, image and text, and achieved rich results [17, 18]. With the rise of artificial intelligence-related technologies, computers can realize complex emotion analysis and calculation, and automatically output emotion analysis results through algorithms. Scholars' researches on music emotion feature extraction and classification model are also gradually carried out. Hizlisoy et al. [19] proposed a music emotion recognition method based on CNN-LSTM [19]. The experimental evaluation on the constructed emotional music database effectively showed the good performance of the proposed method. However, this method ignores the timing features of audio itself. Sorussa et al. [20] proposed a digital music emotion classification system with different emotion categories, which used supervised machine learning technology to identify the acoustic features and create prediction models [20]. This method effectively improves the accuracy of the algorithm classification, but the efficiency of machine learning needs to be improved. Gan [21] proposed a recurrent neural network method with channel-attention mechanism to classify the music features [21]. The above machine learning methods have achieved good results in the field of music emotion classification, but in the process of dealing with lyrics and melody, the relationship between lyrics and melody emotions is separated in different ways, without considering the consistency of emotion between lyrics and melody [22], so there is room for further optimization of the detailed classification of music emotion.

Aiming at the problem that most existing classification methods are difficult to deal with multi-dimensional and complex music texts, a music emotion classification method based on deep learning and improved attention mechanism is proposed. Its innovations are summarized as follows:

(1) Aiming at the problem of high dimension and sparsity of word vector, the proposed method combines CNN and LSTM to construct emotion classification model, and integrates the matching attention mechanism to further improve the classification accuracy.

(2) In order to solve the problem of insufficient performance of single feature classification, the proposed method uses CNN-LSTM model and deep neural network to process word vector and word frequency weight vector, respectively, and carries out feature concatenation to ensure the reliability of emotion classification.

2. Lyrics Feature Extraction

2.1. TF-IDF Feature Extraction. Term Frequency-Inverse Document Frequency (TF-IDF) is a feature extraction method that represents the weights according to the frequency of word items in the text. TF-IDF can calculate the number of word occurrences by means of probability statistics, evaluate the proportion of word items in the text to determine the importance of the word, and use this to represent the emotional polarity of the lyric text. The more times an emotional representative word appears in a lyrics text, the higher the importance of the emotional word in the emotional classification evaluation. Integrating all word frequency information, the emotional tendency of the whole lyrics text can be evaluated [23].

TF is the word frequency of a word, indicating the number of times a word item appears in the text. TF is calculated as follows:

$$\mathrm{tf}(i, j) = \frac{n(i, j)}{\sum_k n(k, j)}, \tag{1}$$

where $n(i, j)$ represents the number of times that word w_i appears in document d_j, and its denominator represents the total number of words in the document.

IDF is the inverse text frequency. The fewer times the current text contains word items, the stronger the classification ability of the word items to the text. It can be obtained by dividing the total number of words in the data set by the number of samples containing word items and through logarithmic operation. IDF is calculated as follows:

$$\mathrm{idf}(i) = \log\frac{|D|}{\left\{j\colon t_i \in d_j\right\}}, \tag{2}$$

where |D| represents the number of all documents, and the denominator represents the number of documents containing the word w_i.

The TF-IDF calculation result is represented by the product of TF and IDF. If the current word item appears less in the current category and more in the overall sample, the larger the TF-IDF value, the higher the classification ability of the feature item. To sum up, the core of TF-IDF text feature extraction method is to remove the influence of common words and retain important features with text resolution.

TF-IDF is a simple and convenient text word frequency feature extraction method, but it also has some defects. The words in the text are regarded as independent feature items,

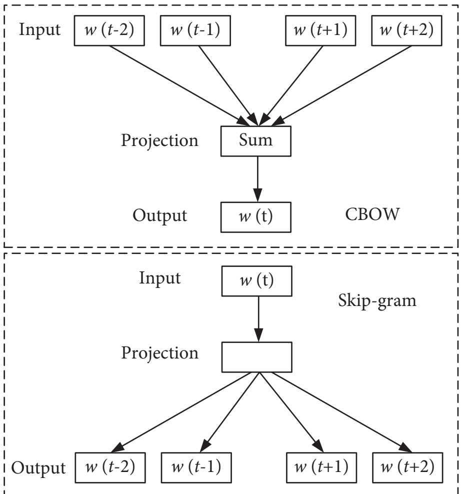

Figure 1: Word2vec training word vector model.

ignoring the relationship between words and ignoring the relationship between words and the whole article. This representation method has good statistical significance for local content, but ignores the integrity of the text, resulting in the loss of fine-grained emotional semantic content. For example, a certain emotion polar word only appears in the song lyrics text of this emotion, but less in other emotion types, which will lead to the error of emotion evaluation.

2.2. Word2vec Word Vector. Word2vec is a distributed text representation method, which maps each word item in the text to a word vector. Word2vec improves the shortcomings of the traditional deep learning word embedding model, with faster training speed and fewer vector dimensions. Word2vec usually includes two model structures: Continues Bag of Words (CBOW) and Skip-Gram, as shown in Figure 1.

The model includes input layer, projection layer, and output layer. In CBOW method, the surrounding words are used to predict the central word, so as to use the prediction results of the central word to represent the a priori probability; Skip-Gram uses the central word to predict the surrounding words, so as to predict the overall result and represent a posteriori probability. Therefore, CBOW will be faster than Skip-Gram in practical use. The parameter dimension of Word2vec-generated word vector is related to the number of hidden layer units in the network. The default value of the program is 100 dimensions.

Word2vec also has some defects: because words and vectors are one-to-one, the problem of polysemy cannot be solved; a static word vector representation, although it has strong universality, it cannot be dynamically optimized for specific tasks. For special text types such as lyrics, text information is different from evaluation text, which can be expressed directly through the emotion polar words. The implicit semantic expression in lyrics is often difficult to summarize emotion through separated word frequency information. The word vector method integrating context semantic information has better classification performance [24].

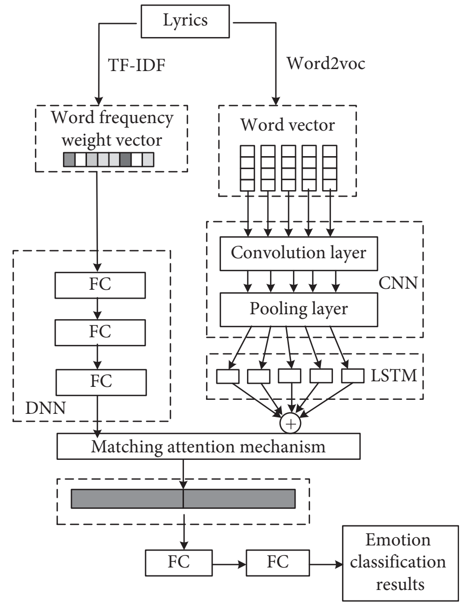

Figure 2: Emotion classification model of lyrics based on CNN-LSTM.

3. Proposed Lyrics Emotion Classification Model

3.1. Model Construction. After preprocessing the lyrics text, two emotion feature vectors, vector space model and distributed vector representation, can be extracted. Word2vec is extracted as word vector representation, which can be applied to deep learning methods, but it often has the characteristics of high dimension and sparsity. A single network model cannot deal with the features well. The architecture of CNN-LSTM not only has the advantage of CNN extracting local features, but also has the advantage of LSTM connecting the extracted features in sequences. Although TF-IDF representation method based on word frequency statistics has some defects in the semantic representation, it also has good distinguishing ability for text information with prominent keywords. In order to integrate the emotional feature representation of two kinds of text, a lyric emotion classification model based on CNN-LSTM is constructed. The model architecture is shown in Figure 2.

The proposed model is divided into two parts: word vector + CNN-LSTM and word frequency weight + Deep Neural Network (DNN). First, CNN is used to extract multiple sets of word vector features of the input text, and the extracted features are integrated into the input of LSTM neural network to output a new set of word vector feature representation. Then, the word bag model vector extracted by TF-IDF is processed by DNN. The features of the two categories are concatenated as the fusion representation of lyrics text, which is finally classified and output by Softmax to obtain the text emotion classification results.

The lyrics emotion classification model based on CNN-LSTM is similar to the audio emotion classification model in network structure. The inputs of the audio classification model are spectrogram and low-level descriptor features, respectively, while the inputs of the text classification model are word vector and word frequency weight vector, respectively [25]. The proposed model also has some performance differences when applied to audio features and text features. Because the audio feature dimension depends on the extracted spectrum description feature, the sequence length depends on the segmentation mode and frame interval of the original music; the text feature dimension depends on the distributed representation dimension set in the feature extraction stage, and the length of the text sequence is directly related to the number of word items. For the theme of song audio classification, CNN plays a leading role in the CNN-LSTM combined network. CNN is used to extract spectrum feature, which requires deeper convolution operation. The size of convolution kernel and stride will affect the classification performance. For the propose of lyrics text classification, the original serialized text feature word vector is difficult to train due to its high dimension and sparsity. CNN mainly provides feature compression ability. Bidirectional LSTM and matching attention mechanism have a greater impact on classification accuracy than convolution layer.

BiLSTM is a structure composed of forward LSTM and backward LSTM, which can well complete the extraction of data features. BiLSTM can well analyze bidirectional data information and provide more fine-grained calculation. The calculation process is as follows:

$$\begin{aligned}\overrightarrow{h}_t &= f\left(\overrightarrow{W}\cdot x_t + \overrightarrow{W}\cdot \overrightarrow{h}_{t-1} + \overrightarrow{b}\right),\\ \overleftarrow{h}_t &= f\left(\overleftarrow{W}\cdot x_t + \overleftarrow{W}\cdot \overleftarrow{h}_{t-1} + \overleftarrow{b}\right),\\ y_t &= g(U\cdot[\overleftarrow{h};\overrightarrow{h}] + c),\end{aligned} \tag{3}$$

where, one LSTM layer processes the sequence from left to right, and the other LSTM layer processes the sequence from right to left. $\overrightarrow{W}$ and $\overleftarrow{W}$ represent the network hidden layer parameters, x_t represents the input data, $\overleftarrow{h}_t$ and $\overrightarrow{h}_t$ represent the output results of the two LSTM layers at time t, $\overrightarrow{b}$ and $\overleftarrow{b}$ represent the offset value, and y_t represents the output of BiLSTM. The BiLSTM structure is shown in Figure 3.

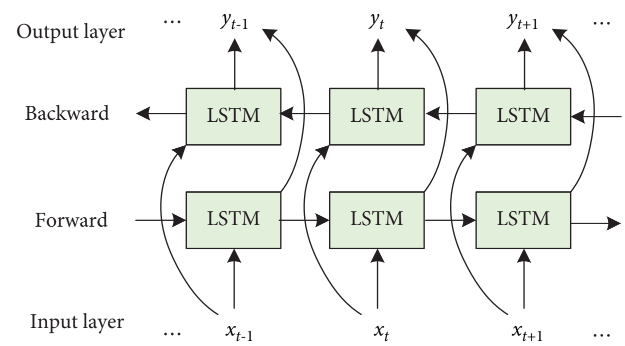

Figure 3: BiLSTM structure.

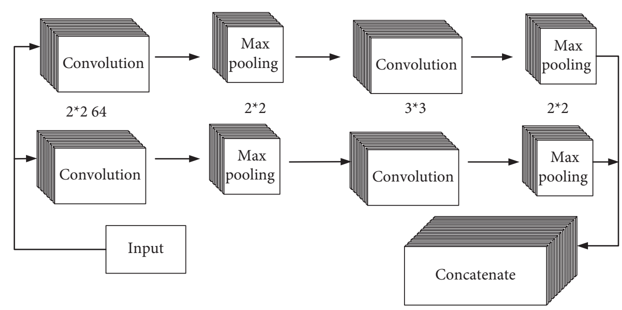

Figure 4: CNN model.

3.2. Model Description

3.2.1. Input Layer. The input of the model is audio feature data. The original music file is preprocessed, and the word vector and word frequency weight vector are obtained, respectively. The feature size of each spectrogram is normalized to $256\times256\times3$, where 256 is the width and height of the image, and 3 represents the number of channels (RGB) of the color spectrogram.

3.2.2. CNN Layer. The detailed view of the CNN layer model is shown in Figure 4. In the model implementation, CNN layer includes two convolution layers and two pooling layers. The input of first convolution is the word vector, the convolution operation is performed through 64 convolution kernels with size of 2×2 and step of 1, and Relu is used as the activation function [26].

The output vector size H of CNN depends on G (input size), κ (convolution kernel size), P (padding size), and τ (step size). The calculation is as follows:

$$H = \frac{(G-\kappa+2P)}{\tau+1}. \tag{4}$$

During the convolution feature extraction, first, use a single convolution kernel to calculate each local feature of the input. Then, concatenate the calculated features vertically, and finally perform nonlinear calculation on the concatenated features through the activation function to obtain the final convolution feature. The mathematical expression is as follows:

$$\begin{aligned}h_{1\kappa}(i) &= f\left(J_\kappa\cdot X(i\colon i+\kappa-1)+b\right),\\ h_{1\kappa} &= [h_{1\kappa}(1);h_{1\kappa}(2);\cdots;h_{1\kappa}(H);],\\ hr_{1\kappa} &= \mathrm{Relu}[h_{1\kappa}],\end{aligned} \tag{5}$$

where, J_κ represents the convolution kernel with height κ, H is the size of the output vector, $h_{1\kappa}(i)$ is the i-th local feature, $hr_{1\kappa}$ is the output c8onvolution feature, X is the input, and f is the tanh activation function.

3.2.3. LSTM Layer. In order to fuse different features to improve the classification accuracy, cascade is used to connect the merged results as the input of LSTM layer. The mathematical expression is as follows:

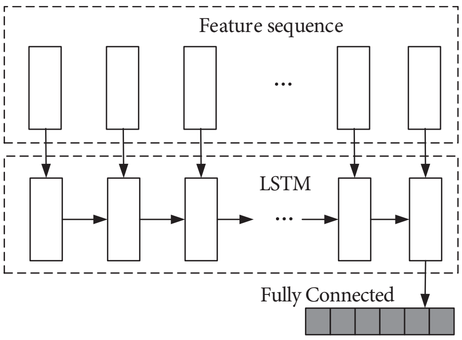

Figure 5: LSTM model.

$$\begin{aligned} hp_{1\kappa} &= \max[hr_{1\kappa}], \\ h_1 &= \varphi(hp_{1\kappa}, hp_{2\kappa}), \end{aligned} \tag{6}$$

where, $\mathrm{hp}_{1\kappa}$ is the result of pooling operation; φ is the merge connection function, and h_1 is the input of LSTM.

The word vectors generated from the sample set are further extracted by the CNN layer. Specifically, for the lyrics sample represented as $[v_{(1)}, v_{(2)}, \ldots, v_{(T)}]$, where T is the number of frames after lyrics segmentation. After passing through the CNN layer, a sequence vector $[c_{(1)}, c_{(2)}, \ldots, c_{(T)}]$ is obtained as the input of the LSTM layer. The detailed view of LSTM model is shown in Figure 5.

Input the vector output from the previous layer and selected by the feature into the bidirectional LSTM. The LSTM layer in the model has 128 units, and the output results can be expressed as $[l_{(1)}, l_{(2)}, \ldots, l_{(T)}]$.

3.2.4. Matching Attention Mechanism. For fine-grained emotion analysis, the ordinary attention mechanism cannot accurately extract the target words of fine-grained elements, resulting in the low accuracy of emotion analysis. Therefore, based on the original attention mechanism, a matching attention mechanism is built to improve this problem. The input of attention matching mechanism includes two parts. One part is the weighted word vector after the feature fusion of Word2vec word vector feature and TF-IDF feature based on word frequency statistics; the other part is the word vector generated after the fine-grained feature information in the data set is sent to Word2vec. First, these two parts of input are fed into the matching attention mechanism, and the context information and fine-grained element information q_s are captured at the same time. The calculation is as follows:

$$q_s = \mathrm{Average}\left(\frac{1}{m}\sum_{i=1}^{m} e_{a_i}, \frac{1}{n}\sum_{j=1}^{n} e_{\omega_j}\right), \tag{7}$$

where, Average represents the average value of the input vector, e_{a_i} is the word vector, e_{ω_j} is the weight word vector, and m and n are the numbers of word vectors and weight word vectors, respectively. In order to make the information of fine-grained elements meaningful, only the dimensions related to fine-grained elements will be retained in the Q_t, while other dimensions will be deleted. The calculation process is as follows:

$$Q_t = \omega_t \cdot q_s + b_t, \tag{8}$$

where Q_t is the weight vector of k fine-grained elements. It mainly looks for the dimensions related to fine-grained elements by looking at the words nearby in the word vector space. ω_t and b_t represents the weight matrix and offset vector, respectively. After the loss function is determined, the parameters in ω_t and b_t can be updated by gradient descent method. When the loss function converges, the optimal solution can be obtained. Then multiply Q_t by a randomly initialized matrix ψ to obtain the target word a_s matching the fine-grained elements identified by matching attention, which is expressed as follows:

$$a_s = \psi \cdot Q_t, \tag{9}$$

where, the dimension of ψ is $k \times d$. It can be updated by gradient descent method.

Finally, matching attention weight p_i is calculated according to a_s. The calculation is as follows:

$$p_i = \frac{\exp\left(\tanh\left(h_i^T \cdot \omega_0 \cdot a_s\right)\right)}{\sum_{j=1}^{n} \exp\left(\tanh\left(h_j^T \cdot \omega_0 \cdot a_s\right)\right)}, \tag{10}$$

where $\omega_0 \in \mathfrak{R}^{d\times d}$ is a trainable weight matrix, h is the output of LSTM hidden layer.

Finally, the weighted sum of the hidden vector h_i generated by the bidirectional LSTM and the matching attention weight p_i is used for the sentence representation Z_s of emotion classification, which is expressed as follows:

$$Z_s = \sum_{i=1}^{n} p_i h_i. \tag{11}$$

Take Z_s as the feature of the final emotion classification and put it into the fully connected layer for linear transformation, and Softmax classifier is used for emotion classification to obtain the final emotion ϕ. The mathematical expression is as follows:

$$\phi = \mathrm{softmax}\left(\omega_Z \cdot Z_s + b_Z\right). \tag{12}$$

3.2.5. DNN Layer. The input of DNN layer is the word frequency weight vector, which contains three hidden layers, also known as FC (fully connected layer). All nodes of FC in the network are connected with the nodes of the previous layer to achieve the purpose of integrating feature information and reducing dimension. The number of nodes of the three FCs in the model is 256, 128, and 64, respectively. The dimension of the input feature is further compressed after passing through the DNN layer.

3.2.6. Output Layer. The output layer consists of FC and Softmax. First, the output of word vector features through CNN layer, LSTM layer, and attention mechanism layer and the output of word frequency weight vector features through

DNN layer are concatenated as the final classification feature vector representation. Output classification is through FC and Softmax layers. The Softmax layer is a loss function, which is used to map the output to the probability interval to obtain the classification probability distribution, so as to output the classification results. The model is actually classified into four emotional categories: happy, sad, healing, and calm.

4. Experiments and Analysis

In order to build a parallel corpus of Chinese audio and lyrics, the data source is locked on the domestic music platform, and the data is collected based on the target of the task. In order to select the songs with higher quality, the songs with more credibility are selected, that is, the songs with a playback times of more than 2.5 million. In order to further carry out the task of music emotion classification, four kinds of emotion labels with happy, sad, healing, and calm were selected as candidates. A total of about 6000 music were collected. After further screening of song length, audio quality and language, 5286 music were finally retained as the candidate data set. On this data set, it is divided into two parts: training set and test set. The specific information of each data set is shown in Table 1.

In the experiment, the lyric text is preprocessed. First, the word segmentation is carried out to remove the invalid information related to music composition and stop words, and constructs a pure lyric text word item combination representation. Then, the text is transformed into a digital vector recognized by the computer through different feature extraction methods, and the feature dimension of the text vector is set to 100 dimensions. Finally, input them to the classifier to output the emotion classification results. The parameters of LSTM model are shown in Table 2.

4.1. Classification Accuracy of Different Text Features. The experiment adopts different word frequency weight vector feature extraction methods to verify the emotional classification performance of lyrics. First, the preprocessed text is represented by text vector through TF-IDF and Word2vec feature extraction methods, and then the same SVM classifier is used to output the emotion classification results. The classification accuracy of different text extraction methods is shown in Table 3.

As can be seen from Table 3, TF-IDF is completely based on the features of word frequency. When facing the sample data with implicit emotional semantics such as lyrics, the emotional classification performance is slightly insufficient, and the average classification accuracy is only 0.701. At the same time, the distributed word vector feature representation extracted by Word2vec tool has also achieved good accuracy in SVM classifier. The classification accuracy of happy emotion is as high as 0.801 and the average classification accuracy is 0.746. This distributed vector can be well used as the input of deep network method.

Table 1: The size of the data set and the number of songs contained in each type of emotion.

	Training set	Test set	Total
Happy	1078	194	1272
Sad	1267	317	1584
Calm	882	221	1103
Healing	1061	266	1327
Total	4288	998	5286

Table 2: Parameter setting of LSTM network model.

Parameter	Value
Loss function	Softmax
Optimizer	Adam
Learning rate	0.01
Activation function	Tanh
Dropout	0.03
Batch size	50
Epoch	30

Table 3: Classification accuracy results of different text features.

Text features	TF-IDF	Word2vec
Classification method	SVM	
Happy	0.762	0.801
Sad	0.735	0.779
Calm	0.647	0.698
Healing	0.661	0.703
Average	0.701	0.746

Table 4: Experimental results of three attention mechanisms.

Model	Classification accuracy
Traditional attention mechanism	0.753
Matching attention mechanism	0.826

4.2. Classification Accuracy of Different Attention Mechanisms. In order to study whether the matching attention mechanism can further improve the performance, it is compared with the traditional attention mechanism. The evaluation results of the joint training model on the selected data set are shown in Table 4, in which the average classification accuracy is used for performance evaluation.

It can be seen from Table 4 that the matching attention mechanism significantly improves the classification performance of the model, and its average classification accuracy is 0.826, which is 0.073 higher than that of the traditional attention mechanism. The traditional attention mechanism cannot accurately extract the target words of fine-grained elements, resulting in the low accuracy of emotion analysis. The matching attention mechanism can solve this problem, and greatly improve the classification accuracy combined with the context information.

4.3. Experimental Comparison and Analysis with Other Methods. In order to demonstrate the performance of the proposed method, it is experimentally analyzed with

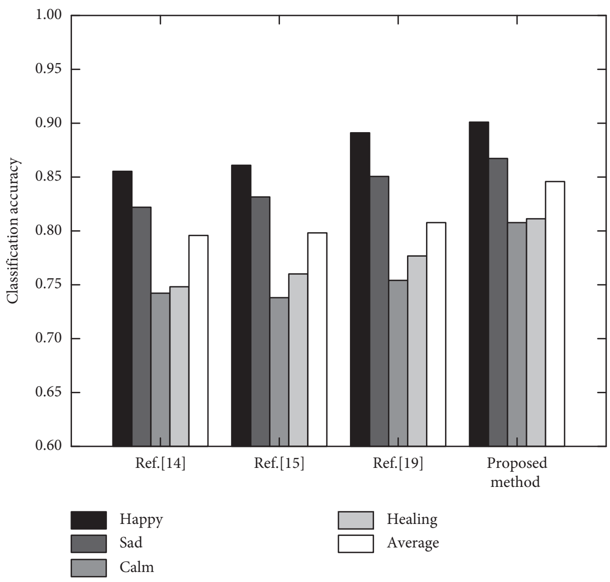

Figure 6: Classification accuracy of different methods.

Table 5: Classification results of different methods.

Method	Reference [14]	Reference [15]	Reference [19]	Proposed method
Happy	0.853	0.861	0.887	0.903
Sad	0.828	0.837	0.849	0.864
Calm	0.742	0.739	0.753	0.809
Healing	0.751	0.766	0.771	0.816
Average	0.794	0.801	0.815	0.848

Reference [14, 15, 19] on the selected data set. The classification accuracy of different emotions in lyrics is shown in Figure 6 and Table 5.

As can be seen from Figure 5 and Table 5, the proposed method combines the characteristics of CNN and LSTM, constructs an emotion analysis model based on CNN-LSTM, and combines DNN network learning to greatly improve the accuracy of music emotion classification, with an average classification accuracy of 0.848. The fusion processing of deep learning network improves the classification performance, especially integrates the matching attention mechanism, accurately extracts the target words of fine-grained elements, and significantly improves the classification accuracy of emotional types such as calm and healing, which are 0.056 and 0.045 higher than those in reference [19]. Reference [19] uses CNN-LSTM architecture to complete music emotion recognition. Although the average classification accuracy reaches 0.815, it is easy to confuse emotion types such as calm and healing, and the performance needs to be improved. Reference [14] classifies emotions based on gradient descent SNN classifier, and reference [15] classifies emotions based on stacking multi-modal ensemble learning method. Both of them are difficult to accurately distinguish massive and complex music types, and the average classification accuracy is about 0.800. In conclusion, the proposed method uses the comprehensive feature extraction ability of CNN and the ability of LSTM to process the serialized data to obtain better classification results, and has stable performance and high robustness under each subclassification.

5. Conclusion

Music contains rich human emotional information. The study of music emotional classification is helpful to organize and retrieve massive music data. Because of the large number and multiple dimensions of music, it is difficult and incomplete to extract emotional features. Therefore, a music emotion classification method based on deep learning and improved attention mechanism is proposed. The word frequency weight vector obtained based on TF-IDF is input into DNN for feature analysis, and the word vector obtained by Word2vec method is sent into the emotion analysis model based on CNN-LSTM. After the output of the two feature extraction channels are fused, the output layer outputs the emotion type. The experimental results based on the selected data set show that matching attention mechanism can more accurately extract the target words of fine-grained elements and improve the classification performance. Compared with the traditional attention mechanism, its average classification accuracy is improved by 0.073.

The processing of audio features in this paper is still a little rough. Only using the existing common features cannot fully reflect the relationship between music structured information and human emotion. Therefore, the feature extraction method with more music emotion classification ability can be further explored.

Data Availability

The data used to support the findings of this study are included within the article.

Conflicts of Interest

The author declares that there are no conflicts of interest regarding the publication of this paper.

References

[1] M. Z. I. Ahmed and N. Sinha, "EEG-based emotion classification using LSTM under new paradigm," *Biomedical Physics & Engineering Express*, vol. 7, no. 6, pp. 065018–065027, 2021.

[2] P. T. Krishnan, A. N. Joseph Raj, and V. Rajangam, "Correction to: emotion classification from speech signal based on empirical mode decomposition and non-linear features," *Complex & Intelligent Systems*, vol. 8, no. 1, 703 pages, 2021.

[3] J. S. Rahman, T. Gedeon, S. Caldwell, and R. Z. Jones, "Towards effective music therapy for mental health care using machine learning tools: human affective reasoning and music genres," *Journal of Artificial Intelligence and Soft Computing Research*, vol. 11, no. 1, pp. 5–20, 2021.

[4] K. Yang, C. Wang, Z. Sarsenbayeva et al., "Benchmarking commercial emotion detection systems using realistic distortions of facial image datasets," *The Visual Computer*, vol. 37, no. 6, pp. 1447–1466, 2020.

[5] R. J. R. Kumar, M. Sundaram, and N. Arumugam, "Facial emotion recognition using subband selective multilevel

stationary wavelet gradient transform and fuzzy support vector machine," *The Visual Computer*, vol. 37, no. 8, pp. 2315–2329, 2020.
[6] M. Khateeb, S. M. Anwar, and M. Alnowami, "Multi-domain feature fusion for emotion classification using DEAP d," *IEEE Access*, vol. 9, no. 6, pp. 12134–12142, 2021.
[7] Y. R. Pandeya and J. Lee, "Deep learning-based late fusion of multimodal information for emotion classification of music video," *Multimedia Tools and Applications*, vol. 80, no. 2, pp. 2887–2905, 2021.
[8] L. J. Zheng, J. Mountstephens, and J. Teo, "Four-class emotion classification in virtual reality using pupillometry," *Journal of Big Data*, vol. 7, no. 1, pp. 1–9, 2020.
[9] O. Akbulut, "Feature normalization effect in emotion classification based on EEG signals," *Sakarya University Journal of Science*, vol. 24, no. 1, pp. 60–66, 2020.
[10] K. Sui and K. Hyung-Gi, "Innovative methods in planning, design and lighting of music visual buildings in modern architectural," *Open House International*, vol. 44, no. 3, pp. 17–19, 2019.
[11] Q. Kong, Y. Cao, T. Iqbal, and Y Wang, "PANNs: large-scale p audio neural networks for audio pattern recognition," *IEEE/ACM Transactions on Audio, Speech, and Language Processing*, vol. 28, no. 6, pp. 2880–2894, 2020.
[12] Y. Rao Veeranki, N. Ganapathy, and R. Swaminathan, "Electrodermal activity based emotion recognition using time-frequency methods and machine learning algorithms," *Current Directions in Biomedical Engineering*, vol. 7, no. 2, pp. 863–866, 2021.
[13] P. Kumar and M. Vardhan, "PWEBSA: t," *International Journal of Information Technology*, vol. 14, no. 1, pp. 69–77, 2022.
[14] B. Tiple and M. Patwardhan, "Multi-label emotion recognition from Indian classical music using gradient descent SNN model," *Multimedia Tools and Applications*, vol. 81, no. 6, pp. 8853–8870, 2022.
[15] C. Chen and Q. Li, "A multimodal music emotion classification method based on m combined network classifier," *Mathematical Problems in Engineering*, vol. 3, no. 6, pp. 1–11, 2020.
[16] Y. Dong, X. Yang, X. Zhao, and J. Li, "Bidirectional convolutional recurrent sparse network (BCRSN): an efficient model for music emotion recognition," *IEEE Transactions on Multimedia*, vol. 21, no. 12, pp. 3150–3163, 2019.
[17] M. U. Salur and I. Aydin, "A novel hybrid deep learning model for sentiment classification," *IEEE Access*, vol. 8, no. 6, pp. 58080–58093, 2020.
[18] Q. Cheng, L. Gao, and A. Abdelmouty, *Journal of Maternal-Fetal and Neonatal Medicine*, vol. 39, no. 9, pp. 1–9, 2020.
[19] S. Hizlisoy, S. Yildirim, and Z. Tufekci, "Music emotion recognition using convolutional long short term memory deep neural networks," *Engineering Science and Technology, an International Journal*, vol. 24, no. 3, pp. 760–767, 2021.
[20] K. Sorussa, A. Choksuriwong, and M. Karnjanadecha, "Emotion classification system for digital music with a cascaded technique," *ECTI Transactions on Computer and Information Technology (ECTI-CIT)*, vol. 14, no. 1, pp. 53–66, 2020.
[21] J. Gan, "Music feature classification based on recurrent neural networks with channel attention mechanism," *Mobile Information Systems*, vol. 2021, no. 1, pp. 1–10, 2021.
[22] Y. Zhu, W. Zheng, and H. Tang, "Interactive dual attention network for text sentiment classification," *Computational Intelligence and Neuroscience*, vol. 2, no. 3, pp. 1–11, 2020.
[23] M. B. Dastgheib, S. Koleini, and F. Rasti, "The application of deep learning in Persian documents sentiment analysis," *International Journal of Integrated Supply Management*, vol. 18, no. 1, pp. 1–15, 2020.
[24] W. Li, F. Qi, M. Tang, and Z. Yu, "Bidirectional LSTM with self-attention mechanism and multi-channel features for sentiment classification," *Neurocomputing*, vol. 387, no. 6, pp. 63–77, 2020.
[25] H. T. Nguyen and L. M. Nguyen, "ILWAANet: an Interactive Lexicon-Aware Word-Aspect Attention Network for aspect-level sentiment classification on social networking," *Expert Systems with Applications*, vol. 146, no. 5, pp. 113065.1–113065.11, 2020.
[26] S. Feng, K. Song, D. Wang, and W. Y. Gao, "InterSentiment: combining deep neural models on interaction and sentiment for review rating prediction," *International Journal of Machine Learning and Cybernetics*, vol. 12, no. 2, pp. 477–488, 2021.

Hindawi
Computational Intelligence and Neuroscience
Volume 2022, Article ID 2419175, 9 pages
https://doi.org/10.1155/2022/2419175

Research Article

Analysis of the Style Characteristics of National Dance Based on 3D Reconstruction

Dongqi Zhang

Yangtze University, Jingzhou 434020, China

Correspondence should be addressed to Dongqi Zhang; 13593848251@163.com

Received 11 April 2022; Revised 3 May 2022; Accepted 4 May 2022; Published 20 June 2022

Academic Editor: Xin Ning

National dance is an important symbol of national spiritual culture, as it embodies each nation's unique history, living habits, ideology, and culture. Many Chinese ethnic groups have developed their own dance forms and styles, each with their own set of charms. Strengthening our understanding of its style and characteristics is critical to our understanding of the national dance. To begin with, this paper proposes a patch-based multiview stereo reconstruction scheme that can accurately reconstruct 3D character models. The movement capture system then collects national dance movement data and uses them to drive a three-dimensional character model that generates dance visual animation. In the human skeleton model, a spatial-temporal HMM (hidden Markov model) is proposed that not only studies the temporal information of human movements but also the spatial information of adjacent connection points. The recognition rate of this algorithm increases to 95.68 percent when the number of setting points is increased to ten and to 98.28 percent when the number of setting points is increased to twenty, according to the research. The experimental results show that the 3D reconstruction model of ethnic dance developed in this paper is capable of meeting the goal of ethnic dance digitalization while being simple to use, being low in cost, and with a good display effect.

1. Introduction

Three factors make up the essence of dance style: formal characteristics, thoughts, and images of dance works. They are concerned not only with the expression of the external form of dance works but also with the transmission of spiritual ideas. Many factors influence the formation and development of a dance style, including the social environment, history, and culture, as well as the personal preferences and aesthetics of the dancers. The styles and characteristics of different national dances are obviously different, influenced by regional, national psychology, culture, and other factors. People will gain a better understanding of ethnic dance style characteristics by comparing the style characteristics of different ethnic dances. National dancers use special costumes or auxiliary props such as a stage to assist dancers in performing and silk to express dance images, in addition to using body movements to express national dance culture. The effective arrangement of dance movements and efforts to use the arrangement and flexible design of shapes to form a good dance performance image share many similarities with national dance art and painting art. The lines produce products that satisfy the aesthetics, interesting dance steps, and emotional resonance of the audience.

National dance has a long and ancient history as a phenomenon of dance culture and embodies a specific style and a specific form, as well as historical changes and the development of the times in a specific period, i.e., the development of the times has a far-reaching impact on the national dance culture. To demonstrate the national dance, Piniés et al. used 3D modeling and human motion capture technology, and the model used in the dance was an animation model drawn by hand [1]. Ma et al. proposed a dance training system that combines motion capture and virtual reality by capturing imitation motion, projecting it on the screen using virtual reality technology, and providing feedback, but there occurred a large error in capturing motion [2]. Jones et al. proposed to perform three-dimensional convolution in the CNN (Convolutional Neural

Network) convolution layer, in order to capture the distinguishing features of spatial and temporal dimensions [3]. By extracting 16 joint points, Liu et al. were able to perform motion tracking and attitude analysis. Because the human body's movements are flexible, simply changing the joints will result in a large error in recognizing the movements of the human body [4]. Werner et al. used the metric learning algorithm twice during the time-consuming model training stage. This means that achieving the real-time recognition effect for an unfamiliar action is difficult for the algorithm [5]. Furthermore, because this type of algorithm must make complex decisions in order to eliminate a large number of false 3D graphics primitives, the search volume is too large and the efficiency is too low, making it unsuitable for widespread use. It is the most effective means of improving the efficiency of the bottom-up recognition algorithm by aligning it with engineers' drawing methods and starting from a higher level of graphic semantics.

Video technology research has become one of the hottest topics in academia in recent years. Video motion recognition is one of the most important video technologies for the application of video intelligence, and it is widely used in many fields [6, 7]. As a result, using 3D reconstruction technology to protect Chinese national dance art and culture is critical. The national dance artists are reconstructed using 3D reconstruction technology [8], their images are saved in digital form on the computer, and a model of national dance artists driven by dance scores is imported. The underlying data are selected and analyzed in the feature extraction stage, and the action information is modeled on the data to obtain the human action pattern. It is a crucial component of human motion recognition that has a direct impact on the accuracy and robustness of the system. It investigates not only the time series data of human movement but also the spatial data of adjacent connection points in the human skeleton model, in order to better reflect the fundamental law of feature distribution.

1.1. Main Research Contributions

(1) This document combines camera image array and Kinect principle to collect depth images and calculates the 3D point cloud coordinates and normal vectors of depth images. Then, this paper uses the camera pose matrix estimation method with edge feature points as the auxiliary relationship to realize point cloud matching, and the generated point cloud is triangulated to form a triangular surface model.

(2) People should not only judge the type of action according to the image when the action is still but also pay attention to the whole changing process of the action from the beginning to the end. In this paper, a human motion recognition algorithm based on 3D joint space-time information is proposed. The algorithm extends the one-dimensional hidden Markov model, which studies time series information, to spatial time series HMM, which not only studies the time series information of actions but also studies the spatial information of events.

1.2. Structural Arrangement. Section 1 introduces the research background and significance and then gives the main work of this paper. Section 2 mainly introduces the related technologies of 3D reconstruction. Section 3 puts forward the concrete methods and implementation of this research. Section 4 verifies the superiority and feasibility of this research model. Section 5 is the summary of the full text.

2. Related Work

2.1. Research on 3D Reconstruction Technology. 3D reconstruction is an important part of the field of artificial vision, in which the recovery of 3D structures of objects and scenes from 2D image sequences based on motion information has always been an important research content of 3D reconstruction. In order to get more detailed information from the model, it is necessary to reconstruct a dense point cloud. Therefore, it is very important to solve the problem of dense pixel matching in image sequences.

Ma et al. proposed an energy function, which contains not only a constant brightness term but also a regularization term, which can supplement the optical flow information of weak texture areas [9]. Hernando et al. adopted effective duality based on optimization scheme and extended it to video registration of multiframe optical streams by establishing a long-term temporal coherence model with subspace constraints [10]. Han et al. proposed that the subspace constraint should be regarded as an implicit long-term trajectory regularization term in the whole video, and the time-consistent optical flow can be obtained [11]. Lu et al. proposed using subspace constraints to build a multiframe optical flow model and made a clear reasoning on occlusion [12]. However, this method is limited by the hard subspace constraint of the known principal component analysis base, which is calculated by sparse feature tracking.

The method of model reconstruction through the software can provide abundant components and functions by the software itself, and it is convenient to construct the Wang Wei model, which provides convenience for the design of the article model. Kottkamp et al. proposed an automatic surface generation system [13]. The system uses a handheld camera to collect image sequences, and through multiview feature matching, it can automatically complete camera calibration and layered reconstruction of object surface. Boden et al. constructed the RGB-D mapping system by using the depth and color information collected by Kinect [14]. The system combines battery correction and visual feature matching and realizes the postregistration of three-dimensional point clouds. Then, through closed-loop detection and global optimization, the indoor scene can be reconstructed in real time. Chen et al. realized real-time 3D reconstruction by using mobile Kinect and studied the physical interaction and multitouch of the reconstructed scene [15].

2.2. Research on Human Motion Recognition Technology. The features of human motion recognition learned by traditional methods cannot cope with the troubles caused by complex scenes, and the problems to be solved are limited. The way of deep learning conforms to the mechanism of human perception of the world. When there are enough samples, the features learned through deep network often have certain semantic features.

Yin et al. divided the human skeleton into five parts, represented by five subnetworks, and then fused them at the high level. An end-to-end recurrent neural network method based on the skeleton is proposed for human body recognition [16]. Iosifidis et al. put forward a new cyclic attention neural network, which uses separated spatial attention to improve the accuracy in the data set [17]. Almazán et al. put forward a dance training method based on systematic desensitization, defined the function of systematic desensitization training, and concluded that this method can help athletes to master sports dance skills [18]. Wang applied support vector machine to motion recognition, and they classified the extracted local feature vectors linearly. Later, many researchers used support vector machine in the recognition process [19]. Wang et al. combined the features of skeleton and contour, considered the boundary of contour itself, and used the background removal method to obtain contour [20]. Then, the histogram of human body shape is calculated by a radial algorithm centered on silhouette, and the final descriptor is obtained by combining the two features. Chang et al. used inertial sensors and depth cameras to capture the actions of cooking food (such as cutting food, subpackaging food, and eating food) [21]. Referring to the acceleration measured with the wearable inertial sensor, the coordinates and displacements of the human wrist, elbow, and shoulder can be estimated according to the depth data.

3. Methodology

3.1. Three-Dimensional Reconstruction of the National Dance Style Characteristics

3.1.1. Overall Framework. The primary goal of the national dance deductive process is to use the image deductive process to allow the audience to truly experience and feel the allure of dance as an art form. Each nation's physical formation and dynamic characteristics are not only closely related to the nation's historical development but also the result of artistic creation. Dance is thus not only an artistic expression but also a symbol of traditional culture and customs. Every feature of each historical stage is reflected in national dance, which has always been the carrier of popular culture. In a unique way, it preserves and accumulates cultural factors at various historical stages. The model's accuracy is always inversely proportional to the amount of data stored. A portion of the storage space will be sacrificed in order to achieve high accuracy, and the compression of the storage space will inevitably result in a decrease in accuracy. As a result of the discrepancy between the amount of data and the model's accuracy, the strain reference template is chosen for the measured point cloud. The first box's point cloud template is arbitrary and can be a standard template. The previous frame's point cloud is used as the reference template for the next frame after nonrigid body registration, and then, the rigid body's point cloud registration method with two viewpoints is used for preregistration. This is to strike a balance between accuracy and data volume so that the final model can satisfy both computers and users.

Using the depth data collected by mobile Kinect, high-quality 3D models can be reconstructed in real time. The technical framework of the Kinect Fusion system is shown in Figure 1.

Firstly, the system collects the original depth data through Kinect and then calculates the unit coordinates and normal vectors from the spatial point cloud. Then, the absolute camera pose is calculated by iterative algorithm, and the point cloud registration operation is carried out. In the process of point cloud merging, different from the previous simple point cloud merging methods, the system uses truncated symbolic distance function to map the point cloud data into a global cube to realize the merging. Finally, the ray tracing method is used to model the surface according to the current camera pose.

Because the obtained depth map contains some holes, it is necessary to repair the depth map in order to improve the quality of subsequent reconstruction. In this paper, the method of joint bilateral filtering is used to draw depth data. Its basic idea is to use the RGB image as the guide map and fill the missing information in the depth map with its full-edge information.

The filtered depth map is expressed as

$$D'_x = \frac{\sum_{ij} w^s_{i,j} w^c_{i,j} w^z_{i,j}}{\sum_{ij} w_{i,j}}, \tag{1}$$

where $w^s_{i,j}$, $w^c_{i,j}$, and $w^z_{i,j}$ is the spatial weight, color weight, and depth weight, respectively.

The data processing flow of the system mainly includes three parts: calibration, acquisition, and registration, as shown in Figure 2.

After the system is started, first initialize the system parameters, setting the Kinect depth frame resolution to 650×460 and the frame rate to 20 frames per second, and initialize Kinect Fusion-related parameters. In the acquisition stage, Kinect Fusion integrates them into their global surface model system and uses the ICP (Iterative Closest Point) algorithm.

Estimation of the current position of Kinect: in the registration stage, two point clouds are fitted to the same coordinate system, which provides a good starting position for the subsequent ICP algorithm and improves the registration accuracy. In the calibration stage, the point clouds obtained by two Kinect cameras are adjusted to the same coordinate system. The calibration process only needs to be done once after the hardware platform of the system is built.

3.1.2. Point Cloud Registration. Point cloud registration is the key link of network reconfiguration technology, and the accuracy of point cloud registration directly affects the quality of the reconfiguration model. Because the accuracy of image processing is usually high, this step needs a lot of calculations, so the execution efficiency becomes one of the

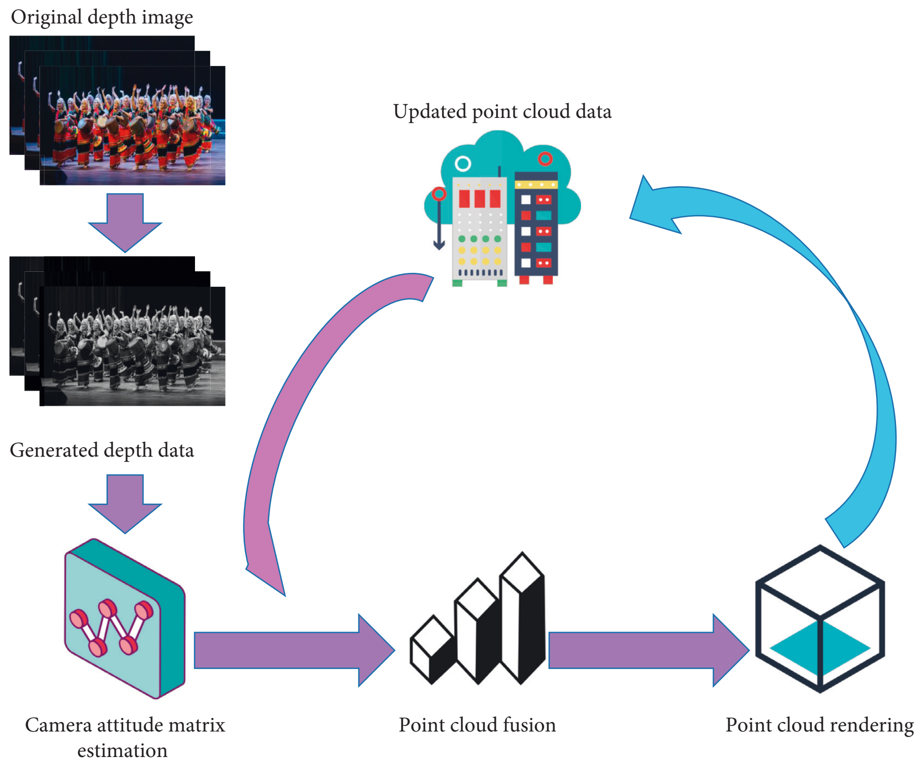

FIGURE 1: System framework.

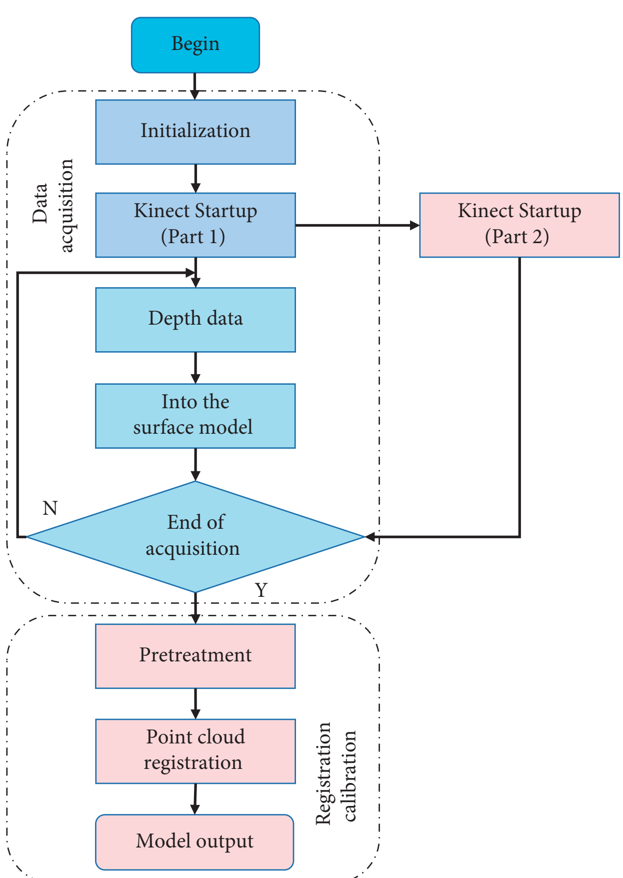

FIGURE 2: Data processing flow.

criteria to judge the algorithm. Besides efficiency, the accuracy and completeness of reconstruction must also be considered, because these factors determine the quality of the point cloud. In the process of recording consecutive frames, the body shape parameters of the same measured object must be the same. Firstly, the shape parameters of the standard model are selected as reference elements and then optimized according to the cost function, which is optimized frame by frame.

PMVS (Patch-Based Mufti View Stereo) algorithm is the best multiview stereo reconstruction algorithm at present. In addition, in order to distinguish between rendering and sparse reconstruction, this step is also called dense reconstruction. PMVS only reconstructs rigid structures. It will automatically ignore nonrigid structures, such as pedestrians in front of buildings. Given a set of oriented 3D points, the 3D coordinates and normal of each point are estimated. When the Kinect acquisition scene is mainly composed of walls and other planes, the ICP algorithm adopted by Kinect Fusion will terminate the iteration problem ahead of time, and the camera pose cannot be accurately estimated at this time, which will affect the results. It is not difficult to imagine that this problem can be solved by adding other corresponding nearest point pair selection methods. Therefore, this paper adopts the method of adding the edge features corresponding to the nearest points to avoid this problem.

Because the number of edge feature points in the registration process is much smaller than the number of nearest points corresponding to the original method, the error function between the nearest points of the edge is relatively weak. Here, the weight coefficient α is used to amplify the edge characteristic error function and increase its proportion in the total error function. So the final error function is shown in the following equation:

$$E'\left(T_{g,i}\right) = E_1 + \alpha E_2, \quad (2)$$

where it is the error function before modification, namely,

$$\begin{aligned} E_1 &= \sum_u \left\| \left(T_{g,i}\dot{V}_i(u) - \widehat{V}_{i-1}^g(\widehat{u})\right)^T \cdot N_{i-1}^g(\widehat{u}) \right\|_2, \\ E_2 &= \sum_q \left\| T_{g,i}\dot{V}_i(q) - \widehat{V}_{i-1}^g(\widehat{q}) \right\|_2. \end{aligned} \quad (3)$$

From the operations given above, we can get the final error function $E'(T_{g,i})$, which is consistent with the original error function of Kinect Fusion, and $E'(T_{g,i})$ can also be transformed into linear equations for least square optimization.

The center coordinate and normal vector of the patch are optimized to maximize the average correlation coefficient. In the optimization process, the center point of the patch is fixed on the ray of the reference image and the optimization degree of freedom is 3. The z coordinate of the center of the patch represents the two angles α and β of the normal vector. The equation of the slope is shown as follows:

$$a\left(X - X_c\right) + b\left(Y - Y_c\right) + c\left(Z - Z_c\right) = 0. \quad (4)$$

The relationship between normal and direction angle is $a = \cos\alpha\cos\beta, b = \sin\alpha\cos\beta,$ and $c = \sin\beta$.

3.1.3. Body Shape and Posture Estimation. The Poisson reconstruction method is used to reconstruct the surface of the recorded point cloud. Poisson reconstruction can consider all sampling points globally and has good robustness. After the surface is reconstructed, texture mapping is performed according to the vertices of the human mesh and the nearest neighbors of the human point cloud. For the vertex of each patch in the model, we find the nearest point in the point cloud, calculate the distance between the corresponding points, and assign the texture coordinates of that point to the vertex if it is less than the threshold. Considering the extensive research value and application prospect of the 3D human body model, this section proposes a method of human body model reconstruction combined with the human body model for nonrigid reconstruction of the dynamic human body. SMPL (Skinned Multiperson Linear) can accurately represent various postures and body shapes of the human body according to the deformation of skin apex, can simulate the bulge and depression of human muscles and other tissues during limb movement, so as to avoid surface deformation during movement, and can accurately describe the human body. Stretched and contracted muscles show the same soft tissue movement as real people.

Through rigid body registration, the two models are preregistered, and then the shape and posture parameters of SMPL are optimized to obtain the final model. The cost parameters are constructed as follows:

$$E(\beta,\theta) = \lambda_{m2s}E_{m2s} + \lambda_\beta E_\beta(\beta) + \lambda_\theta E_\theta(\theta). \quad (5)$$

Among them, E_β in the cost function is the prior constraint term of body shape and E_θ in the cost function is the constraint of posture, which helps to prevent unnatural posture. The obtained body shape parameters and posture parameters are input into the SMPL generation model, and a complete three-dimensional human body model is obtained.

The constraint term E_{m2s} represents the sum of the distances of the corresponding points between the reconstructed points and the standard model:

$$E_{m2s}(M,P) = \sum_{m_i\in vis(M)} \rho\left(\min\left\|m_i, v\right\|\right). \quad (6)$$

Here, M is the model surface, P is the scanning point cloud, function $vis(M)$ represents the effective visible model vertex, m_i is the effective point on P, ρ is the robust Geman–McClure function, and v is the point corresponding to m_i point on the SMPL model. λ_{m2s} is its weight term.

3.2. Dance Movement Recognition

3.2.1. Feature Extraction. National dance is a form of time and space coexistence art. It, like other straight tree arts, has cultural and individual characteristics that are connected through communication. The passage of time and space has brought about significant changes in people's lives and cultures. National dance should be based on current events. At the same time, folk dance follows the rhythm of the times and incorporates its characteristics. The theme and dance form were innovated and arranged in accordance with China's different revolutionary histories and modern opening periods, reflecting the characteristics of the times at the time. The goal of extracting local features in human motion recognition is to pique people's curiosity. In the part of a motion that changes significantly, there is no need to locate and track the entire human body. External environmental factors such as the change in human body shape, the change in shooting angle, the change in illumination, and the problem of occlusion have strong anti-interference properties.

In the experiment of this chapter, (x_i, y_i, z_i) is used to represent the three-dimensional coordinate of the ith bone joint and $J = [J_1, J_2, \ldots, J_M]$ represents the selected M bone joints. The calculation method of displacement vector features is as follows:

$$d_i^t = \frac{J_i^{t+1} - J_i^{t-1}}{\Delta T}, \quad t = 1,2,\ldots,N,\ i = 1,2,\ldots,M, \quad (7)$$

whereJ_i^t represents the coordinate of the ith bone joint in the t frame, N represents the serial number of the frame in which the bone joint is located, and M represents the corresponding label of the selected bone joint. ΔT represents the time interval between the $t+1$ frame and the $t-1$ frame.

Content-based retrieval technology has been proved to be very effective and fast in similarity search of large-scale data. Therefore, this section is devoted to extending the retrieval technology to real-time motion recognition.

General templates representing various categories can be used as template patterns to directly match and identify test actions.

Assume that x and y represent a frame of the test sample and the general template, respectively, to support the similarity calculation:

$$h_p(x, y) = \begin{cases} 1, & x_p \in y_p, \\ 0, & \text{otherwise}. \end{cases} \quad (8)$$

Here, if the two x and y do not match, $s(x, y)$ is no longer assigned to zero, but a negative value, and $h_p(x, y) - 5$ is given as punishment, thus enhancing the difference between different actions.

In the process of recognition, each part of it is searched in its corresponding key table in turn. The accumulated scores of these results can be used as the identification basis, and the specific identification process is shown in Figure 3.

After the previous steps, the key frame is represented by a five-dimensional vector, where each dimension represents the pose mapping of a part of the frame. For each dimension, we look for its match on its corresponding key. Therefore, five sets of search results are returned for these five dimensions. Therefore, we need to further analyze these search results and find the matching results from the intermediate frames. The input frame can always find as many matches as possible, which leads to the accurate classification of similar actions. Finally, input action recognition is determined by the general template with the highest performance score.

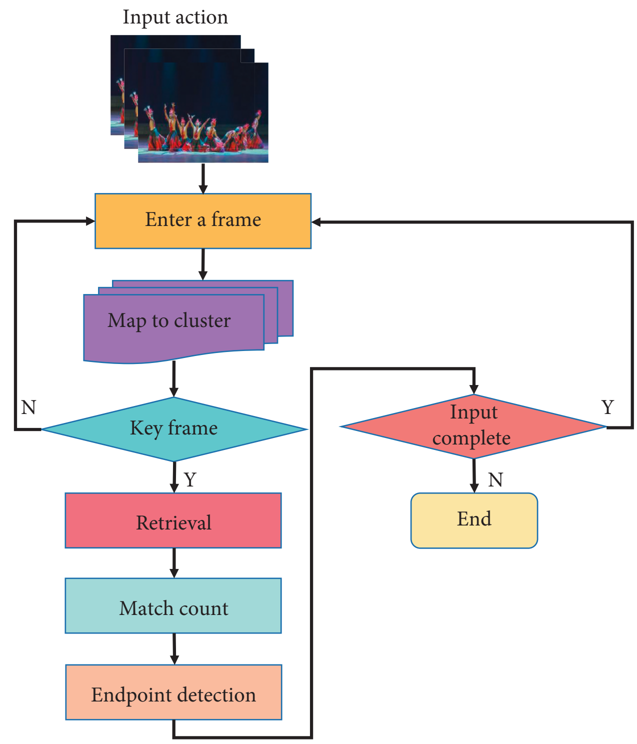

FIGURE 3: Real-time motion recognition process.

3.2.2. Action Classifier Design. HMM (hidden Markov model) is a dynamic model based on stochastic process and probabilistic observation. It is widely used in the recognition of various dynamic process systems involving state transition, such as speech recognition, handwriting recognition, and motion recognition. Its basic assumptions include the output independence hypothesis and the Markov hypothesis. The value is implicit, and it is one of some finite sequence of states. Markov hypothesis means that the current state completely depends on the state of the previous moment, and there is a fixed probability of this dependence between states.

Evaluation is the first problem to be solved in the motion recognition algorithm based on HMM, because given the observation sequence O and multiple HMMs, it is necessary to judge which HMM produced the observation sequence O according to the evaluation results.

There are two solutions to the evaluation problem: the forward algorithm and the backward algorithm. The Markov hypothesis is extended to the two-dimensional case. The state of the feature block depends on the state of the left feature block and the state of the upper feature block. There is a fixed probability between these states.

Both forward probability and backward probability can be calculated effectively by recursion. Unlike the new forward algorithm proposed in this paper, the iterative sequence of backward algorithm is from right to left and from bottom to top. The backward algorithm iteratively calculates $\phi_i^{w+1}(m, x)$ and $\beta_{i+1}^{w}(m, n)$, which represents the backward probability of the joint state of adjacent feature blocks. Their definitions are as follows:

$$\begin{aligned} \beta_{i+1}^{w}(m, n) &= p\left(o_{i+1}^{w+1,\ldots,W}, O_{t+2}, \ldots, O_T | q_i^w = s_m, q_{i+1}^w = s_n\right), \\ \phi_i^{w+1}(m, x) &= p\left(O_{i+1}, \ldots, O_T | q_i^w = s_m, q_i^w = s_x\right). \end{aligned} \quad (9)$$

4. Experiment and Results

In order to quantitatively compare the 3D SMPL human body models reconstructed by this method, this section uses the shadow recovery shape 3D reconstruction method to establish the standard 3D human body template and adds additional illumination constraints on the basis of this method. In order to optimize the depth value, this method integrates the illumination information of the object surface and the generated 3D model is smoother and contains more detailed information of the object surface.

Then, the three-dimensional human body model reconstructed by the first two methods is registered with the standard template, and the nearest geometric distance between the reconstructed model point and the standard template is calculated and represented by pseudo-color. By comparing the root mean square values of the generated model and template, the similarity between the model and template can be effectively reflected. The error comparison of the former two methods is shown in Figure 4.

According to the calculation of Figure 4, the average root mean square error of this method is 2.23 times that of this method and the reconstruction effect of this method is better.

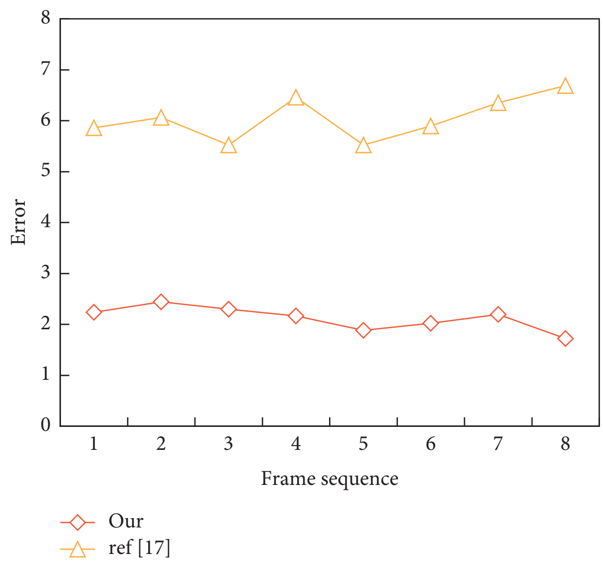

Figure 4: Error comparison of algorithms.

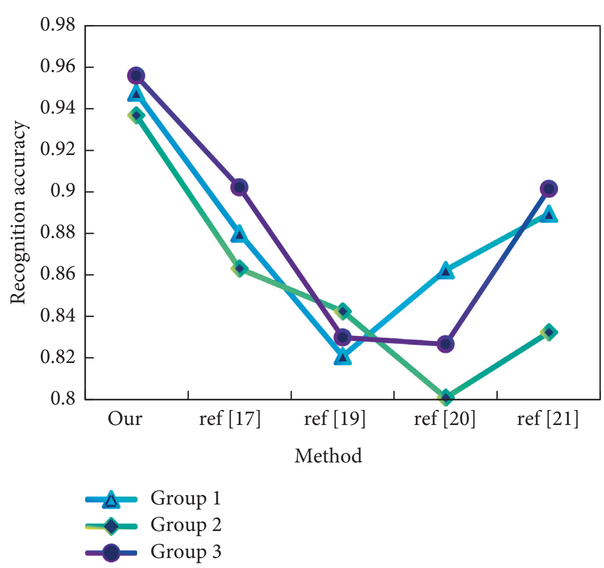

Figure 5: Recognition accuracy (data set 1).

For each group of data sets, we conduct a user-independent group action pattern recognition experiment, and we select three collected samples as training sets and the other two as test samples. As shown in Figures 5 and 6, for each action type, only the first two training samples are selected for each captured topic for training; that is, there are only 6 training samples for each action type.

It can be seen from the results that the recognition accuracy of this method is the highest among all methods. As far as human perception is concerned, they belong to the same action category, but due to different arm actions, the action data values may be quite different. Therefore, when these actions are calculated and recognized as a whole, the recognition accuracy will be seriously affected and our limb-based segmentation method can avoid this shortcoming.

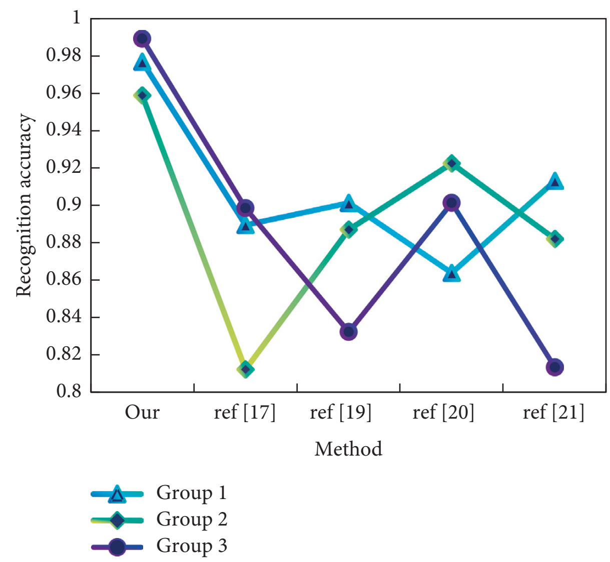

Figure 6: Recognition accuracy (data set 2).

In this section, on the basis of the above experiments, some extended experiments are made. Table 1 gives the comparison of the algorithm proposed in this paper and the training time of a single sample in each stage of reference [19–21].

It can be seen from Table 1 that the average training time of the model in [19] for a single sample is more than 20 times higher than that of the algorithm in this paper. The amount of data in this database is relatively small, so this time cannot be ignored for a database with a relatively large amount of data. It can be concluded that the algorithm in this paper can basically recognize human movements in real time. More importantly, the algorithm in this document does not need human intervention. According to different databases, the parameter values can be automatically adjusted according to the input data, and the adaptability is strong.

In order to reduce the randomness of the clustering process, nine people are used for training and one person is used for testing in the database, which is a one-time cross-validation method. Table 2 shows comparison with the other literature studies.

As can be seen from Table 2, the recognition rate of this algorithm basically exceeds that of all the current literature. It is easy for an algorithm to achieve a high recognition rate in the database, but it is very difficult to increase it by a few percentage points on the existing basis.

The auxiliary training method collects the coordinate points of each trainer's motion joints and compares them with the standard movements. The Kinect is used to collect the position of the trainer's motion coordinates, and the error values of the motion joint coordinates obtained by the three methods are compared to assist the dance method. Compared with the data collected by Kinect, the detailed analysis of joint angle capture in motion capture shows the experimental results in Figure 7.

In Figure 7, the method designed in this paper is more accurate in angle capture than other comparison methods. It can be known that the analysis method of folk dance style characteristics based on 3D reconstruction designed in this

Table 1: Training time comparison.

Method	Feature extraction (ms)	Feature processing (ms)	Training classifier (ms)
Methods of this paper	6.693	0.524	6.632
Literature [19]	6.358	6.012	2012.214
Literature [20]	10.332	18.324	1869.367
Literature [21]	7.213	9.668	2231.47

Table 2: Comparison between identification results and mainstream methods.

Method	Recognition rate (%)
Methods of this paper	88.6
Literature [19]	93.2
Literature [20]	90.7
Literature [21]	97.8

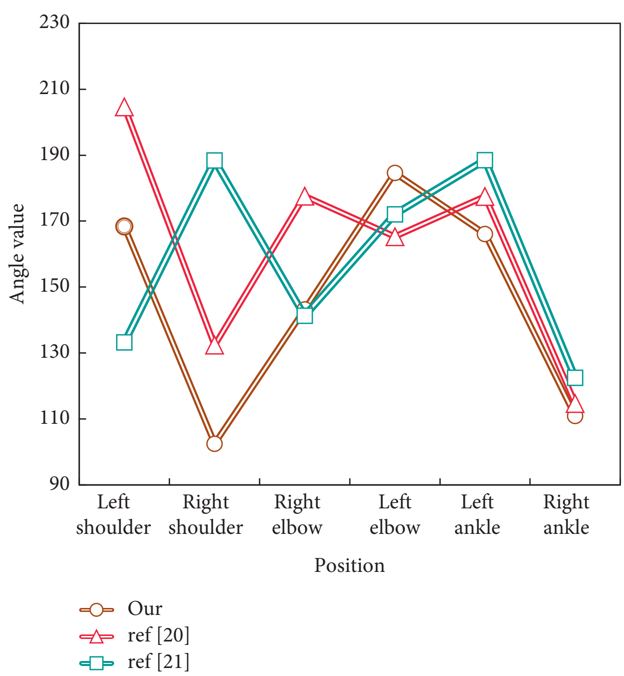

Figure 7: Comparison of joint angle values of trainers.

paper has higher accuracy in capturing the trainer's movement position and can form a more accurate contrast with the standard movement, thus realizing error correction in auxiliary training.

The experiment will investigate the influence of test sample noise on spatio-temporal HMM recognition performance. The test sample feature space is composed of Gaussian noise with different signal-to-noise ratios. At this time, the number of training samples is set to 50% of the total number of samples. In the experiment, feature information from different joint points is used to represent the features of the human body model and the influence of feature dimensions on the recognition rate of the model is tested. The results are shown in Figure 8.

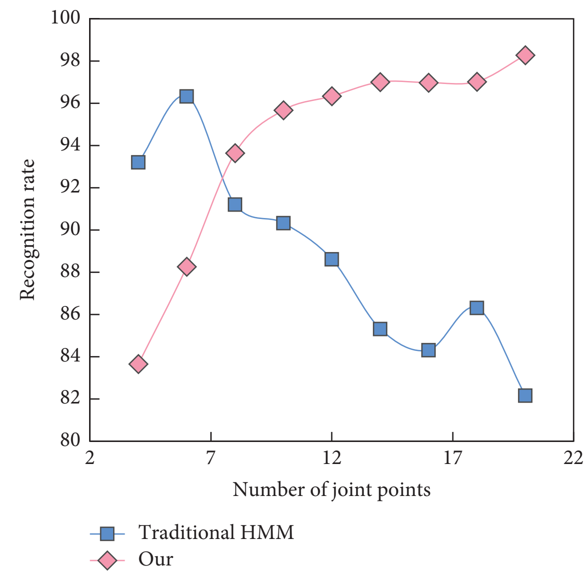

Figure 8: Influence of feature information of different number of joints on recognition rate of different algorithms.

The change of curve reflects the influence of the dimension change of skeleton model features on the recognition algorithm. The larger the dimension, the richer the skeleton model features. When the feature dimension increases, the recognition rate increases, while the recognition rate of one-dimensional Markov model algorithm decreases. When the number of joints increases to 10, the recognition rate of our algorithm increases to 95.68%, and when the number of joints increases to 20, the recognition rate of our algorithm increases to 98% and 28%. When the feature dimension is small, the reason for the low recognition rate of our algorithm in this paper is that the spatial dependency between low-dimensional feature blocks is fuzzy and the dependency is easily affected by noise in the training feature space, which will affect the performance of our algorithm. Experimental results show that the proposed algorithm is superior to the one-dimensional Markov model algorithm in recognition rate and robustness in solving high-dimensional human motion recognition problems.

5. Conclusions

Ethnic dance is a powerful reflection of a country's culture, national identity, and historical tradition. Dances of various nationalities have their own distinct styles as an important cultural card of a nation. It is necessary to understand the style characteristics of national dance in order to better understand its performance characteristics and improve its performance effect. This is done by first understanding its basic characteristics. The upper and lower parts of the human body are scanned with two Kinect depth cameras, and the two 3D point clouds obtained by scanning are spliced to create a complete 3D model of the human body. The one-dimensional hidden Markov model is extended to the spatial time series HMM in order to solve the dimension disaster caused by the three-dimensional representation of the human body. The recognition rate of this algorithm increases to 95.68 percent when the number of joints is increased to ten and to 98.28 percent when the number of joints is increased to twenty, according to the experimental results. This method is quick and simple to use, and it can be applied to augmented reality, ethnic dance style analysis, and other applications.

Data Availability

The data used to support the findings of this study are available from the author upon request.

Conflicts of Interest

The author declares no conflicts of interest.

References

[1] P. Piniés, L. M. Paz, D. Gálvez-López, and J. D. Tardos, "CI-Graph simultaneous localization and mapping for three-dimensional reconstruction of large and complex environments using a multicamera system," *Journal of Field Robotics*, vol. 27, no. 5, pp. 561–586, 2010.

[2] S. Ma, R. Zhu, C. Quan, L. Chen, C. J. Tay, and B. Li, "Flexible structured-light-based three-dimensional profile reconstruction method considering lens projection-imaging distortion," *Applied Optics*, vol. 51, no. 13, p. 2419, 2012.

[3] H. G. Jones, K. P. Mingard, and D. C. Cox, "Investigation of slice thickness and shape milled by a focused ion beam for three-dimensional reconstruction of microstructures," *Ultramicroscopy*, vol. 139, pp. 20–28, 2014.

[4] M. Liu, L. Zhang, and C. Li, "Nonuniform three-dimensional configuration distributed SAR signal reconstruction clutter suppression," *Chinese Journal of Aeronautics*, vol. 25, no. 3, pp. 423–429, 2012.

[5] H. Werner, J. Lopes, G. Tonni, and E. Araujo Junior, "Plastic reconstruction of fetal anatomy using three-dimensional ultrasound and magnetic resonance imaging scan data in a giant cervical teratoma. Case report," *Medical Ultrasonography*, vol. 17, no. 2, pp. 252–255, 2015.

[6] Y. Hu, J. Zhan, G. Zhou et al., "Fast forest fire smoke detection using MVMNet," *Knowledge-Based Systems*, vol. 241, Article ID 108219, 2022.

[7] X. Ning, K. Gong, W. Li, L. Zhang, X. Bai, and S. Tian, "Feature refinement and filter network for person Re-identification," *IEEE Transactions on Circuits and Systems for Video Technology*, vol. 31, no. 9, pp. 3391–3402, 2021.

[8] W. Cai, D. Liu, X. Ning, C. Wang, and G. Xie, "Voxel-based three-view hybrid parallel network for 3D object classification," *Displays*, vol. 69, Article ID 102076, 2021.

[9] H. Ma, Z. G. Liu, Y. Bao, P. X. Ran, and N. S. Zhong, "Morphology and three-dimensional reconstruction of the digestive system of *Periplaneta americana*," *Journal of Medical Entomology*, vol. 46, pp. 165–168, 2009.

[10] J. Hernando, D. Geijo, I. O. Leizaola-Cardesa et al., "Reconstruction of liposarcoma resection defect with a made-to-measure polyethylene prosthesis using three-dimensional digital technology," *Journal of Craniofacial Surgery*, vol. 29, no. 1, pp. 16-17, 2018.

[11] Q. Han, A. Zhang, C. Wang, K. Yang, and J. Wang, "Application of three-dimensional reconstruction to improve the preoperative measurement accuracy and applicability of femoral neck torsion angle," *Medicine*, vol. 98, no. 45, Article ID e17727, 2019.

[12] M. Lu, Y. Li, Y. Luo, W. Zhang, Y. Zhou, and C. Tu, "Uncemented three-dimensional-printed prosthetic reconstruction for massive bone defects of the proximal tibia," *World Journal of Surgical Oncology*, vol. 16, no. 1, p. 47, 2018.

[13] H. Kottkamp, G. Hindricks, G. Breithardt, and M. Borggrefe, "Three-dimensional electromagnetic catheter technology: electroanatomical mapping of the right atrium and ablation of ectopic atrial tachycardia," *Journal of Cardiovascular Electrophysiology*, vol. 8, no. 12, pp. 1332–1337, 1997.

[14] S. Boden, M. Bieberle, G. Weickert, and U. Hampel, "Three-dimensional analysis of macroporosity distributions in polyolefin particles using X-ray microtomography," *Powder Technology*, vol. 188, no. 1, pp. 81–88, 2008.

[15] J. Chen, S. Huang, and W. Zhao, "Three-dimensional defect inversion from magnetic flux leakage signals using iterative neural network," *IET Science, Measurement & Technology*, vol. 9, no. 4, pp. 418–426, 2015.

[16] H. Yin, J. Wang, J. Lin, D. Han, C. Ying, and Q. Meng, "A memory-attention hierarchical model for driving-behavior recognition and motion prediction," *International Journal of Automotive Technology*, vol. 22, no. 4, pp. 895–908, 2021.

[17] A. Iosifidis, A. Tefas, and I. Pitas, "Multi-view action recognition based on action volumes,fuzzy distances and cluster discriminant analysis," *Signal Processing*, vol. 93, no. 6, pp. 1445–1457, 2013.

[18] J. Almazán, E. Valveny, A. F. ornés et al., "Pattern recognition and image analysis," *Lecture Notes in Computer Science*, vol. 45, no. 9, p. 3047, 2013.

[19] P. Wang, "Research on sports training action recognition based on deep learning," *Scientific Programming*, vol. 2021, no. 7, pp. 1–8, 2021.

[20] L. Wang, J. Lan, and W. Wei, "Application of acceleration sensor in upper body motion information acquisition and attitude recognition," *Revista de la Facultad de Ingenieria*, vol. 32, no. 11, pp. 191–196, 2017.

[21] Z. Chang, X. Ban, Q. Shen, and J. Guo, "Research on three-dimensional motion history image model and extreme learning machine for human body movement trajectory recognition," *Mathematical Problems in Engineering*, vol. 2015, Article ID 528190, 15 pages, 2015.

Hindawi
Computational Intelligence and Neuroscience
Volume 2022, Article ID 7277742, 10 pages
https://doi.org/10.1155/2022/7277742

Research Article

Comparative Study of Physical Education Teaching in Middle Schools at Home and Abroad Using Clustering Algorithm

Dejun Tan

Huizhou University, Huizhou 516001, China

Correspondence should be addressed to Dejun Tan; 2017107142@ctgu.edu.cn

Received 20 March 2022; Revised 8 May 2022; Accepted 11 May 2022; Published 18 June 2022

Academic Editor: Xin Ning

Physical education in middle school is very important for teenagers, so it is also crucial to understand the differences between PET (Physical Education Teaching) systems in middle schools at home and abroad. The frontier and hotspot of PET research in middle schools at home and abroad are examined in this paper using citation analysis, information visualization, and cluster analysis, as well as CiteSpace software. The findings show that PET method research in China is qualitative, whereas PET method research in middle schools around the world is quantitative evaluation and empirical research. Domestic research hotspots focus on classroom instructional design, whereas foreign countries focus on load identification theory's application in instructional design. Frontier research in the United States is dispersed and covers a wide range of topics, whereas research in other countries focuses on cognitive load theory. The classification time of this improved algorithm is reduced by 190.97 seconds when compared to the traditional KNN algorithm, and the total time is increased by more than 50%. According to the findings, nonsports or nonsports influencing factors should be given more consideration in the study of adolescent physical fitness decline in China.

1. Introduction

Physical education is one way for schools to implement comprehensive education, and physical education in all levels and types of schools plays an important role in sports development. The purpose of the physical education curriculum is to assist students in mastering the fundamental theoretical knowledge of physical education as well as the fundamental skills of scientific exercise, as well as to establish a correct view of physical education, in order to achieve the goal of improving physical fitness and health. It can help us understand and discuss the interaction of various factors and their various forms in the overall process of Physical Education Teaching, which is conducive to dynamically grasping the essence and law of the process [1]. In general, there are many PET (Physical Education Teaching) systems in middle schools that can help to develop the teaching system in middle schools. Physical education is an important part of our country's middle school education, with a focus on the combination of physical education and fitness, as well as the function of leisure and entertainment [2]. With China's middle school physical education reform progressing, developing a scientific and effective middle school physical education model is becoming more important in addressing the practical issues that the current social environment imposes on the development of school physical education in the country. It is critical to study the PET model abroad because it is at the forefront of the development of high-level theory of school physical education.

PET mode is a teaching program that encapsulates a set of teaching principles. It consists of a relatively stable teaching process structure and teaching method system, which is primarily reflected in the design and implementation of units and teaching courses [3]. Teaching, according to Xiong et al. [4], is a step toward transforming learning experiences into units, courses, and procedures. Alternatively, it is the process by which teachers teach students to absorb knowledge and skills [4]. Alves et al. [5] believe that education is a form of social power and that knowledge allows some people to control others [5]. Oliveira et al. [6] believe that the social environment plays an important role in the development of children and that social activities can explain cognitive changes in children [6]. Learning, according to Barker et al. [7], is a process of reorganizing the cognitive system as well as a series of processes of acquiring knowledge from the media, imitating knowledge, and incorporating it into the knowledge framework [7]. It is stated that classroom learning motivation is a natural characteristic of students, not a result of teacher manipulation. By drawing concept maps, Kim et al. [8] developed a teaching tool to help us check whether students truly integrate new knowledge into their cognitive structure [8]. This methodology and conceptual relationship framework are extremely useful. PET theory and practice are linked by the fact that the PET model is not only theoretical but also operable. A comparison of Chinese and foreign PET models will aid us in absorbing the positive aspects of foreign PET models and serve as a useful reference for China's PET model reform.

Sports and PET are both effective ways to encourage teenagers' healthy development. Excellent PE teachers play a critical role in assisting students in developing their physical fitness, competitiveness, and self-confidence. Physical education majors bear the burden of training future physical education teachers, and the quality of that training is directly related to whether or not the training plan for undergraduate talents of physical education majors is scientific, reasonable, and in line with national conditions. The main goal of comparing PET schemes in middle schools in the United States and other countries is to see if foreign models and experiences can help improve the quality of domestic physical education professionals.

The main creative points of this paper are as follows: (1) By using the method of citation analysis, the knowledge maps of the development of PE teaching design in middle schools at home and abroad were constructed, respectively, and the development of PET design in middle schools at home and abroad was comprehensively compared and analyzed. By looking for the key nodes in the process of cluster analysis of cocited documents, this paper compares the key documents that have changed the research field in the history of PET design in middle schools at home and abroad in recent ten years. (2) Through the comparative analysis of physical training research at home and abroad, this paper finds out the shortcomings of physical training research in China and the gap between China and foreign countries, then provides new ideas and methods for the development of physical training in China, and at the same time provides some references for theoretical research of physical training in China.

2. Related Work

2.1. Study on PET. Brian et al. started with the concept of curriculum, pedagogy, and evaluation as interrelated school information system, put forward and discussed "quality sports" with curriculum, pedagogy, and evaluation as basic dimensions and the meaning of sports quality in each dimension, and thought that to realize quality education in PET, it is necessary to pursue and demonstrate quality education within and between curriculum, pedagogy, and evaluation [9]. Roure and Pasco [10] believe that physical ability is the athletic ability of the human body through the nerve-muscle system based on the energy metabolism of the three energy supply systems [10]. Ayers and Woods [11] regarded citation network as a directed acyclic network formed by a series of events and papers in time series, used a search algorithm to explore the events that can represent the mainstream direction and the connection paths that play a key role in the formation of citation network, and put forward the critical path algorithm in citation network [11]. Giordano and Christopher [12] pointed out that British universities implement the training goal of "thick foundation and wide caliber." The training of sports talents in Japanese middle schools is adjusted and improved according to the social demand for sports talents [12].

Amatori et al. [13] pointed out that, with the change in social demand for sports talents, the training goal of physical education major in colleges and universities has changed from specialized training of physical education teachers to training comprehensive talents and applied talents with strong adaptability [13]. Li and Fan's [14] research focuses on the analysis of childhood feelings. It is necessary to carry out education, which is the way for every individual to feel the world [14]. Sui [15] thinks that the influence of social factors and cultural factors is very important in the personal learning process. It should be emphasized that people will internalize their social environment and their cultural expression in the process of learning [15]. Osborne et al. [16] have proved that physical education class is regarded as a secondary course in many middle schools, so it has not been highly valued, the teaching equipment of this course is backward, and the concern of leaders at all levels has not been fully implemented [16]. Garnham [17] believes that the rapid development of modern society has greatly improved people's living standards, people pay more and more attention to physical and mental health, and people's attention has gradually turned to physical exercise [17]. We should put the reform of physical education at the top of the government's education department and actively promote the reform of physical education.

2.2. Overview of Clustering Algorithm Research. Clustering algorithm [18, 19] has achieved remarkable results since it was applied to data mining analyzed some clustering methods from the perspective of data mining (such as strict distinction between similarity and distance measurement and relevant optimization criteria applied to clustering) put forward a method to determine the initial clustering center by using the neighbor information of data points, which also has a certain reference value. Chen and Qiu [20]used the multidimensional grid data structure of attribute space to divide the space into multiple cell grids [20]. According to different levels of resolution, it stores multiple levels of cell grids, which form a hierarchical structure, and each high-level cell grid is divided into multiple lower-level cell grids.

Qin et al. [21] proposed a method to automatically optimize parameters. Clustering algorithm based on a synchronous model can alleviate some difficult problems of clustering analysis and noise detection on traditional data and has the characteristics of dynamic, local, and multiscale analysis, which can solve the difficulties faced by clustering analysis of large-scale data to a certain extent [21]. Yang et al. [22] proposed a simple nearest neighbor clustering algorithm based on statistics, which can eliminate background noise and isolated points and detect clustering areas with different densities from some data sets [22]. Baracchini et al. [23] showed how to reduce the time cost of clustering algorithm by using the idea and method of nearest neighbor. This idea based on nearest neighbor can still be applied to the clustering method based on the synchronous model. Therefore, we think this problem has certain research significance [23].

3. Methodology

3.1. Design of Clustering. Data mining technology has been widely used in finance, commerce, medicine, and other fields. In recent years, educational informatization has been popularized continuously. It is an inevitable trend to develop data mining technology in the field of education, analyze these complicated educational data, study teachers' teaching methods, and improve students' learning effect. Applying data mining analysis technology to analyze and predict mixed teaching behavior in middle schools and providing powerful decision-making or guidance for teachers and learners is the focus of current research, and it is also a realistic problem to be solved urgently. Data mining is a process of extracting data information that meets different business objectives and feeding back the information to users based on massive data analysis. In order to obtain potentially effective information to meet the needs of users, it is necessary to fully tap the surface information, remove redundant data, and display key data to users intuitively. Prediction and description are two goals of data mining. Prediction refers to the use of some information fields and variables in the database to predict hidden useful information, and description refers to the description of data into understandable patterns.

Because clustering is done without knowing the data structure of data pattern, it is difficult to judge what is a good transformation of feature space and the selection of feature subset. In fact, for some data sets, one standard can produce good results, while other data sets show the opposite results. The problem of pooling high-dimensional data comes from different angles. Besides designing new dimensionality reduction algorithms, we should also study the integration method of dimensionality reduction of high-dimensional data. Figure 1 shows the general steps of this method.

Clustering consists of two parts: set constructor $\prod$ and consensus function Γ. For a given data set, the set constructor generates a set of clustering schemes, and the consensus function analyzes and processes multiple clustering schemes of the set and finally outputs an optimized clustering scheme.

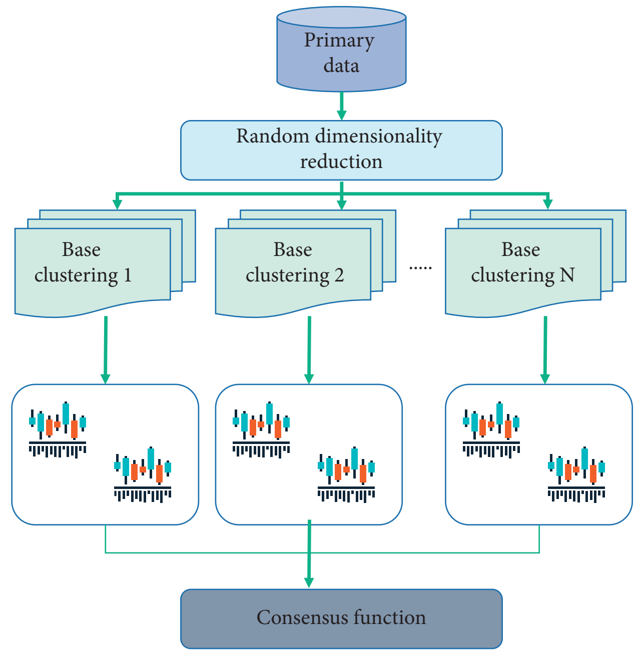

Figure 1: High-dimensional data clustering set process.

When there is a certain degree of linear correlation between variables in matrix X, the change of data X will be mainly reflected in the direction of the first few load vectors, and the projection of data matrix X on the last few load vectors will be very small, which is mainly caused by measurement noise. In this way, the matrix X_s can be written into the following formula after principal component decomposition:

$$X_s = t_1 p_1^T + t_2 p_2^T + \cdots + t_k p_k^T + E = \widehat{X}_s + E, \qquad (1)$$

where E is the residual matrix, which represents the change of X in the direction of p_{k+1} to p_m load vector, and it explains the measurement noise and model error factors. If only the reserved k principal component vectors $(k < m)$ are used to reconstruct the original data, the estimated data matrix $\widehat{X}_s$ and residual matrix E can be expressed as

$$\begin{aligned}\widehat{X}_s &= \sum_{i=1}^{k} t_i p_i^T,\\ E &= \sum_{i=k+1}^{m} t_i p_i^T.\end{aligned} \qquad (2)$$

The consensus function analyzes and processes according to the pooled set to generate the final pooled result. Because there is no clear correspondence between groups in a cluster and those supervised set combination methods cannot be directly applied, it is difficult to combine cluster sets.

There are two advantages of using the consensus function to partition graphs in this section:

(1) Graph division has a good learning area, and the algorithm of clustering to spectrum has been successfully applied in a large number of applications.

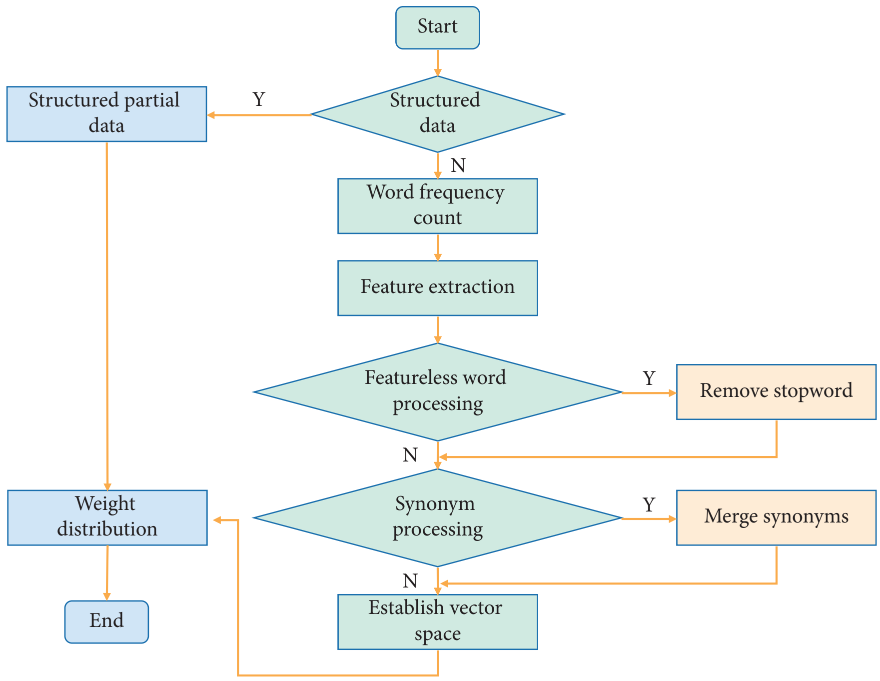

FIGURE 2: Text feature selection.

(2) When calculating the weight of edges in a graph, the clustering set gives a simple and effective measurement method to define similarity, which is a prerequisite for the success of graph division.

For simplicity, we only use the grouping set part of this method. In the process of building a cluster set, every time the base clustering algorithm is executed, a similarity matrix will be generated. Finally, all similarity matrices will be combined into a main similarity matrix to generate a similarity map. The graph is divided into several subgraphs, and each subgraph is connected and can be labeled as a group. The similarity matrix is constructed as follows according to the probability density function:

$$P\left(s_j \mid x_i\right) = \frac{p\left(x_i \mid s_j\right) \times P\left(s_j\right)}{\sum_{k=1}^{m} p\left(x_i \mid s_k\right) \times P\left(s_k\right)}, \tag{3}$$

where m is the number of clusters, Σ_j is the covariance matrix of relative cluster j, and u_j is the mean value of data objects in cluster j. The probability includes two parts: input data and clustering results. Therefore, the density vector is a good method for similarity measurement.

3.2. Feature Selection and Dimension Reduction. The general method of feature dimension reduction is to evaluate each original feature with an evaluation function, calculate its weight, and select features with high weight to form feature subsets. The basic process is as follows (Figure 2).

(1) Initially, the feature set includes all original features.

(2) Calculate the evaluation function value of each feature in the feature set.

(3) Sort features according to the value of the feature evaluation function.

(4) Select the first k features as feature subsets.

(5) According to the selected feature subset, the dimension of the text vector is compressed to simplify the representation of the text vector.

Generally speaking, the feature item set should have three characteristics: a complete feature item can truly represent the target content. According to the difference in feature vectors, objects can be distinguished from other documents. The dimension of the refined feature vector should be as small as possible.

The idea of possibility matching is to attach a membership function of the fuzzy set to each element in the sample based on the possibility theory so as to limit the evaluation values compatible with the elements, which represent the range values of attributes represented by atoms. The elements in the sample are described by a probability distribution, which indicates the inaccuracy and uncertainty of the data. The similarity of two samples is calculated by calculating the matching degree between sample objects.

Let the sample space be $U, p \in U, q \in U$, $\mu_p(u)$ as the membership function of p and $\pi(p)$ as the probability distribution of p, both of which are functions from U to [0,1]. In order to calculate the similarity between sample p and sample q, two measurement functions are introduced: possible similarity and necessary similarity.

The possible similarity of p to q is as follows:

$$\begin{aligned} f(p) &= \pi(p,q) \\ &= \operatorname*{Sup}_{u \in p} \min\left(\mu_p(u), \pi_q(u)\right). \end{aligned} \tag{4}$$

$f(p)$ gives the possible similarity between sample p and sample qq, that is, the degree of matching between the set tone of values compatible with sample p and the set of sample q values.

The necessary similarity between p and q is as follows:

$$g(p) = N(p,q) = \operatorname*{Inf}_{u\in p} \max\left(\mu_p(u), 1 - \pi_q(u)\right). \quad (5)$$

$g(p)$ gives the degree of certainty of $p-q$ compatible values, that is, the degree to which the set of possible values of q is contained by the set of p compatible values.

Probabilistic clustering analysis is the application of probabilistic matching in clustering analysis. Traditional fuzzy clustering analysis can be roughly divided into two categories: one is based on fuzzy equivalence relationships, and the other is based on fuzzy similarity relationships. A clustering method based on fuzzy equivalence relations is known as probabilistic clustering. When the sample space is a finite set, a fuzzy equivalence matrix represents the fuzzy equivalence relation, while a Boolean equivalence matrix represents the ordinary equivalence relation. The fuzzy equivalence matrix is then converted to a Boolean equivalence matrix, resulting in a clustering analysis process.

3.3. Text Classification of PET Research in Middle Schools at Home and Abroad. Because cluster analysis can aid in the exploration of unknown data structures, the results of its analysis can provide the best sample set for classification and other tasks and reduce the workload of empirical analysis such as manual annotation, and it has become the starting point for a series of data analyses. It is widely used in descriptive and predictive models to help analyze the known data structure. Clustering analysis and classification fall under the category of machine learning when it comes to developing a learning model. As a result, studying arbitrary family shape processing and large-scale text classification through clustering is extremely important from the perspective of machine learning.

Calculate the Euclidean distance or cosine similarity between the sample to be classified and the known training sample, find the K nearest neighbor texts with the closest distance or the greatest similarity to the text to be classified, and then judge the K nearest neighbor texts of the text to be classified according to the category of the text to be classified [19]. Considering the distance and angle between two vectors, the representative function is defined. The defined representative function is applied to KNN weight calculation instead of the category attribute function.

Let the known category of training text d_i be C_j, and define the importance of d_i to category C_j as the representative function $u(d_i, C_j)$, as shown in (6).

$$u\left(d_i, C_j\right) = \frac{1}{\operatorname{Dist}\left(d_i, \overline{C}_j\right)} \times \operatorname{Sim}\left(d_i, \overline{C}_j\right), \quad (6)$$

where $\overline{C}_j$ represents the center vector of category C_j, which is to add all the text vectors of category C_j and then average them. $\operatorname{Dist}(d_i, \overline{C}_j)$ represents the Euclidean distance from the training text d_i to the center of the category C_j to which it belongs, and $\operatorname{Sim}(d_i, \overline{C}_j)$ is the cosine similarity between the training text d_i and the center of the category C_j to which it belongs.

The value of K is determined by the spatial distribution of all points and can only be adjusted by the experimental results. Common methods for calculating distance include cos distance and Euclidean distance. In this paper, the cos distance formula is used to calculate the distance. Assuming there is a vector A, B, the cos distance between them is calculated by the following formula:

$$D_{\cos} = \frac{A \cdot B}{|A| \cdot |B|}. \quad (7)$$

A, B and the denominator is the product of the length of the vector A, B.

In this paper, the naive Bayes classifier is used for comparative experiments. It is a classification method based on the Bayes rule, which is expressed as follows:

$$P(h|D) = \frac{P(D\,|\,h)P(h)}{P(D)}. \quad (8)$$

$P(h)$ is the prior probability of assuming h, $P(D)$ represents the prior probability of training data D, $P(D\,|\,h)$ represents the probability of observing data D when h holds, and $P(h\,|\,D)$ is called the posterior probability of h.

The category attribute function $y(d_i, C_j)$ in the KNN algorithm will be replaced by the following formula:

$$y\left(d_i, C_j\right) = \begin{cases} u\left(d_i, C_j\right), & d_i \in C_j, \\ 0, & d_i \notin C_j. \end{cases} \quad (9)$$

In the KNN text classification algorithm, the improved K-medoids algorithm is applied to cut the training text. In the classification process of the KNN algorithm, the representative degree $u(d_i, C_j)$ is used to replace the category attribute function $y(d_i, C_j)$. The flow of this improved algorithm is shown in Figure 3.

4. Experiment and Results

4.1. Analysis and Comparison of PET Research Hotspots at Home and Abroad. In this paper, CiteSpace software is used to analyze the literature data with similar themes. Because the research methods used in this paper (word frequency analysis and cocitation analysis) have certain requirements for references and keywords in literature data, this index mainly checks literature data and CSSCI, and the database does not contain bibliographic data. During the operation, 15 items of bibliographic information and related information were counted, as shown in Figure 4. These 15 items reflect the most concerned hot topics in the field of PET research abroad.

Among these 15 papers, the papers involved the research of the combination of self-determination theory and PET. Therefore, the self-determination theory is also one of the hottest research points in the field of PET research abroad. Emphasis is placed on the influence of language and behavior of PE teachers on students and their professional development. Physical education courses are also studied according to the characteristics of girls. It can be seen that

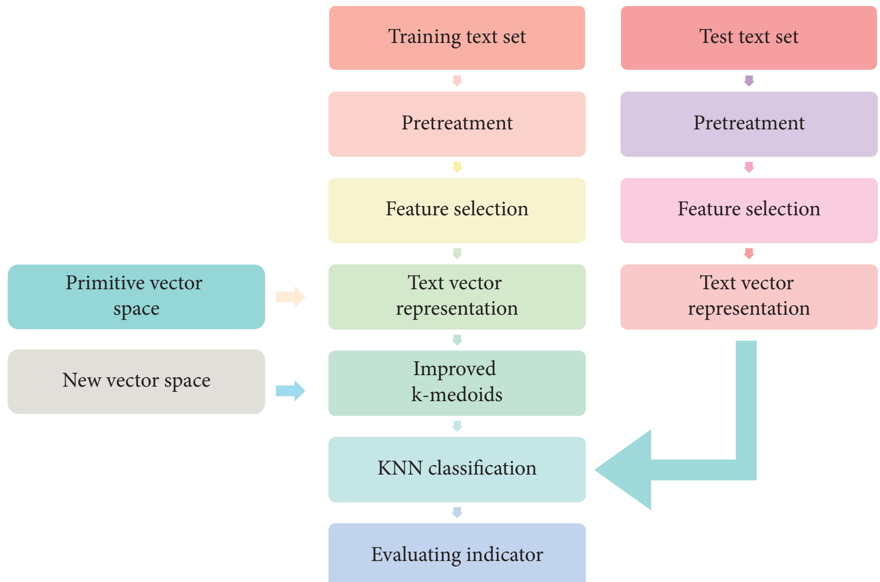

Figure 3: Improved algorithm flow.

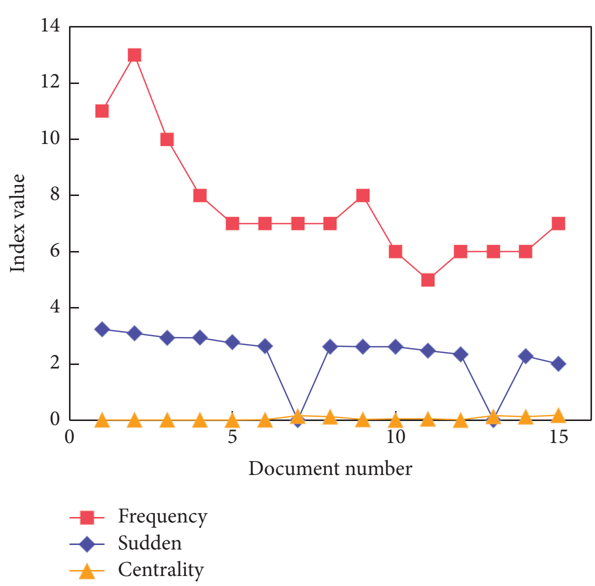

Figure 4: Literature of PET research hotspots abroad cocited network literature information.

the research field of PET abroad is biased toward women. The keyword frequency statistics in a specific period is the concentrated expression of the research focus in a specific field in that period. Therefore, keyword frequency is an important index to reveal research hotspots in specific fields. In this work, the information of 10 articles cited twice is counted, as shown in Figure 5. These 10 documents will reflect the most concerned hot topics in the field of PET research in China.

It can be seen that the research hotspots represented by keywords in the keyword cooccurrence network mainly focus on school physical education, physical education, physical education curriculum, middle school physical education, physical education teachers, PET methods, physical education concepts, traditional physical education, national physical education, physical education, and health curriculum standards and educational theories. This conclusion is generally consistent with the key research points reflected in the previous highly cited literature.

China's PET practice research should appropriately increase the research on sports from the perspective of public health. At present, the research on PET practice in China is mostly biased toward students' physical condition, and the research on sports from the perspective of public health should be appropriately increased. China's physical education curriculum survey should pay more attention to the details of the physical education class program. At present, China's physical education curriculum research tends to pay more attention to the standards or reforms of physical education and health curriculum and should appropriately increase the research on the details of physical education curriculum (such as students' physical activity level).

4.2. Comparative Analysis of Research Hotspots of PET Design in Middle Schools at Home and Abroad. Comparing the hot keywords at home and abroad, we can see that there are some similarities between them. The same hot field reflects the intersection of teaching design research at home and abroad, and it is also the mainstream research field at home and abroad. Due to the different degrees of attention paid to some hot keywords, the research enthusiasm and depth will be different (Figure 6).

From the ontology of instructional design, foreign countries pay more attention to the research of teaching strategies, while domestic countries pay more attention to the research of teaching methods and models. The frequency of attention to constructivism theory research in China is relatively high and central, while that in foreign countries is relatively low, which shows that the attention to constructivism theory in China is higher than that in foreign

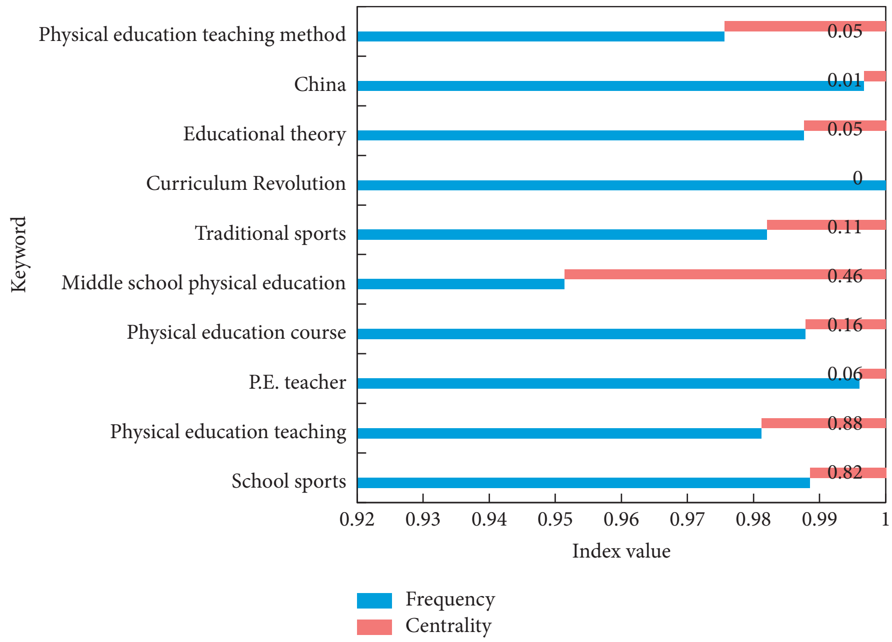

FIGURE 5: Keyword frequency in periodical cooccurrence network.

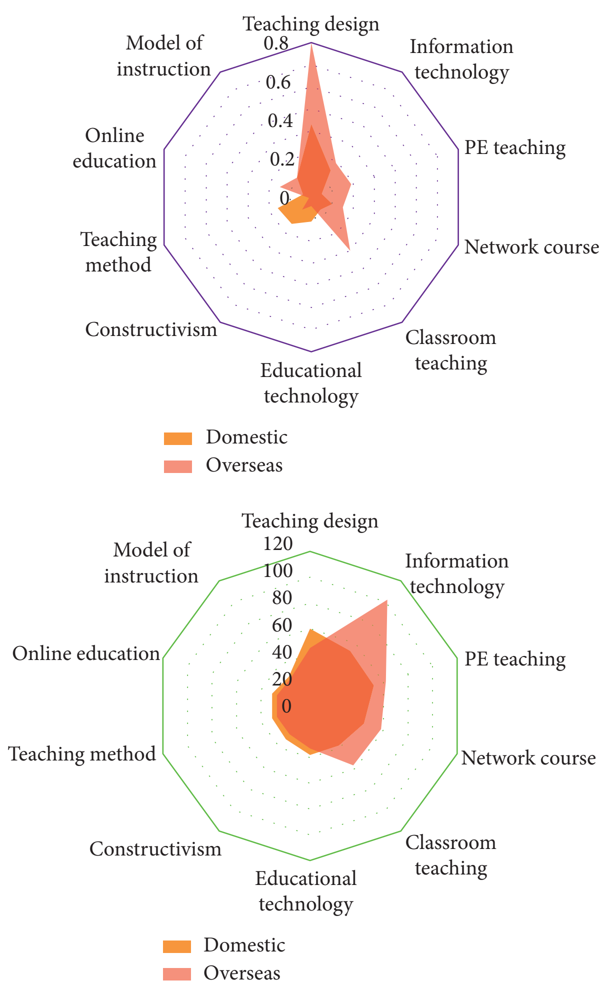

FIGURE 6: Hot keywords at home and abroad.

countries in the past decade. In addition, foreign countries gradually pay attention to the influence of emotional factors on students' learning effect, and the study of learning motivation is highly valued. However, the frequency of student-centered middle school students' hot words in China is only 7. In recent years, the domestic educational circles have vigorously advocated the design concept of constructivism, but in practice, the dominant position of students is often neglected.

Foreign countries focus on the research of teaching strategies, while domestic countries focus on the research of teaching methods and models. There are many discussions on the ontology of instructional design in China. At present, in the information age, informational instructional design and networked instructional design have become hot spots, while foreign countries focus on performance technology research.

Using the mutation word detection technology and CiteSpace software algorithm, combined with the time distribution characteristics of word frequency, keywords with high-frequency change rate are detected from subject words, which are called mutation words. Determine the frontier research and development trend of specific disciplines or fields. After importing the data into CiteSpace, 41 domestic variant words and 3 foreign variant words can be detected, and their time zone views can be obtained by running them separately. The statistics of variant words in domestic instructional design are shown in Figure 7. Statistics of variant words in foreign instructional design are shown in Table 1.

It is clear that domestic research has progressed in the area of exploration, which is consistent with the findings of other national researchers. Every year, hot research topics in

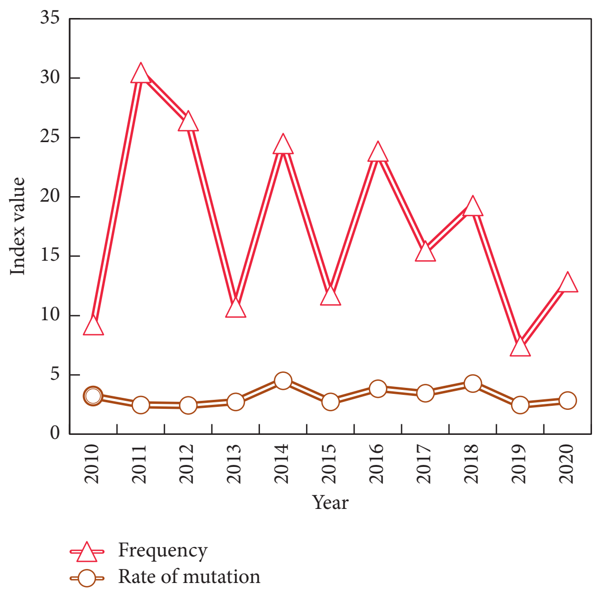

Figure 7: Statistics of abrupt words in domestic instructional design automation.

Table 1: Statistics of abrupt words in foreign instructional design.

Year	Rate of mutation	Frequency	Keyword
2011	2.36	13	Curriculum practice
2012	2.88	21	Information-based instructional design

instructional design are identified, but the research is not innovative. Since then, the focus of instructional design theory research has shifted to cognitive science, particularly distraction research, and no new research topics have emerged. When compared to domestic research, foreign boundary research, cognitive load, and distraction effect have not piqued domestic researchers' interest. More practical research closely related to national instructional design appears to be more important to national researchers. Localization of instructional design theory research entails combining foreign culture with traditional Chinese culture and social needs, as well as reconstructing and internalizing theoretical achievements in instructional design from other countries that do not meet China's needs. In reality, what exists is a theoretical system with Chinese characteristics. Teaching design research is inherently boring, and any research results necessitate the investment of time and energy by researchers, which can be exchanged through hard work. It is commendable that researchers pay attention to the latest trends, new theories, new models, and new technologies. The original research can be abandoned, and researchers must pay attention to the application of new hotspots.

Physical training is an important part of physical training. In recent years, some domestic scholars have conducted many valuable theoretical and empirical studies on the research status, existing problems, and future development trends of physical training, most of which are based on local conditions. There are relatively few researches

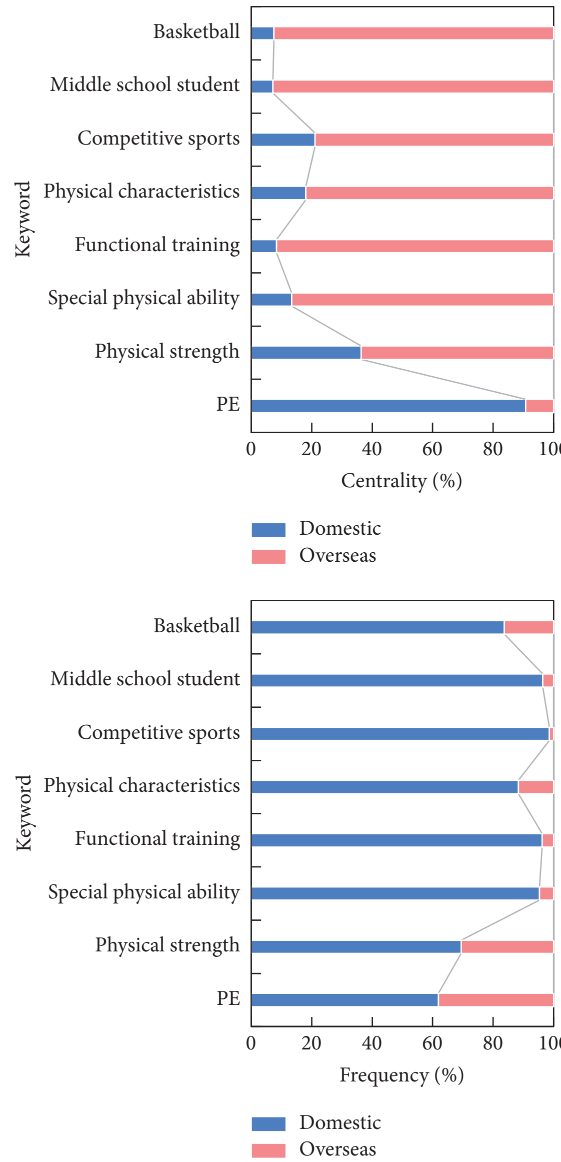

Figure 8: Distribution of keywords in physical training research at home and abroad.

on visual angle, subjective thinking, and qualitative analysis, as well as macroscopic understanding and quantitative analysis of physical exercise theory and practice at home and abroad. According to the visualization results, the keyword distribution of physical exercise research at home and abroad is drawn, as shown in Figure 8.

From the time distribution point of view, China's physical training research started late, but with the rapid development of modern competitive sports and the vigorous promotion of national fitness, China's physical training has undergone tremendous changes compared with the past. Foreign countries have a wide range of research objects on physical training, while China's research objects on physical training are relatively limited, mostly concentrated on a few elite athletes of various competitive sports.

The research field of physical exercise in China is mainly concentrated in the field of competitive sports. Compared

Table 2: Time performance.

Time/min	Before improvement	Before improvement
Training time	0	72.43
Classification time	346.58	155.61
Total time	346.58	228.04

with foreign countries, there is less research on physical training in other aspects such as mass fitness and national physique; that is, the development of physical training in competitive sports and mass fitness is uneven. Foreign countries pay more attention to the synchronous development of theory and practice, while domestic theoretical research of physical training lags behind practice, with competitive sports as the main theoretical research and certain repetitiveness of research contents. Pay attention to the physical health, mental health, and cognitive status of teenagers and the elderly in order to improve their physical health and quality of life. However, many empirical studies in China have the largest number of athletes among them, and their main purpose is to improve the recovery quality and achieve better quality of life and good results.

4.3. Performance Analysis of Clustering Algorithm. The experimental Chinese corpus is used, and the training set and the test set do not overlap. The selected text categories include 30 categories, like art, education, history, law, transportation, politics, and so on. The training text set contains 9809 texts, and the test text set contains 9813 texts. The comparison results of algorithm time performance are shown in Table 2.

It can be seen from Table 2 that, compared with the traditional KNN algorithm, the sorting time is reduced by 190.97, and the total time is increased by more than 50%. To sum up, compared with the traditional KNN algorithm, the improved KNN algorithm in this paper has a significant improvement in time performance.

5. Conclusions

In this study, the frontier and key points in the field of PET research in middle schools at home and abroad are investigated, scientometrics and clustering algorithms are comprehensively applied, and quantitative analysis and qualitative analysis are combined. Self-determination theory has been discovered to be one of the hottest research hotspots in the field of PET research in other countries. Physical education curriculum research in China has a tendency to focus on the standard or reform of physical education and health curriculum. The frequency and centrality of constructivism theoretical research in China are higher, whereas the frequency and centrality of constructivism research abroad are lower. Both at home and abroad, emphasis is placed on the methods, steps, and scheme design of the teaching process, with foreign countries placing a greater emphasis on teaching strategy research. Physical training research in China is primarily focused on competitive sports, and the development of physical training in competitive sports, mass fitness, and other areas is uneven. Foreign countries place a greater emphasis on the simultaneous development of theory and practice, whereas domestic physical training theoretical research lags behind practice. When compared to the traditional KNN algorithm, this algorithm reduces classification time by 190.97 seconds while increasing total time by more than 50%. Improving one's ability to face the educational world necessitates a large number of teaching resources in order to improve classroom teaching quality.

Data Availability

The data used to support the findings of this study are available from the corresponding author upon request.

Conflicts of Interest

The author declares no conflicts of interest.

References

[1] B. Bordel, R. Alcarria, and T. Robles, "Industry 4.0 paradigm on teaching and learning engineering," *International Journal of Engineering Education*, vol. 35, no. 4, pp. 1018–1036, 2019.

[2] S. Hu and B. Yu, *Big Data Analytics for Cyber-Physical Systems*, Springer International Publishing, Berlin, Germany, 2020.

[3] Z. Xu, K. K. R. Choo, A. Dehghantanha, R. Parizi, and M. Hammoudeh, *Cyber Security Intelligence and Analytics*, Vol. 928, Springer, , Berlin, Germany, 2019.

[4] Y. Xiong, X.-Y. Sun, X.-Q. Liu, P. Wang, and B. Zheng, "The influence of self-efficacy and work input on physical education teachers'creative teaching," *Frontiers in Psychology*, vol. 102856 pages, 2019.

[5] L. F. Alves, D. Brandão, and M. A. Oliveira, "A multi-process pilot plant as a didactical tool for the teaching of industrial processes control in electrical engineering course," *International Journal of Electrical Engineering Education*, vol. 56, no. 1, pp. 62–91, 2019.

[6] P. S. d. Oliveira, M. d A. v. Munster, J. V. d. Souza, and L. J. Lieberman, "Adapted physical education collaborative consulting: a systematic literature review," *Journal of Teaching in Physical Education*, vol. 39, no. 2, pp. 165–175, 2020.

[7] D. Barker, G. Nyberg, and H. Larsson, "Exploring movement learning in physical education using a threshold approach," *Journal of Teaching in Physical Education*, vol. 39, no. 3, pp. 415–423, 2020.

[8] I. Kim, P. Ward, O. Sinelnikov et al., "The influence of content knowledge on pedagogical content knowledge: an evidence-based practice for physical education," *Journal of Teaching in Physical Education*, vol. 37, no. 2, pp. 133–143, 2018.

[9] A. Brian, A. D. Meester, A. Klavina et al., "Exploring children with visual impairments'physical literacy: a preliminary investigation of autonomous motivation," *Journal of Teaching in Physical Education*, vol. 38, no. 2, pp. 1–24, 2018.

[10] C. Roure and D. Pasco, "The impact of learning task design on students'situational interest in physical education," *Journal of Teaching in Physical Education*, vol. 37, no. 1, pp. 24–34, 2018.

[11] S. F. Ayers and A. M. Woods, "Chapter 5: recruitment in PETE: survey results and discussion," *Journal of Teaching in Physical Education*, vol. 38, no. 1, pp. 37–44, 2019.

[12] A. N. Giordano and C. R. Christopher, "Repurposing best teaching practices for remote learning environments: chemistry in the news and oral examinations during COVID-19," *Journal of Chemical Education*, vol. 97, no. 9, pp. 2815–2818, 2020.

[13] S. Amatori, S. D. Zeppa, A. Preti et al., "Dietary habits and psychological States during COVID-19 home isolation in Italian college students: the role of physical exercise," *Nutrients*, vol. 12, no. 12, 3660 pages, 2020.

[14] W. Li and X. Fan, "Construction of network multimedia teaching platform system of college sports," *Mathematical Problems in Engineering*, vol. 202111 pages, Article ID 6304703, 2021.

[15] Y. Sui, "Employment education research integrity of college sports majors," *International technical management*, vol. 33 pages, 2014.

[16] H. Osborne, L. Anderson, P. Burt, M. Young, and D. Gerrard, "Australasian college of sports physicians-position statement," *Clinical Journal of Sport Medicine*, vol. 26, no. 2, pp. 87–95, 2016.

[17] A. P. Garnham, "The wide spectrum of sport and exercise medicine: an Australasian college of sports physicians theme issue," *British Journal of Sports Medicine*, vol. 46, no. 13, 895 pages, 2012.

[18] J. Chen, C. Du, Y. Zhang, P. Han, and W. Wei, "A clustering-based coverage path planning method for autonomous heterogeneous UAVs," *IEEE Transactions on Intelligent Transportation Systems*, vol. 1, pp. 1–11, 2021.

[19] Y. Jiang, X. Gu, D. Wu et al., "A novel negative-transfer-resistant fuzzy clustering model with a shared cross-domain transfer latent space and its application to brain CT image segmentation," *IEEE/ACM Transactions on Computational Biology and Bioinformatics*, vol. 18, no. 1, pp. 40–52, 2020.

[20] X. Chen and Y. Qiu, "A combined clustering algorithm based on ESynC algorithm and a merging judgement process of micro-clusters," *International Journal of Uncertainty, Fuzziness and Knowledge-Based Systems*, vol. 29, no. 3, pp. 463–495, 2021.

[21] X. Qin, J. Li, W. Hu, and J. Yang, "Machine learning K-means clustering algorithm for interpolative separable density fitting to accelerate hybrid functional calculations with numerical atomic orbitals," *The Journal of Physical Chemistry A*, vol. 124, no. 48, pp. 10066–10074, 2020.

[22] P.-L. Yang, G.-Q. Xu, Q. Yu, and J.-W. Guo, "An adaptive heuristic clustering algorithm for influence maximization in complex networks," *Chaos: An Interdisciplinary Journal of Nonlinear Science*, vol. 30, no. 9, Article ID 093106, 2020.

[23] E. Baracchini, L. Benussi, S. Bianco et al., "A density-based clustering algorithm for the CYGNO data analysis," *Journal of Instrumentation*, vol. 15, no. 12, Article ID 12003, 2020.

Hindawi
Computational Intelligence and Neuroscience
Volume 2022, Article ID 2586716, 12 pages
https://doi.org/10.1155/2022/2586716

Research Article

Biomechanical Analysis of Arm Manipulation in Tai Chi

Xiaoyan Dong,[1] Xiaofan Hu,[1] and Biqing Chen[2]

[1]*NingboTech University, Zhejiang, Ningbo 315100, China*
[2]*Jinhua Polytechnic, Zhejiang, Jinghua 321000, China*

Correspondence should be addressed to Biqing Chen; 2016056001@stu.gzucm.edu.cn

Received 26 April 2022; Revised 25 May 2022; Accepted 3 June 2022; Published 17 June 2022

Academic Editor: Xin Ning

In order to explore the kinematics and muscle force characteristics of competitive Taijiquan arm manipulation, and solve the problems of arm trajectory and control in the process of manipulation, this study puts forward the sports biomechanical analysis of arm manipulation in competitive Taijiquan. The technical characteristics and muscle force characteristics of 15 athletes from the competitive Taijiquan team of Xi'an Institute of physical education were studied. Use Excel 2007 and SPSS17.0 to statistically analyze and process the original data. According to the actual needs, the data indicators are summarized. The combined movements of competitive Taijiquan arm manipulation are captured through high-speed photography, and the kinematic data are statistically analyzed, mainly from the two aspects of action amplitude change and action braking. The results show the action track length, relative track length, and action track length of each plane of the two combined hands. The order of the two combined action tracks is: combination 1 > combination 2, in which the action track in the sagittal plane is the longest in combination 1, and it can also be considered that the motion amplitude in the sagittal plane is the largest in combination 1. The average acceleration of group A in the first beat is 0.51 m/s^2 smaller than that of group B, and the value is 0.22 m/s^2 smaller. Therefore, the deceleration of group A is larger than that of group B, and the braking capacity of group A is slightly stronger than that of group B. In the second beat, the average acceleration of group B is 1.5722 m/s^2 larger than that of group A, and the value is 0.210 m/s^2 larger. The average acceleration of group A in the third, fourth, fifth, and sixth beats is 0.9, 3.728, 0.57, and 0.837 m/s^2 smaller than that of group B, and the values are 0.466, 0.174, 0.250, and 0.003 m/s^2 smaller, indicating that the braking capacity of group A in the third, fourth, fifth, sixth, and eighth beats is slightly stronger than that of group B. In the braking of each beat in combination 1 and combination 2 of group AB, the braking ability of arm manipulation of group A is stronger than that of group B. In competitive Taijiquan, the movement techniques of manipulation include: bouncing technology, braking technology, and control technology. For arm manipulation, athletes should have the ability of "braking" technology. In the correlation analysis of movement track length, RMS and I EMG, the score of athletes in group A is high, and there is no correlation between movement track length and RMS. There is a significant correlation between RMS and movement track length in group B, and the correlation degree is moderate. This shows that when the movement of group B athletes is completed, the muscles are in a state of tension, the movement skills are not mastered well, and the energy saving is not achieved. During training, we should pay more attention to the proprioception of muscles and form a correct way of muscle exertion.

1. Introduction

After years of experience in the field, the success rate of competitive Taijiquan difficult movements gradually tends to be stable. In the application of difficult movement training methods, professional teams in various provinces and cities are different, but they are developing towards scientific and systematic training. Because the difficult movement of competitive Taijiquan requires one foot landing support, and the connection difficulty coefficient is very large, so that when competitive Taijiquan competition is carried out in the competitive field, there will still be mistakes and points deducted in the difficult movement. Through the investigation on the selection and completion of difficult movements of competitive Taijiquan, this study explores the training methods of difficult movements, so as to contribute to the scientific and sustainable development of competitive Taijiquan in China [1]. From the situation of Chinese competitive Taijiquan competition, the problems of athletes in difficult movements mainly include jumping, shaking, foot rolling, incoherent connection between front and back movements, and so on [2]. Therefore, we should understand the basic characteristics of difficult movements and fully realize the significance of the success of difficult movements for athletes to achieve excellent results. On this basis, the training system of difficult movements of competitive Taijiquan is designed, which has high research value and practical significance for enriching the training methods of difficult movements of competitive Taijiquan. This study summarizes the influencing factors involved in the difficult movement training of competitive Taijiquan, scientifically summarizes and systematically summarizes the methods and steps of difficult movement training of competitive Taijiquan according to the results of questionnaire and interview survey, hoping to provide theoretical basis for improving the overall level of difficult movement completion, find and make up for the shortcomings of difficult movement training methods, and provide theoretical reference for the training practice of competitive Taijiquan [3, 4]. Dynamic analysis is not carried out independently, and it often needs kinematic means to assist it. Synchronous measurement of kinematics and dynamics will better and more scientifically collect and analyze experimental data. Generally, the force value on the body ground or the peak value of flexion and extension muscle group when overcoming resistance can be measured by means of force measuring platform, isokinetic muscle strength tester, and plantar pressure. It is generally used to study the force value at a certain time of a sports event and the explosive power of athletes. Figure 1 shows the biomechanical factors affecting the economy of running [5].

2. Literature Review

Ding et al. used Ariel kinematics video fast feedback analysis system to analyze the three-dimensional kinematics of the rotating shot put technology of two excellent male shot putters in China. The whole action process was divided into six space-time points, and each space-time point was quantitatively analyzed [6]. Acosta and others used the three-dimensional image analysis method to analyze the kinematic characteristics of Chinese professional football players throwing long-distance out of bounds, and came to the conclusion that they want to throw long-distance and high-quality out of bounds. Athletes need to mobilize their body muscles as much as possible for orderly swing from bottom to top, and can release the ball within a reasonable and effective angle range [7]. Lee and others used six optical cameras to obtain the lower limb technical action images of 10 men's volleyball players during the take-off period of front and rear buckle. Through the analysis and research on the kinematic characteristics of the obtained data, it is concluded that the rear spike has shorter take-off time and larger parallel distance than the front buckle. The technical requirements of the front and rear breasting are different in the take-off stage [8]. Peng and others used the biomechanical principle to study and analyze the volleyball spiking action, and concluded that the force order of spiking action [9]. Rodrigues and others believe that testing and analyzing the indexes of kinematics, dynamics, and biology is the main research method and means of sports biomechanics, and the kinematics research method is one of its main research methods [10]. Kim and others have summed up the mechanical principles and requirements of the Taijiquan push hand technical action of "its root is in the foot, hair is in the leg, dominates the waist and shape is in the finger" with mechanical common sense and empirical perception [11]. Sun and others define Taijiquan pushing hand as a competitive skill project that follows certain rules and uses techniques such as hugging, stroking, squeezing, pressing, picking, eight, elbow, and leaning. Both sides stick together, judge each other's strength through the feeling of muscles, and then push each other out with strength to determine the outcome [12]. Anderson and others interpreted Taiji pushing hand as: two people are opponents of each other. According to the principle of "sacrificing themselves to others, calling for smooth delivery, sticking to each other, and not losing the top", they use the methods of shed, stroking, squeezing, pressing, picking, eight, elbow, leaning, advancing, retreating, looking, looking, and fixing to find out each other's strength and intention through the feeling of their skin, and achieve the form of sports to win each other in an effective way when they have the opportunity and power [13]. Wampler and others described in detail the technical movements of Taijiquan hand pushing, and summarized that the four techniques of holding, stroking, squeezing, and pressing are the main technical movements of Taijiquan hand pushing, which also explains the importance of shed, stroking, squeezing, and pressing in the process of Taijiquan hand pushing [14]. Ahmed and others proposed that Taijiquan push hand is based on the principle of "stick with touch, do not lose, do not top, do not be too short, bend and stretch with bending", using eight techniques and strength of "shed, stroke, squeeze, press, pick, clear, elbow, and lean", to practice the sensitivity of skin touch and inner body feeling of limbs, and find out the changes of each other's strength, such as direction, size, rigidity, reality, length, speed, and so on [15].

Based on the current research, this study puts forward the sports biomechanical analysis of arm manipulation in competitive Taijiquan. Using the synchronous measurement method of three-dimensional high-speed camera (casio-fh25) and *s* EMG (megawin6000), this study studies the hand movements of 15 teams in a sports college, evaluates the quality of 15 athletes, and carries out two groups of combined movements. The scores were divided into AB group and statistically analyzed by Excel 2007 and spss170. The results show that in the braking of each beat in combination 1 and combination 2 of group AB, the braking ability of arm manipulation of group A is stronger than that of group B. In competitive Taijiquan, the movement techniques of manipulation include: bouncing technology, braking technology and control technology. For arm manipulation, athletes should have the ability of "braking" technology. In the correlation analysis of movement track length, RMS and *i* EMG, the score of athletes in group A is high, and there is no

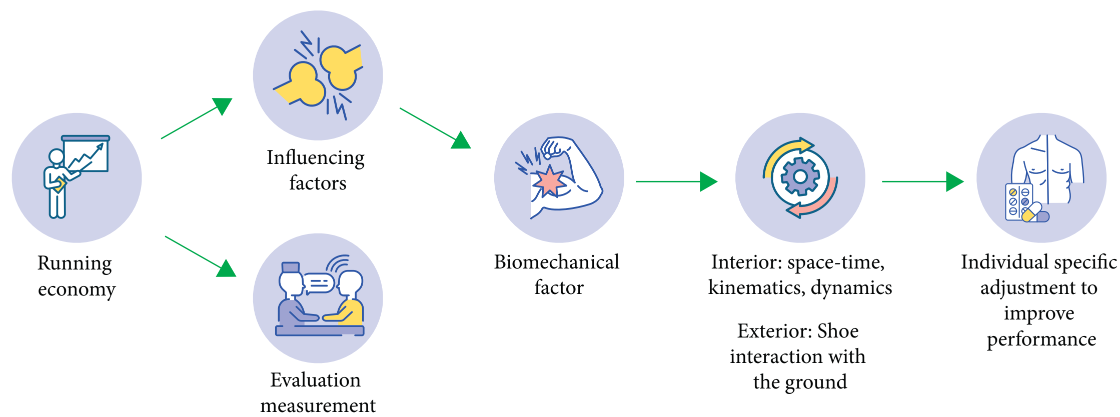

Figure 1: Biomechanical factors affecting running economy. It is generally used to study the force value at a certain time of a sports event and the explosive power of athletes.

correlation between movement track length and RMS. There is a significant correlation between RMS and movement track length in group B, and the correlation degree is moderate.

3. Method

3.1. Research Object. This study takes the technical characteristics and muscle force characteristics of 15 athletes from the competitive Taijiquan team of Xi'an Institute of Physical Education to complete the arm manipulation of competitive Taijiquan.

3.2. Research Methods

3.2.1. Subjects. About 15 athletes from the competitive Taijiquan team of a sports college were divided into 4 athletes with grade and 11 athletes without grade, including 10 males and 5 females. And the special years of the subjects were more than 3 years. The height of all subjects was 1.77 ± 0.09 m, the weight was 62.59 ± 8.85 kg, the age was 20.94 ± 1.44 years old, there was no medical history, and the test was in good condition without muscle fatigue. Finally, the athletes are grouped according to the scoring results of the athletes' arm manipulation.

3.2.2. Test Action. The exercise of competitive Taijiquan is complex and changeable, with certain innovation. In the competitive Taijiquan competition, they all appear in the form of combination, so the actions tested in this study are reflected in the form of combination. The arm manipulation of competitive Taijiquan can be divided into: take the shoulder joint as the axis, lift the arm in a certain direction and stop at a certain position, and the range of motion is no more than 180° [16, 17]. Flexion and extension: the upper arm is fixed and the elbow joint is the axis. The elbow joint is extended from straight to curved or from curved to straight. Winding/looping: arc movement of both arms or one arm with the shoulder as the axis or the forearm with the elbow joint as the axis. In the daily training of competitive Taijiquan, the basic arm manipulation movement combination will be practiced, and combined with the basic arm manipulation movement of competitive Taijiquan, so these basic movements are divided into two combination movements. Since the rhythm of the single action structure of winding/looping is not easy to control, the combined action test is not carried out for the action structure of winding. The main actions of combination 1 are: front lift, up lift, side lift, and down lift. The action of combination 2 is also a lift, including side up lift and side down lift. Among them, chest crossing is only a connecting action [18]. In the test, under the unified beat, the beat is 120 beats/minute, and the athletes complete two movements with heel lifting, and take the best group of movements for analysis.

3.2.3. Experimental Equipment. Equipment required for kinematics: 2 CASIO-FH25 high-speed cameras in Japan; Stereo calibration frame; lampstand; Tape measure; 1 synchronous lamp; American APAs image analysis system.

Equipment required by sEMG: Finland megawin6000 surface electromyography wireless remote tester, sampling frequency of 1000 Hz, 17 packs of electromyography, 1 bottle of 75% medical alcohol, 1 shaving knife, and 1 pack of medical tampon.

Equipment required for sEMG standardized test: use Lifefitness and purelength fitness equipment, including pastor chair biceps trainer; Gantry comprehensive trainer; Dumbbells; Sitting high tension back muscle trainer [19].

3.2.4. Experimental Content. Test of high-speed camera: in this test, two high-speed cameras are used for synchronous shooting, and the shooting frequency is 30 Hz to analyze the kinematics of the action image.

Test of actual action sEMG. sEMG test muscles include biceps brachii, triceps brachii, middle bundle of deltoid and latissimus dorsi on the left and right sides, with a total of 8 muscles.

sEMG standardized test.

The maximum random isometric contraction (MIVC) strength test was performed on the tested muscles, and the test results were taken as the standardized value (100%).

3.2.5. Indexes Selected in the Experiment. Kinematic indexes and *s* EMG indexes are selected in this study.

Kinematic index:

Original coordinates: in this study, the original coordinates of each athlete's hand on the X, y and Z axes are selected to calculate the athlete's action track length [20].

Linear speed, this study selects the linear speed from the upper arm to the forearm, and obtains the arm braking effect of each athlete through the change of linear speed.

sEMG indicators:

RMS index, RMS is selected in this study to explore the rhythmicity of motor unit recruitment and excitation of each muscle. The calculation formula of RMS is as follows:

$$RMS = \sqrt{\frac{1}{N}\sum_{i=1}^{N} X_i}. \tag{1}$$

I EMG index, this study selects iEMG to explore the participation of muscle fibers. The calculation formula is

$$iEMG = \int_{N2}^{N1} X(t)\mathrm{d}t, \tag{2}$$

$N2$ is the starting point of integration; $N1$ is the end point of integration; X(t) is the function value of EMG curve; DT is the sampling interval, in millivolts per second.

3.2.6. Mathematical Statistics. Use Excel 2007 and SPSS17.0 to statistically analyze and process the original data. Summarize various data indicators according to the actual needs. Excel 2007 makes statistics and summary of the data, and uses independent sample t-test and correlation analysis to analyze the correlation and difference of the data. If $P < 0.05$, there is significant difference between the mean values of the two samples; if $P < 0.01$, there is very significant difference between the mean values of the two samples [21, 22].

3.3. Experimental Process. Two high-speed cameras (casio-fh25, Japan) were used to shoot in the gymnasium of Xi'an Institute of Physical Education by using the method of three-dimensional fixed camera photography. The two cameras and the subjects were in an isosceles right triangle [23]. The shooting distance is 7 m, the machine height is 1.0 m, the focal length is 49 mm, and the shooting frequency is 30 Hz. Use the Finnish MegaWin6000 surface electromyography wireless telemetry system to test it synchronously, and carry out standardized test for each muscle tested.

3.3.1. Test the Main Muscles of the Movement. Analyze the participating muscles of the test action from human anatomy, and analyze the actions of the two combinations, respectively. The results are as follows.

The participating muscles of each action in combination 1: Front lift, up lift, and side lift: biceps brachii, triceps brachii, deltoid, latissimus dorsi, extensor digitorum, extensor ulnaris lateralis, and pectoralis major. Downward lift: biceps brachii, triceps brachii, deltoid, latissimus dorsi, extensor digitorum, and extensor ulnaris lateralis [24].

Participating muscles of each action in combination 2: Chest cross, side down lift: biceps brachii, triceps brachii, deltoid, latissimus dorsi, extensor digitorum, and extensor ulnaris lateralis. Side lift: biceps brachii, triceps brachii, deltoid, latissimus dorsi, extensor digitorum, extensor ulnaris lateralis, and pectoralis major.

3.3.2. Basis of Muscle Selection. The muscles selected in this study are selected according to the structure of human anatomy, muscle function, and the characteristics of surface electromyography wireless remote test system. The biceps brachii spans the shoulder joint, elbow joint, and proximal radioulnar joint, so it has an effect on these three joints. The biceps brachii is divided into long head and short head. The main function is to bend the elbow joint and turn the forearm back [25]. Triceps brachii is located behind the humerus. Its main function is to extend the elbow joint and help the shoulder joint extend back and adduct. The middle bundle of deltoid muscle is located at the shoulder joint, and its main functions are shoulder abduction, flexion and pronation, extension and pronation. Latissimus dorsi is located at the back of the waist and the posterolateral sternum. Its main functions are shoulder joint extension, adduction, and internal rotation.

4. Results and Analysis

4.1. Kinematic Characteristics of Arm Manipulation. Through high-speed photography, the combined movement of competitive Taijiquan arm manipulation is captured, analyzed by the American APAs image system, and the kinematic data are statistically analyzed, mainly from the two aspects of action amplitude change and action braking. The results are as follows.

4.1.1. Change of Arm Manipulation Range. In competitive Taijiquan, the range of movement is one of the standards to judge the quality of athletes' movement completion. Action trajectory refers to the spatial characteristics of the action composed of the route that a part of the body passes from the starting position to the end. In kinematics, the length of action trajectory can be used to reflect the size of action amplitude. In arm manipulation, there are "route" requirements for combined action. The "route" of an action is the trajectory from one action to another. If the combination of manipulation action is straight arm, it is required to take the farthest "route". If the arm action is from bending arm to straight arm, it is required to take the shortest "route". In this study, because the athletes have a long sports life and the action routes of combined actions meet the above requirements, the action amplitude of combined actions of groups A and B is analyzed by the length of action track in biomechanics. The calculation of the length of the action track is based on the original coordinates of the athlete's completion of the action. The length from the second coordinate point to the first coordinate point is obtained, then it is superimposed, and finally the sum is obtained to obtain the track length of the complete action. Available formula is as follows:

$$L = \sum \sqrt{(X_{n+1} + X_n)^2 + (Y_{n+1} - Y_n)^2 + (Z_{n+1} - Z_n)^2}, n = 1, 2, 3, \ldots, \quad (3)$$

where L is the length of action track.

The hand is the limb end of the arm, and the movement track of the hand can be regarded as the movement track of each combined action. The track length of an athlete can also represent the range of motion of the athlete. In this study, the movement trajectory of the hand is selected, the trajectory length of the left and right hands is calculated, respectively, and then the average value is taken to reflect the trajectory length of the athlete's movement in the combination. Due to the difference of gender and height, the relative track length is obtained by the ratio of action track length to height. In order to more intuitively understand the movement trajectory changes of each combined action, select the movement trajectory of Jiang's left and right hands in group A and Niu's left and right hands in group B.

It can be seen from Table 1 that there is no significant difference between the two groups from the results of t-test. According to the action structure, the combined actions include flexion, abduction, adduction, and so on. In terms of numerical value, group A was longer than group B in terms of track length in horizontal plane, sagittal plane, frontal plane, and relative track length. In terms of relative track length, group A is 19.2 cm longer than group B on the sagittal plane, 7.5 cm longer than group B on the frontal plane, and 13.5 cm longer than group B on the horizontal plane. The longest length of group A is in the sagittal plane, and the longest length of group B is in the frontal plane. In combination I, the action amplitude of group A is greater than that of group B. It can be considered that the combined action has a long trajectory in the frontal and sagittal planes.

This is due to the action structure. The first four beats and the last four beats of the combined action of combination I are symmetrical actions, in which the front lift (the first beat and the seventh beat) and the up lift (the second beat and the sixth beat) mainly move in the frontal plane and horizontal plane, and the side lift (the third beat and the fifth beat) and the down lift (the fourth beat and the eighth beat) mainly move in the sagittal plane and horizontal plane. Combined with the relative track length, the action amplitude of group A in front lift and up lift is greater than that in side lift and down lift. The range of side lift and down lift in group B was greater than that in front lift and side lift.

The action trajectories of the two groups of hands are different on each plane, so the statistical analysis of the trajectories of XY (horizontal plane), XZ (frontal plane), and YZ (sagittal plane) on each plane is shown in Table 2.

It can be seen from Table 2 that there is no significant difference between the two groups from the results of t-test. According to the action structure, the actions of combination 2 include flexion, external rotation, adduction, and so on. In terms of numerical value, group A was longer than group B in terms of track length in horizontal plane, sagittal plane, frontal plane, and relative track length. From the perspective of relative trajectory, the longest is in the horizontal plane. On the horizontal plane, group A is 34.8 cm longer than group B. Secondly, in the sagittal plane, group A was 11 cm longer than group B. The shortest length was on the frontal plane. Group A was 8.1 cm longer than group B. It can be considered that in combination 2, the trajectory of motion on the horizontal plane is the longest. This is due to the structure of the action. The combination two has four beats, in which the chest cross two beats (the first beat and the third beat) mainly move in the horizontal plane and sagittal plane. The action structure of side up lift and side down lift is the same, but the end position of the action is different. One is side up (45° inclined up) and the other is side down (45° inclined down). Its moving surface is the same. The two beat actions move on the frontal plane and horizontal plane. Combined with the action structure and research results, it shows that the combined action of combination 2 has the longest trajectory on the horizontal plane, that is, the maximum motion amplitude on the horizontal plane.

Based on the above, the action track length, relative track length, and action track length of each plane of the two combined hands. The order of the two combined action tracks is: combination 1 > combination 2, in which the action track in the sagittal plane is the longest in combination 1, and it can also be considered that the motion amplitude in the sagittal plane is the largest in combination 1. The action track of combination 2 is the longest on the horizontal plane, and it is considered that the movement amplitude of combination 2 is the largest on the horizontal plane. In the action trajectories of these two combinations, the action trajectories of group A are longer than those of group B, and the action range of group A is larger than that of group B in the three combinations, which is consistent with the score results of the referee. Therefore, the length of action trajectories can be used as one of the criteria for judging the arm manipulation of athletes. The reason for the difference between the action trajectories of the two combined actions is that the beat is inconsistent: among them, combination 1 is an eight beat action and combination 2 is a four beat action. Difference of action structure: because each combined action structure has its own characteristics, the motion trajectory of each combination is different. Combined with the height difference between the two groups of athletes, there is no significant difference. The difference between the mean values is only 0.94 cm, and the movement structure is consistent. The reason for the difference in the length of movement track between the two groups of AB is that the movement of group B athletes is not "in place". In particular, the action of lifting requires a certain angle of arm action. For example, the forward lift requires the arm to be parallel to the ground when the action is in place, and the upward lift requires the arm to be located on the ear side. In training, the coach requires the "arm to clamp the ear". The action route is not clear: in competitive Taijiquan, the action of lifting requires taking the "farthest route". For example, in combination 1, the "farthest route" should be taken from the front lift to the upper lift, and the same is true from the upper lift to the side lift. Some of these movements require the most

Table 1: Track length of group AB hand.

	XY	*XZ*	*YZ*
Group a track length	6.076 ± 0.531	7.467 ± 0.442	7.572 ± 0.456
Group B track length	5.869 ± 0.29	7.382 ± 0.357	7.278 ± 0.344
Difference (A-B)	0.194	0.086	0.275
Group a relative track length	3.545 ± 0.384	4.362 ± 0.330	4.424 ± 0.349
Group B relative track length	3.412 ± 0.175	4.285 ± 0.202	4.24 ± 0.255
Difference (A-B)	0.136	0.076	0.193

Table 2: Action track length of group AB hands.

	XY	*XZ*	*YZ*
Group A track length	5.182 ± 0.576	4.548 ± 0.288	4.598 ± 0.53
Group B track length	4.617 ± 0.476	4.386 ± 0.387	4.428 ± 0.472
Difference (A-B)	0.568	0.163	0.169
Group A relative track length	3.032 ± 0.400	2.658 ± 0.238	2.689 ± 0.238
Group B relative track length	2.684 ± 0.299	2.548 ± 0.23	2.577 ± 0.318
Difference (A-B)	0.349	0.12	0.082

recent route. Flexibility of shoulder: from the results, the movement track length of group B is smaller than that of group A, indicating that the flexibility of group A's shoulder is better than that of group B. When athletes do movements, they shrug and pinch their shoulders, especially when their arms are up. Some athletes are used to shrugging their shoulders. For this phenomenon, athletes should strengthen the practice of proprioception, always remind when doing actions, and slowly correct this wrong habit.

4.1.2. Arm Action Braking Effect. In competitive Taijiquan, whether the arm manipulation action of a single action or the combined arm manipulation action, each beat action needs to have "braking". In the kinematic index, the change of midline speed can be reflected from the moment of maximum online speed to the end of the action or the moment when the speed drops to zero. The speed change during this period is the "braking" of the arm, which is expressed by Δv and the average acceleration $\overline{a}$, according to the formula

$$\overline{a} = \frac{\Delta v}{\Delta t}. \tag{4}$$

Through the index of linear speed, the Δv value and average acceleration of each athlete's left hand and right hand in each beat are calculated, and then the average value is taken. The mean value can be considered as the speed change during the braking of the athlete's arm movement. The results of Δv and average acceleration of each beat between the two groups are shown in Tables 3 and 4.

The arm braking changes and t-test results of each beat in combination I are shown in Table 3. It can be seen from Table 3 that in terms of speed change, the minus sign only represents the deceleration process. In terms of value, the change trend of the two groups of speeds is consistent with the acceleration. The average acceleration of group A in the first beat is $0.51\,\mathrm{m/s^2}$ smaller than that of group B, and the Δv value is $0.22\,\mathrm{m/s^2}$ smaller. Therefore, the deceleration of group A is larger than that of group B, and the braking capacity of group A is slightly stronger than that of group B. In the second beat, the average acceleration of group B is $1.5722\,\mathrm{m/s^2}$ greater than that of group A, and the Δv value is $0.210\,\mathrm{m/s^2}$ greater. The average acceleration of group A in the third, fourth, fifth, and sixth beats is 0.9, 3.728, 0.57, and $0.837\,\mathrm{m/s^2}$ smaller than that of group B, and the V value is 0.466, 0.174, 0.25,0 and $0.003\,\mathrm{m/s^2}$ smaller, indicating that the braking capacity of group A in the third, fourth, fifth, sixt,h and eighth beats is slightly stronger than that of group B. The Δv value and average acceleration of group B in the seventh beat are less than those of group A. It can be considered that the braking capacity of group B in the seventh beat is slightly stronger than that of group A. The Δv value and average acceleration of group A in the eighth beat are smaller than those of group B, the deceleration of group B in the eighth beat is larger than that of group A, and the braking capacity of group A is slightly stronger than that of group B. It can be seen from the above that in the eight beat action of combination 1, the braking ability of group A is stronger than that of group B in the six beat action, and the braking ability of group B in the two beat action is stronger than that of group A. It can be considered that in the combination action of combination 1, the braking ability of athletes in group A is stronger than that of group B. The braking action of the second and seventh beats is the change between the front lift and the up lift. The braking action of the second beat is the braking action from the front lift to the upper lift, and the braking action of the seventh beat is the braking action from the upper lift to the front lift. The changes between the two movements of the athletes in group A are not as good as those in group B. The braking capacity of other actions of group B is not as good as that of group A.

In combination 2, the braking changes of the arm at each beat are shown in Table 4. It can be seen from Table 4 that from the numerical point of view, the change trend of the two groups of speeds is consistent with the acceleration. The Δv value and average acceleration of the first, second, and

Table 3: Arm action braking of group AB.

Rhythm	1	2	3	4	5	6	7	8
Group A Δv	-3.498 ± 0.704	-2.869 ± 0.737	-3.404 ± 0.843	-3.809 ± 0.775	-3.938 ± 1	-3.12 ± 0.76	-3.16 ± 1.2	-3.51 ± 1.02
Group B Δv	-3.269 ± 0.663	-3.054 ± 0.376	-2.941 ± 0.531	-3.635 ± 0.517	-3.681 ± 10.61	-3.13 ± 0.3	-3.1 ± 0.41	-3.21 ± 0.39
Difference A-B Δv	−0.228	0.186	−0.466	−0.172	−0.258	−0.002	0.06	−0.29
Group A $\overline{a}$	-17.643 ± 12.356	-13.422 ± 7.461	-16.877 ± 9.708	-22.936 ± 9.374	-18.772 ± 11.67	-17.91 ± 10.78	-16.43 ± 11.04	-16.04 ± 12.34
Group B $\overline{a}$	-17.143 ± 5.862	-14.993 ± 3.215	-16.173 ± 5.328	-19.207 ± 11.54	-18.21 ± 5.33	-17.08 ± 4.48	-17.99 ± 6.36	-14.71 ± 3.24
Difference A-B $\overline{a}$	−0.6	1.572	−0.8	−3.726	−0.57	−0.837	1.567	−1.335

Table 4: Arm action braking of group AB.

Rhythm	1	2	3	4
Group A Δv	-3.498 ± 0.31	-3.72 ± 2.44	-9.8 ± 0.44	-5.18 ± 1.29
Group B Δv	-4.09 ± 0.99	-3.26 ± 0.49	-8.56 ± 0.43	-4.72 ± 0.8
Difference A-B Δv	-0.7	-0.46	-1.24	-0.45
Group A $\overline{a}$	-14.88 ± 6.12	-23.82 ± 17.47	-13.42 ± 7.46	-19.67 ± 9.38
Group B $\overline{a}$	-13.46 ± 5.32	-18.22 ± 7.94	-14.7 ± 4.44	-19.18 ± 8.58
Difference A-B $\overline{a}$	-1.41	-5.6	-1.27	-4.99

fourth beat actions of group A are less than those of group B. from the perspective of braking effect, the braking ability of the arm manipulation combination actions of group A of the first, second, and fourth beat is stronger than that of group B. The Δv value and average acceleration of group B in the third beat are less than that of group A. From the perspective of braking effect, the braking ability of group B in the third beat is better than that of group A. The braking of the third beat is the action of lifting from the side up to the chest cross. In this beat, the braking of group A is stronger than that of group B. On the whole, in combination 2, the braking ability of arm manipulation in group A is stronger than that in group B, and the arm manipulation braking technology in group A is better than that in group B.

Based on the above data results, from the results of t-test, there is no significant difference between AB and ab groups ($P > 0.05$). From the numerical point of view, in the braking of each beat in combination 1 and combination 2 of group AB, the braking ability of arm manipulation of group A is stronger than that of group B. In competitive Taijiquan, the movement techniques of manipulation include: bouncing technology, braking technology and control technology. For arm manipulation, athletes should have the ability of "braking" technology. Through the braking technology, we can see the athlete's control over the action, and through the action control ability, we can evaluate the athlete's ability and level. Generally speaking, athletes with good action braking ability also have a good grasp of action control and understanding. The braking ability of the movement also reflects the athlete's control of muscle tension and relaxation. From the formation process of motor skills, it shows that the inhibition of motor center in cerebral cortex has been established and the formation of motor skills is automatic. The braking ability of group B athletes is weaker than that of group A. the main reasons are: the muscle exertion mode is wrong: the main exerting muscles of group AB athletes may be different, so there are differences in the muscle parts of action exertion. There are differences in muscle tension and relaxation ability: in competitive Taijiquan, athletes need to exert force and brake quickly, and have high requirements for muscle tension and relaxation ability. The ability of muscle tension and relaxation can be called energy saving in physiology. The ability of excellent athletes in this aspect is greater than that of ordinary athletes. There are some wrong movements: because the sports years of the two groups of athletes are more than three years, the movements have been automated. The original wrong action has also become automatic and difficult to correct.

4.2. s EMG Analysis. The *s* EMG of this study was carried out simultaneously with high-speed photography to explore the muscle force characteristics of athletes in each combination. The main muscles tested are: left biceps brachii, left triceps brachii, left deltoid middle bundle, left latissimus dorsi, right biceps brachii, right triceps brachii, right deltoid middle bundle, and right latissimus dorsi. RMS and EMG were selected to judge the strength of each muscle activity. Considering the difference of sebum thickness among athletes, it is impossible to make a direct comparative analysis. In the process of the experiment, each muscle is standardized, and then the standardized value of each athlete is obtained, and of each athlete is compared and analyzed.

4.2.1. Combination 1 s EMG Feature. The standardized value of RMS of combination 1 is shown in Figure 2.

As can be seen from Figure 2, the maximum muscles of the two groups are different. Group A is 118.87% of the right latissimus dorsi, group B is 75.78% of the left triceps brachii, and the minimum muscles are the left biceps brachii, group A is 12.87%, and group B is 10.78%. From the above figure, we can see that the standardized values of the muscles and standardized actions on the right are larger than those on the left. In group A, the latissimus dorsi and triceps brachii on both sides and biceps brachii were larger than those in group B, and the RMS standardized values of other muscles in group B were larger than those in group A.

The *i* EMG features of the combination are shown in Figure 3.

It can be seen from Figure 3 that in the combined arm manipulation, the standardized values of latissimus dorsi on both sides of group A are larger than those of other muscles, and the standardized values of triceps brachii on the left and biceps brachii on the right in group B are larger than those of other muscles. The lowest standardized value of the two groups was the left biceps brachii.

Based on the above standardized values of RMS and I EMG, the muscle standardized values of the two groups changed, but the change trend of their standardized size was unchanged. In the exercise of combination 1, the arms on both sides start to act at the same time. It is found that the standardized value of athletes in group AB is greater on the right than on the left. This is because the dominant hand of most athletes is the right hand, which is related to personal sports habits. Combined with the standardized values of RMS and I EMG in Figures 3 and 4, it is found that the recruitment ability and excitation rhythm of motor units of latissimus dorsi muscle in group A are stronger than those of

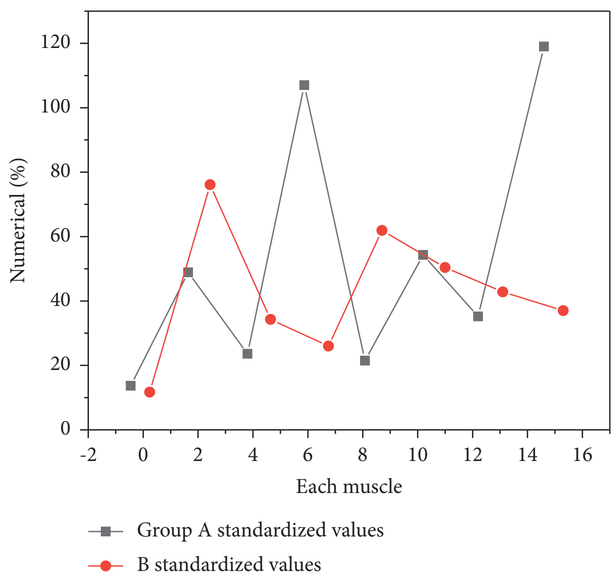

Figure 2: RMS standardized values of muscles in group AB. In group A the latissimus dorsi and triceps brachii on both sides and biceps brachii were larger than those in group B and the RMS standardized values of other muscles in group B were larger than those in group A.

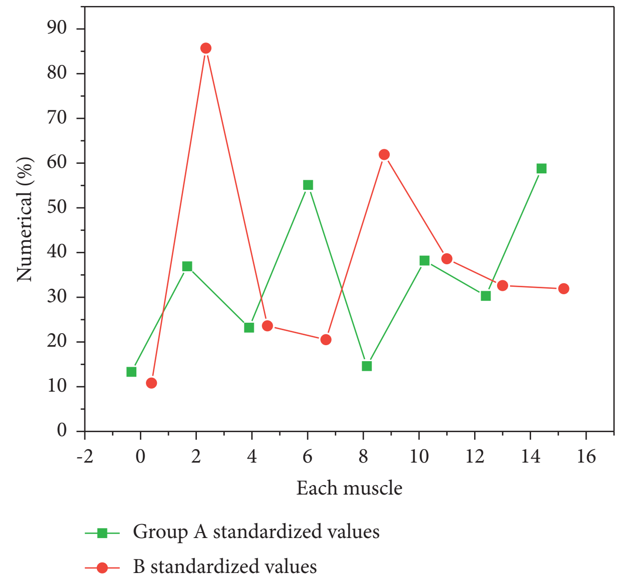

Figure 3: Standardized values of I EMG of muscles in groups B and AB. The lowest standardized value of the two groups was the left biceps brachii.

other muscles, and the participation of muscle fibers is also more than that of other muscles. It can be considered that the latissimus dorsi muscle is the main muscle involved in the arm manipulation of group A, and the triceps brachii on the left and biceps brachii on the right in group B have stronger recruitment ability and excitation rhythm of motor units than other muscles, and the participation of muscle fibers is also more than other muscles. It can be considered that the main muscles in group B are the triceps brachii on the left and the biceps brachii on the right. Combined with the scoring results of the referees on the athletes' arm manipulation movement, the athletes in group A are higher than those in group B, which shows that the action completion quality of group A is high, and it can be considered that the action force mode of this group of athletes is more correct than that of group B. Therefore, the main muscles of combined arm manipulation are latissimus dorsi on both sides. The athletes in group B should improve the way of exertion, no longer take the left triceps brachii and the right biceps brachii as the main exerting muscles, but change to latissimus dorsi.

4.2.2. sEMG Characteristics of Combination 2. The standardized value of RMS of combination 2 is shown in Figure 4.

As can be seen from Figure 4, among the standardized values of all muscles in group A, the maximum value is 89.61% of the latissimus dorsi on the right, and the minimum value is 11.32% of the biceps brachii on the left. Among the standardized values of all muscles in group B, the maximum value was 56.31% of the biceps brachii on the right and the minimum value was 17.69% of the latissimus dorsi on the left. The RMS standardized values of bilateral latissimus dorsi, right triceps brachii, and middle bundle of right deltoid in group A were higher than those in group B. In general, the standardized value of the right muscle in group A was greater than that in group B, and the standardized value of the left muscle in group B was greater than that in group A.

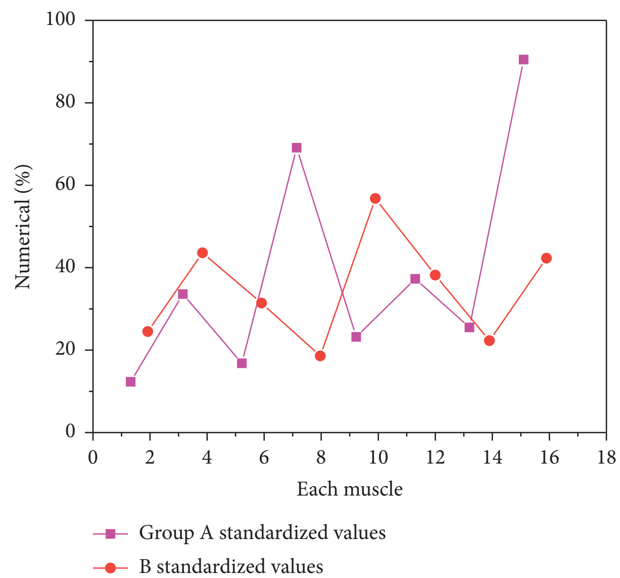

Figure 4: RMS standardized values of muscles in group AB. Among the standardized values of all muscles in group (B) the maximum value was 56.31% of the biceps brachii on the right and the minimum value was 17.69% of the latissimus dorsi on the left.

The *i* EMG characteristics of combination II are shown in Figure 5.

As shown in Figure 5, in the combined second-hand arm manipulation, the standardized value of latissimus dorsi on

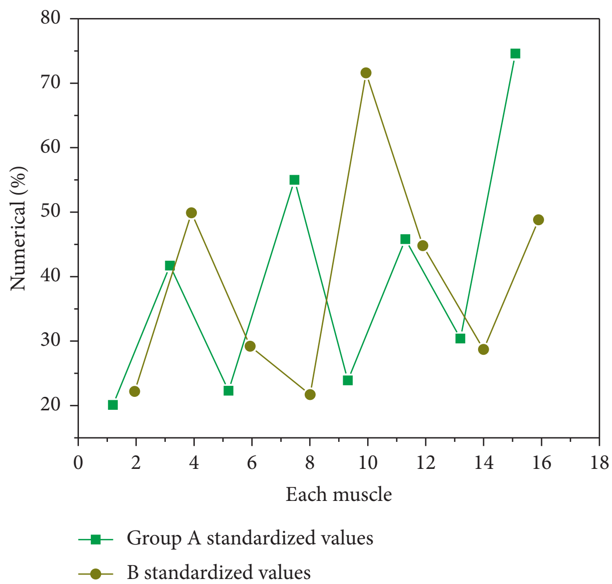

Figure 5: Standardized values of i EMG of muscles in group AB. In group B the standardized values of the left triceps brachii and the right biceps brachii were greater than those of other muscles, and the smallest value was the left latissimus dorsi.

both sides of group A is the largest, and the lowest standardized value is the left biceps brachii. In group B, the standardized values of the left triceps brachii and the right biceps brachii were greater than those of other muscles, and the smallest value was the left latissimus dorsi.

Based on the above standardized values of RMS and I EMG, the muscle standardized values of the two groups changed, but the change trend of their standardized size was unchanged. It is found that the muscle force on the right side of the athletes in group AB is greater than that on the left, indicating that the dominant hand of both groups is the right hand. This is because the dominant hand of most athletes is the right hand, which is related to personal sports habits. Combined with the standardized values of RMS and I EMG of latissimus dorsi in Figures 4 and 5, it is found that the recruitment ability and excitation rhythm of motor units of latissimus dorsi in group A are stronger than those of other muscles, and the participation of muscle fibers is also more than that of other muscles. It can be considered that in the arm manipulation of combination 2, the latissimus dorsi muscle is the main muscle involved in group A, and the recruitment ability and excitation rhythm of motor units of right biceps brachii and left triceps brachii in group B are stronger than those of other muscles, and the participation of muscle fibers is also more than that of other muscles. It can be considered that the main muscles in group B are the right biceps brachii and the left triceps brachii. Combined with the score results of the referee on the athletes' arm manipulation movement, it shows that the movement completion quality of group A is high, and it can be considered that the movement force mode of this group of athletes is more correct than that of group B. Therefore, the main muscles for the arm manipulation of combination 2 are the latissimus dorsi muscles on the left and right sides.

According to the characteristics of RMS and *i* EMG in these two combinations, the latissimus dorsi muscle is the main muscle in group A in the three combinations. The main muscles involved in group B in combinations 1 and 2 are the right triceps brachii and the left biceps brachii. In competitive Taijiquan, the basic form requirements for athletes are: lift the heels of both feet, clamp the legs and hips inward, clamp the shoulder blades backward, straighten the spine, sink the shoulders, center the head, open both hands, straighten the arms, put the five fingers together, and force to the fingertips. The control of athletes' basic posture also reflects the control ability of athletes to a certain extent. Combined with the structure and function of muscles and the research results, it can be considered that the basic shape of group A is better than group B, and the control ability of group A is stronger than group B. From the perspective of sports skills, the athletes in group A have a high degree of energy saving, good nerve control over muscles, and less redundant actions. It is suggested that athletes and coaches should mainly focus on the training of latissimus dorsi muscle in the training of arm manipulation, instead of the traditional arm muscle strength training.

In the correlation analysis of motion trajectory length, RMS and *i* EMG, there was no linear correlation in group A and moderate correlation in group B. The correlation between action track length and RMS and *i* EMG in group B was greater than that in group A. Combined with the referee's score results, the athletes in group A have high scores, and there is no correlation between the three indexes of action track length and RMS. There is a significant correlation between RMS and movement track length in group B, and the correlation degree is moderate. This shows that when the movement of group B athletes is completed, the muscles are in a state of tension, the movement skills are not mastered well, and the energy saving is not achieved. During training, we should pay more attention to the proprioception of muscles and form a correct way of muscle exertion.

5. Conclusion

This study provides a biomechanical analysis of the movements of Taijiquan hands. In this study, biomechanical research methods and tools were used to analyze the arm manipulation of competitive Taijiquan, and the problems of kinematics and muscle strength characteristics were solved. Pull and control arm movement during adjustment. Using the synchronous measurement method of three-dimensional high-speed camera (casio-fh25) and *s* EMG (megawin6000), this study studies the hand movements of 15 teams in a sports college, evaluates the quality of 15 athletes, and carries out two groups of combined movements. The scores were divided into AB group and statistically analyzed by Excel 2007 and spss170. The kinematic characteristics of arm exercise and the strength characteristics of eight muscles (biceps, triceps, middle deltoid, and major muscle) were studied in the two groups of athletes. The results show that in the competitive Taijiquan movement combining hand and chemistry, the movement of group a athletes is close to the music rhythm, and the movement coordination conforms to the rhythm of group A, which is more than that of group B. The larger the relative trajectory, the greater the motion amplitude and the higher the elongation. The length of track a is longer than that of group B, which is consistent with the scoring results. The "braking" method is very important. Comparing the normal values of RMS and I EMG during ab exercise between the two groups, the right muscle load was greater than the left. When combined with arm exercises, the core muscles use the left and right back muscles. The main muscles in group A are back muscles, and the main muscles in group B are triceps and biceps. In order to further brake the hand action, you can switch the hand action from two times to one blow, and feel the braking process. For athletes who have completed the action automation, special attention should be paid to the "in place" of the action.

Data Availability

The data used to support the findings of this study are available from the corresponding author upon request.

Conflicts of Interest

The authors declare no conflicts of interest.

Acknowledgments

This work was supported by Humanities and Social Sciences (Pedagogy) Youth Fund Project from Ministry of Education "Research on the Influence of Public Welfare Sports on College Students' Sports Interest and Behaviors and the Construction of Long-Term Mechanism" (17YJC880020).

References

[1] D. J. Diangelo, C. Chung, D. Hoyer, T. Carson, and K. T. Foley, "164. biomechanical analysis of the endplate fixation methods of cervical total disc replacement (tdr) prostheses to shear force expulsion," *The Spine Journal*, vol. 21, no. 9, pp. S82–S83, 2021.

[2] I. Villagrán, C. Moënne-Loccoz, V. Aguilera et al., "Biomechanical analysis of expert anesthesiologists and novice residents performing a simulated central venous access procedure," *PLoS One*, vol. 16, no. 4, Article ID e0250941, 2021.

[3] N. Nishida, M. Mumtaz, S. Tripathi, A. Kelkar, T. Sakai, and V. K. Goel, "Biomechanical analysis of posterior ligaments of cervical spine and laminoplasty," *Applied Sciences*, vol. 11, no. 16, p. 7645, 2021.

[4] S. E. Bayramoğlu, N. Sayın, D. Y. Ekinci, N. Aktay Ayaz, and M. Çakan, "Anterior segment analysis and evaluation of corneal biomechanical properties in children with joint hypermobility," *Turkish Journal of Orthodontics*, vol. 50, no. 2, pp. 71–74, 2020.

[5] O. A. Ezeukwu, C. P. Ojukwu, A. J. Okemuo, C. F. Anih, I. T. Ikele, and S. C. Chukwu, "Biomechanical analysis of the three recommended breastfeeding positions," *Work*, vol. 66, no. 1, pp. 183–191, 2020.

[6] J. Ding, F. Wang, F. Jin, Z.-k. Wu, and P.-q. Shen, "Finite element and biomechanical analysis of risk factors for implant failure during tension band plating," *Journal of International Medical Research*, vol. 48, no. 11, Article ID 030006052097207, 2020.

[7] J. Acosta, J. M. Rinaldi, J. J. Guth, and S. Akhavan, "The loop 'n' tack knot: biomechanical analysis of a novel suture technique for proximal biceps tenodesis," *Orthopaedic Journal of Sports Medicine*, vol. 8, no. 9, Article ID 232596712095231, 2020.

[8] J.-S. Lee, M.-H. Lim, and J.-H. Back, "A biomechanical analysis of the turn leap in modern dance," *Korean Journal of Sports Science*, vol. 29, no. 1, pp. 813–822, 2020.

[9] X. Peng and L. Tang, "Biomechanics analysis of real-time tennis batting images using internet of things and deep learning," *The Journal of Supercomputing*, vol. 78, no. 4, pp. 5883–5902, 2021.

[10] A. A. Rodrigues, T. D. D. Silva, E. A. Soares et al., "Analysis of biomechanical properties of tibias after bone failure and ozone treatment in rats," *Research, Society and Development*, vol. 9, no. 9, Article ID e530997474, 2020.

[11] K. Kim, B. Davaasambuu, R. Wei, and Y. H. Kim, "Biomechanical investigation of anterior cruciate ligament injury risk in pivoting leg during taekwondo kicks using motion analysis system," *Journal of Mechanical Science and Technology*, vol. 36, no. 2, pp. 1051–1056, 2022.

[12] X. Sun, X. Gao, B.-k. Mu, and Y. Wang, "Understanding the role of corneal biomechanics-associated genetic variants by bioinformatic analyses," *International Ophthalmology*, vol. 42, no. 3, pp. 981–988, 2021.

[13] S. T. Anderson, M. Dorris, M. Littles, T. Rodriguez, and M. Spear, "Working out the woes: an analysis of the impact of exercise on depression," *Plastic Surgical Nursing*, vol. 41, no. 1, pp. 54–60, 2021.

[14] D. A. Wampler, R. M. Stewart, R. Summers et al., "Biomechanical motion analysis of cervical and thoracolumbar spine during ambulance transport: a healthy volunteer study," *Journal of Neurology Research*, vol. 10, no. 3, pp. 73–79, 2020.

[15] M. Ahmed and G. D. Ghai, "Joints activity and its role in the upper extremity in badminton strokes: a biomechanical perspective of sports education," *Humanities & Social Sciences Reviews*, vol. 8, no. 4, pp. 522–529, 2020.

[16] R. Taiar, M. Bernardo-Filho, and Mario, "Editorial "biomechanical spectrum of human sport performance"," *Applied Sciences*, vol. 10, no. 5, p. 1898, 2020.

[17] N. Kurpiers, P. Mcalpine, and U. G. Kersting, "A biomechanical field testing approach in snow sports: case studies toward a detailed analysis of joint loading," *Proceedings of the Institution of Mechanical Engineers - Part P: Journal of Sports Engineering and Technology*, vol. 234, no. 4, pp. 337–346, 2020.

[18] W. Wei and L. Yalong, "Study on treatment and rehabilitation training of ligament injury of javelin throwers based on sports biomechanics," *Measurement*, vol. 171, no. 4, Article ID 108757, 2021.

[19] A. V. Shpakov, A. V. Voronov, A. A. Artamonov, D. O. Orlov, and A. A. Puchkova, "Biomechanical characteristics of walking and running during unloading of the musculoskeletal system by vertical hanging," *Human Physiology*, vol. 47, no. 4, pp. 419–428, 2021.

[20] F. D. Villa, M. Buckthorpe, A. Grassi, A. Nabiuzzi, and S. D. Villa, "Systematic video analysis of acl injuries in professional male football (soccer): injury mechanisms, situational patterns and biomechanics study on 134 consecutive cases," *British Journal of Sports Medicine*, vol. 54, no. 23, 2020.

[21] R. N. Rekik, R. Bahr, F. Cruz, P. D'Hooghe, P. Read, M. Tabben et al., "059 the mechanisms of anterior cruciate ligament injuries in male professional football players in the

middle east: a systematic video analysis of 15 cases," *British Journal of Sports Medicine*, vol. 54, no. Suppl 1, p. A26, 2020.

[22] F. Roggio, S. Ravalli, G. Maugeri et al., "Technological advancements in the analysis of human motion and posture management through digital devices," *World Journal of Orthopedics*, vol. 12, no. 7, pp. 467–484, 2021.

[23] L. Ernstbrunner, R. El Nashar, P. Favre, S. Bouaicha, K. Wieser, and C. Gerber, "Chronic pseudoparalysis needs to be distinguished from pseudoparesis: a structural and biomechanical analysis," *The American Journal of Sports Medicine*, vol. 49, no. 2, pp. 291–297, 2020.

[24] S. Coppola, D. Albano, I. Sivoccia, and R. Vastola, "Biomechanical analysis of a rhythmic gymnastics jump performed using two run-up techniques," *Journal of Physical Education and Sport*, vol. 20, no. 1, pp. 37–42, 2020.

[25] R. M. Palmieri-Smith, M. T. Curran, S. A. Garcia, and C. Krishnan, "Factors that predict sagittal plane knee biomechanical symmetry after anterior cruciate ligament reconstruction: a decision tree analysis," *Sport Health: A Multidisciplinary Approach*, vol. 14, no. 2, pp. 167–175, 2022.

Hindawi
Computational Intelligence and Neuroscience
Volume 2022, Article ID 3054587, 10 pages
https://doi.org/10.1155/2022/3054587

Research Article

Analysis of the Role of Continuous Early Intervention in Improving the Quality of Life of Breast Cancer Patients

Xiufang Ding and Lijie Chen

Huzhou Maternity & Child Health Care Hospital, Huzhou 313000, Zhejiang Province, China

Correspondence should be addressed to Lijie Chen; clj961001@163.com

Received 5 May 2022; Accepted 25 May 2022; Published 16 June 2022

Academic Editor: Xin Ning

In order to improve the quality of life of breast cancer patients, this paper will apply continuous early intervention to the nursing of breast cancer patients. The continuous early intervention nursing model can propose countermeasures for the health problems faced by patients with postoperative chemotherapy. In order to analyze the effect of continuous early intervention nursing on negative emotions and quality of life in breast cancer patients, the effect of continuous early intervention in improving the quality of life of breast cancer patients is analyzed by means of experimental research. The control group is given routine nursing, and the observation group is given continuous early intervention nursing intervention. Moreover, this paper obtains data statistics in combination with statistical analysis. Through the comparison of the test results, it can be seen that the implementation of continuous early intervention nursing intervention in breast cancer patients can improve the nursing effect, effectively relieve the negative emotions of patients, and improve the quality of life of patients.

1. Introduction

With the progress of modern medicine and the enhancement of people's awareness of health care, most breast cancer patients can get early diagnosis and early treatment and the long-term survival rate after surgery is also gradually improved. Therefore, how to improve the quality of life of breast cancer patients has attracted widespread attention in the medical community. Quality of life, a multidimensional concept, is people's subjective experience of goals, values, expectations, and living conditions. Clinically, quality of life is commonly used to evaluate the impact of disease and treatment on the physical, psychological, and social functions of patients. The quality of life of breast cancer patients is a dynamic indicator that changes with lifetime and is affected by many factors. Existing studies have shown that patients' physical symptoms, self-esteem, psychological stress, self-efficacy, and ability to cope with and adapt to diseases are all influencing factors of quality of life. First of all, the fact of having breast cancer is a serious stress and crisis event for both the patient and the family members. The diagnosis and surgical treatment of breast cancer is a process that most breast cancer patients have to go through. This process will have a huge impact on the patient's psychological, social, and family functions and then seriously affects the quality of life of breast cancer patients. Secondly, modified radical mastectomy for mastalgia can improve the cure rate of tumors, but it also damages the patient's skin, breast, fascia, muscle, and other tissue structures. This can easily lead to pathophysiological conditions such as soft tissue fibrosis, decreased muscle contractility, disruption of lymphatic pathways, and increased nerve sensitivity. After modified radical mastectomy for breast cancer, the skin lymphedema of the affected limb, the functional impairment of the loyal limb, and the movement disorder of the shoulder joint caused serious distress to the patient and seriously affected the quality of daily life of the patient. Third, the absence of breasts after surgery results in physical defects and changes in women's self-image, resulting in serious damage to the patient's self-esteem. At the same time, changes in self-efficacy and social adaptability affect the patient's normal work and life and reduce the patient's quality of life.

The perioperative period is a dangerous period in terms of the occurrence of negative emotions and abnormal adaptive behavior, which seriously affects the patient's compliance with surgical treatment and greatly affects the patient's prognosis, quality of life, and survival time. The perioperative period is a critical period for the treatment of breast cancer patients, and it is also a period of concentrated outbreaks of various physiological dysfunctions and psychological crises. Studies have shown that breast cancer patients have more psychological problems during the perioperative period and negative emotions such as anxiety are prominent, which is much higher than that of healthy people. However, at the same time, the perioperative period is also a critical period for functional exercise, prevention of complications, psychological adjustment, obtaining more social support, and establishing a good social adaptation function. The early postoperative period of breast cancer is the best time to start functional exercise, which can effectively prevent postoperative upper limb dysfunction. At the same time, family is the most important source of support for perioperative patients. The care, understanding, and support of family members, especially spouses, can enhance the patient's expectation of life, improve self-esteem, effectively enhance the patient's confidence in coping with difficulties, and better maintain their social adaptation function, thereby improving the quality of life of breast cancer patients.

2. Related Work

In [1], a survey of 200 breast cancer patients showed that a total of 14 symptoms were significantly negatively correlated with the quality of life of patients. Among them, the top five symptoms were lack of vitality, hair loss, mental stress, sweating, and anxiety. The top 5 most distressing symptoms for patients were hair loss, feeling "I do not look like myself," poor sleep, loss of appetite, and lack of energy. The research in literature [2] shows that the pain and edema of the affected limb after surgery have a certain degree of influence on the quality of life of loyal patients and the painful mouth maggots will also affect the quality of life of patients. In improving the quality of life of patients, the first thing to do is to maximize the control of symptoms [3]. Medical staff should pay enough attention, because these symptoms will accompany patients through every day; if these symptoms improve, the quality of life of patients will naturally improve. Literature [4] investigated the quality of life of 70 cancer patients before and after cancer pain treatment. The results showed that pain can comprehensively affect the quality of life of patients and effective analgesic treatment can significantly improve the quality of life of patients. Literature [5] systematically evaluated the effect of functional rehabilitation training in patients after breast cancer surgery, and the results showed that progressive limb rehabilitation training and whole body rehabilitation exercise in patients after breast cancer surgery can effectively improve the function of the affected limb and improve the quality of life. Relief of fatigue symptoms in patients with chemotherapy and radiotherapy has a certain effect. Individualized aerobic exercise can improve the patient's fatigue state and improve the patient's quality of life [6]. Postoperative breast cancer patients experience heaviness, swelling, tenderness, and numbness before developing upper extremity lymphedema, so early guidance and intervention are imperative. Clinical nurses should provide patients and their families with personal care guidance for lymphedema, so that patients and their families can master the correct long-term supportive treatment methods for the prevention of lymphedema [7]. Breast cancer patients have more psychological problems in the process of diagnosis, treatment, and rehabilitation, which has been proved by more and more studies [8]. Suffering from cancer is a strong stress stimulus for most people. Breast cancer and its surgical treatment can lead to obvious stress reactions in patients, such as anxiety, depression, anger, fear, and other negative emotions, which affect treatment and recovery. To a certain extent, the quality of life of patients and the whole family decreases [9]. Literature [10] studies have shown that systematic psychological intervention for breast cancer patients can effectively alleviate their negative emotions and improve their quality of life. Literature [11] believes that negative life events, social support, depression, and other psychosocial factors have a greater impact on the immune function of cancer patients. Most breast tumor patients have a strong stress response, and their immune function is significantly inhibited, and the stronger the stress response, the more severely inhibited their immune function. After timely psychological intervention, providing spiritual comfort, support, persuasion, and hints, the patient can quickly control the chaotic thinking and feelings and the psychological response and immune function can be effectively improved. Perioperative breast cancer patients have serious negative emotions, and psychological intervention can significantly improve the treatment of their physical diseases and their quality of life. The results of the study also showed that through psychological intervention, the negative emotions such as anxiety and depression in different cancer patients were significantly reduced and the quality of life was significantly improved. Yang Qiaoju's psychological intervention research confirmed that social psychological factors are closely related to the occurrence and development of malignant tumors, which is why the psychological intervention for patients with malignant tumors received better results. The main reason is that psychological intervention can better relieve some of the patients' psychological pressure and mental burden. It enables patients to receive treatment under a good emotional experience, and at the same time, a healthy psychological condition and a good mood can improve immunity and improve the quality of life through the role of the neuroendocrine immune system, forming a virtuous circle, which further enhances the patient's confidence in treatment. On the other hand, health education before and during chemotherapy enables patients to understand a lot of chemotherapy knowledge, eliminate patients' doubts and worries, help patients establish positive coping strategies, enhance self-care awareness, and actively help them cooperate with treatment. Finally, psychological intervention, such as one-on-one conversation and communication, enables patients to feel the greatest support and care from medical staff and helps patients adjust to problems caused by diagnosis and treatment [12]. The psychological intervention measures used in the study can effectively promote the improvement of the quality of life of patients with breast cancer after chemotherapy and contribute to the overall recovery of the patients. Clinical medical staff should understand the poor psychology of patients undergoing chemotherapy after breast cancer surgery, master the methods of psychological intervention, and actively carry out psychological intervention to improve the quality of life of patients undergoing chemotherapy after breast cancer surgery [13]. The results of literature [14] show that the psychological disorders of postoperative patients are closely related to age. The older they are, the lighter the psychological barrier, because they and their husbands have high hopes for quality of life and prolonging life and have little requirements for sex. The younger the age, the more severe the mental disorder. Improvement can be achieved to a large extent through psychological care. Unilateral mastectomy did not affect the postoperative quality of sexual life. In this process, medical staff's sense of responsibility and psychological communication ability and skills play a leading role. Correct psychological guidance has a significant effect on reducing postoperative sexual dissatisfaction. The main reasons for patients' anxiety and low self-esteem before and after surgery were concerns about affecting their sexual life. It is advised to inform the patient that postmastectomy will not affect the couple's sexual life. However, it should also be noted that the operation will bring inconvenience and embarrassment to the sexual life of the patient and her husband. The patient will be ashamed to expose herself due to physical defects, and at the same time, she will worry that sexual life will have adverse effects on her body. In response to this problem, patients and their husbands should be informed that this deficiency can be compensated by nonphysical love at this stage [15]. After a period of time, the psychology of both parties adapts to this reality and it will naturally get better. Psychological care can help patients adapt to the physical changes caused by mastectomy as soon as possible, influence patients to establish a correct understanding and evaluation of such changes, help them adjust to their psychological state in a timely manner, and help them to be confident in their future life. Psychological counseling and guiding intervention are very important to eliminate the anxiety and inferiority of patients through enlightenment. Psychological intervention can transform the spouse's sexual attitude and improve the quality of sexual life. Therefore, as long as the patients and their families are relieved of their ideological concerns, psychological intervention can reduce the occurrence of postoperative sexual life dissatisfaction [16].

Studies have shown that 30% of breast cancer patients show varying degrees of anxiety and depression and their quality of life is significantly lower than that of the normal population. Although the American Society of Clinical Oncology (ASCO) has developed assessments and measures to manage symptoms such as anxiety and depression in cancer patients, many breast cancer patients undergoing chemotherapy still report a high number of unmet needs, including physical, psychological, and social support and spiritual care [17]. A survey of support needs for breast cancer patients undergoing chemotherapy showed that younger patients had more information needs about the health care system and sexuality and that unmet needs were positively associated with patient symptom distress scores. The results of a survey on the quality of life of long-term breast cancer survivors in literature [18] show that the quality of life of breast cancer survivors is relatively satisfactory, but there are still physical and psychological diseases, and anxiety and depression are related to the reduction of quality of life. Literature [19] shows that the longer the breast cancer chemotherapy patients continue early care, the better their cognition, behavior, and status of the disease and the more confident they are to complete the treatment. During hospitalization, cancer patients can be cared for by medical staff, but their treatment time in the hospital is not long, and most of the patients recuperate at home during the intermittent period of treatment. Corresponding support and guidance are of great significance. Patients are eager to return to normal life after discharge, and they need to be managed to prevent tumor recurrence, symptom control, rehabilitation exercises, etc., to reduce physical and psychological discomfort. Rehabilitation will be of great benefit.

3. Materials and Methods

3.1. Research Object. In the experiment, breast patients who are admitted to the hospital were selected as the research objects. Inclusion criteria are as follows: female patients, who were conscious and normal, underwent pathological and imaging examinations, met the diagnostic criteria for breast cancer, received chemotherapy after surgery, had complete clinical data, provided informed consent, and obtained approval by the medical ethics committee. Exclusion criteria are as follows: showed poor active cooperation ability during treatment or withdrawal from the study for some reason; had systemic chronic disease or liver and kidney dysfunction; had nonprimary breast cancer; had speech, communication, audio-visual, behavioral, and other obstacles. They are equally divided into the observation group and control group completely by the random number table method. There is no significant difference in general data between the two groups ($P > 0.05$), which is comparable. There is no statistical difference in the age composition and educational level composition of the two groups of patients ($P > 0.05$), which are comparable. This study was approved by the hospital ethics committee.

3.2. Experiment Method. When the patients in the two groups are discharged from the hospital after the operation, the responsible nurses provided health guidance for discharge after the modified radical mastectomy for breast cancer. It includes dietary guidance, key points of limb protection, functional exercise of the affected limb, guidance on identifying flap necrosis and subcutaneous effusion, maintenance of drainage tubes, monitoring of drainage

Table 1: Comparison of SAS of patients.

Number	Control group	Test group	Number	Control group	Test group
1	42.71	35.35	16	53.08	39.05
2	52.64	41.91	17	56.50	48.48
3	54.83	40.62	18	47.36	40.73
4	45.49	44.22	19	57.99	39.12
5	53.51	35.59	20	58.50	36.87
6	54.95	45.78	21	56.38	43.08
7	56.53	38.86	22	43.46	40.06
8	53.35	36.30	23	57.13	37.50
9	47.60	44.38	24	53.85	34.71
10	51.82	42.15	25	55.27	47.48
11	51.85	35.95	26	52.82	38.31
12	54.46	41.98	27	48.29	34.58
13	57.91	39.14	28	52.59	47.44
14	43.61	47.36	29	49.47	37.11
15	52.22	44.63	30	56.12	38.84

fluid, and guidance on taking medicines for discharge. At the same time, the patients on every Monday afternoon (control group) or every Wednesday afternoon (observation group) made an appointment to return to the hospital to observe the wound. One month after the patients are discharged from the hospital, the recovery status of the skin flap and the functional recovery of the upper limb on the affected side were evaluated.

On this basis, the observation group implemented diversified continuous early interventions. (1) 1–3 days before discharge, the patients and their families will be evaluated for their psychosocial status, a personalized continuous early intervention plan will be developed, and hospital contact information will be issued. The specific methods and contents of continuous early intervention are shown in Table 1. (2) Composition and training of successive early intervention teams: The ward has 32 beds and 13 nurses. The continuous early intervention group consisted of 2 deputy chief physicians of breast surgery, 2 nurses in charge, and 5 nurses who had worked for more than 5 years. Among them, there is 1 lymphedema therapist and 1 psychological counselor. The training content includes breast cancer-related disease knowledge, wound management, physical function assessment, common complication assessment and coping strategies, listening and talking skills, guidance education on negative emotions, service awareness, nutrition, etc. (3) Establishment of a patient basic information table: the main contents of the control group information table include the patient's name, hospital number, age, admission date, operation date, discharge date, discharge diagnosis, phone number, diet, sleep, mood, flap recovery, incision suture removal time, amount of drainage fluid, upper limb swelling, and upper limb function recovery. On this basis, the observation group information table adds the follow-up date, follow-up content, and answers to difficult questions. (4) Items of continuous early care.

(1) Incision Management. ① It is necessary to observe the color, temperature, and tension of the wound flap to identify flap necrosis and subcutaneous effusion. If it is found that the incision is red and swollen, there is a sense of fluctuation under the skin, or if the color of the skin flap is purple, we should contact the management physician in time and deal with it in time. ② It is necessary to keep the incision dressing clean and dry, and it is advised not to scratch it with the hands to avoid infection.

(2) Drainage tube management. ① It is necessary to squeeze the drainage tube correctly to keep the drainage smooth. ② It is necessary to maintain the effective negative pressure suction of the negative pressure drainage bottle. ③ It is necessary to pour the drainage fluid regularly every day. If it is found that the drainage fluid suddenly decreases sharply, combined with chest wall pain or more fluid leakage from the drainage tube orifice, the patient needs to go to the hospital in time. At the same time, patients need to be informed of the dangers of not pouring the drainage fluid in time and the importance of recording the drainage fluid to improve their compliance.

(3) Process of Functional Exercise of the Affected Limb. It is necessary to formulate a personalized functional exercise plan for the affected limb for the patient according to the patient's description, postoperative days, and wound healing. At the same time, it is necessary to invite family members to participate in the plan and inform patients and family members of the purpose and significance of functional exercise of the affected limbs, so as to improve patients' compliance and family members' awareness of supervision.

(4) Guidance on Diet and Emotional State. It is necessary to distribute small prescriptions for breast cancer nutrition diets, instruct patients to arrange meals reasonably, and fast from greasy, estrogen-rich foods, or drugs.

(5) Psychosocial Support. It is necessary to assist patients in discovering social support resources around them, so that they can obtain support effectively, encourage family members, especially spouses, to provide psychological support, and maintain emotional stability. At the same time, patients need to be informed that they can consult follow-up

Table 2: Comparison of SDS of patients.

Number	Control group	Test group	Number	Control group	Test group
1	48.14	36.17	16	53.55	41.48
2	54.89	40.81	17	44.41	44.10
3	47.03	42.96	18	47.72	38.37
4	41.76	35.70	19	54.18	35.71
5	43.37	34.31	20	48.03	40.14
6	43.33	36.20	21	40.95	35.58
7	52.35	42.92	22	49.46	40.02
8	53.98	44.00	23	54.90	37.15
9	46.87	42.09	24	47.66	33.27
10	48.35	35.37	25	54.51	33.76
11	53.90	38.04	26	52.98	40.77
12	52.16	36.29	27	41.77	38.54
13	46.79	39.43	28	40.45	43.13
14	45.08	37.38	29	50.03	35.72
15	51.38	37.74	30	42.75	36.00

staff if they have anxiety, depression, and other emotions or poor sleep. In addition, it is necessary to encourage participation in the activities of the Pink Ribbon Club and the promotion of rehabilitation-themed salons to provide patients with more information and psychological support.

The adverse mood changes of the two groups of patients were recorded. Adverse mood changes were evaluated using the Self-Rating Anxiety Scale (SAS) and Self-Rating Depression Scale (SDS). They are performed before treatment and 3 months after patient care. The scales include 20 items, and the cutoff value is 50 points. The higher the score, the more severe the anxiety or depression. Changes in the quality of life of patients before and after nursing are recorded, and the European Organization for Cancer Treatment and Research is used to develop the RTC-QOL-C30 scoring scale. The higher the functional score, the better the quality of life of the patients. The nursing satisfaction of the two groups of patients is compared using a self-made questionnaire, which is divided into satisfied and dissatisfied levels. Before and after nursing, the health knowledge mastery of the two groups of patients is measured. In this experiment, we design a questionnaire on health knowledge of patients after chemotherapy, including five dimensions, representing the most basic chemotherapy support, skin reaction, and diet. The score adopts a three-level scoring method, and the patient never understands complete mastery of 3 points. The higher the score, the higher the patient's mastery of health knowledge.

4. Results

After nursing, the SAS and SDS scores of the two groups are significantly decreased (both $P < 0.05$). There are statistically significant differences in the SAS and SDS scores between the two groups (both $P < 0.05$), as shown in Tables 1 and 2. The corresponding statistical chart is shown in Figure 1 and 2.

After nursing, the quality of life scores of the two groups are improved (both $P < 0.05$). The quality of life scores of the observation group after intervention are significantly better than those of the control group (all $P < 0.05$), as shown in Tables 3–9. The corresponding statistical chart is shown in Figures 3–9.

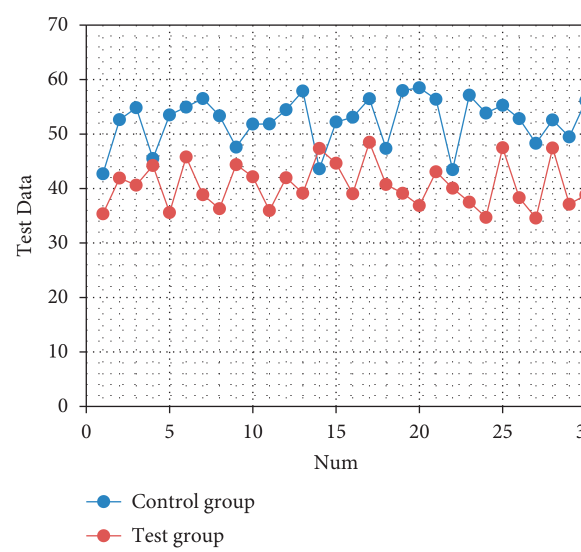

Figure 1: Statistical chart of comparison of SAS of patients.

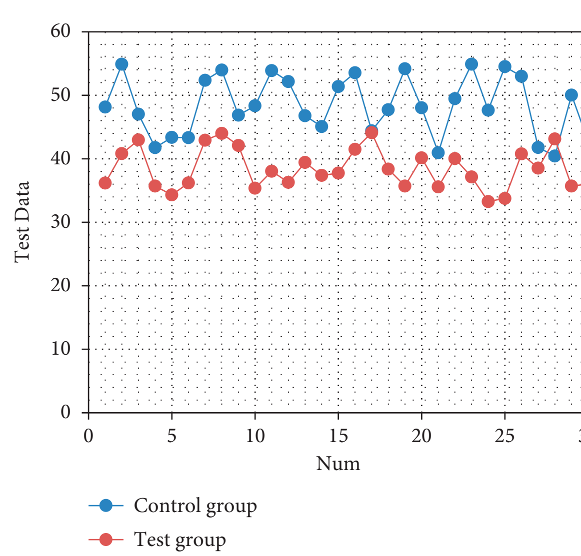

Figure 2: Statistical chart of comparison of SDS of patients.

Table 3: Comparison of physical functions.

Number	Control group	Test group	Number	Control group	Test group
1	60.22	62.51	16	16	89.80
2	67.52	60.65	17	17	80.71
3	85.66	67.10	18	18	88.88
4	75.84	74.12	19	19	89.17
5	89.19	84.65	20	20	75.13
6	74.98	60.44	21	21	75.65
7	84.85	74.88	22	22	68.21
8	65.66	64.02	23	23	76.10
9	70.70	56.68	24	24	62.12
10	72.31	79.06	25	25	89.54
11	79.44	78.62	26	26	86.62
12	79.27	73.09	27	27	63.12
13	88.72	69.26	28	28	85.95
14	66.41	82.70	29	29	78.77
15	65.72	73.12	30	30	67.66

Table 4: Comparison of role functions.

Number	Test group	Control group	Number	Test group	Control group
1	72.51	25.14	16	58.78	20.80
2	42.11	10.61	17	55.06	41.51
3	63.22	23.69	18	84.62	9.58
4	38.19	12.13	19	82.83	67.74
5	60.72	21.27	20	63.07	71.45
6	85.54	10.77	21	62.56	35.48
7	73.24	66.44	22	44.92	12.55
8	55.21	67.04	23	58.52	19.52
9	66.24	64.99	24	62.66	37.47
10	47.34	10.27	25	52.63	57.30
11	75.41	10.98	26	49.80	32.81
12	86.77	16.20	27	42.40	69.36
13	50.82	8.90	28	76.56	44.75
14	40.35	16.97	29	44.35	45.52
15	84.68	35.54	30	56.09	68.39

Table 5: Comparison of emotional functions.

Number	Test group	Control group	Number	Test group	Control group
1	73.59	70.26	16	86.55	50.07
2	86.60	61.65	17	58.86	30.22
3	64.98	42.94	18	87.15	60.08
4	64.27	55.82	19	49.14	64.89
5	80.67	59.25	20	68.96	51.92
6	75.90	27.73	21	76.09	43.44
7	69.10	58.39	22	51.02	53.99
8	59.84	57.25	23	76.64	34.23
9	55.37	40.99	24	66.98	55.92
10	59.22	73.88	25	73.31	47.99
11	63.28	33.96	26	47.62	67.64
12	50.06	63.85	27	66.81	28.48
13	85.04	74.15	28	86.94	52.39
14	52.09	46.12	29	75.52	74.05
15	81.02	65.31	30	50.51	38.18

5. Analysis and Discussion

In recent years, the incidence of breast cancer in China has shown a gradually increasing trend and the affected population is getting younger. Statistics show that breast cancer has acquired the third place among all malignant tumors. Although the diagnosis and treatment techniques have been improved, the functional rehabilitation of nurses

Table 6: Comparison of social functions.

Number	Test group	Control group	Number	Test group	Control group
1	77.77	16.88	16	49.94	37.74
2	41.33	23.55	17	78.33	42.01
3	65.44	48.09	18	51.93	13.18
4	30.19	18.93	19	68.79	9.50
5	76.75	53.52	20	41.46	54.55
6	33.90	52.69	21	49.72	53.34
7	55.92	35.04	22	36.42	25.83
8	31.43	39.29	23	72.48	51.37
9	46.87	38.26	24	57.09	56.74
10	47.74	36.09	25	51.37	16.48
11	40.73	35.25	26	53.79	42.50
12	52.18	41.80	27	42.09	21.45
13	49.85	53.99	28	43.54	10.56
14	37.80	49.83	29	34.89	44.72
15	59.40	22.96	30	68.69	39.99

Table 7: Comparison of cognitive functions.

Number	Test group	Control group	Number	Test group	Control group
1	90.34	89.35	16	89.60	74.65
2	80.79	82.24	17	97.91	84.85
3	84.33	55.42	18	70.67	64.41
4	81.20	87.95	19	79.90	79.35
5	72.15	94.52	20	67.34	83.56
6	69.23	93.60	21	67.91	83.40
7	69.16	83.73	22	85.52	55.87
8	88.36	62.65	23	89.13	88.35
9	90.19	78.73	24	89.55	91.59
10	95.94	62.32	25	72.36	58.24
11	74.94	83.89	26	94.34	78.49
12	73.20	53.63	27	68.27	88.63
13	77.61	69.02	28	70.09	57.36
14	79.42	60.01	29	94.04	92.74
15	92.74	80.68	30	95.80	52.62

Table 8: Comparison of overall functions.

Number	Test group	Control group	Number	Test group	Control group
1	31.64	53.99	16	42.71	23.39
2	24.70	23.35	17	59.09	54.13
3	68.43	31.32	18	71.18	35.44
4	73.46	36.03	19	33.71	43.98
5	62.70	23.88	20	33.07	41.21
6	25.57	35.05	21	20.95	48.32
7	39.83	28.19	22	61.42	29.16
8	69.83	38.27	23	24.72	23.74
9	40.12	23.99	24	70.87	38.72
10	47.08	32.65	25	58.63	21.97
11	42.73	30.57	26	48.09	22.39
12	25.31	50.02	27	49.42	44.41
13	56.77	38.41	28	32.59	43.38
14	28.58	50.82	29	67.90	31.31
15	60.00	45.00	30	56.40	38.79

after surgery will inevitably lead to the loss of hope for many patients. Therefore, it is of great practical significance to study which nursing methods are used to improve patients' negative emotions and quality of life. The adverse reactions of breast cancer patients during treatment not only affect the patients' recovery but also affect their psychological status, resulting in a decline in the patients' quality of life. In the analysis of this group, the focus is on the application of

Table 9: Comparison of nausea and vomiting.

Number	Test group	Control group	Number	Test group	Control group
1	71.95	96.44	16	67.51	87.69
2	83.21	75.07	17	46.71	64.25
3	71.57	94.08	18	82.57	91.64
4	43.23	62.72	19	77.94	75.06
5	71.94	64.00	20	50.80	64.78
6	75.31	93.38	21	55.16	71.32
7	89.72	61.94	22	46.77	67.39
8	59.10	86.00	23	50.23	66.08
9	82.30	68.92	24	94.41	83.64
10	41.97	65.84	25	68.52	63.21
11	71.04	85.39	26	95.22	74.30
12	71.35	73.55	27	95.94	73.18
13	57.62	78.71	28	93.88	65.43
14	73.52	75.45	29	80.60	66.22
15	76.92	65.44	30	73.32	94.98

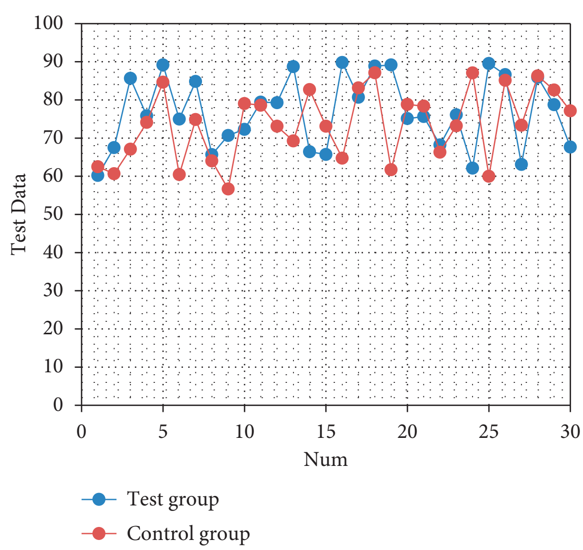

Figure 3: Statistical chart of comparison of physical functions.

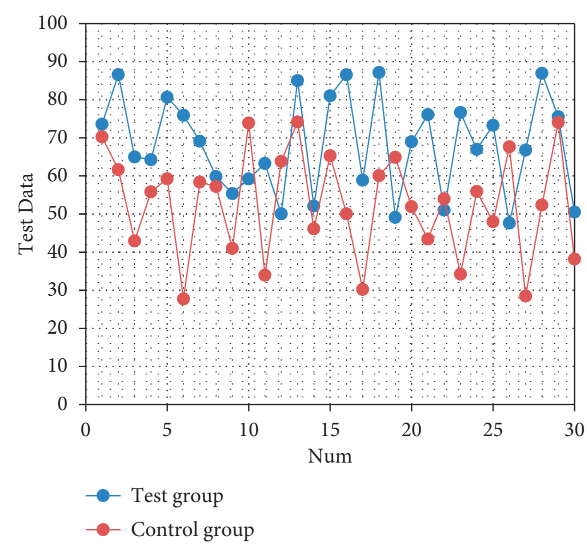

Figure 5: Statistical chart of comparison of emotional functions.

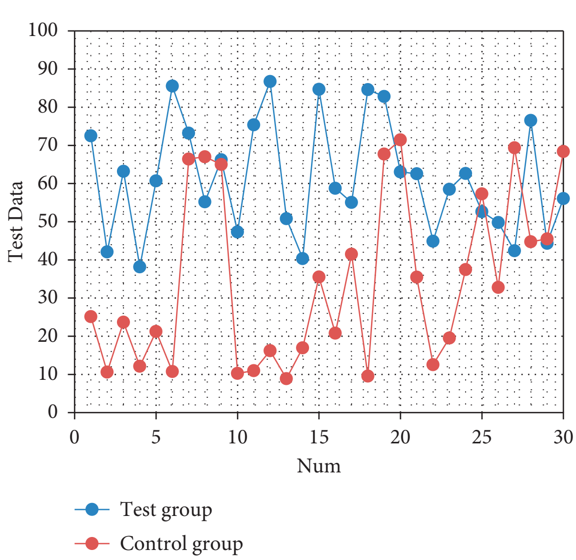

Figure 4: Statistical chart of comparison of role functions.

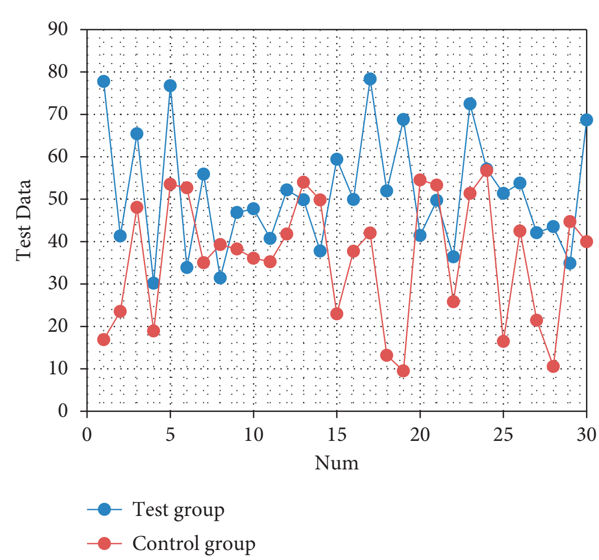

Figure 6: Statistical chart of comparison of social functions.

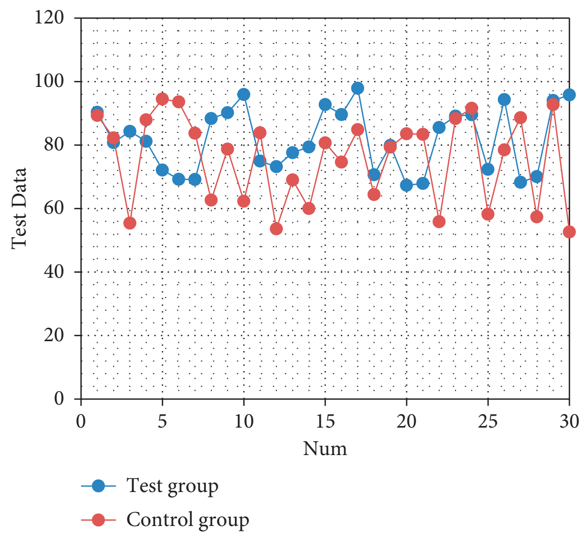

Figure 7: Statistical chart of comparison of cognitive functions.

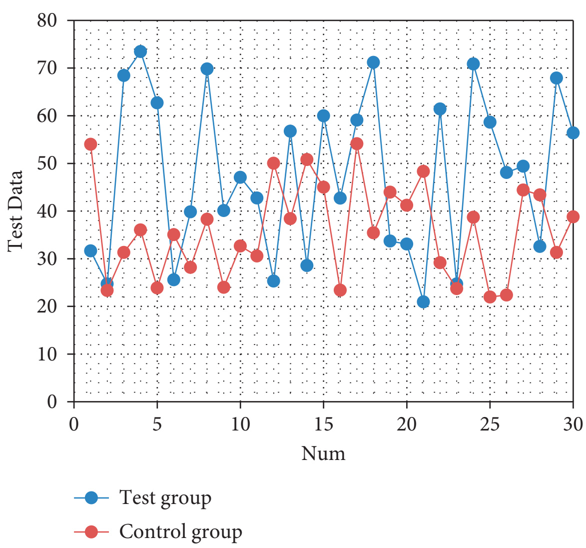

Figure 8: Statistical chart of comparison of overall functions.

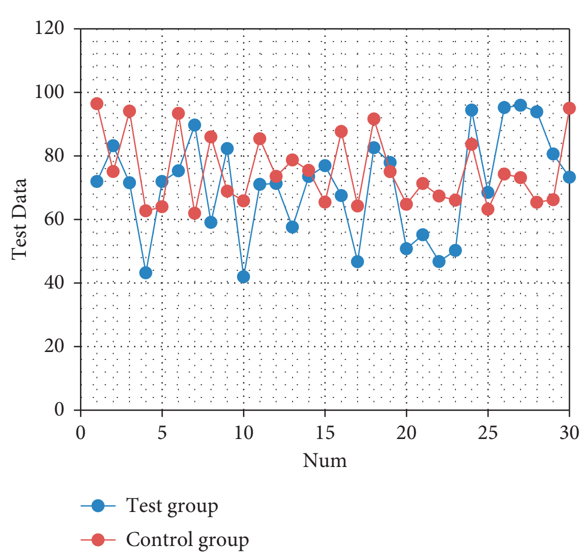

Figure 9: Statistical chart of comparison of nausea and vomiting.

continuous early care in breast cancer. With the rapid development of nursing disciplines, a lot of efforts have been made in the nursing work of breast cancer chemotherapy at home and abroad. Continuous early care is given to implement discharge care on the basis of overall care, to ensure that patients can receive the same care as inpatient care after hospitalization, to effectively ensure the rehabilitation of patients with humerus, and to reduce the case fatality rate of patients. Continuous early care for breast cancer patients can effectively reduce CRF during chemotherapy and improve patient satisfaction. It shows that the implementation of continuous early nursing care for breast cancer patients is helpful for the mastery of patients' health knowledge and has an important effect on improving the relationship between nurses and patients, which is consistent with the results reported in previous studies. Moreover, various adverse reactions after breast cancer treatment seriously affect the quality of life of patients. As patients spend most of their time recovering at home, this prevents continuation of care. The implementation of continuous early care can ensure the continuity and integrity of nursing intervention and, at the same time, can improve the nursing ability of patients themselves and their families and improve the quality of life of patients. Before nursing, there is no significant difference in the SAS score and SDS score between the two groups ($P < 0.05$). After nursing, the SAS and SDS scores of the two groups are significantly decreased (both $P < 0.05$) and the SAS and SDS scores of the observation group are significantly lower than those of the control group at the same time after nursing (both $P < 0.05$). Moreover, the quality of life of the patients in the observation group after intervention is significantly better than those in the control group except for loss of appetite, constipation, diarrhea, economy, and other dimensions (all $P < 0.05$). The research results show that the implementation of continuous early care can improve the role function and emotional function of patients, indicating that the implementation of continuous early care can effectively reduce the adverse symptoms of patients and extend clinical intervention from the hospital to the family.

It is necessary to standardize the way of continuous early care and improve the professional quality of nursing staff. Moreover, continuous early care needs to organically combine the enthusiasm of patients for self-care and the enthusiasm of nurses by carrying out a variety of health education activities, which increases the trust of patients in nursing staff and makes the satisfaction of patients improve. In this study, continuous early care team members were trained once a week on breast cancer specialist knowledge, prevention and countermeasures for common complications after breast cancer surgery, identification of common psychological problems and emotional management, and other related subjects to improve their professional quality. At the same time, relevant guidelines and standards are formulated for the content and operation procedures of continuous early care, to standardize the professional behavior of nursing staff and to improve the quality of continuous early care. At the same time, it is necessary to use a convenient and economical network platform to provide consultation services, implement health guidance, and facilitate the implementation of continuous early care for patients in various places. Through face-to-face guidance and communication, the patients' compliance with treatment and functional rehabilitation of the affected limbs after discharge can be effectively improved and their emotions can be relieved in time. However, the disadvantage is that it is limited by time; through telephone follow-up, patients can feel the humanistic care of the hospital and improve nursing satisfaction. To sum up, continuous early nursing can effectively reduce postoperative complications of breast cancer and promote functional recovery of the upper limbs on the affected side. The establishment of a high-quality continuous early care team is the guarantee of continuous early care. Therefore, we need to develop a personalized continuous early care program and use a variety of continuous early care pathways. For example, carrying out continuous early care by means of appointment follow-up time, setting up QQ group, WeChat group, online consultation and answering questions, follow-up consultation, telephone follow-up, etc., is conducive to achieving good results.

Data Availability

The labeled datasets used to support the findings of this study are available from the corresponding author upon request.

Conflicts of Interest

The authors declare no conflicts of interest.

Acknowledgments

This study was sponsored by Huzhou Maternity & Child Health Care Hospital.

References

[1] K. Zeng, B. He, B. B. Yang et al., "The pro-metastasis effect of circANKS1B in breast cancer," *Molecular Cancer*, vol. 17, no. 1, p. 160, 2018.

[2] A. B. Hanker, D. R. Sudhan, and C. L. Arteaga, "Overcoming endocrine resistance in breast cancer," *Cancer Cell*, vol. 37, no. 4, pp. 496–513, 2020.

[3] F. J. Couch, H. Shimelis, C. Hu et al., "Associations between cancer predisposition testing panel genes and breast cancer," *JAMA Oncology*, vol. 3, no. 9, p. 1190, 2017.

[4] K. L. Britt, J. Cuzick, and K.-A. Phillips, "Key steps for effective breast cancer prevention," *Nature Reviews Cancer*, vol. 20, no. 8, pp. 417–436, 2020.

[5] H. Pan, R. Gray, J. Braybrooke et al., "20-Year risks of breast-cancer recurrence after stopping endocrine therapy at 5 years," *New England Journal of Medicine*, vol. 377, no. 19, pp. 1836–1846, 2017.

[6] A. E. Giuliano, S. B. Edge, and G. N. Hortobagyi, "Eighth edition of the AJCC cancer staging manual: breast cancer," *Annals of Surgical Oncology*, vol. 25, no. 7, pp. 1783–1785, 2018.

[7] N. Mavaddat, K. Michailidou, J. Dennis et al., "Polygenic risk scores for prediction of breast cancer and breast cancer subtypes," *The American Journal of Human Genetics*, vol. 104, no. 1, pp. 21–34, 2019.

[8] H. W. Jackson, J. R. Fischer, V. R. T. Zanotelli et al., "The single-cell pathology landscape of breast cancer," *Nature*, vol. 578, no. 7796, pp. 615–620, 2020.

[9] T. O. Nielsen, S. C. Y. Leung, D. L. Rimm et al., "Assessment of Ki67 in breast cancer: updated recommendations from the international Ki67 in breast cancer working group," *Journal of the National Cancer Institute: Journal of the National Cancer Institute*, vol. 113, no. 7, pp. 808–819, 2021.

[10] P. Schmid, J. Cortes, L. Pusztai et al., "Pembrolizumab for early triple-negative breast cancer," *New England Journal of Medicine*, vol. 382, no. 9, pp. 810–821, 2020.

[11] A. Bardia, I. A. Mayer, L. T. Vahdat et al., "Sacituzumab govitecan-hziy in refractory metastatic triple-negative breast cancer," *New England Journal of Medicine*, vol. 380, no. 8, pp. 741–751, 2019.

[12] H. J. Burstein, G. Curigliano, S. Loibl et al., "Estimating the benefits of therapy for early-stage breast cancer: the St. Gallen International Consensus Guidelines for the primary therapy of early breast cancer 2019," *Annals of Oncology*, vol. 30, no. 10, pp. 1541–1557, 2019.

[13] R. E. Hendrick, J. A. Baker, and M. A. Helvie, "Breast cancer deaths averted over 3 decades," *Cancer*, vol. 125, no. 9, pp. 1482–1488, 2019.

[14] H. Wang, Z. Tan, H. Hu et al., "microRNA-21 promotes breast cancer proliferation and metastasis by targeting LZTFL1," *BMC Cancer*, vol. 19, no. 1, pp. 1–13, 2019.

[15] M. E. Gatti-Mays, J. M. Balko, S. R. Gameiro, R. G. Sofia, D. B. Harry, and P. Sangeetha, "If we build it they will come: targeting the immune response to breast cancer," *NPJ breast cancer*, vol. 5, no. 1, pp. 1–13, 2019.

[16] K. B. Kuchenbaecker, J. L. Hopper, D. R. Barnes et al., "Risks of breast, ovarian, and contralateral breast cancer for BRCA1 and BRCA2 mutation carriers," *JAMA*, vol. 317, no. 23, pp. 2402–2416, 2017.

[17] A. C. Garrido-Castro, N. U. Lin, and K. Polyak, "Insights into molecular classifications of triple-negative breast cancer: improving patient selection for treatment," *Cancer Discovery*, vol. 9, no. 2, pp. 176–198, 2019.

[18] Z. Anastasiadi, G. D. Lianos, E. Ignatiadou, H. V. Harissis, and M. Mitsis, "Breast cancer in young women: an overview," *Updates in surgery*, vol. 69, no. 3, pp. 313–317, 2017.

[19] M. M. S. Obradović, B. Hamelin, N. Manevski et al., "Glucocorticoids promote breast cancer metastasis," *Nature*, vol. 567, no. 7749, pp. 540–544, 2019.

Hindawi
Computational Intelligence and Neuroscience
Volume 2023, Article ID 9803532, 1 page
https://doi.org/10.1155/2023/9803532

Retraction

Retracted: Probabilistic Statistics-Based Endurance Life Prediction of Bridge Structures

Computational Intelligence and Neuroscience

Received 25 July 2023; Accepted 25 July 2023; Published 26 July 2023

This article has been retracted by Hindawi following an investigation undertaken by the publisher [1]. This investigation has uncovered evidence of one or more of the following indicators of systematic manipulation of the publication process:

(1) Discrepancies in scope
(2) Discrepancies in the description of the research reported
(3) Discrepancies between the availability of data and the research described
(4) Inappropriate citations
(5) Incoherent, meaningless and/or irrelevant content included in the article
(6) Peer-review manipulation

The presence of these indicators undermines our confidence in the integrity of the article's content and we cannot, therefore, vouch for its reliability. Please note that this notice is intended solely to alert readers that the content of this article is unreliable. We have not investigated whether authors were aware of or involved in the systematic manipulation of the publication process.

Wiley and Hindawi regrets that the usual quality checks did not identify these issues before publication and have since put additional measures in place to safeguard research integrity.

We wish to credit our own Research Integrity and Research Publishing teams and anonymous and named external researchers and research integrity experts for contributing to this investigation.

The corresponding author, as the representative of all authors, has been given the opportunity to register their agreement or disagreement to this retraction. We have kept a record of any response received.

References

[1] Y. Zhang, "Probabilistic Statistics-Based Endurance Life Prediction of Bridge Structures," *Computational Intelligence and Neuroscience*, vol. 2022, Article ID 8035028, 12 pages, 2022.

Hindawi
Computational Intelligence and Neuroscience
Volume 2022, Article ID 8035028, 12 pages
https://doi.org/10.1155/2022/8035028

Research Article

Probabilistic Statistics-Based Endurance Life Prediction of Bridge Structures

Yanan Zhang

School of Mathematics and Computer Science, Shaanxi University of Technology, Hanzhong 723001, China

Correspondence should be addressed to Yanan Zhang; zhangyanan@snut.edu.cn

Received 21 April 2022; Revised 13 May 2022; Accepted 14 May 2022; Published 15 June 2022

Academic Editor: Xin Ning

With the massive construction of bridge infrastructures, bridge health monitoring systems have gradually matured in application and research, but previous research has primarily focused on structural damage detection and bridge safety warnings based on valid data. The structural details of steel bridge panels and structural systems are determined by the coupling effects of many intrinsic and extrinsic uncertainties, such as material properties, structural characteristics, manufacturing processes, and random traffic loads. The evaluation of fatigue is a difficult task. This article first builds a big data platform, utilizing its high-efficiency parallel computing capability and highly fault-tolerant distributed file system to achieve second-level monitoring data processing; ensuring real-time data cleaning, data analysis, and safety warning; and building a big data analysis and processing platform with high reliability, high availability, high storage efficiency, and high scalability of bridge health monitoring. The big data platform chooses HDFS for offline data storage and Spark for data analysis and modelling after comparing and analysing the benefits and drawbacks of various big data technologies. Kafka is used for caching real-time data, and Spark-streaming is used for reading data and real-time processing. Finally, the platform's superiority and reliability in terms of offline computing performance, real-time online performance, scalability, and fault tolerance are confirmed through experimental analysis; the optimal data cleaning method is derived by comparing and analysing monitoring data noise, jump point, and drift phenomena. This part of the research is based on bridge temperature data with stable signals and bridge strain data with fluctuating signals, taking into account the influence of different data types; the corresponding data missing repair algorithms are proposed for different types of data to form a complete and general data patching method process. The probabilistic fracture mechanics theory, in comparison to the traditional deterministic fatigue assessment method, can better reflect the essential uncertainty of fatigue problems and is an effective way to assess the fatigue performance of orthotropic steel bridge decks. The goal of data patching is to ensure data recovery accuracy of over 90%, with no patching repair required for monitoring data with too much missing data. The endurance life of bridge structures is predicted using a big data probabilistic statistics approach based on a variety of factors such as material properties, construction characteristics, manufacturing processes, and random traffic loads.

1. Introduction

Bridges are the key nodes in the traffic lifeline project, and also show the strength of the country in social and economic development. In recent times, as the number of bridges increases and the age of bridges increases, the focus of bridgework is changing from "reconstruction rather than maintenance" to "construction and maintenance," and even "management and maintenance." However, compared with the breakthrough achievements in the fields of super flexible structure analysis, deep-water foundation design and construction, and super span bridge construction, there is a serious lack of research in bridge maintenance technology, and a weak reserve of bridge safety and health technology, resulting in the structural performance of bridges decaying before they get old, and the service life is generally much lower than the design life, and even safety accidents occur frequently. According to statistics, 60% of the actual life of the bridge is less than 25 years, nearly 800,000 highway bridges, the proportion of dangerous bridges is close to 15%, and the hidden danger is huge.

Large steel bridges are critical nodes and hubs in road traffic engineering, and orthotropic anisotropic steel bridge deck panels as the preferred deck structure for their main girders are required to ensure their safety and reliability in high-quality service during the design life. The fatigue cracking problem and secondary diseases such as deck pavement damage caused by the coupling influence of multiple factors such as structural characteristics and force system, material properties, environmental effects, and construction quality run through the entire process of application and development of orthotropic steel bridge panels, according to engineering application practice and research at home and abroad. It is difficult to repair and raise the overall cost of ownership, making it a management issue and a technical bottleneck that stymies the long-term development of steel bridges.

After large-scale new construction, developed countries have shifted their focus to the repair, reinforcement, and renovation of old buildings, and reconstruction is not only less expensive than new construction but also recovers the investment faster. Because of the current state of bridges, infrastructure investments should be directed toward the expansion and reconstruction of old and dangerous bridges. Durability assessment and life prediction are needed to develop scientifically developed repair, strengthening, and renovation plans for existing service structures. On the one hand, durability assessment and service life prediction can reveal the structure's potential hazards, and based on the results, the structure can be repaired and strengthened at an early stage of structural performance degradation, extending the structure's service life, reducing economic loss, and mitigating the serious energy and environmental problems caused by durability failure. On the other hand, it can reveal internal and external factors that affect the structure's life span. The existing deterministic methods are difficult to accurately consider the influence of the random characteristics of the abovementioned key factors and may obtain unsafe fatigue performance evaluation results. Aiming at the shortcomings of the existing deterministic evaluation methods, this article conducts systematic research on key issues such as fatigue load, crack growth, and fatigue reliability model and introduces the theory of random process and elastic-plastic fracture mechanics respectively to explore the effect of constant amplitude and random load. Based on the fatigue crack propagation characteristics, the probability and statistics theory and reliability theory are unified into the fatigue evaluation framework based on fracture mechanics, and a fatigue reliability evaluation method based on probabilistic fracture mechanics is proposed. Thus, targeted investments can be made according to the surrounding environment, usage, economic conditions, etc., which helps to improve the design level and construction quality of the project and improve the theory and method of new structural durability design.

2. Related Works

The research results of bridge health monitoring are becoming more mature, and some large bridges in the United States and abroad are equipped with various monitoring instruments and monitoring devices, as shown in Figure 1 for factors affecting bridge endurance life, primarily to monitor these factors. The first health monitoring systems were installed and researched in foreign countries in 1922 on the Ironton-Russell suspension bridge in the United States, which had undergone several repairs and reinforcements, so the relevant units installed health monitoring systems to monitor the stress changes of the bridge structure, and the bridge was operated safely for the next decades until it was demolished [1]. In addition to the installation of bridge health monitoring, research in the field of health monitoring has tended to be rich and mature, and bridge health monitoring has evolved in the direction of intelligence and digitalization in the current era of big data.

The material fracture prediction is closely related to the material type, chemical composition, and manufacturing process, and its magnitude is the key factor determining the fatigue crack propagation characteristics of the structural details of the steel bridge deck. The fracture parameter values of different steels are quite different and show significant random characteristics due to the influence of the inhomogeneity of the material microstructure. In foreign studies, literature [2] designed a bridge health monitoring system based on strain monitoring data, using the strain monitoring data collected to determine the stresses generated by live loads, to identify valuable parameters such as live load distribution factors and peaks, and to evaluate the structural health state of the bridge. Literature [3] investigated the improvement in the existing bridge monitoring system and proposed a method for information integration. The method uses a Bayesian probability model to obtain data and information from the structural health monitoring system to predict the probability of extreme values generation. This bridge health monitoring system has been applied to bridges in Wisconsin with good results. A method for adaptive identification of truss structures based on the Lyapunov method is proposed in the literature [4]. The Lyapunov method provides guaranteed convergence for parameter estimation in the identification. The finite element analysis method is used to identify the simulation model. The simulation results show that the adaptive estimation method can track the changes over time, thus providing monitoring of the degraded structure. Literature [5] utilized an enhanced structural health monitoring system using stream processing and artificial neural network techniques (SPAN Net) and applied it to a bridge in Bangkok. The system provides real-time monitoring and early warning mechanisms for bridge structures by applying wireless sensor networks, real-time data stream processing, and weighted attack maps based on measured bending strains.

Although Chinese bridge monitoring research is lagging behind that of other countries, bridge health monitoring researchers have conducted scientific research on health monitoring systems and practical research on various major bridge structures in China. Bridge health monitoring combined with machine learning and big data platforms are gradually emerging in today's wave of big data and artificial intelligence. Literature [6] proposed a method to evaluate the service status of bridge structures using a five-layer deep learning network and built an accurate finite element model of bridge structures based on bridge monitoring data. The pattern classification technique using neural networks was analysed using dynamic networks and genetic algorithms in literature [7], and its effectiveness in identifying structural damage of bridges was analysed in real tests, demonstrating the technique's feasibility.

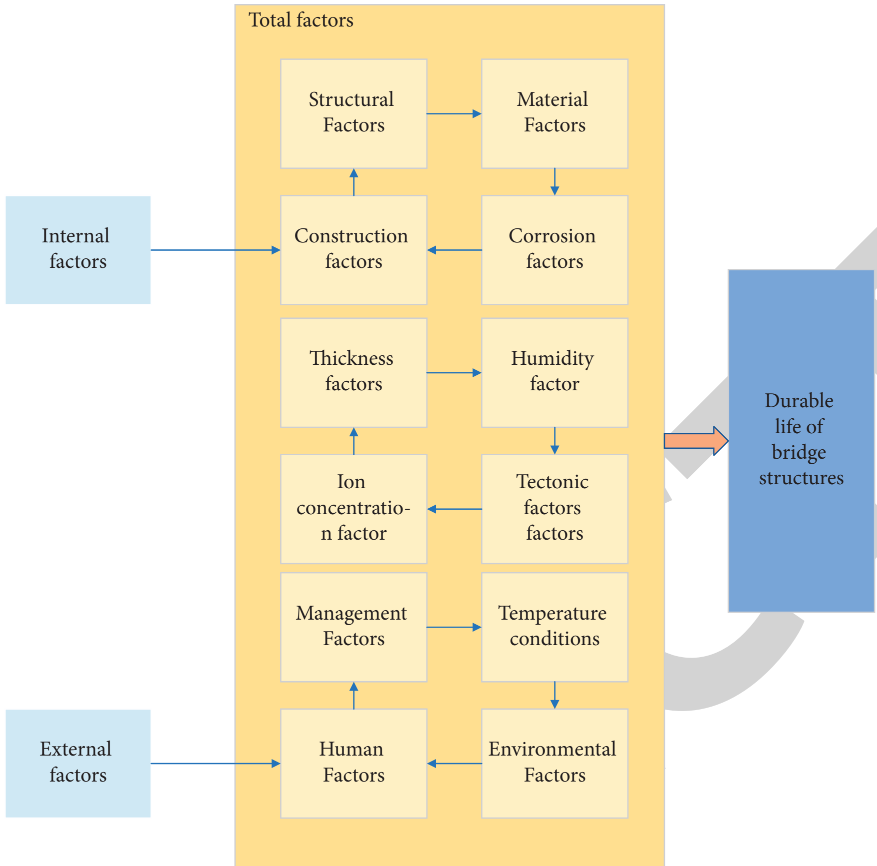

Figure 1: Factors affecting the durability life of bridges.

Literature [8] used radial basis function (RBF) neural networks to identify bridge damage and established guidelines for locating judged damage as well as an evaluation method for the identification effect. Literature [9] looked into a two-step method for damage detection based on a generalized regression neural network (GRNN), which is a variant of the radial basis (RBF) network with a faster training speed and a stronger nonlinear mapping capability, and network training can be completed instantly with high fitting accuracy. However, only a few typical simple bridge structures have been numerically simulated in the experimental validation stage, and there is still a significant gap in applying it to the damage identification of large bridge structures. The Korhonen clustering network was used in literature [10] to analyse isolated points of bridge monitoring data, as well as the analysis and early warning reference of bridge structure abnormalities based on this; the a priori model for bridge condition assessment was also established to explore the potential association rules among the attributes of bridge data, providing a data-supported basis for bridge condition assessment.

3. A Probabilistic Statistics-Based Approach to Bridge Life Prediction

3.1. Bridge Structure Durability Life Prediction Method. The service life of bridge structures has certain uncertainty due to the environment they are in and the level of corrosion stress. However, how to accurately predict the reliability of bridge structures during service; guide, overhaul, and improve their reliability; and ensure their service life under harsh environments is a concern for bridge durability researchers [11]. The establishment of a reliable theoretical relationship between the durability deterioration process and time, based on which the service life of bridge structures can be assessed qualitatively and quantitatively, is referred to as life prediction of bridge structures. Empirical prediction, comparative performance prediction, accelerated test prediction, mathematical model prediction, and probabilistic analysis (stochastic process) prediction are the main methods for life prediction of bridge structures in general, and these methods are often used interchangeably in practice, rather than just one. Due to the drawbacks of empirical and performance comparison prediction methods [12], such as low prediction reliability, large errors, and significant limitations in the application of new materials, three bridge structure durability prediction methods are widely used.

3.1.1. Accelerated Test Prediction Method. Accelerated testing is based on test simulations to increase the level of corrosion stress, such as increasing the temperature, humidity, and concentration of corrosive ions, to accelerate the deterioration process of bridge structure durability and shorten its actual service life. This method can predict the service life of reinforced concrete very well if the acceleration mechanism is reasonably designed, the test operation is reasonable, and the data collection method is correct [13]. But often in practice, due to the acceleration test mechanism and corrosion stress level and the actual engineering corrosion stress in the process of durable deterioration of reinforced concrete between the match to be clear, whether too high or too low scholars question the attitude, that is, the precise value of the acceleration factor (K) has ambiguity. According to the fatigue damage characteristics of orthotropic steel bridge decks, the effects of key factors such as materials, loads, and defects are comprehensively considered, and the fatigue reliability and time-varying laws of typical structural details during service as well as fatigue crack propagation characteristics are reasonably predicted. The evaluation method of the orthotropic steel bridge deck is the primary issue in fatigue evaluation. Figure 2 shows the accelerated experimental prediction method process.

3.1.2. Mathematical Model Prediction Method. The mathematical model prediction method is the most widely used in today's study of bridge structure life prediction, and it is primarily based on the steel corrosion model, which is embodied primarily through the carbonation and chloride ion diffusion theory and other calculation models, and it has now become an important life prediction tool. The accuracy and reliability of life prediction, on the other hand, are closely linked to the logic of mathematical models, the selection of material-related parameters, and the compatibility of environmental factors, and the results are somewhat absolute.

3.1.3. Probabilistic Analysis and Prediction Method. The probabilistic analysis prediction method expresses the relationship between the service life of bridge structures and time through the function of development evolution, and the prediction result is the non-mean service life (deterministic model), but the service life with a stochastic process, that is, the probability that the durability of bridge structures will fail at a certain service time point. The durability degradation of bridge structures is a changing process during the service life of bridge structures because it is the result of the coupling of various factors. For example, the hydration of $MgSO_4$ and cementitious materials has a double effect on bridge durability degradation. According to the need for durability assessment, the environment in which the structure is located should be investigated. Temperature, humidity, aggressive material gases, liquids and solids, freeze-thaw cycles and scouring, wear and tear, and other factors are all taken into account. The corresponding original design data and the survey of the completed acceptance data should both be completed at the same time. Meanwhile, the initial durability of the bridge structure is a continuous strengthening process with the addition of admixtures and dopants, and given this, the probabilistic analysis-based method of predicting the life of bridge structures is more reasonable than other methods. Furthermore, the service life prediction based on a deterministic model has certain ambiguity in the process of bridge structure life prediction, so it is necessary to use a probabilistic method to predict its service life. The probabilistic analysis prediction method is depicted in Figure 3.

The durability of bridge structures has always been the focus of scholars' attention. With the continuous research, scholars at home and abroad have a profound understanding of the durability degradation process and deterioration mechanism of bridge structures, and most of them adopt the methods related to accelerated corrosion and have achieved fruitful results [14]. However, the research on the durability of bridge structures is mostly concentrated in the field of general bridges, and relatively little research has been done on new construction materials. Along with the improvement in people's environmental awareness and the requirements of sustainable development, the research on the durability of green bridge structures and accelerated corrosion also needs to be further clarified, to lay a solid theoretical foundation for the promotion and application of green building materials.

Current methods of accelerated corrosion of bridge structures, particularly carbonation and chloride ions under the action of the accelerated corrosion mechanism, are more mature, and more research results based on the acceleration of steel corrosion method have also attracted more and more attention from scholars. However, the electrolyte used in the existing accelerated corrosion process is mostly an aggressive solution, but due to the lack of oxygen supply in the acceleration process, the deterioration mechanism of the reinforcing steel is distorted, and the model of reinforcing steel corrosion is questioned to some extent. There are many models for predicting the service life of bridge structures, but the majority of current research findings are based on a deterministic model, that is the service life under a specific corrosive environment or stress level. There is no denying that the erosion environment in which the bridge structure is situated changes over time, and that the corrosion stress level is also influenced by uncertainties. At the same time, the durability deterioration of the bridge structure is changing. For example, under the action of a single factor, durability is a gradual accumulation of the deterioration process, whereas under the action of multiple factors, the coupling of various factors sometimes slows down the deterioration rate, and sometimes accelerates it, both have a degree of uncertainty, so based on the deterministic model to predict the service life of the bridge, the use of the probabilistic analysis method as a reliability model for life prediction can better reflect the randomness of bridge structure durability deterioration due to various factors.

Overall, the main problems in the current study are as follows:

(1) At present, the research on the durability deterioration mechanism of bridge structures is mostly focused on ordinary silicate bridges, while there is little research based on green building materials, such as recycled bridge structures and magnesium chloride cement bridge structures to accelerate corrosion.

(2) In the accelerated corrosion study of bridge structures, especially based on the accelerated corrosion

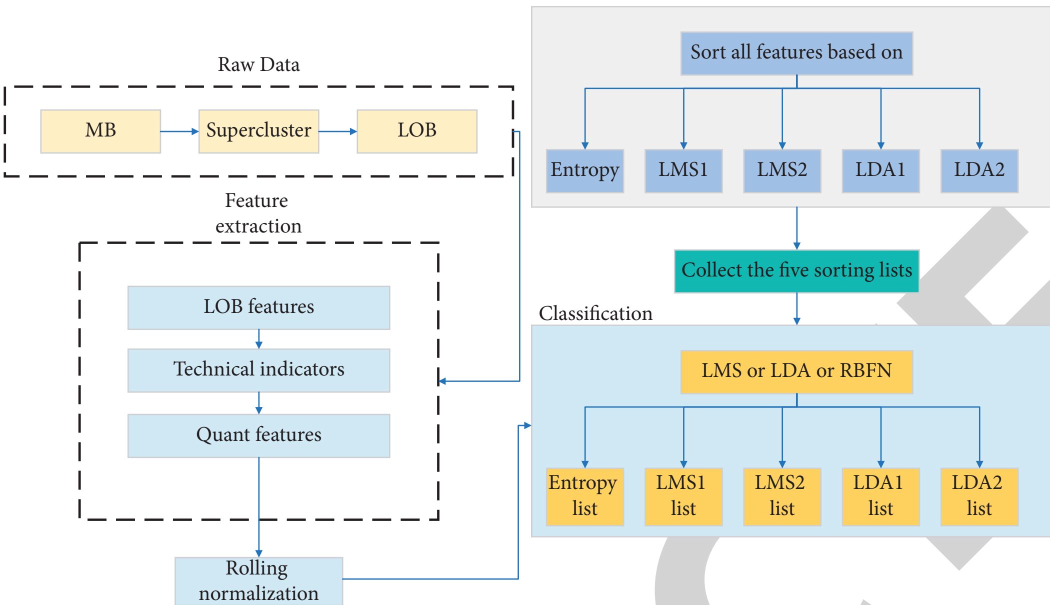

Figure 2: The flow of accelerated experimental prediction method.

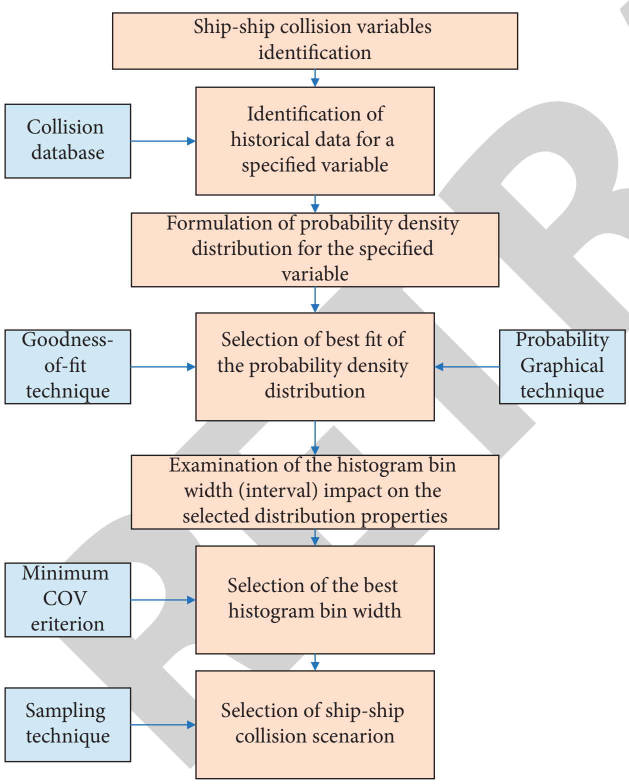

Figure 3: Probabilistic analysis prediction method flow.

test by electricity, the electrolyte mostly uses aggressive solutions; however, in the accelerated process with the bridge expansion and cracking, the solution is easy to penetrate the cracks resulting in the outflow of rust products, resulting in a certain ambiguity of the durability deterioration process of bridge structures under the effect of accelerated corrosion by electricity.

(3) There are many methods for life prediction of bridge structures, and the life prediction model based on stochastic analysis is practical, but the applicability of the probability function in the stochastic analysis method, the calculation of relevant parameters, and the accuracy of the prediction model need to be further determined.

(4) The model of the accelerated test prediction method has certain conditions of applicability, so under the premise of improving the accelerated corrosion mechanism, it will be more practical to explore the applicability and accuracy of life prediction of bridge structures based on the reliability analysis model.

Probabilistic statistical methods can reflect the factors affecting the durability life of bridge structures in a multi-level and all-around way; therefore, this article focuses on the application of probabilistic statistical methods in the durability prediction of bridge structures.

3.2. Probabilistic Statistical Methods. Considering the random nature of endurance life data, the correlation between before and after data, and the effectiveness of probabilistic statistics in the face of data and lack of theoretical models, this section will introduce models and methods based on probabilistic statistics used in the problem of predicting the endurance life of bridge structures. These include traditional probabilistic models, such as Bayesian classification models, conditional random field models, etc., and statistical learning theory, which is the basis of machine learning theory [15–17].

Based on the Bayesian formulation, numerous related theories have been developed. In this section, we introduce Bayesian decision theory in statistical pattern recognition and the Bayesian parameter estimation techniques [18] and

Bayesian learning techniques used to apply this decision theory in intrusion detection. The statistical decision theory with Bayesian decision-making as the core component is an important foundation of statistical pattern recognition, and the classifier designed based on it has the lowest classification error rate or risk, so it is often used as a criterion to measure the merits of other classifier design methods. When using this method to build a classification model, the following two prerequisites must be met: (1) the probability of the overall of each category of the sample needs to be known; and (2) the number of categories to be classified for decision-making needs to be known. The problem it solves is to determine the class to which the d-dimensional feature vector observed on the feature space $X = [x_1, x_2, x_3, ..., x_d]^T$ belongs, so it can be said that the Bayesian decision model-based intrusion detection technique combines both the feature space-based intrusion detection technique and the probabilistic statistics-based intrusion detection technique.

Bayesian decision-making based on the minimum error rate considers the posterior probability $P(x_i \mid X)$, which x_i denotes the category to which it belongs, and for the binary classification problem, $i = 1,\ 2$; then, based on the known probability of the overall of each category, this posterior probability is calculated by the Bayesian formula, to determine the category to which it belongs by the probability magnitude. The Bayesian formula is shown as follows:

$$P(x_i \mid X) = \frac{P(X \mid x_i)P(x_i)}{P(X)}, \tag{1}$$

where $P(x_i)$ is the prior probability x_i of the class, and $P(x_i \mid X)$ is the conditional probability of the observation X x_i under the class, $P(X)$ is a constant and generally need not be considered. In practice, the prior and conditional probabilities of each class are the premises of Bayesian decision theory. This requires estimation of the probability density function, that is, it requires the use of Bayesian parameter estimation or Bayesian learning to infer the overall distribution given a known sample set $P(x_i \mid D)$. Although the fuzzy-means clustering method based on soft partition can evaluate the durability of multiple samples to be evaluated and multiple evaluation indicators, due to the problem of data resources, although there are multiple samples, each sample has only two durability. The evaluation index can only show the durability of the component to a certain extent. Unlike traditional parameter estimation, which treats the parameter θ to be estimated as a constant, Bayesian parameter estimation treats θ as a random variable with a priori distribution. The basic idea is to use the past knowledge of θ to give a more realistic estimate of θ.

The Bayesian parameter estimation problem can be described as follows: first, the posterior probability density of the parameter θ under known data Y is calculated using the following Bayesian formula:

$$P(\theta \mid Y) = \frac{P(Y \mid \theta)P(\theta)}{P(Y)}, \tag{2}$$

where $P(\theta)$ is the known θ prior distribution and is the conditional probability of the sample Y under $P(Y \mid \theta)$ the parameters θ; then, the estimate $\theta = E(\theta \mid Y)$ is calculated according to the θ theorem.

Bayesian learning, on the other hand, solves directly for the overall distribution $P(x_i \mid Y)$ by finding the posterior probability of the parameter θ, which is expressed as follows:

$$P(x_i \mid Y) = \int P(x_i \mid X)P(X \mid Y)\mathrm{d}x_i. \tag{3}$$

Its learning process is roughly encapsulated as follows: for a fixed, it will completely determine the probability density of x; when the sample is observed; as the number of samples increases, the uncertainty of inference on will decrease. The basic theory of statistical pattern recognition is Bayesian decision theory, which has important implications for modelling and designing classifiers for bridge durability life prediction. Because Bayesian parameter estimation and Bayesian learning are both basic probabilistic statistical methods, they can be used in a variety of other durability life prediction models.

3.3. Experimental Design and Analysis of Results. For durability assessment of actual projects, the reliability of the current structural system should be evaluated not only from the system level but also considering the time effect and evaluating the reliability of the system at different moments [19]. The carbonization rate of different parts is different due to various factors, and considering the complexity of the carbonization process, if a single time-varying model is used to deal with the carbonization of the members, the results are too subjective and difficult to match with the specific actual project. Therefore, the Bayesian dynamic carbonation model can be used to make dynamic corrections to the respective carbonation based on the historical inspection data of each part of the real bridge and then calculate the reliability of the structural system based on the corrected carbonation depth (Figure 4).

In the figure $A_i(\alpha, \beta)$, it indicates the carbonation depth correction value of member i at the α moment after the moment update; $M_i(\alpha, \beta) = F[A_\mathrm{i}(k, k-1)]$ is the detection value of member i at the moment β; $N_i(\alpha, \beta)$ is the reliability index of member i at the moment α after the moment β update; $N(\alpha, \beta) = F[M_1(\alpha, \beta), \ldots, M_i(\alpha, \beta)]$ is the system reliability index at the moment α after the moment β update. From the flow chart, it can be seen that the Bayesian dynamic linear model completes the dynamic update correction of the carbonation depth, that is

$$A_i(\alpha, \beta) = F[A(k, k-1), M(i, k)]. \tag{4}$$

The component reliability calculation can be expressed as follows:

$$M_i(\alpha, \beta) = F[A_i(k, k-1)]. \tag{5}$$

And the differential equivalence recursive algorithm completes the calculation of the component reliability to the system reliability, that is

$$N(\alpha, \beta) = F[M_1(\alpha, \beta), \ldots, M_i(\alpha, \beta)]. \tag{6}$$

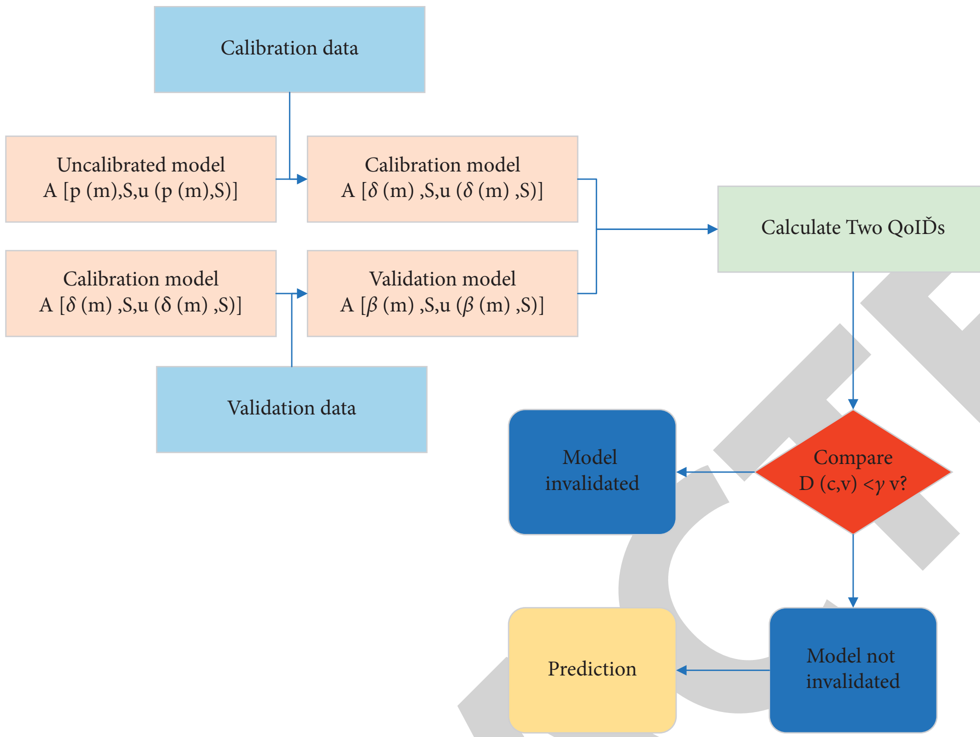

FIGURE 4: Flow chart of dynamic reliability assessment.

A top-bearing reinforced concrete box arch bridge with a calculated span of 81 m and a calculated vector height of 13.5 m was selected here. Due to the lack of bridge inspection data, it is difficult to collect the same bridge inspection data for the past years, so the rapid carbonation test of concrete was carried out in the laboratory to replace the actual measured data of the bridge with the test data. The stress state of the members in the test was determined according to the computational model, and Figure 5 shows the comparison of the carbonation depth of each specimen.

For reinforced concrete arch bridges, the main components can be divided into bridge tunnel system, arch column, main arch ring, etc. The carbonization model of different components is different due to different environments. The speed should be greater than the carbonization speed when there is no stress; while the main arch ring and the columns on the arch are mostly eccentric compression members, under appropriate compressive stress, the concrete is denser, which hinders the entry of carbon dioxide to a certain extent and slows down the carbonization speed. However, if the compressive stress is too large, cracks will occur inside, which may facilitate the entry of carbon dioxide and increase the carbonization rate instead.

The Bayesian dynamic linear model is used to correct and predict the carbonization depth. Taking the updated carbonization depth as the effect and the corresponding protective layer thickness as the resistance, according to the reliability calculation method, the reliability index of the component can be obtained at any time. The reliability index of the bridge system is obtained, and then the differential and equivalent recursive algorithm is used to obtain the reliability index of the bridge system after each update. It can be seen from Figure 6 that with the introduction of their respective test data, the reliability indicators of each component have been revised to different extents. On the one hand, some members become more reliable after the update, and some members become less reliable, which has little effect on the overall correction. It can also be seen from Figure 6 that the reliability changes of different components are different. If we use the reliability of components to evaluate the reliability of the system, not only because of the different selection of components, the evaluation results will also be

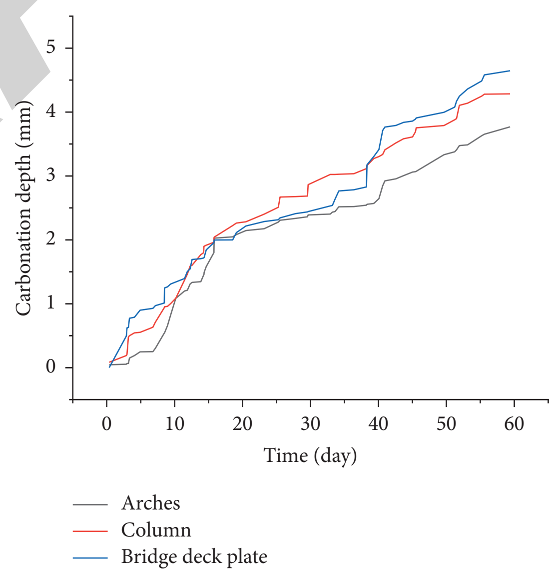

FIGURE 5: Comparison of the carbonization depth of specimens in each part.

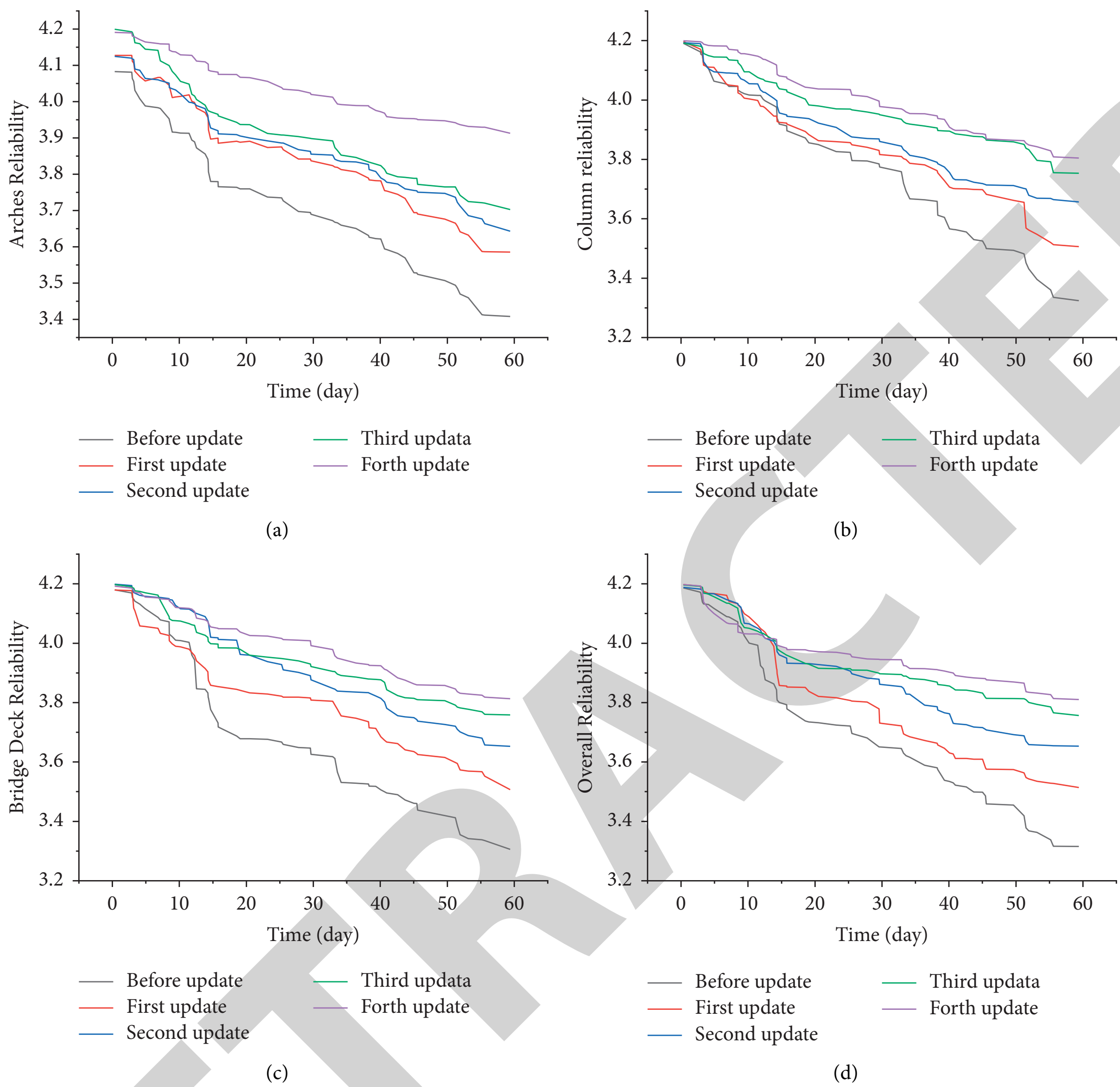

Figure 6: Comparison of the reliability of each component of the bridge.

different, and no matter how you choose, the reliability of components is always greater than the reliability of the system, which is dangerous to a certain extent.

Therefore, when evaluating the durability of bridge structures, it is not only necessary to start from the system level to solve the bias brought by replacing the system with the components, but also to reduce the subjective error by making comprehensive use of previous empirical models and engineering actual measurement data. In the absence of a large amount of statistical information on carbonation, this method can be effectively adapted to each specific project to make a more reliable assessment, and also has an important guiding role for the later maintenance and strengthening.

The reliability of the system is influenced by many factors, not only the reliability of each member, but also its correlation coefficient, which depends on the limit state equation of each member and is influenced by the thickness of the protective layer and the depth of carbonation. The influence of the reliability of each member on the reliability of the system is studied to determine the sensitivity of each member to the system and to provide guidance for the design and testing of reinforcement. The material fracture prediction is closely related to the material type, chemical composition, and manufacturing process, and its magnitude is the key factor determining the fatigue crack propagation characteristics of the structural details of the steel bridge deck. The fracture parameter values of different steels are quite different and show significant random characteristics due to the influence of the inhomogeneity of the material microstructure. The thickness of the protective layer of the members directly affects the reliability of the members. The thickness of the protective layer of each member is changed from 24 mm to 36 mm, and the thickness of the protective layer of one member is changed each time, and the reliability index is calculated on the 30th day after the fourth update. $\beta = 3.24$.

From Figure 7(a), it can be seen that when the thickness of the protective layer is 30 mm, the change in the thickness

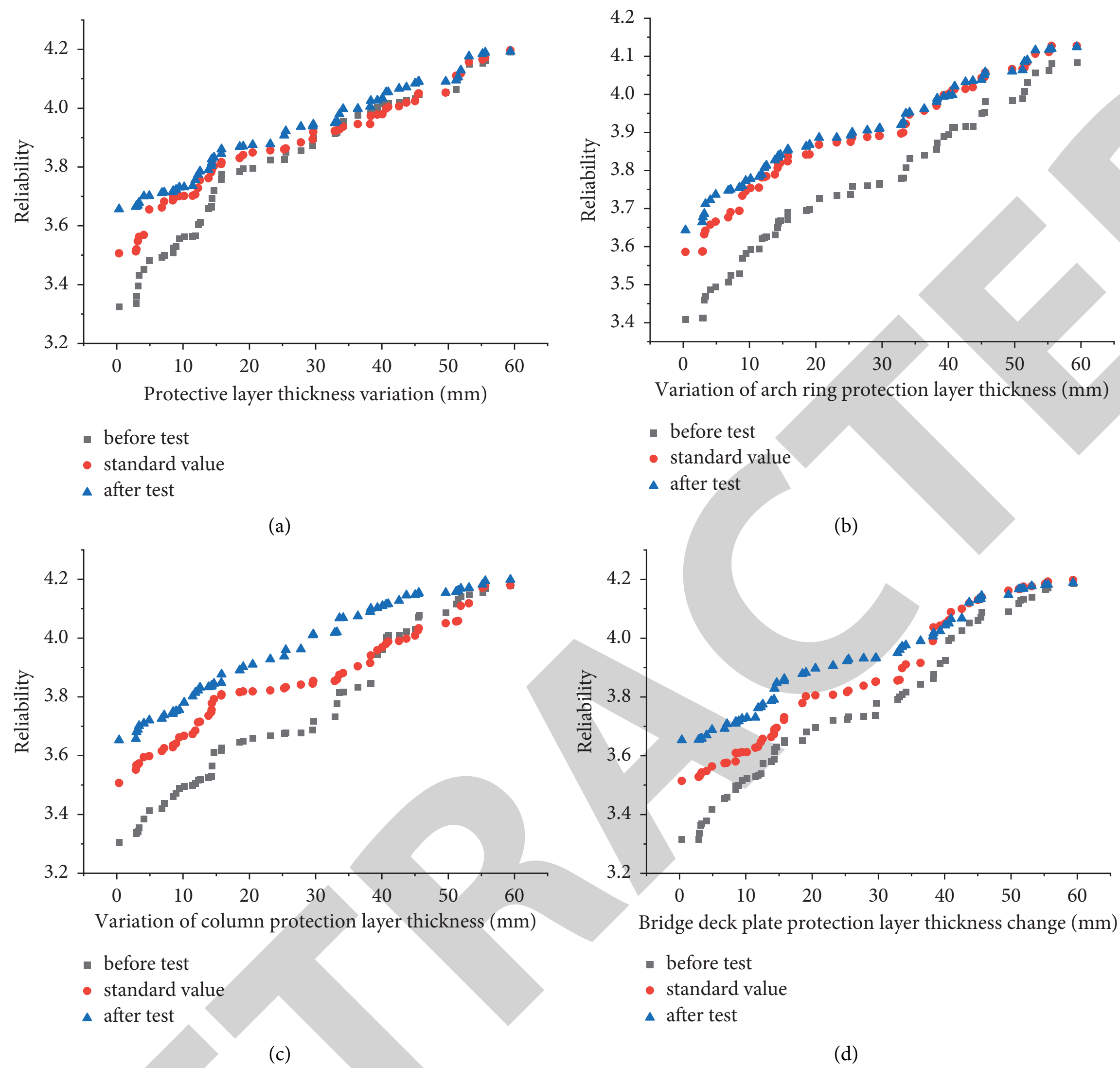

Figure 7: Effect of the thickness of the protective layer on the reliability of the system. (a) Protective layer thickness variation (mm), (b) variation of arch ring protection layer thickness (mm), (c) variation of column protective layer thickness (mm), and (d) bridge deck plate protection layer thickness change (mm).

of the protective layer of the bridge deck has the greatest influence on the reliability of the system and increasing the thickness of the protective layer of the bridge deck within a certain range can improve the reliability of the system, while increasing the thickness of the protective layer of the arch ring and column, the reliability of the system is not obvious; if the thickness of the protective layer of the bridge deck is reduced, the reliability of the system will be reduced immediately, while the thickness of the protective layer of the arch ring and column will be reduced by a certain amount before the reliability of the system decreases sharply. After a certain amount, the reliability of the system will drop sharply. When the thickness of the protective layer remains unchanged, the reliability index of the bridge deck is the lowest, and the reliability change of the bridge deck has the greatest influence on the reliability of the system, and the component with the greatest influence on the reliability of the system or the component with the lowest reliability, in order to further investigate the change law, makes the change of the reliability caused by the thickness of the respective protective layer and the change of the reliability of the corresponding system, as shown in Figures 7(b)–7(d), where Figures 7(b) and 7(c) make the auxiliary line $y =$. From the graph, it can be seen that the system reliability index is always lower than the reliability index of each member, according to the analysis of Figures 7(c) and 7(d), when the thickness of the protection layer of column or arch ring increases, the reliability index of the bridge deck remains unchanged, and the lowest reliability index is the bridge deck; therefore, when the thickness of the protection layer of column and arch ring increases, the system reliability can only be infinitely close to that of the bridge deck. The reliability of the system can only be infinitely close to the reliability index of the bridge deck; while the reliability of the

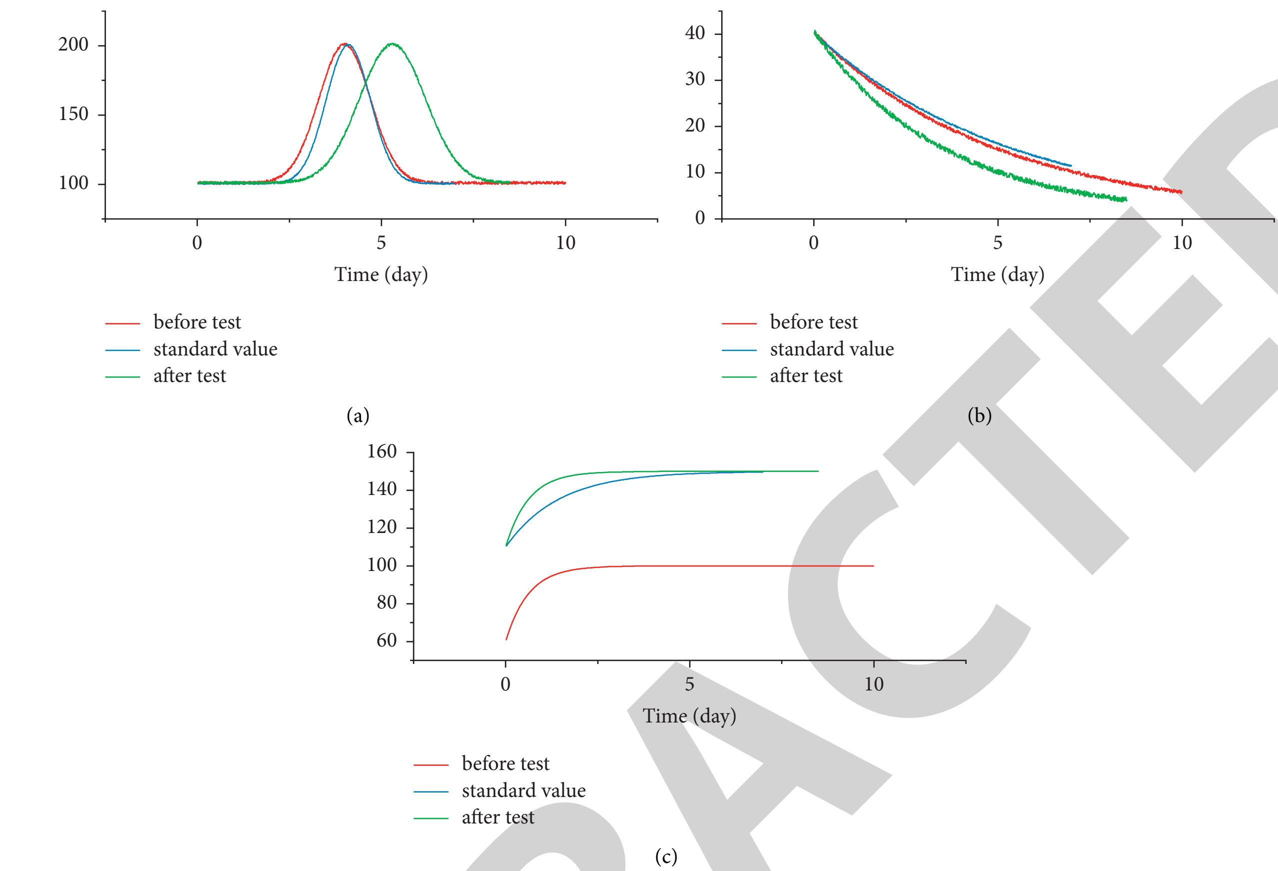

Figure 8: Comparison of reliability indicators after the maintenance of different components. (a) Maintenance of bridge deck, (b) maintenance of column, and (c) maintenance of arches.

bridge deck is still the lowest when the thickness of the protective layer of the column or the arch ring is reduced, and the change of the system reliability is not much when the thickness of the protective layer is reduced to the reliability index lower than that of the bridge deck, the system reliability index will be reduced with the reliability of the arch ring or the column; from Figure 7(d), it can be seen that for the bridge deck, the reliability is lower than that of the arch ring and the column because the reliability is lower than that of the bridge deck. Therefore, the change of protection layer thickness directly affects the system reliability index, and when the protection thickness increases to the extent that the reliability index of the deck plate is larger than that of the column, the change in system reliability gradually becomes smaller and lower than that of the column, which has the lowest member reliability at this time.

It can be seen from Figures 8(a) and 8(b) that when there is arch or column maintenance, although the member reliability can be temporarily stopped, the improvement in the system is not large, because at this time the system has the greatest impact on the components for the lowest reliability of the bridge deck, so the arch and column maintenance on the system is not much, and from Figure 8(c), it can be seen that when there is bridge deck maintenance, the system reliability decreases significantly slower, indicating that the maintenance of the bridge deck plate has a certain slowing effect on the system, but the system reliability is still decreasing at this time, which also shows that the members are only part of the system, and the influence of a single member on the system is limited. The maintenance of the deck slab has a more obvious improvement on the system's durability. According to the calculation results, the system reliability index is improved by 2.55% after the maintenance of the deck slab, while the arch ring and column are improved by 0.15% and 0.29%, respectively, after the maintenance. Therefore, when maintaining the bridge, the deck plate should be considered first, and if the reliability is no longer the lowest after the deck plate maintenance, the member with the lowest reliability at that moment should be considered for maintenance if maintenance is still needed.

Because the maintenance of the bridge deck plate has a more obvious impact on the system's reliability, the reliability index comparison is calculated separately when the bridge deck is maintained at different carbonation times, as shown in the experiment above, to investigate the impact of the maintenance time point on the change in reliability. The a priori model is modified by combining the testing data, based on the Bayesian dynamic linear model, so that the initial general a priori model can continuously incorporate the individual characteristics of the structure and the results are closer to the actual conditions. According to the analysis, the reliability index change curve shifts to the right after maintenance, and because the distance shifted is the same, the final effect of maintenance remains the same as long as maintenance is performed before the failure of the member; however, the system's reliability still decreases when maintenance is performed on a single member, so maintenance of the member before the system's failure does not guarantee.

4. Conclusion

The ability of a structure or member to maintain its safety and serviceability within the design life is reflected in its durability. In this article, a combination of experimental analysis, finite element simulation, and theoretical analysis is used to investigate how to incorporate the carbonation model of concrete members with individual characteristics, the durability and reliability of members and their time-varying properties, and the system durability and reliability dyads, all while considering the working conditions of concrete bridges in actual services, such as loading, cracking, and even acid rain erosion. The research looked into dynamic reliability assessment methods. The following are the main conclusions: (1) The carbonation rate of concrete decreases under compressive stress, and the degree of reduction is related to the ratio of compressive stress to ultimate compressive stress; tensile stress facilitates carbonation, and the higher the tensile stress, the faster the carbonation rate. (2) The similarity of the mechanism of action between the carbon dioxide diffusion model and the heat conduction equation is revealed by comparing the two, allowing a finite element model of concrete with cracks to be constructed and the effects of crack width and depth on the carbonation of concrete to be discussed. (3) The a priori model is modified based on the Bayesian dynamic linear model by combining the testing data, so that the initial general a priori model can continuously incorporate the individual characteristics of the structure, and the results are closer to the actual conditions; in the meantime, in response to the finding that the traditional Bayesian dynamic linear model may have a shortage of gradually increasing deviation between the predicted data and the measured data, the a priori model is modified by combining the testing data, so that the initial general idea of stepwise correction of the a priori model and prediction model is proposed, the error correction expression is given, and the idea's effectiveness is tested using the algorithm. (4) By combining the Bayesian dynamic model and the differential equivalence recursive algorithm, a dynamic assessment method for the bridge system's durability is presented, which can dynamically update the structure's durability condition at any time based on inspection data feedback. The algorithm's analysis reveals that there is a risk of replacing system evaluation with component evaluation, and that the components with the lowest reliability in tandem mode have the greatest influence on the system, which should be considered during inspection and maintenance.

Data Availability

The data used to support the findings of this study are available from the author upon request.

Conflicts of Interest

The author does not have any possible conflicts of interest.

References

[1] F. Shen, C. Xu, and J. Zhang, "Statistical behavior guided block Allocation in hybrid cache-based edge computing for cyber-physical-social systems," *IEEE Access*, vol. 8, pp. 29055–29063, 2020.

[2] M. Rajalakshmi and W. Razia Sultana, "Intelligent hybrid battery management system for electric vehicle," *Artificial Intelligent Techniques for Electric and Hybrid Electric Vehicles*, pp. 179–206, Wiley Online Library, Hoboken, NJ, USA, 2020.

[3] J. F. Arinez, Q. Chang, R. X. Gao, C. Xu, and J. Zhang, "Artificial intelligence in advanced manufacturing: current status and future outlook," *Journal of Manufacturing Science and Engineering*, vol. 142, no. 11, Article ID 110804, 2020.

[4] F. Davidson, A. Alvera-Azcárate, A. Barth et al., "Synergies in operational oceanography: the intrinsic need for sustained ocean observations," *Frontiers in Marine Science*, vol. 6, p. 450, 2019.

[5] Z. Wei and K. Eriguchi, "Analytic modeling for nanoscale resistive filament variation in ReRAM with stochastic differential equation," *IEEE Transactions on Electron Devices*, vol. 64, no. 5, pp. 2201–2206, 2017.

[6] Z. Wang, H. Xiong, J. Zhang et al., "From personalized medicine to population health: a survey of mhealth sensing techniques," 2021, https://arxiv.org/abs/2107.00948.

[7] S. Puerto Tchemodanova, M. Mashayekhi, M. Sanayei, and E. Santini Bell, "Multiaxial fatigue assessment of complex steel connections: a case study of a vertical-lift gussetless truss bridge," *Engineering Structures*, vol. 235, Article ID 111996, 2021.

[8] S. A. Mirfarhadi and H. E. Estekanchi, "Value based seismic design of structures using performance assessment by the endurance time method," *Structure and Infrastructure Engineering*, vol. 16, no. 10, pp. 1397–1415, 2020.

[9] Z. Liu, J. Correia, H. Carvalho et al., "Global-local fatigue assessment of an ancient riveted metallic bridge based on submodelling of the critical detail," *Fatigue and Fracture of Engineering Materials and Structures*, vol. 42, no. 2, pp. 546–560, 2019.

[10] E. Ghaffari, H. E. Estekanchi, and A. Vafai, "Application of endurance time method in seismic analysis of bridges," *Scientia Iranica*, vol. 27, no. 4, pp. 1751–1761, 2020.

[11] B. S. Saini and S. P. Singh, "Flexural fatigue strength prediction of self compacting concrete made with recycled concrete aggregates and blended cements," *Construction and Building Materials*, vol. 264, Article ID 120233, 2020.

[12] W. Cai, Y. Song, and Z. Wei, "Multimodal data guided spatial feature fusion and grouping strategy for E-commerce commodity demand forecasting," *Mobile Information Systems*, vol. 2021, Article ID 5568208, 14 pages, 2021.

[13] M. R. Garcez, L. C. Meneghetti, and R. M. Teixeira, "The effect of FRP prestressing on the fatigue performance of strengthened RC beams," *Structural Concrete*, vol. 22, no. 1, pp. 6–21, 2021.

[14] P. Ovchynnykov, O. Dubinchyk, O. Tiutkin, V. Kildieiev, V. Sedin, and K. Bikus, "Predicting changes of the state of a bridge reinforced with concrete superstructures in view of operational changes," *Civil and Environmental Engineering Reports*, vol. 29, no. 3, pp. 134–152, 2019.

Hindawi
Computational Intelligence and Neuroscience
Volume 2022, Article ID 7483454, 9 pages
https://doi.org/10.1155/2022/7483454

Research Article

Optimization Model of Financial Market Portfolio Using Artificial Fish Swarm Model and Uniform Distribution

Yao Xiao

Chongqing Industry Polytechnic College, Chongqing 400000, China

Correspondence should be addressed to Yao Xiao; xiaoyaokk2022@163.com

Received 4 April 2022; Revised 4 May 2022; Accepted 5 May 2022; Published 15 June 2022

Academic Editor: Xin Ning

The central issue in finance is how to select a portfolio in the financial market. The traditional artificial fish swarm algorithm (AFSA) is optimized in this paper, and the improved AFSA is used to solve the portfolio model. This model generates a uniform distribution operator using uniform distribution and combines it with the basic fish swarm algorithm. Uniform variation occurs when the variance of the optimal value of continuous convergence is within the allowable error. In this manner, the fish can escape the trap of the local extremum, obtaining the global optimal state. To validate the feasibility of improving AFSA, this paper conducts simulation experiments on portfolio problems using MATLAB tools. Experiments show that this model has an accuracy of 93.56 percent, which is 8.43 percent higher than that of the NSGA-II model and 3.76 percent higher than that of the multiobjective optimization model. The experiment shows that the algorithm in this paper can solve these types of problems well and that, using this model, the optimal portfolio investment decision scheme satisfying investors can be obtained. The optimized AFSA presented in this paper can serve as an important reference for investment portfolios and has a wide range of application possibilities in the investment market.

1. Introduction

With the increasing trend of economic globalization and financial integration, the regional economy has become more market-oriented and transparent. Market competition is all around us, and it is becoming more fierce and diverse [1]. While considering the enormous benefits that investment can bring, business should be prepared for the potential risks that come with it. During the capital investment process, rational investors will consider how to allocate a certain amount of capital to thousands of risky securities in order to spread the risk as widely as possible and obtain the greatest benefit [2]. The securities market, on the other hand, is a financial trading market where risks and interests coexist. Its risk changes are influenced by a variety of factors, including politics, economic fluctuations, policy regulation, and company development, making it difficult to grasp its essential characteristics [3]. Because of the volatile economic environment, the types of risks faced by investors in investment also exhibit diversification and variability, and the investment risk is increasing day by day. Individual investors and financial institutions face a central problem in determining how to allocate resources optimally in an uncertain environment in order to maximize income or minimize risk, that is, how to make portfolio selection in the financial market [4]. With the ongoing development of the market economy, investors from all walks of life are frequently confronted with the portfolio problem when engaging in asset investment activities. Portfolio optimization is extremely important in the financial field and has an incalculable impact on the growth of the market economy. Many scholars are currently concerned about it [5]. In today's volatile market, how to assist investors in effectively avoiding risks has gradually become the focus of portfolio research.

The central issue in finance is how to select an investment portfolio in the financial market. The goal of investors is to maximize benefits in a low-risk environment or to bear the least amount of risk while maximizing returns as much as possible. This establishes the need for investors to evaluate the benefits of securities investment and diversify asset risk as much as possible through portfolio model optimization [6]. Because of their high inspiration, effectiveness, and high matching with computer language, artificial intelligence algorithms have piqued the interest and application of researchers in recent years. AFSA (artificial fish swarm algorithm) is a swarm intelligence algorithm made up of many simple autonomous bodies. Each autonomous body is self-contained and can interact with information in its environment, utilizing a novel bottom-up search concept [7]. AFSA employs a novel concept that distinguishes it from other optimization algorithms. AFSA differs from traditional design and solution methods from the specific implementation of the algorithm to the overall design concept, but it can be well integrated with other traditional algorithms at the same time. AFSA's search process is divided into four stages: foraging behavior, tail chasing behavior, clustering behavior [8], and default behavior. The characteristics of AFSA, such as low initial requirements, strong robustness, strong ability to get rid of local extremum, and global optimization, can bring us an opportunity to solve the portfolio optimization problem. It is precisely because of the superior characteristics of AFSA that AFSA has attracted great interest and extensive attention of scholars from all walks of life at home and abroad since it was proposed. With the deepening of the research on this algorithm, many improved algorithms are applied, and the application field is gradually expanded. Therefore, this paper applies AFSA to the optimization of portfolio model. The innovations of this paper are as follows:

(1) The AFSA algorithm is applied to financial market portfolio optimization in this paper, and the original AFSA is improved. The adaptive improvement concept is used in this paper to improve the field of view and step size in the traditional AFSA. The field of view and step size gradually change from large to small to meet the needs of various states of algorithm optimization. Simultaneously, AFSA is integrated with a free search algorithm, allowing it to be applied to data in a portfolio problem to produce a better portfolio.

(2) In this paper, AFSA is used to solve the portfolio optimization problem in the investment field, and the algorithm can jump out of the trap of local extreme value in the optimization process, so as to achieve the optimal value. At the same time, the classical test function is used for simulation verification, and a variety of investment decision-making schemes that meet the requirements of investors are obtained. This study broadens the research field of portfolio and AFSA to a certain extent.

2. Related Work

As a nonlinear programming problem, the research goal of portfolio problem is to allocate the weight to the individuals of a specific asset set, so as to maximize the total return or minimize the total risk. Nowadays, many scholars use swarm intelligence method to solve this kind of problems. At present, the research and application of AFSA have penetrated into many disciplines and were used to solve practical problems. The algorithm has become a cutting-edge research topic with high research value. Some scholars have studied the application of AFSA in combinatorial optimization, but the research in this field needs to be further deepened.

For solving the nonlinear foreign exchange portfolio multiobjective optimization problem, Neumuller and Rothschild added liquidity conditions and proposed a unified method for solving portfolios [9]. Howton et al. carried out measurement research on the risk of investment portfolio, but there is still strong uncertainty in the measurement of investment return and risk [10]. Vikas et al. proposed the optimal portfolio model under the probability criterion. However, there is no explicit discussion on investment risk, and investment risk is implicitly described by the covariance of returns [5]. Au-Yeung and Chan used a compromise algorithm to solve portfolios with linear transaction costs [11]. Low et al. studied the relative effectiveness of proxy securities, the equilibrium and disequilibrium of portfolio investment, the interaction between investment decision-making and capital structure optimization, and portfolio selection under financing constraints [12]. Bekiros et al. studied a multiperiod portfolio optimization problem and algorithm with feedback control in a fuzzy environment [13]. Sabine finally established a multiobjective nonlinear programming model with transaction fees by adding another objective to generate a multiobjective function of nonlinear programming under the premise of including the objectives of rate of return, risk, liquidity, and so forth [14]. In order to improve the deficiencies of variance model, Eslamloueyan and Jafari introduced conditional value-at-risk to measure asset investment risk and established a multiobjective investment optimization model. Experiments show that the model can improve the ability of investors to manage investment risks [15]. Based on the subjective expected utility theory, Corradin constructed the dynamic prospect theory value objective function model by using the dynamic aversion coefficient and the wealth reference point; at the same time, considering the opportunity constraints to ensure the capital security of investors, the multifrequency vibration mutation particle swarm algorithm was used to analyze the model. Experiments have proved that it has good feasibility in the formulation of practical investment decisions [16]. In order to simplify the covariance matrix, Luque et al. introduced a multifactor tool. Experiments have verified that the method can effectively solve the large-scale investment portfolio problem [17]. Jappelli and Padula reviewed the evolution, improvement, integration with other algorithms, and applications of AFSA in various fields in recent years [18].

The research of these algorithms has played a positive role in promoting the solution of portfolio model. This paper makes a relatively in-depth study on the relevant literature and puts forward the financial market portfolio optimization model based on AFSA. In this paper, the field of vision and step size in traditional AFSA are improved by self-adaptation, and the field of vision and step size are gradually reduced from large to small, so that it can meet the different state needs of algorithm optimization. Try to use standardized and random selection behavior to add variation factors and improve the search strategy of foraging behavior, and then iterate through roulette to select the best of the whole fish school, so as to solve the problem of accuracy and stability. The simulation results show that the algorithm in this paper has good performance and can solve the problem of portfolio optimization.

3. Methodology

3.1. Financial Market Portfolio. The rational allocation of various assets to best meet the investors' trade-off between risks and benefits is referred to as portfolio management. In finance, portfolio theory is a key asset management theory. During the early stages of portfolio theory development, investors primarily used diversification as an investment strategy, making decisions based on their understanding of market information as well as their historical experience and skills [19]. According to this theory, the risks in portfolio problems decrease as the number of assets in the portfolio decision increases, and a diversified portfolio of assets with very low correlation can effectively reduce the risks. Investing behavior is frequently a long-term process for investors. In general, a portfolio is a research method that allows investors to correctly choose the distribution ratio of capital investment when confronted with multiple capital options in order to maximize profits while minimizing risks. Modern finance and modern portfolio theory are built around the portfolio problem [20]. This problem discusses how to rationally distribute an investor's wealth among various assets in order to achieve the goal of stable and rapid capital growth while also controlling investment risks. Effective portfolio must meet the two following conditions: ① Risk is minimized under the given expected rate of return. ② Under the condition of given risk, the expected rate of return is maximized. All efficient portfolios constitute efficient boundaries or efficient frontiers.

Investment risk is the possibility that the expected investment income will be lost due to the fluctuation of the invested assets as a result of objective factors such as the market environment. The manner in which an investment is made determines the risk of the investment. According to the causes of the risk, we can usually divide the risk into market risk, credit risk, liquidity risk, and operational risk. In a stochastic uncertain investment environment, the return on risky assets is typically assumed to be a random variable. Based on historical asset return data, investors can accurately predict the probability distribution of their future returns. The term "risk" refers to the fact that the rate of return on assets is uncertain [21]. The term "risk-free assets" refers to assets with a guaranteed rate of return. Risk-free assets have at least two characteristics: fixed income and no risk of default. In actual investment activities, portfolio investment, as opposed to single asset investment, can play a role in dispersing overall investment risk, so portfolio investment is a common problem in financial activities. The goal of an investor's investment is to realize consistent and rapid growth of their funds while effectively managing investment risks. During this time, investors must constantly readjust their wealth in order to realize their investment intention, that is, to minimize risks and maximize returns. Any investor wants to maximize his return on investment, but higher returns come with higher risks. The investment decision-making process is a trade-off between yield and risk, which is a decision-making problem with two objectives. The reason for building a portfolio is to reduce the investment risk to a certain extent. Investors can find a trade-off point between the investment income and the corresponding investment risk in the form of portfolio, so as to maximize the total income as much as possible when the investment risk is certain or minimize the investment risk as much as possible when the income is certain.

3.2. Portfolio Optimization. The so-called optimization algorithm, in fact, describes a search process or rule, and it is based on a certain idea or mechanism, and through certain search rules and ways, it can obtain the solution to the problem that users want. Combinatorial optimization is one of the optimization problems. It usually refers to the optimization process of finding the optimal arrangement, grouping, sequence, or screening of discrete events through the study of mathematical methods or finding the optimal solution of the objective function from a limited number of feasible solutions. When optimizing the objective function, the objective function with constraints is often involved, so the solution process is complicated. With the development of global economy, the risk of financial market is also increasing. At the same time, with the development of computer technology and the explosive growth of data in solving practical problems, the traditional mathematical solution has been unable to solve practical problems. Therefore, the use of artificial intelligence technology to solve combinatorial optimization problems arises at the historic moment. At present, AFSA has been widely used. In the research field of mathematical theory, some progress has been made in optimizing the objective function by AFSA, and people have paid attention to solving constrained combinatorial optimization problems. AFSA is a new swarm intelligence optimization algorithm based on simulating biological behavior. In the optimization algorithm, the concept of animal autonomy is introduced, and the bottom-up design idea is used, thus forming a new intelligent algorithm.

The intelligent algorithm not only reduces the labor of solving by hand but also lacks the precision of solving by hand. We can quickly find useful information hidden in a large number of data sets, including rules, concepts, patterns, and rules, by combining computer technology and a combinatorial optimization model. Traditional portfolio models are based on probability theory and treat problem uncertainty as a random phenomenon. However, there is a lot of uncertainty in the securities market. Fuzziness is more important than randomness in the field of subjective cognition. The modern portfolio invests in risk diversification and employs quantitative research methods to determine the optimal portfolio investment ratio. The risk of the portfolio decreases as the number of investment types in the portfolio increases. The primary goal of studying portfolio models is to learn how to control the distribution ratio of a portfolio in order to maximize its return. The algorithm is primarily used to rigorously describe a program's iterative steps to solve problems, and it is a generalized general program to solve problems step by step. For an arbitrary given problem, we say it can solve the example if there is such a method that can find the answer to the given problem after a certain step. During the investment process, investors must consider the expected return rate as well as the potential risk rate of purchasing securities. The portfolio model must be optimized in order to provide more objective and optimal decisions. The schematic diagram of optimization algorithm in this paper is shown in Figure 1.

In order to diversify the investment risk and obtain appropriate investment income, investors often use portfolio investment, that is, invest a sum of money in several different securities at the same time. The expression of mean-variance plays a very important role in the construction of portfolio model, providing an objective research tool for rational investors, and is the representative of current portfolio theory. In the mean-variance model, the expected return rate is the expected value of the return rate of the portfolio, and the expected risk refers to the variance of the return rate of the portfolio. Although the mean variance has laid the foundation of modern portfolio theory and has been widely recognized and applied, it still has some limitations. For example: ① Variance or standard deviation cannot determine the direction of income deviation and the possibility of future risks of investment, which are more concerned by investors. ② Generally, the return on assets in the actual market cannot meet the condition that it must conform to the normal distribution, which is a strict premise. ③ The investment portfolio model based on this theory has a large amount of calculation. The main innovation of the statistical analysis method of mean-variance probability is to quantify the income risk in the portfolio problem. Because the income and risk in the investment process are random and uncertain, it is better to use random variables in mathematical statistics for statistical analysis. The mean-variance model assumes that investors are risk-averse. Rational investors always hope to obtain the maximum expected return under the condition of restraining the risk and minimize the investment risk under the condition of restraining the expected return. A portfolio with this nature is called an effective portfolio. Compared with allowing short selling, when using Markowitz mean-variance model to select the optimal investment proportion vector under the condition of not allowing short selling, the opportunity space of portfolio will often be reduced. However, to a certain extent, not allowing short selling can reduce market risks and investors' risks. Therefore, short selling is often not allowed in underdeveloped markets.

3.3. Construction of Portfolio Optimization Model in Financial Market Based on AFSA. Artificial fish can realize the mutual conversion of these behaviors at different times through perception of the environment; that is, they can realize their own behavior through behavior evaluation. The food concentration and crowding distance are used to evaluate behavior. Artificial fish continue to move towards areas with high food concentration but are not overcrowded; then choose the best or better behavior, and finally realize the fish swarm convergence. Traditional AFSA has a number of flaws. For example, a fixed field of vision and step size may cause convergence speed to be slow or convergence accuracy to fail, and it may sometimes fall into the local extreme value and fail to reach the global optimum. Furthermore, the algorithm's mathematical foundation is lacking as is the corresponding theoretical analysis. Based on the shortcomings of the traditional AFSA, this section improves the financial market portfolio one by one. The basic strategy for artificial fish movement in this paper is no longer applicable. As a result, this paper proposes a normalization process to address the overflow problem of feasible solutions and employs dynamic vision and step size to improve the search ability of the fish swarm algorithm, avoiding local extremum and increasing optimization accuracy. When a typical transaction cost function is introduced, the model's constraint function becomes nonlinear, and the effective solution set becomes nonconvex and nonconcave, indicating that the search space is irregular. This necessitates using a highly robust algorithm that avoids falling into the local optimum. The flow chart of the improved free search algorithm of artificial fish swarm is shown in Figure 2.

The basic alternate behavior is foraging behavior. If you cannot find a better state than the current one in the process of clustering or rear-end collision, you will do foraging behavior. In foraging behavior, if you cannot find a better state than yourself, you will randomly select a location to update. This will lead to retrogression in the process of optimization. In view of this situation, the solution of this paper is to regard the current solution as a vector, and the next position is no longer obtained randomly, but offset the random angle based on the original direction. The point where AFSA triggers the uniform mutation of the fish school is that when the difference of the global optimal value in the bulletin board for several consecutive times is very small and the number of optimization iterations is not reached, the fish school begins to produce uniform mutation and generates a new fish school state. In this paper, the fitness of individuals is measured by an evaluation function based on ranking. Evaluation function is used to set a probability for each chromosome in the population, so that the probability of this chromosome being selected is proportional to its adaptability to other chromosomes in the population. That is, through roulette, the chromosome with strong adaptability is selected to have a greater chance of producing offspring. In the process of applying the algorithm, this paper tries to reduce the number of individuals and scale of the fish school as much as possible on the premise of ensuring the convergence of the stable algorithm. In this algorithm, with more fish swarm individuals set, the frequency of information exchange between artificial fish individuals will increase, and the convergence speed of the algorithm will be accelerated, so as to better jump out of the local extreme value. However, the amount of calculation and optimization

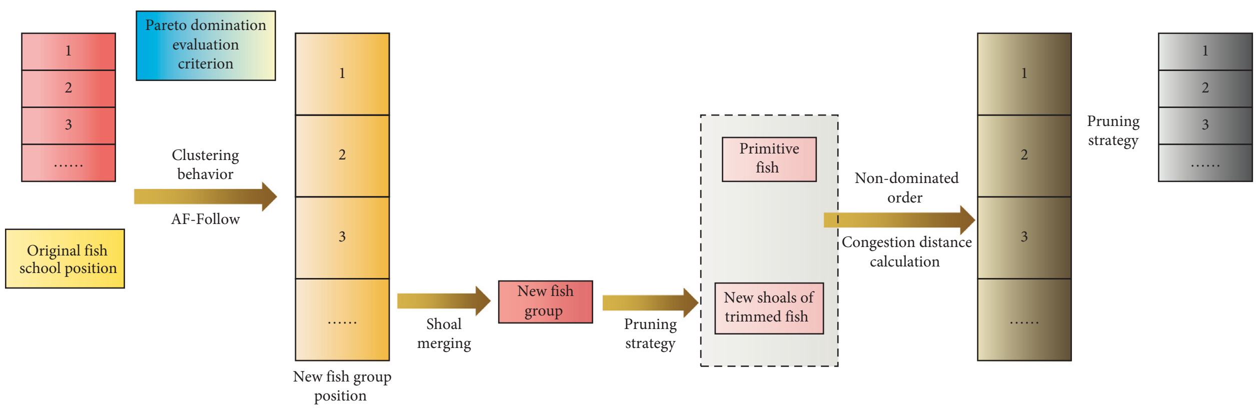

Figure 1: Schematic diagram of the optimization algorithm in this paper.

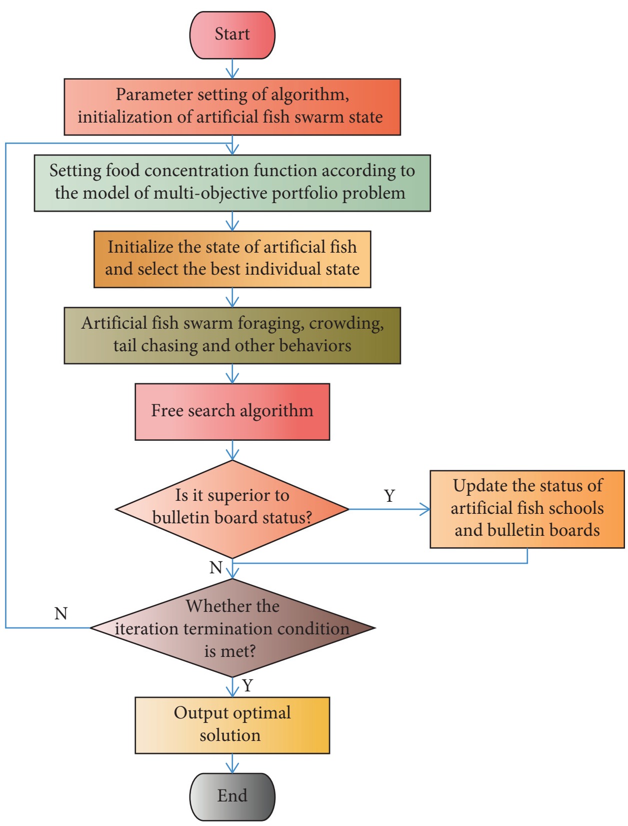

Figure 2: Process of the improved artificial fish free search algorithm.

time in each optimization iteration of the algorithm are also increased. Therefore, reasonably specifying the size of fish swarm is the key to improve the efficiency of the algorithm. In the past, artificial fish swarms did not consider individuals with poor search effect in the population. In this regard, this paper uses roulette to screen according to the fitness function value of each individual and seeks individuals with strong ability to iterate to the next generation with a large probability. AFSA embodies the natural law of survival of the fittest for all fish groups throughout the evolution of animals. Suppose that the i-th individual x_i in the artificial fish swarm is given a probability P_b of mutation; randomly select the subelement x_{ij} at position j in x_i to mutate it.

$$\begin{aligned} &\text{if } rand < P_b,\\ &x_{ij} = rand \\ &x_{i/\text{next}} = \text{norm}\left(x_{i/\text{next}}\right). \end{aligned} \tag{1}$$

The basic fish swarm algorithm selects and randomly generates a new solution after it is not optimized, which may lead to the regression of the solution. This paper uses the following formula to deal with it:

$$\begin{aligned} x_{i/\text{next}} &= \begin{cases} x_i + \left(x_v - x_i\right) * \text{dis}\left(x_v - x_i\right); & \text{if } Y_i > Y,\\ \text{ob}\left(x_i\right); & \text{else if } Y_{ob\left(x_i\right)} > Y,\\ x_i; & \text{else,} \end{cases}\\ x_{i/\text{next}} &= \text{norm}\left(x_{i/\text{next}}\right).. \end{aligned} \tag{2}$$

In the above formula, $ob\left(x_i\right)$ is the vector obtained by taking x_i as a direction vector and offsetting it by a certain angle. According to the fitness function value, the artificial fish individuals with strong optimization ability are screened out by roulette to enter the next generation.

$$\text{fish} - \text{swarm}_{i/\text{next}} = \text{roullete}\left(\text{fish} - \text{swarm}_i\right). \tag{3}$$

Suppose that investors consider four decision-making factors: wealth, risk, skewness, and kurtosis of the portfolio terminal. It is required to maximize the terminal wealth and cumulative skewness of the portfolio and minimize the cumulative risk and kurtosis of the portfolio. According to the uniform mutation operator in genetic algorithm, the mutation characteristics are combined with AFSA, so that the fish swarm algorithm has the same mutation ability, and it can avoid falling into local extremum, which is more conducive to the fish swarm reaching the global optimum in the shortest time. A single error index cannot fully evaluate the prediction effect of the model. Therefore, MAE (mean absolute error), RMSE (root mean square error), and CTR (correct trend rate) are introduced to evaluate the prediction accuracy, and the running time of the algorithm is used to evaluate the convergence speed. Its calculation formula is as follows:

$$\mathrm{MAE}=\frac{\sum_{i=1}^{n}\left|y_i'-y_i\right|}{n},$$
$$\mathrm{RMSE}=\sqrt{\frac{1}{n}\sum_{i=1}^{n}\left(y_i'-y_i\right),n} \qquad (4)$$
$$\mathrm{CTR}=\frac{\sum_{i=1}^{n}\mathrm{CTR}_i}{n}.$$

In the above formula, y_i and R_i are the income of the asset on the current day and the previous day, respectively, and i is the return of the asset on the i day; namely,

$$R_i=\frac{y_i-y_i-1}{y_i-1}\quad i=2,\ldots,n=220. \qquad (5)$$

The expected rate of return is

$$\frac{y_i'-y_i-1}{y_i-1}. \qquad (6)$$

Combined with the portfolio model constraint function studied in this paper, an outlier penalty function is introduced:

$$\max F(x)=\delta\sum_{i=1}^{n}\left(Kx_iR_i-\prod_i\right)+(1-\delta)\left\{\max_{1\le i\le n}\{Kx_iS_i\}\right\}-\gamma\left(\sum_{i=1}^{n}x_i-1\right). \qquad (7)$$

In the above formula, $\gamma=8^k\,(k=1,2,3,\ldots)$.

The perception of artificial fish's range or distance is known as vision. The algorithm's convergence speed is generally determined by the value of the visual field. As a result, in order to observe the search space more thoroughly, the sensing range should be expanded, making it easier for artificial fish to locate and converge on the global extremum. For multiobjective decision-making problems, there is usually no optimal solution in the traditional sense due to the incommensurability and contradiction of objectives. A common method for resolving this type of problem is to convert the multiobjective decision-making problem into the corresponding single-objective decision-making problem. The traditional AFSA is limited in its search for the optimal solution of the objective function in the solution space of its research problem because the vision and step size of the fish swarm algorithm are typically fixed and artificially set before the experiment begins. In AFSA, each parameter's setting is not sensitive, and there is no strict theoretical basis for selecting the optimal parameter. The algorithm is extremely robust. However, because the algorithm is random, the value of each parameter has some influence on the algorithm's convergence process and optimization results. In this paper, adaptive field of vision and step size are used, which means that, in the early stage of convergence, a larger field of vision and step size are used so that it can be quickly positioned in the global optimal state; in the late stage of convergence, a smaller field of vision and step size are used to improve the algorithm's convergence accuracy.

4. Result Analysis and Discussion

The experimental data of this paper are the trading data of 25 stocks from the stock market for 450 trading days. The rate of return is the relative average rate of return. The data sent by the sample can minimize the interference caused by relevant errors in the experiment and can accurately demonstrate the performance of the algorithm. In this chapter, Matlab software is used for experiments. Run a 64-bit operating system with 16 GB of memory. Before the simulation, initialize the parameters. The experimental parameters for testing the performance of the algorithm are set as follows: the number of artificial fish school is 100; the initial visual field size is 1; the maximum number of attempts is 80; the mutation operator is 0.05; and the visual field distance is 1; the maximum number of iterations is 100. CTR, MAE, and RMSE experiments are carried out with different algorithms, and the results of three indexes are shown in Table 1.

It can be seen from the data in the table that the MAE and RMSE of the algorithm in this section are lower than those of other algorithms, and the CTR of the algorithm in this paper is the highest. In order to verify the effectiveness of this algorithm, we run the algorithm 100 times and test the influence of cardinality constraint and confidence value on the optimal value of this paper. The influence of cardinality constraint on the optimal value is shown in Figure 3. The influence of confidence on the optimal value is shown in Figure 4.

Figure 3 shows that the overall trend is that the value of conditional risk value decreases with the increase of base constraint. This is in line with the principle that diversified investment can reduce nonmarket risks. As can be seen from Figure 4, when the expected return is constant, with the increase of confidence value, the conditional risk value also increases correspondingly. This shows that investors' aversion to risks has increased. Figure 5 shows the comparison results of Pareto frontier distribution of different algorithms.

It can be seen from Figure 5 that the result obtained by the improved AFSA has the lowest risk under the same expected rate of return, and it approaches the optimal solution of linear programming well, and a group of Pareto optimal solutions are found. The improved AFSA and the traditional AFSA were tested by the test function, and the test was repeated 50 times in an independent environment. The test results are shown in Table 2.

Table 1: Comparison of the results of three indicators of different algorithms.

Algorithm	CTR	MAE	RMSE
Support vector machine algorithm	0.878	0.501	0.649
Multiobjective optimization algorithm	0.623	0.279	0.387
Particle swarm optimization	0.807	0.328	0.416
NSGA-II algorithm	0.745	0.496	0.485
Basic fish swarm algorithm	0.815	0.287	0.389
Algorithm in this paper	0.647	0.213	0.347

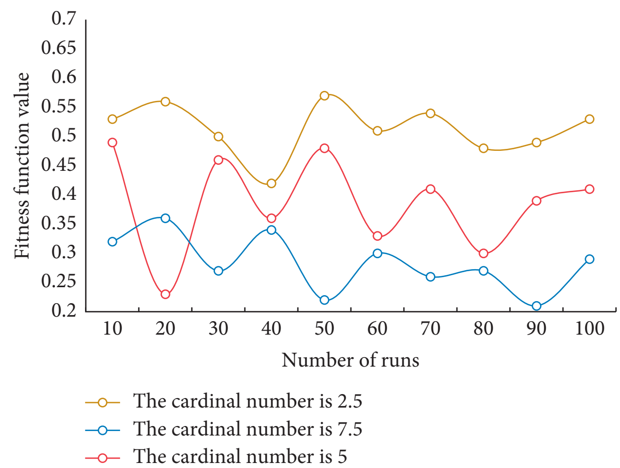

Figure 3: Influence of cardinality constraint on optimal value.

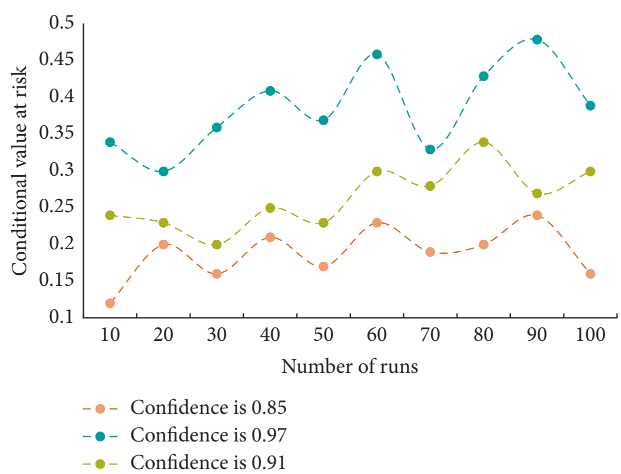

Figure 4: The effect of confidence on the optimal value.

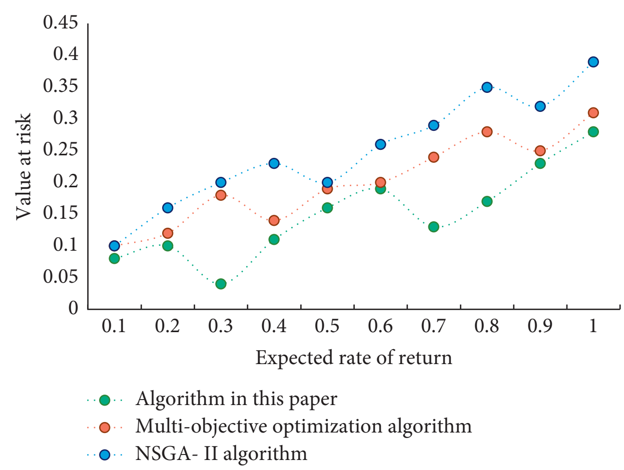

Figure 5: Comparison of pareto frontier distributions for different algorithms.

It can be seen from Table 2 that the improved AFSA has stronger overall optimization solution ability and better robustness than the traditional AFSA. The success rate of the improved algorithm in optimizing the test function has been greatly improved. To verify the effectiveness and reliability of the improved method, the precision experiment of the model is carried out, and the results are shown in Figure 6.

It can be seen that the accuracy of the improved model is obviously higher than those of the other two models. The accuracy of this model can reach 93.56%, which is 8.43% higher than that of NSGA-II model and 3.76% higher than that of multiobjective optimization model. This result verifies the effectiveness and reliability of the improved method in this paper. Using this model, NSGA-II model, and multiobjective optimization model to test the performance, the results are shown in Figure 7.

From the data analysis in Figure 7, it can be concluded that most of the total returns of the optimized portfolio model in this paper are higher than those of other models. It can obtain a better portfolio decision scheme, make the investment income as large as possible, and minimize the risk and provide investors with a certain investment direction. This shows that the portfolio model in this paper is

Table 2: Optimization results of test functions for different algorithms.

Index	Test 1		Test 2	
	Traditional AFSA	Improved AFSA	Traditional AFSA	Improved AFSA
Optimal solution	0.994	1	164.72	174.97
Worst solution	0.978	1	163.57	174.92
Average function value	0.983	1	163.98	174.96
Average number of convergence iterations	20	8	18	12
Success rate (%)	74.5	99.6	82.6	99.2

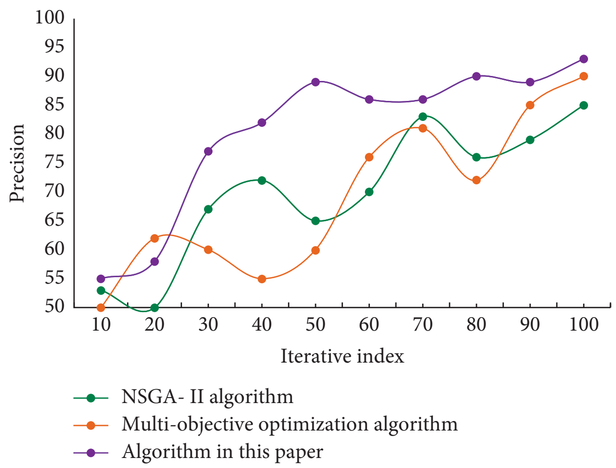

Figure 6: Comparison of the accuracy results of different models.

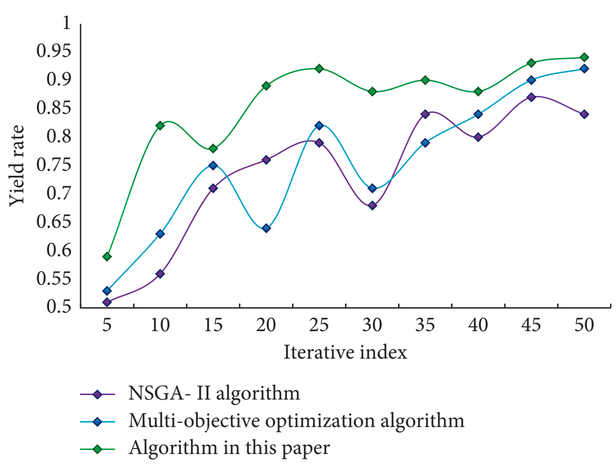

Figure 7: Model performance test.

effective, and its optimal investment strategy can be applied to actual investment.

The improved AFSA shows more reliable convergence performance than the traditional AFSA because it refers to the solution strategy with strong theoretical basis in genetic algorithm. At the same time, due to the inherent advantages of AFSA, it also overcomes the problems such as the sensitivity of genetic algorithm to initial value. The experimental results show that it can eliminate the local extremum and finally obtain the global optimal state, which effectively solves the problem of low convergence accuracy of the algorithm optimization problem.

5. Conclusions

Market competition is prevalent at the moment, and it is becoming increasingly intense and diverse. Investors should be prepared for potential risks while also considering the numerous advantages that investment can provide. As a result, the current research focus is on how to select an investment strategy to maximize profits. The related literature are studied fairly thoroughly in this paper, and a financial market portfolio optimization model based on AFSA is built. Simultaneously, the corresponding improvement methods are proposed to address the shortcomings of traditional AFSA, such as low convergence accuracy, slow speed, and the tendency to fall into local extremum. Combining AFSA with a free search algorithm improves the optimization performance of traditional AFSA and, as a result, strengthens the overall algorithm's global ergodicity and local delicacy. According to empirical evidence, this model's accuracy can reach 93.56 percent, which is 8.43 percent higher than that of the NSGA-II model and 3.76 percent higher than that of the multiobjective optimization model. Simultaneously, the Pareto frontier obtained by improving AFSA is more uniform and diverse, indicating that the Pareto optimal solution is of higher quality. This demonstrates the improved algorithm's effectiveness and applicability. The optimal decision optimized by the improved fish swarm algorithm has a higher investment benefit, a higher expected return, and a lower risk of portfolio investment. This is beneficial to the prosperity and development of the securities trading market because it promotes investors' investment and trading activities. According to the findings of the preceding research, AFSA is a viable option for addressing the portfolio problem. AFSA has significant development potential, which merits our thorough and extensive investigation. By improving and perfecting it, AFSA is expected to have a better application prospect. The improved AFSA in this paper achieved good optimization results, but the index selection of the investment portfolio is not detailed and comprehensive enough, and how to improve the stability of AFSA performance without sacrificing efficiency will be researched further in the future.

Data Availability

The data used to support the findings of this study are available from the author upon request.

Conflicts of Interest

The author does not have any possible conflicts of interest.

References

[1] D. Wang, Q. Huang, T. Ye, and S. Tian, "Research on the two-way time-varying relationship between foreign direct investment and financial development based on functional data analysis," *Sustainability*, vol. 13, no. 11, p. 6033, 2021.

[2] T. Stoilov, K. Stoilova, and M. Vladimirov, "Explicit value at risk goal function in Bi-level portfolio problem for financial sustainability," *Sustainability*, vol. 13, no. 4, p. 2315, 2021.

[3] O. Stoddard and I. Noy, "Fire-sale FDI? The impact of financial crises on foreign direct investment," *Review of Development Economics*, vol. 19, no. 2, pp. 387–399, 2015.

[4] S. G. Hanson, D. S. Scharfstein, and A. Sunderam, "Social risk, fiscal risk, and the portfolio of government programs," *Review of Financial Studies*, vol. 32, no. 6, pp. 2341–2382, 2019.

[5] A. Vikas, S. Ruenzi, and F. Weigert, "Tail risk in hedge funds: a unique view from portfolio holdings," *Journal of Financial Economics*, vol. 125, no. 3, pp. 610–636, 2017.

[6] S. G. Chule, M. D. Beer, and S. Moyo, "Computations and performance analysis of self-financing fixed-mix investment portfolio strategies in a South African financial market," *Research Policy*, vol. 41, no. 51, pp. 201–215, 2015.

[7] P. R. Junior, E. Pamplona, L. Rocha, V. E. de Mello-Valerio, and A. P. Paiva, "Stochastic portfolio optimization using efficiency evaluation," *Management Decision*, vol. 53, no. 8, p. 1698, 2015.

[8] J. Chen, C. Du, Y. Zhang, P. Han, and W. Wei, "A clustering-based coverage path planning method for autonomous heterogeneous UAVs," *IEEE Transactions on Intelligent Transportation Systems*, vol. 1, pp. 1–11, 2021.

[9] S. Neumuller and C. Rothschild, "Financial sophistication and portfolio choice over the life cycle," *Review of Economic Dynamics*, vol. 26, pp. 243–262, 2017.

[10] S. D. Howton, S. W. Howton, and B. Scheick, "Financial flexibility and investment: evidence from REIT at-the-market (ATM) equity offerings," *Real Estate Economics*, vol. 46, no. 2, pp. 334–367, 2018.

[11] T. C. Au-Yeung and K. K. Chan, "Crafting the financial-subject: a qualitative study of young workers' experiences in financialised pension investment in Hong Kong," *Journal of Social Policy*, vol. 49, no. 2, pp. 1–19, 2019.

[12] R. K. Y. Low, Y. Yao, and R. Faff, "Diamonds vs. precious metals: what shines brightest in your investment portfolio? [J]," *International Review of Financial Analysis*, vol. 43, no. 1, pp. 1–14, 2016.

[13] S. Bekiros, D. K. Nguyen, G. S. Uddin, and B. Sjo, "On the time scale behavior of equity-commodity links: implications for portfolio management," *Journal of International Financial Markets, Institutions and Money*, vol. 41, no. 3, pp. 30–46, 2016.

[14] D. Sabine, "Strategic nodes in investment fund global production networks: the example of the financial centre Luxembourg," *Journal of Economic Geography*, no. 4, p. 4, 2015.

[15] K. Eslamloueyan and M. Jafari, "Do better institutions offset the adverse effect of a financial crisis on investment? Evidence from East Asia," *Economic Modelling*, vol. 6, no. 6, pp. 154–172, 2019.

[16] S. Corradin, R. Gropp, H. Huizinga, and L. Laeven, "The effect of personal bankruptcy exemptions on investment in home equity," *Journal of Financial Intermediation*, vol. 25, pp. 77–98, 2016.

[17] A. Luque, S. Junqueira Junior, H. A. Cabra, P. Andrade, and F. Oliveira, "Peripheral arterial disease management program: screening-risk factor management program and financial return on investment," *Value in Health*, vol. 18, no. 3, p. 251, 2015.

[18] T. Jappelli and M. Padula, "Investment in financial literacy, social security, and portfolio choice," *Journal of Pension Economics and Finance*, vol. 14, no. 4, pp. 369–411, 2015.

[19] C. R. Dunn, T. E. Dorsch, M. Q. King, and K. J. Rothlisberger, "The impact of family financial investment on perceived parent pressure and child enjoyment and commitment in organized youth sport," *Family Relations*, vol. 65, no. 2, pp. 287–299, 2016.

[20] E. Dardati and J. Riutort, "Cap-and-Trade and financial constraints: is investment independent of permit holdings?" *Environmental and Resource Economics*, vol. 65, no. 4, pp. 841–864, 2016.

[21] T. Kikuchi and G. Vachadze, "Minimum investment requirement, financial market imperfection and self-fulfilling belief," *Journal of Evolutionary Economics*, vol. 28, no. 2, pp. 305–332, 2018.

Hindawi
Computational Intelligence and Neuroscience
Volume 2022, Article ID 7228833, 9 pages
https://doi.org/10.1155/2022/7228833

Research Article

The Recommendation System of Innovation and Entrepreneurship Education Resources in Universities Based on Improved Collaborative Filtering Model

Li Geng

Xi'an Physical Education University, Xian 710068, China

Correspondence should be addressed to Li Geng; 102015@tea.xaipe.edu.cn

Received 8 May 2022; Revised 18 May 2022; Accepted 25 May 2022; Published 14 June 2022

Academic Editor: Xin Ning

In the huge number of online university education resources, it is difficult for learners to quickly locate the resources they need, which leads to "information trek." Traditional information recommendation methods tend to ignore the characteristics of learners, who are the main subjects of education. In order to improve the recommendation accuracy, a recommendation algorithm based on improved collaborative filtering model is proposed in this paper. Firstly, according to the student behavior data, consider the behavior order to create the behavior graph and behavior route. Then, the path of text type is vectorized by the Keras Tokenizer method. Finally, the similarity between multidimensional behavior path vectors is calculated, and path collaborative filtering recommendations are performed for each dimension separately. The MOOC data of a university in China are introduced to experimentally compare the algorithm of the article as well as the control group algorithm. The results show that the proposed algorithm takes better values in evaluation indexes, thus verifying that this algorithm can improve the effectiveness of innovation and entrepreneurship education resources recommendation in universities.

1. Introduction

In recent years, the use of online education platform is more and more accepted by learners [1]. Especially, after the outbreak of New Coronavirus, online learning is the preferred learning mode when offline learning cannot be carried out normally. Faced with the huge demand for online learning, online education institutions are providing free online courses and sharing online teaching resources, and the online education industry is showing an explosive growth trend. With the widespread use of online learning platforms, the number of educational resources for innovation and entrepreneurship in universities has also increased dramatically.

In the huge number of online college education resources, learners are difficult to quickly locate the resources they need, resulting in "information trek" [2]. Information recommendation is a method for students to quickly and effectively screen out the objects that meet their preference characteristics from the mass objects. At present, information recommendation technology is widely used in many fields [3]. It is an effective way to solve the problem of "information trek" to apply information recommendation technology to online education and realize personalized recommendation of innovation and entrepreneurship education resources in universities in the process of online education.

With the upgrading of Internet technology, the scale of online education services, represented by Massive Open Online Courses (MOOC), Net Ease Cloud Classroom, and innovation and entrepreneurship education resource platforms built by universities, continues to expand. Meanwhile, teaching data through social media such as Weibo, forum, and post bar also constitute a massive amount of online education resources [4]. These abundant online education service resources not only expand students' knowledge scope and supplement the deficiency of offline learning, but also bring a lot of inconvenience to students. First, complicated online education resources cause "information trek," and the quality of online education services is uneven, which makes it difficult for students to identify and compare, resulting in poor learning experience and effects. Second, faced with the same high-quality educational resources, students with high information literacy can easily obtain relevant information, while students with low information literacy can hardly access such resources, resulting in new educational inequities in the information environment. Third, all kinds of teaching resources are not pushed to students with the same probability. Mainstream education resources are pushed to students more frequently due to their high frequency of use, thus covering the minority and high-quality education resources. As a result, it is difficult for students to obtain such resources, resulting in "information cocoon."

How to help learners acquire the knowledge they are interested in quickly and accurately is an urgent problem to be solved by online education service platforms of universities [5]. Educational recommendation services are based on learners' personalized network information and learning behavior. The recommendation algorithm is used to quickly recommend precise college innovation and entrepreneurship education resources that meet students' potential learning needs from the massive educational information resources. It can enhance the experience and effectiveness of online learning [6].

The development of the Internet has broadened the channels for students to obtain information, but not all online information is valuable. Therefore, in the era of information overload, helping students efficiently and accurately screen out the resources they are interested in has become the key to the development of the Internet [7]. Collaborative filtering algorithm is the main technology to solve this problem [8]. As a widely recognized recommendation technology, collaborative filtering can effectively process structured information without studying the content and attributes of the recommendation information. At the same time, it can combine some concepts that are not easy to embody to complete information filtering, and the recommendation has a high degree of intelligence, which fully meets the requirements of personalized recommendation.

Relevant scholars further improve the collaborative filtering recommendation effect by using different methods. A personalized system filtering recommendation method based on coverage minimalism is proposed. According to the method of coverage reduction and student reduction in coverage rough set, the matching of redundant elements and redundant students is realized. Redundant students are removed from the target student set by reduction algorithm to ensure the effectiveness of collaborative filtering. Under the open data set, personalized recommendation services are provided for target students. The literature [9] proposed a method based on the clustering of student interest degree. Combining with the frequency of the target students scoring keywords, the degree of students' preference for keywords is obtained, and the student-keyword preference matrix is constructed, through which the clustering is realized. Logistic function is used to obtain students' interest in the project, determine students' preferences, find out students' similar students in the cluster, and collect some information about neighbours' hobbies to realize the recommendation of target students. However, the above recommendation method has some limitations, such as the serious problem of cold start, and it is difficult to accurately reflect the relationship between students and education resources.

In the era of big data, information overload is a huge problem we are faced with. It is extremely difficult for students to acquire the content they are interested in in time and accurately from massive data [10]. Recommendation system can alleviate the problem of information overload well and has been widely used in e-commerce, online news, and social networking sites.

Personalized recommendation system mainly uses the historical interaction information between students and projects to establish a model to predict students' evaluation of the project. In the traditional recommendation system, the recommendation based on collaborative filtering is the most classic [11]. An intuitive interpretation of collaborative filtering recommendations is that a student's rating of a project can be predicted by the rating of other students who are similar to him. Matrix decomposition is a common collaborative filtering method [12]. The idea of recommendation is to map the student vector and the project vector to a common vector representation space, in which the implicit vector is used to represent the student and the project, and then the score of the project can be directly obtained by calculating the similarity between the implicit vector of the student and the project. The successful application of matrix decomposition model in the recommendation field has led to the emergence of many improved methods based on matrix decomposition in the research field of recommendation system, such as the integration of neighbourhood model in matrix decomposition in the literature [13]. Factorization machine is used for feature interaction to generate more features and add them to model training. The literature [14] improves the effect of matrix decomposition by introducing auxiliary information such as project content. In recent years, the application of deep learning in image, natural language processing, and other fields has achieved good results, and many studies have begun to introduce deep learning into the field of the recommendation system [15]. Deep learning is usually introduced from two perspectives: (1) neural network is used to learn the representation vectors of students and projects, such as the deep matrix factorization (DMF) model proposed in the literature [16]. Dual-path neural network is used to replace the traditional matrix decomposition to learn the representation vectors of students and projects, and then score prediction is made. (2) The neural network is used as the matching function of the recommendation model, and the student vector and the project vector are fed into the matching function to directly obtain the scores of the students on the project, such as the neural collaborative filtering (NCF) model proposed in reference [17]. NeuMF in NCF simply concatenates the student vector and the project vector into a multilayer perceptron (MLP) to calculate the student's rating of the project. The literature [18] comprehensively considered the above two aspects and proposed a deep collaborative filtering model (DeepCF) combining representation learning and function learning. The above collaborative filtering recommendation model and deep learning recommendation model only extract the interaction features between students and projects from a single perspective, and the feature extraction is not comprehensive enough, which will limit the model's recommendation ability.

The essence of recommendation is a continuous decision-making process, and students' interest degree is not constant, so resource recommendation cannot be carried out from a static perspective. Therefore, this paper proposes a recommendation system of innovation and entrepreneurship education resources in universities based on the improved collaborative filtering model.

The innovations and contributions of this paper are listed as follows:

(1) According to the student behavior data, consider the behavior order to create the behavior graph and behavior route.
(2) Use Keras Tokenizer to vectorize the path of text type.
(3) The similarity between multidimensional behavior path vectors is calculated, and path collaborative filtering recommendations are performed for each dimension separately.

This paper consists of five main parts: the first part is the introduction, the second part is state of the art, the third part is methodology, the fourth part is result analysis and discussion, and the fifth part is the conclusion.

2. State of the Art

In order to improve the expansibility of the recommendation system, a scholar proposed Spark Hierarchical CF, which uses the student preference model and clustering algorithm to divide students into different student clusters according to different preference characteristics. And then it makes collaborative filtering recommendations for different student clusters. Compared with the algorithm based on MapReduce, the recommendation accuracy is improved and the operation time is saved, but the centre point of clustering is difficult to determine.

At present, there are four kinds of research on student behavior path, including methods based on reinforcement learning, methods based on statistical analysis, methods based on activity trajectory clustering, and methods based on the ant colony algorithm.

In order to improve the problem that the collaborative filtering algorithm ignores item attributes, a dynamic individual recommendation method based on reinforcement learning was proposed in the literature [19]. Firstly, students' attribute labels are mined from the operation behaviors, and then the reward and punishment models of attribute labels are adjusted according to the operate path and recall path to achieve dynamic adjustment of label weight. Finally, reinforcement learning is used to achieve label recommendation. The disadvantage of this method is that only recent behaviors are considered. Student preference information implied by behavioural pathways is not fully utilized.

The literature [20] proposed that students' experience perception can improve the recommendation effect. According to the behavioural data, analyse the student behavior path and create the student experience perception model. The behavioural path is defined as continuous indicators such as attracting attention, expressing interest, clicking intention, and watching video, which can better show the development trend of students' interest. However, this method has the problems of cold start and sparse data.

Considering the similarity between student visit and ant foraging, the ant colony algorithm was introduced in the literature [21] to realize recommendation, and the transition probability was calculated according to students' browsing behavior and preferred browsing path, so as to dynamically make recommendation. However, there are cold start problem and Matthew effect in this method, and there is occasional error in recommendation based on transfer probability. The literature [22] imitates the concept of pheromone in the ant colony algorithm and proposes pheromone-based algorithm to combine students' browsing behavior with reading behavior through commodity pheromone, and then recommend students according to their browsing trajectory. However, the properties of resource pheromones lead to the Matthew effect.

3. Methodology

This paper proposes a behavior path collaborative filtering recommendation algorithm based on knowledge graph. First, t behaviors in user behavior data are initialized to t nodes $= g_1, g_2, \ldots, g_t$, each node g stores the attribute of this behavior. And these nodes are constructed into a behavior knowledge map in Neo4j, which is referred to as the behavior map. Second, define the behavior path for the user against the same target entity in long weeks $\text{Route}_{\text{uid,iid}} = (h_1, h_2, \ldots, h_t)$, and construct it according to the behavior sequence in the behavior graph. Uid and iid indicate the student ID and education resource ID, respectively. Then, the behavior path is derived for vectorization. Finally, the similarity between multidimensional behavior paths is calculated. The flow of this algorithm is shown in Figure 1. This section describes the specific steps of the algorithm.

3.1. Construct Behavior Map. Taking each behavioural datum as a node, w genera of each behavior $(f_1, f_2, \ldots, f_w)$ is sealed as nodes and stored in the Neo4j data library. The construction algorithm is shown in

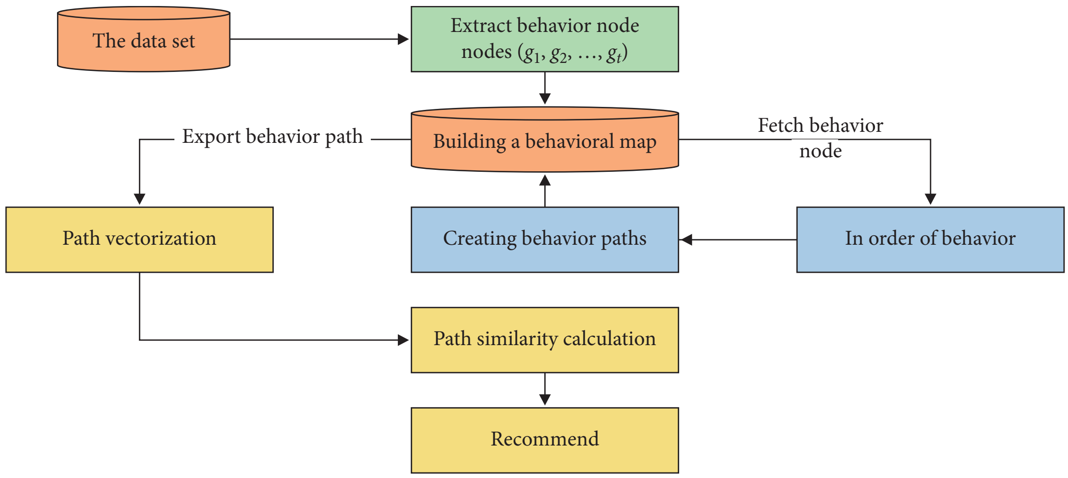

Figure 1: Flowchart of the BR-CF algorithm.

$$
\begin{aligned}
g &= \text{Graph}(\text{host}, \text{http\_port}, \text{user}, \text{password}),\\
\text{node} &= \text{Node}({}'f1' = f1, {}'f2' = f2, \ldots, {}'fm' = fm),\\
&\quad g.\text{create}(\text{node}),\\
&\quad g.\text{create}(\text{node}),
\end{aligned}
\tag{1}
$$

where host, http_ port, user, and password represent host address, port address, database user name, and password, respectively, which are used to connect to the neo4j database. Node encapsulates each behavior datum into a node, and the create (node) command stores each node in the neo4j database. The preliminarily constructed behavior map is shown in Figure 2.

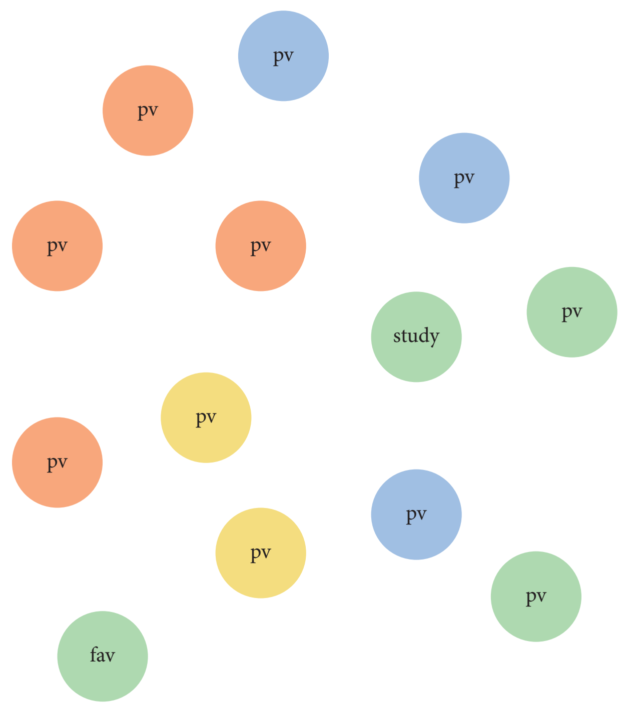

Figure 2: Preliminarily constructed behavior map.

3.2. Creating a Behavior Path. First, prioritize your actions. According to t behavior types contained in the behavior map, the behavior priority is defined $(h_1, h_2, h_3, \ldots, h_t)$, h represents a single behavior, h_1 has the lowest priority, and h_t has the highest priority.

Then, define the behavior path. This paper defines the behavior path as an ordered set of all behaviors generated by students for the same educational resource in a long period. $\text{Route}_{\text{uid,id}} = (h_1, h_2, \ldots, h_t)$. Uid and iid represent the student ID and education resource ID, respectively.

Finally, create a behavior path. According to the behavior sequence, traverse the behavior map, create a "continuous action" relationship for the continuous behavior made by the same student about the same educational resources, skip the single node that does not constitute a path, and get the $\text{Route}_{\text{uid, iid}}$ of all students about different educational resources after completing the traversal. The specific steps are shown in Figure 3. The created behavior path is shown in Figure 4.

3.3. Path Vectorization. Because the data type of the behavior path created in the previous step is text, and the similarity calculation requires digital data. The next is the vectorization and alignment of paths.

Firstly, classify the behavior paths by behavior priority, as listed in Table 1.

Secondly, vectorize each path in each class from text format to digital format. In this paper, Keras's Tokenizer class is used for vector transformation.

Finally, vector alignment is required. Because the path length is different, the length of each vector is also different, which means that the spatial dimension of the vector is not unified, and the similarity cannot be calculated. Calculate the maximum path length of all behavior paths and use Keras's kps.pad_sequences method to make the spatial dimension of each path the same as the maximum length, with the principle of complement 0. The data change process is listed in Table 2.

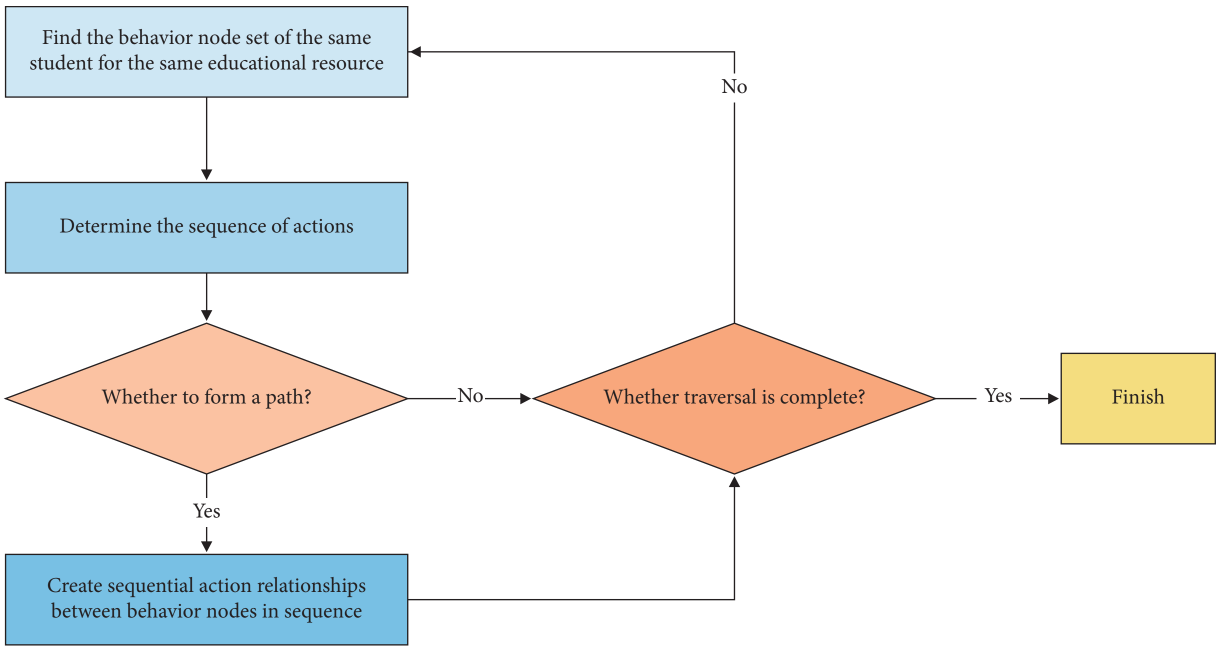

FIGURE 3: Steps to create a behavior path.

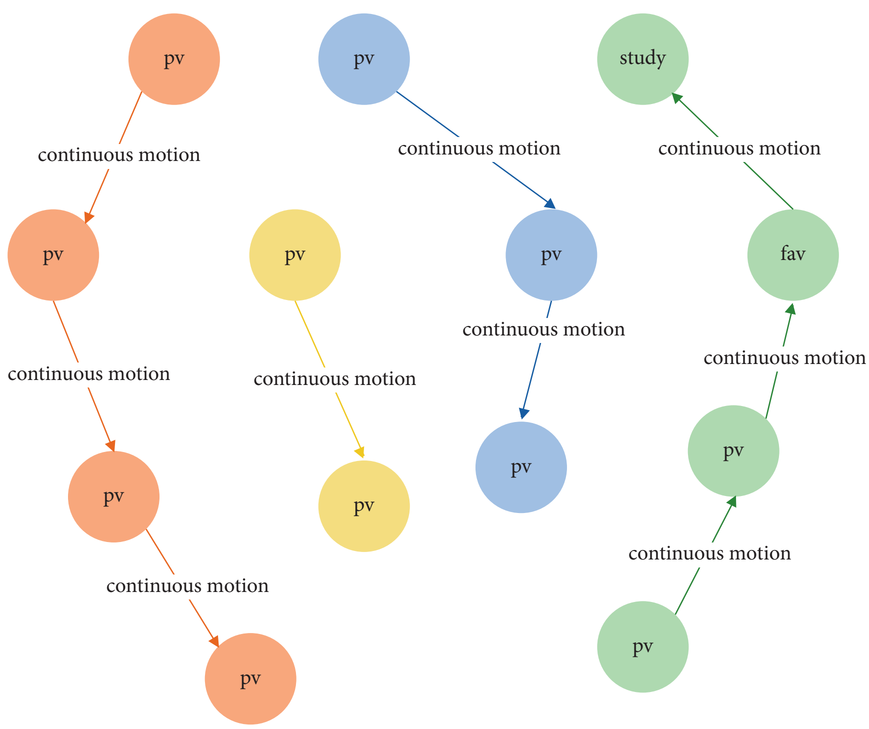

FIGURE 4: Behavior path diagram.

TABLE 1: Path classification.

Classification	Classification basis
Class h_1	The highest behavior priority in the path is h_1
Class h_2	The highest behavior priority in the path is h_2
...	...
Class h_t	The highest behavior priority in the path is h_t

3.4. Calculation of Path Similarity. Here, the path similarity is measured by the sum of the distances between a path in class G and each path in class H. As shown in equation (3), the smaller the total distance, the greater the similarity.

As shown in Table 2, the array of class h_2 and class h_3 is empty, it can be seen that there may be empty classes in the path classification. Direct calculation of similarity will lead

Table 2: Example of data change process.

Path status	Numerical value
Initial behavior path set	{"h_1–h_2–h_4–h_1–h_1" "h_1–h_1–h_1"} {h_1:["h_1–h_1–h_1"]
After path classification	h_2:[ ], h_3:[ ], h_4:["h_1–h_2–h_4–h_1–h_1"]} {h_1:[[1, 1, 1]]
After path steering	h_2:[ ], h_3:[ ], h_4:[[1, 2, 4, 1, 1]]} {h_1:[[1, 1, 1, 0, 0]],
After path alignment	h_2:[ ], h_3:[ ], h_4:[[1, 2, 4, 1, 1]]}

Table 3: Path category combination.

Possible combination of route categories	
1	(h_1)
2	(h_2)
3	(h_3)
4	(h_4)
5	(h_1, h_2)
6	(h_1, h_3)
7	(h_1, h_4)
8	(h_2, h_3)
9	(h_2, h_4)
10	(h_3, h_4)
11	(h_1, h_2, h_3)
12	(h_1, h_2, h_4)
13	(h_1, h_3, h_4)
14	(h_2, h_3, h_4)
15	(h_1, h_2, h_3, h_4)

to empty objects. Therefore, it is necessary to distinguish which classes are empty in the path classification and finally decide which behaviors can be recommended.

According to the permutation and combination principle, there are 2^T-1 types of classification for T types of behavior. For example, there are 15 types of classification for 4 types, as listed in Table 3, where combination (h_1) means that all classes except fot h_1 are empty, and combination (h_2, h_3, h_4) means that h_2, h_3, and h_4 are not empty. The h_1 class is empty, and so on.

After the path combination is determined, the path similarity is calculated. In this paper, Euclidean distance is used to calculate the similarity of paths. The calculation formula of Euclidean distance in t-dimensional space is shown in

$$d(i,j)=\sqrt{\sum_{x=1}^{t}\left(i_x-j_x\right)^2}. \tag{2}$$

Secondly, the sum of the distance between each path in class_1 and the path in class_2 is calculated, as shown in (3), where class_1 and class_2 represent two classes in the path subclass. The classification of other paths is similar:

$$\text{distances}=\sum_{i=1}^{t} d\left(i,j_x\right),\quad i\in\text{class}_1,\ j\in\text{class}_2. \tag{3}$$

Finally, the corresponding total distance list can be obtained for h_t class path, as shown in

$$\text{List\_distances\_}h_t=\left[\text{distances}_1,\text{distances}_2,\ldots\right],\quad t\in[1,t]. \tag{4}$$

If the combination is (h_2, h_3, h_4), the total distance list can be obtained by calculation, as shown in

$$\begin{aligned}\text{List\_distances\_}h_2&=\left[\text{distances}_1,\text{distances}_2,\ldots,\text{distances}_w\right],\\ \text{List\_distances\_}h_3&=\left[\text{distances}_1,\text{distances}_2,\ldots,\text{distances}_t\right],\end{aligned} \tag{5}$$

where w and t are the number of paths in h_2 and h_3, respectively. List_distances_h_2 represents the total distance list between each path in h_2 and all paths in h_3. And List_distances_h_3 represents the total distance list between each path in h_3 and all paths in h_4.

3.5. Multidimensional Recommendation. In this paper, the definition is derived from the multidimension $(d_1, d_2, d_3, \ldots, d_{t-1})$. D represents a set of recommendations that may be generated in line h. The d_1 pair should be able to generate the h_2 recommendation set. D_{t-1} corresponds to the possible recommendation set of h_t, which can be divided into possible_h_t table. D is the set of target entities corresponding to min (List_distances), that is, the set of target entities corresponding to the path with the minimum total distance. The results of recommendation obtained are shown in

$$\left\{d_1,d_2,\ldots,d_{n-1}\right\}=\left\{\text{possible\_}h_2{}'':\ [\cdots\cdots],{}''\text{possible\_}h_3{}'':\ [\cdots\cdots],\cdots\cdots{}''\text{possible\_}h_t{}'':\ [\cdots\cdots]\right\}. \tag{6}$$

According to the example results in equation (5), there are two recommendation dimensions d_2 and d_3. The returned recommendation results are shown in equation (7), which, respectively, represents the set of educational resources where the user recommended by this algorithm may have behaviors h_3 and h_4, and the value is the ID or other unique identification of the educational resource:

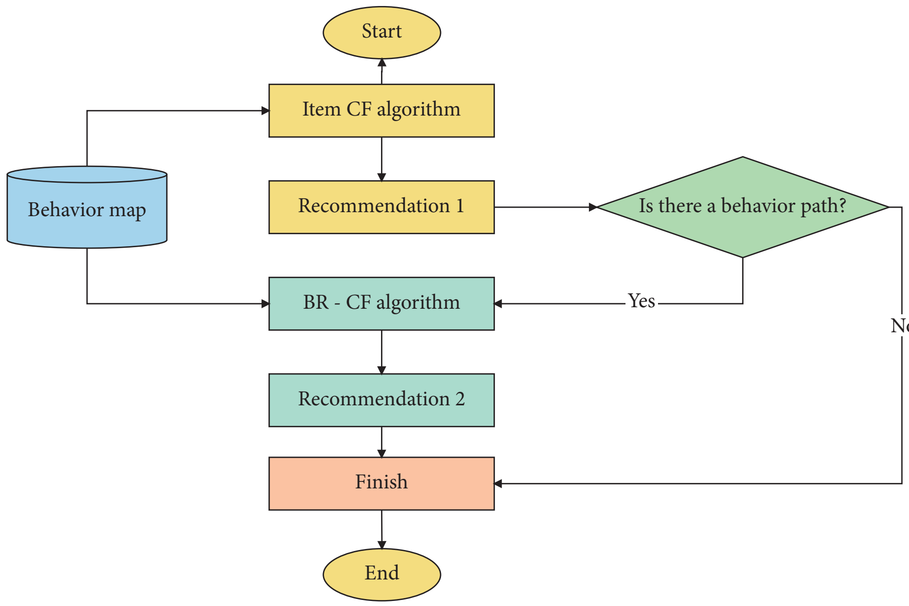

FIGURE 5: Flowchart of combine the item CF and BR-CF algorithm.

TABLE 4: Comparison of experimental results of four recommended algorithms with different TOP-N.

TOP-N	Index	Literature [23]	Literature [24]	Literature [25]	Proposed
5	Precision (%)	30.61	28.42	32.05	31.21
	Recall (%)	41.24	39.94	43.21	42.92
	RMSE	0.88	0.93	0.85	0.86
20	Precision (%)	28.16	26.96	28.08	29.98
	Recall (%)	44.37	43.65	46.78	47.58
	RMSE	0.79	0.91	0.78	0.72
35	Precision (%)	26.12	24.94	24.06	28.73
	Recall (%)	46.82	45.42	48.88	49.11
	RMSE	0.75	0.81	0.72	0.65
50	Precision (%)	23.24	22.25	21.78	25.97
	Recall (%)	50.16	48.9	51.34	51.79
	RMSE	0.68	0.72	0.61	0.57

$$\{d_3, d_4\} = \{"\text{possible\_}h_3" [\,2733371, 332733\,], "\text{possible\_}h_4": \ [124451]\}. \tag{7}$$

The item collaborative filtering recommendation algorithm, referred to as item CF, is used to recommend educational resources similar to those they liked before to college students.

In order to further analyse the recommendation performance of BR-CF, item CF and BR-CF are cascaded and mixed, respectively, in this section, and an improved algorithm based on the combination of item CF and BR-CF is proposed.

The cascade recommendation algorithm of item CF and BR-CF is referred to as Combine item CF and BR-CF. In the recommendation result of resource collaboration, the algorithm further calculates the set of target entities with behavior paths and the minimum total distance from the behavior paths of all target entities in the verification set. The flowchart is shown in Figure 5.

4. Result Analysis and Discussion

The experimental data in this paper are from a MOOC of a university in China bound by QQ account, and the crawler tool is used to directly obtain student information and innovation and entrepreneurship education resource data of universities. A total of 36,967 pieces of online learner information were obtained, including major, educational background, geographical location, friend relationship, learning time, course name, and evaluation content. After data screening, the dormant accounts and abandoned accounts whose monthly login times are less than 3 are excluded. Finally, the effective data set obtained contains 2400 students. The students were divided into two data sets in the ratio of 8 : 2. Among them, 1920 students' information constituted the training data set, and the other 480 students' information constituted the test data set.

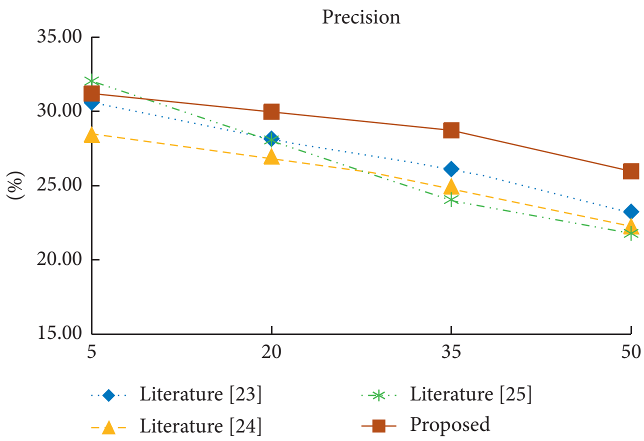

Figure 6: Accuracy of four recommendation algorithms under different recommendation numbers.

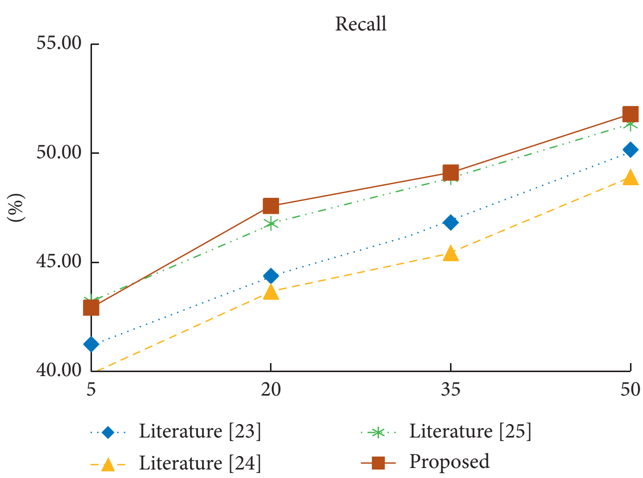

Figure 7: Recall rate of four recommendation algorithms under different recommendation numbers.

In order to test the quality of the proposed algorithm, the proposed algorithm based on the improved collaborative filtering model is compared with the literature [23], literature [24], and literature [25]. The number of adjacent recommendation students is set as 5, and the value is increased by 15 until it is 50. The Precision, Recall, and RMSE values of the four recommendation models under different number of recommendation students are listed, as shown in Table 4.

As shown in Figures 6–8, when the number of recommended students is greater than 20, the accuracy and root mean square error of the proposed algorithm in experimental data are better than those of the other three recommendation algorithms. In terms of recall rate, when the number of recommended students is greater than 35, there is not much difference between the proposed algorithm and the knowledge-based recommendation algorithm, but it is significantly better than the other two algorithms. Compared with the currently commonly used recommendation algorithm, the proposed algorithm takes into account student information, social relationship, and online learning behavior, so the recommendation quality is higher.

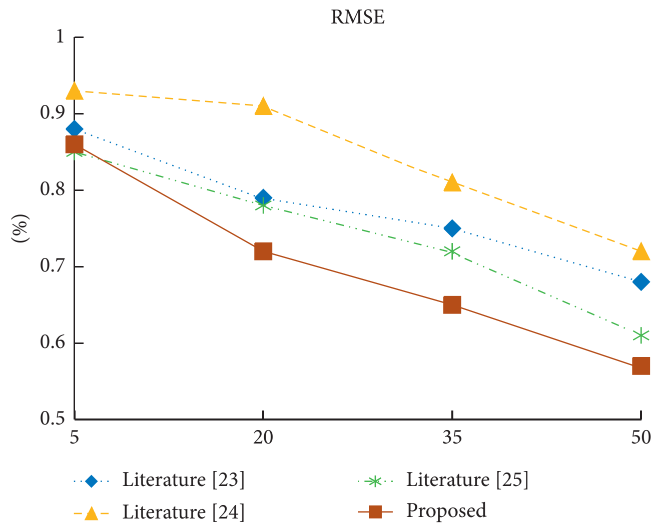

Figure 8: Root mean square error of four recommendation algorithms under different recommendation numbers.

5. Conclusion

At present, there are a lot of learning resources in online education learning platform, but the personalized service is not high. The target of online education services is learners. The commonly used personalized recommendation algorithm of education services only considers static information or dynamic characteristics of users, resulting in low recommendation quality. The collaborative filtering algorithm is the mainstream of information recommendation technology at present. However, the traditional recommendation system based on collaborative filtering algorithm has some limitations, such as low accuracy and cold start. And it is difficult to accurately reflect the relationship between students and educational resources. In order to improve the recommendation accuracy, this paper proposes a recommendation algorithm based on the improved collaborative filtering model for innovation and entrepreneurship education resources in universities. This paper uses 20,059 real behavior data and successfully creates 2,266 behavior paths according to the sequence of students' behaviors, which enriches the semantic information of the data. In addition, students' behavior data are fully used to make recommendations from three dimensions, which improves the data utilization rate and the diversity of recommendations. In particular, this paper puts forward the concept of behavior path, which can well represent the evolution and development process of students' behavior and better predict students' learning preferences by creating associations between behaviors. In order to test the quality of the recommendation algorithm, the proposed algorithm and other three recommendation algorithms were used as the control group in the experiment, and the Precision, Recall, and RMSE of these four recommendation algorithms were calculated under different recommended users. It shows the recommendation the proposed algorithm has more advantages in three evaluation indicators, and can be applied to online education services to better provide students with high-quality recommendation of college innovation and entrepreneurship education resources. Since the experimental platform and data in this paper are relatively single, in order to further verify and improve the personalized recommendation effect of the algorithm in this paper, other online education service platforms will be introduced in the future to verify the scalability and accuracy of this method.

Data Availability

The labeled dataset used to support the findings of this study are available from the corresponding author upon request.

Conflicts of Interest

The author declares no conflicts of interest.

Acknowledgments

This study was sponsored by Xi'an Physical Education University.

References

[1] L. P. Dinh and T. T. Nguyen, "Pandemic, social distancing, and social work education: students' satisfaction with online education in Vietnam," *Social Work Education*, vol. 39, no. 8, pp. 1074–1083, 2020.
[2] Q. Yang, "Research on active service model with personalized education resources," *Asian Journal of Contemporary Education*, vol. 3, no. 1, pp. 95–104, 2019.
[3] M. C. Urdaneta-Ponte, A. Mendez-Zorrilla, and I. Oleagordia-Ruiz, "Recommendation systems for education: systematic review," *Electronics*, vol. 10, no. 14, Article ID 1611, 2021.
[4] N. A. Albelbisi and F. D. Yusop, "Factors influencing learners' self -regulated learning skills in a massive open online course (MOOC) environment," *The Turkish Online Journal of Distance Education*, vol. 20, no. 3, pp. 1–16, 2019.
[5] W. Zhang, Y. Wang, L. Yang, and C. Wang, "Suspending classes without stopping learning: China's education emergency management policy in the COVID-19 outbreak," *Journal of Risk and Financial Management*, vol. 13, no. 3, p. 55, 2020.
[6] S. Ali, Y. Hafeez, M. Humayun, N. S. M. Jamail, M. Aqib, and A. Nawaz, "Enabling recommendation system architecture in virtualized environment for e-learning," *Egyptian Informatics Journal*, vol. 23, no. 1, pp. 33–45, 2022.
[7] S. McGrew, J. Breakstone, T. Ortega, M. Smith, and S. Wineburg, "Can students evaluate online sources? Learning from assessments of civic online reasoning," *Theory & Research in Social Education*, vol. 46, no. 2, pp. 165–193, 2018.
[8] Q. Wang, C. Zeng, and W. Zhou, "Online interactive collaborative filtering using multi-armed bandit with dependent arms," *IEEE Transactions on Knowledge and Data Engineering*, vol. 31, no. 8, pp. 1569–1580, 2018.
[9] S. Wan and Z. Niu, "A hybrid e-learning recommendation approach based on learners' influence propagation," *IEEE Transactions on Knowledge and Data Engineering*, vol. 32, no. 5, pp. 827–840, 2019.
[10] P. G. Roetzel, "Information overload in the information age: a review of the literature from business administration, business psychology, and related disciplines with a bibliometric approach and framework development," *Business research*, vol. 12, no. 2, pp. 479–522, 2019.
[11] Z. Cui, X. Xu, F. Xue et al., "Personalized recommendation system based on collaborative filtering for IoT scenarios," *IEEE Transactions on Services Computing*, vol. 13, no. 4, pp. 685–695, 2020.
[12] R. M. Sallam, M. Hussein, and H. M. Mousa, "An enhanced collaborative filtering-based approach for recommender systems," *International Journal of Computer Application*, vol. 176, no. 41, pp. 9–15, 2020.
[13] X. Ma, D. Dong, and Q. Wang, "Community detection in multi-layer networks using joint nonnegative matrix factorization," *IEEE Transactions on Knowledge and Data Engineering*, vol. 31, no. 2, pp. 273–286, 2018.
[14] Y. Pan, F. He, and H. Yu, "Learning social representations with deep autoencoder for recommender system," *World Wide Web*, vol. 23, no. 4, pp. 2259–2279, 2020.
[15] Z. Batmaz, A. Yurekli, A. Bilge, and C. Kaleli, "A review on deep learning for recommender systems: challenges and remedies," *Artificial Intelligence Review*, vol. 52, no. 1, pp. 1–37, 2019.
[16] B. Yi, X. Shen, H. Liu et al., "Deep matrix factorization with implicit feedback embedding for recommendation system," *IEEE Transactions on Industrial Informatics*, vol. 15, no. 8, pp. 4591–4601, 2019.
[17] W. Chen, F. Cai, H. Chen, and M. D. Rijke, "Joint neural collaborative filtering for recommender systems," *ACM Transactions on Information Systems*, vol. 37, no. 4, pp. 1–30, 2019.
[18] Y. Zhang, C. Yin, and Q. Wu, "Location-aware deep collaborative filtering for service recommendation," *IEEE Transactions on Systems, Man, and Cybernetics: Systems*, vol. 51, no. 6, pp. 3796–3807, 2019.
[19] T. T. Nguyen, N. D. Nguyen, and S. Nahavandi, "Deep reinforcement learning for multiagent systems: a review of challenges, solutions, and applications," *IEEE Transactions on Cybernetics*, vol. 50, no. 9, pp. 3826–3839, 2020.
[20] M. Mailizar, D. Burg, and S. Maulina, "Examining university students' behavioural intention to use e-learning during the COVID-19 pandemic: an extended TAM model," *Education and Information Technologies*, vol. 26, no. 6, pp. 7057–7077, 2021.
[21] H. Liu and X. Li, "Learning path combination recommendation based on the learning networks," *Soft Computing*, vol. 24, no. 6, pp. 4427–4439, 2020.
[22] S. Shamshirband, M. Babanezhad, A. Mosavi et al., "Prediction of flow characteristics in the bubble column reactor by the artificial pheromone-based communication of biological ants," *Engineering Applications of Computational Fluid Mechanics*, vol. 14, no. 1, pp. 367–378, 2020.
[23] J. Shu, X. Shen, H. Liu, B. Yi, and Z. Zhang, "A content-based recommendation algorithm for learning resources," *Multimedia Systems*, vol. 24, no. 2, pp. 163–173, 2018.
[24] H. Jia, L. Yang, and B. Cui, "Collaborative filtering recommendation of online learning resources based on knowledge association model," *International Journal of Emerging Technologies in Learning (iJET)*, vol. 17, no. 2, pp. 158–172, 2022.
[25] J. K. Tarus, Z. Niu, and G. Mustafa, "Knowledge-based recommendation: a review of ontology-based recommender systems for e-learning," *Artificial Intelligence Review*, vol. 50, no. 1, pp. 21–48, 2018.

Hindawi
Computational Intelligence and Neuroscience
Volume 2023, Article ID 9767693, 1 page
https://doi.org/10.1155/2023/9767693

Retraction

Retracted: MOOC and Flipped Classroom Task-Based English Teaching Model for Colleges and Universities Using Data Mining and Few-Shot Learning Technology

Computational Intelligence and Neuroscience

Received 26 September 2023; Accepted 26 September 2023; Published 27 September 2023

This article has been retracted by Hindawi following an investigation undertaken by the publisher [1]. This investigation has uncovered evidence of one or more of the following indicators of systematic manipulation of the publication process:

(1) Discrepancies in scope
(2) Discrepancies in the description of the research reported
(3) Discrepancies between the availability of data and the research described
(4) Inappropriate citations
(5) Incoherent, meaningless and/or irrelevant content included in the article
(6) Peer-review manipulation

The presence of these indicators undermines our confidence in the integrity of the article's content and we cannot, therefore, vouch for its reliability. Please note that this notice is intended solely to alert readers that the content of this article is unreliable. We have not investigated whether authors were aware of or involved in the systematic manipulation of the publication process.

In addition, our investigation has also shown that one or more of the following human-subject reporting requirements has not been met in this article: ethical approval by an Institutional Review Board (IRB) committee or equivalent, patient/participant consent to participate, and/or agreement to publish patient/participant details (where relevant).

Wiley and Hindawi regrets that the usual quality checks did not identify these issues before publication and have since put additional measures in place to safeguard research integrity.

We wish to credit our own Research Integrity and Research Publishing teams and anonymous and named external researchers and research integrity experts for contributing to this investigation.

The corresponding author, as the representative of all authors, has been given the opportunity to register their agreement or disagreement to this retraction. We have kept a record of any response received.

References

[1] Y. Gong and J. Zhou, "MOOC and Flipped Classroom Task-Based English Teaching Model for Colleges and Universities Using Data Mining and Few-Shot Learning Technology," *Computational Intelligence and Neuroscience*, vol. 2022, Article ID 9770747, 11 pages, 2022.

Hindawi
Computational Intelligence and Neuroscience
Volume 2022, Article ID 9770747, 11 pages
https://doi.org/10.1155/2022/9770747

Research Article

MOOC and Flipped Classroom Task-Based English Teaching Model for Colleges and Universities Using Data Mining and Few-Shot Learning Technology

Yujuan Gong [1] and Jie Zhou [2]

[1]Jiangxi Police Institute, Nanchang, Jiangxi 330013, China
[2]East China Jiaotong University, Nanchang, Jiangxi 330013, China

Correspondence should be addressed to Yujuan Gong; gongyujuan123456@163.com

Received 1 April 2022; Revised 26 April 2022; Accepted 27 April 2022; Published 13 June 2022

Academic Editor: Xin Ning

As a revolutionary education model, the flipped classroom teaching model has unique advantages over the traditional education model. How to change the teaching method of flipped classroom into a teaching method suitable for college English courses is a problem. The goal of this research is to investigate how to use data mining and few-shot learning technology to investigate the impact of MOOC and flipped classroom task-based college English teaching modes. This work provides a data mining-based decision tree algorithm and examines the enhanced decision tree method. The experimental results of this study demonstrate that two students in each of the two groups believe that the English teaching mode, which is mostly taught by traditional teachers, is very favorable to a thorough understanding of basic knowledge, accounting for 4% of the total. There are 17 students that believe the new teaching methodology is really beneficial, accounting for 34% of the total. This mode was determined to be effective for in-depth knowledge of the basics by a total of 25 students. It can be seen that the flipped classroom model is more popular with students.

1. Introduction

Since human beings entered the information society, with the rapid development of information technology, the amount of data generated by human society has also increased dramatically. However, how to turn complicated data into knowledge that people can easily accept and understand is a difficult problem for data researchers. Faced with the situation of "a large amount of data, but little knowledge," data mining technology came into being. This discipline, which originated in the field of database and artificial intelligence [1], has formed a system and has begun to play a huge role in practical applications.

At present, most mathematics classroom teaching is still not free from the shackles of traditional educational ideas. It has disadvantages such as dogmatization, unification, static, isolation, and separation from the real life of students. The dominant position of students in classroom teaching has not yet been established, lacking due freedom and choice, and there is still a large market for indoctrination education. In recent years, MOOCs and flipped classrooms have entered people's field of vision, which is a new form of educational resources and educational models, which has aroused strong repercussions in the education community around the world. MOOCs mainly use online platforms to display the main educational content in the form of microcourses. The flipped classroom is an innovative and personalized education model. The flipped classroom teaching mode based on MOOC mainly uses network technology and resources to reverse the educational purpose and educational form, educational subjects, and the role of teachers, which has attracted great attention in the field of education.

The innovations of this paper are as follows: (1) It introduces the relevant theoretical knowledge of data mining technology and MOOC and flipped classroom task-based college English teaching mode. It also uses decision tree algorithm based on data mining technology to analyze how data mining plays a role in MOOC and flipped classroom task-based college English teaching mode. (2) Based on the decision tree algorithm, it carried out experiments and analysis on MOOC and flipped classroom task-based college English teaching mode. Through investigation and analysis, it found that the task-based college English teaching model based on MOOCs and flipped classrooms can stimulate students' more interest in learning and enthusiasm for learning.

2. Related Work

The rapid development of information technology has brought people a convenient life that was unimaginable before and also impacted the traditional way of cognition of knowledge and information. Jovanovic found that learning strategies are related to flipped classrooms, and he also found that students tend to change the strategies that they employ and switch to less effective strategies. Although the scholar used clustering to discover the problems that students have in learning, he did not propose corresponding solutions based on the students' problems. Yilmaz found that the flipped classroom (FC) teaching model was associated with student satisfaction and motivation. The purpose of his research was to investigate the impact of students' e-learning readiness on student satisfaction and motivation in the FC teaching model. Research was conducted among 20 undergraduate students. They learn using the FC teaching model. The results show that the more satisfied students are, the more active they will be in preparing for the preclass preview. Although the scholar has specific experimental objects, he did not analyze the experimental data [2]. Baytiyeh tried to find out whether the flipped classroom model works in teaching and whether students can acquire skills in this model. Using a qualitative case study design, he found that this type of teaching enriches students' learning experience and helps them develop the skills they need. The scholar proposed a qualitative case study design, but he does not address an actual case [3]. Mcnally et al. found that although the flipped classroom is widely used, it lacks experience and is not easy to be accepted. He surveyed 5 students under the flipped classroom model and the results showed that students can have positive attitudes towards flipped classroom elements according to them. But the scholar came to the result directly, without explaining the whole process [4]. Kostaris et al. found that the emerging flipped classroom method has been widely used in teaching practice and achieved many good results. His main purpose is to design and implement an action study to study the effect of flipped classroom approach in teaching and learning. The scholar did not introduce what this action research is for [5]. Jin et al. found that body recognition is crucial in a variety of applications, including pursuit, defense, and more. Traditional human recognition methods are usually based on vision, biometrics, etc. They proposed a recognition method based on radar micro-Doppler features. The method uses deep convolutional neural networks (DCNNs) [6–8] and can recognize people in contactless, remote, and unilluminated states. But the scholar did not explain why he chose this method.

3. Decision Tree Algorithm before and after Improvement Based on Data Mining

3.1. The Process and Tasks of Data Mining. Network courses have steadily become an important teaching method in remote education due to the rapid growth of network technology. Students generate a tremendous amount of data about education and learning while taking online courses. Because the knowledge concealed behind the data cannot be mined, the linkages and laws that exist in the data cannot be uncovered when confronted with such a vast data collection. Teachers are unable to comprehend the impact of students' online learning, and studying diverse information points does not enable students to make judgments for themselves. Teachers are unable to improve the content of online courses or the effect of distant education due to their incapacity to alter targeted assistance and the pedagogical structure of online courses in a short amount of time.

Data mining, also known as knowledge discovery in databases, is a hot research topic in the field of artificial intelligence and databases. The so-called data mining refers to the nontrivial process of revealing implicit, previously unknown, and potentially valuable information from a large amount of data in the database. Data mining technology [9] provides an excellent solution to this problem. Data mining is the extraction of hidden data from practical application data that many people do not know in advance and are incomplete and ambiguous. However, it is also a potentially useful information process. Its application of data mining for online course learning is undoubtedly practical. The unearthed knowledge helps teachers to complete higher-level decision-making, adjust the educational structure of online courses in time, and improve the content and educational effects of online courses. The data mining architecture is shown in Figure 1.

As shown in Figure 1: Data mining is the process of mining interesting patterns and knowledge from large amounts of data. The data source is generally a database, data warehouse, Web, etc., and the obtained data is called a data set. Data mining is not a simple job. It does not mean that, with data, using a certain method and building several models, it can get the desired information. Data mining should be a multistep process. Before its implementation, a detailed plan should be made to determine what needs to be done at each step and how to do it. Only in this way can data mining be carried out in an orderly manner and be successful. Different environments and different projects may have different data mining processes [10].

In general, the data mining process goes through the following steps, as shown in Figure 2.

As shown in Figure 2: Knowledge is discovered for application. Now people are using knowledge of the following two methods. One is to look only at the relationships or results described by the knowledge itself to support decision-making, and the other is to analyze knowledge. The knowledge gained will be integrated into the organizational structure of information systems to guide practice. The data

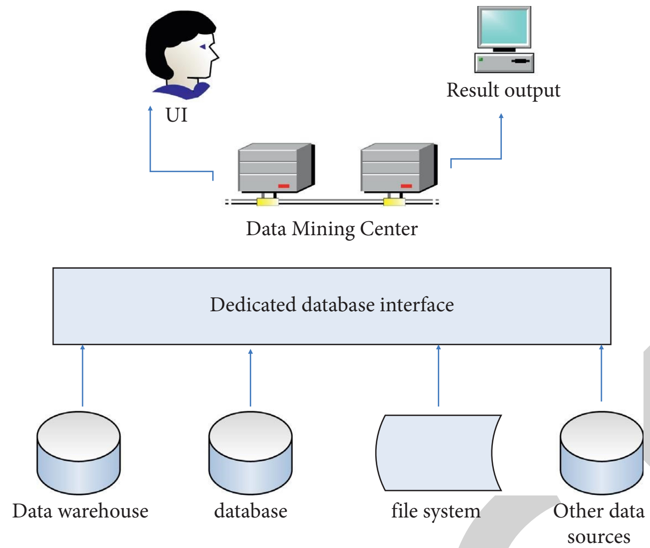

Figure 1: Data mining architecture.

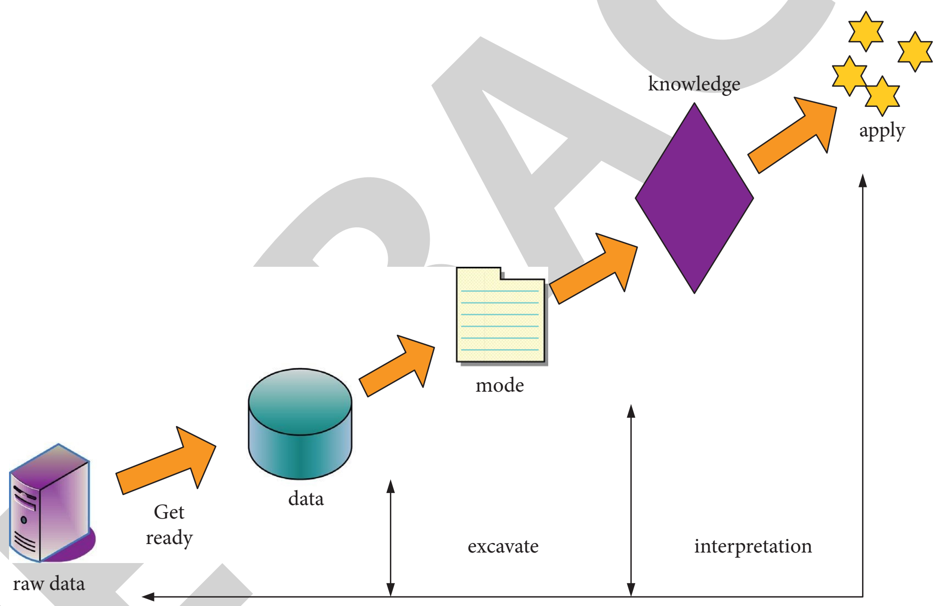

Figure 2: Steps of data mining.

mining process is a cyclic process. It will constantly approach the essence of things and achieve the purpose of optimizing and solving problems. It turns useful data into information, information into action, and action into value.

3.2. Decision Tree and Related Algorithm Theory. Decision tree is one of the classic methods of data mining. It clearly and completely shows the decision and classification process in a tree structure. The algorithm is simple and intuitive. Decision tree is a decision analysis method to obtain the probability that the expected value of the net present value is greater than or equal to zero by forming a decision tree based on the known probability of occurrence of various situations, to evaluate the project risk, and to judge its feasibility. It is a graphical method that uses probability analysis intuitively. Since this decision branch is drawn as a graph like the branches of a tree, it is called a decision tree.

The properties of a decision tree are that it has a clear hierarchy and logic. The entire decision-making process is straightforward, intuitive, and simple to comprehend, with a good classification effect. However, because the data mining technique involves so many association rules, it is not ideal for clustering [11, 12] and is instead employed for classification. The decision tree method is well suited to processing nonnumeric data, particularly on a large scale. This article is primarily concerned with the use of information such as enrollment sources and college entrance examination results in college and university enrollment. As a result, it primarily describes the information theory-based decision tree classification technique. The schematic diagram of decision tree generation is shown in Figure 3.

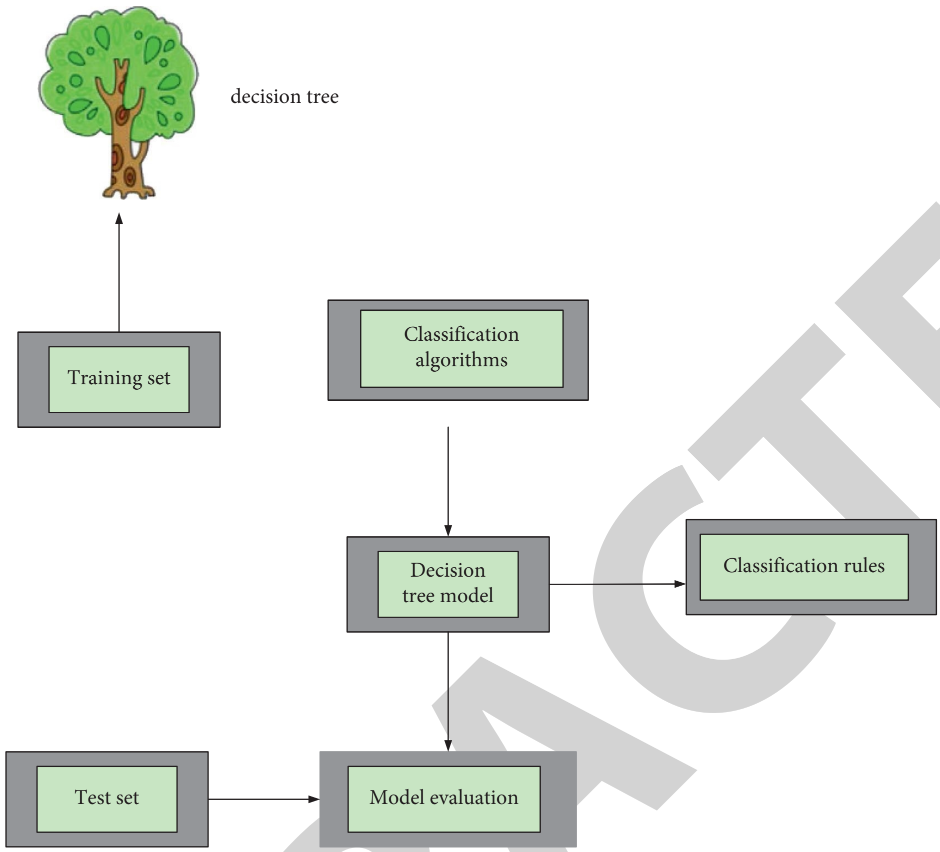

FIGURE 3: Schematic diagram of decision tree generation.

As shown in Figure 3: The related concepts in decision tree correlation information theory are as follows:

Information gain reflects the characteristics of the sample [13], and there is a close relationship between the two and a proportional relationship. In probability theory and information theory, information gain is asymmetric, which is used to measure the difference between two probability distributions P and Q. Information gain describes the difference between coding with Q and coding with P. Usually P represents the distribution of samples or observations, or it may be a theoretical distribution that is precisely calculated. Q represents a theory, model, description, or approximation to P. The entropy $\mathrm{Info}(D)$ of data D is as formula (1):

$$\mathrm{Info}(D) = -\sum_{i=1}^{m} P_i \log(P_i), \tag{1}$$

P_i is the nonzero probability that any information in D is contained in class C_i.

Attribute A is divided into D and contains n different attribute values 1. From this, it can be obtained that the attribute A is divided into D into a branch node with $A = \{a_1, a_2, \ldots, a_n\}$, $A = \{d_1, d_2, \ldots, d_n\}$ is a tuple in D, and its value in A is a_i, so the calculation formula of entropy can be obtained as

$$E(A) = -\sum_{i=1}^{m} \frac{|d_i|}{D} \times \mathrm{Info}(d_i). \tag{2}$$

The information gain is the difference between the amount of information before and after, and the calculation formula is

$$\mathrm{Gain}(A) = \mathrm{Info}(D) - E(A). \tag{3}$$

The information gain rate regulates the information gain through the parameter value, and the calculation formula is

$$\mathrm{SplitInfo}(D) = -\sum_{i=1}^{n} \frac{|S_i|}{S} \times \log\left(\frac{|d_i|}{D}\right). \tag{4}$$

It divides the n partitions corresponding to each subset in attribute A into the corresponding D. The calculation formula of the gain rate can be obtained as

$$\mathrm{GainRation}(A) = \frac{\mathrm{Gain}(A)}{\mathrm{SplitInfo}(A)}. \tag{5}$$

There are many algorithms for generating decision trees in data mining. The following focuses on several typical decision tree generation algorithms.

ID3 algorithm is the most influential and typical in decision tree mining [14]. Decision trees classify data for prediction purposes. The decision tree method first forms a decision tree according to the training set data. If the tree cannot give the correct classification for all objects, it selects some exceptions to add to the training set data and repeats the process until the correct decision set is formed. A decision tree represents the tree structure of a decision set.

It sets G to be a collection of training instance samples. It assumes that there are m classes in G; then the expected information to classify a given sample is

$$\operatorname{Inf}\left(g_1, g_2, \ldots, g_m\right) = -\sum_{i=1}^{m} \frac{g_i}{g} \log_2 \frac{g_i}{g}. \quad (6)$$

The expected information obtained by dividing according to the B attribute is called the entropy $E(B)$ of the B attribute, which is defined as

$$E(B) = \sum_{j=1}^{n} \left[\frac{\left(g_{1j} + g_{2j} + \cdots + g_{mj}\right)}{g} \right] \times \operatorname{Inf}\left(g_{1j,\ldots,}g_{mj}\right). \quad (7)$$

The obtained information gain for this partition on the B attribute is defined as

$$\operatorname{Gain}(B) = \operatorname{Inf}\left(g_1, g_2, \ldots, g_m\right). \quad (8)$$

The ID3 algorithm has the attribute of high information gain, which is the attribute with the highest partition purity in the given attribute set. Therefore, it can calculate the information gain of each attribute of the sample in G and obtain the attribute with the maximum information gain as the division attribute [15].

The ID3 algorithm is powerful and easy to use. It seems that this algorithm has been able to cope with most cases of classification applications, but a careful study can find that ID3 is more inclined to generate multibranched attributes when selecting split attributes. In extreme cases, the classification of ID3 algorithm becomes very unreasonable [16]. To this end, some scholars have introduced an extended parameter called segmentation information. It uses this parameter mainly to correct the information gain in the ID3 algorithm. The definition of the extended parameter is as

$$\operatorname{ExInf}_B(G) = -\sum_{i=1}^{v} \frac{\left|G_i\right|}{|G|} \log_2 \frac{\left|G_i\right|}{|G|}. \quad (9)$$

It also introduces the gain ratio metric to replace the information gain metric in the ID3 algorithm. It is defined as

$$\operatorname{GainRatio}(B) = \frac{\operatorname{Gain}(B)}{\operatorname{ExInf}_B(G)}. \quad (10)$$

It can be seen that the gain rate not only considers the information gain of the training samples in attribute B, but also considers the amount of information generated by the v branches generated by the v attribute values of attribute B [17]. So in the above example, due to the existence of extended parameters, its gain rate tends to be reasonable. The improved algorithm uses the highest gain rate as the splitting attribute, which is more scientific and reasonable [18, 19].

3.3. C4.5 Algorithm. C4.5 is a classification decision tree algorithm in machine learning [20]. It combines the advantages of the ID3 algorithm and is continuously improved to better realize the construction of decision trees. C4.5 is a family of algorithms used in classification problems in machine learning and data mining. Its goal is supervised learning. The goal of C4.5 is to learn to find a mapping from attribute values to categories, and this mapping can be used to classify new entities with unknown categories.

It gets the minimum value of the continuity property and stores it in MIN. It also stores the maximum value in MAX and divides the breakpoints A_i in [MIN, MAX] in the continuous attribute:

$$A_i = \mathrm{MIN} + \frac{\mathrm{MAX} = \mathrm{MIN}}{N} \times i. \quad (11)$$

Assuming that each variable in the database has two distinct values A and B, the uncertainty assessment of the optimal amount of data, i.e., the information entropy is as

$$S = -\sum_{I} \left(p_i \times \lg\left(p_i\right)\right). \quad (12)$$

There are V different data values in the attribute A in the set S, and A is used to divide S into v subsets, and the information gain rate is calculated during the division as

$$\operatorname{Gain}\left(A_i\right) = \operatorname{Gain}(A) \times \sum_{j \in [1, v]} p_i \log_2 p_i. \quad (13)$$

In the data mining algorithm, in order to improve the enthusiasm of the students in class and the learning efficiency, the students' learning progress data set is taken as the research object. This can scientifically apply these potential relevant influencing factors to provide key decision-making basis for future college English teaching [21].

The advantages of the decision tree method include a simple and straightforward analysis, high classification accuracy, and high execution efficiency. As a result, the decision tree technique is highly suited for data mining on a wide scale. ID3 chooses the classification standard for the data it collects. The ID3 algorithm can only mine nonlinear data; hence it chooses split attributes based on the number of attribute values. The C4.5 assessment classification criteria are used to determine the rate of information gain. By gradually increasing the information according to the information gain formula, C4.5 effectively eliminates the issues that emerge in ID3.

3.4. C4.5 Algorithm Improvement. The C4.5 decision algorithm has better advantages for mining massive data, and the improved algorithm of the classic C4.5 decision algorithm in the decision tree construction will better construct the decision tree. It places some restrictions on the rules and conventions of data: First, it performs classification based on the constructed new attributes, so it is necessary to centrally process and manage the classification attributes in the dataset. Second, it uses the last generated new attribute to classify, so it needs to pay attention to the approximate accurate rule management with high attribute degree.

The core step of the C4.5 decision tree size algorithm is the attribute selection metric calculation. It needs to compare the information gain of each attribute and select the attribute with the largest value to split the tree. Unfortunately, the logarithmic function is used a lot in entropy calculation, and the calculation of the logarithmic function in almost all programming languages requires a lot of computer computing time. Therefore, the computational efficiency of the algorithm is greatly reduced in each attribute selection. Therefore, the key to solving the problem of computing efficiency is how to optimize the entropy value operation and shorten its operation time. To solve this problem, this paper introduces Taylor's mean value theorem and McLaughlin expansion.

Using the Taylor expansion as a substitution to find the limit of the function is the most widely used. At this time, the Taylor formula containing the Peano remainder is generally used. Other equivalent infinitesimals can also be found using Taylor's formula. Taylor's mean value theorem is

$$f(n) = f(n_0) + f'(n_0)(n - n_0) + \cdots + \theta_t(n). \tag{14}$$

It assumes that function $f(n)$ has a derivative value of order $t + 1$ in a narrow interval around n_0, and $\theta_t(n)$ is Tay's remainder.

Maclaurin's expansion: when $n_0 = 0$, Tay's mean value theorem can be converted into Maclaurin's formula, which is

$$f(n) = f(n_0) + f'(n_0) + \cdots + \theta_t(n). \tag{15}$$

Among them, when $\theta_t(n)$ is negligible, the following approximate expression is obtained, which is

$$f(n) \approx f(n_0) + f'(0)m + \cdots + f'(0)\frac{m^t}{t}!. \tag{16}$$

McLaughlin's formula is a special form of Taylor's formula. It can be seen that, for the logarithmic operation in the entropy value, one can use the approximate expression of McFarland's formula instead. Since there is only the logarithmic operation on the base e in the java language, the logarithmic operation in the entropy value needs to be transformed as follows, that is,

$$\mathrm{Log}_2(n) = \frac{Ln(n)}{Ln(2)}, \tag{17}$$

$Ln(2)$ is a constant and only needs to be calculated once, while $Ln(n)$ needs to be improved.

Because $Ln0 = \infty$, function $Ln(n)$ cannot be directly expanded by McFarland's formula, so people set

$$f(n) = Ln(1 + n). \tag{18}$$

Formula (19) is expanded by the approximate expression 18 of McFarland's formula:

$$f(n) = Ln(1 + n) \approx \frac{n - n^2}{2 + n^3} + \cdots + \frac{(-1)^t n^{t+1}}{(t + 1)}. \tag{19}$$

Further approximately, the polynomial $(-1)^t n^{t+1}/(t + 1)$ can be used to replace the $Ln(n)$ operation, so as to reduce the computational complexity of the entropy value in the C4.5 algorithm.

3.5. The Flipped Classroom Teaching Mode Based on MOOC. With the continuous deepening of reform and opening up, the demand for foreign languages, especially international talents proficient in English, from various industries in society continues to increase. Although the proportion of English in various exams is decreasing, the requirement of English proficiency in the actual fierce competition has not decreased. According to the actual situation, China's college English education reform is being implemented.

In this mode, teachers will use screen recording software to create 10-minute video teaching points and upload them to the Internet. Students can watch in their free time and discover their own problems in time. The video contains a simple class review to deepen students' understanding of the knowledge. The unique method of "students study by themselves before class and practice together in class" is contrary to the previous "teacher lectures in class, students practice after class," so it is called flipped classroom, as shown in Figure 4.

As shown in Figure 4: The biggest difference between the flipped classroom education model and the previous classroom education model is that, in the flipped classroom, students complete knowledge learning outside the classroom, and the classroom becomes an interactive place between teachers and students. The flipped classroom teaching mode means that students watch teachers' video explanations before or outside of class, and they learn independently, and teachers no longer occupy classroom time to teach knowledge. The classroom becomes a place for teacher-student and student-to-student interaction. It includes answering questions and doubts, cooperative exploration, completing studies, etc., so as to achieve better educational effects. With the support of the network, students can use high-quality educational resources to learn knowledge without relying on teachers. The learning mode of the MOOC is shown in Figure 5.

As shown in Figure 5, a MOOC is a newly imported online course learning medium. It integrates a variety of educational resources, learning management systems, and open network resources, but it differs in several respects from previous online courses. MOOC platforms are open to the general public for free learning as well as formal learners in specialized schools and educational institutions. The construction of curricula and the organization of events are both examples of openness. Anyone can take part in a variety of learning and exchange activities, as well as providing educational resources and themes to the MOOC.

Traditional online course video software is frequently recorded with reference to the classroom teaching form, and the length of the video generally increases. Learners in MOOCs do not receive information passively.

3.6. Construction Model of Flipped Classroom Based on MOOC. In a typical flipped classroom teaching mode, preclass activities and in-class activities are the main sections, but these two sections are not separated by the flipped classroom teaching mode. Each section contains specific implementation links. These links reasonably connect the preclass activities with the in-class activities to form a complete and smooth teaching mode. The flipped classroom teaching mode based on MOOC is shown in Figure 6.

As shown in Figure 6, MOOC, a large-scale open online course, is the product of "Internet + education." It is a newly

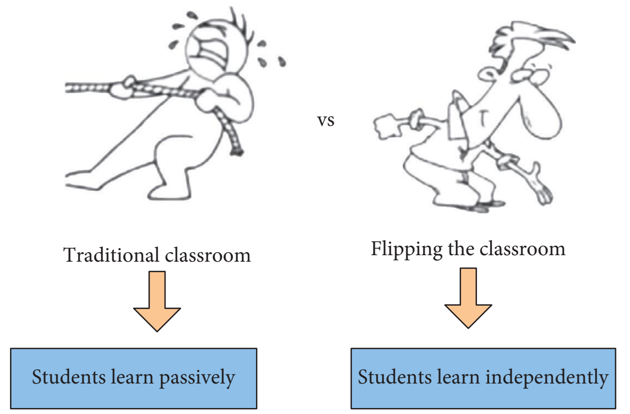

Figure 4: The difference between the flipped classroom education model and the previous classroom education model.

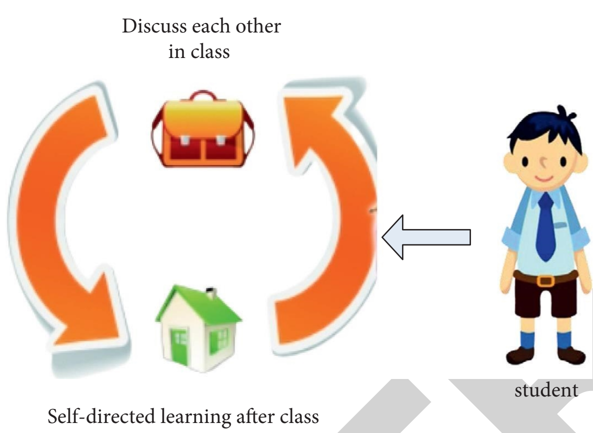

Figure 5: The learning model of MOOCs.

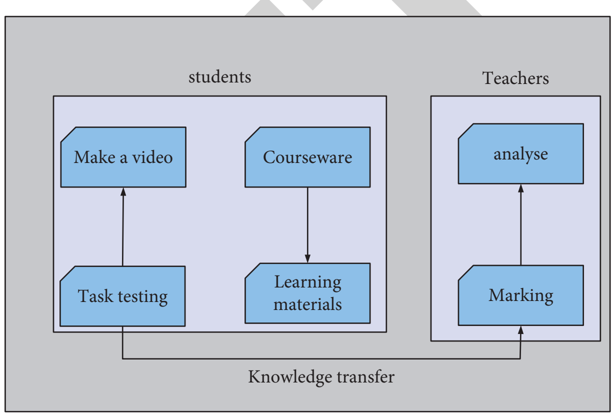

Figure 6: The flipped classroom teaching mode based on MOOC.

emerging online course development model. In a typical flipped classroom teaching model, the activities before class and the activities during class are the main parts. These two parts are not separated by the flipped classroom teaching mode. The autonomous learning based on the MOOC platform before class is mainly composed of task bar guided learning module, autonomous learning module, and group module. In the classroom, teachers create appropriate instructional situations based on instructional content, and students complete knowledge internalization through coinvestigation and interaction.

4. Decision Tree Algorithm and Experiment and Analysis of Flipped Classroom

4.1. Experimental Analysis of Improved Decision Tree Algorithm. In order to simplify the operation, this experiment chooses the first method. It uses the C4.5 original algorithm improved by the previously described improvement scheme. The data used in the experiment comes from the information of 50 students in college English teaching, and the total number of sample instances is 50. In this experiment, the original algorithm and the improved algorithm are compared and analyzed for 5 divisions of the sample instance set, namely, 10, 20, 30, 40, and 50 sample instances. The experimental results are shown in Figure 7.

As shown in Figure 7: It can be seen that, with the increase of the number of data sample instances, the execution efficiency of the improved algorithm is higher. At the same time, in the case of large data sample instance sets, the classification accuracy of the improved algorithm has also been improved to a certain extent. The practice of data mining itself is often faced with the mining of large data set instances. Therefore, using this improved C4.5 algorithm can greatly shorten the waiting time of data analysis and improve work efficiency without sacrificing the classification accuracy. The improved C4.5 algorithm overcomes the deficiencies of choosing attributes with many values when using information gain to select attributes and can complete the discretization processing of continuous attributes.

By comparing the decision trees generated by the two algorithms, it can be known that the improved decision tree shortens the attributes far from the root node by the balance coefficient. This increases the importance of teaching information and makes the classification results more accurate and reasonable. Only a partial decision tree is shown here. The final displayed results are shown in Table 1.

The revised C4.5 method is employed in the subsequent decision tree construction since the improved approach is more reasonable and accurate, as shown in Table 1. The average proportion of leaf node samples of the C4.5 algorithm is 6.6%. The average proportion of leaf node samples of the improved C4.5 algorithm is 7.7%. Because the data used to determine the training set is so tiny, the resulting mining model may have certain flaws. It then validates the training set model against the test set to see if it is accurate. This enables the mining model to be refined and revised further. The decision tree analysis function module of the system module analysis will be used to investigate this.

4.2. Experiment and Analysis of Traditional Teaching Mode and MOOC-Based Flipped Church Teaching Mode. This paper analyzes the development trend of English learning in recent years, as shown in Figure 8.

As shown in Figure 8: The study of college English is very important for expanding students' international horizons.

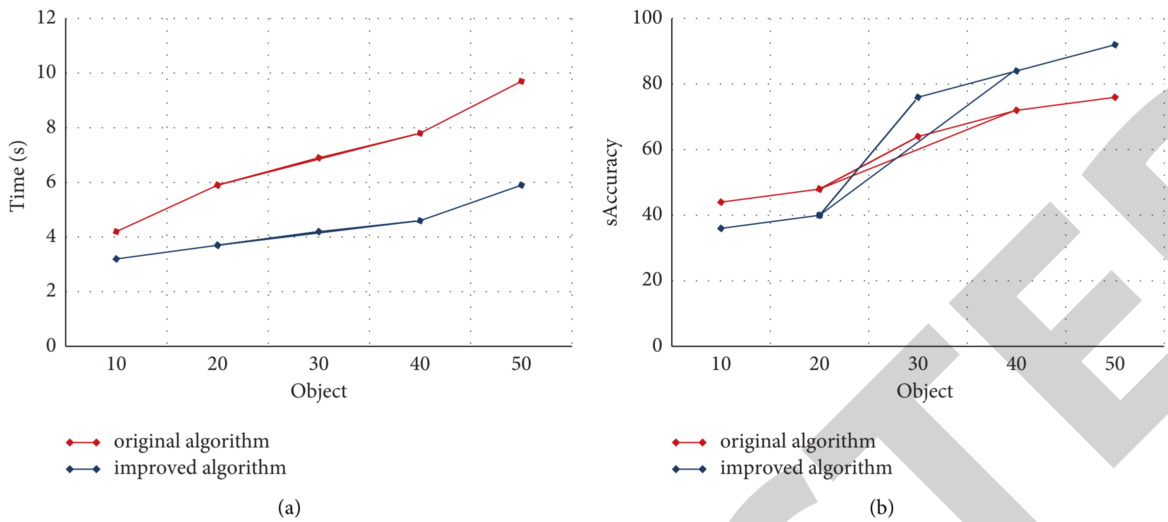

Figure 7: Comparison of algorithms before and after improvement. (a) Comparison of the efficiency of the C4.5 algorithm before and after the improvement. (b) Comparison statistics of C4.5 algorithm classification accuracy before and after improvement.

Table 1: Advantages of the improved decision tree.

Model	C4.5 algorithms	Improved C4.5 algorithm
Tree level	5	5
Number of leaf nodes	15	13
Leaf node sample proportion average	$(20/15)/20 * 100\% = 6.6\%$	$(18/13)/18 * 100\% = 7.7\%$

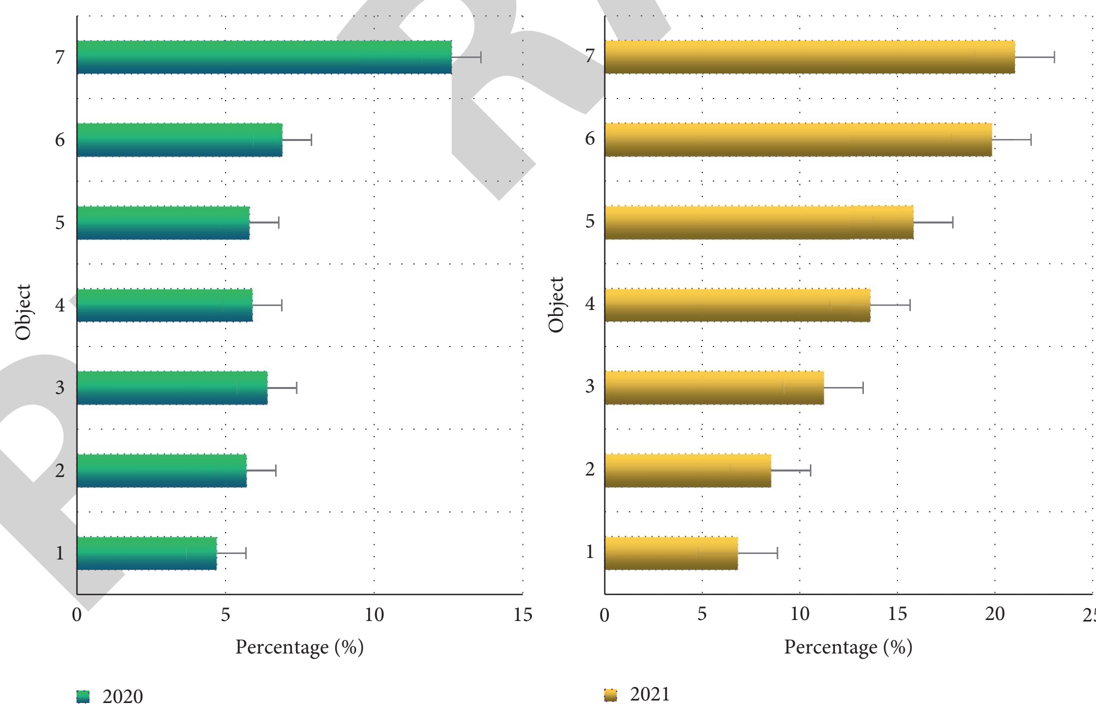

Figure 8: The development trend of learning English from 2020 to 2021.

The traditional education mode of college English education faces the problems of students' participation and educational effects.

The experimental subjects selected in this experiment are students majoring in English in a university, with a total of 50 people. There are 15 boys and 35 girls. It is divided into two groups, one group is conducted in the traditional teaching mode, which is group A, and the other group is conducted in the flipped classroom teaching mode based on MOOC, which is group B. There are 20 people in each group,

Table 2: Popularity of traditional teaching mode.

Object of investigation	Number of people	Percentage (%)	Effective percentage (%)
Like very much	2	10	10
Generally like	3	15	15
Neither like nor hate	5	25	25
Dissatisfied	8	32	32
Dislike very much	2	10	10

Table 3: Popularity of traditional teaching mode.

Object of investigation	Number of people	Percentage (%)	Effective percentage (%)
Like very much	9	45	45
Generally like	8	40	40
Neither like nor hate	2	10	10
Dissatisfied	1	5	5
Dislike very much	0	0	0

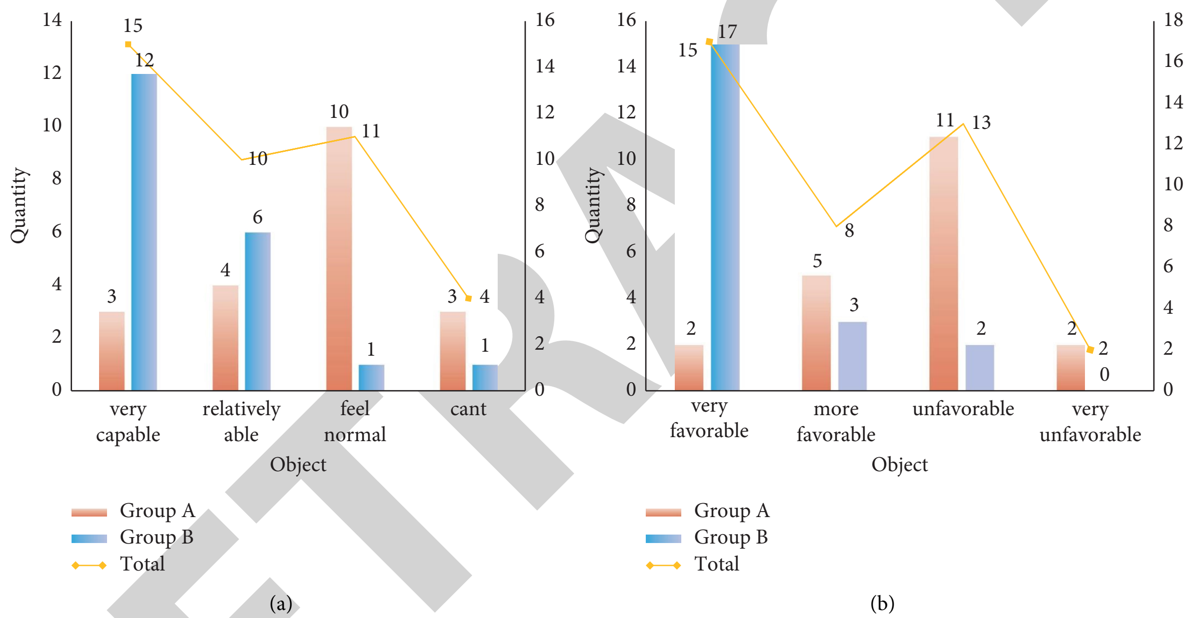

Figure 9: Statistical chart of pre- and posttests of the benefits of the two modes to the mastery of basic knowledge. (a) The traditional teaching mode can stimulate interest in learning. (b) Statistical graph of whether the MOOC-based flipped classroom teaching model can stimulate interest in learning.

and the purpose of this experiment is to change the students' learning attitude and improve the learning enthusiasm of the students in the college English classroom by applying the MOOC-based flipped classroom education model in the college English classroom. After a week of teaching, it first analyzes the students in the traditional teaching mode, as shown in Table 2.

As demonstrated in Table 2, the current teaching mode, which is mostly dependent on instructors' instruction, is unable to pique students' interest in learning, and the majority of students believe that this mode will not improve their learning efficiency or autonomy. Second, the students in group B, who are in the flipped classroom teaching style based on MOOC, are analyzed, as shown in Table 3.

As can be seen from Table 3, there are 9 people who like the MOOC-based flipped classroom teaching model very much, accounting for 45%. Generally, there are 8 people who like it, accounting for 40%. There are 2 people who neither like nor dislike, accounting for 10%. This paper investigates and analyzes two groups of students, as shown in Figure 9.

As shown in Figure 9: Through the summary of the results of the student interview survey, it can be known that the students are more accepting of the new teaching model and have higher satisfaction. This model has improved the overall teaching effect. After the teaching experiment, it tested 2 groups. The weekly test scores of the 2 groups are shown in Tables 4 and 5.

As shown in Tables 4 and 5, the students whose weekly scores in group B were higher than 70 points were significantly higher than those in group A. It can be seen that the new teaching mode has a good teaching effect compared with the traditional teaching mode. The learning ability of

Table 4: Weekly test scores of group A.

Fraction	Number of people	Percentage (%)	Effective percentage (%)
50–60	3	15	15
60–70	9	45	45
70–80	4	20	20
80–90	3	15	15
90–100	1	5	5

Table 5: Weekly test scores of group B.

Fraction	Number of people	Percentage (%)	Effective percentage (%)
50–60	0	0	0
60–70	1	5	5
70–80	7	35	35
80–90	7	35	35
90–100	5	25	25

group B students has been improved. At the same time, it can also indicate that the students in group B have a significant improvement in the application of knowledge compared with the students in group A.

5. Conclusion

Information is becoming a more important driver of humanity's progress in the natural and social sciences. Data mining is a technique for extracting information from seemingly unrelated data that is strongly related to people's lives. The fine-tuning teaching mode is a combination of computer-aided education and network platform technology that compensates for some of the deficiencies of the traditional teaching mode's teacher education mode. The importance of English in worldwide communication is growing, as is the importance of English teaching. MOOCs and flipped classroom task-based college English teaching modes have begun to appear as the traditional teaching mode can no longer match the needs of students. The main focus of this study is on the fundamental concepts of data mining technology, as well as the usefulness of MOOCs and flipped classroom task-based college English teaching modes for future local investigation. It offers a decision tree method based on data mining technology and discovers that decision trees are useful for mining and classifying students' information, resulting in improved English instruction. It conducts experiments on students using various teaching methods in the experimental section. The findings reveal that students prefer the task-oriented collegiate English education strategy based on MOOCs and flipped classrooms. This teaching method boosts students' learning initiative and excitement, as well as their English proficiency.

Data Availability

The data used to support the findings of this study are available from the corresponding author upon request.

Conflicts of Interest

The authors do not have any possible conflicts of interest.

Acknowledgments

This study was supported by the Department of Education Jiangxi Province with title of "Research on Application and Practice of Task-Based Teaching Mode Based on MOOC + SPOC—Take Police English Course of Jiangxi Police Institute as an Example," no. JXJG-18-19-2.

References

[1] X.-B. Jin, W.-T. Gong, J.-L. Kong, Y.-T. Bai, and T.-L. Su, "PFVAE: a planar flow-based variational auto-encoder prediction model for time series data," *Mathematics*, vol. 10, no. 4, p. 610, 2022.

[2] R. Yilmaz, "Exploring the role of e-learning readiness on student satisfaction and motivation in flipped classroom," *Computers in Human Behavior*, vol. 70, pp. 251–260, 2017.

[3] H. Baytiyeh, "The flipped classroom model: when technology enhances professional skills," *The International Journal of Information and Learning Technology*, vol. 34, no. 1, pp. 51–62, 2017.

[4] B. Mcnally, J. Chipperfield, P. Dorsett, L. D. Fabbro, and R. Andrea, "Flipped classroom experiences: student preferences and flip strategy in a higher education context," *Higher Education*, vol. 73, no. 2, pp. 1–18, 2017.

[5] C. Kostaris, S. Sergis, D. G. Sampson, M. N. Giannakos, and L. Pelliccione, "Investigating the potential of the flipped classroom model in K-12 ICT teaching and learning: an action research study," *Educational Technology & Society*, vol. 20, no. 1, pp. 261–273, 2017.

[6] X. Jin, J. Zhang, J. Kong, T. Su, and Y. Bai, "A reversible automatic selection normalization (RASN) deep network for predicting in the smart agriculture system," *Agronomy*, vol. 12, no. 3, p. 591, 2022.

[7] Y. Liu, K. Tang, W. Cai et al., "MPC-STANet: Alzheimer's disease recognition method based on multiple phantom convolution and spatial transformation attention mechanism," *Frontiers in Aging Neuroscience*, vol. 530, 2021.

[8] Y. Wang, Y. Chen, and R. Liu, "Aircraft image recognition network based on hybrid attention mechanism," *Computational Intelligence and Neuroscience*, vol. 2022, Article ID 4189500, 2022.

[9] J. Zhou, X. Wei, J. Shi, and W. W Chu, "Underwater image enhancement method with light scattering characteristics," *Computers & Electrical Engineering*, vol. 100, Article ID 107898, 2022.

[10] Y. Cheng, D. Wang, P. Zhou, and T. Zhang, "Model compression and acceleration for deep neural networks: the principles, progress, and challenges," *IEEE Signal Processing Magazine*, vol. 35, no. 1, pp. 126–136, 2018.

[11] J. Chen, C. Du, Y. Zhang, P. Han, and W. Wei, "A clustering-based coverage path planning method for autonomous heterogeneous UAVs," *IEEE Transactions on Intelligent Transportation Systems*, vol. 99, pp. 1–11, 2021.

[12] J. Chen, Y. Zhang, L. Wu, T. You, and X. Ning, "An adaptive clustering-based algorithm for automatic path planning of heterogeneous UAVs," *IEEE Transactions on Intelligent Transportation Systems*, vol. 99, pp. 1–12, 2021.

[13] Y. Ding, X. Zhao, Z. Zhang, and W. N Cai, "Graph sample and aggregate-attention network for hyperspectral image

Hindawi
Computational Intelligence and Neuroscience
Volume 2022, Article ID 4125833, 10 pages
https://doi.org/10.1155/2022/4125833

Research Article

Formation and Schema Analysis of Oil Painting Style Based on Texture and Color Texture Features under Few Shot

Yuanyuan Zhao

Guangxi Normal University for Nationalities, Chongzuo 532200, China

Correspondence should be addressed to Yuanyuan Zhao; zhaoyuanyuan@gxnun.edu.cn

Received 13 April 2022; Revised 8 May 2022; Accepted 9 May 2022; Published 13 June 2022

Academic Editor: Xin Ning

Texture has strong expressiveness in picture art, and color texture features play an important role in composition. Together with texture, they can convey the artistic connotation of portrait, especially in oil painting. Therefore, in order to make the picture form oil painting style and oil painting schema, we need to study the texture and color texture in combination with the previous oil painting art images. But now, there are few samples of good oil paintings, so it is difficult to study the texture and color texture in oil paintings. Therefore, in order to form a unique artistic style of modern oil painting and promote the development of modern oil painting art, this paper studies the texture and color texture characteristics in the environment of few oil painting works. This paper establishes a model through deep neural network to extract the image incentive and color texture of oil painting art works, which provides guidance for promoting the development of oil painting art. The experiments in this paper show that the depth neural network has high definition for the extraction of texture and color texture of small sample oil painting images, which can reach more than 85%. It has high guiding significance for the research and creation of oil painting art.

1. Introduction

For artistic creation, the first thing is to be based on the shoulders of predecessors. Therefore, it is very necessary to study the works created by predecessors, but it is also a difficult problem to fully study the previous works of art, especially the development of oil painting art. From the perspective of iconography, the texture that can best reflect the artistic language in oil painting art can deeply convey the painter's creative thought and emotion [1]. The second is the color texture, which can reflect the beauty of oil paintings, especially the combination of color can give people a visual impact. But at present, there are not many excellent oil painting works left by predecessors. In order to carefully extract the incentive and color texture in the image in a few works and play its role in oil painting art creation, it is necessary to establish the recognition model of image texture and color texture in a small sample environment, study the internal structure and formation elements of texture and color texture, and promote the formation and schema analysis of oil painting style in modern art.

In this paper, the extraction and analysis of texture and color texture features in the image can not only promote the development and creation of modern art, but also promote the development of modern art education. It makes the development of art more rapid but also has internal meaning. Furthermore, the study of texture and color texture features can help to integrate modern and traditional oil painting art, transforming modern painting into an oil painting style. It is more vibrant and creative. The importance of exploring texture in contemporary oil painting is enormous. The texture composition can reflect the creator's style and spirit while also increasing the aesthetic value of the work. From previous people's oil paintings, the logical relationship between texture, color, and texture features is examined. In their respective systems, they create styles. It can aid students in their exploration and creation of oil painting art. It allows people who practise painting to self-diagnose problems with their work and improve their aesthetic ability after viewing the article.

In order to make modern art images from oil painting style, many people have studied the texture, color, and texture of images. Liu's image oil painting style transfer reconstruction algorithm based on generative countermeasure network was difficult to train. He proposed an improved generative countermeasure network based on gradient punishment and constructed the total variance loss function to study the migration and reconstruction of image oil painting style. The experimental results show that the algorithm has better performance of image oil painting style migration and reconstruction and better effect of image oil painting style migration and reconstruction [2]. However, his research does not specifically explain how the oil painting style is transferred. Yang had proposed a joint domain image stylization method for portrait oil painting. From the perspective of art appreciation, a large number of oil painting works have been analyzed. Three key factors are summarized: texture, structure, and other image. Based on this, a sample-based color adjustment method is proposed. A large number of experimental results show that this method has achieved good results in maintaining the consistency of given image content [3]. His research only studied the color of the image, and the research has a certain one sidedness. El Mehdi et al. proposed a fast and efficient image indexing and search system based on color and texture features in content-based image retrieval system. The experimental results show that the combination of color features and texture features of brightness components can obtain similar results, and the efficiency is higher [4]. His research lacks experimental data and cannot reflect the accuracy of his conclusions. Do et al. proposed a CBIR system based on semantic features to retrieve images from databases. Their method divides the query image into 100 regions and uses K-means clustering algorithm and KNN classification algorithm for semiautomatic annotation. The experimental results showed that the image retrieval efficiency of the system is more than 98% [5]. His research has no specific theoretical support and is not convincing. In order to improve the efficiency of oil painting creation, the pyramid reference image sequence was established by using bilateral reference filtering and mathematical morphology operations by Chen. The experimental results show that the new reference image sequence has clearer texture direction, clear boundary, and is easy to draw. At the same time, this method can be well applied to oil painting teaching [6]. His research has studied the texture features of images, but the construction process of pyramid reference image sequence is not very systematic. Based on the research of these people, this paper reconstructs the recognition model of texture and color texture features in the image under a few samples so as to promote the formation of image oil painting style and graphic analysis.

In this paper, the research on the formation of oil painting style and graphic analysis has the following innovations: (1) this paper applies deep neural network to how to analyze the texture and color texture features in the image, and constructs a model system based on neural network, which can recognize more accurate texture and color texture features in the case of few samples. (2) In this paper, the texture and color texture of the image are analyzed with the help of neural network model, and then the image schema is analyzed with the algorithm. It enables the oil painting style to be transmitted and promotes the formation of oil painting style. (3) In this paper, a series of experiments are carried out on the research of color texture features. It proves that the model of this paper can promote the development of art biography and the formation of oil painting style.

2. Methods of Oil Painting Style Formation and Schema

2.1. Texture, Color, and Texture Characteristics of Oil Painting. No matter how a painting is handled, it will produce brush texture, so texture is one of the important formal elements of constructing portraits. With its rich artistic expression, it plays an important role in the field of painting and exists in oil painting in a unique form. Through the expression form of its own unique attributes, it shows the aesthetic feeling of vision and form in oil paintings [7]. The texture of different materials can show the characteristics of artistic language and image on the picture. In oil painting texture, texture can be said to be a kind of texture. Texture refers to the aesthetic feeling caused by the real expression of texture in the image of plastic arts. It is not only the texture of oil painting materials themselves but also the formation of new image texture after integration with texture materials. It is the combination of oil painting materials and texture materials [8]. In addition, the combination of texture materials and optimized materials will inevitably produce new different visual effects, so it will make people who look at images form different visual or tactile feelings. Texture characteristics refer to the special properties of all actual object surfaces, such as clouds, trees, bricks, hair, and buildings. People are used to some local disordered features in the image, but the whole has regular features, which are also called textures. It also contains important information about the arrangement of surface structure and its relationship with the environment. Texture is also a very important but difficult feature in the image, as shown in Figure 1.

In Figure 1, it can be seen that the Figure on the left is visually different from the Figure on the right. The Figure on the left is visually a water vortex image. The picture on the right is a water grain image, which has different visual effects. And from the perspective of feeling, the picture on the left will be more fresher, while the picture on the right will be heavier. In terms of feeling, in addition to the different effects of texture, we can also see the direction of the painter from the texture. It shows the traces left intentionally and unintentionally in the process of painting. These painting traces can obviously feel the emotional changes in the process of painter's creation. The rich and strong collocation of colors will make people form a completely different vision. Therefore, the color feature is not only the most direct and prominent feature of the image but also one of the most important sensory features of graphic vision [9, 10], as shown in Figure 2.

The contrast before and after colouring can be seen clearly in Figure 2. The portrait in the picture does not match the real human image when it is not painted, but after painting, it can see the skin color and hair color clearly and has a better sense of hierarchy. As a result, texture can reflect

Figure 1: Oil painting texture.

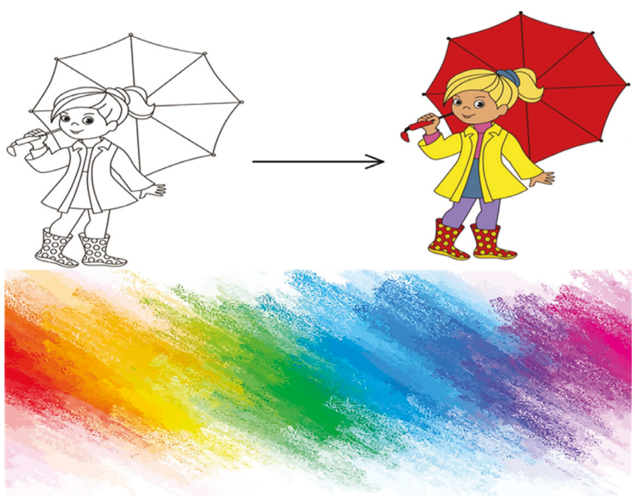

Figure 2: Image color.

the painter's emotional changes, and texture and color features can provide people with visual effects. At the same time, the painter's thoughts and feelings will be conveyed through color intensity. Its bright, warm color expresses the painter's inner love. Texture composition is how you express texture. Its concave, thick, and light surface will evoke a variety of emotions in those who view it. The introduction and creation of texture effects in painting art have opened up a whole new world for the expression of form and color. It has a natural, fresh, and flexible appearance, as well as the ability to be skillfully borrowed. It has evolved into a one-of-a-kind language for artists to express their emotions. It makes natural beauty and subjective feelings blend harmoniously in artistic creation [11]. Therefore, in order to make a breakthrough in modern art creation, we need to analyze the texture and color texture of previous art works.

2.2. Oil Painting Style Formation and Schema. Schema is to serve the formal beauty in painting. Schemata can be divided from time, regional environment, cultural background, personal artistic language, and so on. In all paintings, personal artistic language is to combine the things to be painted in the picture according to their feelings, and strengthen their feelings by using the basic rules of composition [12]. Painting is to match dots, lines, faces, black, white, gray, color blocks, etc. It uses the feeling to mix the elements such as points, lines, and surfaces with scattered, size, rhythm, straightness, cold, and warm. The art of painting must fully understand a pair of contradictions such as virtual reality, square and round, black and white, density, rhythm and charm, and experience the aesthetic principles contained here.

The three-dimensional characteristics [13] of natural objects should be transformed into two-dimensional through both eyes, and the painter's composition ability is fully reflected in this sensitivity. The position of the object image in the picture and the size proportion of the object image will have different visual and psychological feelings. How to form the characteristics of the image in the composition on the basis of clarifying the modeling system and color system becomes very important [14]. There is also an important portrait skill in the image, that is, the placement of portrait modeling. Modeling is how the painter deals with the placement of objects in the painting. Modeling system refers to a unique way formed by the painter's unique treatment of various factors constituting the picture. Modeling is not a single visual grasp, simple object reproduction. Graphic appearance writing is the active pursuit of perceptual psychology and an activity of the interaction between subject consciousness and object spiritual essence [15]. The establishment and improvement of the modeling system is a sign of the maturity of a painter. The modeling system does not take whether the picture has an image as the judgment basis of whether there is a modeling system. Conceptualizing the image is by no means the establishment of a modeling system. Because the painter's quality and taste determine his aesthetic ability and artistic appreciation. The establishment of modeling system requires painters to have high quality and taste, and they can also take this as a breakthrough point to form their own artistic style. The arrangement of composition and shape is shown in Figure 3.

The oil painting style is both traditional and contemporary. We must first understand the oil painting style in order to form it in the transmission of modern art. Oil painting styles and genres are diverse, and there have been countless styles since its inception [16]. Every painter will absorb the essence of the classic paradigm in order to create something new. It defies convention by employing open

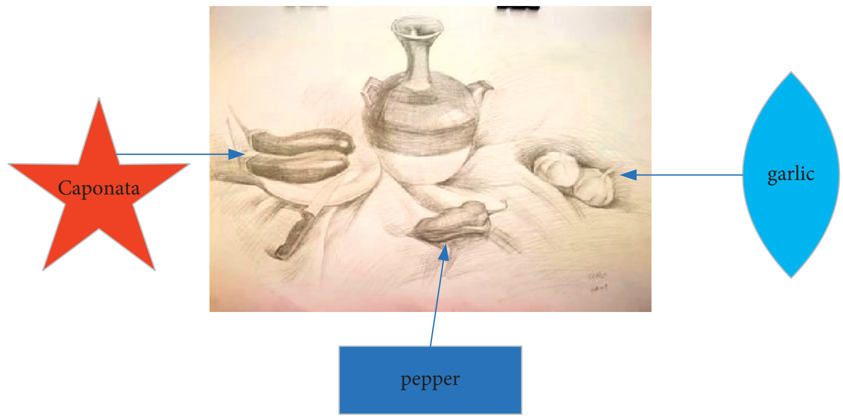

Figure 3: Placement of composition and shape.

reading and its own oil painting creation style, discussing new artistic connotations and expression forms, and attempting to establish its own independent painting style. As a result, when creating modern art, we must consider the style of classic oil paintings. It defies convention by incorporating practical research into the composition, color treatment, and texture effect of the image during the creative process. It attempts to learn from and integrate the schema in order to create modern works in a modern style and oil painting style [17].

2.3. Oil Painting Texture and Color Texture Feature Extraction and Principle. In the previous article, we know the importance of texture and color texture to the image, so if we want to form the oil painting style, we need to extract the texture and color texture features of the classic oil paintings. The specific process of extraction is shown in Figure 4.

As shown in Figure 4, the feature extraction process first inputs the pictures into the gallery, then compares the similarity of the oil paintings in the gallery, extracts the places with low similarity, and then improves it.

For the extraction of color texture features in the image, the histogram method of RGB space is generally adopted. The RGB model is the most commonly used color representation method in the computer, and the statistical histogram of the image is a function, which is usually expressed as

$$G(v) = \frac{A_v}{m}, \quad v = 0, 1, 2, \ldots, N. \tag{1}$$

In the upper form, v represents the color texture features that need to be extracted in the image, and m is the feature dimension of the feature in the RGB model. In order to make the size change of the picture not affect the image feature recognition, this paper normalizes the function. For the color of the image, the RGB model will obtain the statistical histogram of three different colors: R, G, and B, as shown in Figure 5.

If the histograms intersect, the horizontal axis is generally used to classify each color. The level depends on the depth of the color, and the vertical axis represents the proportion of the color in the Figure. If AG (v) and AW (v) are similar features of the two pictures, then the color similarity of the two images is calculated as follows: G and the characteristic histogram of the image W in the image library.

$$S(G, W) = \frac{\sum_{v=0}^{l-1} \min\left[A_G(v), A_W(v)\right]}{\sum_{v=0}^{l-1} H_Q(v)}. \tag{2}$$

In the query matching system, the efficient and accurate similarity matching degree of the query system makes the two methods restrict each other. At the same time, in order to improve efficiency, it also needs to reduce the cost of calculating the same distance. The original search method based on color features filters out the pictures with completely different colors and then introduces the similarity with the texture features of the image. It realizes the search based on texture characteristics, which further improves the accuracy of the search [18]. The fastest matching method is the distance between objects of different colors in the same picture, which roughly represents the color features on the three axes of R, G, and B. Then, the image color features can be represented by vectors:

$$F = \left[\kappa_R, \kappa_G, \kappa_B\right]. \tag{3}$$

At this time, the matching degree between image G and image W is as follows:

$$\begin{gathered} S(G, W) = \sqrt{\left(F_G - F_W\right)^2}, \\ \sqrt{\left(F_G - F_W\right)^2} = \sqrt{\sum_{R,G,B} \left(\kappa_G - \kappa_W\right)^2}. \end{gathered} \tag{4}$$

However, the RGB model histogram cannot effectively measure the fuzziness of people's perception of color features. In order to accurately measure the similarity of two different images, it is necessary to retrieve people's visual color similarity so as to integrate modern art creation into oil painting style. Therefore, it is necessary to refer to the color Table [19]. Assuming that people can feel the same reference color visually, and the number of this group of reference colors is more than the color features of the image to be

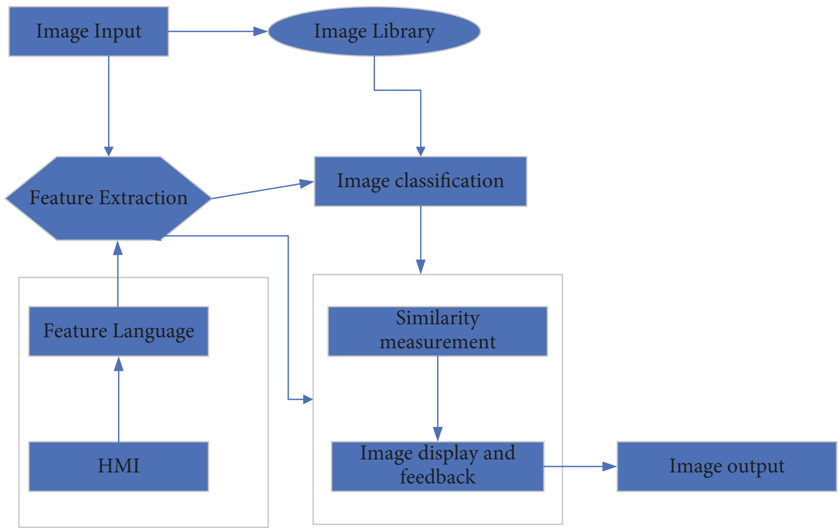

Figure 4: Flowchart of feature extraction.

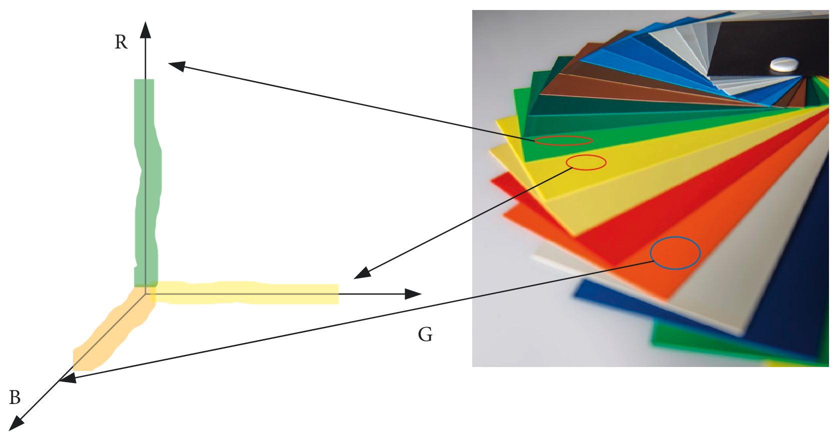

Figure 5: Statistical histogram.

retrieved, the matched feature vector in the cumulative histogram is

$$F = [e_1, e_2, \sigma, e_N]^T. \tag{5}$$

Among them, e_1 represents the frequency of the reference color in the image, and N is the dimension coefficient of the color reference Table, then the similarity matching degree between the test image A and the image W in the image library is

$$\begin{aligned} S(G,W) &= \sqrt[N]{(F_G - F_W)^2}, \\ \sqrt[N]{(F_G - F_W)^2} &= \sqrt{\sum_{i=1}^{N} N_1 (e_{iG} - e_{iW})^2}. \end{aligned} \tag{6}$$

In modern art creation, we need to match the similarity between the newly created image and the color of classic oil painting in the gallery step by step. The closer the similarity is, the deeper the integration of color and texture in classical oil painting is, and the oil painting style is forming [20]. Of course, in order to form the more perfect oil painting style, it is necessary to extract and recognize the texture features in classical oil painting [21]. At present, the commonly used texture analysis methods are statistical analysis method and spectrum analysis method. The measurement of texture has four feature quantities, namely contrast, energy, entropy, and correlation [22].

The so-called contrast refers to the moment of inertia of the main diagonal. The calculation method is generally as follows:

$$CON = \sum_G \sum_W (G - W)^2 d_{GW}. \tag{7}$$

Texture is divided into thickness. For coarse texture, the value of d_{GW} is a value concentrated on the diagonal of the image. If the value of $(G\text{-}W)$ is smaller, the value of image contrast is smaller, otherwise, it is larger. The calculation of energy will be affected by the gray value of the image, so assuming that the energy is t, the formula is

$$T = \sum_G \sum_W (d_{GW})^2. \tag{8}$$

Because the gray value of the image will affect the recognition of the texture features of the image, it is necessary to measure the uniformity of the gray value distribution of the image. When d_{GW} is more concentrated on the diagonal of the image, the value of T will be larger, and vice versa. When the dispersion degree of d_{GW} value distribution in the gray level co-occurrence matrix is different, the entropy value will change. The more dispersed d_{GW} is, the greater the entropy value will be. The calculation formula is as follows:

$$C = -\sum_{G}\sum_{W} d_{GM} \log d_{GM}. \tag{9}$$

The correlation is a measure of the linear relationship between image gray levels. Assuming that the mean value in matrix d_{GW} is λ_a and λ_b, and the standard deviation is χ_a and χ_b, the formula for calculating the correlation is

$$COR = \frac{\left[\sum_G \sum_W GW d_{GM} - \lambda_a \lambda_b\right]}{\chi_a \chi_b}. \tag{10}$$

Therefore, as an example, features can be basically extracted, and then roughness is the measurement of texture granularity, fine or rough. The finer the texture, the finer the image, and the grain size is the size of the basic grain of the texture [23], which can be defined as

$$R = \left[\left(\frac{1}{X_{ps}} \sum_{l,v\in N_t} [\vartheta(R,l,j)]^2\right) > Y\right]. \tag{11}$$

In the above formula, $\vartheta(R,l,j)$ represents the window with coordinates (I, J) as the center, R as the radius, Npt represents the clarity of the image, and Y is the threshold, so the image texture features can be extracted through granularity. Therefore, the extraction principles of color texture features and texture texture features are integrated into the depth neural network model. It integrates the color texture features and texture features of the image into the depth neural network model. Through the autonomous learning ability of the model, it no longer needs to extract step by step according to the above principle. It can not only improve the extraction efficiency of image features but also improve the accuracy of similarity and texture roughness. In the depth neural network model, the image contrast is defined as

$$CTS = \left(\frac{H}{a_4}\right)^{1/4}. \tag{12}$$

Among them, A4 = λ_a / H^4, H is the standard deviation, and the calculation method is as follows:

$$\begin{aligned} H &= \sqrt{\left(\lambda_b - \chi_b^2\right)}, \\ &= \sum_{i=0}^{U} p, \\ H_4 &= \sum_{i=0}^{U} p_4. \end{aligned} \tag{13}$$

In the upper form, H is the intensity of image brightness, and P represents the probability of texture appearing in the image with the same roughness. Therefore, in the deep neural network model, the classical oil painting is put into the neural network model, and then the modern works are transmitted to the deep neural network model for comparison. Then, the similarity between color texture and texture characteristics is obtained, and modern works are constantly adjusted to form oil painting style.

3. Experiment of Oil Painting Texture and Color Texture Feature Extraction

3.1. Experiment of Texture Feature Extraction and Recognition. This experiment will take two pictures as samples and use the depth neural network model constructed in this paper to recognize the texture of the two pictures. One of the samples is a classic oil painting in the model, while the other is a work of modern art. The sample picture is shown in Figure 6.

The specific data of each picture in Figure 6 is shown in Table 1.

Therefore, the texture of the picture is recognized and extracted in this experiment, and the texture is shown in Figure 7.

Figure 7 shows that the sample picture's texture is delicate, and it is clear that the painter is attempting to depict a peaceful landscape. The painter is very light when it comes to texture in the painting process. The image on the left is a classic gallery piece, while the image on the right is a contemporary art piece. Because the picture on the right cannot reflects the painter's emotion during the painting process, the similarity in texture should be around 85 percent. The image on the left is more delicate, particularly the texture of the waterfall, which will convey more vivid thoughts and feelings downstream.

3.2. Color Texture Feature Extraction Experiment. Taking the pictures in the above experiment as samples, the above A, B, C, and D pictures have different brightness. Therefore, this experiment first identifies the color similarity of the same picture under different brightness. Taking the diagonal of the picture as the benchmark, the measurement data record of similarity is shown in Figure 8.

In Figure 8, seven color points are tested from the diagonal of the picture, and the color similarity of the same picture under different brightness is identified. It can be found that the color similarity of the color taking points of the same diagonal in the picture is basically the same. In particular, although the same picture has different clarity, the color similarity is very similar and basically the same. Therefore, the model constructed in this paper has high accuracy for the extraction of color similarity, and it is of great help to the formation of oil painting style. Therefore, we extract and recognize the texture features and color features in the sample image, as shown in Figure 9.

In order to better measure the recognition of color features and texture features in this model, this experiment also makes similarity statistics on the color and texture

Figure 6: Experimental sample.

Table 1: Picture data.

Picture	Luminance (%)	Pixel
a	85	128 * 138
b	80	192 * 192
c	90	384 * 384
d	95	640 * 640

features of the same picture of different pixels in the sample, as shown in Table 2.

In combination with Figure 9 and Table 2, the pixels of the image will affect the similarity of the image, so it is necessary to ensure the clarity of the image during image comparison. In addition, from Figure 9, there will be some gaps between the color and texture of classic oil paintings and modern art works. However, it can be constantly revised according to the gap to guide the final formation of oil painting style.

3.3. Experimental Summary. Through the experiment of this paper, the model constructed in this paper plays a very important role in the formation of oil painting style. The texture extraction of oil painting is in place, which can clearly see how the painter writes in the process of painting. This model can find out the gap between classical oil paintings and modern art works by comparing the color characteristics, texture, and texture characteristics. It can help painters approach the oil painting style purposefully and promote the formation of oil painting style in modern art creation. At the same time, the analysis of the texture and other characteristics of the image is the analysis of the schema, and the model in this paper has a good effect on the schema analysis.

4. Discussion

This paper understands the texture characteristics of oil painting. The texture of oil painting can clearly see the trend of painters' brushes in their creation. A careful study of the texture of classic paintings can be of great help to artistic creation. The artistic expression of oil painting is very strong, especially in the matching of colors. The collocation is very strong, and some have a great visual impact. In the painting materials of oil painting, the roughness of texture produced by the thickness of pigment is different. Therefore, some that need to be distinguished can be reflected by the thickness of the pigment. Therefore, the integration and development of oil painting style and modern art can promote the development of modern art. Schema is very important in portrait, and point, line, and surface lighting constitute the basic structure of portrait. In addition, illustration is essential to the art of painting, especially in the modeling and placement of things in the portrait. This reflects the overall artistic effect of the portrait, so the schema can also be carefully analyzed to promote the development of modern art. Through the experiment of this paper, it can extract and recognize the texture and color texture features in oil paintings, and analyze the schema composition in oil paintings. This model can further compare the gap between classical oil painting and modern art works, and automatically make modern works close to oil painting style and promote the formation of oil painting style. It can also make a very detailed analysis of the schema.

Figure 7: Sample picture texture.

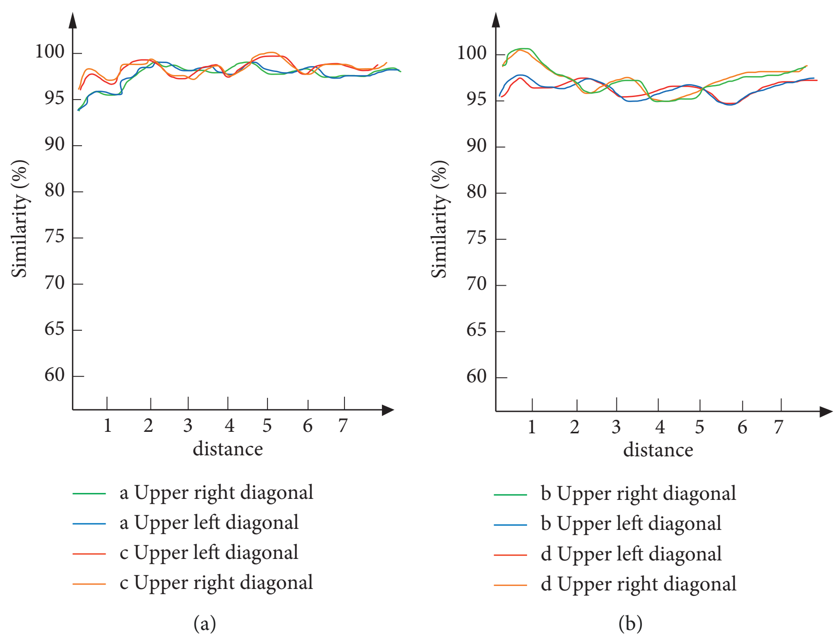

Figure 8: Diagonal color similarity. (a) Similarity between A and C. (b) Similarity between B and D.

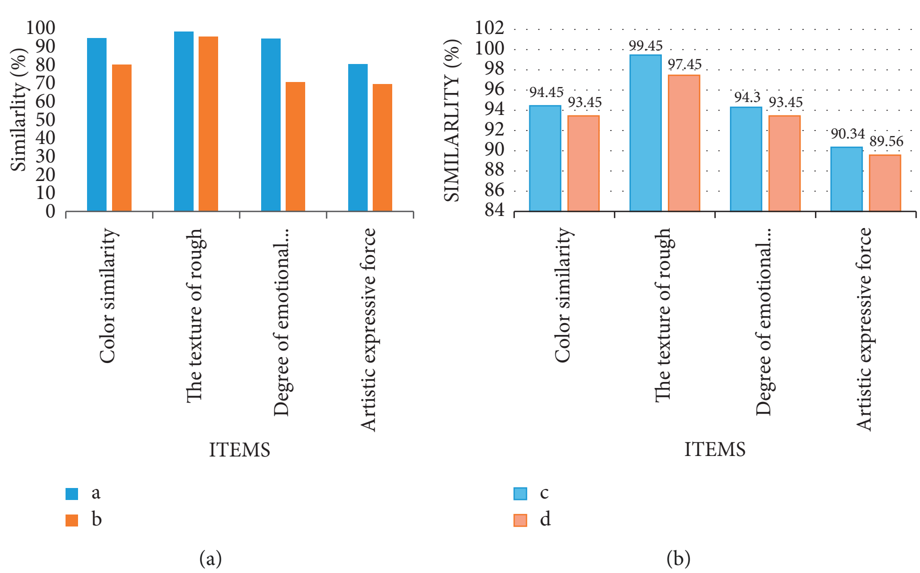

Figure 9: Similarity of different pictures. (a) Comparison of A and B. (b) Comparison of C and D.

Table 2: Similarity of color and texture features of the same image with different pixels.

	Gallery images		Image	
	a	*c*	*b*	*d*
Color similarity	99.45	97.45	89.45	94.45
The texture of rough	94.5	94.5	84.45	95.67
Degree of emotional communication	93.23	98.34	93.45	96.45
Artistic expressive force	94.56	95.45	94.34	98.45

5. Conclusion

This paper explores the role of texture and color texture in the portrait. Texture is the most direct way for oil painting to convey the painter's thoughts and feelings, and it is also the best way to convey the artistic effect of portrait. Color texture can bring great visual impact to people. Therefore, this paper makes a theoretical reasoning on how to form oil painting style and graphic analysis. This paper also constructs a deep neural network model to facilitate the extraction of image texture and color texture features so as to facilitate the graphic analysis in modern creative art and the formation of oil painting style. And the experiment of this paper proves that through the combination of the recognition principle of image color and texture features and the depth neural network model, we can well compare the gap of modern art in oil painting style and promote the formation of oil painting style. However, the research on oil painting texture and color texture features in this paper will still be affected by many uncertain factors. It is hoped that future research can overcome the influence of uncertain factors.

Data Availability

The data used to support the findings of this study are available from the corresponding author upon request.

Conflicts of Interest

The author declares conflicts of interest.

Acknowledgments

This study was supported by Young and Middle-aged Teachers in Colleges and Universities in Guangxi Scientific Research Basic Ability Improvement Project "Painting creation and Research of Comprehensive materials with Guangxi major Festival folklore as the theme" research project Number: 2020KY20028.

References

[1] X. Gu, W. Cai, and M. Gao, "Multi-source domain transfer discriminative dictionary learning modeling for electroencephalogram-based emotion recognition," *IEEE Transactions on Computational Social Systems*, 2022.

[2] Y. Liu, X. Zhu, Y. Xie, J. Yan, and Q. Guo, "Respiratory roller coaster ride following ambulatory surgery in a young woman: a case report," *International journal of surgery case reports*, vol. 75, no. 2, pp. 104–107, 2020.

[3] J. Zhou, X. Wei, J. Shi, W. Chu, and W. Zhang, "Underwater image enhancement method with light scattering characteristics," *Computers & Electrical Engineering*, vol. 100, Article ID 107898, 2022.

[4] E. A. El Mehdi, S. Hassan, and E. Nourddine, "A fast and efficient image indexing and search system based on color and texture features," *Indian Journal of Science and Technology*, vol. 10, no. 39, pp. 1–7, 2017.

[5] A. M. Do, A. Noura, and H. Hala, "An efficient semantic image retrieval based on color and texture features and data mining techniques," *International Journal of Computer Application*, vol. 158, no. 7, pp. 34–39, 2017.

[6] M. A. Jan, *Application of Big Data, Blockchain, and Internet of Things for Education Informatization*, Springer Nature, Berlin. Germany, 2021.

[7] Z. Jiang and J. Yin, "Performance evaluation of texture analysis based on kinetic parametric maps from breast DCE-MRI in classifying benign from malignant lesions," *Journal of Surgical Oncology*, vol. 121, no. 8, pp. 1181–1190, 2020.

[8] Z. Xin, C. Jintian, W. Weisheng, and L. Chao, "A study for texture feature extraction of high-resolution satellite images based on a direction measure and gray level Co-occurrence matrix fusion Algorithm," *Sensors*, vol. 17, no. 7, pp. 1474-1475, 2017.

[9] J. Zhang, W. Feng, T. Yuan, J. Wang, and A. K. Sangaiah, "SCSTCF: spatial-channel selection and temporal regularized correlation filters for visual tracking," *Applied Soft Computing*, vol. 118, Article ID 108485, 2022.

[10] J. Zhou, D. Liu, X. Xie, and W. Zhang, "Underwater image restoration by red channel compensation and underwater median dark channel prior," *Applied Optics*, vol. 61, no. 10, pp. 2915–2922, 2022.

[11] K. Seetharaman, "Melanoma image classification based on color, shape, and texture features using multivariate statistical tests," *Journal of Computational and Theoretical Nanoscience*, vol. 16, no. 4, pp. 1717–1724, 2019.

[12] B. Kumar, N. Janu, S. Vishnoi, and V. Jain, "Analysis on CBIR with color and texture-based feature extraction using SVM," *International Journal of Computer Application*, vol. 178, no. 46, pp. 30–35, 2019.

[13] W. Cai, D. Liu, X. Ning, C. Wang, and G. Xie, "Voxel-based three-view hybrid parallel network for 3D object classification," *Displays*, vol. 69, Article ID 102076, 2021.

[14] N. Niloofar, "Texture analysis and development of ultrafine grained structure during thermo-mechanical treatment in a gamma-TiAl intermetallic," *Materials Science & Engineering, A. Structural Materials: Properties, Misrostructure and Processing*, vol. 711, no. 23, pp. 259–267, 2018.

[15] O. t. Ejofodomi and G. Ofualagba, "Detection and classification of land crude oil spills using color segmentation and texture analysis," *Journal of Imaging*, vol. 3, no. 4, 47 pages, 2017.

[16] D. Helbing, G. Tröster, and M. Wirz, "Recognition of crowd behavior from mobile sensors with pattern analysis and graph clustering methods," *Networks and Heterogeneous Media*, vol. 6, no. 3, pp. 521–544, 2017.

[17] B. S. Nabawy, M. A. Rashed, A. S. Mansour, and W. S. M. Afify, "Petrophysical and microfacies analysis as a tool for reservoir rock typing and modeling: rudeis Formation, off-shore October Oil Field, Sinai," *Marine and Petroleum Geology*, vol. 97, no. 23, pp. 260–276, 2018.

[18] X. Zhong, H. Shi, Q. Ming, D. Dong, X. Zhang, and S. Yao, "Whole-brain resting-state functional connectivity identified major depressive disorder: a multivariate pattern analysis in two independent samples," *Journal of Affective Disorders*, vol. 218, pp. 346–352, 2017.

[19] A. Spiessberger, D. R. Vogt, J. Fandino, and S. Marbacher, "Formation of intracranial de novo aneurysms and recurrence after neck clipping: a systematic review and meta-analysis," *Journal of Neurosurgery*, vol. 132, no. 2, pp. 1–9, 2019.

[20] M. Wu, X. Chen, K. Cui, H. Li, and Y. Jiang, "Pigmentation formation and expression analysis of tyrosinase in Siniperca chuatsi[J]," *Fish Physiology and Biochemistry*, vol. 46, no. 6, pp. 67–69, 2020.

[21] K. M. Hwang, D. J. Lee, H. Yun, S. C. Yoo, and J. H. Kim, "Analysis of material loss behavior according to long-term experiments on LDIE-FAC multiple degradation of carbon steel materials," *World Journal of Nuclear Science and Technology*, vol. 12, no. 1, pp. 1–10, 2022.

[22] X. Zhang, G. Shen, C. Li, and J. Gu, "Analysis of interface migration and isothermal martensite formation for quenching and partitioning process in a low-carbon steel by phase field modeling," *Modelling and Simulation in Materials Science and Engineering*, vol. 27, no. 7, pp. 075011–075013, 2019.

[23] H. Sun, Y. Zhang, H. Liu, R. Xie, and Y. Ren, "Typological analysis and genetic mechanism of dolomite in the lower Cambrian Longwangmiao Formation, eastern Sichuan Basin," *Oil & Gas Geology*, vol. 39, no. 2, pp. 318–329, 2018.

Hindawi
Computational Intelligence and Neuroscience
Volume 2022, Article ID 7986426, 10 pages
https://doi.org/10.1155/2022/7986426

Research Article

Intelligent Structure Design of Learning Seats in University Smart Classroom under the Background of Intelligent Education

Yang Gao and Li Li

College of Materials Science and Technology, Beijing Forestry University, Beijing 100083, China

Correspondence should be addressed to Li Li; 210014@sdjtu.edu.cn

Received 16 March 2022; Revised 3 May 2022; Accepted 4 May 2022; Published 13 June 2022

Academic Editor: Xin Ning

Under the background of intelligent education, the study chairs of intelligent classrooms in colleges and universities should reflect humanistic care and design and guide students to establish a healthy learning style. To realize the intelligent classroom learning, the intelligent seat can be applied to different sitting positions or different heights and weights. This paper designs a control system based on MC9S08DZ60 and realizes the communication between the control system and the mobile app by combining the Bluetooth module based on CSR8670. At the same time, this paper proposes an intelligent design that can adjust the seat height by voice. LD3320 speech recognition module is used for voice control, and a push rod motor with a rising speed of 7 mm/s is used to complete the lifting to meet the requirements of different sitting positions and different heights and weights. Then, the folding design of the intelligent seat for classroom learning is carried out. Infrared detectors are used at the armrests on both sides of the seat. When people have a tendency to sit down, they will speed up deployment. When a person leaves the seat, the seat will automatically retract. Finally, the objective evaluation method of pressure distribution test experiment is compared with the subjective scale evaluation of students, which verifies the effectiveness of the shape design of the chair in keeping students' healthy sitting posture for a long time.

1. Introduction

Under the background of intelligent education, it presents new opportunities and challenges for university education informationization. Universities must actively promote the development of educational management informationization, deepen the integration of information technology and education and teaching, innovate educational concepts and teaching models, promote the integration and sharing of educational management data, and improve fine management and scientific decision-making capability. Learning in the context of intelligent education is characterized by an autonomous learning process, interconnected learning methods, and intelligent learning support [1], resulting in a new intelligent learning paradigm. The premise and guarantee for achieving intelligent learning is to create a good intelligent learning environment. The main research contents of intelligent learning environment [2, 3] are how to fully utilize the new generation of information technology to support the realization of the core features of intelligent learning and how to design intelligent learning environment according to different learning occasions to support different activity modes.

Teaching smothering chair, also known as class chair, refers to the chair used by students in class, which is the most frequently used seat in campus life. It is not only the main category of school chairs but also the focus of educational furniture. It also reflects the related characteristics of smothering products and public services. A healthy chair is one that can ensure students' healthy sitting posture, and a healthy chair can maintain the health of lumbar vertebrae. In design, the shape of the chair is very important because a reasonable shape can maintain the normal physiological curve of lumbar vertebrae [4]. Literature [5] pointed out that if you keep sitting forward for a long time, it will cause great physiological pressure on the intervertebral disc, muscles, and ligaments. In general, it is generally believed that a good sitting position means sitting very straight, and the back support can make the back muscles support the trunk. If there is no back support, the time for the back muscles to support the trunk will be greatly shortened. Therefore, few people can keep their backs straight for a long time. There are two ways to solve this problem: either by providing a backrest or by increasing the angle between the torso and thighs. Literature [6–8] evaluates and analyzes the differences between the current human body sitting posture and healthy sitting posture, and then according to the relevant principles of sitting posture, discriminates six common sitting postures, which are: leaning right (left), leaning head, bending spine, leaning forward, and leaning back. These contents provide a theoretical basis for the study of sitting behavior. The algorithm of face, eyes, mouth, and shoulder detection has been improved, however, no specific product design scheme has been put forward, and the detection of the most sitting positions has been explored theoretically and experimentally. Literature [7], from the perspective of ergonomics, summarizes the main parameters of a healthy sitting posture for students. The angle of the body in a better sitting posture is 4 at 90 degrees, and the angle of the body in the best sitting posture is 2 at 90 degrees and 2 at 135 degrees. Literature [8] found that when the neck of human body bends more than 20 degrees, it will cause different degrees of musculoskeletal diseases.

In the case that the chairs in the modern market cannot meet the needs of students, the study has improved the design of the learning chairs in the intelligent classrooms of colleges and universities from the perspective of health. After repeated tests and experiments, various scientific and reasonable design indexes are constantly explored, and the design ideas and methods of intelligent structure of learning chairs in intelligent classrooms of colleges and universities based on human factors engineering are put forward.

2. Learning Seat Design Principles in Smart Classroom

2.1. Comfort Principle. In the intelligent classroom, the comfort of the chair has an impact on the learning experience. Human factors, seat factors, and human-seat interaction are the three types of factors that affect comfort. Gender, height, weight, and BMI are just a few examples of human factors. Individual preferences influence seat comfort [9]. Size, material, and appearance are all factors to consider when choosing a seat. The pressure distribution on the seat surface is related to seat factors, and the seat back should conform to the human spine curve [10]. Table and chair height ratios, as well as color matching, are important factors to consider. The height ratio of tables and chairs varies according to the user. The height of seats should be easily adjustable to meet the needs of the majority of users. Colors used in moderation can help reduce visual fatigue and provide a pleasant visual experience [11, 12].

2.2. Functional Principle. To cater to the intelligent classroom, tables and chairs should not be limited to the basic functions of sitting, writing, and receiving. The functional design of seats can be improved in many aspects, such as material, size, function, and color. In addition to the conventional physical improvement means, such as height adjustment, desktop tilt, roller addition, folding, or deformation of tables and chairs, we can also focus on technical improvement means, such as classroom interaction and resource sharing. For example, the application of Bluetooth transmission, virtual desktop technology, VR (Virtual Reality), AR (Augmented Reality), and other information technologies can optimize management, improve efficiency, facilitate data transmission, help students better integrate into the classroom, and improve students' participation and experience [13].

2.3. Interaction Principle. Wisdom class deviates from the traditional teaching model by emphasizing teacher-student interaction. We can consider the teaching mode and the realization of interactivity when designing seats for interactivity. There are four different types of teaching modes: the traditional teaching method, in which the teacher speaks and the students listen, is the first. The second type of discussion is group discussion, in which students are divided into groups of varying sizes. Thirdly, there are class meetings or other group gatherings that require everyone to sit together for deliberation, voting, and other activities [14, 15]. Fourth, to conduct activities in the classroom, tables and chairs must be removed. The implementation of interactivity in the smart classroom necessitates more technical means. Seats should be placed in a convenient and uniform manner, and they should be able to be adjusted as the class mode changes.

3. Intelligent Structure Design of Seat

3.1. Seat Shape Deduction. The design of the seat surface is based on the principle that different parts of the buttocks bear different pressures. The pressure is the greatest at the ischial tuberosity of the human body, gradually decreases to the periphery, and the pressure is the lowest at the thigh of the human body. The body pressure of the seat back is mainly distributed in the scapula and lumbar vertebrae of the back of the human body [16]. The supporting positions of these two parts are called "shoulder rest" and "waist rest." The seat "lumbar support" is approximately between the third and fourth lumbar vertebrae, and the seat "shoulder support" is approximately between the fifth and sixth thoracic vertebrae. In the design of seats, "lumbar support" is very important.

This paper mainly focuses on the medium-sized seats. As the design of a seat cushion is the key part of the seat to maintain students' healthy sitting posture, three types of seat cushion are designed: I, II, and III. The edge of the I seat cushion is raised, and the ischial tuberosity is raised with emphasis, and the legs have certain support. The overall shape of the B seat cushion is sleek, mainly heightening the hips and thighs. Type III cushion is relatively square, only heightening the rear side of the buttocks. The purpose of heightening the two sides and the rear edge of the cushion is to fix and limit the buttocks and thighs of the user and to correct the sitting posture of the user using the above methods.

As the cushion part is the key design part of the whole seat, firstly, the three preliminary designs are verified, and the most suitable cushion is selected. Then, the subsequent shape design and verification test are continued. Figure 1 below shows the hot zone diagram of the sitting and pressing comparative experiment of the three seat cushions I, II, and III.

As shown in the comparison of the hot zone diagrams of the three seat cushions in the above figure, the hot zone of the thigh part of the II seat cushion is red, which indicates that the pressure value here is too high, the pressure on the thigh is relatively large, and the stress on the sitting surface is uneven, which is not conducive for maintaining a healthy sitting posture. There are many red areas on the rear side of the buttocks of Type III seat cushion, and the red area at the ischial tuberosity is large and mainly concentrated on the right side, which shows that the above areas exert great pressure on the human surface and are unevenly stressed, and the curved surface design of the sitting surface is reasonable, which does not meet the requirements of maintaining sitting posture. Although the pressure distribution of type I cushion is not ideal, the pressure distribution of type I cushion is relatively balanced among the three cushions. Therefore, type I cushion is selected as the initial seat shape, which provides a basis for the subsequent shape deduction and verification test.

3.2. Design and Composition of the Mechanical Structure of Intelligent Seat in Intelligent Classrooms. The mechanical structure of the intelligent seat for learning in the intelligent classroom is shown in Figure 2. The design inspiration comes from the seats with high utilization rate in the market, which mainly includes the floor bracket part, the control armrest part, the reversible seat cushion, the locking part, and the chair back part [17].

The floor support part is used to support the seat cushion, connect the seat cushion with the chair back, and make the whole chair be placed on the ground completely and reliably.

Back part: the design of the back part is made of wooden strips and is polished. Considering ergonomics and according to the data provided by references, the backrest and waist are designed [18] to make users have perfect riding experience as much as possible. At the same time, the main control board is placed at the back of the fixed backrest, which makes reasonable use of the space and facilitates the later program debugging and maintenance.

Control handrail part: used for placing fingerprint reading module, LED lights for displaying the status of attendees, and interactive buttons. It is connected with the main control board at the back of the backrest through the slot on the armrest, which ensures the stability of the flat cable and makes rational use of the space. Armrests allow users to place their arms to adjust their sitting posture, relieve fatigue, and improve their riding experience and comfort [19].

This part is inspired by the common reversible seat cushion and locking mechanism. This part, however, is equipped with a controlled electromagnetic locking device, unlike ordinary seats. The iron core in the locking device is in a pop-up state before the fingerprint signal is input. The iron core is inserted into the pin hole of the rotary seat cushion at this point, preventing the seat from being turned over, achieving the function of one person and one seat. The electromagnet is electrified after receiving the fingerprint unlocking signal, the iron core is adsorbed, the pin hole is unlocked, and the seat cushion can be turned over [20], completing the intelligent unlocking function.

3.3. Design of Intelligent Seat Control System in Intelligent Classroom

3.3.1. Circuit Design. To realize that the intelligent classroom learning intelligent seat can be used for different sitting positions or different heights and weights, this paper designs a control system for intelligent classroom learning intelligent seat, which realizes the above functions by controlling two stepping motors and one steering gear in the adjusting mechanism. There are many integrated circuits in the control system, which need to be powered by 24 V, 5 V, 3.3 V, and 1.5 V. TPS54386 is a converter with dual voltage outputs and nonstep down, with the maximum output current reaching 3 A, and the output voltage range can be selected between 0.8 V and 90% of the input voltage [21]. Therefore, TPS54386 is selected in this paper to step down 12 V to 5 V for position detection sensor, operational amplifier BA4558F, power amplifier NS4150, and steering gear and step down to 3.3 V for main processor MC9S08DZ60 and Bluetooth module CSR8670. The circuit diagram is shown in Figure 3.

To facilitate the operation, the control system adopts the way of mobile phone APP to realize the automatic adjustment of the intelligent seat in the intelligent classroom, and the mobile phone APP communicates with the control circuit board through the Bluetooth module [22]. With reference to the power consumption, transmission distance, transmission speed, and chip cost of different versions of Bluetooth, this paper uses the Bluetooth molding set BT86 based on CSR8670, which has a power rate equal to Class2 10, and it is packaged with the size of 20 mm (L) $*$ 10 mm (W) $*$ 1.8 mm (H). Its main features are as follows:

(1) It fully supports Bluetooth V4.0 technical specification and is compatible with Bluetooth V5.0 technical specification.

(2) 80 MHz RISC MCU and 80MIPS Kalimba DSP.

(3) With integrated balun radio frequency module, the transmitting power of the radio frequency module is 10 dBm, and the receiving sensitivity is −90 dBm.

(4) 16 Mb internal Flash memory, which can support external expansion to 64 Mb SPI flash memory.

(5) Dual-channel ADC stereo audio decoder can support up to 6 microphone inputs.

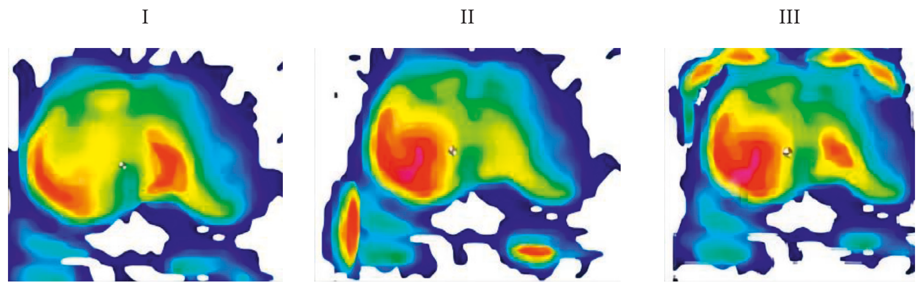

Figure 1: Hot zone map of three seat cushions.

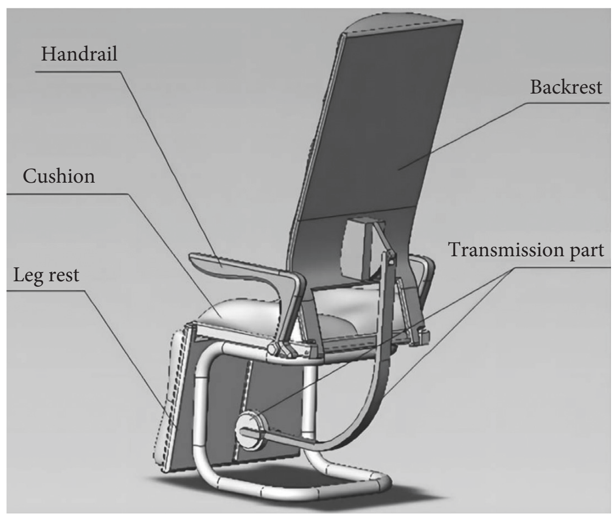

Figure 2: Learning 3D modeling of intelligent seat in intelligent classroom.

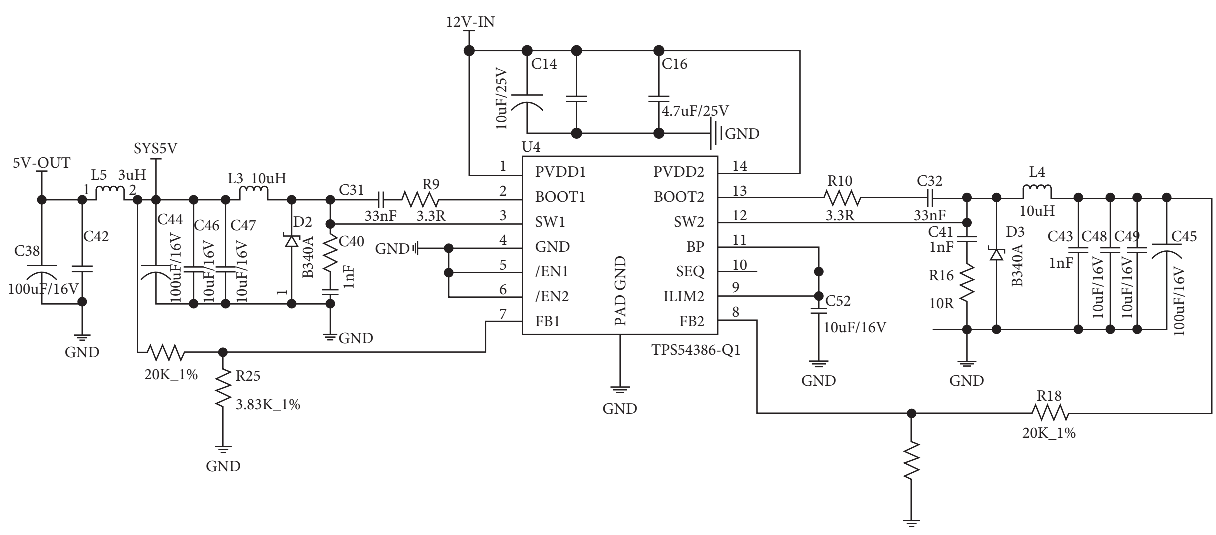

Figure 3: Circuit diagram of TPS54386 buck conversion.

(6) The audio interface supports I2S, PCM, and SPDIF.
(7) Support CSR's latest CVC noise reduction technology.

According to the above characteristics, it can fully meet the functional requirements of intelligent classroom learning intelligent seat control system. The circuit schematic diagram of Bluetooth module BT86 based on CSR8670 is shown in Figure 4.

3.3.2. Voice-Adjusted Seat Height Design. This paper proposes the design of intelligent seat height adjustment by voice based on the previous design to meet the needs of smart seats for various sitting positions, heights, and weights. The design of the voice-adjusted seat height in this section is based on STM32C8T6 single chip microcomputer, as well as the motor drive module, power supply module, and voice recognition module, which integrates the path planning algorithm and performs voice-controlled lifting.

(1) Top Management System. The STM32F103 series based on Cortex-M3 core should be used as the main control chip, with the highest working frequency of 72 MHz, including 32–512 kB Flash memory and 6–64 kB SRAM memory. There are 11 timers inside, with 3 12 bit ADCs, 2 IIC interfaces, and 5 USART interfaces and CAN interfaces. In addition, the chip is powered by a low voltage of 1.7~3.6 V. The schematic diagram of the minimum system core is shown in Figure 5.

(2) Lifting System. The lifting is completed by adopting a putter motor with a rising speed of 7 mm/s, which is in line with the time difference from voice recognition to processing and issuing instructions by the voice module. The lifting is driven by DC, which transfers the horizontal rotation to the vertical lifting. By changing the positive and negative poles of the motor to ascend and descend, there is a travel limit switch at both ends of the push rod, and the telescopic rod will automatically lock when it reaches the bottom or reaches the top, thus avoiding the idling burning of the motor.

(3) Voice Control Adjusts Seat Height. LD3320 speech recognition module is used in speech control, and it has the function of double password control recognition: password mode + I/O control mode, which increases the recognition accuracy. The voice feature information we extracted is the input voice spectrum data. After setting the primary password, the next secondary password can be used for control operation. Furthermore, LD3320 supports speaker-independent speech recognition technology and does not need recording training. Speak specific speech recognition instructions (which have been entered in advance) through MIC microphone, carry out signal processing and judgment, and transmit the obtained results to STC slave control system for processing.

This module has a 5V TTL serial port and 16 I/O ports, which can communicate with external single-chip microcomputer, exchange information, and can also control relay and other equipment. Therefore, the voice recognition module is directly connected with the relay to control the lifting of the push rod motor.

(4) Adaptive Weight Regulation. The original purpose of the weight adjustment mechanism was to accommodate students of various weights in seats. When students of various weights sit in the seats, the upper and lower floors of the seats drop to varying degrees. Different students' weights can be quite different. Chinese students' weight can range from 45 to 100 kilograms. As a portion of a student's weight should be supported by their arms and legs, which do not act on the seat suspension system, 75 percent of them, according to experience, are supported by the suspension system. The seat's estimated dead weight is 10 kg. As a result, the possible variation range of the effective mass acting on the seat suspension system can be estimated to be 45–85 kg. Because each student's weight varies, the equivalent spring-loaded mass will vary as well. The compression amount of the vertical spring is different, and the length of the vertical spring is different when the seat suspension is in equilibrium. To make the seat suspension suitable for students of various weights, the lower end point of the vertical spring should change with the weight of the students, ensuring that the upper end point of the vertical spring is always in the same position when the seat suspension is balanced.

3.3.3. Folding Design of Seat. The automatic folding seat with infrared sensor includes backrest, cushion, chain wheel, chain, limit switch, and control structure. The passive infrared sensor installed on the head of the seat senses whether someone exists, which has the following three functions [23]:

(1) When someone approaches the seat, the seat will control the motor to rotate and slowly open the seat.
(2) When a person stands temporarily and has not left the seat, the seat will not fold automatically.
(3) When a person leaves, the seat will be folded slowly without perceiving the existence of the person.

The structural design of the folding seat is shown in Figure 6 below.

The control structure comprises a controller, a brake, and a motor, wherein the controller is electrically connected with the brake and the motor, respectively. The motor is connected with the brake shaft through a coupling. The hardware of infrared foldable seat includes the following: core processor STC15w408AS, single chip microcomputer, active infrared sensor, passive infrared sensor, and motor. The hardware design block diagram is shown in Figure 7 below.

Select STC15w408AS single chip microcomputer, which integrates high-precision RC oscillation circuit and high-reliability reset circuit internally, so that the direct external crystal oscillator and reset circuit can be omitted, and the chip can work directly after being powered on, can output multichannel PWM to control the rotation of the motor, and sense whether someone approaches by reading the level change of the passive infrared sensor. By reading the level change of the active infrared sensor, we can sense whether someone has the tendency to sit down to speed up the rotation of the motor and open the seat.

Active infrared sensor has strong adaptability to ambient light. It has a pair of infrared transmitting and receiving tubes, which emit infrared rays with a certain frequency. When there are no obstacles in the transmitting and

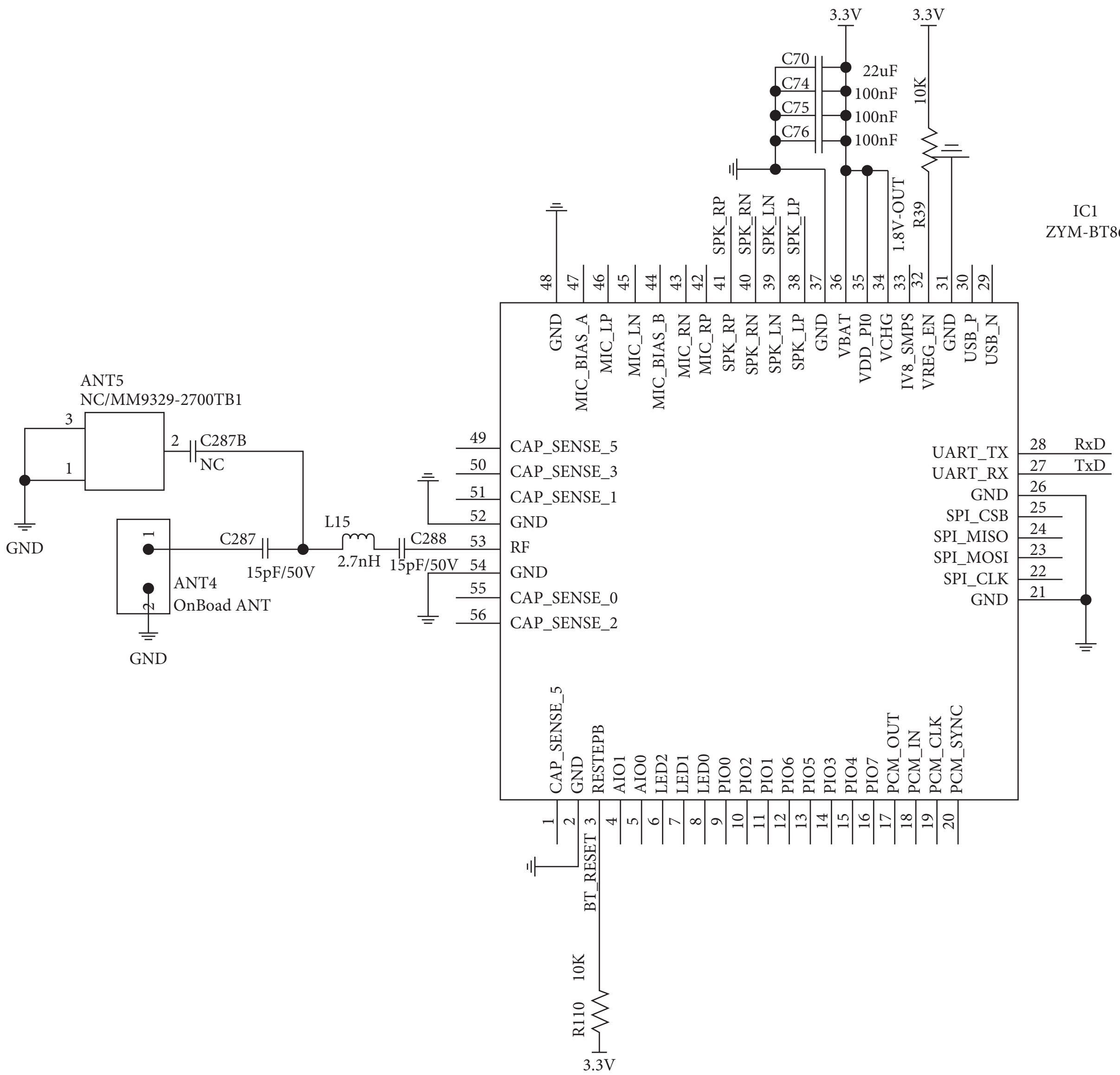

Figure 4: Circuit diagram of BT86 module.

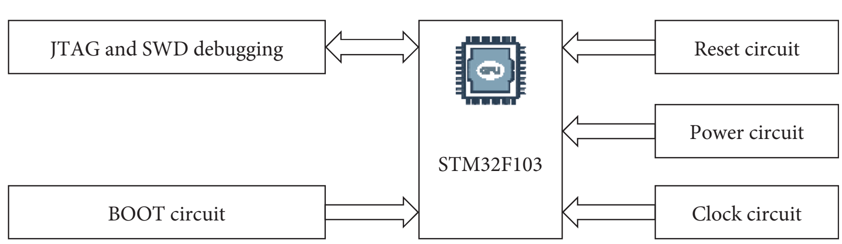

Figure 5: Structure diagram of STM32 core circuit.

receiving tubes, the receiving tube receives the infrared rays emitted by the transmitting tubes, and the green indicator lights up. At the same time, the signal output interface outputs a digital signal and a low-level signal, and the sensitivity can be adjusted by a potentiometer knob.

The sensing module adopts a binary probe, the window of which is rectangular, and the binary is located at both ends in the longer direction. When the human body walks from left to right or from right to left, there is a difference in the time and distance when the infrared spectrum reaches the binary. The larger the difference, the more sensitive the sensing. When the human body walks from the front to the probe, from top to bottom, or from bottom to top, the binary cannot detect the change of infrared spectrum distance, and

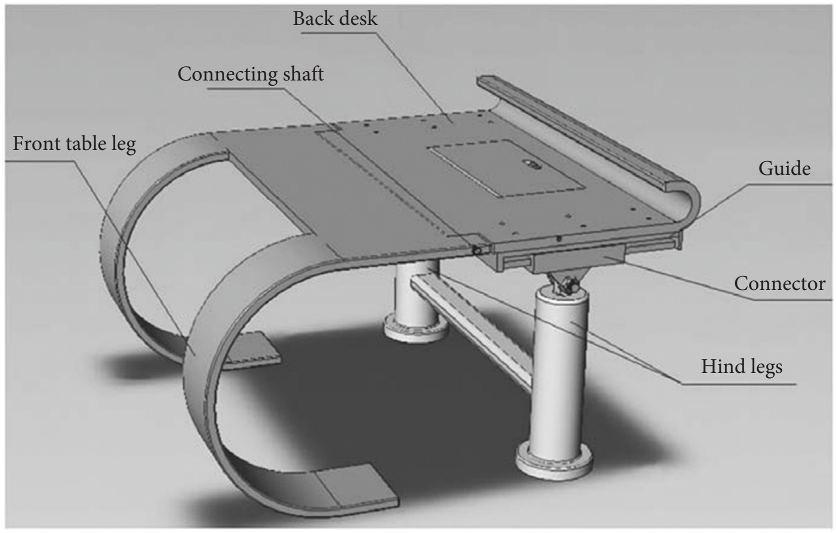

Figure 6: Structural design drawing of folding seat.

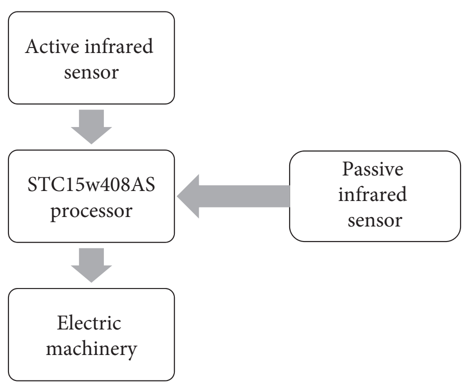

Figure 7: Hardware design block diagram.

there is no difference. Hence, the sensing is insensitive or not working.

The procedure of infrared automatic folding seat is shown in Figure 8.

(1) Start running the program, initialize all parameters and functions, and judge whether the seat is folded.
(2) The program senses whether someone exists by receiving the level change of the passive infrared sensor installed on the head of the seat. When someone approaches the seat, the level changes from high level to low level, and the MCU outputs PWM to control the motor to rotate and slowly open the seat.
(3) The program judges whether people have a tendency to sit down by receiving the level change of the active infrared sensor, and if so, the MCU outputs PWM to control the motor to rotate and quickly deploy the seat.
(4) When both the passive infrared sensor and the active infrared sensor are at high level, no user exists, and the seat is automatically folded.

4. Experimental Analysis

The medium seat is used as the research object for seat deduction in this paper. In this chapter, a comparison experiment is conducted between study seats in a university smart classroom and seats in a regular classroom to determine the effectiveness of the smart seat prototype designed in this paper in maintaining students' healthy sitting posture. Following the shape verification deduction of seat design, the design scheme of learning seat in the smart classroom of university is chosen to make physical products, and the prototype is made based on the short-time static test results. This chapter mainly verifies the two prototypes and assesses the subjective scale of the students. The effectiveness and rationality of the intelligent seat designed in this paper to maintain students' healthy sitting posture are confirmed through these two prototypes, and the effectiveness of the seat shape design and whether it meets the original purpose of designing the seat is confirmed through the pressure distribution experiment.

Experimentation: the subjects' body sizes were measured using a weight scale and a body size measuring ruler before the experiment began. Then, in a table, record the measured

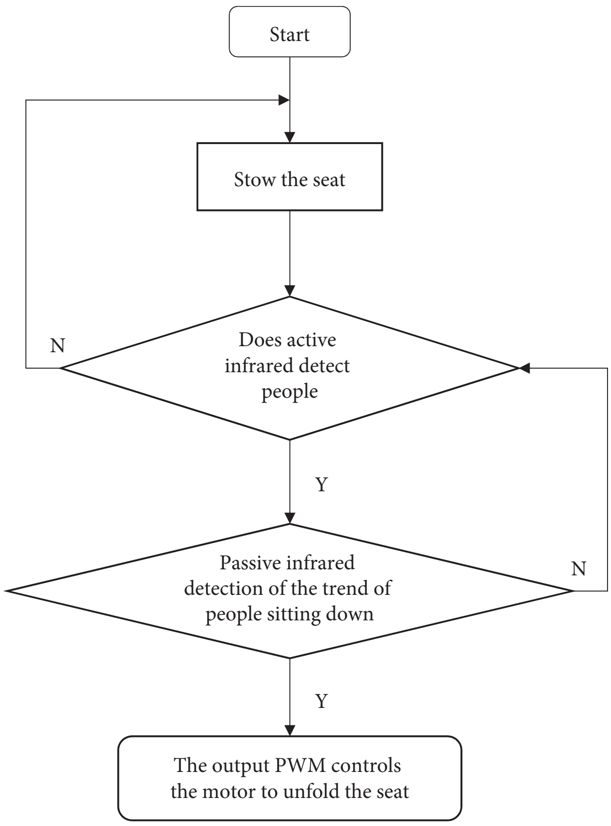

Figure 8: Flow chart.

data. Students' classroom environment is simulated in the laboratory to make the experiment more scientific and reasonable. The students will sit in the standard sitting position while a computer plays the video of the teacher's lecture. The subject is asked about his or her subjective body feeling of seat comfort after the pressure distribution is measured. Complete the subject evaluation scale on a subjective scale.

After the experiment is completed, the experimental data are sorted and made into a data sample database, and then a set of data is randomly selected for comparative analysis according to the experimental comparison items. To observe the displacement of the subjects when using the seat for a long time more intuitively, a set of data is obtained through experiments, which is the plane displacement coordinate data of the pressure center points of the subjects' backs and buttocks, and the data are sorted out, as shown in Figures 9 and 10.

Figure 9 shows the fluctuation diagram of the pressure distribution center point of the common seat back, and Figure 10 shows the fluctuation diagram of the pressure distribution center point of the common seat surface. The broken line Row in the diagram represents the lateral displacement, and the broken line Col represents the longitudinal displacement.

When the subjects started the experiment, their sitting position and position shifted, and with the passage of time, the range of displacement became larger, especially the movement of the backrest was more obvious, which

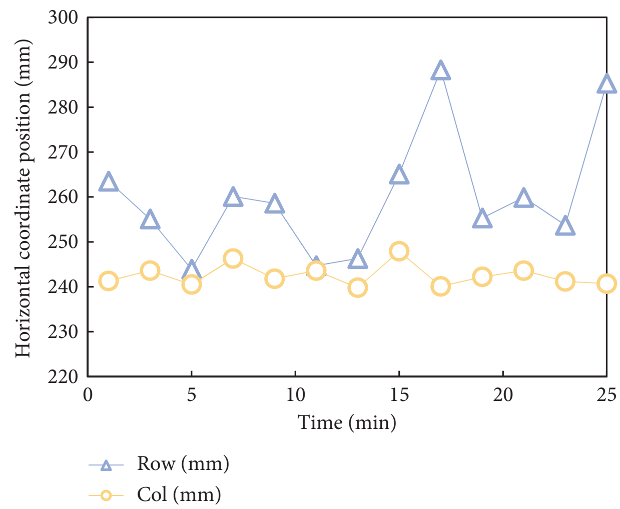

Figure 9: Line chart of the fluctuation of the central point position of common backrest pressure distribution.

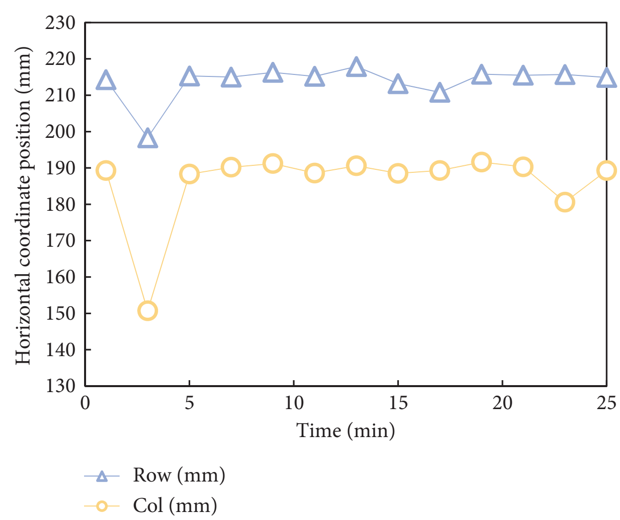

Figure 10: Line chart of the fluctuation of the central point position of pressure distribution on common chair surface.

indicated that the ordinary seats had poor binding force on the subjects' sitting position and could not maintain their healthy sitting position.

Then, the pressure distribution of the intelligent seat designed in this paper is tested. To observe the displacement of the subjects when using the seat for a long time more intuitively, a set of data is obtained through experiments, which is the plane displacement coordinate data of the pressure center points of the subjects' backs and buttocks, and the data are sorted out, as shown in Figures 11 and 12.

It can be seen from the fluctuation of the pressure distribution center position in the above Figure 12 that the body displacement of the subjects is slight during the whole 25-minute test. These phenomena indicate that the intelligent seat designed in this paper can play a certain role in maintaining a healthy sitting posture and can maintain well

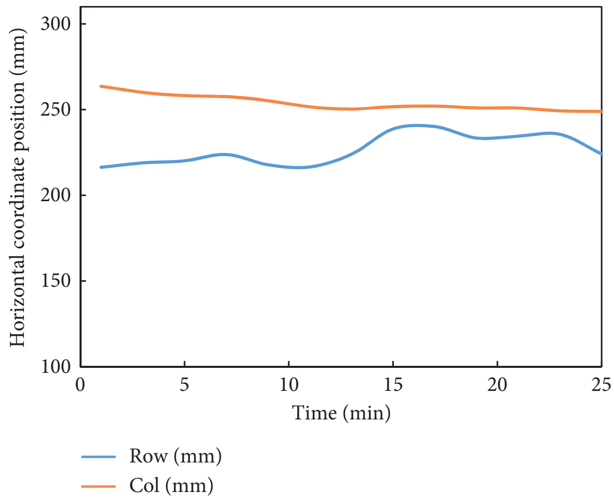

Figure 11: In this paper, a line chart of pressure distribution center point fluctuation of intelligent seat backrest is designed.

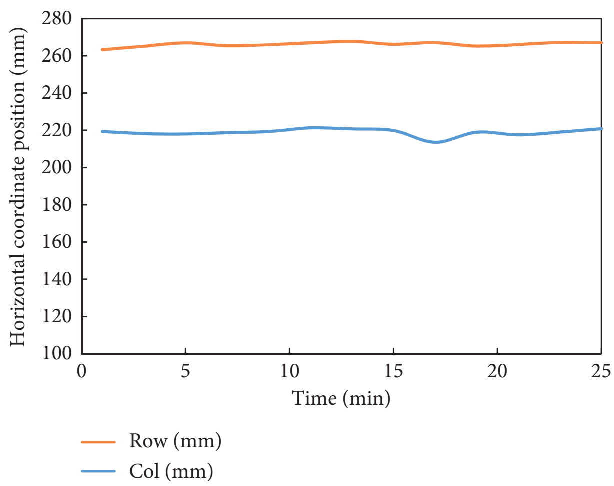

Figure 12: In this paper, the fluctuation line chart of the center point of pressure distribution on the seat surface of intelligent seat is designed.

Table 1: Evaluation system of subjective scale for students' seat use feeling.

Classification of discomfort	No (1)	Slight (2)	Moderate (3)	Serious (4)	Very serious (5)
			Body parts		
Seat type	Shoulder	Back	Waist	Hip	Thighs
Ordinary seat	3	4	3	5	4
This paper designs an intelligent seat	1	2	1	2	1

the healthy sitting posture of the subjects. After the experiment, the subjective evaluation forms filled in by five students were sorted and analyzed. The statistical results are shown in Table 1.

From the comfort point of view, the comfort of ordinary seats is the worst. The intelligent seats designed in this paper feel better overall comfort. The shape design of the intelligent seat designed in this paper not only restricts the sitting behavior of students but also supports the back and waist to ensure a certain degree of comfort. Experiments show that the smart seat designed in this paper has reasonable comfort and can be used for a long time.

5. Conclusion

The research on the design of study seats in smart classrooms should be based on the construction and development status of smart classrooms, which can be considered from the perspectives of interactivity, functionality, and comfort and rely on Bluetooth, virtual desktop technology, VR, AR, and other information technologies to realize the automatic arrangement of seats, data transmission, classroom feedback, and efficient management, so that students can better integrate into the classroom and ensure teaching quality. Through the mechanical analysis of the chair, the intelligent student chair is designed with infrared folding structure, so that the backrest and cushion can move according to the rest needs of students at the same time. The antioverturning base ensures that the seat will not tilt backward and fall over when the students rest. The self-locking seat wheel can move freely when the seat is not stressed by a simple braking mechanism, and the seat wheel cannot move after the student sits down. In addition, the design of voice-adjusted seat height meets the needs of different sitting positions and different heights and weights. Compared with the seats in ordinary classrooms, the intelligent seats designed in this paper basically achieve the function of maintaining a healthy sitting posture, have a certain restraining effect on students' sitting posture, and provide a more reasonable pressure distribution. The shape design of the intelligent seat designed in this paper not only constrains the students' sitting behavior but also supports the back and waist, ensuring a certain degree of comfort. In the bionic modeling design, the size of the seat and the man-machine data are not sufficient. Hence, it is necessary to improve the data analysis of students' sitting posture. With the development of automation technology, all kinds of products serving human beings tend to be intelligent. Therefore, it is also the general trend to realize the intelligentization of learning seats.

Data Availability

The data used to support the findings of this study are available from the corresponding author upon request.

Conflicts of Interest

The authors do not have any possible conflicts of interest.

References

[1] Y. Zhang, K. Xia, Y. Jiang, C. Weiwei, Q. Chengyu, and K. Lai, "Multi-modality fusion & inductive knowledge transfer underlying non-sparse multi-kernel learning and distribution adaption," *IEEE/ACM Transactions on Computational Biology and Bioinformatics*, 2022.

[2] X. Jiang, X. Ma, C. Wang, and G. Jian, "Design and implementation of intelligent library seat management system," *Digital Technology and Application*, vol. 37, no. 6, pp. 158-159, 2019.

[3] J. Chang and F. Feng, "Design and research of intelligent health monitoring chair system based on multi-sensor data fusion algorithm," *Electronic Test*, vol. 11, no. 11, pp. 56–58, 2019.

[4] T. Hyman and W. Li, "Engineering intelligent racing concepts using design research methods," *World Journal of Engineering and Technology*, vol. 6, no. 2, pp. 420–440, 2018.

[5] P. P. Angelov and X. Gu, "Empirical fuzzy sets," *International Journal of Intelligent Systems*, vol. 33, no. 2, pp. 362–395, 2018.

[6] D. Ma and J. Xu, "Design of the intelligent poct network architecture," *Zhongguo yi liao qi xie za zhi = Chinese journal of medical instrumentation*, vol. 42, no. 6, pp. 428–430, 2018.

[7] L. Xue, "Seat or sit: way of thinking in seat design," *Design Art Research*, vol. 9, no. 4, pp. 61–68, 2019.

[8] X. Yang, E. Mao, J. Zhang, Z. Song, and W. Li, "Design and analysis of comfortable cab of high-power tractor based on creo-manikin," *International Agricultural Engineering Journal*, vol. 27, no. 2, pp. 42–50, 2018.

[9] J. B. Du, Z. Y. Wu, C. W. Cai, and H. Liu, "Design of intelligent home system based on arduino," *World Scientific Research Journal*, vol. 5, no. 8, pp. 12–21, 2019.

[10] F. Winjaya and A. Darmawan, "Design of wheel chair up stairs at station for disability people," *Jurnal Perkeretaapian Indonesia (Indonesian Railway Journal)*, vol. 4, no. 2, pp. 99–104, 2020.

[11] D. Zhang, "Analysis and research on the images of drivers and passengers wearing seat belt in traffic inspection," *Cluster Computing*, vol. 22, no. 2, pp. 1–7, 2019.

[12] X. Shi, H. Lu, and Z. Chen, "Design and analysis of an intelligent toilet wheelchair based on planar 2dof parallel mechanism with coupling branch chains," *Sensors*, vol. 21, no. 8, p. 2677, 2021.

[13] Y. Chen, Z. Ding, and J. Liu, "Life cycle assessment of environmental emissions and scenario simulation of an automotive power seat considering scrap recycling," *Environmental Engineering Science*, vol. 36, no. 10, pp. 1349–1363, 2019.

[14] F. P. Chee, S. F. Angelo, A. Asmahani, D. Jedol, and C. Jackson, "An intelligent safety warning and alert system (iswas) for automobile vehicle," *ASM Science Journal*, vol. 11, no. 3, pp. 7–17, 2018.

[15] J. Jalaney and R. S. Ganesh, "Review on iot based architecture for smart public transport system," *International Journal of Applied Engineering Research*, vol. 14, no. 2, pp. 466–471, 2019.

[16] N. X. J. Pan, D. Pan, and Y. Liu, "Study of the bullet rifling linear traces matching technology based on deep learning," *Journal of Intelligent and Fuzzy Systems*, vol. 40, no. 4, pp. 1–6, 2021.

[17] V. Alexei and B. Arthur, "The history of the decline and fall of the glial numbers legend," *Neuroglia*, vol. 1, no. 1, pp. 188–192, 2018.

[18] X.-M. Du, M. Yu, J. Fu, Y.-X. Peng, H.-F. Shi, and H. Zhang, "H∞ control for a semi-active scissors linkage seat suspension with magnetorheological damper," *Journal of Intelligent Material Systems and Structures*, vol. 30, no. 5, pp. 708–721, 2019.

[19] U. Mellstrm and D. Balkmar, "Masculinity and autonomous vehicles a degendered or resegregated future system of automobility?" *Transfers*, vol. 8, no. 1, pp. 44–63, 2021.

[20] G. Bajaj and P. Singh, "Understanding preferences of Delhi metro users using choice-based conjoint analysis," *IEEE Transactions on Intelligent Transportation Systems*, vol. 22, no. 99, pp. 1–10, 2019.

[21] I. Zahirović, D. Danilović, and B. Martinović, "Application of esp pump with intelligent control system in well x," *Podzemni Radovi*, vol. 2020, no. 37, pp. 51–59, 2020.

[22] J. Wang, R. Li, and X. Tianwei, "Research on intelligent soccer robot motion control system," *Green technology*, vol. 22, no. 22, pp. 176–180, 2018.

[23] Q. Wu, F. He, and X. Fan, "The intelligent control system of traffic light based on fog computing," *Chinese Journal of Electronics*, vol. 27, no. 6, pp. 1265–1270, 2018.

Hindawi
Computational Intelligence and Neuroscience
Volume 2022, Article ID 6386360, 10 pages
https://doi.org/10.1155/2022/6386360

Research Article

Tourism Information Management System Using Neural Networks Driven by Particle Swarm Model

Xuan Gao [1,2] **Yuan Qi** [2,3] **Yong Chai**,[1,2] **Chun Lei**,[3,4] **and Jiefei Wang**[1]

[1]*School of International Hospitality Management, University of Sanya, Sanya 572022, China*
[2]*Research Institution of Hainan Silk Road Commercial Civilization, University of Sanya, Sanya 572022, China*
[3]*School of Tourism Management, University of Sanya, Sanya 572022, China*
[4]*School of Hospitality, Tourism and Event, Taylor's University, Penang, Malaysia*

Correspondence should be addressed to Xuan Gao; xuangao@sanyau.edu.cn

Received 23 April 2022; Revised 15 May 2022; Accepted 16 May 2022; Published 13 June 2022

Academic Editor: Xin Ning

Based on the concept of "smart tourism," this paper designs and implements a tourism management information system based on PSO-optimized NN. The foreground tourism web page of the system adopts DIV + CSS mode for page planning and layout, PHP as the client script language, and SQL server as the database to store and analyze user information. At the same time, the system adds personalized components to the user's search ranking results, so that the routes and scenic spots presented in front of users in the result interface are more in line with users' consumption habits. In order to verify the performance of the model and algorithm constructed in this paper, several experiments were carried out in this paper. Experimental results show that the prediction accuracy of this algorithm is 94.67% and the recall rate is 96.11%. This algorithm can overcome the disadvantages of traditional algorithms and provide some effective suggestions for tourism management. At the same time, this paper applies the concept of "smart tourism" to specific tourism informatization, which can promote the transformation and upgrading of tourism industry structure and further enhance the overall development level of tourism industry.

1. Introduction

Tourism informatization contributes significantly to the growth of tourism and is increasingly becoming a key competitive advantage in global resource allocation [1]. The three major industries in the world are tourism, automobiles, and oil, and tourism is also known as the "smokeless industry." The tourism industry has grown rapidly in tandem with the improvement of people's living standards, but it has also brought many problems. Travel agencies currently deal with a large amount of data, with low efficiency and significant errors. With the advancement of the economy and the improvement of people's living standards, many people are turning to holiday tourism to relieve stress and relax [2]. As a result, people's demand for tourism will continue to rise. It is critical to develop a tourism management information system that meets application requirements and has comprehensive functions in order to better adapt to the current market situation. Wisdom tourism is a higher-level and more comprehensive guiding strategy for tourism informatization development, as well as a more profound embodiment of the value of tourism informatization development. With the rapid advancement of computer technology, database management systems are becoming increasingly sophisticated [3]. People are gradually paying attention to modern enterprise management as a result of the establishment of scientific management systems and the popularisation of modern computer management mode, particularly due to the rapid development of computer technology and modern communication technology [4]. The use of computer-assisted management emerged and grew quickly. The importance of carrying out informatization construction in the tourism industry is both theoretical and practical.

People's office efficiency and cost savings can be greatly improved with a tourism management system. However, tourism development is currently slow, and there is no effective management strategy in place. Enterprises with poor information management are less efficient. It is not smooth due to a lack of informatization, a single management mode, and limited communication channels in the tourism administrative department. The tourism industry's development is hampered by these issues. Simultaneously, how to quickly and accurately find high-quality information from the vast amount of Internet data; how to thoroughly analyze customers' consumption habits and formulate user strategies is an important field of Internet technology research [5]. As an information processing system that mimics biological neurons, the ANN (Artificial Neural Network) offers non-linear approximation, parallel processing, self-learning, self-organization, and fault tolerance. As a result, it has some advantages in terms of practical application. The most widely used NN (Neural network) model is the Bpnn (Back propagation neural network) [6]. To adjust the weight, BPNN typically uses the gradient descent method. However, it has some flaws, such as the ability to fall into local minima, slow convergence speed, and easy oscillation [7]. This paper introduces PSO (Particle Swarm Optimization), which is used to train the weights and thresholds of NN in order to address these flaws. This paper builds a tourism management information system based on PSO-optimized NN based on the concept of "smart tourism." The following are some of its innovations:

(i) This paper mainly researches and develops the system according to the idea of software engineering design, and uses a variety of cutting-edge technologies to complete the establishment of tourism management information system. Aiming at the time-consuming problem faced by users in choosing tourist routes, this paper puts forward a brand-new price comparison decision method. It can help users easily get all kinds of travel route information of various travel websites. In addition, the security and reliability of this system are effectively verified by testing.

(ii) BPNN generally adopts gradient descent method to adjust weights. In this paper, an improved PSO-optimized NN algorithm is proposed, aiming at its inherent defects of falling into local minima, slow convergence and easy oscillation. Compared with the traditional NN algorithm, the results show that the performance of PSO-optimized NN algorithm is better.

This paper will be divided into five sections based on the content of the paper and the needs of the article structure, with the following contents for each section: the introduction is the first section. This section provides an overview of the paper's research background, significance, and innovation. The work in the second section is related. This section describes the current state of research on the research topic both at home and abroad, as well as the research work and ideas presented in this paper. There are two parts to the third section. Section 3.1 examines the tourism management information system and the NN algorithm in general. Section 3.2 A tourism management information system is built and implemented using a PSO-optimized NN algorithm. Many experiments are carried out in the fourth section to investigate the performance of the proposed system and the improved algorithm. Summary and prospects are covered in the fifth section. This chapter summarises the paper's research findings. Finally, the paper's shortcomings are discussed, as well as future research directions.

2. Related Work

With the fierce competition of more and more tourism industries, how to improve the service quality and management of tourism is becoming more and more important. At the same time, with the rapid development of mobile Internet, cloud computing, AI and other technologies, the integration of tourism industry and IT industry is getting closer and closer. among them, ANN has been well applied in many fields. At present, many scholars have combined NN with tourism and made some achievements.

In order to improve the prediction accuracy of popular tourist attractions, Du et al. proposed a prediction model of popular tourist attractions based on genetic algorithm optimization [8]. Zhou et al. used use cases for travel service recommendation [9]. This model organizes the user's historical data into case forms and stores them; when the user has a demand, the system will search through the case by the method of similarity calculation to find the case that is close to the user's needs; The case is adjusted according to local needs and a recommended solution is generated. Liu et al. introduced the radial basis function NN with strong non-linear modeling ability to describe the non-linear change characteristics of popular tourist attractions, and optimized the parameters of the radial basis function NN to establish the optimal prediction model of tourist attractions [10]. Bai and Han made dynamic prediction of tourist attractions based on grey system and NN [11]. Lv uses the improved genetic algorithm to optimize the structure and initial weight of the BPNN in the research of improving the genetic algorithm to optimize the BPNN for prediction [12]. In the PSO optimization NN prediction model, Zhao et al. used PSO to optimize the weight parameters of the BP network [13]. This method improves the problem that the BP network is easy to fall into the local minimum value, and improves the convergence speed. The system proposed by Sundriyal et al. uses demographic information to recommend tourist attractions, and classifies users by using Bayesian methods and support vector machines; and assumes that users in the same class have similar interests and preferences, recommending similar Other attractions of interest to users to solve the cold start problem [14]. It has a certain effect. Du achieves a balance between the global search and local search of particles through the linear decrease of the inertia weight and acceleration factor of the PSO, and improves the optimization performance [15]. Behjaty and Monfared proposed a PSO-optimized NN ensemble tourism prediction model based on support vector machines [16]. Zhang designed a tourism demand forecasting system based on

BPNN. The system can dynamically predict tourism demand and has good prediction accuracy [17].

This paper discusses the mode of "smart tourism" and builds a tourism management information system based on PSO optimized NN based on an in-depth review of relevant literature. To begin, an improved PSO optimization algorithm is used to optimize the weight parameter combination of the BPNN model repeatedly. The algorithm is then used to precisely optimize the obtained network parameters. Finally, for prediction, the most accurate optimal parameter combination is used. Customer receipt management module, customer information management module, management module, customer group, tourism resource management module, and functional module have all been completed through design and practise. Finally, the experimental simulation demonstrates that the improved method presented in this paper improves the accuracy of prediction results while requiring few parameters and being simple and effective.

3. Methodology

3.1. Tourism Management Information System and NN Algorithm. The brain is the most complex, perfect and effective information processing system known in the universe. The number of nerve cells in the brain is huge, and these nerve cells are also called neurons. It is hundreds of millions of such neurons that make up our human brain through complex connections. Neurons are the only cells in human body that can sense stimulation and conduct shock, and are also the basic units of nervous system in morphology, structure, function and nutrition. Inspired by the bionics research of ANN [18–20], the operation mode of brain neurons was simulated. NN has the characteristics of massive parallelism, learning autonomy, high nonlinearity and self-organization, and is widely used in many fields. ANN is a complex network composed of a large number of simple components connected to each other. It has a high degree of nonlinearity, and is a system that can perform complex logical operations and realize non-linear relationships. ANN can process information, and its core idea is to adjust the connection relationship between internal nodes according to the different complexity of the system. It has all the characteristics of non-linear dynamic system, such as irreversibility, various types of attractors, chaos and so on. BPNN is the most commonly used NN model at present. Because of its good adaptability and strong non-linear mapping ability, BPNN has been widely used, but it also has some shortcomings. For example: ① the random initialization assignment of BP network connection weight and threshold before network model training makes the network easy to fall into local extreme points and affects the accuracy of prediction. ② For the determination of BPNN structure, there is no exact formula for the number of hidden layer nodes. Improper selection is prone to over fitting or insufficient learning ability, which affects the generalization ability of the network. BPNN model generally has input layer, hidden layer and output layer. The neurons in adjacent layers are fully connected, and there is no connection between neurons in each layer. The structure of NN is shown in Figure 1.

BPNN is a multilayer feedforward NN with two processes: forward transmission of input signals and error back propagation. Various neurons in a feedforward network accept the previous layer's input and output to the next layer without receiving feedback. There are two types of nodes: input cells and calculation cells. There can be any number of inputs, but only one output per computing unit. The basic idea behind the BPNN algorithm is to first initialise the weight and threshold of NN, and then calculate the corresponding output value using the transfer function between NN layers; finally, calculate the error between the output value and the expected output value, and then reverse the weight and threshold of NN. NN is trained by performing forward and reverse error corrections repeatedly. The operation is terminated when the error value reaches the set standard. The neuron state of each layer only affects the neuron state of the next layer in the BPNN model. To approach any rational function with any accuracy, the network structure usually only requires a single hidden layer. The number of neural nodes in the input and output layers of the network is determined by the dimension of the input and output vectors of training samples. The characteristics of neurons, the form of neuron interconnection, and learning rules are the three factors that determine NN's overall performance. We must improve the BPNN model's inherent flaws in order to better apply it. PSO stands for swarm intelligence optimization. The algorithm is simple to use and is used in a variety of optimization problems. This paper will build a tourism management information system using a PSO optimized NN algorithm.

The development of information and Internet technology has completely changed people's life, and the intellectualization of tourism management has also become a trend. At present, the websites of travel agencies all over the country are in their own array in terms of function, information service and business operation, and the phenomenon of "information island" is serious [21]. The tourism management information system is convenient, which can manage, store and share resources through the network and various types of tourism resources. It greatly saves the labor cost, reduces the work difficulty and improves the intelligent level of the tourism industry. Continuously improve the level of tourism informatization management, optimize the allocation of resources, and realize the industrial chain of enterprises; It can promote the development of enterprises, expand employment and realize the positive role of tourism economic development. Therefore, developing a tourism management information system that can not only store but also update and query data is critical. The requirements for building various formats of informatization in smart tourism are extensive. The creation of a smart travel agency, for example, necessitates the network realization of various functions such as data collection and resource procurement, product planning and release, product sales, tourist service, order management, team management, statistical settlement, and so on. However, in the current reality, only a few tourism businesses use the network to carry out the aforementioned functions. The tourist route can be inquired by inputting tourist places; Travel agency management route; Recommended by popular

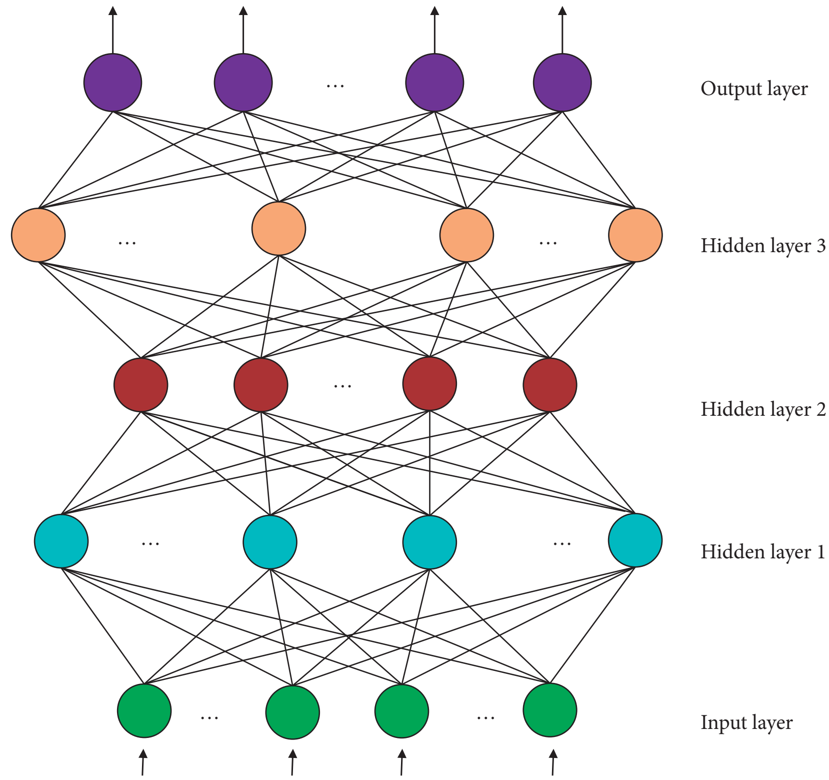

FIGURE 1: NN structure.

scenic spots; Scenic spot reservation; Order processing, and so on are the main functions of a tourism management information system that can satisfy the application. It should also have a user-friendly interface and provide appropriate operation tips. Decision-making is central to management, and prediction [22, 23] is the foundation of decision-making. In tourism development and planning research, we should employ appropriate forecasting methods and models to determine the tourism economy's development law, as well as predict and speculate on tourism's future development trend, direction, and possibility, in order to better serve tourism planning, project decision-making, and management. Before developing an application system, we must understand the design and actual requirements of the system, assess the technology and principle's feasibility, and plan for development. The system should be simple to use once it has been launched, and most ordinary users with Internet experience should be able to use it without difficulty. At the same time, system administrators must have a thorough understanding of computers. General computer-related professionals can become competent after reading the instruction book. The paper then provides an overview of the system's overall design and implementation functions, as well as the system's overall test and trial operation, using an example design.

3.2. Construction of Tourism Management Information System Based on PSO-Optimized NN. This system combines NN and PSO to create a tourism management information system. It is concerned with network applications. The function, or purpose, of a network management system should be the first step in its development [24]. The functional requirements are usually to clearly express a network management theme, to accommodate various types of content, and to adapt to various resolutions. Second, the design structure should be obvious. Because there are so many databases in this system, the databases must be designed ahead of time. It is the foundation of the data tourism management information system, the core content of the smart tourism city construction, and it provides crucial data support for the application service system construction. A data dictionary is made up of data items, data storage, data flow, data structure, and data processing, with data items being the smallest unit of the data dictionary. Data items make up the data structure. Data structure and data items are used to describe the data dictionary. A solution system for industry-wide data perception is proposed in this planning scheme, which is integrated into tourism intelligence data based on industry-wide data. Many weight adjustment methods for BPNN algorithms based on gradient descent exist, but they all have drawbacks, such as slow convergence, long training times, and global convergence. PSO's optimization process is independent of gradient information, and it does not require that the function be differentiable or that the derivative be excessive. PSO is used as the NN training method in this paper to reduce NN training time and improve search efficiency. The flow chart of optimizing PSO NN algorithm is shown in Figure 2.

A perfect system should have good stability, reliability, security and scalability, and can run efficiently. Therefore,

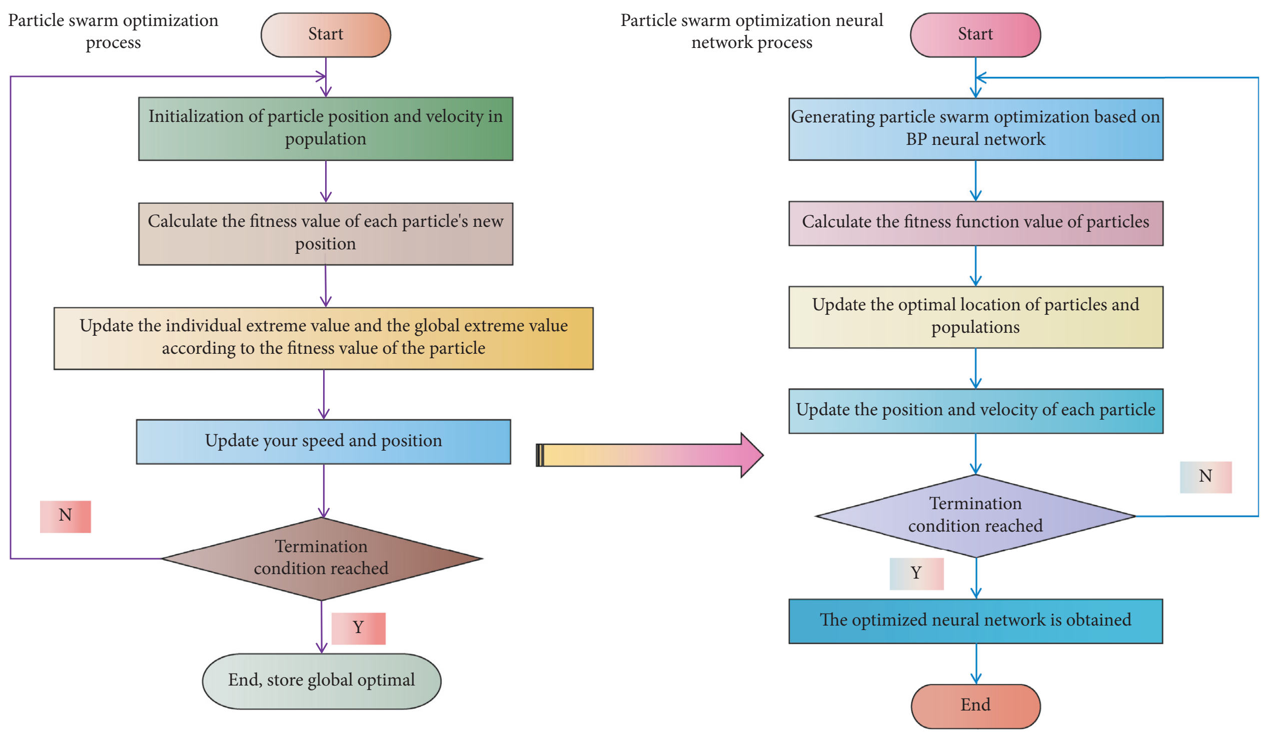

Figure 2: PSO optimization NN algorithm flow.

this system meets the following performance requirements: ① correctness. ② Reliability. ③ Easy practicality. ④ Maintainability. ⑤ Reusability. ⑥ Understandability. ⑦ Safety. ⑧ Effectiveness. The system's basic information data for users primarily consists of gender, age, occupation, city, and historical comment items, while the comment data primarily consists of the user's comment text information on previous tourism service items and the corresponding scores. The system covers all end users based on the characteristics of the online travel network. The system also allows for real-time online operation, and the front page of timeliness and variability consistently sets high standards. The establishment of tourism data security standards ensures the security of data circulated in the tourism industry. Data transmission security standards, data storage security standards, and data exchange security standards are all included in the construction. Traditional linear modeling methods cannot accurately describe influencing factors and tourist attractions because they have a strong non-linear relationship. In order to fit the non-linear relationship between influencing factors and tourist attractions, this paper uses PSO to optimize NN. This paper uses a three-layer NN with only one hidden layer for the topological structure of NN in order to balance the algorithm's simulation and prediction accuracy, and because the more hidden layers, the more over-fitting of practical problems will occur. The number of nodes in the input layer represents the dimension of the original data, while the number of prediction indexes represents the number of nodes in the output layer. The activation function of a neuron and a network is what determines the network's function. Its primary function is to control the activation of input to output and to perform functional conversion on input and output in order to transform an infinite domain input into a limited range output. S-type function is used in this paper. The output formula of NN is

$$Y(X_n) = \sum_{i=1}^{I} W_i \Phi(X_n, t_i). \tag{1}$$

In the formula, W_i represents the weight between the nodes of the hidden layer and the output layer; t_i represents the center of the NN function; Φ represents the NN function, which is defined as follows:

$$\Phi(x) = \exp\left(\frac{\|x - c_i\|^2}{\delta_i^2}\right), \tag{2}$$

where δ_i represents the radius of the radial basis, and c_i represents the center of the response function. For the three-layer BPNN used in this paper, the optimization dimension is

$$D = m \times n + n \times k + n + k. \tag{3}$$

Set the threshold vector from the input layer to the hidden layer as

$$A_1 = [a_{11}, a_{12}, a_{13}, \ldots, a_{1n}]^T. \tag{4}$$

Set the threshold vector from hidden layer to output layer as

$$A_2 = [a_{21}, a_{22}, a_{23}, \ldots, a_{2k}]^T. \tag{5}$$

Set the encoding on each particle dimension in the algorithm to

$$x = [IW_{11}, \ldots, IW_{mn}LV_{11}, \ldots, LV_{nk}a_{11}, \ldots, a_{1n}a_{21}, \ldots, a_{2k}]. \tag{6}$$

The adjustment of weights and thresholds in BPNN is based on the mean square of errors. The fitness function optimized by PSO is used as the back-propagation function of the BP network error, and the equivalence relationship between the mean square value of the error and the fitness function of PSO is established. The objective function expression is

$$f_i = \frac{1}{N}\sum_{k=1}^{n}[y(k) - y_m(k)]^2. \tag{7}$$

In the formula, N represents the total number of training samples, f_i represents the square error sum of the objective function; $y(k)$ and $y_m(k)$ represent the target output value and actual output value of the objective function, respectively.

The related parameters are coded based on the setting of the NN structure, and the optimization dimension is represented by the weights and thresholds of the NN connection. Using cyclic iteration, the number of hidden layers is determined, and the optimal number and weight of NN hidden layers are found. The optimal position of the current particle and PSO is updated based on the fitness function value. Then, to generate a new group of PSO, update each particle's position and velocity. The individuals in the improved PSO optimization algorithm are coded into the weights and thresholds of the three-layer feedforward NN structure. Set the variable value intervals in the improved PSO optimization algorithm, then randomly initialise PSO's position and speed within the initialization range. The performance of particle local search and global search will decrease if the inertia factor of PSO is linearly adjusted, according to the basic PSO. The non-linear method is used to overcome the limitations of the linear decreasing method. At this time, the inertia factor expression is

$$w(k) = w_{\min} + (w_{\max} - w_{\min})\exp\left(-\frac{25k}{T_{\max}}\right). \tag{8}$$

For the problem of network evaluation, the widely used evaluation indicators include MSE (Mean squared error), RMSE (Root mean square error), MAE (Mean absolute error) and MAPE (Mean absolute percentage error). The specific expressions of these four indicators are given here:

$$\begin{aligned}
\text{MSE} &= \frac{1}{n}\sum_{k=1}^{n}\left(y_k - \hat{y}_k\right)^2,\\
\text{RMSE} &= \sqrt{\frac{1}{n}\sum_{k=1}^{n}\left(\left|y_k - \hat{y}_k\right|\right)^2},\\
\text{MAE} &= \frac{1}{n}\sum_{k=1}^{n}\left|y_k - \hat{y}_k\right|,\\
\text{MAPE} &= \frac{1}{N}\sum_{k=1}^{n}\left|\frac{y_k - \hat{y}_k}{y_k}\right|.
\end{aligned} \tag{9}$$

Table 1: Settings of simulation test environment parameters.

Serial number	Test parameters	Set up
1	Hidden layer	One
2	CPU	4 nuclear
3	RAM	64 GN
4	Hard disc	1T
5	Display card	512G
6	Operating system	Windows

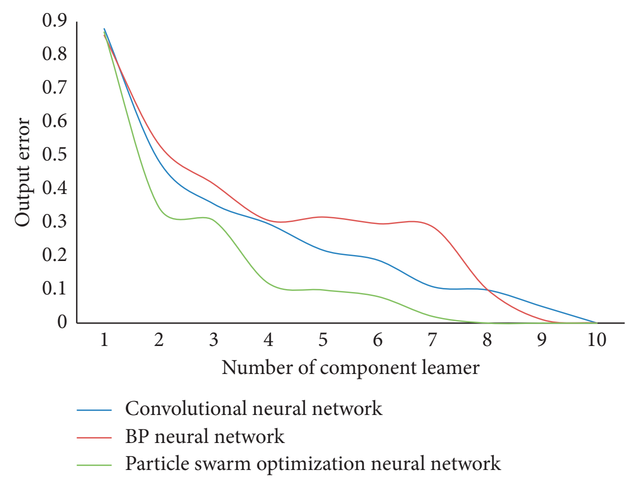

Figure 3: Training results of different networks.

Among them, y_k is the actual value, and $\hat{y}_k$ is the output value.

Using the system's HTML page, manage and maintain the online travel network. The customer and logical interface are displayed using the presentation layer. The presentation layer represents users, and the presentation layer also represents the link between users and the system. The presentation layer realises the client's request, and the data is transmitted, primarily in the business layer, with the results displayed. The goal of the data exchange interface design is to create a system that is open, extensible, adaptable, efficient, and stable. The data exchange interface has its own hierarchical authority management mechanism, and it also manages the security authentication of data acquisition and storage for other data exchange application systems, as well as effectively encrypting the data during transmission. The goal of this paper is to promote online tourism, and the principle of serving users is used to design a tourism management system that meets the actual needs of tourism management. Furthermore, the goal of a simple and clear interface, stable functionality, low implementation cost, and meeting a variety of service tourism demands has been met. Provide assistance to tourism businesses in making decisions.

4. Result Analysis and Discussion

This system is developed in B/S mode, and the interface of presentation layer is realized through WEB browser, mainly for the realization of text, Flash, pictures and other functions. Through the client browser HTML form, URL and Flash request realization, the data is given to the

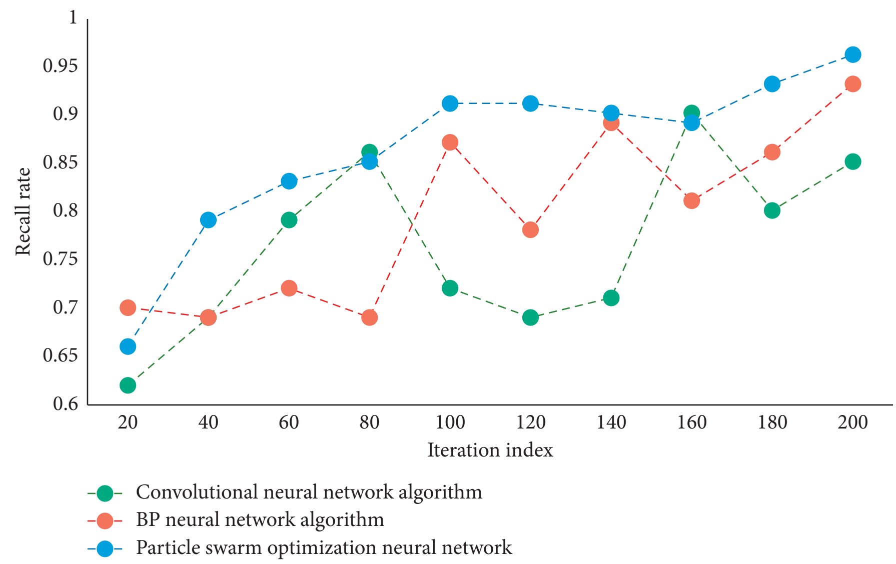

Figure 4: Comparison of recall rates of different algorithms.

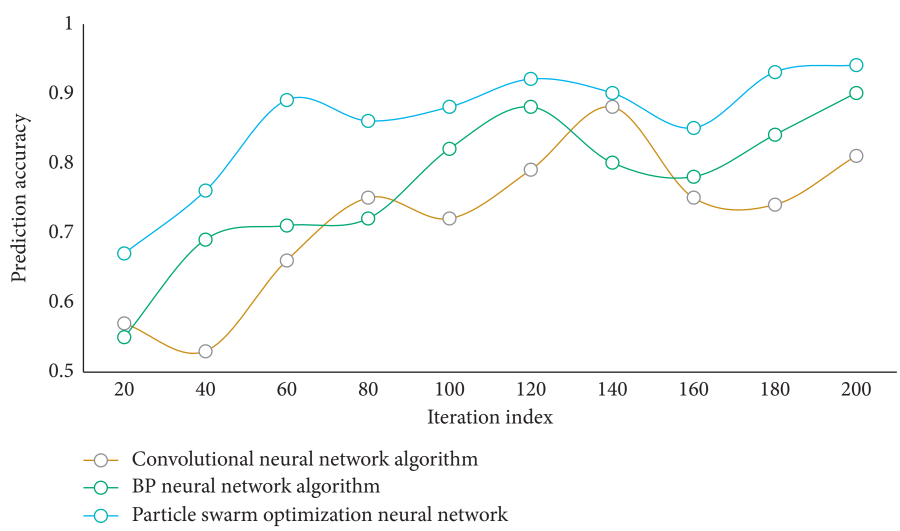

Figure 5: Comparison of prediction accuracy of different algorithms.

programming model, and the system provides J2EE realization to develop and realize the system. In order to verify the practical application effect of the system, simulation experiments are carried out in this chapter. Table 1 shows the parameter settings of simulation test environment.

Tansig function is used as the conversion function between the input layer and the hidden layer, and Purelin is used as the conversion function between the hidden layer and the output layer. The maximum training step is 1000, and the number of particles in the parasitic group and host group in the improved PSO is set to 50. The network is trained and the results are shown in Figure 3.

It can be seen that the convergence speed of this network is faster. In this paper, PSO is combined with NN, and the weight and threshold of NN are determined by using improved PSO instead of BPNN based on gradient descent. Therefore, the optimal parameter combination is obtained for NN to forecast the tourist volume in tourist areas. Three different models are used to predict the test set, and the prediction results are compared and the performance is analyzed. Test the recall results of different algorithms at the same time. The comparison results of recall rates of different algorithms are shown in Figure 4. The prediction accuracy results of different models are shown in Figure 5.

Table 2: Test index values of different methods.

Algorithm	MSE	RMSE	MAE	MAPE
Convolution algorithm	0.154	0.499	0.803	0.614
BPNN algorithm	0.108	0.279	0.627	0.512
Traditional ANN algorithm	0.094	0.301	0.614	0.487
Improved PSO algorithm	0.057	0.213	0.551	0.369

According to the data analysis in Figure 4, the recall rate of this algorithm is the highest, and it is better than the

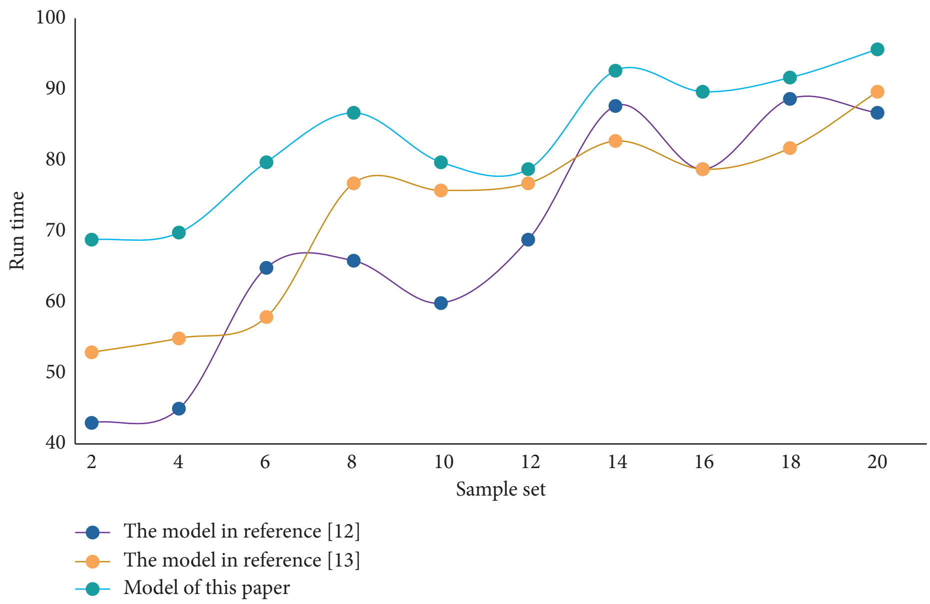

Figure 6: Running time results of different systems.

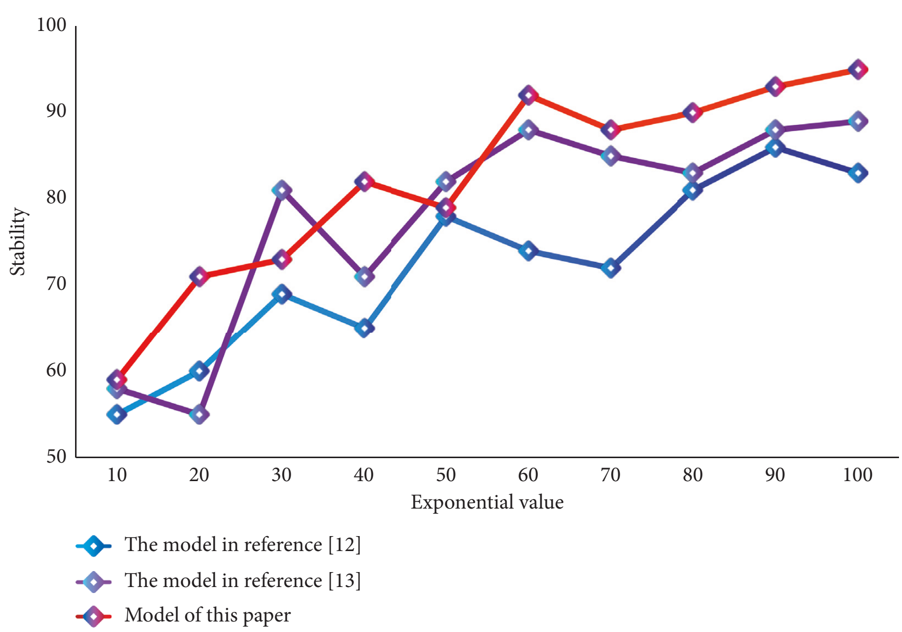

Figure 7: Stability test of different systems.

comparison algorithm. According to the data analysis in Figure 5, the prediction accuracy of this algorithm is at a high level, up to 94.67%. It shows that the model in this paper can be well applied to forecast the number of tourists in tourist areas. This further verifies the feasibility and effectiveness of this method. Table 2 shows the test index values of different methods.

It can be seen from the data results in the table that the fitting accuracy of BPNN algorithm is much higher than that of cluster analysis algorithm; However, the accuracy of improved ANN is better than that of BPNN algorithm and traditional ANN. Comparing the performance of different systems, the running time results of different systems are shown in Figure 6.

Considering the migration of different database management systems, SQLSERVER database replication is adopted. Through the data layer, it mainly operates the query, database storage, transaction processing and update of the system; Realize the return of database data results through the data layer. Test the stability of different systems as shown in Figure 7.

According to the data analysis in the figure, the stability of this system is higher than that of the other two comparison systems. It has the highest stability. Moreover, the response time of the system in this paper is short, which can achieve high efficiency. This data verifies that the system in this paper has certain superior performance. It can be applied to tourism information management. In this chapter, to verify the performance of the tourism management information system based on PSO-optimized NN proposed and designed in this paper, a simulation experiment is carried out. The simulation results show that the prediction accuracy of this algorithm is 94.67% and the recall rate is 96.11%. The performance of this system can meet the practical application requirements and provide some effective suggestions for tourism management decision-making.

5. Conclusions

The development of the tourism industry has been accelerated by the rapid development of computer technology, and the traditional tourism industry has changed dramatically. As a result, a tourism management information system with high availability, expandability, and ease of maintenance is required. This paper completes the construction and application of a tourism management information system using a PSO-optimized NN algorithm. The improved PSO is used to optimize BPNN in this paper, and the PSO's optimization performance is improved by nonlinearly decreasing the inertia factor. Simultaneously, the system provides end-to-end service, including system setup, management personnel analysis of tourism resource management, and statistical category reports. This can provide a great deal of convenience for visitors and have a significant positive impact on tourism benefits. Several experiments were conducted in order to verify the performance of the model and algorithm developed in this paper. The prediction accuracy of this algorithm is 94.67 percent, and the recall rate is 96.11 percent, according to experimental results. This system uses the Scrapy framework to crawl travel website route information, allowing it to efficiently and accurately capture travel route information; providing a user registration interface, clustering users based on user information, and storing user clicks in different categories on different lines; and rearranging route information to make search results more personalized and accurate. The system's performance is adequate for the application's needs. At the same time, this paper applies the concept of "smart tourism" to specific tourism informatization, which can help the tourism industry transform and upgrade its structure, as well as improve its overall development level. This research has made some achievements, but due to the time problem and the limitation of knowledge level, there are still many deficiencies in this system. In the future, distributed crawling and distributed storage should be considered to improve the system performance. At the same time, a more humanized interface should be designed.

Data Availability

The data used to support the findings of this study are available from the corresponding author upon request.

Conflicts of Interest

The authors do not have any possible conflicts of interest.

Acknowledgments

This study was supported by the Research Fund for Hainan Federation of Humanities and Social Sciences Circles, Research on the Impact of the Entry of International High-End Hotel Brands on the Promotion of Tourism Image in Hainan and Their Image Fit (HNSK(ZC)21-134), and Research Fund for Hainan Federation of Humanities and Social Sciences Circles, Research on Kinetic Energy System Optimization of High-Quality Tourism Development in Hainan (JD(ZC)21-60).

References

[1] T. Ma, "Identification of new media technology factors and research on big data in the tourism industry," *ICIC Express Letters*, vol. 13, no. 4, pp. 279–285, 2019.

[2] L. Peng and Y. Chen, "Tourism safety monitoring information service system based on internet of things and block-chain," *Journal of Intelligent and Fuzzy Systems*, vol. 10, pp. 1–7, 2021.

[3] S. Liu, "Advanced hybrid information processing," in *Proceedings of the 5th EAI International Conference, ADHIP 2021, Virtual Event, October 22–24, 2021, Proceedings, Part II*, October 2021.

[4] K. Luu, M. Noble, A. Gesret, N. Belayouni, and P.-F. Roux, "A parallel competitive particle swarm optimization for non-linear first arrival traveltime tomography and uncertainty quantification," *Computers & Geosciences*, vol. 113, no. 4, pp. 81–93, 2018.

[5] Z. Liao, M. Jin, P. Ren, and Y. Luo, "Research on scenic spot's sustainable development based on a sd model: A case study of the jiuzhai valley," *Sustainability*, vol. 6, no. 7, pp. 4632–4644, 2014.

[6] G. Anfuso, A. T. Williams, G. C. Martinez, C. M. Botero, J. A. C. Hernández, and E. Pranzini, "Evaluation of the scenic value of 100 beaches in Cuba: Implications for coastal tourism management," *Ocean & Coastal Management*, vol. 142, no. 6, pp. 173–185, 2017.

[7] J. Xi, X. Wang, Q. Kong, and N. Zhang, "Spatial morphology evolution of rural settlements induced by tourism," *Journal of Geographical Sciences*, vol. 25, no. 4, pp. 497–511, 2015.

[8] S. Du, H. Zhang, H. Xu, J. Yang, and O. Tu, "To make the travel healthier: A new tourism personalized route recommendation algorithm," *Journal of Ambient Intelligence and Humanized Computing*, vol. 10, no. 9, pp. 3551–3562, 2018.

[9] X. Zhou, Y. Zhan, G. Feng, D. Zhang, and S. Li, "Individualized tour route plan algorithm based on tourist sight spatial interest field," *ISPRS International Journal of Geo-Information*, vol. 8, no. 4, p. 192, 2019.

[10] J. Liu, N. Liu, Y. Zhang, Z. Qu, and J. Yu, "Evaluation of the non-use value of beach tourism resources: A case study of Qingdao coastal scenic area, China," *Ocean & Coastal Management*, vol. 168, no. 3, pp. 63–71, 2019.

[11] S. Bai and F. Han, "Tourist behavior recognition through scenic spot image retrieval based on image processing," *Traitement du Signal*, vol. 37, no. 4, pp. 619–626, 2020.

[12] F. Lv, "Study on the development of web GIS technology-based tourism geographic information service system,"

Revista de la Facultad de Ingenieria, vol. 32, no. 15, pp. 423–427, 2017.

[13] X. Zhao, C. Zhang, and D. Xue, "Geographic information system application in evaluating forest tourism resources based on tourism experience perspective," *Boletin Tecnico/Technical Bulletin*, vol. 55, no. 4, pp. 260–266, 2017.

[14] S. Sundriyal, V. Shridhar, S. Madhwal, K. Pandey, and V. Sharma, "Impacts of tourism development on the physical environment of Mussoorie, a hill station in the lower Himalayan range of India," *Journal of Mountain Science*, vol. 15, no. 10, pp. 191–206, 2018.

[15] J. Du, "Research on intelligent tourism information system based on data mining algorithm," *Mobile Information Systems*, vol. 2021, Article ID 5727788, 10 pages, 2021.

[16] M. Behjaty and Z. Monfared, "Modeling and dynamic behavior of a discontinuous tourism-based social-ecological dynamical system," *Filomat*, vol. 33, no. 18, pp. 5991–6004, 2019.

[17] X. Zhang, "Characteristics of mountain climate change and optimization of agricultural tourism management based on satellite Internet of Things," *Arabian Journal of Geosciences*, vol. 14, no. 16, pp. 1–14, 2021.

[18] W. Cai, Y. Song, H. Duan, Z. Xia, and Z. Wei, "Multi-Feature fusion-guided multiscale bidirectional attention networks for logistics pallet segmentation," *Computer Modeling in Engineering and Sciences*, vol. 131, no. 3, pp. 1539–1555, 2022.

[19] J. Kong, H. Wang, C. Yang, X. Jin, M. Zuo, and X. Zhang, "A spatial feature-enhanced attention neural network with high-order pooling representation for application in pest and disease recognition," *Agriculture*, vol. 12, no. 4, p. 500, 2022.

[20] Y. Wang, Y. Chen, and R. Liu, "Aircraft image recognition network based on hybrid attention mechanism," *Computational Intelligence and Neuroscience*, vol. 2022, Article ID 4189500, 9 pages, 2022.

[21] Y. Xing-Zhu and W. Qun, "Exploratory space-time analysis of inbound tourism flows to China cities," *International Journal of Tourism Research*, vol. 16, no. 3, pp. 303–312, 2014.

[22] W. Cai, Y. Song, and Z. Wei, "Multimodal data guided spatial feature fusion and grouping strategy for E-commerce commodity demand forecasting," *Mobile Information Systems*, vol. 2021, Article ID 5568208, 14 pages, 2021.

[23] X. Jin, J. Zhang, J. Kong, T. Su, and Y. Bai, "A reversible automatic selection normalization (RASN) deep network for predicting in the smart agriculture system," *Agronomy*, vol. 12, no. 3, p. 591, 2022.

[24] X. Ferràs, E. L. Hitchen, E. Tarrats-Pons, and N. Arimany-Serrat, "Smart tourism empowered by artificial intelligence: The case of lanzarote," *Journal of Cases on Information Technology*, vol. 22, no. 1, pp. 1–13, 2020.

Hindawi
Computational Intelligence and Neuroscience
Volume 2022, Article ID 3276696, 10 pages
https://doi.org/10.1155/2022/3276696

Research Article

Dynamic Recognition and Analysis of Gait Contour of Dance Movements Based on Generative Adversarial Networks

Junlin Ren and Jae-Keun Park

Sangmyung University, Seoul 03016, Republic of Korea

Correspondence should be addressed to Jae-Keun Park; 201936014@sangmyung.kr

Received 2 April 2022; Revised 26 April 2022; Accepted 27 April 2022; Published 8 June 2022

Academic Editor: Xin Ning

With the generation of images, videos, and other data, how to identify the gait of the action in the video has gradually become the focus of research. Aiming at the problems of complex and changeable movements, strong coherence, and serious occlusion in dance video images, this paper proposes a dynamic recognition model of gait contour of dance movements based on GAN (generative adversarial networks). GAN method is used to convert the gait diagrams in any state into a group of gait diagrams in normal state with multiple angles, which are arranged in turn. In order to retain as much original feature information as possible, multiple loss strategy is adopted to optimize the network, increase the distance between classes, and reduce the distance within classes. Experimental results show that the average recognition rates of this model at 50°, 90°, and 120°are 93.24, 98.24, and 97.93, respectively, which shows that the recognition accuracy of dance movement recognition method is high. And this method can effectively improve the dynamic recognition of gait contour of dance movements.

1. Introduction

The posture and movement of a person walking is referred to as gait. The majority of today's gait research focuses on human gait movement. Gait is the only noninvasive method that can be employed, unlike fingerprints, face, and iris. Gait recognition, when compared to other long-distance biometric recognition technologies, has the benefits of long-distance recognition, noncontact, difficult concealment, and so on and has a lot of potential and application possibilities. Few universities or institutions have studied dance movements among the many studies on human body movement recognition, mainly because dance is a way of expressing emotions to the public through body movements, and dance movements in this category also include many dance movements with their own characteristics [1]. As a result, dance movement research is still in the stage of dance movement analysis. Most of the time, the gathered dance movements are gesture analyzed and then adapted to animated character performances utilizing animation processing software.

In order to solve the problem that the training gait cannot meet the training requirements of dance action steps, domestic and foreign scholars have successively carried out research on the generation method of personalized training gait. Qin et al. established the motion trajectory generation models of hip, knee, and ankle joints with multilayer perceptron, respectively [2]; Rida et al. established an ellipse model, which divided the human body into seven parts according to the proportional relation of the center of mass of the ellipse, and modeled each part [3]. Deng et al. proposed the method of deep gait and used the pretraining model VGG-16 to obtain the feature representation of gait map [4]. Li et al. proposed to learn the similarity between gait diagrams directly through the depth CNN (convolutional neural network) and extract the features of gait diagrams through CNN for matching recognition [5]. Zhao et al. extracted the information of human motion shape by Canny edge detection to represent the information of motion edge and then achieved the purpose of human motion recognition by matching similar edges [6]. Hnatiuc et al. changed the traditional separate training and combined attitude estimation and action recognition in order and put forward a framework for combining attitude estimation and action recognition [7]. Luo et al. reconstruct the 3D structure of human beings to generate views and 3D models that can be generated in any 2D by projection, but they usually need to fully control and cooperate in multiple camera environments [8]. However, there are still some shortcomings in the personalized gait generation experiment in the above research: the research object is limited to single or local joints, lacking comprehensive consideration of joint coupling relationship and overall coordination of motion. It is difficult to accurately describe the walking characteristics of human body only by the difference of gait parameters.

The input for recognizing human dance movements must be a series of motions, yet dance movements are similar to other sorts of movements. The activities in the video contain a lot of redundant information, and while the directions of the actions may alter, they can all be considered the same action based on the sequence of events. Traditional dynamic recognition methods based on the approach have a low identification rate, are unable to distinguish joint changes in precise dance motions, and have a poor recognition effect. In light of this shortcoming, this research investigates a GAN-based dynamic recognition and analysis method for dance movement gait contour (generative adversarial networks). The global coordination of the generated gait and whether it fits the standards of naturalness, adaptability, and stability are investigated using the gait stability criterion, which is based on the notion of human balanced perception. We intend to develop a tailored gait generation approach that can accurately represent distinct human gait features and give theoretical support for personalized training as a result of this research.

1.1. Innovation of This Paper

(1) In order to extract effective gait features for cross-view gait recognition, this paper proposes a cross-view gait feature extraction method based on GAN, which only needs to train a model to transform the gait template into any view. Retain the original identity information to the greatest extent, thus improving the accuracy of gait recognition.

(2) In this paper, GAN is used to transform the gait map, and a GAN recognition model is proposed to make full use of the feature information of the gait map, thus improving the accuracy of gait recognition.

1.2. Organizational Structure of This Article. The first chapter introduces the research background and significance, and then introduces the main work of this paper. The second chapter mainly introduces the related technologies of gait contour dynamic recognition of dance movements. The third chapter puts forward the specific methods and implementation of this research. The fourth chapter verifies the superiority and feasibility of this research model. The fifth chapter is the summary and prospect of the full text.

2. Related Work

2.1. Overview of GAN Research. With the innovation of information technology and the constant replacement of computing power of hardware devices, artificial intelligence [9–11] is developing vigorously in the information society, and the field of machine learning represented by generative model continues to attract researchers' attention.

The performance of GAN model proposed by Vma and others in generating image data surprised researchers. At present, its research in computer vision, medicine, natural language processing, and other fields has been active. It shows that there are few summary papers on the structure and performance of GAN at present, and other research work mainly focuses on the performance verification of different types of GAN architectures. Because the benchmark data set cannot reflect the diversity well, the comprehensive discussion of GAN in these works is limited. Paulo et al. proposed a GAN framework based on FC layer modeling, which only showed high performance in a few groups of data distribution. The deep convolution GAN model proposed by Switonski et al. can smooth the training process of generator and discriminator and contribute to improving the stability. Creswell et al. proposed a framework based on GAN, called Fu-sionGAN, which generates a fused image by controlling two input images [12]. Experiments show that the fusion method can change the shape and features of the input image and generate a new image while retaining the main content of the input image. Wang et al. summarized the image super-resolution technology based on deep learning and divided it into three types: supervised, unsupervised and specific application fields, and provided systematic super-resolution theory and practical methods [13]. Lei et al. proposed a framework that can be used to decipher passwords, so that GAN can be applied to decipher passwords [14]. In addition to the above areas, GAN has been successfully applied in other directions, such as domain adaptation, sequence generation, semi-supervised learning, semantic segmentation, attack resistance, machine translation, automatic driving, and so on.

2.2. Research Status of Gait Recognition. In recent years, gait recognition has attracted more and more attention in video surveillance and computer vision fields such as crime prevention and forensic identification, and its development will greatly promote the development of application, society, and computer vision. Therefore, gait recognition will become more and more important in the future. Unfortunately, gait recognition is still a challenging task because it has many potential sources of change, such as angle change, transportation, and clothes change.

Mosser et al. put forward the application of single linear projection, called view invariant discriminant projection, whose single property enables cross-view gait recognition without knowing the query gait view [15]. Lu et al. used the stacked progressive automatic encoder to convert the angle and converted the arbitrary angle of gait features into a single side view angle [16]. Yao et al. used 2D stick map obtained by connecting nine body points extracted from gait to simulate human movement [17]. Cai and others simulated human legs and used them to analyze human walking and running [18]. The research of Gadaleta et al. also simulates human legs, in which the legs are represented by many thick lines connected at one point [19]. Connie et al. put forward a method to predict 3D pose from 2D pose matching database, which predicts 3D pose according to the mutual constraint relationship of every joint in human body [20].

Gait is periodic, coordinated, and balanced, and the analysis in one cycle of gait can reduce the calculation amount of gait recognition and improve the operation efficiency. Gait periodicity can be analyzed according to the changes of the features of the graphic areas in each frame of binary images, such as area, centroid, and external rectangle. Risi et al. analyzed the periodicity of gait sequence according to the width signal of the binding frame of human body area and proposed a cycle calculation method under the condition of large lateral angle and lateral angle deviation [21]. Zhao et al. used PSO (particle swarm optimization) algorithm to optimize the pattern recognition method of SVM (support vector machine) [22], and the experimental results showed that the recognition rate of PSO-SVM classifier was higher than that of nonparameter optimized SVM classifier for lower limb analysis of five normal walking gait. Mannini et al. used k-nearest neighbor method to classify and recognize gait [23]. DTW (dynamic time warping) is to regularize the motion feature templates with different time lengths according to a certain time warping curve, so as to make the feature templates have the same length and then match them. This method has the advantage of solving the similarity measurement and matching problems of dynamic patterns.

3. Methodology

3.1. Gait Image Preprocessing. Gait recognition mainly analyzes and processes moving image sequences containing people, which usually includes four stages: target segmentation, feature extraction, feature processing, recognition, and classification. It should be noted that gait itself and compared with other biometric technologies also have many shortcomings, which are mainly influenced by emotion, object use, and gait angle. At present, most gait recognition algorithms use cameras to acquire gait data and use two-dimensional methods for gait recognition. In order to improve the recognition effect, the application of multicamera gait recognition algorithm and 3D method can be studied. By using multiple cameras, the problem of feature extraction caused by occlusion can be improved, and 3D modeling of human motion can extract the gait features [18] of human body more accurately and realize more complex feature matching. Multicameras and 3D methods are also the trend of human body recognition. If a motion sequence does not have a separate background picture, we must get the backdrop of motion sequence images [20] in order to collect some local photographs as background images in preparation. It should be noted that the light intensity has a significant impact on the background map selection, and the data of the background map vary substantially depending on the light intensity. Multiple backdrop photos should be picked and collected for optional use to eliminate this influence.

The volume contour area also appears in its own contour area, so there will be repetition in the calculation. Because of the noise in these small areas, the edge tracking algorithm cannot work smoothly, so we must use image connectivity algorithm to remove these small areas and get pure object images. There are many marked points to be extracted in the image sequence and other background noises. In order to extract the target points from multivalued digital images, binarization must be performed.

That is, by setting a threshold T [11], the image data are divided into pixel groups larger than T and pixel groups smaller than T with different values, respectively, so as to extract the feature points we care about, as shown in formula 1:

$$I_B(u,v)=\begin{cases}255, & I_P(u,v)>T,\\ 0, & I_P(u,v)<T,\end{cases} \tag{1}$$

where $I(u,v)$ represents the pixel value of a certain point in the image.

After binarization, the image sequence has only two areas: bright and dark, in which the marked points are bright. By programming and calling the function library, we can get the coordinates (u,v) of the center of each marked point in the forward process. In the sagittal plane of human body, the distance between waist and hip joint is measured as D_{mm}, and the number of pixels between these two points is obtained as d in the image plane, and the corresponding proportional relationship between the two coordinate planes is obtained as follows:

$$s=\frac{D}{d}. \tag{2}$$

Therefore, the coordinates of the image plane are converted to the coordinates x, y of the sagittal plane of the human body, and the change curve of the displacement of the subject's arch in x, y direction is obtained, as shown in Figure 1:

In this paper, the gait energy map is used as the gait template [16], and the gait energy map can be obtained by averaging the gait contour maps in the gait sequence, which can effectively retain the feature information during walking. As shown in Figure 2, the brightest pixel in the gait energy map represents the highest frequency of the position in the whole gait sequence.

The degree of coordination of human joint movement directly affects the stability of gait when walking, so the author's previous results are used to analyze the stability of the generated gait [18], thus reflecting its overall coordination. With the passage of time, the coordinates of the soles of the feet in two directions are extracted, and then the trajectory of the soles of the feet in two directions is fitted by the least square curve fitting method. The trajectory described by polynomial is to calculate the first derivative to get the gait speed curve of normal walking.

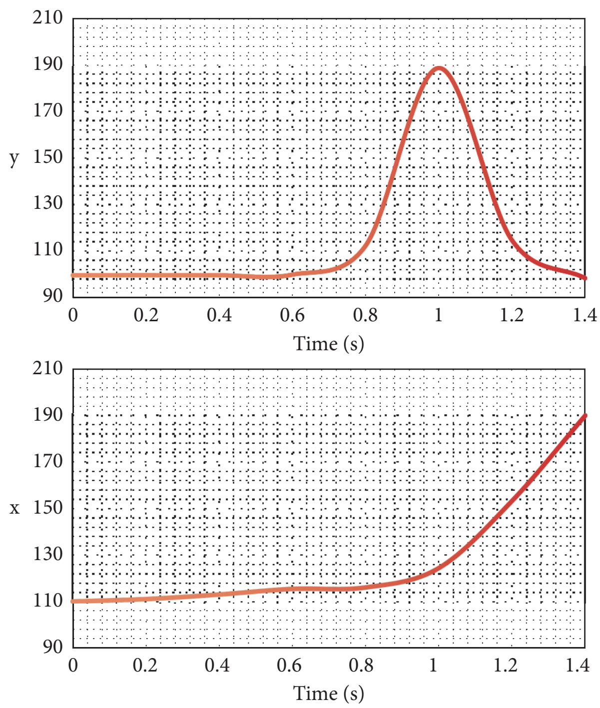

Figure 1: Change diagram of arch x, y displacement.

3.2. Dynamic Recognition of Gait Contour of Dance

3.2.1. Gait Feature Extraction Based on GAN. Human posture characteristics are derived from human posture information, which can be obtained in two methods. The first is to use attitude estimation on the test set to retrieve the position of human joints and calculate the joint angle; the second is to utilize the coordinates of each joint of the human body received when the motion capture equipment gathers the dance video. Most dance moves involve two arms and two legs, although there is no definite correlation between arms, arms and legs, and legs. The full-body region was chosen because various activities, such as those performed by the actor from bottom to top as a whole, turning about, strolling around, and so on, should be judged and identified by the motion information of the actor's entire body. By partitioning the human body area by the human body position, the impact of garment occlusion on motion recognition can be decreased. The background information with little or no change in the image can also be filtered according to the optical flow value in the process of optical flow feature extraction, so the areas where the information is finally retrieved are the upper body, lower body, and the entire actor's body. As a result, some features of the source gait map may not be effectively reflected in the gait map generated after the conversion due to angle conversion. As the angle difference grows, more feature information in the source gait map is masked, and the amount of feature information in the source gait map that can be expressed by the converted gait map decreases, resulting in a lower recognition rate.

In the experiment, the camera is stationary, and people walk in front of the camera without being blocked by objects. Therefore, contour extraction is essentially to eliminate the background from the sequence images to obtain the contour of the moving target. Its implementation steps are as follows:

(1) Because the scene is approximately still in the whole video sequence, the background corresponds to low-frequency information. Therefore, the average value of pixels in sequential images can be used to estimate the static background.

(2) Background difference method is used to detect moving targets in sequence images, and binary segmentation of images is performed under a set threshold.

(3) The contour information of the moving person in the sequence image is further extracted by the inner boundary tracking algorithm.

In order to eliminate the inconvenience of feature extraction caused by motion change, the centroid points of human body contour are calculated, respectively, and used as the coordinate origin of the image.

Let (x_c, y_c) be the centroid coordinate, N_b be the total number of boundary pixels, and (x_i, y_i) be the pixels on the boundary, then

$$\begin{cases} x_c = \dfrac{1}{N_b} \displaystyle\sum_{i=1}^{N_b} x_i, \\ y_c = \dfrac{1}{N_b} \displaystyle\sum_{i=1}^{N_b} y_i. \end{cases} \tag{3}$$

In order to eliminate the influence of image scale and signal length on the training and recognition process, the minimum-maximum normalization method and equally spaced resampling method are used to reduce the amplitude and length of the signal, respectively. The prediction of 3D pose mainly depends on the identification and planning of each person's crossing angle. It is difficult for us to predict 3D posture, which requires a lot of work and research. The 2D pose is drawn on the image plane. When the view changes, the 2D pose will change greatly, so it will not resist the change of viewpoint. The solution proposed in this paper is to estimate 3D pose from 2D pose.

After getting the 3D pose, we still need to do normalization, and there are 14 3D joint points. The length unit is the distance from the neck to the center of the hip, the position of the hip is in the center of the left and right hips, and the neck is at the origin of the plane coordinate system. So the joints of the body are normalized as follows:

$$J_i' = \frac{J_i - J_{\text{neck}}}{H_{nh}}, \tag{4}$$

where $J_i \in R^2$ is the position i of body joints, J_i' is the position of J_i after normalization, J_{neck} is the position of neck, and H_{nh} is the distance between neck and hip.

The postures from three different individuals after normalization are shown in Figure 3, from which we can find

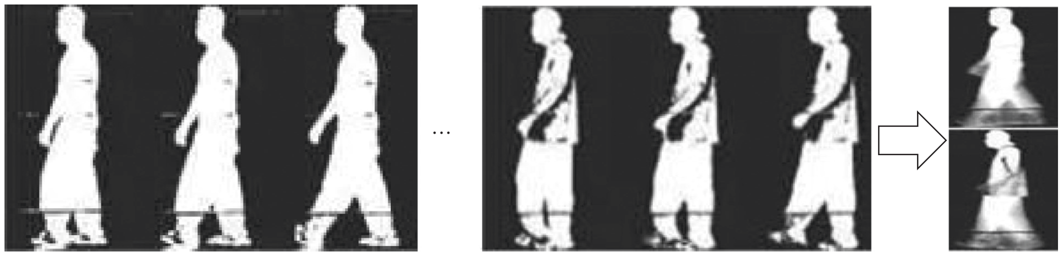

Figure 2: Synthesis of gait energy diagram.

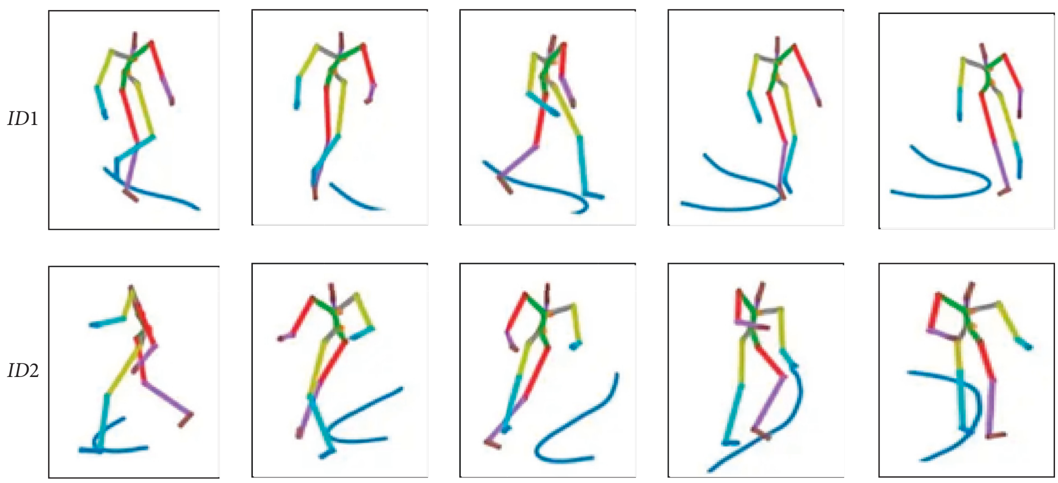

Figure 3: Example figure of posture after returning to one.

the differences of leg movement patterns among three different individuals.

Figure 4 shows the flow chart of the whole algorithm.

First, all the gait video sequences of test set, training set, and verification set are uniformly processed into the same gait template. Then, z^p is converted from perspective a to perspective b through a perspective converter V and the feature implicit representation $z^g = V(z^p, a, b)$ after perspective conversion is obtained.

Finally, it is determined that the identity of p^a is in the verification set of perspective b, and the calculation formula of nearest neighbor classifier is as follows:

$$x = \arg\min \left\| \tilde{z}^g - z_i^g \right\|_2, i \in \{1, 2, \cdots, n\}. \quad (5)$$

Here, $\| \cdot \|_2$ stands for L_2 norm.

3.2.2. Motion Gait Contour Tracking. An important clue to determine the intrinsic movement of pedestrians is the change of human body contour with time. In order to eliminate the information redundancy and reduce the computational complexity, we convert the two-dimensional contour shape changes into one-dimensional distance signals to approximate the spatiotemporal change pattern of gait movement.

The target movements of the dance gait contour extracted during the dance process are divided into heel strike stage, load-bearing reaction stage, middle support stage, end support stage, start stage, prestart stage, swing

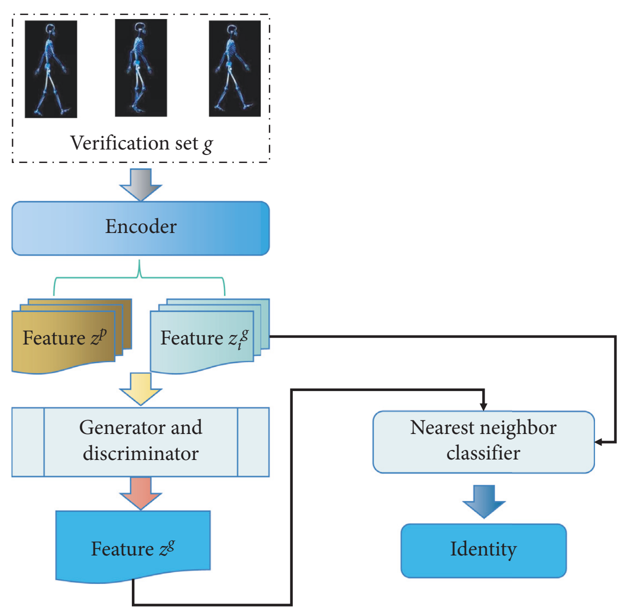

Figure 4: Algorithm flow chart.

stage, initial swing stage, middle swing stage, and finally swing stage, when the heel touches the ground again and waits for 9 time periods [7]. In the actual dance process, these nine time periods will appear repeatedly with each point in Figure 5, showing certain regularity and periodicity.

Taking the top edge point as the reference starting point, the contour boundary is expanded counterclockwise to

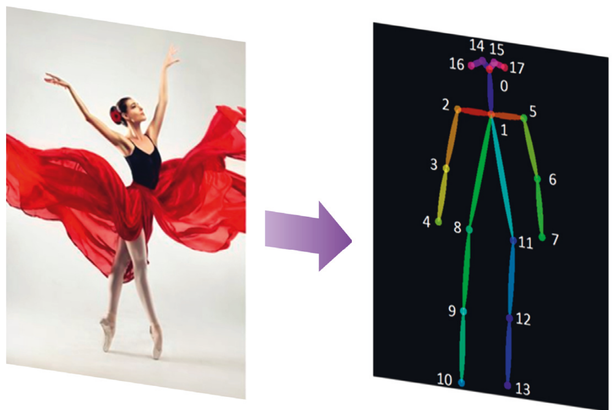

Sample dancer image

Outline of the dancer's gait

Figure 5: Divide the gait contour points of dancers based on.

become a one-dimensional signal composed of the distance from the boundary pixel point to the centroid.

$$d_i = \sqrt{(x_i - x_c)^2 + (y_i - y_c)^2}. \tag{6}$$

In order to eliminate the influence of image size and signal duration on the training and recognition process, we normalize the signal amplitude and duration, respectively. When normalizing the amplitude, we divide each distance signal by the maximum value of the distance, so that its value is between 0 and 1. For length normalization, we use equally spaced sampling to make the number of edge points within a certain range, such as 400.

3.2.3. Dynamic Contour Recognition. The input of the authenticity discriminator network is an image, which can come from the sample generated in the target domain or the image in the source domain. The goal of this discriminant model is to learn a classifier to separate the two types of samples as much as possible. Through the contradiction training between the generated model and the generated model, the generated model can generate samples with source domain attributes as much as possible.

That is, the authenticity discriminator acts on the generation network to generate realistic images, where I^i is the source image and $\widehat{I}^i$ is the sample image generated by the generator. Here, the discriminator generates a probability to indicate whether the image is true or not, and its loss function L_D^R is expressed in the form of cross entropy as follows:

$$\begin{aligned} &L_D^R(I) = -t \cdot \log\left[D_R(I)\right] + (t-1)\cdot \log\left[1 - D_R(I)\right], \\ &s\cdot t\cdot \quad t = \begin{cases} 1 & \text{if } I \in \left\{I^i\right\}, \\ 0 & \text{if } I \in \left\{\widehat{I}^i\right\}. \end{cases} \end{aligned} \tag{7}$$

Because of the uncertainty of the target, an extra loss function is needed at the top of the generator to restrict the generated target image, and an independent network named domain discriminator is connected at the top of the converter. The discriminator takes the source image and the target image as inputs and is trained to generate the scalar probability of input-to-correlation.

Gait is a space-time movement, so we expect to use STC (spatiotemporal correlation) to capture its spatial structure characteristics and time translation characteristics.

For any two gait sequences, after the above processing, they are converted into distance signal sequences $I_1(t), I_2(t)$; The feature space $[\ell_1, \cdots, \ell_k]$ is constructed, and their projection trajectories $P_1(t), P_2(t)$ in the feature space are as follows:

$$\begin{aligned} P_1(t) &= [\ell_1, \cdots, \ell_k]^T I_1(t), \\ P_2(t) &= [\ell_1, \cdots, \ell_k]^T I_2(t). \end{aligned} \tag{8}$$

Then the similarity measure between them can be defined as

$$d^2 - \min_{ab} \sum_{i=1}^{T} \left\| P_1(t) - P_2'(at+b) \right\|^2. \tag{9}$$

Among them, $P_2'(at+b)$ is the vector trajectory that is dynamically normalized according to time expansion and shift, and the selection of parameter a, b depends on the change of velocity and phase between different sequences, respectively.

For the training of generators and discriminators, we adopt the common confrontation loss, and the formula is as follows:

$$\min{}_G \max{}_D L_{\text{adv}} = E\left[\log D\left(\widehat{y}^b\right)\right] + E\left[\log\left(1 - D\left(G\left(V\left(E\left(p^a\right)a, b\right)c\right)\right)\right)\right]. \tag{10}$$

Among them, E, V, G, D represents encoder, angle converter, generator, and discriminator, respectively, p^a is the original input gait energy map from a angle of view, c represents the unique thermal coding of walking state, and $\widehat{y}^b$ is the real gait energy map.

Universal templates representing various categories can be used as template patterns to directly match with test actions for identification. Assume that x, y represents a certain frame of the test sample and the general template, respectively, which supports the similarity calculation $s(x, y)$:

$$h_p'(x, y) = \begin{cases} 1 & \text{if } x_p \in y_p, \\ 0 & \text{otherwise.} \end{cases} \tag{11}$$

In its calculation process, if the x, y of the two frames does not match, then $s(x, y)$ is no longer assigned to zero, but a negative value, $h(x, y) - 5$, is given as a punishment, thus enhancing the differentiation between different actions.

In the process of recognition, each frame of input action should be divided into five parts in turn, and each part should be mapped to the trained cluster. If the key frame is the key frame, we will search the results of each part in its corresponding key table in turn. The real-time action recognition process is shown in Figure 6.

The accumulated scores of these results can be used as the basis for identification, and the end point of the input

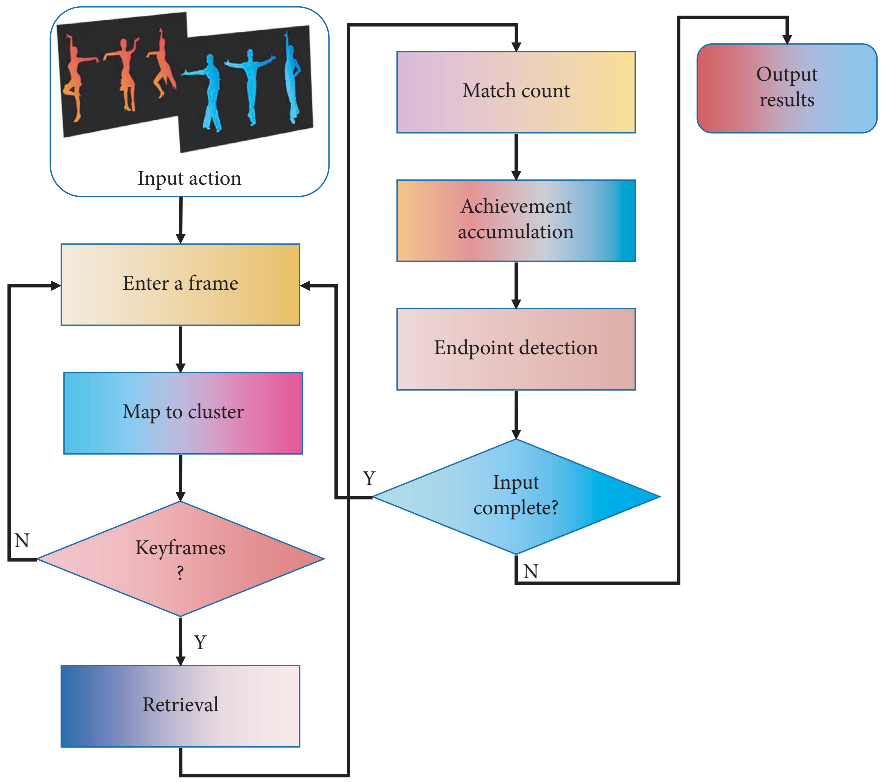

Figure 6: Real-time action recognition process.

action pattern and whether it is a legal action can also be judged by matching.

4. Experiment and Results

4.1. Experimental Data Set and Its Settings. In order to better verify the accuracy of the dance action recognition method designed in this paper, the most commonly used PASCAL VOC 2011-val (Data_P) and Stanford 40 actions (Data_S) data sets [14, 15] and the dance image to be executed (Data_D) are used. After the data collection is completed, use ipi Mocap Studio software to preprocess and correct each frame of the captured contour data. It is defined that the right heel leaves the ground as the gait cycle and the right heel touches the ground as the gait cycle. The gait contour data of 70 dancers were collected.

The generator in this model is an end-to-end unified network, which can be divided into two parts, an encoder and a decoder. The encoder part consists of four convolution layers, which extract features from the source image into a new spatial expression z. The extracted features z are sent to the decoder, so as to construct the correlation generation target through four decoding layers. We use the generated gait energy map as gait feature. In the testing stage, we trained many models to generate gait energy maps for the test data set and used the nearest neighbor algorithm to calculate the feature recognition rate. The detailed information of encoder and decoder structure is shown in Table 1 and Table 2. The discriminator structure uses four convolution layers.

4.2. Experimental Result. After the experiment on the Data_P data set, we selected three methods (ref [17], ref [19], ref [20]) to achieve better recognition results without cross-viewing and compared the average rank-1 accuracy on the same data set. The average rank-1 accuracy in three walking states and all cases is shown in Figure 7.

From Figure 7, it can be seen that the method proposed in this paper has no great advantages over the other three methods in the “running” and “walking” state, but the recognition accuracy is improved in the “jumping” state, which proves that the method proposed in this paper has better adaptability to the interference factor of clothing. In order to verify that actions are divided according to human body structure and consider their advantages, respectively, we have also implemented a case of treating human body actions as a whole in Data_S and Data_D data sets. When the action data are treated as a whole, we choose $\theta = 45$ as the quantization error of K-means clustering, and the two action data sets after clustering generate an average of 210 and 150 clusters, respectively, in three groups of experiments. Table 3 compares the recognition results of this method and the method based on whole-body segmentation under two whole-body segmentation schemes.

It can be seen that the classification performance of our method on these two data sets is better than the general body-based pattern, especially on the Data_D data set. This is because the Data_D data set covers basic daily actions, such as running and jumping, which may lead to more changes in the class. Therefore, when these actions are calculated and recognized as a whole, the recognition accuracy will be

Table 1: Settings of encoder in generator.

Layers	Number of convolution kernels	Convolution kernel size	Step length	Batch processing	Activation function
Conv.1	98	5× 5× [1, 3]	4	N	L-ReLU
Conv.2	188	5 × 5 × 99	4	Y	L-ReLU
Conv.3	364	5 × 5 × 193	4	Y	L-ReLU
Conv.4	779	5 × 5 × 384	4	Y	L-ReLU

Table 2: Settings of decoder in generator.

Layers	Number of convolution kernels	Convolution kernel size	Step length	Batch processing	Activation function
F-Conv.1	779	5 × 5 × 384	1/4	Y	L-ReLU
F-Conv.2	364	5 × 5 × 193	1/4	Y	L-ReLU
F-Conv.3	188	5 × 5 × 99	1/4	Y	L-ReLU
F-Conv.4	98	5 × 5 × 3	1/4	N	Tanh

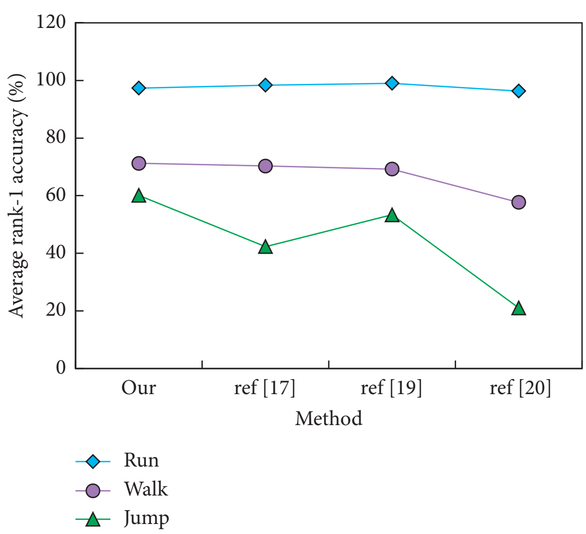

Figure 7: Walking state.

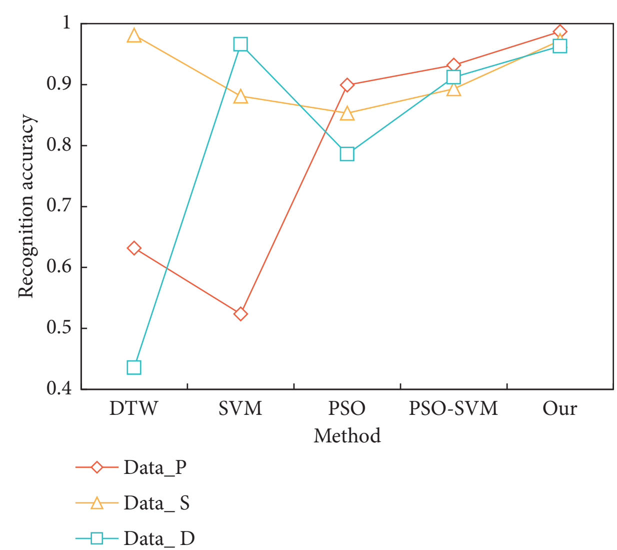

Figure 8: Comparison of the results of several recognition methods in the recognition of segmented actions.

Table 3: Recognition result under two scheme.

Data set	Plan	Recognition accuracy
Data_ S	Method base on whole-body segmentation	0.869
	Methods of this paper	0.941
Data_ D	Method base on whole-body segmentation	0.712
	Methods of this paper	0.924

seriously affected, and our limb-based segmentation method can avoid this shortcoming.

In order to further prove the effectiveness of our method, we also compare it with other commonly used motion recognition methods (DTW, SVM, and PSO). The recognition results of the above methods on the data set are shown in Figure 8.

On the Data_ S data set, the result demonstrates that DTW has the highest recognition accuracy. On these three data sets, the classification performance of SVM and PSO is not as good as this technique. PSO-accuracy SVM's on these three data sets is extremely near to the best score, demonstrating the method's stability and efficacy once again. Figure 9 shows the experimental results of this strategy on the Data_ D data set. In the experiment depicted in Figure 9, the registration set consists of four normal walking sequences from each sample, while the verification set consists of the latest two normal walking sequences.

The experimental recognition rate of Data_ *D* data set is shown in Figure 10. The experimental results in Figure 10 are used to evaluate the single angle of view.

The results show that the method proposed in this paper has obvious advantages for gait recognition with view changes. This means that the GAN model can generate better features and is robust to the change of viewing angle.

In order to better verify the performance of the model, several methods with better recognition effect (SVM, PSO, and PSO-SVM) were selected for comparison, and the experimental results are shown in Figure 11.

Compared with other methods, the model in this paper achieves better results from every angle, and the recognition rate is better than other methods. Under all test set angles,

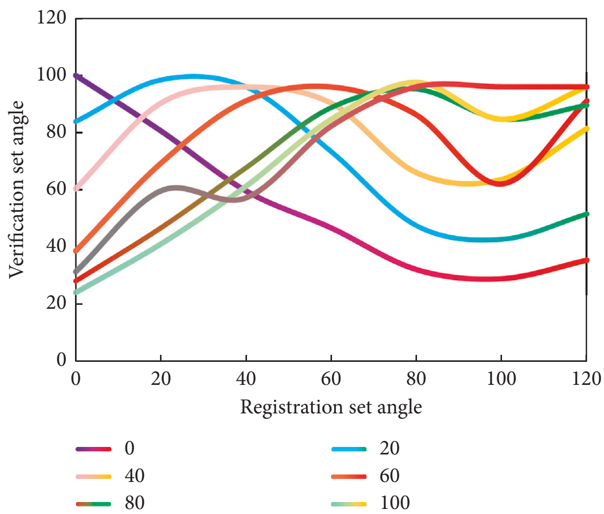

Figure 9: The training set includes three walking conditions.

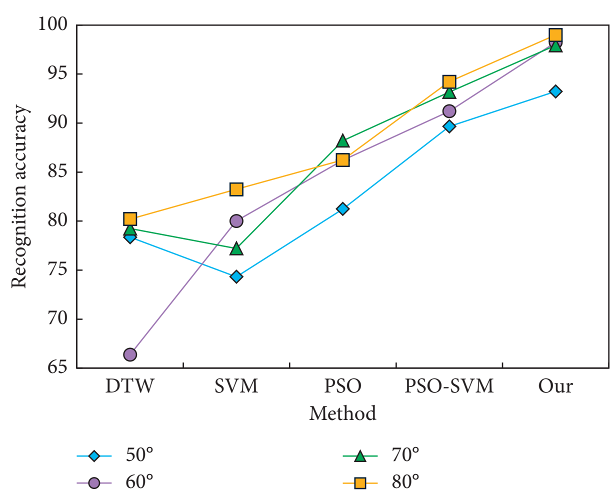

Figure 10: Recognition rate from four perspectives on Data_ D data set.

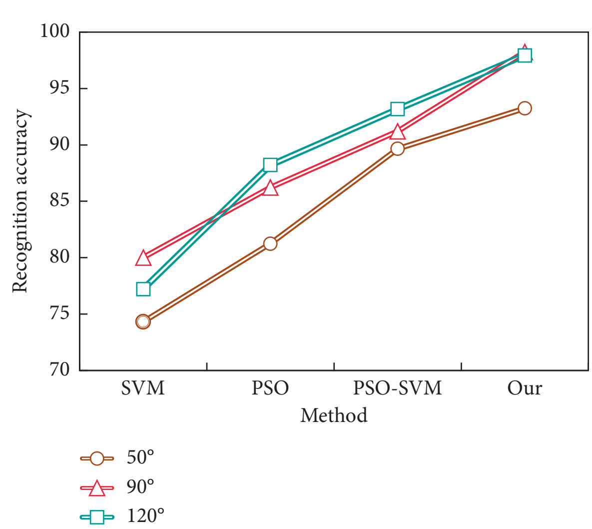

Figure 11: Recognition rate under different test set angles.

compared with the three methods in Figure 11, the best average recognition rate is obtained. The average recognition rates of the model in this paper are 93.24, 98.24, and 97.93 at 50°, 90°, and 120°, respectively, which shows that the model in this paper has good stability, can effectively deal with various test set angles, and maintains a high recognition rate.

5. Conclusions

Gait recognition, as a biometrics research center, has a wide range of applications in intelligent monitoring, human-computer interaction, security, and other fields, each with its own set of benefits. Computer vision technology can be used by experts in a variety of settings, such as competition refereeing, beginner dancer teaching, and dancer motion correction, to recognize motion in dance video images. In this research, we propose using GAN to dynamically recognize the gait contour of dancing motions. The average identification rates of this model at 50°, 90°, and 120°, respectively, are 93.24, 98.24, and 97.93, indicating that the recognition accuracy of the dance movement recognition approach is good. Simultaneously, a comparison of this strategy to other existing ways demonstrates that it is both successful and practicable. Although GAN is good at extracting contour data, dynamic features are crucial for gait identification. This paper suggests studying between frames, and I believe there is a bright future ahead.

Data Availability

The data used to support the findings of this study are available from the corresponding author upon request.

Conflicts of Interest

The authors do not have any possible conflicts of interest.

References

[1] M. Balazia and K. N. Plataniotis, "Human gait recognition from motion capture data in signature poses," *IET Biometrics*, vol. 6, no. 2, pp. 129–137, 2016.
[2] T. Qin, Y. Yang, B. Wen et al., "Research on human gait prediction and recognition algorithm of lower limb-assisted exoskeleton robot," *Intelligent Service Robotics*, vol. 14, no. 3, pp. 445–457, 2021.
[3] I. Rida, X. Jiang, and G. L. Marcialis, "Human body Part Selection by group lasso of motion for model-free gait recognition," *IEEE Signal Processing Letters*, vol. 23, no. 1, pp. 154–158, 2016.
[4] M. Deng, C. Wang, and Q. Chen, "Human gait recognition based on deterministic learning through multiple views fusion," *Pattern Recognition Letters*, vol. 78, no. 15, pp. 56–63, 2016.
[5] G. Li, Y. Gong, and W. Yuan, "Human gait recognition based on earth movers distance and zernike moments," *Procedia CIRP*, vol. 56, pp. 461–464, 2016.
[6] L. Zhao, Z. Wang, X. Wang, Y. Qi, Q. Liu, and G. Zhang, "Human fatigue expression recognition through image-based dynamic multi-information and bimodal deep learning," *Journal of Electronic Imaging*, vol. 25, no. 5, p. 053024, 2016.

[7] M. Hnatiuc, O. Geman, A. G. Avram, D. Gupta, and K. Shankar, "Human signature identification using IoT technology and gait recognition," *Electronics*, vol. 10, no. 7, p. 852, 2021.
[8] J. Luo and T. Tjahjadi, "View and clothing invariant gait recognition via 3D human semantic folding," *IEEE Access*, vol. 8, pp. 100365–100383, 2020.
[9] Y. Ding, X. Zhao, Z. Zhang, W. Cai, N. Yang, and Y. Zhan, "Semi-supervised locality preserving dense graph neural network with ARMA filters and context-aware learning for hyperspectral image classification," *IEEE Transactions on Geoscience and Remote Sensing*, vol. 60, 2021.
[10] J. Chen, C. Du, Y. Zhang, P. Han, and W. Wei, "A clustering-based coverage path planning method for autonomous heterogeneous UAVs," *IEEE Transactions on Intelligent Transportation Systems*, vol. 1, pp. 1–11, 2021.
[11] D. Yao, Z. Zhi-li, Z. Xiao-feng et al., "Deep hybrid: multi-graph neural network collaboration for hyperspectral image classification," *Defence Technology*, 2022.
[12] A. Creswell, T. White, V. Dumoulin, K. Arulkumaran, B. Sengupta, and A. A. Bharath, "Generative adversarial networks: an overview," *IEEE Signal Processing Magazine*, vol. 35, no. 1, pp. 53–65, 2018.
[13] K. F. Wang, C. Gou, Y. J. Duan, L. Yilun, X.-H. Zheng, and F.-Y. Wang, "Generative adversarial networks: the state of the art and beyond," *Acta Automatica Sinica*, vol. 43, no. 3, pp. 321–332, 2017.
[14] L Bi, J. Kim, A Kumar, D Feng, and M Fulham, "Synthesis of positron emission tomography (PET) images via multi-channel generative adversarial networks (GANs)," *Lecture Notes in Computer Science*, vol. 1055, pp. 43–51, 2017.
[15] L. Mosser, O. Dubrule, and M. J. Blunt, "Stochastic reconstruction of an oolitic limestone by generative adversarial networks," *Transport in Porous Media*, vol. 125, no. 1, pp. 81–103, 2018.
[16] P Lu, M Morris, S Brazell, C Comiskey, and Y Xiao, "Using generative adversarial networks to improve deep-learning fault interpretation networks," *The Leading Edge*, vol. 37, no. 8, pp. 578–583, 2018.
[17] N. M. Yao, Q. P. Guo, F. C. Qiao, H. Chen, and H.-A. Wang, "Robust facial expression recognition with generative adversarial networks," *Zidonghua Xuebao/Acta Automatica Sinica*, vol. 44, no. 5, pp. 865–877, 2018.
[18] S. Yu, H. Chen, E. B. Garcia Reyes, and N. Poh, "Gaitgan: invariant gait feature extraction using generative adversarial networks," in *Proceedings of the IEEE conference on computer vision and pattern recognition workshops*, pp. 30–37, Honolulu, HI, USA, July 2017.
[19] M. Gadaleta and M. Rossi, "IDNet: smartphone-based gait recognition with convolutional neural networks," *Pattern Recognition*, vol. 74, pp. 25–37, 2018.
[20] T. Connie, M. K. O. Goh, and A. B. J. Teoh, "A grassmannian approach to address view change problem in gait recognition," *IEEE Transactions on Cybernetics*, vol. 47, no. 6, pp. 1395–1408, 2017.
[21] R. Chhatrala and D. V. Jadhav, "Multilinear Laplacian discriminant analysis for gait recognition," *IET Computer Vision*, vol. 11, no. 2, pp. 153–160, 2017.
[22] L. Zhao, L. Guo, R. Zhang, X. Xie, and X. Ye, "mmGaitSet: multimodal based gait recognition for countering carrying and clothing changes," *Applied Intelligence*, vol. 52, no. 2, pp. 2023–2036, 2021.
[23] A. Mannini, D. Trojaniello, U. D. Croce, and A. M. Sabatini, "Automatic recognition of altered gait using wearable inertial sensors," *Gait & Posture*, vol. 49, no. 9, p. S9, 2016.

Hindawi
Computational Intelligence and Neuroscience
Volume 2022, Article ID 2683008, 12 pages
https://doi.org/10.1155/2022/2683008

Research Article

Sharing of Teaching Resources for English Majors Based on Ubiquitous Learning Resource Sharing Platform and Neural Network

Lijuan Zhang

Shanghai Jian Qiao University, Shanghai 201306, China

Correspondence should be addressed to Lijuan Zhang; 19215@gench.edu.cn

Received 18 April 2022; Revised 9 May 2022; Accepted 10 May 2022; Published 8 June 2022

Academic Editor: Xin Ning

Teachers in traditional English education devote a great deal of time and effort to developing excellent English teaching courseware and other teaching materials. However, because the network's powerful sharing capability was not fully utilized, poor resource sharing hampered the school's overall teaching efficiency. The goal of this paper is to investigate how to use a ubiquitous learning resource sharing platform and a neural network to analyze the method of English major education resource sharing. Because the BP neural network algorithm has better classification and prediction functions, it was proposed because it can classify and predict information in the sharing of teaching resources for English majors. This allows for seamless sharing of teaching materials. According to the findings of this study, there were 562.13 million people learning English in China in 2015, accounting for 37% of the population. By 2018, 945.61 million people were learning English, accounting for 85 percent of the population. Almost every student is learning English, demonstrating the language's importance. As a result, the importance of English instruction is clear, and the sharing of teaching resources should be prioritized.

1. Introduction

Colleges and universities are educational institutions and departments with the most resources. The level of sharing of teaching resources for English majors in China is largely determined by the sharing of teaching resources for English majors. However, there are numerous issues with China's current resource construction and sharing that are impeding the growth of co-construction and sharing of teaching resources for English majors in China. As a result, the theoretical and practical implications of how to solve these problems and realize the co-construction and sharing of digital teaching resources among colleges and universities are significant. The resource sharing class provides rich resources, including video resources, but also these resources cannot be copied. Basic resources are provided for free, and teachers in different schools should be based on the actual situation of the school. They need to refer to relevant practices to construct courses suitable for their students and truly teach students in accordance with their aptitude.

The ubiquitous learning environment is a comprehensive learning environment produced from the physical, social, information, technological environment, and other aspects. In particular, various educational institutions, seminars, communities, and families are organically linked through networked devices. In addition, in a common learning environment, many scattered smart devices such as computers, mobile phones, and PDAs are used. Anyone can access the right source of information from any device at any time.

The innovation of this paper is that (1) it introduces related theoretical knowledge of English teaching resource sharing and neural networks, and proposes a neural network-based BP neural network (BPNN) algorithm. It examines the role of the BPNN algorithm in teaching resource sharing. (2) The effects of the BPNN algorithm and the other two algorithms on classification and prediction are compared and analyzed in this paper. The BPNN algorithm's classification and prediction effect are higher than the other two algorithms, as demonstrated by the experiment. This allows for data analysis in teaching resource sharing, resulting in increased efficiency.

2. Related Work

Rich and attractive teaching resources are the core link to make English professional education efficient. The sharing of teaching resources for English majors has begun to attract attention. Therefore, Yuan found that the intelligent network teaching system provides learners with rich teaching resources and an efficient learning environment. However, online teaching resources are widely distributed and difficult to concentrate. Resource sharing has become a key problem to be solved urgently in the network environment. Based on this, he studied link prediction methods in online education and builds a model suitable for online education. He used neural network sorting algorithm to realize online learning knowledge prediction [1]. Guichon proposed a method for creating multimodal corpora. This corpus can be shared to analyze simultaneous online teaching interactions. He described an analysis of the steps involved in creating a multimodal and shareable corpus [2]. Yan discovered that the university video management system has evolved into one of the most important video communication platforms. He created a microgrid-based teaching video resource management system to improve the storage and sharing of teaching video resource systems in colleges and universities. He realized video network storage and improved network sharing efficiency by constructing micro-technology network storage [3]. Tucker et al. found that one of the main difficulties in achieving effective online teaching was the difficulty of accessing the vast teaching resources of teachers. He also discovered the speech and language repository as a central repository for sharing, managing, and developing resources for science teaching [4]. The main purpose of Liu R's analysis of the fusion of network media and secondary English was to better play the function of secondary English. He discovered that using resource integration technology to manage distributed teaching resources helped colleges and universities improve their level of informatization [5]. Bai and Li designed a platform for statistical analysis of educational data and studied the storage of educational multidimensional data models in order to meet the rapid growth of educational data and improve operational efficiency and scientific decision-making. He then used educational big data to test query efficiency and storage space, demonstrating the utility of the Hadoop-based educational big data platform [6].

With the rapid advancement of education in recent years, teaching resources have expanded as well. Modern education is no longer limited to textbooks and individual teachers. Many developed countries encourage the sharing of educational resources, and many universities and primary and secondary schools in China are doing so as well. China's English professional education began late, but it has a brief history. Many aspects must be standardized and improved. As a result, traditional teaching resources are limited to teachers, and they are unable to meet the information-based teaching needs of modern society. Teacher resources can be shared to make teaching more efficient and the classroom more colorful.

3. Sharing of Teaching Resources for English Majors Based on Neural Network

3.1. Ubiquitous Learning Resource Sharing Platform Based on Web2.0 Environment. The importance of English is growing due to the informatization of social life and the globalization of the economy. English has become the most widely used language in all aspects of human life as one of the most important information carriers. English is now considered a necessary skill. If a student can learn a foreign language, he can open the door to a new world of learning and ultimately achieve the goal of multiple learning and value. With the progress of globalization, English is very important especially for those who want to communicate with foreigners. On the other hand, English is a necessary factor for understanding the outside world. In today's world, most of the communication of cultural confidence is achieved through the linguistic form of English, especially through high information [7]. The number and percentage of English learners in recent years are shown in Table 1.

The number of people learning English is increasing, as shown in Table 1. The term "ubiquitous learning network" refers to a technology that allows users to freely access and exchange information over broadband and wireless networks at any time, from any location, using any tool. The Internet, digital TV networks, satellite networks, wireless networks, and 3G mobile communication networks are all part of it. The communication network is the backbone of the entire learning environment and is in charge of basic data transmission [8]. Intelligent terminals are linked together to allow for the transmission and sharing of information and resources, and they help to create a ubiquitous learning environment. Figure 1 depicts the creation of the ubiquitous learning network.

As shown in Figure 1, ubiquitous learning is also referred to as seamless learning, pervasive learning, and ubiquitous learning, among other terms. It refers to all forms of communication and learning at all times. It is a way for anyone, anywhere, at any time, to get any information they require. In human learning, the important part of ubiquitous computing technology is to provide learners with a ubiquitous learning environment. The most obvious feature of a universal learning environment is the universality and conditionality of learning [9].

For example, a teacher may use a computer in the classroom to look for additional teaching materials, assign homework to students using a mobile phone, or better organize his teaching schedule. A learner in the park can use his phone to get information from his friends and classmates, such as learning tasks [10].

In recent years, China's scientific and information technology has developed faster and faster. Among them,

Table 1: Number and percentage of English learners from 2015 to 2018.

years	Number of people (thousands)	Percentage (%)	Effective percentage (%)
2015	56,213	37	37
2016	63,890	49	49
2017	67,583	52	52
2018	94,561	85	85

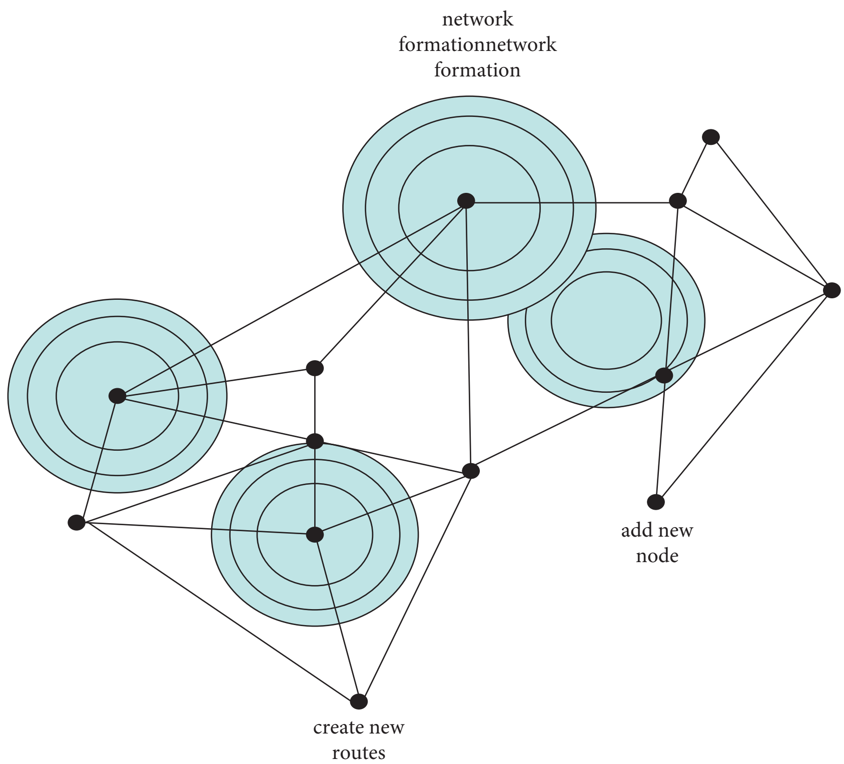

Figure 1: Ubiquitous learning network construction.

Web2.0 and other related information technologies are used more and more widely, and the information resources are also more and more abundant. This also makes the information-based teaching constantly improved in recent years. From the point of view of system design and technology, Web2.0 has the characteristics of adaptability for user interaction, main participatory architecture, open architecture for other systems, multiple nonlinear mechanisms, and sociality [11]. The Web2.0 teaching resource sharing platform is shown in Figure 2.

Traditional network resource construction has some flaws, as shown in Figure 2. Meeting user needs, such as user participation, creating or adding content, forming a community, and so on, is insufficient. And some Web2.0 application commonalities can just about satisfy it. It facilitates communication between those who have resources and those who require them, and it makes network resources social and open [12]. The free sharing and integration of information resources is the source of Web2.0. To achieve this goal on the web, a mechanism and technology must be in place to support resource exchange and matching, and these mechanisms and technologies are sufficient to meet the needs of Web2.0 sites.

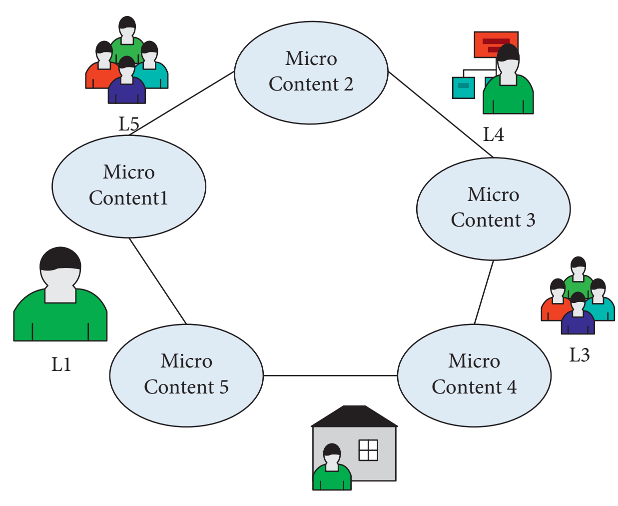

Figure 2: Web2.0 teaching resource sharing platform.

3.1.1. *Open API.* API generally refers to an application programming interface. The main purpose of the API is to provide applications and developers with the ability to access

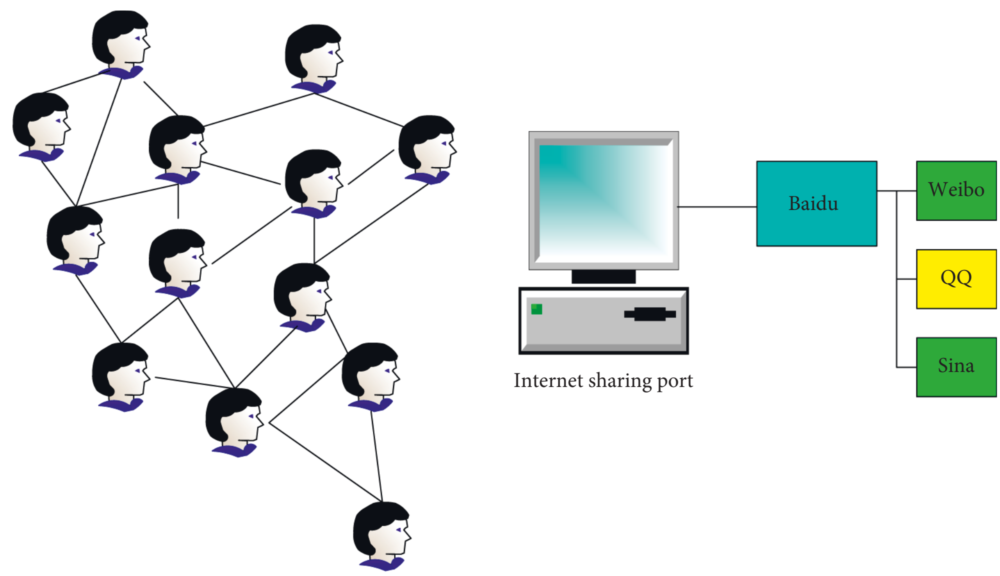

Figure 3: Internet sharing API.

a set of routines without having to access the source code or understand the details of the inner workings. Software that provides the functionality defined by an API is called an implementation of that API. The application of Web2.0 is becoming more and more popular, and this open architecture gradually emerges in the application process. From API to open API in other various websites and social software programmable web, the system pays more and more attention to the interaction and integration with other systems. Whether it is open and can form good writing with other systems becomes the key to whether web information resources can attract and be reused by users [13]. The Internet sharing API is shown in Figure 3.

As shown in Figure 3, the opening of all APIs makes the sharing, acquisition, and service of a large number of network information resources simple and easy, reducing the threshold of user experience. Simultaneously, these open platforms also bring greater value to users, developers, and small and medium-sized websites [14].

3.1.2. RSS. RSS is a data exchange method and distribution protocol for individuals to share content among other websites and is an XML form for distributing and aggregating web content. RSS builds a technical platform for the rapid dissemination of information, making everyone a potential information provider. RSS is widely used in major websites and blogs. To realize the sharing and recompilation of information resources, its significance lies in the realization of machine readability of information content, synchronization, and integration of content between systems [15].

3.2. Problems Faced by the Sharing of Teaching Resources for English Majors. The main resource builder should make detailed plans for the construction of course resources to ensure shared use of teaching resources for English majors. Participating in resource development should result in useful teaching materials [16]. A special English teaching resource library can be established to meet the needs of different teachers and students when it comes to this subject's teaching resources. Accessing the teaching resource library, as shown in Figure 4, allows college teachers and students to find and use the teaching resources they require.

As shown in Figure 4, prosperous English teaching resources have brought benefits to people. Not only colleges and universities themselves have made huge profits, but more importantly, college users can enjoy more and richer resources. It also provides an effective development method for the development of lifelong education and distance education in China [17]. But after years of resource construction, the consequences of blindness and disorder have become more and more obvious. It is mainly reflected in the following aspects:

(1) Scattered resources, lack of normative and systematic

Many universities are now developing their own resources, and university students have access to some digital resources as well. However, the majority of these resources are dispersed, and many of those created by universities lack a unified classification standard and plan. The amount of resource data grows as the number of resources built increases, and the interface problem becomes more apparent. The sharing of digital educational resources has been greatly hampered, and the resource utilization rate has been significantly reduced, due to the lack of various resource technology platforms and tools to provide users with services.

(2) The phenomenon of "information island" is serious, and repeated construction leads to a lot of waste

Because the interconnected functions and advantages are not fully utilized, and the human, material, and financial resources invested in the process of resource construction, universities are rarely willing to provide free resources to others. This will greatly

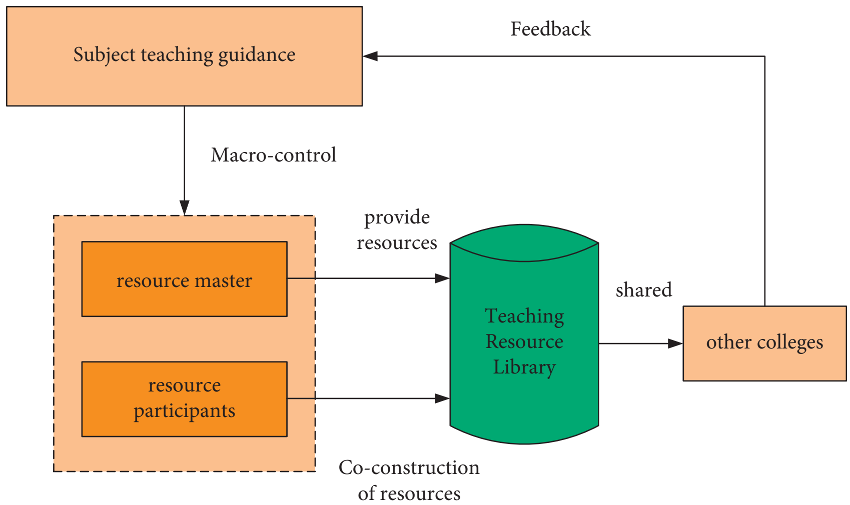

FIGURE 4: Shared structure diagram of subject teaching resource library.

limit resource sharing. Despite significant progress in the development of educational resources, there are still numerous issues. Co-construction resources are scarce, sharing coverage is limited, construction duplication is common, resource quality is poor, and resource inhomogeneity caused by platforms and data forms is on the rise. People should use BP neural networks [18] to better understand educational resource information classification [19, 20] and prediction [21], as well as to share educational resources more effectively [22].

3.3. The Classification Function of BP Neural Network. Large-scale parallel processing, decentralized storage and processing, self-organization, self-adaptation and self-learning ability, nonlinear approximation characteristics, and so on are all advantages of neural networks as one of the classic methods for dealing with classification and prediction problems. It is appropriate for dealing with inaccurate data, but there are a few things to consider. Retraining the network takes a long time when the trained learning system needs to learn new knowledge from new samples. On the premise of preserving the majority of previously learned knowledge, incremental learning can partially adjust network parameters to adapt to new knowledge.

The BP neural network is a multi-layer feedforward network with error backpropagation training (referred to as error backpropagation). It uses the BP algorithm, which is based on the gradient descent method. The complex network structure and repeated learning process of BP neural network make it not affected by random or unknown factors, and it has outstanding fitting ability to complex chaotic systems. The fitting ability of the BPNN is shown in Figure 5.

Figure 5 shows that the neural network has strong self-adaptive learning and parallel processing capabilities, but it is difficult to properly represent the input-output relationship obtained. One of the most widely used and successful artificial neural networks is the BP neural network model. It can be used in a variety of fields, including image and sound,

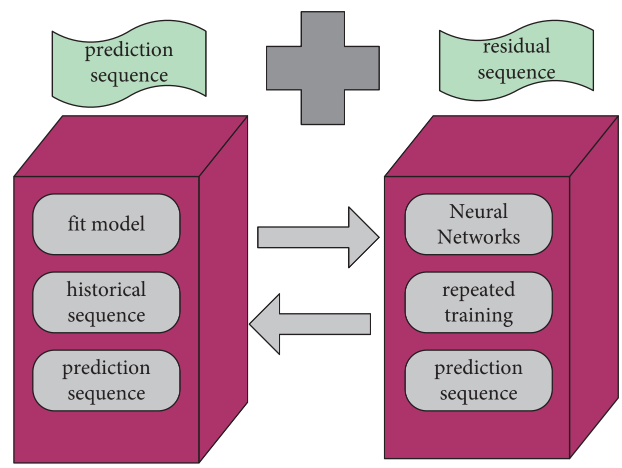

FIGURE 5: Fitting ability of BP neural network.

due to its powerful nonlinear mapping capability. When the BPNN is applied to time series data, a large amount of data preprocessing is not required, allowing the previous time to be effectively reduced. As shown in Figure 6, the sequence classification algorithm is designed to improve classification performance while extracting features.

The number of nodes in the output layer, as shown in Figure 6, is set according to the needs of the actual problem. The number of nodes in the hidden layer determines the neural network's complexity. In general, the more nodes in the network's hidden layer, the more difficult the problem is to solve. A neural network is known to have n input layer nodes, m hidden layer nodes, and one output layer node. It can update the weights of each connection chain using formula (1) to describe the neural network's training process:

$$\mathrm{net}_j = \sum_{i=0}^{n} v_{ij} a_i, \quad j = 1, 2, \ldots, m. \tag{1}$$

net_j represents the excitation value of the first node, a_i represents the output value of any node in the hidden layer, and v_{ij} represents the excitation function of the hidden layer node. It generally uses the sigmoid function, such as formula

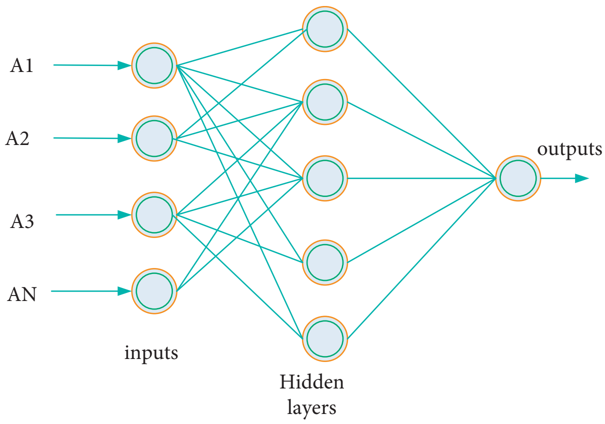

FIGURE 6: BP neural network structure diagram.

$$f_H(a) = \frac{1}{1+\exp(-a)}. \quad (2)$$

The output value of the output layer node is shown in formula

$$O = f_0\left(\sum_{j=0}^{m} w_{jk} b_i\right). \quad (3)$$

f_0 is the excitation function.

Compared with a single classifier or predictor, ensemble learning can achieve better performance and generalization ability. The main methods of ensemble learning include bagging, boosting, AdaBoost (adaptive boosting), and other algorithms. Bagging algorithm constructs different training sets by sampling samples with replacement, thereby generating different learners. It finally gets the final result by voting.

The principle of AdaBoost algorithm is to adjust the sample weight and weak classifier weight. It selects the weak classifiers with the smallest weight coefficients from the trained weak classifiers and combines them into a final strong classifier. The AdaBoost algorithm assigns different weights to different sub-models under the same training set. The algorithm first assigns the same initial weight to each input sample. In each round of iteration, it adds new base classifiers until a preset small enough accuracy is reached or all base classifiers are used for training to determine the final classifier.

AdaBoost. HM algorithm is an improved algorithm of AdaBoost algorithm. AdaBoost algorithm calculates the error of the classifier on the initial weight distribution by calculating the classification error rate of the base classifier. The AdaBoost. HM algorithm calculates the error of the classifier on the initial weight distribution by calculating the classification accuracy of the base classifier. Its calculation formula is

$$u(a_z) = h^{y_z}(a_z) - \max_y h^y(a_z). \quad (4)$$

Among them, $z = 1, \ldots, Z$ is the total number of input data, and h^y represents the class label data consisting of multiple 0 s and 1 s. The formula for calculating the weight of the base classifier in the final classifier is also different. The formula for the AdaBoost algorithm to calculate this weight is formula

$$\gamma = \frac{1}{2}\text{in}\left(\frac{1-r}{r}\right). \quad (5)$$

The formula for the AdaBoost.HM algorithm to calculate this weight is

$$\gamma = \frac{1}{2}\text{In}\left(\frac{1+r}{1-r}\right). \quad (6)$$

r is the error of the base classifier.

In this paper, improvements are made to the AdaBoost.HM algorithm. The classifier coefficients calculated by the formula are often not optimal. Therefore, people add a coefficient to the formula for calculating the weight coefficient of the base classifier in the final classifier and use the particle swarm optimization (PSO) algorithm to optimize the coefficient. People use the result of the base classifier as a kind of weight. It uses the direct output of the base classifier to compute the final classifier instead of converting it to class label data. It selects a classifier with the lowest current error rate as the first base classifier. It calculates the accuracy of this classifier as formula

$$u_l(a_z) = \begin{cases} 1, & b_z = f_l^z, \\ -1, & b_z \neq f_l^z. \end{cases} \quad (7)$$

f_l^z represents the actual output class of the lth base classifier relative to input a_z. The error of this base classifier on the d_l-distribution is formula

$$r_l = \sum_{z=1}^{Z} d_l(z) u_l(a_z). \quad (8)$$

The weight of the base classifier in the final classifier is calculated as formula

$$r_l = p\text{In}\left(\frac{1+r_l}{1-r_l}\right), \quad p \in [0,1]. \quad (9)$$

It updates the weight distribution of training samples as formula

$$d_{l+1}(z) = \frac{d_l(z)\exp(-\gamma_l u_l(a_z))}{\sum_{z=1}^{z} d_l(z)\exp(-\gamma_l u_l(a_z))}. \quad (10)$$

It combines each base classifier according to the weight of the base classifier to obtain the final classifier as formula

$$H(A) = \arg\max_o \sum_{l=1}^{M} \gamma_l H_l^o(A). \quad (11)$$

$H_l^o(A)$ represents the direct output of the lth base classifier.

3.4. Naive Bayes Algorithm. The Bayesian method is based on the Bayesian principle and classifies the sample dataset using probability and statistics knowledge. The Bayesian classification algorithm has a very low false-positive rate due to its solid mathematical foundation. The principle of the

Naive Bayes algorithm is simple. It assumes that the various characteristic attributes of the sample have independent effects on the classification of the sample. It can more accurately estimate the necessary parameters when the amount of data is small. In addition, the classification model is characterized by simple installation, fast classification speed, and high accuracy.

The training process of the Naive Bayes classifier is to estimate the class prior probability $P(c)$ based on the training set D.

$$P(c) = \frac{|D_C|}{|D|}. \tag{12}$$

It estimates the conditional probability that the ith feature in the training sample appears in class c as formula

$$P(a_i|c) = \frac{D_{c,a_i}}{D_c}. \tag{13}$$

Although the Naive Bayes classifier is simple and efficient, when the labeled data are small, the number of samples much larger than the training will cause the problem of over-adaptation, which will lead to insufficient classification effect.

3.5. Prediction Model of Teaching Resource Sharing Based on BP Neural Network. Using neural network as the base classifier or predictor of ensemble learning can improve the generalization ability of the network and the effect of classification or prediction.

Prediction usually works through classification or valuation. That is, predictions are usually modeled by classification or estimation, and the models are applied to predictions of unknown variables. The target of prediction is to predict the unknown variables in the future, which often takes time to verify. The process of modeling and training using neural network is as follows:

Since the impact factor units are inconsistent, people first normalize the data to the [−1, 1] interval. Its formula is

$$a_k = \frac{a_k - a_{\min}}{a_{\max} - a_{\min}}. \tag{14}$$

The output of the BP rule in the BP wavelet neural network is the wavelet function. The network not only has the self-learning and self-adaptive ability of BP neural network, but also has the characteristics of wavelet function. In this section, the wavelet function used is expressed as formula

$$\varphi_{il}(a_i) = -\zeta_{il}\exp\left(\frac{-\zeta_{il}^2}{2}\right). \tag{15}$$

ζ_{il} is the translation factor and scaling factor of the wavelet function.

The first layer is the input layer, and the ith output can be expressed as formula

$$f_1(a_i) = a_i, \quad i = 1, \ldots, n. \tag{16}$$

The second layer is the pooling layer. Each node of this layer is used to calculate the membership function of the BP subset corresponding to input variable a_i. In this section, the Gaussian BP function is used to input the neural network, and the output of the neuron node of this layer can be expressed as formula

$$\mu_{il} = \exp\left(-\frac{(a_i - m_{il})^2}{2\sigma_{il}^2}\right), \quad (i = 1, \ldots, n). \tag{17}$$

The third layer is the regular aggregation layer. It uses the multiplication operator to calculate the membership of each rule. The output expression of this layer is formula

$$\mu_l = \prod_{i=1}^{n} \mu_{il}. \tag{18}$$

The fourth layer is the normalization layer, whose main function is to normalize the membership degree of each BP rule to formula

$$v_l = \frac{\mu_l}{\sum_{l=1}^{L}\mu_l}. \tag{19}$$

Here are $0 < v_l \le 1$ and $\sum_{l=1}^{L}\mu_l = 1$.

This paper uses a learning rate based on the idea of variable universe for parameter learning. This paper uses the classification accuracy of the network with the training sample set to construct the scaling factor. It can adaptively adjust the size of the learning rate according to the training effect of the network. Its expression is as formula

$$\eta(k) = \left(\frac{100 - \text{accuracy\_train}(k-1)}{\text{acc\_const}}\right)^T \eta(k-1). \tag{20}$$

Among them, k is the number of iterations, and $100 - \text{accuracy\_train}(k-1)$ is the percentage value of the classification accuracy of the training set samples predicted by the network after the last iteration.

When the values of acc_const and T are determined, it is not difficult to see from the expression of the scaling factor that at the beginning of the iteration or when the number of iterations is small, the value of the model classification accuracy $100 - \text{accuracy\_train}(k-1)$ is very small, and the value of T is greater than 1. The learning rate for the k-th iteration is increased relative to the previous iteration. This can improve the global search ability of the model and speed up the network convergence speed.

Before dealing with the time series forecasting problem, it first divides the time series data into training set and test set. It converts the predicted input and output data into a matrix representation. It is assumed that the first s sequence values are used to predict the sequence value at the next moment, and the formula is

$$\begin{bmatrix} a_1 & \cdots & a_s \\ a_t & \cdots & a_{t+s-1} \\ a_T & \cdots & a_{T+s-1} \end{bmatrix} \longrightarrow \begin{bmatrix} a_{s+1} \\ a_{t+s} \\ a_{t+s} \end{bmatrix}. \tag{21}$$

Table 2: Experimental data.

Data name	Data length	Number of training sets	Number of test sets	Number of categories
Beef	470	30	30	5
Gun-Point	150	20	150	2
Trace	270	20	100	4
ItalyPowerDemand	20	10	1000	2
Lightning-7	319	30	70	7
OSU Leaf	420	25	240	6
Wafer	150	10	6100	2
WordSynonyms	265	120	620	125
Yoga	420	10	2500	2

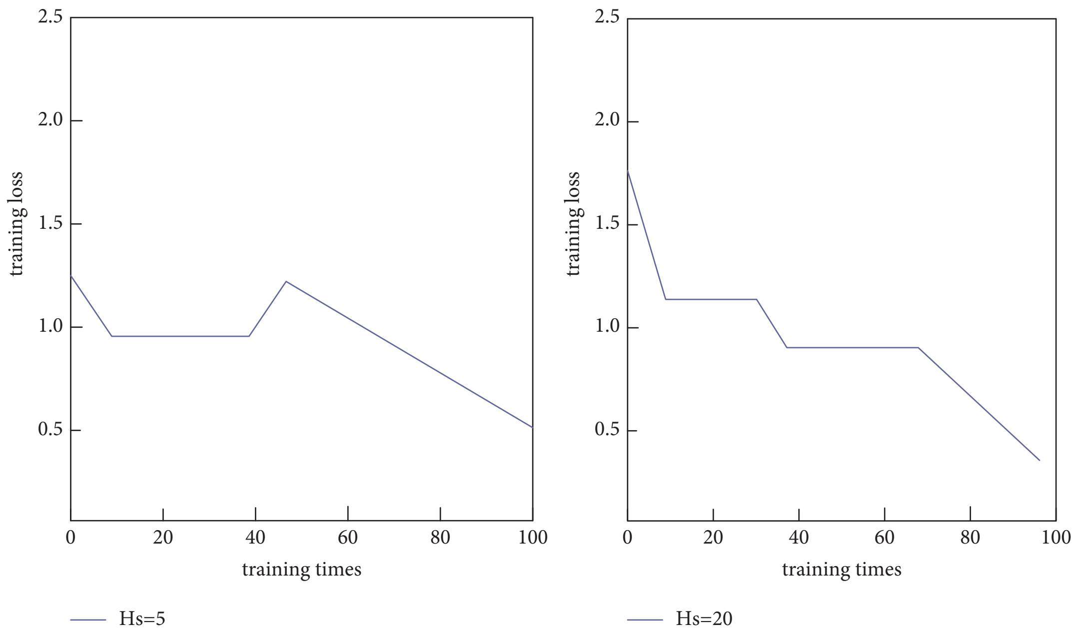

Figure 7: Training loss of BP neural network on Beef dataset.

Matrix A represents the input to the model, a_{s+1} represents the output of the model, and T is the number of rows in matrix A. The arithmetic mean of the results of the two base predictors is directly taken as the integrated prediction result; that is, each base predictor is given a weight of size N_f and then weighted and summed. The integration result is as formula

$$b_{\text{ensemble}} = \frac{\sum_{l=1}^{N_f} b_i}{N_f}. \tag{22}$$

b_{ensemble} is the result after ensemble, b_i is the result based on the lth predictor, and N_f is the number of base models participating in the ensemble.

4. Experiment and Analysis of Classification and Prediction of BP Neural Network

4.1. Classification Function Experiment of BP Neural Network. In the experiments, 9 sets of time series data were selected from various data sources in the UCR time series classification software house. The specific information of the experimental data selected from the UCR time series classification software house is shown in Table 2.

As shown in Table 2, the BPNN constructed in this paper has a three-layer structure. The amount of nodes in the input layer is the data length of the time series data, and the number of nodes in the output layer is the number of data categories.

The setting of neural network training time usually needs to be manually adjusted according to the experimental results. If there is insufficient labeled data, the training loss of the neural network may converge faster due to fewer training samples. The training loss of the neural network in the datasets Beef and Gun-Point is shown in Figure 7.

As shown in Figures 7 and 8, the neural network's training time setting must usually be manually adjusted based on the experimental results. A neural network is a distributed parallel information processing algorithmic mathematical model that mimics the behavioral characteristics of animal neural networks. Due to fewer training samples, the neural network's training loss may converge faster if there are insufficient labeled data.

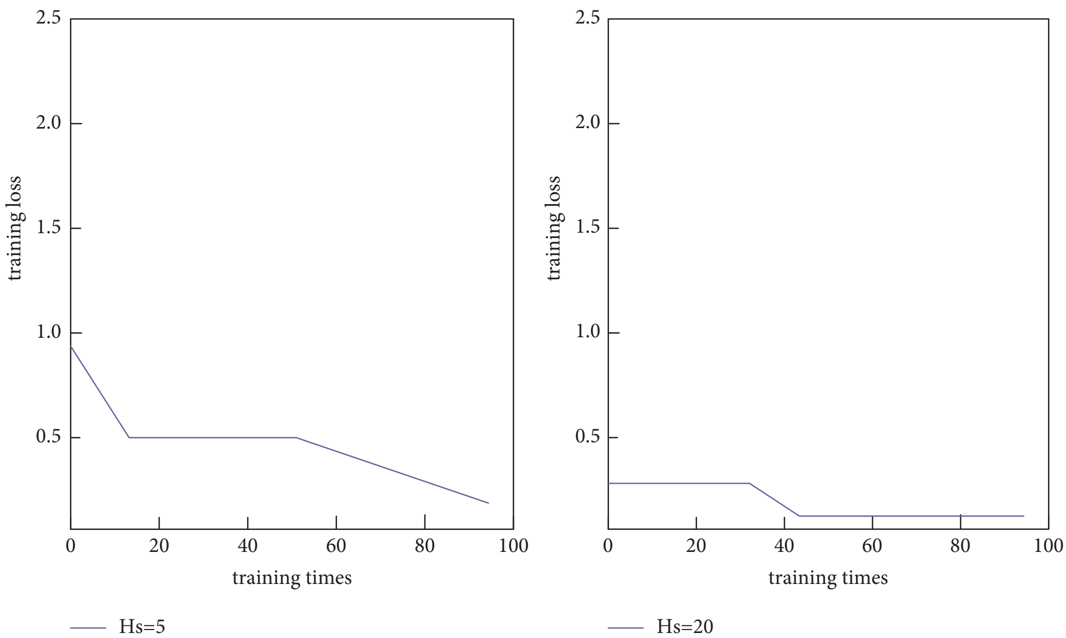

Figure 8: Training loss of BP neural network on Gun-Point dataset.

Table 3: Classification accuracy of different methods on different datasets.

Data name	Naive Bayes	Support vector machine classification algorithm	BP classification algorithm
Beef	0.89	0.750	0.932
Gun-Point	0.654	0.473	0.790
Trace	0.703	0.648	0.743
ItalyPowerDemand	0.926	0.732	0.964
Lightning-7	0.583	0.549	0.674
OSU Leaf	0.269	0.216	0.315
Wafer	0.894	0.809	0.932
WordSynonyms	0.237	0.251	0.367
Yoga	0.518	0.437	0.522

For the above 9 datasets, the proposed BP classification algorithm is compared to the conventional SVM classification algorithm and the simple Bayes algorithm in this paper, as well as the classification effect of the classifier using only a limited number of labels. The accuracy of classification is used to assess the strengths and weaknesses of various algorithms. The best classification results of various parameter settings are BPNN classification algorithm, support vector machine classification algorithm, and Naive Bayes algorithm. Table 3 illustrates this.

Table 3 shows the following: the highest accuracy is 0.964 for the BP neural network classification algorithm, while the highest accuracy is 0.809 and 0.926 for the support vector machine classification algorithm and the Naive Bayes algorithm, respectively. The BPNN classification algorithm outperforms the support vector machine and Naive Bayes classification algorithms. The best classification effect is achieved by the BP algorithm proposed in this paper. The BP algorithm and the Naive Bayes algorithm proposed in this chapter are used as benchmark classifiers in this experiment. It expands the label set with the AdaBoost algorithm and compares the classification effects by building a temporal classification model. Figure 9 depicts the experimental results.

As shown in Figure 9, in the Beef dataset and Gun-Point dataset, if the BP algorithm proposed in this paper is used as the benchmark classifier, the simple Bayes algorithm has matching rate, recurrence rate, and metric values. If the BP algorithm proposed in this paper is used as a benchmark classifier, unlabeled data can be labeled more accurately. The AdaBoost algorithm can take into account unlabeled data and make better use of unlabeled data information for improvement.

4.2. Prediction Experiment and Analysis of BP Neural Network. This part compares the accuracy of the prediction model through experiments and evaluates the performance of English major teaching resource sharing prediction based on BP neural network. In the following comparative experiments, it selects the BPNN prediction model and the Naive Bayesian model as the experimental comparison object and selects the error index of the prediction sequence as the model evaluation standard.

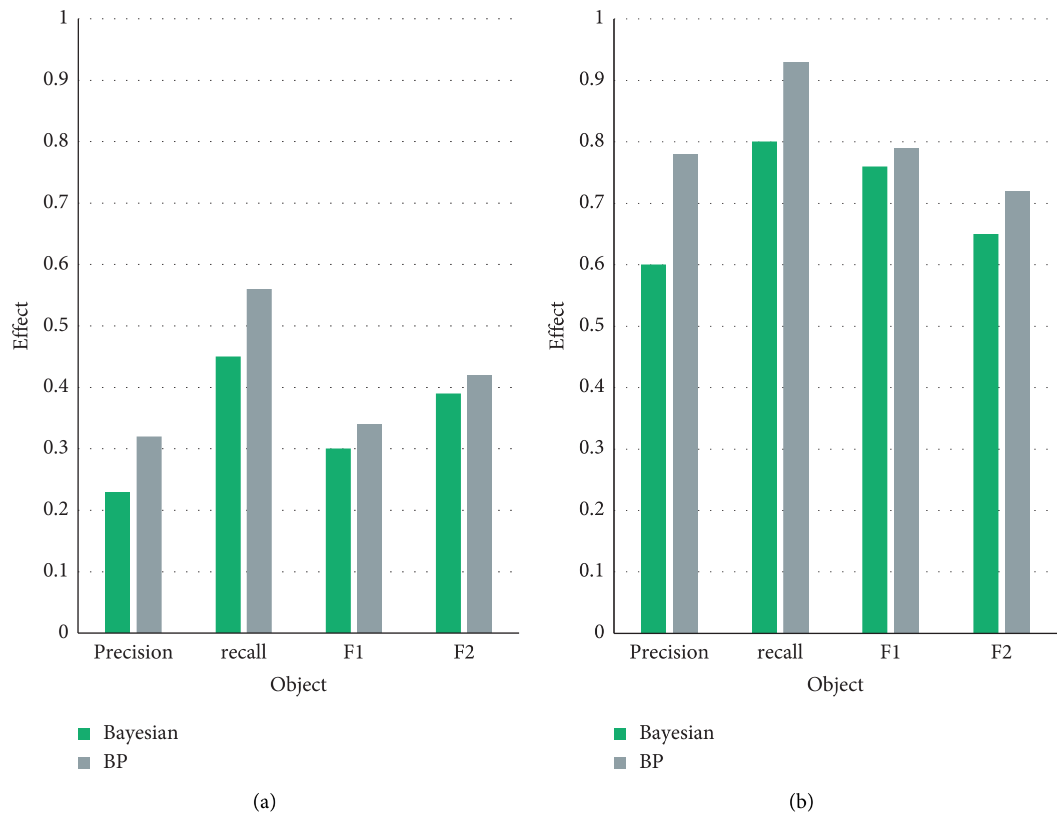

FIGURE 9: Comparison of the classification effects of the two algorithms on different datasets. (a) Comparison of classification effect of Beef dataset. (b) Comparison of classification effect of Gun-Point dataset.

In order to better explain the experimental results, on the one hand, it shows the error rate of the prediction results, and on the other hand, it visually shows the fitting effect and prediction results of each prediction model to the experimental data. In general, it evaluates the performance of forecasting models according to the following three generally applicable error measures: mean absolute error (MAE), mean percentage error (MAPE), and root mean square error (RMSE).

$$\begin{aligned} \mathrm{MAE} &= \frac{\sum_{i=1}^{n}\left|b_t - b_l\right|}{n}, \\ \mathrm{MAPE} &= \frac{\sum_{t=1}^{n}\left|b_t - b_l\right|}{n \times \left|b_t\right|} \times 100\%, \\ \mathrm{RMSE} &= \sqrt{\frac{\sum_{t=1}^{n}\left(b_t - b_l\right)^2}{n}}. \end{aligned} \tag{23}$$

Among them, b_t is the actual value of the time series at time t, and b_l is the predicted value of the time series at time t.

This experiment is to compare the Naive Bayesian model and the BP neural network prediction model. The datasets are the data of teaching resources of English majors in College A and the data of teaching resources of English majors in College B.

In this experiment, under the setting of the same neural network structure, the fitting effect of the two models on historical data and the prediction results for a period of time in the future are, respectively, shown. It also compares the model's performance on datasets with significantly different lengths and features, as shown in Figure 10.

As shown in Figure 10, the BPNN has a very good fitting effect on historical data and can basically reproduce the real data. The fitting effect of the Naive Bayesian model on historical data is slightly worse than that of the BP neural network. It cannot accurately recover the short-term numerical fluctuations in historical data, but it can still grasp the trend of time series movement. The prediction results of the Naive Bayes model and the BP neural network on the data are shown in Table 4.

As shown in Table 4, the prediction error of the Naive Bayesian model is between 0.69 and 0.75, and the error of the BP neural network is between 0.21 and 0.43. The Naive Bayesian model has a bigger gap than the BPNN in the prediction results of time series data. With the increase of the prediction step, the Naive Bayes model will be limited to the periodicity of local fluctuations, and there will be periodic

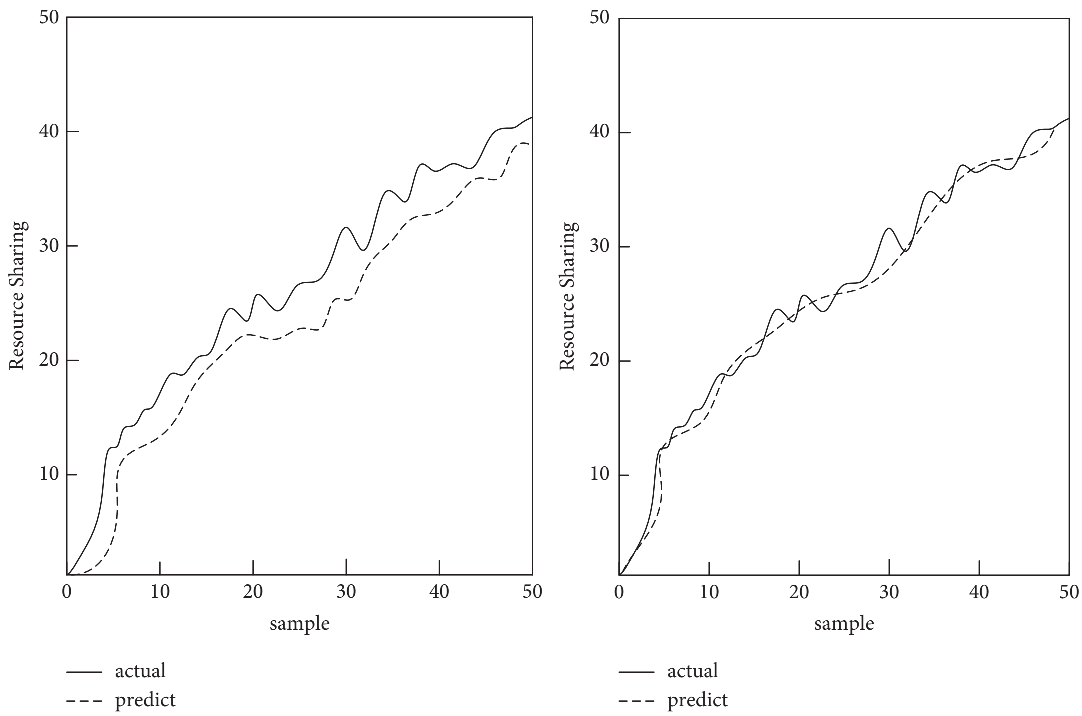

Figure 10: Fitting diagram of Naive Bayes model and BP neural network prediction.

Table 4: Prediction results of the two algorithms.

Error	Naive Bayes model	BP neural network
MAE	0.75	0.43
MAPE	0.70	0.36
RMSE	0.69	0.21

repeated numerical fluctuations. The BPNN model can basically predict the change of the shock trend in time.

5. Conclusions

The contradiction between the shortcomings and unbalanced development of the educational needs of colleges and universities has made all sectors of society focus more and more on this. This also makes the sharing of higher education resources an important requirement to promote the rapid development of China's higher education. Teachers rely on computers for education as a result of the advancement of modern computer technology, and the distribution of many software and assignments is dependent on networks and computers. This can improve resource sharing efficiency, expand educational resource content, and maximize the use of educational content. In recent years, the English major has grown in popularity, and major colleges and universities have increasingly focused on teaching English majors. This paper focuses on how to use teaching resource sharing responsibly and deliver effective instruction. The ubiquitous learning resource sharing platform is described in detail in this paper, and it is discovered that the platform has numerous advantages. It not only enables teachers to share resources at any time and from any location, but it is also very efficient. This paper briefly discusses the challenges of sharing teaching resources for English majors before highlighting the neural network's function. The neural network is used primarily for classification and prediction in this paper. The classification and prediction effects of the BP neural network are higher than those of the Bayesian classification algorithm, according to a series of experiments. There are still some errors in the data due to the experiment's technical and environmental factors. The author will continue to learn from his mistakes and strive to improve his work in the future.

Data Availability

The data used to support the findings of this study are available from the author upon request.

Conflicts of Interest

The author does not have any possible conflicts of interest.

References

[1] Q. Yuan, "Network education recommendation and teaching resource sharing based on improved neural network," *Journal of Intelligent and Fuzzy Systems*, vol. 39, no. 4, pp. 5511–5520, 2020.

[2] N. Guichon, "Sharing a multimodal corpus to study webcam-mediated language teaching[j]," *Language, Learning and Technology*, vol. 21, no. 1, pp. 56–75, 2017.

[3] Q. Yan, "Design of teaching video resource management system in colleges and universities based on micro-technology," *Security and Communication Networks*, vol. 2021, no. 4, 11 pages, Article ID 9914048, 2021.

[4] B. V. Tucker, M. C. Kelley, and C. Redmon, “A place to share teaching resources: Speech and language resource bank,” *Journal of the Acoustical Society of America*, vol. 149, no. 4, p. A147, 2021.

[5] Y. Li, “Psychological stress detection and early warning system based on wireless network transmission,” *Scientific Programming*, vol. 2021, no. 3, 9 pages, Article ID 3739045, 2021.

[6] X. Bai and J. Li, “Intelligent platform for real-Time page view statistics using educational big data digital resource sharing,” *Journal of Intelligent and Fuzzy Systems*, vol. 40, no. 1, pp. 1–10, 2020.

[7] L. Liang, Q. Yin, and C. Shi, “Exploring proper names online and its application in English teaching in university,” *ASP Transactions on Computers*, vol. 1, no. 1, pp. 24–29, 2021.

[8] H. He, F. Gang, and C. Jinde, “Robust state estimation for uncertain neural networks with time-varying delay,” *Journal of Jishou University (Natural Sciences Edition)*, vol. 19, no. 8, pp. 1329–1339, 2019.

[9] Y.-G. Jiang, Z. Wu, J. Wang, X. Xue, and S.-F. Chang, “Exploiting feature and class relationships in video categorization with regularized deep neural networks,” *IEEE Transactions on Pattern Analysis and Machine Intelligence*, vol. 40, no. 2, pp. 352–364, 2018.

[10] L.-F. Wang, H. Wu, D.-Y. Liu, D. Boutat, and Y.-M. Chen, “Lur’e Postnikov Lyapunov functional technique to global Mittag-Leffler stability of fractional-order neural networks with piecewise constant argument,” *Neurocomputing*, vol. 302, pp. 23–32, 2018.

[11] J. Cheng, P. S. Wang, L. I. Gang, H. U. Qing-Hao, and L. U. Han-Qing, “Recent advances in efficient computation of deep convolutional neural networks,” *Frontiers of Information Technology & Electronic Engineering*, vol. 19, no. 1, pp. 64–77, 2018.

[12] S. Mei, A. Montanari, and P.-M. Nguyen, “A mean field view of the landscape of two-layer neural networks,” *Proceedings of the National Academy of Sciences*, vol. 115, no. 33, pp. E7665–E7671, 2018.

[13] Y. Dong and H. Wang, “Robust output feedback stabilization for uncertain discrete-time stochastic neural networks with time-varying delay,” *Neural Processing Letters*, vol. 51, no. 1, pp. 83–103, 2020.

[14] A. Lucas, M. Iliadis, R. Molina, and A. K. Katsaggelos, “Using deep neural networks for inverse problems in imaging: beyond analytical methods,” *IEEE Signal Processing Magazine*, vol. 35, no. 1, pp. 20–36, 2018.

[15] P. Yin, S. Zhang, J. Lyu, S. Osher, Y. Qi, and J. Xin, “BinaryRelax: a relaxation approach for training deep neural networks with quantized weights,” *SIAM Journal on Imaging Sciences*, vol. 11, no. 4, pp. 2205–2223, 2018.

[16] Y. Guo, “Globally robust stability analysis for stochastic cohen-g neural networks with impulse control and time-varying delays,” *Ukrainian Mathematical Journal*, vol. 69, no. 8, pp. 1220–1233, 2018.

[17] R. Liu, “Analysis on the stratified intervention of mental health education in colleges and universities,” *ASP Transactions on Psychology and Education*, vol. 2, no. 1, pp. 17–23, 2021.

[18] L. Huang, G. Xie, W. Zhao, Y. Gu, and Y. Huang, “Regional logistics demand forecasting: A BP neural network approach,” *Complex & Intelligent Systems*, vol. 1, pp. 1–16, 2021.

[19] M. Gao, R. Liu, and J. Mao, “Noise robustness low-rank learning algorithm for electroencephalogram signal classification,” *Frontiers in Neuroscience*, vol. 15, 2021.

[20] Y. Ding, X. Zhao, Z. Zhang, W. Cai, and N. Yang, “Semi-supervised locality preserving dense graph neural network with ARMA filters and context-aware learning for hyperspectral image classification,” *IEEE Transactions on Geoscience and Remote Sensing*, vol. 60, 2021.

[21] W. Cai, Y. Song, and Z. Wei, “Multimodal data guided spatial feature fusion and grouping strategy for E-commerce commodity demand forecasting,” *Mobile Information Systems*, vol. 2021, Article ID 5568208, 14 pages, 2021.

[22] M. Atiquzzaman, N. Yen, and Z. Xu, *Big Data Analytics for Cyber-Physical System in Smart City, BDCPS 2019*, Computer Systems Applications, Shenyang, China, 2019.

Hindawi
Computational Intelligence and Neuroscience
Volume 2022, Article ID 1559099, 12 pages
https://doi.org/10.1155/2022/1559099

Research Article

Dance Fitness Action Recognition Method Based on Contour Image Spatial Frequency Domain Features and Few-Shot Learning

Qinglong Chi [1] and Lifeng Li [2]

[1] *Dance Teaching and Research Office, Shandong Sport University, Jinan 250000, China*
[2] *Music Teaching and Research Group, Xiamen Foreign Language School, Xiamen 361000, China*

Correspondence should be addressed to Qinglong Chi; chiqinglong@sdpei.edu.cn

Received 11 February 2022; Revised 24 March 2022; Accepted 25 March 2022; Published 8 June 2022

Academic Editor: Xin Ning

In recent years, the research work of artificial intelligence technology has progressed rapidly, and various classic Few-Shot learning models have achieved unprecedented success in many artificial intelligence application fields. These include face recognition, object classification detection and tracking, speech recognition, and natural language processing, which greatly facilitate our lives. This paper aims to identify dance fitness movements based on contour image spatial frequency domain features and Few-Shot learning technology. This paper proposes a Few-Shot learning method based on contrastive average loss for Few-Shot learning. This method makes the learned model more representative by improving the loss function and performing a normalization process, and it proposes a feature extraction algorithm that combines improved LBP and HOG for action recognition technology. The experimental results show that the recognition accuracy of the algorithm in this paper is 93.10%, 90.30%, and 92.70% for walking, opening hands, and running, respectively. This illustrates the effectiveness of the fusion feature algorithm.

1. Introduction

In the early days, research based on images and videos was an important part of human action recognition methods. With the continuous development of computer technology, intelligent machines and equipment have gradually attracted widespread attention from human beings. These methods mainly take the RGB information collected by the camera equipment as the research object and use the features such as texture and color information in the two-dimensional image to perform action recognition. However, the changes of lighting conditions, background interference, and occlusion and self-occlusion problems cannot be solved well, which has become the bottleneck of this type of research method. In order to enable deep learning models to overcome the problem of relying on large-scale data and obtain the ability to quickly learn new categories of things similar to humans, Few-Shot learning came into being.

The general action recognition method works by extracting features from the original input and then training a classifier using those features. Robust feature representations must be obtained to ensure the accuracy of the final algorithm, which necessitates a significant amount of computational and testing effort. Massive labeled data are usually difficult to obtain in real-world applications. On the one hand, some industries find it difficult to collect image data for a variety of reasons, including privacy and security; on the other hand, even if image data are collected, labelling it is often costly. These disadvantages severely limit the application of image classification models. As a result, for dance fitness action recognition, it is necessary to investigate the spatial frequency domain features of contour images as well as Few-Shot learning technology.

On the basis of predecessors, this paper has the following two innovations for human body recognition research: (1) a contrastive average loss-based Few-Shot learning method is proposed. Few-Shot learning is a commonly used method in human action recognition research, but the traditional Few-Shot learning method will be hampered by the action's noise and background processing. This problem can be solved using the Few-Shot learning method based on contrastive average loss proposed in this paper. (2) The three movements of running, walking, and opening hands are used to research dance fitness movement recognition. Because these three movements are the most common in dance and fitness, and because other movements are based on their extensions, research on these three movements can better represent the entire movement.

2. Related Work

There are numerous studies on human action recognition that are related. To compensate for the flaws of traditional algorithms, Tarn C et al. used the Few-Shot learning method to fit data online. Their proposed method was tested on ten datasets using different collision energy settings and instruments such as Velos, QE, Lumos, and Sciex. Their findings show that Few-Shot learning can improve prediction accuracy while using virtually no computational resources [1]. Research performed by Szcs and Németh aims to aid medical workers' work by analyzing pathological X-ray recordings with only a few images. They propose the Deep Neural Network-based Dual View Matching Network (DVMN), an improved method that addresses the problem of Few-Shot learning and different views of pathological records in images. Its main contribution is the use of convolutional neural networks in image representation for feature extraction and multiview processing [2]. Li et al. proposed Joint Distance Maps, a simple and effective method for encoding the spatiotemporal information of skeleton sequences into color texture images, based on the good performance of deep learning (JDMs). They also used convolutional neural networks to extract distinguishing features from JDMs for recognizing human action and interaction. The proposed method has been validated by state-of-the-art results in single-view and cross-view settings on the large RGB + D dataset and the small UTD-MHAD dataset [3]. SkeletonNet, a deep learning framework for skeleton-based 3D action recognition, was investigated by Ke et al. They begin by extracting features based on body parts from each frame of the skeleton sequence. When compared to the original coordinates of the skeletal joints, the proposed features are translation, rotation, and scale invariant [4]. Wang et al. analyzed human activity recognition from videos using multimedia and convolutional neural network features. They feed frame-level CNN sequence features to a long short-term memory (LSTM) model for video activity recognition, treating video as a sequence of frames [5]. To process video data, Ullah et al. proposed an action recognition method using convolutional neural networks and deep bidirectional LSTM-LSTM networks. First, every six frames of video are analyzed for deep features, which helps to reduce redundancy and complexity. Then, using a DB-LSTM network, order information between frame features is learned, with multiple layers stacked together in the forward and reverse passes to increase the depth of the network. By analyzing features within specific time intervals, the method can learn long-term sequences and process lengthy videos. On three benchmark datasets, UCF-101, YouTube 11 Actions, and HMDB51 [6], their experimental results show that the proposed method achieves significant improvement in action recognition compared to existing action recognition methods.

Many studies on human actions are based on machine learning methods, and the extraction of video information is emphasized, as evidenced by a review of related research. These kinds of processing methods are quite complicated.

3. Few-Shot Learning Based on Contrastive Average Loss

3.1. Introduction to Few-Shot Learning. In recent years, Few-Shot learning is a subfield of machine learning [7, 8]. The definition of machine learning is that a computer program learns from experience (experiences, E) to solve a certain task (task, T) and perform a certain performance measure (performance, P). Performance P on task T improves with experience E. While Few-Shot learning is a class of machine learning problems (specified by E, T, and P), where E contains little supervision information for the target T. Specific to the image classification [9, 10] task based on Few-Shot learning, T is the image classification task, E is a small number of labeled pictures and prior knowledge used for the classification task, and the performance measure P is the accuracy rate. According to the definition of machine learning, the classification task should be to improve the experience E based on the measured accuracy, while the few labeled images are fixed. Therefore, only the part corresponding to the prior knowledge can be improved. Specifically, the prior knowledge may be some original images of other categories or a pretrained model. Figure 1 is an example of rooster single-sample recognition. The model only needs to judge which birds on the right are roosters based on the rooster image on the left.

Therefore, the training method of Few-Shot learning is different from the training method of conventional deep learning models [11–13]. Specific to the image classification problem, the training process usually contains two datasets, namely the support dataset and the query dataset. Formally, the training set learned by Few-Shot contains multiple samples of different classes. The model is required to learn how to distinguish the c classes from the Few-Shot with the number of training sets *ck*. Such a task is called a c-way k-shot classification task. The value of k is usually 1 or 5. When k is 1, this Few-Shot learning is called one-shot learning, as shown in Figure 2:

The core problem of Few-Shot learning is insufficient sample size. In order to "learn" from a small number of samples to a deep learning model that can be generalized, the current main solutions can be divided into three categories: Few-Shot learning methods based on data augmentation, metric learning, and meta-learning. As stated in Chapter 1, the current research status at home and abroad, the probability-based generative model in the nondeep learning stage is the mainstream of the Few-Shot classification task; and the current mainstream is the deep learning-based discriminative model. So far, there are three main methods for using discriminative models to solve the Few-Shot classification

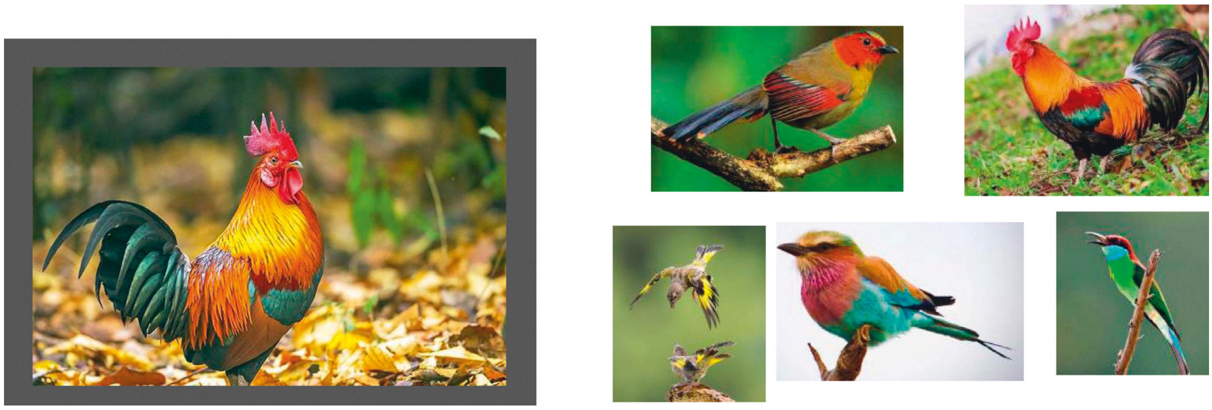

Figure 1: Example of rooster single-sample image classification.

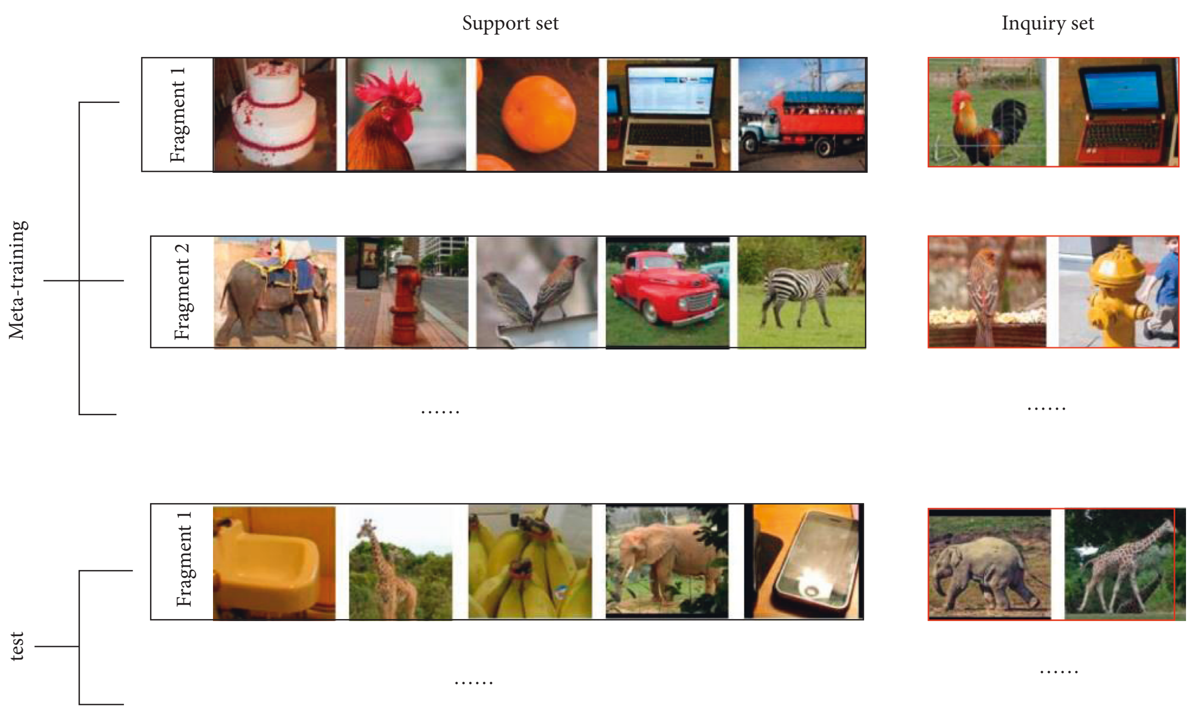

Figure 2: Schematic diagram of segment training mechanism for c-way k-shot image classification, where $c = 5$ and $k = 1$.

problem: data augmentation, metric learning, and meta-learning. They solve the problem of Few-Shot image classification from three aspects: directly expanding the diversity of label samples, using prior knowledge (training set data) to learn better feature models, and optimizing hyper-parameters to make the model learn quickly. The following three methods are briefly introduced.

3.1.1. Few-Shot Learning Based on Data Augmentation. The data augmentation method based on Few-Shot learning is a method to enhance data and improve data diversity through prior knowledge. There are two types of data augmentation methods, one is a generative model that generates new samples through transformation; the other is a transduction model that uses the model to label unlabeled samples and then further trains the model. The specific working method is shown in Table 1. The converter inputs the unlabeled image u and the reference sample image x, and its label y and outputs the synthesized image x and label y, which are used to enhance the training dataset of Few-Shot.

Table 1: Few-Shot image classification method based on data augmentation.

Type	Input (u, x, y)	Converter t	Output (x, y)
Generating model	Original (u_i, x_i, y_i)	Transformation model based on training set learning	$(t(u_i), y_i)$
Transduction model	Unmarked picture	Classifier based on training set learning	(x_i, y_i)

Image processing [14, 15], zoom-in and zoom-out, random cropping, adding noise, mirror flipping, and other

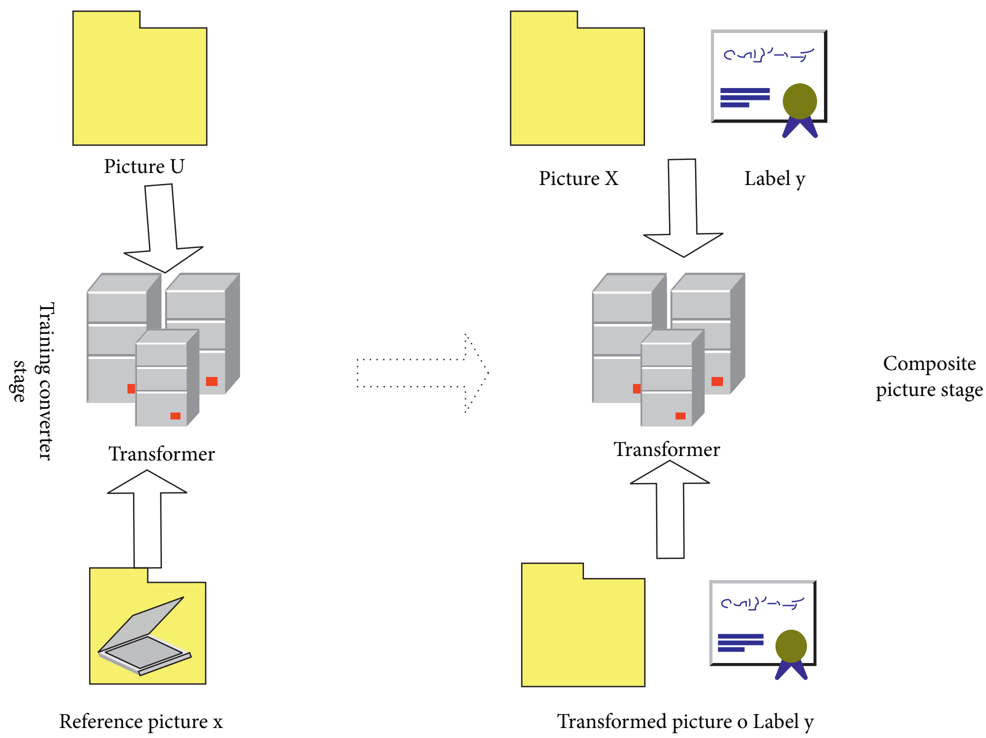

FIGURE 3: Schematic diagram of data synthesis method based on generative model.

basic data augmentation methods based on generative models are among the most basic. These manual transformers can create new images that have the same tags as the old ones. The amount of data generated above for Few-Shot learning is far insufficient to improve the model's generalization ability. Many new methods have been developed as a result of the development of deep learning, the majority of which are based on autoencoders (AE) or adversarial generative networks (GAN) [16]. DAGAN learns on the training set using a generator that combines U-Net and ResNet, as well as a discriminator that uses DenseNet. This trained GAN model is then used to generate new sample images for Few-Shot image classification on the test set [17, 18].

It can be seen that the difference between this type of data expansion method and other Few-Shot learning methods is that there are two more steps before training image classification, as shown in Figure 3, which are training converters (generators), and then synthesizing new data.

3.1.2. Metric-Based Few-Shot Learning. Metric learning refers to extracting features from samples and embedding them into a feature space with a small dimension, and then using the distance between two features to measure the similarity of two samples. Commonly used distances in feature space include Euclidean Metric and Cosine similarity [19, 20].

(1) Siamese Network. Siamese network is the first to introduce metric learning into Few-Shot learning. As shown in Figure 4, the network structure consists of two convolutional neural networks (CNNs), which input a pair of samples (x_i, y_i). At the same time, the two CNNs share the convolution kernel weight, then output two feature vectors through the fully connected layer, and finally output the similarity score $p(x_i, y_i)$ of the two samples according to the distance between the two vectors. The distance metric function of the two features is directly a weighted 1 function, and the loss function of the network structure is shown in the following equation:

$$\nabla = \sum_{q} y_{ij} \log p(x_i, y_i) + (1 - y_{ij}) \log (1 - p(x_i, y_i)). \tag{1}$$

Among them, $y_{ij} = 1$ when x_i and x_j belong to the same category. After the model is trained, the parameters of the Siamese network are fixed and tested on the Few-Shot task, and then, the nearest neighbor classifier (NearestNeighborClassifier) is used for classification.

(2) Matching Network. Unlike Siamese networks, which share parameters for training and test sets, matching networks are the first to design a piecemeal training mechanism. The matching network adds a support set attention model. Specifically, in the training process, the convolutional neural network is used to extract features for the support set and the query set, and then, the attention weight corresponding to each support set is calculated according to the sample features of the query set, and then calculate the possible labels of the query set samples according to the attention weights, and finally use the cosine similarity to measure the matching degree of the support set samples and the query set

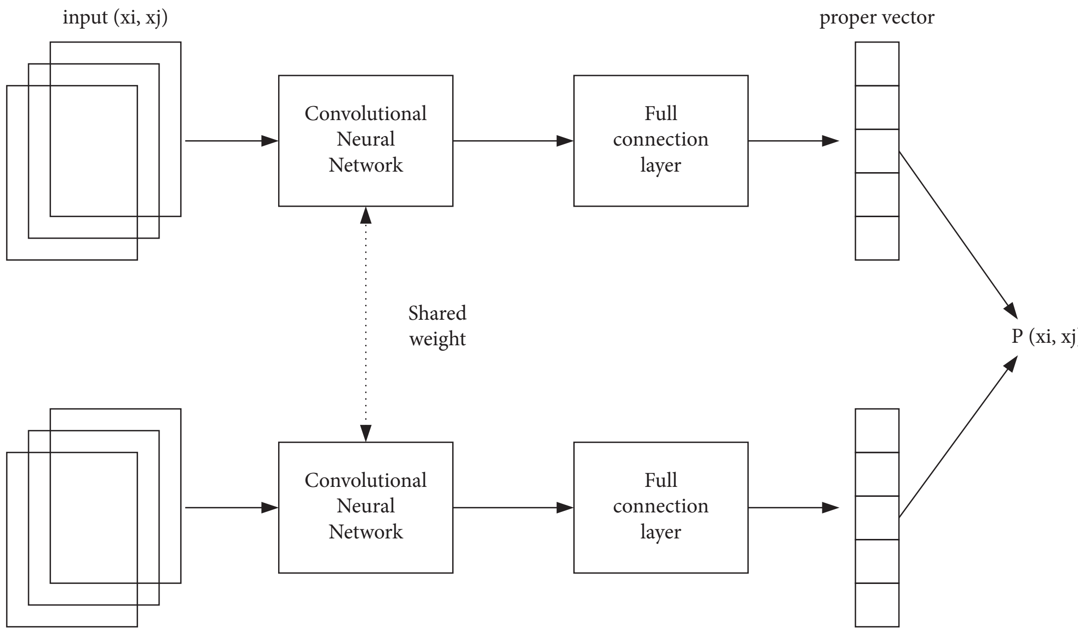

FIGURE 4: Siamese network structure diagram.

samples. The calculation formula of attention is shown in the following equation:

$$\alpha(x, x_i)\frac{\exp[c(f(x), g(x_i))]}{\sum_{i=1}^{k}\exp[c(f(x), g(x_i))]}, \tag{2}$$

where x represents the query set sample, x_i represents the i-th support set sample, $c(,)$ represents the cosine distance, and $f()$ and $g()$ represent the feature extraction function of the query set and support set, respectively.

(3) Prototype Network. Since the matching network studies the single-sample problem, the number of each sample learned by Few-Shot is less than 20. In order to solve the problem of solving the similarity of feature space in the case of multiple samples of each type, the prototype network has designed the concept of prototype. First, the support set samples are embedded in the feature space, and then, the center of each class of the support set is designed as a prototype. The prototype calculation formula is shown in the following equation:

$$C_k = \frac{1}{S_k(x_i, y_i)}\sum_{(x_i, y_i)\in S_k} f_\varphi(x_i). \tag{3}$$

Among them, $f_\varphi(x_i)$ represents the feature extraction function, and S_k represents the support set containing k samples for each class.

Then, the similarity is calculated by calculating the Euclidean distance $d(,)$ between the query set and the prototype. In the test, the normalized exponential function is used to calculate the distance between the test sample and the prototype of the support set. The specific formula is shown in the following equation.

$$p_\varphi(y = k|x) = \frac{\exp\left[-d\left(f_\varphi(x_i), c_k\right)\right]}{\sum_k \exp\left[-d\left(f_\varphi(x_i), c_k\right)\right]}. \tag{4}$$

Prototype networks do not suffer from class imbalance since there is only one prototype per class. Also since the prototype can only capture the mean of the support set, naturally its variance information will be lost. The features extracted from the support set are updated by extracting the features from the query set of the task as environmental features, so that each task has its own different feature output, so as to solve the problem that the variance information will be lost.

(4) Relationship Network. As shown in Figure 5, the relational network model mainly includes two modules: an embedded module and a relational module. The former is the feature extraction module that every metric learning must have; and the relational module is the metric module, which directly connects the sample features of the query set and the support set, and then input into a convolutional neural network and directly classify and score through the fully connected layer. The classification scoring formula is shown in the following equation:

$$r_{i,j} = g_\phi\left[C\left(f_\phi(x_i), f_\phi(x_j)\right)\right], \quad i = 1, 2, \ldots, C. \tag{5}$$

Among them, x_i and x_j represent the support set and query set samples, respectively; $f_\varphi(x_i)$ represents the embedding function; $c(,)$ represents the concatenation of the embedded feature maps; and $g_\phi(x_i)$ represents the relation function.

3.1.3. Few-Shot Learning Based on Meta-Learning. Metric learning, hyper-parameter optimization-based meta-learning, and model-based meta-learning are some of the meta-learning-based methods for Few-Shot image classification. Metric learning, and thus its widespread use, has become a separate branch among them. Model-based meta-learning

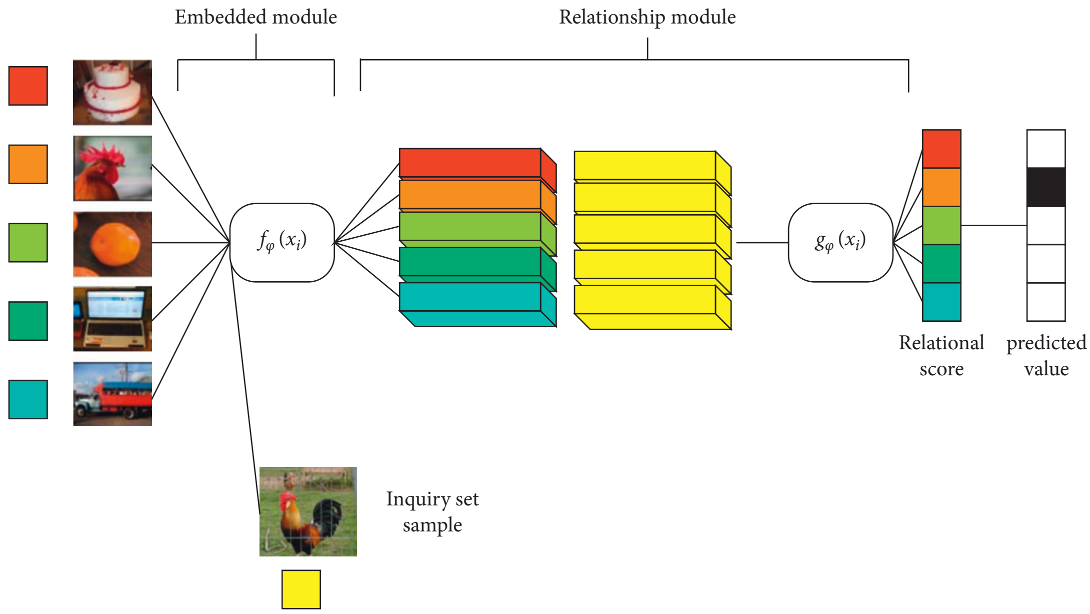

FIGURE 5: Schematic diagram of the relationship network structure.

methods are frequently combined with metric learning and hyperparameter optimization meta-learning. As a result, the following sections focus on hyperparameter optimization-based meta-learning methods.

The core idea of MAML (Model-Agnostic Meta-Learning) model is to set initialization parameters suitable for fast learning for basic learning model parameters through cross-task training strategy. In this way, the base learning model can generalize well to new tasks using only a few samples of the support set. Specifically, the parameter update formula for the basic learner of task T is shown in the following equation:

$$\theta_b^T = \theta_b - \alpha \nabla_{\theta_b} L\left(D^T, \theta_b\right), \tag{6}$$

where α is the learning rate, $L(D^T, \theta_b)$ is the loss function of task T on the support set, and θ_b is the initialization parameter of the basic learner.

In the meta-learning stage, MAML optimizes the meta-learner model by balancing the loss corresponding to parameter θ_b^T of the basic learning model on multiple tasks. The specific formula is shown in the following equation:

$$\theta_m = \theta_m - \beta \nabla_{\theta_m} L\left(D^T, \theta_b^T\right). \tag{7}$$

It is worth noting that the meta-learning model and the basic learning model in MAML in Table 2 are the same model, that is, parameter $\theta_m = \theta_b$. In fact, there are many MAML-based variant models. The MAML-based variant models and their improvement points in recent years are shown in Table 2.

TABLE 2: Improved model based on MAML framework.

way	Improvement point
MAML	
BMAML	A parameter-free reasoning model based on MAML is designed to solve the uncertainty problem of MAML model.
MT-net	Simplify the parameter space of MAML meta-learning model into a subspace composed of each layer of activation space, thus reducing the difficulty of fast learning.
TAML	Unbiased task unknowable experience is added to the initial model to solve the problem of poor performance of MAML framework in meta-training.
LEO	Combining MAML with metric learning, the model can quickly learn hyperparameters in low-latitude embedded space.

3.2. Few-Shot Learning Based on Contrastive Average Loss. In metric learning, a prototype network is a representative algorithm framework. It uses the feature embedding module to process the data and represent it as a prototype for a specific category. The metric module is a parameter-free module that compares query set samples to all prototypes and chooses the prototype category with the shortest distance as its own category. When the algorithm creates category prototypes, however, it only takes into account the relationship between samples and similar prototypes, which can cause issues in more complex situations.

This paper proposes a new loss function based on the prototype network. In comparison with the average loss (CDM), the loss function compares the difference between the sample and different prototypes at the same time, reducing the difference between Few-Shot and the same type of prototype while increasing the differences between samples and different types of samples. This will improve the feature embedding function's ability to represent features, making the learned prototypes more representative. Prototypes of various categories are more differentiated, which improves the model's generalization ability. The method is tested on a benchmark dataset for image classification, and the results show that it can effectively improve the model's performance.

The loss function proposed in this paper will consider the relationship between samples and prototypes of different categories at the same time. Through the adjustment of hyperparameters, it can flexibly convert between the overall category and some categories. Experiments show that this method can improve the performance of the model on the dataset. Note the training dataset $D = \left\{ (x_i, y_i)_{i=1}^{N} \right\}$. For a support set sample, the number of categories is k, and the prototype of a category is denoted as C_k. The class prototype to which sample x_i belongs is C_i, and the distance between sample x_i and class prototype C_j is denoted by d. The measurement method of distance can be selected by yourself. The distance contrast is recorded as l, and the optimization goal is to minimize it, as shown in the following equation:

$$l = d^2 (x_i, c_i) - \frac{1}{m} \sum_{j \neq i} d^2 (x_i, c_i). \tag{8}$$

In the formula, m is an adjustable hyperparameter. Its function is to adjust the number of comparisons between a single sample and different types of prototypes, and its maximum value is $k - 1$. In machine learning, gradient descent is a commonly used optimization algorithm. According to the amount of data used to update the parameters each time, it is divided into batch gradient descent, mini-batch gradient descent, and stochastic gradient descent (SGD). After the model training is completed, given a query set sample, the corresponding prediction is as shown in the following equation:

$$y_q = \arg\ \min_k d\left(f_\theta \left(x_q, c_k \right) \right). \tag{9}$$

That is, the sample will be marked as the class of the closest prototype to it. The distance metric part of this loss function consists of two parts. Considering that the proportion of the difference between the two may have a certain impact on the results, parameters can be added before the two parts to control, such as the following formula:

$$l = \alpha \times d^2 (x_i, c_i) - (1 - \alpha) \frac{1}{m} \sum_{j \neq i} d^2 (x_i, c_i). \tag{10}$$

The value range of α is between 0 and 1. By adjusting the value, the numerical proportion of different parts in the loss can be adjusted. However, after experiments, the effect of α is very limited, and the addition or not has little effect on the experimental results. And α is a hyperparameter, and the adjustment of the parameters must be considered after adding it. Taking it into consideration, it is more secure to remove it; that is, the part of the lost contrast remains unchanged.

4. Contour Image Spatial Frequency Domain Feature Extraction Algorithm

4.1. HOG Feature Extraction Algorithm. The essence of HOG is to rely on the statistics of gradients in the image. This gradient information is usually at the edge of the image, and the directional density distribution at the edge can better reflect the information and shape of the local target in the image. The primary basis of HOG is to segment the image and divide it into connected regions called cell units; next, we need to collect the edge or gradient direction histogram of each pixel in the segmented cell unit above, and finally combine them to obtain the feature descriptor we need. These combined directional gradient histograms need to be diffused from the local area, and the contrast normalization operation is performed in a larger area in the image. This larger area is called a block, which is an interval. The main operation steps are to first calculate the density of the histogram of each direction in the whole area, and then normalize the whole cell unit according to the calculated density, so as to reduce the influence of light and shadow on the detection result.

The concept of directional gradient histogram (HOG) was proposed earlier, and it has many advantages compared with other algorithms. First, it is not very sensitive to the effects of optical and geometric distortions in the image, because all its operations are performed in local grid cells. The second point is that under the condition that the local optical normalization is relatively high, the sampling in the spatial domain is relatively coarse, and the sampling in the direction is relatively fine, and some relatively small movements of the human body can be allowed. Usually, these relatively small actions are ignored and have little effect on the final result. Through the above content, we can find that the directional gradient histogram will have a wide range of applications in human body recognition in images.

4.1.1. Calculate the Image Gradient. The gradients of the horizontal and vertical coordinates in the image are calculated, respectively, to obtain the value of the gradient direction of each pixel in the image. Through this derivation method, we can reduce the sensitivity to light and obtain information such as human contours and textures in the image.

The gradient component of the pixel point (x, y) is shown in following equations:

$$G_x (x, y) = H(x + 1, y) - H(x - 1, y), \tag{11}$$

$$G_y (x, y) = H(x, y + 1) - H(x, y - 1). \tag{12}$$

The gradient magnitude and direction of the (x, y) point are as shown in following equations:

$$G(x, y) = \sqrt{G_x (x, y)^2 + G_y (x, y)^2}, \tag{13}$$

$$\alpha(x, y) = \tan^{-1}\left(\frac{G_y (x, y)}{G_x (x, y)} \right). \tag{14}$$

In the directional gradient histogram, the following methods are often used: in the first step, the gradient operator is used to perform convolution calculation to obtain

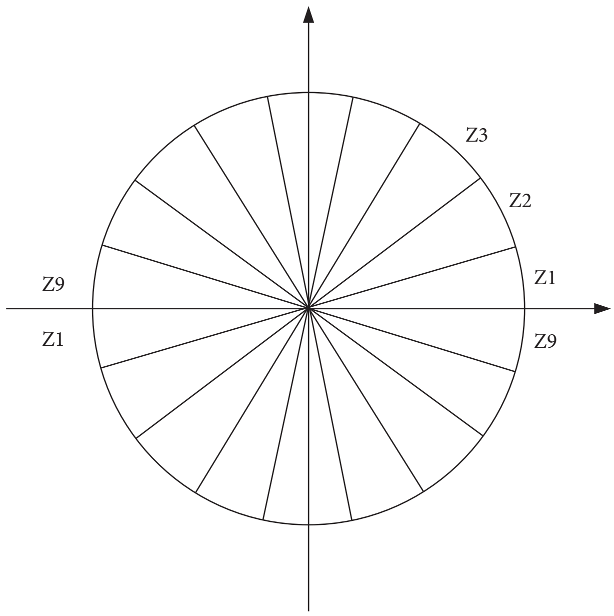

Figure 6: Schematic diagram of gradient direction segmentation.

the gradient component in the horizontal direction; the second step is to use the gradient operator to perform convolution calculation to obtain the gradient component in the vertical direction; and finally, formula (13) and (14) are used to calculate the gradient direction and size at the pixel position.

4.1.2. Construct the Gradient Direction Histogram for Each Unit. This step is mainly to provide a code to the local area, but without destroying the weak sensitivity to human targets while encoding. First, the processed image is divided into several units called cells. Here, we assume that a cell contains 36 pixels, that is, 6×6, and the gradient information of these 36 pixels is counted through the histogram. A cell has a gradient direction of 360 degrees, and we divide it into 9 parts, as shown in Figure 6.

4.2. Classifier. Now add the following explanation: SVM is an effective method to solve the problem of Few-Shot pattern recognition. Finding the generalized optimal classification hyperplane is in high-dimensional space. In order to realize the recognition of multiple categories, it is necessary to make corresponding improvements to the SVM.

At present, many researchers have extended SVM and proposed many excellent algorithms to solve multiclass classification problems. For example, using multiple two-class classifiers and other methods in action recognition, the commonly used kernel functions of SVM include linear kernel and histogram. In this paper, the two factors of SVM classification accuracy and computational complexity are comprehensively considered, and through experimental comparison, the histogram cross-kernel is used as the kernel function of the classifier. Its expression is as in the following equation:

$$K\left(X_i, X_j\right) = \sum_{n=1}^{m} \min\left(a_n, b_n\right). \tag{15}$$

Among them, X_i, X_j is two arbitrary eigenvectors, a_n, b_n is the eigenvalue of the nth dimension, and m is the dimension of the eigenvector. Compared with the other two kernel functions, the histogram cross-kernel has the characteristics of low computational complexity and good classification effect. Then, we input the previously obtained feature vector based on the histogram cross-kernel SVM to obtain the final classifier. After obtaining the test set features, we use the classifier just obtained to make corresponding predictions on the results, and finally achieve action recognition.

4.3. Improved LBP Algorithm. When the improved LBP encodes, firstly, the difference between the gray value of the pixel at the center position and the gray value of its adjacent pixels is taken separately, and then, the difference is added and the average value is obtained to obtain the threshold M, as shown in the following equation:

$$M = \frac{1}{p} \sum_{i=0}^{p-1} \left|g_i - g_c\right|. \tag{16}$$

Then, we use the gray value of the neighboring pixels and the gray value of the center pixel to perform a subtraction operation in a certain order (clockwise or counterclockwise) to get the absolute value, and then add it compare with the threshold M. If the value is greater than M, it is coded as 1; otherwise, it is coded as 0. Its coding formula is shown in the following equation:

$$S\left(g_p - g_c\right) = \begin{cases} 1, & \left|g_p - g_c\right| > M, \\ 0, & \left|g_p - g_c\right| \leq M. \end{cases} \tag{17}$$

Finally, we convert the encoding. Since the computer encoding system uses binary data, we convert it into decimal data that are easy to calculate, as shown in the following equation:

$$\mathrm{LBP}_{P.R}^{*} = \sum_{i=1}^{p-1} S\left(g_p - g_c\right) 2^{p}. \tag{18}$$

4.4. Feature Fusion. Multifeature fusion can retain the effective identification information of various features and can also remove the redundant and invalid parts of various features to a certain extent. Many current feature fusion methods directly merge two sets of feature vectors into a new feature vector in a serial manner. In order to solve this problem, this paper compresses the two features extracted at the beginning and performs weighted fusion, so as to achieve effective fusion of feature vectors, and at the same time appropriately reduce the dimension of feature vectors.

At present, there have been many related researches on multifeature fusion, including the fusion of HOG features and SIFT features, the fusion of HOG features and ordinary LBP features, and the fusion of SIFT features and LBP features. The SIFT feature is a scale-invariant feature transform. SIFT features remain invariant to rotation, scale scaling, brightness changes, etc., and maintain a certain degree of stability for viewing angle changes, affine transformations, occlusions, and noise, and are relatively stable local features. However, it detects too few feature points for blurred images and images with smooth edges, resulting in a low recognition accuracy. In the follow-up experiments, the proposed algorithm is also compared with these existing fusion methods.

Due to the above shortcomings of a single feature, this paper proposes a method based on the fusion of HOG features and improved LBP features. Feature fusion first needs to extract a large amount of feature information and then compares the information. Although this can enhance real-time performance, it will lead to missing information and inaccurate results. However, if we adopt serial fusion, although the recognition accuracy can be improved, it will lead to an increase in the amount of data and reduce the detection efficiency. Select a video from Weizmann and YouTube, respectively, and then extract the video frame image, and perform grayscale and normalization processing on the image. It is mainly to standardize Gamma and color space and also to reduce the influence of lighting and other factors on the detection results. Therefore, this paper adopts the method of weighted fusion of HOG features and improved LBP features. The algorithm flowchart is shown in Figure 7.

(1) In an image, the exposure of the local surface layer accounts for a large proportion of the texture intensity. By normalizing the image, we can greatly reduce the lighting and the effect of shadows on the local part of the image. Typically, we first convert the image to grayscale. The Gamma compression formula is shown in equation (19), and Gamma is represented by 1. In this experiment, the value of 1 is taken as 0.5.

$$I(x, y) = I(x, y)^{\gamma}. \tag{19}$$

(2) Normalize the scale of the two feature sets obtained.

(3) Use a weighted method to perform feature fusion to obtain the final feature set, as shown in equation (20). Among them, $\alpha, \beta \geq 0$ is the weight, which satisfies $\alpha + \beta = 1$.

$$T(l) = \alpha L(I) + \beta H(I). \tag{20}$$

(4) Use the SVM classifier to identify in which the SVM kernel function adopts the histogram cross-kernel.

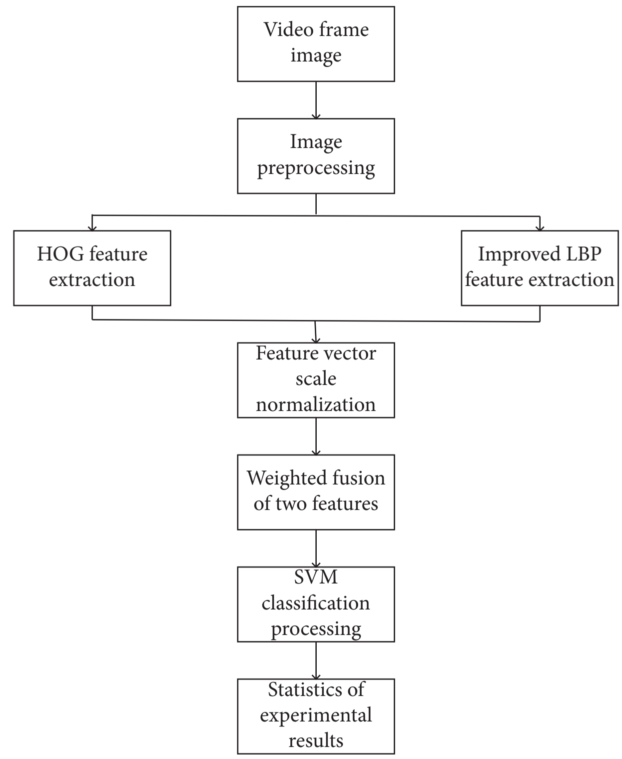

Figure 7: Flowchart of feature fusion algorithm.

5. Recognition and Analysis of Dance Fitness Movements

Dance fitness movements are complex, especially under high-speed movement, various movements are difficult to capture and cannot achieve good results. In this paper, three common movements in dance fitness are selected for identification and analysis. The three movements are walking, opening hands, and running. The feature extraction structure of a single frame is shown in Figure 8.

As shown in Figure 8, in different actions, the contours extracted from the two feature maps are relatively clear, but some details are still blurred. Therefore, the action recognition for dance fitness still needs to be optimized.

For the Omniglot dataset, the training epoch = 100, the learning rate is 0.001, and the dynamic adjustment strategy is adopted, and the learning rate is adjusted to one-half of the original every 20 rounds. The value of episode is set to 100 in one epoch, and the number of categories in each episode is set to 60. By adjusting the number of samples for each category in the support set to 1 and 5, and the number of categories to 5 and 20, the corresponding n-way k-shot training is completed. For the miniImageNet dataset, due to the large amount of data, the total number of training rounds is set to 200, that is, epoch = 200, and the learning rate is 0.001. The dynamic adjustment strategy of the learning rate is the same as above, and the value of episode in each epoch is also 100. When the image is input, it will be scaled to a size of $84 * 84$. In order to speed up the convergence, the RGB channels of the image will be normalized. During SeProtNet training, the value of γ is set to 16.

The training process under the 5-way 5-shot setting is shown in Figure 9. When the number of iterations is 161,000, the image classification model based on Transformer Few-

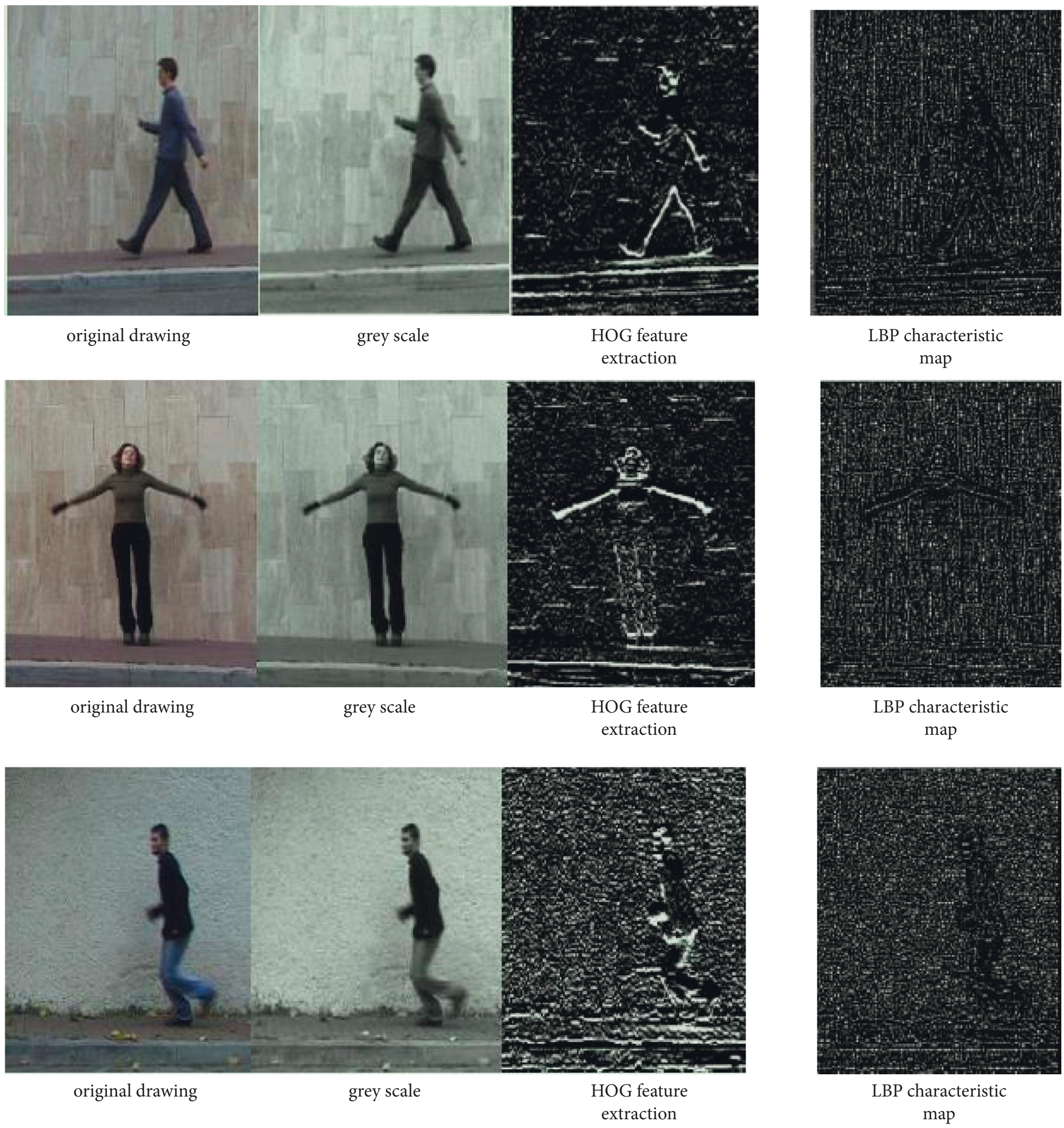

Figure 8: HOG and LBP feature maps under different actions.

Shot learning achieves the highest accuracy rate of 85.28% on the validation set. It can be seen from Figure 9 that the image classification model based on Transformer Few-Shot learning in the case of 5-shot, when the accuracy rate and loss basically converge, the fluctuation range is much smaller than the 1-shot setting.

As shown in Table 3, in the testing phase, the trained model performance is measured by randomly building 600 segment tasks. The accuracy of the Transformer Few-Shot-based learning model is better than the other methods in both settings, with 66.75% accuracy under 1-shot setting and 82.05% under 5-shot setting. Among them, the prototype network, that is, the model without Transformer and group regularization, is the basic network of this model. Compared with the prototype network, the accuracy of this model has been greatly improved, with an increase of 6.43% under the 1-shot setting and 4.03% under the 5-shot setting.

As shown in Figure 10, the three actions of walking, opening hands, and running are analyzed under the dataset. The accuracy of different algorithms is different, but the recognition efficiency of the feature extraction algorithm that combines HOG and improved LBP algorithm has always been high. The recognition accuracy rates of walking, opening hands, and running are 93.10%, 90.30%, and 92.70%, respectively. This illustrates the effectiveness of the fusion feature algorithm.

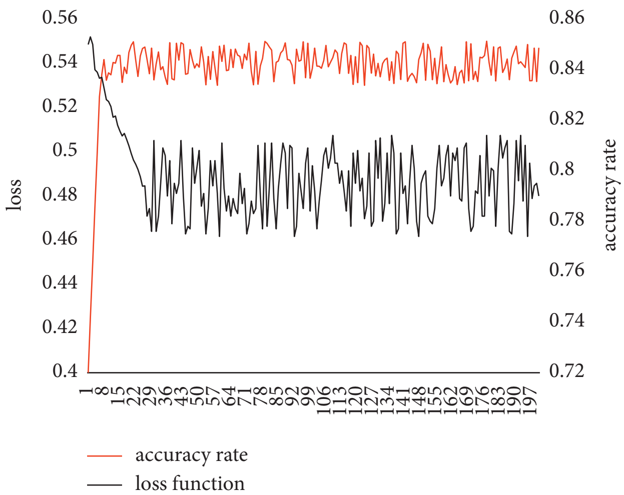

Figure 9: Iterative curve of accuracy loss in 5-way 5-shot.

Table 3: Few-Shot classification results based on different methods.

way	1-Shot (%)	5-Shot (%)
HOG	60.37	78.02
LBP	62.08	78.63
Improved LBP	62.64	80.51
HOG + LBP	64.60	79.51
HOG + Improved LBP	66.87	82.44

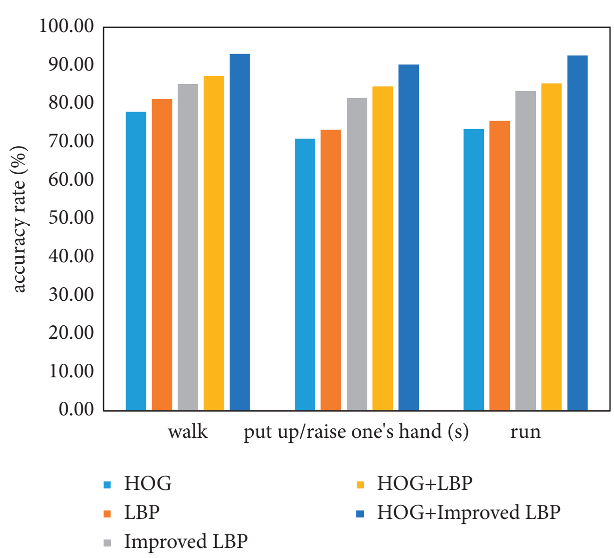

Figure 10: Recognition accuracy of different feature extraction algorithms.

6. Conclusions

Few-Shot and data imbalance are frequently symbiotic in practical applications. Data augmentation, knowledge transfer between similar categories, data synthesis, structured knowledge graph, domain adaptive learning, and model solvability are all strategies that can help Few-Shot learn better. At the moment, Few-research Shot's is primarily focused on image data modeling and processing. Many fields of supervised learning, such as video object detection and semantic segmentation, have an urgent need for Few-Shot learning, and other directions are also worth exploring. Furthermore, in the future, directions such as natural language processing and recommendation systems will be important application scenarios for Few-Shot learning.

Data Availability

The data used to support the findings of this study are available from the corresponding author upon request.

Conflicts of Interest

The authors do not have any possible conflicts of interest.

References

[1] C. Tarn and W.-F. Zeng, "pDeep3: Toward more accurate spectrum prediction with fast few-shot learning," *Analytical Chemistry*, vol. 93, no. 14, pp. 5815–5822, 2021.
[2] G. Szcs and M. Németh, "Double-view matching network for few-shot learning to classify covid-19 in X-ray images," *Infocommunications Journal*, vol. 13, no. 1, pp. 26–34, 2021.
[3] C. Li, Y. Hou, P. Wang, and W. Li, "Joint distance maps based action recognition with convolutional neural networks," *IEEE Signal Processing Letters*, vol. 24, no. 5, pp. 624–628, 2017.
[4] Q. Ke, S. An, M. Bennamoun, F. Sohel, and F. Boussaid, "SkeletonNet: mining deep Part Features for 3-D action recognition," *IEEE Signal Processing Letters*, vol. 24, no. 6, pp. 731–735, 2017.
[5] X. Wang, L. Gao, J. Song, and H. Shen, "Beyond frame-level CNN: Saliency-aware 3-D CNN with LSTM for video action recognition," *IEEE Signal Processing Letters*, vol. 24, no. 99, pp. 510–514, 2017.
[6] A. Ullah, J. Ahmad, K. Muhammad, M. Sajjad, and S. W. Baik, "Action recognition in video sequences using deep Bi-directional LSTM with CNN features," *IEEE Access*, vol. 6, no. 99, pp. 1155–1166, 2018.
[7] L. You, H. Jiang, J. Hu et al., "GPU-accelerated Faster Mean Shift with euclidean distance metrics," 2021, https://arxiv.org/abs/2112.13891.
[8] Y. Zhang, K. Xia, Y. Jiang et al., "Multi-modality fusion & inductive knowledge transfer underlying non-sparse multi-kernel learning and distribution adaption," *IEEE/ACM Transactions on Computational Biology and Bioinformatics*, 2022, in press.
[9] D. Yao, Z. Zhi-li, Z. Xiao-feng et al., "Deep hybrid: multi-graph neural network collaboration for hyperspectral image classification," *Defence Technology*, 2022.
[10] W. Cai and Z. Wei, "Remote sensing image classification based on a cross-attention mechanism and graph convolution," *IEEE Geoscience and Remote Sensing Letters*, vol. 5, 2020.
[11] J. Kong, H. Wang, C. Yang, X. Jin, M. Zuo, and X. Zhang, "A spatial feature-enhanced attention neural network with high-order pooling representation for application in pest and disease recognition," *Agriculture*, vol. 12, no. 4, p. 500, 2022.
[12] Z. Huang, Y. Liu, C. Zhan, C. Lin, W. Cai, and Y. Chen, "A novel group recommendation model with two-stage deep learning," *IEEE Transactions on Systems, Man, and Cybernetics: Systems*, 2021, In Press.

[13] M. Gao and J. Mao, “A novel active rehabilitation model for stroke patients using electroencephalography signals and deep learning technology,” *Frontiers in Neuroscience*, vol. 1459, 2021.
[14] J. Zhou, D. Liu, X. Xie, and W. Zhang, “Underwater image restoration by red channel compensation and underwater median dark channel prior,” *Applied Optics*, vol. 61, no. 10, pp. 2915–2922, 2022.
[15] J. Zhou, T. Yang, W. Chu, and W. Zhang, “Underwater image restoration via backscatter pixel prior and color compensation,” *Engineering Applications of Artificial Intelligence*, vol. 111, Article ID 104785, 2022.
[16] Y. Zhao, H. Di, J. Zhang, Y. Lu, F. Lv, and Y. Li, “Region-based Mixture Models for human action recognition in low-resolution videos,” *Neurocomputing*, vol. 247, pp. 1–15, 2017.
[17] S.-L. Cheng, H.-F. Sun, and M.-L. Yeh, “Effects of an 8-week aerobic dance program on health-related fitness in patients with schizophrenia,” *Journal of Nursing Research*, vol. 25, no. 6, pp. 429–435, 2017.
[18] N. Sato, “Injury surveillance in street dance in Japan,” *Japanese Journal of Physical Fitness and Sports Medicine*, vol. 67, no. 6, pp. 431–437, 2018.
[19] S.-E. Lee, “Effects of individualized korea dance program for elderly women,” *Korean Journal of Sports Science*, vol. 26, no. 1, pp. 993–1000, 2017.
[20] A. Nain and N. Yurievna, “Implementation of “fitness mix” dance fitness program in physical education for senior preschool children,” *Science & Sports: Current Trends*, vol. 8, no. 2, pp. 129–136, 2020.

Hindawi
Computational Intelligence and Neuroscience
Volume 2022, Article ID 7971904, 11 pages
https://doi.org/10.1155/2022/7971904

Research Article

Analysis of Human Exercise Health Monitoring Data of Smart Bracelet Based on Machine Learning

Xiaoge Ma

School of Sports and Leisure, Guangdong Ocean University, Zhanjiang, Guangdong,524088, China

Correspondence should be addressed to Xiaoge Ma; tyxymxg@gdou.edu.cn

Received 11 April 2022; Revised 4 May 2022; Accepted 5 May 2022; Published 8 June 2022

Academic Editor: Xin Ning

The smart bracelet has become a hot-selling commodity, according to a daily consumption survey. Based on people's interest and concern for their health, the smart bracelet, as a design and application for achieving healthy weight loss monitoring, is quickly becoming a popular new favorite. This bracelet detects fat using the near-infrared diffuse reflection principle, with the goal of assisting people in controlling and maintaining a healthy weight. A large amount of data has been accumulated in all walks of life due to the development of the Internet network and data storage technology. As a result, the emergence of machine learning plays a critical role in the data analysis of human sports health monitoring of smart bracelets. Based on machine learning, this paper investigates the data analysis of human sports health monitoring smart bracelets. When the population index reaches 50 in the analysis of health monitoring data, the average accuracy of data mining is 86.8 percent, the average accuracy of the association rule algorithm is 85.9 percent, the average accuracy of the collaborative filtering algorithm is 84.3 percent, and the average accuracy of the machine learning algorithm is 90.1 percent in this paper. Among the four algorithms, the method presented in this paper is clearly the most effective, stable, and accurate. The system's stability and accuracy have been greatly improved by the addition of GPS-assisted and hand-up misjudgment algorithms. Because the smart bracelet is inexpensive, easy to wear, and consistent with consumer psychology, it is becoming increasingly popular to use it to monitor the human body's sports health.

1. Introduction

With the increasingly fierce social competition, young people's work pressure is gradually increasing, and they have little time to pay attention to the travel activities and vital signs of the elderly and children, such as obesity caused by less exercise, falling alarm of the elderly, exercise monitoring and calorie consumption, and measurement of heart rate and exercise [1, 2]. The smart bracelet has become a hot-selling commodity, according to a daily consumption survey. Based on people's current interest and focus on health, the smart bracelet, as a design and application for achieving healthy weight loss monitoring, is quickly becoming a popular new favorite. This bracelet detects fat using the near-infrared diffuse reflection principle, with the goal of assisting people in controlling and maintaining a healthy weight [3]. Currently, scientific researchers in the field of sports health use the traditional acceleration motion sensor worn at the waist to monitor physical activity, obtain effective data for analysis and processing, provide a scientific foundation for mass sports fitness, and increase the scientificity of mass sports fitness. However, the bracelet must use its own algorithm to calculate the acceleration vector length changes in three directions of wrist movement during human movement. However, because the wrist's movement direction cannot be determined, calculating the number of steps of the bracelet in software requires high accuracy. Because the traditional acceleration motion sensor is small and convenient and does not require subject review, it can effectively reduce recall bias and accurately provide information about energy consumption, frequency, intensity, and duration of physical activities through the validity tests of various methods, and it has been widely accepted and applied in scientific research.

With the development of the Internet network and data storage technology, a large amount of data has been accumulated in all walks of life. The application of health monitoring data mainly refers to the use of Internet technology and big data technology [4, 5] for data mining and analysis, the analysis and integration of health information and data at all levels, and the improvement of health services, to make the operation of various medical industries at all levels more efficient and make the services of various medical industries at all levels better under the background of China's informatization. Machine learning [6–8] can not only be applied to the preprocessing stage of monitoring data but also, more importantly, it is necessary to establish a learning model and actively learn the information contained in the data to evaluate the safety of the structural state and reflect the health state in time. In the face of a large amount of information generated all the time, the traditional manual method is simply unable to make efficient and rapid judgment [9, 10]. Machine learning first appeared in the last century. Learning in machine learning actually wants to express learning from data. It consists of three parts: unsupervised learning, semisupervised learning, and supervised learning. Machine learning uses computers to simulate human learning activities. Today, machine learning is the main way to deal with big data. As a multidisciplinary field, machine learning is widely used [11].

The use of machine learning in the analysis of human exercise health monitoring data from a smart bracelet is reflected not only in the preprocessing of raw data and the efficient operation of the learning model but also in the "iterative optimization" of the machine learning model. The most significant difference between machine learning and traditional manual quantitative and qualitative analysis is that the algorithm has the property of "iterative optimization," which means that the learning model established by machine learning can be optimized step by step. The more data samples there are, the more effective the information the learning model has, and the model's accuracy and precision can be continuously improved [12, 13]. To accurately and efficiently synthesize existing motion capture data into a new motion sequence, three basic problems must be solved: how to establish a mathematical model of human motion, how to reduce the dimension of the motion data, and how to quickly and accurately synthesize a new motion sequence [14]. Because these three fundamental problems are so closely related, the applicable dimensionality reduction method and synthesis algorithm are determined by the specific mathematical model. Simultaneously, the specific synthesis algorithm and dimensionality reduction method require the assistance of specific mathematical models. The accelerometer principle is also used by the smart bracelet to monitor physical activity. By connecting with the corresponding mobile phone application software, the public can intuitively obtain physical activity index data such as energy consumption and daily steps, thus effectively monitoring the realization of long-term or short-term physical activity goals. In addition, because the smart bracelet is affordable, easy to wear, and in line with the public's consumption psychology, it is becoming more and more popular to apply the smart bracelet to monitor the level of human sports health [3]. The innovations of this paper are as follows:

(1) Based on machine learning, this paper builds an intelligent Bracelet human motion health monitoring data model. The machine learning process entails training the model on a large number of task-related data sets; iterating the training model continuously to obtain a reasonable model fitting the data set; applying the training adjusted model to the real scene. The selection of input parameters, output parameters, and learning algorithm is part of the process of developing a predictive GRF learning model.

(2) A data collection system for intelligent Bracelet human movement health monitoring is built. Although researchers are dedicated to testing the validity of sports intelligent Bracelet monitoring physical activities, the intelligent Bracelet human sports health monitoring data system is still in its early stages. This paper analyzes and summarizes existing research results and research progress by combing the relevant literature on the validity of sports intelligent Bracelet evaluation steps, energy consumption, distance, and physical activity intensity, in order to serve as a reference for future research.

The following sections comprise the overall structure of this paper: The first chapter discusses the history and significance of human movement in intelligent bracelets before moving on to the main work of this paper. The second chapter focuses primarily on the related work of intelligent Bracelet human movement both at home and abroad. The algorithm and model of machine learning are introduced in the third chapter. The fourth chapter describes the implementation of human motion health monitoring data from an intelligent bracelet, as well as the experimental part's analysis. The fifth chapter is a synopsis of the entire document.

2. Related Work

2.1. Research Status at Home and Abroad. Ciocca Gianmarco proposed that the health monitoring system of human movement of the intelligent bracelet is indeed much more efficient than the traditional manual method, but it also brings many challenges while providing real-time data: How to transform the noisy original data into processable and effective information, and how to further improve the computing power of the algorithm model to process the increasing real-time monitoring data [15]. Tang et al. proposed that while adding some new functions, the design and development of an intelligent bracelet will take the advantages and disadvantages of the 37-degree bracelet as a reference. On the basis of avoiding similar disadvantages, some design improvements have been added to the bracelet developed this time [16]. Garofolini a et al. proposed that human motion recognition technology based on acceleration sensors has been a hot research topic in the field of human motion recognition and health monitoring data analysis for a long time. It aims to use various information or data processing technologies to establish a behavior perception platform for the purpose of finding the representation, modeling, and prediction methods of health monitoring data movement [17]. GFA B et al. proposed that the core of the health monitoring system of human movement of the intelligent bracelet is a set of systems that analyzes the output response state based on structural information, historical records, and real-time data collected by sensors to evaluate the use and safety [18]. Vaz *d* v et al. proposed that in recent years, artificial intelligence technology is in the stage of rapid development, and the big data analysis industry is booming. Borrowing artificial intelligence technology is not only the trend of human motion recognition but also the inevitable result of the development of the motion recognition field [19]. Aerenhouts Dirkdirk proposed that there are two kinds of posture recognition technologies: wearable and nonwearable. As the name implies, wearable technology refers to the human body posture recognition technology, such as image recognition, in which the posture recognition device is not in direct contact with the human body. Compared with nonwearable, wearable human posture recognition technology has the advantages of unlimited space and has a better development space in research and application [20]. Julie M et al. proposed that for common physical activities, using the acceleration and gyroscope in smartphones to recognize human motion can achieve good accuracy. It has great potential to develop timely action classification and recognition and feedback programs with intelligent mobile terminals [21]. Higueras-Fresnillo S et al. proposed a PHM system based on Bayesian estimation theory and general particle swarm filtering framework, which integrated the modules of human motion data processing, eigenvalue extraction, fault diagnosis, and failure prognosis of the smart bracelet. Purdue University's Intelligent Process System Laboratory has put forward different solutions based on knowledge discovery, neural networks, and statistical analysis in the field of risk identification of complex systems [22]. Yanci Javier proposed to use the smart bracelet to recognize human motion, which is basically the processing of the information of human motion captured by sensors in the bracelet. Considering that the research object of this subject is people, which have wide differences and the quality of smart bracelets worn is also different, the acceleration sensor equipped with each smart bracelet is used as the human motion data acquisition module based on human motion recognition of smart bracelets [23]. Monajati Alireza Larumbe proposed that the basic human motion recognition method of a smart bracelet is the threshold detection method. That is, by judging whether the sensor value exceeds the set value, several kinds of actions can be distinguished. For example, several ongoing basketball playing actions can be identified by the data interval and vibration amplitude collected by the acceleration sensor [24].

2.2. Research Status of Human Motion Health Monitoring Data of Intelligent Bracelet Based on Machine Learning. This paper uses machine learning to analyze the human movement health monitoring data of an intelligent Bracelet. In comparison to previous studies, this method has the functions of step counting, positioning, and vital sign monitoring. It can calculate the number of steps a person walks using the pedometer function and the movement distance using the GPS positioning function to calculate the number of calories consumed, making it easy for people to understand their own and family members' movements. A heart rate sensor is a sensor that detects the rate of the heart. Accurate motion analysis can be achieved by collaborating with other sensors. Typically, three methods are used: photoelectric transmission measurement, test ECG signal measurement, and vibration measurement. When the heart is bleeding, the blood absorbs light of a specific wavelength. This characteristic of blood is used by the photoelectric transmission measurement method to determine heart rate. In light of this phenomenon, this paper performs hardware circuit design and software debugging, relying on the intelligent bracelet as the medium, so that the bracelet can not only realize indoor high-precision positioning but also upload the carrier's vital signs information to the positioning server, so that family members can accurately understand the internal position and physical condition in time. Furthermore, people may feel uneasy in the continuous monitoring environment for an extended period of time. This uneasy state will impair a person's activity performance and lead to inaccurate behavior detection. Furthermore, the video acquisition results will contain information about the life of the monitoring object, and improper use will result in the disclosure of users' personal information. Researchers have increasingly introduced various methods in machine learning into the research of human motion health monitoring of intelligent bracelets due to the high-dimensional characteristics and great temporal and spatial correlation of human motion data, which has made great progress in the research of human motion health monitoring of intelligent bracelets.

3. Algorithm and Model of Machine Learning

Simulated learning is another name for machine learning. In layman's terms, this means that computers are learning how to think like humans. It stimulates the human learning process in order to achieve learning. Computers are used to simulate human learning activities in machine learning. Following the computer learning process, it will acquire data information and new knowledge in order to continuously improve its performance. Machine learning is defined as "a process in which a model learns and explores the existing connections and potential information among data based on the existing information set, in order to continuously optimize its own performance." When compared to traditional computing methods, the most distinguishing feature of machine learning is its "self-learning and self-adaptation." It has achieved great success in many fields such as finance and biology by fully drawing on the working mechanism of the human brain "neurons are connected hierarchically and information is updated iteratively." The decision tree algorithm is a popular machine learning algorithm that is used not only for classification but also for regression. This algorithm serves as the foundation for many other advanced algorithms. Machine learning is classified into two types: supervised learning and unsupervised learning, depending on whether the training samples are labeled manually in advance. Supervised learning is a learning method that uses labeled data as the training data set, learns the rules for dividing objects from the training data set's characteristics, applies this rule to predict classification results on the test data set, and outputs the labeled results. Unsupervised learning is a learning method that is used to deal with data that has not been labeled or classified. Its goal is to discover potential relationships and statistical laws between data in order to determine the characteristics of the sample data. A decision tree is an inverted tree structure composed of a root node, an inner node, a leaf node, and an edge. The root node is the highest node, the leaf node provides the judgment conclusion, and the internal node is a relative concept. The purpose of building a decision tree is to perform classification or regression. The purpose of this paper is to investigate classification or the relationship between target variable categories and attributes. We can predict the category of the test data set once the relationship is built. At the moment, more research is needed on the high integration of "data collection, data preprocessing, data analysis, model evaluation, information visualization, and early warning mechanism." Figure 1 depicts the basic structure of a common structural health monitoring system, which is made up of five major components: "online test, real-time analysis, damage identification, condition assessment, and maintenance decision."

The main information about each meal in the file has two parts. One is the position and rotation information of the root joint. The second is the rotation information of each joint. Therefore, each frame of human motion can be expressed as follows:

$$f_i = \left(p_i, r_i^1, r_i^2, \ldots r_i^n\right), \tag{1}$$

where f_i represents the data of the i, p_i represents the position and rotation information of the root joint in the frame, $r_i^1, r_i^2, \ldots r_i^n$ represents the rotation angle $r \in R^3$ of each joint, and n is the number of joints defined in the ASF file.

Therefore, a motion sequence defined by the $ASF - AMC$ capture data file can be expressed as follows:

$$\text{motion} = \left(f_1^T, f_2^T, \ldots f_m^T\right), \tag{2}$$

where f_i^T is the transpose of i frame data f_i, and m is the number of rounds of the motion sequence.

Mathematicians have proved that the connection of a rotation sequence is equivalent to a single rotation. Therefore, any angular displacement can be expressed as a single rotation of an object around a certain axis. That is, a corner of the axis is used to describe (n, θ) s orientation, n represents the unit vector of the axis, and θ represents the angle of rotation around the axis. This method is seldom used in implementation, usually replaced by Euler angle or quaternion.

$$\begin{aligned} q &= \left[\cos\frac{\theta}{2}, n\sin\frac{\theta}{2}\right], \\ q &= \left[\cos\frac{\theta}{2}, \left(n_x\sin\frac{\theta}{2}\right) n_y\sin\frac{\theta}{2} n_x\sin\frac{\theta}{2}\right]. \end{aligned} \tag{3}$$

Therefore, if the quaternion $p = [0, (x, y, z)]$ is used to represent a standard point in the three-dimensional space, and the corner of the rotating axis is (n, θ), let the quaternion $q = [\cos\theta/2, n\sin\theta/2]$, and the formula can show that the point p rotates by θ degrees around the n axis.

$$p' = qpq^{-1}. \tag{4}$$

According to the connectivity of rotation, if the point p rotates through quaternions a , b , according to the associative law of quaternions, it can be expressed as follows:

$$\begin{aligned} p' &= b\left(apa^{-1}\right)b^{-1} \\ &= (ba)p\left(a^{-1}b^{-1}\right). \end{aligned} \tag{5}$$

Therefore, the rotation of a certain point in three-dimensional space can be expressed by the connection of multiple quaternions.

Let two similar motion sequences T, R, whose sequence lengths are t, r, respectively. Normally, $t \neq r$ can be known from the following formula:

$$\begin{aligned} T &= \left[T_1 T_2 \ldots T_t\right], \\ R &= \left[R_i R_2 \ldots R_r\right]. \end{aligned} \tag{6}$$

Among them, the dimension of $T_i, R_j (i \in [1, t], j \in [1, r])$ is P . The purpose of $DT\ W$ algorithm is to find an optimal synchronization path by pattern matching the two motion sequences, so that the two motion sequences have the same length and retain the most complete data information, that is, to find the sequence F^* in a grid

$$F^* = \{c(1), c(2), \ldots, c(k), \ldots, c(K)\}, \max(t, r), \tag{7}$$

where $c(k)$ can be expressed as follows:

$$c(k) = [i(k), j(k)]. \tag{8}$$

$c(k)$ means that when the k frame is matched, comparing the $i(k)$ frame of sequence T with the $j(k)$ frame of sequence R , $c(k)$ can be regarded as a point in $t \times r$ grid. With the increase of k , it moves in $t \times r$ grid, and the curve formed by its moving track is the matching path. Therefore, F^* is also called time bending function.

Since the generated shortest matching path must be equal to the length of motion sequence T , $k = t$ and $k = i$ can be obtained

$$F^* = \{c(1), c(2), \ldots c(i), \ldots, c(t)\}. \tag{9}$$

Obtain the shortest matching path F^* , an asymmetric algorithm called $DT\ W$. Including all frames of the standard reference sequence T , and some posts in the sequence R to be aligned are compressed or stretched due to different local

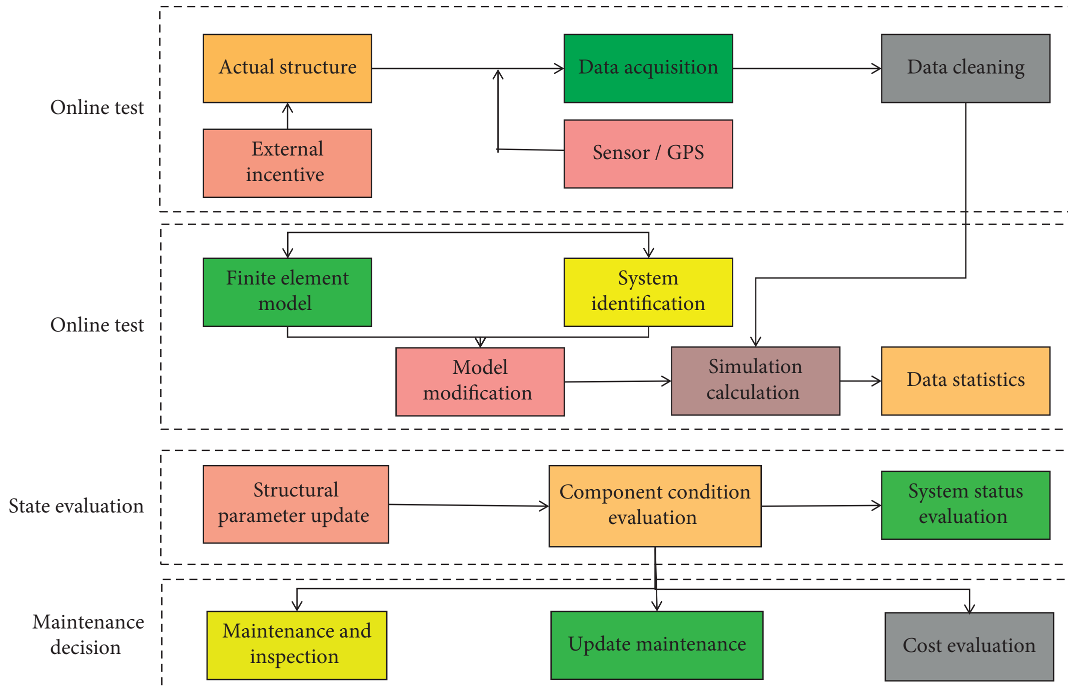

Figure 1: Machine learning health monitoring model.

features from the standard reference sequence. After this processing, the motion data before and after alignment are different, resulting in the following effects.

In the algorithm of machine learning, the artificial neural network is a mathematical model which can imitate brain neurons to a certain extent. In the algorithm of machine learning, artificial neural network processes data in this way, and the application of an artificial neural network is also very much. The process of machine learning includes using a large number of task-related data sets to train models. Through the error of the model on the data set, the model is repeatedly trained, and a model that fits the data set reasonably is obtained. Apply the trained and adjusted model to the real scene. A process of building a predictive GRF learning model includes the selection of input parameters, output parameters, and learning algorithm. Decision tree algorithm has the general characteristics of machine learning algorithms, which build models based on specific data, so it is different from traditional statistical models. It does not need prior assumptions, and it does not need data to obey any probability distribution. This is actually a very good feature because the actual data is generally difficult to meet the settings of those boxes. The core idea of deep learning is that unsupervised learning from bottom to top trains the data layer by layer and extracts the statistical characteristics nonlinearly, constantly updates and establishes the mapping relationship in the calculation, establishes the initialized network, and iteratively updates and optimizes the network parameters by using supervised learning from top to bottom, thus achieving the expected effect. Different from the shallow network structure, the multihidden layer structure of deep learning can break through the parity problem of the shallow structure, can complete the approximation of complex functions, realize the accurate processing of complex problems, and has good generalization ability. The smart bracelet system designed in this paper consists of two parts: smart bracelet and ultrawideband positioning system. The smart bracelet can be divided into six modules according to its functions, and the relationship between the components of the modules and the sensors is shown in Figure 2.

The power management module, which consists of a charging chip and a voltage stabilizing chip, is one of the six modules of the smart bracelet: A microcontroller can control data acquisition and processing; There is a mobile node and low-power Bluetooth communication module; Gyroscopes are used to realize the motion state module of step counting and motion state analysis. TFT-LCD display screen is used in the display module. A sign sensor module includes a heart rate and blood pressure sensor, a blood oxygen sensor, and a temperature sensor. The sensor's data can be transmitted to the mobile app via low-power Bluetooth, and it can also be viewed on the display screen. Second, the mobile node in the UWB positioning system can communicate with the basic positioning wireless network to master the accurate location of the bracelet carrier in real time. Traditional signal processing and kinematics methods have lost their advantages in these technologies due to the rise of machine learning methods because traditional methods cannot well model some complex characteristics of the above motion data, whereas appropriate machine learning methods can not only model them but also effectively use these characteristics to complete specific tasks. Although the tasks of motion restoration and motion denoising differ slightly, the former is dedicated to regaining the lost joint position during the capture process, while the latter is dedicated to combating noise, but their methods are similar. As a result, they are not

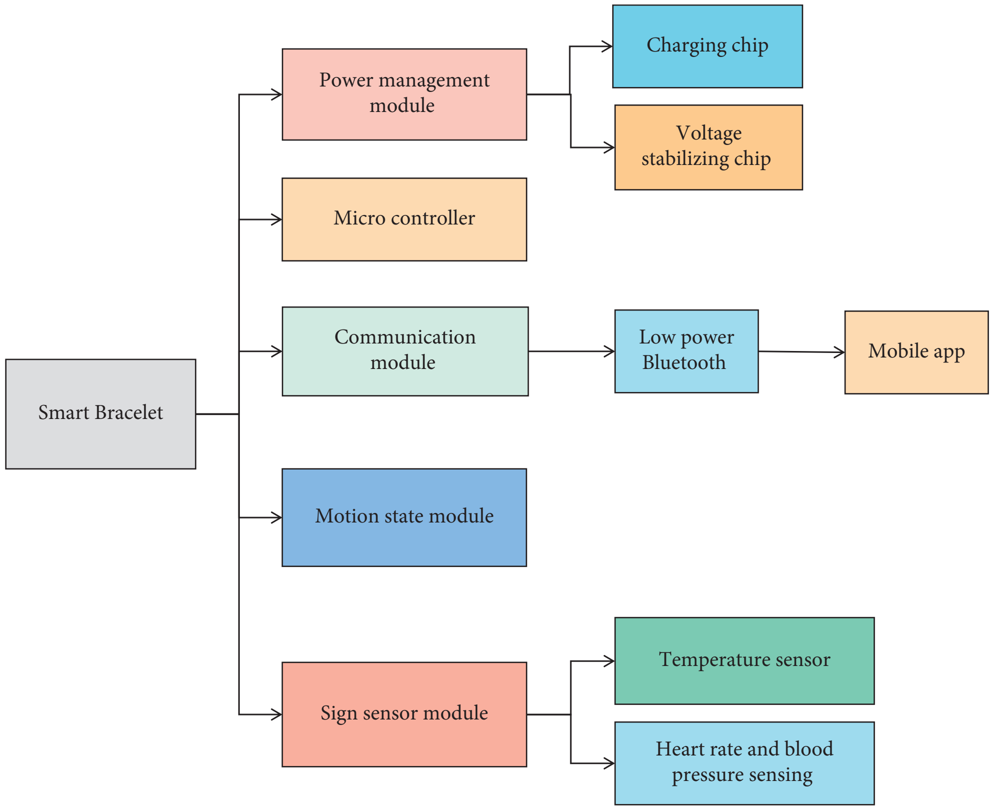

Figure 2: Functional module diagram of intelligent Bracelet system.

deliberately distinguished when introducing the current state of motion restoration research.

4. Realization of Monitoring Data of Human Exercise Health with Intelligent Bracelet

4.1. Design of Intelligent Bracelet Human Exercise Health Monitoring Data System. The monitoring data of human exercise health of intelligent bracelets is the key technology and the most difficult link in the process of exercise data reuse. The analysis of human exercise health monitoring data system under machine learning has high dimensions, a large amount of information, and a complex structure, all of which bring challenges to exercise synthesis. The synthesized motion data will eventually be used for viewing, and the human eye is very good at finding out the incongruities in the motion, which puts forward higher requirements for motion synthesis. Usually, there are many physical quantities in the data of human motion recognition, and different physical quantities have different measurement methods, so they cannot be directly compared with each other. Therefore, it is necessary to normalize the feature vectors so that different feature vectors are in an equal and comparable position. In this paper, the normalization function map minmax in Matlab is used to normalize the characteristic data. After normalization, the restriction of units between different eigenvalues is eliminated, and the differences between different individuals are also reduced, and they are converted into pure values to facilitate feature extraction and comparative analysis. In the data system of human exercise health monitoring with an intelligent bracelet based on machine learning, users can switch measurement functions and observe data through touch screen, so three interfaces are designed according to bracelet functions. One is a clock interface to display real-time time. The main menu interface allows users to independently select the functions to be measured. The other is the display interface to display the measured data in real time. The structure of the sports bracelet includes a system processor module, sensor module, GPS module, and OLED display module. MK60DN512ZVLQ10 chip is adopted as the processor, which is a 32-bit processor with ARM-CORTEX-M4 as the core introduced by NXP. Whether it is used for scientific research or mass fitness, it is very important to evaluate its validity.

At present, under the intelligent Bracelet human sports health monitoring data system, although researchers are committed to testing the validity of sports intelligent Bracelet monitoring physical activities, it is still in its infancy. This paper analyzes and summarizes the existing research results and research progress by combing the relevant literature on the validity of sports intelligent Bracelet evaluation steps, energy consumption, distance, and physical activity intensity, so as to provide reference for further research. The sensor module includes an acceleration sensor mpu6050, which includes a multichannel ad, which can convert the obtained analog data into digital signals and transmit them to the processor through IIC. Through processing, it can obtain the human motion state, realize the step measurement function and control the OLED on and off function. The pulse heart rate sensor pulse sensor outputs analog signals, which are processed by ad to detect human heart rate data in real time. The GPS module sends data to the processor in the form of serial port to obtain position coordinate information. Therefore, motion synthesis has always been a very hot research topic. With the deepening of research, some excellent motion synthesis algorithms have emerged. Among them, the data-driven motion synthesis method can maintain the temporal and spatial characteristics of motion data, so it has been widely studied and applied. According to its different implementation methods, it can be divided into four categories: motion mixing, motion synthesis based on graph search and motion transition, parametric motion synthesis, and motion synthesis based on deep learning. Then machine learning is used to analyze the acceleration data of the smart bracelet to realize the attitude recognition on the mobile device. Finally, the comparative analysis of human motion based on various methods verifies that the analysis system of human motion health monitoring data system of intelligent bracelet based on machine learning is more accurate than traditional recognition methods such as support vector machine, more convenient and more practical than computer-based analysis platform.

4.2. Experimental Results and Analysis. The type of SVM selected in this study is C-SVC. When studying the effect of the RBF kernel, the loss function C of C-SVC and the gamma function G of the RBF kernel have a major impact on the recognition accuracy. The labeled test set is brought into the classifier for verification, and the classification accuracy rate is 94.4652%. The results expressed in are shown in Table 1. The training time is 45.702 seconds, and the testing time is 0.0242 seconds.

As the gamma function does not need to be set for the linear kernel, this study only needs to set the loss function C of C-SVC when testing with linear kernel and bring the labeled test set into the classifier for verification, and the classification accuracy rate is 93.0495%. The results are shown in Table 2. The training time is 60.885 seconds, and the testing time is 0.023 seconds.

From Tables 1 and 2, it can be seen that both RBF kernel SVM algorithm and linear kernel algorithm can achieve more than 90% recognition rate for the problems studied in this paper, and the recognition accuracy of RBF kernel SVM classification algorithm is slightly higher than that of linear kernel SVM algorithm, and the memory occupation and training time of the former are better than those of the latter. It can be seen that the RBF kernel is more suitable for the human motion recognition algorithm studied in this paper.

In this experiment, the human movement health monitoring data of intelligent bracelets are analyzed, and the data mining algorithm, association rule algorithm, collaborative filtering algorithm, and machine learning algorithm are used to compare the steps of left and right hands wearing bracelet randomly and test walking and running, respectively. The experimental results are shown in Figures 3–5.

Figures 3–5 show that when the population index reaches 50 in the analysis of health monitoring data, the average accuracy of data mining is 86.8 percent, the average accuracy of the association rule algorithm is 85.9 percent, the average accuracy of the collaborative filtering algorithm is 84.3 percent, and the average accuracy of the machine learning algorithm is 90.1 percent. Among the four high-accuracy algorithms, this method is clearly the most effective and stable. The addition of GPS assistance and a hand raising misjudgment algorithm improves the system's stability and accuracy significantly. The monitoring data of human exercise health of smart bracelets are analyzed in this experiment, and the curves of time consumption increasing with the sequence length of the data mining algorithm, association rule algorithm, collaborative filtering algorithm, and machine learning algorithm are used in this paper, respectively. The experimental results are shown in Figures 6 and 7.

As can be seen from Figures 6–7, the time consumption curve of the machine learning algorithm in this paper is the highest among the four algorithms, and the linear complexity of the algorithm is verified from an experimental point of view. The time consumption curves of the data mining algorithm, association rule algorithm, and collaborative filtering algorithm indicate that they have quadratic complexity, and the linear complexity is another advantage of the algorithm in this chapter. Because accelerometer data and gyroscope data are three-dimensional data, and there are many sampled data, the extracted feature dimensions are too large, which is not conducive to the subsequent classification and recognition. At the same time, more redundant features will also reduce the classification accuracy so that the most effective features can be selected to achieve the effect of dimension reduction and improve the classification accuracy.

Table 1: Forecast details of RBF core test set.

	Walk	Go upstairs	Sit-up	Run	Go downstairs	Wipe	%
Walk	102	6	1	2	1	4	85.82
Go upstairs	3	61	1	0	3	1	88.56
Sit-up	2	0	82	0	0	0	98.82
Run	0	1	0	114	1	0	102
Go downstairs	6	4	0	0	104	2	89.73
Wipe	0	2	1	1	0	1	98.58

Table 2: Prediction details of linear kernel SVM test set.

	Walk	Go upstairs	Sit-up	Run	Go downstairs	Wipe	%
Walk	96	12	1	2	3	4	70.28
Go upstairs	8	55	0	1	4	1	80.03
Sit-up	2	0	83	1	1	0	101
Run	1	1	1	112	0	1	102
Go downstairs	5	2	0	0	107	0	92.33
Wipe	3	2	1	1	0	131	102

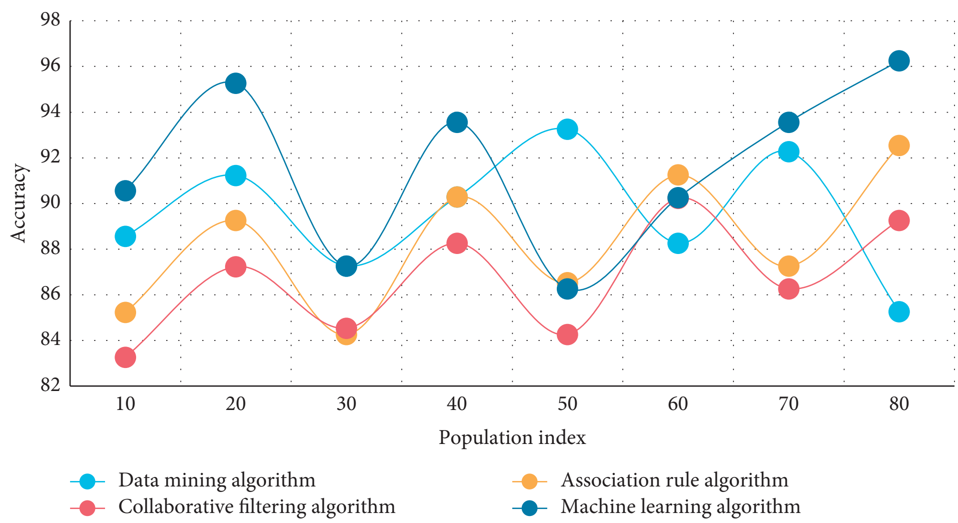

Figure 3: Comparison of several algorithms in health monitoring data analysis.

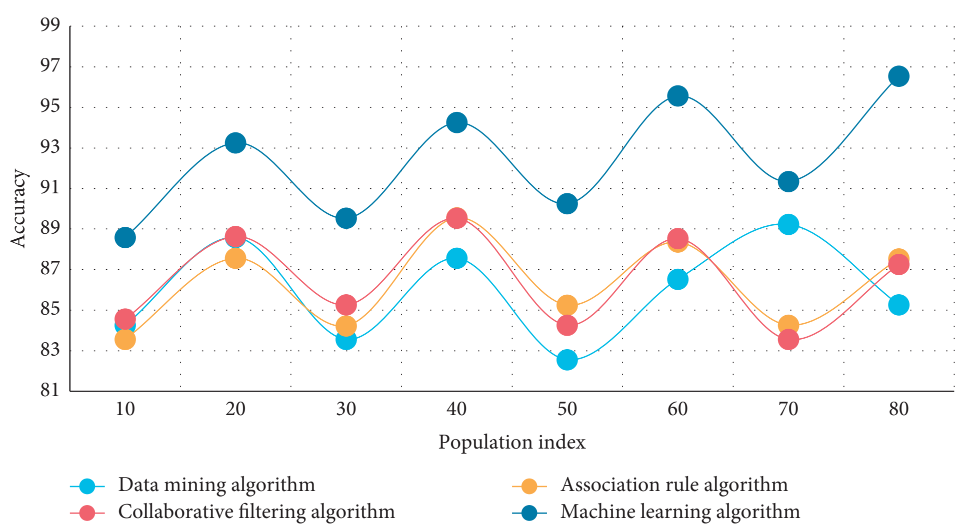

Figure 4: Comparison of several algorithms in health monitoring data analysis.

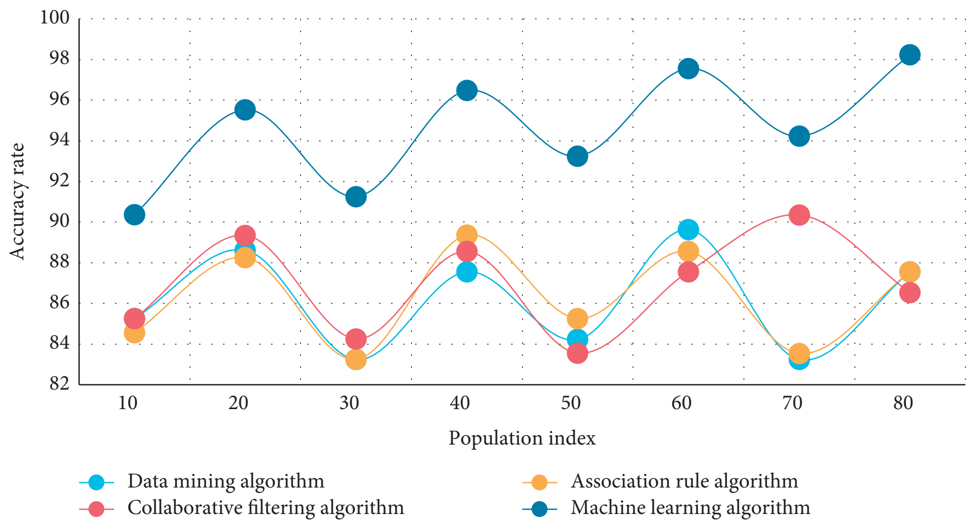

FIGURE 5: Comparison of several algorithms in health monitoring data analysis.

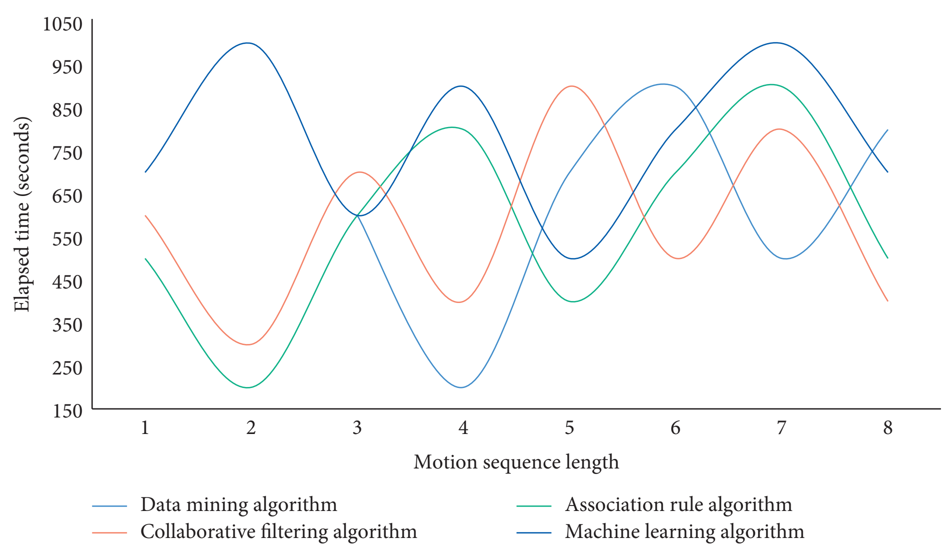

FIGURE 6: Time curves consumed by different algorithms on different length motion sequences.

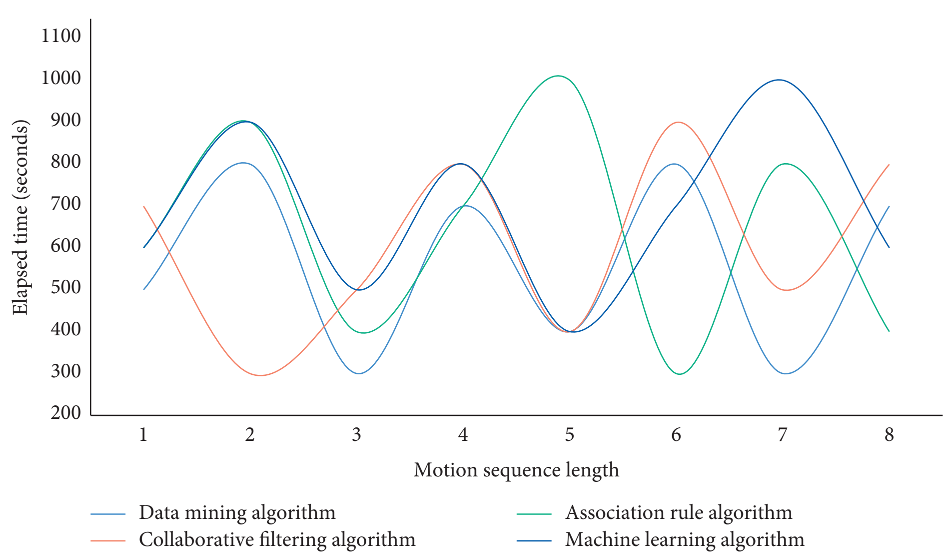

FIGURE 7: Time curves consumed by different algorithms on motion sequences of different lengths.

5. Conclusions

In this paper, a set of human motion recognition systems is developed using the intelligent bracelet's built-in acceleration sensor. In this paper, machine learning is used as a human motion recognition algorithm, and for the first time, this method is realized by an intelligent bracelet on a mobile terminal. This method is then contrasted with the data mining algorithm, the association rule algorithm, and the collaborative filtering algorithm. When the population index reaches 50 in the analysis of health monitoring data, the average accuracy of data mining is 86.8 percent, the average accuracy of the association rule algorithm is 85.9 percent, the average accuracy of the collaborative filtering algorithm is 84.3 percent, and the average accuracy of the machine learning algorithm in this paper is 90.1 percent. This method is clearly the most effective and stable of the four high-accuracy algorithms. The addition of GPS assistance and a hand raising misjudgment algorithm greatly improves the system's stability and accuracy. With the rapid advancement of science and technology in recent years, we believe that the development of smart bracelets will be extremely beneficial. The combination of smart bracelets with sports, medical treatment, and mobile payment will make our lives more convenient and fast in the future. Current machine learning models, on the other hand, are based on smaller data sets. Data sharing can provide larger data sets for developing a comprehensive learning model for a broader range of people. Simultaneously, the current learning model is primarily used for walking, running, and a few special movements. Its wide range of applications in various human movements warrants further investigation.

Data Availability

The data used to support the findings of this study are available from the corresponding author upon request.

Conflicts of Interest

The author does not have any possible conflicts of interest.

Acknowledgments

This work was sponsored in part by Guangdong Ocean University 2017 Innovation strong school project "Model study of coastal water sports projects in Athletic Training Services" (GDOU2017052616).

References

[1] B. Fang, F. Sun, Z. Quan, H. Liu, and J. Shan, "Smart bracelet system for temperature monitoring and movement tracking analysis," *Journal of Healthcare Engineering*, vol. 2021, p. 11, Article ID 8347261, 2021.

[2] D. Yazhu and G. Junqi, "A new approach of intelligent physical health evaluation based on GRNN and BPNN by using a wearable smart bracelet system - ScienceDirect," *Procedia Computer Science*, vol. 147, pp. 519–527, 2019.

[3] J. Qu, N. Qiao, H. Shi, C. Su, and A. Razi, "Convolutional neural network for human behavior recognition based on smart bracelet," *Journal of Intelligent and Fuzzy Systems*, vol. 38, no. 5, pp. 5615–5626, 2020.

[4] X.-B. Jin, W.-T. Gong, J.-L. Kong, Y.-T. Bai, and T.-L. Su, "PFVAE: a planar flow-based variational auto-encoder prediction model for time series data," *Mathematics*, vol. 10, no. 4, p. 610, 2022.

[5] X.-B. Jin, W.-T. Gong, J.-L. Kong, Y.-T. Bai, and T.-L. Su, "A variational bayesian deep network with data self-screening layer for massive time-series data forecasting," *Entropy*, vol. 24, no. 3, p. 335, 2022.

[6] Z. Huang, Y. Liu, and C. Zhan, "A novel group recommendation model with two-stage deep learning," *IEEE Transactions on Systems, Man, and Cybernetics: Systems*, In Press, 2021.

[7] J. Chen, C. Du, Y. Zhang, P. Han, and W. Wei, "A clustering-based coverage path planning method for autonomous heterogeneous UAVs," *IEEE Transactions on Intelligent Transportation Systems*, vol. 1, pp. 1–11, 2021.

[8] X. Gu, W. Cai, and M. Gao, "Multi-source Domain Transfer Discriminative Dictionary Learning Modeling for Electroencephalogram-Based Emotion recognition," *IEEE Transactions on Computational Social Systems*, In Press, 2022.

[9] A. Öztekin, Ö. F. Ertuğrul, E. Aldemir, and E. Acar, "Determining the most relevant frequency bands in motion identification by accelerometer sensors," *Multimedia Tools and Applications*, vol. 81, no. 8, p. 11639, 2022.

[10] J.-R. Zhang, G. Huang, and X.-M. Gou, "An optimum metamodel for safety control of operational subway tunnel during underpass shield tunneling," *Structural Control and Health Monitoring*, vol. 25, no. 8, Article ID e2195, 2018.

[11] Y. Zhang, P. He, and M. Luo, "Highly stretchable polymer/silver nanowires composite sensor for human health monitoring," *Nano Research*, vol. 13, no. 4, pp. 919–926, 2020.

[12] Self-Repairing, "Large linear working range shape memory carbon nanotubes/ethylene vinyl acetate fiber strain sensor for human movement monitoring," *ACS Applied Materials and Interfaces*, vol. 12, no. 37, Article ID 42179, 2020.

[13] D. Bacciu, G. Bertoncini, and D. Morelli, "Topographic mapping for quality inspection and intelligent filtering of smart-bracelet data," *Neural Computing & Applications*, vol. 2, no. 2, pp. 1–15, 2021.

[14] S. A. Yu, A. Hw, and A. Xc, "High-efficiency self-charging smart bracelet for portable electronics - ScienceDirect," *Nano Energy*, vol. 55, pp. 29–36, 2019.

[15] G. Ciocca, H. Tschan, and A. Tessitore, "Effects of post-activation performance enhancement (PAPE) induced by a plyometric protocol on deceleration performance," *Journal of Human Kinetics*, vol. 80, no. 1, pp. 5–16, 2021.

[16] L. Tang, T. Nagashima, K. Hasegawa, T. Ohara, K. Sudo, and N. Itsubo, "Development of human health damage factors for PM2.5 based on a global chemical transport model," *International Journal of Life Cycle Assessment*, vol. 23, no. 12, pp. 2300–2310, 2018.

[17] A. Garofolini and S. Taylor, "The effect of running on foot muscles and bones: a systematic review," *Human Movement Science*, vol. 64, pp. 75–88, 2019.

[18] B. Gfa, A. Hm, and A. Vf, "Locomotor pattern and mechanical exchanges during collective load transport," *Human Movement Science*, vol. 66, pp. 327–334, 2019.

[19] D. V. Vaz, P. L. Silva, M. C. Mancini, C. Carello, and J. Kinsella-Shaw, "Towards an ecologically grounded functional practice in rehabilitation," *Human Movement Science*, vol. 52, pp. 117–132, 2017.

[20] D. Aerenhouts, L. Chapelle, P. Clarys, and E. Zinzen, "Hydration status in adolescent alpine skiers during a training camp," *Journal of Human Kinetics*, vol. 79, no. 1, pp. 55–63, 2021.

[21] M. Julie, "Kapp MPH, PhD, FACE a b, Ws C. Kombucha: a systematic review of the empirical evidence of human health benefit," *Annals of Epidemiology*, vol. 30, pp. 66–70, 2019.

[22] S. Higueras-Fresnillo, M. Á De la Cámara, V. Cabanas-Sánchez, and D.-S Martínez-Gómez, "Associations of frailty and physical function with a daily activities measured by a pattern-recognition activity monitor: an isotemporal substitution analysis in the IMPACT65+ study," *The Journal of Nutrition, Health & Aging*, vol. 24, no. 1, pp. 55–62, 2020.

[23] J. Yanci, A. Los Arcos, D. Castillo, and J. Cámara, "Sprinting, change of direction ability and horizontal jump performance in youth runners according to gender," *Journal of Human Kinetics*, vol. 60, no. 1, pp. 199–207, 2017.

[24] A. Monajati, E. Larumbe-Zabala, M. Goss-Sampson, and F. Naclerio, "Analysis of the hamstring muscle activation during two injury prevention exercises," *Journal of Human Kinetics*, vol. 60, no. 1, pp. 29–37, 2017.

Hindawi
Computational Intelligence and Neuroscience
Volume 2022, Article ID 6341852, 9 pages
https://doi.org/10.1155/2022/6341852

Research Article

Analysis of Biomechanical Parameters of Martial Arts Routine Athletes' Jumping Difficulty Based on Image Recognition

Mengjie Qiao and Shibiao Dong

School of Physical Education, Xuchang University, Xuchang 461000, China

Correspondence should be addressed to Shibiao Dong; 12001043@xcu.edu.cn

Received 4 April 2022; Revised 3 May 2022; Accepted 4 May 2022; Published 8 June 2022

Academic Editor: Xin Ning

This paper uses image segmentation technology to examine the biomechanical parameters of martial arts routine athletes' whirlwind legs and backflips, two difficult jumping sports. The successful completion of the whirlwind leg, a typical martial arts jumping difficulty, during the buffer period of the take-off stage, the left knee angle flexion, the drop of the body's center of gravity, and the drop of the horizontal speed of the center of gravity are all significantly correlated, so it is only necessary to grasp airborne altitude and speed from landing. The 720-degree cyclone foot has a flying height of 0.470.11 m, which is 4 cm higher than the 540-degree cyclone foot (0.430.11 m). The antigravity of the last foot is greater than about 1.3 kgf/kg of the left foot during the run-up stage, which allows for a higher rotational angular velocity and completion of the 720-degree difficulty of the whirlwind foot. As a result, it is crucial to pay attention to how you step with your right foot. In the backflip, the coordination of the two legs and the upper body is crucial. The right foot's effective braking can help to increase the body's rising angle. The trunk inclination angle in the flying stage is between 110° and 120°, the knee angle is between 60° and 70°, and the angle between the two legs is between 35° and 35°. When lifting off the ground and landing, the tibialis anterior muscle discharge is greater than the gastrocnemius muscle discharge, which helps to maintain the balance between the fulcrums. As a result, it is necessary to let the non-supporting leg fall first in order to achieve the goal of a smooth landing.

1. Introduction

With the advancement of the athletes' competitive level, competitive martial arts is gradually evolving in the direction of "high, difficult, beautiful, new, stable, and refined." The movement difficulty in competitive martial arts routine competition is increasing, and the movement between the movements is becoming more difficult. Athletes must complete difficult movements delicately, steadily, and with high quality in order to achieve excellent competition results, especially as the trend of changing connections becomes more complex. These difficult movements include not only the fast rotation of the trunk around the sagittal and coronal equiaxes during the jumping process, but also the stable balance of the connection after the difficult jumping movements have been completed [1]. The difficulty of the movements from fast movement to sudden stillness and stable support, as well as the high-difficulty and graceful posture shown by the jumping movements, adds color to the viewing of competitive martial arts routines. On the other hand, as sports science and technology advance, and training quality improves, the gap between athletes' physical fitness and competitive level narrows [2]. The success of any action has a significant impact on the evaluation of the quality of the athlete's entire set of actions and the final score, especially when the level and strength are similar. In competitive martial arts routine competitions, the error rate of athletes' jumping movements is quite high, and athletes of any level have certain deficiencies in the completion time and quality of their balance movements. Therefore, the mastery and stable performance of jumping movements are also the decisive criteria for judging the level of athletes' competitive level.

In order to make the technical practice of the athlete's balance movement more scientific and effective, this paper has a preliminary understanding of the balance movement by visiting relevant experts, watching on-site, or watching martial arts competitions and other aspects. According to factors such as the frequency of occurrence, difficulty level, and share of balance movements in martial arts competitions in recent years, two movements of backflip and whirlwind leg were selected for analysis. Using image segmentation technology to analyze the biomechanics method reveals its movement law. It provides a reference for improving the rationality and optimization of the balance movements of martial arts routine athletes, so as to solve the technical difficulties of balance movement practice encountered in daily training, so as to achieve the purpose of improving the athletes' competitive level and refining and perfecting technical movements.

Analysis systems based on modern digital image processing technology [3, 4] are becoming increasingly important in the process of analyzing martial arts routines. Because of its intuitive and rapid characteristics, it can effectively overcome the drawbacks of traditional martial arts teaching, assist learners in quickly mastering the fundamentals of martial arts movements, and attract an increasing amount of attention from martial arts enthusiasts. The research on identification, detection, and analysis technology in the jumping process has a lot of potential due to the unique movement mode of martial arts routines. A set of Wushu routine movement analyzer systems is developed in this paper using image recognition technology [5–7] on the basis of video acquisition and video processing. Through the front-end camera and the capture card, the system collects and records the martial arts routine motion video into the specified file, adds a variety of line drawing analysis tools to the video playback and comparison process, and uses graphics and lines to aid in the action video analysis. This paper investigates a set of image recognition algorithms that use the background difference method to grayscale captured image sequences, extract edges, median filtering, and binarization, based on the premise that basic video acquisition and analysis functions can meet the needs of martial arts teaching. The movement trajectory of the jumping process is finally obtained after processing; using the frame-to-frame difference method to compare the change trend of the two frames before and after, the analyzer system can assist martial arts practitioners in correcting swinging and jumping movements, and cooperate with the later developed man-machine interface and simple file management module, which makes the analysis of high-difficulty jumping movements in martial arts more convenient. The system meets the requirements for analyzing and using high-difficulty jumping movements in martial arts after a large number of field experiments.

The innovation of this paper: this paper analyzes the actual needs of martial arts routine athletes training and the particularity of martial arts high-difficult jumping movements. Image recognition technology can intelligently identify the details of martial arts athletes' jumping movements and gradually analyze the biomechanical parameters of each environment.

The structure of the article: first, we introduce some international researches on the analysis of the physical force of sports movements based on image recognition technology; the biomechanical parameters of the whirlwind leg and backflip in the jumping action are analyzed; finally is a summary of the full text.

2. Related Work

In today's social production and life, the application value produced by the combination of video processing technology and image recognition technology is more and more concerned by the majority of scientific researchers, and the fields involved are also very wide. Human motion detection and tracking system is mainly used to deal with image sequences including moving human body. Motion detection extracts foreground motion regions from the background from an image sequence. Motion detection is the basis for the classification and tracking of moving objects, as well as the analysis and understanding of moving human movements. The processing results at this stage directly affect the effect of subsequent processing. With the continuous progress of the development of sports science and technology, the technical research on jumping movements also tends to use electronic and digital scientific instruments for analysis and research [8]. Tripodi et al. [9] mainly focused on the study of its "backward jumping" action, using close-range dynamic stereo photogrammetry as the research method, and using the Aijie motion image analysis system to analyze technical movements, respectively. The speed change, the center of gravity displacement change, and the torso displacement change have been comprehensively studied. The analysis results show that the strength of the legs is the key factor affecting the stability of the back jump. The small muscle group of the right supporting leg of the martial arts routine athletes is weak, and strength training should be strengthened [9]. Li and Zhang [10] also used this method to study the jumping movements of "sidekicking and holding the feet upright" of martial arts routine athletes. The technical indicators such as the swinging leg, the opposite side arm of the swinging leg, the speed of the center of gravity, and the displacement of the center of gravity are selected as parameters, and the swing speed of the swinging leg and the opposite side arm of the swinging leg in the X-axis direction is changed. The maximum swing speed of the swing leg is slightly greater than the swing of the opposite arm of the swing leg, but when it swings over the central axis of the body, the swing speed of the arm is faster than the speed of the leg. At the same time, reach the best jumping state to complete the action. In addition, it can be seen from the comparison curve of the center of gravity speed and displacement that martial arts routine athletes change evenly in the center of gravity speed during the entire movement process, which lays the foundation for their stable jumping support [10]. Through a series of data analysis, Mastalerz et al. [11] concluded that, in the practice of martial arts jumping movements based on muscle strength, attention should be paid to strengthening the coordinated development of upper and lower limb muscle strength and the flexibility of the legs [11]. In the study by Tagaev et al. [12], the kinematics comparative analysis of the sidekicks and the upright jumps of the martial arts routine athlete and Zhang Yanan, the two champions, was found in the comparison. Sex is closely related to the swing speed of the right arm and the swing sequence of the two [12]. Strengthening the rapid arm swing exercises to form a rapid cooperation between the arms and the legs can greatly enhance the stability of the jumping action. In the study of other martial arts jumping movements, Lewis et al. [13] conducted a technical analysis of the sea-exploring jumping and lying-fishing jumping movements in swordsmanship routines to clarify the principle of maintaining the stability of jumping movements. Find the difficult points of the jumping action. It calculates and draws the coordinates of the center of gravity of each link of the body and the coordinates of the total center of gravity of the body with reference to the Japanese body model of Hideji Matsui to evaluate the stability of the jumping action. At the same time, it also pointed out the main muscle groups involved in the movement of the sea-exploring jumping movement and studied the stability regulation of the flexion and extension muscle groups of the body on the sea-exploring jumping [13]. In Atalay et al.'s [14] article on the muscle EMG analysis of Sanda's sidekick action, the EMG test was performed on seven muscles including the rectus femoris, medial vastus, biceps femoris, and semitendinosus, which are mainly involved in the movement of the contralateral kick action. Analysis and research show that the time sequence and sequence of muscle force exerted by excellent Sanda athletes in the sidekick action are relatively close and evenly concentrated, while the time and sequence of muscle force exerted by ordinary athletes when they complete the same action are uneven, uniform, and scattered. The importance of strengthening muscle coordination exercises during training was emphasized [14]. The attacking leg of the whipping technique was studied simultaneously by three-dimensional kinematics analysis and surface electromyography measurement to explore the movement speed of each link of the attacking leg, the contraction mode of the main muscle groups, and the order of force at the attacking moment [15]. The study found that when the knee angle of the attacking leg presents about 140° in the preparation moment of the whip leg attack, it is beneficial to move quickly on the ring and maintain the angle of each joint to achieve better results. Through the analysis of the electromyography tester, it was found that, in the stage of knee flexion and leg raising, sartorius, tensor fascia lata, biceps femoris, and gastrocnemius participated in the muscle contraction, and the rectus femoris EMG contributed the most, and the tensor fascia lata muscle contributed the most. It is the smallest, but it is mainly done by the tensor fascia lata in the stage of widening the knee [15].

With the combination of martial arts and computer technology, more and more martial arts-related equipment has introduced information technology. However, professional golf swing analysis systems are still relatively rare in the world, and the difficulty of jumping martial arts routines using image recognition technology is even rarer, and some martial arts routine sports coaching software that simply uses video processing and analysis technology is available in some countries. The particularity of Wushu sports determines the special requirements for equipment of Wushu sports teaching analysis system. The existing teaching system has shortcomings such as low software intelligence, poor image quality, single video angle, etc., and there is currently no professional golf course. The swing analysis system cannot well complete the Wushu sports teaching task. Therefore, the analysis of the jumping difficulty of Wushu routine athletes based on image recognition in this paper is very meaningful for the research in this field.

3. Image Segmentation-Based Feature Extraction Method for Jumping Action

This paper proposes a method to calculate the period based on the geometric shape of the signal. Before extracting the signal, the original signal should be median-filtered to make the period clearer. It is worth pointing out that, due to the median filtering, horizontal lines may appear in the signal. Since the minimum point of the signal is required to extract the period, when a horizontal line appears, there may be several consecutive identical minimum points, which will interfere with determining the distance between each minimum point, so the horizontal line in the signal should also be removed. The lowest point of each cycle appears in cycles, and the cycle in which the lowest point appears can be regarded as the cycle of the signal [16]. The steps to determine the cycle of the signal are shown in Figure 1.

Motion regions are extracted by thresholding pixel-based temporal differences between adjacent images in successive image sequences [17]. The early temporal difference method is to use the difference of two adjacent images to obtain the motion area, as shown in

$$D_k(x, y) = \left|f_k(x, y) - f_{k-1}(x, y)\right|, \tag{1}$$

where $f_k(x, y)$ is the gray value at the midpoint (x, y) in the k-th frame and $f_{k-1}(x, y)$ is the grayscale value at the midpoint (x, y) in the $k-1$-th frame. The D_k binarization of the difference result is shown in

$$R_x(x, y) = \begin{cases} 1, & D_k(x, y) > T, \\ 0, & D_k(x, y) \leq T. \end{cases} \tag{2}$$

Pixels with values of 1 and 0 correspond to the foreground (moving object area) and background (non-moving area), respectively [18]. The differenced D also includes the change of the scene between two consecutive frames. This change is composed of many factors, including the movement of the target, lighting, shadow, noise, etc. It can be considered that the change of the moving target is obvious. Set a threshold T; when the difference of a certain pixel value in the difference is greater than the given threshold T, the pixel is considered as a foreground pixel; otherwise, it is considered as a background pixel. The interframe difference method is the simplest method to detect changes between adjacent frame images. It directly compares the difference in gray value of corresponding pixels in two or three

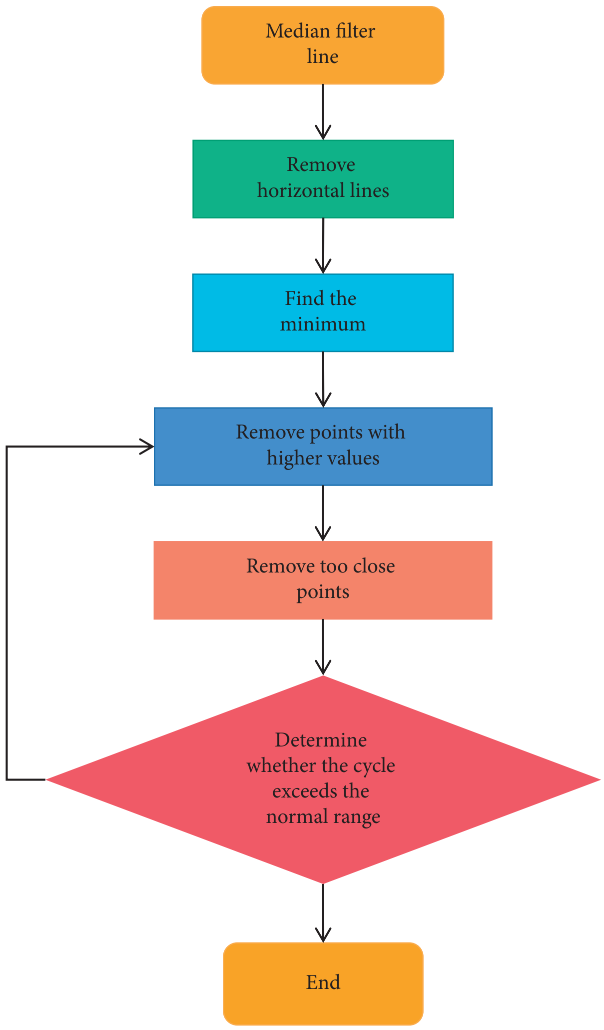

Figure 1: Flowchart of the cycle algorithm.

consecutive frames of images in a video sequence and then sets a threshold to extract motion regions in sequence images [19, 20]. The main advantages of the interframe difference method for target detection are that the algorithm is simple to implement, the programming complexity is low, and it is easy to realize real-time monitoring. Based on the adjacent frame difference method, since the time interval between adjacent frames is generally short, the method is generally less sensitive to changes in scene light. The most basic interframe difference method can detect changes in the scene and extract the target, but in practical applications, the result of the interframe difference method is not very accurate, and it is difficult to obtain an accurate description of the target area [21].

The background subtraction method is a motion detection method that uses the difference between the current image and the background image to extract the motion area, and it is also a widely used method at present [22], which can generally provide complete data of the target. The principle of the background difference method is to use the current image and the background model to differentiate and then threshold to obtain the moving object. In practical application, it is difficult to get the background directly from the monitored area because of the movement of objects or the change of environment, such as the moving target becoming a part of the background, the local background becoming a moving target, etc. Therefore, it is very necessary to acquire, reconstruct, and update the background [23].

The background difference method assumes that the background is stationary, so the background does not change with the number of frames. First, the difference D_k between the current f_k and the background b_k is obtained by using

$$D_k(x, y) = \left|f_k(x, y) - b_k(x, y)\right|. \tag{3}$$

Then, the difference is also binarized according to formula (2). Whether the threshold T is selected accurately or not directly affects the quality of the binary dipper. If the threshold T is selected too high, the area determined as a moving target in the binary value will be fragmented; on the contrary, if the threshold T is selected too low, a lot of noise will be introduced. The most common method for selecting the threshold T is to use the grayscale histogram with double peaks or multiple peaks and select the grayscale value at the bottom of the valley between the two peaks as the threshold value. The background subtraction method is simple to calculate and fast, and the obtained result directly gives the position, size, shape, etc. of the target, so that a complete and accurate description of the moving target area can be obtained [24].

4. Case Study of Jumping Action

4.1. Analysis of Biomechanical Parameters of Cyclone Foot Movement. Approach, take-off, air, and landing make up the 720-degree cyclone foot. When starting, the right foot is buckled in, and the right leg is bent and squatted and quickly pushes the ground, while the left leg swings to the left and the body is twisted counterclockwise; when taking off, the right foot is buckled in, and the right leg is bent and squatted and quickly pushes the ground. After the right leg completes the straight swing and the body's center of gravity is near the highest point, the left hand taps the right sole, the two legs are completed in the air, the limbs are kept vertical, and the arms are close to the body. After rotating in the air for nearly two weeks, spread the limbs and slow down the rotation speed, touch the ground with both feet, take the horse step or drop the vertical fork, and finish the landing action. The subjects for this study were seven martial arts routine athletes. The average vertical distance between the right swing leg and the lowest shoulder point was 0.180.16 m after the subjects completed the strike in the air. The results are shown in Figure 2.

During the flying stage, the subjects completed the 720-degree cyclone foot with an average flying height of 0.47 ± 0.11 m, which was 4 cm higher than the 540-degree $(0.43 \pm 0.11\ \text{m})$ cyclone foot. This is a comparison of the overall samples that completed the C-level and B-level jumping difficulty movements of the cyclone feet. The paired t-test was used to find that the same athletes completed the

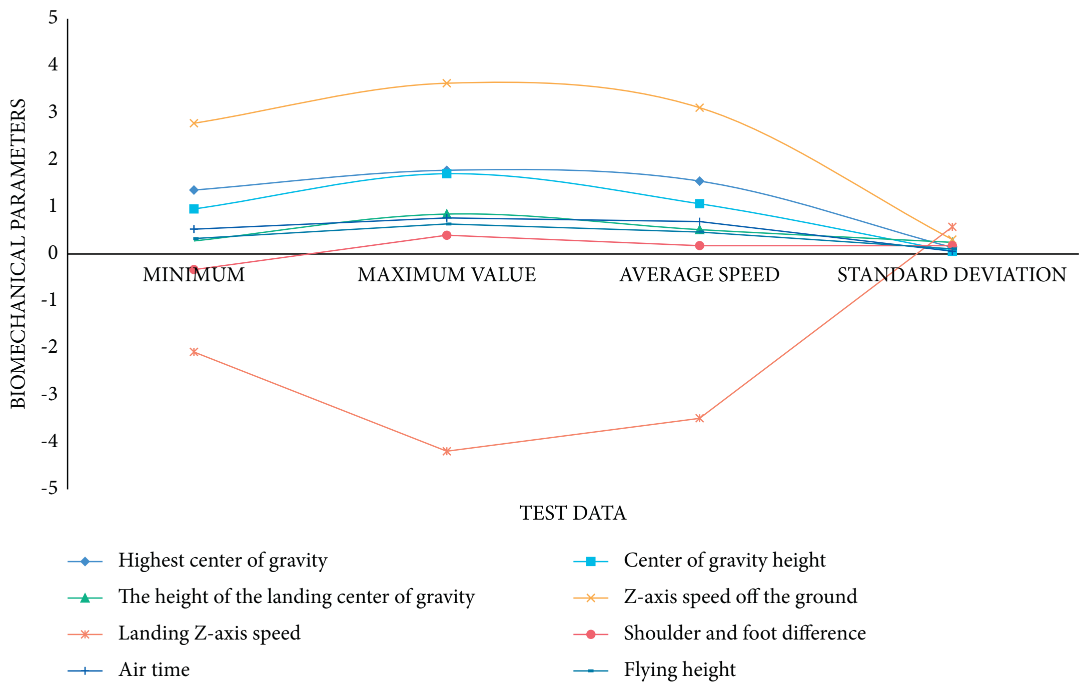

Figure 2: Kinematic parameters of the cyclone foot at 720°.

C-level and *B*-level jumping difficulty movements of the cyclone feet, respectively, and the flying heights of the two were not significant. It can be considered that the same athlete has no difference in the height of the air when completing the *B*-level and *C*-level jumping difficulty movements of the whirlwind foot, and the main reason is that the rotation speed in the air is increased. The comparison of kinematic parameters of cyclone feet with different difficulties is shown in Figure 3.

The average maximum ground reaction force of the left foot in the final step of the approach stage is 2.151.03 kgf/kg body weight, while the average maximum ground reaction force of the right foot in the final step is 3.500.76 kgf/kg body weight, which is significantly greater than the starting braking. The action of the left foot indicates that the last step's ground reaction force should be high in order to help raise the air's height. The turning moment around the body's longitudinal axis is large, allowing for a higher rotational angular velocity and completing the whirlwind foot's 720-degree difficulty. As a result, it is important to pay attention to how you walk with your right foot.

The EMG signal strength of the vastus medialis muscle is the strongest in the take-off and landing stages; the EMG signal of the vastus lateralis muscle is stronger in the take-off and landing stages; the EMG signal of the rectus femoris in the take-off stage is average, and there is a discharge signal in the flight stage, which is consistent with the discharge time of the adductor magnus. It shows that this stage is the clicking action when flying, and there is also an EMG signal when landing; the gastrocnemius discharge time is the earliest, because the right leg has a certain angle with the ground when taking off, and the triceps of the calf keeps the ankle joint through isometric contraction. At a certain joint angle,

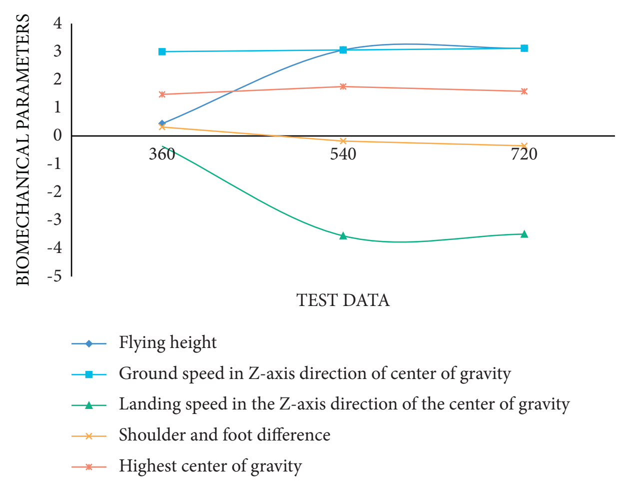

Figure 3: Comparison of kinematic parameters of cyclone feet with different difficulties (mean value).

the ground reaction force is transmitted through the calf to the thigh. In training, attention should be paid to the exercises of calf strength, especially the isometric strength exercises to strengthen the calf.

Athletes who use one foot to perform a 720-degree take-off with a whirlwind foot should obtain a certain degree of rotation as much as possible before leaving the ground; that is, the human body has already rotated part of the body before it is in the air, so as to improve the height of the air and complete the degree of rotation. The training methods for the *B* and *C*-level jumping difficulty of the whirlwind foot include the click of the legs together, the legs together, and the landing technique. In the flying stage, when the center of gravity of the human body rises close to the highest point, the click must be completed, and the time from take-off to the completion of the click should be as short as possible, so as to achieve the corresponding degree of leg rotation in the flying stage as soon as possible. Athletes choose horse stance in the dynamic and static connection of Changquan and Nanquan. Although individual athletes avoid landing with both feet, foot movement, or jumping in sequence, they focus on one leg in order to stabilize the movement. In the action quality score, points are deducted if the squatting legs are not level and the distance between the feet is too small. Therefore, the 720-degree stance of the whirlwind foot must strengthen the awareness of movement norms and training requirements. Figures 4 and 5 show the kinematic parameter diagrams of the athlete's front extension.

It can be seen from Figure 4 that the left knee angle of the seven athletes is $(119.74 \pm 20.83)^{\circ}$ at the lowest point of the center of gravity of the body. At this time, the left leg is firmly supported by the inside of the foot and actively stretches, and the knee angle begins to increase. When the right foot hits the ground, the angle is $(139.26 \pm 14.17)^{\circ}$, when the left foot is off the ground, the knee angle is $(164.93 \pm 4.19)^{\circ}$, the kicking range is $(45.19 \pm 21.48)^{\circ}$, and the vertical velocity of the center of gravity is (1.91 ± 0.35) m/s. After inspection, the left knee extension during the front extension period is significantly positively correlated with the vertical speed of the center of gravity when the left foot leaves the ground, indicating that the greater the left knee extension during the front extension period, the higher the vertical speed of the center of gravity when the left foot leaves the ground. In addition, the active stretch action of the left leg can quickly push the hip and body weight forward, which is of great significance for obtaining a larger impulse during take-off and quickly stepping on the right leg to the take-off point. The horizontal distance of the body's center of gravity moving forward and the horizontal speed of the center of gravity were (0.18 ± 0.08) m and (2.21 ± 0.81) m/s, respectively, during the forward stretch. After testing, the horizontal distance of the body's center of gravity moving forward during the forward stretch is significantly correlated with the horizontal speed of the center of gravity when the left foot is off the ground, indicating that the more fully the left leg is stretched during the forward stretch, the greater the horizontal distance of the body's center of gravity forward, and the more it is beneficial to obtain a larger horizontal velocity of the center of gravity when the left foot is off the ground. 1, 2, 5, and 6 give full play to the left leg's positive role during the forward stretch period, allowing the right leg to quickly transition to the stretch action and the early swing of the left leg after stepping on the take-off point. The main reason for the disparity among athletes is that the left leg is not actively stretched, which is extremely detrimental to improving center of gravity speed and maintaining good body posture when taking off. Figure 6 depicts the swing speed of the two arms during the front kicking and extension period.

It can be seen from Figure 6 that the swing of the left and right arms shows different changing laws during the front kicking and extension period. From the lowest point of the center of gravity to the moment when the right foot hits the ground, the swing speeds of the left and right arms continue to increase. When the right foot hits the ground, the swing speeds of the left and right arms are (8.64 ± 1.47) and (9.33 ± 1.73) m/s, respectively. Based on the previous analysis, it can be seen that, from the moment of the lowest point of the center of gravity to the moment when the right foot hits the ground, the athlete pushes the center of gravity forward through the active stretch of the left leg and the accelerated swing of the two arms, creating a favorable situation for the right leg to move towards the take-off point actively and quickly. condition. 1, 2, 5, and 6 have more sufficient kicking and stretching actions, and the swing speed of the left and right arms is higher than that of other athletes, which indicates that the athletes such as Zhou can make full use of the swing of the arms to take-off better than other athletes. After the right foot touched the ground, the swing speed of the left arm continued to increase. When the left foot was off the ground, the swing speed reached the maximum (10.21 ± 2.24) m/s, while the swing speed of the right arm showed a decreasing trend. After kicking off the ground, the swing speed of the right arm drops to (7.01 ± 1.51) m/s. After inspection, when the left foot leaves the ground, the swing speed of the left arm has a significant positive correlation with the horizontal speed of the center of

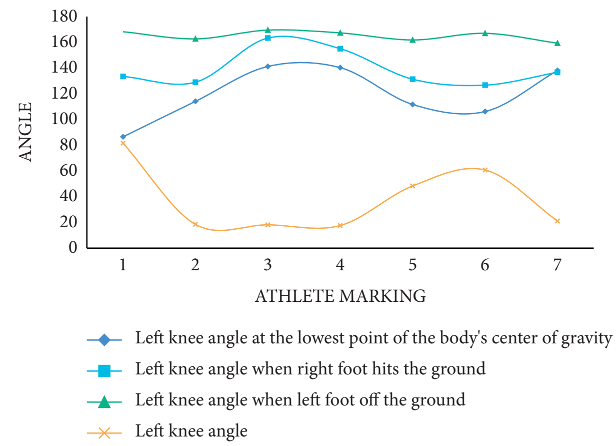

Figure 4: Kinematic parameters of the athlete's front extension.

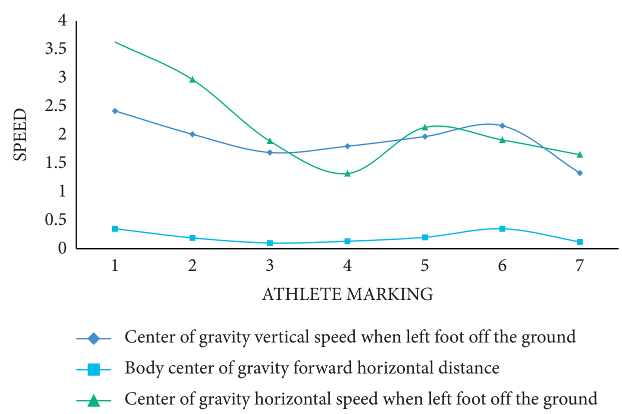

Figure 5: Kinematic parameters of the athlete's front extension.

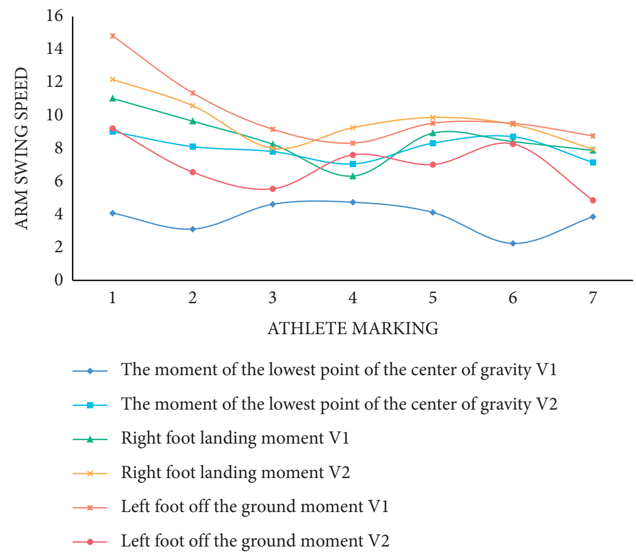

Figure 6: The variation characteristics of the swing speed of the athlete's arms during the forward extension period.

gravity at this moment. It shows that the greater the swing speed of the left arm, the greater the horizontal speed of the center of gravity when the left foot leaves the ground. It can be seen that, from the moment when the right foot hits the ground to the time when the left foot leaves the ground, the horizontal speed of the center of gravity of the body is maximized by the rapid swing of the left arm, and the body balance is maintained by reducing the swing speed of the right arm.

4.2. Analysis of Biomechanical Parameters of Backflip. The backflip consists of four steps: run-up, take-off, flying, and landing. In the run-up stage, try to keep the balance of the body and run in a straight line; in the take-off stage, the right heel brakes on the ground, the upper body is leaned back, and the left leg is raised and the left leg swings up. Raise your legs and swing your knees to your chest, and tuck your legs in the air; in the landing stage, after your body has completed a 360-degree backward rotation in the air, land both feet on the ground at the same time, landing in a single butterfly step. In this paper, 6 martial arts athletes are selected for action analysis, and key information is proposed based on image segmentation technology. The torso anteversion is the angle between the torso and the supporting leg. The inclination angle of the non-supporting leg is the angle between the non-supporting leg and the horizontal position as shown in Figure 7.

The angle of the ankle joint of the supporting leg is controlled at about 90° when the backflip is stable, which means that, in the leaning-over balance, the body's center of gravity is moving forward. In the upright position, there is no discernible difference; however, the center of gravity is projected onto the support legs, making balance easier to control. The backflip's torso inclination angle is between 110° and 120°. Because the action requirements of each link differ, one requires raising the chest while the

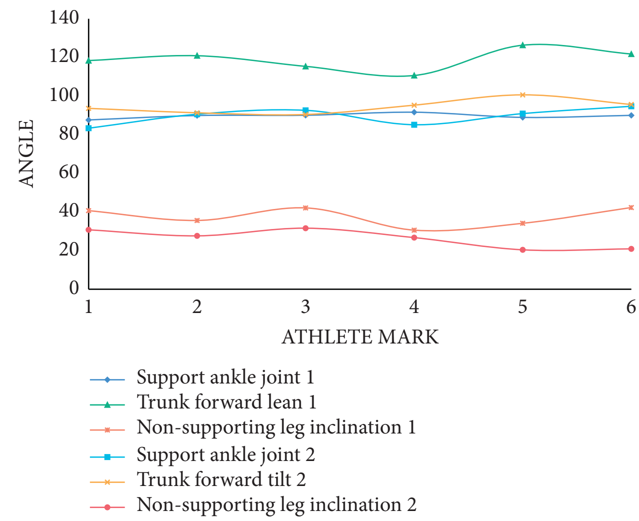

Figure 7: The angle of each link of the backflip.

other requires leaning forward. As a result, the trunk's forward inclination angle becomes the primary basis for the two groups' balance. The inclination of the non-supporting leg of the backflip, on the other hand, is found to be the same as the inclination of the supporting leg using statistical technical parameters of image segmentation. When the fulcrum stays the same, the forward probe of the torso causes the center of gravity to move forward, resulting in a change in the gravitational distance and an increase in the gravitational arm. The non-supporting leg compensates for the change in gravitational distance due to the forward movement of the center of gravity and ensures that the total external moment is zero in order to maintain the balance position with the torso in the air. The non-supporting leg's horizontal angle decreases, increasing the moment arm between the non-supporting leg and gravity and achieving the goal of maintaining balance and stability. As a result, the backflip's non-support leg angle is slightly reduced, as shown in Figure 8.

In the process of observing the support leg movement of the backflip action, the support leg of the backflip action is all the pelvis flexed at the hip joint and is in a forward tilted position. The support leg is always in the upright phase. The support leg is always in the upright phase. In both balanced stabilization movements, the torso and non-supporting legs are rotated counterclockwise to a horizontal position about the hip joint. In this state, the rectus femoris muscle contracts concentrically, the biceps femoris muscle contracts eccentrically, and the moment arm of the rectus femoris muscle is shorter than the moment arm of the biceps femoris muscle, and the movement balance is maintained under the condition of equal muscle force distance, so the discharge of the rectus femoris is greater than that of the biceps femoris. The calf is flexed at the ankle joint, the tibialis anterior muscle performs eccentric contraction, the gastrocnemius muscle contracts concentrically, and the muscle arm of the tibialis anterior muscle is much smaller than that of the

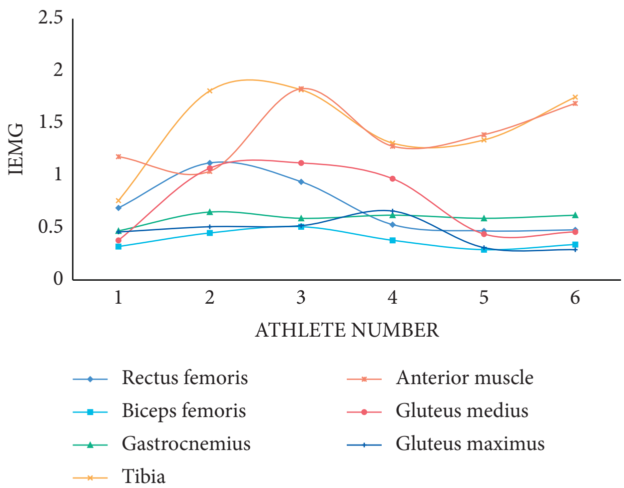

FIGURE 8: Muscle IEMG of backflip test of martial arts athletes.

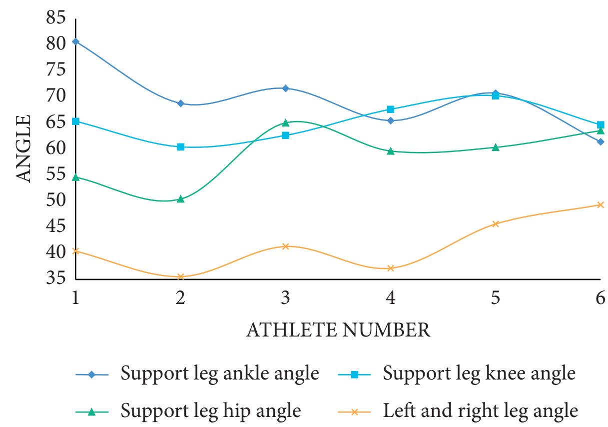

FIGURE 9: Body part angle of backflip.

gastrocnemius muscle, so the discharge of the tibialis anterior muscle is more than that of the gastrocnemius muscle. The gluteus maximus and gluteus medius do eccentric contraction in the hip flexion movement in the bending part, and the muscle arm of the gluteus medius is smaller than that of the gluteus maximus, so the discharge of the gluteus medius is more than that of the gluteus maximus. Figure 9 shows the angle of the body part of the backflip buckle leg link.

It can be seen from the figure that the ankle joint angle of the support leg becomes smaller in the stable stage of the backflip than in the upright stage, because the bending of the support leg causes the body's center of gravity to drop and move forward. At this time, the angle of the ankle joint decreases with the forward movement of the center of gravity, which increases the projected area of the center of gravity on the support surface, which is beneficial to control the stability of the center of gravity. Buckling balance requires the support leg and thigh to be kept as level as possible. According to the principle of parallel lines, the range of the knee angle is controlled between 60 and 70° to compensate for the increased moment arm due to hip flexion and squatting, so that the action can be balanced between the fulcrums. The trunk leans forward from the hip joint, so that the head is close to the vertical line of the center of gravity, which increases the balance and stability and makes the movement more graceful and stretched. The angle between the two legs is between 35 and 50°, which is to balance the component forces on the left and right sides of the action, so that the combined external force is zero, so as to achieve the purpose of landing smoothly. The swing speed and swing sequence of the non-supporting leg and the heterolateral arm have a great relationship with the stability of the movement. The swing of the opposite side arm should be prior to the swing of the non-supporting leg, which is conducive to improving the side swing speed, shortening the time to complete the action, and enhancing the stability of the balance while improving the quality of the action.

5. Conclusions

The results of image segmentation technology's biomechanical analysis of all martial arts high-difficulty jumping movements show that, whether the whirlwind foot jumps with one foot or two, the two feet should form a certain angle with the approaching route, which is conducive to the rotation in the air and the sound of the strike. The movement should be performed while the center of gravity is rising. The faster the run-up speed, the better in the warm-up phase. When the right foot touches the ground during the forward stretch phase of take-off, the sole of the foot is buckled inward, and the right foot pushes and stretches in a timely manner, with almost no concessional work. The range of leg extension is greater, and the key technology is the "orange pendulum combination" of the two legs and upper limbs. When the martial arts routine athletes slam their legs together in the vacant stage, the body's center of gravity rises, approaching the highest point of the body's center of gravity. The key to achieving a stable stance on the ground is to stretch the limbs as soon as possible after completing the rotation in the powder, in order to increase the human body's rotational inertia. When taking off, the backflip should increase the amplitude and speed of the upper body slanting downwards, and the possibility of adjusting the position of the left foot when the left foot is pushing the ground should be minimized. It is crucial to get the body and the running route to form a certain angle, and the backflip's running braking technology and group body technology are crucial. In terms of image processing technology, although motion detection-related algorithms can extract the motion trajectory of the jumping action process, it is still very difficult to recognize the hands and feet of the system. It is necessary to consider the operation time of the system and ensure the accuracy of the detected target. In future research, you can try to add some advanced algorithms of image matching and perform template matching for hands and feet.

Data Availability

The data used to support the findings of this study are available from the corresponding author upon request.

Conflicts of Interest

The authors do not have any possible conflicts of interest.

References

[1] J. R. Yoon and H. Sun, "Analysis of physiological parameters for new combined event in modern pentathletes," *Kinesiology*, vol. 19, pp. 11–16, 2017.

[2] J. Zhang, "Biological analysis of trunk support strength training in sports training," *Network Modeling Analysis in Health Informatics and Bioinformatics*, vol. 10, no. 1, p. 15, 2021.

[3] J. Zhang, J. Sun, J. Wang, Z. Li, and X. Chen, "An object tracking framework with recapture based on correlation filters and Siamese networks," *Computers & Electrical Engineering*, vol. 98, Article ID 107730, 2022.

[4] J. Zhang, W. Feng, T. Yuan, J. Wang, and A. K. Sangaiah, "SCSTCF: spatial-channel selection and temporal regularized correlation filters for visual tracking," *Applied Soft Computing*, vol. 118, Article ID 108485, 2022.

[5] W. Cai and Z. Wei, "Remote sensing image classification based on a cross-attention mechanism and graph convolution," *IEEE Geoscience and Remote Sensing Letters*, vol. 19, pp. 1–5, 2022.

[6] D. Yao, Z. Zhi-li, Z. Xiao-feng et al., "Deep hybrid: multi-graph neural network collaboration for hyperspectral image classification," *Defence Technology*, vol. 2022, p. 007, 2022.

[7] X. Gu, K. Xia, Y. Jiang, and A. Jolfaei, "Multi-task fuzzy clustering-based multi-task TSK fuzzy system for text sentiment classification," *ACM Transactions on Asian and Low-Resource Language Information Processing*, vol. 21, no. 2, pp. 1–24, 2022.

[8] f Chen, "Athlete muscle measurement and exercise data monitoring based on embedded system and wearable devices," *Microprocessors and Microsystems*, vol. 82, no. 5, Article ID 103901, 2021.

[9] D. Tripodi, D. Fulco, A. Beraldi, P. Ripari, G. Izzi, and S. D'Ercole, "Custom-made mouthguards: electromyographic analysis of masticatory muscles and cardiopulmonary tests in athletes of different sports," *Health*, vol. 11, no. 04, pp. 428–438, 2019.

[10] H. Li and B. Zhang, "Application of integrated binocular stereo vision measurement and wireless sensor system in athlete displacement test," *Alexandria Engineering Journal*, vol. 60, no. 5, pp. 4325–4335, 2021.

[11] A. Mastalerz, P. Szyszka, W. Grantham, and J. Sadowski, "Biomechanical analysis of successful and unsuccessful snatch lifts in elite female weightlifters," *Journal of Human Kinetics*, vol. 68, no. 1, pp. 69–79, 2019.

[12] X. Tagaev, N. Zafar, and M. Akmal, "The analysis of the athlete's speed capability – an important factor in increasing the efficiency of physical training," *Journal of Manegementences in China*, vol. 12, p. 38, 2015.

[13] A. Lewis, W. Robertson, and E. J. Phillips, "Mass distribution of wheelchair athletes assessssed using dxa scans and Bio-Mechanical simulations," *Journal of Biomechanical Engineering*, vol. 141, p. 10, 2019.

[14] E. S. Atalay, D. Tarakci, and C. Algun, "Are the functional movement analysis scorers of handball players?" *Journal of Exercise Rehabilitation*, vol. 14, no. 6, pp. 954–959, 2018.

[15] V. Zagrevskiy and O. Zagrevskiy, "Syntheses of program and finite laws of motion in analytical models of control of the final state of biomechanical systems," *Human Sport Medicine*, vol. 19, no. 1, pp. 93–99, 2019.

[16] M. Oh, N. Bonina, and S. Tuhec, "Comparative biomechanical analysis of the hurdle clearance technique of colin jackson and dayron robles: key studies," *Applied Sciences*, vol. 10, no. 9, p. 3302, 2020.

[17] Y. Li, "Biomechanical analysis of stability of palmar lateral joint capsule ligament complex of A track and field athlete," *Indian Journal of Pharmaceutical Sciences*, vol. 83, pp. 203–206, 2021.

[18] L. Gastaldi, S. Mauro, and S. Pastorelli, "Analysis of the pushing phase in Paralympic cross-country sit-skiers - class LW10," *Journal of Advanced Research*, vol. 7, no. 6, pp. 971–978, 2016.

[19] Y. Jiang, Y. Zhang, C. Lin, D. Wu, and C.-T. Lin, "EEG-based driver drowsiness estimation using an online multi-view and transfer TSK fuzzy system," *IEEE Transactions on Intelligent Transportation Systems*, vol. 22, no. 3, pp. 1752–1764, 2021.

[20] J. Zhou, D. Zhang, and W. Zhang, "Underwater image enhancement method via multi-feature prior fusion," *Applied Intelligence*, vol. 2022, pp. 1–23, 2021.

[21] M. Fröhlich, H. Felder, and M. Reuter, "Training effects of plyometric training on jump parameters in D- and D/C-squad badminton players," *Journal of Sports Research*, vol. 1, no. 2, pp. 22–33, 2014.

[22] J. Baus, J. R. Harry, and J. Yang, "Jump and landing biomechanical variables and methods: a literature review," *Critical Reviews in Biomedical Engineering*, vol. 48, no. 4, pp. 211–222, 2020.

[23] B. K. Német, T. Terebessy, and Z. Bejek, "Biomechanical and functional comparison of kayaking by abled-disabled athletes," *Orvosi Hetilap*, vol. 160, no. 52, pp. 2061–2066, 2019.

[24] Y. Jiang, X. Gu, D. Wu et al., "A novel negative-transfer-resistant fuzzy clustering model with a shared cross-domain transfer latent space and its application to brain CT image segmentation," *IEEE/ACM Transactions on Computational Biology and Bioinformatics*, vol. 18, no. 1, pp. 40–52, 2021.

Hindawi
Computational Intelligence and Neuroscience
Volume 2022, Article ID 8679748, 10 pages
https://doi.org/10.1155/2022/8679748

Research Article

Optimization Simulation of Dance Technical Movements and Music Matching Based on Multifeature Fusion

Liusha Dong

Yangtze University, JingZhou 434020, China

Correspondence should be addressed to Liusha Dong; 2016217230@smail.jsut.edu.cn

Received 1 April 2022; Revised 29 April 2022; Accepted 30 April 2022; Published 8 June 2022

Academic Editor: Xin Ning

Music and dance videos have been popular among researchers in recent years. Music is one of the most important forms of human communication; it carries a wealth of emotional information, and it is studied using computer tools. In the feature engineering process, most present machine learning approaches suffer from information loss or insufficient extracted features despite the relevance of computer interface and multimedia technologies in sound and music matching tasks. Multifeature fusion is widely utilized in education, aerospace, intelligent transportation, biomedicine, and other fields, and it plays a critical part in how humans get information. In this research, we offer an effective simulation method for matching dance technique movements with music based on multifeature fusion. The initial step is to use music beat extraction theory to segment the synchronized dance movements and music data, then locate mutation points in the music, and dynamically update the pheromones based on the merits of the dance motions. The audio feature sequence is obtained by extracting audio features from the dancing video's accompanying music. Then, we combine the two sequences to create an entropy value sequence based on audio variations. By comparing the consistency of several approaches for optimizing dance movement simulation trials, the optimized simulation method described in this research has an average consistency of 87%, indicating a high consistency. As a result, even though the background and the subject are readily confused, the algorithm in this research can keep a consistent recognition rate for more complicated dance background music, and the approach in this study can still guarantee a certain accuracy rate.

1. Introduction

The most common form is that the dance form evolves in response to the music [1]. Music theme information is communicated through a variety of dance expressions. Dance action matching technology in music arrangement [2] is the process of determining the shape of dance works based on the music style. Effective dance video clip retrieval can assist dance teachers in organizing dance and supporting dance teaching activities [3]. The emotional expression of dancers' works is intimately linked to musical comparison [4]. The dance team's variable or scattered arrangement and creation are similarly difficult to distinguish from the music's production and design [5]. Music is one of the most essential forms of auditory data in multimedia. Computers have carefully studied music as a strong analytical tool in today's digital music era, which has become an unavoidable trend.

In the field of computer vision research [6–8], optimization simulation is currently a highly difficult problem. Its purpose is to analyze dance video data utilizing image processing [9, 10], classification [11], and recognition technology to distinguish motions. With tens of thousands of new songs released each year and the rapid emergence of millions of digital songs that were previously unclassified, existing matching approaches are unable to keep up with the changing times. Because real-world human behavior is based on three-dimensional space, three-dimensional information is critical for music matching optimization simulation. However, extracting 3D information about the human body from RGB dancing photos is difficult. To gather 3D information about the human body, some traditional methods use a depth camera or a laser scanner. The development of matching optimization simulation has been considerably aided by research into human behavior recognition technologies based on artificial intelligence [12] and computer vision. It takes a series of keyframes from a dancing video sequence, generalizes the original video content from high-level semantic information to low-level visual features, and retrieves the original video content using the keyframes as the index, which has a direct impact on video quantity and quality. Final search results in efficiency and accuracy [13].

By annotating the written description of each video frame and matching query keywords with annotations, the multifeature fusion completes the video search [14]. This method begins by incorporating picture band decomposition theory, extracting low-frequency grass-roots information and high-frequency detail information from the dance, and then mapping the corrected grass-roots image. It incorporates multiple functions such as speech, motion, face recognition, and others in a new way, collects diverse human body movements using RGB and infrared cameras, analyzes and recognizes them, and enables intelligent human-computer interaction [15]. It has been discovered that the multifeature fusion of dance and music matching optimization simulation approach may not only aid dance experts assess dance videos but can also be used for teaching, cultural heritage protection, and excavation. The following are the study's unique features: (1) because too many repetitive dance moves in dance motions reduce the retrieval rate, this research provides a method for extracting crucial frames from music and dance videos. (2) In order to improve the classification effect of multimodal features, a multifeature fusion-based optimization simulation method for matching dance and music is proposed, with the goal of transforming low-level audio features into a bag-of-words model that is unified to the lyric text regardless of time or frequency domain. (3) In this study, a multifeature fusion strategy is utilized to learn the implied links between higher-order features recovered by the feature encoding network, allowing for early detection of information interactions between distinct features.

The research framework of this study consists of five major parts, which are organized as follows:

The first part of this study introduces the background and significance of the research and then describes the main work of this study. The second part introduces the work related to the optimal simulation of dance movement and music matching, and multifeature fusion. The third part of the study introduces the design methods of music and dance movement feature extraction and multifeature fusion dance-music matching simulation, so that the readers of this study can have a more comprehensive understanding of the multifeature fusion-based dance-music matching simulation method. The fourth part is the core of the thesis, which completes the description of the multifeature fusion-based optimization simulation analysis from two aspects: optimization simulation and multifeature fusion of dance and music. The last part of the study is the summary of the whole work.

2. Related Work

2.1. Optimization Simulation of Match between Dance and Music. Music is a kind of artistic expression that is more powerful than images but less so than words. Dance, on this premise, transforms the rich information of dance images buried in music into rich three-dimensional and multidimensional visual images, presenting the meaning of dance to its fullest extent. The significance of music emotion analysis can be seen in the following ways: the study ideas of the music emotion model can be applied to artificial intelligence in emotion recognition, and this research can also be applied to other domains of pattern recognition. Domestication technology and intelligent human-computer interaction have advanced rapidly. The analysis of these music and dance videos is performed using matching optimization simulation, and organically related music and dance action segments are obtained, which not only reduces the work intensity of dance professionals but also facilitates the retrieval of music and dance video data and dance arrangement automation.

Zhou and Zhang developed an application software to improve the content-based matching function on the Internet and make the matching or optimization of music and dance more intelligent [16]. Hong et al. proposed an optimization method based on genetic theory to match the technical movements of dance and music. This method first determines the music style, obtains the basic style characteristics of music and dance, and then analyzes the correlation between the basic characteristics of music and dance to remove the repeated feature pairs [17]. Sun and Ruan used the depth and bone information obtained by the camera for dance action recognition [18]. The recognition accuracy is improved by using the information obtained from the offline data set, including RGB information and available depth and bone information. Ng et al. proposed an optimization method based on machine learning to match dance technical movements and music in music arrangement [19]. First, combined with machine learning theory, this method constructs the mapping relationship between dance action and music based on historical sample data set and obtains the evaluation function of the harmonious relationship between dance action and music. Wang et al. proposed a method to quickly and accurately predict the 3D position of dance movements in a single depth image without using time information [20].

2.2. Research on Multifeature Fusion. In the human perception of music, a music category refers to a group of songs that usually feel the same interpretation. Music genres provide important emotional descriptions and are used to classify music. In recent years, many domestic and foreign scientific research institutes and relevant scholars are committed to the research of dance movement recognition, which has made great contributions to the development of movement recognition research. However, how to classify dance movements and music in the music genre classification system is an arduous task.

Zhang and Zhao proposed an optimization method for matching dance technique movements to music based on greedy theory [21]. The method now adapts a given dance movement and that movement to the beat of the music, and then performs music-dance movement matching based on this. According to Pandeya and Lee motion recognition based on static RGB image features, in videos dealing with complex backgrounds, static features are susceptible to factors such as background, illumination, and human motion, making feature extraction difficult [22]. Huang et al. focused on dynamic scene understanding, target tracking, and motion recognition through multifeature fusion and successfully applied it to applications such as real-time surveillance, teleconferencing, and intelligent robot navigation [23]. López-Ortega proposed an optimal matching method for multifeature fusion images based on correction and balancing techniques in dance [24]. The method first maps the luminance of each pixel in the dance correction and balance technique image to the luminance range that can be output by the display device according to a one-to-one correspondence. Roy et al. developed an intelligent video surveillance system based on multifeature fusion that overcomes the interference of scene illumination changes and can automatically detect music in the video with the function of automatically matching the dance [25].

The dance competition is not only a competition for dancers' skills but also a competition for general arts other than dance, such as music creation, theme script, and stage art. As an important part of dance, dance music is unparalleled in dance works.

3. Optimization Simulation Method of Dance and Music Matching Based on Multifeature Fusion

3.1. Feature Extraction of Music and Dance Movements. The variability of dance movements and too many overlapping movements leads to major problems in extracting movement features [26]. The movements of music and dance videos are complex, changeable, and repetitive, which makes it difficult to analyze and identify dance movements [27]. The artistic form of music is stronger than abstraction and weaker than an image, but its rigid organizational logic, artistic structure, and rich symbolic meaning strengthen people's thoughts and connect and synthesize metaphors into moving sounds [28]. On this basis, a genetic algorithm is used to train the corresponding relationship of different music and dance movements, and its accuracy is taken as the fitness function to obtain the optimal music and dance movement matching. People are greatly inspired by the research in the field of art and music psychology. The analysis model of music emotion perception is shown in Figure 1.

First, in the process of dance action matching and optimization in music arrangement, the synchronized dance action and music data are segmented through music beat extraction theory to obtain multiple short action music fragment combinations. After calculating the entropy value of each image in the image sequence, the entropy value corresponding to the current frame is compared with the previous frame. If it is greater than the threshold, it is considered as a keyframe. The following formula is often used to calculate the entropy between samples. The smaller the entropy, the greater the similarity between samples. For an n dimensional space, the Minkowski distance between point X and point Y can be expressed as follows:

$$dis(X,Y) = \sqrt[p]{\sum_{i=1}^{n} |x_i - y_i|^p}, i = 1, 2, ..., n, \tag{1}$$

where x_i is the i dimensional characteristic data of point X and y_i is the$i$ dimensional characteristic data of point Y.

Using the keyframe sequence as input, the RGB image information of the keyframes is input to the spatial convolutional neural network to extract the video shape information and the optical flow information of the keyframes and adjacent frames, which is used to extract the temporal convolutional network motion information of the video frames. Therefore, in this study, each joint point of the image is assigned a motion contribution weight, and the joint contribution weight formula of the feature vector can be expressed as follows:

$$\mathrm{dis}\left(x^{(m)}, x^{(n)}\right) = \sqrt{\sum_{i=1}^{N} \omega_i \left(x_{ix}^{(m)} - x_{ix}^{(n)}\right)^2 + \left(x_{iy}^{(m)} - x_{iy}^{(n)}\right)^2}. \tag{2}$$

Before the comparison, in order to select more representative features and reduce the computational complexity, the CHI feature selection method based on the difference mentioned above is used to select features for both audio words and text words. Generally, the feature extraction process is shown in Figure 2.

Second, the transition point of music is detected, the beat prediction position obtained in each stage is aligned, the correlation coefficient between dance action and music part is calculated, and the dance action matching optimization objective function is obtained. The dance action is represented by the dispersion of different coordinate positions in the whole video. The more active the action is, the higher the dispersion degree is. The dispersion degree of dance action i is measured by the variance of coordinates:

$$\sigma_i^2 = \frac{\sum_{f=0}^{n} \left(x_i^{(f)} - x_i\right)^2 + \left(y_i^{(f)} - y_i\right)^2}{n}. \tag{3}$$

Here, $x_i^{(f)}, x_i$ are the abscissa and ordinate positions of joint point i in frame f, x_i, y_i are the average abscissa and ordinate positions in the whole video sequence, and n is the video frames.

Then, the motion contribution weight of joint point i can be expressed as follows:

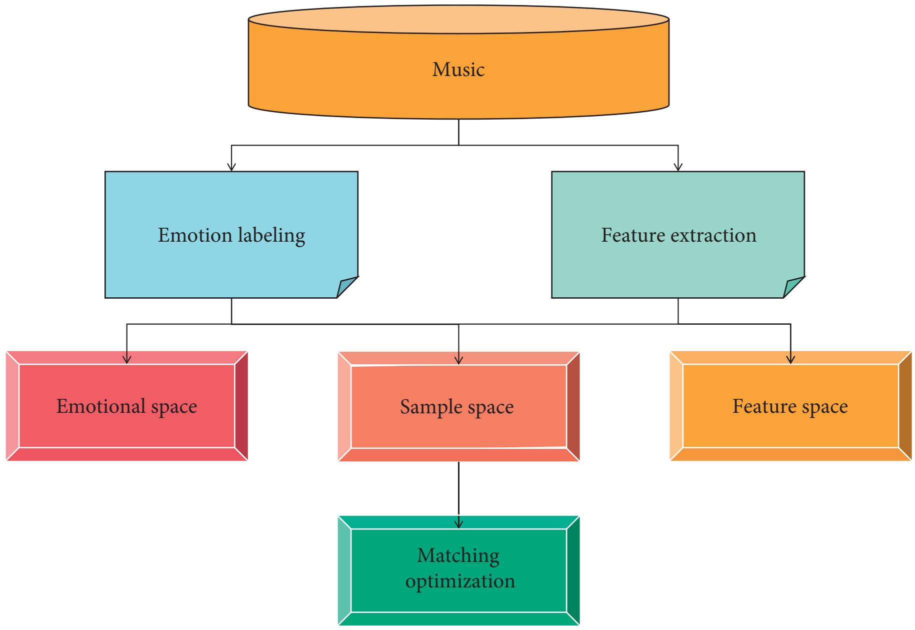

Figure 1: Analysis model of music emotion recognition.

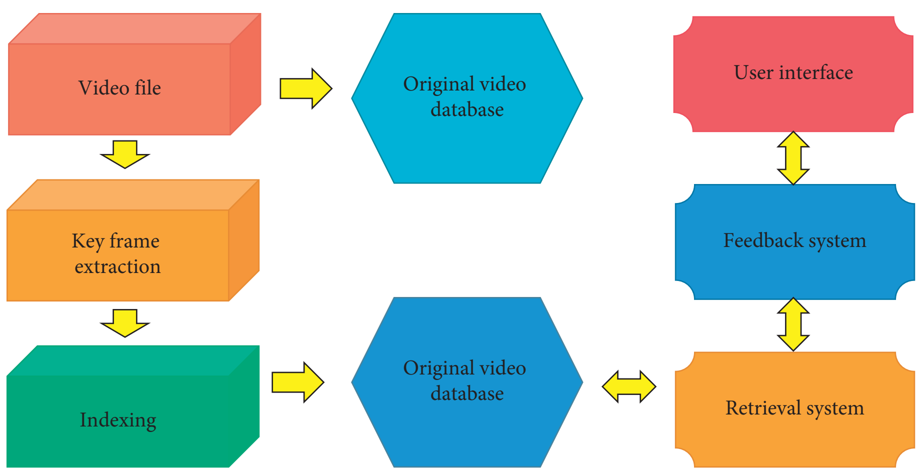

Figure 2: Feature extraction process diagram.

$$\omega_i = \frac{\sigma_i^2}{\sum_{k=0}^{n} \sigma_k^2}. \quad (4)$$

The duration of the dance video, the number of frames in the image, and the frame rate of the video are all known during these audio and dance movements, and interval operations are performed using standard deviations, corresponding to audio and audio values computed once per second. Entropy value sequences and functions are combined [29]. The contrast and visual quality of the image are increased by mapping pixels concentrated in several grayscales to other grayscales and distributing them uniformly by dividing the color gamut point by point by the chromaticity priority of the standard layer image [30].

Finally, to achieve dance action matching in music arrangement, all music and dance action parts of the music arrangement are adaptively adjusted to pheromone fluctuation factors according to pheromone concentration, and pheromones are dynamically updated according to the optimal solution of dance action matching. The order of entropy values is calculated after feature fusion. In comparison, the difference in entropy values between two adjacent frames is not utilized as a benchmark for determining keyframes, but instead, it is determined by comparing this value with the threshold using the following formula:

$$\mathrm{V} = \frac{\left| H_{\text{current}} - H_{\text{key}} \right|}{H_{\text{key}}}. \quad (5)$$

Here, $H_{current}$ is the entropy value of current frame and H_{key} is the entropy of the current keyframe.

For the skeleton 3D coordinate data in each frame of the video sequence, k frame is randomly selected as the sample center, and then the 30 3D coordinate data in k extracted at last are unchanged or less than a certain threshold through iteration in turn by using the above algorithm.

3.2. Specific Design of Multifeature Fusion Dance and Music Matching Optimization Simulation. In the first mock exam of video, there are many modes in its content, such as appearance, optical flow, and depth. These modes complement each other, convey important information, and integrate these modes, which can effectively solve the problem of insufficient expression of single modal video information. The distance between the keyframe sequence KF and the original video sequence set F can be expressed by the maximum semi Hausdorff, which is defined as follows:

$$D = (F, KF) = \max\{D(F_i, KF)|i = 1, 2, \ldots, N\}. \tag{6}$$

Music in a narrow sense refers to the basic elements of music sound, including pitch, length, intensity, and timbre. These basic elements combine to form the "formal elements" of common music. After extracting low-level features from audio's auditory and visual features, we use feature coding network to study the low-level features to obtain high-level features. Emotion recognition presents a hierarchical feature, as shown in Figure 3.

Because music genres are often distributed in local and repeated audio clips, if the music is divided into segments that are too short, it will be difficult to reflect the relationship between local characteristics. The specific design method of multifeature fusion music recognition method is shown below.

First, the optical flow information in the video is extracted by the denseflow software, and the video is divided into frames. Recall (R) is used to measure the missing detection of extracted keyframes and can be expressed as follows:

$$R = \frac{N_c}{N_c + N_m} \times 100\%. \tag{7}$$

Here, N_c is the number of keyframes correctly extracted from the extracted results and N_m is the number of missed keyframes.

The open pose posture estimation tool is used to extract the coordinate information of human joints in the image and normalize it. First, the collected music data are divided, and the movement segments are connected and constructed in the dance movement database, so as to obtain the basic features of historical music and dance movements, extract some feature pairs by correlation analysis, and calculate the gender coefficient by the correlation between music and dance features. In order to avoid the situation that the weight tends to be long text, which is not conducive to short text, this study normalizes the weight of the calculated feature words, and the formula is as follows:

$$W(t, d) = \frac{1 + \log_2 tf(t, d) \times \log_2 (N/n_l)}{\sqrt{-\sum_{t\epsilon d}[(1 + \log_2 tf(t, d) \times \log_2 (N/n_l))]}}. \tag{8}$$

Here, $W(t, d)$ is the weight, $tf(t, d)$ is the frequency, N is the total number of all videos in the training set, and n_t is the number of documents, in which the feature word t appears.

In the actual work process, if the length of the lens and the complexity of the video content under the lens are not considered, if the lens is too long, it is difficult to summarize the content of the lens with only a few music clips. Therefore, relevant features are extracted from the original data according to the needs and analyzed and processed in combination with the differences of various feature information. The difference here is defined as follows:

$$\Delta\ dis(w) = \frac{abs\left(chi_i - chi_j\right)}{\sqrt{\max\left(chi_i, chi_j\right)}}. \tag{9}$$

Second, we constructed temporal and spatial convolutional network models based on the Res Net152 structure, respectively, and then fine-tuned the dual-stream network model by migration learning to obtain high-level semantic features, image functions, and optical stream functions of RGB. In this system, audio features and lyric features are fused at the feature level, and the fusion is done in a linked manner. That is, the features of the two modes are directly linked to form a new feature vector. Unlike semi-infinite linear programming, it exploits the smoothing property of the objective function and uses gradient descent to update the kernel function weights. The kernel function weights are given by the following equation:

$$D_m = \begin{cases} 1, \left(\text{if} dm = 1, \text{and} \dfrac{\partial J}{\partial d_m} - \dfrac{\partial J}{\partial d_\mu} > 0\right), \\[2ex] -\dfrac{\partial J}{\partial d_m} + \dfrac{\partial J}{\partial d_\mu}\ (if dm\ > 1, \text{and}\, m \neq \mu), \\[2ex] \displaystyle\sum_{i=1} \dfrac{\partial J}{\partial d_v} - \dfrac{\partial J}{\partial d_\mu}\ (if m = \mu)\,. \end{cases} \tag{10}$$

Here, D_m is the direction of gradient descent.

To keep the input sample size sufficient and increase the number of input samples, the original audio stream is separated into continuous segments. The trajectories created by SIFT matching between video frames are one type, while the trajectories obtained by optical flow tracking sampling points are the other. The sampling sites are sampled near each sift point. Finally, we construct a spatiotemporal graph convolutional neural network model based on the graph convolutional neural network structure to capture the spatial information of the joint points in the time series. Then, based on the extracted audio sentiment features, these features are used to obtain a pixel-value representation of the lyrics based on the codebook. The new pixel value is considered as a background pixel when the nearest Gaussian distribution belongs to any of the above B Gaussian distributions; otherwise, it is a foreground pixel. Then, a sector template with a circular angle of 70° is rotated and slid in a circular area to obtain the vector formed by the sum of the Harr responses in each sliding window, and the direction corresponding to the maximum of the sum of the sums is chosen as the reference direction of the feature.

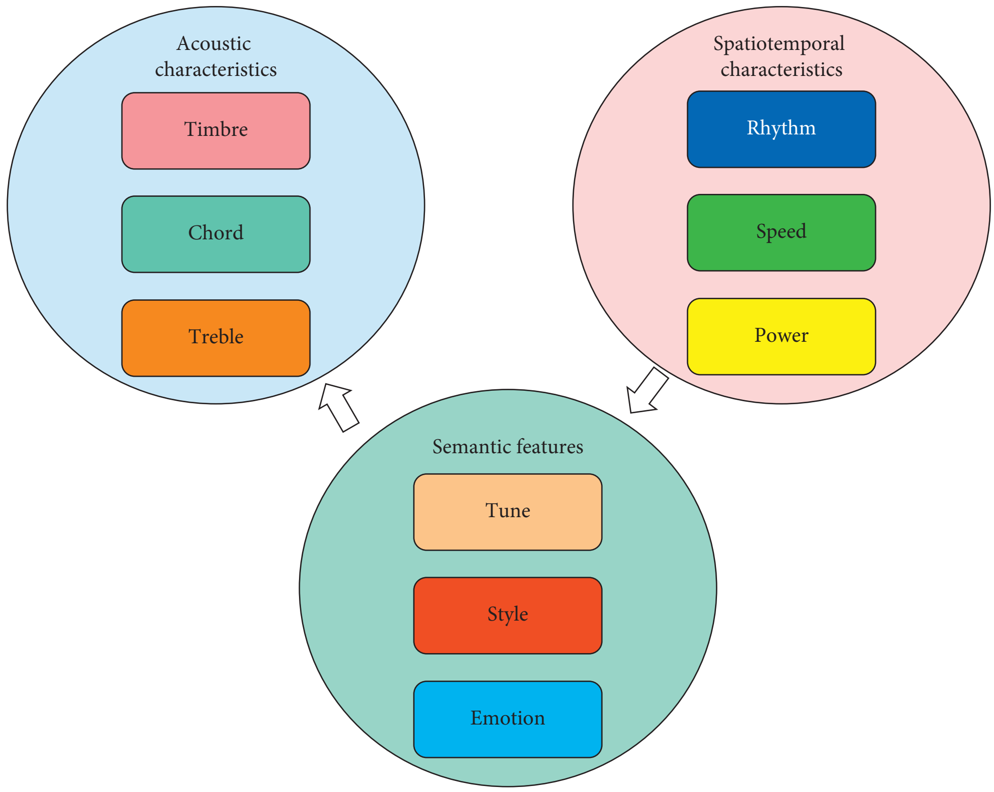

Figure 3: Hierarchical characteristics of music emotional cognition.

4. Simulation Analysis of Matching Optimization Based on Multifeature Fusion

4.1. Optimization Analysis. When we appreciate dance (especially the artistic dance carefully created by choreographers), music and its melody, harmony, rhythm, mode, and texture are indispensable components of dance works. In the process of music and dance movement matching optimization, based on the objective function of dance movement matching optimization, combined with the optimization simulation theory, the objective function is optimized. The concentration adaptively adjusts the pheromone volatilization factor, dynamically updates the pheromone according to the advantages and disadvantages of the optimal dance action matching scheme, and completes the dance action matching optimization in music choreography. Since the features extracted here are exactly the same as those in the single-mode music emotion recognition based on audio, the main factor to judge whether the two clips are similar is the feature factor, which is the feature value video obtained by matching the information. It is the principal component to measure whether two things are consistent with one result. Therefore, the characteristic factors should occupy a high weight. The accuracy of video clips in the two dance data sets under different weights is shown in Figure 4.

First, we create a sliding window containing many pixels in the window and use the median of all these pixels as the new value for the center of the window. Viewing a band in this window, the harmonic content remains fairly constant, while the shock structure is shown as a peak. Low-level music features usually use statistical function variables to summarize the variance or central tendency in the music. Among them, the boundary direction histogram is a boundary-based shape analysis method that is independent of the size and location of the image object, simple to compute, and can better describe the shape of the object boundary. In this section, the Mel spectrogram of the dataset is used as an input to select the appropriate size of music segments and the number of heads in the feature encoding network, and the results are shown in Figure 5.

Second, it sorts the gray values of all pixels in the window. After sorting, the median of the array is taken as the new value of the gray value of the central pixel of the window. According to the comparison results between the ratio of the nearest distance and the next nearest distance and the threshold, a pair of matching points is accepted, then one-way matching is completed, whether to obtain a group of candidate matching pairs is judged, and the same method of using the matching points of the next frame is used to inverse match with the previous frame to obtain a pair of inverse matching feature points. Because it is difficult to describe and measure an image frame accurately and comprehensively by relying on only one image feature, it is necessary to integrate several different image features to measure the similarity in order to describe the original image content more comprehensively and accurately. This study compares the different λ values that affect the experiment. The results show that the best test accuracy can be obtained when the value of λ is set to 0.05. The influence of self-

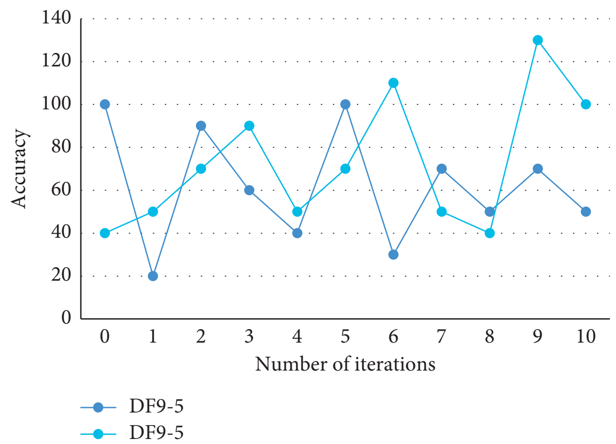

Figure 4: Accuracy of video clips in two dance datasets under different weights.

attention mechanism and net VLAD on a feature coding network is shown in Figure 6.

Finally, the directional gradient histogram feature used to describe the dance movement information is extracted from the image. Features are described as the boundary direction histogram, and texture features are described as wavelet transform containing various image features.

This is because the method in this study first incorporates music beat extraction theory to segment the synchronized dance movement and music data to obtain multiple short movement-music fragment combinations and calculate the correlation between the dance movement-music fragments. It is used to obtain the optimal objective function for dance movement matching, which improves the degree of dance movement-music matching in the music choreography performed by the method of this study.

4.2. Multifeature Fusion Analysis of Dance and Music. The smallest unit of any fully structured music is a part. The phrases and parts in a part are the internal building blocks of the structural unit. Similarly, the features of dance images provide other information for motion recognition, and image features provide appearance information closely related to the human movement in the image in the process of motion recognition. The comprehensive effectiveness of this method needs to be verified by simulation. The experimental data are from the dance action capture database provided by Carnegie Mellon University Laboratory, and the length of each music segment is about 5 seconds. Using the methods of this study and references [17] and [19], the optimization experiment of dance action matching in music choreography is carried out, and the matching degrees (%) of the three methods are compared. Figure 7 shows the comparison results of dance movements in music arrangement.

The results show that the average matching degree between the optimized simulation methods in this study is 87%, and the matching degree is very high. This is mainly because the method in this study first detects the transition point of a music segment, aligns the beat prediction position obtained in each stage, and adaptively adjusts the pheromone fluctuation factor according to the pheromone concentration of all music dance motion segments. The music arrangement uses the method of this study to match the dance movements well.

The calculation procedure is to use the k vectors clustered out in each video sequence about the sample centers of 3D joint node positions, the clustering centers of the joints in each vector, and the coordinates of the corresponding 3D joints in each frame of the video sequence to calculate the Euclidean distance, respectively. The appearance information of objects in an image can be well described by the direction of gradients or edges, and the method generates descriptors by calculating the statistical information of local image gradient directions. Two images can be generated by using a median filter to filter in the horizontal and vertical directions of the magnitude spectrogram of the descriptor. If the median filter is applied at the frequency, the shock events are enhanced and the harmonic components are suppressed. The best combination of features is input to the meta-CNN and the training process is visualized on the model GTZAN and Extended Ballroom datasets. The results are shown in Figure 8.

Second, in the training process, the feature pyramid network (FPN) extracts features and returns to the key points of human skeleton, and the simple key points will be basically completed in the FPN stage. The detailed network structure of FPN is listed in Table 1.

Multicore learning can be understood as having great interpretability when learning the weighted convex combination of several cores, and the weight coefficient is crucial for extracting features from different modes. It is possible that such a probability value is zero. To avoid the occurrence of zero probability, it is a common practice to apply various data smoothing procedures. A pixel with a significant difference value in two orthogonal directions is particularly unique and ideal for tracking, even if it is on an edge. As a result, the RGB picture data recovered from the keyframe, as well as the stacked optical flow generated by the keyframe and its surrounding 10 frames, are fed into the spatial and temporal convolution networks for testing. The results are listed in Table 2.

Finally, the strong and weak edges and details of each layer are separated by limiting the number of strong edges, then the layered mapping function is constructed for each layer, and point-by-point mapping is performed for each layer by enhancing the details of each layer and the contrast of the weak edges and keeping the strong edges, thus realizing the remapping process for each layer. The video frame with the largest C value is calculated, the index of the frame with that C value is obtained, and finally, the keyframes are sorted by index value, and if the number of indexes is the same, the keyframes are determined based on the sum of the calculated distance between the nodes in the frame and the nodes corresponding to the clustering center, and the one with the smallest sum is the keyframe. Thus, the edge features of each image of a video frame are accumulated in a single image, and finally, the directional gradient histogram features are extracted from the image of the accumulated edge features.

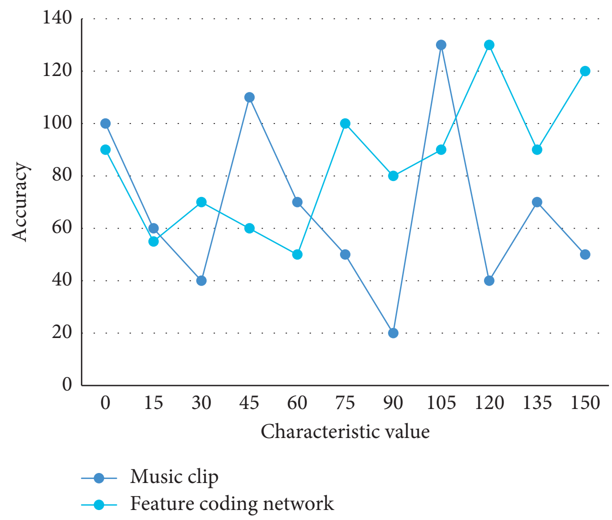

Figure 5: Test accuracy of music segment and feature coding network.

Figure 6: Influence of self-attention mechanism and net VLAD on feature coding network.

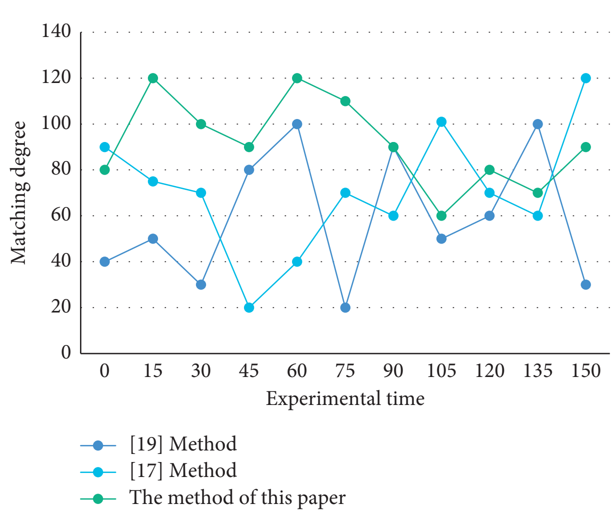

Figure 7: Comparison chart of matching degree of different methods of dance movements.

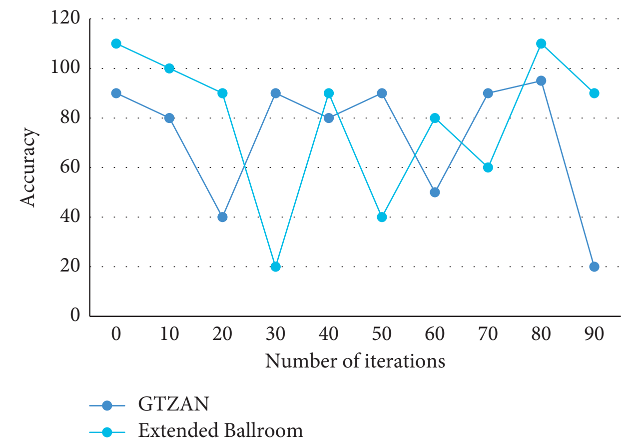

Figure 8: Training results.

Table 1: Detailed structure of FPN network.

Type of layer	Step size and number of fills	Output size	Nuclear size
Conv1D	3.0	(10, *b*, 84)	(34, 969)
ReLU	2.5	(28, 76, 32)	(27, 1004)
Dense	1.8	(27, 47, 44)	(29, 1863)
Maxpooling1D	2.2	(43, 34, 38)	(63, 548)

Table 2: Accuracy of different keyframes on ufc101 split1.

Number of keyframes	10	20	30
Accuracy (%)	44.8	52.9	89.8
Average consumption time (s)	3.6	4.2	2.1

5. Conclusions

Unique or expressive rhythms, such as strength, weight, and melody, are primarily used to define the integration of music and dance. Music sentiment analysis, such as music sentiment expression models, music review feature identification, emotional music classification, and emotional music search, is a hot trend in artificial intelligence. Music and dance matching is crucial in music discovery and can be used to manage and tag music content on websites and device music engines. On the basis of multifeature fusion, a strategy is given for optimizing dance technology movement and music matching simulation. By obtaining optimal performance on a dataset, multifeature fusion illustrates a good application case. The multifeature fusion-based dance and music matching optimization simulation approach, which includes feature extraction of music and dance movements, is described in this work. The dance music multifeature fusion and multifeature fusion-based matching optimization simulations are thoroughly examined. This aggressive and comprehensive matching approach is more universal and scalable, and it can give a platform for additional distinct songs and dances besides chime music and dance. In this way, the same cultural isomorphism, emotional isomorphism, affective isomorphism, and imagery synthesis of music and dance matching can both express the music's sensual characteristics and reach the audience's mind. Music expresses emotion, while music ultimately reproduces the form of space through dance, ultimately creating an audience through audio-visual fusion.

Data Availability

The data used to support the findings of this study are available from the corresponding author upon request.

Conflicts of Interest

The author declares that there are no conflicts of interest.

References

[1] L. Xiong, R. S. Chen, X. Zhou, and C. Jing, "Multi-feature fusion and selection method for an improved particle swarm optimization[J]," *Journal of Ambient Intelligence and Humanized Computing*, no. 8, 2019.

[2] S. Chen, "Chinese mosuo "playing dance" music analysis," *Review of Educational Theory*, vol. 3, no. 1, p. 38, 2020.

[3] G. Sun, Y. Wong, Z. Cheng et al., "Deep dance: music-to-dance motion choreography with adversarial learning[J]," *IEEE Transactions on Multimedia*, vol. 23, no. 99, p. 1, 2020.

[4] B. Liu, "Simulation research based on ant colony theory of music and dance technical movement matching optimization [J]," *Revista de la Facultad de Ingenieria*, vol. 32, no. 11, pp. 641–646, 2017.

[5] F. J. Karpati, C. Giacosa, N. E. Foster, V. B. Penhune, and K. L. Hyde, "Dance and music share gray matter structural correlates," *Brain Research*, vol. 1657, pp. 62–73, 2017.

[6] D. Yao, Z. Zhi-li, Z. Xiao-feng et al., "Deep hybrid: multi-graph neural network collaboration for hyperspectral image classification," *Defence Technology*, 2022.

[7] Y. Wang, T. Wang, X. Zhou et al., "Trans EffiDet: aircraft detection and classification in aerial images based on EfficientDet and transformer[J]," *Computational Intelligence and Neuroscience*, vol. 2022, Article ID 2262549, 2022.

[8] Y. Ding, X. Zhao, Z. Zhang, Wei Cai, Nengjun Yang, and Ying Zhan, "Semi-supervised locality preserving dense graph neural network with ARMA filters and context-aware learning for hyperspectral image classification[J]," *IEEE Transactions on Geoscience and Remote Sensing*, vol. 60, pp. 1–12, 2021.

[9] J. Zhou, Y. Wang, and W. Zhang, "Underwater image restoration via information distribution and light scattering prior," *Computers & Electrical Engineering*, vol. 100, Article ID 107908, 2022.

[10] J. Zhou, D. Liu, X. Xie, and W. Zhang, "Underwater image restoration by red channel compensation and underwater median dark channel prior," *Applied Optics*, vol. 61, no. 10, pp. 2915–2922, 2022.

[11] W. Cai and Z. Wei, "Remote sensing image classification based on a cross-attention mechanism and graph convolution," *IEEE Geoscience and Remote Sensing Letters*, vol. 19, pp. 1–5, Article ID 8002005, 2022.

[12] J. Chen, Y. Zhang, L. Wu, T. You, and X. Ning, "An adaptive clustering-based algorithm for automatic path planning of heterogeneous UAVs," *IEEE Transactions on Intelligent Transportation Systems*, pp. 1–12, 2021.

[13] J. Cong and B. Zhang, "WITHDRAWN: multi-model feature fusion for human action recognition toward sport sceneries," *Signal Processing: Image Communication*, Article ID 115803, 2020.

[14] H. Wang and J. Li, "Human action recognition algorithm based on multi-feature map fusion[J]," *IEEE Access*, no. 99, p. 1, 2020.

[15] S. Yu, Y. Cheng, L. Xie, Z. Luo, M. Huang, and S. Li, "A novel recurrent hybrid network for feature fusion in action recognition," *Journal of Visual Communication and Image Representation*, vol. 49, no. nov, pp. 192–203, 2017.

[16] E. Zhou and H. Zhang, "Human action recognition toward massive-scale sport sceneries based on deep multi-model feature fusion," *Signal Processing: Image Communication*, vol. 84, no. 1, p. 115802, 2020.

[17] L. I. Hong, J. Chen, and H. U. Ruimin, "Multiple feature fusion in convolutional neural networks for action recognition[J]," *Wuhan University Journal of Natural Sciences*, vol. 22, no. 01, pp. 78–83, 2017.

[18] P. Sun and D. Ruan, "Virtual simulation design and effect of high jump technology action optimization based on complex embedded system," *Microprocessors and Microsystems*, vol. 81, no. 2, p. 103646, 2021.

[19] W. Ng, W. Zeng, and T. Wang, "Multi-level local feature coding fusion for music genre recognition[J]," *IEEE Access*, no. 99, p. 1, 2020.

[20] Y. Wang, W. Zhang, D. Huang, and Y. Liu, "Multi-level feature fusion and multi-loss learning for person Re-Identification," *Signal Processing: Image Communication*, vol. 94, no. 10, p. 116197, 2021.

[21] C. Zhang and H. Zhao, "Lip reading using local-adjacent feature extractor and multi-level feature fusion," *Journal of Physics: Conference Series*, vol. 1883, no. 1, Article ID 012083, 2021.

[22] Y. R. Pandeya and J. Lee, "Deep learning-based late fusion of multimodal information for emotion classification of music video," *Multimedia Tools and Applications*, vol. 80, no. 2, pp. 2887–2905, 2021.

[23] Z. Huang, X. Jia, and Y. Guo, "State-of-the-Art model for music object recognition with deep learning," *Applied Sciences*, vol. 9, no. 13, p. 2645, 2019.

[24] O. López-Ortega, F. Castro-Espinoza, and O. Pérez-Cortés, "An intelligent multi-agent system to create and classify fractal music," *Computing*, vol. 100, no. 7, pp. 671–688, 2018.

[25] S. Roy, D. Sarkar, and D. De, "Entropy-aware ambient IoT analytics on humanized music information fusion," *Journal of Ambient Intelligence and Humanized Computing*, vol. 11, no. 1, pp. 151–171, 2020.

[26] Y. Dong, X. Guo, and Y. Gu, "Music recommendation system based on fusion deep learning models," *Journal of Physics: Conference Series*, vol. 1544, no. 1, Article ID 012029, 2020.

[27] K. V. V. Kumar, P. V. V. Kishore, and D. Anil Kumar, "Indian classical dance classification with adaboost multiclass classifier on multifeature fusion," *Mathematical Problems in Engineering*, vol. 2017, pp. 1–18, 2017.

[28] P. Hua, L. D. Jing, C. Hh, Liping Zhao, Sheng Feng, and Keli Hu, "Feature fusion based automatic aesthetics

evaluation of robotic dance poses - ScienceDirect[J]," *Robotics and Autonomous Systems*, vol. 111, pp. 99–109, 2019.

[29] J. Li, H. Peng, H. Hu, Z. Luo, and C. Tang, "Multimodal information fusion for automatic aesthetics evaluation of robotic dance poses," *International Journal of Social Robotics*, vol. 12, no. 1, pp. 5–20, 2020.

[30] S. L. Carter, A. R. Bryant, and L. S. Hopper, "An analysis of the foot in turnout using a dance specific 3D multi-segment foot model," *Journal of Foot and Ankle Research*, vol. 12, no. 1, p. 10, 2019.

Hindawi
Computational Intelligence and Neuroscience
Volume 2022, Article ID 4318962, 10 pages
https://doi.org/10.1155/2022/4318962

Research Article

Integration and Optimization of British and American Literature Information Resources in the Distributed Cloud Computing Environment

Mei Chen

Nanchong Vocational and Technical College, Nanchong 637000, China

Correspondence should be addressed to Mei Chen; chenmei163163@163.com

Received 1 April 2022; Revised 28 April 2022; Accepted 29 April 2022; Published 7 June 2022

Academic Editor: Xin Ning

One of the most effective approaches to improve resource usage efficiency and degree of resource collecting is to integrate resources. Many studies on the integration of information resources are also available. The search engines are the most well-known. At the same time, this article intends to optimize the integration of British and American literature information resources by employing distributed cloud computing, based on the needs of British and American literature. This research develops a model for the dispersed nature of cloud computing. It optimizes the method by fitting the mathematical model of transmission cost and latency. This article analyzes the weaknesses of the current British and American literature information resource integration and optimizes them for the integration of British and American literature resources. The Random algorithm has the longest delay, according to the results of this paper's experiments (maximum user weighted distance). The algorithms NPA-PDP and BWF have longer delays than the algorithm Opt. The percentage decline varies between 0.17 percent and 1.11 percent for different algorithms. It demonstrates that the algorithm presented in this work can be used to integrate and maximize information resources from English and American literature.

1. Introduction

In the past ten years, cloud computing has experienced rapid development and has been widely used. Many commercial cloud computing service providers (cloud service providers, CSPs) began to provide a variety of public cloud computing services. More enterprises and organizations have also built their own private cloud infrastructure or built hybrid cloud facilities. Achieving efficient utilization and management of cloud computing resource pool resources can not only reduce service costs, but also improve service quality and competitiveness. The current problem is how to allocate resources to meet the service quality requirements of diversified businesses, reduce costs, and increase profits. Therefore, resource allocation is one of the most basic and core issues in cloud computing service deployment.

At the same time, the research on British and American literature is becoming more and more enthusiastic, and the demand for British and American literature resources is increasing. Whether it is a literary worker or the general public, the thirst for literary knowledge is getting higher and higher. However, the resources of British and American literature are widely distributed in archives, websites, and libraries around the world, which makes it difficult and costly to obtain. In addition, the language of British and American literature includes Old English, confused language, and other mixed languages, which are not easy to read. Therefore, combined with the characteristics of distributed cloud computing, it is necessary to integrate and optimize the global British and American literature resources.

The main innovations of this paper are as follows: it optimizes the delay and cost of migrating distributed big data of British and American literature to the cloud. Firstly, the selection target of data center during data migration is analyzed. It proposes an approximate algorithm for fair data placement and optimal data placement. It simultaneously extends the traditional k-supplier problem, the capacity-unlimited facility location problem, and the k-middle point problem. Aiming at the two goals of minimizing data placement for transmission cost and minimizing data placement for total cost, a nearest data center priority heuristic algorithm is proposed. The proposed algorithm can effectively reduce latency, save costs, and solve the problem that some data centers are unavailable due to regulatory restrictions or user preferences during data migration.

2. Related Work

In order to maximize the profits of CSPs and optimize the user experience, in recent years, it has become a trend to use multiple cloud networks to provide services in a unified manner. In the multi-cloud structure, cloud broker service has been recommended as a basic cloud service and has attracted extensive attention from industry and academia. Tsai and Lo proposed an efficient distributed mobile cloud computing service authentication scheme. His scheme reduces the authentication processing time required for communication and computation between cloud service providers and traditional trusted third-party services. Formal security proofs and performance analysis show that the scheme is both secure and efficient [1]. Hirai et al. modeled the task scheduling server as a single-server queue, where the server consists of many workers. When a task enters the server, the task is split into subtasks. Each subtask is served by its own worker and an alternate different worker [2]. Xiong et al. believed that, with the rapid development of mobile services, mobile cloud computing (MCC) has received great attention from researchers in academia and industry. He will design an enhanced and provably secure authentication scheme for distributed MCC services [3]. Kakade et al. eliminated the need for an uninterruptible power supply (UPS) in the data center by connecting direct current voltage from a backup power source directly to the motherboards of multiple servers in the data center. The alternating current power received from the electric utility service is converted to a lower voltage by on-site transformers and then supplied to one or more power distribution units on-site [4]. Liao et al. proposed an active data prefetching scheme on the storage server of the distributed file system for cloud computing. Experiments demonstrate that their proposed active prefetching technique can benefit distributed file systems in cloud environments to achieve better I/O performance [5]. Deng et al. proposed a distributed intrusion detection based on hybrid gene expression programming and cloud computing (DID-HGEP Cloud) for the massive and high-dimensional intrusion data behavior in cyber-physical power systems. Through comparative experiments, it is shown that the algorithm they proposed has obvious advantages in false attack rate, DAR, average time consumption, etc. Furthermore, the proposed algorithm has excellent parallel performance [6]. Alhazmi et al. believed that cloud computing provides on-demand IT services through large distributed data centers on high-speed networks. Virtualization is a key cloud computing technology. It allows service providers to offer computing services in a cloud environment without platform compatibility differences. He formulated the virtual network configuration in a geographically distributed cloud computing data center supporting SDN as a mixed integer linear programming (MILP) problem. The formulation of the proposed Optimal Virtual Network Provisioning (OVNP) model is studied by simulation. The experimental results verify the effectiveness of his proposed method [7]. However, through the summary of related research, it can be found that although the current research on distributed cloud computing is very in-depth, there is no research on resource integration for British and American literature. This is detrimental to the development of the resource integration of English and American literature in China.

3. Distributed Cloud Computing

Cloud computing has become the preferred platform for big data analysis [8, 9]. Especially when data is generated from multiple geographically distributed locations, local users need to use local data frequently, and sometimes all local data need further joint analysis. Therefore, it is more appropriate to use a cloud platform. For example, for a multinational sales company with many subsidiaries around the world, subsidiaries in each country need to analyze data generated by local users in a timely manner for business purposes. At the same time, all data should be aggregated and analyzed to report to headquarters or support cross-border transactions. For example, US demographic data is stored by state. Huge remote sensing data are stored in data centers across regions. Although these data are managed regionally, they may also require collaborative analysis for a common goal [10, 11]. Generally speaking, large-scale cloud computing is networked in a distributed manner. It has multiple geographically distributed data centers (Amazon has at least 11 DC1s across 4 continents; Google has at least 13 DC2s across 4 continents). Each DC configures computing and storage resources on a pay-as-you-go basis. This kind of infrastructure can provide nearby services and is especially suitable for data processing distributed across regions.

In order to process big data in cloud computing, the prerequisite is to migrate and store the data on a suitable data center (DC) [12]. Moving hardware directly is an optional way to move large-scale data. The Amazon Import/Export service, for example, recommends using removable storage devices to transport data, and sometimes it is even possible to move entire machines. But this is only suitable for infrequent, or one-time, bulk data movement. This method has a large delay and cannot meet the growing demand for real-time analysis of data. It also contradicts the idea of automated management and requires more labor participation. Transferring data over the Internet is very expensive and impractical due to the large delays. For example, it takes roughly 13 days to transmit 1 TB of data through a 10 MB internetwork. It is generally recommended to transfer real-time data over a high-speed dedicated connection (such as AWS Direct Connect1), which can speed up the transfer. But even relying on high-speed dedicated connections, transferring data across continents is difficult. For example, AWS

Direct Connect does not provide cross-continental service, and international private lines are too expensive. This limits the movement of all large-scale data across the globe to the same DC [13, 14]. Also, using a DC to store data results in more frequent local data analysis delays. Especially in some regions, data security laws require that some data must be stored locally (e.g., some countries in the European Union). All in all, it is necessary for users to follow some rules to choose a suitable storage location for their data. As Amazon suggests, being closer to the user can reduce latency in data usage, meet specific legal and regulatory requirements, or reduce costs, etc.

Figure 1 simulates the distribution of DCs and users (for simplicity, users are used to represent subsidiaries or data owners).

There are a total of 10 DCs and 9 users in Figure 1, spanning 4 continents. Different users can use different DC services or prefer different DCs. For example, users 4, 5 in Europe can only be scheduled to DC5, 6 in Europe. Users in Asia only prefer DCs in Asia Pacific.

Cross-DC data analysis is now possible with various MapReduce-based frameworks, such as G-Hadoop and G-MR [15, 16]. A lower-cost cross-data center big data processing method is also proposed in this research. Using numerous DCs instead of just one can meet the needs of comprehensive data analysis while also ensuring faster local data analysis and cheaper expenses.

Considering the underlying incomplete graph,

$$G = (U, V, E). \tag{1}$$

Among them, the side length

$$e_{ij} \in E, \quad (i \in U, j \in V). \tag{2}$$

It satisfies trigonometric inequalities, as well as positive integers $k\,(k \le |U|, k \le |V|)$. This chapter aims to find a DC subset D ($|D| \le k$) from the available DC set V to store the data of all users in U according to different goals. For any $i \in U$ and $j \in V$, if user i's data can be moved to DC j (at least not restricted by regulations or excluded by users), there is an edge between them. This problem assumes that all i are adjacent to at least one j; otherwise the problem has no solution. Also it assumes that

$$|E| = m. \tag{3}$$

Among them,

$$m \le |U| * |V|. \tag{4}$$

Each user is assigned a weight w_i, which represents the activation level of current or foreseeable future data generation, or the importance of local users. w_i increases with the amount of data or the importance of the user. The activation level rather than the data volume is used because it can tolerate the dynamic changes in the data while providing a modest approximation to the data volume. The activation level can be based on the amount of data uploaded per day. For example, for a typical company uploading 200 GB per day [17], 10 GB can be used as the threshold for determining the activation level. If a subsidiary generates less than 10 GB of data per day, a weight of 1 can be assigned. For subsidiaries between 20 and 30 GB, a weight of 3 is assigned. By analogy, for user i with activation level w_i, a fee $w_i e_{ij}$ will be charged to move data to DC j.

Each DC has a different price for compute and storage resources. For more economical storage and processing of data, lower prices are of course preferred. Given DC j, assume that the price of one VM instance processing data per hour is a_j. On average, such instances are able to analyze b_j GB of data per hour. Then, the price for processing 10 GB of data is

$$p_j' = \frac{10 * a_j}{b_j}. \tag{5}$$

If the storage cost for 10 GB of data is p_j'', then the total cost on the DC side for a user with activation level 1 is

$$p_j = p_j' + p_j''. \tag{6}$$

For user i with activation level p_j', if it wants to store and process data at DC j, it needs to pay $w_i p_j$.

Because of the high scalability of cloud computing, this chapter assumes that the DC has no computing and storage capacity constraints. For data integrity, a user's data is only stored in one DC. The target data center selection problem can be summarized as follows: it selects at most k target DCs and assigns each user to a target DC such that it satisfies the following objectives.

Fair data placement (FDP): the maximum distance between the user and the assigned DC is minimized so that each local user can access data with minimal delay:

$$\min D \subseteq V, |D| \le k^{\max}; i \in U, j \in D\left(e_{ij}\right). \tag{7}$$

Preferred data placement (PDP): the maximum weighted distance between the user and the assigned DC is minimized, allowing local users with more data to access data with minimal delay:

$$\min D \subseteq V, |D| \le k^{\max}; i \in U, j \in D\left(w_i e_{ij}\right). \tag{8}$$

If needed, it also uses

$$w(i, j) = w_i e_{ij}, \tag{9}$$

to represent the weighted distance.

Transmission cost minimization data placement (TCMDP): transmission cost is defined as the minimization of the sum of the weighted distances between all users and the DC to which they are assigned:

$$\min D \subseteq V, |D| \le k\left(\sum_{i \in U} j \in D\left(w_i e_{ij}\right)\right). \tag{10}$$

Total cost minimization (cost minimization data placement, CMDP): the total cost is defined as the minimization of the sum of the costs for all users:

$$\min D \subseteq V, |D| \le k\left(\sum_{i \in U} j \in D\left(c_{ij}\right)\right). \tag{11}$$

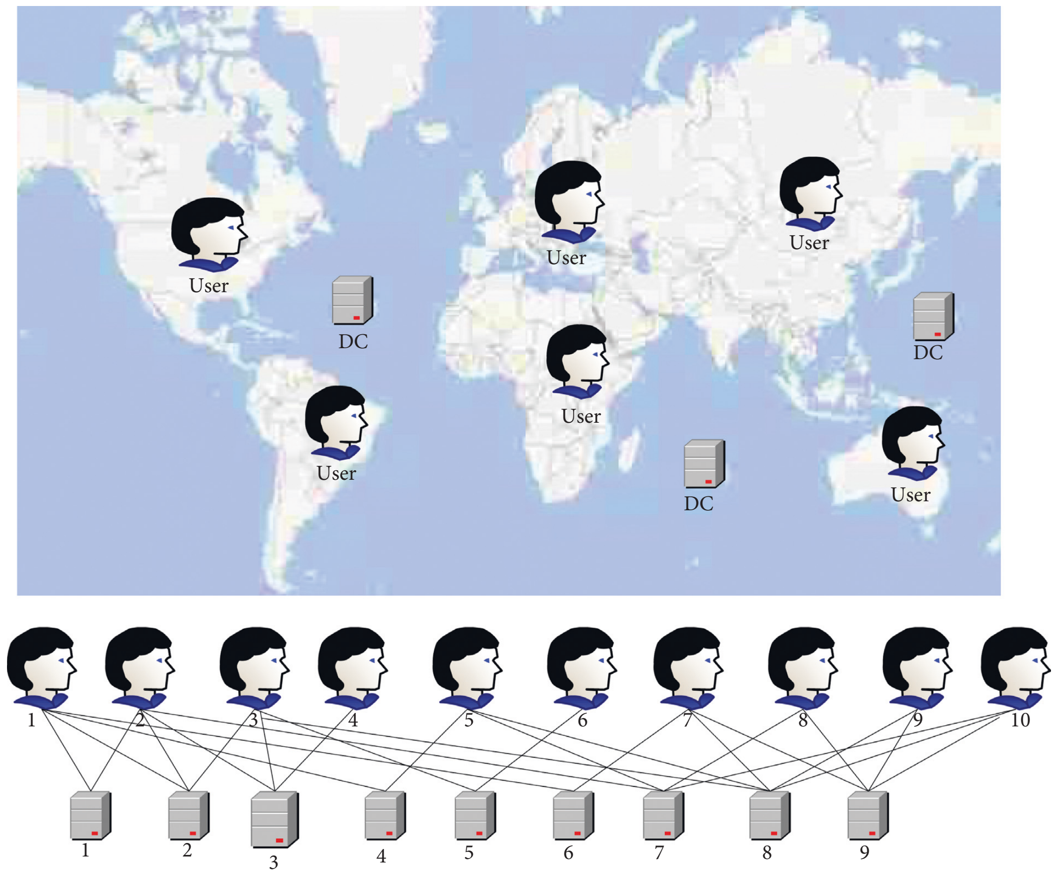

Figure 1: Data centers and users distributed across geographies.

It needs to note that goal 1 is a special case of goal 2 when $w_i = 1$. Goal 3 is a special case of Goal 4 when $p_j = 0$, and subsequent discussions will focus on goals 2 and 4. The corresponding results can be directly applied to objectives 1 and 3, respectively.

Suppose x_{ij} is a Boolean variable that indicates whether user i is assigned to DCj. It is 1 if i is assigned to j, and 0 otherwise. y_j is also a Boolean variable that indicates whether DCj is used. It is 1 if used, and 0 otherwise.

The PDP problem wants to minimize the largest weighted distance z, where

$$w_i e_{ij} x_{ij} \leq z \; \forall i \in U, j \in V. \tag{12}$$

PDP can be formalized as the following 0–1 mixed integer program:

$$\begin{aligned} &\min z \\ &\text{s.t} \end{aligned}, \tag{13}$$

$$\sum_{j \in V} x_{ij} = 1, \quad \forall i \in U, \tag{14}$$

$$y_j \geq x_{ij} \; \forall i \in U, j \in V, \tag{15}$$

$$x_{ij} \in \{0,1\}, y_j \in \{0,1\}, \tag{16}$$

$$x_{ij} = 0 \text{ for some } i \in U, j \in V. \tag{17}$$

Constraint (13) guarantees that every user must be assigned to at least 1 DC. Constraint (14) guarantees that this DC must be used. And the number of selected DCs cannot exceed k (Constraint (15)). Moreover, not all DCs can be used by every user (Constraint (16)); that is, the underlying bipartite graph is incomplete.

CMDP can be formalized as the following 0–1 integer linear program:

$$\begin{aligned} &\min \sum_{i \in U, j \in V} \left(w_i e_{ij} + w_i p_j\right) x_{ij} \\ &s.t \;\; (13), (14), (15), (16), (17) \end{aligned}. \tag{18}$$

In the objective function, both e_{ij} and p_j are in normalized form. The first half $\sum_{i \in U, j \in V} w_i e_{ij} x_{ij}$ is the transmission cost. The second half, $\sum_{i \in U, j \in V} w_i e_{ij} x_{ij}$, is the cost of storing and processing data in the data center.

PDP is an extension to the k-vendor problem, while CMDP is a common extension to the UFL and k-middle point problem. Because of the k-vendor problem, both UFL and k-middle point problems are NP-insoluble [18, 19]. So both PDP and CMDP are NP-insoluble. This section presents an approximation algorithm for PDP and a heuristic algorithm for CMDP. For the convenience of reading, the special summary abbreviation table is shown in Table 1.

4. Strategies and Methods for Integrating Information Resources of British and American Literature

4.1. Engine Search Aspects. The search engine is mainly composed of four parts, namely, the information collector (robot or spider or crawler), the analysis indexer (indexer), the searcher (searcher) and the query interface. The composition and structure of the current mainstream search engines generally include miners for data mining and user information mining [20]. Its connection mechanism is shown in Figure 2:

The availability of engine search is poor, and it is difficult to cope with the challenge of information islanding. The countermeasures include improving the ranking of mainstream engine search and improving the daily management system of engine search by improving the intelligent search engine. One of the major reasons why users cannot find the information they need is that they are not familiar with literature classifications; that is, users may not understand the classification information of English and American literature websites. Or the literary works recommended by the website are too professional, so that users cannot find the information they need when searching in plain language.

A better solution is to filter the correspondence between the vernacular words and the official words according to semantic analysis and probability statistics by collecting the search keywords of users on British and American literature websites. And according to the corresponding relationship, a lexicon of common people is generated. After receiving the vernacular words input by the user, the intelligent search engine system will query the Baiqiao style thesaurus, obtain official words matching the vernacular words input by the user, and search the website according to the obtained official words. Intelligent guidance, keyword association, and other technologies used in business engines such as Baidu are widely used to intelligently correct and sort retrieval results, so as to facilitate user retrieval. At the same time, box calculation can also be used to optimize the user's search results. The difference between this approach and the traditional approach is that, in the traditional search, users need to filter the search results. This kind of search system displays application services on the search result page by formulating association rules and engine search application containers.

When users use the search system to retrieve the information they need, they often do not search the system through the engine on the homepage of the English and American literature website but directly retrieve the required information in the mainstream search engine. Therefore, the search for British and American literature can improve the ranking of website information resources by purchasing services on mainstream engines such as Baidu. It can learn from the relatively mature engine search optimization guidelines in the United States and the United Kingdom and strive to enhance the visibility of information resources.

In the engine search of English and American literature websites, the latest search is empty, the information resource structure is single, and the update is not timely, which will cause the poor search function of the engine. Therefore, this article recommends that an experienced and first-class technical information management professional team be responsible for the maintenance of the search system, and to update and maintain the system in time. At the same time, English and American literature websites can consider using information integration and real-time monitoring procedures for user experience to achieve automatic integration and manual integration, daily integration and emergency integration, individual integration, and coordinated integration. In this way, a complete management chain such as real-time information monitoring, crisis early warning, and emergency response can be realized, and the search ranking of information resources on Chinese English and American literature websites can be improved.

In the face of the impact of emerging information technologies such as big data and the threat of information islanding, the website management department should put the needs of citizens first. This is also the core of the new

Table 1: Algorithm abbreviation correspondence table.

Name	Abbreviate
Fair data placement	FDP
Preferential data placement	PDP
Transmission cost minimization data placement	TCMDP
Cost minimization data placement	CMDP

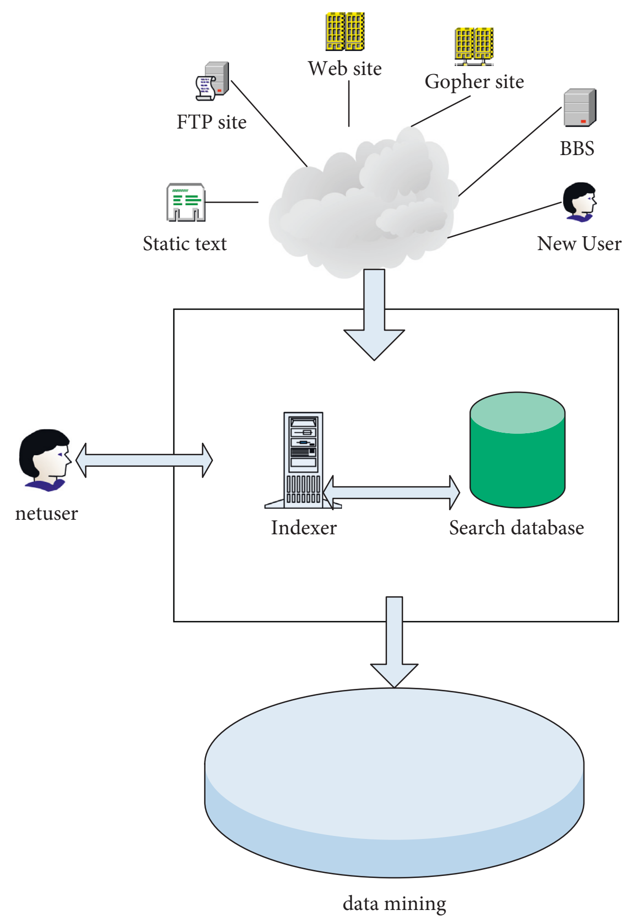

Figure 2: Search engine basic structure process.

public service theory; that is, the engine search design of the website should be more humanized and intelligent. The website content should show more hotspots that are closely related to civic life. The management department should take citizen satisfaction as the basis for evaluating website performance. Open data should be more concerned with fulfilling citizens' needs for specific data. On this basis, website management can consider strengthening the top-level design to improve the information resource management system. Website management should continue to improve the intensive construction of infrastructure, avoid duplication of construction, and improve the efficiency of equipment use.

4.2. Content Integration of British and American Literature. Internet search and information disclosure are the core and private content of Chinese British and American literature websites. It examines website content integration from the perspective of web search. It conducts an online survey on the online search services of English and American literature websites across the country. The current network search services are summarized as follows: (1) based on the account of the English and American literature website at the same level, the Internet search service of Bukou is integrated. The main feature of this model is that the service interface is unified and easy to integrate. However, this form of integration only guides users to the websites of various ministries, districts, and counties through address links for online search service requirements and does not actually integrate service resources on a unified platform. (2) Relying on brick-and-mortar bookstores, the online center at the same level is integrated. The advantage of this mode is to provide users with a unified login entry, and to realize the combination of the front-end service and the back-end service system; that is, the English and American literature website already has a service system. However, there are problems such as inconsistency in the handling process and service content between the newly built service integration platform and the already built service integration platform.

From the angle of information disclosure of English and American literature websites, the integration of website content is investigated. By analyzing the search, download, and reading usage of British and American literature websites, it finds that the biggest shortcoming is that although the number of British and American literature websites has been increasing actively, the number of applications for disclosure has not decreased accordingly but has continued to increase. In the software evaluation, the websites of districts and counties within the range of 600 were also tested. It found that about 90% of the websites were blocked and the updates were not timely enough. More than 80% of the websites have the phenomenon that the page cannot be opened or the function cannot be used. 90% of websites have fake links, dark links, and unusable links. The operation, maintenance, and management of grassroots websites need to be improved.

4.3. Open Data Integration of British and American Literature. The evaluation report on the construction of English and American literature websites of the State Information Center believes that, in the construction of open data, the situation of information islanding is serious. In a research evaluation of the practice of open data on British and American literature websites across the country, it was found that, as of May 2019, 86.25% of the data were updated annually or not at all. Only 13.75% of the data are updated monthly or daily.

From the problems of open data platforms, it can be seen that the number of data applications provided by open data platforms in various places is poor. Although some platforms have opened data application channels, the existing "applications" on the platform are not downloadable and useable data applications, but only the results of functional tests. Although some platforms provide downloadable and useable data applications, most of them do not use the data of this site or only use basic data such as geographic location in a shallow level. Or even if the data of this site is used, it does not explain which data is used. Some platforms offer "data apps" that do not live up to their name. In fact, it is the business processing system of local literature, and it is the source of open data, not the practical application after data opening, which greatly dampens the enthusiasm and creativity of users.

First of all, many British and American literature websites lack the awareness of change and do not realize the impact of big data and other information technologies on Chinese British and American literature websites. The main problem is that information technology such as big data is only understood as a common technical means. It did not realize that big data would improve the integration efficiency of information resources of English and American literature websites and promote the reform of literature administration. Many developers are not clear about the trend of e-government reform such as open data and even have resistance. Developers' awareness of technological innovation needs to be enhanced. Secondly, it is difficult for the laws and regulations of China's informatization standards to keep up with the pace of technological change. The laws and regulations of electronic technology informatization and big data construction are relatively lagging behind. The information integration of Chinese English and American literature websites requires the personnel in charge of British and American literature websites to strengthen the top-level design, enhance the efficiency of Chinese big data to promote the information integration of British and American literature websites, and improve the pertinence of problems. Finally, the talent construction of Chinese English and American literature websites cannot meet the impact of big data and other information technologies. The phenomenon of insufficient innovative talents and professional and technical talents, low level of internationalization of talents, and serious loss always exists. The key reason lies in the disconnection between China's e-government personnel training system and selection system. This requires China's public service department to reform its management system, select the right talent in an unorthodox way, and break down the identity barrier. Only in this way can it form an open, inclusive, and orderly pattern of talent selection.

5. British and American Literature Information Resource Integration System

Aiming at the problems existing in English and American literature websites and search platforms, this paper focuses on three aspects: engine search optimization, content integration optimization, and public information integration optimization. Combined with the low cost and high efficiency of distributed cloud computing, combined with the problems of wide distribution of English and American literature websites and many kinds of languages, it optimizes the experiment and cost of the website.

5.1. Optimization of Engine Search. To evaluate the impact of DC size on the BWF algorithm, it is assumed that users 1~9 can be served by different numbers of candidate DCs. It adds one DC at a time to DCs 1~10 in order from 11 to 14. The performance of each algorithm is shown in Figure 3.

As shown in Figure 4, the time delay (maximum user weighted distance) of the Random algorithm is the largest. The delays of the algorithms NPA-PDP and BWF are larger than those of the algorithm Opt. First, the algorithms NPA-PDP and BWF both choose DC2, 6, 9. When the number of DCs increases from 10 to 13, the delays of the algorithms NPA-PDP and BWF and the assignment relationship from users to DCs are the same. This is because none of the 3 DCs added subsequently are better than the preceding DCs, so none of the 3 DCs are chosen. When DC14 (Beijing) is added, the delays of algorithms NPA-PDP and BWF both increase. The reason is that user 8 (Xian) has the largest user weight, so the algorithm selects it as the user representative for the Asia-Pacific region. Because user 8 is closest to DC14 (Oakland), the algorithm abandons DC9 and chooses DC14 instead. Users originally assigned to DC9 are reassigned to DC14. This causes the delay to rise as the weighted distance between Beijing and Oakland.

The Opt. algorithm has the smallest delay. Although the number of DCs has increased, the delay has remained the same. Although the delay solved by the BWF algorithm is slightly larger than that solved by the Opt. algorithm, the average is about 5%. Experiments show that the Opt. algorithm can only optimize the main objective function value but cannot optimize the delay of other clusters. For example, the algorithms NPA-PDP and BWF both choose DC2, 6, and 9. Algorithm Opt. chooses 2, 5, 7. Among the three algorithms, the users served by DC2 are the same, namely, users 1, 2, and 3. NPA-PDP and BWF assign users 4, 5 to DC6. And Opt. assigns them to DC5. Users 6, 7, 8, and 9 are assigned to DC9 by algorithms NPA-PDP and BWF, and assigned to DC7 by algorithm Opt. The delays for each user are compared in Table 2. Obviously, the total delay of the Opt. algorithm is larger than that of the other two algorithms. This is because the Opt. algorithm cannot consider all clusters.

The experiment also increased the number of users from 9 to 19. It joins two users at a time in numerical order. The delay results are shown in Figure 5.

When users 18, 19 join, the delay changes because their minimum weighted distance is greater than the current delay. This also reveals that even if the number of users increases, it is not necessary to use more DC. Only when more distant users join is it possible to cause greater delays and thus require more DCs. Although the Opt. algorithm finds the optimal solution, the experiment again observes that the total delay of the Opt. algorithm is larger than that of the BWF algorithm. Although limited by the randomness of user location selection, a purely increasing delay curve cannot be drawn, but the simulation results still reveal a trend: the delay will not decrease as users join.

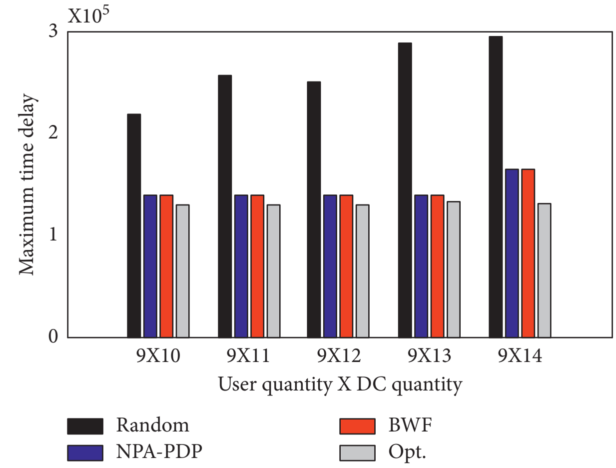

Figure 3: Comparison of the maximum delay obtained by the algorithm when the number of DCs increases.

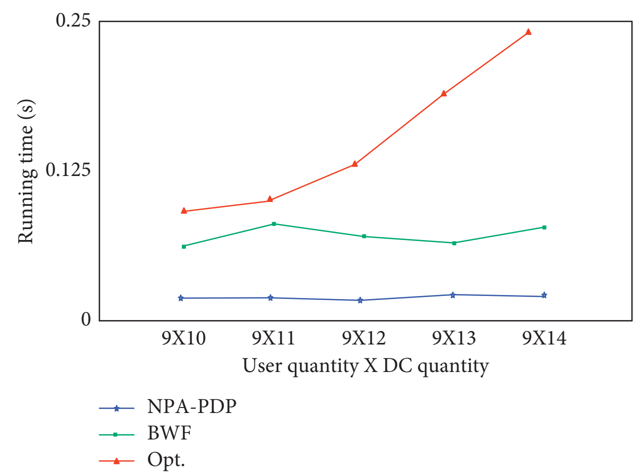

Figure 4: Comparison of algorithm running time when the number of DCs increases.

Table 2: Opt. algorithms cannot optimize every cluster.

User	BWF	Opt.
User 4	6679	25189
User 5	5137	23172
User 6	17893	9496
User 7	18542	54108
User 8	38263	88790
User 9	141337	134541

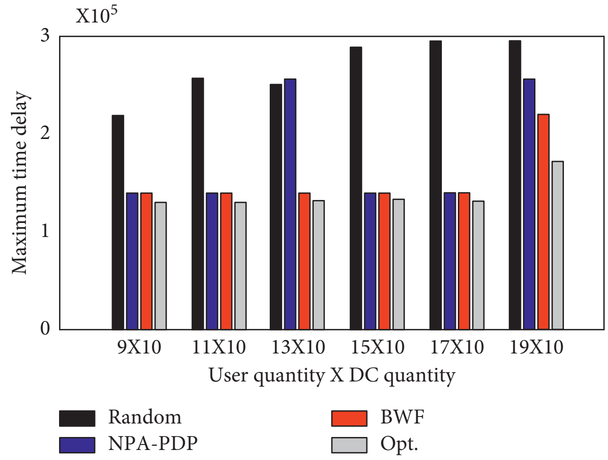

Figure 5: Comparison of the maximum delay obtained by the algorithm when the number of users increases.

It is worth noting that when users 12 and 13 join in, the delay of NPA-PDP algorithm increases sharply. This is because the NPA-PDP algorithm simply deletes a DC without considering the user's grouping attributes. This also reflects the instability of NPA-PDP algorithm.

In terms of running time, Random algorithm and NPA-PDP algorithm are faster than the other two algorithms. All in all, the Opt. algorithm requires more time than the BWF algorithm. With the addition of DCs and users, the time consumption of the Opt. algorithm increases rapidly. The time consumed by the BWF algorithm is much slower, so it is more suitable for large-scale applications.

5.2. Content Integration and Optimization. In order to make full use of the various dimensions of PM resources, this section introduces the "similarity" boxing mechanism. Figure 6 reveals the effectiveness of this mechanism. Simulation experiments are carried out for three scenarios, and the three sets of experiments include 450, 900, and 1500 VMs, respectively. In each set of experiments, the residual resources of each dimension of PM used were compared in the order of network bandwidth (N), CPU (C), memory (M), and hard disk storage (D). It can be seen from Figure 6 that the algorithm achieves a balanced use of resources in each dimension.

In order to save resource costs without compromising quality of service requirements, this section formalizes the problem as a stochastic multi-objective nonlinear programming. It targets a common situation (that is, VMs can be independent or related, and PMs can be heterogeneous and networked in a tree topology), while optimizing server and network bandwidth, which account for most of the data center cost. VM partitioning, statistical multiplexing, and "similarity" methods are used to implement a new offline algorithm and a new online algorithm. The effectiveness of the algorithm is verified through extensive simulation experiments. Experiments show that the algorithm proposed in this section is more effective. Not only do they drastically reduce PM and network-related resource costs, but they also guarantee a suitable quality of service.

5.3. Integration and Optimization of Public Information. The number of PM in each DC follows a U(3050) distribution. And the type of PM is uniformly chosen from four options. PM's configuration is based on the IBM SystemxM5 and Systemx3300M4 server types. The resource configuration requirements of the VMs in this chapter are based on the setup of four types of VMs from Amazon EC2's m3-series (for consistency with PM, GB is used to replace GiB). The M3-series is the most representative and is designed for general use. The number of logical cores per PM is equal to or at most twice the number of physical cores, according to VMWare8. The number of logical cores in a PM cannot exceed the number of vCPUs in a VM. Assume that vCPUs and physical cores have a one-to-one connection; the details are provided in Table 3.

Table 4 reflects resource pricing as well. Experiments strive to use Amazon as much as possible to expose data in order to maintain prices consistent. Because of the complex interaction between PM setup and VM resource requirements, only the medium type resource pricing is shown here. The prices of the remaining categories are expected to have the same multiplier relationship; for example, the price of xLargeVM with 4 vCPUs is four times that of the medium type. The pricing for storage is from Amazon S3. It may be computed that transferring 1 GB of data costs $0.0243 using the Amazon Import/Export service pricing.

TLGGA convergence is seen in Figure 7 when there are four DCs (DC1DC4). The value of the objective function decreases rapidly and the curve is highly steep in the first 200 iterations (including crossover, mutation, and local optimization of all populations), according to simulation experiments. The curve begins to flatten down over the next 800 cycles. The goal function value declined extremely slowly after roughly 1,000 times, despite the fact that the method took longer. In less than two seconds, a good solution can be found.

There is a similar convergence pattern for different numbers of DCS. The cost values for 1,000 and 10,000 iterations are shown in Figure 8. It demonstrates that multiple repetitions do not result in a proportional reduction in the goal value. The decrease in percentage was merely 0.17 percent to 1.11 percent.

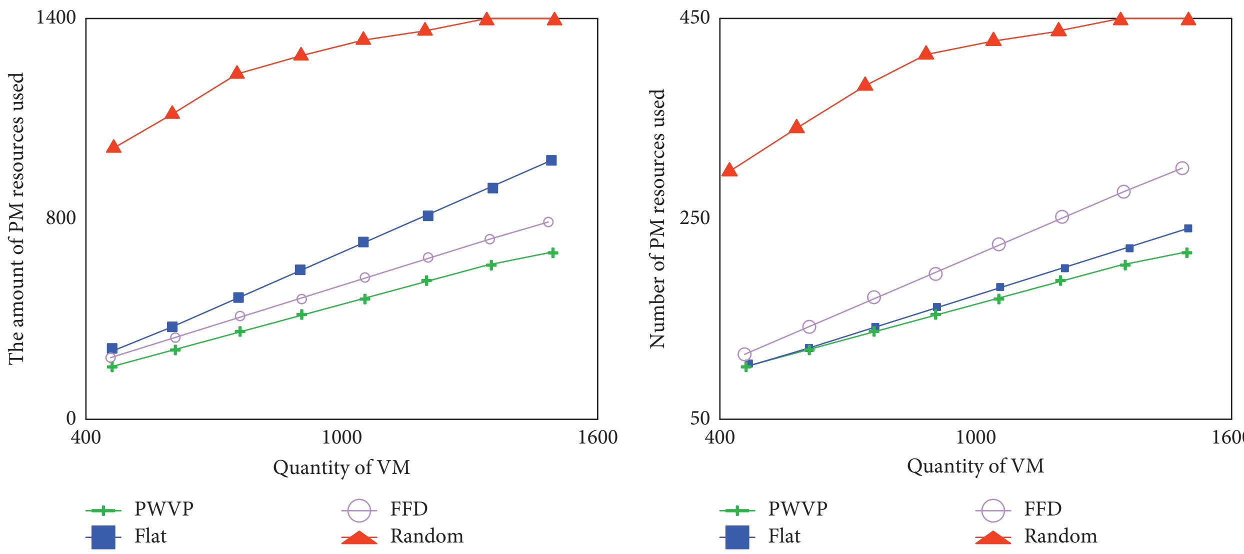

FIGURE 6: Physical node cost.

TABLE 3: PM resource configuration and VM resource requirements.

PM	Cores	Memory	VM	vCPUs	Memory
Medium	4	32	Medium	2	3.75
Large	8	64	Large	4	7.50
Xlarge	24	192	Xlarge	8	15.00
2xlarge	32	256	2xlarge	vCPUs	30.00

TABLE 4: Serial numbers and resource prices of data centers in different regions.

Data center location	California	Frankfurt	Singapore	Sao Paulo	Oregon	Ireland	Sydney
Medium PM	0.408	0.400	0.498	0.480	0.480	0.380	0.472
Medium VM	0.077	0.075	0.098	0.095	0.095	0.073	0.093
Save	0.033	0.0324	0.030	0.0408	0.0408	0.030	0.033
Power	11.910	9.490	15.470	14.370	14.370	8.900	15.470

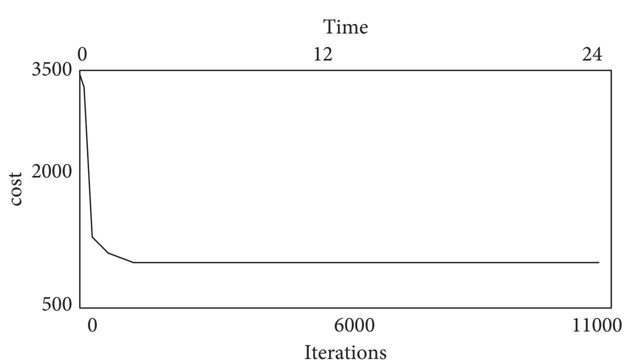

FIGURE 7: Convergence of TLGGA with 4 DCS.

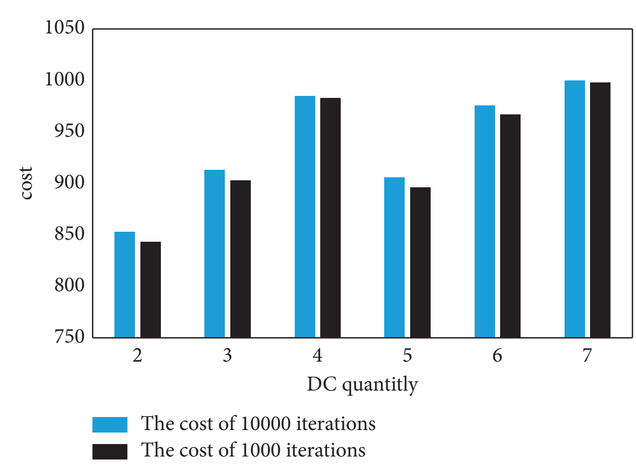

FIGURE 8: Cost comparison for different iterations of different numbers of DCS.

The use of Reducer deployment in Hadoop for big data processing across data centers is examined in this study. It first formalizes the challenge as a two-tier plan to keep expenses down and follow typical Hadoop localization principles. Layer 2 planning can take into account the co-selection of a DC and a server at the same time. The new architecture is then used to offer a novel cross-data center large data processing technique based on key distribution. The Reducer can be deployed to the DC with the greatest data to process and the lowest cost of other resources with this approach. Finally, the system is implemented using a two-layer grouping genetic algorithm (TLGGA). The approach employs a local optimization strategy and a customized starting population creation mechanism. TLGGA's efficiency is demonstrated through simulation results. It outperforms both the baseline Hadoop method and the most recent G-MR algorithm.

6. Conclusion

This paper focuses on the global British and American literature websites and studies the resource allocation algorithm in distributed cloud computing. Firstly, based on the sequence of cloud computing service deployment, it adopts the top-down engineering theory method to divide cloud computing deployment into three stages: cloud network selection, data center selection, and server selection. Then, based on the specific business, it systematically studies the resource allocation methods in cloud computing according to the different goals and resources required by the business in each stage. Resource allocation based on distributed cloud computing still has many problems to be solved. The next step will focus on the research of distributed cloud computing algorithm.

Data Availability

The data used to support the findings of this study are available from the author upon request.

Conflicts of Interest

The author does not have any possible conflicts of interest.

References

[1] J.-L. Tsai and N.-W. Lo, "A privacy-aware authentication scheme for distributed mobile cloud computing services," *IEEE Systems Journal*, vol. 9, no. 3, pp. 805–815, 2015.

[2] T. Hirai, H. Masuyama, H. Masuyama, S. Kasahara, and Y. Takahashi, "Performance analysis of large-scale parallel-distributed processing with backup tasks for cloud computing," *Journal of Industrial and Management Optimization*, vol. 10, no. 1, pp. 113–129, 2014.

[3] L. Xiong, D. Peng, and T. Peng, "An enhanced privacy-aware authentication scheme for distributed mobile cloud computing services," *KSII Transactions on Internet and Information Systems*, vol. 11, no. 12, pp. 6169–6187, 2017.

[4] V. S. Kakade, A. Kirve, A. Bhoir, and S. Kadam, "Enhancing distributed data storage security for cloud computing using AES algorithm," *IJARCCE*, vol. 6, no. 3, pp. 752–755, 2017.

[5] J. Liao, F. Trahay, G. Xiao, and L. Y. Li, "Performing initiative data prefetching in distributed file systems for cloud computing," *IEEE Transactions on Cloud Computing*, vol. 5, no. 3, pp. 550–562, 2017.

[6] S. Deng, A. H. Zhou, D. Yue, and B. L. P. Hu, "Distributed intrusion detection based on hybrid gene expression programming and cloud computing in a cyber physical power system," *IET Control Theory & Applications*, vol. 11, no. 11, pp. 1822–1829, 2017.

[7] K. Alhazmi, A. Shami, and A. Refaey, "Optimized provisioning of SDN-enabled virtual networks in geo-distributed cloud computing datacenters," *Journal of Communications and Networks*, vol. 19, no. 4, pp. 402–415, 2017.

[8] X.-B. Jin, W.-T. Gong, J.-L. Kong, Y.-T. Bai, and T.-L. Su, "PFVAE: a planar flow-based variational auto-encoder prediction model for time series data," *Mathematics*, vol. 10, no. 4, p. 610, 2022.

[9] W. Cai, Y. Song, and Z. Wei, "Multimodal data guided spatial feature fusion and grouping strategy for E-commerce commodity demand forecasting," *Mobile Information Systems*, vol. 2021, Article ID 5568208, 10 pages, 2021.

[10] E. G. Chung, "Bob dylan and American literature songs floating on the desolation row," *In/Outside English Studies in Korea*, vol. 46, no. 42, pp. 116–145, 2017.

[11] M. Strauss and S. Kraus, "Prag in der amerikanischen Literatur: cynthia Ozick und Philip Roth [Prague in American literature: cynthia Ozick and Philip Roth]. Frankfurt am Main: lang," *English and American Studies in German*, vol. 6, no. 1, pp. 61–63, 2017.

[12] E. Di Pascale, I. Macaluso, A. Nag, M. Kelly, and L. Doyle, "The network as a computer: a framework for distributed computing over IoT mesh networks," *IEEE Internet of Things Journal*, vol. 5, no. 3, pp. 2107–2119, 2018.

[13] R. Talavera-Llames, R. Pérez-Chacón, A. Troncoso, and F. Martínez-Álvarez, "Big data time series forecasting based on nearest neighbours distributed computing with Spark," *Knowledge-Based Systems*, vol. 161, no. DEC.1, pp. 12–25, 2018.

[14] K. C. Okafor, C. C. Udeze, and A. A. Obayi, "Dependent reliability of distributed cloud computing network (DCCN)," *International Journal of Applied Engineering Research*, vol. 13, no. 9, pp. 6551–6586, 2018.

[15] F. Wu, X. Li, L. Xu, and A. K. Sangaiah, "Authentication protocol for distributed cloud computing: an explanation of the security situations for internet-of-things-enabled devices," *IEEE Consumer Electronics Magazine*, vol. 7, no. 6, pp. 38–44, 2018.

[16] V. M. Mohan, "Application level resource scheduling with optimal schedule interval filling (RS-OSIF) for distributed cloud computing environments," *International Journal of Applied Engineering Research*, vol. 12, no. 24, pp. 15746–15753, 2017.

[17] J. Zhang, X. Wang, H. Huang, and S. Chen, "Clustering based virtual machines placement in distributed cloud computing," *Future Generation Computer Systems*, vol. 66, no. jan, pp. 1–10, 2017.

[18] C. Li, C. Zhang, B. Ma, and Y. Luo, "Efficient multi-attribute precedence-based task scheduling for edge computing in geo-distributed cloud environment," *Knowledge and Information Systems*, vol. 64, no. 1, pp. 175–205, 2022.

[19] Y. Li, H. Li, G. Xu, T. Xiang, X. Huang, and R. Lu, "Toward secure and privacy-preserving distributed deep learning in fog-cloud computing," *IEEE Internet of Things Journal*, vol. 7, no. 12, pp. 11460–11472, 2020.

[20] J. Zhou, D. Zhang, and W. Zhang, "Underwater image enhancement method via multi-feature prior fusion," *Applied Intelligence*, vol. 223, pp. 1–23, 2022.

Hindawi
Computational Intelligence and Neuroscience
Volume 2022, Article ID 1092383, 10 pages
https://doi.org/10.1155/2022/1092383

Research Article

Algorithm Composition and Emotion Recognition Based on Machine Learning

Jiao He

Wuhan Sports University, Wuhan 430079, China

Correspondence should be addressed to Jiao He; 2008020@whsu.edu.cn

Received 16 April 2022; Revised 11 May 2022; Accepted 12 May 2022; Published 6 June 2022

Academic Editor: Xin Ning

This paper proposes a new algorithm composition network from the perspective of machine learning, based on an in-depth study of related literature. At the same time, this paper examines the characteristics of music and develops a model for recognising musical emotions. Using the model's information entropy of pitch and intensity to extract the main melody track, note features are extracted from bar features. Finally, the cosine of the vector included angle is used to judge the similarity between feature vectors of several adjacent sections, allowing the music to be divided into several independent segments. The emotional model of music is used to analyze each segment's emotion. By quantifying music features, this paper classifies and quantifies music emotion based on the mapping relationship between music features and emotion. Music emotion can be accurately identified by the model. The model's emotion recognition accuracy is up to 93.78 percent, and the algorithm's recall rate is up to 96.3 percent, according to simulation results. The recognition method used in this paper has a higher recognition ability than other methods, and the emotion recognition result is more reliable. This paper can not only meet the composer's auxiliary creative needs, but it can also help intelligent music services.

1. Introduction

With the development of economy and society, people put forward higher requirements for spiritual life. In today's society, people's entertainment life is richer and more diverse, and music is a special social ideology, which can not only cultivate sentiment and regulate emotions, but also develop thinking and glow emotions, and it has a strong appeal [1]. Music is becoming increasingly important in human life as a spiritual food. Simultaneously, digitalization, as the core of information technology, has aided the rapid development of a variety of emerging technologies; digitalization of audio has become the digital trend's intermediate force. As a result, the marriage of computer and music has become a research hotspot [2]. "Computer music" is a new technology that combines music art and computer technology. It is an important component of multimedia technology. Music has a higher scientific and technological content, as well as its own distinct and colourful artistic expression. The use of algorithms to create musical works is known as computer composition. One method of composing music is to use an algorithm set [3]. More researchers have devoted themselves to the research field of algorithmic composition because concrete music and random music differ greatly from the theoretical system and creative thinking of traditional composition techniques. Probability model, rule system model, genetic algorithm model, and NN (neural network) model are the most commonly used algorithm composing methods today. The motivation of composition and the development of motivation are precisely the application of these thoughts as the guidance of technological innovation in the universal law of music creation. The composition algorithm is both a simple mathematical operation and an expression of the artistry that exists in human thought. Computer automatic composition will greatly improve music creativity as machine learning advances, while also assisting composers in generating new creative ideas. However, as the amount of music produced grows, it is becoming increasingly important to classify and manage it.

The application of algorithms to solve specific problems is at the heart of algorithmic composition on a theoretical level, and the knowledge contained therein comes from musicology, mathematics, computer science, and other disciplines. These levels encompass not only specific technical methods of theoretical techniques and mathematical operations, but also a deeper expression of human thought. Music comes from life and reflects the creators' emotions [4]. Music is a psychological process that includes a variety of human emotional factors that are produced when people interact with music. Because of its heavy workload, difficult description, and impersonality, the early text annotation method has some limitations. Furthermore, as digital music production technology advances and the number of different types of music styles grows, text-based music retrieval becomes obsolete, and people begin to investigate new classification retrieval methods to aid in the retrieval of target music from massive data. The advantages of digital music over traditional music are primarily in the areas of production, storage, dissemination, and retrieval. Users' demand for music emotion can be met by emotion-based retrieval. In addition, a real-time soundtrack for multimedia video should be created based on the emotion conveyed by the video content. Music emotion recognition is a pattern recognition task, and the mapping of data from high-dimensional music feature space to low-dimensional emotion space must be done correctly. However, most musical emotion studies are limited to categorising an entire piece of music into one emotional category. Music's emotion, on the other hand, is not static. This paper uses a machine learning algorithm to create a model of music composition and emotion recognition. The following are some of its innovations:

(1) There is basically no complete set of music data expression rules in algorithmic composition system. Based on the in-depth study of related literature, this paper proposes a new algorithm composition network from the perspective of machine learning algorithm [5–7]. It restrains the style and quality of generated music by using music theory rules to construct a reasonable Reward function. At the same time, the general machine learning methods created by deep learning network in the field of algorithm are summarized, so as to generate music with polyphonic structure. It can meet the composer's auxiliary creative needs and provide more support for intelligent music services.

(2) In this paper, the average pitch, average sound intensity, speed, and other characteristics are analyzed, and the classification model of emotion feature vector input is constructed. It can select an appropriate formula according to the applied scene; at the same time, several adjustable parameters are set to adjust the similarity. This paper classifies and quantifies music emotion according to the mapping relationship between music characteristics and emotion by quantifying music characteristics. The model can accurately identify the emotion of music.

2. Related Work

Computer-aided music creation and algorithm-based music creation have a long history since computers and digital systems were widely used. At present, researchers have put forward various methods for computer composition, among which the influential ones are hidden Markov chain, rule-based system, music grammar, genetic algorithm, NN technology, etc.

Zheng and Lu used LSTM (long short term memory network) to process blues music of twelve bars and realized the generation of chords and melody in blues music [8]. The hidden layer of the model uses four LSTM modules, the input is the current note, and the output is the predicted note at the next moment. Jenke et al. mainly introduced the related research on algorithmic composition using recursive NN. For the possible gradient vanishing problem, the LSTM algorithm that avoids the gradient vanishing problem is used [9]. Zhang et al. applied generative adversarial networks to algorithmic composition and created the MidNet popular melody generation system [10]. In this network structure, the CNN (convolutional neural network) used by both the generator and the discriminator is trained by converting the midi format data set into a piano roll and inputting it into the network. Then the generator inputs random noise and generates music melody, and then the discriminator will make a true or false judgment on the generated melody. Majumder et al. mainly used the sampling of audio data and mainly designed and innovated the structure of NN [11, 12]. However, this method has certain limitations on the accuracy of preprocessing of music data. Hong et al. adopted a trained LSTM to predict the next note in a monophonic melody and used reinforcement learning to enhance it [13].

With the continuous development of various disciplines, scholars have done a lot of work in the research of music emotion. People gradually recognise people's response mechanism to emotion, establish a unified emotional standard, and establish an open and correct corpus. The unified algorithm evaluation system has continuously promoted the development of emotion recognition technology.

Jiang et al. used the SVM (support vector machine) classification algorithm to extract the spectral features of music and perform sentiment classification [14]. Mattei et al. studied a variety of acoustic features, including low-level features and features such as melody, pitch, and high-level genre, style, etc.; these features were then reduced to a D-dimensional space and associated with semantic features. Finally, automatic recognition of music emotion was done using k-nearest neighbor algorithm [15]. Kaya and Salah explored the effectiveness of random forest classification algorithm in music emotion recognition [16]. Compared with the SVM classification algorithm, this method has greater advantages in generalization and robustness against noise and is very suitable for audio classification tasks. Nordström and Laukka used a continuous emotional mental model and used regression modeling to predict the emotional value of music, using two fuzzy classifiers to measure the emotional intensity to identify the emotional content of music [17]. Yun et al. completed music emotion classification by extracting the pitch, width, and brightness features of music frequency domain [18]. Wang et al. used the SVM method to identify the emotional type of music by extracting the spectral features of music and training these features [19].

The related literature of algorithmic composition and emotion recognition is thoroughly examined in this paper, and a composition and emotion recognition model based on a machine learning algorithm is proposed. According to the information entropy of pitch and intensity, this paper extracts the main melody track. Second, take note features and extract bar features. Finally, the cosine of the vector included angle is used to judge the similarity between feature vectors of several adjacent sections, allowing the music to be divided into multiple segments. The speed, melody direction, intensity, tempo, rhythm change, major third degree, minor third degree, and timbre of each segment are extracted using digital music feature extraction technology, and the emotion of each segment is analyzed using a music emotion model. This paper employs a two-layer filtering mechanism in order to improve retrieval speed. To begin, dissimilar music is quickly filtered out based on time length and category vector. The user is then presented with the most similar music, which is calculated using the exact similarity calculation formula. The study found that the model's retrieval speed is faster, its accuracy is higher, and all indexes are high.

3. Methodology

3.1. Algorithm and Emotion Recognition. The regular vibration of the vocal body produces music, which is a type of sound art. The composer's inspiration and music creation rules, which primarily include the melody, interval, harmony, chord, mode, and form of music [20], are used to create music. Music's allure stems from the unpredictable nature of creative motivation, and the new auditory experience it provides can often elicit emotional resonance. Music can convey emotions and regulate the mood of listeners as an important part of human life. It is an important aspect of emotional music, and the relationship between computer music, music, and emotion has sparked a lot of research. The various elements of music work together and have a constantly changing expressive force. Melody is the foundation of music, while other elements are the branches and leaves. The image of music will change to varying degrees as each element changes. Melody is a musical sound movement that is organised and harmonious according to certain rules. It is the most common way for musical works to express their feelings. Melody is the heart of music, the foundation of its creation, and the expression of music's image and thought. The pitch relationship between two tones is indicated by the interval. It measures the auditory distance between sounds in degrees, which is a normalised representation method. A sound combination in which multiple tones are arranged according to certain rules is referred to as harmony. The vertical combination of three or more pitches is known as a chord. When it comes to overlapping, it can be done in a third-degree or non-third-degree relationship. The absolute height of a sound is expressed by its phonetic name, which is the expression of its pitch frequency. Every song has a tonic, whose tuning height is represented by key signature and whose height is the key of the scale. Form is a musical structure that combines people's cognition of certain music works in a specific cultural context, and it is a summary of the theoretical laws of music. The smallest unit of sound behaviour in music is the note. A note is a sound that has a specific time length and frequency. In addition, the intensity and timbre of notes should be taken into account when describing them. We can derive the basic characteristics of notes from this: pitch, dynamics, duration, and timbre. Digital music is a new genre of music created with computer technology, stored in digital format, and distributed via digital media technologies like the Internet. Digital music, in comparison to traditional music, has taken on new characteristics as a result of the rapid advancement of digital technology.

The algorithm is a logical and systematic instruction for solving a problem that represents the description of a specific problem and the strategy for solving it. Through normative data input, an excellent algorithm can produce effective and standardized output results in a specified amount of time. Musical elements, writing logic, algorithm, structural model or rule system, and a series of composing techniques formed by matching algorithm thinking with the smallest decision-making model in composition thinking are all examples of algorithm concepts. Computer music differs from traditional music in terms of how it deals with sound, as well as the principles of sound creation and organisation. The creator's perspective and the computer's automatic learning of big data are two common approaches to computer composition. From the perspective of the creator, it is necessary to condense a large number of music-making rules into a single routine. This method produces high-quality music, but it takes a lot of manpower to establish rules and routines in the early stages. Big data [21, 22] automatic learning composition allows computers to learn the laws in music data and then compose music using calculators. Using a computer to learn from big data music can save time and money, and the music generated is more diverse. The way music is processed, manufactured, and organised differs significantly from traditional music. The irrelevance between playing method and timbre breaks through the quantitative limit of timbre [23]. Digital music has various sound effects, and its sound is produced by a point oscillator. However, at this time, the computer is unable to create music that reflects subjective emotion and thought. It is even more difficult to meet people's requirements for pleasant music by simply using a computer to compose music using an algorithm. And, like words, music has emotional connotations. The process of establishing music characteristics and music database is shown in Figure 1.

Music emotion is an essential feature of music, and more research on music information behaviour shows that emotion is an important standard used by people when retrieving music. In fact, there is no such thing as pure musical emotion, and emotion is only meaningful when it is associated with people. When it comes to the same emotion, everyone has different reactions. As a result, if you want to share your musical emotional experience with others, you

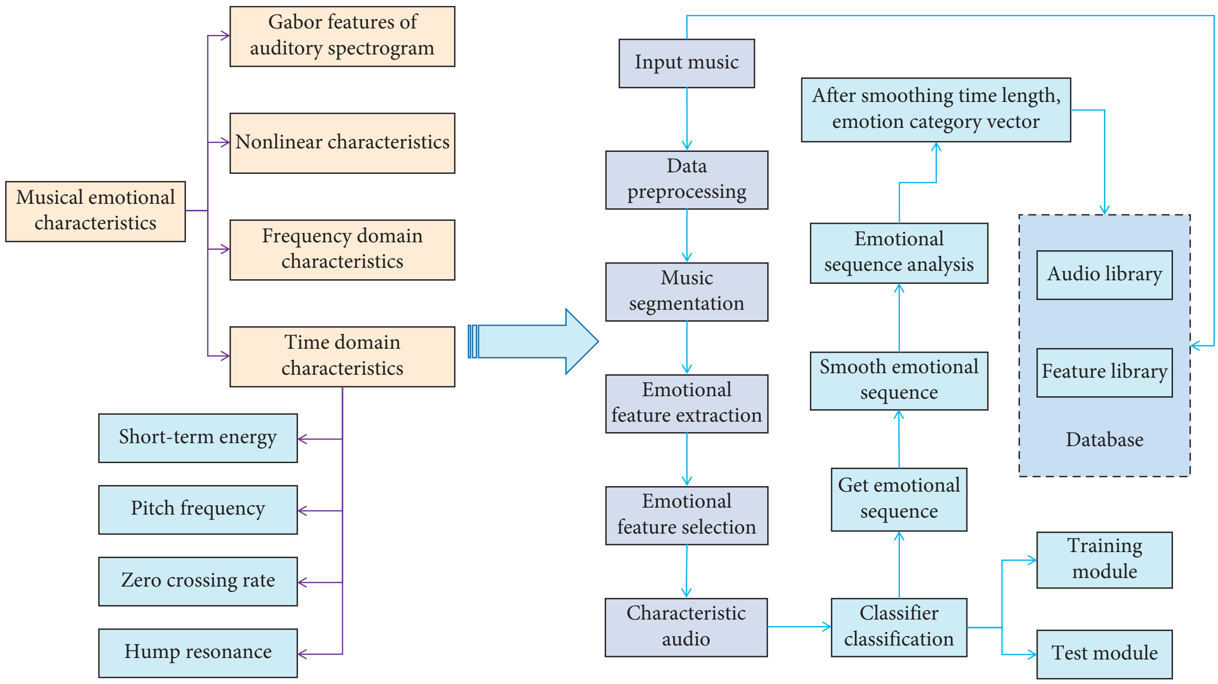

Figure 1: Emotional characteristics of music and the establishment process of music database.

must express music using a specific rule and symbol, and the same rules and symbols represent the same emotional expression in different types of music. Music emotion recognition, which is one of the important research directions in digital music, is at the heart of emotion-based music retrieval. Computers are unable to perceive the emotions contained in music. As a result, we should summarize the related elements of music into mathematical models and conduct quantitative analysis of them, so that the computer can recognise the emotional connotation of music based on its musical characteristic parameters and rules. Everyone's emotional response to music is a series of brain reactions following the acquisition of characteristic information from the music, with the results reflected in expression and psychological feelings. We must first understand the classification and expression of emotion types in order to study the relationship between music and emotion. Individual needs and desires mediate emotion, which is a psychological state. Emotion is difficult to quantify because it is complex and subjective, and different people have different levels of understanding of it. People have deepened their understanding of emotional types by constantly exploring the changing rules of emotions. At different points in time, a complete piece of music may have emotional changes. Music can be divided into two types of rhythms: fast and slow. Gentle rhythm refers to a slow-changing rhythm. The abrupt rhythm, on the other hand, is a rapidly changing rhythm. Music with a smooth rhythm can evoke a sense of calm, whereas music with an abrupt rhythm can evoke a strong sense of emotion.

3.2. Algorithm Composition and Emotion Recognition Model Construction Based on Machine Learning. Based on the deep learning theory [24], aiming at the problems existing in the current algorithmic composition system, this chapter puts forward a new NN structure of music creation from the perspectives of machine learning and music theory creation and constructs a music emotion recognition model. Different music formats have different structural characteristics and extraction methods [3, 25]. This section determines the format of music, making preparations for the extraction of emotional features of music. Generally, music files include three categories: sound files, MIDI files, and module files. MIDI file is a binary file that records the sequence of MIDI instructions. Its basic structure consists of header file and data description. In this paper, MIDI files are selected as experimental objects. The reasons are as follows: ① accurate sampling; ② easy feature extraction; ③ occupying less space; ④ high utilization rate. To begin, obtain the corresponding music score data and music data in MIDI format; after obtaining the music data, it is necessary to create a music data set in accordance with the standard; then, data normalisation, note extraction from music in MIDI format, and other preprocessing operations must be performed on the data input into the network. Multiple audio channels are usually used in MIDI music production because the music is more stereo and beautiful. The main melody is first identified from the MIDI format files in this paper. Input a classical music database in MIDI format, set initial notes to randomly generate music, collect the generated music, and construct a music generation sample database, marked as 0; mark the training data set as 1. Simultaneously, a binary classification model is built to pretrain the CNN network. The music sequence is generated by the LSTM network by setting the initial notes. LSTM, Dropout, Dense, Softmax, and other network layers are commonly used in this paper. After creating the appropriate music generation network, the network must be trained using the appropriate deep learning framework. The specific training scheme is to iteratively optimize it using cyclic operations until a satisfactory result is obtained or the specified number of iterations is reached. Figure 2 depicts the algorithm's emotion recognition flow.

This model is based on the chess game concept. The generated model is optimized by the Reward function, so that the generated music and the training sample have as much confusion as possible, and the recognition output probability of the classification network CNN is closer to 1; that is, the difference between the generated sample and the training sample cannot be distinguished, and music with similar style and theme to the training sample cannot be distinguished. The music feature analysis model is divided into two sections: one for extracting the main melody and another for extracting the musical emotional features from the main melody and constructing the musical emotional feature vector. The process of NN training is essentially the updating of weights. To update the weight between each neuron, the samples propagate forward through NN to get the output of the output layer and then backward to minimise the difference between the output of the output layer and the sample label. In this paper, a music evaluation function, Reward, is proposed, which can monitor and adjust the generated music in real time, make up for the deficiency of using LSTMNN alone for algorithm composition, make it closer to the composer's creative thinking, and meet the needs of the audience. In most music, the pitch of the main melody is generally higher than that of the accompaniment melody, and the basic contour algorithm is applicable to most music. However, for a small number of music with higher accompaniment melody, we cannot just use the pitch feature as the criterion to judge the main melody, so the basic contour algorithm has limited effect. To solve this problem, this paper proposes an improved contour algorithm based on track features to extract the main melody.

In order to improve the effectiveness of Reward function introduced in this paper, the reference value 1 is subtracted when calculating the probability, as shown in the following formula:

$$p_{(\mathrm{CNN})} = \begin{cases} 0, & \mathrm{fort} < T, \\ D_{\varphi}\left(a_{1:T}\right) - 0.5, & \mathrm{fort} = T. \end{cases} \quad (1)$$

If a piece of music has the interval difference between the adjacent notes in the a group greater than the octave, the remaining b group is less than or equal to the octave. It can be expressed by the following formula:

$$g_1(x) = \frac{a * 0 + b * 1}{a + b}. \quad (2)$$

In order to make the generated music more aesthetic, the following standards are set here:

$$\begin{aligned} I_b &\in \{0, 2, 3, 4, 5\}, \\ I_{bb} &\in \{0, 2, 3, 4, 5, 7\}, \\ I_{\longrightarrow p} &\in \{6, 7, 9, 10, 12\}, \\ N_{i=1} &\in \{1, 2\}. \end{aligned} \quad (3)$$

Among them, I_b, I_{bb}, and $I_{\longrightarrow p}$, respectively, represent the interval sample values corresponding to the measures within the measure, between the measures, and to the climax. $N_{i=1}$ is the number of minor second intervals in a piece, and the minor second can highlight the tension of the interval. If there are more than four consecutive notes at the same pitch and duration in a piece, this parameter will be recorded as 0; otherwise it will be 1.

$$g_3(x) = \begin{cases} 1, & \dfrac{1}{n-1}\left|\sum_{i=1}^{n-1} \mathrm{interval}_i \leq 4\right|, \\ 0, & \mathrm{else}. \end{cases} \quad (4)$$

The normalisation strategy in this system adopts the Min-Max scaling method, as follows:

$$X_{\mathrm{normal}} = \frac{X - X_{\min}}{X_{\max} - X_{\min}}, \quad (5)$$

where X_{normal} represents the normalised value of the digitized note data. X represents the digitized note data, $X_{\min}$ represents the digitized minimum value of note data, and $X_{\max}$ represents the digitized maximum value of note data.

The algorithm's quality evaluation mechanism plays an important role in improving the quality of music generation in the next step. This paper evaluates the quality of music from both subjective and objective perspectives in order to test the generating effect of algorithmic composition. The learning rate indicates how quickly weights are updated during the training process. The larger the amplitude of updating weights each time, and the faster the initial convergence speed, the higher the learning rate. However, an excessively high learning rate may cause the network to cross the minimum point, making convergence difficult. With the right learning rate, the objective function can converge to the local minimum in a reasonable amount of time. Music emotion recognition is the process of associating music with specific emotions based on the characteristics of the music and given reasoning rules. Emotion recognition is a mathematical mapping process that converts the features of dimensional music into dimensional emotion space. The main melody's relevant features are extracted from the melody of the alternative tracks in this paper to determine the likelihood of each track channel containing the main melody. The higher the score is, the more likely the main melody will be included. Six features of the alternative track melody are extracted based on the musical theory characteristics of the main melody when the related features of the main melody are extracted. These six characteristics are sound source balance, main volume, pronunciation area, loudness area, average pitch, and average sound intensity. Music is a kind of time series. In this paper, LSTM network is used to generate music series. LSTM has a special function of sequential memory. On the basis of ordinary multilayer NN, the structure adds the horizontal connection among the units in the hidden layer. Through a weight matrix, the

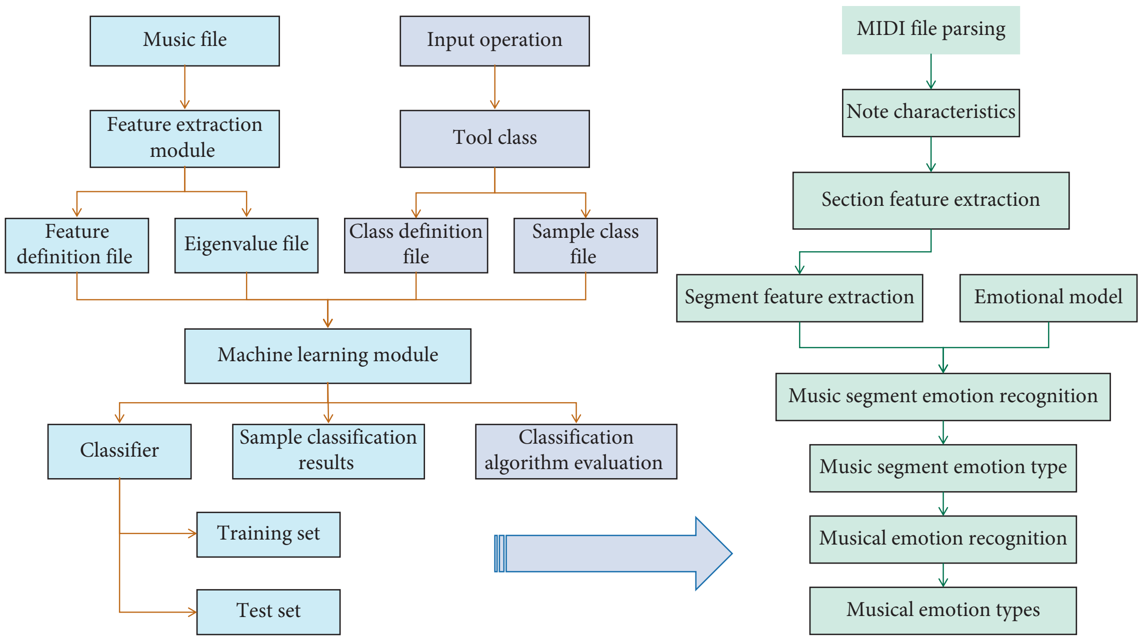

Figure 2: The algorithm emotion recognition flow in this paper.

previous information can be connected to the current task; that is, the next sequence action can be predicted by the previous generated sequence. After the data set is made, the data preprocessing of the data set will be carried out. Its purpose is to make the note data input to NN have a unified standardization standard, thus effectively reducing the number of event types in huge data and effectively improving the generalization ability of the system. It contains many core musical data expressions.

In this paper, we use information entropy to evaluate the amount of information in each track of MIDI file. The formula of entropy is as follows:

$$H(p(x)) = -\sum p(x)\log_2^{p(x)}, \tag{6}$$

where $p(x)$ is the probability density function. The input s_j of each intermediate layer unit is calculated by using the input sample $X = (x_1, x_2, x_3 \ldots, x_n)$, the connection weight W_{ij}, and the threshold θ_j, and then the output b_j of the intermediate layer unit is calculated.

$$\begin{aligned} s_j &= \sum_{i=1}^{n} w_{ij}x_i - \theta_j, \quad j = 1, 2, 3, \ldots, p, \\ b_j &= f(s_j) = \frac{1}{1 - e^{-s_j}}, \quad j = 1, 2, 3, \ldots, p. \end{aligned} \tag{7}$$

Global error of the calculated network:

$$E = \frac{1}{2}\sum_{i=1}^{q}(y_i - c_i)^2. \tag{8}$$

The changing intensity of rhythm can be expressed by the length and intensity of notes in a passage, and the formula is as follows:

$$\text{Rhy} = \sum_{i=1}^{n-1}\left|\frac{I_{i+1} - I_i}{D_i}\right|. \tag{9}$$

The main melody track typically has a large number of notes, and the number of notes in the main melody track should not be less than half of the average number of notes in each track. As a result, before determining the main melody track, tracks with less than half the average number of notes should be eliminated. Musical emotion cannot be expressed solely through the basic information contained in musical notes, and musical emotion analysis must take into account the organisational structure and changing rules of musical notes. As a result, we divide music features into two levels: high-level features and note features, based on the composition form of music features and the audience's hierarchical cognitive process of music features. Following the division of the music into segments with distinct emotions, the forms and methods of music expression are investigated, and some features that have a significant impact on music emotions are chosen to represent music. For each segment, feature extraction is performed, and the extracted features are used to create the segment's feature vector. In this paper, the introduction of attention mechanism will assign different attention sizes to each part of the frame, reflecting the influence degree of each original information on the current information. This number is also the attention size assigned to each word by attention mechanism when learning the current information. When new information is introduced, the training efficiency will be improved.

4. Result Analysis and Discussion

This section conducts an experimental comparison of various models in order to verify the performance of the algorithm composition and emotion recognition model based on machine learning proposed in this paper. The network model in this paper is created using Matlab. To begin, create two large loops. After that, the data blocks are then input into the set network model, and the output results are obtained after weight calculation. To ensure the experiment's objectivity, the same training set is used for all algorithms, and the number of network layer units is set to 512 with 200 iterations. Tansig and Logsig are the excitation functions for the network's hidden layer and output layer, respectively. Each note sequence corresponds to a one-hot vector and is 192 characters long. Table 1 shows the parameter values set by the network in the training process.

The loss value specifies how the difference between the prediction result and the actual label should be calculated. Because note prediction is a multiclassification problem, the categorical cross-entropy function is chosen because of its high performance. The distance between the predicted value and the real value can be minimised by minimising the cross-entropy, achieving the ultimate goal of training. This chapter examines the impact of network parameters on experimental results by looking at the number of iterations. The influence of the number of iterations on the loss value is shown in Figure 3.

The findings show that the longer iteration times are, the more weight parameters are learned and adjusted, which can improve the model's accuracy to some extent. And as the number of iterations increases, the loss function decreases more slowly. When learning and training a NN, the numerical distribution changes dramatically as the number of layers increases, accompanied by error accumulation. The resulting layer-by-layer superposition will drastically alter the high-level input distribution. As a result, the normalisation strategy can be used to process the data distribution to the [0, 1] interval in order to reduce the impact of distribution change. The training set is processed using feature analysis, the emotional feature quantity is used as the model's input, and the classification result is used as the model's output. The error results of different music algorithms are shown in Figure 4.

It can be seen that the error of the music algorithm generated in this paper is the smallest, and its performance is better. In this network, the more units in the hidden layer, the stronger the network's ability to learn abstract data features. The dimension of hidden layer has an important influence on the experimental results, but the more layers there are, the larger the calculation amount of NN will be. Comparison of algorithm recall results is shown in Figure 5.

According to the data analysis in Figure 5, the recall rate of this algorithm is higher than that of the other two algorithms. This algorithm has certain reliability. This chapter verifies the quality of music generation through professional evaluation. 100 music professionals from a university were invited to comprehensively grade 30 samples generated by each model. The results are shown in Table 2.

As can be seen from Table 2, the music generation algorithm in this paper has more advantages in results. This proves the effectiveness of the model in music generation, and it can be seen that the network model constructed in this paper has stronger practical value. In this paper, the emotional classification of music is realized by fusing the time domain features, frequency domain features, auditory spectrogram features, and nonlinear Hurst parameters of music. Through experiments, the accuracy of emotion classification of different algorithms is shown in Figure 6.

It is clear that this model has a higher retrieval accuracy. The results confirm the model proposed in this paper's validity and correctness. In this paper, choose an appropriate training set as the network's input and constantly revise the network's connection weights and thresholds to

Table 1: Parameter values of network settings in this paper.

Serial number	Parameter	Set value
1	Input layer-neuron	9
2	Hidden layer-neuron	20
3	Output layer-neuron	7
4	Epochs	200
5	Batch_ size	64
6	Loss	Categorical_crossentropy
7	Optimizer	Rmsprop
8	Save_ number	20
9	Activation	Softmax activation function

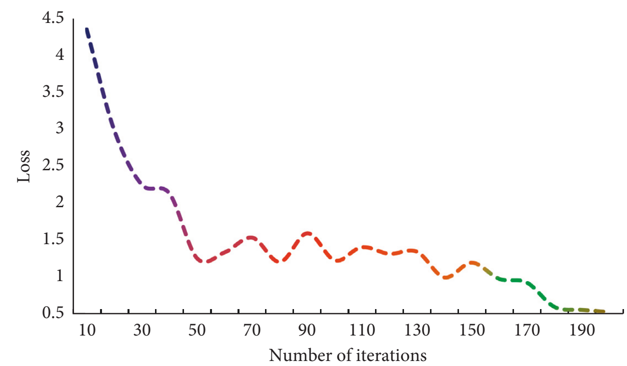

Figure 3: Influence of iteration times on loss value.

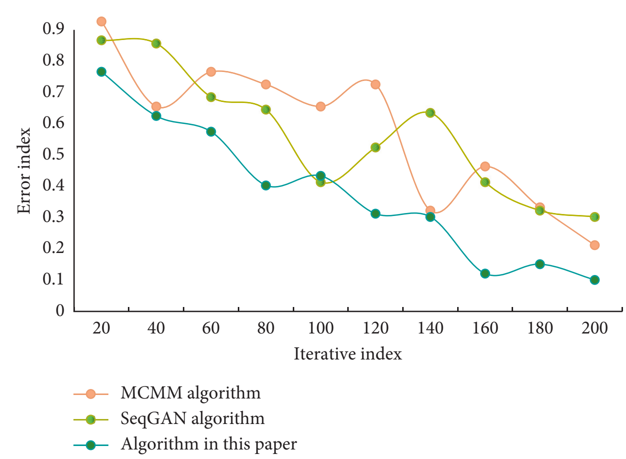

Figure 4: Generate error results of different music algorithms.

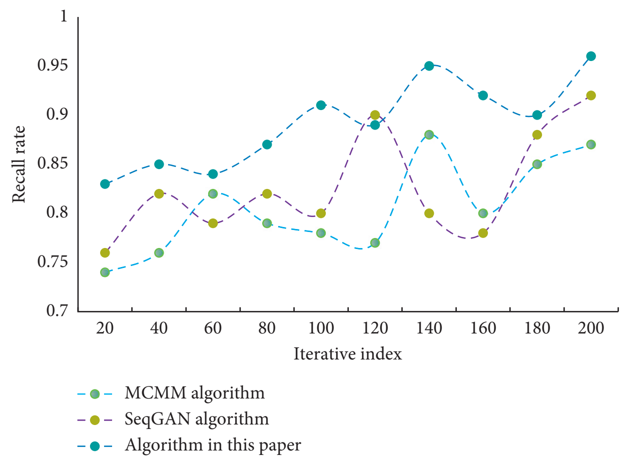

Figure 5: Comparison of algorithm recall results.

Table 2: Evaluation of music generation quality.

Model	Melody	Rhythm	Harmony	Expressive force	Satisfaction (%)
HMM model	6.36	7.15	6.47	6.18	65.03
MCMM model	7.59	7.34	8.01	7.03	69.34
Seq GAN model	6.28	6.84	7.78	6.35	63.17
RL-RNN model	6.54	6.58	6.97	5.84	59.93
RFCM model	5.89	5.13	6.74	6.62	58.46
Model of this paper	7.76	7.45	8.03	7.16	74.89

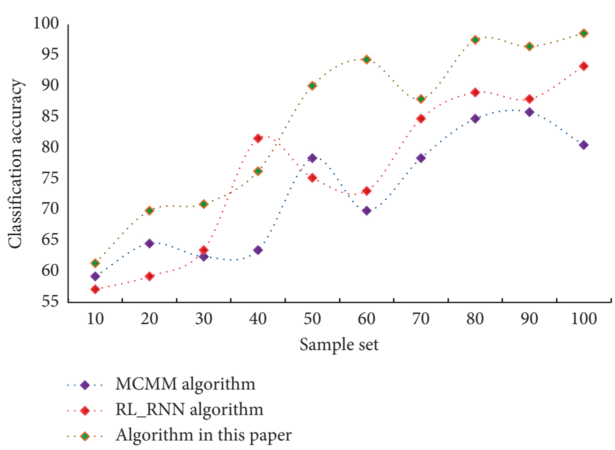

Figure 6: Comparison of accuracy of different algorithms in emotion classification.

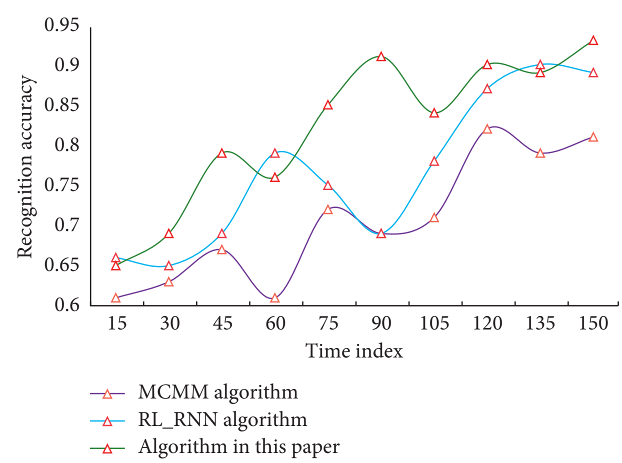

Figure 7: Different accuracy of emotion recognition algorithm.

make it converge. Finally, the emotion recognition model is used to identify the emotion of the music in the test set, and the algorithm's accuracy is evaluated. The emotion recognition accuracy of different algorithms is shown in Figure 7.

When compared to the results of three different algorithms for accurately recognising emotion samples, the algorithm in this paper has a better effect, with higher generalization, stability, recognition rate, and practical value. Several experiments are carried out in this chapter to verify the performance of the algorithm and model proposed in this paper. The model's emotion recognition accuracy is up to 93.78 percent, and the algorithm recall rate is up to 96.3 percent, according to the experimental analysis. The model's retrieval speed is quick, and its accuracy is excellent. Many results show that the recognition method used in this paper is superior to other recognition methods in terms of recognition ability, and the emotion recognition results are reliable.

5. Conclusions

Research on an efficient music generation algorithm and emotion recognition model has become a research hotspot as artificial intelligence technology matures. The construction of an emotion recognition model of composition is a multidisciplinary research topic. This paper builds an algorithm composition and emotion recognition model based on an in-depth study of machine learning. This paper examines the workflow of a music emotion recognition system and summarizes the contents of digital music emotion recognition and music features. The features are used to represent music, and then algorithms are used to analyze the features to determine the emotional categories of music. The model's emotion recognition accuracy is up to 93.78 percent, and the algorithm recall rate is up to 96.3 percent, according to the experimental analysis. The segmented emotion recognition method proposed in this paper can better show the movement of music than the whole music emotion recognition method. It has a strong ability to recognise emotions. The experimental results show that this recognition method has superior recognition ability, fast retrieval speed, and certain reliability when compared to other recognition methods. The method proposed in this paper is feasible and effective, and it produced the expected outcomes. On the level of computer-aided music creation, artificial intelligence music is expected to help creators fill the thinking gap in creation in the future, and users will be able to choose the most appropriate candidate sequence to increase creator inspiration. You can also recreate entirely new music in the style of specific musicians and composers. This study, however, has some flaws due to the influence of our knowledge level and time constraints. We can continue to research the emotional model in order to more scientifically represent the emotional categories of music in future work.

Data Availability

The data used to support the findings of this study are available from the corresponding author upon request.

Conflicts of Interest

The authors do not have any possible conflicts of interest.

Acknowledgments

This article is the phased achievement of the Key Project of Hubei Province Educational Science Planning, Study on the "Double Creation" Artistic Talent Training Model under the Collaborative Education Mechanism (Project no. 2020GA052).

References

[1] G. Korvel and B. Kostek, "Discovering rule-based learning systems for the purpose of music analysis," *Journal of the Acoustical Society of America*, vol. 146, no. 4, p. 2947, 2019.

[2] M. Russo, L. Kraljević, M. Stella, and M. Sikora, "Cochleogram-based approach for detecting perceived emotions in music," *Information Processing & Management*, vol. 57, no. 5, Article ID 102270, 2020.

[3] N. Wang, H. Xu, F. Xu, and L. Cheng, "The algorithmic composition for music copyright protection under deep learning and blockchain," *Applied Soft Computing*, vol. 112, Article ID 107763, 2021.

[4] W. Cai, M. Gao, R. Liu, and J. Mao, "MIFAD-net: multi-layer interactive feature fusion network with angular distance loss for face emotion recognition," *Frontiers in Psychology*, vol. 12, p. 4707, 2021.

[5] L. You, H. Jiang, J. Hu et al., "GPU-accelerated faster mean shift with euclidean distance metrics," 2021, http://arXiv.org/abs/2112.13891.

[6] J. Kong, H. Wang, C. Yang, X. Jin, M. Zuo, and X. Zhang, "A spatial feature-enhanced attention neural network with high-order pooling representation for application in pest and disease recognition," *Agriculture*, vol. 12, no. 4, p. 500, 2022.

[7] Y. Zhang, K. Xia, Y. Jiang et al., "Multi-modality fusion & inductive knowledge transfer underlying non-sparse multi-kernel learning and distribution adaption," *IEEE/ACM Transactions on Computational Biology and Bioinformatics*, vol. 13, p. 1, 2022.

[8] W. L. Zheng and B. L. Lu, "Investigating critical frequency bands and channels for EEG-based emotion recognition with deep neural networks," *IEEE Transactions on Autonomous Mental Development*, vol. 7, no. 3, p. 1, 2015.

[9] R. Jenke, A. Peer, and M. Buss, "Feature extraction and selection for emotion recognition from EEG," *IEEE Transactions on Affective Computing*, vol. 5, no. 3, pp. 327–339, 2014.

[10] L.-k. Zhang, S.-q. Sun, B.-x. Xing, R.-m. Luo, and K.-j. Zhang, "Using psychophysiological measures to recognize personal music emotional experience," *Frontiers of Information Technology & Electronic Engineering*, vol. 20, no. 7, pp. 964–974, 2019.

[11] A. Majumder, L. Behera, and V. K. Subramanian, "Emotion recognition from geometric facial features using self-organizing map," *Pattern Recognition*, vol. 47, no. 3, pp. 1282–1293, 2014.

[12] C. S. Ooi, K. P. Seng, L.-M. Ang, and L. W. Chew, "A new approach of audio emotion recognition," *Expert Systems with Applications*, vol. 41, no. 13, pp. 5858–5869, 2014.

[13] Y. Hong, C.-J. Chau, and A. Horner, "An analysis of low-arousal piano music ratings to uncover what makes calm and sad music so difficult to distinguish in music emotion recognition," *Journal of the Audio Engineering Society*, vol. 65, no. 4, pp. 304–320, 2017.

[14] W. Jiang, Z. Wang, J. S. Jin, X. Han, and C. Li, "Speech emotion recognition with heterogeneous feature unification of deep neural network," *Sensors*, vol. 19, no. 12, p. 2730, 2019.

[15] T. A. Mattei, A. H. Rodriguez, and J. Bassuner, "Selective impairment of emotion recognition through music in Parkinson's disease: does it suggest the existence of different networks for music and speech prosody processing?" *Frontiers in Neuroscience*, vol. 7, no. 7, p. 161, 2013.

[16] H. Kaya and A. A. Salah, "Combining modality-specific extreme learning machines for emotion recognition in the wild," *Journal on Multimodal User Interfaces*, vol. 10, no. 2, pp. 139–149, 2016.

[17] H. Nordström and P. Laukka, "The time course of emotion recognition in speech and music," *Journal of the Acoustical Society of America*, vol. 145, no. 5, pp. 3058–3074, 2019.

[18] W.-h. Yun, D. H. Kim, C. Park, and J. Kim, "Hybrid facial representations for emotion recognition," *ETRI Journal*, vol. 35, no. 6, pp. 1021–1028, 2013.

[19] S.-H. Wang, P. Phillips, Z.-C. Dong, and Y.-D. Zhang, "Intelligent facial emotion recognition based on stationary wavelet entropy and Jaya algorithm," *Neurocomputing*, vol. 272, no. 1, pp. 668–676, 2018.
[20] Y. Dong, X. Yang, X. Zhao, and J. Li, "Bidirectional convolutional recurrent sparse network (BCRSN): an efficient model for music emotion recognition," *IEEE Transactions on Multimedia*, vol. 21, no. 12, pp. 3150–3163, 2019.
[21] W. Cai, Y. Song, and Z. Wei, "Multimodal data guided spatial feature fusion and grouping strategy for E-commerce commodity demand forecasting," *Mobile Information Systems*, vol. 2021, Article ID 5568208, 14 pages, 2021.
[22] X.-B. Jin, W.-T. Gong, J.-L. Kong, Y.-T. Bai, and T.-L. Su, "PFVAE: a planar flow-based variational auto-encoder prediction model for time series data," *Mathematics*, vol. 10, no. 4, p. 610, 2022.
[23] V. Chaturvedi, A. B. Kaur, V. Varshney, A. Garg, G. S. Chhabra, and M. Kumar, "Music mood and human emotion recognition based on physiological signals: a systematic review," *Multimedia Systems*, vol. 2021, no. 3, pp. 1–24, 2021.
[24] Z. Huang, Y. Liu, and C. Zhan, "A novel group recommendation model with two-stage deep learning," *IEEE Transactions on Systems, Man, and Cybernetics: Systems*, vol. 2021, 2021, In Press.
[25] S. Rho and S.-S. Yeo, "Bridging the semantic gap in multimedia emotion/mood recognition for ubiquitous computing environment," *The Journal of Supercomputing*, vol. 65, no. 1, pp. 274–286, 2013.

Hindawi
Computational Intelligence and Neuroscience
Volume 2022, Article ID 2615153, 10 pages
https://doi.org/10.1155/2022/2615153

Research Article

Development and Supervision of Financial Technology Based on Blockchain

Rui Yang

College of Economic and Management, Chongqing Industry Polytechnic College, Chongqing 401120, China

Correspondence should be addressed to Rui Yang; yangrui@cqipc.edu.cn

Received 17 April 2022; Revised 28 April 2022; Accepted 29 April 2022; Published 1 June 2022

Academic Editor: Xin Ning

Decentralization, stability, security, and immutability are all features of blockchain technology. Blockchain, as the underlying technology of Bitcoin's digital monetary system, is currently sweeping the globe. Blockchain is a revolutionary decentralized database technology that employs encryption, a timestamp chain data structure, a distributed consensus mechanism, and other technologies to achieve decentralization, tamper resistance, easy tracking, and programmable smart contracts. In the face of rising financial technology, we must maintain inclusive, technological, and invasive regulatory principles that not only foster financial innovation, but also conduct dynamic supervision to avoid systemic financial hazards. The consensus algorithm is one of the main blockchain technologies that has a direct impact on the system's functioning. As a result, in this paper, we propose a blockchain-based development and supervision method for financial technology, as well as an application of this technology to commercial settlement, which can significantly reduce data complexity, time consumption, and the structural chain phenomenon in existing transaction settlement. We bring the idea of pow competition into DPoS, construct a consensus algorithm with an upgrade mechanism, and call it delegated proof of work, based on an in-depth investigation of the working principle of pow (proof of work) (dDPoS). The blocking efficiency of the dDPoS consensus method is around one block every 10 seconds, which is significantly higher than the blocking efficiency of the POW and POS consensus algorithms. As a result, it offers a potential answer to traditional centralized institutions' concerns of high brokerage costs and insecure central storage, as well as a wide range of application possibilities.

1. Introduction

Financial English "Fin Tech" is an abbreviation for "Financial Technology," which refers to the integration of finance and IT, as well as the use of various scientific and technological techniques to improve efficiency and successfully cut operating costs in the traditional financial industry [1]. Financial liberalization and globalization, on the other hand, make the entire financial system more vulnerable. Financial supervision has become a focal point of concern, particularly during the 1990s, as a result of massive, devastating, and recurring financial crises [2]. The price of Bitcoin has witnessed two strong surges and falls in recent years, owing to the progressive popularization of the notion of Bitcoin and the influence of investor mood and government supervision, which has sparked broad discussion and interest [3]. Although technology is transforming China's financial industry, it is also posing new challenges to legal concepts, norms, and regulatory structures [4]. The financial legal system is experiencing new issues as a result of decentralization, as represented by blockchain, and legal supervision reform, as represented by supervision technology [5].

The legislation of financial supervision and the financial industry is complementary. The financial industry's growth encourages financial supervision law innovation, and the financial supervision legislation ensures the financial industry's healthy growth [6]. On the other hand, if the legal structure of financial supervision cannot keep up with the financial industry's expansion, the financial business outside of supervision may provide unanticipated hazards [7]. Blockchain has a strong basis of trust as a sharing technology

[8]. However, the blockchain technology development cycle is short, and the technology's evaluation is mixed [9]. The existing calculating methods may lead to a complex conversion procedure and low efficiency of long-term encryption and decryption process [10], yet all nodes in the blockchain network maintain the same block sequence and attain agreement according to the accepted norms [11]. In this research, we present the dDPoS algorithm and compare the experience with existing methods to verify the performance of the proposed method. This study examines the development and oversight of blockchain technology in financial settlements, as well as the associated concepts of blockchain technology, and explains, summarizes, and summaries them.

People began to recognize the usefulness of blockchain technology as the basic underlying technology when the price of bitcoin fluctuated dramatically [12]. Although blockchain is undeniably appealing to the banking industry, most banks are still in the early stages of adopting it, and many financial businesses are currently proving the concept and developing their own blockchain strategies or are only now becoming aware of it [13]. Furthermore, financial technology has altered the manner in which the financial industry operates, rather than the nature of the industry [14, 15]. Financial regulatory authorities in industrialized nations have been exploring how to monitor complex financial institutions, which has become the most significant responsibility, in order to achieve financial stability and avert financial crises. We should be aware of new hazards as a result of financial technology, not just the changes in the financial business. The efficient and complete evaluation of consensus algorithm is realized in this paper's financial technology development and supervision method based on blockchain, in order to discuss its working principle on private blockchain platform and how it affects the overall performance of blockchain, as well as the efficient and complete consensus algorithm, complete analysis and comparison of performance characteristics of various consensus algorithms, and a complete evaluation of consensus algorithms.

(1) This study analyzes and describes the technological model, advantages and disadvantages of blockchain technology in as much detail as possible, based on a complete analysis of the existing academic literature, various research reports, and white papers in the industry.

(2) The selected nodes can be the initial permanent nodes with resources and the right to vote in the DPoS process, and the PoW is used to "screen" the node sets with a specific computational capacity to vote in the election.

(3) The use of blockchain technology in financial technology development and supervision can improve the loan quality and procedure in the financial industry, as well as ensuring loan business efficiency and endorsement transparency.

This paper's research framework is divided into five sections, which are as follows:

The first section of this paper introduces the research background and significance before moving on to the paper's primary work. The second section introduces the work on financial technology development and oversight, as well as blockchain and related algorithms. The third section analyzes the combination of financial efficiency and supervision, as well as structural optimization methodologies, to provide readers with a better knowledge of visual composition and semantic expression. The fourth section is the meat of the study, and it covers two areas of blockchain technology: blockchain core technology and consensus algorithm analysis. The final section of the paper is a recap of the entire study's work.

2. Related Work

2.1. Financial Technology Development and Supervision. Financial technology refers to financial innovations that create new business models, applications, processes, or products through technology. These innovations can have a significant impact on financial markets, financial institutions, or financial service delivery methods. Although deregulation and self-regulation can maintain market competitiveness, it is difficult to cope with the actual financial crisis, and international arbitrage has increased due to deregulation. In the face of the crisis, it has become an important topic for Chinese and foreign legal circles to have some thoughts, opinions, and constructive opinions, and how to improve the current financial supervision mode.

Zachariadis and others believe that regulatory adjustment is necessary because there are external influences that lead to serious information asymmetry, natural monopoly, and market failure in the financial market [16]. Kabra et al. analyzed the mechanism and application of blockchain consensus algorithm in the field of financial supervision, chose Java Spring framework as the implementation framework of the platform, and adopted Dockers technology to realize multi-node private chain deployment [17]. Cretarola and others systematically studied the supervision mode of world commercial banks and its relationship with financial development. However, the effectiveness of various financial supervision theories has not been systematically verified in the existing literature [18]. Egelund Muller and others believe that the public interest theory lacks empirical support, and the reason why many industries are regulated is not because of the higher degree of monopoly or easier to trigger monopoly [19]. The public interest theory of financial supervision proposed by Yu et al. is based on three assumptions: sufficient government information, contribution to the overall welfare of society, and sufficient credit. It allows individuals to supervise powerful financial institutions [20].

The financial supervision law needs to determine the future financial supervision reform plan from the perspective of national historical development. In terms of respecting and understanding China's actual situation, this paper attempts to explore a practical legal system of financial supervision, so as to create a platform for others and themselves to continue their research in the future.

2.2. Blockchain and Its Related Algorithms. In order to meet the needs of social development, the blockchain is constantly changing, and the core technology of blockchain-consensus algorithm also needs to be innovated. For example, Ping An Yizhang chain solution, Wanxiang blockchain laboratory baas platform, Zhonghui interbank joint loan clearing project, ant financial service social welfare project, etc. all show that domestic financial technology enterprises attach importance to blockchain technology application research and consensus algorithm. Many scholars at home and abroad have done a lot of in-depth research on financial supervision and investigated in detail the impact of various specific financial supervision measures on financial development.

Sun et al. proposed a technical model for the first time. Aiming at the problem of repeated payment of existing third-party electronic payment, this paper attempts to establish a decentralized point-to-point direct transaction e-cash system based on P2P network technology and uses cryptography, timestamp, and consensus mechanism to ensure that the data is easy to trace but not easy to tamper [21]. Zhu and Zhou analyzed the security and performance of different consensus mechanisms and network parameters in public by introducing a new quantitative framework [22]. The framework can objectively analyze the trade-off between the performance and security of public blockchain under the conditions of network propagation, block size, block generation interval, information propagation mechanism, and network malicious attack. Nathan and Jacobs proposed a private blockchain evaluation framework [23]. At present, the design of BLOCKBENCH is carried out through three most mature blockchain platforms that can support smart contract functions: Hyperledger Fabric, ETHEREUM, and PARITY. Cong and He put forward the model of Ethereum and developed a programming script language with complete Turing and more complex intelligent contracts for the first time based on technology [24]. delegated Byzantine fault tolerance (DBFT) is an improved Byzantine fault tolerance algorithm initiated by domestic small ant team, which has been applied to its original ant shares (NEO) project [25].

Therefore, through a unified input-output interface, the underlying code of performance simulation evaluation of consensus algorithm is integrated into the platform visualization management module, which is convenient for blockchain practitioners to start performance simulation by inputting certain specific parameters.

3. Combination of Financial Efficiency and Supervision and Structural Optimization Method

3.1. Combination Method of Financial Efficiency and Financial Supervision. In the current credit economy, financial resources are fresh resources required to maintain social and economic progress [26]. The Pareto optimality criterion is extended and applied to resource allocation [27]. The Pareto optimal allocation of financial resources is then the so-called financial efficiency. As a result, advancements in financial technology not only raise the risk of consumer information disclosure and fraud, but also make customer personal information protection and remedy more difficult. These are regulatory concerns that need to be addressed as financial technology develops. Data layer, network layer, consensus layer, incentive layer, contract layer, and application layer are the six levels that the blockchain system separates its infrastructure into, from low to high, according to distinct functions. The blockchain infrastructure model is shown in Figure 1.

Firstly, according to the Pareto condition of optimal distribution of commodities among consumers, when there are two or more consumers and two or more commodities, when the marginal substitution rate between two commodities is the same for any one consumer, and when it is equal to the ratio of product price, the distribution of commodities will reach Pareto optimal. Financial regulators are responsible for supervision. Select the appropriate key generation function according to the different encryption methods of each part, which must meet the conditions under the following formula:

$$K_{2i} = f_i\left(U_i R_i, H_i(CF)\right). \tag{1}$$

The blockchain is distributed and stored at each node of the network in the form of encryption. All transaction records of each node of the whole network are stored on the chain, so the blockchain can be regarded as an account book recording all bitcoin transactions [28]. The cost of regulators' hard work will be significantly higher than the cost of laziness, while the benefits of hard supervision and laziness are not obvious. Therefore, the net benefits of regulators' hard work will be significantly lower than the net benefits of laziness, that is,

$$\left(R_2 - C_2\right) > \left(R_i - C_i\right), \left(R_2^*, C_2^*\right) > \left(R_1^*, C_1^*\right). \tag{2}$$

Blockchain technology has a natural trust advantage, because it cannot be tampered with, is easy to trace, and is very suitable for scenarios where some information is opaque, credit risk is high, and losses may be high [29]. Set up various financial supervision departments corresponding to different types of financial institutions and delimit the jurisdiction of each financial supervision department, and the supervision departments of one type of financial institutions shall not supervise other types of financial institutions beyond their authority. At this time, there is also a refined Bayesian Nash equilibrium, where regulators choose to be lazy, and the public choose to pay low remuneration when

$$p = \frac{\left(R_p^* - C_p^*\right) - \left(R_p^* - C_p^*\right)}{\left(R_\mathrm{q} - C_q\right)}. \tag{3}$$

Secondly, according to the Pareto condition of the optimal allocation of producer input factors, the input

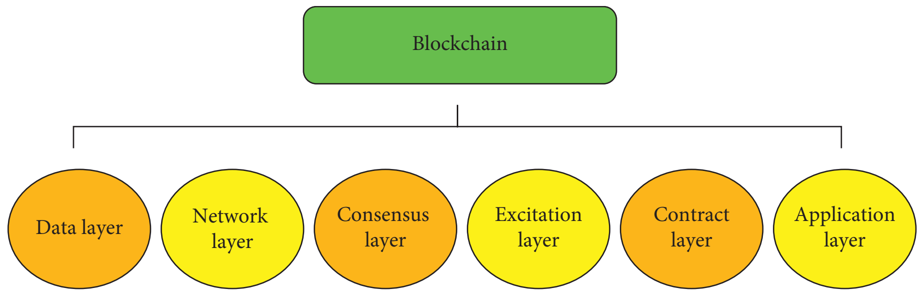

Figure 1: Blockchain infrastructure model.

combination of the optimal allocation of producer input factors is an input combination that meets the equal marginal rate of technology substitution of any two inputs and is equal to the ratio of input factor prices. Through multiple transaction intermediaries, the transaction efficiency is greatly reduced, the transaction cost is increased, and the moral hazard is high. The application of blockchain technology can realize point-to-point direct transactions with high trust of all trading parties, so as to improve efficiency and reduce costs. Use performance indicators to express the expected objectives of the system:

$$J = f_{t0}^{tf} L[x(t), u(t), t] \mathrm{d}t. \tag{4}$$

Then, combined with the encryption algorithm, the transaction results are made public (that is, the prototype of blockchain), and a decentralized property authentication system is established. Due to the specialized operation of the supervised subjects, the supervision level is highly specialized, which greatly guarantees the stability and security of the financial system in a certain period of time. The method of selecting the optimal process and strategy can be solved by establishing Hamiltonian function:

$$H(x, u, \lambda, t) = L(x, u, t) + \lambda(t) f(x, u, t). \tag{5}$$

Finally, for financial resources, if the supply and demand of financial resources are to be roughly balanced, that is, to meet the distribution of financial resources among financiers and financial commodities among investors, the marginal financing conversion rate of financiers must be equal to the marginal commodity substitution rate of investors. If the business scope of financial institutions is clearly and strictly divided, and the responsibility of financial supervision is relatively clear, the separate supervision system of institutional supervision is feasible. Since financial institutions only need to accept the supervision of one regulatory department, they can avoid the cross supervision and overlapping supervision of regulatory departments, reduce the cost of regulators, and indirectly reduce the cost of consumers. Any authorized person can see the records of the whole data chain at any node, so that the audit department and regulatory department will celebrate warmly.

3.2. Optimization Method of Financial Supervision Structure. Vulnerability is the fundamental motivation of financial supervision and the core and springboard of long-term historical development of financial supervision [30]. With the increasingly blurred division of business among heterogeneous financial institutions, institutional supervision is likely to lead to gaps in financial supervision and potential risks, especially the subsidiaries controlled by financial groups can carry out banking, securities, and insurance business separately. Therefore, it is necessary to realize the stability of monetary function and financial function, including the stability of financial market function and the stability of financial enterprises. The optimal control problem is defined by mathematical language; that is, the state equation of the given continuous-time economic system is

$$x^{\circ}(t) = f[x(t), u(t), t]. \tag{6}$$

That is, under the background of computer-driven trading, the trading frequency and trading volume are rising rapidly. Therefore, the structure of financial supervision needs to be optimized. On the basis of giving full play to the role of basic services, the party applying funds, the party providing funds, and other participants in the supply chain are constructed together, as shown in Figure 2.

First, handle the relationship between financial supervision and financial supervision structure adjustment. Under the condition of modern financial economy, the investment of financial resources comes from savers' savings in a broad sense, including the financial assets investment behavior of individuals and enterprises. When implementing the institutional supervision mode, even if the main supervision system is adopted for the business approval and supervision of a certain type of financial institutions, and several financial supervision institutions are responsible for coordination, the supervision objectives are diverse, not a single one. The real economic system, in addition to its constantly changing environment, will also change its internal structure, thus affecting the performance of the economic system. The general equation of adaptive control is

$$\mathrm{A}\left(Z^{-1}\right) Y(t) = Z^{-d} B\left(Z^{-1}\right) u(t) + C\left(Z^{-1}\right) W(t). \tag{7}$$

Before extracting the main features of distributed big data from the database, set the evaluation criteria of distributed data features, and apply them when evaluating the importance of features to determine the ability to distinguish feature classes. When publishing data on the blockchain, everyone can access it and issue transactions waiting to be

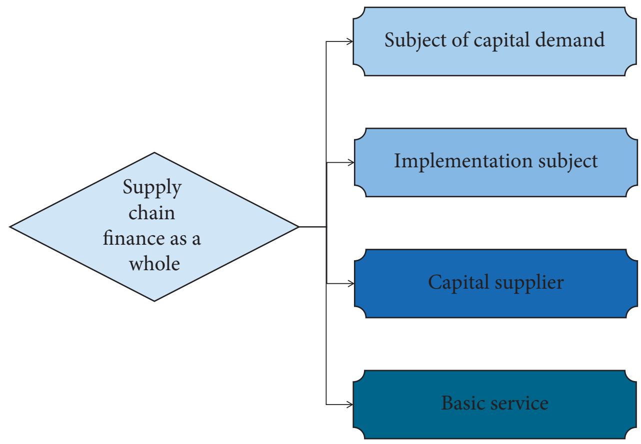

Figure 2: Overall financial application structure model of supply chain.

written into the blockchain. Suppose that $S = S(i)$ represents the surplus of consumers or investors of financial products, and $\Pi = \pi(i)$ represents the profit of financial enterprises. They are all functions of financial market price. Then, the political production function is as follows:

$$M = M(S, \pi). \tag{8}$$

Secondly, the compatibility between regulatory structure and regulatory objectives: the setting of regulatory structure should ensure the smooth realization of regulatory objectives and reduce the interference of structure to regulatory objectives. This condition shows that the marginal substitution rate between any two commodities is equal to the marginal product conversion rate of producers between these two commodities. Therefore, a possible boundary of political production can be deduced:

$$S = S(i(\Pi)) = S\left[\pi^{-1}(\Pi)\right]. \tag{9}$$

Since one of the purposes of blockchain is to reduce excessive human interference, it emphasizes automation. Through the setting of mathematical algorithms and the formulation of some rules, transactions should be automated. We should not only maximize the number of votes, but also make the marginal substitution rate of politics equal to the marginal substitution rate of mutual transfer between enterprise profits and consumer surpluses, so as to achieve a balance. Therefore, the interest rate of financial supervision is solved as follows:

$$\max_i M(S(i), (i)). \tag{10}$$

Less than 51% of the nodes in the system can intervene and verify the transaction; otherwise, a single node cannot play any role in data tampering, and at the same time, the nodes of the whole network will be alert to it, and it will be automatically rejected by the system. The financial supervision structure model is shown in Figure 3.

Finally, the financial supervision system must be based on market law and cannot substitute subjective administrative intent for the market mechanism. Its goal should be to support financial innovation, financial efficiency, and financial stability. Anyone may find the information they need thanks to binary value (hash value) query entries, which make the system's data information more transparent. The use of blockchain in bitcoin is to use the blockchain to validate blocks containing transaction data in order to achieve the goal of irreversible and undisputed transaction confirmation. Each regulatory authority's jurisdiction is determined by the kind of regulated financial institutions such as commercial banks, securities firms, and insurance firms. The regulatory structure optimization is based on cryptographic algorithm technology, which ensures the unique direction of account address and has some application potential in the areas of authentication and company identity certificate.

4. Blockchain and Consensus Algorithm Analysis

4.1. Analysis of Blockchain Core Technology. When the blockchain was first proposed, it was designed to solve the problem of safe transaction between the two parties in the unknown network environment without a third-party certification authority, that is, to create a payment mechanism through communication channels without a trusted party. Therefore, only by using blockchain to supervise financial institutions can the government overcome the negative impact of market failure, improve the governance level of financial institutions, improve the efficiency of financial operation, and maintain the stability of the financial system.

Firstly, distributed ledger refers to the accounting technology of data sharing, data replication, and data synchronization among nodes in computer network. Pow, namely, workload proof, is a consensus mechanism, which first appeared in bitcoin. An input value of any length can be calculated into a binary value of a specified length. For example, the SHA-256 algorithm applied in the blockchain system can calculate the fixed length output with the growth of 256 bits for transactions or other data of any length, and the output binary value is hash value (also known as hash value). Learn from the data processing mechanism of separate storage of cold and hot data and separate storage of

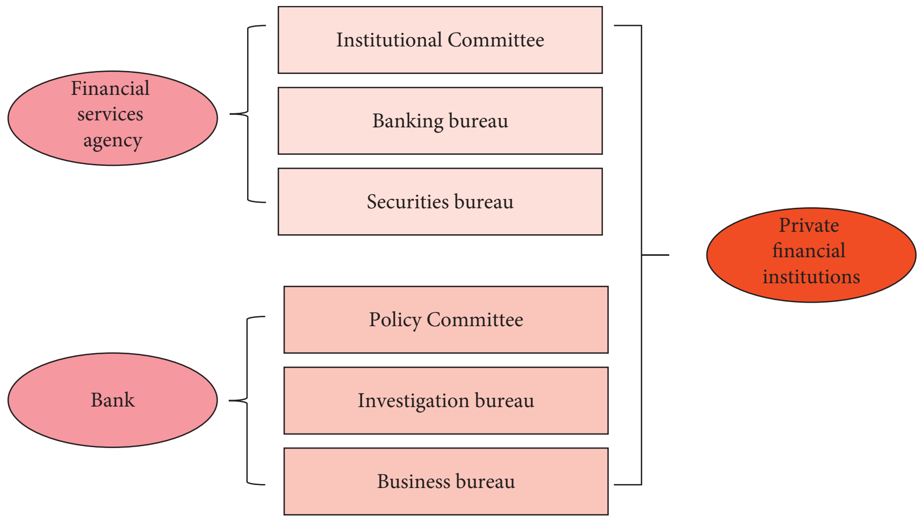

Figure 3: Financial supervision structure model.

cold and hot data in traditional financial data processing methods to realize the effective storage of a large number of node data. When a node reaches the target value, it will broadcast the block to other nodes, and all other nodes must confirm the correctness of the hash value with each other. The specific transaction information is stored in blocks, and the data structure of blocks is shown in Table 1.

Secondly, in the blockchain system, all transaction data is publicly visible, but the personal identity information of the nodes is encrypted, and only after the information owner authorizes the nodes to access the information, which is to protect the security of transaction data and the privacy of personal identity information. The data structure of the header is shown in Table 2.

Blockchain system is a point-to-point network composed of a large number of nodes. There is no centralized hardware or management organization. The whole system depends on the cooperation of all nodes in the network, and all nodes have the same business mode, rights, and obligations. POW collects all pending transactions on the network after creating the last block. Then, the transaction data received within a certain period of time forms a Merkle tree data structure through hash operation at each distributed node, encapsulates the nodes that have obtained the consensus mechanism, connects the current longest main chain, and creates the nearest main chain. The Merkle root of these transactions is then calculated and filled with block serial number, 256-bit hash of the previous block, current target hash, random number, and other information. In order to release data uniformly and avoid problems between the two armies, some specific data processing links can only be processed in serial mode, not in parallel.

Finally, the consensus mechanism is a method to prove the correctness and legitimacy of a block by reaching consensus among all the nodes participating in the consensus in the blockchain network environment. Since there is only one "Merkel root" at the end of processing a large amount of transaction data, it is not necessary to encapsulate all the underlying data in the block header, which greatly improves the operation efficiency and scalability of the blockchain. The consensus mechanism depends on the ability of the kernel, using CPU and memory resources to isolate the operating system's view of applications through a separate namespace.

4.2. Consensus Algorithm Analysis. POW competes for the computing power of each node and then competes for the power of generating blocks, which greatly consumes computer resources and power resources. The submodule will regularly poll the status of the sent transaction request until all the unconfirmed transactions in the local sequence are confirmed and removed from the sequence, and all the transaction requests sent by the client are completed. The network environment composed of consensus nodes is called consensus network. In the dDPoS algorithm, the consensus network changes with the change of consensus nodes. In addition, the consensus efficiency of pow is too slow. It takes 10 minutes to generate a block. Among them, the web module provides basic web-oriented integration features. The web servlet module package contains the spring MVC implementation of web applications. The number of consensus nodes elected by DPoS consensus algorithm is 100, which has the advantages of reducing the number of consensus nodes, improving consensus speed, and reducing energy consumption in the consensus process. This indicator represents the transaction response time of the blockchain and can directly reflect the performance of the consistency algorithm. The number of blocks generated by the three consensus algorithms pow, POS, and dDPoS in 0–100 minutes and under nodes with different sizes of 500–5500 is shown in a broken line diagram, as shown in Figures 4 and 5.

Firstly, select the consensus node module: functionalize all nodes in the blockchain system, and different types of nodes undertake different tasks, which are mainly divided into consensus nodes and transaction nodes. During the change of transaction request rate from 20 times per second to 200 times per second, the average

Table 1: Block data structure.

Field	Describe	Size (byte)
Block size	The size of all information after this field	1–10
Block head	The general name of all the information constituting the block header	92
Number of transactions	The number of transaction information stored in the block	1–20

Table 2: Data structure of block header.

Field	Resource consumption	Size (byte)
Pervious block hash	Enormous	20
Merkle tree root	Big	87
Timestamp	Small	20–30

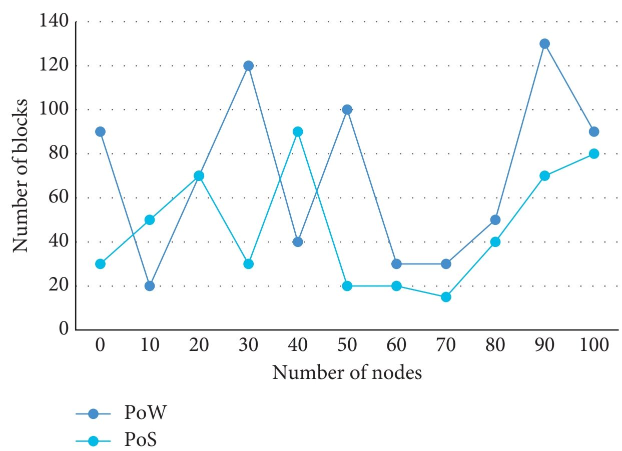

Figure 4: Comparison diagram of block broken lines generated by PoW and PoS within 100 minutes.

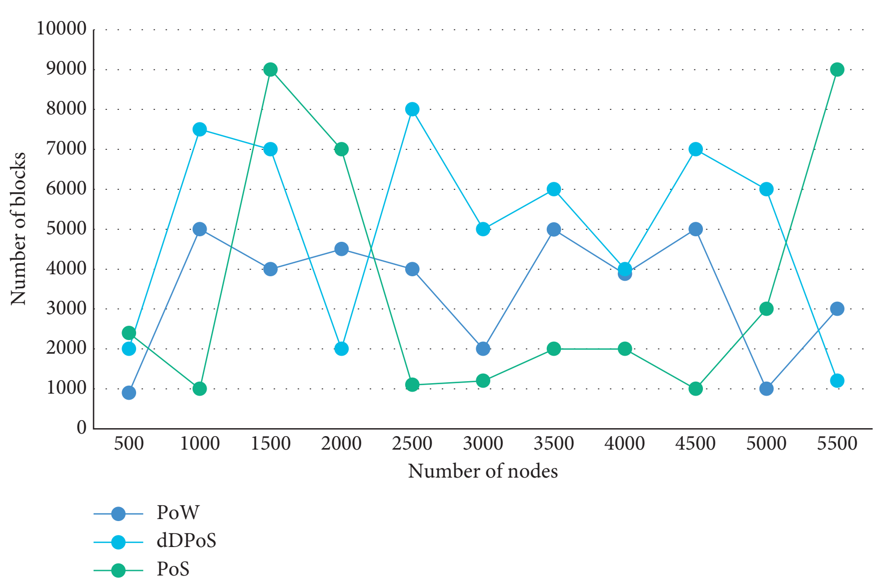

Figure 5: Comparison diagram of block broken lines generated by PoW, PoS, and dDPoS under 5000 nodes.

delay of PoW first increased and then decreased, while the delay of DPoS fluctuated around 5 seconds, during which the peak delay of PoW reached 50 times that of DPoS. The logarithmic graph of average delay of PoW and DPoS consensus algorithms at different transaction request rates is shown in Figure 6.

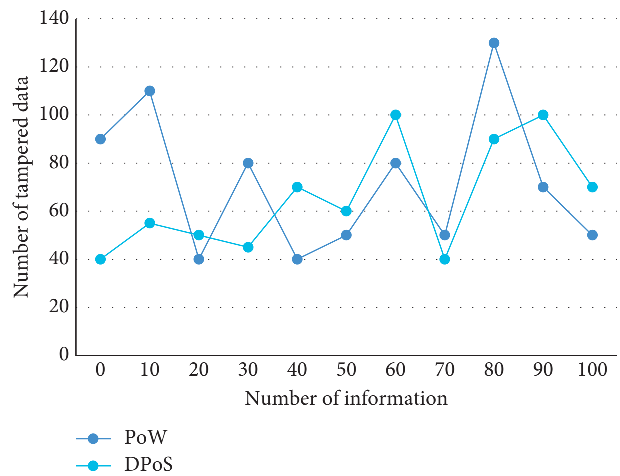

Figure 6: Comparison line chart of average delay of consensus algorithm under different transaction requests.

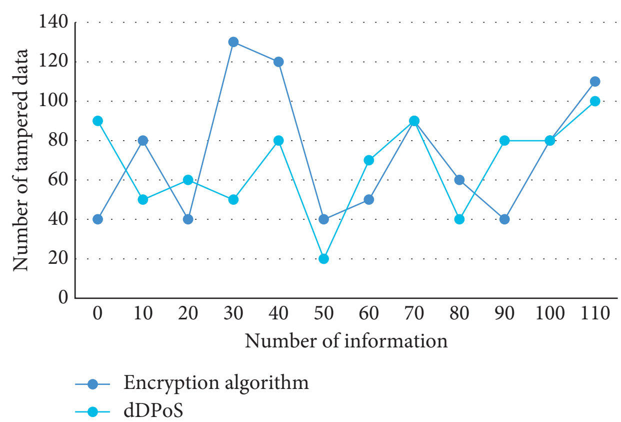

Figure 7: Comparison of antiattack performance between encryption algorithm and dDPoS algorithm.

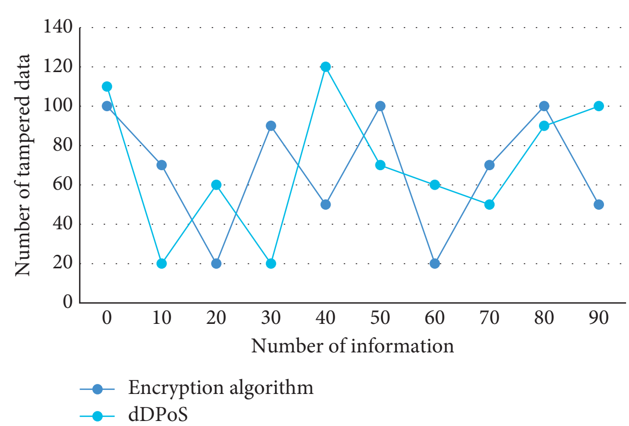

Figure 8: Comparison of protocol security in distributed network.

The blocking efficiency of the dDPoS consensus algorithm is about one block every 10 seconds, which is much higher than that of the pow consensus algorithm. Data entry permission can set multiple users in a unified account and provide users with different work permissions according to their different work needs, so as to meet the use scenarios under the control of multiple users. All data are extracted from the financial database of decentralized supply chain and mapped into a multidimensional space. This is because some interest groups may not make public support or opposition after cost-benefit comparison. On the one hand, the demand for financial supervision system depends on the comparison between the number of beneficiary groups n and the number of damaged groups $(N - n)$; on the other hand, it depends on the degree of support f expressed by beneficiary groups and the degree of opposition h expressed by damaged groups. The security and integrity of information and data in the decentralized supply chain financial network can be better protected. Figure 7 shows the antiattack performance comparison of encryption algorithm and dDPoS algorithm.

Secondly, remove the malicious node module: when the malicious node appears, dDPoS algorithm enters the malicious node removal mode and introduces the upgrade mechanism to complete the upgrade conversion between the malicious node and the candidate node. During data processing, ECDG, PCI, and R DTP protocols were tested, and the final test results are shown in Figure 8.

Filter much transaction information of blockchain finance through artificial intelligence, big data, and cloud computing technology, and write algorithms and models that can automatically calculate and analyze these data to capture, identify, and analyze abnormal behaviors of regulatory objects. One of the problems to be solved in the initial design of blockchain system is the problem of repeated payment in electronic transactions; that is, a sum of money cannot appear in two transactions. It is a method of filtering data features using split equation and a feature extraction method for calculating the score corresponding to size features. In particular, it should be noted that some damaged groups may evade regulation, which mainly depends on the comparison between the net income of publicly opposing the success of regulation and the net income of evading regulation.

5. Conclusions

The rapid advancement of financial technology may provide significant benefits to regulators. Blockchain technology, as opposed to the old centralized approach, uses cryptography, distributed consensus, and economic incentives to achieve the benefits of decentralization, nontampering, data traceability, and programmable smart contracts. We can create a blockchain-based evidence retention and collection system based on this characteristic of blockchain technology. Financial supervision not only necessitates a genuine increase in the enthusiasm for nongovernmental financial industry oversight, but also actively improves the independence of financial supervision organizations. The goal of effective supervision is to reduce the expense of supervision while increasing the contribution to social welfare.

This study proposes a strategy for integrating financial efficiency and oversight, as well as a method for structural optimization, based on blockchain. In addition, the blockchain's underlying technology and consistency algorithm are thoroughly examined. This paper effectively integrates relevant theories and knowledge of financial supervision and financial efficiency, with the goal of improving financial efficiency. It attempts to reveal the mechanism of financial supervision on financial efficiency and discusses the impact of financial supervision on improving financial efficiency. It can not only assist blockchain practitioners understand the characteristics of consistency algorithm and make acceptable decisions, but it can also improve the performance simulation efficiency of consistency algorithm and promote further research into consistency algorithm. It can help related businesses develop and process information more quickly, allowing for the effective and practical application of blockchain technology. It can also help solve problems with the original model, allowing the new model to be implemented and popularized more quickly, contributing to the development of a good trade settlement environment in China. This can help financial organizations fix their financial transaction data, prevent tampering and data loss, and preserve the integrity of their financial data.

Data Availability

The data used to support the findings of this study are available from the corresponding author upon request.

Conflicts of Interest

The author does not have any possible conflicts of interest.

References

[1] J. Li, Y. Chen, and H. Song, "Research on digital currency supervision model based on blockchain technology," *Journal of Physics: Conference Series*, vol. 1744, no. 3, Article ID 032112, 2021.

[2] Z. Zhao, S. K. C. F. Yao, W. Zhao et al., "Real-time functional connectivity-informed n of amygdala-frontal pathways reduces anxiety," *Psychotherapy and Psychosomatics*, vol. 88, no. 1, pp. 5–15, 2019.

[3] J. Xiang, "Research on the problems and governance of live E-commerce based on blockchain technology," *Business and Economic Research*, vol. 4, no. 2, p. 4, 2021.

[4] W. Zhao, "Blockchain technology:development and prospects," *National Science Review*, vol. 6, no. 2, pp. 193–197, 2019.

[5] Y. Ding, X. Zhao, Z. Zhang, W. Cai, N. Yang, and Y. Zhan, "Semi-supervised locality preserving dense graph neural network with ARMA filters and context-aware learning for hyperspectral image classification," *IEEE Transactions on Geoscience and Remote Sensing*, vol. 60, 2021.

[6] S. Meunier, "Blockchain 101: what is blockchain and how does this revolutionary technology work? - ScienceDirect," *Transforming Climate Finance and Green Investment with Blockchains*, vol. 2, pp. 23–34, 2018.

[7] Z. Cheng, S. Jiang, and Z. Zhou, "Substrate access tunnel engineering for improving the catalytic activity of a thermophilic nitrile hydratase toward pyridine and pyrazine nitriles," *Biochemical and Biophysical Research Communications*, vol. 575, no. 4, pp. 8–13, 2021.

[8] F. Yang, W. Zhou, Q. Wu, R. Long, N. N. Xiong, and M. Zhou, "Delegated proof of stake with downgrade: a secure and efficient blockchain consensus algorithm with downgrade mechanism," *IEEE Access*, vol. 7, pp. 118541–118555, 2019.

[9] U. Tariq, A. Ibrahim, T. Ahmad, Y. Bouteraa, and A Elmogy, "--things: a necessity framework for security, reliability, transparency, immutability and liability," *IET Communications*, vol. 13, no. 19, pp. 3187–3192, 2019.

[10] S. Li, N. Wang, X. Du, and X. Li, "Supervisable anonymous management of digital certificates for blockchain PKI," *Proceedings of the International Conference on computer frontier*, vol. 1257, no. 1, p. 15, 2020.

[11] R. Toledo, "Upgraded supervision facilitates financial technology," *Beijing weekly: English version*, vol. 61, no. 51, p. 1, 2018.

[12] L. Michaels and M. Homer, "Regulation and supervision in a digital and inclusive world," *Handbook of Blockchain, Digital Finance, and Inclusion*, vol. 1, pp. 329–346, 2018.

[13] K. Fanning and D. P. Centers, "Blockchain and its coming impact on financial services," *Journal of Corporate Accounting & Finance*, vol. 27, no. 5, pp. 53–57, 2016.

[14] J. Chen, Y. Zhang, L. Wu, T. You, and X. Ning, "An adaptive clustering-based algorithm for automatic path planning of heterogeneous UAVs," *IEEE Transactions on Intelligent Transportation Systems*, vol. 1, pp. 1–12, 2021.

[15] J. Zhou, T. Yang, W. Chu, and W. Zhang, "Underwater image restoration via backscatter pixel prior and color compensation," *Engineering Applications of Artificial Intelligence*, vol. 111, Article ID 104785, 2022.

[16] M. Zachariadis, G. Hileman, and S. V. Scott, "Governance and control in distributed ledgers: understanding the challenges facing blockchain technology in financial services," *Information and Organization*, vol. 29, no. 2, pp. 105–117, 2019.

[17] N. Kabra, P. Bhattacharya, S. Tanwar, and S. Tyagi, "MudraChain : blockchain-based framework for automated cheque clearance in financial institutions," *Future Generation Computer Systems*, vol. 102, pp. 574–587, 2020.

[18] A. Cretarola, G. Figà-Talamanca, and C. Grunspan, "Blockchain and cryptocurrencies: economic and financial research," *Decisions in Economics and Finance*, vol. 44, no. 2, pp. 781–787, 2021.

[19] B. Egelund-Muller, M. Elsman, F. Henglein, and O. Ross, "Automated execution of financial contracts on blockchains," *Business & Information Systems Engineering*, vol. 59, no. 6, pp. 457–467, 2017.

[20] T. Yu, Z. Lin, and Q. Tang, "Blockchain: the introduction and its application in financial accounting," *Journal of Corporate Accounting & Finance*, vol. 29, no. 4, pp. 37–47, 2018.

[21] J. Sun, J. Yan, and K. Zhang, "Blockchain-based sharing services: what blockchain technology can contribute to smart cities," *Financial Innovation*, vol. 2, no. 1, pp. 1–9, 2016.

[22] H. Zhu and Z. Z. Zhou, "Analysis and outlook of applications of blockchain technology to equity crowdfunding in China," *Financial Innovation*, vol. 2, no. 1, p. 29, 2016.

[23] J. Nathan and B. Jacobs, "Blockchain consortium networks: adding security and trust in financial services," *Journal of Corporate Accounting & Finance*, vol. 31, no. 2, 2020.

[24] L. W. Cong and Z. He, "Blockchain disruption and smart contracts," *Review of Financial Studies*, vol. 32, no. 5, pp. 1754–1797, 2019.

[25] C. Jonathan and T. V. Koeppl, "Blockchain-based settlement for asset trading[J]," *Review of Financial Studies*, vol. 32, no. 5, pp. 1716–1753, 2019.

[26] G. Xie, L. Huang, H. Bin et al., "Sustainable entrepreneurship in rural E-commerce: identifying entrepreneurs in practitioners by using deep neural networks approach," *Frontiers in Environmental Science*, vol. 370.

[27] I. D. . Motsi-Omoijiade, "Financial ic markets – regulation, gaps and bridges," *Handbook of Blockchain, Digital Finance, and Inclusion, Volume 1*, vol. 1, pp. 207–223, 2018.

[28] B. Hu, Z. Yin, and L. Zheng, "Development of China\"s financial supervision and regulation || research on the financial reform and innovation and corresponding regulation in China (shanghai) pilot free trade zone," vol. 16, p. 189, 2016.

[29] Y. Li, W. Li, C. Fu, Y. Song, and Q. Fu, "Lonicerae japonicae flos and Lonicerae flos: a systematic review of ethnopharmacology, phytochemistry and pharmacology," *Phytochemistry Reviews: Proceedings of the Phytochemical Society of Europe*, vol. 19, no. 10, pp. 1–61, 2019.

[30] "Blockchain Technologies and applications," *China Communications: English Version*, no. 6, pp. I0004–I0006, 2019.

Hindawi
Computational Intelligence and Neuroscience
Volume 2022, Article ID 4796075, 11 pages
https://doi.org/10.1155/2022/4796075

Research Article

Commercial Bank Credit Grading Model Using Genetic Optimization Neural Network and Cluster Analysis

Yunpu Bai and Dunlin Zha

School of Management, Nanjing University of Posts and Telecommunications, Nanjing 210003, China

Correspondence should be addressed to Yunpu Bai; baiyunpu@njupt.edu.cn

Received 4 April 2022; Revised 4 May 2022; Accepted 5 May 2022; Published 31 May 2022

Academic Editor: Xin Ning

Commercial banks are facing unprecedented credit risk challenges as the financial market becomes more volatile. Based on this, this study proposes and builds a credit risk assessment model for commercial banks based on GANN from the standpoint of commercial banks. In order to provide commercial banks with an effective and dependable credit risk assessment method, the indicators in this study are classified using cluster analysis, and then various representative indicators are chosen using a factor model, which takes into account the comprehensiveness of the information and reduces the complexity of the subsequent empirical analysis. On this basis, the network structure, learning parameters, and learning algorithm of commercial banks' credit risk assessment models are determined. Furthermore, advancements in data preprocessing and genetic operation have been made. According to simulation results, the highest accuracy rate of this method is 94.17 percent, which is higher than the BPNN algorithm 89.46 percent and the immune algorithm 90.14 percent. The optimization algorithm presented in this study improves the convergence speed and search efficiency of traditional algorithms, and the final experimental results show that the scheme is feasible and effective and can be used for commercial bank credit risk assessment.

1. Introduction

Commercial banks, as the financial institution with the most influence, the greatest number, and the broadest coverage in the financial market, play a variety of roles, including financing monetary capital, guiding capital flow, and regulating the balance of social supply and demand [1]. It holds a unique and crucial position in the entire financial system, as well as the national economy. At the moment, the rate of economic globalization is gradually accelerating, and financial market volatility is increasing by the day. Commercial banks face increasing financial risks as the "general hub" and "regulator" of a country's economic development [2]. Commercial banks' credit risk refers to the risk of economic losses caused by the customer's failure to perform the obligations in the agreed contract, that is, the possibility of the borrower defaulting due to the borrower's failure to repay the bank loan on time and in full for a variety of reasons [3]. Commercial banks' credit activities are divided into two categories: obtaining funds and using funds. If the risk of capital utilization is not effectively managed, the bank will face difficulties in obtaining funds, making it impossible for the bank to continue operations. Credit risk management is the most critical and difficult aspect of commercial banks' financial risk management. Effectively preventing and reducing credit risk has become the primary function of commercial bank operations and management. Simultaneously, in the context of interest rate marketization, commercial banks' pricing of loan interest rates is essentially the pricing of credit risk. As a result, credit risk is the most significant risk that commercial banks face. The ability to effectively control credit risk has become critical to commercial banks' profitability. Accurate and scientific credit risk evaluation is critical for providing a better basis for loan pricing. At present, most commercial banks, especially urban commercial banks with a short establishment time, mainly rely on manual work to complete credit risk assessment, which is unable to assess all enterprises with loan needs, and the assessment results are difficult to update in time. The development of ANN (artificial neural network) [4–6] and GAs (genetic algorithms) provides a new direction for credit risk analysis and evaluation of commercial banks.

ANN is a parallel distributed mode processing system developed by applying mathematical methods based on the research results of neuropsychology and cognitive science. It has high parallel computing ability, self-study ability, and fault tolerance. The basic constituent elements of ANN are neurons, which are connected together in the form of nodes through some mode, and nodes can communicate with each other. The output information will be transmitted to other nodes through the connection right, which can inhibit or excite the information being transmitted, just like a real neuron. ANN can carry out complex logic operations and deal with nonlinear problems and abstract, simplify, and simulate biological NN (neural network). ANN is not strict about the distribution of data, and it is not necessary to describe the functional relationship between independent variables and dependent variables in detail. These characteristics make it a hotspot of credit risk analysis methods. Although NN has been widely used, it also has its own shortcomings, which are mainly reflected in the uncertainty of the training process. The emergence of GA makes the training of NN have a new look. Using GA instead of NN algorithm to search the connection weight of NN can solve the problem of NN falling into the local minimum. Therefore, this study constructs a credit risk assessment model for commercial banks based on GANN (genetic algorithm neural network). The specific innovations are as follows:

(1) Aiming at the shortcomings of BPNN (back-propagation neural network), such as easy to fall into the local minimum and slow convergence speed, this study introduces GA to design a practical GA coding scheme. In addition, reasonable fitness function, crossover operator, and mutation operator are used in genetic operation to optimize BPNN.

(2) This study establishes a credit risk evaluation index system based on industry classification, with quantitative indicators as the main factor and qualitative indicators as the auxiliary factor. And the improved technology and method of credit index data pre-processing are given. On the basis of discussing the related theories of credit risk assessment of commercial banks, this study focuses on the in-depth study of credit risk assessment methods and makes empirical analysis by using the constructed model and evaluation index system to verify the rationality and feasibility of the evaluation system constructed in this study.

The study is organized as follows: Section 1 introduces the background and significance of the topic selection and puts forward the research innovation and structural arrangement of this study. Section 2 describes the related works and analyzes the research status of NN and commercial bank credit risk at home and abroad and gives the research content and work of this study. Section 3 summarizes the relevant theoretical basis, constructs the bank credit risk assessment model based on GANN, and introduces its software implementation method in detail. Section 4 makes an empirical analysis of the index system and the improved GANN model, verifies the scientificity and rationality of the evaluation system, and shows that the algorithm model constructed in this study has certain practical value. Section 5 summarizes the conclusions and limitations of the full-text research and puts forward the future research direction.

2. Related Works

With the advancement of global economic integration, financial security has become a global concern. How to achieve financial security and how to ensure commercial banks' credit risk management are also common issues discussed by countries all over the world. Many aspects of ANN make it a popular credit risk analysis method. In recent years, with the advancement of information technology, an artificial intelligence method [7–9] with machine learning [10] capability has been introduced into credit risk assessment. The main goal of this stage is to develop a quantitative credit risk assessment model.

Cole and others studied the credit risk assessment of commercial banks by using genetic programming method and tested the model empirically by using the actual data of commercial banks in China. The test results show that this model is superior to a traditional statistical model, NN model, and decision tree model in prediction accuracy, practical value, and robustness. Masoudik et al. analyzed the microscopic and easily quantified non-systematic risks in the financial risks of commercial banks. On the basis of identifying types and root causes, referring to international practices and international financial regulations, and combining with the reality of Chinese commercial banks, this study systematically designs the non-systematic risk monitoring and early warning index system and corresponding early warning signals of commercial banks [11]. Eckert et al. and others can make efficient and timely judgments by introducing domain knowledge and using specific artificial intelligence methods such as GA, NN, and decision tree and provide effective decision support for decision makers [12]. The research of Yu et al. and others showed that under the same data environment, the accuracy of credit risk assessment by NN is higher than other assessment methods [13]. Huang et al. compared the early warning model based on ANN with the early warning model based on probability and reduced the rate of occurrence errors by reconstructing the data set. The results show that the NN model is superior to the probabilistic model in discrimination accuracy [14]. Soui et al. and others discussed and compared the application of the expert system in the field of credit risk analysis from the perspective of knowledge acquisition [15]. Labriola used a fixed-length code to represent the risk identification criteria and solved the credit risk assessment problem by using GA [16]. Plosser and Santos and others thought that when using GA to solve practical problems, operators need to have a deep knowledge of algorithms and a comprehensive understanding and good judgment of the problem itself, and the limitations of genetic coding itself hinder the application of GA to a certain extent [17]. Zhang et al. and others used NN to predict the failure of a company, and the results showed that NN-like prediction had better prediction ability than discriminant analysis [18]. Zhang et al. and others suggested that GA should be used to screen the input indicators and combine them with ANN to work together. They used this method to analyze the data of bankrupt enterprises 3 years before the bankruptcy, and the results showed that the discrimination accuracy of ANN network model was much better than that of comparison model [19]. Wang et al. and others used a rough set and NN method to predict credit risk, and the rough set was used to screen financial variables, thus improving the explanatory ability of the NN method, and the prediction accuracy was correspondingly improved [20]. Based on the research of previous relevant literature and GANN, this study puts forward and constructs the credit risk evaluation model for commercial banks. Aiming at the shortcomings of BPNN, such as easy to fall into the local minimum and slow convergence speed, GA is introduced to design a practical GA coding scheme. A credit risk assessment index system classified by industry, dominated by quantitative indicators, and supplemented by qualitative indicators has been established. It also gives the improved technology and method of credit index data preprocessing. In genetic operation, more reasonable fitness function, crossover operator, and mutation operator are used to optimize BPNN. Experiments verify that the evaluation system constructed in this study has certain accuracy and feasibility.

3. Methodology

3.1. GANN. The three elements of ANN are (1) synapse or connection weight: the connection degree between different neurons is given by the connection weight, negative value indicates inhibition and positive value indicates excitation; (2) summation unit or adder: similar to linear combiner, it obtains the weighted sum of input information; and (3) activation function or transfer function: nonlinear mapping, which can distribute the output value within a certain range, such as [0, 1] or [−1, 1]. As a powerful tool to study complexity, the ANN method has shown its unique advantages in pattern recognition and classification, automatic control, financial distress prediction, etc. It can deal with a series of ratio type information input, and then find its law from a large number of complex data of unknown mode through continuous learning and produce corresponding output, so as to generate a mode that successfully reflects the corresponding relationship between input and output variables. According to the information flow and network topology, the ANN model can be divided into feedforward network and feedback network. Each layer of neurons in feedforward NN receives input information from the previous layer and transmits it to the next layer. There is only one direction and there is no feedback of information. It is the most common and easy to program network structure. A feedforward network includes two basic forms: single-layer feedforward network and multilayer feedforward NN [21]. A single-layer feedforward network consists of an input layer and an output layer. There is no hidden layer in the middle. It can only solve the classification problem of linear separability. A multilayer feedforward NN is composed of an input layer, several hidden layers, and an output layer. It can be used to solve nonlinear classification problems. A single-layer feedforward network is the simplest layered network, whereas a multilayer feedforward network is the most widely used network structure in NN. In the feedback NN, the output information of some neurons is fed back to the upper layer or the same layer, and the information flow is interleaved in the forward and reverse directions.

The role of ANN in credit risk analysis is carried out through the classification function of ANN [22]. That is to say, firstly, a group of factors that affect the classification is found, which are used as the input of ANN, and then an ANN credit risk analysis model is formed through training with or without tutors. For the new sample input, this model can produce the discrimination of credit risk. The NN model includes two processes: training and testing. Firstly, the neurons are trained with training set data, so that different input vectors can get corresponding output values. By repeatedly adjusting and modifying the parameters and thresholds until the error is within the specified range, the training process of NN is completed. The test process is to input a group of data of non-training indicators into the model generated in the training process to test the accuracy of model classification. The ANN method overcomes the complexity of traditional analysis process, especially the establishment of model function and brings great convenience to modeling and analysis. BPNN is a kind of multilayer feedforward NN. BPNN is considered to be the most suitable approximate relationship for analog input and output. It is one of the most widely used ANNs with mature algorithm. BPNN is a multilayer feedforward NN according to the backward propagation of errors, and its learning process consists of forward propagation of signals and backward propagation of errors. Although BPNN has been widely used, it also has its own shortcomings, which are mainly manifested in the uncertainty of the training process.

GA is a relatively new and effective optimization technology. GA is the most well-known evolutionary algorithm at the moment, and it is widely used in machine learning, engineering technology, data mining, computer science, pattern recognition, image processing, social science, and other fields. GA is a global random search algorithm that solves complex problems by simulating the genetic and long-term evolution processes of biology. GA is a group optimization algorithm with the ability to perform global searches due to its multipoint search, allowing the search results to avoid converging to the local optimal solution. As a result, the global optimal solution is obtained, and the accuracy of network evaluation is improved. Some criteria can be used to determine the termination condition of GA, and the algorithm's running process can be terminated when it is determined that the population has matured and there is no evolutionary trend. There are two commonly used criteria:

(1) reaching the preset number of iterations and (2) the difference of average fitness of successive N generations of individuals is less than a certain minimum threshold. The evolutionary nature of GA makes it possible to search for excellent structure in parallel, thus reducing the possibility of falling into local optimum, and this method is also sensitive to the change of credit index. The emergence of GA makes the training of NN have a brand-new look. Using GA instead of BP algorithm to search the connection weight of NN is expected to solve the problem that BPNN falls into the local minimum.

3.2. Credit Risk of Commercial Banks. Credit risk can be defined in two ways: broadly and narrowly. Generalized credit risk refers to the uncertainty or volatility of the future impact of various uncertain factors on commercial banks, such that actual income deviates from expected income, suffers losses, or gains additional income. Narrow credit risk perception means that in the credit business, if the debtor or borrower fails to perform the contract and repay the loan principal and interest, the creditor or bank will incur financial losses because it will not receive the expected benefits. Commercial banks are credit-based industries with high debt and risk, with the profit point of settlement business and money management lending. Commercial banks' operating characteristics, as well as their important position and key role in maintaining national economic stability, have resulted in the characteristics of concealment and diffusion of bank operating risks. Credit risk arises from the asymmetry of information between the two parties to the transaction. This phenomenon occurs before the two parties sign the contract, which is referred to as asymmetric information beforehand, and it is easy to produce adverse selection. Customer credit risk has a direct impact on the quality of bank credit assets, and it can even lead to bank bankruptcy.

Credit risk management process is the concrete implementation of credit risk management policy, the refinement and embodiment of credit risk management, and the main content of credit risk management. Credit management reflects the core competitiveness of commercial banks, and directly or indirectly affects the quality of bank assets, asset growth, income level, and financing strategy. The main goal of credit management is to evaluate the credit risk so as to effectively supervise and control the risk. In the transaction activities in the financial market, for commercial banks, there are intricate credit and interest relationships with borrowers, and the interrelated borrower enterprises form a credit chain. Once an enterprise in the credit chain defaults and fails to repay its accounts payable on schedule, it will cause a series of enterprises in the credit chain to default. Credit risk and credit risk for commercial banks, their subjects are the same, and all of them are due to the change of the debtor's credit status, which leads to the emergence of the value risk of bank credit assets. The difference lies in the range of financial assets they cover. The general framework of the commercial bank credit risk assessment model is shown in Figure 1.

Commercial banks develop relevant policies in order to create an efficient risk management organizational structure and to identify, analyze, evaluate, and respond to credit risks. Credit risk is an unavoidable risk in the day-to-day operations of commercial banks because banks themselves are in high-risk industries, and the asset market is volatile. The goal of improving credit risk management is to reduce the likelihood of such losses occurring. Credit risk assessment refers to the qualitative analysis and quantitative calculation of credit risk influencing factors using appropriate technical means, as well as the assessment and calculation of the borrower's default probability, in order to provide a decision-making basis for commercial banks' credit activities. The overall framework of the credit risk management system primarily consists of the organizational structure, management process, internal control, and credit risk management information reporting and disclosure. After nearly a century of evolution, the basic methods of commercial bank credit risk evaluation have progressed from simple to complex, including proportional analysis, statistical analysis, and artificial intelligence analysis. The methods used in the proportional analysis and statistical analysis stages, for example, can also be referred to as traditional credit risk assessment methods. Despite the fact that the traditional credit risk assessment method has significant limitations, it serves as a valuable reference for modern credit risk assessment.

3.3. Construction of Bank Credit Risk Evaluation Model Based on GANN. In this section, GA is used to optimize BPNN, which is easy to fall into the local minimum and slow in convergence. Before modeling, the data should be standardized to eliminate the influence of different dimensions and improve the accuracy of the model. The basic idea of the optimization algorithm in this study is: firstly, GA is used to globally optimize the weights and thresholds of NN, and then BPNN is used to accurately solve the problem, so as to realize complementary advantages and better solve the problem. Because the system is always developing and changing, the selected learning samples should not only reflect the characteristics of the system when it develops steadily, but also reflect the characteristics of the system when it suddenly changes, and at the same time, take into account all stages of the system development. According to the differences of financial indicators of different enterprises, this study divides the samples into different sets according to the comparability and similarity of financial characteristics of enterprises, and each such set is called a model. The division of patterns is related to the financial characteristics of enterprises and is limited by the number of valid samples under this pattern. If the number of pattern samples meets the requirements of building an evaluation model, the pattern is called an effective pattern; otherwise, it is called an invalid pattern. When establishing the index system, this study selects 18 financial and nonfinancial secondary indicators reflecting the status of loan enterprises. According to whether these indicators have significant differences

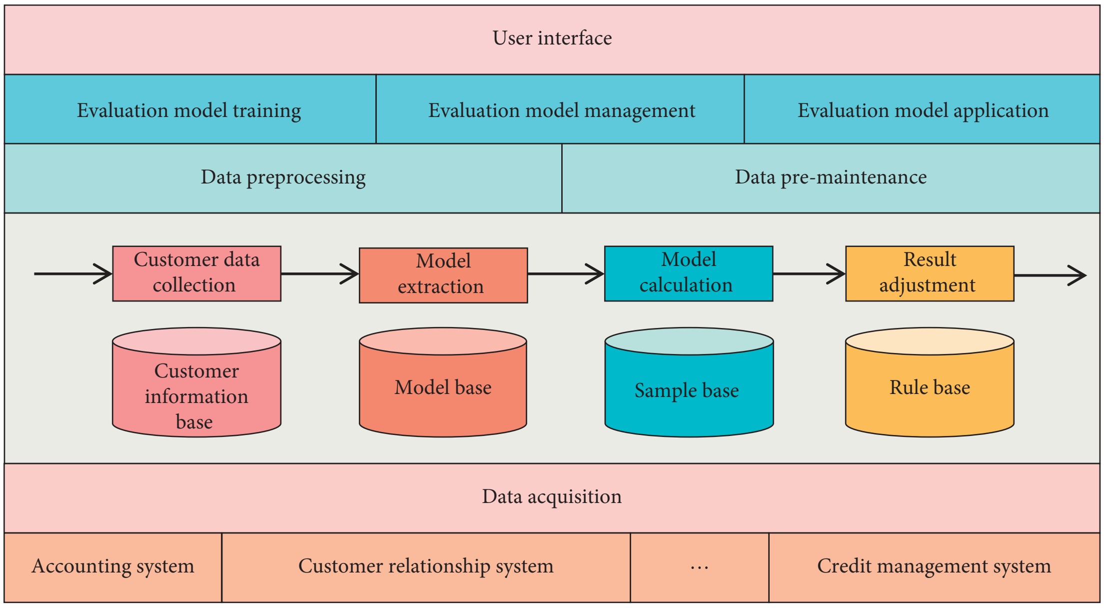

FIGURE 1: Overall structure of the credit risk assessment model for commercial banks.

between normal loans and loss loans, it is determined whether the indicators can be used as input index vectors. This study constructs the index system and follows the following basic principles: scientificity, comprehensiveness, pertinence, and applicability. Considering the availability of data, it constructs a credit risk evaluation index system suitable for commercial banks. The flow of genetic algorithm optimization is shown in Figure 2.

The article chooses three-layer BPNN structure. The input layer contains 19 input units, the hidden layer has 10 nodes, and the output layer contains 4 output units. Since the input initial values and initial weights have a great relationship with whether the learning can reach the local minimum and converge, it is necessary to preprocess the input initial values, that is, normalize them. For the continuous data in qualitative indicators, the feature discretization technology can be used for reduction. The advantage of this technology is that it simplifies the data description, not only greatly reduces the complexity of data mining calculation, but also makes the relationship between data and the final data mining results easier to understand. Data discretization is the process of merging attribute values. By scientifically merging attribute values, the number of attribute values is reduced, thus reducing the complexity of the problem. It is beneficial to improve the classification performance of rule sets obtained in the process of knowledge learning. Generally, when determining the number of neurons in the hidden layer, it is usually necessary to satisfy the following two formulas:

$$\begin{aligned} m &= \sqrt{x+y} + R(10), \\ 2^m &> y, \end{aligned} \tag{1}$$

where m is the number of neurons in the hidden layer, x is the number of neurons in the output layer, and y is the number of neurons in the input layer. $R(10)$ represents any integer between 1 and 10. Assuming that the set $X = \{U_2, U_3, U_4, U_5\}$ and the conditional attribute set $C = \{A_1, A_2\}$, the roughness calculation process of the set X is as follows:

$$\begin{aligned} R^{-}(X) &= \{x \in U | R(x) \subseteq X\} = \{U_2, U_3, U_4, U_5, U_7\}, \\ R_{-}(X) &= \{x \in U | R(x) \cap X \neq 0\} = \{U_2, U_4, U_5\} \neq \varnothing. \end{aligned} \tag{2}$$

Therefore:

$$\rho(X) = 1 - \frac{|POS_C(X)|}{|R^{-}(X)|} = 0.6. \tag{3}$$

If $X = \{U_2, U_3\}$, it is not definable because:

$$\begin{aligned} R^{-}(X) &= \{x \in U | R(x) \subseteq X\} = \{U_2, U_3, U_5, U_7\}, \\ R_{-}(X) &= \{x \in U | R(x) \cap X \neq \varnothing\} \neq \varnothing. \end{aligned} \tag{4}$$

Because there are redundant attributes and noise data in training data, it will affect the efficiency and convergence speed of GA. Therefore, attribute reduction of raw data is needed to improve the algorithm efficiency. This study uses the attribute reduction algorithm based on attribute importance. This method can accurately reduce redundant attributes and maintain the original correlation between data, which provides a strong guarantee for the performance and accuracy of GA. The output layer of this study adopts a neuron, and the output value is close to indicate that the enterprise is classified as a high-risk category, and the closer the output value is, it indicates that the enterprise belongs to a low-risk category. Suppose that in the qth iteration, the output error p of the $e_p(q)$th node at the output end:

$$\begin{aligned} e_p(q) &= t_p(q) - y_p(q), \\ p &= 1, 2, \ldots, k, \end{aligned} \tag{5}$$

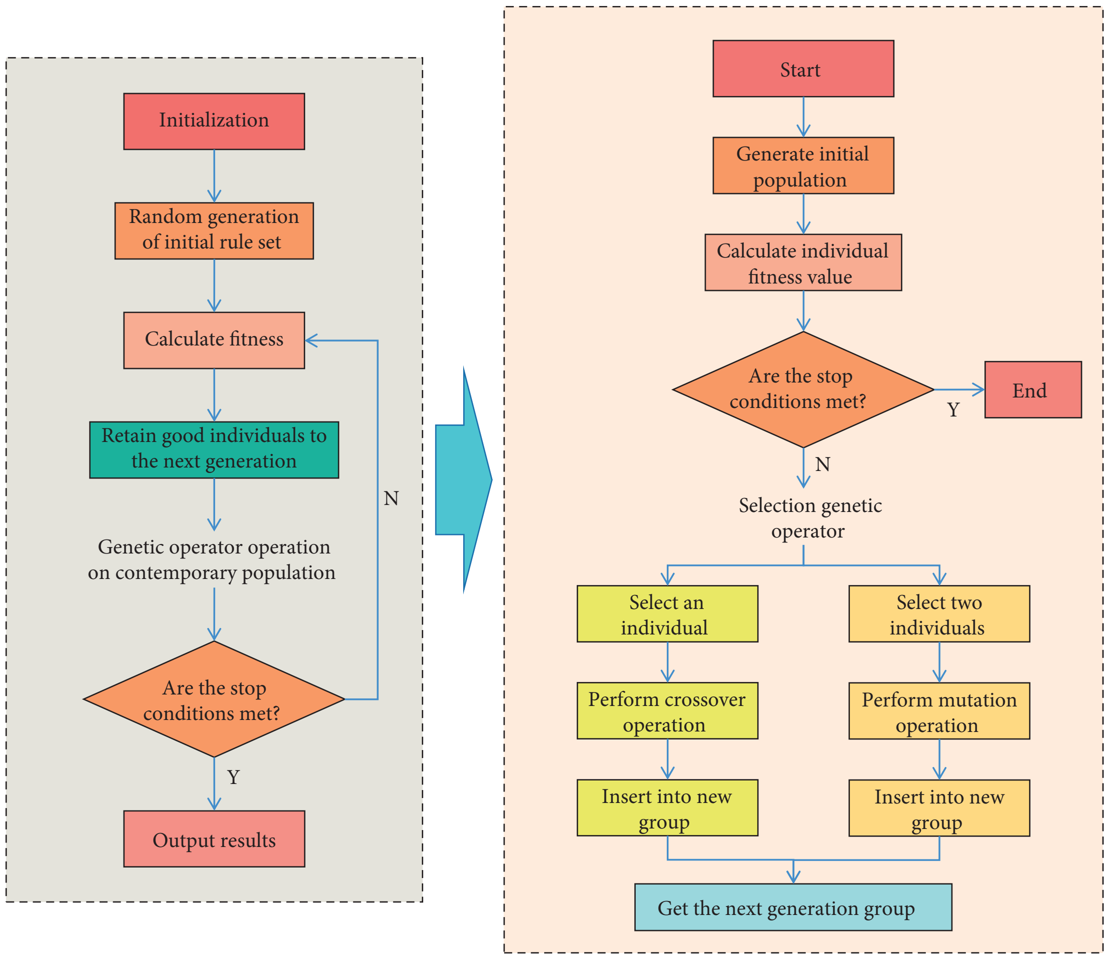

Figure 2: Genetic algorithm optimization process.

where $t_p(q)$ is the target output value, $y_p(q)$ is the actual output value, and the mean square error signal is:

$$\begin{aligned}\xi_p(q) &= \frac{1}{M}\sum_{s=1}^{M}\left(\frac{1}{k}\sum_{l=1}^{k} e_p(q)^2\right)\\ &= \frac{1}{M}\sum_{s=1}^{M}\left(\frac{1}{k}\sum_{l=1}^{k}\left(t_p(q)-y_p(q)\right)^2\right).\end{aligned} \tag{6}$$

The above formula can be expressed as a vector:

$$\xi_p(q) = \frac{1}{M}\sum_{s=1}^{M}\left(\frac{1}{k}\sum_{l=1}^{k}(T(q)-Y(q))^2\right). \tag{7}$$

The gradient of $\xi(q)$ with respect to $v(q)$ is:

$$\begin{aligned}\nabla(\xi(q)) &= \frac{\partial\xi(q)}{\partial v(q)}\\ &= \frac{\partial\xi(q)}{\partial Y(q)}\cdot\frac{\partial Y(q)}{\partial v(q)}\\ &= -E(q)g(U(q))\left[g\left(W(q)^T\right)X + B_1(q)^T\right]^T.\end{aligned} \tag{8}$$

The initial parameters are set as follows: initial threshold θ, initial weight W, and momentum term α. The values of Z_j and y_k are calculated according to the following formulas:

$$\begin{aligned}z_j &= f\left(\sum_{i=1}^{n} w_{jk}x_i - \theta_j\right),\\ y_k &= f\left(\sum_{j=1}^{l} w_{jk}z_j - \theta_k\right),\end{aligned} \tag{9}$$

where n is the number of samples, θ_i is the threshold between the hidden layer and the input layer, θ_k is the threshold between the output layer and the hidden layer, and l is the number of neurons in the hidden layer. The error between the layers is found according to the following formula:

$$\begin{aligned}\delta_{jk}^{\phi} &= \left(t_l^{\phi}-y_l^{\phi}\right)y_l^{\phi}\left(1-y_l^{\phi}\right),\\ \delta_{ij}^{\phi} &= z_j^{\phi}\left(1-z_j^{\phi}\right)\sum_{k=0}^{m}\delta_{jk}^{\phi}w_{jk},\end{aligned} \tag{10}$$

where m is the number of neurons in the output layer.

When using GANN model for credit risk assessment and analysis, we should first set the corresponding parameters of NN to ensure the effective operation of the assessment model. Then the credit risk evaluation index value and target value of the evaluation sample are inputted, and the network to make the output value close to the target value is trained. In this study, in the process of optimizing BPNN by GA, the main functions and parameters of GA are: determining 800 generations of genetic algebra. Using real coding method, the fitness function is selected according to the error. The larger the error, the smaller the fitness. The selection is based on the fitness scale method. Single point crossing, the crossing rate is 1. Uniform variation, the variation rate is 0.08. The fitness function will directly affect the efficiency of solving problems with GA. A good evaluation function should better reflect the background knowledge of solving the problem, which is more conducive to guiding GA to search for a better solution space. In this study, every training data are matched with every rule of the solution. If any rule matches the training data, it is considered as a correct classification of the solution. The fitness of each individual can be defined as the square of the ratio of the number of times it correctly classifies training data to all training data. Learning rate is the magnitude of weight adjustment after each step of training. The greater the learning rate, the greater the magnitude of weight adjustment and the faster the error curve converges. The gradient descent method used in NN operation may cause the error plane to fall into the local minimum, and the additional momentum model constructed in this study can effectively solve this problem.

4. Result Analysis and Discussion

In the simulation experiment, the number of nodes in the input layer is determined by the number of sample indexes. Different number of hidden layer nodes will form different NN models, which need constant and repeated debugging to obtain appropriate network parameters, thus forming an effective credit risk assessment network model. In this study, the company that has been specially treated is called ST company, and the company that has not been specially treated is called non-ST company. It means that the company's credit risk is relatively poor, which means that the company has fallen into debt repayment or has a high possibility of credit risk. Non-ST company means that the company operates normally and the possibility of default is very small. It is used to represent the sample with good credit. ST is used to represent the default sample, and the output value in the model is represented by 1. The output value of non-ST company in the model is represented by 0. The number of output layer nodes is 1. With 0.5 as the critical point, when the output value is less than 0.5 and close to 0, it belongs to ST enterprise. When the output value is greater than 0.5 and close to 1, it is a non-ST enterprise.

This study selects 350 listed companies as test samples, including 56 ST companies and 294 non-ST companies. After the data of 350 companies in the test sample are standardized, the value of credit risk evaluation index can be used as the input mode. The 350 companies selected in this study cover the electronics industry, chemical industry, paper industry, wine industry, chemical fiber industry, science and technology industry, pharmaceutical industry, automobile manufacturing, and other industries, which are quite representative. The specific settings are shown in Table 1.

Table 1: Performance comparison of different algorithms.

Industry	ST company	Non-ST company
Electronic industry	39	8
Chemical industry	51	4
Paper industry	28	7
Brewing industry	17	10
Chemical fiber industry	45	6
Technology industry	42	4
Pharmaceutical industry	26	5
Automobile manufacturing industry	34	9
Other industries	12	3
Total	294	56

This study uses MATLAB tools to build GANN, and then uses VisualC++, which can develop applications with good interactive functions, compatibility, and expansibility, to write user interface programs. In the standardized test sample input, the network model is used to simulate the operation, without setting the target expectation value, and the output value of the model is compared with the sum to check the accuracy of the simulation. The function of gradient descent backpropagation algorithm with adaptive adjustment of learning rate and momentum factor is a combined optimization algorithm of gradient descent method and adaptive adjustment of learning rate method. In this study, the training function chooses traingdx algorithm. Figure 3 shows the training of different models.

It can be seen from the Figure 3 that the traditional NN algorithm evaluation model took 912 steps to achieve the accuracy requirement, the BPNN algorithm evaluation model took 742 steps to achieve the accuracy goal, and the improved BP algorithm evaluation model only took 523 steps to achieve the accuracy goal.

In order to further illustrate the accuracy and reliability of the model constructed above, we also need to verify it with test samples. The training errors of traditional NN algorithm, BPNN algorithm, and GANN algorithm on data set A are shown in Figure 4. The mean absolute error of traditional NN algorithm, BPNN algorithm, and GANN algorithm on data set B is shown in Figure 5.

It can be seen from Figures 4 and 5 that the MAE values of GANN algorithm on different data sets are all at a low level. Compared with the contrast algorithm, the error is smaller, which shows that this algorithm has certain accuracy. In this study, the initial weight, learned weight, training data set, test data set, application data set, and other data are established into files to facilitate program call. The performance comparison of immune algorithm, traditional NN algorithm, BPNN algorithm, and GANN is shown in Table 2.

From the data in the table, it can be seen that BPNN with GA optimized weights has greater advantages in time and accuracy than other three different models. It can be

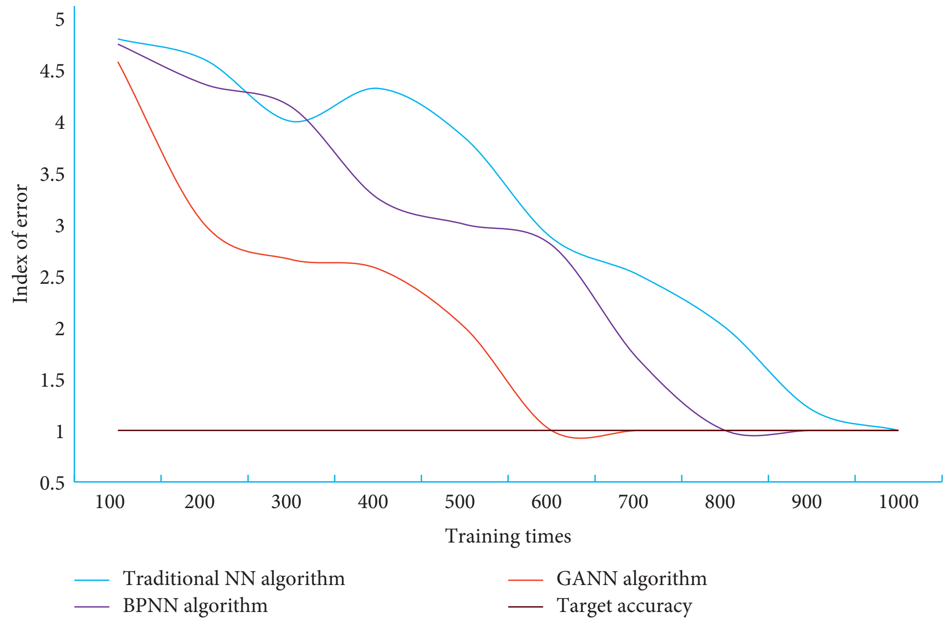

Figure 3: Training of different models.

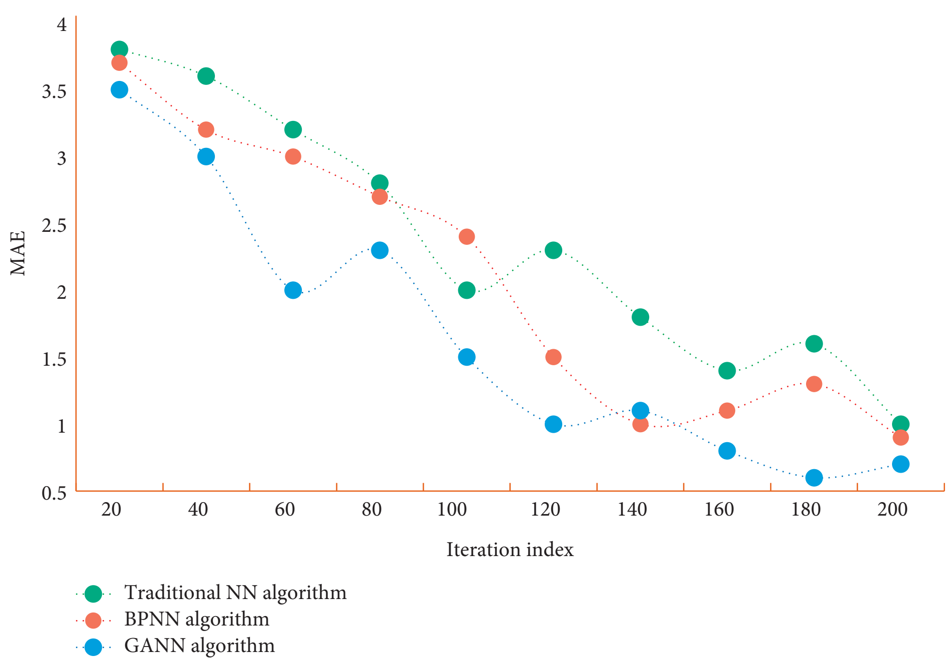

Figure 4: MAE of different algorithms on data set A.

seen that GANN has strong advantages in evaluating the credit risk of commercial banks. In order to ensure the reliability and credibility of the obtained results, this study draws the accuracy performance of different algorithms on different data sets into data graphs, as shown in Figures 6 and 7.

It can be seen that the accuracy of this method is always at a high level, whether on data set A or B. The highest accuracy rate of this method is 94.17%, which is higher than that of BPNN algorithm 89.46% and immune algorithm 90.14%. The accuracy of GANN in this study is better than the other two algorithms, and this result shows the accuracy

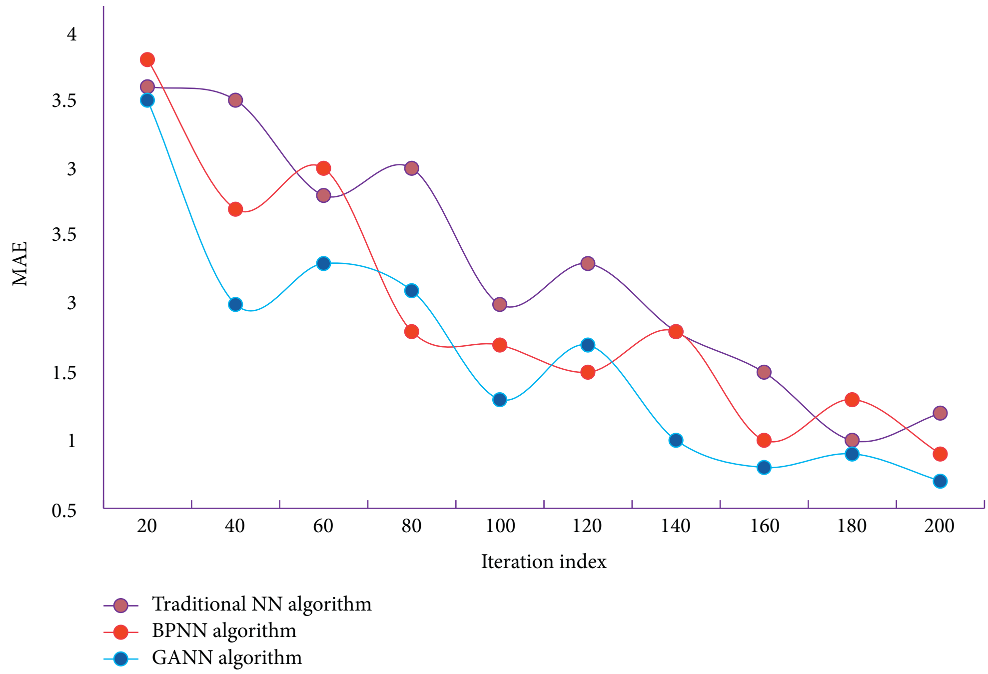

Figure 5: MAE of different algorithms on data set B.

Table 2: Performance comparison of different algorithms.

Algorithm	Accuracy (%)	Training time
Immune algorithm	90.14	7.412
Traditional NN algorithm	86.73	8.293
BPNN algorithm	89.46	7.014
GANN algorithm	94.17	6.154

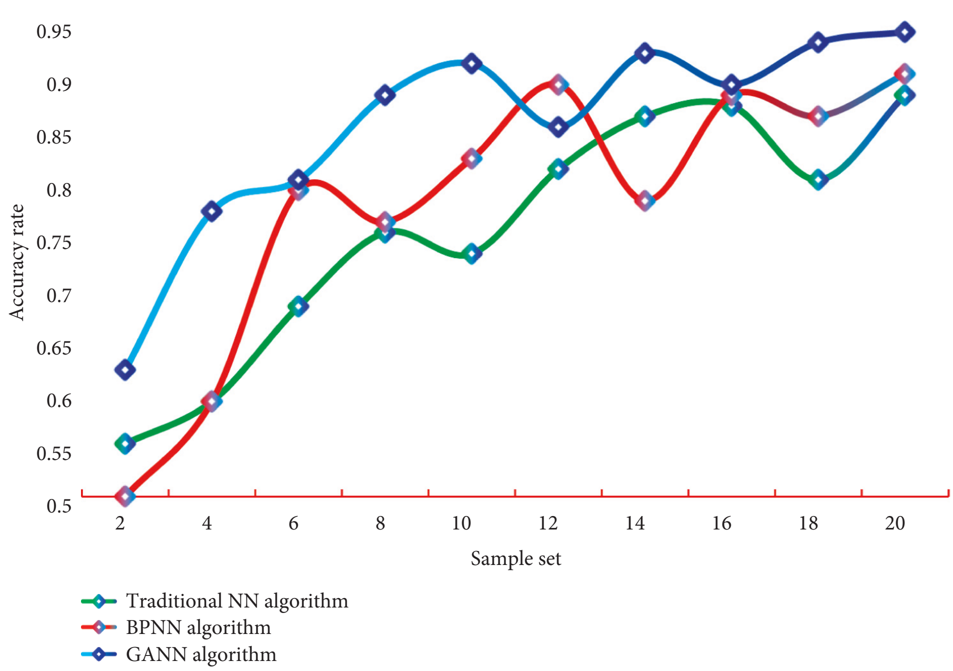

Figure 6: Accuracy performance of different algorithms on data set A.

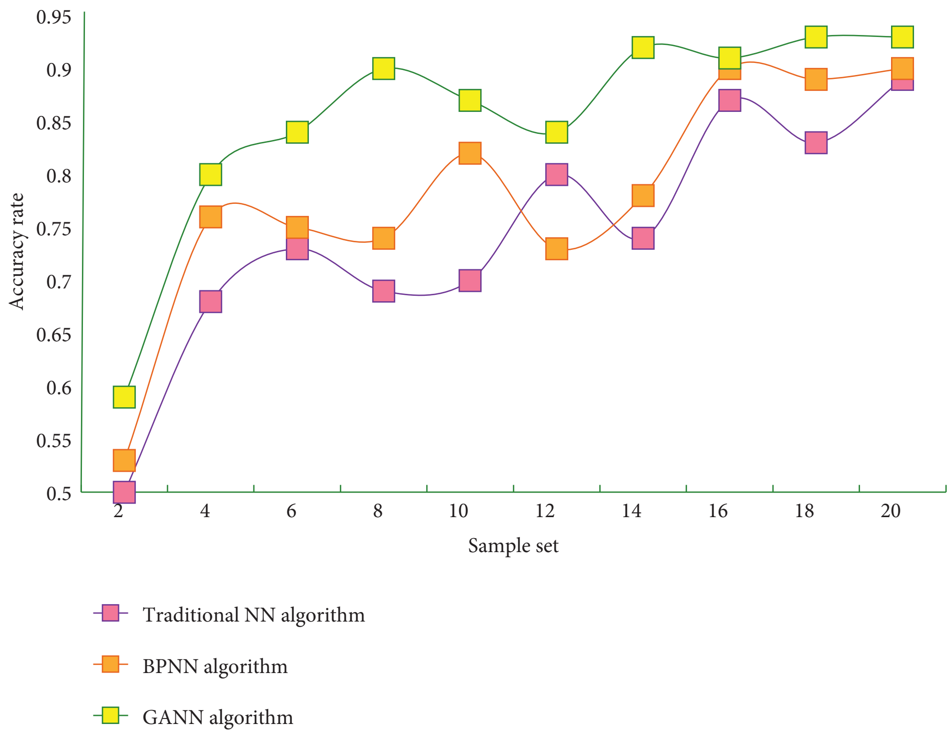

FIGURE 7: Accuracy performance of different algorithms on data set B.

and reliability of the optimization algorithm in this study. It can be seen that the model constructed in this study has certain practicability and practical significance.

5. Conclusions

Commercial banks play an important role in the implementation of financial policies and social investments. Credit risk identification, evaluation, monitoring, reporting, and control are the main components of commercial banks' credit management. The assessment of credit risk is the cornerstone of all of them. This study builds a credit risk assessment model for commercial banks using GANN based on credit risk research. In this model, GA is used to create a practical GA coding scheme that addresses the shortcomings of BPNN, such as its tendency to fall into the local minima and slow convergence speed. In addition, a credit risk evaluation index system is established, which is classified by industry and is primarily based on quantitative indicators, with qualitative indicators supplemented. In addition, improved credit index data preprocessing technology and methods are presented. According to simulation results, this method has a higher accuracy rate of 94.17 percent than the BPNN algorithm (89.46 percent) and the immune algorithm (90.14 percent). Traditional algorithms' convergence speed and search efficiency are improved by the optimization algorithm presented in this study. It has some practical value and significance, and it provides a method for commercial banks to assess credit risk that is both effective and reliable. However, due to time and level constraints, some parts of this study continue to have flaws: the improvement in the fitness function and the correlation analysis of credit risk assessment indicators are insufficient. The following step in this study will optimize the improvement in the fitness function and investigate the correlation of credit risk assessment indicators in depth.

Data Availability

The data used to support the findings of this study are available from the corresponding author upon request.

Conflicts of Interest

The authors do not have any possible conflicts of interest.

Acknowledgments

This study was supported by the National Social Science Foundation of China (Grant no. 20CGL061), MOE (Ministry of Education in China) Project of Humanities and Social Sciences (Grant no. 19YJC790002), and the National Statistical Research General Project of China (Grant no. 2018LY21).

References

[1] M. Minnis and A. Sutherland, "Financial statements as monitoring mechanisms: evidence from small commercial loans[J]," *SSRN Electronic Journal*, vol. 55, no. 1, pp. 197–233, 2016.

[2] C.-C. Huang and G. Gombola, "The effect of leverage and liquidity on earnings and capital management: evidence from US commercial banks[J]," *International Review of Economics & Finance*, vol. 43, no. 5, pp. 35–58, 2016.

[3] R. Florez-Lopez and J. M. Ramon-Jeronimo, “Enhancing accuracy and interpretability of ensemble strategies in credit risk assessment. A correlated-adjusted decision forest proposal[J],” *Expert Systems with Applications*, vol. 42, no. 13, pp. 5737–5753, 2015.
[4] Y. Ding, X. Zhao, and Z. Zhang, “Semi-supervised locality preserving dense graph neural network with ARMA filters and context-aware learning for hyperspectral image classification[J],” *IEEE Transactions on Geoscience and Remote Sensing*, vol. 2021, 2021.
[5] X. B. Jin, W. Z. Zheng, J. L. Kong et al., “Deep-learning temporal predictor via bidirectional self-attentive encoder–decoder framework for IOT-based environmental sensing in intelligent greenhouse[J],” *Agriculture*, vol. 11, no. 8, p. 802, 2021.
[6] D. Yao, Z. Zhi-li, and Z. Xiao-feng, “Deep Hybrid: Multi-Graph Neural Network Collaboration for Hyperspectral Image classification,” *Defence Technology*, 2022.
[7] J. Chen, C. Du, Y. Zhang, P. Han, and W. Wei, “A clustering-based coverage path planning method for autonomous heterogeneous UAVs,” *IEEE Transactions on Intelligent Transportation Systems*, vol. 2021, pp. 1–11, 2021.
[8] Z. Huang, Y. Liu, and C. Zhan, “A novel group recommendation model with two-stage deep learning[J],” *IEEE Transactions on Systems, Man, and Cybernetics: Systems*, vol. 2021, 2021.
[9] J. Zhang, W. Feng, T. Yuan, J. Wang, and A. K. Sangaiah, “SCSTCF: Spatial-Channel Selection and Temporal Regularized Correlation Filters for Visual Tracking,” *Applied Soft Computing*, vol. 118, Article ID 108485, 2022.
[10] L. You, H. Jiang, J. Hu et al., “GPU-accelerated Faster Mean Shift with Euclidean Distance Metrics,” 2021, https://arxiv.org/abs/2112.13891.
[11] K. Masmoudi, L. Abid, and A. Masmoudi, “Credit risk modeling using Bayesian Network with a latent variable[J],” *Expert Systems with Applications*, vol. 127, no. 8, pp. 157–166, 2019.
[12] J. Eckert, N. Gatzert, and M. Martin, “Valuation and risk assessment of participating life insurance in the presence of credit risk,” *Journal of Insurance: Mathematics and Economics*, vol. 71, pp. 382–393, 2016.
[13] S. A. Yu, A. Yw, and Y. A. Xin, “Multi-view ensemble learning based on distance-to-model and adaptive clustering for imbalanced credit risk assessment in P2P lending[J],” *Information Sciences*, vol. 525, pp. 182–204, 2020.
[14] X. Huang, X. Liu, and Y. Ren, “Enterprise credit risk evaluation based on neural network algorithm[J],” *Cognitive Systems Research*, vol. 52, no. 12, pp. 317–324, 2018.
[15] M. Soui, I. Gasmi, S. Smiti, and K. Ghédira, “Rule-based credit risk assessment model using multi-objective evolutionary algorithms[J],” *Expert Systems with Applications*, vol. 126, no. 7, pp. 144–157, 2019.
[16] J. LaBriola, “Risky business: institutional logics and risk taking at large U.S. Commercial banks[J],” *Social Science Quarterly*, vol. 100, no. 1, pp. 389–404, 2019.
[17] M. C. Plosser and J. A. C. Santos, “Banks’ incentives and inconsistent risk models[J],” *Review of Financial Studies*, vol. 31, no. 6, pp. 2080–2112, 2018.
[18] Y. Zhang, X. Chen, X. Liu, and N. Zhu, “Exploring trust transfer between internet enterprises and their affiliated internet-only banks: an adoption study of internet-only banks in China[J],” *Chinese Management Studies*, vol. 12, no. 1, pp. 56–78, 2018.
[19] Q. Zhang, J. Wang, A. Lu, S. Wang, and J. Ma, “An improved SMO algorithm for financial credit risk assessment - evidence from China’s banking[J],” *Neurocomputing*, vol. 272, no. 1, pp. 314–325, 2018.
[20] Z. Wang, Q. Zhao, M. Zhu, and T. Pang, “Jump aggregation, volatility prediction, and nonlinear estimation of banks’ sustainability risk[J],” *Sustainability*, vol. 12, no. 21, p. 8849, 2020.
[21] Y. Guo, W. Zhou, C. Luo, C. Liu, and H. Xiong, “Instance-based credit risk assessment for investment decisions in P2P lending[J],” *European Journal of Operational Research*, vol. 249, no. 2, pp. 417–426, 2016.
[22] A. T. Shiri, S. Chirume, and Z. Fields, “Determinants of commercial bank profitability from prior-to post-hyperinflation: evidence from Zimbabwe[J],” *Journal of Economics*, vol. 6, no. 2, pp. 129–139, 2015.

Hindawi
Computational Intelligence and Neuroscience
Volume 2023, Article ID 9783816, 1 page
https://doi.org/10.1155/2023/9783816

Retraction

Retracted: Design of Teaching Quality Analysis and Management System for PE Courses Based on Data-Mining Algorithm

Computational Intelligence and Neuroscience

Received 26 September 2023; Accepted 26 September 2023; Published 27 September 2023

This article has been retracted by Hindawi following an investigation undertaken by the publisher [1]. This investigation has uncovered evidence of one or more of the following indicators of systematic manipulation of the publication process:

(1) Discrepancies in scope
(2) Discrepancies in the description of the research reported
(3) Discrepancies between the availability of data and the research described
(4) Inappropriate citations
(5) Incoherent, meaningless and/or irrelevant content included in the article
(6) Peer-review manipulation

The presence of these indicators undermines our confidence in the integrity of the article's content and we cannot, therefore, vouch for its reliability. Please note that this notice is intended solely to alert readers that the content of this article is unreliable. We have not investigated whether authors were aware of or involved in the systematic manipulation of the publication process.

Wiley and Hindawi regrets that the usual quality checks did not identify these issues before publication and have since put additional measures in place to safeguard research integrity.

We wish to credit our own Research Integrity and Research Publishing teams and anonymous and named external researchers and research integrity experts for contributing to this investigation.

The corresponding author, as the representative of all authors, has been given the opportunity to register their agreement or disagreement to this retraction. We have kept a record of any response received.

References

[1] S. Li and Y. Luo, "Design of Teaching Quality Analysis and Management System for PE Courses Based on Data-Mining Algorithm," *Computational Intelligence and Neuroscience*, vol. 2022, Article ID 6830375, 9 pages, 2022.

Hindawi
Computational Intelligence and Neuroscience
Volume 2022, Article ID 6830375, 9 pages
https://doi.org/10.1155/2022/6830375

Research Article

Design of Teaching Quality Analysis and Management System for PE Courses Based on Data-Mining Algorithm

Sen Li and Yanrui Luo

School of Physical Education and Health, Shanghai Lixin University of Accounting and Finance, Shanghai 201620, China

Correspondence should be addressed to Yanrui Luo; luoyr@lixin.edu.cn

Received 16 April 2022; Revised 7 May 2022; Accepted 9 May 2022; Published 31 May 2022

Academic Editor: Xin Ning

Advances in network technology have led to extensive information technology construction work in all walks of life; universities, as a key component of national development, cannot be overlooked in this regard. In today's universities, the Web-based integrated academic management information system is widely used, promoting higher education management system innovation and improving the management level of education departments and teaching management. The traditional management mode is incapable of locating "knowledge" in the mountains of student transcripts, and the original management mode must be improved. In business, finance, insurance, marketing, and other fields, digital exploration technology is widely used. This article describes the design approach for a data mining-based analysis and management system for PE course teaching quality, as well as the application of information technology and data mining technology in PE by combining actual PE teaching in schools, with the goal of realizing a data mining-based PE performance management system to serve PE teaching in schools and improve PE teaching quality. The results show that the time required to find frequent itemsets using a traditional algorithm running on a single machine, as well as the time required to scan the database several times for frequent itemset search in a distributed cluster of 20 computing nodes, is significantly longer than that required by the data mining algorithm. As a result, the proposed sports performance management system is functional, simple, and scalable, with each functional module operating independently and cooperatively, reflecting the concept of "high cohesion and low coupling."

1. Introduction

Along with the expansion of college operations, the number of students is increasing year by year, and the teaching of physical education, which is an important part of school education, has sparked a wave of pedagogical reform [1]. Classroom teaching is the primary means of achieving educational goals in schools, and its effectiveness has a direct impact on the learning quality of students [2]. Colleges use improving higher education quality and cultivating special talents as the purpose of school operation in order to respond to the national call and achieve the state's higher education development goals [3]. The original grade data analysis method, on the other hand, is unable to thoroughly analyse and capture information useful for teaching and learning from large amounts of grade data, resulting in inefficient use of teaching information resources. This has resulted in grade management based primarily on simple statistical analysis, such as processing student identity. Data mining [4, 5] is a vital information processing technique [6, 7] that has been widely adopted in a variety of industries around the world, generating significant economic and social value.

The service that universities provide to students as a "service-oriented enterprise" is "education." We can only "produce" a high-quality product—graduates—and establish a brand name in the education market by continuously and effectively improving education quality [8]. Knowledge and rules in the knowledge base are created by experts or programmers using external input in traditional decision support systems [9]. Data mining is an automatic process of acquiring knowledge from within a system with the goal of discovering undiscovered knowledge in a large amount of data [10]. Online query and analysis can be used to process information that is clearly understood by decision-makers [11]. It is beneficial to motivate teachers, improve teaching quality, and strengthen faculty construction and scientific management by establishing a good teaching quality evaluation mechanism [12].

Many schools now conduct physical activity and achievement tests for their students [13]. The majority of these post-test scores, however, are only saved as data or files in school computers, and these students are unaware of their physical condition despite having completed the relevant physical fitness tests [14]. Analysing and processing these massive amounts of data using traditional data analysis and data query validation methods are not only computationally intensive but also completely reliant on pre-assumed and estimated data relationships. In data, there is a growing demand for tacit knowledge [15]. The use of parallel computing and data-mining arithmetic can help to solve this problem to a large extent, because parallel computing can provide the computational power required to process large amounts of data, and clusters can scale up the computational power as the data grows. In response to the problems and current state of PE in universities, relevant information is compiled, and modern data mining techniques are fully employed to automate the processing and analysis of large amounts of sports data in order to assist students. Professors and consultants analyse statistical data. In this paper, technology for digital exploration is introduced into the performance analysis of the university teaching system, with the goal of identifying factors affecting students' performance and specifically improving teaching quality. The innovative points of this paper are as follows:

(1) Using data mining techniques to uncover possible hidden relevant factors that affect teachers' teaching level, provide specific indications for improving teaching level, and apply them to teaching practice.

(2) Research and analysis of existing student data information using association rule extraction technology, and statistical analysis of some factors affecting teaching quality in schools using scientific methods, so as to evaluate teaching quality and student learning quality.

(3) The purpose of the analysis and management system of PE curriculum with quality according to data mining algorithm is to enhance the productivity and accuracy of PE teachers in schools, free them from tedious and boring work, and then improve their management-level teaching quality.

The first part of this paper introduces the background and significance of the study, and then introduces the main work of this paper. The second part introduces the work related to the teaching quality analysis and management system of PE courses, data-mining arithmetic. In the third part, the system functional module design and the logical system design of the physical education database are explained so that the readers of this thesis can have a more comprehensive understanding of the design idea of the physical education curriculum teaching quality analysis and administration system based on the data mining algorithm. The fourth part is the core of the thesis, which describes the usage of data mining algorithm in the quality control system of physical education from two aspects: data point set compression and discard analysis and large-scale data set clustering process analysis. The last part of the thesis is the summary of the full work.

2. Related Work

2.1. Quality Analysis and Management System of PE Course Teaching. To enhance the cultural qualification of all the people, China's higher education has made rapid progress, with major breakthroughs in system reform, successive expansion of various colleges and universities, and leapfrog development in the scale of college operation. However, it is impossible to implement the national education policy, let alone to implement quality education, if the physical health training of young people is neglected. Therefore, classroom teaching quality monitoring has great significance as an essential component of the university's education quality supervision mechanism, and the study and improvement of the teacher classroom teaching quality evaluation system is one of the hot spots and priorities of the current higher education evaluation of quality management.

From the perspective of effectiveness, Cao defined teaching quality evaluation as the evaluation process, which is essentially the process of determining the extent to which curricula and learning programmes actually achieve educational goals [16]. Cui and Yoon proposed a decision tree data extraction method that combines this algorithm with the SLIQ algorithm and applies it to a database of student grades to analyse various data and build a decision tree model through analysis [17]. Parmezan et al. proposed a teacher teaching quality assessment questionnaire that includes nine dimensions such as teaching quality, value of learning, enthusiasm for teaching, teaching organization and clarity, group interaction, interpersonal harmony, breadth of knowledge, examinations and test scores, homework, and other reading materials [18]. Zhang et al. conducted an in-depth study on mining techniques and proposed the ID3 algorithm to manage the university faculty-related data was extracted and analysed to discover correlations between various course environments with a view to providing data university decision reference [19]. Yin discussed the application of distortion-resistant algorithms in mining association rules. This algorithmic technique significantly reduces the number of database scans by a factor of even less than two. The algorithm with the shortest scanning time is the use of sampling to collect relevant data [20].

Teaching quality analysis is an important tool for evaluating teaching and learning. Data-mining arithmetic is used to analyse data generated from examination processes and teaching sessions at multiple levels and perspectives. Utilizing the analysis results to assist teaching decisions is an inevitable requirement for assuring teaching excellence and enhancing the quality as well as the overall competence of students and teachers.

2.2. Data-Mining Arithmetic. Given the current rapid development of higher education, self-monitoring of school teaching quality has become an important guarantee for scientific administration, and the development and implementation of teaching quality evaluation systems has become an important tool for implementing teaching control. Currently, digital exploration technology is widely used in telecommunications, commerce, banking, and enterprise production and marketing, but it has a limited use in education. As a result, this research focuses on the performance analysis characteristics of PE courses and integrates them with practical work to propose a data mining-based algorithm for identifying the keys that have the greatest impact on students and enhancing their learning experience. Dan and Li classify the original data set for large-scale data sets, analyse the OS virtual memory implementation mechanism, and improve the original FP-GROWTH algorithm in terms of spatial and temporal locality to make it a mining algorithm with perceptual input and output [21]. Gong and Lin proposed a multivariate strategy, which combines previous mining and discovery techniques and applies them to the qualification database to help universities make better decisions. To assist teachers in making teaching decisions, the results of each subject are computed, as well as a performance analysis report and related analysis table [22]. The hardware and software infrastructures for distributed association rule mining algorithms were investigated by Atta-ur-Rahman and DaSh. They looked at distributed data mining algorithms, parallel mining algorithms, and distributed parallel databases [23]. Li et al. discussed the Apriori association rule algorithm and the well-known decision tree ID3 algorithm, as well as their application scope [24]. Huang used a similar algorithm, Random-kmeans [25], to sample the original data set statistically and pool the smaller data set after sampling. The relationships and trends that are hidden in large amounts of data are beyond the ability of even the experts who manage these data to discover, and this information is potentially and critically important for decision-making, which is what data mining aims to solve.

3. Design Ideas of Teaching Quality Analysis and Management System of PE Courses Based on Data-Mining Arithmetic

3.1. System Functional Module Design. An important task of the generic system design phase is to determine how the system will accomplish the intended functionality using a more abstract and generic approach [26]. Thus, the overall design phase has three main subphases, starting with the test type management module, followed by the test project management module, and finally the result management module. Data mining is the complete process of extracting previously unknown, valid, and useful information from a database through data mining tools and using this information for decision-making or knowledge enrichment. The system functional module diagram is shown in Figure 1.

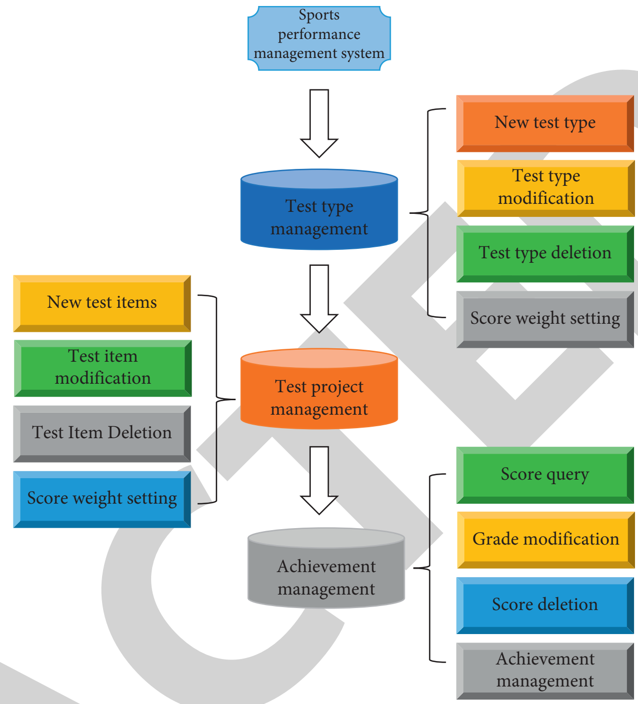

Figure 1: System function module.

First, the test type management module completes data preprocessing [27] and management of sports event types, including adding, modifying, deleting, and configuring the weights of event types. Data preprocessing is mainly done by cleaning, integrating, selecting, transforming, and conceptually layering data attributes to form tuples from the data training set. The information entropy of sample classification is as follows:

$$I(x_1, x_2, \ldots, x_n) = -\sum_{i=1}^{n} p_i \log_2 p_i. \tag{1}$$

The construction of the teaching quality evaluation system includes two aspects: the determination of indicators and the determination of weights. Indicators are specific, measurable operational and behavioural goals of a particular aspect; that is, they do not reflect the complete goal, but only one aspect of the goal. Simultaneous comparative analysis of factor data of different dimensions requires their standardization. The value of i factor j in all samples is as follows:

$$Z_{i,j} = \frac{X_{i,j} - \mu_j}{\sigma_j}, \tag{2}$$

where μ_j is the mean value of the i th factor and σ_j is the standard deviation of the j th factor.

The business problems to be mined are identified by a detailed understanding of the raw data to be extracted and the business problems to be applied in practice before starting data mining. In data mining, determining the purpose of mining is crucial. Mining produces unpredictable results, but the problem to be mined must be predictable, and mining blindness must be minimized. It is necessary to determine whether the test type contains test elements. It is impossible to remove something that already exists. Otherwise, the deletion procedure is carried out. Figure 2 depicts the programme flow for performing this function.

Secondly, the evidence project management module completes the operations of adding, modifying, deleting, and setting weights of sports evidence items. Due to the large amount of data, among these data, the required data suitable for this data mining are selected to establish a data mining library [28]. It generally includes data selection, selection of relevant data, noise, data purification and elimination, inference of missing data, conversion of discrete-valued data to continuous-valued data, grouping, and classification of data values. Each itemset needs to carry a decision attribute d, and when performing a join to produce a candidate $k+1$ itemset, two frequent k itemsets that can undergo the join operation must satisfy

$$(l_a, l_h) \in \{(l_1, l_2)|\text{diff}\,(l_1, l_2) = 1, d_1 = d_2\}. \tag{3}$$

As a result, the test management module enables the administration and maintenance of classroom quality assessment programmes, as well as the adjustment of the number of test questions or test content as needed. An independent internal hierarchy to describe the functions or characteristics of the system is created based on the requirements of the questions, and a judgement matrix of higher-level elements is created by comparing the relative importance of factors or objectives, criteria, and plans. To get a sequence of relative importance of relevant elements to higher level elements, a recursive hierarchy is built. Confidence thresholds must be set in order to extract rules from a set of frequent items and calculate the confidence level of the bar rule when extracting sports databases using the active search mining algorithm.

$$\text{Confidence} = \frac{\text{support}}{|\text{matched}|}. \tag{4}$$

Finally, the score management module completes the operations of adding, modifying, deleting, querying, exporting, and grading system conversion of students' sports test scores. The incomplete, noisy, and random data are sorted out, and the unwanted data are cleaned. Suppose S is the set of s data specimens, and the expected amount of information required to classify a given sample assuming that the class label attribute has a distinct value

$$I(s_1, s_2, \ldots s_m) = -\sum_{i=1}^{m} \log^{2}\frac{s_i}{s}. \tag{5}$$

Then, according to the data mining objectives and data characteristics, appropriate analysis models are selected for the data-mining arithmetic and the data are transformed. The module can classify courses. Different assessment items can be set for each course type. For courses that do not require assessment, you can also set up multiteacher classes to allow for more specific assessment of students. Relevant factors are broken down into levels based on their attributes

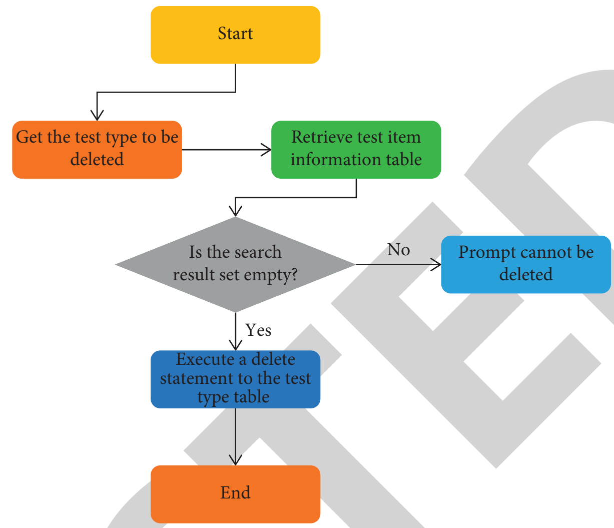

Figure 2: Process of test type deletion programme.

from top to bottom, with each factor at the same level being subordinate to, or having an influence on, the higher level factor, while dominating the lower level or being influenced by the lower level factor. Then, using a prototype system, developers brainstorm with users to iteratively modify and expand the prototype until the final system is formed.

3.2. PE Database Logic Design. The database logical design determines the overall performance of the database and its applications, tuning location [29]. If the database logic is poorly designed, all tuning methods will have limited effect on improving the database performance. The flow of data mining is shown in Figure 3.

First, the conceptual structure is transformed into the corresponding data model, such as relational model, network model, and hierarchical model. The data are cleaned, synthesized and filtered from data sources, and then entered into the database for data mining, pattern evaluation, and knowledge representation. According to the level of abstraction of datum in the proposed rule, association rules can be classified into single-level correlations and multiple-level correlations. KL scatter, also known as relative entropy, is used in the field of statistics to calculate the degree of agreement of two probability distributions, and in the area of machine knowledge to measure the closeness of two functions, and is calculated as follows:

$$KL(pq) = \sum p(x)\log\frac{p(x)}{q(x)}. \tag{6}$$

Single-level association rules do not consider the hierarchical nature of the actual data attributes, but simply describe the attributes of the data [30]. Metadata is the core of the data warehouse and is used to store data models, define data structures, transformation planning, data warehouse structure, and control information. The management part includes data security, archiving, backup, maintenance, and recovery. The index interval $[a, b]$ of the soft constraint is given based on empirical data and detects whether there exists

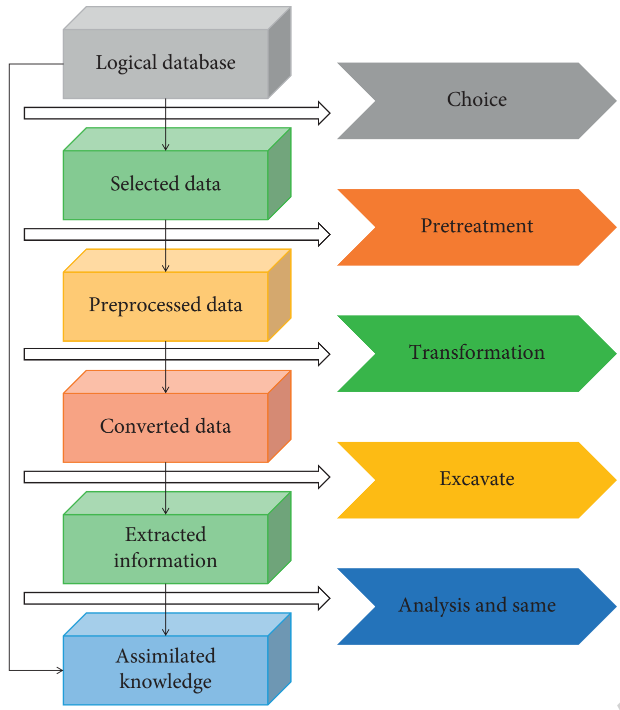

FIGURE 3: Process of data mining.

a solution within the initial solution set T that meets the requirements of the soft constraint. If it exists, it is marked as a feasible solution; otherwise, the parameter range of the constrained indicator interval is adjusted until a feasible solution exists; assuming that B is a diagonal matrix, the above formula can be transformed into the following form.

$$e(y,z) = \left[\sum_{j=1}^{p} b_{ij}\left|y_j - z_j\right|^s\right]^{(1/2)}, \tag{7}$$

where b_{ij} represents the i, j data attribute in the database.

In this step, data will be extracted and integrated from the operational environment, semantic ambiguities will be resolved, dirty data will be removed, etc. The process of summing data and calculating data averages are both statistical methods, and the results of these calculations are represented by certain graphs, such as histograms and pie charts. The absolute value function of the factor coefficients in the regression equation is added to the model as a penalty term to make some regression coefficients smaller. By regression, the coefficients of factors whose absolute values are not sufficient to explain the dependent variable can be changed directly to 0. The expression of the LASSO method can be written as follows:

$$\overline{\beta} = \arg\min\left\{\|Y - X\beta\|^2 + \lambda\sum_{j=1}^{p}\left|\beta_j\right|\right\}. \tag{8}$$

Next, these data models are converted into data models that can be supported by the corresponding database management system. First, all frequent itemsets in the data set are found, and the itemsets that satisfy the minimum support threshold are called frequent itemsets, and then, association rules are generated from these frequent itemsets, mainly by extracting frequent itemsets from all the generated high confidence levels. As a large amount of detailed and descriptive data is stored in the data warehouse, the data set is relatively large and requires a large number of join operations between relational tables to respond to the user's analysis request, increasing the response time user. But the data are stored only once, saving space compared to MOLAP, and analysis can get more detailed data; that is, the granularity of analysis can be relatively fine. So, the branching of attributes is carried out cyclically, and the information gain is the entropy compression expected after knowing the value of the attributes, which is given by the formula:

$$\text{Gain}(A) = I(s_1, s_2, \ldots s_m) - E(A). \tag{9}$$

The database is logically divided into several disconnected blocks, each of which is considered individually and for which all frequency sets are generated. The generated frequency sets are then combined to generate all possible frequency sets, and finally, the support of these element sets is calculated. It is possible to distinguish the similarity of tedious repetitive data in the database, and feature vectors can describe the relevant data with high similarity in the database. The variation parameters of the different features of the data attributes can be calculated using the following formula:

$$e(y,z) = \left[\sum_{j=1}^{p}\left|y_j - z_j\right|^s\right]^{(1/s)}. \tag{10}$$

Finally, the association rules are verified and the transformed model is optimized. If the extracted rules meet the evaluation mechanism's requirements, the knowledge is sent to the evaluation system and stored in the knowledge base. The knowledge is also stored in the knowledge base if the extracted rules do not meet the evaluation system's requirements. The indexing strategy, data storage location, and storage allocation operation are all determined. Data modelling is needed after determining the data warehouse information to be searched to determine the process of extracting, cleaning, and transforming data from data sources to data warehouse, analysing and dividing dimensions, and determining the physical data storage structure. The primary goal of grade data processing in the academic affairs system is to unify and disambiguate data types. Data decomposition reads data from segmented blocks into memory for processing and then merges all processing results, overcoming the memory bottleneck and improving data set extraction efficiency.

4. Analysis of Data-Mining Arithmetic in PE Teaching Quality Analysis and Management System

4.1. Data Point Set Compression and Discard Analysis. When the data-mining arithmetic performs in-memory clustering, the data point set is clustered in general and the resulting clusters are marked as the main clusters, and then, the data set in the main clusters is discarded and compressed for deletion. The main memory space reads the data to be clustered again and continues clustering until all clustering work is completed. By setting the maximum available size of the programme, it is shown that this data-mining arithmetic can extract association rules for large data sets in a small memory space. A comparison of the system CPU and GC activity is shown in Figure 4.

First, the discarding process is completed in two steps, which are called primary discarding and secondary discarding. The IP of the data node is obtained from the configuration file, so each node must be a static IP address. The specific configuration table of IP of this system is shown in Table 1.

The main idea of these two discard processes is to move the points that do not change the cluster attributes out of the main storage and store them in the discarded data set. The points in the marker set are not involved in this process and always guide the mining process. Information entropy, called entropy in information theory, is used to measure the average value of the transmitted information. Here, since the process of generating frequent itemsets from candidate itemsets must pass through the database, the most critical part of this process is how to generate the minimum number of candidate itemsets correctly. Therefore, for processing, users classify the data according to their needs and then extract the different parts, thus increasing the extraction speed. The statistical experiment time also does not include the time to write the discovered itemsets to disk in order to accurately count the running time of each algorithm. The support levels are set to 5 and 10, and each algorithm is executed 5 times at each support level, and the average of the statistical record execution time is shown in Figure 5.

Secondly, the main idea of the compression process is to replace high-density regions during the pooling process to clean up the main storage space. It divides the recommendation process into two parts: offline and online. The offline part constructs a cluster using the similarity between users and uses the average rating value of the users in the group as the centre of the group. The set of data points within this region has the same category affiliation and the categories change as a whole. The breast cancer data set was preprocessed, and files of different sizes were obtained by backup. Each file size is approximately 150 million and contains 2 million transaction records. Three D_1 to D_3 data sets were defined, and their specific configurations are described in Table 2.

While the traditional algorithm for finding frequent itemsets using a single machine running a distributed cluster of 20 compute nodes requires multiple scans of the database, the data-mining arithmetic can complete the task of finding frequent itemsets with little time consumption. It only needs to scan the transactional database twice, and does not generate a large number of temporary intermediate key-value pairs, and takes advantage of parallelization very efficiently.

Thus, it can be considered as a whole and can keep its grouping information and have sufficient statistical information. According to the rules defined by the data definition component, the data from the data source are extracted into the data warehouse, cleansing, and transformation; integration work is done; the data are loaded into the data warehouse; the data warehouse data are periodically cleansed; inconsistencies between data are eliminated data storage and source databases; and invalid data are eliminated. A basic principle is that when a transaction does not contain a large set of length k, it should not contain a large set of length $k + 1$. The information transferred at the source consists of a limited number of mutually exclusive joint

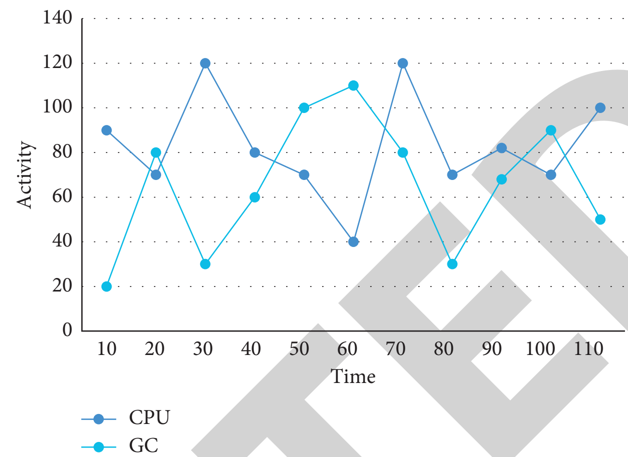

Figure 4: Comparison of CPU and GC activities.

Table 1: IP-specific configuration table.

Machine name	Masker	Slave 1	Slave 2	Slave 3
IP address	192.168.5.23	192.168.5.34	192.168.5.25	192.168.5.31
Attribute	Name node	Data node	Data node	Data node

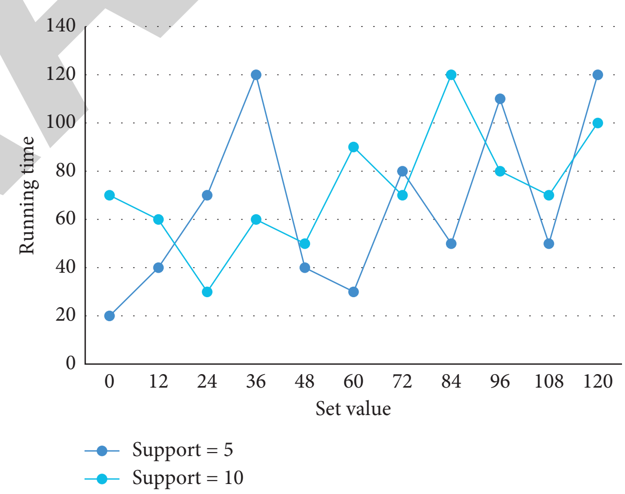

Figure 5: Running time of the system with different durations.

Table 2: Data set size based on mining association rules.

Data set	D_1	D_2	D_3
Average number of items	35	41	49
Number of data files	5	10	12
Transaction record number	6000	13000	13000

complete events, all of which occur with a certain probability. The effect of the size of the data set on the clustering algorithm is tested by varying the size of the data set and fixing the size of the storage space. The results are shown in Figure 6.

Finally, when semisupervised clustering is performed for the data points, labels, SS, and OUTS in the main memory, the data points contained in them are not involved in the compression and discard, thus allowing the set to guide the mining in the main memory all the time. If the description is a model of linking relationships between pages, the logical description can be in the form of a matrix. When mining with aggregate data not only does the mining time increase accordingly, the useful rules are drowned in a sea of rules that are not of interest to the user, but there may be rules that cannot be mined due to the "dilution" of the overall data. Each element of the matrix indicates whether the node represented by the matrix row label to the node represented by the matrix column label is related, which is the hyperlink between the pages in the domain. If the consistency index test passes, the consistency design of the judgement matrix is reasonable, and the corresponding weights reflected by the feature vector are also relatively reasonable.

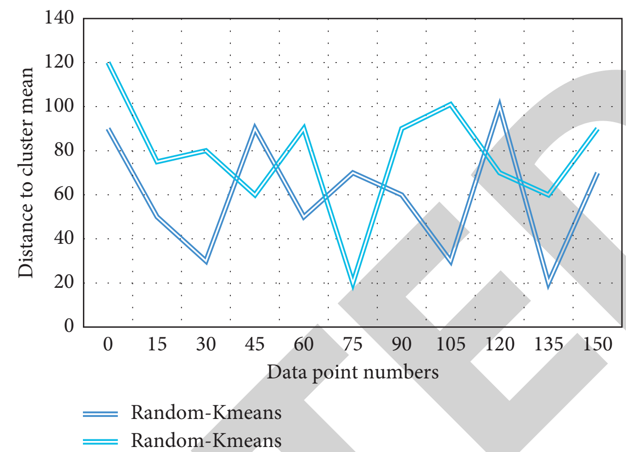

Figure 6: Quality scene of each cluster when the real data set is increasing.

4.2. Analysis of Clustering Process of Large-Scale Data Sets.

For a certain scale of transaction database, which contains a particularly large number of candidate itemsets, a transaction can also contain many candidate itemsets, so the number of candidate itemsets will be the main factor limiting the performance of the algorithm. Therefore, it is necessary to choose a large-scale data set clustering process to abstractly describe the various network linkage relationships in reality. At the same time, it is necessary to find a suitable data structure in a high-level language to store the mathematical model in a structured way in the computer, which is easy to analyse and process in the high-level language. To compare the performance of DISK-MINE, DRBFP-MINE, and data mining test algorithms on large-scale data sets, experiments were conducted using a combination of records generated from 2000 different items, and the comparison results are shown in Figure 7.

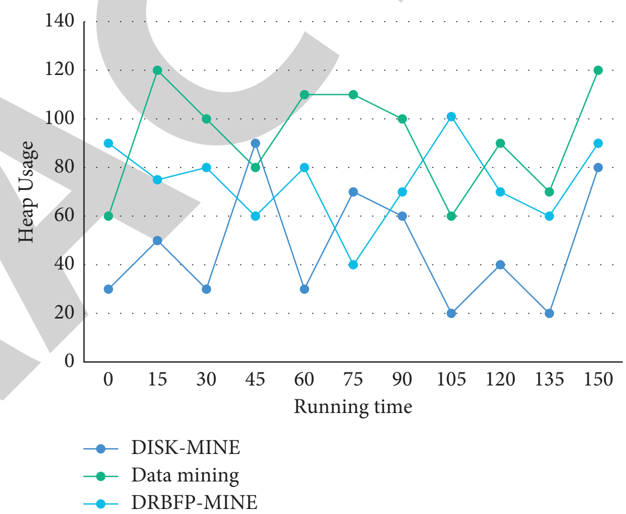

Figure 7: Performance comparison and analysis of large-scale data set algorithms.

First, data points from the data set are sequentially read (or otherwise read) into a finite memory called a pipeline until the pipeline's space is filled. The distance between data points is calculated, the data's neighbourhood is determined, the sample's centroid is determined based on the density of the neighbourhood, and the data's global centroid is determined for sampled data. Based on the sample centroids' data, the criterion for selecting the attribute is the information entropy. The information entropy value is calculated based on the data, and then, the sizes of each information entropy are compared, with the largest information entropy being chosen as the selection criterion. The element's information entropy is calculated, and it serves as the decision tree's root node. While all variants of the one-level correlation rule ignore the fact that practical data are multilevel, the multilevel character of the data has been adequately taken into account in the multilevel correlation rule.

The data points in the pipeline are then subjected to semisupervised clustering on finite primary storage until convergence. The entropy value of the system is minimized after using this property to divide the example set into subsets, and the average path from the nonleaf nodes to each descendant leaf node is expected to be the shortest, resulting in a small decision tree. The proposed data to be handled will be related to multiple dimensions using multidimensional correlation rules. In addition, the set of points removed from the main storage goes through a triad after each stage of the discard and compression process, preserving the data point information and grouping information. Density validation and sampling centroids can be done in order, but this takes a long time with large sample sizes and long sampling times, and the sample validation centroids are useless. As a result, it is necessary to consider various influencing factors and compensate each factor appropriately, integrate factors with similar influence, and consider the distribution width and representativeness of factors appropriately during the actual evaluation operation. The comparative analysis of clustering

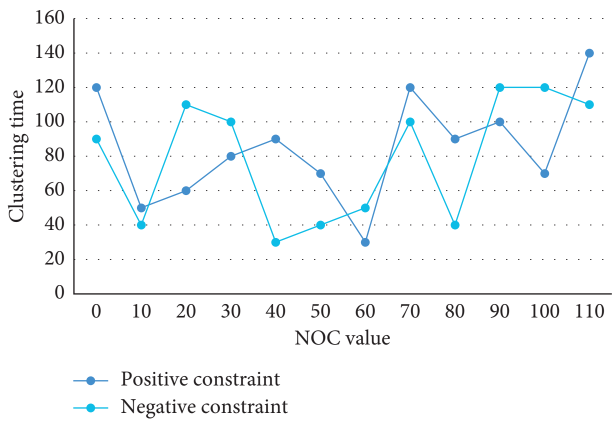

Figure 8: Comparison of clustering time between positive constraints and negative constraints.

time with positive and negative constraints is shown in Figure 8 to study the influence of the amount of information of equivalent partial constraints on the quality of clustering results and clustering efficiency.

Finally, the data points in the pipeline are compressed and discarded. The data point sets that satisfy the compression conditions are replaced and the corresponding data points are removed from the main memory. The higher the entropy of a training sample set in terms of target classification, the messier and messier it is; the lower the entropy of a training sample set in terms of target classification, the clearer and more ordered it is. The correctness of the algorithm is guaranteed by all possible frequencies established at least in the given block. The online part first calculates the similarity between the target user and the centre of the cluster, then divides the target user into the most similar clusters, and finally finds the nearest neighbours of the target user in the cluster, and then performs item recommendation. In this process, the data points in the algorithm design set can change the attributes of the clusters and also allow new clusters that were not originally in the original set to appear, avoiding wrong labels in the initial set and making the algorithm somewhat fault-tolerant.

5. Conclusions

PE to serve the daily physical education in school is an integral step in today's information age. Student evaluation is the system that makes up the most of the teaching quality monitoring system at universities and plays the most important role. The common practise is to use information technology and network technology to assess and predict teaching quality. The ability to apply complex statistical methods and calculations to these data and the rapid access to big data by data mining provide exciting reasons for the rapid development of data mining. Data mining techniques in teaching management, particularly in teaching quality evaluation systems, will provide some data support for university administrators, allowing them to improve teaching quality and make more effective decisions. Using computers to evaluate teaching quality can simplify and improve management. In this paper, we propose a data-mining arithmetic-based design of a teaching quality analysis and management system for PE courses, with the goal of standardizing the workflow related to sports performance management, achieving scientific management and information management, transforming the traditional complex teachers' workplace, and increasing work efficiency through the application of the target system. The system can mine the correlations between PE course grades, analyse these relationships scientifically, provide good decisions for educators and teachers and teacher management, better guide teaching work, and make students' teaching quality assessment data a truly important resource.

Data Availability

The data used to support the findings of this study are available from the corresponding author upon request.

Conflicts of Interest

The authors do not have any possible conflicts of interest.

Acknowledgments

This study was supported by the Young Scholar of Xulun Training Program of Shanghai Lixin University of Accounting and Finance.

References

[1] Y. Fan, Y. Liu, H. Chen, and J. Ma, "Data mining-based design and implementation of college physical education performance management and analysis system," *International Journal of Emerging Technologies in Learning (iJET)*, vol. 14, no. 6, p. 87, 2019.

[2] Y. Zeng, "Evaluation of physical education teaching quality in colleges based on the hybrid technology of data mining and hidden markov model," *International Journal of Emerging Technologies in Learning (iJET)*, vol. 15, no. 1, p. 4, 2020.

[3] X. Zhang and P. Luo, "Analysis of psychological education factors based on computer software and hardware collaboration and data mining," *Microprocessors and Microsystems*, vol. 81, Article ID 103744, 2021.

[4] X. Jin, J. Zhang, J. Kong, T. Su, and Y. Bai, "A reversible automatic selection normalization (RASN) deep network for predicting in the smart agriculture system," *Agronomy*, vol. 12, no. 3, p. 591, 2022.

[5] J. Kong, H. Wang, C. Yang, X. Jin, M. Zuo, and X. Zhang, "A spatial feature-enhanced attention neural network with high-order pooling representation for application in pest and disease recognition," *Agriculture*, vol. 12, no. 4, p. 500, 2022.

[6] W. Cai, Y. Song, and Z. Wei, "Multimodal data guided spatial feature fusion and grouping strategy for E-commerce commodity demand forecasting," *Mobile Information Systems*, vol. 2021, Article ID 5568208, 14 pages, 2021.

[7] J. Zhang, W. Feng, T. Yuan, J. Wang, and A. K. Sangaiah, "SCSTCF: spatial-channel selection and temporal regularized correlation filters for visual tracking," *Applied Soft Computing*, vol. 118, Article ID 108485, 2022.

Hindawi
Computational Intelligence and Neuroscience
Volume 2022, Article ID 6799633, 11 pages
https://doi.org/10.1155/2022/6799633

Research Article

Adaptive Spatial Division-Guided Resource-Based Economic Transformation with Synergistic Resource, Economic, and Environmental Health

Jiangong Yang

School of Economics Lanzhou University, Lanzhou 730000, China

Correspondence should be addressed to Jiangong Yang; yangjg16@lzu.edu.cn

Received 16 April 2022; Revised 7 May 2022; Accepted 9 May 2022; Published 31 May 2022

Academic Editor: Xin Ning

Relying on the advantages of its input factors, the resource-based economy has achieved rapid development. However, with the global emphasis on scientific development, various contradictions have sharply reduced the competitiveness of the resource-based economy. In the process of a new round of changes in the world economic pattern and the adjustment of China's development strategy, most resource-based economies have begun to implement transformation actively or passively. Resource-based economy was mostly established and developed in the period of planned economy, which made great contributions to national construction and accomplished brilliant achievements in regional economic and social development. However, the development of natural resources always goes through stages of development, growth, maturity, and decline. Therefore, resource-based cities also have problems of rise, prosperity, and decline. From the perspective of adaptive space division, this paper analyzes and studies the teaching of the coordinated development of resource-based economy in the transformation of the resource-based economy and environment economy and puts forward the panel data model, logistic curve, and other algorithm models. After optimization, the collaborative development model is designed. Based on the analysis of the model, it is found that the error analysis of the model has improved by 77.3% and the average growth rate of transformation benefits is generally 56.8%.

1. Introduction

As the source of basic energy and important raw materials in my country, resource-based economy has made outstanding contributions to the development of the national economy [1]. The question of how to avoid repeating the mistakes; develop high-efficiency industries based on resource advantages; scientifically demonstrate, optimize, and adjust economic development from the source of decision making; and protect economic ecology and environment while developing the economy has become a key problem that needs to be solved in the development of the emerging resource-based economy [2]. Resource-based economy is mostly established in the desolate backcountry, which is mostly old, small, and poor areas [3]. My country is a rare resource-rich country in the world, with a wide variety of resources, among which coal, iron, oil, and other resources are exploited on a relatively large scale, which plays an important role in the formation and development of their corresponding resource-based economy [4]. Since the establishment of New China, due to the large-scale demand for energy and raw materials in national economic construction, the construction of the resource development base has received great attention [5]. The rise and development of the resource-based economy has provided a large number of employment opportunities for these areas and accelerated the process of economization [6]. The high concentration and large-scale development of resource-based industries have greatly changed the economic development mode and lifestyle of their surrounding areas and promoted the development of regional economy [7].

The transformation of resource-based economy is a worldwide issue. This type of economy rises or develops due to the exploitation of natural resources and also stagnates or even declines due to the reduction and depletion of natural resources [8]. The operability of sustainable development is based on regional sustainability. Resource-based economy plays an important role in China's national economic and social development [9]. The nonrenewable nature of natural resources makes the development of resource-based economy face more difficulties than other economies [10]. My country is now in an important period of economic development and transformation. It is necessary to guide the direction of economic development with the concept of green and ecological projects and to build an ecologically civilized society as the goal of economic development. Only when the economic development model is successfully transformed can we build an ecological civilization. This strategic goal has become a reality [11]. In general, the environmental scheduling problem is to optimize the economic minimization of resource scheduling as a single objective by analyzing and using the constraint model of power scheduling. However, these methods cannot effectively solve the nonconvex Pareto optimal problem. At present, the multiobjective optimization algorithm that simultaneously processes two or more objectives in parallel has been applied to the multiobjective environmental and economic scheduling problem [12]. The core of building a conservation-minded society is to conserve resources, that is, in all aspects of production, circulation, consumption, and other fields, through the adoption of comprehensive measures such as technology and management, strict conservation, continuous improvement of resource utilization efficiency, and reduction of resource consumption and environmental costs as much as possible. A development model that meets people's growing material and cultural needs was needed [13]. Environment-friendly society is a social form of harmonious coexistence between man and nature. The relevant research mainly adopts the research means of economic geography, and the application of management theory and economic analysis methods is very few. The research method is relatively single, so it is urgent to strengthen the normative theoretical research [14]. In addition, the resource-based economy relies too much on the resource-based industries and forms a tie relationship with the resource-based industries.

This paper will examine the special problems and special laws in the sustainable development of resource-based economy, as well as the theory and method of sustainable development of the resource-based economy and the main methods of implementation, based on the basic theory of sustainable development and the actual development of resource-based economy. From the standpoint of sustainable development, it will present theoretical foundations and operational decision-making suggestions for my country's resource-based economy [15]. However, in the transformation of resource-based economy based on adaptive space division, the previous research did not perform a good optimization analysis on the coordinated development of resource-based economy and environment. However, in the transformation of the resource-based economy, it is critical to solve or improve the problem or process of coordinated development of resource-based economy, environment, and economy. As a result, the following innovations are proposed in this paper:

(1) This paper puts forward a new mode of industrial development of resource-based economy: intensive-green-chain network development mode. Based on the analysis of the coordinated development of resources, environment, and economy in resource-based economy transformation, this paper studies the connotation and characteristics of transformation based on the theory of sustainable development, analyzes the feasibility of transformation and the theoretical conditions of sustainable development, and designs a dynamic development model on this basis.

(2) This paper makes a multiobjective analysis on the coordinated development of resources, environment, and economy in the resource-based economy transformation in the adaptive space division because the adaptive space division solves the problem of different subspaces in the multiobjective optimization problem. In the experimental analysis, it can be divided into a large number of subspaces, and several important theories such as the panel data model algorithm are proposed in the algorithm to obtain the comparison of these algorithms in detection.

2. Related Work

In order to improve the level of intensive and friendly use of the construction land in the Chang Zhu Tan area and realize the sustainable use of land resources, Feng et al. [16] first analyzed the relationship between "two oriented" social construction and intensive and friendly use of construction land, explained the connotation of saving and friendly use of construction land, and then constructed the evaluation index system of intensive and friendly use of construction land. The factor analysis method is used to dynamically analyze the evolution trend of intensive and friendly utilization of construction land in the Chang Zhu Tan area [16]. Stevenson et al. [17] proposed a multiobjective particle swarm optimization algorithm based on bi-local optimization and combined it with the constraint processing method with the best feasible solution to solve the multiobjective EED problem [17]. Halder et al. [18] and others believe that efforts should be made to form a scientific form of economic development mode, social development mode, rational economic structure, and spatial pattern of resources and environment that do not waste resources and rather improve environmental quality. On the basis, the waste of resources and environmental damage are completely reduced [18]. The study by Morais et al. [19] shows that improving the quality of social development is the objective requirement of social development under the background of the new normal. Only by improving the quality of economic development can we promote the smooth transformation and optimization of social and economic structure, the improvement of development quality, and the improvement of ecological civilization construction performance [19]. Song et al. [20] and others think that after entering the post-industrialization, the status of natural resources as the main factor of production has been shaken, and the dependence of resource-based economy on resources and the constraints of resources on economy have become the bottlenecks of this economic growth. Due to the restriction of the life cycle of natural resources development and the gradual shrinking of the traditional product market, the resource-based economy began to decline, even faced with extinction, and the resource-based economy gradually changed from "core economy" to "marginal economy" [20]. Wang et al. [21] proposed that in multitarget tracking systems, the number of targets is usually unknown and constantly changing, and each target is in constant motion. The MTT algorithm plays a vital role in the multitarget tracking system. Through the target information obtained from sensors, such as position information, target attributes, and target strength, it can achieve stable positioning and tracking of multiple targets [21]. The research results of Chen and Guo [22] show that if economic growth continues at the expense of environment and quality, it will be difficult for resources and environment to bear its weight. After experiencing the rapid growth and re-industrialization since this century, China's economy has also reached an important juncture of transformation and upgrading [22]. Yu et al. [23] and others think that "the practical goal of building socialist ecological civilization is to build a sustainable modern economic model that is coordinated between ecology and economy, which is mainly manifested in developing circular economy, building an eco-safe economy and society, and realizing the development of ecological green civilization" [23]. The research of Chatterjee and Dutta [24] explained that the economy is an inevitable product of the development of human society and economy. The process of industrialization and economization in our country is accelerating, and a large number of rural surplus labor are transferred to the economy, which makes the economy quickly gather a large number of people. The rapid expansion of the economic scale and the rapid expansion of the population have brought problems such as water and soil resources' shortage and ecological damage [24]. Babamiri and Marofi [25] analyzed the country as a whole. The results show that the problems of forest land loss and sustainable forest management are related to the number of state-owned public stops and the differences between developed and developing countries. This gap is also an important factor affecting the sustainable development of state-owned forests [25]. Vondolia et al. [26] think that under the multitarget system, due to the problems of missed detection, clutter measurement, the emergence and extinction of targets, the simultaneous matching of motion models for multiple targets, and the unknown correspondence between multiple targets and measurements, all these will have a great impact on the performance of multitarget estimation [26]. The research of Pang et al. [27] and others shows that the leading industries of resource-based economy are developed on the basis of local advantageous resources. This resource-oriented development model is in the early stage of industrialization and economization, and the resource market supply has its practical significance under the condition of shortage [27]. Marin G, Marino M, and Pellegrin C believe that the two oriented development of industry refers to taking technological innovation and management innovation as the means and for the purpose of improving economic, social, and ecological environmental benefits, promoting the development of the industrial system in the direction of low resource consumption and less environmental pollution, so as to optimize the industrial structure, enhance the sustainable development capacity of the industry, and make it meet the requirements of the construction of two oriented society; we further constructed the evaluation index system of the development level of two oriented industry and conducted an empirical analysis [28].

On the basis of the above related research, the positive role of adaptive spatial division of labor in the coordinated development of resources, environment, and economy in the transformation of resource-based economy is determined, and a new strategy for coordinated development of resources, environment, and economy is constructed. Based on the spatial adaptive division of the resource-based economy in transition, in-depth analysis and research were conducted on the coordinated development of resources, environment, and economy, with a view to making more effective use of resources, exploring the hidden value behind resource data, and identifying potential problems affecting the coordinated development of resources, environment, and economy in the transformation of a resource-based economy.

3. Methodology

3.1. Research and Analysis of Related Theories

3.1.1. Adaptive Spatial Partitioning. The adaptive multiobjective evolutionary algorithm based on the division of solution space solves the multiobjective optimization problem. First, the solution space of the multiobjective optimization problem is divided into a large number of subspaces. In the process of algorithm evolution, each subspace retains a nondominated solution set to ensure the diversity of the population. From this, we can know the general continuous multiobjective optimization model:

$$\text{Minimize}\, F(x) = \left(f_1(x), f_2(x), \ldots, f_m(x)\right). \tag{1}$$

$x = (x_1, x_2, \ldots, x_n) \in R^n$. represents a decision vector, Ω is the decision space, and $F\colon \Omega \longrightarrow R^m$ is an objective space composed of m objective functions $f_1, f_2, \ldots, f_m$. For adaptive space partitioning, all the original frames are basically closed, and all the objective functions are continuous functions of their decision vectors. The completion time and cost of workflow are two conflicting optimization objectives, which we call multiobjective optimization problems. According to the value characteristics of variables, multiobjective optimization problems can be roughly divided into continuous multiobjective optimization problems and discrete multiobjective optimization problems. The multidimensional search space is divided into multiple grids. The particles in the grid adjust their speed and position by sharing the empirical information of "guiding" particles.

3.1.2. Resource-Based Economy and Resource-Environment-Coordinated Economy. Generally speaking, a resource-based economy is a kind of specialized functional economy, which refers to the economy that rises with the development of resources, or the economy that thrives again due to the development of resources in its development process. As a special type of economy, an economy built or developed basically relying on resource development, its leading industries are extractive industries and primary processing industries built around resource development. The industrial development mode of "high consumption, high investment, and high pollution" of the resource-based economy has many disadvantages. While developing the economy, it leads to the excessive consumption of natural resources and the destruction of ecological environment. It is an unsustainable production and consumption mode. The mechanism behind the course of resources is actually very simple, that is, under severe pressure, resource-poor economies have to abandon the traditional growth mode, adopt technological innovation and institutional innovation, and embark on a new economic development route. The sustainable development theory, system theory, and self-organization theory have provided us with good inspiration for understanding and managing economic problems and provided us with basic ideas, directions, and guiding principles for the study of the resource-based economy. Figure 1 shows the basic connotation of sustainable development.

Sustainable development is a comprehensive concept involving economy, society, culture, technology, and natural environment. It refers to the development that not only meets the needs of contemporary people but also does not endanger the ability of future generations to meet their own needs. The coordinated operation of the regional system will be affected by multiple factors, which can be divided into two categories: beneficial factors and limiting factors, collectively referred to as nuclear factors and factors. The relationship between these two factors is different, and the development situation is also different. When the leading factors play a dominant role, the development process is reflected in the competition of human activities for the leading factors, and a large number of people have invested in obtaining sufficient material and environment. Due to the stimulation of competition, this stage of development has grown rapidly; the leading factor is gradually consumed, and the emergence of a series of limiting factors hinders the regional development. This generally refers to the economic structure and a form of coordinated development of resources and environment. In order to realize the coordinated development of environmental resources and economy, it is necessary to understand the value measurement of environmental resources. Only by clarifying the value of environmental resources can we better protect environmental resources and realize coordinated development in practice. According to the adaptive spatial division theory, the value of environmental resources lies in its usefulness, scarcity, and conditions of development and utilization.

3.2. Research and General Mechanism Analysis of Economic Development in Transition. The transformation of the resource-based economy is a long-term and complex systematic project. It takes the industrial transformation of the resource-based economy as the starting point and leads and thus triggers social, economic, environmental, and other multifaceted and multilevel changes. Therefore, the transformation of the resource-based economy should be based on the transformation of the industrial structure, change the mode of economic development, and then carry out a comprehensive transformation of the system. In terms of structure, the basic structure of the regional resource environment economic system should be a complex system composed of a resource subsystem, environment subsystem, and economic subsystem. The coupling of the regional resource environment economy system is formed by three levels of system coupling development. First, the internal coupling and coordinated development of a single subsystem. Second, the coupling and coordinated development between the two subsystems. Third, the coupling and coordinated development among the three subsystems. Figure 2 shows the structure of the resource-based economy.

As shown in Figure 2, a resource-based economy consists of a resource subsystem, an economic subsystem, an environmental subsystem, a social subsystem, and several other factors. Each subsystem is interconnected, influenced, and restricted by human activities, resulting in a crisscross network structure. Furthermore, people are the main body and core of a resource-based economy. People are at the heart of any economic transformation or theory of sustainable development and they are the most important factor in achieving it. As a result, people control the production and distribution of all resources in the network structure depicted in Figure 2. The multiobjective evolutionary algorithm is simple, effective, and has a high degree of generality, making it appealing for solving multiobjective optimization problems. Multiobjective evolutionary algorithms, such as NSGA-II, MOEA/D, MOPSO, and others, are widely used in many fields, including data mining, cloud computing resource management and task scheduling, engineering project scheduling optimization, and Earth observation satellite task planning. This is an evaluation index that is used to determine whether Pareto's optimal solution is reasonable and reliable under self-use space division. Therefore, the objective function is generally introduced to achieve the requirement constraint of space division:

$$\min\left[\sum_{i=1}^{N_G} F_i\left(P_{Gi}\right), \sum_{i=1}^{N_G} E_i\left(P_{Gi}\right)\right]. \tag{2}$$

Among them: $F_i(P_{Gi})$ is the resource consumption function, $E_i(P_{Gi})$ is the pollution amount function $i = 1, 2, \ldots, N_G, N_G$ are the total number of all resources in the space. The Pareto optimal solution of a continuous multiobjective optimization problem is a piecewise continuous dimensional manifold in the objective space. In the process of evolving $m-1$, if the population lacks diversity, the algorithm may ignore some key search areas

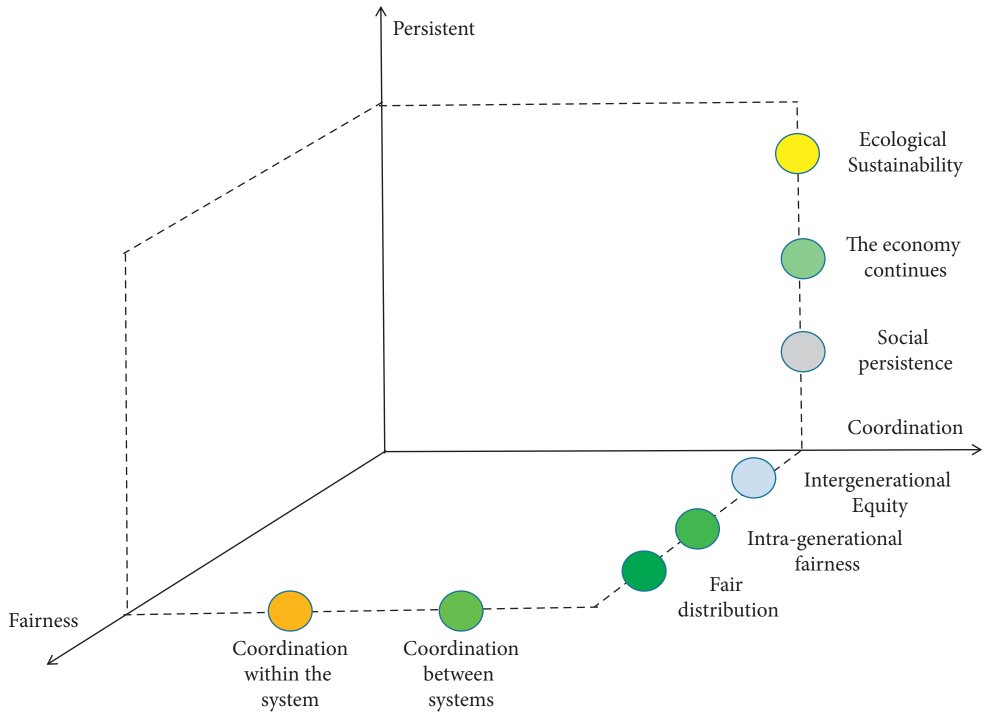

Figure 1: Basic connotation of sustainable development.

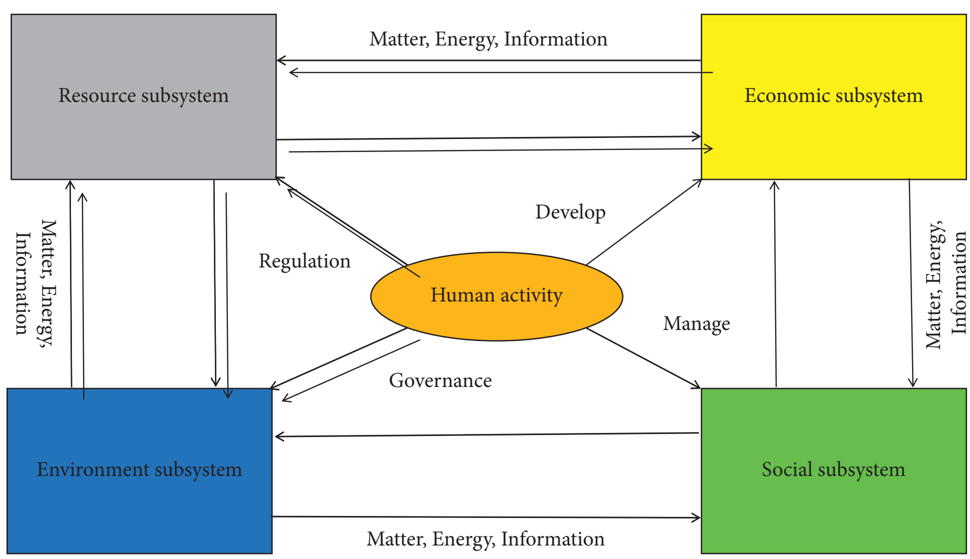

Figure 2: Resource-based economy structure diagram.

and weaken its search ability, making the convergence ability of the algorithm weak or even unable to converge to the real *PF*. Therefore, the general mechanism of resource-based economic transformation can be proposed as shown in Figure 3.

The resource-based economy needs to evolve harmoniously under the action of internal and external forces in order to achieve a successful transformation. Figure 3 lists several key elements of internal and external forces of the resource-based economy. First of all, we should know that scientific and technological strength and innovation are extremely helpful to the promotion of the economy. Different from the mechanism by which capital and labor promote economic growth, a technological progress has an accelerating effect, a delaying effect, a magnifying effect, or a leading effect on economic growth. The infrastructure affects the industrial scale and industrial structure of the economy by affecting the rate of return of economic industries and shaping the ability of the economy to attract talents, technology, capital, resources, and other elements. The construction and improvement of the infrastructure can provide transportation, communication, energy, and power facilities for the optimization of economic and industrial structure and economic development.

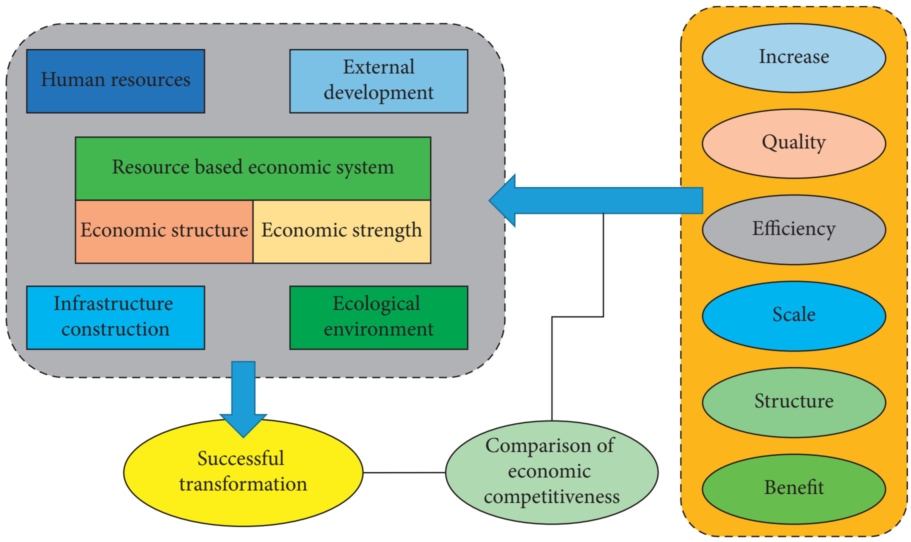

FIGURE 3: Schematic diagram of the general mechanism of resource-based economic transformation.

3.3. Dynamic Model Design for Coordinated Development. Because collecting transition economy samples is difficult, an algorithm model that can expand data processing in the same period must be introduced. As a result, this paper proposes the panel data model for designing and processing the algorithm portion of the model in order to meet the model's design requirements. The panel data model can effectively weaken the mutual influence and differences between various economies, as well as be described in very specific terms in dynamic changes. The model's design accuracy can be improved when multicollinearity weakens. As a result, the following is the fundamental model proposed in this paper:

$$\mathrm{TRA}_{it} = c + \alpha_2 \mathrm{MAR}_{i,t} + \alpha_4 \mathrm{URB}_{it} + \alpha_5 \mathrm{EDU}_{i,t} + \alpha_6 \mathrm{INF}_{i,t} + \varepsilon_{it}, \tag{3}$$

where i, t represents the i region and t year, respectively, and ε represents the random interference term. The meaning of each variable and coefficient standard are as follows. TRA in the model represents the transformation degree of the resource-based economy. In this paper, the vector angle is used to calculate the industrial structure transformation coefficient, which makes the model quite operable. It not only takes into account the change degree of the same industrial proportion in different years but also reflects the average change degree of the ratio of different industries, which is difficult to achieve by the general coefficient standard. Its specific expression is as follows:

$$\theta = \arccos\left[\frac{\sum_{i=1}^{n} s_i(t_1) s_i(t_2)}{\sqrt{\sum_{i=1}^{n} s_i(t_1)^2 \sum_{i=1}^{n} s_i(t_2)^2}}\right]. \tag{4}$$

In the formula, n is the number of industrial sectors, $s_i(t_1)$ refers to the share of the added value of i industrial sector in t years in the GDP of t years, and θ is the angle between $s(t)$ and $s(t-1)$ vectors, which generally becomes the transformation coefficient of the industrial structure. Generally, TEC is expressed as the level of technological progress, and the measurement formula is as follows:

$$\mathrm{TEP} = G - \alpha k - \beta l. \tag{5}$$

In the formula (5), G represents the average annual growth rate of GDP, $k \cdot l$ represents the average annual growth rate of capital and labor input, respectively, and $\alpha \cdot \beta$ is the elasticity coefficient of capital and labor, respectively. Generally, in economics, the two values are 0.56 and 0.44. If you need to calculate the value of k, you need to calculate the capital stock K. Its basic formula is as follows:

$$K_t = K_{t-1}(1 - \delta_t) + I_t, \tag{6}$$

where $K_t \cdot K_{t-1}$ represents the capital stock in the t year and the $t-1$ year, I_t represents the material capital investment in the t year, and δ_t represents the depreciation rate in the t year. Among the many economic factors, the two main factors, labor and capital, should be emphasized. This paper adopts the transformation of the Douglas function:

$$Y = A_t K^{\alpha} L^{\beta}. \tag{7}$$

By deriving and simplifying both sides of the equation at the same time, we obtain the following:

$$Y = a + \alpha K + \beta L. \tag{8}$$

The specific meaning of formula (8)$\mathrm{d}Y/\mathrm{d}t/Y = Y, \mathrm{d}A_t/\mathrm{d}t/At = a, \mathrm{d}k/\mathrm{d}t/K = K, \mathrm{d}L/\mathrm{d}t = L$ is that the growth rate of

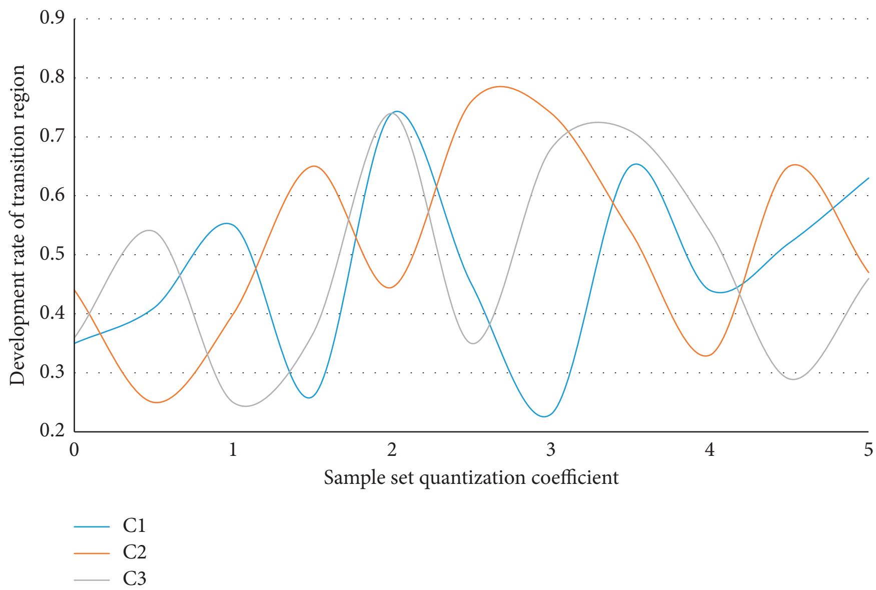

Figure 4: Analysis of the development speed of transitional regions.

economic benefits is determined by technological progress a, labor input L, and capital K. After observation, it can be found that the economic benefits of transformation are proportional to technological progress. After knowing formula (8), the contribution rate can be calculated as follows:

$$E_A = \frac{a}{y} \times 100\%, \tag{9}$$

where E_A represents the ratio between the annual technological innovation speed and the economic benefit growth speed in transition. The logistic curve is also checked for the transformation of the resource-based economy. Therefore, if $X(t)$ represents the transformation process of the resource-based economy, the development speed of the model is $\mathrm{d}X/\mathrm{d}t$. Due to the restriction of resource set and environmental capacity, the resource-based economy generally shows a nonexponential growth, which is generally in the form of the following curve:

$$\frac{\mathrm{d}X}{\mathrm{d}t} = \pi X\left(1 - \frac{X}{X_m}\right). \tag{10}$$

Among them, π is the growth rate required for development and X_m is the saturated capacity of the development factor. Generally speaking, if the threshold value of the capacity is found, the entire economic system will collapse directly. Therefore, X_m is a key element of transformation and represents reasonable development. The importance of, so continue to discuss X_m, which can be obtained after scoring it as follows:

$$X = \frac{X_m}{1 + Ce^{-m}}, \tag{11}$$

where C is a constant $C = X_m - X_0/X_0 > 0$ and when $t \longrightarrow \infty$, X converges to the threshold X_m. When the derivative is 0, we know that,

$$\begin{aligned} X_1, X_2 &= X_m, \\ X_3 &= \frac{X_m}{2}. \end{aligned} \tag{12}$$

It can be found that X_1, X_2 is an extreme situation. When $X = 0$, it indicates that the factor base of resource economic development is 0 and $X = X_m$ indicates that the development has reached the threshold of the economic system. Through the above algorithm design and improvement, the dynamic change trend of main parameters under the transformed economic model can be obtained, which will be helpful for analysis and decision making.

4. Result Analysis and Discussion

The foundation for the coordinated development of resource-based and resource-environmental economies is the establishment of a scientific, feasible, and practical model system. The coordinated development model of resources, environment, and economy proposed in this paper will examine and address a number of key parameters, including the transition region's development speed, the transition logistics' change rate, the model estimation error rate, the benefit rate of coordinated development, and coordinated development efficiency. Let C1, C2, and C3 be the analysis and comparison data charts of three sample sets of the resource-based economy transformation resource environment economic system in terms of transformation region development speed, transformation logistic change rate, and model estimation error rate as shown in Figures 4–6.

The abovementioned three indicators are in a stage of greater volatility between 1 and 3 in the above graph due to interference items in the transformation. Of course, this is also foreseeable, and the economic transformation may necessitate a variety of policy adjustments. Market

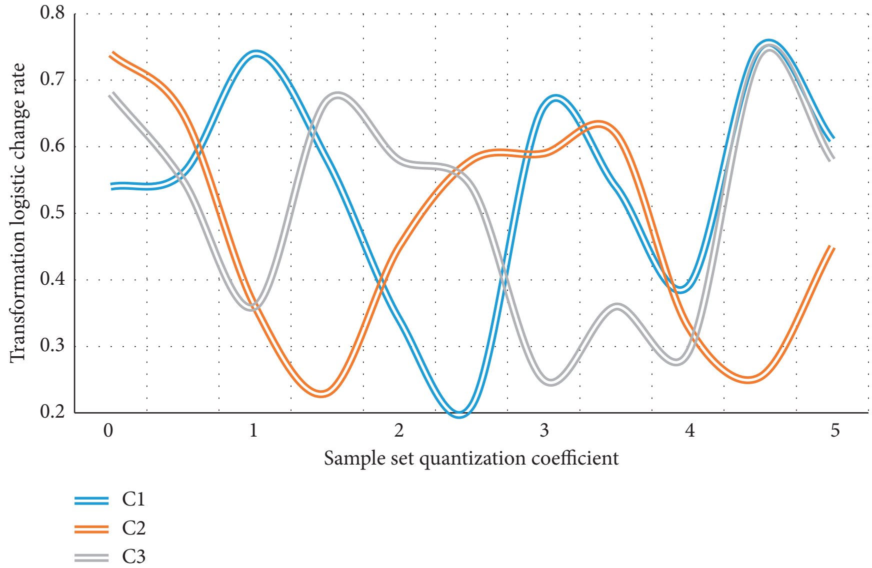

Figure 5: Analysis of the transformation rate of the logistic change.

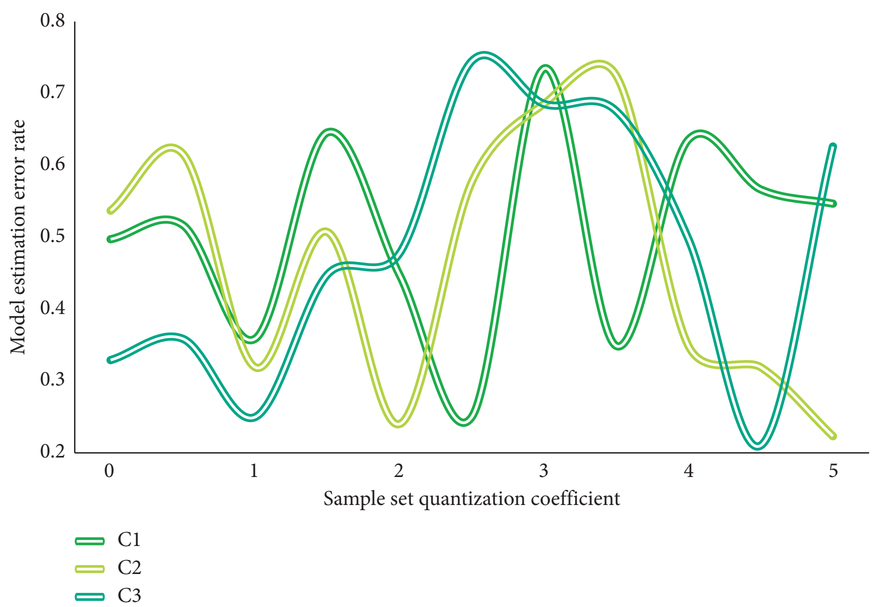

Figure 6: Analysis diagram of the model estimation error rate.

fluctuations, for example, can stymie the transformation process. As a result, while the transformation is risky in practice, the overall trend in the transformation area is upward, implying that despite the presence of interference items, the economic situation is improving. The system will benefit as a whole if it begins to transit from a resource-based economy to a resource-environmental economy with co-ordinated development. In terms of the logistic change rate, it is discovered that three different sample sets in the entire change process, especially in the 0-1 and 4-5 stages, have the same trend change tendency, proving that the model designed in this paper is universal, and the control of change rate reaches 87.4 percent, greatly improving the model's capture and mastery of unfavorable factors in the transition process. The model's error is analyzed intuitively in the experiment. In the three sample sets, it can be found that the overall error analysis state of sample set C2 is good. It is found that due to the existence of evaluation models for different risks in sample set C2, this also makes the model designed in this paper more accurate after comparing the other two sample sets and having better control over the risk, with a 77.3% improvement in error analysis. Assuming that $X1$ and $X2$ are two different sample sets of coordinated development benefit rate and coordinated development efficiency, Figures 7 and 8 are the analysis diagrams of the two.

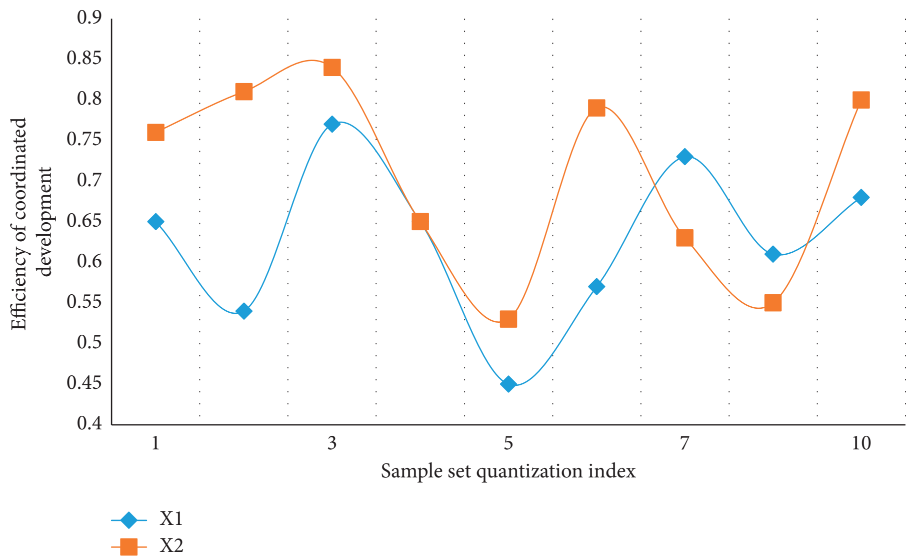

Figure 7: Analysis of the benefit rate of coordinated development.

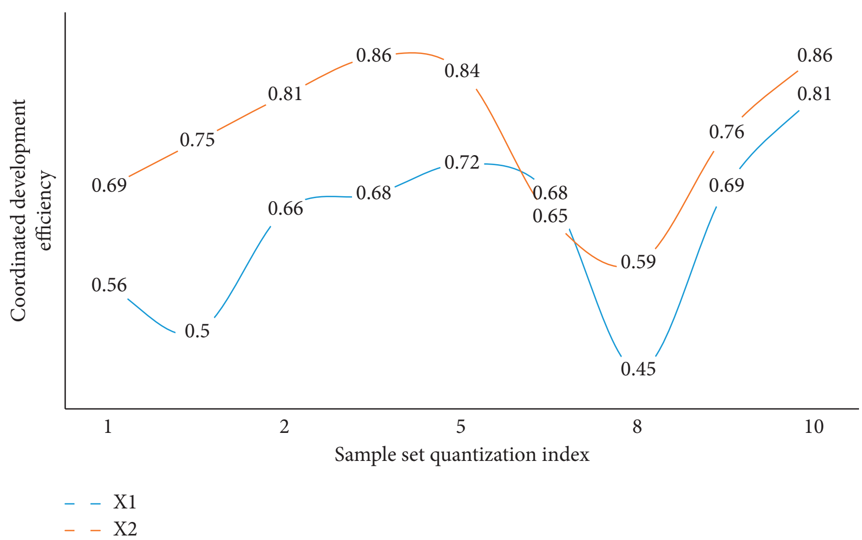

Figure 8: Analysis of coordinated development efficiency.

From Figures 7 and 8, it can be concluded that the benefit rate of coordinated development is basically kept at a high level, which reflects that the model designed in this paper has a very good promoting effect, and it promotes its rapid growth in the coordinated development of resources, environment and economy in the transformation of the resource-based economy. Although the benefits fluctuate in the 3–5 stages, they quickly return to the high-speed growth level, and the average growth rate of the transformation benefits generally reaches 56.8%. The efficiency of coordinated development is an important reference index. For the region after adaptive spatial division, under the constraints of the model, it basically promotes the development efficiency of the economic system after coordinated transformation. It is worth noting that the stability is basically maintained on the entire quantization axis, which is generally difficult to achieve in practice, but because the panel data model is embedded in the model designed in this paper, the stability of the model is greatly enhanced.

5. Conclusions

This paper conducts a systematic, selective, and focused exploratory research and analysis on the sustainable development of a resource-based economy, based on systematically summarizing related research results at home and abroad, with the goal of constructing a theoretical research framework and platform for the coordinated development of resources, environment, and economy in resource-based economy transformation. The goal of resource-based economy industrial development model innovation is to achieve sustainable development, long-term competitiveness, a reasonable economic structure, a healthy ecological environment, and social harmony and stability.

We must follow the principles of sustainable development, intensification, environmental protection, and efficiency to achieve this. To achieve a coordinated transformation from disorder to order, the resource-based economy requires a combination of internal and external factors. Three levels of analysis are used to examine the resource-environment-economic subsystem. To begin with, the resource-environment-economy subsystem's basic status is examined from four perspectives: natural environment, resources, economy, and environmental conditions. In terms of adaptive space division, the collaborative model is designed based on important theoretical algorithms such as the panel data model. The error analysis is improved by 77.3% and the average growth rate of transformation benefits is 56.8%.

Data Availability

The data used to support the findings of this study are available from the corresponding author upon request.

Conflicts of Interest

The author does not have any possible conflicts of interest.

References

[1] N. Antheaume, D. Thiel, F. de Corbière, and F. H. Rowe, "An analytical model to investigate the economic and environmental benefits of a supply chain resource-sharing scheme based on collaborative consolidation centres," *Journal of the Operational Research Society*, vol. 69, no. 12, pp. 1888–1902, 2018.

[2] G. Xie, L. Huang, H. Bin et al., "Sustainable entrepreneurship in rural E-commerce: identifying entrepreneurs in practitioners by using deep neural networks approach," *Frontiers in Environmental Science*, vol. 370.

[3] N. Gu, Z. Zhang, and Y. Li, "Adaptive iron-based magnetic nanomaterials of high performance for biomedical applications," *Nano Research*, vol. 15, no. 1, pp. 1–17, 2022.

[4] C. Guan, "Design of a coupling model for sustainable development in industry 4.0," *IETE Journal of Research*, pp. 1–12, 2022.

[5] D. D. T. Pham, P. Paillé, and N. Halilem, "Systematic review on environmental innovativeness: a knowledge-based resource view," *Journal of Cleaner Production*, vol. 211, no. 20, pp. 1088–1099, 2019.

[6] H. Wang, "Robust waveform optimization for MIMO-OFDM-based STAP in the presence of environmental uncertainty," *Circuits, Systems, and Signal Processing*, vol. 38, no. 3, pp. 1301–1317, 2018.

[7] J.-C. Chen, Y. Qin, H.-Y. Wang, and C. Xu, "Simulation might change your results: a comparison of context-aware system input validation in simulated and physical environments," *Journal of Computer Science and Technology*, vol. 37, no. 1, pp. 83–105, 2022.

[8] J. Liu and X. Chen, "Adaptive control based on neural network and beetle antennae search algorithm for an active heave compensation system," *International Journal of Control, Automation and Systems*, vol. 20, no. 2, pp. 515–525, 2022.

[9] Z. Zhongtang Zhao and R. Ruixian Li, "Bayesian cellular automata fusion model based on dual-stream strategy for video anomaly action detection," *Pattern Recognition and Image Analysis*, vol. 31, no. 4, pp. 688–698, 2021.

[10] I. Kaliukh and O. Lebid, "Constructing the adaptive algorithms for solving multi-wave problems," *Cybernetics and Systems Analysis*, vol. 57, no. 6, pp. 938–949, 2021.

[11] S. V. Zaitsev, N. V. Sokorinskaya, V. M. Vasylenko, and A. N. Y. N. Trofimchuk, "Optimization of turbo code encoding/decoding processes for development of 5G mobile communication systems," *Radioelectronics and Communications Systems*, vol. 64, no. 8, pp. 440–450, 2021.

[12] Y. Zhang, Z. Zhang, Y. Wang et al., "Dual-constrained deep semi-supervised coupled factorization network with enriched prior," *International Journal of Computer Vision*, vol. 129, no. 12, pp. 3233–3254, 2021.

[13] W. Qu, T. Qian, G. Deng, and Y. C. Li, "Analytic phase retrieval based on intensity measurements," *Acta Mathematica Scientia*, vol. 41, no. 6, pp. 2123–2135, 2021.

[14] M. A. Álvarez, C. Dafonte, M. Manteiga, D. Garabato, and R. Santoveña, "GUASOM: an adaptive visualization tool for unsupervised clustering in spectrophotometric astronomical surveys," *Neural Computing & Applications*, vol. 34, no. 3, pp. 1993–2006, 2021.

[15] Z. Chen, K. Li, and X. Xiang, "An adaptive high-order unfitted finite element method for elliptic interface problems," *Numerische Mathematik*, vol. 149, no. 3, pp. 507–548, 2021.

[16] Z. Feng, Y. Zheng, and M. Xu, "Integrated strategy of stationkeeping, autonomous navigation, and real-time geodetical recovery of gravity fields: application into asteroid Lutetia mission," *Nonlinear Dynamics*, vol. 106, no. 4, pp. 3247–3263, 2021.

[17] R. Stevenson, R. van Venetië, and J. Westerdiep, "A wavelet-in-time, finite element-in-space adaptive method for parabolic evolution equations," *Advances in Computational Mathematics*, vol. 48, no. 3, pp. 17–43, 2022.

[18] S. Halder, K. H. Lim, J. Chan, and X. Zhang, "Efficient itinerary recommendation via personalized POI selection and pruning," *Knowledge and Information Systems*, vol. 64, no. 4, pp. 963–993, 2022.

[19] R. G. Morais, N. Nedjah, and L. M. Mourelle, "A novel metaheuristic inspired by Hitchcock birds' behavior for efficient optimization of large search spaces of high dimensionality," *Soft Computing*, vol. 24, no. 8, pp. 5633–5655, 2019.

[20] K. Song, Y. Zhang, X. Zhuang, and X. B. Yu, "Reliability-based design optimization using adaptive surrogate model and importance sampling-based modified SORA method," *Engineering with Computers*, vol. 37, no. 2, pp. 1295–1314, 2019.

[21] F. Wang, Z. Q. Chao, L. b. Huang, H. Y Li, and C. Q. Zhang, "Trajectory tracking control of robot manipulator based on RBF neural network and fuzzy sliding mode," *Cluster Computing*, vol. 22, no. S3, pp. 5799–5809, 2017.

[22] J. Chen and J. Guo, "Static response of a layered magneto-electro-elastic half-space structure under circular surface loading," *Acta Mechanica Solida Sinica*, vol. 30, no. 2, pp. 145–153, 2017.

[23] W. Yu, M. A. Jacobs, R. Chavez, and M. Feng, "The impacts of IT capability and marketing capability on supply chain integration: a resource-based perspective," *International Journal of Production Research*, vol. 55, no. 14, pp. 4196–4211, 2017.

[24] S. Chatterjee and S. Dutta, "Assessment of groundwater potential zone for sustainable water resource management in south-western part of Birbhum District, West Bengal," *Applied Water Science*, vol. 12, no. 3, pp. 1–16, 2022.

[25] O. Babamiri and S. Marofi, "A multi-objective simulation–optimization approach for water resource planning of

reservoir–river systems based on a coupled quantity–quality model," *Environmental Earth Sciences*, vol. 80, no. 11, pp. 1–19, 2021.

[26] G. K. Vondolia, W. Chen, C. W. Armstrong, and M. D. Norling, "Bioeconomic modelling of coastal cod and kelp forest interactions: Co-benefits of habitat services, fisheries and carbon sinks," *Environmental and Resource Economics*, vol. 75, no. 1, pp. 25–48, 2019.

[27] X. J. Pang, S. S. Li, L. Qin, Y. L. Pei, and S. K. Gong, "Effect of trace Ce on high-temperature oxidation behavior of an Al-Si-coated Ni-based single crystal superalloy," *Journal of Iron and Steel Research International*, vol. 26, no. 1, pp. 78–83, 2019.

[28] L. Cheng, Y. Wang, Q. Liu et al., "Network-aware locality scheduling for distributed data operators in data centers," *IEEE Transactions on Parallel and Distributed Systems*, vol. 32, no. 6, pp. 1494–1510, 2021.

Hindawi
Computational Intelligence and Neuroscience
Volume 2022, Article ID 4991244, 9 pages
https://doi.org/10.1155/2022/4991244

Research Article

Neural Network Technology-Based Optimization Framework of Financial and Management Accounting Model

Yan Zeng

Wuhan College, Wuhan 430000, China

Correspondence should be addressed to Yan Zeng; 9088@whxy.edu.cn

Received 14 April 2022; Revised 8 May 2022; Accepted 9 May 2022; Published 31 May 2022

Academic Editor: Xin Ning

Traditional financial accounting has gradually evolved into management accounting in order to adapt to changing times and developments. To avoid being obliterated by the times, accountants must gradually improve their professional and comprehensive abilities in order to create greater value for businesses in the AI (Artificial Intelligence) era. This article presents an AI-based financial management optimization design and proposes an AI-based accounts receivable management optimization framework based on the existing information system. A typical financial distress early-warning model is built using the BPNN (BP Neural Network) model, and the training samples of listed companies' financial data are processed iteratively using the neural network algorithm to realize the visual modeling of the object-oriented neural network and learn the training samples. Finally, the network's ability to provide early warning is put to the test. The results show that BPNN's prediction accuracy is significantly higher than that of other types, especially after years of data, with prediction results exceeding 90%. The results show that the BPNN-based financial early-warning method is feasible.

1. Introduction

Accounting is the statistical analysis of an enterprise's financial data using professional recording methods in accordance with the accounting financial system's basic principles and the use of financial data to reflect a company's financial transactions and business information at a given point in time. Accounting is a management information system that employs systematic methods to analyze, evaluate, and manage the financial and economic data generated by an enterprise's business activities and assists management in providing supporting data for management decisions and operations. With the advancement of economic levels, generating more value in order to achieve sustainable development has become a problem that every business will face. The gradual implementation of AI (Artificial Intelligence) technology [1, 2] has a significant impact on social development and accounting work, with some traditional financial personnel potentially losing their jobs. In light of this, financial accounting must keep up with the times and strive to transform into management accounting in order to adapt to the transformation and development of the times. AI has accelerated the transformation and promotion of accounting work in the field of accounting. Financial robots can independently identify financial data, making large amounts of data processing simple and quick. At the same time, it imposes more stringent requirements on businesses.

In recent years, some issues in the company's economic activities, financial management, and high-risk fields have been exposed, whether through external audit or internal special inspection. It is necessary to research and develop perfect financial audit system functions and establish a unified financial audit management method and mode, in order to find and solve problems as soon as possible. To achieve centralized financial system management, Eckles et al. proposed that each member unit's financial business be concentrated in the financial sharing service center or rely on the financial organization [3]. Powell et al. emphasized that if an enterprise wants to improve its competitiveness, it must fully exploit its own advantages and devote its limited resources to its core business [4]. Kobrak stated that shared service is the first step in financial transformation, and financial shared service is an excellent practice of shared service, and he created a detailed and feasible optimization design for the organizational framework, process, financial information system, operation management, specific implementation, and other aspects of financial shared service [5]. Rau pioneered data warehouse technology in the banking industry as the primary tool for centralized data management [6]. Liu improved the BP neural network (BP neural network) and used it to predict financial distress, with good results [7]. Kirk et al. found that the data had an ideal effect of 89.16% using a nonlinear combination model of fuzzy neural networks [8].

Data in financial accounting can be automatically identified under AI conditions, accounting information can be efficiently recorded and reflected, and data can be analyzed with the help of a network and processing programme, which is more timely than traditional financial accounting. In the AI era, the accounting department should not only do a good job accounting monetary funds but also record relevant data resources based on the data of other companies in order to exert greater labour value and make greater contributions to the company. Although financial exchanges' accounts receivable business has been continuously optimized in line with the trend in recent years, issues such as too many manual operations, long working hours, low invoicing efficiency, and uncontrollable errors have not been adequately addressed. Despite its powerful functions in data calculation, reasoning, and pattern recognition, the intelligent prediction model lacks stability. This article discusses the specific steps in the transformation process by analyzing the differences between management accounting and traditional financial accounting.

1.1. Contribution of the Subject

(1) Based on the existing information system, this article designs an optimization framework of accounts receivable management based on AI, describes the application of BPNN in accounts receivable risk management in detail, analyzes the optimization contents, and puts forward concrete implementation suggestions from three aspects of financial team transformation.

(2) Using a neural network model and combinatorial thinking method, this article constructs the financial distress notification model of listed companies in China. The neural network method can reveal the nonlinear relationship contained in data samples, and a large number of processing units form a nonlinear adaptive dynamic system, which has good adaptability, self-organization, strong learning, relevance, fault tolerance, and capacity, and can flexibly and conveniently model complex unknown coefficients with various reasons.

1.2. Organizational Structure of the Article. The first chapter introduces the research background and significance and then introduces the main work of this article. The second chapter mainly introduces the related technologies of financial management. The third chapter puts forward the specific methods and implementation of this research. The fourth chapter verifies the superiority and feasibility of this research model. The fifth chapter is the summary of the full text.

2. Related Work

2.1. Financial Management Research. To construct the enterprise financial management and decision-making system, the technical route based on theory is to first establish a data warehouse and take the original data collection of the data warehouse as the main task. At present, the original data of the data warehouse established by the survey object come from relevant text information such as enterprise financial information platform.

Basic financial work is an important foundation to improve the level of financial management, covering accounting, system construction, process design, accounting supervision, performance evaluation, and other aspects of management. Dale pointed out that companies with scattered organizational structure or less hierarchical structure can gain management advantages by sharing human resources and technical resources [9]. Byrne defines the essence of a shared service center as an independent organizational entity and emphasizes that the objects of shared services should be molecular companies and business departments within the enterprise [10]. James believed that shared services can integrate all the resources of the company, reduce operating costs, and provide high-quality and professional services for different regions and internal partners, so as to realize enterprise value [11]. Luca and Meschieri believed that in the case of organizational failure, enterprises can gather many basic businesses in a semi-market organizational entity [12]. Tinoco et al. explained the mode of financial sharing service mainly from three aspects: entry management, outflow management, and comprehensive control [13].

2.2. Research on Early Warning of Financial Distress. At present, China has not yet established a complete financial early-warning system, and only some financial forecast information is disclosed in the financial statements, which is only a simple extension of the historical and present financial trends. The artificial neural network is a parallel distributed pattern processing system developed from the research results of neuropsychology and cognitive science by applying mathematical methods.

Huang et al. used multivariate discriminant analysis to discuss the prediction of financial distress of enterprises [14]. Gudmunson et al. put forward that the early-warning system is mainly composed of three subsystems: evaluation, warning, and response, in which evaluation is the evaluation and prediction of the existing alarm situation [15]; warning is to transform the forecast of the previous step into information and communicate with each department. Besancenot and Vranceanu used multivariate discriminant analysis to study the early warning of the financial crisis and adopted 22 financial ratios to establish the famous 5-variable Z-Score model through mathematical statistics screening. According to the discriminant score, the financial crisis of the research object was discriminated with a certain critical value [16]. The results of Olafsson's research show that factors such as enterprise size, financial structure, operating performance, and liquidity are highly correlated with the probability of financial distress [17]. Li et al. synthesized the academic definition of financial distress and divided it into four situations: failure, insolvency, default, and bankruptcy [18].

The financial early-warning system is an organizational operation system for analysis, early warning, monitoring, and implementation, which is established to prevent business errors. It adopts the information management method, selects appropriate early-warning indicators according to various financial analysis data, makes a comprehensive and systematic analysis of the company's related financial indicators, and timely informs the company's management about the risks of the company's financial operation system and other stakeholders, so as to take early action to prevent losses.

3. Methodology

3.1. Optimization of Financial Management Process Based on AI. In the process of transition from traditional accounting to management accounting, it is necessary to start with accountants' own quality, combine the advanced ideas of management accounting with the actual situation, and make good use of AI to cultivate a set of management accounting that can meet the needs of the new era. Accounting can use AI financial system to fully understand the company's cost management information, understand the linkage of cost differences through data analysis, and finally realize effective cost control through problem rectification. In order to make greater contributions, accountants must constantly improve their professional ability, expand their knowledge, and enhance their comprehensive ability to adapt to the development and progress of the times.

In the aspect of accounts receivable management, the main risks faced by enterprises include margin risk and settlement risk, which involve both owner's credit management and accounts receivable risk management. The original documents are mainly composed of manual documents and electronic documents, and the business departments of subsidiaries sort out the original invoices generated by various businesses. Through bill image scanning technology [19, 20], the original bill is converted into image data and stored in the database. Regarding the risk management of accounts receivable, as the damage of overdue accounts receivable to the company is directly reflected in bad debt risk, which damages the company's operating profit, the company should evaluate the risk of accounts receivable in time and guide the business personnel to choose an appropriate payment management method according to the evaluation results.

Relying on information technology such as cloud computing, financial services scattered in various departments with high repeatability, high turnover rate, and high standardization will be integrated into a new business service platform so as to realize process reengineering and standardization and provide users with quality products. According to the analysis in Figure 1, this document adopts "basic finance, financial management and strategic finance." Furthermore, the first step of building the platform is completed in collaboration with various departments of the company.

Most employees and users have access to financial information, which primarily includes online payment and reimbursement. The settlement and financial accounting modules, as well as the treasury payment system and banking system, are all linked; the budget management module is linked to the financial department to ensure one-to-one budget item correspondence. It will promote the most profound change in enterprise financial management and provide comprehensive and effective decision support for management while ensuring the efficient operation of the enterprise financial communication platform. Platform business process strategy should be in line with platform strategy. Business process strategy is a shared platform strategy, and business process goal is a shared platform goal, which guides business process optimization and design. After the auditor confirms the original paper receipt, the system will automatically generate the electronic accounting receipt, print the paper version, and begin the electronic payment programme. If the audit fails, the data will be returned in the same manner, with an e-mail sent to remind the refund staff to make the necessary changes.

Accounts receivable have high liquidity and high risk, and their safety and quality will have a significant impact on the company's resources, excess losses, cash flow, etc. and have an important impact on improving the business level of enterprises. Because of its strong fault-tolerant ability, BPNN can ensure that the accuracy of its training results remains at a high level. Assume that the number of nodes in the input layer of BPNN is c, the number of nodes in the output layer is d, the number of nodes in the hidden layer is e, the weights between the hidden layer and the input layer are V_{iw}, and the weights between the hidden layer and the output layer are V_{jw}. Let the hidden layer function be f_1 and the output layer function be f_2.

Among them, the output of the hidden layer node is as follows:

$$Z_k = f_1\left(\sum_{i=0}^{n} V_{ik} X_i\right), \quad k = 1, 2, \ldots, q. \tag{1}$$

For P sample sizes, the overall error value is as follows:

$$E = \frac{1}{2} \sum_{P=1}^{P} \sum_{j=1}^{m} \left(t_j^p - y_j^p\right)^2. \tag{2}$$

Accounts receivable system is a part of the financial management system, which can work independently or cooperate with other subsystems to transmit relevant data and vouchers. The relationship between the credit system and other subsystems of listed companies' financial participation system mainly includes the following four aspects:

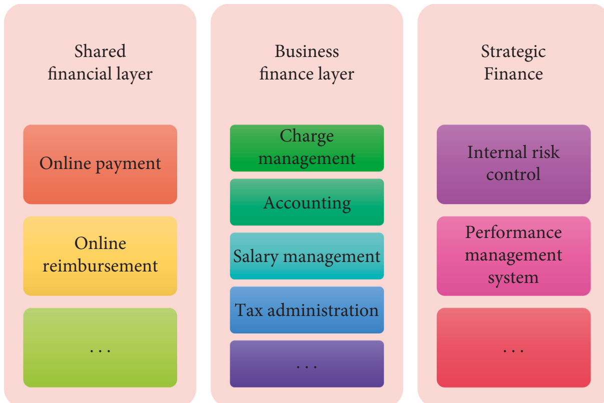

Figure 1: Organizational structure of enterprise financial sharing platform.

(1) The relationship between A/R management and sales management: A/R management and sales management share A/R balance information, and sales invoices issued by sales management will be fed back to the A/R system in a timely manner; (2) relationship between A/R management and A/P management: write-off of A/R and A/P is supported; (3) relationship between collection management and budget management: budget revenue and expenditure items can be entered in A/R management; (4) relationship between A/R management and fund management: the collection document can generate the fund system collection notice.

Based on the BPNN default risk prediction model, the automation of finance improves the efficiency of the clearing house and automates the processes with a high repetition rate but is prone to problems, such as invoicing, accounts receivable reconciliation, and collection cancellation, and theses processes have been optimized and improved. The optimization framework of accounts receivable management of listed companies is shown in Figure 2.

DT (decision tree) is an important classification technology [21, 22] in data mining. Its main function is to classify and process the data in the existing training set according to the attributes and class labels of the training dataset and to establish a model according to the algorithm and use it to classify new data. The core content of this algorithm is the process of constructing the DT model. Firstly, the data samples of the training set are analyzed, and then DT is constructed. The DT model is established to analyze the data and then predict and analyze the data.

An improved algorithm of DT algorithm is proposed: DT is actually an improved DT that combines a linear classifier and DT classifier. DT construction method is used to reduce the number of layers in the tree. This method is a measure of DT, which can better improve the efficiency of DT classification. The algorithm used is a supervised algorithm, in which the labeled classification training set is performed in advance.

Compared with the obvious Mahalanobis distance measurement method, all linear methods have the invariance of scale transformation. Let $y = Ax$, then, the vector be x_1, x_2, m_x, and the transformed distance between them be y_1, y_2, m_y. Mahalanobis distance is as follows:

$$\|x - m\|_M = (x - m)^T C^{-1} (x - m). \tag{3}$$

Under the Mahalanobis distance scale, this method provides the basis for distance judgment.

This algorithm introduces the concept of measurement method when calculating information drop gain, which can be used as a reference when selecting and classifying. The following Figure 3 shows the process of improving the algorithm.

(1) For a superset $C \in T$, C contains several categories of samples. They will wait until the next level to continue the classification.
(2) Choosing the best case for classification is the classification method adopted when no attribute set can be found.
(3) At the end of the process, all samples are classified or the sample classification cannot be continued.

3.2. Research on Financial Distress Prediction. The application and advancement of AI technology has gradually altered the traditional financial accounting function. Accounting work is no longer a single data record, and more financial accountants are needed to effectively organize and extract data. Accounting is an organization's internal accounting, and it focuses on providing information to help management make informed decisions. Financial accounting must be prepared according to strict accounting standards, and management is more flexible than financial accounting. AI can help businesses process financial data more quickly and efficiently and guide them through internal production processes. It can also serve as a reference for managers making predictive decisions. The transition from financial to management accounting is accelerated by AI.

When developing accounting functions, businesses are paying more attention to the integration of other departments and financial departments. As a result, when financial accounting becomes management accounting, the financial department's personnel must meet higher standards. We must start with the company's information construction when transitioning from financial accounting to management accounting. The old enterprise information system equipment should be replaced as soon as possible, and the entire system should be properly optimized to meet intelligence demand. With the advancement of information globalisation, the demand for the transition from financial accounting to management accounting is becoming more apparent, and the trend of enterprise and finance integration is becoming more apparent, which is more conducive to the innovation of the financial management mode of enterprises and increases market share. The unexpected occurrence of financial distress determines the uncertainty of financial distress management. Financial distress is influenced by a variety of factors, some of which can be understood and controlled and others of which are explosive and unexpected. With the advancement of economic globalisation, an increasing number of businesses rely solely on traditional management methods, leaving them unable to plan for rapidly

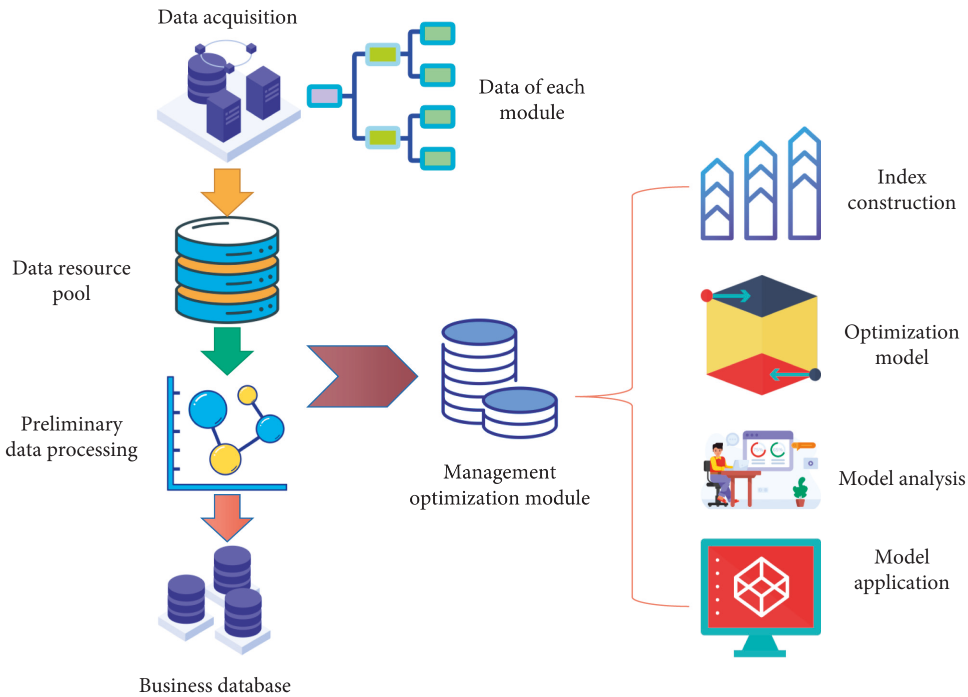

Figure 2: AI-based optimization framework for accounts receivable management of listed companies.

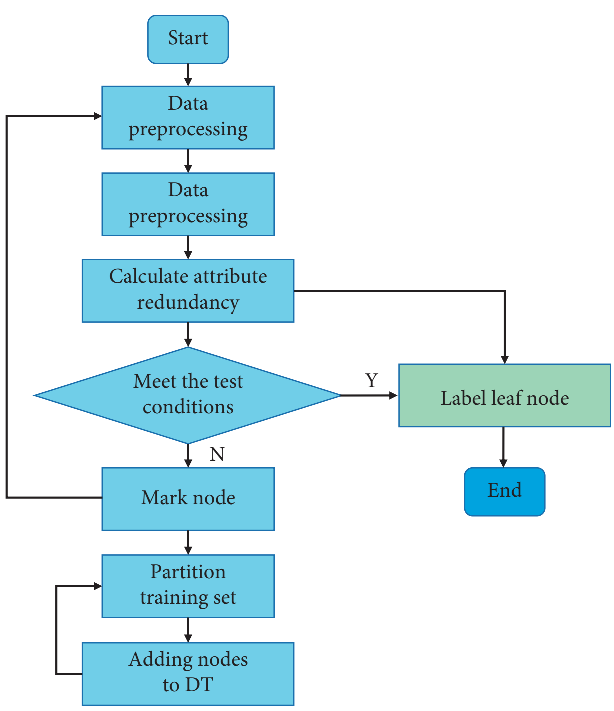

Figure 3: Improve algorithm flow.

changing activities and market dynamics, and deal with a variety of new problems. More importantly, business leaders are paying increasing attention to the prevention and management of financial difficulties and financial early warning.

Up to now, most of the samples used to test the prediction efficiency of the model have used paired samples, and there is no clear sample pairing rule. As the number of companies in financial distress is very small, the most diversified self-test models can always be found in a large number of nonfinancial distress companies, so the universality of the models is questionable. From the perspective of the neural network mapping relationship, the variable selection method based on the neural network not only avoids the practical difficulty of how to set the shape of function correctly in the modeling process but also expands the function types in regression modeling. Research that makes variable selection research more common and opens up an additional way for variable selection when the structure of the response function is unknown. Choosing forecast variables according to economic and financial theories can make up for this.

Theoretically, three-layer BPNN can approximate any function. In this article, we use a three-layer BPNN with only one hidden layer. The weight is adjusted according to the general gradient descent method: i represents the input layer, j represents the hidden layer, k represents the output layer, and l represents the learning step; w_{ij}, w_{jk} represents the weights of input to the hidden layer and hidden layer to output layer, respectively; $E(n)$ is the sum of error energies.

$$\begin{aligned}\Delta w_{ij}(n) &= -\frac{\partial E(n)}{\partial w_{ij}(n)},\\ \Delta w_{jk}(n) &= -\frac{\partial E(n)}{\partial w_{jk}(n)}.\end{aligned} \tag{4}$$

Here, we combine dynamic principal component analysis with BPNN to construct a BP prediction model, as shown in Figure 4.

Assuming that the ensemble is composed of N independent neural network classifiers, adopting the voting

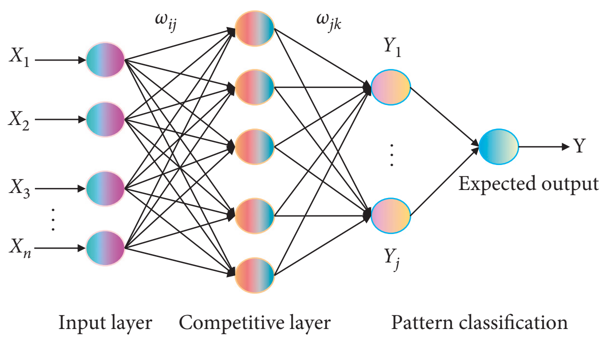

Figure 4: Schematic diagram of BPNN working principle.

method of an absolute majority, and assuming that each network gives the correct classification result with the probability of $1-p$, the errors among the networks are uncorrelated and the probability of errors in the ensemble neural network is P_{error}:

$$P_{\text{error}} = \sum_{k>N/2}^{N} \binom{N}{k} p^k (1-p)^{N-k}. \tag{5}$$

At $p<1/2$, P_{error} decreases monotonically with the increase of N. Therefore, if the prediction accuracy of each neural network is higher than 50%, and the errors among the networks are uncorrelated, the more the networks in neural network integration, the higher the integration accuracy. When N tends to infinity, the error rate of integration tends to zero.

Aiming at these shortcomings of the BPNN algorithm, this paper improves the original BPNN algorithm. The adaptive learning method and momentum summation method are used to modify the standard BPNN algorithm, which can effectively avoid the problem that the network falls into local minima. The artificial neural network can be mapped in any form, and financial early warning provides a new way of thinking.

The concrete improvement method of the BPNN algorithm is shown as follows.

In fact, the traditional BPNN algorithm is a simple high-speed descending static optimization algorithm. When correcting the weight $w(k+1)$, it is only corrected according to the negative gradient direction at time k, without considering the previous accumulated experience. Its weight correction function is written as follows:

$$w(k+1) = w(k) + \eta(k), \tag{6}$$

where the weight of $w(k)$ connection is the negative gradient of k moment:

$$D(k) = \frac{-\partial V}{\partial w(k)}, \tag{7}$$

where V is the square error between the actual output and the desired output of the network, and η is the learning rate.

A good learning rate at the beginning of training may not be suitable for later training. In order to solve this problem, it is natural to think of automatically adjusting the learning rate during the training process, so an improved algorithm of self-adaptive adjusting the learning rate appears, and its calculation formula is as follows:

$$\begin{aligned} w(k+1) &= w(k) + \eta(k)D(k), \\ \eta(k) &= 2^{\lambda}\eta(k-1). \end{aligned} \tag{8}$$

It can be seen that when the gradient direction of two successive iterations is the same, it means that the descent is too slow and the step size can be doubled; when the gradient directions of two successive iterations are opposite, it means that the descent time is too long, and the step size can be halved. Therefore, the network convergence can be accelerated by constantly adjusting the learning rate.

4. Experiment and Results

In order to analyze the progress of the company's financial budget implementation and the past years, it is necessary to extract the past years' budget data from the financial data warehouse and achieve the purpose by data aggregation and other calculation methods. The implementation of intelligent decision-making in financial budget management is divided into two steps:

(1) For analysis and application, firstly, intelligent decision-making based on the company's financial data warehouse and multidimensional analysis is established;

(2) Data mining is used to perform intelligent decision-making function.

The calculation of information gain depends on the attributes with more values, and the information gain depends on the number of attribute values, but in fact, this choice is meaningless in some cases. For example, the identification number is the identification attribute of a piece of data, and the identification attribute is the unique identification of the corresponding information. As the data value becomes larger and larger, the information gain corresponding to the port attribute is finally maximized.

In the process of DT construction, the key step is the splitting of nodes. Algorithm C4.5 uses information gain rate to measure the advantage of split nodes. In the formula of information entropy and information gain, the ratio of information gain is information gain and information entropy.

ID3, C4.5, and improved DT algorithms are run on different datasets, and the experimental data are obtained. The improved DT algorithm, ID3 algorithm, and C4.5 algorithm are compared, respectively, and the classification performance of the improved DT algorithm is compared. The error rate of the improved DT algorithm is significantly higher than that of the ID3 algorithm and C4.5 algorithm. The DT constructed by the improved algorithm is compared with the DT constructed by the traditional algorithm ID3 and C4.5, as shown in Figure 5.

The improved DT produces three layers of DT, according to the experimental results. Only one dataset is misclassified in each classification structure. When you examine the

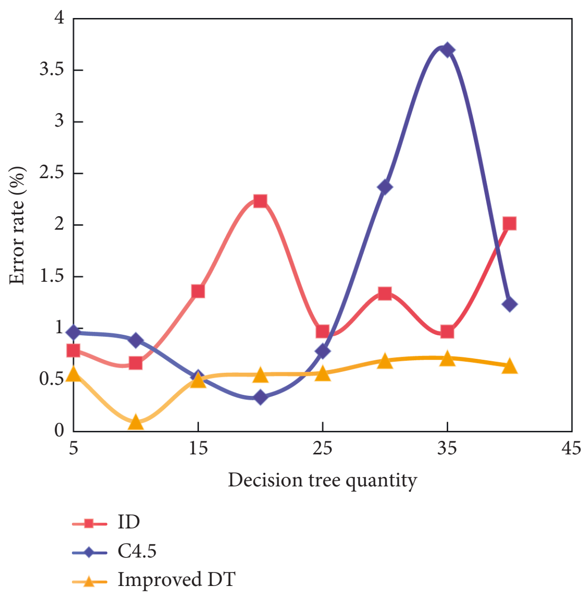

Figure 5: Comparison between DT constructed by the improved algorithm and traditional DT.

misclassified data, you will notice that each characteristic value is very similar to the misclassified class, not its own. The accuracy of the improved algorithm has improved. There is no guarantee that the final results will be the best, and the relationship between them is not linear. The tree hierarchy can be reduced effectively in order to improve the classification result.

The focus of accounts receivable analysis should be on the liquidity analysis of accounts receivable. Through trend analysis and structure analysis, we can find out the changing rules of accounts receivable, then pay attention to accounts receivable in abnormal situations, and analyze the economic essence that causes abnormal changes. The p value of the Bartlett spherical test is close to 0, which indicates that there is a linear correlation between indicators, which is suitable for factor analysis. When the factor reaches the fourth place, the cumulative variance contribution rate is 95.32%, indicating that almost all the information of the original variable is retained. At this time, the number of factors is only 2/3 of the original, thus achieving the purpose of simplifying the indicators. Therefore, this article selects three factors for analysis, and the total explanatory variance is shown in Table 1.

Firstly, according to the comprehensive score of the owner unit, this article classifies the accounts receivable risk of the owner unit in the model sample and then finds out the dividing points of each level. The cluster analysis results are shown in Table 2.

After obtaining the evaluation results, carry out a risk assessment and select the appropriate collection strategy. Overdue accounts collection is the joint responsibility of the subsidiary business department and the legal department, and the legal department takes the lead in cooperation with the business department. Through various channels, we can fully and truly understand the reasons why the owner cannot pay the project payment on time. And the legal department of the business department shall adopt appropriate nodes to collect according to the split result and collection policy.

Table 1: Total variance of interpretation.

Component part	Total	Variance percentage	Cumulative%
1	2.201	36.252	36.252
2	1.936	30.287	68.632
3	1.002	15.642	85.241
4	0.425	8.869	93.368
5	0.225	4.213	99.012

Table 2: Cluster analysis results.

Central point	Sample size
−12.363	3
72.541	20
−69.283	1
30.325	14
−28.736	5

In order to easily reflect the role of dynamic principal component analysis in financial forecasting, we conducted three groups of experiments on three models. The first model: the original data are directly predicted by BPNN without any processing (called BP_A). Model 2: Firstly, the data are standardized to eliminate the industry differences, then the original data are processed by static PCA, and a new variable combination (called BP_B) is obtained. The third model is the same: the industry differences are corrected; first, the original data are processed by dynamic principal component analysis, and then the prediction is made by BPNN (called BP_C). The empirical results of the BP model are shown in Figure 6.

It can be seen from the experimental results that there is no difference between BP_B and BP_C, so there is no difference between their results. Compared with the BP_A model, the prediction accuracy is not greatly improved, but the stability is improved. However, because the BP_C model increases the amount of information without increasing the network input and the complexity of the network structure, it not only improves the accuracy but also keeps the stability. When using three-year data, although the complexity of the BP_A model is reduced and the accuracy is improved, it is still not as accurate as when using one-year data. Compared with BP_A, BP_B itself greatly reduces the input dimension, and its accuracy is also in the BP_C model. The input dimension and network complexity do not increase, which shows that the data have little impact on the business.

Here, we combine the dynamic principal component analysis with two network models to obtain two prediction models. In these two models, we select the single bound function and its first, second, and third derivatives to form the mapping function of network nodes. For the output node, we choose a single limiting function. For empirical data, we still use the three groups used above. The detailed results of the three datasets are shown in Figure 7.

Judging from the prediction results, compared with other types, the prediction accuracy of BPNN has been

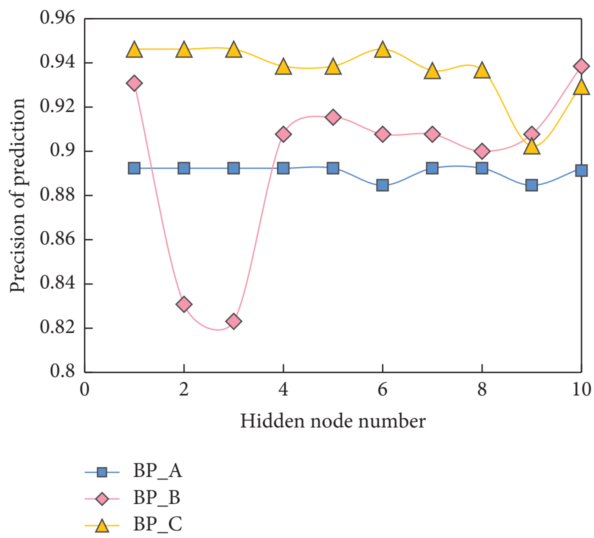

Figure 6: Empirical results of BP model.

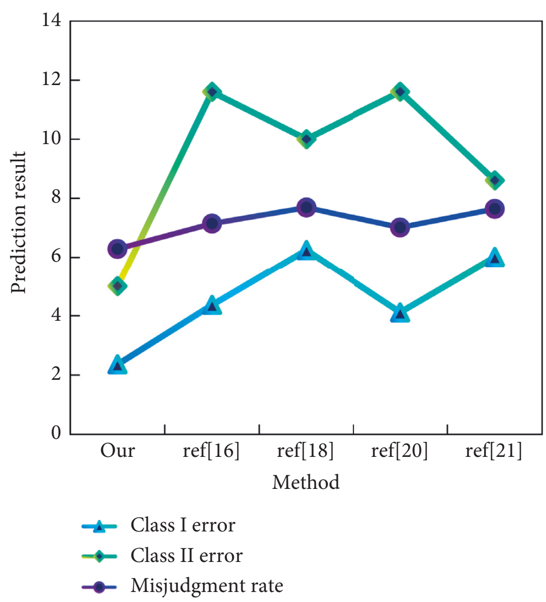

Figure 7: Detailed empirical results of three groups of data.

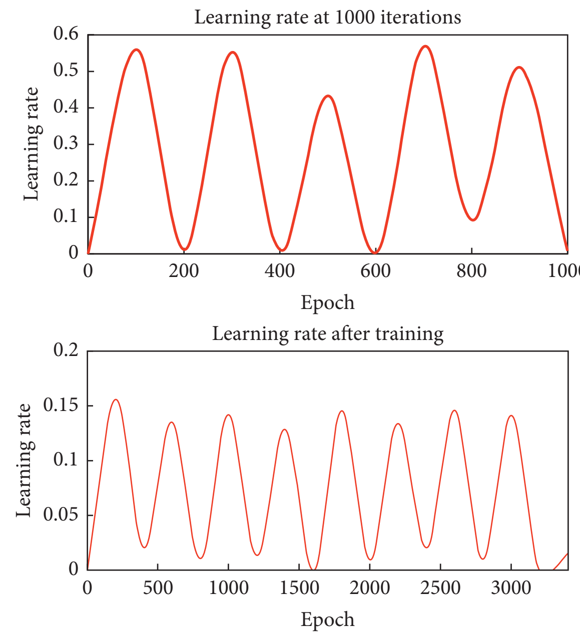

Figure 8: Learning rate curve after the training of financial distress early warning model.

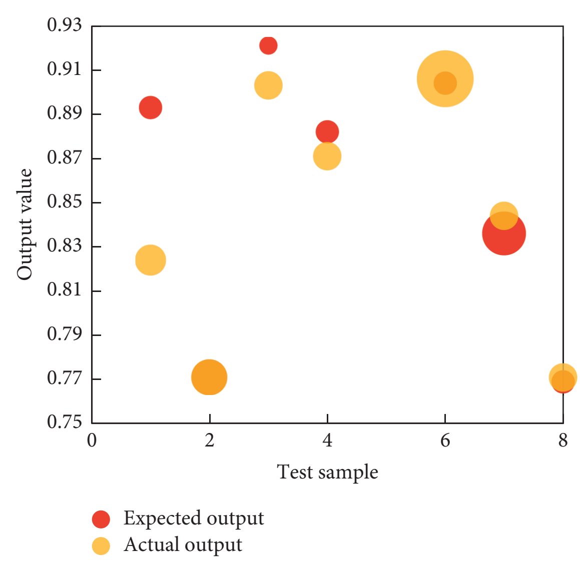

Figure 9: Judgment result of the neural model test.

significantly improved, especially after using data for many years; the prediction results have reached more than 90%, which is unmatched by other methods. Theoretically speaking, dynamic principal component analysis is used to select the variables of financial distress prediction, and an integrated network is used to predict the financial distress of listed companies, all of which have achieved ideal results. MATLAB is used to analyze and design the neural network system. First, a new M-File is created, and then a program is written in the editing bar. Because the input of this network model is a continuous variable, the premnmx function of MATLAB is used to normalize the training and unify the network output before processing. The learning rate curve of this network is shown in Figure 8.

Then the test sample is used for testing. See Figure 9 for the training and testing results.

The empirical research on the training, testing, and evaluation of the financial early-warning method model established in this article shows that the established neural network model has a good prediction effect and the actual results of the sample are close to the expected results, which are quite consistent, and its financial early-warning results are completely in line with its financial situation, which also shows that the application of BPNN in FinTech has a good prediction effect. On the other hand, the use of the BPNN algorithm and network topology configuration can be studied further, and a neural network and expert system combination can be used to see if the ability to predict financial difficulties can be improved. Naturally, this model has flaws, one of which is the number of nodes in the hidden layer. Constant training and sample testing are required to determine the number of nodes, and once convergence is achieved, the number of nodes meets the requirements. This procedure necessitates a significant amount of effort.

5. Conclusions

The shift from accounting to management accounting is a general trend that is unavoidable, given the new era's economic situation and the industry's long-term development. The role of enterprise accounting is changing, and the transition from financial to management accounting is speeding up, thanks to the advancement of modern information technology in the financial field. At the same time, management accounting is becoming more computerised. The government and other relevant departments must supervise the company internally. This document uses AI technology as the foundation for optimizing accounts receivable management in the integration mode and adopts a financial management optimization design based on AI to meet listed companies' accounts receivable management needs. The financial distress early-warning model of publicly traded companies is built using the BP neural network method. The empirical results show that, when compared to other types, BPNN has a significantly higher prediction accuracy. It has the potential to help operators take effective actions early in the financial crisis, improve their operating conditions, and avoid business failures.

Data Availability

The data used to support the findings of this study are available from the author upon request.

Conflicts of Interest

The author does not have any possible conflicts of interest.

References

[1] Y. Huang, L. Cheng, L. Xue et al., "Deep adversarial imitation reinforcement learning for QoS-aware cloud job scheduling," *IEEE Systems Journal*, vol. 5, 2021.

[2] J. Chen, C. Du, Y. Zhang, P. Han, and W. Wei, "A clustering-based coverage path planning method for autonomous heterogeneous UAVs," *IEEE Transactions on Intelligent Transportation Systems*, vol. 1, pp. 1–11, 2021.

[3] D. L. Eckles, R. E. Hoyt, and S. M. Miller, "Reprint of: the impact of enterprise risk management on the marginal cost of reducing risk: evidence from the insurance industry," *Journal of Banking & Finance*, vol. 49, pp. 409–423, 2014.

[4] M. Powell, A. Gillett, and B. Doherty, "Sustainability in social enterprise: hybrid organizing in public services," *Public Management Review*, vol. 21, no. 2, pp. 159–186, 2018.

[5] C. Kobrak, "Family finance: value creation and the democratization of cross-border governance," *Enterprise and Society*, vol. 10, no. 1, pp. 38–89, 2009.

[6] S. Hu and B. Yu, Eds., *Big Data Analytics for Cyber-Physical Systems*, Springer International Publishing, New York, USA, 2020.

[7] C. Liu, "Failures of enterprise-level unionization in China: implications for coalmine safety and beyond," *International Labour Review*, vol. 150, no. 1-2, pp. 163–175, 2011.

[8] G. Kirk and S. Beth Nolan, "Nonprofit mission statement focus and financial performance," *Nonprofit Management and Leadership*, vol. 20, no. 4, pp. 473–490, 2010.

[9] A. R. Bell and R. S. Dale, "The medieval pilgrimage business," *Enterprise and Society*, vol. 12, no. 3, pp. 601–627, 2011.

[10] T. Byrne, "Debating enterprise social software," *EContent*, vol. 32, no. 7, p. 29, 2009.

[11] J. James, "Plight of the fortune tellers: why we need to manage financial risk differently," *Financial Analysts Journal*, vol. 65, no. 2, pp. 86-87, 2009.

[12] F. D. e. Luca and E. Meschieri, "Financial distress pre-warning indicators: a case study on Italian listed companies," *The Journal of Credit Risk*, vol. 13, no. 1, pp. 73–94, 2017.

[13] M. H. Tinoco, P. Holmes, and N. Wilson, "Polytomous response financial distress models: the role of accounting, market and macroeconomic variables - ScienceDirect," *International Review of Financial Analysis*, vol. 59, pp. 276–289, 2018.

[14] J. Huang, H. Wang, and G. Kochenberger, "Distressed Chinese firm prediction with discretized data," *Management Decision*, vol. 55, no. 5, pp. 786–807, 2017.

[15] C. G. Gudmunson, S. Son, J. Lee, and J. W. Bauer, "EITC participation and association with financial distress among rural low-income families," *Family Relations*, vol. 59, no. 4, pp. 369–382, 2010.

[16] D. Besancenot and R. Vranceanu, "Financial distress and banks' communication policy in crisis times," *Romanian journal of economic forecasting*, vol. 1, pp. 5–20, 2008.

[17] A. Olafsson, "Household financial distress and initial endowments: evidence from the 2008 financial crisis," *Health Economics*, vol. 25, no. S2, pp. 43–56, 2016.

[18] S. Li, W. Shi, J. Wang, and H. Zhou, "A deep learning-based approach to constructing a domain sentiment lexicon: a case study in financial distress prediction," *Information Processing & Management*, vol. 58, no. 5, Article ID 102673, 2021.

[19] J. Zhou, X. Wei, J. Shi, W. Chu, and W. Zhang, "Underwater image enhancement method with light scattering characteristics," *Computers & Electrical Engineering*, vol. 100, Article ID 107898, 2022.

[20] J. Zhou, D. Liu, X. Xie, and W. Zhang, "Underwater image restoration by red channel compensation and underwater median dark channel prior," *Applied Optics*, vol. 61, no. 10, pp. 2915–2922, 2022.

[21] W. Cai and Z. Wei, "Remote sensing image classification based on a cross-attention mechanism and graph convolution," *IEEE Geoscience and Remote Sensing Letters*, vol. 19, pp. 1–5, 2022, Art no. 8002005.

[22] J. Zhang, W. Wang, C. Lu, J. Wang, and A. K. Sangaiah, "Lightweight deep network for traffic sign classification," *Annals of Telecommunications*, vol. 75, no. 7-8, pp. 369–379, 2020.

Hindawi
Computational Intelligence and Neuroscience
Volume 2022, Article ID 6492410, 11 pages
https://doi.org/10.1155/2022/6492410

Research Article

Analysis and Correction of Wrong Technical Actions in Juvenile Sports Training Based on Deep Learning

Xuefeng Zhao

College of Physical Education, Shaanxi Normal University, Xi'an, Shaanxi 710100, China

Correspondence should be addressed to Xuefeng Zhao; zxf1993@snnu.edu.cn

Received 4 April 2022; Revised 5 May 2022; Accepted 6 May 2022; Published 31 May 2022

Academic Editor: Xin Ning

Scientific analysis of students' incorrect actions in class, as well as timely and effective correction, is frequently an important link in the PE process. At the same time, it is an important symbol for assessing a teacher's teaching level and quality. In this paper, the analysis and correction model of sports wrong technical movements is built using DCNN to address shortcomings in the process of detecting wrong movements in PE and training. This article is based on CNN and has been enhanced by DL. The model learns both manual and DL features; the manual features use an improved dense trajectory, the DL features use CNN based on motion information, and the generalization ability of the kernel support vector machine is used to fuse the two. The simulation results show that the accuracy of the wrong action judgment of this method can reach 92.16 percent, which is 4.6 percent higher than the method of combining NN with region prediction and 5.7 percent higher than the method of detecting image matching score. This method can accurately describe the characteristics of human motion and identify incorrect movements, improve the ability of judging and correcting incorrect movements in sports training, and help athletes improve their sports level.

1. Introduction

With the continuous improvement of the technical level of sports, in the teaching process of sports technology, the demonstration of correct movements of sports has become a key research topic in the field of sports teaching [1]. Generally speaking, in the process of mastering motor skills, learners make mistakes, which can be prevented but cannot be absolutely avoided. Thus, correcting wrong actions has become an important task of PE (Physical education) and training [2]. In the actual PE teaching process, due to the obvious differences between students' cognition and understanding levels, some students have more wrong movements and are slow to master the correct movements of PE [3]. At the same time, in all kinds of sports, the technical specifications of movements are more complicated. Especially for some highly technical sports, it is necessary to carry out standardized training with correct movements to improve the level of sports training. In this state, how to effectively correct the wrong movements in sports has become the main problem to be solved urgently in this field. Due to the further development of research in related fields, computer image processing technology has been widely used in sports movement recognition. However, at present, there are various complex movements in sports training, and it is difficult to accurately judge the wrong movements by relying solely on traditional contour detection methods, which leads to the athletes' inability to get movements corrected in time.

With the continuous progress of computer science and technology, artificial intelligence technology [4, 5] has gradually matured. Once the concept of DL (Deep learning) [6, 7] was put forward, a large number of scholars devoted themselves to studying DL and made great progress and innovation. Nowadays, DL has been widely used in the process of human motion recognition and target detection. DL comes from the study of artificial NN (Neural network). In DL, it includes CNN (Convolutional neural network), cyclic NN, Boltzmann machine, etc., but now CNN is the most widely used one. Deep NN can automatically learn data features so as to discover sparse and distributed big data features. However, due to the poor hierarchy of the depth NN constructed in the current research and the failure to further process the action samples, the applicability of this method to the detection of wrong actions in PE teaching and training is poor. This technology can not be directly applied to capture human motion data. Scientific analysis of students' wrong actions in teaching, and timely and effective correction, is often an important link in the process of PE. It is also an important symbol to measure a teacher's teaching level and teaching quality. Based on the idea of improving the teaching quality, this paper improves the shortcomings of the current methods one by one, and builds a technical action analysis and correction model of sports errors based on DCNN (Deep convolution neural network). In order to quickly and accurately detect the wrong movements in PE and training and further improve the sports level of athletes. The innovations of this article are as follows:

(1) In view of the shortcomings in the process of detecting the wrong actions in PE and training, this paper is based on CNN and improves it through DL, adding a batch classification layer in the middle of the convolution layer and pool layer, and processing the wrong action samples in PE and training through batch normalization. Given the previous frame, the network can learn to predict the future moving frame and train the time encoder of human motion.

(2) In order to meet the needs of large-scale data sets and small-scale motion recognition at the same time, a human motion recognition algorithm based on multifeature fusion and motion information is designed. Through data enhancement, feature optimization, and transfer learning, the detection model in this paper is optimized to improve the detection accuracy and realize the real-time detection of the target. And through self-designed visual calibration objects, the uniqueness detection of multiperson identity can be realized. Experiments show that the algorithm can effectively identify large-scale data sets and small-scale actions.

The article is divided into five parts, which are arranged as follows: The first chapter is the introduction. This part summarizes the background and research significance of this paper and gives the organizational structure and innovation of this paper. The second chapter is related work. This chapter briefly describes the research status of motion recognition methods and target detection and analysis at home and abroad. And the research work and methods of this paper are introduced. The third chapter is divided into two parts. Section 3.1 outlines the concept of DL and related theoretical basis and introduces the related content of human motion detection based on DL. Section 3.2 puts forward and constructs the technical action analysis and correction model of sports errors based on DCNN. In chapter 4, the model proposed in this paper is simulated for many times, and the results are analyzed. The fifth chapter is the conclusion. This chapter summarizes the research work of this paper and looks forward to the future.

2. Related Work

Accurate recognition and analysis of human body posture can provide effective data support for sports training. By obtaining the relevant data of human movement and correcting the details of athletes' movements with the data of standard database, the athletes' sports level can be improved. Because of the far-reaching development significance, the detection and correction of wrong movements in sports have also become the focus of research in the industry, which has received extensive attention, and many detection methods have also appeared.

Miao et al. designed an action recognition method based on depth images. The algorithm projects the depth image in three projection planes, extracts features from the three projection images, and uses these features to train the extreme learning machine classifier. The algorithm is computationally efficient, but its performance is not ideal for small-amplitude action recognition [8]. Arrieta et al. proposed a temporal deep belief network that can complete online human action recognition [9]. Kluding et al. proposed a gesture feature extraction and recognition method based on acceleration trajectory images. The algorithm converts unknown gesture trajectory features into low-dimensional subfeature sequences by establishing an acceleration gesture trajectory map, which improves the accuracy and time efficiency of gesture recognition [10]. Ullah et al. model human motion information through asymmetric systematic bias [11]. The recognition algorithm proposed by Yao et al. achieves high recognition accuracy for small-amplitude movements, but the amount of features to be analyzed is large, which is difficult to apply to large-scale data sets [12]. Yassine et al. used two-dimensional wavelet packet technology and spatial clustering technology to analyze human behavior and actions and improved the accuracy of wrong action detection by analyzing PE training images. However, the features extracted by the two-dimensional wavelet packet technology are not comprehensive enough, so the subsequent detection results deviate greatly from the actual ones, while the spatial clustering technology is too extensive, ignoring the detailed features of the image edges, and the detection results are prone to errors [13]. Belczak et al. proposed a 3D modeling and detection method for wrong action images in sports without background information [14]. Department et al. proposed an image reconstruction method for wrong action images in sports based on feature moving frame differential scanning and adaptive compensation. In this method, infrared projection and edge contour feature extraction are performed on the wrong action images collected in sports, and the box filtering method is used for image filtering to improve the accuracy of image detection. This method is susceptible to disturbances, resulting in a high error rate for false action detection [15]. Mi et al. proposed a 3D modeling detection method for wrong actions in sports based on 3D contour feature decomposition [16]. The method proposed by Cai et al. uses edge contour reconstruction to repair the missing information of the image and uses the zero-cross point feature segmentation and corner detection method to perform adaptive positioning and detection of wrong actions in sports, image classification, and screening. This method improves the detection and recognition ability of wrong actions [17].

In this paper, the traditional methods of moving target detection and motion recognition are summarized, and their advantages and disadvantages are analyzed. Given the shortcomings in the current detection process of incorrect movements in PE teaching and training, a model for analyzing and correcting incorrect technical movements in PE is built using DL. The model learns both manual and DL features; the manual features use an improved dense trajectory, the DL features use CNN based on motion information, and the generalization ability of the kernel support vector machine is used to fuse the two. The detection model in this paper is optimized through data enhancement, feature optimization, and transfer learning to improve detection accuracy and achieve real-time detection of the target. Furthermore, the detection of multiperson identity uniqueness can be realized using self-designed visual calibration objects. This method can accurately describe the characteristics of human motion, identify incorrect movements in sports training, and improve the ability to judge and correct incorrect movements. It has theoretical and practical implications in the field of sports action recognition and correction.

3. Methodology

3.1. Human Motion Detection Based on DL. Artificial NN is an algorithm model inspired by nature and constructed by simulating human brain nerve activity. The basic unit of artificial NN is the neuron, which is also the most basic unit for processing all information. By simulating the process of the human neuron processing external stimuli, the neuron appears as a many-to-one nonlinear mapping unit. DL comes from the research of artificial NN [18]. There are four basic models of DL. Specifically: (1) Automatic encoder, sparse automatic encoder, and noise reduction automatic encoder with their variants. (2) Limiting Boltzmann machine. (3) Convolution Boltzmann machine. (4) Circulation NN. Action recognition is influenced by different lighting conditions, diverse perspectives, complex backgrounds, and great changes within a class. In this field, the improved dense trajectory method is the best method of traditional methods. It has good stability and the highest reliability, but the algorithm is very slow. The appearance of DL provides a new idea for action recognition and achieves good results.

DCNN is a multilayer backpropagation artificial NN designed for shape recognition in DL. Each layer of neurons is linked to the local visual field area where the front layer network intersects, but there are no connections between neurons in the same layer. DCNN is primarily a type of NN that employs DL to improve CNN by displaying changeable levels and backward propagation direction, allowing for error action detection [19]. Weight sharing and local connection are features of DCNN, which greatly reduce network complexity and improve algorithm performance. As a result, DCNN is the most popular NN [20]. The pooling layer is usually connected after the convolution layer. Then the convolution layer is alternated with the full connection layer. Convolution kernels of various sizes can be used to improve the overall generalization performance of the network during the convolution process. A classifier will be connected at the end of the network to classify the input data. The process of object detection based on deep learning is shown in Figure 1.

DCNN has certain advantages. It includes the following: (1) Minimize pretreatment. Most of the input data are raw data that have not been processed many times, and there is no accurate mathematical expression between input and output. Its feature extraction is trained within the network, which avoids the subjectivity and limitations of manual feature extraction. (2) DCNN is influenced by time delay NN and adopts the network structure of weight sharing, which reduces the computational complexity in the process of network training and makes it more suitable for time series data. DCNN weights are shared and the calculation during training is relatively simple, which can be widely used in the process of time series data analysis, and it can change the capacity of the wrong action detection model in PE and training through the depth and breadth of the network structure. The structure of the dual-flow network is that two NN mix features before the final decision. For the spatial information feature extraction network, only the intercepted video frames need to be grouped into network training to get the spatial features. For the time information feature, the optical flow information of several consecutive frames is usually selected as the input of the network and then added to the network for training. The intrinsic characteristics of the signal, the statistical characteristics of one part may be the same as those of other parts. Therefore, a small subimage can be randomly selected from the image for feature learning, and then the feature can be used as a filter to scan the whole image, and a different feature activation value can be extracted at each position of the whole image, thus realizing feature extraction of the image.

Intercepting video frames according to a set frame rate is the simplest way to deal with video for motion recognition. Processing video frames requires significantly less computation than directly processing video data. Pooling the feature map obtained from the convolution layer through the pooling layer yields the corresponding pooled feature map. A feature extractor is analogous to a convolution kernel. Different convolution kernels can be designed to extract features at different levels in the image, and all of the features processed by convolution kernels are then combined as the output of the convolution layer, so convolution kernel design is crucial. Convolution kernel size, number, and step size can all be customized. The convolution operation is carried out in the cube by combining several consecutive video frames into a video frame cube. The sequential convolution operation involves performing three consecutive video frames at the same time, and the time dimension of the convolution kernel is three, making it a three-dimensional convolution kernel. The video frame

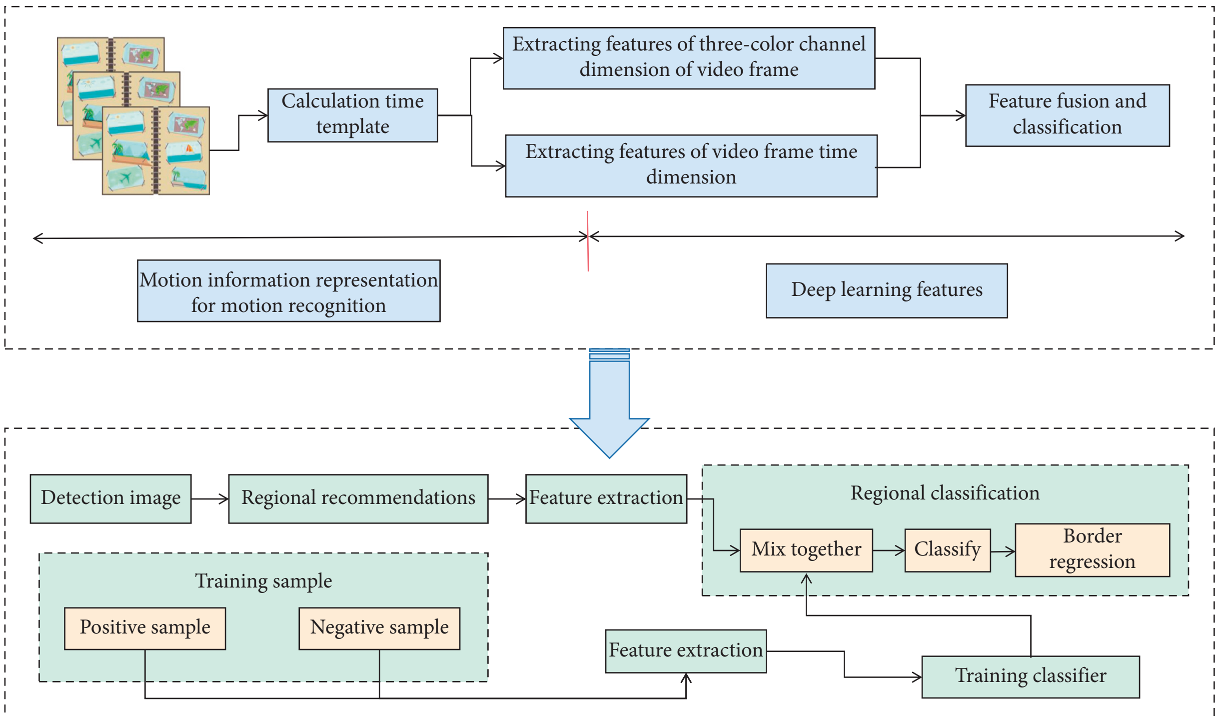

Figure 1: Target detection process based on deep learning.

cube's convolution kernel weights are shared. A variety of convolution kernels are used for convolution layer operation in order to better obtain the information in the video frame.

3.2. Analysis and Correction Model of Technical Action of Sports Errors. DCNN weight sharing has a network structure that is more similar to biological perception NN, and it can adjust model capacity by changing the depth and breadth of the network structure, which has strong statistical stationarity and pixel local correlation for natural images. Convolution and pooling are two important DCNN links. As a result, one of the key factors that determine the performance of a DCNN structure is the choice of convolution kernel size and sliding step size, pool kernel size, and sliding step size. The model's parameter training is also a critical factor in determining the network structure's performance. Because CNN requires a large number of training parameters, the model's complexity is high, which could lead to the trained model's error rate on the training set decreasing while the error rate on the verification set increases. The main reason is that in the training process, every input must be considered, and there are numerous parameters to consider. A small change in the input data has a big impact on the outcome, so keeping the parameters as small as possible is the problem that needs to be solved right now.

In this paper, the regularization method is frequently used in the full connection layer to prevent overfitting due to the small size of the data set used in the DCNN process. Because of the randomness of this method, the network structure corresponding to each transmitted data set will be inconsistent, but all network weights will be shared, greatly improving the stability of the wrong action detection model in PE and training and making it easier for neurons to adapt to one another. Every pixel in a video frame or image is made up of three primary colors. The amount of data read at one time during network training is large, which has a significant impact on the computer's computing speed. When training the model, end-to-end training can be done when the two pieces of information match, and the corresponding real frame can be chosen from a list of default frames with various aspect ratios, scales, and positions. The batch normalization algorithm is used in the batch normalization layer in this paper, which integrates the network layer input processing operation into the wrong action detection of PE and training. It processes the wrong action samples of PE and training through microbatch normalization. The flow of sports movement detection and analysis using this method is shown in Figure 2.

The size of convolution kernel has obvious influence on image processing. If the convolution kernel used is too small, the enhancement effect of the action information of interest to the image is not obvious, but it may increase the noise in the same frequency band and cover up some original details of the image. If the convolution kernel used is too large, the calculation amount of convolution will also increase, resulting in higher computational complexity. According to a large number of applications of DCNN structures in human motion recognition, this paper finds that the convolution kernel size is 3×3 convolution network structure. ResNet residual network is an improvement to solve the problem of deep network structure degradation. ResNet is based on the cross-layer connection structure of Highway Network. The number of layers of residual network is usually

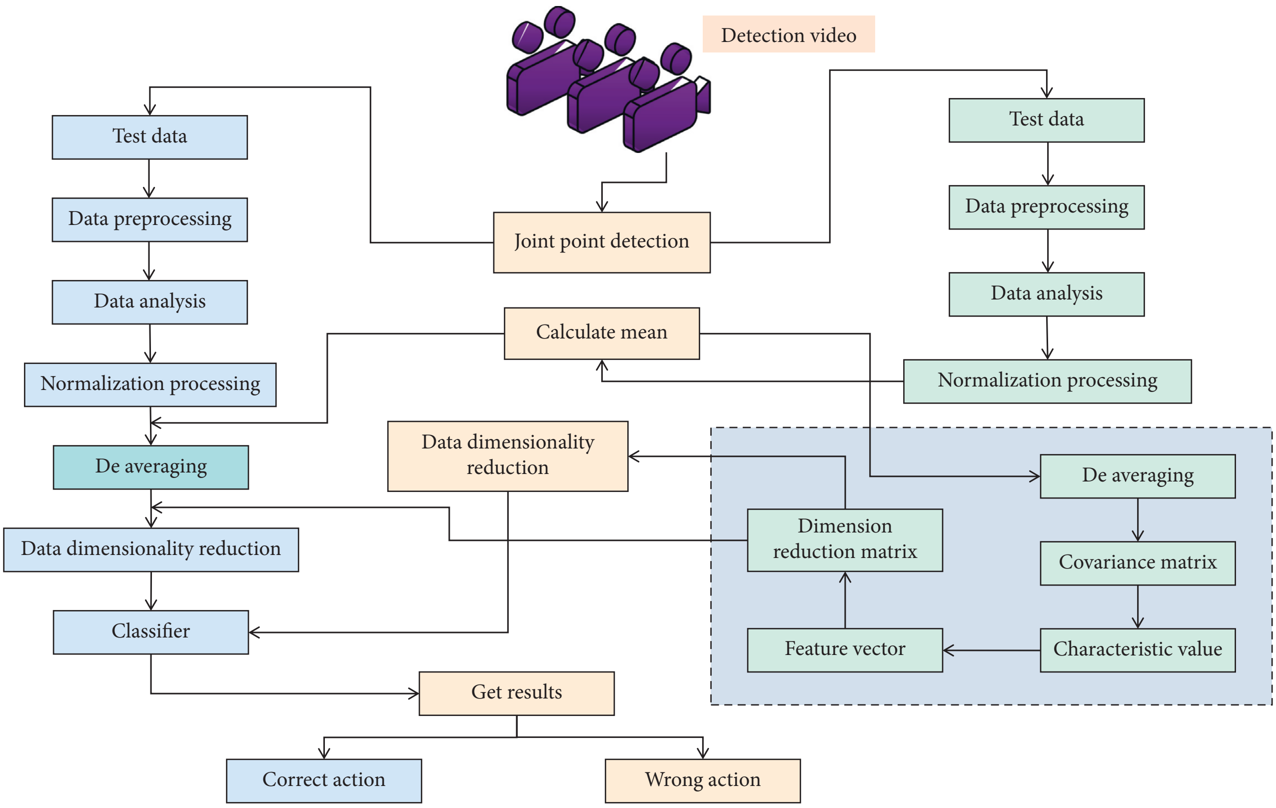

FIGURE 2: Sports action detection and analysis process.

very large, up to 100 layers, but this fast connection method makes the actual depth of the network not too deep. Experiments show that residual network can well solve the problem of deep network degradation. When the auxiliary features are used as input to pass through the last hidden layer of the proposed model and connected with the auxiliary output points, and the extracted features are closer to the output of the auxiliary features in the training stage of the proposed network model, the regularization of the model is completed. The convolution layer of DCNN applies the weight sharing method, and at the same time, it reduces the structural parameters and difficulty, prevents NN from overfitting in the early stage, makes it have better generalization ability, and ensures the stability of NN through pooling. Suppose the formula of the fully connected layer feature output $x^{(l)}$ of the l layer is as follows:

$$x^{(l)} = f\left(w^{(l)} x^{(l-1)} + b^{(l)}\right). \tag{1}$$

Among them, $w^{(l)}$ represents the weight parameter, and $b^{(l)}$ is the bias term. The Softmax regression classifier needs to iteratively update and learn, and the functions to be learned are as follows:

$$h_w(\overrightarrow{x}) = \frac{1}{\sum_{i=1}^{k} e^{\overrightarrow{w_i}\cdot\overrightarrow{x}+b_i}} \begin{bmatrix} \overrightarrow{w_1}\cdot\overrightarrow{x}+b_1 \\ \overrightarrow{w_2}\cdot\overrightarrow{x}+b_2 \\ \cdots \\ \overrightarrow{w_k}\cdot\overrightarrow{x}+b_k \end{bmatrix}. \tag{2}$$

Among them, k represents the number of categories to be classified, and b_i and $\overrightarrow{w_i}$ represent the offset vector and weight vector corresponding to the i th category. (3) represents the probability value that the sample $\overrightarrow{x}$ is the j class.

$$P(y=j\,|\,\overrightarrow{x}) = \frac{\overrightarrow{w_j}\cdot\overrightarrow{x}+b_j}{\sum_{i=1}^{k} e^{\overrightarrow{w_i}\cdot\overrightarrow{x}+b_i}}\ \sum_{j=1}^{k} P(y=j\,|\,\overrightarrow{x}) = 1. \tag{3}$$

After training and learning to get $\overrightarrow{w_i}$ and b_i, the objective loss function can be expressed as follows:

$$J(w,b) = -\frac{1}{m}\sum_{j=1}^{m}\sum_{l=1}^{k} 1\left\{y^{(j)} = l\right\}\log\frac{e^{\overrightarrow{w_l}\cdot\overrightarrow{x}+b_l}}{\sum_{i=1}^{k} e^{\overrightarrow{w_i}\cdot\overrightarrow{x}+b_i}}. \tag{4}$$

Among them, m represents the number of samples in the training set, k represents the number of classification categories, and $1\{\cdot\}$ is an indicative function. When $y^{(j)} = l$, the function value is 1. Otherwise, it is 0. Optimized by an autoencoder for high-dimensional input data $x \in R^N$:

$$\min_{f,g} \|x - f(g(x))\|. \tag{5}$$

Among them, the encoder $y = g(x)$ maps the input data to the low-dimensional space $y \in R^M, N > M$. Let $x \in R^N$ be the observations of time t. The optimization function of the time encoder is as follows:

$$\min_{f,g}\left\| X_{(t+1):\ (t+\Delta t)} - f\left(g\left(X_{(t-\Delta t+1):\ t}\right)\right)\right\|, \tag{6}$$

where the encoder $y = g(X_{(t-\Delta t+1):t})$ maps the input data to the low-dimensional space $y \in R^M$, $(N \times \Delta t)n!/r!(n-r)! > M$. The decoder $\widehat{X}_{(t+1):(t+\Delta t)} = f(y) \in R^{N\times\Delta t}$ is used to map back to the data space.

Neurons appear with a certain probability in each layer of the network structure, causing the training network to change every time, reducing the correlation between neurons and increasing the generalization and robustness of the entire network. The depth of NN affects the detection accuracy of incorrect movements in sports, and the features are related to representation ability. The NN depth will calculate all of the features of incorrect movements, and the deeper the final output, the better the feature extraction ability. The extreme learning machine is divided into two layers: the first calculates two feature cores, then fuses the two to form a fused feature core, and finally outputs the predicted scores of the three feature cores. All of the predicted scores are mapped to the final action classification by the second training classifier. This method's manual and DL features complement each other, and the video's human motion information is described from various perspectives. The independent batch normalization process replaces the joint normalization process of each dimension of data, and the formula is as follows:

$$\widehat{X}^{(k)} = \frac{x_i^{(k)} - E\left[x^{(k)}\right]}{\sqrt{\operatorname{var}\left[x^{(k)}\right]}}. \tag{7}$$

Among them, the k th dimension of the input sample is denoted by $x^{(k)}$, the expectation is denoted by $E[x^{(k)}]$, and the variance is denoted by $\operatorname{var}[x^{(k)}]$. Adding parameters $\lambda^{(k)}$ and $\beta^{(k)}$ to the k dimension of each input sample, the following formula is obtained:

$$y^{(k)} = \lambda^{(k)}\widehat{X}^{(k)} + \beta^{(k)}. \tag{8}$$

Among them, $\lambda^{(k)}$ and $\operatorname{var}[x^{(k)}]$ are equal and both are variances. The local binary fitting method is used to complete the information collection and the reconstruction of the feature database, and the regional pixel information can be obtained:

$$L = J(w,e) - \sum_{i=1}^{N} a_i\left\{w^T \varnothing(x_i) + b + e_i + y_i\right\}. \tag{9}$$

Among them, $J(w,e)$ refers to the repeated pixels of the motion position; x_i and y_i are the correct action and wrong action feature vectors of the i th Gaussian unit, respectively; a_i is the standard action configuration sequence; $\varnothing(x_i)$ is the contour feature distribution function. By estimating the probability of the motion feature obtained by dimensionality reduction in the Gaussian unit i, we can get the following:

$$r(i) = \frac{w_i p_i - v_i}{\sum_{i=1}^{k} w_i p_i(v_i)}. \tag{10}$$

Among them, p_i refers to the probability of being assigned to the i th Gaussian unit, and w_i is the mixing weight.

A low-dimensional mapping, that is, a fixed-length feature vector, is generated for each $n \times n$ sliding window position, and then these feature vectors are sent to two fully connected layers, respectively, one for border regression and the other for predicting the category of the sliding window target; that is, the transformation parameters of the border position are given. Because the gray-scale data and the original data are identical in video length, data set size, action types, etc., except for the single pixel data of the image, the gray-scale image is chosen to preliminarily determine the training parameters of the network structure. In the process of deepening the network depth, it is easy for the gradient to disappear, which leads to a decline in network performance. To solve this problem, the basic network used to extract features by DCNN is ResNet101, which can extract the subtle features of PE training sample data faster and better. At the same time, in the middle of the convolution layer and pooling layer, the normalized layer and residual block are added in batches through ResNet, which can speed up the network training and adjust the data transmission strategy to further optimize the network performance.

4. Result Analysis and Discussion

In DL, the more effective samples are produced, the better the robustness of the trained model will be. Therefore, this paper uses some data enhancement strategies at the beginning of the network and carries out some random operations for each input sample picture, including using the original input sample picture; Sampling the original picture at random; Cut the original picture randomly, etc. After the above operation, the sample sizes of all samples are normalized, and the samples are randomly flipped horizontally with a certain probability. In order to determine the batch size of network training, the network training is carried out at every 10 groups of samples based on the batch data from 10 to 100 under the condition of 10 iterations, 20 iterations, and 100 iterations, respectively. Among them, the parameter settings of DCNN are shown in Table 1.

In order to comprehensively evaluate the performance of this algorithm, experiments were carried out on video dataset A and video dataset B, respectively. Data set A has a low resolution and a large amount of data, which can test the recognition performance of this algorithm for large-scale data sets. The video data set B has a high resolution, including 35 actions, all of which are local actions of the human body, with a small range of actions. This data set can test the recognition effect of this algorithm for small-amplitude actions. During the experiment, the data set used in this paper is a nonpublic data set. All experimental data are divided into two groups on average, one for DCNN training and the other for experimental testing. The accuracy of action recognition of different methods on two data sets is shown in Figures 3 and 4.

In this paper, we sort the confidence of the default boxes of negative samples, then select some default boxes in the front as samples, and discard all other negative samples, so that the final ratio of positive and negative samples is about 1 : 3. Experiments show that this operation can accelerate the

Table 1: Parameter settings of DCNN.

Number of plies	Function
1	Input layer
2	Convolution layers 3-64
3	Maximum pool layer
4	Convolution layers 3-128
5	Convolution layers 3-128
6	Maximum pool layer
7	Convolution layers 3-256
8	Convolution layers 3-256
9	Maximum pool layer
10	Convolution layers 3-512
11	Convolution layers 3-512
12	Maximum pool layer
13	Convolution layers 3-512
14	Convolution layers 3-512
15	The full connection layer 3072
16	Output layer

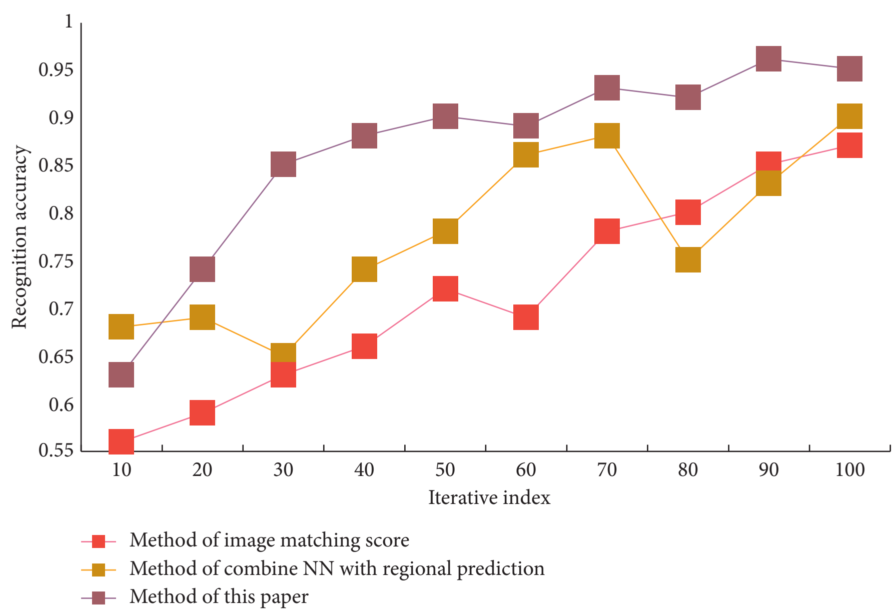

Figure 3: Action recognition accuracy of different algorithms—dataset A.

convergence speed, and the training process is more stable, which is a very effective optimization strategy. In this paper, representative F1 indicators are plotted as data as shown in Figure 5.

In the process of recognition, the processing of different frames will also occupy different sizes of computing resources. In order to reduce the use of computing resources, before the network training, firstly, the key area of human motion is detected by the method of target detection, and this area is cut out, which is used as new data to join the network for training. The method in this paper, the method of combining NN with regional prediction and the method of image matching score are used to detect the wrong actions in the process of PE teaching and training, and the effects of the three methods in detecting the wrong actions in PE teaching and training are compared with the increasing number of experiments. The effects of three different methods on detecting the wrong actions in PE teaching and training on two data sets are shown in Figures 6 and 7.

From the data analysis in Figure 7, it can be seen that the method in this paper has a certain accuracy in judging wrong actions. Among them, the error judgment accuracy of this method is about 92%, the error judgment accuracy of the method combining NN with regional prediction is about 87%, and the error judgment accuracy of the image matching score method is about 86%. The problem of small target detection is addressed in this paper by adding another layer to the feature selection layer, selecting lower-level features, and retaining more lower-level detail features. The video data is preprocessed as network input and the network parameters are effectively trained. The extracted motion features are then convolutioned and

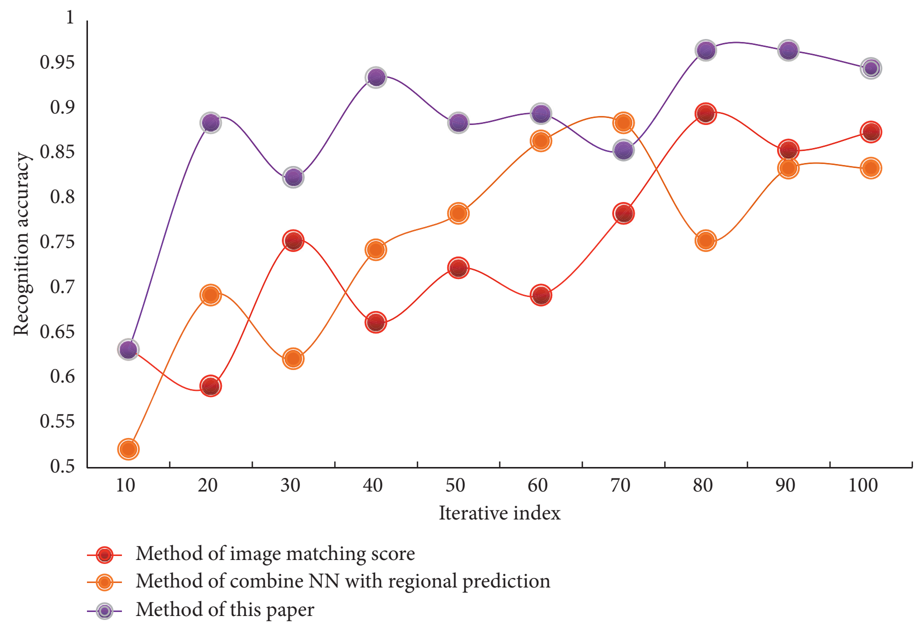

Figure 4: Action recognition accuracy of different algorithms—dataset B.

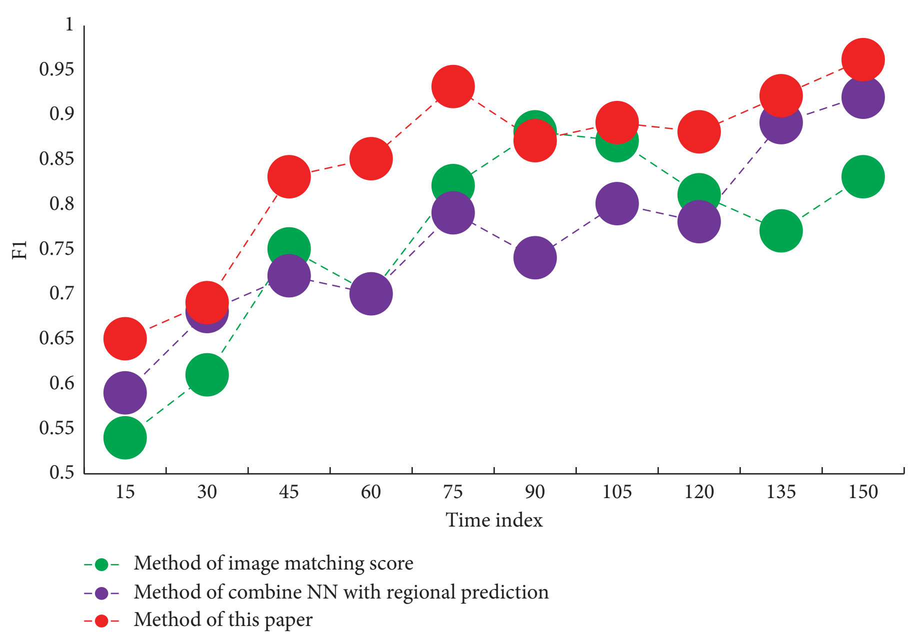

Figure 5: F1 value comparison.

pooled to add more time and space dimension information. Finally, it passed through the softmax classifier, which improved the accuracy of human motion recognition and better adapted to different changes in video data scenes, thanks to two layers of full connection. Six test indexes, namely accuracy, recall, sensitivity, complexity, specificity, and positive prediction rate were used for quantitative comparison in order to verify the effectiveness and robustness of this method in the detection of incorrect movements in sports training. The comparison results are shown in Table 2.

The data analysis in the table shows that among the three methods of detecting incorrect actions in PE teaching and training, the six parameters of this method are better than the method of combining NN with regional prediction and the method of image matching score. The model in this paper has fewer parameters, which reduces overfitting and reduces structural redundancy, resulting in a faster convergence speed and a shorter training period. It improves the accuracy of recognizing sports incorrect actions and reduces running time to some extent. This confirms the superior performance of the DCNN proposed in this paper.

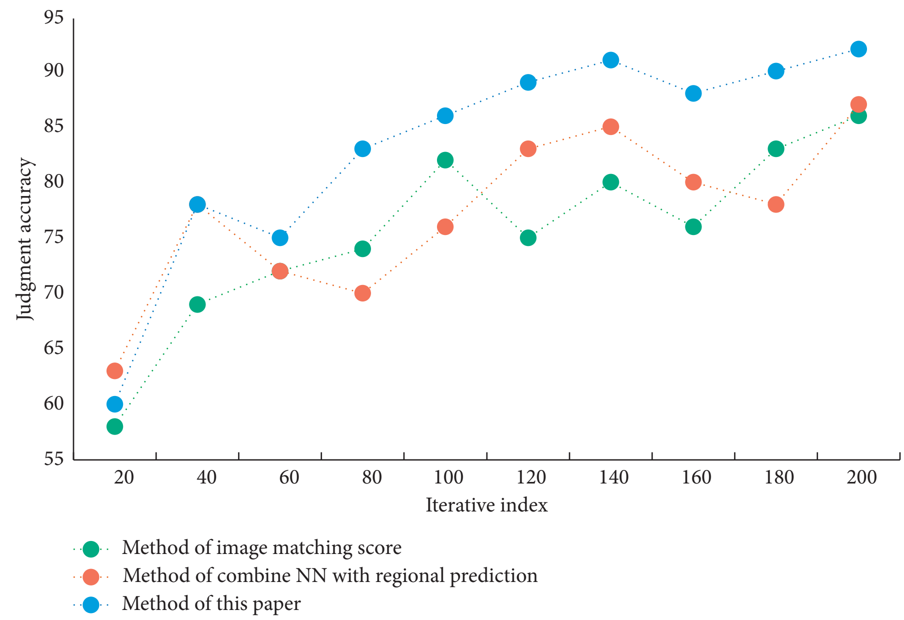

Figure 6: The effect of different algorithms for detecting wrong actions in PE training—dataset A.

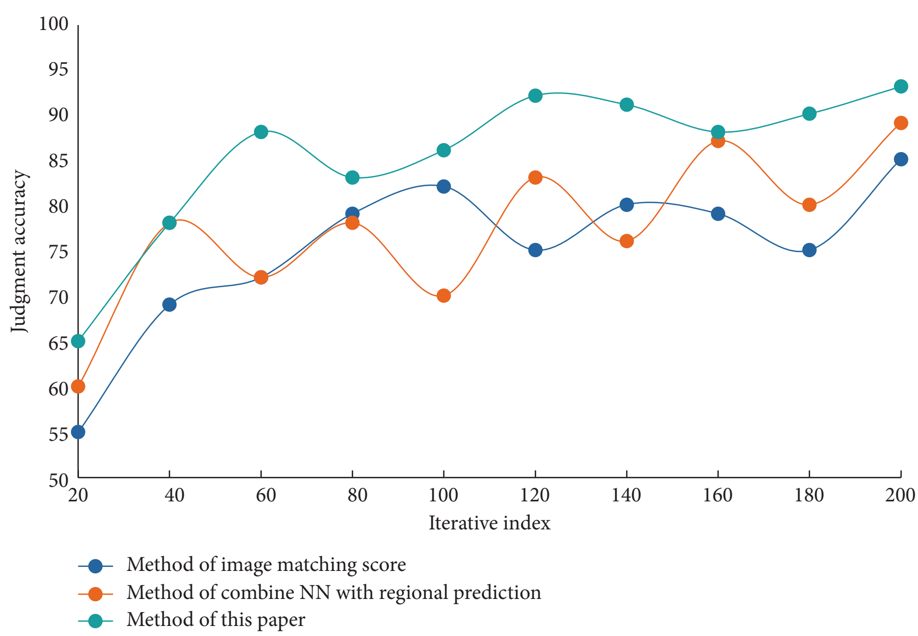

Figure 7: The effect of different algorithms for detecting wrong actions in PE training—dataset B.

Table 2: Detection results of wrong actions in PE training with different methods.

Test index	Methods of this paper	Method of combining NN with regional prediction	Method of image matching score
Accuracy rate	0.927	0.879	0.861
Recall rate	0.948	0.906	0.874
Sensitivity	0.948	0.891	0.876
Complexity	0.642	0.726	0.774
Specificity	0.026	0.054	0.113
Positive predictive rate	0.098	0.214	0.239

5. Conclusions

It is natural for students to make mistakes when learning new movements in technology classes, and teachers should prevent and correct these errors. Preventing and correcting incorrect movements in technology teaching is a necessary condition for effectively exercising and avoiding sports injuries. However, due to the variety of complex movements in sports training, it is difficult to accurately judge the incorrect movements using traditional contour detection methods, resulting in athletes being unable to correct the movements in a timely manner. Traditional methods, on the other hand, are unable to accurately capture the incorrect movement characteristics of PE teaching and training, resulting in decreased detection accuracy. This paper proposes a DCNN-based detection model of incorrect actions in PE teaching and training based on this information. The model learns manual and DL features, with the manual features using an improved dense trajectory and the DL features using a CNN based on motion information, and the two features are fused using the generalization ability of a kernel support vector machine. Simulation experiments are conducted in this paper to demonstrate the efficacy of the method proposed in this paper for detecting incorrect actions in PE teaching and training. The results show that the accuracy of wrong action judgment can reach 92.16 percent, which is higher than the 4.6 percent accuracy of the method that combines NN and region prediction and the 5.7 percent accuracy of the method that detects image matching score. The accuracy and robustness of human motion feature analysis are improved because the network structure used in this paper can directly classify actions on features without fine-tuning. The findings show that this method can accurately detect athletes' incorrect movements during PE and training, control detection errors, and judge incorrect movements quickly and accurately. For the field of sports action recognition and correction, this study has some theoretical and practical relevance. Despite the fact that this paper yielded some research findings, it still has some flaws that need to be investigated and improved. We will continue to research how to improve timeliness and immediacy while also increasing recognition accuracy in future work. In PE teaching and training, provide strong technical support for detecting incorrect movements.

Data Availability

The data used to support the findings of this study are available from the author upon request.

Conflicts of Interest

The author does not have any possible conflicts of interest.

References

[1] H. Jiang and S.-B. Tsai, "An empirical study on sports combination training action recognition based on SMO algorithm optimization model and artificial intelligence," *Mathematical Problems in Engineering*, vol. 2021, Article ID 7217383, 11 pages, 2021.

[2] Y. Bai and Y. Chen, "Human motion analysis and action scoring technology for sports training based on computer vision features," *Journal of Intelligent and Fuzzy Systems*, vol. 2021, no. 34, pp. 1–9, 2021.

[3] X. Wang, L. Gao, J. Song, and H. Shen, "Beyond frame-level CNN: saliency-aware 3-D CNN with LSTM for video action recognition[J]," *IEEE Signal Processing Letters*, vol. 24, no. 99, pp. 510–514, 2017.

[4] D. Yao, Z. Zhi-li, Z. Xiao-feng et al., "Deep hybrid: multi-graph neural network collaboration for hyperspectral image classification[J]," *Defence Technology*, vol. 2022, 2022.

[5] J. Chen, C. Du, Y. Zhang, P. Han, and W. Wei, "A clustering-based coverage path planning method for autonomous heterogeneous UAVs," *IEEE Transactions on Intelligent Transportation Systems*, vol. 2021, pp. 1–11, 2021.

[6] Z. Huang, Y. Liu, and C. Zhan, "A novel group recommendation model with two-stage deep learning[J]," *IEEE Transactions on Systems, Man, and Cybernetics: Systems*, vol. 145, 2021.

[7] W. Cai, Y. Song, and Z. Wei, "Multimodal data guided spatial feature fusion and grouping strategy for E-commerce commodity demand forecasting," *Mobile Information Systems*, vol. 2021, Article ID 5568208, 14 pages, 2021.

[8] X. Miao, Z. Hong, H. Wang, M. Sun, and D. Yuan, "ARCH: adaptive recurrent-convolutional hybrid networks for long-term action recognition[J]," *Neurocomputing*, vol. 178, no. 4, pp. 87–102, 2015.

[9] H. Arrieta, C. Rezola-Pardo, S. M. Gil, J. Irazusta, and A. Rodriguez-Larrad, "Physical training maintains or improves gait ability in long-term nursing home residents: a systematic review of randomized controlled trials," *Maturitas*, vol. 109, pp. 45–52, 2018.

[10] P. M. Kluding, S. K. Bareiss, M. Hastings, R. L. Marcus, C. R. Sinacore, and M. J. Mueller, "Physical training and activity in people with diabetic peripheral neuropathy: a paradigm shift[J]," *Physical Therapy*, vol. 97, no. 1, pp. 31–43, 2017.

[11] A. Ullah, J. Ahmad, K. Muhammad, M. Sajjad, and S. W. Baik, "Action recognition in video sequences using deep Bi-directional LSTM with CNN features," *IEEE Access*, vol. 6, no. 99, pp. 1155–1166, 2018.

[12] G. Yao, T. Lei, and J. Zhong, "A review of convolutional-neural-network-based action recognition[J]," *Pattern Recognition Letters*, vol. 118, no. 2, pp. 14–22, 2018.

[13] N. Yassine, C. Helmi, S. Senda et al., "Effects of plyometric training on physical fitness in prepuberal soccer athletes[J]," *International Journal of Sports Medicine*, vol. 38, no. 05, pp. 370–377, 2017.

[14] S. Belczak, G. C. Mulatti, and A. Sergio Ricardo, "Effects of combined resistance training and plyometrics on physical performance in young soccer players[J]," *International Journal of Sports Medicine*, vol. 94, no. 11, pp. 906–914, 2015.

[15] P. Department of, "Perceived skills and abilities required by athletic trainers in hospital and clinical management positions: a delphi study[J]," *Journal of Athletic Training*, vol. 48, no. 1, pp. 87–91, 2017.

[16] C. Mi, Z. Zhang, X. He, Y. Huang, and W. Mi, "Two-stage classification approach for human detection in camera video in bulk ports[J]," *Polish Maritime Research*, vol. 22, no. 1, pp. 163–170, 2015.

[17] J. Cai, J. Hu, S. Li, J. Lin, and J. Wang, "Combination of temporal channels correlation information and bilinear feature for action recognition," *IET Computer Vision*, vol. 14, no. 8, pp. 634–641, 2020.

[18] Y. Wang, Y. Chen, and R. Liu, "Aircraft image recognition network based on hybrid attention mechanism," *Computational Intelligence and Neuroscience*, vol. 2022, Article ID 4189500, 9 pages, 2022.
[19] R. Diniz, F. D. Tourino, L. Lacerda et al., "Resistance training intervention performed with different muscle action durations influences the maximal dynamic strength without promoting joint-angle specific strength gains[J]," *Journal of Sports Sciences*, vol. 2021, no. 3, pp. 1–7, 2021.
[20] J.-K. Tsai, C.-C. Hsu, W.-Y. Wang, and S.-K. Huang, "Deep learning-based real-time multiple-person action recognition system," *Sensors*, vol. 20, no. 17, p. 4758, 2020.

Hindawi
Computational Intelligence and Neuroscience
Volume 2022, Article ID 1362272, 12 pages
https://doi.org/10.1155/2022/1362272

Research Article

Quantitative Morphology of Polder Landscape Based on SOM Identification Model: Case Study of Typical Polders in the South of Yangtze River

Zhe Li,[1] **XinYi Lu**,[1] **Xiao Han**,[1] **LiYa Wang**,[1] **XiaoJian Tang**,[2] **and XiaoShan Lin**[1]

[1]*School of Architecture, Southeast University, Nanjing, Jiangsu 210096, China*
[2]*Architects & Engineers Co., Ltd. of Southeast University, Nanjing, Jiangsu 210096, China*

Correspondence should be addressed to Zhe Li; lizheseu@seu.edu.cn

Received 3 March 2022; Revised 12 April 2022; Accepted 13 April 2022; Published 29 May 2022

Academic Editor: Xin Ning

Landscape morphology is a significant area of landscape architecture research. One of the scientific and technological issues in recent landscape morphology research is the use of quantitative analysis technology driven by morphology indexes and computational models to describe, compare, and analyze form features. This article focuses on the form features of the polder landscape, based on existing theoretical and practical achievements in landscape morphology. First, we choose five landscape morphology indexes based on the morphological constituent units of the landscape (elongation, rectangular compactness, concavity, ellipse compactness, and fractal dimension). Then, using the self-organizing map (SOM), we create an identification model for clustering the types of constituent units. The experimental results show that the identification model can classify polder morphology and analyze the distribution of units using typical polders in the Yangtze River's south bank as study cases. This article presents a technical approach to polder landscape morphology classification as well as a reference and developable quantitative analysis method for landscape morphology research.

1. Introduction

Landscape morphology is an organic part of the landscape environment that condenses the landscape material space in a plane, which is one of the crucial representatives in distinguishing the landscape feature of different regions [1]. Digital identification and quantitative analysis of representative regional landscapes are of great significance for continuing and reshaping the features of regional landscape morphology [2]. With the support of landscape morphology and typo-morphology theories, developing quantitative analysis technologies suitable for identifying and analyzing polder landscape morphology has become one of the practical problems in the current landscape morphology research.

Contemporary studies on landscape morphology have gradually shown a trend of quantitative research, driven by emerging digital landscape research methods and technologies [3]. The analysis foundation for this type of study is to combine spatial information based on the morphological characteristics of the research object, and then obtain operable and comparable values and intervals. A crucial step is to keep optimizing the morphology index in order to achieve the mathematical translation of objective morphology. Exploring the morphological features of a research question requires building a quantitative analytical model that fits the research question. A landscape morphology analysis model created based on the machine learning model can transform traditional qualitative cognition into quantitative judgment [4]. Related research has been carried out in the fields of landscape classification [5], simulation prediction [6], landscape efficiency, and evaluation [7]. Exploring theoretical methods and technical means in the investigation of a typical zonal landscape morphological feature will effectively respond to the theoretical and practical needs of the refined development of landscape morphology. Meanwhile, it can provide a research basis and technical reference for quantitative research and digital development of landscape morphology [8].

2. Relevant Research

2.1. Polder Landscape Morphology. Polders are agricultural production environments formed by artificial water conservancy projects, mainly distributed in low-lying and water-rich river banks [9], estuary deltas, and coastal lowlands [10]. In the long-term production evolution process, the morphological features of the wetland polders are integrated with production methods, intertwining the landscape paddy fields, dry land, canals, ponds, and fields and ridges (Figure 1). One of the main difficulties in studying polder landscape is accurately describing and analyzing its morphological features.

In the study of interpretation, historical evolution, planning, and design of polder landscape, the unique landscape morphology of polder has the fundamental significance for regular summary and retrospective tracking. In terms of morphological interpretation and historical evolution, Steenbergen et al. analyzed and illustrated the development and distribution of polder morphology in the Netherlands, and then classified and analyzed the features of the polder from aspects of nature, water conservation, agriculture, and settlement [11]. Missiaen et al. summarized the landscape evolution of polders in northern Belgium [12]. Li et al. used remote sensing images to sort out the spatiotemporal distribution and development of polders in the Dongting Lake Plain in China [13]. In terms of planning and design, Velde and Wit summarized the methods of polder management and planning strategies of polder urban based on morphological research [14]. Nijhuis and Pouderoijen based on the GIS platform to visualize various polder data, introducing a digital orientation to the study and management of the polder landscape morphology [15]. The morphology of the polder also impacts the realization of its production, life, and ecological functions. Optimizing the polder morphology can improve flood management and the capacity for disasters in this area [16, 17]. The landscape morphology element is also a critical research indicator in evaluating the effectiveness of the polder transformation scheme [18] and the value of polder ecosystem services [19].

The polder form has gotten a lot of attention in landscape architecture research because of its distinguishing characteristics and crucial role in polder landscape research. Upgrading morphological classification from empirical cognition to quantitative judgment, as part of the digital landscape research trend, will aid in the promotion of polder landscape research.

2.2. Theory and Method of Landscape Morphology. American geographer C. O. Sauer first proposed landscape morphology in 1925 [20]. As an intuitive reflection of landscape environment on a two-dimensional plane, the specific syntagmatic relation and composition methods presented by landscape morphology are an essential carrier for exploring the feature of the landscape. As a branch of morphology research, landscape morphology research closely relates to the trend of morphology research. Since the 1950s, academic circles have paid increasing attention to the inheritance and protection of typical forms. Guided by the theory of morphology and graphical analysis, under the joint influence of Conzen [21] and Muratori-Caniggia [22] produced a morphological research method named typo-morphology, which provides a framework for the study of typical features of complex morphological systems. Specifically, it takes the basic constituent units of the research object's morphology as the entry point and selects geometric morphology indexes to describe the morphological features of the units. Then, identify the research object's morphological types and typical features by analyzing, comparing, and classifying the index value.

Current research continues to verify the applicability of morphology-type analysis to identify morphological features in the built environment and natural environment from multiple perspectives and scales. The perfection and development of digital landscape theory and technical methods also provide new research and practice tools for exploring the feature of morphological [23]. In research of urban morphology [24], settlement pattern [25], and landscape morphology [26] have accumulated a large number of indexes. Meanwhile, statistical and machine learning models are applied to morphology index analysis, expanding the visual analysis capabilities of multidimensional morphological data with large sample sizes. For example, Gil et al. used the K-means algorithm to analyze the typical urban block morphological dataset, realizing the objective classification of block morphology types [27]. SEM [28] and hierarchical clustering [29] also provide practical tools for a comprehensive analysis of morphological data. Machine learning methods such as back propagation neural network [30, 31] and convolutional neural network [32] can also achieve identification and classification of morphological unit types by learning morphological data [33]. On this basis, exploring data-driven landscape morphology research methods with the help of landscape morphology index and mathematical analysis model has positive significance for analyzing the feature of polder morphology.

2.3. Application of SOM in Landscape Architecture and Related Research. SOM is an unsupervised machine learning algorithm [34], which does not need to form an evaluation standard by learning samples with existing classification labels. It can perform competitive learning on the potential laws and fundamental attributes of the input samples after independently adjusting the connection weights of the network structure. Therefore, in the analysis without pre-classification criteria, often use SOM.

SOM is commonly combined with quantitative indexes and applied in element identification, comprehensive evaluation, and scheme optimization in landscape architecture and related disciplines research. It can be applied to SOM to hierarchical classification studies of building form [35], building space [36], and land use [37] in terms of

Polders in the Yangtze River in China | Seaside polders in Netherland | Coastal polders in Indonesia | Riverside polders in Bangladesh

Figure 1: Morphology features of the polders.

element recognition. When it comes to comprehensive evaluation, SOM is frequently used to analyze multifactor datasets and solve complex classification problems, such as a comprehensive analysis of tourist motivation and behavior in protected areas [38]. SOM can also be used to investigate relationships between research elements, such as correlations between river ecological indicators [39], pattern associations between different environmental conditions and physiological responses [40], and links between residents' lifestyles and their choice of residence within the city [41]. Using SOM to create a parametric building model can optimize the architectural design scheme [42].

In summary, SOM has substantial autonomy and a low degree of manual intervention. It can adapt to the high-dimensional data [43], which is highly suitable for polder landscape morphological identification's application scenario. In this sense, a polder landscape morphological identification model based on SOM will promote the refinement and intellectual development of polder landscape morphological identification and provide a quantitative analysis method for the research of landscape morphology.

3. Methods and Materials

3.1. Technology Roadmap. Under the guideline of landscape morphology and typo-morphology theory, we took polder landscape morphology as the research object, attempting to make a quantitative research process to analyze its landscape morphology feature based on the constituent units. The process combined landscape morphology index, SOM, and statistical methods to characterize the overall morphological features and internal differences of the polder units. This article conducted an empirical study on typical polders in the South of the Yangtze River, and the specific research steps are as follows (Figure 2):

(1) *Morphological Quantitative Translation*. Select suitable landscape morphology indexes, and convert the polder morphological constituent units into operable, analyzable, and comparable index values.

(2) *Morphological Data Processing*. Use factor analysis to integrate the multi-index into several common factors. Then, use common factors value for the subsequent cluster identification of the polder landscape morphology type.

(3) *Morphology-Type Clustering*. Use SOM to build a polder landscape morphological identification model. Then, realize the typo-morphology and distribution pattern analysis of the research area through self-learning and clustering of the common factors extracted by factor analysis.

(4) *Morphological Quantitative Analysis*. Use the ArcGIS platform to visualize the identification results. Then, establish a polder landscape morphological database, realizing the management, display, retrieval, and quantitative analysis of polder units [44].

3.2. Morphology Index Translation. Describing the polder morphology with the landscape morphology index is crucial for identification and classification of the polder morphology types. Based on the two-dimensional plane of the polder landscape constituent morphological unit [45], the morphology indexes selection according to the geometric features of the constituent units. Index selection principles combined scientificity, representativeness, comprehensiveness, and operability. The indexes abstractly translated the two-dimensional morphology of the polder units into the indexes value, providing primary data for subsequent morphology-type classification and feature analysis.

Long-term agricultural production and natural evolution have occurred in the polder landscapes studied in this article. Polder unit boundaries were originally almost regular geometric shapes. The polder units' boundary morphology tends to be tortuous as the water network expands and current scouring occurs, and some water network extends to the interior of the units. The morphology of polder unit boundaries then becomes diversification. A complex and diverse polder landscape morphology is formed by various constituent units. It is difficult to fully reflect the morphological features of the boundary morphology with a single landscape morphology index because the boundary morphology is complex and self-similar. As a result, an index system with comprehensive description dimensions and easy data acquisition is required to describe its morphological features.

We used an interdisciplinary perspective to summarize related index systems in typo-morphology, geoscience, computer vision, and pattern recognition. Then, selected landscape morphology indexes have been empirically effective for two-dimensional morphology measurements in related research. Extended degree, squareness, morphological concavity, and tortuosity were four angles to choose appropriate landscape morphology indexes in this article.

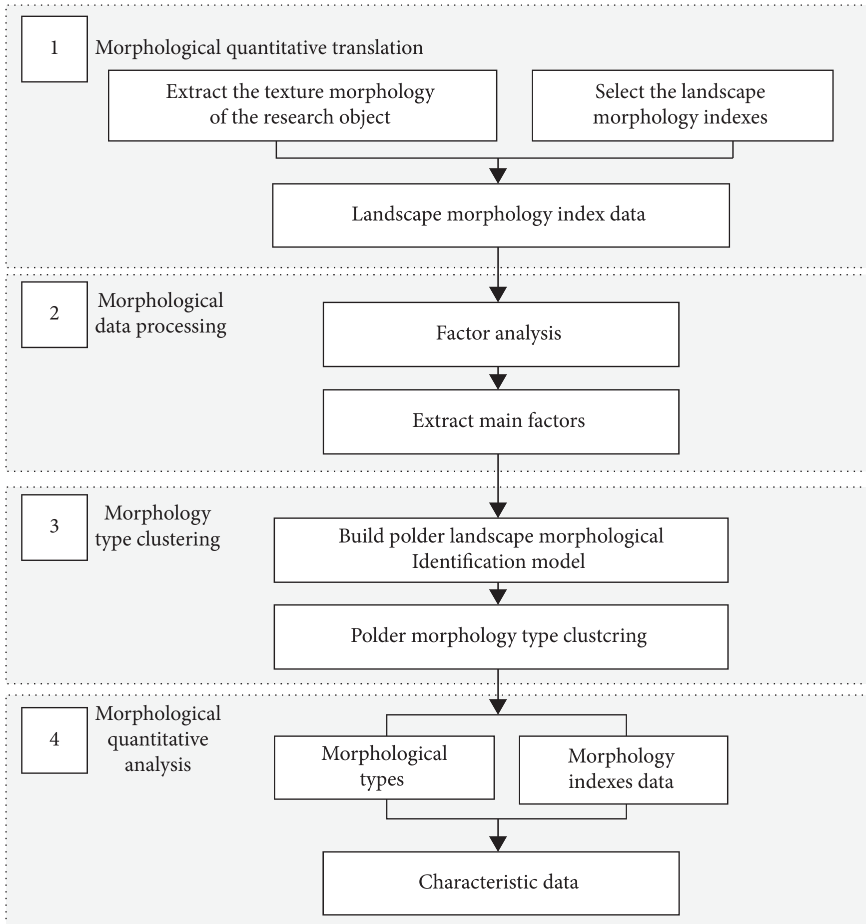

Figure 2: Technology roadmap.

Elongation (λ) is used to measure extended degree [46], rectangular compactness (S_1) is used to describe squareness [47], the concavity (V) is used to characterize morphological concaveness [48], and the ellipse compactness (S_2) and fractal dimension (D) jointly represent tortuosity [49] (Table 1). Then, we obtained the geometric attribute data to calculate the selected indexes value, such as area (A), perimeter (P), area of minimum bounding rectangle ($A_{\text{min\_ref}}$), area of the minimum convex hull ($A_{\text{min\_h}}$), long axis ($a_{\text{min\_ref}}$), and short axis ($b_{\text{min\_ref}}$). Landscape morphology indexes are linked and complementary to each other, which can jointly describe the boundary morphological features of the polder units.

3.2.1. Elongation (λ). Its geometric meaning is the ratio of the long axis to the short axis of the polder units. In the actual operation, use the ratio of the length of the long side ($a_{\text{min\_ref}}$) to the length of the short side ($b_{\text{min\_ref}}$) of the minimum bounding rectangle to reference it. We use this index to define the extended degree of the shape of the constituent units. The closer the ratio is to 1, the more likely the constituent units appear as equilateral shapes. The ratio is higher, the morphology of the constituent units is more likely to extend in a stripe shape:

$$\lambda = \frac{a_{\text{min\_ref}}}{b_{\text{min\_ref}}}, \tag{1}$$

where $a_{\text{min\_ref}}$ represents the length (m) of the long side of the minimum bounding rectangle of the constituent units and $b_{\text{min\_ref}}$ represents the length (m) of its short side.

3.2.2. Rectangular Compactness (S_1). Rectangular compactness (S_1) is the ratio of the polder morphological constituent unit area (A) to the minimum bounding rectangle area ($A_{\text{min\_ref}}$), and its numerical value ranges from 0 to 1. The closer the ratio is to 1, the more similar the constituent unit boundary to its minimum bounding rectangle. $S_1 = (A/A_{\text{min\_ref}})$, where S_1 represents the rectangular compactness, A represents the area of the polder units (m^2), and $A_{\text{min\_ref}}$ represents the area of the minimum bounding rectangle of the polder units (m^2).

3.2.3. Concavity (V). This article use concavity to define the degree of the concave shape of the polder morphological constituent units. A convex hull is the smallest convex polygon that can contain two-dimensional geometry. The concavity value ranges range from 0 to 1. The concavity is more similar to 1, and the boundary of the unit is less

Table 1: Summary table of morphology indexes and schematic diagram.

Name of morphology index	Elongation	Rectangular compactness	Concavity	Ellipse compactness	Fractal dimension
Formula of morphology indexes	$\lambda = a_{\min\_ref}/b_{\min\_ref}$	$S_1 = A/A_{\min\_ref}$	$V = ((A_{\min\_h} - A)/A_{\min\_h})$	$S_2 = (P/(1.5\lambda + 1.5 - \sqrt{\lambda}))\sqrt{\lambda/A\pi}$	$D = 2\ln(P)/\ln(A)$
Schematic diagram of morphology indexes	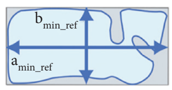	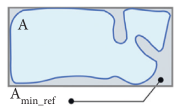	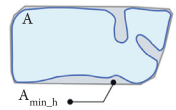	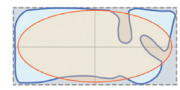	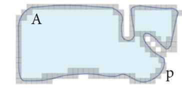

concave. When $V = 0$, the shape of the polder unit is a convex polygon:

$$V = \frac{A_{\min\_h} - A}{A_{\min\_h}}, \quad (2)$$

where V represents the concavity, A represents the area of the polder units (m^2), and $A_{\min\_h}$ represents the minimum convex hull area of the polder units (m^2).

3.2.4. Ellipse Compactness (S_2). The ellipse compactness takes the ellipse with the same area (A) and the same elongation (λ) as the polder shape units as the reference figure. Calculating the ratio of the ellipse perimeter to the perimeter of the constituent units (P) can reflect the complexity of the constituent units. Due to the introduction of elongation, this index is more suitable for quantitative analysis of complex boundary patterns. The larger the value of S_2 is, the more tortuous the boundary is:

$$S_2 = \frac{P}{1.5\lambda + 1.5 - \sqrt{\lambda}}\sqrt{\frac{\lambda}{A\pi}}, \quad (3)$$

where S_2 represents the ellipse compactness, P represents the polder unit perimeter (m), A represents the polder unit area (m^2), and λ represents the elongation.

3.2.5. Fractal Dimension (D). The shape of the polder units tends to be complex and fragmented in the long-term evolution process, which shows a specific self-similar shape. Thus, we introduce the fractal geometry index to supplement the description of tortuosity. The fractal dimension (D) is the most important parameter for describing fractal geometry. Researchers often use it to study irregular shapes in natural and built environments. Since the polder morphology is a two-dimensional figure, the theoretical value of fractal dimension is 1-2. The fractal dimension is closer to 2, the shape of the polder unit is more complex.

$$D = \frac{2\ln(P)}{\ln(A)}, \quad (4)$$

where D represents fractal dimension, P represents the polder unit perimeter (m), and A represents the polder unit area (m^2).

3.3. Data Processing and Analysis Methods of Landscape Morphology. This article selects factor analysis to integrate the polder landscape morphology index value to avoid repeated information and explore the relationship between different indexes. Factor analysis is a standard multivariate dimensionality reduction statistical method in statistics. Analyzing the internal structural relationship of the original data correlation coefficient matrix converts multiple indicators with complex relationships into a few combinations of random variables, namely, the common factors, which can reproduce the mutual relationship between the original variables and the common factors [50]. The common factor value will be used as input data to identify the morphology type of polder units.

To identify the polder morphological features, selecting an appropriate machine learning model according to the research needs and data characteristics is necessary. We apply unsupervised machine learning for clustering analysis to identify the morphology types of polder units. SOM is a kind of unsupervised artificial neural network similar to the brain neural network. It consists of an input layer and a computational layer. When receiving external information input, different input samples activate various neurons. Through "autonomous learning," SOM can enable each neuron to form a specific response pattern, thus facilitating the grouping of input samples [51]. Therefore, SOM can directly use the input samples to complete the whole process from network training to sample clustering (Figure 3).

3.4. Research Object Extraction. We select the typical polders in China as the research object to explore the validity of the polder landscape morphological identification model. The research object is located in Gaochun District, Nanjing city, in the middle and lower reaches of the Yangtze River, with a total area of 3507 hectares (Figure 4). It belongs to the local typical agricultural production environment, with flat terrain and dense water network characteristics. The agricultural production there is closely related to the water network. The polder units formed under the limitation of natural river channels and artificial canals are the primary constituent units of the polder morphology in this area.

The data extraction for this research is based on the drawings surveyed in 2019. It combined the impact of Landsat 8 satellite remote sensing and field surveys for review and proofreading. We extracted the polder morphological constituent unit boundary as the basis for the study, took the water network and polder dykes as the boundary of the unit morphology, and retained the canals that extend into the polder units (Figure 5).

The study area extracted 381 polder unit samples; the sample size can meet the data requirements of SOM for

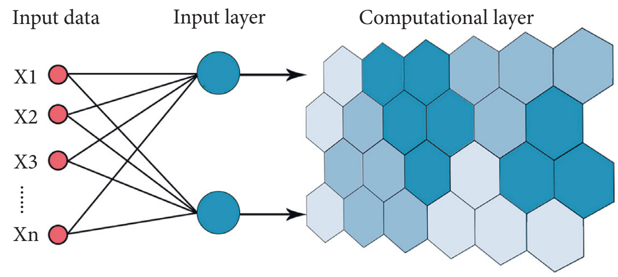

Figure 3: Structure of SOM.

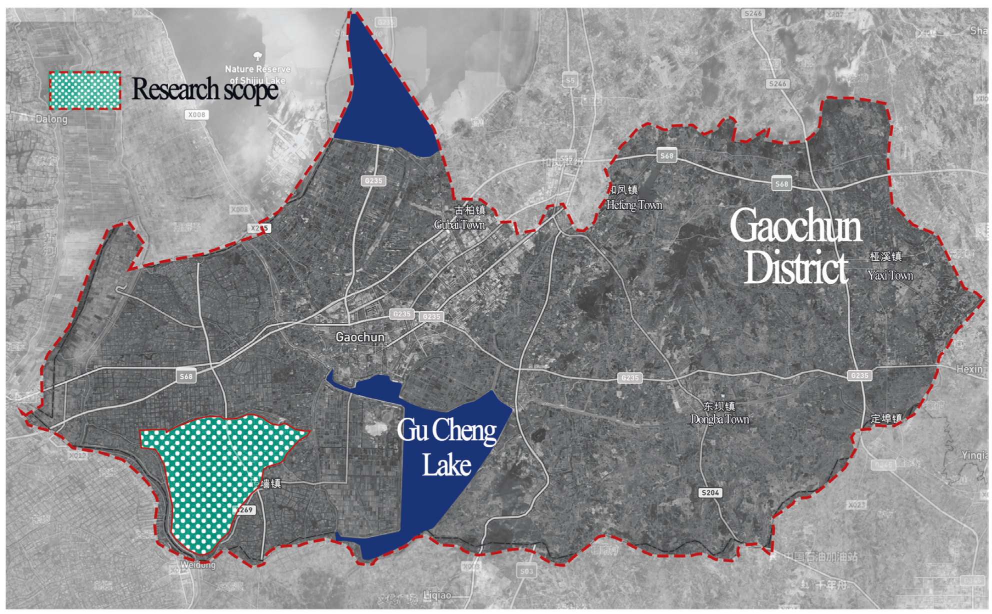

Figure 4: Location and scope of the research object.

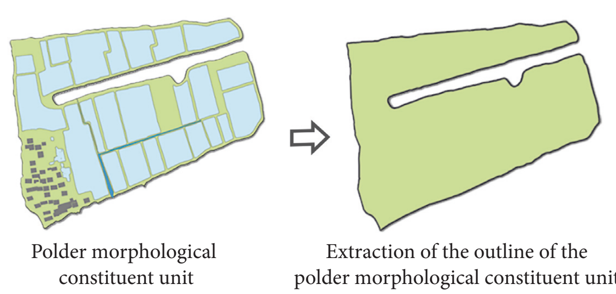

Figure 5: Schematic diagram of morphology extraction and optimization of the research object.

forming stable and reasonable classification results (≥100). Then, moderately smooth the boundary shape to avoid the measurement error. Store the data on the ArcGIS platform to generate the morphological unit's minimum bounding rectangle and convex hull. After that, extract the fundamental geometric values required for the polder landscape morphology index calculation. The final landscape morphology index statistics of each sample are shown in Table 2. The landscape morphology index statistics of each samples are shown in Table 2.

4. Quantitative Results of Polder Landscape Morphology

4.1. Data Processing Results. This article used SPSS (26.0) for factor analysis. First, standardize the morphology index data of the polder landscape and conduct moderate analysis by KMO and Bartlett's test. According to the test results, the KMO sampling adequacy is more significant than 0.5, and the significance level of the Bartlett test is less than 0.01, indicating that the tested data are suitable for factor analysis (Table 3).

Table 2: Descriptive statistics of landscape morphology indexes.

Landscape morphology index	Maximum	Minimum	Average value	Standard deviation
Elongation	11.10	1.00	2.42	1.65
Rectangular compactness	0.99	0.42	0.78	0.12
Concavity	0.67	0.00	0.10	0.12
Ellipse compactness	4.28	1.00	1.22	0.30
Fractal dimension	1.47	1.24	1.30	0.04

Note. Sample size $n = 381$.

Extract the first two factors with a characteristic root greater than 1 as the common factors, and the cumulative variance contribution rate is 80.79% (Table 4). It showed that the two common factors contain more than 80% of the original information of the landscape morphology indexes, which is enough to represent the main content of the variable information. The characteristic value of the first factor after rotation is 2.385, and the variance contribution rate is 47.706%. The characteristic value of the second factor after rotation is 1.654, and the variance contribution rate is 33.086%. These two common factors used linear combinations to replace the original landscape morphology indexes. The common factors jointly described the morphology of the polder unit for the following types of clustering (Table 5).

4.2. Clustering Analysis Based on SOM. The SOM model was driven by the two common factors to realize the polder landscape morphology-type clustering. The number of neurons in the input layer, computational layer, and total number of learning times are all important parameters to set when building a model. The input layer's number of neurons is determined by the data it receives. The requirement for morphological clustering is related to the number of neurons in the computational layer. We must determine the specific number combination, universality, and interpretability of the classification results based on the distribution characteristics of the input data. The neural network must reach a point of stability within the allotted learning time. This article used MATLAB R2019b to create a SOM model to achieve the clustering of the polder morphology types after several experiments to determine the parameters. Connect the results to the ArcGIS platform for visual display, and create a polder landscape morphological database to serve as the data and image foundation for polder morphology-type analysis. The specific clustering results are shown in Figure 6.

4.3. Morphology Clustering Results of Polder Landscape. From the SOM cluster results, the polder units' morphological features in the same clusters have consistency, and the features in different clusters have significant differences. A comprehensive analysis of the identification results of polder landscape morphology shows that the average value of the landscape morphology index of each category has a logical law, which indicates that SOM can autonomously make the clustering results of polder morphology types highly interpretable (Table 6).

Table 3: KMO and Bartlett's test.

KMO sampling adequacy		0.580
Bartlett's test	Approximate chi-square	894.835
	df	10
	Sig.	.000

(1) From an individual perspective, rectangular and polygonal units constitute the polder feature. From the landscape morphology index perspective, the morphological constituent units identified by SOM can classify into two categories: rectangular (Type A) and polygonal (Type B). The former has high squareness, low concavity, and low tortuosity, so this type of unit presents a relatively simple and square overall shape. The latter has low squareness, high concavity, and high tortuosity, so the morphological features are complex and tortuous. In the rectangular unit, due to the difference in elongation, the morphology type of the constituent units can further divide into low elongation rectangle (Type A1), medium elongation rectangle (Type A2), and high elongation rectangle (Type A3). In polygonal types, the concavity, ellipse compactness, and fractal dimension increase simultaneously as the rectangular compactness decreases. The morphology type of constituent units can divide into low complexity polygon (Type B1), medium complexity polygon (Type B2), and high complexity polygon (Type B3). In terms of the morphology of polder units, their boundary shapes tend to be complex, and the number and length of concave channels gradually increase.

(2) From an overall perspective, the distribution pattern of the polder units is closely linked to the morphological feature. Regarding the proportion and distribution of morphological units, the number of rectangular and polygonal units is basically the same: rectangular units accounted for 51.4% of the total polder morphological units, and polygonal units accounted for 48.6%. From the perspective of morphological distribution, the morphological composition of the polder shows the combination of different types of morphological units, which makes the polder in the studied area present a multicomplex morphological feature.

Table 4: Total variance explained.

Initial eigenvalues				Extraction sums of squared loading			Rotation sums of squared loading		
Component	Total	% of variance	Accumulative %	Total	% of variance	Accumulative %	Total	% of variance	Accumulative %
1	2.520	50.397	50.397	2.520	50.397	50.397	2.385	47.706	47.706
2	1.520	30.396	80.792	1.520	30.396	80.792	1.654	33.086	80.792
3	.525	10.504	91.296						
4	.247	4.949	96.245						
5	.188	3.755	100.000						

Table 5: Common factor coefficient matrix.

	Landscape morphology index	Before rotation	After rotation
Factor 1	Zscore (Rectangular compactness)	−0.845	−0.860
	Zscore (Concavity)	0.752	0.845
	Zscore (Fractal dimension)	0.905	0.901
Factor 2	Zscore(Elongation)	0.920	0.936
	Zscore (Ellipse compactness)	0.671	0.848

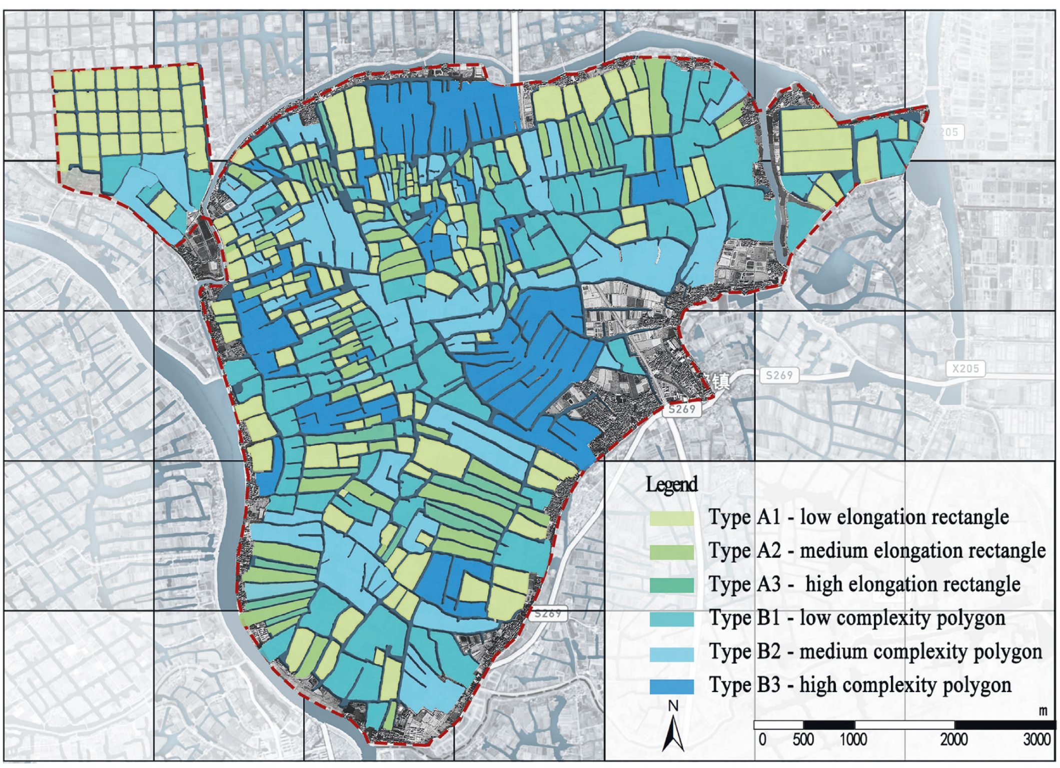

Figure 6: Results of polder landscape morphological clustering.

5. Analysis and Discussion

In this article, the identification of the polder landscape morphology based on the SOM identification model can effectively classify the types of polder landscape morphology in the research area. The results have application value for quantitative research and analysis on the morphology of the polder landscape. This technical route is suitable for in-depth development and horizontal expansion in the field of landscape morphology research.

(1) At the level of research effectiveness, the SOM identification model effectively classified the polder morphology in the studied area and obtained relatively stable six types of polder units, realizing the division of polder landscape morphology types in the individual perspective. We integrated and applied five landscape morphology indexes such as elongation and rectangular compactness, which can effectively translate the polder landscape morphology of the studied area. Thus, this technical system has

Table 6: The results of polder landscape morphology types and the average value of morphology indexes.

Type A—rectangular units	Type A1—low elongation rectangle 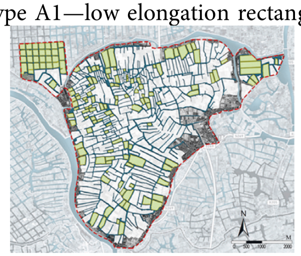	$n = 119$ $\lambda = 1.68$ $S_1 = 0.87$ $V = 0.03$ $S_2 = 1.09$ $D = 1.28$	Type A2—medium elongation rectangle 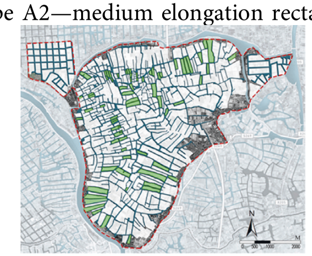	$n = 61$ $\lambda = 3.51$ $S_1 = 0.81$ $V = 0.07$ $S_2 = 1.08$ $D = 1.28$	Type A3—high elongation rectangle 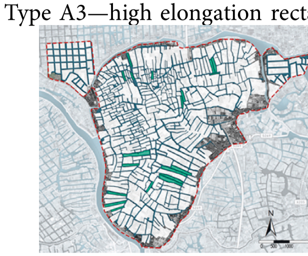	$n = 16$ $\lambda = 7.83$ $S_1 = 0.80$ $V = 0.12$ $S_2 = 1.04$ $D = 1.37$
Type B— polygonal units	Type B1—low complexity polygon 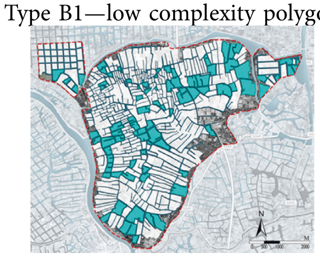	$n = 123$ $\lambda = 1.59$ $S_1 = 0.72$ $V = 0.10$ $S_2 = 1.25$ $D = 1.28$	Type B2—medium complexity polygon 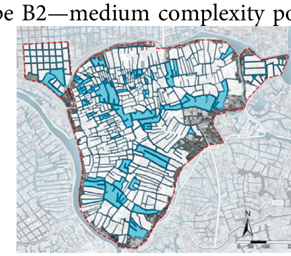	$n = 41$ $\lambda = 2.48$ $S_1 = 0.65$ $V = 0.21$ $S_2 = 1.49$ $D = 1.33$	Type B3—high complexity polygon 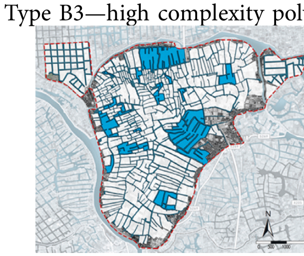	$n = 21$ $\lambda = 2.20$ $S_1 = 0.51$ $V = 0.47$ $S_2 = 1.95$ $D = 1.35$

specific reference significance and application value for the quantitative analysis of complex and wide-area landscape morphology such as polder.

(2) At the application level, we quantitatively translated and clustered the polder unites to achieve advanced research on polder landscape morphology. From an individual perspective, the technical system can quantitatively study the geometric properties of various polder units and the threshold of the morphology index. From an overall perspective, the technical system can present the units' composition features of the polder landscape morphology. Combined with morphology index value in different periods, it can play a role in tracking the morphological evolution of polders.

(3) At the level of research expansion, the technical route can further expand research and perfect. The landscape morphology indexes used in this article mainly focus on the two-dimensional plane. Follow-up research can further be developed by selecting landscape morphology indexes from other perspectives such as facade and space. It can also expand and enrich the research samples to improve the cognition of the polder landscape morphology type at different research levels and scales.

6. Conclusions and Prospects

This article took the quantitative analysis method of polder landscape morphology as the critical issue, constructed an index system to describe its morphological features, and formed an identification model based on SOM to classify its types. Taking the typical polders in the South of Yangtze River as the research object, we explored and verified machine learning classification, visualization, and quantitative analysis methods of the morphological features of the polder landscape. This article realized the research and development of automatic identification and quantitative judgment of polder landscape morphology, providing an analysis method and analysis technology that can be referred to and developed for landscape architecture morphology research.

Combining quantitative indexes and machine learning models is one of the quantitative research methods of landscape architecture. For landscape morphology research, the quantitative research process can not only enrich the theory and technical system, but also provide a data basis for analysis, comparison, summary, and traceability. Computer technology has brought a series of cutting-edge analysis methods such as machine learning to the development of landscape architecture. While promoting in-depth scientific research, the technology promotes the iterative development of professional theories, methods, and technologies. Thus, it is an inevitable choice for landscape architecture's informatization and intellectual development.

Data Availability

The data presented in this study are available on request from the corresponding author. The data are proprietary or confidential in nature and may only be provided with restrictions.

Ethical Approval

This article does not contain any studies with human participants performed by any of the authors.

Conflicts of Interest

The authors declare no conflict of interest.

Authors' Contributions

Li Z. and Lu X.Y. conceived the study; Li Z. helped with the methodology; Lu X.Y. helped with software; Han X., Wang L.Y., and Lin X.S. validated the study; Lu X.Y. and Lin X.S. investigated the study; Han X. helped with the resources; Wang L.Y. curated the data; Li Z. prepared the original draft of the manuscript; Lu X.Y. and Wang L.Y. reviewed and edited the manuscript; Lu X.Y. and Han X. visualized the study; Lin X.S. supervised the study; and Li Z. and Lu X.Y did in the funding acquisition of the study.

Acknowledgments

Our research was supported by the National Key R&D Program of China (No. 2019YFD1100405), the Postgraduate Research & Practice Innovation Program of Jiangsu Province(No. SJCX20_0053), and the Fundamental Research Funds for the Central Universities (No. 3201002112D). The authors thank Cheng YuNing, Edoardo Curra, Yuan FuTian, Gao Ying, Huang RuoXuan, Zhou Zheng, and Shi JiaYing for their indispensable help with this research, and the Digital Landscape Laboratory of Southeast University for the RS and GIS data support.

References

[1] B. Martín, E. Ortega, P. Martino, and I. Otero, "Inferring landscape change from differences in landscape character between the current and a reference situation," *Ecological Indicators*, vol. 90, pp. 584–593, 2018.

[2] G. Cillis, A. Lay-Ekuakille, V. Telesca, D. Statuto, and P. Picuno, "Analysis of the evolution of a rural landscape by combining SAR geodata with GIS techniques," in *Proceedings of the International Mid-Term Conference 2019 of the Italian Association of Agricultural Engineering (AIIA)*, Matera, Italy, September 2019.

[3] Y. Deng, L. Xie, C. Xing, and L. Cai, "Digital city landscape planning and design based on spatial information technology," *Neural Computing & Applications*, vol. 33, pp. 1–12, 2021.

[4] Z. Li, Y. N. Cheng, S. Song, and Y. K. He, "Research on the space cognitive model of new Chinese style landscape based on the operator optimization genetic algorithm," *Fresenius Environmental Bulletin*, vol. 28, no. 6, pp. 4483–4491, 2019.

[5] F. Riccioli, T. El Asmar, J.-P. El Asmar, C. Fagarazzi, and L. Casini, "Artificial neural network for multifunctional areas," *Environmental Monitoring and Assessment*, vol. 188, no. 1, p. 67, 2016.

[6] D. Buscombe and A. Ritchie, “Landscape classification with deep neural networks,” *Geosciences*, vol. 8, no. 7, p. 244, 2018.
[7] S. Aboufazeli, A. Jahani, and M. Farahpour, “A method for aesthetic quality modelling of the form of plants and water in the urban parks landscapes: an artificial neural network approach,” *MethodsX*, vol. 8, no. 2, Article ID 101489, 2021.
[8] Z. Li, Y. He, X. Lu, H. Zhao, Z. Zhou, and Y. Cao, “Construction of smart city street landscape big data-driven intelligent system based on industry 4.0,” *Computational Intelligence and Neuroscience*, vol. 2021, Article ID 1716396, 11 pages, 2021.
[9] B. Tang, X. Zhan, and J. Zhang, “The agricultural heritage value of the polder system in gaochun, nanjing,” *Built Heritage*, vol. 3, no. 1, pp. 47–58, 2019.
[10] W. Reh, C. M. Steenbergen, and D. Aten, *Sea of Land; the Polder as an Experimental Atlas of Dutch Landscape Architecture*, Architectura & Natura, Stichting Uitgeverij Noord Holland, 2007.
[11] C. M. Steenbergen, W. Reh, S. Nijhuis, and M. T. Pouderoijen, *The Polder Atlas of The Netherlands: Pantheon of the Lowlands*, Uitgeverij Thoth, Netherlands, 2009.
[12] T. Missiaen, I. Jongepier, K. Heirman et al., “Holocene landscape evolution of an estuarine wetland in relation to its human occupation and exploitation: waasland scheldt polders, northern Belgium,” *Netherlands Journal of Geosciences*, vol. 96, no. 1, pp. 35–62, 2017.
[13] Y. Li, Y. Ye, J. Li, C. Zhang, and X. Fang, “Reconstructing the spatiotemporal distribution of polders in modern dongting plain, hunan province,” *Applied Geography*, vol. 123, no. 4, Article ID 102250, 2020.
[14] R. Velde and S. Wit, “The landscape form of the metropolis,” *Footprint*, vol. 3, no. 5, 2009.
[15] S. Nijhuis and M. Pouderoijen, “The polder map of The Netherlands: an instrument for spatial development of the lowlands,” *KNOB Bulletin*, vol. 112, no. 3, pp. 137–151, 2013.
[16] S. Yadav, M. K. Mondal, A. M. Shew et al., “Community water management to intensify agricultural productivity in the polders of the coastal zone of Bangladesh,” *Paddy and Water Environment*, vol. 18, no. 2, pp. 331–343, 2019.
[17] A. L. Nillesen and M. Kok, “An integrated approach to flood risk management and spatial quality for a Netherlands’ river polder area,” *Mitigation and Adaptation Strategies for Global Change*, vol. 20, no. 6, pp. 949–966, 2015.
[18] I. Laks and Z. Walczak, “Efficiency of polder modernization for flood protection. case study of golina polder (Poland),” *Sustainability*, vol. 12, no. 19, 8056 pages, 2020.
[19] Z. Zhang, J. Gao, X. Fan, M. Zhao, and Y. Lan, “Assessing the variable ecosystem services relationships in polders over time: a case study in the eastern chaohu lake basin, China,” *Environmental Earth Sciences*, vol. 75, no. 10, 856 pages, 2016.
[20] C. O. Sauer, *The Morphology of Landscape*, Berkeley: University Press, San Francisco, 1925.
[21] M. R. Conzen, *Thinking about Urban Form: Papers on Urban Morphology, 1932-1998*, Peter Lang, Germany, 2004.
[22] G. Caniggia and G. L. Maffei, *Architectural Composition and Building Typology:Interpreting Basic Building*, Alinea Editrice, Italy, 2001.
[23] Z. Li, Y. Cheng, and R. Xiao, “Electroencephalogram experiment based analysis of aesthetic fatigue on Chinese traditional garden,” *NeuroQuantology*, vol. 16, no. 5, 2018.
[24] R. Ma, X. Li, and J. Chen, “An elastic urban morpho-blocks (EUM) modeling method for urban building morphological analysis and feature clustering,” *Building and Environment*, vol. 192, Article ID 107646, 2021.
[25] T. Figlus and Ł. Musiaka, “Analysis of morphological changes of rural settlement patterns after World War II in the metropolitan area of Łódź using a graph theory based method,” *Environmental & Socio-economic Studies*, vol. 8, no. 4, pp. 57–72, 2020.
[26] A. Moura and D. M. D. Magalhes, “Landscape morphology metrics for urban areas: analysis of the role of vegetation in the management of the quality of urban environment,” *Disegnarecon*, vol. 6, no. 11, pp. 82–92, 2013.
[27] J. Gil, J. N. Beiro, N. Montenegro, and J. P. Duarte, “On the discovery of urban typologies: data mining the many dimensions of urban form,” *Urban Morphology*, vol. 16, no. 1, pp. 27–40, 2012.
[28] Z. Li, X. Han, X. Lin, and X. Lu, “Quantitative analysis of landscape efficacy based on structural equation modelling: empirical evidence from new Chinese style commercial streets,” *Alexandria Engineering Journal*, vol. 60, no. 1, pp. 261–271, 2021.
[29] J. Dong, L. Li, and D. Han, *New Quantitative Approach for the Morphological Similarity Analysis of Urban Fabrics Based on a Convolutional Autoencoder*, IEEE Access, no. 99, , 1 page, New Jersey, NY, USA, 2019.
[30] C. Cai and B. Li, “Training deep convolution network with synthetic data for architectural morphological prototype classification,” *Frontiers of Architectural Research*, vol. 10, no. 2, pp. 304–316, 2021.
[31] C. Cai, Z. Guo, B. Zhang, X. Wang, B. Li, and P. Tang, “Urban morphological feature extraction and multi-dimensional similarity analysis based on deep learning approaches,” *Sustainability*, vol. 13, no. 12, 6859 pages, 2021.
[32] R. Prabhu, B. Parvathavarthini, and A. R. Alaguraja, “Integration of deep convolutional neural networks and mathematical morphology-based postclassification framework for urban slum mapping,” *Journal of Applied Remote Sensing*, vol. 15, no. 1, 2021.
[33] Z. Li, X. Han, L. Wang, T. Zhu, and F. Yuan, “Feature extraction and image retrieval of landscape images based on image processing,” *Traitement du Signal*, vol. 37, no. 6, pp. 1009–1018, 2020.
[34] J. Vesanto, J. Himberg, E. Alhoniemi, J. Parhankangas, S. O. M. T. Team, and L. Oy, “SOM toolbox for Matlab 5,” vol. 572 pages, Helsinki University of Technology, Finland, 2000, , Technical report. ISBN:9512249510.
[35] C. Derix and P. Jagannath, “Near futures: associative archetypes,” *Architectural Design*, vol. 84, no. 5, pp. 130–135, 2014.
[36] Z. Wang and Q. Liu, “The cluster of city buildings based on the SOM neural network,” *IOP Conference Series: Earth and Environmental Science*, vol. 57, no. 1, Article ID 012047, 2017.
[37] P. Xiao, C. Zhao, Y. Zhou, H. Feng, X. Li, and J. Jiang, “Study on land consolidation zoning in hubei province based on the coupling of neural network and cluster analysis,” *Land*, vol. 10, no. 7, 756 pages, 2021.
[38] K. Taczanowska, X. González, L.-M. García-Massó et al., “Nature-based tourism or mass tourism in nature? segmentation of mountain protected area visitors using self-organizing maps (som),” *Sustainability*, vol. 11, no. 5, 1314 pages, 2019.
[39] S.-R. Park, S.-J. Hwang, K. An, and S.-W. Lee, “Identifying key watershed characteristics that affect the biological integrity of streams in the han river watershed, korea,” *Sustainability*, vol. 13, no. 6, 3359 pages, 2021.
[40] V. K. Ojha, D. Griego, S. Kuliga et al., “Machine learning approaches to understand the influence of urban

environments on human's physiological response," *Information Sciences*, vol. 474, pp. 154–169, 2019.
[41] A. Frenkel, E. Bendit, and S. Kaplan, "The linkage between the lifestyle of knowledge-workers and their intra-metropolitan residential choice: a clustering approach based on self-organizing maps," *Computers, Environment and Urban Systems*, vol. 39, no. 2, pp. 151–161, 2013.
[42] J. Harding, "Dimensionality reduction for parametric design exploration," in *Advances in Architectural Geometry*, Elsevier, Amsterdam, Netherlands, 2016.
[43] C. Gielen, "Neural computation and self-organizing maps, an introduction," *Neurocomputing*, vol. 5, no. 4-5, pp. 243-244, 1993.
[44] Z. Li, Y. Cheng, and Y. Yuan, "Research on the application of virtual reality technology in landscape design teaching," *Educational Sciences: Theory and Practice*, vol. 18, no. 5, 2018.
[45] P. Bosselmann, "Metropolitan landscape morphology," *Built Environment*, vol. 37, no. 4, pp. 462–478, 2011.
[46] C. Bo, H. Xu, and Y. Liu, "Examination of the relationships between urban form and urban public services expenditure in China," *Administrative Sciences*, vol. 7, no. 4, 39 pages, 2017.
[47] X. Li, S. Cheng, Z. Lv, H. Song, T. Jia, and N. Lu, "Data analytics of urban fabric metrics for smart cities," *Future Generation Computer Systems*, vol. 107, pp. 871–882, 2020.
[48] Y. H. Ang, Z. Li, and S. H. Ong, "Image retrieval based on multidimensional feature properties," *SPIE Proceedings*, vol. 2420, pp. 47–57, 1995.
[49] B. B. Mandelbrot and B. B. Mandelbrot, *The Fractal Geometry of Nature*, Vol. 1, W. H. Freeman, , New York, 1982.
[50] X. Tan, X. Li, and Y. Peng, "Aesthetic evaluation of plant landscape based on principal factor Analysis and sbe in wetland park - a case study of jinlong lake wetland park (China)," *Journal of Environmental Engineering and Landscape Management*, vol. 29, no. 1, pp. 40–47, 2021.
[51] F. Bação, V. Lobo, and M. Painho, "The self-organizing map, the geo-som, and relevant variants for geosciences," *Computers & Geosciences*, vol. 31, no. 2, pp. 155–163, 2005.

Hindawi
Computational Intelligence and Neuroscience
Volume 2022, Article ID 1062223, 11 pages
https://doi.org/10.1155/2022/1062223

Research Article

Measurement of the Correlation Degree between Rural Family Fertility Willingness and the Development of China's Labor Original Equipment Manufacturing Industry

Liangshan Li

Faculty of Public Administration, Shanxi University of Finance & Economic, Taiyuan 030006, Shanxi, China

Correspondence should be addressed to Liangshan Li; lls@sxufe.edu.cn

Received 20 March 2022; Revised 4 May 2022; Accepted 6 May 2022; Published 26 May 2022

Academic Editor: Xin Ning

At present, China is facing problems such as the decline of fertility rate, gender imbalance, serious aging, and the reduction of youth and working population, which will have an adverse impact on the long-term development of social economy. Based on the literature review, combined with China's financial family data, combined with the innovative calculation model of the correlation between rural family fertility willingness and labor original equipment manufacturing (OEM) industrial development, through the empirical analysis of rural families, this paper investigates the relationship between fertility willingness and the development and endogeneity of labor OEM industry and finds that female labor participation has a significant negative impact on the number of children in rural families. Spouse labor participation has a negative effect on the number of children in rural families. The regression coefficient of women's willingness to have two children for career development is significant and negative ($c_1 = -0.181, P = -0.003 < 0.01$), and that of women's family status is significant and negative ($c_1 = -0.998, P = 0.031 < 0.01$). The relative opportunity cost of birth of individual operators is more concentrated in the range of 50%–80%. The results show that the development of labor OEM industry is significantly influenced by the fertility willingness of rural families. This paper concludes that differentiated policies and measures should be taken according to the type of industrial promotion.

1. Introduction

The introduction of the comprehensive three-child policy has greatly reformed the family planning policy that has been implemented for more than 30 years, which has attracted the attention of academia and the public. Some scholars worry that if the policy is liberalized, the pressure of fertility rate will still be great, and there will be another "population explosion." Some scholars have high hopes for the two-child policy, which will significantly increase the fertility rate. The aging population will aggravate the decline of labor supply [1]. The working-age population is gradually decreasing, and the population distribution is gradually disappearing, as a result of the aging society. In this case, increasing the labor force participation rate of the working-age population, including women, is a key strategy for reversing the demographic dividend decline [2]. Population aging and disparities are becoming global concerns. Population decline and rapid aging result from a fertility rate below the replacement level. According to the World Bank database, the proportion of people under the age of 14 in the total population fell to 25.94 percent in 2017, while the proportion of people aged 65 and up rose to 8.70 percent [3, 4], indicating that the world is becoming an aging society. In this case, increasing the participation rate of the age-appropriate population, including women, in economic activities is an important way to offset the current decline in the demographic dividend, while increasing the fertility rate is an important way to offset future economic growth declines.

As the main body of reproductive behavior, women bear the dual roles of work and family, which is not only an important part of the labor market, but also an indispensable human resource for China's economic development and is responsible for the future labor supply and human resources. Fatima and others believe that the fertility rate depends on the balance between the income effect and the substitution effect of reproductive demand [5]. Devaro and others found that young women can delay or give up childbearing by learning the skills of reducing unemployment risk and increasing income [6]. Long believes that demographic dividend promotes economic growth by stimulating investment expansion, because it reduces the burden of dependence on the productive population and can spend more time and energy on productive activities, thus increasing investment and promoting the expansion of economic reproduction [7]. The research results of Mao et al. show that there is no direct relationship between female labor participation and fertility rate, and it is found that female labor participation has a positive impact on fertility rate [8]. The existing literature pays more attention to the relationship between female labor force participation and fertility rate in developed countries, but less attention to developing countries, especially China. China's fertility rate has been lower than the population replacement rate for many years, so there is concern about this phenomenon. Labor force participation rate and number of births: we do not pay attention to the comprehensive influence of women's labor participation on childbearing age and number of births.

Child support, fertility willingness, support, and other factors all play a role in the decision-making process for family fertility in rural areas. This paper adds to the explanation for the discrepancy between them, which is primarily due to women's reproductive choices in the labor market. The goal of this paper is to use the model in conjunction with data on female employment and fertility in China to better understand the impact of rural families' desire for children on the development of China's original equipment manufacturing industry, as well as to theoretically support the practical importance of family economic theory. Exploring how to eliminate the negative impact of women's employment on fertility through policy measures is useful for providing a theoretical foundation and decision-making reference for the government's employment policy direction and focus in the context of the current human dividend's disappearance.

Possible innovations of this paper are as follows:

(1) A possible innovation of this paper is to link the influence of rural families' fertility willingness on the development of China's labor OEM industry with the demographic dividend, which is the growth source of the demographic dividend itself.

(2) According to the research object, this paper adopts a variety of research methods, using probit and logit analysis methods as explanatory variables of children's binary variables, and the number of children is an ordinal variable analyzed by OLS. For different research objects, adopt more scientific analysis methods.

2. Related Work

2.1. Study on the Relationship between Fertility Willingness and Fertility Behavior. Fertility desire is people's desire and pursuit for fertility, and it is also the individual's desire and requirement for fertility, which is reflected in the expectation of the quantity, time, gender, and quality of fertility. Because there is a strong correlation between fertility behavior and fertility willingness, the three-dimensional thinking of fertility behavior is applied, in which fertility willingness, number of children, and gender of willing children are the main components.

In a high fertility environment, unexpected births often occur, and the actual number of children born is larger than the expected number. They think that the level of fertility willingness is much higher than the actual fertility rate. Yakita believes that the deviation degree of fertility will and behavior is influenced by the life cycle of women [9]. Tian et al. found that the implementation of the "two-child policy" gradually converged the willingness and fertility, and the proportion of "willingness is the same as action" and "willingness is less than action" gradually increased [10]. Erten and Metzger believe that men at the middle level of gender role equality are in the transitional stage from the traditional concept of gender role to the modern concept of gender role, facing a higher level of family and workplace conflicts [11]. This also means that both the concept of gender role equality and the traditional concept of gender role are helpful in increasing the fertility rate. Codazzi and others found that increasing women's labor force participation and educational opportunities would reduce women's willingness to have children, and at the same time strengthen women's position in rural families and give them more choices [12]. Shen et al. believe that unwanted fertility rate, gender preference, children's substitution effect and female age have significant influence on fertility rate [13]. Fin and others believe that the fertility rate will affect the employment of rural women, and the number of children will affect the working hours and income of rural women [14]. Rong and others believe that a family-friendly policy that only considers women's fair social status from the family perspective will have a negative impact on women's social status and further reduce the fertility rate [15].

2.2. Research on Labor OEM Industry. OEM industry, as its name implies, is an agent processing industry, also known as outsourcing industry, which is composed of many companies engaged in OEM industry. Its main business is to share the processing and assembly defects in other enterprises' industrial chains, and the main types are processing with incoming materials, processing with imported materials and processing with incoming samples. Labor cost is the main component of production cost. If the level of labor cost or labor wage rises, the production cost of enterprises will also rise. Industrial transfer is a process in which the market continuously allocates resources. Maximizing the allocation of resources through industrial transfer can promote the industrial structure of a country or region, improve efficiency, and ultimately promote economic development.

Harrison and others studied many companies and multinational corporations on the basis of empirical analysis and thought that, in the highly industrialized open economy, labor-intensive industries were easier to transfer than before [16]. Through historical and theoretical analysis, it can be seen that the industrial overlap formed by international industrial trade and international industrial investment is the basic condition of international industrial transfer, and international industrial transfer requires that the technical composition of goods produced be similar and different. In terms of the composition of values, Han et al. established a two-step game analysis framework and concluded that if the game was repeated twice, the refined Nash equilibrium result of the subgame of urban cooperation between the former industries could be obtained [17]. Yan and others suggested that local government transfer should not only consider regional economic interests, but also update ideas and build industrial parks on the basis of cooperation to achieve win-win results [18]. Huang pointed out that enterprises may "escape" from the investment competition among local governments and emphatically analyzed the dynamic game process between local governments and enterprises and between local governments in the investment competition [19].

3. Methodology

3.1. Model Design. Analyzing the factors affecting fertility will help systematically understand the three child policy support needs of people of childbearing age. Through the analysis of the "three-child" policy and the wishes of children of childbearing age groups, it can be seen that the "three-child" policy is an important measure to solve the problems of China's population structure and population aging. The three-child policy is facing the dilemma of low fertility willingness, which is not conducive to the healthy development of China's society and economy [20].

I can divide the influencing factors into the following:

(1) The main economic factors are high economic pressure and high cost of raising three children.

(2) Social factors, including raising children to prevent old age, giving birth to elders, happy and complete family, unattended children, affecting the development of work and career, etc.

(3) Cultural factors, such as the hope of both children and children to satisfy parent-child feelings.

Due to the needs of China's actual national conditions, the family planning policy is China's basic national policy, and the influence of policy factors on fertility willingness of fertility families is also worth investigating. Therefore, this study divides the influencing factors of childbearing families into four dimensions: policy factors, economic factors, social factorsm and cultural factors. The theoretical framework of this paper is shown in Figure 1.

In order to observe the influence of rural families' fertility desire on the development of China's labor OEM industry, it is assumed that women decide both the employment situation and the childbearing time and that she has not changed her employment situation after giving birth to her first child, and she decides whether to work at the same time as giving birth to her child. Assume that the number of children and women employed in a given period is the result of this decision-making process.

The independent variable is the number of children in rural families, represented by Y_{th}, t is the time variable, and h is the family variable. The expectation of Y_{th} based on the exogenous feature z_{th} is represented by $E[Y_{\mathrm{th}}|Z_{\mathrm{th}}, \theta]$ and θ. According to the above model and iterative expectation law, the conditional expectation of Y_{th} can be obtained as follows:

$$E[Y_{th}|Z_{th}, \theta] = E_{I_{(Y_{th}>0)}, W_{th}}\left[E\left[Y_{th}|I_{(Y_{th}>0)}, W_{th}, Z_{th}; \theta\right] Z_{th}; \theta\right], \tag{1}$$

W_{th} represents the situation of women's employment ($W_{th} = 1$ means women's employment, 0 means other). $I_{(Y_{th}>0)}$ is the index function of children's existence.

Basically, the fact that the unobservable factors that determine women's employment status have nothing to do with whether they have children or not is not included in this model. Different from the case of univariate (probability and logarithm), the comparison between bivariate linear and multinomial logarithmic models is complicated, and there is no direct connection between the parameter estimates obtained from the two models. When children enter rural families, their conditional expectations are

$$E\left(Y_{\mathrm{th}}|W_{\mathrm{th}} = 1, I_{(Y_{\mathrm{th}}>0)} = 1; Z_{\mathrm{th}}, \beta_1\right) = 1 - \exp\left(Z_{\mathrm{th}}\beta_1\right). \tag{2}$$

For the existence of the second child, this setting always has an expected value greater than 1, which is limited by the existence of the child.

First, we examine the variables related to the number of children in rural families. The variable described in this paper is the fertility rate, which is a binary dummy variable with a value of 1 when a child is born. The model of logit, probit regression, is

$$\begin{aligned} Y_{th} = {} & \alpha_0 + \alpha_1 \mathrm{jobstatus}_h + \alpha_2 \mathrm{fjobstatus}_h + \alpha_3 \mathrm{fincome}_h \\ & + \alpha_4 \mathrm{wage}_h + \alpha_5 \mathrm{family}_h + \mu_h. \end{aligned} \tag{3}$$

The variables in the model are explained in Table 1:

There is a causal relationship between rural family fertility willingness and the development of Chinese labor OEM industry. The choice of female reproductive behavior mainly includes the choice of reproductive age and the choice of the number of children, which is also a process of mutual decision and influence. Based on this, this paper constructs the following simultaneous equations to evaluate the influence of women's labor participation behavior on the childbearing age and the number of children.

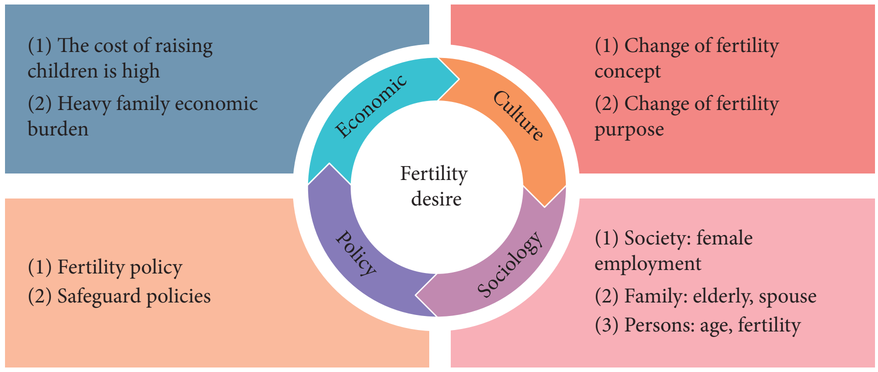

FIGURE 1: An analysis framework of influencing factors of childbearing family's fertility willingness.

$$\begin{aligned}\text{Number}_{\text{it}} &= \alpha_0 + \alpha_1 \text{Labor}_{\text{it}} + \alpha_2 \text{Age}_{\text{it}} + \alpha_3 X_{\text{it}} + \alpha_4 U_{\text{it}} + \alpha_5 P_{\text{it}} + \mu_{\text{it}},\\ \text{Age}_{\text{it}} &= \beta_0 + \beta_1 \text{Labor}_{\text{it}} + \beta_2 \text{Number}_{\text{it}} + \beta_3 Y_{\text{it}} + \beta_4 U_{\text{it}} + \mu_{\text{it}}.\end{aligned} \tag{4}$$

Among them:

$\text{Number}_{\text{it}}$, Age_{it}—Representing the number and age of women's childbearing respectively is the main index of reproductive behavior choice.

Labor_{it}—Variables reflecting women's labor participation, in this study, we will mainly consider whether women participate in labor and the nature of labor as variable indicators.

X_{it}—Personal characteristics affecting the number of births.

Y_{it}—Personal characteristics that affect the reproductive age.

U_{it}—Other controlled variables, mainly including the characteristics of family and community.

P_{it}—Virtual variable of family planning policy.

It can provide nonagricultural employment opportunities for surrounding women as a leader in economic development, and because of its proximity, it can also promote rural women's participation in nonagricultural work, which is beneficial to local rural women's participation in nonagricultural work. It is a problem that women should not consider when making reproductive decisions, just as it is a problem that women should not consider when making transportation facilities such as bus stops, development zones, and special economic zones. It only has to do with labor participation in decision-making and has nothing to do with reproductive choices.

We constructed a dynamic two-person and three-level game with complete information [21]. The competing government A and the company are located in the middle, and the company has three optional operations: requirement and default, A. The government adopts two selective measures to increase the preferential margin and maintain the status quo.

If the enterprise fails to ask government A to provide more preferential treatment, otherwise, it will move to Zhengzhou. Government A learns that government B has also implemented preferential policies for attracting investment. At this time, the economic aggregate of the enterprise is $(R + E_3)$, the economic aggregate of government A changes to $(G_1 - E_3)$, and the economic aggregate of government A does not change to G_2, with zero change.

In the third stage, the enterprise's strategies are migration, default, and requirements. At the time of migration, the economic aggregate of enterprises is $(R + E_2 - C)$, the economic aggregate of government A is $(G_1 - R)$, and that of government B is $(G_2 + R - E_2)$.

If the enterprise chooses the default at this time, the economic aggregate of the enterprise is $(R + E_1)$, the economic aggregate of government A is $(G_1 - E_1)$ at this time, and the economic aggregate of government B remains unchanged. This cycle continues until a certain local government withdraws from the game process. The whole game process is shown in Figure 2:

A^0 is defined as the game in which government A starts bidding. Because the whole game process is repeated indefinitely, A^0 does not affect the game analysis process at any stage. In this game, enterprises can freely choose whether to suspend negotiations with government A and turn to other regional governments.

Let π^0 be the upper bound of the payment that enterprises can get in this game equilibrium. We use A to represent the game that the enterprise has stopped the negotiation and turned to government B to renegotiate, and also let π represent the upper bound of the payment that the enterprise can get in equilibrium. We can clearly show the process of the stage game we intercepted with Figure 3 below.

In this model, we also need the following two constraints:

After bidding, the enterprise must wait for the counteroffer of government A, which is in the position of "insider," before deciding whether to suspend negotiations with it and start negotiations again with new "insider." The negotiation between an enterprise and a certain government must last at least T time periods.

Table 1: The variables in the model.

Variable	Explaining variables
Y_{th}	The number of children in rural families, h is the family variable
jobstatus	Female labor participation
fjobstatus_h	Employment of fathers in rural families
fincome_h	Per capita household income of the sample
wage_h	Binary explanatory variable
family_h	Other influencing factors in rural families that affect fertility rate
μ_h	The number of children in rural families is an orderly variable.

In game A^0, enterprises choose their own payment maximization, so there are

$$\pi^0 = \max\left(\sigma_1\left(1 - \sigma_2 + \sigma_2\pi^0, \pi\right)\right). \tag{5}$$

Because π is the supremum of the solution in game A equilibrium, so

$$\pi = \frac{\left(1 - \sigma_2\right)\left[1 - \left(\sigma_1\sigma_2\right)^{T+1/2}\right]}{1 - \sigma_1\sigma_2} + \sigma_1^{T-1/2}\sigma_2^{T+1/2}\pi^0. \tag{6}$$

According to (5), if $\pi^0 = \sigma_1\left(1 - \sigma_2 + \sigma_2\pi^0\right)$, there is

$$\pi^0 = \frac{\sigma_1\left(1 - \sigma_2\right)}{1 - \sigma_1\sigma_2}. \tag{7}$$

Substituting (7) into (6) results in

$$\pi = \frac{1 - \sigma_2}{1 - \sigma_1\sigma_2}. \tag{8}$$

If $\pi^0 = \pi$ is substituted into formula (6), the maximum payment of the enterprise is

$$\pi = \frac{\left(1 - \sigma_2\right)\left[1 - \left(\sigma_1\sigma_2\right)^{T+1/2}\right]}{\left[1 - \sigma_1\sigma_2\right]\left[1 - \sigma_2\left(\sigma_1\sigma_2\right)^{T-1/2}\right]}. \tag{9}$$

At this time, the payment of government A is $1 - \pi$.

Through the analysis in the last part, we compare the labor cost, land cost, and tax preference of the two places to illustrate the main differences of the expected profits of enterprises in the two places.

Random forest (RF) algorithm is an ensemble learning algorithm based on decision tree. Decision tree is a single learning method, called "Basic Learner," which combines multiple decision trees into a "Forest." By forming a strong learner in the integrated learning method, the predictive ability of the algorithm can be effectively improved. Create RF model:

$$y_n = f^*(\cdot) = \sum_{b=1}^{B} f^b \frac{\left(n, x, x_i, t_i, T, \lambda\right)}{B}. \tag{10}$$

Among them, x_i, t_i are the characteristic variable and the corresponding splitting critical value of each decision tree when splitting at the i-layer in RF algorithm according to the principle of "minimizing the sum of squares of residuals."

λ—The punishment intensity of complexity T obtained by cross-validation method;

n—Core characteristic variables;

x—Other characteristic variables;

B—Number of decision trees contained in RF.

After obtaining the results of parameters such as x_i, t_i, T, λ through algorithm training and verification, the relative opportunity cost of childbearing can be combined with the level of living burden to measure the degree that the opportunity cost of childbearing can be borne.

3.2. Data Source and Variable Description. The data used in this paper is the panel data of CFPS 2015–2021. In this study, the variables used in the equivalence scale method include income satisfaction, total family income, family size, and number of children. This paper chooses income satisfaction as the explanatory variable. We need to filter data and delete missing items and outliers of families with children under 20 years old. Because the answer of income satisfaction is set to 1 to 5, 1 means "unsatisfied," and 5 means "very satisfied," and the variable is discrete.

Compared with cross-sectional data, panel data has certain advantages: first, it can use the difference between groups to multiply the time trend, so as to eliminate the possible deviation caused by small samples; secondly, the endogenous problem can be overcome by using lag data. Table 2 reports the descriptive statistics of the main variables.

Among the basic elements of social support, this paper takes into account the respondents' maternity insurance status, peer reproductive pressure, and local infant community service facilities. Table 3 shows descriptive statistics of independent variables of basic state characteristics of social support.

From Table 1, we can see that most people still choose to enjoy maternity insurance, which may be because many people in this survey are in economically developed areas, and maternity protection in these provinces and cities is in place. According to Table 2, it is found that many respondents have fertility pressure. When processing the data, the author assigns the answers of "absolute influence," "greater influence," and "general" as 1. Infant service facilities have a great influence on fertility willingness, otherwise, 2. Infant service facilities have little influence on fertility willingness.

4. Experiment and Results

Increasing the female labor force participation rate can revitalize the current economy, but it will significantly reduce the female fertility rate, further affect the national

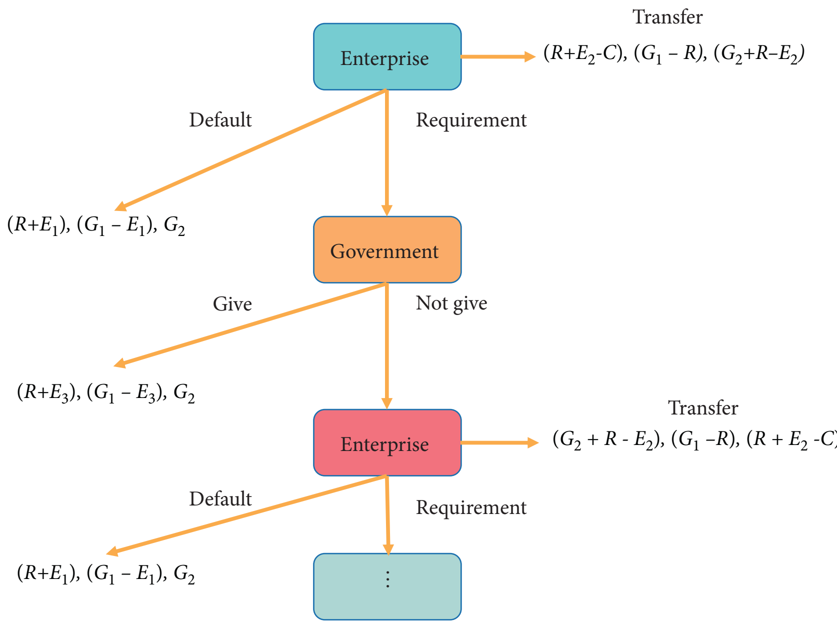

Figure 2: The second stage game process.

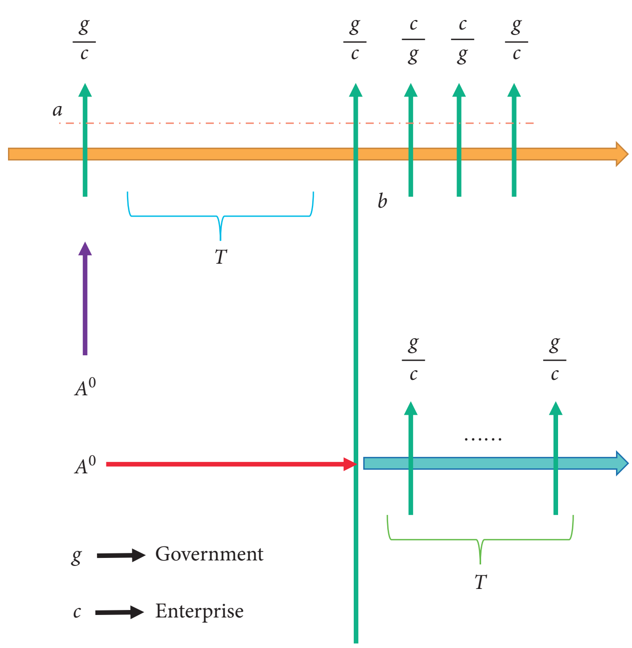

Figure 3: The process of intercepting stage game.

fertility rate, and affect the future labor supply and economic development. Therefore, it is the goal of all countries to maintain a high female labor force participation rate without affecting the fertility rate. Asian countries, especially some East Asian countries and Southeast Asian countries, should constantly improve policies to encourage women to bear children, such as parental leave and flexible working system.

The regression results in Figure 4 show that women's career development has a significant negative impact on the fertility willingness of the two children, and the rise of women's family status plays a part of the intermediary role.

The regression coefficient between women's career development and their willingness to have two children is significant and negative ($c_1 = -0.181, P = -0.003 < 0.01$), indicating that the better the career development, the lower the probability that women intend to have two children. The regression coefficient between women's family status and the willingness to have two children is significant and negative ($c_1 = -0.998, P = 0.031 < 0.01$), indicating that the higher the family status, the lower the probability that women intend to have two children. This means that the impact of a woman's professional advancement on her desire to have two children is at least

Table 2: Descriptive statistics of main variables.

Variable	Mean value	Standard deviation	Observation and measurement
Total fertility rate *T*	3.15	1.32	1136
Female labor participation rate *F*	44.1	20.01	1427
Proportion of urban population to total population *C*	50.31	25.68	1427
Neonatal mortality rate *B*	33.21	27.14	1427
Female primary school enrollment rate *S*1	95.32	20.63	1021
Female secondary school enrollment rate *S*2	72.4	26.74	886
Enrolment rate of female colleges and universities *S*3	22.17	17.16	653

Table 3: Support independent variable description statistics of basic social situation characteristics.

Independent variable	Variable assignment	Minimal	Maximum	Mean value	Standard deviation
Is there maternity insurance *Q*	1 = yes 2 = No	1	2	1.33	0.412
Peer fertility pressure *W*	1 = yes 2 = No	1	2	1.06	0.364
Influence of infant service facility on fertility willingness *E*	1 = greater impact 2 = minor impact	1	2	1.27	0.428

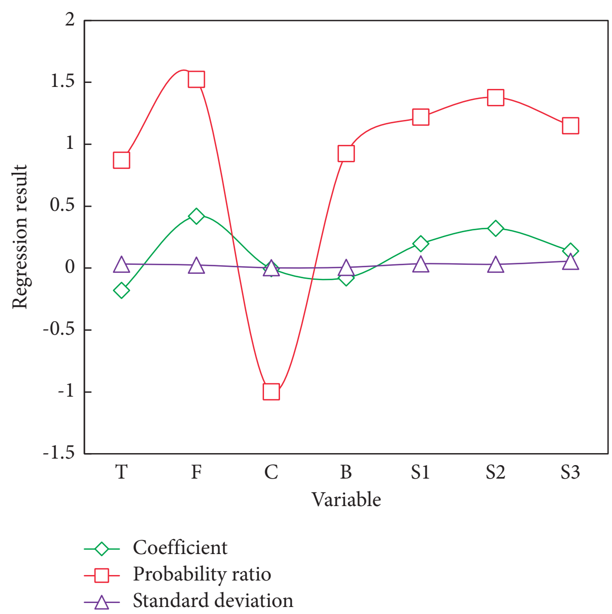

Figure 4: The influence of women's career development and family status on the fertility willingness of two children.

partially realized through the parameters of her family status. The improvement of women's family status is one of the negative effects of their career advancement on their willingness to have a second child. We made a comparison by age in Figure 5 to explain in detail the fertility wishes, current fertility behaviors, and future fertility plans of these women.

The following points can be observed from Figure 5:

(1) There are differences in women's fertility wishes of all ages, but the differences are not too great, fluctuating around 1.5.

(2) Compared with women in other age groups, the 20–24 age group has the lowest willing fertility rate.

(3) The gap between the maximum and minimum target fertility rate of women gradually narrows with the increase of age, which indicates that the younger the women, the greater the variability of family planning.

(4) With the increase of age and the distance between women's fertility ideal and future fertility plan, the possibility of realizing fertility ideal also increases. Women of different ages were born in different ages, and their fertility wishes, current fertility behaviors, and future fertility plans all reflect the differences among women of different ages.

From the calculation results of social support status factor model, it can be seen that the social support factors selected in this study have no significant influence on the

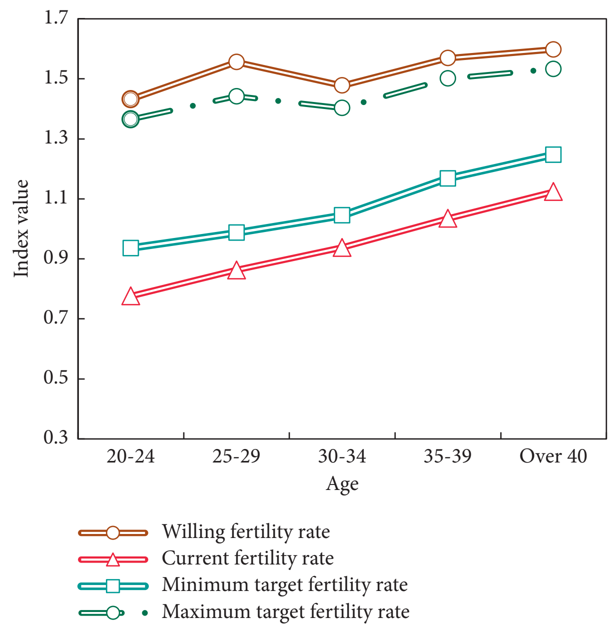

Figure 5: Women's will, current and target age-specific fertility rate in line with the two-child policy.

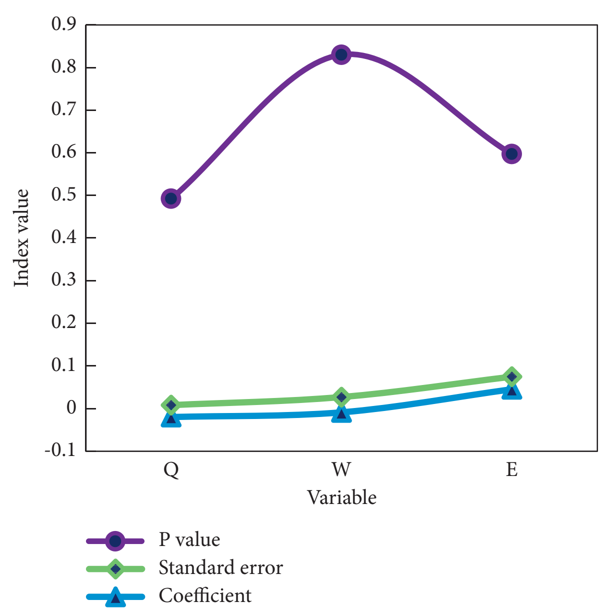

Figure 6: Social support condition factor model.

fertility desire of childbearing age families. The coefficient of maternity insurance coefficient is negative, and respondents without maternity insurance are more likely to have children, which may be because people without maternity insurance are often distributed in rural areas.

Age can have relatively traditional thinking. In addition, the above results can be obtained because the coverage rate and wages of maternity insurance are generally low, which can not be used as the guarantee of fertility (Figure 6).

Peer pressure factors have no significant influence on the willingness of families to bear children, and the absolute value of the coefficient is very small, which is 0.009, which may be the reason for sample selection. In addition, as shown above, it is found that the factors of infant service facilities in local communities have no significant influence on the family's fertility desire, which may be due to the imperfect infant service facilities in China. Many families of childbearing age with better economic conditions look for private kindergartens and other childcare facilities at their own expense, while families with poorer economic conditions often choose families. Therefore, for families of childbearing age, the factors of infant service facilities in local communities are very important, and the fertility will has no significant influence.

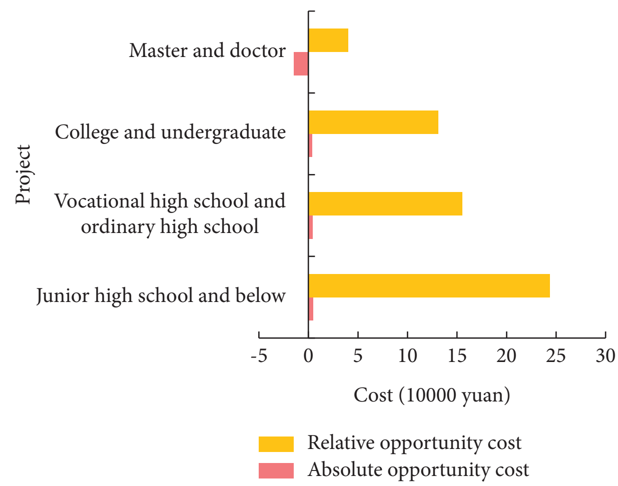

FIGURE 7: Differences in reproductive opportunity cost of women with different educational levels.

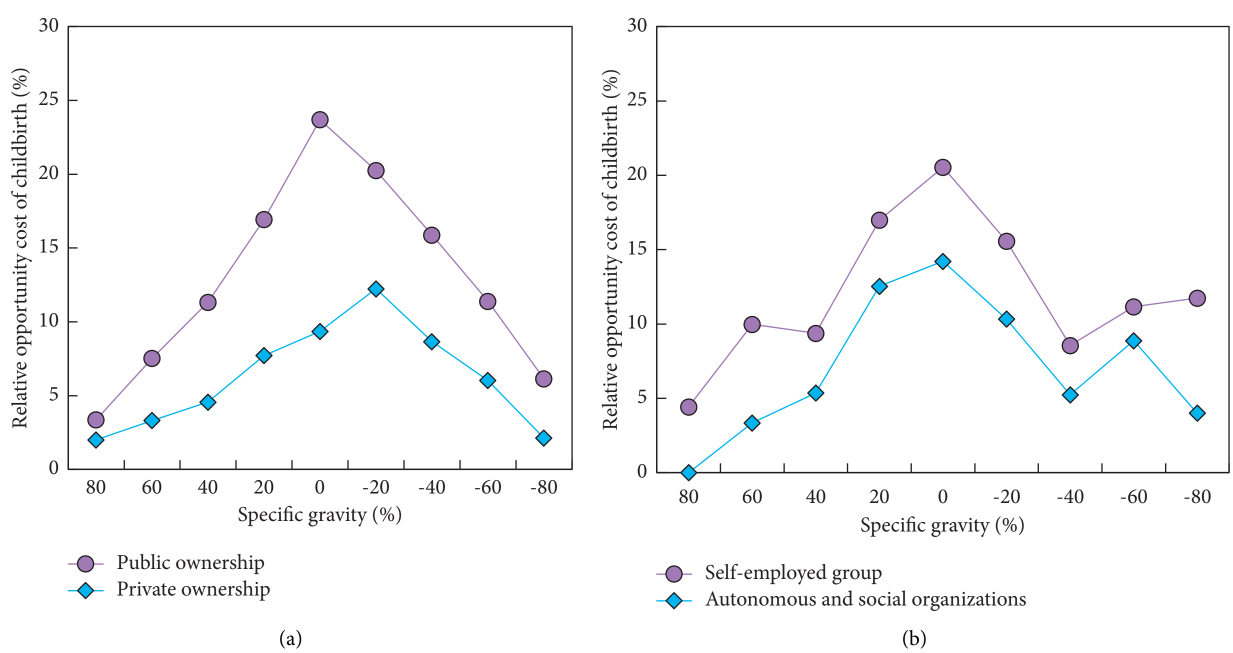

FIGURE 8: Comparison of reproductive opportunity cost of women in different employment units.

The difference of reproductive opportunity cost of women in different education levels and employment units also confirms the role of maternity insurance. As shown in Figure 7, on average, women with lower education level have higher absolute and relative opportunity cost of childbirth.

Women with master's and doctor's degrees have the lowest absolute and relative opportunity cost of childbirth, and this group of women is more likely to engage in high-paying jobs with high working threshold and high maternity insurance coverage. Because of the high opportunity cost of fertility rate, social security is not perfect.

Figure 8 shows the reproduction opportunity cost of employers according to the nature of legal entities. Figures 8(a) and 8(b) show that the relative opportunity cost of female fertility rate in public units is more obviously concentrated in the range of 0–10%, while that in private units is concentrated in the range of 10%–20%. The relative opportunity cost of female fertility rate of local governments and social organizations is concentrated in the range of 0~10%, which is distributed symmetrically around 0. However, the relative opportunity cost of female fertility rate of self-employed households is concentrated in the range of 50%~80%. Compared with other types of units, self-employed households cannot protect their own rights and interests because they do not buy maternity insurance.

According to the regression results, female labor participation has a significant negative impact on the fertility level of one and two children. In the regression process, the regression results obtained by probit and logit are consistent. In order to ensure the reliability of regression results, this paper uses OLS to test the robustness of probit regression results. The obtained test results are shown in Table 4, and

Table 4: Influence of labor supply on fertility level.

Variable	A family with one child	Families with a second child
T	−0.06***	−0.097***
F	0.121	0.041***
C	−0.002***	−0.066
B	−0.006	−0.001*
S1	0.017	−0.017
S2	−0.009	0.068
S3	−0.047	−0.087***
Q	−0.367***	−0.201
W	0.001*	−0.002***
E	−0.038	−0.047

Note: *, ** and *** are significant at the level of 10%, 5% and 1% respectively.

Table 5: Influence of labor supply on fertility level.

Variable	A family with one child	Families with a second child
Number of elderly people in rural families	2.318***	2.217***
Labor supply	−0.036	−0.863***
Average personal household income	−0.128	−0.221
Is there any wage income	−0.001	−0.003*
Total cash and deposits	−0.068**	−0.012***
Account status	−0.042	−0.076
Age	−0.033***	−0.038**
Gender	0.168	−0.156

the obtained results are remarkably consistent, and the regression results are stable.

Combined with the research direction of this paper and the availability of selected data, this paper chooses the number of elderly people in rural families as the tool variable of female labor supply model. The results are shown in Table 5.

The endogenous relationship between women's labor participation rate and fertility rate is solved using the instrumental variable method, and the rural elderly population is used as an instrumental variable in regression estimation. Female labor participation has a significant negative impact on one or two child fertility rates. The negative impact of women's labor on the two children is particularly significant in the empirical findings. An important reference is how to improve the three-child fertility rate in the context of China's three-child policy liberalization.

5. Conclusions

The research of this paper mainly focuses on the measurement of the correlation degree between rural families' fertility willingness and the development of China's labor OEM industry and investigates the main influencing factors of different children in rural families. The main findings are as follows:

(1) The regression analysis results considering the influence of female labor participation on fertility rate show that female labor participation has a significant negative effect on the number of children in rural families, and female labor participation will lead to the decrease of the number of children in rural families.

(2) The regression coefficient between women's career development and their willingness to have two children is significant and negative ($c_1 = -0.181, P = -0.003 < 0.01$), indicating that the better the career development, the lower the probability that women intend to have two children. The regression coefficient between women's family status and the willingness to have two children is significant and negative ($c_1 = -0.998, P = 0.031 < 0.01$), indicating that the higher the family status, the lower the probability that women intend to have two children.

(3) The relative opportunity cost of unit female fertility rate is more obviously concentrated in the range of 0–10%, while that of private ownership is concentrated in the range of 10%–20%. The relative opportunity cost of female fertility rate in local governments and social organizations is concentrated in the range of 0~10%, and distributed symmetrically around 0, but the relative opportunity cost of self-employed fertility rate is in the range of 50%–80%.

Data Availability

The data used to support the findings of this study are available from the corresponding author upon request.

Conflicts of Interest

The author does not have any possible conflicts of interest.

Acknowledgments

This study was supported by Philosophy and Social Science Planning Office of Shanxi Province: "Research on the Organizational Strategy of Labor Service Export in Shanxi Province" (2020YJ094).

References

[1] F. Droller, M. Cripps, and A. Galeotti, "Migration, population composition and long run economic development: evidence from settlements in the pampas," *The Economic Journal*, vol. 128, no. 614, pp. 2321–2352, 2018.

[2] M. Bratti, T. Frattini, F. Scervini, and F. Scervini, "Grandparental availability for child care and maternal labor force participation: pension reform evidence from Italy," *Journal of Population Economics*, vol. 31, no. 4, pp. 1239–1277, 2018.

[3] F. Cai, "The second demographic dividend as a driver of China's growth," *China and World Economy*, vol. 28, no. 5, pp. 26–44, 2020.

[4] M. T. Choudhry, P. Elhorst, and A. Ziderman, "Female labour force participation and economic development," *International Journal of Manpower*, vol. 39, no. 7, pp. 896–912, 2018.

[5] S. T. Fatima and A. Q. Khan, "Globalization and female labor force participation: the role of trading partners," *Journal of International Trade & Economic Development*, vol. 28, no. 3, pp. 365–390, 2019.

[6] J. Devaro and O. Gürtler, "Advertising and labor market matching: a tour through the times," *Journal of Labor Economics*, vol. 36, no. 1, pp. 253–307, 2018.

[7] R. Shrestha, "Early life exposure to air pollution, cognitive development, and labor market outcome," *Asian Economic Papers*, vol. 18, no. 2, pp. 77–95, 2019.

[8] R. Mao, J. Xu, and J. Zou, "The labor force age structure and employment structure of the modern sector," *China Economic Review*, vol. 52, pp. 1–15, 2018.

[9] A. Yakita, "Female labor supply, fertility rebounds, and economic development," *Review of Development Economics*, vol. 22, no. 4, pp. 1667–1681, 2018.

[10] F. Tian, J. Gao, and K. Yang, "A quantile regression approach to panel data analysis of health-care expenditure in Organisation for Economic Co-operation and Development countries," *Health Economics*, vol. 27, no. 12, pp. 1921–1944, 2018.

[11] B. Erten and M. Metzger, "The real exchange rate, structural change, and female labor force participation," *World Development*, vol. 117, pp. 296–312, 2019.

[12] K. Codazzi, V. Pero, and A. Albuquerque Sant'Anna, "Social norms and female labor participation in Brazil," *Review of Development Economics*, vol. 22, no. 4, pp. 1513–1535, 2018.

[13] J. Shen, C. Chen, M. Yang, and K. Zhang, "City size, population concentration and productivity: evidence from China," *China and World Economy*, vol. 27, no. 1, pp. 110–131, 2019.

[14] J. E. Finlay, "Women's reproductive health and economic activity: a narrative review," *World Development*, vol. 139, Article ID 105313, 2021.

[15] Z. Rong and C. Zhao, "Research on the correlation model of vocational talents, population structure and economic development," *Wireless Personal Communications*, vol. 102, no. 2, pp. 1–12, 2018.

[16] G. Xie, L. Huang, H. Bin et al., "Sustainable entrepreneurship in rural E-commerce: identifying entrepreneurs in practitioners by using deep neural networks approach," *Frontiers in Environmental Science*, vol. 6, p. 370, 2022.

[17] H. Han, L. Guo, J. Zhang, and K. N. Zhang, "Spatiotemporal analysis of the coordination of economic development, resource utilization, and environmental quality in the Beijing-Tianjin-Hebei urban agglomeration," *Ecological Indicators*, vol. 127, no. 8, Article ID 107724, 2021.

[18] S. Yan, Z. Ming, and Z. Min, "Study on the decoupling relationship between CO2 emissions and economic development based on two-dimensional decoupling theory: a case between China and the United States - ScienceDirect," *Ecological Indicators*, vol. 102, pp. 230–236, 2019.

[19] C. Huang, "Why are U.s. Women decreasing their labor force participation if their wages are rising?" *Economic Inquiry*, vol. 56, no. 4, pp. 2010–2026, 2018.

[20] D. Salehi-Isfahani and M. H. Mostafavi-Dehzooei, "Cash transfers and labor supply: evidence from a large-scale program in Iran," *Journal of Development Economics*, vol. 135, pp. 349–367, 2018.

[21] D. Baerlocher, S. L. Parente, and E. Rios-Neto, "Female labor force participation and economic growth: accounting for the gender bonus," *Economics Letters*, vol. 200, Article ID 109740, 2021.

Hindawi
Computational Intelligence and Neuroscience
Volume 2022, Article ID 4391491, 16 pages
https://doi.org/10.1155/2022/4391491

Research Article

A Graph-Related High-Order Neural Network Architecture via Feature Aggregation Enhancement for Identification Application of Diseases and Pests

Jianlei Kong,[1] **Chengcai Yang**,[1] **Yang Xiao**,[1] **Sen Lin**,[2] **Kai Ma**,[3] **and Qingzhen Zhu**[4]

[1]*School of Artificial Intelligence, Beijing Technology and Business University, Beijing 100048, China*
[2]*Research Center of Intelligent Equipment Technology, Beijing Academy of Agriculture and Forestry Sciences, Beijing 100097, China*
[3]*School of Engineering, Beijing Forestry University, Beijing 100086, China*
[4]*School of Agricultural Equipment Engineering, Jiangsu University, Zhenjiang, Jiangsu 212013, China*

Correspondence should be addressed to Sen Lin; linseng@nercita.org.cn and Kai Ma; makai2015@bjfu.edu.cn

Received 23 March 2022; Accepted 5 April 2022; Published 26 May 2022

Academic Editor: Xin Ning

Diseases and pests are essential threat factors that affect agricultural production, food security supply, and ecological plant diversity. However, the accurate recognition of various diseases and pests is still challenging for existing advanced information and intelligence technologies. Disease and pest recognition is typically a fine-grained visual classification problem, which is easy to confuse the traditional coarse-grained methods due to the external similarity between different categories and the significant differences among each subsample of the same category. Toward this end, this paper proposes an effective graph-related high-order network with feature aggregation enhancement (GHA-Net) to handle the fine-grained image recognition of plant pests and diseases. In our approach, an improved CSP-stage backbone network is first formed to offer massive channel-shuffled features in multiple granularities. Secondly, relying on the multilevel attention mechanism, the feature aggregation enhancement module is designed to exploit distinguishable fine-grained features representing different discriminating parts. Meanwhile, the graphic convolution module is constructed to analyse the graph-correlated representation of part-specific interrelationships by regularizing semantic features into the high-order tensor space. With the collaborative learning of three modules, our approach can grasp the robust contextual details of diseases and pests for better fine-grained identification. Extensive experiments on several public fine-grained disease and pest datasets demonstrate that the proposed GHA-Net achieves better performances in accuracy and efficiency surpassing several other existing models and is more suitable for fine-grained identification applications in complex scenes.

1. Introduction

Agriculture is an industry that integrates technology, economy, politics, and national security, supporting the entire history of human evolution, and is increasingly multifunctional with social development and progress. Agriculture is an essential source of basic living materials for human society, which provides the primary products and material basic conditions for developing the global economy and feeding humanity [1, 2]. Plant pests and diseases affect the overall functioning of the plant, and it can lead to slowed growth, reduced fruit yield, leaf drop, and many other diseases. The sources of plant diseases are multifaceted. Sometimes, the diseases are spread from one crop to another caused by some fungus or other bacteria. Moreover, some viruses hidden in the seeds are transferred from one place to another place, resulting in outbreaks of diseases [3]. Due to the complex generation and transmission mechanism, pests and diseases have become one of the most challenging questions faced by global agricultural production. According to statistics, the annual loss of plant yields due to diseases and pests accounts for more than 50% [4]. Therefore, the accurate identification of disease and pest species is of great significance to controlling plant diseases and pests as well as improving crop yield.

Identifying diseases and pest maintenance in traditional agricultural production relies on some agronomy experts with professional knowledge and experience through their naked eyes [5, 6]. This approach is usually a time-consuming, uneconomical, and repeated job when invasive species appear or the production farmlands are changed, which affects the subsequent production operations. In recent years, modern agriculture is striving to make full use of innovative systems and methods to achieve intelligent production and management, including Internet of Things (IoT), automated robots, big data cloud computing, and artificial intelligence modelling [7–11]. With the development of information and intelligent technologies, the automatic and accurate identification methods handling various diseases and pests have become one of the important issues in the modern agricultural production process, which attracts many agricultural experts and enterprises to carry out related research [2, 12–14]. An efficient and reasonable solution is using some machine learning-based methods to identify the species of plant pests and diseases [15–17]. On basis of enough image data collected by visible sensors or devices, those methods firstly apply some classical statical learning or machine learning methods to identify the varieties of plant pest and diseases. Those classical methods mainly rely heavily on complex statical analysis and designed feature engineering to gain a modest performance, which occupy massive computing power and human resources to cover time-consuming model training process, leading to a lack of recognition ability in complex practical applications.

With the development of information technology and intelligent approaches, deep learning neural networks have made significant improvement in solving many intelligent applications, including image classification, object detection, and video tracking, which provide a promising candidate for a generalizable approach for complex environment practices. At present, several deep learning models, including convolutional neural network (CNN), recurrent neural network (RNN), and generative adversarial networks (GAN), have been introduced into the visual recognition of plant's disease and pest species [18–20]. With multilayer structure and massive majorization modules, deep learning methods could automatically learn the multidimensional feature expressions from a large amount of raw data and mine more potential rules at an abstract perspective, which obtained better accuracy and stronger robustness over traditional technologies in identifying different plant pest and disease types.

Although many studies provide credible references to demonstrate the superiority of deep learning approaches, accurately classifying plant diseases and pests is still challenging in a natural scene. The main problem is that the practical identification process of different diseases and pests is a typical fine-grained visual classification (FGVC) problem [21]. As a research hotspot of artificial intelligence in recent years, FGVC is mainly to identify image samples belonging to multiple sublevel classes via retrieving objects under a meta-level category, which is more complicated than simple coarse-grained identification of existing deep learning methods [22–25]. There are many fine-grained difficulties that need to be addressed in identifying plant diseases and pests. On the one hand, the same meta-level category contains vast sublevel samples with viewpoints, illumination, positions, growth periods, and environmental factors, which are easy to confuse the model, resulting in incorrect identification. On the other hand, there is a certain similarity among different meta-level categories. Different genera or subspecies of the same biological subject often have a highly similar overall appearance except for several critical local parts. Thus, deep learning models based on coarse-grained representation learning are generally lacking the effective and accurate ability to handle the identification puzzle for plant disease and pest.

To overcome the above problems, this study proposes a novel graph-related high-order architecture with feature aggregation enhancement to establish a fine-grained deep learning neural network (GHA-Net), aiming to promote the rapid identification of plant pests and diseases in complex natural applications. There are two main innovations in this proposed method. Firstly, a feature aggregation module is designed to improve the fine-grained feature perception capability of the cross stage partial network stage (CSP-stage) backbone network, which filters out multiscale discriminating features and pays more attention to local parts. Secondly, the graphic convolution module is constructed to analyse the graph-correlated representation of part-specific interrelationships by regularizing semantic features into the high-order tensor space. With collaborative learning and global optimization, our approach can achieve better fine-grained identification performance for massive plant diseases and pests in terms of accuracy and robustness, which is more suitable for practical recognition applications.

The rest of the paper is organized as follows: Section 2 introduces the related research of computer vision and machine learning techniques for plant pest and disease identification. Then, the details of the proposed algorithm and experimental datasets are explained in Section 3. Section 4 presents contrastive experimental results and performance evaluation. Finally, Section 5 concludes the whole work with future research prospects.

2. Related Work

Plants infected with diseases and pests usually exhibit visible marks or lesions on the leaves, stems, and fruits, which generally present unique visible patterns for intelligent diagnosis. Nowadays, lots of researchers apply machine learning and information processing techniques to identify different pest and disease species on controllable environmental conditions or public competition datasets. In this section, we review and summarize some relevant studies on machine learning technologies and coarse-grained deep learning methods for plant disease and pest classification, as well as some fine-grained recognition approaches, which is also a key issue of our work.

2.1. Machine Learning Technology for Plant Disease and Pest Identification. In order to guarantee the amount of training data for training complicated deep learning models, many studies have collected various public datasets of plant disease and pest categories. In the first stage of intelligent algorithm modelling, a sufficient amount of image data is necessary for feature extraction, including texture, shape, color, and motion-related attributes. Islam et al. [22] used a dataset of 300 potato leaves from the PlantVillage dataset [26] to design a classifier capable of identifying healthy leaves and leaves affected by late blight and early blight. Then, a multiclass support vector machine was used to classify leaf images based on ten colors and texture features. Qin et al. [27] proposed a solution to identify four leaf diseases affecting alfalfa grass by cropping the image to generate a subimage with one or more lesions. At the same time, the principal component analysis (PCA) method was used to reduce the dimension of *45* feature vectors, which offers the Naïve Bayes classifier to achieve good classification results. Similarly, Wu et al. [23] collected over *75,200* images covering *102* types of crop pests and framed more than 19,000 photos to handle visual classification and detection. Recently, some public competitions also provided public pest and disease datasets, such as AI Challenger 2018, which provided nearly 50,000 photos of plant leaves classified into 61 categories. Cassava Leaf Disease Classification competition provided a dataset of *21,367* labeled images of cassava, divided into four disease classes and health states [28]. These datasets often contain disease and pest infestations, providing a good foundation for intelligent algorithm modelling and optimization.

Meanwhile, several statistical learning and machine learning approaches have been widely introduced to the image identification of plant diseases and pests, including support vector machine (SVM), K-nearest neighbour (KNN), decision tree (DT), and artificial neural network (ANN). For example, Kumar et al. [29] designed an exponential spider-monkey algorithm to optimize an SVM-based classifier, which selects the high-dimensional essential features from the images of pests and diseases by eliminating unimportant features. Zhang et al. [30] proposed a hybrid clustering-based method for plant disease and pest identification. Through KNN clustering, the entire image is divided into several compact and approximately uniform superpixels, providing valuable clustering clues for guiding image segmentation, which effectively detects plant diseases and pests. Similarly, Khule et al [31] attempted to apply different machine learning methods for the classification of tomato diseases. Using image processing techniques combined with SVM, DT, and ANN algorithms, the proposed work achieves good identification performance with an accuracy of 93.75% for all leaf diseases. However, these traditional methods based on simple shallow structures need to rely heavily on manual feature design engineering to obtain satisfactory identification performance. Moreover, these methods lack good performance in the face of large-scale data and complex environment applications. Therefore, more and more researchers have begun to turn their attention to new technologies such as popular deep learning.

2.2. Coarse-Grained Deep Learning Recognition Approaches. Deep learning neural networks with multilayer structure and comprehensive optimization strategies have achieved better performance surpassing human recognition or traditional machine learning methods on different visual research aspects. At present, several deep learning-based convolutional neural networks (CNNs), such as AlexNet [26], VGG [32], ResNet [33], and GoogLeNet [34], have been applied in the image recognition of pest and disease species with considerable performance. For example, Mohanty et al. [35] employed the AlexNet and GoogLeNet models to identify various pest categories on the PlantVillage dataset, which obtained a better accuracy rate than other machine learning methods with shallow structures. Chen et al. [36] added a new batch normalization to the VGG network and replaced the fully connected layer with a global pooling layer, improving identification accuracy. Similarly, Yan et al. [37] replaced all fully connected layers of ResNet with global average pooling layers to identify apple leaf disease and pest categories. The experimental results show that the optimization algorithm improves the whole recognition rate of diseases and pests and dramatically shortens the training and recognition time of the model.

In order to improve the generalization of deep learning algorithms in practical applications, many researchers attempted to combine various machine learning strategies to optimize original CNN models with fixed network architecture. For example, Hu et al. [38] firstly introduced the SVM to design an improved conditional deep convolutional generative adversarial network (C-DCGAN) for local area segmentation. Taking lesion images as input, the proposed method could generate new training samples automatically to train the VGG16 model for identifying tea pests and diseases, which achieves better accuracy while relying on only a little image data. From similar thinking, Argüeso et al. [39] studied the identification problem of leaf diseases and pests to handle a small amount of data. Based on the Siamese network with a few-shot learning approach, the proposed method reduced dependence on data quantity while achieving relatively good recognition results.

Moreover, some studies have attempted to apply some knowledge distillation and structural lightweight methods to reduce recognition model parameters, in order to accommodate the real-time application requirements in natural practices. Take Liu et al. [40] for instance; MobileNet and Inception-V3 models with light-weighted structures are migrated simultaneously to construct the deep learning model for plant pest identification. Experimental results show that the optimal method can be transplanted to the Android system on mobile phones, effectively balancing the model's parameters and accuracy. Similarly, Zhang et al. [41] proposed a global pool dilated convolutional neural network (GPDCNN) for plant pest identification. The deep learning network replaces the global convolution of AlexNet with dilated convolution, aiming to reduce the computational complexity and parameter quantity, which are demonstrated to obtain enough recognition performance on cucumber leaf disease and insect images. Although existing coarse-grained methods have achieved some applications in the meta-level identification of plant pests and diseases, they lack the adequate perception for fine-grained features in the absence of particular designs or modules. It is still challenging to implement plant pest and disease recognition in natural settings meeting practical requirements.

2.3. Fine-Grained Visual Recognition Methods. Unlike coarse-grained image recognition, fine-grained visual recognition aims to correctly distinguish different sublevel samples within a sizeable meta-level class, which is a significant difficulty in pattern recognition. The critical link of fine-grained identification is discovering some powerful features or local regions, which could represent the potential rules for effectively distinguishing different subclasses with similar appearance and tolerating sample differences of the same class. Fine-grained identification methods are mainly divided into two categories depending on the local labeling approach. The first category is the strongly supervised learning method, which adds extra labels such as label boxes to the image, improving fine-grained identification ability. However, adding extra labels to massive images is a very labor-intensive and time-consuming process, which is not suitable for large-scale datasets. The second kind is the weak supervision method [9], which only relies on the attention method without extra labels to adaptively locate the discriminating part of the target. Such methods have attracted the attention of many researchers. For example, Cruz et al. [20] reduced the number of network layers by modifying convolution blocks as attention modules to contrast the proposed path aggregation network (PANet). This method obtains fine-grained positioning information on different receptive fields to enhance the multiscale features, which is conducive to detecting apple pests and diseases in complex scenes. Similarly, Hughes and Salathé [42] proposed a feature compensation model based on residual neural network (MDFC-ResNet), which grabs multidimensional local information from different granularities into fusing recognition results, achieving a better recognition performance than contrastive deep learning models.

In the above fine-grained methods, the discrimination parts of targets are often used independently. Considering that plant pests and diseases have obvious physiological spatial situations, learning the relationship between different discrimination characteristics can further enhance the discrimination ability. The relationship representation of different local parts can be regarded as a graph structure. Thus, graph neural network plays a vital role in applying non-Euclidean data to analyse the interpretable characteristics, which has excellent research significance in defining the intrinsic relevance of deep learning network nodes and parameters. Recently, deep learning-based graphic networks have developed several model variants, such as graph convolution neural network [43], gated graph neural network [44], graph attention network [45], and graph spatiotemporal network. In the aspect of fine-grained image recognition, Wang et al. [46] proposed the GCL model to exploit and utilize the semantic correlation between regional features fully, designed a cross graph to spread from the network to learn the correlation semantics between different regions, and then enhanced each region by cross-weighted aggregation of other regions. Zhao et al. [25] proposed an effective graph-based relationship discovery method to establish context understanding of high-order relationships. This method regularizes the high-dimensional feature library using high-order constraints of semantic awareness. It embeds the high-order tensor library into the low-dimensional space, which can grasp the context details of fine-grained objects.

In summary, due to the challenging fine-grained problems, traditional machine learning and coarse-grained deep learning methods are unsuitable for plant pest and disease recognition in practical applications. Inspired by graphic neural networks, this paper proposes a graph-related high-order approach via feature aggregation enhancement for fine-grained plant disease and pest identification, aiming to solve the existing identification problems of low accuracy and efficiency. For detailed method descriptions, refer to the following sections.

3. Materials and Methods

This section will introduce the details of the graph-based high-order model constructed for fine-grained plant disease and pest identification. Our proposed GHA-Net consists of three main parts: (1) improved backbone network based on the CSP-stage operations is subjected to extract rich coarse-grained feature maps; (2) feature aggregation enhancement module is proposed to learn more slight features of different parts; and (3) graph-related feature extractor is designed to explore intrinsic relationship among various local features and further mine hidden higher-order features of graph nodes and edges. The overall architecture is shown in Figure 1.

3.1. CSP-Based Backbone Network. According to actual application requirements, we apply some data enhancement operations, such as rotate, flip, random crop, Gaussian noise adding, and HSV changing, to enlarge existing image samples before model training. These preprocessing operations can ensure that the deep learning models have sufficient data volume to achieve good generalization and noise resistance to internal and external factor changes. Subsequently, all images are subjected to an improved CSP-based backbone network with the superiority of residual structure. After so many years of theoretical and application demonstrations, a basic knowledge has been recognized by everyone, that is, as the level of the deep neural network is deeper, the model can obtain more scales of receptive fields and rich features, leading to better identification performance. As network structures become more complex and deeper, there is a rapidly growing demand for more training data to fit the explosion of model parameters. However, too many model parameters will not only waste a lot of computing resources but also have little effect on improving model accuracy; due to this, the single path of information propagation in the complex network structure is easy to cause gradient vanishing or explosion.

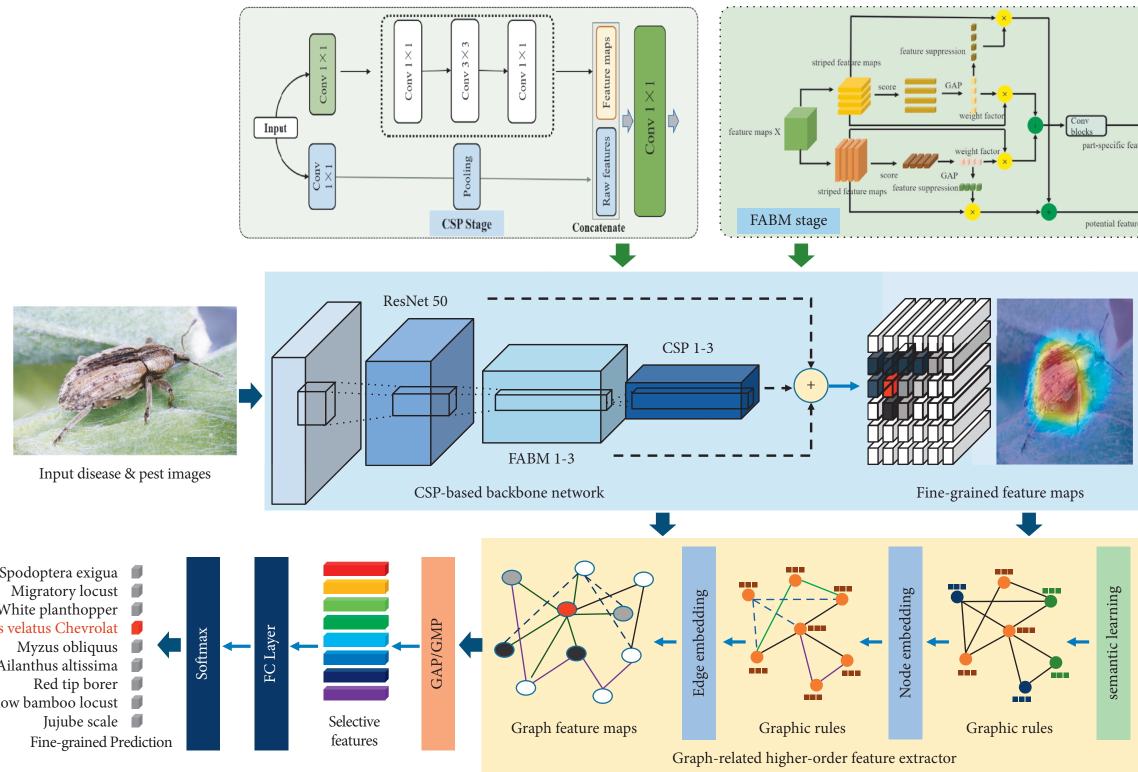

Figure 1: Schematic diagram of the proposed model structure.

Thus, the CSPNet50 [47], a new variant network of ResNet family, is selected as the backbone network in this paper. The backbone network consists of three CSP stages. Each stage adds several cross-channel branches on the primary residual block, so that a portion of features can directly skip all computational processes, which ensures network performance while reducing the number of parameters. As shown in Figure 2, the CSP-stage module firstly divides the input flow into two parallel parts, X1 and X2. The X2 branch is convolved as the feature of normal convolution to pass through the residual operation. Then, the primary branch X1 is connected to the spanning branch X2 by a 1×1 convolution layer. We replace the 1×1 convolution of the original model as a channel attention operation to realize the feature interaction, which further enhances the feature extraction ability of the proposed network. After passing through several ResNet layer structures, X1 is aggregated to enhance the learning capability as well as prevent excessive repetitive gradient information, which effectively reduces computational and resource costs. Each CSP-stage module could be combined with any CNN network structure, such as ResBlock or DenseBlock.

3.2. Feature Aggregation Enhancement Module. To further improve the backbone network's performance and to apply it to fine-grained image classification tasks, we also propose a novel feature aggregation enhancement module on basis of the attention mechanism, which makes the network more focused on the parts with discrimination information in the image. Usually, attention methods can be divided into two categories: strong attention methods and weak attention methods. The strong attention method relies on extra annotation boxes or other annotations, which requires much manual work. The weak attention method is more inclined to automatically add submodules to the network to locate the target position automatically. Our approach focuses on the weak attention method, which only uses the image-level label without adding additional annotations. However, the process of weak attention tends to pay attention to the most significant part, so other inconspicuous but distinguishable parts will be ignored. However, when the essential part is shielded or suppressed, the network will be forced to explore other potential parts. Inspired by Song and Yang [24], we designed a novel structure of weak-supervised attention named as the feature aggregation enhancement module (FABM), which includes an enhanced feature extraction module (EFEM) and feature fusion. In the FABM module, the EFEM module highlights the most prominent part of feature mapping in the current stage to obtain part-specific representations, suppress the representations, and force other potential features to be excavated in the next step. The unique fusion part fuses different elements learned in multiple stages and then obtains feature maps with numerous prominent features. The detailed illustration of FABM module is shown in Figure 3.

Consider feature maps $X \in R^{C \times W \times H}$ from a specific layer, where C, W, and H denote the number of channels, width, and height, respectively. In the next step, X is evenly split into k parts along the width and height dimensions, and the parts along the width and height are the same except for the division direction. Take the width division as an example:

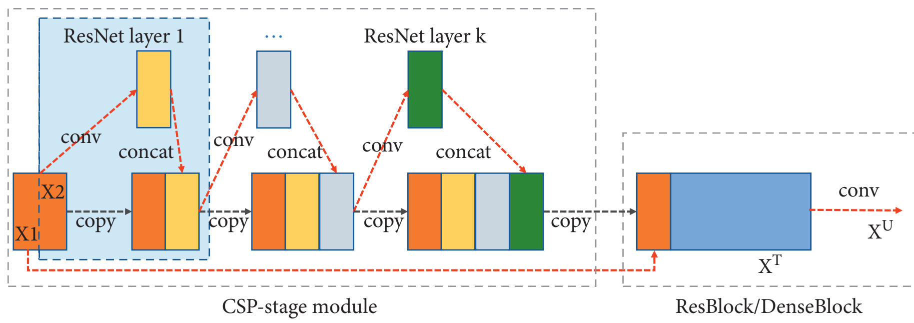

Figure 2: Illustrations of CSP-stage module.

each striped part is denoted as $X_i \in R^{C\times(W/k)\times H}$, $i \in [1,k]$. Then, we use a 1×1 convolution φ to explore the importance of each part:

$$A_{(i)} = \mathrm{Relu}\Big(\Phi\big(X_{(i)}\big)\Big) \in R^{1\times(W/k)\times C}. \tag{1}$$

The non-linear function Relu is applied to remove the negative activation. Φ is shared in different stripes, which plays the role of a grader. Then, we take the average of $A_{(i)}$ as an important factor b_0 of $X_{(i)}$, i.e.,

$$b_i' = \mathrm{GAP}\big(A_{(i)}\big) \in R, \tag{2}$$

where GMP denotes global maximum pooling. We use softmax to normalize $B\prime = (b_1',\ldots,b_k')^T$:

$$b_i = \frac{\exp\big(b_j'\big)}{\sum_{j=1}^{k}\exp\big(b_j'\big)}. \tag{3}$$

With the normalized importance factor $B\prime = (b_1',\ldots,b_k')^T$, the most significant part can be immediately determined. Then, the most significant part of the enhancement feature enhancement is obtained:

$$X_b = X + \alpha(B\otimes X), \tag{4}$$

where α is a hyperparameter, which controls the degree of enhancement, and $\otimes$ denotes the multiplication calculated by various elements. Then, a 1×1 convolution layer h is applied to X_b to get a specific partial representation X_p:

$$X_p = h(X_b). \tag{5}$$

By multiplying the parts with the most stripes, the suppression features X_s are obtained:

$$X_s = S\otimes X,$$
$$s_i = \begin{cases} 1-\beta, & \text{if } b_i = \mathrm{MAX}(B), \\ 1, & \text{otherwise,}\end{cases} \tag{6}$$

where $S = (s_1, s_2, \ldots, s_k)$ and β is a hyperparameter, which controls the degree of suppressing.

The data information carried by multilevel features is very high-dimensional. If each multilevel feature is calculated, it will lead to a large amount of calculation. Therefore, to reduce the amount of calculation, we fuse the multilevel feature information by means of feature addition, to obtain a feature vector with multiple discriminant information:

$$F = \theta\left(\sum_{i=1}^{3} X_i\right) \in \mathbb{R}^{W_1\times H_1\times C_1}, \tag{7}$$

where F denotes the feature obtained after fusion, X_i denotes the i-th extracted enhancement feature, and θ is 1×1 convolution.

After multistage fusion, the features obtained already aggregate multiple discriminant parts but ignore the relationship between different semantic channels. In order to increase the interaction between channels, we use the following methods to establish the relationship matrix between channels.

$$M = B\left(\frac{1}{WH}\sum_{i=1}^{WH} F^T\varphi(F_i)\right) \in R^{C_1\times C_2}, \tag{8}$$

where B denotes normalization, ϕ denotes convolution, and C_2 represents the number of channels after convolution.

3.3. Graph-Related Higher-Order Feature Extractor. From the FABM module, we can get the feature map with multiple discrimination parts, which can be extracted and processed by a downsampling operation. However, the feature map is still a matrix with high latitude. The high latitude matrix embedded into the low margin using the full connection layer will lead to training many learnable parameters. At the same time, by consulting relevant agricultural pest experts, we know that different pests and diseases have certain hidden information in space, and various pests and diseases have their spatial distribution and shape laws. Based on this, we think that the isolated use of discriminant features cannot learn this information. Inspired by Zhao et al. [25], we used a semantic learning module (SRL) which can further mine higher-order feature maps from raw images. Firstly, the module filters the massive information according to the previous network's feature map to obtain the critical discriminant features representing local parts. Then, we introduce the graph-related convolution network to learn the higher-order semantics between different discrimination parts. The nodes in the graph do not exist in isolation in graph data, so we can build a relationship between different sampling points through a graph convolution network. We construct a graphic dataset using sampling nodes as points and the correlation between points as an adjacency matrix.

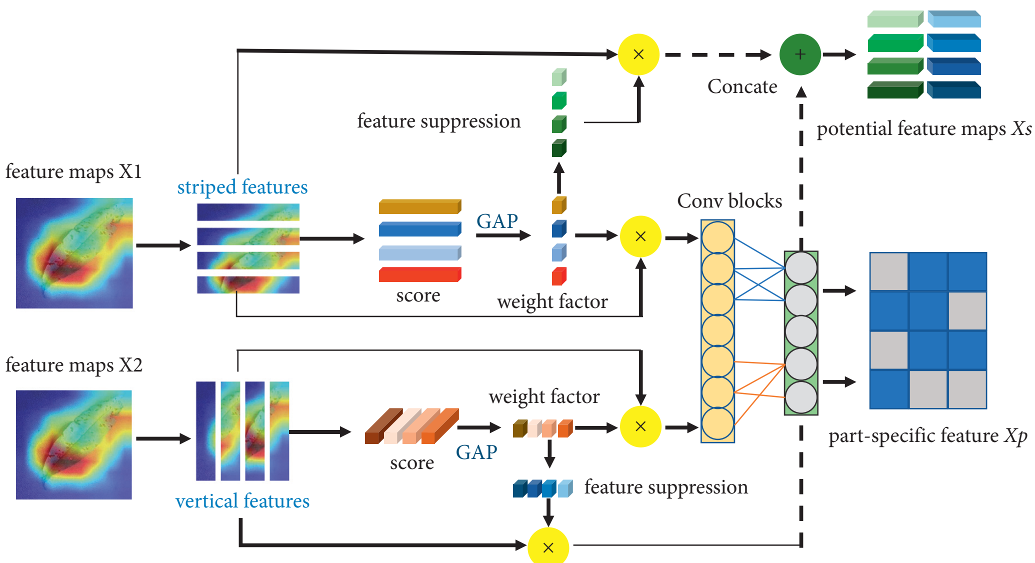

Figure 3: FABM attention module.

The higher-order features between parts are implicitly learned and discriminated by spreading on graph convolution network.

Inspired by Zhao et al. [25], we designed a sampler to sample the discrimination parts, which can extract the discrimination parts in the feature map. After obtaining the residual feature map, which aggregates the related features with the original input features, it is sent to the discrimination response layer. Specifically, we introduce a $1 \times 1 \times C_1$ convolution layer and a sigmoid function σ to learn discriminative probability maps $S \in \mathbb{R}^{N \times H \times W}$, which express the impact of discriminative regions on the final classification. C_1 is the number of channels in the feature map. Then, each selected patch will be assigned a corresponding discrimination probability value P_{ijk}. The formulation is as follows:

$$P_{ijk} = \left[t_x, t_y, t_k, s_{ijk}\right], \tag{9}$$

where $[t_x, t_y, t_k]$ represent the coordinates of each patch and s_{ijk} denotes the discrimination probability value of the i^{th} row, the j^{th} column, and the k^{th} channel.

After sampling discriminant feature, a discriminant feature library $\mathcal{K} \in \mathbb{R}^{C_1 \times C_2}$ can be constructed. Furthermore, the discriminant feature library $\mathcal{K} = \{f_1, f_2, \ldots, f_C\}$ can be described as a graph with C_2 nodes of C_1 channels as shown in Figure 4. These nodes share many information in essence, so we use graph convolution network to aggregate these features [43]. The relationship between pairs of adjacencies can be defined as

$$A_{i,j} = \frac{\tau(f_i)^T \cdot \tau(f_j)}{\left\|\tau(f_i)\right\|\left\|\tau(f_j)\right\|}, \tag{10}$$

where τ denotes the 1×1 convolution for dimension transformation, the last adjacency matrix is defined by self-circulation $\widetilde{A} = A + I$, and $\mathrm{I} \in \mathbb{R}^{C_1 \times C_2}$ is an identity matrix. Through this similarity aggregation, the update mode of each node is as follows:

$$H = \mathrm{ReLu}\left(D^{-\frac{1}{2}}\widetilde{A}D^{-\frac{1}{2}}KW^g\right), \tag{11}$$

where $W^g \in \mathbb{R}^{C_2 \times d_h}$ represent the learnable graph weights with a dimension d_h and $D = \sum_j \widetilde{A}_{i,j}$ is the diagonal matrix for normalization. K denotes the matrix of $\mathcal{K}$.

This operation can update the information of each node. At the same time, another purpose of graph embedding is to learn the context understanding of different discrimination parts. We use the following methods to form multiple groups to learn the relationship between contexts:

$$H = \mathrm{ReLu}\left(D^{-1/2}\widetilde{A}D^{-1/2}KW^e\right), \tag{12}$$

where $\mathrm{W}^e \in \mathbb{R}^{d_h \times C_r}$ represent the learnable graph weights. $G \in \mathbb{R}^{C_1 \times C_r}$ indicates the mapping function of each node from the original space to form a new graph node:

$$\begin{aligned} Z &= H^T \frac{e^{G_{i,j}}}{\sum_{j=1}^{C_r} \in R^{d_h \times C_r}}, \\ Z &= H^T \frac{e^{G_{i,j}}}{\sum_{j=1}^{C_r} \in R^{d_h \times C_r}}, \end{aligned} \tag{13}$$

where C_r represents the number of new embedded graph nodes. We design the softmax layer with the group dimension to accomplish the C_r by the calculation formula C_1/r.

This method can efficiently allocate a high-order feature library in low-dimensional manifold and map channel dimension and node dimension at the same time. Then, the remaining connections are grouped and characterized to construct the final embedding $\widetilde{Z} = Z + H$. Finally, these

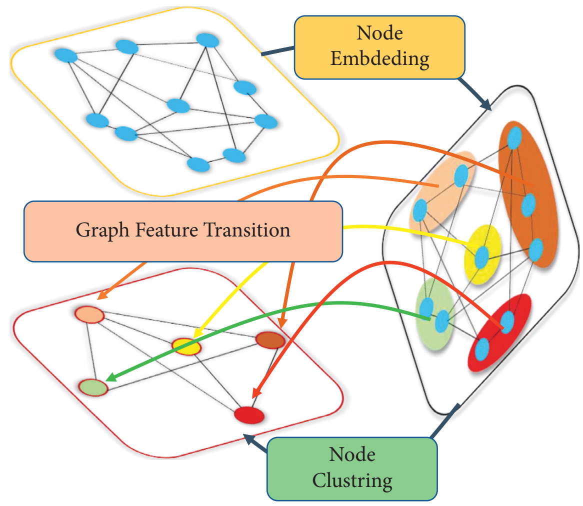

FIGURE 4: Schematic diagram of graph feature description.

embeddings can be finally predicted by applying a GMP or GAP and a classifier.

An obvious problem of infinite granularity classification is overfitting under challenging cases [25]. A preferable class clustering should be based on representative sample sets, while ignoring remote hard samples. This means that we use the centre of multiple samples of a specific class as the average feature to update the network parameters, so the loss function can be defined as follows:

$$L_{\text{loss}} = \frac{1}{NK} \sum_{n=1}^{N} \sum_{k=1}^{K} L_{CE}\left(\left(\frac{y_n}{y_n}\right)\right) y_n, \tag{14}$$

where y_n denotes the sample labels, N denotes the number of class, K denotes the samples in each class, and L_{CE} represents the cross-entropy function. The representative samples are applied to update the complex parameter features of the whole network, which help improve the model's identification performance with better generalization.

4. Experimental Results and Analysis

4.1. Experiment Setup. We use three datasets publicly available on the web for experiments: AI Challenger agricultural pest and disease dataset, Cassava leaf disease dataset (Cassava leaves), and IP102 dataset.

4.1.1. AI Challenger Agricultural Disease Dataset. This data contains 27 disease categories on 10 kinds of plant hosts, including apple, cherry, grape, citrus, peach, strawberry, tomato, pepper, corn, and potato. The entire dataset has a total of 47637 image samples. However, the data distribution is highly unbalanced, and the number of pictures in some categories is tiny. Therefore, we cleaned the dataset, eliminated the types with a few images in the dataset, and finally got 31,027 training sets and 4,739 test sets.

4.1.2. Cassava Leaves. This dataset consists of leaf images of cassava plants and contains 21397 cassava leaves. The disease types include cassava brown streak disease (CBSD), cassava mosaic disease (CMD), cassava bacterial blight (CBB), and cassava green mite (CGM). In this paper, the annotated image data are re-divided, including 17,115 images in the training set and 4,282 images in the test set.

4.1.3. IP102. This dataset has a total of 75,222 images, covering 102 different types of pests, including *corn borer*, *red spider mites, whitefly,* and *Spodoptera litura.* At the same time, the crops in the dataset images also contain a variety of crops, including rice, corn, grapes, citrus fruit trees, and mango trees. All images in the classification task are divided into the training set, validation set, and test set. The detection task uses 18,983 annotated images containing bounding boxes, including 15,178 photographs in the training set and 3,798 images in the test set. Since the dataset includes many image data crawled from the network, some of these image data contain some situations such as text occlusion and watermark. These factors will interfere with the training effect of the network, so we culled some parts and finally obtained the training.

In our experiments, the model we used uses ImageNet for pretraining. The images are processed before entering the network, including random cropping, random flipping, and brightness enhancement, to enhance the anti-interference ability of the model. In addition, all images are also normalized, and the image size is set to 448 × 448. In the network training process, the number of iterations is set to 150, and a checkpoint is set every 10 times. The optimizer is SGD, using momentum processing, the weight decay is set to 0.001, and the initial learning rate is set to 0.001. Our experiments are trained end-to-end on 4 NVIDIA P40 GPUs without adding additional part or bounding box annotations, only using image-level labels. In the network structure design, we use the CSPNet50 structure as the backbone network and use the three-stage FABM module in the network structure to extract the features of three different stages for aggregation enhancement.

4.2. Evaluation Indicators. In order to objectively evaluate the prediction results of different algorithms, four performance indicators of accuracy, precision, recall, and F1 score are selected to compare the prediction results of each model. ACC is the ratio of the number of correctly labeled items to the total number of observations. PRE is the number of true positives divided by the total number of items belonging to that category. Meanwhile, REC is defined as the number of true positives divided by the total number of items belonging to the category, also known as sensitivity. Through the above three indicators, the number of results in the confusion matrix can be converted into a ratio between 0 and 1, which can be calculated based on true positive (TP), true negative (TN), false positive (FP), and false negative (FN). In addition, another high-level indicator, F1 score, is adopted in this paper, which is the harmonic mean of ACC and REC with a better comprehensive evaluation of multiclass recognition problems. Here are the formula definitions for each indicator:

$$\begin{aligned} \mathrm{ACC} &= \frac{\mathrm{TP}+\mathrm{TN}}{\mathrm{TP}+\mathrm{TN}+\mathrm{FP}+\mathrm{FN}}, \\ \mathrm{PRE} &= \frac{\mathrm{TP}}{\mathrm{TP}+\mathrm{FP}}, \\ \mathrm{REC} &= \frac{\mathrm{TP}}{\mathrm{TP}+\mathrm{FN}}, \\ F_1 &= 2\times\frac{\mathrm{PRC}\times\mathrm{REC}}{\mathrm{PRE}+\mathrm{REC}}. \end{aligned} \tag{15}$$

The proposed model first selects several regions with the most robust feature performance according to the FABM module. Then, the SRL module tries to extract the discriminative features to construct the correlation between different discriminative parts. Finally, the designed GCN implicitly learns the high-order feature vector to achieve better fine-grained recognition performance. Therefore, to comprehensively evaluate the improvement effect of each module on the proposed method, this paper selects various indicators to analyze the experimental results of our model.

4.3. Comparative Results. To verify that the proposed method can identify crop pest species, we set up some experiments to compare the performance of deep stacking networks and other methods. In this section, some coarse-grained image recognition network methods are selected, including VGG [32], Inception [34], ResNet [33], DenseNet [48], CSPNet50 [49], and SeNet [50]; at the same time, several other fine-grained image recognition networks are selected for comparison, including LIR [51], WSAP [52], and FBSM [24]; these networks are trained separately on the three datasets using the same strategy.

The experimental results of AI Challenger are shown in Table 1. The experimental results of the model proposed in this paper are better than those of the commonly used coarse-grained recognition networks, indicating that our network can extract more features than coarse-grained networks. Our network considers learning the discriminative part features of multiple targets as much as possible and suppresses useless features. Therefore, our model is better than other models by comparing coarse-grained networks and some fine-grained methods. In AI Challenger, the best results have been achieved on the dataset, with an accuracy rate of 96.4%, a precision rate of 88.3, a recall rate of 86.7, and an F1 score of 0.87, all of which are optimal.

The experimental results on the Cassava dataset are shown in Table 2. Our experimental results are better than those of other models, except slightly lower than FBSM and LIR. We think this is because the Cassava dataset is more straightforward than the IP102 and AI Challenger. There is one plant category in the Cassava dataset, and the number of pests and diseases is also less. Specifically, the method proposed in this paper focuses more on locating the location of pests and diseases in complex backgrounds. In data with simpler backgrounds, the discriminant parts' enhanced parts receive significant gains. At the same time, since the SRL module learns, the spatial relationship depends on the complexity of the pests. The results show that LIR and FBSM benefit from simpler backgrounds on the Cassava dataset, while in complex environments, such as IP102 and AI Challenger, the method proposed in this paper is more dominant (Table 3).

In addition to this, we visually compare the F1 scores of ten models, as shown in Figure 5. It can be seen intuitively that compared with the coarse-grained method, the F1 score of our model is better than that of the coarse-grained method, indicating that our model has better recognition performance and is comparable to other fine-grained methods. In comparison, the F1 score of our model is also comparable to the rest of the fine-grained algorithms, indicating that our model is capable of fine-grained recognition.

As shown in Figure 6, we compared the loss trend of different models on the three datasets. We can see that the loss rate of the proposed model in the early catenary stage is lower than that of other models, since the FABM model and the high-order relation learning module added to the model structure are not pretrained. Hence, the convergence rate in the early stage is relatively slow, but after reaching a certain number of training times, the loss of our model also tends to converge.

To further illustrate the performance of our model, we plotted the confusion matrix of the accuracy rates of the three models, as shown in Figure 7. Our model has a high accuracy rate on each class on the Cassava dataset with the best effect. The worst is the third category, but the accuracy rate has also reached 95%, and the best impact is the 0th category.

To further judge the model's performance proposed in this paper, we visualized part of the model. We considered whether the model played a role through a visual operation. The visualization results are shown in Figure 8. We selected two different samples from each of the three datasets for a total of 6 image samples for visualization. The compared models are VGG19, ResNet50, and FSBM. The heat map shows that the features learned by VGG and ResNet50

Table 1: AI Challenger experiment results of agricultural pests and diseases.

Methods		Accuracy (%)	Precision (%)	Recall (%)	F1
Coarse-grained	VGG19 [32]	94.1	86.2	85.7	0.86
	ResNet50 [33]	94.5	86.4	85.8	0.86
	Inception [34]	95.0	86.9	86.0	0.86
	DenseNet [48]	95.3	86.8	86.3	0.87
	CSPNet50 [49]	95.6	86.9	86.3	0.87
Fine-grained	Senet [50]	95.8	86.9	86.2	0.87
	LIR [51]	95.9	87.0	86.1	0.87
	WSAP [52]	96.2	87.1	86.3	0.87
	FBSD [24]	96.4	87.3	86.4	0.87
	GHA-Net	96.4	88.3	87.4	0.89

Table 2: The experimental results of cassava agricultural diseases and pests.

Methods		Accuracy (%)	Precision (%)	Recall (%)	F1
Coarse-grained	VGG19 [32]	88.0	79.0	77.8	0.78
	ResNet50 [33]	89.7	77.0	74.5	0.76
	Inception [34]	88.5	79.3	78.2	0.78
	DenseNet [48]	89.1	79.6	78.4	0.79
	CSPNet50 [49]	92.3	80.1	80.1	0.81
Fine-grained	Senet [50]	94.5	84.3	80.2	0.82
	LIR [51]	98.5	88.3	86.6	0.88
	WSAP [52]	98.4	88.4	87.2	0.88
	FBSD [24]	98.6	87.2	86.5	0.87
	GHA-Net	97.4	89.2	87.9	0.90

Table 3: IP102 pest test results.

Methods		Accuracy (%)	Precision (%)	Recall (%)	F1
Coarse-grained	VGG19 [32]	54.1	43.1	42.0	0.43
	ResNet50 [33]	54.7	43.4	42.1	0.43
	Inception [34]	55.3	43.4	42.3	0.43
	DenseNet [48]	55.4	43.6	42.4	0.43
	CSPNet50 [49]	55.6	43.9	42.4	0.44
Fine-grained	Senet [50]	54.3	45.1	42.6	0.44
	LIR [51]	56.9	45.4	42.9	0.44
	WSAP [52]	56.8	45.6	43.3	0.45
	FBSD [24]	56.4	45.4	43.1	0.44
	GHA-Net	57.1	46.7	45.3	0.48

contain a lot of background, which is unfavorable for the classification results. At the same time, our model focuses more on the discriminative parts of the target itself, indicating that our model can play the role of learning more discriminative features.

4.4. Ablation Analysis. To verify the effectiveness of our model, we conduct ablation experiments on each dataset. The results of our ablation experiments are shown in Table 4, including a feature enhancement module and a spatial higher-order relation learning module. In the absence of fine-grained classification of extra labels or local annotations, we perform feature extraction on the entire image through ResNet50, set it as the baseline network, and then improve the discrimination by eliciting features learned at different residual stages. Finally, the classification accuracy of the network is improved by further extracting and sampling the discriminative features and learning the spatial high-order semantic features between the discriminative parts through the graph. Xia Rong's experiments show that the FABM module can learn more features, and the model accuracy of the FABM module is improved by 1.5%, 5.5%, and 1.7% on the AI Challenger, Cassava, and IP102 datasets, respectively, compared to the baseline network accuracy.

Finally, we introduce the SRL module to learn the implicit relationship between features further, and the network progress is further improved. Ablation experiments prove that the proposed network can understand the discriminative regions, enhance the discriminatory feature values, and improve accuracy. Moreover, we also added a comparison of experimental results using ResNet50 as the backbone network. The experimental results show that after adding the FABM module and the SFL module to ResNet,

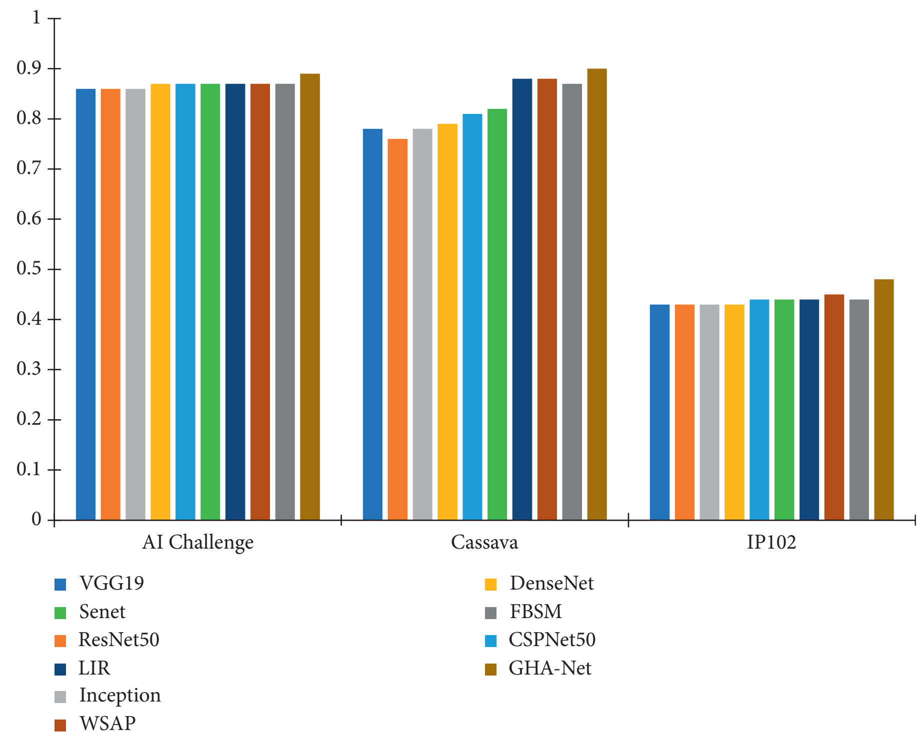

Figure 5: F1 scores of different models on different datasets.

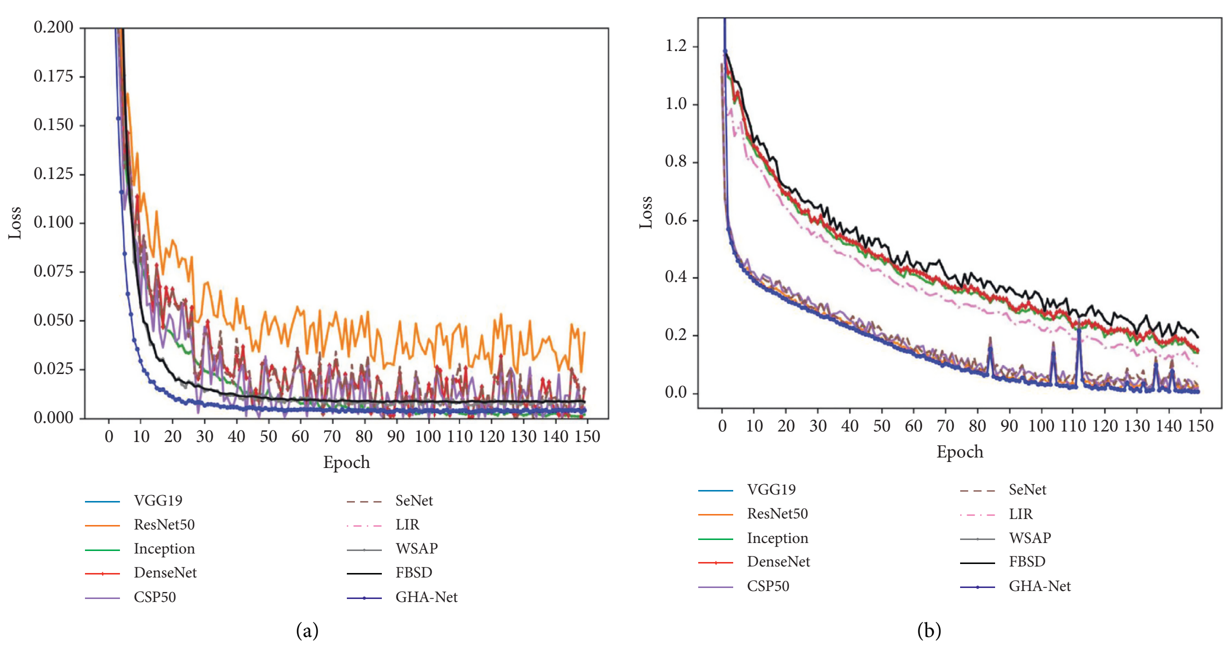

Figure 6: Continued.

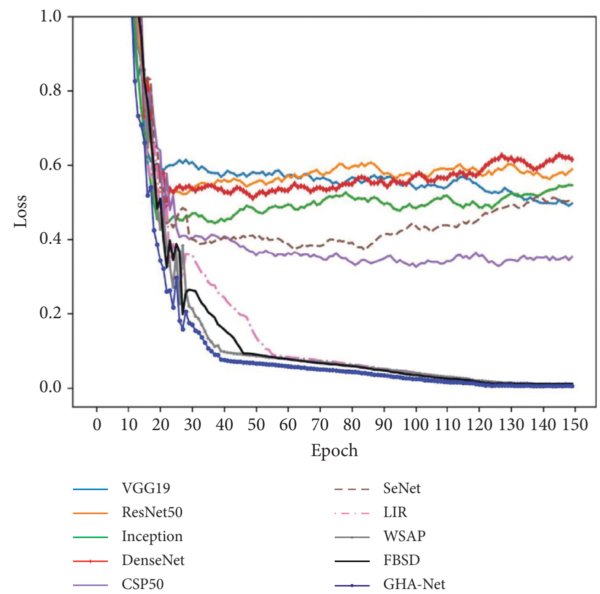

(c)

FIGURE 6: (a) Loss function curves on AI Challenger. (b) Loss function curves on Cassava. (c) Loss function curves on IP102.

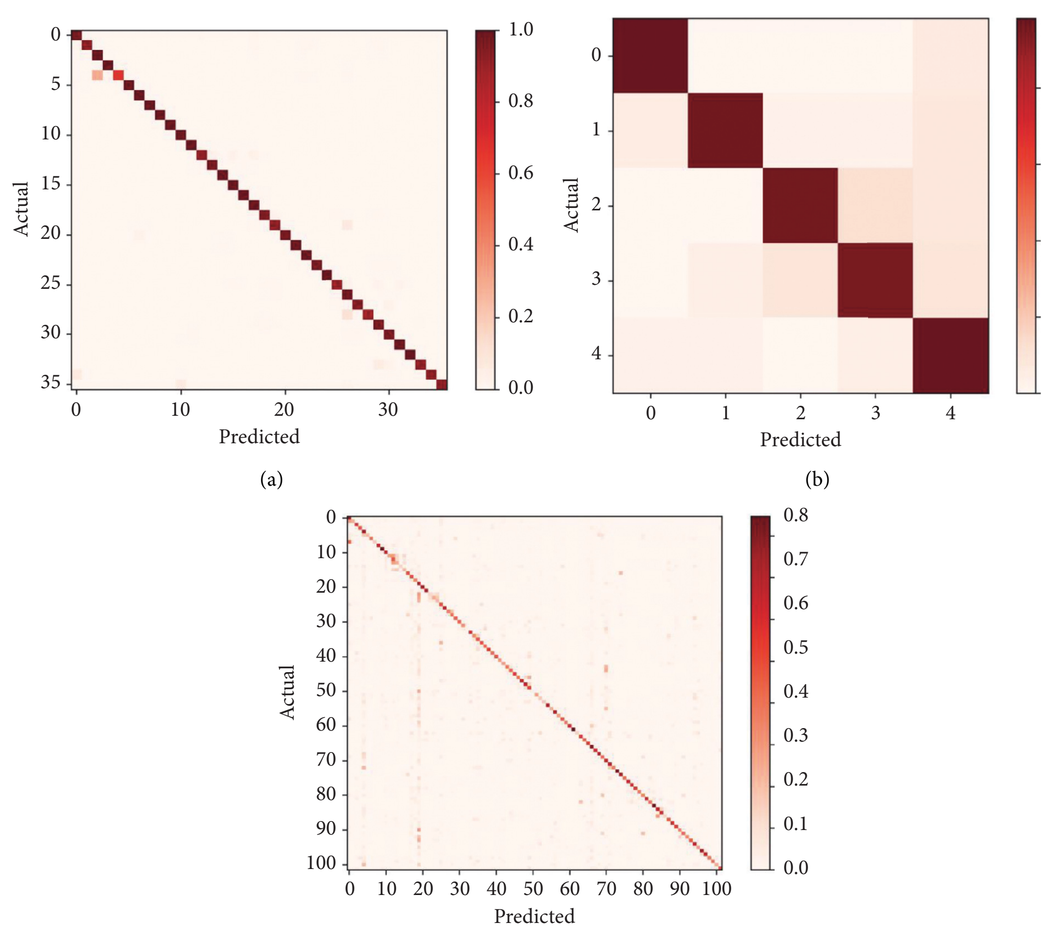

(c)

FIGURE 7: (a) Confusion matrix on AI Challenger. (b) Confusion matrix on Cassava. (c) Confusion matrix on IP102.

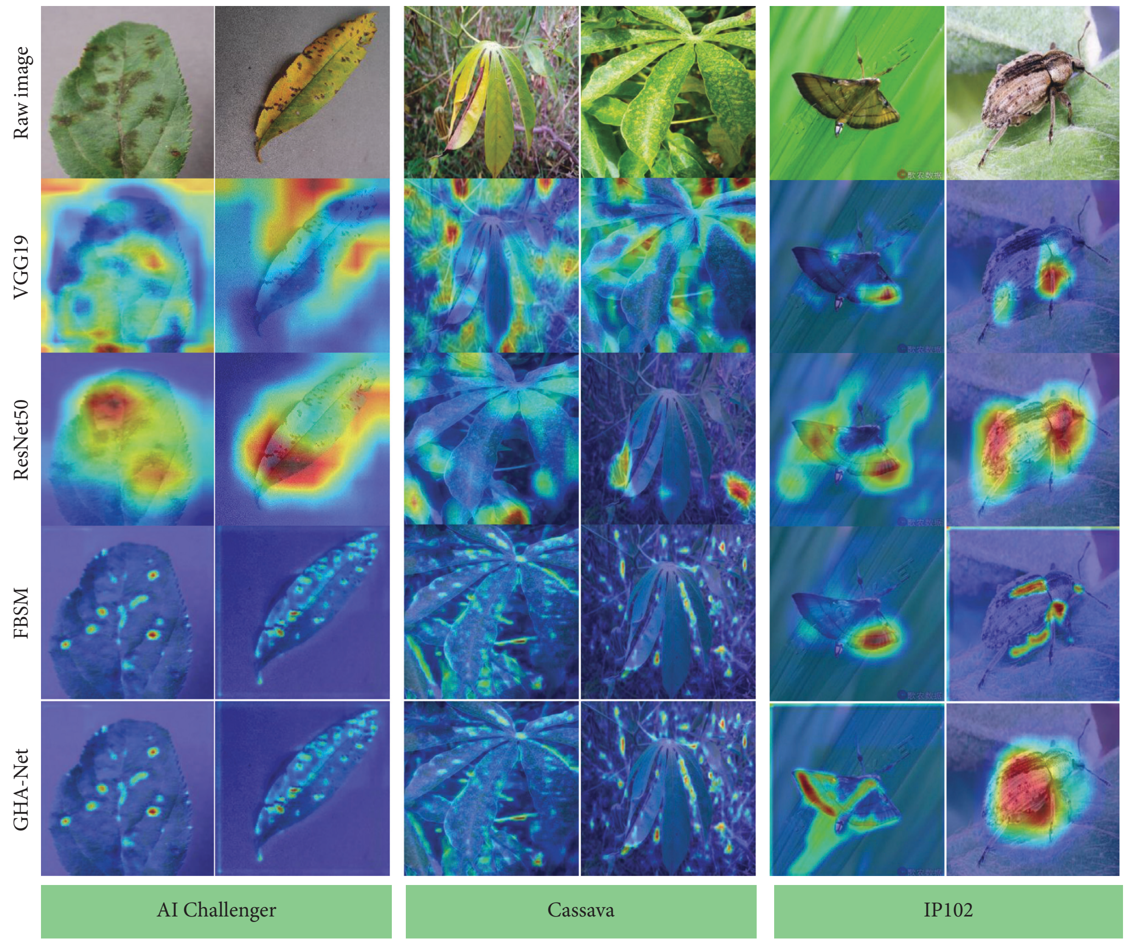

Figure 8: Attention visualization of different models.

Table 4: Ablation experiment results.

Method	ACC (%)		
	AI Challenger	Cassava leaves	IP102
ResNet50	94.5	89.7	54.7
ResNet50+FABM	95.3	94.2	55.9
ResNet50+ SFL	95.0	92.8	55.4
ResNet50+ FABM + SFL	96.0	96.1	56.9
CSP	95.6	92.3	55.6
CSP + FABM	96.0	95.2	56.4
CSP + SFL	95.9	93.6	56.0
CSP + FABM + SFL	96.4	96.4	57.1

the experimental results are improved to varying degrees, which shows that our module can be used on other backbone networks, further illustrating the effectiveness of our model.

To further illustrate the effectiveness of our model, we visualize the different stages of the attention module FABM. As shown in Figure 9, our model has three FABM modules, which are denoted as FABM-1, FABM-2, and FABM-3. The aggregation of the three modules is characterized as FABM-Con, as shown in Figure 9. The non-stage FABM can focus on the features of different parts, and the fused FABM can locate multiple discriminative features of the target.

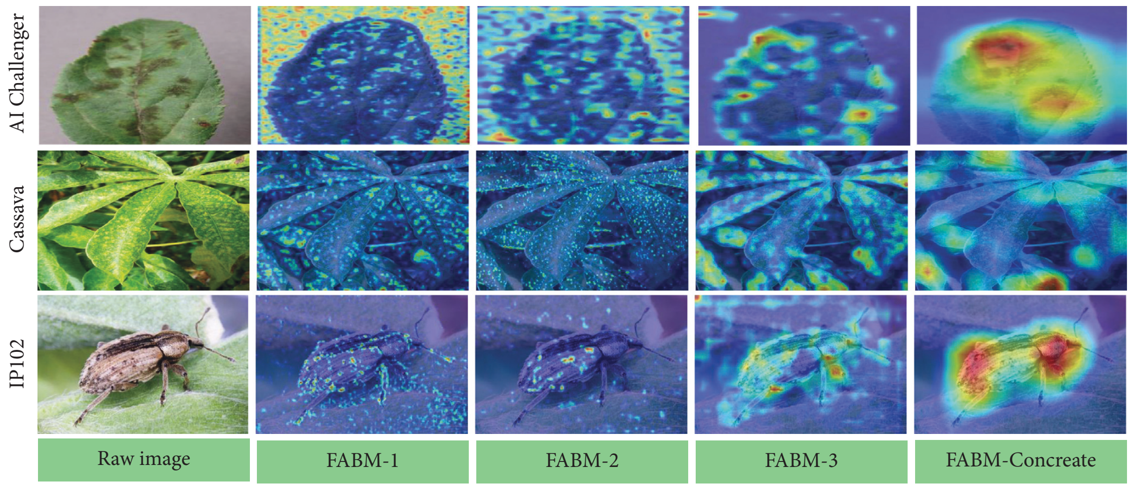

Figure 9: Heat map visualization of different FABM stages.

5. Conclusion

Aiming to solve the fine-grained identification problem of plant diseases and pests, this research proposes an effective graph-related high-order network with feature aggregation enhancement (GHA-Net) to promote the fine-grained recognition performance of deep learning technology. Based on the improved CSP-stage backbone network, the feature aggregation enhancement module is firstly designed to enhance multilevel attention for learning multiple discriminant features. Meanwhile, the graphic convolution module is constructed to analyse the graph-correlated representation of part-specific inter-relationships by regularizing semantic features into the high-order tensor space. Experiments on AI Challenger, Cassava, and IP102 datasets have demonstrated robust and accurate performance in terms of fine-grained plant disease and pest identification. Compared with other deep learning models, the proposed GHA-Net achieves the identification accuracy of 96.4%, 97.4%, and 57.1% on three public datasets, overperforming all compared methods with a minor error, which is verified more suitable for fine-grained identification applications in complex scenes.

The model structure will be optimized to improve the identification performance in further work. The related technologies will be investigated to expand the application scope of the proposed model in intelligent greenhouses and grain warehouses. Also, they can be applied to other fields such as temporal prediction, signal modelling, and control systems [53, 54].

Data Availability

The datasets presented in this study are available from the following links: AI Challenger—https://aistudio baidu com/aistudio/datasetdetail/76075; Cassava—https://www kaggle.com/c/cassava-disease/overview; and IP102—https://github com/xpwu95/IP102.

Conflicts of Interest

The authors declare that they have no conflicts of interest to report regarding the present study.

Acknowledgments

This research was financially supported by the National Key Research and Development Program of China (no. 2021YFD2100605), National Natural Science Foundation of China (no. 62006008, 62173007, and 61903009), Beijing Municipal Natural Science Foundation (no. 4202014), and 2022 Graduate Research Ability Improvement Program of Beijing Technology and Business University.

References

[1] X. Zhang, "On the relationship between agriculture and economic development," *Modern state-owned enterprise research*, vol. 0, no. 22, p. 36, 2016.

[2] X.-B. Jin, W.-Z. Zheng, J.-L. Kong et al., "Deep-learning temporal predictor via bidirectional self-attentive encoder-decoder framework for IOT-based environmental sensing in intelligent greenhouse," *Agriculture*, vol. 11, no. 8, p. 802, 2021.

[3] V. Singh, N. Sharma, and S. Singh, "A review of imaging techniques for plant disease detection," *Artificial Intelligence in Agriculture*, vol. 4, pp. 229–242, 2020.

[4] J. Lu, L. Tan, and H. Jiang, "Review on convolutional neural network (CNN) applied to plant leaf disease classification," *Agriculture*, vol. 11, no. 8, pp. 707–725, 2021.

[5] P. Mishra, G. Polder, and N. Vilfan, "Close range spectral imaging for disease detection in plants using autonomous platforms: a review on recent studies," *Current Robotics Reports*, vol. 1, no. 2, pp. 43–48, 2020.

[6] L. Liu, Y. Dong, W. Huang et al., "A disease index for efficiently detecting wheat Fusarium head blight using sentinel-2 multispectral imagery," *IEEE Access*, vol. 8, no. 99, pp. 52181–52191, 2020.

[7] X.-B. Jin, W.-Z. Zheng, J.-L. Kong et al., "Deep-learning forecasting method for electric power load via attention-based

encoder-decoder with bayesian optimization," *Energies*, vol. 14, no. 6, pp. 1596–1614, 2021.

[8] J. Kong, C. Yang, J. Wang et al., "Deep-stacking network approach by multisource data mining for hazardous risk identification in IoT-based intelligent food management systems," *Computational Intelligence and Neuroscience*, vol. 2021, Article ID 1194565, 16 pages, 2021.

[9] J. Kong, H. Wang, X. Wang, X. Jin, X. Fang, and S. Lin, "Multi-stream hybrid architecture based on cross-level fusion strategy for fine-grained crop species recognition in precision agriculture," *Computers and Electronics in Agriculture*, vol. 185, Article ID 106134, 2021.

[10] X.-B. Jin, W.-T. Gong, J.-L. Kong, Y.-T. Bai, and T.-L. Su, "PFVAE: a planar flow-based variational auto-encoder prediction model for time series data," *Mathematics*, vol. 10, no. 4, p. 610, 2022.

[11] A. Voulodimos, N. Doulamis, and S. A. Doulami, "Deep learning for computer vision: a brief review," *Computational Intelligence and Neuroscience*, vol. 2018, Article ID 7068349, 13 pages, 2018.

[12] X. Jin, J. Zhang, J. Kong, T. Su, and Y. Bai, "A reversible automatic selection normalization (RASN) deep network for predicting in the smart agriculture system," *Agronomy*, vol. 12, no. 3, p. 591, 2022.

[13] X.-B. Jin, W.-T. Gong, J.-L. Kong, Y.-T. Bai, and T.-L. Su, "A variational bayesian deep network with data self-screening layer for massive time-series data forecasting," *Entropy*, vol. 24, no. 3, p. 335, 2022.

[14] N. Nandhini and R. Bhavani, "Feature extraction for diseased leaf image classification using machine learning," in *Proceedings of the 2020 International Conference on Computer Communication and Informatics (ICCCI)*, pp. 1–4, Coimbatore, India, January 2020.

[15] N. Ahmad, H. M. S. Asif, G. Saleem, M. U. Younus, S. Anwar, and M. R. Anjum, "Leaf image-based plant disease identification using color and texture features," *Wireless Personal Communications*, vol. 121, no. 2, pp. 1139–1168, 2021.

[16] K. P. Panigrahi, H. Das, A. K. Sahoo, and S. C. Moharana, "Maize leaf disease detection and classification using machine learning algorithms," *Progress in Computing, Analytics and Networking*, Springer, Singapore, 2020.

[17] Y. Guo, J. Zhang, C. Yin et al., "Plant disease identification based on deep learning algorithm in smart farming," *Discrete Dynamics in Nature and Society*, vol. 2020, no. 7, 11 pages, Article ID 2479172, 2020.

[18] Y. A. Nanehkaran, D. Zhang, J. Chen, Y. Tian, and N. Al-Nabhan, "Recognition of plant leaf diseases based on computer vision," *Journal of Ambient Intelligence and Humanized Computing*, vol. 2020, pp. 1–18, 2020.

[19] A. Fuentes, S. Yoon, S. Kim, and D. Park, "A robust deep-learning-based detector for real-time tomato plant diseases and pests recognition," *Sensors*, vol. 17, no. 9, p. 2022, 2017.

[20] A. Cruz, Y. Ampatzidis, R. Pierro et al., "Detection of grapevine yellows symptoms in Vitis vinifera L. with artificial intelligence," *Computers and Electronics in Agriculture*, vol. 157, pp. 63–76, 2019.

[21] J. Kong, H. Wang, C. Yang, X. Jin, M. Zuo, and X. Zhang, "A spatial feature-enhanced attention neural network with high-order pooling representation for application in pest and disease recognition," *Agriculture*, vol. 12, no. 4, p. 500, 2022.

[22] M. Islam, A. Dinh, and K. Wahid, "Detection of potato diseases using image segmentation and multiclass support vector machine," in *Proceedings of the 2017 IEEE 30th canadian conference on electrical and computer engineering (CCECE)*, pp. 1–4, Windsor, Ontario, May 2017.

[23] X. P. Wu, C. Zhan, and Y. K. Lai, "Ip102: a large-scale benchmark dataset for insect pest recognition," *Computer Vision and Pattern Recognition (CVPR) IEEE*, vol. 2019, pp. 8787–8796, 2019.

[24] J. Song and R. Yang, "Feature boosting, suppression, and diversification for fine-grained visual classification," in *Proceedings of the 2021 International Joint Conference on Neural Networks (IJCNN)*, vol. 2103, Article ID 02782, Shenzhen, China, July 2021.

[25] Y. Zhao, K. Yan, and F. Huang, "Graph-based high-order relation discovery for fine-grained recognition," in *Proceedings of the IEEE/CVF Conference on Computer Vision and Pattern Recognition*, pp. 15079–15088, June 2021.

[26] K. Alex, S. Ilya, and E. H. Geoffrey, "ImageNet classification with deep convolutional neural networks," *Advances in Neural Information Processing Systems*, vol. 25, pp. 1097–1105, 2012.

[27] F. Qin, D. Liu, B. Sun, L. Ruan, Z. Ma, and H. Wang, "Identification of alfalfa leaf diseases using image recognition technology," *PLoS One*, vol. 11, no. 12, Article ID e0168274, 2016.

[28] E. Mwebaze, T. Gebru, and A. Frome, "ICassava 2019 fine-grained visual Categorization challenge," 2019, http://arXiv.org/abs/2019.

[29] S. Kumar, B. Sharma, V. K. Sharma, H. Sharma, and J. C. Bansal, "Plant leaf disease identification using exponential spider monkey optimization," *Sustainable Computing: Informatics and Systems*, vol. 28, Article ID 100283, 2020.

[30] S. W. Zhang, Y. J. Shang, and L. Wang, "Plant disease recognition based on plant leaf image," *Journal of Animal and Plant Sciences*, vol. 25, pp. 42–45, 2015.

[31] S. Khule and K. R.S., "Tomato plant disease detection using image processing," *IJARCCE*, vol. 6, no. 6, pp. 293–297, 2017.

[32] K. Simonyan and A. Zisserman, "Very deep convolutional networks for large-scale image recognition," in *Proceedings of the International Conference on Learning Representations*, pp. 5048–5057, San Diego, CA, USA, May 2015.

[33] K. He, X. Zhang, S. Ren, and J. Sun, "Deep residual learning for image recognition," in *Proceedings of the 2016 IEEE Conference on Computer Vision and Pattern Recognition (CVPR)*, pp. 770–778, Las Vegas, NV, USA, June 2016.

[34] C. Szegedy, V. Vanhoucke, S. Ioffe, J. Shlens, and Z. Wojna, "Rethinking the inception architecture for computer vision," in *Proceedings of the 2016 IEEE Conference on Computer Vision and Pattern Recognition (CVPR)*, pp. 2818–2826, IEEE, Las Vegas, NV, USA, June 2016.

[35] S. P. Mohanty, D. P. Hughes, and M. Salathé, "Using deep learning for image-based plant disease detection," *Frontiers of Plant Science*, vol. 7, 2016.

[36] J. Chen, J. Chen, D. Zhang, Y. Sun, and Y. A. Nanehkaran, "Using deep transfer learning for image-based plant disease identification," *Computers and Electronics in Agriculture*, vol. 173, Article ID 105393, 2020.

[37] Q. Yan, B. Yang, W. Wang, B. Wang, P. Chen, and J. Zhang, "Apple leaf diseases recognition based on an improved convolutional neural network," *Sensors*, vol. 20, no. 12, p. 3535, 2020.

[38] G. Hu, H. Wu, Y. Zhang, and M. Wan, "A low shot learning method for tea leaf's disease identification," *Computers and Electronics in Agriculture*, vol. 163, Article ID 104852, 2019.

[39] D. Argüeso, A. Picon, U. Irusta et al., "Few-Shot Learning approach for plant disease classification using images taken in

the field," *Computers and Electronics in Agriculture*, vol. 175, Article ID 105542, 2020.
[40] Y. Liu, F. Ding, and Y. Shi, "An efficient hierarchical identification method for general dual-rate sampled-data systems," *Automatica*, vol. 50, no. 3, pp. 962–970, 2014.
[41] S. Zhang, S. Zhang, C. Zhang, X. Wang, and Y. Shi, "Cucumber leaf disease identification with global pooling dilated convolutional neural network," *Computers and Electronics in Agriculture*, vol. 162, pp. 422–430, 2019.
[42] D. Hughes and M. Salathé, "An open access repository of images on plant health to enable the development of mobile disease diagnostics," 2015, http://arXiv.org/abs/preprint arXiv.
[43] B. Yang, H. Pan, and J. Yu, "Classification of medical images with synergic graph Convol.utional networks," in *Proceedings of the 2019 IEEE 35th International Conference on Data Engineering Workshops (ICDEW)*, pp. 253–258, Macao, China, April 2019.
[44] K. S. Tai, R. Socher, and C. D. Manning, "Improved semantic representations from tree-structured long short-term memory networks," in *Proceedings of the 53rd Annual Meeting of the Association for Computational Linguistics and the 7th International Joint Conference on Natural Language Processing (Volume 1: Long Papers)*, vol. 1, pp. 1556–1566, Beijing, China, July 2015.
[45] T. Zhang, B. Liu, D. Niu, K. Kai, and Y. Xu, "Multiresolution graph attention networks for relevance matching," in *Proceedings of the 27th ACM International Conference on Information and Knowledge Management*, pp. 933–942, Beijing, China, November 2019.
[46] Z. Wang, S. Wang, H. Li, Z. Dou, and J. Li, "Graph-propagation based correlation learning for weakly supervised fine-grained image classification," in *Proceedings of the AAAI Conference on Artificial Intelligence*, vol. 34, no. 07, pp. 12289–12296, New York, NY, USA, February 2020.
[47] Z. Hu, H. Yang, and J. Huang, "Fine-grained tomato pest identification based on attention residual mechanism," *Journal of South China Agricultural University*, vol. 40, no. 9, 2019.
[48] G. Huang, Z. Liu, L. Van Der Maaten, and K. Q. Weinberger, "Densely connected convolutional networks," in *Proceedings of the 2017 IEEE Conference on Computer Vision and Pattern Recognition (CVPR)*, pp. 4700–4708, Honolulu, HI, USA, July 2017.
[49] Y. Wang, Y. Liao, Y. H. Wu, and P. Y. Chen, "CSPNet: a new backbone that can enhance learning capability of CNN," in *Proceedings of the IEEE/CVF conference on computer vision and pattern recognition workshops*, pp. 390-391, Seattle, WAS, USA, June 2020.
[50] J. Hu, L. Shen, and G. Sun, "Squeeze-and-excitation networks," in *Proceedings of the IEEE conference on computer vision and pattern recognition*, pp. 7132–7141, Salt Lake City, UH, USA, June 2018.
[51] P. Zhuang, Y. Wang, and Y. Qiao, "Learning attentive pairwise interaction for fine-grained classification," in *Proceedings of the AAAI Conference on Artificial Intelligence*, vol. 34, no. 07, pp. 13130–13137, New York, NY, USA, February 2020.
[52] Y. Ding, Z. Ma, S. Wen et al., "AP-CNN: weakly supervised attention pyramid convolutional neural network for fine-grained visual classification," *IEEE Transactions on Image Processing*, vol. 30, pp. 2826–2836, 2021.
[53] Y.-Y. Zheng, J.-L. Kong, X.-B. Jin, X.-Y. Wang, and M. Zuo, "CropDeep: the crop vision dataset for deep-learning-based classification and detection in precision agriculture," *Sensors*, vol. 19, no. 5, p. 1058, 2019.
[54] R. Ji, L. Wen, L. Zhang, and D. Du, "Attention convolutional binary neural tree for fine-grained visual categorization," in *Proceedings of the 2020 IEEE/CVF Conference on Computer Vision and Pattern Recognition (CVPR)*, pp. 10468–10477, Seattle, WT, USA, June 2020.

Hindawi
Computational Intelligence and Neuroscience
Volume 2022, Article ID 1343358, 9 pages
https://doi.org/10.1155/2022/1343358

Research Article

A Data-Driven Adaptive Emotion Recognition Model for College Students Using an Improved Multifeature Deep Neural Network Technology

Li Liu ,[1,2] Yunfeng Ji,[1] Yun Gao,[1] Tao Li,[1] and Wei Xu[1]

[1]*Jiangsu Vocational College of Information Technology, Wuxi, Jiangsu 214153, China*
[2]*Jiangsu Key Laboratory of Media Design and Software Technology (Jiangnan University), Wuxi 214122, China*

Correspondence should be addressed to Li Liu; liul2@jsit.edu.cn

Received 22 April 2022; Revised 11 May 2022; Accepted 13 May 2022; Published 26 May 2022

Academic Editor: Xin Ning

With the increasing pressure on college students in terms of study, work, emotion, and life, the emotional changes of college students are becoming more and more obvious. For college student management workers, if they can accurately grasp the emotional state of each college student in all aspects of the whole process, it will be of great help to student management work. The traditional way to understand students' emotions at a certain stage is mostly through chats, questionnaires, and other methods. However, data collection in this way is time-consuming and labor-intensive, and the authenticity of the collected data cannot be guaranteed because students will lie out of impatience or unwillingness to reveal their true emotions. In order to explore an accurate and efficient emotion recognition method for college students, more objective physiological data are used for emotion recognition research. Since emotion is generated by the central nervous system of the human brain, EEG signals directly reflect the electrophysiological activity of the brain. Therefore, in the field of emotion recognition based on physiological signals, EEG signals are favored due to their ability to intuitively respond to emotions. Therefore, a deep neural network (DNN) is used to classify the collected emotional EEG data and obtain the emotional state of college students according to the classification results. Considering that different features can represent different information of the original data, in order to express the original EEG data information as comprehensively as possible, various features of the EEG are first extracted. Second, feature fusion is performed on multiple features using the autosklearn model integration technique. Third, the fused features are input to the DNN, resulting in the final classification result. The experimental results show that the method has certain advantages in public datasets, and the accuracy of emotion recognition exceeds 88%. This proves the used emotion recognition is feasible to be applied in real life.

1. Introduction

With the development of the times, the environment in which college students live is also constantly changing. The transformation of the identity of college students is accelerating, and they are faced with problems in study, work, interpersonal communication, and life. Most of the current college students were born after 1995. They have a strong sense of independence, have their own ideas, and are emotionally sensitive. In addition, in the current summer of the epidemic, students' learning and employment have been greatly affected. The epidemic not only affects the physical health of college students but also affects their emotions. On the one hand, when college students surf the Internet, they will be confronted with a variety of epidemic-related information, which will have a psychological impact. On the other hand, college students need to adapt to the comprehensive online teaching state and complete various learning tasks arranged by the school. College students will experience stressful emotions for an extended period of time under these conditions, and negative emotional states such as loneliness, anxiety, depression, and fear will emerge. If you do not pay attention and adjust in a timely manner, it may result in more serious consequences. As a result, whether it is college students or colleges and universities, they should pay close attention to the emotional state and mental health of college students while focusing on the epidemic and their studies.

For college student management workers, the traditional methods to understand students' emotions mainly include interviews, questionnaires, and oral presentations by class informants. The main problems in these methods are as follows: first, some students are worried that telling the truth will cause adverse effects and other reasons to falsely report information, resulting in inaccurate information collected. Second, some students are disgusted or impatient to fill in the questionnaire, so they fill in the content at will, resulting in inaccurate information collected. Third, some students' emotions are not exposed, so it is difficult to obtain accurate information through the observation of classmates and teachers. Therefore, in order to obtain accurate and effective emotional data, it is best to obtain it based on objective physiological data. Since the emotion recognition results based on physiological signals are more objective, various emotion recognition methods based on physiological signals emerge as the times require. These physiological signals are noninvasive in nature, easily obtained from the individual, and largely reflect the influence of emotion on the automatic nervous system. Electrocardiogram (ECG) [1], electromyography (EMG) [2], ElectroSkin (GSR) [3], respiration rate (RR) [4], and EEG [5] are all commonly used for emotion recognition. Physiological signals: in particular, EEG signals are most often used for emotion recognition [6, 7]. EEG signals have been widely used to study swallowing, analyze mental states, and assist in diagnosing neuropsychiatric diseases [8–10].

EEG-based emotion recognition research is mainly carried out from the following aspects. one is the research based on the recognition model, mainly based on machine learning algorithms and based on deep learning algorithms. Reference [11] applies Support Vector Machine (SVM) to binary classification tasks or to few classifications and achieves good results. In SVM, by calculating the distance between each support vector, a maximum interval space is optimized to realize the distinction of different categories [12]. Reference [13] annotates the feature information of the ECG signal according to the local features and overall features of the ECG signal, and SVM is used to identify the ECG. However, when the data scale becomes large, using SVM for classification will consume a lot of machine memory and computing time. Reference [14] classified four kinds of ECG signals through a decision tree ensemble algorithm, and the classification Fl-score exceeded 0.81. Reference [15] uses a one-dimensional convolutional neural network to perform feature extraction on ECG signals, and the accuracy rate reaches 86% in the ECG four-classification task. Reference [16] proposes to combine a convolutional neural network (CNN) with a recurrent neural network (RNN) to achieve a multiscale representation of ECG signals. However, due to the limited depth, the ECG signal feature extraction is incomplete, and the improvement of the classification effect is not obvious. Reference [17] extracted a set of ECG signal features to describe the morphological features of the entire ECG signal and improved the classification accuracy based on XGBoost. Reference [18] used DNN to classify 12 kinds of signals in single-lead ECG signal, and its classification performance accuracy was as high as 83.7%. The second is research based on different emotion expression models. There are mainly continuous emotional expression models that represent emotions, mainly two-dimensional [19], three-dimensional [20], 4-dimensional [21], and discrete emotional expression models [22–24]. The third is based on different EEG feature extraction. Methods of research include the power spectrum feature [25] and wavelet energy entropy feature [26].

At present, EEG-based emotion recognition is mainly carried out from the above three aspects. Multifeature extraction strategies are mostly combined with machine learning algorithms for research. Most of the research on deep learning algorithms focuses on improving the algorithm itself. Inspired by this, this study combines a multi-feature fusion strategy with a deep learning algorithm to further increase the emotional EEG′ recognition accuracy. Considering that different features can represent different information from the original data, in order to express the original EEG data information as comprehensively as possible, various features of the EEG are first extracted. Second, feature fusion is performed on multiple features using the autosklearn model integration technique. Third, the fused features are input to the DNN, resulting in the final classification result. The experimental results show that the method has certain advantages in public datasets, and the accuracy of emotion recognition exceeds 88%. This proves that the used emotion recognition method is feasible to be applied in real life.

2. Relevant Background Knowledge

2.1. Emotional Characteristics of College Students

(1) Anxiety and loss due to employment and higher education pressure: in addition to academic pressure, some senior students feel anxious when faced with the pressure of employment and further education. In order to protect the health of college students, the government requires college students not to return to school and colleges to reopen until the epidemic is effectively controlled. This means that many recent university graduates cannot improve their employability through internships. Due to the severe epidemic situation, many companies have not resumed work in time or have not resumed normal production and operations after the resumption of work, and corporate recruitment will inevitably be affected. Affected by this, college students who are applying for jobs generally show negative emotions such as anxiety and loss.

(2) Under the epidemic environment, online learning at home has led to burnout and anxiety. Affected by the epidemic, colleges and universities have delayed the start of school, and domestic colleges and universities have adopted online teaching methods to enable college students to study courses at home. The school arranges a week's class schedule according to

the students' course selection, and the teacher selects the appropriate online platform for teaching and assignments according to the needs of the course. Many college students are taking online classes for the first time. Coupled with the influence of factors such as irregular work and rest during the holidays, they have a lot of discomfort with online teaching, which in turn has an impact on their emotional state. Some students expressed their rejection of online classes and even thought of dropping out. Each teacher has different requirements and needs to use many software programs such as QQ, WeChat, and Tencent Conference. Due to problems such as network or software capacity, there are often problems such as freezes and flashbacks during class, which affect the status of the class. Teachers are worried about the effect of students studying at home, and they will assign more homework. Students feel that they are either taking online classes or rushing to do homework every day and feel exhausted.

(3) Sadness and anger caused by following all kinds of news: sudden emergencies will greatly stimulate the public's information exchange and dissemination behavior. With the help of Internet technology, the spread of epidemic-related information has become very fast. But for the recipient of the information, it can be difficult to discern which is credible and which is a rumour from the dizzying array of information. The prevention and control of the epidemic require the public to reduce going out. College students respond to the government's call to stay at home for a long time, and they can only obtain information through TV news, online media, and various social software. College students should be concerned about current affairs, but 24-hour reports on the epidemic, closed home isolation environment, etc. will make individuals pay too much attention to the epidemic. In addition, there are some negative news on the Internet that are exaggerated to attract attention. If you are too immersed in negative social information, you will have negative emotions that are not good for your physical and mental health.

2.2. Emotion Expression Model. The representation of discrete emotions is derived from basic emotion theory. The basic emotion theory divides emotion into basic emotion and secondary emotion. Basic emotion is determined by the human physiological autonomic nervous system. Assuming that there are various neural channels in the human body system, each basic emotion corresponds to its own functional channel and presents certain physiological feedback to the surrounding environment and situation. Such feedback may be physiological electrical signals, body movements, voice intonation, natural language expressions, and facial expressions. Secondary emotion is no longer restricted by basic emotion; it can reflect individualized emotion through the combination of different basic emotions or the fusion of cognition and inner needs. There are three typical evaluation criteria for discrete emotions, namely: Scherer affective state model [27], OCC affective model [28], and Roseman affective model [29].

Some scholars believe that emotional states do not exist in isolation but are distributed in multiple dimensional spaces. Therefore, any two affective states in a continuous affective space can be brought together by the continuity of dimensions. Emotions that are closer in space have a greater similarity. Conversely, the farther the distance in the space is, the smaller the similarity is, and the easier it is to distinguish. In addition, the continuous emotional space can also be measured by Euclidean distance, and the similarity of emotions can be quantified according to the distance, which makes it easier to analyze the emotional state. Typical continuous emotional expression models include Wundt emotional space [30], Schlosberg 3D cone emotional space [31], 3D emotional space for PAD [32], and Plutchik emotional wheel continuous space [33]. The relationship between the above two types of emotion expression models is not completely independent but an inclusive relationship. Continuous types of emotion models include discrete types of emotion expression models. Moreover, even within a certain type of emotion expression model, there is an inclusive relationship between several typical emotion expression models.

2.3. EEG Features. Before the EEG raw data are input to the classifier, it needs to perform preprocessing, feature extraction, and dimensionality reduction. Based on preprocessed EEG data such as denoising, multidomain feature extraction is required. Generally, effective features are extracted from the time domain, frequency domain, and spatial domain, respectively. A brief introduction to the features of each domain is shown in Table 1.

3. Emotion Recognition Models

3.1. Emotion Recognition Architecture. In order to maximize the use of feature data in various fields of EEG, the classification performance of the model can be improved as much as possible. This article extracts 8 features in the three domains of time domain, frequency domain, and spatial domain given in Section 2.3. The eight features are Hurst, sample entropy (SE), Hjorth complexity (HC), vector autoregression (VAR), wavelet entropy (WE), spectral entropy (SE), power spectral density (PSD), and complex network (CN). Although the increase of feature dimension can convey the features of EEG more comprehensively and objectively, the number of redundant and invalid features it contains also increases. While increasing the computational complexity, it also reduces the classification accuracy. Therefore, feature selection is very necessary. Feature selection is to filter out the most effective feature subsets from the original features. Model fusion aggregates the classification results of many models to improve single-model performance. Under the assumption that a single model produces uncorrelated errors, deep learning models based on multidomain features may allow incorrect models to be

Table 1: EEG features.

Domain	Feature
Time domain	Skewness, kurtosis, zero-crossing rate, instability index, Hurst's index Detrended fluctuation analysis, Pearson's fractal dimension, sample entropy, HFD, Hjorth activity, hjorth mobility, hjorth complexity Energy, RMS, vector autoregression (VAR)
Frequency domain	Power, wavelet entropy, spectral entropy, PSD, partial directed coherence (PDC) Band power (BP)
Spatial domain	Index of asymmetry, complex network (CN)

rejected in decision-making. Based on DNN, this article proposes a DNN model that combines multifeature input and applies it to the recognition of emotion EEG. Figure 1 illustrates the architecture of the used recognition method.

As shown in Figure 1, firstly, eight features are extracted from the input raw EEG data. Second, the importance of the features is sorted using a random forest (RF) algorithm, and the top 3 most important features are selected. Third, use the autosklearn model integration technology to perform feature fusion on the three features; fourth, input the fused features into the DNN to obtain the final classification result.

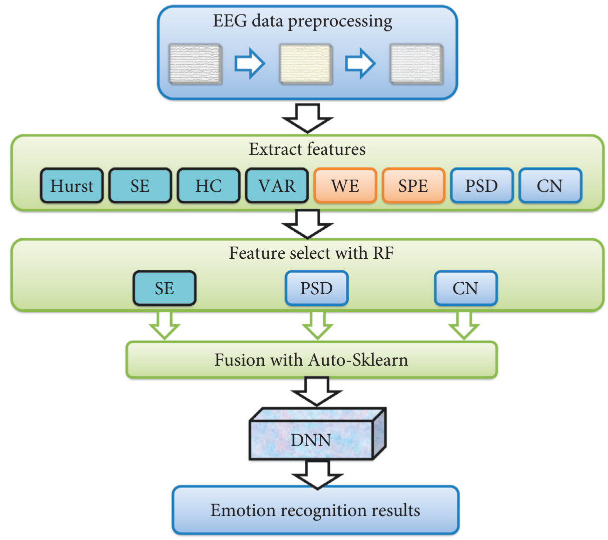

Figure 1: Emotion recognition architecture diagram.

3.2. Feature Selection Strategy. When filtering feature information based on RF, the importance value (IV) of all feature information can be calculated to sort the features according to their importance. Taking a decision tree *i* as the initial point, based on equation (1), the out-of-bag data error (OD_{error}) is obtained. After that, the value of the feature information H^j in the out-of-bag data is rearranged, keeping other eigenvalues unchanged. Then a new out-of-bag data set can be obtained, denoted as $OD_{error'}$. Similarly, use equation (1) to obtain a new out-of-bag data error (OD_{error}). The IV of the feature information F^j in the ith decision tree can be derived by subtracting the results of the two calculations.

$$\mathrm{OD}_{\mathrm{error}} = \frac{1}{n}\sum_{i=1}^{n}\left(x_f - x_c\right)^2, \tag{1}$$

where n represents the total amount of data, x_f represents the actual value of data, and x_c represents the classification value of data.

$$\mathrm{IV}\left(H^j\right) = \mathrm{OD}_{\mathrm{error}_i'} - \mathrm{OD}_{\mathrm{error}_i}. \tag{2}$$

According to the same principle, the corresponding IV is obtained for each decision tree in the random forest, and finally all the obtained IV are averaged to obtain the IV of the feature information H^j:

$$\mathrm{IV}\left(H^j\right) = \frac{1}{m}\sum_{i=1}^{m}\mathrm{IV}_i\left(H^j\right), \tag{3}$$

where m is the number of decision trees in random forests. It can be seen that if feature information is very important, its numerical value varies greatly among different samples. When the feature values in the out-of-bag dataset are reordered, the difference between different samples will be reduced so that OD_{error} will increase. Then according to (2) and (3), it can be concluded that the larger the IV of the feature information, the stronger its importance.

By calculating the IV of all feature information, combined with the reverse search method of the sequence, a set of optimal prediction feature information subsets can be obtained. Considering the high dimension of the track feature information, if the reverse search method of the sequence is used directly, the operation time will be too long, thus reducing the operability of the algorithm. Therefore, this article uses an improved sequence reverse search algorithm. Specifically, a rough selection stage is added before the reverse search method is applied to the feature information set. Specific steps are as follows:

Step 1. Train the random forest using the extracted eight kinds of feature data. After the training is completed, *IV* of all feature information can be obtained. At this time, the test set is used to evaluate the classification accuracy e_{all} of the random forest algorithm, and this value is set as the classification threshold.

Step 2. Sort the *IV* of all feature information in descending order. After the sorting is completed, the feature information corresponding to the first 15 *IV* is imported into the rough selection feature information set S_{pre}, which is initially an empty set, and this feature information is deleted from the initial feature set K at the same time.

Step 3. The RF is retrained based on S^i_{pre}, and the classification error e^i_{pre} of the test is obtained. The upper right corner mark i in the formula represents the number of feature information of the information set S_{pre}.

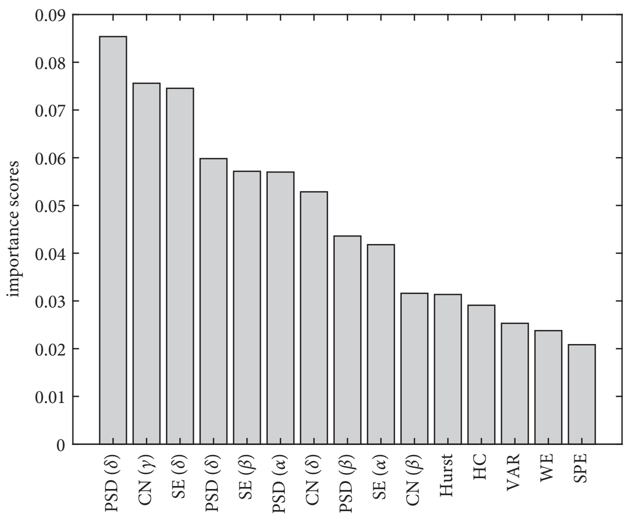

Figure 2: Feature sorting.

Step 4. Determine the size relationship of e_{pre}^{i}. If $e_{\text{pre}}^{i} \geq e_{\text{all}}^{i}$, then add 15 more feature information to the feature information set S_{pre}^{i} to form a new set S_{pre}^{i+15}. If $e_{\text{pre}}^{i+15} \leq e_{\text{pre}}^{i}$, do not add feature information to S_{pre}; otherwise, continue to select the top 15 feature information in K to add.

After the rough selection information set S_{pre} is determined, the reverse sequence search method is used for this set. The IV corresponding to all feature information in set S_{pre} are sorted from small to large, and then a feature information variable corresponding to the smallest IV is eliminated. The RF is trained again based on this set, and the classification results in the test set are saved.

After the above operations are completed, the feature information variable corresponding to the next IV is eliminated, and training, testing, and recording are repeated until the initial set S_{pre} becomes an empty set. Finally, considering the classification accuracy of each scheme comprehensively, determine the appropriate feature information set S_{best}.

4. Experimental Simulation and Discussion

4.1. Feature Selection Experiment. The PI value corresponding to each feature information is calculated based on RF and arranged in descending order. This selects features that play an important role in the classification decision-making process. The number of populations in RF is 500 by default. In order to better compare the importance of each feature, the calculated PI value is normalized to represent the importance of each feature. Figure 2 gives the top 15 features based on RF.

It can be seen from Figure 2 that the feature importance of each frequency band of the PSD ranks first, indicating that its importance is the greatest. It is speculated that the classification results of PSD in CNN may be good, so PSD is selected as one of the optimal feature subsets. After the PSD is the CN, and after the CN is the SE. Behind SE is Hurst. Considering that the more the features are, the longer the model training takes, and the classification results are not necessarily good. Therefore, this article finally selects the top 3 features, namely PSD, CN, and SE.

Table 2: Description of experimental software and hardware environment.

Name	Details	Name	Details
CPU	I9 9900 K	Editor	PyCharm COMMUNITY 2018.3
RAM	32G DDR4 3200 MHz	Locales	Python 3.6
GPU	GTX 1070	Deep learning framework	Tensorflow 1.12
Graphics card	NVIDIA GeForce RTX2080	Operating system	Windows10

Table 3: Experimental results of each model on different emotional dimensions.

Model	Index	Valence	Arousal	Liking
SVM	Accuracy	0.6587	0.5882	0.5643
	Precision	0.6174	0.5612	0.5144
	*F*1	0.5693	0.5610	0.4757
CNN	Accuracy	0.7596	0.6716	0.6685
	Precision	0.7396	0.6586	0.6285
	*F*1	0.7264	0.6659	0.6217
DNN	Accuracy	0.8773	0.8606	0.8457
	Precision	0.8338	0.8316	0.8182
	*F*1	0.8163	0.8573	0.8383
RNN	Accuracy	0.7196	0.7016	0.6985
	Precision	0.7047	0.6644	0.6891
	*F*1	0.7160	0.6254	0.6850
LSTM	Accuracy	0.8924	0.8841	0.8572
	Precision	0.8501	0.8744	0.8459
	*F*1	0.8346	0.8282	0.8244
Reference [39]	Accuracy	0.7288	0.7469	0.7475
	Precision	0.7069	0.7413	0.7346
	*F*1	0.6767	0.7769	0.7235
Reference [40]	Accuracy	0.7697	0.7830	0.7550
	Precision	0.7367	0.7571	0.7064
	*F*1	0.7583	0.7983	0.7022
Proposed	Accuracy	0.9078	0.9002	0.8865
	Precision	0.8926	0.8841	0.8677
	*F*1	0.8903	0.8782	0.8559

4.2. Model Evaluation Experiment. The dataset used in this article is the public DEAP dataset. The tenfold cross-validation strategy was adopted, and 70% of the EEG sample set was used as the training set to build the emotion recognition model. Use the established emotion recognition model to test the remaining 30% of the test samples to perform emotion recognition. The comparison models include SVM [34], CNN [35], DNN [36], RNN [37], LSTM [38], [39], and [40], and the parameter settings of each comparison model are consistent with those in the article. To make the model converge quickly, the Adam optimizer employs the adaptive learning rate method so this model employs the Adam

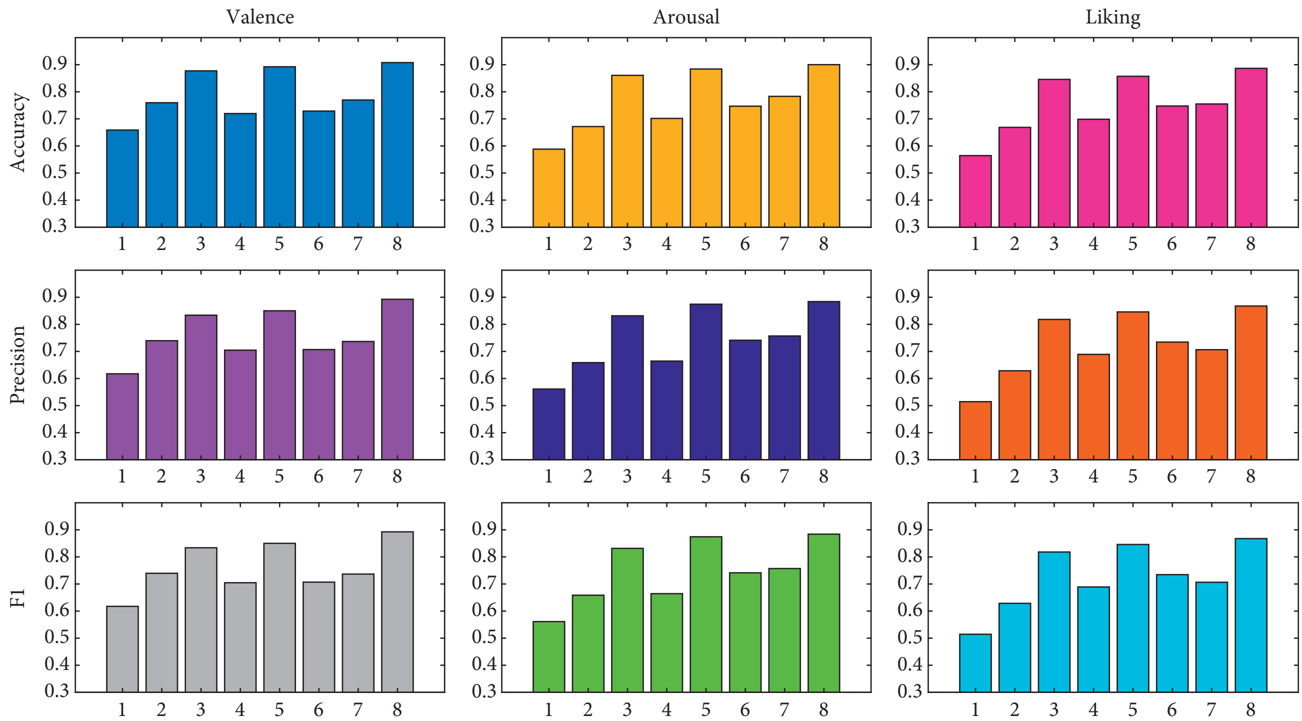

Figure 3: Comparison of experimental results.

optimizer, the initial learning rate is set to 0.001, the Dropout layer ratio is set to 0.2, and the batch size is set to 32. The epoch is 80, and for each epoch, a full training process is performed on all training sets. Table 2 depicts the experimental environment for this article. The accuracy rate, precision rate, and F1 score are the quantitative indicators used to assess the model's effectiveness. The three indicators' calculation formulas are as follows:

$$\begin{aligned} \text{Accuracy} &= \frac{\text{TP} + \text{TN}}{\text{TP} + \text{TN} + \text{FP} + \text{FN}}, \\ \text{Precision} &= \frac{\text{TP}}{\text{TP} + \text{FP}}, \\ \text{Recall} &= \frac{\text{TP}}{\text{TP} + \text{FN}}, \\ F1 &= \frac{2 * \text{Precision} * \text{Recall}}{(\text{Precision} + \text{Recall})}. \end{aligned} \tag{4}$$

The experimental results of each algorithm on the DEAP dataset are shown in Table 3. Since the presentation method in the form of a table cannot visually show the small gap between the numbers, this article compares and displays the experimental data of each method on different indicators and different emotional dimensions in the form of legends, as shown in Figure 3.

The above simulation data illustrate that the overall recognition effect on the Valence dimension is the best, followed by Arousal, and the worst is Liking. Comparing the recognition results of each model, first of all, the machine learning representative algorithm SVM performs the worst, which shows that for EEG-based classification tasks, the deep learning algorithm has more advantages in terms of recognition accuracy. Second, comparing each deep learning model, the classification accuracy of each model is between 0.7 and 0.9. CNN, RNN, [39], and [40] are all below 0.8. The classification performance of LSTM is good. This is due to the fact that, despite being an RNN variant model that inherits most of the RNN model's characteristics, LSTM solves the vanishing gradient problem caused by the gradual reduction of the gradient backpropagation process, thereby improving model classification performance. The recognition accuracy of DNN has risen to more than 0.8. This demonstrates that increasing the number of network layers can improve the model's classification accuracy. Based on DNN, the model in this article has increased Accuracy, Precision, and $F1$ by 3.48%, 7.05%, and 9.07%, respectively, in the Valence dimension. In the Arousal dimension, Accuracy, Precision, and $F1$ increased by 4.6%, 6.31%, and 2.44%, respectively. In the Liking dimension, Accuracy, Precision, and $F1$ increased by 4.82%, 6.05%, and 2.1%, respectively. It can be seen that no matter which dimension it is, the recognition effect of the model in this paper is improved by more than 4 points compared with DNN. This fully demonstrates the effectiveness of this method in processing the input feature data.

This experiment records the classification accuracy and loss of the proposed method in the Valence dimension of the training set and the test set at different epochs. Figure 4 illustrates that when the training round reaches about 25 in the training set, the model gradually tends to be stable. At this time, the loss value is reduced to 0.082, and the accuracy rate reaches 0.9124. In the test set, when the number of training rounds reaches about 40, the model gradually

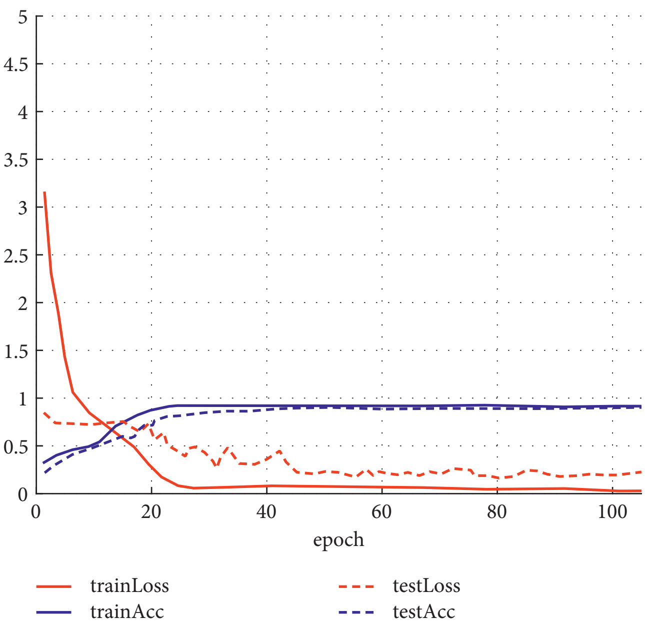

FIGURE 4: Loss and accuracy of training and test sets in Valence dimension.

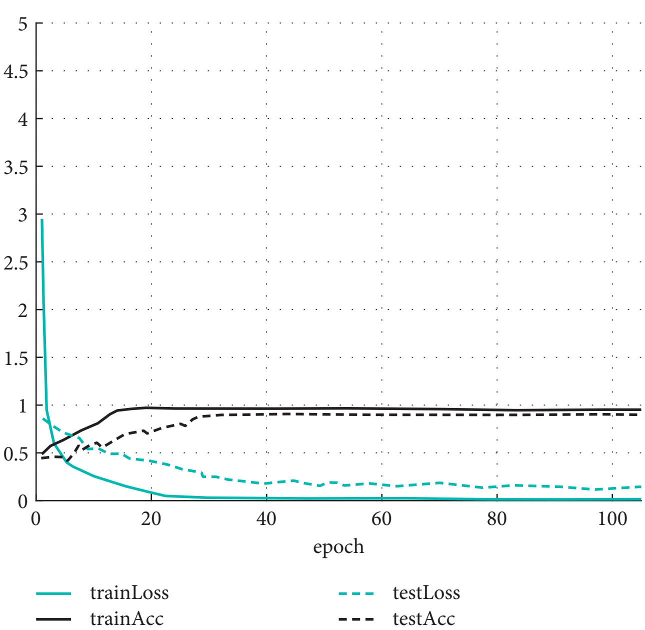

FIGURE 5: Loss and accuracy of training and test sets in the Arousal dimension.

stabilizes. At this time, the loss value is 0.2633, and the accuracy reaches 0.9078.

The experiment also records the classification accuracy and loss of the model in the training set and the test set in the Arousal dimension under different epochs. Figure 5 shows when the training round reaches about 20 in the training set, the model gradually tends to be stable. At this point, the loss value is 0.086, and the accuracy is 94.79%. In the test set, when the number of training rounds reaches about 30, the model gradually stabilizes. At this time, the loss value is 0.1703, and the accuracy reaches 90.21%.

Figures 4 and 5 show that the training set's classification accuracy and model convergence speed are greater than those of the test set. However, there is still overfitting, which has an impact on the final classification effect. Therefore, the improvement of the overfitting phenomenon will also be the content that needs further research in this article in the future. It can be expanded by increasing the amount of data, regular terms, or reducing the complexity of the model.

5. Conclusion

The identity and characteristics of college students are not the same as other students. They are relatively independent and have a certain rudimentary understanding of society and their own responsibilities. They are under increasing pressure in their studies, life, work, and other aspects as society and technology develop. College students' mental health is receiving increasing attention. The emergence of the epidemic in recent years has caused the global economy to suffer. Employment has dropped sharply, and college students' job-hunting and living pressures have intensified. Multiple internal and external pressures make the number of students with mental health problems increase year by year. If students with psychological problems can be identified as soon as possible and given timely and appropriate psychological counseling and help, many tragedies can be reduced. In order to detect students with mental health problems as early as possible, it is necessary to grasp the psychological state of each classmate as accurately as possible and be very clear about the emotional changes of students. Therefore, this article proposes an emotion recognition method based on EEG data. Considering that different features can represent different information from the original data, in order to express the original EEG data information as comprehensively as possible, various features of the EEG are first extracted. Second, use the autosklearn model integration technology to perform feature fusion on the screened features. Third, input the fused features into the DNN to get the final classification result. The experimental results demonstrate that the method in this article has a good effect on the emotion recognition of college students. The method shows certain advantages in public datasets, and the accuracy of emotion recognition exceeds 88%. The advantage of this method is that the recognition results based on physiological data are more accurate, and the recognition results are close to 90%, which can be applied in real life. However, there is still room for further improvement in this study, such as continuing to improve the recognition accuracy and how to easily collect EEG data in real life. The emotion recognition results of college students should not be limited to the application of mental health but can also be extended to classroom teaching. In the process of classroom teaching, if teachers can obtain real-time emotional changes in students, they can better promote the improvement of teaching methods. For example, when the teacher explains a certain knowledge point, some students are obviously anxious, indicating that these students do not understand the content of the teaching, then the teacher can change the teaching method at this time. When the teacher explained a certain knowledge point, the students' emotion recognition results were happy and positive, indicating that the students were very interested in this part of the content. Through the emotion recognition results, the students' learning situation can be sensed in real time in the classroom, and teachers can dynamically adjust their teaching methods and teaching progress according to the obtained results. On the other hand, although the EEG-based emotion recognition system is accurate, the data collection is inconvenient. Therefore, it is also important to develop a collection device that is convenient, fast, and low-cost and does not affect students' classroom learning.

Data Availability

The labeled dataset used to support the findings of this study is available from the corresponding author upon request.

Conflicts of Interest

The authors declare that there are no conflicts of interest.

Acknowledgments

This work was supported by the Open Project from Jiangsu Key Laboratory of Media Design and Software Technology (Jiangnan University) under Grant 21ST0203, Jiangsu Province Higher Vocational Education High-level Professional Group Construction Project under Grant Su Jiaozhi Letter [2021] No. 1, Jiangsu Province Higher Vocational Education Industry-Education Integration Platform Construction Project under Grant Su Jiaozhi Letter [2019] No. 26, Natural Science Research Project of Jiangsu Province Colleges and Universities under Grant 18KJD510011, Jiangsu Province High-level Key Professional Construction Project Funding under Grant Su Jiaogao [2017] No. 17, and Jiangsu Province Education Science "14th Five-Year Plan" 2021 Annual Project under Grant D/2021/03/03.

References

[1] M. K. Elliott, J. Blauer, V. S. Mehta et al., "Comparison of electrical dyssynchrony parameters between electrocardiographic imaging and a simulated ECG belt," *Journal of Electrocardiology*, vol. 68, pp. 117–123, 2021.

[2] H. Namazi and N. Pakniyat, "Investigation of the effect of walking speed on leg muscle reaction by complexity-based analysis of electromyogram (emg) signals," *Fractals.* vol. 29, no. 05, pp. 2150201–2150209, 2021.

[3] Y. Nagai, C. I. Jones, and A. Sen, "Galvanic skin response (GSR)/Electrodermal/Skin conductance biofeedback on epilepsy: a systematic review and meta-analysis," *Frontiers in Neurology*, vol. 10, p. 377, 2019.

[4] M. E. Eisenberg, D. Givony, and R. Levin, "Acoustic respiration rate and pulse oximetry-derived respiration rate: a clinical comparison study," *Journal of Clinical Monitoring and Computing*, vol. 34, no. 1, pp. 139–146, 2020.

[5] M. Savadkoohi, T. Oladunni, and L. Thompson, "A machine learning approach to epileptic seizure prediction using Electroencephalogram (EEG) Signal," *Biocybernetics and Biomedical Engineering*, vol. 40, no. 3, pp. 1328–1341, 2020.

[6] S. M. Venothanee and F. M. A. Mohd, "Yuhanim hani yahaya, emotion classifications in electroencephalogram (EEG) signals," *International Journal of Recent Technology and Engineering*, vol. 8, no. 3, pp. 2736–2740, 2019.

[7] D. S. Naser and G. Saha, "Influence of music liking on EEG based emotion recognition," *Biomedical Signal Processing and Control*, vol. 64, Article ID 102251, 2021.

[8] R. Andrade-Machado, B. C. Vanesa, K. M. Irshad, and I. K. Muhammad, "Recognition of interictal and ictal discharges on EEG. Focal vs generalized epilepsy," *Epilepsy and Behavior*, vol. 117, Article ID 107830, 2021.

[9] T. Tuncer, S. Dogan, G. R. Naik, and P. Pławiak, "Epilepsy attacks recognition based on 1D octal pattern, wavelet transform and EEG signals [J]," *Multimedia Tools and Applications*, vol. 80, no. 16, pp. 25197–25218, 2021.

[10] I. Zawar and E. M. Pestana Knight, "An overview of the electroencephalographic (EEG) features of epilepsy with eyelid myoclonia (jeavons syndrome)," *The Neurodiagnostic Journal*, vol. 60, no. 2, pp. 113–127, 2020.

[11] M. Balachandran and L. Jooyoung, "SVMQA:Support-vector-machine-based protein single-model quality assessment [J]," *Bioinformatics*, no. 16, p. 2496, 2017.

[12] N. Peng, Y. Zhang, and Y. Zhao, "Selecting quasar candidates using a support vector machine classification system [J]," *Monthly Notices of the Royal Astronomical Society, 2015*, vol. 425, no. 4, pp. 2599–2609.

[13] S. Radovan, H. Jakub, and R. Marina, "Multi-stage SVM approach for cardiac arrhythmias detection in short single-lead ECG recorded by a wearable device [J]," *Physiological Measurement*, vol. 39, no. 9, Article ID 094003, 2018.

[14] M. Rizwan, B. M. Whitaker, and D. V. Anderson, "AF detection from ECG recordings using feature selection, sparse coding, and ensemble learning," *Physiological Measurement*, vol. 39, no. 12, Article ID 124007, 2018.

[15] B. Pyakillya, N. Kazachenko, and N. Mikhailovsky, "Deep learning for ECG classification," *Journal of Physics: Conference Series*, vol. 913, no. 1, Article ID 012004, 2017.

[16] P. A. Warrick and M. Nabhan Homsi, "Ensembling convolutional and long short-term memory networks for electrocardiogram arrhythmia detection," *Physiological Measurement*, vol. 39, no. 11, Article ID 114002, 2018.

[17] T. Teijeiro, C. A. Garcia, D. Castro, and P. Fe´lix, "Abductive reasoning as the basis to reproduce expert criteria in ECG atrial fibrillation identification [J]," *Physiological Measurement, 2018*, vol. 39, no. 8, Article ID 084006.

[18] A. Y. Hannun, G. H. Tison, C. Bourn, M. P. Turakhia, P. Rajpurkar, and M. Haghpanahi, "Cardiologist-level arrhythmia detection and classification in ambulatory electrocardiograms using a deep neural network," *Nature Medicine*, vol. 25, no. 1, pp. 65–69, 2019.

[19] R. Plutchik, "The nature of emotions," *American Scientist*, vol. 89, no. 4, p. 344, 2001.

[20] J. Posner, J. A. Russell, and B. S. Peterson, *Development and Psychopathology*, vol. 17, no. 3, pp. 715–734, 2005.

[21] M. P. Alice and F. Russo, "Multimodal recognition of emotions in music and language," *Psychology of Music*, vol. 50, no. 1, pp. 54–68, 2022.

[22] P. J. Lang and J. Peter, *American Psychologist*, vol. 50, no. 5, pp. 372–385, 1995.

[23] Z. Zhu, F. Hector, U. Blanke, A. Perez-Uribe, and G. Troster, "Naturalistic recognition of activities and mood using wearable electronics," *IEEE Transactions on Affective Computing*, vol. 7, no. 3, pp. 272–285, 2016.

[24] O. Bălan, G. Moise, A. Moldoveanu, M. Leordeanu, and F. Moldoveanu, "Fear level classification based on emotional dimensions and machine learning techniques," *Sensors*, vol. 19, no. 7, p. 1738, 2019.

[25] M. Hashemi, A. Hutt, L. Buhry, and Jamie Sleigh, "Optimal model parameter estimation from EEG power spectrum features observed during general anesthesia," *Neuroinformatics*, vol. 16, no. 2, pp. 231–251, 2018.

[26] M. Sharma, S. Patel, and U. R. Acharya, "Automated detection of abnormal EEG signals using localized wavelet filter banks," *Pattern Recognition Letters*, vol. 133, pp. 188–194, 2020.

[27] K. R. Scherer, "On the nature and function of emotion: a component process approach," in *Proceedings of the Approaches to Emotion*, pp. 293–318, Psychology Press, London, England, 13 July 1984.

[28] A. Ortony, G. L. Clore, and A. Collins, *The Cognitive Structure of Emotions*, Cambridge University Press, no. 2, , pp. 15–33, Cambridge, USA, 1990.

[29] I. J. Roseman, "Appraisal determinants of emotions: constructing a more accurate and comprehensive theory," *Cognition & Emotion*, vol. 10, no. 3, pp. 241–278, 1996.

[30] K. Wagner and J. Blower, "Animating architecture: empathy and architectonic space," *Art in Translation*, vol. 6, no. 4, pp. 399–435, 2014.

[31] H. Schlosberg, "Three Dimensions of Emotion," *Psychological Review*, vol. 61, no. 2, pp. 81–88, 1954.

[32] R. Plutchik, "Ageneral psychoevolutionary theory ofemotion," *Emotion Theory Research & Experience*, vol. 21, no. 4-5, pp. 529–553, 2000.

[33] J. A. Russell, "A circumplex model of affect," *Journal of Personality and Social Psychology*, vol. 39, no. 6, pp. 1161–1178, 1980.

[34] S. Behera and M. N. Mohanty, "Classification of EEG signal using SVM," *Advances in Electrical Control and Signal Systems*, vol. 665, pp. 859–869, 2020.

[35] W. M. Shalash, "A deep learning cnn model for driver fatigue detection using single EEG channel," *Journal of Theoretical and Applied Information Technology*, vol. 99, no. 2, pp. 462–477, 2021.

[36] M. S. Fahad, A. Deepak, G. Pradhan, and J. Yadav, "DNN-HMM-Based speaker-adaptive emotion recognition using MFCC and epoch-based features," *Circuits, Systems, and Signal Processing*, vol. 40, no. 1, pp. 466–489, 2021.

[37] M. A. Asghar, M. J. Khan, H. Shahid, M. Shorfuzzaman, N. N. Xiong, and M. M. Raja, "Semi-skipping layered gated unit and efficient network: hybrid deep feature selection method for edge computing in EEG-based emotion classification," *IEEE Access*, vol. 9, pp. 13378–13389, 2021.

[38] W.-H. Hwang, D.-H. Kang, and D. H. Kim, "Brain lateralisation feature extraction and ant colony optimisation-bidirectional LSTM network model for emotion recognition," *IET Signal Processing*, vol. 16, no. 1, pp. 45–61, 2022.

[39] A. Mert and A. Akan, "Emotion recognition from EEG signals by using multivariate empirical mode decomposition," *Pattern Analysis & Applications*, vol. 21, no. 1, pp. 81–89, 2018.

[40] X. Xing, Z. Li, T. Xu, L. Shu, B. Hu, and X. Xu, "SAE+LSTM: a new framework for emotion recognition from multi-channel EEG," *Frontiers in Neurorobotics*, vol. 13, p. 37, 2019.

Hindawi
Computational Intelligence and Neuroscience
Volume 2022, Article ID 4675181, 10 pages
https://doi.org/10.1155/2022/4675181

Research Article

Application Research of Tooth Arrangement Based on Rotation Matrix Calculation and Resistance Detection in Oral

Mingming Wu

Engineering Laboratory for Biomaterials and Tissue Regeneration, Ningbo Stomatology Hospital, Ningbo 315000, China

Correspondence should be addressed to Mingming Wu; doubleming0808@163.com

Received 16 March 2022; Revised 18 April 2022; Accepted 28 April 2022; Published 20 May 2022

Academic Editor: Xin Ning

The goal of this research was to provide a new approach for analyzing orthodontic teeth arrangement inside oral depending on the rotation matrix computation and resistance detection. The present method includes the following operations within a certain therapy period: first three-dimensional positions of the tooth were evaluated with a pierced laser beam and a three-dimensional system of surface-scanning. Second, the three-dimensional shape data was automatically registered at maxillary 1st molars, and methods of coordinate had been normalized. Third, a translation vector and rotation matrix had been evaluated from automatic registration of two position data of a particular tooth. Fourth, the limited spiral axes of teeth had been measured as the zero rotational dislocation locus; and impressions for a model of the dental cast had been taken at five different points: shortly before and after device was fitted, and ten days, one month, and two months after the treatment started. The results showed that existing analysis approach could more quickly classify a specific tooth's movement by spinning all over and translating along a finite helical axis. It can provide statistical visual three-dimensional data on complex tooth arrangement throughout orthodontic therapy.

1. Introduction

The orthodontic tooth arrangement is a complicated biological process characterized by the periodontal tissue's gradual reactions towards the biomechanical stimuli [1, 2]. The size, direction, and moment–force ratio of the force applied and physiological state of each patients' periodontal tissue substantially influence tooth arrangement [3–5]. Even though such studies only used a one or 2-D investigation, other morphometrical and theoretical studies about tooth arrangement have provided considerable information [6–9]. Moreover, all these investigations only explain the first tooth arrangement even before periodontium undergoes degenerative modification [10–13]. A statistical analysis utilizing the finite-element method produces a three-dimensional stress distribution throughout periodontal tissue and three-dimensional tooth dislocation under different loading conditions [13, 14].

The aim of this research had to create a new approach to evaluate the orthodontic teeth arrangement focusing on the calculation of rotation matrix, focusing on the precision of three-dimensional surface measurement and analysis of limited helical axis, for providing health-care professionals with accurate visual information [15, 16]. The main features of orthodontic treatment include jaw relation, tooth size, and tooth alignment [17, 18]. An oral cavity is examined, radiographs are evaluated, and dental casts are evaluated in order to collect the essential data for treatment decisions [19, 20]. However, from the perspective, there are limitations in correctly seeing the palate, lingual surface, and occlusal [21]. Furthermore, imprint treatments may be painful for the patient and need more chair duration [22, 23]. In addition to the logistical and financial challenges, the plaster casts require physical storage space. Furthermore, dental plaster casts visual examination does not allow physicians to check, measure, or monitor orthodontic tooth arrangement and the root region of surrounding bone [24, 25]. With each subsequent activation of the device, the application of orthodontic force via the appliance adjusts the teeth in progressive stages [26]. As shown in (Figure 1), symmetrical characteristics of the dentition are used in the reconstructed-based identical matrix point approach, a novel method of analyzing tooth arrangement [27].

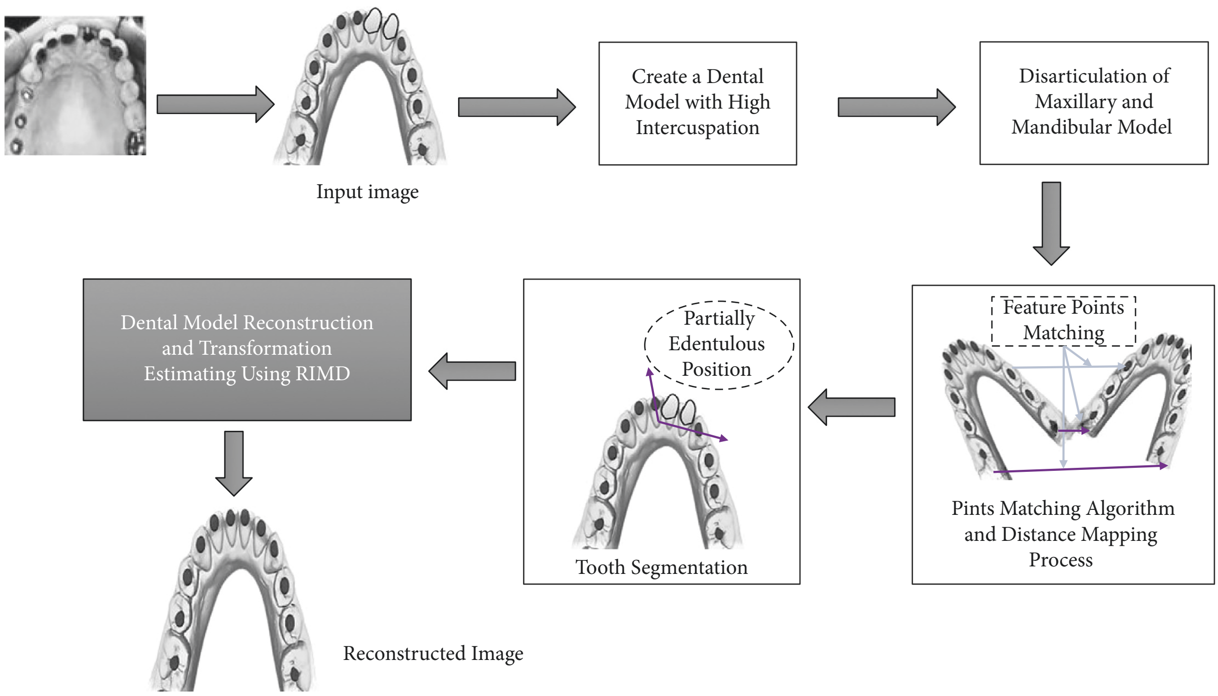

Figure 1: Overall design of reconstructed-based identical matrix point.

2. Literature Review

Saratti et al. [28] conducted a comprehensive literature search employing PubMed, a database of Cochrane Library, and Google Scholar. They provided up-to-date details on two issues. The first one was how natural tooth tissues combined to make architecture as strong, tough, and resistant to strain faults the tooth. The second was how 'bio-inspiration' was being implemented to develop and manufacture restorative dentistry while considering the limitations of existing dental methods. They expressed that bio-inspired principles had previously been effectively employed to improve the strength and toughness of artificially made materials in various engineering sectors. They highlighted that three-dimensional printing techniques also provide a novel and promising avenue for rebuilding dental tissues. Anil et al. [27] used a reconstructed-based identical matrix point (RIMP) approach to build a new way for re-establishing dental occlusion. They rebuilt the curvature of dental areas utilizing distance mapping to save calculation time. They also employed a technique of iterative point matching for precise re-establishment. They used a setup of dental experimental with high-quality digital camera pictures to examine satisfactory restoration and occlusion testing. Their suggested RIMP outperformed traditional approaches like GLCM, Fuzzy C Means, PCR, OGS, and OPOS in terms of the overall accuracy of 91.50 percent and an efficiency of 87.50 percent.

Schneider et al. [29] proposed optical coherence tomography, a revolutionary image-based approach that had significant potential in aiding regular tooth examination. They expressed that the cross-sectional pictures acquired were simple to comprehend and process. They observed that multiple uses of OCT in cariology had been studied, ranging from detecting various problems to restoration monitoring and reporting or the visualization of therapy processes. Their review based on chosen cases described the potential and limits of their approach in cariology and restorative dentistry, which were the most clinically essential domains of dentistry. Patil et al. [21] focused on polylactic acid, acrylonitrile styrene acrylate, polymethylmethacrylate, and limpet teeth (a mixture of chitin and goethite). They investigated the performance of novel materials using analytical and experimental approaches. However, they expressed that J-OCTA software had overcome experimentation-related difficulties such as costs and time. They concluded that compared to other simulation tools, this approach worked on the molecular dynamics principles to study the efficiency of the soft materials having more precision. They highlighted that the experimental techniques provide erroneous findings, while the analytical methods are confined to smaller materials because each particle has rotational and translational velocities.

Cho et al. [25] used atomistic simulations and sole fiber/microdroplet pull-out experiments in micro-scale to undertake a comparative study on the behavior of interfacial adhesion of short glass fiber and matrix of dental resin. They determined the interfacial shear strength at the molecule level by adding a factor of scale to the glass fiber. They compared the simulation findings to experimental findings of pull-out experiments. They expressed that both results confirmed the improved, reinforcing effects of modifying the surface with agents grafting of silane coupling on glass fibers. Furthermore, they investigated the mechanical characteristics and dynamic behavior of dental materials under transverse and longitudinal tension loadings that were using free volume variations. The results of their study provided optimum design recommendations for accurately predicting the mechanical properties of short fiber-reinforced dental composites using simulations, molecular dynamics, and testing. Lopez et al. [30] used a laboratory test that replicated the clinically apparent wear aspects to investigate wear processes inside a dental materials suite with a ceramic element and tooth enamel. They employed a tetrahedral ball-on-3-specimen analyzer with a revolving challenging opponent zirconia sphere to induce circular wear marks on the surface of dental composites using artificial saliva. They expressed that wear scars images allowed for the analysis of wear processes, while measurements of scar dimension quantify abrasive wear. They explained that Zirconia ceramics had the lowest rates, while lithium disilicate had the highest, having feldspathic ceramics and ceramic–polymer composites in the middle. They discussed that examination of fatigue scars showed surface residues, indicating a material removal process at the microstructural level. They accounted for mild and severe wear zones for utilizing microcracking and microplasticity models. They also used w ear models to assess the possible lifespan of various dental materials. They concluded that wear damage would produce significant material loss, resulting in early tooth or prosthesis failure.

Tahir et al. [31] suggested and tested a simulator of mechanical mastication that would simulate the force cycle of human rumination and record the requisite interactive loading via specially constructed force sensors. Their suggested method made the tooth-replacement surgery easier. They discussed that PKM completed a mastication cycle with six degrees of freedom, allowing any movement and rotation in the horizontal, vertical, and sagittal planes. Their proposed mechanism had a force transmission range of approximately 2000 N and would imitate the mastication cycle of humans. Their constructed load-sensing device would capture interactive forces ranging from 200 N to 2000 N using rapid reaction and high sensitivity to establish a simulator mechanical mastication using custom-made modules. Wei et al. [26] presented a learning-based strategy for quickly and automatically arranging teeth. They constructed the task of tooth arrangement as a unique structural 6-DOF pose estimation problem and resolved it by presenting a novel neural network structure to train from a vast number of clinical studies encoding successful orthodontic treatment instances. They claimed that extensive studies had confirmed their strategy, which yields promising descriptive and analytical results.

Zhang et al. [32] proposed a multi-manipulator tooth arrangement approach for full denture production. They suggested a revolutionary entire denture production method using a generator of dental arch and a multi-manipulator. They used an analytical technique to build the kinematics version of tooth arrangement of a multi-manipulator robot based on the concept of tooth arrangement for a complete denture. Their proposed multi-manipulator tooth-arrangement robot was used for preliminary tooth-arrangement tests. As per the jaw arch specifications, their multi-manipulator tooth-arrangement robot can autonomously design and produce a set of complete dentures for a patient. Their experimental findings confirmed the validity of the kinematics concept of the multi-manipulator tooth-arrangement robot and the viability of the whole denture manufacturing strategy implemented by the multi-manipulator tooth-arrangement robot. Cheng et al. [33] explained a newly created virtual, customized, and precise tooth arrangement mechanism based on comprehensive dental root and skull information. They made a feature-limited database of a three-dimensional tooth model. Second, they established anatomical points of reference, the reference lines and planes for tooth movement computational simulation. They thoroughly exploited the corresponding mathematical formalism of the tooth pattern and the concept of the stiff body's unique posture transformation. Their experimental findings suggested that the approach of virtual tooth arrangement would successfully arrange aberrant teeth and was suitably flexible. Their newly designed method was distinguished by its high-speed processing and quantitative measurement of each tooth's level of three-dimensional movement.

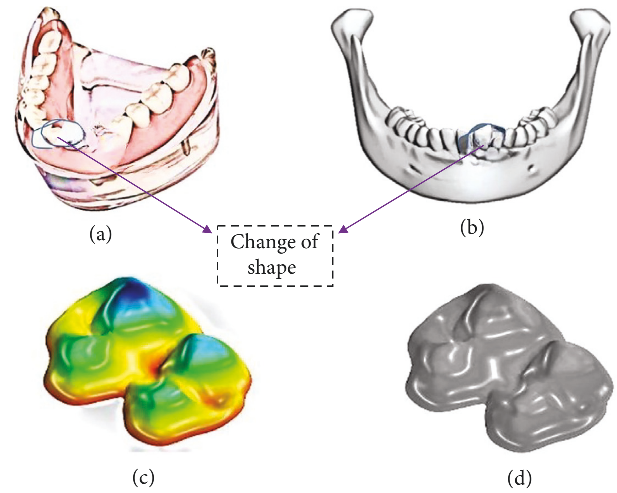

Figure 2: (a) Full mandibular model. (b) A component of mandibular model chosen. (c) The triangular mesh's foundation. (d) Cloud point as seen with the MATLAB-based toolbox.

3. Methods

To put the existing procedure to the test, a male patient of 22 yr two months had been examined in the Dental Hospital. The hospital treated the patient's Angle Class III malocclusion with anterior teeth modest crowding with a tool of multi-bracket. Conventional hooks with edge of 0.460.64 mm standard slot size were used for the primary leveling and arrangement, together with 0.41 mm hardened Ni–Ti round wire as well as a rectangular wire of 0.41 mm to 0.410.56 mm. The paired maxillary initial molars related to a bar of transpalatal to improve anchoring as well as provide immovable reference features for superimposition. The models of d dental cast were generated at each step employing alginate impressions made by die stone. A model of complete mandibular is presented in Figure 2.

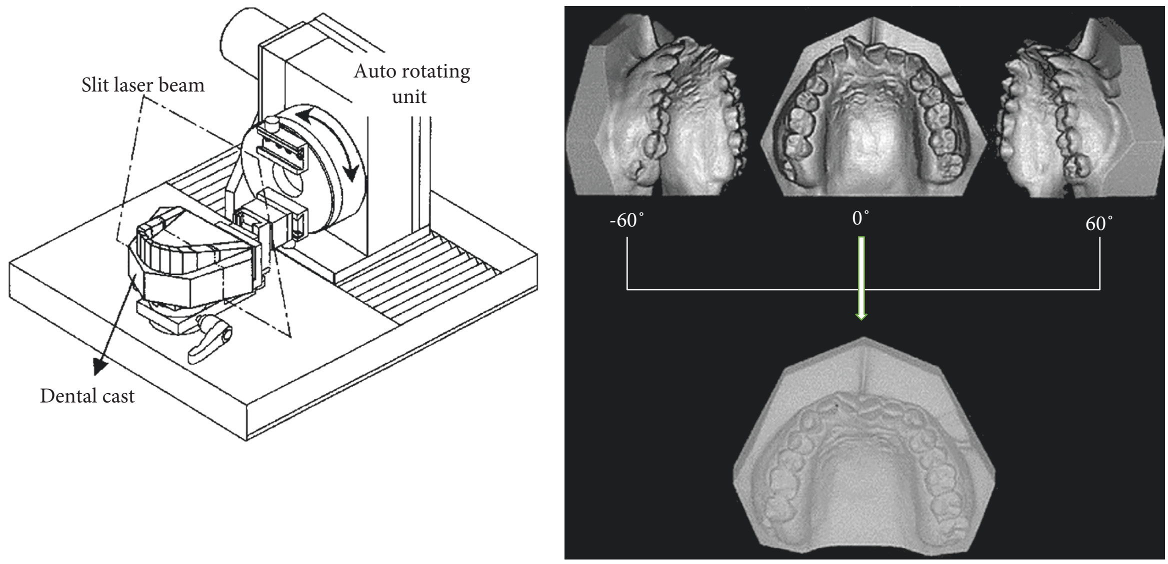

(a) (b)

Figure 3: (a) Three-dimensional strategy of surface scanning and a three-dimensional scanned shape of maxillary dental casts (b).

3.1. Printing Models of Dental Cast. Prints for models of the dental cast took 5 times: instantly before and after the appliance has been implanted (T0 and T1), ten days (T2), one month (T3), and two months with (T4) right after treatment started. To test the dental cast reproducibility, a model of proxy dental with the marks of hemisphere (reentrants; 3 mm in diameter) to the maximal incisor of right central and bilateral maximal first molars has been used as a template. A point of reference was placed inside the center point of every re-entrant. We created five alginate impressions, as well as die stone cast replicas. The points of reference distance were calculated 5 times on prototype as well as five duplicate models using a three-dimensional CNC of high-precision measurement machine. The average distance disparities between the duplicate models and prototype were calculated. The dental castings were calculated with a three-dimensional surface-scan machine equipped with the splitting laser beam known as VMS-150RD, UNISN, Japan. The system included a slicing laser projector, 2 CCD (charge-coupled device) cameras, a mounting unit with the auto-rotating feature, and one PC (Figure 3(a)). An X-axis resolution had been 0.01 mm, while the 0.1 mm resolution of the Y-axis.

A three-dimensional shape system of data-analysis composed of (Zx1, Intergraph) graphic workstations (Surfacer, Image ware) data-processing and -analyzing software and (Visual C++ 5.0, Microsoft), a newly constructed numerical and analytical program was utilized to demonstrate the limited helix axis.

Dental casts were scanned with three orientations to decrease blind areas by rotating the auto-rotational positioning unit of the computational tools. The post-processor combined the three data files into a single file (Figure 3(b)). It was used to test the measurement precision of the three-dimensional measuring equipment by measuring a calibration plane plate, and the best-fitted equation for plane was derived on all data inside about 73 seconds utilizing the least-squares approach. The most significant divergence between the projected plane and the actual data was used to assess the measurement accuracy. The placement of dental cast on auto-rotating modules remained random while scanning. A standard coordinate system must be built to predict tooth-arrangement three-dimensionally relying on the three-dimensional shape. Many fixed components known to every model had been chosen as superimposition points of reference. This study selected the maxillary 1st molars as registered components as they had been relatively stable after treatments. Registration conducted automatically (automatically, registration was built-in Surfacer software function). Figure 4 depicts the pre- and post-treatment normalized three-dimensional shape data for maxillary teeth.

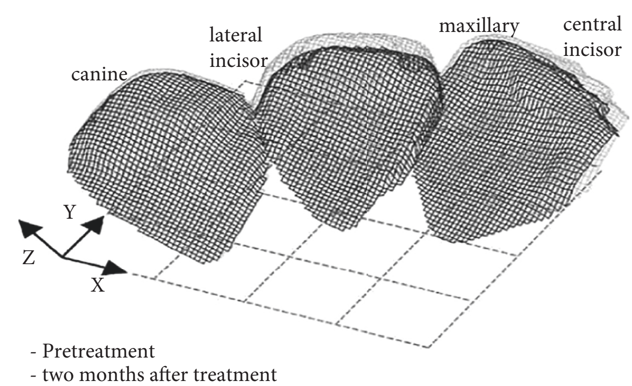

Figure 4: Before and after treatment view of a normalized three-dimensional anterior teeth. Black represents before treatment, and gray represents two months after the therapy.

3.2. Difference between Maxillary and Frontal Teeth Normalized Images. The difference between maxillary and

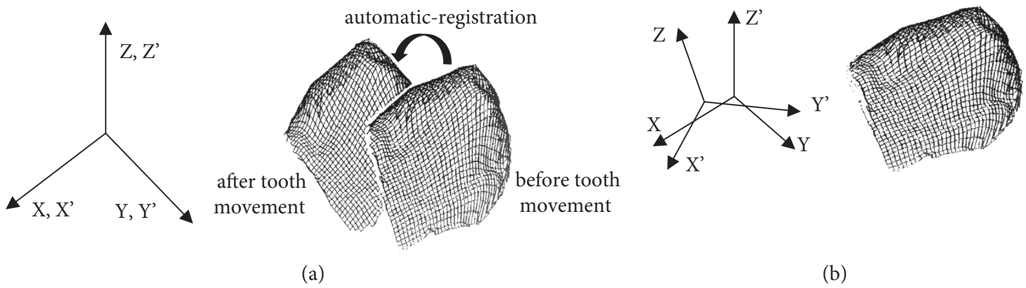

FIGURE 5: A coordinate system of automatic registration for assessing tooth arrangement is known as before-&-after registration. The coordinate systems ($x0$, $y0$, $z0$) and $P(x,y,z)$ adhere to tooth arrangement before-&-after.

frontal teeth normalized photos was defined as the tooth arrangement. A vector of translation and a matrix of rotation generated by adding the three-dimensional shapes before as well as after tooth arrangement could be utilized in (Figure 5) to represent the arrangement of a single tooth. Employing the least-squares technique to investigate the error of mean fitting for an automated registration of three-dimensional structures, a mean three-dimensional distance with every tooth point towards its closest neighboring point seen between points' sequences on the two registered forms was determined for every treatment point [34]. In the existing investigation, we employed a minimization strategy utilizing commercially using software to build a rotation matrix from autonomously recorded location data, and after, we also used the resulting matrix to predict the helical axis. After movement, every point of P (x^0, y^0, z^0) on the three-dimensional form was represented in the system of coordinate X, Y, and Z as a factor of six translations as well as rotation constants. So, Figure 3 depicts the three-dimensional dislocation of $P(x,y,z)$ with three-dimensional form prior to movement.

The formula is determined by

$$m = An + o, \tag{1}$$

where A depicts the 33-rotation matrix, m represents the arbitrary point position vector after the tooth arrangement, n shows the position vector of arbitrary point before arrangement, and o depicts translation vector. After that, tooth arrangement in three-dimensional space was identified as a p displacement vector with $(x' - x)$, $(y' - y)$, & $(z' - z)$ components. This motion includes both rotation and translation. Equation (2) is used to describe the (P) displacement vector.

$$p = (A - K)n + o. \tag{2}$$

K depicts the unit matrix that is also an initial coordinate's function. The 33 matrix A represents the all-around rotation axis that passes through the origin as well as parallel to a limited helical axis. Because the displaced vector p only runs parallel towards the limited helical axis and therefore is undisturbed by rotations for locations on this axis, this axis position has been given by

$$p = A^T p. \tag{3}$$

As a result, Equation (2) is multiplied by the AT and also applying the relationship within Equation (3).

$$(A - K)n + o = (A - K)n + A^T o. \tag{4}$$

Equation (4) becomes

$$\left(A + A^T - 2K\right)n + \left(K - A^T\right)o = 0. \tag{5}$$

Equation (5) becomes

$$\frac{d}{db} = \left\{\left((A - K)n + o^T (A - K)n + o\right)\right\} = 0. \tag{6}$$

This produces the locations n with the smallest displacements and resides on the limited helical axis. The relationship in Equation (6) holds at all positions along the helix axis. Though not distinct, the solution may be achieved by swapping the value for the component of Z.

When the b has been selected on a limited helix axis, as calculated by Equation (1), it is also on the same axis. A translation p with a limited helical axis equals to the distance between a and b. Following that, an arbitrary point d_0 was picked outside of a helix axis, and also its location after arrangement of tooth d_1 had been determined once again using Equation (1):

$$d_1 = Ad_0 + o. \tag{7}$$

Further, the d_0 and d_2 ($d_2 = d_1 - v$) orthogonal projection on helical axis calculated as

$$q' = q + \frac{(d - q).h}{h.h} h, \tag{8}$$

wherein q^0 is a point's position vector on the helical axis, q depicts any point's position vector on helix axis, d is either d_0 or the d_2, and the helical axis direction. Thus, this angle of rotation within space around a limited helical axis is just like angle among d_0, q^0, and d_2.

4. Results

Dental cast means the error was 0.07 mm from the incisor of right-center towards right 1st molar, 0.05 mm towards left 1st molar, and 0.04 mm for both the right and left 1st molars, showing that the die stone had slightly expanded during the setting process. Their standard deviations remained 0.04 mm or less. The three-dimensional measuring instrument has a

Table 1: Maximum errors also known as fitting error for the automated registration employing the method of least squares (mm).

Stages	Canine	Central incisor	Lateral incisor
T0–T1	0.05	0.05	0.05
T1–T2	0.04	0.04	0.04
T2–T3	0.03	0.02	0.02
T3–T4	0.02	0.03	0.03
Mean	0.04	0.05	0.05

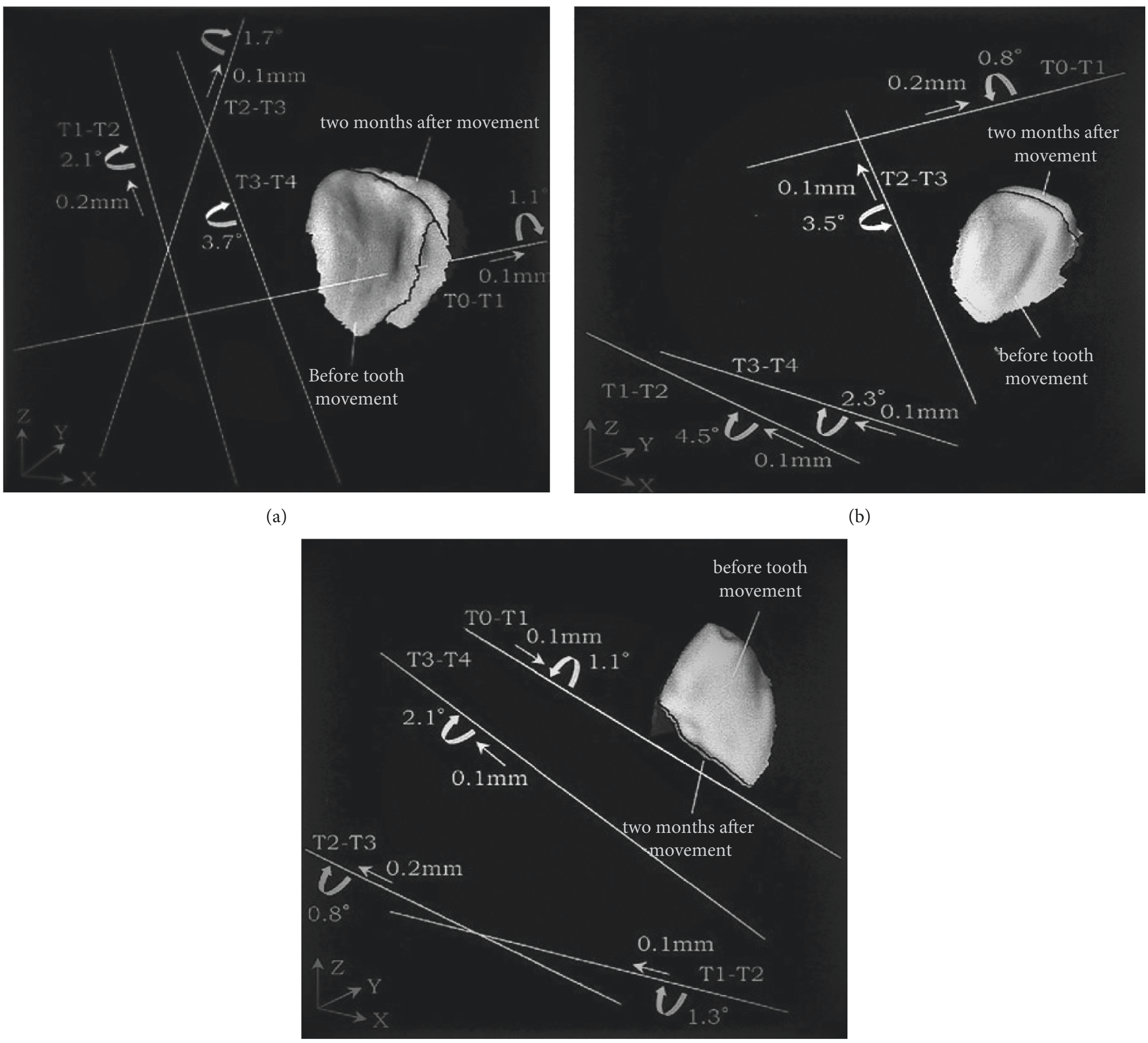

Figure 6: Graph depicting the three-dimensional displacement of the maxillary right centralized incisor, canine as well as lateral incisor during two months of therapy. The angle of rotation and amount of translation with a helical axis is++ used to indicate tooth movement. T0: shortly before device application; T1: instantly after device implementation; T2: Ten days of treatment; T3: one month of treatment; T4: Two months after therapy. The white bar represents the rotation axis; the curved arrow represents the rotation angle; and the little straight arrow represents the translation amount.

seven 0.05-mm measurement accuracy. The lateral incisor, centralized incisor, and canine had to mean fitting errors of 0.05, 0.05, and 0.04 mm, correspondingly (Table 1). The helix axis of the right central incisor would be within the crown and almost orthogonal to lingual surface of crown throughout T0 to T1 (Figure 6(a)). An angle of helical axis

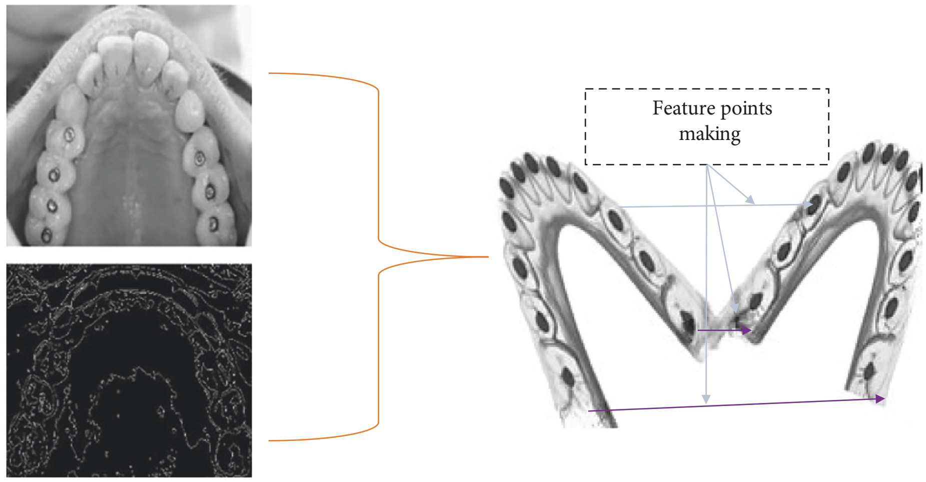

Figure 7: Proper articulation of dental prototypes.

rotation had been 1.11, and the lingual translation became 0.1 mm. In the first ten days of therapy, this helical axis migrated almost orthogonal to the occlusal plane (T1 to T2). Their occlusal translation approximated 0.2 millimeters and 2.11 degrees of the rotation angle. From ten days to one month after therapy (T2 to T3), the helix axis migrated labially and was almost parallel to tooth's long axis. The occlusal displacement gave 0.1 millimeters and 1.71° rotation angle. Their helical axis migrated palatially from one to two months after therapy (T3 to T4) and was approximately parallel to a helical axis through T1 to T2.

The translation was minimal, and the angle of rotation was 3.71. These data imply that immediately after the device was implanted, the center incisor translated considerably labially along with palatal tilt, then twisted histologically and pointed labially with the intrusion. The maxillary helical axis of the right lateral incisor was outside from crown and also was about 451 to the tooth's long axis from T0 to T1 (Figure 6(b)). The labio-occlusal translation measured value was 0.2 millimeters, and the rotation angle became 0.81°. From T1 to T2, a lateral incisor migrated significantly. At the root surface, the helix axis changed and nearly paralleled to the occlusal plane. Their distal translation approximated 0.1 millimeters, and the rotation angle was 4.51°. The helix axis of the tooth migrated towards the disto-palatal axis with a twist of 3.51 and an occlusal movement of 0.1 millimeters from T2–T3. T3–T4 saw a similar shift in the helical axis of T1–T2. The distal translation approximated 0.1 millimeters, and the angle of rotation became 2.31°. Its lateral incisor first inclined palatal, later labially by the intrusion, twisted mesio-labially, and ultimately slanted labially with invasion with these data. The helical axis of maxillary right canine was nearly parallel towards an occlusal plane during T0–T4, while direction of rotation and translation altered after T1 (Figure 6(c)). These actions included jiggling of labio-lingual.

5. Discussion

In this work, we used a screw axis, also known as a helical axis, to measure the three-dimensional motion of a solid body to investigate the arrangement of specific teeth compared to standard teeth [35, 36]. Woltring cross-validation method [37] illustrated that the angle of rotation and translation has become relatively well-focused. Still, the direction and position of the helix axis has been greatly sensitive to calculations errors of landmarks, particularly for the little rotations, the long distances towards the center of gravity mean of the monuments, and also small monument sizes of distribution. In the current work, we studied dental cast repeatability, the measurement precision of three-dimensional system of surface scanning, and a maximum superimposition error employing least-squares technique, and all errors would be within 0.05 millimeter range.

The number of orthodontic tooth arrangements differs across patients and therefore is determined by the force direction, moment–force ratio, force magnitude, and periodontal tissue quality [31]. The horizontal arrangement of a buccal cusp points of the maxillary premolars under a constant force of 0.5 N was calculated towards being 1.7 mm (ranging 0.5–3.4 mm) and 4.3 mm (range 2.7–7.1 mm), correspondingly, after 4 and 7 weeks. After four weeks, the tooth arrangement varied from 0.2 to 2.2 mm when a pressure of 1 to 1.5 N had been implemented towards the maxillary canine [38]. As a result, the current method's accuracy is enough to examine the orthodontic tooth arrangement. As shown in (Figure 7), when the feature points of camera photos are matched, the dental prototypes are appropriately articulated.

Translation (movement of the body), rotation (tipping motion), or a mixture of the two is caused by orthodontic force. The model of tooth arrangement is established by how the force's route of action correlates to the teeth's center of reluctance [27]. Traditionally, 1 or 2 two locations in the teeth were selected as points of reference [39], and the center of rotation position defined the final tooth arrangement [40]. When a horizontal force is given to the lingual surface, it induces simple rotation (tipping) along the root's bottom half. The present research clearly shows that the arrangement of orthodontic tooth is complex and varies greatly from past study data, specifically in severe crowding. The original tooth position and force applied to the teeth, and the

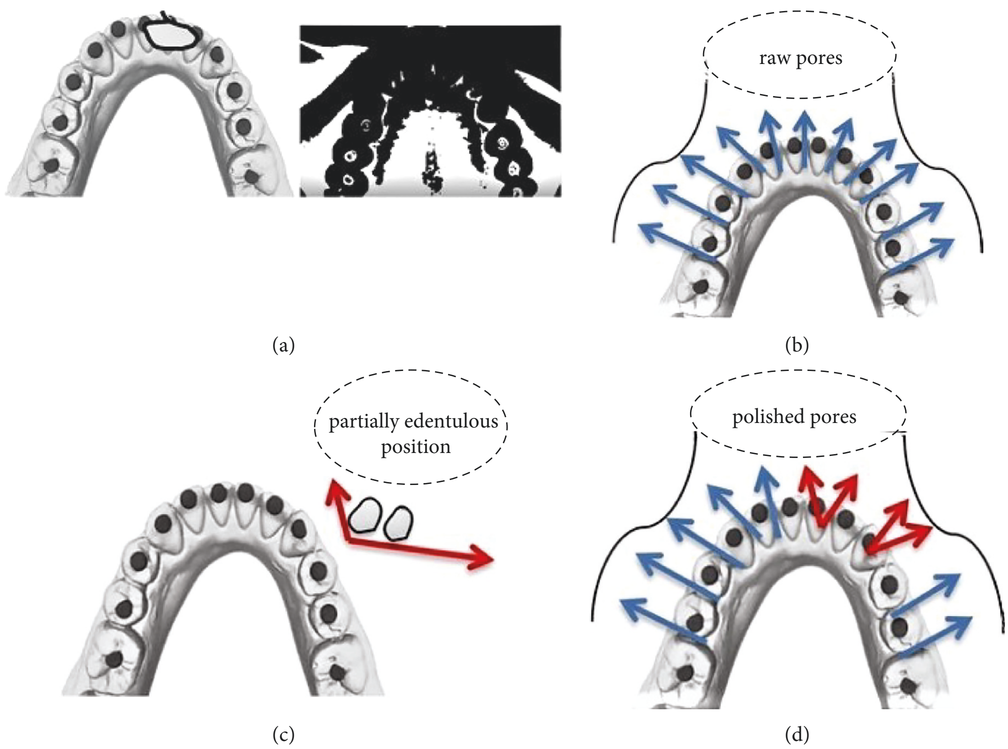

Figure 8: (a) Image selection for dental image classification. (b) Unprocessed image. (c) Edentulous area. (d) Extensive sequence.

contact conditions and movement behavior of surrounding teeth all influence orthodontic tooth arrangement. Surprisingly, the rotational axis position changed significantly throughout treatment stages, even though this was assumed that the rotational axis location would change gradually and consistently during tooth arrangement. Nevertheless, part of the axis variability might be attributable to measurement mistakes. A complete investigation of the accuracy of the axis parameters utilizing a new setup of the experiment would be required. The four stages of tooth arrangement and sequences are shown in Figure 8.

In this work, we created a new way to analyze orthodontic tooth arrangement that may provide orthodontists with accurate visual data on the tooth arrangement and may be a helpful strategy for developing an orthodontic technique. Moreover, three-dimensional data on teeth arrangement during therapy would enable orthodontic tooth-arrangement modeling, which might be included in treatment planning. The better architecture and the cheap treatment of orthodontic tooth arrangement would be an area of interest in future.

Data Availability

The labeled datasets used to support the findings of this study are available from the corresponding author upon request.

Conflicts of Interest

The authors declare no competing interests.

Acknowledgments

This work was supported by the Ningbo Stomatology Hospital.

References

[1] H. Jokar, G. Rouhi, and N. Abolfathi, “The role of PDL-cementum enthesis in protecting PDL under masticatory loading: a finite element investigation,” *Journal of Mechanics in Medicine and Biology*, vol. 21, no. 7, 2021.

[2] Z. Usmanova and E. Sunbuloglu, “An in-silico approach to modeling orthodontic tooth movement using stimulus-induced external bone adaptation,” *Journal of the Mechanical Behavior of Biomedical Materials*, vol. 124, Article ID 104827, 2021.

[3] Y. Jiang, Y. Guan, Y. Lan et al., “Mechanosensitive Piezo1 in periodontal ligament cells promotes alveolar bone remodeling during orthodontic tooth movement,” *Frontiers in Physiology*, vol. 12, 2021.

[4] V. Krishnan and Z. e. Davidovitch, “Biological basis of orthodontic tooth movement,” *Biological Mechanisms of Tooth Movement*, John Wiley & Sons, Ltd, Hoboken, NJ, USA, pp. 1–15, 2021.

[5] M. Yamaguchi and G. G.-B. M. of Tooth, *Inflammatory Response in the Periodontal Ligament and Dental Pulp during Orthodontic Tooth Movement*Wiley Online Libr, 2021, https://onlinelibrary.wiley.com/doi/abs/10.1002/9781119608912.ch4.

[6] M. Kaneko, “Spatiotemporal profiles of somatosensory and insular cortical responses to mechanical stimulation of the periodontal ligament during experimental tooth,” 2019, https://m.repository.nihon-u.ac.jp/xmlui/bitstream/handle/11263/1549/Kaneko-Mari-3.pdf?sequence=3&isAllowed=y.

[7] T. Gong, B. C. Heng, J. Xu et al., "Decellularized extracellular matrix of human umbilical vein endothelial cells promotes endothelial differentiation of stem cells from exfoliated deciduous teeth," *Journal of Biomedical Materials Research Part A*, vol. 105, no. 4, pp. 1083–1093, 2017.

[8] K. L. Hughes and D. D. Gaffin, "Investigating sensory processing in the pectines of the striped bark scorpion, Centruroides vittatus," *Invertebrate Neuroscience*, vol. 19, no. 3, p. 9, 2019.

[9] M. Kaneko, S. Fujita, N. Shimizu, and M. M.-B. Research, *Experimental Tooth Movement Temporally Changes Neural Excitation and Topographical Map in Rat Somatosensory Cortex*Elsevier, 2018, https://www.sciencedirect.com/science/article/pii/S0006899318303500.

[10] K. R. Moss, A. E. Johnson, T. S. Bopp et al., "SARM1 knockout does not rescue neuromuscular phenotypes in a Charcot-Marie-Tooth disease Type 1A mouse model," *Journal of the Peripheral Nervous System*, vol. 27, no. 1, pp. 58–66, 2022.

[11] A. Alagu Rathi Bharathi, K. Yuvaraj Babu, and K. G. Mohanraj, "Vestigiality of wisdom teeth in relation to human evolution and lifestyle modification: a cross-sectional study," *Drug Invention Today*, vol. 10, no. 10, p. 1899, 2018, https://search.ebscohost.com/login.aspx?direct=true&profile=ehost&scope=site&authtype=crawler&jrnl=09757619&AN=131602159&h=3CQattnUMOuWZcuTtS6rgy0dXCbBvgHdfjSnj4lLczBLgOU6VNjKp2JRziZwL6d1CKH28l6Z5XBJxXAy61VoAQ%3D%3D&crl=c.

[12] A. Asif, K. Meenakshi, P. Vikas, M. Saransh, and A. Professor, "Prosthodontic care for edentulous patients with Parkinson disease," *Case Ser. Ann. Essences Dent.*vol. IX, 2017.

[13] W. E. Roberts and C. J. Goodacre, "The temporomandibular joint: a critical review of life-support functions, development, articular surfaces, biomechanics and degeneration," *Journal of Prosthodontics*, vol. 29, no. 9, pp. 772–779, 2020.

[14] K. Nakakura Ohshima, *The Effects of Reducing the Root Length by Apicoectomy on Dental Pulp Revascularization Following Tooth Replantation in Mice*Wiley Online Libr, 2021, https://onlinelibrary.wiley.com/doi/abs/10.1111/edt.12679.

[15] M. G. Sghaireen, "Effect of verbal and visual information on the level of anxiety among dental implant patients," *The Journal of Contemporary Dental Practice*, vol. 21, no. 8, pp. 846–851, 2020.

[16] M. S. Sommers, "Santa claus, the tooth fairy, and auditory-visual integration," *The Handbook of Speech Perception*, John Wiley & Sons, Ltd, Hoboken, NJ, USA, pp. 517–539, 2021.

[17] R. Bjering, L. Sandvik, M. Midtbø, and V. Vandevska-Radunovic, "Stability of anterior tooth alignment 10 years out of retention," *Journal of Orofacial Orthopedics/Fortschritte der Kieferorthopaedie*, vol. 78, no. 4, pp. 275–283, 2017.

[18] M. Huang, H. Ye, H. Chen et al., "Evaluation of accuracy and characteristics of tooth-color matching by intraoral scanners based on Munsell color system: an in vivo study," *Odontology*, pp. 1–10, 2022.

[19] L. Gao, T. Xu, G. Huang, S. Jiang, Y. Gu, and F. Chen, "Oral microbiomes: more and more importance in oral cavity and whole body," *Protein & Cell*, vol. 9, no. 5, pp. 488–500, 2018.

[20] J. Brandt, S. Nelson, H.-C. Lauer, U. von Hehn, and S. Brandt, "In vivo study for tooth colour determination-visual versus digital," *Clinical Oral Investigations*, vol. 21, no. 9, pp. 2863–2871, 2017.

[21] A. Y. Patil, N. R. Banapurmath, B. B. Kottershettar, K. Lekha, and M. Roseline, "Limpet teeth-based polymer nanocomposite: a novel alternative biomaterial for denture base application," *Fiber-Reinforced Nanocomposites: Fundamentals and Applications*, pp. 477–523, 2020.

[22] M. Alcañiz, F. Chinesta, S. Albalat, V. Grau, and C. Monserrat, "A new system for 3D planning of orthodontic treatment and 3D tooth movement simulation," *Computer Methods in Biomechanics and Biomedical Engineering*, vol. 2, pp. 645–654, 2020.

[23] P. Plugmann, "Digitalization in dentistry," *Digitalization in Healthcare*, Springer, Berlin, Germany, pp. 65–71, 2021.

[24] M. Gund, J. Isack, M. Hannig et al., "Contamination of surgical mask during aerosol-producing dental treatments," *Clinical Oral Investigations*, vol. 25, no. 5, pp. 3173–3180, 2021.

[25] K. Cho, J.-H. Sul, M. H. Stenzel, P. Farrar, and B. G. Prusty, "Experimental cum computational investigation on interfacial and mechanical behavior of short glass fiber reinforced dental composites," *Composites Part B: Engineering*, vol. 200, Article ID 108294, 2020.

[26] G. Wei, Z. Cui, Y. Liu et al., "TANet: towards fully automatic tooth arrangement," *Computer Vision - ECCV 2020*, vol. 12360, pp. 481–497, 2020.

[27] L. Hua and P. S. Ungar, "A brief description of the application of dental micro-scar research in paleophagy reconstruction," *Chinese Journal of Anthropology*, vol. 40, no. 2, pp. 292–306, 2021.

[28] C. M. Saratti, G. T. Rocca, and I. Krejci, "The potential of three-dimensional printing technologies to unlock the development of new 'bio-inspired' dental materials: an overview and research roadmap," *Journal of Prosthodontic Research*, vol. 63, no. 2, pp. 131–139, 2019.

[29] H. Schneider, K.-J. Park, M. Häfer et al., "Dental applications of optical coherence tomography (OCT) in cariology," *Applied Sciences*, vol. 7, no. 5, pp. 472–5, 2017.

[30] O. Borrero-Lopez, F. Guiberteau, Y. Zhang, and B. R. Lawn, "Wear of ceramic-based dental materials," *Journal of the Mechanical Behavior of Biomedical Materials*, vol. 92, pp. 144–151, 2019.

[31] A. M. Tahir, M. Jilich, D. C. Trinh, G. Cannata, F. Barberis, and M. Zoppi, "Architecture and design of a robotic mastication simulator for interactive load testing of dental implants and the mandible," *The Journal of Prosthetic Dentistry*, vol. 122, no. 4, pp. e1–389, 2019.

[32] G. Tan, J. Zhang, L. Zheng et al., "Nature-inspired nacre-like composites combining human tooth-matching elasticity and hardness with exceptional damage tolerance," *Advanced Materials*, vol. 31, no. 52, Article ID 1904603, 2019.

[33] Z. Liang, J. Cheng, Q. Zhao et al., "High-performance flexible tactile sensor enabling intelligent haptic perception for a soft prosthetic hand," *Advanced Materials Technologies*, vol. 4, no. 8, Article ID 1900317, 2019.

[34] N. Dai, X. Yu, Q. Fan, F. Yuan, L. Liu, and Y. Sun, "Complete denture tooth arrangement technology driven by a reconfigurable rule," *PLoS One*, vol. 13, no. 6, Article ID e0198252, 2018.

[35] F. Ghazvinian Zanjani, D. Anssari Moin, F. Claessen, T. Cherici, T. Tan, and P. H. N de With, "Deep learning approach to semantic segmentation in 3D point Cloud intra-oral scans of teeth bas verheij 2 BAS@PROMATON.COM," 2019, https://proceedings.mlr.press/v102/ghazvinian-zanjani19a.html.

[36] V. T. Hoang, J. A. Al-Tawfiq, and P. Gautret, "The Tokyo Olympic Games and the risk of COVID-19," *Current Tropical Medicine Reports*, vol. 7, no. 4, pp. 126–132, 2020.

[37] S. Sasaki, H. Koga, T. Krosshaug, S. Kaneko, and T. Fukubayashi, "Kinematic analysis of pressing situations in female collegiate football games: new insight into anterior cruciate ligament injury causation," *Scandinavian Journal of Medicine & Science in Sports*, vol. 28, no. 3, pp. 1263–1271, 2018.

[38] J.-l. Wu, Y.-f. Liu, W. Peng, H.-y. Dong, and J.-x. Zhang, "A biomechanical case study on the optimal orthodontic force on the maxillary canine tooth based on finite element analysis," *Journal of Zhejiang University - Science B*, vol. 19, no. 7, pp. 535–546, 2018.

[39] L. Huanca Ghislanzoni, G. Jonasson, and S. Kiliaridis, "Continuous eruption of maxillary teeth and changes in clinical crown length: a 10-year longitudinal study in adult women," *Clinical Implant Dentistry and Related Research*, vol. 19, no. 6, pp. 1082–1089, 2017.

[40] M. Landova Sulcova, O. Zahradnicek, J. Dumkova et al., "Developmental mechanisms driving complex tooth shape in reptiles," *Developmental Dynamics*, vol. 249, no. 4, pp. 441–464, 2020.

Hindawi
Computational Intelligence and Neuroscience
Volume 2022, Article ID 2872965, 6 pages
https://doi.org/10.1155/2022/2872965

Research Article

The Relationship between Urban Public Art and Regional Environment Based on Wireless Network Technology

Juan Li

College of Art and Design, Shanghai Normal University Tianhua College, Shanghai 201815, China

Correspondence should be addressed to Juan Li; lj2355@sthu.edu.cn

Received 2 March 2022; Revised 5 April 2022; Accepted 6 April 2022; Published 19 May 2022

Academic Editor: Xin Ning

The relationship between urban public art and regional environment based on wireless network technology is studied. Combining domestic specific cases and referring to sociology, art, and design thinking, combing about the relationship between the city's public art and the regional environment, and further integration of its relationship components, at the same time, the planning study of Changning district, Shanghai, and the actual operation of the Shanghai Pudong International Airport, which incorporates the regional mesolevel background, are examples for case analysis. In reference cases and practical cases, they are deduced in sequence, starting from the environmental context of urban areas to the evolution model of public art. Moreover, the specific event background also constitutes a special opportunity period for the sudden growth of public art.

1. Introduction

There are two phases to the development of public art in contemporary China. The first is Hong Kong and Taiwan's earlier experience of absorbing the development of foreign public art and establishing independent institutions to promote the development of urban public art [1]. Furthermore, in recent years, major cities on the Mainland, such as Shenzhen, Beijing, and Shanghai, have actively conducted public art theoretical research and preliminary practical projects. Taiwan began researching and promoting public art such as fire and tea in the early 1990s, and in 1992, the "Regulations on Cultural and Arts Awards" were passed, defining the percentage of public art policies in Taiwan [2]. Every year since 1998, the competent authorities in charge of Taiwan's public art policy and implementation have compiled a "Yearbook of Public Art." Simultaneously, he paid close attention to public art cultural studies, actively organized social resources, and published a large number of related works during Taiwan's development of public art. Hong Kong's public art has followed Taiwan's lead, and it has grown rapidly in the first decade of this century. The Hong Kong Arts Centre serves as the implementing agency for Hong Kong's "Public Art," which was established in 2005 to promote the interaction of the arts, space, and the public. Its goal is to transform Hong Kong into a culturally vibrant metropolis. Interiorly, modern public art was enlightened in the late 1990s and has accelerated development in the last five years [3]. On the one hand, the advancement of public arts is linked to the advancement of the social environment, and on the other hand, it develops rapidly in the context of major historical events such as the Olympics and the World Expo [4].

2. State of the Art

The related topics of public art in China are based on the practical process of combining art with architecture and urban environment in the modernization after the reform and opening up. Whether it is the construction of murals or the development of urban sculptures, public art is involved in contemporary urban construction in various ways. In the face of vigorous development of practice, public art has lagged far behind in theory, breadth, and depth of research. Until the end of the 1980s, a group of well-known artists have conducted in-depth reflection on issues encountered in public art practice. The study of public art theory was first incorporated into the overall framework of contemporary social and cultural development [5]. Despite the fact that there are no monographs on regional environmental and public art relations studies in the publications related to public art, they provide a wealth of argumentation basis and can be roughly divided into four categories based on their contents: textbooks, thematic series, works, and doctoral student publications. Textbooks, whether they are monographs or other monographs, do not place a strong emphasis on problem exploration [6]. Its research aims to guide students in understanding the public consciousness in the social crowd through the concept and characteristics of public art and the design teaching of public art works so that students master a complete theoretical system and design method of public art design and then serve as a public art for students and the foundation of design ability and continuous research ability training [7]. As far as the research of this topic is concerned, these contents are the basic theory and case reference basis for the expansion of public art research. At the same time, from the compilation of a large number of public art related textbooks, it can be seen that public art is becoming a focus of training in domestic universities [8].

3. Methodology

3.1. Performance Analysis Algorithm Based on Key Chain Wireless Sensor Network Management Solution. It is possible that the above system will satisfy the security requirements of group key management in sensor networks [9–11], such as group key confidentiality, forward secrecy, and backward secrecy. We select k objects from n data objects to serve as the initial clustering centers and then group the other objects together based on how similar (or how far they are from these cluster centers) they are to these cluster centers (represented by the cluster center). Following that, the new cluster center value should be calculated (that is, the average of the objects in each cluster). This is repeated until the criteria function is no longer divergent. K objects $c_1, c_2, \ldots, c_K$ are randomly selected from the set of n objects $\{x_1, x_2, \ldots, x_n\}$ as the center of the initial K sets of clusters. Taking K objects $c_1, c_2, \ldots, c_K$ as the center, each object is divided into the most similar collection. The specific division principle is as follows: if $\|x_i - c_j\| < \|x_i - c_m\|, \quad m = 1, 2, \ldots, K; i = 1, 2, \ldots, n$ and $j \neq m$ divide x_i into the collection C_j. We calculate the average of the objects in each newly-collected object collection: $\overline{x_i} = 1/n_i \sum_{x \in C_i} x, i = 1, 2, \ldots, K$, where n_i is the number of objects in the collection C_i, so $C_i = \overline{x_i}, i = 1, 2, \ldots, K$. Calculation criterion function E is

$$E = \sum_{i=1}^{k} \sum_{x \in C_i} \left\| x - \overline{x_i} \right\|^2. \tag{1}$$

As a last resort, it is proceeded through step 2 until E does not appear to be changing any more. Because it is simple and rapid, the K-means algorithm [12] is a common solution for tackling the clustering problem. As a result, the approach is very scalable and efficient for processing big data sets, with a complexity of (n.k.t), where n is the total number of objects processed, k is the total number of clusters processed, and t is the total number of iterations processed. In the vast majority of circumstances, $k + n$ and $t + n$ are employed. The K-means method, on the other hand, has some shortcomings, including the following: because of the initial cluster center selection, it is possible that the K-means algorithm will converge to the local optimal solution before it is ready. When dealing with "noise" and outlier data, it is extremely sensitive, and even a small bit of it can have a significant impact on the average. The frequency distribution is defined as the distribution of the number of random events that occur in a certain number of trials (n trials in total). Variance is defined as the arithmetic mean of the square of dispersion. Specifically, the difference between each data in a group of data and the average of the group squared, summed, and divided by the number of data, represented by σ_X^2. Its definition formula is

$$\sigma_X^2 = \frac{\sum (X - \overline{X})^2}{N}. \tag{2}$$

Among them, $X - \overline{X}$ represents the dispersion (that is, the difference between each data and the average), $\sum (X - \overline{X})$ represents the sum of deviations, and N represents the total frequency. The standard deviation is the square root of the dispersion and the average square root. The square root of the variance, represented by σ_X. Its definition formula is

$$\sigma_X = \sqrt{\frac{\sum (X - \overline{X})^2}{N}}. \tag{3}$$

The standard deviation and variance are two fundamental markers of variation between two groups. It is important to square and make the variance a positive number since the dispersion of each data point and the average is positive and negative, but the unit of data is also squared; therefore, the variance must be made positive. It is necessary to reopen the square in order to make the unit of difference quantity consistent with the original data. The skewness and kurtosis coefficients are statistics that are used to describe the characteristics of a data distribution. This has resulted in the inability to recover the group session key that existed prior to its inclusion. A steady-state distribution model of the Markov chain [13] is first provided in order to examine the computational overhead of the sensor nodes in the scheme, as well as the communication overhead between the key server and the nodes. A wireless sensor network's channel instability, which occurs when a node gets the key distribution message, might result in the loss of group key distribution message packets or the failure of authentication. These two events are deemed to have the same probability of occurring and can be treated as separate random events in this scenario. Because of this, it is simple to describe the key buffer status of each sensor node using a one-dimensional Markov chain, as seen in Figure 1. The state of the node $\alpha = (\sum (X - \overline{X})^3/N)/\sigma_X^3$ represents the key buffer in the node, among other things.

When a key distribution message packet is lost or when a key update message event is successfully received [14], the node status is passed to the receiving node. If the frequency distribution is not normal, then the skewness coefficient and the kurtosis coefficient can be used to determine whether or not the distribution is normal. The following is the formula for determining the skewness coefficient when working with raw data:

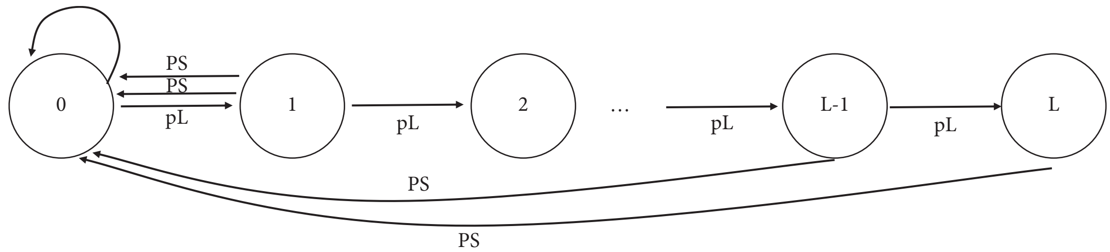

Figure 1: Diagram of sensor node state transitions.

$$\alpha = \frac{\sum (X - \overline{X})^3 / N}{\sigma_X^3}. \tag{4}$$

Among them, α denotes the skewness coefficient, X denotes the original data, $\overline{X}$ denotes the average number, N denotes the total frequency, and σ_X denotes the standard deviation when $\alpha = 0$, indicating that the frequency distribution is in a symmetrical shape, which is in accordance with the normal distribution. When $\alpha > 0$, the frequency distribution was positively skewed. When $\alpha < 0$, it shows that the frequency distribution is negatively skewed. When using the raw data to calculate the kurtosis coefficient, the formula is

$$\beta = \frac{\sum (X - \overline{X})^4 / N}{\sigma_X^4} - 3. \tag{5}$$

Among them, β represents the kurtosis coefficient, X represents the original data, $\overline{X}$ represents the average number, N represents the total frequency, σ_X represents the standard deviation, and the distribution has a normal peak. When $\beta > 0$, the distribution showed a high narrow peak, at which time the average frequency around the ratio was large. The distribution pattern is highly narrow. The relationship between the urban public art and the regional environment is first considered in its entirety, and it is related to the development of the city. Different periods of urban appeal and development have a great influence on the degree of public art. The specific integration into the urban system, with the driving force as the reference point, reflects the relationship between the urban public art and the environment. There are mainly several modes: the government-planned policy promotes the development of the regional cultural image. The method of shaping public art as an image is concentrated in the municipal squares, streets, and parks. Here, the public art represents the regional environmental aesthetics business card and the values of regional culture; the specific events are temporary breakout points. At the emergence of public art sprawl in specific areas, such core areas of public art are mainly associated with specific space backgrounds such as the Olympic Park and Expo landscape belt; there is also a combination of specific cultural site backgrounds, such as universities and monumental parks, with cultural self-building and social communication as the driving force, from the inside out public art divergent setting.

3.2. The Constitutive Relationship between Public Art and Regional Environment. John Ayer and Rigoberto Tols have been creating public art in the South Bronx of New York for 13 years. This community is the poorest area in New York City. Violence, drug abuse, and home destruction are commonplace here. Aahan and Tols used the method of living to overturn and convert the most common residents of the community into a single statue, and part of it was permanently hung on the walls of the neighborhood. Residents are honored to be able to reappear in the works of the artist and have a new experience and understanding of their own life. Maybe art does not change the living habits of these people. However, they have changed the narrow and closed concept of space here, which has transformed the residents here towards openness. Obviously, what Ai Heng and Tols pursued was not the "artistic" effect of the work but the "social" effect; the problem they were trying to solve was not the issue of beautifying the city and beautifying the environment, but rather a social issue that was due to race. The artist advocated both the affirmation of cultural diversity and the spirit of tolerance for different cultures through this creative activity, as well as demonstrating profound humanistic care for society's bottom population. The civil society places a premium on the exercise of public rights. On the people's petition, the "oblique arc" sculpture on the welfare square in front of the Manhattan Federal Office Building mentioned in Chapter 2 was demolished. Designer Serra, on the other hand, filed a lawsuit in court, claiming that this was a violation. The First Amendment Act guarantees the right to freedom of expression. The Court of Appeal, on the other hand, recognized Serra's right to freedom of expression in principle while also arguing that Serra had already relinquished his right to freedom of expression when he turned the work over to the General Services Administration. The term "slope arc" refers to property rather than expression. Some important issues in public art are addressed in the "oblique arc" debate, such as the artist's right to express, public choice, and artistic expression under the constraints of property rights. This kind of property rights and public rights awareness not only drew attention in the United States several decades ago, but it is now increasingly influencing the realization of public art in today's domestic situation. Although most people were familiar with Shanghai Pudong International Airport's "Day at the Airport" series of scene sculptures, some passengers

Table 1: Population characteristics of Changning district.

Classification	Population	Percentage of total population (%)	Compared to the previous census (%)	Ratio of the whole city (%)
65 and older	9.75 million	14.12	1.38	4
0–14 years old	4.80 million	6.95	4.24	1
All ethnic minorities	0.99 million	1.43	0.57	0.2
University level (college or above) population	25.73 million	37.26	18.04	1
Resident population	17.54 million	25.39	7.82	13

reported to the appropriate departments that one set of sculptures placed in chairs was occupying passengers. The rest, space, although the sculpture was not removed under the interpretation of coordination, it can be seen that the public is more sensitive to their own awareness of social rights, which also necessitates more careful consideration of space in the design and implementation process of public art. In China, the composition of human rights provides a more respected artistic experience for the general public. Citizens' spiritual needs are met first and foremost by contemporary urban public arts, which also promote the interaction of artistic needs. That is to say, artists use public works that are full of artistic appeal and cultural thinking to materialize social culture and public civilization in the form of public art. The public's cultural cognition is enhanced by people's cultural understanding, resulting in a socialized cultural artwork.

4. Result Analysis and Discussion

The relationship between public works of art and the environment is concerned, because the nature of the environment derived from the creation of public art is important, but this environment linkage does not need to be stereotyped as the inevitable requirements. The key is whether the installation of the work is to create a social significance for the public for the purpose of the aesthetic environment. As a result, this paper investigates and calculates using Shanghai as an example. Changning District has a permanent population of 690,600 people, 242,900 households, and an average household population of 2.49 people, according to the 2010 National Population Census results; daily residents are 334,600 men. There were 356,000 females, 21,400 more than males.

In addition to displaying basic population density data, these basic demographic data also provide some characteristics of the population environment in Changning District for the study of the project: the aging population tends to show a growing trend; the education level of the population is high; the population environment is diversified. The population has increased, the population of ethnic minorities has increased, and there is a relatively concentrated foreign population; the female population is high; the family size is small (Table 1). Therefore, focusing on the cultural life of the middle-aged and elderly people in the community as a background is a focus of public art; the protection of the local culture and the cultural context display will constitute a useful bridge between nonwoodland residents and communication; the scale of the family shows that the residents' attention to outdoor cultural life will be higher. As the East Hongqiao Business District has grown mature, its personnel education background should be higher than this average plan, which means that Hongqiao Business Centre as the energy of smart highlands will be more abundant; therefore, the artistic construction of this region also has a higher potential demand market. The promotion of public art as a means of promotion in high-quality population activity areas is also a choice to increase the satisfaction of residents in the area, and it is conducive to the formation of a virtuous cycle of comprehensive integration of talents. As is shown in Figure 2, Changning District is a comprehensive residential area with a wide range of areas and nature. From Xinli Residence to Garden House, from the grassroots community to the high-end villa area, the residential category and the nature of the residents are also distinct.

"Public art is the art of planning," says the artist. One of the ways in which it differs from conventional contemporary art and contemporary art in general is that it incorporates conscious methodological knowledge into the design process. This is the first topic to look at the interaction between public art and the surrounding environment in depth. The fundamental conclusion is concerned with the logical chain of this relationship, and the continuation is concerned with the public art methodology that is employed in urban planning. In this article, the program's overall performance is assessed and reviewed. When compared to existing schemes, the key advantage of the suggested system is that group members can choose their own personal secret information without the need for the group administrator to communicate it through a secure channel. Each member of the group is simply required to keep the identity of the persons he or she chooses a secret from the others. When it comes to storage overhead, communication overhead, and security, the performance of this project compares favorably to that of analogous solutions, as shown in Table 1; t is the maximum number of collaborators that can be accommodated by the system, m is the total number of sessions that can be accommodated by the group life cycle, and q is a prime number that matches the cryptographic key specifications. The fundamental mechanism of the layer μ UTESLA protocol is depicted in Figure 3.

Our group members can choose their own personal secret information, as seen in Figure 2, and as a result, each

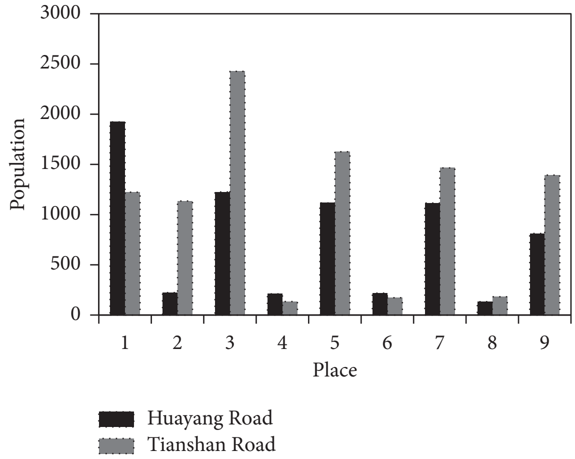

Figure 2: Comparison of population living in different streets in Changning District.

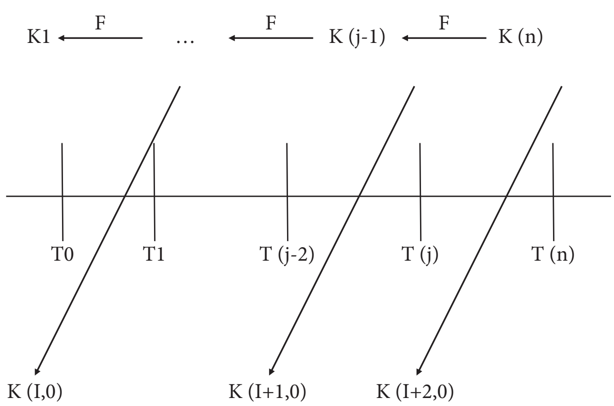

Figure 3: Layered μ TESLA protocol basic mechanism.

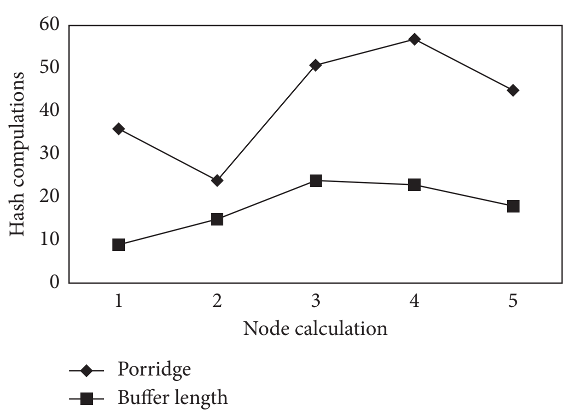

Figure 4: Schematic diagram of calculation cost results of sensor nodes.

group member only needs to keep a personal key of their choice throughout the self-healing key distribution process [15, 16]. It is necessary for scheme group members to maintain individual secret polynomial values that have been distributed by the group administrator, hence keeping the scheme's storage overhead to a minimum. After the parameter p_L changing to a different value, the graph of $E[N^H]$ as a function of the key buffer length l in Figure 4 can be seen in more detail. The average node update per key requires less computing overhead even when the channel packet loss rate is high (for example, $p_L = 0.5$), as illustrated in the diagram.

5. Conclusion

The results of public art reflected in different field backgrounds also have a symmetrical relationship with the environmental background. First of all, from the perspective of the city, the image language of the regional culture conveyed by the public art works depicts a certain aspect of the city image and is a label for the positioning of the city art; furthermore, from the specific regional environment, the public art often defines the vitality center of the region, infecting the public's sense of the environment with cultural cohesion; secondly, the positive energy that public art can transmit is also an important way of guiding social values. The exploration of the mode of public art also drives the corresponding discipline construction; essentially, the most important value of public art is the shaping of social cultural characters and the positive power of citizens' self-value recognition. The public experience is an important criterion for judging the value of public art in the environment. Public perception is a double-edged sword. On the one hand, public experience reflects the social value of public art. On the other hand, it is not enough for public perception. It may also hinder the realization of public art. Therefore, in the practice of public art and environment, we should pay attention to the value of the people's experience, but we should also do a good job of active cultural guidance.

Data Availability

The data used to support the findings of this study are available from the corresponding author upon request.

Conflicts of Interest

The authors declare that they have no conflicts of interest.

Acknowledgments

This research was financially supported by the Key Scientific Research Projects in Shanghai "Practical research on improving the innovation and entrepreneurship ability of students majoring in Arts and design under the background of Digitalization" (No. 2016-SHNGE-12ZD).

References

[1] Y. Wang, "Cultural creation of urban public art from the perspective of environmental aesthetics," *Art and Design*, vol. 3, no. 2, pp. 567–722, 2017.

[2] X. U. Qiwen, W. Luo, and X. Long, "On the urban and rural integration and the construction of regional ecological culture in lianyungang city," *Journal of Huaihai Institute of Technology (Natural Sciences Edition)*, vol. 4, no. 1, pp. 8–30, 2017.

[3] E. Aguirre, P. Lopez-Iturri, and L. Azpilicueta, "Design and implementation of context aware applications with wireless sensor network support in urban train transportation environments," *IEEE Sensors Journal*, vol. 8, no. 9, pp. 1–13, 2016.

[4] Y. Deng, “Research on the relationship between the public art design of the urban subway and the red historical culture——taking nanchang, jiangxi as an example,” *Journal of Jiangxi Science & Technology Normal University*, vol. 6, no. 2, pp. 46–82, 2016.

[5] D. D. Wang, K. B. Lu, and S. O. Business, “Construction of urban vegetable retail distribution network under the environment of regional electricity suppliers——taking Hefei city as an example,” *Journal of Jiamusi Vocational Institute*, vol. 6, no. 1, pp. 574–723, 2016.

[6] R. Tao and W. A. University, “A probe into the functions of urban public environment landscapes,” *Journal of Beijing City University*, vol. 8, no. 2, pp. 458–732, 2016.

[7] T. Guo and S. A. University, “Design of public facilities in urban public environment,” *Packaging Engineering*, vol. 7, no. 12, pp. 5578–5622, 2018.

[8] T. Naumann and S. Golz, “Environmental risks in urban and regional development—assessing the effects of flood resilient technologies,” *Corporate Finance*, vol. 55, no. 4, pp. 77–183, 2018.

[9] M. Eltoweissy, M. Moharrum, and R. Mukkamala, “Dynamic key management in sensor networks,” *IEEE Communications Magazine*, vol. 44, no. 4, pp. 122–130, 2006.

[10] X. He, M. Niedermeier, and H. De Meer, “Dynamic key management in wireless sensor networks: a survey,” *Journal of Network and Computer Applications*, vol. 36, no. 2, pp. 611–622, 2013.

[11] F. Anjum, “Location dependent key management in sensor networks without using deployment knowledge,” *Wireless Networks*, vol. 16, no. 6, pp. 1587–1600, 2010.

[12] K. Krishna and M. Narasimha Murty, “Genetic K-means algorithm,” *IEEE Transactions on Systems, Man and Cybernetics, Part B (Cybernetics)*, vol. 29, no. 3, pp. 433–439, 1999.

[13] C. Nemeth and P. Fearnhead, “Stochastic gradient Markov chain Monte Carlo,” *Journal of the American Statistical Association*, vol. 116, no. 533, pp. 433–450, 2021.

[14] M. Zhang, “Application and research of automatic password update technology based on the development of wireless network,” *Journal of Intelligent and Fuzzy Systems*, vol. 37, no. 3, pp. 3357–3363, 2019.

[15] T. J. Tsitaitse, Y. Cai, and A. Ditta, “Secure self-healing group key distribution scheme with constant storage for SCADA systems in smart grid,” *Wireless Personal Communications*, vol. 101, no. 3, pp. 1749–1763, 2018.

[16] I. Nape, E. Otte, A. Vallés et al., “Self-healing high-dimensional quantum key distribution using hybrid spin-orbit Bessel states,” *Optics Express*, vol. 26, no. 21, pp. 26946–26960, 2018.

Hindawi
Computational Intelligence and Neuroscience
Volume 2023, Article ID 9804502, 1 page
https://doi.org/10.1155/2023/9804502

Retraction

Retracted: Influencing Factors and Improvement Path of Synergistic Value Creation Efficiency of Emerging Enterprises

Computational Intelligence and Neuroscience

Received 25 July 2023; Accepted 25 July 2023; Published 26 July 2023

This article has been retracted by Hindawi following an investigation undertaken by the publisher [1]. This investigation has uncovered evidence of one or more of the following indicators of systematic manipulation of the publication process:

(1) Discrepancies in scope
(2) Discrepancies in the description of the research reported
(3) Discrepancies between the availability of data and the research described
(4) Inappropriate citations
(5) Incoherent, meaningless and/or irrelevant content included in the article
(6) Peer-review manipulation

The presence of these indicators undermines our confidence in the integrity of the article's content and we cannot, therefore, vouch for its reliability. Please note that this notice is intended solely to alert readers that the content of this article is unreliable. We have not investigated whether authors were aware of or involved in the systematic manipulation of the publication process.

Wiley and Hindawi regrets that the usual quality checks did not identify these issues before publication and have since put additional measures in place to safeguard research integrity.

We wish to credit our own Research Integrity and Research Publishing teams and anonymous and named external researchers and research integrity experts for contributing to this investigation.

The corresponding author, as the representative of all authors, has been given the opportunity to register their agreement or disagreement to this retraction. We have kept a record of any response received.

References

[1] M. Liu, G. Wang, and H. Huang, "Influencing Factors and Improvement Path of Synergistic Value Creation Efficiency of Emerging Enterprises," *Computational Intelligence and Neuroscience*, vol. 2022, Article ID 8075349, 10 pages, 2022.

Hindawi
Computational Intelligence and Neuroscience
Volume 2022, Article ID 8075349, 10 pages
https://doi.org/10.1155/2022/8075349

Research Article

Influencing Factors and Improvement Path of Synergistic Value Creation Efficiency of Emerging Enterprises

Mingzheng Liu, Guohong Wang, and Hao Huang

School of Economics and Management, Dalian University of Technology, Dalian, Liaoning, China

Correspondence should be addressed to Guohong Wang; wanggh@dlut.edu.cn

Received 16 March 2022; Revised 6 April 2022; Accepted 8 April 2022; Published 16 May 2022

Academic Editor: Xin Ning

The cooperation between emerging enterprises and different enterprises can stimulate innovation enthusiasm and realize synergistic value creation. At present, there is no regular pattern and rules for synergistic value creation among emerging enterprises, which cannot achieve effective synergistic value creation. Based on the complex network relationship and dynamic model of game evolution among multiple entities of value creation within emerging enterprises, the factors that affect the efficiency of synergistic value creation in the aspect of input, benefit assignment, and interaction mechanism of synergistic value creation are analyzed and then the path of the promotion of synergistic value creation among the entities of new enterprises is studied. The results show that the core enterprises play a leading role in the cooperation input among emerging enterprises, and if the balance of interests among cooperative enterprises is guaranteed, the revenue effect is the best, and the network cooperation density is the strongest. The game evolution shows that, in order to improve the efficiency of synergistic value creation, it is necessary to improve the expected coefficient and number of synergies between enterprises and establish a mechanism for equitable distribution of synergies by strengthening information exchange among enterprises in emerging industries, so as to build an atmosphere of synergies, the complementarity of assets and synergies.

1. Introduction

With the development of economy and society, the demand of the people and the market for different industries are constantly innovating, and different emerging industries are derived. Effective allocation of innovation resources and improvement of innovation efficiency can promote the development of relevant industries [1]. In the process of industrial development, the innovation ability of a single enterprise is limited, and the emergence of synergistic value creation effectively solves this problem. Synergistic value creation in emerging industries is an innovation behavior similar to an alliance, which is based on competition and cooperation between enterprises and mainly includes research and development cooperative innovation, product innovation, and market innovation [2]. Synergistic value creation of emerging industries has the advantage of saving technology transfer and technology exchange costs [3]. When technology spills over between and within industries, enterprises can form innovation alliances to tackle key problems and monopolize the technology within the alliances [4]. As a result, many emerging industries have a very strong motivation on synergistic value creation, and the main causes of competition between enterprises is now more emphasised on the customer knowledge economy, flexibility, rapid response, and the value chain of the internalization and unstructured. However, limited resources will inevitably lead to competition within and among synergistic value creation systems. Different subjects adopt corresponding strategies based on their own development interests, so the strategies of other relevant innovation subjects will also change accordingly [5].

The innovation of emerging industries needs the cooperation of various parties. There are important innovation resources within the industry such as scientific research institutions, governments, and universities. The flow and allocation of resources are the necessary conditions for innovation. Since the process of establishing industrial competitiveness is a process of competing for resources in essence, the innovation subjects must go through a process of evolutionary game. Innovation resources are mainly concentrated in enterprises, while heterogeneous resources such as talents and latest scientific research achievements are concentrated in universities and scientific research institutions. Therefore, in order to fundamentally improve the overall innovation capacity of the industry, effective flow and allocation of resources must be realized first. The emerging industries of China are still in the embryonic stage, so a series of help from the government and intermediary agencies is needed to achieve faster development. Of course, as the subject of innovation itself, strategic emerging industries should learn from each other and develop together. The innovations and contributions of this study are as follows:

(1) Based on the complex network relationship and dynamic model of game evolution among the multiagents of value creation within emerging enterprises, the influencing factors and upgrading path of synergistic value creation among the agents of emerging enterprises are studied.

(2) According to the analysis of historical data, the factors influencing the synergistic value creation of different types of enterprises from the aspects of initial investment, enterprise attributes, and profit distribution are analyzed.

(3) The trajectory of synergistic value creation among different enterprises is studied by means of game evolution and puts forward the path of synergistic value creation according to the changes of different variables, and it has certain practicality.

2. Related Work

In recent years, many experts have studied the theories and measures of synergistic value creation and value enhancement in enterprises. The present situation of synergistic value creation, synergistic method research, and complex network application is studied.

2.1. Collaborative Value Innovation of Enterprises. Frank and Piller believe that synergistic value creation can be defined as the active integration of different parties in the process of value creation within an organization, aiming to bring different parties together to create common valuable results [6]. Schreier proposed that enterprises have unique tangible and intangible resources, which can reduce the risk of failure and the cost of innovation when combined with the resources of service providers [7]. Stephan and Hankammer introduced customer groups and believed that synergistic value creation encourages customers (service consumers) to actively participate in the design and delivery of innovative customized services to meet customers' performance goals, thus greatly reducing the risk of service delivery failure [8]. Doren et al. studied Indian offshore service providers and found that Indian organizations can improve customer retention rate and attract new customers by promoting the acquisition and utilization of network resources through high-quality synergistic value creation with customers and maintaining innovation through close cooperation with customers [5].

2.2. Method and Framework of Enterprise Collaborative Development. Schweizer proposes a framework that facilitates the execution of successful collaborations. Schweizer proceeds to propose a ratio-driven approach and a value-adjustment mechanism, enhancing the probability of successes in pharmaceutical research collaborations [9]. Chesbrough considers open innovation requires collaboration among distributed but interdependent actors who rely on each other's capabilities for value creation and capture. Value in open innovation is driven not only by actors' value creation but also by their ability to capture value [10].

2.3. Complex Network Application. A complex network has a strong application background in the cooperative development of enterprises and government affairs. Arellano proposes a new algorithm to select the relevant nodes that maintain the cohesion of the network of the complex network. The result shows that the proposed approach outperforms degree, PageRank, and betweenness in most of the several real complex networks [11]. Meng proposes a Spearman coefficient reconstruction network (SCRN) method based on the Spearman correlation coefficient. In the SCRN method, we select entities in the real world as the nodes of the network and determine the connection weights of the network edges by calculating the Spearman correlation coefficients among nodes [12].

From the point of the current research status, different countries and enterprise development patterns vary, experts often seek emerging from the successful case enterprise synergy creation combining site and advantage, and it is not the professional model which combined with the actual enterprise development present situation, and it leads the study to one-sided. At the same time, synergistic value creation among emerging enterprises is usually carried out from enterprise types and product business, without analyzing the specific implementation process and influencing factors, resulting in an unclear promotion path of synergistic value creation and a lack of data analysis of evolutionary nature.

3. Analysis on the Influencing Factors of Synergistic Value Creation Efficiency of Emerging Enterprises

3.1. Construction and Evolution of the Complex Network Model. There are two types of emerging enterprises: one is the core enterprise that plays a leading role and the other is the general enterprise that has a certain research and development capability [13]. The connection mechanism of its network architecture is the synergistic relationship between enterprises. The partial schematic diagram of synergistic value creation network of emerging enterprises is shown in

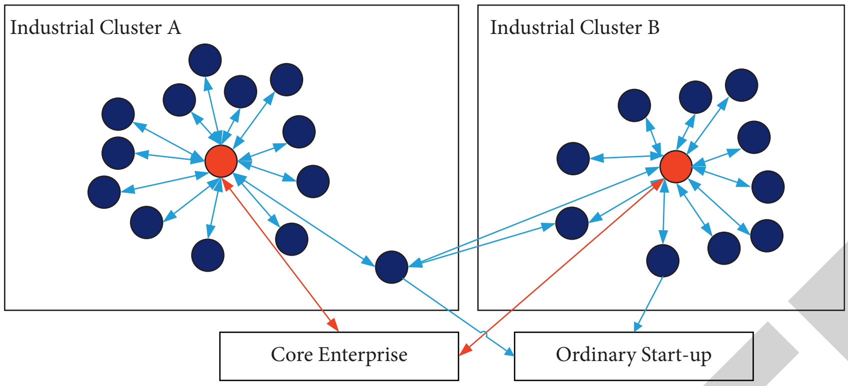

Figure 1: The partial schematic diagram of synergistic value creation network of emerging enterprises.

Figure 1. The blue line represents the coordination and cooperation between ordinary enterprises and core enterprises, while the red line represents the interaction and cooperation between core enterprises.

The evolution process of innovation network mainly includes initial network construction, node entry, and generation of edge and gradually evolves into the corresponding complex system through the continuous growth of network scale. Therefore, based on the initial network formed randomly, this study constructs the synergistic value creation network of emerging enterprises with three types of nodes, namely, $G(V, E)$. V is the set of all nodes in the network, and E is the set of all edges in the network. The evolution rules are as follows:

Step 1. Build the initial network. An initial network with m_0 nodes and edges is generated randomly.

Step 2. For each time step, a new node joins the network. First, set the parameter q, and $0 < q < 1$, then randomly generate the real numbers q', and $q' \in (0, 1)$. When $q < q' < 1$, the probability of this new node connecting to $m_1 (m_1 < m_0)$ node in the global network G is as follows:

$$\prod_i = \frac{k_i}{\sum_{j\in G} k_j}, \tag{1}$$

when $0 < q < q'$, randomly select M node from the current global network to form the LAN. In addition, the probability that the new node preferentially connects to $m_2 (m_2 < M)$ nodes in the LAN L is as follows:

$$\prod_i = \frac{k_i}{\sum_{j\in L} k_j}, \tag{2}$$

where k_i is the degree of any node in the network.

Step 3. Repeat the second step, and do not allow repeated edges and self-connection. Until the network node scale reaches N, the evolution ends.

In this study, the evolutionary mechanism of synergistic value creation of emerging enterprises is shown in Figure 2, which mainly includes synergistic value creation input, benefit assignment, and interaction mechanism.

In the synergistic value creation network of emerging enterprises, the interaction modes between different types of innovation subjects are diverse, which makes the innovation network present a nonlinear cooperative behavior evolution form. In fact, there are cooperative relations and competitive relations between innovation subjects in the network [14]. Cooperative relations are the premise of collaborative innovation activities between subjects, while competitive relations promote game behaviors between subjects. However, in the initial stage of innovation activities, because of the limited rationality of innovation individuals, their game decisions may not be optimal, and they need to constantly adjust and optimize their decisions by learning and imitating other individuals who are better than them, thus forming a dynamic evolutionary game process. From the individual point of view, the game decisions adopted by each innovation subject will affect the benefits obtained by other subjects, which makes the innovation subject with preference characteristics change their own strategies to maximize their own interests. From the overall point of view, innovation subjects are based on a certain learning and imitation mechanism, which makes excellent strategies gradually spread in the innovation network, thus promoting the evolution of the overall cooperative behavior of the network.

3.2. Game Evolution Model of Complex Network Evolution. The evolution of complex networks is influenced by input and benefit assignment. Production input is the basis of cooperation and can analyze the importance of the enterprise. Profit distribution describes the results of synergistic value creation, and the two factors describe the purpose and results of cooperation, respectively. Therefore, the above two factors are selected as evolutionary variables in this model.

3.2.1. Synergistic Value Creation Input Model Construction. In this study, cost and early income jointly determine the production input of game subjects in the cooperation process, and the production input of enterprises in each neighborhood is determined by the following formulas:

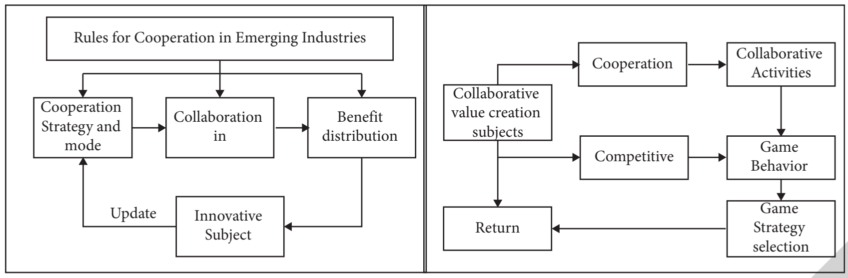

Figure 2: Evolutionary and dynamic mechanisms of synergistic value creation of emerging enterprises.

$$a_{x,y}(t_n) = (1 - w_1)\frac{e^{\alpha \cdot m_{x,y}(t_{n-1})}}{\sum_{i=0}^{k_x} e^{\alpha \cdot m_{x,y}(t_{n-1})}} + w_1 \frac{e^{\alpha \cdot k_x}}{\sum_{i=0}^{k_x} e^{\alpha \cdot k_i}}, \quad (3)$$

$$\sum_{y=0}^{k_x} a_{x,y}(t_n) = C, \quad (4)$$

where the benefit index is $e^{\alpha \cdot m_{x,y}(t_{n-1})} / \sum_{i=0}^{k_x} e^{\alpha \cdot m_{x,y}(t_{n-1})}$, which is the standardized ratio of the income of node x in the neighborhood y to the total income in the neighborhood y; the enterprise importance index is $e^{\alpha \cdot k_x} / \sum_{i=0}^{k_x} e^{\alpha \cdot k_i}$, which is the standardized ratio of the degree of the node x to the sum of the degrees of all nodes in the neighborhood y, reflecting the importance of the node x in the neighborhood. $t_n = 2, 3, \ldots, T$ represents the number of rounds of the game.

3.2.2. Benefit Assignment Model Construction. This study uses the utilization allocation model created by Chen [16]. In this study, the cost and innovation input jointly determine the benefit assignment of the game subjects in the cooperation process, and in order to simplify the model, the evaluation error of enterprise innovation input is ignored here. After the end of the t_nth round of game, the net income of the node x in the neighborhood y is determined by the following formula:

$$m_{x,y}(t_n) = \left[w_4 \frac{e^{\beta \cdot a_{x,y}(t_n)}}{\sum_{i=0}^{k_x} e^{\beta \cdot a_{x,y}(t_n)}} + w_3 \frac{e^{\beta \cdot b_{x,y}(t_n)}}{\sum_{i=0}^{k_x} e^{\beta \cdot b_{x,y}(t_n)}} + w_2 \frac{e^{\beta \cdot k_x}}{\sum_{i=0}^{k_x} e^{\beta \cdot k_i}} \right] \pi_y(t_n) - a_{x,y}(t_n) - b_{x,y}(t_n). \quad (5)$$

According to formula (5), the income distributed by node x in the neighborhood y is jointly determined by its production input index, cooperation input index, and degree index in the neighborhood. β is the regulation coefficient, w_2, w_3, and w_4 respectively represent the degree weight, cooperation input weight, and production input weight of the node x, and $w_2 + w_3 + w_4 = 1$.

After the end of the t_n round of game, the total income of node x in each $k_x + 1$ neighborhood is as follows:

$$M_x(t_n) = \sum_{y=0}^{k_x} m_{x,y}(t_n). \quad (6)$$

3.2.3. Innovation Model Construction. Innovation can reflect the vitality of new enterprises and the value of cooperation. This study evaluates the effect of enterprise cooperation by combining enterprise value cocreation with innovation ability. At present, it is generally accepted at home and abroad to judge the innovation ability of enterprises by measuring the international patent classification number. According to the previous research results of some scholars, innovation ability is often related to "the number of technological innovation projects," "product update speed," "the number of patents," and "customer satisfaction." In this study, the number of patents obtained by enterprises in the recent five years is selected as the standard to measure the innovation capability of enterprises.

3.2.4. Design of Policy Update Rules. At the end of each round of game, each node x randomly selects its neighbor nodes y and compares its total income $M_x(t_n)$ with $M_y(t_n)$ of its neighbor nodes. If $M_x(t_n) \leq M_y(t_n)$, the node will adjust the game strategy and follow the strategy of the node x in the neighborhood y according to a certain probability W. In this study, Fermi updating rule is used to determine the imitative probability.

The variable description is listed in Table 1.

Table 1: The variable description of the model.

Variable	Description
$e^{\alpha \cdot m_{x,y}(t_{n-1})} / \sum_{i=0}^{k_x} e^{\alpha \cdot m_{x,y}(t_{n-1})}$	Benefit index
$e^{\alpha \cdot k_x} / \sum_{i=0}^{k_x} e^{\alpha \cdot k_i}$	Enterprise importance index
y	Neighborhood
$M_x(t_n)$	Total income of x
α, β	Regulation coefficient
t_n	Number of evolution

3.3. Evolutionary Simulation and Analysis of Complex Network Evolutionary Game. The MATLAB simulation platform is used to simulate the evolutionary game model of

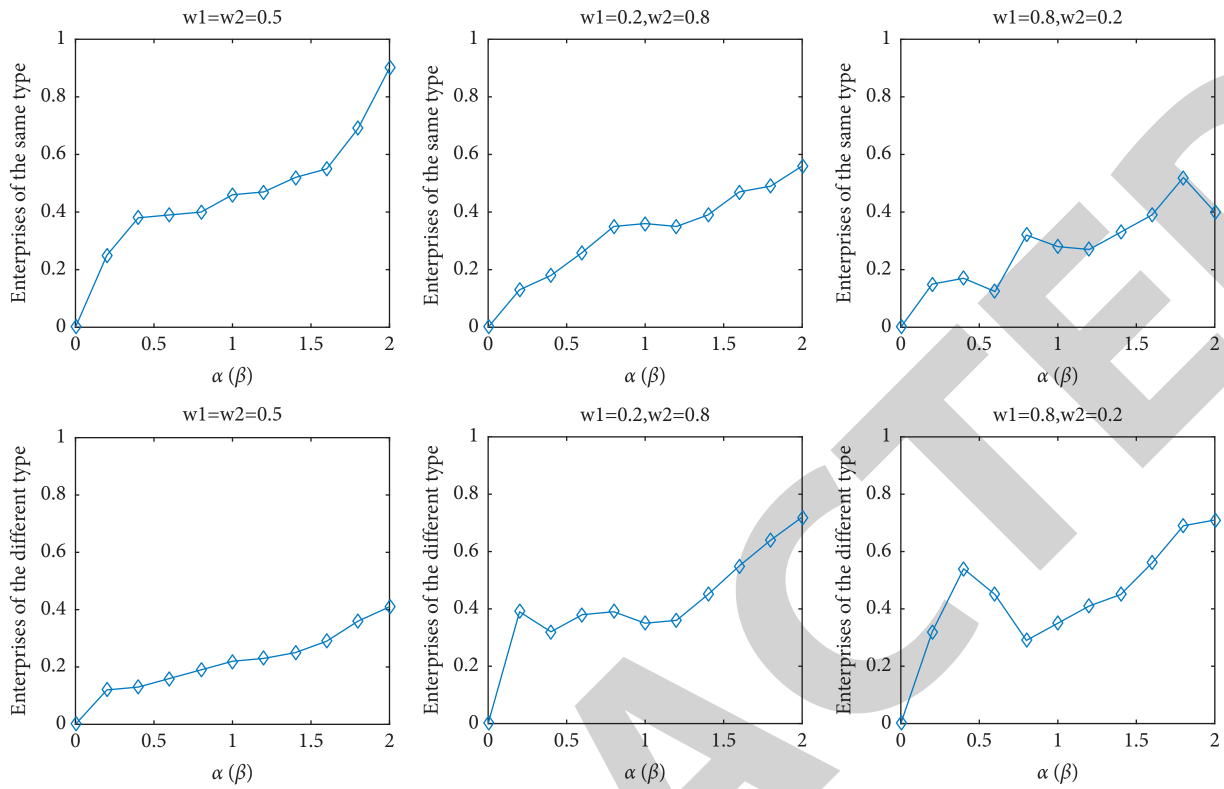

FIGURE 3: Influence of input on network density.

synergistic value creation network of emerging enterprises. The simulation algorithm and related parameters are set as follows.

Step 4. Set the initial parameters of the synergistic value creation network for emerging enterprises. $r = 2$, $\alpha = \beta = 0.5$, $w_1 = w_2$, $w_3 = w_4$, $B = C = 1$, noise factor $K = 0.1$, and total number of rounds of game $T = 400$.

Step 5. Determine the initial game state of the synergistic value creation network of emerging enterprises. In the beginning, the total production input that can be paid by each node is evenly distributed among its participating neighborhoods, and the initial cooperation rate of each node is 0.5, which is randomly distributed.

Step 6. The game players in the synergistic value creation network of emerging enterprises determine their innovation input according to the established rules and determine the benefits of all game players according to the benefit assignment rules.

Step 7. The strategy updating process of game subjects in the synergistic value creation network of emerging enterprises. The game subject updates the strategy according to the established strategy updating rules.

Step 8. Repeat Steps 6 and 7, and the simulation will be terminated when the set game iterations are reached. The simulation results of the innovation network achieving dynamic equilibrium are the average values of the last 50 rounds under each group of parameters, and several independent experiments are conducted respectively.

Two experimental scenarios are designed in this study, which is the comparison of network density between two cooperative enterprises with different input ratios and different income distribution ratios. The experimental results are shown in Figures 3 and 4.

The test results show that if the two companies are the same kind of enterprises, and the disparity of the property and asset size is small, then the network density rises, and as the disparity of enterprises gradually increases, the network density is reduced. The result suggests that synergistic value creation of the same kind of enterprises tends to be homogeneous. At the same time, if the two enterprises are of different types, such as the core enterprise and the general enterprise, and the disparity of enterprises is small, then the network density decreases, and as the disparity of enterprises gradually increases, the network density increases instead, and it shows that synergy value creation of the same kind of companies tends to be dependent.

By selecting the number of cooperative patents between enterprises of different orders of magnitude as a parameter variable, the network density of emerging enterprises is counted. The impact of innovation on network density is listed in Table 2. It can be seen from the results that with the increasing number of cooperative patents between enterprises, the degree of cooperation is closer and the easier it is to produce industrial clusters.

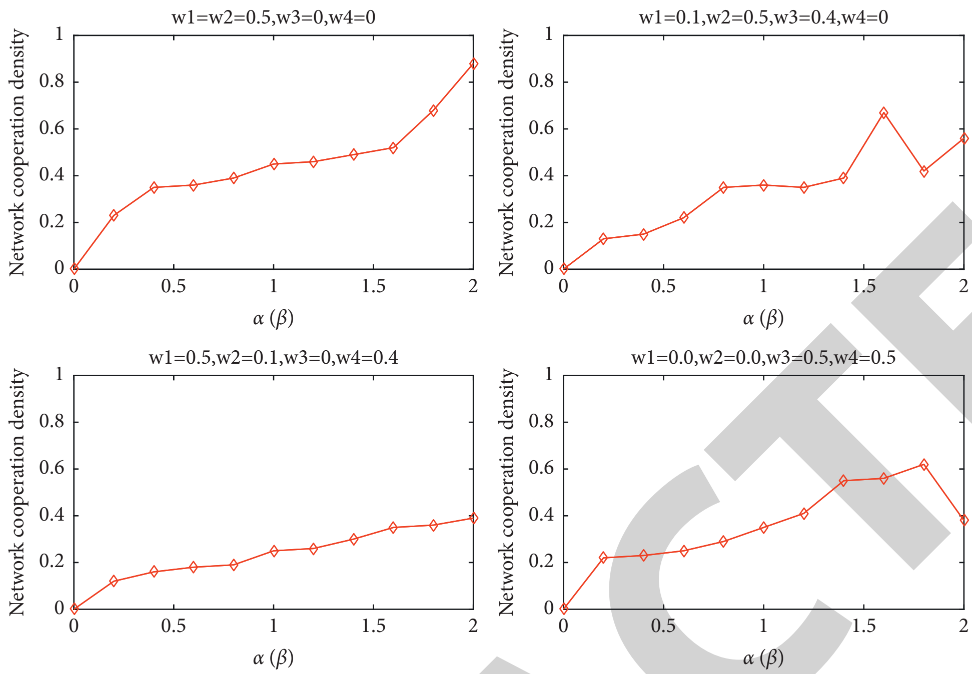

Figure 4: The effect of revenue distribution on network density.

Table 2: The impact of innovation on network density.

Cooperative patents	0	5	10	15
Network density	0.12	0.19	0.23	0.31
Cooperative patents	20	30	40	50+
Network density	0.42	0.56	0.67	0.82+

It can be seen from Figure 4 that when emerging enterprises cooperate with each other, the profit effect is the best and the network cooperation density is the strongest. The reason is that the high degree weight will make many ordinary enterprises choose not to cooperate, which leads to the serious loss of interests of core enterprises with high degree, while the damage degree of backbone enterprises is less than that of core enterprises. At the same time, with the increase of and coefficient, the network cooperation density between enterprises gradually increases.

3.4. Analysis on the Influencing Factors of Synergistic Value Creation Efficiency. Through the analysis of the evolutionary dynamics of the cooperative behavior of the cooperative value creation network of emerging enterprises, it can be seen that the benefits gained by the innovation subjects can be an important driving factor of whether they change the game strategy through a learning mechanism. However, as the innovation subject, benefits obtained through collaborative innovation actually only play a certain guiding role in the self-organization evolution of synergistic value creation of emerging enterprises [14]. As for the factors that affect the evolution of network cooperative behavior, it is necessary to investigate the root, which can be analyzed from external factors and internal factors, respectively.

According to the data analysis results, we build the synergistic value creation network operation mechanism of emerging enterprises and make the distribution of interests between innovation subjects consider the innovation investment and important degree. However, the different types of enterprises in the process of collaborative innovation input will exist a certain difference of importance, which makes the innovation main body produce an obvious income gap, leading to cooperation between the players to change. As for the equitable benefit assignment structure, it can promote the stable development of innovation activities in the collaborative innovation network, thus attracting a large number of subjects to participate in the collaborative innovation to share the benefits. However, the unfair profit distribution structure will lead the innovation subject with low income to produce negative cooperative behaviors and transfer them to other innovation subjects in the network, thus inhibiting the positive evolution of network cooperative behaviors. Over time, more and more innovation subjects will withdraw from cooperation. Therefore, whether the benefit assignment structure is reasonable or not will directly affect the development of synergistic relationship between participants, and thus it has an impact on the evolution of cooperative behavior of synergistic value creation network of emerging enterprises.

4. Evolutionary Game and Promotion Path of Synergistic Value Creation of Emerging Enterprises

4.1. Model Construction of Game Equilibrium. To build the model and simplify the calculation, the following game elements are considered:

(1) *Participants of the Game.* It is assumed that the proportion of the assets of the two enterprises X, Y

participating in innovation in the emerging industry in the total assets of the emerging industry is X_1, and the proportion W_1 of the input in synergistic value creation is directly proportional to the total assets. The total input (including the input of human resources, material resources, financial resources, technical resources, and other factors, which can be converted into currency) is I, where the share of enterprise X input is $X = X_1 W_1$, the proportion of enterprise input in the total assets is W_2, and the input share is $Y = Y_1 W_2$.

(2) *Behavior*. If enterprises trust each other and adopt synergistic value creation behaviors, then the enterprise synergistic income c is distributed according to the proportion of input, and the enterprise income is ac. The size of revenue c is positively correlated with the expected synergy coefficient $\eta\,(\eta > 1)$ of the two enterprises. If both enterprises A, B do not trust each other and both parties betray each other, then it is considered that there is no synergy and no income. In this case, the payment of both parties is 0. If company A cooperates with each other and B is selfish, it can be considered that the input of new industry companies is completely taken by the company B, which leads to no further cooperation.

Suppose that the probability of A cooperative behavior is p, the probability of selfish behavior is $1 - p$, the probability of enterprise B taking collaborative behavior is q, the generalization of selfish behavior is $1 - q$, and suppose that the collaboration between enterprises A, B is motivated by a positive feedback, expressed by θ $(\theta > 0)$. The more times of collaboration can cause the more tacit collaboration and make the rational increase. Synergy is cumulative, and every success of synergy will receive a positive incentive on the original basis.

(3) If the enterprises in the emerging industry trust each other and cooperate before the synergistic value creation for n times, each enterprise will continue to adopt the strategy of cooperation. However, once one enterprise in the emerging industry betrays in the n th stage, the enterprises in the emerging industry will not cooperate in the future.

According to the above assumptions, the payment matrix of the enterprises A and B in the nth synergistic value creation can be constructed, as listed in Table 3.

Table 3: The payoff matrix.

Enterprise A	Enterprise B		
	State (probability)	Synergy (q)	Betrayal ($1-q$)
	Synergy (q)	G_{1A}, G_{1B}	0, G_{2B}
	Betrayal ($1-q$)	G_{3A},0	0,0

4.2. Analysis of Synergistic Value Creation Conditions in Game Balance

4.2. Analysis of Synergistic Value Creation Conditions in Game Balance. Whether an enterprise A chooses synergy or betrayal, it depends on the difference ΔG_A between its expected payment when it chooses synergy $(p = 1)$ and betrayal $(p = 0)$, because it has incomplete information for the enterprise and can only consider the problem from its own interests:

$$\Delta G_A = \sum_{i=1}^{4} G_{iA}(p = 1) - \sum_{i=1}^{4} G_{iA}(p = 0), \tag{7}$$

$$\Delta G_A = qI\left[a\eta(1+\theta)^{n-1} - 1\right]. \tag{8}$$

The condition for enterprise A to choose synergy is $\Delta G_A \geq 0$, and according to the above formula, there is $a\eta(1+\theta)^{n-1} - 1 \geq 0$, as $a \geq 0$, so

$$a \geq \frac{1}{\eta(1+\theta)^{n-1}}. \tag{9}$$

Based on the above model construction results, the following can be seen:

(1) When η and θ are certain, if the η value is relatively large, then a can be relatively small, and if the η value is small, then the requirement is relatively large. That, result of the first cooperation conditions show that the synergistic effect of enterprises of innovation, also willing to adopt cooperative behavior, and it suggests the less resources and ability to make synergistic value creation. The synergistic effect of innovation is small, and enterprises only adopt cooperative behavior when they are dominant in the process of innovation.

(2) When η is certain, if η and θ are relatively large, then a can be relatively small, and if η and θ are small, then the requirement is relatively large. Thus, the second cooperation condition is obtained:

When there are more times of collaboration and trust relationship is established, enterprises are willing to take cooperative innovation behavior even though they have less dominance in the innovation process. When there are fewer times of cooperation and trust relationship is not established, enterprise A is willing to take cooperative behavior only when they are dominant in the innovation process.

As mentioned above, in theory, the game behavior of enterprise B and the game behavior of enterprise A have the same rational choice in the same strategic environment. Therefore, it can be concluded that the conditions for enterprise B to choose synergy are as follows:

$$b \geq \frac{1}{\eta(1+\theta)^{n-1}}. \tag{10}$$

When $a = b = 1/2$, it means the two enterprises have equal input, equal undertaking of innovation risks, and equal separation of innovation benefits, and both parties have the

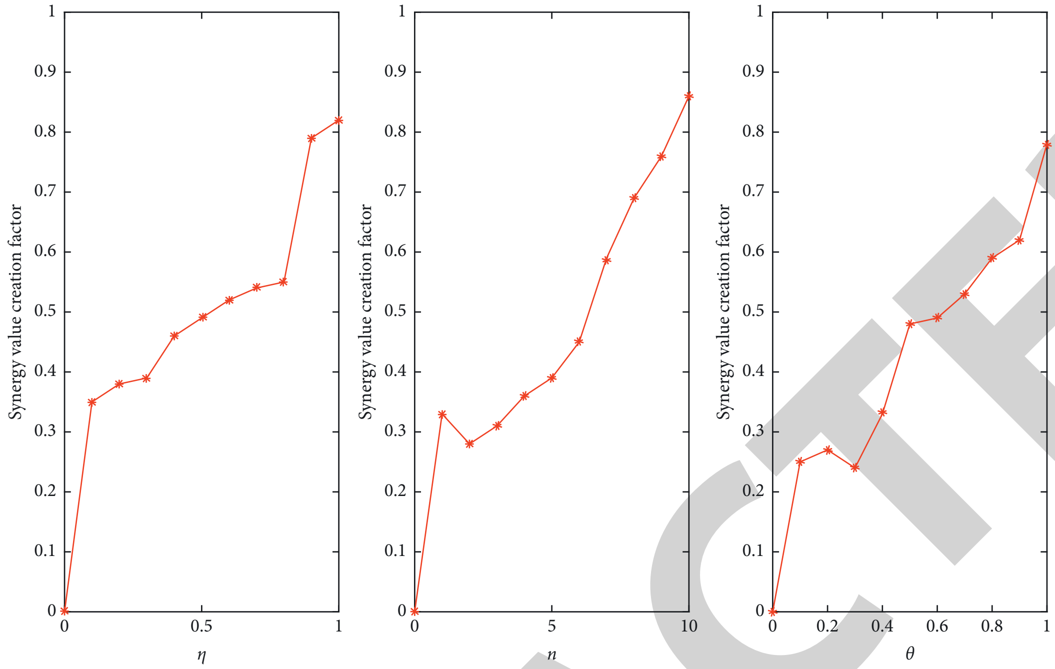

Figure 5: Comparison results of models with different η values, n values, and θ values.

Table 4: Results of network cooperation density under different ratios.

Ratios	Network cooperation density	Synergistic value creation goal probability
$a = 0 \cdot 1,\ b = 0 \cdot 9$	0.34	0.32
$a = 0 \cdot 2,\ b = 0 \cdot 8$	0.46	0.49
$a = 0 \cdot 3,\ b = 0 \cdot 7$	0.56	0.62
$a = 0 \cdot 4,\ b = 0 \cdot 6$	0.67	0.71
$a = 0 \cdot 5,\ b = 0 \cdot 5$	0.87	0.92
$a = 0 \cdot 6,\ b = 0 \cdot 4$	0.77	0.79
$a = 0 \cdot 7,\ b = 0 \cdot 3$	0.67	0.71
$a = 0 \cdot 8,\ b = 0 \cdot 2$	0.62	0.67
$a = 0 \cdot 9,\ b = 0 \cdot 1$	0.45	0.59

greatest desire to carry out long-term or repeated cooperative innovation.

4.3. Promotion Path and Experiment of Cooperative Competition Game Analysis. According to the above game analysis of collaborative competition, the essence of collaborative competition is incomplete information repeated game, so enterprises in emerging industries need to pay attention to balance. The comparison results of models with different η values, n values, and θ values are shown in Figure 5. The synergistic value creation of enterprises in emerging industries needs to start from the following aspects:

(1) *Improved η Value*. The higher the expected synergy coefficient between enterprises, the more inclined enterprises are to long-term synergy. The value can be improved by improving the way and structure of collaboration and strengthening the communication between enterprises in the process of collaboration.

(2) *Improved n Value*. In other words, the more times of synergistic value creation, the more mutual understanding and trust between enterprises, so as to establish a long-term stable synergistic value creation relationship.

(3) *Improved θ Value*. We should strengthen the information exchange of enterprises in emerging industries, establish the mechanism of equitable distribution of collaborative achievements, and develop a good collaborative institutional environment, legal environment, and cultural environment.

Table 5: Results of network cooperation density under different ratios based on empirical data.

Ratios	Cooperation density (2019)	Goal probability (2019)	Cooperation density (2020)	Goal probability (2020)
$a = 0 \cdot 1, b = 0 \cdot 9$	0.33	0.34	0.33	0.34
$a = 0 \cdot 2, b = 0 \cdot 8$	0.45	0.55	0.46	0.55
$a = 0 \cdot 3, b = 0 \cdot 7$	0.57	0.64	0.55	0.64
$a = 0 \cdot 4, b = 0 \cdot 6$	0.68	0.77	0.68	0.77
$a = 0 \cdot 5, b = 0 \cdot 5$	0.86	0.94	0.86	0.95
$a = 0 \cdot 6, b = 0 \cdot 4$	0.79	0.82	0.81	0.82
$a = 0 \cdot 7, b = 0 \cdot 3$	0.68	0.72	0.68	0.72
$a = 0 \cdot 8, b = 0 \cdot 2$	0.67	0.68	0.66	0.67
$a = 0 \cdot 9, b = 0 \cdot 1$	0.48	0.62	0.48	0.64

(4) *Improved q Value*. In other words, it can effectively promote the synergistic value creation of emerging industries by improving the potential synergistic benefits, asset complementarity, and synergistic atmosphere and increasing the punishment for betrayal.

Meanwhile, under different ratios of a and b, the synergistic value creation has different effects. The specific simulation results are listed in Table 4.

The empirical data selected in this study are the sample data of new energy emerging enterprises, and the times of synergistic value creation, degree of knowledge collaboration, and innovation data are collected. Innovation is based on patent data based on the Patsnap database. The sample data include a total of 200 enterprises from 2019 to 2020. Results of network cooperation density under different ratios based on empirical data are listed in Table 5.

Based on the constructed model and experimental results, it can be theoretically proved that when $a = b = 1/2$, two enterprises are most likely to adopt synergistic value creation behavior. In the same way, the case of individual enterprises can be deduced. When $a = b = c = \ldots = 1/n$, n, enterprises are most likely to adopt synergistic value creation behavior. Therefore, it is necessary to create synergy conditions so that enterprises in emerging industries can make an equal investment and equal separation of innovation benefits and risks.

5. Conclusions

Based on the complex network relationship and dynamic model of game evolution among multiple entities of value creation within emerging enterprises, the factors that affect the efficiency of synergistic value creation in the input, benefit assignment, and interaction mechanism are analyzed, and then the path of the promotion of synergistic value creation among the entities of new enterprises is proposed. The model test results show that the core enterprises play a leading role in the cooperation input among emerging enterprises, and if the balance of interests among cooperative enterprises is guaranteed, then the revenue effect is the best, and the network cooperation density is the strongest. To enhance synergistic value creation, it is necessary to improve the expected coefficient and number of synergies between enterprises and establish a mechanism for equitable distribution of synergies by strengthening information exchange among enterprises in emerging industries, so as to build an atmosphere of synergies, the complementarity of assets and synergies.

Finally, based on the above research findings and combined with the realistic situation, countermeasures and suggestions are provided for synergistic value creation of emerging enterprises in China, and reference basis is provided for the government to support the development of synergistic value creation activities of emerging enterprises. However, due to the lack of more data support and technical support tools, the subsequent research will combine the collaboration data of typical emerging enterprises for value creation data analysis.

Data Availability

No data were used to support this study.

Conflicts of Interest

The authors declare that they have no conflicts of interest.

References

[1] B. Leavy, "Collaborative innovation as the new imperative – design thinking, value co-creation and the power of "pull"," *Strategy & Leadership*, vol. 40, no. 2, pp. 25–34, 2012.

[2] V. Hlupic and S. Qureshi, *A Research Model for Synergistic Value Creation from Intellectual capital[C]//International Conference on Information Technology Interfaces*, IEEE, Piscataway, NJ, USA, 2003.

[3] M. J. Xavier, R. Krishnan, and N. Borin, *An Integrated Model of Synergistic Value Creation for Strategic Innovation: The Case of Retail Automation in India*, IIMB Management Review, Bengaluru, 2005.

[4] S. Mei, "Research on collaborative B2B e-business model and value creation," *Journal of Management Sciences in China*, vol. 16, no. 5, pp. 55–68, 2013.

[5] D. Chadee, R. R. Sharma, and B. Roxas, "Linking and leveraging resources for innovation and growth through collaborative value creation: a study of Indian OSPs," *Asia Pacific Journal of Management*, vol. 34, no. 4, pp. 777–797, 2016.

[6] N. Franke and F. Piller, "Value creation by toolkits for user innovation and design: the case of the watch market," *Journal of Product Innovation Management*, vol. 21, no. 6, pp. 401–415, 2004.

Hindawi
Computational Intelligence and Neuroscience
Volume 2022, Article ID 7295834, 10 pages
https://doi.org/10.1155/2022/7295834

Research Article

Network Extraction and Analysis of Character Relationships in Chinese Literary Works

Chao Fan [1,2] and Yu Li [1,2]

[1] *The School of Artificial Intelligence and Computer Science, Jiangnan University, Wuxi 214122, China*
[2] *Jiangsu Key Laboratory of Media Design and Software Technology, Jiangnan University, Wuxi 214122, China*

Correspondence should be addressed to Chao Fan; fanchao@jiangnan.edu.cn

Received 1 April 2022; Revised 27 April 2022; Accepted 30 April 2022; Published 14 May 2022

Academic Editor: Xin Ning

Character relationships in literary works can be interpreted and analyzed from the perspective of social networks. Analysis of intricate character relationships helps to better understand the internal logic of plot development and explore the significance of a literary work. This paper attempts to extract social networks from Chinese literary works based on co-word analysis. In order to analyze character relationships, both social network analysis and cluster analysis are carried out. Network analysis is performed by calculating degree distribution, clustering coefficient, shortest path length, centrality, etc. Cluster analysis is used for partitioning characters into groups. In addition, an improved visualization method of hierarchical clustering is proposed, which can clearly exhibit character relationships within clusters and the hierarchical structure of clusters. Finally, experimental results demonstrate that the proposed method succeeds in establishing a comprehensive framework for extracting networks and analyzing character relationships in Chinese literary works.

1. Introduction

Classic literary works are passed down to the present day because imaginative virtual worlds created by the authors can reflect many characteristics of our society. Character relationships in a novel indirectly reflect the writer's experiences and feelings about social life, cultural beliefs, and habits. Traditional analysis tries to discover the value of a literary work and compares similarity between the social structure in the work and real-world structure. However, recent analysis paid more attention to social relationships of characters. For example, the relationships of characters portrayed by a novel often carry a large amount of social information which is important for scholars when interpreting a literary work. Hence, extracting a social network and analyzing intricate character relationships will help to better understand the internal logic of plot development and explore the significance of a literary work. For instance, it can ease the process of reading a novel with too many characters, because readers are often confused about complicated character relationships while reading a long novel.

This paper attempts to extract networks of character relationships for several Chinese literary works by performing network analysis, cluster analysis, and data visualization. By applying these technologies and refining shared features in literary works, we succeeded in building a framework for studying network extraction and character relationship analysis of the Chinese literature. Initially, a Chinese lexical analysis on the novel text is used to resolve character names. Co-word network analysis is then employed to extract a network of character relationships. By analyzing the created network, we are able to grasp the basic characteristics of important characters in the specified Chinese novel. Finally, a variety of data visualization techniques are proposed to display character relationships in the novel.

This article is arranged as follows: Related researches are discussed in Section 2. Section 3 elaborates the methodology of character relationship extraction and analysis in Chinese literary works. Datasets and experimental results are described in detail in Section 4. The conclusion is drawn in Section 5.

2. Related Work

Analyzing literary works quantitatively by using scientific tools is one of the current research hotspots. The research approach is mainly divided into three categories: language analysis, text analysis, and comprehensive analysis [1]. Experts in both literature and computer science have recently focused on comprehensive analysis, which will be the main direction for literary research in the future. Zhao et al. [2] established a model of character graphs based on emotional polarity and gave general procedures to comprehend the Chinese literature. Huang et al. [3] developed a Chinese person entity relation extraction technology utilizing distant supervision, which can automatically identify and extract semantic relationships. Li and Liu [4] divided the corpus of a classical Chinese novel into training data and test data. Based on an N-gram language model and a random forest algorithm, they extracted features and performed a classification experiment to identify the authorship of the novel.

Social networks have also been introduced to analyze literary works. A growing number of scholars have begun to research literary character relationships based on social networks. Muhuri et al. [5] devised a means of annotation and character categorization to extract social networks. They applied it to two Bengali dramas and successfully found the protagonist and antagonist in the literature. Chowdhury et al. [6] investigated character relationships in a novel and its adapted film based on social network. They exploited many network features such as centrality metrics to analyze the difference in the character categorization within two expressions of art. Wang et al. [7] utilized co-word and social network analyses to study old Chinese literature in the Qing Dynasty. Fan et al. [8] examined character relationships in a classical Chinese novel by combining social network and cluster analysis.

A scheme for constructing a social network is using the co-word analysis technique. It measures the strength of relationships by counting the co-occurrence of words in a text. In recent years, co-word analysis has been widely employed in several fields. Chen et al. [9] conducted research by collecting the scientific literature with the topic of medical image processing. In order to explore research hotspots in this field, keywords of papers were used for co-word and cluster analysis. Huang et al. [10] chose industrial symbiosis as their research topic, using co-word and social network analysis to evaluate the current status and trends. They found that this research direction showed an interdisciplinary characteristic. Another research [11] built and visualized a co-word network in the Night-Time Light remote sensing field according to data from the Web of Science. Hu et al. [12] adopted scientometrics and co-word analysis to study bibliographic data in food safety from 1991 to 2018. Their work focused on food safety in agriculture and industry and revealed global research trends in this field. Xie et al. [13] predicted the evolution of academic research and hotspots in bioacoustics and ecoacoustics based on bibliometric analysis and network-based methods such as co-word network analysis, co-author network analysis, and co-citation network analysis.

3. Methodology

Manual analysis is a choice when the number of characters is small in a literary work. Nevertheless, it is unacceptable to manually process a novel with hundreds and thousands of characters. Thus, this paper focuses on automatically extracting and analyzing character relationships with the help of social networks and natural language processing technologies. The main framework of character relationship analysis can be illustrated in Figure 1. At first, a corpus of the Chinese literature and its corresponding character name list are loaded. Chinese lexical analysis is then performed so that character names can be correctly resolved. After building a social network based on co-word analysis, we calculate the number of network features and implement the visualization of network data in many ways.

3.1. Preprocessing. Before preprocessing, a full-text collection of Chinese literary works has to be collected from open datasets on the Internet. A selected literary work should contain the standardized Chinese text with high quality. Besides, a corresponding character name list downloaded from the web has to be provided for co-word analysis. Data cleansing is also done to correct some mistakes and remove unclear data in a raw corpus.

A Chinese natural language processing tool, ICTCLAS (https://ictclas.nlpir.org/), was used to perform lexical analysis, including segmentation, part-of-speech (POS) tagging, and named entity recognition (NER). Combining the character name list and character names resolved by NER, we succeeded in preparing the data for constructing a character relationship network.

3.2. Network Extraction of Character Relationships. Literary character relationships can be described as an undirected network. The character name is recognized as the node, and co-appearance of two names in a sentence or a paragraph is deemed as the link. Then, the weight of a link can be calculated by counting the number of times that the two names co-occur in the text. By performing co-word analysis, we can extract a weighted network of character relationships for the Chinese literature.

When dealing with Chinese character names, it is necessary to identify a character with different types of names: full name, nickname, and abbreviated name. A powerful algorithm should handle it correctly and effectively. We set a series of rules to convert names of different forms into full names.

3.3. Network Analysis for Character Relationships. Performing network analysis requires calculating multiple network features. The network features involve degree distribution, density, clustering coefficient, average clustering coefficient, shortest path length, average shortest path length, diameter, and centrality.

The degree of a node represents the number of its neighbors in the network. Degree distribution [14] is defined

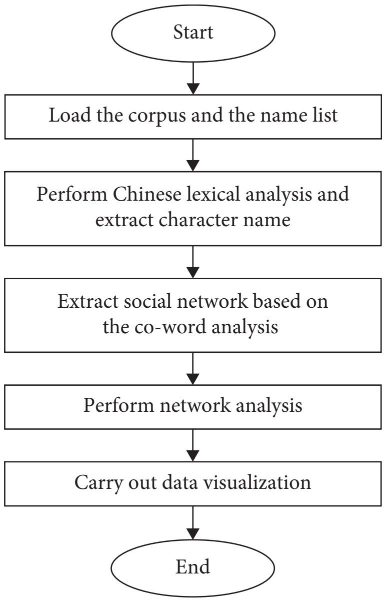

Figure 1: Research framework for analyzing character relationships in Chinese literature.

as the distribution of node degree, showing how links are distributed among nodes. Many researchers inspect whether a character relationship network has the power-law distribution, which is a common pattern discovered in numerous real networks [15].

Network density assesses the relative denseness of a network from the perspective of connected links. In a network, density is the portion of potential links which actually exist in the network [8]. It is often used in social networks to measure the intensity of social relationships and trends in evolution.

As a local feature of a network, the clustering coefficient [16] reflects the degree of clustering from the perspective of the nodes. It is the number of existing connections within a node's neighbors divided by the number of potential connections [17]. If all neighbors of a node are connected to each other, the clustering coefficient of this node will be 1. The average clustering coefficient, also known as the clustering coefficient of a network, is an average of all nodes' clustering coefficients. This value indicates the probability that friends of a person are also friends in real social connections.

The shortest path length [18] between two nodes refers to the number of links that connects two nodes by the shortest path. Thus, the average shortest path length is defined by the average number of links along the shortest paths. It measures information transmission efficiency within a network. Another indicator related to the shortest path is the diameter of a network, which is the maximum value of all shortest path lengths.

Centrality [15] is a measurement of significance for each node in the network. Three centralities are often discussed in network science involving degree centrality, betweenness centrality [19], and closeness centrality [20]. They are calculated based on the concept of degree, betweenness, and degree of closeness.

3.4. Cluster Analysis for Character Relationships. The weight of a link between two nodes in a social network can be used to represent the similarity of two characters. The larger the weight is, the more likely the two characters will be related to each other. At the beginning, a co-occurrence matrix is created by counting the weights of links, which are frequencies of character names appearing together. Furthermore, Ochiai coefficients [21] are calculated to implement the normalization of the co-occurrence matrix for the purpose of eliminating the influence of frequency of a character existing in a literary work. The formula of the Ochiai coefficient is described by

$$\mathrm{Och} = \frac{\mathrm{freq}\,(X \cap Y)}{\sqrt{\mathrm{freq}\,(X) \times \mathrm{freq}\,(Y)}}, \tag{1}$$

where $\mathrm{freq}\,(X)$ is the frequency of character X and $\mathrm{freq}\,(X \cap Y)$ is the frequency that X and Y co-occur in the literary work. In addition, a similarity matrix can be produced by applying the mathematical formula to the co-occurrence matrix. The elements of the similarity matrix range from 0 to 1. A large value implies a high similarity between the two characters, which means they incline to gather together in cluster analysis.

After taking the similarity matrix of character relationships as input, we exploit a bottom-up agglomerative hierarchical clustering method to organize characters into groups. The algorithm treats each character as a cluster at first. Two most similar clusters are merged at each iteration until only one cluster remains or it reaches the specified threshold. Finally, a hierarchical tree structure of character relationships is obtained through cluster analysis.

3.5. Data Visualization. Data visualization offers a graphical representation of data, helping us better understand the pattern within the data. Character relationships can be visualized in many different types. In this paper, clustering results of characters are portrayed in the form of a dendrogram. Since the output of hierarchical clustering is a binary tree, a tree-like dendrogram is an effective structure for visualizing character relationships.

Furthermore, the binary tree can be illustrated by a Venn diagram [22] as shown in Figure 2. In Figure 2, a red leaf node is also a node in the Venn diagram. The red node represents a character in the literary work, whereas a branch node stands for a larger group involving characters or small groups. Using the Venn diagram to display the result of hierarchical clustering has the following advantages: for one thing, nodes can be connected by links in the Venn diagram, which cannot be done in a tree structure; for another, the Venn diagram can clearly express a hierarchical structure. According to Figure 2(b), cluster A contains cluster B and character C, whereas characters D and E are included in cluster B.

However, application of a simple Venn diagram has some limitations. For instance, a novel with n characters incorporates $n-1$ clusters in the hierarchical clustering result. When the number of characters is too large, there will be a plethora of nodes and groups in the Venn diagram. It

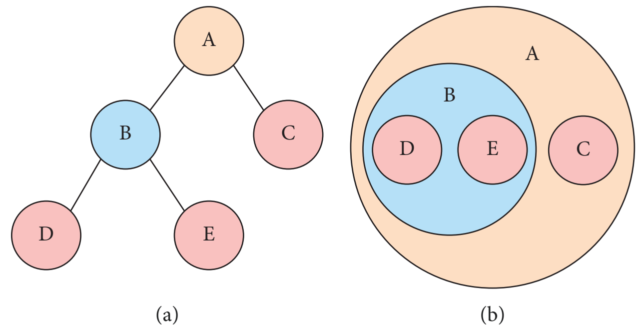

Figure 2: Visualization of the outcome of hierarchical clustering. (a) A binary tree. (b) A Venn diagram.

leads to a poor visualization of clustering results. There is no need to depict all clusters in the hierarchical structure, because researchers only pay attention to several important clusters. This paper improves the representation of target clusters by removing internal small clusters and retaining all character nodes. As shown in Figure 3, inner cluster B will be omitted if we are interested in cluster A, which results in a simplified visualization. The simplification of the Venn diagram is very useful when we visualize a multitude of characters with a small number of clusters.

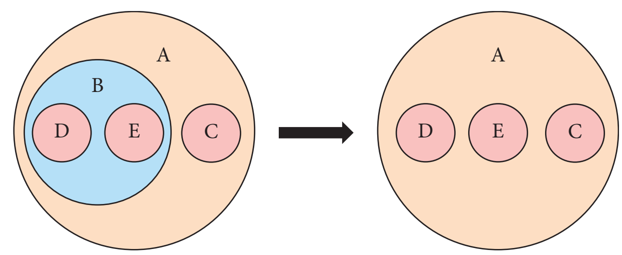

Figure 3: Removal of internal clusters in the Venn diagram.

4. Experimental Results

4.1. Datasets of Chinese Literary Works. A myriad of e-books of the Chinese literature can be downloaded from the Internet. In this paper, four classical Chinese novels are chosen as datasets to be analyzed. The novels' names and their abbreviations are presented in Table 1. Original texts are preprocessed to meet the experimental criteria. Cleaned data are available from the authors upon request. As character names are indispensable to extract social network from a literary work, character name lists of novels are also collected through the Internet. The number of characters for each novel is given in Table 1.

4.2. Results of Network Extraction and Analysis. Based on the character name list and co-word analysis, a social network of character relationships is extracted for each Chinese novel. Taking Demi-Gods and Semi-Devils (DGSD) as an illustration, a network with 169 nodes and 1,559 links is established in this paper. Figure 4 gives the visualization of the DGSD network by showing the top-50 nodes in degree distribution. It is a weighted undirected network where the size of a node denotes the frequency of a character name appearing in DGSD and the strength of a link represents the co-occurrence of two names in different semantic contexts.

The degree distribution of four networks and their log-log plots are depicted in Figures 5 and 6, respectively. According to the figures, only the degree distribution of the RTK network follows a power-law distribution—a significant property of the real-world network. In the log-log plot of Figure 6, we can fit a linear equation to the data of RTK well. However, other datasets of literary works fail to capture power-law properties because their authors only write a small number of core characters and neglect most low-frequency characters.

The average degree of a character relationship network means how many neighbors does a character connect on average. The indices for the 4 Chinese novels are listed in Table 2. The DRM network has the largest average degree. It means that characters in DRM are closely joined together in comparison with other novels. On the contrary, the RTK network has the smallest average degree because its author describes a large number of characters who appear only once or twice in the novel.

According to Table 2, densities of the four networks are less than 0.3, so they are sparsely connected networks, especially the RTK network. The average shortest path length is more than 3 for the RTK network but less than 2 for the DRM and LCH networks. Distribution of the shortest path length between two nodes is displayed in Figure 7. As for diameter which represents the distance of the largest-shortest path, only the RTK network has a diameter of 9, which is much larger than 4. Therefore, it has to afford a high cost of reaching another node in the RTK network in comparison with the other three networks.

The clustering coefficient reflects the local characteristics of a node. In a Chinese literary work, a character with the largest clustering coefficient does not necessarily have the most important role. The average clustering coefficients for 4 novels are given in Table 2. Moreover, we compare the character relationship network with a randomized version of a network with the same number of nodes and links, obtainable with a configuration model [23] that keeps the same degree distributions. This type of a random model is better than a simple ER model [24, 25]. From the results obtained in Table 3, the average shortest path length of each character relationship network is smaller than that of a random

Table 1: Four Chinese novels selected as datasets.

Number	Chinese novel name	Abbreviation	Number of characters
1	Dream of the Red Chamber	DRM	265
2	Romance of the Three Kingdoms	RTK	1,133
3	Legend of the Condor Heroes	LCH	90
4	Demi-Gods and Semi-Devils	DGSD	169

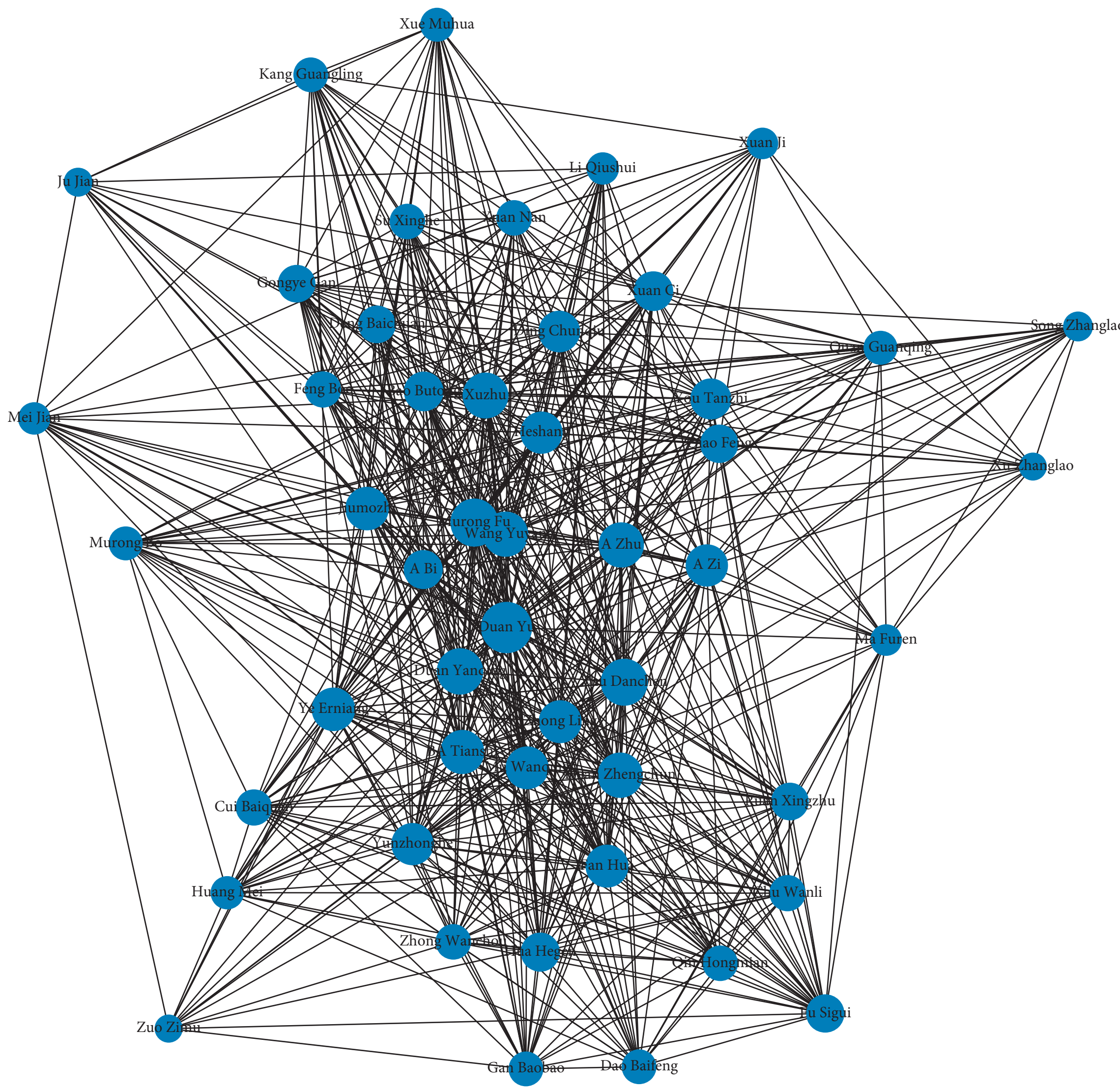

Figure 4: A visualization of the DGSD network with the top-50 nodes in degree distribution.

network except for the RTK network. The exception may be originated from an apparent three-group structure existing in the RTK network. All character relationship networks have larger average clustering coefficients. Hence, the social network of character relationships in a literary work is often a small-world network.

Three centralities can be calculated to measure significance of characters in a novel. Degree centrality is proportional to the degree of a node, which highlights the pivotal position of a node. Betweenness centrality reflects the "communication" ability of a node in the network. A high-betweenness node has a stronger ability to communicate with others. Closeness centrality represents the degree of accessibility from one node to other nodes in the network. Taking the example of DGSD, the top ten characters in centrality are shown in Table 4. Eight of the ten characters appear in three rankings, incorporating Duan Yu, Xu Zhu, Heshang, Murong Fu, Wang Yuyan, Qiao Feng, A Zhu, and A Zi.

4.3. Results of Cluster Analysis and Visualization. In order to discover clusters from data, the co-occurrence matrix should be first created by counting the weights of links. An example

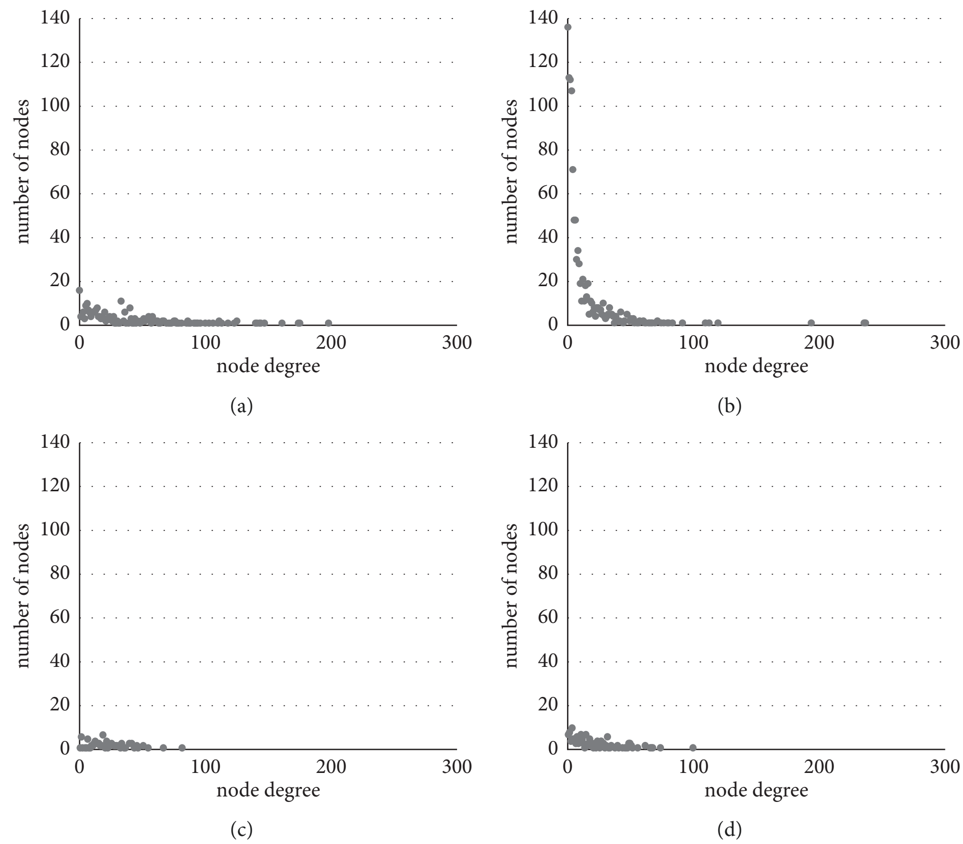

FIGURE 5: Degree distribution of the character relationship network. (a) DRM. (b) RTK. (c) LCH. (d) DGSD.

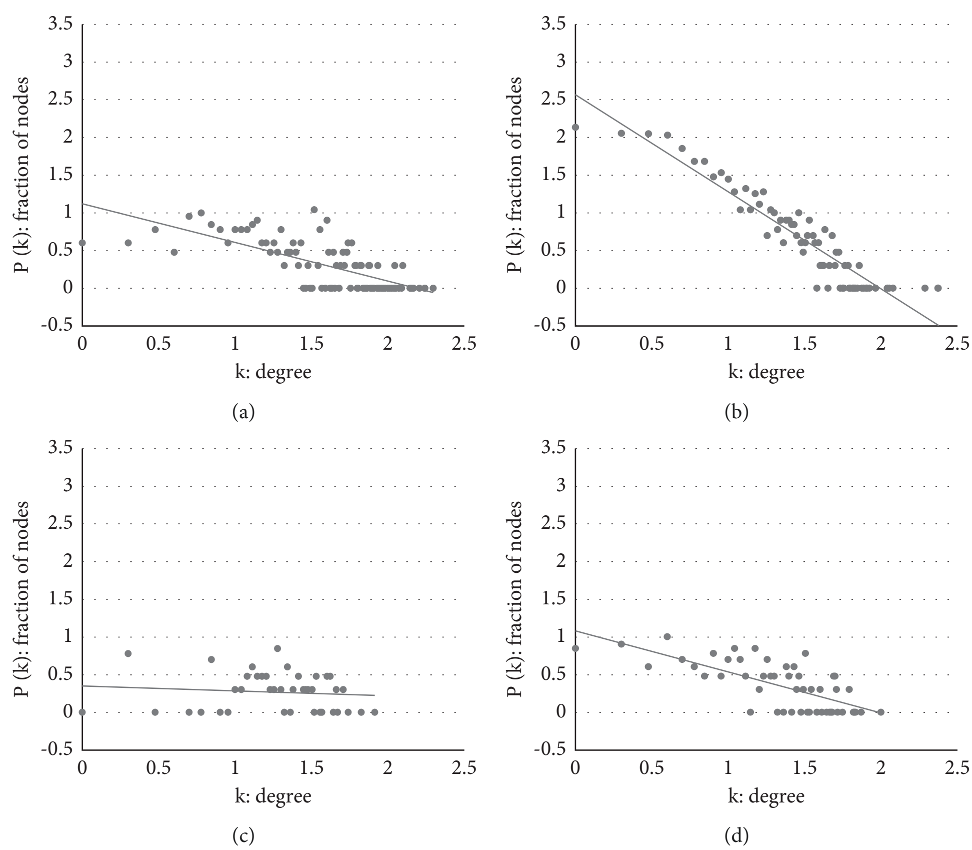

FIGURE 6: Log-log plot of degree distribution. (a) DRM. (b) RTK. (c) LCH. (d) DGSD.

Table 2: Basic network features of character relationship networks.

Network features	DRM network	RTK network	LCH network	DGSD network
Number of nodes	265	1,133	90	169
Number of links	4,748	5,844	1,013	1,559
Density	0.1357	0.0091	0.2529	0.1098
Average degree	35.83	10.31	22.51	18.45
Average shortest path length	1.9512	3.1743	1.7958	2.0889
Average clustering coefficient	0.7209	0.5306	0.7262	0.5907
Diameter	4	9	4	4

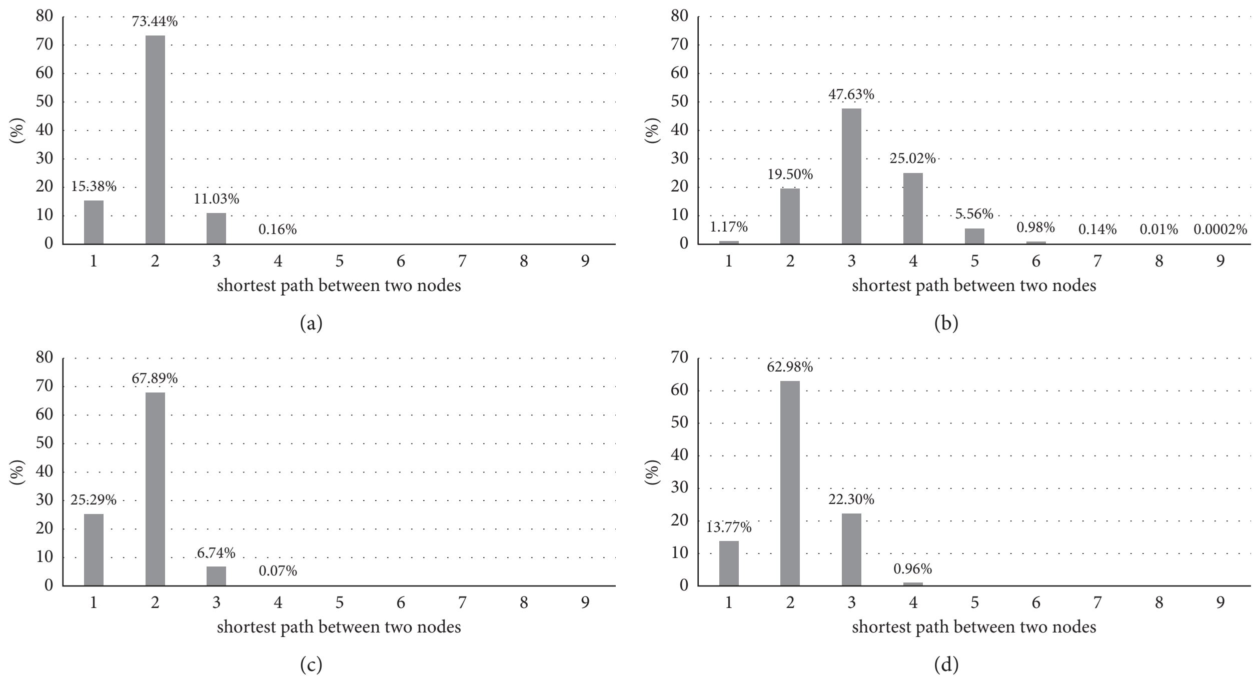

Figure 7: Distribution of the shortest path length. (a) DRM. (b) RTK. (c) LCH. (d) DGSD.

Table 3: Comparison with random networks generated by using configuration models.

Network	Type	Number of nodes	Number of links	Average shortest path length	Average clustering coefficient
DRM	Original	265	4,748	1.9512	0.7209
	Random			2.0345	0.3349
RTK	Original	1,133	5,844	3.1743	0.5306
	Random			3.0212	0.0824
LCH	Original	90	1,013	1.7958	0.7262
	Random			1.9034	0.3308
DGSD	Original	169	1,559	2.0889	0.5907
	Random			2.1423	0.2690

of five characters in DGSD is presented in Table 5. The diagonal number is the frequency of a character's name appearing in the novel.

Normalization of the above co-occurrence matrix is finished by computing the Ochiai coefficient. Then, the co-occurrence matrix is converted into a similarity matrix as shown in Table 6.

Similarity of any two characters can be used for cluster analysis. In this research, a bottom-up hierarchical algorithm employing the similarity matrix is implemented to cluster character names in the literary work. As the result of hierarchical clustering is a binary tree, a dendrogram is drawn to describe character relationships in the novel. Figure 8 depicts a dendrogram of the clustering result for 33 main characters in DRM. Four large clusters can be identified by the clustering algorithm, including the Jia family of the Rongguo Mansion (H1), the Jia family of the Ningguo Mansion (H2), the Xue family (H3), and a group of noble people (H4). In our algorithm, H1 and H2 are clustered together in the hierarchy, which is called the "Jia family."

Table 4: Top ten characters of DGSD in centrality.

Ranking	Degree centrality	Betweenness centrality	Closeness centrality
1	Duan Yu (0.5952)	Duan Yu (0.1599)	Duan Yu (0.6696)
2	Xu Zhu (0.4405)	Xu Zhu (0.0833)	Xu Zhu (0.5874)
3	Heshang (0.4048)	Qiao Feng (0.0710)	Wang Yuyan (0.5675)
4	Murong Fu (0.3988)	Wang Yuyan (0.0508)	Heshang (0.5675)
5	Wang Yuyan (0.3929)	Heshang (0.0436)	Murong Fu (0.5627)
6	Qiao Feng (0.3690)	A Zi (0.0370)	A Zhu (0.5534)
7	A Zhu (0.3690)	Murong Fu (0.0332)	Qiao Feng (0.5511)
8	Duan Zhengchun (0.3333)	A Zhu (0.0323)	Duan Zhengchun (0.5379)
9	Duan Yanqing (0.3095)	Yelv Hongji (0.0244)	A Zi (0.5315)
10	A Zi (0.3036)	Bao Butong (0.0204)	Duan Yanqing (0.5315)

Table 5: An example of the co-occurrence matrix for DGSD.

Co-occurrence	Qiao Feng	Xu Zhu	Duan Yu	Xu Zhanglao	Xi Zhanglao	Jiumozhi
Qiao Feng	104	2	41	50	8	3
Xu Zhu	2	162	116	1	0	43
Duan Yu	41	116	286	1	1	127
Xu Zhanglao	50	1	1	53	1	0
Xi Zhanglao	8	0	1	1	10	0
Jiumozhi	3	43	127	0	0	173

Table 6: An example of the similarity matrix for DGSD.

Co-occurrence	Qiao Feng	Xu Zhu	Duan Yu	Xu Zhanglao	Xi Zhanglao	Jiumozhi
Qiao Feng	1	0.015408	0.23773	0.673466	0.248069	0.022366
Xu Zhu	0.015408	1	0.538912	0.010792	0	0.256855
Duan Yu	0.23773	0.538912	1	0.008122	0.018699	0.570949
Xu Zhanglao	0.673466	0.010792	0.008122	1	0.043437	0
Xi Zhanglao	0.248069	0	0.018699	0.043437	1	0
Jiumozhi	0.022366	0.256855	0.570949	0	0	1

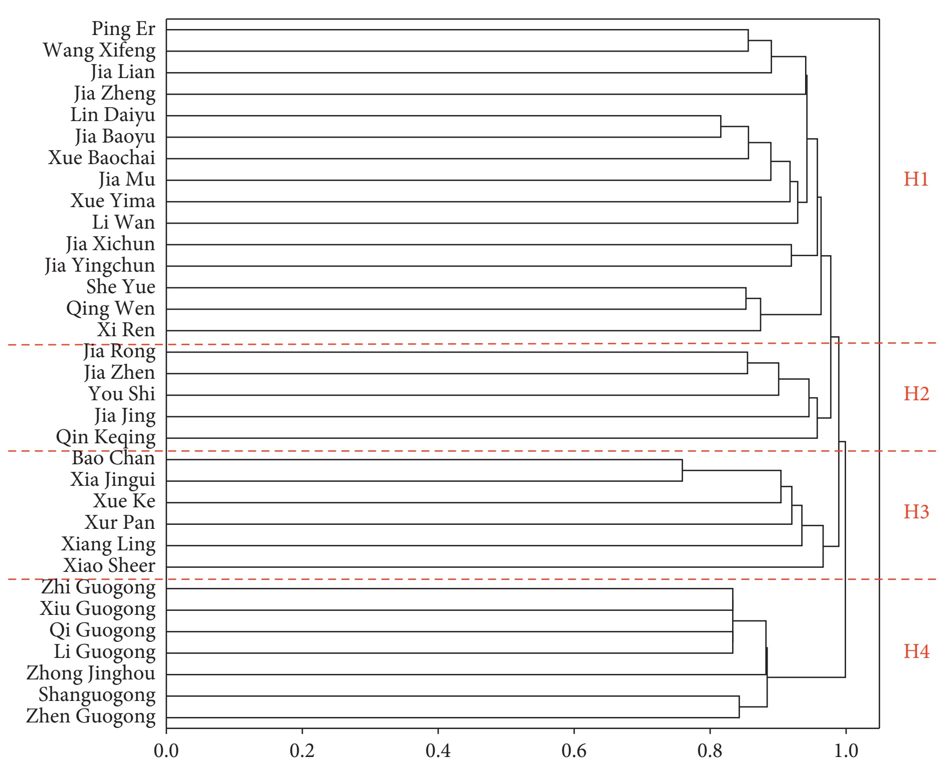

Figure 8: Dendrogram of clustering result for the DRM network.

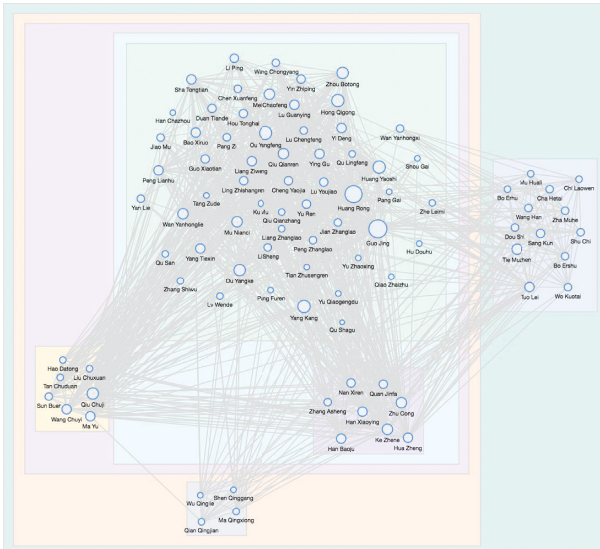

Figure 9: Improved Venn diagram visualizing the clustering result of LCH.

Furthermore, the Jia family (H1 and H2) and the Xue family (H3) are combined to form a bigger cluster due to marriage. H4 is a group of noble people with titles that are closely connected. Finally, all the clusters are aggregated into one cluster.

Besides the dendrogram, an improved Venn diagram is also proposed to depict the hierarchical clustering result. Figure 9 gives an instance of LCH using an improved method and reveals a visualization result by setting the number of clustering as 5. In this figure, small groups within 5 clusters are eliminated so that clusters can be clearly presented. Also, the hierarchical structure of 5 clusters is exhibited by filling different clusters with different colors. Moreover, we can control the number of clusters and merge nodes with the same cluster label in hierarchical clustering. The proposed visualization method can not only draw connections between nodes but also show the hierarchical structure of clusters. For example, four groups on the left side of Figure 9 are different gangs in mainland China. They cluster together to form a large group with leading Chinese characters. The group on the right side of Figure 9 is composed of Mongolian characters. Five groups are aggregated to build a small world of LCH with a hierarchical framework.

5. Conclusions

This article focuses on network extraction and analysis of character relationships in Chinese literary works. Four classical Chinese novels are selected as datasets to be analyzed. Initially, semantic segmentation and POS tagging were completed to process the raw corpus. A co-word analysis was then used to extract social networks of character relationships from Chinese literary works. Furthermore, a network analysis was performed by calculating degree distributions, network density, average clustering coefficient, centrality, and so forth. In order to implement cluster analysis, a co-occurrence matrix and similarity matrix were calculated to measure the similarity (or distance) between two characters in the network. Besides, data visualization was applied to explore character relationships. On the one hand, a tree-like dendrogram was used to display the result of hierarchical clustering. On the other hand, an improved Venn diagram was proposed to simplify graphical visualization. Finally, a dendrogram for DRM and a Venn diagram for LCH were visualized in our experiments.

In future, pronouns will be translated into character names using the coreference resolution so as to improve the extraction effect of character relationships. Introducing other network features and visualization approaches is another direction in the following research.

Data Availability

The original dataset used in this paper is available from the corresponding author on request.

Conflicts of Interest

The authors declare that they have no conflicts of interest.

Acknowledgments

This work was supported by the Youth Foundation of Basic Science Research Program of Jiangnan University, 2019 (no. JUSRP11962), and the High-Level Innovation and Entrepreneurship Talents Introduction Program of Jiangsu Province of China, 2019 (no. 30710).

References

[1] J. Zhao, Z. Li, Q. Zhu, and G. Zhou, "Extracting and analyzing social networks from Chinese literary," *Journal of Chinese Information Processing*, vol. 31, no. 2, pp. 99–106, 2017.

[2] X. Zhao, X. Liang, F. Tang, X. Zhang, X. Zhou, and X. Guo, "Building character graphs and dividing communities in Chinese novels based on graph data extraction: community division for character emotional polarity networks," *IEEE Access*, vol. 8, pp. 95559–95573, 2020.

[3] Y. Huang, Y. Jia, L. Gan, J. Xu, and Z. He, "Multi-factor person entity relation extraction model based on distant supervision," *Journal on Communications*, vol. 39, no. 7, pp. 103–112, 2018.

[4] H. Li and Y. Liu, "Language models and classification analysis for dream of the red chamber," in *Proceedings of the 2nd Conference on Cloud Computing & Intelligence Systems*, pp. 1459–1464, Hangzhou, China, September 2012.

[5] S. Muhuri, S. Chakraborty, and S. N. Chakraborty, "Extracting social network and character categorization from Bengali literature," *IEEE Transactions on Computational Social Systems*, vol. 5, no. 2, pp. 371–381, 2018.

[6] T. Chowdhury, S. Muhuri, S. Chakraborty, and S. N. Chakraborty, "Analysis of adapted films and stories based on social network," *IEEE Transactions on Computational Social Systems*, vol. 6, no. 5, pp. 858–869, 2019.

[7] Y. Wang, J. Yu, and C. Zhao, "Research on application of co-word analysis on relationships of characters in the romance of the three kingdoms," *Information Research*, no. 7, pp. 52–56, 2017.

[8] C. Fan, Z. Yang, and Y. Yuan, "Cluster Analysis and visualization for the legend of the condor heroes based on social network," *Scientific Programming*, vol. 2021, Article ID 9439583, 10 pages, 2021.

[9] W. Chen, Y. Wang, Z. Ouyang, W. Guo, and H. Chi, "A bibliometrics study of literature on medical image processing for the past ten years," *Sheng wu yi xue gong cheng xue za zhi = Journal of biomedical engineering = Shengwu yixue gongchengxue zazhi*, vol. 31, no. 1, pp. 113–119, 2014.

[10] M. Huang, Z. Wang, and T. Chen, "Analysis on the theory and practice of industrial symbiosis based on bibliometrics and social network analysis," *Journal of Cleaner Production*, vol. 213, pp. 956–967, 2019.

[11] K. Hu, K. Qi, Q. Guan et al., "A scientometric visualization analysis for night-time light remote sensing research from 1991 to 2016," *Remote Sensing*, vol. 9, no. 8, p. 802, 2017.

[12] K. Hu, J. Liu, B. Li et al., "Global research trends in food safety in agriculture and industry from 1991 to 2018: a data-driven analysis," *Trends in Food Science & Technology*, vol. 85, pp. 262–276, 2019.

[13] J. Xie, K. Hu, M. Zhu, and Y. Guo, "Data-driven analysis of global research trends in Bioacoustics and Ecoacoustics from 1991 to 2018," *Ecological Informatics*, vol. 57, 2020.

[14] A.-L. Barabási, H. Jeong, Z. Néda, E. Ravasz, A. Schubert, and T. Vicsek, "Evolution of the social network of scientific collaborations," *Physica A: Statistical Mechanics and Its Applications*, vol. 311, no. 3-4, pp. 590–614, 2002.

[15] M. E. J. Newman, *Networks*, Oxford University Press, Oxford, UK, 2nd edition, 2018.

[16] L. Baumgarten and S. Bornholdt, "Critical excitation-inhibition balance in dense neural networks," *Physical Review*, vol. 100, no. 1, Article ID 010301, 2019.

[17] C. Fan, "Research on relationships of characters in the dream of the red chamber based on co-word analysis," *ICIC Express Letters Part B: Applications*, vol. 11, no. 5, pp. 1–8, 2020.

[18] J. Davidsen, H. Ebel, and S. Bornholdt, "Emergence of a small world from local interactions: modeling acquaintance networks," *Physical Review Letters*, vol. 88, no. 12, Article ID 128701, 2002.

[19] D. Corrales-Garay, M. Ortiz-De-Urbina-Criado, and E.-M. Mora-Valentín, "Knowledge areas, themes and future research on open data: a co-word analysis," *Government Information Quarterly*, vol. 36, no. 1, pp. 77–87, 2019.

[20] D. Nguyen, "Mapping knowledge domains of non-biomedical modalities: a large-scale co-word analysis of literature 1987-2017," *Social Science & Medicine*, vol. 233, pp. 1–12, 2019.

[21] Q. Zhou and L. Leydesdorff, "The normalization of occurrence and Co-occurrence matrices in bibliometrics using-Cosinesimilarities andOchiaicoefficients," *Journal of the Association for Information Science and Technology*, vol. 67, no. 11, pp. 2805–2814, 2016.

[22] B. Nair B J and S. M S, "Evolutionary clustering annotation of Ortho-paralogous gene in a multi species using Venn diagram visualization," *International Journal of Engineering & Technology*, vol. 7, no. 1.9, pp. 162–166, 2018.

[23] A. Lancichinetti, S. Fortunato, and F. Radicchi, "Benchmark graphs for testing community detection algorithms," *Physical Review*, vol. 78, no. 4, Article ID 046110, 2008.

[24] B. Bollobás, *Random Graphs*, Cambridge University Press, Cambridge, UK, 2nd edition, 2001.

[25] T. G. Kolda, A. Pinar, T. Plantenga, and C. Seshadhri, "A scalable generative graph model with community structure," *SIAM Journal on Scientific Computing*, vol. 36, no. 5, pp. C424–C452, 2014.

Hindawi
Computational Intelligence and Neuroscience
Volume 2022, Article ID 1847981, 14 pages
https://doi.org/10.1155/2022/1847981

Research Article

Emerging Feature Extraction Techniques for Machine Learning-Based Classification of Carotid Artery Ultrasound Images

S. Latha,[1] **P. Muthu**,[2] **Samiappan Dhanalakshmi**,[1] **R. Kumar**,[1] **Khin Wee Lai**,[3] **and Xiang Wu**[4]

[1]*Department of Electronics and Communication Engineering, SRM Institute of Science and Technology, Kattankulathur, Chennai 603203, India*
[2]*Department of Biomedical Engineering, SRM Institute of Science and Technology, Kattankulathur, Chennai 603202, India*
[3]*Department of Biomedical Engineering, Faculty of Engineering, University Malaya, Kuala Lumpur 50603, Malaysia*
[4]*School of Medical Information Engineering, Xuzhou Medical University, Xuzhou 221000, China*

Correspondence should be addressed to Samiappan Dhanalakshmi; dhanalas@srmist.edu.in, Khin Wee Lai; lai.khinwee@um.edu.my, and Xiang Wu; wuxiang@xzhmu.edu.cn

Received 21 March 2022; Revised 7 April 2022; Accepted 9 April 2022; Published 12 May 2022

Academic Editor: Xin Ning

Plaque deposits in the carotid artery are the major cause of stroke and atherosclerosis. Ultrasound imaging is used as an early indicator of disease progression. Classification of the images to identify plaque presence and intima-media thickness (IMT) by machine learning algorithms requires features extracted from the images. A total of 361 images were used for feature extraction, which will assist in further classification of the carotid artery. This study presents the extraction of 65 features, which constitute of shape, texture, histogram, correlogram, and morphology features. Principal component analysis (PCA)-based feature selection is performed, and the 22 most significant features, which will improve the classification accuracy, are selected. Naive Bayes algorithm and dynamic learning vector quantization (DLVQ)-based machine learning classifications are performed with the extracted and selected features, and analysis is performed.

1. Introduction

Cardiovascular illnesses are the chief reason for death as per the World Health Organization. Accurate measurement and analysis of the carotid artery provide early identification of stroke and atherosclerosis diseases, which are caused by plaque deposit. In clinical diagnosis, plaque morphology and stenosis severity characterization may be diagnosed using noninvasive ultrasound imaging [1]. Experienced radiologists outline the layer thicknesses and plaque deposition buy may vary depending on the person. Automatic segmentation and classification of the carotid artery ultrasound images are necessary for accurate and early assessment of the disease.

Biochemical risk factors and vital signs include high C-reactive protein, glycohemoglobin, low-density lipoprotein cholesterol, serum creatinine, factor alpha, platelet-to-lymphocyte ratio, and neutrophil-to-lymphocyte ratio. Biomechanical risk factors include increased plaque area, low stenosis grade, increase in IMT, presence of in-plane curvature, abnormal shear stress, C-shaped ICA, low wall shear stress, and reversal flow. The related diseases because of plaque formation in the carotid artery are diabetes, hypertension, plaque hemorrhage, head and neck radiotherapy, chemotherapy, coronary artery diseases, peripheral artery diseases, and low ankle-brachial index [2, 3].

Feature extraction reduces the data dimensionality by removing the redundant features, hence improving the training and inference speed. Nonredundant significant features from the ultrasound images of the carotid artery are extracted and used by machine learning (ML) algorithms to classify the image as abnormal or normal. Using additional features might cause overfitting, and less count features may make the data underfit. A good machine learning model may be built with relevant extracted and selected features from the image. Blood flow features like end-diastolic height, resistivity index (RI), maximum systolic height, pulsatility index (PI), spectral broadening index, and height width index help in plaque identification. Texture, grayscale median (GSM), entropy, coarseness, Hurst coefficient, etc. are some of the useful features [4, 5]. The feature mapping to the classes in a computer-assisted diagnostic (CAD) system is called classification.

Loizou et al. proposed a texture feature variation in carotid artery ultrasound video to recognize the biomarkers of the plaque [6]. Followed by denoising and segmentation, the systole and diastole features were extracted from the video sequence. For the normal, symptomatic, and asymptomatic groups, a higher grayscale median was observed in systole and diastole cardiac cycles. Plaque texture features and grayscale median (GSM) were considerably diverse for the two classes. A multiresolution texture classification technique was proposed by Nikolaos et al. to classify the B-mode carotid artery ultrasound image as with or without plaque deposit [7]. Wavelet packet, stationary wavelet, discrete wavelet, Gabor transform, and other basis function decomposition schemes showed effectiveness in identifying the disease. Appropriate features were selected using deviation in values of the features and using a nonlinear correlation coefficient for thresholding. He proved that biomechanical forces affected texture analysis, and they showed horizontal directionality.

Prostate cancer inventions in transrectal ultrasound images by an automatic segmentation approach were proposed by Wang et al. [8]. The low layers of the convolutional neural network (CNN) are suppressed, and the prostate features in the deep layers are increased to identify, select, and influence the multilevel features from the various layers so that each layer features are enhanced. Layer-wise attention is used for enhancing the features in individual layers. The steps are generating attentive maps in layers, concatenate single-layer feature map to multilayer feature maps, and kernel arrangement in the three convolutional layers. The kernels used in the first two convolutional layers are $3 \times 3 \times 3$, and the last kernel has $1 \times 1 \times 1$ layer. From the learned samples in the folds, hyperparameters were identified by cross validation.

A feature-guided denoising CNN was proposed by Dong et al. [9] for removing noise and improving the image quality of portable ultrasound images. A feature masking layer was proposed for hierarchical noise removal in layers. Feature extraction was performed by an explainable artificial intelligence procedure. The highest important features were observed, and the other less important features were also partially preserved by guided backpropagation to map the neural network's choice. The feature images were combined with the Laplacian pyramid fusion method. BI-RADS feature extraction for characterizing the breast cancer lesion, which is continuously varying during the ultrasound sequence, was proposed by Sellami et al. [10]. The analysis was performed for the varying images with morphological and texture features. They concluded that the feature extraction should be performed in many slices of similar mass to get the optimal segmentation results. Slice selection depends on the radiologist, and another slice may have the necessary useful information, which should not be missed for diagnosis.

Siavash et al. proposed a method to quantify morphological features, which helped in classifying tumor cells and disease identification [11]. By conserving the bigger vessel trunks, morphological parameters like tortuosity were measured. They developed an approach to augment the tumor microvessels with ultrafast ultrasound imaging. Wang et al. used a pretrained deep convolutional neural network (DCNN) and developed a multinetwork feature extraction model, which also performed dimensionality reduction and trained an ensemble support-vector machine [12]. Followed by preprocessing of the histological data by scale variation and color improvement, features in many levels were extracted by four trained DCNN. Using dual-network orthogonal low-rank learning, feature selection is performed for overfitting modifications and performance boosting of the method.

Zhou et al. proposed an involuntary measurement with phase images for spine curvature using three-dimensional ultrasound volume projection images [13]. Bony feature extraction by twofold thresholding strategy with asymmetric and symmetric measures information using phase congruency was performed. When the signal Fourier components are hugely in-phase, they can extract Mach bands, roof, line edges, and step edges.

Li and Liu proposed a genetic algorithm using information flow for the Naive Bayes classifier. From the view of correlation and angle of causality, a new weight measure criterion is produced by information flow. The approach provided improved classification accuracy compared with other attribute-weighting approaches with Bayes classifiers. The first, third quartile, and median values were higher for the proposed classifier [14]. Zhang et al. proposed a LVQ with a modular reconfigurable pipelining architecture for object recognition and image compression [15]. The method was verified in a 65 nm CMOS prototype chip. Reduced computation time and integration density efficiency were achieved by the approach.

Feature extraction and selection of the carotid artery ultrasound images are performed to assist ML-based classification. The best significant features are selected by a divergence approach and principal component analysis (PCA). The images are classified as with or without plaque deposit, for early identification of the presence of stroke. This study's layout is as follows. Section 2 gives the methodology of feature extraction, selection, and classification, Section 3 explains the results and discussions, and Section 4 concludes the study.

2. Methodology

This segment describes the feature extraction of the carotid artery ultrasound images. Appropriate features are selected after extracting the image features. The selected features are classified using Naive Bayes and DLVQ machine learning algorithms, and the classification performances are analyzed.

2.1. Carotid Artery Ultrasound Images. Ultrasound imaging is economically affordable, noninvasive, and continuously improving in image quality that will provide early diagnosis of arterial disease. Intima-media layer thickness, lumen diameter, and texture characterization are necessary for the assessment of cardiovascular illnesses. The ultrasound images are affected by speckle noise and should be effectively denoised, so that image quality is preserved and the useful features are not lost. Curvelet decomposition-based denoising is performed for noise removal.

The carotid artery is an artery in the neck region, which transports pure blood from the heart to the brain and the front of the face. It contains the common carotid artery (CCA), which splits into external carotid artery (ECA) and internal carotid artery (ICA). Figure 1(a) presents the carotid artery structure, where ICA provides blood to face and ECA to the brain. The bifurcation is a more plaque-prone area.

Figure 1 presents the sample carotid artery ultrasound image with and without plaque deposit. The deepest smooth layer is intima, muscular middle layer media, and the outer layer is adventitia. Lumen is the inner core of the artery. Atherosclerosis is the narrowing of the artery lumen because of fat and calcium deposit in the artery wall, which may lead to thinning of blood flow as indicated. The local thickening in the artery because of fat deposition is called plaque formation. The intima-media thickness (IMT), lumen-intima (LI) interface thickness, and media-adventitia (MA) interface thickness influence the carotid plaque thickening. IMT measurements for a healthy person are from 0.2 to 0.25 mm.

Carotid artery disease identification includes plaque characterization and layer thickness measurements on age, gender, environmental conditions, and other habits of the person. The increased plaque thickness in the carotid is considered as an early indicator of future cardiovascular risks like stroke and atherosclerosis. The artery is at distance of 1 to 3 cm from the skin and so can be analyzed with imaging techniques.

2.2. Database Creation. Ethical clearance is obtained from SRM Medical College Hospital and Research Centre, Kattankulathur, Tamil Nadu, India, to get carotid artery ultrasound images. Carotid artery ultrasound B-mode image datasets are collected from SRM Medical College Hospital and Research Centre, Kattankulathur, Chennai, and Bharat Scans, Chennai.

Three hundred and sixty-one carotid artery ultrasound images were obtained, out of which 202 are normal images without plaque deposit and 159 images are with plaque deposit in the artery layers. About 75% (270) of data are used for training and 25% (91) for testing the machine learning algorithms.

2.3. Feature Extraction. Feature extraction and selection prevent overfitting of the training data and poor generalization of the new samples as given in Figure 2. Effective model construction for machine learning depends on the suitable optimized features. For a given feature set $F = \{f_1, f_2, \ldots, f_n\}$, the features to be selected should maximize the learner algorithms' ability to classify the carotid image as symptomatic or asymptomatic. F should be a function maximizing the scoring function. The features are normalized or translated in the range [0 1]. Thus, the data are aligned with similar distributions and help in model fit. Z score normalization procedure is used, which is a standard score technique. Population mean is deducted from the individual data and uniformly divided by the population standard deviation.

Despite variations in class, a useful feature should remain unchanged. Feature extraction categories are based on nontransformed and transformed structural characteristics, and structural and graph descriptors. For high-dimensional feature space, computational complexity increases [16]. A kernel function is made to record the nonlinear data into a higher dimensional space. Kernel is a dot product in high-dimensional space. Thus, all computations are made in the low space dimension. The kernel function is given by

$$K(x, x') = \vartheta(x)^T \vartheta(x)', \tag{1}$$

K is the inner product of the vectors x and x' in the low-dimensional feature space for a function ϑ. At an instant y, with slope w_0, the input's hyperplane is given by

$$y(x) = \operatorname{sign}\left[\sum_{i=1}^{M} y_i K(x, x') + w_0\right]. \tag{2}$$

Feature selection is to identify the relevant properties of the image for data reduction and reduction in feature set, and to improve accuracy for performance improvement and proper understanding of the data for image analysis. Features may be subdivided based on their relevance.

The extracted features may belong to any of the following categories, which assist in deciding whether it is a significant feature.

(i) A feature X_i is irrelevant for all the subsets belonging to S_i.

$$P\left(X_i, Y \mid S^{-i}\right) = P\left(X_i \mid S^{-i}\right) P\left(Y \mid S^{-i}\right). \tag{3}$$

These are the features with very less or zero probability calculated by Kullback-Leibler divergence.

(ii) A feature X_i is nearly unrelated with approximation value $\mu > 0$, for subsets S_i

$$\mathrm{EMI}\left(X_i, Y\right) \leq \mu. \tag{4}$$

For $\mu = 0$, the feature is surely irrelevant.

(iii) A feature X_i is separately inappropriate if the significance threshold $\varphi \geq 0$.

$$\mathrm{MI}\left(X_i, Y\right) \leq \phi. \tag{5}$$

(iv) A feature i is possibly nearly inappropriate based on D index computed with n number of examples, with approximation $\phi \geq 0$ and risk $\delta \geq 0$.

$$P(C(i, m) > \phi(\delta, m)) \leq \delta. \tag{6}$$

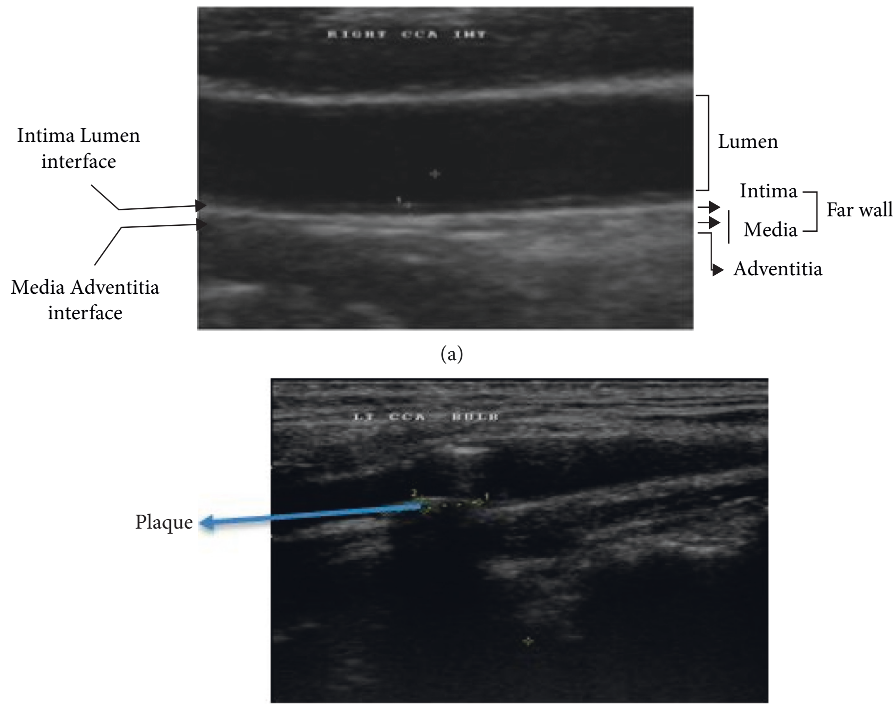

FIGURE 1: Sample carotid artery ultrasound image (a) with plaque and (b) without plaque.

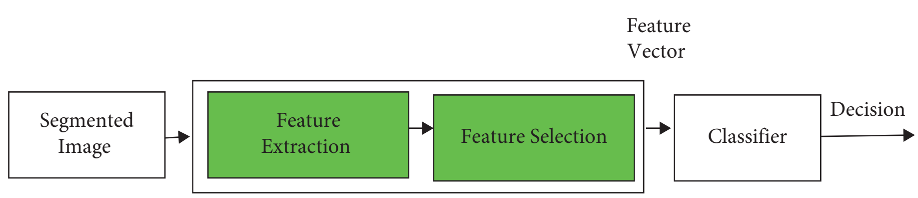

FIGURE 2: Block diagram of classification system.

(v) A subgroup V of features is certainly adequate if it also belongs to the complementary of the subset.

$$ {}^{i}_{v} P(Y \mid V) = P(Y \mid X). \tag{7}$$

(vi) A subgroup V of features is roughly adequate with approximation level $\phi \geq 0$ when

$$\mathrm{DMI}(V) \leq \phi. \tag{8}$$

If $\phi = 0$, the subset is surely sufficient.

(vii) A subset V of features is minimally approximately sufficient with approximation level $\phi \geq 0$, and other smaller subsets of ϕ does not exist.

From the carotid artery dataset, more artery characteristic-related features along with the standard features are extracted to analyze the image and identify whether the person has plaque deposit. The dataset was enhanced and labeled by radiologists for accuracy [17], and 63 shape, texture, morphology, histogram, and correlogram-based features are extracted and analyzed with the machine learning techniques.

Along with the existing features, plaque morphology-based features extracted are plaque power spectra for all the three intensity variations (low, medium, and high), namely, shape, connectivity, convexity, plaque size, lipid core, presence of intraplaque hemorrhage, smooth lumen surface indicating no risk, and rough lumen, which may lead to stroke and plaque volume. Figure 3 gives the procedure followed for feature extraction, selection, and classification of the carotid artery ultrasound images.

2.4. Extracted Features. Features are extracted from the carotid artery images in the database following preprocessing followed by segmentation steps. The image is noise-free and contrast enhanced, assisting in the quantization of the image features. The below sixty-three features are extracted from the carotid artery ultrasound image database.

Table 1 gives the list of the extracted features. Thirty-three texture features, five shape features, ten histogram- and

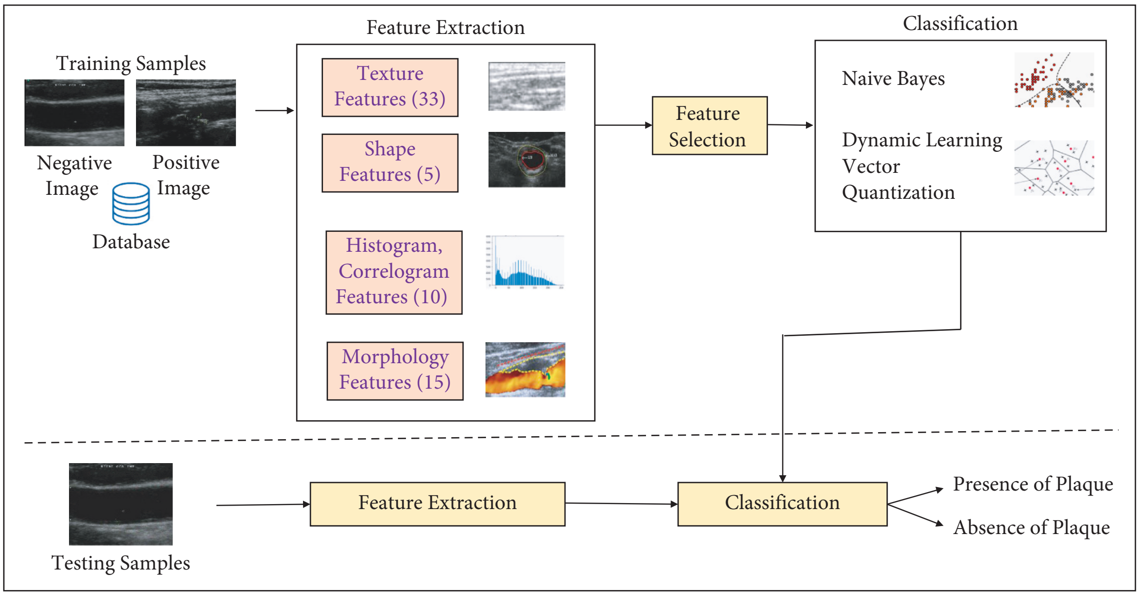

FIGURE 3: Feature extraction, selection, and classification of carotid artery ultrasound images.

TABLE 1: List of extracted features.

Sl. no	Feature type	Features
1	Texture features (33)	Gray-level co-occurrence matrix (GLCM)—inertia, energy, correlation, contrast, entropy, and homogeneity Gabor wavelet Statistical features—mean, median, kurtosis, and skewness Local binary pattern (LBP)—textures spatial structure Gray-level difference statistics (GLDS)—mean, entropy, contrast, angular second moment, and homogeneity Fractal dimension texture analysis (FDTA) Radial and angular sum of discrete Fourier transform for Fourier power spectrum Neighborhood gray-tone difference matrix (NGTDM), given by strength, complexity, coarseness, and contrast Absolute gradient—mean, variance
2	Shape features (5)	Sharpness Complexity Length irregularity Aspect ratio and circularity
3	Histogram and correlogram features (10)	Gray-level histogram of segmented ROI of the carotid image—for 32 same measurements, bins were computed Plaque histogram represents plaque characterization Multiregion histogram—to check whether plaque outer region signifies disease progression Grayscale median (GSM) derived from the histograms first-order statistics, and entropy represents echogenicity Histogram of oriented gradient (HOG)—gradient magnitude and orientation Correlogram—statistics and spatial distribution of the features Texture and shape features—normalized; histogram and correlogram features—used without normalization
4	Morphology features (15)	Mean probability density functions (PDFs), mean cumulative distribution functions (CDFs) Plaque power spectra for all the three intensity variations (low, medium, and high) Shape, connectivity, and convexity Plaque size, lipid core, and presence of intraplaque hemorrhage Smooth lumen surface—no risk; rough lumen—leads to stroke Plaque volume

correlogram-based features are extracted. Fifteen plaque morphology-based features were extracted from the carotid artery ultrasound image database. A detailed explanation of the extracted image features is given below.

2.4.1. Texture Features. Texture in the image is computed from the gray-level co-occurrence matrix (GLCM), which uses spatial difference among the pixels, which are in pairs with a certain distance, relation, and direction [18, 19]. Inertia, energy, correlation, entropy, and homogeneity information are extracted from the matrix. It is proved that the directions 0°, 45°, 90°, and 135° are less dominant for GLCM in medical images, requiring less computation at these angles. For image $I(k, k)$, the co-occurrence matrix is given by

$$C_M = \sum_{i=1}^{k}\sum_{j=1}^{k}\begin{cases} 1, \text{ if } I(i, j) = k, I\left(j + D_x, j + D_y\right) = k, \\ 0, \text{ otherwise,} \end{cases} \tag{9}$$

where $D_x = D.\cos(\theta)$, and $D_y = D.\sin(\theta)$, θ being the offset defining matrix direction from the central pixel, and D, the distance from the central pixel. For the given angle θ, the parameters computed are as follows:

$$\begin{aligned} \text{contrast} &= \sum_{a=1}^{L}\sum_{b=1}^{L}(a-b)^2 C_M, \\ \text{correlation} &= \sum_{a=1}^{L}\sum_{b=1}^{L} C_M\left[\frac{\left(a-\mu_a\right)\left(b-\mu_b\right)}{\sqrt{\left(\sigma_a^2\sigma_b^2\right)}}\right], \\ \text{energy} &= \sum_{a=1}^{L}\sum_{b=1}^{L} C_M^2, \\ \text{homogenity} &= \sum_{a=1}^{L}\sum_{b=1}^{L}\frac{C_M}{1+|a-b|}. \end{aligned} \tag{10}$$

Gabor wavelet texture features are computed in precise directions and frequencies. Statistical features like mean, median, kurtosis, and skewness were computed. LBP gives the characteristics of the texture's spatial structure. GLCM analyzes the pixel pair's gray-level distribution and is known as a second-order histogram. Gray-level difference statistics (GLDS) extracts the texture features mean, entropy, angular second moment, contrast, and homogeneity representing the difference between the pairs of average gray levels. For $d = 1$, the mean displacement values were computed.

The following are the relation between texture and statistical characteristics.

(i) For dis-similar pixel pair in coarse texture region, contrast is high, representing considerable variation in gray level.

(ii) A high-energy feature value represents the textural uniformity of the image.

(iii) Uniform GLCM is represented by a large entropy value, which represents nonhomogeneity or degree of disorder.

(iv) Homogeneity of the pixel pair is small for different gray-level pixel pairs.

(v) Pixel's neighborhood influence represents the correlation.

The pixel statistical properties given by the statistical feature matrix (SFM) are coarseness, roughness, periodicity, and contrast. Pixel's self-similarity is represented by fractals in Euclidean space for a bounded set A for N overlapping copies of itself. For a scaling ratio s, the fractal dimension is given by

$$D = \frac{\log N(s)}{\log(1/s)}. \tag{11}$$

A rough texture has less fractal dimension texture analysis (FDTA) at image resolution 4. Radial and angular sum of discrete Fourier transform for Fourier power spectrum textural feature is computed [20]. The texture's visual properties are projected in the neighborhood gray-tone difference matrix (NGTDM), given by strength, complexity, coarseness, and contrast. The absolute gradient value is more when the pixel intensity moves from black to white, and it is less when it moves from dark gray to a lighter shade. Dark to light shade movement is indicated by a positive gradient, and light to dark shade is represented by a negative gradient [21]. Mean and variance are computed from the absolute gradient texture feature. It measures the mean gray-level changes through the image and how far the pixels are from the mean deviation. Pixels of the same gray level in a certain route are given by the run-length matrix.

2.4.2. Shape Features. Shape-based similarity among the pixels is extracted by shape features. It is a content description based on and performed by feature extraction and likeness measurement among the extracted features. Region-centered shape feature projects the contour characteristics in the entire image region, and contour-based shape feature gives the shape in the contour alone. Contour-based shape features extracted are sharpness, complexity, length irregularity, aspect ratio, and circularity. Contour detection from the edges is possible with these rotation, translation, and scale-invariant shape features [22–24].

$$\begin{aligned} \text{sharpness} &= \sum\frac{\max\left(0, 1-\left(\left(2|\theta-\pi|/\pi\right)^2\right)\right.}{n}, \\ \text{complexity} &= \frac{10^{-3}}{n}, \\ \text{length irregularity} &= \frac{\sum\left|L_i - L_{i+1}\right|}{K}. \end{aligned} \tag{12}$$

For $n > 3$, $K = 2P$ and for $n = 3$, $K = P$, which is the length of the polygon segment and the next segment.

$$\text{aspect ratio} = \frac{p_1 + p_2}{C},$$
$$\text{circularity} = \frac{4\,pA}{P^2}, \tag{13}$$

where the segment boundary enclosed polygon sides n, discontinuity angle θ, the perimeter of the polygon bounded by segment border P, and the most significant perpendicular distances to the boundary p_1 and p_2. X and Y coordinates of the picture frame, area of ROI, perimeter, and perimeter^2/ area of ROI were computed to find whether the complexity and size of the carotid image shape help in identifying plaque deposit.

2.4.3. Histogram and Correlogram Features. For the continuous pixel data, the histogram is its frequency distribution representation. Gray-level histogram of segmented ROI for the carotid image for thirty-two same width bins was computed. The plaque histogram feature effectively represents the plaque characterization. The multiregion histogram is computed for equidistant ROI to check whether the plaque outer region signifies disease progression. Grayscale median (GSM) derived from the histograms first-order statistics and entropy represents the echogenicity and arterial wall ROI's randomness. For the image array Y, T_2 histogram is computed for a known mean scalar A. Image data are obtained from the first-order histogram with n^{th} feature $y_n(i, j)$ in the local region M. Let us consider y_n constitute discrete values only. The distance vector, which is the gray-level difference between the two pixels, is given by

$$d = \left(\Delta_x, \Delta_y\right), \tag{14}$$

for integers Δ_x and Δ_y. At distance d, the gray-level difference is given by

$$Y(d) = |\, I(i, j) - I\left(i + \Delta_x, j + \Delta_y\right) |. \tag{15}$$

The HOG feature derived from DCT gives the details about corners and edges in the image. Gradient and orientation information of the artery layer localized region is extracted after separating the image into smaller regions. The histogram of each region is separately computed from the gradients and orientations of pixel values. For directions G_x and G_y, the gradient magnitude is given by

$$\text{gradient magnitude} = \sqrt{G_x^2 + G_y^2}. \tag{16}$$

The orientation of each pixel is given by

$$\tan\phi = \frac{G_y}{G_x}. \tag{17}$$

The number of HOG features is dynamic based on the size of each region. Based on the gradient and direction, the weighted HOG is generated. To prevent aliasing problems, in orientation and position centers, bilinear vote interpolation is performed.

Statistics and spatial distribution of the features are represented by a type of histogram called correlogram [25]. Pixel gray intensity from the center is computed to get the correlogram of the image. The distance of each pixel from the center is identified from which equidistant pixels histograms were computed. The calculated distance to the maximum distance difference is divided by the normalization factor, which gives the correlogram comparison. The texture and shape features are normalized, whereas histogram and correlogram features are used without normalization.

2.4.4. Morphology Features. The presence of structural elements at different scales is identified by morphological features. The near-isotropic detection structural elements are represented by + in the structural pattern of the plaque. At the two morphological sets, mean cumulative distribution functions (CDFs) and the mean probability density functions (PDFs) are computed. Plaque component-based multilevel decomposition describes the morphology of the image [26, 27]. The normalized image is thresholded at low, medium, and high intensities. The unstable plaque is indicated by low dark components, and the bright region indicates stable plaque. The plaque power spectra for all the three intensity variations are used as a feature for plaque classification. The hypergeometric function used to capture the morphology of the image by the n_{th}-order Krawtchouk classical polynomial k is given by

$$k_m(x; p, N) = \sum_{k=0}^{N} a_{k,m,p} x^k = \mathrm{aF}_1\left(-m, -x; -N; \frac{1}{P}\right). \tag{18}$$

For a given x, with $m = 0$ to N, $N > 0$, $p \in (0, 1)$ if the hyperbolic function F_1. This represents the geometrical structure of the artery and the carotid plaque with details of shape, connectivity, and convexity. Clinical diagnosis depends on the artery wall morphology as a weighted map of the weighted original image. If the segmentation results are poor, the contour morphology may miss some details, leading to improper diagnosis. The morphological stream of feature extraction selects all the morphological features required for learning and classification like plaque size, lipid core, and presence of intraplaque hemorrhage [28]. Plaque destabilization leads to plaque rupture, and the disrupted plaque constitutes a thrombus in the distal artery layers. The volume of plaque in the carotid artery is not a clear indicator of the degree of stenosis. Ischemic symptoms can be identified by the plaque morphological features. In spite of any stenosis degree, the features may cause stroke risk. Thus, the morphological features and the degree of stenosis together give the plaque vulnerability characteristics. A smooth lumen surface indicates no risk, and a rough lumen is considered to lead to stroke.

Blood pressure and plaque rupture cause intraplaque hemorrhage, and it is closely related to cerebrovascular events. The susceptible plaque has a thin fibrous cap, which covers a lipid-rich necrotic core containing inflammatory cells. The artery attempts to maintain a uniform plaque diameter concerning the lumen. Positive remodeling tends to increase the diameter, and adverse remodeling tends to decrease the diameter, which is called stenosis [29, 30]. Plaque volume is proved to be a more significant feature to identify the disease progression and vulnerability than the degree of stenosis.

Echolucent plaque, which contains big white blobs, is considered to be dangerous. Calcified and collagen-stuffed plaque is stable and has very less chance of rupture with a tiny high-intensity image. A lipid with scattered components in the low-intensity image can be characterized as asymptomatic. Thus, unstable plaque is an effect of the thin fibrous cap. From the morphological features extracted, it is understood that plaque instability may not lead to stenosis but reduces blood flow in the artery.

2.5. Feature Selection. A robust subset of the extracted features is selected to reduce computational complexity and improve classification accuracy. Feature selection aims at dimensionality reduction, retaining the discriminatory information from the images. The maximum discriminant features from the extracted features are carefully chosen depending on the subsequent method.

The distance among two classes for all the features are generated as below for mean m_1, m_2 and standard deviation σ_1, σ_2.

$$\text{distance} = \frac{|m_1 - m_2|}{\sqrt{\sigma_1^2 + \sigma_2^2}}. \tag{19}$$

Significant features are identified using the distance measure, and increased distance means more the significance. Sixty-five features are extracted, from which twenty-two most relevant features are considered for the classification process. Along with this method, the principal component analysis (PCA) method for the selection of features is performed. Eigenvalues are used for deriving the principal components. Uncorrelated feature set and principal components are achieved from the correlated ones, orthogonal transformation.

The steps in PCA feature reduction are as follows:

(1) The mean value of the dataset D is computed.

(2) A new matrix S is formed by subtracting the mean value from D.

(3) From S, covariance is estimated at $C = \text{AAT}$. For data 1 to l,

$$S_k \in R^N, \sum_{k=1}^{l} S_k = 0 \, \text{covariance c} = \frac{1}{l} \sum_{i=1}^{l} S_i S_i^T. \tag{20}$$

(4) Eigenvalues derived from the covariance matrix are $[V_1, V_2, \ldots, V_n]$.

(5) Eigenvectors are found from the covariance matrix.

(6) Vector $D - \overline{D}$, a linear function of eigenvectors, is given by

$$D - \overline{D} = b_1 u_1 + b_2 u_2 + \cdots b_n u_n. \tag{21}$$

The symmetric covariance matrix is $[V_1, V_2, \ldots, V_n]$.

(7) Large eigenvalues reduce the dataset to $D - \overline{D} = \sum_{i=0}^{l} b_i u_i$, $1 < N$.

For a normally distributed dataset, the principal components are independent. The PCA depends on the individual variable screening. The PCA reduces the dimensionality of the dataset and increases interpretability with a reduction in loss of information. The variances are maximized one after the other by developing variables, which are uncorrelated.

2.6. Classification. The extracted features were given to machine learning classification algorithms, namely, the Naive Bayes algorithm and dynamic learning vector quantization (DLVQ), for a more accurate classification of the carotid artery ultrasound images.

2.6.1. Naive Bayes Algorithm. Bayes theorem considers an event probability based on prior knowledge of the related conditions with statistical interference. The Naive Bayes classification algorithm is a supervised approach, which depends on the Bayes theorem and assumes that the occurrence of a feature is not dependent on other features in the image. Frequency tables are generated from the dataset, followed by probability-based likelihood table generation and posterior probability calculation based on the Bayes theorem that are performed. Since the dataset followed a normal distribution, Gaussian-based Naive Bayes classification is performed for the dataset images. Weighting the features and structure extension is used to overcome the drawback of the complete feature independence assumption. A kernel function is used to estimate the data distribution instead of following a normal distribution.

For the two-class problem C_1, C_2, samples are indicated by n dimensional vectors.

$\overrightarrow{Y} = \{Y_1, Y_2, \ldots Y_m\}$ containing m attributes A_1 to A_m projecting m measured values. $\overrightarrow{Y}$ needs to be found with the highest a posteriori probability. Y lies inside the class C based on the following condition.

$$P\left(C_i \mid \overrightarrow{Y}\right) = \frac{P\left(\overrightarrow{Y} \mid C_i\right) P(C_i)}{P(\overrightarrow{Y})}. \tag{22}$$

The numerator value should be maximized to get a higher probability, since the probability of getting the Y vector is a constant. The assumption that the classes are conditional independent is performed [31, 32].

$$P\left(\overrightarrow{Y} \mid C_i\right) \approx \prod_{s=1}^{m} P(Y_s \mid C_i). \tag{23}$$

The Y_1 and Y_2 probabilities can be obtained from the training set.

Since Naive Bayes assumes that all the dimensions are independent, the classification accuracy is minimum compared to the LVG algorithm.

2.6.2. Dynamic Learning Vector Quantization (DLVQ). The LVQ is a winner take all Hebbian learning-based supervised learning approach. The algorithm classifies the sample with the same label as the codebook prototype, similar to the nearest neighbor classification. In the training phase, LVQ iteratively goes through the training sample y_j, shifted to the nearest available prototype $n_{m(j)}$ nearer or farther from y_j. This depends on if the $n_{m(j)}$ is in the same class as y_j.

$$n_{m(j)} = \begin{cases} n_{m(j)} + \rho\left(y_j - n_{m(j)}\right), \text{if } n_{m(j)} \text{has label } x_j, \\ n_{m(j)} - \rho\left(y_j - n_{m(j)}\right), \text{otherwise}, \end{cases} \tag{24}$$

ρ is between 0 and 1, and it is a step size, which is monotonically reducing [33, 34]. An adaptive version of LVQ is DLVQ, which can acclimate the neuron count to the dataset. It is a computationally less cost approach that has two layers of the fully connected network. The output parallels to one of the classes and matches to a reference vector with weights assigned. The output value is the consolidation of the outcomes of all the output neurons, which signifies the distance between the input sample and the reference vector. The distance helps in weight updating during the training phase and assigning the neuron to the corresponding output during the classification [33]. The frequency-sensitive competitive learning approach is used for training the network. DLVQ is used with global average pooling so that the model parameter count is minimized, thus reducing overfitting.

3. Results and Discussions

For the carotid artery ultrasound images, feature extraction, selection, and classification are performed. The results are analyzed with the classification performance measures.

3.1. Feature Extraction and Selection. The features extracted from the carotid artery ultrasound images are normalized and plotted for normal images without abnormalities and abnormal images with plaque deposit. From the bar plot, if a particular feature records significant variation for normal and abnormal images, it is considered as a significant feature. If a feature does not show variations for normal and abnormal images, it is considered not a significant feature and is omitted.

Figure 4 shows sample discriminant features such as skewness, kurtosis, histogram, HOG, and correlogram. Features with more variance help in machine learning classification since the values are far apart for normal and abnormal cases. For sample features such as correlation, contrast, entropy, and variance, the normalized feature values are indiscriminate and are hence not useful for machine learning classification. Table 2 gives the selected features based on discriminant and PCA feature reduction technique for the carotid artery ultrasound images.

The statistical PCA model identifies the discrete pattern in the data and thus selects only the required features. The input neurons of the classification algorithms are powered by the potential features.

3.2. Classification Performance Measures. The selection of appropriate performance measures for evaluating the machine learning classification algorithms provides faith for its real-time application. Since the data are imbalanced, applying more measures provides a clear insight into the algorithm usage. Classification of the carotid artery ultrasound images is a binary class problem, correct classification as fitting to the class being true positive (TP), correct classification as not fit in the class as true negative (TN), wrongly categorized to a class false positive (FP), and misclassified to a class as false negative (FN). The general efficiency of the model is given by

$$\text{accuracy} = \frac{\text{TP} + \text{TN}}{\text{TP} + \text{TN} + \text{FP} + \text{FN}}. \tag{25}$$

Agreement of the labels with positives is given by

$$\text{precision} = \frac{\text{TP}}{\text{TP} + \text{FP}}. \tag{26}$$

Sensitivity and recall give the efficiency of identifying positive labels. The data out of the classifier and the positive labeled ones' relationships are measured by F score. Negative label identification performance is measured by specificity. Recall is given by TPR, and probability is given by FPR. Area under the ROC curve (AUC) gives false classification identification presentation of the model, where 1 depicts a *n* ideal model [35, 36].

$$\begin{aligned} \text{recall} &= \frac{\text{TP}}{\text{TP} + \text{FN}}, \\ \text{precision} &= \frac{\text{TP}}{\text{TP} + \text{FP}}, \\ \text{f score} &= 2 \times \frac{\text{precision} \times \text{recall}}{\text{precision} + \text{recall}}, \\ \text{specificity} &= \frac{\text{TN}}{\text{TN} + \text{FP}}, \\ \text{AUC} &= \left(\frac{1}{2}\right)\left(\frac{\text{TP}}{\text{TP} + \text{FN}} + \frac{\text{TN}}{\text{TN} + \text{FP}}\right), \\ \text{Accuracy} &= \frac{\text{TP} + \text{TN}}{\text{TP} + \text{TN} + \text{FP} + \text{FN}}. \end{aligned} \tag{27}$$

These parameters denote the classification model performance. The classification models used ReLU activation function. ReLU is a nonlinear activation function, which does not activate all neurons at the same time. It is fast and easy and converges faster compared to other activation functions.

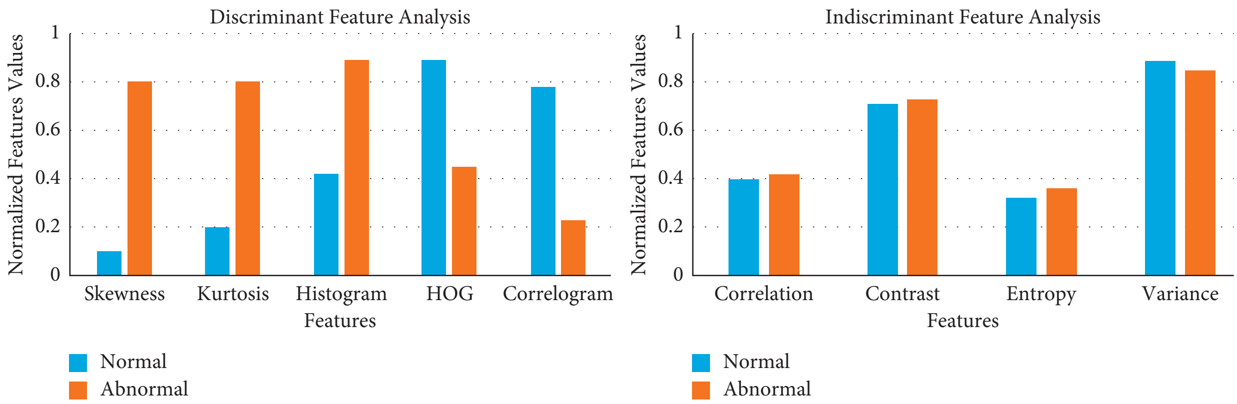

Figure 4: Feature analysis.

Table 2: List of selected significant features.

Sl. no	Selected features	Description
1	Texture	Spatial arrangement of image intensity
2	Spatial structure	Exploit location information
3	Skewness	Extent to which a distribution differs from a normal distribution
4	Kurtosis	Pixel intensity distribution
5	Histogram	Pixel distribution as a function of tonal variation
6	Correlogram	Spatial correlation of intensity changes with distance
7	HOG	Count incidences of gradient alignment in localized regions of an image
8	Gabor wavelet	Frequency-wise intensity variation check in specific direction
9	Angular 2nd moment	Textural uniformity in image
10	Shape	Shape characteristics
11	Sharpness	Degree of clarity in both coarse and fine image detail
12	Length irregularity	Irregularities of the length of structures in an image
13	Mean probability density function	Probability that the region brightness is less than or equal to a specified brightness value
14	Grayscale median	Median of grayscale intensities
15	Multiregion histogram	Checks whether plaque outer region signifies disease progression
16	Arterial wall ROI's randomness	Randomness present in the artery wall
17	Absolute gradient	Directional change in intensity
18	Angular and radial sum of discrete Fourier transform for Fourier power spectrum	Fourier power spectrum's Fourier transform
19	Coarseness	Type of texture feature
20	Convexity	Convex curves present in an image
21	Connectivity	Connectivity among pixels
22	Plaque volume	Plaque volume measure

3.3. Machine Learning. The database comprised of 202 normal images without any plaque deposit and 159 images with plaque deposit. The selected features are provided as the input neurons of the ML approaches. Box-Cox plot transforms the data so that it can be similar to a normal distribution. Considering the presence of normally distributed errors, a hypothesis test can be performed. The gain curve gives the performance of the machine learning models with randomly taken data. The curve analyzes the percentage of the target compared with a group with the highest probability. The receiver operating characteristic (ROC) curve provides the sensitivity vs. specificity relation for the

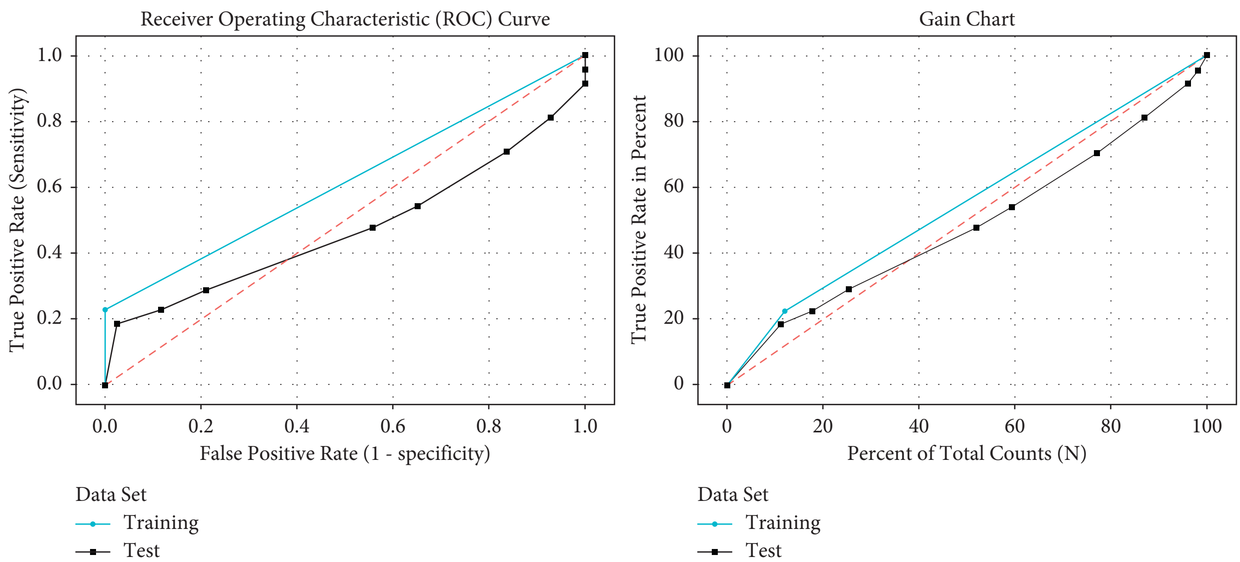

Figure 5: ROC curve and gain chart of Naive Bayes algorithm.

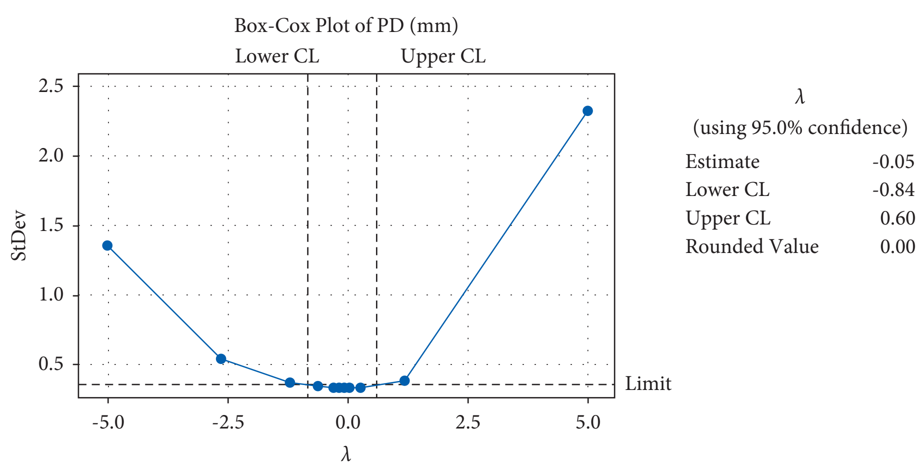

Figure 6: Box-Cox plot of plaque diameter.

probable cutoff values in all classification thresholds. The ordinal curve gives the contribution of the features and their significance. It helps in the data to rely on one final side.

Figure 5 gives the ROC curve and gain chart of the Naive Bayes classification. It has recorded an area under the curve training of 61.46% and 47.50% for testing. The gain chart gives the whole positive rate percentage to the total count percentage.

Figure 6 gives the Box-Cox plot for the plaque diameter, which is a linearity plot giving the correlation between the transformed StDev and the given lambda values. Figure 7 gives the pure ordinal curve for sample features meangl (mean gray level), kurtosis, contrast, and skewness.

Table 3 provides the confusion matrix of the applied ML techniques, namely, Naive Bayes and DLVQ, performed in 361 carotid artery ultrasound images.

Table 4 gives the comparison of the Naive Bayes and dynamic learning vector quantization approaches using the classification performance measures.

Table 5 separately gives the accuracy of the Naive Bayes and DLVQ algorithms with the extracted sixty-three features and the selected twenty-two features. Improved accuracy is found in both the machine learning algorithms on using only the selected features.

Classification of hard and soft plaques will aid in diagnosing dangerous plaque types and may be implemented as a

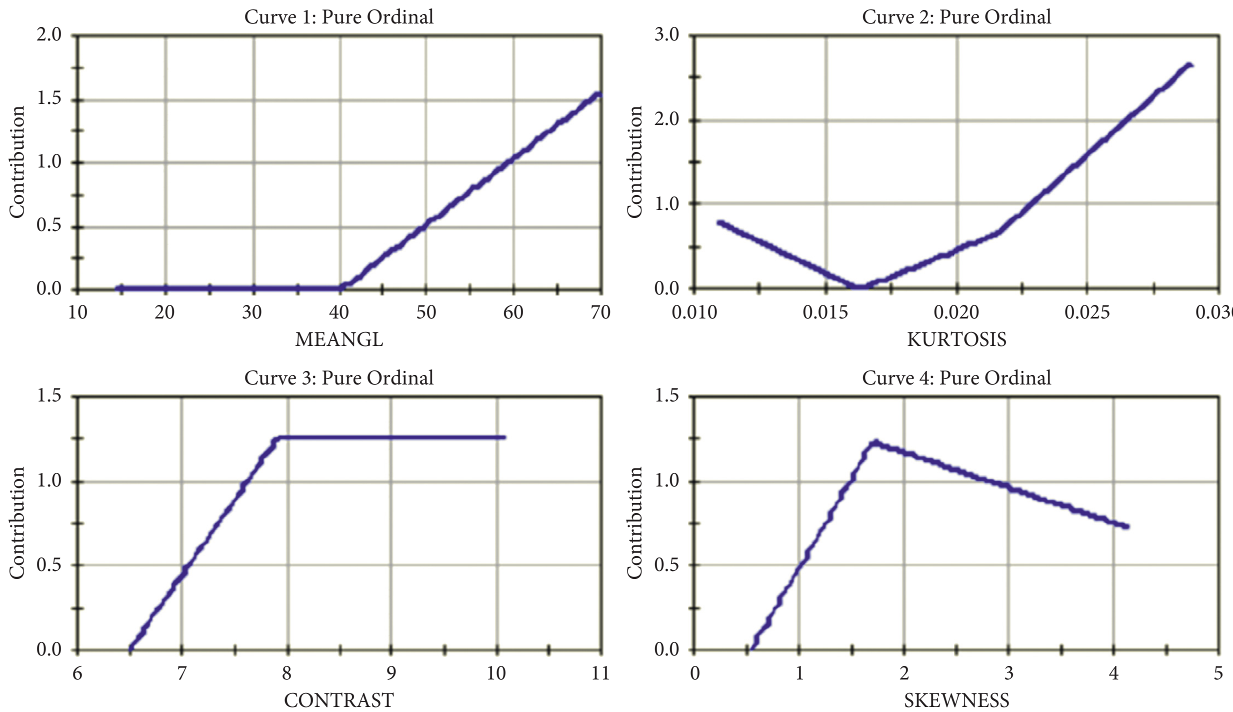

Figure 7: Pure ordinal curve.

Table 3: Confusion matrix of the ML algorithms.

	Naive Bayes		DLVQ	
	Actual positive (1)	Actual negative (0)	Actual positive (1)	Actual negative (0)
Predicted positive (1)	121	24	132	3
Predicted negative (0)	38	178	27	199

Table 4: Performance comparison of classification of carotid artery ultrasound images using ML approaches.

Algorithm	Accuracy	Specificity	Sensitivity	Precision	F score	AUC
Naive Bayes	82.82	88.11	76.1	83.44	79.60	85.77
DLVQ	91.68	98.51	83.01	97.77	89.78	98.14

DLVQ has recorded improved performance in terms of AUC, F score, precision, sensitivity, specificity, and accuracy compared with the Naive Bayes algorithm.

Table 5: Comparison of DLVQ performance with all extracted and selected features.

Accuracy	With all extracted features	With selected features
Naive Bayes	80.91	82.82
DLVQ	88.72	91.68

future work. A patient-specific model with more measurements from a single patient including boundary conditions, pressure, geometry, 3D images, and thermal images may be implemented to improve diagnostic performance.

4. Conclusions

Sixty-three features consisting of texture, shape, histogram, correlogram, and morphology were extracted from the carotid artery ultrasound images. Principal component analysis (PCA) and feature analysis by feature significance-based feature reduction were performed to minimize overfit and underfit problems. The robust subset from the extracted features reduces model complexity and computation and improves the efficiency of the classification task. Classification of Naive Bayes and DLVQ algorithms is performed using the extracted and selected features. DLVQ with the selected features recorded an accuracy of 91.68%, specificity 98.51%, sensitivity 83.01%, precision 97.77, F score 89.78%, and AUC 98.14%. DLVQ has proven to give improved performance compared to the DLVQ classification approach, on using the selected extracted features.

Data Availability

The data are not from any public database. So the authors will not be able to share the data.

Ethical Approval

Ethical clearances were obtained from SRM Medical College Hospital and Research Centre, India, number: 1736/IEC/2019.

Conflicts of Interest

The authors declare no potential conflicts of interest.

Acknowledgments

The authors are grateful to the SRM Institute of Science and Technology, Universiti Malaya, and Xuzhou Medical University. This work was supported in part by Universiti Malaya, and ACU UK under project no. IF063-2021.

References

[1] E. G. Sifakis and S. Golemati, "Robust carotid artery recognition in longitudinal B-mode ultrasound images," *IEEE Transactions on Image Processing*, vol. 23, no. 9, pp. 3762–3772, 2014.

[2] J. Vouillarmet, M. Helfre, D. Maucort-Boulch, B. Riche, C. Thivolet, and C. Grange, "Carotid atherosclerosis progression and cerebrovascular events in patients with diabetes," *Journal of Diabetes and Its Complications*, vol. 30, no. 4, pp. 638–643, 2016.

[3] D. M. Gujral, B. N. Shah, N. S. Chahal et al., "Carotid intima-medial thickness as a marker of radiation-induced carotid atherosclerosis," *Radiotherapy & Oncology*, vol. 118, no. 2, pp. 323–329, 2016.

[4] C. P. Loizou, C. S. Pattichis, M. Pantziaris, and A. Nicolaides, "An integrated system for the segmentation of atherosclerotic carotid plaque," *IEEE Transactions on Information Technology in Biomedicine*, vol. 11, no. 6, pp. 661–667, 2007.

[5] S. Latha, D. Samiappan, and R. Kumar, "Carotid artery ultrasound image analysis: a review of the literature," *Proceedings of the Institution of Mechanical Engineers-Part H: Journal of Engineering in Medicine*, vol. 234, no. 5, pp. 417–443, 2020.

[6] C. P. Loizou, C. S. Pattichis, M. Pantziaris, E. Kyriacou, and A. Nicolaides, "Texture feature variability in ultrasound video of the atherosclerotic carotid plaque," *IEEE Journal of Translational Engineering in Health and Medicine*, vol. 5, pp. 1–9, 2017.

[7] N. Tsiaparas, S. Golemati, I. Andreadis, J. S. Stoitsis, I. Valavanis, and K. S. Nikita, "Comparison of multiresolution features for texture classification of carotid atherosclerosis from B-mode ultrasound," *IEEE Transactions on Information Technology in Biomedicine*, vol. 15, no. 1, pp. 130–137, 2011.

[8] Y. Wang, D. Ni, H. Dou et al., "Deep attentive features for prostate segmentation in 3D transrectal ultrasound," *IEEE Transactions on Medical Imaging*, vol. 38, no. 12, pp. 2768–2778, 2019.

[9] G. Dong, Y. Ma, and A. Basu, "Feature-guided CNN for denoising images from portable ultrasound devices," *IEEE Access*, vol. 9, pp. 28272–28281, 2021.

[10] L. Sellami, O. B. Sassi, k. Chtourou, and A. B. Hamida, "Breast cancer ultrasound images' sequence exploration using BI-rads features' extraction: towards an advanced clinical aided tool for precise lesion characterization," *IEEE Transactions on Nano Bioscience*, vol. 14, no. 7, pp. 740–745, 2015.

[11] S. Ghavami, M. Bayat, M. Fatemi, and A. Alizad, "Quantification of morphological features in non-contrast-enhanced ultrasound microvasculature imaging," *IEEE Access*, vol. 8, pp. 18925–18937, 2020.

[12] Y. Wang, B. Lei, A. Elazab et al., "Breast cancer image classification via multi-network features and dual-network orthogonal low-rank learning," *IEEE Access*, vol. 8, pp. 27779–27792, 2020.

[13] G.-Q. Zhou, W.-W. Jiang, K.-L. Lai, and Y.-P. Zheng, "Automatic measurement of spine curvature on 3-D ultrasound volume projection image with phase features," *IEEE Transactions on Medical Imaging*, vol. 36, no. 6, pp. 1250–1262, 2017.

[14] M. Li and K. Liu, "Causality-based attribute weighting via information flow and genetic algorithm for naive bayes classifier," *IEEE Access*, vol. 7, pp. 150630–150641, 2019.

[15] X. Zhang, F. An, L. Chen, I. Ishii, and H. J. Mattausch, "A modular and reconfigurable pipeline architecture for learning vector quantization," *IEEE Transactions on Circuits and Systems I: Regular Papers*, vol. 65, no. 10, pp. 3312–3325, 2018.

[16] S. Latha, P. Muthu, K. Wee Lai, A. Khalil, and S. Dhanalakshmi, "Performance analysis of machine learning and deep learning architectures on early stroke detection using carotid artery ultrasound images," *Frontiers in Aging Neuroscience*, vol. 13, 2022.

[17] C. I. Christodoulou, C. S. Pattichis, E. Kyriacou, and A. Nicolaides, "Image retrieval and classification of carotid plaque ultrasound images," *The Open Cardiovascular Imaging Journal*, vol. 2, no. 1, pp. 18–28, 2010.

[18] J. Yang, Y. Jiang, and Y. Zhang, "Edge fuzzy clustering by eliminating undesirable features in garment texture image segmentation," *IEEE Access*, vol. 8, pp. 45368–45377, 2020.

[19] M. Li, X. Sun, W. Chen, Y. Jiang, and T. Zhang, "Classification epileptic seizures in EEG using time-frequency image and Block texture features," *IEEE Access*, vol. 8, pp. 9770–9781, 2020.

[20] K. Bommanna Raja, M. Madheswaran, and K. Thyagarajah, "Ultrasound kidney image analysis for computerized disorder identification and classification using content descriptive power spectral features," *Journal of Medical Systems*, vol. 31, no. 5, pp. 307–317, 2007.

[21] G. Castellano, L. Bonilha, L. M. Li, and F. Cendes, "Texture analysis of medical images," *Clinical Radiology*, vol. 59, no. 12, pp. 1061–1069, 2004.

[22] Li. Ce, Z. Dong, Du. Shaoyi, and T. Zhiqiang, "Deformation and refined features based lesion detection on chest X-ray," *IEEE Access*, vol. 8, p. 14675, 2020.

[23] J. L. Bruse, M. A. Zuluaga, A. Khushnood et al., "Detecting clinically meaningful shape clusters in medical image data: metrics analysis for hierarchical clustering applied to healthy and pathological aortic arches," *IEEE Transactions on Bio-Medical Engineering*, vol. 64, no. 10, pp. 2373–2383, 2017.

[24] D. Samiappan and V. Chakrapani, "Classification of carotid artery abnormalities in ultrasound images using an artificial neural classifier," *The International Arab Journal of Information Technology*, vol. 13, no. 6A, pp. 756–762, 2016.

[25] E. C. Kyriacou, C. S. Pattichis, M. A. Karaolis et al., "An integrated system for assessing stroke risk," *IEEE Engineering in Medicine and Biology Magazine*, vol. 26, no. 5, pp. 43–50, 2007.

[26] E. Kyriacou, M. S. Pattichis, C. S. Pattichis et al., "Classification of atherosclerotic carotid plaques using morphological analysis on ultrasound images," *Applied Intelligence*, vol. 30, no. 1, pp. 3–23, 2009.

[27] Q. J. A. Van den Bouwhuijsen, M. W. Vernooij, B. F. J. Verhaaren et al., "Carotid plaque morphology and ischemic vascular brain disease on MRI," *American Journal of Neuroradiology*, vol. 38, no. 9, pp. 1776–1782, 2017.

[28] L. Saba, C. Yuan, T. S. Hatsukami et al., "Carotid artery wall imaging: perspective and guidelines from the ASNR vessel wall imaging study group and expert consensus recommendations of the American society of neuroradiology," *AJNR American Journal of Neuroradiology*, vol. 39, no. 2, p. E9, 2018.

[29] J. Amores and P. Radeva, "Medical Image Retrieval Based on Plaque Appearance and Image Registration," *Plaque Imaging: Pixel to Molecular Level*, pp. 26–54, 2005.

[30] D. Samiappan, S. Latha, T. R. Rao, D. Verma, and C. Sriharsha, "Enhancing machine learning aptitude using significant cluster identification for augmented image refining," *International Journal of Pattern Recognition and Artificial Intelligence*, vol. 34, no. 09, Article ID 2051009, 2020.

[31] X. Liu, R. Lu, J. Ma, L. Chen, and B. Qin, "Privacy-preserving patient-centric clinical decision support system on naïve Bayesian classification," *IEEE Journal of Biomedical and Health Informatics*, vol. 20, no. 2, pp. 655–668, 2016.

[32] A. Faisal, S.-C. Ng, S.-L. Goh, and K. W. Lai, "Knee cartilage segmentation and thickness computation from ultrasound images," *Medical, & Biological Engineering & Computing*, vol. 56, no. 4, pp. 657–669, 2018 Apr.

[33] Z. Zhaowen Wang, N. M. Nasrabadi, and T. S. Huang, "Spatial-spectral classification of h images using discriminative dictionary designed by learning vector quantization," *IEEE Transactions on Geoscience and Remote Sensing*, vol. 52, no. 8, pp. 4808–4822, 2014.

[34] Md B. Hossain, K. W. Lai, B. Pingguan-Murphy, Y. Chai, M. I. Mohd Salim, and Y. Miin Liew, "Contrast enhancement of ultrasound imaging of the knee joint cartilage for early detection of knee osteoarthritis," *Biomedical Signal Processing and Control*, vol. 13, 2014.

[35] C. D'Elia, S. Ruscino, M. Abbate, B. Aiazzi, S. Baronti, and L. Alparone, "SAR image classification through information-theoretic textural features, MRF segmentation, and object-oriented learning vector quantization," *IEEE Journal of Selected Topics in Applied Earth Observations and Remote Sensing*, vol. 7, no. 4, pp. 1116–1126, 2014.

[36] S. Latha, D. Samiappan, P. Muthu, and R. Kumar, "Fully automated integrated segmentation of carotid artery ultrasound images using DBSCAN and affinity propagation," *Journal of Medical and Biological Engineering*, vol. 41, no. 2, pp. 260–271, 2021.

Hindawi
Computational Intelligence and Neuroscience
Volume 2022, Article ID 8239905, 8 pages
https://doi.org/10.1155/2022/8239905

Research Article

Identification Model of Writhing Posture of Classical Dance Based on Motion Capture Technology and Few-Shot Learning

Ning Zhang

Shandong University of Arts, Jinan 250000, China

Correspondence should be addressed to Ning Zhang; 20155060@qlnu.edu.cn

Received 16 March 2022; Revised 8 April 2022; Accepted 9 April 2022; Published 10 May 2022

Academic Editor: Xin Ning

Chinese classical dance is cut into the inner verve from a grasp of external form in dance instruction, and the aesthetic fashion and artistic norms of classical dance are established with historical depth. The "professional specificity" of characters and the "language description" of plots are eliminated in Chinese classical dance creation, highlighting the contemporary spirit of classical dance creation. Chinese classical dance was born during the early years of the People's Republic of China. The term "classical dance" did not refer to all Chinese classical dances at the time; rather, it referred to a dance form that embodied China's national spirit and had a classical cultural heritage based on Chinese traditional dance. The average frequency of step-over was 0.9, which was higher than the average rate of basic turnover of 0.75 and step-by-step turnover of 0.5, according to the results of the SPSS19.0 analysis. As a result, except for a few points with loud noise, it can be concluded that stepping over is an effective feature. The recognition model of the somersault posture of classical dance is studied in this paper, a database for real-time acquisition of three-dimensional data of human motion is established, and the Google model of human body characteristics is obtained based on feature plane matching of human body posture, all using motion capture technology and few-shot learning. The above data has good reference and application value for improving teachers' teaching level and arousing students' learning enthusiasm in the dance teaching process when applied to posture teaching and analysis. The captured data can convert human motion in real three-dimensional space into data in virtual three-dimensional space. Motion capture technology converts human motion information into a technology that can be recognized by computers.

1. Introduction

Chinese classical dance is made up of traditional Chinese opera, dance, martial arts, and ancient art resources that are mined, screened, and integrated. "Twist, tilt, circle, curve, form, spirit, strength, and law" are the overall requirements and prominent features of Chinese classical dance, and these eight words evolve into posture and movement law through waist movement [1]. Second, in dance creation, Chinese classical dance should be cut from the understanding of external form to the understanding of internal charm, and the aesthetic fashion and artistic norms of classical dance have been established with historical depth; third, in dance teaching, Chinese classical dance should be cut from the understanding of external form to the understanding of internal charm, and the aesthetic fashion and artistic norms of classical dance have been established with historical depth; and fourth, in dance creation [2, 3], Chinese classical dance should be cut from the "profession specificity" of character images and the " Opera," which contains the living fossil of dance inheritance, was studied and learned by the founders of Chinese classical dance. The development of opera is perhaps a tributary in the great Chinese culture, but it is the most clear and complete [4]. The origins of Chinese classical dance can be traced back to the early days of the People's Republic of China. At the time, the term "classical dance" did not refer to all Chinese classical dances; rather, it referred to a dance form that embodied China's national spirit and had a classical cultural heritage based on Chinese traditional dance. When we consider that history, we cannot help but think of Mr. Ouyang Yuqian. He actively advocated for dancers learning the fundamental skills of Chinese opera, as well as studying and distinguishing Chinese classical dance from basic opera dance, and this suggestion was taken into consideration and implemented in the curriculum of the first dance school in New China [5, 6].

Motion capture system can track, monitor, and record human motion data. At present, it has been preliminarily applied and developed in entertainment effectiveness, health record, rehabilitation training, and other aspects [7, 8]. Motion capture is a process of acquiring the size measurement, position, and direction information of moving objects so as to realize further research. Since the 1970s, motion capture has been an important method of photographic image analysis in biomechanics research, and since then, this technology has been more and more widely used in animation, robot control, human-computer interactive games, sports training, and other fields [9]. The motion capture system is mainly composed of sensors, signal acquisition equipment, data transmission, and data processing, including mechanical, electromagnetic, and optical. The adopted motion capture equipment is an optical motion capture system with high precision and good stability, which has achieved ideal results in the process of collecting Xinjiang Uygur dance data [10, 11]. The dance data collected by the motion capture system is input into the 3D animation software and can be displayed perfectly through the virtual display engine [12]. Motion capture technology is a rapidly developed technology in the last 20 or 30 years. Many domestic and foreign researchers have invested a lot of scientific research efforts in this field and obtained advanced scientific research results and rich theoretical support in many aspects, including the way and application of motion capture, the analysis of real-time motion data, and the analysis of motion posture.

This paper proposes to apply the motion capture technology to the tumbling posture recognition model of classical dance, establish a database to obtain the three-dimensional data of human motion in real time, and match the human posture based on the feature plane to obtain the Google model of human characteristics. Applying the above data to the posture teaching and analysis in the process of dance teaching is helpful to improve the teaching level of teachers, Mobilizing students' learning enthusiasm has good reference and application value [13, 14]. Human motion posture analysis first rose abroad. With the advent of the new century, Chinese domestic research experts also began the research and analysis of three-dimensional posture [15].

This paper studies and innovates the above problems from the following aspects:

(1) A writhing gesture recognition model of classical dance based on motion capture technology is proposed. This paper studies the identification model construction of the tumbling posture of classical dance. The combination of motion capture technology and the tumbling posture of classical dance will make up for the deficiency of traditional dance forms and has advantages that traditional dance does not have in the acquisition and transmission of movement skills. According to one's own state, one can study and demonstrate actions purposefully and then compare the analysis results of 3D motion data with the standardized action posture so as to correct the standardization of actions in time, which greatly improves students' learning and teachers' teaching efficiency.

(2) Build the database of the identification model of the tumbling posture of classical dance based on motion capture technology. Based on the application of motion capture technology to the identification of the tumbling posture content of classical dance, firstly, set the performer's dance movements and their range of motion; then, capture the three-dimensional data of the performer's dance movements and establish a three-dimensional dance teaching model database. Finally, make the dance movement database into a three-dimensional animation and apply it to the identification model of the tumbling posture of classical dance.

The paper is divided into five parts, and the organizational structure is as follows:

The first chapter introduces the research background and present situation of the tumbling posture of classical dance and puts forward and summarizes the main tasks of this paper. The second chapter introduces the domestic and foreign related work of the somersault posture of classical dance. The third chapter introduces the principle and model of motion capture technology. In chapter 4, the realization of the recognition model of tumbling posture of classical dance based on motion capture technology is introduced, and the performance of the model is compared through experiments. The fifth chapter is the full text summary.

2. Related Work

2.1. Research Status at Home and Abroad. Gaglio et al. proposed that the first trouble for Chinese classical dance to recognize the posture from opera is the contradiction between "stylized dance and functional training," which is the basic contradiction in the construction of Chinese classical dance teaching materials, which has not been completely solved until today [16]. TNA B proposed that the formation of "form" of Chinese classical dance was fundamentally influenced by ancient traditional concepts, mainly the concept of nature, and human natural activities affected the formation of artistic aesthetics and aesthetic ideas [17]. Shiqi et al. proposed that Mr. Mei Lanfang, an opera performing artist, is known as a male actress. When limited by certain clothing, props, and roles, how to shape the stage image of women's posture through a beautiful, "exquisite," delicate, and "language" orchid palm has become an art form integrating the song, dance, and music of the previous generation [18]. Nai et al. proposed that classical dance comes from the burst of emotion, and Oriental people have formed a unique way of posture expression under the influence of traditional ideas. Easterners are not used to expressing their feelings directly like the West, but in a gentle and implicit way, which stems from the naive, simple, and restrained emotional thinking of farmers in the bones of Easterners [19]. The authors proposed that Chinese classical dance is a genuine domestic product and a new kind of dance comparable to modern dance and ballet. Most of its soundtrack is played with musical instruments with Chinese characteristics, such as pipa, erhu, guzheng, and Xiao, and the clothing usually has a smell of ancient fragrance [20]. Deng et al. proposed that the historical and cultural spirit precipitated in opera and dance is in the same line with the spirit of China's 5000-year-old traditional culture. We absorbed the orchid palm from it and drew lessons from and cited the "nonphysical performance" in the drama dance performance, which uses hand movements and human body posture with eyes, body method, pace, and so on [21]. Pope et al. put forward that the traditional poetry contains the ancient people's aesthetic thought activities in the aspects of appreciation and creation, which has a certain influence on the formation and development of Chinese classical dance [22]. Maheu et al. proposed to stand on the vision of the discipline construction of Chinese classical dance. The original intention of the course construction of body rhyme is to deepen the national attributes of Chinese classical dance styles, but it is still the historical mission of the discipline to cultivate the actors' body posture, and it is also an important project for the discipline to continuously inherit and spread the faculty with cultural heritage and professionalism [23]. Christopher et al. put forward that "the basic ability training of Chinese classical dance refers to the basic ability training and special quality training of all parts of body posture." The basic skills training of Chinese classical dance mainly focuses on three aspects: strengthening the training of softness, training of quality and ability, and training of technical skills. From the ground, the lever, and the middle three parts, the soft opening strength of students and their technical skills can be solved [24]. Xuan et al. put forward that the body rhyme of Chinese classical dance should not only have the style of Chinese traditional body culture, but also conform to the scientific nature of human posture. Therefore, for the study of body rhyme of Chinese classical dance, discussing the principle of body rhyme capacity, the principle of style, and its practical application can provide important reference for the discipline to consolidate and deepen the theoretical foundation [25].

2.2. Research Status of Tumbling Posture Recognition in Classical Dance Based on Motion Capture Technology. This paper investigates the recognition of classical dance tumbling postures using motion capture technology. This paper examines the origin and transmission mechanism of the body rhyme movement power of Chinese classical dance from the perspective of human movement, in conjunction with traditional Chinese Dantian theory and the core of modern human physiological anatomy. This paper examines the principles of body rhyme movement in Chinese classical dance in terms of local form, overall movement law, and philosophical category from the standpoint of style; it then moves on to the application stage of action principle, which includes the application of principle in classroom teaching and the application of principle on stage. Human posture recognition and capture technology is currently the most widely used. The method for implementing it is to place the camera in a fixed position in space and then capture the object's real-time action and posture using light spots in this area. Classical art charm meets the rhythmic essence of traditional Chinese dance in China's classical dance. We must first determine the recognition target of human posture and the corresponding data acquisition scheme before recognizing the tumbling posture of classical dance. The main principle of attitude recognition and capture technology is to attach inertial sensors to the joints, such as a gyroscope and an accelerometer, to collect human attitude and action data, and then use data analysis and calculation to determine the amplitude and angle of human joint motion. The following are some of the advantages of this method: low price; there are no issues with the environment, such as light shielding, and the precision is excellent. This paper examines the significance of combining motion capture technology and dance teaching and verifies through experiments that using capture technology in teaching can improve students' subject status, as well as bring enlightenment and innovation to contemporary teaching research.

3. Principle and Model of Motion Capture Technology

The motion capture system records the movement process of moving targets using tracking devices with special marks placed at key positions. After that, computer processing is used to obtain three-dimensional space parameters, and finally, the matching of skeleton models used in animation is completed. The motion capture sensor's human behavior recognition technology is a multidisciplinary system that combines sensor technology, human dynamics, computer graphics, pattern recognition, and other disciplines. Front-end hardware and back-end software make up the technology. The front-end hardware's main functions and contents include gathering human motion data using motion capture sensors and transmitting that data to the computer. The back-end software's main purpose and content is to use the computer to efficiently process the collected exercise data so that the computer can automatically identify the action category of the captured object, allowing for action reproduction and human-computer interaction. First and foremost, the dancers' dance movements and range of motion should be established. The dance pose flowchart of the action capture technology of instructional design is shown in Figure 1.

While watching the animation, they draw posture movements in their mind. The actions that they do not understand or do not know can be demonstrated repeatedly from multiple angles. Secondly, students conduct practical demonstration, capture their own actions with high-precision three-dimensional camera, and compare them with teachers' standard actions. By comparing the dance movements with the teacher's standard movements in sections through the motion capture system, the shortcomings can be quickly found out, which is convenient for local correction.

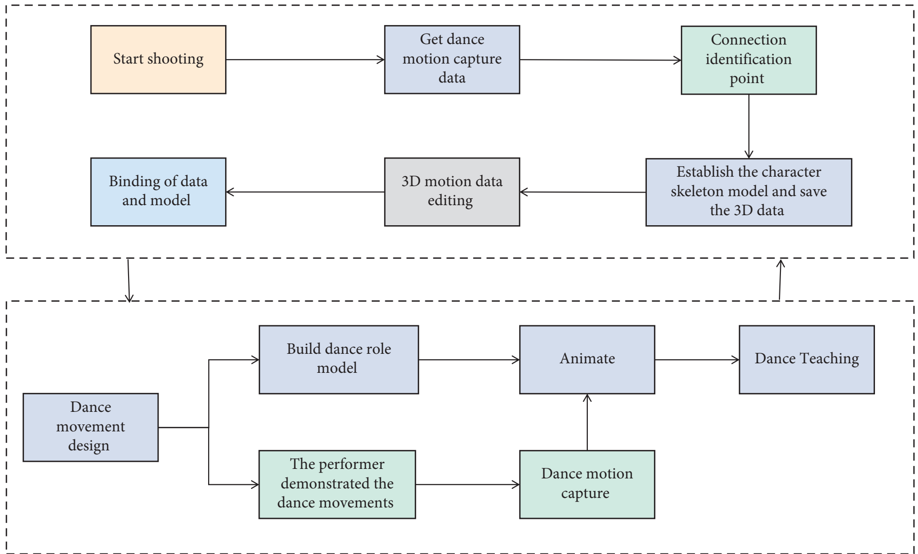

Figure 1: Dance posture flowchart of motion capture technology.

Motion capture technology is used to assist the teaching and research of dance. The early motion capture was proposed by American Polish Fisher in 1915. His "rotoscope" technology is considered to be the pioneer of motion capture technology. The main principle of this technology is to initially take the action video image taken in reality as the bottom sample of animation depiction, and then the animators depict the required actions frame by frame on this basis. The virtual display platform collects all kinds of dance materials, performs by actors, collects data through motion capture devices, and converts them into data recognizable by 3D animation software, and finally displays the dance content perfectly through the virtual display engine. The motion capture technology is applied to the data acquisition in the tumbling posture process of classical dance, the skeleton motion route of human body is extracted, and then the posture discrimination is obtained by using the feature vector matching method so as to establish the tumbling posture model of classical dance. It is easy to know that the depth of the whole bone tree is 3. The human body can be roughly divided into 11 bone trees, as shown in Figure 2.

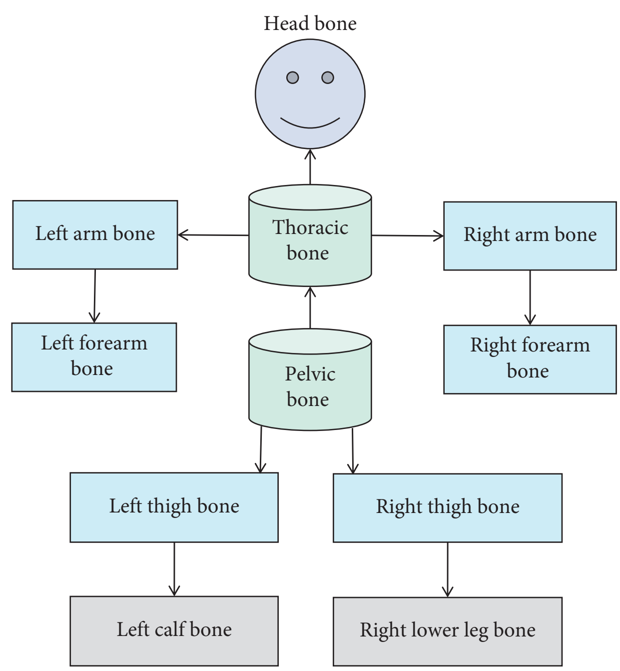

Figure 2: Basic skeleton structure of human body.

The matrix algorithm is proved to be a feasible BVH analytical algorithm, as shown in formula (1), on how to convert the correct position and dynamic of bones into animation.

$$v' = Mv. \quad (1)$$

Type v indicates said transformation point; v indicates the original point; and M indicates the transformation matrix.

This formula is especially important when the matrix multiplication is three independent Euler angles, which are not exchangeable to construct the rotation matrix. Rotation matrix R is based on the rotation parameters of each axis of the individual rotation matrix, R_x, R_y, R_z, as shown in formula (2), where the composition order is "XYZ."

$$R = R_x R_y R_z, \quad (2)$$

where R is rotation matrix; R_x $y$is$y$-axis rotation parameter; R_y $z$is$z$-axis rotation parameter; and R_z $x$is$x$-axis rotation parameter.

The movement of a single bone consists of translation, rotation, and proportional components, which can be combined together and transformed by using homogeneous coordinates. Unless otherwise stated, the order of combination of these different transformations is stated in the form that sufficient transformations will always follow, such as the following formula.

$$M = TRS. \tag{3}$$

Type S is said bone size and T is translation matrix.

In most motion capture file formats, the data is derived in a hierarchical way and formula, and formula (3) only gives the local transformation of a certain bone. The local transformation of the skeleton describes its direction in the local coordinate system, which in turn is influenced by the direction of its parent skeleton. Formula (4) lists this combination sequence, in which $n-1$ is the current bone, its mother bone is $n=0$, and EE represents the root bone of the bone hierarchy.

$$M_{\text{global}}^{n} = \prod_{i=0}^{n} M_{\text{local}}^{i}. \tag{4}$$

Using formula (4) and the derivation of local transformation, we can calculate the global position of the origin of each bone and obtain the position of the bone of the origin from the offset information of the hierarchy.

The function interval changes proportionally with the change of w, b, while the physical interval is fixed. When $\|w\| = 1$, the function interval is equal to the physical interval. The final optimization we need to complete is to select the classification plane that can maximize the minimum physical interval, as shown in

$$\begin{aligned} &\arg\max_{r,w,b} \frac{\hat{y}}{w}, \\ &s.t.\, y_n\left(w^T x_n + b\right) \geq \hat{y}. \end{aligned} \tag{5}$$

In the formula, *s.t.* is abbreviated as constraint condition, where $n = 1, \ldots, N$.

The direct operation here will be very complex. We set the function interval of the sample closest to the classification interface to 1 by using the characteristic that the function interval changes in proportion to the change of w, b without affecting the physical interval. Then, we transform the original problem into a quadratic programming problem that is easier to solve:

$$\begin{aligned} &\arg\min_{w,b} \frac{1}{2} w^2, \\ &s.t.\, y_n\left(w^T x_n + b\right) \geq 1, \end{aligned} \tag{6}$$

where $n = 1, \ldots N$.

To solve such problems, we usually combine the constraints and optimization problems into one formula through Lagrange factor. The Lagrange equation obtained is as follows:

$$L(w, b, a) = \frac{1}{2} w^2 - \sum_{n=1}^{N} a_n \left\{ y_n\left(w^T x_n + b\right) - 1 \right\}. \tag{7}$$

Pay attention to the order of solution here, which is still to get the minimum physical interval according to w, b first, and finally to maximize the minimum physical interval. First, we find the partial derivative of Lagrange equation to w, b and make it equal to 0. Get the following two equations:

$$\begin{aligned} w &= \sum_{n=1}^{N} a_n y_n x_n, \\ \sum_{n=1}^{N} a_n y_n &= 0. \end{aligned} \tag{8}$$

After the above two equations are introduced, we get the duality problem of maximizing the physical interval. This dual problem only contains a, and after solving a, we can get w^*, b^* by bringing it into the formula. The optimal interface is $w^{*T} x + b^* = 0$.

$$\begin{aligned} \hat{L}(a) &= L(w, b, a), \\ &= \sum_{n=1}^{N} a_n - \frac{1}{2} \sum_{n=1}^{N} \sum_{m=1}^{N} a_n a_m y_n y_m x_n^T x_m, \\ &s.t.\, a_n \geq 0, \\ &\sum_{n=1}^{N} a_n y_n = 0. \end{aligned} \tag{9}$$

Type middle $n = 1, \ldots N$.

Finally, the 3D data acquired by using motion capture technology needs to be presented on the computer in a concrete model, and animation is generated for teaching and playing. Students can compare the learned dance movements with the teacher's standard movements by segments through the motion capture system, which can quickly find out the shortcomings and facilitate local correction.

4. Design of Recognition Model of Tumbling Posture in Classical Dance

4.1. Tumbling Posture Recognition of Classical Dance Based on Motion Capture Technology. The data acquisition in the tumbling posture process of classical dance is done using motion capture technology, and the skeleton motion route of the human body is extracted, followed by posture discrimination using the feature vector matching method to create the tumbling posture model of classical dance. The different postures of the human body are divided into two categories: static posture and dynamic posture; the recognition process of static action and dynamic action is carried out in the second level, respectively. The disadvantage of this structure is that it has a problem with error transmission, which means that misclassification samples from the first level will flow into the second level, resulting in a second-level classification error. The key to solving this problem is whether the system's design fully considers the inherent differences between static and dynamic posture, as well as the relative ease with which they can be distinguished. It is possible to interpret and classify multiple sensors at the same time. The results show that the first-grade classification error can be largely ignored, effectively suppressing the error propagation problem. Install 20 data identification points on each part of the dance trainer's body; then start the high-speed 3D data dynamic capture system while remaining well within the preset space range. The controller recognizes that the trainer has completed all of the preprogrammed basic movements. The dynamic capture system will track the dance movements and match them to the model in this process. The real-time acquisition of human action is completed when the computer successfully identifies and enters 20 data acquisition points into the system.

Based on the application of motion capture technology to the identification of the tumbling posture content of classical dance, various postures of human body are divided into two categories: one is static posture, and the other is dynamic posture. In the second level, the recognition process of static action and dynamic action is carried out respectively. The writhing gesture recognition form of classical dance based on motion capture technology is the intersection of computer science, educational technology, and educational psychology. By absorbing and learning from new theories, technologies and methods in other fields, the disadvantages of traditional recognition mode can be solved. The virtual display platform collects all kinds of dance materials, performs by actors, collects data through motion capture devices, and converts them into data recognizable by 3D animation software, and finally displays the dance content perfectly through the virtual display engine. After the motion capture system is successfully matched, the data of human motion posture is recorded, and the natural characteristics of human motion from different perspectives can be analyzed by the system software. In this paper, the motion model database uses key joint points to mark the movement changes of human body. At present, the connection between key points is mainly rigid connection, which can ensure the stability of dance posture. By comparing the dance movements with the teacher's standard movements in sections through the motion capture system, the shortcomings can be quickly found out, which is convenient for local correction. Motion capture technology is used to assist the teaching and research of dance.

4.2. Experimental Results and Analysis. In this experiment, taking the left arm movement of the dance trainer as an example, taking the left arm characteristic plane p_1 as the basic calculation plane, three discriminant parameters $\{\mathrm{Sim}(V_1, V_{\mathrm{stand}}), \mathrm{Corr}(\theta_1), \mathrm{Corr}(\theta_8)\}$ can be obtained, respectively, and the overall motion posture of the left arm can be determined by the above three parameters. Experiments show that the calculation error is effectively reduced, and the results are shown in Table 1.

After completing all teaching hours, the learning situation of the two groups of students is verified through assessment. The college dance teacher scores the range, strength, consistency, and technical standardization of aerobics actions of the two groups of students. The results are determined by SPSS19.0 analysis. The test results are shown in Table 2.

p represents the significance of the experimental effect, and $p < 0.04$ is generally the most significant. According to the experimental results, the students who learn by motion capture have a better grasp of dance movements than those who learn by routine.

This experiment was completed on a PC with Core (TM) i5-34703.2 GHz CPU and 5 GB memory, and MATLAB was used as the development environment. The created motion database contains 20 sets of dance action segments, each of which has about 1,300 frames. The subjects are randomly selected college students, and all subjects have dance foundation. Three experiments were carried out respectively, and the difference of left arm movement posture was compared. From Figures 3–5, the difference between the movement to be measured and the standard movement was clearly seen.

Through the comparison and verification of the experimental results in Figures 3–5, using the feature plane similarity matching method to analyze the motion posture can clearly and efficiently detect the differences and standards between moving objects and has high robustness, which lays a foundation for the scientific training of dance. Coordination is the basic quality of a dancer. The teaching of turning over covers the correct turning of the waist, the orientation training of hand posture, and the joint cooperation of crotch, leg, knee, foot, and step below the waist. It is a great test and exercise for the cultivation of coordination. If the body, especially turning over, is difficult to complete without coordination; even if it is completed, it will lack the corresponding beauty. Therefore, the coordination of turnover movement training dancers is a key point. Physical training can be divided into three stages: initial stage, middle stage, and later stage.

In this experiment, the peak frequency points in the tumbling posture of classical dance, such as basic turning, step-by-step turning, and step-by-step turning, were compared in two experiments. The experimental results are shown in Figures 6 and 7.

From Figures 6 to 7, it can be seen that this feature shows a high degree of discrimination in the three categories of classical dance tumbling posture. At the 8th frame of the sample, the average frequency of step turn is 0.9, which is higher than the average rating of basic turn of 0.75 and that of point turn of 0.5. Therefore, it can be concluded that stepping over is an effective feature, except for some points with loud noise, which is generally stable. In the environment of motion capture equipment, students may have some adaptability problems, which are relatively restrained. However, students can make greater progress by simulating the posture of learning dance training and constantly revising their own learning process, especially in the standardization of dance movements, and students can realize their own shortcomings faster.

Table 1: Relevant parameters of left arm action attitude.

Experimental object	$Sim(V_1, V_{stand})$	$Corr(\theta_1)$	$Corr(\theta_8)$
Standard object	0.6847	0.9758	1.0124
Object to be tested	0.7125	0.8314	0.9847

Table 2: Comparison of experimental results.

Group	Movement range	Strength of action	Action coherence	Action standardization
General group	83.3 ± 6.5	79.7 ± 7.3	81.3 ± 7.8	78.5 ± 6.4
Experimental group	81.4 ± 6.8	81.7 ± 5.2	83.2 ± 3.3	82.3 ± 4.3
Significant p	0.032	0.027	0.024	0.041

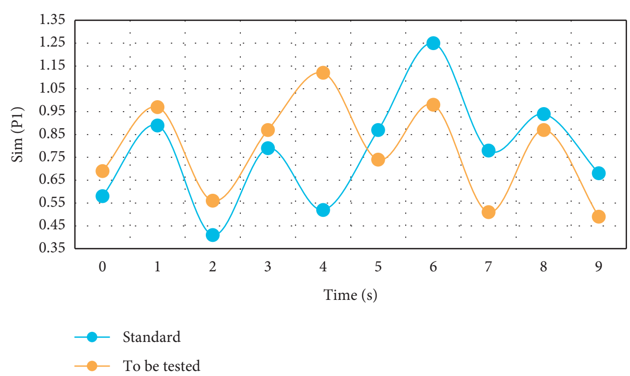

Figure 3: Difference of left arm movement direction.

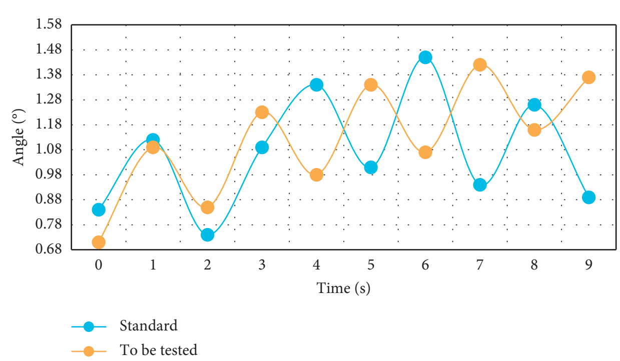

Figure 4: Difference of included angle motion of left arm joint.

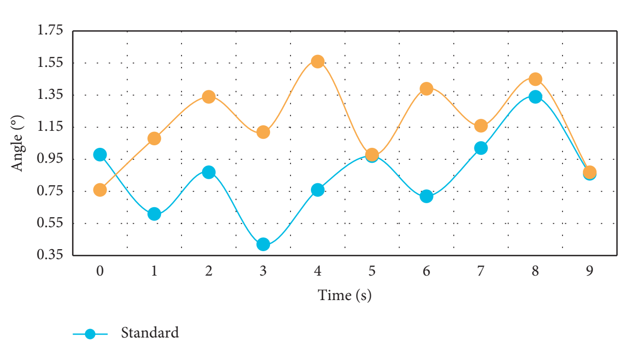

Figure 5: Angle difference between left arm and trunk.

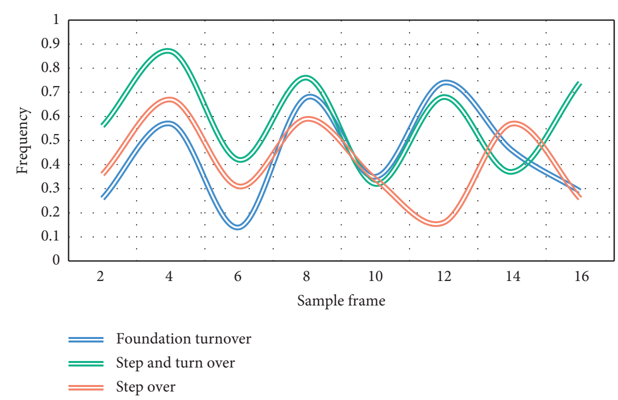

Figure 6: Comparison chart of multisample peak frequency points.

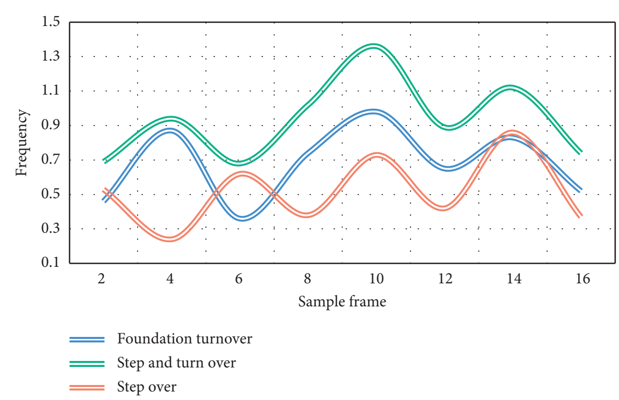

Figure 7: Comparison chart of multisample peak frequency points.

5. Conclusions

The motion capture system-based tumbling posture recognition of classical dance will not only play an important role in the protection of national dance, but also in the long-term development of national dance. The display of dances from various cultures can help with dance research, learning, development, and application. This paper examines human motion posture using the real-time characteristics of motion capture technology, proposes a tumbling posture recognition model for classical dance based on motion capture technology, examines the characteristics of human motion posture, examines the development prospects and research significance of using motion capture technology in classical dance, and provides an effective theoretical basis for scientific training. The range, strength, consistency, and technical standardization of aerobics actions of the two groups of students were scored by the dance teacher. The average frequency of step somersault is 0.9, which is higher than 0.75 of the average evaluation rate of basic somersault and 0.5 of point somersault, according to SPSS19.0 analysis. In addition to the large noise, it can be concluded that the overall turning point is effective. The motion capture technology proposed in this paper can recognize basic classical dance tumbling postures with high precision. The system's ability to achieve higher-precision recognition of more types of posture on this basis is critical. Dance teaching and research benefit from the use of motion capture technology. The captured specific three-dimensional motion data is transformed into digital abstract motion, the three-dimensional human body motion posture database is established, and the teaching animation video is generated, which helps to optimize the traditional dance learning form, according to the characteristics of real-time tracking, detection, and recording of motion capture technology. The importance of improving educational quality cannot be overstated.

Data Availability

The data used to support the findings of this study are available from the corresponding author upon request.

Conflicts of Interest

The author does not have any possible conflicts of interest.

References

[1] D. Rodriguez-Martin, A. Samà, C. Perez-Lopez, A. Català, J. Cabestany, and A. Rodriguez-Molinero, "SVM-based posture identification with a single waist-located triaxial accelerometer," *Expert Systems with Applications*, vol. 40, no. 18, pp. 7203–7211, 2013.

[2] A. Manfrè, I. Infantino, F. Vella, and S. Gaglio, "An automatic system for humanoid dance creation," *Biologically Inspired Cognitive Architectures*, vol. 15, pp. 1–9, 2016.

[3] A. Javier, "See how atoms dance," *National Science Review*, vol. 7, no. 5, pp. 7-8, 2020.

[4] P. Chen, "On traditional Chinese culture: common rhythmical point between traditional opera and classical dance," *Symposium on Health and Education (SOHE 2018)*, Atlantis Press, , pp. 44–48, 2018, May.

[5] D. Risner and J. Anderson, "Digital Dance Literacy: an integrated dance technology curriculum pilot project1," *Research in Dance Education*, vol. 9, no. 2, pp. 113–128, 2008.

[6] G. Sharma, J. Nikolai, S. Duncan, and J. Carter, "Observing the delivery of a curriculum-integrated dance programme across four New Zealand primary schools," *New Zealand Journal of Educational Studies*, vol. 55, no. 1, pp. 29–47, 2020.

[7] S. Corazza, L. Mündermann, A. M. Chaudhari, T. Demattio, C. Cobelli, and T. P. Andriacchi, "A markerless motion capture system to study musculoskeletal biomechanics: visual hull and simulated annealing approach," *Annals of Biomedical Engineering*, vol. 34, no. 6, pp. 1019–1029, 2006.

[8] S. W. Park, H. S. Park, J. H. Kim, and H. Adeli, "3D displacement measurement model for health monitoring of structures using a motion capture system," *Measurement*, vol. 59, pp. 352–362, 2015.

[9] M. Zhao, A. Jha, Q. Liu et al., "Faster mean-shift: GPU-accelerated clustering for cosine embedding-based cell segmentation and tracking," *Medical Image Analysis*, vol. 71, Article ID 102048, 2021.

[10] S. L. Carter, R. Duncan, A. L. Weidemann, and L. S. Hopper, "Lower leg and foot contributions to turnout in female pre-professional dancers: a 3D kinematic analysis," *J Sports*, pp. 1–9, 2018.

[11] C. Swain, E. J. Bradshaw, C. L. Ekegren, and D. G. Whyte, "The epidemiology of low back pain and injury in dance: a systematic review," *Journal of Orthopaedic & Sports Physical Therapy*, vol. 49, no. 4, pp. 1–41, 2019.

[12] Y. Kim, S. Baek, and B. C. Bae, "Motion capture of the human body using multiple depth sensors," *ETRI Journal*, vol. 39, no. 2, pp. 181–190, 2017.

[13] N. F. Bernardi, A. Bellemare-Pepin, and I. Peretz, "Dancing to 'groovy' music enhances the experience of flow," *Annals of the New York Academy of Sciences*, vol. 1423, pp. 415–426, 2018.

[14] S. L. Carter, R. Duncan, A. L. Weidemann, and L. S. Hopper, "Lower leg and foot contributions to turnout in female pre-professional dancers: a 3D kinematic analysis," *J Sports*, pp. 1–9, 2018.

[15] X. Liu, M. Xu, S. J. Peng, and J. X. Du, "Efficient human motion capture data annotation via multi-view spatiotemporal feature fusion," *IET Signal Processing*, vol. 12, no. 3, pp. 269–276, 2017.

[16] S. Gaglio, G. L. Re, and M. Morana, "Human activity recognition process using 3-D posture data," *IEEE Transactions on Human-Machine Systems*, vol. 45, no. 5, pp. 586–597, 2017.

[17] O. J. Urakova, "The philosophical and aesthetic meaning of abdulhamid chulpan's idea of «if literature is alive, so nation will live," *Asian Journal of Multidimensional Research (AJMR)*, vol. 8, no. 4, pp. 179–184, 2019.

[18] H. Chen, B. E. Garcia, Y. Huang, and N. Poh, "GaitGANv2: invariant gait feature extraction using generative adversarial networks," *Pattern Recognition*, vol. 87, pp. 179–189, 2019.

[19] W. Nai, L. Yue, D. Rempel, and Y. Wang, "Fast hand posture classification using depth features extracted from random line segments," *Pattern Recognition*, vol. 65, pp. 1–10, 2017.

[20] E. C. Warburton, "Emotional character: the prospects for a personality-based perspective on embodied learning in dance," *Theatre, Dance and Performance Training*, vol. 11, no. 1, pp. 76–92, 2020.

[21] W. Deng, J. Hu, N. Zhang, B. Chen, and J. Guo, "Fine-grained face verification: FGLFW database, baselines, and human-DCMN partnership," *Pattern Recognition*, vol. 66, pp. 63–73, 2017.

[22] J. Pope, K. Helwig, S. Morrison, A. Estep, and S. Caswell, "Multifactorial exercise and dance-based interventions are effective in reducing falls risk in community-dwelling older adults: a comparison study," *Gait & Posture*, vol. 70, pp. 370–375, 2019.

[23] M. Maheu, L. Bethani, M. Nooristani, B. Jemel, and A. Delcenserie, "Influence of dance training on challenging postural control task," *Gait & Posture*, vol. 69, pp. 31–35, 2019.

[24] T. V. S. Christopher, G. W. Douglas, L. E. Christina, and T. Paul, "Multi-segment spine kinematics: relationship with dance training and low back pain - ScienceDirect," *Gait & Posture*, vol. 68, pp. 274–279, 2019.

[25] T. N. Xuan, T. D. Ngo, and T. H. Le, "A spatial-temporal 3D human pose reconstruction framework," *Journal of Information Processing Systems*, vol. 15, no. 2, pp. 399–409, 2019.

Hindawi
Computational Intelligence and Neuroscience
Volume 2022, Article ID 8015681, 11 pages
https://doi.org/10.1155/2022/8015681

Research Article

An Inclusive Entrepreneurial Path Model Based on Rural Digital Entrepreneurship Data in Zhejiang Province Using Few-Shot Learning

Xiangmin Meng[1,2] **Jie Zhang**,[1] **and Min Sun**[2]

[1]*College of Economics and Management, Nanjing University of Aeronautics and Astronautics, 29 Jiangjun Avenue, Nanjing, Jiangsu 211100, China*
[2]*Zhejiang Wanli University, 8 Qianhu South Road, Ningbo, Zhejiang 315100, China*

Correspondence should be addressed to Xiangmin Meng; mengxiangmin@zwu.edu.cn

Received 14 March 2022; Revised 14 April 2022; Accepted 18 April 2022; Published 9 May 2022

Academic Editor: Xin Ning

The main strategic direction of promoting rural revitalization is to achieve high-quality rural development, maintain the dominant position of farmers, and promote common prosperity of farmers. In recent years, the sustainable development of economy has raised farmers' awareness of starting their own businesses, and their entrepreneurial enthusiasm has been heating up. Based on the empirical survey data of typical rural areas in the Zhejiang Province and structural equation model analysis technology, this paper makes an empirical analysis of the relationship among network embeddedness, entrepreneurial resources, and entrepreneurial ability. The results show that knowledge resources have a significant negative impact on farmers' inclusive entrepreneurial behavior. The dual embedment of social network and industrial network has a significant positive impact on migrant workers' access to knowledge resources and operational resources needed for entrepreneurship, and the entrepreneurial ability of migrant workers mainly depends on operational resources. Under the background of common prosperity, we should continue to implement the policy of supporting farmers' inclusive entrepreneurship and encouraging industrial and commercial capital to enter rural areas, and at the same time, provide rural areas with agricultural knowledge, agricultural skills, and market guidance to promote employment.

1. Introduction

In China's "new normal" stage, entrepreneurship is one of the most important ways to promote the stable operation of the economic system and long-term economic development. However, as there is a common threshold for capital entry to participate in entrepreneurial innovation, the credit exclusion of countries and regions has become a key factor affecting the entrepreneurial activities of small- and medium-sized enterprises and ordinary families. Inclusive development combines economic development with the needs of vulnerable groups, putting people first and achieving social justice and fairness [1, 2]. Since then, "inclusive development" has supplanted "inclusive growth" as the compass for the new era's detailed economic development [3]. Inclusive innovation is defined as a type of innovation that promotes inclusive development, "reduces poverty," and it is "most directly related to the needs of the poor." The will, motivation, and vitality of rural entrepreneurship have been boosted to unprecedented levels by the Common Prosperity Strategy, and more rural entrepreneurs have emerged as the protagonists of poverty alleviation, industrial integration, social governance, and rural areas [4]. As a result, tapping the rural social network and understanding the impact of network embedding on the acquisition of entrepreneurial resources and the improvement of farmers' entrepreneurial ability is critical for farmers' employment and inclusive entrepreneurship.

Farmers' self-employment consciousness gradually emerges as the economy continues to develop. The development of this self-employment consciousness has a more positive impact on farmers' income and employment prospects. Farmers' needs for resources and employment methods in the process of starting their own businesses are also posing a challenge to China's original urban-rural dual system [5]. The revitalization of farmers and rural areas is an important part of common prosperity in the traditional concept, as well as the focus and difficulty of common prosperity [6]. According to Ma and others, China's rural governance should be focused on resolving interdependence and cooperation among people, resolving contradictions and conflicts, and improving people's public services [7]. In academic circles, most small-scale entrepreneurship research focuses on regional differences in small-scale entrepreneurs, as well as the impact of training and entrepreneurial intent on small-scale entrepreneurship. The government's role is to make timely and effective institutional arrangements to create and improve entrepreneurial conditions, optimize the entrepreneurial environment of microsubjects, and improve the overall quality of the entrepreneurial environment. Creating a strong entrepreneurial atmosphere and mature entrepreneurial conditions is the goal of creating an entrepreneurial environment. This paper makes some recommendations to the government based on the research on inclusive entrepreneurial paths to improve the overall entrepreneurial environment, promote the popularization of typical inclusive entrepreneurial paths, and improve the quality of rural entrepreneurial activities.

Highly developed social wealth and social productivity are the premise and foundation of common prosperity. It is difficult to achieve common prosperity unless productivity is highly developed. Despite the fact that farmers' wages and operating income have increased, the income structure still needs to be optimized. Wages and operating income are excessively high, and property income is also rising, however, it is rising only as a small percentage of total income. Supporting the entrepreneurial environment, encouraging farmers to start their own businesses, and focusing on optimizing the rural entrepreneurial environment are the keys to success. This paper can help farmers learn from the research results, obtain the most effective entrepreneurial resources in limited circumstances, maximize their abilities, and complete business creation with quality and policy support factors by studying and analyzing the impact of resource acquisition on farmers' inclusive entrepreneurial path.

The innovations of this paper are as follows:

(1) Innovation from the perspective of research: the evolution of entrepreneurial enterprises has its own life cycle. This paper examines a comprehensive entrepreneurial path based on the life cycle of entrepreneurial enterprises, i.e., selecting existing research from the perspective of enterprise life cycle will gain more targeted characteristics of inclusive entrepreneurial path.

(2) Innovation of research content: the existing research literature on farmers' entrepreneurship mainly focuses on the entrepreneurial environment, and the research on farmers' entrepreneurial access to resources is insufficient. Based on the household survey of typical farmers in the Zhejiang Province, this paper collected the data needed for the research. The form of investigation solves the limitation of time and space well. The investigation can be conducted in different places at the same time, and the quantity and quality of samples can be guaranteed using network tools.

The research framework of this paper consists of five parts, which are arranged as follows: the first chapter introduces the research background and significance, and then, it introduces the main work of this paper. The second chapter mainly introduces the related research status of inclusive entrepreneurship. The third chapter puts forward the concrete method and implementation of this research. The fourth chapter verifies the superiority and feasibility of this research model. The fifth chapter is the summary and prospect of the full text.

2. Related Work

2.1. Inclusive Entrepreneurship Research. Individuals who are entrepreneurs start businesses in one of the two ways: as new ventures or as derivatives of existing ventures. Early academic circles believed that the success or failure of entrepreneurs was determined by their personal characteristics and talents, however, later research has shown that it is the position of individuals in the organization, not the characteristics of entrepreneurs, that determines whether they seek opportunities and engage in entrepreneurial activities [8]. As a result, situational factors and mechanisms become the main ideas to explain entrepreneurial activities in the process of entrepreneurship, which is also the theoretical framework on which this paper is built, i.e., it examines the key features of the overall entrepreneurial process before moving on to the background factors that may influence entrepreneurial activities.

Yu and others believe that inclusive entrepreneurship is actually a collective entrepreneurial activity carried out by ordinary grassroots people in specific areas, and it is a self-employed group [9]. Essougong and others believe that a key feature of inclusive entrepreneurship is the realization of equal opportunities. Inclusive entrepreneurial opportunities are different from entrepreneurial opportunities in general sense. Opportunities appear in specific areas and are strongly influenced by background factors, such as regional cluster environment and government [10]. Oladele et al. think that natural conditions, history, accidental factors, economies of scale and externalities, enterprise organizational structure, competition, and innovation are the key factors for the formation of industrial clusters [11]. Deller et al. established the indicator system of inclusive development and found that inclusive development had an indirect impact on urban-rural income gap using the intergenerational overlap model [12]. From the perspective of microfamily, Ab et al. established a multivalue response model and analyzed inclusive finance from the supply side and demand side [13].

According to the empirical results, the optimal level of inclusive finance is not necessarily the same as the level of demand and supply and is also different from the macrolevel and microlevel. Nie et al. conducted a study based on panel data to further confirm the importance of entrepreneurship and policy support to long-term economic growth [14]. Therefore, although work experience has a positive impact on entrepreneurship, the influence of personal education and the family background of public officials on entrepreneurship is uncertain. Empirical research shows that households with high risk aversion are more inclined to choose agricultural entrepreneurship, households with risk preference are more inclined to start business in industry and commerce, and the income of industrial and commercial entrepreneurial enterprises shows a reciprocal U-shaped relationship.

2.2. Farmers' Entrepreneurship. In the process of farmers' entrepreneurship, farmers rely on family organizations (or informal organizations composed of relatives and friends) or create new organizational forms to form large-scale production and operation scale and pursue the growth and development of wealth. Zhao et al. divided small-scale entrepreneurship into group entrepreneurship and individual entrepreneurship and pointed out that the content of small-scale entrepreneurship referred to the expansion of processing agriculture, and so on [15]. Liu et al. regarded farmers' entrepreneurship as an unbalanced game process that involved the transformation of various resources, and it is also the decisive factor of policy and market in the game [16]. In terms of the influence of farmers' entrepreneurial behavior on society and economy, Phiri et al. explained the importance of farmers' entrepreneurial behavior to rural development [17]. Zhang and Han also made clear the strategic significance of farmers' entrepreneurial actions to the harmonious development of new countryside [18].

More academics are looking at the growth of migrant workers' entrepreneurship through the lens of the entrepreneurial network. The importance of enterprise growth includes scale expansion and capability improvement, and entrepreneurship can be divided into social networks and industrial networks. Shah et al. discovered that migrant workers who engage in growth-oriented and value-oriented entrepreneurship outperform migrant workers who engage in survival-oriented entrepreneurship, implying that higher value pursuit yields better results [19]. The number of families reduces the likelihood of migrant workers returning home to start a business, and the accumulation of family wealth (economic and social capital) has a positive impact on entrepreneurial performance. Sher et al. believe that because they have more knowledge and skills, better education and training, stronger adaptability to the environment, higher self-pursuit, and the new generation of farm tools, they are more willing to return home and start their own businesses [20]. Apart from the difficulty of policy factors, Blevins and Ragozzino have shown that human capital and the individual psychological state of entrepreneurs have a significant impact on farmers' entrepreneurial performance [21]. According to Gans et al., if a company's information capability is low, it will lack the necessary market information and information processing mechanisms [22].

3. Methodology

3.1. Theoretical Model. Entrepreneurship is a form of work that necessitates the development of management, organizational, and service skills, as well as the ability to think, reason, and make decisions. Entrepreneurship is a branch of business that studies how individuals create, discover, or create opportunities to create new things, and how they use those opportunities in various ways to produce different outcomes. With the continued development of our economy and society, an increasing number of people will join the middle class. Many farmers will be present, particularly those who are most likely to enter the middle class. To achieve universal prosperity, we must not only make rural residents the primary beneficiaries of common prosperity but also assist them in achieving material and spiritual prosperity.

Entrepreneurial motivation is the goal or vision that entrepreneurs demonstrate when starting a business based on their internal and external needs. It drives entrepreneurial behavior and influences entrepreneurial performance during the startup process. Regardless of the aforementioned influences on entrepreneurship, entrepreneurs decide whether to start a business based on their own internal needs. Furthermore, outstanding employees from successful peer companies frequently start their own businesses. They are well-versed in the industry's operations and are well-versed in the most critical aspects of the industry's operations. They can grasp the important points when starting a business and achieve twice the result with half the effort, lowering the cost of the enterprise's startup period. Entrepreneurs are well aware of the flaws and drawbacks of running a business, and they can avoid the risks of starting one as soon as possible.

However, unlike the inherent characteristics of other entrepreneurial groups' networks, migrant workers fall into the predicament of leaving the social and industrial networks in the process of entrepreneurship. As they are far away from their hometown, they are hard to integrate into the city, forming a social network, while migrant workers who return home to start their own businesses are far away from the city. Hence, it is difficult for them to obtain external economy in terms of industrial division of labor and cooperation through participation. The purpose of this study is to explore the influence path of dual networks embedded in farmers' inclusive entrepreneurial ability on the acquisition of entrepreneurial resources. Based on this, this paper puts forward the theoretical model as shown in Figure 1.

Entrepreneurship is the process of creating new products or services and realizing their potential value in the absence of resources. Except for the donation of entrepreneurial

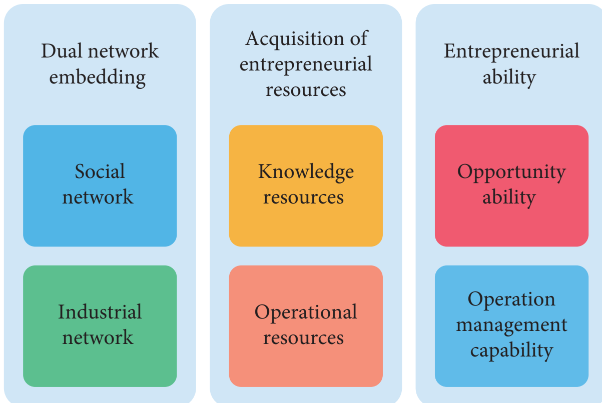

Figure 1: Theoretical model of farmers' inclusive entrepreneurial ability.

resources and entrepreneurial opportunities, entrepreneurs often have nothing. There is a "resource gap" between the huge number of resources needed for starting a business and the limited resources actually controlled by new enterprises. At the initial stage of entrepreneurship, the inherent resource holding of entrepreneurs in the entrepreneurial environment is the basis of entrepreneurial behavior, and the heterogeneity of resource holding composition determines the randomness and diversity of entrepreneurial behavior at the externalized microlevel. With the new creation of some entrepreneurs, the performance of enterprises is obviously better than that of other entrepreneurs. At this stage, entrepreneurs should have the following related skills: integrate resources and start and operate enterprises.

3.2. Life Cycle Model of Enterprise. The age of a company is the basis of its life cycle, which is mainly reflected in the relationship between two factors: adaptability and controllability. Adaptability refers to the response speed and controllability of enterprises to changes in internal and external environment. Controllability refers to the ability of a company to control its external and internal environment. The "youth" of an enterprise refers to its adaptability, which is relatively easy to change and adjust, however, its control is relatively small, and its behavior is generally unpredictable. Therefore, adaptability and controllability are two main factors. The growth of enterprises is the common growth of quality and quantity. Any model that only explains the growth of a company in terms of quality or quantity is one-sided and incomplete. In the three-dimensional enterprise life cycle model, the company life cycle is determined by the age and scale of the company. This model not only reflects the quality of enterprises but also reflects the change of enterprise scale. Hence, it can describe the growth trajectory of enterprises more comprehensively.

A typical enterprise life cycle refers to the whole continuous process of an enterprise from birth to growth, aging, and final decline, however, the enterprise is not an organism. Hence, we cannot apply the biological point of view. Theoretically speaking, it is meaningful to study the growth model of a company. Figure 2 shows the growth model of enterprises in the two models.

For a successful small company, it generally adopts the Ivy enterprise development model. A company can maintain adaptability and flexibility until its heyday. The company can maintain stable growth while extending its scale if it can achieve controllable equilibrium and keep up with the changing market (Figure 2(a)). There is also a meteor model. When a company's life develops to infancy or adolescence, the scale of the company expands rapidly and then suddenly dies, and the growth curve is like the trajectory of a meteorite falling from the sky (Figure 2(b)).

Every stage of the life cycle is very important. Enterprises have different strategic priorities at different stages, and failure at any stage will destroy entrepreneurial enterprises. During the growth of a new enterprise, there may be several problems one after another. Therefore, we need the influx of entrepreneurs, teams, resources, and other factors to constantly overcome various difficulties in the growth process of entrepreneurial enterprises. Entrepreneurs should constantly adapt to the environment, adjust team members, integrate accumulated resources, and improve the overall quality.

3.3. Data Source. The data of this paper comes from the survey of farmers' entrepreneurship and employment in the Zhejiang Province. In terms of regional selection, the survey samples are selected from farmer entrepreneurs in the typical villages of the Zhejiang Province. The questionnaire is distributed in-person and is filled on the spot. A total of 300 questionnaires were distributed and 285 were returned, with an effective rate of 95%. The contents of the survey mainly include personal and family information of farmers, characteristics of farmers' entrepreneurial environment, characteristics of farmers' entrepreneurial behavior, etc. When studying the personal information and family information of farmers, the most important thing is whether they will communicate with public officials and have good relations with state-owned banks and other government agencies to determine whether there are key factors for obtaining resources from resource acquisition. The main gender and age of entrepreneurs are shown in Figure 3.

3.4. Mathematical Model Establishment and Variable Selection. This paper aims to investigate how migrant workers' inclusive entrepreneurial activities can acquire the necessary knowledge and management resources for entrepreneurship via the dual embedding of social and industrial networks, as well as influence farmers' inclusive entrepreneurial ability. The structural equation model (SEM) is a multivariate statistical technique that combines factor and path analysis. It can incorporate some difficult-to-measure variables directly into the model for analysis, as well as analyze the complex relationship between multiple observed variables and latent variables all at once, which traditional regression analysis cannot. The structural model's formula is as follows:

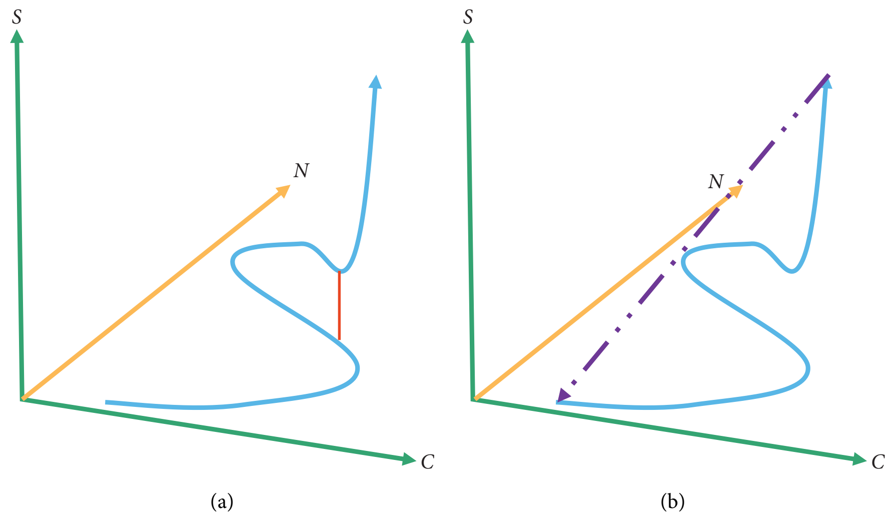

Figure 2: Enterprise growth model based on the (a) Ivy growth model and the (b) Meteor pattern.

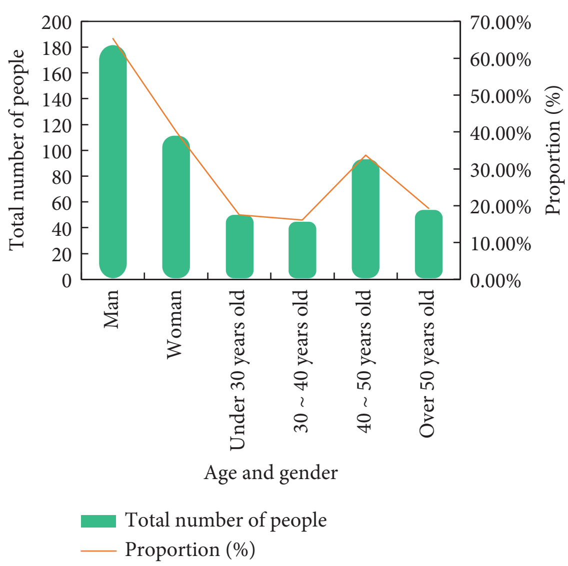

Figure 3: Basic information of sample farmer entrepreneurs.

$$X = \Gamma_X \xi + \sigma, \tag{1}$$

$$Y = \Gamma_Y \tau + \varepsilon. \tag{2}$$

Equations (1) and (2) are measurement models. Among them, X, Y represent exogenous and endogenous observed variables, respectively. ξ, τ, respectively, represent exogenous latent variables (i.e., potential independent variables) and endogenous latent variables (i.e., potential dependent variables). Γ_X is the relationship matrix between the exogenous latent variable and its observed variable, which is composed of a factor load of X on ξ. Γ_Y is the relationship matrix between the endogenous latent variables and their observed variables, which is composed of the factor load of Y on τ. σ, ε is the error term of the measurement model.

$$\tau = A\tau + \Lambda\xi + \gamma. \tag{3}$$

Formula (3) is a structural model in which A is the coefficient matrix of the endogenous latent variables, describing the relationship between endogenous latent variables, Λ is the coefficient matrix of exogenous latent variable, describing the influence of exogenous latent variable ξ on endogenous latent variable τ, and γ is the error term of the structure.

Farmers' entrepreneurial behavior has two possibilities: starting a business and not starting a business. However, in the existing regression model, the value range of dependent variable is between negative infinity and positive infinity, while the value range of the dependent variable affected by entrepreneurial behavior is within [0, 1]. The form of binary dependent variable model is as follows:

$$\hat{y}_1 = x_i\beta + \mu_i, \tag{4}$$

where μ_i is the interference term.

Assuming that $\hat{y}_1$ is greater than the critical value of 0, $y_i = 1$. When $\hat{y}_1 \leq 0$, $y_i = 0$. The relationship is as follows:

$$y_i = \begin{cases} 1 & \hat{y}_1 > 0, \\ 0 & \hat{y}_1 \leq 0. \end{cases} \tag{5}$$

Here, the critical value is chosen as 0. In fact, as long as x_i contains a constant term, the critical value is irrelevant. Hence, at this point,

$$\begin{aligned} P(y_i = 1|x_i, \beta) &= P(\hat{y}_1 > 0) = P(\mu_i > -x, \beta) = 1 - F(-x, \beta), \\ P(y_i = 0|x_i, \beta) &= P(\hat{y}_1 \leq 0) = P(\mu_i \leq -x, \beta) = F(-x, \beta), \end{aligned} \tag{6}$$

where F is the distribution function of μ_i, which requires that it is a continuous function and monotonically increasing. Hence, the regression model can also be regarded as follows:

$$y_i = 1 - F(-x, \beta) + \mu_i. \tag{7}$$

At this point, it becomes the mean regression model of y_i.

112 data obtained from the questionnaire were used as expert opinions. Establish fuzzy number $\widetilde{A}$.

$$\begin{aligned}\widetilde{A} &= (\alpha_i, \beta_i, \gamma_i),\\ \alpha_i &= \min\left(B_{ij}\right),\\ \beta_i &= \left(\prod_{k=1}^{n} B_{ij}\right)^{1/n},\\ \gamma_i &= \max\left(B_{ij}\right).\end{aligned} \tag{8}$$

In the above formula: i—Index number, $i = 1, 2, \cdots, n$; j—Expert number, $i = 1, 2, \cdots, n$; α_i—The minimum value of index i scored by experts; β_i—Geometric mean value of expert scoring index i; γ_i—The maximum value of expert's score on index i; B_{ij}—j expert's scoring value of index i.

When using the fuzzy Delphi method to evaluate risk indicators, we need to convert linguistic variables into fuzzy numbers. Hence, we import expert scoring data into our model and get triangular fuzzy numbers. The fuzzy number is obtained by inverse clearing triangular fuzzy number by the arithmetic average method.

$$A = \frac{\alpha_i + \beta_i + \gamma_i}{3}. \tag{9}$$

In this study, to ensure the validity and reliability of the measurement indicators, some items were modified and supplemented according to the characteristics and actual situation of farmers' inclusive entrepreneurs using the maturity scale used in existing domestic and foreign literatures. The questionnaire was designed by Likert's 5-point scoring method, and the description of the items was described as "strongly agreed," "comparatively agreed," "moderate," "slightly disagreed," and "very different," as shown in Figure 4.

3.4.1. Dual Network Embedding. As migrant workers start their own businesses mainly in industries with low skill content, it is difficult for new enterprises to have the power to establish cooperative relations with universities and research institutes. It represents a group of related partnerships among subsidiaries, financial institutions, intermediaries, and government agencies, excluding universities and scientific research institutions.

3.4.2. Entrepreneurial Resources. This paper investigates the acquisition of knowledge resources by farmers' inclusive entrepreneurs from four aspects: new product or service development, market development, production and management, and related policy system.

3.4.3. Operating Resources. The existing research mainly inspects business resources from the aspect of resource availability, focusing on whether entrepreneurs can obtain capital, human resources, technical resources, plant, equipment, and other physical resources at low cost.

3.4.4. Entrepreneurial Ability. This paper describes entrepreneurs' management ability from four dimensions: organizational ability, strategic ability, relationship ability, and commitment ability. Farmers' inclusive entrepreneurs should have the same relationship and commitment skills as other entrepreneurial groups, however, their newly started enterprises are small in scale and simple in organization, and their requirements for organizational and strategic capabilities are slightly lower than those of other entrepreneurs.

4. Experiment and Results

The estimated coefficients in the binary choice model cannot be interpreted as the marginal effect of symbols on dependent variables only. If the sign is evidence, the probability that the dependent variable is 1 increases. If the sign is negative, the probability that the dependent variable is 1 decreases. Considering that the dependent variable is the implementation of farmers' entrepreneurial behavior in variable selection, i.e., the dependent variable can take the values of "1" and "0" as "entrepreneurship" and "for entrepreneurship." In this study, resource acquisition mainly starts with policy resources, financial resources, and information resources. Hence, the selection of variables is shown in Table 1.

SPSS software is used to analyze the influence of resource acquisition on farmers' inclusive entrepreneurial behavior, and the regression results are shown in Figure 5.

$A4$ has a significant positive correlation with farmers' entrepreneurial behavior of acquiring information resources, which is significant at the statistical level of 1%. The regression coefficient is 0.196 and Exp(B) is 1.21, which means that the probability of farmers' entrepreneurial behavior will increase by 0.196 for each additional unit in contact with civil servants, other things being equal. At the level of 5%, $A1$ has a significant impact on farmers' entrepreneurial behavior, with the coefficient of 0.569 and Exp(B) of 1.806, which means that the probability of farmers' entrepreneurial behavior will increase with each unit of $A1$. Therefore, the probability of entrepreneurial behavior of married farmers is higher than that of unmarried farmers.

$A3$ has a significant negative impact on farmers' entrepreneurial behavior. It passed the 1% significance test, and the coefficient was −0.215 and Exp(B) was 0.774. It means that the higher the education level of farmers, the lower the possibility of entrepreneurial action. Studies have shown that industrial structure adjustment will affect regional innovation activities [23]. The research shows that the optimization and upgrading of industrial structure has a positive effect on inclusive entrepreneurship [16]. Research shows that the rapid change of industrial structure will affect entrepreneurship in the short term, however, it will promote local entrepreneurial innovation activities in the long-term [20]. Therefore, this paper selects the proportion of the tertiary industry in GDP to investigate to control the industrial structure of each region. Descriptive statistics of each variable are shown in Figure 6.

The scale design of this paper refers to the mature scale used by scholars in the past, which ensures the validity of the

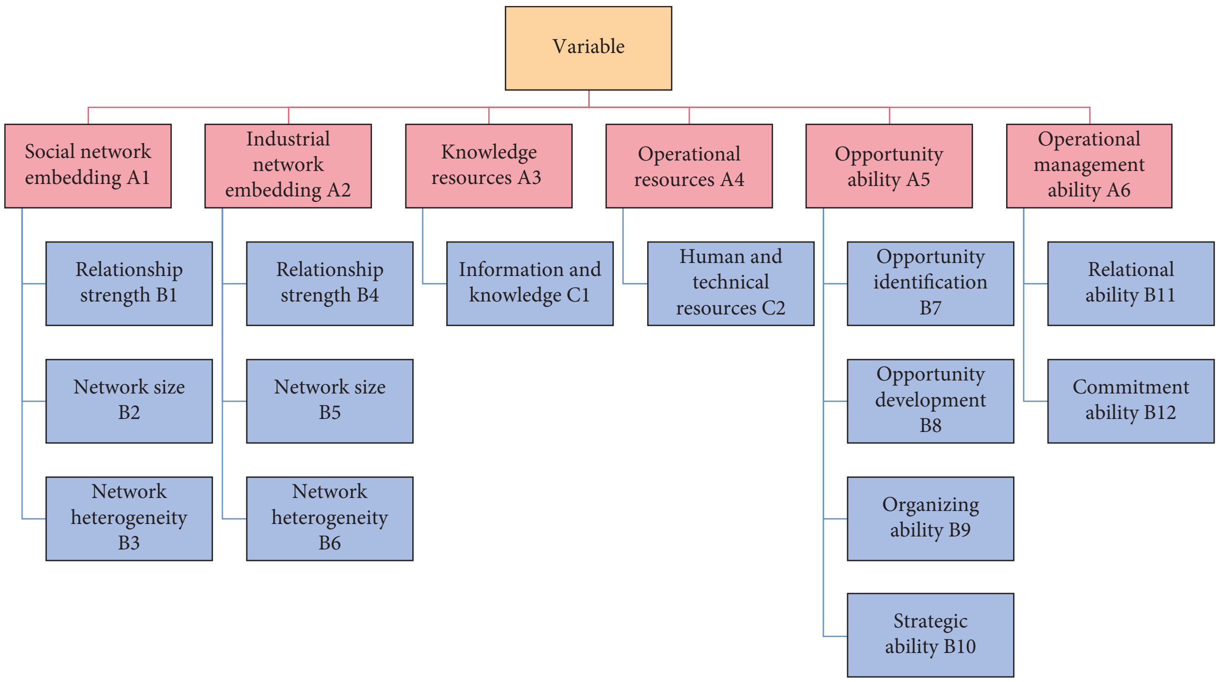

Figure 4: Variable measurement item.

Table 1: Selection of variables influencing access to resources on farmers' inclusive entrepreneurial path.

First-order variable	Secondary variable	Mean value
	$B1$	3.36
$A1$	$B2$	2.25
	$B3$	3.04
	$B4$	2.21
$A2$	$B5$	3.88
	$B6$	2.96
$A3$	$C1$	2.36
$A4$	$C2$	3.32
	$B7$	3.01
$A5$	$B8$	2.88
	$B9$	3.63
	$B10$	2.41
$A6$	$B11$	2.88
	$B12$	3.71

content of this scale. Constructive validity, also known as structural validity, is mainly used to indicate whether the actual measurement result of a scale is consistent with the research concept, which usually consists of convergence validity and discrimination validity. Specifically, $A1$ and $A2$ can extract three factors, $A3$ and $A4$ can extract a single factor, $A5$ can extract two factors, and $A6$ can extract four factors. These extracted factors are measured by a scale, and the variables are the same. At the same time, the factor loading values of all measures after orthogonal rotation are greater than the threshold value of 0.5, which indicates that the convergence validity of the measure scale is ideal. The discriminant validity test results (see Table 2) show that the square root of latent variables on the diagonal is larger than the correlation coefficient between latent variables on off-diagonal, which indicates that the scale has good discriminant validity.

The result of building structural equation model with AMOS is shown in Figure 7. All the test indexes of the overall goodness-of-fit of the model are higher than the threshold, which indicates that the overall goodness-of-fit of the model is good.

In this paper, SPSS20.0 statistical software is used to analyze the impact of resource acquisition on farmers' business performance. In the process of processing, firstly, all variables are introduced into the regression equation. Then, the significance test is carried out, and finally, the regression method is refitted, and this principle is repeated until the regression coefficient of each variable in the equation is significant.

We introduce all the above independent variables into the regression equation, as shown in Figure 8 below.

It can be seen in $A2$, $A4$ and $A6$, $B1$ that it is not obvious. After removing the above variables, a two-step regression analysis is introduced, which shows that insignificant variables are equal to $C1$ and $B10$. So far, in the third step, we used two variables $A1$ and $B9$ and brought all the remaining variables into the regression analysis method to continue the regression analysis. The regression results of the third stage model are shown in Figure 9.

It is significant with $B3$ at the level of 5% in the statistical test, and the estimation coefficient is positive. When other factors remain constant, contact with senior civil servants improves the effectiveness of farmers' entrepreneurial performance. The difficulty level of high government function, relevant market system establishment, market policy guidance, financing convenience, contact with bank staff, access to information from other channels, overall access to

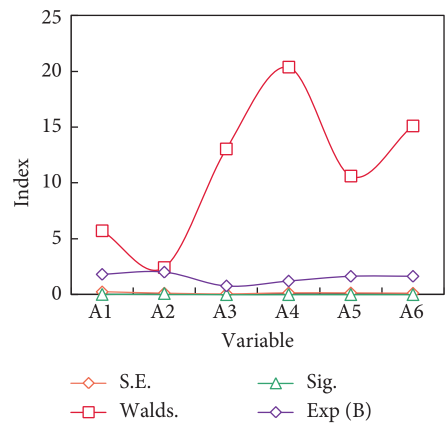

Figure 5: Influencing factors of various variables.

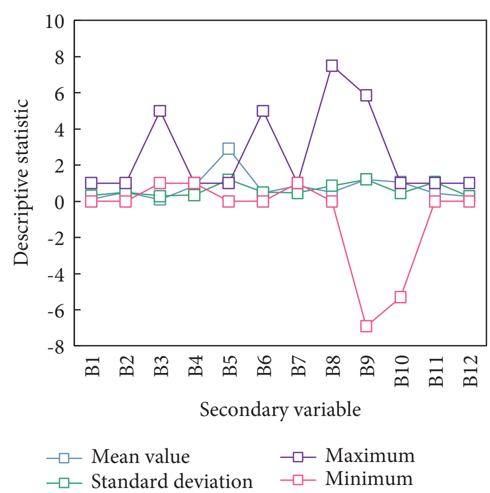

Figure 6: Descriptive statistics of related variables of secondary variables.

Table 2: Test results of discrimination validity.

Variable	*A*1	*A*2	*A*3	*A*4	*A*5	*A*6
*A*1	0.771					
*A*2	0.413	0.762				
*A*3	0.501	0.501	0.821			
*A*4	0.263	0.336	0.461	0.743		
*A*5	0.459	0.428	0.502	0.418	0.874	
*A*6	0.337	0.367	0.424	0.442	0.426	0.769

information resources, policy convenience, and no resources is significant and failed the test.

Farmers' entrepreneurs in China are clearly affected by information restrictions in the process of starting a business because of the limited information channels available to them and the high cost of obtaining information. Business operations and maintenance are no longer limited by information channels. The educational level is statistically significant at 10%. Information channels are becoming more diversified and efficient. The estimated coefficients of age and educational background are positive among the three variables, while the estimated coefficient of gender is negative. Farmers' entrepreneurial performance is significantly influenced by their representative life experience and accumulation of experience. Although operational resources serve a greater purpose than knowledge resources, both have a negligible impact. This result demonstrates that current migrant worker entrepreneurship is still survival-oriented, and the industry entry threshold is low. Inclusive entrepreneurs are relatively simple, and they have not yet attained

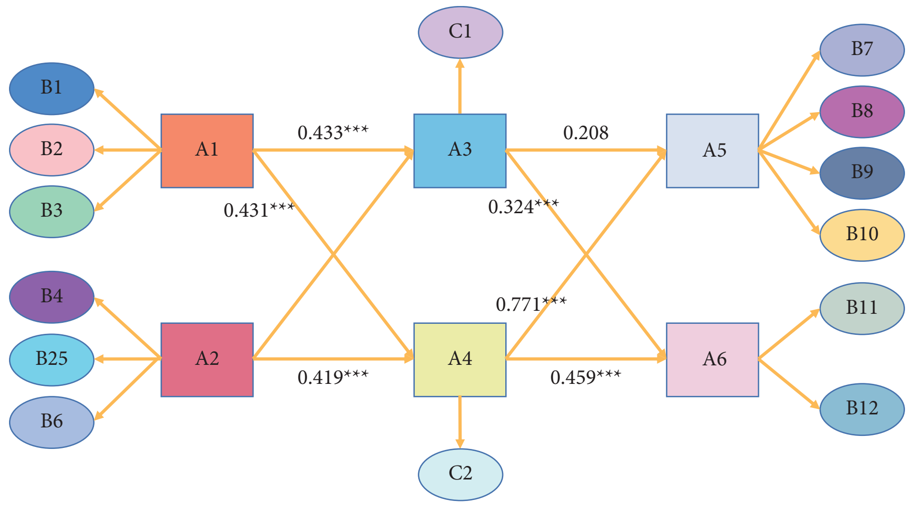

FIGURE 7: Structural equation model diagram of the influence of farmers' inclusive entrepreneurship.

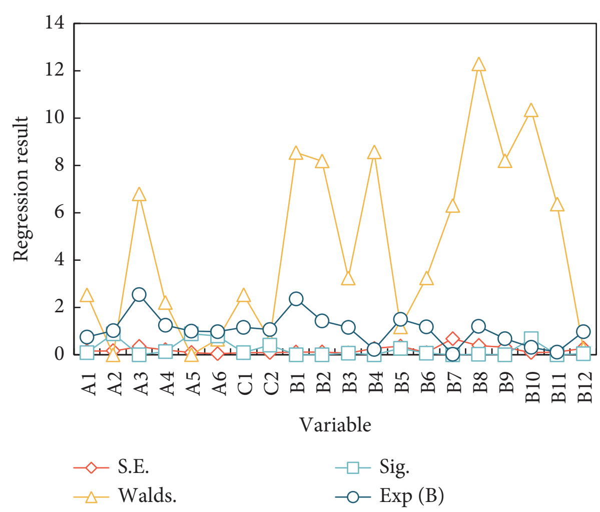

FIGURE 8: The first step model regression results.

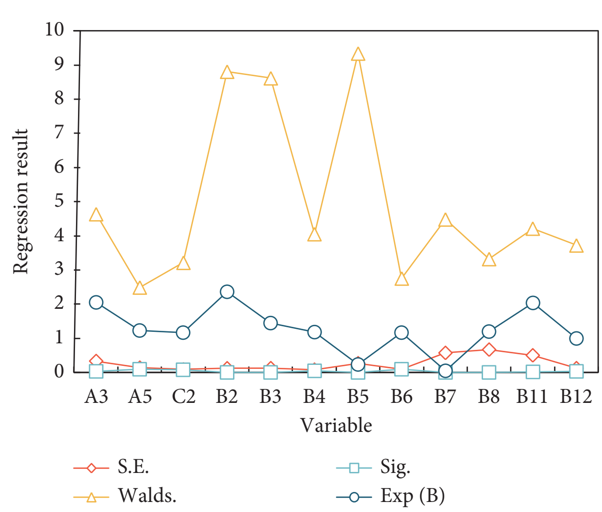

FIGURE 9: The third step model regression results.

the level of knowledge acquisition resources and operational resources required to improve a company's ability to operate and manage. At the moment, Chinese migrant workers are still self-employed, and their new entrepreneurial management mode differs significantly from the modern enterprise management mode that reflects migrant workers' entrepreneurial spirit.

5. Conclusions

Based on the empirical research data of typical villages in the Zhejiang Province, this paper analyzes and summarizes the process and mechanism of inclusive entrepreneurs' development path from the perspective of common prosperity. We find that there is a significant positive correlation between business resources and farmers' entrepreneurial behavior in obtaining information resources. At the statistical level of 1%, knowledge resources have a significant negative impact on farmers' entrepreneurial behavior. The dual embedment of social network and industrial network has a positive impact on migrant workers' acquisition of knowledge resources and business resources needed for starting a business, however, the acquisition of knowledge resources is mainly influenced by the embedded industrial network. Therefore, under the vision of common prosperity, when building various systems, the government fully considers the needs of people of different classes and actively introduces policies to encourage and guide farmers so that more farmers can choose entrepreneurship, employment, and settlement.

Data Availability

The dataset used to support the findings of this study are available from the corresponding author upon request.

Conflicts of Interest

The authors do not have any possible conflicts of interest.

Acknowledgments

This work was supported by the project of Ningbo Wanli Counterpart Cooperation and Anti-Poverty Research Institute—Research on inclusive entrepreneurship path from the perspective of common prosperity (Taking Ningbo farmers' Entrepreneurship and prosperity as an example), the Ningbo Soft Science Project (Research on the construction path and operation performance evaluation of Ningbo entrepreneurship Incubation Platform) under Grant 2021r029, the project on Youth and Youth Work in Zhejiang Province in 2022 under Grant zq202254, the Scientific Research and Innovation Team Project of Zhejiang Wanli University in 2020 and 2021, the New School Level Project of College Students' Ideological and Political Exploration in the New Situation of 2020, the Ningbo University Ideological and political project of Zhejiang University Graduates' science and Technology Entrepreneurship Model and promotion mechanism research project under Grant sgxsz150052021, the National Social Science Fund Project of China (Research on the logic, Dilemma and Countermeasures of big data intervention in the governance of public health emergencies) under Grant 21bgl228, 2022 Cixi Social Science Research Project (inclusive entrepreneurship research from the perspective of common prosperity—Taking Digital entrepreneurship and prosperity in typical rural areas of Cixi as an example), the 2022 Research Project on Strengthening the Consciousness of the Chinese Nation Community in Zhejiang Province (inclusive entrepreneurship research from the perspective of common prosperity—research results of the exploration and practice research project on entrepreneurship and prosperity of ethnic minority floating population in Zhejiang Province), and the 2022 Zhejiang Women's Research Project (Entrepreneurship under inclusiveness from the perspective of common prosperity—taking women's entrepreneurship in Zhejiang Province as an example).

References

[1] R. V. Bianchi and F. de Man, "Tourism, inclusive growth and decent work: a political economy critique," *Journal of Sustainable Tourism*, vol. 29, no. 2-3, pp. 353–371, 2021.

[2] E. Y. Naminse, J. Zhuang, and F. Zhu, "The relation between entrepreneurship and rural poverty alleviation in China," *Management Decision*, vol. 57, no. 9, pp. 2593–2611, 2019.

[3] B. Garner, "Sustainability marketing at the farmers' market: An ethnographic analysis of ambiguous communication," *International Journal of Consumer Studies*, vol. 43, no. 1, pp. 14–22, 2018.

[4] C. Ingram Bogusz, R. Teigland, and E. Vaast, "Designed entrepreneurial legitimacy: the case of a Swedish crowdfunding platform," *European Journal of Information Systems*, vol. 28, no. 3, pp. 318–335, 2019.

[5] J. Gugler, "Life in a dual system revisited: Urban-rural ties in Enugu, Nigeria, 1961-87," *World Development*, vol. 19, no. 5, pp. 399–409, 1991.

[6] Y. Guo and Y. Liu, "Poverty alleviation through land assetization and its implications for rural revitalization in China," *Land Use Policy*, vol. 105, Article ID 105418, 2021.

[7] X. Ma, J. Wang, L. Zhao, and J. Han, "The effects of social capital on farmers' wellbeing in China's undeveloped poverty-stricken areas," *China Agricultural Economic Review*, vol. 12, no. 1, pp. 108–121, 2019.

[8] E. Nigussie, T. Olwal, G. Musumba, T. Tegegne, A. Lemma, and F. Mekuria, "IoT-based irrigation management for smallholder farmers in rural sub-saharan africa," *Procedia Computer Science*, vol. 177, pp. 86–93, 2020.

[9] L. Yu and G. M. Artz, "Does rural entrepreneurship pay?" *Small Business Economics*, vol. 53, no. 1, pp. 1–22, 2019.

[10] U. P. Kenfack Essougong, G. H. Fongang Fouepe, and A. Degrande, "Can community-based organisations deliver adequate agricultural information to farmers? Evidence from rural resources centres in Cameroon," *Information Development*, vol. 35, no. 3, pp. 435–446, 2019.

[11] O. Oladele, M. Gitika, F. Ngari et al., "Adoption of agro-weather information sources for climate smart agriculture among farmers in Embu and Ada'a districts of Kenya and Ethiopia," *Information Development*, vol. 35, no. 4, pp. 639–654, 2019.

[12] S. Deller, M. Kures, and T. Conroy, "Rural entrepreneurship and migration," *Journal of Rural Studies*, vol. 66, pp. 30–42, 2019.

[13] A. Ab, A. Ab, and B. Cad, "Modeling cereal farmers' intended and actual adoption of integrated crop management (ICM) practices - ScienceDirect," *Journal of Rural Studies*, vol. 70, pp. 58–65, 2019.

[14] X. Nie, J. Zhou, P. Cheng, and H. Wang, "Exploring the differences between coastal farmers' subjective and objective risk preferences in China using an agent-based model," *Journal of Rural Studies*, vol. 82, no. 5, pp. 417–429, 2021.

[15] Q. Zhao, G. Jiang, W. Ma, Z. Dingyang, Q. Yanbo, and Y. Yuting, "Social security or profitability? understanding multifunction of rural housing land from farmers' needs: spatial differentiation and formation mechanism-based on a survey of 613 typical farmers in Pinggu District," *Land Use Policy*, vol. 86, pp. 91–103, 2019.

[16] R. Liu, C. Yu, J. Jiang, Z. Huang, and Y. Jiang, "Farmer differentiation, generational differences and farmers' behaviors to withdraw from rural homesteads: evidence from chengdu, China," *Habitat International*, vol. 103, Article ID 102231, 2020.

[17] A. Phiri, G. T. Chipeta, and W. D. Chawinga, "Information needs and barriers of rural smallholder farmers in developing countries," *Information Development*, vol. 35, no. 3, pp. 421–434, 2019.

[18] X. Zhang and L. Han, "Which factors affect farmers' willingness for rural community remediation? a tale of three rural villages in China," *Land Use Policy*, vol. 74, pp. 195–203, 2018.

[19] F. Shah and J. Wang, "Farmers' risk perception, vulnerability, and adaptation to climate change in rural Pakistan," *Land Use Policy*, vol. 79, pp. 301–309, 2018.

[20] A. Sher, S. Mazhar, F. Zulfiqar, D. Wang, and X. Li, "Green entrepreneurial farming: a dream or reality?" *Journal of Cleaner Production*, vol. 220, no. 20, pp. 1131–1142, 2019.

[21] D. P. Blevins and R. Ragozzino, "An examination of the effects of venture capitalists on the alliance formation activity of entrepreneurial firms," *Strategic Management Journal*, vol. 39, no. 7, pp. 2075–2091, 2018.

[22] J. S. Gans, S. Stern, and J. Wu, "Foundations of entrepreneurial strategy," *Strategic Management Journal*, vol. 40, no. 5, pp. 736–756, 2019.

[23] Y. Wang, L. Chen, and K. Long, "Farmers' identity, property rights cognition and perception of rural residential land distributive justice in China: Findings from Nanjing, Jiangsu Province," *Habitat International*, vol. 79, pp. 99–108, 2018.

Hindawi
Computational Intelligence and Neuroscience
Volume 2022, Article ID 7002249, 9 pages
https://doi.org/10.1155/2022/7002249

Research Article

Study on Economic Significance of Rare Earth Mineral Resources Development Based on Goal Programming and Few-Shot Learning

Shuxian Zhang

School of Earth Sciences and Resources, China University of Geosciences (Beijing), Beijing 100083, China

Correspondence should be addressed to Shuxian Zhang; 3001170127@cugb.edu.cn

Received 16 March 2022; Revised 4 April 2022; Accepted 5 April 2022; Published 9 May 2022

Academic Editor: Xin Ning

Rare earth is one of the most important strategic minerals in the world today. The wide application of new products and technologies in the global market has made the world's demand for rare earth resources grow rapidly. As an important basic resource of high technology, rare earth plays a significant role in national security and strategy. As rare earth mineral resources are irreplaceable in civil, military, and nuclear industries, they have become national strategic resources of various countries in the world. Although China's rare earth industry has occupied a leading position in the world, with the continuous expansion of the scale of the rare earth industry, the pollution problem of "three wastes" produced in the recovery of rare earth mineral resources is becoming more and more serious. From the perspective of resource endowment, China is rich in rare earth resources, but the declining trend of resource reserves is obvious, and the advantages and disadvantages of resources are more prominent. Based on the goal planning and few-shot learning, this paper studies the economic significance of rare earth resource development, aiming at solving some problems in the development of rare earth mineral resources in China, and thus promoting the scientific and healthy development of the rare earth industry.

1. Introduction

Rare earth elements have unique electronic structure, which makes them have excellent magnetic, optical, and electrical characteristics. They are widely used in metallurgical machinery, petrochemical industry, electronic information, energy and transportation, national defense and military industry, high-tech materials, and other industries [1]. As an important high-tech basic resource, rare earth plays an important role in national security and strategy. The most important feature of the raw material base developed so far in the world is that its structure is conducive to large or even super large deposits. China has basically formed a legal system for the protection and management of mineral resources guided by the Constitution and dominated by laws, administrative regulations and departmental rules, which provides a clear legal basis for the management of rare earth resources according to law [2]. Many experts believe that these deposits will be relocated according to the special characteristics of rare earth mineral composition [3]. Due to the progress of China's rare earth metallurgy technology and low cost, foreign rare earth smelting and separation enterprises have closed down one after another and the relevant research is gradually reduced [4]. Although China's rare earth industry has occupied a leading position in the world, with the continuous expansion of the scale of the rare earth industry, the pollution problem caused by the recycling of rare earth resources is becoming more and more serious [5]. This situation has affected the healthy, sustainable, and stable development of China's industrial system. It is urgent to develop an efficient and practical green mining and smelting process to solve the problem of environmental pollution caused by three wastes.

Rare earth is an indispensable strategic resource for countries all over the world to transform traditional industries and develop high-tech and cutting-edge national defense technology. We need to re-examine China's mineral resources legal system, explore the root causes of the problems from the theoretical basis and system design, and make up for the insufficient theoretical preparation and unreasonable system design [6]. Then, put forward the feasible countermeasures to improve China's legal system of mineral resources and then study the management of rare earth according to law [7]. China is not only a big country in rare earth resources but also a big country in rare earth production, export, and consumption in the world. Some countries and regions have listed it as a key element for the development of high-tech industries and a national strategic element, which is called an indispensable "industrial vitamin" [8]. From the perspective of resource endowment, China is rich in rare earth resources, but the declining trend of resource reserves is obvious, and the advantages and disadvantages of resources are more prominent [9]. Starting from the theoretical level, this paper abandons the theory that administrative license is the direct allocation of resources and insists that administrative license is only the franchise qualification granted by the government to the opposite party.

Heavy rare earth mineral raw materials mainly include phosphorus manganese ore, brown yttrium ore, ion adsorption rare earth ore, and uranium ore [10]. The rare earth industry is China's advantageous industry. The comprehensive management of the rare earth industry will greatly promote the healthy development of China's rare earth industry and better serve China's high-tech industry, new energy, aerospace, and national defense [11]. In the part of rare earth exploration license, closely follow the pace of China's geological exploration pattern reform, grasp the latest reform trends, put forward suggestions to speed up the establishment of mineral exploration financing market, and promote the exploration of rare earth and other strategic minerals [12]. As rare earth resources are irreplaceable in civil, military, and nuclear industries, they have become national strategic resources of countries all over the world [13]. Although China has obvious advantages in rare earth resources, due to lack of understanding, China's rare earth industry started late and the long-term development and management of rare earth resources are extensive [14]. In practice, the phenomenon of indiscriminate mining and blind competition among enterprises has become increasingly prominent, resulting in a large outflow of resources at low prices [15]. Based on the goal planning, this paper studies the economic significance of the development of rare earth resources, aiming to solve some problems in the development of rare earth resources in China, coordinate the development and utilization of rare earth resources with the ecological environment, and promote the scientific and healthy development of rare earth industry.

Section 2 analyzes the general situation of China's rare earth resources from two aspects: the characteristics of resource endowment and the characteristics of resource trade. Section 3 discusses the economic significance of rare earth resources through the goal planning method. Section 4 summarizes the content of the full text.

2. Overview of Rare Earth Resources in China

2.1. Characteristics of Resource Endowment. From the perspective of resource trade, the export-oriented and primary

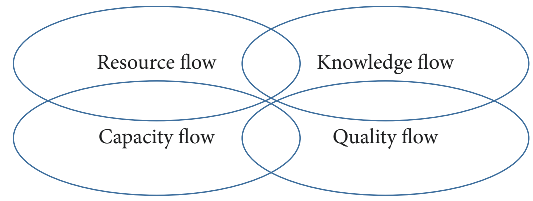

Figure 1: Extension Manufacturing Capability Unit model.

product-oriented trade structure has further weakened China's advantage of large quantity and variety of rare earth resources and intensified excessive competition in the rare earth industry. Between the upstream and downstream of the rare earth industry chain is a process of increasing value. At present, the profits of the rare earth industry are concentrated at the back end of its industry chain. Although rare, rare earth elements have not been known and used for a long time. It was not until the end of the 18th century that people discovered the existence of rare earth elements. Through research, people gradually realized its value and applied it to people's production and life. While China's rare earth is overexploited and its reserves continue to decline, foreign rare earth is being strategically protected and proven reserves are also increasing, leading to the gradual loss of China's rare earth reserve advantage [16]. Rare earth minerals in our country are mainly distributed in remote areas. A large number of small enterprises are engaged in rare earth resources development. The management mode is extensive and destructive mining, resulting in a large amount of rare earth resources loss and destruction [17]. Ultrahigh purity rare earth metals are the material basis for studying the intrinsic properties of rare earth and developing new rare earth materials. The purity of rare earth metals is also one of the key factors affecting and restricting the properties of rare earth functional materials.

With the increasing demand for rare earth resources in China's high-speed economic growth, the export volume of rare earth is decreasing year by year, but the export volume of rare earth and other dominant minerals in China still occupies an important position in the world mineral trade. The rapid establishment, integration, reconfiguration, and dissolution of the Extension Manufacturing Capability Unit, as well as the rapid diffusion, rapid remodeling, and rapid transformation of manufacturing capability. There are four kinds of flows in the diffusion process of the Extension Manufacturing Capability Unit. The combined effect of these four streams enables large engineering equipment manufacturing systems to emerge rapidly expanding manufacturing capabilities in a short time. Figure 1 is a model of the Extension Manufacturing Capability Unit.

The smuggling of rare earth resources in China is very serious, disrupting the order of the rare earth market, invalidating the national rare earth control policy, and failing to achieve industrial integration goals. Although rare earth resources are stored in large quantities in the world, due to the difficulty in industrial smelting and purification in practical applications, rare earth resources are still extremely rare. According to the geographical area, the geographical distribution of rare earth resources is broad and there is no

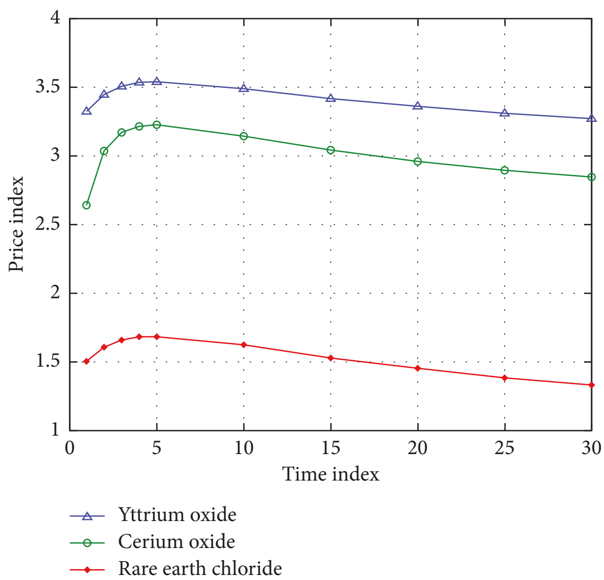

Figure 2: Changes in export prices of rare earth products.

monopoly of a certain region. Rare earth minerals are nonrenewable resources. Although major developed countries have been striving to develop alternatives, the harvests are minimal and some of the so-called alternatives are difficult to achieve the desired results in application. Therefore, rare earth resources are more precious [18]. The vast geographical distribution of rare earth resources determines that it is unrealistic to want to obtain a dominant say in rare earth resources for a long time by tightening supply ports. Compared with energy and basic metals, rare earthconsumption is very small and under the current visible application, the increment in various consumption fields is also limited. The strategic reserve system of resources should be implemented. Once the price of important mineral resources fluctuates abnormally and there is an interruption or shortage of supply, the strategic reserve resources can be put into the market to adjust the relationship between supply and demand in the market, thus greatly improving the right to speak on the price of mineral resources. Generally speaking, the price of rare earth resources has been low for a long time and the economic benefits are limited. At the same time, the environmental cost of rare earth resources development is high, which makes the overall benefits of rare earth resources export low. Figure 2 shows the changes in export prices of rare earth products in China.

There are n indicators for evaluating the independent innovation capability of rare earth enterprises. Based on this part of the indicators, the independent innovation capability of enterprises is quantitatively divided into T grades, which are described as the following quantitative comprehensive evaluation matter element models:

$$Q(u_{ij}) = \sum_{i=1}^{n} \underset{1\le j\le m}{\mathrm{Max}}\left\{g_{ij}(T)\right\}. \quad (1)$$

The matter-element model formed by the comprehensive evaluation of the independent innovation ability and the

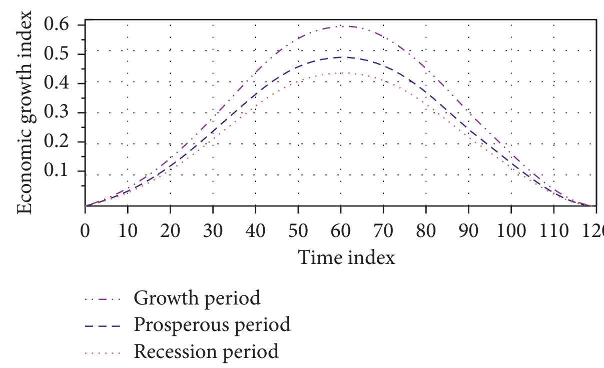

Figure 3: General law of resource-based urban development.

allowable value range of each indicator is called the domain matter element.

$$y_{f-n_m} = \sum_{i=1, i\neq n}^{N} \sum_{l=1}^{M} \sqrt{p_{i_l}} \mathbf{h}_{i,n_m}^{T} \mathbf{W}_{i,i_l} s_{i_l}. \quad (2)$$

For the enterprise to be evaluated, the data or analysis result obtained by the evaluation is represented by the matter element P.

$$P_{f-n_m} = \sum_{i=1, i\neq n}^{N} \sum_{l=1}^{M} p_{i_l} \left\| \mathbf{h}_{i,n_m}^{T} \mathbf{W}_{i,i_l} \right\|_2^2. \quad (3)$$

2.2. Characteristics of Resource Trade. A large number of foreign-funded enterprises have evaded the export quota of rare earth resources in China by investing in factories and other ways and have carried out predatory mining. Only simple processing can be exported, resulting in a large amount of waste of rare earth resources. The abundance of rare earth elements in the earth's crust is not barren, even relatively rich, and the abundance of some elements is higher than that of common metals such as copper and zinc. Rare earth elements are widely distributed in the Earth's crust and there are many mineral occurrences. However, there are no more than 30 large companies that control rare earth resources in the world. If you master the trends of these 30 companies, you can directly understand the global supply and demand of rare earth and the industrial chain [19]. The protection and management of rare earth resources in China have been gradually implemented with the breakthrough of rare earth application technology and the development of the rare earth industry. We should strengthen macrocontrol and give full play to the leading role of the government. The establishment of a rare earth industry enterprise alliance to control the price and usage of concentrate and to control the price and sales of primary products. Formulate relevant policies to encourage rare earth enterprises to go abroad and participate in or take control of the development of foreign rare earth resources, so that China's rare earth industry will truly go international.

Although China prohibits the export of rare earth raw ores, the economic benefits brought to China by the export structure dominated by rare earth separation products are

Table 1: Performance indicator structure parameter estimation and significance test.

Path description	t value	Path coefficient
Market learning ability ⟶ influence performance	3.46	1.57
Marketing ability ⟶ marketing performance	3.24	1.49
Customer management capabilities ⟶ marketing performance	4.37	1.45

Table 2: Characteristic values corresponding to each feature.

Features	A1	A2	A3	A4	A5	A6	A7	A8	A9
Characteristic value	75.6	88.5	87.3	95.2	74.8	74.7	86.2	91.7	76.5

relatively low, and rare earth smelting separation will cause serious pollution. From the beginning, two mechanisms with the nature of compensation and assistance were proposed, i.e., compensation mechanism for resource development and the assistance mechanism for declining industries. Sustainable development is based on natural assets and coordinated with environmental carrying capacity. Sustainable development aims at providing quality of life and is compatible with social progress. Research in any discipline or field should be supported by scientific methods that meet the needs of its research objects and contents and are determined by its research purposes. At the same time, any scientific research method is not exclusive but universal. Figure 3 is a schematic illustration of the general law of the development of resource-based cities.

The relevant data are substituted into the system to run, and the original model is repeatedly corrected to obtain a series of fitting indexes of the corrected model. When the significance level is low, the customer management ability has a relatively large impact on the marketing performance. However, the other two subindicators market learning ability and marketing promotion ability have a significant impact on marketing performance but to a lesser extent. In Table 1, the structural parameter estimation and significance test of performance indicators is shown.

Although the absolute amount of rare earth is large, the content is low and the average abundance in the Earth's crust is only 200 ppm, and the distribution is very uneven. In the matter element, A is an evaluation feature, that is, an indicator. Some feature values can be calculated by the system, and the feature values corresponding to each feature are shown in Table 2. Figure 4 shows the relationship between eigenvalues and matter elements in three sets of experimental data.

China's political system, economic system, and the development of the rare earth industry determine the legal system and policy measures for the management of rare earth resources. At present, almost all oxidizing roasting-hydrochloric acid leaching method is used in the industry. The rare earth ore is oxidized and calcined, and the bastnasite is decomposed to form rare earth oxide, rare earth fluoride, or rare earth oxyfluoride which is soluble in hydrochloric acid [20]. Rare earth elements are mostly in the form of oxides or symbiotic forms of oxoacid minerals, and the degree of enrichment is low. There are not many deposits with mining value at the current technical level, so rare earth

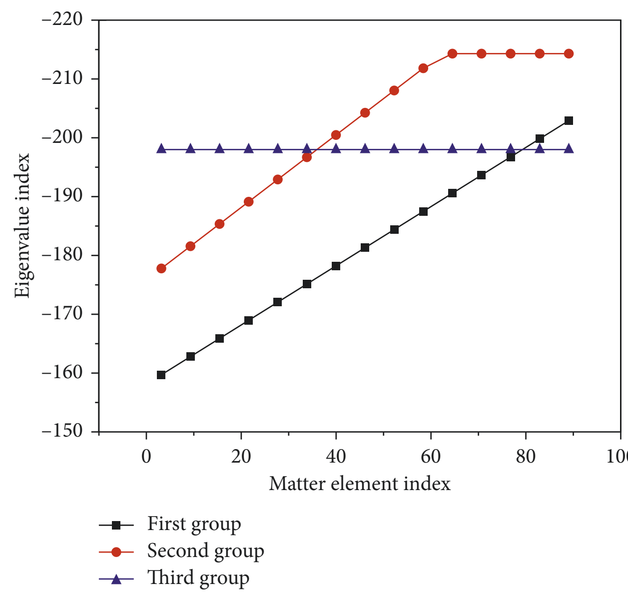

Figure 4: Relationship between eigenvalue and matter element.

resources have been proven in the world. The amount of exploitation is scarce. The in situ leaching process does not requires excavation of ore bodies, has little impact on the ecological environment, and has high resource utilization [21]. However, the in situ leaching process developed in the early stage is only applicable to mines with intact ore bodies. For mines with complex geological conditions, leaching liquid leakage often occurs, resulting in a significant reduction in rare earth recovery.

3. Economic Significance of Rare Earth Resources

Whether the political and legal system of rare earth resources protection and management can adapt to the development requirements of the rare earth resources industry determines the success or failure of China's rare earth resources strategy. Rare earth enterprises should develop new products to meet the domestic demand for rare earth consumption. Rare earth, as a special mineral resource, is greatly different from other mineral resources in terms of resource structure, resource use, and spatial distribution. In view of the problems of high consumption of chemical materials, the low comprehensive utilization rate of resources and serious pollution of the three wastes in the rare earth smelting and separation process, various research institutions, and enterprises have developed a series of efficient, clean, and environmentally friendly smelting and separation processes. In order to reduce dependence on foreign rare earth resources and prevent being controlled by others, some developed countries have begun to develop substitutes for rare earth resources. Judging from the current scientific and technological achievements, although some scientific and technological progress has been made, the results are not good. In order to better protect rare earth resources, China's established rare earth strategic resource reserve system should be implemented and perfected as soon as possible [22]. The unified export of rare earth products has also better maintained the reasonable price of rare earth, but there are also unreasonable problems, such as neglecting the management and protection of light rare earth and failing to adjust the relationship between rare earth development and environmental protection. Rare earth enterprises should seize the market opportunity, follow closely the market demand, and strive to develop the domestic market.

Under the current economic situation, small mining companies should adhere to the principle of large and small, superior and inferior, and follow the laws of the market economy according to the natural occurrence of resources. The social network formed by resource-based urban clusters is a complex and dynamic network. A social implementation mechanism such as a cluster network can establish a cluster trust mechanism to improve the resource environment. At different stages, the strength of urban cluster competitiveness and the specific performance of urban cluster competitiveness at different stages are shown in Figure 5.

The market learning ability has no significant influence on the accounting effect and brand assets. It actively promotes the construction of modern characteristic resource-based industries and the modernization of production methods, production methods, and production concepts. Speed up the transformation of industrial development mode, save natural resources and production factors, optimize the economic structure of resource-based cities, and realize sustainable development. Figure 6 is a schematic structure for strategic adjustment and guidance of industrial structure in resource-based cities.

The mode of unified purchase and sales of rare earth products was severely impacted by the market economy and withdrew from the historical stage. Therefore, the state's policy of controlling rare earth mainly focuses on mining and export. Through orderly mining, effective protection of resources is realized, and at the same time, local regional economic transformation and industrial upgrading are also supported. China's failure to enact a superior mineral protection law in time to meet the requirements of the development of the market economy has put the country's protection of rare earth resources into a dilemma. Most of the rare earth minerals in the world contain only a few rare earth elements, which are incomplete. The rest of the rare earth elements that do not exist still depend on imports [23]. China Nonferrous Engineering Design and Research Institute and Rare Earth Material Factory have improved the

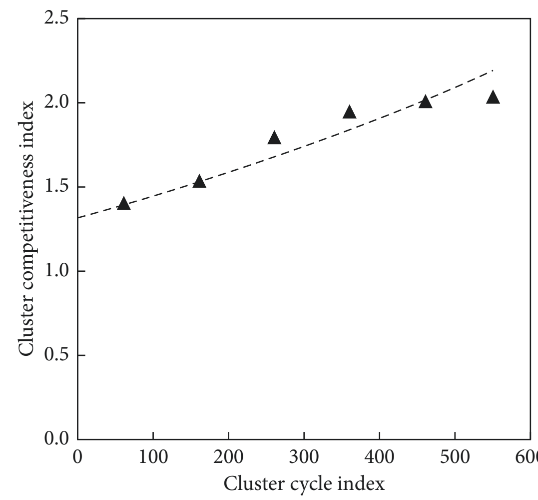

Figure 5: Trends in the competitiveness of resource-based clusters.

low-temperature roasting process to solve the problem of wall formation. Continuous low-temperature dynamic roasting can be realized by using low-temperature curing technology. Although the abundance of rare earth elements in the Earth's crust is not poor or even higher than that of some common metals, due to the technical conditions, some rare earth ores have low mining value and high cost, which are difficult to meet the mining standards and cannot be applied by human beings.

No resource can function independently as a factor of production. Only when natural resources are combined with social resources can they be transformed into productive forces with use value and value. Rare earth enterprises should base themselves on the domestic market and expand domestic demand. Figure 7 shows the contribution of different resources at different stages of economic development.

After the establishment of the comprehensive evaluation of the material-element model of independent innovation capability, it is necessary to evaluate the index value of each characteristic of the independent innovation capability of the enterprise and the approximation degree of each level. Applying the proximity of classical domain matter elements in the following extension set:

$$\mathrm{cell}_{ps-1} = \arg\max_{n} \left(\sum_{m=1}^{M} P_{f-n_m} \right). \tag{4}$$

The extension distance is

$$\mathrm{cell}_{ps-n_{s1}} = \mathop{\arg\min}_{i,i\neq \mathrm{cell}_{ps-1},\ldots,\mathrm{cell}_{ps-n_s}} \left(\sum_{m=1}^{M} \sum_{l=1}^{M} p_{i_l} \left\| \mathbf{h}_{i,ps-1_m}^{T} \mathbf{W}_{i,i_l} \right\|_2^2 \right). \tag{5}$$

Calculate the degree of association of the company to be evaluated with the weight coefficient of each feature.

$$R_{n_i}^{C} = \log_2 \left(1 + \frac{p_{\mathrm{mac},n_i} \left\| \mathbf{h}_{\mathrm{mac},n_i}^{T} \mathbf{W}_{\mathrm{mac},n_i} \right\|_2^2}{\sigma^2} \right). \tag{6}$$

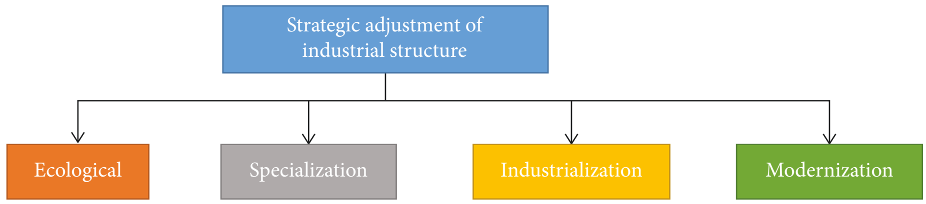

Figure 6: Strategic adjustment structure of the resource-based urban industrial structure.

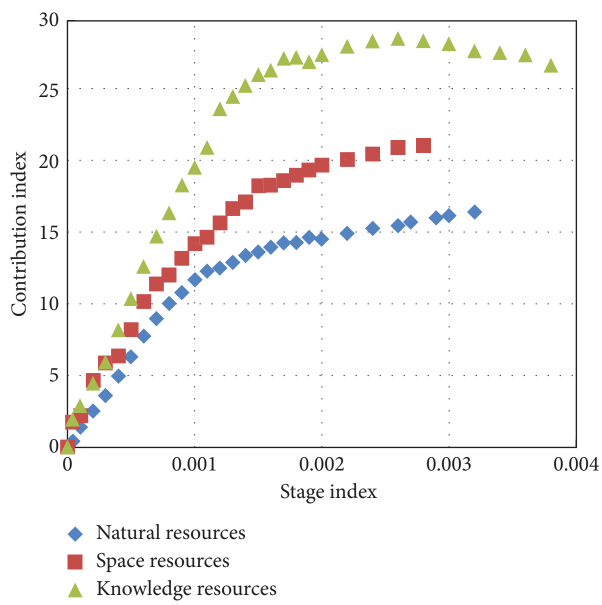

Figure 7: Different resources contribute to different stages of economic development.

Table 3: Price competition degree division.

Degree of decrease (%)	0–20	20–40	40–60	60–80	80–100
Normalized value	0.2	0.4	0.6	0.8	1

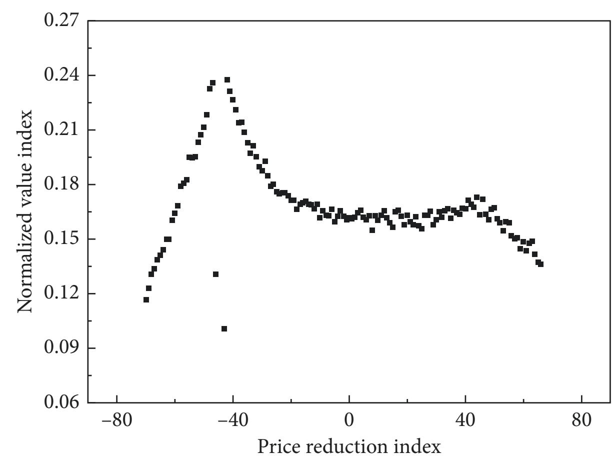

Figure 8: Relationship between normalized value and price reduction.

Through the deep processing of rare earth resources and the extension of the industrial chain, the pace of development of rare earth resources from upstream primary raw materials to deep processed products, high-tech new materials, functional components, and end-use products will be accelerated. After the various influencing factors have been uniformly measured to the four-point system, in order to better study the impact of price competition on various factors, the argumentation part adopts the idea of normalization of price competition. The price competition is divided into five sections, each of which has a length of 20%. The specific division is shown in Table 3. The relationship between the normalized value and the price reduction range is shown in Figure 8.

Sustainability is a measure of the sustainability criteria for resource-based urban transformation systems and the development of subsystems. Using the development rate of each subsystem as a measure, the following can be obtained:

$$Q\left(u_{ij}\right) = \sum_{i=1}^{n} \underset{1\le j\le m}{\mathrm{Max}}\left\{g_{ij}(T)\right\}. \tag{7}$$

Using the fuzzy membership function method to obtain the following:

$$y_{f-n_m} = \sum_{i=1,i\neq n}^{N} \sum_{l=1}^{M} \sqrt{p_{i_l}}\,\mathbf{h}_{i,n_m}^{T}\mathbf{W}_{i,i_l} s_{i_l}. \tag{8}$$

Calculate the trend degree as follows:

$$P_{f-n_m} = \sum_{i=1,i\neq n}^{N} \sum_{l=1}^{M} p_{i_l}\left\|\mathbf{h}_{i,n_m}^{T}\mathbf{W}_{i,i_l}\right\|_2^2. \tag{9}$$

In the impact on the other three indicators, although there is a certain degree of positive impact, but the impact is less than the customer management ability. But it is very close, so its impact on brand equity can not be ignored. The impact of marketing capabilities on customer value and product innovation is not significant, and the positive impacts on the other three indicators are significant. Similarly, the factor load of the corresponding indicators is also less than the factor load associated with the customer. The structural parameter estimation and significance test of the impact of marketing subcategories on marketing performance subindicators are shown in Table 4.

The selection of resource-based city indicators should cover the content of the evaluation as much as possible and comprehensively reflect all aspects of the city's sustainability

Table 4: Significant test of the impact of marketing subcategories on marketing performance subindicators.

	Value of customer	Competitive result	Brand equity	Product innovation
Market promotion ability	0.76	0.59	0.64	0.69
Customer management ability	0.37	0.44	0.49	0.51
Market learning ability	0.39	0.32	0.47	0.45

Table 5: Value of the correlation function of the evaluation level.

Grade indicator	1	2	3	4
S1	0.386	0.556	0.742	0.457
S2	0.943	0.796	0.297	0.362
S3	0.348	0.653	1.569	0.794

capacity. The correlation value of each level indicator is shown in Table 5.

To measure the degree of price competition between a company's homogeneous product and the market average price, you can simply write the price competition between a single company's product pricing and the market average price as follows:

$$c_1(t) = c_{11} + (c_{1T} - c_{11})\frac{t}{T},$$
$$c_2(t) = c_{21} + (c_{2T} - c_{21})\frac{t}{T}. \tag{10}$$

Initialize, calculate the connection weight and threshold, and assign any value.

$$I_i = \left[\sum_{j=1}^{p} \omega_j^m y_{ij}^m\right]^{(1/m)}. \tag{11}$$

Provide input samples and expected output to obtain the following equation:

$$I_\omega \ddot{\delta} = F_r d - K_\omega \dot{\delta} - C_\omega \delta - K_1 e \delta. \tag{12}$$

Calculate the output of each unit in the hidden layer.

$$T = \frac{M}{R} = \frac{i\eta_e M_e}{r}. \tag{13}$$

Enterprises need to improve their independent innovation ability and promote the upgrading of industrial structures. Strengthen the research on the development strategy of the rare earth industry and formulate policies and measures to further promote the development of rare earth technology and industry. Rare earth minerals are China's dominant mineral resources. In the early stage of reform and development, it is historically inevitable to obtain considerable economic income by supplying a large amount of rare earth products to the international rare earth market. Compared with the world's large multinational enterprises, China's enterprises in related industries are not strong in independent innovation, market competitiveness, and ability to resist international market risks. Cultivating a number of large enterprises with strong comprehensive strength is an important goal. Heavy and light rare earth products are sharply divided, and the proportion of heavy rare earth products in the mines that have been put into production is relatively low, so they cannot impact the medium and heavy rare earth market. China will continue to maintain its leading position in this field [24].

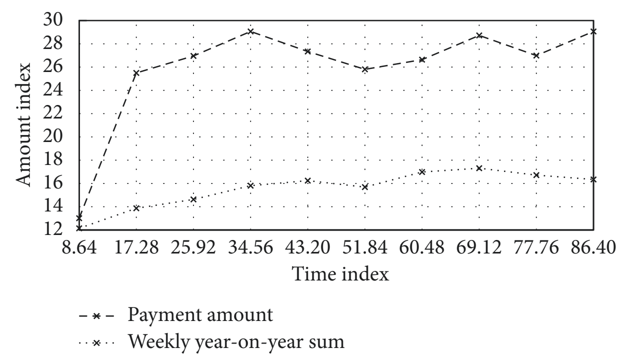

Figure 9: Preview of the transaction overview.

Rare earth resources are widely used in modern industrial development. Rare earth elements play a key role in some aspects. In the overall sales analysis, it is necessary to specifically analyze the customer unit price, year-on-year month-on-month changes, and other links. A preview of the transaction is shown in Figure 9.

China needs to fulfill relevant international commitments and obligations. The supply of rare earth products cannot be controlled by administrative means. Even through the means of environmental protection, its supervision system and law enforcement methods are not perfect and lack of supporting measures. The strategic value of rare earth resources is outstanding, and its supply directly affects the national defense industry, national competitiveness, and even the economic security of the entire country. The development of the rare earth resource industry not only provides a large number of jobs but also solves the problem of insufficient supply of mineral products in rapid economic development. In order to balance the interests of the central, local, and enterprise and properly handle the relationship between different regions and upstream and downstream industries, it is recommended to reconfigure mining licenses for state-led enterprises on the basis of the joint of national large-scale rare earth enterprise groups and resource regions [25]. We must first clearly understand the problems of China's rare earth resources in mining, processing, and export trade and find out the reasons through careful analysis and research, and then we can propose solutions to the problems. In order to enable China's rare earth industry to develop healthily and sustainably, it is recommended to increase investment in science and technology and environmental protection, strengthen research on efficient and clean production processes, industrial development and promotion, and strictly implement the "Rare Earth Industrial Pollutant Emission Standards." You can choose several key links for key management to effectively manage the valuable rare earth resources that protect the country.

4. Conclusions

Rare earth minerals are the strategic resources of the country. Therefore, the distribution and use of rare earth mining rights should not be allowed to be bought and sold arbitrarily as ordinary metal mining rights, so as to realize the effective control of rare earth strategic resources by the country. At a time when the socialist market economy system is gradually improving, the reimplementation of comprehensive planning and control of rare earth and other advantageous mineral resources no longer meets the fundamental requirements of the market economy era but also violates the basic development trend of mining development and operation mechanism and management system. While rare earth development benefits mankind, the accompanying problems of resources and environment are becoming increasingly prominent. With the in-depth development of economic globalization, China's international exchanges and cooperation in the field of rare earth resources are increasing day by day. At the system level, different legal procedures should be applied to the grant of rare earth development and management rights and the assignment of rare earth mining rights, respectively, to clarify the differences between the franchise rights and property rights. Mining rights can be taken as state-owned capital and included in the asset management scope of central enterprises. The exploration right should be granted to large enterprise groups on a regional, limited, and limited basis to avoid the loss of new rare earth resources. It is suggested that departments of land and resources at all levels should clean up and rectify their registration in the name of polymetallic minerals, actually demarcate rare earth mineral resources, and re-examine the exploration licenses and mining licenses that have been issued in rare earth mineral resources areas. In terms of process innovation management, China should attach importance to the nonrenewable nature of rare earth resources and increase the capital investment for rare earth deep processing and process innovation as soon as possible.

Data Availability

The data used to support the findings of this study are available from the author upon request.

Conflicts of Interest

The author declares that there are no conflicts of interest.

References

[1] S. Jaireth, D. M. Hoatson, and Y. Miezitis, "Geological setting and resources of the major rare-earth-element deposits in Australia," *Ore Geology Reviews*, vol. 62, pp. 72–128, 2014.

[2] G. J. Simandl, "Geology and market-dependent significance of rare earth element resources," *Mineralium Deposita*, vol. 49, no. 8, pp. 889–904, 2014.

[3] S. M. Jowitt, V. N. L. Wong, S. A. Wilson, and O. Gore, "Critical metals in the critical zone: controls, resources and future prospectivity of regolith-hosted rare earth elements," *Australian Journal of Earth Sciences*, vol. 1, pp. 1–10, 2017.

[4] H. Guo, J. Zhang, L. Ma, and J. L. L. H. Z. W. Chavez, "White light phosphors: a nonrare-earth ions self-activated white emitting phosphor under single excitation (adv. Funct. Mater. 44/2015)," *Advanced Functional Materials*, vol. 25, no. 44, p. 6826, 2015.

[5] S. Maes, W.-Q. Zhuang, K. Rabaey, L. Alvarez-Cohen, and T. Hennebel, "Concomitant leaching and electrochemical extraction of rare earth elements from monazite," *Environmental Science & Technology*, vol. 51, no. 3, pp. 1654–1661, 2017.

[6] C. Wetzel and T. Detchprohm, "Rare-earth-free direct-emitting light-emitting diodes for solid-state lighting," *IEEE Transactions on Industry Applications*, vol. 50, no. 2, pp. 1469–1477, 2014.

[7] W. K. Dodds, K. Gido, M. R. Whiles, M. D. Daniels, and B. P. Grudzinski, "The Stream Biome Gradient Concept: factors controlling lotic systems across broad biogeographic scales," *Freshwater Science*, vol. 34, no. 1, pp. 1–19, 2015.

[8] T. Dutta, K.-H. Kim, M. Uchimiya et al., "Global demand for rare earth resources and strategies for green mining," *Environmental Research*, vol. 150, pp. 182–190, 2016.

[9] B. W. Stewart, R. C. Capo, B. C. Hedin, and S. H. Robert, "Rare earth element resources in coal mine drainage and treatment precipitates in the Appalachian Basin, USA," *International Journal of Coal Geology*, vol. 169, pp. 28–39, 2017.

[10] L. Kaizhong, L. Huiping, L. Fuguo et al., "Migration of natural radionuclides in the extraction process of the ion-adsorption type rare earths ore," *Hydrometallurgy*, vol. 171, pp. 236–244, 2017.

[11] Z. Zhang, G. Zheng, Y. Takahashi, and C. Wu, "Extreme enrichment of rare earth elements in hard clay rocks and its potential as a resource," *Ore Geology Reviews*, vol. 72, pp. 191–212, 2016.

[12] L. Fangwen, M. Li, C. Guanqiang, and Y. Wen, "The rare earth element geochemistry of surface sediments in four transects in the South China Sea and its geological significance," *Environmental Earth Sciences*, vol. 74, no. 3, pp. 2511–2522, 2015.

[13] C. Huang, K. Wang, J. Sun, and J. Jiang, "Planar binuclear phthalocyanine-containing sandwich-type rare-earth complexes: synthesis, spectroscopy, electrochemistry, and NLO properties," *European Journal of Inorganic Chemistry*, vol. 2014, no. 9, pp. 1546–1551, 2014.

[14] L. Wang and T. Liang, "Accumulation and fractionation of rare earth elements in atmospheric particulates around a mine tailing in Baotou, China," *Atmospheric Environment*, vol. 88, pp. 23–29, 2014.

[15] Z. Hao, Y. Li, H. Li et al., "Levels of rare earth elements, heavy metals and uranium in a population living in Baiyun Obo, Inner Mongolia, China: a pilot study," *Chemosphere*, vol. 128, pp. 161–170, 2015.

[16] R. T. Nguyen and D. D. Imholte, "'China's rare earth supply chain: illegal production, and response to new cerium demand," *Journal of Occupational Medicine*, vol. 68, no. 7, pp. 1948–1956, 2016.

[17] Z. Y. Mao, F. Wang, J. J. Chen, and D. J. Wang, "Rare-earth free phosphors with ultra-broad band emission application for high color rendering index lighting source," *Journal of the*

American Ceramic Society, vol. 98, no. 12, pp. 3856–3862, 2015.

[18] Z. Zhu, Y. Pranolo, and C. Y. Cheng, "Separation of uranium and thorium from rare earths for rare earth production – a review," *Minerals Engineering*, vol. 77, pp. 185–196, 2015.

[19] L. Wang, T. Liang, Q. Zhang, and K. Li, "Rare earth element components in atmospheric particulates in the Bayan Obo mine region," *Environmental Research*, vol. 131, pp. 64–70, 2014.

[20] V. S. Jacqueline, P. C. Buenaventurada, H. Mihoko et al., "Flotation of rare earth minerals from silicate–hematite ore using tall oil fatty acid collector," *Minerals Engineering*, vol. 89, pp. 52–62, 2016.

[21] N. Kim, A. C. Cheong, K. Yi, Y. J. Jeong, and S. M. Koh, "Post-collisional carbonatite-hosted rare earth element mineralization in the Hongcheon area, central Gyeonggi massif, Korea: ion microprobe monazite U-Th-Pb geochronology and Nd-Sr isotope geochemistry," *Ore Geology Reviews*, vol. 79, pp. 78–87, 2016.

[22] J. Wang, D. Zhu, X. Fang, T. Qiu, Y. Liu, and H. Zhu, "Enhanced characteristics and mechanism of static magnetic field on ion-absorbed rare earth precipitation," *International Journal of Mineral Processing*, vol. 158, pp. 13–17, 2017.

[23] P. J. Thomas, D. Carpenter, C Boutin, and J. E. Allison, "Rare earth elements (REEs): e," *Chemosphere*, vol. 96, pp. 57–66, 2014.

[24] M. Bau, K. Schmidt, A. Koschinsky, J. Hein, T. Kuhn, and A. Usui, "Discriminating between different genetic types of marine ferro-manganese crusts and nodules based on rare earth elements and yttrium," *Chemical Geology*, vol. 381, pp. 1–9, 2014.

[25] C. J. Kim, H. S. Yoon, K. W. Chung et al., "Leaching kinetics of lanthanum in sulfuric acid from rare earth element (REE) slag," *Hydrometallurgy*, vol. 146, pp. 133–137, 2014.

Hindawi
Computational Intelligence and Neuroscience
Volume 2022, Article ID 6101368, 8 pages
https://doi.org/10.1155/2022/6101368

Research Article

Cultural Confidence on "Art & Engineering" Construction of Product Design under "New Liberal Arts"

Lijun Xu,[1] **Jun Gao**,[2] **Lu Chen**,[1] **Guodong Liang**,[1] **and Hailong Feng**[1]

[1]*Institute of Art and Design, Nanjing Institute of Technology, Nanjing, Jiangsu 211167, China*
[2]*ABB Beijing Drive System Co., Ltd., Beijing, China*

Correspondence should be addressed to Lijun Xu; xulijun@njit.edu.cn

Received 31 March 2022; Revised 18 April 2022; Accepted 21 April 2022; Published 9 May 2022

Academic Editor: Xin Ning

A master's degree program in "new liberal arts" is a great opportunity to strengthen cooperation between art colleges and universities, to promote the construction of product design and digital molding majors, and to promote teaching and research on the "integration" of the theoretical foundations of engineering intelligent manufacturing. To take advantage of cooperative universities' advantageous disciplines and professional platforms, we should construct new art and emerging interdisciplinary majors, as well as promote the construction and exploration of joint training of doctors and masters in relevant disciplines in the interdisciplinary direction of art and engineering. The foregoing approaches are intended to create a new "art and engineering" model for the establishment of a product design speciality at our university. In order to meet the requirements of "Art & Engineering" advocated by the national new engineering construction, art disciplines have their own inherent rules and characteristics. We should actively create disciplinary and professional characteristics, help universities cooperate with each other in high-quality development, and share and win together, in order to continuously achieve new academic results.

1. Introduction

China's "Six Excellences and One Top" Plan 2.0 was launched in Tianjin on April 29, 2019, with the goal of boosting universities' capacity to serve economic and social development by promoting the construction of new engineering, new medicine, new agriculture, and new liberal arts. When it comes to the growth of higher education, "new liberal arts" has become a subject that needs to be taken seriously [1].

It is necessary to grasp the new requirements for the development of philosophy and social sciences in order to strengthen the construction of new liberal arts. It is also necessary to cultivate new cultures with Chinese characteristics, such as Chinese style and Chinese style in the new era, as well as philosophical and social scientists. It is also necessary to establish a Chinese school of philosophy and social sciences in order to strengthen the construction of new liberal arts. The construction of "new liberal arts" has as its primary goal the adaptation to the new requirements of the development of philosophy and social science in the new era as well as the promotion of cross-fertilization between philosophy and social science with the new round of scientific and technological revolution and industrial change. As a result, the "new liberal arts" have emerged as a topic that must be properly studied and explored in the development of higher education in the contemporary day. For the "new liberal arts," efforts should be made to cross disciplines, form and expand new fields of knowledge at the boundaries between disciplines, particularly in conjunction with science and technology, and realize the intersection of arts and science. This, for the liberal arts, entails enhancing the scientificity of liberal arts and thus promoting the construction of "new liberal arts."

It was Bauhaus principal Walter Gropius who introduced the educational concept of "Art & Engineering" product design for the first time. Gropius insisted on the new unification of art and technology, which resulted in the formation of a new educational system that combined art education with handicraft. With its approach of merging "pure art" with "useful technology" [2, 3], the Bauhaus provided inspiration for the future "Art & Engineering" teaching model.

The term "engineering" in the "Art & Engineering" mainly refers to engineering in science, which is a discipline in which people study and apply theories and knowledge of natural science, sociology, economics, logic, and other disciplines to innovate or improve the design and use of solutions in various fields [4]. It also includes the meaning of "engineering technology," in which people use engineering technology to make practical objects or tools to extend or compensate for human capabilities and change people's way of life, with the intention of being practical.

Product design is a kind of industry that is about innovation, and without innovation, there is no vitality. The educational concept of product design should also include the concept of innovation. Since the Bauhaus pioneered the innovative educational concept and mode of "Art & Engineering," institutions across the world are following suit [5]. However, in this new era, if we adhere to this concept and follow the trend without seeking innovation, the design talents we cultivate will be out of step with the society. Based on the diversified, informative, and intelligent conditions of the times, the educational concept of "Art & Engineering" in product design must keep pace with the times and make the concept of design education have new thinking characteristics.

Rather than just rehashing the old buzzwords of "intersection of disciplines" or "intersection of arts and sciences," the concept of the new liberal arts should be understood from the perspective of China's intrinsic requirements for postsecondary education [6]. The investigation and practice of "Art & Engineering" of product design in the context of "New Liberal Arts" are still in the early stages of its development and implementation.

Problems

(1) The engineering technology category of product design majors does not have sufficient teaching qualifications, and it is difficult to connect the more artistic design majors with the more technical engineering technology at this time. Product design majors will concentrate on the design of rail transportation class and intelligent product class, which will be based on the application of big data, cloud computing, and artificial intelligence technology, allowing the design to be more scientific, rational, and extensive in the context of the "New Liberal Arts." As a result of this rapidly changing development environment, the knowledge structure, cognitive ability, and thinking mode requirements of designers will undergo significant shifts in the near future. As a result, design education will need to adapt quickly in order to meet the changing needs of society.

(2) There is a difference between the training for talents and the education of design as well as the most recent technology available on the market. (2) Product design teachers must convert their art backgrounds and engineering teaching concepts into product design teaching concepts. The talents cultivated by design education will be unable to meet the needs of social development and will eventually be eliminated if design education does not adapt to the changing times in order to adjust the goal of talent training and does not use engineering technology to complement the design practice. It will also be difficult to implement the employment of design education students. In order to better support product design teaching, it is urgently necessary to investigate how "Art & Engineering" can promote the reform of product design education from a systematic and holistic perspective as well as to clarify the ideas for "Art & Engineering" to better support product design education and cultivate more professional product design applied talents.

Solutions

(1) "Art & Engineering" should reflect the personalization and diversity of interdisciplinary

To further strengthen the construction of product design discipline, give full play to disciplinary strengths, and concentrate disciplinary characteristics; to strengthen interdisciplinary crossover and integration with art colleges and engineering majors and take the construction of a special master's degree in art as an opportunity to build the disciplinary characteristics of "Art & Engineering"; to do a good job of training product design talents with high quality and establish an application-oriented education training system that serves the needs of economic and social development.

(2) "Art & Engineering" should pay attention to talent training

To further boost the creation of product design majors and the training of future product design talent. Taking the construction of new engineering and new liberal arts as a model, establish and improve the dynamic adjustment mechanism of majors, optimize the structure and connotation of majors, expand the enrollment scale of majors, and establish new majors in art; concentrating on the cross-fertilization of art and engineering to form the cultivation characteristics of art and design talents, promote the in-depth reform of project-based teaching, and strengthening the internationalization of art and design talents; focusing on the cross-fertilization of it is necessary to continue to increase the construction of teaching staff at the "Art and Engineering" school. It is also important to develop a high-level professional teaching and research team with a worldwide perspective through training, further training, and study visits, in addition to expanding the channels for the entry of high-level talents into the product design industry.

(3) Research on the new platform of discipline construction in College of Arts and Design

> To adapt to the requirements of "Art & Engineering" advocated by the national new engineering construction, art disciplines have their own inherent rules and characteristics, should actively create disciplinary and professional characteristics, and help universities cooperate in high-quality development to help each other and share and win together, in order to continuously achieve new academic results.

At this stage of the school's development ideas and goals, the status of the School of Art and Design is increasingly important, directly related to the comprehensive and coordinated development of the school's related disciplines, the important indicators of the school's name change, and the core content of the school's future sustainable development. Therefore, the great development of art and design disciplines should fully rely on the school's traditional advantageous disciplines, build a new platform for discipline construction of the College of Art and Design, and strive to form a number of characteristic high-level research results around the direction of discipline construction of the College, with the common ideal of "building a first-class art and design college of the same kind with domestic influence and provincial status" [7, 8], form the mainstream value orientation common to all the faculty and students, and concentrate our efforts to create a college culture atmosphere that emphasizes discipline and professional development, academic research and artistic creation, harmonious construction and quality improvement, and continuous deepening, expansion, and ascension.

2. New Thinking and New Forms of Cultural Confidence Research of "Art & Engineering"

According to the "new liberal arts" theory and practice, the Jiangsu brand-product design major establishes a new pattern of "Art & Engineering" in accordance with the investigation and practice of the development of national first-class products. It will be developed in conjunction with the master's degree program at the College of Art and Design in order to strengthen cooperation between art colleges and universities, cooperation with engineering practice majors, and practical teaching of intelligent design and will strive to promote a close connection between knowledge transfer and production practice. It will also be developed in conjunction with the master's degree program at the College of Art and Design in order to promote "integration" of theory and practice in the field of product design and digital molding. It is necessary to establish a design research and development platform with innovation as the goal, a practical platform with engineering training as the means, and a social crowdfunding or school-enterprise cooperation platform with market demand as the guide in order to explore and practice "Art & Engineering" in product design education, resulting in the formation of a new way of thinking about and practicing "Art & Engineering" in product design education. It is shown in Figure 1.

As part of this effort, the college will make better use of the advantageous disciplinary and professional platforms of the partner institutions to carry out the construction of new art and emerging cross-disciplinary disciplines and professions. It will also work to promote the construction and exploration of joint training programs for PhDs, Master of Arts, and Master of Engineering degrees in relevant disciplinary fields as well as joint training programs in engineering-related cross-disciplinary directions. A number of initiatives will be undertaken by the two sides to benefit from their respective disciplines, such as the development of new art and emerging interdisciplinary disciplines and majors, the establishment and sharing of internship and practical training teaching practice bases, the cultivation of PhDs and Master of Art and Engineering-related interdisciplinary directions within relevant disciplinary fields, as well as the collaboration in the development of an innovative and entrepreneurial education system. The partnership will be translated into practical measures to support the development of the school in a timely manner, as well as to promote the quick expansion of the school's business, and work toward the establishment of a new pattern of "Art & Engineering."

2.1. Research on the Construction of Cultural Confidence Majors with "Art & Engineering"

(1) Research on new thinking and new forms of "Art & Engineering" in the era of "New Liberal Arts"

(2) Research on teacher training for "Art & Engineering" talents in the field of design in universities and research on leading the cultivation of product design talents

(3) Research on the construction of product design talent training objectives and curriculum system with "Art & Engineering"

2.2. Investigation into the "Art & Engineering" Teaching Mode and the Use of Abilities in Intelligent Design

(1) To investigate the current state of product design higher education in both China and abroad, as well as the characteristics and applications of intelligent technology, in order to predict the future development trend of intelligent product design education and to establish a fundamental theoretical system for intelligent product design education in China and abroad

(2) To redefine the training objectives of product design talents in the new liberal arts era, improve the talent training program, and establish the core curriculum system of "Art & Engineering"

(3) To study the changes in the teaching resource environment, teaching and learning methods, teaching management and evaluation methods, personalized teaching mode, and teacher training in the "Art & Engineering," to propose the reform direction of product design education, and then to build the education system of product design in the era of "New Liberal Arts"

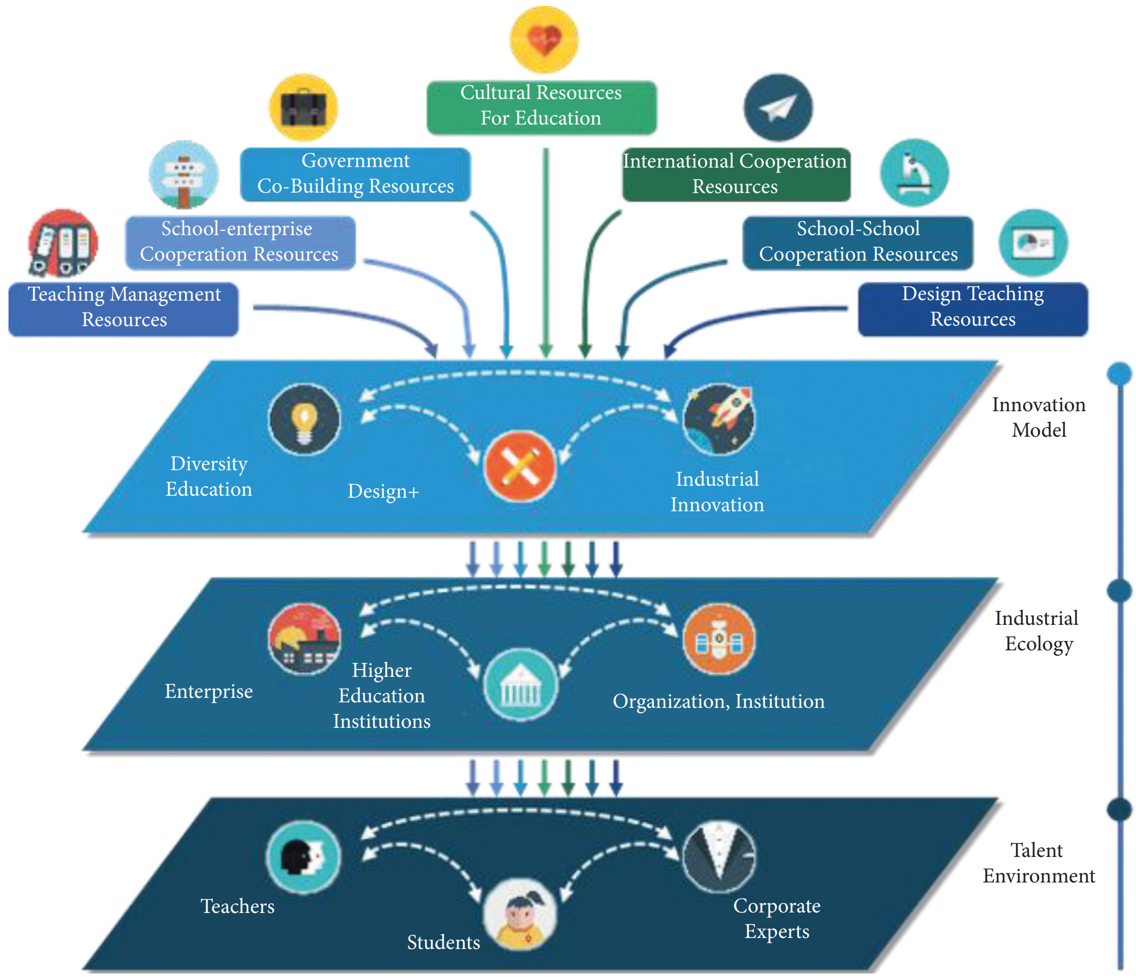

Figure 1: New thinking and new forms of education in "Art & Engineering" cultural confidence theory research.

2.3. Research on the Construction of a Teaching and Research Platform for Product Design and Digital Molding of "Art & Engineering"

(1) Research on courses that are closely linked to the "Art & Engineering": Human-Computer Interaction Design Research at master's level, Advanced Manufacturing Technology and Artistic Design, Thematic Studies in Electromechanical Product Design, Product and Interaction Design Project Practice, Design competitions and exhibitions.

(2) Research on computer-aided design series courses, product design series core courses, model making, thematic design series courses, CG production of animation characters, cultural and creative design of animation, model making of craft products, jewelry design, environmental model making, and many other professional basic courses and professional courses in the undergraduate stage of "Art & Engineering".

(3) Researchers at home and abroad are investigating intelligent educational platforms for "Art & Engineering" in a variety of contexts, including the platform characteristics and operation system of educational robots and platforms, teaching software and teaching tools, intelligent virtual assistants, among other things; they are also investigating the teaching and research platform of intelligent product design and digital molding.

3. Diversification of "Art & Engineering" Practice Research with Cultural Confidence

When placed in the context of the "new liberal arts," product design majors' educational thinking must seek innovation and keep up with the times; as a result, the educational mode of "Art & Engineering" tends to be market-oriented, internationalized, personalized, and manifesting the characteristics of regionalization [9–11].

3.1. Enhancing Students' Interest and Skills in "Art and Engineering" Intellectual Creation. Students' real-world experience with a variety of material processing techniques and skills is enhanced through the use of the basic molding system, which increases the means of expression and the ability of intelligent product design for art and design students, which is conducive to activating students' creative thinking, encouraging students to carefully observe the surrounding living environment and the current social situation, and combining objective natural laws and their own unique thin-film technology. The measures outlined above can assist us in cultivating a diverse pool of high-quality applied talents to satisfy the needs of economic and social development.

3.2. Improving the Quality of Talent Cultivation of "Art & Engineering" and Sharing Teaching Resources with Cultural Confidence. Students can conduct experiments at any time and from any location because of the development of this project, which overcomes the limitations of time and space. At the same time, the software has a variety of learning functions that allow pupils to practice over and over again. "Observation, recording, and combination-making exercises" [12] of virtual experimental items in a variety of virtual experimental contexts have helped students to improve their design skills. When this initiative is put into practice, it significantly improves the scientific approach to learning as well as the professionalization of students' practical skills. Using the Internet, participants can easily access and use large-scale class experiments, and the project is open to the general public as well as educators. As of now, not only do the virtual simulation teaching materials serve the staff and students at this college but they also assist in the virtual simulation experimental teaching of other related majors.

3.3. "Art & Engineering" Should Be Personalized and Diversified Teaching. When it comes to improving students' design ability, the design education process is critical because it cultivates strong hands-on practical skills while also growing high theoretical literacy and the capacity to make full use of regional cultural resources to enrich their design concepts. In addition, professional craftsmen who are engaged in design and production work in the field of traditional crafts should be hired to teach at the institution. At the same time, in order to realize the purpose of assisting social production, the school should develop an industry-university-research platform in collaboration with businesses. A design that has not been translated into a product and the value of that design has not been realized are impossible if pupils do not grasp the manufacturing process. Students from all directions study professional basic courses together in the freshman year, such as design aesthetics, design composition, design expression techniques, the history of world arts and crafts, the history of Chinese arts and crafts, and other basic courses [13–15]; in the sophomore year, we implement discipline subdivision and choose discipline direction, such as curriculum of ceramics, wood carving, leather design, furniture design, and other disciplines [16–18].

3.4. "Art & Engineering" Should Implement Industrialization. The industrial transformation of design works, as well as the capacity to follow up in the process of product manufacture, processing, and sales, is an important element of the product design profession and one that can drive students to pursue a degree in product design which includes: (1) establishing craft design factories or studios on campus, as well as crowdfunding platforms on various commercial websites to publicize the works and raise funds for the processing and production of design works; (2) establishing school-enterprise partnerships with enterprises, in which the school commissions enterprises to process design works and provide them with marketing, as depicted in Figure 2; and (3) establishing school-enterprise partnerships with enterprises, as depicted in Figure 2.

3.5. "Art & Engineering" Should Be Internationalized. Design, like art, has no geographical boundaries. It is also necessary to integrate and cross borders in the "Art and Engineering" approach to product design education in order to better portray the spirit of product design education. Internationalization of the "Art and Engineering" approach to product design education is recommended in order to establish a broader and more diverse sector of design education [16–18]. The process of "Art & Engineering" product design education, such as the teaching of ceramics courses, must combine ceramic engineering and art, and it is necessary to cultivate advanced composite applied talents who understand both ceramic engineering and have excellent artistic design ability in order to meet the needs of China's ceramic industry development. Studying abroad, getting to know oneself and one's adversary, and learning the essence are all essential for standing out in design education.

4. Innovation and Prospect of "Design+" Multidisciplinary Cross-Fertilization with Cultural Confidence

In the context of the "New Liberal Arts," the educational thinking of product design majors must be innovative and keep up with the times so that the educational mode tends to be industrialized, internationalized, and personalized in the market, as well as manifesting the characteristics of regionalization, as shown in the following diagram. It is necessary to establish a design research and development platform with innovation as the goal, a practical platform with engineering training as the means, and a social crowdfunding or school-enterprise cooperation platform with market demand as the guide in order to explore and practice "Art and Engineering" in product design education, resulting in the formation of a new way of thinking about and practicing "Art and Engineering" in product design education. The following are examples of specific innovations.

4.1. Research on the Innovative System of Cultivating Intelligent Applied Talents in Product Design under the "Art & Engineering". The product design major, which is a combination of art and engineering in the context of "New Liberal Arts," should adhere to the principles of moral education, establish cultural self-confidence, support the high-quality development of the regional economy, and cultivate innovative and applied product design professionals who can comprehensively develop "moral, intellectual, physical, aesthetic, and labor" and grasp the elements

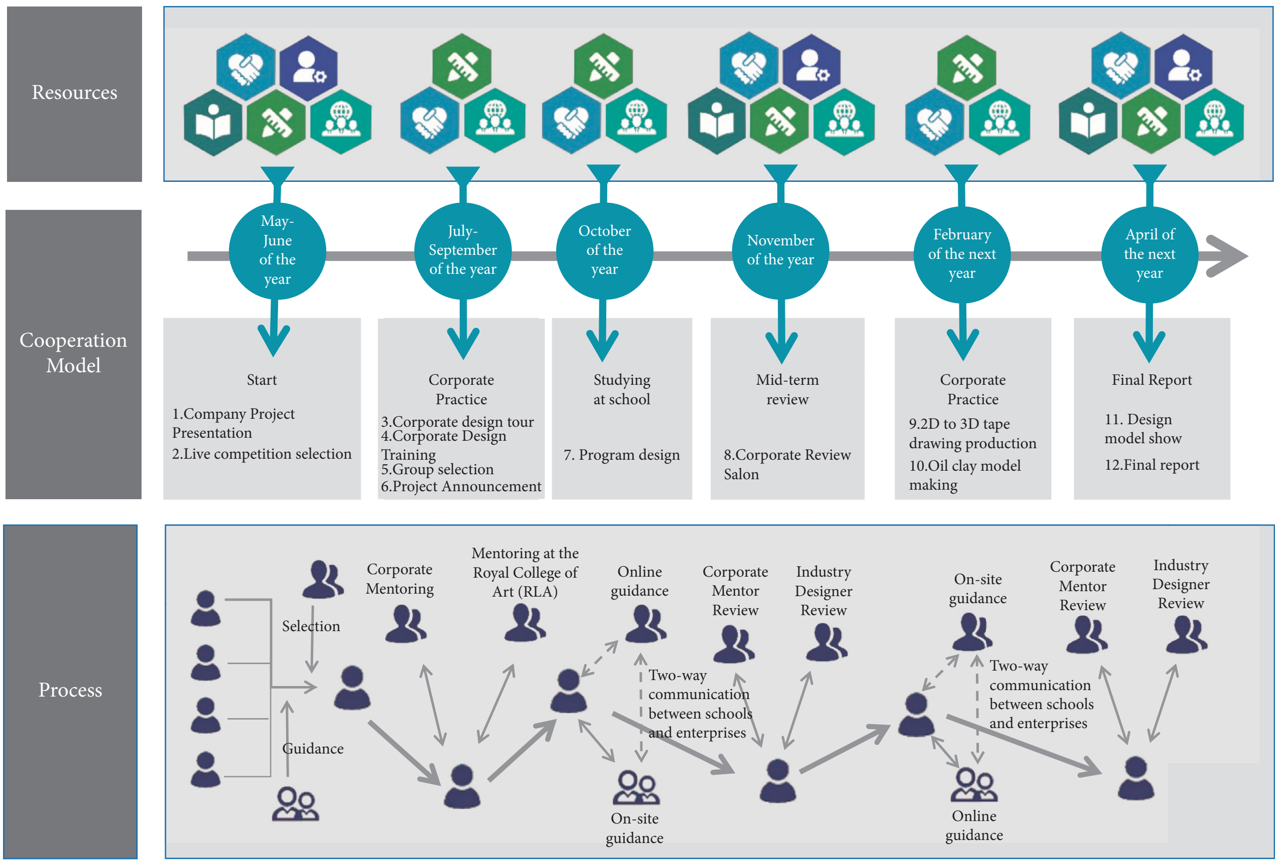

Figure 2: The "Art & Engineering" school-industry partnership project follows a logical progression.

of product function, form, material, structure, and color in the context of "New Liberal Arts."

(1) The practice of "Art & Engineering" product design and professional construction in the context of "New Liberal Arts" is being explored and researched.

It is necessary to emphasize the core purpose of "Art & Engineering" in design majors' curriculum and teaching system and introduce this learning concept to students early in the teaching process [19] so that students realize that they are product designers with comprehensive professional qualities rather than conceptual designers who can only draw concept drawings. We use the case analysis method to examine the current situation of product design education at home and abroad, as well as the nature, connotation, and construction ideas of the "New Liberal Arts." We also investigate the development trend of "Art & Engineering" in product design education, and we establish the fundamental theoretical system of product design education under the umbrella term of "New Liberal Arts."

(2) "Art & Engineering" is a teaching style that focuses on the application of intelligent design applied talents

When faced with the challenges of diversity, information technology, and intelligence, the education concept of "Art & Engineering" for product design majors must evolve to keep up with the times so that the design education concept possesses new thinking characteristics as well. By adopting a new model of product designers' "Art & Engineering" skills, we can reevaluate the training objectives of product design talents, improve the training program, and establish a core teaching model that meets the innovative consciousness and creative ability of "Art & Engineering" skills in the context of "New Liberal Arts."

4.2. Construction of Industry-Education-Research Platform for Product Design under the "Art & Engineering". As required by the discipline's talent cultivation goal, and in order to satisfy the needs of modern design and manufacturing firms, the College of Art and Design is collaborating with the College of Design to declare a master's degree in the field of art and design. A new teaching and research platform for product design and digital molding will be established in order to promote the "integration" of theory and practice in smart manufacturing. This will help to improve the quality of practical instruction while also promoting the close connection between knowledge transfer and manufacturing practice. The development of digital molding technology has altered the rigid standard of traditional manufacturing, allowing for greater design flexibility as the technology advances. In addition, the development of digital molding technology has increased the design dimension while

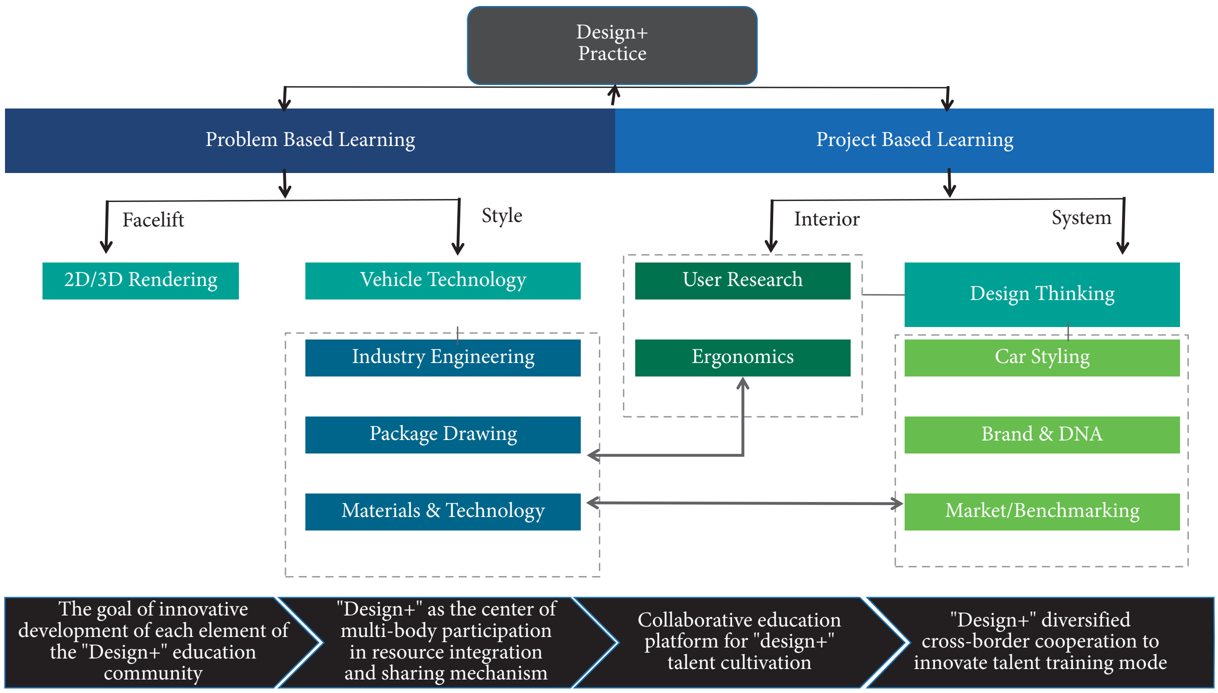

Figure 3: Reform and practice plan of design interdisciplinary graduate education.

simultaneously enriching the design means and presentation level. It encourages the development of teachers' scientific research abilities while also providing substantial technological and physical assistance for the collection of scientific research results in the classroom.

Innovative research on the construction of a teaching and research platform for product design and digital molding of the "Art and Engineering". An important feature of the product design profession and an important aspect that can motivate students to learn is the industrial transformation of design works and the ability to follow up during the production, processing, and sales of products. This teaching and research platform is composed of basic molding system, digital molding system, and reverse design system and is centered on three major master's specialties: product and interaction design, environment and landscape design, and visual and information design, to purchase relevant research instruments and equipment, create a research platform, support relevant basic theory and key technology research, promote the development of relevant disciplines in the university, and help local industries transform and upgrade.

4.3. Establishing a Design Education System of "Vision Sharing-Resource Sharing-Platform Building-Effectiveness Co-creation" as a Linked Evolutionary Mechanism. As a result of technological advancement, social transformation, and international rivalry, new needs for the growth of design education have been established. Specifically, we investigate the objectives, processes, methods, and resources of professional talent training for design graduate students. We also examine the elements and their mutual relationships among them; categorize the elements according to the logical relationship between the domain layer, platform layer, and subject layers [20, 21]; construct an interdisciplinary education system for design majors; follow the basic ideas of interdisciplinary professional construction; form the key tasks of profession; and make the interaction between the many levels of the system and the talent, industry, and innovation chains more comprehensible and understandable. A linking evolution mechanism of "vision sharing-resource sharing-platform building-effectiveness co-creation" is proposed to carry out professional education reform and practice, based on our findings. The reform and practice plan can be seen in Figure 3.

5. Conclusion

As our school's development ideas and goals progress, the status of our design majors has become increasingly important, as it is directly related to the comprehensive and coordinated development of the school's related disciplines, to the important indicators of the school's name change, and to the heart of the school's long-term sustainable growth. The great development of design interdisciplinary disciplines should, as a result, fully rely on the school's traditional advantageous disciplines, create a new platform for the construction of interdisciplinary disciplines in the college, and strive to form several characteristic high-level research results centered on the college's discipline construction direction. The common ideal of "constructing a first-class college of art and design with domestic influence and provincial status" should serve as a guide for all faculty and students, and we should concentrate our efforts on developing a college culture that emphasizes discipline and professional development, academic research and artistic creation, harmonious construction and quality improvement, and continuous deepening, expansion, and ascent. In addition, we will further explore how to combine the new teaching mode system of artificial intelligence in the near future.

Data Availability

The data set used to support the findings of this study is available from the corresponding author upon request.

Conflicts of Interest

The authors declare no conflicts of interest.

Acknowledgments

This work was supported by Innovation Fund General Project. The authors project was proposed by Nanjing University of Technology in 2021, "Research on the Design and Application of Intelligent Interaction Platform based on 5G Technology" (Project no. CKJB202111); Teaching Reform and Construction Project of Nanjing University of Technology in 2021, " Exploration and practice of 'Art and Engineering' in product design under the background of new liberal arts" (Project no. JXGG2021032); "Product Design" in 2021 University-level "Curriculum ideological and political" demonstration major construction point (cultivation) (Project no. SFZY2021P07); and Nanjing Lanju Information Technology Co., Ltd. Ministry of Education Industry-Science Cooperation Collaborative Education Project in 2021 "Product design and digital molding teaching and research platform practice and base construction" (Project no. 202102355023).

References

[1] P.-H. Su, "Case studies of applying electronic flexible material and technology to create the new media arts," *Multimedia Tools and Applications*, vol. 76, no. 23, pp. 25529–25543, 2017.

[2] T. Schoormann, M. Stadtländer, and R. Knackstedt, "Designing business model development tools for sustainability—a design science study," *Electronic Markets*, pp. 1–23, 2021.

[3] C. Filippo, B. Paola, and F. Gualtiero, "Data science for engineering design: state of the art and future directions," *Computers in Industry*, vol. 129, 2021.

[4] L. Marko and N. Suvi, "Design science and Co-designing of hybrid workplaces," *Buildings*, vol. 11, no. 3, p. 129, 2021.

[5] P. Grace, D. Lewis, T. Pollack et al., "Employing user-centered design and learning science theory to enhance remote delivery of diabetes education and survival skills at hospital discharge," *Journal of the Endocrine Society*, vol. 5, p. A447, 2021.

[6] L. Guo, "A system design method for cloud manufacturing application system," *International Journal of Advanced Manufacturing Technology*, vol. 84, no. 1-4, pp. 275–289, 2016.

[7] D. Meng, L. Yan, C. He, J. Guo, Z. Lv, and P. Wu, "Multidisciplinary design for structural integrity using a collaborative optimization method based on adaptive surrogate modelling," *Materials & Design*, vol. 206, 2021.

[8] H. Chen, W. Li, W. Cui, P. Yang, and L. Chen, "Multi-objective multidisciplinary design optimization of a robotic fish system," *Journal of Marine Science and Engineering*, vol. 9, no. 5, p. 478, 2021.

[9] S. Wang, M. Yang, W. Niu et al., "Multidisciplinary design optimization of underwater glider for improving endurance," Structural and Multidisciplinary Optimization," *Structural and Multidisciplinary Optimization*, vol. 63, pp. 1–17, 2021.

[10] Y.-H. Chien, C.-K. Yao, and Y.-H. Chao, "Effects of multidisciplinary participatory design method on students' engineering design process," *Engineering Times*, vol. 1, no. 2, pp. 112–121, 2020.

[11] S. G. Kontogiannis and M. A. Savill, "A generalized methodology for multidisciplinary design optimization using surrogate modelling and multifidelity analysis," Optimization and Engineering," *Optimization and Engineering*, vol. 21, pp. 1–37, 2020.

[12] E. Fredrik, H. Tim, and J. Joel, "Multidisciplinary design automation – a conceptual framework for working with product model extensions," *International Journal of Agile Systems and Management*, vol. 13, no. 1, p. 28, 2020.

[13] M. Prestes Joly, J. G. Teixeira, L. Patrício, and D. Sangiorgi, "Leveraging service design as a multidisciplinary approach to service innovation," *Journal of Service Management*, vol. 30, no. 6, pp. 681–715, 2019.

[14] M. Mengoni and M. Germani, "Reverse Engineering and restyling of aesthetic products based on sketches interpretation," *Research in Engineering Design*, vol. 20, no. 2, pp. 79–96, 2009.

[15] M. Milazzo, A. Spezzaneve, A. Persichetti et al., "Digital and experimental synergies to design high-heeled shoes," *International Journal of Advanced Manufacturing Technology*, vol. 109, no. 1-2, pp. 385–395, 2020.

[16] C. Relvas, A. Ramos, A. Completo, and J. A. Simões, "Accuracy control of complex surfaces in reverse engineering," *International Journal of Precision Engineering and Manufacturing*, vol. 12, no. 6, pp. 1035–1042, 2011.

[17] A. Fischer and S. Park, "Reverse engineering: multilevel-of-detail models for design and manufacturing," *International Journal of Advanced Manufacturing Technology*, vol. 15, no. 8, pp. 566–572, 1999.

[18] A. W. L. Yao, "Applications of 3D scanning and reverse engineering techniques for quality control of quick response products," *International Journal of Advanced Manufacturing Technology*, vol. 26, no. 11-12, pp. 1284–1288, 2005.

[19] S. K. Curtis, S. P. Harston, and C. A. Mattson, "The fundamentals of barriers to reverse engineering and their implementation into mechanical components," *Research in Engineering Design*, vol. 22, no. 4, pp. 245–261, 2011.

[20] L. Iuliano and P. Minetola, "Enhancing moulds manufacturing by means of reverse engineering," *International Journal of Advanced Manufacturing Technology*, vol. 43, no. 5-6, pp. 551–562, 2009.

[21] S. Vijayan, Z. Xu, and H. Zhou, "Application of intelligent systems in multi-modal information analytics," in *Proceedings of the 2020 International Conference on Multi-model Information Analytics (MMIA2020)*, vol. 2, pp. 1–10, Changzhou, China, March 2020.

Hindawi
Computational Intelligence and Neuroscience
Volume 2022, Article ID 3990216, 12 pages
https://doi.org/10.1155/2022/3990216

Research Article

An Intelligent Identification and Repair Method for Annular Holes in 3D Printing

Shanhui Zhang,[1] **Wei Wu**,[2] **and Wei Wei**[2]

[1]*School of Control Science and Engineering, Shandong University, Jinan, Shandong 250061, China*
[2]*Shandong Shanda Hoteam Software Co., Ltd., Jinan, Shandong 250101, China*

Correspondence should be addressed to Shanhui Zhang; zsh@sdu.edu.cn

Received 10 March 2022; Revised 25 March 2022; Accepted 9 April 2022; Published 5 May 2022

Academic Editor: Xin Ning

With the popularization of 3D printing in the consumer goods field, there is a specific type of hole named annular hole in the narrow features, surface bumps, or folded parts of products. The traditional triangular mesh repair method is not effective for such holes. The structural characteristics of the annular hole are analyzed in this research, and the definition and identification method for annular holes is presented through the shape and position relationship of two closed hole lines. To improve the repair efficiency and the applicability of the algorithm, the traditional hole repair method and process are ameliorated. A repair strategy of hole boundary stitching and filling, triangulation optimization, implicit surface construction based on Radial Basis Function, and surface integral deformation is adopted to achieve a smooth joint of the repaired hole surface with the original triangular mesh surface. The method can ensure surface smoothness and accuracy. Finally, two experiments are carried out to verify the repair quality and efficiency of our method. Compared with Geomagic software, the proposed method can automatically identify and repair annular holes with fewer defects and similar efficiency. Compared with a traditional hole repair method, the evaluation results demonstrate that the proposed method is much faster, and the repair quality is higher without the influences of human operations. It is shown that our method can be applied to annular hole repair of 3D printing models without the participation of technicians.

1. Introduction

3D printing is an emerging manufacturing technology based on digital models, which manufactures physical items by stacked bondable materials such as powdered metals or plastics. Having made a profound impact on the traditional process, production line, factory model, and industry chain combination, 3D printing is a representative disruptive technology in manufacturing [1–3]. Currently, with the rapid development and popularity of 3D printing, consumers have also turned to and experienced 3D printing. For example, the platform created by Shapeways in the United States, which integrates design, customization, and sales, has more than 21,000 online stores, having served more than 1 million consumers and printed over 21 million products [4]; in China, Haier Group has built an online open innovation and entrepreneurship platform, which has more than 300,000 registered users and created successful cases such as the Tianzun air conditioner [5].

As 3D printing is applied in the consumer goods field, various types of holes often occur in constructing and acquiring mesh models, which would seriously affect the appearance and quality of 3D printed models. At present, the identification and repair of holes in triangular mesh models are mostly carried out through user interaction, which has low efficiency and requires certain skills of operators. However, most consumers do not have professional skills in hole identification and repair, which poses difficulties for the development of 3D printing in the consumer goods field. The repair of holes like simple holes and island holes has been focused on and researched, but the repair of specific annular holes in the consumer goods field has not been reasonably solved. To this end, it is necessary to research and classify the characteristics of annular holes according to their topology, and corresponding annular hole identification and repair methods could be provided with high repair quality and less professional operation requirement.

The paper is organized as follows. After reviewing some related work in Section 2, the main types and characteristics of annular holes are studied and an intelligent identification method for annular holes is proposed in Section 3. In Section 4, an improved implicit surface repair method for annular holes based on Radial Basis Function (RBF) is presented. In Section 5, compared with the results of internationally well-known commercial software and a traditional hole repair method, experimental results and discussion are given. Finally, our summary, evaluation, and direction for further research are discussed in Section 6.

2. Related Work

Originating as early as the 1980s, 3D printing has boomed again with the promotion of the Internet since 2010. Having made positive progress on the market application in fields including aerospace, automotive, and healthcare, it got started in 3D printed cars, airplanes, and artificial liver tissues. It can be seen that 3D printing is continuing to promote and expand its application. In 2012, the British Magazine the Economist evaluated 3D printing as "an important symbol of the third industrial revolution," which would become a new creative technology to change the future world [6]. Since then, 3D printing has also gained the attention of the average consumer. In October 2013, the world's first successful auction of a 3D printed artwork named "ONO God" was held [7]. 3D printed shoes, jewelry, dolls, and other products have also gradually entered the vision of ordinary consumers, as shown in Figure 1.

Along with the wide application of 3D printing, many scholars at home and abroad have researched the rapid reconstruction and repair of 3D printed models. The simple and flexible structure, high stability, and topology of triangular mesh models lead to the rapid and mature development of the hole-filling technique based on triangular mesh models [11]. A more typical repair method is the surface-based hole-filling algorithm, which repairs holes on the surface with the help of data near the holes by directly detecting and identifying the hole information of the input 3D model. It mainly includes the mesh growth method based on adding new sampling points and the method based on implicit surface fitting [12–14].

The mesh growth method based on adding new sampling points generates new sampling points from hole triangle boundaries to hole area and constructs new triangular patches by edge swapping and triangle refining until the whole hole is covered. Pernot et al. [15] proposed the curvature minimization principle to repair holes by adding new triangles under the premise of minimizing the curvature variation between the surrounding and inserted meshes, which is applicable to holes with a simple shape. Marchandise et al. [16] used the hole boundary points as well as the neighboring vertices as the basis for establishing surface patches and sampling on the surface patches. The method had a relatively high hole-filling accuracy, but it was not applicable to the case where the curvature variation of the hole area was large. Wang et al. [17] first repaired the hole with the advancing front method and then used the data such as normals of the boundary vertices to determine optimal vertices, so as to adjust the position of the pre-repaired hole triangular surface patch. However, for complex holes, especially for the hole boundary area with large curvature variation, the geometric features of the original model would be lost, and the repair result would be too flat.

The hole-filling algorithm based on implicit surface fitting repairs holes with an implicit surface established with original model data. Lévy [18] parametrized the entire model data to the plane for processing, and the algorithm is less efficient when the area of the repaired holes is small. and the number of triangles is large. Brunton et al. [19] first flattened the hole boundaries without self-intersection onto the reference plane for filling and then used the minimum energy method to embed the patched mesh back into the spatial mesh. Fortes et al. [20] proposed a shape feature determination method on top of Brunton's. Based on the minimization of an energy function, the holes were filled by inheriting the local information of the holes in the original model. The method required better local data quality of holes. Du et al. [21–25] all used RBF to fit the implicit surface of holes and then adjusted new vertices to the implicit surface. The method was suitable for repairing simple holes and island holes. For island holes with large curvature variation, a bridging method was proposed to connect the island boundary and hole boundary. Zhao et al. [26] carried out a preliminary repair with the advancing front method and then finished the repair by solving Poisson equation to adjust positions of added vertices. This method was not applicable to the repair of large holes.

Through the above analysis on hole-filling techniques, it is proved that the mesh growth-based repair method is a simple idea, easy to implement, and more effective for repairing holes in flat areas with simple structures and no significant features. The implicit surface fitting method produces a smoother repair surface, inherits the original mesh data information during the repair process, and has little interference with the original mesh model and more accurate repair results. However, it asks for a harsher scenario and would always smooth sharp features. Both methods can obtain ideal results for simple holes, but there may be mapping failure or mapping error for complex holes, resulting in poor hole-filling effects.

For the segmentation and repair of complex holes, Jun [27] proposed an algorithm to split a complex hole into simple holes and then fill each divided simple hole, which helped in triangulating and repairing holes with self-intersecting boundaries in the projection process but was not ideal in filling complex holes of other types, especially the problem of self-intersecting boundaries in the nonprojection process. Inspired by this method, Li et al. [28] presented an algorithm based on the concept of edge expansion to split complex holes into simple holes and then perform hole-filling with due consideration of the neighboring mesh morphology. Lai and Hsu [29] further considered the treatment of island holes and proposed a hole-filling algorithm based on B-sample surfaces to fit the vertices near the holes to the B-sample surfaces, emphasizing the topological accuracy and smoothness of the joint between the new mesh

Figure 1: 3D printed consumer goods [8–10]. (a) 3D printed shoes STRVCT. (b) Nike 3D printed football shoes. (c) Faux Russian big crown. (d) 3D printed table. (e) Custom doll. (f) Flower lampstand.

and the existing mesh. Feng et al. [30] introduced a fast filling method for triangular meshes based on hole size, which classified holes into small-sized, middle-sized, and large-sized holes according to their size and used different filling algorithms for different hole types. However, the classification method, which only considered the hole size and ignored the complex topological morphology, would hardly achieve satisfactory results in filling complex holes. Wen et al. [31] presented a surface-repairing method with automatic identification of defective holes and maintenance of detail features in the hole region, but the method was only applicable to repair defective holes in simply connected domains, ignoring the topology of complex missing regions. By analyzing the hole boundaries and topology, Li [12] classified holes into ordinary holes, interstitial voids, island holes, and semiclosed holes and proposed a hole-filling algorithm based on Poisson equation, which can repair large-scale complex 3D models containing a large number of holes and a variety of hole types. The method was applied to the restoration of heritage models with slightly insufficient repair efficiency. Centin et al. [32] proposed a Poisson-driven approach, which allowed to close complex holes, islands, gaps, and missing parts with a seamless integration of the patching triangles along the mesh boundaries, with guaranteed and homogeneous mesh quality. But its repair quality was seriously influenced by the boundary curves user selected. Based on the above analysis, the intelligent identification and repair method for annular holes is still a challenge.

3. Annular Holes and Their Intelligent Identification Method

3.1. Generation of Annular Holes. In the consumer goods field, due to the complex and varied structures of most products such as handicrafts, doll models, and bionic products, there are many narrow features, surface bulges, hollow-carved structures, or folds, as shown in Figure 2. They can easily cause fracture, local loss, or separation of the triangular mesh model during model construction, scanning, and acquisition. So, a specific type of hole always occurs, namely, an annular hole. Using the existing repair methods, it is easy to cause the fillings of hollow-carved structures or folds, and they lead to high differences from the original structure. In addition, most users for consumer goods are ordinary people lacking the ability to operate specialist repair software, so the result of hole repair is not satisfactory.

3.2. Annular Holes. The annular hole is formed by two boundary lines with similar shape and no common point, whose positional relationship is approximate coplanar or parallel, as shown in Figure 3. Annular holes are commonly found in sections, cross-sections, or folds of models. Two types of annular holes are summarized through analysis.

Coplanar annular hole: the positions of two annular closed curves are approximately coplanar, and the normal directions are similar, as shown in Figure 3(a). It is a common type of annular holes occurred in the surface bulges or hollow-carved structures.

Parallel annular hole: the positions of two annular closed curves are approximately parallel, and the normal directions are nearly contrary, as shown in Figure 3(b). It is an uncommon type of annular holes occurred in narrow features, hole features, and folds. There are few repair methods to deal with such holes.

The annular hole has two annular closed curves. The application of simple hole filling methods to an annular hole will repair all the interior of the two annular closed curves, resulting in a large number of self-intersecting patches. As for island hole repair methods, the number of internal triangular surface patches of annular holes is too large, and

FIGURE 2: The example products prone to annular holes.

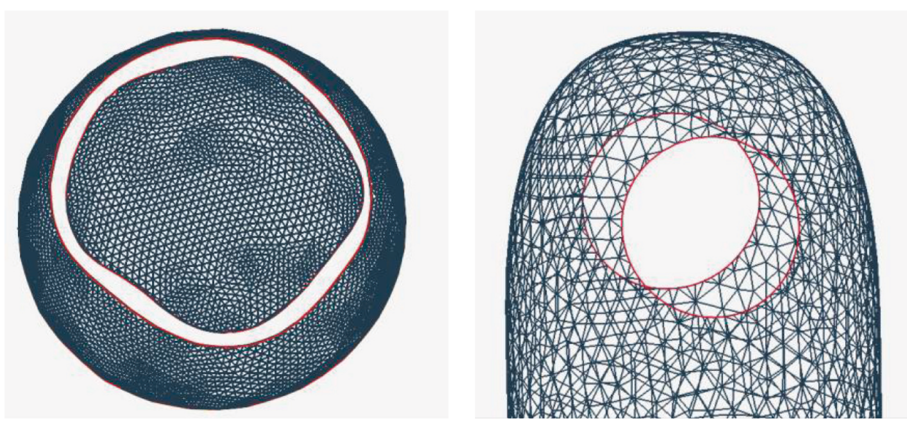

(a) (b)

FIGURE 3: Two types of annular holes. (a) Coplanar annular hole. (b) Parallel annular hole.

the hole normal directions of parallel annular holes are nearly contrary. So, it is not appropriate to simply use the surface deformation repair method of deleting island fragments or selecting some islands as constraint points, which is easy to affect the repair quality or destroy the original structure of the model. For this reason, the repair of annular holes needs to be treated separately.

3.3. Intelligent Identification Method for Annular Holes. As the annular hole is made up of two boundaries that are similarly located and shaped, the hole connects two discontinuous triangular mesh sections of the model. The two boundaries of the annular hole can be identified by detecting the distance between the boundaries of different combinations of triangular facets; that is, an annular hole is composed of the free boundaries of two sets of triangular meshes. Therefore, the following determination method for annular holes is presented.

We set the hole boundary points as $P_1, P_2, P_3, \ldots, P_n$, and O as the gravity center of hole boundary points, i.e.,

$$O(\overline{X}, \overline{Y}, \overline{Z}) = \frac{1}{n}\sum_{i=1}^{n} P_i\,, \quad i = 1, 2, \ldots, n. \tag{1}$$

Using the coordinates of the hole boundary points and the gravity center O, a 3×3 covariance matrix C can be defined as

$$C = \begin{bmatrix} \mathrm{cov}(X,X) & \mathrm{cov}(X,Y) & \mathrm{cov}(X,Z) \\ \mathrm{cov}(Y,X) & \mathrm{cov}(Y,Y) & \mathrm{cov}(Y,Z) \\ \mathrm{cov}(Z,X) & \mathrm{cov}(Z,Y) & \mathrm{cov}(Z,Z) \end{bmatrix}, \tag{2}$$

where

$$\mathrm{cov}(X,Y) = \frac{\sum_{i=1}^{n}(X_i - \overline{X})(Y_i - \overline{Y})}{n-1}. \tag{3}$$

The eigenvalues and eigenvectors of the matrix can be calculated through Jacobi method. We set the three eigenvalues as the first vector $\overrightarrow{V_1}$ and the eigenvector corresponding to the smallest eigenvalue as the second vector $\overrightarrow{V_2}$. The eigenvalues and eigenvectors of the Jacobi matrix represent the distribution direction of the points, and the main feature that distinguishes an annular hole from an island hole is the approximation of the distribution pattern of the points between two boundaries. Therefore, the characteristic distance between two boundaries of the annular hole is defined as

$$Dis_{ab} = \overrightarrow{V_{a1}} \times \overrightarrow{V_{b1}} + \overrightarrow{V_{a2}} \times \overrightarrow{V_{b2}}. \tag{4}$$

In this equation, a and b represent the two boundaries of an annular hole. Dis_{ab} is the characteristic distance between boundaries a and b. $\overrightarrow{V_{a1}}$ and $\overrightarrow{V_{b1}}$ are the first vectors of boundaries a and b. $\overrightarrow{V_{a2}}$ and $\overrightarrow{V_{b2}}$ are the second vectors of boundaries a and b. Then, we screen a large number of annular holes and island holes and calculate their characteristic distances. An empirical value of the characteristic distance is found to distinguish an annular hole from an island hole. When $Dis_{ab} < 0.15$, an annular hole is formed between the two boundaries. At this point, the corresponding repair method can be used to achieve optimal results. Accordingly, an intelligent identification process for annular holes is planned as in Figure 4.

Step 1. Model preprocessing. Segment all the complex holes to single holes without common points.

Step 2. Calculate all the closed hole boundaries, and exclude crack holes and dislocation holes. The method in Steps 1 and 2 has been researched in another thesis [33].

Step 3. Judge whether the number of closed boundaries is less than 2. If yes, this indicates that there is no annular hole, and it ends; if no, proceed to next step.

Step 4. Calculate the nearest boundary of each boundary. It is measured by the distance between the nearest points between two boundaries.

Step 5. Judge whether they are mutually nearest boundaries, and the boundary feature distance is less than 0.15. Mutual nearest boundary means that the nearest boundary of boundary a is b, and the nearest boundary of boundary b is a. At the same time, in order to eliminate the case that two simple holes are adjacent (as shown in Figure 5), it is also necessary to meet the following conditions: on the fitting plane of the boundary, the gravity center of boundary a is within b, and the gravity center of boundary b is within a. If the above conditions are met, it is an annular hole. Otherwise, there is no annular hole.

Step 6. End.

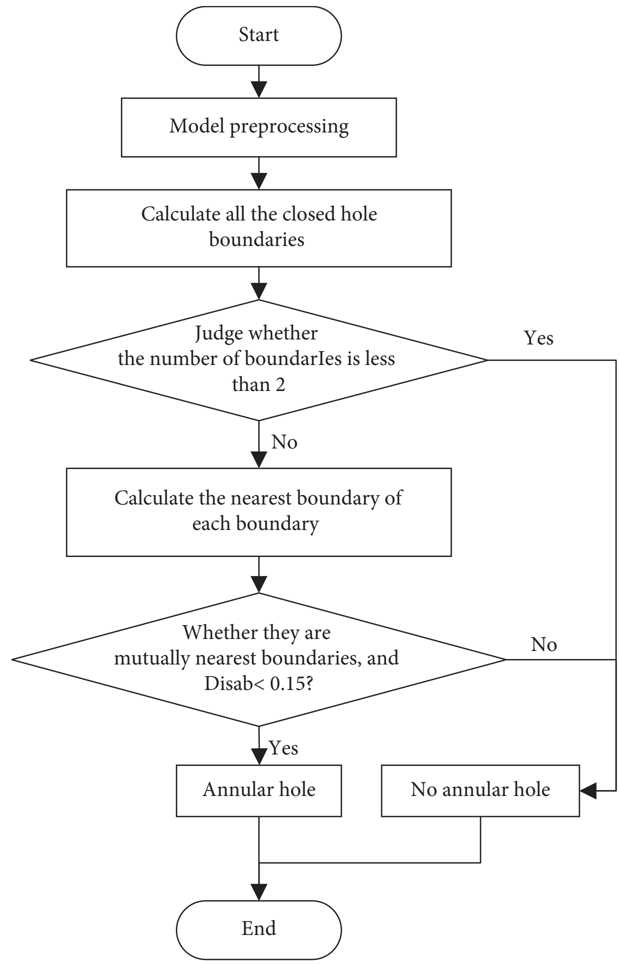

Figure 4: Intelligent identification process for annular holes.

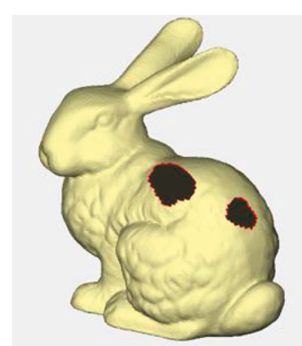

Figure 5: Example of adjacent simple holes.

4. Repair Method for Annular Holes

Traditional hole-filling methods generally require a process of surface fitting, surface cutting, and surface stitching. The annular hole has two boundaries and two sets of corresponding cutting and stitching boundaries, with narrow or flat hole lines and massive boundary points. Using traditional hole-filling methods, it always has low repair efficiency and a high failure rate. Besides, various consumer products lead to a variety of annular holes, and the systematicness and robustness of the above method are also insufficient. Therefore, we propose a method that stitches and fills the holes, optimizes the triangulation, constructs implicit surface, and finally carries out surface integral deformation. The method can solve the repair issue of diversified annular holes and extend the application range in consumer products.

4.1. Hole Boundary Stitching and Filling. First of all, an initial stitching surface patch is constructed as the basis for surface fitting. In this paper, the method of connecting the nearest points is used to stitch annular holes, as shown in Figure 6. The specific steps are described as follows.

Step 1. Reorient hole lines. As the two types of annular holes have different hole line directions, the two hole lines of an annular hole need to be adjusted to the same direction. The same direction refers to the fact that, on the best-fit plane of the two hole lines, the polygons formed by the projection of the hole lines are all clockwise or counterclockwise. Herein, the counterclockwise direction is taken as positive.

Step 2. Connect initial triangles. Start from the starting point P_0 of the hole line L_0 with fewer points, calculate the nearest point Q_0 of P_0 on the other hole line L_1, and connect P_0 and Q_0. Find the next point Q_1 of L_1 and its nearest point Q_2 on L_1, and connect P_1 and Q_2. Triangulate the area composed of P_0-P_1-Q_2-Q_0 to obtain triangles $P_0Q_1Q_0$, $P_0P_1Q_1$, and $P_1Q_2Q_1$.

Step 3. Connect the remaining triangles. Repeat the above steps for the points on L_0 until all boundary points on L_0 are calculated.

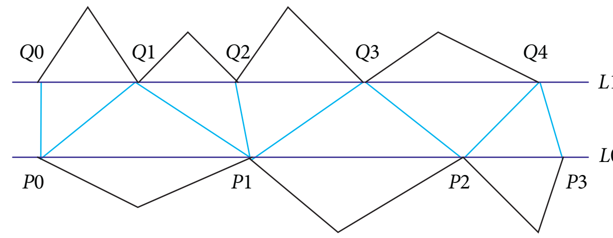

FIGURE 6: Stitch annular hole boundaries.

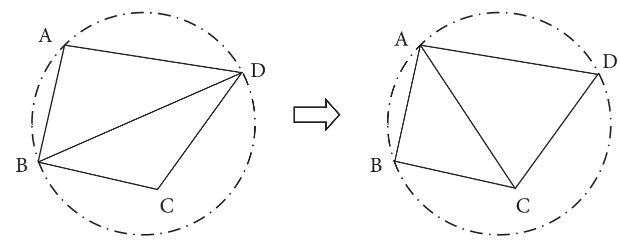

FIGURE 7: Illustration of the edge-swap method.

4.2. Triangulation Optimization. Before the surface is fitted, the stitched triangle patches need to be refined, so that it can be smoothly connected to the original model. The specific optimization principle and method are as follows: (1) for a triangular patch with an area larger than the specified area, divide the patch into three triangular patches by taking a point at the center of the triangle and connecting that point to its three vertices. (2) If two triangles are connected by an edge, and one triangle is inside the circumscribed circle of the other triangle, the edge is called a long and narrow edge. The edge-swap method should be used for optimization. Edge-swap is achieved by swapping the diagonals of the convex quadrilateral formed by two adjacent triangles, so that the narrow triangle converges to a positive triangle, as shown in Figure 7.

4.3. Implicit Surface Construction. The initial repair surface has been created by stitch and refined triangulation of the two hole lines of the annular hole, but it is not yet smoothly integrated with the whole surface. For that, the RBF is used to establish an implicit surface equation for annular holes, to ensure as much continuity and smoothness as possible between the repaired surface and the original surface.

Firstly, to ensure a smooth and continuous joint between the hole boundary and its surrounding original triangular surface, we use the vertex of the two boundaries of an annular hole and the multiplet neighboring points of its neighboring triangular patches (typically 3–5 multiplet neighboring points, depending on the size of the hole) to build a collection $V = \{P_i, i = 1, 2, \ldots, n\}$ (n is the number of hole boundary vertices and neighboring points) of interpolation constraint points. The interpolation constraint points on the surface satisfy

$$f(P_i) = 0, \quad i = 1, 2, \ldots, n. \tag{5}$$

In order to avoid useless solutions of $f \equiv 0$, while keeping the positions of the boundary points of stitched patches unchanged, we calculate the normal information of the refined mesh model boundaries and add additional constraint points in the normal direction. They are located in the inner or outer directions of the surface. The additional constraint points should satisfy

$$f(P_i + h_i N_i) = h_i, \tag{6}$$

where N_i is the normal vector of the surface located at the vertex P_i, and h_i is a normal constraint value with a small positive value. It can be assumed that all additional constraint points are located at the same distance from the surface, and they are on an equivalent surface to the hole surface. The value of the constraint does not affect the solution of the implicit equation for the hole surface, so the implicit equation for the hole surface can be taken to have a value of $h_i = 1$ at all additional constraint points.

From this, we combine all interpolated constraint points and additional constraint points to create a set of constraint points $V = \{P_i, i = 1, 2, \ldots, N\}$ (N is the number of all the hole constraint points) and form the following constraint:

$$f(P_i) = h_i, \quad i = 1, 2, \ldots, N. \tag{7}$$

From the constraint points, we can define the implicit surface equation $f(\mathbf{r}) = 0$. The energy function [22, 34] for a thin plate with its second-order differentiable function is

$$E=\int_{R^3}\left(\frac{\partial^2 f}{\partial x^2}+\frac{\partial^2 f}{\partial y^2}+\frac{\partial^2 f}{\partial z^2}+2\frac{\partial^2 f}{\partial x\partial y}+2\frac{\partial^2 f}{\partial x\partial z}+2\frac{\partial^2 f}{\partial y\partial z}\right)\mathrm{d}x\mathrm{d}y\mathrm{d}z. \tag{8}$$

This energy function reflects the smoothness of the function f in three dimensions, and it has lower energy values in regions of the surface where there are no sharp changes in curvature such as folds. The interpolation function is solved under the interpolation constraint of $f(P_i)=h_i$ such that the value of the energy function is minimized. At this point, the form of the interpolation function f is obtained as the RBF form [13]:

$$f(\mathbf{r})=\sum_{j=1}^{N} w_j\phi\left(\mathbf{r}-P_j\right)+Q(\mathbf{r}). \tag{9}$$

In this equation, $\mathbf{r}$ denotes any point on the generated surface, $\mathbf{r}=(x,y,z)$; P_j denotes the points defining the equation, $P_j=(P_j^x,P_j^y,P_j^z)$; w_j denotes the real weight corresponding to each constraint point; $Q(r)$ is a first order polynomial. For any point $\boldsymbol{r}$, the form of $Q(r)$ is $Q(r)=q_0+q_1x+q_2y+q_3z$, where q_0, q_1, q_2 and q_3 are real coefficients of the polynomial. $\phi(r-P_j)$ is the RBF. In three-dimensional space, as functions with three variables need to be fitted, the more effective form of RBF is a triharmonic spline function $\phi(\mathbf{r})=\mathbf{r}^3$.

In order to solve for the weights and polynomial coefficients, each constraint point must satisfy both the interpolation constraint and the orthogonality conditions.

$$\begin{gathered}f(P_i)=\sum_{j=1}^{N} w_j\phi\left(P_i-P_j\right)+Q(P_i),\\ \sum_{j=1}^{N} w_j=\sum_{j=1}^{N} w_jP_j^x=\sum_{j=1}^{N} w_jP_j^y=\sum_{j=1}^{N} w_jP_j^z=0.\end{gathered} \tag{10}$$

Let $\phi_{ij}=\phi(P_i-P_j)$. From the above conditions, we obtain the following set of linear equations:

$$\begin{bmatrix}\phi_{11} & \phi_{12} & \cdots & \phi_{1n} & 1 & p_1^x & p_1^y & p_1^z\\ \phi_{21} & \phi_{22} & \cdots & \phi_{2n} & 1 & p_2^x & p_2^y & p_2^z\\ \vdots & \vdots & \ddots & \vdots & \vdots & \vdots & \vdots & \vdots\\ \phi_{N1} & \phi_{N2} & \cdots & \phi_{NN} & 1 & p_N^x & p_N^y & p_N^z\\ 1 & 1 & \cdots & 1 & 0 & 0 & \cdots & 0\\ p_1^x & p_2^x & \cdots & p_N^x & 0 & 0 & \cdots & 0\\ p_1^y & p_2^y & \cdots & p_N^y & 0 & 0 & \cdots & 0\\ p_1^z & p_2^z & \cdots & p_N^z & 0 & 0 & \cdots & 0\end{bmatrix}\begin{bmatrix}w_1\\ w_2\\ \vdots\\ w_N\\ q_0\\ q_1\\ q_2\\ q_3\end{bmatrix}=\begin{bmatrix}h_1\\ h_2\\ \vdots\\ h_N\\ 0\\ 0\\ 0\\ 0\end{bmatrix}. \tag{11}$$

For the annular hole repair surface, as the constraint points taken are data points around the hole boundary, the solution time is shorter with the Gauss elimination method, and a unique set of solutions $(w_1,w_2,\ldots w_N,q_0,q_1,q_2,q_3)$ can be obtained directly. Bring the obtained results into the interpolation function $f(\mathbf{r})$, and the implicit surface equation for the hole established by the RBF can be given as

$$f(x,y,z)=\sum_{j=1}^{n} w_j\left(\sqrt{\left(x-P_j^x\right)^2+\left(y-P_j^y\right)^2+\left(z-P_j^z\right)^2}\right)^3+q_0+q_1x+q_2y+q_3z=0. \tag{12}$$

4.4. Surface Integral Deformation. Once the implicit equation for the annular hole surface has been established, the vertices of triangular patches from the triangulation optimization in 4.2 need to be adjusted to the fitted implicit surface, that is, integral deformation of the surface. In this paper, the classical gradient descent method is used to adjust the vertices of triangular patches after triangulation, where all the repaired vertices of triangular patches are gradually approximated towards the implicit surface along the gradient direction of the implicit equation $f(x,y,z)$, until they are adjusted to the fitted hole implicit surface within the allowed error range.

Gradient descent is an iterative optimization-seeking algorithm for some criterion function. Let $f(r)$ be some criterion function and $\boldsymbol{r}$ a vector, and then the negative gradient direction of $\boldsymbol{r}$ is the direction, where $f(r)$ decreases fastest, along which the approximation point can be reached fastest [35]. The gradient of the implicit function $f(x,y,z)$ is denoted as $\nabla f=(\partial f/\partial x,\partial f/\partial y,\partial f/\partial z)$ [22]. From the implicit surface equation for holes, we get

$$\begin{aligned}\frac{\partial f}{\partial x}&=3\sum_{j=1}^{N} w_j\left(x-P_j^x\right)\sqrt{\left(x-P_j^x\right)^2+\left(y-P_j^y\right)^2+\left(z-P_j^z\right)^2}+q_1,\\ \frac{\partial f}{\partial y}&=3\sum_{j=1}^{N} w_j\left(y-P_j^y\right)\sqrt{\left(x-P_j^x\right)^2+\left(y-P_j^y\right)^2+\left(z-P_j^z\right)^2}+q_2,\\ \frac{\partial f}{\partial z}&=3\sum_{j=1}^{N} w_j\left(z-P_j^z\right)\sqrt{\left(x-P_j^x\right)^2+\left(y-P_j^y\right)^2+\left(z-P_j^z\right)^2}+q_3.\end{aligned} \tag{13}$$

Depending on the vertex of each triangulated patch, the new position to which it is adjusted needs to be calculated. Considering the iteration efficiency and the optimization effect, we chose the following equation as the iteration formula:

$$r_{k+1}=r_k-\frac{f(r_k)}{\left\|\nabla f(r_k)^2\right\|}\nabla f(r_k), \tag{14}$$

where k denotes the number of iterations. Calculate the difference $r_{k+1}-r_k$ between the new position of the vertex and the position before stretching. If $r_{k+1}-r_k\le\varepsilon$ (ε is a given limited error), it can be considered that the new position of the vertex r_{k+1} is on the hole surface and the iteration ends. Otherwise, r_{k+1} replaces r_k and the iteration continues.

The implicit surface equation of the hole describes the surface formed by the hole boundaries and their multiplet neighboring triangular patches, so the vertices of the

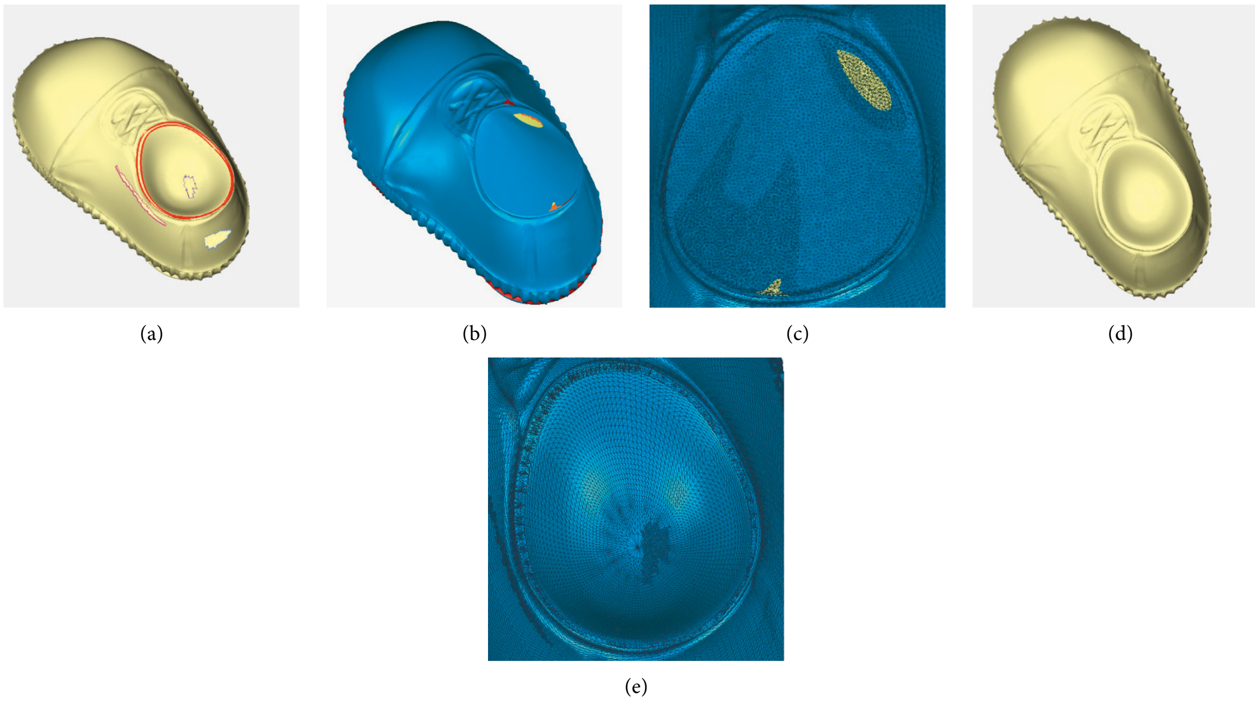

Figure 8: Comparison of repair effect of shoe model. (a) Original annular hole model. (b) Repair result of Geomagic. (c) Repair details of Geomagic. (d) Repair results of the proposed method in this paper. (e) Repair details of the proposed method in this paper.

adjusted triangles are located on the same surface as the vertices of the triangular patches around the hole boundary. It is ensured that the repaired hole surface is well stitched to the original triangular mesh surface and maintains a consistent surface form and continuity.

5. Experimental Results and Discussion

As few scholars have researched automatic identification and repair methods for annular holes, it is difficult to find a targeted algorithm for comparison. For this reason, this paper selects and compares the repair results with the well-known commercial software Geomagic and a traditional hole repair method to determine the identification and repair effect of the research method. All the developed algorithms were implemented in C++ by using Visual Studio 2013 and tested on a PC equipped with an Intel®Core i7-4790 processor and 8 GB of RAM on Windows 10. In the comparison process, three types of consumer-oriented models are selected, such as shoe, bone, and tooth, because these models are prone to the presence of annular holes.

Figure 8 compares the repair effect of shoe model between Geomagic and the proposed method. Figure 8(a) shows that an annular hole exists at the folding location of the shoe mouth, and the annular hole lines are indicated by red lines. When using Geomagic to repair, the two hole lines of the shoe model are repaired, respectively, resulting in the closure of the shoe mouth, and the repaired surface differs greatly from that of the original model, shown in Figures 8(b) and 8(c). With the proposed method, the annular hole of the shoe model is accurately identified and repaired between the hole boundaries, as shown in Figure 8(d). The repair details are displayed in Figure 8(e). It can be seen that triangular meshes are evenly divided, and the surface fitted between the two separated surfaces is smooth.

Figure 9 shows the comparison of repair effect of bone model. An annular hole exists at the fracture location of the bone, as shown in Figure 9(a), and the annular hole lines are also indicated by red lines. Geomagic repairs the broken holes, respectively, resulting in the formation of two independent parts, as Figures 9(b) and 9(c) depict. With the proposed method, the annular hole of the bone model is accurately identified and repaired, leading to regular triangular meshes and smooth surfaces, as shown in Figures 9(d) and 9(e).

When repairing the annular hole on the tooth surface, the result is similar to the shoe and bone models, as shown in Figure 10. Through the above cases, we can draw the following conclusions. Geomagic cannot automatically identify annular holes. Without human intervention, the software fills the inside of two closed hole boundaries, leading to discrepancies between the restoration and the actual requirements, and even to the separation of the model. Geomagic destroys the original structure of the model. With the proposed method, annular holes in the model are all accurately identified and repaired between the hole boundaries. As can be observed through the detailed graphs, the structures of the repaired model match the original models, and the triangular mesh density, the continuity with the edge meshes, and the smoothness are all ideal.

After repairing by the proposed method and Geomagic, the three repaired models were checked by a grid doctor. In terms of the six types of repair defects including nonmanifold

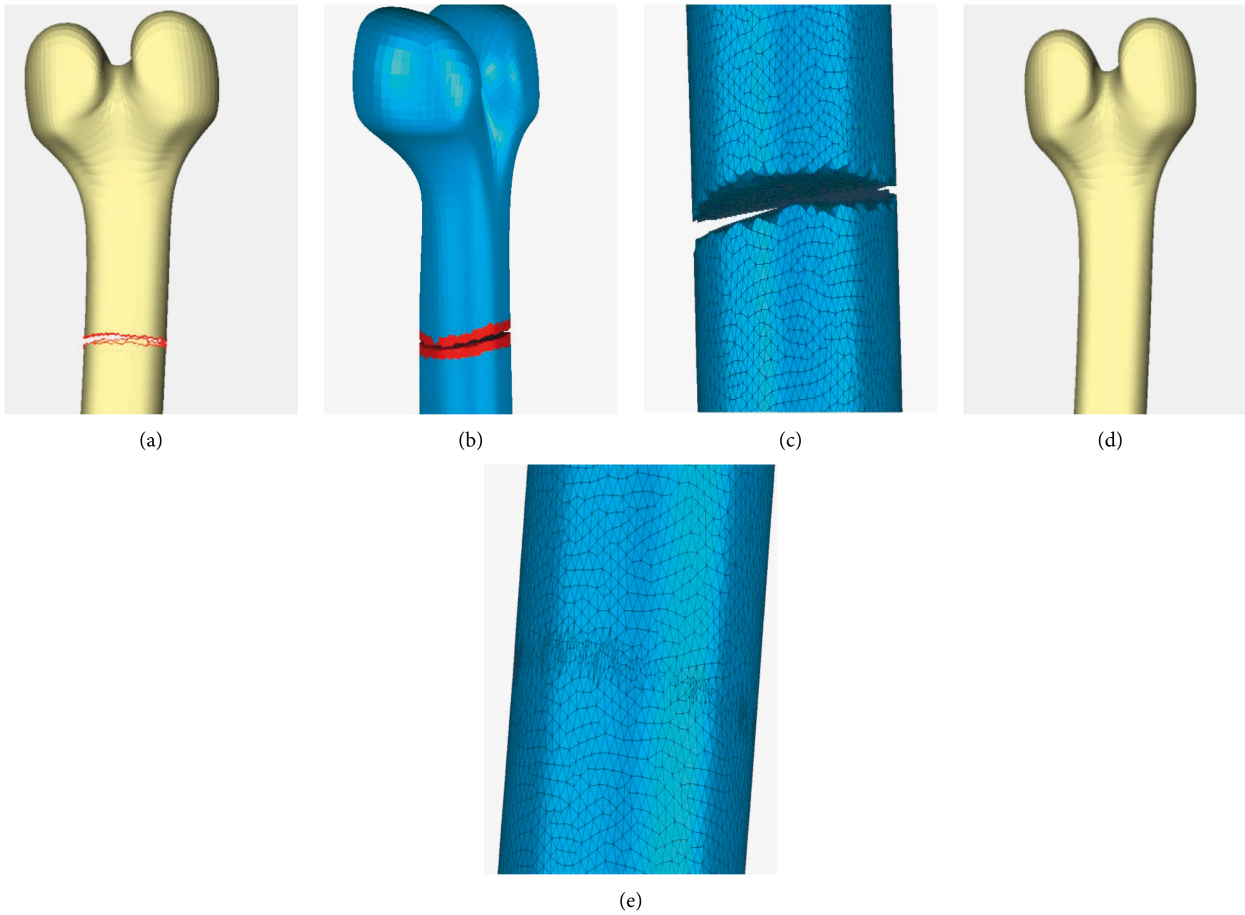

Figure 9: Comparison of repair effect of bone model. (a) Original annular hole model. (b) Repair result of Geomagic. (c) Repair details of Geomagic. (d) Repair results of the proposed method in this paper. (e) Repair details of the proposed method in this paper.

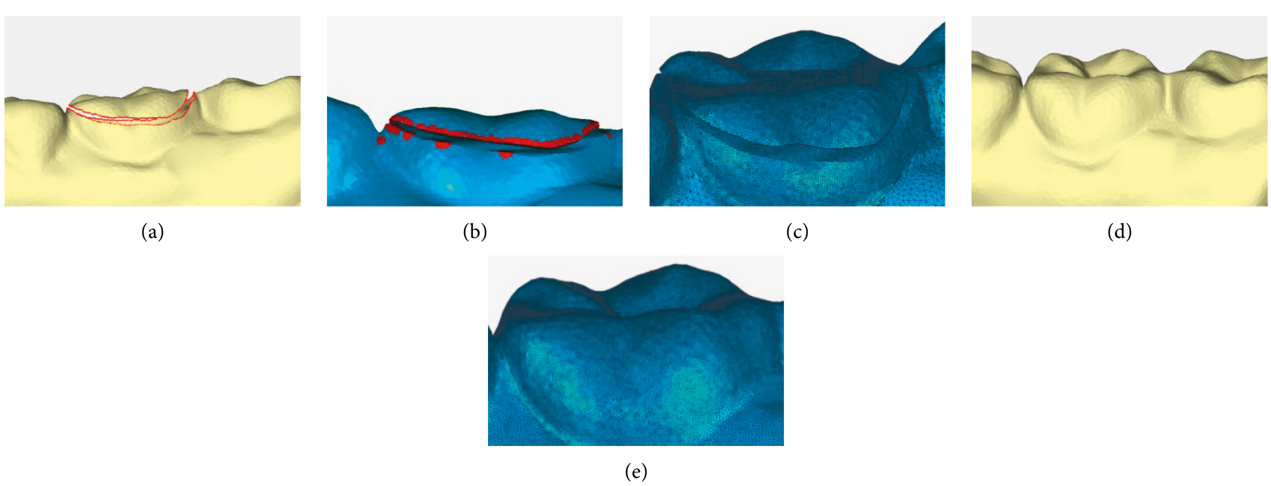

Figure 10: Comparison of repair effect of tooth model. (a) Original annular hole model. (b) Repair result of Geomagic. (c) Repair details of Geomagic. (d) Repair results of the proposed method in this paper. (e) Repair details of the proposed method in this paper.

edges, self-intersections, highly-creased edges, spikes, small components, and small holes, Geomagic is found to have more defects like spikes, highly creased edges, and self-intersections, while the model repaired by the proposed method has fewer defects and higher repair quality. The repair time of our method is equivalent to Geomagic, so the repair efficiency is acceptable. Specific comparison information is shown in Table 1.

Table 1: Comparison of repair results after inspection.

Objects	Methods	Nonmanifold edges	Self-intersections	Highly creased edges	Spikes	Small components	Small holes	Repair time (s)
Shoe	Geomagic	0	102	503	453	0	0	0.077
	Method in this paper	0	11	39	136	0	0	0.086
Bone	Geomagic	0	0	0	357	0	0	0.056
	Method in this paper	0	0	0	0	0	0	0.062
Tooth	Geomagic	0	90	62	1398	0	0	0.046
	Method in this paper	0	8	48	479	0	0	0.058

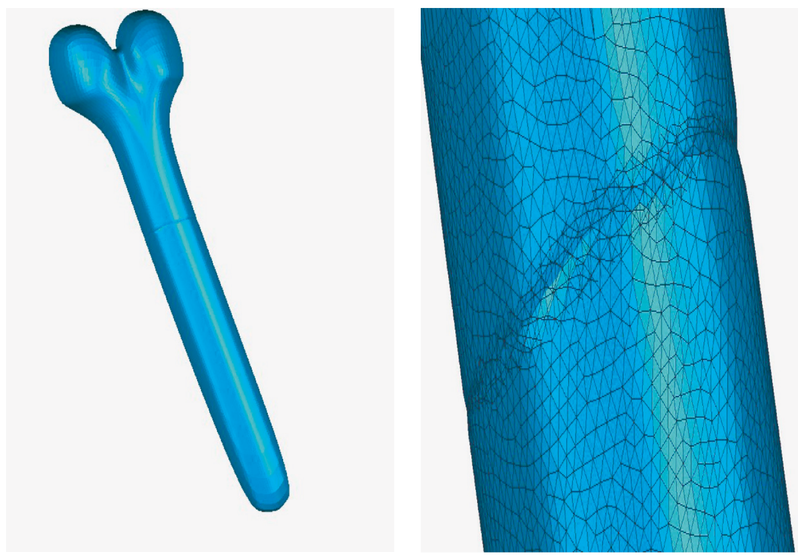

(a) (b)

Figure 11: Repair result of bone model with the method proposed by Centin. (a) The overall repair result of bone model with the method proposed by Centin. (b) Repair details of bone model with the method proposed by Centin.

The existing repair methods, when applied to the repair of annular holes, mostly require manual involvement. Taking the algorithms proposed by Centin [32] as an example, the user input for their method must be a set of boundary curves without defects, and holes or gaps, which are not selected should not be filled. So, the repair quality is seriously affected by the input boundaries. For the bone model, we selected boundaries with slight defects to repair. An obvious dent defect appeared, as shown in Figure 11(a). With their restricted Delaunay triangulation and tailoring routine, there is a high quality mesh in the repair area, as shown in Figure 11(b). But the repair time was significantly increased to 1.278 s without considering time spent on the manual selection of boundary lines, and our time was 0.062 s with the automatic identification of boundary lines. Therefore, our method has the advantage of high repair efficiency.

In summary, as repair algorithms or software like Geomagic cannot independently identify and process annular holes, manual repair method is needed. The use of manual repair requires the selection of two closed hole boundary curves, complex manual bridging, and splitting of annular holes into ordinary holes. The result and quality are affected by the skills of technicians, and the efficiency is drastically reduced, which also makes the operation difficult for average consumer users. Therefore, the above comparison shows that the proposed method can automatically determine whether two closed hole boundary lines form an annular hole by their shape and distance relationships and provide intelligent repair methods of stitching and filling, triangulation optimization, and surface integral deformation. The method can meet the repair needs of various types of consumer-oriented models, reduce the operational difficulties of nonspecialist technicians, and improve repair efficiency.

6. Conclusion

In the field of consumer goods such as handicrafts and bionic products, narrow features, surface bulges, and folds can easily lead to annular holes in the triangular mesh model during the process of construction, scanning, and acquisition. However, the traditional repair method for common holes is unsuitable for annular holes, which would cause defects such as self-intersecting patches, or even alteration of the original structure of the model.

To this end, we propose an intelligent identification and repair algorithm for annular holes. From the structural characteristics of the annular hole, we give the definition and the automatic identification method for annular holes through analysis of the shape and position relationships between the two closed hole lines. Referring to the traditional implicit surface repair method of single hole, we propose a new improved method. In order to optimize the systematicness and robustness of the repair method, we first stitch and fill the two annular hole lines, then optimize triangulation, construct a variational implicit surface based on RBF, and finally deform the surface integrally based on gradient descent. The proposed method achieves a smooth joint of the repaired hole surface with the original triangular mesh surface, and the repaired surface is smooth and accurate. Finally, we verify the feasibility of the method by examples, proving that it can replace the manual repair methods and significantly improve the repair quality and efficiency.

There are two important improvements in our method. Firstly, it retains all the facet information in the annular hole and stitches the facet between two closed hole lines, instead of filling a single hole boundary in sequence or using the artificial bridging repair method of technicians. The repair quality is also ensured. Secondly, the routine of stitching and filling, triangulation optimization, and surface integral deformation has higher repair efficiency. Especially for parallel annular holes, it avoids possible stitching errors caused by the inconsistent normal vectors of holes. But the errors always appear in other repair methods or software.

In the repair process, the implicit surface repair method based on RBF can obtain smoother repair surfaces, but it also smooths out sharp features. In the future, we will provide corresponding repair methods for more special features. The narrow features, surface bulges, hollow-carved structures, or folds occurring in consumer products will be identified and repaired more accurately. When the method is applied to the repair of 3D printed models in the consumer goods field, it will not require the participation of technicians. The easy operation characteristics of the method will attract the attention and attempt of a large number of consumers. It will promote the widespread use of 3D printing technology.

Data Availability

The data used to support the findings of this study are included within the article.

Conflicts of Interest

The authors declare that there are no conflicts of interest regarding the publication of this paper.

Acknowledgments

This research was funded by the National Key R&D Program of China, grant no. 2018YFB1106200.

References

[1] M. H. Ali, S. Batai, and D. Sarbassov, "3D printing: a critical review of current development and future prospects," *Rapid Prototyping Journal*, vol. 25, no. 6, pp. 1108–1126, 2019.

[2] I. Karakurt and L. Lin, "3D printing technologies: techniques, materials, and post-processing," *Current Opinion in Chemical Engineering*, vol. 28, pp. 134–143, 2020.

[3] Rahito, D. Wahab, and A. Azman, "Additive manufacturing for repair and restoration in remanufacturing: an overview from object design and systems perspectives," *Processes*, vol. 7, no. 11, p. 802, 2019.

[4] shapeways, "3D printing service," 2021, https://www.shapeways.com/business/3d-printing-services.

[5] "3D printing innovation and creativity platform," 2021, http://tmxk3d.com/.

[6] T. Economist, "The third industrial revolution," *Economist*, vol. 21, pp. 3–16, 2012.

[7] H. Zhang, "Preface to the selection plan "customized cultural and creative design services for 3D printing"," *Packaging Engineering*, vol. 40, p. 1, 2019.

[8] F. Yu, "3D printing, "customize" the life," *China Public Science*, vol. 6, pp. 23–25, 2014.

[9] Y. Zou, "The various forms of arbitrary objects converging" -- innovation research of 3d printing technology in the interior design," Master Degree Thesis, Hunan Normal University, Changsha, China, 2016.

[10] G. A. Rundle, *Revolution in the Making: 3D Printing, Robots and the Future*, pp. 26–58, Machinery Industry Press, Beijing, China, 2015.

[11] M. Attene, M. Campen, and L. Kobbelt, "Polygon mesh repairing: an application perspective," *ACM Computing Surveys*, vol. 45, pp. 3472–3476, 2013.

[12] Y. Li, *Research on hole-filling algorithm on meshes for digitalization of cultural relic*, Northwest University, Xian, China, 2017.

[13] G. Turk and J. F. O'Brien, "Modelling with implicit surfaces that interpolate," *ACM Transactions on Graphics*, vol. 21, no. 4, pp. 855–873, 2002.

[14] X. G. Jin, H. Q. Sun, and Q. S. Peng, "Subdivision interpolating implicit surfaces," *Computers & Graphics*, vol. 27, pp. 763–772, 2003.

[15] J.-P. Pernot, G. Moraru, and P. Véron, "Filling holes in meshes using a mechanical model to simulate the curvature variation minimization," *Computers & Graphics*, vol. 30, no. 6, pp. 892–902, 2006.

[16] E. Marchandise, C. Piret, J. F. Remacle, and J.-F. Remacle, "CAD and mesh repair with radial basis functions," *Journal of Computational Physics*, vol. 231, no. 5, pp. 2376–2387, 2012.

[17] X. C. Wang, J. J. Cao, X. P. Liu, and B. J. Li, "Advancing front method in triangular meshes hole-filling application," *Journal of Computer-Aided Design & Computer Graphics*, vol. 23, pp. 1048–1054, 2011.

[18] B. Lévy, "Dual domain extrapolation," *ACM Transactions on Graphics*, vol. 22, pp. 364–369, 2003.

[19] A. Brunton, S. Wuhrer, C. Shu, P. Bose, and E. D. Demaine, "Filling holes in triangular meshes by curve unfolding," in *Proceedings of the IEEE International Conference on Shape Modeling and Applications*, pp. 26–28, Beijing, China, June 2009.

[20] M. A. Fortes, P. González, A. Palomares, and M. Pasadas, "Filling holes with shape preserving conditions," *Mathematics and Computers in Simulation*, vol. 118, pp. 198–212, 2015.

[21] J. Du, L. Y. Zhang, H. T. Wang, and S. L. Liu, "Hole repairing in triangular meshes based on Radial Basis Function," *Journal of Computer-Aided Design & Computer Graphics*, vol. 17, pp. 1976–1982, 2005.

[22] H. T. Wang, J. Du, S. L. Liu, and L. Y. Zhang, "A novel algorithm for repairing various holes in mesh surfaces based on Radial Basis Function," *Mechanical Science and Technology*, vol. 24, pp. 744–747, 2005.

[23] J. Morel, A. Bac, and C. Véga, "Surface reconstruction of incomplete datasets: a novel Poisson surface approach based on CSRBF," *Computers & Graphics*, vol. 74, pp. 44–55, 2018.

[24] G. Song, J. Riddle, G. E. Fasshauer, and F. J. Hickernell, "Multivariate interpolation with increasingly flat Radial Basis Functions of finite smoothness," *Advances in Computational Mathematics*, vol. 36, no. 3, pp. 485–501, 2012.

[25] S. Liu and C. C. L. Wang, "Quasi-interpolation for surface reconstruction from scattered data with radial basis function," *Computer Aided Geometric Design*, vol. 29, no. 7, pp. 435–447, 2012.

[26] W. Zhao, S. Gao, and H. Lin, "A robust hole-filling algorithm for triangular mesh," *The Visual Computer*, vol. 23, no. 12, pp. 987–997, 2007.

[27] Y. Jun, "A piecewise hole filling algorithm in reverse engineering," *Computer-Aided Design*, vol. 37, no. 2, pp. 263–270, 2005.

[28] G. Li, X.-Z. Ye, and S.-Y. Zhang, "An algorithm for filling complex holes in reverse engineering," *Engineering with Computers*, vol. 24, no. 2, pp. 119–125, 2008.

[29] J. Y. Lai and S. H. Hsu, "On the development of a hole filling algorithm for triangular meshes," *Journal of the Chinese Institute of Engineers*, vol. 30, no. 5, pp. 877–889, 2007.

[30] C. Feng, J. Liang, M. Ren, G. Qiao, W. Lu, and S. Liu, "A fast hole-filling method for triangular mesh in additive repair," *Applied Sciences*, vol. 10, no. 3, p. 969, 2020.

[31] P. Z. Wen, Y. Q. Lei, and M. L. Sun, "Defective hole identification and hole-filling for 3D reconstruction mesh models," *Application Research of Computers*, vol. 37, pp. 1234–1238, 2020.

[32] M. Centin, N. Pezzotti, and A. Signoroni, "Poisson-driven seamless completion of triangular meshes," *Computer Aided Geometric Design*, vol. 35-36, pp. 42–55, 2015.

[33] S. H. Zhang, W. Wu, W. Wei, and J. Bian, "Research on partitioning method of complex holes in triangle meshes for hole repair," *Electronic Technology and Software Engineering*, vol. 4, pp. 135–137, 2021.

[34] Q. Wang, "Research and application of triangle mesh models transition hole repairing algorithm," Master Degree Thesis, Nanjing University of Aeronautics and Astronautics, Nanjing, China, 2007.

[35] T. Karkanis and A. J. Stewart, "Curvature-dependent triangulation of implicit surfaces," *IEEE Computer Graphics and Applications*, vol. 21, no. 2, pp. 60–69, 2001.

Hindawi
Computational Intelligence and Neuroscience
Volume 2023, Article ID 9870280, 1 page
https://doi.org/10.1155/2023/9870280

Retraction

Retracted: Online and Offline Interaction Model of International Chinese Education Based on Few-Shot Learning

Computational Intelligence and Neuroscience

Received 25 July 2023; Accepted 25 July 2023; Published 26 July 2023

This article has been retracted by Hindawi following an investigation undertaken by the publisher [1]. This investigation has uncovered evidence of one or more of the following indicators of systematic manipulation of the publication process:

(1) Discrepancies in scope
(2) Discrepancies in the description of the research reported
(3) Discrepancies between the availability of data and the research described
(4) Inappropriate citations
(5) Incoherent, meaningless and/or irrelevant content included in the article
(6) Peer-review manipulation

The presence of these indicators undermines our confidence in the integrity of the article's content and we cannot, therefore, vouch for its reliability. Please note that this notice is intended solely to alert readers that the content of this article is unreliable. We have not investigated whether authors were aware of or involved in the systematic manipulation of the publication process.

Wiley and Hindawi regrets that the usual quality checks did not identify these issues before publication and have since put additional measures in place to safeguard research integrity.

We wish to credit our own Research Integrity and Research Publishing teams and anonymous and named external researchers and research integrity experts for contributing to this investigation.

The corresponding author, as the representative of all authors, has been given the opportunity to register their agreement or disagreement to this retraction. We have kept a record of any response received.

References

[1] F. Cao and J. Cai, "Online and Offline Interaction Model of International Chinese Education Based on Few-Shot Learning," *Computational Intelligence and Neuroscience*, vol. 2022, Article ID 8281670, 11 pages, 2022.

Hindawi
Computational Intelligence and Neuroscience
Volume 2022, Article ID 8281670, 11 pages
https://doi.org/10.1155/2022/8281670

Research Article

Online and Offline Interaction Model of International Chinese Education Based on Few-Shot Learning

Fei Cao [1] and Jing Cai [2]

[1] *School of Humanities, Hangzhou Normal University, Hangzhou 311121, China*
[2] *Rotterdam Business School, Rotterdam University, University of Applied Science, Kralingse Zoom 91 3063, ND Rotterdam, Netherlands*

Correspondence should be addressed to Fei Cao; caof@hznu.edu.cn

Received 16 March 2022; Revised 3 April 2022; Accepted 6 April 2022; Published 5 May 2022

Academic Editor: Xin Ning

Few-shot learning is a method to acquire learning ability in a small amount of sample data scenarios. This paper aims to study an online and offline interaction model applied to international Chinese education and teaching based on the few-shot learning method. It first expounds an overview of international Chinese education, including the connotation and characteristics of the hybrid mode of online teaching and offline teaching in international Chinese education, then designs an online and offline interactive model, and finally compares it with a baseline model and a traditional single teaching model. The experimental data shows that the accuracy and recall rate of the international Chinese education online and offline interaction model based on few-shot learning both reach 70%, which verifies its effectiveness.

1. Introduction

Language is not only one of the important media for the transmission of culture, but also an indispensable part of the expression of human thoughts and ideas. With the diversified development of world culture and the rapid increase of China's economic and technological strength, Chinese has become another popular language after English. The charm and connotation of Chinese are more and more appreciated and valued by many countries. According to research data released by the Ministry of Education, more than 70 countries around the world have incorporated Chinese language education into their educational systems and structures. The number of people studying Chinese overseas has also exceeded 20 million, and the number of overseas Chinese education institutions is also increasing every year, as shown in Figure 1. International Chinese education has entered a period of vigorous development. However, with the outbreak of the new crown epidemic, traditional offline education has been hit. International Chinese education has transformed from offline to online development. However, due to the particularity of Chinese teaching, and because online education is still in the early stage of exploration, there are still many limitations in the current international Chinese education. For example, online classroom learning is full of difficulties, low flexibility, and the interactive experience between students and teachers, which has brought many negative effects [1].

The Chinese interpretation of few-shot learning is small sample learning. As the name implies, it is to master the ability of learning and generalization in a small number of samples. Learning in this way can enable humans to obtain an initial target set for learning in a very small number of individual categories. Humans can not only learn object permanence through this target set, but also generalize and apply it to other objects based on this target set. This type of method often plays its own role in task scenarios where data or supervision information is difficult to obtain. It can not only find suitable models for scarce sample tasks, but also assist in data- and computing-intensive data collection, such as image retrieval, object tracking and language modeling, and one-shot architecture search.

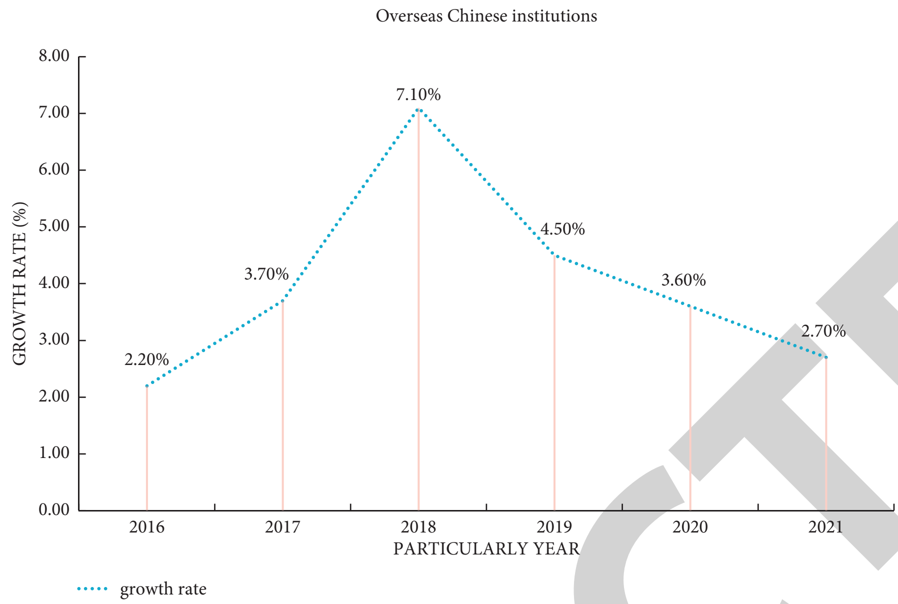

Figure 1: Growth and changes of overseas Chinese education institutions.

Many academics have studied the subject of more-shot training in recent years. Shi Y proposed a self-determination training-based multishot modeling algorithm. The algorithm has a large number of resources and a simple network design. Finally, simulation results show that this algorithm can improve model recognition by 5% to 10%. Chen M proposed a novel diversity transfer network generation framework to address the lack of diversity in few-shot learning. He also confirmed that the generation framework has state-of-the-art results in the few-shot learning method based on feature generation [2] through experimental results. Lv Q proposes the new more-shot learning method in conjunction with programming observation and replaces the mean square error loss function with L1Loss and BCEloss. The test's final results show that the method has an average accuracy of 97.25 percent in the data set, indicating that it is effective [3]. In manipulated microbot systems, Zhang D proposed a data-driven approach to stability and depth analysis. It also demonstrates the method's generality by adapting to microrobots of various shapes using a multishot learning curve [4]. Aharchaou M gives an example of machine learning in action. This example is based on recent advancements in deep learning systems, as well as Siamese networks' few-shot learning capability, which has been shown to generalize well to new datasets [5]. Deng S used meta-learning and unsupervised language models to solve the problem of negating common language features implicit across tasks in few-shot tasks and confirmed that pretraining is a promising solution in many few-shot tasks [6]. Few-shot learning was proposed by Wang Y to address the problem of machine learning being hindered in applications with small datasets. He also looks into the setting, technical, applied, and theoretical aspects of the few-shot learning problem in order to give researchers ideas for future research [7]. Silver T proposes a powerful but general prior and a learning algorithm that, when combined, can learn interesting policies from few shots and shows that this method is a good fit for tasks with sparse training data [8]. In the field of civil aviation emergency management, Hong W proposed a few-shot learning method. Finally, experiments show that the method can solve the problem of automatic updating of concepts and relationships in large-scale domain ontologies while also providing good data support, and using few-shot machine learning [9–11] to train general neural network models in cell lines also has many advantages for high-throughput screening of individual patients. To summarize, many scholars have studied the few-shot learning method and application in depth after several years of research. However, there are few studies that integrate it with the international Chinese education model of online and offline interaction, and previous studies still have some flaws, as shown in Table 1.

Therefore, this paper incorporates the few-shot learning method to establish an online and offline interaction model in order to further promote the long-term development of international Chinese education. It also investigates the current state of international education and teaching, as well as problems and practical teaching strategies. It proposes a novel educational interaction research direction that can effectively improve the quality of Chinese education and teaching, offer suggestions for improvement and improvement for international Chinese communication, and generate new ideas for Chinese education and teaching research.

2. International Chinese Education Based on Few-Shot Learning

2.1. Overview of International Chinese Education. On the basis of the first Chinese international education, international Chinese education is being developed. It is primarily written in the form of a second language for foreigners and foreign Canadians who do not speak English as their first

Table 1: Weaknesses of previous studies.

Sequence	Insufficiency	Influence
1	More qualitative discussions, less quantitative research	Not objective enough
2	More micro research, less macro research	Not comprehensive enough
3	More experience summaries, less theoretical discussions	Not deep enough

language. Although international Chinese education and teaching have an offline component, traditional offline education cannot be adapted in the face of the new epidemic. Traditional education should keep up with the times, build digital and networking, and develop online teaching and learning, as shown in Figure 2, in order to promote the healthy and sustainable development of international Chinese education. Of course, this does not imply that international education and teaching in Canada will replace traditional schooling, nor that offline education will become the predominant teaching method. Modern technology and techniques will not completely replace traditional face-to-face instruction, but they are more likely to introduce a variety of teaching positions in various combinations and sizes. It is believed that it will be able to fully benefit from Chinese online education and that online education can be used as an aid and complement to offline education if the level of international online education in Canada is raised and the quality of education is improved.

2.1.1. The Connotation of the Mixed Mode of Online Teaching and Offline Teaching. The hybrid teaching mode that combines online and offline is an organic combination of online teaching and traditional face-to-face classroom teaching, which integrates multiple elements (teacher, student, classroom, environment, etc.). It is through the transformation of modern information technology means and teaching methods. On the basis of conforming to the laws of language communication, the complementarity between online learning and offline classroom teaching can be realized, so as to achieve the best learning effect. Pure online teaching or offline teaching can no longer fully meet the current Chinese learning needs. Compared with traditional face-to-face classroom teaching and fully online teaching, the online-offline hybrid teaching mode has a deeper meaning. This teaching model neither unilaterally emphasizes the dominant position of students and ignores the dominant position of teachers, nor unilaterally emphasizes online teaching and ignores the emotional communication between teachers and students in traditional face-to-face classrooms. The blended teaching combining online and offline may become a normalized teaching mode in the postepidemic era.

2.1.2. Characteristics of the Hybrid Mode of Online Teaching and Offline Teaching

(1) Multichannel Teaching. At present, the online and offline teaching modes of international Chinese education and teaching are still not closely connected, and the two have not been organically combined. The hybrid teaching mode that combines online and offline teaching cannot simply separate the two, and online Chinese teaching can not only be used as an auxiliary to offline teaching, but must be a necessary teaching link. The offline Chinese teaching in the blended teaching should not just copy the teaching activities in the traditional face-to-face classroom teaching, but should further develop the teaching activities based on the previous results of online Chinese teaching.

(2) Complete Teaching Links. The first stage of the learner's learning process is mainly information transmission, and the second stage is mainly the absorption and internalization of the teaching content. The blended teaching mode of Chinese online teaching optimizes the classroom structure and promotes the rationalization of teaching content distribution. The flipped classroom teaching mode adopts the teaching form of "learning knowledge before class—consolidation and practice in class", and learners can conduct autonomous learning of target knowledge by watching videos online. Practical language practice is carried out in the offline classroom, and the target knowledge is applied in practice.

(3) Targeted Teaching. The online Chinese teaching in the online and offline hybrid teaching can make up for the lack of offline classroom teaching time to a certain extent. However, due to the lack of deep participation of teachers, the effect of learners will be difficult to guarantee; teachers should pay attention to the design of teaching content and target language environment in offline Chinese classroom teaching. By recording the learner's Chinese learning situation, the teacher supervises the learner's learning progress, which is helpful for the teacher to better grasp the teaching progress of the offline classroom and make the teaching activities more targeted.

(4) Interactive Teaching. Training Canada online and offline can not only affect the quality of teachers, but also reflect the high position of students. Teachers teach relevant target knowledge online and complete information transfer; offline practice is a specific exercise of language points. By strengthening the interaction between teachers and students in the classroom, learners can complete the absorption and internalization of knowledge, so that online teaching can better serve offline teaching. At the same time, offline education can be better adapted to online education, in order to achieve a positive attitude and improve the quality of teaching and learning.

2.2. Design of Online and Offline Interactive Model Based on Few-Shot Learning. Few-shot learning is used in this paper to identify the features of intent classification and semantic

Figure 2: Online and offline teaching of international Chinese education.

understanding in international Chinese education, and the two models are combined with algorithms to create a complete online and offline interaction model. The sample input model of the support set and query set must first be encoded, and the data must then be converted into a sample semantic vector that contains semantic information and is more conducive to model learning for the task of intent classification. The class vector of each class in the support set is then obtained by extracting some intentional category features from the semantic vector of the support set sample. Finally, they calculate the loss function and finish the backpropagation by comparing the class vector with the query set sample semantic vector. The few-shot intent recognition model is divided into three parts based on these three basic steps, as shown in Figure 3: encoding module, induction module, and relation module.

The main task of the encoding module is to receive the sample input of support set and query set and encode them into sample semantic vectors. In this study, a bidirectional long-term and short-term memory network with self-attention mechanism was used to form the encoder. Given a set of input text $x = (x_1, x_2, \ldots, x_T)$ represented by a sequence of word embedding, use $Bi - \text{LSTM}$ to process this set of text:

$$\begin{aligned} \overrightarrow{h_t} &= \overrightarrow{\text{LSTM}}(x_t, h_{t-1}), \\ \overleftarrow{h_t} &= \overleftarrow{\text{LSTM}}(x_t, h_{t+1}). \end{aligned} \tag{1}$$

Connect $\overrightarrow{h_t}$ and $\overleftarrow{h_t}$ to obtain a hidden state h_t, and record all T hidden states as $H = (h_1, h_2, \ldots, h_T)$. The length of each text sample is different, and we need to encode it as a fixed-size embedding, which can be achieved by choosing a linear combination of T latent vectors LSTM in H [12]. Computing the linear combination requires a self-attention mechanism that takes the entire hidden state H of LSTM as input and outputs a weight to a:

$$a = \text{soft max}\left(W_{a2}\tanh\left(W_{a1}H^T\right)\right). \tag{2}$$

The definitions of all parameters in (2) are shown in Table 2.

From this, the semantic vector e of an input sample is finally expressed as the weighted sum of H for the self-attention weight a:

$$e = \sum_{t=1}^{T} a_t \cdot h_t. \tag{3}$$

The sample semantic vector of all samples in the support set and query set can be obtained through the encoding module. Among them, the sample semantic vector e^s of the support set needs to be input into the induction module, while the sample semantic vector e^q of the query set is directly input to the relation module [13]. The induction module needs to summarize some essential characteristics of the intent category according to the K samples of each class in the support set, that is, according to the sample semantic vector of the support set, abstract a class vector c of each class, so this part is called the induction module:

$$\left\{e_{ij}^s \in R^{2u}\right\}_{i=1,\ldots,C,\, j=1,K} \leftrightarrow \left\{C_i \in R^{2u}\right\}_{i=1,\ldots,C}. \tag{4}$$

In previous studies, there have been some computational methods, for example, directly adding the semantic vectors of each sample, or taking the average value of the semantic vectors of the samples as a class vector to obtain abstract class vectors. But in few-shot learning, because the number of samples is too small, it is not enough to cover a wider and general situation. This kind of simple algorithm will bring great chance, and the noise brought by each sample is huge, and the capsule network can solve this problem very well [14]. The capsule network adopts an idea of inverse rendering, which can predict the overall features of the high-level from the local features of the bottom layer, so that the model has better generalization, as shown in Figure 4.

In the task of intent classification, the sample semantic vector can be regarded as a local feature, while the class vector that needs to be abstracted can be regarded as the overall feature. Through the dynamic routing algorithm, the coupling coefficient between the sample vector and the same kind of vector is increased, and the coupling coefficient with other class vectors is reduced, so as to obtain a class vector that can dynamically change according to the sample vector and has better generalization. According to the dynamic routing algorithm, it is first necessary to multiply the sample vector by a transformation matrix to obtain the prediction vector:

$$\widehat{e}_{ij}^s = W_s e_{ij}^s. \tag{5}$$

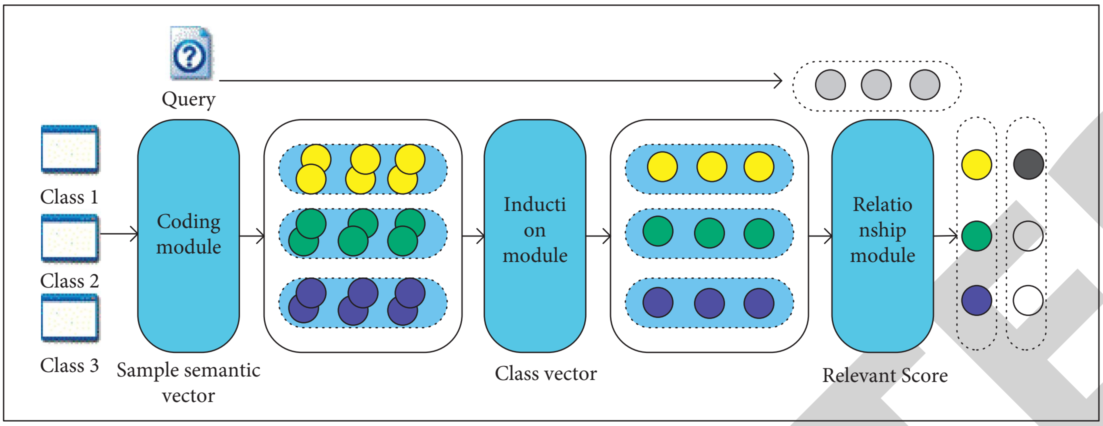

Figure 3: Few-shot intent recognition model structure.

Table 2: Definition of formula parameters.

Sequence	Parameter	Paraphrase
1	$W_{a1} \in R^{d_a \times 2u}$	Weight matrix
2	$W_{a2} \in R^{d_a}$	Weight matrix
3	d_a	Hyperparameters
4	u	The size of the hidden state vector for each one-way LSTM

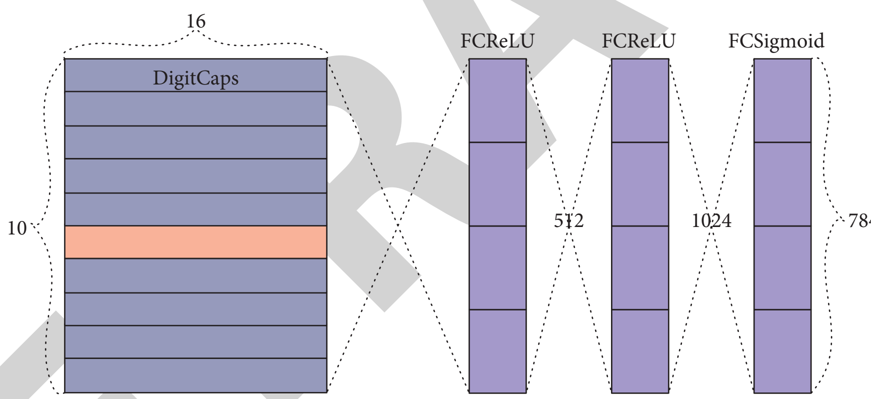

Figure 4: Capsule network structure diagram.

Here is a slight change to the original dynamic routing algorithm: In order to be able to support sets of various sizes (that is, C and K can take any value), let all sample semantic vectors in the support set share a transformation matrix $W_s \in R^{2u\times 2u}$, instead of setting a W_{ij} for each sample. This transformation matrix W_s can encode important spatial and other relations between low-level features (sample semantics) and high-level features (intent categories), and it is also learned to update through backpropagation.

Next, the coupling coefficient d needs to be learned, which is used to represent the probability that each sample semantic vector is routed to each class. And the size of d will be automatically corrected in multiple iterations of the dynamic routing algorithm, and the sum of the coupling coefficients for each class of sample vectors is guaranteed to always be 1 by the softmax function:

$$d_i = \text{soft max}\left(b_i\right), \tag{6}$$

where b_i is the logarithm of the coupling coefficient, initialized to 0 in the first iteration.

A weighted sum is performed on all the predicted vectors obtained in each class, so that the predicted class vector is obtained:

$$\hat{c}_i = \sum_j d_{ij} \cdot \hat{e}^s_{ij}. \tag{7}$$

The modulus of $\hat{c}_i$ represents the probability of the existence of the class it represents, so the nonlinear function squash is used in the capsule network to replace the activation function relu in the traditional neural network, as shown in Figure 5.

It is ensured that short vectors can be compressed to lengths close to 0 and long vectors to lengths close to 1, and the direction of the vectors remains unchanged [15].

$$\text{squash}\left(x\right) = \frac{\|x\|^2}{1 + \|x\|^2}\frac{x}{\|x\|}. \tag{8}$$

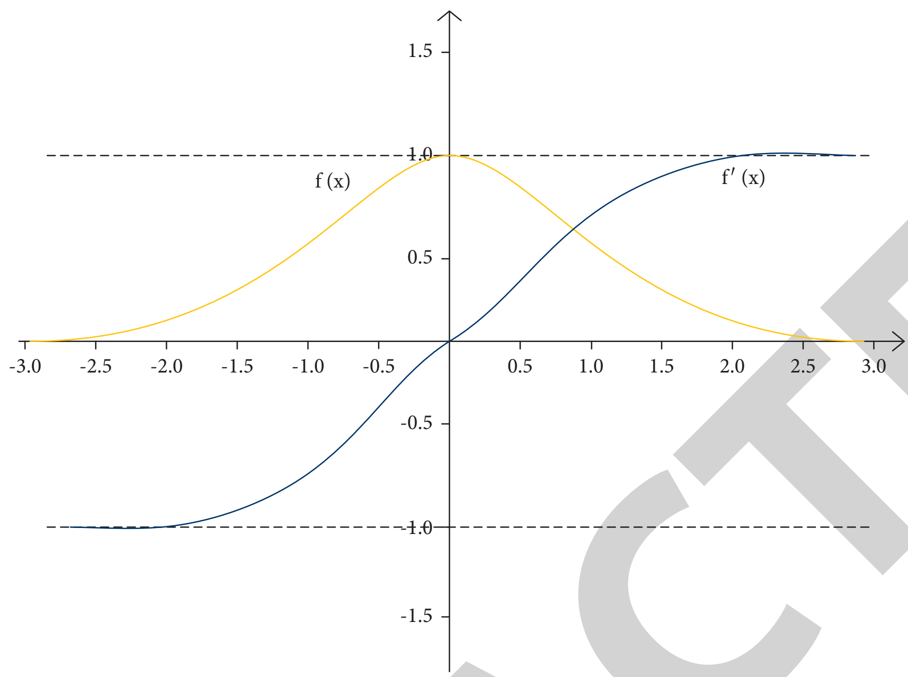

Figure 5: Activation function distribution map.

Finally get the class vector c_i:

$$c_i = \text{squash}(\hat{c}_i). \quad (9)$$

The final step of each iteration of the dynamic routing algorithm is to update the logarithm of the coupling coefficient of b. If the dot product of c_i and b_{ij} is large, there is a top-down feedback, which increases the coupling coefficient of this sample and decreases the coupling coefficient of other samples. Each b_{ij} is updated by

$$b_{ij} = b_{ij} + \hat{e}_{ij}^{s} \cdot c_i. \quad (10)$$

To sum up, the entire algorithm process is shown in Table 3, where r is a hyperparameter representing the number of iterations of the algorithm. The algorithm finally outputs a class vector c_i for each class.

The relation module measures the correlation between each sample semantic vector e_i^q in the query set and each class vector c_j output by the induction module, and it outputs a scalar between 0 and 1 to represent this correlation score. The calculation formula of the scoring function is as follows:

$$r_{ij} = \text{sigmoid}\left(\text{SIM}\left(e_i^q, c_j\right)\right). \quad (11)$$

Among them, SIM is a similarity function, which can choose cosine similarity, dot product similarity, and so on. Cosine similarity measures the similarity of two vectors by calculating the cosine value of the angle between the two vectors and pays more attention to the similarity in direction, while the dot product similarity directly calculates the dot product of the two vectors, which can directly measure the similarity of the length and direction of the two vectors. The higher the similarity of two vectors, the larger their dot product. Moreover, compared with the calculation steps of cosine similarity, dot product similarity is simpler to implement, and it is the simplest similarity measurement method, which can improve the efficiency of the model. For the above two reasons, this paper uses the dot product similarity to calculate the similarity of two vectors, namely:

$$\text{SIM}\left(e_i^q, c_j\right) = e_i^q, c_j. \quad (12)$$

In this paper, the mean square error (MSE) is used as the loss function. For matching query set samples (x_q, y_q) and intent categories, the closer the correlation score r_{iq} is to 1, the better it will be, while for unmatched samples and categories, the closer r_{iq} to 0, the better. In episode, for the input support set S_{support} and query set S_{quiry}, the loss function of C classes is defined as

$$L\left(S_{\text{support}}, S_{\text{quiry}}\right) = \sum_{j=1}^{C}\sum_{i=1}^{n}\left(r_{ij} - 1 \cdot \left(y_i == j\right)\right)^2. \quad (13)$$

The loss function is derived and backpropagated, and all parameters in the above three modules are updated until the best parameters are learned.

The few-shot semantic understanding joint model is improved on the basis of the structure of the few-shot intent recognition model. The overall structure is also divided into three parts: cocoding module, separate induction module, and fusion scoring module. Figure 6 is the basic structure of the joint model of few-shot semantic understanding.

The coencoding module is one of them, and it is used to coencode the input model's support and query set samples not only to get the sample semantic vector, but also to get the sample sequence vector for the semantic slot filling task. The class vectors for the intent and semantic slots are inducted separately using a separate

Table 3: Algorithmic process.

Dynamic routing algorithms in induction modules		
Sequence of steps	1:	For all samplesk $j = 1, \ldots, K$, in class i:
	2:	$b_{ij} = 0$
	3:	$\hat{e}_{ij}^{s} = W_s \hat{e}_{ij}^{s}$
	4:	for r: iterations do
	5:	$d_i = \text{softmax}(b_i)$
	6:	$\hat{c}_i = \sum_j d_{ij} \cdot \hat{e}_{ij}^{s}$
	7:	$c_i = \text{squash}(\hat{c}_i)$
	8:	For all samples $j = 1, \ldots, K$, in class i:
	9:	$b_{ij} = b_{ij} + \hat{e}_{ij}^{s} \cdot c_i$
	10:	return c_i

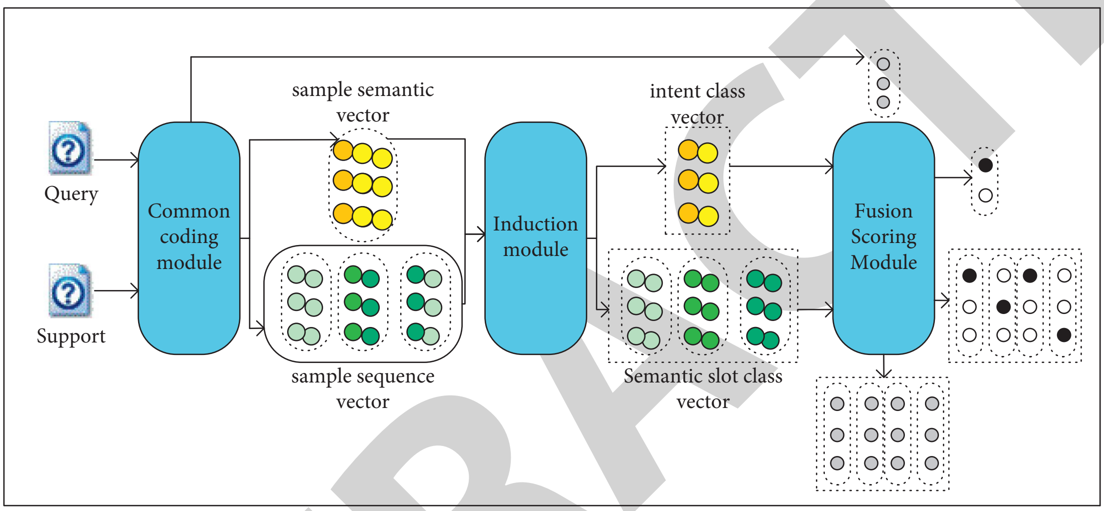

Figure 6: Few-shot semantically understands the basic structure of the federated model.

induction module. The fusion scoring module scores the intent and semantic slot matching based on the similarity between the sample vector and the class vector, but the semantic slot scoring is not done separately, but rather combines the results of the intent classification, so that the sample intent category provides some support for semantic slot annotation. Finally, the backpropagation loss is reduced by combining the loss functions of the two tasks. The coencoding module's primary function is to receive support and query set sample input. For semantic slot prediction and intent classification, they are encoded to produce a sample sequence vector and a sample semantic vector for each sample. The sample semantic vector is an attention-based vector obtained by weighting and calculating the sample sequence vector, which can better focus on the important information in the sample, and the sample sequence vector incorporates the context information of the entire sample during the encoding process.

Given a set of input text $x = (x_1, x_2, \ldots, x_T)$ represented by a sequence of word embedding, first process this set of text using $Bi-\mathrm{LSTM}$:

$$\begin{aligned} \overrightarrow{h_t} &= \overrightarrow{\mathrm{LSTM}}(x_t, h_{t-1}), \\ \overleftarrow{h_t} &= \overleftarrow{\mathrm{LSTM}}(x_t, h_{t+1}). \end{aligned} \tag{14}$$

Connect $\overrightarrow{h_t}$ and $\overleftarrow{h_t}$ to obtain a hidden state h_t, and record all T hidden states as $H = (h_1, h_2, \ldots, h_T)$. Among them, each h_T is a word vector representation that obtains the information before and after the current word, and H is used as the sample sequence vector e^s of this input sample, namely:

$$e^s = H = (h_1, h_2, \ldots, h_T). \tag{15}$$

The attention calculation is performed on H, and the calculation method is the same as that of the few-shot intent recognition model, and the sample semantic vector e^I of each sample is obtained:

$$e^I = \sum_{t=1}^{T} a_t \cdot h_t. \tag{16}$$

Finally, the sample sequence vector e^{S_S} and the sample semantic vector e^{S_I} of each sample of the support set and the sample sequence vector e^{Q_S} and the sample semantic vector e^{Q_I} of each sample of the query set are output to the common coding module.

Input e^{S_I} and e^{S_S} of the support set samples output by the coencoding module into the induction module, which are used to calculate the class prototype representation c^I for each intent category and the semantic slot label class vector c^S for each semantic slot label category:

$$\begin{aligned}\left\{e_i^{S_I} \in R^{2u}\right\}_{i=1,\ldots,s} &\longrightarrow \left\{c_j^{I} \in R^{2u}\right\}_{j=1,\ldots,C_I},\\ \left\{e_i^{S_S} \in R^{2u}\right\}_{i=1,\ldots,s} &\longrightarrow \left\{c_j^{S} \in R^{2u}\right\}_{j=1,\ldots,C_S}.\end{aligned} \tag{17}$$

Among them, the class prototype vector is still obtained by the dynamic routing algorithm, and the semantic slot label class vector is obtained by TapNet.

3. Online and Offline Interactive Model Test

This paper evaluates and tests the online and offline interaction model of international Chinese education based on few-shot learning. Then it is used in teaching practice to verify the validity of the model from the aspects of teaching quality and learning effect, students' experience, and acceptance.

3.1. Evaluation Test. The online and offline interactive model evaluation test of international Chinese education based on few-shot learning uses the FewJoint dataset as the experimental dataset. The parameters it uses in the process of building the model and training the model are shown in Table 4

Table 4: Experimental parameter settings.

Serial number	Parameter name	Parameter value
1	Batch size	4
2	Learning rate	L $e-5$
3	Balance parameters α	0.7

The performance evaluation index of the interactive model adopts the internationally common PRF evaluation index, namely, the precision rate (Precision, P), the recall rate (Recall, R) and the F value. In order to verify the effect of the model, this experiment uses the prototype network as the baseline model and conducts training tests in the six fields of idiomsDic, drama, timesTable, length, story, and constellation of the dataset, and the test results are shown in Figures 7 and 8.

Figure 7(a) shows the accuracy test results of the model proposed in this paper.

Figure 7(b) shows the accuracy test results of the prototype network model.

It can be seen from Figure 7 that the model proposed in this paper has an overall training accuracy of 71.31% in the six fields of the dataset: idiomsDic, drama, timesTable, length, story, and constellation; the training accuracy of the prototype network in the six fields of idiomsDic, drama, timesTable, length, story, and constellation of the dataset is 60.03%.

Figure 8(a) shows the recall test results of the model proposed in this paper.

Figure 8(b) shows the recall test results of the prototype network model.

It can be seen from Figure 8 that the model proposed in this paper has an overall training recall rate of 70.15% in the six fields of idiomsDic, drama, timesTable, length, story, and constellation of the dataset; the recall rate of the prototype network training in the six domains of idiomsDic, drama, timesTable, length, story, and constellation of the dataset is 57.99%.

3.2. Teaching Practice. This experiment takes foreign students majoring in international Chinese education in a university as the experimental object, with a sample size of 50 people, who are divided into two classes. Class A adopts the online and offline interactive teaching mode proposed in this paper for Chinese learning, and class B adopts a single online mode for Chinese learning. The students of the two classes have basically the same level of Chinese proficiency and related theoretical knowledge and are at the same starting point. Through a semester of teaching practice, the test data of the teaching quality and learning effect, students' experience, and acceptance of the four key stages of teaching were compared and analyzed. The analysis results are shown in Figures 9 and 10.

Figure 9(a) shows the test of teaching quality and learning effect under the online and offline interactive teaching mode.

Figure 9(b) shows the test of teaching quality and learning effect under a single online teaching mode.

It can be seen from Figure 9 that, under the online and offline interactive teaching mode, the overall average of the teaching quality of the four key teaching stages reached 86.28 points, and the overall average of the learning effect reached 82.85 points; under the single online teaching mode, the overall mean of teaching quality in the four key stages of teaching is 78.65 points, and the overall mean of learning effect is 73.68 points.

Figure 10(a) is the test of students' experience and acceptance under the online and offline interactive teaching mode.

Figure 10(b) is a test of students' experience and acceptance under a single online teaching mode.

As can be seen from Figure 10, under the online and offline interactive teaching mode, the overall average score of students' experience in the four key stages of teaching reached 86.23 points, and the overall average score of students' acceptance reached 90.38 points; under the single online teaching mode, the overall average score of students' experience in the four key stages of teaching is 80.75 points, and the overall average score of students' acceptance is 76.70 points.

4. Discussion

Through the evaluation test data of the online and offline interaction model based on few-shot learning and the prototype network baseline model, the following conclusions can be drawn:

(1) In terms of the accuracy of the model, the overall mean of the online and offline interactive model based on few-shot learning in the training and testing of the dataset is 11.28% higher than the overall mean of the prototype network baseline model in the training and testing of the dataset, which shows that the online-

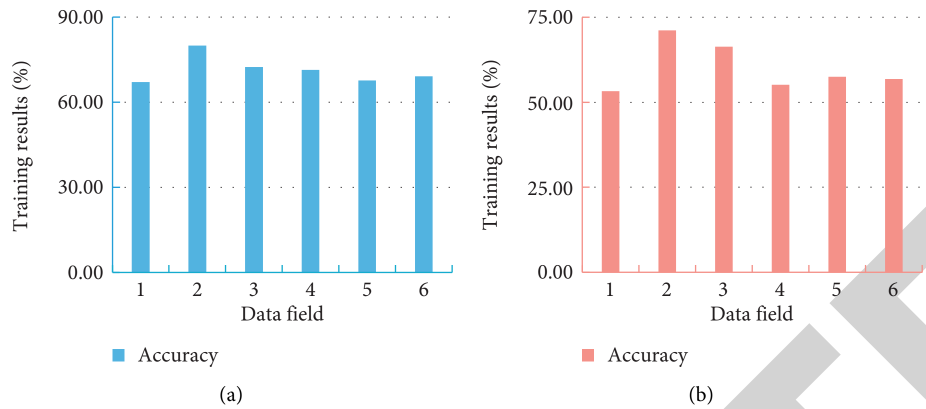

Figure 7: Model accuracy evaluation test.

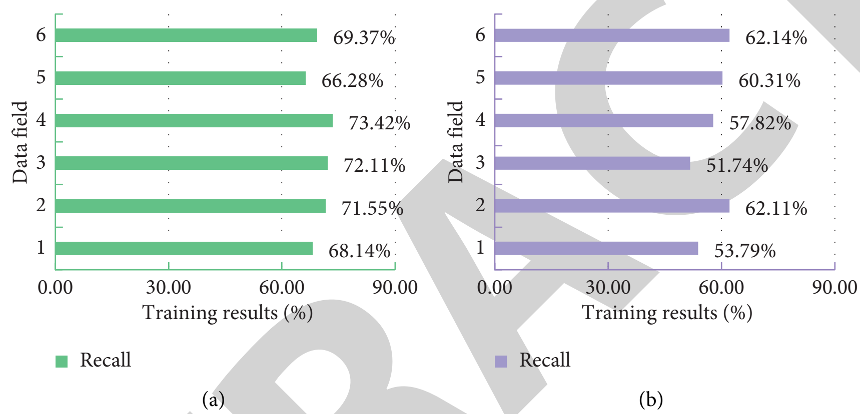

Figure 8: Model recall evaluation test.

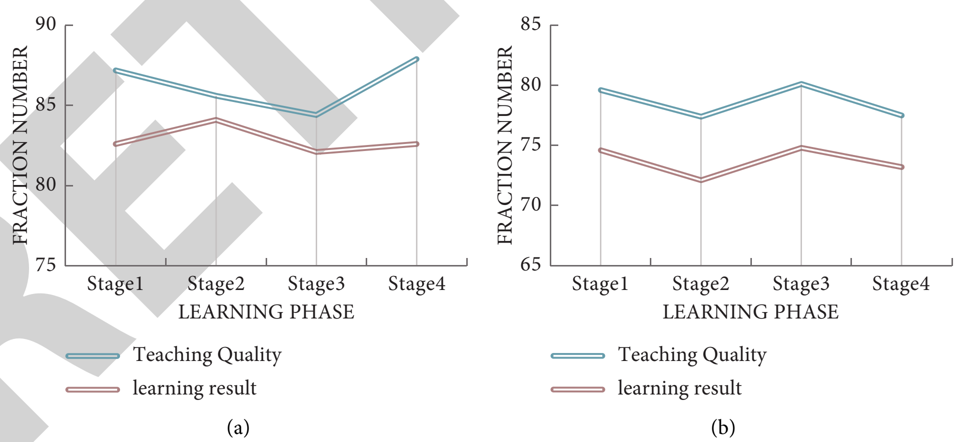

Figure 9: Teaching quality and learning effectiveness test.

offline interaction model based on few-shot learning has superior accuracy.

(2) At the model recall level, the overall mean of the online and offline interaction model based on few-shot learning in the training and testing of the dataset is 12.16% higher than the overall mean of the prototype network baseline model in the training and testing of the dataset, which shows that the online-offline interactive model based on few-shot learning is also superior in retrieval performance.

(i) Through the teaching practice data of the online and offline interactive teaching mode based on few-shot learning and the traditional single online teaching mode, the teaching quality and learning effect, students' experience, and acceptance, the following conclusions can be drawn.

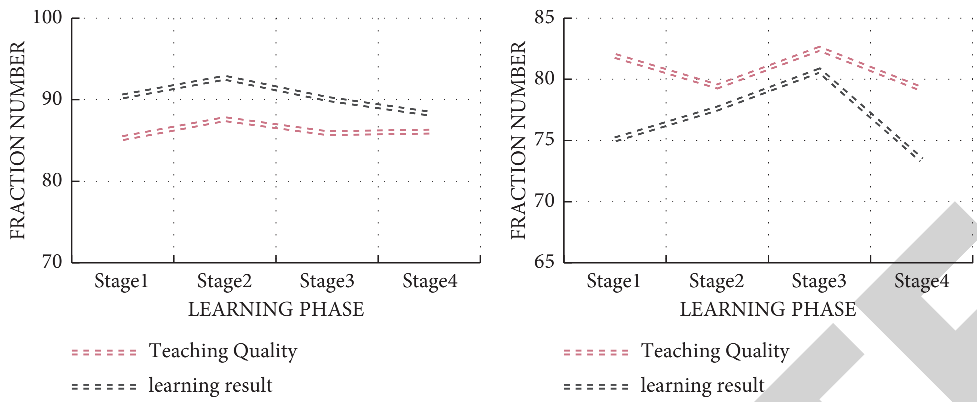

(a) (b)

Figure 10: Student experience and acceptance test.

(3) In terms of teaching quality and learning effect, the overall mean of teaching quality under the online and offline interactive model teaching mode based on few-shot learning is 7.63 points higher than the overall mean of teaching quality under the single online teaching mode; the overall mean of the learning effect is 9.17 points higher than the overall mean of the learning effect under the single online teaching mode.

(4) In terms of student experience and acceptance, the overall mean of students' experience under the online and offline interactive model teaching mode based on few-shot learning is 5.48 points higher than the overall mean of students' experience under the single online teaching mode; the overall mean of student acceptance is 13.68 points higher than the overall mean of student acceptance under the single online teaching mode; and the overall mean of student acceptance is 13.68 points higher than the overall mean of student acceptance under the single online teaching mode.

The entire comparative experimental data shows that when all other experimental conditions are held constant, the online and offline interactive model test data based on few-shot learning performs better in terms of model accuracy and teaching practice results after model scoring and teaching practice test. It demonstrates that the few-shot learning-based online and offline interaction model can improve the level and quality of international Chinese education and teaching, thereby promoting the development of international Chinese education.

5. Conclusion

The continuous updating and development of information technology have promoted the modernization of international Chinese education. A new round of Chinese teaching has begun to change, and online and offline Chinese teaching will become an important development direction for international Chinese education. The combination of few-shot learning method and international Chinese education and teaching is beneficial not only to its own diversified development, but also to international Chinese education to solve the teaching restrictions caused by the epidemic and improve the level of intelligent teaching.

There are still many deficiencies in the research of this paper. The depth and breadth of the research in this paper are not enough, without taking into account some interfering factors involved in the teaching practice process, and the evaluation of the teaching mode is also restricted by many factors. And our academic level research is also limited; the research on the online and offline interaction model of few-shot is still in the preliminary stage. In the future work, the model performance will be improved from more angles based on the existing technology and level, and the teaching methods of international Chinese education will be continuously optimized.

Data Availability

There is no data availability in statement.

Conflicts of Interest

The authors do not have any possible conflicts of interest.

Acknowledgments

This study was supported by Chinese National Funding of Social Sciences (20BYY123).

References

[1] M. A. Jan, *Application of Big Data, Blockchain, and Internet of Things for Education Informatization*, Springer Nature, London, UK, 2021, https://rd.springer.com/book/10.1007/978-3-030-87903-7.

[2] M. Chen, Y. Fang, X. Wang et al., "Diversity transfer network for few-shot learning," *Proceedings of the AAAI Conference on Artificial Intelligence*, vol. 34, no. 7, Article ID 10559, 2020.

[3] Q. Lv and Y. Song, "Few-shot learning combine attention mechanism-based defect detection in bar surface," *ISIJ International*, vol. 59, no. 6, pp. 1089–1097, 2019.

Hindawi
Computational Intelligence and Neuroscience
Volume 2022, Article ID 2128370, 10 pages
https://doi.org/10.1155/2022/2128370

Research Article

Establishment of Economic Forecasting Model of High-tech Industry Based on Genetic Optimization Neural Network

Kai Gao,[1] Tingting Liu ,[2] Bin Hu,[1] Miao Hao,[1] and Yueran Zhang[1]

[1]*School of Management, Shanghai University of Engineering Science, Shanghai 201620, China*
[2]*School of International Trade and Economics, Shanghai Lixin University of Accounting and Finance, Shanghai 200030, China*

Correspondence should be addressed to Tingting Liu; 20190045@lixin.edu.cn

Received 14 March 2022; Revised 2 April 2022; Accepted 4 April 2022; Published 30 April 2022

Academic Editor: Xin Ning

Scientific and accurate prediction of high-tech industries is of great practical significance for government departments to grasp the future economic operation and formulate development strategies. In this paper, aiming at some shortcomings of neural network (NN) applied in economic forecasting, GANN was introduced to construct the economic forecasting model of high-tech industry. Genetic algorithm (GA) has simple calculation and strong robustness and can generally ensure convergence to the global optimum, which effectively overcomes the shortcomings of NN using gradient descent method. In order to verify the feasibility of the economic forecasting model in this paper, the comparative experiments of different models are carried out in this paper. Experimental results show that the proposed algorithm has faster convergence speed and greater generalization ability, and the average error rate is reduced to about 1%. The prediction accuracy of this model reached 95.14%, which was about 11.93% higher than the previous model. Applying the economic forecasting model in this paper to the economic forecasting of high-tech industries can provide the means and reference value for the government to formulate regional future economic development plans, forecast, and control the economic growth and development direction.

1. Introduction

With the rapid development of information technology, the pace of economic development is also accelerating [1]. The rise and growth of high-tech industry has become an important industry to promote economic growth in today's world, which has a great influence on the position and role of a country or region in the world pattern in economic, political, military, and other aspects [2]. In the era of the "knowledge economy," high-tech industry is at the heart of all industries, the most important motivator for a country or region to gain a long-term competitive advantage, and the engine of social economy development. The advancement of high-tech industry is not only an important tool for optimizing and upgrading industrial structure but it is also a critical factor in achieving economic multiplication [3]. As a result, in countries and regions all over the world, the development of high-tech industries has become a strategic focus of economic and social development. One of the topics that the Chinese government and economists are paying increasing attention to is how to accurately and reasonably predict the industrial economic situation based on relevant industrial economic indicators [4]. Prediction is a study that compares the results of things that will happen with reality, and it is an estimate and speculation of things that have not yet happened and are not clear at this time. Economic forecasting, as an important branch of forecasting, has gotten a lot of attention in the economic field [5]. For government departments to grasp the future economic operation and formulate development strategies, scientific and accurate predictions of high-tech industries are critical.

The economic forecast of high-tech industry plays a vital guiding role in implementing effective economic macro-control by national departments at all levels and making specific production and delivery by various enterprises under the market economy. Although traditional economic forecasting and early warning methods have their own advantages, with the complication of economic management problems, these traditional methods are increasingly unsuitable for scientific management and precise management. Therefore, it is particularly important to find a more general and accurate economic forecasting model. Neural network (NN) [6–8] is an important Artificial intelligence (AI) technology [9–11]. NN is also one of the fastest-growing research achievements in AI field recently. It has been successfully used in scientific calculation and automatic control. In recent years, domestic and foreign scholars have carried out a lot of applied research on NN in economic fields such as economic prosperity analysis, economic time-series prediction, portfolio optimization and stock prediction, and achieved good application results. The most widely used NN in the economic field is BPNN (back-propagation neural network). As it is essentially a gradient descent method, and the objective function to be minimized is complex, it has some shortcomings. For example: (1) The learning process converges slowly. (2) It is easy to fall into local minima and the algorithm is incomplete. (3) Poor robustness and poor network performance. Therefore, this paper introduces genetic algorithm (GA). GA is a computational model developed in recent years, which opens up a new way to solve complex problems. GA is an algorithm model to simulate the evolution process or evolution process in nature. It simulates the evolution process of species from low level to high level, adopts the natural law of survival of the fittest to select individuals, generates the next-generation population through mating and mutation and evolves from generation to generation until individuals who meet the conditions are produced [12]. GA is based on strict theory. It has strong adaptability and robustness and is especially suitable for searching for optimal solutions in high-dimensional, multipole, nondifferentiable, continuous, or discrete space. In this paper, based on genetic algorithm neural network (GANN), the economic prediction model of high-tech industry is constructed, and its innovations are as follows:

(1) In this paper, GANN is introduced to overcome some shortcomings of NN in economic forecasting. Combining the two methods, GA, with its unique characteristics, effectively overcomes the shortcomings brought by NN using gradient-descent method. In this paper, GANN is applied to the economic forecast of high-tech industries and good results are obtained.

(2) In view of the large scale of modern industrial economy and the uncertainties such as nonlinearity and time-varying brought about by globalization, this paper puts forward the research assumption of intelligent modeling and prediction. Combining structural self-organizing genetic optimization NN with reinforcement learning theory and method, the economic prediction model of high-tech industry is studied. The growth rate data and time-window series data of economic indicators are introduced into the constructed NN input layer unit, which improves the generalization ability of the established NN model.

The research content and structure of this paper are mainly divided into five chapters:

The introduction is the first chapter. This section introduces the paper's research background, significance, contents, and methods. The second chapter primarily summarizes and examines related literature from both within and outside the United States. Based on these documents, the second chapter introduces the innovation and research methods in general. The third chapter focuses on related theoretical high-tech industry development research and the development of a genetic optimization economic forecasting model. Section 3.1, for example, examines the concept connotation of high-tech industry and summarizes the basic theories relating to its development. In addition, the contents of artificial neural network (ANN) and GA were introduced. The construction method and implementation of the GANN model are discussed in Section 3.2. The experimental analysis section is covered in the fourth chapter. The actual test is carried out in this section, and the test results are obtained, based on the relevant data. The model's performance is evaluated in comparison to the experimental results of other models. The fifth chapter concludes with a prognosis. This section primarily reviews the main contents and findings of economic forecasting model research, summarizes the findings, and suggests future research directions.

2. Related Work

The scope of China's high-tech industries and their products was determined by Zeng et al., who also analyzed the characteristics of high-tech industries, as well as the conditions and methods of developing high-tech industries and outlined the basic theories related to high-tech industry development [13]. Kuo et al. proposed a construction scheme for a stock price forecasting system based on the vector error correction model [14] based on previous research in the field of economic forecasting and early warning. Liu et al. proposed a rolling grey model economic forecasting algorithm based on particle swarm optimization [15] to address the uncertain subjective factors in economic forecasting and control. To predict the industrial economy, Yuan et al. developed a GA-based BPNN model and compared it to a regression analysis model [16]. Claveria et al. used special processing methods to create a general economic forecasting model by combining the characteristics of economic time series. And then use this model to forecast economic data [17]. For the control and prediction of regional macroeconomics, Rossi et al. developed a prediction model based on the intelligent NN algorithm. Modeling and predictive control methods are proposed to be improved [18]. The NN model is used for multivariate time-series forecasting, according to Zhao et al., and its accuracy and trend are better than traditional statistical methods. The experimental results show that the method is feasible and that it has a higher prediction accuracy than one-shot modeling [19]. The use of NN for multivariate time-series forecasting and multivalue forecasting was investigated by Qiu et al., who discussed the modeling mechanism and multivalue forecasting of this method, as well as its application in stock price forecasting [20]. Ince et al. discussed the NN-based time-series prediction model's establishment mechanism, then proposed adaptive time-series modeling and prediction based on a combination of the time difference method and the BPNN method and experimented with the foreign exchange rate problem as an example [21]. According to Fameliti et al., there is currently little systematic evidence that NN methods are better than traditional time-series forecasting methods in some areas. As a result, before using NN for prediction, it must be rigorously compared to traditional statistical methods to demonstrate that NN is indeed superior and then it is a wise decision to use it [22]. Shang et al. investigated the economic forecasting method, classification, and forecasting accuracy evaluation index, as well as developing a forecasting model for key macroeconomic indicators [23]. Talaat et al. proposed a new load-forecasting algorithm, the GANN optimization forecasting method [24], by combining GA and ANN. Using corporate financial data, Ding et al. developed a new discrete grey multivariate model to predict the output value of China's high-tech industries [25].

In this paper, some opinions and ideas are presented based on the predecessors' research on NN and economic forecasting models, and a high-tech industry economic forecasting model based on GANN is established. The structure and weights of GANN are used in this paper, and the NN learning algorithm is used to iterate several steps, with the network average error after iteration being used to calculate individual fitness values. Near this point, the NN learning algorithm is in charge of some quick local searches, and GA is in charge of global searches. The competition mechanism is used to adjust the structure of NN automatically. The distribution and adjustment of weights are further optimized while adjusting the structure, demonstrating more intelligence and better self-organization, self-adaptation, and self-learning ability. It not only eliminates the large approximation error caused by the fixed network model structure, but it also improves control and prediction. In this paper, GA is used to combine NN models, which overcomes the problem that NN models are prone to local minima. The simulation results show that this model's economic forecasting of the high-tech industry has a high predictive effect.

3. Methodology

3.1. High-Tech Industry and GANN Algorithm. High-tech industry refers to an industry with high knowledge and technology density, rapid industrial development, high added value and high benefit, and a certain market scale and great influence on related industries. High-tech industry is the core of all industries in the era of "knowledge economy", the most important motive force for a country or region to gain long-term competitive advantage, and the driver of sustainable development of social economy. High-tech industry is the crystallization of the highest scientific wisdom and technology of mankind, reflecting the highest level of human production activities and management [26]. At present, the high-tech industry is developing well, and it has become an important force for mode change, structure adjustment, and steady growth. There are usually two ways to develop high-tech industries: first, based on high-tech, develop the high-tech products and form new high-tech industries. The second is to transform traditional industries with high technology. At present, we should give full play to the leading role of high-tech industries in stabilizing growth and restructuring and promote the rapid and healthy development of high-tech industries. Therefore, scientific and accurate prediction of high-tech industries is of great practical significance for government departments to grasp the future economic operation and formulate development strategies.

With the development of high-tech industries and the constant changes of society, how to establish a scientific economic forecasting system for high-tech industries, improve forecasting efficiency and accurately predict the possible development trend of industrial economy in the future has become the main goal of current research [27]. As a nonlinear calculation model, ANN expands the concept and approach of "calculating" the possibility of nonlinear systems. Its basic principle of simulating human brain and its high dimension, distributed storage and processing of neurons, self-organization, self-adaptation, and learning ability are especially suitable for economic information processing in complex modern social and economic systems [28]. The basic structural unit of ANN is neuron, which is also called node. It simulates the structure and function of biological neuron. According to the different connection modes of neurons, NN with various structures can be formed. ANN has four basic characteristics: (1) Parallel distributed processing, (2) learn through training, (3) nonlinear mapping, and (4) adaptation and integration.

Economic forecasting is essentially the forecasting of economic time series, which is a collection of unique data. The previous number will have an influence on the latter number in this set of data, and this influence can be expressed as a certain trend change or periodic change, for example. The influence relationship is usually nonlinear, and establishing a quantitative and fixed mathematical relationship is difficult. ANN is a nonlinear science. It has parallel processing, fault tolerance, and self-learning capabilities, which distinguishes it from traditional statistical methods and allows it to effectively solve such problems. This paper introduces GA as a solution to NN's shortcomings. GA refers to a collection of random search heuristic parallel algorithms [29]. The GA algorithm selects several search points at random and then conducts parallel searches from each of these search points, with the goal of obtaining points with higher-objective function values. Only the fitness guides and executes the search process repeatedly. The search points have high fitness and are close to the optimal solution after many times or generations of evolution. In NN, feed-forward NN is a common hierarchical structure. NN with various functional characteristics can be formed using various neuron transfer functions, hidden layers, and weight adjustment rules. An input layer, an output layer, and a hidden layer between the input and output layers comprise the BPNN [30]. Only one hidden layer exists in the most common NN. The goal of applying GA to BPNN is to improve learning accuracy and iteration speed, as well as to better match biological systems. Figure 1 depicts the flow of the GANN algorithm.

By learning and training the samples, NN can constantly change the connection weights and topology of the network, ensuring that the network's output is close to the expected output. The forward NN algorithm has good local searching and climbing abilities, but it is easy to converge to the local minimum, so it is necessary to improve global convergence. To find a solution that can jump out of the local extremum and converge to the global optimal solution, the GA crossover operator and mutation operator are used. In this paper, we combine GA and NN to create an algorithm that converges quickly and finds the global optimal solution. Encoding is the process of mapping the representation of a search space solution to the representation of a genetic space solution in GA; decoding is the process of mapping the representation of a search space solution to the representation of a genetic space solution. Individuals or chromosomes are the solutions of genetic space, and multiple individuals form a group. In GA, there are several key parameters to consider, including population capacity, replacement ratio, and crossover operator. We must adjust the parameter values for different problems because the optimal values of these parameters vary from problem to problem and cannot be obtained using fixed rules.

3.2. Construction of Economic Forecast Model of High-Tech Industry. The system applied in this paper is nonlinear, and the selection of initial weights follows the following principles: take random values and ensure that the weights are relatively small, and the output value of each neuron after initial weighting is close to zero, which can ensure that the weights of each neuron can be adjusted where their S-shaped activation function changes the most. The system is time-varying and time-delayed, so each data sample should have a different weight. For economic forecasting, the data close to the year to be forecasted should have a greater weight. In the concrete implementation, GA is used to learn the weights and offsets between layers of feed-forward network. Arrange the weights and offset values in order and generate chromosomes according to certain coding rules. In addition to the change of the connection coefficient with other neurons, the number of neurons in the middle layer can also be randomly adjusted within a certain range according to the specific situation. Once the prediction NN is preliminarily determined, its input layer and output layer will not change. GANN-based economic forecasting system and its subsystems are shown in Figure 2.

The learning rate adaptive gradient-descent method with additional momentum term is used to train the network. For each NN and its training data, there is a suitable learning rate. However, different learning rates may be required in different parts of the error surface for complex network models. When there is a large prediction error and the network needs to be corrected, the middle hidden layer is the first thing to adjust and change. A sufficient data supply is required for the establishment of multilayer forward NN. The data are primarily used to train the network and determine weights, but it is also used to check and verify the network's correctness. As a result, the information provided must be divided into two sections: training and experiment. After the decoded weights and offset values of chromosomes are substituted into the network, the fitness function is defined as the difference between the actual output and the expected output. Through GA, a new generation of people will be created on a regular basis, while those who are not fit will be weeded out. The inheritance is terminated if a specific termination condition is met. The weight and offset corresponding to the chromosome with the best fitness are currently the network's optimal solution.

Let the number of neurons in the input layer be n, the output layer be m, and the hidden layer be p. Then the output formula of the hidden layer is as follows:

$$x_i^1 = f\left(\sum_{j=1}^{n} w_{ij}^0 x_j + w_{i0}^0\right), \quad i = 1, 2, \ldots, p. \tag{1}$$

Among them, x_i^1 is the output of neurons in the hidden layer, and $\sum_{j=1}^{n} w_{ij}^0 x_j + w_{i0}^0$ is the weighted sum of all neurons in the input layer. w_{ij}^0 is the weight coefficient of input neuron j to i. w_{i0}^0 is the threshold of neuronal i. f is a nonlinear excitation function. The calculation formula of the neuron output value of the output layer is as follows:

$$y^k = f\left(\sum_{j=1}^{p} w_{jk}^1 x_j^1 + w_{k0}^0\right), \quad k = 1, 2, \ldots, m. \tag{2}$$

In addition, the output layer neuron error function is as follows:

$$E = \frac{1}{2} \sum_k \left(d^k - y^k\right). \tag{3}$$

Among them, d^k is the target value. After calculating the error value of each node by layer-by-layer back-propagation error, the error is corrected. The weighted correction formula is as follows:

$$\Delta w_{ij}^m = \eta \delta_j^m y_j^{m-1}. \tag{4}$$

Among them, w_{ij}^m is the weight coefficient; y_j^{m-1} is the output value of the neuron, η is the learning rate, and δ_j^m is the error signal. Define the error function E_p as the sum of squares of errors between the expected output d_{pi} and the actual output y_{pi}:

$$\begin{aligned} E_p &= \frac{1}{2} \sum_{i=1}^{N_{L+1}} \varepsilon_{pi}^2 \\ &= \frac{1}{2} \sum_{i=1}^{N_{L+1}} \left(d_{pi} - y_{pi}\right)^2. \end{aligned} \tag{5}$$

It is hoped that E_p can be reduced as much as possible, so that the actual output value can be as close to the expected

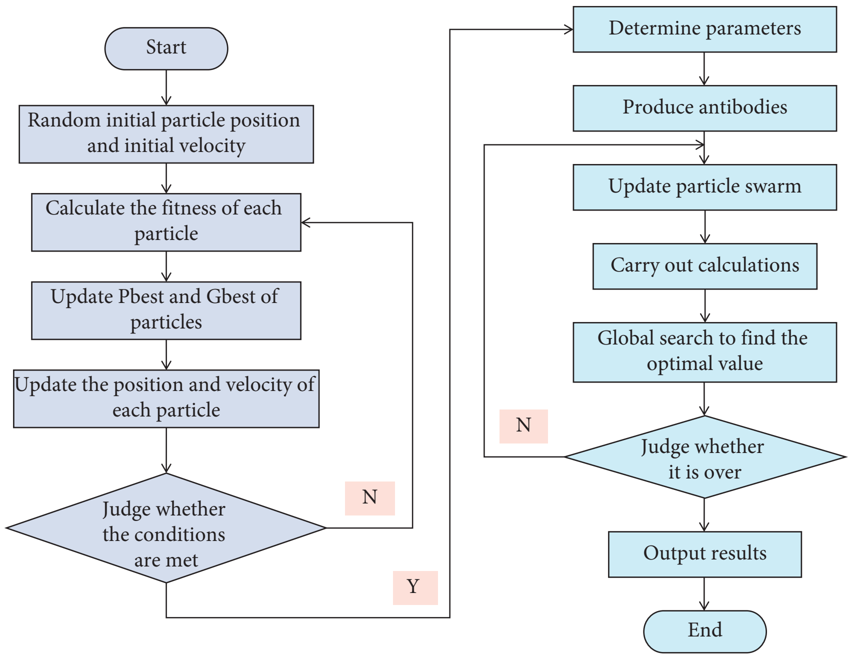

Figure 1: GANN algorithm flow.

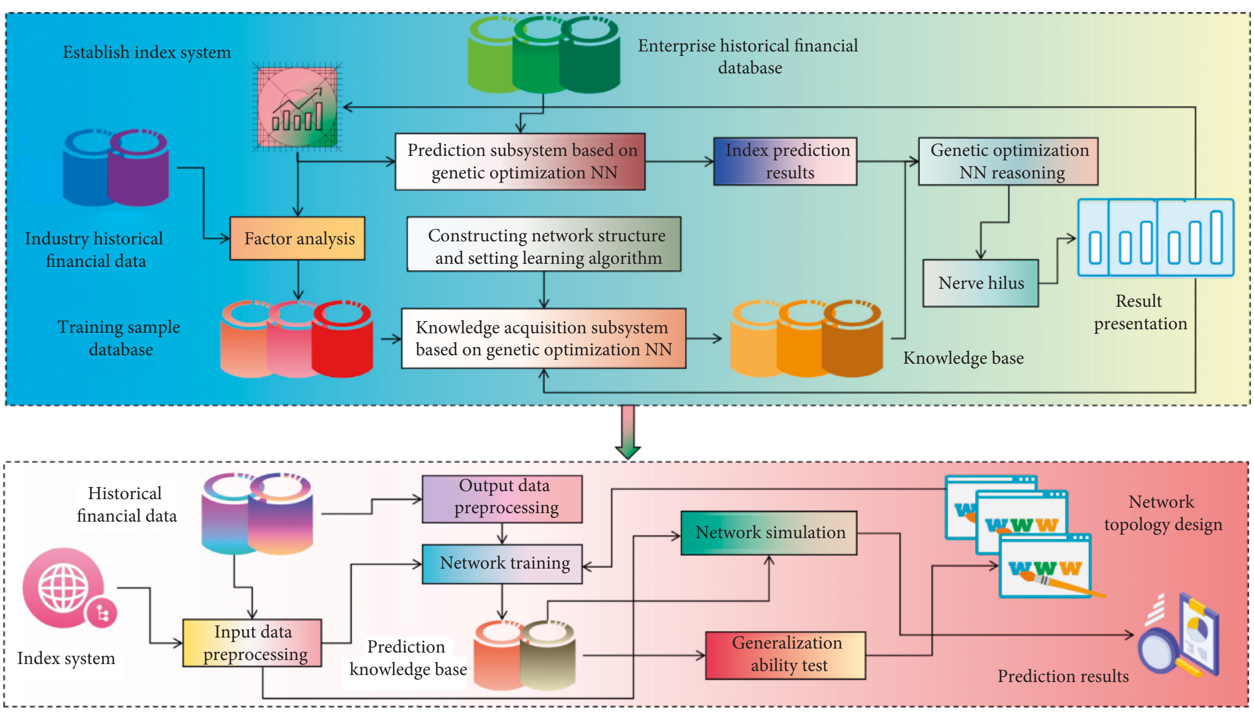

Figure 2: The composition of the GANN-based economic forecasting system and its subsystems.

output value as possible. This is actually the problem of finding the minimum value of the error function, and the steepest descent algorithm can be used to make the weight coefficients change along the negative-gradient direction of the error function. The adjustment amount of the weight coefficient $W_{ij}^{(l)}$ can be calculated as follows:

$$\Delta_p W_{ij}^{(l)} = -a \frac{\partial E_p}{\partial W_{ij}^{(l)}}, \quad a > 0, \tag{6}$$

In the formula, a is the learning stride, which changes with the learning process. $l = 1, 2, \ldots, L$; $i = 1, 2, \ldots, N_{l+1}$; $j = 1, 2, \ldots, N_{l+1}$.

The test data are used to determine the prediction error of the established network, and the training data are used to establish the network. The middle layer should be adjusted if the error exceeds the allowable range. When correcting the network's weight, the additional momentum method takes into account not only the effect of error on the gradient but also the influence of changing trend on the error surface. The network may fall into shallow local minima without additional momentum, but it is possible to slip through these minima with additional momentum. At the same time, making the middle layer dynamic is critical for accurate economic time-series prediction. Unlike when using NN in scientific calculations, the prediction point of NN prediction is always outside the training data, making it difficult to control the error. Furthermore, some economic fields, such as stock market fluctuations, change at a rapid pace, necessitating dynamic models to keep up.

When calculating the fitness of genetic algorithm, the reciprocal of neural network error is used to evaluate the fitness of the network, namely,

$$\begin{aligned} \text{fitness} &= \frac{1}{S_{se}}, \\ S_{se} &= \frac{1}{2}\sum_{i=1}^{k}\sum_{j=1}^{n}\left(d_{ij} - o_{ij}\right)^2, \end{aligned} \tag{7}$$

where d is the standard output, o is the actual output, k is the number of input patterns contained in the training set, and n is the number of neurons in the output layer.

Establish an initial group. The number of individuals in the population is between 45 and 65, and the length of individuals is the product of the sum of weights and offsets of NN and the number of digits occupied by a code, and the genes of individuals are randomly selected within a predefined range. The information provided by an input neuron is not enough to establish an accurate network model to simulate complex nonlinear relationships. At the same time, the input values should show the curve characteristics of fluctuation. Therefore, in addition to expanding the one-dimensional time series, the input data should be preprocessed. On the contrary, the goal of prediction determines the single output characteristic of the network. If the total input of neurons is too far from the threshold, the modification of weights will be very small, which will not only slow the learning speed, but also make it difficult for the network to converge. At the same time, small numerical information may be overwhelmed by large numerical information. Therefore, before NN prediction, in order to avoid network paralysis caused by too large raw data, the raw data should be normalized. For the predicted value, it is not suitable to be directly used as the output of NN because of the large change range. GA algorithm is used to optimize the combination of weights and parameters of ANN model repeatedly. The goal is to set a small load error, with the hybridization rate of 0.4 and the variation rate of 0.005. According to the value range of the parameter set and the set number of individuals, the initial population is randomly generated, and the fitness value of each individual is calculated. Through systematic cluster analysis, the population is divided into several populations, and the average fitness of each population is calculated, and some individuals with the best fitness value are selected as the representatives of the population to breed the next generation.

For the same forecast project, the size of the mean square error can be used to measure the quality of different forecasting methods. For different forecast items, due to their different actual values, only comparing the size of the mean square error cannot explain the problem. At this time, $E(|e|/x)$ should be used as the comparison standard, which is called the predicted mean absolute percent error (MAPE). It is estimated by retrospective forecasting, and its estimator is as follows:

$$\text{MAPE} = \frac{1}{n}\sum_{i=1}^{n}\frac{|e_i|}{x_i}. \tag{8}$$

In the NN model, in order to prevent the situation that the fitting of the learned data is good and the fitting of the nonlearned data is not good, rolling learning and prediction are adopted, and the minimum sum of the error of learning and prediction is the evaluation mark of the success of the model. Generally, the quality of prediction results is measured by MAPE. Table 1 gives the prediction accuracy range of MAPE.

Select the individual with the best fitness value in each population to continue the genetic operation until the fitness of the solution is no longer significantly increased. At this time, the decoded parameter combination is close to the best combination that meets the application needs. On this basis, the BP algorithm of ANN is used to further accurately optimize the network parameters obtained above, until the optimal network parameters are found, and then the precise optimal parameter combination can be obtained. Owing to the singularity in NN training, the results of each training will be slightly different. This also means that the prediction result of NN will be a range value, so it is necessary to evaluate the prediction result, and get the reliability and risk degree of the prediction. As GA replaces the initial optimization of NN, the network only optimizes the parameters on the basis of approaching the optimal solution, thus effectively improving the optimization speed and accuracy of the network. GA-based NN model is used in prediction. That is, the model prediction result is used as input and the actual value is used as output, and a mapping relationship is established between the model prediction result and the actual value. After continuous learning and testing, the network is applied to the economic forecast of high-tech industry to get the final forecast result.

4. Result Analysis and Discussion

Through theoretical analysis, the economic factors related to the GDP of high-tech industries are: labor input and capital input. Based on the GDP data of high-tech industries in a province from 2010 to 2020, this paper establishes a prediction model. MATLAB software has powerful functions of numerical calculation, data visualization, graphic drawing,

Table 1: Prediction evaluation based on MAPE.

Scope of MAPE	Prediction and evaluation
MAPE ≤ 8%	High precision prediction
8% ≤ MAPE ≤ 25%	Good prediction
25% ≤ MAPE ≤ 55%	Feasible prediction
MAPE ≥ 55%	Misprediction

and so on, which brings great convenience to users. In this paper, the NN toolbox based on MATLAB is implemented in full software. The network training involves the generalization ability of the network. The so-called generalization ability refers to the ability of NN to correctly reflect the new sample data other than the training samples. In this paper, the available samples of the training set are randomly divided into two parts: one part as the training set and the other part as the test set. Taking eight samples from 2010 to 2017 as training samples and three samples from 2017 to 2020 as test samples, the established prediction model is tested.

The fitness function is used to evaluate the superiority and inferiority of individual solutions, so as to breed or select individuals. The fitness function is not bound by continuously differentiable condition, and the domain of the function can be any set. The only requirement for the fitness function is that the input can be compared with the output. For time-series prediction, the number of input nodes can be obtained by the following methods: changing the number of input nodes from small to large, and training and testing its accuracy. When the error does not decrease further with the increase of the number of input nodes, the critical value of the change of the number of input nodes is the numerical value to be adopted. We use various forecasting methods, such as Arima model, Stepar model, and Winters model, to forecast the economy, respectively. These prediction methods are compared with this GANN prediction method, and the results are shown in Table 2.

Draw representative MAPE results into line charts, as shown in Figure 3.

As a result, this algorithm outperforms the others. Dynamic NNs are those that have feedback, whether local or global. The weights and thresholds of the network can be changed, and the structure of the network, that is, the number of nodes in the input layer, hidden layer, and output layer, can be changed, so that the network is not only dynamic, but also the retained system information is more complete. After the BPNN has been generated and initialized, the network can be trained using the existing "input-output" sample vector data. The train function completes the BP network training, and the network training parameters are properly set prior to training. The train function is used to train the BP network after the training parameters have been set. The network training will alternate between training and testing, with the mean square error of each training recorded. The network weight will then be left unchanged, and the network simulation will be run forward with the test data, with the test mean square error recorded once. The curves of two kinds of mean square errors with training times can be drawn using the two types of data, as shown in Figure 4.

From the error curve, it can be seen that before a certain number of training times, with the increase of training times, the two curves decrease simultaneously. When this number of training times is exceeded, the training error continues to decrease, while the test error begins to rise. This training number is the best training number.

Mutation operation refers to the change between 0 and 1 in some bits when an individual generates the next generation. It plays the role of local search in GA, which increases the ability of GA to search the optimal solution. Appropriate mutation strategy can improve the diversity of individuals in the population, thus preventing GA from falling into local solution and terminating evolution. The preprocessing of input data is the key step to effectively train NN, which directly affects the performance of the trained network. In this paper, the mean and variance of the sample set data are standardized so that the mean is zero and the variance is 1. When there is new data input, we think it has the same distribution as the training sample data, so we can convert it according to the aforementioned formula. In this paper, some measures are taken to improve NN from the learning rate adaptive network learning with additional momentum term, the principle of minimizing empirical risk and the principle of minimizing structural risk, and so on, so as to make the NN model closer to the actual economic operation. Figure 5 shows the comparison result of recall rate of the algorithm.

It can be seen from Figure 5 that the recall rate of the algorithm in this paper is higher than that of the other two algorithms, and the recall rate of the algorithm in this paper is better. Research and analyze the factors that affect the industrial technical and economic indicators, and determine some important factors as the input elements of the network. Analyze and determine some main technical and economic indicators of the enterprise as the output elements of the network, that is, the indicators that need to be predicted. Taking the influencing factors of the industry to be predicted as the input elements of the grid, input them into the model for pattern matching inference, and finally output the expected predicted value of technical and economic indicators. According to various typical rules for modifying network weights and the network training process, various network design and training subroutines are written in MATLAB language. We can call the NN design and training in the toolbox according to our own needs. Program, so that you can free yourself from tedious programming and concentrate on thinking and solving problems, thereby improving efficiency and the quality of problem solving. We compare the economic forecast results using our model with the actual values, and the results are shown in Figure 6.

In order to ensure the generalization ability of the network, the error accuracy cannot be improved only by the number of training, and the test of the test data error is appropriately added in the training process, which can stop the network training in advance and prevent over-training. Although this method sometimes cannot achieve the preset error accuracy, it ensures the good generalization ability of the network, thus making the prediction more effective.

Table 2: Comparison of different methods.

Method	Square sum error	Mean absolute error	Mean square deviation	Average percentage error	Mean square percentage error
Arima model	2216.8	4.59	0.54	3.11	0.53
Stepar model	2119.6	3.78	0.29	3.63	0.55
Winters model	1987.2	3.96	0.37	2.26	0.42
GANN model	214.9	2.13	0.21	1.01	0.31

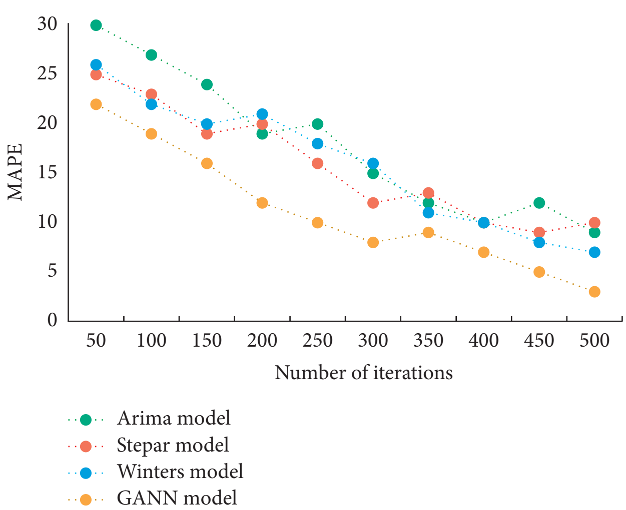

Figure 3: Comparison of MAPE results of different algorithms.

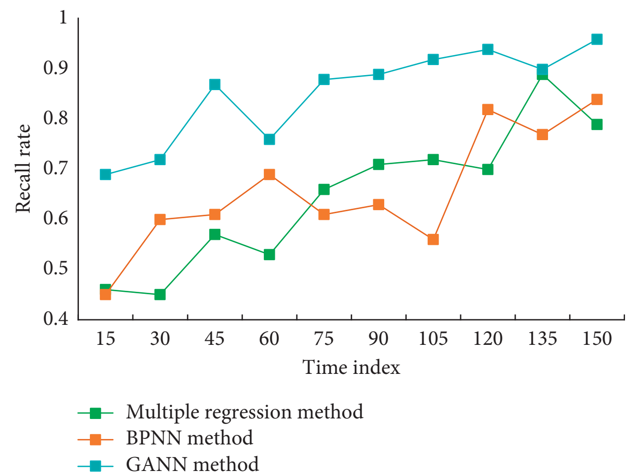

Figure 5: Comparison of recall rates of algorithms.

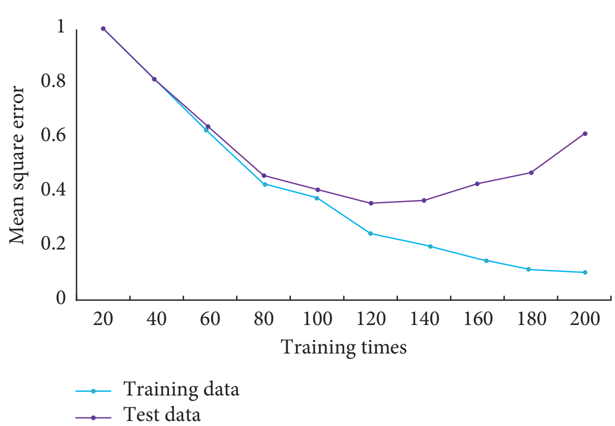

Figure 4: Network output error change diagram.

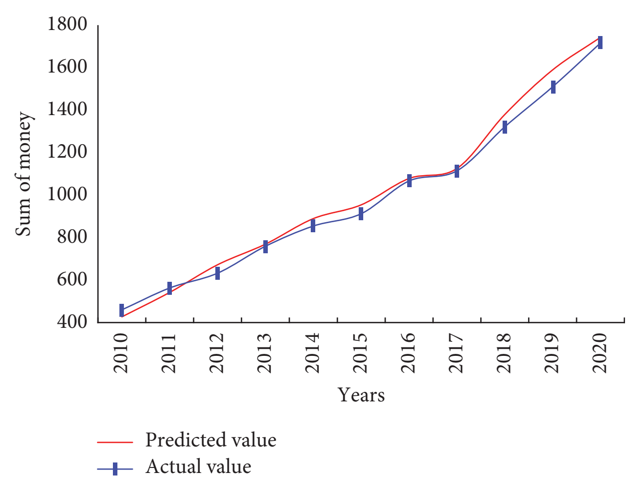

Figure 6: Comparison of predicted and actual values.

Owing to the increasing trend of economic system index data year by year, it is easy to fall into the blind spot of prediction using historical data values to train network models and applying the trained models for prediction. Therefore, we introduce an economic indicator growth rate input node in the network input unit to improve the generalization ability of the NN. As long as the input data of the validation sample set is predicted, it can ensure that the nerve does not fall into the training blind spot. The multiple regression method, BPNN method, and GANN method are used to compare the economic forecasts of high-tech industries. The results are shown in Figure 7.

The comparative analysis of the prediction results shows that the prediction accuracy of the multiple regression method is low, and the highest is only 83.21%. The prediction accuracy of BPNN method is better, the highest is 89.17%. The GANN method proposed in this paper has the best prediction accuracy, up to 95.14%. This result further verifies the feasibility and practicability of the method in this paper. From the comparison of system modeling and prediction results, it can be seen that after using GANN, expanding the sample set, and introducing time-series data input units, the NN model meets the requirements of economic system

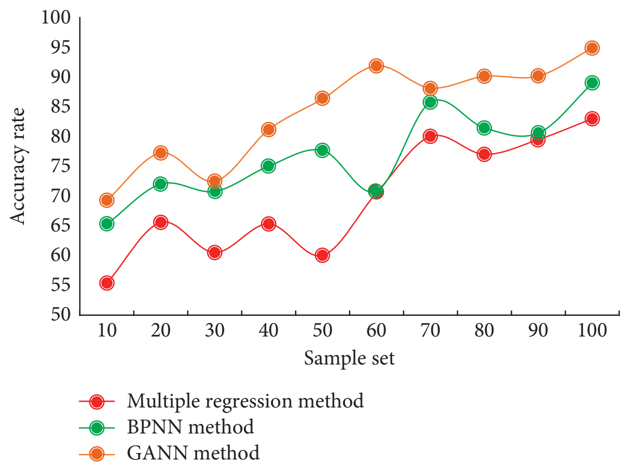

Figure 7: Economic forecast results of different models.

modeling and prediction. The generalization ability of the GANN constructed in this paper has been greatly enhanced, and the system time-varying delay problem has been solved. The experimental results show that the prediction accuracy of the model in this paper reaches 95.14%, and a satisfactory prediction effect is achieved.

5. Conclusion

At present, the development of high-tech industry has become an important indicator to measure the comprehensive national strength, economic strength, and scientific and technological strength of a country or region. Therefore, scientific and accurate prediction of high-tech industries is of great practical significance for government departments to grasp the future economic operation and formulate development strategies. This paper adopts NN modeling method to study the establishment of economic forecasting model of high-tech industry, introduces GA to optimize NN and gives specific implementation steps. The construction scheme of this paper fully reflects the advantages of combining GA and NN technology in economic forecasting and has strong normative and operability. In order to verify the performance of the model, through simulations, predictions are made for the instances. The results show that the algorithm in this paper has faster convergence speed and greater generalization ability, and the average error rate is reduced to about 1%. The algorithm improves the learning and prediction accuracy of NN, and its accuracy reaches 95.14%. At the same time, the good flexibility makes it well suited to many economic forecasting fields. The research of this paper provides a certain basis for the economic forecast of the high-tech industry and the government's regulation of economic growth and has certain practical significance. The construction idea of this paper has certain reference value for most enterprises to construct their own economic forecasting system. However, due to the limitation of knowledge level, time and energy, there are still some problems in this paper. For example, the entire economic forecasting system is based on the authenticity of the data. If the original data are not true, the final forecast result will not have a reference. Value; since the network is dynamic, the number of neuron nodes and the number of hidden layers are adjusted during the training process, which also makes it difficult to prove the stability of the network. These problems need to be expanded and further researched to solve.

Data Availability

The data used to support the findings of this study are available from the corresponding author upon request.

Conflicts of Interest

The authors do not have any possible conflicts of interest.

Acknowledgments

This research was funded by the Shanghai Sailing Program (grant no. 20YF1433800).

References

[1] M. D. Mainar-Toledo, M. A. Castan, G. Millán et al., "Accelerating sustainable and economic development via industrial energy cooperation and shared services - a case study for three European countries," *Renewable and Sustainable Energy Reviews*, vol. 153, Article ID 111737, 2022.

[2] J. Zhao, H. Tian, and D.-a. Li, "Channel prediction based on BP neural network for backscatter Communication networks," *Sensors*, vol. 20, no. 1, p. 300, 2020.

[3] G. Xie, L. Huang, C. Apostolidis, Z. Cai, W. Li, and G. au, "Assessing Consumer Preference for Overpackaging solutions in E-commerce," *International Journal of Environmental Research and Public Health*, vol. 18, no. 15, p. 7951, 2021.

[4] L. Huang, Y. Huang, R. Xie, G. Cai, and W. au, "Factors influencing Returning Migrants' Entrepreneurship Intentions for Rural E-commerce: An empirical investigation in China," *Sustainability*, vol. 14, no. 6, p. 3682, 2022.

[5] D. Wang, H. Luo, O. Grunder, Y. Lin, and H. Guo, "Multi-step ahead electricity price forecasting using a hybrid model based on two-layer decomposition technique and BP neural network optimized by firefly algorithm," *Applied Energy*, vol. 190, no. 3, pp. 390–407, 2017.

[6] J. Kong, H. Wang, C. Yang, X. Zuo, M. Zhang, and X. au, "A Spatial Feature-enhanced Attention neural network with high-order Pooling representation for Application in pest and Disease recognition," *Agriculture*, vol. 12, no. 4, p. 500, 2022.

[7] D. Yao, Z. Zhi-li, Z. Xiao-feng et al., "Deep hybrid: multi-graph neural network collaboration for hyperspectral image classification," *Defence Technology*, 2022, In press.

[8] Y. Ding, X. Zhao, Z. Zhang, W. Cai, N. Yang, and Y. Zhan, "Semi-supervised locality preserving dense graph neural network with ARMA filters and context-aware learning for hyperspectral image classification," *IEEE Transactions on Geoscience and Remote Sensing*, vol. 60, 2021.

[9] J. Zhou, Y. Wang, and W. Zhang, "Underwater image Restoration via information distribution and light scattering prior," *Computers and Electrical Engineering*, vol. 100, Article ID 107908, 2022.

[10] X. Gu, W. Cai, M. Gao, Y. Jiang, X. Ning, and P. Qian, "Multi-source domain transfer discriminative dictionary learning modeling for electroencephalogram-based emotion

recognition," *IEEE Transactions on Computational Social Systems*, In Press, 2022.
[11] J. Zhou, X. Wei, J. Shi, and W. Zhang, "Underwater image enhancement method with light scattering characteristics," *Computers and Electrical Engineering*, vol. 100, Article ID 107898, 2022.
[12] W. Xiao, J. Dai, H. Wu, and G. Cheng, "Effect of meteorological factors on photovoltaic power forecast based on the neural network," *RSC Advances*, vol. 7, no. 88, pp. 55846–55850, 2017.
[13] L. Zeng, "Analysing the high-tech industry with a multivariable grey forecasting model based on fractional order accumulation," *Kybernetes*, vol. 48, no. 2, 2018.
[14] C.-Y. Kuo, "Does the vector error correction model perform better than others in forecasting stock price? An application of residual income valuation theory," *Economic Modelling*, vol. 52, no. 1, pp. 772–789, 2016.
[15] L. Liu, Q. Wang, J. Wang, and M. au, "A rolling grey model optimized by particle swarm optimization in economic prediction," *Computational Intelligence*, vol. 32, no. 3, pp. 391–419, 2016.
[16] Z. Yuan, W. Wang, H. Wang, and S. au, "Combination of cuckoo search and wavelet neural network for midterm building energy forecast," *Energy*, vol. 202, Article ID 117728, 2020.
[17] O. Claveria, E. Monte, and S. Torra, "Economic forecasting with evolved confidence indicators," *Economic Modelling*, vol. 93, pp. 576–585, 2020.
[18] B. Rossi, "A review ofEconomic forecasting," *The Econometrics Journal*, vol. 19, no. 3, pp. B1–B3, 2016.
[19] J. Zhao, X. Li, Y. Liu, X. Zhou, and C. au, "Ionospheric foF2 disturbance forecast using neural network improved by a genetic algorithm," *Advances in Space Research*, vol. 63, no. 12, pp. 4003–4014, 2019.
[20] M. Qiu and Y. Song, "Predicting the direction of stock market index Movement using an optimized Artificial neural network model," *PLoS One*, vol. 11, no. 5, Article ID e0155133, 2016.
[21] H. Ince, A. F. Cebeci, and S. Z. Imamoglu, "An Artificial neural network-based Approach to the Monetary model of exchange rate," *Computational Economics*, vol. 53, no. 2, pp. 817–831, 2019.
[22] S. P. Fameliti and V. D. Skintzi, "Predictive ability and economic gains from volatility forecast combinations," *Journal of Forecasting*, vol. 39, no. 2, pp. 200–219, 2020.
[23] Y. Shang and T. Zheng, "Fitting and forecasting yield curves with a mixed-frequency affine model: evidence from China," *Economic Modelling*, vol. 68, no. 1, pp. 145–154, 2018.
[24] M. Talaat, M. A. Farahat, N. Mansour, and A. Y. Hatata, "Load forecasting based on grasshopper optimization and a multilayer feed-forward neural network using regressive approach," *Energy*, vol. 196, no. 4, pp. 117087.1–117087.12, 2020.
[25] S. Ding, "A novel discrete grey multivariable model and its application in forecasting the output value of China's high-tech industries," *Computers & Industrial Engineering*, vol. 127, no. 1, pp. 749–760, 2019.
[26] J. Wu and X. Xing, "Rainfall forecast and computer data algorithm optimization in coastal areas based on improved neural network," *Arabian Journal of Geosciences*, vol. 14, no. 15, 2021.
[27] Y. Zhang, "Application of improved BP neural network based on e-commerce supply chain network data in the forecast of aquatic product export volume," *Cognitive Systems Research*, vol. 57, no. 10, pp. 228–235, 2019.
[28] P. Singh and P. Dwivedi, "Integration of new evolutionary approach with artificial neural network for solving short term load forecast problem," *Applied Energy*, vol. 217, no. 5, pp. 537–549, 2018.
[29] Q. Cai, B. Yan, B. Su, and S. Liu, "Short-term load forecasting method based on deep neural network with sample weights," *International Transactions on Electrical Energy Systems*, vol. 30, no. 5, 2020.
[30] A. S. Khaniani, H. Motieyan, and A. Mohammadi, "Rainfall forecast based on GPS PWV together with meteorological parameters using neural network models," *Journal of Atmospheric and Solar-Terrestrial Physics*, vol. 214, no. 1-2, Article ID 105533, 2021.

Hindawi
Computational Intelligence and Neuroscience
Volume 2023, Article ID 9783759, 1 page
https://doi.org/10.1155/2023/9783759

Retraction

Retracted: An Entity Relationship Extraction Model Based on BERT-BLSTM-CRF for Food Safety Domain

Computational Intelligence and Neuroscience

Received 25 July 2023; Accepted 25 July 2023; Published 26 July 2023

This article has been retracted by Hindawi following an investigation undertaken by the publisher [1]. This investigation has uncovered evidence of one or more of the following indicators of systematic manipulation of the publication process:

(1) Discrepancies in scope
(2) Discrepancies in the description of the research reported
(3) Discrepancies between the availability of data and the research described
(4) Inappropriate citations
(5) Incoherent, meaningless and/or irrelevant content included in the article
(6) Peer-review manipulation

The presence of these indicators undermines our confidence in the integrity of the article's content and we cannot, therefore, vouch for its reliability. Please note that this notice is intended solely to alert readers that the content of this article is unreliable. We have not investigated whether authors were aware of or involved in the systematic manipulation of the publication process.

Wiley and Hindawi regrets that the usual quality checks did not identify these issues before publication and have since put additional measures in place to safeguard research integrity.

We wish to credit our own Research Integrity and Research Publishing teams and anonymous and named external researchers and research integrity experts for contributing to this investigation.

The corresponding author, as the representative of all authors, has been given the opportunity to register their agreement or disagreement to this retraction. We have kept a record of any response received.

References

[1] Q. Zhang, M. Li, W. Dong et al., "An Entity Relationship Extraction Model Based on BERT-BLSTM-CRF for Food Safety Domain," *Computational Intelligence and Neuroscience*, vol. 2022, Article ID 7773259, 13 pages, 2022.

Hindawi
Computational Intelligence and Neuroscience
Volume 2022, Article ID 7773259, 13 pages
https://doi.org/10.1155/2022/7773259

Research Article

An Entity Relationship Extraction Model Based on BERT-BLSTM-CRF for Food Safety Domain

Qingchuan Zhang[1,2] **Menghan Li**[1,2] **Wei Dong**[1,2] **Min Zuo**[1,2] **Siwei Wei**[1,2] **Shaoyi Song**[1,2] **and Dongmei Ai**[3]

[1]*National Engineering Research Centre for Agri-Product Quality Traceability, Beijing Technology and Business University, Beijing 100048, China*
[2]*School of E-Business and Logistics, Beijing Technology and Business University, Beijing 100048, China*
[3]*Basic Experimental of Natural Science, University of Science and Technology Beijing, Beijing 100083, China*

Correspondence should be addressed to Wei Dong; dongwei2019@btbu.edu.cn and Min Zuo; zuomin@btbu.edu.cn

Received 14 March 2022; Accepted 5 April 2022; Published 28 April 2022

Academic Editor: Xin Ning

Dealing with food safety issues in time through online public opinion incidents can reduce the impact of incidents and protect human health effectively. Therefore, by the smart technology of extracting the entity relationship of public opinion events in the food field, the knowledge graph of the food safety field is constructed to discover the relationship between food safety issues. To solve the problem of multi-entity relationships in food safety incident sentences for few-shot learning, this paper adopts the pipeline-type extraction method. Entity relationship is extracted from Bidirectional Encoder Representation from Transformers (BERTs) joined Bidirectional Long Short-Term Memory (BLSTM), namely, the BERT-BLSTM network model. Based on the entity relationship types extracted from the BERT-BLSTM model and the introduction of Chinese character features, an entity pair extraction model based on the BERT-BLSTM-conditional random field (CRF) is established. In this paper, several common deep neural network models are compared with the BERT-BLSTM-CRF model with a food public opinion events dataset. Experimental results show that the precision of the entity relationship extraction model based on BERT-BLSTM-CRF is 3.29%~23.25% higher than that of other models in the food public opinion events dataset, which verifies the validity and rationality of the model proposed in this paper.

1. Introduction

Food is the paramount necessity of the people and the material basis for human survival. Food safety is closely related to human health and has always been a concern of the society. With the development of the Internet and the wide application of computers, the Internet has penetrated into people's daily life. People have been accustomed to expressing their opinions on the Internet, so online public opinion has become an important channel to reflect social problems. Especially in recent years, food safety issues, such as dyed steamed buns, expired meat, poisoned bean sprouts, and other incidents have aroused high public concern. Some food safety incidents were not noticed until they were exposed on the Internet and finally solved. It can be seen that online public opinion is particularly important for the governance of food safety issues.

With the progress of society and the awakening of people's health consciousness, people's demand for improving medical technology and enhancing health is more urgent. In the actual industrial development, China's smart healthcare is still in its infancy [1]. Smart health management is the application of artificial intelligence technology to specific scenarios of health management [2–6]. In terms of risk identification, through the acquisition of information and the use of artificial intelligence technology for analysis, we identify the risk of disease occurrence and provide risk reduction measures. In addition, virtual nurses can collect personal habit information about patients, such as eating habits, exercise cycles, and medication habits, and use artificial intelligence technology to analyze data and evaluate patients' overall status to help plan their daily life.

Therefore, by constructing the knowledge graph of public opinion events in the field of food safety, we can find food safety problems, prompt public opinion problems and give risk warnings, to make the connection between diseases clearer, and patients can receive treatment before complications occur, thus improving the health of patients. Extraction of public opinion events in the field of food safety is one of the important basic tasks in the construction of a knowledge graph in the field of food safety. Tao et al. [7] proposed crowdsourcing and machine learning approaches for extracting entities indicating potential food-borne outbreaks from social media using the dual-task BERTweet model. Mitra et al. [8] adopted a multiview deep neural network model for chemical-disease relation extraction from imbalanced datasets.

However, due to the diversity and universality of diseases caused by food safety incidents, there is a lack of a large number of available corpus in the field of food safety. Therefore, few-shot learning has become an effective method for information extraction. Gao et al. [9] proposed a multitask graph neural network based on few-shot learning for disease similarity measurement. Lu et al. [10] built a few-shot learning-based classifier by limiting training samples for food recognition. Sainz et al. [11] proposed a method of label verbalization and entailment for effective zero and few-shot relation extraction.

Extraction of public opinion events in the field of food safety is one of the important basic tasks in the construction of a knowledge graph in the food safety domain. The purpose is to extract semantic relationships between entities marked in sentences. Entity relationship extraction is mainly used to transform text unstructured data into structured data. The complexity of the entity relationship extraction task and the small sample of corpus lead to the difficulty to complete the task with few-shot learning. For the supervised deep learning model, the model is prone to underfitting due to the small sample corpus. On the other hand, the model is easy to fall into the local optimal solution, resulting in the poor actual effect of the model.

This paper mainly studies an entity relationship extraction method based on BERT-BLSTM-CRF for the food safety domain. Based on few-shot learning, the whole model adopts the pipeline-type extraction method, which is divided into two tasks: entity relationship extraction and entity pair extraction. In the entity relationship extraction network model, the BLSTM network joined the BERT network trains on Chinese corpora, preprocessed to complete the entity relationship extraction task. In the entity pair extraction network model, to add feature information in the BLSTM network, this model puts the entity relationship extracted from the entity relationship extraction model to both ends of the character vector to reinforce the semantic features and obtain the radical feature to join the character vector. The model can not only handle entity overlap well but also effectively use the information of Chinese characteristics.

The rest of the article is organized as follows: Section 2 describes the related work. Section 3 introduces the algorithm proposed in this paper. Section 4 describes the environment we used to validate the algorithm as well as the experimental results and analysis. Finally, Section 5 summarizes this paper.

2. Related Work

The pipeline relationship extraction method [12–15] is popular in entity relationship extraction methods based on deep learning. In recent years, the problem of extracting multi-entity relationships in sentences has attracted the attention of researchers.

Bai et al. [16] proposed to extract local semantic features through word embedding and designed a new fragment attention mechanism based on CNN (convolutional neural network). Compared with the CNN model, the RNN (recurrent neural network) model can deal with distant patterns, so it is particularly suitable for learning relationships in longer contexts. Socher et al. [17] applied the matrix-recursive neural network model (MV-RNN) to natural language processing for the first time, which effectively solved the problem that the word vector model could not capture the constituent meaning of long phrases or sentences.

The long short-term memory (LSTM) network model [18] has the same general framework as the RNN model, which has both forward pathways to transmit information and a self-feeding pathway to process information. However, LSTM allows each neural unit to forget or retain information. To some extent, the problem of vanishing or explosion gradient of RNN is solved. Zhang et al. [19] proposed a location-aware attention mechanism based on the LSTM sequence, which is combined with a kind of entity location-aware attention, to achieve better performance of relationship extraction. Huang et al. [20] proposed a new Chunk Graph LSTM network to learn the representation of solid blocks and infer the relationship between them. Chen and Hu [21] transformed the BLSTM-CRF deep learning model and improved sequence labeling rules.

In the latest research on natural language processing, the BERT model is a kind of network model which performs well in the present research stage. Instead of the traditional one-way language model or the method of shallow splicing of two one-way language models for pretraining, the algorithm adopts the new marked language model, which can generate deep two-way language representation and fine-tune specific downstream tasks [22]. At present, BERT has played an essential role in the research field of natural language processing, such as entity relationship extraction, text emotion analysis, and text classification [23]. Gao et al. [24] proposed a medical relationship extraction model based on BERT, which combined the whole sentence information obtained from the pretrained language model with the corresponding information of two medical entities to complete the relationship extraction task. Qiao et al. [25] proposed an agricultural entity relationship extraction model based on BERT-BLSTM-LSTM, which can effectively extract the relationship between agricultural entities.

In terms of the improvement of the model, Zhang et al. [26] proposed a new multi-label relationship extraction method based on a capsule network, which performed better than existing convolutional networks or cyclic networks in identifying highly overlapping relationships in a single sentence. Hang et al. [27] proposed an end-to-end neural network model for joint extraction of entity and overlap relations. Li et al. [28] proposed a new lightweight neural network framework to solve the problem of remote supervised relationship extraction. Xu et al. [29] proposed a new DocRE code-classifier-reconstruction model to extract document-level relationships and give more attention on the related entity pairs and path reconstruction. Sun and Wu [30] studied joint entity relationship extraction under remote supervision and developed a new adaptive algorithm that could deliver high-quality but heterogeneous entity relationship annotations robustly and consistently.

However, in the papers mentioned above, most studies on entity relationship extraction are based on a large-scale corpus, while in the field of food safety, there is a lack of a large corpus. Moreover, in the literature given above, word vectors are used to represent semantic features of sentences, but unlike the foreign corpus, Chinese entities are usually grouped together in the form of characters. Furthermore, the radical feature of Chinese characters, which can reflect the semantics to some extent, has not been well used.

3. Methods

In Section 3.1, how to carry out manual annotation is introduced. Section 3.2 describes how to construct the radical feature. In Section 3.3, the structure of the BERT-BLSTM-CRF model is introduced and the operating mechanism of the model is shown. In Section 3.4, this paper explains the detail of the extraction process of relationships of Chinese food public opinion event sentences. Section 3.5 introduces the entities extraction model of food public opinion events sentences.

3.1. Manual Annotation. Firstly, entity relationship triples in sentences are extracted as shown in Figure 1, and then, sentences are processed into sequence labels as shown in Figure 2.

Sequence label in single relationship entity extraction consists of three parts, namely, entity boundary, entity relation, and entity role label. The entity boundary label is used by BIO to represent the location information of the element in the entity, where B indicates that the element is at the beginning of the entity, I indicates that the element is in the middle or end of the entity, and O indicates that the element is not an entity. Entity relationship labels in the corpus are shown in Table 1 in Section 4.1. The entity role tag represents the role of the entity in the triple, denoted by 1, 2, 1 for the subject and 2 for the object, for example, (metronidazole in edible duck egg exceeding bid, adverse reaction, nausea).

3.2. Construction of the Radical Feature. At first, Chinese sentences are divided into character units and then converted to radicals according to the correspondence defined

Input sentence: Metronidazoleinedible duck egg exceedingbid can cause nausea.

↓

Extracting result: (Metronidazole in edible duck egg exceeding bid, adverse reaction, nausea)

Figure 1: Manual annotation instance.

in "Specification for Identifying Indexing Components of GB 13000.1 Chinese Characters Set," as shown in Figure 3. For the problem that the simplified radicals are not defined in the word list of the pretrained model during the experiment, some of the simplified radicals are converted into normal Chinese characters by referring to the work of "Specification for Identifying Indexing Components of GB 13000.1 Chinese Characters Set" and the study by Chen and Hu [31].

Formally, each Chinese character f in the sentence is added to Cr. And then, according to the rule of the radical decomposition, the radicals of the input sentence are generated and the radical f_{iv} of each character in the input sentence is added to Cr_v.

$$\begin{aligned} Cr &= [f_1, f_2, f_3, \ldots, f_n], \\ Cr_v &= [f_{1v}, f_{2v}, f_{3v}, \ldots, f_{nv}]. \end{aligned} \tag{1}$$

Then, the vector representation G_r corresponding to the input Cr_v can be obtained through the one-hot method. Finally, we get the radical feature G_r of the input sentence.

$$\begin{aligned} G_r &= \left[g_v^1, g_v^2, g_v^3, \ldots, g_v^n\right] \\ &= \text{one} - \text{hot encoder}\left(Cr_v\right). \end{aligned} \tag{2}$$

3.3. Framework of the BERT-BLSTM-CRF Model. Figure 4 shows the structure of the BERT-BLSTM-CRF network model. The model is divided into left and right parts. Among them, the left half part of the figure shows the relationship extraction process of Chinese food public opinion events sentences. The right half part of the figure shows the extraction process of the entity pair of food public opinion events sentences.

In the relationship extraction model, as shown in the left half of Figure 4, after the sentence is put through the BERT, the character vector is obtained. Then, the BLSTM model which receives the character vector as input outputs the hidden layer vector, and finally, under the activation function of the sigmoid, the multirelationships can be obtained. The implementation details of the model are explained in Section 3.4.

In the entity pair extraction model, as shown in the right half of Figure 4, firstly, we obtain Chinese radicals in the field of Chinese food public opinion events and then get the Chinese radical feature representation by the one-hot method. In the BLSTM model, the character vector participates with the Chinese radical feature representation in the calculation of the intermediate hidden layer, and the entity relationships extracted by the model in left

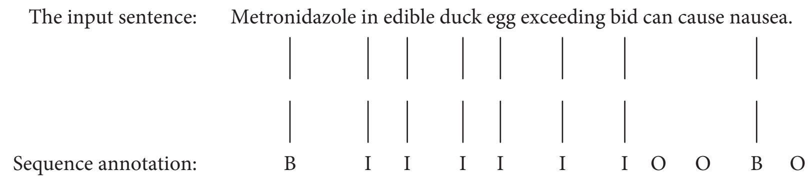

Figure 2: Sequence annotation instance.

Table 1: Definition of relationships for the BBC dataset.

ID	Relation name	Abbreviations
1	Time	TI
2	Scene	SC
3	Name of food	NF
4	Food contaminant	FC
5	Adverse reaction	AR
6	Manufacturer	MF
7	Inspection body	IB

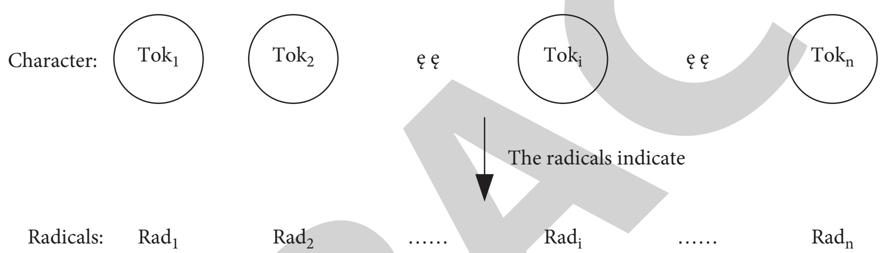

Figure 3: The radical feature construction.

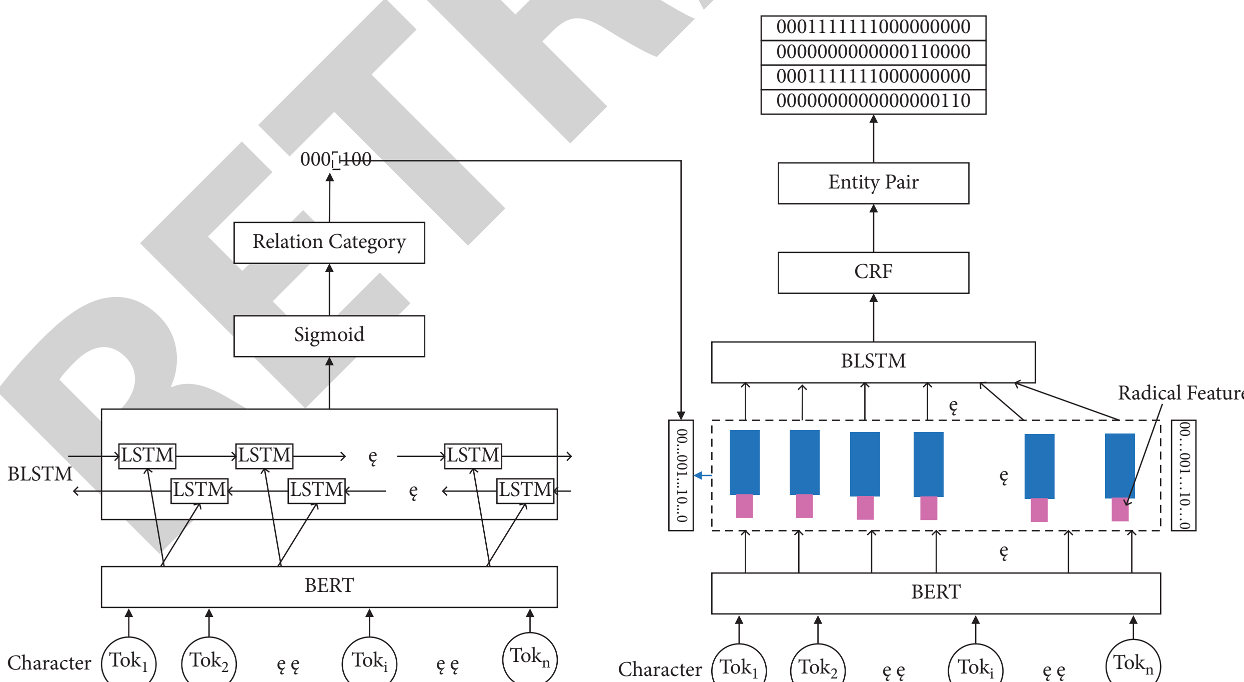

Figure 4: Structure diagram of the BERT-BLSTM-CRF model.

half part are added to the front and end of the hybrid character vector. After the BLSTM model outputs the hidden layer vector, the entity pairs are finally labeled under the function of the CRF method. Section 3.5 will explain the specific implementation process of the model in detail.

3.4. Structure of the Relationship Extraction Model. The internal structure of the relationship extraction model is shown in Figure 5.

In order to strengthen the semantic features of Chinese, this paper chooses the way of character annotation, that is, the character is input as the basic unit.

BERT is a language model trained by using a large number of unmarked texts in an unsupervised way. The encoder part based on the transformer carries out bidirectional coding. By constructing a marking language model, BERT can randomly cover or replace any word in a sentence, so that the model can predict the part that is randomly covered by the context and get the distributed context representation of the word. In addition, BERT performed the next sentence prediction task at the same time in the pretraining stage to make the model understand the relationship between the two sentences. Therefore, in order to enhance contextual semantic relevance, the BERT model is adopted in this paper. In the model of relational extraction, firstly, in the BERT, the characters loop through the Token Embedding layer, the Segment Embedding layer, and the Position Embedding layer. In the Token Embedding layer, [CLS] is put at the beginning of the sentence as the mark to be used for follow-on tasks to determine the kind of relationship.

The BLSTM receives the character vector generated by the BERT as input. In the BLSTM network, the character vector propagates forward and backward and the output layer outputs the final hidden layer vector. Finally, the sigmoid function is used to predict the multirelationship types, as shown in (3). The threshold value is trained by the neural network. When the value of the activation function is greater than the threshold value, it is judged to have a correlation and marked as 1; otherwise, it is judged to have no correlation and marked as 0. Finally, we get the relationship types.

$$\text{Sigmoid} = \frac{1}{1 + e^{x}}. \tag{3}$$

In this paper, we labeled seven types of relationships. We adopt seven bits to indicate whether there is a relevant correlation, where 1 represents correlation and 0 represents no correlation.

3.5. Structure of the Entity Extraction Model. The internal structure of the entity pair extraction model is shown in Figure 6.

To enhance the accuracy of entity recognition, entity semantics in statements need to be enforced. Firstly, the identified relationships are added to the hybrid vector to highlight the entities that need to be recognized. Secondly, Chinese characters have their own characteristics and radical features can represent a certain degree of Chinese meaning. Therefore, for the BLSTM model, the hybrid vector input is adopted.

At the input end of the BLSTM model, there are three kinds of inputs. The first one is the character vector generated by the BERT, and the second one is the Chinese radical feature representation. And then, one of the relationships extracted from the relational extraction model is constructed as the vector as long as the character vector which joins the Chinese radical feature and is added to the front and end of the hybrid character vector.

The Chinese radical features of character have been obtained according to formula (2) as in Section 3.2. The character vectors are generated when Chinese characters pass through the BERT model, as shown in the following formula:

$$\begin{aligned} T &= \left[t_r^1, t_r^2, t_r^3, \ldots, t_r^N\right] \\ &= \text{BERT encoder}\,(Cr). \end{aligned} \tag{4}$$

Then, the character vectors are spliced with the radical features, as shown in the following formula:

$$R = \left[G_r \odot T\right]. \tag{5}$$

Next, we take one of the relations obtained in Section 3.4 and construct a relation vector $H(i)$ as long as the splicing vector R, as shown in formula (6). Then, we divide the relation vectors into t parts, which are the kinds of relationship types, and the length of each part can be obtained by dividing the length of the splicing vectors by the kinds of relationship types. At last, we get the vector of the i^{th} relationship: the vector of the i^{th} segments are 1_i^k, and the vector of the other segments are 0_i^k.

$$H(i) = \left[0_1^k, 0_{2,}^k \ldots 1_i^k, \ldots, 0_t^k\right]. \tag{6}$$

Finally, the hybrid vector K is constructed by integrating G_r, T, and $H(i)$, as shown in the following formula:

$$K = \left[\left[G_r \odot T\right], H(i)\right]. \tag{7}$$

After the sentence passes through the BERT and BLSTM models, only the relationship between the text sequence and tags can be obtained and the relationship between tags cannot be considered, so there will be many invalid predictive tags. Through the CRF layer, the obtained prediction tags are constrained to reduce the number of invalid prediction tags and obtain the global optimal tag sequence.

There are two types of scores in the CRF layer; one type is the tag probability P obtained through the BLSTM layer and the size of the matrix P is n*m. N is the number of sentences, m is the type of tags, and $P_{i,j}$ is the probability of the label of the word in the sentence. And, the other type is the transition matrix T, and $T_{i,j}$ represents the transition probability from tag i to tag j. The sentence sequence $x = \{x_1, x_2, \ldots, x_n\}$ corresponding to the tag sequence $y = \{y_1, y_2, \ldots, y_n\}$ shown in the following equation:

$$s(x, y) = \sum_{i=1}^{n} \left(W_{yi-1,yi} + P_{i,yi}\right). \tag{8}$$

The loss function of CRF consists of the real path score and the total score of all possible paths, as shown in the following equation:

$$\text{loss function} = \frac{e^{s(x,y)}}{\sum_{\tilde{y} \in Y_x} e^{s(x,\tilde{y})}}. \tag{9}$$

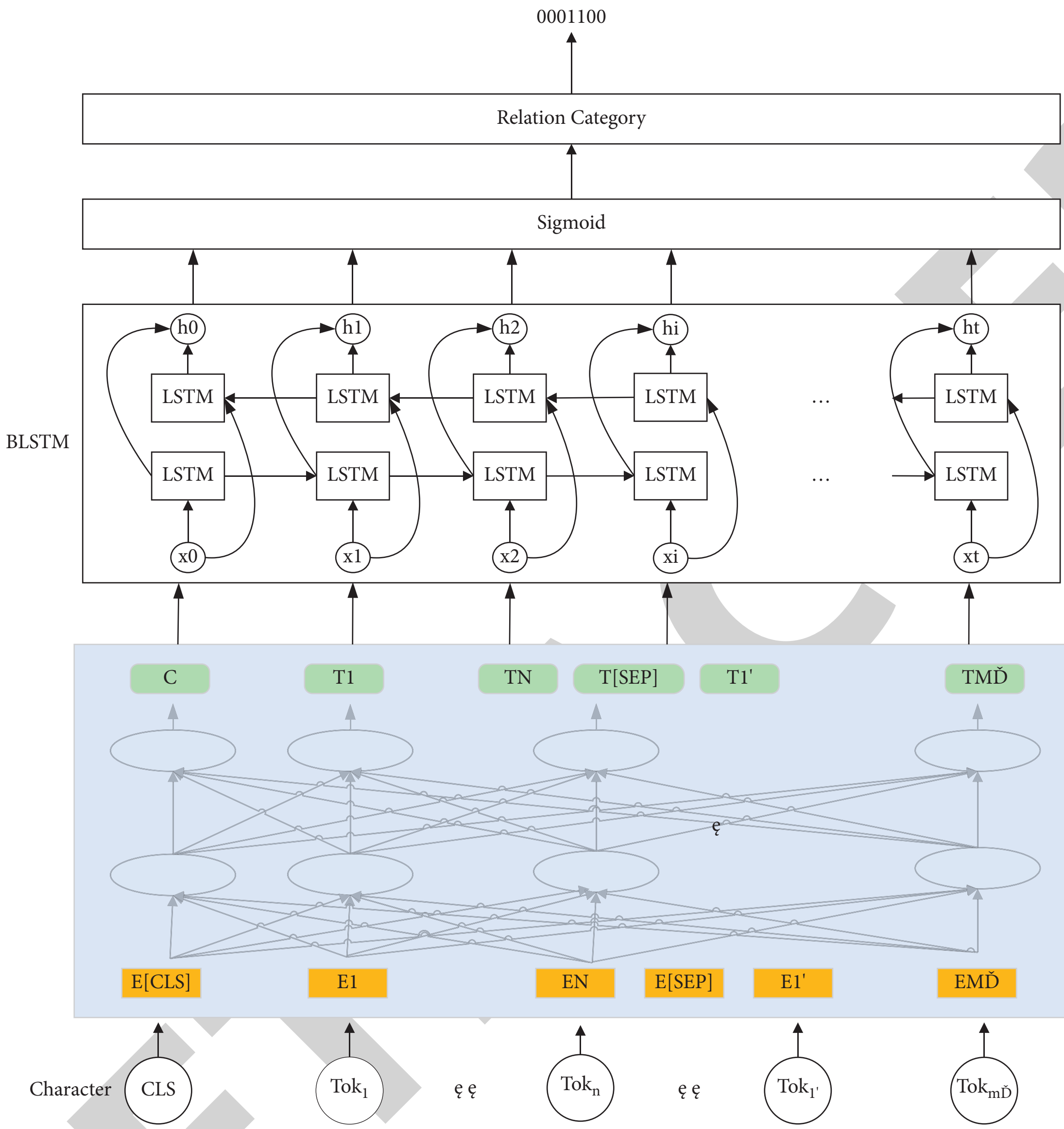

Figure 5: The framework of the relationship extraction model.

After the label probability and transfer probability in the CRF layer are obtained, the Viterbi algorithm is used to find the shortest path and the prediction label of each word in the sentence is obtained. The final hidden layer vector as the input passes through the conditional random field layer to mark whether the character is a subject or an object.

The outputs of the BERT-BLSTM-CRF network model consist of four layers of output vectors. Two layers are the output vectors of subject labels in entity annotation, and the other two layers are the output vectors of object labels in entity annotation. Vector labels have no order and depend on input.

4. Results and Discussion

In Section 4, we introduce our experimental environment and parameter settings and compare the experimental results of entity relationship extraction with different models.

4.1. Experimental Dataset. In this paper, a field dataset (BBC) of food public opinion events in China is constructed as an experimental dataset. The corpus of the experimental dataset is from authoritative and professional websites in the field of food safety (such as China Quality News Network and Baidu Information about Food-Borne Diseases and Food Safety Events). In addition, another open (OP) dataset is used for comparison experiments to ensure the fairness of the experimental results. Among them, the corpus contains seven kinds of relationships. Table 1 lists the seven relationship types, as well as their names and abbreviations.

The experimental dataset and open-source dataset are divided into three parts: training set, validation set, and test set. The data volume size of each subset is shown in Table 2, and the details of the experimental dataset are given in Figure 7

In addition, to evaluate the effectiveness of BERT-BLSTM-CRF in different entity overlap scenarios, sentences

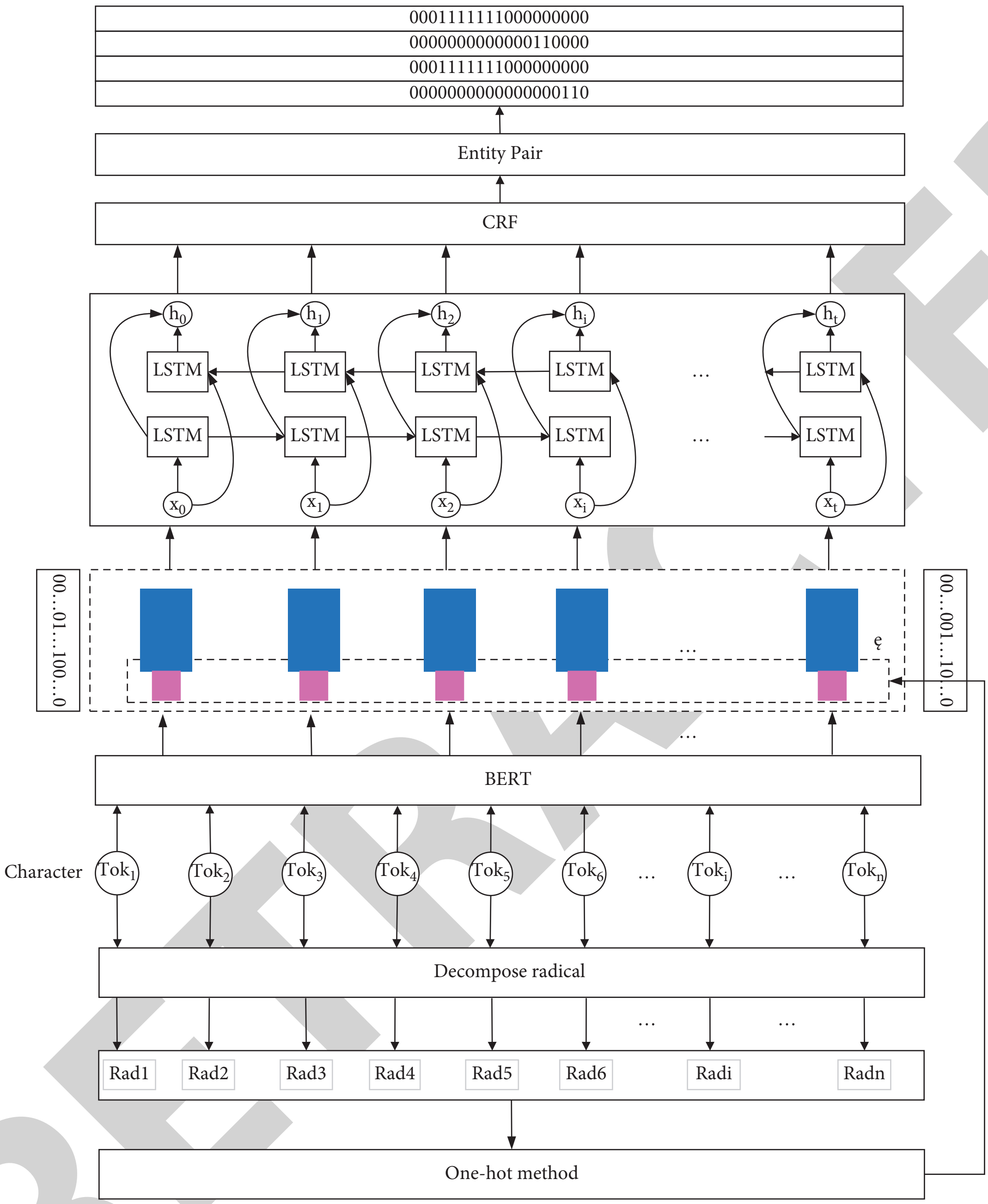

Figure 6: Entity extraction model structure diagram.

Table 2: Experimental dataset.

Dataset	Training	Validation	Test	Label
BBC-DATA	1500	300	400	7
OP-DATA	180000	50000	50000	35

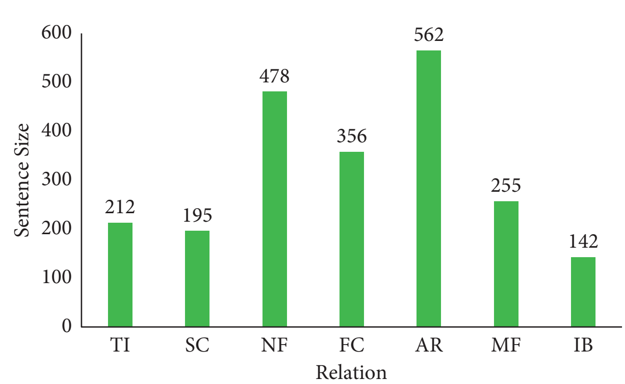

Figure 7: Details of the BBC experimental dataset.

in the BBC dataset are divided into normal (normal), entity pair overlap (EPO), and single entity overlap (SEO) according to different overlap types of relational triple, as shown in Figure 8. The normal class contains only one triple. In the SEO scene, only a single entity is shared at both ends of the relationship, such as the entity “excessive drug residues in turbot” in the sentence related to the entities

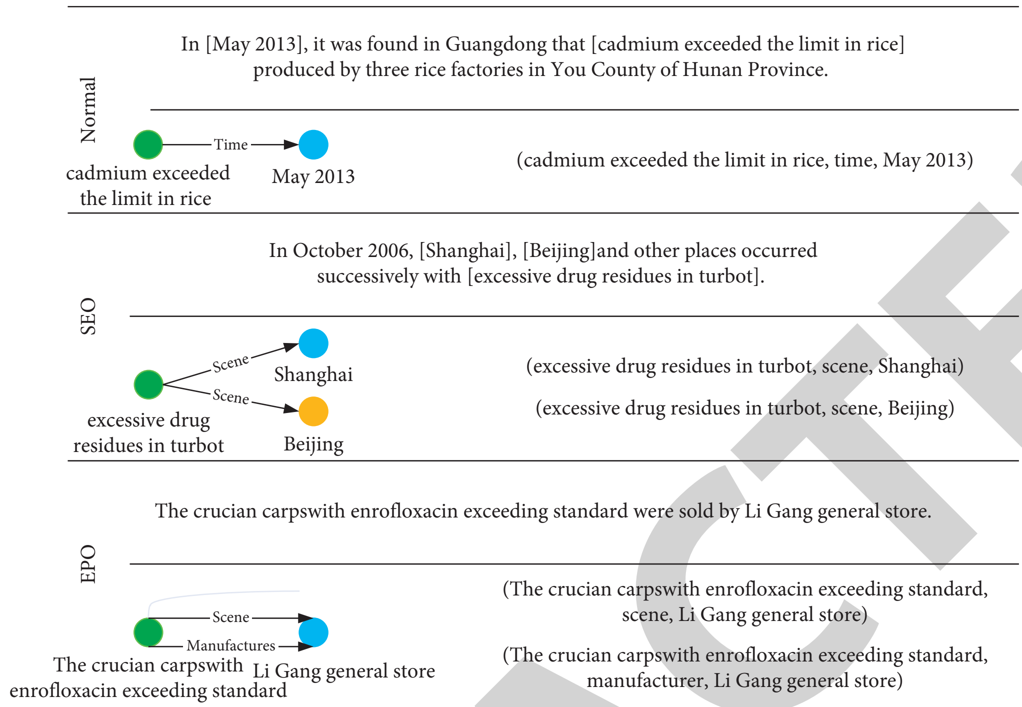

Figure 8: Different overlap types of relational triple.

Shanghai and Beijing. In the EPO scenario, the entities at both ends of the relationship are consistent, such as the entities in the triple < the crucian carps with enrofloxacin exceeding standard, Li Gang general store > overlapping. Table 3 describes BBC experimental dataset division for different entity overlap scenarios.

Table 3: BBC experimental dataset division for different entity overlap scenarios.

Dataset	Training	Validation	Test
Normal	573	96	143
EPO	281	35	79
SEO	646	169	178

4.2. Evaluation Standard Setting. In this paper, three experimental results of precision, recall rate, and $F1$ value are used as performance measurement standards. The calculation formulas are shown as follows:

$$P_i = \frac{TP_i}{TP_i + FP_i}. \tag{10}$$

In precision calculation formula (10), the precision as shown previously is referred to as P. TP_i represents the number of positive classes predicted by the model correctly and FP_i represents the number of positive classes predicted by the model from negative classes.

$$R_i = \frac{TP_i}{TP_i + FN_i}. \tag{11}$$

In recall calculation formula (11), the recall as shown previously is referred to as R. TP_i is as the same as the above-mentioned formula and FN_i represents the number of negative classes predicted by the model from positive classes.

$$F1 = \frac{P * R * 2}{P + R}. \tag{12}$$

The dataset of BBC-DATA constructed in this paper is a balanced dataset. Since precision and recall are a pair of contradictory indicators, to evaluate the performance of the classifier better, the harmonic mean $F1$ score of precision and recall rate is adopted as the evaluation standard to evaluate the comprehensive performance of the model.

4.3. Experimental Parameter Settings. In terms of experimental parameter setting, the main parameter information of the model in this experiment is determined by training the model and adjusting the parameters constantly. Among them, the BERT model's hidden layer has 12 layers, the vector has 768 dimensions, and the BLSTM model's hidden layer has 256 dimensions. An open-source deep learning framework based on PyTorch (https://pytorch.org/) is used to construct a deep learning model for experimental platform development. The main parameter information of the model proposed in the experiment is shown in Table 4 The hyperparameters in the experiment are determined by experiment and corpus, in which the dimension of character embedding is based on the experiment, the pad size is based on the maximum length of the sentence, and the learning rate is adjusted by the experiment.

4.4. Experimental Results and Analysis. In this paper, the proposed BERT-BLSTM-CRF model is experimentally compared with several other classical neural network models

Table 4: Experimental parameter setting.

Model	Parameters	Value
BERT	Layer	12
	Dimensions	768
	Learning rate	$5e-5$
	Pad size	128
	Function	Tan$h$
BLSTM	Layer	2-Layer
	Dimensions	256
	Learning rate	$1e-3$
	Pad size	128
	Function	ReLu Tan$h$

and models with an added attention mechanism. As shown in Table 5, the BERT-BLSTM-ATT model was proposed in [15]. In this experiment, seven annotated relationships are selected to conduct comparative experiments on independently constructed datasets and open datasets. The experimental results of each model relationship identification, including precision, recall rate, and $F1$ score, are shown in Table 5.

The experimental results in Table 5 show that in the food public opinion events corpus and the open-source dataset, the precision of the BLSTM-ATT model is better than that of the CNN-ATT model, but CNN-ATT is better than BLSTM-ATT in recall rate and the overall effect of BLSTM-ATT is better. It can be seen from experiments 1, 2, 3, and 4 that the extraction precision of the neural network model is greatly improved after the attention mechanism is added. In the latest research on relation extraction, BERT learned a better text feature through the deep learning model, which further improved the overall performance of the model. In experiment 4, the BERT model is introduced into the BLSTM-ATT model and its accuracy is significantly higher than in the original model, which further verifies this point. The BERT-BLSTM-CRF model with no attention mechanism proposed in this paper adopts the BLSTM network model and the BERT network model. It is shown that the relational extraction precision and recall rate of the BERT-BLSTM-CRF model adopted in this paper have been greatly improved in the small sample dataset of the food public opinion events corpus and open-source dataset of large-scale corpus. Furthermore, its $F1$ value is the best.

After extracting the relationship, to test the effectiveness of entity pair extraction of the model proposed in this paper in the field of entity recognition of food public opinion events in China, this paper uses the same neural network model mentioned above for comparative experiments. The specific experimental results are shown in Table 6.

After extracting multiple relationships, the BLSTM model is only used to extract entity pairs. Experiments showed that the BERT-BLSTM-CRF model performs better with datasets. BERT-BLSTM-CRF offers significant improvements in precision and recall rate, and F1 also offers the best performance. For entity recognition, the BERT-BLSTM-CRF network model makes use of extracted relationships and Chinese radical features to reinforce the semantics of entities in sentences and enhance the entity recognition ability of the whole network. It is worth noting that the BERT-BLSTM-CRF network model constructed in this paper has good performance in both precision and recall rate, because not only BLSTM in the model can deal with the long-distance dependency problem in time series modelling but also BERT can introduce a deep learning model to learn a better text feature.

This paper also verifies the BERT-BLSTM-CRF model's ability to extract relational triples from sentences with different numbers of triples. The sentences in the dataset are divided into five categories according to the number of different triples in the sentence, and the number of triples in the sentences is denoted by N. Figure 9 shows the results of each model with different numbers of triples. It is obvious that the performance of the baseline model, including precision, recall rate, and $F1$ score, decreases with the increase of the number of triples included in sentences. Here, precision, recall rate, and $F1$ score are calculated according to the number of correctly extracted triples. Although the BERT-BLSTM-CRF model also showed a downward trend, it achieved excellent performance in all five classes. Compared with the baseline models, the model in this paper is least affected by the increasing complexity of input sentences, which also proves that the BERT-BLSTM-CRF model has achieved considerable improvement. At the same time, the biggest improvement of the BERT-BLSTM-CRF model in the BBC dataset comes from the most difficult cases ($N \geq 5$), which also indicates that the model in this paper is more suitable for complex scenarios than the baseline model.

To further investigate the ability of the BERT-BLSTM-CRF model to extract overlapping triples, experiments are carried out on different types of sentences and the performance is compared with that of the baseline model. Figure 10 shows the detailed experimental results of three different sentence types. It can be seen that the performance of all models in normal, EPO, and SEO sentence classification shows a decreasing trend, which also reflects that with the increase in sentence complexity, the difficulty of extracting relational triples from these three overlapping patterns is increasing. In other words, among the three overlapping cases, the normal class is the easiest sentence form to extract, while the EPO class and SEO class are relatively difficult cases to extract. In contrast, the BERT-BLSTM-CRF model achieves better performance in the extraction of three

Table 5: Experimental results of relationship extraction.

Model	BBC-DATA			OP-DATA		
	P%	*R*%	*F*1%	*P*%	*R*%	*F*1%
CNN	68.77	69.22	68.99	66.37	67.65	67.00
CNN-ATT	72.37	73.33	72.39	71.65	73.25	72.44
BLSTM-ATT	77.37	71.33	74.23	75.25	70.37	72.72
BERT-BLSTM-ATT	86.65	86.25	87.44	84.22	83.37	83.79
BERT-BLSTM-CRF	95.48	95.12	95.30	96.15	95.82	95.98

Table 6: Experimental results of entity extraction.

Model	BBC-DATA			OP-DATA		
	P%	*R*%	*F*1%	*P*%	*R*%	*F*1%
CNN	69.23	69.72	69.47	66.37	67.65	67.00
CNN-ATT	72.89	73.88	73.38	71.65	73.25	72.44
BLSTM-ATT	77.85	71.87	74.74	75.25	70.37	72.72
BERT-BLSTM-ATT	89.19	86.78	87.97	84.22	83.37	83.79
BERT-BLSTM-CRF	92.48	91.82	92.15	93.15	92.42	92.78

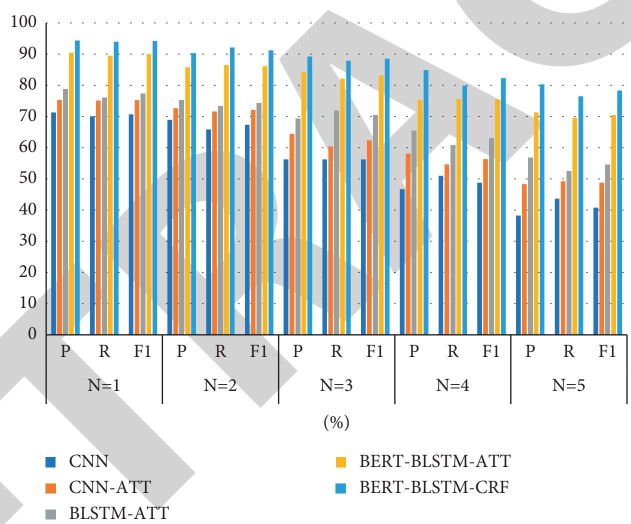

Figure 9: Precision, recall rate, and *F*1 scores for different number of triples.

sentence types. It is worth noting that the experimental effect of the EPO scenario is better than the effect of the SEO scenario on the BERT-BLSTM-CRF model. The reason is that the model adopts the pipeline-type extraction method, which extracts the relationship first and then the entity. Therefore, the improvement of the relationship extraction can improve the extraction effect of the entity to a certain extent and thus improve the extraction effect of the triplet.

The decreasing trend of the loss function of the BERT-BLSTM-CRF model proposed in this paper is shown in Figure 11. At the beginning of model training, many

Figure 10: Precision, recall rate, and *F*1 scores of relational triples in different overlapping patterns.

parameters of BERT have just been initialized and have not been adjusted for many iterations, so BERT does not have a good effect and the loss function has a large value. However, as the number of iterations of model training increases and the parameters are adjusted to a better state, the performance of the BERT-BLSTM-CRF network is gradually improved and the value of the loss function is gradually reduced.

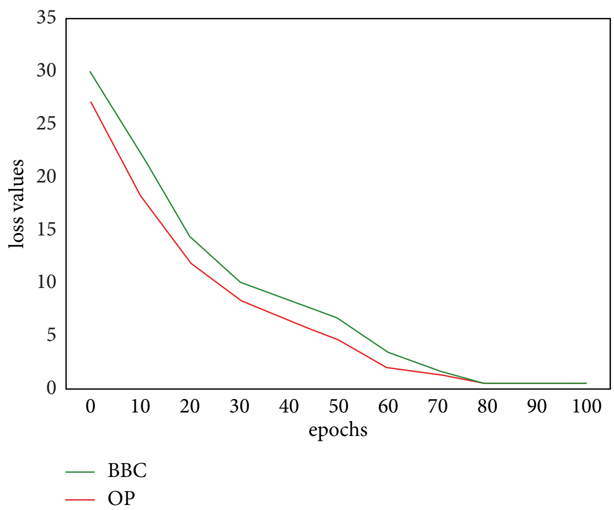

Figure 11: The loss function trending graph.

5. Conclusions

This paper proposes a BERT-BLSTM-CRF relationship entity extraction model based on the corpus of food public opinion events in China. This model adopts the BLSTM model, BERT model, and CRF algorithm and performs training on a small sample corpus to complete the entity relation extraction task of transforming unstructured data into structured data. By constructing the BERT network model and the BLSTM network model, we predict the multirelationship in one sentence. Then, the splicing character vector is constructed by the character vector generated by the BERT joining the Chinese radical feature in the field of food safety events. One of the multirelationships is put on the front and the end of the splicing character vector of the sentence. Finally, CRF is used to mark the entity pair. The comparison experiment results show that the model proposed in this paper performs better than the previous deep neural network model.

The BERT-BLSTM-CRF model can solve the problem of entity relationship in the field of food safety by few-shot learning, which provides the basis for smart healthcare and security guarantees for human health. The model in this paper can not only have a good performance for multirelationship and multi-entity extraction problems but also handle entity overlap well. However, it has a limit for the number of entity pairs. Therefore, we will further explore how to solve more entity problems in Chinese entity relation extraction, such as the improvement of annotation methods, and transfer the proposed method to other application fields such as agricultural image recognition, greenhouse environmental time-series prediction, food safety risk assessment, and image recognition [32–40].

Data Availability

The datasets used in this paper are available from the corresponding author upon request.

Conflicts of Interest

The authors declare that they have no conflicts of interest.

Acknowledgments

This research was supported by the National Key Technology R&D Program of China (grant no. 2021YFD2100605), Beijing Natural Science Foundation (grant no. 4202014), Natural Science Foundation of China (grant nos. 62006008 and 61873027), Humanity and Social Science Youth Foundation of Ministry of Education of China (grant no. 20YJCZH229), Open Project Program of National Engineering Laboratory of Agri-Product Quality Traceability (grant no. AQT-2020-YB6), Social Science Research Common Program of Beijing Municipal Commission of Education (grant no. SM202010011013), and Research Foundation for Youth Scholars of Beijing Technology and Business University (grant no. QNJJ2020-28).

References

[1] Y. U. Qi, S. Jing, Y. Tai, S. Wu, J. Chang, and P. He, "Multidimensional analysis of the healthcare big data policy documents in China," *Chinese General Practice*, vol. 22, no. 26, p. 3209, 2019.

[2] B. Zhou, G. Yang, Z. Shi, and S. Ma, "Natural language processing for smart healthcare," 2021, https://arxiv.org/pdf/2110.15803.pdf.

[3] M. Shah, C. Li, M. Sheng, Y. Zhang, and C. Xing, "Smarter smart contracts: efficient consent management in health data sharing," in *Web and Big Data*Springer International Publishing, New York, NY, USA, 2020.

[4] K. Yu, L. Tan, L. Lin, X. Cheng, Z. Yi, and T. Sato, "Deep-learning-empowered breast cancer auxiliary diagnosis for 5GB remote E-health," *IEEE Wireless Communications*, vol. 28, no. 3, pp. 54–61, 2021.

[5] K. Yu, L. Tan, S. Mumtaz et al., "Securing critical infrastructures: deep-learning-based threat detection in IIoT," *IEEE Communications Magazine*, vol. 59, no. 10, pp. 76–82, 2021.

[6] L. Tan, K. Yu, F. Ming, X. Chen, and G. Srivastava, "Secure and resilient artificial intelligence of things: a HoneyNet approach for threat detection and situational awareness," *IEEE Consumer Electronics Magazine*, p. 1, 2021.

[7] D. Tao, D. Zhang, R. Hu, E. Rundensteiner, and H. Feng, "Crowdsourcing and machine learning approaches for extracting entities indicating potential foodborne outbreaks from social media," *Scientific Reports*, vol. 11, no. 1, 2021.

[8] S. Mitra, S. Saha, and M. Hasanuzzaman, "A multi-view deep neural network model for chemical-disease relation extraction from imbalanced datasets," *IEEE Journal of Biomedical and Health Informatics*, vol. 24, no. 11, pp. 3315–3325, 2020.

[9] J. Gao, X. Zhang, L. Tian et al., "MTGNN: multi-Task Graph Neural Network based few-shot learning for disease similarity measurement," *Methods*, vol. 198, pp. 88–95, 2022.

[10] Y. Lu, T. Stathopoulou, M. F. Vasiloglou, S. Christodoulidis, Z. Stanga, and S. Mougiakakou, "An artificial intelligence-based system to assess nutrient intake for hospitalised patients," *IEEE Transactions on Multimedia*, vol. 23, pp. 1136–1147, 2021.

[11] O. Sainz, O. Lopez de Lacalle, G. Labaka, A. Barrena, and E. Agirre, "Label verbalization and entailment for effective

Hindawi
Computational Intelligence and Neuroscience
Volume 2022, Article ID 3138413, 18 pages
https://doi.org/10.1155/2022/3138413

Research Article

Is Resilient Transportation Infrastructure Low-Carbon? Evidence from High-Speed Railway Projects in China

Zheng He[1,2], Genda Wang[1], Huihua Chen[1], and Hongyan Yan[2]

[1]Central South University, Shaoshan Rd, Railway Campus, Changsha 410075, Hunan, China
[2]Hunan University of Finance and Economics, Fenglin Rd, Changsha 410205, Hunan, China

Correspondence should be addressed to Huihua Chen; chh@csu.edu.cn

Received 16 February 2022; Revised 16 March 2022; Accepted 21 March 2022; Published 28 April 2022

Academic Editor: Xin Ning

Establishing resilient transport infrastructure is an effective way for cities to deal with external disturbances and uncertainties during rapid urbanization. However, human society is presently facing a series of sustainable development obstacles, where the energy shortage and environmental pollution are catching significant concerns. Hence, it is imperative to investigate the carbon emission of the growing number of resilient transportation infrastructure (RTI) projects. Through extracting the carbon emission factor (CEF), this study built the carbon emission measurement model (CEMM) to evaluate the carbon emission of 26 resilient high-speed railway construction projects in China. The results indicated that the carbon emissions of the entire high-speed railway infrastructure projects in China show regional and social environmental differences. Meanwhile, there are potential correlations and positive relationships between the resilience of the high-speed railway infrastructure projects and their carbon emission. Suggestions and recommendations for governments and construction enterprises are put forward to further improve the resilient and low-carbon development of transportation infrastructure in China.

1. Introduction

In the past decade, China is undergoing a rapid urbanization process with a high increasing rate of 1.46%. Under this background, a large number of people have poured into the megacities and the capitals of the provinces of China, such as Beijing, Shanghai, Guangzhou, and so on. To effectively alleviate the pressures on the urban caused by the concentration of the large populations, these cities are promoting and improving infrastructure construction. However, the construction projects of urban transport infrastructure, which are served as the lifeline, are challenged by a series of natural or man-made disasters, such as the natural hazards of hurricanes, fires, earthquakes, public security problems, and so on. These disasters act as the most significant uncertainties and disturbances that bring severe damage to the infrastructure, which thus will result in huge economic and social losses for the urban residents [1].

The concept of "resilience," which owns the unique advantages of the traditional disaster management framework, is one of the efforts made to overcome the challenges [2]. A resilient transport infrastructure with the characteristic of absorption, adaptation, recovery, and upgrading can withstand the external uncertainties and disturbances and maintain the basic function and performance, which finally guarantee the lives and property safety of the residents.

However, the urban transport infrastructure that required huge investments is of both high energy and resource consumption. Can the resilient transport infrastructure meet the current requirements for low-carbon emission? In 2018, global carbon emissions reached the historic high record of 33 billion tons, an increase of 1.7% over the last year [3]. At the same time, China's carbon emissions reached 9.5 billion tons, an increase of 2.5%, accounting for about 28% of the world [4]. China became the country with the largest carbon dioxide emissions in the world, and it is the key area for carbon emission reduction and low-carbon development. Thereafter, China has implemented a series of national strategies to actively respond to climate change achieve low-carbon and sustainable development and promote carbon emission reduction in infrastructure construction [5]. At the end of 2019, China's carbon emissions have been reduced by about 48.1% compared with 2015, reversing the rapid growth of carbon dioxide emissions. In 2021, China aims to "strive to achieve carbon peaks by 2030 and carbon neutrality by 2060." The "14th Five-Year Plan" has also made comprehensive arrangements for achieving carbon peaking, carbon neutrality, and addressing climate change [6, 7].

On these bases, the resilient transport infrastructure and the low carbon emission share the crucial strategic goals that both are expected to enhance the performance of the city, maintain the steady of the city system, reduce losses bring benefits, and improve the life quality of the residents. Hence, when the transport infrastructure is designed to be resilient, it must also be planned to meet the needs of low carbon emissions.

However, scarce prior studies have investigated the connections between resilient transport infrastructure and low carbon emission. The existed literature focused on making an independent discussion of the resilient transport infrastructure and the low carbon emission separately. Hence, this study aims to investigate the relationship between resilient transport infrastructure and low carbon emissions from this perspective. The tasks of this study are as follows.

2. Literature Review

2.1. Transport Infrastructure Resilience. The infrastructure is acknowledged as the most critical lifeline of the cities [8–10] which is of great significance for the flow of commerce, city residents, goods and information, and even the daily activities of society [11]. Infrastructure can be considered to include everything from the physical infrastructure of roads, bridges, airports, rail, water supply, telecommunications, and energy services to the social infrastructure of health care, education, banking, and financial services, emergency services, and the justice system [12–15].

The main responsibility of the department of traffic management is to give priority to ensuring that the physical engineering of the transportation infrastructure is intact and that the social services provided by the transportation infrastructure can operate continuously, stably, and safely [16–19]. Compared with traditional risk defensive measures, this demand for the transportation infrastructure system level will attract special attention from the decision-makers and the researchers [20, 21]. Therefore, the resilience proposal helps define, measure, and improve the traditional paradigm in the entire transportation system [22, 23].

From the perspective of the function of the transportation infrastructure construction project, the social and urban producing activities depend on the availability of the transportation network [24–27]. When the transportation infrastructure project operates under uncertain conditions and disturbances and the ability to quickly restore an acceptable level of service after a disruptive event occurs, it is the basis for the survival of the whole city [28, 29].

2.2. Carbon Emission

2.2.1. Greenhouse Gas and Environmental Problems. With the progress of human civilization, production activities have become increasingly frequent. Large-scale industrialization activities require the consumption of a large number of fossil fuels, resulting in a large number of cumulative emissions of carbon dioxide [30]. The global accumulation of large amounts of carbon dioxide emissions will cause the concentration of greenhouse gases in the Earth's atmosphere to increase rapidly and significantly, eventually causing a series of environmental problems such as global warming and rising sea levels [31, 32].

These environmental problems will have a significant negative impact on the global natural ecosystem. In addition to global temperature rise and sea-level rise, extreme climate events are also typical climate disaster events, posing a huge threat to human survival and development [33].

The generally accepted view in theoretical circles is that carbon dioxide (CO_2) is the main greenhouse gas (GHG). If carbon dioxide emissions cannot be controlled and active and effective actions are taken, a series of environmental problems caused by the global climate will bring huge losses to the global economy (about 5% of global GDP each year). Therefore, achieving carbon emission reduction should be the consensus and top priority of everyone.

2.2.2. Carbon Emissions. Carbon emissions refer to the average greenhouse gas emissions produced by byproducts during the life cycle of production, transportation, use, and recycling [34, 35]. In actual research, the total amount of carbon emissions in a certain area can be measured in a certain period. Carbon footprint is usually used to measure the total amount of greenhouse gases released by an organization or product each year. Carbon efficiency is used to quantify carbon footprint efficiency. It is the ratio of carbon dioxide emissions to the company's annual revenue [36, 37].

2.2.3. Carbon Emissions Factor. Carbon emission factor (CEF) refers to the number of carbon emissions produced per unit of energy during combustion or use. The IPCC believes that the carbon emission factor of a certain energy source is fixed. But, every year, the Chinese government announces the carbon emission factors for the six major regions of China.

2.2.4. Carbon Emission Intensity. Carbon emission intensity (CEI) aims to reveal the internal relationship between the level of economic development and carbon emissions in different countries and regions. Its calculation formula is the ratio of carbon emissions to GDP, that is, carbon emission intensity is inversely proportional to GDP. High carbon emission intensity indicates carbon emissions in the region. High energy consumption or low GDP value and low carbon emission intensity indicate that the region's energy use efficiency is high. Per capita, carbon emission is the ratio of the total carbon emissions of a country or region to the population of the region. Per capita, carbon emission can generally measure the level of development of a country or region.

2.2.5. Carbon Emission Measurement Method. Based on applicable objects and measurement scales, carbon emission measurement methods can be divided into four types: field measurement method, carbon emission coefficient method, input-output method, and material balance algorithm [38].

The site measurement method is the most accurate carbon emission measurement method, and its measurement objects are specific and specific carbon emission units [39]. The site measurement method requires the use of specific professional equipment to monitor the emission flow rate and speed of the research gas and then calculate the output carbon emissions. The site measurement method is generally applied to the carbon emission measurement of the ecosystem, and the industrial carbon emission measurement is less used.

The carbon emission coefficient method, also known as the IPCC inventory method, was first proposed by the IPCC (United Nations Intergovernmental Panel on Climate Change). It refers to the establishment of a carbon emission factor database containing all emission units, combing the carbon emission inventory, and obtaining the carbon emission units of activities or products [40]. Multiply the carbon emission unit data on the carbon emission inventory with the corresponding carbon emission factor to obtain the carbon emission of the emission unit and sum them up to obtain the total carbon emission of the research object. This method is similar to the domestic railway engineering quantity inventory pricing method, and the key to its use is to accurately calibrate the carbon emission factor. Many experts and scholars worldwide have calculated and analyzed the carbon emission coefficients of various energy and materials and constructed a rich database of carbon emission factors. Due to the simple calculation logic, strong operability, and relatively easy acquisition of carbon emission data, the carbon emission coefficient method has become the most widely used carbon emission measurement method [41].

The material balance algorithm, also known as the material balance method or the mass balance method, is a method of measuring the material consumption of the research object according to the law of conservation of mass [42]. Material balance refers to the principle of conservation of quality or "four-pillar inventory" in the system per unit time, that is, the original amount of material + the amount of new material = the amount of material consumption + the remaining amount of material. In the actual industrial production process, the use of this method requires first determining the process flow, to obtain the internal connection between the raw materials and the product [43, 44]. The products include the final product, the semi-finished product that has not been processed, and the byproducts produced together with the main product. It is necessary to comprehensively control the material consumption, physical and chemical reactions, and the impact of the environment on the production of products in each production stage and finally analyze and calculate carbon emissions. Because this method needs to master the physical and chemical reactions and energy consumption in each production stage, the calculation logic is complicated and involves a lot of content, and the measurement workload is relatively large.

The input-output method is different from the first three measurement methods. It uses the macro input-output table data to build a model; analyzes the internal connections between different industries, different economic sectors, and macroeconomic data; and combines them to reflect the characteristics of the industry [45]. The environmental impact data of the company estimate the environmental impact of a product. The input-output method has low requirements on the data accuracy and data range of the research object. Using the input-output method does not need to spend a lot of time and energy sorting out the carbon emission inventory. As long as the macro input-output table data are used, the environmental impact of a product can be determined for quick evaluation [46]. In summary, the input-output method is a macroevaluation method that analyzes the overall environmental impact of a certain industry or department and cannot accurately measure the carbon emissions of specific products or objects [47].

2.2.6. Carbon Emission Factor Calibration Method. The key to using the carbon emission coefficient method is to accurately calibrate the carbon emission factor. There are currently the following three mainstream carbon emission factor calibration methods:

(1) The carbon emission factor is calibrated based on the equivalent carbon dioxide value produced per unit of energy. This law applies to the calibration of energy carbon emission factors. For example, the carbon emission factors of fossil energy and electricity can be calibrated with the amount of fossil energy consumed per unit mass (volume) and the carbon dioxide emissions produced by consuming 1 kWh of electricity;

(2) The carbon emission factor is calibrated based on the equivalent carbon dioxide value produced by the production unit product. This method is applicable to the calibration of carbon emission factors of materials and construction machinery. According to the production process, the carbon dioxide emissions produced by the production unit materials and equipment are measured to achieve the purpose of carbon emission factor calibration;

(3) The carbon emission factor is calibrated based on the equivalent carbon dioxide value produced by the direct carbon source consumed. This method is suitable for direct carbon source carbon emission factor calibration. For example, coal can be used to measure the amount of carbon dioxide, nitrogen oxide, and other gases produced after full combustion based on the element composition to achieve carbon emission factor calibration.

This study uses the first two methods to calibrate the carbon emission factor.

3. Methodology

As mentioned above, there are many carbon emission measurement methods, and multiple methods are used for accurate measurement in many studies. Since the carbon emission coefficient method has obvious advantages in carbon emission measurement in the fields of construction and engineering, this study chooses the carbon emission coefficient method as the carbon emission measurement method. The carbon emission coefficient method is adapted in this study as the carbon emission measurement method.

3.1. Defining the Boundary of Carbon Emission Measurement. The determination of the carbon emission measurement boundary is the first step in the construction of the carbon emission measurement model. The definition of the measurement boundary is subjective, and its breadth and depth directly determine the accuracy and difficulty of carbon emission measurement.

Railway engineering can generally be divided into eight subsystems of bridges and culverts, tunnels, subgrades, tracks, traction power supply, electricity, signal, and communication (the latter four systems are generally collectively referred to as the four-electric system). This paper takes all subsystems into the carbon emission measurement. Meanwhile, we select the "bid section Y of railway X" as the studied cases. However, due to the large amount of railway construction projects and many majors involved, it is difficult to consider all aspects. Therefore, this article only measures the carbon emissions of major energy sources, materials, machinery, and equipment. The carbon emissions of energy, materials, and machinery that do not account for a large proportion are no longer considered. The specific selection criteria are as follows:

(1) Quality standards: Classify all building materials consumed in railway construction and sort all types of materials from large to small according to their quality. Materials whose cumulative mass exceeds 80% of the total mass of the materials are included in the measurement range.

(2) Cost standard: Classify all materials consumed in railway construction and sort all kinds of materials according to cost from largest to smallest. Building materials whose cumulative cost exceeds 80% of the total material cost are included in the measurement range.

(3) Carbon emission standards: Classify all machinery and equipment used in railway construction and sort all types of machinery according to carbon emissions from largest to smallest. Machinery and equipment with cumulative carbon emissions exceeding 80% of the total carbon emissions are included in the measurement scope.

3.2. Source of Data. The railway construction process involves a large amount of energy consumption, the use of materials and construction equipment, and a large amount of relevant data is generated, which causes the railway construction carbon emission measurement to rely heavily on data, and the accuracy of the data directly affects the accuracy of the carbon emission measurement results. This study divides the carbon emission measurement data into two major categories: railway engineering quantity data and carbon emission factor data, and explains their data sources and selection methods.

3.2.1. Railway Engineering Volume. Railway engineering volume data is the basis of railway construction carbon emission measurement. Railway engineering volume data mainly includes two parts.

(1) Railway construction materials and construction equipment data

Railway construction materials and construction equipment data include the types and consumption of construction materials, the types of construction equipment and the number of mechanical shifts, and the energy consumption per mechanical shift. As a large amount of data is involved in the process of railway construction, data accuracy and data availability are considered comprehensively when selecting.

The data sources of materials and construction equipment include railway project budget documents, cost software such as Glodon, and engineering drawings. Budget documents generally refer to construction quotas or budget quotas; the built-in quota data in the cost software depend on the productivity levels of different regions, and there may be differences in consumption of the same equipment or process.

(2) Railway construction material transportation data

The carbon emission generated by the energy consumption during the transportation of a large number of building materials is an important part of the carbon emission of railway construction. The transportation objects in the transportation stage include the building materials, prefabricated components that constitute the railway engineering entity, and turnover materials used in amortization during the construction stage. In the construction material transportation stage, carbon emission measurement should collect data such as the transportation distance, transportation weight, and transportation method of the building materials.

It is generally believed that the transportation process includes three parts: one is the raw material mining place to the raw material processing place. The carbon emission factor for building materials calibrated in this paper considers the transportation process of raw materials from the mining place to the processing place, so it is no longer considered in the transportation data. The second is the construction material production site (raw material processing site) to the construction site. This transportation process includes the transportation of turnover materials and prefabricated components used in railway construction. The third is the waste from the construction site to the landfill. The railway construction phase involves the transportation of a large number of wastes such as tunnel slag and abandoned formwork.

In summary, the transportation data in this study need to consider the transportation process of building materials production site (raw material processing site) to a construction site and waste from the construction site to the landfill.

3.2.2. Identification of the Carbon Emission Factor. Carbon emission factor calibration is the core part of carbon emission measurement using the carbon emission coefficient method. Accurate carbon emission factors are the key to achieving accurate carbon emission measurement. The carbon emission factors are identified from the literature (Table 1).

3.3. Calibration of the Carbon Emission Factor. Carbon emission factor calibration is the core part of carbon emission measurement using the carbon emission coefficient method. Accurate carbon emission factors are the key to achieving accurate carbon emission measurement. This research sorts out the carbon emission factors of energy, transportation, building materials, and construction machinery and establishes a reliable carbon emission factor database.

3.3.1. Energy CEF. In the railway construction stage, direct consumption of energy or indirect consumption of energy through machinery produces a large number of carbon emissions. Energy carbon emission factors are the basis for the calculation of carbon emission factors for building materials and machinery, so it needs to be clarified first. This article divides energy into fossil energy, electricity, and water.

(1) Fossil energy CEF

Regarding the hot issue of carbon emissions, many institutions actively participate in the research and calculate and publish carbon emission factor data. Among them, the IPCC (United Nations Intergovernmental Panel on Climate Change), as a climate change assessment agency with international influence, published assessment reports five times in 1990, 1995, 2001, 2007, and 2013 and issued research systems, computing science, and comprehensive energy carbon emission factor data. However, since the IPCC's latest assessment report was released in 2013 (IPCC WGI Fifth Assessment Report), the timeliness is poor, and the energy carbon emission factor in the IPCC assessment report is determined based on international data, which is different from China's carbon emission data. Therefore, this cultural stone energy carbon emission factor data does not directly quote the relevant data in the IPCC assessment report but draws on the calculation method of the IPCC energy carbon emission factor and calculates it by China's national conditions. Since the carbon emissions of fossil energy mainly come from the use (consumption) stage and the carbon emissions in the production and transportation stage are difficult to measure, this article only measures the carbon emissions generated during the use (consumption) stage.

According to the benchmark method published in the energy section of the 2006 IPCC National Greenhouse Gas Inventory Guidelines 2019 Revised Edition, the calculation formula for the carbon emission factor of this cultural stone energy (combustion) is

$$\begin{aligned} \text{Fossil energy CEF} &= \text{default net calorific value} \times \\ &\quad \text{default carbon content} \times \text{default carbon oxide factor} \\ &\quad \times \text{molar conversion coefficient of carbon and carbon dioxide}. \end{aligned} \tag{1}$$

In the formula, the default net calorific value is derived from the "China Energy Statistical Yearbook 2018"; the default carbon content is quoted from the "2006 IPCC National Greenhouse Gas Inventory Guidelines 2019 Revised Edition"; the default carbon oxidation factor is 100% (the degree of carbon oxide combustion does not affect its carbon content); the molar conversion coefficient of carbon and carbon dioxide is 44/12. The calculation results of fossil energy carbon emission factors are shown in Table 2.

(2) Electricity CEF

As clean energy, electricity does not directly produce carbon emissions during its use but consumes energy to produce carbon emissions during its production process. Therefore, the carbon emission factor of electricity is affected by the energy structure of power generation. The Climate Change Department of the National Development and Reform Commission has clarified two types of marginal emission factors, OM (marginal emission factor for electricity) and BM (marginal emission factor for capacity) in the "2019 China Regional Grid Baseline Emission Factors," and unifies the grid boundaries. It is divided into regional power grids in North China, Northeast China, Northwest China, East China, Central China, and South China, excluding Tibet Autonomous Region, Taiwan Province, Hong Kong, and Macau Special Administrative Regions. The carbon

Table 1: Carbon emission factor from the literature.

Factor	Unit	CEF	Production processes: Fossil energy mining	Raw material acquisition	Raw material transportation	Processed into lumber	Building materials transportation	Regeneration treatment	Source of data
Sand	m^3	72.5		✓	✓	✓			[48]
Stone	m^3	31.2		✓	✓	✓			[49]
Fly ash	kg	0.0015		✓	✓	✓			[50]
Bentonite	kg	0.041		✓	✓	✓			[51]
Mineral powder	kg	0.05692		✓	✓	✓			[52]
32.5#cement	t	677.68	✓	✓	✓	✓			[52]
42.5# cement	t	920.03	✓	✓	✓	✓			[53]
52.5# cement	t	1,041.56	✓	✓	✓	✓			[54]
C20 concrete	m^3	239.19		✓	✓	✓	✓		[55]
C25 concrete	m^3	289.44		✓	✓	✓	✓		[56]
C30 concrete	m^3	346.95		✓	✓	✓	✓		[57]
C35 concrete	m^3	382.11		✓	✓	✓	✓		[58]
C40 concrete	m^3	432.29		✓	✓	✓	✓		[59]
C50 concrete	m^3	563.89		✓	✓	✓	✓		[60]
C60 concrete	m^3	644.85		✓	✓	✓	✓		[61]
1:1 cement mortar	m^3	730.20		✓	✓	✓			[62]
1:2 cement mortar	m^3	531.52		✓	✓	✓			[63]
1:2.5 cement mortar	m^3	469.41		✓	✓	✓			[64]
1:3 cement mortar	m^3	393.65		✓	✓	✓			[65]
Large steel	kg	1.72		✓	✓	✓		✓	[66]
Small and medium steel	kg	1.38		✓	✓	✓		✓	[67]
Hot rolled steel bar	kg	2.21		✓	✓	✓		✓	[68]
Cold rolled steel bar	kg	2.76		✓	✓	✓		✓	[69]
Iron product	kg	1.53		✓	✓	✓		✓	[70]
Wood	m^3	144.5		✓	✓	✓			[71]
Waterproof coating	kg	1.21	✓	✓	✓	✓	✓		[72]
		1.01	✓	✓	✓	✓			[73]
		0.89		✓	✓	✓			[74]
Modified asphalt waterproof materials	m^2	4.28	✓	✓	✓	✓	✓		[75]
		4.01	✓	✓	✓	✓			[76]
PVC waterproof board	kg	8.69		✓	✓	✓			[77]
Rubber waterstop	kg	0.5		✓	✓	✓			[78]

emission factors of power in each region are shown in Table 3.

(3) Water CEF

Water does not contain carbon elements, so water is not a direct carbon emission unit but indirectly produces carbon emissions during its production and transportation. Therefore, its carbon emission factor refers to the energy consumption per unit volume (mass) of water production and transportation. Carbon emissions are generated. This study quotes the value of 0.91 kg CO_2/m^3 in the literature. Since the density of water is 1,000 kg/m^3, the water carbon emission factor can be converted to 0.00091 kg CO_2/kg.

3.3.2. Materials CEF

(1) Silicon-Containing Materials. Sand and gravel are indispensable building materials for railway construction, but there are relatively few studies on carbon emissions during sand and gravel mining and processing. As the carbon emission measurement process for production and mining without sand and gravel in the reference, assuming that the measurement range is the same as this article, it can be

Table 2: Fossil energy CEF.

Fossil energy	Net calorific value	Carbon content	Carbon dioxide factor (%)	Unit	CEF
Raw coal	20,908	25.8	100	kg	1.978
Washed coal	26,344	25.8	100	kg	2.492
Coke	28,435	29.2	100	kg	3.044
Crude	41,816	20.0	100	kg	3.067
Kerosene	43,070	19.5	100	kg	3.080
Gasoline	43,070	18.9	100	kg	2.985
Diesel fuel	42,652	20.2	100	kg	3.159
Liquefied petroleum gas	50,179	17.2	100	kg	3.165
Natural gas	38,931	15.3	100	m^3	1.996
Coke oven gas	16,726	12.1	100	m^3	0.770

Table 3: Fossil energy CEF.

Region	OM electricity CEF	BM electricity CEF
North China power grid	0.9419	0.4819
Northeast power grid	1.0826	0.2399
Northwest power grid	0.8922	0.4407
East China power grid	0.7921	0.3870
Central China power grid	0.8587	0.2854
China southern power grid	0.8042	0.2135

Table 4: Silicon-containing materials CEF.

Silicon-containing materials	Bulk density (kg/m^3)	CEF ($kg\ CO_2/m^3$)	CEF ($kg\ CO_2/kg$)
Stone	1,560	31.2	0.02
Sand	1,450	72.5	0.05

directly quoted. The specific numerical calculations are shown in Table 4.

(2) Blended Materials. Since there is no carbon emission measurement process for bentonite, mineral powder, and fly ash in the references, assuming that the measurement range is the same as this article, it can be directly quoted, then the carbon of bentonite, mineral powder, and fly ash. The emission factors are 0.041 kg CO_2/kg, 0.05692 kg CO_2/kg, and 0.0015 kg CO_2/kg.

(3) Cement Materials. The total carbon emission factor of cement can be obtained by summing the carbon emission factors of the raw material production stage, raw material transportation stage, and cement production and processing, as shown in Tables 3–8, that is, the cement carbon emission factors of PS32.5, PO42.5, and PI52.5 are, respectively, 802.259 kg CO_2/t, 1,103.707 kg CO_2/t, and 1,254.874 kg CO_2/t.

(4) Concrete Materials. The production amount and processing energy consumption of different strength concrete raw materials are used to calculate the CEF in this study, namely C20, C25, C30, C35, C40, C50, and C60.

In the raw material production stage, five strength grades of concrete (C20, C25, C30, C35, and C40) use 42.5# cement, and two strength grades (C50 and C60) use 52.5# cement. The consumption of raw materials for concrete production is shown in Table 6.

The carbon emission factors of raw materials consumed in concrete production are shown in Table 7.

The carbon emission factors of the raw material production stage, the raw material transportation stage, and the concrete processing production stage are added together to obtain the concrete carbon emission factor, as shown in Table 8, that is, the carbon emission factors of the seven strength grades of concrete (C20–C60) are 306.192 kg CO_2. /m^3, 336.680 kg CO_2/m^3, 371.654 kg CO_2/m^3, 389.568 kg CO_2/m^3, 419.599 kg CO_2/m^3, 502.819 kg CO_2/m^3, and 549.342 kg CO_2/m^3.

(5) Mortar Materials. The carbon emission factor of cement mortar is obtained by adding the carbon emission factors of the raw material production phase, the raw material transportation phase, and the cement mortar processing production phase. As shown in Table 9, the carbon emission factors of the four different ratios of cement mortar are 829.388 kg CO_2/m^3, 636.038 kg CO_2/m^3, 581.347 kg CO_2/m^3, and 532.518 kg CO_2/m^3.

(5) Steel Materials. A large amount of steel is used in the railway construction stage, and the steel production stage consumes a lot of resources and energy to generate carbon emissions. Steel materials can be classified according to processes and uses, and there are large differences in the carbon emission factors of steel products of different uses and processes. Steel materials can be divided into screw steel, angle steel, section steel, round steel, and so on according to

Table 5: Cement materials CEF.

CEF	Raw material production stage	Raw material transportation stage	Cement production and processing stage	Total
P.S.32.5	517.100	40.498	244.661	802.259
P.O.42.5	729.200	44.211	330.296	1,103.707
P.I.52.5	835.550	46.092	373.232	1,254.874

the purpose. As is presented in Table 10, the classification of steel in this study is that the four types of steel are large steel, medium and small steel, hot-rolled steel, and cold-rolled steel.

(6) Wood Materials. Timber is a commonly used turnover material for railway construction, such as wooden formwork, wooden support, and so on. This article believes that turnover wood is difficult to regenerate, that is, the turnover rate of turnover wood is 0. According to the above formula of turnover material carbon emission factor calculation formula, the turnover wood carbon emission factor can be obtained as 120.924 kg CO_2/m^3. Turnover timber amortization frequency is taken as 10 times, and its amortization uses CEF = 120.924/10 = 12.092 kg CO_2/m^3. Table 11 presented the CEF of wood material.

The construction materials CEF of railway engineering are shown in Table 12.

3.3.3. Facility CEF. The CEF of commonly used construction equipment for railway construction is shown in Table 13.

3.4. Measuring Model of the Carbon Emission. The carbon emissions from railway construction should include three aspects: carbon emissions from the transportation of building materials, carbon emissions from the use of building materials, and carbon emissions from construction. However, the use of construction machinery to assemble building materials does not directly generate carbon emissions. Carbon emissions related to building materials occur in the process of production, that is, carbon emissions from railway construction are "transferable."

In this study, the production of building materials is listed separately before the construction phase, that is, it is divided into the building material production phase, the building material transportation phase, and the construction and construction phase. Based on the carbon emission measurement boundary, this research clarifies the content of carbon emission measurement at each stage and combs the carbon emission calculation formula.

(1) The calculation model of CEs during the production stage of building materials is shown in the following formula:

$$C_{sc} = \sum_{i=1}^{n} m_i \times (1 + \mathscr{U}_i) \times C_i, \tag{2}$$

where C_{sc} represents the carbon emissions during the production phase of building materials, m_i represents the consumption of building materials, $\mathscr{U}_i$ denotes the building material loss rate, c_i represents the CEF of the building material production stage, and n represents the types of the building materials.

(2) The calculation model of CEs during the building materials transportation stage is shown in the following formula:.

$$C_{ys} = \sum_{i=1}^{n} \sum_{j=1}^{k} m_{ij} \times (1 + \mathscr{U}_i) \times d_{ij} \times C_i, \tag{3}$$

where C_{ys} represents the carbon emissions during the building materials transportation stage, d_{ij} denotes the average transportation distance of type j for construction materials (waste) i,m_i represents the consumption of building materials (amount of waste engineering), $\mathscr{U}_i$ denotes the building material loss rate, and c_i represents the CEF of the building material production stage.

(3) The calculation model of CEs during the construction stage is shown in formula (4).

During the construction phase, carbon emissions are composed of two parts: the operation of construction machinery consumes energy (gasoline, diesel, electricity, etc.) to produce carbon emissions, the amortization of revolving materials produces carbon emissions, and the direct consumption of energy produces carbon emissions.

$$C_{js} = C_{js1} + C_{js2}, \tag{4}$$

where C_{js} represents the carbon emissions during the construction phase, C_{js1} denotes the construction machinery carbon emissions, C_{js2} represents the energy carbon emissions, $\mathscr{U}_i$ denotes the building material loss rate, and c_i represents the CEF of the building material production stage.

The C_{js1} and C_{js2} can be obtained through the following equations:

$$C_{is1} = \sum_{l=1}^{a} h_l \times c_l = \sum_{m=1}^{b} r_m \times c_m, \tag{5}$$

$$C_{is2} = \sum_{t=1}^{f} r_t \times c_t. \tag{6}$$

Table 6: Consumption of raw materials for concrete production.

Materials	C20	C25	C30	C35	C40	C50	C60
Cement	135	170	210	235	270	320	370
Fly ash	70	70	70	75	80	80	80
Mineral powder	80	80	80	80	80	80	90
Sand	843	825	805	755	732	723	682
Stone	1,020	1,020	1,020	1,020	1,020	1,025	1,000
Water	185	185	180	180	180	165	170
Admixture	1.18	1.38	3.64	4.1	4.9	7	8.3

Table 7: Concrete raw material CEF.

Raw materials	42.5# cement	52.5# cement	Admixture	Stone	Sand	Water	Mineral powder	Fly ash
CEF	1.104	1.255	0.02849	0.02	0.05	0.00091	0.05692	0.0015

4. Determining the Samples Implementing the MCDM

We collected 188 high-speed railway infrastructure construction projects in China using the average sampling method to complete the empirical research. These samples are China's important high-speed railway infrastructure construction projects. The Delphi method was used to determine whether these samples are resilient. MCDM selection techniques were used to determine the suitable MCDM methodology tailored to the decision process [79, 80]. The techniques adapted totally 9 alternatives for determining the required abilities from a set of 78 MCDM databases where the specific descriptors for the properties of the decision process are presented. For instance, qualitative, quantitative, and relative are regarded as the general standards for the alternative type of weights [81–83]. Finally, 26 samples are identified as resilient high-speed railway infrastructure construction projects.

The proposed measuring model was implemented to calculate the carbon emissions of the selected 26 projects.

5. Results and Discussions

We separately calculated the carbon emissions of these 26 resilient high-speed rail projects. Taking section A of the Huaihua-Hengyang (HH) high-speed railway project in China as an example, the measurement for the sample is adapted as follows.

The length of section A of the HH high-speed railway project is 66.95 km, including 44.36 km of tunnels, 9.65 km of bridges, and 12.94 km of roadbeds and stations; the proportion of bridges and tunnels is 80.7%; and the contract period is 60 months. The main project quantities are shown in Table 14.

(1) The value of carbon emissions

The total carbon emission is calculated from the two dimensions of the construction stage and carbon emission source. The total carbon emission of materials is 1,253,677.42 t, of which the carbon emission in the production stage is 1,124,700.91 t and the carbon emission in the transportation stage is 128,976.52 t. The total carbon emission of construction equipment is 158,279.70 t. The total energy carbon emission is 7,167.56 t.

(2) Comprehensive assessment of the carbon emissions

The results presented that the material production stage is the largest source of carbon emissions in the case of railway construction, accounting for 79%; the construction stage carbon emissions account for 12%; and the construction stage carbon emissions are the least, accounting for 9%. Moreover, the carbon emission contribution of materials is 88%; the carbon emission contribution of construction equipment is 11%; and the carbon emission of direct energy use only accounts for 1%. A comprehensive analysis of the data showed that reducing carbon emissions during material production is of great significance for controlling carbon emissions in high-speed railway construction.

The carbon emissions of cement and stone materials are higher than those of other building materials in the material production stage and material transportation stage. The high-speed railway construction in this study uses ready-mixed concrete. Cement, as the main building material for concrete production, consumes a huge amount of carbon, accounting for 54.38% and 25.83% of carbon emissions in production and transportation, respectively. As an important building material for concrete production, sand and gravel account for 16.80% of carbon emissions, second only to cement carbon emissions. The consumption of stone is smaller than that of cement, so the proportion of carbon emissions in the production process is lower than that of cement. However, due to the high density, a large amount of carbon emissions is generated in the transportation process. In summary, reducing carbon emissions from cement and sand production and transportation is the key to controlling carbon emissions from building materials.

Among the construction equipment, the top four contributors to carbon emissions are power machinery; transportation machinery; earth-rock machinery; foundation and pump machinery, with carbon emissions accounting for 37%, 26%, 17%, and 9%, respectively; hoisting machinery; and paving machinery. The carbon emissions from

Table 8: Concrete material CEF.

CEF	C20	C25	C30	C35	C40	C50	C60
Raw material production	184.051	213.396	247.016	266.137	295.257	375.593	422.704
Raw material transportation stage	119.431	120.574	121.928	120.721	121.632	124.516	123.928
Concrete production and processing stage	2.710154	2.710154	2.710154	2.710154	2.710154	2.710154	2.710154
Total	306.192	336.680	371.654	389.568	419.599	502.819	549.342

machinery, processing, and other machinery are relatively small. From this, it can be seen that the carbon emission reduction of construction equipment such as power machinery and transportation machinery with a large carbon emission contribution is the focus of carbon emission control of construction equipment.

Among the direct energy carbon emissions, electricity carbon emissions account for up to 73%, and water carbon emissions account for 26%. Direct consumption of fossil energy produces the least carbon emissions, accounting for only about 1%. Therefore, the energy and carbon emission reduction of construction sites can start by saving electricity and water resources.

After obtaining the carbon emissions of 26 resilient high-speed rail projects, we investigated the relationship between the resilience of the high-speed railway projects and the low-carbon emission. The results of the statistical analysis revealed that the resilience of the high-speed railway projects has a significant positive influence on low-carbon emissions.

6. Suggestions and Recommendations

6.1. Carbon Emission Control Strategy for the Government. Some scholars have called the climate change caused by excess carbon emissions, “the most serious and wide-ranging market failure in history,” and pointed out that only the coordinated efforts of the government and enterprises can avoid the irreversible consequences of excess carbon emissions. According to externality theory, effective government regulation can compensate for market failures. As a typical market failure, carbon emission requires effective government control to achieve its externality internalization. Based on literature research and domestic and foreign practice, it is concluded that carbon emission control strategies widely recognized at home and abroad mainly include carbon auditing, carbon tax collection, and carbon emission trading.

Railway construction carbon auditing refers to tracking and measuring the carbon emissions generated in the process of railway construction, reviewing the management of carbon emissions in the process of railway construction, and achieving the purpose of external intervention in carbon emissions. Carbon audit not only can realize the supervision of carbon emission reduction activities and promote the rational allocation of resources but also can contribute to the coordinated development of the economy and environment.

The participants in the carbon audit process of railway construction include the audit client, the carbon audit subject, and the carbon audit object. Among them, the principal-agent relationship between the audit client and the carbon audit object is the fundamental reason for carbon audit activities, and the audit content is the carbon emissions generated in the process of railway construction. The main body of carbon audit plays an important role in audit activities and can be divided into three categories: government audit subject, social audit subject, and internal audit. In the early stage of the development of carbon auditing in railway construction, China lacked relevant practical experience in carbon auditing in railway construction, and the audit risk was relatively high. Government auditing mainly assumed the main role of carbon auditing. Moreover, the government audit is highly authoritative, which is conducive to promoting the carbon audit of railway construction on the right track. With the gradual improvement of the carbon emission trading market, the participation of social audit subjects has gradually increased, which can play an important role in the carbon audit of railway construction. When the carbon emission trading market is relatively complete, the carbon emission audit of railway construction will become a routine audit business. At this time, the main body of internal audit was derived, and the role of carbon emission management in the process of railway construction was brought into full play.

Since it is currently impossible to implement mandatory carbon audits for all railway construction processes, this paper proposes the implementation framework of railway construction carbon audits concerning the “Kyoto Protocol.” Railway projects can be divided into three categories according to the priority of railway construction. The first category is the railway projects with mandatory carbon audit. The second category is the railway projects that are ready to implement carbon audit, and the third category is all the remaining railway projects. Then carbon audits are carried out for these three types of railway projects in three steps. Under the condition of gradual improvement, the implementation of carbon audits for the second type of railway projects has been promoted, and the construction of related systems such as carbon tax has been promoted. Furthermore, the carbon audit system is promoted in the construction process of all railway projects to achieve energy saving and emission reduction in the process of railway construction.

Based on the relevant economic theories, the negative external effects of carbon emissions originate from the coupling effect of government failure and market failure. To solve this problem, we must make full use of market instruments, which leads to carbon emission trading, a carbon emission response measure widely recognized and used by all countries in the world. The carbon audit of railway projects and the carbon emissions trading system promote and complement each other and can work together to help reduce carbon emissions. The attestation role of carbon audit

Table 9: Concrete material CEF.

CEF	1:1 cement mortar	1:2 cement mortar	1:2.5 cement mortar	1:3 cement mortar
Raw material production	712.694	514.127	457.936	409.636
Raw material transportation stage	115.086	120.303	121.803	121.274
Mortar production and processing stage	1.608	1.608	1.608	1.608
Total	829.388	636.038	581.347	532.518

Table 10: Steel material CEF.

Steel type	CEF	Categories
Large steel	3,612.011	Section steel, I-beam
Small and medium steel	2,895.229	Channel steel, angle steel, steel plate, steel support, steel formwork, steel support
Hot rolled steel bar	3,041.139	Rebar, round steel
Cold rolled steel bar	3,786.384	Cold drawn steel wire

can regulate market transactions and provide a basis of trust for both parties to the transaction. At the same time, carbon emission trading will also promote the development of carbon auditing, and the economic benefits brought by carbon emission trading will attract more carbon emission entities to participate. Finally, the market means to guide the construction unit's carbon audit activities.

To ensure the sustainable, long-term, and healthy development of the carbon audit system for railway projects, we should also build a friendly audit environment for carbon audit of railway projects from the perspectives of politics, economy, law, and social environment.

The economic principle of carbon emission trading involves three classic theories of resource scarcity, externality, and property rights. The theory of resource scarcity reveals the deep root of carbon emissions trading. The negative externality of carbon emissions is the direct cause of emissions trading, and the definition and trading of carbon emissions provide solutions for the internalization of negative externalities of carbon emissions. According to economic theory, carbon emission behaviors enter the market without clear property rights, resulting in significant negative external effects. Economists believe that based on the initial allocation of carbon emissions within the quota, carbon emission rights can be regarded as a tradable commodity and allowed to circulate freely, to achieve the purpose of controlling carbon emissions and achieving economic benefits. In the exploration of carbon emission rights trading in the past 10 years, China has laid a solid foundation for the construction of a unified national carbon emission rights trading market and has also contributed to the early establishment of a carbon emission rights trading system. This study explores key regimes for rail carbon emissions trading.

Government regulation can be divided into two stages: carbon emission reduction regulation and carbon emissions trading regulation, which are implemented through the following mechanisms. The first is the quota allocation supervision mechanism. Whether the allocation of carbon emission allowances is fair and effective is directly related to the normal operation of the carbon emission trading market. The competent department of carbon emission allowance allocation should set up a reasonable and effective supervision system and take measures such as introducing a notary public for supervision and implementing allowance allocation through an online carbon emission allowance allocation system to ensure fair distribution. The second is the regulatory mechanism for trading market behavior. The government should supervise the carbon emission trading process strongly to ensure the trading order. On the one hand, qualification checks can be set up. The carbon emission rights exchange should conduct qualification examinations on carbon emission rights trading entities and set membership criteria. Only those who meet the standards can join the membership. On the other hand, transaction monitoring is possible. Exchanges can establish a transaction monitoring platform to monitor transaction information in real time. The third is the performance offset supervision mechanism. Carbon emission compliance and write-off directly affect the emission reduction results of railway projects, so they must be taken seriously. The carbon emission rights trading authority should formulate a time scale for compliance and urge emission reduction units to submit carbon emission quotas promptly. Competent authorities should also focus on carbon emissions trading volumes in carbon emissions trading and conduct data verification. After the implementation of the contract, the competent department should cancel the quota that has been implemented in time to lay the foundation for the next round of carbon emission reduction implementation.

In addition to supervision, the carbon emission rights trading of railway projects should also set up a penalty mechanism to achieve constraints on emission reduction units. The punishment mechanism should not only punish those who fail to meet the emission reduction targets but also cannot affect the enthusiasm of carbon emission entities to participate in carbon emission trading. In practice, a combination of various punishment methods can be considered.

The first is to set up a mechanism for the disclosure of energy efficiency of railway projects. The key to carbon emission trading of railway projects is the lack of accurate energy consumption and carbon emission data. At present, the energy consumption data of railway projects are not

Table 11: Wood material CEF.

Production process	Log harvesting	Log transportation	Timber processing
Energy	Gasoline	Diesel fuel	Electricity
Number	16.487 (kg/m^3)	4.844 (kg/m^3)	70.142 (kWh/m^3)
CEF (kg/CO_2)	2.985	3.159	0.8042
CEF (m^3/CO_2)	49.214	15.302	56.408

public, which is not conducive to the promotion of carbon emission reduction of railway projects. China can learn from the practical experience of developed countries, set up a special carbon emission information disclosure agency, and require enterprises to include emission reduction information in their annual reports to facilitate supervision by the competent authorities. The second is to set up an overquota price increase mechanism. For small projects, when the carbon emission exceeds the allocated carbon emission quota, the overquota price increase system can be adopted concerning the electricity price. This kind of pricing utilizes a progressive price lever, which is conducive to guiding emission reduction entities to conduct spontaneous emission reductions. In the specific implementation process, relevant departments need to coordinate and cooperate to jointly determine the data such as the price increase rate.

The incentive system is the opposite of the penalty system, and positive incentives are used to promote the development of the carbon emissions trading market. In the early stage of the establishment of the market, the relevant system is not perfect, and the participants are limited. The role of the incentive system should be brought into full play to encourage carbon emission entities to actively participate in carbon emission trading so that the role of the carbon emission trading market can be brought into full play.

On the one hand, it can make full use of market adjustment funds. In the early stage of the establishment of the carbon emission rights market, a unified national normative system has not yet been established, and the participation of carbon emission entities is less, resulting in a shortage of demand. The government should play a role at this time to stimulate the demand for carbon emissions trading, allocate funds to set up special funds, and stimulate market vitality. When the market develops gradually, the government can buy or sell the carbon emission allowances it holds according to the actual market conditions, to achieve the purpose of market regulation. After the market matures, it is no longer necessary for the government to fully invest in the establishment of special funds, which can be composed of various sources such as fines for violations and social donations, to achieve the sustainability of funds. On the other hand, support should be provided for railway energy-saving technologies. The carbon emission of railways is relatively large, and the realization of carbon emission reduction requires long-term continuous promotion, and the key to realizing carbon emission reduction is the research and development and promotion of energy-saving technologies. The government should fully support the technical needs of emission reduction entities, carry out research on energy conservation and emission reduction in relevant national or

Table 12: Construction materials CEF of the high-speed railway project.

Types	Materials	Unit	CEF
Nonturnover material	Stone	m^3	31.2
	Sand	m^3	72.5
	Bentonite	kg	0.041
	Mineral powder	kg	0.05692
	Fly ash	kg	0.0015
	32.5#cement	t	802.259
	42.5# cement	t	1,103.707
	52.5# cement	t	1,254.874
	C20 concrete	m^3	306.192
	C25 concrete	m^3	336.680
	C30 concrete	m^3	371.654
	C35 concrete	m^3	389.568
	C40 concrete	m^3	419.599
	C50 concrete	m^3	502.819
	C60 concrete	m^3	549.342
	1:1 cement mortar	m^3	829.388
	1:2 cement mortar	m^3	636.038
	1:2.5 cement mortar	m^3	581.347
	1:3 cement mortar	m^3	532.518
	Large steel	t	3,612.011
	Small and medium steel	t	2,895.229
	Hot rolled steel bar	t	3,041.139
	Cold rolled steel bar	t	3,786.384
	Iron product	t	2,084.565
	Wood	m^3	120.924
	Waterproof coating	kg	0.89
	Modified asphalt	m^2	3.53
	Waterproof materials	m^2	19.553
	PVC waterproof board	m	4.608
Reusable materials	Rubber water stop	t	1,331.805
	Turnover steel	m^3	12.092

local research centers, increase financial support, and vigorously promote low-carbon railway technology research and railway low-carbon equipment upgrades.

6.2. Carbon Emission Control Strategies of Construction Enterprises. The carbon emission control strategies of construction enterprises focus on low-carbon materials, environmental protection construction techniques, and clean energy. The carbon emission information integrated management platform and various information tools can effectively help reduce carbon emissions. As an important participant in railway engineering construction and the main promoter of carbon emission reduction in railway construction, the construction unit should implement the concept of low-carbon construction and optimize on-site management; it can also make full use of information tools

Table 13: Facility CEF of the high-speed railway project.

Types	Construction equipment	Energy consumption			CEF
		Gasoline (kg)	Diesel fuel (kg)	Electricity (kWh)	
Earthwork machinery	Crawler hydraulic single bucket excavator ≤0.4 m^3	—	35.48	—	112.08
	Crawler hydraulic single bucket excavator ≤0.6 m^3	—	44.08	—	139.25
	Crawler hydraulic single bucket excavator ≤1 m^3	—	62.90	—	198.70
	Crawler bulldozer ≤75 kW	—	49.73	—	157.10
	Crawler bulldozer ≤300 kW	—	197.57	—	624.12
	Self-propelled vibratory roller ≤12 t	—	75.00	—	236.93
	Frog ram ≤700 Nm	—	—	20.40	16.41
	Wheel loader ≤2 m^3	—	56.45	—	178.33
Lifting machinery	Truck crane ≤8 t	—	35.28	—	111.45
	Truck crane ≤16 t	—	57.15	—	180.54
	Gantry crane ≤10 t–22 m	—	—	61.44	49.41
	Gantry crane ≤20 t–22 m	—	—	109.44	88.01
	Gantry crane ≤50 t–40 m	—	—	176.64	142.05
	Crawler crane ≤10 t	—	31.75	—	100.30
	Crawler crane ≤15 t	—	38.81	—	122.60
	Crawler crane ≤40 t	—	47.63	—	150.46
	Crawler crane ≤250 t	—	352.80	—	1,114.50
	Single drum slow speed winch ≤30 kN	—	—	38.40	30.88
	Single drum slow speed winch ≤50 kN	—	—	56.32	45.29
Transportation machinery	Dump truck ≤4 t	—	34.27	—	108.26
	Dump truck ≤8 t	—	47.58	—	150.31
	Dump truck ≤12 t	—	61.29	—	193.62
	Truck ≤4 t	26.61	—	—	79.43
	Truck ≤6 t	34.56	—	—	103.16
	Sprinkler ≤5,000 L	34.56	—	—	103.16
	Small transport vehicle ≤1 t	—	7.26	—	22.93
	Belt conveyor ≤10 m	—	—	15.36	12.35
	Concrete mixing truck ≤6 m^3	—	88.70	—	280.20
	Concrete mixing truck ≤8 m^3	—	100.80	—	318.43
	Concrete mixing truck ≤10 m^3	—	106.85	—	337.54
Concrete and mortar machinery	Concrete mixer ≤250 L	—	—	15.68	12.61
	Concrete mixer ≤400 L	—	—	21.56	17.34
	Concrete mixer ≤800 L	—	—	86.24	69.35
	Concrete mixing station ≤60 m^3/h	—	—	636.16	511.60
	Concrete mixing station ≤100 m^3/h	—	—	913.92	734.97
	Concrete mixing station ≤120 m^3/h	—	—	1,008.00	810.63
	Concrete plug-in vibrator	—	—	5.38	4.33
	Concrete attached vibrator	—	—	6.72	5.40
	Suspended pulp lifting and leveling machine	—	—	105.28	84.67
	Concrete wet spraying machine ≤5 m^3/h	—	—	24.64	19.82
	Hydraulic grouting pump ≤50 L/min	—	—	30.80	24.77
	Concrete pump ≤60 m^3/h	—	—	492.80	396.31
	Concrete pump truck ≤90 m^3/h	—	61.74	—	195.04
	Concrete placing machine ≤21 m	—	—	21.84	17.56
	Mortar mixer ≤200 L	—	—	13.44	10.81
	Mortar mixer ≤400 L	—	—	20.16	16.21
	Prestressed steel bar hydraulic tensioning equipment ≤1,200 kN	—	—	38.40	30.88

Table 13: Continued.

Types	Construction equipment	Energy consumption Gasoline (kg)	Diesel fuel (kg)	Electricity (kWh)	CEF
Foundation and pump machinery	Hydraulic vibration pile driver ≤320 t	—	650.92	—	2,056.26
	Hydraulic static pile driver ≤1,200 kN	—	—	138.60	111.46
	Hydraulic static pile driver ≤1,600 kN	—	—	189.00	151.99
	Impact hole forming machine $d \leq 1.5$ m	—	—	177.60	142.83
	Crawler hydraulic grab grooving machine ≤1.2 m	—	194.04	—	612.97
	Dynamic compaction machinery ≤1,200 kNm	—	56.70	—	179.12
	Dynamic compaction machinery ≤2,000 kNm	—	69.30	—	218.92
	Single-stage centrifugal clean water pump ≤12.5 m^3/h–20 m	—	—	8.98	7.22
	Single-stage centrifugal clean water pump ≤50 m^3/h–38 m	—	—	44.88	36.09
	Multi-stage centrifugal clean water pump ≤85m^3/h–180m	—	—	224.40	180.46
	Multi-stage centrifugal clean water pump ≤155 m^3/h–185 m	—	—	538.56	433.11
	Sewage pump ≤90 m^3/h–26 m	—	—	89.76	72.18
	Centrifugal mud pump ≤108 m^3/h–21 m	—	—	89.76	72.18
	Mud water treatment centrifuge ≤100 m^3/h	—	—	326.40	262.49
	Mud water separation equipment ≤1,500 m^3/h	—	—	1,836.00	1,476.51
	Mud production cycle equipment ≤500 m^3/h	—	—	136.00	109.37
Welding machinery	AC arc welding machine ≤42 kVA	—	—	144.00	115.80
	DC arc welding machine ≤32 kW	—	—	102.40	82.35
	Butt welding machine ≤100 kVA	—	—	288.00	231.61
Pavement machinery	Track laying machine 25 m	—	193.64	—	611.71
	Long rail laying unit for ballastless track 500 m	—	94.25	—	297.74
	Turnout tamping car	—	298.17	—	941.92
	Long rail line laying and rolling mill	—	182.50	—	576.52
	Bridge erecting machine ≤900 t	—	642.03	—	2,028.17
	Box beam transport vehicle ≤900 t	—	913.92	—	2,887.07
	Wheel-rail beam moving machine ≤900 t	—	188.50	—	595.47
	Wheel rail type beam lifting machine ≤2 × 450 t	—	188.50	—	595.47
	Rail slab reinforcement tensioning equipment	—	—	105.60	84.92
	Type I double-block sleeper concrete pouring production line	—	—	384.00	308.81
Processing and other machinery	Steel bar straightening machine, $d \leq 14$	—	—	18.70	15.04
	Rebar cutting machine, $d \leq 40$	—	—	33.32	26.80
	Rebar bending machine, $d \leq 40$	—	—	14.28	11.48
	Woodworking circular saw machine, $d \leq 500$	—	—	16.32	13.12
	Jaw crusher, ≤250 × 400	—	—	81.60	65.62
	Vertical drilling machine, $d \leq 25$	—	—	8.98	7.22
	Pipe cutting machine, $d \leq 150$	—	—	13.60	10.94

Table 14: Categories of subprojects of section A of the HH project.

No.	Categories	Projects	Numbers
1	Earthworks	Subgrades	1.69 million m^3
2		Stations	2.2 million m^3
3	Bridges	Mega bridge	3,517 m
4		Large bridge	5,580 m
5		Middle bridge	557 m
6		Small bridge	49 m
7		Culverts	1,638 m
8	Tunnels		44,057 m
9	Buildings		14,404 m^2

such as BIM to achieve integrated management of railway carbon emissions information.

Due to the huge volume of railway projects, carbon emission measurement needs to call a large amount of engineering data. Manually exporting engineering quantities and then performing carbon emission measurement is time-consuming and inefficient, and carbon emission measurement cannot be correlated with information such as construction progress and cost. BIM technology can meet the above requirements at the same time. Therefore, a BIM model of railway engineering construction should be constructed to integrate various information such as railway construction project quantity, progress, cost, and carbon emissions to provide information technology support for railway carbon emissions management.

The integrated management of carbon emission information in railway engineering construction refers to the combination of low-carbon information in the railway engineering construction stage and the BIM model to build a low-carbon information database in the railway engineering construction stage and at the same time integrate construction data (construction progress, railway cost, etc.) with low-carbon information, realize the real-time measurement of carbon emissions in the construction phase of railway projects, and analyze the influencing factors of carbon emissions accordingly. Its essence is to add progress information, cost information, and carbon emission information based on the 3D BIM model to build a 6D BIM model. The carbon emission information integrated management model can realize the carbon emission management in the construction process. By monitoring the progress, cost, carbon emission, and other data displayed in the model in real-time, the influencing factors of carbon emission in the construction process can be analyzed, which can provide a reference for the selection of schemes and promote railway construction carbon emission management.

The implementation steps of the railway carbon emission integrated management model are as follows: first, collect carbon emission data. Carbon emission data are the prerequisites for the integrated management of carbon emission information in the construction phase of railway projects, including railway engineering volume data and carbon emission factor data. The railway engineering quantity data can be obtained directly from the railway BIM model, and the carbon emission factor can be queried in the authoritative carbon emission factor database. Second, integrate schedule data, cost data, and carbon emissions data in the BIM model. The construction progress plan is imported into the BIM model as construction progress information, and the on-site construction progress of the railway construction stage is controlled in real-time; the price information of different regions has been included in the BIM software, and the bill of quantities can be coded to summarize the railway construction cost data. The carbon emission data of the BIM model is added to the BIM model as a resource, and the carbon emission generation process is regarded as the resource consumption process, and the resource consumption curve diagram of the construction schedule is obtained.

7. Conclusion

We collected 188 high-speed railway infrastructure construction projects in China using the average sampling method to complete the empirical research. These samples are China's important high-speed railway infrastructure construction projects. The Delphi method was used to determine whether these samples are resilient. Finally, 26 samples are identified as resilient high-speed railway infrastructure construction projects.

The proposed measuring model was implemented to calculate the carbon emissions of the selected 26 projects. Achieving a resilient transport infrastructure is imperative to building a modern society. At the same time, the resilient transport infrastructure requires a combination and investment of multiple resources that have caused concern about the carbon emissions of resilient transportation infrastructure. Therefore, from this perspective, this study developed a carbon emission measurement framework for evaluating the carbon emission of several selected resilient transport infrastructure projects. Twenty-six samples are finally identified as resilient high-speed railway infrastructure construction projects. The results revealed a relatively high carbon emission in these resilient high-speed railway infrastructure construction projects. Resilient transport infrastructure with lower carbon emissions is located in remote cities.

The findings could help investigate the carbon emission of resilient transport infrastructure projects. The correlation between resilience and carbon emission is useful for policy-makers to conduct an effective plan for the cities.

Data Availability

All data sets generated for this study are included in the article.

Disclosure

Zheng He and Genda Wang are the co-first authors.

Conflicts of Interest

The authors declare that there are no conflicts of interest.

Acknowledgments

The study was funded by the Natural Science Foundation of Hunan Province (2021JJ30861). The authors are very grateful for the time the reviewers voluntarily spent reviewing the manuscript. The authors would like to thank the constructive comments and suggestions, which have helped them improve the manuscript.

References

[1] M. A. Ahad, S. Paiva, G. Tripathi, and N. Feroz, "Enabling technologies and sustainable smart cities," *Sustainable Cities and Society*, vol. 61, Article ID 102301, 2020.

[2] S. A. Argyroudis, S. A. Mitoulis, L. Hofer, M. A. Zanini, E. Tubaldi, and D. M. Frangopol, "Resilience assessment framework for critical infrastructure in a multi-hazard environment: case study on transport assets," *The Science of the Total Environment*, vol. 714, Article ID 136854, 2020.

[3] M. A. Islam, Y. Gajpal, and T. Y. Elmekkawy, "Mixed fleet based green clustered logistics problem under carbon emission cap," *Sustainable Cities and Society*, vol. 72, Article ID 103074, 2021.

[4] Y. Zhou, M. Chen, Z. Tang, and Z. Mei, "Urbanization, land use change, and carbon emissions: quantitative assessments for city-level carbon emissions in Beijing-Tianjin-Hebei region," *Sustainable Cities and Society*, vol. 66, Article ID 102701, 2021.

[5] C.-W. Chen, "Clarifying rebound effects of the circular economy in the context of sustainable cities," *Sustainable Cities and Society*, vol. 66, Article ID 102622, 2021.

[6] Z. He and H. Chen, "Critical factors for practicing sustainable construction projects in environmentally fragile regions based on interpretive structural modeling and cross-impact matrix multiplication applied to classification: a case study in China," *Sustainable Cities and Society*, vol. 74, Article ID 103238, 2021.

[7] B. Cheng, K. Lu, J. Li, H. Chen, X. Luo, and M. Shafique, "Comprehensive assessment of embodied environmental impacts of buildings using normalized environmental impact factors," *Journal of Cleaner Production*, vol. 334, Article ID 130083, 2022.

[8] D. V. Achillopoulou, S. A. Mitoulis, S. A. Argyroudis, and Y. Wang, "Monitoring of transport infrastructure exposed to multiple hazards: a roadmap for building resilience," *The Science of the Total Environment*, vol. 746, Article ID 141001, 2020.

[9] M. Ibrahim, A. El-Zaart, and C. Adams, "Smart sustainable cities roadmap: readiness for transformation towards urban sustainability," *Sustainable Cities and Society*, vol. 37, pp. 530–540, 2018.

[10] S. H. Otuoze, D. V. L. Hunt, and I. Jefferson, "Neural network approach to modelling transport system resilience for major cities: case studies of lagos and kano (Nigeria)," *Sustainability*, vol. 13, no. 3, p. 1371, 2021.

[11] W. Sun, P. Bocchini, and B. D. Davison, "Resilience metrics and measurement methods for transportation infrastructure: the state of the art," *Sustainable and Resilient Infrastructure*, vol. 5, no. 3, pp. 168–199, 2020.

[12] P. Marana, C. Eden, H. Eriksson et al., "Towards a resilience management guideline - cities as a starting point for societal resilience," *Sustainable Cities and Society*, vol. 48, Article ID 101531, 2019.

[13] H. J. Liu, P. E. D. Love, M. C. P. Sing, B. Niu, and J. Zhao, "Conceptual framework of life-cycle performance measurement: ensuring the resilience of transport infrastructure assets," *Transportation Research Part D: Transport and Environment*, vol. 77, pp. 615–626, 2019.

[14] N. Bešinović, "Resilience in railway transport systems: a literature review and research agenda," *Transport Reviews*, vol. 40, no. 4, pp. 457–478, 2020.

[15] Z. He and N. Elhami Khorasani, "Identification and hierarchical structure of cause factors for fire following earthquake using data mining and interpretive structural modeling," *Natural Hazards*, pp. 1–30, 2022.

[16] S. Marasco, A. Cardoni, A. Zamani Noori, O. Kammouh, M. Domaneschi, and G. P. Cimellaro, "Integrated platform to assess seismic resilience at the community level," *Sustainable Cities and Society*, vol. 64, Article ID 102506, 2021.

[17] D. Patrman, A. Splichalova, D. Rehak, and V. Onderkova, "Factors influencing the performance of critical land transport infrastructure elements," *Transportation Research Procedia*, vol. 40, pp. 1518–1524, 2019.

[18] A. Quinn, E. Ferranti, S. Hodgkinson, A. Jack, J. Beckford, and J. Dora, "Adaptation becoming business as usual: a framework for climate-change-ready transport infrastructure," *Infrastructure*, vol. 3, no. 2, p. 10, 2018.

[19] Z. Xu, S. S. Chopra, and H. Lee, "Resilient urban public transportation infrastructure: a comparison of five flow-weighted metro networks in terms of the resilience cycle framework," *IEEE Transactions on Intelligent Transportation Systems*, 2021.

[20] J.-M. Cariolet, M. Vuillet, and Y. Diab, "Mapping urban resilience to disasters - a review," *Sustainable Cities and Society*, vol. 51, Article ID 101746, 2019.

[21] B. Balaei, S. Wilkinson, R. Potangaroa, and P. McFarlane, "Investigating the technical dimension of water supply resilience to disasters," *Sustainable Cities and Society*, vol. 56, Article ID 102077, 2020.

[22] K. Rasoulkhani, A. Mostafavi, J. Cole, and S. Sharvelle, "Resilience-based infrastructure planning and asset management: study of dual and singular water distribution infrastructure performance using a simulation approach," *Sustainable Cities and Society*, vol. 48, Article ID 101577, 2019.

[23] N. Habermann and R. Hedel, "Damage functions for transport infrastructure," *International Journal of Disaster Resilience in the Built Environment*, vol. 13, 2018.

[24] Y. Yang, S. T. Ng, F. J. Xu, and M. Skitmore, "Towards sustainable and resilient high density cities through better integration of infrastructure networks," *Sustainable Cities and Society*, vol. 42, pp. 407–422, 2018.

[25] K. Hoterová and N. Chovančíková, "Methodical procedure for creating a new methodology for assessing the resilience of transport infrastructure," *Transportation Research Procedia*, vol. 55, pp. 1431–1435, 2021.

[26] S. A. Mitoulis, M. Domaneschi, G. P. Cimellaro, and J. R. Casas, "Bridge and transport network resilience - a perspective," in *Proceedings of the Institution of Civil Engineers-Bridge Engineering*, pp. 1–12, Thomas Telford Ltd, London SW1P 3AA, 2021.

[27] K. Pitilakis, S. Argyroudis, K. Kakderi, and J. Selva, "Systemic vulnerability and risk assessment of transportation systems under natural hazards towards more resilient and robust infrastructures," *Transportation Research Procedia*, vol. 14, pp. 1335–1344, 2016.

[28] M. D. Hendricks, M. A. Meyer, N. G. Gharaibeh et al., "The development of a participatory assessment technique for infrastructure: neighborhood-level monitoring towards sustainable infrastructure systems," *Sustainable Cities and Society*, vol. 38, pp. 265–274, 2018.

[29] D. H. K. Mohammed, F. Külahcı, and A. Muhammed, "Determination of possible responses of Radon-222, magnetic effects, and total electron content to earthquakes on the North Anatolian Fault Zone, Turkiye: an ARIMA and Monte Carlo Simulation," *Natural Hazards*, pp. 1–20, 2021.

[30] A. Akande, P. Cabral, P. Gomes, and S. Casteleyn, "The Lisbon ranking for smart sustainable cities in Europe," *Sustainable Cities and Society*, vol. 44, pp. 475–487, 2019.

[31] S. Di Dio, M. La Gennusa, G. Peri, G. Rizzo, and I. Vinci, "Involving people in the building up of smart and sustainable cities: how to influence commuters' behaviors through a mobile app game," *Sustainable Cities and Society*, vol. 42, pp. 325–336, 2018.

[32] S. E. Bibri and J. Krogstie, "Smart sustainable cities of the future: an extensive interdisciplinary literature review," *Sustainable Cities and Society*, vol. 31, pp. 183–212, 2017.
[33] C. Hou, Y. Wen, Y. He et al., "Public stereotypes of recycled water end uses with different human contact: evidence from event-related potential (ERP)," *Resources, Conservation and Recycling*, vol. 168, Article ID 105464, 2021.
[34] L.-Y. He and H.-Z. Zhang, "Spillover or crowding out? The effects of environmental regulation on residents' willingness to pay for environmental protection," *Natural Hazards*, vol. 105, no. 1, pp. 611–630, 2021.
[35] Z. He and H. Chen, "An ism-based methodology for interrelationships of critical success factors for construction projects in ecologically fragile regions: take korla, China as an example," *Applied Sciences*, vol. 11, no. 10, p. 4668, 2021.
[36] A. D. Boloorani, M. S. Najafi, and S. Mirzaie, "Role of land surface parameter change in dust emission and impacts of dust on climate in Southwest Asia," *Natural Hazards*, pp. 1–22, 2021.
[37] Q. Sheng, X. Zheng, and N. Zhong, "Financing for sustainability: empirical analysis of green bond premium and issuer heterogeneity," *Natural Hazards*, pp. 1–11, 2021.
[38] H. Huang, H. Cui, and Q. Ge, "Assessment of potential risks induced by increasing extreme precipitation under climate change," *Natural Hazards*, pp. 1–21, 2021.
[39] S. Gopikumar, S. Raja, Y. H. Robinson, V. Shanmuganathan, H. Chang, and S. Rho, "A method of landfill leachate management using internet of things for sustainable smart city development," *Sustainable Cities and Society*, vol. 66, p. 102521, 2021.
[40] A. Tiwari, M. Shoab, and A. Dixit, "GIS-based forest fire susceptibility modeling in Pauri Garhwal, India: a comparative assessment of frequency ratio, analytic hierarchy process and fuzzy modeling techniques," *Natural Hazards*, vol. 105, no. 2, pp. 1189–1230, 2021.
[41] R. Ali, K. Bakhsh, and M. A. Yasin, "Impact of urbanization on CO2 emissions in emerging economy: evidence from Pakistan," *Sustainable Cities and Society*, vol. 48, Article ID 101553, 2019.
[42] Y. Wang, X. Fang, S. Yin, and W. Chen, "Low-carbon development quality of cities in China: evaluation and obstacle analysis," *Sustainable Cities and Society*, vol. 64, Article ID 102553, 2021.
[43] Y. Cao and D. Shen, "Contribution of shared bikes to carbon dioxide emission reduction and the economy in Beijing," *Sustainable Cities and Society*, vol. 51, Article ID 101749, 2019.
[44] S. T. Hassan, M. A. Baloch, N. Mahmood, and J. Zhang, "Linking economic growth and ecological footprint through human capital and biocapacity," *Sustainable Cities and Society*, vol. 47, Article ID 101516, 2019.
[45] S. E. Bibri, "The IoT for smart sustainable cities of the future: an analytical framework for sensor-based big data applications for environmental sustainability," *Sustainable Cities and Society*, vol. 38, pp. 230–253, 2018.
[46] R. Ulucak and S. U.-D. Khan, "Determinants of the ecological footprint: role of renewable energy, natural resources, and urbanization," *Sustainable Cities and Society*, vol. 54, Article ID 101996, 2020.
[47] T. Yigitcanlar, M. Kamruzzaman, M. Foth, J. Sabatini-Marques, E. da Costa, and G. Ioppolo, "Can cities become smart without being sustainable? A systematic review of the literature," *Sustainable Cities and Society*, vol. 45, pp. 348–365, 2019.
[48] S. Keita, C. Liousse, V. Yoboué et al., "Particle and VOC emission factor measurements for anthropogenic sources in West Africa," *Atmospheric Chemistry and Physics*, vol. 18, no. 10, pp. 7691–7708, 2018.
[49] A. Victor, N. Valery, and Z. Louis, "Carbon storage and emission factor of Savanna ecosystems in soudano-sahelian zone of Cameroon," *Journal of Botanical Research*, vol. 2, no. 1, pp. 60–67, 2020.
[50] S. R. Cho, S. T. Jeong, G. Y. Kim, J. G. Lee, P. J. Kim, and G. W. Kim, "Evaluation of the carbon dioxide (CO2) emission factor from lime applied in temperate upland soil," *Geoderma*, vol. 337, pp. 742–748, 2019.
[51] Y. F. Nassar, M. A. Salem, K. R. Iessa, I. M. AlShareef, K. A. Ali, and M. A. Fakher, "Estimation of CO2 emission factor for the energy industry sector in Libya: a case study," *Environment, Development and Sustainability*, vol. 23, no. 9, pp. 13998–14026, 2021.
[52] K. Du, C. Xie, and X. Ouyang, "A comparison of carbon dioxide (CO2) emission trends among provinces in China," *Renewable and Sustainable Energy Reviews*, vol. 73, pp. 19–25, 2017.
[53] N. Novita, N. S. Lestari, M. Lugina, T. Tiryana, I. Basuki, and J. Jupesta, "Geographic setting and groundwater table control carbon emission from Indonesian peatland: a meta-analysis," *Forests*, vol. 12, no. 7, p. 832, 2021.
[54] L. Qin, M. Wang, J. Zhu, Y. Wei, X. Zhou, and Z. He, "Towards circular economy through waste to biomass energy in Madagascar," *Complexity*, p. 2021, 2021.
[55] H. Wang, Y. Wu, and B. Cheng, "Mechanical properties of alkali-activated concrete containing crumb rubber particles," *Case Studies in Construction Materials*, vol. 16, Article ID e00803, 2022.
[56] J.-C. Feng, X.-L. Zeng, Z. Yu, Y. Bian, W.-C. Li, and Y. Wang, "Decoupling and driving forces of industrial carbon emission in a coastal city of Zhuhai, China," *Energy Reports*, vol. 5, pp. 1589–1602, 2019.
[57] Y. Sihui, L. Jing, and W. Mengjie, "Study on influencing factors of carbon emission of civil buildings based on regional differences," in *Proceedings of the IOP Conference Series: Earth and Environmental Science*, vol. 647, no. 1, p. 012194, March 2021.
[58] B. Peng, X. Fan, X. Wang, and W. Li, "Key steps of carbon emission and low-carbon measures in the construction of bituminous pavement," *International Journal of Pavement Research and Technology*, vol. 10, no. 6, pp. 476–487, 2017.
[59] Y. Lou, Y. Ye, Y. Yang, and W. Zuo, "Long-term carbon emission reduction potential of building retrofits with dynamically changing electricity emission factors," *Building and Environment*, vol. 210, Article ID 108683, 2022.
[60] J.-w. Doe, W.-g. Lim, H.-k. Kang, I.-h. Hwang, J.-h. Ha, and B.-k. Na, "Study on characteristics of change in calorific value and carbon emission factor of domestic petroleum energy source," *Journal of the Korean Applied Science and Technology*, vol. 34, no. 4, pp. 1046–1057, 2017.
[61] G. Zhang, M. Sandanayake, S. Setunge, C. Li, and J. Fang, "Selection of emission factor standards for estimating emissions from diesel construction equipment in building construction in the Australian context," *Journal of Environmental Management*, vol. 187, pp. 527–536, 2017.
[62] C. Quan, X. Cheng, S. Yu, and X. Ye, "Analysis on the influencing factors of carbon emission in China's logistics industry based on LMDI method," *The Science of the Total Environment*, vol. 734, Article ID 138473, 2020.

[63] M. Wang, X. Mao, Y. Gao, and F. He, “Potential of carbon emission reduction and financial feasibility of urban rooftop photovoltaic power generation in Beijing,” *Journal of Cleaner Production*, vol. 203, pp. 1119–1131, 2018.

[64] M. Cossutta, D. C. Y. Foo, and R. R. Tan, “Carbon emission pinch analysis (CEPA) for planning the decarbonization of the UK power sector,” *Sustainable Production and Consumption*, vol. 25, pp. 259–270, 2021.

[65] X. Zhao, X. Zhang, N. Li, S. Shao, and Y. Geng, “Decoupling economic growth from carbon dioxide emissions in China: a sectoral factor decomposition analysis,” *Journal of Cleaner Production*, vol. 142, pp. 3500–3516, 2017.

[66] X. Pan, S. Guo, H. Xu, M. Tian, X. Pan, and J. Chu, “China’s carbon intensity factor decomposition and carbon emission decoupling analysis,” *Energy*, vol. 239, Article ID 122175, 2022.

[67] W. Li, C. An, and C. Lu, “The assessment framework of provincial carbon emission driving factors: an empirical analysis of Hebei Province,” *The Science of the Total Environment*, vol. 637, pp. 91–103, 2018.

[68] S. Kang, S.-D. Kim, and E.-C. Jeon, “Emission characteristics of ammonia at bituminous coal power plant,” *Energies*, vol. 13, no. 7, p. 1534, 2020.

[69] J. Röder, D. Beier, B. Meyer, J. Nettelstroth, T. Stührmann, and E. Zondervan, “Design of renewable and system-beneficial district heating systems using a dynamic emission factor for grid-sourced electricity,” *Energies*, vol. 13, no. 3, p. 619, 2020.

[70] M. M. Haque, J. C. Biswas, N. Salahin et al., “Tillage systems influence on greenhouse gas emission factor and global warming potential under rice-mustard-rice cropping system,” *Archives of Agronomy and Soil Science*, vol. 43, pp. 1–16, 2022.

[71] X. Zeqiong and H. Junfei, “Decomposition and sector aggregation analysis of indirect household carbon emission indicators: a case study of Guangdong Province in China,” *Environment, Development and Sustainability*, vol. 20, pp. 1–22, 2021.

[72] W. Sun and C. Huang, “Predictions of carbon emission intensity based on factor analysis and an improved extreme learning machine from the perspective of carbon emission efficiency,” *Journal of Cleaner Production*, vol. 338, Article ID 130414, 2022.

[73] P. Yang, L. Luo, K. W. Tang et al., “Environmental drivers of nitrous oxide emission factor for a coastal reservoir and its catchment areas in southeastern China,” *Environmental Pollution*, vol. 294, Article ID 118568, 2022.

[74] Y. Zhang, Z. Yuan, M. Margni et al., “Intensive carbon dioxide emission of coal chemical industry in China,” *Applied Energy*, vol. 236, pp. 540–550, 2019.

[75] X. Chen, C. Shuai, Y. Wu, and Y. Zhang, “Analysis on the carbon emission peaks of China’s industrial, building, transport, and agricultural sectors,” *The Science of the Total Environment*, vol. 709, Article ID 135768, 2020.

[76] X. Ma, C. Wang, B. Dong et al., “Carbon emissions from energy consumption in China: its measurement and driving factors,” *The Science of the Total Environment*, vol. 648, pp. 1411–1420, 2019.

[77] H. Ye, X. Hu, Q. Ren et al., “Effect of urban micro-climatic regulation ability on public building energy usage carbon emission,” *Energy and Buildings*, vol. 154, pp. 553–559, 2017.

[78] B. J. Wang, J. L. Zhao, and Y. X. Wei, “Carbon emission quota allocating on coal and electric power enterprises under carbon trading pilot in China: mathematical formulation and solution technique,” *Journal of Cleaner Production*, vol. 239, Article ID 118104, 2019.

[79] Z. He, H. Chen, H. Yan, Y. Yin, Q. Qiu, and T. Wang, “Scenario-based comprehensive assessment for community resilience adapted to fire following an earthquake, implementing the analytic network process and preference ranking organization method for enriched evaluation II techniques,” *Buildings*, vol. 11, no. 11, p. 523, 2021.

[80] Z. Stević, D. Pamučar, A. Puška, and P. Chatterjee, “Sustainable supplier selection in healthcare industries using a new MCDM method: measurement of alternatives and ranking according to COmpromise solution (MARCOS),” *Computers & Industrial Engineering*, vol. 140, Article ID 106231, 2020.

[81] Z. He, G. Wang, H. Chen, Z. Zou, H. Yan, and L. Liu, “Measuring the construction project resilience from the perspective of employee behaviors,” *Buildings*, vol. 12, no. 1, p. 56, 2022.

[82] A. Kumar, B. Sah, A. R. Singh et al., “A review of multi criteria decision making (MCDM) towards sustainable renewable energy development,” *Renewable and Sustainable Energy Reviews*, vol. 69, pp. 596–609, 2017.

[83] H.-C. Lee and C.-T. Chang, “Comparative analysis of MCDM methods for ranking renewable energy sources in Taiwan,” *Renewable and Sustainable Energy Reviews*, vol. 92, pp. 883–896, 2018.

Hindawi
Computational Intelligence and Neuroscience
Volume 2022, Article ID 4248778, 9 pages
https://doi.org/10.1155/2022/4248778

Research Article

Application Optimization of University Aesthetic Education Resources Based on Few-Shot Learning from the Perspective of Ecological Aesthetic Education

Yang Liu

Hubei University of Education, Wuhan, Hubei 430205, China

Correspondence should be addressed to Yang Liu; lisiyu201113@163.com

Received 3 March 2022; Revised 20 March 2022; Accepted 21 March 2022; Published 22 April 2022

Academic Editor: Xin Ning

The idea of EAE (Ecological Aesthetic Education) is put forward on the basis of the mature development of ecological aesthetics and AE theory. Starting with EAE, establishing people's aesthetic attitude and improving people's spiritual realm will help to reverse people's hostile attitude towards nature and rebuild the harmonious relationship between man and nature. This paper studies the application optimization of AE (aesthetic education) resources in universities based on ML (machine learning) from the perspective of resource development. The recommendation algorithm based on ML is the main idea of the classification of AE resources, and the classification model of AE resources is constructed. Through deep learning, we can learn the effective features of items from the content data in advance and then transform the learned features into CF (Collaborative Filtering) target learning task. Optimize the voting mechanism of the algorithm, and compare the RF_VM (random forest with optimized voting mechanism) algorithm with the traditional RF (random forest) algorithm. Experiments show that the algorithm proposed in this paper can effectively classify texts and has high feasibility.

1. Introduction

The core of basic education reform is curriculum reform, and AE is an aspect that cannot be ignored in curriculum reform. The development and utilization of AE curriculum resources is an important part of AE. The essence of EAE (Ecological Aesthetic Education) is AE with vivid ecological beauty, which exerts a subtle influence on college students, which is unmatched by other ecological education and AE forms [1]. It should be emphasized that the implementation of EAE is mainly realized through art education. That is to say, art education in our school must also examine its own value and function from the perspective of EAE. The effective implementation of EAE will help young people enjoy the fun of life no matter what stage they are in, and they will not give up easily no matter what adversity they face in the future [2]. School living resources are the foundation and premise of school EAE, and the development and utilization level of school EAE resources determines the effectiveness of school EAE.

The smooth implementation of education requires a well-designed school curriculum. Process is a means and tool for achieving educational and teaching objectives, as well as an important link in determining educational quality [3]. AE (Aesthetic education) is frequently based on theoretical research or individuals in terms of a comprehensive and systematic analysis of history, current situation, tasks, and in these papers [4–7], but there is still a lack of research on how to systematically and comprehensively apply AE elements. The content and quality inspection of the scientific AE process is the key to the development of college AE [8–10], while rationality is the issue that college AE does not play its role. This is a crucial reason, and more in-depth and systematic research and discussion on the use of AE resources in universities is required.

Generally speaking, the university AE started later than other education, so we have some knowledge of university AE, but there is still a big gap compared with other education. Although some university leaders attach importance to AE and care about building AE, not all university leaders attach importance to it and there is no general consensus. EAE development aids in the cultivation of people's ecological awareness, the realization of harmonious coexistence between man and nature, the improvement of people's spiritual world, and the realization of people's poetic existence. The active development of EAE is a key component of current AE. The goal of this study is to more objectively analyze and evaluate the selection, organization, and implementation of university AE resource support by looking into the current status of AE resources in universities and identifying problems with the support. Recognize the current state of AE resources in universities and propose countermeasures and suggestions that are appropriate for the goal.

Innovation:

(1) Taking resource development as a breakthrough, this study makes theoretical thinking on the main topic of youth education-school EAE. In the study of school EAE, we should focus on resource development, explore the elements of EAE resources, choose an effective implementation path of school EAE, and develop and construct AE resources ecologically.

(2) Personalized recommendation is very common on commercial websites, but it is rarely used in university AE resources. In this paper, the similarity of course and user attributes is calculated, specific algorithms are designed, and personalized recommendations are made so as to put forward reasonable suggestions for the application optimization of AE resources in universities.

The organizational structure of the paper is as follows:

The first chapter introduces the research background and significance before moving on to the paper's main work. The second chapter focuses on the technologies associated with university AE resource application optimization. The research's specific methods and implementation are presented in the third chapter. The fourth chapter verifies the research model's superiority and feasibility. The fifth chapter is a synopsis and preview of the entire text.

2. Related Work

2.1. Present Situation of AE Research in Universities. The fundamental goal of higher education is to promote the high-level development of college students, and the ultimate goal is the all-round development of morality, intelligence, physique, beauty, and labor. Among them, AE is not only one of the important goals of quality education, but also one of the important contents of school education. With the continuous promotion of quality education strategy in China, more and more scholars begin to pay attention to and study the AE in universities.

Aesthetic course research must be grounded in AE theory research. All students, regardless of their background or talent, should have the resources and conditions to learn art and exercise their right to art education, according to Leanne and others [11]. According to AFBY and others, professional art education in universities has advanced to unprecedented levels in the new era, with universities establishing art departments, offering art courses, organizing art activities in schools, and promoting a positive artistic environment in schools [12]. Many universities have not included AE in their education plans, but AE still exists, according to Jianlin et al. and this has had an impact on the development of AE practice [13]. Because of its own characteristics, Lvdn and others believe that AE, as one of the methods for achieving quality education, has an inherent and inevitable connection with moral education, intellectual education, and physical education and pervades all education, games, and people's spiritual worlds, and plays a significant role in comprehensive influence. Freedom, communication, experience, honesty, and extensiveness, according to Krainer and others, are the operating principles of modern AE. Yan and colleagues looked at teaching aesthetics from three perspectives: language, posture, and rhythm.

Although the research on the basic theory of AE has achieved fruitful results, the existing research on AE in universities has little penetration into the new achievements of AE theory and lacks the support for college students' AE theory.

2.2. Research Status of ML. ML (machine learning) [14–17] is the core of artificial intelligence and the fundamental way to make computers intelligent. Using effective artificial intelligence technology to obtain abstract information from big data and turn it into useful knowledge is one of the main challenges facing big data analysis today [18]. In the era of big data, how to effectively analyze complex data, reflect its value, and make rational use of it is an urgent task to be solved and considered.

Stein et al. conducted a study to eliminate heterogeneous influence by removing sensitive attributes from the decision-making process and adding fairness constraints to avoid heterogeneous processing. Observe that the standard fairness constraint is nonconvex; then use covariance to turn the nonconvex problem into a convex problem. Finally, measure the output results and sensitive attributes of parameters to investigate the sensitive attributes of multiple classification and analysis. Some scholars looked at the fairness metrics of a variety of algorithms to see how they correlated with different definitions and discovered that they were very closely related. The transformed data retains most of the characteristic signals of insensitive attributes, intersection-sensitive attributes are proposed, and the effects of two sensitive attributes do not overlap [19]. Nguyen et al. modified each attribute so that the marginal distribution of a given subset of sensitive attributes is the same, and this change will not affect other variables, and the transformed data retains most of the characteristic signals of insensitive attributes and intersection-sensitive attributes are proposed, and the effects of two sensitive attributes do. To control identification, limit the degree of distortion of a single data sample, and maintain utility, Nguyen et al. proposed a convex optimization for learning data conversion [20]. Nguyen et al. improved the logistic regression and support vector machine algorithms without bias based on historical data and provided a flexible balance between fairness and accuracy according to various false alarm rates. When sensitive attribute information is unavailable, this method works well [21]. In social networks, Wang et al. proposed a random walk push model. In the trust relationship, this model uses the traditional CF (Collaborative Filtering) method, which can define and measure the reliability of recommendations [22]. Lang et al. experimented with a number of online recommendation systems [23] and found that when both online systems and friends recommended them, users preferred the latter. The difference between content-based and user-based recommendations demonstrates that users prefer the latter. However, their model's goal is to predict users' and items' scores rather than personalized preference ranking, so the goal does not align with the recommendation system's ultimate goal, resulting in low recommendation accuracy.

3. Methodology

3.1. Analysis of the Application of AE Resources in Universities. Ecological problems are closely related to people, and ecological imbalance is the deviation of people's ideas and consciousness. To solve ecological problems, we must first solve the problem of people's ideology, which is actually a problem of people's education. AE aims to establish people's aesthetic attitude and create aesthetic living conditions, as an education to improve people's living standards. Starting with AE, it is of great significance to establish people's aesthetic attitude for solving ecological problems and improving people's living conditions, and EAE is still a new field of AE in China.

EAE's mission is to educate and infect people through art and various forms of EAE so that they can achieve true enlightenment, good education, and emotional edification in a pleasant spirit and gradually develop people's ecological aesthetic sensibility and consciousness. Realize the survival of ecology and aesthetics and perform a one-of-a-kind and irreplaceable role. On the one hand, we should focus on infecting and educating people about the aesthetic method of perceptual freedom so that they can consciously educate beauty or "give freedom with freedom." On the other hand, understanding the natural laws of the ecosystem should be a priority in the implementation of EAE so that people can correctly apply the natural laws and realize the harmonious unity between man and nature. EAE imbues educated people with a sense of beauty and encourages them to pursue and yearn for ecological beauty. Colorful ecological landscapes, endless back and forth, and endless phenomena make people feel a new rhythm of life, ideal living conditions, and a stirring sense of life, which makes them indulge and miss. Ecological beauty education will have a positive impact if we can make conscious use of these resources and educate people about ecological beauty.

The difference of EAE resources in schools is caused by the imbalance of social economy, the difference of management system and supply mode, and the information asymmetry of social demand for talents. The difference of school EAE resources constitutes the difference of school EAE process and effect. The diversity and complexity of school EAE resources determine the instability of education resources, among them are human factors, material factors, policy orientation, development and changes of social and economic conditions, and other factors. Its mobility is mainly manifested in the flow of teachers' resources and students' resources and funds.

The aesthetic course of university is mainly realized through aesthetic activities, so the appreciation and creation of various kinds of beauty is an important part of the course content. If you want to appreciate various forms of beauty, you must know and understand the basic knowledge of various forms of beauty. Through the study of various meanings, features, forms, elements, and other knowledge of beauty, we can accumulate certain theoretical knowledge and become the basis of aesthetic practice. The forms of beauty can be divided into natural beauty, social beauty, and artistic beauty, and the aesthetic practice part of the application of university AE resources is also selected from these four parts. It can be concluded that the basic framework of university AE resource application is shown in Figure 1.

The frame diagram only shows what the AE courses in universities should have, which can be emphasized or supplemented in the implementation of specific courses. For example, in the part of aesthetic practice, you can appreciate and create natural beauty, artistic beauty, and social beauty at the same time, or you can choose one kind of beauty as the main part of the course and another form. Even in the part of basic theory, theoretical study can be appropriately increased or decreased according to class time, students' aesthetic quality, classroom content arrangement, and so on.

3.2. University AE Resources Application Optimization

3.2.1. Hybrid Recommendation System. Social ecological beauty is the beauty reflected in the social ecosystem, which widely exists in all fields of people's production and life, is reflected in the harmonious and orderly social life, and embodies people's ecological aesthetic ideal. Therefore, we can cultivate people's sensibility and ecological aesthetic consciousness through various social and ecological aesthetic forms. In the implementation of EAE in schools, the development of material resources such as educational environment resources should reflect the spirit of the times, and the architectural style should fully reflect the characteristics of vitality and simplicity. At the same time, we should also pay attention to the nationalized and localized material resources, which contain our precious culture and fine traditions, and embody the harmonious unity between man and nature, tradition and modernity, and ideas and modernity.

The world, including humans, is an interconnected life ecosystem that appears as an organic whole. The concept of ecological science highlights the inseparable relationship between man and nature, breaking the existing concept of separation and opposition between man and nature. Everything in this place is connected. Life and life, life and

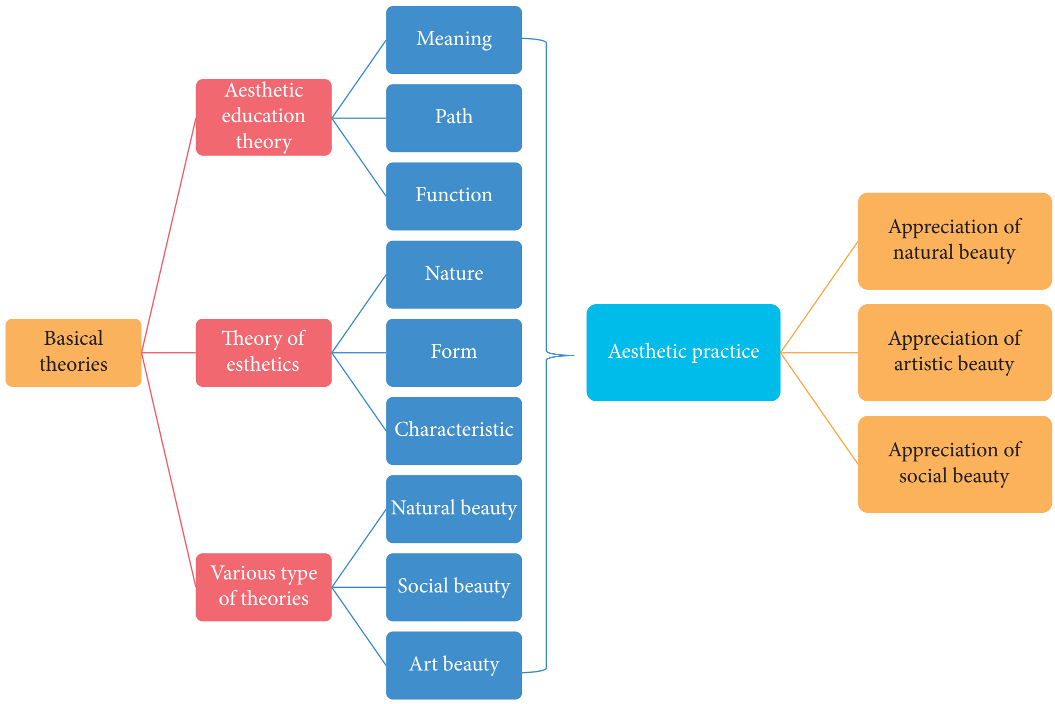

FIGURE 1: Basic framework of AE resource application in universities.

environment, life and environment, and life and environment, communicate and coordinate with one another, cooperate with one another, displaying a beautiful form. The use of a recommendation system [24] is one of the most important and effective ways to reduce information overload, and it is crucial to the success of various Internet application platforms. Most existing recommendation algorithms are based on the CF algorithm, which analyzes historical interactive information, such as scoring, browsing, and collecting, to provide products that users are most likely to be interested in. The evaluation matrix, on the other hand, is very sparse in the face of very sparse real-world data, and the CF-based model frequently fails to provide reliable recommendations. To reduce data sparseness, cold start, and scale, the HHR_L (Learning-based Hash Hybrid Recommendation) model constructs a loss function aimed at predicting ranking and learns the effective hash codes of users and projects by adding individual constraints to users and projects.

The HHR_L model is proposed to solve the data sparseness, cold start, and scalability problems in recommendation system. HHR_L constructs a recommendation algorithm based on hash, which enables the recommendation system to handle large-scale data recommendation, improves the recommendation efficiency, and provides an effective method for scalable recommendation. The model framework as an example of HHR_L is shown in Figure 2.

At first, we initialize the hidden layer feature representation of the project by DAE (Denoising Autoencoder); then we fine-tune the DAE network by combining the paired sorting objective function based on CF, and finally get the hash codes and items of users, and the top-k suggestions are given by Hamming distance sorting.

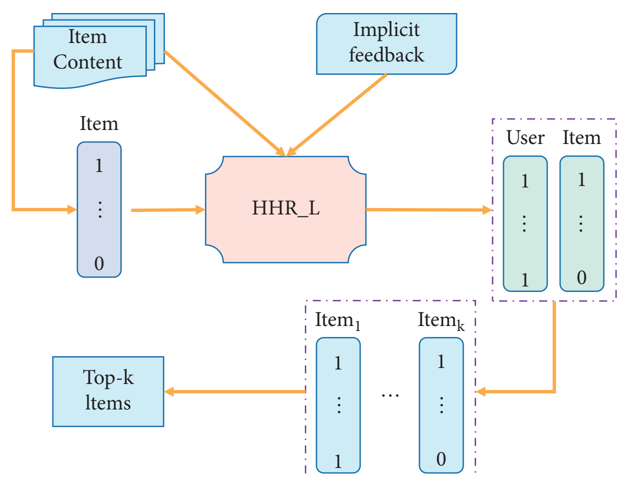

FIGURE 2: Framework diagram of HHR_L model.

The basic idea of hashing algorithm is to compress input data of arbitrary length and map it to data output of fixed length. A key skill is dimension reduction. For test samples, if the information from adjacent samples and related markers is known, the maximum posterior criterion is used to predict a group of markers in the test samples.

Then, through the maximum posterior probability criterion, it can be shown that the ith mark of sample x is

$$y_x(i) = \underset{b\in\{0,1\}}{\arg\max}\, P\left(H_i^b|x\right), \quad i \in Y. \tag{1}$$

Among them, $y_x(i)$ represents the posterior probability of the label corresponding to sample x. Because the posterior probability is difficult to be directly calculated, it can be converted into prior probability and conditional probability according to Bayesian theorem. Therefore, if the label of the sample is unknown, the labeled sample can be expressed as

$$y_x(i) = \underset{b\in\{0,1\}}{\arg\max}\, P\left(H_i^b\right)P\left(x|H_i^b\right), \tag{2}$$

$P(H_i^b)$ represents the prior probability of H_i^b, $P(x\,|\,H_i^b)$ represents the conditional probability that the tag belongs to sample x when H_i^b is known, and $P(H_i^b)$ and $P(x\,|\,H_i^b)$ can be obtained from a given data set.

And change the distribution of hashed points on the machine by selecting a specific hash function. First, given the parameter $D > 0$, the hash function $R^k \longrightarrow Z$ satisfies the formula

$$G(v) = \left[\frac{\alpha \cdot v + \beta}{D}\right], \tag{3}$$

$\alpha \in R^k$ represents a K-dimensional feature vector that obeys $N(0,1)$ standard normal distribution, $\beta \in R$ represents a feature vector randomly selected from the range of $[0, D]$, and D represents the width of the bucket.

From the above steps, we can get the quantization result from k groups $s = \{s_1, \cdots, s_k\}$. For example, the ith group will have a cluster center point μ_i. We distinguish data points based on the median points of two neighboring groups, and the median plane between them is hyperplane. The definition of the vertical plane is as follows:

$$\left(x - \frac{\mu_i + \mu_j}{2}\right)^T \left(\mu_i - \mu_j\right) = 0. \tag{4}$$

Given B, D, Y, Θ, when the intermediate variable X is updated, the items unrelated to X in formula equation (4) are eliminated, and the objective function becomes the following subobjective about X:

$$\begin{aligned} &\max_{X\in R^{d\times n}} tr\left(B^T X\right),\\ &\text{s.t}\, X1_n = 0,\ XX^T = nI_d. \end{aligned} \tag{5}$$

The above model can be optimized by SVD (Singular Value Decomposition). In particular, the update rules of X are as follows:

$$X = \sqrt{n}\left[U_b, \widehat{U}_b\right]\left[V_b, \widehat{V}_b\right]^T. \tag{6}$$

U_b, V_b is a stack of left singular vector and right singular vector of matrix $\overline{B} : \overline{b}_{ui} = b_{ui} - 1/n\sum_{u=1}^{n} b_{ui}$ centered on row mean, respectively. $\widehat{U}_b$ is a matrix of zero singular vector stack, and $\widehat{V}_b$ represents Gram–Schmidt orthogonal complement of V_b, which can be determined by $[V_b, 1]^T \widehat{V}_b = 0$.

3.2.2. Text Classification. A collection of natural languages is referred to as a document set. To classify and organize the document set, all that is required is to extract elements from the document set that can express the content of each document. Because "word" is a fully expressible semantic object in Chinese documents, it is frequently chosen as the metadata of text features. The metadata of text features must first be extracted before text mining can begin. Currently, all types of text representation methods suffer from the same issue. There are many dimensions that can be used to represent a document, and many documents that are not useful for text clustering. As a result, text features must be extracted twice. After the text feature vectors have been dimension reduced, they can be clustered, and the clustering results can be analyzed in light of the current situation.

"Thesaurus," or machine dictionary, has as many entries as possible. Word segmentation based on Thesaurus is the most commonly used, the simplest operation method and the most effective method. Match the item to be processed with Thesaurus, and if the match is successful, display the item string as a word. If they appear more at the same time, they are most likely to form a word. Therefore, the confidence of two adjacent words can usually be obtained by calculating their co-occurrence frequency. The mutual information M is

$$M(X,Y) = \log \frac{P(X,Y)}{P(X)P(Y)}, \tag{7}$$

where $P(X,Y)$ is the adjacent co-occurrence probability of X, Y, and X, Y represent two Chinese characters. $P(X), P(Y)$ are the probability of X, Y appearing separately in the text. This can indicate the tightness between Chinese characters. When the value of M is greater than a certain threshold, it can be considered that X, Y can form a word.

CI (Conceptual index) is a simple and effective dimension reduction method. For supervised learning, CI constructs CI subspaces, takes the cyclic vector composed of these CI subspaces as the base vector, and projects the text cyclic vector onto this subspace.

Classified prototype vector: assuming that the prototype vector of the ith classification is Center_i, its calculation method is as follows:

$$\text{Center}_i = \frac{1}{N}\sum_{j=1}^{N_i} \text{Doc}_{ij}, \tag{8}$$

where N_i is the number of texts in category C_i and Doc_{ij} represents the j prototype vector in category C_i.

PCA (principal component analysis) is a widely used method of pattern recognition and signal processing, which is especially effective for data compression and feature extraction. In this paper, we apply PCA method to text classification, hoping to obtain low-dimensional representation of text vectors.

Assuming that there are M categories in the training set sample, the following is how to calculate the covariance matrix of each internal document category separately:

$$X_i = E\left[(x-\mu)(x-\mu)^T\right]. \tag{9}$$

Among them, X_i is the covariance matrix of the internal document classification in the ith classification, x is the text vector in the ith classification, and μ_i represents the prototype vector in the ith classification.

The essence of PCA method is that you can always get the best linear mapping from M-dimensional space to

D-dimensional space. This is because the sum of error squares of the data obtained by the algorithm can always be kept to a minimum. At the same time, the mutual information between the original vector x and the mapping vector y is the largest.

When dealing with multiclassifier combinations in classification problems, the voting mechanism is frequently used in machine learning. In the above rules, the relative majority voting rule, which selects the class with the highest output among all machine classification algorithms, is a commonly used voting rule. The RF (random forest) algorithm must aggregate the classification results of each DT in the forest and vote on classification categories when determining the classification results. The DT (decision tree) model's similarity can be calculated from two perspectives: DT semantics and DT structure. The concrete implementation idea for improving the voting mechanism is to combine the DT classification effect with the weighted voting method of class probability to improve the RF voting mechanism. The accuracy of data classification outside the bag reflects the classification effect of DT. The DT classification effect improves as classification accuracy improves.

Before making the classification decision, it is necessary to calculate the accuracy rate of each DT's out-of-bag data. If the total number of samples is X and the number of correctly classified samples is X^{correct}, then the accuracy rate of DT's out-of-bag data is the ratio of the two. The accuracy of DT data outside the bag is used to weight DT, and the weight of DT in RF algorithm is

$$W_i = \frac{X^{\text{correct}}(i)}{X}. \tag{10}$$

Remember that the probability that DT outputs that the sample belongs to each class is P_i, the probability that the sample belongs to class y is $P_i(y)$, the weight of DT is w_i, and the number of DTs in RF is k. The weighted value $z(y)$ of the sample belonging to class y is obtained by the formula

$$z(y) = \sum_{i=1}^{k} w_i * P_i(y). \tag{11}$$

The probability that the sample belongs to each class is calculated by the above method, and the class with the largest weighted value is selected as the classification result.

The RF_VM (Random Forest Classification Using Optimized Voting Mechanism) model can be divided into three modules: learning module, weight calculation module, and decision module. The algorithm flow is shown in Figure 3.

First, we implement a training module, which is almost the same as the traditional RF algorithm. Next, the weight calculation module calculates the weight of each DT according to formula (10). Finally, the decision-making module uses the DT set obtained by the learning module and the DT weight obtained by the weight calculation module to classify the samples and calculates the probability weight that the samples belong to a specific category as formula (11). Compare the probabilities of all classes, and get the classification results by weighted values.

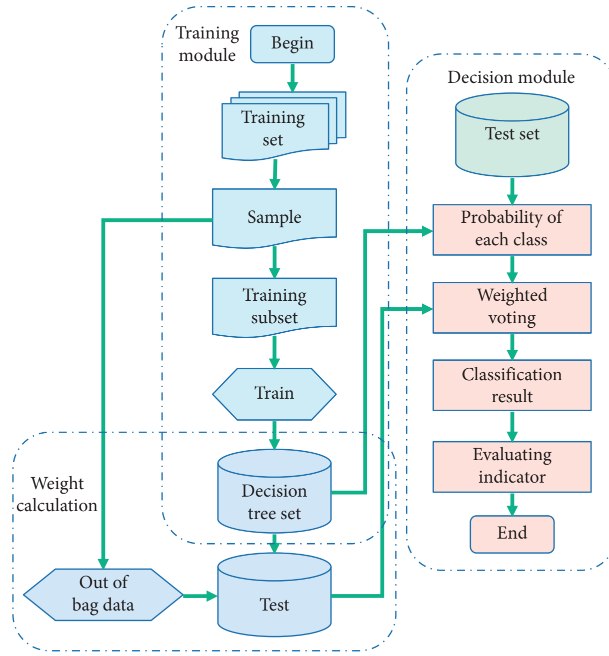

Figure 3: RF algorithm for optimizing voting mechanism.

4. Experiment and Results

4.1. Experimental Environment Setting. The computer used in the experiment is running Microsoft Windows 10. In this article, we choose Python as the development language of our experiment. Try PyCharm software to make Python language development more efficient.

As an excellent Python integrated development software, PyCharm can provide intelligent Python support through intelligent code completion, code inspection, and navigation. PyCharm supports project and file management and various scientific packages, such as Anaconda, matplotlib, and NumPy. Table 1 shows the main hardware configuration of the computer used in this experiment.

In order to verify the effectiveness of the proposed algorithm in cold start and sparse scenarios, we choose to experiment on two public datasets (Amazon dataset and Yelp 9th round dataset), and the sparsity is as high as 99.9%. For content data, first, delete punctuation marks and numbers. And words with stop words and length less than 2 usually have no clear meaning, so the remaining words are processed by English word segmentation.

4.2. Result Analysis. In this paper, Accuracy and MRR (Mean Reciprocal Rank) are used to evaluate the recommendation performance of HHR_L in cold start environment. The experimental results are shown in Table 2 and Figure 4.

It can be seen that the recommendation accuracy of HHR_L is higher than that of comparison method. This is because [18] and [20] are hash recommendation algorithms based on CF, and no project content data is used for modeling. However, in a highly sparse environment, the recommendation accuracy of [18] and [20] will be reduced

Table 1: Use the main hardware configuration of the experimental computer.

Project	Deploy
CPU	Intel Core i5 2.5 GHz
Internal storage capacity	8 GB
Hard disc capacity	300 GB

Table 2: Comparison of recommended accuracy at sparsity of 20% and 30%, respectively.

Method	Amazon		Yelp	
	20%	30%	20%	30%
Ref [18]	0.0123	0.0169	0.0196	0.0341
Ref [20]	0.0114	0.0102	0.0192	0.1162
Ref [21]	0.0463	0.0266	0.0154	0.0128
HHR_L	0.0452	0.0511	0.0288	0.0286

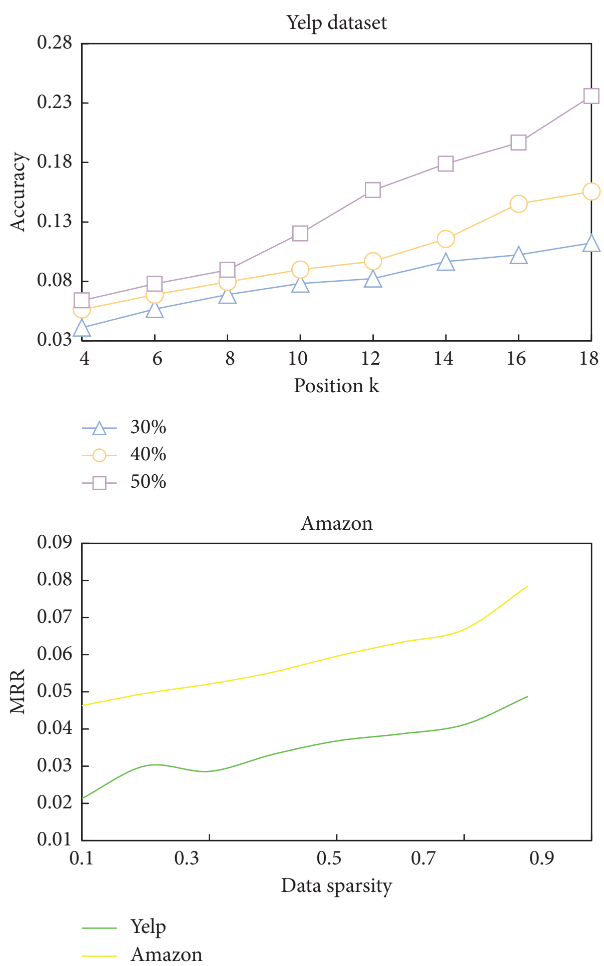

Figure 4: The recommendation accuracy of HHR_L in sparse environment varies with data sparsity.

because the content data plays a key role in improving the recommendation accuracy.

In addition, although the recommendation accuracy of HHR_L increases steadily with the increase of data density, the performance of [21] is unstable, because [21] is based on score prediction rather than ranking. Because the prediction goal is consistent with the ultimate goal of the recommendation system, the recommendation performance is more reliable.

Keep more commonly used words in text documents to improve classification accuracy. CI_PCA and DF (Document frequency) are compared in dimension reduction effect, so KNN (*K*-Nearest Neighbors) algorithm is used for classification, where $K = 10$ is shown in Figure 5.

In Figure 5, except for the 0 dimension, we can see that the accuracy of CI_PCA proposed in this paper is much higher than that of the conventional DF method. When the last 110 dimensions are reached, the accuracy of the algorithm is as high as 80%, and the accuracy of DF method is only 70%. Increasing the dimension to 5 significantly improves the accuracy of the text frequency method.

Another problem in this example is how to choose the appropriate K value when using KNN algorithm for classification. The choice of K value has a great influence on the classification effect. If the K value is too small, the similarity vector may be ignored. If the K value is too large, a large number of noise vectors will seriously affect the classification result. The results are shown in Figure 6.

The experimental results show that the small K value is better than the large K value, and the accuracy rate can reach 81% when $K = 10$ is 110. That is to say, after the CI_PCA process, we prove that similar documents are closer in subspace, prototype vector can weaken the negative influence of synonyms and semantics, and projection of original text vector can partially filter "document vector."

In this paper, the existing RF classification algorithm and RF_VM algorithm are used for the comparative experiment of text classification. Different DT numbers are selected for text classification. In the experiment, the number of DT trees is selected as 20, 50, 60, 90, 150, 220, and 300, and other hyperparameters are used as default values for comparative experiments. The time for performing text classification is shown in Figure 7.

It can be seen from Figure 7 that the number of DTs in RF classification algorithm has a certain influence on the text classification time of both algorithms. Most of the text classifications using these two algorithms will increase accordingly. Although the RF_VM algorithm in this paper is more complicated than the existing RF algorithm in voting, each DT is given a constant weight according to the prediction accuracy of the trained out-of-pocket data. However, the probability that the output samples belong to each category does not significantly increase in the required time resources. Figure 8 shows the prediction accuracy of the existing RF classification algorithm and the RF_VM algorithm in this paper for text classification experiments.

It can be seen that the number of DTs in the algorithm has a great influence on the accuracy of the algorithm. Generally speaking, the higher the number of DTs, the higher the prediction accuracy of the algorithm. For other DT trees, the prediction accuracy of RF_VM algorithm in this paper is improved compared with the existing RF algorithm. The RF_VM algorithm in this paper improves the prediction accuracy of text classification based on the

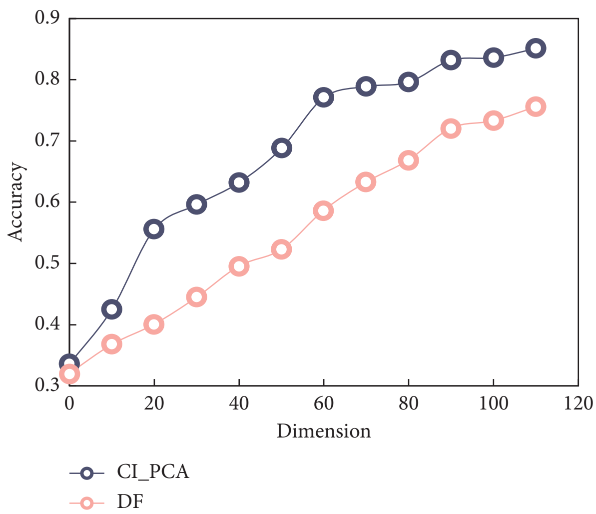

Figure 5: Comparison of dimension reduction effects.

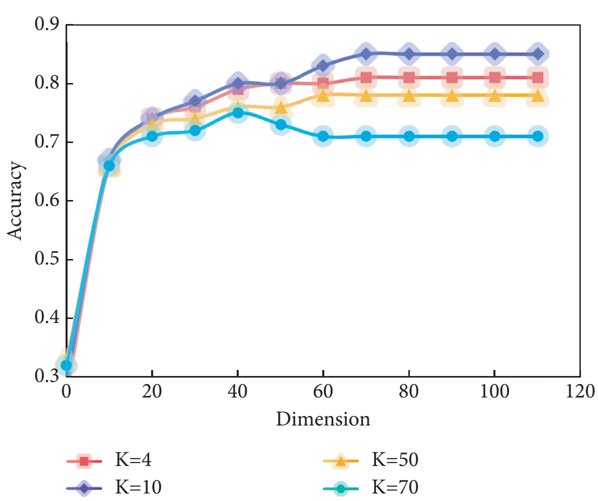

Figure 6: Influence of K value on accuracy.

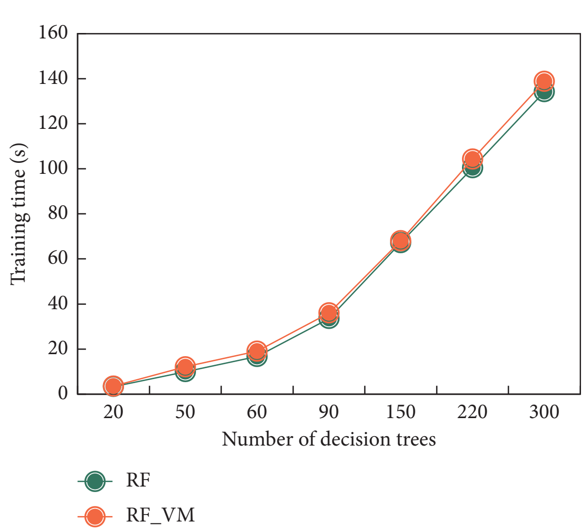

Figure 7: Algorithm time comparison.

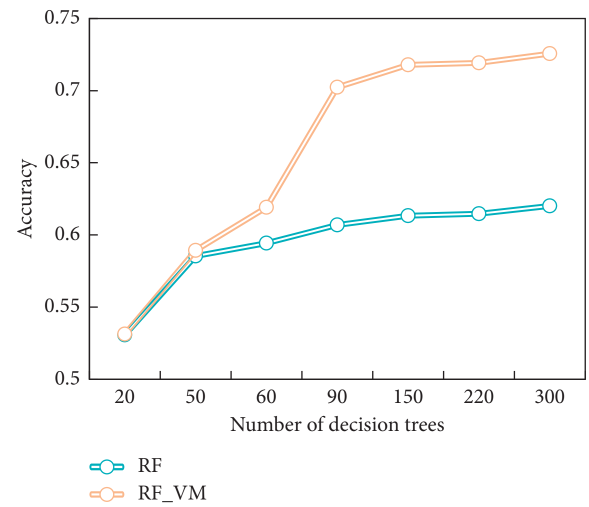

Figure 8: Comparison of prediction accuracy of algorithms.

characteristics of less increase of time resources and better performance than existing RF algorithms. In addition, the prediction accuracy of the two algorithms failed to reach a high level, which was related to the use of default values (excluding DT number) for the superparameters of the algorithms, which also proved the importance of value optimization.

5. Conclusions

EAE is extremely important for environmental protection and improving human living conditions. The EAE educational method should focus on aesthetics, psychological discipline, and infection, and its practical implementation should be integrated with all aspects of school operations. Teachers' human resources are the main body, curriculum resources are the foundation, and material resources are the carrier in the development of school EAE resources, in order to create a humanized environment, build an information platform, and carry out various activities. When designing an ML algorithm, try to avoid data sparsity and a cold start. Data scarcity is not a big deal because of the curriculum limitations, so we pay attention to the new curriculum. By projecting the high-dimensional prototype text onto a low-dimensional subspace and then reducing the dimension according to the classification covariance matrix, the CI PCA algorithm significantly reduces the classification cost. When the proposed RF algorithm is combined with the optimized voting mechanism, the algorithm's classification ability can be greatly improved.

Data Availability

The data used to support the findings of this study are included within the article.

Conflicts of Interest

The author does not have any possible conflicts of interest.

Acknowledgments

This study was supported by 2021 Philosophy and Social Sciences Research Project of Colleges and Universities in Hubei Province (Project no. 21d123): research on the integration of Hubei intangible cultural heritage into the art design education system of local colleges and universities (key project).

References

[1] C. M. Smith, "The aesthetics of john dewey and aesthetic education," *Educational Theory*, vol. 21, no. 2, pp. 131–145, 2010.

[2] D. J. Elliott, "Jazz education as aesthetic education," *Journal of Aesthetic Education*, vol. 20, no. 1, pp. 41–53, 1986.

[3] P. Zheng, X. Wang, and J. Li, "Exploration and practice of curriculum ideological and Political Construction Reform --Take "information security" course as an example," *ASP Transactions on Computers*, vol. 1, no. 1, pp. 1–5, 2021.

[4] W. Liang and Y. Yu, "Research on the improvement of Teachers' Artistic accomplishment based on the status quo of contemporary aesthetic education," *Contemporary educational research*, vol. 5, no. 12, p. 4, 2021.

[5] Yu Xu, "Aesthetic education in the age of artificial imagination," *New Art*, vol. 039, pp. 79–84, 2018.

[6] Y. Zhou, "Discussion on the theoretical guidance and practical exploration of the integrated development of aesthetic education and moral education in colleges and universities," *Journal of Education Theory and Management*, vol. 4, no. 2, p. 24, 2020.

[7] H. Shams, G. Garmaroudi, S. Nedjat, and M. S. Yekaninejad, "Effect of education based on socio-ecological theory on bullying in students: an educational study," *Electronic Physician*, vol. 10, no. 7, pp. 7046–7053, 2018.

[8] S. Kahn and D. L. Zeidler, "A conceptual analysis of perspective taking in support of socioscientific reasoning," *Science & Education*, vol. 28, no. 6-7, pp. 605–638, 2019.

[9] M. Crocker and A. Baur, "Connecting loose ends: integrating science into psychoanalytic theory," *Clinical Social Work Journal*, vol. 2, pp. 1–11, 2020.

[10] A. Thorwart and H. Lachnit, "Inhibited elements model — implementation of an associative learning theory," *Journal of Mathematical Psychology*, vol. 94, p. 102310, 2019.

[11] B. Leanne, D. V. Shaheem, G. Rushaana et al., "Paramedics, poetry, and film: health policy and systems research at the intersection of theory, art, and practice," *Human Resources for Health*, vol. 17, no. 1, p. 64, 2019.

[12] F. B. Yahia, H. Essid, and S. Rebai, "Do dropout and environmental factors matter? A directional distance function assessment of tunisian education efficiency - ScienceDirect," *International Journal of Educational Development*, vol. 60, pp. 120–127, 2018.

[13] H. Jianlin, W. Zhifeng, L. Youhui, J. C. Kolars, and Q. Meng, "China's private institutions for the education of health professionals: a time-series analysis from 1998 to 2012," *Human Resources for Health*, vol. 16, no. 1, p. 40, 2018.

[14] J. Zhou, T. Yang, W. Chu, and W. Zhang, "Underwater image restoration via backscatter pixel prior and color compensation," *Engineering Applications of Artificial Intelligence*, vol. 111, p. 104785, 2022.

[15] W. Cai, B. Zhai, Y. Liu, R. Liu, and X. Ning, "Quadratic polynomial guided fuzzy C-means and dual attention mechanism for medical image segmentation," *Displays*, vol. 70, p. 102106, 2021.

[16] J. Zhou, D. Zhang, and W. Zhang, "Underwater Image Enhancement Method via Multi-Feature Prior fusion," *Applied Intelligence*, pp. 1–23, 2022, in Press.

[17] L. You, H. Jiang, J. Hu et al., "GPU-accelerated Faster Mean Shift with Euclidean Distance Metrics," 2021, https://arxiv.org/abs/2112.13891.

[18] X. Jin, J. Zhang, J. Kong, T. Su, and Y. Bai, "A reversible automatic selection normalization (RASN) deep network for predicting in the smart agriculture system," *Agronomy*, vol. 12, no. 3, p. 591, 2022.

[19] R. A. Stein, P. A. Jaques, and J. F. Valiati, "An analysis of hierarchical text classification using word embeddings," *Information Sciences*, vol. 471, pp. 216–232, 2019.

[20] B. H. Nguyen, B. Xue, P. Andreae, H. Ishibuchi, and M. Zhang, "Multiple reference points-based decomposition for multiobjective feature selection in classification: static and dynamic mechanisms," *IEEE Transactions on Evolutionary Computation*, vol. 99, p. 1, 2019.

[21] B. Nguyen, C. Morell, and B. De Baets, "Distance metric learning for ordinal classification based on triplet constraints," *Knowledge-Based Systems*, vol. 142, no. 15, pp. 17–28, 2018.

[22] B. Wang, X. Hu, P. Li, and P. S. Yu, "Cognitive structure learning model for hierarchical multi-label text classification," *Knowledge-Based Systems*, vol. 218, no. 3, p. 106876, 2021.

[23] S. Lang, F. Bravo-Marquez, C. Beckham, M. Hall, and E. Frank, "WekaDeeplearning4j: a deep learning package for Weka based on Deeplearning4j," *Knowledge-Based Systems*, vol. 178, no. 15, pp. 48–50, 2019.

[24] Z. Huang, Y. Liu, C. Zhan, C. Lin, W. Cai, and Y. Chen, "A novel group recommendation model with two-stage deep learning," *IEEE Transactions on Systems, Man, and Cybernetics: Systems*, 2021, in Press.

Hindawi
Computational Intelligence and Neuroscience
Volume 2022, Article ID 7261551, 9 pages
https://doi.org/10.1155/2022/7261551

Research Article

Image Shadow Detection and Removal Based on Region Matching of Intelligent Computing

Junying Feng ,[1,2] Yong Kwan Kim ,[2] and Peng Liu [1]

[1] *School of Intelligent Manufacturing, Weifang University of Science and Technology, Shandong, Weifang 261000, China*
[2] *Department of Information and Communication Engineering, Hoseo University, Chungcheongnam-do, Asan, 31499, Republic of Korea*

Correspondence should be addressed to Junying Feng; fengjunying@wfust.edu.cn

Received 8 March 2022; Revised 17 March 2022; Accepted 2 April 2022; Published 20 April 2022

Academic Editor: Xin Ning

Shadow detection and removal play an important role in the field of computer vision and pattern recognition. Shadow will cause some loss and interference to the information of moving objects, resulting in the performance degradation of subsequent computer vision tasks such as moving object detection or image segmentation. In this paper, each image is regarded as a small sample, and then a method based on material matching of intelligent computing between image regions is proposed to detect and remove image shadows. In shadow detection, the proposed method can be directly used for detection without training and ensures the consistency of similar regions to a certain extent. In shadow removal, the proposed method can minimize the influence of shadow removal operation on other features in the shadow region. The experiments on the benchmark dataset demonstrate that the proposed approach achieves a promising performance, and its improvement is more than 6% in comparison with several advanced shadow detection methods.

1. Introduction

Although the shadow in the image is a kind of image information, it often interferes with object recognition, image segmentation, and other image processing work. Therefore, the detection and removal of shadow have been widely concerned. The difficulty of shadow detection lies in the complexity of background and light in the image, as well as the interference of dark objects in the image. The difficulty of shadow removal is to ensure that only the shadow is removed without changing other image features in the shadow region.

Inspired by the relevant articles on shadow detection and removal through region matching and other methods [1, 2], this paper proposes a shadow detection and removal method based on interarea material matching without training. This method can accurately detect the shadow region and minimize the impact of shadow removal on other features in the shadow region.

The contributions of this paper are as follows. (1) In shadow detection, based on the mutual restriction between image region features and matching region, this method can detect directly without training. (2) In shadow removal, the shadow region is restored according to the region matching. The calculation time is very short. Other features in the shadow region can be kept unchanged to a great extent, and only the shadow is restored.

The remainder of this paper is organized as follows. Section 2 introduces the related works of our proposed approach. In Section 3, we present the processes of shadow detection and removal. The experiments and experimental results' analysis are described in Section 4, and finally, this paper is briefly summarized in Section 5.

2. Related Works

At present, the commonly used shadow detection and removal methods are divided into three directions: the method based on a physical model, the method based on basic image features, and the method based on machine learning. At the same time, there are many ways to combine these directions.

2.1. Shadow Detection

2.1.1. Shadow Feature. At present, shadow detection based on image features is widely studied, mainly to extract some changing and invariant features in shadow. Zhu et al. [3] proposed a variety of features that change and remain unchanged under the shadow in the gray image, including the features of distinguishing dark objects from shadow regions. Lalonde et al. [4] emphasized the local features of the image and determined the shadow boundary quickly by comparing the features of adjacent regions. Chung et al. [5] proposed a single feature threshold method for directly distinguishing shadow regions. Dong et al. [6] proposed the characteristics of brightness and change rate. Some color-related features were mentioned in [1, 7] to distinguish shadow regions.

2.1.2. Machine Learning Method. Currently, a lot of works combined the direct distinction of original features with machine learning algorithms to train classifiers to distinguish shadow regions under the premise of data-driven [1, 3, 4, 8]. At the same time, for the models that distinguish each pixel separately, most of the works used CRF, MRF, and other similar models to maintain regional consistency [3, 9–11]. With the development of deep learning algorithms in recent years, deep learning models have also been applied to shadow detection [9, 10, 12]. Deep learning models make the original feature engineering no longer necessary, but these algorithms are often based on a large amount of data and need a long time for model training.

2.2. Shadow Removal. User assistance shadow removal can be completed under two conditions: automatic image shadow detection and input of some image information with user assistance. Different from the earlier user assistance that requires users to clearly input various complex information such as shadow contour [13–15], at present, some user assistance methods only need to input a small amount of information to obtain good results [16–18].

2.2.1. Shadow Removal Algorithm. At present, many shadow removal algorithms are based on shadow matting [1, 9], that is, to decompose the image into the form of some parameters acting on the original unshaded image, and then remove the shadow by calculating these parameters. On the basis of shadow detection, shadow boundary and image reorganization with shadow can be used to remove shadow [19–21]. Vicente and Samaras [2] proposed a method to restore the shadow by using the adjacent region of the shadow region, but this method required the shadow region to have the same material as its adjacent region. At the same time, some recent machine learning algorithms and deep learning methods also have good performance in shadow removal [9, 12, 22].

3. The Proposed Method

The proposed method in this paper is based on image region matching and image optical features. Firstly, the Meanshift [23] algorithm is used to segment the image into a total of n regions. Each region is recorded as S_i, and the center is C_i. Then, match the region with the closest material for each region (see Section 3.1). Shadow detection (see Section 3.2) and shadow removal (see Section 3.3) are realized according to region matching. The overall pipeline is shown in Figure 1.

3.1. Region Matching Calculation. Since the color, saturation, and other features will change in the shadow region and the target is looking for the region with the most similar materials, the features used in region matching are the two shadow-invariant features mentioned in reference [3]: gradient feature and texture feature.

3.1.1. Gradient Feature. The gradient change of the image region is hardly affected by shadow. The gradient similarity between regions with similar materials is stronger. In order to extract this feature, a histogram is calculated using the gradient value of each region in the image, and the similarity between regions is measured through the Euclidean distance of the histograms between two regions.

3.1.2. Texture Feature. Image surface texture features are almost independent of shadows. Specifically, the method in reference [24] is used to extract texture features. Similarly, the similarity between regions is measured by calculating the Euclidean distance of the histograms of two regions.

3.1.3. Distance between Regions. In order to ensure the local consistency, the distance between the central points of the two regions is added as the factor to judge the regional similarity. The calculation of similarity between regions is shown in the following equation:

$$D_{i,j} = D_{\text{gradient}_{i,j}} + D_{\text{texture}_{i,j}} + D_{\text{distance}_{i,j}}, \tag{1}$$

where $D_{\text{gradient}_{i,j}}$, $D_{\text{texture}_{i,j}}$, and $D_{\text{distance}_{i,j}}$, respectively, represent gradient feature similarity, texture feature similarity between regions i, j, and distance between center points of regions i, j.

3.2. Shadow Detection. In shadow detection, on the one hand, the shadow is judged by the shadow features; on the other hand, the shadow is judged by the mutual restriction between regions.

3.2.1. Feature Selection. In color images, color tone is a powerful descriptor that simplifies and dominates feature identification and extraction in visual pattern recognition applications. Shadow detection and removal require separate chrominance and luminance information. Since the image represented by the RGB color space is a mixture of

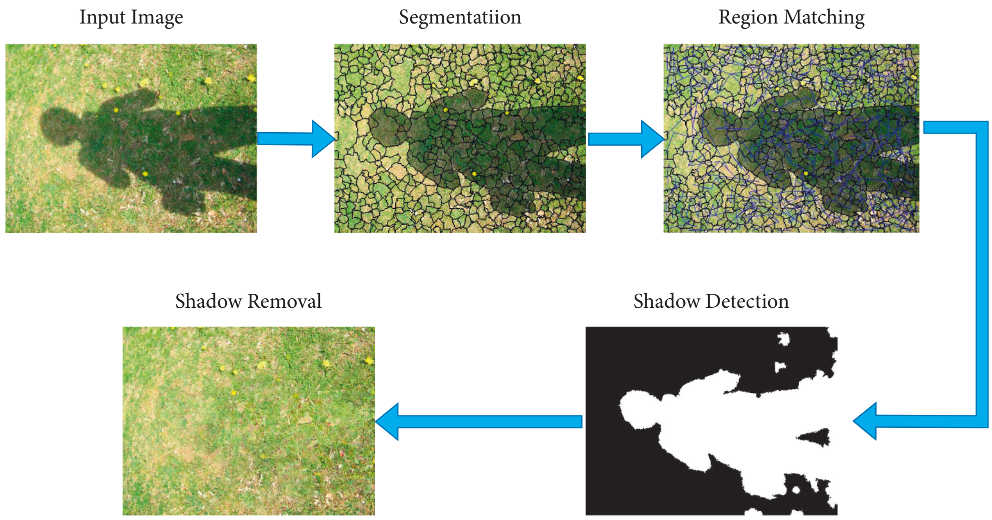

Figure 1: Pipeline of the proposed method.

chrominance and luminance information into the three components of R, G, and B, we need some other color models to handle shadow. There are five invariant color models, HSI model, HSV model, HCV model, YIQ model, and YCbCr model. All of the models consist of independent chromaticity and luminance. We select three common color space models to detect and remove shadows.

(1) Y-channel information in YCbCr color space: convert the original image from RGB color space to YCbCr color space. According to the method mentioned in reference [25], when the value of a pixel on the Y-channel in YCbCr space is less than 60% of the average value of the Y-channel of the whole image, it can be directly considered that the pixel is in shadow. In the algorithm introduced in Section 3.2.2, when the average value of the Y-channel of a region is less than 60% of the average value of the Y-channel of the whole image, this region is considered in the shadow. Take the average value from the region S_i and record the feature as Y_i.

(2) HSI color space information: convert the original image from RGB space to HSI space and then normalize the values on H and I channels to the [0, 1] interval to obtain H_e and I_e. According to the method in reference [5], the value in equation (2) is extracted for each pixel as another feature of the image. Take the average value from the region S_i and record the feature as R_i.

$$R(x, y) = \frac{H_e(x, y) + 1}{I_e(x, y) + 1}. \tag{2}$$

$R(x, y)$, $H_e(x, y)$, and $I_e(x, y)$ represent pixel at position (x, y) in R, image H_e, and image I_e, respectively.

(3) HSV color space information: convert the original image from RGB space to HSV color space. We utilize the chrominance channel H as the other feature. Take the average value from the region S_i and record the feature as H_i.

3.2.2. The Proposed Algorithm. Figure 2 shows the flowchart of the shadow detection approach.

The specific implementation steps of the proposed shadow detection method are as follows.

Variable Preparation.

(1) Segment image with Meanshift algorithm and then obtain n regions; each region is remarked as S_i. The center of each region is C_i.

(2) Compute the disparity between S_i and S_j and get the corresponding region with the highest similarity for a given region which is denoted as Near_i. At the same time, record the information label_i of whether the region i is in shadow and initialize label_i to 255. The similarity of regions i and j is computed as equation (1).

(3) For all R_i, $1 < i < n$, use K-means algorithm to calculate two centers C_{shadow} and C_{lit} which, respectively, represent whether it is the feature center of the shadow region. Suppose R follows a normal distribution; the standard deviations $\text{Std}_{\text{shadow}}$ and Std_{lit} are calculated, which correspond to C_{shadow} and C_{lit}, respectively. Then, for every R_i, F_{shadow} and F_{lit} corresponding to C_{shadow} and C_{lit} are computed.

(4) For each region S_i, Refuse_i represents whether S_i is forbidden to be a shadow region because of other regions, and Refuse_i is initialized to 0.

Steps.

(1) Extract features Y_i and R_i and prepare relevant variables.

(2) If $Y_i < 60\% * \text{mean}(Y_{\text{image}})$, $\text{label}_i = \text{shadow}$.

(3) Select the region S_i with the greatest F_{shadow} and $\text{Refuse}_i = 0$, and set $\text{label}_i = \text{shadow}$.

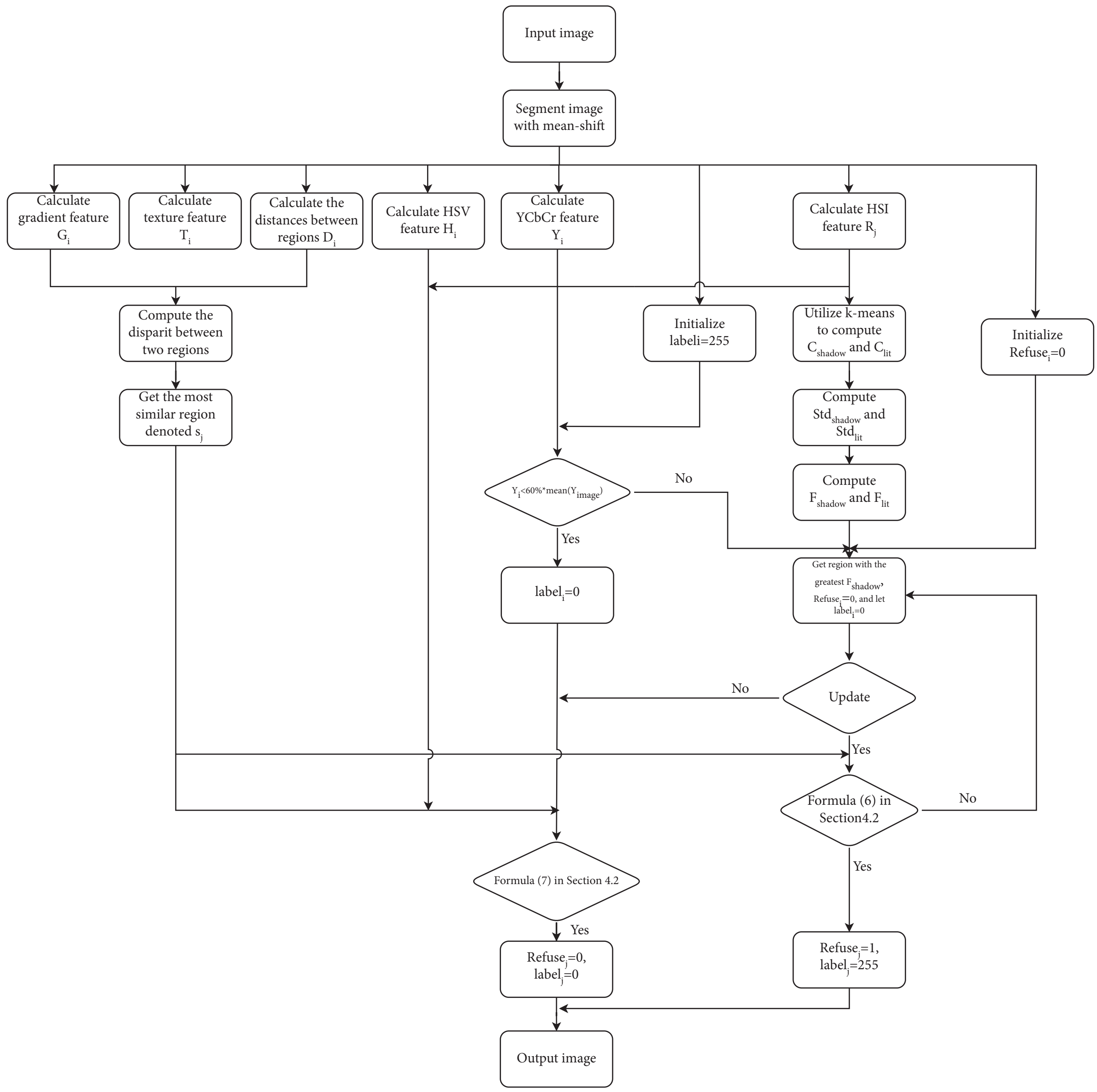

Figure 2: The flowchart of the shadow detection.

(4) Denote the nearest region Near_i of S_i as S_j. Check whether S_i and S_j are brightness opposite regions by comparing R_i and R_j, and if so, then judge $\text{Refuse}_j = 1$.

(5) Iteratively execute steps (3) and (4) until no update.

(6) For the region S_i of label_i = shadow, if the brightness of S_i is similar to S_j and $\text{Refuse}_j = 0$ by comparing Y_i, Y_j, R_i, R_j, set $\text{label}_j = 0$.

3.3. Shadow Removal. Shadow removal is mainly carried out in HSV color space. The overall idea is to find the corresponding region S_j for the shadow region S_i to meet $\text{label}_j = 1$ and minimize $D_{i,j}$. Therefore, S_j is the most similar non-shaded region of S_i. Consider using S_j to adjust the brightness of S_i, remove the shadow on the S_i through the histogram matching algorithm, and minimize the impact of the operation on other features. The flowchart of shadow removal is shown in Figure 3.

3.3.1. Histogram Matching. Supposing the feature of region S_i as Feature_i, given template histogram Hist_T, the purpose of histogram matching is to ensure that the overall offset conforms to the distribution of the template T under the condition of ensuring the minimum change of mutual distributions between Feature_i. The specific methods are as follows.

(1) Calculate the histogram Hist_i of Feature_i with the number of bins equal to T.

(2) The cumulative histograms Acc_i and Acc_T are calculated for Hist_i and Hist_T, respectively.

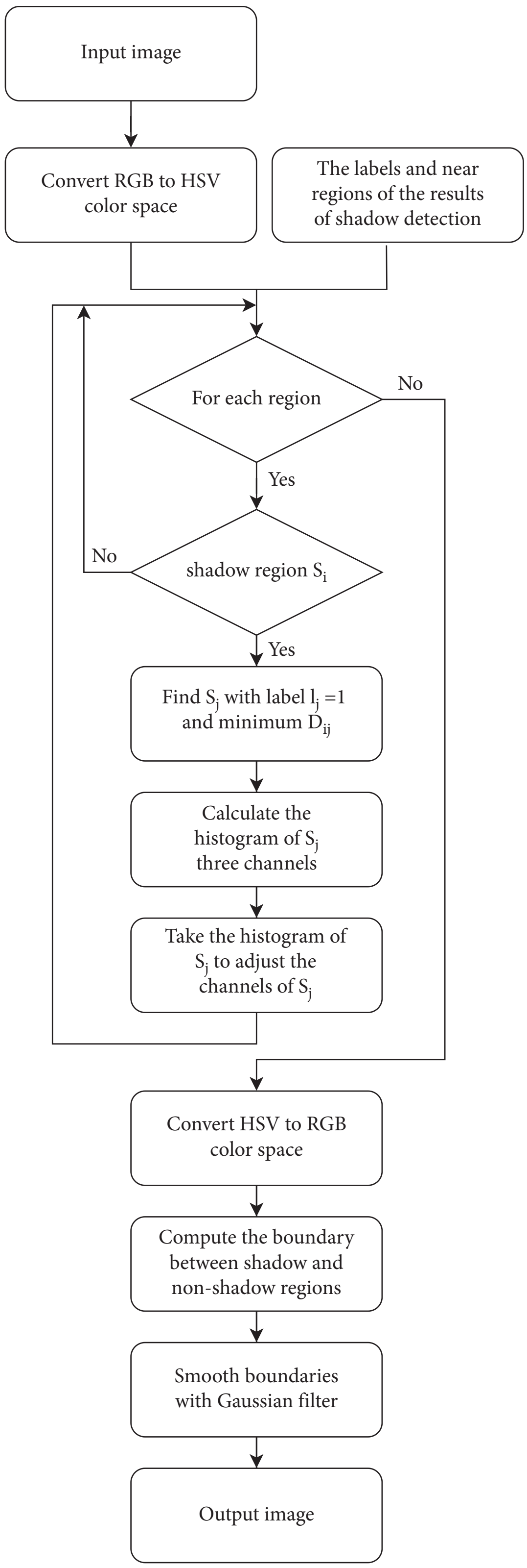

Figure 3: The flowchart of the shadow removal.

(3) For each stripe p in Acc_i, calculate the bin number q with the smallest interpolation among Acc_i.

(4) Move each bin p to the position q.

3.3.2. The Proposed Algorithm. The specific implementation steps of the proposed shadow removal method are as follows.

(1) Calculate the shadow detection result label and convert the image to HSV space at the same time.

(2) Repeat steps (3)–(5) for each shadow region S_i.

(3) For region S_i, find S_j with label$_j$ = 1 and minimum $D_{i,j}$, and use S_j to relight S_i.

(4) In the HSV color space, compute the histograms $\text{Hist}_{H,j}$, $\text{Hist}_{S,j}$ and $\text{Hist}_{V,j}$ of S_j in the three channels H, S, and V, respectively..

(5) Take $\text{Hist}_{H,j}$, $\text{Hist}_{S,j}$, $\text{Hist}_{V,j}$ as the template of histogram matching and adjust the three features of S_i, so that the feature distribution is close to the template.

(6) Convert the image to RGB space.

(7) Calculate the intersection boundary of all shadow regions and non-shaded regions in the image and then smooth all boundaries using a Gaussian filter.

4. Experiments

Experiments are conducted on the shadow dataset SBU [26]. SBU dataset is a large shadow detection dataset, which contains 4727 images, and each image has a ground truth based on pixel markers. In order to quantitatively evaluate the effectiveness of the proposed method and comparative methods, the commonly used indexes such as recall, specificity, and balanced error rate (BER) are used as the evaluation indexes, which are defined as follows:

$$\begin{aligned} \text{recall} &= \frac{\text{TP}}{\text{TP} + \text{FN}}, \\ \text{specificity} &= \frac{\text{TN}}{\text{TN} + \text{FP}}, \\ \text{BER} &= 1 - 0.5 * (\text{recall} + \text{specificity}), \end{aligned} \tag{3}$$

where *TP* indicates that the real shadow is correctly classified, *FN* indicates that the real shadow is incorrectly classified as non-shaded, *TN* indicates that the non-shaded pixels are correctly classified, and *FP* indicates that the non-shaded pixels are incorrectly classified as shadow pixels. The higher the recall is, the more the shadow pixels are found. The higher the specificity is, the more the non-shaded pixels are recalled. Recall and specificity are considered a pair of contradictions. The comprehensive performance of the algorithm is tested by BER. The smaller the BER, the better the shadow detection performance.

4.1. Region Matching. Region matching is shown in Figure 4. The blue line in the figure connects the center of each pair of matching regions. It can be seen that when the image segmentation is more accurate, the nearest region matching is also more accurate.

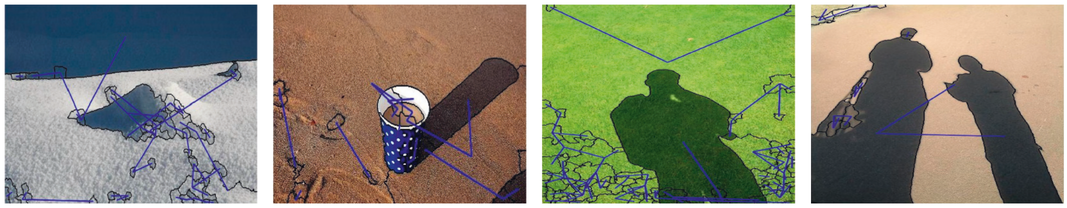

FIGURE 4: Most similar region matching.

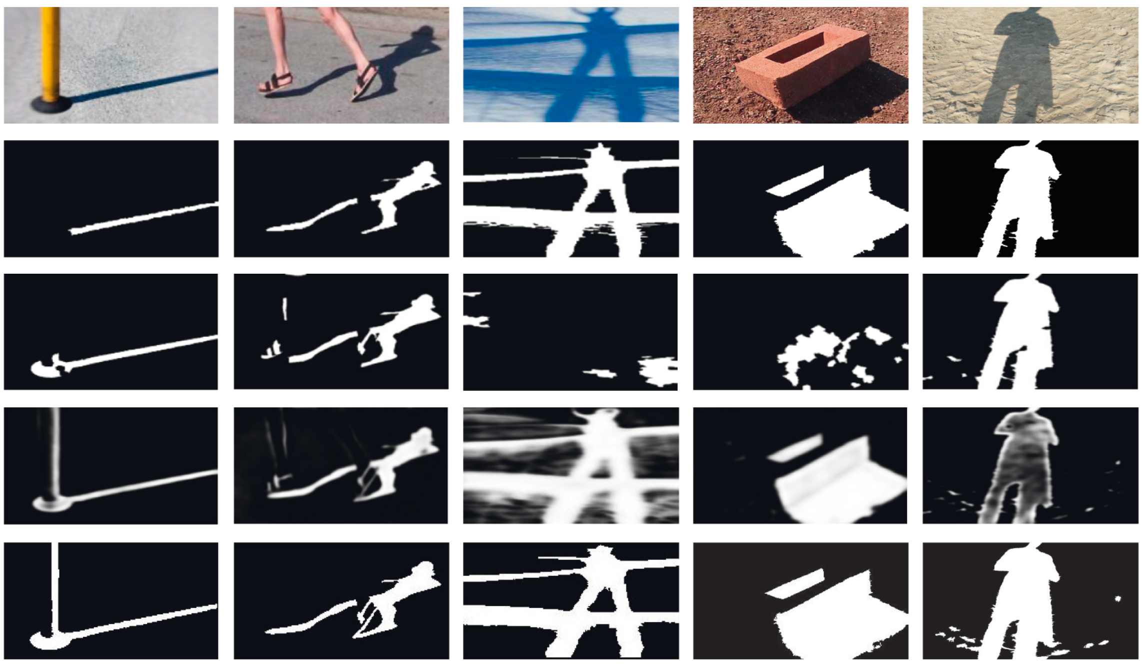

FIGURE 5: Qualitative comparison of the proposed method with other methods. Rows from top to bottom: input images, ground truths, results of the Unary-Pairwise method, results of the Stacked-CNN method, and results of the proposed method.

4.2. Shadow Detection. The parameter setting of shadow detection is mainly in steps (4) and (6) of Section 3.2.2.

In step (4), when equation (4) is satisfied between S_i and S_j, it is considered that the label properties of R_i and R_j are opposite, and set $\text{Refuse}_j = 1$.

$$\frac{R_i - C_{\text{shadow}}}{\text{Std}_{\text{shadow}}} - \frac{R_j - C_{\text{shadow}}}{\text{Std}_{\text{shadow}}} > 3, \tag{4}$$

where R_i and R_j are the features of shadow detection in the region S_i and S_j. The value of R_i ado R_j can be computed by equation (2). C_{shadow} is the feature center of the shadow areas, and $\text{Std}_{\text{shadow}}$ is the standard deviation corresponding to the C_{shadow}. Step (3) of Section 3.2.2 describes the details.

In step (6), when equation (5) is satisfied between S_i and S_j, it is considered that the label properties of S_i and S_j are the same, and set $\text{label}_j = 0$.

$$\frac{\min\left(H_i, H_j\right)}{\max\left(H_i, H_j\right)} + \frac{\min\left(Y_i, Y_j\right)}{\max\left(\left(Y_i, Y_j\right)\right.} + \frac{\min\left(R_i, R_j\right)}{\max\left(R_i, R_j\right)} > 2.5, \tag{5}$$

where H_i, Y_i, R_i, H_j, Y_j, and R_j are the shadow detection features of regions S_i and S_j, respectively.

TABLE 1: Evaluation of shadow detection methods on SBU dataset.

Method	Recall	Specificity	BER
Unary-Pairwise	0.5636	0.9357	0.2504
Stacked-CNN	**0.8609**	0.9059	0.1166
Our method	0.8460	**0.9361**	**0.1090**

The bold entries indicate the best result in a given column.

TABLE 2: Time complexity of shadow detection methods on the SBU dataset.

Method	Testing (hours)	Testing (sec/image)	Training (hours)
Unary-Pairwise	9.13	51.56	~
Stacked-CNN	25.08	141.56	9.4
Our method	**3.08**	**17.40**	~

The bold entries indicate the best result in a given column.

3 and 2.5 are empirical constants. Tuning of the parameters is outside the scope of the current work.

The performance of the proposed shadow detection method is evaluated by comparing it with two commonly used methods: Unary-Pairwise [27] and Stacked-CNN [26].

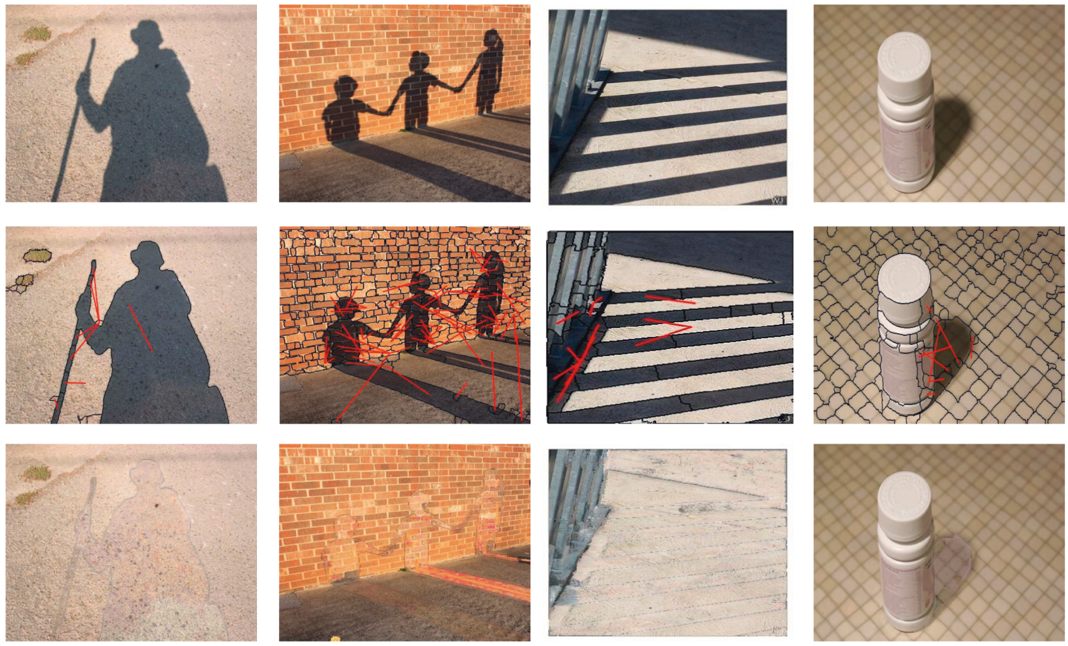

Figure 6: Qualitative analysis results of the proposed shadow removal method on the SBU dataset. Rows from top to bottom: input images, shadow removal matching regions, and shadow removal images.

Figure 7: Failed images for shadow removal on the dataset.

The Unary-Pairwise method is one of the best statistical methods to detect shadows from a single image. The Stacked-CNN method is a shadow detection method based on the deep learning framework using shadow prior map.

4.2.1. Qualitative Analysis. Figure 5 shows the shadow detection results of some images in the SBU dataset.

It can be seen from the third line of Figure 5 that the Unary-Pairwise method has good shadow detection results in some images, but almost no shadow is detected in columns 3 and 4. The fourth line of Figure 5 shows the shadow detection results of the Stacked-CNN method, which can detect all correct shadows, but the visual effects of some results are blurred.

As can be seen from the last line of Figure 5, the proposed method has relatively small error in image shadow detection, but the detection is basically correct. The consistency of shadow regions is ensured by region matching. It should be noted that in the images in column 1, the black base of the pole is detected as a shadow, which is caused by the similar color features between the black base and the shadow. Objects with color features similar to shadow will reduce the precision of shadow detection.

4.2.2. Quantitative Analysis. Table 1 shows the results of quantitative analysis on the SBU dataset. The proposed method can improve the detection rate of shadow and non-shaded regions. Obviously, recall and specificity are considered a pair of contradictions. Considering the performance of shadow detection, the BER metric is used, and the proposed method effectively reduces the BER.

The Stacked-CNN method can detect most shadow pixels in the dataset, but it also causes pixels in non-shaded areas to be insufficiently recalled. Some non-shaded pixels are wrongly classified as shadow pixels, resulting in blurred shadow detection images, which is consistent with the results of qualitative analysis. The Unary-Pairwise method has the lowest recall of shadow pixels on a large-scale shadow detection dataset. This is because of the false pairing between regions due to the loose constraints. Although the recall of the proposed method is lower than that of the Stacked-CNN method, the precision is higher. On average with BER, the improvement made by the proposed method is more than 6% which is impressive.

In Table 2, we show the execution time of testing phases of the proposed approach. Our method does not need training, and it works faster than the statistical method and one order of magnitude faster than the deep learning method.

4.3. Shadow Removal. The parameters of shadow removal are set in step (7) of Section 3.3.2, in which Gaussian blur is applied to the points whose distance from the edge pixel is less than or equal to 2, and the parameters of Gaussian blur are set to $h$size = 15, $\sigma = 15$.

The second line of Figure 6 shows the shadow removal process of some images in SBU dataset, in which the red lines connect and match the corresponding shadow region S_i and non-shaded region S_j. Use S_j to relight S_i through the algorithm in Section 3.3.2.

The third line of Figure 6 shows the shadow removal results of the images. It can be seen that the regions after removing shadow through region matching maintain the original texture features, but the brightness changes. The image after removing shadow has an obvious boundary around the original shadow region, but the edge effect is significantly weakened after Gaussian smoothing.

Through experiments, it is found that not all the shadows of the image can be removed correctly. Two failed shadow removal scenarios are shown in Figure 7. In the first image, the shadow occupies most of the image, and the shadow is evenly distributed in the image, which will lead to the uniform distribution of image feature histogram, and the non-shaded region is not enough to remove the shadow region. In the second image, the shadows of multiple objects are complex, and the fire hydrant is almost completely in shadow, resulting in the wrong shadow removal matching, so the shadows cannot be removed correctly.

In this work, the experiments are run on a PC with a 3.6 GHz CPU and 8G RAM in the Matlab 2018b environment under Windows 10.

5. Conclusion

Experiments show that the shadow detection and removal algorithm based on region matching is effective. In the aspect of shadow detection, the consistency of images can be guaranteed to a certain extent through the mutual restriction of regions with the same material; in the aspect of shadow removal, the method of brightening the shadow by the region with similar material can minimize the impact of shadow removal on the non-shaded features in the shadow region.

The limitation of the method proposed in this paper is that it is difficult to ensure the accuracy of region matching for complex images. Therefore, in shadow detection and shadow removal, it will bring wrong constraints due to wrong matching or restore the region to the wrong material. At the same time, this algorithm is based on Meanshift image segmentation technology, which is difficult to segment accurately in complex images.

The further improvement mainly lies in the calculation of the material matching region. First, using more and more datasets, the matching region is given by training classifiers and other methods. Second, adding more shadow-invariant features to improve the accuracy of region matching in complex images will be taken into account.

Data Availability

The data used to support the findings of this study are included within the article.

Conflicts of Interest

The authors declare that there are no conflicts of interest regarding the publication of this paper.

References

[1] R. Guo, Q. Dai, and D. Hoiem, “Paired regions for shadow detection and removal,” *IEEE Transactions on Pattern Analysis and Machine Intelligence*, vol. 35, no. 12, pp. 2956–2967, 2013.

[2] T. F. Y. Vicente and D. Samaras, “Single image shadow removal via neighbor-based region relighting,” in *Proceedings of the European Conference on Computer Vision*, pp. 309–320, Munich, Germany, September, 2014.

[3] J. Zhu, K. G. Samuel, S. Z. Masood, and M. F. Tappen, “Learning to Recognize Shadows in Monochromatic Natural Images,” in *Proceedings of the 2010 IEEE Computer Society conference on computer vision and pattern recognition*, pp. 223–230, San Francisco, CA, USA, June, 2010.

[4] J.-F. Lalonde, A. A. Efros, and S. G. Narasimhan, “Detecting ground shadows in outdoor consumer photographs,” in *Proceedings of the European Conference on Computer Vision*, pp. 322–335, Heraklion, Crete, Greece, September, 2010.

[5] K.-L. Chung, Y.-R. Lin, Y.-H. J. I. T. o. G. Huang, and R. sensing, “Efficient shadow detection of color aerial images based on successive thresholding scheme,” vol. 47, no. 2, pp. 671–682, 2008.

[6] Q. Dong, Y. Liu, Q. Zhao, H. Yang, and graphics, “Detecting soft shadows in a single outdoor image: from local edge-based models to global constraints,” *Computers & Graphics*, vol. 38, pp. 310–319, 2014.

[7] A. Panagopoulos, C. Wang, D. Samaras, and N. Paragios, “Estimating shadows with the bright channel cue,” in *European Conference on Computer Vision*, pp. 1–12, Springer, Berlin, Heidelberg, 2010.

[8] T. F. Y. Vicente, M. Hoai, and D. Samaras, “Leave-one-out kernel optimization for shadow detection and removal,” *IEEE Transactions on Pattern Analysis and Machine Intelligence*, vol. 40, no. 3, pp. 682–695, Mar 2018.

[9] S. H. Khan, M. Bennamoun, F. Sohel, R. J. I. t. o. p. a. Togneri, and m. intelligence, “Automatic shadow detection and removal from a single image,” vol. 38, no. 3, pp. 431–446, 2015.

[10] S. H. Khan, M. Bennamoun, F. Sohel, and R. Togneri, “Automatic feature learning for robust shadow detection,” in *Proceedings of the 2014 IEEE Conference on Computer Vision and Pattern Recognition*, pp. 1939–1946, IEEE, Columbus, OH, USA, June, 2014.

[11] T. F. Y. Vicente, C.-P. Yu, and D. Samaras, “Single Image Shadow Detection Using Multiple Cues in a Supermodular

MRF," in *Proceedings of the BMVC*, Aberystwyth, UK, January, 2013.

[12] L. Qu, J. Tian, S. He, Y. Tang, and R. W. Lau, "Deshadownet: a multi-context embedding deep network for shadow removal," in *Proceedings of the IEEE Conference on Computer Vision and Pattern Recognition*, pp. 4067–4075, Honolulu, HI, USA, July, 2017.

[13] E. Arbel, H. J. I. t. o. p. a. Hel-Or, and m. intelligence, "Shadow removal using intensity surfaces and texture anchor points," vol. 33, no. 6, pp. 1202–1216, 2010.

[14] F. Liu and M. Gleicher, "Texture-consistent shadow removal," in *European Conference on Computer Vision*, pp. 437–450, Springer, Berlin, Heidelberg, 2008.

[15] Y.-F. Ya-Fan Su and H. H. J. I. T. o. I. P. Chen, "A three-stage approach to shadow field estimation from partial boundary information," *IEEE Transactions on Image Processing*, vol. 19, no. 10, pp. 2749–2760, 2010.

[16] Y. Shor and D. Lischinski, "The shadow meets the mask: pyramid-based shadow removal," in *Computer Graphics Forum*, vol. 27, no. 2, pp. 577–586, Wiley Online Library, 2008.

[17] H. Gong and D. Cosker, "Interactive Shadow Removal and Ground Truth for Variable Scene Categories," in *Proceedings of the BMVC*, pp. 1–11, Nottingham, September, 2014.

[18] X. Yu, G. Li, Z. Ying, and X. Guo, "A new shadow removal method using color-lines," in *Proceedings of the Computer Analysis of Images and Patterns*, pp. 307–319, Seville, Spain, July, 2017.

[19] G. D. Finlayson and C. Fredembach, "Fast Re-integration of shadow free images," *Color and Imaging Conference*, vol. 2004, no. 1, pp. 117–122, 2004.

[20] C. Fredembach and G. Finlayson, "Hamiltonian path-based shadow removal," in *Proceedings of the 16th British Machine Vision Conference (BMVC)*, vol. 2, pp. 502–511, CONF, Oxford, UK, September, 2005.

[21] G. D. Finlayson, S. D. Hordley, and M. S. Drew, "Removing shadows from images," in *European Conference on Computer Vision*, pp. 823–836, Springer, Berlin, Heidelberg, 2002.

[22] L. Fu, "Auto-exposure fusion for single-image shadow removal," in *Proceedings of the IEEE/CVF Conference on Computer Vision and Pattern Recognition*, pp. 10571–10580, Nashville, TN, USA, June, 2021.

[23] D. Comaniciu, P. Meer, and m. intelligence, "Mean shift: a robust approach toward feature space analysis," *IEEE Transactions on Pattern Analysis and Machine Intelligence*, vol. 24, no. 5, pp. 603–619, 2002.

[24] D. R. Martin, C. C. Fowlkes, J. Malik, and m. intelligence, "Learning to detect natural image boundaries using local brightness, color, and texture cues," *IEEE Transactions on Pattern Analysis and Machine Intelligence*, vol. 26, no. 5, pp. 530–549, 2004.

[25] C. Blajovici, P. J. Kiss, Z. Bonus, and L. J. P. o. t. S. Varga, "19th summer school on image processing," *Shadow Detection and Removal from a Single Image*, pp. 7–16, Springer, Szeged, Hungary, 2011.

[26] T. F. Y. Vicente, L. Hou, C.-P. Yu, M. Hoai, and D. Samaras, "Large-scale training of shadow detectors with noisily-annotated shadow examples," in *European Conference on Computer Vision*, pp. 816–832, Springer, Berlin, Heidelberg, 2016.

[27] R. Guo, Q. Dai, and D. Hoiem, "Single-image shadow detection and removal using paired regions," in *Proceedings of the CVPR 2011*, pp. 2033–2040, IEEE, Colorado Springs, CO, USA, June, 2011.

Hindawi
Computational Intelligence and Neuroscience
Volume 2022, Article ID 4204644, 9 pages
https://doi.org/10.1155/2022/4204644

Research Article

Human Health Activity Recognition Algorithm in Wireless Sensor Networks Based on Metric Learning

Dejie Sun ,[1] Jie Zhang ,[2] Shuai Zhang,[1] Xin Li,[1] and Hangong Wang[1]

[1]*School of Mathematics and Information Science and Technology, Hebei Normal University of Science and Technology, Qinhuangdao 066004, China*
[2]*School of Information Science and Engineering (School of Software), Yanshan University, Qinhuangdao 066000, China*

Correspondence should be addressed to Jie Zhang; zhangjie@ysu.edu.cn

Received 20 January 2022; Revised 8 February 2022; Accepted 10 February 2022; Published 18 April 2022

Academic Editor: Xin Ning

Wireless sensor network is an ad hoc network with sensing capability. Usually, a large number of sensor nodes are randomly deployed in an unreachable environment or complex area for data collection and transmission, which can realize the perception and monitoring of the target area or specific objects and transmit the obtained data to the remote end of the system. Human health activity recognition algorithm is a hot topic in the field of computer. Based on the small sample problem and the linear indivisibility of real samples encountered in metric learning, this paper proposes a human activity recognition algorithm for wireless sensor networks. Human activity recognition algorithm for wireless sensor networks uses human activity recognition algorithm to solve the singularity of intraclass divergence matrix, so as to reduce the impact of small sample problem. The algorithm maps two different feature spaces to the high-dimensional linearly separable kernel space through the corresponding kernel function, calculates the distance between samples in the two projected feature subspaces to obtain two distance measurement functions, and finally linearly combines them with weights to obtain the final distance measurement function.

1. Introduction

The recognition of human health activities is a hot topic in the computer field. Human activities, like language, play an important role in human communication. With the rapid development of mobile terminals, as well as the intelligent development of mobile terminals, today's mobile phones, tablets, and other devices can accurately judge simple human activities using gyroscopes and gravity sensors and send them to opposite target terminals via the network [1]. A wireless sensor network [2, 3] is a distributed network system in which a series of microsensor nodes collect and transmit data using wireless communication. Because of the characteristics and viability of this technology, this paper develops a set of human activity recognition algorithms for mobile terminals and employs wireless sensor networks to implement a series of complex commands for controlling computer terminals from mobile terminals. A wireless sensor network is a sensor-capable ad hoc network. Typically, a large number of sensor nodes are randomly deployed in environments or complex areas that are inaccessible to humans to collect and transmit data, realize perception and monitoring of target areas or specific objects, and transmit the acquired data to the system's remote end [4, 5]. For the elderly living alone, using the behavior recognition technology based on wireless sensor network to build an intelligent monitoring system indoors can not only send alarm signals in time to prevent accidents of the elderly, but also make intelligent decision-making and behavior recommendation by monitoring their daily activities [6]. For example, we can monitor the user's behavior of boiling water and then use the previous life records to find out from the data that the user has the behavior of boiling water from 8 : 00 to 9 : 00 every morning. According to this rule, we can set the electric water heater to work at 8 : 00 a.m. [7, 8].

Based on the small sample problem encountered in metric learning and the linear indivisibility of real samples, a human activity recognition algorithm for wireless sensor networks is proposed [9]. Human activity recognition algorithm for wireless sensor networks uses human activity recognition algorithm to solve the singularity of intraclass divergence matrix, so as to reduce the impact of small sample problem. The human activity recognition algorithm maps the samples from the linear nonseparable original feature space to the linearly separable high-dimensional feature space through the chi-square kernel function, then constructs the divergence matrix describing the proximity relationship between samples in the high-dimensional space, and finally obtains the projection matrix from high-dimensional to low-dimensional space by regularized linear discriminant analysis, so that the samples can still maintain the separability of high-dimensional space in low-dimensional shadow space, so as to improve the classification effect. The purpose of the method based on metric learning is to design a representation model of human activity recognition algorithm with wireless sensor networks [10, 11]. The extracted features should be robust to changes such as illumination and viewing angle and can distinguish different human activities. The most commonly used features in human activity re-recognition are color features and texture features [12, 13].

The essence of human activity recognition algorithm in wireless sensor networks based on metric learning is to learn a distance metric function through training samples, which can effectively classify samples, and make the distance between similar samples as small as possible and the distance between different samples as large as possible. Considering the difference of descriptive ability of different features, a pedestrian re-recognition algorithm based on kernel regularization linear discriminant analysis is proposed by using the idea of multifeature subspace [14]. In this algorithm, two different feature spaces are mapped to the high-dimensional linearly separable kernel space through the corresponding kernel functions, and then the projection matrices of the two feature spaces are obtained by performing regularized linear discriminant analysis in the kernel space, and the distances between samples are calculated in the two projection feature subspaces to obtain two distance measurement functions, and finally the final distance measurement function is obtained by linearly combining them with weights [15]. However, in actual research, the human activity recognition algorithm is complicated and its accuracy is low, and the effect will be even worse when processing a large amount of data, so improving recognition accuracy has become the most important task of human activity recognition at the moment. This paper focuses on a metric learning-based algorithm for human activity recognition, with the goal of learning the relationship between data using this method, making the relationship more beneficial to the recognition task, and thus improving the accuracy of human activity recognition.

2. Related Work

Binary sensors and motion sensors, according to [16], are used to identify ADL in the elderly. Human behavior recognition research can be divided into two categories: the first is image vision recognition, which uses image equipment to generate pictures or videos and monitor user behavior. Reference [17] employs a convolutional neural network to learn behavior data automatically using a big data analysis method to select the best features. A feature fusion method is proposed in light of the overfitting phenomenon of data labels in the learning process, which strengthens the ability of feature learning and improves the discrimination of behavior features. Although this method solves the problem of data label overfitting, it adds to the data complexity and slows down the process. Taking the video data provided by the image equipment as input, [18] proposes a moving human body segmentation algorithm based on interframe difference and an improved C-V model. The algorithm can solve the problem of recognizing moving human body behavior in complex situations and provide real-time alarms for security and monitoring systems. According to [19], wireless sensor networks have a solid business foundation as well as theoretical research significance, whether in astronomy, basic people's livelihood, or human activities. Many applications requiring the location of nodes in wireless sensor networks on a large scale, such as animal survival ecology monitoring, activity range monitoring, and so on, must solve the problem of obtaining the location of nodes in the network. Literature [20] through the big data analysis method and wireless sensor networks, with their ad hoc characteristics, further expands human vision, enables people to obtain information more safely and conveniently, enables people to explore areas unsuitable for human activities or inaccessible to human beings, and directly and efficiently obtains the information needed by human beings. The research in [21] shows that the hidden Markov model is used to segment the user's daily behavior sequence. According to the characteristics of continuity of actual actions and multisensor data fusion, a dynamic segmentation method of continuous action sequence based on hidden Markov model is proposed, and the result directly affects the accuracy of action recognition. Finally, the average recognition accuracy is 89%. This method only carries out time sequence segmentation for continuous actions and does not take into account discontinuous action sequences. Literature [22] suggests that the process of monitoring by sensors is completely transparent to users and will not affect the daily life and work of the monitored person. Sensor data is collected through a computer network and stored in a database for pattern recognition and prediction. Literature [23] proposes a design framework for data transmission scheduling and a data aggregation scheduling strategy in the network, with the goal of reducing energy consumption and data transmission delay in wireless sensor networks using big data analysis. According to [24], a wireless sensor network can transmit relevant information from the battlefield to a remote terminal without causing a network footprint due to the loss or failure of some nodes in the network, ensuring information acquisition continuity. The method of improving user behavior characteristics is presented in [25]. It proposes an algorithm for enhancing sensor data characteristics and uses the feature enhancement coefficient to express the feature recognition ability of behaviors, addressing issues such as behavior concurrency and peer diversity. Time series features are added to behavior characteristics to highlight features in the data, and the physical meaning of behavior data is improved to make it easier to understand. Although this method solves the behavior concurrency problem, it ignores the behavior similarity problem.

Based on metric learning, this paper studies the human activity recognition algorithm in wireless sensor networks. In this case, the divided time slice is used to represent the activities that occupy most of the time. However, the result is that the situation after the discretization is different from the actual situation. In order to express the difference, the discretization accuracy is introduced. When there is a rejection task, the difficulty of recognition will be increased, because it limits a part of the samples, which will make the training model unstable. Human activity recognition algorithm module is the preprocessing module of this system, which is mainly used to complete the function of human activities. It can disassemble the relationship between specific points, lines, and surfaces of human activities according to specific algorithms, and transmit these data to the calculation module.

3. Human Activity Recognition Algorithm Based on Metric Learning in Wireless Sensor Networks

Measurement Learning: By training and learning the wireless sensor network, we can get the appropriate Markov matrix M, treat the characteristics of different emotional contributions in the wireless sensor network data samples differently, and then measure the similarity of the wireless sensor network data samples more accurately, and finally achieve the goal of improving the accuracy of emotional recognition. The discretization accuracy based on metric learning indicates the percentage of correct labels in the discretized data set, and the data after discretization is used to calculate the performance metric of the model. In this paper, 1 s discrete data is used as the comparison data to evaluate the performance of the model. The algorithm of human activity recognition in wireless sensor networks based on metric learning is based on the solution set of a problem, which is called population, and there are individuals with certain gene coding properties in the solution set, and the individuals can also be considered as chromosomes. Individual chromosomes contain important information, which is expressed by a human activity recognition algorithm through gene combination. Human hair color features, for example, are determined by a gene combination of this feature. If it is to be applied to real-world problems, the first step must be coding, or expressing the characteristics of things through gene coding. A global optimization can be achieved using a human activity recognition algorithm. It differs from a general optimization algorithm in that it starts with the problem's solution set rather than a single solution at the beginning of the search. The search range is initially broad, which can serve as a good foundation for the subsequent steps and make finding the best solution easier. Metric learning is a projective space-friendly non-Euclidean metric. By finding a human activity recognition algorithm in wireless sensor networks, metric learning can reflect the fractional linear transformation of spatial structure information or semantic information of samples and model the potential relationship of training samples; it can improve discrimination. The structure of human activity recognition algorithm is given as shown in Figure 1.

The metric learning algorithm of human activity recognition algorithm draws lessons from the idea of maximum interval of SVM and learns the Markov matrix with the goal that the same sample points are as close as possible, and the different sample points are away from and maintain a large interval. It optimizes the K target nearest neighbors and intrusion samples of the target sample, so that the new feature space and space obtained from the original sample features are mapped. The K samples closest to the target sample belong to the same class, while they maintain a large interval distance from heterogeneous samples. In the process of evaluating individuals, human activity recognition algorithm only needs to calculate the fitness function value without other information. The form of fitness function can also be set for different problems, which increases the application scope of human activity recognition algorithm. In terms of recognition, clustering, and retrieval performance, although the Mahalanobis metric obtained by metric learning is better than Euclidean metric or original Mahalanobis metric, the limitations of the transformation of human activity recognition algorithm make it unable to describe the potential nonlinear relationship of training samples, which limits its application in practice. Because the expression form of the potential Riemannian manifold of the training sample is not known in advance, and the type of nonlinear transformation is also unknown, the Riemannian metric can only be approximately calculated by Euclidean metric on the training data, and the calculation efficiency is very low. In practical applications, Riemannian metric learning is not always better than Markov metric learning in recognition, clustering, and retrieval. As far as we know, there is no important breakthrough research progress in Riemannian metric learning. The framework of human activity recognition is shown in Figure 2.

The pedestrian re-recognition method based on metric learning mainly includes three stages: feature extraction, distance metric learning, and re-recognition. These advantages of human activity recognition algorithm make it widely used in parameter optimization. But its problems can not be ignored, such as nonstandard population coding, premature convergence, local optimum, and so on. In this paper, the distance measurement learning stage is studied, and the algorithm of human activity recognition is proposed. The kernel method is used to map the training samples to the linearly separable feature space, in which the divergence matrix describing the neighborhood relationship between samples is constructed, and finally a projection matrix is obtained. The flowchart analysis of human activity

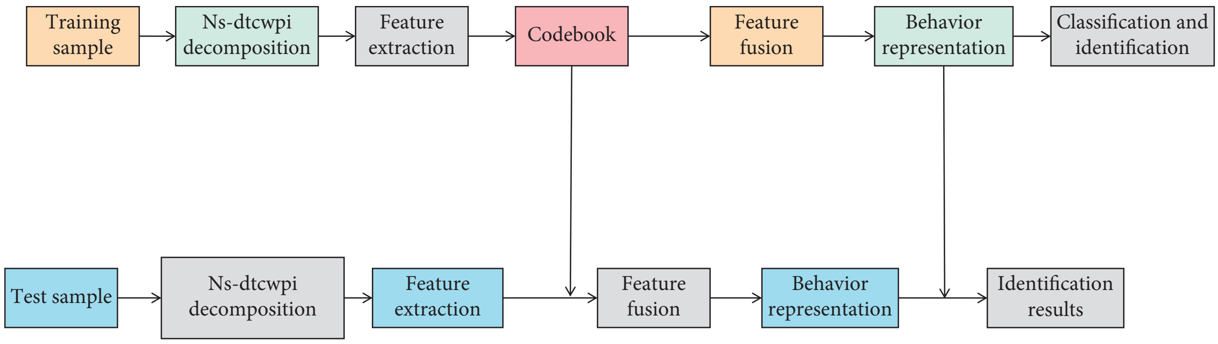

Figure 1: Structure diagram of human activity recognition algorithm.

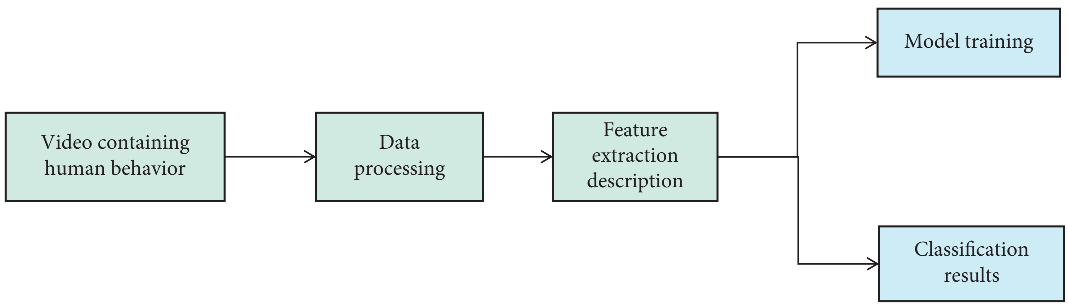

Figure 2: Framework diagram of human activity recognition.

recognition algorithm in wireless sensor networks based on metric learning is shown in Figure 3.

The process of human activity recognition can be divided into two subprocesses: one is to extract human behavior features and fully express human behavior through feature data; the other is to construct recognition algorithm or recognition model according to the obtained features. Although the human activity recognition algorithms based on metric learning proposed in this paper have high recognition rate, in each data set with very little human activity knowledge, the kernel regularized linear discriminant analysis can not well reflect the intraclass and interclass changes of samples due to the very small number of samples in each human activity knowledge during training. Thus, the performance of the algorithm is greatly affected. Distance measurement plays a very important role in many application tasks in the field of wireless sensor network understanding and pattern recognition. The most widely used is Euclidean metric, which regards the input sample space as isotropic, so instinct has been well used.

Given a reversible symmetric matrix $\Psi \in R^{(n+1)\times(n+1)}$, its bilinear form can be represented by $\psi(x, y)$.

$$\psi(x,y) = \left(x^T, 1\right)\Psi\begin{pmatrix} y \\ 1 \end{pmatrix}, \forall x, y \in R^n. \tag{1}$$

If the matrix Ψ is positive semidefinite, let $E^n = \{x \in R^n\colon \psi_{xx} > 0\}$ define

$$\rho_E(x,y) = \frac{k}{2_i}\log\left(\frac{\psi_{xy} + \sqrt{\psi_{xy}^2 - \psi_{xx}\psi_{yy}}}{\psi_{xy} - \sqrt{\psi_{xy}^2 - \psi_{xx}\psi_{yy}}}\right)(k > 0). \tag{2}$$

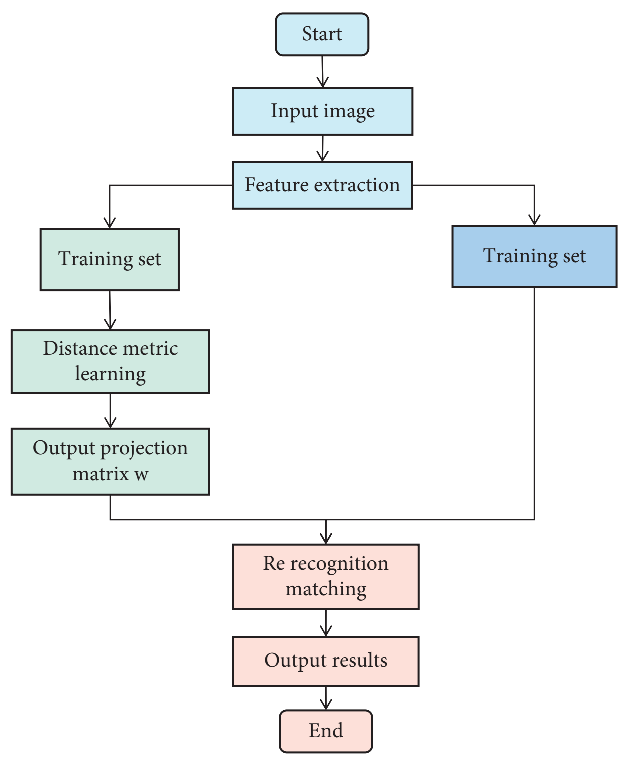

Figure 3: Flowchart of human activity recognition algorithm in wireless sensor networks based on metric learning.

If the matrix Ψ is indefinite, let $B^n = \{x \in R^n | \psi_{xx} < 0\}$ define

$$\rho_H(x,y) = -\frac{k}{2}\log\left(\frac{\psi_{xy} + \sqrt{\psi_{xy}^2 - \psi_{xx}\psi_{yy}}}{\psi_{xy} - \sqrt{\psi_{xy}^2 - \psi_{xx}\psi_{yy}}}\right)(k > 0). \tag{3}$$

On En and Bn, $\rho_E(x,y)$ and $\rho_H(x,y)$ forces both satisfy the metric axiom, so they are metrics on En and Hn. (R^n, ρ_E) is called elliptic geometry space, (B^n, ρ_H) is called hyperbolic geometry space, k is a constant related to CC, $1/k$ is the curvature of elliptic geometry space, and $-1/k$ is the curvature of hyperbolic geometry space. They are all special Riemann geometry, collectively called Kelley Klein metric geometry and can be unified into

$$\rho(x,y) = \frac{k}{2}\left|\log\left(\frac{\psi_{xy} + \sqrt{\psi_{xy}^2 - \psi_{xx}\psi_{yy}}}{\psi_{xy} - \sqrt{\psi_{xy}^2 - \psi_{xx}\psi_{yy}}}\right)\right|(k > 0). \tag{4}$$

The abovementioned Kelley Klein metric only depends on the symmetric matrix Ψ; that is, given a symmetric matrix, there can be a specific Kelley Klein metric.

Given a symmetric positive definite matrix G, its bilinear form in Kelley Klein metric can be expressed as

$$\sigma(x_i, x_j) = (x_i^T, 1)G\begin{pmatrix} x_j \\ 1 \end{pmatrix} \stackrel{\Delta}{=} \sigma_{ij}. \tag{5}$$

Ellipse Kelley Klein measures as follows:

$$d_{ck}(x_i, x_j) = \frac{k}{2i}\log\left(\frac{\sigma_{ij} + \sqrt{\sigma_{ij}^2 - \sigma_{ij}\sigma_{ij}}}{\sigma_{ij} - \sqrt{\sigma_{ij}^2 - \sigma_{ij}\sigma_{ij}}}\right)(k > 0). \tag{6}$$

The V support vector machine method is used as a reference in this chapter to make the Cayley-Klein metric between data points of the same class smaller and the Cayley-Klein metric between data points of different classes larger, and the following Cayley-Klein metric learning optimization model is given:

$$\begin{aligned}
&\min \quad \sum_{i,j \longrightarrow i}\left(d_{CK}(x_i, x_j) - \nu\beta + \mu\sum_i \zeta_{ijl}\right),\\
&s.t. \quad (a)d_{CK}(x_i, x_l) - d_{CK}(x_i, x_j) \geq \beta - \zeta_{ijl},\\
&(b)\zeta_{ijl} \geq 0, \beta \geq 0,\\
&(c)G > 0,
\end{aligned} \tag{7}$$

where the symbol $j \longrightarrow i$ represents X_j and X_i, which are data points belonging to the same category. The first term of the objective function punishes the large distance between the input sample and its samples of the same category, the V in the second term controls the proportion of misclassified sample points, the third term punishes the small distance between heterogeneous samples, and μ is the equilibrium constant.

With the mark $C_{ij} = (x_i^T, 1)^T \ (x_j^T, 1)$, there is

$$\sigma(x_i, x_j) = tr(C_{ij}G) = tr(C_{ij}(L^T L)). \tag{8}$$

In order to improve the iterative efficiency, this chapter uses small batch random gradient descent algorithm to solve the above optimization problems. Assume that the total number of samples is that, at each iteration, only B samples are selected to update the gradient value, where B is far less than the total number of samples N. The pedestrian re-recognition method based on metric learning needs labeled sample data in the training process to learn a metric model with good discrimination and generalization ability. However, in practical application, the cost of labeling samples is relatively high, which leads to the lack of enough training samples in metric learning and the problem of small samples.

4. Research on Human Activity Recognition Algorithm in Wireless Sensor Networks

4.1. Human Activity Recognition Algorithm for Wireless Sensor Networks Based on Metric Learning. Metric learning can be traced back to some early research. Metric learning, on the other hand, first appeared in Xing et al's 2002 proposal for the first Markov distance measurement method. It uses the nonregularized convex formula to maximize the sum of distances between points while keeping the distance between similar examples as small as possible. Some existing studies have introduced mobility into wireless sensor networks in order to maximize the network life cycle and reduce the delay in wireless sensor networks. Because rejection processing is required after measurement learning, we must manually select the rejection radius in order to achieve the same accuracy in discrimination and rejection tasks. To achieve the expected trade-off between identification and rejection tasks, the rejection radius can be selected using the cross validation method. Mobility in wireless sensor networks has a number of benefits, including improved connectivity, lower deployment costs, higher reliability, and lower energy consumption. However, using the human activity recognition algorithm, the average recognition accuracy of the human activity process is 97.42, which is 2.58 higher than the decision tree algorithm. Sensors and activity tags both use the same discrete time length, so two or more activities can happen at the same time. For example, one activity could be stopped in the middle of the time period while the other could begin right away.

Human activity recognition in wireless sensor networks based on metric learning can be divided into visual activity recognition and nonvisual activity recognition. Vision-based human activity recognition focuses on the field of computer vision, using imaging devices such as cameras and video cameras to collect information, and tracking, identifying, analyzing, and understanding activities through related processing technologies of graphics and images. Non-vision-based activity recognition mainly obtains human information through sensors such as gyroscope, gravity accelerator, and GPS. However, the feature extraction of the above methods is mostly carried out in time domain, and it is not robust compared with feature extraction in frequency domain. Another important point is that the above methods are basically based on SVM to classify different group behaviors. Human health activity recognition in wireless sensor networks can be divided into four aspects according to the complexity of the research object: posture, individual behavior, interactive behavior, and group behavior, in which interactive behavior is an action completed by two or more people, and group behavior refers to an action completed by a group of people. Measuring group behavior is influenced by complex semantics and environment, and there are relatively few studies, most of which focus on posture and individual behavior. All nodes in this architecture are static, and the receiver is mobile here. Once the receiver reaches a given sensor node and the sensor detects the existence of the receiver, data collection is completed. This architecture is beneficial to better connect to WSNs deployed in the area of interest. The process of learning human activity recognition algorithm in wireless sensor networks can usually be simplified to the classification of time-varying data; that is, the test sequence is matched with the reference sequence of typical behaviors calibrated in advance. At present, the algorithms of human behavior recognition in wireless sensor networks based on metric learning mainly include template matching method and state space method. Frame-to-frame matching method, fusion frame matching method, and key frame matching method all belong to template matching method.

4.2. Experimental Results and Analysis. The following is the experimental results of the measurement learning-based wireless sensor network human activity recognition algorithm model implemented in MATLAB language on the data set. This experiment adopts four algorithms, namely, decision tree algorithm, data mining algorithm, machine learning algorithm, and human activity recognition algorithm in this paper. Three experiments are carried out, as shown in Figures 4–6.

On three data sets, the recognition accuracy of the fast nearest neighbor component analysis algorithm is clearly improved when compared to the 1NN and NB algorithms, according to the experimental results. On the Weizmann data set, the average recognition accuracy of decision tree and data mining algorithms is 92.86 and 94.61, respectively, which is higher than decision tree algorithm. However, using the human activity recognition algorithm, the average recognition accuracy of the human activity process is 97.42, which is 2.58 higher than the decision tree algorithm. Sensors and activity tags both use the same discrete time length, so two or more activities can happen at the same time. For example, one activity could be stopped in the middle of the time period while the other could begin right away. The divided time slice is used to represent the activities that take up the majority of the time in this case. However, as a result of the discretization, the situation afterward differs from the actual situation. The discretization accuracy is introduced to express the difference. When a rejection task is used, the difficulty of recognition is increased because a portion of the samples is limited, making the training model unstable. In this case, however, the average recognition accuracy of the machine learning algorithm is 83.68, while the average recognition accuracy of the human activity recognition algorithm is 89.63, which is 5.45 higher than the

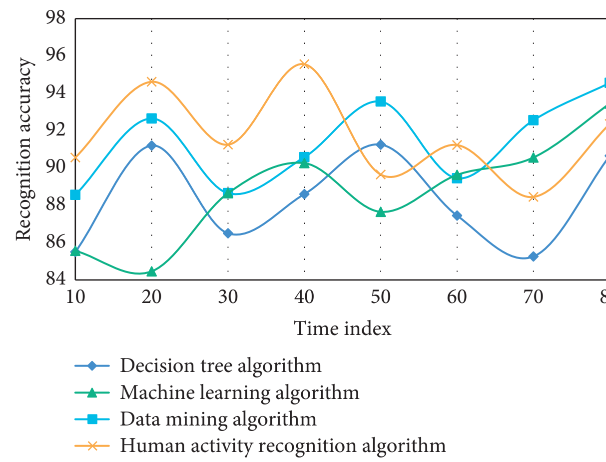

Figure 4: Data results of different algorithms in wireless sensor networks based on metric learning.

no rejection task. Individual behavior recognition research results can be fully utilized in group behavior recognition based on individual behavior recognition. However, feature extraction in the above methods is primarily done in the time domain, which is less robust than feature extraction in the frequency domain. Another important point to note is that the methods described above use SVM to classify various group behaviors. Because SVM is difficult to apply to large samples and sensitive to missing data, metric learning is used to classify different group behaviors due to its advantages.

In this experiment, in order to evaluate the advantages and disadvantages of the human activity recognition algorithm of wireless sensor networks based on metric learning proposed in this chapter, two types of group behaviors are mainly considered, each of which is completed by individuals. The wireless sensor networks are selected, in which six segments are used as training samples and two segments are used as test samples, including frames of group target images. The group behavior corresponding to each frame is manually calibrated as a reference value. The recognition rate obtained by this method is low. The main reason is that the background is complex and the interference to recognition is large. On the other hand, only hog features are relatively single and the ability to describe behavior is limited. In general, the human activity recognition algorithm based on metric learning in wireless sensor networks has a high recognition accuracy. This experiment adopts four algorithms, namely, decision tree algorithm, data mining algorithm, machine learning algorithm, and human activity recognition algorithm in this paper. Four experiments are carried out, as shown in Figures 7–10.

The experimental results show that these methods are all based on the feature extraction of human activity recognition in wireless sensor networks based on metric learning. They need to be processed accurately in the early stage, and complex models need to be built in the later stage, which makes the whole algorithm less robust. In this paper, feature extraction in complex frequency domain can effectively suppress the influence of noise, and the whole model is

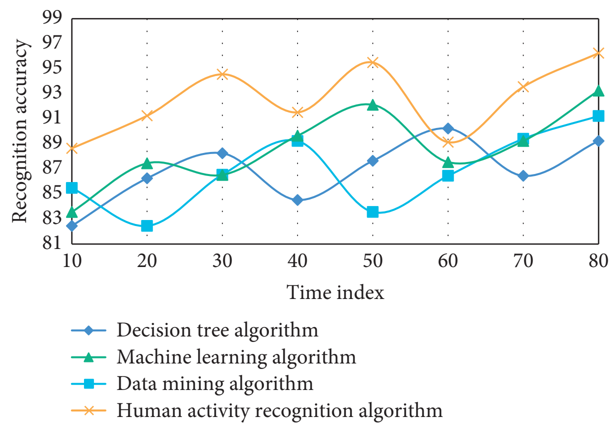

FIGURE 5: Data results of different algorithms in wireless sensor networks based on metric learning.

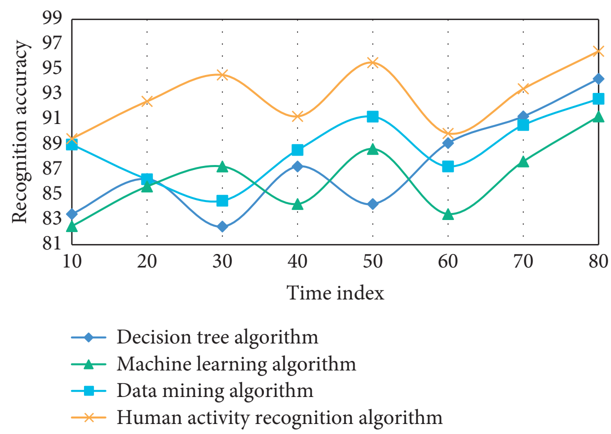

FIGURE 6: Data results of different algorithms in wireless sensor networks based on metric learning.

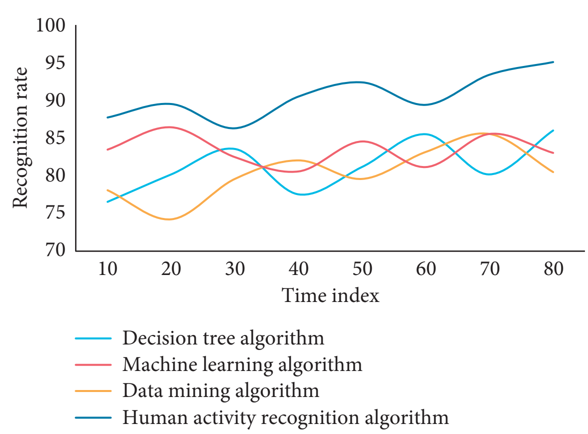

FIGURE 7: Recognition rate of different algorithms in wireless sensor networks.

simple and robust. In addition, on the sum video set, using basic methods to identify group behaviors, the recognition rates can reach 64.58% and 56.87%, respectively. Human activity recognition method based on metric learning uses linear method to classify human activity recognition samples. However, the real pedestrian sample data is often nonlinear, so it is obviously inappropriate to use linear method to solve nonlinear problems. Finally, most of the human activity recognition algorithms based on distance metric learning encounter the problem of small samples due to the lack of enough training samples. However, in this case, the average recognition accuracy of machine learning algorithm is 83.68, and that of human activity recognition algorithm is 89.63, which is 5.45 higher than that of no

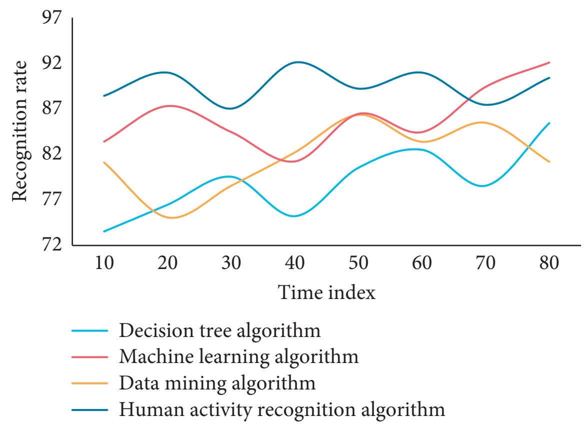

Figure 8: Recognition rate of different algorithms in wireless sensor networks.

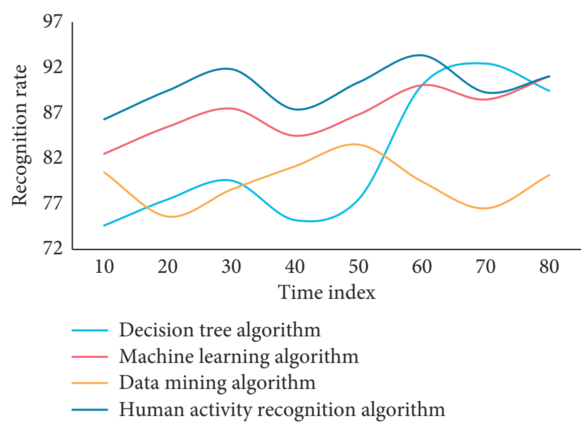

Figure 9: Recognition rate of different algorithms in wireless sensor networks.

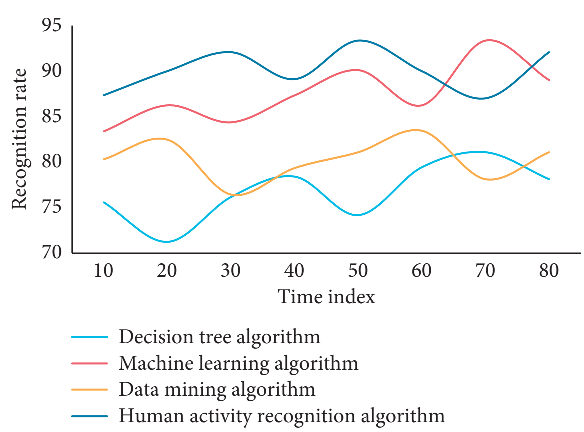

Figure 10: Recognition rate of different algorithms in wireless sensor networks.

rejection task. Group behavior recognition based on individual behavior recognition can make full use of the existing research results of individual behavior recognition.

5. Conclusions

Measurement: Some existing research has introduced mobility into wireless sensor networks in order to maximize the network life cycle and reduce the delay. Because we must deal with rejection after metric learning, we must manually select the rejection radius to achieve the same accuracy in task identification and rejection. Wireless sensor networks have become increasingly popular in recent years because they are nonintrusive, private, and simple to set up. Contact switches, for example, are used to monitor how well doors and cupboards open and close. Mercury contacts are for measuring the movement of objects or the switch state of drawers. Passive infrared sensor is for detecting the movement of specific areas. The status of the flushing device is measured by a floating sensor. The human activity recognition algorithm of wireless sensor networks based on metric learning, on the other hand, uses the chi-square kernel function to map samples from the linearly indivisible original feature space to the linearly separable high-dimensional feature space, then constructs the divergence matrix describing the neighborhood relationship between samples in the high-dimensional space, and finally obtains the projection matrix from the high-dimensional space to the low-dimensional space.

Data Availability

The data used to support the findings of this study are included within the article.

Conflicts of Interest

The authors do not have any possible conflicts of interest.

References

[1] M. Lv, L. Chen, T. Chen, and G. Chen, "Bi-view Semi-Supervised learning based semantic human activity recognition using Accelerometers," *IEEE Transactions on Mobile Computing*, vol. 17, no. 9, pp. 1991–2001, 2018.

[2] Q. Liu, L. Cheng, A. L. Jia, and C. Liu, "Deep Reinforcement learning for Communication flow control in wireless Mesh networks," *IEEE Network*, vol. 35, no. 2, pp. 112–119, 2021.

[3] H. Shota, I. Daiki, and A. Kiyoharu, "Significance of Softmax-based features in comparison to distance metric learning-based features[J]," *IEEE transactions on pattern analysis and machine intelligence, 2021*, vol. 42, no. 5, pp. 1279–1285, 2020.

[4] A. Titaev, "Energy-saving routing metric for aggregate low-rate wireless sensor networks," *Wireless Networks*, vol. 26, no. 3, pp. 2037–2050, 2020.

[5] H. Zhang, R. Nie, M. Lin, and M. Mokayef, "A deep learning based algorithm with multi-level feature extraction for automatic modulation recognition[J]," *Wireless Networks*, vol. 1, pp. 1–12, 2021.

[6] L. Chen, X. Liu, L. Peng, and M. Wu, "Deep learning based multimodal complex human activity recognition using wearable devices[J]," *Applied Intelligence*, vol. 1, no. 6, pp. 1–14, 2020.

[7] M. M. Hassan, S. Ullah, M. S. Hossain, and A. Alelaiwi, "An end-to-end deep learning model for human activity recognition from highly sparse body sensor data in Internet of Medical Things environment[J]," *The Journal of Supercomputing*, vol. 4, no. 4, 2020.

[8] S. Dang, S. Chaudhury, B. Lall, and P. K. Roy, "The dynamic programming high-order Dynamic Bayesian Networks learning for identifying effective connectivity in human brain from fMRI," *Journal of Neuroscience Methods*, vol. 285, pp. 33–44, 2017.

[9] Please provide the complete details for this reference.

[10] Please provide the complete details for this reference.

[11] G. Satat, M. Tancik, O. Gupta, B. Heshmat, and R. Raskar, "Object classification through scattering media with deep learning on time resolved measurement," *Optics Express*, vol. 15, no. 15, pp. 17466–17479, 2017.

[12] X. Jin, J. Zhang, J. Kong, T. Su, and Y. Bai, "A reversible automatic selection Normalization (RASN) deep network for Predicting in the Smart Agriculture system," *Agronomy*, vol. 12, no. 3, p. 591, 2022.

[13] Y. Zhang, K. Xia, Y. Jiang et al., "Multi-modality fusion & Inductive knowledge transfer Underlying non-sparse multi-kernel learning and distribution Adaption[J]," *IEEE/ACM Transactions on Computational Biology and Bioinformatics*, 2022.

[14] W. Cai, Y. Song, H. Duan, and Z. Xia, "Multi-feature fusion-Guided Multiscale Bidirectional Attention networks for Logistics Pallet segmentation[J]," *Computer Modeling in Engineering and Sciences*, vol. 131, 2022.

[15] O. Akbarzadeh, M. R. Khosravi, and L. T. Alex, "Design and Matlab Simulation of Persian License plate recognition using neural network and image Filtering for intelligent Transportation systems," *ASP Transactions on Pattern Recognition and Intelligent Systems*, vol. 2, no. 1, pp. 1–14, 2022.

[16] A. Dabrin, J.-P. Ghestem, E. Uher et al., "Metal measurement in aquatic environments by passive sampling methods: lessons learning from an in situ intercomparison exercise," *Environmental Pollution*, vol. 208, pp. 299–308, 2016.

[17] L. Li, F. Zhu, H. Sun, Y. Hu, Y. Yang, and D. Jin, "Multi-source information fusion and deep-learning-based characteristics measurement for exploring the effects of peer engagement on stock price synchronicity," *Information Fusion*, vol. 69, no. 3, pp. 1–21, 2021.

[18] S. Shirmohammadi and H. Al Osman, "Machine learning in measurement Part 1: Error contribution and Terminology Confusion," *IEEE Instrumentation and Measurement Magazine*, vol. 2, pp. 84–92, 2021.

[19] M. Khanafer and S. Shirmohammadi, "Applied AI in instrumentation and measurement: the deep learning revolution," *IEEE Instrumentation and Measurement Magazine*, vol. 23, no. 6, pp. 10–17, 2020.

[20] W. Xu, J. Zhang, C. Zhong, J. Chang, and B. Wen, "Noise-suppressed Temperature measurement based on machine learning in a Scramjet Combustor[J]," *AIAA Journal*, no. 10, pp. 1–12, 2021.

[21] J. W. Mcgrath, J. Neville, T. Stewart, H. Clinning, B. Thomas, and J. Cronin, "Quantifying cricket fast bowling volume, speed and perceived intensity zone using an Apple Watch and machine learning," *Journal of Sports Sciences*, vol. 39, no. 1, pp. 1–8, 2021.

[22] V. S. Sreekanth, K. Raghunath, and D. Mishra, "Dictionary learning technique and penalized maximum likelihood for extending measurement range of a Rayleigh lidar[J]," *Journal of Applied Remote Sensing*, vol. 14, no. 3, pp. 34529–34521, 2021.

[23] X. Zou, "Analysis of consumer online resale behavior measurement based on machine learning and BP neural network," *Journal of Intelligent and Fuzzy Systems*, vol. 40, no. 2, pp. 2121–2132, 2021.

[24] Q. Lin, J. Yang, B. Zhang, R. Wang, N. Ye, and M. Yan, "Distributed Face recognition in wireless sensor networks," *International Journal of Distributed Sensor Networks*, vol. 2014, pp. 1–8, 2016.

[25] G. Han, J. Shen, L. Li, and L. Shu, "BRTCO: a Novel Boundary recognition and tracking algorithm for continuous objects in wireless sensor networks," *IEEE Systems Journal*, vol. 12, no. 3, pp. 1–10, 2016.

Hindawi
Computational Intelligence and Neuroscience
Volume 2022, Article ID 5333589, 14 pages
https://doi.org/10.1155/2022/5333589

Research Article

OTO-Net: An Automated MRA Image Segmentation Network for Intracranial Aneurysms

Jianming Ye,[1] **Xiaomei Xu**,[2] **Liuyi Li**,[2] **Jialu Zhao**,[2] **Weiling Lai**,[1] **Wenting Zhou**,[1] **Chong Zheng**,[3] **Xiangcai Wang**,[1] **and Xiaobo Lai**[2]

[1]*First Affiliated Hospital, Gannan Medical University, Ganzhou, China*
[2]*School of Medical Technology and Information Engineering, Zhejiang Chinese Medical University, Hangzhou, China*
[3]*Longyan First Affiliated Hospital, Fujian Medical University, Fuzhou, China*

Correspondence should be addressed to Chong Zheng; zhengchong2005163@163.com, Xiangcai Wang; wangxiangcai@csco.ac.cn, and Xiaobo Lai; dmia_lab@zcmu.edu.cn

Received 10 February 2022; Revised 8 March 2022; Accepted 17 March 2022; Published 14 April 2022

Academic Editor: Guangming Zhang

Intracranial aneurysms are local dilations of the cerebral blood vessels; people with intracranial aneurysms have a high risk to cause bleeding in the brain, which is related to high mortality and morbidity rates. Accurate detection and segmentation of intracranial aneurysms from Magnetic Resonance Angiography (MRA) images are essential in the clinical routine. Manual annotations used to assess the intracranial aneurysms on MRA images are substantial interobserver variability for both aneurysm detection and assessment of aneurysm size and growth. Many prior automated segmentation works have focused their efforts on tackling the problem, but there is still room for performance improvement due to the significant variability of lesions in the location, size, structure, and morphological appearance. To address these challenges, we propose a novel One-Two-One Fully Convolutional Networks (OTO-Net) for intracranial aneurysms automated segmentation in MRA images. The OTO-Net uses full convolution to achieve intracranial aneurysms automated segmentation through the combination of downsampling, upsampling, and skip connection. In addition, loss ensemble is used as the objective function to steadily improve the backpropagation efficiency of the network structure during the training process. We evaluated the proposed OTO-Net on one public benchmark dataset and one private dataset. Our proposed model can achieve the automated segmentation accuracy with 98.37% and 97.86%, average surface distances with 1.081 and 0.753, dice similarity coefficients with 0.9721 and 0.9813, and Hausdorff distance with 0.578 and 0.642 on these two datasets, respectively.

1. Introduction

Intracranial aneurysms are abnormal projections that occur on the walls of cerebral arteries. Such hemorrhage is common among relatively young people, with a higher mortality and incidence rate and about 3% in healthy adults [1]. The main threat comes from subarachnoid hemorrhage (SAH) caused by the rupture of an intracranial aneurysm [2], which accounts for more than 85% [3, 4]. According to the survey, SAH is a catastrophic event, with a mortality rate as high as 25%–60% after rupture [5]. Therefore, accurate measurement and evaluation of the shape of intracranial aneurysms are crucial in daily clinical work so that we can monitor and analyze the growth and rupture risks of aneurysms, making it easier to intervene or treat early [6, 7].

According to the current form of technological development, combined with the actual clinical situation, we found that the inspection methods for intracranial aneurysms include invasive and noninvasive. Compared with invasive Digital Subtraction Angiography (DSA), Computed Tomography Angiography (CTA), magnetic resonance angiography (MRA), and Transcranial Doppler (TCD) have been advocated as the best detection methods for intracranial aneurysms [8]. MRA is a noninvasive angiographic method that does not require radiation exposure. With the introduction of new technologies such as 3D imaging, contrast enhancement, and 3T magnetic field, its sensitivity can reach the detection of aneurysms less than 3 mm [9]. Therefore, based on the simple operation and accurate imaging characteristics of MRA technology, radiologists usually use it to perform 3D visualization and quantitative analysis of small intracranial aneurysms [10]. However, the MRA image of a particular part usually contains part of normal tissue, and it may have a relatively large proportion. Therefore, currently in clinical practice, experts often use manual segmentation to separate the tumor tissue regions. In this context, the segmentation results are greatly affected by the subjective experience of experts, and the repetition rate is low and time-consuming. With the development of emerging technologies such as deep learning, some automated segmentation algorithms have gradually emerged, which have initially solved the problem of manual segmentation. However, the accuracy of these algorithms is still to be discussed.

Under the background of the current era of big data, driven by artificial intelligence, it automatically recognizes complex pattern features in image data and provides quantitative data evaluation results [11]. In particular, the application of Convolutional Neural Network (CNN) [12] in deep learning has shown superior performance in a series of image recognition tasks [13], including medical image processing [14–17]. At present, the research on intracranial aneurysms is not in-depth, but some researchers have made courageous attempts. Park et al. developed and applied a neural network segmentation model called the HeadXNet model, which can generate accurate voxel prediction of intracranial aneurysms on head CTA images [18]. Wang et al. presented a multilevel segmentation method based on the lattice Boltzmann method (LBM) and level set with ellipse for accurate segmentation of intracranial aneurysms, making it potential for clinical assessment of the volume and aspect ratio of the intracranial aneurysms [19]. However, these studies focused on unruptured intracranial aneurysms (UIAs) and did not include patients with Aneurysmal subarachnoid hemorrhage (aSAH). Hence, it remains unclear how deep learning model (DLM) algorithms perform on patients with acutely ruptured intracranial aneurysms (RIAs) and whether the extent of hemorrhage impedes detection sensitivity. Moreover, there still has room for performance improvement due to the significant variability of lesions in the location, size, structure, and morphological appearance.

Based on this, we propose a novel automated MRA image segmentation network for intracranial aneurysms, which can quickly locate intracranial aneurysms and accurately segment its three 3D shapes to help radiologists quantitatively evaluate MRA examinations. The contributions are as follows:

(1) A novel 3D image preprocessing scheme is designed to correlate the structural information between data blocks through overlap and partition operations. If the Graphic Processing Unit (GPU) is large enough, the kind of processing is not necessary;

(2) A new One-Two-One Fully Convolutional Network (OTO-Net) for intracranial aneurysms automated segmentation in MRA images is proposed, which is based on the idea of fully convolutional networks with three consecutive encoding and decoding structures to detect and segment intracranial aneurysms more efficiently and accurately;

(3) Aiming at the severe imbalance of categories caused by small intracranial aneurysms, a loss ensembles objective function is proposed, which improves the segmentation accuracy and dramatically enhances the stability of the backpropagation of the network structure.

After reviewing the state-of-the-art in the field of traditional machine learning-based segmentation methods, deep learning-based methods, and the current intracranial aneurysms segmentation methods in Section 2, we introduce in detail the structure and method of our proposed model in Section 3. Then, we describe the details and results of the experiment in Section 4. Finally, we present a discussion in Section 5 and draw the conclusions in Section 6.

2. Related Work

2.1. Traditional Machine Learning-Based Segmentation Methods. For a long time in the past, traditional machine learning algorithms have occupied a significant position in image segmentation. Traditional machine learning algorithms include decision tree, random forest, extra tree, ridge classifier, logistic regression, K-Nearest Neighbor [20], Naive Bayes (Gaussian) [21], and Kernel Support Vector Machine (polynomial, Gaussian) [22], and other algorithms. Yang et al. used the random forest method to build a predictive model of cardiovascular disease and achieved significant results, referencing cardiovascular disease prediction and treatment [23]. In addition, Bender used regression models to analyze epidemiological statistics so that an adjusted effect estimate can be obtained that takes into account the impact of potential confounding factors [24]. On the other hand, as the advancement of high-throughput technology had resulted in the generation of a large amount of genomic and epigenome data, the classification features of support vector machines were expanding their applications in cancer genomics, leading to the development of new biomarkers and new drug targets [25].

2.2. Deep Learning-Based Segmentation Methods. With the application of image segmentation in biomedical image processing, relevant characteristics of this field are also exposed, such as small sample dataset, high segmentation accuracy, and fast segmentation speed. In order to solve this series of problems, new algorithms such as deep learning were born. However, because CNN loses image details in convolution and pooling, the size of the feature map gradually decreases. It does not provide a good indication of the precise contour of the target body. To solve this problem, Shelhamer et al. proposed a Fully Convolutional Network

(FCN) [26], which became the basic framework for semantic segmentation tasks. Most of the subsequent networks are improved on this basis. In 2015, Ronneberger et al. proposed the U-Net structure [27], which has the advantages of supporting a small number of data samples, classifying each pixel and high image segmentation efficiency. In 2016, the V-Net structure was introduced [28], a volume segmentation algorithm based on FCN. Due to its 3D convolution, the introduction of Dice objective function, novel data expansion method, and residual learning, this model showed superior performance in the prostate MRI segmentation task. Especially in recent years, image segmentation has been widely used in medical image processing [29].

2.3. Intracranial Aneurysms Segmentation Methods. With the development of modern medical imaging technology, it is possible to understand further the structure, size, and other characteristics of the diseased tissue in a noninvasive way to diagnose the progress of the disease. In 1895, the German physicist Wilhelm Konrad Rontgen discovered X-rays [28, 30], which had opened the door to medical imaging. Medical imaging methods commonly used in clinical practice include X-ray imaging, X-ray computed tomography (CT), emission computed tomography (ECT), magnetic resonance imaging (MRI), etc., and various medical imaging equipment are widely used in hospitals [31]. Based on literature reading and clinical experience, MRA is a relatively good imaging method for diagnosing intracranial aneurysms. We learned that relevant scholars had explored the intracranial aneurysms' automatic segmentation and analysis. However, the accuracy of its segmentation and other indicators cannot be fully guaranteed. This means that aneurysm detection proves to be challenging and time-consuming.

Shahzad et al. [32] developed and evaluated a Deep Learning Model (DLM) to automatically detect and segment aneurysms in patients with aneurysmal subarachnoid hemorrhage (aSAH) on computed tomography angiography. The results prove that this method is highly sensitive and can potentially assist treating physicians in aSAH by providing automated detection and segmentation of aneurysms. Law et al. [33] proposed a novel intensity-based algorithm to segment intracranial vessels and the attached aneurysms, which can handle the low-contrast aneurysmal regions affected by turbulent flows. It is grounded on multirange filters and local variances to extract intensity-based image features. Prior to this, the team also designed a new method based on multirange filters and local variance to segment blood vessels and intracranial aneurysms on PCMRA images that achieves an excellent segmentation effect [34]. Even though there are related research results in this field, there is still no systematic system to solve this problem. This shows that in order to achieve the effect of accurately and efficiently segmenting the tumor area, new methods are being explored continuously.

2.4. Our Work. Facing the vast challenge of precise segmentation, how to segment the intracranial aneurysm structure from the complex brain tissue structure has become an urgent problem that we need to overcome. Aiming at the characteristics of the existing technology, we proposed a novel model for intracranial aneurysms segmentation in MRA images. We used datasets from the First Affiliated Hospital of Gannan Medical University (GMU) and Aneurysm Detection and segMentation Challenge 2020 (Adam2020, https://adam.isi.uu.nl/). The specific process of our method is as follows: first, the original MRA images of desensitized intracranial aneurysm patients were pretreated. Next, an OTO-Net for intracranial aneurysms automated segmentation in MRA images was proposed. Then, the OTO-Net model was trained on the preprocessed datasets. Finally, the generalization ability of the OTO-Net model is validated by model testing and evaluation indexes. The flow chart of this experimental research is shown in Figure 1.

3. Methodology

The purpose of this paper is to realize the accurate and automated segmentation of intracranial aneurysms in MRA images. Therefore, we designed a novel OTO-Net model, which was based on the idea of fully convolutional networks with three consecutive encoding and decoding structures. The process of data preprocessing, OTO-Net network structure, and loss function used were introduced in this section.

3.1. Data Preprocessing. MRA image is a 3D data structure, and the 2D network-based segmentation model needs to slice it. The sliced data is 2D data, making the model unable to learn the structural relationship between layers in the data, leading to insufficient network model learning. Therefore, to preserve the spatial expression of intracranial aneurysms, we decided to use 3D data as the model's input. For radiologists' observation and analysis of images, 3D data has significant value in clinical diagnosis and treatment. Below we will elaborate on the 3D image preprocessing method.

3.1.1. Overlapping Blocks. Due to the limitation of GPU memory resources, MRA images cannot be input into the original size network, so the 3D MRA images must be processed in blocks. The paper introduces two chunking methods, namely nonoverlapping block and overlapping block, the structure of which is shown in Figure 2.

The dimension size of the input data of the network structure we designed is $128 \times 128 \times 64$. Here, an MRA image with a size of $512 \times 512 \times 128$ in the dataset is taken as an example. If the same nonoverlapping partitioning processes the original image and the label image, then the step size of each partitioning operation in the X and Y directions is equal to 128. Furthermore, there is no overlap between the data blocks, so the X and Y directions are divided into four blocks, respectively. Similarly, if the Z step equals 64, it is split into two pieces.

Although 3D data as input solves the structural relationship between the layers of the learning model, nonoverlapping block processing contains up to 64 layers of image information, and the data blocks are still disconnected

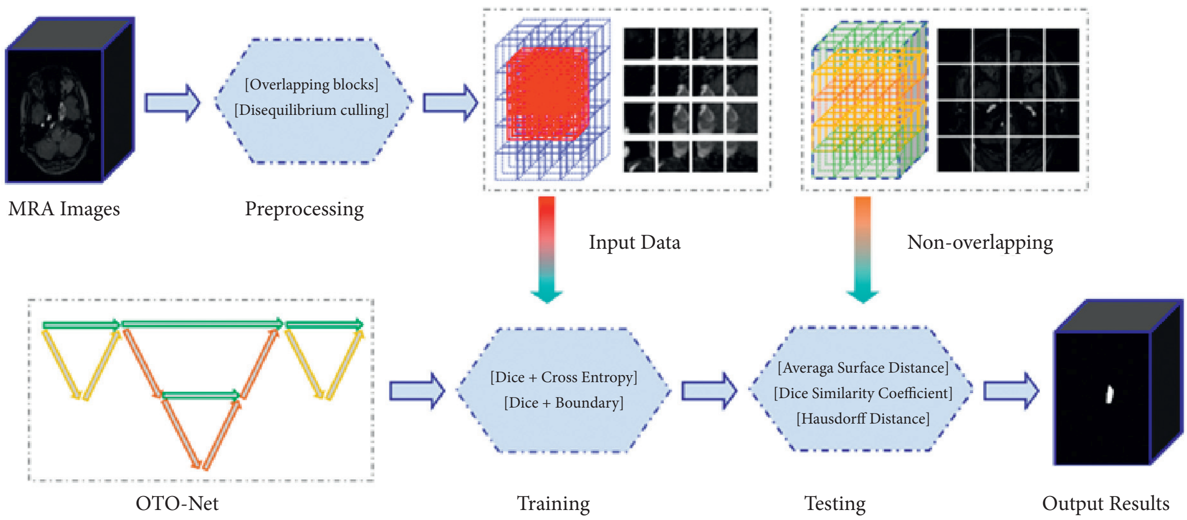

Figure 1: Procedures of our OTO-Net for intracranial aneurysms automated segmentation in MRA images.

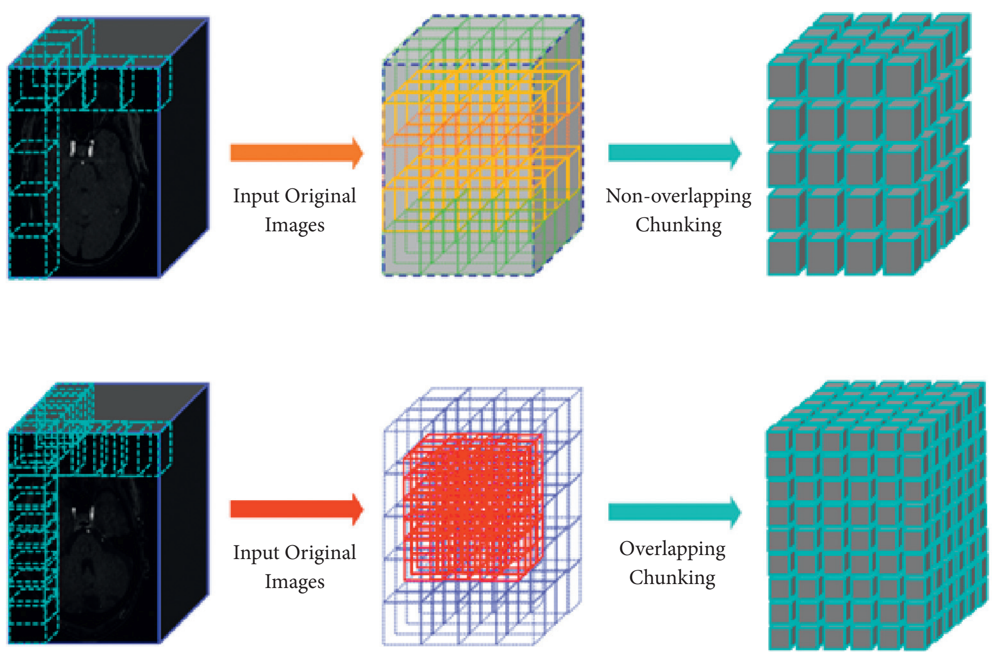

Figure 2: Nonoverlapping chunking and overlapping chunking.

from each other, making the complete structure unable to be learned. It is similar to the slice image input from the 2D network model. Therefore, we propose an overlapping division method to alleviate this problem. The size of the block remains the same. The step size of the original image and the label image that move simultaneously in the X, Y, and Z directions is smaller than the block size. Although it increases the number of blocks, the advantage is that there is absolute information correlation between blocks.

3.1.2. Disequilibrium Culling. After the block processing, a 3D original image and label image are cut into many $128 \times 128 \times 64$ data blocks. Since the lesion area only occupies a small part of the brain, the block processing partnership will contain the nonlesion blocks. If these data blocks are used together as input data for the model, the class imbalance will be caused, and the model's learning process will be troubled.

Therefore, to mitigate category imbalance in this study, the label image data block is further screened after the chunking process. If there is no data more significant than 0 in the data block, the lesion area is not included, the original image and label image data block would be discarded.

3.2. Model Design. The OTO-Net is a model based on 3D fully convolutional networks. Its main structure takes advantage of the encoder-decoder proposed by Hinton et al. [35] in 2006. The most significant feature of the OTO-Net

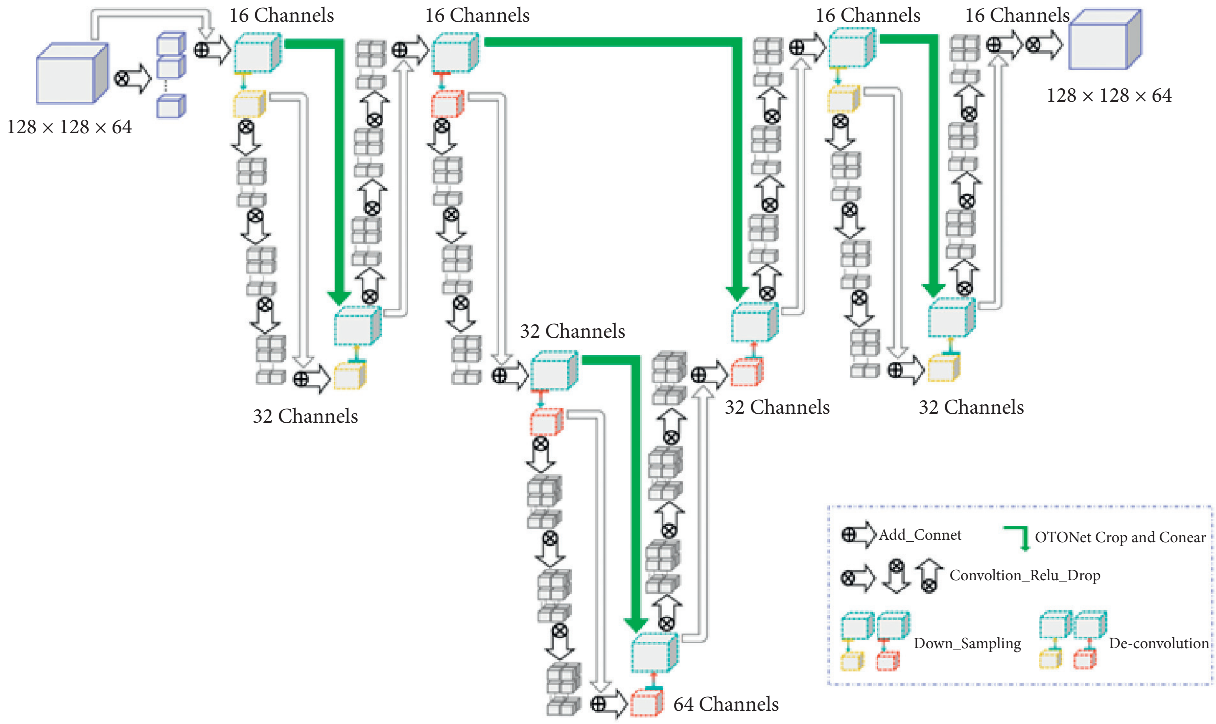

Figure 3: Overall architecture of our proposed OTO-Net.

structure is the continuous use of three complete encoding and decoding structures to achieve the purpose of accurate detection and segmentation of intracranial aneurysms. The whole network still presents an entirely symmetrical design. The schematic diagram of OTO-Net is shown in Figure 3.

In the OTO-Net structure designed by us, the convolution kernel uses $3 \times 3 \times 3$ voxels, assigns 'SAME' mode to supplement data, and selects ReLU as the activation function. The three complete encoding and decoding structures in OTO-Net are used in downsampling, upsampling, and skip connection. First, the input data of $64 \times 128 \times 128 \times 1$ was received. And then, the convolution check with $3 \times 3 \times 3$ voxels with the convolution step of [1] was performed for two convolution operations. Finally, Layer 1 was obtained by adding the first and second convolution layers.

After being downsampled with a convolution kernel step size of [1, 2], the network structure of Layer1 changes from 16 channels to 32, and then, perform three successive convolution operations and add the downsampled layer and the third convolutional layer to get Layer2. Subsequently, deconvolve Layer2. Moreover, the convolution kernel size was still [1, 2], so the channels changed from 32 to 16. After skip connection between the deconvolution layer and Layer1 stack operation, three consecutive convolution operations and the deconvolution layer are added to obtain Layer3, whose size is the same as Layer1. At this point, the first complete encoding and decoding structure is completed.

Except for the second encoding and decoding structure is different from the first structure, two consecutive downsampling and then two successive upsampling are used, while the third is the same as the first structure. When the OTO-Net structure enters Layer 9, the layer's size is the same as that of Layer1 again. Finally, it passes through the output layer's convolution operation and uses the Sigmoid activation function to map out the prediction result of the size of $64 \times 128 \times 128 \times 1$. The theoretical calculation of network parameters of the OTO-Net structure is shown in Table 1.

Table 1: Parameter details of the proposed OTO-Net.

Layer	Input size	Kernel
O^{I}-Stage1	128	$3 \times 3 \times 3 \times 16 \times 16$
O^{I}-Stage2	64	$3 \times 3 \times 3 \times 32 \times 32$
T-Stage1	128	$3 \times 3 \times 3 \times 16 \times 16$
T-Stage2	64	$3 \times 3 \times 3 \times 32 \times 32$
T-Stage3	32	$3 \times 3 \times 3 \times 64 \times 64$
T-Stage4	64	$3 \times 3 \times 3 \times 32 \times 32$
T-Stage5	128	$3 \times 3 \times 3 \times 16 \times 16$
O^{II}-Stage1	64	$3 \times 3 \times 3 \times 32 \times 32$
O^{II}-Stage2	128	$3 \times 3 \times 3 \times 16 \times 16$

3.3. Loss Ensembles. The loss function, also known as the objective function, solves and evaluates the model by minimizing it, so it is crucial for model construction. Medical images usually have a characteristic that the target area to be segmented is unbalanced with the background area. To solve this problem, Milletari et al. proposed a new objective function in the V-Net structure, which had an immediate effect because the Dice coefficient was cited [36]. Since then, Dice loss has become one of the most critical evaluation indexes of medical image segmentation.

Nevertheless, as Figure 4 shows, intracranial aneurysms account for a tiny proportion of the entire brain, and the

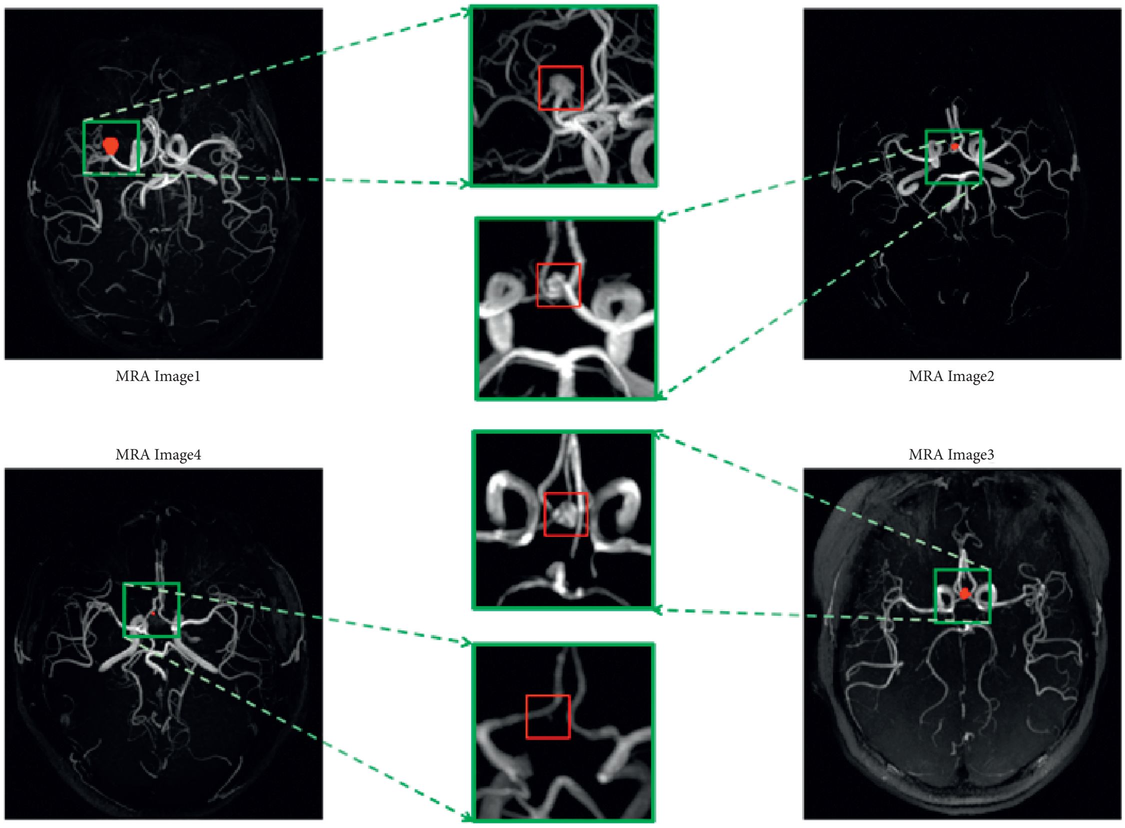

Figure 4: Morphology of intracranial aneurysm at high magnification.

foreground and the background are highly imbalanced. Therefore, we propose an objective function optimization for loss ensembles, including the comparative experiment between Dice loss + Cross-Entropy loss and Dice loss + Boundary loss. The principles of each are described in detail in the following sections.

3.3.1. Dice Loss. Dice coefficient is a set similarity measurement function, which is usually used to calculate the similarity between two samples, and its value ranges between [0, 1]. The formula is as follows:

$$s = \frac{2|\mathbf{A} \cap \mathbf{B}|}{|\mathbf{A}| + |\mathbf{B}|}, \tag{1}$$

where $|\mathbf{A} \cap \mathbf{B}|$ represents the intersection of set $\mathbf{A}$ and set $\mathbf{B}$, $|\mathbf{A}|$ and $|\mathbf{B}|$ represents the number of elements of set $\mathbf{A}$ and set $\mathbf{B}$, respectively. And the coefficient 2 in the numerator is to eliminate the common component of double calculation in the denominator. For semantic segmentation, p represents the predicted image and g represents the label image. Thus, Dice loss can be expressed as follows:

$$L_{dice} = 1 - \frac{\left(2\sum_{i=1}^{N} p_i g_i\right) + w}{\left(\sum_{i=1}^{N} p_i^2 + \sum_{i=1}^{N} g_i^2\right) + w}, \tag{2}$$

where w is known as the smoothing coefficient, a minimal number. And it is used to prevent the denominator from being 0. Although Dice loss has a good performance in the scenario where there is a severe imbalance between positive and negative samples and focuses more on the mining of foreground area in the training process, it also has disadvantages. Loss is prone to be unstable, especially in small targets, which will lead to gradient saturation in extreme cases. Therefore, we propose a loss ensembles optimization method to solve these problems.

3.3.2. Cross-Entropy Loss. Suppose two different probability distributions, $P(x)$ and $Q(x)$, for the same random variable X. In that case, we can use relative entropy (KL divergence) [37] to measure the difference between these two probability distributions. The formula is expressed as follows:

$$D_{KL}(PQ) = \sum_{i=1}^{N} P(x_i)\log\left(\frac{P(x_i)}{Q(x_i)}\right), \tag{3}$$

$$D_{KL}(PQ) = -H(P(x)) + \left[-\sum_{i=1}^{N} P(x_i)\log(Q(x_i))\right]. \tag{4}$$

KL divergence formula (4) can be obtained by further deformation from (3), where the former represents information entropy and the latter represents cross-entropy, that is, KL divergence = cross-entropy − information entropy.

In the model training process, since the input data and labels have been determined, and the true probability distribution $P(x)$ has also been determined, the information entropy is constant. In addition, since the value of KL

Table 2: Experimental design of image segmentation for intracranial aneurysms.

Experiment	Dataset	Algorithm	Loss function
Ex1	GMU	V-Net	Dice
Ex2	GMU	V-Net	Dice + cross-entropy
Ex3	GMU	V-Net	Dice + boundary
Ex4	GMU	OTO-Net	Dice
Ex5	GMU	OTO-Net	Dice + cross-entropy
Ex6	GMU	OTO-Net	Dice + boundary
Ex7	ADAM2020	V-Net	Dice
Ex8	ADAM2020	V-Net	Dice + cross-entropy
Ex9	ADAM2020	V-Net	Dice + boundary
Ex10	ADAM2020	OTO-Net	Dice
Ex11	ADAM2020	OTO-Net	Dice + cross-entropy
Ex12	ADAM2020	OTO-Net	Dice + boundary

Table 3: The hyperparameters of each experiment.

Experiment	Inputable data	Learning rate	Dropout	Epoch	Batch size
Ex1	597	0.001	0.5	200	4
Ex2	597	0.001	0.5	200	4
Ex3	597	0.001	0.5	200	4
Ex4	597	0.001	0.5	200	2
Ex5	597	0.001	0.5	200	2
Ex6	597	0.001	0.5	200	2
Ex7	1613	0.001	0.5	150	4
Ex8	1613	0.001	0.5	150	4
Ex9	1613	0.001	0.5	150	4
Ex10	1613	0.001	0.5	150	2
Ex11	1613	0.001	0.5	150	2
Ex12	1613	0.001	0.5	150	2

divergence represents the difference between the true probability distribution $P(x)$ and the predicted probability distribution $Q(x)$, the smaller the value, the better the prediction result. Therefore, it is necessary to minimize the KL divergence to obtain the best results. It is easier to calculate using the cross-entropy loss function as the objective function. Replace $P(x)$ with $g(x)$ and $Q(x)$ with $Q(x)$. The formula of cross-entropy loss can be expressed as follows:

$$L_{ce} = -\sum_{i=1}^{N} g(x_i)\log(p(x_i)), \tag{5}$$

where the former represents the KL divergence, and the latter is a constant.

3.3.3. Boundary Loss. Boundary loss is an objective function proposed by Kervadec et al. to solve the difficulty of highly unbalanced segmentation [38]. The core of the method is to calculate the distance between the predicted image and the boundary of the marked image through calculus. The calculation formulas are as shown in (6) and (7), respectively:

$$\mathrm{Dist}(\partial G, \partial S) = \int_{\partial G} \left\| y_{\partial S}(p) - p \right\|^2 \mathrm{d}p, \tag{6}$$

$$\mathrm{Dist}(\partial G, \partial S) \approx 2\int_{\Delta s} D_G(q)\mathrm{d}p. \tag{7}$$

Since the distance differential expression (6) cannot be used as a loss function, the integral expression (7) is adopted. The crucial region $\triangle S$ is divided into S and G, and the binary indicators function $s(q)$ and $g(q)$ about segmentation and ground truth are introduced so that the integral region extends from S and G to the entire image domain.

$$\Delta S = \left(\frac{S}{G}\right) \cup \left(\frac{G}{S}\right), \tag{8}$$

$$\begin{aligned}\frac{1}{2}\mathrm{Dist}(\partial G, \partial S) &= \int_S \phi G(q)dq - \int_G \phi G(q)dq \\ &= \int_\Omega \phi G(q)s(q)dq - \int_\Omega \phi G(q)g(q)dq.\end{aligned} \tag{9}$$

Then we replaced $s(q)$ in formula (9) with $S(q)$, which established a connection with the softmax output of the network. At this point, we can obtain the Boundary loss function expression (11):

$$\min_\theta Di\ st(\partial G, \partial S_\theta) \approx \int_\Omega \phi G(q)S_\theta(q)dq - \int_\Omega \phi G(q)g(q)dq, \tag{10}$$

$$L_B(\theta) = \int_\Omega \phi G(q)S_\theta(q)dq. \tag{11}$$

4. Experiments

4.1. Datasets. In the study, we evaluated the proposed OTO-Net on one public benchmark dataset and one private dataset used to train, evaluate and objectively compare the performance of standardized intracranial aneurysm MRA data segmentation algorithms. First, we use the Adam2020 dataset. A set of 255 representative intracranial aneurysm MRA data is shared on the challenge website (https://adam.isi.uu.nl/) [2]. Adam2020 dataset includes 113 training data and 142 test data, and about 32 epochs are needed for training the model. In addition, the second in-house private dataset is provided by the First Affiliated Hospital of Gannan Medical University (GMU dataset). In total, 65 clinical intracranial aneurysm MRA data are provided with manual segmentation labels to verify the model, including 30 training data and 35 test data. It takes about 27 epochs to train the proposed OTO-Net with GMU dataset.

4.2. Evaluation Metrics. In order to have a more systematic evaluation of the effect of segmentation, we have stipulated the following indicators as the evaluation metric. The Average Surface Distance (ASD) refers to the average surface distance of all points in the 3D data block. It is a commonly used evaluation index in medical image segmentation tasks, and its mathematical definition can be expressed by the following formula:

Table 4: Evaluation index and a comprehensive score of each experimental model.

Experiment	Time (h)	ASD	DSC	95% HD	Comprehensive ranking
Ex1	11.5	3.562 ± 0.77	0.9391 ± 0.023	7.332 ± 2.31	12/12 + 11/12 + 12/12 = 2.91
Ex2	11.7	2.409 ± 0.26	0.9502 ± 0.032	3.053 ± 1.11	9/12 + 10/12 + 8/12 = 2.25
Ex3	12.1	**0.706 ± 0.05**	0.9672 ± 0.020	2.751 ± 1.29	1/12 + 7/12 + 7/12 = 1.25
Ex4	10.4	2.014 ± 0.20	0.9701 ± 0.017	1.242 ± 2.68	7/12 + 5/12 + 6/12 = 1.50
Ex5	11.0	1.989 ± 0.62	0.9721 ± 0.005	**0.578 ± 0.43**	6/12 + 3/12 + 1/12 = 0.83
Ex6	11.3	1.081 ± 0.27	0.9710 ± 0.013	0.942 ± 0.87	4/12 + 4/12 + 3/12 = 0.91
Ex7	43.6	3.194 ± 0.31	0.9362 ± 0.020	7.116 ± 9.84	11/12 + 12/12 + 11/12 = 2.83
Ex8	43.9	2.113 ± 0.09	0.9586 ± 0.031	5.583 ± 1.92	8/12 + 9/12 + 10/12 = 2.25
Ex9	44.1	2.991 ± 0.31	0.9621 ± 0.017	1.131 ± 0.31	10/12 + 8/12 + 5/12 = 1.91
Ex10	39.8	1.953 ± 0.71	0.9699 ± 0.042	4.112 ± 0.94	5/12 + 6/12 + 9/12 = 1.66
Ex11	40.1	0.905 ± 0.11	0.9761 ± 0.007	1.041 ± 0.31	3/12 + 2/12 + 4/12 = 0.75
Ex12	40.6	0.753 ± 0.03	**0.9813 ± 0.008**	0.642 ± 0.17	**2/12 + 1/12 + 2/12 = 0.33**

$$ASD = \frac{\sum_{a\in S(A)} \min_{b\in S(B)} \|a-b\| + \sum_{b\in S(B)} \min_{a\in S(A)} \|b-a\|}{|S(A)| + |S(B)|}. \quad (12)$$

Next, since Dice Similarity Coefficient (DSC) is equivalent to equation (1), and the sum of Dice loss and DSC is 1. Based on the above conditions, DSC can be expressed as follows by the following formula:

$$\mathrm{DSC} = \frac{2\sum_{i=1}^{N} p_i g_i}{\sum_{i=1}^{N} p_i^2 + \sum_{i=1}^{N} g_i^2}. \quad (13)$$

If DSC is sensitive to internal filling, Hausdorff distance (HD) focuses on calculating segmentation boundaries. Hausdorff distance is a maximum function describing set A to set B. And the general definition can be expressed by the following formula:

$$\mathrm{HD}(C,D) = \max\{h(C,D), h(D,C)\}, \quad (14)$$

where $h(C,D)$ is called the directed Hausdorff distance and given by $h(C,D) = \max_{a\in C}\min_{b\in D}\|a-b\|$, where $\|a-b\|$ is some norm. In all HD calculations, the maximum distance quantile is set to 95%. The purpose is to eliminate the little distance caused by some outliers to ensure the overall value's stability.

4.3. Experimental Details. We use the V-Net model and the OTO-Net model for comparative experiments. As mentioned in the previous article, we used the comprehensive objective function of Dice loss + Cross-entropy loss and Dice loss + Boundary loss in the training process. The intracranial aneurysm segmentation study provided two datasets, so we designed Table 2 that shows the experimental protocol.

4.4. Training Process. As shown in Table 3, to meet the experimental conditions of the control group without limiting the optimal performance of the model, we reasonably set the training parameters of each group of experiments, such as learning rate, dropout, epoch, and batch size.

In this study, we used the python-based PyCharm framework to implement the preprocessing and our proposed OTO-Net model, including the software packages such as 1.19.2 NumPy, 3.1.1 Nibabel, 2.0.0 SimpleITK, 1.1.2 Pandas, 4.4.0 OpenCV, and the GPU version of 1.13.1 TensorFlow. The workstation is installed with the Window10 system, equipped with two Intel(R) Xeon(R) Silver 4210 CPU @2.20 GHz, one NVIDIA TITAN RTX 24 GB GPUs, and 128G running memory. All different modes were tested under the same GPU and environment.

5. Results and Discussion

5.1. Results. After completing the model's training process, we tested its segmentation detection performance. Evaluation indicators can be considered as the most intuitive manifestation of results. As shown in Table 4, we used the ASD, DSC, and HD three indicators introduced in the previous article to compare and evaluate the effects of all experimental groups. The last column of the table—comprehensive ranking is the cumulative sum of the scales of each group in the three indicators. It can be implied by its definition that the smaller the value, the higher the overall performance of the corresponding model.

By observing and comparing the experimental data, it can be concluded that Ex3, Ex5, and Ex12 rank first in the three indicators of ASD, HD, and DSC, respectively, and Ex12 is the best in the overall ranking. Combined with the experimental model design, they use all OTO-Net. Therefore, we have reason to believe that O's segmentation effect on V has been further improved. In addition, for another experimental variable loss function, we found that the overall rankings of Ex1, Ex4, Ex7, and Ex10 that only use the dice objective function are relatively low, and the loss ensembles play a critical role in improving the segmentation performance.

We comprehensively analyze and calculate the results of 6 sets of experiments and finally conclude that the accuracy of the OTO-Net model on the GMU and Adam2020 datasets is 98.37% and 97.86%, respectively. The accuracy is the ratio of the correct prediction area to the target area. Ex5 ranked first in the GMU dataset, with ASD reaching 1.989, DSC reaching 0.9721, and HD reaching 0.578 mm; Ex12 ranked first on the Adam2020 dataset with ASD of 0.753, DSC of 0.9813, and HD of 0.642 mm. We have noticed that this model performs better on the Adam2020 dataset and believe

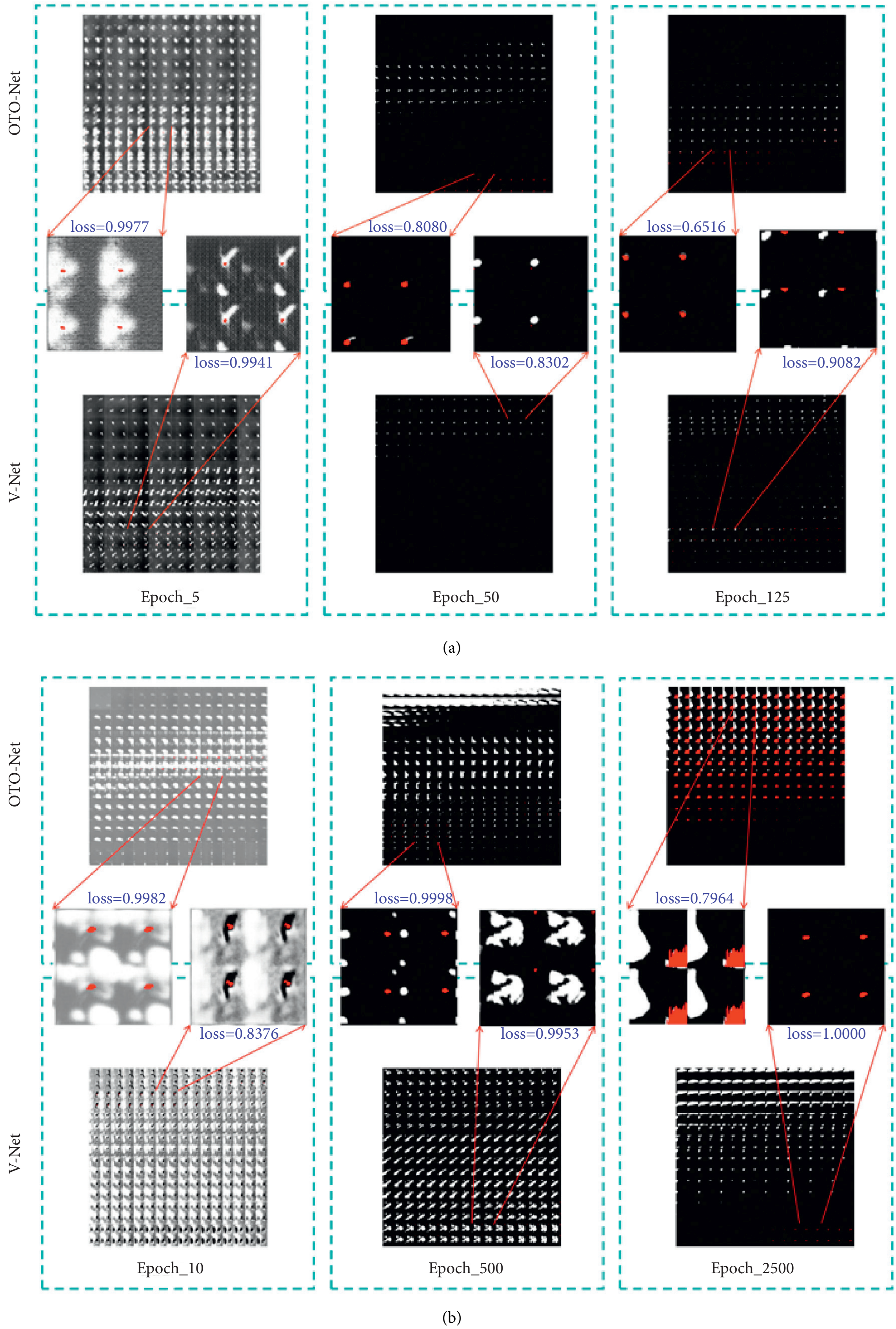

Figure 5: Prediction results comparison between the OTO-Net and V-Net: (a) GMU dataset, (b) Adam2020 dataset.

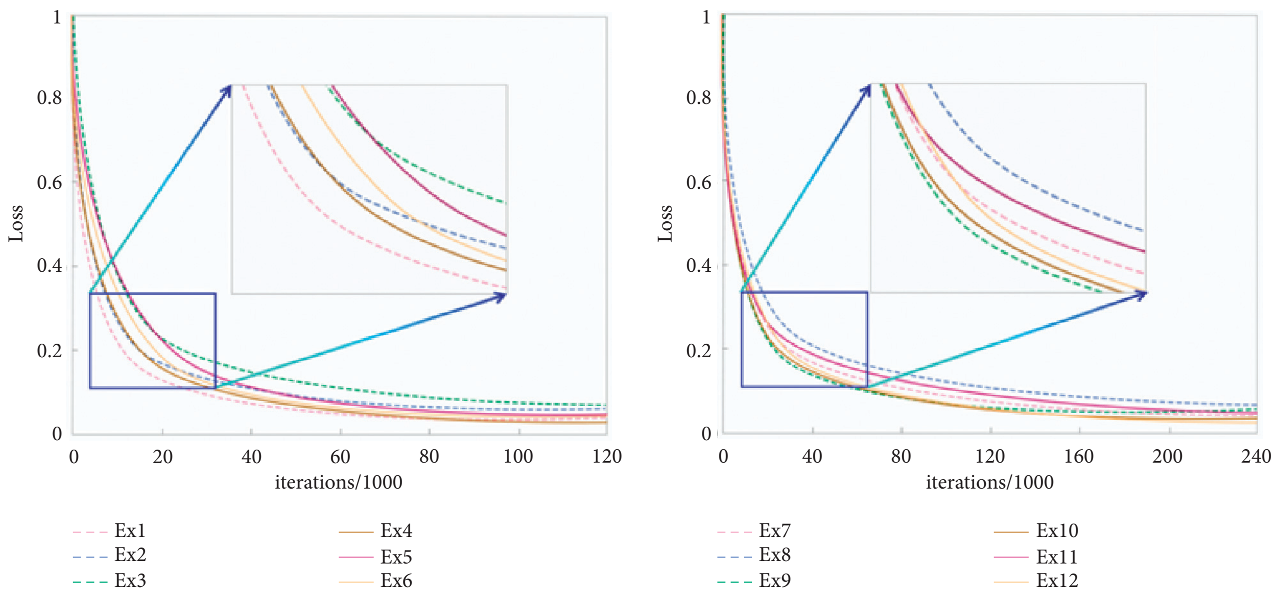

Figure 6: Training loses per group of experiments on GMU dataset and Adam2020 dataset.

Table 5: RSS calculation results for each loss curve.

	Ex1/Ex7	Ex2/Ex8	Ex3/Ex9	Ex4/Ex10	Ex5/Ex11	Ex6/Ex12
Residual sum of squares (RSS)	17.7597	17.0351	18.1124	15.9172	**15.1319**	17.0053
	19.8024	19.0271	21.9512	16.3814	18.7011	**16.1217**

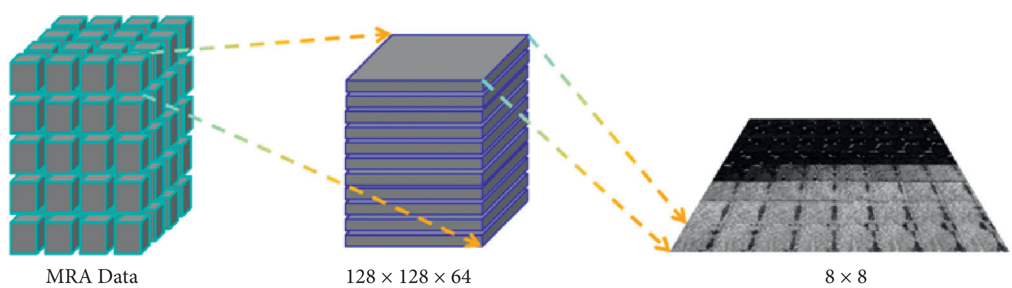

Figure 7: Test set nonoverlapping block processing.

that the reason is that the data contained in it is more standardized.

For the clinician's diagnosis, the most intuitive and effective way of presentation is the visualization of the segmentation results. Both OTO-Net and V-Net mentioned in this article have end-to-end characteristics, so the output data size is still $128 \times 128 \times 64$. To preserve the predicted results in the model training process, we converted the $128 \times 128 \times 64$ 3D data blocks into 64 128×128 2D images and then merged them into 8×8 images. The smaller the inference cycle of the model is, the faster the inference speed is, and the stronger the model's performance is. When the reasoning cycles are the same, the reasoning cycles' size can be evaluated by comparing the value of dice loss, and then the performance of the model can be judged.

As shown in Figure 5(a), (a) is the comparison between the prediction results of OTO-Net and V-Net on the GMU dataset in the 5th, 50th, and 125th rounds of the inference period and the standard; (b) is the comparison between the prediction results of OTO-Net and V-Net on the Adam2020 dataset in the 10th, 500$^{\text{th}}$, and 2500th rounds of the inference period and the standard. By comparing the four groups of data, it can be found that the dice loss values of Ex5 and Ex12 are significantly smaller, indicating that their predicted results are more similar to the standard. Therefore, the model structure of Ex5 and Ex12 is superior.

On this basis, to observe the loss values of each group of experiments in the training process, Figures 6(a) and 6(b) recorded and described the dynamic change curves of training loss of 12 groups of experiments GMU and Adam2020 datasets, respectively. The volatility of the loss curve is one of the important indexes to measure the model's stability. As shown in Table 5, by calculating the residual sum of squares (RSS) of each loss curve, the volatility of the loss's discrete value was characterized by a quantity that measured

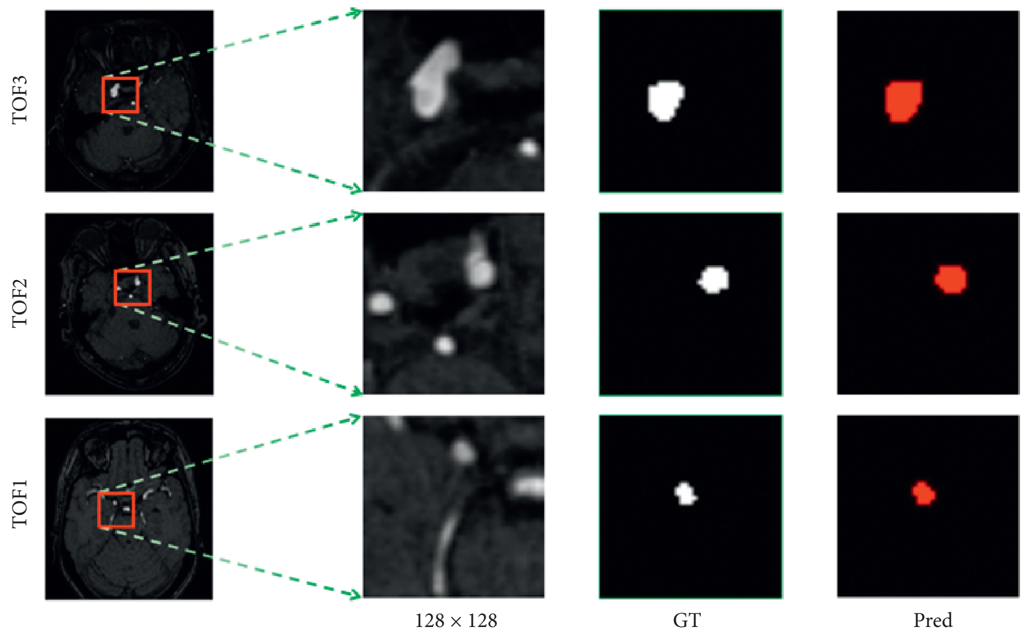

Figure 8: Visualization results of the intracranial aneurysms segmentation using the proposed OTO-Net on GMU dataset.

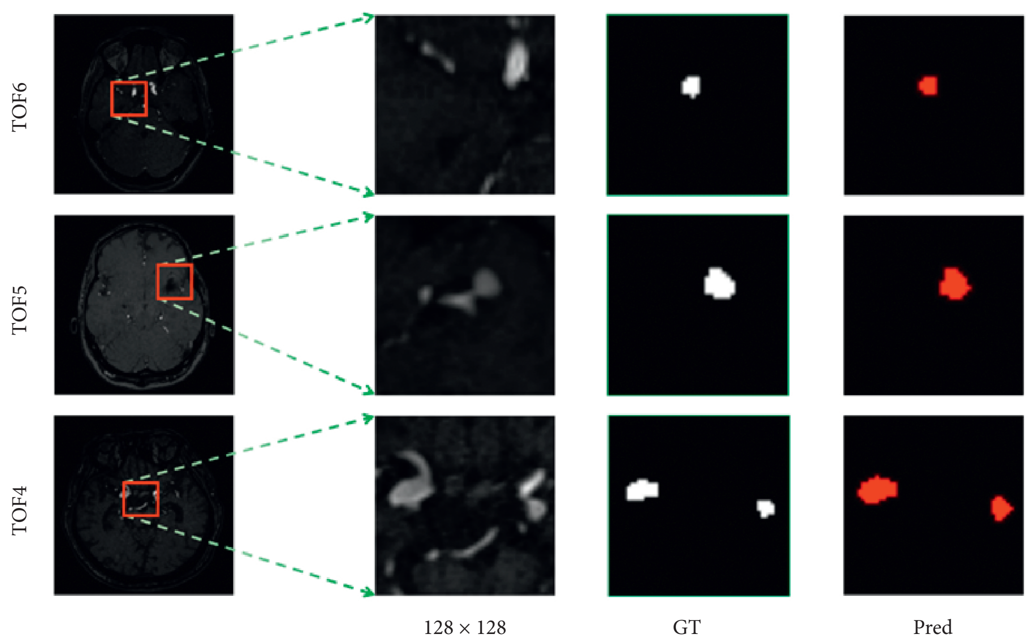

Figure 9: Visualization results of the intracranial aneurysms segmentation using the proposed OTO-Net on Adam2020 dataset.

Table 6: Evaluation indexes of six MRA image test sets.

Test	Dataset	ASD	DSC	95% HD
TOF1	GMU	0.982	0.9604	0.812
TOF2	GMU	**0.699**	0.9711	0.640
TOF3	GMU	0.704	0.9622	**0.506**
TOF4	ADAM2020	1.105	0.9730	0.618
TOF5	ADAM2020	0.786	**0.9803**	0.574
TOF5	ADAM2020	1.032	0.9705	0.713

the degree of model fit in the linear model. The smaller the matter is, the smaller the fluctuation is, which means that the model tends to be more stable. By comparing the data in the table, it can be seen that the RSS values of Ex4~6 and Ex10~12 are small, so the model structure is more stable.

To sum up, all the experimental data, respectively, reflect the excellent effects of training stability, segmentation accuracy, and generalization ability, which effectively verify the advancement of the OTO-Net structure and loss ensembles proposed by us.

5.2. Discussion. After introducing the process and results of this experiment, it can be seen that OTO-Net with loss ensembles shows high overall accuracy and robustness in the segmentation of highly unbalanced intracranial aneurysms. As shown in Figure 7, the test samples divided in advance by GMU and Adam2020 datasets were first processed by nonoverlapping block processing, respectively, to obtain multiple test datasets with the size of $128 \times 128 \times 64$, and then input them into OTO-Net, respectively, for prediction.

Figures 8 and 9 respectively, show the three groups of MRA image results predicted by the OTO-Net model on the GMU dataset and the Adam2020 dataset. Because the intracranial aneurysm was too small, we enlarged and clipped the target region to have a precise observation of each result. Observation of the predicted results shows that OTO-Net can still achieve pixel-level segmentation requirements, but for tiny intracranial aneurysms, it is difficult for OTO-Net to achieve absolute precision segmentation in some marginal areas. In order to quantitatively discuss the prediction results, three indicators of ASD, DSC, and HD of the six groups of test data were counted, respectively. As shown in Table 6, ASD of TOF2 reached 0.699 and HD of TOF3 reached 0.506 mm, both of which were higher than the maximum values of the training results. The maximum value of DSC is 0.9803, which is slightly inferior to the maximum value of training.

In order to increase the persuasiveness of the results of the article, we must effectively compare it with the results of previous studies. However, by reading a large number of documents, we can see that few studies overlap entirely with the research field of this article, which fully proves that the idea of the article is quite innovative. The model proposed by Sichtermann et al. has a system with a maximum overall accuracy of 90% for detecting intracranial aneurysms and an accuracy of 96% for aneurysms with a diameter of 3–7 mm, which is lower than the segmentation result obtained by this model [39].

Therefore, it can be seen from the whole that the current research results show that OTO-Net has a high level of segmentation accuracy for large, medium, and small regions and multiregions. OTO-Net is fully competent to assist radiologists in quantitative analysis and evaluation of MRA examination in patients with intracranial aneurysms. Accuracy is the most important index in the field of medical image processing. There is no upper limit to this index, so our current research needs to be more in-depth and detailed.

6. Conclusion

This study proposed the OTO-Net model for intracranial aneurysms automated segmentation in MRA images and performed experiments on the Adam2020 dataset and GMU dataset, respectively. We designed a novel 3D image preprocessing scheme to correlate the structural information between data blocks through overlap and partition operations. At the same time, we proposed the OTO-Net for intracranial aneurysms automated segmentation in MRA images. The OTO-Net uses full convolution to achieve intracranial aneurysms automated segmentation through the combination of downsampling, upsampling, and skip connection. In addition, loss ensemble is used as the objective function to steadily improve the backpropagation efficiency of the network structure during the training process. We evaluated the proposed OTO-Net on one public benchmark dataset and one private dataset. Our proposed model can achieve the automated segmentation accuracy with 98.37% and 97.86%, average surface distances with 1.081 and 0.753, dice similarity coefficients with 0.9721 and 0.9813, and Hausdorff distance with 0.578 and 0.642 on these two datasets, respectively. Therefore, our proposed OTO-Net plays an essential role in radiologists' assisted discovery and diagnosis of intracranial aneurysms and brings substantial value to intelligent medicine's advancement and development. The next research direction is to better use the transformer and 3D information to segment intracranial aneurysms in MRA images.

Data Availability

The raw/processed data required to reproduce these findings cannot be shared at this time as the data also forms part of an ongoing study.

Ethical Approval

The studies involving human participants were reviewed and approved by Institutional Review Board (IRB), Gannan Medical University.

Consent

The patients/participants provided their written informed consent to participate in this study.

Conflicts of Interest

No conflicts of interests, financial or otherwise, are declared by the authors.

Authors' Contributions

J. Ye, X. Xu, X. Wang, and X. Lai conceived and designed the study. J. Ye, L. Li, J. Zhao, W. Lai, and X. Lai contributed to the literature search. J. Ye, X. Xu, W. Zhou, and X. Lai contributed to data analysis and data curation. J. Ye, X. Xu, C. Zheng, X. Wang, and X. Lai contributed to data visualization. J. Ye and X. Xu contributed to software implementation. J. Ye, L. Li, J. Zhao, W. Lai, W. Zhou, and X. Lai contributed to the tables and figures. J. Ye, X. Xu, J. Zhao, W. Lai, C. Zheng, X. Wang, and X. Lai contributed to the writing of the report. J. Ye, L. Li, X. Wang, and X. Lai contribute to reviewing and editing. All the authors have read and approved the publication of this work.

Acknowledgments

This work was funded by the Science and Technology Research Project of the Education Department of Jiangxi Province (No. GJJ211512) and also supported in part by the

Guiding Science and Technology Project of Ganzhou City (No. GZ2017ZSF042).

References

[1] M. H. Vlak, A. Algra, R. Brandenburg, and G. J. Rinkel, “Prevalence of unruptured intracranial aneurysms, with emphasis on sex, age, comorbidity, country, and time period: A systematic review and meta-analysis,” *The Lancet Neurology*, vol. 10, no. 7, pp. 626–636, 2011.

[2] A. Keedy, “An overview of intracranial aneurysms,” *McGill Journal of Medicine*, vol. 9, no. 2, pp. 141–146, 2006.

[3] M. Koide, I. Sukhotinsky, C. Ayata, and G. C. Wellman, “Subarachnoid hemorrhage, spreading depolarizations and impaired neurovascular coupling,” *Stroke Research and Treatment*, vol. 2013, Article ID 819340, 2013.

[4] B. N. R. Jaja, M. D. Cusimano, N. Etminan et al., “Clinical prediction models for aneurysmal subarachnoid hemorrhage: A systematic review,” *Neurocritical Care*, vol. 18, no. 1, pp. 143–153, 2013.

[5] F. Olubajo, S. Stavropoulos, M. M. Hussain, C. Rowland-Hill, and S. Achawal, “Cranial subarachnoid and subdural haemorrhage caused by spinal melanoma metastasis,” *British Journal of Neurosurgery*, vol. 33, no. 1, pp. 110-111, 2019.

[6] M. J. H. Wermer, I. C. van der Schaaf, A. Algra, and G. J. E. Rinkel, “Risk of rupture of unruptured intracranial aneurysms in relation to patient and aneurysm characteristics,” *Stroke*, vol. 38, no. 4, pp. 1404–1410, 2007.

[7] J.-S. Nam, S.-B. Jeon, J.-Y. Jo et al., “Perioperative rupture risk of unruptured intracranial aneurysms in cardiovascular surgery,” *Brain*, vol. 142, no. 5, pp. 1408–1415, 2019.

[8] J. M. Wardlaw and P. M. White, “The detection and management of unruptured intracranial aneurysms,” *Brain*, vol. 123, no. Pt 2, pp. 205–221, 2000.

[9] E. Z. Kapsalaki, C. D. Rountas, and K. N. Fountas, “The role of 3 Tesla MRA in the detection of intracranial aneurysms,” *International journal of vascular medicine*, vol. 2012, Article ID 792834, 2012.

[10] M. H. Li, Y. D. Li, H. Q. Tan et al., “Contrast-free MRA at 3.0 T for the detection of intracranial aneurysms,” *Neurology*, vol. 77, no. 7, pp. 667–676, 2011.

[11] A. Hosny, C. Parmar, J. Quackenbush, L. H. Schwartz, and H. J. W. L. Aerts, “Artificial intelligence in radiology,” *Nature Reviews Cancer*, vol. 18, no. 8, pp. 500–510, 2018.

[12] Y. Lecun, B Boser, J. S. Denker et al., “Backpropagation applied to handwritten zip code recognition,” *Neural Computation*, vol. 1, no. 4, pp. 541–551, 2014.

[13] A. Krizhevsky, I. Sutskever, and G. Hinton, “ImageNet classification with deep convolutional neural networks,” *Advances in Neural Information Processing Systems*, vol. 25, no. 2, pp. 84–90, 2012.

[14] S. Soffer, A. Ben-Cohen, O. Shimon, M. M. Amitai, H. Greenspan, and E. Klang, “Convolutional neural networks for radiologic images: a radiologist’s guide,” *Radiology*, vol. 290, no. 3, pp. 590–606, 2019.

[15] D. Killock, “AI outperforms radiologists in mammographic screening,” *Nature Reviews Clinical Oncology*, vol. 17, no. 3, p. 134, 2020.

[16] A. M. Rauschecker, J. D. Rudie, L. Xie et al., “Artificial intelligence system approaching neuroradiologist-level differential diagnosis accuracy at brain MRI,” *Radiology*, vol. 295, no. 3, pp. 626–637, 2020.

[17] K. Muhammad, S. Khan, J. D. Ser, and V. H. C. d. Albuquerque, “Deep learning for multigrade brain tumor classification in smart healthcare systems: a prospective survey,” *IEEE Transactions on Neural Networks and Learning Systems*, vol. 32, no. 2, pp. 507–522, 2021.

[18] A. Park, C. Chute, P. Rajpurkar et al., “Deep learning-assisted diagnosis of cerebral aneurysms using the HeadXNet model,” *JAMA Network Open*, vol. 2, no. 6, Article ID e195600, 2019.

[19] Y. Wang, Y. Zhang, L. Navarro et al., “Multilevel segmentation of intracranial aneurysms in CT angiography images,” *Medical Physics*, vol. 43, no. 4, pp. 1777–1786, 2016.

[20] J. Y. Jiang, S. C. Tsai, and S. J. Lee, “FSKNN: multi-label text categorization based on fuzzy similarity and k nearest neighbors,” *Expert Systems with Applications*, vol. 39, no. 3, pp. 2813–2821, 2011.

[21] H.-C. Kim, J.-H. Park, D.-W. Kim, and J. Lee, “Multilabel naïve Bayes classification considering label dependence,” *Pattern Recognition Letters*, vol. 136, pp. 279–285, 2020.

[22] D. Wang, J. Jiang, J. Mo, J. Tang, and X. Lv, “Rapid Screening of thyroid dysfunction using Raman spectroscopy combined with an improved support vector machine,” *Applied Spectroscopy*, vol. 74, no. 6, pp. 674–683, 2020.

[23] L. Yang, H. Wu, X. Jin et al., “Study of cardiovascular disease prediction model based on random forest in eastern China,” *Scientific Reports*, vol. 10, no. 1, p. 5245, 2020.

[24] R. Bender, “Introduction to the use of regression models in epidemiology,” *Methods in Molecular Biology*, vol. 471, pp. 179–195, 2009.

[25] S. Huang, N Cai, P. P. Pacheco, S. Narrandes, Y. Wang, and W. Xu, “Applications of support vector machine (SVM) learning in cancer genomics,” *Cancer genomics & proteomics*, vol. 15, no. 1, pp. 41–51, 2018.

[26] E. Shelhamer, J. Long, and T. Darrell, “Fully convolutional networks for semantic segmentation,” *IEEE Transactions on Pattern Analysis and Machine Intelligence*, vol. 39, no. 4, pp. 640–651, 2017.

[27] O. Ronneberger, P. Fischer, and T. Brox, *U-net: Convolutional Networks for Biomedical Image Segmentation*, Springer International Publishing, Switzerland, 2015.

[28] F. Milletari, N. Navab, and S. A. Ahmadi, “V-Net: fully convolutional neural networks for volumetric medical image segmentation,” in *Proceedings of the 2016 Fourth International Conference on 3D Vision (3DV)*, October 2016.

[29] W. K. Röntgen, “On a new kind of rays,” *CA: A Cancer Journal for Clinicians*, vol. 22, no. 3, pp. 153–7, 1972.

[30] W. K. Röntgen, “A new form of radiation,” *Science*, vol. 3, no. 72, pp. 726–729, 1896.

[31] R. Smith-Bindman, M. L. Kwan, E. C. Marlow et al., “Trends in use of medical imaging in US health care systems and in Ontario, Canada, 2000-2016,” *JAMA*, vol. 322, no. 9, pp. 843–856, 2019.

[32] R. Shahzad, L. Pennig, L. Goertz et al., “Fully automated detection and segmentation of intracranial aneurysms in subarachnoid hemorrhage on CTA using deep learning,” *Scientific Reports*, vol. 10, no. 1, Article ID 21799, 2020.

[33] M. W. K. Law and A. C. S. Chung, “Segmentation of intracranial vessels and aneurysms in phase contrast magnetic resonance angiography using multirange filters and local variances,” *IEEE Transactions on Image Processing*, vol. 22, no. 3, pp. 845–859, 2013.

[34] M. W. Law and A. C. Chung, “Vessel and intracranial aneurysm segmentation using multirange filters and local variances,” *Medical Image Computing and Computer-Assisted Intervention*, vol. 10, no. Pt 1, pp. 866–874, 2007.

[35] G. E. Hinton and R. R. Salakhutdinov, “Reducing the dimensionality of data with neural networks,” *Science*, vol. 313, no. 5786, pp. 504–507, 2006.

[36] L. R. Dice, "Measures of the amount of ecologic association between species," *Ecology*, vol. 26, no. 3, pp. 297–302, 1945.
[37] A. Gofman and M. Kelbert, "Un upper bound for Kullback-Leibler divergence with a small number of outliers," *Mathematical Communications*, vol. 18, no. 1, pp. 75–78, 2013.
[38] H. Kervadec, J. Bouchtiba, C. Desrosiers, E. Granger, J. Dolz, and I. Ben Ayed, "Boundary loss for highly unbalanced segmentation," *Medical Image Analysis*, vol. 67, Article ID 101851, 2021.
[39] T. Sichtermann, A. Faron, R. Sijben, N. Teichert, J. Freiherr, and M. Wiesmann, "Deep learning-based detection of intracranial aneurysms in 3D TOF-MRA," *American Journal of Neuroradiology*, vol. 40, no. 1, pp. 25–32, 2019.

Hindawi
Computational Intelligence and Neuroscience
Volume 2022, Article ID 5866922, 13 pages
https://doi.org/10.1155/2022/5866922

Research Article

Electronic User Authentication Key for Access to HMI/SCADA via Unsecured Internet Networks

Amer Tahseen Abu-Jassar,[1] Hani Attar ,[2] Vladyslav Yevsieiev ,[3] Ayman Amer,[2] Nataliia Demska,[3] Ashish Kr. Luhach ,[4] and Vyacheslav Lyashenko [5]

[1]*Faculty of Computer Science and Information Technology, Ajloun National University, Ajloun, Jordan*
[2]*Faculty of Engineering, Department of Energy Engineering, Zarqa University, Zarqa, Jordan*
[3]*Department of Computer-Integrated Technologies, Automation and Mechatronics, Kharkiv National University of Radio Electronics, Kharkiv, Ukraine*
[4]*The PNG University of Technology, Lae, Papua New Guinea*
[5]*Department of Media Systems and Technology, Kharkiv National University of Radio Electronics, Kharkiv, Ukraine*

Correspondence should be addressed to Ashish Kr. Luhach; ashish.kumar@pnguot.ac.pg

Received 5 December 2021; Revised 5 February 2022; Accepted 9 March 2022; Published 13 April 2022

Academic Editor: Xin Ning

This paper discusses the development of new hardware and software for protecting access to HMI/SCADA systems via Unprotected Internet Networks (UPN), mainly when working remotely with confidential information. Based on the analysis carried out, it is shown that the existing vulnerabilities can be exploited by cybercriminals to steal passwords and user authentication logins. Modern protection technologies based on the OTP method have been investigated. Moreover, a new concept of information security for user authentication in UPNs when working with information remotely is proposed. The structure of the electronic key and the connection diagram based on the selected hardware modules have been developed. In addition, the two-level user identification algorithms and the firmware program code for the ATmega32U4 microcontroller are considered. Finally, to show the reliability and stability of the of the developed electronic user authentication key against any unexpected software hacking, a number of experiments have been performed.

1. Introduction

Industry 4.0 is a new vision in production associated with the introduction of modern digital technologies, such as Industrial Internet of Things (IIoT), Machine-to-Machine (M2M), Operation 4.0 (Ops 4.0), Big Data (BD), Cloud Computing (CC), and integration of Robotic Process Automation (RPA) with Artificial Intelligence (AI) [1]; these technologies facilitate the achieving of implementing new models for managing the production processes. One of the current ideas about modern production has found its reflection in the concept of Smart Manufacturing (SM). SM is a production concept that implements computer integration, and a high level of adaptability and a rapid change in production levels, which depends on the demand and the required tasks to solve [2]. Moreover, [2] showed that for the usage of digital information techniques that can be implemented for more flexible multiscale dynamic production systems, a single end-to-end industrial network based on IIoT is required. Indeed, the single end-to-end industrial network provides the access to the global Internet network, which supports the connection to all information control actions, besides the interaction with all constituent elements of the SM. However, implementing end-to-end systems may worsen the vulnerability of the MS systems, as a result of the information loss risk and distortion that carried out by the cyberattacks from the Internet uncontrolled sources, which could cause high economic losses and even man-made disasters. Therefore, when applying the end-to-end systems, protecting production information from the cyberattacks becomes a priority; as an example, the Stuxnet worm affected the access to the information from industrial systems Simatic WinCC SCADA [3]. Another example is the Bushehr nuclear power plant in Iran, where a worm disabled a large number of uranium enrichment centrifuges controlled by the Variable-Frequency Drive (VFD). Similarly, [4] presented the theft of IIoT production files from a Korean nuclear power plant in 2014. Indeed, the examples in [3, 4] show the urgent need to protect the access to the production SCADA/HMI information from external unprotected IoT networks during far-distance work of enterprise employees.

The work of Ali Süzen indicates that a threat of cyberattack is always present as long as there is available digital data [5]; consequently, the need for high level of cyber security is increasing. Moreover, [5] conducts valuable research into the threat of the cyberattacks sources in the Industry 4.0 ecosystem, which are listed below:

(i) Unsecured device connections in the control system protocols.
(ii) The lack of regular penetration tests.
(iii) The lack of ability to effectively manage network devices, mainly by untrained personnel, resulting in the shortage of complete prevention of the cyberattacks in the Industry 4.0 ecosystem [5].

Pang et al. proposed a new two-stream structure of SM includes specifications, organizational architecture, security, user access, databases, and hardware and software requirements [6]. However, [6] indicated that the standard solutions are left for enterprise cyber security.

The authors Efe and Isik in their publications classify the types of vulnerabilities that need to be considered and resolved in an enterprise to counter cyberattacks and increase cybersecurity [7]. However, the authors consider solutions to SM cyber security issues, only on the basis of case studies, which are not specific, but generalized in nature.

Mullet et al. evaluate methodologies and technical solutions from classic countermeasures to cyberattacks to innovative ones, for example, based on decoys and digital twins [8]. As a result, the authors have given recommendations on the cyber protection of SM, which are of a general nature without a specific solution.

The proposed new methodology for the semantic expansion and improvement of cyber security models is presented in the work of Laković et al. [9], which allows quantifying the level of existing cyber security SM, through adapted methods. At the same time, the authors do not consider security issues at the SCADA/HMI, MES, and ERP levels.

In Ferencz et al.'s article, the authors conduct MS research from a security perspective, focusing on the integration of IoT devices, and propose a theoretical architecture for the integration of SOC and IoT [10].

On the other hand, Sharma introduces the vulnerabilities and defines a cyber-defense strategy for corporate and end users, who are instructed to simultaneously implement preventive protection measures [11].

Naanani and Humayun in their work carried out a detailed review of possible cyberattacks targeting each level of Industry 4.0, as well as the consequences of these attacks and the corresponding countermeasures [12]. In addition, a multilayered framework is presented that can provide end-to-end protection against cyberattacks; however, this structure has a minimum level of protection on the Application Layer, against theft of usernames and passwords using the Phishing and Social Engineering methods to access the SCADA/HMI, MES, and ERP levels [13, 14], besides the ability to cyberattack the PLC, SCADA/HMI levels, which can lead to disruption of physical production processes.

In the work of Gómez et al., the issues of PLC, SCADA/HMI protection are considered by finding anomalies in control networks [15].

Based on the analysis of [15], it can be seen that they are aimed at tracking the possibility of a cyberattack within the IIoT network, while not paying attention to the issue of protecting the username and password from theft when logging into the SCADA/HMI system. So if the username and password are stolen, the system will consider that the user is identified with certain access parameters, resulting in making the system to be insecure and vulnerable to industrial espionage and cyberattacks.

Based on the above, in order to prevent the above commented-on errors and take into account possible other errors, the proposed work in this paper is directed to the following guidelines:

(i) Analyzing modern methods and technologies for user authentications; taking into account the positive aspects and identifying flaws; and developing a new concept of protecting user authentication information using modern software and hardware.
(ii) Considering the possibility of minimizing the influence of the human factor on the loss and disclosure of the username and password content and conducting researches to resist the hacking.

2. General Concept of Information Protection Using Electronic Keys for User Authentication

Cracking a password is one of the most common types of attacks on any information system that uses password or username-password pair authentication. The essence of the attack boils down to the seizure of the password of the user who has the right to enter the system. In this case, the following approaches can be used [16]:

(i) Direct search: Enumeration of all possible combinations of characters allowed in the password.
(ii) Selection by dictionary: The method is based on the assumption that existing words of any language or their combinations are used in the password.
(iii) Method of social engineering: Based on the assumption that the user used personal information as a password, such as the first or last name, date of birth, and so on.

The attackers' goal is to obtain the password to guarantee granting all the rights that the original user holds. At the same time, logging in under an existing account that does not arouse suspicion among system administrators and enterprise security systems.

Therefore, the reliability of the authentication using a password or a "username-password" pair is determined by the following criteria:

(i) Length (the number of characters that the password contains).

(ii) Complexity (the usage of the combinations: letters, symbols, and numbers).

(iii) Unpredictability (the usage of the publicly available data, nicknames, dates, or any information available on social networks).

The most common cracking methods of an authentication password or username-password pair are presented in Table 1.

The presented methods of cracking an authentication password or a "username-password" pair are implemented in the following software tools; some of the most common are presented in Table 2.

By analyzing the methods of cracking the password for authentication or username/password pairs, it can be seen that reusable passwords can be compromised. As a consequence, for the safety of working with industrial information via remote SCADA/HMI, it is necessary to consider alternative security methods, which are presented in Table 3.

Let's analyze alternative authentication methods from the point of view of their application for access to industrial SCADA/HMI in unsecured networks:

(i) Biometrics Method: in 2017, it was proved that it is possible to recreate a fingerprint pattern from photographs taken with a digital camera from a distance of three meters [36]. In 2014, the fingerprints of the Minister of Defense of Germany were shown, which recreated from official high-resolution photographs from open sources [37]. Thus, the use of biometrics methods to implement access to industrial SCADA/HMI can be considered irrelevant and easily vulnerable.

(ii) The Single Sign-On (SSO) method is based on setting up a trust relationship between an application known as a service provider and an access control system. The software snippet assumes local installation. This allows implementing a password store, where a single username and a single password are allowed; however, they must be entered every time to access a new application or a new site. Such a system simply stores the credentials for other applications and enters them when needed. Within the framework of these studies, this method is not suitable, since access to industrial data via SCADA/HMI is carried out through a trust relationship, and they are possible only within the industrial IIoT. Therefore, this method is not suitable for the proposed work in this paper.

(iii) The OpenID Connect method allows Internet resources to verify the identity of the user based on the authentication performed by the authorization server. For work, the RESTful API described in the specification is used. Also, OpenID Connect defines additional mechanisms for strong encryption and digital signatures. But at the same time, some researchers believe that the OpenID protocol is vulnerable to phishing attacks, when, instead of the provider, attackers direct the end user to a site with a similar design. If the user does not notice the substitution, then he enters the authentication data (login, password). As a result, attackers can present themselves to Internet resources as a given user and gain access to the information stored on these resources. Phishing attacks are also possible when a site that supports OpenID authorization is forged in order to obtain information about the user from the provider. Using the "hidden redirect" vulnerability, attackers can create the illusion for the user that the information is being requested by this site [38].

(iv) One-Time Password (OTP) is a one-time password method valid for only one authentication session. The one-time password can also be limited to a certain period of time. The advantage of a one-time password over a static password is that the password cannot be reused [39]. However, in some cases, the use of one-time passwords increases the risk of compromising the data of the entire system, since when an attacker accesses the OTP authentication server all system components will trust this server. However, this may increase the risk of transferring one-time passwords to attackers if the token is lost. It is worth mentioning here that often in the application, in addition to a one-time password, a reusable password should be entered, but it can also be compromised in the same way as a regular password. Finally, when OTP does not function correctly, the security of the system becomes vulnerable, such as increasing the validity period of a one-time password, which increases the possibility to guess the password, which what happened at the Banks of Sweden in 2005, and Citibank (USA) in 2006, where one-time passwords were obtained as a result of phishing attack [40].

The resynchronization of OTP tokens and authentication servers in time, as a result of which, at a certain moment, the server may have several "correct" one-time passwords. Suppose, for example, that the approximate desync time is 5 minutes and the OTP changeover period is 30 seconds. In such a situation, up to 10 "correct" passwords can exist simultaneously, which increases the likelihood of unauthorized access.

Table 1: Methods for cracking the authentication password or username-password pair.

Method	Description
Dictionary attack [17]	The method involves using a list of words to compare with user passwords.
Brute force attack [18]	The method uses algorithms that combine alphanumeric characters and symbols to come up with passwords for the attack. For example, a password with the value "password" can also be used like the word p @ $$ using a brute force attack.
Rainbow attack [19]	The method uses precomputed hashes (md5), a ready-made database of hashes is generated or bought, and then it is compared with the hashes to be cracked.
Guessing [20]	The method assumes guessing the most common passwords (qwerty, password, and admin). Usually used or set as default passwords. If they have not been changed or the user is careless when choosing passwords, then they can be easily compromised.
Spidering [21]	The method of social engineering. Most organizations use passwords that contain company information. This information can be found on company websites and social networks, such as Facebook, Twitter, and so on. Spidering collects information from these sources to compile word lists. The wordlist is then used to carry out dictionary and brute force attacks.

Table 2: Software tools for cracking authentication passwords.

Name of the tool	Description
John the Ripper [22, 23]	Uses command line to crack passwords. This makes it suitable for advanced users who are comfortable working with teams. It uses a wordlist to crack passwords. The program is free, but the wordlist is not.
Cain and Abel [24, 25]	Used for password cracking methods: dictionary attack, brute force, and cryptanalysis. Unlike John the Ripper, Cain and Abel uses a graphical user interface.
Ophcrack [25–27]	Is a cross-platform, Windows password cracker that uses rainbow tables to crack passwords. It works on Windows, Linux, and Mac OS. It also has a module for brute force attack attacks among other features.

Table 3: Alternative authentication methods.

Method	Description
Biometrics [28, 29]	These are unique biological and physiological characteristics that make it possible to establish a person's identity. There are five most common types of biometrics: fingerprint, facial, voice, eye iris, and palm and finger vein patterns.
Single sign-on (SSO) [30, 31]	An authentication method that allows users to securely authenticate to multiple applications and sites at once using a single set of credentials.
OpenID Connect (OIDC) [32, 33]	Describes a metadata document RFC that contains most of the information needed for any application to sign in. This includes information such as the used URLs and the location of the service signing public keys.
One-time password (OTP) [34, 35]	It is a password that is valid for only one authentication session. The one-time password can also be limited to a certain period of time. The advantage of a one-time password over a static password is that the password cannot be reused. Thus, an attacker who intercepted data from a successful authentication session cannot use the copied password to gain access to the protected information system.

3. The Proposed Mythology and the Hardware

Based on the analysis of alternative authentication methods presented in Table 3, this paper proposes to modify the OTP method by using new concepts of protecting the access to the production information through unprotected networks, which are as follows:

(i) Implementing access in such a way that the user does not know the password and identification login.

(ii) Complicating the password and not associating it with specific dates or associative concepts of the user (i.e., automatic generation of the username and password).

(iii) Changing of the username and the password once a week automatically or more often without notifying the user. The period of changing the username and the password depends on the required protection level of the information and the level of security of the internal IIoT networks.

(iv) Providing information for automatic login without using the keyboard, thus avoiding the use of key-loggers and similar spyware.

(v) Automatically checking of the URL, which the user visits for the protection against phishing attacks.

(vi) Implementing two-factor user authentication.

(vii) Providing connections to the HMI, HMI/SCADA terminal via modern USB/Tape-C/OTG interfaces, and so on, considering the protection against malicious Trojan viruses transmitted via INF/Autorun.

The structural diagram and the components' selection for the implementation of the proposed electronic key to improve the user authentication through unsecured Internet networks is illustrated in Figure 1, which shows how to implement the concept of information protection during user authentications to access HMI and HMI/SCADA systems via unprotected Internet networks.

During the development of the structural diagram, an analysis was also carried out of modern interfaces that can be used to connect to PCs, laptops, tablets, mobile phones, or external and internal terminals, through which a physical connection could be applied to ensure the authentication of user access rights to the production HMI and HMI/SCADA systems [41].

The proposed work in this paper suggests implementing the most common USB (Universal Serial Bus) 1.0–3.0 interface and its compatible Type-C and OTG counterparts. Serial interface for connecting peripherals is divided into USB 1.x (average speed 12 Mb/s); USB 2.x (average speed 25–480 Mb/s); USB 3.x (average speed 2.5 Gb/s); and Type-C or USB 3.1. All listed serial interfaces are used on 98% of industrial control systems and PCs, laptops, and modern mobile phones (except for Apple corporation). To combine these serial interfaces, adapters are used, which are free for sale and which allow you to connect the developed electronic dongle even to a hardware device of Apple corporation.

As a consequence, it is necessary to use a microcontroller with built-in extended USB functions to provide universal access to all kinds of devices, resulting in the developing of the access key that consists of three main elements: a control board, based on the ATmega32U4 microcontroller [42], was chosen due to the peculiarities of its CPU architecture, inside which, on a chip, a usb <> uart converter is implemented. Thanks to this, no drivers are required when connecting to a PC. And the computer itself recognizes the Arduino Pro Micro ATmega32U4 as a Human Interface Device (HID) device, an LCD display for displaying the necessary information [43], and a push-button control unit [44]. Analyzing the modern element base and the characteristics to solve the assigned tasks, the following hardware components of the electronic key were selected, which are shown in Figure 2.

The main characteristics of the selected hardware items are taken from the Datasheet: Arduino Pro Micro (ATmega32U4) where the Micro has built-in USB communication, eliminating the need of a secondary processor, operating voltage 5 V microUSB, Flash ROM-4Kb with dimensions of 18×33 mm [42], and 0.91 OLED display module with I2C connection interface; the viewing angle is more than 160°; the operating voltage is 3.3-6V with dimensions of $12 * 12 * 38$ mm [43] and Clock button model A24 with number of contacts 4, with dimensions of $12 * 12 * 7.3$ mm [44].

Based on the selected hardware modules, the following wiring diagram has been developed, which is shown in Figure 3.

To connect the 0.91 OLED display module, the I2C connection interface is used that requires connecting the SCL c D3 and SDA c D2 connectors to the Arduino Pro Micro. This display module was chosen because of its support for the I2C interface, which allows data transmission over two connectors (SCL, SDA) and two power supplies (5V, GND), as opposed to the Serial Peripheral Bus (SPI) interface, which uses four connectors (MISO, SCK, SS, and MOSI) for data transmission and two for power supply (5 V, GND). The 5 V power supply for the display can be taken from the VCC and GND connectors on the Arduino Pro Micro and connected to the corresponding connectors on the display. Based on the proposed structural diagram, the A24 clock model buttons is connected through a common ground, to the digital connectors (D6, D7, and D8). Accordingly, the "<<" button for menu control is connected to the D6 connector, the selection confirmation button "OK" to the D7 connector, and the menu control button ">>" to the D8 connector.

To assemble an experimental dummy of the electronic authentication key, the size form factor of a USB flash drive was chosen. The placement of all hardware modules is done on a breadboard with dimensions of $30 \times 40 \times 20$ mm (WxDxH). When designing the topology of the printed circuit board of the electronic key, the authentication was carried out using modern CAD systems EDA Altium Designer, which reduces the overall dimensions. The obtained result of assembled prototype of the proposed electronic authentication key is shown in Figure 4.

The next step is to develop an algorithm for two-factor authentication of access to SCADA/HMI. To simplify perception, the proposed algorithm was divided to several levels.

At the first level, user authentication is performed to provide the access to the main menu of the electronic key, where a 4-digit digital access pin must be entered. Depending on the security requirements and the level of user access to the production HMI or HMI/SCADA, the minimum number of attempts in the Attempt counter, can be equal to one attempt. If pin is entered incorrectly, the electronic key is blocked for in the interval of 30 seconds before the new firmware by the security administrator is created. The algorithm of the first level of the electronic key user authentication is shown in Figure 5.

The second level of user authentication is automatic, where the electronic key management menu (Main Menu) of the user offers the name of the domains needed to perform the necessary actions. In this case, the name of the domains can be any name that is convenient for the user's association. After choosing the HMI/SCADA domain name, the electronic key copies the address line in the Web browser for verification and compares it with the domain name stored in the memory of the electronic key; if they do not match, the site is considered as "fake," and hence the work stops, and the user receives a warning about the danger. If the domain addresses are the same, then the user puts italics on the login field and clicks the "OK" button on the key. This allows the user of the electronic key not to remember the login and password for accessing Cloud Storage of the enterprise. After automatic filling of the authentication fields, the user performs the standard action to enter in the form of clicking the "Sign in" button. Further, the received data is transferred to the enterprise's Cloud Storage server, where the user's level

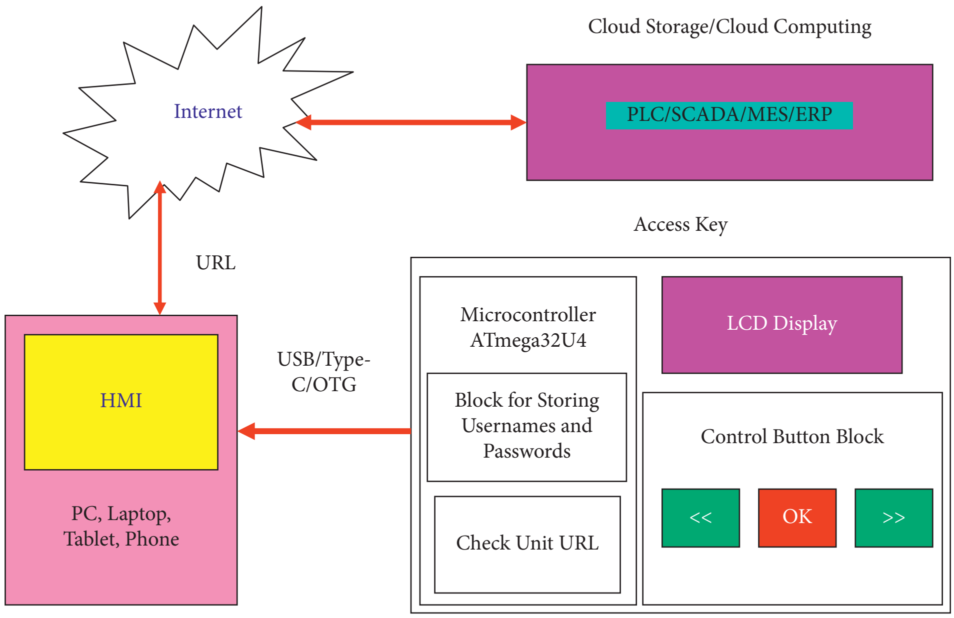

Figure 1: Block diagram of the electronic key for user authentication in HMI/SCADA.

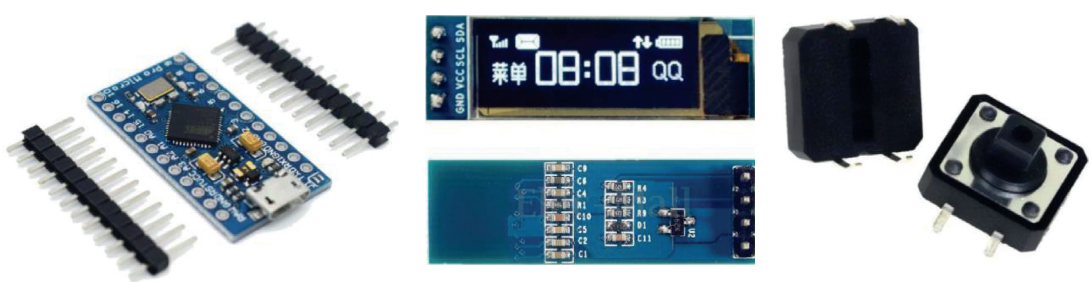

(a) (b) (c)

Figure 2: Hardware components of the electronic key. (a) Arduino Pro Micro (ATmega32U4) [42]; (b) 0.91 OLED display module 128×32 [43]; and (c) button clock model A24 [44].

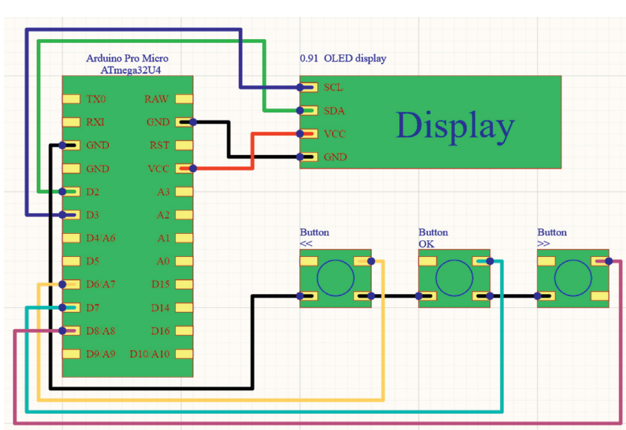

Figure 3: Electrical connection diagram.

of the access to the information is checked on the server. If the user is defined on the server, then in accordance with his priorities and permissions, the access to information is given that is displayed in the Web browser window. The algorithm of the second level of automatic user authentication is shown in Figure 6.

The next step in the development of the HMI/SCADA user authentication electronic key is the development of software for the ATmega32U4 microcontroller. To be able to understand the required software, it is necessary to analyze the existing software development environments for microcontrollers of the whole family, which considers the following development environments: AVRStudio [45], MPLAB [46], and Arduino IDE [47]. All of the above development environments, a C ++ language or a subset of it, can be implemented. However, it is worth noting that for software development in Atmel Studio, it is necessary to additionally install the Atmel Toolchain [48]. At the same time, there is no confusion when compiling software, due to the fact that for different versions of Atmel Studio two types of compiler Atmel Toolchain and WinAVR are used [49], which complicates the perception of the compilation process. Therefore, the Arduino IDE to develop the HMI/SCADA user authentication electronic key software is chosen. The selection was based on the following factors:

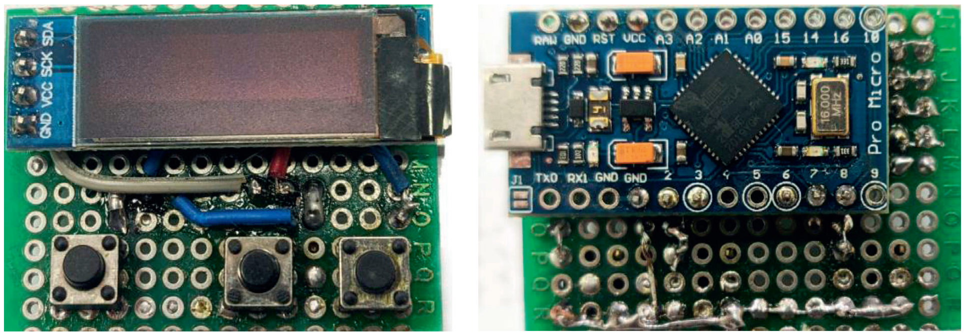

(a) (b)

Figure 4: Assembled prototype of the electronic authentication key. (a) Top view. (b) Bottom view.

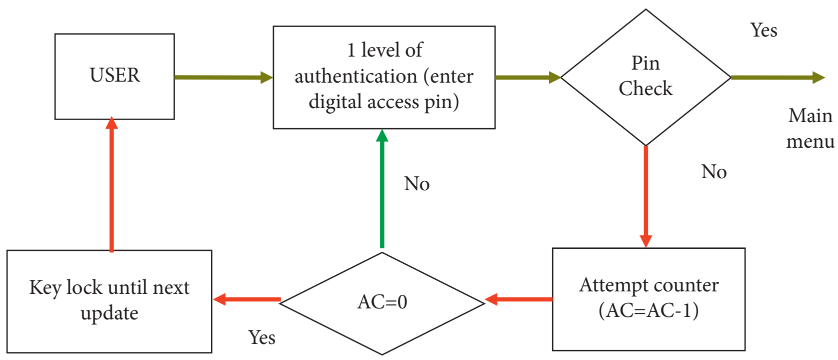

Figure 5: Algorithm of the first level of user authentication with an electronic key.

simplicity and ease of software development, ease of library integration, support from official Arduino developers, and a Freeware license. The enlarged logic of the firmware for the electronic key in the form of an algorithm is shown in Figure 7.

At the first stage of program development, it is necessary to connect the libraries necessary and sufficient to implement the specified functions and work with hardware modules, such as 0.91 OLED display modules 128×32 or tact button model A24.

In the form of constants, the password of the first level of authentication of the electronic key user to implement the algorithm (Figure 5) is set, where a 4-digit numeric password from 0 to 9 is required:

const int pas_1 = 0;

const int pas_2 = 0;

const int pas_3 = 0;

const int pas_4 = 0.

In later steps, flashing electronic access keys in secure IIoT and hence generating a random new password for the first level of electronic key automatically is required, and automatically sent to the user's phone or mail, with information about the time of its validations in the system.

The pins for connecting the clock buttons is inserted into the navigation menu for controlling the electronic key of the Arduino Pro Micro, in accordance with the connection diagram (Figure 3):

const int pin_OK = 8;

const int pin_UP = 6;

const int pin_DOWN = 7.

A limit on the number of HMI/SCADA access accounts used (the maximum can be 25) is created:

int max_account_number = 5;

A function that allows dividing the key's array into columns, in the record format: site—username—login—password, is created.

typedef struct {char* site; char* name; char* login; char* password;} State;

An array in accordance with the division suggested above is created.

The flags "menu" and work with Electrically Erasable Programmable Read-Only Memory EEPROM (EEPROM) is set, where EEPROM is a type of memory that allows writing and reading data from a program, while it is not possible to clear it by rebooting the electronic key. Accordingly, implementing the storage of settings that changes "from the menu" of the device, without flashing is required, as well as a counter of attempts to maintain the first level of authentication and a counter of the timer for blocking the electronic key:

int pas_ST_1 = 0, pas_ST_2 = 0, pas_ST_3 = 0, pas_ST_4 = 0, flag_menu = 60, flag_RES_DISP = 0, msecs = 300;

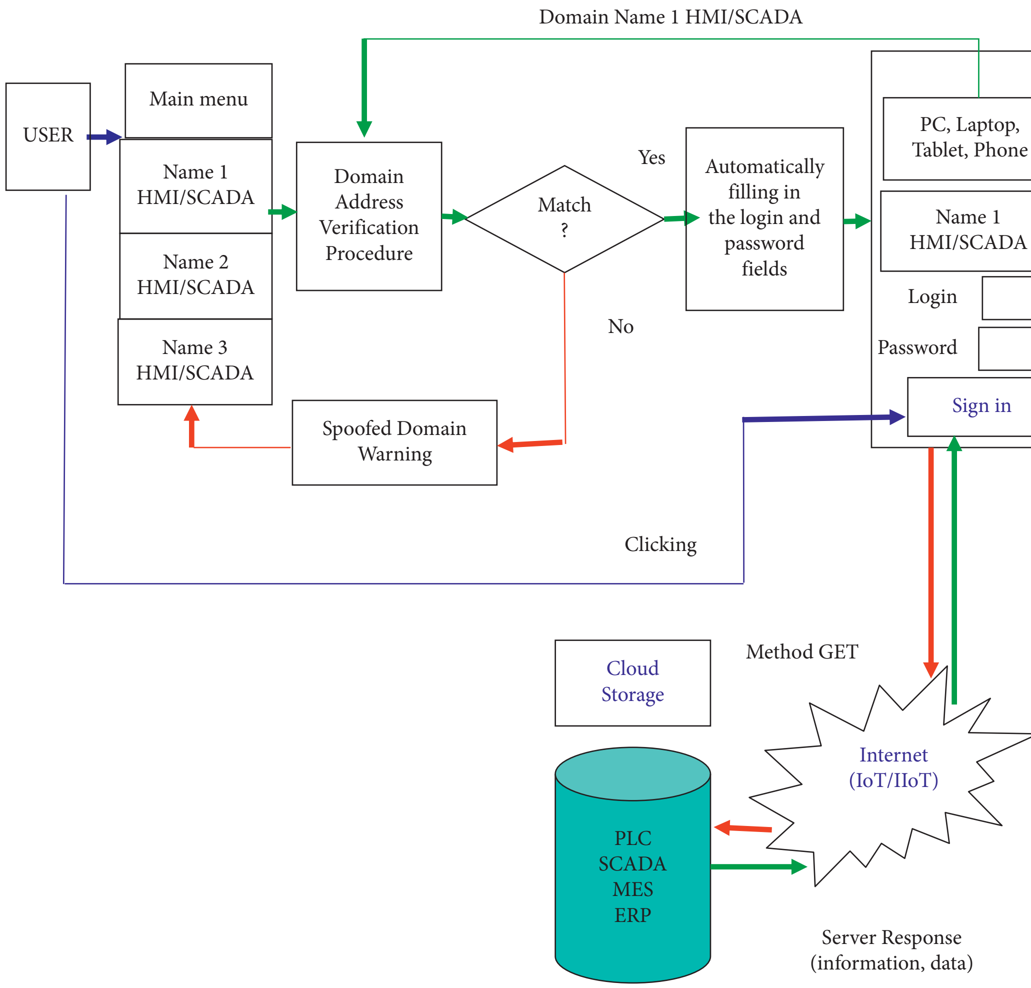

FIGURE 6: Algorithm of the second level of automatic user authentication with an electronic key to access information in HMI/SCADA IV. Development of the software for the functioning of the proposed electronic key.

```
int pin_OK_st = 0, pin_UP_st = 0, pin_DOWN_st = 0, account_number = 0, flag_RES_ACC = 0, timer = 0;
int address_FLAG = 1, flag_EEPROM = 125, seconds = 0;
int seconds1 = 10, seconds2 = 20;
```

To enter the 4-digit password of the first level of user authentication of the electronic key on the OLED display, the following function is implemented.

The function of scanning tact buttons on an electronic key is implemented by the following function:

```
void scan_buttons(){
  pin_OK_st = digitalRead(pin_OK);
  pin_UP_st = digitalRead(pin_UP);
  pin_DOWN_st = digitalRead(pin_DOWN);
}
```

Using the void setup () function, the settings for the electronic authentication key is described.

The main program for the operation of the electronic key using the void loop () cyclic function is implemented.

To flash the layout of the electronic key for user authentication in HMI/SCADA, configuration of the following Arduino IDE settings is required to work with the ATmega32U4 microcontroller (Arduino Pro Micro). In the Tools menu, in the Board section, select “Arduino Micro” and specify the Com port number, as shown in Figure 8.

After the configuration, the firmware with an ATmega32U4 microcontroller (Arduino Pro Micro) is carried out. When the electronic key is turned on for the first time, the user of the electronic key must enter a 4-digit pin to enter the main menu, as shown in Figure 9(a), and the implementation of the selection menu is shown in Figure 9(b).

The developed prototype of the electronic key for user authentication in HMI/SCADA has the following characteristics:

(i) The ability to memorize up to 25 pairs “username-password,” while the user is not obliged to know the “pair” username and does not know the “password,” which avoids the leakage of the disclosure of access data to HMI/SCADA, in contrast to software protection: Google Authenticator, SafeNet Trusted Access (STA), Microsoft MFA, and GateKeeper Enterprise, which displays the token number on the

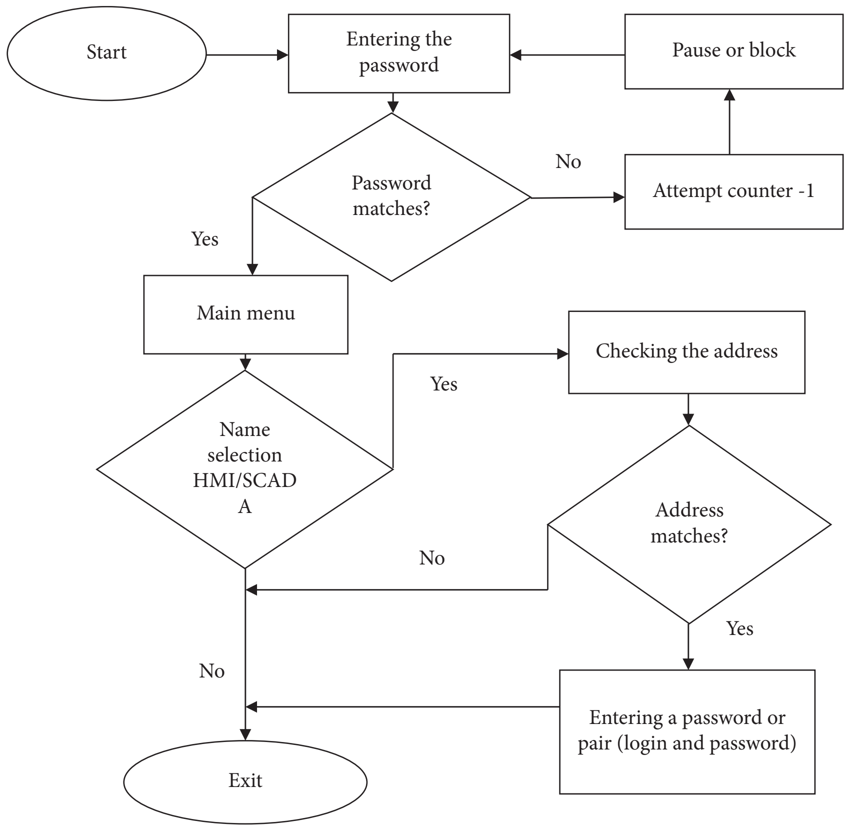

Figure 7: Enlarged algorithm of the electronic key firmware operation.

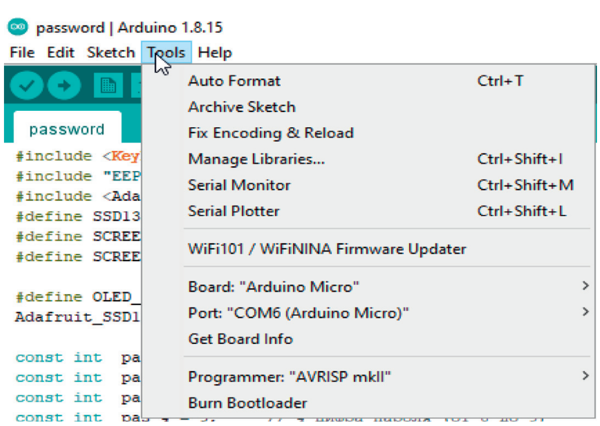

Figure 8: Arduino IDE settings for flashing user authentication electronic key in HMI/SCADA.

smartphone display, hardware protection: RSA token, SafeNet OTP from Thales, which displays the token number on the key display, and the visual access data, which is vulnerable.

(ii) The implemented access concepts in the developed electronic key for user authentication in HMI/SCADA, in contrast to OTP technologies, avoid the desynchronization of OTP tokens and authentication servers in time; as a result of which at a certain moment, there can be several "correct" one-time passwords on the server. For example, suppose the approximate desync time is 5 minutes and the OTP changeover period is 30 seconds; in such a situation, up to 10 "correct" passwords can exist simultaneously, which increases the likelihood of unauthorized access.

(iii) Input of information about the "username-password" pair, on public devices, occurs without using data input devices (keyboards), the data is filled in automatically, and the user simply sends them for verification to the server. This solution avoids the theft of information for a username-password pair using keyloggers, which record the sequence of typing data from the keyboard.

(iv) In case of loss and theft of the user electronic key authentication in HMI/SCADA, a "rigid system" of regulations has been developed according to the following steps:

(1) The action of the key and passwords is limited in time, depending on the security requirements, the change of the "username-password" pair occurs automatically on the server without human involvement, using random symbol generators, which reduces the likelihood of accidental disclosure to zero.

(2) If the notable four-code pin is entered incorrectly at the first level, the user authentication level, the authentication key is blocked for the set time by the administrator, during this time a new "username-password" pair is automatically

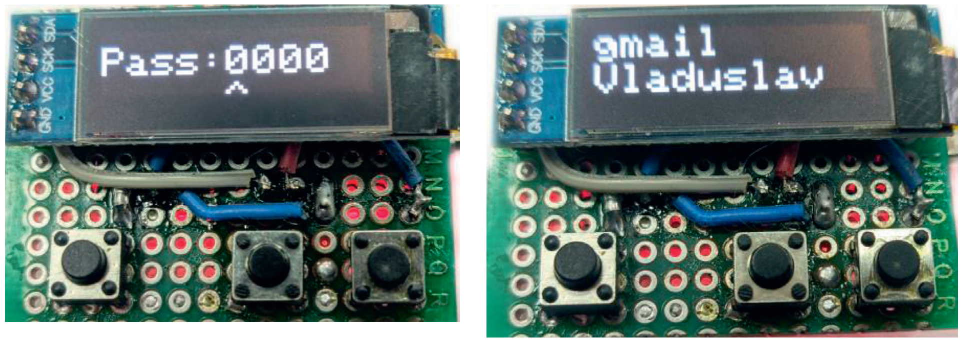

(a) (b)

Figure 9: Checking the functionality of the electronic user authentication key in HMI/SCADA. (a) The first level of user authentication. (b) Main menu for electronic key control.

```
:100000000C9418060C9440060C9440060C94400680
:100010000C9440060C9440060C9440060C94400648
:100020000C9440060C9440060C943A190C94A919AF
:100030000C9440060C9440060C9440060C94400628
:100040000C9440060C9440060C9440060C94400618
:100050000C9440060C9440060C9440060C94DB1B58
:100060000C9440060C9440060C9440060C944006F8
:100070000C9440060C9440060C9440060C944006E8
:100080000C9440060C9440060C9440060C944006D8
:100090000C94251C0C9440060C9440060C944006CD
:1000A0000C9440060C9440060C9440065E0050618F
:1000B00073733A000000000000000000002A2B2800A3
:1000C0000000000000000000000000000000000030
:1000D00000000002C9EB4A0A1A2A434A6A7A5AE47
:1000E000362D3738271E1F2021222324252 6B333FF
:1000F000B62EB7B89F8485868788898A8B8C8D8E2B
:100100008F909192939495969798999A9B9C9D2FF6
:100110003130A3AD35040506070809 0A0B0C0D0E96
:100120000F101112131415161718191A1B1C1DAFD6
:10013000B1B0B500000103070F1F3F7F0080C0E092
:10014000F0F8FCFE0000000003E5B4F5B3E3E6BA3
:100150004F6B3E1C3E7C3E1C183C7E3C181C577D61
:10016000571C1C5E7F5E1C00183C1800FFE7C3E7AD
```

(a)

```
.sec1:00000000 0c    db 0ch
.sec1:00000001 94    db 94h
.sec1:00000002 18    db 18h
.sec1:00000003 06    db 06h
.sec1:00000004 0c    db 0ch
.sec1:00000005 94    db 94h
.sec1:00000006 40    db 40h
.sec1:00000007 06    db 06h
.sec1:00000008 0c    db 0ch
.sec1:00000009 94    db 94h
.sec1:0000000a 40    db 40h
.sec1:0000000b 06    db 06h
.sec1:0000000c 0c    db 0ch
.sec1:0000000d 94    db 94h
.sec1:0000000e 40    db 40h
.sec1:0000000f 06    db 06h
.sec1:00000010 0c    db 0ch
.sec1:00000011 94    db 94h
.sec1:00000012 40    db 40h
.sec1:00000013 06    db 06h
.sec1:00000014 0c    db 0ch
.sec1:00000015 94    db 94h
.sec1:00000016 40    db 40h
.sec1:00000017 06    db 06h
.sec1:00000018 0c    db 0ch
.sec1:00000019 94    db 94h
.sec1:0000001a 40    db 40h
.sec1:0000001b 06    db 06h
```

(b)

Figure 10: An attempt to hack the firmware of the electronic key. (a) A fragment of the firmware in hex. (b) Disassembling the firmware fragment.

generated on the server, as a result of which information about access to the HMI/SCADA is deprecated. The selection of pin by the combinatorial method is 10,000 combinations; it is not possible to perform it manually and this is provided for by the key.

(v) A high degree of protection against "dumping" information is conditionally possible only in the case of the physical theft of an electronic key, and at the same time, an attacker is not very likely to receive a firmware file in a hexadecimal format, which must be disassembled.

4. Practical Experiments to Test the Burglary Resistance of the Proposed Key Security

We will conduct a number of studies to check the stability of the developed electronic key against theft of information in HMI/SCADA user authentication. When introducing the developed electronic key into mass use, it is possible to use a three-level protection for reading the firmware by known methods: protection against opening the case, hidden internal breakage of the leg used by the programmer for reading, and hidden on-chip removal of the leg control logic used for reading. The first level is a refractory polymer that is resistant to acids and solvents, which does not allow reaching the crystal. The second level makes it impossible to read the programmer without special expensive tools. The third level performs a function similar to the second, but at the same time on-chip restoration of the control logic on the inner layers is practically impossible, or it requires very expensive equipment. When introducing the developed electronic key into operation, the authors recommend using the unpackaged ATmega32U4 microcontroller. In the course of an attempt to hack the firmware of an electronic key, in laboratory conditions, the authors of the article were unable to remove the "firmware clone" through the AVRDUDE

```
.data:00000000  e2402001        sub r2, r0, #1
.data:00000004  e0612002        rsb r2, r1, r2
.data:00000008
.data:00000008              loc_00000008:
.data:00000008  e4d13001        ldrb r3, [r1], #1
.data:0000000c  e3530000        cmp r3, #0
.data:00000010  e7c13002        strb r3, [r1, r2]
.data:00000014  1afffffb        bne loc_00000008
.data:00000018  e12fff1e        bx lr
```

Figure 11: Fragment of the electronic key firmware in assembly language.

Table 4: Comparative characteristics of the developed approach and existing approaches.

Hacking methods (software and hardware)	Authentication methods				
	Biometrics	Single sign-on (SSO)	Open ID connect (OIDC)	One-time password (OTP)	Developed approach
John the Ripper	+	−	−	−	+
Spidering	±	−	−	−	+
Cain and Abel	+	−	−	+	±
Dictionary attack	+	−	−	−	+
Brute force attack	+	−	−	−	+
Ophcrack	+	−	−	+	+
Create a clone	−	+	+	+	+

+ not vulnerable, ± partially vulnerable, and − vulnerable.

program [50], since the firmware is copy-protected. Therefore, a situation when attackers managed to steal an electronic key and copy a firmware file from it in *.hex format will be simulated. A hex file is a hexadecimal file containing source code, configuration information, setting information, or other data. The format is commonly used in low-level programming when developing microcontrollers. A fragment of the firmware file of the electronic key in hex format is shown in Figure 10(a) and in Figure 10(b), in an attempt to disassemble it.

As an example, an attempt to disassemble the resulting fragment is presented in Figure 10(b), using the strcpy functions (the standard library of the C programming language, for copying a null-terminated string into a given buffer) for the ARM architecture. A fragment of the resulting assembly language code is shown in Figure 11.

The presented fragment contains the command for calculating registers and the processing, and then the cycle can be observed; however, from the presented fragment, it is impossible to understand the essence of the execution of commands and the purpose, which does not allow to open and understand the authentication passwords and the purpose; as a result, this gives an opportunity to make sure that the software hacking the electronic user authentication key in HMI/SCADA is a difficult task, even if the attackers have a source file in *hex format, the maximum that allowed to be viewed is the firmware code.

We can also note the strengths and weaknesses of the developed approach. This is presented in Table 4, which gives a comparative description of the developed approach and existing approaches.

5. Conclusions

In this paper, the processes of developing authenticating user access to industrial information through unsecured Internet networks were introduced in detail. Moreover, a number of vulnerabilities for cyberattacks were identified, such as phishing and social engineering, which are based on the human factor.

The authors analyzed the proposed new method for organizing user access to industrial SCADA/HMI. The analysis based on the concept of an unknown authentication parameters. Consequently, an electronic key based on ATmega32U4 microcontroller was developed as well. All the necessary information to enter the industrial SCADA/HMI is stored inside the firmware in accordance with the company's internal cyber security regulations, which allows generating a powerful automatic passwords and user logins without involving the user's information to remove the risk of accidental transmission of the authentication parameters to a third part. Accordingly, the authors developed a structure, selected electronic components, developed a connection diagram, and assembled an experimental model of an electronic key for user authentication of industrial HMI, HMI/SCADA. On the other hand, to protect the access to the main menu of the electronic key, the authors have developed an algorithm for the first level of user authentication and an algorithm for the second level of automatic user authentication with an electronic key for accessing information in HMI/SCADA. The firmware for the ATmega32U4 microcontroller has been developed as well, which can store up to 25 logins and passwords. To testify the proposed algorithm, a number of experiments were carried out to simulate the hacking of an electronic key, which showed high stability and reliability of the stored information, compared to the same parameters without applying the proposed development. The future work is planned to be directed to apply the proposed algorithm on more complicated networks where the information is transmitted in broadcast manor, such as the networks introduced in [51–55].

The authors are confident that the method proposed in the article will protect data with high reliability from hacking by social engineering. But this requires the implementation of all the recommendations in the proposed concept. This is based on the fact that the strength of the password is due to the fact that the user does not know the access passwords, which are automatically generated and remotely recorded on the electronic key. Moreover, depending on security requirements, access passwords can be changed each time the dongle is connected to a secure device (PC, etc.) in the local network without warning the user. The authors are also confident that if the developed key is stolen, the data will be protected from hacking during the first 24 hours. This is based on the fact that during this time you can change access passwords or block an account. At the same time, the authors understand that there is a possibility of physical hacking of the prototype microcontroller. But this method of hacking requires expensive equipment. Moreover, this hacking method leads to the destruction of the key.

Data Availability

The data used to support the findings of this study are included in the article.

Conflicts of Interest

The authors declare that they have no conflicts of interest to report regarding the publication of the present study.

References

[1] A. Martinelli, A. Mina, and M. Moggi, "The enabling technologies of industry 4.0: examining the seeds of the fourth industrial revolution," *Industrial and Corporate Change*, vol. 30, no. 1, pp. 161–188, 2021.

[2] É. Marcon, M. Soliman, W. Gerstlberger, and A. G. Frank, "Sociotechnical factors and Industry 4.0: an integrative perspective for the adoption of smart manufacturing technologies," *Journal of Manufacturing Technology Management*, vol. 33, 2021.

[3] D. Kushner, "How Kaspersky Lab Tracked Down the Malware that Stymied Iran's Nuclear-Fuel Enrichment Program," 2013, https://spectrum.ieee.org/the-real-story-of-stuxnet.

[4] E. Bajramovic, D. Gupta, Y. Guo, K. Waedt, and A. Bajramovic, "Security challenges and best practices for IIoT," in *INFORMATIK 2019: 50 Jahre Gesellschaft für Informatik – Informatik für Gesellschaft (Workshop-Beiträge)*, pp. 243–254, Gesellschaft für Informatik e, Germany, 2019.

[5] A. Ali Süzen, "A risk-assessment of cyber attacks and defense strategies in industry 4.0 ecosystem," *I. J. Computer Network and Information Security*, vol. 1, pp. 1–12, 2020.

[6] T. Y. Pang, J. D. Pelaez Restrepo, C.-T. Cheng, A. Yasin, H. Lim, and M. Miletic, "Developing a digital twin and digital thread framework for an 'industry 4.0' shipyard," *Applied Sciences*, vol. 11, no. 3, p. 1097, 2021.

[7] A. Efe and A. Isik, "A general view of industry 4.0 revolution from cybersecurity perspective," *International Journal of Intelligent Systems and Applications in Engineering*, vol. 8, no. 1, pp. 11–20, 2020.

[8] V. Mullet, P. Sondi, and E. Ramat, "A review of cybersecurity guidelines for manufacturing factories in industry 4.0," *IEEE Access*, vol. 9, no. 9, pp. 23235–23263, 2021.

[9] L. Laković, I. Ognjanović, R. Šendelj, and O. Injac, "Semantically enhanced cyber security model for industry 4.0: methodological framework," in *Proceedings of the 25th International Conference on Information Technology (IT)*, pp. 16–20, Zabljak, Montenegro, February 2021.

[10] K. Ferencz, J. Domokos, and L. Kovács, "Review of industry 4.0 security challenges," in *Proceedings of the IEEE 15th International Symposium on Applied Computational Intelligence and Informatics (SACI)*, pp. 19–21, Timisoara, Romania, May 2021.

[11] S. Sharma, "Cybersecurity – vulnerability assessment of attacks, challenges and defence strategies in industry 4.0 ecosystem," *International Journal of Modern Agriculture*, vol. 10, no. 2, pp. 203–210.

[12] A. Naanani and M. Humayun, "Security in industry 4.0: cyber-attacks and countermeasures," *Turkish Journal of Computer and Mathematics Education (TURCOMAT)*, vol. 12, no. 10, 2021.

[13] M. Lezzi, M. Lazoi, and A. Corallo, "Cybersecurity for Industry 4.0 in the current literature: a reference framework," *Computers in Industry*, vol. 103, pp. 97–110, 2018.

[14] R. Prasad and V. Rohokale, "Internet of Things (IoT) and machine to machine (M2M) communication," *Springer Series in Wireless Technology*, pp. 125–141, 2019.

[15] Á. L. P. Gómez, L. F. Maimó, A. H. Celdrán, F. J. G. Clemente, M. G. Pérez, and G. M. Pérez, "SafeMan: a unified framework to manage cybersecurity and safety in manufacturing industry," *Journal of: Software: Practice and Experience*, vol. 51, no. 3, pp. 607–627, 2020.

[16] T. Alladi, V. Chamola, and S. Zeadally, "Industrial control systems: cyberattack trends and countermeasures," *Computer Communications*, vol. 155, pp. 1–8, 2020.

[17] E. Aarón, C. Cevallos, I. Ortiz-Garces, and R. O. Andrade, "Cybersecurity model based on hardening for secure Internet of Things implementation," *Applied Sciences*, vol. 11, no. 7, 2021.

[18] S. Zhang, X. Xie, and Y. Xu, "A brute-force black-box method to attack machine learning-based systems in cybersecurity," *IEEE Access*, vol. 8, pp. 128250–128263, 2020.

[19] C. Seong-Min, K. Jane, and S. Seung-Hyun, "Analysis of attacks and security level for multivariate quadratic based signature scheme rainbow," *Journal of the Korea Institute of Information Security & Cryptology (정보보호학회논문지)*, vol. 31, no. 3, pp. 533–544, 2021.

[20] L. Li, K. Thakur, and M. L. Ali, "Potential development on cyberattack and prospect analysis for cybersecurity," in *Proceedings of the 2020 IEEE International IOT, Electronics and Mechatronics Conference (IEMTRONICS)*, September 2020.

[21] I. Charles, L. Nnadi, I. Okpala, M. Onuoha, A. Emmanuel, and G. Chukwudebe, "A focused Web crawler for strengthening cyber security and building a knowledge-based domain," in *Proceedings of the International Conference on Emerging Applications and Technologies for Industry 4.0 (EATI 2020)*, pp. 157–162, Abuja, September 2020.

[22] Openwall, "John the Ripper password cracker," 2019, https://www.openwall.com/john/.

[23] N. Dharavath, S. V. Nalla, and G. Padmavathi, "Analysis of password protected document," COMPUSOFT," *An international journal of advanced computer technology*, vol. 9, no. 7, pp. 3762–3767, 2020.

[24] A. Mohamed, “Password cracking using Cain & Abel,” 2018, https://resources.infosecinstitute.com/topic/password-cracking-using-cain-abel/.
[25] S. Islam, “Security auditing tools: a comparative study,” *International Journal of Computing Sciences Research*, vol. 5, no. 1, pp. 407–425, 2021.
[26] ophcrack, “What is ophcrack?,” 2018, https://ophcrack.sourceforge.io/.
[27] ophcrack, “All You Need to Know about Ophcrack Windows 10,” 2022, https://passper.imyfone.com/windows-10/ophcrack-guide-how-to-use-ophcrack-for-windows-10-password-recovery/.
[28] L. K. McGoldrick and J. Halámek, “Recent advances in noninvasive biosensors for forensics, biometrics, and cybersecurity,” *Sensors*, vol. 20, no. 21, p. 5974, 2020.
[29] N. A. Alanezi, N. H. Alharbi, Z. S. Alharthi, and O. H. Alhazmi, “POSTER: a brief overview of biometrics in cybersecurity: a comparative analysis,” in *Proceedings of the 2020 First International Conference of Smart Systems and Emerging Technologies (SMARTTECH)*, Riyadh, Saudi Arabia, November 2020.
[30] M.-J. Sule, M. Zennaro, and G. Thomas, “Cybersecurity through the lens of digital identity and data, protection,” *Issues and Trends,” Technology in Society*, vol. 67, 2021.
[31] D. Anand, V. Khemchandani, M. Sabharawal, O. Cheikhrouhou, and O. B. Fredj, “Lightweight technical implementation of single sign-on authentication and key agreement mechanism for multiserver architecture-based systems,” security and communication networks,” *Special Issue Application-Aware Multimedia Security Techniques*, vol. 2021, Article ID 9940183, 2021.
[32] B. O. Kose, O. Buk, H. A. Mantar, and V. Coskun, “An identity management system based on OpenID connect protocol,” in *Proceedings of the 2020 4th International Symposium on Multidisciplinary Studies and Innovative Technologies (ISMSIT)*, pp. 22–24, Istanbul, Turkey, October 2020.
[33] T. Saito, S. Shibata, and T. Kikuta, “Comparison of OAuth/OpenID connect security in America and Japan,” *Advances in Networked-Based Information Systems*, Springer, vol. 1264, Cham, 2021.
[34] “What is a one-time password (OTP)?,” 2020, https://www.okta.com/blog/author/teju-shyamsundar/https://www.okta.com/blog/2020/06/what-is-a-one-time-password-otp/.
[35] K. Richards, “One-time password (OTP),” 2021, https://searchsecurity.techtarget.com/definition/one-time-password-OTP.
[36] Physorg, “Japan researchers warn of fingerprint theft from ’peace’ sign,” 2017, https://phys.org/news/2017-01-japan-fingerprint-theft-peace.html.
[37] Z. Kleinman, “Politician’s fingerprint ’cloned from photos’ by hacker,” 2014, https://www.bbc.com/news/technology-30623611.
[38] M. Bilal, C. Wang, Z. Yu, and A. Bashir, “Evaluation of secure OpenID-based RAAA user authentication protocol for preventing specific Web attacks in Web apps,” in *Proceedings of the 2020 IEEE 11th International Conference on Software Engineering and Service Science (ICSESS)*, pp. 16–18, Beijing, China, October 2020.
[39] InWebo, “What is an OTP - one-time password?,” 2011, https://www.inwebo.com/en/mfa-otp-one-time-password/.
[40] Citi Bank, “One time password,” 2020, https://www.citibank.co.uk/personal/one-time-password.do.
[41] Examguides.com, “CompTIA®A+ exam notes: various PC connection interfaces, their characteristics and purpose,” 2022, https://www.examguides.com/Aplus-Essentials/aplus-essentials5.htm.
[42] Atmel, “ATmega16U4/ATmega32U4,” 2016, https://ww1.microchip.com/downloads%20/en/DeviceDoc/Atmel-7766-8-bit-AVR-ATmega16U4-32U4_Datasheet.pdf.
[43] Waveshare, “0.91inch OLED Module,” 2022, https://www.mcielectronics.cl/website_MCI/static/documents/0.91inch_OLED_Module_User_Manual_EN.pdf.
[44] components101, “Push Button Switch,” 2020, https://components101.com/switches/push-button.
[45] Microchip, “Microchip Studio for A. V. R. ® and S. A. M. Devices,” 1959, https://www.microchip.com/en-us/development-tools-tools-and-software/microchip-studio-for-avr-and-sam-devices.
[46] Microchip, “Mplab® X. Integrated Development Environment (Ide),” 1959, https://www.microchip.com/en-us/development-tools-tools-and-software/mplab-x-ide.
[47] Arduino Web Editor, “Arduino I. D. E 1.8.1.9,” 2021, https://www.arduino.cc/en/software.
[48] Microchip, “AVR® and Arm® Toolchains (C Compilers),” 2019, https://www.microchip.com/en-us/development-tools-tools-and-software/gcc-compilers-avr-and-arm.
[49] WinAVRTM, 1996, http://winavr.sourceforge.net/.
[50] AVRDUDE, “AVRDUDE-AVR Downloader/UploaDEr,” 2022, https://www.nongnu.org/avrdude/.
[51] Y. Liu, Z. Song, X. Xu et al., “Bidirectional GRU networks-based next POI category prediction for healthcare,” *International Journal of Intelligent Systems*, pp. 1–21, 2021.
[52] Y. Liu, D. Li, S. Wan et al., “A long short-term memory-based model for greenhouse climate prediction,” *International Journal of Intelligent Systems*, vol. 37, no. 1, pp. 135–151, 2021.
[53] Y. Liu, A. Pei, F. Wang et al., “An attention-based category-aware GRU model for the next POI recommendation,” *International Journal of Intelligent Systems*, vol. 36, no. 7, pp. 3174–3189, 2021.
[54] H. H. Attar, A. A. A. Solyman, and A. Alrosan, “Deterministic cooperative hybrid ring-mesh network coding for big data transmission over lossy channels in 5G networks,” *EURASIP Journal on Wireless Communications and Networking*, vol. 159, 2021.
[55] H. H. Attar, A. A. A. Solyman, M. R. Khosravi, L. Qi, M. Alhihi, and P. Tavallali, “Bit and Packet Error Rate evaluations for Half-Cycle stage cooperation on 6G wireless networks,” *Physical Communication*, vol. 44, Article ID 101249, 2021.

Hindawi
Computational Intelligence and Neuroscience
Volume 2022, Article ID 7365544, 8 pages
https://doi.org/10.1155/2022/7365544

Research Article

Generation of Human Micro-Doppler Signature Based on Layer-Reduced Deep Convolutional Generative Adversarial Network

Mahdi Ostovan ,[1] Sadegh Samadi,[1] and Alireza Kazemi[2]

[1]*Department of Electrical and Electronics Engineering, Shiraz University of Technology, Shiraz 71557-13876, Iran*
[2]*Mathematics Department, College of Science, Shiraz University, Shiraz 71348-14336, Iran*

Correspondence should be addressed to Mahdi Ostovan; m.ostovan@sutech.ac.ir

Received 1 March 2022; Revised 16 March 2022; Accepted 21 March 2022; Published 12 April 2022

Academic Editor: Xin Ning

Human activity recognition (HAR) using radar micro-Doppler has attracted the attention of researchers in the last decade. Using radar for human activity recognition has been very practical because of its unique advantages. There are several classifiers for the recognition of these activities, all of which require a rich database to produce fine output. Due to the limitations of providing and building a large database, radar micro-Doppler databases are usually limited in number. In this paper, a new method for the generation of radar micro-Doppler of the human body based on the deep convolutional generating adversarial network (DCGAN) is proposed. To generate the database, the required input is also generated by converting the existing motion database to simulated model-based radar data. The simulation results show the success of this method, even on a small amount of data.

1. Introduction

Human activity recognition (HAR) has been a popular field of study in the last decade [1–5]. This field of research has attracted the attention of data scientists since the 1980s. HAR is a technology that tries to recognize the activities or movements of the human body through a computer. The purpose of HAR is to recognize the activity of an individual using a series of observations of human behaviors and environmental conditions. In recent decades, various methods have been used to recognize human activities. The methods used can be divided into two main categories: those based on wearable sensors and those based on nonwearable sensors. Wearable sensors require some markers to be attached to a part of the human body for their functionality [6–8]. In applications such as clinical care of the elderly and disabled people, the sensor must be attached to the patient's body and cause inconvenience to them, which is their disadvantage. In contrast, nonwearable sensors such as video surveillance cameras, infrared sensors, and radars do not encounter these problems.

Among the nonwearable sensors, radar has shown its application as well. The advantages of using radar for HAR are as follows:

(1) Radar is resistant to light and weather conditions. Therefore, it can be used in environments with adverse conditions.
(2) The radar sensor maintains the visual privacy of people. Because instead of extracting the visual form of the body, it uses target-modulated return signals that contain valuable information about the range and speed of the moving target.
(3) Radar can detect humans even through walls, which makes it useful in more scenarios.
(4) Radar does not need to attach a marker to a human target for its operation. This makes it more user-friendly.

The human body is a nonrigid target. In addition to the translational motion of the whole body, the locomotion of the body parts is also significant. The instantaneous distance of the body parts to the radar changes with micromotions, and it induces the effects of micro-Doppler on the echo signal [9]. The radar micro-Doppler signature carries unique and valuable information about moving targets, which has received much attention in the classification, recognition, and identification of human targets.

An issue that has always been a major concern in machine learning-based classification problems is how to prepare a standard, large, and diverse enough database. In camera-based classification methods, the camera sensor is publicly available, many images and videos of people's daily lives and activities are recorded, and usually many databases are available for these sensors [10, 11]. However, radar is not a typical sensor and is accessible only to certain people. So, the radar databases are very limited and sometimes not available due to some security issues. Lack of sufficient volunteer humans, costly radar data recording tests, long preparation time of the test environment, and such issues make providing radar database very difficult and rather challenging. Therefore, the challenge we are dealing with is the collection of diverse and appropriate data. Attempts have been made to increase the data in a way other than direct testing.

One of the methods used in various literature is the computer simulation method. In this method, data are generated statistically from scratch using human kinematic models. The most famous kinematic model of the body is the Boulic gait model [12]. In this model, given a limited number of body parameters such as height and thigh length, the human gait model can be simulated. This method has been validated many times, including [13, 14]. It has been used as a reference for walking simulation. Although this method can generate an unlimited amount of data for deep network training, it is limited to the walking model and can also be used for running with little modification, but it is not applicable for other activities, such as crawling and sitting. In [15], a method for simulating micro-Doppler signatures of running and crawling in addition to walking activity has been proposed using virtual reality animation. However, the diversity of models is not significant.

The most widely used method is using the Kinect sensor for Microsoft's Xbox game console [16, 17]. This camera has two optical sensors and an IR sensor. By integrating the data from these three cameras, it has been able to measure the depth and instantaneous location of the joints in the human body with an accuracy of better than 1 cm. Thus, a model provides a simplified point of the human body at about 18 to 30 frames per second (depending on software and hardware conditions) in 3D space.

The locations of these body joints can be used to simulate the radar echo signal [9, 18], which is a widely used method that is close to reality. In this method, a 17-point model equivalent to the Boulic model is extracted from the joints of the test object. Each limb is then assigned a simple geometric shape. All body parts (except the head) are assigned an ellipse, and a sphere is assigned to the head. By calculating the RCS of each limb according to physical relations, the radar echo can be simulated. After that, the echo in the time domain is transformed to the time-frequency domain by a transform such as the STFT. This method has also proven its efficiency and closeness to reality. The use of the Kinect will be limited due to the very short operational range (less than 2 meters) and the missed detection of some limbs, such as the legs [17].

Another method to solve the problem of data shortages is using a method known as transfer learning. In this technique, a few network layers that have already been trained on a large database are used in the designed network. The initial database should be somewhat close to our desired task. Usually, the primary layers of the deep grid are responsible for extracting general and basic features, and therefore, a series of general features can be extracted regardless of the input contents. In contrast to deeper layers, they extract minor features. So, if we maintain the primary layers of a deep network trained with a large database and retrain and replace the deep layers with a database of related data, which is called "fine-tuning," then we will be able to achieve the required accuracy with a small amount of data. References [19–25] have used this method to improve classification with a small amount of data. However, it is often difficult to find a database close enough to the radar micro-Doppler problem. Although using heterogeneous and irrelevant databases can train the primary layers of the network, they can also take us away from our destination. Radar micro-Doppler images are composed of several lines and curves and using natural pictures to train the transferred network will produce unpromising results as they contain completely different content.

A new method that has recently been discussed to produce a realistic image [26–29] is the use of generating adversarial networks, or GAN for short. The faces in Figure 1 are simulated using the DCGAN network trained with the CelebA database [30]. This database contains more than 200,000 faces of Hollywood actors and singers around the world. The faces in Figure 1 do not exist in the real world, but they look like real faces, and that shows the power of GAN.

Due to the weakness of the mentioned methods and the novelty and power of GAN networks in making realistic images, in this paper, we have proposed a new method for generating human body radar micro-Doppler based on the deep convolutional generative adversarial network (DCGAN) using a simulated database. The structure of the paper is as follows: Section 2 describes how to generate our database. Section 3 provides an overview of GANs. Section 4 introduces the proposed GAN network. Section 5 presents the results of the simulations. Finally, Section 6 is devoted to the discussion and conclusion.

2. Database Preparation

We used the MoCap motion capture database of CMU [31] to simulate radar echo. In this relatively rich database, various activities have been performed by volunteers, and their body locomotions, have been recorded by very accurate multi-modal motion sensors. They are a combination of cameras and inertial sensors like gyroscopes and

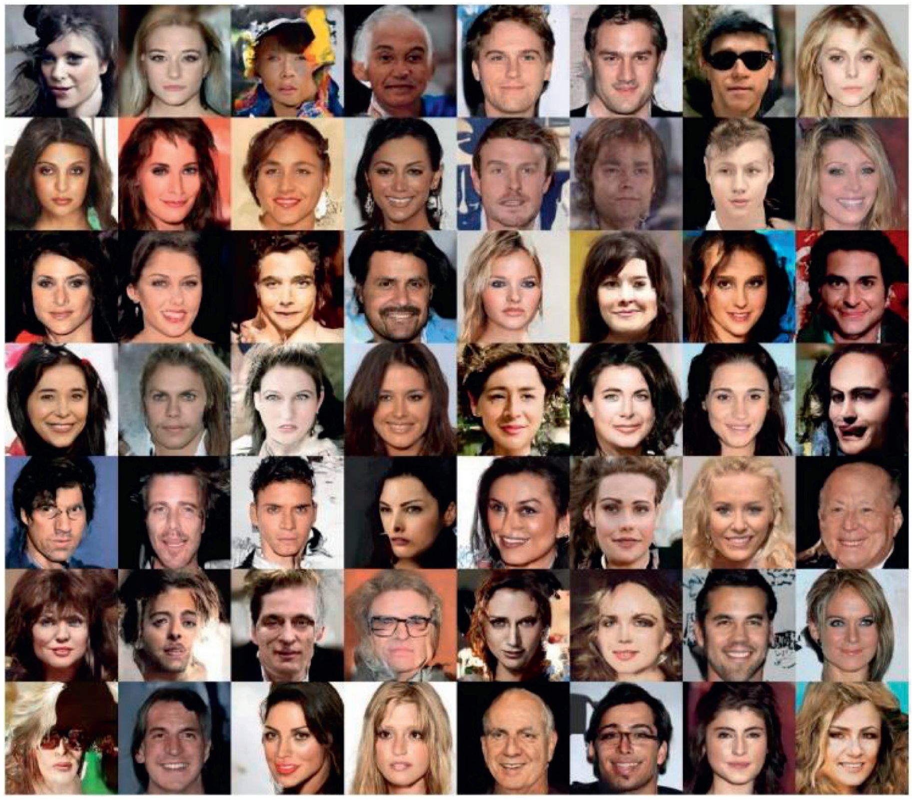

Figure 1: Simulated faces with DCGAN [29].

accelerometers. We have focused only on walking activities. The data recorded in the MoCap output related to the bodies of walking people was first extracted in the point model. The number of points is up to 40, but we used only 17 points, according to [9]. Figure 2 shows a frame of the 17-point body model extracted from the CMU database and simulated by the routine of [9].

According to this method, an ellipsoid is assigned to each limb except for the head, which is spherical. These geometric shapes move according to the instant locations of body joints. The temporal coordinates of the body parts are extracted from data provided by [32] in the form of $[x(t), y(t), z(t)]^T$. By micromotion of these shapes, radar echo data is simulated. The signal at this stage is generated in the range-time domain. Finally, the simulated echo signal is transformed into the time-frequency domain. We used the FSST transform introduced in [33], whose time-frequency resolution is better than STFT. A synchro-squeezing process is applied to the time-frequency domain to make it sharper along the frequency axis. A comparison of FSST and STFT is performed in [34] and is depicted in Figure 3. As we can see, the resolution of FSST is better than that of STFT.

After transforming into the T-F domain, the echo signal of each trial is stored as an image like Figure 3(a). In this way, the initial data were generated to enter the DCGAN.

3. Generative Adversarial Networks

The GAN network, first introduced in [26], implements the game theory method by training two different networks, one as a generator and the other as a discriminator. The generator network is represented by the G function and is parameterized by θ_g and initialized with an input noise vector z, which consists of samples of a normal distribution. (P_{noise} (z)) and its output is $\tilde{I}$.

The discriminator network is a convolutional neural network (CNN) represented by the D function and is parameterized by θ_d. Its input is a real image I or a fake image $\hat{I}$, and its output is a number between 0 and 1 that indicates the probability that the input is real or fake. Training of the GAN includes a minimax game [35] in which the generator tries to fool the discriminator so that it cannot recognize fake images from real ones. Meanwhile, the discriminator is trying to identify them correctly.

D is trained to maximize the probability of assigning the correct label to both training samples and generated samples of G. At the same time, G is trained to minimize the $\log(1-D(G(z))$, in other words, D and G play the minimax game with the value of the $V(G, D)$ as given inthe following equation:

$$\min_G \max_D V(D,G) = E_{x\sim p_{\text{data}}(x)}[\log D(x)] + E_{z\sim p_z(z)}[\log(1-D(G(z)))], \tag{1}$$

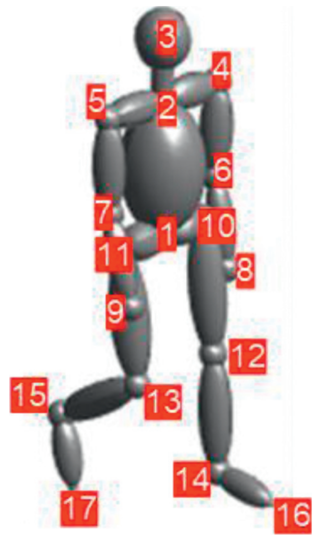

Figure 2: 17-point simulated body.

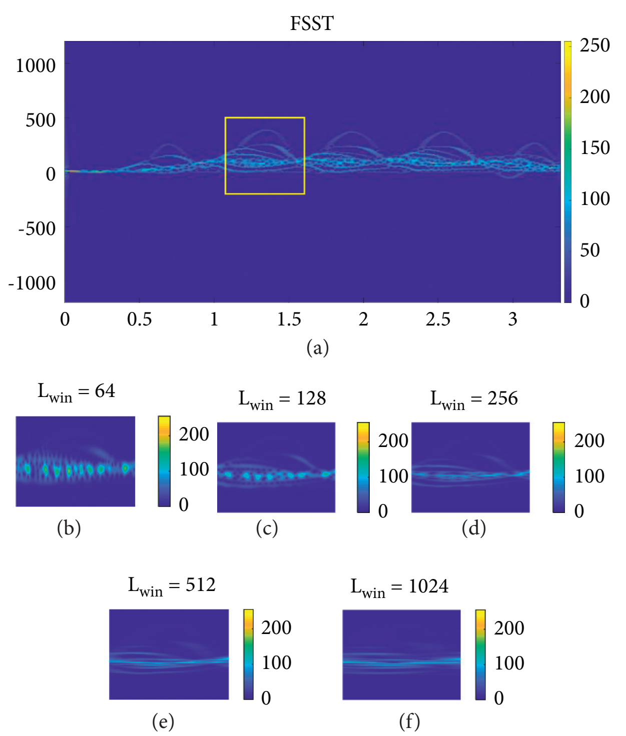

Figure 3: Comparison of (a) FSST and (b)–(f) STFT with different window lengths [32].

where P_g is the probability distribution of G on set x, $G(z, \theta_g)$ is a differentiable function with parameters θ_g, and $D\ (x;\theta_d)$ is a differentiable function with parameters θ_d.

After several training iterations, if G and D have enough training capacity, they will reach a final point in which the training error does not decrease further. At this point, $P_g = p_{data}$ and the discriminator does not have enough power to discriminate between two distributions. Now network G is ready to generate fake samples with maximum similarity to real samples and with the same statistical distribution. A basic GAN block diagram is depicted in Figure 4.

4. Proposed DCGAN Network

In [29], a kind of convolutional GAN network called DCGAN is used to produce realistic images. Due to the success of GAN networks in various studies, in this paper, we have used a kind of DCGAN to generate the micro-Doppler signal of the walking human in the T-F domain. The original DCGAN was trained on the LSUN database [36], Imagenet-1k [37], and CelebA [30]. The contents of these databases are about natural scenes, which have many details. Our proposed discriminator network structure has only four convolutional layers. The purposes for reducing the convolutional layers are as follows:

(1) The network is trained to generate the micro-Doppler signal in the time-frequency domain, which is composed of some periodic curves, and unlike natural images, it does not have much detailed information.

(2) Computational load could be reduced by the simplification of network structure.

The architecture of the generator network is shown in Figure 5 and the discriminator network in Figure 6.

The generator network is composed of five transposed convolutional layers followed by a batch normalization layer for the stability of training progress and an activation layer of type rectified linear unit (ReLU). Table 1 lists the parameters of the generator network.

The parameters of discriminator network are listed in Table 2.

These two networks are trained simultaneously on our database using the Adam optimization method. The output images from the simulated database described in Section 2 will enter into the discriminator network of Figure 5. Simultaneously, noise with a length of 100 samples enters the generator network of Figure 6. As a result of the training described previously, the statistics of the data generated by the generator network gradually approach the statistics of the samples within the database.

5. Simulation Results

In this section, we have reported the simulation results of generating curves by the proposed DCGAN network.

5.1. Simulation Platform. Training of deep neural networks usually encounters challenges. The first challenge is the high computational load, which forces us to use powerful processing platforms. In the simulations presented in this paper, due to the modifications that are performed on the network structure and the small number of input trials in the database, a CPU-based platform has been used.

5.2. Training Options. Hyperparameters of training are selected as in Table 3.

According to Table 1, the number of trials in the simulated database is only 81. However, the output is very close to reality and promising. In the simulation process, as the

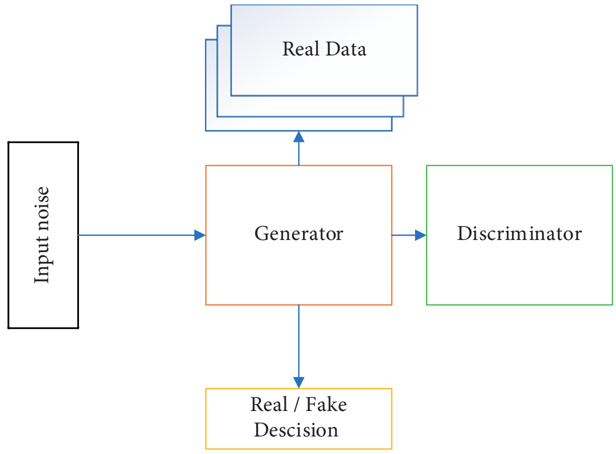

Figure 4: Block diagram of a basic generative adversarial network.

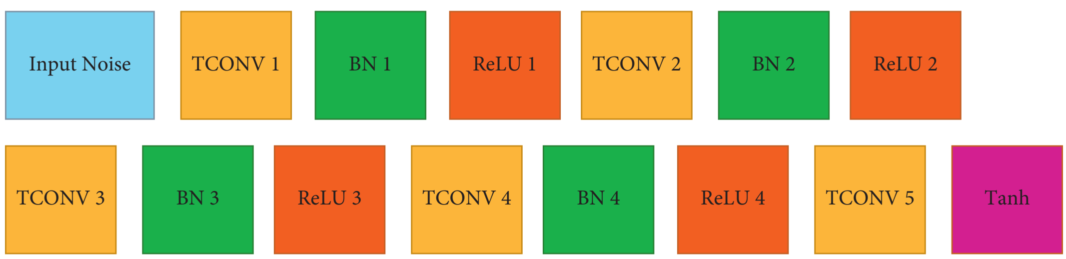

Figure 5: Generator network.

Figure 6: Discriminator network.

Table 1: Parameters of generator network.

Row	Layer name	Layer type	Attribute
1	Input noise	Image input	$1 \times 1 \times 100$ noise vector
2	TConv 1	Transposed convolutional	512 tconv filters of size 4×4 with stride [2, 2] and cropping [0, 0]
3	BN1	Batch normalization	—
4	ReLU 1	ReLU	—
5	TConv 2	Transposed convolutional	512 tconv filters of size 4×4 with stride [2, 2] and cropping [0, 0]
6	BN2	Batch normalization	—
7	ReLU 2	ReLU	—
8	TConv 3	Transposed convolutional	512 tconv filters of size 4×4 with stride [2, 2] and cropping [0, 0]
9	BN3	Batch normalization	—
10	ReLU 3	ReLU	—
11	TConv 4	Transposed convolutional	512 tconv filters of size 4×4 with stride [2, 2] and cropping [0, 0]
12	BN4	Batch normalization	—
13	ReLU 4	ReLU	—
14	TConv 4	Transposed convolutional	512 tconv filters of size 4×4 with stride [2, 2] and cropping [0, 0]
15	tanh	Hyperbolic tangent	—

training epochs increase, the input noise gradually proceeds to true form. Figures 7(a) to 7(c) show the network output at different stages of training. As the training progresses, the output gets closer to the expected shape. Figure 7(d) shows a comparison of one of the real samples of the database, which is very close to output 5c.

Table 2: Parameters of discriminator network.

Row	Layer name	Layer type	Attribute
1	Input image	Image input	$64 \times 64 \times 3$ images
2	Conv 1	Convolutional	64 conv filters of size 4×4 with stride [2, 2] and padding [1, 1]
3	Leaky ReLU 1	Leaky ReLU	Scale of 0.2
4	Conv 2	Convolutional	128 conv filters of size 4×4 with stride [2, 2] and padding [1, 1]
5	BN2	Batch normalization	—
6	Leaky ReLU 2	Leaky ReLU	Scale of 0.2
7	Conv 3	Convolutional	256 conv filters of size 4×4 with stride [2, 2] and padding [1, 1]
8	BN3	Batch normalization	—
9	Leaky ReLU 3	Leaky ReLU	Scale of 0.2
10	Conv 4	Convolutional	1 conv filter of size 8×8 with stride [1, 1] and padding [0, 0]

Table 3: Training hyperparameters.

Parameter	Value
Epoch	1000
Mini batch size	8
Generator learning rate	2×10^{-4}
Discriminator learning rate	1×10^{-4}
Gradient decay factor	0.5
Squared gradient decay factor	0.999
Number of samples	81

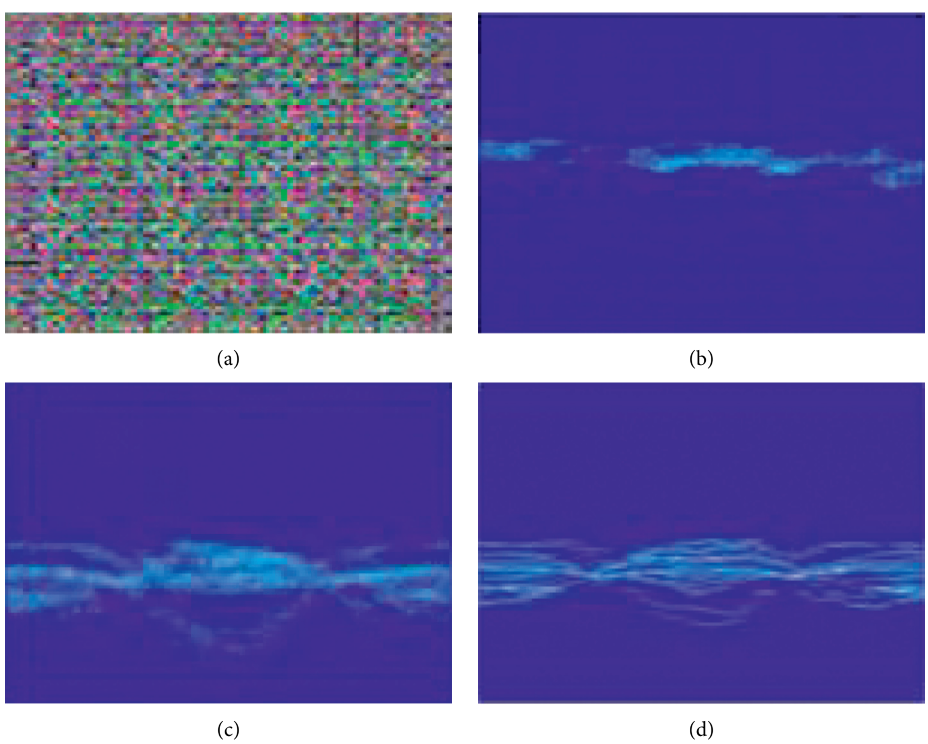

Figure 7: (a) Input noise to GAN. (b) Output after 150 epochs. (c) Output after 1000 epochs. (d) A real sample.

5.3. Evaluation. Because the output of the DCGAN network is random, it cannot be evaluated in terms of traditional image comparison criteria such as PSNR because the ground truth could not exist. However, it is important to note that the matching of generated data statistics and database statistics is the optimization criterion of the adversarial learning process, and it converges when these statistics are matched. Thus, the adversarial network ensures that the output image statistics and the database images are the same, which can be considered a quantitative evaluation and a complement to the visual evaluation.

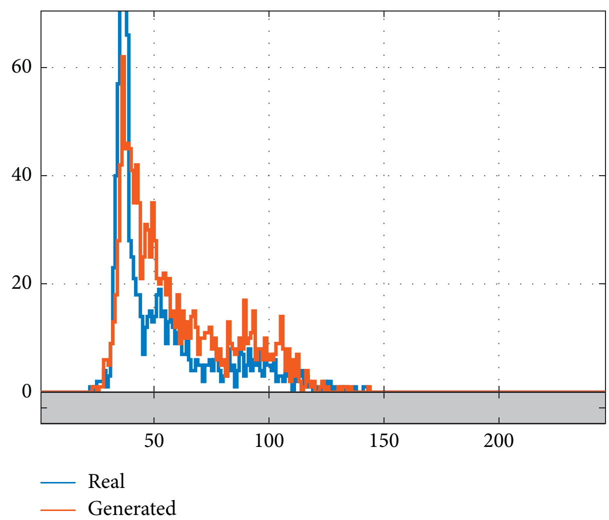

Figure 8: Comparison of the histograms of the real and generated samples.

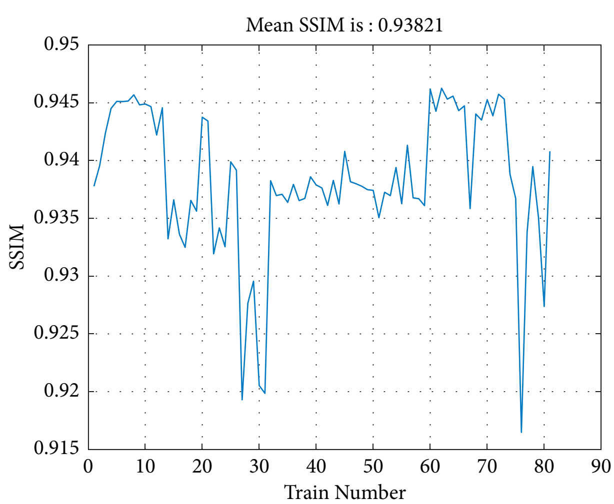

Figure 9: SSIM calculated over generated samples and real samples.

The histogram of an image is a demonstration of the intensity levels and can represent the distribution of these intensities. To show that the trained network is able to generate good fake results, we have compared the average histogram of some samples in the database with some generated samples. Figure 8, shows the results. The result demonstrates the similarity of statistics.

As a second metric for similarity measurement of the real and fake images, we used the structural similarity index measure (SSIM) [38]. SSIM is a good metric to show perception and saliency-based errors. Therefore, we can conclude that SSIM could be comparatively a better metric than mean square error (MSE) and PSNR metrics from a human visual perspective. The term structural information emphasizes pixels of the image that are strongly interdependent or pixels that are spatially interconnected. Highly dependent image pixels provide more valuable information than visual objects in the image domain [39]. The SSIM metric is an index in [0,1] with 0 indicating no similarity and one indicating maximum similarity.

For comparison, we have calculated SSIM between 100 generated images and every image in the database and averaged them, as shown in Figure 9. The consequent average value is about 0.94, which represents a very high similarity between generated images and real samples.

6. Conclusions

In this paper, a new method based on the use of the DCGAN for the production of micro-Doppler of the human body is presented. The database required for this work was generated using a computer simulation of the radar echo signal based on the 17-point body model while considering the system parameters of a typical radar. Motion data of 17 body parts and their kinematics are taken from the MoCap database of CMU University. The production database for the input of the proposed method has only 81 members, but the result is very promising. In the future, we will seek to increase the database and train this network with more diverse data. The results of this work provide a valuable tool for future research in the field of classification of human activities based on radar micro-Doppler.

Data Availability

The data we have used is given from the publicly available online Carnegie Mellon University (CMU) motion capture database [32], [online] available from https://mocap.cs.cmu.edu/.

Conflicts of Interest

The authors declare that they have no conflicts of interest with this study.

References

[1] M. Cristani, R. Raghavendra, A. Del Bue, and V. Murino, "Human behavior analysis in video surveillance: a Social Signal Processing perspective," *Neurocomputing*, vol. 100, pp. 86–97, 2013.

[2] W. Qian, Y. Li, C. Li, and R. Pal, "Gesture recognition for smart home applications using portable radar sensors," in *Proceedings of the 36th Annual International Conference of the IEEE Engineering in Medicine and Biology Society*, pp. 6414–6417, Chicago, IL, USA, August 2014.

[3] J. J. Wang and S. Singh, "Video analysis of human dynamics-a survey," *Real-Time Imaging*, vol. 9, no. 5, pp. 321–346, 2003.

[4] L. Chen, M. Zhou, M. Wu et al., "Three-layer weighted fuzzy support vector regression for emotional intention understanding in human-robot interaction," *IEEE Transactions on Fuzzy Systems*, vol. 26, no. 5, pp. 2524–2538, 2018.

[5] P. Molchanov, S. Gupta, K. Kim, and J. Kautz, "Hand gesture recognition with 3D convolutional neural networks," in *Proceedings of the IEEE Conference on Computer Vision and Pattern Recognition*, pp. 1–7, Boston, MA, USA, June 2015.

[6] J. Sun, Y. Fu, S. Li, J. He, C. Xu, and L. Tan, "Sequential human activity recognition based on deep convolutional network and

extreme learning machine using wearable Sensors," *Hindawi Journal of Sensors*, vol. 2018, Article ID 8580959, 10 pages, 2018.

[7] F. J. Ordóñez and D. Roggen, "Deep convolutional and LSTM recurrent neural networks for multimodal wearable activity recognition," *Sensors*, vol. 16, p. 115, 2016.

[8] O. D. Lara and M. A. Labrador, "A survey on human activity recognition using wearable sensors," *IEEE Communications Surveys & Tutorials*, vol. 15, no. 3, pp. 1192–1209, 2013.

[9] V. C. Chen, D. Tahmoush, and W. L. Miceli, *Radar Micro-doppler Signatures: Processing and Applications*, Institution of Engineering and Technology, London, UK, 2014.

[10] K. Soomro, A. R. Zamir, and M. Shah, *UCF101: A Dataset of 101 Human Action Classes from Videos in the Wild*, CRCV-TR-12-01, 2012, https://arxiv.org/abs/1212.0402.

[11] H. Kuehne, H. Jhuang, E. Garrote, T. Poggio, and T. Serre, *Hmdb: A Large Video Database for Human Motion Recognition*, ICCV, Seoul, Republic of Korea, 2011.

[12] R. Boulic, N. M. Thalmann, and D. Thalmann, "A global human walking model with real-time kinematic personification," *The Visual Computer*, vol. 6, no. 6, pp. 344–358, 1990.

[13] P. van Dorp and F. C. A. Groen, "Human walking estimation with radar," *IEE Proceedings - Radar, Sonar and Navigation*, vol. 150, no. 5, pp. 356–365, 2003.

[14] S. S. Ram, C. Christianson, Y. Youngwook Kim, and H. Hao Ling, "Simulation and analysis of human micro-Dopplers in through-wall environments," *IEEE Transactions on Geoscience and Remote Sensing*, vol. 48, no. 4, pp. 2015–2023, 2010.

[15] S. Ram and H. Ling, "Simulation of human micro-Dopplers using computer animation data," in *Proceedings of the 2008 IEEE Radar Conference*, pp. 1–6, Rome, Italy, May 2008.

[16] B. Erol, C. Karabacak, S. Z. Gürbüz, and A. C. Gürbüz, "Simulation of Human Micro-doppler Signatures with Kinect Sensor," in *Proceedings of the 2014 IEEE Radar Conference*, pp. 863–868, Cincinnati, OH, USA, May 2014.

[17] B. Erol and S. Z. Gürbüz, "A Kinect-Based Human Micro-doppler Simulator," *IEEE A&E SYSTEMS MAGAZINE*, vol. 30, 2015.

[18] V. C. Chen, F. Fayin Li, S. S. Shen-Shyang Ho, and H. Wechsler, "Micro-Doppler effect in radar: phenomenon, model, and simulation study," *IEEE Transactions on Aerospace and Electronic Systems*, vol. 42, no. 1, pp. 2–21, 2006.

[19] Z. Chen, G. Li, F. Fioranelli, and H. Griffiths, "Personnel recognition and gait classification based on multistatic micro-Doppler signatures using deep convolutional neural networks," *IEEE Geoscience and Remote Sensing Letters*, vol. 15, no. 5, pp. 669–673, 2018.

[20] M. S. Gurbuz and S. Z. Gürbüz, "Deep neural network initialization methods for micro-Doppler classification with low training sample support," *IEEE Geoscience and Remote Sensing Letters*, vol. 14, no. 12, pp. 2462–2466, Dec. 2017.

[21] M. S. Seyfioglu, B. Erol, S. Z. Gurbuz, and M. G. Amin, "DNN transfer learning from diversified micro-Doppler for motion classification," *IEEE Transactions on Aerospace and Electronic Systems*, vol. 55, no. 5, pp. 2164–2180, Oct. 2019.

[22] H. Du, Y. He, and T. Jin, "Transfer Learning for Human Activities Classification Using Micro-doppler Spectrograms," in *Proceedings of the 2018 IEEE International Conference on Computational Electromagnetics (ICCEM)*, pp. 1–3, Chengdu, China, March 2018.

[23] Y. Lang, Q. Wang, Y. Yang, C. Hou, D. Huang, and W. Xiang, "Unsupervised domain adaptation for micro-Doppler human motion classification via feature fusion," *IEEE Geoscience and Remote Sensing Letters*, vol. 16, no. 3, pp. 392–396, 2019.

[24] Y. Jiang, X. Gu, D. Wu et al., "A novel negative-transfer-resistant fuzzy clustering model with a shared cross-domain transfer latent space and its application to brain CT image segmentation," *IEEE/ACM Transactions on Computational Biology and Bioinformatics*, vol. 18, no. 1, pp. 40–52, 2021.

[25] Y. Jiang, Y. Zhang, C. Lin, D. Wu, and C.-T. Lin, "EEG-based driver drowsiness estimation using an online multi-view and transfer TSK fuzzy system," *IEEE Transactions on Intelligent Transportation Systems*, vol. 22, no. 3, pp. 1752–1764, 202.

[26] I. Goodfellow, J. Pouget-Abadie, M. Mirza et al., "Generative adversarial nets," *Advances in neural information processing systems*, (NIPS 2014), vol. 27, 2014.

[27] A. Dosovitskiy, J. T. Springenberg, M. Tatarchenko, and T. Brox, "Learning to generate chairs, tables and cars with convolutional networks," *IEEE Transactions on Pattern Analysis and Machine Intelligence*, vol. 39, no. 4, pp. 692–705, 2017.

[28] D. Wang, Y. Yuan, and Q. Wang, "Early action prediction with generative adversarial networks," *IEEE Access*, vol. 7, Article ID 35795, 2019.

[29] A. Radford, L. Metz, and S. Chintala, "Unsupervised representation learning with deep convolutional generative adversarial networks," 2015, https://arxiv.org/abs/1511.06434.

[30] Z. Liu, P. Luo, X. Wang, and X. Tang, "Deep learning face attributes in the wild," in *Proceedings of the IEEE international conference on computer vision*, pp. 3730–3738, Santiago, Chile, 2015.

[31] F. De la Torre, H. Jessica, B. Adam et al., "Guide to the Carnegie Mellon University Multimodal Activity (cmu-mmac) Database," 2009.

[32] C Mellon University (Cmu), "Motion capture database," 2021, http://mocap.cs.cmu.edu/.

[33] I. Daubechies, J. Lu, and H. T. Wu, "Synchrosqueezed wavelet transforms: an empirical mode decomposition-like tool," *Applied and Computational Harmonic Analysis*, vol. 30, no. 2, pp. 243–261, 2011.

[34] M. Ostovan, S. Samadi, and A. Kazemi, "DecompNet: deep context dependent decomposition network for micro-Doppler signature of walking human," *IEEE Sensors Journal*, vol. 21, no. 22, Article ID 25862, 2021.

[35] M. Michael, S. Eilon, and Z. Shmuel, "Game Theory. Cambridge University Press," pp. 176–180, Cambridge, England, 2013.

[36] F. Yu, A. Seff, Y. Zhang, S. Song, T. Funkhouser, and J. Xiao, "Lsun: construction of a large-scale image dataset using deep learning with humans in the loop," 2015, https://arxiv.org/abs/1506.03365.

[37] O. Russakovsky, J. Deng, H. Su et al., "ImageNet large scale visual recognition challenge," *International Journal of Computer Vision*, vol. 115, no. 3, pp. 211–252, 2015.

[38] Z. Wang, A. C. Bovik, H. R. Sheikh, and E. P. Simoncelli, "Image quality assessment: from error visibility to structural similarity," *IEEE Transactions on Image Processing*, vol. 13, no. 4, pp. 600–612, 2004.

[39] U. Sara, M. Akter, and M. S. Uddin, "Image quality assessment through FSIM, SSIM, MSE and PSNR—a comparative study," *Journal of Computer and Communications*, vol. 7, no. 3, 2019.

Hindawi
Computational Intelligence and Neuroscience
Volume 2022, Article ID 2256522, 9 pages
https://doi.org/10.1155/2022/2256522

Research Article

Kinect and Few-Shot Technology-Based Simulation of Physical Fitness and Health Training Model for Basketball Players in Plateau Area

Xijun Hong

Teaching and Research Section of Basketball, College of Sports Science, Dali University, Dali 671003, China

Correspondence should be addressed to Xijun Hong; hongxijun@dali.edu.cn

Received 4 February 2022; Revised 20 February 2022; Accepted 21 February 2022; Published 11 April 2022

Academic Editor: Xin Ning

Players in modern basketball have a lot of physical contact, a lot of bumps, and a lot of physical struggles. The competition for the ball, whether in the air or on the ground, is fierce, putting higher demands on the players' physical abilities. Coaches frequently use plateau physical training, which is very effective in developing athletes' cardiopulmonary function, among many other training methods. The proportional length and active area of arms are obtained using the skin color model of the human body, the angle and posture information of each joint is extracted from dynamics, and the 3D posture of arms and dynamic arms is trained and recognized in this paper, which is based on Kinect. The findings revealed that mild hypoxia in the plateau significantly lowered basketball players' performance and that basketball players' maximum heart rate and 1-minute heart rate recovery in high-intensity exercise were lower than those in flat area training.

1. Introduction

Altitude training refers to a special training method that uses the double stimulation of altitude hypoxia and exercise hypoxia to deepen the stress reaction of the body and improve the various functions and sports ability of the body [1]. Basketball is a combination of walking, sports, and running at various speeds based on the anaerobic decomposition of high-energy phosphate compounds, which is characterized by the mixture of anaerobic metabolism and aerobic metabolism [2]. Athletes' physical examinations are an important part of their physical development, and they help to promote their physical development to some extent. The collection, collation, and analysis of training data have become an important link with continuous scientific training [3, 4], which is the main reason for including physical training in the basketball training plan, improving the physical fitness of basketball players to a certain level, ensuring the improvement of athletes' physical fitness, and establishing a certain physical reserve in competition to ensure the use of more effective tactics and commands [5].

With the rapid development of the intelligent industry, the application scope of robots in various industries is constantly expanding, and artificial intelligence technology [6–8] has penetrated into people's work and life. 3D gesture recognition in dynamic arm is an important way to improve the technical level of artificial intelligence, and it is also a major problem to be solved urgently in the field of intelligent technology. The use of RGB-D sensors like the Microsoft Kinect is a convenient and effective way to obtain a diverse and realistic 3D human model, but existing methods of extracting whole body point cloud information for 3D modeling are complicated in terms of operation, equipment, and subsequent processing, and the modeling effect is not suitable for 3D crowd animation [9]. With the introduction of Kinect technology, a new type of disease rehabilitation system has emerged, allowing athletes to select the appropriate exercise mode based on their current situation, allowing for more targeted and planned rehabilitation and a desire to recover as quickly as possible [10]. The new rehabilitation exercise system adds a variety of exercise methods, allowing players to customize their workouts based on their preferences and improving their real-world experience. The new system can also help doctors make more accurate and scientific exercise plans, reduce workload, improve the efficiency of doctors' diagnosis and treatment, and help athletes achieve faster health recovery.

Although the recent research on plateau training has made some achievements, due to the different characteristics of each event, there is no plateau training model suitable for all sports and athletes [11], which has great theoretical and practical value. Kinect equipment has achieved interdisciplinary and has a good development prospect and economic value. After the introduction of Kinect technology, the overall functions of the training system can become more powerful and rich. When athletes use the training system, they can choose their own training mode in a targeted way and get the best results with proper exercise. In order to scientifically explore the high-level physical training of high-level basketball players, the changes of body function and body shape before and after the plateau were deeply studied.

2. Related Work

Some basketball players have competed in terms of training quantity and intensity, and their mutual cooperation has been strained. In general, there is a negative correlation between basketball players and their training. That is, as the training amount increases, the training intensity decreases [12, 13], and as the training intensity increases, the training amount decreases as well [12, 13]. The difference between basketball and other sports, according to literature [14], is that it is the same game in which space, ground, time, and speed compete with each other around the basket in the air. Basketball is a speed-strength, confrontation-endurance-skill event aimed at fast and changeable attack and defense [15]. According to literature [16], anaerobic metabolism and anaerobic and aerobic mixed metabolism are the primary sources of energy for elite female basketball players in competition, with aerobic metabolism and aerobic metabolism as backups. According to literature [17], short-term actions in basketball games such as fast layups, jumping, shooting, dribbling, and rebounding are primarily dependent on energy conversion from ATP (adenosine triphosphate) to CP (creatine phosphate), but this energy supply is not limited to 10–15 seconds and is primarily triggered by the system during continuous attack and defense conversion. Basketball players should have tall, well-proportioned, slender limbs; big hands; and big feet [18]. Other related works' qualitative descriptions of basketball players' physical characteristics are mostly similar to those mentioned above, so I will not repeat them here.

Nowadays, Kinect technology researched and designed by Microsoft Corporation is more and more used in medical care. Reference [19], in conjunction with Kinect technology and system, proposes a system for assisting upper-limb recovery in stroke athletes that has shown to be effective. Reference [20] has conducted professional research on the rehabilitation assistant robot, focusing on the intensity control of the robot and the training scheme implementation. Literature [21] has created a new type of equipment that uses Kinect technology to obtain athletes' bone data, creates the best recovery training plan for athletes, and monitors their training results and disease recovery. The factors affecting the random error of depth data when using Kinect are discussed in [22]. Reference [23] proposes a method for reconstructing a 3D model of the human body that involves using 24 Kinect devices to collect registration and fusion of local point clouds from various parts of the body, followed by template fitting. Reference [24] proposes a method to measure human morphological parameters by using the depth information of the front and side of human body obtained by the second generation Kinect equipment and creates a new model by modifying the standard human body model. In [25], RGB-D sensor based on Kinect extracts the information of human point cloud from 6 directions, 3 pitch angles, and a total of 18 viewing angles and uses it in 3D human reconstruction method combined with improved point cloud alignment algorithm. Reference [26] proposes a 3D gesture recognition method of dynamic arm based on D-S evidence theory algorithm, which uses gesture sensor to acquire and analyze 3D gesture information from human dynamic arm. Reference [27] puts forward a 3D gesture recognition method of dynamic arm based on classification feature extraction. The background model of dynamic arm is built based on adaptive Gaussian mixture model, and the human arm region is divided by fusion background subtraction method. The limited scanning accuracy and range of Kinect equipment limit the accuracy of 3D mannequin to a certain extent. Multiple devices or multiple small scans are used to improve the scanning accuracy and reduce the scanning range. This will lead to hardware environment, operation methods, and problems. The algorithm is very complicated to implement.

Indoor strength training, aerobic endurance training on land, exercises after strength conversion, and coordination and relaxation exercises make up the majority of the regular physical education class, which lasts about 2 hours. Prior to technical training, 40–60 minutes of special preparation activities is required. According to the literature [28], the 5000 m and 10000 m swimming events are 8% lower than sea level, and the 100 m swimming events are 2–3% lower, with the decline becoming more apparent as the movement distance increases [28]. Working at a 2000 m altitude increased the heart rate by 10–20% when compared to working on the plain; according to literature [29, 30], when the altitude is 1000 meters or higher, the maximum oxygen uptake drops by 10.5 percent. The decrease in VO_2 max was linked to an increase in oxygen tolerance as altitude was increased, according to research. Blood flow and oxygen saturation are also involved. Basketball players can benefit from altitude training not only in terms of aerobic endurance, but also in terms of lactic acid energy supply. As a result, team sports like basketball require altitude physical training to enhance athletes' physical fitness during the pre-match preparation stages.

3. Research Method

3.1. Research Design

3.1.1. Research Objects. All the players took part in and completed the test. The average age of the subjects was 26.5 years, average body weight 70.4 kg, and average height 174.8 cm.

3.1.2. Literature Data Method. Through China Journal Network and National Library, a lot of literature on basketball selection, physiology, physical education, and modern training theory was retrieved and collected, basically focusing on the research and development of basketball in China. By reading and classifying various papers, relevant data were analyzed, classified, and synthesized according to the physical characteristics of basketball players.

3.1.3. Expert Interview Method. I had the opportunity to take part in the physical fitness test of Chinese basketball players in winter training and interviewed five coaches according to the prepared interview outline, so as to understand the specific situation of physical fitness training of Chinese basketball players and do more in-depth research.

3.1.4. Test Method. The complete test lasted two months and was divided into two parts. All subjects underwent elevation and routine electrocardiogram (ECG) before the experiment, and all subjects' ECGs were normal. During the whole testing process of the two sites, ECG samples of the subjects were obtained and no abnormal ECGs were found. Physical function test finger blood was collected on an empty stomach at around 7:00 a.m., and body composition test was conducted at around 7:00 a.m. to complete the tester analysis.

3.2. Physical Training Process. Fitness should be defined as the combination of various physical abilities required of athletes in order to maximize the flexibility of various organs and systems of the body, overcome fatigue, and produce exceptional performance under the stress of special training and competition. Physical and intangible physical strength are included. Physical ability is referred to as tangible physical ability, while psychological ability is referred to as intangible physical ability. Physical quality is divided into three categories: physical structure, physical function, and mental willpower. There are two types of stretching: static and dynamic. Basketball is a type of high-intensity anaerobic exercise that causes muscles to produce a lot of lactic acid. As a result, athletes should do warm-up and relaxation exercises to improve their health and performance in sports. The comprehensive principle, ladder principle, goal principle, proper subordinate principle, and recovery principle should be followed when developing a basketball plan.

Physical training at altitude is a well-thought-out method. It is a good pre-competition training method for improving athletes' performance by assembling athletes in a large enough area and conducting routine special sports training under anoxia and anoxia conditions. Altitude training helps to stimulate and unlock the body's full potential, allowing the body's absorption, transportation, and utilization of oxygen to be improved and enhanced, and thus the body's functions and athletic performance to be maximized. As a result, sports performance in training and competition will improve.

Physical training is the process of transferring athletes' physical strength from the actual state to the target state. According to the training cycle, the whole physical education process from training to retirement can be regarded as a complete process, which is linked to multiple stages, such as multiyear training courses, annual training courses, and step-by-step training. Every stage of the training process, regardless of the duration, should theoretically cover the basic knowledge: diagnosing the situation of athletes (or sports teams), determining the training objectives, making training plans, and implementing and checking the training plans. The results of the performance evaluation can be found in Figure 1.

In the training process, it can be seen that there are four key steps to effectively change the physical fitness from a relatively chaotic reality state to a relatively orderly target state, realize the effective coordination of all components of physical fitness, accurately grasp the actual situation of athletes (or sports teams), scientifically determine the training objectives, make a careful training plan, ensure the effective implementation of the training plan, and establish a perfect training process monitoring system.

For the training participants, the training goal describes the ultimate goal of the sports training process, and all training activities aid in achieving this ultimate goal. By ensuring that all links and training activities in the training process can be fully developed around the realization of the target state [12], the determination of this ultimate goal provides a basis for the formulation and implementation of training plans and competition plans in the training process. Physical fitness goals, on the other hand, are horizontally related to technical and psychological training goals, so adjustments to other training goals, such as physical fitness requirements, should be taken into account when determining physical fitness goals. Innovation in technology physical training is a subgoal that is made up of several separate goals that must all work together to achieve the desired result.

3.3. Kinect-Based Physical Training Model for Basketball Players. Kinect is one of the most popular somatosensory devices on the market. The functional design of this product is mainly to enhance the real experience of gamers in the game. Community interaction is also a key function of Kinect, allowing people to play games together and communicate with others instantly through voice and text [17]. Kinect is far beyond the traditional concept of human-computer interaction in function. It does not need to use other devices to capture the user's physical information in sight, manipulate objects in the interface, provide intelligent

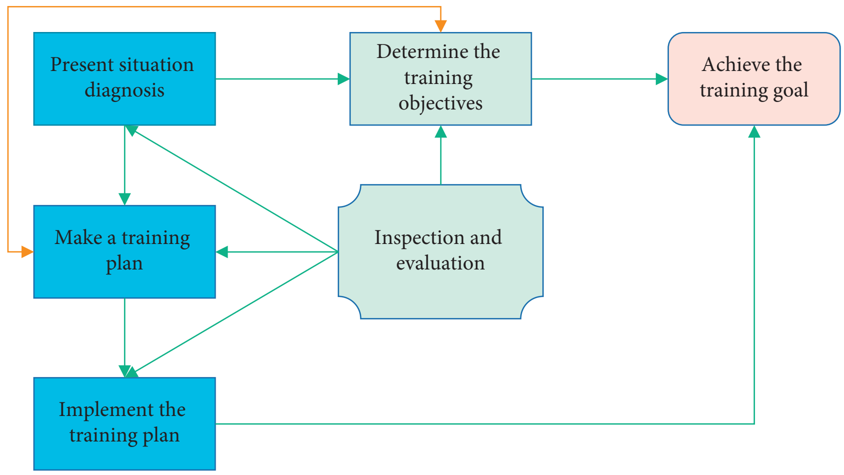

Figure 1: Basic structure of exercise training process.

and flexible human-computer interaction, realize work functions, and have strong human characteristics.

Kinect somatosensory device has many functions such as speech recognition, microphone input, and advanced sensing technology. The sensing technology of Kinect somatosensory device can fully acquire the video and audio images in the field of vision and use this information to identify the user's identity and voice information and track the bones. For users, Kinect can provide unprecedented interactive experience and achieve four goals: first, bone tracking; second, gesture recognition; third, face recognition; and fourth, voice recognition.

Practice shows that database design is software engineering, and the principles, techniques, and methods of software engineering can be applied. Compared with general software engineering, database design has a wider range and is closely related to the application environment, so database design has its own characteristics and training. The database design mainly includes some parts: demand analysis, conceptual structure design, logical structure design and physical structure design, database management, physical fitness test database system design (logical structure design and physical structure design), and database management (Figure 2).

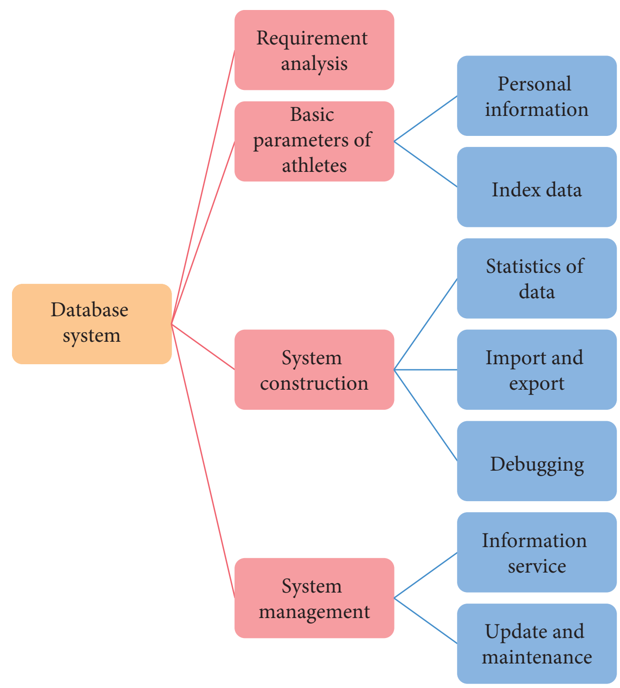

Figure 2: System design process.

The database of athletes' test data needs to include the functions of summary, input, modification, deletion, storage, download, backup, update, statistical analysis of physical test data, and system security. The system's ease of use is ensured by the integrated friendly operation interface. The DTW (dynamic time warping) method is primarily used to compare two unrelated time series. Different from other methods, when the lengths of two sequences are different or the X axis cannot judge them, this method can explain the relationship between the current two sequences by time warping function under certain conditions. In this calculation process, firstly, a matrix of m rows and n columns should be established, and the distance between points in two sequences should be stored in the matrix to observe the matrix effect. The smaller the value, the higher the similarity between the two sequences. When the calculation reaches the end point, the accumulated value reflects the similarity of the two sequences to a certain extent. The cumulative distance $\operatorname{dist}(i, j)$ can be expressed as the following formula:

$$\operatorname{dist}(i, j) = \min \begin{cases} \operatorname{dist}(i-1, j-1) + d(A(i), B(j)), \\ \operatorname{dist}(i-1, j) + d(A(i), B(j)), \\ \operatorname{dist}(i, j-1) + d(A(i), B(j)), \end{cases} \tag{1}$$

where $\operatorname{dist}(i, j)$ represents the cumulative distance, which represents the sum of the distance between data column $A(i)$ and data column (j) plus the cumulative distance of the element closest to the end point.

If each frame of motion data is regarded as a point in 16-dimensional space, then an action sequence can be regarded as a curve in this space. The similarity between two action sequences can be obtained by calculating the distance between the two sets of data, which is usually referred to as

Euclidean distance. Then, the Euclidean distance between them is as follows:

$$D(M_1, M_2) = \sqrt{\sum_{i=0}^{N-1} (G_i - G_i')^2}. \quad (2)$$

The smaller the calculation result, the closer the two groups of actions are.

In covariance probability theory and statistics, this parameter represents the total error of variables. Assuming that the two quantities have the same changing trend, they must be both greater than or less than their expected value, in which the calculated covariance is positive. For the same reason, if the two trends are opposite, the calculated covariance is negative.

$$\operatorname{cov}(X, Y) = E((X - \mu)(Y - \upsilon)). \quad (3)$$

μ represents the expectation $E(X)$ of X, and υ represents the expectation $E(Y)$ of Y.

The evaluation of rehabilitation training in this system adopts triple evaluation algorithm (DPL algorithm for short), which combines dynamic time warping algorithm, human correlation coefficient, and longest common subsequence algorithm. The data streams of patient motion applying DPL algorithm are sent to DTW algorithm, Pearson correlation coefficient evaluation, and longest common subsequence (LCS) algorithm to obtain the similarity evaluation data with the standard template.

The specific formula of DPL algorithm is as follows:

$$\begin{aligned} D = {} & \frac{C_1}{C_1 + C_2 + C_3} \times S_1 + \frac{C_2}{C_1 + C_2 + C_3} \\ & \times S_2 + \frac{C_3}{C_1 + C_2 + C_3} \times S_3. \end{aligned} \quad (4)$$

By setting three confidence variables in advance to a certain extent, the problem that the accuracy of the three fusion algorithms decreases according to the actual situation can be solved, and it can also be adjusted by professional medical staff according to the treatment experience, which is suitable for the rehabilitation of some patients.

In the process of 3D posture recognition in dynamic arm, assuming that x, y represent two joint points of the arm, first calculate the difference between the coordinates of the arm and the shoulder node, then judge whether the joint points of each arm are in approximately the same position according to the difference, and then use (5) to calculate the angle (Euclidean distance) between the connection lines of the joint points in dynamic arm:

$$d = K \tan(Hd_{\text{raw}} + L) - O. \quad (5)$$

In (5), d_{raw} represents the depth value of the three-dimensional posture image in the dynamic arm, and H, L, O represent the constants of the depth value.

According to the distance between the two joint points, calculate the angle between the two joint points of the arm and the X axis of the reference point, use the angle of the reference point on the X axis to obtain the coordinates of the specified point, and then use (6) to obtain the angular constraint conditions of the arm joint points:

$$P_A = \frac{\{P_1, P_2, \theta, \tau\}}{D(X, Y)} \times d, \quad (6)$$

where P_1 represents the reference point of the arm, θ represents the angle between the arm joint point P_2 and the X axis, and τ represents the set angle threshold.

In the process of three-dimensional posture optimization recognition in dynamic arm, the feature vector sets of angle between arm joint points with different postures are obtained by the following formula:

$$\text{Ktr} = K_i \times \frac{\{K_1, K_2, \ldots, K_n\}}{\text{Str}} \text{Str}. \quad (7)$$

Among them, $\{K_1, K_2, \ldots, K_n\}$ represents the feature vector of the angle between arm joints in different postures. Str stands for training sample set.

4. Result Analysis and Discussion

4.1. Physical Training Plan and Load Arrangement. Special preparation activities before technical training are also selected according to the content of technical training, mainly including elastic belt shoulder wrist joint maintenance, weight-bearing water bag basketball footwork practice, ball practice, and dynamic stretching. In the definition of load intensity and load quantity in this study, the load intensity is determined as the maximum of the main load indexes (bench push, squat, high pull) in the last two weeks of flat land. The relationship between load intensity and load weight during training is reflected in the percentage of each training index relative to the maximum load value and total training weight (Figure 3).

There is no restricted load applied, the load is only close to the level of flat ground, and the load strength is only about 80% of the maximum strength. A three-day break between two high-intensity strength workouts can help athletes recover completely. The men's basketball team in this study used the plateau to perform strength training, aerobic endurance training, and special skill training, with fat being one of the challenges of this plateau training. Because the waist-hip ratio has changed dramatically, this plateau training can be considered a training goal for body fat reduction.

4.2. Analysis of Physical Fitness Test of Basketball Players in Winter Training. Quantitative quality ensures the physical fitness of basketball players and is the material basis for rapidly changing skills and tactics. Modern basketball players need highly developed comprehensive strength. Comprehensive strength is the comprehensive strength of athletes who are engaged in special basketball activities due to the coordination of various sports links. It is the foundation of athletes' special abilities. Improving the overall strength in training is the development trend of modern basketball strength training. In strength training, the

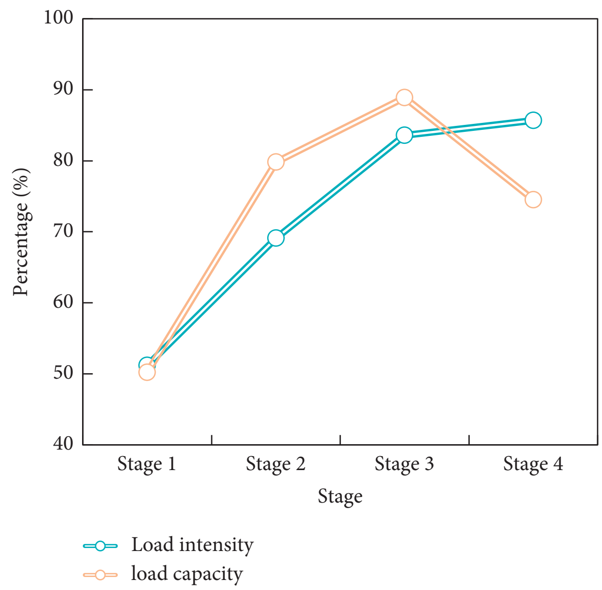

Figure 3: The relationship between altitude train load and intensity change.

training methods of adults are not completely suitable for young athletes, so the physiological characteristics of young athletes must be taken into account in training, based on moderate load, comprehensive and gradual.

Figure 4 shows the main physical indexes of young male basketball players in China. Among them, indicators 1~8, respectively, represent comprehensive running (s), in situ touching height (m), run-up touching height (m), sit-ups, standing long jump (m), 1-minute bench press, turn-back running (s) and 3,200 meters (s).

Generally speaking, the aerobic endurance of Chinese basketball players has obviously decreased, and other indexes have not improved. This shows that the physical training of Chinese youth men's basketball team is not systematic and has not produced good results. Speed endurance and aerobic endurance training can improve other physical qualities of athletes every year, laying the foundation for athletes to reach a higher level.

4.3. Comparison of HR Recovery after Exercise in Different Regions. In order to further observe the ability of basketball players to recover cardiovascular function after altitude exercise, the heart rate (HR) recovery at different times after exercise was compared, so as to understand the influence of altitude hypoxia on cardiovascular function. That is, immediately after exercise, the difference between the peak HR of warm-up activity and normal HR is 100%, and the net recovery of HR at different times after two activities in different regions is compared. As a result, the heart rate recovery in 1 minute after high-intensity 10-minute running is obviously faster than that in flat and highland areas, and there is no significant difference between the two places after 4-minute exercise.

It can be seen that, even in the 10-minute curve executed in Figures 5 and 6, the change of the individual's normal

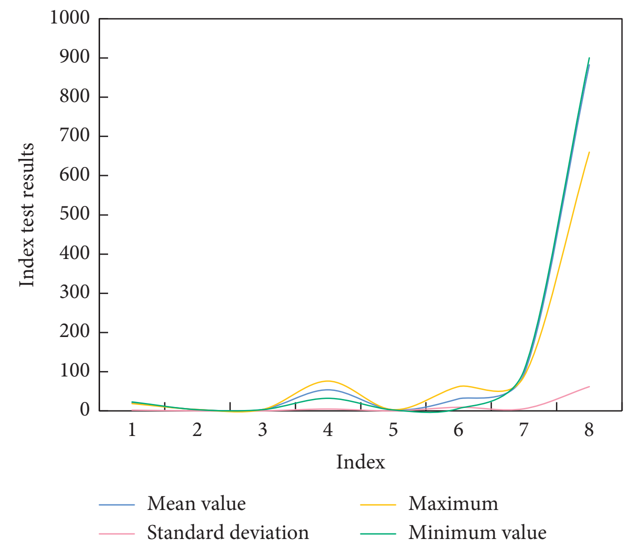

Figure 4: Test and analysis of main physical indexes of Chinese basketball players in winter training.

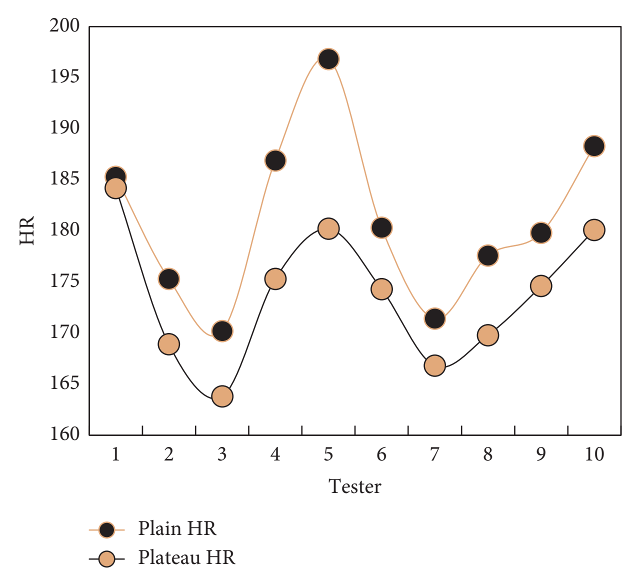

Figure 5: Comparison of HR recovery between plain and plateau immediately after 10 min running.

heart rate is relatively stable. The HR at high altitude is generally higher than normal HR, but individuals with lower HR in plain areas still keep lower HR in high altitude areas.

After running for 4 minutes and 10 minutes, HR basically returns to the HR level of the preparation activities, whether in flat or highland areas. It is found that the heart recovery ability of basketball players is not affected by the local altitude (see Figure 7).

The heart is different from other organs in human body. The nutritional system and functional system of different organs are two different systems. The heart not only performs its own functions, but also nourishes the organs themselves. Therefore, insufficient oxygen supply to myocardium is one of the reasons why the heart works at a high level for a long time. On the one hand, increased myocardial

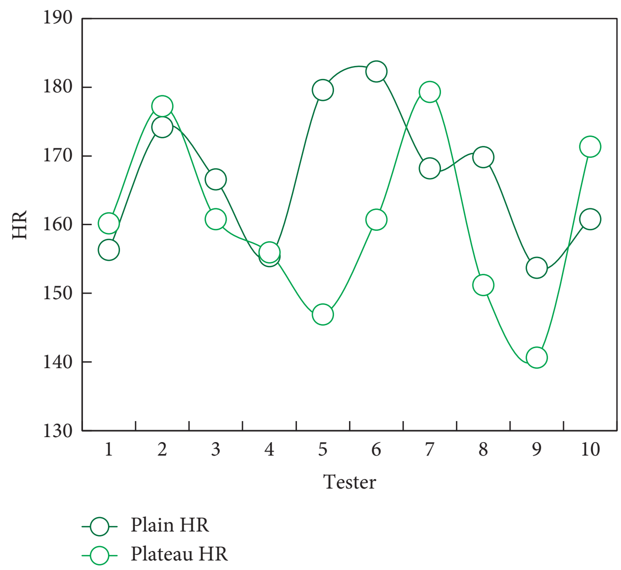

Figure 6: Comparison of 1 min HR recovery after 10 min running.

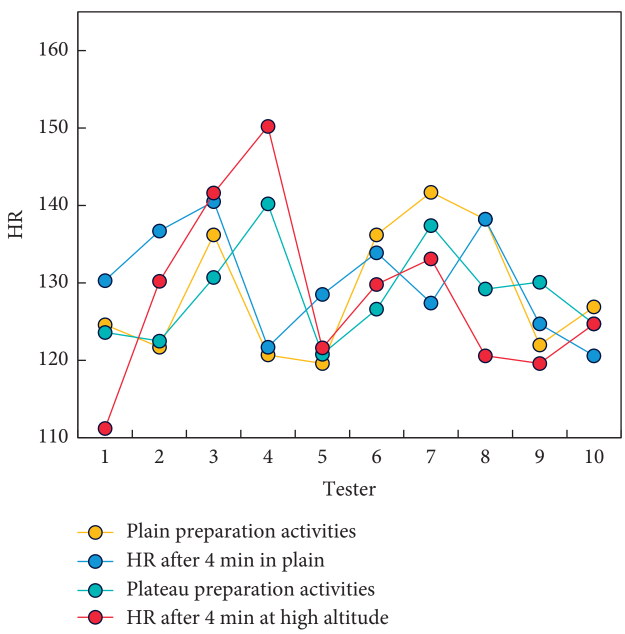

Figure 7: Comparison of 4 min HR after preparation and exercise.

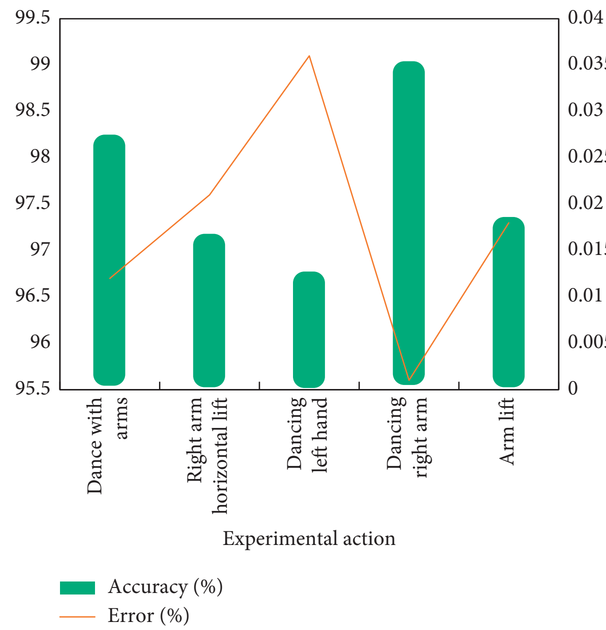

Figure 8: Improve the effectiveness of algorithm identification.

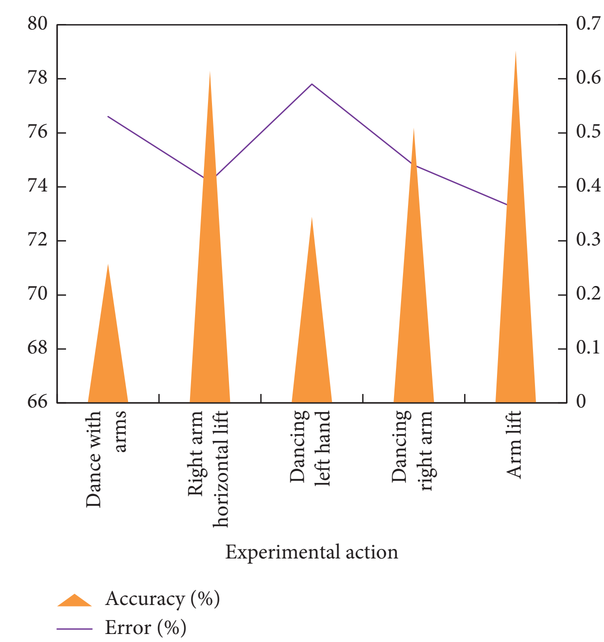

Figure 9: Effectiveness of traditional algorithm identification.

contractility raises oxygen consumption and necessitates more blood to perfuse myocardial tissue. Because myocardial tissue relies almost entirely on oxidative metabolism for energy, coronary artery oxygenation is critical [19]. On the other hand, a high HR reduces the diastolic time of the myocardium and makes the coronary artery insufficient in blood supply. Because most coronary artery branches are deeply embedded in the myocardium, the intense compression of myocardial contraction causes a sharp decrease in coronary blood flow.

HR can maintain a relatively stable change in both plain and plateau. Although the overall HR level in the plateau area is higher than that in the plain area, individuals with lower HR in the plain area still maintain a lower HR level during the plateau training period. Therefore, the heart rate can be said to be a very effective index to monitor the changes of cardiovascular function during actual exercise, and it is not affected by the altitude of the area, but only related to exercise intensity, so it can objectively reflect the status of cardiovascular system. During the exercise, the heart deformation and function of athletes of different levels adapt to the training course of specific functions.

4.4. Comparison of Algorithm Identification Effectiveness. Simulation verification is needed to prove the effectiveness of 3D gesture recognition method in boom based on Kinect.

A virtual platform for 3D gesture recognition experiment in boom is built with Windows 7 operating system, and the experimental computer is a personal computer. The number of participants in the experiment was five. Using the improved algorithm and the existing algorithm, 3D postures of dynamic arms were identified, and each person created five kinds of dynamic arm postures. The recognition accuracy and error rate of the two algorithms are compared, and the results are shown in Figures 8 and 9.

The analysis shows that the improved 3D gesture recognition algorithm of dynamic arm has higher accuracy than the existing algorithms and ensures higher accuracy and fewer recognition errors. Using the improved algorithm, in 3D gesture recognition rendering of dynamic arm, the direction, position, and some specific details of human dynamic arm can be well displayed, and the recognition effect is better than that of the existing algorithm, which can effectively meet the requirements.

5. Conclusion

Altitude physical training can help basketball players lose weight, but its effect on muscle circumference is dependent on their height, body shape, and training load. Athletes' aerobic metabolism can be improved, allowing them to tap into their full potential and better adapt to high-intensity training and competition. The DTW algorithm is used to evaluate sports, and the DTW distance is calculated as the similarity evaluation index between two sports groups. This method compensates for the traditional Euclidean distance's shortcomings in determining the similarity of nonconformal data. Simulation results show that a 3D gesture recognition method based on the Kinect boom has a high recognition accuracy and can meet intelligent technology application requirements.

Data Availability

The data used to support the findings of this study are included within the article.

Conflicts of Interest

The author declares that there are no conflicts of interest regarding the publication of this paper.

Acknowledgments

This study was supported by the Teaching Model Project of Dali University (2015).

References

[1] C. C. Erickson, "Discrimination of the "Athlete's Heart" from real disease by electrocardiogram and echocardiogram," *Cardiology in the Young*, vol. 27, no. 1, pp. S80–S88, 2017.

[2] V. M. Meyer, "Sport psychology for the soldier athlete: a paradigm shift," *Military Medicine*, vol. 183, no. 7-8, 2018.

[3] C.-H. Chang, Y.-J. Hsu, F. Li et al., "Reliability and validity of the physical activity monitor for assessing energy expenditures in sedentary, regularly exercising, non-endurance athlete, and endurance athlete adults," *PeerJ*, vol. 8, no. 2, Article ID e9717, 2020.

[4] T. J. Gabbett, G. P. Nassis, E. Oetter et al., "The athlete monitoring cycle: a practical guide to interpreting and applying training monitoring data," *British Journal of Sports Medicine*, vol. 51, 2017.

[5] B. Desbrow, "Youth athlete development and nutrition," *Sports Medicine*, no. 5, pp. 1–10, 2021.

[6] X.-B. Jin, W.-T. Gong, J.-L. Kong, Y.-T. Bai, and T.-L. Su, "PFVAE: a planar flow-based v auto-encoder prediction model for time series data," *Mathematics*, vol. 10, no. 4, p. 610, 2022.

[7] Z. Huang, Y. Liu, C. Zhan, C. Lin, W. Cai, and Y. Chen, "A novel group recommendation model with two-stage deep learning," *IEEE Transactions on Systems, Man, and Cybernetics: Systems*, 2021.

[8] X. Jin, J. Zhang, J. Kong, T. Su, and Y. Bai, "A reversible automatic selection normalization (RASN) deep network for predicting in the smart agriculture system," *Agronomy*, vol. 12, no. 3, p. 591, 2022.

[9] C. Montanaro and G. Limongelli, "Exercise in adult with congenital heart disease: not a chimaera anymore," *International Journal of Cardiology*, vol. 243, pp. 209-210, 2017.

[10] L. E. Heaton, J. K. Davis, E. S. Rawson et al., "Selected in-season nutritional strategies to enhance recovery for team sport athletes: a practical overview," *Sports Medicine*, vol. 47, no. 11, pp. 2201–2218, 2017.

[11] S. S. Rodrigo, A. Ferreira, T. H. Nakagawa, J. E. Santos, and F. V. Serrão, "Rehabilitation of patellar tendinopathy using hip extensor strengthening and landing-strategy modification: case report with 6-month follow-up," *Journal of Orthopaedic & Sports Physical Therapy*, vol. 45, no. 11, pp. 899–909, 2017.

[12] L. Ding, L.-m. Yuan, Y. Sun, X. Zhang, J. Li, and Z. Yan, "Rapid assessment of exercise state through athlete's urine using temperature-dependent NIRS technology," *Journal of Analytical Methods in Chemistry*, vol. 2020, no. 1, pp. 1–7, 2020.

[13] S. Hendricks, K. Till, J. L. Oliver et al., "Rating of perceived challenge as a measure of internal load for technical skill performance," *British Journal of Sports Medicine*, vol. 53, no. 10, 2018.

[14] A. J. Arnold, C. A. Thigpen, P. F. Beattie, M. J. Kissenberth, J. M. Tokish, and E. Shanley, "Sport specialization and increased injury frequency in youth baseball players: a prospective study," *Journal of Athletic Training*, vol. 54, no. 10, pp. 1115–1122, 2019.

[15] N. Keay and R. M. Bracken, "Managing type 1 diabetes in the active population," *British Journal of Sports Medicine*, vol. 54, 2019.

[16] H. Yang, T. Luo, L. Li, H. Liang, and H. Zhang, "Athlete's respiratory state monitoring method based on inertial measurement unit," *Zhongguo Guanxing Jishu Xuebao/Journal of Chinese Inertial Technology*, vol. 26, no. 5, pp. 591–596, 2018.

[17] R. -G. Markel, L. A. Asier, R. V. Daniel, F. Clemente, and J. Pino-Ortega, "A survey to assess the quality of the data obtained by radio-frequency technologies and microelectromechanical systems to measure external workload and collective behavior variables in team sports," *Sensors*, vol. 20, no. 8, 2020.

[18] H. Wang and H. Yuan, "Training project arrangement for tennis athletes based on BP neural network model," *International Journal of Reasoning-Based Intelligent Systems*, vol. 9, no. 3-4, pp. 144–148, 2017.

[19] H. Shi, H. Zhao, X. C. Chen, and D. Li, "A judgment method of athlete's movement state based on pulse wave mathematical model," *Dongbei Daxue Xuebao/Journal of Northeastern University*, vol. 39, no. 12, pp. 1697–1701, 2018.

[20] K. He, "Prediction model of juvenile football players' sports injury based on text classification technology of machine learning," *Mobile Information Systems*, vol. 2021, no. 2, pp. 1–10, 2021.

[21] Z. Huang, Q. Chen, L. Zhang, and X. Hu, "Research on Intelligent Monitoring and Analysis of Physical Fitness Based on the Internet of Things," *IEEE Access*, vol. 7, no. 99, p. 1, 2019.

[22] Y. Guo, "Pattern recognition and neural network-driven roller track analysis via 5G network," *Mobile Information Systems*, vol. 2020, pp. 1–8, 2020.

[23] L. Tao, "Application of data mining in the analysis of martial arts athlete competition skills and tactics," *Journal of Healthcare Engineering*, vol. 2021, no. 4, pp. 1–6, 2021.

[24] M. S. Xanthopoulos, T. Benton, J. Lewis, J. A. Case, and C. L. Master, "Mental health in the young athlete," *Current Psychiatry Reports*, vol. 22, no. 11, p. 63, 2020.

[25] C. Cremin and B. C. Anderson, "Commitment and satisfaction in the classroom and on the field: evidence from a Division I liberal arts college," *Applied Economics*, vol. 51, no. 7-9, pp. 858–880, 2019.

[26] V. Sarlis, V. Chatziilias, C. Tjortjis, and M. Dimitris, "A data science approach analysing the impact of injuries on basketball player and team performance," *Information Systems*, vol. 99C, no. 1, p. 16, 2021.

[27] M. Bayramoğlu and N. Ünlütürk, "Nonhealing, progressive stress fractures of the foot in a 13-year-old basketball player: is vitamin K deficiency a risk factor?" *Journal of Physical Therapy Science*, vol. 29, no. 4, pp. 763–766, 2017.

[28] Z. Y. Kerr, R. C. Lynall, K. G. Roos, S. L. Dalton, A. Djoko, and T. P. Dompier, "Descriptive epidemiology of non-time-loss injuries in collegiate and high school student-athletes," *Journal of Athletic Training*, vol. 52, pp. 1062–6050-52.2.15, 2017.

[29] R. Liu, Z. Liu, and S. Liu, "Recognition of basketball player's shooting action based on the convolutional neural network," *Scientific Programming*, vol. 2021, no. 3, pp. 1–8, 2021.

[30] P. Wang and W. Gao, "Image detection and basketball training performance simulation based on improved machine learning," *Journal of Intelligent and Fuzzy Systems*, vol. 40, no. 2, pp. 2493–2504, 2021.

Hindawi
Computational Intelligence and Neuroscience
Volume 2022, Article ID 7487452, 14 pages
https://doi.org/10.1155/2022/7487452

Research Article

Application of PRP in Chloasma: A Meta-Analysis and Systematic Review

Tinghan Deng,[1] **Fengrui Cheng**,[2] **Shanshan Guo**,[1] **Hongbin Cheng**,[3] **and Jingping Wu**[2]

[1]*Clinical Research on Skin Diseases School of Clinical Medicine, Chengdu University of TCM, Chengdu 610072, China*
[2]*Department of Medical Cosmetology, Hospital of Chengdu University of Traditional Chinese Medicine, Chengdu 610072, China*
[3]*Dermatology of Department, Hospital of Chengdu University of Traditional Chinese Medicine, Chengdu 610072, China*

Correspondence should be addressed to Jingping Wu; wujingping@cdutcm.edu.cn

Received 18 January 2022; Revised 10 March 2022; Accepted 11 March 2022; Published 7 April 2022

Academic Editor: Xin Ning

Background. Chloasma is a common skin pigment disorder. Treatment of chloasma has been challenging, often unsatisfactory, and difficult to avoid recurrence. PRP is a new treatment for chloasma, but there is no consensus on its use. Lingyun Zhao's team recently reported a systematic evaluation and meta-analysis of the efficacy and safety of PRP in the treatment of chloasma, which is consistent with our ideas, but we will elaborate on the application of PRP in chloasma from a deeper and more comprehensive perspective. Before we started this study, we had registered with Prospero as CRD42021233721. *Methods*. The authors searched the public medical network, MEDLINE, EMBASE, Cochrane Central Register of Controlled Trials, ScienceDirect, Scopus, and Science Network. The clinical trials registry ClinicalTrials.gov databases were searched for relevant publications to June 2021. The results showed the area and severity of chloasma (MASI) or revised MASI (mMASI) score. *Results*. Three RCTs, one nonrandomized controlled study, and four were prospective before and after self-controlled studies met the inclusive criteria. Intradermal PRP injections significantly improved chloasma as indicated by the significant decrease MASI (average balance -6.71, 95% CI -8.99 to -4.33) and mMASI scores (average balance -2.94, 95% CI -4.81 to -1.07). The adverse reactions were mild, and there were no significant long-term adverse events. *Conclusive*. The data can reflect the effectiveness and safety of PRP therapy for chloasma. RCTs are needed to determine effective treatment parameters, and long-term follow-up should be included to better clarify the efficacy and side effects of PRP in treating chloasma.

1. Background

Chloasma is a pigmentation disorder that mostly affects women's faces. The cheeks, forehead, chin, lips, and neck are the most common areas exposed to the sun, but other areas are not uncommon [1]. The main clinical manifestation of brown facial patches has a significant impact on the patient's appearance and quality of life [2]. It is a disfiguring dermatosis that affects a large number of people all over the world, and it is difficult to treat because the pathogenesis is still unknown [3]. Many studies have recently confirmed that contraceptive pills, ultraviolet radiation, genetic predisposition, and sex hormone levels are all strongly linked to the occurrence of chloasma. In addition, skin destruction, barrier vascular factors, and inflammatory factors all play a role in chloasma pathogenesis. Drug therapy, chemical peeling, and laser are the most commonly used treatment methods today. Despite the fact that there are numerous ways to treat chloasma, data obtained through general methods cannot reach the ideal state. Because of its recurrence, chloasma can cause complications like irritation, excessive pigmentation after inflammation, and excessive pigmentation after rebound, making it an unsolvable problem in the field of beauty [4].

The main problems to be solved in chloasma are facial pigmentation and pigmentation after drug treatment. As a new technique used in dermatology and plastic surgery, PRP has been confirmed in the latest studies in its potential role in pigmented dermatitis. PRP is an autologous blood product defined as a platelet concentrate obtained by centrifuging blood to a concentration 3 to 5 times above the basal platelet concentration [5]. As for the mechanism of PRP in the treatment of pigmentation diseases such as chloasma, the present research can be divided into three aspects [6]. On the one hand, the key elements of platelets are contained in alpha particles. Alpha-granules contain more than 30 cytokines and growth factors. These include PDGF, TGF-β1 and β2, EGF, and MGF [7]. Of these, the most important reduction in pigmentation is TGF-β1 [8]. It has already been shown to reduce melanogenesis by delaying activation of extracellular signal-regulated kinases [9]. On the other hand, some recent studies show that the key pathology needs to control melanin production by adjusting the activities of extracellular kinase and prostaglandin E2 (PGE2). In addition, it guides extracellular matrix remodeling, strengthens the expression of matrix metalloproteinases, eliminates extracellular matrix elements damaged by light, and stimulates fibroblast proliferation and collagen synthesis [1]. In summary, PRP can reduce pigmentation and brighten skin tone [10], which is also the primary need of patients with chloasma.

In recent years, PRP is a novel treatment option for chloasma and has shown significant clinical improvement. However, there is no consensus on its use [11]. The safety, efficacy, and prognosis of PRP have not been fully confirmed. Zhao et al. [12] recently reported a systematic review on PRP in the treatment of chloasma, which included studies without controlled experimental designs. We will elaborate on the application of PRP in chloasma under more stringent inclusion and exclusion criteria and bias evaluation and try to explore the evaluation of efficacy and safety by multiple factors including ethnic differences and pharmacological effects. This study was registered with PROSPERO as CRD42021233721.

2. Method

A systematic review and meta-analysis were conducted according to the PRISMA (Preferred Reporting Items for Systematic reviews and Meta-Analysis) statement [13].

2.1. Search Strategy. A literature search was conducted in PubMed (1966 until acquisition time), MEDLINE (1966 until acquisition time), EMBASE (1974 to until acquisition time), ScienceDirect (until acquisition time), Scopus (until acquisition time), and Web of Science (until acquisition time). From 2000 to 2021, the clinical trial registry of ClinicalTrials.gov (http://ClinicalTrials.gov/) was searched.

The analytical strategy is to fuse the terms associated with chloasma with the terms identifying platelet rich plasma. Text and mesh term searches cover the words "platelet rich plasma," "platelet concentrate," "melanosis," "chloasma," "chloasma," "chlodue to the factma," "plaque," "spot," "chlosimilar Toma," "color," "photo," "stain," "stain," "pigment" "And word variants and similar words combined with Boolean operators" or "and."

We will review the list of documents that have been identified for similar tests or reviews to clarify the next research ideas. A complete article attachment of references reporting potential qualified tests will be obtained. If this is not possible, we will try to contact the author of the study to get some relevant information.

2.2. Sample. Inclusive criteria were as follows:

(1) Participants were diagnosed with chloasma.

(2) Intervention was any form of platelet-rich plasma, alone or as an adjunct in chloasma.

(3) Control was placebo, standard care, or alternative topical therapies.

(4) Pre- and post-treatment chloasma area and severity index (MASI) or modified MASI (mMASI) scores completed by dermatologists, as well as objective skin imaging analysis data. Other valid methods of evaluating the effects of PRP therapy include physician assessment, participants' subjective self-assessments, participant-reported outcomes, or satisfaction level. Additional outcomes included adverse effects reported during and after treatment.

(5) Study type was RCTs. Without a random trial, well-designed non-RCTs and prospective before-and-after self-control research will be regarded as a narrative embodiment of the present facts.

2.3. Study Quality and Risk of Bias Assessment. Two authors independently assessed the risk of bias of each study in the field of sequence generation using the criteria suggested in the Cochrane Handbook of Systematic Reviews of Interventions [14]: occupational concealment, blindness for healthcare professionals, participants and evaluators, incomplete outcome data, and other potential threats to outcomes and validity. For nonrandomized and before-and-after studies, risk of bias was assessed using the ROBINS-I bias tool [15]. The tool includes assessments in seven areas: bias due to obscure, bias in choice of study participants, bias in intervention classification, bias in expected interventions, missing data bias, outcome measurement bias, and reporting outcome selection bias.

2.4. Data Extraction. The data was collected and given to two reviewers to complete on their own. The discrepancy will be repaired through discussion or negotiation with the third reviewer. The following blinded and structured stratification strategy will be used by reviewers. First, the title and abstract should be filtered. Second, read the first article you chose. Third, choose research that satisfies the predetermined inclusive and exclusionary criteria. The author name, study duration, location, year of publication, journal, study design, sample, patient characteristics, dose and type of PRP used, concomitant interventions and outcomes, duration of follow-up, evidence level, and quality of research were all listed in a standard format.

2.5. Data Synthesis and Statistical Analysis. Results are combined unless diversity indicates that the combination is unreasonable. If some studies reported results as continuous measures, while others used dichotomous methods of the same structure, we would convert the previous results from continuous measures to binary. If results were reported at different times throughout the year, data from each time were aggregated and combined with data from other trials from similar times. After data collection is complete, the final analysis point is determined by consensus.

ReviewManager version 5.3 was used for meta-analyses. A meta-analysis was performed as suggested by the Cochrane Collaboration [16]. For continuous data with the same measurement unit, the weighted average difference and 95% confidence interval are used. For continuous data with different measurement units, the standardized average balance and 95% confidence interval are used. The difference is represented by 95% confidence interval. When there was no heterogeneousness ($I^2 = 0$), a fixed-effects model was used. We also used a random effects model. When heterogeneousness was high ($I^2 \geq 70\%$), except for the lowest quality studies, sensitivity analyses were performed to account for heterogeneousness and to confirm the stability of the results, with $p \leq 0.05$ considered statistically significant.

3. Results

From the database, a total of 101 records were retrieved (Figure 1). Following the deletion of 66 duplicate records, 35 articles were screened based on title and abstract. There is no other literature available from other sources. Eight studies were considered appropriate and included in the qualitative meta-analysis, while three studies were included in the quantitative meta-analysis after dragging through studies that did not meet inclusive criteria. Three RCTs, one non-randomized controlled study, and four prospective before-and-after self-controlled studies were among the studies included.

3.1. Characteristics of Included Studies. Tables 1 and 2 summarize study characteristics and patient demographics. A total of 8 articles published between 2017 and 2021 were included in this study, which included a total of 277 patients with chloasma. All of the study patients were adults, patient age-bracket from 20 to 58 years of age, and about 80 percent of them were women. Of the eight studies included, three were from Egypt, two were from Pakistan, one was from Thailand, and the remaining two were from India. All studies used the MASI or mMASI score to assess the severity of patients' chloasma conduct an initial assessment. Of the 8 studies, 3 had subjects with skin types III and VI, 1 had subjects with skin types II, III and VI, 1 had subjects with skin types IV and V, 1 had subjects with skin types III and V, and the other 2 were not mentioned. In 4 of the studies, the type of chloasma in patients was epidermal and mixed, while the remaining 4 were not mentioned. The mean follow-up time of patients was 97 days (range 14–180 days). All studies have demonstrated the significant efficacy of PRP in the treatment of chloasma. The specific quality results of RCT and non-RCT studies are shown in Figure 2 and Table 3.

4. MASI

Four of the eight included studies comparing the MASI between experimental (PRP treatment) group and control group were reviewed [1, 3, 18, 20]. The baseline MASI were comparable between experimental and control groups in all included studies ($p > 0.05$). In MASI, the random-effect model showed significant differences between the experimental group and the control group (average balance −6.71, 95% CI −8.99 to −4.33; $p < 0.05$; $I^2 = 55\%$) (Figure 3).

4.1. mMASI. Four studies comparing the mMASI between experimental (PRP treatment) group and control group were enrolled in the meta-analysis [3, 4, 18, 19]. The baseline mMASI were comparable between experimental and control groups in all included studies ($p > 0.05$). A REM yielded a significant difference in mMASI between experimental and control groups (average balance −2.94, 95% CI −4.81 to −1.07; $p < 0.05$) (Figure 4). The heterogeneousness was substantial ($p < 0.05$; $I^2 = 87$ percent). The study by Sirithanabadeekul et al. [4] was conducted in Thailand, whereas other studies were conducted in Egypt [3, 18, 19]. The racial difference may account for the heterogeneousness. The heterogeneousness decreased from 87% to 26%, and the average balance increased slightly to −3.66 (95 percent CI −4.74 to −2.57; $p < 0.05$) (Figure 5).

4.2. Degree of Improvement. A description of the extent of improvement can be found in five of the included studies [3, 17, 19, 20] (Table 4). The degree of improvement is mainly determined by referring to the decline ratio of MASI or mMASI score; among them, the most important values as dividing stages are 0%, 25%, 50%, and 75%, respectively. In most studies, the degree of improvement was rated as follows: 0: no feedback; 1: partial feedback (decrease 0%–25%); 2: good feedback (26%–50% reduction); 3: very good feedback (51%–75% reduction); 4: near perfect (75% reduction). Among the five studies, only one study chose the decrease ratio of MASI score as the evaluation criterion. Faiz and Meng [20] found that more than 60% of patients showed fair improvement, but no patient (0%) showed excellent response. Among them, 2 studies only used the decrease ratio of mMASI score as the basis for evaluating degree of Improvement. Tuknayat et al. [17] found that more than 80% of patients had mild or greater improvement, and about 40% of patients showed significant improvement. Topical tranexamic acid alone and topical tranexamic acid combined with PRP both showed some improvement in both groups, according to Gamea et al. [19]. PRP-treated patients, on the other hand, improved significantly more than the control group. MASI and mMASI were chosen as the improvement degree evaluation indexes for the remaining two groups. Hofny et al. [3] found that both the MASI and mMASI scores decreased and that more than 80% of patients improved mildly or significantly but that the difference

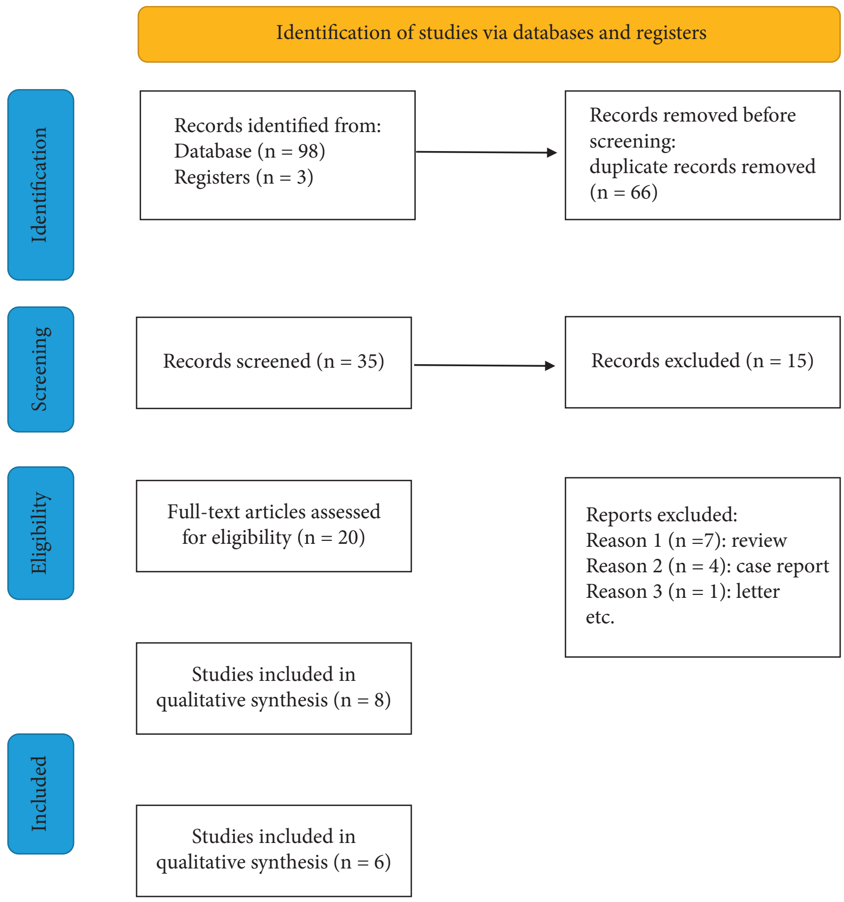

Figure 1: Flow diagram of included studies.

between two different PRP injections was insignificant. According to Adel et al. [18], clinical efficacy of PRP alone or PRP combined with IPL was improved, but there was no significant difference between the two groups.

4.3. Patient Satisfaction. A total of five studies reported patients' satisfaction after treatment. In two of the RCTs looking at PRP versus other therapies, patient satisfaction was significantly higher under PRP than in the control group [4, 19]. In the study of the effect of two different injection methods of PRP and the randomized controlled study examining the efficacy of PRP alone and in combination with PRP and IPL, there was no significant difference in satisfaction with the efficacy between the experimental group and the control group [3, 18]. And in another prospective before-and-after self-control studies, more than 90% of patients were satisfied with the efficacy of PRP [2] (Table 4).

4.4. Adverse Events. Adverse events were mentioned in 6 studies. Faiz et al. [20] found the presence of temporary transient erythema at the injection site of PRP (13% of the patients). Hofny et al. [3] noted swelling, redness, and pain at the injection site of PRP. Sirithanabadeekul et al. [4] noted bruising at the injection site of PRP (the number was not mentioned). Tuknayat et al. [2] noted xerosis and hyperpigmentation at the injection site of PRP (the number was not mentioned). Gamea et al. [19] reported hyperpigmentation (5% of the patients), erythema (50% of the patients), and pain (60% of the patients) at the injection site of PRP (Table 4). Tuknayat et al. reported xerosis (35% of the patients) and pruritus (25% of the patients) at the injection site of PRP (Table 4).

4.5. Other Outcomes. In the RCTs conducted by Sirithanabadeekul et al. [4] on the efficacy of PRP in the treatment of chloasma, not only were MASI and mMASI score used as the efficacy criteria, but also indicators such as melanin levels, skin wrinkle levels, and erythema levels were used. However, based on the disease characteristics of chloasma and the requirements of this study, only melanin level was included in the analysis. They found a significant drop in melanin levels in the skin of patients treated with PRP, but there was no significant change in melanin levels in the skin of patients injected with normal saline (Table 4).

5. Discussion

Chloasma is a common skin pigment disorder characterized by brown patches on the face, which sometimes becomes a chronic distressing condition on the patient. Chloasma is caused by a complex interplay of factors such as sunlight,

Table 1: Characteristics of included studies.

Author, year	Study design	Location	Number assigned/evaluated	Age	Control	PRP preparation	Treatment	Treatment time	Follow-up
Hofny et al. 2019 [3]	Prospective before-and-after self-control studies	Egypt	23/23	21–50	before-and-after self-control	(1) Double centrifugation (2) 10 minutes at 1600 rpm (3) 10 minutes at 4000 rpm	(1) Used PRP alone (2) Hemi-face study (3) Intradermal injections on the left side and microneedling before and after PRP application on the right side	Three sessions (four-week intervals)	1 month
Sirithanabadeekul et al. 2020 [4]	Randomized, split-face, single-blinded prospective trial	Thailand	10/10	33–58	Intradermal normal saline injection	(1) Single centrifugation 2.4 minutes at 3200 rpm	(1) Used PRP and saline (2) Hemi-face study (3) Unilateral intradermal injection of PRP and the other side was injected with saline	Four times every two weeks	1 month
Tuknayat et al. 2020 [17]	Prospective before-and-after self-control studies	India	64/65	—	before-and-after self-control	(1) Single centrifugation (2) 8 minutes at 3500 rpm	(1) Used PRP alone (2) Autologous PRP injections	Three sessions (four-weeks intervals)	3 months
Mumtaz et al. 2021 [1]	Nonrandomised controlled trial	Pakistan	64/64	20–40	Intradermal tranexamic acid	(1) Double centrifugation (2) 10 minutes at 1500 rpm (3) 10 minutes at 4000 rpm	(1) Used PRP and tranexamic acid (2) Grouping study (3) Experimental group: intradermal injection of PRP Control group: intradermal tranexamic acid	Three sessions (four-week intervals)	6 months
Adel et al. 2021 [18]	Randomized prospective split-face study	Egypt	20/20	—	Intradermal injection of PRP vs intradermal injection of PRP + IPL	—	(1) Used PRP and IPL (2) Hemi-face study (3) One side: intradermal injection of PRP The other side: intradermal injection of PRP + IPL	Four sessions (two-week intervals)	1 month
Gamea et al. 2020 [19]	Randomized controlled trial	Egypt	40/40	32–58	Topical 5% tranexamic acid	(1) Double centrifugation (2) 3 minutes at 2000 rpm (3) 5 minutes at 5000 rpm	(1)Used PRP and tranexamic acid (2)Grouping study (3) Experimental: topical tranexamic acid and intradermal injection of PRP Control group: topical tranexamic acid	Topical tranexamic acid (twice daily for 12 weeks	1 month

Table 1: Continued.

Author, year	Study design	Location	Number assigned/ evaluated	Age	Control	PRP preparation	Treatment	Treatment time	Follow-up
Tuknayat et al. 2021 [2]	Prospective before-and-after self-control studies	India	40/40	—	—	(1) Double centrifugation (2) 10 minutes at 1600 rpm (3) 10 minutes at 4000 rpm	(1) Used PRP alone (2) Intradermal injection of PRP	Three sessions (one-week intervals)	3 months
Faiz and Meng 2018 [20]	Prospective before-and-after self-control studies	Pakistan	20/15	21–42	before-and-after self-control	(1) Double centrifugation (2) 3 minutes at 1500 rpm (3)5 minutes at 4000 rpm	Intradermal injection of PRP	Five sessions (two-week intervals)	2 weeks

PRP: platelet-rich plasma; IPL: intense pulse light.

Table 2: Demographic and clinical characteristics of participants.

Study	Gender (M/F)	Grouping	Fitzpatrick skin type	Depth	Distribution	Baseline score	Duration of illness	Triggering factor
Hofny et al. 2019 [3]	4/19	A: microneedling with Dermapen	Types III: 7	Epidermal: 18	Malar: 1	MASI:A: 6.13 ± 2.73	1–3 years: 12 patients	Sun exposure:16 Hormonal Contraception: 3
		B: microinjections using mesoneedles	Types IV: 16	Mixed: 5	Centrofacial: 22	B: 5.73 ± 2.77 mMASI:5.71 ± 2.56	˃3 years: 11 patients	Pregnancy: 4
Sirithanabadeekul et al. 2020 [4]	0/10	A: intradermal PRP B: intradermal normal saline	Types III: 2 types V: 8	Mixed: 10	—	A: 4.92 ± 0.96 B: 4.98 ± 0.86	—	—
Mumtaz et al. 2021 [1]	35/29	A: intradermal PRP	—	—	—	A: 29.84 ± 5.14	A: 24.63 ± 9.87 months	—
		B: intradermal tranexamic				B: 29.56 ± 4.39	B: 23.94 ± 8.93 months	
Adel et al. 2021 [18]	0/20	A: IPL	Types II: 3	Epidermal: 6	Centrofacial: 19	MASI:16.3 ± 7.7 mMASI:	2 months-18 years	Sun exposure: 13
		B: PRP-IPL	Types III: 9 types V: 8	Mixed: 14	Malar: 1	A:19 ± 6.4B: 19.8 ± 5.8		Pregnancy:0
Gamea et al. 2020 [19]	0/40	A: topical 5% Tranexamic acid + PRP	Types III (A: 11 B:12)	Epidermal: (A: 12 B:8)	—	mMASI: A: 12.1 ± 2.9	A:12–72 months	—
		B: topical 5% tranexamic acid	Types IV (A: 9 B:8)	Mixed: (A:8 B: 12)		B: 11.7 ± 2.98	B: 18–80 months	
Faiz and Meng 2018 [20]	12/3	—	Types III: 4 Types IV: 11	—	—	MASI: 15.71 ± 6.81	—	—
Tuknayat et al. 2021 [2]	36/4	—	Types IV and V	Epidermal: 29 Mixed: 11	Malar: 8 Centrofacial: 31 Mandibular: 1	mMASI:13.7	—	—

*PRP: platelet-rich plasma; IPL: intense pulse light; MASI: melasma area severity index; mMASI: modified melasma area severity index.

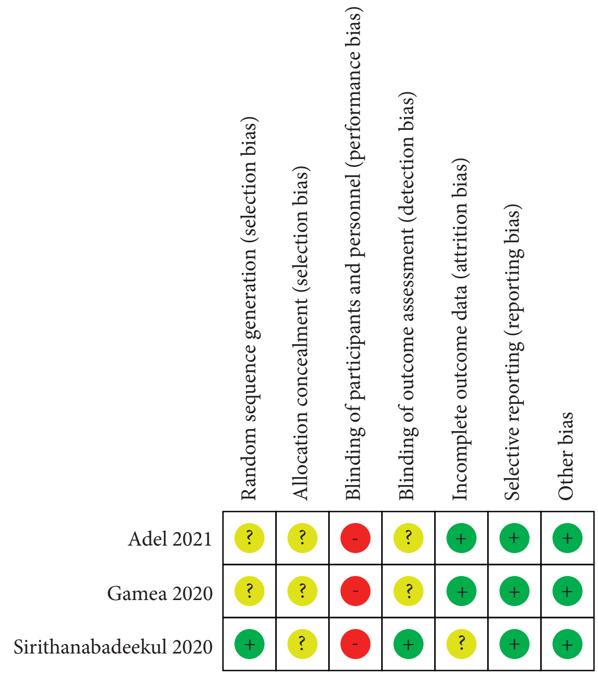

FIGURE 2: Cochrane risk of bias assessment of RCTs [4, 18, 19].

TABLE 3: ROBINS-I risk of bias summary for nonrandomized controlled studies and before-after studies.

Author, year	Domain						
	Obscure	Choice of participants	Classification of intervention measures	Deviations from intended interventions	Missing data	Comparison of results	Choice of the reported result
Hofny et al. 2019 [3]	Mild	Lower	Lower	Lower	Lower	Mild	Lower
Tuknayat et al. 2020 [17]	Mild	Lower	Lower	Mild	Uncertain	Mild	Uncertain
Mumtaz et al. 2021 [1]	Mild	Lower	Lower	Lower	Lower	Mild	Lower
Tuknayat et al. 2021 [2]	Mild	Lower	Lower	Lower	Lower	Mild	Mild
Faiz and Meng 2018 [20]	Mild	Lower	Lower	High	Mild	Mild	Mild

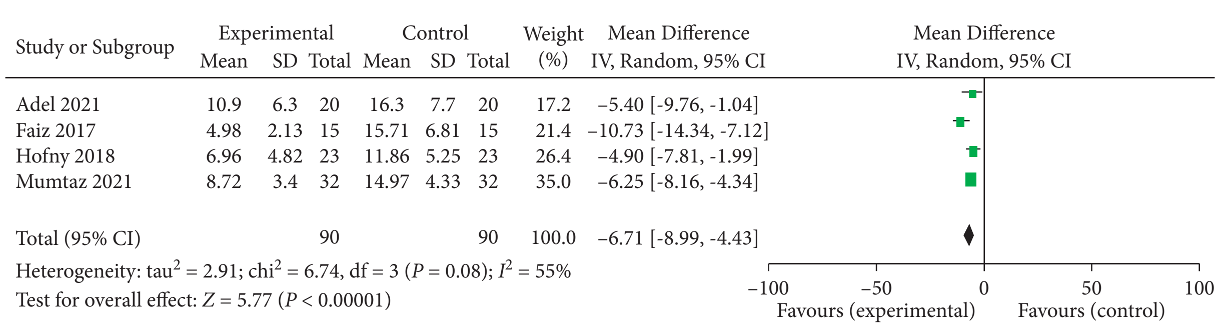

FIGURE 3: Forest plot comparing the chloasma area and severity index (MASI) of patients accepting PRP treatment and control group. IV: interval variable, CI: confidence interval.

Study or Subgroup	Experimental Mean	Experimental SD	Experimental Total	Control Mean	Control SD	Control Total	Weight (%)	Mean Difference IV, Random, 95% CI
Adel 2021	14.2	5.8	20	19	6.4	20	13.8	−4.80 [-8.59, -1.01]
Gamea 2020	3.6	1.9	20	7.8	1.9	20	28.3	−4.20 [-5.38, -3.02]
Hofny 2018	2.9	2.05	23	5.71	2.56	23	27.4	−2.81 [-4.15, -1.47]
Sirithanabadeekul 2019	3.5	0.67	10	4.53	0.96	10	30.4	−1.03 [-1.76, -0.30]
Total (95% CI)			73			73	100.0	−2.94 [-4.81, -1.07]

Heterogeneity: tau^2 = 2.85; chi^2 = 23.60, df = 3 ($P < 0.0001$); I^2 = 87%
Test for overall effect: Z = 3.08 (P = 0.002)

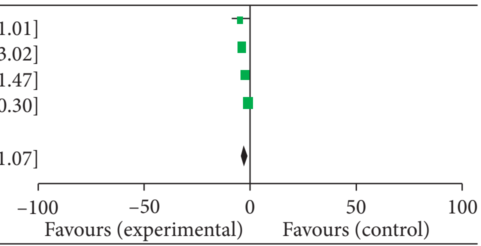

Figure 4: Forest plot comparing the modified melasma area and severity index (mMASI) of patients accepting PRP treatment and control group. IV: interval variable, CI: confidence interval.

Study or Subgroup	Experimental Mean	Experimental SD	Experimental Total	Control Mean	Control SD	Control Total	Weight (%)	Mean Difference IV, Random, 95% CI
Adel 2021	14.2	5.8	20	19	6.4	20	7.7	−4.80 [-8.59, -1.01]
Gamea 2020	3.6	1.9	20	7.8	1.9	20	49.9	−4.20 [-5.38, -3.02]
Hofny 2018	2.9	2.05	23	5.71	2.56	23	42.5	−2.81 [-4.15, -1.47]
Sirithanabadeekul 2019	3.5	0.67	10	4.53	0.96	10	0.0	−1.03 [-1.76, -0.30]
Total (95% CI)			63			63	100.0	−3.66 [-4.74, -2.57]

Heterogeneity: tau^2 = 0.25; chi^2 = 2.70, df = 2 (P = 0.26); I^2 = 26%
Test for overall effect: Z = 6.62 ($P < 0.00001$)

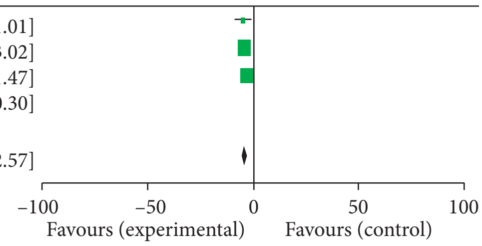

Figure 5: Forest plot of sensitive analysis of the modified MASI of patients accepting PRP treatment and control group using sensitive analysis. IV: interval variable, CI: confidence interval.

endocrine, hepatopathies, ovarian tumors, parasitic infestations, cosmetics, and stressful life events in a genetically predisposed individual [21–24]. However, the exact etiology of chloasma is still not well elucidated yet.

Although there are various treatments including drug therapy, chemical peeling, laser, etc., finding a cure for chloasma has always been challenging, often unsatisfactory, and hard to avoid recurrence [24].

In order to provide a reference for clinical treatment, we conducted a systematic review and meta-analysis to assess the safety and efficacy of PRP in the treatment of chloasma. The key finding of this systematic review was that intradermal PRP injections significantly improved chloasma, as evidenced by significant decreases in MASI and mMASI scores in various patient populations over a 12-week period. The systematic analysis found no serious or significant long-term negative effects. The effectiveness and safety of PRP therapy for chloasma were also demonstrated by the reported degree of improvement and patient satisfaction in enrolled studies. The following are some of the benefits of our research: (1) we focus on the efficacy and safety of intradermal PRP injection to improve chloasma, providing clear conclusions for other clinicians; (2) The conclusions are true and reliable due to rigorous and serious inclusion and exclusion by two professionals, and reasonable and standardized inclusion of relevant research and analysis; (3) the topic and possibility of the corresponding direction are analyzed and discussed based on the relevant professional knowledge of the team.

Our discovery is in line with a few previous studies. Cayırlı et al. [5] reported a case of a 27-year-old woman who accepted three PRP injections sessions with 15-day intervals for skin rejuvenation, and regression of chloasma achieved more than 80%. Farag et al. [25] reported a case with resistant chloasma. After six sessions of PRP injection, her MASI score came down from 17.7 to 7.5, and after a three-month follow-up, no relapse of chloasma was examined. In another case report, PRP was used as an adjuvant with Q-switched Nd-YAG laser and alpha arbutin therapy with hopeful lightening [26].

PRP is a high concentration of platelet plasma. Platelets are cellular fragments of megakaryocytes of the bone marrow. They are characterized by the absence of nuclei, organelles, and three types of granules in the cytoplasm: alpha, dense, and lambda [27]. Green fluorescence can regulate the biological medium of cell turnover and regeneration, exert influence on target cells and extracellular matrix, and thus realize the stimulation of repair and tissue regeneration. At present, the most widely studied green fluorescent factors include PDGF, TGF, and vascular endothelial growth factor, insulin-like growth factor, and EGF. Among them, TGFβ and PDGF play the biggest role in PRP treatment of chloasma. TGF-β1 and PDGF present in PRP could have led to chloasma reduction [15]. TGF-1 inhibits melanogenesis by downregulating the expression of the paired-box homotypic c gene of the ommatidium-associated transcription factor (MITF) promoter in a concentration-dependent manner. PDGF not only promotes collagen

Table 4: Treatment outcomes of included studies.

Study	Group	MASI		mMASI		Degree of improvement N (%)	Patient satisfaction N (%)	Adverse effects N (%)	Other outcomes
		Before	After	Before	After				
Faiz and Meng 2018 [20]	—	15.71 ± 6.81	4.98 ± 2.13			MASI: Poor (0–25% decrease) 4 (26.7) Fair (26–50% decrease) 9 (60) Good (51–75% decrease) 2 (13.3) Excellent (>75% decrease) 0 (0)	—	Temporary Mild erythema: 2(13.3)	—
Hofny et al. 2019 [3]	A: microneedling with Dermapen B: microinjections using mesoneedles	11.86 ± 5.25	6.96 ± 4.82	5.71 ± 2.56	2.90 ± 2.05	mMASI: Excellent (>75–100% decrease): 3 (13) Significant (>50–75% decrease): 8 (34.8) mild (>25–50% decrease): 9 (39.2) Slight (0–25% decrease): 3 (13.0) MASI: Excellent (>75–100% decrease): 3 (13.1) Significant (>50–75% decrease): 5 (21,7) mild (>25–50% decrease): 10 (43.5) Slight (0–25% decrease): 5 (21.7)	Very satisfied: 9 (39.1) Satisfied: 9 (39.1) Slight satisfaction: 3 (13.1) Unsatisfied: 2 (8.7)	Swelling, redness and soreness	
Sirithanabadeekul et al. 2020 [4]	A: intradermal PRP injection B: intradermal saline injection	A: 4.92 ± 0.96 B: 4.98 ± 0.86	A: 3.5 ± 0.67 B: 4.53 ± 0.96	—	—	—	From baseline to the end of treatment, the patients' satisfaction under PRP condition was significantly improved at the time of visit	Bruising	Mean melanin levels; A: Before: 256.73 ± 17.68 After: 238.63 ± 16.4 B: 246.57 ± 22.88 (before) 249.47 ± 21.36 (after)

Table 4: Continued.

Study	Group	MASI		mMASI		Degree of improvement N (%)	Patient satisfaction N (%)	Adverse effects N (%)	Other outcomes
		Before	After	Before	After				
Tuknayat et al. 2020 [17]	—	—	—		47.3% reduction	mMASI: Excellent (>75% decrease): 4 (6.25) Significant (51–75% decrease): 21 (32.8) mild (26–50% decrease): 27 (42.1) Slight (1–25% decrease): 10 (15.6) No minimal (0% decrease): 2 (3.1)	—	Xerosis Hyperpigmentation	
Mumtaz et al. 2021 [1]	A: intradermal platelet-rich plasma B: intradermal tranexamic	A: 29.84 ± 5.14 B: 29.56 ± 4.39	A: 8.72 ± 3.40 B: 14.97 ± 4.33	—	—	—	—	—	—
Adel et al. 2021 [18]	A: PPL B: PRP + IPL	16.3 ± 7.7	10.9 ± 6.3	A: 19 ± 6.4 B: 19.8 ± 5.8	A: 14.2 ± 5.8 B: 14.6 ± 5.5	MASI: 33.13% improvement mMASI: No significant difference between both sides	No significant difference between both sides	—	—
Gamea et al. 2020 [19]	A: topical5% B: topical 5% tranexamic acid	—	—	A: 12.1 ± 2.9	A: 3.6 ± 1.9	mMASI: A: Excellent (75–100% decrease): 3 (15) Significant (50–74% decrease): 4 (20) mild (25–49% decrease): 12 (60) Slight (0–24% decrease): 1 (5) B: Excellent (75–100% decrease): 1 (5) Significant (50–74% decrease): 3 (15) mild (25–49% decrease): 7 (35) Slight (0–24% decrease): 9 (45)	A: Highly satisfied: 5 (25) mildly satisfied: 10 (50) Partially satisfied: 3 (15) Not satisfied: 2 (10) B: Highly satisfied: 3 (5) mildly satisfied: 2 (10) Partially satisfied: 4 (20) Not satisfied: 11 (55)	Hyperpigmentation: A: 1 (5) B: 2 (10) Erythema: A: 10 (50) B: 0 (0) Pain: A:12 (60) B: 0 (0)	

Table 4: Continued.

Study	Group	MASI		mMASI		Degree of improvement N (%)	Patient satisfaction N (%)	Adverse effects N (%)	Other outcomes
		Before	After	Before	After				
Tuknayat et al. 2021 [2]	—	—	—	13.7	6.258	—	Excellent: 4 (10) Very pleased: 19 (47.5) Pleased: 16 (40) Satisfied: 1 (2.5) Not satisfied: 0 (0)	Xerosis: 14 (35) Pruritus: 10 (25)	

PRP: platelet-rich plasma; IPL: intense pulse light; MASI: melasma area severity index; mMASI: modified melasma area severity index.

production, synthesis, and extracellular matrix formation, but also promotes angiogenesis, collagen, and hyaluronic acid synthesis. The rationale is that EGF reduces melanin production by inhibiting the expression of prostaglandin E2 and the activity of tyrosinase. They can further improve the pigmentation of the spots.

PRP treats chloasma not only through the action of platelets themselves, but also through biological stimulation at the time of injection. Biological stimulation can activate the anabolic function of fibroblasts and collagen production, thus restoring the metabolism and normal function of the skin [27], which also has a certain effect on delaying the process of chloasma.

PRP appears to be a potential new therapy with significant efficacy for chloasma, as a monotherapy as well as an adjuvant therapy. Gamea et al. [19] used PRP therapy in combination with topical 5% tranexamic acid, compared to topical 5% tranexamic acid monotherapy, which showed significantly better treatment results and patient satisfaction was detected in patients of combination therapy group. Adel et al. [18] compared PRP alone versus intense pulsed light (IPL) plus PRP, proving an obvious improvement of chloasma after PRP treatment ($p < 0.05$). However, no statistically significant difference was found between the two groups regarding mMASI score or patient satisfaction ($p > 0.05$).

The clinical stage and classification of chloasma can be divided into active stage and stable stage according to the results of slide pressure diagnosis, the number and morphology of inflammatory cells and dendritic cells under the reflection confocal microscope (RCM), and the changes of the number and morphology of blood vessels under the skin microscope and the erythema index. In addition, melasma was examined by slide pressure and wood lamp. Combined with its pathogenesis, melasma can be divided into four types: pigment type (m, melanin); vascular type (V, vessel); pigment dominant type (M > V); vascular dominant type (V > m). For typing treatment, simple type M: oral chloromethylnaphthoic acid, combined with fruit acid or Q-switched laser; Type V: to improve microcirculation, Nd: YAG/KTP can be used for treatment. M > V type and V > M type: both types are formed by both pigment and vascular factors. The treatment plan should take into account the inhibition of melanin production and the improvement of blood circulation. At present, PRP can not only inhibit the synthesis of melanin, but also have a variety of repair functions, such as its antibacterial or anti-inflammatory effect and skin vascular remodeling function, which play a role in a variety of main pathological and pathogenic mechanisms of chloasma. However, more and more data are needed to support and analyze whether the efficacy of PRP combined with the above treatment schemes is better.

What we can know is that chloasma is more common among Hispanic and Oriental people, but unfortunately we have not retrieved or understood the treatment of PRP in Indochina. However, there are exact reports on the efficacy of PRP for chloasma in the Middle East, India, East Asia, and other countries included in this study.

In terms of delivery methods, Hofny et al. [3] evaluated the efficacy of PRP treatment on chloasma via two different delivery methods. A statistically significant decrease was detected in both groups after treatment ($p < 0.05$), while no significant difference was found between two delivery methods.

6. Limitations

This review and meta-analysis established a foundation for using PRP to treat chloasma patients. It does, however, have some limitations. First, RCTs and prospective self-controlled before-and-after studies were combined, increasing the risk of choice bias. Furthermore, the current meta-analysis is constrained by a lack of high-quality studies, and biases hampered the interpretation of study findings. Furthermore, the small sample sizes and short follow-up periods in this study may have hampered the ability to detect clinically significant differences in outcome measures. Even if we use REM, the disparity in curative effect could be due to differences in research design, population, preparation technology (centrifugal/anticoagulant), treatment (volume/frequency/method), baseline patient characteristics (age, sex, skin type, or chloasma depth), and research methods.

7. Conclusion

To summarize, people are becoming more aware of and interested in PRP treatment for chloasma. In light of the findings discussed above, PRP therapy is a safe and effective treatment option for chloasma, regardless of the MASI or mMASI score, the degree of clinical improvement, or patient satisfaction. To establish optimal treatment parameters, more RCTs with an adequate control group, controlling for obscure factors, and larger sample sizes are required. Furthermore, the negative effects of PRP were not fully understood, limiting clinicians' use of PRP as a first-line treatment for chloasma. Long-term follow-up for effectiveness and side-effect profiles would be beneficial.

Data Availability

All data are available upon request to the corresponding author.

Ethical Approval

This work is based on reported studies and does not include any studies conducted by the authors on human participants or animals.

Consent

Consent is not applicable.

Disclosure

All authors meet the standards of the International Medical Journal Editorial Board (ICMJE) on the identity of the author of this article and are responsible for their works.

Conflicts of Interest

The authors declare that they have no conflicts of interest.

Authors' Contributions

Deng Tinghan and Cheng Fengrui contributed equally to this paper.

Acknowledgments

This work was supported by grants from "Hundred Talents Project" of the Affiliated Hospital of Chengdu University of Traditional Chinese Medicine, under No. P2020042; San Huang Zeng Mian Decoction Treatment Mild-to-Mild SLE Randomized Controlled Clinical Studies, under No. 2020ZD03; and Clinical Study on Optimization of Treatment of Simple Obesity by Combination of Shu and Bi Acupoint Embedding Thread and Traditional Chinese Medicine, under No. 2021MS068.

References

[1] M. Maryam, T. H. Chandio, M. K. Shahzad, N. Hanif, S. Anwar, and S. Rafique, "Comparing the efficacy of patelet-rich plasma (PRP) versus tranexamic acid (4mg/mL) as intradermal treatments of chloasma," *Journal of the College of Physicians and Surgeons--Pakistan*, vol. 30, no. 5, pp. 502–505, 2021.

[2] A. Tuknayat, G. P. Thami, M. Bhalla, and J. K. Sandhu, "Autologous intralesional platelet rich plasma improves chloasma," *Dermatological therapy*, vol. 34, no. 2, 2021.

[3] E. R. M. Hofny, A. A. Motaleb, A. Ghazally, A. M. Ahmed, and M. R. A. Hussein, "Platelet-rich plasma is a useful therapeutic option in melasma," *Journal of Dermatological Treatment*, vol. 30, no. 4, pp. 396–401, 2019.

[4] P. Sirithanabadeekul, A. Dannarongchai, and A. Suwanchinda, "Platelet-rich plasma treatment for melasma: a pilot study," *Journal of Cosmetic Dermatology*, vol. 19, no. 6, pp. 1321–1327, 2020.

[5] M. Cayırlı, E. Çalışkan, G. Açıkgöz, A. H. Erbil, and G. Ertürk, "Regression of Chloasma with platelet-rich plasma treatment," *Annals of Dermatology*, vol. 26, no. 3, pp. 401-402, 2014.

[6] A. Tuknayat, M. Bhalla, and G. P. Thami, "Platelet-rich plasma is a promising therapy for melasma," *Journal of Cosmetic Dermatology*, vol. 20, no. 8, pp. 2431–2436, 2021.

[7] W. Merchán, L. A. Gómez, M. E. Chasoy, C. A. A. Rodríguez, and A. L. Muñoz, "Platelet-rich plasma, a powerful tool in dermatology," *J Tissue Eng Regen Med*, vol. 13, no. 5, pp. 892–901, 2019.

[8] E. R. M. Hofny, M. R. A. Hussein, A. Ghazally, A. M. Ahmed, and A. A. Motaleb, "Increased expression of TGF-β protein in the lesional skins of Chloasma patients following treatment with platelet-rich plasma," *Journal of Cosmetic and Laser Therapy*, vol. 21, no. 7-8, pp. 382–389, 2019.

[9] M. M. Gamea, D. A. Kamal, A. A. Donia, and D. S. Hegab, "Comparative study between topical tranexamic acid alone versus its combination with autologous platelet rich plasma for treatment of melasma," *Journal of Dermatological Treatment*, pp. 1–7, 2020.

[10] M. Y Lin, C. S Lin, S Hu, and W. H Chung, "Progress in the use of platelet-rich plasma in aesthetic and medical dermatology," *The Journal of clinical and aesthetic dermatology*, vol. 13, no. 8, pp. 28–35, 2020.

[11] H. Kim, S. Moon, S. Cho, J. Lee, and H. Kim, "Efficacy and safety of tranexamic acid in melasma: a meta-analysis and systematic review," *Acta Dermato-Venereologica*, vol. 97, no. 7, pp. 776–781, 2017.

[12] L. Zhao, M. Hu, Q. Xiao et al., "Efficacy and safety of platelet-rich plasma in melasma: a systematic review and meta-analysis," *Dermatologic Therapy*, vol. 11, no. 5, pp. 1587–1597, 2021 Oct.

[13] D. Moher, fnm au, L. Shamseer et al., "Preferred reporting items for systematic review and meta-analysis protocols (PRISMA-P) 2015 statement," *Systematic Reviews*, vol. 4, no. 1, pp. 1–9, 2015.

[14] J. P. Higgins and S. Green, *Cochrane Handbook for Systematic Reviews of Interventions*, Cochrane, Chichester, England, 2009.

[15] J. A. Sterne, M. A. Hernán, B. C. Reeves et al., "ROBINS-I: a tool for assessing risk of bias in non-randomised studies of interventions," *BMJ*, vol. 355, p. i4919, 2016.

[16] J. Higgins and S. R. Green, *Cochrane Handbook for Systematic Reviews of Interventions*, Cochrane Collaboration, Chichester, England, 2011.

[17] A. Tuknayat, M. Bhalla, and G. Pal Thami, "Clinical efficacy of platelet rich plasma in Chloasma," *Journal of the Dermatology Nurses' Association*, vol. 12, no. 2, 2020.

[18] S. Adel, A. Serri, and T. Abd El-Raheem, "Study of autologous platelet-rich-plasma versus its combination with intense pulsed light in treatment of Chloasma," *Dermatologic Therapy*, p. e15008, 2021.

[19] M. M. Gamea, D. A. Kamal, A. A. Donia, and D. S. Hegab, "Comparative study between topical tranexamic acid alone versus its combination with autologous platelet rich plasma for treatment of melasma," *Journal of Dermatological Treatment*, pp. 1–7, 2020.

[20] F. Faiz and K. Meng, "Efficacy of platelet-rich plasma in the treatment of Chloasma: a pilot study," *Journal of Pakistan Association of Dermatologists*, vol. 28, no. 3, pp. 348–353, 2018.

[21] A. Achar and S. K. Rathi, "Chloasma: a clinico-epidemiological study of 312 cases," *Indian Journal of Dermatology*, vol. 56, no. 4, 2011.

[22] "Epidemiology of Chloasma in Brazilian patients: a multicenter study," *International Journal of Dermatology*, vol. 53, no. 4, 2014.

[23] "A global survey of the role of ultraviolet radiation and hormonal influences in the development of Chloasma," *Journal of the European Academy of Dermatology and Venereology*, vol. 23, no. 11, pp. 1254–1262, 2009.

[24] R. Sarkar, P. Ailawadi, and S. Garg, "Chloasma in men: a review of clinical, etiological, and management issues," *Journal of Clinical & Aesthetic Dermatology*, vol. 11, no. 2, pp. 53–59, 2018.

[25] M. Farag, F. Mostafa, and K. Gharib, "Therapeutic effect of dermapen with PRP versus dermapen with tranexamic acid," in *Chloasma Cases*Zagazig University Medical Journal, 2020.

[26] C. H. Yew, T. S. Ramasamy, and F. Amini, *Response to Intradermal Autologous Platelet Rich Plasma Injection in Refractory Dermal Chloasma*, Report of two cases, 2015.

[27] W. H Merchán, L. A Gómez, M. E Chasoy, C. A Alfonso-Rodríguez, and A. L Muñoz, "Platelet-rich plasma, a powerful tool in dermatology," *Journal of tissue engineering and regenerative medicine*, vol. 13, no. 5, pp. 892–901, 2019.

Hindawi
Computational Intelligence and Neuroscience
Volume 2022, Article ID 9441375, 9 pages
https://doi.org/10.1155/2022/9441375

Research Article

An Inquiry-Based Teaching Model for Nursing Professional Courses Based on Data Mining and Few-Shot Learning Technology

Fuling Fan

Nursing Department, Luohe Medical College, Luohe 462000, China

Correspondence should be addressed to Fuling Fan; 0277@lhmc.edu.cn

Received 9 February 2022; Revised 14 March 2022; Accepted 15 March 2022; Published 4 April 2022

Academic Editor: Xin Ning

Teaching is defined as a relatively stable structural framework and activity process of teaching activities established under the guidance of specific teaching concepts and theories. It serves as a link between teaching theory and practice, as well as between the teaching system's static and dynamic conditions. The ITM (Inquiry-Based Teaching Model) has received a lot of attention and has been used in a lot of classrooms. Data mining (DM) is a method for discovering knowledge in databases and a technology for mining information in large data sets. It is primarily used to discover unknown relationships and patterns in related data. This paper applies DM's core technology, particularly the decision tree algorithm, to give hospital managers more comprehensive and in-depth data analysis capabilities, as well as strong technical support for hospitals in developing management plans. Furthermore, due to the scarcity of research data in the nursing profession, this paper introduces the few-shot learning technology to improve the model's analysis ability.

1. Introduction

At present, nursing students in China have low information quality, unclear information behavior, low information demand, weak learning awareness, poor literature retrieval ability, and weak information ethics awareness [1–5]. Moreover, the teaching method of nursing major is mainly classroom teaching; the teaching methods and teaching methods are relatively simple, with little contact with practice and little cultivation of students' management ability, which is not conducive to cultivating high-quality students [6]. It is an important part of nursing medicine, providing health and health services for human beings and taking the road of multicultural nursing to adapt to the changes of globalization and pluralism. Nursing education is the cornerstone of nursing career development, and how to adapt to the changes of pluralistic society is an important issue that modern nursing education should pay attention to and solve.

Data mining (DM) is an important method for discovering knowledge in databases. Data collection, processing, analysis, and interpretation are all part of the DM technology process [7, 8]. However, a study to improve the suitability and efficiency of curriculum resources is looking into how to organically combine these vast educational resources and apply them to classroom teaching according to students' interests. ITM (Inquiry Teaching Mode) emphasizes students' independent inquiry spirit, with the goal of cultivating students' innovative ability and thinking and ultimately guiding them to learn for life [9]. ITM has made significant progress in China in terms of reforming traditional teaching methods. In this case, it is decided to use DM technology to extract hidden but useful information and knowledge from these huge, incomplete, disturbing, noisy, and random data. By classifying and analyzing this potential basic information, potential problems can be identified with professional care planning and management [10, 11].

Under the guidance of modern nursing education thought, how to make full use of DM skills, integrate DM skills into subject education, and combine with the characteristics of nursing subjects to build a new education model is an important topic of education reform. In this study, DM technology is used to create a realistic scene of nursing management, provide abundant network resources, transform a single theoretical education into a rich activity experience, transform an isolated classroom space into a realistic scene of active reconstruction and closure between teachers and students, and accept open and interactive communication passively. Furthermore, because the Internet has abundant information resources and a human-computer interface that allows students to access a large amount of knowledge and information that matches their associative thinking and associative memory characteristics, students can use the Internet to generate interest in learning and encourage exploration and discovery learning [12]. Applying ITM to the course of educational research methods and exploring the innovation and practice of university teaching methods has a lot of practical implications.

2. Related Work

In the traditional teaching process, teachers pay more attention to the relevance, accuracy, emphasis, and difficulty of teaching content, and students are in a completely passive learning state [13]. Literature [14] puts forward the course of "inquiry learning" and points out that students' active participation in the process of scientific inquiry is the best way to learn scientific research. Literature [15] holds that science education should not require students to learn knowledge from textbooks but should master the process or method of scientific inquiry. Literature [16] holds that the content of textbooks should no longer emphasize students' passive knowledge learning but should involve them directly in the learning process, so as to cultivate students' inquiry ability and enable them to understand and master the inquiry process. According to [17], most nursing colleges do not provide multicultural nursing education, but only a few universities provide multicultural nursing education. Literature [18] holds that textbooks are an important carrier for spreading knowledge, and there is no development of education without textbooks. Therefore, it is particularly important to improve the compiling ability of multicultural nursing teaching materials and enable nursing students to acquire knowledge related to multicultural nursing in the process of nursing education. In [19], multiculturalism is regarded as a wide-ranging content, which has no clear connection and influence with the actual nursing practice. Therefore, only focus on professional knowledge education, ignoring the guidance of students' humanistic quality and cross-cultural ability. Literature [20] holds that foreign-related nursing talents should have competent humanistic professional knowledge, skilled operation skills, and nursing talents in medical and health institutions and community posts and have a high level of English to meet international nursing requirements. Literature [21] puts forward the "quality-oriented" training mode of foreign-related nursing talents in higher vocational colleges and constructs a nursing professional education program based on nursing professional ability and dominated by cross-cultural nursing ability.

In recent years, with the increasing amount of data and the increasing demand for data storage, management, and analysis, DM has gradually attracted the attention of academic and business circles. DM has been widely used in the fields of finance, commerce, and medicine to date, with positive results. Reference [22] is a rudimentary model for predicting and analyzing student dropout. It builds a university data warehouse and improves the ID3 decision tree algorithm by using educational administration and student information systems as data sources. Students' dropout can be predicted by factors such as major, percentage of failed subjects, and attendance records. The spectral clustering method is used in [23] to classify courses based on their degree of correlation, align existing courses, build an intuitive curriculum association system, and apply association rule mining to courses. Reference [24] proposed an algorithm to combine multiple subclusters based on connectivity, with the goal of improving the quality and accuracy of clustering results by focusing on the local optimality of the K-means algorithm and the sensitivity to the initial cluster centroid. Reference [25] proposes an algorithm for determining the number of clusters in a data set based on object stability. Reference [26] examines 11 widely used clustering validity evaluation indexes in depth, assessing their performance as well as the limitations of application scenarios in five aspects of the clustering algorithm.

3. Research Method

3.1. Application of DM Technology in the Nursing Field. Constructivism holds that the interaction between learners and the surrounding environment plays an important role in the understanding of learning content (that is, the construction of knowledge meaning). Under the teacher's organization and guidance, students discuss and communicate together, form a study group, analyze and discuss nursing management issues together, and conduct counseling discussion. This collaborative learning environment enables the whole group to share the ideas and wisdom of students and teachers.

With the development of nursing field, the nursing function is greatly expanded, and nursing is gradually developing towards specialization. DM technology from these huge, incomplete, noisy, fuzzy, and random data is used to discover the relationship between things through hidden but useful extracted information and knowledge to build a professional nursing quality management platform [1].

C4.5 algorithm is evolved from ID3 algorithm. An item called split information is introduced into the gain ratio. Split information is used to measure the width and balance of attribute split data. The formula is

$$SplitInfo(A) = -\sum_{i=1}^{w} \frac{s_i}{s} \log_2 s_i. \tag{1}$$

The formula for calculating the gain ratio is

$$GainRatio(A) = \frac{Gain(A)}{SplitInfo(A)}. \tag{2}$$

The information entropy of classification with attribute as root node is $Entroy(A)$, and its calculation formula is as follows:

$$Entroy(A) = \sum_{i=1}^{v} \frac{p_i + n_i}{p + n} Entroy(p_i, n_i). \quad (3)$$

Therefore, the formula $Gain(A)$ for calculating the information gain divided with A as the root node can be obtained as follows:

$$Gain(A) = Info(p, n) - Entroy(A). \quad (4)$$

After the calculation of the judgment criterion, that is, the information gain, a set of data can be obtained, which is the information gain of all attributes on the initial root node to divide the data set S.

The ID3 decision tree algorithm is a common decision tree learning algorithm. Its essence is to select all of the attributes of decision tree nodes based on information gain, so that all of the largest class classification nodes can have gain and the entropy of the classification data set is minimized when testing on each nonleaf. By reducing the average depth of the tree, this method effectively improves classification efficiency. To create the best decision management plan, the platform first uses a decision tree algorithm to mine and analyze these data [2]. Create a tree using this algorithm. Each node in the tree represents a single instance of a column, with the algorithm determining the node's placement, whereas each column in another instance is represented by nodes of varying depths. As a result, the algorithm is a classification form, with nodes represented as tree structures that represent additional data classification.

The implementation of decision tree can not only help nurses analyze the influencing factors of various clinical symptoms and implement targeted nursing actions according to the analysis results, but also effectively reduce patients' complications and improve nursing quality. It supports clinical decision-making by establishing predictive evaluation model, thus reducing medical cost and saving medical resources. Skilled nursing platform is a basic functional module, which is consistent with the clinical management of patient information through peripheral central venous catheter, including initiating clinical nurse consultation, checking professional nurse consultation table and writing consultation opinions, adding catheterization records for patients, arranging the next maintenance time, adding maintenance records, and adding complications, statistical reports, and other functions. The structure is shown in Figure 1.

Patient records in the data warehouse can be used to classify the prognosis of patients with various catheters at first and then analyze the indicators such as catheter consultation history, catheter maintenance, incidence of adverse events, etc., so as to improve related treatment schemes. In patients with catheterization, disease prognosis evaluation is an important means to promote medical quality control [6].

3.2. ITM Construction of Nursing Specialty Course. All teaching methods are developed by continuously verifying and fine-tuning the ideas, theoretical guidance, and teaching practice of specific teaching methods. Cognitive structuralism and constructivism are primarily at the heart of ITM's theory. The constructivist teaching theory emphasizes the fact that knowledge evolves over time. Professors cannot ignore students' prior experience because learning is active construction of knowledge based on one's own experience background. Simultaneously, the roles of teachers and students are clear: teachers serve as guides and supporters of learning, while students are active knowledge builders. As a result, constructivism theory emphasizes the importance of "situation" and "collaborative learning" in students' learning, particularly in learning environment design.

Through the mining and analysis of learning behavior data, the characteristics of students in the learning process are extracted and the learning process portrait is established. Analyze the learning time and learning quality of different students, establish a unified process description method, and make a formal description. Analyze the behavior information of students in process learning, determine the learning characteristics of the process, and set up the process portrait. Use the degree of understanding and difficulty of knowledge points embodied in learning behavior to optimize curriculum design and curriculum planning and improve existing deficiencies and improvement plans. Through the comprehensive analysis of the above two methods, data related to subject learning can be obtained, which is convenient for students to accurately get the subject learning situation and learning effect. Teachers can teach plan coordination without frequent interactive surveys and classroom tests.

By summarizing, analyzing and mining the data of various learning behaviors of the course, the learning situation of course learners can be obtained to form personalized labels. This label reflects the learner's learning ability and mastery of knowledge points in the course learning. The active time for learners to explore the course content on the information education platform can reflect the demand level for the expansion and renewal of learning resources. And dynamic and static information analysis are shown in Figure 2.

Because the classroom is the main part of classroom activities, the main component of ITM is to explore the classroom through group activities. Generally speaking, the team leader should be recommended democratically, and it is better not to be appointed by the teacher. This will allow students who are responsible and supported by students to organize and lead group activities. The team leader is responsible for coordinating within the group, supervising and inspecting the team members, and contacting the teachers during the investigation. The composition of student groups can usually be determined in the first two weeks of the new school year and will not change in the next semester or even the first year. Of course, if necessary, this will change according to the specific situation, for example, after a unit or chapter is completed.

The improved K-means algorithm designed in this paper firstly defines the sample density according to the local spatial distribution of samples. You can set a density threshold to identify outliers and temporarily delete them

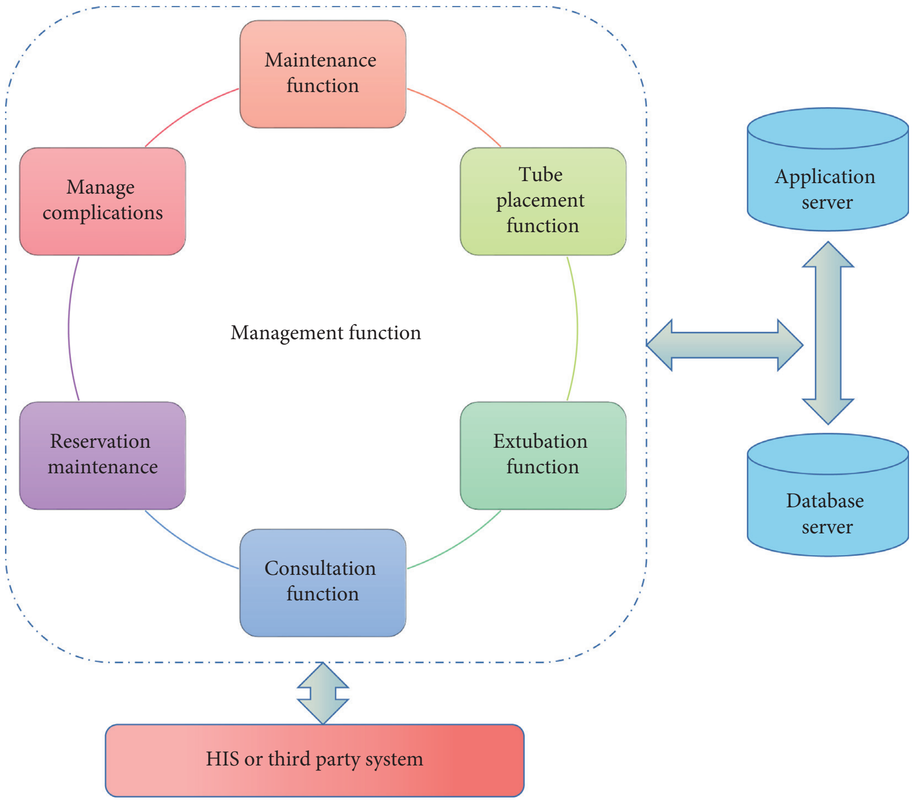

Figure 1: Platform architecture.

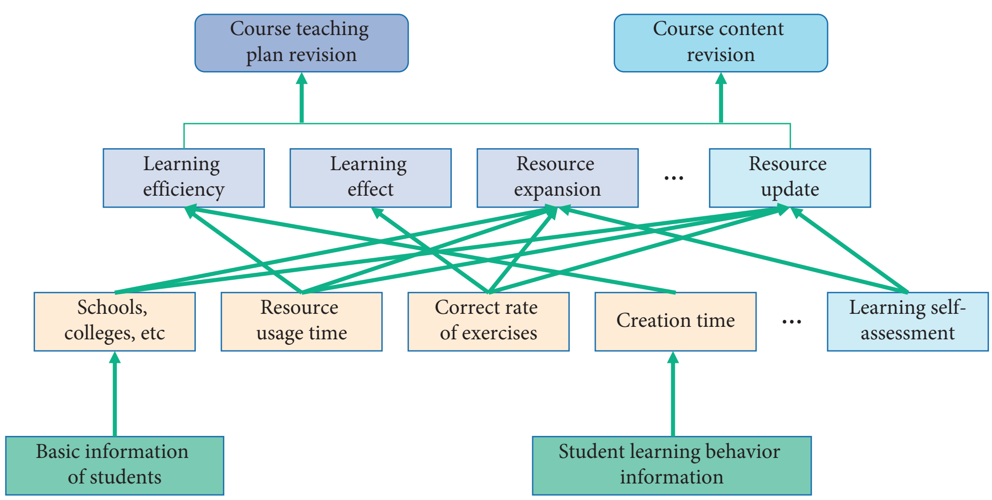

Figure 2: Dynamic and static data acquisition and analysis.

from the data set. Then it selects an initial cluster centroid according to the density of sample distribution.

The achievement data of students in a certain course and session are represented by data set $X = \{x_1, x_2, \cdots, x_n\}$, and the data object $x_i = \{i = 1, 2, \cdots, n\}$ in the data set is one-dimensional achievement data. n is the number of data points in the data set, and k is the number of clusters.

The distance between data points x_i, x_j is

$$d\left(x_i, x_j\right) = \sqrt{\left(x_i - x_j\right)^2} i = 1, 2, \cdots, n; \quad j = 1, 2, \cdots, n. \tag{5}$$

Sample distribution density of data point x_i is defined as the number of data points within the radius r around the data point:

$$density\left(x_i\right) = count\left\{x | x \in X, \left|x - x_i\right| < r\right\}. \tag{6}$$

Because there are a large number of overlapping data points in the score data, the number of overlapping data points is directly taken as the sample density value of this data point; that is, $r = 1$ is taken.

The threshold value of sample density is determined by multiplying the average value of sample density of all data points by a coefficient c:

$$threshold = c \times \frac{1}{n} \sum_{i=1}^{n} density(x_i). \tag{7}$$

Pay attention to cultivating students' innovative spirit and practical ability through examination, cultivating good psychological quality, learning interest and positive emotional experience, respecting individual differences, recognizing the uniqueness of individual development, giving positive evaluation, and giving full play to students' multiple potentials [20].

Teachers play an important role in assisting and guiding students in inquiry learning, which is centered on students' self-exploration process. Teachers should assist and guide students as needed throughout the learning process and fully reflect their leadership abilities. Students' time and homework must be carefully planned by teachers. Inquiry learning in the context of an inquiry-based teaching management platform relieves teachers' workload while also testing their professional abilities. Teachers' primary role in inquiry-based classroom instruction is to guide and inspire students, as well as to improve their learning and problem solving abilities. In a timely manner, summarize and evaluate the discussion and communication process, as well as the outcomes of the discussion and communication. Teachers and students collaborate in inquiry classroom teaching. They are clearly teachers and masters when they enter the inquiry classroom [13].

4. Results Analysis and Discussion

4.1. ITM Application Analysis. All kinds of teaching methods have relatively fixed teaching methods, and the active exploratory learning course is not static, but flexible and diverse. Let students study and discuss problems through independent thinking, group discussion and group communication, find solutions to problems, acquire relevant knowledge and resources, and combine and summarize classroom teaching applications and student feedback. Through the teaching system, abundant knowledge and information resources are provided, so that teachers and students can easily obtain the required information from the system, and at the same time, the natural and convenient navigation system can be exchanged to enable students to quickly complete self-study activities. In this way, teachers can avoid spending a lot of time and energy to master deep network computer knowledge and making educational software, so that teachers can concentrate on educational design and students will not get lost and struggle, in addition to the influence of bad information.

QQ chart and QQ residual were used to test the normality of evaluation results of nursing management knowledge and skills of nursing students. From QQ chart and QQ residual chart, the evaluation scores of nursing students obey normal distribution. Figure 3 shows the test results of the evaluation results of nursing management knowledge and skills of two groups of nursing students.

According to the evaluation scores of EG (experimental group) and CG (control group) nursing management knowledge and skills, as well as statistical tests, the total score, comprehension level, and application analysis level of EG nursing students, are higher than those of CG nursing students, with no significant difference in memory scores. Inquiry-based learning is based on the principle of interaction between two subjects, emphasizing learners' active participation, teachers' proper guidance, and students' active participation in the learning process. A learning method for gathering, organizing, and actively mining knowledge is included in the materials. Students can develop not only scientific knowledge, but also scientific thinking and attitude in this way. In general, teachers incorporate knowledge and skills into problems, allow students to learn knowledge while solving problems, and use knowledge to improve skills, all of which exemplify the concept of "hands-on learning."

Figure 4 shows the comparison between the total score of self-study ability before experimental teaching (before intervention) and scores of various dimensions of EG and CG nursing students.

According to the statistical test, there was no significant difference between the scores of self-study ability of EG nursing students and CG nursing students before the intervention. Step-by-step explanation of new knowledge points put forward by students aims at combining and discussing new knowledge points and practical teaching methods with students, instead of completely brainwashing and gradually injecting new knowledge into students' learning process. The ultimate goal of group exploration is to complete the general tasks stipulated in this chapter and require students to plan and design in various aspects after mastering the basic knowledge. They must perform a set of specific steps, such as division of labor, time planning, provision of materials, data collection, running experiments, and writing reports. The students' ability to accomplish the activity objectives is evaluated by concrete demonstration and project description.

After the intervention, the scores of self-learning ability, information ability, and cooperation ability between EG nursing students and CG nursing students were significantly different, but there was no significant difference in the scores of self-management ability (see Figure 5).

Nursing is a discipline with strong theoretical knowledge, which contains many concepts, principles, and abstract theories, which makes students feel bored. The research shows that most CG students who adopt traditional teaching methods lack interest and enthusiasm in nursing management. ITM of nursing specialty courses based on DM skills has significantly increased students' interest in learning, enhanced their learning enthusiasm and initiative, and increased the fun and intuition of education. This stimulates students' interest in learning and makes learning more active. Based on the course ITM of DM skill nursing specialty, this study makes full use of DM skill simulation to create a realistic nursing management scene, and students use the knowledge they have learned to conduct nursing

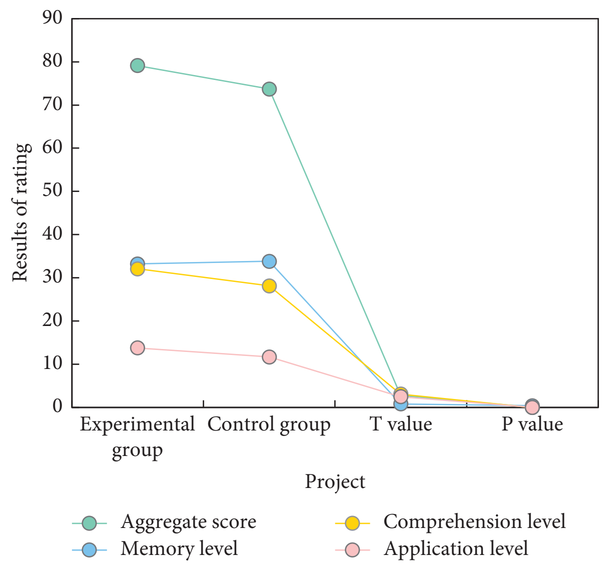

Figure 3: Examination results of nursing management knowledge and skills of nursing students.

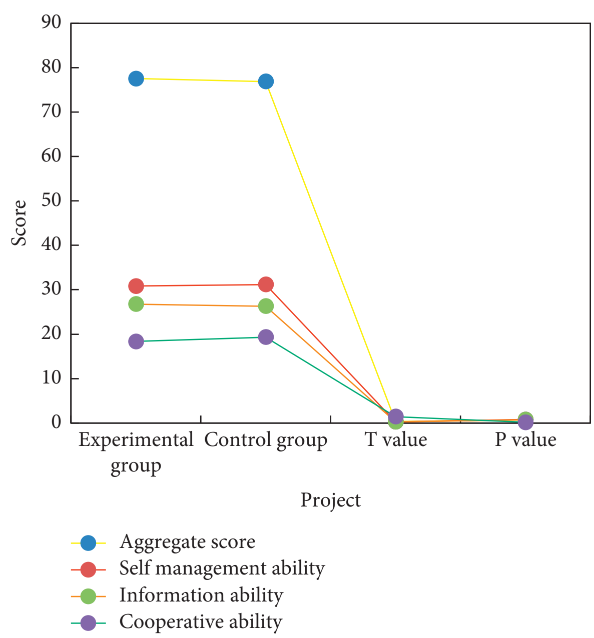

Figure 4: Comparison results of total scores and scores of all dimensions of autonomous learning ability of nursing students (before intervention).

management activities in the simulation situation, thus transforming into a single theoretical teaching, with rich experience in activities in class. Therefore, the nursing professional course ITM based on DM skills can improve students' problem analysis ability and practical problem solving ability and help to cultivate nursing management skills.

The network-based education has clear learning objectives and content, as well as related tasks and problem situations. Students are primarily responsible for learning objectives throughout the educational process, aside from

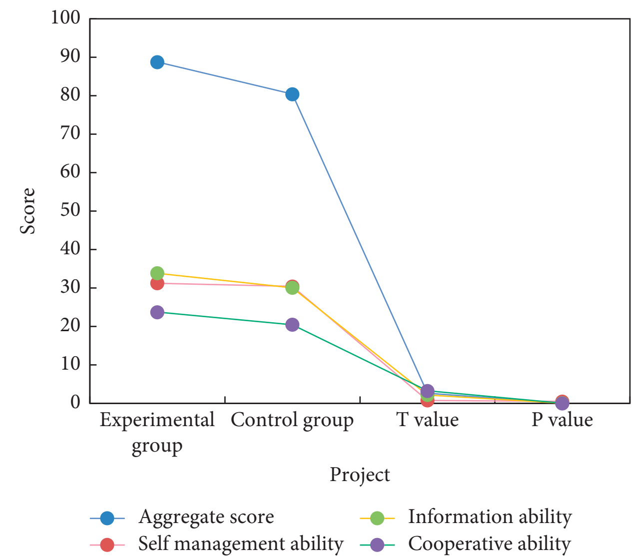

Figure 5: Comparison results of total scores and scores of each factor of independent learning ability of nursing students (after intervention).

the appropriate inspiration, guidance, and assistance from teachers. It conducts independent exploratory learning in a variety of ways, actively refers to and collects reasonable data, combines and processes it, and finally achieves the goal of solving problems and acquiring knowledge and ability, all while being guided and driven by problems or tasks. Students have a lot of freedom to study independently with this multichannel problem solving method. As a result, an ITM-based nursing professional course based on DM technology can help students improve their autonomy and discipline awareness. Consider internal medicine, which is at the heart of the nursing process. In terms of the knowledge system and curriculum requirements, ITM does not contradict nursing education [4, 5]. This model integrates the cultivation of innovative ability, clinical thinking ability, and cooperation ability into nursing education in the new era, trains innovative applied nursing talents with innovative spirit and adapting to the development of the times, promotes nursing education's innovative development, and thus produces better teaching effect for nursing students (Figure 6).

From these analysis results, the comprehensive inquiry-based teaching concept can improve the innovative thinking of undergraduates. In the interview, students thought that inquiry education provided a platform for innovation, guided scientific research, and helped innovation. This is basically consistent with many scholars' research on providing an innovation platform for college students to improve their innovation ability [6, 7].

The concept of inquiry teaching supporting nursing practice education puts forward a higher level of professional test for teachers. Teachers should organize and carefully consider all aspects of educational activities. In the whole process of maker education, teachers should learn to integrate and help students innovate and share their successful creation. This will greatly develop and improve teachers' abilities and improve the quality of comprehensive

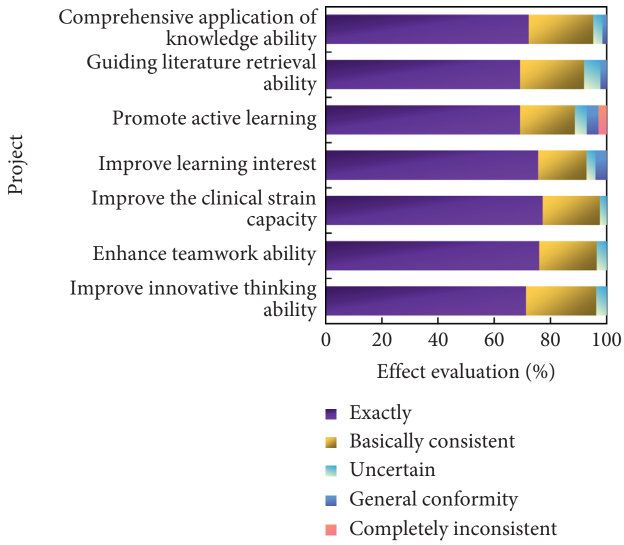

FIGURE 6: EG students' evaluation of the effect of inquiry-based teaching.

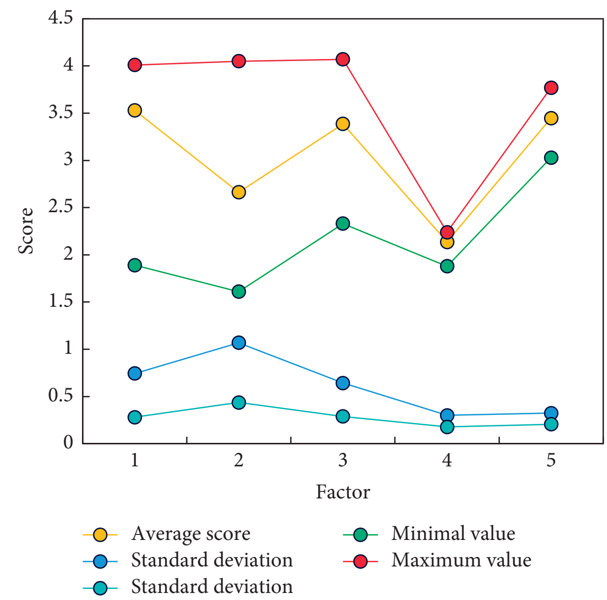

FIGURE 7: Scores of various factors in cross-cultural sensitivity scale.

education for nursing teachers. In order to analyze the poor cross-cultural sensitivity of the interviewees in more detail, the multicultural sensitivity was counted according to the factors shown. See Figure 7 for details. Among them, 1~5, respectively, represent communication participation, difference of identity, communication confidence, communication pleasure, and communication concentration.

The results show that the scores of each factor from high to low are communication participation, communication concentration, communication trust, discriminatory identity, and communication pleasure. Among them, the scores of communication participation and communication focus are relatively separated, indicating that modern nursing students are willing and able to engage in cross-cultural communication seriously. But differences in identity and communicative enjoyment were relatively poor, suggesting that, despite cross-cultural communication, students were less able to distinguish between cultural differences due to a lack of understanding of other cultural differences, affecting the pleasure of communication. Therefore, it is suggested that follow-up research work should focus on cross-cultural knowledge learning.

4.2. DM Analysis. The distribution of scoring data has the following characteristics: First, the distribution of scores in the same subject may fluctuate greatly due to changes in subject content, question types, examination difficulty, and so on. Secondly, in the case of different subjects in the same academic year, the distribution of scores may be quite different due to the great differences in subject contents and examination methods. Third, the scores of most subjects are distributed continuously, without obvious flaws, and the number of intermediate students is large. Fourth, the scores of individual students in most subjects are not good, so they are separated from the scores of most students and become outliers in the data set. Calculate the standard deviation of sample size and contour coefficient for the discretization results of the three algorithms.

Figure 8 shows the standard deviation of the result sample size of three methods of discretizing the result data of some courses according to the score value by using the K-means algorithm and the improved K-means algorithm.

As can be seen in Figure 9, the result of fractional discretization is not good in data similarity and does not meet the requirement of discretization, so as to maximize the data similarity within clusters and the data difference between clusters.

The improved K-means algorithm of data discretization can make the data similarity within segments and data differences between segments as large as possible and make the number of data points more uniform, meeting the requirements of class discretization.

It is worth noting that ITM injects a lot of color into teaching and teacher evaluation methods, as well as raising the bar for teachers, students, the educational environment, and educational conditions. Teachers' knowledge scope, classroom control, students' understanding, and instructional design skills are all put to the test in ITM. And teaching methods are not set in stone. Teachers must pay attention to course effectiveness, integrate various teaching methods based on the actual teaching situation in the classroom, and fully exploit the benefits of each teaching method. ITM, on the other hand, is time-consuming and labor-intensive, making it unsuitable for classes with a large number of students. As a result, teachers should adapt it to the situation at hand. Dynamic data differs from static data in that it can be changed. Bring course learners' learning habits into the information-based teaching platform. Compare the time spent browsing course content, the correct rate of answering course matching questions, and the knowledge point feedback scores. These data reflect students'

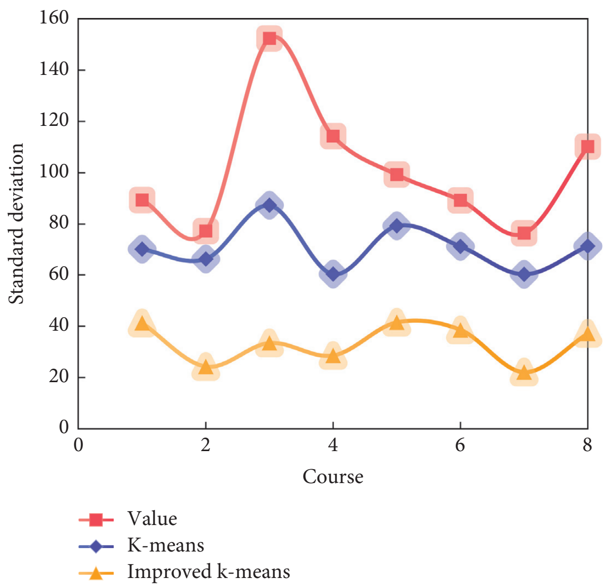

Figure 8: Standard deviation of the sample number of results of data discretization.

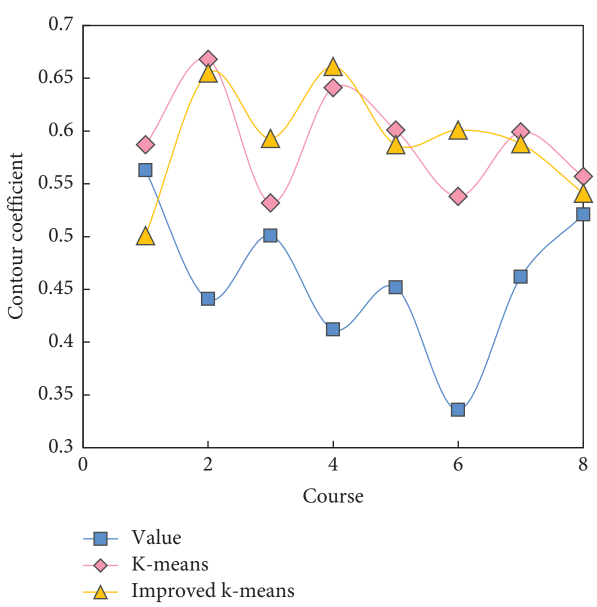

Figure 9: Contour coefficient of result of data discretization.

interest in and mastery of the course, and self-tests and other tests can be used to achieve the online learning effect. The learner's self-evaluation of the mastery degree of the learning content, such as complete mastery, basic mastery, and unclear places, is referred to as a self-test. It comes with knowledge test questions that the system evaluates based on the answers to the test questions.

The ITM course of nursing specialty constructed by researchers has achieved relatively successful results. In the inquiry teaching of nursing major courses, researchers guide students to learn independently, adopt flexible and diverse teaching methods around the teaching content, and make the teaching content more colorful, thus stimulating students' learning subjectivity and learning better and constantly deepening students' understanding of multicultural nursing, so that students can enhance their memory and absorption of multicultural nursing knowledge through multiangle and novel ways. According to the evaluation results of teaching methods, students have a high degree of recognition of the teaching methods and means adopted in this study, which has produced positive and effective results.

5. Conclusion

In the era when DM realizes personalized learning with big data, big data is influencing and changing the ecological environment of education and the operation mode of teaching. Using various related technologies of DM to deeply process the massive data of the platform can make the information system get rid of the previous mode which can only be used as electronic data entry tool, simple query function, and statistical report. Evaluation feedback in each teaching stage is used to continuously improve and perfect teaching activities, promote students to better understand and apply DM knowledge and concepts, and improve the quality of engineering education. Under DM technology, the nursing professional course ITM has changed the teaching concept, established a brand-new modern nursing education concept, effectively cultivated the nursing professional students' autonomous learning ability, auxiliary learning ability, and practical problem solving ability, laid a solid foundation for the full implementation of student-centered quality education, and provided reference for the development of inquiry teaching.

Data Availability

The data used to support the findings of this study are included within the article.

Conflicts of Interest

The author declares no conflicts of interest.

Acknowledgments

This study was supported by Henan Higher Education Teaching Reform Research and Practice Project "Research and Project of Live Teaching Method in Nursing Teaching with Teaching Hospital as the Second Classroom" under no. 2017SJGLX591.

References

[1] F. Zhang, L. Zhao, Y. Zeng, K. Xu, and X. Wen, "A comparison of inquiry-oriented teaching and lecture-based approach in nursing ethics education," *Nurse Education Today*, vol. 79, pp. 86–91, 2019.

[2] R. Wu, J. Xu, and P. Qian, "Situational inquiry method in the research teaching mode for ideological and political courses," *Journal of Intelligent and Fuzzy Systems*, vol. 40, no. 2, pp. 1–12, 2020.

[3] O. Smadi, S. J. Parker, and D. Gillham, "The applicability of community of inquiry framework to online nursing

education: a cross-sectional study," *Nurse Education in Practice*, vol. 34, pp. 17–24, 2018.

[4] T. Dombrowsky, K. Gustafson, and D. Cauble, "Service-learning and clinical nursing education: a delphi inquiry," *Journal of Nursing Education*, vol. 58, no. 7, pp. 381–391, 2019.

[5] R. R. Chan and M. Schaffrath, "Participatory action inquiry using baccalaureate nursing students: the inclusion of integrative health care modalities in nursing core curriculum," *Nurse Education in Practice*, vol. 22, pp. 66–72, 2017.

[6] M. S. Mousavi, M. Mahmoudi, and D. H. Pou, "Comparison of problem solving and participatory teaching methods on clinical learning, anxiety, and satisfaction of nursing students in arak," *Journal of Nursing Education*, vol. 7, no. 1, pp. 54–62, 2021.

[7] X.-B. Jin, W.-T. Gong, J.-L. Kong, Y.-T. Bai, and T.-L. Su, "PFVAE: a planar flow-based variational auto-encoder prediction model for time series data," *Mathematics*, vol. 10, no. 4, p. 610, 2022.

[8] Y. Zhang, K. Xia, and Y. Jiang, "Multi-modality fusion & inductive knowledge transfer underlying non-sparse multi-kernel learning and distribution adaption," *IEEE/ACM Transactions on Computational Biology and Bioinformatics*, vol. 1, p. 1, 2022.

[9] T. M. T. Valiga, "Do schools of nursing truly value excellence in teaching? Actions speak louder than words," *Journal of Nursing Education*, vol. 56, no. 9, pp. 519-520, 2017.

[10] P. L. Schultz and J. Baker, "Teaching strategies to increase nursing student acceptance and management of unconscious bias," *Journal of Nursing Education*, vol. 56, no. 11, pp. 692–696, 2017.

[11] M. Prince, M. Vigeant, and K. Nottis, "Teaching concepts using inquiry-based instruction: how well does learning stick?" *International Journal of Engineering Education*, vol. 34, pp. 304–315, 2018.

[12] L. S. Lewis, "The stories of nursing student repeaters: a narrative inquiry study," *Nurse Education in Practice*, vol. 28, pp. 109–114, 2018.

[13] A. E. Patterson, T. M. Mason, and P. Duncan, "Enhancing a culture of inquiry," *The Journal of Nursing Administration: The Journal of Nursing Administration*, vol. 47, no. 3, pp. 154–158, 2017.

[14] J. White, K. Costilow, J. Dotson, R. Mauldin, M. Schanandore, and D. Shockley, "Guided-inquiry experiment for teaching the calibration method of standard addition in the analysis of lead with graphite furnace atomic absorption spectroscopy," *Journal of Chemical Education*, vol. 98, no. 2, pp. 620–625, 2021.

[15] J. R. Burkett and T. M. Dwyer, "Combining inquiry-based and team-teaching models to design a research-driven, cross-disciplinary laboratory course," *Journal of Chemical Education*, vol. 96, no. 4, pp. 660–667, 2019.

[16] J. C. Goeltz and L. A. Cuevas, "Guided inquiry activity for teaching titration through total titratable Acidity in a general chemistry laboratory course," *Journal of Chemical Education*, vol. 98, no. 3, pp. 882–887, 2021.

[17] J. Gao, X. G. Yue, and L. Hao, "Optimization analysis and implementation of online wisdom teaching mode in cloud classroom based on data mining and processing," *International Journal of Emerging Technologies in Learning (iJET)*, vol. 16, no. 1, p. 205, 2021.

[18] S. Lu, "Development and research of university sports teaching information management system based on data mining technology," *Revista de la Facultad de Ingenieria*, vol. 32, no. 13, pp. 501–506, 2017.

[19] Y. Zeng, "Evaluation of physical education teaching quality in colleges based on the hybrid technology of data mining and hidden markov model," *International Journal of Emerging Technologies in Learning (iJET)*, vol. 15, no. 1, p. 4, 2020.

[20] W. Ye, "Teaching effectiveness evaluation of physical education and aerobics training based on data mining method," *Revista de la Facultad de Ingenieria*, vol. 32, no. 2, pp. 727–733, 2017.

[21] P.-h. Liu and S.-b. He, "Analysis of teaching reform mode based on cognitive computing system - an example of dragon boat teaching," *Cognitive Systems Research*, vol. 52, pp. 978–984, 2018.

[22] Y. Zhang and D. Yi, "A new music teaching mode based on computer automatic matching technology," *International Journal of Emerging Technologies in Learning (iJET)*, vol. 16, no. 16, p. 117, 2021.

[23] N. Wang, "A teaching mode for art anatomy based on digital virtual technology," *International Journal of Emerging Technologies in Learning (iJET)*, vol. 13, no. 8, p. 225, 2018.

[24] L. Zhang, "Illustration design teaching mode based on virtual wall painting technology," *International Journal of Emerging Technologies in Learning (iJET)*, vol. 14, no. 3, p. 190, 2019.

[25] X. Li, J. Wei, and S. Ding, "Teaching mode of mechanical design course based on simulation analysis technology," *International Journal of Emerging Technologies in Learning*, vol. 12, no. 7, p. 112, 2017.

[26] X. Yang, X. Jiang, and L. Rong, "A sports teaching mode based on social networking service teaching resources," *International Journal of Emerging Technologies in Learning (iJET)*, vol. 15, no. 8, p. 180, 2020.

Hindawi
Computational Intelligence and Neuroscience
Volume 2022, Article ID 7688985, 10 pages
https://doi.org/10.1155/2022/7688985

Research Article

College Sports Decision-Making Algorithm Based on Machine Few-Shot Learning and Health Information Mining Technology

Rui Zhang

Heilongjiang Bayi Agricultural University, Heilongjiang, DaQing 163319, China

Correspondence should be addressed to Rui Zhang; zhangrui@byau.edu.cn

Received 26 January 2022; Revised 10 March 2022; Accepted 11 March 2022; Published 31 March 2022

Academic Editor: Xin Ning

Few-Shot Learning has had a significant influence on how people live, work, and learn. Physical education is a requirement for a college diploma. Sports management systems, which focus on data collection, organization, and analysis, as well as timeliness and guidance, are one of the current challenges in the field of physical education at the country's top colleges and universities. The amount of sex in the room is minimal. Time is money when it comes to making college sports decisions, and this paper uses data from physical fitness tests to illustrate this point. Use Few-Shot Learning technology to extract relevant data from the data, allowing teachers to provide more scientific and effective guidance and suggestions to students. The design and implementation of this paper collect data from physical fitness tests in real-time using mobile edge computing, analyze the data, and display the results using machine learning technology, which mines deep features and displays analysis results, can be used to evaluate students' physical fitness. The data and information in the physical fitness analysis system are more readable and time-saving, allowing students to better understand their true level of physical fitness. Because of the results of data mining, teachers can provide more specific guidance and recommendations for each student's physical characteristics.

1. Introduction

With the deepening of the practical application and theoretical research of big data, big data has become a new growth point of the economy and society, as well as an emerging analytical tool for humanities and social science research, which has put forward innovative requirements for decision support of college sports in the era of big data [1]. The rapid development of big data and the Internet, cloud computing, and other technologies have prompted the growth of data in the information age, and the accumulation of data has become more and more massive, with the consequent generation of industry data in massive areas. Sports can improve people's physical and mental health, as well as guide them toward developing scientific and healthy lifestyles and habits and promoting their overall development. It is conducive to deepening sports reform, enabling the sports industry to be developed more systematically and comprehensively, and enhancing the vitality and momentum of the sports industry's development; it is conducive to increasing employment opportunities and raising the employed population; it is conducive to deepening sports reform, enabling the sports industry to be developed more systematically and comprehensively, and enhancing the vitality and momentum of the sports industry's development. The main shortcomings of such tools are manifested in the manual way of input work intensity; form stacking complex, inefficient, weak analysis, data readability is poor. Traditional physical education adopted statistical tools, often taking Excel office software and comprehensive class education office system. It not only adds to administrators' and teachers' daily workloads but it also makes data processing and analysis more difficult. Daily teaching activities and physical fitness tests cannot provide students with real-time and effective feedback [2]. In terms of analysis methods, the analysis methods used in the above tools are still stuck on simple variance, mean, and reliability calculations, resulting in the conclusions obtained from the analysis staying on the surface and failing to bring the full value of a large amount of data into play. However, the data and conclusions that administrators, teachers, and students care about are precisely these less easily discovered and valuable hidden information. To meet the development needs of big data analytics and to facilitate the deep integration of big data and its applications in various fields, research on big data analytics process modeling techniques is conducted to fully consider the ease of data analysis, domain complexity, and efficiency of execution of big data analytics. To improve the efficiency of big data analysis, to allow users to focus on domain business analysis logic rather than tool usage in big data analysis, to establish a domain-oriented reusable, well-structured processing framework for big data analysis processes, and to rely on the Hadoop platform with distributed storage scale and parallel computing capabilities. This aids big data analysis and value discovery in a variety of fields, and it is critical for developing scalable and user-friendly big data intelligent analysis software systems. The integration of existing resources and the development of a professional university sports decision support system can solve problems and issues encountered on the road to sports development, provide advice and strategic support for the development of sports, and accelerate the construction process of physical education in the context of globalisation and informatization [3].

In this paper, I attempt to use data mining techniques to study and analyze data on college students' physical fitness, develop a new college sports decision support system, and mine and analyze data on college physical fitness in order to uncover more valuable hidden information. This will assist students in better understanding their physical fitness status and teachers in initiating appropriate teaching activities on time. It improves the quality of university physical education by making physical education more timely, effective, and relevant; it also assists students in improving their physical fitness and developing good exercise habits.

2. Related Work

With the in-depth research of data mining technology, the application of data mining technology has been gradually extended to different fields, and some of the scholars have applied data mining technology to the education industry.

The literature [4] systematically discusses the importance of data mining techniques applied to education and teaching. The literature [5] employs crude sugar set theory and mining analysis to determine the relationship between improved student performance and active learning IM's dominant factors. There is still a lot of data in the university education system that can be mined, such as teaching evaluations, student performance, student information, and so on. However, data mining research in college education is currently primarily theoretical, and there are few shaped products that apply to data mining technology. The number of students and data managed by colleges and universities is growing year by year, and the manual processing mode in dealing with student information and student achievement can no longer meet the current needs. More scholars and researchers are applying data mining techniques to college education and physical ability analysis in this environment. Literature [6] uses the classification method of a decision tree, applies data mining technology to the student performance information, and constructs a professional ability decision tree model to help teachers gain more accurate and efficient insight into the problems that exist in the teaching process, and achieve the effect of optimizing teaching quality by using performance information. The literature [7] adopted the decision tree ID3 algorithm, and the association rules Apriori algorithm for data mining analysis based on student performance data. The ID3 algorithm was analyzed to get which factors are related to students' good grades; the association rules Apriori algorithm was analyzed to dig out the degree of influence of course excellence on other courses. The literature [8] used the FP-Growth algorithm to study the student physical fitness test data from a deeper level based on the physical fitness test data from six colleges and universities. The results showed that nearly half of the students in the six colleges were not at the standard weight and the results of the algorithm run observed that the students lacked training for lower body strength in their physical training and had significantly weaker lung capacity rating and endurance rating, suggesting that the students should strengthen their aerobic training. The literature [9] used the association rule Apriori algorithm to filter out five strong association rules about male and female students, respectively, based on the physical test data of college students in a university. The results showed that under the condition of "total score = pass," more female students failed in the test item standing long jump, and more male students failed in the test item pull-up. This identifies sports that need further attention in the future at the university to strengthen the overall physical fitness of students. The literature [10] used student data from a US university to develop an early warning system for students. The literature [11] proposes a method for predicting students' knowledge of the necessary skills for their majors by mining information from their academic performance once the students' bias in the learning process has been compensated for. Literature [12] uses the Hadoop big data platform to mine the data of informative campus applications in order to recommend campus information based on learning characteristics. The literature [13] examines the innovation of graduate physical education's deep evaluation mechanism in the era of big data from three perspectives: student-oriented value logic, practical logic with the goal of theory implementation, and problem-oriented reality logic. The literature [14] examines the general idea of reforming the evaluation method of college physical education based on big data from a theoretical perspective before delving into the specific application of big data evaluation on a practical level. The literature [15] begins with the current state of operation and growth trend of the big data platform for physical education in colleges and universities, analyses its goals and values, and investigates its architecture and characteristics in order to develop an excellent scheme to promote the construction, operation, and management of the big data platform for physical education.

It can be seen that a large number of research findings on big data have aided in the development of quantitative analysis methods in physical education. These findings seize big data's innovation opportunity and examine the innovation of quantitative analysis methods of physical education promoted by big data from multiple perspectives, based on a comprehensive analysis of big data's characteristics and mining its value; However, the majority of big data and physical education research is based on a general perspective of physical education or a more general study on the overall grasp of physical education, and the relevance of theoretical guidance, as well as the operability of the application of theoretical results, must be improved. Simultaneously, research into the integration and innovation of big data and quantitative analysis methods in physical education is primarily based on theoretical or empirical feasibility analyses, with the realistic path of how to apply it not being sufficiently explored.

3. Research and Construction of a Decision Support System for University Sports Based on Big Data Analysis Technology

3.1. Big Data Analytics Technology. In the current network era, the value of data as the core of big data does not arise out of thin air and requires the help of certain mining techniques.

Data mining usually has the following eight steps: (1) information collection: abstract the analyzed object, get the characteristic information of the analyzed object, and use reasonable information collection methods to load the characteristic information of the analyzed object into the database. (2) Data integration: the information collected from various objects is centralized to facilitate the subsequent correlation analysis work. (3) Data statute: The data volume after data integration is generally large and difficult to handle. The data set obtained can be statutorily represented, and the data volume after the statute is much smaller than the original data, but still maintains the integrity of the original data, and the data mining result after the statute is the same as a result before the statute. (4) Data cleaning: Some of the data collected in the database may be incomplete, noisy, or have conflicts, etc., so data cleansing work is needed to improve the data in the database and eliminate all kinds of illegal data. (5) Data transformation: the data in the database will be transformed into a form that is convenient for data mining, and the common ways and means are smooth aggregation, data generalization, etc. (6) Data mining: the data information stored in the data warehouse, the use of appropriate analytical tools and statistical methods, processing data, and finally getting the analysis results. (7) Pattern evaluation: Validate the data mining results from the business perspective and analyze whether the data mining results are correct. (8) Knowledge representation: presenting data mining results to users, which can use various visualization tools, reporting tools, etc.

Deep learning [16–18] is one of the key technologies for tapping the value of data at the level of big data; at the level of deep learning, the collection and use of a large amount of data has the potential to improve the accuracy of machine models. The meanings of TP and TN when classifying a class in a machine model both represent the case where the classification result is correct: TP is a positive class, and TN is a negative class. FP denotes that the incorrect category is divided into the correct, while FN denotes that the correct category is divided into the incorrect. As a result, the support of big data is required to develop machine learning, and the assistance of machine learning is required to mine the value of big data, and the two are mutually reinforcing and interdependent. The study's main algorithm is machine learning, which is a broad term for a specific type of algorithm. Machine learning algorithms [19, 20] attempt to intervene or classify a large amount of raw data in order to uncover hidden laws in the data and discover the data's value, allowing data models to be built. As shown in Figure 1, it mainly consists of three types, and this study is chosen to implement model building with supervised learning.

Concerning the machine models in this study, they are all practically similar to decision tree classification models, and all amount to a combination of multiple dichotomous classification problem models. Therefore, before proceeding to model generation, the first task is to gain a detailed understanding of the binary classification problem. The next example will be picture content discrimination: there is a picture stored in a certain computer gallery. The task of the computer at this point is to determine the specific content in the current picture. After making the relevant determination, the computer has to check whether the judgment output meets the expected effect. Therefore, a feature vector X can be set in the computer for representing the result. Then, the current computer can use the computer language $Y = 0$ or $Y = 1$ to indicate the right and wrong results of the judgment, the main formula used as shown below:

$$Y_i^{l+1} = \left[X_{i,j,c}^{l+1}\right]_{s^*s^*32}. \tag{1}$$

$$\prod_i X(\oplus| > i) = \prod_i Y(\, > i\oplus) \tag{2}$$

CRM, as a cascade regression model, usually requires first integrating the predictions of each decision tree and calculating the average as the final prediction; however, the classification problem employs a different strategy: the plural voting method, which requires counting the number of votes received for each type of label and selecting the one with the most votes. As the final prediction result, the classification labels are output. According to the previous analysis, some factors tend to influence the combined classifier's generalization ability, which is mainly related to the classification performance of individual metaclassifiers from the perspective of individual metaclassifiers; from the perspective of the set of metaclassifiers, the size of the correlation between metaclassifiers is also an important influencing factor.

The boundary function of a decision forest is described as follows:

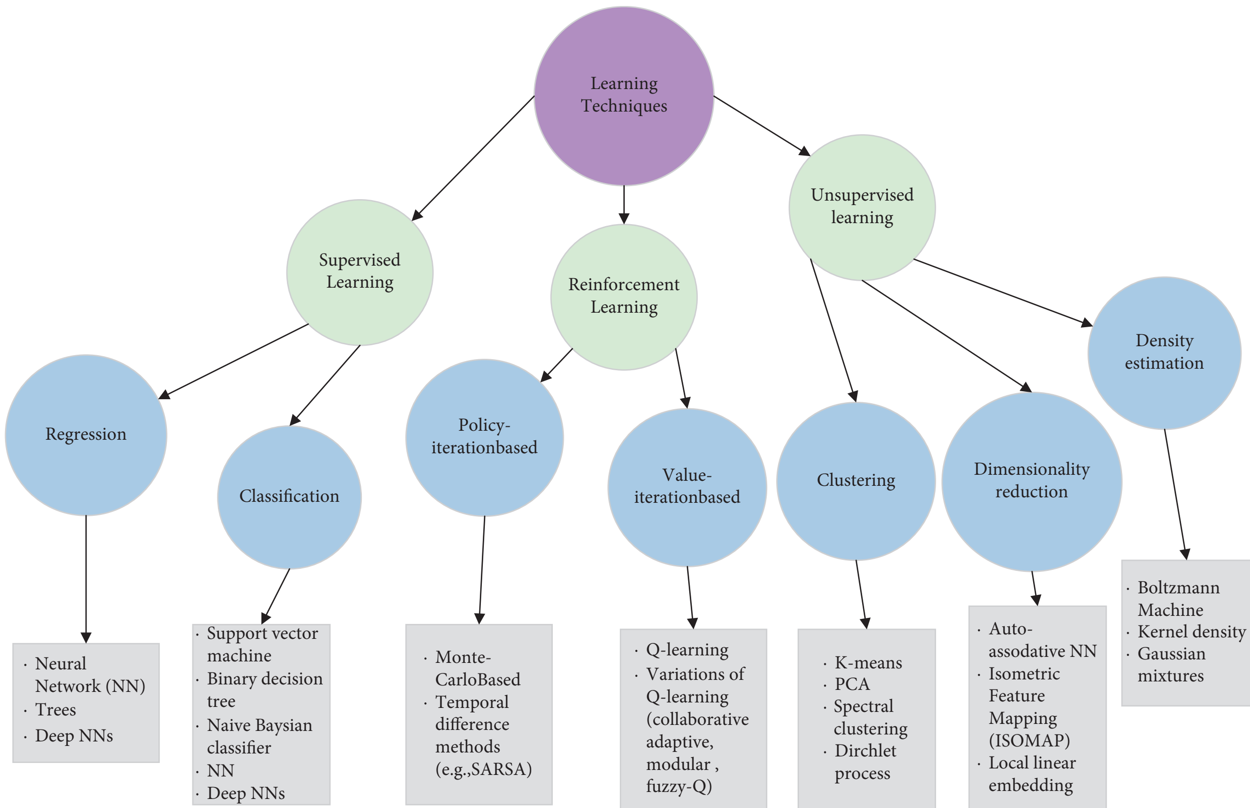

FIGURE 1: Machine learning classification graph.

$$g_{i,j,f}^{1} = \mathrm{ReLU}\left(b_1 + \sum_{a=1}^{m}\sum_{b=1}^{n} g_{i,j,f} + b\cdot t_{a,b,c}^{1}\right). \tag{3}$$

The categorical efficacy of decision forests is defined as follows:

$$r(h_i) = Nh_i(1)\left(Nh_i(1) + Nh_i(-1)\right)^{-1}. \tag{4}$$

Define the original prime function of the decision forest as $rm(\theta, x, y)$, and the boundary function as the mathematical expectation of the original prime function on $m(x, y)$, whose expression is as follows:

$$rm(\theta, x, y) = m(x, y)\cdot I(x, \theta) + k(y, \theta)\cdot j(\theta, x) \tag{5}$$

Since the mathematical expectation of the variance satisfies the following:

$$g^{\mathrm{n}}(x) = \lim_{a\longrightarrow 0}\frac{1}{a^n}\sum g(x - ak)\binom{n}{k}(-1)^k. \tag{6}$$

Therefore, it can be obtained that the generalization error of the decision forest PE^* satisfies the inequality

$$PE^* = \bigcup_{i=1}^{n} X_i\left(1 - s^{\mu}\right) + C. \tag{7}$$

The decision tree's definition and principle have been explained. The decision tree is essentially a process of growing data from the root node to the leaf nodes in a continuous split. The branching direction of nodes is currently determined in the construction of decision trees primarily based on the judgment criteria of the classified nodes, which cannot be changed once the direction has been established. Following VGGNet, 3 ∗ 3 small convolution kernels became the standard for network design. Most general neural networks start with a 7 ∗ 7 large convolution and then use 3 ∗ 3 convolution stacking (ResNet, DenseNet), whereas lightweight neural networks start with a 3 ∗ 3 convolution and then use 3 ∗ 3 convolution stacking. This method can make the network classify the best at the current node, but it cannot guarantee the best final classification result, according to the Info-Gain principle. A "probabilistic" decision tree is designed to balance the current optimum and the final classification result. This tree does not determine the split of each node but rather describes it in a probabilistic manner. Because the number of labeled samples in practical recognition tasks is usually limited, using ISM for target detection tasks has some drawbacks.

Figure 2 explains the structural framework of the decision tree algorithm, where the voting codebook is obtained by sliding windows and extracting feature channels (feature descriptions), and in the training process, a series of decision trees are formed by supervised target training and heuristic algorithms, and further formed into a decision forest; in the target detection process, the voting codebook obtains numerous target locations by weighted voting, and the greedy algorithm is used to solve for the maximum target probability to obtain the final target location.

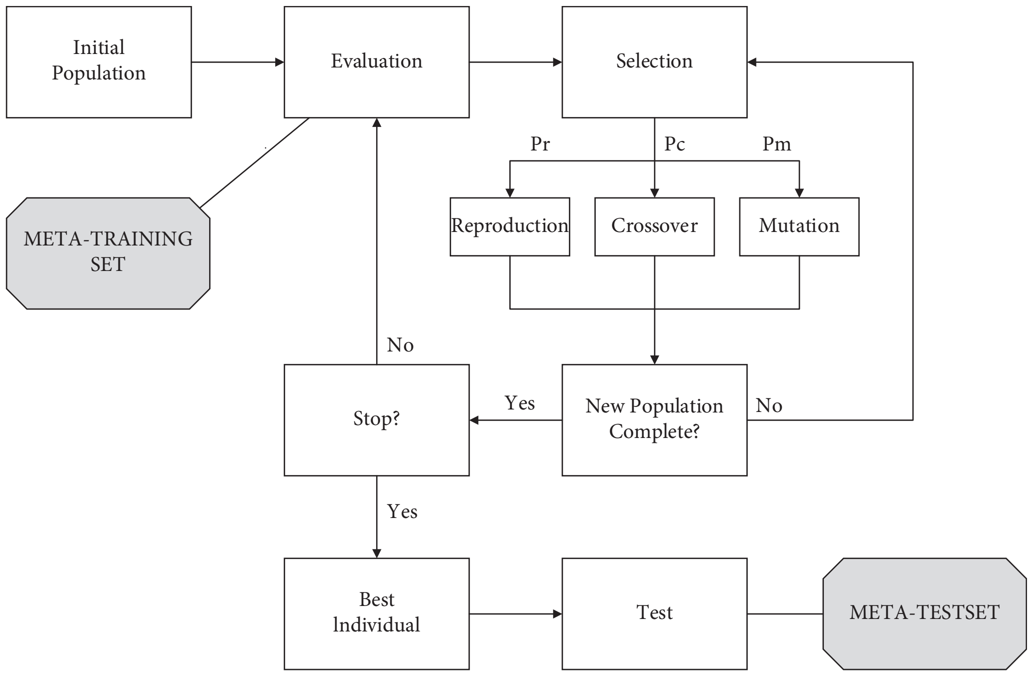

Figure 2: The structural framework of the decision tree algorithm.

3.2. Research and Construction of a Decision Support System for University Sports Based on Big Data Analysis Technology. Colleges and universities provide physical education in the form of college physical education courses for physical exercise, education, and guidance. The issue is primarily focused on the fact that physical education in China is still a teaching system centered on physical education teachers and that the quality of physical education is influenced to some extent by the disparity in physical education teacher quality. Simultaneously, the physical education system's and statistical tools' backwardness lowers the quality of teaching and learning in three ways: first, the traditional method of performance evaluation and statistics makes teachers' work tasks cumbersome and inefficient; second, the traditional method of performance evaluation and statistics makes teachers' work tasks cumbersome and inefficient. Second, the single system for evaluating physical education results and physical tests makes it difficult to apply the results to each student's problems of physical fitness and health. Third, based on the above two points, the heavy workload of teachers makes it difficult to give students effective guidance advice immediately; the single sports assessment makes it difficult to come up with professional guidance and feedback. For the above problems, data mining methods can be adapted to analyze the sports test data of college students and the whole process. After determining the content and purpose of the project, then the relevant data are collected and preprocessed, where the data preprocessing includes data selection, data cleaning, data integration, and data specification, in four steps. Finally, data mining processing is then performed on the data set using relevant data mining models to obtain data mining results. The actual content of the project is linked to getting the corresponding value knowledge. The process is shown in Figure 3.

The personal data analysis module can realize the detection and analysis of personal physical fitness test data and judge the comprehensive evaluation of individual users and fitness methods. Test indicators include three major indicators of body shape, body function, and physical quality. Morphological indicators mainly include waist circumference, scapular skinfold thickness, height, hip circumference, weight, chest circumference, abdominal skinfold thickness, and upper arm skinfold thickness; functional indicators mainly include step index, veins, systolic blood pressure, vital capacity, and diastolic blood pressure. Qualities mainly include choosing reaction time, push-ups, back strength, grip strength, sitting forward bends, sit-ups, vertical jumps, standing on one foot with eyes closed. Secondly, adults are grouped by age and gender, each group is 5 years old, and there are 16 groups of men and women in total. 10 test indicators are used to analyze individual physical fitness test results, which is convenient for the rapid processing of physical fitness test data. Potential value analyze the needs of individual users and managers, provide specific implementation methods for each module, and complete the overall design of the service application platform.

After performing machine learning, the result obtained from the learning is often an optimal decision tree, which leads to the establishment of a comprehensive evaluation model of college students' physical fitness. Next, the performance of the model needs to be evaluated using the sample data of the physical fitness test. Only when the evaluation result is good using the sample data of the physical fitness test, the comprehensive evaluation model of university students' physical fitness has the most "optimal" set of functions to solve the problem.

The personalized fitness mode recommendation service solution based on machine learning mainly includes three

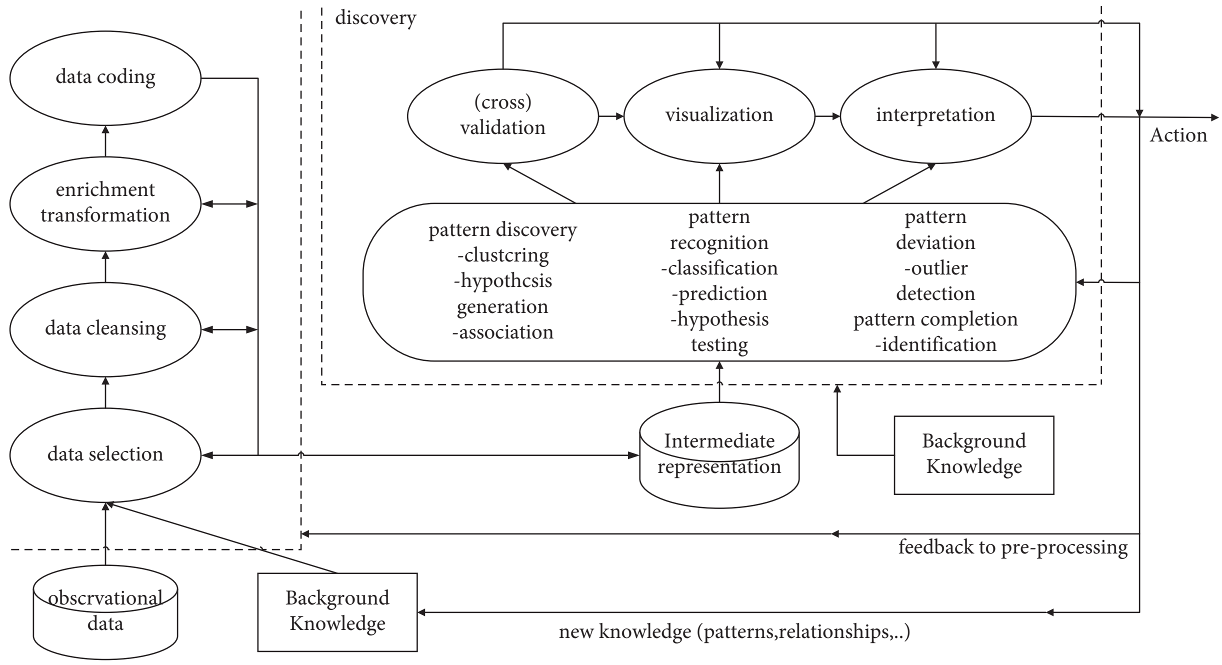

Figure 3: Data mining process for student physical tests in universities.

parts: the collection of basic user data, the discovery of fitness modes that match personal fitness test data and interest needs, and the recommendation of personalized fitness modes that match personal fitness test information and so on. For the generation of the fitness mode recommendation model based on machine learning, machine learning is then mainly applied to tap the value of personal fitness test information and carry out fitness mode recommendations suitable for individual users' fitness test information. Using the fitness test data uploaded by the administrator or the personal fitness test data stored in the database by the service application platform as input, the fitness test data is classified by the machine learning algorithm after entering the model, and the corresponding fitness mode categories are extracted from the fitness resource library, and the fitness modes of the corresponding categories are called through the Web UI module in the recommendation list and presented to the individual user through the service application platform presented to individual users.

The scale transformation mechanism makes the variable scale cluster analysis method capable of automatic execution, ensuring that the decision-maker is almost not required to participate in the method execution process, i.e., the decision-maker only needs to subjectively select the type of scale transformation strategy and deterrence. This method can directly obtain all college students' physical test results that satisfy decision preferences and their performance on the appropriate analysis level, assisting the university sports director in making the best sports training decision for the students. Because the traditional cluster analysis method can only perform cluster analysis at a single scale level, and the management business itself has multilevel characteristics, i.e., competition support groups made up of various participating students each have their own appropriate levels of decision analysis, the traditional cluster analysis method can only perform cluster analysis at a single scale level. All three scale levels have unsatisfactory classes in the single-scale clustering results. Although unsatisfactory classes are always present in the traditional cluster analysis method's clustering results, as the scale hierarchy grows, the number of unsatisfactory classes decreases significantly. This is strong evidence that scales can link decision-making activities to subjective and objective data and that scale transformation can add more valid information and knowledge to operational data, reducing decision complexity.

In addition to the basic scale hierarchy, the variable scale cluster analysis method can obtain more accurate scale characteristics of satisfaction classes than the traditional cluster analysis methods at the same level. Since the scale transformation process of variable scale cluster analysis starts from the basic scale level and takes the lowest scale level of each satisfaction class as its appropriate decision analysis level, the satisfaction class consistency theorem ensures that the clustering results are consistent among different data analysis levels so that each satisfaction class retains its most detailed scale characteristics, allowing analysts to have more accurate information and thus improve the quality of decision results [21]. For the traditional clustering analysis method, even if it can find the partial satisfaction class in the process of single-scale data analysis, it does not guarantee that the scale characteristics of the satisfaction class reach a better analysis level at this time, which leads to the problem that the result class characteristics are often not significant in solving practical problems in management.

4. Experimental Verification and Conclusions

Clustering validity can be evaluated in terms of internal validity evaluation and external validity. Since there is a scale transformation iterative transformation process in the execution of the variable scale clustering analysis method, and the set of objects (thesis domain) decreases with the increase of the number of iterations, there is a situation that the results of variable scale clustering analysis are distributed in different analysis levels. The internal validity index can only evaluate the quality of clustering results on the same analysis level, so to ensure the objectivity and fairness of the evaluation results; this paper adopts the external validity evaluation method to verify the variable scale clustering analysis method. The experiments are conducted on the premise of satisfying the methods and principles of multiscale data model construction and randomly generating multiscale data models, and the main purpose is to conduct relevant experimental analysis on the validity and parameter sensitivity of the variable-scale clustering analysis method. Since the experiments take an external validity evaluation index to test the clustering effect, data labels are added to this data model. The basic task of the experiments on the validity of the variable-scale cluster analysis method is to test the clustering effect of the variable-scale cluster analysis method compared with the traditional single-scale cluster analysis method. Because the meta-partitioning cluster analysis algorithm's initial class center selection is random, this paper first repeats the class analysis work 50 times on each of the 54 single-scale data models obtained from the multiscale data model and then takes the mean, maximum, minimum, and standard deviation of the results of these 50 experiments, as well as the maximum value, minimum value, and standard deviation to complete the full-scale spatial clustering analysis. The variable scale clustering analysis method's validity is tested by comparing its results to those of the traditional single scale clustering analysis method at the basic scale level to see if the variable scale clustering analysis method can meet the clustering results' quality requirements. The results of the clustering validity index evaluation between the variable-scale cluster analysis method and the traditional single-scale cluster analysis method at the optimal scale level are compared to see if the variable-scale cluster analysis method can improve clustering analysis efficiency. The clustering validity index evaluation results are shown in Figure 4.

Sensitivity analysis of satisfaction determination thresholds for variable scale cluster analysis methods. The basic task of the experimental analysis of satisfaction determination thresholds & sensitivity for variable scale cluster analysis methods is to test the clustering effect of variable scale cluster analysis methods under the conditions of different satisfaction determination thresholds. It is the maximum granularity deviation taken from all the basic scale clustering results that satisfy the business requirements. In this experiment, the clustering effect of the variable scale clustering analysis method under all possible values is examined by setting the experimental analysis range of the satisfaction determination threshold parameter. As can be seen from Figure 4, among the 50 clustering experiments of the variable scale cluster analysis method, the average clustering validity results of the variable scale cluster analysis method for all the above evaluation indexes are better than the average validity results achieved by the traditional single

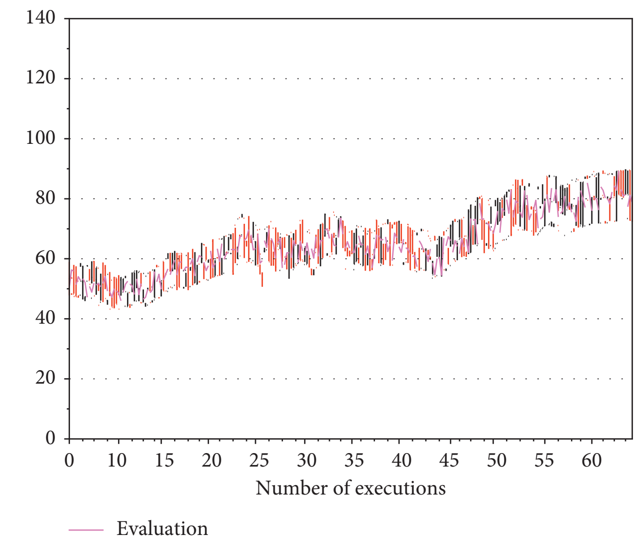

Figure 4: Results of the evaluation of clustering validity indicators.

scale cluster analysis method at the basic scale level, and the quality improvement rate of the clustering results is more than 10%, among which the quality improvement rate of the results under the NMI evaluation index reaches 1. 5. 63%. 5.63%, proving that the variable scale clustering analysis method can better meet the validity requirements of the clustering results of the traditional single scale clustering algorithm.

According to the basic task of the sensitivity experiment of the variable scale cluster analysis method's satisfaction threshold R, the experiment compares the results of the external validity evaluation indicators of the variable scale cluster analysis method under different satisfaction threshold R0 and investigates the degree of influence of the satisfaction threshold R 0on the validity of the variable scale cluster analysis method. To investigate the relationship between satisfaction determination thresholds and the effectiveness of the variable scale clustering analysis method and to compare the trends of the clustering effect of the variable scale clustering analysis method under various satisfaction determination thresholds, the satisfaction threshold R0, which was determined subjectively by the analyst, was 3.8 in the above-mentioned experiments on the effectiveness of the variable-scale cluster analysis method. The satisfaction threshold's experimental analysis range was set to a region around 3.8, which was specifically set to [3.0, 6.0] in this experiment, and the step of change was 0.1. Each satisfaction threshold was subjected to 50 runs of the variable-scale cluster analysis method. The cluster result validity evaluation indicators were averaged to perform a satisfaction determination threshold sensitivity analysis.

Figure 5 shows the results of the sensitivity analysis of the parameters of the scale cluster analysis method. By comparing the experimental results, it is found that the variable scale clustering analysis method is less affected by the satisfaction determination threshold R_0 and the results have stability, as discussed below: although the results of all evaluation indicators of the variable scale analysis method

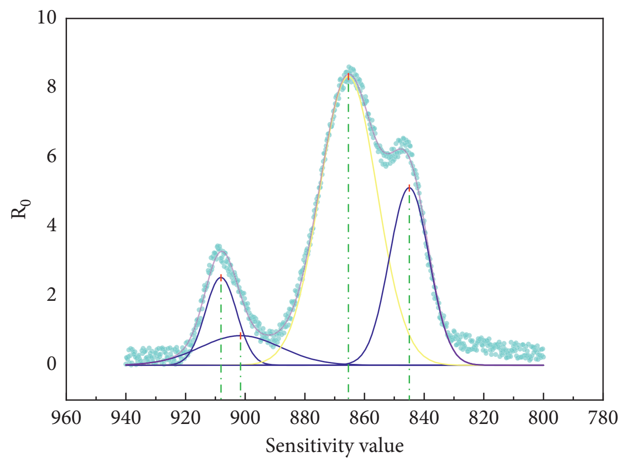

FIGURE 5: Results of sensitivity analysis of parameters of the scale cluster analysis method.

fluctuate in the range of the satisfaction determination threshold parameter, the maximum fluctuation does not exceed 1%, indicating that the validity of the clustering results of the variable scale clustering analysis method is not sensitive to the satisfaction determination threshold. The overall trend of the evaluation index results of the variable scale cluster analysis method increases slightly with the increase in the value of the satisfaction determination value parameter, indicating that the overly strict initial satisfaction constraint is not conducive to the optimal solution of the variable scale cluster analysis method.

After obtaining valuable data based on machine learning decision trees and multiscale cluster analysis methods, the data can be applied to the actual curriculum for decision support. Classroom monitoring is mainly achieved through wearable sports bracelets, which can monitor various indicators such as student exercise intensity, exercise density, heart rate curve, and heart rate warning. The sports bracelet has four colors: green, blue, orange, and red, and it can be used to guide teaching by monitoring students' heart rates. When the red logo appears, it means the student's heart rate is higher than normal, and the sports watch will sound an alarm, alerting the teacher to reduce the intensity and volume of exercise. The teacher can then use big data to analyze the movement of students through the class's background and determine whether the class has met the teaching objectives. The use of the decision support system by teachers is depicted in Figure 6.

According to the research, 94.4 percent of students believed the decision support system could achieve targeted teaching, while 5.6 percent believed it could not. This means that the majority of physical education teachers still believe that decision support systems can help them deliver more targeted instruction and learning. At the same time, the decision support system can make intelligent statistical analyses of students' learning performance, as shown in Figure 7. Based on the conversion scores of students' indicators, and statistical comparison and analysis based on items, gender, grade level, and other degrees, the system can continuously track students' physical development trends, quickly grasp students' physical and athletic qualities, and conduct targeted teaching according to students' differences, to solve the problems of students' "not being able to eat" and the problem of "not being able to eliminate." And through intelligent statistics out of the student results can not only be viewed by individual students, but also for classmates, teachers, school leaders, and other views. The percentage of teachers who often use the decision support system to push PE homework to students is 35.2%, the percentage of PE teachers who use it occasionally is 53.7%, and 11.1% of PE teachers will not use the platform to push homework to students, with teachers occasionally assigning homework accounting for the largest percentage. This indicates that physical education teachers do not frequently use the decision support system to assign physical education homework to students. Physical education is now gradually being paid attention to in junior high school teaching, recognizing that cultivating students' physical quality cannot be accomplished overnight, that a few minutes in the classroom is insufficient, and that teachers must reasonably arrange students' physical education homework to ensure that students can develop good physical exercise habits whether in classroom teaching or at home. This will help junior high school students grow in a healthy way. It is a new trend in physical education to assign "physical education homework," which will serve as a strong motivator for students to engage in physical activity. PE homework will not only encourage students to engage in physical activity after school, but it will also draw parents' attention to their children's physical development and improve their physical performance.

As can be seen in Figure 8, the use of decision support systems for learning by students grows steadily with grade level. The lowest usage rate is among the first-year students, with 24.1%. The next highest usage rate is among sophomores, with 33.2%. The highest rate of use was among third-year students, with 42.7%. The move of junior high school students to use the decision support system for learning makes it possible to deeply integrate "Internet+" with college sports. The decision support system is a manifestation of the integration of Internet+ with sports, which breaks the traditional way of learning sports. For example, the learning space has changed a lot. Physical education is traditionally taught by teachers in physical education classes, and students learn the content from the teachers. The learning space must be set up in a specific location on campus. Schools with better hardware facilities have more indoor learning space and are less affected by weather, but schools with poor hardware implementation may not be so fortunate and will be impacted by weather. When it rains, for example, physical education classes are canceled, and the physical education program in junior high schools has only one class per week, so there is not much physical education left in a semester after holidays and rainy days. Physical education teaching tasks in high schools cannot be completed on time, in a high-quality and quantity manner, and students' physical health will not improve but will deteriorate as they grow older. The advent of the decision support system allows schools to overcome

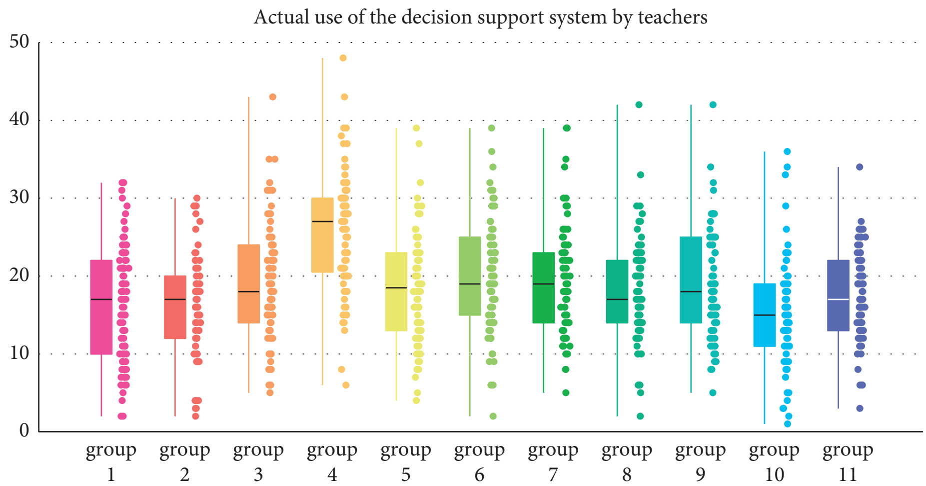

FIGURE 6: Actual use of the decision support system by teachers.

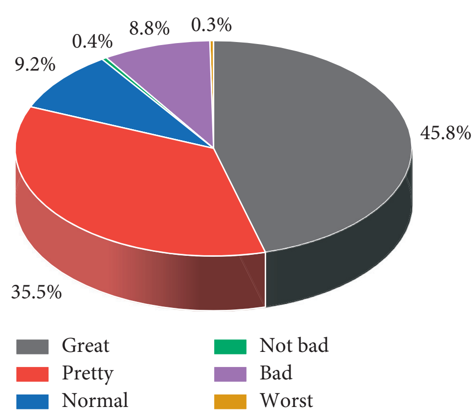

FIGURE 7: Results of intelligent analysis of learning achievement.

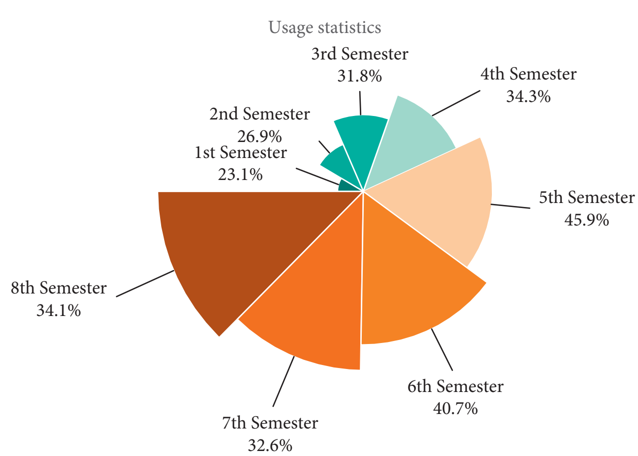

FIGURE 8: Usage statistics of the decision support system.

learning space constraints; the transformation of students' learning spaces adds color to the traditional way of physical education learning, while the decision support system also contributes to college physical education innovation.

5. Conclusions

While data mining techniques have made significant progress in a variety of fields, the use of fitness analysis in conjunction with data mining techniques is less common. The main reason for this is the limitations of physical education in colleges and universities, where major institutions have vastly different curricula and evaluation criteria. This has resulted in a physical fitness and health management system based on data collection and statistics, making guidance and educational significance difficult to achieve. With the advent of the big data era, the problem of data support for college physical education decision-making guidance has been solved, and the "online + offline" hybrid teaching model has emerged and permeated the college physical education teaching model, which is not only innovation of the college physical education teaching model, but also an important reflection of the new curriculum concept. Furthermore, the rapid development of big data has aided the development of multifunctional school teaching instruments. Teaching can benefit from a web page with a larger capacity and faster page updates, which provides richer and more specialized information resources. The research objects in this paper are physical test data and physical health self-assessment data, and the physical test data have uniform standardization and guidance but are not strong for readability and guidance. In order to achieve better physical fitness health education goals, this paper employs data mining technology and design to implement a physical fitness analysis system. The theory of data mining is discussed, as well as data mining algorithms such as the decision tree and association rule algorithms and the decision tree C4.5 algorithm and association rule algorithm. To mine the physical fitness data information, the apriori algorithm and multiscale clustering algorithm are chosen, and the results of big data analysis are also used to design, implement, and verify the physical fitness analysis system for college students.

Data Availability

The data used to support the findings of this study are included within the article.

Conflicts of Interest

The author does not have any possible conflicts of interest.

References

[1] X.-B. Jin, W.-T. Gong, J.-L. Kong, Y.-T. Bai, and T.-L. Su, "A Variational Bayesian deep network with data self-screening layer for massive time-series data forecasting," *Entropy*, vol. 24, no. 3, p. 335, 2022.

[2] K. H. Leung, C. C. Luk, K. L. Choy, H. Y. Lam, and C. K. M. Lee, "A B2B flexible pricing decision support system for managing the request for quotation process under e-commerce business environment," *International Journal of Production Research*, vol. 57, no. 20, pp. 6528–6551, 2019.

[3] Y. Yang, "College physical education teaching methods under the background of big data," in *Innovative Computing*, pp. 967–974, Springer, Singapore, 2022.

[4] P. B. Keenan and P. Jankowski, "Spatial decision support systems: three decades on," *Decision Support Systems*, vol. 116, pp. 64–76, 2019.

[5] O. Enaizan, A. A. Zaidan, N. H. M. Alwi et al., "Electronic medical record systems: decision support examination framework for individual, security and privacy concerns using multi-perspective analysis," *Health Technology*, vol. 10, no. 3, pp. 795–822, 2020.

[6] J. Zagorskas and Z. Turskis, "Setting priority list for construction works of bicycle path segments based on eckenrode rating and aras-f decision support method integrated in gis," *Transport*, vol. 35, no. 2, pp. 179–192, 2020.

[7] M. M. Baig, H. GholamHosseini, A. A. Moqeem, F. Mirza, and M. Lindén, "Clinical decision support systems in hospital care using ubiquitous devices: current issues and challenges," *Health Informatics Journal*, vol. 25, no. 3, pp. 1091–1104, 2019.

[8] C. Bai, S. Kusi-Sarpong, H. Badri Ahmadi, and J. Sarkis, "Social sustainable supplier evaluation and selection: a group decision-support approach," *International Journal of Production Research*, vol. 57, no. 22, pp. 7046–7067, 2019.

[9] A. Awaysheh, J. Wilcke, F. Elvinger, L. Rees, W. Fan, and K. L. Zimmerman, "Review of medical decision support and machine-learning methods," *Veterinary pathology*, vol. 56, no. 4, pp. 512–525, 2019.

[10] C. Kadar, R. Maculan, and S. Feuerriegel, "Public decision support for low population density areas: an imbalance-aware hyper-ensemble for spatio-temporal crime prediction," *Decision Support Systems*, vol. 119, pp. 107–117, 2019.

[11] H. Song, C. E xiu-ying Han, C. E. Montenegro-Marin, and S. krishnamoorthy, "Secure prediction and assessment of sports injuries using deep learning based convolutional neural network," *Journal of Ambient Intelligence and Humanized Computing*, vol. 12, no. 3, pp. 3399–3410, 2021.

[12] F. R. Goes, L. A. Meerhoff, M. J. O. Bueno et al., "Unlocking the potential of big data to support tactical performance analysis in professional soccer: a systematic review," *European Journal of Sport Science*, vol. 21, no. 4, pp. 481–496, 2021.

[13] M. M. Chupin, A. S. Katasev, A. M. Akhmetvaleev et al., "Neuro-fuzzy model in supply chain management for objects state assessing[J]," *International Journal of Supply Chain Management*, vol. 8, no. 5, pp. 201–208, 2019.

[14] J. Wang, Y. Yang, T. Wang et al., "Big data service architecture: a survey[J]," *Journal of Internet Technology*, vol. 21, no. 2, pp. 393–405, 2020.

[15] L. Gordon, T. Grantcharov, and F. Rudzicz, "Explainable artificial intelligence for safe intraoperative decision support," *JAMA surgery*, vol. 154, no. 11, pp. 1064-1065, 2019.

[16] X. Gu, W. Cai, M. Gao, Y. Jiang, X. Ning, and P. Qian, "Multi-source domain transfer discriminative dictionary learning modeling for electroencephalogram-based emotion recognition," *IEEE Transactions on Computational Social Systems*, 2022, In Press.

[17] Z. Huang, Y. Liu, C. Zhan, C. Lin, W. Cai, and Y. Chen, "A novel group recommendation model with two-stage deep learning," in *IEEE Transactions on Systems, Man, and Cybernetics: Systems*Press, 2021.

[18] W. Cai and Z. Wei, "Remote sensing image classification based on a cross-attention mechanism and graph convolution," *IEEE Geoscience and Remote Sensing Letters*, vol. 19, pp. 1–5, 2022, Art no. 8002005.

[19] D. Yao, Z. Zhi-li, Z. Xiao-feng et al., *Deep Hybrid: Multi-Graph Neural Network Collaboration for Hyperspectral Image classification[J]*, Defence Technology, 2022.

[20] L. You, H. Jiang, J. Hu et al., *GPU-accelerated Faster Mean Shift with Euclidean Distance Metrics*, arXiv preprint arXiv: 2112.13891, 2021.

[21] L. Chen, A. Baird, and D. Straub, "Why do participants continue to contribute? Evaluation of usefulness voting and commenting motivational affordances within an online knowledge community," *Decision Support Systems*, vol. 118, pp. 21–32, 2019.

Hindawi
Computational Intelligence and Neuroscience
Volume 2022, Article ID 7193234, 9 pages
https://doi.org/10.1155/2022/7193234

Research Article

An Adaptive Human Posture Detection Algorithm Based on Generative Adversarial Network

Zhiming Xu,[1] **Wenzheng Qu**,[2] **Hanhua Cao**,[1] **Meixia Dong**,[1] **Danyu Li**,[1] **and Zemin Qiu**[1]

[1]*Guangzhou Xinhua University, Guangzhou 510000, Guangdong, China*
[2]*University of Edinburgh, Edinburgh EH9 3JN, UK*

Correspondence should be addressed to Zemin Qiu; qiuzemin@xhsysu.edu.cn

Received 22 January 2022; Revised 19 February 2022; Accepted 21 February 2022; Published 31 March 2022

Academic Editor: Xin Ning

Human posture equipment technology has advanced significantly thanks to advances in deep learning and machine vision. Even the most advanced models may not be able to predict all body joints accurately. This paper proposes an adaptive generative adversarial network to improve the human posture detection algorithm in order to address this issue. GAN is used in the algorithm to detect human posture improvement. The algorithm uses OpenPose to detect and connect keypoints and then generates heat maps in the GAN system model. During the training process, the confidence evaluation mechanism is added to the system model. The generator predicts posture, while the resolver refines human joints over time. And, by using normalization technologies in the confidence evaluation mechanism, the generator can pay more attention to the prominent body joints, improving the algorithm's body detection accuracy of nodes. In MPII, LSP, and FLIC datasets, the proposed algorithm has shown to have a good detection effect. Its positioning accuracy is about 95.37 percent, and it can accurately locate the joints of the entire body. Several other algorithms are outperformed by this one. The algorithm described in this article has the best simultaneous runtime in the LSP dataset.

1. Introduction

The goal of human posture estimation is to predict positions from the input images of body joints. At the moment, human posture estimation relies on a variety of methods [1–6], such as Google's G-RMI, which uses target detection to open a human posture estimation method. The OpenPose system [7–9] proposed by Carnegie Mellon University (CMU) greatly improved the construction of human posture. OpenPose is an open-source library written in the Caffe programming language that can track human facial expressions, torsos, limbs, and even fingers. It is based on convolutional neural networks and supervised learning, not only for a single person, but also for a group. The introduction of AlphaPose has significantly improved the accuracy of human pose detection. The AlphaPose system [10,11] is a highly accurate real-time multiplayer posture estimation system. The algorithm uses a top-down structure, that is, to detect the inverted human body first and then obtain the key points and skeleton. Therefore, his accuracy and Ap values are higher than OpenPose. But the disadvantage is that as the number of people on the picture increases, his calculations increase and the speed becomes slower. These algorithms still have the problem of being frustrated in the face of occlusion problems—problems such as high accuracy, obstruction of real time, and limited small size images.

This article proposes an adaptive generative adversarial network to improve the human pose detection algorithm in order to address the aforementioned issues. Based on the robustness of the generative adversarial network (GAN) in occlusion conditions, the coherence of the shape, and the fidelity of the details, the algorithm improves the generative adversarial network (GAN) model [12–16]. The generator generates the human body posture, the discriminator distinguishes the actual heat map, and the human joint is gradually improved. The existing posture resolution effect is improved through continued training. Finally, the normalization technology is used to perform confidence processing on the generator's generated data in order to keep the correct key nodes, improving the algorithm's body node detection accuracy. Through experiments, compared with the existing methods, the proposed algorithm can improve the accuracy of the position of known people and search for poses in these areas through the GAN model.

2. This Article Algorithm

Human posture estimation is a very basic problem in computer vision. From the perspective of the name, it can be understood as an estimate of the position of the posture of the "human body" (key points, such as head, left hand, right foot, etc.). The traditional human skeleton key point detection algorithm is basically based on the idea of template matching on the basis of geometric a priori, so the core lies in how to use the template to represent the entire human body structure, including the representation of key points, the representation of limb structure, and the representation of the relationship between different limb structures. A good template matching idea can simulate more attitude ranges, so that it can better match and detect the corresponding human posture.

Human posture estimation can be divided into two lines of thought:

(1) "top-down," which refers to the detection of human body areas first and then the detection of key points in the human body in the area.

(2) "bottom-up:" which refers to detecting all the key points of the human body in the picture first and then corresponding these key points to different individual characters. It should be mentioned here that the first scheme is slower because it needs to detect each area of the human body separately for forward key point detection, while OpenPose uses the second scheme.

There are disadvantages of the "bottom-up" method: (1) the priori information of the global context is not used, that is, the key points of other people's bodies in the picture. (2) Corresponding key points to different individuals, the algorithm complexity is too high.

OpenPose improvement point: in the proposed "Part Affinity Fields (PAFs)," each pixel is a 2D vector for characterizing position and direction information. Based on the detected joint nodes and joint connection areas, using the greedy inference algorithm, these joint nodes can be quickly corresponded to different individual characters.

2.1. Heat Map

2.1.1. Critical Point Detection. Calculate the ground truth of S through the 2D points $x_{j,k}$ and $x_{i,k}$ marked in the image. Among them, $x_{j_1,k}$ and $x_{j_2,k}$ represent the real pixels corresponding to the two key points j_1 and j_2 of a certain person k in Figure 1. Calculation method: when the pixel point p is close to the annotation points $x_{j,k}$ and $x_{i,k}$, it reaches the peak of the normal curve. Then the S of the j-th joint in each image is the peak of the normal distribution of k individuals in the image.

Figure 1 is the heat map of each joint point. The first picture on the left is the input image and the final predicted joint position. The second picture is the probability result predicted by the channel responsible for the neck node. Red and yellow represent the high probability that the corresponding pixel location is the neck. The other blue areas mean that it will hardly be the neck location. The following pictures, respectively, represent the p probability results of different nodes predicted by different channels of heat map.

$$S^*_{j,k} = \exp\left(-\frac{\left\|p - x_{j,k}\right\|_2^2}{\sigma^2}\right),$$
$$S^*_j(p) = \min_k S^*_{j,k}(p). \tag{1}$$

2.1.2. Joint Connections. If a pixel p is located on this torso, the value of $L^*_{c,k}(p)$ represents the unit vector from the key point j_1 to the key point j_2. For pixels not on the torso, the corresponding vector is the zero vector.

Then the value of $L^*_{c,k}(p)$ is as follows:

$$L^*_{c,k}(p) = \begin{cases} v, & \text{if p on c}, k, \\ 0, & \text{otherwise}. \end{cases} \tag{2}$$

Among them, $v = (x_{j_2,k} - x_{j_1,k})/|x_{j_2,k} - x_{j_1,k}|_2$ represents the unit direction vector corresponding to this torso.

Pixels belonging to this torso satisfy the following function:

$$0 \le v\left(p - x_{j_1,k}\right) \le l_{c,k},$$
$$\left|v_{\perp}\left(p - x_{j_1,k}\right)\right| \le \sigma_l. \tag{3}$$

The inner table σ_l shows the distance between pixels. The length of the torso is $l_{c,k} = |x_{j_2,k} - x_{j_1,k}|_2$, $v_{\perp}$ represents the vector perpendicular to v. The whole image is the average value corresponding to all people in the image. $n_c(p)$ is the number of nonzero vectors corresponding to k persons at pixel p in the image.

$$L^*_c(p) = \frac{1}{n_c(p)} \sum_k L^*_{c,k}(p). \tag{4}$$

Figure 2 is an image of the key nodes of the human body extracted by the above algorithm. The article extracts the key points of the image and then connects the key points to the image of the human body posture.

2.2. Generative Adversarial Network (GAN). The generative adversarial network (GAN) was proposed by GOOdfellOw, using two convolutional neural networks using game training to generate samples similar to the original pictures [17–19].

Figure 1: Key point probability distribution plot.

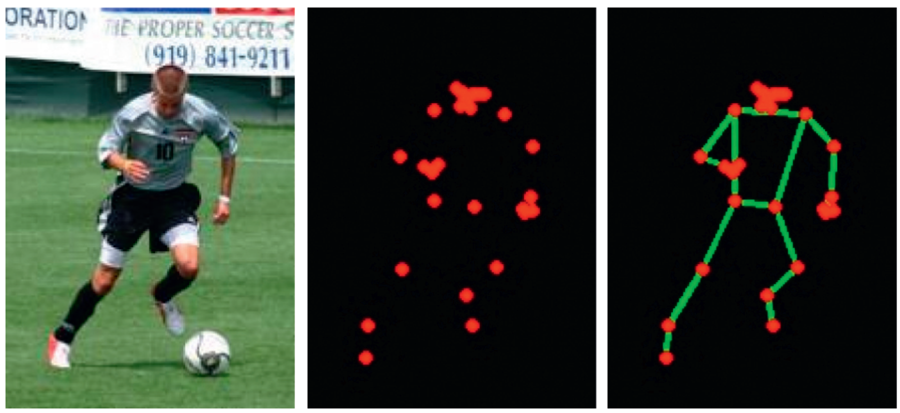

Figure 2: Human body posture design diagram.

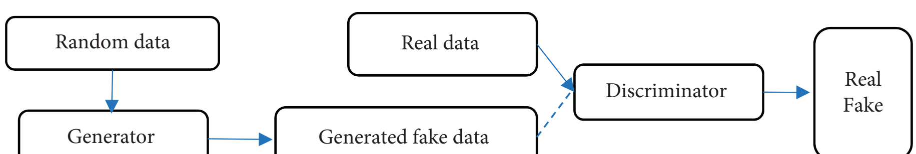

Figure 3: Generative adversarial network structure.

Figure 3 shows the structure of the generated confrontation network, which shows that GAN is primarily made up of a generating network *G* and a discriminating network D. It makes use of a conflicting relationship. The goal is for the generator to be able to generate data that is similar to real data distribution while giving the impression of being fake. GAN, which is aimed at the problem of data prediction, trains the generator to learn the data distribution and predicts the image distribution data. The success of confrontational ideas benefits the GAN network as well. Machine learning and artificial intelligence are two fields where the concept of confrontation has been introduced. Confrontation is present in the two behaviors of "game" and "competition." Game machine learning is the result of combining game theory and machine learning.

The advantages and disadvantages of GAN: compared with other generative models, GAN has the following four advantages:

(a) From the actual results, GAN seems to produce better samples than other models.

(b) Most other frameworks require the generator network to have a certain functional form; for example, the output layer is Gaussian. It is important that all other frameworks require that the generator network be distributed with nonzero quality. The generative confrontation network framework can train any type of generator network and can learn to generate points only on thin manifolds close to the data.

(c) Any generator network and any discriminator will be useful because it does not need to design a model that follows any type decomposition.

(d) There is no need for reasoning during the learning process and no need to use Markov chain for repeated sampling (inference), thus avoiding difficult approximate calculation problems of probabilities.

2.3. The Generative Adversarial Network of Pose. The model in this paper is divided into two networks, the generator and the discriminator, similar to the traditional GAN model [20, 21]. A convolutional network is the first network generator. The generator generates a set of heat maps that show the confidence score of each position of each key point after forward calculation. The second network discriminator uses the same architecture as the generator, but it encodes the input heat map along with the RGB image and decodes it into a new set of heat maps in order to distinguish between the real and fake heat maps. The generator is strengthened to generate the human body posture as a result of the game between the generator and the discriminator, and the discriminator's human joints are gradually improved. The existing pose estimation model is improved through continuous training, as shown in Figure 4.

2.3.1. Generator. The generator is responsible for predicting the posture, and its role is to generate accurate information about the key points of the human body. Of course, as part of the generational confrontation, the main function of the generator is to allow the generated key points to fool the final discriminator, so that the discriminator cannot distinguish whether the current key point heat map is actual or generated by the generator.

That is to say, the purpose of the counter loss is to make the key points generated by the generator conform to a more reasonable posture. More directly, the purpose of L_{adv} is to make the false heat map generated by the generator fool the discriminator as much as possible, making it impossible to distinguish between the GT heat map and the false heat map. The process of generating confrontation is reflected here. Finally, the loss shown in formula 3 is used to optimize the generator. λ is a hyperparameter. The generator loss function is as follows:

$$\begin{aligned} L_{\text{MSE}} &= \sum_{i=1}^{N}\sum_{j=1}^{M}\left(C_{ij}-\widehat{C}_{ij}\right)^2,\\ L_{\text{adv}} &= \sum_{i=1}^{N}\left(\widehat{C}_j - D\left(\widehat{C}_j, X\right)\right)^2,\\ L_G &= L_{\text{MSE}} + \lambda L_{\text{adv}}, \end{aligned} \tag{5}$$

where L_{MSE} is the loss of the generator, L_{adv} is the counter loss from the resolver, and λ is a hyperparameter.

2.3.2. Differentiator. The discriminator's goal is to improve human joints over time. The goal is to determine whether the input heat map is the real thing or a forgery created by the generator. The discriminator's ultimate training goal is to be able to tell the difference between the data generated by the generator and the real heat map as much as possible. As a result, a confrontation game with the generator is formed.

The encoded new heat map is obtained by inputting the false heat map generated by the generator into the discriminator. And calculate the distance between the new heat map and the fake heat map generated by the generator to calculate the L_{fake} loss. As mentioned above, the purpose of the discriminator is to distinguish the false heat map from the actual heat map as much as possible. That is to say, the classifier hopes that the output reconstructed heat map after the actual heat map input is as close as possible to the actual one. The loss function of the discriminator is as follows:

$$\begin{aligned} L_{\text{real}} &= \sum_{j=1}^{N}\left(C_j - D\left(C_j, X\right)\right)^2,\\ L_{\text{fake}} &= \sum_{j=1}^{N}\left(\widehat{C}_j - D\left(\widehat{C}_j, X\right)\right)^2,\\ L_G &= L_{\text{real}} + k_t L_{\text{fake}},\\ k_{t+1} &= k_t + \lambda_k\left(L_{\text{real}} - L_{\text{fake}}\right). \end{aligned} \tag{6}$$

The *kt* in the above formula is used to constrain the capability of the discriminator. Constraining *kt* through the formula can make the network easier to train. But GAN is unstable and difficult to train because the discriminator converges too fast. This will cause the network to easily collapse and train an invalid generator. In response to this problem, in order for the network to be able to generate enough truth to deceive the discriminator. By studying the relationship between L_{fake} and L_{real}, it can be found that, with the increase of kt, L_{fake} has more advantages, which makes the discriminator more training to recognize the generated heat map. But *kt* is not an infinite stack. To this end, this paper extracts the confidence heat map information from the discriminator and feeds it back into the generator, thereby enhancing the generator's accurate prediction of the key nodes of the human body on the ground.

2.4. Confidence Evaluation Mechanism. The generator can pay more attention to prominent body joints because the confidence evaluation mechanism uses normalization technology. As a result, the algorithm's body node's detection accuracy increases. To determine the key points' credibility, compare the generated heat map with the actual heat map. Following that, improve the algorithm's key point extraction accuracy. The following are the techniques.

The discriminator is used to process the generated heat maps and truth heat maps in this paper—confidence heat maps that were derived from the data. The pose resolver requires two tags to calculate two losses. The identification network marks the real samples as 1 and the pseudosamples as 0, in the traditional work of image conversion using GAN. We discovered that using only 0 or 1 as the label for the human body pose estimation problem makes convergent network difficult. As a result, this paper relies on the discriminator's confidence heat maps to direct the generator's data generation.

Set the initial setting of the generator to a low-confidence heat map. Then the confidence discriminator classifies the result as fake. The generator will self-optimize based on this result error to generate a higher degree of confidence until it can make the discriminator think that the result of the generator is true. Therefore, even if there is occlusion, this process will help the generator to generate a high-confidence heat map.

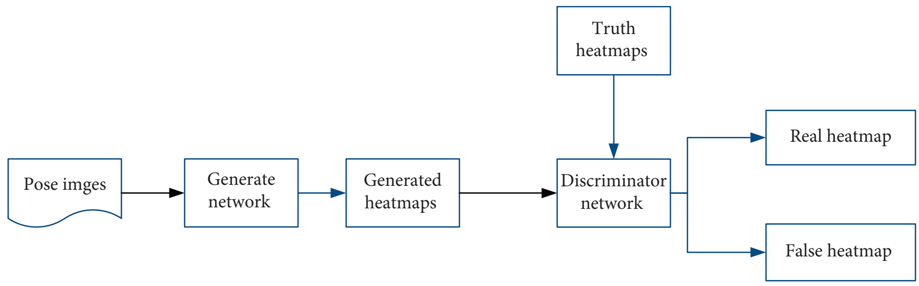

Figure 4: Human pose generation confrontation network structure model.

The vector corresponding to the feature map with the corresponding key point value is 1, and the vector corresponding to the feature map without the key point is 0, where *di* is the normalized distance between the predicted position of the i-th body part and the true position. For fake samples, if the predicted body part is far away from the real position, then the posture in this image is obviously not believable to the body structure. Therefore, if the distance is relatively close, the corresponding vector is 1; otherwise the corresponding vector is 0.

Then the corresponding value of C_{fake} is shown in the following formula. When the generated key point heat map is relatively close to the actual heat map (the distance is less than the threshold), the corresponding vector is 1. Otherwise, the corresponding vector is 0.

$$C_{\text{fake}} = \begin{cases} v, & \text{if } \left\| d_i - \hat{d}_i \right\| < \tau, \\ 0, & \text{if } \left\| d_i - \hat{d}_i \right\| \geq \tau. \end{cases} \quad (7)$$

Among them, for the feature map, first transform x into feature space f and g. And make it satisfy

$$\begin{aligned} f(x) &= W_f(x), \\ g(x) &= W_g(x). \end{aligned} \quad (8)$$

$W_f(x)$ is the weight matrix of generated heat maps. $W_g(x)$ is the weight matrix of confidence heat maps.

The distance is normalized to [0, 1] through element transformation.

$$d_i = \frac{e^{\|f(x_i) - g(x_i)\|_2} - 1}{e^{\|f(x_i) - g(x_i)\|_2} + 1}. \quad (9)$$

In the end, the best key points are obtained, and the network model of the algorithm in this paper is shown in Figure 5.

Figure 6 is the result of adopting the human body pose generation confrontation network structure that introduces confidence. The human body posture is generated by the generator, and the discriminator is gradually improving the human joints. Finally, the normalization technology is used to perform confidence processing on the generator's generated data to retain the correct key nodes. In turn, the detection accuracy of the body node of the algorithm is improved. The effect is shown below.

Through observation, it can be seen that the above method can accurately locate the characters of the image and can accurately locate all key nodes of the whole body. In order to better verify the feasibility of the algorithm, the following is a detailed experiment.

3. Simulation Experiments

3.1. Experimental Environment and Datasets. The experimental environment of this article: Ubuntu 16.04.4 platform is implemented by Python programming with open CV 3.4 and Tensorflow 1.5 frameworks, processors: Intel Core i7 7700 HQ (up-to 3.8 GHz), 16 GB Memory, nVidia Geforce GTX 1060 6 GB VGA, training with a total of 20,000 images, training time of 80 hours.

Dataset: this paper selects three widely used human posture datasets as follows.

3.1.1. LSP Human Posture Estimation Dataset (Address: https://sam.johnson.io/research/lsp.html). Leeds Sports Pose is a dataset of sports postures divided into categories such as athletics, badminton, baseball, gymnastics, parkour, soccer, volleyball, and tennis, all of which are images from physical activity and thus very challenging in terms of appearance, particularly joints. The dataset consists of 2,000 annotated images of postures primarily sourced from Flickr and labeled with the labels shown above. The length of the most prominent person has been scaled to approximately 150 pixels in these images. Each image has 14 joint positions labeled.

3.1.2. FLIC Human Detection Dataset (Address: https://bensapp.github.io/flic-dataset.html). FLIC is a dataset of images that label people in frames of movies, which contains 5,003 images collected from mainstream Hollywood movies. The training images are derived from a character detector running in 30 movies and are manually annotated for them after the pictures are taken, including 10 upper body joints. In addition, there are 5 median markers in the image to ensure that the outlier annotation is robust. Publishers voluntarily reject images that are obscured or have too low picture clarity and reserve 20% of about 1016 images for testing.

3.1.3. MPII Human Posture Estimation Dataset (Address: https://human-pose.mpi-inf.mpg.de/). MPII is a dataset for evaluating human posture estimates and related

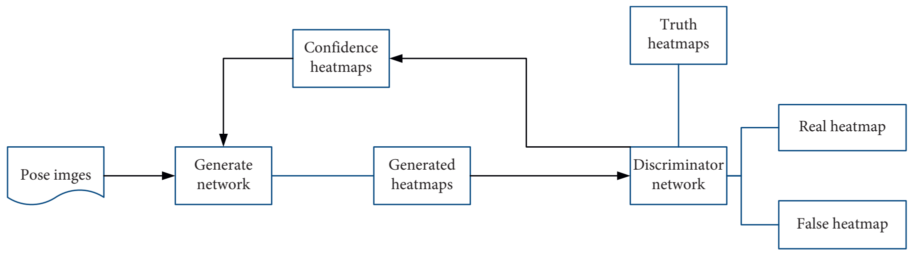

Figure 5: Introduces confidence in human posture generation of adversarial network structures.

Figure 6: Human posture setting effect.

benchmarks, with approximately 25,000 images and more than 40,000 people with annotated joints, systematically collecting images using established taxonomies of human activity.

Overall, the dataset covers 410 human behaviors and each image provides an activity tag, each image is from a YouTube video, and provides a related unnoticed framework. In addition, the test set's annotations include body part occlusion, 3D torso, and head orientation.

3.2. Evaluate Metrics. The article selects the LSP human pose estimation data set for verification and uses the percentage of correct key points (PCK) to measure the performance of the LSP data set. We choose the traditional OpenPose algorithm; [20] algorithm, and [21] algorithm to verify the accuracy of the algorithm by calculating the percentage of correct detections that fall within the normalized distance and recording the data results. Table 1 shows the data obtained by measuring the key nodes of the whole body using the abovementioned algorithms, as shown in the table.

This article selects head, shoulder, elbow, wrist, hip, knee, and ankle as 7 nodes for data comparison; through the observation of the data, it can be seen that the proposed algorithm synthesis data is better than several other algorithms. Among them, the algorithm of this paper has achieved the best results in head, shoulder, elbow, and ankle of 96.64%, 95.16%, 95.97%, and 95.16%, respectively. The average values of each algorithm were 89.83%, 92.30%, 94.71%, and 95.37%, respectively; you can see that using the algorithm of this article in the key point extraction effect is the best. We aimed to verify whether the algorithm can still maintain good results in different environments. In this paper, we use LSP human pose estimation data set to verify that the difference is motion pictures. After testing, the result of the test is shown in Figure 7.

Through observation, it can be seen that the data obtained by the algorithm of this paper can accurately locate the characters in the image. And in the key extraction renderings of the human body, the key points will not appear to be missing and elegant. The algorithm can accurately locate according to the different actions of the characters. It further verifies the key point extraction accuracy of the algorithm.

By collecting the iterative data of each algorithm, and according to the number of iterations of the algorithm, the data curve shown in Figure 8 can be obtained, which is marked according to the number of iterations and accuracy of each algorithm, as shown in Figure 8.

By observing the curve data graph in Figure 8, it can be seen that the final accuracy of the algorithm in this paper is higher than the other three algorithms, but the cost is that the number of iterations required by the algorithm is higher than that of other algorithms. It can be seen that the accuracy of the algorithm in this paper is stable at about 96.20%, and the number of iterations needs to meet more than 350 times to achieve. In contrast, the number of iterations of other algorithms can reach the highest value of the algorithm at about 200 times.

3.3. Qualitative Analysis. The article selects the LSP human pose estimation data set for qualitative analysis. And on the basis of the above, the key points are connected and displayed in the actual image. At the same time, combined with target detection, on the basis of human posture, the detection effect of target detection is strengthened. Reflect in the following. The detection image is shown in Figure 9.

By observing Figure 9, it can be seen that using the algorithm in this paper, good key point extraction and target locking can be maintained in different motion environments. This method strengthens the processing of extraction and confidence through high-performance network architecture and loss function. In turn, the high-precision human body posture positioning effect is obtained, and the pedestrian detection capability is better.

3.4. Comparison of Average Running Time. In this paper, we train on the MPII human body pose estimation data set, LSP human body pose estimation data set, and FLIC human

Table 1: Correct detection percentage.

Method	Head	Shoulder	Elbow	Wrist	Hip	Knee	Ankle	Average value
Traditional algorithms	89.01	85.40	91.72	89.06	89.90	91.45	92.30	89.83
Literature [20] algorithms	91.96	91.57	88.32	90.21	94.65	94.90	94.51	92.30
Literature [21] algorithms	93.81	98.76	93.57	94.51	95.68	93.05	93.56	94.71
This article algorithm	96.64	95.16	95.97	94.73	94.88	95.08	95.16	95.37

Figure 7: Key point extraction rendering.

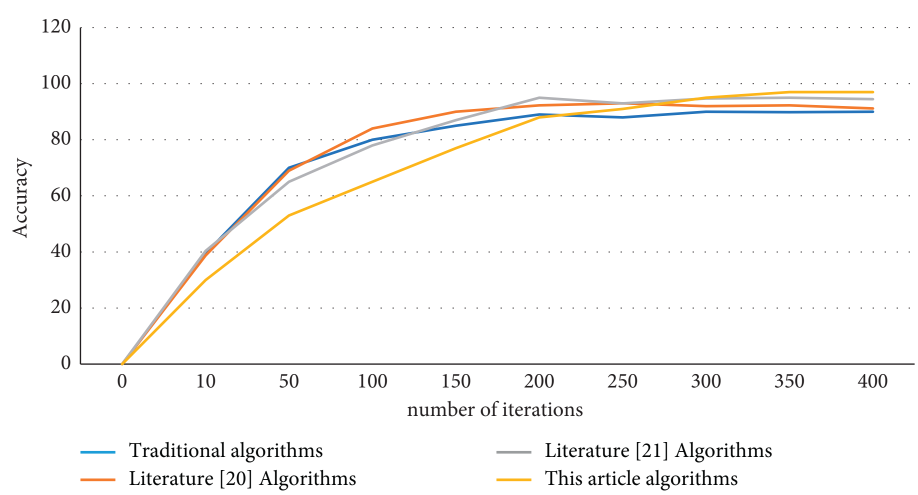

Figure 8: The number of iterations and the accuracy of each algorithm into the data curve.

body detection data set. And the various running times are compared, and the results are shown in Table 2.

Verify the algorithm's running time in various environments by observing the data differences to see if the algorithm can maintain a stable running effect. We can see

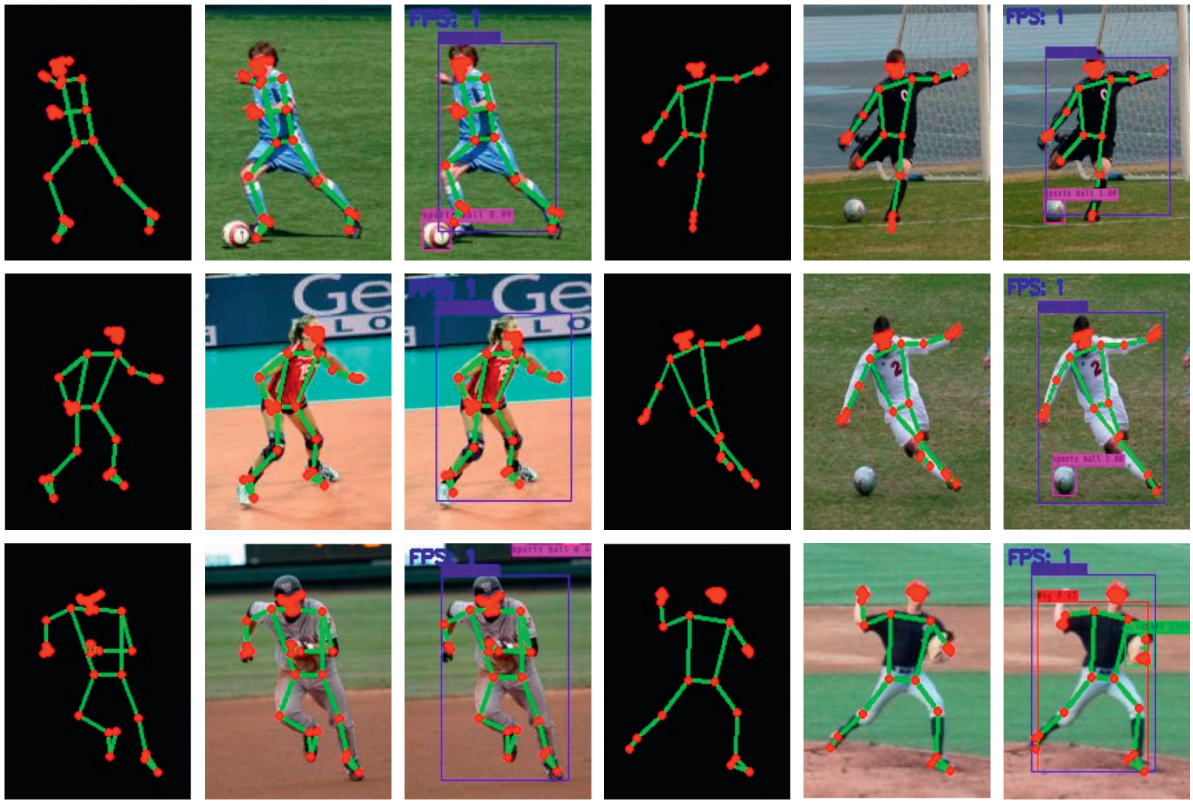

Figure 9: Human body posture design effect figure.

Table 2: Average running time under each data set.

Method	Model size (M)	Runtime(s) on MPII test set	Runtime(s) LSP test set	Runtime(s) FLIC test set
Traditional algorithms	162.1	1.242	0.234	1.07
Literature [20] algorithms	157.3	1.201	0.325	0.921
Literature [21] algorithms	196.21	1.266	0.238	0.951
This article algorithm	201.2	1.191	0.229	0.806

that the algorithm in this paper performs well in each data set by comparing the data in Table 2. The model used in this paper is the largest of them all, but in terms of running time, it can be applied to a variety of other algorithms. The effect expressed in the LSP data set is the best, with a time of only 0.229 s, effectively proving the algorithm's feasibility.

4. Conclusion

The article proposes an adaptive generative adversarial network to improve human pose detection algorithm. In the algorithm model of this article, the generator is responsible for predicting the posture, and the discriminator is for the gradual improvement of the human joints. However, in the actual training process, the predicted nodes generated by the generator sometimes deviate from reality. Therefore, this paper introduces a confidence evaluation mechanism into the system to determine the credibility of the generated key points, so that the generator can pay more attention to the prominent body joints, thereby improving the detection accuracy of the algorithm. Finally, by using three standard data sets to evaluate the algorithm, it can be seen that the algorithm is superior to other algorithms in terms of detection accuracy and running time. This effectively proves the effectiveness of our method. Compared with the existing methods, the algorithm in this paper can use the GAN model to search for the positions of known persons and search for poses in these areas and improve the prediction of subsequent poses based on the existing data, and the accuracy is greatly improved. In the next step, we will conduct in-depth research on the improvement of model training stability and how to improve the resolution of generated images.

Data Availability

The data used to support the results of this study need to be obtained with the consent of the corresponding author.

Conflicts of Interest

The authors declare that there are no conflicts of interest regarding the publication of this paper.

Authors' Contributions

The authors have equally contributed to the manuscript. All authors read and approved the final manuscript.

Acknowledgments

This research was supported by the Science and Technology Project of Guangzhou under Grant No. 202002030273, Guangzhou Xinhua University Teaching Quality and Teaching Reform Project, No. 2021JYS003, and Guangzhou Xinhua University School-level Scientific Research Project, No. 2019KYQN12.

References

[1] H. Liu, Y. Chen, W. Zhao, S. Zhang, and Z. Zhang, "Human pose recognition via adaptive distribution encoding for action perception in the self-regulated learning process," *Infrared Physics & Technology*, vol. 114, Article ID 103660, 2021.

[2] M. Kruis, *Human Pose Recognition Using Neural Networks, Synthetic Models, and Modern Features*, Oklahoma State University, Stillwater, OK, USA, 2010.

[3] H. Wang, F. Zhou, W. Zhou, and L. Chen, "Human pose recognition based on depth image multifeature fusion," *Complexity*, vol. 2018, Article ID 6271348, 12 pages, 2018.

[4] Y. K. Zhou, Y. Wang, and Y. F. Zhao, "Human pose recognition based on CNN," *Computer and Modernization*, vol. 2, pp. 49–54+92, 2019.

[5] F. Sajjad, A. F. Ahmed, and M. A. Ahmed, "A study on the learning based human pose recognition," in *Proceedings of the 2017 9th IEEE-GCC Conference and Exhibition (GCCCE)*, pp. 1–8, Manama, Bahrain, May 2017.

[6] C.-W. Wang and A. Hunter, "Robust pose recognition of the obscured human body," *International Journal of Computer Vision*, vol. 90, no. 3, pp. 313–330, 2010.

[7] A. P. Yunus, N. C. Shirai, K. Morita, and T. Wakabayashi, "Time series human motion prediction using RGB camera and OpenPose," *International Symposium on Affective Science and Engineering*, vol. ISASE2020, pp. 1–4, 2020.

[8] D. Zhou, "OpenPose combined with BP network behavior detection method," *Journal of Guizhou University: Natural Science Edition*, vol. 37, no. 3, p. 6, 2020.

[9] K. Fujiwara and K. Yokomitsu, "Video-based tracking approach for nonverbal synchrony: a comparison of Motion Energy Analysis and OpenPose," *Behavior Research Methods*, pp. 1–12, 2021.

[10] Y. L. Jin, "Fall detection technology based on alphapose bone key points and GRU neural network," *Computer Science and Application*, vol. 11, no. 4, pp. 840–848, 2021.

[11] W. Shaojie and Y. Zhou, "Human body fall detection model combining alphapose and LSTM," *Small Microcomputer System*, vol. 40, no. 9, 2019.

[12] M. N. Allahyani, R. M. Alsulami, T. H. Alwafi et al., "SD2GAN: A siamese dual discriminator generative adversarial network for mode collapse reduction," vol. 1, pp. 1–9, 2021.

[13] H. Chen, "Challenges and corresponding solutions of generative adversarial networks (GANs): a survey study," *Journal of Physics: Conference Series*, vol. 1827, no. 1, Article ID 012066, 2021.

[14] Y. Wang, D. Chang, and Y. Zhao, "A new blind image denoising method based on asymmetric generative adversarial network," *IET Image Processing*, vol. 15, no. 6, pp. 1260–1272, 2021.

[15] Y. Zhou, P. Zhao, W. Tong, and Y. Zhu, "CDL-GAN: contrastive distance learning generative adversarial network for image generation," *Applied Sciences*, vol. 11, no. 4, p. 1380, 2021.

[16] L. Huang, J. Zhuang, and X. Cheng, "STI-GAN: multimodal pedestrian trajectory pre-diction using spatiotemporal interactions and a generative adversarial network," *IEEE Access*, no. 99, pp. 1–9, 2021.

[17] I. J. Goodfellow, J. Pouget-Abadie, and M. Mirza, "Generative adversarial networks," *Advances in Neural Information Processing Systems*, vol. 3, no. 1, 2014.

[18] F. Lateef, Y. Ruichek, and M. Kas, "Saliency heat-map as visual attention for autonomous driving using generative adversarial network (GAN)," *IEEE Transactions on Intelligent Transportation Systems*, vol. 99, no. 1, pp. 1–14, 2021.

[19] F. Wang, Z. Xu, W. Ni, J. Chen, and Z. Pan, "An adaptive learning image denoising algorithm based on eigenvalue extraction and the GAN model," *Computational Intelligence and Neuroscience*, vol. 2022, Article ID 5792767, 10 pages, 2022.

[20] A. Nambiar, A. Bernardino, and J. C. Nascimento, "GAN-based pose-aware regulation for video-based person Re-identification," *ACM Computing Surveys*, vol. 52, no. 2, pp. 1–34, 2019.

[21] X. Wang, Z. Cao, R. Wang, Z. Liu, and X. Zhu, "Improving human pose estimation with self-attention generative adversarial networks," *IEEE Access*, vol. 7, 2019.

Hindawi
Computational Intelligence and Neuroscience
Volume 2023, Article ID 9805282, 1 page
https://doi.org/10.1155/2023/9805282

Retraction

Retracted: Study of Trunk Morphological Imbalance and Rehabilitation Outcome of Adolescent Idiopathic Scoliosis with Intelligent Medicine

Computational Intelligence and Neuroscience

Received 25 July 2023; Accepted 25 July 2023; Published 26 July 2023

This article has been retracted by Hindawi following an investigation undertaken by the publisher [1]. This investigation has uncovered evidence of one or more of the following indicators of systematic manipulation of the publication process:

(1) Discrepancies in scope
(2) Discrepancies in the description of the research reported
(3) Discrepancies between the availability of data and the research described
(4) Inappropriate citations
(5) Incoherent, meaningless and/or irrelevant content included in the article
(6) Peer-review manipulation

The presence of these indicators undermines our confidence in the integrity of the article's content and we cannot, therefore, vouch for its reliability. Please note that this notice is intended solely to alert readers that the content of this article is unreliable. We have not investigated whether authors were aware of or involved in the systematic manipulation of the publication process.

In addition, our investigation has also shown that one or more of the following human-subject reporting requirements has not been met in this article: ethical approval by an Institutional Review Board (IRB) committee or equivalent, patient/participant consent to participate, and/or agreement to publish patient/participant details (where relevant).

Wiley and Hindawi regrets that the usual quality checks did not identify these issues before publication and have since put additional measures in place to safeguard research integrity.

We wish to credit our own Research Integrity and Research Publishing teams and anonymous and named external researchers and research integrity experts for contributing to this investigation.

The corresponding author, as the representative of all authors, has been given the opportunity to register their agreement or disagreement to this retraction. We have kept a record of any response received.

References

[1] Q. Zhao, Y. Huang, M. Wu et al., "Study of Trunk Morphological Imbalance and Rehabilitation Outcome of Adolescent Idiopathic Scoliosis with Intelligent Medicine," *Computational Intelligence and Neuroscience*, vol. 2022, Article ID 6775674, 8 pages, 2022.

Hindawi
Computational Intelligence and Neuroscience
Volume 2022, Article ID 6775674, 8 pages
https://doi.org/10.1155/2022/6775674

Research Article

Study of Trunk Morphological Imbalance and Rehabilitation Outcome of Adolescent Idiopathic Scoliosis with Intelligent Medicine

Qin Zhao,[1,2] Yiming Huang,[3] Maodong Wu,[1,2] Longying Shen,[1,2] Yu Lu,[1,2] Xingyue Fan,[1,2] and Qinglun Su[1,2]

[1]*The First affiliated Hospital of Kangda College of Nanjing Medical University, Lianyungang, Jiangsu 222000, China*
[2]*Department of Rehabilitation Medicine The First People's Hospital of Lianyungang, Lianyungang,, Liaoning 222000, China*
[3]*Jinzhou Medical University Rehabilitation Medicine and Physiotherapy, Jinzhou 121001, Liaoning, China*

Correspondence should be addressed to Qinglun Su; suqinglun@njmu.edu.cn

Received 26 January 2022; Revised 17 February 2022; Accepted 24 February 2022; Published 28 March 2022

Academic Editor: Xin Ning

In recent years, artificial intelligence technology has been widely used in various medical fields to effectively assist physicians in patient treatment operations. In this paper, we design and implement a deep biblical network model-based orthotic design for adolescent idiopathic scoliosis to quickly and effectively assist physicians in designing orthotics for adolescent idiopathic scoliosis. A fuzzy set is used to express the knowledge of adolescent idiopathic scoliosis orthosis design, and a fuzzy reasoning based on the confidence level is implemented. Finally, the efficiency of the design of adolescent idiopathic scoliosis orthoses was improved by 50% through two cases of adolescent idiopathic scoliosis patients, and the deviation rate between the inference value and the actual operation value of the domain experts was less than 10%.

1. Introduction

Adolescent Idiopathic Scoliosis (AIS) is a skeletal and muscular disorder of unknown etiology that occurs during preadolescence or before skeletal growth and maturation, mostly in females aged 10 to 18 years. The prevalence of scoliosis in adolescents is increasing year by year, and the prevalence of scoliosis in adolescents is reported to be more than 5% in Guangdong and other regions [1–3], and the increase in prevalence is especially obvious in junior high school (12–15 years old).

AIS can cause great physical and psychological harm to the affected adolescents and one of the most easily detected and most important concerns of the patients themselves is the physical appearance deformity. The most easily recognized and most important concern is the deformity of the physical appearance. Since the human torso is an integral part [4], AIS not only manifests as distortion and deformity of the spine but also affects the position of the scapular girdle, thorax, and pelvis, resulting in high and low shoulders, razor backs, thoracic deformities, and pelvic disorders [5, 6].

If left untreated, it can lead to secondary symptoms such as chronic pain and pulmonary dysfunction, and severe scoliosis deformity can also can cause irreversible damage to respiratory function and spinal nerves, bringing great harm to individuals and families [5]. Therefore, the prevention and treatment of the prevention and treatment of AIS has been the focus of attention of experts and scholars in the field of spinal surgery and spinal rehabilitation for patients with idiopathic scoliosis and their corresponding X-ray images, as shown in Figure 1.

Surgery is recognized as an effective treatment for AIS, but according to statistics, only 1% of AIS patients require surgery and surgery can cause limitations in spinal motion. In Europe, exercise therapy interventions for scoliosis were first developed and have resulted in many mature rehabilitation systems; in China, research on AIS rehabilitation started later and there are more case studies and interventions [7, 8]. Therefore, experimental research on the idea or system of AIS rehabilitation therapy is needed.

Since the Cobb angle became the gold standard for scoliosis, the focus of AIS treatment has been on how to reduce the scoliosis angle and slow the progression of the scoliosis curve, while the local or overall morphological imbalance of the trunk caused by scoliosis has been increasingly neglected. Because the visual impact of poor posture is more severe, it is important to assess the trunk imbalance in patients with AIS before developing a rehabilitation program and to design a customized program for the patient [9].

AIS, as shown in Figure 2, is one of the most common types of scoliosis, accounting for approximately 80% of all idiopathic scoliosis, with the prevalence of AIS reaching 1% to 3% in the 10- to 16-year-old risk group. AIS not only affects the physical appearance of adolescents but also impairs their respiratory function, motor function, psychological status, and overall quality of life [10].

It is proposed that the difference of about 5° in scoliosis measurements is usually an error in measurement rather than a difference in the degree of scoliosis itself.

AIS is a common orthopedic disorder of uncertain etiology that affects the normal growth and function of the spine. 1%–3% of the normal population has AIS, and the main principle of clinical intervention is to control the progression of scoliosis using AIS orthoses [11–13]. An expert system contains a large amount of knowledge of domain experts inside and it can simulate the expert's reasoning methods to solve problems in the domain [14–16]. The currently popular expert systems are mainly classified as rule-based reasoning-based expert systems [17–20], artificial neural network-based expert systems [21], and rough set-based expert systems [22]. In [23], a generative-based expert system shell design method was proposed and applied to the treatment of AIS; however, the system could not be fully applicable to the knowledge expression and reasoning of uncertain information in the design of AIS orthoses.

2. Related Work

The authors of [24] found that the Cobb angle measurement error was around 3.2°, and this measurement difference should be taken into account when diagnosing and treating scoliosis. In addition, errors in the Cobb angle measurement can lead to differences in subsequent staging. The typing reliability of radiographs based on a given angle was found by [24]. The authors of [25], only general intraobserver ($\kappa = 0.50$) and interobserver reliability ($\kappa = 0.60$) were found for Lenke typing in cases where the ab initio Cobb angle measurements were required. The authors of [2] proposed that T1 tilt signifies that patients may have upper thoracic segment scoliosis and validated that this method of determining the presence or absence of upper thoracic curvature was included in the King typing, but subsequent studies by [3] reported that patients with AIS with T1 tilt do not necessarily show differences in the appearance of high and low shoulders, and therefore, the T1 tilt direction and T1 tilt angle do not reflect the imbalance of the patient's shoulders. In [14], the angle between the line connecting the highest points of the left and right clavicles and the horizontal plane was defined as the clavicle angle (CA) and used as a parameter to measure the balance of the shoulder. A study by [7] showed a significant correlation between reduced cervical physiological curvature and inadequate thoracic kyphosis in patients with AIS; in addition, cervical curvature correlated with lumbar anterior convexity angle, independent of thoracolumbar lateral bending angle and pelvic parameters. Reference [6] performed an imaging study of sagittal pelvic parameters in normal Chinese adults and concluded that the mean value of PI in Chinese adults was $45.1^\circ \pm 9.6^\circ$.

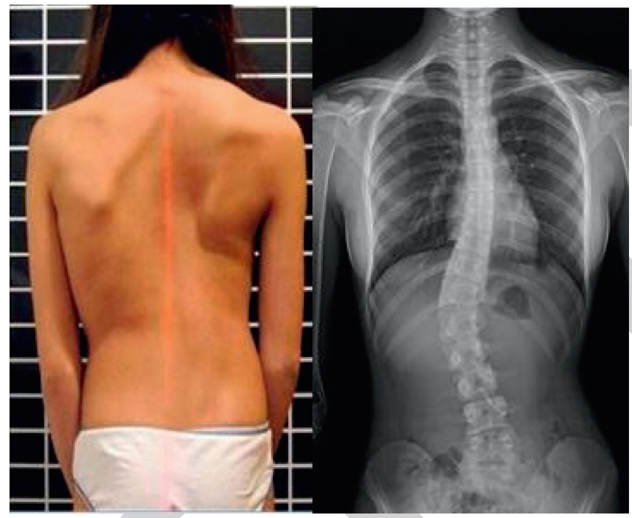

Figure 1: Patients with idiopathic scoliosis and their corresponding x-ray images.

In the field of spinal surgery, AI is widely used for diagnosis of diseases, especially for image processing, measurement, and classification. Theoretically, the successful development and application of AI-based automated measurement systems will provide an objective, accurate, and rapid solution to these problems and improve the diagnosis and treatment of AIS patients.

3. U-Net-Based Scoliosis Typing Algorithms for Idiopathic Scoliosis

The original data set is expanded, and the expanded data set is fed into the network for training and prediction to obtain the segmentation results; then, the segmentation results are fed into the automatic Cobb angle measurement algorithm designed in this paper to obtain the identified upper and lower endplate positions and Cobb angles; finally, the center points of the segmented images are extracted and fitted to obtain the curve fitting coefficient features, and the corresponding Cobb angles are measured by the automatic Cobb angle measurement algorithm. Finally, the center point of the segmented image is extracted and fitted to obtain the curve fitting coefficient features, and the corresponding

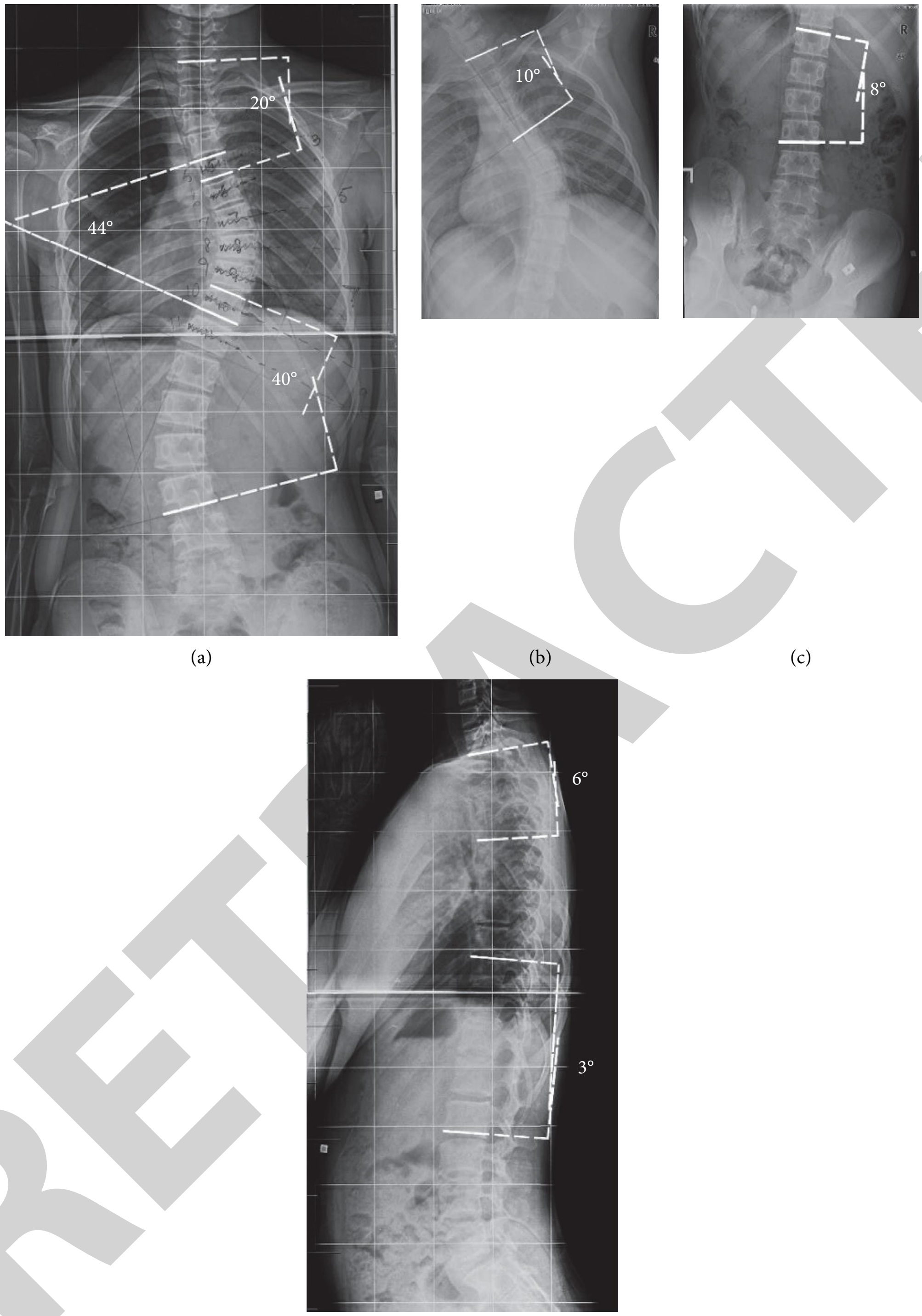

Figure 2: Cobb angle measurement method.

bending bits and Cobb angles of the side slices are measured by the automatic Cobb angle measurement algorithm and used as auxiliary feature materials. The overall framework is shown in Figure 3, and the automatic Lenke typing algorithm based on the U-net partition network can be implemented by experimenting according to the process shown in the overall framework.

4. Overall Design

The AIS expert system infers diagnostic and therapeutic solutions to assist physicians in solving complex medical problems [19]. The method in this paper can reason out the selection and design parameters of the AIS orthosis from patient information, and its structure is shown in Figure 4.

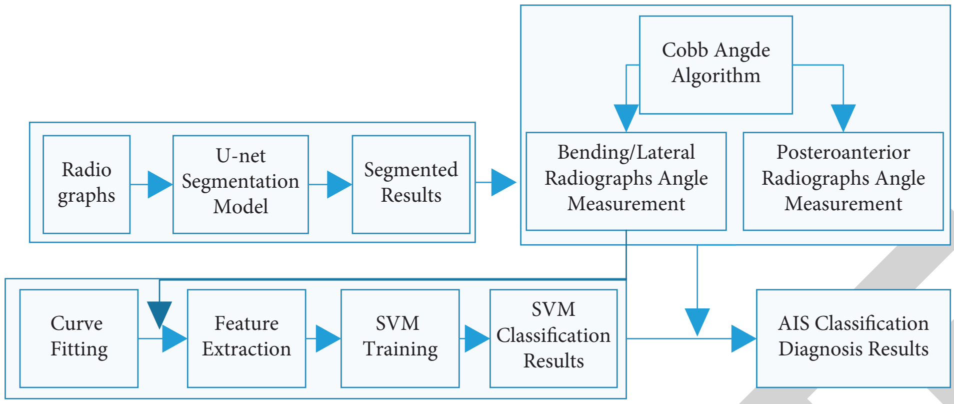

Figure 3: Flowchart of the overall framework of the U-net-based automatic typing algorithm.

The architecture functional modules in this paper include the fuzzy reasoner, knowledge base, knowledge base management system, agenda, interpreter, and human-machine interface. They are described separately as follows. They activate rules from the knowledge base for questions posed by the user according to the established reasoning strategy and process the facts until the end of reasoning. A dynamic storage space containing all facts in the fact base and intermediate results in the reasoning process is present.

Real-time operations such as adding, deleting, modifying, and querying the knowledge base, as well as consistency and integrity checking of the knowledge therein are performed.

A database for storing domain expert knowledge is found. The knowledge base serves as the basis for reasoning and is the foundation of the expert system's reasoning.

A functional module explains the reasoning process of an expert system in a way that is easy to understand by the user. It gives the user a clear understanding of the reasoning process and decision making of the expert system.

The functional module that performs real-time operations such as adding, deleting, modifying, and querying the fact database, as well as displaying the expert system decisions and explanations by the interpreter is present.

The workflow of the method in this paper is shown in Figure 5.

Its fuzzy reasoning unit is shown in Figure 6.

In the fuzzy inference stage of the method in this paper, the confidence degree CFRHS of the right-hand side (RHS) of the activation rule is calculated as [10].

$$CF_{RHS} = CF_{LHS} \times CF_R, \tag{1}$$

where CFLHS is the confidence of the left part of the rule; CR is the confidence of the rule.

In the deblurring stage, the deblurring algorithm of the method in this paper uses the weighted average method [21], which is given as follows:

$$x = \frac{\sum_{i=1}^{n} x_i \mu(x_i)}{\sum_{i=1}^{n} \mu(x_i)}, (n = 1, 2, 3, \cdots), \tag{2}$$

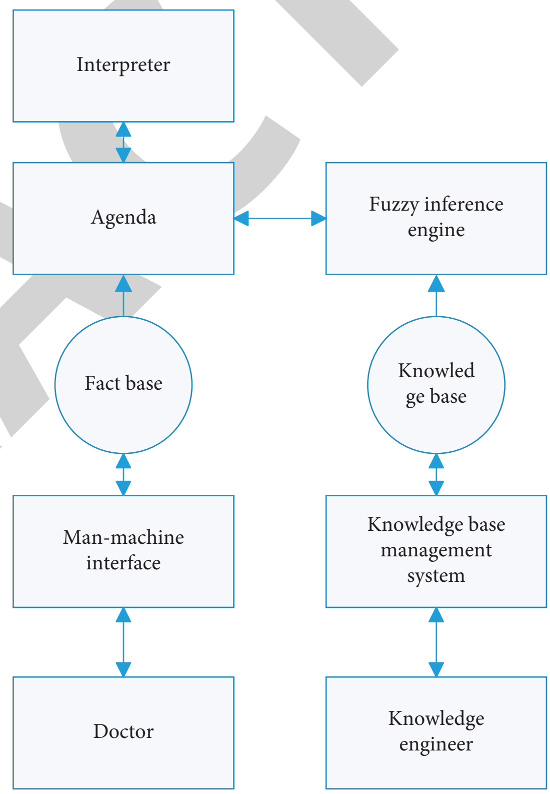

Figure 4: Structure of the scoliosis orthosis design expert system (SODES).

where x is the clear amount of design parameters; x_i is the value of fuzzy subset; $\mu(x_i)$ is the affiliation degree of fuzzy subset.

The AIS orthosis is then shaped and manufactured from the patient's phantom according to the shaping volume. After the patient has tried on the AIS orthosis, the doctor determines the amount of trim adjustment for the AIS orthosis based on the patient's feedback and adjusts the trim of the AIS orthosis according to the amount of trim adjustment. By adjusting the height of the pressure application zone of the AIS orthosis, the orthotic force exerted on the patient is thereby adjusted until the patient no longer experiences discomfort while wearing the orthosis [23]. As

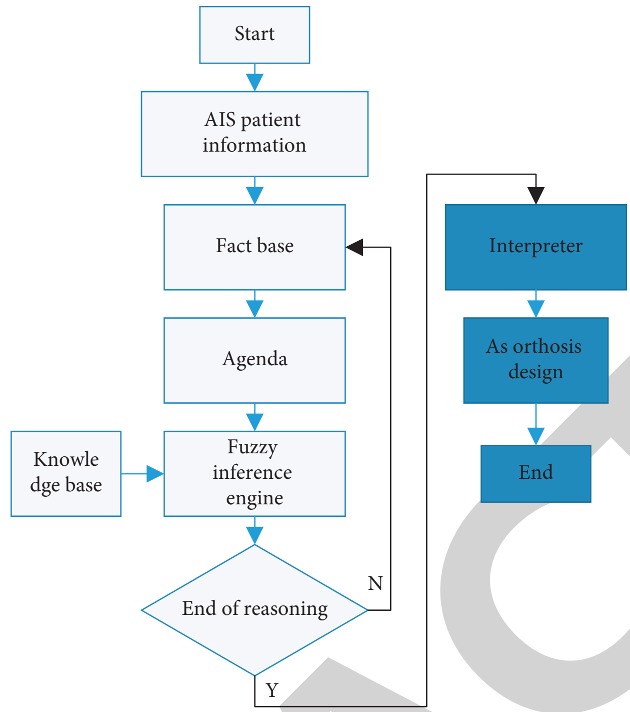

Figure 5: Workflow diagram of the expert system.

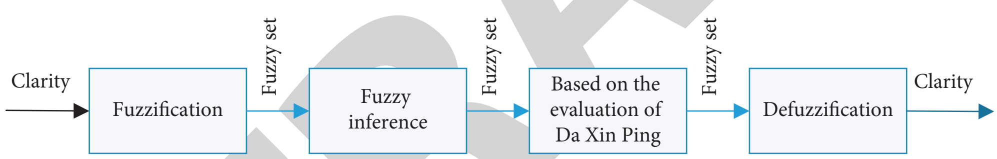

Figure 6: Fuzzy inference unit of the scoliosis orthosis design expert system.

shown in Figure 7, the determination of the amount of trim and trim adjustment is an important factor in ensuring that the AIS orthosis meets the individual needs of the patient.

The fact sheet in the knowledge base management system is used to maintain the known facts in the fact base. The knowledge engineer conceptualized and formalized 848 AIS treatment and AIS orthotic design rules through interviews and case studies with AIS conservative treatment specialists [26].

5. Application Examples

To verify the feasibility of the proposed expert system design method for AIS orthosis design based on the fuzzy reasoning, the method in this paper was applied to the AIS orthosis-assisted design of 2 cases of AIS patients.

The method in this paper was successfully applied to the AIS orthosis-assisted design of 2 AIS patients. The average design time of the AIS orthoses for Patient A and Patient B was reduced from 4 h to 2 h with the aid of this method, which improved the design efficiency of the AIS orthoses by 50% as shown in Figure 8. The deviation rates of some of the methods in this paper are shown in Table 1, and the deviation rates of the inferred values from the actual operational values of the domain experts in the AIS orthosis design of this paper are less than 10%. This shows that the method of this paper can assist physicians in designing AIS orthoses quickly and efficiently.

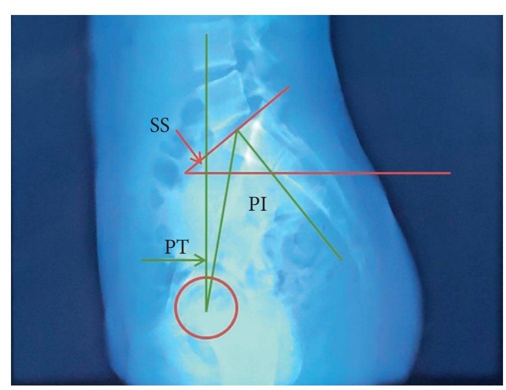

Figure 7: “Three point force” orthopedic diagram.

6. Experimental Analysis

The raw data of the spine were provided by Shenzhen University General Hospital, and the spine segmentation performed in this chapter The experiments were performed for the thoracic, lumbar, and full spine segmentation of the

Figure 8: Patients A and B wearing the scoliosis orthosis design expert system (method in this paper) assisted by the before and after comparison of adolescent idiopathic scoliosis orthoses designed with the aid of the design expert system.

Table 1: Deviation rate of the expert system component.

Project	Patient A				Patient B			
	Opening diameter of release area (CM)	Opening angle of release area (°)	Three-point force modification (CM)	Adjustment amount of three-point force repair (CM)	Opening diameter of release area (CM)	Opening angle of release area (°)	Three-point force modification (CM)	Adjustment amount of three-point force repair (CM)
Inference value	15.8	54.8	6.3	1.5	14.5	48.4	5.1	2
Recommended value	15	60	6	1.6	14.9	52	5.5	1.8
Deviation rate	5%	9.4	4.7	6.7	3.4	7.4	7.8	10

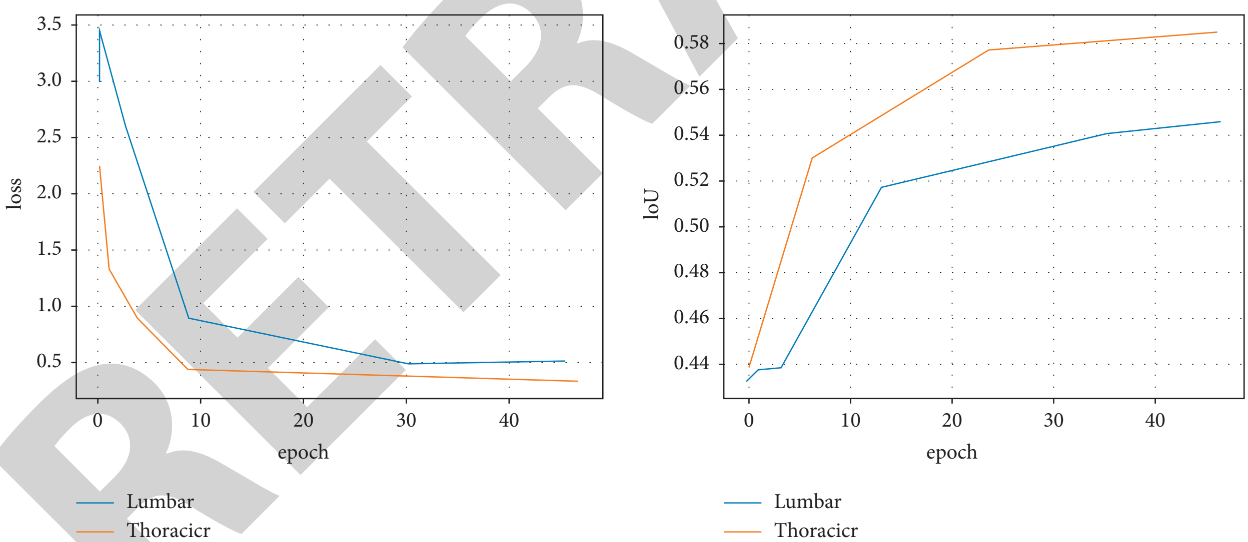

Figure 9: Data display of the thoracolumbar spine training process.

orthopantomographs of the spine. Among them, the original data volume of lumbar spine was 84. The original data volume for the lumbar spine was 84 cases, the original data volume for the thoracic spine was 166 cases, and the original data volume for the coronal position was 88 cases. Each of these cases is derived from different patient x-rays. Since the original data could not be trained for deep learning, the data were expanded by rotation, flip, and offset [27, 28]. The expanded data were 1050 for lumbar spine, 4910 for thoracic spine, and 6302 for coronal spine. The size of the data expansion was determined by the ease of segmentation. The experimental platform is based on the Window 7 system and the Kares deep learning library.

From the training process, in Figure 9, the Loss curves of the training and validation sets show a steady decreasing trend, and the IOU shows an increasing trend overall. After 50 iterations, the loss values of the training and validation sets of the lumbar spine drop to 0.033 and 0.0754, and the loss values of the training and validation sets of the thoracic spine drop to 0.0537 and 0.050. The IOU values of the

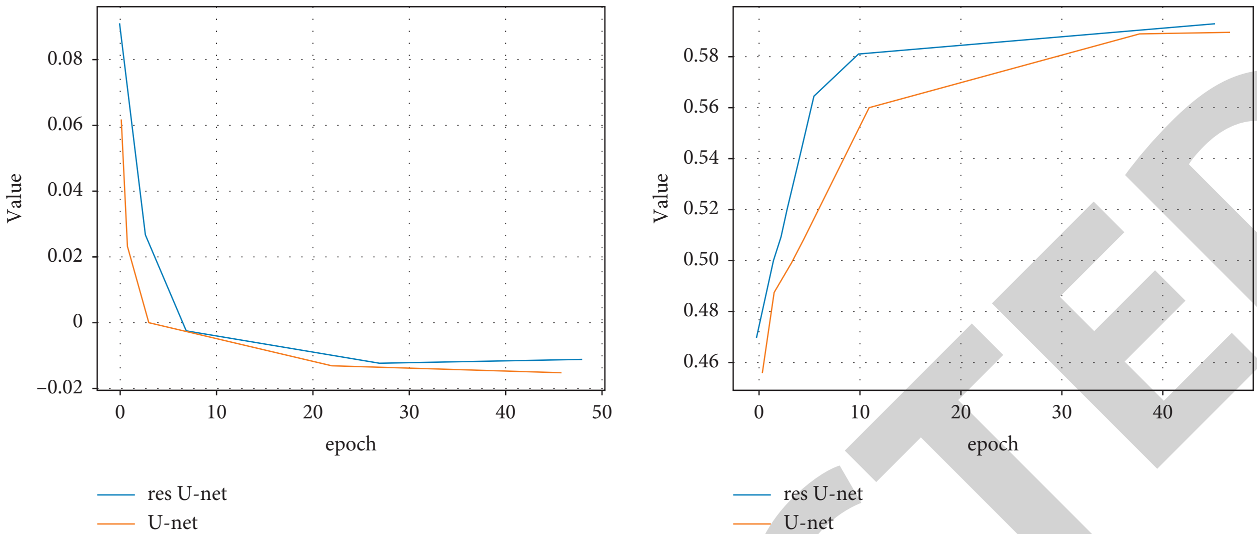

Figure 10: Training results of the U-net network and its improved network in coronal position.

training and validation sets of the thoracic spine can reach 0.6341 and 0.6342, and the IOU values of the training and validation sets of the lumbar spine can reach The training and validation sets for the lumbar spine were 0.5947 and 0.5948, respectively.

The training process of full spine segmentation is shown in Figure 10 below, from which we can see that the red discounted represents the improved U-net model and the blue-dashed line represents the original U-net model. The improved U-net model is able to segment the contours of the coronal spine well, and it is very meaningful for medical diagnosis to be able to achieve the segmentation of the coronal position. With good segmentation results, the accuracy of the subsequent series of automatic measurements will also be improved.

7. Conclusions

The accuracy rate of the system in this paper is more than 80%. The above studies are all applications of the expert system technology in the direction of scoliosis-assisted diagnosis and treatment and have achieved a certain accuracy rate, but their inference models have not yet reached the optimal accuracy rate. The main reason for this is the use of the traditional generative reasoning model, which relies on the physician's empirical knowledge in the treatment of scoliosis and contains a large amount of uncertain information. Fuzzy logic is a method that can effectively handle uncertain information based on multivalued logic and can effectively realize the expression and inference of uncertain knowledge in expert systems. The future research direction should be to further investigate the influence of individual and gender differences on this method by increasing the number of subjects.

Data Availability

The data underlying the results presented in the study are available within the manuscript.

Disclosure

The authors confirm that the content of the manuscript has not been published or submitted for publication elsewhere.

Conflicts of Interest

The authors declare that they have no conflicts of interest.

Authors' Contributions

Qin Zhao and Yiming Huang made equal contributions to the manuscript. They worked together.

Acknowledgments

This study was supported by Lianyungang Science technology and Health Project: 202003, the correlation research between morphology and somatosensory pressure in adolescent idiopathic scoliosis.

References

[1] X. Guo, WW. Chau, CWY. Hui-Chan, CSK. Cheung, WWN. Tsang, and JCY. Cheng, "Balance control in adolescents with idiopathic scoliosis and disturbed somatosensory function," *Spine*, vol. 31, no. 14, pp. E437–E440, 2006.

[2] Y. Zheng, Y. Dang, Y. Yang et al., "Whether orthotic management and exercise are equally effective to the patients with adolescent idiopathic scoliosis in mainland China?" *Spine*, vol. 43, no. 9, pp. E494–E503, 2018.

[3] J. Blundell, S. Scott, D. Harris, J. Huddlestone, and D. Richards, "Workload benefits of colour coded head-up flight symbology during high workload flight," *Displays*, vol. 65, Article ID 101973, 2020.

[4] Z. Gao, G. Zhai, H. Deng, and X. Yang, "Extended geometric models for stereoscopic 3D with vertical screen disparity," *Displays*, vol. 65, Article ID 101972, 2020.

[5] S. He, B. Liang, L. Tähkämö, M. Maksimainen, and L. Halonen, "The influences of tunnel lighting environment

Hindawi
Computational Intelligence and Neuroscience
Volume 2023, Article ID 9872618, 1 page
https://doi.org/10.1155/2023/9872618

Retraction

Retracted: Blockchain-Based Information Supervision Model for Rice Supply Chains

Computational Intelligence and Neuroscience

Received 25 July 2023; Accepted 25 July 2023; Published 26 July 2023

This article has been retracted by Hindawi following an investigation undertaken by the publisher [1]. This investigation has uncovered evidence of one or more of the following indicators of systematic manipulation of the publication process:

(1) Discrepancies in scope
(2) Discrepancies in the description of the research reported
(3) Discrepancies between the availability of data and the research described
(4) Inappropriate citations
(5) Incoherent, meaningless and/or irrelevant content included in the article
(6) Peer-review manipulation

The presence of these indicators undermines our confidence in the integrity of the article's content and we cannot, therefore, vouch for its reliability. Please note that this notice is intended solely to alert readers that the content of this article is unreliable. We have not investigated whether authors were aware of or involved in the systematic manipulation of the publication process.

Wiley and Hindawi regrets that the usual quality checks did not identify these issues before publication and have since put additional measures in place to safeguard research integrity.

We wish to credit our own Research Integrity and Research Publishing teams and anonymous and named external researchers and research integrity experts for contributing to this investigation.

The corresponding author, as the representative of all authors, has been given the opportunity to register their agreement or disagreement to this retraction. We have kept a record of any response received.

References

[1] J. Wang, X. Zhang, J. Xu et al., "Blockchain-Based Information Supervision Model for Rice Supply Chains," *Computational Intelligence and Neuroscience*, vol. 2022, Article ID 2914571, 17 pages, 2022.

Hindawi
Computational Intelligence and Neuroscience
Volume 2022, Article ID 2914571, 17 pages
https://doi.org/10.1155/2022/2914571

Research Article

Blockchain-Based Information Supervision Model for Rice Supply Chains

Jian Wang[1,2], **Xin Zhang**[1,2], **Jiping Xu**[1,2], **Xiaoyi Wang**[1,2], **Haisheng Li**[2,3], **Zhiyao Zhao**[1,2], and **Jianlei Kong**[1,2]

[1]*School of Artificial Intelligence, Beijing Technology and Business University, Beijing 100048, China*
[2]*Beijing Key Laboratory of Big Data Technology for Food Safety, Beijing Technology and Business University, Beijing 100048, China*
[3]*School of Computer Science and Engineering, Beijing Technology and Business University, Beijing 100048, China*

Correspondence should be addressed to Xin Zhang; zhangxin@btbu.edu.cn

Received 13 December 2021; Accepted 7 February 2022; Published 29 March 2022

Academic Editor: Xin Ning

Rice is a major food crop around the world, and its various quality and safety problems are closely related to human health. As an important area of food safety research, the rice supply chain has attracted increasing attention. Based on blockchain technology, this study investigated problems of data privacy and circulation efficiency caused by complex rice supply networks, long circulation cycles, and various risk factors in each link. First, we deconstructed the quality and safety of each link of the rice supply chain at the information level and established a key information classification table for each link. On that basis, we built a rice supply chain information supervision model based on blockchain. Various encryption algorithms are used to secure the sensitive data of enterprises in the supply chain to meet regulators' needs for efficient supervision. Moreover, we propose a practical Byzantine fault-tolerant consensus algorithm that scores the credit of enterprise nodes, optimizes the selection strategy of master nodes, and ensures high efficiency and low cost. Then, we built a prototype system based on the open-source framework of hyperledger fabric, analyzed the model's viability, and implemented the system using cases. The results indicated that the proposed system can optimize the information supervision process of rice supply chain regulators and provide a feasible solution for the quality and safety supervision of grain and oil.

1. Introduction

In recent years, consumers have paid increasing attention to food quality and safety, which provide a basic guarantee for human health and are directly related to improving people's lives [1]. Rice is among the world's major food crops, but in recent years, various quality and safety problems have arisen, such as cadmium-laced rice, mercury-laced rice, and aging grain [2–4]. Such problems can not only affect human health but also threaten social stability. It is necessary, therefore, to establish a safe and efficient rice supply chain information supervision system. Compared with other foods, rice is characterized by long supply chains, complex supply networks, long circulation cycles, and numerous risk factors in all links [5, 6]. Moreover, each link of the rice supply chain is relatively independent, and there is little information exchange between them. It can be difficult, then, for enterprise nodes in the supply chain to trust each other, and supervision efficiency is low [7, 8]. In addition, traditional supervision systems rely on a centralized database to store data. This can give rise to problems such as enterprises tampering with detection data in different links of the supply chain, which compromises the credibility of supervision results [9, 10].

Blockchain technology can provide effective solutions for issues related to centralization, security, and tamperability [11–13]. Blockchain can automatically execute a code according to business rules set by the system and can record the whole process in the chain to reliably transfer information, logistics, and capital flow information in a supply chain [14, 15]. In recent years, researchers have investigated the supervision and management of blockchains combined with food and agricultural product supply chains. They have focused on areas such as establishing product identification through various technologies and developing supply chain management systems for data uploading, real-time monitoring, early risk warning, and information tracing using sensor technologies [16–19]. It has been found that blockchain can improve data security and traceability for food-related supply chains and provide a guarantee for food quality and safety. However, there is still much room for improvement in the areas of blockchain storage modes, consensus overhead, and rice supply chain information supervision.

In light of the above, this study deconstructed and analyzed the quality and safety information of each link of the rice supply chain at the information level and established a key information classification table for each link. Then, a rice supply chain information supervision model was constructed based on blockchain. The model adopts a hierarchical privacy encryption and storage mode, as well as a practical Byzantine fault-tolerant consensus algorithm based on credit scoring (CPBFT). Finally, a prototype system was designed, and the model and system were analyzed to provide a reference for the current theoretical research and actual construction of rice supply chain information supervision system.

2. Related Work

Researchers have investigated the application of blockchain technology in related fields from different perspectives. Baralla et al. [20], for example, developed a blockchain-based system to manage and trace the food supply chain, using smart contracts to ensure the credibility of the whole process. Based on an analysis of the wheat-processing supply chain, Zhang et al. [21] proposed a blockchain-based grain and oil supply chain system architecture using a multimode storage mechanism. Wang et al. [22] proposed a framework based on consensus and smart contracts to achieve traceability and sharing in the agricultural product supply chain and improve the integrity and security of transaction records. In their model, data are stored in an interstellar file system, and the data hash is stored in the blockchain network, which saves storage space and ensures security. Mao et al. [23–25] built a blockchain-based food supply chain trading system to provide more reliable and authentic information. Pigini and Conti [26] used Near Field Communication (NFC) technology to achieve effective traceability and safety tracking to collect product information in all links of the food supply chain. Salah et al. [27] analyzed the traceability and business processes of the soybean supply chain and proposed using smart contracts to control and ensure the safety and credibility of supply chain information.

The aforementioned studies addressed the security problems of food supply chains to a certain extent. However, with the rapid expansion of supply chain nodes, existing traditional consensus modes have too much overhead, and sharp increases in the amount of data have corresponding requirements for consensus security. Researchers have sought to solve this problem by improving the blockchain consensus algorithm. Liu et al. [28], for example, improved the Delegated Proof of Stake (DPOS) consensus algorithm to keep the consensus process from being controlled by a few nodes. Meanwhile, to achieve node consensus in large-scale distributed systems, Li et al. [29] proposed an extensible multilayer PBFT consensus mechanism that groups nodes hierarchically and limits communication within the group, such that PBFT consensus is not limited to small consensus networks. In rice supply chains, however, the key data in each link are complex, and enterprise entities cannot form a unified standard. It is necessary, then, to adopt a targeted consensus scheme, that is, to reduce the consensus cost and ensure consensus reliability at the same time. In addition, because the nodes in the blockchain are not completely anonymous, there are privacy risks, which necessitate privacy encryption for uplink data.

To meet these challenges, this study analyzed the information for each link in the rice supply chain and output a classification table of key information for each link. Combining the principles of cryptography and blockchain, we proposed a data encryption and storage mode that protects the sensitive data of supply chain enterprises and meets the needs of regulators for efficient supervision. In addition, our proposed credit score-based PBFT consensus algorithm reduces the probability that the master node is a Byzantine node and ensures high efficiency and low overhead. In summary, this research can help optimize regulators' information supervision processes in rice supply chains and provide a feasible solution for rice quality and safety supervision in the future.

3. Analysis of Supply Chain Process and Key Information

Many enterprises are involved in each link of the rice supply chain, including growers, purchasers, storage enterprises, processing enterprises, logistics enterprises, and distributors. The rice supply chain is therefore characterized by a long life cycle and complex links. From rice planting to sales, there are many potential safety hazards in the supply chain, which are summarized in the following:

(1) In the planting process, rice needs to absorb a large amount of water, which makes it more vulnerable to pollution than other crops. Farmers' fertilization practices are not always standardized. Some even irrigate farmland using untreated domestic sewage and industrial wastewater, resulting in excessive heavy metal pollution [30].

(2) Rice processing is a lengthy process, and problems such as broken rice and fumigant residue easily arise in the process of impurity removal [31]. China's rice-quality standards stipulate that no flavor or pigment is allowed in rice. Yet, to increase profits, some enterprises in China add fragrance to rice or treat it to increase its brightness. When polishing rice, it not

only adds water but also illegally adds mineral oils, thus processing ordinary rice into “poisonous rice.”

(3) With regard to packaging, the plastic woven bags mainly used for rice commodities offer a simple, low-price packaging method. However, the material has a poor moisture barrier and moisture resistance, resulting in problems such as oxidization and mildew.

(4) Storage and transportation links: improper warehouse storage makes rice prone to mildew. In addition to changing the color of rice, mildew can produce harmful molds and microorganisms [32].

(5) The sales link of rice is widely distributed and contains a large amount of information. As the terminal link of the supply chain, it directly faces consumers. If there is an information supervision problem in this link, it can seriously affect the whole supply chain.

In summary, the types of hazards in each link of the rice supply chain are complex, and safe and efficient supervision is needed. However, traditional blockchain supervision systems generally have problems such as large differences in inspection standards and inconsistent data storage formats in all links of the supply chain. It is difficult to effectively enter the multilink information of a complex supply chain. It is also difficult to build models and systems based on these data in the follow-up process, making it difficult to solve the problem of rice quality in terms of data security.

Based on the rice supply chain process and the business characteristics of enterprises in the supply chain, we divided the rice supply chain into 13 links and five types of key data: main information, basic information, environmental information, hazard information, and transaction and price information (Table 1).

The subject information is the enterprise information in different links of the supply chain, including the enterprise name, the person in charge, and contact information. The basic information is the information recorded by the enterprise staff in each link, such as rice type, sampling inspection record, rice milling method, and whether it is genetically modified. Environmental monitoring information is the information recorded by sensors in the supply chain, including temperature and humidity, carbon dioxide concentration, and real-time photos. Hazard information mainly refers to the content of mycotoxins, pesticide residues, and heavy metals in rice during sampling inspection. Mycotoxins mainly include aflatoxin B1, ochratoxin A, and deoxynivalenol. Heavy metals include lead (Pb), cadmium (Cd), Mercury (Hg), arsenic (As), and chromium (Cr). Pesticide residues include chlorpyrifos, triazophos, carbofuran, and bensulfuron methyl. Transaction records and price information include the commercial information circulating among various links, and their confidentiality is high. Table 1 summarizes the key information in each link. Taking the processing link as an example, processing enterprises accept rice stored in multiple granaries, including storage enterprises. After the rice is transported to the processing plant, the processing plant also needs to carry out various processes, such as removing the husk, rice milling, color selection, and polishing. This study regarded the abovementioned processes as independent links. Detailed information classification can further optimize the process architecture of the supply chain business system and can be used as the basis for establishing an information supervision model for the safety and quality of the rice supply chain.

4. Blockchain-Based Supervision Model for Rice Supply Chain Information

Traditional rice supervision systems store supply chain information in a central database. Its supervision timeliness is poor, data are easily tampered with, flow between enterprises is difficult, and the enterprise data query efficiency is low. A blockchain stores enterprise data with a distributed ledger instead of a central database to achieve data sharing and value transfer between upstream and downstream enterprises in a supply chain. Using blockchain technology, an improved consensus algorithm, and the principle of cryptography, this study built a rice supply chain information supervision model based on supply chain processes and the characteristics of enterprises in the chain. The model includes not only complete supervision of the supply chain but also government agency supervision, as well as the data uploading and data sharing of enterprises. Querying and consumer commodity traceability are employed to achieve integrated supervision. In this way, rice information can be supervised and managed from the supply chain, which ensures the security and authenticity of data circulated in the supply chain. Meanwhile, it reduces the information gap between consumers, regulators, and enterprises in the supply chain and avoids the generation of information islands.

This study regarded each link in the rice supply chain as a node in the blockchain, and each node corresponds to a cloud database. Each node in the supply chain invokes a smart contract deployed in the blockchain network through the supervision system and carries out network consensus through an improved PBFT consensus algorithm. Enterprises in all links can encrypt and store the data in the system through this system. After blockchain network consensus, plaintext and ciphertext data in the supervision system are recorded in a cloud database, and a small part of the plaintext data, information summary, and key are saved in the blockchain network (Figure 1).

Combining regulatory authorities and supply chain enterprises and based on the key information classification table, we standardized the data uploading or traceability of supply chain links (e.g., production, processing, warehousing, transportation, and sales), which can achieve effective information supervision of the entire rice supply chain.

The model mainly includes rice supply chain network nodes, data hierarchical encryption, storage mode, and CPBFT. The data hierarchical encryption and storage mode combined symmetric encryption and hash encryption

Table 1: Key data of each link in the rice supply chain.

Links in rice supply chain		Key data classifications				
		Main information	Basic information	Environmental information	Hazard information	Transaction and price information
Plant		Identity information of growers; planting license information; contact information; business license information (optional)	Seed source; rice varieties; origin information; planting and harvesting time; pesticide and fertilizer information and use records	Pictures of rice growth cycles; real-time ambient temperature; real-time ambient humidity; actual illumination intensity of environment; soil moisture content	Pictures of rice growth cycles; real-time ambient temperature; real-time ambient humidity; actual illumination intensity of environment; soil moisture content	Seed price; fertilizer price; total cost; selling price; collect and store enterprise information
Acquisition and storage	Acquisition	Enterprise name; business address; corporate information; person in charge of relevant links; license information; enterprise contact information	Pesticide sampling inspection records; transgenic or not	None	Mycotoxin: fumigant and insecticide residues	Grower information; purchasing price; drying, impurity removal, storage, and other costs; selling price; processing enterprise information
	Dry		Drying method; moisture content before drying; moisture content after drying	Real-time ambient temperature; real-time ambient humidity		
	Impurity removal		Impurity content; impurity removal rate			
	Storage		Inventory number; product source; warehousing time; delivery time	Ambient temperature, humidity, oxygen concentration, carbon dioxide concentration, and various toxic gas concentrations produced by long-term storage		

Table 1: Continued.

Links in rice supply chain		Key data classifications: Main information	Basic information	Environmental information	Hazard information	Transaction and price information
Machining	Removing the husk	Enterprise name; business address; corporate information; person in charge of relevant links; license information; enterprise contact information	Ridge and valley mode (brand of ridge and valley machine); roughness; shelling rate	Real-time ambient temperature; real-time ambient humidity	Mycotoxin: broken needle foreign body; chemical reagents; heavy metals	Processing cost; processing price
	Rice milling		Rice milling method (chemical method/ mechanical method); whole meter rate; broken rice rate			
	Color selection		Color separation accuracy; bringing out the ratio			
	Polishing		Polishing rate			
	Packing		Product package number; product batch number; product quality information			
Storage		Name of warehousing enterprise; address of storage enterprise; corporate information	Inventory number; product source; warehousing time; delivery time	Ambient temperature, humidity, oxygen concentration, carbon dioxide concentration, and various toxic gas concentrations produced by long-term storage	Mycotoxin	Storage cost; storage price
Transport		Name of logistics enterprise; address of logistics company; information of the person in charge of transportation	Means of transport; place of departure; departure time; destination	Ambient temperature inside the vehicle; ambient humidity in the vehicle; oxygen/carbon dioxide concentration in the vehicle	Fungi and toxins produced by temperature and humidity metamorphosis	Logistics cost; logistics price
Sale		Merchant name; shop address; information of the person in charge of the store; business license information; business contact information	Product name; product quantity; purchase time; purchase number; shipping time	Sales environment photos	None	Purchasing price; selling price

algorithms to ensure the security and privacy of the data uploaded to the blockchain network and the cloud database in the process of circulation and storage. Advanced Encryption Standard (AES) is used to ensure data confidentiality. It is characterized by that both sides of communication use the same key in the process of encryption and decryption. Hash encryption algorithms can compress arbitrary length data into information summary of fixed length to realize digital signature and data integrity. As a partial synchronous pattern consensus algorithm, PBFT has been widely used in the alliance chain. The algorithm can solve the Byzantine problem, which is relatively efficient and widely used [33]. However, when the algorithm is applied to the supervision of agricultural products with many coverage links, there are still some problems, such as high overhead, low throughput, and low performance. CPBFT introduces the credit-scoring mechanism in PBFT, which scores and grades the credit of supply chain enterprise nodes to ensure the efficiency of consensus. At the same time, the algorithm improves the reliability of supply chain supervision. In addition, based on the model, this study designs the information supervision prototype system, constructs the system infrastructure, and analyzes the complete operation process of the system.

4.1. Hierarchical Data Encryption and Storage Mode. Based on the above classification of key information in each link of the rice supply chain, as well as the integration of data privacy, encryption algorithm security, algorithm time complexity, and space complexity in each link, we performed the hierarchical encryption and secure storage of supply chain circulation data. Figure 2 shows the data flow in the encryption and storage mode.

We mainly used the AES encryption algorithm and SM3 password hash algorithm to encrypt and decrypt the supply chain information. The AES encryption algorithm uses ECB and CBC working modes. The difference between AES working modes is reflected in the association between plaintext data blocks, although the processing flow inside the AES encryptor is the same. Algorithm 1 shows the AES encryption process, and Algorithm 2 shows the decryption process. NR is the number of encrypted rounds. For different key lengths, the number of rounds is different, and W is the extended key array. The SM3 hash algorithm is a commercial hash algorithm standard published by the State Encryption Administration of China. The algorithm has excellent anticollision ability and is very suitable for privacy data encryption in a rice supply chain. For a plaintext message m with a length of less than 264 bits, the SM3 hash algorithm generates a hash value (ciphertext) after filling and iterative compression. The hash value length is 256 bits. Algorithm 3 shows the encryption process.

4.1.1. Level I Privacy Data Encryption. Hazard information is defined as level I privacy data. In this mode, the AES algorithm ECB mode is used to encrypt level I privacy data and then transmit it to the cloud database. In this mode, the encryption of each plaintext block is completely independent. The data are grouped with 128 bits, and the remaining insufficient bits are filled to reach the integer multiple of the packet:

$$x_1, x_2, x_3 \ldots . \tag{1}$$

Each group of data and the key of the same length are used as input, and new data packets are generated by independent encryption. The same is true for decryption. The encryption process is

$$y_1 = E_k(x_1), y_2 = E_k(x_2), y_3 = E_k(x_3) \ldots . \tag{2}$$

The decryption process is

$$x_1 = D_k(y_1), x_2 = D_k(y_2), x_3 = D_k(y_3) \ldots . \tag{3}$$

The AES algorithm ECB working mode can carry out a large number of parallel calculations, which is suitable for rice hazard information with large amounts of data. In this mode, the data key is randomly generated by the algorithm and uploaded to the blockchain network for storage to ensure the randomness and security of the key and mitigate the risk of key disclosure in symmetric encryption.

4.1.2. Level II Privacy Data Encryption. Transaction records and price information are defined as level II private data. For level II private data, the AES algorithm CBC mode is used for encryption, and ciphertext data are transmitted to the cloud database.

In the process of privacy data encryption, the first plaintext data packet is XOR with the randomly generated initial vector IV. Then, packet encryption is carried out, and the ciphertext output by this group and the XOR of the next plaintext packet are used as the input of the next packet encryption. In this way, until encryption is completed, the decryption process is the same.

Encryption process:

$$\begin{aligned} y_0 &= IV, \\ y_1 &= E_k(y_0 \oplus x_1), \\ y_2 &= E_k(y_1 \oplus x_2) \ldots . \end{aligned} \tag{4}$$

Decryption process:

$$\begin{aligned} y_0 &= IV, \\ x_1 &= D_k(y_1) \oplus y_0, \\ x_2 &= D_k(y_2) \oplus y_1 \ldots . \end{aligned} \tag{5}$$

The output of each ciphertext in this mode is related to its corresponding plaintext packet and all previous plaintext packets; thus, the ciphertext generated by the same plaintext may be different. Therefore, compared with the ECB mode, the CBC mode has stronger security and is suitable for commodity value guarantee with a higher security level. In addition, in this process, the data key is generated and stored in the same way as with level I privacy data.

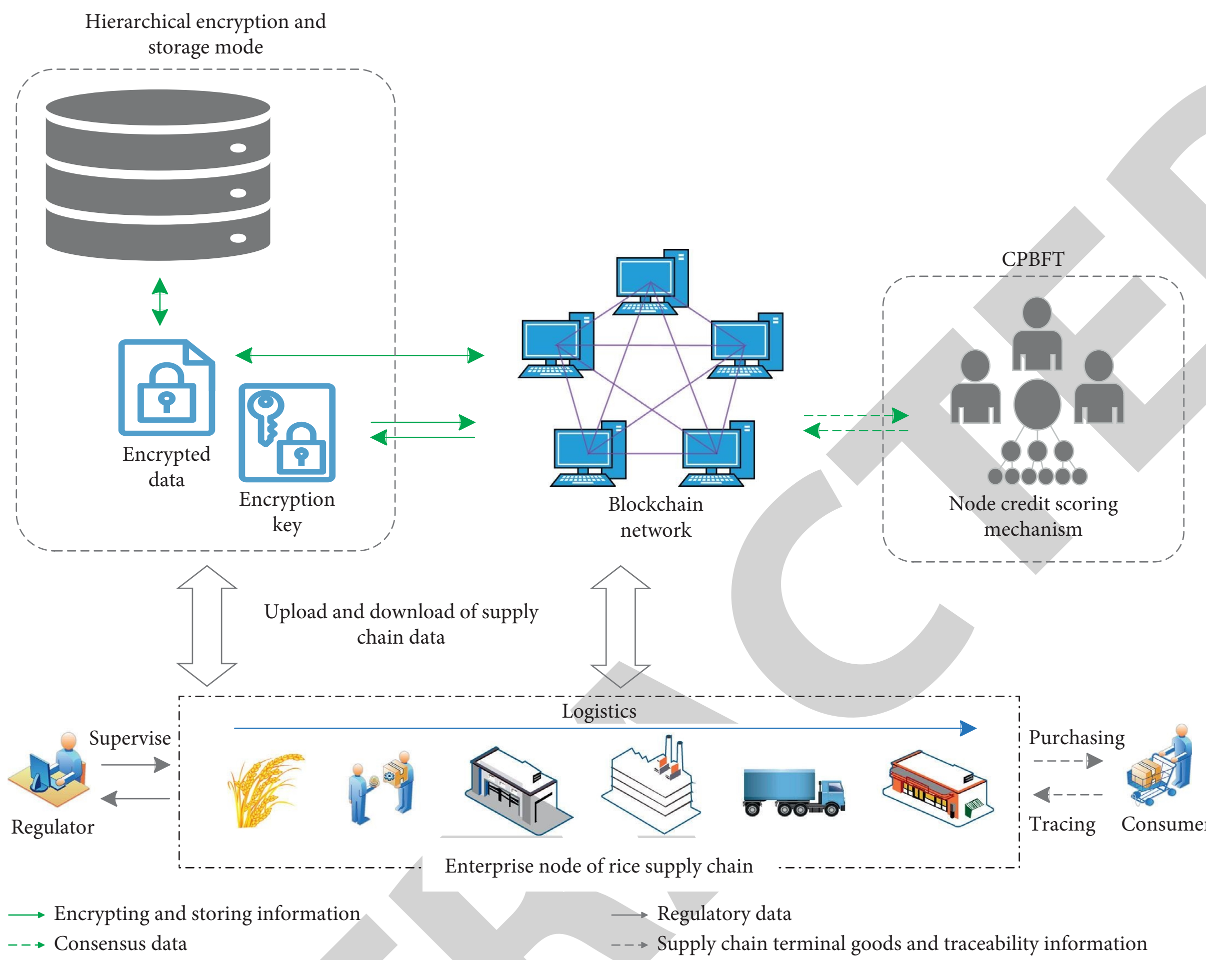

Figure 1: Rice supply chain information supervision model.

4.1.3. Level III Privacy Data Encryption. Subject information, basic information, and environmental information are defined as class III privacy data. For subject information, the amount of data is small, and the degree of importance is high. This mode adopts the method of directly transmitting data to the blockchain network. For all level III privacy data, the SM3 cryptographic hash algorithm is used for encryption. The algorithm first fills the data and then expands the filled data, iteratively compresses the expanded data, and finally generates an information summary with a length of 256 bits. Finally, the encrypted information summary is uploaded to the blockchain network, and the level III privacy data are uploaded to the cloud database in plaintext. The compression function of the SM3 cryptographic hash algorithm has a similar structure to that of SHA-256, but the structure of the compression function of the SM3 cryptographic hash algorithm and the design of the message expansion process are more complex. Each round of the compression function uses two message words, and each round of the message expansion process uses five message words, which can further ensure that high-privacy data are nontamperable.

4.2. Practical Byzantine Fault-Tolerant Consensus Algorithm Based on Credit Score. The PBFT algorithm is a partially synchronous mode consensus algorithm. To ensure that nonfault nodes execute client requests in the same order, third-order broadcast communication is needed to ensure security in the asynchronous mode, resulting in a great deal of communication overhead. At the same time, PBFT lacks the mechanism of troubleshooting nodes, and the selection of master nodes is arbitrary. The probability of selecting Byzantine nodes as master nodes is high, and the frequent replacement of master nodes greatly affects system efficiency [28, 34]. Therefore, this study improved the original PBFT algorithm and designed CPBFT (PBFT based on credit score) according to the characteristics of rice supply chains. Taking the transaction time and honesty of the nodes in the rice supply chain as the main reference factors, we scored the behavior of all nodes participating in consensus in the supply chain. The credit-scoring model divides the nodes into fault, ordinary, supervision, and candidate nodes according to the score and then optimizes the selection strategy of the main node, reduces the possibility of the main node becoming a Byzantine node, reduces the amount of view switching, and improves the efficiency of the information supervision system. Figure 3 shows the classification and conversion mode of consensus nodes.

4.2.1. Credit-Scoring Mechanism of Nodes. In this model, it is necessary to first conduct multiple rounds of PBFT consensus and then select the consensus set, eliminate nodes that fail in the consensus process or send messages inconsistent with most nodes, and conduct node credit scoring to remove most nonsystem interference factors.

After each correct consensus, the credit score of the corresponding node is added β. After n rounds of consensus, all honest nodes will correctly complete the consensus, and the node's credit score will be η. The traditional PBFT consensus algorithm has $3f+1$ nodes, and at least $2f+1$ honest nodes can complete consensus. If a malicious node wants to join the consensus set, it must be honest every time. At this time, the credit score of more than $2f+1$ nodes will be divided into η and is marked as an honest node. This will be reached within specified time η. The node with the score is marked as an ordinary node and can only participate in consensus. A node that fails to reach the score is regarded as a fault node. After multiple consensuses, according to the credit score of the node, the nodes participating in consensus can be divided into ordinary, supervision, candidate, and fault nodes. These nodes perform different functions in the consensus to maintain the stable operation of the rice supply chain information supervision system. Table 2 shows the specific node division method.

In the unimproved PBFT consensus mechanism, the master nodes are randomly selected by formula $p = v\mathrm{mod}|R|$, where p is the master node number, v is the view number, and $|R|$ is the number of nodes. The probability that the selected master node is a Byzantine node is 1/3. In this model, the node with the highest score among the candidate nodes is selected as the master node of the next view. If there is no single node with the highest score, the system randomly selects a node with the highest score among the candidate nodes as the master node. After a period of time t, the master node resets the node credit score and downgrades to an ordinary node to avoid the problem of overcentralization of the system. The main node selection mechanism of this model reduces the possibility of a Byzantine node becoming the main node, reduces the number of attempts to switch, reduces communication overhead, and improves system efficiency and security.

In the process of consensus, there are often objective fault nodes and subjective malicious nodes caused by unavoidable physical conditions, such as enterprise host failure, communication system delay, and supply chain link change. The role of the monitoring node is to eliminate the problem nodes in these situations. In the process of consensus, the monitoring node can record information that has been judged malicious by the system and then deprive it of consensus authority. In addition, the monitoring node can also record the node that does not send feedback information to the client within the specified time, or the feedback information is inconsistent with the feedback information of most nodes. Then, the system will mark the node as a failed node and temporarily deprive it of consensus authority. When the problems of malicious or failed nodes are repaired, the system will initialize them as ordinary nodes. The existence of a supervision node further reduces the possibility of fault nodes in the consensus node, improves consensus efficiency, and reduces system overhead.

4.2.2. Consensus Process. Figure 4 shows the CPBFT algorithm flow. After a consensus is started, all nodes are initialized and classified according to their credit scores. However, since the credit scores of the nodes are all 0, all nodes are ordinary nodes at the beginning, and the primary node is randomly selected according to the $p = v\mathrm{mod}|R|$ formula for consensus. After multiple consensuses, each node receives a corresponding credit score, and the node credit score system is gradually established. The model divides all nodes into four types with different functions and permissions and selects the main node according to the node credit-scoring mechanism. After the client sends the request, the master node broadcasts the proposal. If the replica node does not respond, the mechanism determines that the master node has a problem and records the delayed response information to the monitoring node. Then, the monitoring node judges whether the primary node is a failed node or a malicious node. Then, the mechanism will perform credit score reduction and node consensus authority deprivation for the corresponding nodes. The consensus process then returns to the node classification stage after view switching and finally reclassifies the nodes to select a new primary node for consensus. If the master node is an honest node, the consensus is completed at one time, and the algorithm will add points to the node that successfully records the information to the local node.

4.3. Design of the Information Supervision Prototype System. Based on the above model and the needs of all links in the rice supply chain, we designed a rice supply chain information supervision prototype system. Figure 5 shows the system architecture, which is divided into application layer, consensus layer, storage layer, and perception layer.

As the data-acquisition end of the system, the sensing layer mainly collects the various business data and hazard information of supply chain enterprises through temperature and humidity sensors and infrared scanning and photographing equipment. It then transmits the data to the data storage layer through wireless sensor networks, 4G/5G, Wi-Fi, and other networks. The storage layer includes a cloud database and hyperledger fabric blockchain platform storage, in which data in the blockchain are stored in the form of files. Enterprises first perform data cleaning, transformation, and fusion and then encrypt and store data according to its privacy level through smart contracts. The hierarchical encryption and storage mode can ensure storage efficiency, decentralize data, and make data more secure and reliable. Meanwhile, this mode also facilitates user data query. The consensus layer encapsulates the improved consensus algorithm and mechanism. The credit-scoring model divides the consensus nodes into four categories,

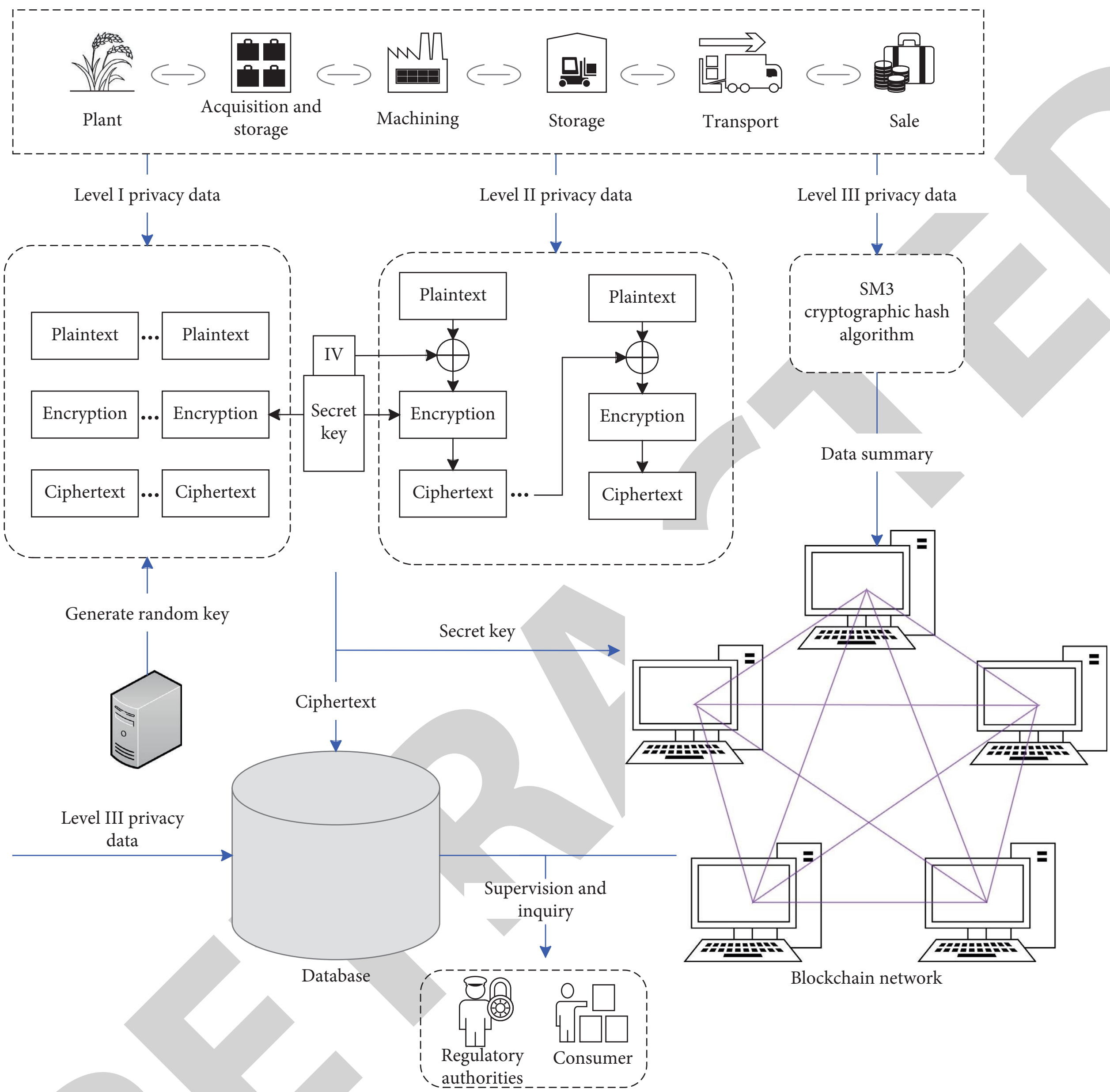

Figure 2: Hierarchical data encryption and storage mode.

which can enable highly decentralized nodes to efficiently reach consensus on the effectiveness of block data in a decentralized blockchain network. The application layer provides corresponding functions to regulatory authorities, enterprises, and consumer users in the form of web pages and mobile apps. Further, it divides authority levels according to different users, mainly including information traceability, enterprise authority management, and supply chain supervision functions. It can also observe the number of nodes and score changes in real time.

The system adopts a hyperledger fabric open-source blockchain platform to construct the supply chain blockchain network. Its essence is the uploading and querying of the blockchain ledger and cloud database by supply chain node users through the client interface. The system adopts a B/S structure, CentOS 7 as the operating system; Docker 18.09 as the container engine; and go, JavaScript, HTML, and CSS for program development. CouchDB, LevelDB, and MySQL are used as database servers. MySQL is the main data storage database, and CouchDB and LevelDB are the status databases in the blockchain network. The state database is just an index view in the transaction log in the chain and can be regenerated from the chain at any time. Before data transactions, the state database will be automatically restored when the peer node starts or is generated as needed. LevelDB stores chaincode data as key value pairs, while CouchDB, which is mainly used in this system, uses JSON to store data, which can support richer queries.

In this study, different users who log in to the system have different permissions, which can be achieved by the

```
Input: plaintext, key
Output: ciphertext
/∗ First, the algorithm expands the input key and stores it in W ∗/
AddRoundKey(state,w) // Bitwise XOR between the extended key in W and the matrix column
state = plaintext
for(r = 1; r <= Nr; r++) {
SubBytes(state) // Find the S-box and output four new bytes to form word
ShiftRows(state) // Each row of the matrix is shifted left circularly in bytes
if(r ! = Nr) {
MixColumns(state) // Column-by-column transformation of matrix
}
AddRoundKey(state, w) // In this round of encryption, XOR each column with the extended key
}
ciphertext = state
```

Algorithm 1: Process of AES encryption.

```
Input: plaintext, key
Output: ciphertext
/∗ First, the algorithm expands the input key and stores it in W ∗/
state = ciphertext
AddRoundKey(state,w) // Bitwise XOR between the extended key in W and the matrix column
for(r = Nr; i >= 0; i--) {
InvShiftRows(state) // Rotate each row of the matrix to the right
InvSubBytes(state) // Find the inverse S-box and output four new bytes to form word
AddRoundKey(state,w) // In this round of decryption, XOR each column with the extended key
if(r ! = Nr) {
InvMixColumns(state) //Inverse column transformation of matrix
}
}
plaintext = state
```

Algorithm 2: Process of AES decryption.

```
Input: plaintext
Output: ciphertext
plaintext = m
/∗ Fill the message m with M1, which is an integer multiple of 512
Group the filled messages, where B (0) B (1)... B (n − 1) where n = (L + K + 65)/512, and l is the plaintext length ∗/
for (i = 0; i < n; i++) {
The packet message Bi is extended to generate 132 words
Carry in the generated word for iterative compression
}
The final hash value is obtained by iterative compression, IV (n) = CF (IV (n − 1), B (n − 1))
ciphertext = V (n)
```

Algorithm 3: Process of SM3 encryption.

hyperledger fabric's own management user ID and membership authentication function for all blockchain participants. Moreover, the fabric access control list can also enable different users to authorize different permissions. Figure 6 shows the system sequence diagram. The personnel of multiple production, processing, transportation, packaging, and sales enterprises and regulatory agencies in the supply chain can use the system, and the user has the authority to upload and query data. Users log in to the system and upload data. At this time, the system calls up the smart contract and encrypts it according to the data privacy level of the rice supply chain. The encryption key is randomly generated by the system. Part of the data is saved to the traditional database, and the other part of the data and the key participate in node consensus and upload to the blockchain. At the same time, the system updates the enterprise node credit score of the supply chain to ensure efficiency consensus.

5. Performance and Effect Analysis

5.1. Model Analysis. In the practical application of a traditional rice supervision model, due to the use of a central database, data are easily tampered with, and enterprise data traceability and query efficiency are low. Blockchain stores enterprise data with a distributed ledger instead of a central database, which can achieve data sharing and value transfer between upstream and downstream enterprises in the supply chain. Based on rice supply chain processes and the business logic of enterprises in the chain, we built an information supervision model using blockchain, an improved consensus algorithm, and cryptography principles to ensure the safe, efficient flow of data in the chain.

In our model, symmetric and hash encryption algorithms are used to encrypt rice supply chain data twice before data connection. The blockchain network stores a small amount of plaintext data, information summary, and keys at a high security level. Most ciphertext and plaintext data are stored in a cloud database, which can ensure the security of information storage and circulation in the whole system. In addition, this mode differentially encrypts different data safely registered in the supply chain information flow, standardizes the data storage and management process of the whole system, completes the hierarchical storage of data, and makes system resource investment proportional to data importance. In this mode, various encryption algorithms are used to ensure the confidentiality, integrity, and availability of sensitive data. This helps protect the key sensitive data of rice supply chain enterprises; the hierarchical structure can also meet the needs of regulators for efficient supervision.

In terms of the safety of the algorithm, the selection of master node is arbitrary in the consensus process of PBFT. The algorithm can select the master node in turn according to the node number. CPBFT uses PBFT as the consensus core, and its intragroup consensus and global consensus antiattack capabilities are consistent with PBFT. The following focuses on the security performance of CPBFT against witch attack and conspiracy attack.

Sybil Attack refers to Byzantine node illegally inventing multiple identities to attack the network. In this study, the credit-scoring method is used to elect high credit nodes to participate in the consensus, while the nodes with low credit will be stripped of the authority of consensus by the system so as to reduce the probability of Sybil Attack.

Collusion attack means that multiple Byzantine nodes give a trust evaluation higher or lower than the actual level, which makes the trust value of the evaluated node deviate from the actual trust value. When the total number of Byzantine nodes in CPBFT does not exceed 1/3 of the total

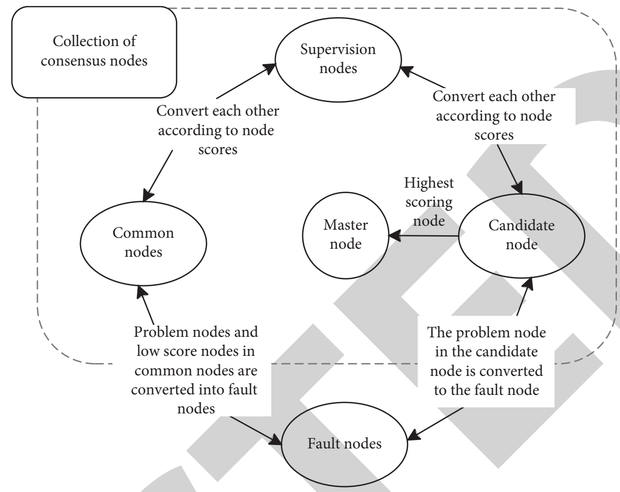

Figure 3: Category and transformation of consensus nodes.

number, even if all Byzantine nodes collude, the system can still reach a correct consensus. And once malicious behavior occurs in the consensus proposal, the node is highly likely to be determined as a Byzantine node, and the monitoring node can record the information that has been determined as a Byzantine node by the system and then deprive its authority of consensus. Therefore, the node collusion attack can only increase the opportunity for Byzantine nodes to enter the set of alternative nodes through voting collusion, and the node credit-scoring mechanism of CPBFT can adjust and divide the credit score in real time according to the situation. When there are great differences in the credit evaluation of the attacked node, the system will change the parameters in the mode of division in Table 2 in real time to reduce the impact of collusion attack on consensus security so as to ensure the high reliability of the candidate node.

In addition, we conducted a system simulation on a hyperledger fabric platform and compared the traditional PBFT algorithm with the proposed CPBFT algorithm in terms of total communication between nodes and throughput. The communication overhead of the node was directly proportional to the number of communications between nodes in the consensus process. The main purpose of the CPBFT algorithm is to reduce the number of failed nodes in the consensus node to reduce communication. In the system simulation, one-third of the nodes were set as fault nodes. As shown in Figure 7, the communication of the CPBFT algorithm increases slowly, while the communication of the PBFT algorithm before improvement increases rapidly. Therefore, it can be seen that the CPBFT algorithm can effectively reduce communication overhead and broadband pressure.

Throughput refers to the number of transactions completed in a unit of time. CPBFT can effectively reduce the number of consensus nodes and shorten communication time. The probability that the master node is a reliable node is higher, the probability of error is smaller, the amount of view switching is reduced, and the time to complete consensus is shortened. For our experiment, we sent 800 requests to the client, recorded the number of transactions that

Table 2: Division mode of nodes.

Node name	Node classification	Node function
Common node	Node that reaches credit score η within time t	Can only participate in consensus
Supervision node	$2(2f+1)/3$ nodes that first reach credit score λ among ordinary nodes	Can participate in consensus and can record the information of the problem node
Candidate node	$2(2f+1)/9$ nodes that first reach credit score μ among ordinary nodes	Can participate in consensus and select the master node from it
Fault node	Nodes that do not reach η score within time t	Cannot participate in consensus

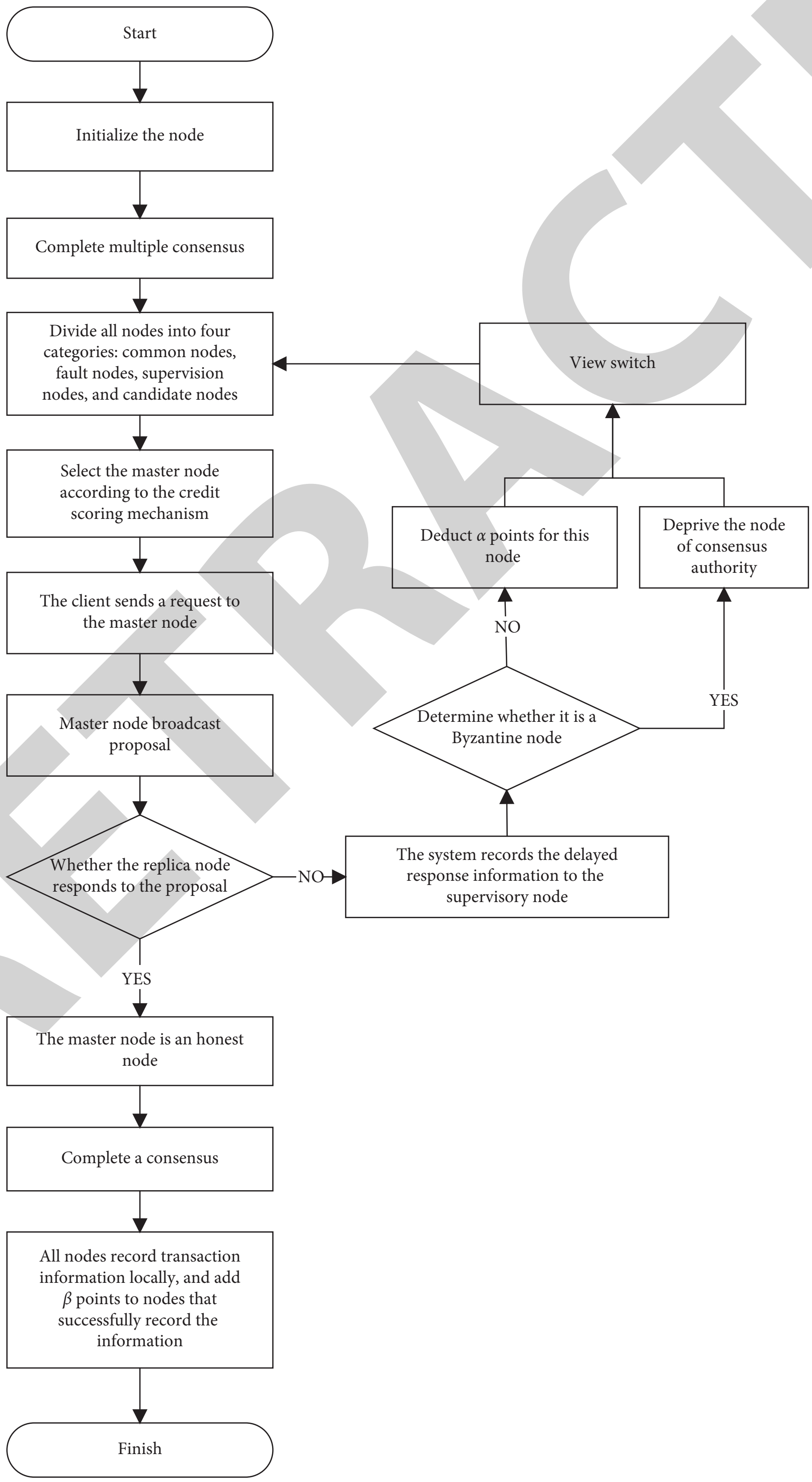

Figure 4: The process of CPBFT.

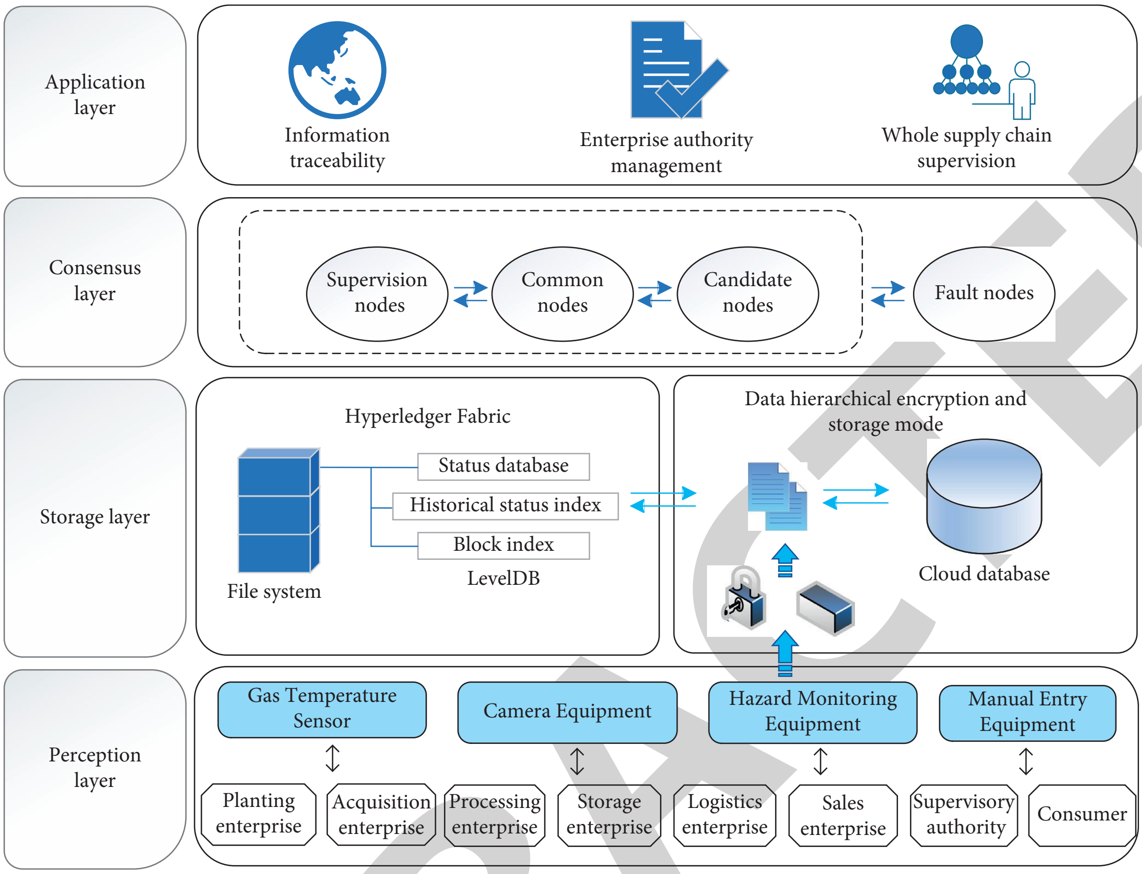

FIGURE 5: The information supervision prototype system architecture.

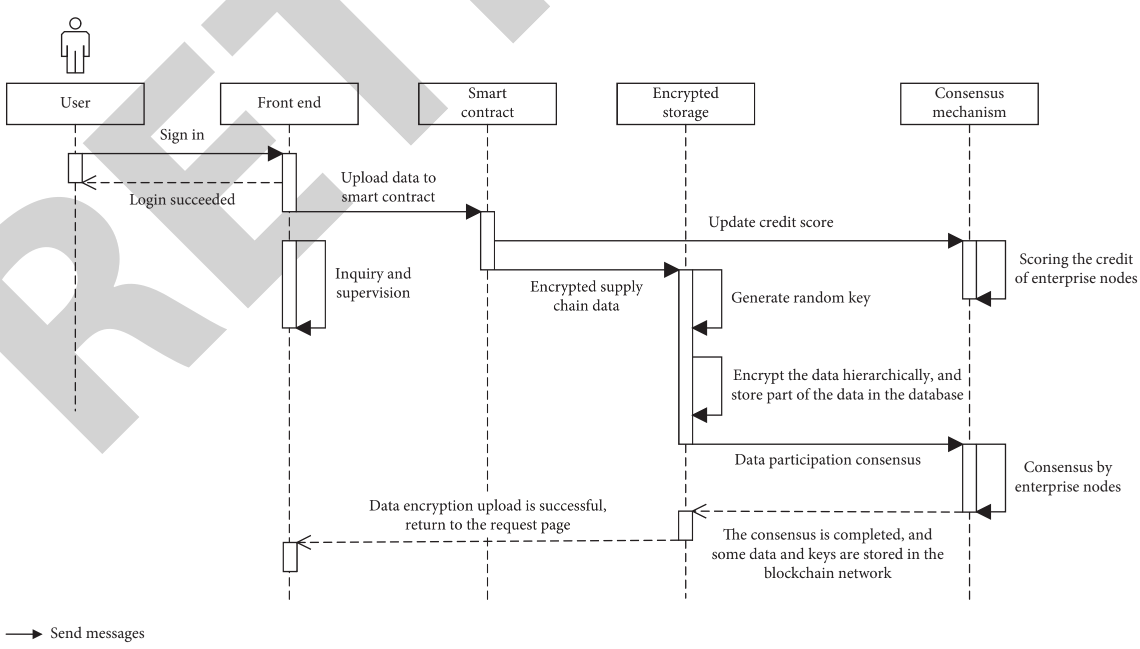

FIGURE 6: Sequence diagram of the information supervision prototype system.

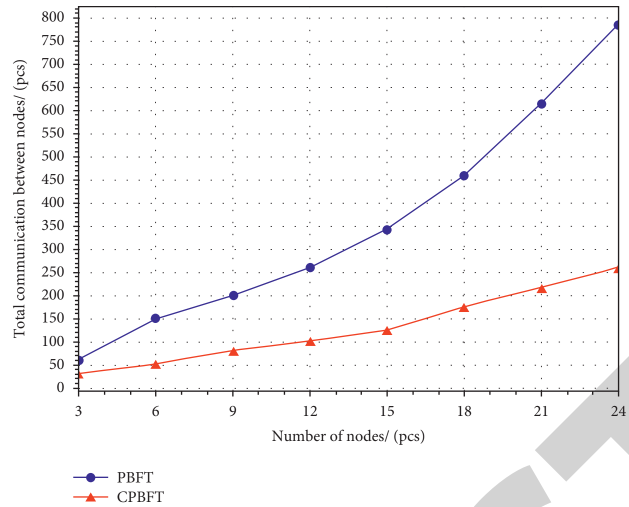

Figure 7: Comparison of communication.

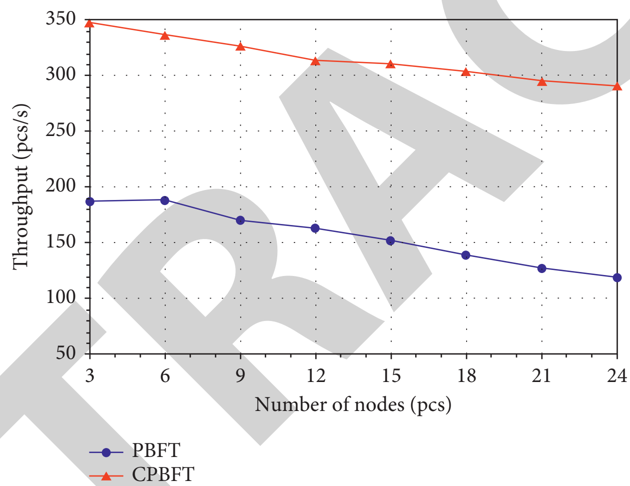

Figure 8: Comparison of throughput.

could complete consensus per second, and tested it with different numbers of nodes. Figure 8 shows the CPBFT algorithm. With the increase in the number of nodes in the network, the throughput of both algorithms shows a downward trend. Overall, however, the throughput of the CPBFT algorithm is much higher than that of the improved algorithm.

5.2. Systematic Analysis. After the field investigation of several rice enterprises, we initially chose to apply the system to a grain and oil enterprise in Changde City, Hunan Province, China, to verify the system's effectiveness. The enterprise's industry involves all links of the rice supply chain. All links have complete monitoring and inspection equipment and stable communication, and all data records are detailed and complete. However, as a result of internal information storage among enterprises and various exchanges between companies, the difficulty of supervision is further increased. In addition, all supply chain data of the enterprise are stored in the central database, and data security is difficult to ensure. Therefore, the proposed rice supply chain supervision system was selected to optimize the supervision and management ability of the enterprise.

Figure 9 shows the system interface. Figure 9(a) is the login interface of the supervision system. After logging in to the system, a supervisor user with administrator authority can supervise and manage all circulating data in the rice supply chain. After logging in to the system, the enterprise user can upload and query information for the entire rice supply chain. The supervision user can search and query all data uploaded by an enterprise in the supply chain supervision interface, including its main information, basic information, hazard information, environmental information, and transaction and price information. As shown in Figure 9(b), all query information is the main data of the supply chain enterprise, which is encrypted and uploaded to the blockchain network and cloud database by the system. The system decrypts the plaintext data again. This mode effectively ensures security and privacy in the process of data storage and transmission. If it is verified as bad data, the

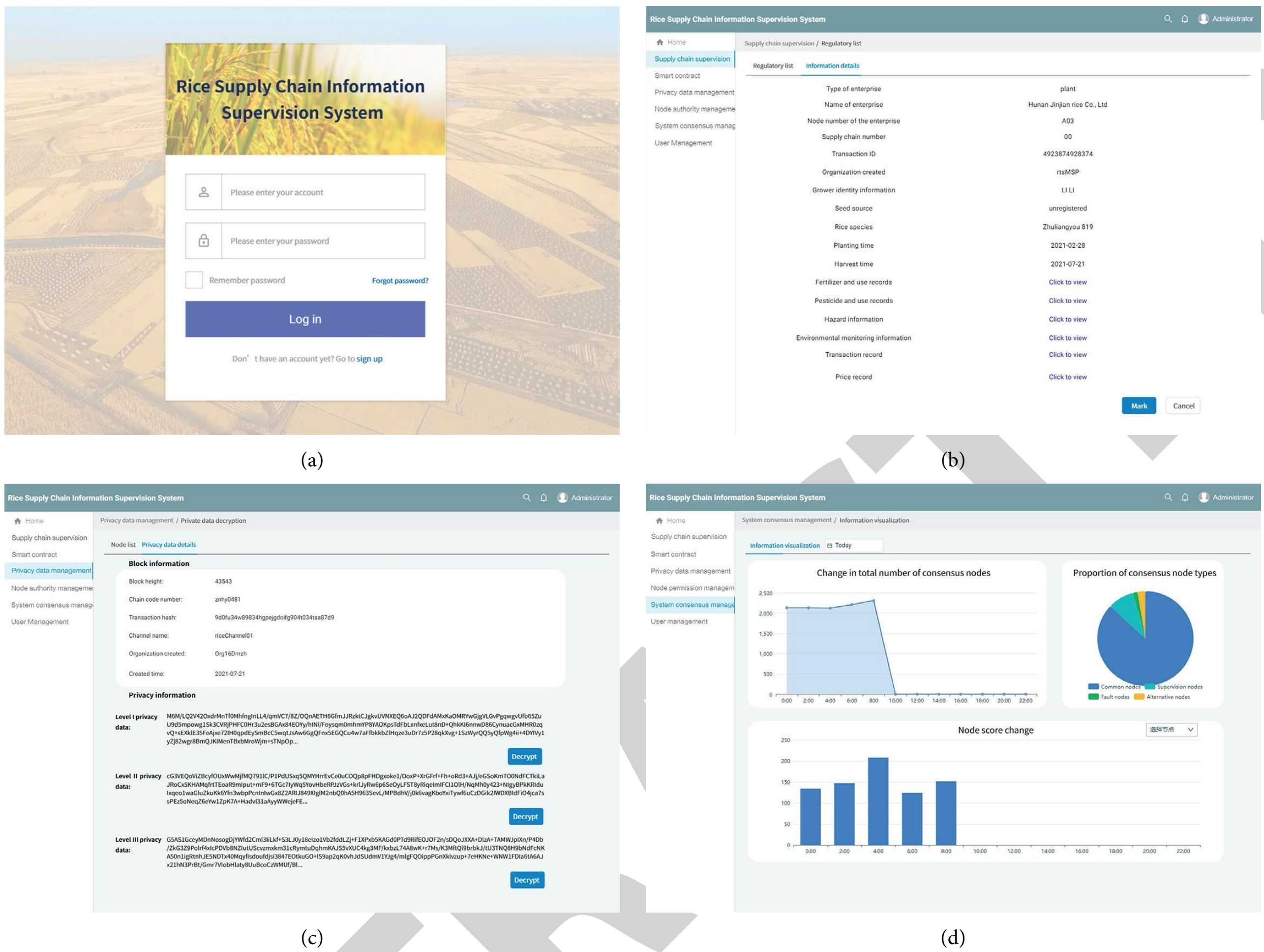

Figure 9: Front-end interface of the prototype system. (a) Supervision system login interface. (b) Supply chain supervision interface. (c) Privacy data management interface. (d) System consensus management interface.

regulator can mark the data and conduct a secondary sampling inspection of the information to finally determine whether the enterprise information is true and reliable and whether the rice quality is good. Users can query the information and stored data of each block in the privacy data management interface of the enterprise. Moreover, the user can decrypt the stored data according to the privacy level, as shown in Figure 9(c). Figure 9(d) shows system consensus management. The main interface is a visual interface. The user can see real-time changes in the total number of consensus nodes and real-time changes in the type proportion of consensus nodes. Users can also select an enterprise node to view real-time changes in the credit scores of the node. Regulators can learn the latest change trend in consensus nodes through the consensus management function and adjust the credit score value in a timely way to improve consensus efficiency.

Compared with traditional systems, the proposed rice information supervision system has a detailed division of permissions. Regulators can query all supply chain circulation data in the system, while enterprise users can upload data and view node consensus. The corresponding permissions are different according to the different supply chain links of the enterprise. In addition, the regulator can query information and analyze privacy in real time according to data privacy level to determine the authenticity of enterprise information and the security of rice-quality data. Moreover, while monitoring the supply chain nodes, the system's visual interface can more intuitively show the data transmission efficiency of the supply chain.

6. Conclusions

The traceability, decentralized, and tamper-resistant characteristics of blockchain technology are in line with the requirements of information supervision system, and blockchain technology has broad development prospects in the field of information supervision system for rice supply chains. This study deconstructs and analyzes the quality and safety information of each link of the rice supply chain at the information level and establishes a key information classification table for each link. Combining cryptography with the characteristics of rice supply chains, a hierarchical data encryption and storage mode is proposed to ensure the security and privacy of data uploaded to the blockchain and cloud database in the process of circulation and storage. In addition, a scoring mechanism is introduced into the consensus process of the blockchain network. Supply chain enterprise nodes are scored to improve consensus efficiency. The improved consensus algorithm also improves the reliability of supply chain supervision.

Verified using practical cases, this research can help optimize regulator information supervision processes in rice supply chains, and the proposed rice supply chain information supervision system can provide a feasible solution for grain and oil supervision. The proposed approaches in the paper can combine other deep-learning algorithms to study the identification and prediction problems, and can be applied to other fields such as signal processing and engineering application systems [35–41].

Data Availability

The data supporting this study are available within the paper.

Conflicts of Interest

The authors declare that they have no conflicts of interest.

Acknowledgments

This work was supported in part by the National Key Research and Development Plan (nos. 2019YFC1605306 and 2017YFC1600605), the Beijing Natural Science Foundation (no. 4222042), and the 2018 Industrial Internet Innovation and Development Project Industrial Internet Identification Resolution System: National Top-Level Node Construction Project (Phase I) and in part by the 2018 Industrial Internet Innovation and Development Project Industrial Internet Identification Overall Architecture: Technical Standard Formulation and Test Verification.

References

[1] F. Yeasmin, I. A. Begum, D. Z. Ethen, and F. A. Happy, "Measurement of farm productivity of rice: a case of Bangladesh," *South Asian Journal of Social Studies and Economics*, vol. 26, no. 4, pp. 1203–1210, 2019.

[2] M. R. Boorboori, Y. Gao, and H. Wang, "Usage of Si, P, Se, and Ca decrease arsenic concentration/toxicity in rice, a review," *Applied Sciences*, vol. 11, no. 17, p. 8090, 2021.

[3] Z. Shi, M. Carey, and C. Meharg, "Rice grain cadmium concentrations in the global supply-chain," *Exposure and Health*, vol. 12, no. 4, pp. 869–876, 2020.

[4] T. Abedi and A. Mojiri, "Arsenic uptake and accumulation mechanisms in rice species," *Plants*, vol. 9, no. 2, p. 129, 2020.

[5] S. Muthayya, J. D. Sugimoto, S. Montgomery, and G. ., F. Maberly, "An overview of global rice production, supply, trade, and consumption," *Annals of the New York Academy of Sciences*, vol. 1324, no. 1, pp. 7–14, 2014.

[6] S. Jifroudi, E. Teimoury, and F. Barzinpour, "Designing and planning a rice-supply-chain: a case study for Iran farmlands," *Decision Science Letters*, vol. 9, no. 2, pp. 163–180, 2020.

[7] B. Lawson, A. Potter, F. K. Pil, and M. Holweg, "Supply chain disruptions: the influence of industry and geography on firm reaction speed," *International Journal of Operations & Production Management*, vol. 39, no. 9/10, pp. 1076–1098, 2019.

[8] P. Kittipanya-Ngam and K. H. Tan, "A framework for food supply chain digitalization: lessons from Thailand," *Production Planning & Control*, vol. 31, no. 2-3, pp. 158–172, 2019.

[9] S. F. Wamba and M. M. Queiroz, "Blockchain in the operations and supply chain management: benefits, challenges and future research opportunities," *International Journal of Information Management*, vol. 52, Article ID 102064, 2020.

[10] L. W. Wong, G. W. H. Tan, V. H. Lee, K. B. Ooi, and A. Sohal, "Unearthing the determinants of Blockchain adoption in supply chain management," *International Journal of Production Research*, vol. 58, no. 7, pp. 2100–2123, 2020.

[11] D. Berdik, S. Otoum, N. Schmidt, D. ., Porter, and Y. Jararweh, "A survey on blockchain for information systems management and security," *Information Processing & Management*, vol. 58, no. 1, Article ID 102397, 2021.

[12] D. Berdik, S. Otoum, N. Schmidt, D. Porter, and Y. Jararweha, "A survey on blockchain for information systems management and security," *Information Processing & Management*, vol. 58, no. 1, Article ID 102397, 2021.

[13] M. Pournader, Y. Shi, S. Seuring, and S. C. Lenny Koh, "Blockchain applications in supply chains, transport and logistics: a systematic review of the literature," *International Journal of Production Research*, vol. 58, no. 7, pp. 2063–2081, 2020.

[14] T. Hidayat and R. Mahardiko, "A review of detection of pest problem in rice farming by using blockchain and IoT technologies," *Journal of Computer Networks, Architecture, and High-Performance Computing*, vol. 3, no. 1, pp. 89–96, 2021.

[15] S. Islam and J. M. Cullen, "Food traceability: a generic theoretical framework," *Food Control*, vol. 123, Article ID 107848, 2021.

[16] J. Duan, C. Zhang, Y. Gong, S. Brown, and Z. Li, "A content-analysis based literature review in blockchain adoption within food supply chain," *International Journal of Environmental Research and Public Health*, vol. 17, no. 5, p. 1784, 2020.

[17] E. Y. Daraghmi, M. Abu Helou, and Y. A. Daraghmi, "A blockchain-based editorial management system," *Security and Communication Networks*, vol. 2021, Article ID 9927640, 2021.

[18] J. Kong, H. Wang, X. Jin, X. Fang, and S. Lin, "Multi-stream hybrid architecture based on cross-level fusion strategy for fine-grained crop species recognition in precision agriculture," *Computers and Electronics in Agriculture*, vol. 185, Article ID 106134, 2021.

[19] Y. Zheng, J. Kong, X. Jin, X. Y. Wang, and M. Zuo, "Crop deep: the crop vision dataset for deep-learning-based classification and detection in precision agriculture," *Sensors*, vol. 19, no. 5, p. 1058, 2019.

[20] G. Baralla, A. Pinna, R. Tonelli, M. Marchesi, and S. Ibba, "Ensuring transparency and traceability of food local products: a blockchain application to a Smart Tourism Region," *Concurrency and Computation: Practice and Experience*, vol. 33, no. 1, Article ID e5857, 2021.

[21] X. Zhang, P. Sun, and J. Xu, "Blockchain-based safety management system for the grain supply chain," *IEEE Access*, vol. 8, pp. 36398–36410, 2020.

[22] L. Wang, L. Xu, and Z. Zheng, "Smart contract-based agricultural food supply chain traceability," *IEEE Access*, vol. 9, pp. 9296–9307, 2021.

[23] D. Mao, F. Wang, Z. Hao, and H. Li, "Credit evaluation system based on blockchain for multiple stakeholders in the food supply chain," *International Journal of Environmental Research and Public Health*, vol. 15, no. 8, p. 1627, 2018.

[24] D. H. Mao, Z. H. Hao, F. Wang, and H. Li, "Innovative blockchain-based approach for sustainable and credible

Hindawi
Computational Intelligence and Neuroscience
Volume 2023, Article ID 9839378, 1 page
https://doi.org/10.1155/2023/9839378

Retraction

Retracted: Application of Artificial Intelligence Computing in the Universal Design of Aging and Healthy Housing

Computational Intelligence and Neuroscience

Received 25 July 2023; Accepted 25 July 2023; Published 26 July 2023

This article has been retracted by Hindawi following an investigation undertaken by the publisher [1]. This investigation has uncovered evidence of one or more of the following indicators of systematic manipulation of the publication process:

(1) Discrepancies in scope
(2) Discrepancies in the description of the research reported
(3) Discrepancies between the availability of data and the research described
(4) Inappropriate citations
(5) Incoherent, meaningless and/or irrelevant content included in the article
(6) Peer-review manipulation

The presence of these indicators undermines our confidence in the integrity of the article's content and we cannot, therefore, vouch for its reliability. Please note that this notice is intended solely to alert readers that the content of this article is unreliable. We have not investigated whether authors were aware of or involved in the systematic manipulation of the publication process.

Wiley and Hindawi regrets that the usual quality checks did not identify these issues before publication and have since put additional measures in place to safeguard research integrity.

We wish to credit our own Research Integrity and Research Publishing teams and anonymous and named external researchers and research integrity experts for contributing to this investigation.

The corresponding author, as the representative of all authors, has been given the opportunity to register their agreement or disagreement to this retraction. We have kept a record of any response received.

References

[1] Q. Shu and H. Liu, "Application of Artificial Intelligence Computing in the Universal Design of Aging and Healthy Housing," *Computational Intelligence and Neuroscience*, vol. 2022, Article ID 4576397, 7 pages, 2022.

Hindawi
Computational Intelligence and Neuroscience
Volume 2022, Article ID 4576397, 7 pages
https://doi.org/10.1155/2022/4576397

Research Article

Application of Artificial Intelligence Computing in the Universal Design of Aging and Healthy Housing

Quanfa Shu [1,2] and Hui Liu [3]

[1] *Shenzhen Grandland Building Decoration Design Institute, Shenzhen, Guangdong 518003, China*
[2] *Graduate School, Hoseo University, Asan, Chungcheongnam-do 31499, Republic of Korea*
[3] *Zhengzhou Business University, Zhengzhou, Henan 451200, China*

Correspondence should be addressed to Quanfa Shu; 20215527@365.hoseo.edu

Received 4 January 2022; Revised 18 February 2022; Accepted 10 March 2022; Published 26 March 2022

Academic Editor: Xin Ning

Intelligent control technology is not only the use of the so-called highly sophisticated technology in the daily life of the elderly but also control services according to the individual needs of the elderly. This paper combines research in psychology and ergonomics to explore how to use the living space to build indoor scenarios that influence the behavioural and psychological changes of the elderly based on satisfying functionality. The external environment influences the user's perception, and the perception determines the user's behaviour. Through the construction of scenarios, objects and people can interact with each other, thus achieving the objective of "solitude but not loneliness" for the elderly living alone and providing a modern ageing environment with high safety, convenience, quality, and comfort for the elderly.

1. Introduction

With the development of ageing population, developed countries such as Europe and the United States are entering an ageing society first. More and more attention is being paid to the issue of elderly people's retirement. With their strong economic strength and the advantages of science and technology, developed countries have been developing their medical and healthcare services. Especially with the rapid development of electronic and information technology, developed countries have taken the lead in exploring the use of information technology to help traditional elderly care [1]. After IBM put forward the concept of "smart city," countries such as the UK, the US, and Japan have also put forward the concept of "intelligent old-age care" or "intelligent care for ageing." The market-oriented operational characteristics of smart old-age care in developed countries are obvious, and the degree of commercialisation is high [2].

Commercial enterprises carefully analyse the needs of the elderly for elderly care services, constantly optimise user experience, and apply new technologies, so as to develop newer and better products for smart elderly care services, including health and medical information sharing data platforms for the elderly, smart elderly community management platforms, emergency call systems, and intelligent elderly care terminal products. A theoretical system and industrial chain for smart elderly care have been initially formed [3].

Old and frail, with children at home, but living alone in a small space or courtyard bungalow is the current situation of the elderly living alone in China. They are relatively capable of taking care of themselves, but can only maintain the status quo for the time being. As they grow old and live alone in small space for long periods of time and rarely leave their homes, they gradually become isolated from their neighbours and society and have a great need for spiritual comfort. The elderly long for companionship, but their families cannot be there for long.

Every family has an elderly person, but not every elderly person has a family member with them. It is easier to know than to do. At least one-third of urban families are of the empty nest type, that is, elderly people living alone or an elderly couple with no children. While paying more attention to these elderly people, the research aims to address the loneliness of the elderly living alone, improve the quality of their lives and living environment, and meet their physical and mental needs through scenario-based design so that they do not feel lonely even when living alone. The study aims to improve the quality of the elderly's living and living environment through scenario-based design, so that they do not feel lonely even when living alone [4].

China has also entered a phase of rapid population ageing. On the whole, the problem of insufficient supply of elderly services and products and the structural imbalance in the supply of social elderly service resources is also becoming increasingly prominent. Taking advantage of the opportunities brought about by the rapid development of the Internet and information technology, it has become an important task to build a well-off society to resolve the contradiction between the growing demand for elderly services and the unbalanced and insufficient development. Compared with developed countries, China is relatively late in the process of population ageing, and the development of the domestic smart elderly care industry is still in the initial exploration stage. Therefore, by comparing and studying the smart ageing in developed countries such as Europe, America, and East Asia and then combining the actual situation of ageing in China, summarising the experience suitable for the development of smart ageing in China will help to build and improve a smart ageing service system with Chinese characteristics [5].

The birth of intelligent device control technology is the result of the mutual reaction between the pursuit of high-quality physical and mental health of the elderly and the rapid development of information technology. Intelligent control technology is not only the use of the so-called highly sophisticated technology in the daily life of the elderly but also control services according to the individual needs of the elderly. This paper combines research in psychology and ergonomics to explore how to use the living space to build indoor scenarios that influence the behavioural and psychological changes of the elderly based on satisfying functionality. The external environment influences the user's perception, and the perception determines the user's behaviour. Through the construction of scenarios, objects and people can interact with each other, thus achieving the objective of "solitude but not loneliness" for the elderly living alone and providing a modern ageing environment with high safety, convenience, quality, and comfort for the elderly.

2. Related Work

Many efforts have relied on existing Internet resources and social forces to build public information platforms and senior care information service network platforms using technologies such as cloud computing and big data to provide community-based care and nursing, health management, rehabilitation, and other home care services. For example, the authors of [6] proposed the concept of "digital community" and "digital elderly care" and conducted research and discussion. The authors of [7] introduced the Hangzhou digital community to realize the livelihood project of "digital elderly care" in the district. Söker et al. [8] proposed a networked home care model. Ostrowski [9] proposed a strategy for the construction of digital elderly care services in the context of new urbanisation. The authors of [10] put forward the concept of smart elderly care, pointing out that smart elderly care is the use of the Internet of Things, cloud computing, and other technologies to carry out comprehensive, online and offline, integrated medical care and all-round elderly care services. Glavič et al. [11] emphasised that smart ageing provides comprehensive services for the elderly in terms of clothing, food, housing, transport, entertainment, and health, helping them to improve their quality of life while not forgetting to help them reflect their value and dignity. The authors of [12] argued that smart ageing is a new model of elderly care services, the core of which lies in taking the needs of the elderly in groups as the guide, mobilising various elderly care resources to coordinate the actions of various elderly care-related parties through the integration of advanced management and information technology, so as to systematically, intelligently, and humanely improve the capacity and level of community elderly care services at home, and strive to provide the lowest cost, highest efficiency, and most convenient services, solving the problem of ageing in place for the elderly in the community.

In response to the characteristics of the scattered population living in the United States, a fleet of medical services for the elderly (mobile medical network) has been established in major cities in the United States, providing a variety of services such as home medical services and home care services in a midbus for the home-bound elderly in need [13]. It adopts market-oriented operation and professional management, so that the elderly can share service resources and reduce the cost of elderly care services. The UK was the first country to introduce the concept of "smart ageing." The UK believes that community-based ageing is the most suitable model for ageing in the country. More old people mainly are in the community, including senior housing, day care centres, senior activity centres, and care institutions. [14]. The UK has a high level of enthusiasm for volunteer participation in community-based ageing. Germany is currently one of the most ageing countries in Europe, with 23% of the elderly over 60 years old. The elderly in Germany do not rely on their children for their old age, but mainly rely on themselves and the support of the state and society. In order to cope with the shortage of manpower, Germany is actively developing smart ageing [15]. Japan has the highest level of ageing in the world. In order to cope with the problem of ageing population, Japan attaches great importance to the development of smart ageing as an economic industry. The Housing Authority of Singapore has tested and developed the "Smart Alert System for the Elderly at Home." The system monitors the lives of the elderly and notifies caregivers in the event of an accident [16].

3. Intelligent Device Control

3.1. Intelligent Equipment Control. Since its introduction, intelligent device control technology has sparked heated discussions in all sectors of society and has been highly respected by many elderly care institutions in particular as a new type of industrial development driver [17]. Intelligent device control technology not only pushes the development and innovation of intelligent elderly care services to a higher level but also allows the elderly to pursue a more comfortable, safe, and convenient living environment as their living standards continue to improve [18].

The birth of intelligent device control technology is the result of the mutual reaction of the elderly group's pursuit of high-quality physical and mental health and rapidly developing information technology. Intelligent control technology is not only the so-called highly sophisticated technology used in the daily life of the elderly but also control services according to the individual need of the elderly group [19]. Intelligent control technology is the product of a high degree of integration of innovative technologies such as Internet of Things technology, deep neural network algorithms [20], intelligent control technology, and elderly service technology, providing a modern elderly environment with high security, convenience, quality, and comfort for the elderly [21].

3.2. Indoor Fall Detection. In this study, it was found that there are two main causes of accidental falls in the elderly population, namely, intrinsic physical factors and extrinsic environmental factors.

A review of the literature on the epidemiology of falls in China revealed that intrinsic factors include dulled senses, reduced vision, slower reflexes, muscle deterioration, reduced balance, and central nervous system disorders, while extrinsic factors include uneven surfaces in the area, poor lighting, cluttered surroundings, and regular use of medications with dizzying side effects. These factors all contribute to the increased likelihood of accidental falls in the elderly population [22]. Reduced balance in older people is a key factor in falling. Factors contributing to unintentional falls in older people are shown in Table 1.

As people walk on their left and right feet, the associated parts of the body work in tandem to maintain balance, and in doing so, they go through a tedious process of musculo-neurotransmission, in which three main mechanisms—perceptual, central, and musculo-organisational—work together. If disturbances in balance occur in the elderly population, such as peripheral neuropathy, vertigo, and visual or muscle strength problems, the risk of accidental falls increases significantly [23].

Falls in older people generally occur when the body's balance mechanisms are accidently disrupted, often within 2 seconds. This is much shorter than normal movements such as squatting, lying down, or standing up. Because the human body falls within a short period of time, the body's centre of gravity is shifted significantly in the direction of the fall, and the fall is accompanied by three specific instantaneous values of acceleration in the X, Y, and Z axes and the angle of tilt in the three axes.

Most studies of accidental falls have used the change in the 3D acceleration and tilt angle values during the fall as a criterion for fall detection. The relationship between the 3D coordinates and the human body is shown in Figure 1.

4. Fall Detection Algorithms

The experiment consisted of 8 normal state transitions and 4 indoor fall states. A total of 1080 simulated data were collected, 720 for daily activities and 360 for falls. It was found that placing the integrated sensor at the waist to obtain the acceleration signal of the human body can more accurately reflect the degree of change of the overall movement state, while the more complex transformation of the wrist or arm cannot fully reflect the information of the human posture transformation. Therefore, the optimal position for the sensor was chosen to be the waist and the sensor was fixed directly in front of the volunteer's waist. The required example data are shown in Tables 2 and 3.

When experimenting with the fall detection algorithm, it is important to first sort out the general idea of the entire algorithm process and visualise it using a flowchart. The general framework of the fall detection experiments is shown in Figure 2, with each part of the experiment module described later.

Through the algorithm flowchart, we have a clear understanding of the process of this study on the detection of accidental falls in elderly people, and each step of the algorithm and its principles will be described in detail next.

Noise reduction: based on the fact that the original signal of the sensor is mixed with a large amount of white noise, which must be removed when applied in practical scenarios, this experiment uses wavelet threshold noise reduction to preprocess the original signal [24]. The wavelet threshold noise reduction process is as follows:

(1) Wavelet transform of the original signal $f(x)$ containing noise to obtain the wavelet coefficients $w(j,k)$

(2) Thresholding the coefficient set $w(j,k)$ to obtain an estimated coefficient set $w(j,k)$ such that the difference between $w(j,k)$ and $w(j,k)'$ is as small as possible

(3) The estimated coefficient $w(j,k)'$ is reconstructed as a wavelet, and the estimated signal $f(k)$ is the noise-free signal required for the experiment

The angular velocity reflects the tilt of the human body in the room, and the angular velocity of the human body on the three axes during movement can also accurately characterise the change in posture of the elderly. The angular velocities in the three axes are also an accurate representation of the changes in the posture of the elderly. The improved formulae for calculating SMA and angular velocity are shown in equations (1) and (2), where the acceleration values in the X, Y, and Z axes are taken and axis(t) is taken as the angular velocity value in the X, Y, and Z axes, respectively.

Table 1: Factors contributing to the occurrence of unintentional falls in older people.

Factor type	Fall inducement
Physical internal factors	Sensory retardation, vision loss, slow response, and central nervous system diseases
External environmental factors	Skeletal muscle degeneration, uneven road surface, insufficient light, disordered environment, inappropriate height of bed and chair, and dizziness and weakness caused by taking some drugs

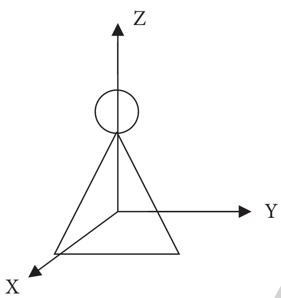

Figure 1: Schematic diagram of the correspondence between 3D coordinates and the human body.

Table 2: Simulated data on daily behavioural activities required for the fall algorithm.

Behaviour type	Human body state transformation	Number of experiments
Daily behaviour activity simulation	From standing to sitting	90
	From sitting to standing	90
	From standing to lying down	90
	From lying down to standing	90
	From sitting to lying down	90
	From lying down to sitting up	90
	Stand and turn left	90
	Stand and turn right	90

Table 3: Simulated data for accidental fall activity required for the fall algorithm.

Behaviour type	Human body state transition	Number of experiments
Indoor fall anomaly simulation	Fall to the left	90
	Fall to the right	90
	Fall forward	90
	Fall back	90

$$SMA(\text{axis}) = \sum_{i=1}^{n} |\text{axis}(i)|, \quad (1)$$

$$ta(\text{axis}) = \int_{t=1}^{\text{timewindow}} w\,\text{axis}(t)\cdot \mathrm{d}t. \quad (2)$$

Kernel principal component analysis first maps the original set of feature vectors to a high-dimensional space through a nonlinear transformation and then achieves linear separability in the high-dimensional space to obtain better feature attributes than in the original space [25].

The set of feature vectors $\{B_n\}_{i=1}^{N}$ represents the normalised set of human feature data, where B_n represents the row vector of the nth human feature data. For each vector in the set of feature vectors, a suitable nonlinear transformation $\Phi(B_i)$: $R^m \longrightarrow H\,B_i \longrightarrow B_i'$ is used to map the feature vector B_i into the high-dimensional space H. In kernel principal component analysis, the nonlinear transformation $\Phi(B_i)$ corresponds to a different kernel function $k(B, B')$. The covariance matrix of the high-dimensional space H is shown as follows:

$$\sum = \frac{1}{N}\sum_{n=1}^{N}\Phi(B_n)\Phi(B_n)^T. \quad (3)$$

The formula for solving the eigenvalues of the covariance matrix $\sum$ and its corresponding eigenvectors is shown as follows:

$$\lambda u = \sum u. \quad (4)$$

The ith eigenvector u_i of the covariance matrix $\sum$ can be represented by a linear combination of $\alpha_n^{(i)}$, where $\alpha_n^{(i)}$ is the summation coefficient, as shown in the following equation:

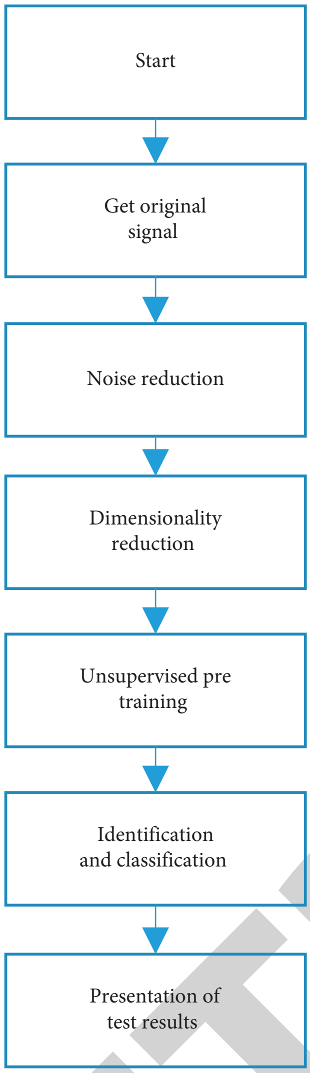

FIGURE 2: General framework of the fall detection experiment.

$$u_i = \sum_{n=1}^{N} \alpha_n^{(i)} \Phi(B_n). \tag{5}$$

Substituting equations (3) and (4) into equation (5) gives

$$\lambda_i \sum_{n=1}^{N} \alpha_n^{(i)} \Phi(B_n) = \frac{1}{N} \sum_{n=1}^{N} \Phi(B_n) \Phi(B_n)^T \sum_{m=1}^{N} \alpha_m^{(i)} \Phi(B_m). \tag{6}$$

The inner product operation in the high-dimensional feature space is replaced by a kernel function to obtain

$$k(B, B') = \Phi(B)^T \Phi(B'). \tag{7}$$

Multiply both sides of the equal sign in equation (6) by $\Phi(B')^T$ at the same time to obtain

$$\lambda_i \sum_{n=1}^{N} \alpha_n^{(i)} k(B', B_n) = \frac{1}{N} \sum_{n=1}^{N} k(B', B_n) \sum_{n=1}^{N} \alpha_m^{(i)} k(B_n, B_m). \tag{8}$$

According to (8), it is possible to calculate the elements of the kernel matrix as shown in the following equation:

$$K_{mn} = k(B_m, B_n). \tag{9}$$

To make the mean $(1/N) \sum_{i=1}^{N} \Phi(B_i) = 0$, the kernel matrix K in the centralized high-dimensional feature space is also needed.

Unsupervised pretraining: for the data feature of accidental indoor falls by elderly people, this topic uses self-encoders for layer-by-layer unsupervised pretraining to solve the gradient diffusion problem. The hidden layers of the deep neural network are pretrained layer by layer, and the parameters obtained from the pretraining are used as initialisation values for the corresponding parameters of the full algorithm.

To facilitate the computation of feature vector sets, the raw signals including all anomalies and daily behaviour are intercepted as time segments in this experiment. The length of the time slice contains enough information about the elderly action transformation for the computation of the feature vector set and does not produce too long a response delay. The calculation of the components of the feature vector set in this experiment is based on the original signal data population within the time window.

Detection and recognition classifier: based on the efficiency and real-time criteria of the fall anomaly detection algorithm, especially the requirement that the fall algorithm can accurately determine the behavioural characteristics of the elderly, this experiment decided to use a deep neural network based on the back propagation algorithm as the detection and recognition classifier for the whole fall algorithm. The deep neural network classifier designed in this experiment has 2 neurons corresponding to the classification output and a forward fully connected pattern between the layers.

5. Assessment of Fall Test Results

Evaluation metrics for determining whether a fall detection algorithm is efficient usually include sensitivity and specificity. In this study, in order to effectively compare the performance of classifiers, it was decided to use an evaluation performance metric commonly used in deep learning and statistics, namely, the error matrix [26]. The error matrix is a standard format for accurate evaluation, and these metrics reflect the performance of the classifier from different aspects. The error matrices are shown in Table 4. Sensitivity refers to the rate at which all fall abnormalities are accurately identified in older people, and specificity refers to the rate at which all normal everyday behaviours are accurately detected in older people.

The experiment was evaluated three times to assess the classification effectiveness of each part of the feature vector group. Using a comparative validation approach, each feature vector group was selected to train the neural network for recognition and classification.

5.1. Single-Variable Controlled Experiments. In this experiment, a single-variable control approach was used, i.e., the selected feature vector sets were not dimensionally reduced

Table 4: Error matrix.

	Positive sample	Negative sample
Correct	Accidental falls	Daily behaviour
Error	False accidental fall	Pseudo-daily behaviour

Table 5: Results of fall detection based on single-variable control method.

Data preprocessing	KPCA dimensionality reduction	Unsupervised training	Recognition classifier	Sensitivity (%)	Specificity (%)
Have	Nothing	Have	Deep neural network	96.32	95.48
Have	Have	Have	Deep neural network	99.21	99.87

Table 6: Results of fall detection based on bivariate control methods.

Data preprocessing	KPCA dimensionality reduction	Unsupervised training	Recognition classifier	Sensitivity (%)	Specificity (%)
Have	Nothing	Nothing	Deep neural network	94.57	93.32
Have	Have	Have	Deep neural network	99.21	99.87

Table 7: Fall detection results for different recognition classifiers.

Data preprocessing	KPCA dimensionality reduction	Unsupervised training	Recognition classifier	Sensitivity (%)	Specificity (%)
Have	Have	Have	Support vector machine	97.36	97.52
Have	Have	Have	Shallow neural network	96.93	95.41
Have	Have	Have	Deep neural network	99.21	99.87

by kernel principal component analysis and then trained for deep neural network recognition classification, all other conditions being identical. The classification recognition results based on the single-variable control are shown in Table 5. According to the data in the table, the sensitivity of the feature vector group without kernel principal component analysis dimensionality reduction reached 90.32% and the specificity reached 93.48%. However, there is still a significant difference between the training results obtained by the algorithm and the results obtained by the algorithm.

5.2. Bivariate Controlled Experiments. This experiment uses a bivariate control approach based on the above to evaluate the effect of kernel principal component analysis down scaling and unsupervised pretraining on the classification of the test set. Each human activity contained 14 coefficient matrices obtained by modelling the preprocessed example data for training the deep neural network and 14 coefficient matrices obtained by the same method for classification tests of fall abnormal and normal behaviour. The recognition classification results are shown in Table 6. The experimental results show that the sensitivity of recognition classification without kernel principal component analysis and unsupervised pretraining can reach about 94.57% and the specificity can reach about 93.32%. This is still a significant difference compared to 99.21% sensitivity and 98.97% specificity of the algorithm. It can be seen that the deep neural network with kernel principal component analysis and unsupervised pretraining is more robust and has better generalization ability.

5.3. Identifying Classifier Experiments. The aim of this experiment was to evaluate the effect of different recognition classifiers on the classification of the test set of fall anomalies. The classifiers selected were support vector machines, shallow feedforward neural networks, and deep neural networks. The tilt angle and signal amplitude were combined into a 14-bit feature vector set, and for each human activity, there were 14 coefficient matrices obtained by modelling the coefficient data after data processing, dimensionality reduction, and unsupervised pretraining for training the three classifiers mentioned above, and 14 coefficient matrices obtained by the same method were used for testing the fall detection classifier. The classification results of the different recognition classifiers are shown in Table 7. According to the experimental results, although the classification results of the first two classifiers have reached a high level of accuracy, there is still a significant gap compared to the deep neural network, which has the advantage of balancing sensitivity and specificity that other classifiers do not have.

6. Conclusions

In this paper, a fall detection algorithm based on kernel principal component analysis and deep neural networks is proposed to address a series of urgent problems such as the vulnerability of elderly people to fall indoors and the potential for multiple injuries after a fall. The algorithm takes the raw signal from the integrated sensor, acceleration, and body tilt as the feature vectors to be input, and after dimensionality reduction by kernel principal component analysis and unsupervised pretraining by self-encoder, a deep neural network based on backpropagation algorithm is

Hindawi
Computational Intelligence and Neuroscience
Volume 2022, Article ID 8633190, 11 pages
https://doi.org/10.1155/2022/8633190

Research Article

Research on Humanistic Quality Higher Medical Education Based on Internet of Things and Intelligent Computing

Rongyu Shang and Yutong Qin

Department of Medical Education, School of Basic Medicine, Army Medical University, Chongqing 400038, China

Correspondence should be addressed to Yutong Qin; qinyt2021@163.com

Received 21 December 2021; Revised 4 January 2022; Accepted 5 January 2022; Published 24 March 2022

Academic Editor: Xin Ning

The importance of the humanities in promoting economic and social development is becoming increasingly clear. Combining humanities with higher medical education in order to meet the needs of medical talent training in the new situation has become a key component of higher medical education reform and development. Adult higher medical education is an integral part of higher medical education, but it has different training objectives and training objects than regular higher medical education. These technological advancements are certain to hasten the continued emergence of education cloud or industry cloud, create a good information-based environment for education informatization improvement, and pose technical challenges to resource allocation in intelligent computing environments. Humanistic quality higher medical education based on the Internet of Things and intelligent computing makes the efficient intelligent information system more open, interactive, and coordinated, allowing students and teachers to perceive a variety of teaching resources more comprehensively.

1. Introduction

With the development of modern science and technology, the role of humanities in promoting all-round economic and social development is becoming more and more obvious. The combination of humanities and higher medical education to meet the needs of medical talent training in the new situation has become an important content of the reform and development of higher medical education. In the era of increasingly prominent humanistic spirit, higher medical education should cultivate talents with all-round development of both humanistic quality and scientific knowledge [1]. For a long time, Chinese medical education has paid attention to the technical training of medical science and ignored the humanistic nature of medicine, resulting in the unreasonable knowledge structure of medical students and the lack of humanistic spirit. From ancient times to the present, the process of world medical education has experienced the initial integration and separation stage of humanistic and professional education and gradually moved towards a new level of integration [2, 3]. The development of medical science also poses a severe challenge to the training mode of new medical talents. The World Health Organization proposed five-star doctors as a global strategy in 1995, stating that doctors should be healthcare providers, decision makers, health educators, community leaders, and service managers in the future [4]. This necessitates not only professional knowledge but also a broad understanding of the humanities and social sciences in today's medical professionals. Adult medical college education is a vital component of higher medical education, but it differs from traditional higher medical education in terms of training objectives and objects. The key points of medical education reform in China are focusing on humanistic quality education and closing the gap between Chinese and developed countries' medical education [5].

Nowadays, with the proposal of the concept of humanistic quality higher medical education, colleges and universities across the country have carried out research on the Internet of Things and big data based on intelligent computing. These technological innovations are bound to accelerate the continuous emergence of education cloud or industry cloud and create a good information-based environment for the improvement of educational informatization. At the same time, it brings technical challenges to resource allocation in intelligent computing environment [6]. The task of the transport layer of the Internet of Things is to reliably transmit the information collected by a large number of terminals to the background central server. However, at present, the construction of the transport layer network is far from reaching the level of welcoming the explosion of the industrial scale of the Internet of Things. The massive data collected by the perception layer will flow into the transport layer network in real time, which will lead to network congestion or node failure. Therefore, how to quickly find network fault nodes is the guarantee for reliable data transmission of the Internet of Things. Intelligent computing is a powerful comprehensive computing method that combines grid computing, parallel computing, and distributed computing. Cloud computing has achieved previously unimaginable results by using server cluster [7, 8]. The campus Internet of Things construction needs to rely on powerful storage and efficient computing technology to realize higher medical education and humanistic quality education [9].

The storage and processing of massive data is the prominent feature and ability of intelligent computing [10, 11]. The intelligent computing mode of humanistic quality education system in higher medical education can ensure the security and normal operation of the data resources of the medical education platform. Students and teachers can access the medical education platform and read data at any time through the Internet [12]. Internet of Things technology, like intelligent computing technology, is network-based. The Internet of Things allows for human-computer interaction as well as human-to-human interaction. As a result, the Internet of Things is a physical Internet that can cover everything in the world [13]. The application benefits of Internet of Things technology in humanistic quality higher education and medical education are primarily manifested in that it makes the efficient intelligent information system more open, interactive, and coordinated and enables students and teachers to perceive all kinds of teaching resources more comprehensively, so as to effectively collect all kinds of required information, realize intelligent learning and teaching modes, and assist in the realization of e-learning.

2. Related Work

Marques et al. [14] assert that, in terms of humanistic quality, higher medical education's mastery of humanistic knowledge is not promising, as evidenced by a lack of literary knowledge, historical knowledge, philosophical knowledge, artistic knowledge, and language skills. Many domestic scholars have recognized the seriousness of the problem, conducted more research on how to inject humanistic spirit into medical science education, discussed some important theoretical problems of humanistic education in medical colleges, and made many positive explorations in methods and means [15] using the big data analysis method. According to literature [16], most higher medical education students have a strong desire and urgent need to strengthen humanistic education, improve self-cultivation and cultural taste, and perfect and realize life ideals and values. The majority of medical students are positive, but their humanistic quality needs to be improved, and humanistic education in medical schools is not given enough attention. There is a significant disparity between investment in humanistic education and the construction of teaching resources, teachers and disciplines, and a campus cultural atmosphere. According to literature [17], most medical courses are interspersed with some strong humanist courses, and the teachers who teach them are mostly former Marxism, Leninism, and ideological politics teachers. They equate humanistic education with ideological education and the cultivation of the humanistic spirit with ideological politicization, causing humanistic education to lose its vitality. Humanistic spirit cannot develop as well as science and technology in medicine. Zhu et al. [18] conducted practical research on the necessity of humanistic spirit in medical colleges from the perspective of curriculum through the method of big data analysis and came to the conclusion that medical courses must be combined with humanistic and social courses in order to cultivate talents meeting social needs. Thibaud et al.'s research [19] shows that only by integrating professional education with humanistic education can the fundamental purpose of medical respect and caring for life be restored. Mao et al. [20] pointed out that higher medical education does not have a deep understanding of the concepts of humanistic quality, humanistic quality education, humanistic spirit, etc. It is thought that the current humanistic education model has to be enhanced because it is primarily focused on a single curriculum and a single teaching technique, neither of which can inspire learning interest. The most significant humanities subjects are psychology, literature, and law, which should be made mandatory. According to the literature [21], students do not pay enough attention to humanistic quality higher education and medical education while using the big data analysis approach. 58.3% of the students are not satisfied with the humanistic quality education courses offered by the school, ignoring humanistic quality education. Due to the lack of teachers' investment, curriculum arrangement, and teaching equipment, students spend most of their time studying professional courses. Wei et al.'s research [22] shows that under the background of diversified socialist values, humanistic quality higher medical education is seriously affected by bad social atmosphere, such as money worship, hedonism, extreme individualism, and some corruption. The value orientation of medical students is somewhat deficient, and humanistic quality education is ignored, and understanding is vague. Khanna and Kaur [23] suggest that more cross courses should be added to medical education and practice in order to achieve the mutual penetration of medical humanities and medical natural sciences.

Based on the Internet of Things and intelligent computing, this paper studies the humanistic quality higher medical education, analyzes the connotation, history, function, influencing factors, and development characteristics of humanistic education in medical education, explores the training strategies of humanistic quality education for medical students under the new situation, and puts forward some suggestions and countermeasures to improve the humanistic education for medical students.

3. Principles and Algorithms of Internet of Things and Intelligent Computing

3.1. Concept and Algorithm of Internet of Things. The concept of Internet of Things was put forward by American scholars. It is a network technology that can identify, locate, track, monitor, and manage information resources. Under the Internet of Things environment, humanistic quality higher medical education is proposed, and a network model is constructed, as shown in Figure 1.

The components of the four-tier architecture of the Internet of Things are as follows.

3.1.1. Perceptual Layer. The perception layer is mainly responsible for identifying objects and collecting information. The work of the perception layer needs to be completed by some terminal devices. At present, the more popular devices include two-dimensional code tags and readers, RFID tags and readers, cameras, GPS, various sensors, and so on.

3.1.2. Transport Layer. The transport layer is mainly responsible for information transmission. The current mainstream technologies include communication network, wireless private network, Internet, and converged network.

3.1.3. Intelligent Processing Layer. The intelligent processing layer creates the dynamic view corresponding to the physical world in the digital/virtual space mainly through processing and services such as dynamic aggregation, decomposition, and merging of sensing information.

3.1.4. Application Layer. The application layer provides rich specific services for users by using the analyzed information. However, at present, the application of the Internet of Things shows the characteristics of "narrow but small," and it is still dominated by single and customized applications, and the sharing and use of item information is not high. The process of humanistic quality higher medical education based on the Internet of Things is shown in Figure 2.

The hierarchical clustering method is used to construct the data acquisition tree. The data sensors in each unit of the Internet of Things are regarded as a class. N classes are divided according to N units. These classes are aggregated one by one according to the distance relationship. The calculation process is shown in the following formula:

$$D_{mn} = \sum_{m-1,n-1}^{a-x,b-y} \frac{d_{ab}}{(x \times y)}. \tag{1}$$

In formula (1), let the classes of hierarchical aggregation be $M = \{m_1, m_2, m_3, \ldots\ldots, m_n\}$, $N = \{n_1, n_2, n_3, \ldots\ldots, n_n\}$, the distance between m_n and n_n is dab, and the distance between classes is D_{mn}. According to formula (1), a data collection tree can be constructed to provide the basis for data collection.

The distribution of data in the entire network has been understood after the data acquisition tree has been constructed using formula (1). The next step is to organize the electronic data. The grouping effect is influenced by two factors: intragroup distance AI and intergroup distance B_i. As a result, the intragroup distance AI and intergroup distance B_i must be calculated in order to determine the grouping data. The following is the procedure for calculating intragroup distance AI. Calculate the total number of nodes in each group first.

$$x = \frac{\sum_{Ljex} d_{ij}}{d_{ab}(i, j)}. \tag{2}$$

In formula (2), it is assumed that there are n data sensors in the network, which can be divided into two categories: A and B, where I is the degree of intragroup separation, J is the number of groups, d_{ab} is the distance between two groups of data, and X is the calculated data node. After calculating the data nodes, calculate the distance variance of two groups of data, as shown in the following formula:

$$y = \frac{\sum_{m,ney} d_{mn}}{d_{ab}(m, n)}, \tag{3}$$

where M represents the number of nodes in the cell, n represents the number of data in the cell, and Y is the variance of data distance. Root work formulas (2) and (3) calculate the distance AI in the data group:

$$AI = \sum_{b}^{a} \frac{x}{y}, \tag{4}$$

where $a = \{a_1, a_2, a_3, \ldots, a_n\}$, $b = \{b_1, b_2, b_3, \ldots, b_n\}$, x is the calculated data node, and y is the variance of data distance. The calculation process of intergroup distance BI is shown in the following formula:

$$BI = \sum_{i-1}^{m} \sum_{j-1}^{n} (x - y). \tag{5}$$

The intragroup distance AI can be calculated by formula (4), and the intergroup distance B_i can be calculated by formula (5). When the number of groups is large, the intragroup distance AI will expand and the intergroup distance B_i will decrease; when the number of groups is small, the intragroup distance AI will be reduced and the intergroup distance B_i will be expanded. The grouping process of electronic data can be completed through the above formula.

If there is at least one path to connect $\forall v_i, v_j \in V$ in a graph G composed of complex networks, then G is called a connected graph. Because there may be many paths between nodes v_i and v_j, the shortest path is called the shortest path connecting v_i and v_j. Assuming that $\sigma(vi, vj)$ is the number of shortest paths between nodes v_i and v_j and $\sigma(v_i, v_j, v_k)$ is the number of shortest paths passing through vertex v_k between nodes v_i and v_k, then the intermediary centrality $B(v_k)$ of node VK in Figure 2 is defined as follows:

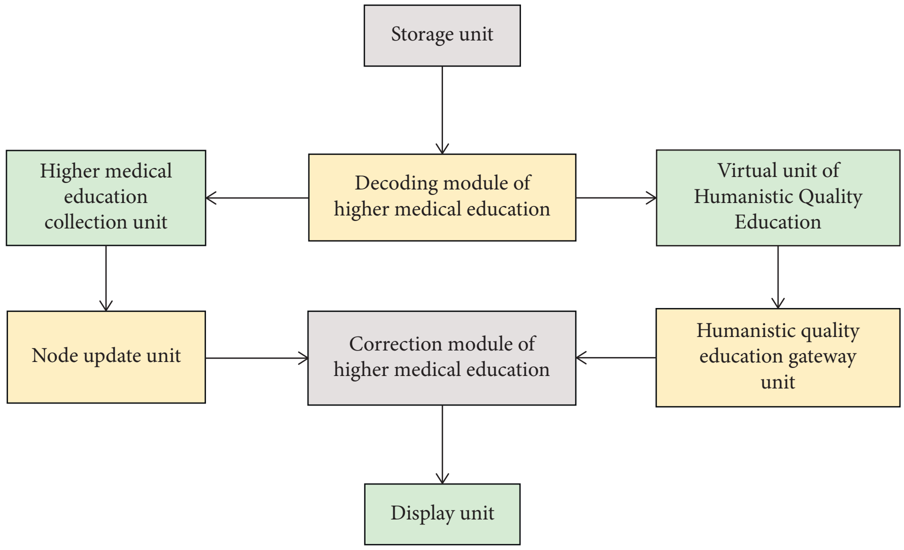

FIGURE 1: Network model of humanistic quality higher medical education.

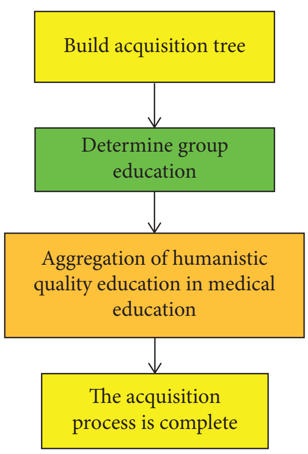

FIGURE 2: Humanistic quality education process in higher medical education.

$$B(v_k) = \sum_{v_i, v_j \in V} \frac{\sigma(v_i, v_j, v_k)}{\sigma(v_i, v_j)}. \tag{6}$$

As can be seen from the above definition, the more the shortest paths passing through a node, the greater its node intermediary centrality, and the shortest path in the network topology is often the path for rapid information transmission. Therefore, node intermediary centrality reflects the bearing degree of nodes on information transmission in the network.

In the figure, assuming that the degree of node v_i is $\deg(v_i)$, then the sum of the degrees of all nodes in the graph is $\sum_{v_i \in V} \deg(v_i)$; then, the degree centrality $D(v_i)$ of node VI is defined as

$$D(v_i) = \frac{\deg(v_i)}{\sum_{v_i \in V} \deg(v_i)}. \tag{7}$$

As can be seen from the definition above, a node is a structure that connects two or more nodes together. The ratio of a node's degree to the sum of all nodes' degrees in a graph is known as degree centrality. The number of nodes directly connected to a node is referred to as its degree centrality. If a node has a high degree of centrality in a computer network, the node could be in the middle of data transmission. After a node is removed, the average shortest path is an important indicator for determining network connectivity, as it reflects the network's reliability and connectivity. The following is the definition:

$$l \equiv (d(v, w)) \equiv \frac{1}{N(N-1)} \sum_{v \in V} \sum_{w \neq v \in V} d(v, w), \tag{8}$$

where $d(v, w)$ is the shortest path length between two dissimilar nodes V and W in the network. In the small-world network, the value of L is around 6; in WWW, the value of L is around 17. After some nodes in the network are removed, some nodes cannot be connected, and the distance between them tends to $+\infty$, which is a value that cannot be calculated conveniently. The concept of reverse average shortest path L is put forward, and its definition is as follows:

$$l \equiv \frac{1}{d(v, w)} \equiv \frac{1}{N(N-1)} \sum_{v \in V} \sum_{w \neq v \in V} \frac{1}{d(v, w)}. \tag{9}$$

When two dissimilar nodes cannot communicate with each other, $1/d(v, w) = 0$. It should be noted that L is not the reciprocal, and the larger the value of L, the better the connectivity of the network.

The size of the largest connected subgraph is the number of nodes in the largest connected subgraph in the graph, which reflects the connectivity among the nodes in the graph and is an important measure of the connectivity within the graph. Assuming that each connected subgraph set of graph

$G = (V, \varepsilon)$ is $\{g_1, g_2, g_3, g_4, \ldots, G_N\}$ and there are paths between any two different nodes in these subgraphs, the relative size of the maximum connected subgraphs is defined as follows:

$$S = \frac{\mathrm{Max}\left\{\left|V_{g1}\right|, \left|V_{g2}\right|, \left|V_{g3}\right|, \ldots, \left|V_{gn}\right|\right\}}{|V|}, \tag{10}$$

where $|V|$ refers to the number of nodes in the whole computer network graph and I% I refers to the number of nodes contained in the connected subgraph GI.

3.2. Concept and Model of Intelligent Computing. The development of intelligent computing technology is based on the development of network information technology. It is a computing mode, which can realize the integrated computing of a large number of data and information resources. Intelligent computing technology architecture mainly depends on three-tier architecture. The relationship among the three is closely related and interdependent, which is progressive step by step, from the bottom hardware to the application software for the end customers. Its concept is developed on the basis of SaaS (Software as a Service). In different levels of intelligent computing, people play the role of users or providers. The process of humanistic quality education in intelligent computing higher medical education involves decision making, comprehensive guarantee, financial management, student management, teaching management, teaching staff management, scientific research management, and application. Combing the business mainly solves the systematic problems of information construction, avoids more complex systematic problems caused by a single process, and provides relevant basis for the intelligent integration of various businesses. Combined with the situation of higher medical education and the development of informatization at home and abroad, Figure 3 shows the relationship between business income and humanistic quality higher education medical education.

Multiple computers can be linked together using intelligent computing technology to create a powerful technical system with massive storage and processing power. Intelligent computing's greatest advantage is that it can customize services to meet the needs of users. It will be able to meet the various network personalized service needs of school teachers, students, and teachers in this way. Intelligent computing does not alter these SAA patterns, but it does provide application providers with more options for delivering SAA products without having to configure the data center. Intelligent computing allows SaaS to be deployed without building or providing data centers, and the scale of SaaS can be scaled according to needs, just as the emergence of semiconductor OEM allows chip companies without production lines the opportunity to design and sell chips.

Intelligent computing is a revolutionary measure, which means that computing power can also be circulated as a commodity; of course, this commodity is transmitted through the Internet. The main goal of intelligent computing is to get all the services we need through network services, even including tasks such as supercomputing, with only a notebook or a mobile phone and other clients. A task space dimension can include many different resource types, and a task space can be divided into many different dimensions, and different dimensions indicate different tasks requested by users. Nowadays, intelligent computing technology has become a very popular and concerned technology in various industries, including academia. With the deepening of educational informatization construction, intelligent computing will play an increasingly important role in the construction of intelligent campus system.

4. Application of Humanistic Quality Higher Medical Education Based on Intelligent Computing and Internet of Things

4.1. Humanistic Quality Higher Medical Education in Intelligent Computing and Internet of Things. Let us compare the time required for intelligent computing and humanistic quality higher medical education. Firstly, the data blocks are divided into 5M, 60M, 120M, and 500M, respectively. On machines with the same configuration environment, serial k-means algorithm and intelligent computing algorithm are used to process these data blocks, respectively. The value of k in the experiment is 5. The experimental results are shown in Table 1.

The experimental results show that the memory occupied by k-means algorithm increases with the increase of the size of data file, until the memory resources are exhausted. However, parallel programs based on intelligent computing are competent, and there will be no shortage of memory. This fully proves that the intelligent computing algorithm has the ability to process large-scale data.

Intelligent computing and k-means algorithm are used to cluster the data of humanistic quality higher medical education, and finally different user groups are obtained. Four different data block sizes were used in this experiment, as shown in Table 2.

Medical education describes the performance of an intelligent computing algorithm as a result of a reduction in running time, which is an important metric for assessing intelligent computing performance. Medical education is the time spent on solving problems at a single node, which is the time spent on solving problems at the same node using P intelligent computing algorithms. In the following experiments, two, four, six, and eight nodes are chosen as different computing resource nodes, and their effects on the processing results are observed. The experimental results are shown in Tables 3–5.

The above table shows that increasing the number of cluster nodes reduces the processing time for the four different datasets A, B, C, and D, demonstrating that increasing the number of cluster nodes can increase the system's processing capacity. We clustered datasets of various sizes in the previous section, and the final results are similar. As a result, we only look at dataset D's clustering results. The dataset's clustering results are shown in Tables 6 and 7.

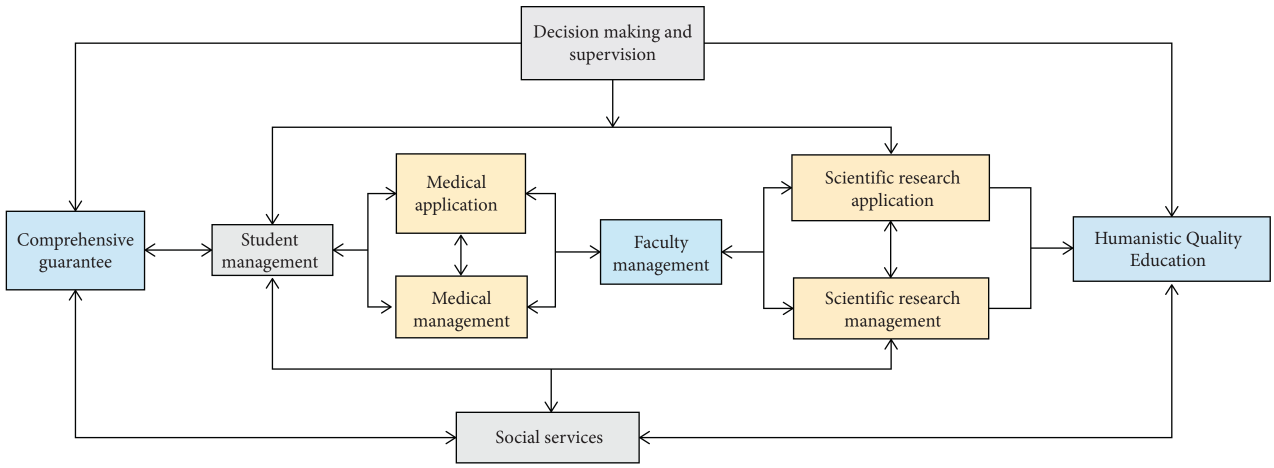

Figure 3: The relationship between humanistic quality education in intelligent computing higher medical education.

Table 1: Comparison of processing time between intelligent computing and k-means algorithm.

Number of experiments	File size (M)	Number of records	t1	t2 (s)
1	5	243145	4.54s	10.368
2	35	1738310	32.76s	38.516
3	125	6953245	98.09s	144.854
4	520	290022854	Insufficient memory	638.810

Table 2: Experimental dataset of intelligent computing and k-means algorithm performance.

Dataset	Dataset size (M)	Number of data items
A	5	243145
B	35	1738310
C	125	6953245
D	520	29022856

Table 3: Performance experiment of humanistic quality education in medical education in Internet of Things and intelligent computing (time unit is ms).

	2	4	6	8
A	7005	4983	4065	4695
B	23258	15258	11281	9725
C	85394	52691	35647	28610
D	356241	188179	130200	98128

Table 4: Performance experiment of humanistic quality education in medical education in Internet of Things and intelligent computing (time unit is ms).

	2	4	6	8
A	7121	4987	4412	4745
B	23456	15245	11293	9796
C	85478	52698	35674	28674
D	356245	188487	130410	98136

Table 5: Performance experiment of humanistic quality education in medical education in Internet of Things and intelligent computing (time unit is ms).

	2	4	6	8
A	7584	4996	4447	4720
B	23635	15287	11345	9895
C	85745	52471	35741	28741
D	356201	188368	130689	98246

Table 6: Clustering result (the center point of each category).

Attribute	1	2	3	4	5
Duration	68121	15395	72036	3198	184
Clicks	34827	1434	3787	377	32
Session num	35	127	140	44	4
Uplink	2371	116	430	32	26
Downlink	825965	9997	20960	2148	167

Table 7: Cluster results of Internet of Things and intelligent computing (number of cases in each category).

	Number of cases in each cluster
1	4690
2	98823
3	26529
4	778333
5	28114377

Through the Internet of Things and intelligent computing clustering, it can be seen that the online time, clicks, and network traffic generated by most mobile Internet users are very low. How to strengthen the loyalty of such users to mobile Internet services has become the primary task of network service providers.

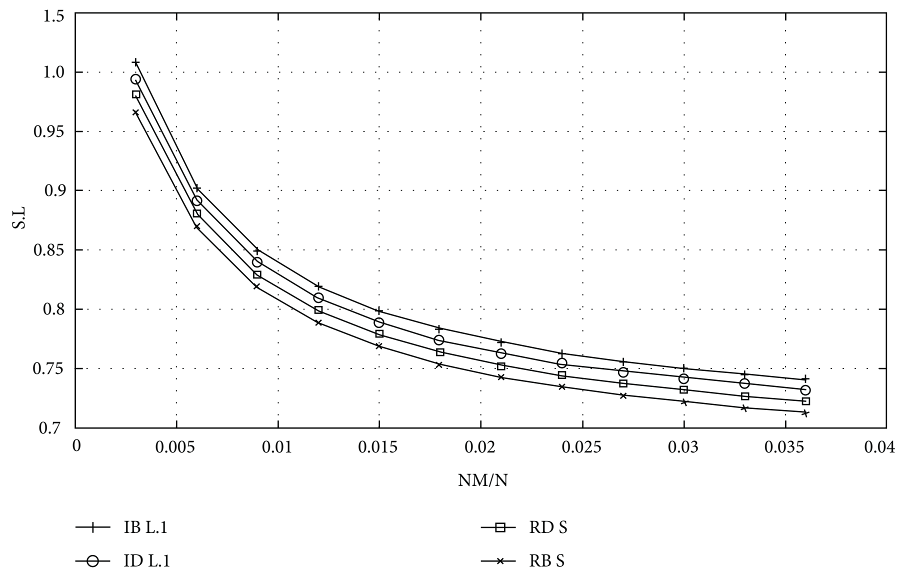

Figure 4: Results of S and L after simulating humanistic quality higher medical education.

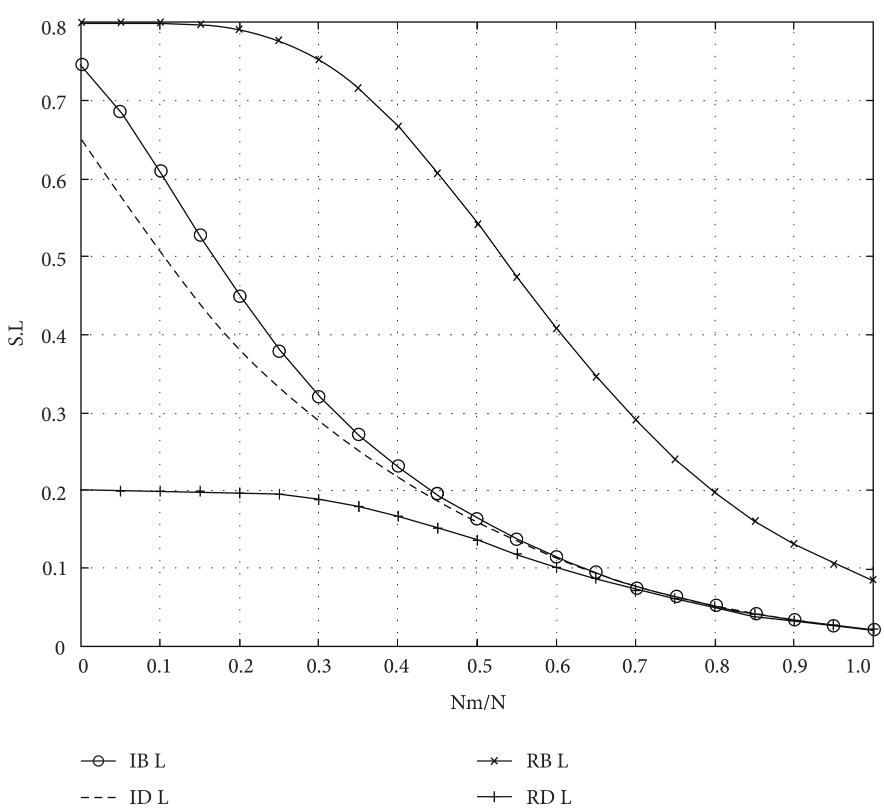

Figure 5: Results of S and L after simulating humanistic quality higher medical education.

4.2. Experimental Results and Analysis. Because the scale-free network accurately depicts the scale-free structure characteristics of higher medical education, it is selected as the higher medical education network simulation data set in this study. In Figure 4, the Y axis represents the relative values of S and L (the ratio of the values of S and L to that of the original graph is recalculated after removing the faulty nodes every time), and the data points on the curve are the results obtained by calculating the values of S and L on 210 networks after removing 51 faulty nodes in the same original BA scale-free network by four different mechanisms, as shown in Figures 4 and 5.

The following conclusions can be drawn from Figure 4. (1) For the BA scale-free network D with 1510 nodes, s

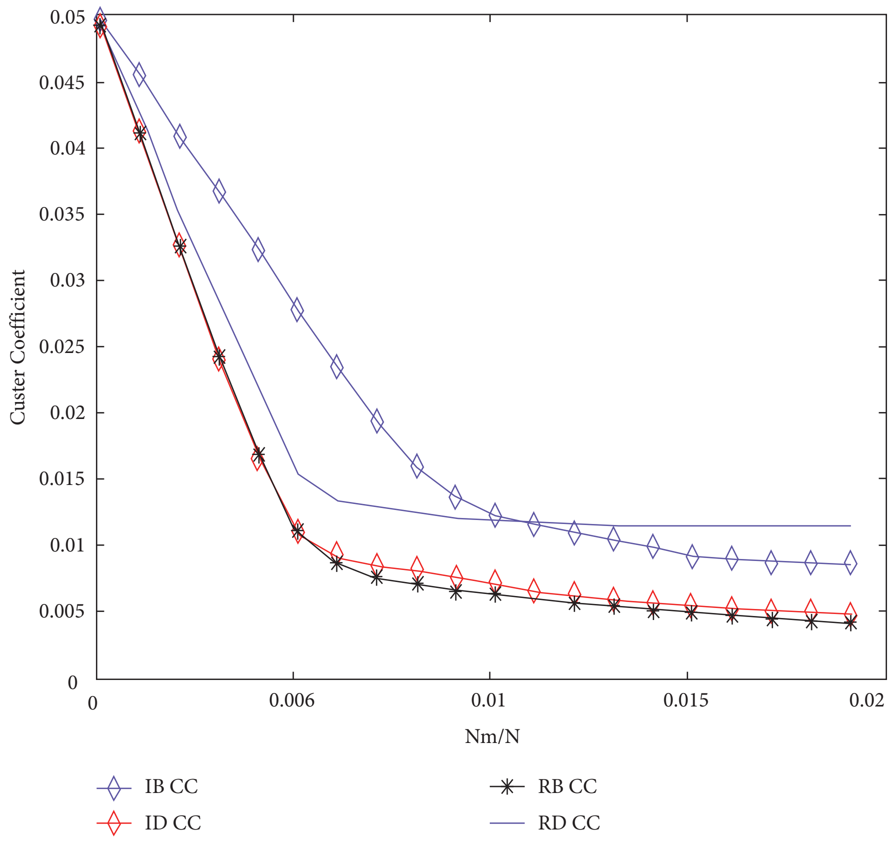

Figure 6: Cluster efficiency results after simulating humanistic quality higher medical education.

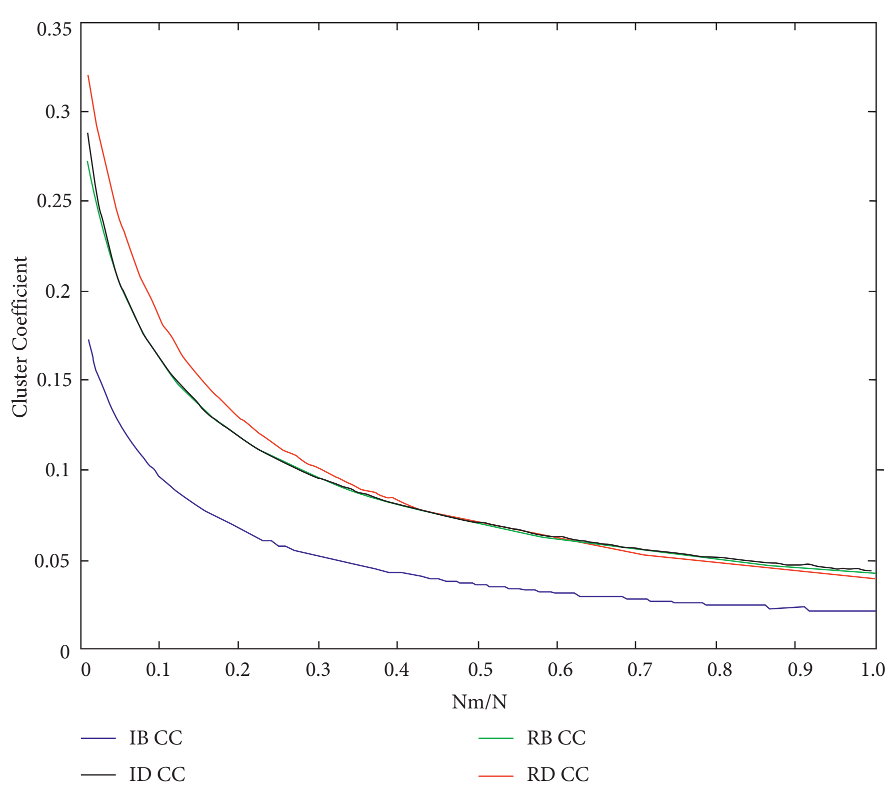

Figure 7: Cluster efficiency results after simulating humanistic quality higher medical education.

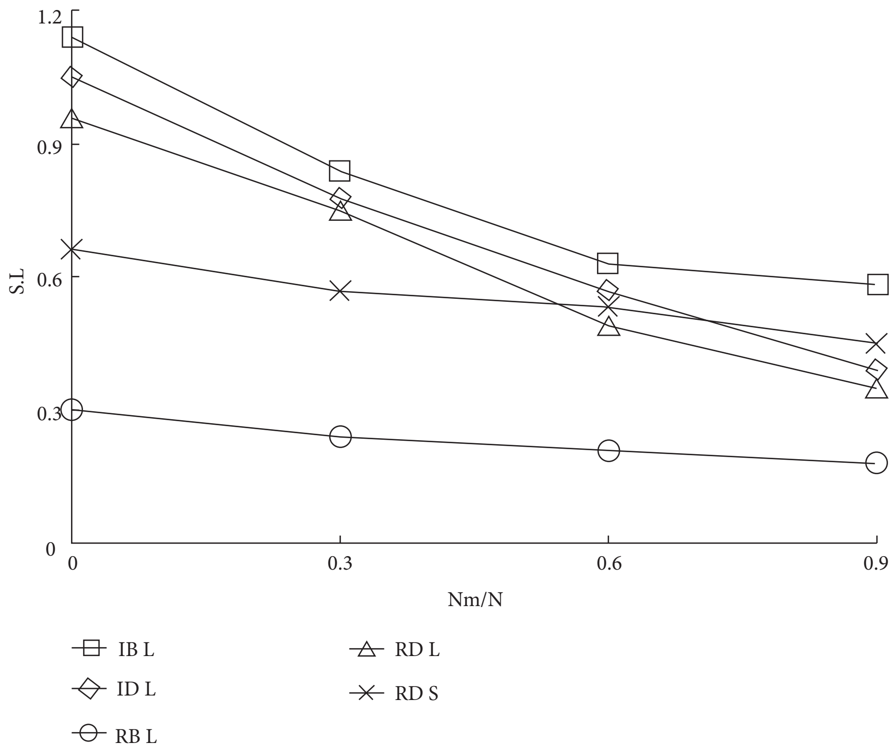

Figure 8: S and L results of humanistic quality higher medical education based on intelligent computing.

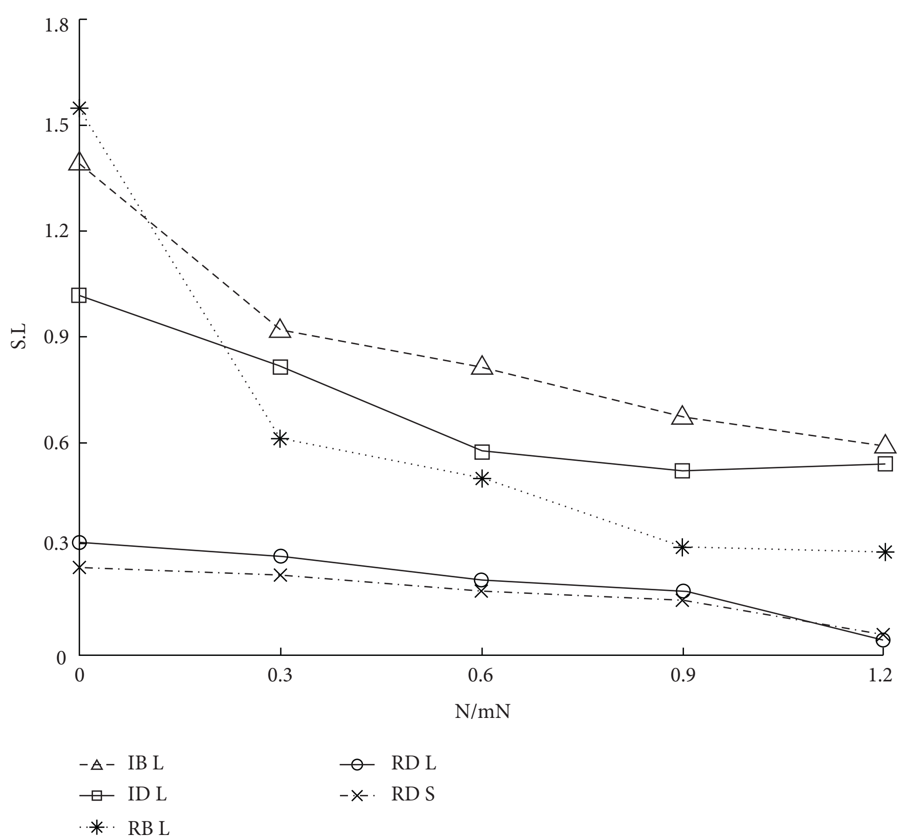

Figure 9: S and L results of humanistic quality higher medical education based on Internet of Things.

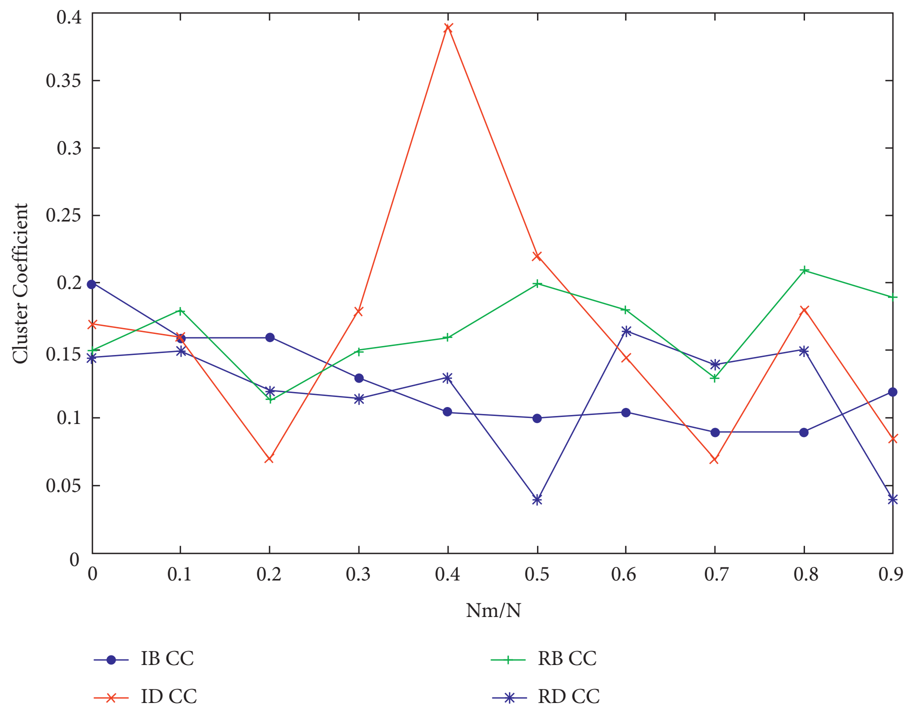

Figure 10: Cluster coefficient results of humanistic quality higher medical education based on Internet of Things.

generated by the four mechanisms is basically the same after the removal of the first 51 failed nodes. (2) When $0.76 < l < 0.93$, the curve of Rb is the lowest after the implementation of the four mechanisms, and the influence of Rb is the largest for L in the whole interval.

Figure 5 shows the graph clustering coefficient corresponding to each data point in the graph. Under normal circumstances, the higher the graph clustering coefficient, the denser the graph; otherwise, the rarer the graph. However, when the graph clustering coefficient of a curve suddenly increases from decreasing all the time, it shows that the graph suddenly produces disconnected subgraphs, which further aggravates the sparseness of the graph, as shown in Figures 6 and 7.

Figure 6 shows the following. (1) On the whole trend, IB has the greatest influence on network performance. (2) When $0.0000 < \mathrm{NRM}/n < 0.0060$, the effects of the four mechanisms are quite consistent. (3) When $0.0060 < \mathrm{NRM}/n < 0.0300$, the mechanism of IB and RB has the greatest influence, and the sudden upward trend caused by IB curve is the most obvious. The graph clustering coefficient corresponding to each data point can be obtained from Figure 7. For the whole curve, when each branch has no upward trend, IB has the greatest influence on the network performance, while for IB, it jumps the most, generates the largest number of disconnected subgraphs, and has the greatest influence.

Three real computer network topologies are introduced to discover and analyze the impact on the actual network. The experimental results of S and L on network A are shown in Figure 8. The network model is one of the few provincial secondary trunk communication network datasets available, which, to some extent, reflects the topology characteristics of the real provincial communication network.

It can be seen from Figure 8 that for L, (1) when $0.1 < l < 1.0$, Rb has the greatest impact and (2) when $0.0 < l < 0.1$, it roughly presents the relationship of Rb > Rd > ID > IB. For the whole curve of S, Rb has the greatest impact. Because the number of nodes in the whole graph is too small, the linear relationship between S and IB is not obvious.

Figures 9 and 10 show the experimental results of S, l, and graph clustering coefficients on network B. In Figure 9, it can be found that RB has the greatest impact on L, and the impact effect relationship is roughly RB > ID > Rd > IB. For the whole curve of S, Rb has the greatest influence, and the linear relationship between S and IB is obvious. In Figure 10, it can be found that IB has the strongest impact on network performance, with the largest number of hops, followed by RB. For the whole clustering coefficient curve, IB > RB > ID > Rd.

5. Conclusion

Higher education should consciously and effectively combine the cultivation of the scientific spirit of seeking truth with the cultivation of the humanistic spirit of seeking goodness, so that students understand with whom to discuss scientific truth. You know how to act when you are studying humanities. Teachers hold the key to providing high-quality humanistic education. Humanistic quality education is meaningless without high-level teaching staff. Basic medical teachers are the strongest in adult medical colleges, while humanities and social sciences teachers are the weakest. This paper examines the humanistic quality of higher medical education, examines the humanistic quality of medical education, and discusses the practicality and participation of students in humanistic education, and finally our curriculum system will incorporate humanistic spirit education into every curricular and clinical practice instruction. Strengthening teaching staff's humanistic quality construction, cultivating a group of teachers with professional skills and humanistic quality through internal training and external introduction, and intensifying cultivation can not only increase students' interest in learning but also strengthen their belief in occupation.

Data Availability

The data used to support the findings of this study are included within the article.

Conflicts of Interest

The authors declare that they have no conflicts of interest.

Acknowledgments

This study was supported by Humanities and Social Sciences Fund of Army Medical University in 2020 (Exploration and implementation path of ideological and political elements in management courses) (project no. 2020XRW07).

References

[1] C. Jiang, Y. Li, J. Su, and Q. Chen, "Research on new edge computing network architecture and task offloading strategy for internet of things," *Wireless Networks*, vol. 2021, no. 2, pp. 1–13, 2021.
[2] X. Liu, Y. Yang, K.-K. R. Choo, and H. Wang, "Security and privacy challenges for internet-of-things and fog computing," *Wireless Communications and Mobile Computing*, vol. 2018, Article ID 9373961, 3 pages, 2018.
[3] B. N. Silva, M. Khan, and K. Han, "Internet of things: a comprehensive review of enabling technologies, architecture, and challenges," *Iete Technical Review*, vol. 35, pp. 1–16, 2017.
[4] Z. Sheng, D. Tian, and V. C. M. Leung, "Toward an energy and resource efficient internet of things: a design principle combining computation, communications, and protocols," *IEEE Communications Magazine*, vol. 56, no. 7, pp. 89–95, 2018.
[5] A. V. Dastjerdi and R. Buyya, "Fog computing: helping the internet of things realize its potential," *Computer*, vol. 49, no. 8, pp. 112–116, 2016.
[6] H. Almajed and A. Almogren, "A secure and efficient ECC-based scheme for edge computing and internet of things," *Sensors*, vol. 20, no. 21, pp. 6158–6160, 2020.
[7] P. Zhang, M. Durresi, and A. Durresi, "Multi-access edge computing aided mobility for privacy protection in Internet of Things," *Computing*, vol. 101, no. 7, pp. 729–742, 2019.
[8] P. Song and W. Tang, "Emphasizing humanities in medical education: promoting the integration of medical scientific spirit and medical humanistic spirit," *BioScience Trends*, vol. 11, no. 2, pp. 128–133, 2017.
[9] M. Mazumder, J. Yun, and S. J. Lee, "Cost-effectiveness of conventional compaction (CC) and intelligent compaction (IC) methods of asphalt pavement overlay," *Sustainability*, vol. 13, pp. 13–15, 2021.
[10] M. Miao, W. Cai, and X. Li, "Parameter estimation of gamma-gamma fading with generalized pointing errors in FSO systems," *Wireless Communications and Mobile Computing*, vol. 2021, Article ID 1301878, 14 pages, 2021.
[11] Y. Huang, L. Cheng, L. Xue et al., "Deep adversarial imitation reinforcement learning for QoS-aware cloud job scheduling," *IEEE Systems Journal*, pp. 1–11, 2021.
[12] M. Nazari Jahantigh, A. Masoud Rahmani, N. Jafari Navimirour, and A. Rezaee, "Integration of Internet of Things and cloud computing: a systematic survey," *IET Communications*, vol. 14, no. 2, pp. 165–176, 2020.
[13] J. Y. Cai, P. P. Zhang, and X. Tan, "A novel physical education environment platform using Internet of Things and multimedia technology," *International Journal of Electrical Engineering Education*, vol. 2019, Article ID 002072091987939, 2019.
[14] G. Marques, N. Miranda, A. Kumar Bhoi, B. Garcia-Zapirain, S. Hamrioui, and I. de la Torre Díez, "Internet of things and enhanced living environments: measuring and mapping air quality using cyber-physical systems and mobile computing technologies," *Sensors*, vol. 20, no. 3, pp. 720–723, 2020.
[15] M. Du, K. Wang, Y. Chen, and Y. Sun, "Big data privacy preserving in multi-access edge computing for heterogeneous internet of things," *IEEE Communications Magazine*, vol. 56, 2018.
[16] J. Yang, M. Liu, J. Lu, and Y. Miao, "Botanical internet of things: toward smart indoor farming by connecting people, plant, data and clouds," *Mobile Networks & Applications*, vol. 23, 2017.
[17] M. Badra, "Preface," *Ad Hoc Networks*, vol. 57, pp. 1-2, 2017.
[18] R. Zhu, L. Liu, H. Song, and M. Ma, "Multi-access edge computing enabled internet of things: advances and novel applications," *Neural Computing & Applications*, vol. 32, no. 19, pp. 15313–15316, 2020.
[19] M. Thibaud, H. Chi, W. Zhou, and S. Piramuthu, "Internet of things (IoT) in high-risk environment, health and safety (ehs) industries: a comprehensive review," *Decision Support Systems*, vol. 108, pp. 79–95, 2018.
[20] W. Mao, Z. Zhao, Z. Chang, and G. Min, "Energy-efficient industrial internet of things: overview and open issues," *IEEE Transactions on Industrial Informatics*, vol. 17, no. 99, pp. 1–3, 2021.
[21] N. Y. Philip, J. J. P. C. Rodrigues, H. Wang, S. J. Fong, and J. Chen, "Internet of things for in-home health monitoring systems: current advances, challenges and future directions," *IEEE Journal on Selected Areas in Communications*, vol. 39, no. 2, pp. 300–310, 2021.
[22] K. Wei, L. Zhang, and S. Wang, "Intelligent channel allocation for age of information optimization in internet of medical things," *Wireless Communications and Mobile Computing*, vol. 2021, Article ID 6645803, 10 pages, 2021.
[23] A. Khanna and S. Kaur, "Internet of things (IoT), applications and challenges: a comprehensive review," *Wireless Personal Communications*, vol. 114, no. 15, pp. 1–76, 2020.

Hindawi
Computational Intelligence and Neuroscience
Volume 2022, Article ID 8040913, 9 pages
https://doi.org/10.1155/2022/8040913

Research Article

Visual Health Analysis of Print Advertising Graphic Design Based on Image Segmentation and Few-Shot Learning

Sen Hu

School of Design,Shandong University of Arts, Jinan,250307, China

Correspondence should be addressed to Sen Hu; z00547@sdca.edu.cn

Received 20 January 2022; Revised 11 February 2022; Accepted 12 February 2022; Published 24 March 2022

Academic Editor: Xin Ning

Graphics innovation must adapt to the changing trends of the times in order to stay ahead of the curve. This article investigates the use of graphic vision in print advertising design, using image segmentation as a starting point and examines the current state of visual innovation in print advertising graphic design and its various expressions and applications. A series of homogeneous regions are generated and outlined using an image segmentation algorithm based on adaptive local threshold. The user then paints different colors on the area sets that make up the various targets. Finally, the image segmentation is completed by merging the color mark region sets. Automatic extraction of the initial curve of an active contour model, construction of an active contour model based on saliency and level set solution, automatic selection of training samples when a classifier is used for image segmentation, and so on are all problems that this method effectively solves. Experiments show that this algorithm not only satisfies users' demands for more intuitive input and more accurate interactive image segmentation results but also enables multiregion and multitarget image segmentation with ease.

1. Introduction

Graphics and image processing [1] has become one of the most active research directions today as a result of the advancement and perfection of computer science and related mathematical theories. Among them, graphic image segmentation has long been a hot topic in this field. Image segmentation is the process of dividing an image into several disjoint regions based on a similarity measurement criterion, with pixels in the same region having similar features and pixels from different regions having low similarity [2]. Graphic image segmentation technology has found widespread use in a variety of fields, including computer animation, medical image processing [3], virtual reality, computational visualization, and so on. Graphics have become synonymous with fashion in the irresistible visual space. Changing time and space gives graphic vision a new lease on life, as well as revealing its glory. Many image processing tasks necessitate the extraction of some image areas. We can divide the pixels by means of image segmentation [4, 5] technology and separate the target areas from the background. At present, many image segmentation methods have been proposed, but there are still some problems, such as poor universality, dependence on user interaction, and inconsistency between segmentation results and human visual perception. With the deepening of the era of reading pictures and the development of artistic interoperability, the aesthetic ability and demand of the public are further improved, and the print advertising design industry is facing new challenges. Graphics in modern print advertisements are intuitive, vivid, lively, distinctive, unique, and changeable. The language displayed by graphics can be our perception of daily life or the trend of the times [6].

Print advertising is an important part of today's social and economic life, and it helps to promote the circulation of goods [7]. Every designer working in print advertisement design is concerned about how to make print advertisements better serve today's society [8]. Currently, issues such as design material simplification and homogenization are more prominent in the industry. Design practitioners are concerned about how to use image processing technology to improve the innovation of print advertising design [9]. The data item established by the local algorithm is the first part of the energy function of the traditional graph cutting algorithm, and the smoothing term of disparity difference between neighboring pixels is the second part. The local algorithm data items will cause relatively large errors due to occlusion and other reasons, and the smoothness assumption of occluded areas is often not valid, so parallax mismatch will occur in some occluded areas [10]. With people's access to images becoming more convenient and quick, more image segmentation algorithms are being used for Internet and mobile device image processing tasks like image classification, marking, retrieval, and thumbnail generation, among others, which necessitates image segmentation algorithms that are fast, accurate, and have the advantages of automatic and real-time processing [11]. Image segmentation is a key step from bottom image processing to image recognition and understanding because the result has a direct impact on subsequent visual tasks [12]. Humans can accurately separate the target area in an image, but computers find it difficult. This article investigates and analyzes the visual innovation of graphic design in print advertisements using image segmentation technology.

At present, in this era of visual transmission everywhere, our sights or thoughts are usually filled with various kinds of graphics [13]. Graphics spread information everywhere in the world, and it has become an expression language without national boundaries. On the one hand, modern print advertising is a new way to promote commercial advertising; on the other hand, it is also the expression of aesthetic symbolism in the market economy [14]. Graphic vision in modern print advertising design, as a combination of technology and art, embodies the diversity and richness of modern culture all the time. As a force that cannot be ignored in visual art, it promotes the development of modern print advertising design and promotes print advertising design to enter a new visual era. This kind of commercial works combined with artistic sense can often stimulate the infinite imagination of the audience, and at the same time, it will leave a deep impression on the audience [15]. This will also greatly promote the products involved in the advertisement. Graphic vision in graphic advertising design is not just a picture to convey information, but a kind of symbolic sentiment, which can deeply attract people, move people, and inspire people. Graphic vision will show different advertising themes according to different advertising concepts [16]. As print commercial advertising is an outstanding performance of innovation, the graphic design of print advertising not only plays the role of information transmission in external publicity but also is a prominent performance of corporate culture. Based on image segmentation, this study analyzes the innovation of graphic design vision in print advertisements and discusses how graphic design vision will face the public. The potential position of the target object is predicted using a saliency map, and the result is further refined using a morphological operation to obtain the target object's contour information. The objective function is defined to quantitatively describe the visual information in an image based on human visual characteristics. The global optimal threshold of each subgraph is obtained by optimizing the objective function. The final threshold segmentation result is then obtained by performing a local adaptive threshold operation using the image's local characteristics. The results of the experiments show that this method is active and adaptive. Furthermore, the segmented binary image has a pleasing visual effect, and its overall visual quality is closer to that of human perception.

2. Related Work

People are tired of traditional marked graphics, according to Zhang et al. [17], and the era of traditional print advertising is over. According to Wang [18], it is necessary to combine innovative ideas in advertising art with technical science, as well as to demonstrate cultural diversity, while considering the economic benefits of advertising. In order to encourage in-depth visual concept innovation in print advertising design, discussing the importance of graphic vision and studying the innovative elements of graphic vision in print advertising design, according to Walter et al. [19], will help graphic vision better serve people and encourage them to use graphic visual language more quickly. Soldow [20] discussed iconology and conducted a pedigree study on the visual images used in print advertisements. The visual images used in print advertisements are systematically classified and studied in groups as a result of this. According to Ramezani et al. [21], graphic image processing is usually based on graphic image segmentation technology, which allows the target area to be accurately separated from the graphic image background. Javan and Zeman [22] proposed a new interactive image segmentation algorithm. This algorithm overcomes the shortcomings of many current interactive algorithms, such as cumbersome operation and ineffective multiobjective segmentation and is very practical. Based on the analysis and research of existing graphics and image segmentation algorithms, combined the characteristics of human vision and related theories with the segmentation process, Miller et al. [23]proposed new graphics and image segmentation algorithms, respectively. Zeller [24] compared the visual images of graphics in print advertising design in different times. At the same time, through the analysis of the development process of print advertising, the connotation of graphic vision in modern print advertising design is interpreted.

This article summarizes the composition and characteristics of the human visual system and comprehensively analyzes the problems that exist in current graphic image segmentation based on an in-depth review of related literature. A new adaptive image segmentation method is proposed that combines the threshold selection process with human visual characteristics. The geometric attributes of the mesh model, which include arc length, angular distance, and correction term, define the distance function between mesh vertices. Visually meaningful segmentation results are obtained by clustering the grid's vertices. This research combines print advertising design with image processing technology, resulting in a unique artistic effect and increased advertising information transmission accuracy. It is also

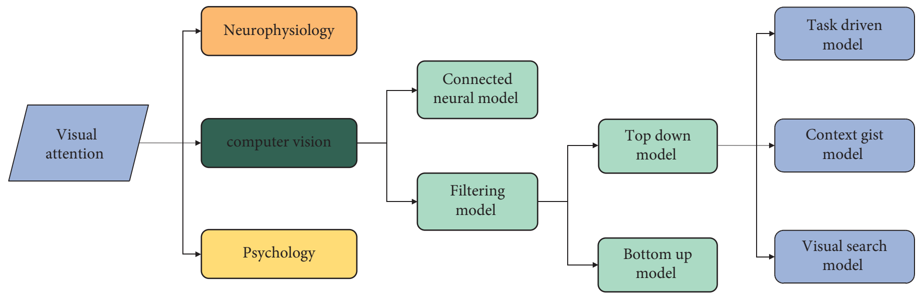

FIGURE 1: The category of attention mechanism.

more in line with the current aesthetic trend, and it is more conducive to the spread of digital network media and other forms of communication.

3. Methodology

3.1. Visual Innovation in Graphic Design of Modern Print Advertisements. Vision is one of the important ways for human beings to obtain information about the surrounding environment. The human visual system generally consists of two parts: the human eye and the central nervous system of vision. Among them, the human eye is responsible for perceiving visible light information, which projects a two-dimensional image on the human retina [25]. The visual central nervous system is responsible for the reconstruction, positioning, discrimination, analysis, and research of two-dimensional images. Visual perception is a highly complex visual perception process, which is from the direct response to the attributes of the target object to the acquisition of its advanced semantic information. At present, many methods in graphics and image processing are based on mathematics, computer, and other disciplines. Because human intuition and analysis of things will play an important role in the process of selecting methods, this selection process is usually based on human subjective visual judgment. Therefore, understanding the composition of human visual system and its visual characteristics is of practical significance for solving the problems in graphic image processing.

In modern society, due to the progress of science and technology, all kinds of images that human beings can see have far exceeded the sum of the visual images of any era after the emergence of human beings. The visual attention mechanism [26] helps the brain to process all kinds of information in the visual field in parallel, and visual salience can help the visual attention system to realize automatic real-time target selection. After calculating the saliency of each object in vision, the vision system will use different eye movement strategies to determine the attention order of several prominent objects in vision, and then transfer attention among these prominent objects [27]. The main feature of human visual concentration is that the human visual system can quickly fix the visual attention on several obvious visual targets that it is interested in and automatically screen out other visual targets when faced with a large number of complicated visual information. When dealing with complex scenes or facing a large amount of visual information, the human visual system can quickly focus on several prominent targets while ignoring other uninterested objects. This process is called visual attention mechanism. The visual mechanism is shown in Figure 1.

In modern print advertising design, the creative elements of graphic vision are important in design expression techniques. Each designer may have different ways and means of conceiving and express the connotation of print advertising works through graphic vision creativity. To study the visual innovation of graphic design, we must analyze it from the most fundamental elements. This kind of element is the tool of creation. Visual creativity refers to the expression of creative ideas [28]. In the graphic design of contemporary print advertisements, the visual innovation elements of graphic design play an important role in the way of expression. Different designers have different ways of thinking and show the specific meaning of advertising works by means of graphic design visual creativity. In the design of modern print advertisements, graphic creative elements commonly used can be divided into abstract graphic creative elements and realistic graphic creative elements.

In a broad sense, visual image refers to all images that human beings see. The premise is to have a normal visual system. Images in nature are complicated and rich. As a specialized visual discipline, the visual image of print advertisement needs more strict classification standards. Classifying all kinds of images will help us to better grasp the fundamentals of image application. Among the graphic design elements, the design of Chinese and English fonts is quite common [29]. Chinese characters are the accumulation of Chinese traditional culture, and characters are one of the best graphic elements to accurately convey information. Usually, designers design graphic visual creativity from the pictographic consciousness of characters. The creativity of Chinese characters is to re-create graphics on this basis. Using the product of modern social development, modern element symbols, and regraphics and creativity in the structure of Chinese characters, people can imagine another meaning after the change in the basis of familiarity with existing Chinese characters.

Graphic vision is an important way of expressing oneself in the graphic creation of contemporary print advertisements, and it is the focus of the audience's attention. Good advertising creation can reveal the ideas to be expressed in advertising creation using its own distinct graphic language and can succinctly and effectively show the theme with profound meaning [30]. Graphic advertisement, as a concrete manifestation of graphic design, bears most of the design features of graphic design, particularly the design innovation of graphics and pictures, which plays a significant role in the design process. Graphic design vision, in particular, is the soul of print advertising design. To fully comprehend the overall design work, start with these subtle elements, consider graphic elements as the building blocks of graphic design, and consider the visual effect of the results as the standard for testing the properties of graphic elements. The premise foundation of this type of advertising product is innovative ideas of vision and creative forms of expression of ideas. With the increasing variety of visual expression creation, graphic design's visual language should use new ways to realize ideas in the creation process. It is clear that graphic vision creation plays a vital role in the graphic creation of contemporary print advertisements. The graphic creation elements in the graphic creation of print advertisements are also investigated, and it can be concluded that graphic vision creation plays a vital role in the graphic creation of print advertisements. In the current graphic design process, the graphic elements involved are abstract and concrete. Analyzing and grasping these two elements will promote the development of the whole print advertisement. The visual information processing model is shown in Figure 2.

Visual traction is a bright spot in the graphic design process of current print advertisements. There are two aspects to draw the visual audience's information: using color and using graphics, the audience can follow the designer's ideas to appreciate the works. Most existing print advertisements are guided by dots, lines, and planes. The subjective initiative quota of people plays an important role in the design process. Different designers often design different graphics to express different artistic feelings as a result of their diverse life experiences, and even the same type of graphic design can be interpreted in different ways depending on the language used. Visual metaphorical expression in graphic works is an extremely important, unique, and inventive expression form in today's print advertising, and we can also use metaphorical expression techniques in graphic design of contemporary works in large quantities. This type of graphic expression can help to advance graphic vision in works, as well as focus the audience's attention, which can benefit businesses financially.

In the design of modern print advertisements, realistic graphics, a creative element, also occupies an important position, which is equally divided with abstract graphics. Although realistic graphics have not changed in various ways, it can make the audience feel the real sense of existence and narrow the sense of distance between audiences. Excellent image creation advertising works do not care how much the graphics change but the extraction and processing of creative thinking. No matter how the graphic design itself changes, we cannot interpret without the two scales of abstraction and concreteness. The correct use of these two tools will not only help the audience to understand the graphic design but also promote the inspiration of designers.

The idea of minimalism comes from the minimalism of contemporary school. The designers of this school all

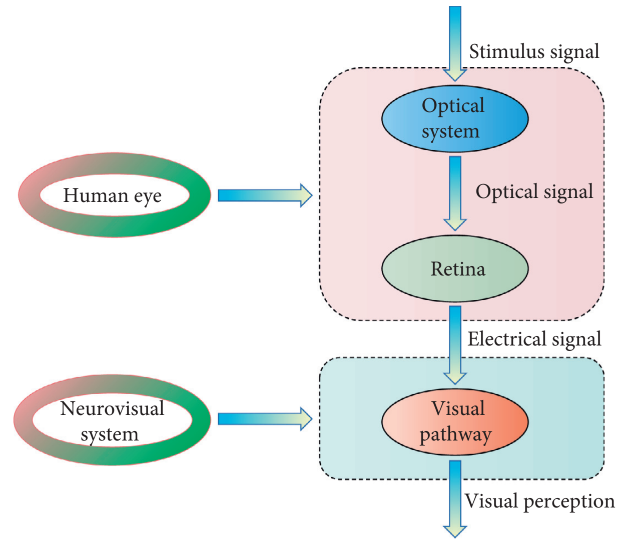

Figure 2: Schematic diagram of visual information processing model.

encourage minimalist drawing methods, and the purpose of the simplest treatment of creation is to find a simple scheme that is rich in content and pure in Chinese and modern classics. In order to create advertising works with more special visual effects, I should pay attention to the existence of minimalist style, master it, and use it properly in the visual creation of graphic works. Learn about graphic effects and how to use them. We should concentrate on displaying the bright spots of graphics during the graphic design and postdecoration processes in order to fully attract the audience's attention and increase their interest in graphic culture and persuade the audience to accept the advertisement's content while admiring and being drawn to the beauty.

3.2. Graphic Design and Implementation of Print Advertisement Based on Image Segmentation. Image segmentation has always been one of the most difficult problems in computer vision, with the ultimate goal of allowing computers to mimic human visual cognition and recognize the meanings represented by different regions in an image. Traditional image segmentation methods and image segmentation methods combined with new theories are the two main types of image segmentation methods. Early image segmentation methods relied on analyzing image features, such as grayscale, orientation, size, and shape. This category includes histogram threshold segmentation methods, region-based segmentation methods, edge-based segmentation methods, and hybrid segmentation methods. With the advancement of computer vision and research into human cognitive ability, the question of how to use human visual characteristics to produce more reasonable image segmentation results has become a hot topic in research.

The basic principle of threshold-based image segmentation method is as follows. Let the original image as f, the image size as $M \times N$, the image grayscale as L, and $f(x, y)$ represents the gray level of the pixel whose coordinates are (x, y),then $x \in [1, M]$, $y \in [1, N]$. The single-threshold segmentation method is to determine a segmentation threshold T, segment the gray levels of all pixels, and obtain the segmentation result $g(x, y)$:

$$g(x, y) = \begin{cases} 0, & 0 \leq f(x, y) \leq T, \\ L - 1, & T < f(x, y) \leq L - 1, \end{cases} \tag{1}$$

where T is a constant that applies to the whole image, the processing method given by this formula is called global thresholding. When the value of T changes constantly and is determined by (x, y) and its neighborhood characteristics, the processing method is local thresholding. The multi-threshold image segmentation method adopts multiple thresholds, set the number of thresholds as n, and denote T_1, T_2, ..., T_n as the segmentation threshold, then the image $g(x, y)$ after segmentation is

$$g(x, y) = \begin{cases} L_0 & 0 \leq f(x, y) \leq T_1, \\ L_1 & T_1 < f(x, y) \leq T_2, \\ \cdots & \cdots \\ L_{n-1} & T_{n-1} < f(x, y) \leq T_n, \\ L_n & T_n < f(x, y) \leq L - 1, \end{cases} \tag{2}$$

where $L_0, L_1, \ldots, L_n$ are the $n + 1$ gray levels of the segmented image.

There are four major flaws in the segmentation of two-dimensional images in the computer image processing process right now. (1) An insufficient number of image segmentation methods are available. (2) Image segmentation has a low level of accuracy. (3) There is no perfect quality evaluation standard for image segmentation. (4) Image segmentation results are difficult to match human visual perception requirements. The threshold segmentation method is a simple image segmentation method that uses the gray level difference between the target object and the background in the image to select one or more thresholds based on the image gray histogram and divides the image into target and background areas with different gray levels. The key to using a threshold segmentation algorithm is to pick the right one. When the gray histogram of an image has a bimodal shape, the gray value corresponding to the valley between two peaks is selected as the threshold, depending on the number of thresholds used in segmentation. Different thresholds or dynamic thresholds can be used in different positions of the image using variable and multiple thresholds. The visual mechanism is still under investigation due to the complexity of the human visual system. Many image segmentation methods currently use visual saliency as a visual mechanism, with the image's saliency map being used to simulate vision.

Interarea contrast GC indicates the gray contrast between the divided areas:

$$\mathrm{GC} = \frac{(f_1 - f_2)}{f_1 + f_2}, \tag{3}$$

where f_1 and f_2 are the average gray levels of pixels in the target area and the background area, respectively. Internal uniformity UM indicates the degree of uniform distribution of pixel characteristics in each area in the segmented image.

$$\mathrm{UM} = 1 - \frac{1}{C}\sum_{i=1}^{2} \sum_{(x,y) \in R_i} \left[I(x, y) - \frac{1}{A_i} \sum_{(x,y) \in R_i} I(x, y) \right]^2. \tag{4}$$

C is the normalization coefficient, and R_1 and R_2 represent the segmented target and background regions, respectively. A_1 and A_2 represent the areas of the target and background areas. Pixel distance error FOM is defined as follows:

$$\mathrm{FOM} = \frac{1}{N} \sum_{i=1}^{N} \frac{1}{1 + p \times d^2(i)}. \tag{5}$$

Among them, N is the number of misclassified pixels, p is the scale coefficient, and $d^2(i)$ represents the distance between the i-th misclassified pixel and its correct position. Pixel segmentation error PE is the number of misclassified pixels due to segmentation errors:

$$\mathrm{PE} = P(o) \times P(b|o) + P(b) \times P(o|b). \tag{6}$$

Among them, $P(b|o)$ and $P(b|o)$ represent the probability of misclassifying the target pixel as the background, and the probability of misclassifying the background pixel as the target, respectively. $P(o)$ and $P(b)$ are the prior probabilities of the object and background in the image, respectively.

The original image is divided into multiple homogeneous connected regions by minimizing the energy function. Using the specific law of the boundary curve of the target object, the homogeneous region with small intensity changes is represented by a piecewise smooth function, although the intensity changes are drastic. The region's boundary is represented by the union of short smooth functions, with the discontinuous point set of the function close to the target object's boundary to achieve effective image segmentation. The algorithm's specific implementation process is divided into three steps: (1) divide the pixels in the image, (2) make a new two-dimensional image, and (3) determine the image segmentation threshold for the corresponding image. It is necessary to determine the corresponding objective function based on human visual characteristics and optimize the corresponding objective function in this link. Finally, it is combined with the image's local pixels to scientifically calculate an image segmentation threshold that is consistent with human visual characteristics, and the image is segmented.

The target area is extracted from the background area of the image by calculating and selecting the image threshold. Although the image separated by the threshold segmentation algorithm has a small amount of data, it occupies less storage space, which significantly simplifies the subsequent image analysis and image processing links, and speeds up the efficiency of image processing. Compared with the original image, the amount of binary image data generated by threshold segmentation is reduced, which can highlight the target area of interest, but the process of thresholding will also cause the loss of many other important information in the original image, thereby reducing the binary value and the visual quality of the image. Therefore, reducing the loss of main information in the threshold segmentation process is the key to improving the quality of the final binary image.

Based on the quality of the reconstructed image, peak signal-to-noise ratio measurement method is given as

$$\mathrm{PSNR} = 10 \times \log_{10}\left(\frac{\mathrm{MAX}_i^2}{\mathrm{MSE}}\right),$$
$$\mathrm{MSE} = \frac{1}{N}\sum_{(x,y)} \|\mathrm{Rco}\,(nx, y) - Or\,(ix, y)\|^2, \tag{7}$$

where MAX_i is the largest pixel in the image, Rcon is the reconstructed image, Ori(x, y) is the real image of the reconstructed image, and N is the total number of pixels.

The active contour model is founded on curve evolution theory and the level set method. The zero level set of the traditional level set function represents the contour curve. By updating the level set function, the model achieves its goal of moving the contour line. The level set function can remain effective even if the contour line undergoes topological changes such as splitting or merging. The algorithm uses human visual characteristics as a starting point for image segmentation, then uses advanced methods to optimize the image's segmentation threshold from a humanized perspective, and finally makes the segmented target 2D image better meet human visual perception needs. The algorithm automatically merges the target region sets according to these marks to complete the separation of the target from the background. Users can clearly and roughly mark the regions that make up the target.

4. Result Analysis and Discussion

Image segmentation gathers pixels in an image into different connected regions according to certain similarity criteria, and its purpose is to simplify the expression form of the image and extract more abstract and compact useful information from complex image information, which is beneficial to subsequent processing and analysis. The key of threshold segmentation method is how to select the appropriate threshold, which will directly affect the final segmentation result. We use the optimization method to solve the optimal threshold of the image, so as to give visual meaning to the threshold and then combine the local properties of the image to produce threshold segmentation results that are more in line with human visual perception.

When people observe a scene, the processing unit is not pixels, but an area or outline composed of many pixels, according to the working principle of the human visual system. Pixels are merely a representation of the transition from continuous to discrete in the image digitization process, and they do not exist in the human visual system or brain. People can only have visual perception significance when pixels are combined. Experiments are used to verify the effectiveness of the adaptive threshold segmentation method proposed in this chapter, and we have verified a large number of images and did subjective visual comparison of the experimental results, as well as quantitative comparison using various image quality evaluation indicators. The process of calculating the global optimal threshold for each subgraph is the most time-consuming part of the algorithm. Before we can calculate the optimal threshold for each subgraph, we must optimize the objective function twice. The time comparison of the algorithm proposed in this article with fuzzy clustering and particle swarm optimization algorithms is shown in Figure 3.

Experiments show that compared with the calculation time of particle swarm optimization algorithm and fuzzy clustering algorithm, the calculation efficiency of the algorithm adopted in this article is obviously improved. The mean shift algorithm is used to divide the color image into several regions. The purpose of this step is to divide the image into related areas according to the color characteristics of the image. Similar to the steps of parallax optimization, the depth map has strict statistical correlation in a segmentation plane, and the plane consistency of the segmentation area of the depth map is used for optimization.

Calculate the image's boundary map, then find the path through the image on the boundary map with the least weight, and segment the image at the location with the lowest boundary cost. The image is continuously divided into two parts by searching for the optimal path in both vertical and horizontal directions, resulting in the superpixel of regular grid. The algorithm uses the minimum cut method and the dynamic programming method to find the best path. The former can generate nonregression paths, whereas the latter can generate arbitrary topological paths. When looking for the best path, make sure that no two vertical and horizontal paths cross and that each vertical and horizontal path crosses only once. We use two indicators, accuracy and recall, to verify the effectiveness of this algorithm and compare it to fuzzy clustering and particle swarm optimization algorithms, yielding the following results. The accuracy of the three algorithms is compared in Figure 4. The recall rates of the three algorithms are compared in Figure 5.

According to the proportion and number of segmentation points corresponding to the confidence matching points, it is divided into reliable areas and unreliable areas. For the reliable region, the template parameters are calculated by the weighted least square algorithm according to the confidence matching points. For the unreliable region, the calculated template parameters are unreliable. Using the adjacent good or bad region as the initial template, the final parameters of the unreliable region are obtained through global template parameter optimization. In each iteration, we first rank all the particles according to their contribution to the global optimal solution. In addition, considering the diversity of the population and the fitness value of the optimal solution cannot exceed the average, we will eliminate the particles that are lower than the average fitness value of the whole population.

The depth plane of each image segmentation area passes through the infrared camera, and the infrared light and the sensor receiving the infrared light are in different positions, so the blocked area has no infrared reflection, so the depth value is useless. In addition, the surface of highly bright

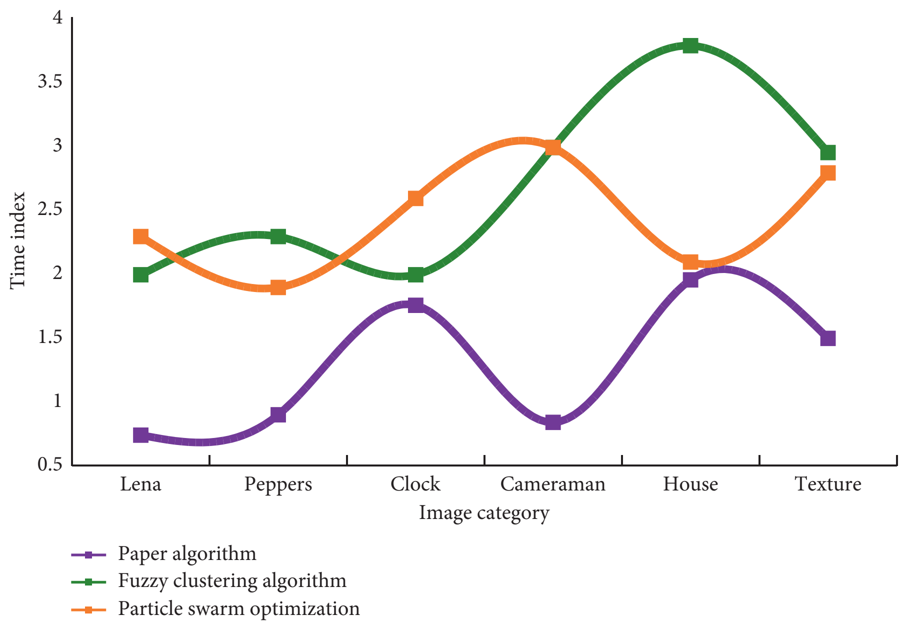

FIGURE 3: Comparison of calculation time of three algorithms.

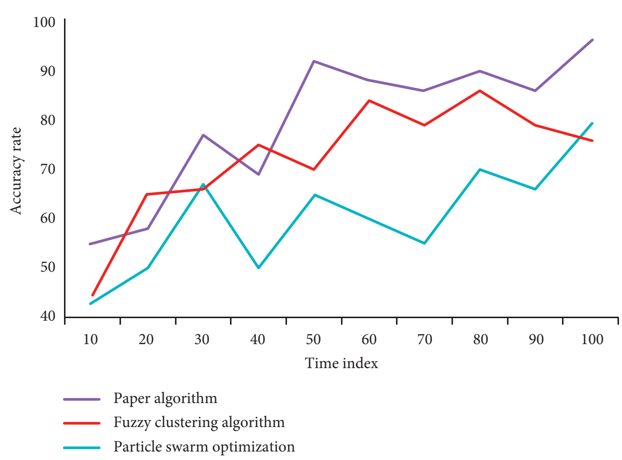

FIGURE 4: Comparison of accuracy of three algorithms.

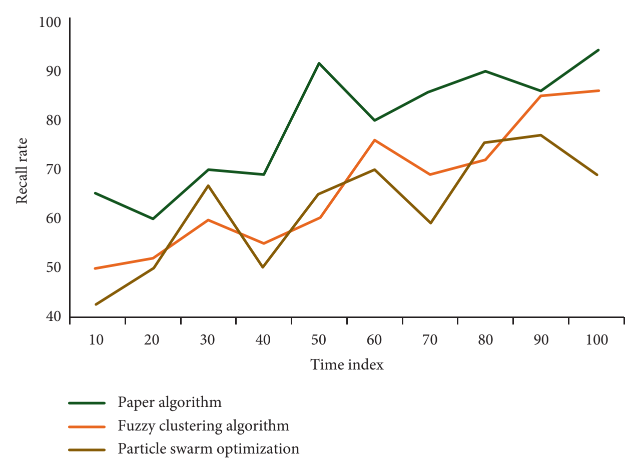

FIGURE 5: Comparison of recall rates of three algorithms.

object does not diffuse the infrared light, which leads to the receiving sensor not receiving the reflected infrared structured light. In order to better test the performance of the algorithm proposed in this article, we compare the proposed method with fuzzy clustering method and Otsu method. Figure 6 shows the comparison of experimental results of test images.

Different from most image threshold segmentation methods, the method proposed in this article combines the human visual characteristics with the threshold calculation process to automatically extract the target area in the image. The experimental results show that the binary image obtained by this method achieves good visual effect, and its overall visual quality is more in line with the visual perception.

Halftone image is essentially a special kind of binary image. Halftone image pays more attention to layering, whereas general binary image pays more attention to boundary information and contrast. In addition, compared with texture information and multiple gray levels of pixels, general binary images have richer structural information. The extraction method is adaptive and active, without user intervention or any prior information of the image to be segmented. Different input images get different initial contours, and the initial contour contains the target object of the image, which corresponds to the region of visual interest and also accords with the visual cognitive characteristics of human beings. Moreover, the saliency detection algorithm based on frequency domain analysis is simple and easy, with fewer adjustable parameters, and it will not add extra operation time when used in the preprocessing stage before image segmentation. The gray value of each pixel represents its significance, that is, the ability of the pixel to attract the attention of the observer. The larger the significance value, the more likely it is that the pixel is the region of interest, that is, the brighter the

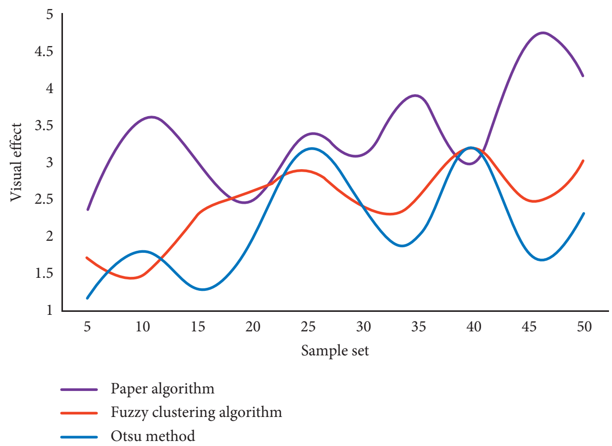

Figure 6: Comparison of image threshold segmentation results.

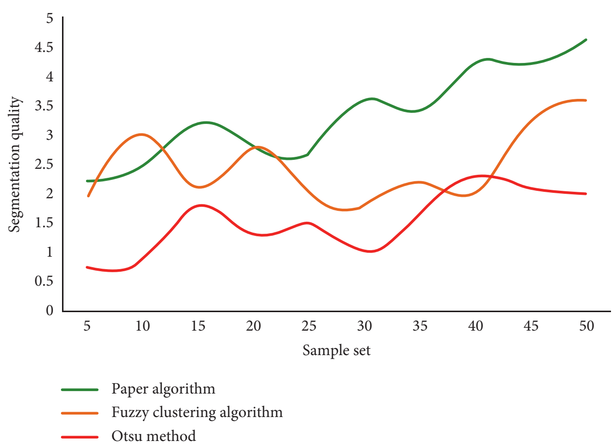

Figure 7: Comparison of segmentation quality of different threshold segmentation methods.

region in the saliency map, the potential position of the target object.

The image pixels are grouped and clustered, and the image plane is divided into a series of "meaningful" areas, based on the similarity criterion of some features or feature sets of images, greatly reducing the amount of data to be processed in later advanced processing stages such as image analysis and recognition, while retaining the information about image structural features. Using the original gray image as a reference image, we compare the visual quality of binary images generated by this method to that of other threshold segmentation methods. Figure 7 shows the segmentation quality evaluation results of different threshold segmentation methods.

It can be seen from the graph that the method proposed in this article achieves better scores compared with the other two image segmentation methods. Its segmentation quality is higher than that of fuzzy clustering method and Otsu method. This shows that this method has certain advantages compared with other methods, and the binary image generated by this image threshold segmentation method is more in line with human visual perception.

In this section, the active contour model and image segmentation application are updated to include the saliency detection mechanism of human visual cognitive characteristics, and the shape features of the target object in the image can be accurately described using knowledge of the image's bottom features. For various image contents and target objects, different initial contours are constructed adaptively. In the process of image segmentation, two subimages are first constructed in order to reduce the loss of main information from the original image during threshold segmentation, and the calculation of the optimal threshold is transformed into solving an optimization problem. After solving the objective function, the final binary image is created by analyzing the local properties of pixels. Various images were examined and compared with other threshold segmentation methods. Experiments and subjective and objective analysis show that the binary image generated by the proposed image threshold segmentation method is more in line with human visual perception.

5. Conclusions

Graphics in modern print advertising design can cross all obstacles, such as language, words, time, space, countries, nationalities, beliefs, and the like, and spread widely all over the world, blending and infiltrating with each other. Graphic vision really realizes the silent spread of advertisements. Modern print advertising plays an increasingly important role in modern political, economic, and social society, and the effect of its advertising communication is closely related to our industry. Only by deeply studying the related elements of print advertising and looking at the development of the whole discipline from the intersection of multiple disciplines, we can have a good grasp of its inherent laws. The visual creation of graphic advertisement is the perfect combination of science and art. Excellent visual creation of graphic advertisement can spread the information of advertisement and can also make the audience get a beautiful visual experience.

This article examines the innovation of graphic design vision in print advertising using image segmentation. From bottom-level image processing to image recognition and understanding, image segmentation is a critical step. Image threshold segmentation is a popular image segmentation method because of its clear physical meaning, high efficiency, and practicality. In the segmentation process, the threshold segmentation method only considers the image's grayscale characteristics and spatial information, ignoring the impact of vision on the segmentation results. In this article, the image's threshold selection process is combined with human vision characteristics, and the original image's information is presented in two subimages. The objective function is optimized by the optimization method to calculate the global optimal threshold of each subimage, and the visual information of each subimage is quantitatively described by human vision characteristics. Finally, the image is subjected to a local adaptive threshold operation based on the image's characteristics, resulting in segmentation results that are more in line with human vision perception. It can handle a wide range of graphics and image segmentation needs.

Data Availability

The data used to support the findings of this study are included within the article.

Conflicts of Interest

The author does not have any possible conflicts of interest.

References

[1] J. Kong, H. Wang, X. Wang, X. Jin, X. Fang, and S. Lin, "Multi-stream hybrid architecture based on cross-level fusion strategy for fine-grained crop species recognition in precision agriculture," *Computers and Electronics in Agriculture*, vol. 185, Article ID 106134, 2021.

[2] S. Fatović-Ferenčić and J. F. Bogdan, "Father and sons: feller family members in the context of the beginnings of advertising in Croatia," *AMHA - Acta Medico-Historica Adriatica*, vol. 16, no. 1, pp. 49–74, 2018.

[3] Q. Liu, P. C. Louis, Y. Lu et al., "Simtriplet: simple triplet representation learning with a single gpu," in *Proceedings of the International Conference on Medical Image Computing and Computer-Assisted Intervention*, pp. 102–112, Springer, Strasbourg, France, September 2021.

[4] W. Cai, Z. Wei, Y. Song, M. Li, and X.-M. Yang, "Residual-capsule networks with threshold convolution for segmentation of wheat plantation rows in UAV images," *Multimedia Tools and Applications*, vol. 80, no. 21, Article ID 32131, 2021.

[5] H. You, L. Yu, S. Tian, and W. Cai, "DR-Net: dual-rotation network with feature map enhancement for medical image segmentation," *Complex & Intelligent Systems*, vol. 8, no. 1, pp. 611–623, 2022.

[6] R. Zeng and T. Deng, "Research on application of graphic unit technology in product structure design," *Revista de la Facultad de Ingenieria*, vol. 32, no. 5, pp. 578–587, 2017.

[7] N. Zhao, Q. Zheng, J. Liao, Y. Cao, H. Pfister, and R. W. H. Lau, "Selective region-based photo color adjustment for graphic designs," *ACM Transactions on Graphics*, vol. 40, no. 2, pp. 1–16, 2021.

[8] T. Teichert, D. Hardeck, Y. Liu, and R. Trivedi, "How to implement informational and emotional appeals in print advertisements," *Journal of Advertising Research*, vol. 58, no. 3, pp. 363–379, 2018.

[9] Y. Wang, "Application of 3d modeling software in landscape planning and design," *Revista de la Facultad de Ingenieria*, vol. 32, no. 11, pp. 659–664, 2017.

[10] P. L. Bartlett, V. Gabillon, and M. Valko, "A simple parameter-free and adaptive approach to optimization under a minimal local smoothness assumption," in *Proceedings of the Algorithmic Learning Theory*, pp. 184–206, PMLR, Chicago, CH, USA, March 2019.

[11] Y. Luo and X. Niu, "Model construction and research of graphic originality influencing factors in film poster design [J]," *Revista de la Facultad de Ingenieria*, vol. 32, no. 11, pp. 967–972, 2017.

[12] Y. Hu, J. Zhan, G. Zhou et al., "Fast forest fire smoke detection using MVMNet," *Knowledge-Based Systems*, vol. 241, Article ID 108219, 2022.

[13] J. Holsanova, N. Holmberg, and K. Holmqvist, "Reading information graphics: the role of spatial contiguity and dual attentional guidance," *Applied Cognitive Psychology*, vol. 23, no. 9, pp. 1215–1226, 2009.

[14] S. Guo, Z. Jin, F. Sun et al., "Vinci: an intelligent graphic design system for generating advertising posters," in *Proceedings of the CHI Conference on Human Factors in Computing Systems*, pp. 1–17, May 2021.

[15] X. Zhao, "Application of computer graphics and image software in the graphic advertisement design of marine industry," *Journal of Coastal Research*, vol. 106, no. SI, pp. 526–530, 2020.

[16] R. Olbrich and C. D. Schultz, "Multichannel advertising: does print advertising affect search engine advertising?" *European Journal of Marketing*, vol. 48, 2014.

[17] Y. Zhang, Y. Yue, and G. Yang, "A method of increasing precision for hand bone models reconstruction of CT images," *Jisuanji Fuzhu Sheji Yu Tuxingxue Xuebao/Journal of Computer-Aided Design and Computer Graphics*, vol. 29, no. 10, pp. 1802–1806, 2017.

[18] S. Wang, "Recursive line-based algorithm for hole-filling in DIBR images," *Jisuanji Fuzhu Sheji Yu Tuxingxue Xuebao/Journal of Computer-Aided Design and Computer Graphics*, vol. 29, no. 8, pp. 1536–1541, 2017.

[19] G. Walters, B. Sparks, and C. Herington, "The effectiveness of print advertising stimuli in evoking elaborate consumption visions for potential travelers," *Journal of Travel Research*, vol. 46, no. 1, pp. 24–34, 2007.

[20] G. F. Soldow, "The processing of information in the young consumer: the impact of cognitive developmental stage on television, radio and print advertising," *Journal of Advertising*, vol. 12, no. 3, pp. 4–14, 1983.

[21] M. Ramezani, S. Li, and S. Golestan, "Analysis and controller design for stand-alone VSIs in synchronous reference frame," *IET Power Electronics*, vol. 10, no. 9, pp. 1003–1012, 2017.

[22] R. Javan and M. N. Zeman, "A prototype educational model for hepatobiliary interventions: unveiling the role of graphic designers in medical 3D printing," *Journal of Digital Imaging*, vol. 31, no. 9, pp. 1–11, 2017.

[23] K. Miller, M. Capan, D. Weldon et al., "The design of decisions: matching clinical decision support recommendations to Nielsen's design heuristics," *International Journal of Medical Informatics*, vol. 117, no. 9, pp. 19–25, 2018.

[24] S. Zeller, "Centering the periphery: reassessing Swiss graphic design through the prism of regional characteristics," *Design Issues*, vol. 37, no. 1, pp. 64–75, 2021.

[25] Y. Shi, C. Feng, and Y. Shen, "Research on graphic design based on digital media," *Acta Technica CSAV (Ceskoslovensk Akademie Ved)*, vol. 62, no. 1, pp. 391–400, 2017.

[26] W. Cai and Z. Wei, "Remote sensing image classification based on a cross-attention mechanism and graph convolution," *IEEE Geoscience and Remote Sensing Letters*, vol. 19, pp. 1–5, Article ID 8002005, 2022.

[27] I. B.-A. Gitler and E. Lachover, "Gendered memory and miniaturization in graphic design: representations of women on Israeli postage stamps," *Design Issues*, vol. 37, no. 3, pp. 18–32, 2021.

[28] Y. Shi, L. Xu, and Y. Zhang, "Research on three-dimensional spatial expansion model of graphic design based on visual aesthetic analysis," *Revista de la Facultad de Ingenieria*, vol. 32, no. 11, pp. 783–788, 2017.

[29] F. He, "Industrial product graphic design based on visual communication concept," *Acta Technica CSAV (Ceskoslovensk Akademie Ved)*, vol. 62, no. 1, pp. 269–278, 2017.

[30] M. Lou, "A virtual reality teaching system for graphic design course," *International Journal of Emerging Technologies in Learning (iJET)*, vol. 12, no. 9, pp. 117–129, 2017.

Hindawi
Computational Intelligence and Neuroscience
Volume 2022, Article ID 5064615, 10 pages
https://doi.org/10.1155/2022/5064615

Research Article

Emotional Experience and Psychological Intervention of Depression Patients Based on SOM

Yuanyuan Zou

College of Health Management, Shangluo University, Shangluo 726000, Shaanxi, China

Correspondence should be addressed to Yuanyuan Zou; 209005@slxy.edu.cn

Received 12 February 2022; Revised 10 March 2022; Accepted 11 March 2022; Published 24 March 2022

Academic Editor: Xin Ning

Depression is a severe mental illness with an unknown pathogenesis. Clinical diagnosis is based primarily on symptoms and does not include objective biological markers. Finding objective markers for diagnosis and treatment from imaging, on the contrary, is becoming increasingly important. The SOM (self-organizing feature mapping) model was used to identify the depression tendency of users in order to investigate the emotional experience and psychological intervention of patients with depression. On this foundation, the concept of depression index is developed further, and the relationship between depression index and the severity of depression in patients is thoroughly investigated. The system can accurately and quickly identify the depression state by applying it directly to the original EEG signals, without any preprocessing or feature extraction. When combined with traditional classifiers, the analysis and comparison results show that SOM can not only effectively select features but also improve the accuracy of depression classification. This research proposes a new research direction for deep learning in the context of large-scale big data analysis.

1. Introduction

Depression is a common emotional disorder with a high occurrence rate, a high recurrence rate, a high suicide rate, a high rate of disability, and a high social burden [1]. Currently, the rate of depression recognition is low, and the proportion of patients who can be identified and treated in a timely, sufficient, and adequate manner is even lower [2]. Depression is a complex negative emotional [3, 4] experience characterised by subjective distress. The most recent findings from the China Mental Health Survey are as follows. The six mental disorders (mood disorders, anxiety disorders, alcohol/drug addiction disorders, schizophrenia and related mental disorders, eating disorders, and impulse control disorders) accounted for 9.3% of the total, with mood disorders accounting for the majority of the cases. The prevalence of depression in the disorder was 3.4 percent over a lifetime and 2.1 percent over a 12-month period, respectively. Domestic and international experts and scholars have made significant progress in the study of depression in recent years [5]. These advancements include the exploration of aetiology and pathogenesis, as well as the development of new diagnostic criteria and the emergence of new and better treatments, particularly the emergence of a large number of new antidepressants, which have given patients with depression good news and enabled clinical doctors to provide more effective treatments.

SOM (self-organizing feature map) neural network [6–8] is an unsupervised learning method that imitates the characteristics of self-organizing signal processing in animal and human cerebral cortex. It can automatically extract the intrinsic important statistical features of samples according to the rules of samples. This makes it widely used in intelligent control, pattern recognition, computer vision, nonlinear optimization, signal processing, etc., and now, it has become one of the important fields of artificial intelligence research [9, 10]. According to the emotional recognition results based on EEG signals, medical staff can accurately judge the current mental state of patients and the real activity of the brain and guess the degree of their illness, so as to realize accurate nursing. Personalized nursing pays more attention to the patient's own characteristics, and a reasonable nursing plan is tailored according to the patient's condition, age, education level, etc., and comprehensive in-depth nursing is implemented to improve the recovery speed of patients. When the neural network makes a correct classification by identifying the key features that can depict brain diseases, the system is considered reasonable. On the contrary, although the final result is correctly identified, the neural network does not analyze the key features, but the peripheral factors even make decisions due to the correct identification of noise or interference. Obviously, the neural network cannot meet the medical requirements due to too high false positives.

At this time, research indicates that the mechanism of depression is primarily related to abnormal activity in emotional regulation brain regions, and a large number of studies have focused on specific brain regions and neural circuits, such as the prefrontal cortex, anterior cingulate cortex, and subcortical amygdala, hippocampus, habenular nucleus, and hypothalamus [11, 12]. Long-term use of antidepressants causes damage to the liver, kidneys, extra-vertebral system, and other organs, and the recurrence rate is very high after stopping antidepressants, so the psychological state of patients has not improved significantly, and patients frequently cannot receive appropriate treatment, and their prognosis is poor. The purpose of this study is to understand the emotional experience and psychological intervention of patients with depression, explore the effect of psychological intervention on their negative emotional experience, provide suggestions for clinical nursing, and provide reference for the majority of clinical medical staff to implement intervention measures for patients with depression.

2. Related Work

China's society is experiencing a high incidence of psychological problems, and depression has become a major social problem that plagues China. Social factors are directly related to the rising prevalence of depression. In [13], studies show that depression is a high-cost disease. Early detection and treatment, especially, early diagnosis and effective treatment by physicians in general hospitals, can reduce the course of depression and suicide and can significantly reduce functional impairment and medical resource consumption, thus reducing the total burden of depression. In [14], the study also found that the negative and rejection attitude of the public towards mental illness has changed little or even worsened over the years. Literature [15] holds that it is necessary to encourage the patient's spirit of tenacious struggle against the disease, mobilize the patient's subjective initiative to fight against the disease, and work with doctors to obtain the patient's cooperation and improve the curative effect. According to [16], identifying the harbinger of disease recurrence can encourage patients to see a doctor sooner rather than later, thereby controlling symptoms, significantly improving discharged mental patients' compliance, and effectively lowering the recurrence rate. Literature [17] examines 241 living relatives of 163 first-episode schizophrenia patients and finds that the proportion of patients with high emotional experience (50.3%) is similar to that reported by foreign countries, which shows that 54 percent of patients live in families with high emotional experience. In [18], the relatives of 56 anxiety disorder inpatients were followed for 9 months, and it was discovered that the recurrence rate of patients in the high emotional experience family group was significantly higher than that of the low emotional experience family group. In [19], the results of a study of 86 psychotic patients and their relatives revealed that patients with a lot of emotional experience had higher depression and anxiety scores, but no significant difference in psychotic symptoms. This study suggests that emotional experience may be more reliable than schizophrenia in predicting depression outcomes. According to [20], patients in the experimental group had a 9.1% one-year recurrence rate, while those in the control group had a 33.3 percent recurrence rate. The two groups differed significantly. Family intervention can help patients with schizophrenia have fewer relapses and improve their social functioning.

Early brain imaging studies based on voxel morphological measurement found that patients with unipolar depression had reduced gray matter volume, which was related to their psychopathology and cognitive dysfunction [21]. Literature [22] collected 40 subjects' emotional self-rating scale data and used Lasso regression to establish a two-category model of depression prediction. In [23], uUsing BPNN (BP neural network), the recommendation algorithm of industrial organization psychology under big data is constructed. Literature [24] has built an intermediary model, which shows that depression factors in families are influenced by family identity factors and insomnia factors. Thus, sleep quality, study, family identity, and other dimensions all have an important influence on depression, indicating that the diversity of dimensions also has a positive effect on the identification of depression. In [25], from the point of view of online healthy community users' comment analysis, this study analyzes how different factors affect users' comments in online healthy communities by building a user voting adoption model. In [26], through research, it is proved that users with mental illness in online healthy communities can get certain medical care decision information by communicating with others. Literature [27] classifies patients into different types for the purpose of using online healthy communities, analyzes the patients' network information behaviors, and finds that there are significant differences in personal health information management behaviors of patients with depression in online healthy communities. Literature [28] holds that family members with high emotional experience are more inclined to attribute the patients' symptoms to personal, internal, and controllable factors and that patients can try their best to change their problem behaviors, thus showing more negative attitudes, criticisms, and controllable behaviors.

To summarise, the emotional experience of depression patients is a multidisciplinary problem, involving medicine, sociology, and psychology. The widespread negative emotional experience of depression patients has had a significant impact on their rehabilitation and quality of life and is a roadblock in the development of health care. Psychotherapy research on emotional experience can gradually be expanded to other related fields of mental diseases, and further and deeper research can be conducted to investigate other factors that affect emotional experience and patient rehabilitation from a variety of perspectives, as well as to demonstrate the characteristics of these influencing factors in the disease progression process.

3. Research Method

3.1. Analysis of Emotional Experience of Patients with Depression. Social learning theory was put forward by American psychologist Bandura. Behavior acquisition is learned by observing and imitating others. Behavior, environment, and personal internal factors interact and influence each other, and environment plays a decisive role. And through the motivation of the group, achieve collective change and driving force. Other family members will adjust themselves to better adapt to life by observing and imitating benign behaviors in daily life.

A good family environment is conducive to the healthy development of every family member's body and mind, and it is the primary environment for one's survival. Family members have an impact on and interact with one another. The behavior, cognition, and emotional changes of one family member will influence the behavior, cognition, and emotional changes of others. The suffering that depression causes patients and their families is difficult to put into words. The emotional experiences of patients and family members have a significant impact on their rehabilitation and physical and mental health. The family emotional experience of depression can be improved, the mental health of family members can be improved, family harmony can be promoted, and depression patients' symptoms can be alleviated through targeted group counseling for family members, which can meet the actual needs of family intervention for depression patients more economically and effectively. It is a novel approach and method for depression patients' family intervention.

To explore the characteristics of brain activation in patients with depression under the task of positive and negative emotion induction and to test the hypothesis of emotional background insensitivity, during the experiment, each picture is presented as an experiment. The experimental process is as follows. First, the gaze point is presented for 2 seconds, reminding the subjects to pay attention to the center of the screen. Then, positive and negative emotional pictures are presented at the top of the screen, and the subjects are asked to pay attention to the emotional pictures and experience emotional arousal for 8 seconds. This study adopts the experimental design of randomized controlled study, and its specific technical route is shown in Figure 1.

After the experiment, the degree of instruction execution was checked, and all the subjects could understand the instruction and implement the instruction requirements during the experiment, including the distribution characteristics of family emotional experience of depression patients, the proportion of high emotional experience and low emotional experience, the mental health status of depression patients and their families, coping styles, and social support,. These studies are the basis of group counseling. Carry out group counseling research on family emotional experience intervention of depression patients, and design targeted group counseling implementation scheme based on the investigation of family emotional experience status of depression patients.

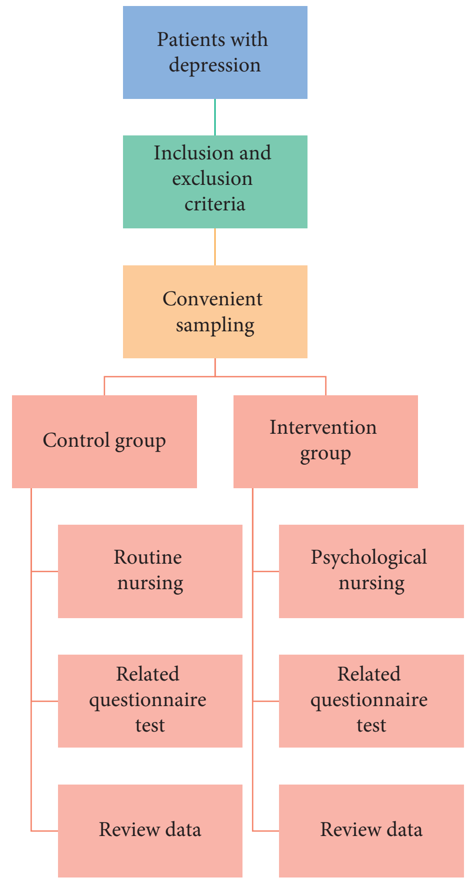

Figure 1: Schematic diagram of research route.

According to the scanning parameters and stimulus presentation mode, the statistical model is selected, the experimental variables and related time and space information are brought into the model, deconvolution is carried out according to the hemodynamic function, and the high-frequency and low-frequency images are filtered out by filtering so that the experimental design is fitted and the parameters are estimated.

Events directly affect a person's mental state, and they are also events that need certain psychological adaptation in individual life, including positive events and negative events. The former refers to events that trigger positive emotions of individuals, while the latter refers to events that trigger negative emotions of individuals. It is found that the frequency and severity of life events within two years are related to the onset of mental disorders. Negative life events and independent events may be important factors for the occurrence or recurrence of depression, while positive life events are obviously related to the occurrence or recurrence of mania. On the one hand, it shows that life events may be one of the causes of depression. On the other hand, it may be that patients' habitual defense style and its characteristics make them experience some negative life events more easily and actively than ordinary people, such as lovelorn or friends turning against each other.

3.2. Psychological Intervention of Depression Patients Based on SOM. As a subconscious response to conflict, a defense mechanism is a set of habitual adaptive behaviors that people use to avoid and relieve mental stress such as anxiety when confronted with a variety of frustrating situations. Patients with depression have different psychological defense styles, according to studies. Neurosis patients, including neurotic depression patients, use immature defense mechanisms more than mature defense mechanisms, according to a comprehensive study [21]. Qualitative research is sensitive to patients' subjective feelings and worldviews, which can elaborate their real experiences of diseases and health. Qualitative research encapsulates the overall concept of nursing and allows nurses to understand and feel the inner world of patients on a deeper level.

SOFM has two characteristics similar to human brain information mapping.

First, the topological mapping structure is not realized by the movement and reorganization of neurons, but a topological structure formed by each neuron in different excited states. Secondly, the formation of this topological mapping structure has the characteristics of self-organization [10]. The topological structure of the network is introduced into SOFM, and the concept of changing neighborhood is further introduced into the structure to simulate the side inhibition phenomenon in the biological neural network, so as to realize the self-organizing characteristics of the network. The SOFM mapping model is shown in Figure 2.

The network consists of an input layer and an output layer. The input layer receives signal input, and the output layer is a two-dimensional grid, which maps the output of network signals by self-organization. Each node in the two-dimensional plane grid is connected with the source node of the input layer. Each neuron in the output layer makes competitive selection in learning. The winning neuron not only strengthens itself but also drives the neighboring neurons around it to strengthen accordingly. Functionally, it can connect the change rules of individual neurons with the group change rules of one layer of neurons. After learning the network, the spatial distribution of the connection weight vectors among neurons in the output layer can correctly reflect the approximate distribution of the input pattern space.

PC (principal construct) projection is the intermediate variable of PC analysis algorithm. It is the projection matrix from the original large sample data to small samples. This method not only reduces the computation of the later algorithm but also retains the original features. Consider the projection of the sample on the PC:

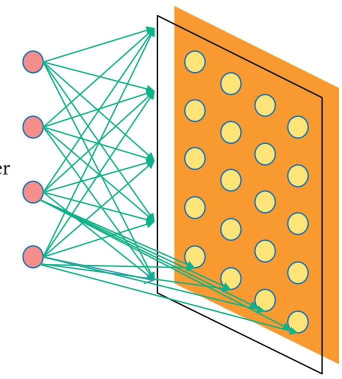

Figure 2: SOFM mapping model.

$$\eta_d = \frac{\lambda_1 + \lambda_2 + \cdots + \lambda_d}{\sum_{i=1}^{n} \lambda_i},$$
$$y_{mi} = x_m p_i = \sum_{k=1}^{n} x_{mk} p_{ki}. \tag{1}$$

It can be seen from the above formula that the projection of each data point in the original dataset on the PC is a linear combination of all the original features, and the effect of each feature on the new features can be expressed by the elements multiplied by it in the projection matrix. Therefore, the projection matrix can also be expressed as

$$C = [v_1, v_2, \cdots, v_n]^T, v_i = \{p_{i1}, p_{i2}, \cdots, p_{i\,d}\}. \tag{2}$$

For each original feature, there is a line component corresponding to it, and the correlation between original features is closely related to the similarity of line components. Therefore, the original data $X_{m\times n}$ are converted into a projection matrix $C_{n\times d}$ by PC projection, the sample size of the original data is reduced from m to d, and the original feature number is maintained.

The learned "distributed feature representation" vector is mapped to the sample tag space by the full connection layer, and the tag $\overline{y}$ of Weibo content text, that is, positive, neutral, and negative probability distribution, is discriminated. The calculation formula is as follows:

$$p(y \mid s) = soft\max(w \cdot v^* + b^*),$$
$$\overline{y} = \arg\max p(y \mid s). \tag{3}$$

Among them, $y \in R$ is the true emotional tag of Weibo content, which is expressed by unique heat coding. $\overline{y} \in R$ is the emotional tag vector of Weibo content obtained through training. For each predicted emotional category probability, the tag with the highest probability is selected as the output.

When judging the depression tendency of online users from the perspective of text analysis, the depression index of users is calculated by the proportion of depression Weibo to the total Weibo number of users, so as to measure the depression tendency of users in a certain period of time. A depression index based on online healthy community is proposed, and the calculation formula is as follows:

$$DI = \frac{N_{cd}}{2N_{ct}} + \frac{N_{md}}{2N_{mt}}, \tag{4}$$

where N_{cd} refers to the number of Weibo posts with depression tendency published by users in other accounts within a certain period of time, N_{ct} refers to the number of Weibo posts published by users in other accounts within a certain period of time, N_{md} refers to the number of Weibo posts with depression tendency distributed and forwarded by users in personal accounts within a certain period of time, N_{mt} refers to the number of Weibo posts distributed and forwarded by users in personal accounts within a certain period of time, and DI is the depression index.

The time complexity of the whole sub-SOFM is calculated as follows:

$$O(S(N, L)) = O\left(\sum_{l=1}^{d} n_{l-1} \cdot s_l^2 \cdot n_l \cdot m_l^2\right), \tag{5}$$

where l is the index of convolution layer and d is the depth, n_l is the number (also called width) of filters in the lth layer, n_{l-1} represents the number of input channels in the lth layer, and s_l^2 and m_l^2 represent the spatial size of the filter and the size of the output feature map, respectively.

LSTM (long short-term memory) network is a special RNN (recurrent neural network), which can learn long-term dependent information. Through a special design, long-term information can be remembered. The core idea of LSTM is similar to a conveyor belt. The characteristic information is placed on the conveyor belt, and there is only a small amount of linear interaction so that the information can circulate on it and remain unchanged. LSTM has a well-designed structure called “gate” to remove or add information.

Besides text information, there are other types of feature information that can be used in the analysis of depression tendency prediction to help improve the recognition rate. Because these features are time-sequential and change with the interview, this section uses LSTM to study the audio features of each time stamp. Finally, combining the prediction results of the three features, the following prediction collaborative classification prediction models are given, as shown in Figure 3.

The predicted results of the test set based on these three characteristics are brought into the function expression, and the results between 0 and 1 are obtained. If the calculated result is greater than or equal to 0.5, it will be counted as 1, and if it is less than 0.5, it will be counted as 0.

4. Results’ Analysis and Discussion

After experiencing the emotional group counseling, members fill in the feedback form of group counseling activities and evaluate the whole group counseling. All members feel that group counseling has a lot of gains, as shown in Figure 4.

It can be seen that the psychological intervention activities of the group members (including the arrangement of psychological intervention game activities and group atmosphere) as well as the group members themselves (including self-expression, satisfaction, and harvest, among other things) have been greatly affirmed. Excel calculates the arousal rating of depression patients and normal CG emotions (1–4 grades, representing “almost no feeling,” “weak,” “strong,” and “very strong”), as well as the average value for each group. There was no significant difference in arousal degree evaluation of neutral, positive, and negative emotional materials and CG in patients with depression, according to the findings (Figure 5). The arousal degree evaluation of positive and negative emotional materials is consistent, and it is higher than the arousal degree evaluation of neutral emotional materials.

The images collected at different time points are corrected at the same time point. Due to the differences of anatomical structures of different individuals, the functional images of individuals are registered with templates, and the brains of individuals are registered into the standard MNI space for functional localization of activation areas. Gaussian smoothing adopts the full width at half maximum of 8 mm to improve the signal-to-noise ratio and make the smoothed image obey the nature of random Gaussian field. For positive emotional stimulation, the differences of brain activation areas induced by two groups of subjects are shown in Figure 6.

Independent double sample T test was used to compare the brain activation areas and their intensity of emotional stimulation materials with a different potency in depression group and normal CG emotional evaluation task. For negative emotional stimulation, the differences of brain activation areas induced by two groups of subjects are shown in Figure 7.

The differences in brain activation of negative emotional stimulus materials between the two groups are as follows: the activation of right posterior cingulate gyrus, anterior cingulate gyrus, and right anterior wedge lobe in depression group are less than that in normal CG. The descriptive statistics of behavioral results show that the arousal degree of positive, medium, and negative emotional materials in the patient group is lower than CG, in which the arousal degree of positive and negative emotions is consistent and higher than that of neutral emotions, and the arousal degree of positive emotions is slightly lower than that of negative emotions.

Only the activated and weakened brain regions were discovered in the patient group when positive emotion induction was used, and only the activated and enhanced brain regions were discovered when negative emotion induction was used. Negative feelings activate the brain more than neutral or positive feelings. Patients with depression may have a negative bias in their emotional responses, but this hypothesis must be tested against normal CG. The anterior cingulate gyrus was activated in normal people under both positive and negative emotional conditions, which is consistent with the previously reported nonselective activation of anterior cingulate gyrus potency [18]. Dorsal cognitive control system includes the anterior cingulate gyrus. The anterior cingulate gyrus and the prefrontal cortex are jointly responsible for cognitive control, with the prefrontal cortex performing the majority of the control process and the anterior cingulate gyrus determining whether the

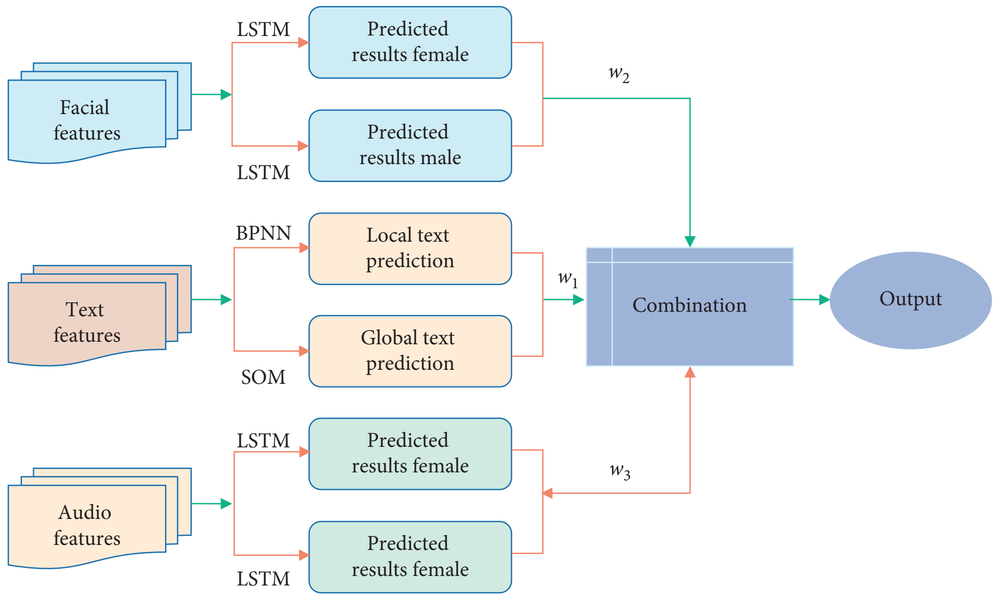

FIGURE 3: Comprehensive model.

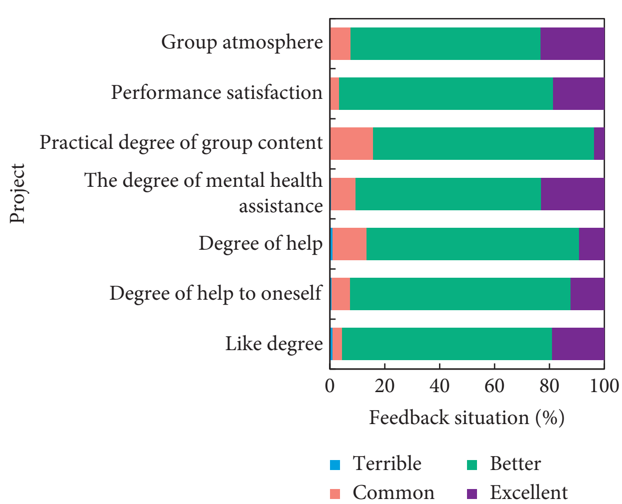

FIGURE 4: Psychological intervention effect feedback.

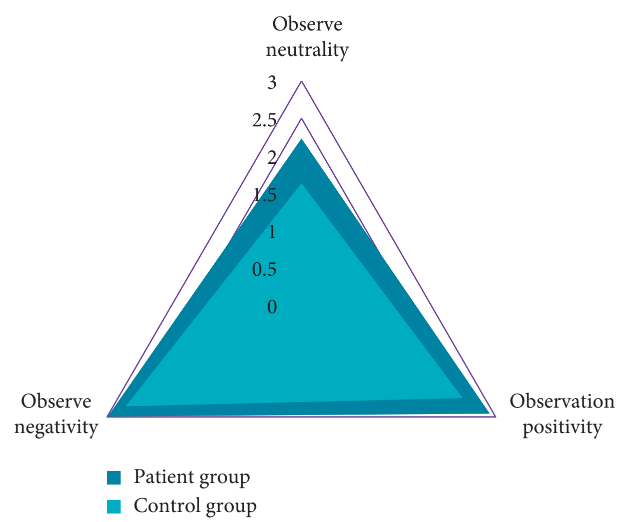

FIGURE 5: Awakening degree evaluation.

control process needs to be changed based on the degree of reaction conflicts and errors.

It was found that the activation of anterior and posterior cingulate gyrus and right anterior cuneiform lobe was weakened under the condition of negative emotion induction in patients with depression. When comparing the positive and negative emotional evoked conditions of depression patients horizontally, it is found that these areas are not activated compared with neutral conditions. Therefore, it is speculated that the activation and weakening of these areas is not caused by emotional valence, but there is abnormality in the level of nerve spontaneous activity or basic activity. This part of the study did not make a deeper discussion about it.

As can be seen from Figure 8, the immature defense style and intermediate defense style of depression group are significantly higher than those of CG, but there is no significant difference between mature defense style and masking factor.

Great changes in the environment are the source of stress for many people. When the stimulus event breaks the balance and load capacity of the organism or exceeds the individual's ability, it will be reflected in stress. These stimulus events include all kinds of situations from outside or inside, collectively referred to as stressors. Researchers have found many ways to study the relationship between life events and health. It is found that the frequency and severity of life events within two years are related to the onset of mental disorders. Negative life events and independent events may be important factors for the occurrence or recurrence of depression, while positive life events are obviously related to the occurrence or recurrence of mania. The results show that the frequency of negative life events and the total intensity of life

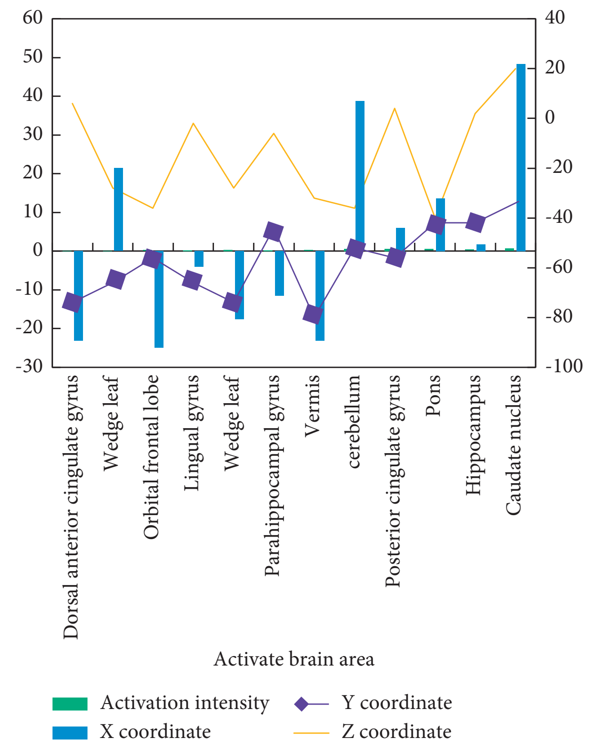

Figure 6: Localization and intensity of brain activation difference in positive emotion evaluation task.

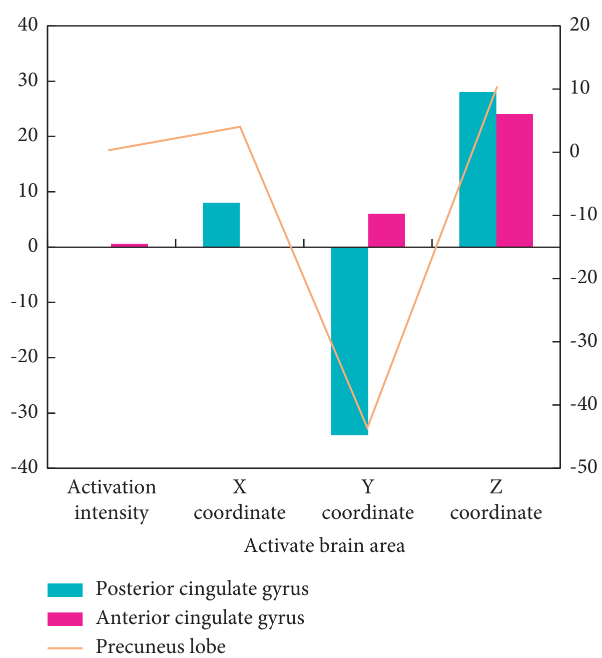

Figure 7: Differences of brain activation differences in negative emotion evaluation tasks.

events in depression group are higher than those in CG, and there are significant differences. This shows that, with the increase of the frequency of negative life events and the total intensity of life events, the possibility of individuals suffering from depression will increase.

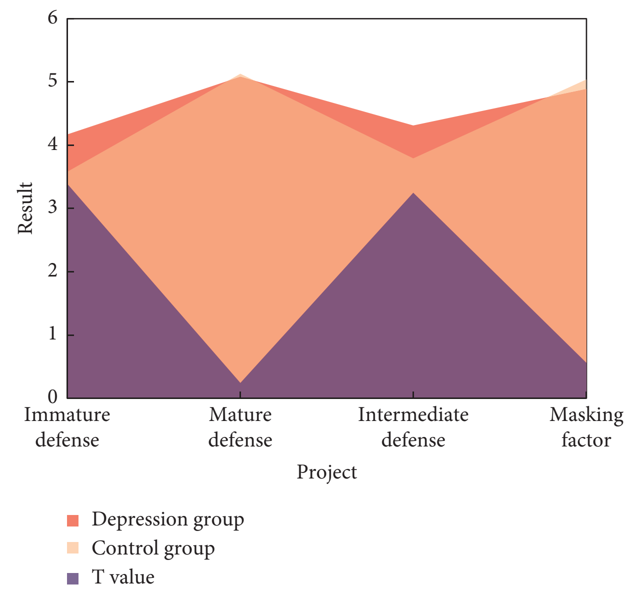

Figure 8: Comparison of the results of two groups of defense style questionnaires.

Some people in the CG have a higher frequency of negative life events and a higher total intensity of life events, whereas some people in the depression group have a lower frequency of negative life events and a lower total intensity of life events, suggesting that the occurrence of negative life events can help us predict or explain the occurrence of depression in general. Any event may have different meanings for different people. The same life events and different cognitive styles will have different effects on individuals. As some scholars have pointed out, life events can affect mental health in two ways: one is direct influence and the other is indirect influence through intermediary variables.

In this study, there is no significant difference between the mature defense mechanisms of depression group and CG, which also show that the defense mechanisms are mixed and not used independently. Even in depression patients, mature defense mechanisms will be used, but the frequency that depression patients may use immature and intermediate defense mechanisms is much higher than that of them. Instead, take these three defense mechanisms as a whole. Psychological problems such as depression are not caused by the obstacles in the use of certain defense mechanisms, but related to the imbalance in the use of immature defense mechanisms, intermediate defense mechanisms, and mature defense mechanisms.

The F1-score of four variants of SOM and the control model in different depression grades are shown in Figure 9.

The classification performance of SOM in this study has obvious advantages over CG. Compared with other models, SOM (especially mul + add) can better and more accurately identify people with severe depression, which is very valuable in the screening of depression. Therefore, by comparing with the control model, it can be seen that the deep neural network model designed in this study shows a good classification ability, and the introduction of factor

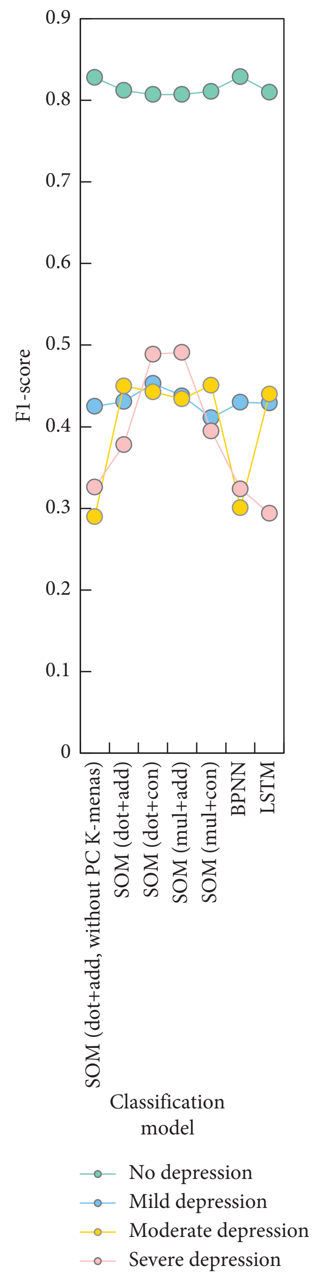

Figure 9: Classification of each depression level F1-score.

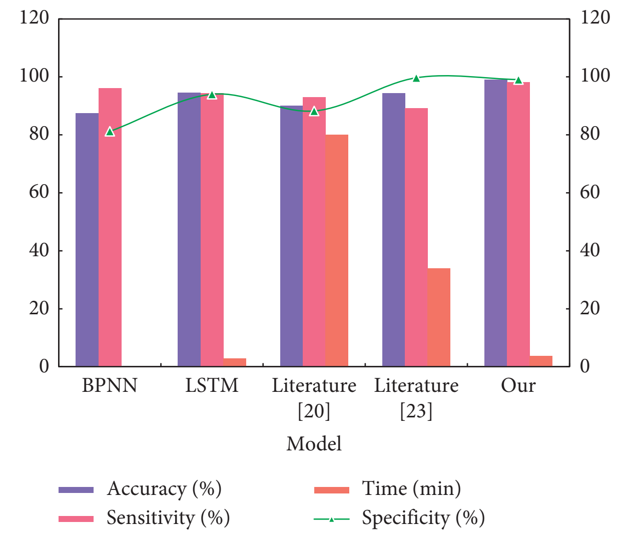

Figure 10: Comparison of classification performance of correlation methods.

decomposition machine also plays a significant role in optimizing the network structure.

On the same dataset (MPHCs emotional experience G data), different classifiers are used to classify depression, and the classification performance indicators are shown in Figure 10.

Figure 10 shows that the classifier proposed in this study is the best in all classification indexes, and the higher sensitivity and specificity also indicate that the classifier can effectively screen out not only depressed patients but also normal people.

According to psychologists, the narrator's process of putting past fragments and scattered experiences into complete stories is a way for the narrator to actively give meaning to changes in his or her life and bring order to disorder, which is therapeutic for the narrator. Hospital administrators should allocate medical human resources appropriately so that medical staff have enough time to sit down and communicate with patients, provide appropriate opportunities for patients to talk about their inner pain, patiently listen to their inner voice when they need it, provide emotional comfort when they are in pain, and truly enter their hearts and earn trust. They walk alongside them to help them overcome depression and pain, stay away from death's edge, and rediscover the meaning and value of life.

5. Conclusion

This study proposes a research method of emotional experience and psychological intervention in patients with depression based on SOM. In the face of depression-scale big data, the SOM algorithm of PC projection automatically selects the optimal feature subset on the basis of retaining the original feature space, thereby eliminating redundant information in depression-scale big data. The identification of the user's depression emotional state is divided into the judgment of the depression emotional tendency of a single text and the judgment of the user's depression state to measure the user's depression and depression. Interpretation results of the complexity of the SOM show that the classifier effectively captures the intrinsic characteristics of depression. The abnormal emotion regulation in patients with depression is mainly manifested in two aspects: one is that it is difficult to use cognitive resources needed to enhance positive emotions through cognitive reappraisal, and the cognitive control ability declines; secondly, cognitive reappraisal weakens negative emotions. It is difficult to call the required cognitive resources, and cognitive control ability declines, but it also fails to effectively reduce the activation of brain regions related to emotional evaluation.

Data Availability

The data used to support the findings of this study are included within the article.

Conflicts of Interest

All the authors do not have any possible conflicts of interest.

Acknowledgments

The work was supported by Special scientific research plan for emergency public health safety of Shaanxi Provincial Department of Education "Research on the Construction of Mental Health Service System in Colleges and Universities in Public Health Emergencies (Grant no. 20JG009)".

References

[1] L. Yang, D. Ling, L. Ye, and M. Zeng, "Psychological nursing intervention on anxiety and depression in patients with urinary incontinence after radical prostatectomy," *Medicine*, vol. 99, no. 48, p. e23127, 2020.

[2] G. Rodin, C. Lo, A. Rydall et al., "Managing cancer and living meaningfully (calm): a randomized controlled trial of a psychological intervention for patients with advanced cancer," *Journal of Clinical Oncology*, vol. 36, no. 23, pp. 2422–2432, 2018.

[3] X. Gu, W. Cai, M. Gao, Y. Jiang, X. Ning, and P. Qian, "Multi-source domain transfer discriminative dictionary learning modeling for electroencephalogram-based emotion recognition," *IEEE Transactions on Computational Social Systems*, pp. 1–9, 2022, In Press.

[4] W. Cai, M. Gao, and R. Liu, "MIFAD-net: multi-layer interactive feature fusion network with angular distance loss for face emotion recognition[J]," *Frontiers in Psychology*, p. 4707, 2021.

[5] S. Yu, H. Liu, and Q. Yan, "Effects of exercise training combined with psychological intervention compared to exercise training alone in prediabetes subjects[J]," *Journal of Public Health*, vol. 42, no. 2, p. 2, 2020.

[6] X. Jin, J. Zhang, J. Kong, T. Su, and Y. Bai, "A reversible automatic selection normalization (RASN) deep network for predicting in the smart agriculture system," *Agronomy*, vol. 12, no. 3, p. 591, 2022.

[7] D. Yao, Z. Zhi-li, Z. Xiao-feng et al., *Deep Hybrid: Multi-Graph Neural Network Collaboration for Hyperspectral Image classification[J]*, Defence Technology, 2022.

[8] W. Cai, Y. Song, H. Duan, Z. Xia, and Z. Wei, *Multi-Feature Fusion-Guided Multiscale Bidirectional Attention Networks for Logistics Pallet Segmentation*, CMES-Computer Modeling in Engineering & Sciences, 2022, In Press.

[9] X.-B. Jin, W.-T. Gong, J.-L. Kong, Y.-T. Bai, and T.-L. Su, "PFVAE: a planar flow-based variational auto-encoder prediction model for time series data," *Mathematics*, vol. 10, no. 4, p. 610, 2022.

[10] L. Cheng, Y. Wang, Q. Liu et al., "Network-aware locality scheduling for distributed data operators in data centers," *IEEE Transactions on Parallel and Distributed Systems*, vol. 32, no. 6, pp. 1494–1510, 2021.

[11] K. A. Campbell, B. C. Healy, C. M. Celano, A. Albanese, R. A. Millstein, and J. C. Huffman, "Predictors of completion of a psychological-behavioral intervention in acute coronary syndrome patients," *Journal of Psychosomatic Research*, vol. 112, pp. 9–12, 2018.

[12] A. A. Modabbernia et al., "Promoting medication adherence among patients with bipolar disorder: a multicenter randomized controlled trial of a multifaceted intervention[J]," *Psychological medicine*, vol. 47, no. 14, pp. 2528–2539, 2017.

[13] V. Tengattini, L. Foschi, P Rucci et al., "Effectiveness of psychological intervention in psoriatic patients relative to standard care[J]," *European Journal of Dermatology*, vol. 29, no. 2, pp. 231–233, 2019.

[14] A. T. Stein, E. Carl, P. Cuijpers et al., "Looking beyond depression: a meta-analysis of the effect of behavioral activation on depression, anxiety, and activation[J]," *Psychological Medicine*, vol. 51, no. 9, pp. 1–14, 2020.

[15] Y. Liu, Y. Zhao, and J. Tian, "The association of depression following percutanous coronary intervention with adverse cardiovascular events: protocol for a systematic review and meta-analysis[J]," *Medicine*, vol. 98, no. 98, p. 2, 2019.

[16] L. Daniela, G. Daniela, and B. E. Corrò, "Psychological characteristics of inflammatory bowel disease patients: a comparison between active and nonactive patients[J]," *Inflammatory Bowel Diseases*, vol. 25, no. 8, p. 1399, 2019.

[17] A. Ghesquiere, K. Wyka, M. Smith, and J. S. Kutner, "Associations between psychological symptoms and treatment outcomes of a massage therapy intervention: secondary analyses of a randomized controlled trial," *Complementary Therapies in Medicine*, vol. 46, pp. 116–122, 2019.

[18] R. Gu, Z. Li, and X. Yan, "Psychological intervention on COVID-19: a protocol for systematic review and meta-analysis[J]," *Medicine*, vol. 99, no. 21, p. e20335, 2020.

[19] A. El-Jawahri, L. Traeger, H. Vandusen et al., "Effect of inpatient palliative care during hematopoietic stem cell transplantation (HCT) hospitalization on psychological distress at six months post-HCT," *Journal of Clinical Oncology*, vol. 35, no. 15_suppl, p. 10005, 2017.

[20] L. Wu and Y. Zou, "Psychological nursing intervention reduces psychological distress in patients with thyroid cancer," *Medicine*, vol. 99, no. 38, p. e22346, 2020.

[21] A. Syw, C. Imlab, and D. Syf, "The effects of alpha asymmetry and high-beta down-training neurofeedback for patients with the major depressive disorder and anxiety symptoms[J]," *Journal of Affective Disorders*, vol. 257, pp. 287–296, 2019.

[22] L. A. Brenner, J. E. Forster, and A. S. Hoffberg, "Window to hope: a randomized controlled trial of a psychological intervention for the treatment of hopelessness among veterans with moderate to severe traumatic brain injury[J]," *The Journal of Head Trauma Rehabilitation*, vol. 33, no. 2, p. 1, 2017.

[23] I. Magán, L. Casado, R. Jurado-Barba et al., "Efficacy of psychological interventions on psychological outcomes in coronary artery disease: systematic review and meta-analysis [J]," *Psychological Medicine*, vol. 51, no. 11, pp. 1–15, 2020.

[24] H. S. Marie, D. Filip, and L. Carina, "Mamma Mia – a randomized controlled trial of an internet-based intervention for perinatal depression[J]," *Psychological Medicine*, vol. 49, pp. 1–9, 2018.

[25] M. L. Brown, J. P. Ospina, and C. M. Celano, "The effects of positive psychological interventions on medical patients' anxiety: a meta-analysis[J]," *Psychosomatic Medicine*, vol. 81, no. 7, p. 1, 2019.

[26] B. Lockwood, A. El-Jawahri, and A. R. Walker, "Psychological distress in young adults with acute myeloid leukemia undergoing induction chemotherapy[J]," *Blood*, vol. 136, no. Supplement 1, pp. 17-18, 2020.

[27] J. Zhang, C. B. Johnson, and B. Weinhaus, "In situ mapping identifies distinct vascular niches for myelopoiesis[J]," *Nature*, vol. 590, no. 18 February 2021, p. 457, 2021.

[28] H. Zhou, H. Zhao, and Y. Zhang, "Nonlinear system modeling using self-organizing fuzzy neural networks for industrial applications," *Applied Intelligence*, vol. 50, no. 5, pp. 1657–1672, 2020.

Hindawi
Computational Intelligence and Neuroscience
Volume 2022, Article ID 4134086, 9 pages
https://doi.org/10.1155/2022/4134086

Research Article

3D Indoor Scene Reconstruction and Layout Based on Virtual Reality Technology and Few-Shot Learning

Huanmei Li

School of Art, Taiyuan University of Science and Technology, Taiyuan, Shanxi 030021, China

Correspondence should be addressed to Huanmei Li; lihuanmei@tyust.edu.cn

Received 18 January 2022; Revised 18 February 2022; Accepted 19 February 2022; Published 24 March 2022

Academic Editor: Xin Ning

Indoor three-dimensional layout has a strong application background, such as virtual office three-dimensional layout planning, museum three-dimensional layout planning, and cave scene three-dimensional layout planning, which have been widely used in telecommuting, education, tourism, and other industries. In view of this, this paper proposes an indoor landscape reconstruction method based on VR (virtual reality) and draws indoor landscape information and images by using VR technology to generate an indoor landscape reconstruction panorama. A model is established to correct the distance error and reflectivity error of depth image, improve the accuracy of the depth image, and finally improve the accuracy of three-dimensional indoor scene TDR (three-dimensional reconstruction). In the process of optimizing layout, the Monte Carlo sampling method is used based on the Markov chain, and constraints are used as density functions to guide layout sampling and generate a number of reasonable scene layout suggestions in the iterative process of the sampler. Experiments show that this method can provide scientific and reasonable guidance to users' scene layout and help them complete the furniture layout quickly.

1. Introduction

With the vigorous development of VR (virtual reality) technology and the continuous emergence of new devices, TDR (three-dimensional reconstruction) has become a hot research topic in the field of computer vision [1]. The main task is to build a three-dimensional model of the real physical world based on the data collected by various sensors, using mathematical tools such as multiview geometry, probability statistics, and optimization theory, and building a bridge between the real world and the virtual world [2, 3]. The design inspiration of three-dimensional indoor scenes often comes not from simple imagination but from the backwardness of existing scene designs, and there happen to be a large number of realistic scene images on the Internet. In practice, when collecting large amounts of scene image data, such as crowded shopping malls, it is inevitable that dynamic objects will appear, which greatly limits the application of the TDR algorithm in real life [4]. Three-dimensional layout planning of indoor scenes is one of the key research contents in the field of computer vision and an important part of autonomous navigation and unknown environment model reconstruction of mobile robots.

At present, three-dimensional point cloud data acquisition methods are based on a three-dimensional laser scanner and RGB-D camera. The former point cloud based on laser scanning is of high quality, less influenced by the surrounding environment, and is usually used in outdoor large-scale scenes. Because the equipment is complex to operate, inconvenient to carry, and expensive, which usually reaches millions of levels, it is not convenient to collect indoor point clouds [5, 6]. The 3D point cloud reconstruction method based on vision camera mainly uses a multiview stereo geometry algorithm [7]. The motion recovery structure algorithm is an important off-line TDR method that uses several images of a scene to recover the pose of each exposure point and create a three-dimensional point cloud at the same time. It is characterized by time-consuming calculations, but the reconstruction results are extremely accurate [8]. It is necessary to develop an information-based interior color design method based on computer VR technology in order to help users better understand the effect of interior color design and to make it easier for designers to create interior color designs that are more in line with customers' wishes and needs. As a result, the current research hotspot is holographic image based on laser technology, and the research foundation is model building of 3D layout planning of 3D indoor scenes. Data collection, automation degree, model building range, and other issues plague traditional model building of 3D layout planning of indoor scenes [9].

At present, the application in 3D indoor scene design is mainly done by VR technology, which has a good reconstruction effect for noisy animated scene images, and also helps to enhance the realism and immersion of scene design, so as to realize the optimal design of 3D indoor scene model. With the development of deep learning research, some researchers have also proposed an end-to-end method based on deep learning, which is used to directly infer indoor 3D layout from image data. This kind of innovative method is very attractive, but the results often lack accuracy and rigor. Compared with traditional methods, there are still some big defects in practical application. In order to facilitate the reasonable reconstruction of 3D indoor scenes, this paper proposes a brand-new 3D scene modeling method based on VR technology, which mainly solves the two core problems of restoring 3D scenes from a single picture and optimizing the layout of scenes. Based on the solutions of these two problems, the corresponding prototype system of picture scene restoration and layout is designed and implemented. The research in this paper not only makes it convenient for users to get pictures from the Internet and restore picture scenes quickly with little interaction but also puts forward diversified layout suggestions on this basis, which enriches the established 3D scenes.

2. Related Work

TDR of the three-dimensional indoor scene based on RGB-d sensor spans many fields such as computer vision and robotics. The author of [10] analyzes the calibration of the Kinect v1 sensor and analyzes its depth image information in terms of accuracy and resolution. This paper studies how to use Kinect v1 to build a dense 3D map of the indoor environment for robot navigation, semantic mapping, and remote presentation. The author of [11] studied the physical measurement principle and capability of TOF technology used in the depth image of Kinect v2 sensor and its error source analysis and put forward a new calibration method of Kinect v2 sensor. The experiment verified that the calibration effect of the two open-source calibration methods was improved, and the reconstruction of a single image was effectively simplified by introducing appropriate interaction. These methods mostly started from the image's own information and realized the geometric reconstruction of a single image by interactively specifying the vanishing point information and any variables, but there were some limitations. The data-driven suggestion method is introduced into 3D modeling in [12], allowing artists to easily use existing 3D models for innovation. To achieve the idea of redesigning a 3D model, their method combines graphics, retrieval, and connection technology among graphics. The improved random sampling consistency algorithm in [13] can effectively eliminate outliers in feature point matching, allowing the SLAM (simultaneous localization and mapping) algorithm to maintain its high robustness in a dynamic environment. The author of [14] proposes Dyna SLAM, which uses a Mask R-CNN network to identify and segment dynamic objects based on prior information, and then repairs the background after removing the dynamic objects. It not only removes dynamic objects but also repairs the background area that has been blocked by dynamic objects and accurately reconstructs the map of pure static scenes. The author of [15] predicted the boundary characteristics of the cavity area using a convolution neural network model combined with a color image and a depth image and realized the filling of the cavity area through function optimization. This method works well and preserves details, but it is heavily influenced by the training data set and takes a long time to learn.

Three-dimensional point cloud is the most basic representation method of three-dimensional scenes, and furthermore, algorithms are needed to mine the scene structure information and semantic information contained in it. The characteristics of buildings in the indoor virtual environment are different from those in the outdoor environment. When building in the indoor environment, the density of the 3D indoor scene needs to be considered. This paper presents a method of constructing solid geometry based on 2D, which can build a more complex indoor layout in layers. The author of [16] focuses on automatic methods to reconstruct the basic semantic information of interior layout, including walls, doors, and windows. The author of [17] proposed a plan reconstruction method based on the Manhattan world hypothesis, so as to reconstruct the visual layout of the room. The author of [18] also proposed an indoor structure reconstruction method based on the Manhattan world hypothesis. The image method is also used in [19] to synthesize the model's facade, and the use of texture allows users to see the real street scene. A data-driven method for generating the room layout of the building plane was proposed in [20]. 120 architectural schemes were used in their study to train a Bayesian network to determine the relationship between rooms. The author of [21] encapsulates architectural design knowledge into an expert system, allowing it to assess the evaluated architectural plane in accordance with government regulations and interior design guidance, and then provides reasonable revision opinions. A similar method for furniture layout is used in [22]. Every furniture object will be connected to its parent, and the constraint relationship between parent and child objects will be specified ahead of time. However, as the number of furniture models in the model library grows, the relationship between parent and child models must be specified on a regular basis, which is a time-consuming task.

3. Research Method

3.1. 3D Indoor Scene Reconstruction Based on VR Technology. Color camera of RGB-D sensor collects color images, while infrared camera collects depth images. They all calibrate based on the pinhole model and establish the transformation relationship from 3D world coordinates to 2D image coordinates. Before using any camera, it is necessary to calibrate it, and so is the RGB-D sensor. It is necessary to get the internal and external parameters and distortion coefficient of the RGB-D sensor.

RGB-D image hardly changes in scenes such as changing illumination and complex background, but the image is affected by environmental noise and equipment noise when shooting, so it is impossible to encode the depth of every point in space. To improve the rationality of segmentation, the following types of points are removed:

Boundary point: in a neighborhood of image pixels, the local normal consistency is used to judge boundary points, which mainly include object edges, high curvature edges, and occluded scene edges.

Missing points of data [2]: when acquiring scene data, there are some areas that are not perceived, which leads to data missing.

According to the above definition, the boundary area is excluded in a neighborhood of each pixel, and the calculation formula is

$$A(c) = F \sin(a, b), \tag{1}$$

where $\sin(a, b)$ represents a pixel; F is the image boundary area.

The input image is over-segmented using an image segmentation algorithm [23, 24]. Although the scene cannot be correctly segmented, the segmentation result can be used as the over-segmentation result. Usually, the corresponding retrieval is completed by calculating the matching degree between the image features of the 2D object and the projected image features of the 3D model in the library. Therefore, the retrieval process will mainly involve the following main issues: how to unify the 2D object and the 3D model into the same representation form and analyze the features; what matching mechanism is used for efficient retrieval?

The viewpoint coordinates are converted to spherical coordinates, and binary $\langle \phi, \theta \rangle$ is used to represent the deflection angle of viewpoint relative to the model, ϕ is used to represent the horizontal deflection angle, and θ is used to represent the rigid deflection angle

$$\begin{aligned} \phi &= \arctan \frac{\sqrt{X_E^2 + Y_E^2}}{Z_E^2}, \\ \theta &= \frac{\pi}{2} - \arctan \frac{Y_E}{X_E}. \end{aligned} \tag{2}$$

To keep all two-dimensional models consistent with the structure of the object to be built, all scene observation viewpoints should be projected under this viewpoint. The basic process of sparse point cloud reconstruction based on incremental TDR is depicted in Figure 1, which is divided into two parts: image feature matching, camera pose recovery, and spatial structure recovery.

To begin, geometric constraints are used to filter out mismatches in the initial feature point matching pairs. Basic and essential matrices are two of the most common geometric constraints. Second, two images must be chosen in order to reconstruct the initial model. The use of two good images for initialization is crucial in the TDR algorithm. The global optimal solution will not be found if the initialization falls into the local minimum. By performing a beam adjustment on the model reconstructed from the two initial images, the initial model can be made more accurate. Because of noise, calculation errors, and certain errors in image feature matching, errors in camera pose estimation and 3D coordinate restoration occur in incremental TDR every time a new image is added. The cumulative error increases as the number of images increases, resulting in poor TDR results.

Assuming that the number of images participating in TDR is n, and C_i is the internal participation and external parameter of the i th image, m three-dimensional space points are reconstructed, the coordinate of the j th three-dimensional space point is X_j, and the objective function optimized by the beam adjustment method is

$$g(C, X) = \sum_{i=1}^{n} \sum_{j=1}^{m} w_{ij} \left\| q_{ij} - P\left(C_i, X_j\right) \right\|^2, \tag{3}$$

where w_{ij} is the indicator variable, which represents whether point j exists in image i, if point j is in image i, w_{ij} is 1; otherwise, it is 0. $P(C_i, X_j)$ is the coordinate of point j on image i after projection transformation, and q_{ij} is the actual image coordinate of point j on image i.

In practice, Levenberg–Marquardt algorithm is usually used to iteratively optimize the minimum reprojection error [10], which is the most widely used nonlinear least square algorithm, and its iterative formula is as follows:

$$\Delta = -\left(J_f^T J_f + \lambda I\right)^{-1} J_f^T f, \tag{4}$$

where λ is the weight parameter; when $y\,\lambda$ is large, the above formula is the gradient descent method with a small step size, and when λ is small, it is the Gauss-Newton method.

The process of solving the optimal value is that after one iteration, when the objective function drops successfully, the value of λ will be reduced; otherwise, the value of λ is increased and iterated again. After several iterations, the optimized parameter variables can be output when the error value is less than a certain threshold.

3.2. Research on 3D Indoor Scene Layout. In reality, it is common for people to need to decorate a new room when they move in. Sofas, coffee tables, televisions, tables, chairs, and benches are frequently arranged in disarray at this time, and people frequently want to know how to arrange these items to create a comfortable, beautiful, simple, and generous new home. There are some established rules to guide experienced designers on how to lay out furniture, such as in a living room, how to lay out furniture to make it easier for people sitting in different positions to talk, how to consider the room layout reasonable, visual balance, and compactness.

The input of this chapter is the furniture model randomly placed by users. Based on the functional rules such as pairing and conversation and visual rules such as balance

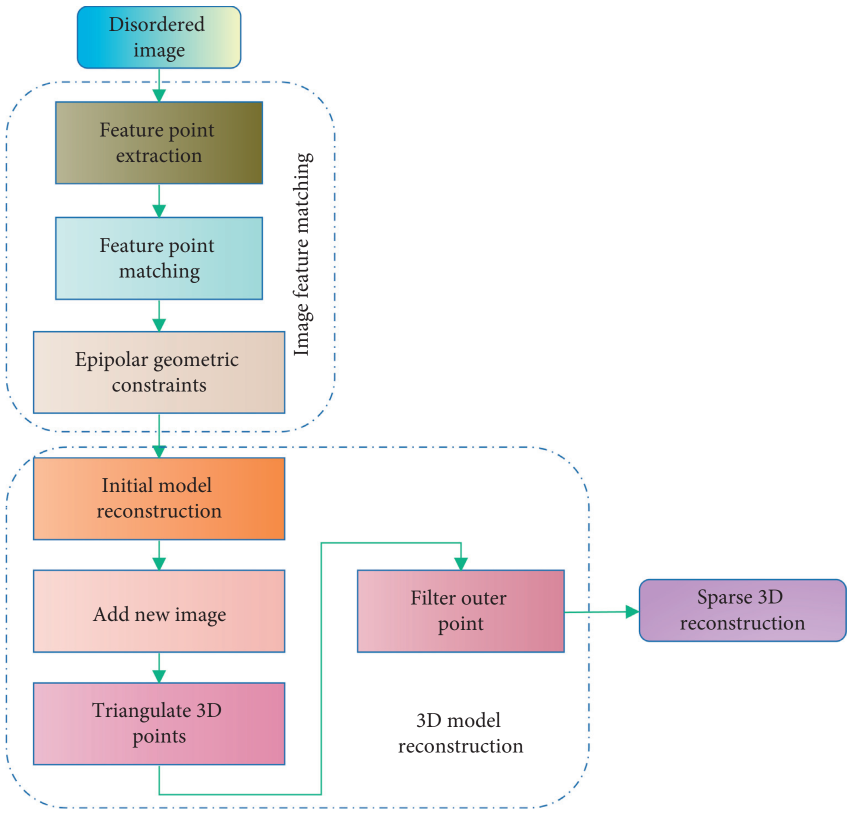

Figure 1: Basic flow chart of sparse TDR.

and neatness, a series of reasonable furniture layout suggestions are obtained through Markov chain Monte Carlo sampling. The flow of the whole algorithm is shown in Figure 2. Next, the algorithm flow of each stage is briefly introduced.

The layout proposal is generated by sampling through the density function, which associates the defined rules and represents the layout state of the furniture collection in the current space. The sampling method adopts the Markov chain Monte Carlo method to optimize and display different furniture layout suggestions through iteration and state transition.

The functional rules of furniture layout are based on human physiological constraints and the influence of spatial layout on human behavior. The statistics of human physical characteristics, such as body size and shape, are called anthropometry. Conversation comfort is often affected by the relative placement of seats, and strong factors such as sight, body orientation, and speaking distance all greatly affect conversation comfort. People's normal walking is similar. It requires that the layout can make a person walk around the room unimpeded without being affected.

For many furniture, it is necessary to reserve a certain space around them so that people can walk to the furniture or make the furniture work normally. The furniture onto a two-dimensional plane is projected, and the constraint space to Minkowski sum of furniture projection is added, thus defining a set of formulas J_F that describe the areas of individual furniture and surrounding space. We use $C_{cv}(I)$ to minimize the overlapping area of the surrounding space of different furniture.

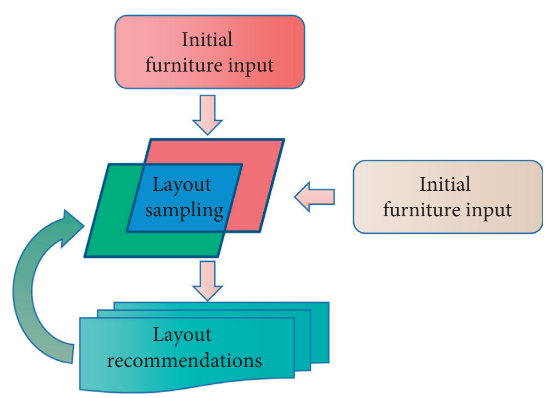

Figure 2: Method is not intended.

$$C_{cv}(I) = \sum_{f,g \in J_F \cup \{\overline{R}\}} A(f \cap g). \quad (5)$$

Among them, $A(\cdot)$ represents the area operator, $\overline{R}$ represents the polygon area of the room, and J_F is estimated from the area of the whole room.

The following are the methods for optimizing and designing indoor color using VR technology: the entire interior scene of a home is modeled, as well as individual models of each room, and then presented in a three-dimensional model. First and foremost, two-dimensional graphics must be collected and input, which is done using cameras. Following the creation of the two-dimensional model, the computer converts it into the corresponding three-dimensional model. The 3D model is then given a second color design and a corresponding light rendering. The final step in creating a 3D indoor scene is to improve the details of all types of furniture. Other objects can be used as an aid to help the 3D indoor scene achieve a more realistic simulation effect, assuming the number of models has been fixed.

u is defined as the distance from floodlight to plane, k is the radius of attenuation distance of long-distance light, and g is the corresponding display lamp distance. If there is a line segment n perpendicular to the light source on the x axis, and the corresponding number of light sources is m, then the corresponding illumination brightness is obtained according to the following formula:

$$W\left(x_j\right) = \sum_{j=1}^{m} W_j\left(x_j, \rho_j\right). \tag{6}$$

The simulation effect corresponding to indirect light is obtained, and the lighting feeling with perfect color brightness in indoor home design is realized.

In order to facilitate more convenient and intuitive color matching, different furnishings and furniture of indoor homes can be colored by establishing different material units to ensure more flexible color matching and higher efficiency. The materials are relatively independent, and they can be superimposed on each other to ensure the richness of colors. The material unit can be widely applied to tables, chairs, sofas, pendants, doors, and windows in indoor home design.

Then, geometric modeling of indoor object models is carried out by using laser holographic images. After mapping and color simulation of the built models, the 3D indoor scenes and models are further optimized to form a 3D layout planning model of example scenes that can be displayed by laser holographic images [8].

Because the RGB-D image sequence is not an accurate result in the layout prediction of new layout instances, there are certain layout conflicts, such as the phenomenon that the functional areas across the wall and the functional areas overlap [10]. Therefore, in the layout planning of 3D indoor scenes, the occlusion edges in RGB-D images are calculated, mainly including no wall penetration, no overlap, and no door blocking. The constraint conditions are set as follows:

$$E = \sum_{i=1} \frac{d\left(a_1, a_2, \cdots, a_n\right)}{A}, \tag{7}$$

where $a_1, a_2, \cdots, a_n$ represents wall-crossing constraint, door-blocking constraint, and overlapping constraint, respectively; $\sum_{i=1} d$ represents the description parameter of layout information.

When planning a path for a more complex indoor environment, it is necessary to browse and switch the indoor environment, determine the path to be planned, select the navigation type that can be used for path planning, and select the key position in the indoor environment and the key position of the data in the holographic image. Then, the set related service parameters are imported into the navigation service item, and the expression state of the result is finally determined so that the holographic image can perfectly express the 3D indoor scene [16].

4. Results Analysis and Discussion

Indoor point cloud reconstruction based on VR technology is an important basic work in this paper. A key improvement point on this issue is the combination of real-time reconstruction and off-line reconstruction. In off-line reconstruction, feature matching and incremental reconstruction processes are enhanced for the prior information of position, and attitude is obtained through real-time reconstruction.

In this paper, four algorithms, 4PCS (4-points congruent sets), PFH (point feature histogram), FPFH (fast point feature histograms), and NDT (normal distribution transform), are used to test two pieces of indoor point cloud data, respectively. At the same time, in order to enhance the comparability, the parameters set by these four algorithms are all the optimal parameters. After running in vs2017 + pcl environment, the result is shown in Figure 3.

From the error analysis in Figure 3, it can be seen that the 4PCS algorithm divides the original two disordered point clouds into upper and lower layers, and the initial attitude of the target point cloud has been well corrected, but the stability of the algorithm is not strong. Through a large number of parameter adjustments, this paper finds that the above-mentioned effects are random, and the generated results will be different every time the program is run. Comparing PFH and FPFH algorithms, although the basic principles of these two algorithms are similar, they can correct the attitude of the target point cloud.

Compared with 4PCS algorithm and NDT algorithm, it is obviously much higher, so it is not suitable for the real-time registration and splicing of point clouds in 3D indoor scenes, which makes it unsuitable for the real-time construction of 3D indoor scenes. Through the above analysis, it can be concluded that although the grid parameters of the NDT algorithm are the key to its registration accuracy, its high registration accuracy and high running efficiency will become the preferred coarse registration algorithm in the construction of 3D indoor scenes.

Through ICP (iterative closest point) fine matching operation, the positions of the point clouds to be matched have been greatly adjusted, and they are more coincident with the corresponding points. As mentioned earlier, a good initial position is the key to determine ICP fine matching. Figure 4 shows the algorithm's time-consuming and error analysis.

It can be seen from Figure 4 that the FPFH algorithm and PFH algorithm are not suitable for the real-time construction of 3D indoor scenes in terms of registration accuracy or running efficiency. Although the registration accuracy of the 4PCS + ICP algorithm is high, when the overlapping area of two point clouds is small, this algorithm runs unsteadily and takes a relatively long time. Experiments show that the NDT + ICP algorithm is obviously superior to other algorithms in registration accuracy and running efficiency, and it is effective for point clouds of 3D indoor scenes.

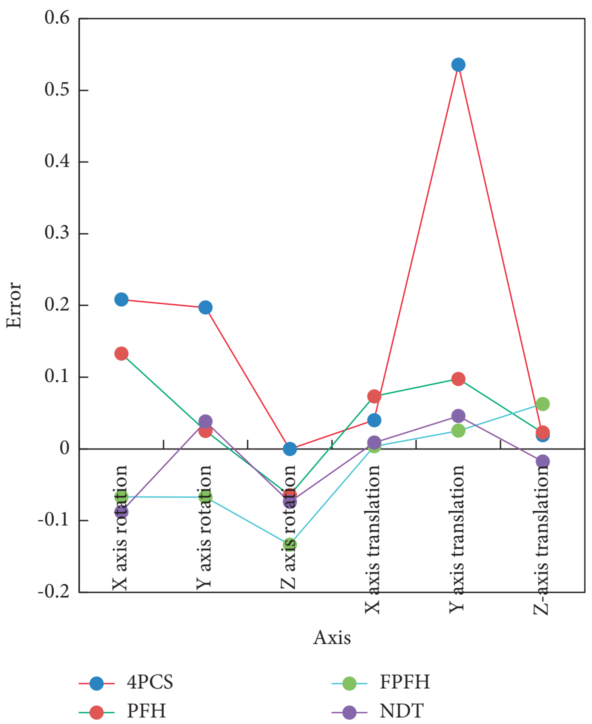

Figure 3: Error analysis.

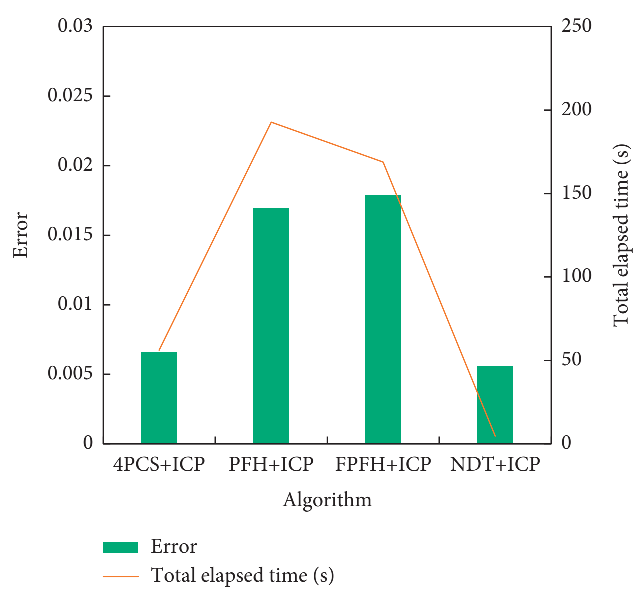

Figure 4: Algorithm time-consuming and error analysis.

The original point cloud scale represents the number of 3D points in the reconstructed dense point cloud, the preprocessed point cloud scale represents the number of 3D points in the point cloud after downsampling, statistical denoising, and smooth resampling, the number of candidate wall faces represents the number of candidate wall faces after plane fitting, plane merging, and plane classification, and the number of reconstructed wall faces represents the number of wall faces in the final room layout after optimal solution.

In order to establish the model of the relationship between reflectivity and depth values captured by different types of sensors, this paper designs and utilizes strip plane templates with six different gray levels. The gray value of the plane is divided into six levels, and the reflectivity of each level is shown in Figure 5.

The proposed neural network-based model is trained by optimizing the polynomial logistic regression objective using the RMSprop algorithm. There are five hidden layers in both Kinect v1 and Kinect v2. This procedure entails adjusting various parameters on a regular basis in order to achieve the desired results. The test set contains 260 data points, based on the above distribution ratio because the total data set used in this paper is 1300. The experimental results are shown in Figures 6 and 7.

Using this more than intelligent postcorrection neural network, for Kinect vl, depth accuracy is increased by 1.1 mm and depth accuracy by 4.3 mm. Meanwhile, for Kinect v2, the depth accuracy is increased by 115.6 mm, and the depth accuracy is increased by 0.3 mm. However, the author of [12] used the most advanced correction method to obtain the depth accuracy of its report. In addition, the results of the previous method are compared with those of this method, and it is found that the accuracy and precision of this method are better than those of the previous methods.

The room is encircled by white walls, storage cabinets, and glass walls, among other things. Many weak textures and repetitive and nondiffuse reflection environments present significant challenges for the motion recovery structure algorithm. Although the visual inertia odometer results are used for spatial local matching, cumulative drift errors are introduced into the incremental motion recovery structure algorithm, causing wall reconstruction artifacts.

The experiment will compare the data collection effects of the two methods in 3D indoor. The two methods not only collect the overall conditions of 3D doors and windows, buildings, and rooms but also collect the details of indoor modules, floors, and network structures, which can more comprehensively reflect the advantages and disadvantages of the two methods in data collection. Figure 8 shows the comparison of the two experimental methods in data collection.

According to the comparison results in Figure 8, it can be seen that the proposed method has a better effect in indoor data collection. It mainly applies a variety of key algorithms to optimize and analyze indoor-related data and also carries out unique data collection ideas according to the characteristics of data, which effectively improves the efficiency of data collection.

The relative motion between the static object in the scene and the camera is caused by the camera's motion, whereas the motion of the dynamic object in the scene is affected by both the camera's relative motion and its own motion at the same time, so the motion of each dynamic object differs from the motion of the static object in the scene. The number of moving objects in the image influences the number of static and dynamic feature points, and the number of dynamic and static feature points influences the estimation of camera internal and external parameters. The effect of the number of moving objects in the scene on the TDR algorithm is discussed using various numbers of moving objects. The

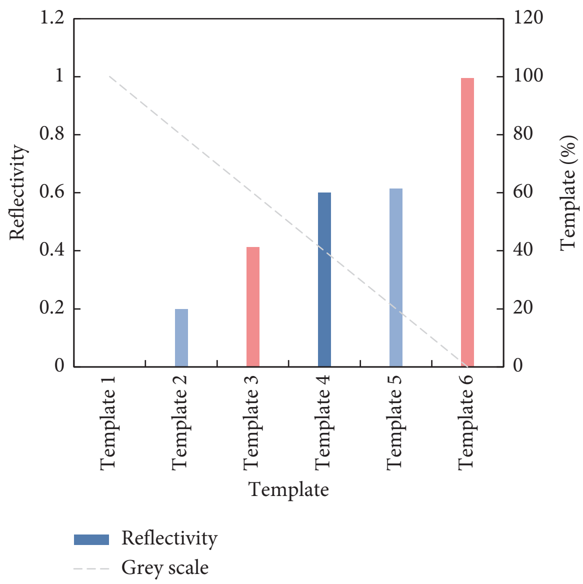

Figure 5: Reflectivity of different gray levels.

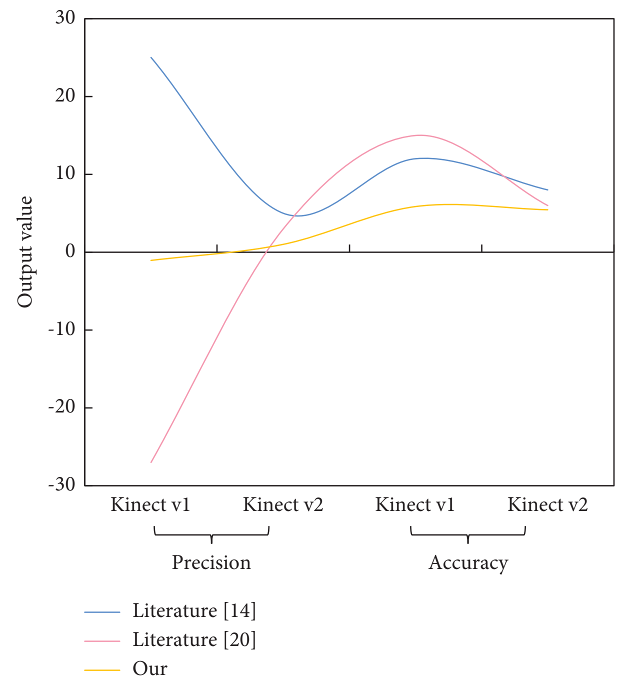

Figure 7: Comparative result.

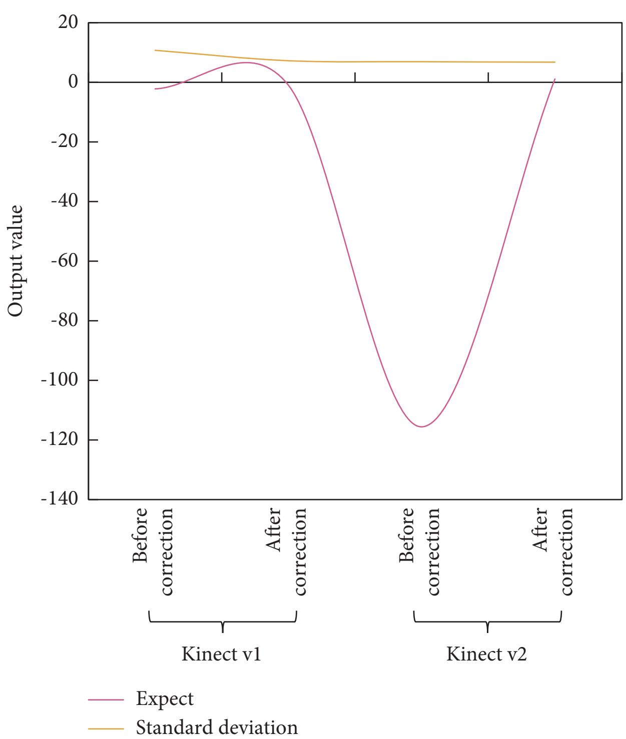

Figure 6: Expected value and standard deviation.

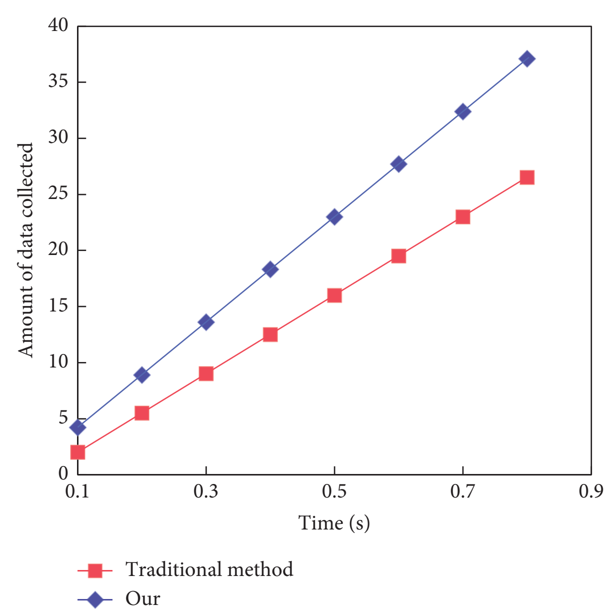

Figure 8: Comparison of effectiveness in data collection.

bedroom group's experimental data were subjected to the same TDR experiment, with 380 images in total. Three experiments were carried out, including 90 single moving targets, 90 multiple moving targets, and no moving targets. Detailed reconstruction data results are shown in Figure 9.

The experimental scenes are the living room and bedroom. Each scene is set with three modes, namely, no dynamic objects, single dynamic objects, and multidynamic objects. TDR is carried out before and after removing dynamic objects. From the experimental results, it can be seen that the reconstruction effect after removing dynamic objects is better than that without removing dynamic objects, and the reconstruction effect of single dynamic objects is better than that of multidynamic objects. In the 3D target test of the reconstructed point cloud model, more accurate recognition results can be obtained.

In the aspect of the indoor effect, not only the indoor path is optimized but also the effects such as details coloring and details perfection are carried out on the already built model. However, the traditional method lacks the adjustment of

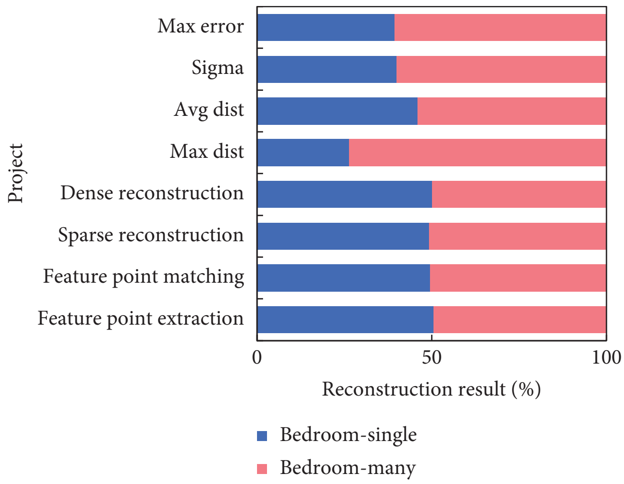

Figure 9: Reconstruction result of bedroom scene after removing dynamic objects.

details, which makes the layout planning of 3D indoor scenes too monotonous to immerse users in images.

5. Conclusion

A digital model of indoor landscape reconstruction can be created using VR technology. Dense TDR is realized in a 3D indoor scene using an RGB-D sensor, and real-time operation is achieved for an extended period of time using only the CPU. Experiments show that when the initial position and pose of the two point clouds are good, the ICP algorithm is ideal, and there is no problem with finding the local optimal solution. Experiments show that, based on the characteristics of indoor point clouds, the NDT + ICP registration scheme can achieve ideal registration and mosaic results in terms of time and accuracy, which can be used to construct 3D scenes in real time. A layout recommendation method based on the Markov chain Monte Carlo sampling method can complete diversified furniture layout recommendations quickly and efficiently with little interaction. However, based on the current research, the model deformation method will be introduced into the modeling process, which will be changed according to the model's own style, in order to obtain a layout result that is more realistic with the actual scene.

Data Availability

The data used to support the findings of this study are included within the article.

Conflicts of Interest

The author declares no conflicts of interest.

Acknowledgments

This study was supported by the Shanxi Province Philosophy and Social Science Planning Project (No. 2020YY157), Investigation and activation strategy of military industrial heritage of the 8th Route Army in southeast Shanxi Province.

References

[1] Y. Ding, Z. Xiaofeng, Z. Zhili, C. Wei, Y. Nengjun, and Z. Ying, "Semi-supervised locality preserving dense graph neural network with ARMA filters and context-aware learning for hyperspectral image classification," *IEEE Transactions on Geoscience and Remote Sensing*, vol. 60, 2021.

[2] S. Xin, M. Adam, and J. Bahram, "Three-dimensional profilometric reconstruction using flexible sensing integral imaging and occlusion removal," *Applied Optics*, vol. 56, no. 9, p. D151, 2017.

[3] J. Lei and Q. Liu, "Three dimensional temperature distribution reconstruction using the extreme learning machine," *IET Signal Processing*, vol. 11, no. 4, pp. 406–414, 2017.

[4] Y. Han, L. Ding, X. L. D. Ben, D. Razansky, J. Prakash, and V. Ntziachristos, "Three-dimensional optoacoustic reconstruction using fast sparse representation," *Optics Letters*, vol. 42, no. 5, p. 979, 2017.

[5] O. Emad, L. Antoine, D. Z. Sandro et al., "Stereo-vision three-dimensional reconstruction of curvilinear structures imaged with a TEM," *Ultramicroscopy*, vol. 184, pp. 116–124, 2017.

[6] A. V. VokhmintceV, A. V. Melnikov, K. V. Mironov, and V. V. Burlutskiy, "Reconstruction of three-dimensional maps based on closed-form solutions of the variational problem of multisensor data registration," *Doklady Mathematics*, vol. 99, no. 1, pp. 108–112, 2019.

[7] E. J. Sellountos, "A single domain velocity - vorticity fast multipole boundary domain element method for three dimensional incompressible fluid flow problems, part II," *Engineering Analysis with Boundary Elements*, vol. 114, no. May, pp. 74–93, 2020.

[8] X. Wang, M. Luo, H. Wu et al., "A three-dimensional magnetic tweezer system for intraembryonic navigation and measurement," *IEEE Transactions on Robotics*, vol. 34, no. 1, pp. 240–247, 2018.

[9] J. Kang, S. Heo, W. J. Hyung, S. L. Joon, and L. Sanghoon, "Three-dimensional active vessel tracking using an elliptical prior," *IEEE Transactions on Image Processing*, vol. 27, no. 12, 2018.

[10] Y. Zhou, L. Wang, and P. Love, "Three-dimensional (3D) reconstruction of structures and landscapes: a new point-and-line fusion method," *Advanced Engineering Informatics*, vol. 42, no. Oct., pp. 1–11, 2019.

[11] N. K. Mangal and A. K. Tiwari, "Kinect V2 tracked body joint smoothing for kinematic analysis in musculoskeletal disorders," in *Proceedings of the 2020 42nd Annual International Conference of the IEEE Engineering in Medicine & Biology Society (EMBC)*, pp. 5769–5772, IEEE, Montreal, CA, USA, 2020 July.

[12] G. Gunasekaran and M. Venkatesan, "An efficient technique for three-dimensional image visualization through two-dimensional images for medical data," *Journal of Intelligent Systems*, vol. 29, no. 1, pp. 100–109, 2017.

[13] I. M. Lochhead and N. Hedley, "Modeling evacuation in institutional space: linking three-dimensional data capture, simulation, analysis, and visualization workflows for risk assessment and communication," *Information Visualization*, vol. 18, no. 1, pp. 173–192, 2019.

[14] Z. Yin and J. Xiong, "Three-dimensional reconstruction of molten pool appearance in GMA additive manufacturing based on ACT stereo matching algorithm," *Hanjie Xuebao/*

Transactions of the China Welding Institution, vol. 40, no. 1, pp. 49–52, 2019.

[15] M. Wang, H. Wang, Y. Yin, S. Rahardja, and Z. Qu, "Temperature field prediction for various porous media considering variable boundary conditions using deep learning method," *International Communications in Heat and Mass Transfer*, vol. 132, Article ID 105916, 2022.

[16] Y. Wang and L. Sun, "Three-dimensional reconstruction of macrotexture and microtexture morphology of pavement surface using six light sources-based photometric stereo with low-rank approximation," *Journal of Computing in Civil Engineering*, vol. 31, no. 2, pp. 4016054–4016061, 2017.

[17] S. Park, H. Lee, S. Lee, and H. S. Yang, "Line-based single view 3D reconstruction in manhattan world for augmented reality," in *Proceedings of the 14th ACM SIGGRAPH International Conference on Virtual Reality Continuum and Its Applications in Industry*, pp. 89–92, New York, NY, USA, 2015 October.

[18] X. Li, J. Sui, and Y. Wang, "Three-dimensional reconstruction of fuzzy medical images using quantum algorithm," *IEEE Access*, vol. 8, pp. 218279–218288, 2020.

[19] J. Kim and C. O. Lee, "Three-dimensional volume reconstruction using two-dimensional parallel slices," *SIAM Journal on Imaging Sciences*, vol. 12, no. 1, pp. 1–27, 2019.

[20] G. Li, H. Song, S. Wang, and J. Kong, "Application of image processing and three-dimensional data reconstruction algorithm based on traffic video in vehicle component detection," *Mathematical Problems in Engineering*, vol. 2017, no. 11, 16 pages, Article ID 4145625, 2017.

[21] Z. Wei, Z. Yi, and Z. Long, "A three-dimensional virtual resource scheduling method for energy saving in cloud computing," *Future Generation Computer Systems*, vol. 69, no. APR, pp. 66–74, 2017.

[22] Z. Z. Wang and C. S. Zhang, "Three-dimensional hand reconstruction by single-shot structured light line pattern," *IEEE Access*, vol. 6, 2018.

[23] W. Cai, Z. Wei, Y. Song, M. Li, and X. Yang, "Residual-capsule networks with threshold convolution for segmentation of wheat plantation rows in UAV images," *Multimedia Tools and Applications*, vol. 80, no. 21, pp. 32131–32147, 2021.

[24] H. You, L. Yu, S. Tian, and W. Cai, "DR-Net: dual-rotation network with feature map enhancement for medical image segmentation," *Complex & Intelligent Systems*, vol. 4, pp. 1–13, 2021.

Hindawi
Computational Intelligence and Neuroscience
Volume 2022, Article ID 3099794, 10 pages
https://doi.org/10.1155/2022/3099794

Research Article

Research on the Construction of a Nursing Education Management Model Based on a Small Data-Driven Model and Its Application

Qingna Lv ,[1] Yanyun Zhang,[2] Yanyan Li,[3] and Yang Yu [1]

[1]*Nursing Department, The Second Affiliated Hospital of Dalian Medical University, Dalian, Liaoning 116023, China*
[2]*College of Nursing, Inner Mongolia Minzu University, Tongliao, Inner Mongolia Autonomous Region 028000, China*
[3]*College of Nursing, Chongqing Medical and Pharmaceutical College, Shapingba, Chongqing 401331, China*

Correspondence should be addressed to Qingna Lv; qingna0522@dmu.edu.cn

Received 18 January 2022; Revised 14 February 2022; Accepted 22 February 2022; Published 24 March 2022

Academic Editor: Xin Ning

Based on the concept of responsible holistic nursing care, a whole-process dual-tutor nursing practice model is established and its application effects are explored. This paper firstly reviews the research progress of nursing workload prediction methods at home and abroad, in order to provide a reference for clinical nursing workers in China to choose a scientific, reasonable, and easy-to-use nursing workload prediction method. It is proposed to construct a nursing education management model based on small data to provide ideas and references for nursing education management to effectively predict the evolutionary trend of students' behaviour and improve the level of accurate services. The experimental group adopted a dual-tutor responsibility system for the whole-process nursing practice model, including a complete three-level supervision system: a dual-tutor teaching system, a PDCA responsibility system for continuous improvement, and a multichannel teacher-student interaction platform; the control group adopted the traditional nursing practice model.

1. Introduction

In recent years, with the acceleration of the internationalization of medical education and the localization of international standards, nursing education has taken on the multiple missions of optimizing the cultivation of talents, leading to the development of disciplines and deepening the connotation of the profession, and the development of education needs to adapt to the development of social economy, the progress of science and technology, and the coordination of health undertakings [1]. The former Ministry of Health and the Ministry of Education jointly put forward the strategic point of building an integrated teaching mode of industry-university-research and clearly defined the development goal of deepening teaching reform and cultivating higher technical application talents [2]. The former Ministry of Health and the Ministry of Education jointly put forward the strategic point of building an integrated teaching model of industry-academia-research, specifying the development goal of deepening teaching reform and cultivating higher technical application-oriented talents. The changes in the clinical environment have put clinical nursing education in a new period of conceptual transformation and practical reform, and it is one of the core issues of nursing higher education to realize an effective interface and buffer between theory and practice and to explore a clinical practice model that fits the cultivation objectives of higher nursing education at this stage [3].

The information system-based nursing workload forecasting method refers to the use of information system retrieval and statistical functions to present medical order entries and nursing project data that reasonably and effectively reflect nursing workload so as to analyse and forecast nursing workload [4]. Currently commonly used in the USA is the GRASP nursing management information system (Grace Reynolds Application and Study of Peto, GRASP), which predicts workload and manpower in advance by forming a database of nursing workload for different categories of patients, depending on the type of patient admitted each day [5].

The GRASP system divides nursing items into 11 categories with 50 nursing operations and assigns a fixed number of points to each operation based on the average time spent on each item, plus a certain percentage of delay or fatigue time points to predict work hours and prospectively arrange manpower [6]. In Singapore, scholars developed a nursing intensity system based on nursing diagnosis, which identifies the type of nursing diagnosis based on the type of intervention performed on the patient, quantifies the relationship between the nursing time required and the type of nursing diagnosis through a regression equation, and obtains the number of patients with different nursing diagnoses to predict the nursing work hours required per shift [7]. In addition, Japan has developed a Nursing Care Assignment Management (NCAM) system to visualise daily workloads and use the quantified workload data to efficiently assign staff and tasks [8]. In China, scholars have used the Hospital Information System (HIS) to obtain and predict workload data. In [9], the HIS system was combined with the work hour measurement method, and the nursing work hours of each operation were correlated with the frequency of HIS medical orders to establish an HIS-based nursing work our database. The relationship between the number of nursing hours and the number of nurses was calculated by linear regression analysis; for example, Nephrology: number of nurses $= 1.577 + 0.030x$ working hours, predicted nursing manpower required for tomorrow $= 1.577 + 0.030x$ total nursing hours of yesterday $\div$ actual number of admissions yesterday $\div$ expected number of admissions tomorrow. By programming the formula into the information system, the manager only needs to enter the number of hospital admissions for tomorrow to predict the number of people who will work on tomorrow.

Nursing projects are mostly derived from doctors' orders and nursing workflows and are selectively retrieved from information systems in a simple and operational way [10]. Overseas information systems mainly quantify the categorisation of patient need and use statistical analysis to identify the relationship between patient categories and workload, thereby predicting the number of nursing hours required for each category of patients and allocating manpower. Domestic information systems are based on the prediction of workload purely statistical nursing items to get nursing workload, but due to the imperfect data dictionary of information systems, in practice there are many non-chargeable items and indirect nursing work that are not included in the dictionary of medical advice, such as health education, linen change, material collection, and so on, which cannot be directly retrieved for statistics. In addition, the different information system environments of individual hospitals, the fact that standard nursing hours have not yet been unified, and the lack of uniform standards for screening nursing items make the results of some scholars' research not universally applicable and externally applicable [11, 12].

The contributions of this article are as follows:

This article proposes to build a nursing education management model based on small data, which provides ideas and references for nursing education management to effectively predict the evolution of student behavior and improve the level of precise service.

Based on the in-depth analysis of the concept and characteristics of small data, we design a dynamic portrait label system from two aspects of student surface behavior and deep driving factors and propose a research method to realize dynamic portrait and form an overall framework model.

The experimental group adopts the whole-course dual-mentor responsibility system holistic nursing practice model and comprehensively evaluates the two groups of nursing students, investigating the professional identity of the nursing students, the evaluation of the internship model, and the satisfaction of patient care services.

2. Related Work

2.1. A Predictor-Based Approach to Nursing Workload Prediction. Predictor-based methods for forecasting nursing workload are based on statistical methods such as regression analysis, which explores the factors inherent in nursing workload data, use the main influencing factors as predictors, and identify parameters to be determined in order to construct a mathematical model, followed by regression modelling of the identified predictors using polynomial Logistic, LASSO, and other methods [13]. Common predictors used overseas include Hours Per Patients Day (HPPD) [14], Case Mix Index (CMI) [12, 14], and International Classification of Function (ICF) [15].

In addition, studies have also shown that the Unit Activity Index (UAI), the number of discharges, transfers, or discharging (Admitting, Transferring, or Discharging Patients (ADT)) [16] have a positive impact on the inclusion of workload prediction. Reference [17] used multiple stepwise linear regression analysis to identify the factors influencing work hours and used them as classification factors to build a query table of direct nursing hours and indirect nursing hours required by different categories of patients. The table was used to identify the factors influencing the working hours and use them to establish a table of direct nursing hours and indirect nursing hours required by different categories of patients for dynamic manpower deployment. In [18], the results of a survey in a general adult ward in a tertiary care hospital showed that there was a linear relationship between the Barthel Index and Simple Clinical Score (SCS) of patients and the 24-hour direct nursing hours of patients, and a mathematical model using least squares and multiple linear regression was developed to identify the nursing hours of patients in different levels of care, thus enabling prediction of nursing workload.

2.2. Grey Dynamic Model. Grey systems theory consists of the use of dynamic predictive models to process incomplete small sample "information-poor" data to establish a quantitative relationship between the present and the future on a timeline, through which things can be predicted [19]. Nursing workload is the result of a combination of internal and external environmental factors, such as patients, environment, and nurses, which are covered by grey information. In contrast, workload measures are specific and defined, covered by white information, and meet the requirements for predictive modelling of data grey systems [20]. Reference [21] used a grey system prediction model to quantitatively predict trends in nurse performance, using 12 nurses in the unit as the study population and selecting four months of performance for each nurse as the basic data for modelling and predicting nurse performance over the next five months. Nursing performance is a quantitative assessment of nurses' workload, and the prediction of performance can indirectly help managers predict workload, scientifically set work standards, and reasonably assign work tasks.

2.3. Time Series Models. Time series models are forecasting methods that apply mathematical models to describe the changes in variables over time and their development patterns, that is, predicting their future values from the past and present values of the time series. The Autoregressive Integrated Moving Average Model (ARIMA) is one of the most widely used and well-known time series forecasting methods, which is able to integrate seasonal, trend, and random disturbance factors and has good forecasting function, and is gradually used in the field of health care [2]. Reference [22] used the ARIMA model to predict daily patient occupancy in a short-term acute care ward for optimal management of human resources, and the results showed that the model predicted with high accuracy for up to one week, which is a good guide for managers. Reference [23] used an ARIMA model prediction combined with linear correlation and regression analysis to obtain a predictive model for the number of obstetric outpatient card builds and deliveries. Reference [24] used time series analysis to construct a time series prediction model for daily nursing workload in the neurology department.

2.4. Discrete Event System Simulation. Discrete event simulation (DES) is a method of experimenting with computer simulation of discrete events for evaluating, predicting, and optimizing the efficiency of existing systems. The DES model was used by [25] to predict caregiver demand in a nursing home. Data on the daily care needs (ADLs) of older people were collected and entered into the DES model to predict the relationship between care workload and staffing to meet the daily care needs of older people so as to determine the optimal staffing for different care needs. Reference [26] collected 1 month of inpatient care data from a general hospital in Canada into the system and logically simulated the impact of different nurse-patient ratios on quality of care as well as nursing workload to help managers predict and optimally manage nursing workload. Discrete event simulation is a nurse-centred approach to workload prediction.

3. Questions to Ask

3.1. Small Data. The concept of small data was first discovered by Professor D. Eestrin of Cornell University, who believed that students' health could be dynamically monitored through the tracking of a full range of data on their daily behaviour [27]. There is no clear definition of small data, but it is accepted that small data is a collection of all data on a person or team-centred, multilevel behavioural pattern, and situational awareness. Over time, these data collections have become richer and richer, providing a powerful support for dynamic mining of student needs and preferences and behaviour patterns. Current research on small data focuses on personalised recommendations and accurate services, interest discovery and prediction, and theoretical discussions on the fusion of small data, but there is a lack of conceptual concepts for building academic app portraits based on small data.

3.2. Nursing Education Management Student Portrait. Traditional student portraits only capture data at a certain point in time; that is, they abstract a static model of a student's reality and history based on their behavioural characteristics, habits, and other data tags. A dynamic portrait of a student in nursing education management is one that introduces a time segment based on a conceptual picture of the student and uses a scientific approach to dynamically and continuously outline trends in the behavioural trajectories of students as they interact with the platform.

4. Overall Design

The dynamic portrait model based on small data proposed in this paper places more emphasis on the relevance and three-dimensionality of the labelling system. Therefore, the process of the small data-based student profiling model for nursing education management should be divided into four segments, as shown in Figure 1:

Step 1. Design a three-dimensional dimensional label that includes deeper drivers of student behaviour from a small data perspective, combined with the characteristics of nursing education management.

Step 2. Collect and preprocess student data-based on the dimension labels.

Step 3. Classify the data according to the temporal information in the student microdata and use clustering algorithm to cluster the data in specific time segments to classify students into different groups and build a time-phased portrait, which will be stored in the database.

Step 4. Based on the time-phased portrait, identify the cluster centres of each time period (the cluster centres can be regarded as the typical representatives of the group of students).

The above design process not only refers to the basic aspects of traditional student profiling, but also incorporates the special features and requirements of the small data based dynamic profiling proposed in this paper, which ensures practical value and innovation.

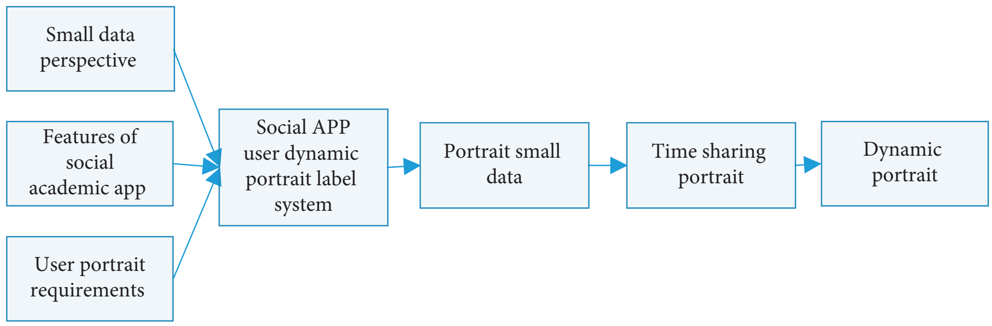

Figure 1: The process of constructing a student portrait for nursing education management based on small data.

5. Nursing Education Management Systems and Small Data Acquisition

5.1. Label Dimension. The psychological activity of students is an intrinsic factor that underpins behaviour, and any behaviour is driven by certain intentions before it occurs. Social psychologist Levin developed the field dynamics theory to analyse the driving forces and behavioural change processes that underpin individual behaviour. Field dynamics theory consists of field theory and dynamics theory, in which field theory defines "field" as the overall form of interdependence between the individual and the environment, also known as individual life space (LS). The individual's psychological and behavioural processes always take place and move within this space, which can be expressed in a functional equation as

$$B = f\left(P^{*}E\right) = f\left(LS\right), \tag{1}$$

where B represents the externalised behavioural expression. P represents the intrinsic needs of the individual, E represents the psychological environment, that is, the situation that stimulates the intrinsic needs of the individual, and f is a function of the interaction between the individual and the environment. Thus, field theory considers individual behaviour as a result of the interaction between the subject and the situation.

5.2. Small Data Collection. Based on the field dynamics theory and the characteristics of nursing education management, this paper argues that the factors driving student behaviour in nursing education management include students' value orientations, cognitive abilities, situational characteristics, and social relationships. Combining the two basic factors of student natural attributes and behavioural preferences, a six-dimensional portrait system is constructed, as shown in Figure 2. The internal relationship of each dimension is as follows: students' natural attributes and behavioural preferences are the basic framework of the portrait, while values, cognitive abilities, situational characteristics, and social relationships drive the production of behaviour, among which values and cognitive abilities are driven by students themselves, that is, internal drive P, and situational and social situations are the stimulus of external situations (i.e., trigger). E. Behavioural preferences are the external effect of the combination of natural attributes, values, cognitive abilities, situational characteristics and social relationships. E. Behavioural preferences are the externalisation of a combination of natural attributes, values, cognitive abilities, situational characteristics, and social relationships.

Basic student information and care data are stored in the administration backend; behavioural preferences can be obtained from behavioural data stored in student logs and student-generated content; value orientations can be obtained by mining student-generated content or through research methods such as questionnaires and interviews (e.g., targeted electronic questionnaires distributed by the platform to understand students' visions and current needs); cognitive abilities can be obtained from authentication data submitted by students and analysis of interaction data. Cognitive skills can be obtained from student submissions and interaction data analysis; situational awareness can be obtained from sensors, location systems, and smart wearable devices; social relationships can be obtained from log mining and social network analysis.

5.3. Small Data Processing. In the past, most of the data used in student profiles were basic attribute data and behavioural data, which could be coded and transformed numerically or simply processed for direct experimental analysis. This paper builds on this foundation by incorporating comment or posting text (i.e., content features). The professional and domain-specific nature of nursing education management and the fact that students' nursing topics are often related to their own specific domains makes it possible to mine and analyse students' areas of interest from the textual content. Therefore, this paper proposes a text data modelling approach based on the LDA topic model (see Figure 3):

Step 1. The text content was collected, stitched, and stored as text documents by student IDs, cleaned and imported into the domain word list for Chinese word separation and deactivation filtering, and the original text was cut into a sequence of feature words; then, the TF-IDF was used to calculate feature word weights from both word frequency and importance perspectives, and important feature words were retained.

Step 2. Use the easy-to-use Gibbs sampling in the LDA (Latent Dirichlet Allocation) topic model to mine the

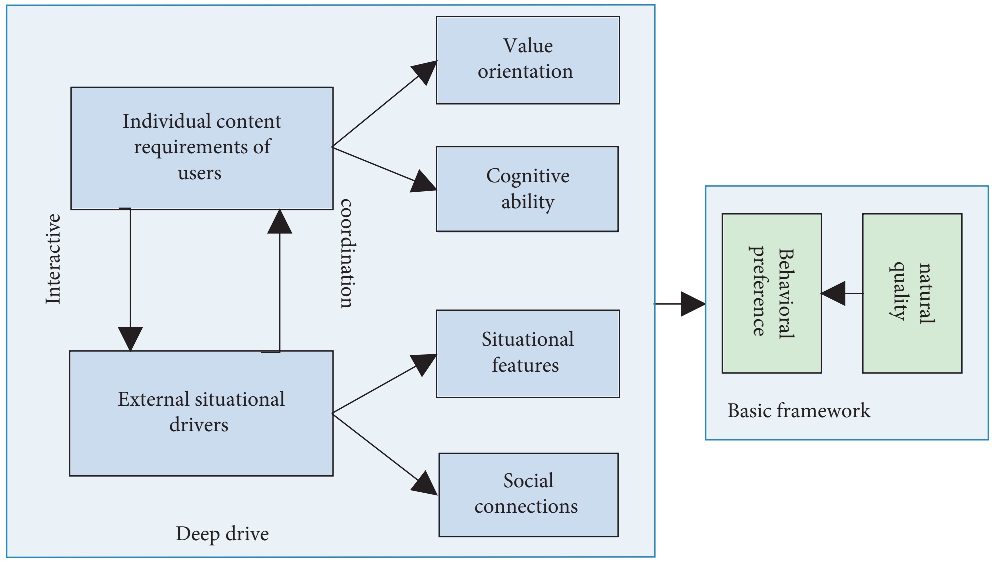

Figure 2: System of nursing education management student portrait dimensions.

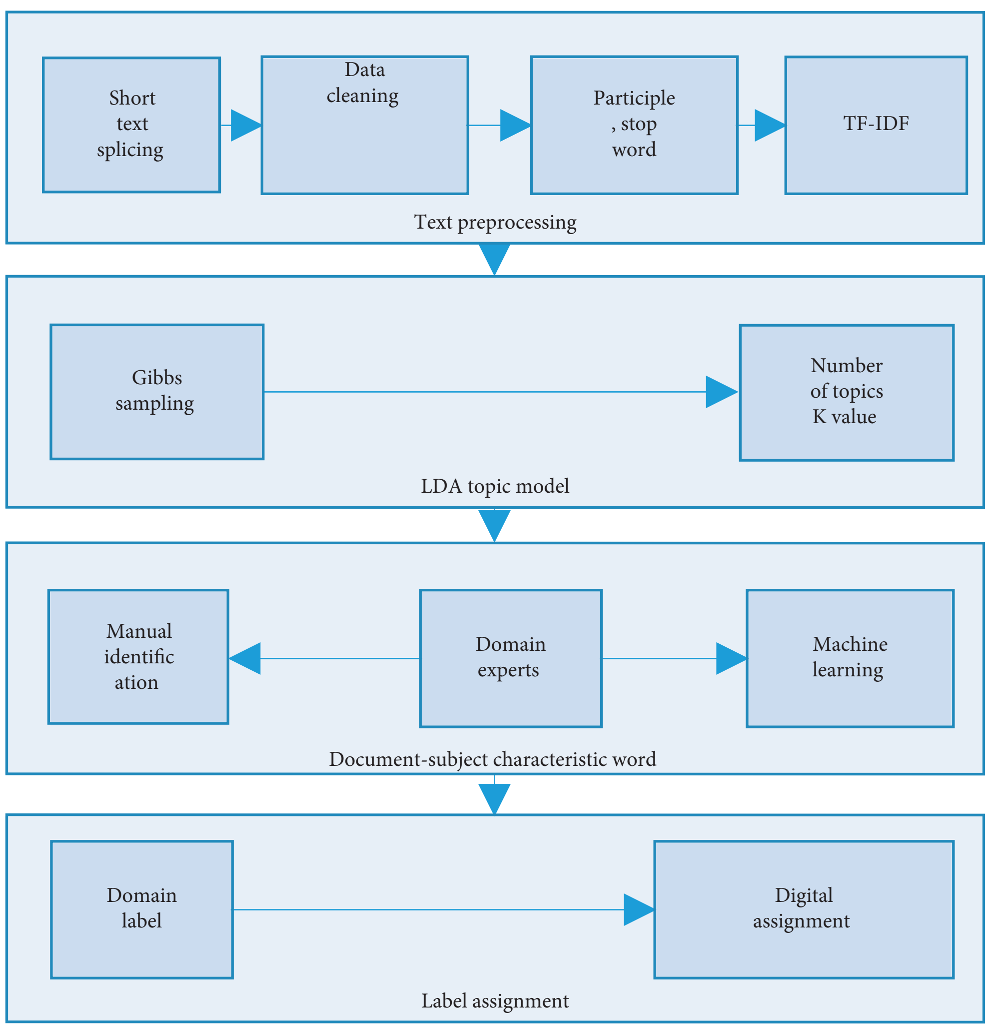

Figure 3: Steps for modelling unstructured text based on LDA topic models.

implied topics of the text; that is, project the complex text into the potential topic space according to the statistical idea, and obtain the "document-topic" distribution θ topic distribution θ and "topic-featured word" distribution:

$$\text{perplexity}(D) = \exp\left[-\frac{\sum_{d=1}^{M}\log(P(W)_d)}{\sum_{d=1}^{U} N_d}\right],$$
$$p(w) = p(z|d) * p(w|z). \quad (2)$$

Step 3. After obtaining the "document-topic-feature word" matrix, if the sample is small, each topic word cluster can be identified manually, taking into account the distribution of words and semantic relationships under the topic. As most of the nursing education management apps are industry vertical platforms, such as the Dingxiangyuan App for the medical field and the House of Economics and Management App for the management field, we can consult with experts in the relevant fields to set a domain label for each document that summarises its characteristics when identifying thematic feature words.

Step 4. After obtaining the domain labels for each document, the labels are digitally assigned, for example, the labels "internal medicine," "surgery," and "Chinese medicine" are assigned {1, 2, 3}, respectively. The result is the identification of student interest areas from student-generated content and their conversion into numerical values.

The above method can quantify the textual data and also reveal the textual characteristics at the thematic level, which is both practical and scientific, and achieves the research goal of combining textual data and other data to portray the portrait, avoiding distortion of the portrait to the greatest extent possible.

6. Case Studies

6.1. Study Subjects. A convenience sampling method was used to include 200 nursing students who underwent a clinical internship in a tertiary care hospital from August 2014 to April 2015. The experimental group consisted of 200 nursing students who underwent clinical internship from August 2014 to April 2015, and the control group consisted of 200 nursing students who underwent an internship in the same hospital, all with bachelor's degree. During the study period, 3 nurses were dropped out of the experimental group and 6 from the control group. The reason for the dropout was that the nursing students were transferred to other hospitals at the end of their internship and were unable to complete the comprehensive assessment and related questionnaires. Therefore, a total of 192 nursing students in the experimental group and 185 in the control group were included in this study [28].

6.2. Evaluation Methods. At the end of the internship, nursing students are assessed in a unified manner, including theoretical and operational assessments, with a score of 100 points each. Each student is evaluated by the first- and second-level managers according to the "Internship Performance Assessment Form," which covers five major categories: professionalism, professional skills, communication skills, study and research skills, and teamwork, each with 20 points, totalling 100 points [29].

A survey of nursing students at the end of their placement was conducted using the "Nurse Professional Identity Scale" developed by the Department of Nursing Management, Faculty of Medicine, University of Tokyo, Japan. The scale consists of 21 items with 7 dimensions: a sense of control, a sense of consistency, a sense of meaningfulness, sense of self-efficacy, sense of self-determination, sense of organisational influence, and sense of patient influence. The items are rated on a 7-point Likert scale, according to "not at all," "less," "less," "not sure," "not sure," "not at all," and "not sure." The dimensional score is the average of the scores of the included items. The higher the score, the higher the degree of professional identity of nursing students. Cronbach's alpha coefficient for the Chinese version of the scale was 0.84 and the content validity was 0.92. In this study, Cronbach's alpha coefficient was 0.817.

A self-made patient care service satisfaction questionnaire was distributed to patients at the end of the practice, including five dimensions of nursing student service quality, professional skills, patient education, humanistic care, and overall evaluation, with a total of 16 items. "Dissatisfied," "average," "satisfied," and "very satisfied" were assigned a score of 1 to 5, respectively. The higher the score, the higher the patient's satisfaction with the nursing student. Six experts in nursing education, nursing management, and clinical nursing were invited to evaluate the relevance of each item to the content expressed in the questionnaire on a 4-point scale (i.e., 1 = not relevant, 2 = weakly relevant, 3 = strongly relevant, and 4 = very relevant). The Cronbach's alpha coefficient for this questionnaire was 0.923.

A self-made questionnaire was used to survey nursing students at the end of the placement, which included five items: rationality, replicability, the quality of teaching, quality of management, and overall evaluation of the placement model.

6.3. Results. Comparison of overall assessment scores of nursing students is presented in Table 1.

Clinical practice is an integral part of higher nursing education, and the quality of clinical teaching is crucial to the overall standard of higher education. It is an innovation and development of the traditional mobility practice paradigm, adhering to the student-centred talent training concept, based on the development of nursing students, based on clinical nursing practice, facing the frontier of discipline development, adapting to the educational market demand, aiming to cultivate excellent nursing students, and devoting to the comprehensive training of nursing students' knowledge, ability, and quality so as to become talents with greater development potential. As shown in Table 1, the experimental group was the first to be trained in nursing. As shown in

Table 1: Comparison of the comprehensive assessment scores of nursing students in the two groups ($\overline{x} \pm s$).

Project	Experimental group ($n = 182$)	Control group ($n = 165$)	t/t' value	P value
Theoretical assessment	79.70 ± 8.12	77.19 ± 6.78	3.108	0.002
Operation assessment	85.48 ± 7.33	82.56 ± 8.25	3.491	<0.001
Practice performance	72.02 ± 10.12	66.58 ± 12.27	4.472	<0.001
Professional quality	14.72 ± 1.92	13.55 ± 1.94	5.621	<0.001
Professional skills	15.04 ± 2.22	14.29 ± 2.98	2.631	<0.001
Communication skills	13.25 ± 2.21	11.48 ± 2.45	5.843	0.009
Learning and scientific research ability	14.81 ± 2.38	13.57 ± 5.24	4.512	<0.001
Teamwork	14.21 ± 2.1	13.26 ± 2.49	3.815	<0.001

Table 2: Comparison of professional identity between the two groups of nursing students ($\overline{x} \pm s$).

Project	Experimental group ($n = 182$)	Control group ($n = 165$)	t value	P value
Sense of grasp	5.86 ± 0.99	5.33 ± 1.04	4.862	<0.001
Sense of consistency	5.52 ± 1.41	4.36 ± 1.68	6.988	<0.001
Sense of meaning	5.88 ± 1.25	5.40 ± 1.36	3.426	<0.001
Self-efficacy	5.91 ± 0.85	5.64 ± 0.93	2.826	0.005
Self-determination	4.35 ± 1.84	3.76 ± 1.92	2.922	0.004
Sense of organisational influence	3.66 ± 1.53	3.38 ± 1.65	1.640	0.102
Patient's sense of influence	5.15 ± 1.20	4.39 ± 1.33	5.465	<0.001

Table 1, the assessment scores and overall practice performance of nursing students in the experimental group were higher than those of the control group ($P < 0.05$), and the comparison was statistically significant in terms of professional quality, professional skills, communication ability, study and research ability, and team writing ($P < 0.05$) [30].

Comparison of professional identity of nursing students is shown in Table 2.

Professional identity is a socialised self-identification of the individual's values, attitudes, behaviour, knowledge, and skills in their professional role, and is the process of integration and development of self-value and professional value that overcomes the sense of professional externalities and alienation. Clinical practice is a critical period for nursing students to strengthen their professional awareness, experience their professional values, and transform their social roles and has an important impact on the formation and development of their professional identity. As shown in Table 2, through the clinical practice of the whole nursing internship model of double censorship, in which the mentor is responsible for the whole process and the nursing students are independently assigned to beds at the end of the internship, the nursing students in the experimental group have a higher sense of grasp and consistency of the professional role of nurses than those in the control group ($P < 0.05$), their clinical skills have been improved, their degree of nursing decision-making and influence on patients has been deepened, and their sense of self-worth has been elevated, and they are higher than those in the control group in the above related dimensions ($P < 0.05$). All comparisons were higher than those of the control group ($P < 0.05$). It is possible that this is due to the limited time spent on rotation in different departments and limited participation in the nursing organisation. The nursing students in both groups scored lower on this dimension, with there was no statistical difference between the two groups ($P > 0.05$). In conclusion, the holistic nursing practice model with dual membership can continuously enhance the professional experience of nursing students and promote the positive transition of nursing students to their social roles [30].

Comparison of patient satisfaction with care services is shown in Table 3.

Table 3 shows that the overall satisfaction of patients with nursing students in the experimental group was higher than that of the control group ($P < 0.05$), and there was a statistical difference in the comparison of satisfaction in terms of service quality, professional skills, patient education, and humanistic care ($P < 0.05$). Patient satisfaction is the evaluation yardstick of quality nursing service and is the starting point and footing point of nursing practice. The nursing students are the new force in the nursing team and should inherit and carry forward the "patient-centred" service concept. Under the dual-tutor system, the tutors focus on the cultivation of nursing students' service consciousness and professional ability, supervising them to implement basic nursing care and health education for patients and guiding them to communicate effectively with patients; the nursing department organises regular humanities lectures and health education competitions to motivate nursing students to provide quality nursing services [31].

Comparison of nursing students' evaluation of placement models is shown in Table 4.

The results of the nursing students' evaluation of the practice model (Table 4) show that the overall nursing practice model with dual tutors is more reasonable than the traditional practice model and is highly scalable. In the construction of this model, a complete three-level supervision system, a dual-tutor teaching system, a PDCA accountability system for continuous improvement, and a multichannel teacher-student interaction platform have been formed after continuous experience summing up and perfecting practice, which is worth promoting at one time.

Table 3: Patient care service satisfaction ($\overline{x} \pm s$).

Project	Experimental group ($n = 182$)	Control group ($n = 165$)	t value	P value
Service quality	3.91 ± 0.84	3.62 ± 0.93	3.056	0.002
Professional skills	4.00 ± 0.88	3.46 ± 0.95	5.496	<0.001
Patient education	4.05 ± 0.92	3.53 ± 0.86	5.425	<0.001
Humanistic concern	3.60 ± 0.89	3.26 ± 0.87	3.592	<0.001
Overall evaluation	3.86 ± 0.94	3.52 ± 0.97	3.314	0.001

Table 4: Evaluation of placement patterns by nursing students in both groups ($\overline{x} \pm s$).

Project	Experimental group ($n = 182$)	Control group ($n = 165$)	t/t' value	P value
Rationality	4.26 ± 0.76	3.70 ± 0.94	6.075	<0.001
Generalizability	4.40 ± 0.73	3.34 ± 0.82	12.760	<0.001
Teaching quality	4.20 ± 0.78	3.62 ± 1.02	5.900	<0.001
Management quality	4.25 ± 0.79	3.55 ± 0.95	7.382	<0.001
Comprehensive evaluation	1.30 ± 0.81	3.53 ± 0.89	8.424	<0.001

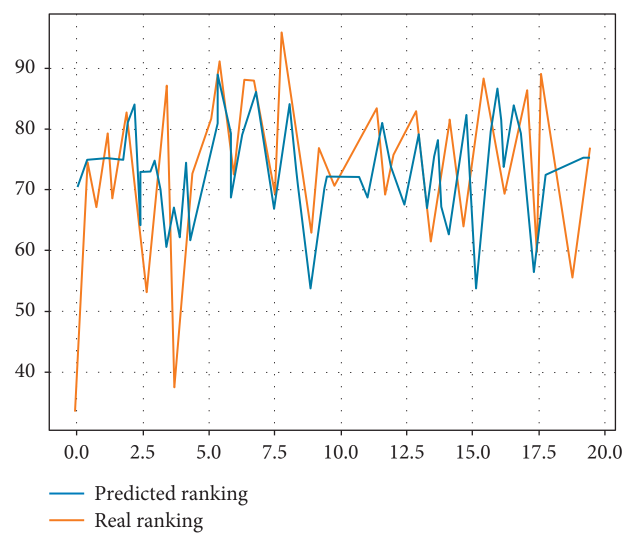

Figure 4: Predicted performance for different management.

7. Experimental Analysis

In the process of data collection and analysis, the metadata that is exchanged as information is standardised in order to fully exploit, share, and utilise information resources. The standardisation of nursing language has been researched earlier overseas, and information systems predict nursing workload based on the Nursing Outcome Classification (NOC), the North American Nursing Diagnostic Association Nursing Diagnosis (NANDA), and other standardised language captures, providing a good basis for full data mining and analysis. As nursing work records in China are still dominated by semistructured, nonstandardised data, the lack of a common standardised nursing language and terminology system has resulted in a large amount of nursing workload data that cannot be directly analysed and processed, and a low rate of sharing and utilisation of data resources across institutions and systems as shown in Figure 4, with different management of prediction models.

In the context of the era of medical informatization, it is urgent for China to establish a unified coordination mechanism, promoted by the state and professional academic organizations, to develop a standardised system of nursing data suitable for China, such as the different prediction modules shown in Figure 5.

As shown in Figure 6 for the short-term nursing effect, the difficulty in achieving the prediction of nursing workload is not in the use of data mining tools, but in choosing which data mining tools are more applicable to the reality of nursing workload in China, which currently presents diverse, complex, and fragmented data. When predicting, the traditional regression approach inevitably leads to errors and even biases, and due to the expanding volume of data, there is an urgent need for working methods that are more in line with the volume of nursing data. Currently, methods such as support vector machines and random forests are increasingly becoming mainstream mining tools, and more suitable research methods should be actively incorporated in the prediction methods of nursing workload.

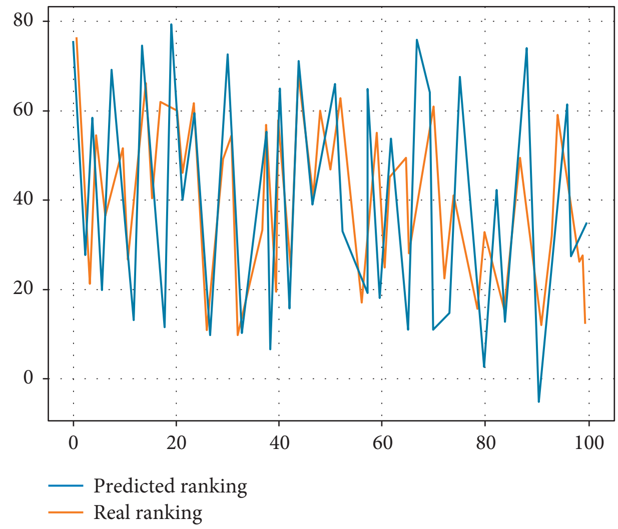

FIGURE 5: Different prediction levels.

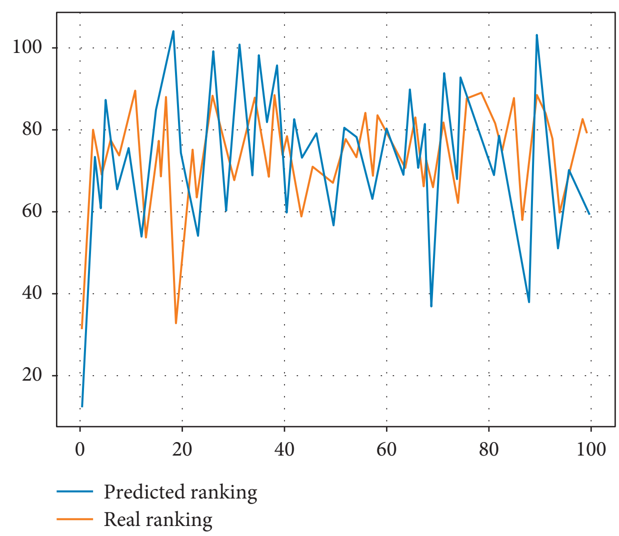

FIGURE 6: Short-term effects of care.

8. Conclusions

This paper proposes the construction of a nursing education management model based on small data to provide ideas and references for nursing education management to effectively predict the evolutionary trends of student behaviour and improve the level of precise services. The experimental group adopted a full dual-mentor responsibility system holistic nursing practice model, specifically including a complete three-level supervision system, dual-mentor teaching system, PDCA responsibility system holistic nursing practice pathway for continuous improvement, and a multichannel teacher-student interaction platform.

Data Availability

The data underlying the results presented in the study are included within the manuscript.

Conflicts of Interest

The authors declare no conflicts of interest regarding the publication of this paper

Authors' Contributions

All authors have read the manuscript and approved to submit for publication.

References

[1] R. Han, W. Mo, and D. Shao, "Research on the construction strategy of information model for manchuria style architecture and its application," *International Journal of Smart Home*, vol. 10, no. 7, pp. 175–184, 2016.

[2] Y. Liu and D. Li, "Research on construction of nursing knowledge portal based on big data," in *Proceedings of the*

International Conference of Educational Innovation Through Technology, pp. 207-208, Osaka, Japan, December 2017.
[3] S. E. Fleming, A. Boyd, M. Ballejos et al., "Goal setting with type 2 d," *The Diabetes Educator*, vol. 39, no. 6, pp. 811–819, 2013.
[4] J. Hu and M. Zhang, "Research on the construction of liberal arts graduate student learning situation-A Case study of the tourism management major in guangdong province," *Higher Education Studies*, vol. 5, no. 2, 2015.
[5] E. J. Randall, "Research and its application in the advanced nursing series," *Journal of Advanced Nursing*, vol. 20, no. 5, p. 975, 2010.
[6] P. S. Appelbaum, M. D. Anatchkova, K. Albert, L. B. Dunn, and C. W. Lidz, "Therapeutic misconception in research subjects: development and validation of a measure," *Clinical Trials*, vol. 9, no. 6, pp. 748–761, 2012.
[7] D. Vanneste, B. Vermeulen, and A. Declercq, "Healthcare professionals' acceptance of BelRAI, a web-based system enabling person-centred recording and data sharing across care settings with interRAI instruments: a UTAUT analysis," *BMC Medical Informatics and Decision Making*, vol. 13, no. 1, p. 129, 2013.
[8] J. R. Frick, J. Goebel, E. Schechtman, G. G. Wagner, and S. Yitzhaki, "Using analysis of gini (ANoGi) for detecting whether two sub-samples represent the same universe: the SOEP experience," *IZA Discussion Papers*, vol. 34, no. 4, pp. 427–468, 2004.
[9] S. Bahn and L. Barratt-Pugh, "Getting reticent young male participants to talk: using artefact-mediated interviews to promote discursive interaction," *Qualitative Social Work*, vol. 12, no. 2, pp. 186–199, 2013.
[10] L. Levin and E. Peled, "The attitudes toward prostitutes and prostitution scale: a new tool for measuring public attitudes toward prostitutes and prostitution," *Research on Social Work Practice*, vol. 21, no. 5, pp. 582–593, 2011.
[11] M. L. Wall and T. E. Carraro, "Kuhn's revolutionary theory and its influence on the construction of nursing knowledge," *Revista Latino-Americana de Enfermagem*, vol. 17, no. 3, pp. 417–422, 2009.
[12] C. Intree, B. Srisa-Ard, and C. Sirisuth, "The development of a knowledge management (KM) model for the faculty of nursing, ratchathani university," *Education Journal of Thailand*, vol. 2, no. 1, 2008.
[13] C. Clark, J. Farnsworth, and E. Landrum, "Development and description of the incivility in nursing education (INE) survey," *Journal of Theory Construction & Testing*, vol. 13, no. 1, pp. 7–15, 2009.
[14] B. Helmig, S. Ingerfurth, and A. Pinz, "Success and fn organizations: theoretical foundations, empirical evidence, and future research," *Voluntas: International Journal of Voluntary and Nonprofit Organizations*, vol. 25, no. 6, pp. 1509–1538, 2014.
[15] R. H. Weisberg and L. Zheng, "Hurricane storm surge simulations comparing three-dimensional with two-dimensional formulations based on an Ivan-like storm over the Tampa Bay, Florida region," *Journal of Geophysical Research: Oceans*, vol. 113, no. C12, 2008.
[16] H. Z. Marzieh, A. M. Reza, A. Suleiman, R. H. Gholizadeh, and H. Karimi-Moonaghi, "Knowledge creation in nursing education," *Global Journal of Health Science*, vol. 7, no. 2, pp. 44–55, 2015.
[17] L. Zhang, X. You, J. Jiao, and P. Helo, "Supply chain configuration with co-ordinated product, process and logistics decisions: an approach based on Petri nets," *International Journal of Production Research*, vol. 47, no. 23, pp. 6681–6706, 2009.
[18] A. Wojna, "Center-based indexing in vector and metric spaces," *Fundamenta Informaticae*, vol. 56, no. 3, 2003.
[19] V. A. Marchman and A. Fernald, "Speed of word recognition and vocabulary knowledge in infancy predict cognitive and language outcomes in later childhood," *Developmental Science*, vol. 11, no. 3, pp. F9–F16, 2010.
[20] K. Vanderven, "The road to intergenerational theory is under construction: a continuing story," *Journal of Intergenerational Relationships*, vol. 9, no. 1, pp. 22–36, 2011.
[21] D. L. Giltrap, S. Saggar, J. S. Singh, M. J. Harvey, A. M. S. Mcmillan, and J. Laubach, "Field-scale verification of nitrous oxide emission reduction with DCD in dairy-grazed pasture using measurements and modelling," *Soil Research*, vol. 49, no. 8, pp. 696–702, 2012.
[22] S. A. Harvey and J. R. Wandersee, "Publication rate of abstracts of papers and posters presented at Medical Library Association annual meetings," *Journal of the Medical Library Association: JMLA*, vol. 98, no. 3, pp. 250–255, 2010.
[23] L. H. Sider, M. P. Heaton, C. G. Chitko-McKown et al., "Small ruminant lentivirus genetic subgroups associate with sheep TMEM154 genotypes," *Veterinary Research*, vol. 44, no. 1, p. 64, 2013.
[24] A. Wallman, S. K. Sporrong, M. Gustavsson, A. K. Lindblad, M. Johansson, and L. Ring, "Swedish students' and preceptors' perceptions of what students learn in a six-month advanced pharmacy practice experience," *American Journal of Pharmaceutical Education*, vol. 75, no. 10, p. 197, 2011.
[25] J. Strijbos, N. Engels, and K. Struyven, "Criteria and standards of generic competences at bachelor degree level: a review study," *Educational Research Review*, vol. 14, pp. 18–32, 2015.
[26] N. Kundakcı and I. Ayşegül Tuş, "Integration of MACBETH and COPRAS methods to select air compressor for a textile company," *Decision Science Letters*, vol. 5, no. 3, pp. 381–394, 2016.
[27] E. A. Gage-Bouchard and K. A. Devine, "Examining parents' assessments of objective and subjective social status in families of children with cancer," *PLoS One*, vol. 9, no. 3, Article ID e89842, 2014.
[28] J. Blundell, S. Scott, D. Harris, J. Huddlestone, and D. Richards, "Workload benefits of colour coded head-up flight symbology during high workload flight," *Displays*, vol. 65, Article ID 101973, 2020.
[29] Z. Gao, G. Zhai, H. Deng, and X. Yang, "Extended geometric models for stereoscopic 3D with vertical screen disparity," *Displays*, vol. 65, Article ID 101972, 2020.
[30] S. He, B. Liang, L. Tähkämö, M. Maksimainen, and L. Halonen, "The influences of tunnel lighting environment on drivers' peripheral visual performance during transient adaptation," *Displays*, vol. 64, Article ID 101964, 2020.
[31] S. Weech, S. Kenny, C. M. Calderon, and M. Barnett-Cowan, "Limits of subjective and objective vection for ultra-high frame rate visual displays," *Displays*, vol. 64, Article ID 101961, 2020.

Hindawi
Computational Intelligence and Neuroscience
Volume 2023, Article ID 9890364, 1 page
https://doi.org/10.1155/2023/9890364

Retraction

Retracted: A New Generation of ResNet Model Based on Artificial Intelligence and Few Data Driven and Its Construction in Image Recognition Model

Computational Intelligence and Neuroscience

Received 25 July 2023; Accepted 25 July 2023; Published 26 July 2023

This article has been retracted by Hindawi following an investigation undertaken by the publisher [1]. This investigation has uncovered evidence of one or more of the following indicators of systematic manipulation of the publication process:

(1) Discrepancies in scope
(2) Discrepancies in the description of the research reported
(3) Discrepancies between the availability of data and the research described
(4) Inappropriate citations
(5) Incoherent, meaningless and/or irrelevant content included in the article
(6) Peer-review manipulation

The presence of these indicators undermines our confidence in the integrity of the article's content and we cannot, therefore, vouch for its reliability. Please note that this notice is intended solely to alert readers that the content of this article is unreliable. We have not investigated whether authors were aware of or involved in the systematic manipulation of the publication process.

Wiley and Hindawi regrets that the usual quality checks did not identify these issues before publication and have since put additional measures in place to safeguard research integrity.

We wish to credit our own Research Integrity and Research Publishing teams and anonymous and named external researchers and research integrity experts for contributing to this investigation.

The corresponding author, as the representative of all authors, has been given the opportunity to register their agreement or disagreement to this retraction. We have kept a record of any response received.

References

[1] H. Wang, K. Li, and C. Xu, "A New Generation of ResNet Model Based on Artificial Intelligence and Few Data Driven and Its Construction in Image Recognition Model," *Computational Intelligence and Neuroscience*, vol. 2022, Article ID 5976155, 10 pages, 2022.

Hindawi
Computational Intelligence and Neuroscience
Volume 2022, Article ID 5976155, 10 pages
https://doi.org/10.1155/2022/5976155

Research Article

A New Generation of ResNet Model Based on Artificial Intelligence and Few Data Driven and Its Construction in Image Recognition Model

Hao Wang,[1] **Ke Li**,[2] **and Chi Xu**[3]

[1]*Shandong Anhui Information Technology Co., Ltd., Jinan 250100, Shandong, China*
[2]*Shandong Anyong Precision Machinery Co., Ltd., Taian 271000, Shandong, China*
[3]*Shandong Kangyuan Technology Innovation Development Co., Ltd., Jinan 250100, Shandong, China*

Correspondence should be addressed to Hao Wang; coldfish_wen@sina.com

Received 12 January 2022; Revised 18 February 2022; Accepted 22 February 2022; Published 19 March 2022

Academic Editor: Xin Ning

The paper proposes an A-ResNet model to improve ResNet. The residual attention module with shortcut connection is introduced to enhance the focus on the target object; the dropout layer is introduced to prevent the overfitting phenomenon and improve the recognition accuracy; the network architecture is adjusted to accelerate the training convergence speed and improve the recognition accuracy. The experimental results show that the A-ResNet model achieves a top-1 accuracy improvement of about 2% compared with the traditional ResNet network. Image recognition is one of the core technologies of computer vision, but its application in the field of tea is relatively small, and tea recognition still relies on sensory review methods. A total of 1,713 images of eight common green teas were collected, and the modeling effects of different network depths and different optimization algorithms were explored from the perspectives of predictive ability, convergence speed, model size, and recognition equilibrium of recognition models.

1. Introduction

Green tea is good for people's physical and mental health and is a popular beverage among consumers. At the same time, green tea is also the most diverse and the most produced tea in China, and appearance is an important basis for its classification and differentiation of grades, as well as an important part of team sensory evaluation. However, the traditional tea sensory review method uses review terminology that has not been perfected [1]. The uncertainty of the objective environment, the low prevalence of standard quantities, the interference of subjective factors by tea evaluators, the poor repeatability, and other limitations do not match the increasing consumer demand for accurate information and safe and high quality tea products in the current new era [2]. Therefore, the development of open, standardized, and intelligent [3] green tea classifications and identification methods is an inevitable trend. New classification and assessment methods for green tea have been emerging, such as physicochemical review methods [4, 5], fingerprinting assessment methods [6, 7], intelligent sensory review methods [8, 9], and infrared spectral imaging technology detection methods [10, 11], but these methods have their limitations to a certain extent, such as relevant instruments and cumbersome and complicated operations, and most of them are based on the overall tea leaves. It is necessary to propose an objective, simple, fast, and low-cost method for green tea classification, since most of them are based on the whole tea leaves for review, which requires specific and time-consuming requirements.

Convolutional neural networks, as an important member of image classification algorithms, have the advantages of high recognition accuracy, fast detection speed, and great development potential [12], have achieved considerable success in image classification [13], object detection [14], pose estimation [15], image segmentation [16], and face recognition [17, 18], have great scaling advantages [19], and have been widely used in agriculture [20], healthcare [21], education [22], energy [23], industrial inspection [24], and other fields [25]. Currently, convolutional neural networks have been used for tea tree pest and disease identification [26], tea grade sieving [7], and the sorting of tea tree fresh leaves [8], but for the recognition and classification of different species of green tea based on ResNet, a typical convolutional neural network is proposed by researchers in recent years to perform computer vision tasks, which minimizes the gradient disappearance problem caused by increasing the depth of the network due to the introduction of the residual module and reduces the redundancy of information in the data while maintaining a high accuracy rate, which is simple and practical.

Based on ResNet convolutional neural network, this study constructs a deep learning model capable of distinguishing 8 kinds of green tea by selecting the appropriate optimization algorithm and model depth, aiming to develop an efficient, accurate, and objective identification model and apply it to mobile, realizing the recognition of green tea pictures in different backgrounds and environments, which can be shared and used by multiple people and devices, saving resources and realizing deep learning in tea recognition. The identification of green tea is a new way of thinking.

2. Materials and Methods

2.1. Data Acquisition and Test Platform Construction. The dataset of this study consists of 8 kinds of green teas, such as Lishui fragrant tea, Xinyang Maojian, Lu'an Guapian, Taiping Monkey Kui, Anji White Tea, Biluochun, Bamboo Leaf Green, and Longjing. The number of images of each kind is shown in Table 1, with a total of 1,713 images. Part of the dataset of this study is shown in Figure 1. The eight kinds of green tea with different appearance and quality characteristics present different states in different scenes with different backgrounds, which better reproduce the actual scenes of tea in life. These images are manually searched from different Internet platforms, such as the shopping platform Jingdong (https://www.jd.com), Tao Bao (https://www.taobao.com), the social platform Weibo (https://weibo.com), and Baidu Post (https://tieba.baidu.com), with different brightness, background, and angle. The higher the resolution of the image is, the more features it contains, and the better it is for model learning. Therefore, the image datasets selected in this study are basically above 100 KB in size, and extended formats are basically JPG and PNG.

The experimental platform for this study was built as shown in Table 2, and the modeling scripts used are available on github (https://github.com/seldas/DL_Beetles).

2.2. Image Preprocessing. The original images obtained in this study vary in size, and conducting some preprocessing of the images can enhance the recognition of the target objects by the model and also avoid overfitting of the network. In this study, the tea images in the training set were first randomly cut into RGB images in the image format of $224 \times 224 \times 3$ and then flipped. The images in the test set are first scaled and then cropped to $224 \times 224 \times 3$ RGB images with the center as the reference. In this study, the preprocessing of the images in the test is a data enhancement operation, which can effectively improve the fitting ability and generalization ability of the model [9].

2.3. Data Processing and Evaluation Indicators. The images were randomly selected and sampled according to the training set : validation set = 3 : 1. The training data were used for parameter learning, and the validation data were used for model performance evaluation. The same preprocessing was strictly followed, and to ensure the accuracy of the validation results, each set of experiments was repeated at least three times, cross-validation was adopted to avoid the arbitrariness in dividing the training and test sets, and the data were analyzed by one-way ANOVA ($p < 0.05$) using SPSS 21.0 software for significant differences, and finally the data were divided into batches of the same size The data were divided into equal-sized batches to facilitate subsequent model training.

In order to evaluate the performance of ResNet model for green tea species classification, accuracy, error rate, precision rate, recall rate, F-value, and the confusion matrix were adopted as the evaluation indexes in this experiment. Taking the eight types of green tea in this study as an example, the accuracy rate is the average of the overall performance of the model in recognizing the eight types of green tea, and the error rate corresponds to the accuracy rate, which can be suitable for the comparison of recognition balance because of its small base. Accuracy, recall, and *F*-value are performance evaluations for each of these categories. Taking Anji white tea as an example, the accuracy rate is the proportion of all samples predicted to be Anji white tea which are predicted correctly; the recall rate is judged on the basis of samples whose true label is Anji white tea, and it is the proportion of those predicted correctly to all samples whose true label is Anji white tea; and the F-value is a composite index, which is the summed average of the accuracy rate and recall rate. The confusion matrix can summarize and compare the classification prediction results and the actual target, and from the presentation in the form of $N \times N$ matrix, the sum of each row is the number of real samples of the category, and the sum of each column is the number of samples predicted as the category, which can directly evaluate the effectiveness of the classification method.

3. Related Theories

3.1. Traditional ResNet Network Structure. Since Alexnet [11], the CNN structure has been deepening, and VGG and GoogLeNet [12] have 19 and 22 convolutional layers, respectively. With the increase of network depth, the existence of gradient disappearance problem makes the network training more difficult and the convergence result is not good, and then the ResNet network [13] is introduced, as shown in Figure 2.

Table 1: Number of pictures of different kinds of green tea.

Name	Number	Size range of each image	The size of dataset	The source of images/piece		
				Shopping platform	Social platform	Portal site
Lishui Xiangcha	210	102–1201	61	117	66	27
Xinyang Maojian	204	100–15751	108	152	47	5
Lu'an Guapian	200	102–9088	110	136	53	11
Taiping Houkui	226	114–17780	256	118	108	0
Anji Baicha	224	100–6226	151	134	88	2
Biluochun	210	101–4409	83	180	28	2
Zhuyeqing	199	100–9646	135	101	72	26
Longjing	240	104–11484	298	37	200	9

Figure 1: Partial display of the dataset.

Table 2: Partial presentation of the dataset.

Operating system	Windows10 professional edition
Test platform	Keras
Hardware environment	Intel(R)Core(TM)i7-7700hq CPU@2.80 GHZ 2.80 GHZ
Basic configuration	Anaconda Python3. Version 7

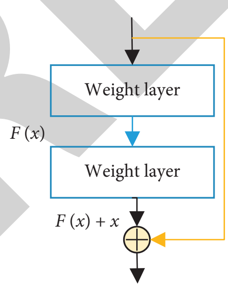

Figure 2: Shortcut connection method.

The output of the residual module in ResNet is obtained by summing the backbone network with the jump connection, and the shortcut connection adopts a constant mapping. ResNet network can better weaken the gradient disappearance phenomenon, retain more original information in the input image, reduce the loss, and also improve the convergence speed in deeper networks compared with the traditional VGG network, essentially reducing the training. The redundancy of data information in the training process is essentially reduced, but the shortcut direct connection makes it less focused on the local target information in multiple categories, which reduces the classification accuracy.

3.2. Dropout Layer. The dropout layer is a layer that is used to temporarily discard neurons with a certain probability during the training process of the network. When the data samples are small, it can prevent the model from overfitting and effectively improve the classification accuracy. Reference [14] introduced the dropout layer into the convolutional neural network, which not only solved the overfitting phenomenon but also obtained good classification accuracy.

3.3. Residual Attention (Attention) Network. Attention networks can highlight local target information and allow the network to focus more on finding useful information related to the output in the input image, thus improving the classification accuracy of image targets [8, 15, 16]. Reference [8] proposed a residual attention network in 2017, which enables the classification accuracy to be improved by focusing more on the target information through residual attention networks. A residual attention network is a convolutional neural network containing an attention mechanism, which is constructed by superimposing an attention mechanism in an end-to-end training approach combined with a forward feedback network architecture.

The residual attention network is composed of several attention modules superimposed on each other, and the attention module is divided into two branches: the main branch and the mask branch. The structure of the attention module is shown in Figure 3.

The mask branch contains both upsampling and downsampling layers, which can be both quickly feed-forward scan to collect global information of the image and top-down feedback to combine the global information with the original image features. Each trunk branch has its corresponding mask branch, which is used to learn the attention information of its corresponding layer features, prevent the trunk branch from updating the wrong weight parameters, and can gradually refine the attention features of complex images by superimposing the network structure. The formula for calculating the residual attention block can be shown in the following equation:

$$H_{i,c} = \left(1 + M_{i,c}(x)\right) * F_{i,c}(x), \tag{1}$$

where $F_{i,c}(x)$ denotes the result of convolutional neural network output and $M_{i,c}(x)$ denotes the result of mask branch weight output, which takes values in the range of [0, 1], and the closer it is to 0, the closer the output is to $F(x)$, which can then represent the network as a residual learning network. $M_{i,c}(x)$ as a feature selector can enhance useful information and suppress undesirable noisy information from the trunk branch, but the increase of attention mechanism makes more parameters in the network, which may cause overfitting and make the training converge slowly.

4. Intersection Based on ResNet Network (A-ResNet)

In order to improve the training convergence speed and classification accuracy, the traditional ResNet network model is improved and the A-ResNet network model is proposed and applied to the traffic sign recognition system.

The A-ResNet network is composed of convolutional layer, pooling layer, residual unit, residual attention unit, and softmax layer. Its structural composition is shown in Table 3.

The input image of A-ResNet network has fixed size 224×224, and the 112×112 feature map is generated after the first convolutional layer and then input to 4 residual units and 3 attention units after the pooling layer is reduced in dimension. Compared with the original ResNet network, we add attention units, adjust the structure of each unit, and add dropout layer, which can speed up the convergence of the loss value of the network training and improve the classification accuracy of the network in recognizing traffic signs.

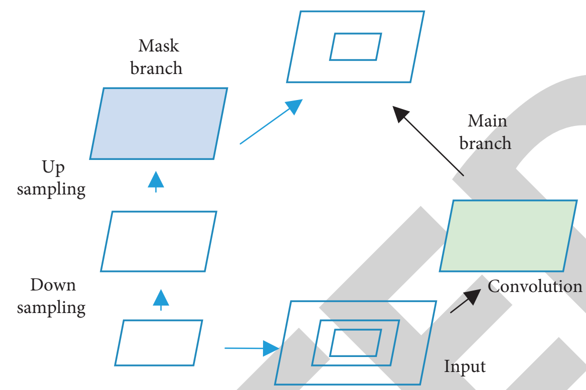

Figure 3: Structure of attention module.

Table 3: A-ResNet network model structure.

Arrangement	Output size	A-ResNet
Input layer	224×224	
Convolution layer 1	112×112	7×7, 64
Maximum pooling	56×56	3×3
Residual element	56×56	$\begin{pmatrix} 3 \times 3, & 64 \\ 3 \times 3 & 64 \end{pmatrix} \times 1$
Attention unit	56×56	Attention ×1
Residual element	28×28	$\begin{pmatrix} 3 \times 3, & 64 \\ 3 \times 3 & 64 \end{pmatrix} \times 1$
Attention unit	28×28	Attention × 1
Residual element	14×14	$\begin{pmatrix} 3 \times 3, & 64 \\ 3 \times 3 & 64 \end{pmatrix} \times 1$
Attention unit	14×14	Attention × 1
Residual element	7×7	$\begin{pmatrix} 3 \times 3, & 64 \\ 3 \times 3 & 64 \end{pmatrix} \times 2$
Average pooling	1×1	7×7
Softmax	43×1	

4.1. Improvement of Residual Module in A-ResNet. The structure of the residual unit in the conventional ResNet network is shown in Figure 4(a). The training speed of the ResNet network composed of this structure is slow, and the recognition accuracy is not high, so the structure of the residual unit after adjusting the network to improve the classification accuracy and training convergence speed is shown in Figure 4(b).

The scale normalization layer (BN layer) and the activation layer (ReLU layer) are adjusted to the convolutional layer before the BN layer to normalize the data for stabilizing the network convergence, and then the processed data are input to the Re-LU activation function for activation, which can not only increase the nonlinear relationship between the layers, but also enhance the network sparsity and prevent the overfitting phenomenon, and the activated data are input to the convolutional layer. The data after activation is input to the convolutional layer, and the dropout layer is added

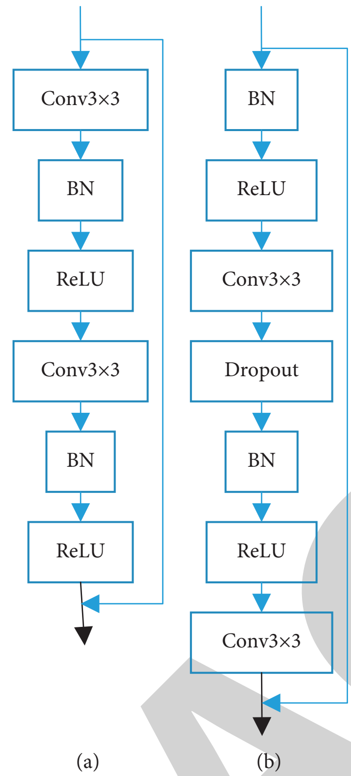

Figure 4: Residual module before and after improvement. (a) Original residual module. (b) Adjusted residual module.

between the convolutional layers to avoid overfitting of the network parameters.

4.2. Improvement of Residual Attention Module in A-ResNet. To address the problem of slow convergence of the residual attention network in the network training phase, an improved residual attention network is proposed in this paper to speed up the convergence of the network training while stabilizing the recognition accuracy. The attention network used is shown in Figure 5.

The basic structures of the residual block, upsampling, downsampling, and jumping branch modules are all consistent with the improved residual unit of this paper. However, the shortcut connection mechanism is not used directly. If the shortcut mechanism is used directly as the structure of the mask branch, it will cause the problem that the gradient of the deep network is not inverted, so the structure of the mask branch is combined with the upsampling and downsampling process, which can obtain the global feature information in the image and convert the extracted global information into a dimensionally consistent feature map. Finally, dimensionally consistent feature maps obtained from the trunk branch and the mask branch are combined by the dot product to form the final output feature map. In the downsampling stage [27], the extracted feature maps are downsampled to a minimum size of 7×7 using the maximum pooling layer, and then in the upsampling stage, the feature map dimensions are expanded layer by layer using bilinear interpolation, and the feature maps obtained from downsampling are summed with them to obtain the final feature maps. The purpose of doing so is to combine global and local features to further enhance the characterization capability.

5. Results and Analysis

5.1. Comparison of Optimization Algorithms. In this study, four algorithms such as SGD, RMSprop, Adam, and Adadelta are compared based on the selection of ResNet-18 as the network model. Due to overfitting, the parameters that converge on the training set are not optimally implemented on the test set [28]. Therefore, in this study, the accuracy and training time of the validation set are chosen as the criteria for comparison, and the experimental data are shown in Figure 6, and it can be seen that SGD performs optimally in both aspects, with the highest average accuracy of 90.99% and the shortest training time of 71.37 min. Therefore, SGD is chosen as the optimal algorithm in this experiment.

5.2. Comparison of Model Depth. ResNet uses constant mapping to avoid the "degradation" problem of deep networks and thus can reach very deep network layers. Usually, the increase in the number of layers of the network leads to an increase in the performance of ResNet, but there are also problems such as larger computation, slower convergence, and increased training time [29].

5.2.1. Model Convergence Speed. Convergence in this study means that the accuracy of the network model is infinitely close to the optimal accuracy of the model as the epochs

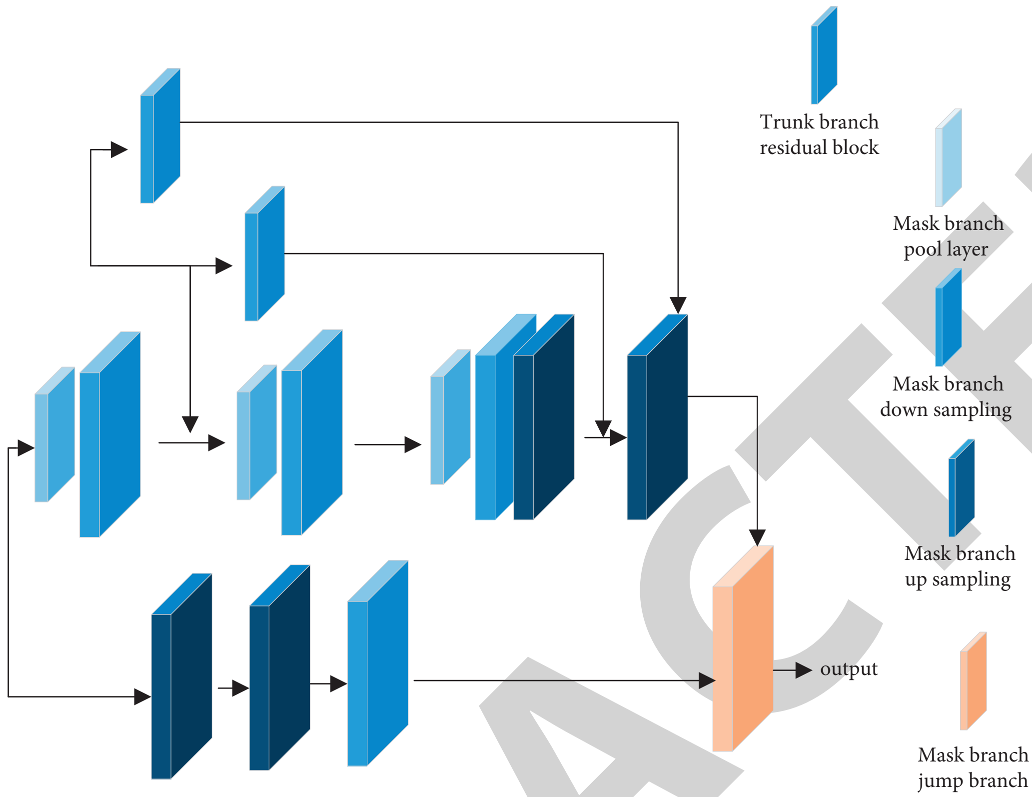

Figure 5: Structure of attention module.

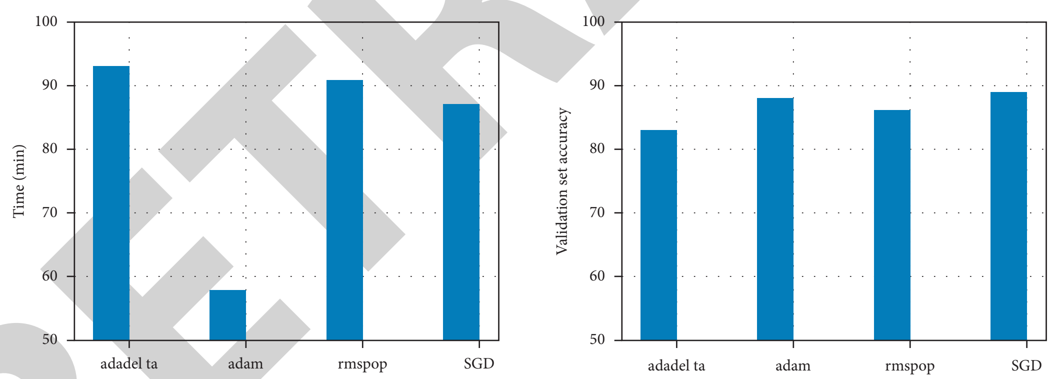

Figure 6: Comparison of different optimization algorithms.

tend to infinity (the maximum value of epochs in this study is 19). ResNet networks of different depths have different rates of approaching their optimal accuracy as epochs become larger. Faster convergence means fast and robust fusion, avoiding overfitting or getting stuck in a local optimum. Progressively deeper colors are used to represent the number of ResNet layers at different depths, and the speed of reaching the optimal accuracy is represented by a line of corresponding color from top to bottom [30]. As shown in Figure 7, all four ResNet models with different depths show no convergence jitter and eventually converge, among which ResNet-18 has the fastest convergence speed and is able to show a stable convergence when the epochs reach 7.

5.2.2. Model Size. At present, as the research on network models continues, the model structure shows a deeper and deeper trend, the complexity of computation deepens, and the size of the model and the amount of memory it occupies increase. Although the hardware facilities of computers are being constantly updated and upgraded, they are still unable to accommodate large-scale complex network models at this stage, which can limit their use on smart devices such as cell phones and computers. Therefore, on the basis of ensuring high accuracy, this study is to find the network models of suitable depth that are lightweight and easy to use on end devices. The sizes of ResNet models with different depths are shown in Table 4. ResNet-18 has a model size of 43.7 MB and requires the least space, which is about 52% of ResNet-34

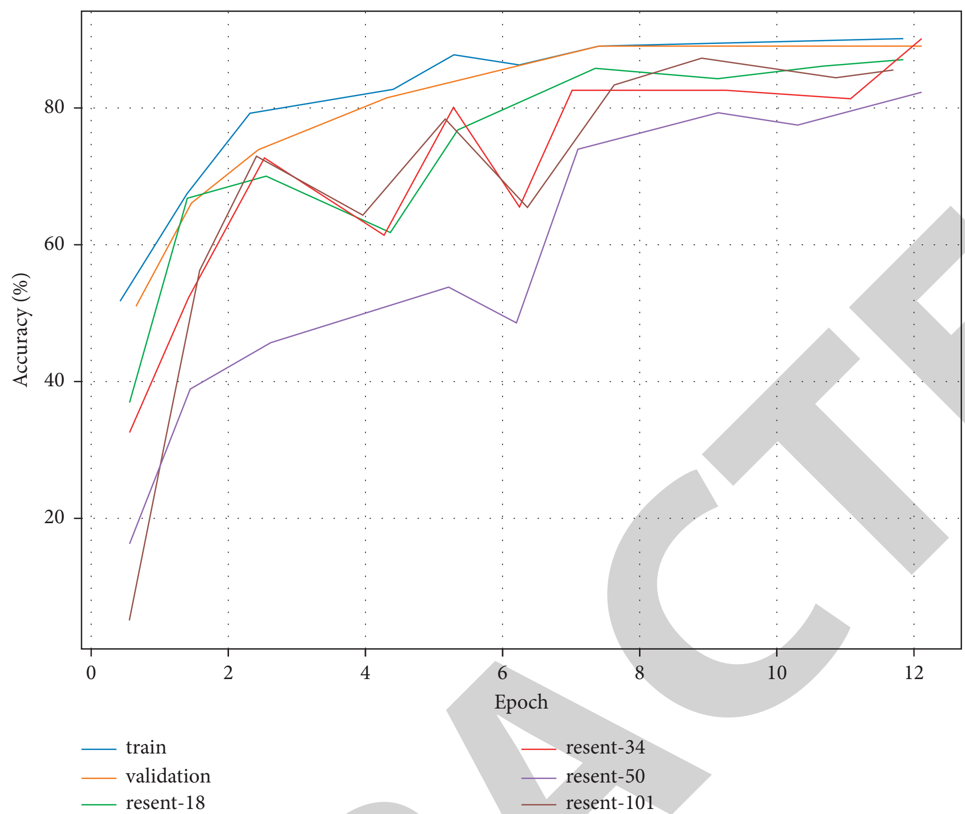

Figure 7: Convergence speed of ResNet models with different depths.

Table 4: Efficiency and size of ResNet models with different depths.

Model	Identification time per graph	Accuracy %	Size/MB
ResNet-18	0.097 ± 0.0011	90.99 ± 0.37	42.1
ResNet-34	0.112 ± 0.0013	90.94 ± 0.95	82.2
ResNet-50	0.134 ± 0.0009	91.47 ± 0.57	90.2
ResNet-101	0.147 ± 0.001	90.05 ± 0.37	154.5

and 26% of ResNet-101, implying that it takes up less memory, has faster computing time, and is more suitable for mobile.

5.2.3. Equilibrium of Model Identification. The improvement of the balance of the model recognition accuracy is more beneficial to the application of the model in practice and can avoid the problem of poor recognition of specific species. As can be seen from Figure 8, using the average deviation of the recognition error rate of the eight tea samples as the measurement index, the smaller the average deviation value, the stronger the recognition balance of the model.

From Figure 8, it can be seen that the ranking of the balance of the training set is ResNet-18>ResNet-101>ResNet-50>ResNet-34, and the ranking of the balance of the validation set is ResNet-34>ResNet-18>ResNet-50>ResNet-101, ResNet-18. The balance of the recognition in both the training and validation sets is better, and the equilibrium of both the training and validation sets is also better.

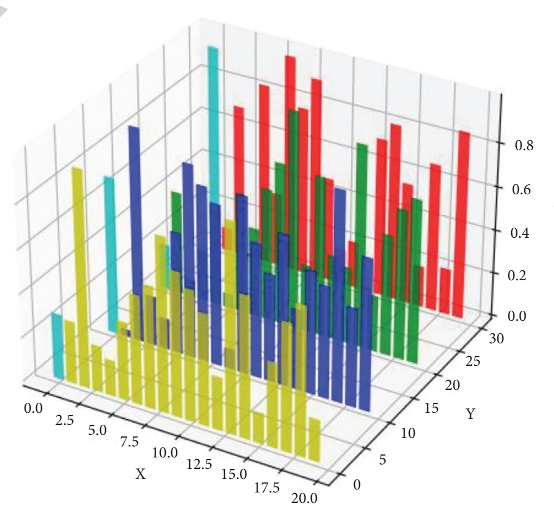

Figure 8: Mean deviation of recognition error rate of 8 green tea species.

In this study, the model performance is measured from four perspectives: convergence speed, size, efficiency, and recognition balance, and finally ResNet-18 is chosen as the basis of the model to build a green tea recognition model, which requires the shortest training time for the fastest convergence speed, effectively maintains the accuracy of

Table 5: Precision, recall, and F-value of the eight green teas.

Classification performance metrics	Precision	Recall	F-value
Lishui Xiangcha	0.85 ± 0.15	0.93 ± 0.008	0.89 ± 0.01
Xinyang Maojian	0.94 ± 0.02	0.95 ± 0.01	0.94 ± 0.01
Lu'an Guapian	0.88 ± 0.01	0.82 ± 0.02	0.85 ± 0.03
Taiping Houkui	0.94 ± 0.03	0.087 ± 0.03	0.91 ± 0.02
Anji Baicha	0.90 ± 0.01	0.88 ± 0.02	0.89 ± 0.04
Biluochun	0.95 ± 0.05	0.97 ± 0.01	0.95 ± 0.02
Zhuyeqing	0.87 ± 0.14	0.95 ± 0.12	0.90 ± 0.12
Longjing	0.98 ± 0.01	0.87 ± 0.02	0.95 ± 0.01

image recognition on the basis of the smallest memory occupation and the fastest recognition speed, and performs better in recognition balance. The problem of poor recognition of specific categories can be avoided. As the dataset of this study is more realistic, it proves that the model has a strong practical application capability and breaks through the limitation of many previous studies that cannot fully reproduce the actual diversity. Based on this, the model can be improved in terms of accuracy by using uniform background and field photography to obtain more valid information. In the classification recognition of species by convolutional neural network, the average recognition accuracy of maize [9], chrysanthemum [4], and pepper [1] with different total datasets (3,600, 6,300, and 65,000) and average number of samples per class (1,200, 1,260, and 13,000) reached 95.49%, 95.9%, and 99.35%, respectively (all with clean scenery, with little noise). Therefore, the model can also be optimized and improved by expanding the dataset and selecting more representative team pictures. Green tea species in China are far more than the eight species in this study and can be extended to other tea types in the next study to achieve intelligent recognition of more tea types [31–33].

5.3. Green Tea Predicted Classification Results. As shown in Table 5, the low precision, recall, and F-value of Lishui fragrant tea, Lu'an Guapian, bamboo leaf green, and Biluochun indicate that they are more easily confused with other teas, and it can be seen from Figure 9 that Anji white tea and bamboo leaf green, Biluochun, and Lishui fragrant tea are easily confused with each other: in the three validation sets with combined statistics, 10 Anji white teas were misconceived as bamboo leaf green, 12 bamboo leaf green teas were misconceived as Anji white tea, 12 Lishui fragrant teas were misconceived as Biluochun, and 18 Biluochun teas were misconceived as Lishui fragrant tea. This may be due to the similarity in the characteristics of the tea, with Anji white tea and bamboo leaf green both having a certain straight shape, and Biluochun and Lishui aroma tea having a similar curly shape.

The above results may also be due to the existence of some interference in the background which makes some of the tea characteristics not well discriminated, and a higher quality and larger quantity of dataset are needed to support the model for further learning. Data is the driving force of deep learning, and quantity, quality, preprocessing rationality, and labeling accuracy are all important factors. You can expand the dataset by random

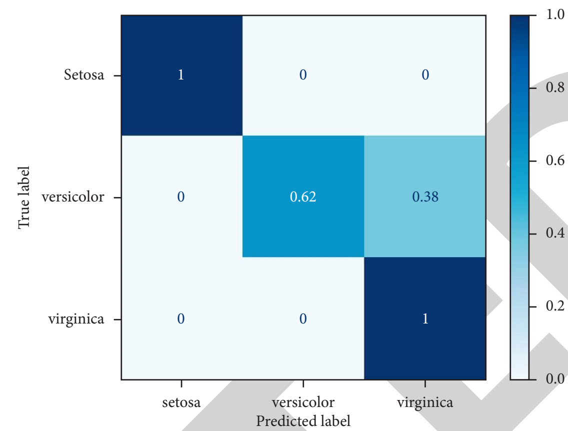

Figure 9: Heat map of confusion matrix for ResNet-18.

cropping, random inversion, random brightness transformation, a clean set to take different angles of field shooting to obtain a higher quality dataset. You can also preprocess cropped into smaller and more focused images, and multiple people check the labels to improve labeling accuracy.

6. Conclusions

In this study, a new model based on ResNet convolutional neural network to recognize different kinds of green tea was constructed by comparing four different optimization algorithms and investigating the effect of the depth of ResNet model from different aspects. The four optimization algorithms, SGD, RMsprop, Adam, and Adadelta, were compared, and it was found that the stochastic gradient descent (SGD) algorithm required the shortest time and had the highest recognition accuracy.

ResNet-18, ResNet-34, ResNet-50, and ResNet-101 were used to investigate the effect of depth of the ResNet model. ResNet-18 lost only 0.15% accuracy (ResNet-50 had the highest average recognition accuracy of 91.14% and ResNet-18 90.99%). In this study, the heat map of confusion matrix and the respective accuracy, recall, and *F*-value of eight tea types were clarified, and it was found that Lishui fragrant tea, Lu'an Guapian, Zhuyeqing, and Biluochun were more easily confused with other tea types, while Anji white tea and Zhuyeqing, Biluochun, and Lishui fragrant tea were easily confused with each other.

The model constructed in this study is a preliminary application of deep learning in the field of tea variety recognition, and through the selection of optimization algorithm and the exploration of model depth, a better recognition effect is achieved overall. It not only provides a simple and efficient new method for the recognition of green tea species, but also lays a corresponding foundation for further application of deep learning in the field of tea.

Data Availability

The dataset used in this paper are available from the corresponding author upon request.

Conflicts of Interest

The authors declare that they have no conflicts of interest regarding this work.

References

[1] M. Owais, M. Arsalan, J. Choi, and K. R. Park, “Effective diagnosis and treatment through content-based medical image retrieval (CBMIR) by using artificial intelligence,” *Journal of Clinical Medicine*, vol. 8, no. 4, p. 462, 2019.

[2] P. C. Pandey, S. Upadhyay, H. C. Pathak, and C. M. D. Pandey, “Studies on ferrocene immobilized sol-gel glasses and its application in the construction of a novel solid-state ion sensor,” *Electroanalysis*, vol. 11, no. 13, pp. 950–956, 2015.

[3] B. Tobias, T. Stephan, and N. Heiko, “On event-based optical flow detection,” *Frontiers in Neuroscience*, vol. 9, p. 137, 2015.

[4] P. Pitchandi, W. Hopper, and R. Rao, “Comprehensive database of Chorismate synthase enzyme from shikimate pathway in pathogenic bacteria,” *BMC Pharmacology and Toxicology*, vol. 14, no. 1, p. 29, 2013.

[5] C. C. Kuo, C. M. Chang, K. T. Liu et al., “Automation of the kidney function prediction and classification through ultrasound-based kidney imaging using deep learning,” *Npj Digital Medicine*, vol. 2, no. 1, 2019.

[6] V. Meana, R. García, A. Bello, I. León, and S. Giganto, “Integrating BIM in Industrial Engineering programs. A new strategy model,” *IOP Conference Series: Materials Science and Engineering*, vol. 1193, no. 1, (8pp), Article ID 012133, 2021.

[7] H. Lu, “Construction of SPOC-based learning model and its application in linguistics teaching[J],” *International Journal of Emerging Technologies in Learning*, vol. 13, no. 02, 2018.

[8] W. Liu, G. Wu, F. Ren, and X. Kang, “DFF-ResNet: an insect pest recognition model based on residual networks,” *Big Data Mining and Analytics*, vol. 3, no. 4, pp. 300–310, 2020.

[9] E. A. Huerta, A. Khan, E. Davis et al., “Convergence of artificial intelligence and high performance computing on NSF-supported cyberinfrastructure,” *Journal of Big Data*, vol. 7, no. 1, pp. 1–12, 2020.

[10] X. Han and R. Jin, “A small sample image recognition method based on ResNet and transfer learning,” in *Proceedings of the 2020 5th International Conference on Computational Intelligence and Applications (ICCIA)*, pp. 76–81, IEEE, Beijing, China, June 2020.

[11] S. Elghamrawy, “An H2O’s deep learning-inspired model based on big data analytics for coronavirus disease (COVID-19) d,” in *Big Data Analytics and Artificial Intelligence against COVID-19: Innovation Vision and Approach*, pp. 263–279, Springer, Cham, 2020.

[12] J. Chen, Q. Liu, and L. Gao, “Visual tea leaf disease recognition using a convolutional neural network model,” *Symmetry Plus*, vol. 11, no. 3, p. 343, 2019.

[13] H. Yang, L. Chen, M. Chen et al., “Tender tea shoots recognition and positioning for picking robot using improved YOLO-V3 model,” *IEEE Access*, vol. 7, pp. 180998–181011, 2019.

[14] X. Sun, S. Mu, Y. Xu, Z. Cao, and T. Su, “Image recognition of tea leaf diseases based on convolutional neural network,” in *Proceedings of the 2018 International Conference on Security Pattern Analysis and Cybernetics (SPAC)*, Jinan, China, December 2018.

[15] L. B. Xie, S. J. Yu, G. Y. Zhou, and H. Li, “Classification research of oil-tea pest images based on BoW model,” *Journal of Central South University of Forestry & Technology*, vol. 35, no. 5, pp. 70–73, 2015.

[16] M. Gao, M. Shi, and C. Li, “Research and implementation of image recognition of tea based on deep learning,” in *Proceedings of the 2021 21st ACIS International Winter Conference on Software Engineering, Artificial Intelligence, Networking and Parallel/Distributed Computing (SNPD-Winter)*, pp. 63–68, IEEE, Ho Chi Minh City, Vietnam, January 2021.

[17] S. U. N. Xiaoxiao, M. U. Shaomin, X. U. Yongyu, C. A. O. Zhihao, and S. U. Tingting, “Image recognition of tea leaf diseases based on convolutional neural network,” in *Proceedings of the 2018 International Conference on Security, Pattern Analysis, and Cybernetics (SPAC)*, pp. 304–309, IEEE, Jinan, China, December 2018.

[18] S. Gayathri, D. J. W. Wise, P. B. Shamini, and N. Muthukumaran, “Image analysis and detection of tea leaf disease using deep learning,” in *Proceedings of the 2020 International Conference on Electronics and Sustainable Communication Systems (ICESC)*, pp. 398–403, IEEE, Coimbatore, India, July 2020.

[19] G. Yang, Y. Bao, and Z. Liu, “Localization and recognition of pests in tea plantation based on image saliency analysis and convolutional neural network,” *Transactions of the Chinese Society of Agricultural Engineering*, vol. 33, no. 6, pp. 156–162, 2017.

[20] L. Yan, L. Pang, H. Wang, and J. Xiao, “Recognition of different Longjing fresh tea varieties using hyperspectral imaging technology and chemometrics,” *Journal of Food Process Engineering*, vol. 43, no. 4, Article ID e13378, 2020.

[21] D. Wu, C. Zhang, L. Ji, R. Ran, H. Wu, and Y. Xu, “Forest fire recognition based on feature extraction from multi-view images,” *Traitement du Signal*, vol. 38, no. 3, pp. 775–783, 2021.

[22] L. Wang, C. Zhang, Q. Chen et al., “A communication strategy of proactive nodes based on loop theorem in wireless sensor networks,” in *Proceedings of the 2018 Ninth International Conference on Intelligent Control and Information Processing (ICICIP)*, pp. 160–167, IEEE, Wanzhou, China, November 2018.

[23] H. Li, D. Zeng, L. Chen, Q. Chen, M. Wang, and C. Zhang, “Immune multipath reliable transmission with fault tolerance in wireless sensor networks,” in *Proceedings of the International Conference on Bio-Inspired Computing: Theories and Applications*, pp. 513–517, Springer, Xian, China, October 2016.

[24] C. H. Cao, Y. N. Tang, D. Y. Huang, G. WeiMin, and Z. Chunjiong, “IIBE: an improved identity-based encryption algorithm for wsn security,” *Security and Communication Networks*, vol. 2021, Article ID 8527068, 8 pages, 2021, https://doi.org/10.1155/2021/8527068.

[25] X. I. E. Tao, C. Zhang, and Y. Xu, “Collaborative parameter update based on average variance reduction of historical gradients,” *Journal of Electronics and Information Technology*, vol. 43, no. 4, pp. 956–964, 2021.

[26] Q. Chen, J. Zhao, and H. Lin, “Study on discrimination of Roast green tea (Camellia sinensis L.) according to geographical origin by FT-NIR spectroscopy and supervised pattern recognition,” *Spectrochimica Acta Part A: Molecular and Biomolecular Spectroscopy*, vol. 72, no. 4, pp. 845–850, 2009.

[27] P. Ye, X. Wu, D. Gao, S. Deng, N. Xu, and J. Chen, “DP3 signal as a neuro-indictor for attentional processing of stereoscopic

Hindawi
Computational Intelligence and Neuroscience
Volume 2022, Article ID 4926124, 12 pages
https://doi.org/10.1155/2022/4926124

Research Article

Image Compression Based on Hybrid Domain Attention and Postprocessing Enhancement

Yuting Bao, Yuwen Tao, and Pengjiang Qian

School of Artificial Intelligence and Computer Science, Jiangnan University, Wuxi 214122, China

Correspondence should be addressed to Pengjiang Qian; qianpjiang@jiangnan.edu.cn

Received 22 January 2022; Revised 14 February 2022; Accepted 15 February 2022; Published 17 March 2022

Academic Editor: Xin Ning

Deep learning-based image compression methods have made significant achievements recently, of which the two key components are the entropy model for latent representations and the encoder-decoder network. Both the inaccurate estimation of the entropy estimation model and the existence of information redundancy in latent representations lead to a reduction in the compression efficiency. To address these issues, the study suggests an image compression method based on a hybrid domain attention mechanism and postprocessing improvement. This study embeds hybrid domain attention modules as nonlinear transformers in both the main encoder-decoder network and the hyperprior network, aiming at constructing more compact latent features and hyperpriors and then model the latent features as parametric Gaussian-scale mixture models to obtain more precise entropy estimation. In addition, we propose a solution to the errors introduced by quantization in image compression by adding an inverse quantization module. On the decoding side, we also provide a postprocessing enhancement module to further increase image compression performance. The experimental results show that the peak signal-to-noise rate (PSNR) and multiscale structural similarity (MS-SSIM) of the proposed method are higher than those of traditional compression methods and advanced neural network-based methods.

1. Introduction

In the age of information technology, pictures have become important information carriers, and massive amounts of image data can lead to enormous transmission and storage pressures. For example, an original RGB image with a resolution of 512×768 has a theoretical storage size of about 1.125 MB, and after compression, the storage size of the image is only one-sixtieth of the original image or even smaller. Therefore, image compression is crucial in computer vision, and the trend of information technology has put forward higher demands on image compression efficiency. Traditional image compression methods [1–3] have achieved better performance through finely designed manual features and complex processing. For example, JPEG [1] employs the discrete cosine transform (DCT) [4] to eliminate redundancy among pixels. Traditional compression algorithms, on the other hand, lack learning capabilities. Thanks to the advancement of deep learning, this also gives new ideas for image compression methods.

In contrast to the traditional methods, where a linear transform module is replaced by a nonlinear neural network, the performance of image compression methods is determined by how the network structure is constructed to produce more compact latent features. In addition, accurate entropy estimation is one of the pivotal factors to improve the performance of image compression. A good entropy model can better suit the true distribution of an image. A further important task is to design the quantization module, which has a significant impact on compression performance.

A classical deep learning-based image compression structure converts images into compressible latent representations by stacking convolutional neural networks [5]. These latent representations are then entropy coded through statistical redundancy, and lossless compression is performed through entropy coding to create bitstreams. At the same time, the joint optimization decoder decodes the latent representations into images. Classical learning-based image compression algorithms [6, 7] use a variational autoencoder structure, and significant progress has been made in various technical components of this architecture, including the use of generalized divisive normalization (GDN) modules in nonlinear transformers, which has been validated for probabilistic modeling and image compression tasks. A nonlocal model was used in the literature [8], and a CNN-based wavelet transform was used in the literature [9] to reduce redundancy among pixels. The entropy estimation model with hyperprior was first proposed in the literature [7] to capture the hidden information of latent representations, aiding the generation of entropy model parameters and improving the mismatch between entropy model and hidden marginal distributions. In the literature [10, 11], the autoregressive module was introduced, and the autoregressive and hyperprior modules complement each other to improve the entropy estimation. The literature [12] proposed a parallelizable checkerboard grid context model and changed the decoding order so as to speed up decoding without breaking performance. The literature [13] used importance maps to guide image compression based on generative adversarial network loss functions for enhancing the subjective image quality. The literature [14] used a manually set distortion weight map to control the bit-rate allocation and assigned a larger distortion weight to the region of interest in the image, thus enhancing the quality of the region of interest. The problem that DNN-based networks cannot be directly used for near-lossless coding is addressed in the literature [15]. It is possible to see that the design and improvement of the deep neural network-based image compression methods focus on improving the main encoder-decoder, the quantization module, and the entropy estimation module structures.

In addition, improving the image compression quality is the eternal theme of image coding and decoding. We need to understand that enhancing the image quality at the decoding end is equivalent to improving the compression efficiency. Moreover, since the actual lossy compression standards are not theoretically optimal, there are information redundancies that can continue to be explored and utilized. Furthermore, we find that there are still some limitations in the existing methods. For example, the information transmitted using a hyperprior is not standardized and fully utilized. This part of the information, which is encoded into the bitstream to construct the entropy model, is not used for image reconstruction. We want to eliminate compression artifacts and blur, despite the fact that existing compression algorithms offer decent compression efficiency. The purpose of this study is to investigate how to build an effective learning-based image compression approach. To summarize, the following are the study's innovations:

(i) This study describes a hybrid domain attention mechanism that was embedded into the transform encoder-decoder and hyperprior module to output latent representations and hyperpriors with channel global context-adaptive activation. Our hybrid domain attention mechanism was embedded into different network layers, which is not only applied to quantized latent representations. The created attention mask dynamically analyzes the relevance of the features to be compressed through the deep learning-based architecture and allocates more bits to more essential features, which will help increase the entropy coding efficiency.

(ii) In addition, because quantization poses a zero-gradient problem, the training of a deep learning-based network cannot be carried out. We use the hybrid quantization approach to fix this problem, that is, the forward propagation adopts the rounding function and the backward propagation adopts the form of straight propagation. Apart from the nondifferentiable problem, quantification also leads to a loss of information. This study proposed an inverse quantization module to alleviate the errors induced by quantization.

(iii) Finally, as our image compression method is lossy, the reconstructed images will inevitably contain compression artifacts. In order to further increase image compression quality, obtain results with rich texture information, and generate vivid details, we perform a filtering process on the compressed image.

2. Related Work

2.1. Traditional Image Methods. Traditional image compression standards use artificially designed encoders, such as the discrete cosine transform used by JPEG [1], separating high-frequency information from low-frequency information and allocating bits according to signal importance to reduce information redundancy. To improve compression performance, entropy coding is also used. The coding of a source according to its probabilities is known as entropy coding. The process of entropy coding is lossless, i.e., there is no loss of image information. Entropy coding includes Huffman coding, tour coding, and arithmetic coding.

2.2. Deep Learning-Based Methods. Deep learning-based image compression is not independent of traditional image compression and is more built on top of it. There are two main approaches, a convolutional neural network-based compression approach using automatic encoders and a compression method with postprocessing filtering combined with traditional encoders. Traditional image compression uses transform coding that introduces block effects and compression artifacts, and while many methods can deal with these issues well, deep learning has a superior ability to solve these types of problems. For the design of transform encoder-decoder, some works [16, 17] used recurrent neural networks (RNNs) to achieve recursive compression of residual information, while other parts of works [6, 7, 10, 11] used stacked convolutional blocks to achieve this. Considering the limited perceptual field of convolutional blocks, Cheng et al. [18] used residual blocks to increase the perceptual field. Rippel and Bourdev [19] proposed the use of feature pyramid pooling (FPN) to obtain more powerful feature representations. In addition, since convolutional operations share features, this would lead to information redundancy. Li et al. [20] proposed using an importance map to adjust the bit allocation of images. The importance map is derived by training a branch of a 3-layer convolutional network. However, according to the method in [20], the explicit learning content needs weight, which increases the computational overhead, and it is difficult to adaptively allocate bits for deep features. Attention mechanisms have demonstrated considerable strength in adaptive learning of feature importance in recent years. In tasks such as natural language processing [21] and semantic segmentation [22], significant results have been made. Furthermore, introducing nonlocal block (NLB) into neural networks can greatly increase image denoising and image super-resolution reconstruction performance [23, 24]. This study, therefore, presents a hybrid domain attention mechanism that is embedded into both main and hyper coders, which allows features to have adaptive responses, reinforcing important features, weakening unimportant ones, and further improving the compression performance. Akbar et al. [25] employed multiplicative convolution. The use of multiplicative convolution is also based on the idea of allocating more bits to important regions and reducing spatial redundancy.

Because deep learning-based methods require network the training, quantization operations are not differentiable. The literature [6] proposed the use of adding uniform noise as an alternative to true quantization. The literature [11] sets the gradient of the quantization operation to a fixed value to ensure that deep learning training takes place. To make the quantization smoother, a soft-to-hard quantization is utilized instead of direct scalar quantization in the literature [26].

In the entropy coding section, different entropy models are proposed for the quantized latent representations. In the earlier literature [6], an entropy model constructed by a linear segmentation function was used for bit-rate estimation, the model has fixed parameters of its probabilistic model at the end of training, and the quantized latent representations are entropically encoded and entropically decoded based on these probabilities. To improve the entropy model, a hyperprior structure was proposed in the literature [7], in which the authors used a Gaussian-scale mixture (GSM) (Gaussian with different means and scales) modeling approach to estimate the probability of latent features. While the parameters needed for GSM modeling are derived by the hyperprior module, the latent features are then encoded into the bitstream and sent to the decoder. This achieves image adaptive coding and also obtains better performance than BPG (4 : 4 : 4) [3]. In the literature [10], an autoregressive context module is proposed to perform parameter prediction of the entropy model in conjunction with the hyperprior structure proposed in the literature [7].

To enhance the image reconstruction quality even more, many research studies [26, 27] used generative adversarial network (GAN) as a distortion measurement in the training phase to guide the decoder to generate more realistic texture structures, resulting in reconstructed images with good subjective quality, but the texture structures generated in this way are not real textures and do not have fidelity. For this reason, TuCode technology in [28] proposed an enhancement module that acts on full-resolution images to reduce compression artifacts in images by building a simple neural network to filter the reconstructed images. The literature [29] investigated the effect of decoding network complexity on image compression performance and concluded that postprocessing networks do not significantly improve compression performance when the network at the decoding end has a strong enough reconstruction capability. When using neural networks for traditional encoding schemes, the auxiliary information generated during the encoding process has a significant effect on image denoising, and ByteDance uses predictive information and coding unit (CU) block segmentation information to assist the neural network in replacing the deblocking (DB) and sample adaptive offset (SAO) modules for loop processing. Qualcomm uses a network of BS-assisted information to replace the DB filter for block filtering.

3. The Proposed Image Compression Method

3.1. Image Compression Architecture. Figure 1 shows the network structure. We deploy a deep learning-based automated encoder network. This method mainly includes the main encoder-decoder, hyper encoder-decoder, autoregressive context module, and postprocessing enhancement module. In particular, given the training images $\mathbf{x}$, a transformer encoder generates corresponding latent features $\mathbf{y}$. The quantization quantizes the latent features to $\widehat{y}$, and subsequently, entropy codes the quantized $\widehat{y}$ into a bitstream for transmission. The autoregressive context module combined with the hyperprior module is used for entropy coding. The entropy coding in this way will first estimate the distribution of latent representations $\mathbf{y}$ through the hyperprior network, and the output of the hyperprior encoder will be then quantized and encoded into bitstream. The reason why it will be encoded into the bitstream is that this part of the bitstream is required during decoding, and the accurate entropy model will improve the compression efficiency. The use of autoregressive prior information to estimate the distribution of latent representations $\mathbf{y}$ is to capture an accurate entropy model.

The attention module is used to adjust bit allocation based on the importance of the information. Considering that the goal of the image compression algorithms is to obtain the highest possible quality reconstructed image for a given bit-rate target, the method in this study adds a postprocessing enhancement module, and the image decoded by the main decoder and the mean information generated for modeling the Gaussian distribution are jointly fed into the postprocessing network to assist in generating the final reconstructed image.

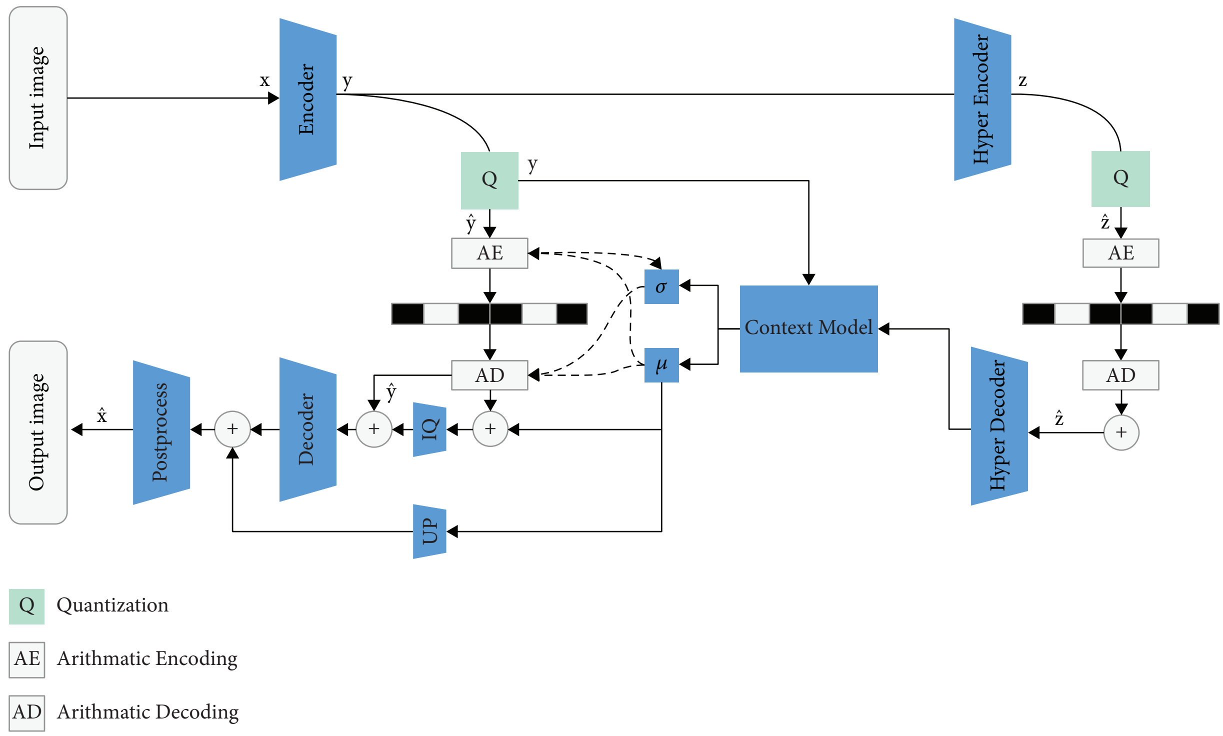

FIGURE 1: Network frame architecture of the proposed method.

We can deduce from our understanding of information theory that when the required coding features are concentrated, the smaller the value of information entropy, the fewer bits are required, and the resulting reconstructed image has more distortion. On the other hand, when the information entropy of the features is higher, the more bits are required, and the image distortion is lower; therefore, we need to use the hyperparameter λ to establish a trade-off between the two. The entire training of the compression method is optimized by means of the following loss function [30]:

$$\text{Loss} = \lambda D(\mathbf{x}, \hat{x}) + R_{\hat{z}} + R_{\hat{y}}, \quad (1)$$

where R refers to the bit rate, and D indicates the distortion between the images before and after compression. There are two commonly used distortion metrics, namely, multiscale structural similarity (MS-SSIM) and mean square error (MSE) [31]. The distortion and bit rate are weighed by. λ.

In training, we use an entropy estimation approach consistent with the model in the literature [10], and we model the latent features as follows:

$$p_{\hat{y}|\hat{z}}(\hat{y}|\hat{z}) = \prod_i \mathrm{N}\left(\boldsymbol{\mu}^i, \boldsymbol{\sigma}^{2(i)}\right) * u\left(-\frac{1}{2}, \frac{1}{2}\right)(\hat{y}_i). \quad (2)$$

Each latent representation $\hat{y}_i$ is modeled as a Gaussian distribution with μ^i and σ^i, which are forecasted by the distribution of the hidden variable $\hat{z}$. $\hat{z}$ is called the hyperprior, $u(\cdot)$ denotes a uniform distribution, and $*$ denotes the convolution operation. Because prior information about $\hat{z}$ does not exist, we model the hyperprior $\hat{z}$ as follows:

$$p_{\hat{z}|\psi}(\hat{z}|\psi) = \prod_i \left(p_{z^i|\psi^{(i)}}\left(\psi^{(i)}\right) * u\left(-\frac{1}{2}, \frac{1}{2}\right)\right)(\hat{z}_i), \quad (3)$$

where $p_{z^{(i)}|\psi^{(i)}}$ represents each univariate's distribution, and $\psi^{(i)}$ represents the parameters of this distribution. Finally, the bit rate in our method consists of the bit rate of the latent representations $\hat{y}$ and the bit rate of the hidden variable $\hat{z}$. These bit rates are denoted as follows:

$$\begin{aligned} R_{\hat{y}} &= \sum_i -\log_2\left(p_{\hat{y}_i|\hat{z}_i}(\hat{y}_i|\hat{z}_i)\right), \\ R_{\hat{z}} &= \sum_i -\log_2\left(p_{\hat{z}_i|\psi^{(i)}}\left(\hat{z}_i|\psi^{(i)}\right)\right). \end{aligned} \quad (4)$$

Table 1 shows the network architecture and related parameters for separate components in our compression method. One of them is the hybrid domain attention mechanism (HDAM), which will be described in Section 3.2. In addition, the inverse quantization module will be described in Section 3.3 and the postprocessing module will be described in Section 3.4.

3.2. Hybrid Domain Attention Mechanism. In previous studies, transform encoders were often implemented using stacks of convolutional neural networks. In learning-based image compression, learning a transform encoder with less redundant information and more critical reconstruction information through convolutional neural networks is one of the keys to better compression performance. While the convolutional layers are limited by the range of perceptual fields and have only local bias induction capabilities, increasing the depth of the network allows for deeper dependencies, but at the same time brings with it a significant increase in computational

Table 1: The proposed method's detailed parameter settings. "CONV" signifies convolutional layer. "2↓" signifies downsampling in the stride of 2. "2↑" signifies upsampling in the stride of 2. HDAM represents the hybrid domain attention module.

Encoder	Decoder	Hyperprior encoder	Hyperprior decoder	Context model
CONV:5 × 5 × 128 2↓	DECONV:5 × 5 × 128 2↑	CONV:3 × 3 × 128	DECONV:5 × 5 × 192 2↑	Masked:5 × 5 × 5 × 24
GDN	IGDN	Leaky ReLU	Leaky ReLU	CONV:1 × 1 × 48
CONV:5 × 5 × 128 2↓	DECONV:5 × 5 × 128 2↑	HDAM	HDAM	ReLU
GDN	IGDN	CONV:5 × 5 × 128 2↓	DECONV:5 × 5 × 288 2↑	CONV:1 × 1 × 96
HDAM	HDAM	Leaky ReLU	Leaky ReLU	ReLU
CONV:5 × 5 × 128 2↓	DECONV:5 × 5 × 128 2↑	CONV:5 × 5 × 192 2↓	DECONV:3 × 3 × 384 2↑	CONV:1 × 1 × 1 × 2
GDN	GDN	HDAM		
CONV:5 × 5 × 192 2↓	DECONV:5 × 5 × 3 2↑			
HDAM	HDAM		HDAM	

effort. Many recent studies have used attention mechanism modules to improve image recovery and compression performance [8, 32], where attention modules were introduced into transformers to model the global dependencies between features, resulting in a less redundant latent representation of the image on the transformer encoder side. The attention mechanism starts from the human visual mechanism by adaptively learning the weights of different features and acquiring the areas that need to be focused on. Previous works have used only spatial information to generate attention maps, which do not allow for good mining of correlations between channels of latent features. As shown in Figure 2, we experimented with the effect of the first 32 channels of the latent representations on the distortion performance of the reconstructed images and came to the conclusion that each channel has a different importance in the final reconstruction effect. Unlike previous works and inspired by [33], we proposed a hybrid domain attention mechanism that works in both the channel and spatial domains. The hybrid attention module is embedded in the transformer encoders and adaptively learns relevant compression features to obtain a transformer encoder with reduced information redundancy and with reconstructed key information. In our hybrid domain attention mechanism module, the input features are first passed through the channel attention module to obtain the channel domain attention map, which is then multiplied element by element with the input features to obtain the features required by the spatial attention mechanism. The output of the channel domain is utilized as the input feature map for the spatial attention mechanism, and then, the spatial domain attention map and the input features are multiplied element by element to obtain the final output. Figure 3(a) depicts the architecture of the channel attention mechanism, and the channel mask can be described as follows:

$$A_c(\mathbf{X}) = \sigma(\mathrm{MLP}(\mathrm{AvgPool}(\mathbf{X}))), \tag{5}$$

where $\mathbf{X}$ is the input feature map, $A_c(\cdot)$ denotes the channel domain attention map, MLP stands for a 2-layer neural network, and σ represents the sigmoid activation function. The spatial information of the aggregated feature map $\mathbf{X}$ is first derived by averaging pooling over spatial dimensions of the feature map, the spatial information is then sent to the MLP to compress its spatial dimensions, and then it undergoes a sigmoid activation operation to create the feature map of channel attention.

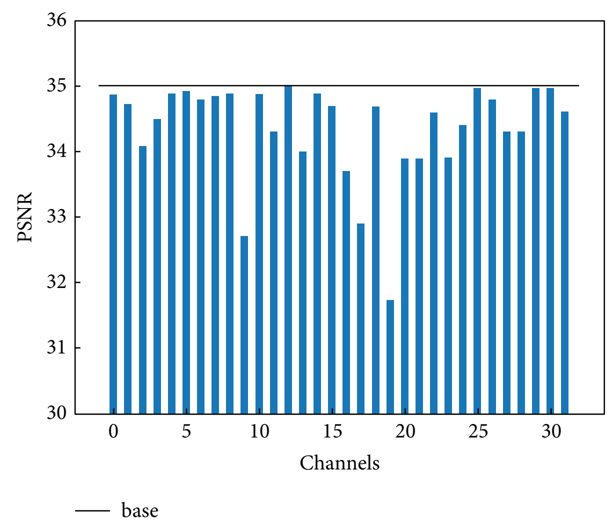

Figure 2: Channel influence on reconstruction distortion (PSNR degradation of the first 32 channels).

The spatial attention module is divided into a backbone branch, which uses traditional residual blocks to generate features, and a mask branch, in which the nonlocal block (NLB) [34] is embedded. Figure 3(b) depicts the spatial attention mechanism (b), and the spatial mask can be described as follows:

$$A_S(\mathbf{X}) = \sigma(F_{\mathrm{NLB}}(\mathbf{X})), \tag{6}$$

where $A_S(\cdot)$ represents the attention mask, and $F_{\mathrm{NLB}}(\cdot)$ denotes the result of utilizing *NLB* and the subsequent residual blocks and convolution.

As shown in Table 1, we integrate hybrid domain mechanisms into the framework of the proposed method. The attention module aids the network's global adaptive response by reinforcing essential features while weakening unimportant ones, thus implicitly learning feature importance mapping and delivering more bits for textured regions, resulting in better visualization with the naked eye at similar bit rates.

3.3. Hybrid Quantization. For lossy image compression, all features need to be quantized into integer form for entropy coding. Deep learning-based training, on the other hand, is

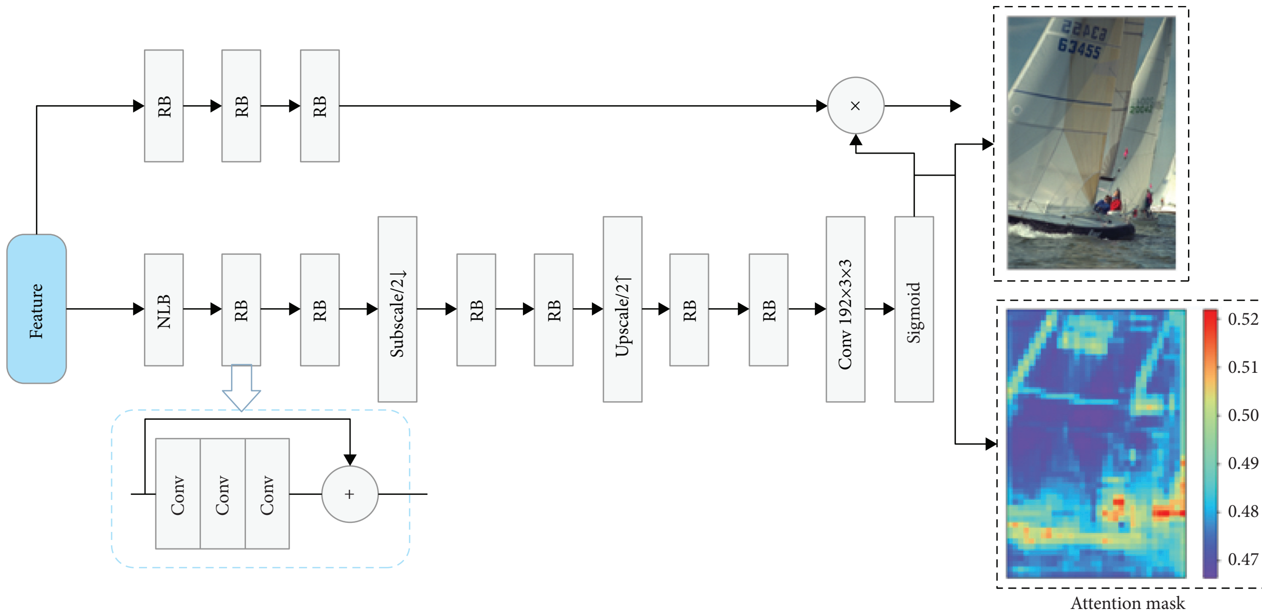

(a)

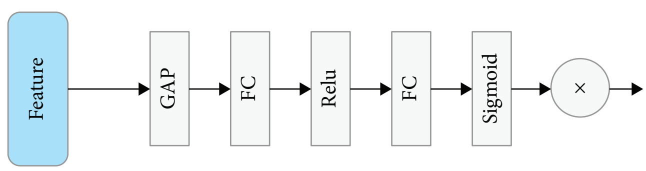

(b)

Figure 3: (a) The structure of spatial attention in hybrid domain attention module. "RB" is for resblock. "NLB" is for nonlocal module proposed in [34]. (b) The structure of channel attention in hybrid domain attention module. "FC" is for 2-layer fully connected layer. "GAP" is for global average pooling.

hampered by the inherently nondifferentiable nature of quantization. In the training phase, quantization methods for deep learning-based image compression methods [6, 7] typically take the form of approximate quantization by adding uniform noise for end-to-end optimization:

$$Q(\mathbf{y}) = \mathbf{y} + \Delta\left(-\frac{1}{2}, \frac{1}{2}\right). \tag{7}$$

The other part of the work uses straight-through estimation (STE) of the gradient and manually sets the backward propagation expression for the rounding function:

$$\begin{aligned} \frac{d}{d_{\mathbf{y}}}\{\mathbf{y}\} &:= \frac{d}{d_{\mathbf{y}}}[\{\mathbf{y}\}] \\ &= \frac{d}{d_{\mathbf{y}}}\mathbf{y} = 1. \end{aligned} \tag{8}$$

In our method, we integrate two quantization methods. For the encoder output $\mathbf{y}$, we use STE quantization to round up and feed the quantized one into the decoder, while for the entropy model network, we use approximate quantization with added noise for entropy modeling. In addition to this, to reduce the loss of information due to quantization, we incorporate an inverse quantization subnetwork. We treat the loss of floating-point numbers due to rounding operations as being added to the noise in the range of (−0.5, 0.5), which is why most compression methods today use an approximate quantization operation in the form of added noise. The inverse quantization network is similar to existing image denoising efforts, making the inverse quantized feature data as close as possible to the prequantization data.

Figure 4 depicts the specific network structure. The addition of uniform noise treats the loss of floating-point numbers due to quantization as a random form of noise, but the loss due to rounding is actually traceable, which also helps the inverse quantization network to perform a more accurate "denoising job."

3.4. Postprocessing Module. Since image compression approaches based on deep learning are lossy, the model in the form of hyperprior needs to ensure that the dimensionality of the latent representation is low; otherwise, the latent representation itself may contain redundancy, which will result in inevitable compression artifacts and poor compression performance. In this case, the hyperprior module may have some loss of information that affects the accuracy of the parameters required to model the entropy rate, especially for high bit rates and high resolutions. Taking into account the degradation information in image compression and the necessity to improve the compressed image's quality and provide better visual effects, we proposed introducing the postprocessing module into the main decoding end. In

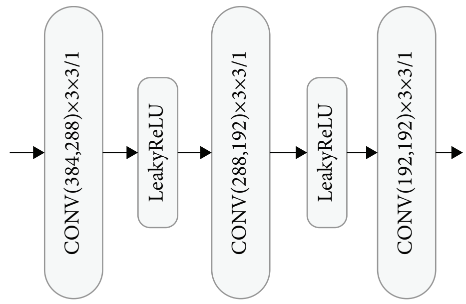

FIGURE 4: The architecture of our dequantization network.

addition, we proposed reuse of the mean information μ derived from the hyperprior module joint autoregression module. As shown in equation (2), through the training of the neural network, μ will capture the hidden information in $\hat{y}$, so μ contains rich structural information. To exploit the full potential of the auxiliary information, we feed the mean information into the postprocessing module to further assist the postprocessing network in removing compression artifacts.

As inspired by image noise reduction and super-resolution network design strategies [35], our postprocessing network uses a residual network structure for quality enhancement of the reconstructed image. As illustrated in Figure 5, we started by adding two convolutional layers to get shallow features, and at the same time, the number of channel dimensions was changed from 6 to 32 and then cascaded through three identical modules for detailed enhancement. Because we are dealing with full-resolution images, we use only three enhancement blocks in order to keep the computational cost from rising as the network depth grows. The enhancement blocks are added with two multiscale residual blocks to extract multiscale features. In addition, three different convolutional kernel sizes are used in these blocks, including 5×5, 3×3, 1×1, and PReLU activation functions, and finally, the convolution is used to change the channel dimension in the image before implementing global residual learning to obtain the enhanced image.

In fact, a general postprocessing module is not necessary because it will fail if the decoder network is powerful enough [29]. However, our postprocessing can increase the quality of the decoded images even further due to the reuse of information from μ. In the ablation experiments in Section 4.3, we proved the effectiveness of the postprocessing module we offered.

4. Experiments

4.1. Operation Details

(1) Experimental environment. We used PyTorch to implement our method, and we ran all of our tests on an NVIDIA-2080TI GPU with 11 GB of video RAM.

(2) Experimental data. To ensure that the recommended technique is effective, we conducted a series of tests. Since image compression tasks are unsupervised tasks that do not require additional label files, most of the image compression methods crawl high-resolution image data on the web as the dataset for the training model. We used 20,745 high-quality images provided by Flick.com. After preprocessing, these images were randomly cropped to size 256×256, and a total of around 800,000 images were obtained as the training set after preprocessing. To assess the efficiency of image compression methods, we tested the performance of various image compression methods using the Kodak Photo CD image dataset [36] as testing data.

(3) Comparison of methods. Our comparative experiments include classical traditional image compression methods (JPEG2000 [2], BPG [3]) and more recent deep learning-based image compression methods (Ballé et al. [6, 7], Minnen et al. [10], Lee et al. [11]). JPEG2000 [2] compression was tested using the official test model OpenJPEG 2000 configured in YUV 420 [37] and was implemented, and BPG [3] compression was tested using the BPG software [9] in the format YUV 440.

(4) Our method. To plot the rate-distortion performance curve, we trained different models according to different distortion measures. In the models with PSNR as the metric, we employed MSE as the distortion function D in the loss function, while in the distortion metric with MS-SSIM, we used (1-MS-SSIM) as a function of D. Six models are trained for each distortion scale based on different bit rates, for a total of twelve models, where the size of the bit rate is controlled by hyperparameter λ, we use different values (256, 650, 2048, 4096, 6144, and 8192) to train our models, and each λ corresponds to a rate-distortion point. The performance of the image compression method is represented by the line obtained by connecting each of the rate-distortion performance points. Initially, we assigned λ to 8192 for training and the model's batch size to 16, we used the Adam optimizer [38] for parameter optimization, the starting learning rate is 1×10^{-4}, and because the learning rate is updated using the callback function 'ReduceLROnPlateau' in the PyTorch framework, it will reduce the learning rate after the loss is no longer reduced. For the other rate-distortion points, we used the initially trained model as the pretrained model for the next training and fine-tuned the initially trained model to obtain the other rate-distortion points while keeping the training settings the same. In the model with MS-SSIM as the distortion metric, we used the original model with PSNR as the distortion metric as a pretraining model and changed the distortion metric in the loss function in this model. In addition, we set λ to 384 and the other rate-distortion points in the model with MS-SSIM as distortion metric on top of this pretraining model. The values of λ are, respectively, 16, 32, 64, 128, 256, and 384.

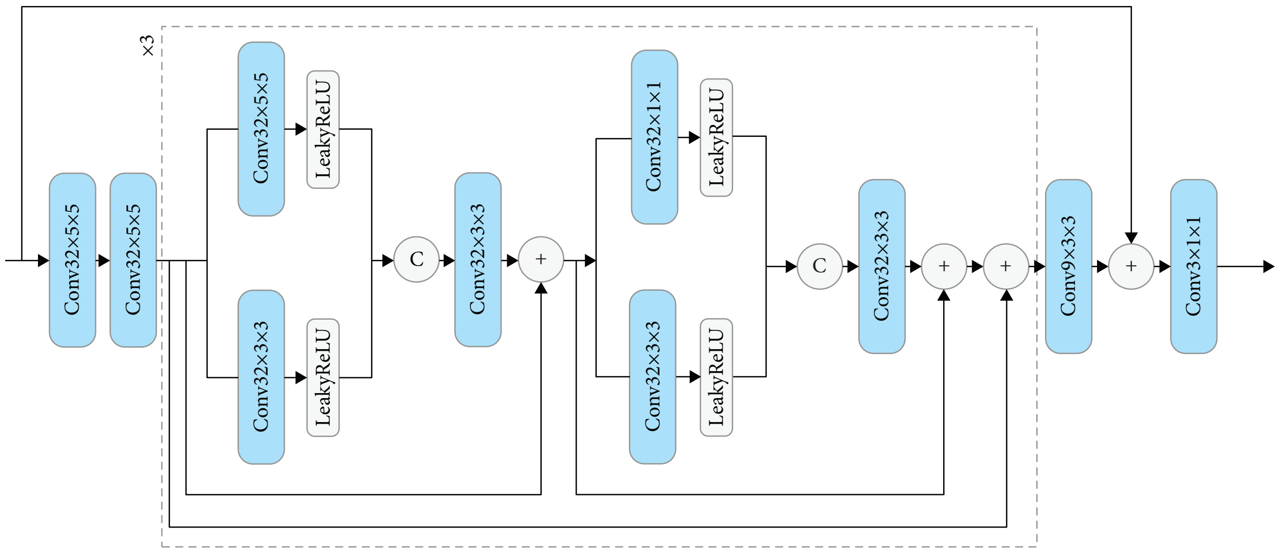

Figure 5: The architecture of our postprocessing module. “C” is for concatenation.

(5) Evaluation metric. Bit per pixel (BPP) reflects an image’s compression ratio. For images with the same aspect ratio, the smaller the BPP, the higher the compression ratio. For the image quality evaluation indicators, PSNR and MS-SSIM indicators are used to evaluate, respectively. PSNR is based on element-by-element comparison of differences, does not take into account human visual perception, and lets alone human esthetics, so PSNR can reflect pixel-level distortion, while MS-SSIM measures image similarity in terms of luminance, contrast, and structure, respectively.

4.2. Compression Performance. The unit of PSNR and MS-SSIM is db, and a higher value means less distortion and better visual impact. As shown in Figure 6 our rate-distortion curves plotted using PSNR (see Figure 6(a)) and MS-SSIM (see Figure 6(b)) as distortion metrics shows that our method has significant performance advantages over JPEG 2000 [2], BPG [3], Ballé2018 [7], and at the same BPP for both of the evaluation indicators mentioned. Our technique exhibits equivalent performance gains to Minnen [10] at low bit rates, and intuitionistic performance increases above Minnen [10] at large bit rates. Furthermore, our method improved performance at all bit rates, demonstrating the efficacy and stability of the suggested method in this study.

We have also conducted ablation studies to validate the effectiveness of each module. As seen in Figure 7, we retrained the model that embeds the hybrid domain attention mechanism into the baseline (four sets of models were trained), and it can see that it produced a rise of around 0.2 db over the baseline model. We also retrained the model by changing the quantization in the baseline to our hybrid quantization (four sets of models were trained), and it can be seen to produce a rise of about 0.2 db over the baseline, with more gain at higher bit rates. We retrained the model with our postprocessing module added to the baseline (four sets of models were trained), and it can be seen to produce a rise of nearly 0.2 db over the baseline as well.

There are four aspects that affect the efficiency of image compression. One is how to extract more compact features. One is the reduction in quantization losses. One is the reconstruction ability of the decoder. One is the accuracy of the entropy estimation. In our method, we improved the baseline model in these four dimensions, and from our ablation experiments, we can conclude that the hybrid domain attention mechanism has the greatest impact on performance.

4.3. Visual Comparison. To make the effectiveness of our framework clearer, we provide some visualization results. Figure 8 shows the visualization of some images compressed using different compression methods in the Kodak Photo CD dataset [36]. Since neural network-based image compression methods cannot strictly limit the BPP of an image, we can only compare different compression methods at similar BPP of the compressed images. As can be seen from the figures, our method has a higher evaluation index at similar BPP.

In terms of qualitative observation, the image compression methods JPEG 2000 [2] and BPG [3] have obvious block effects and blurring phenomena, and the deep learning-based image compression methods of Lee et al. [11] and Minnen et al. [10] have some loss of edge texture information in the reconstructed images, although they do not have as obvious blurring compression artifacts as the traditional compression methods, while the reconstruction quality of the compression methods in this study is higher. This is because our method embeds a spatial channel mechanism that is accordingly globally adaptive, reinforces

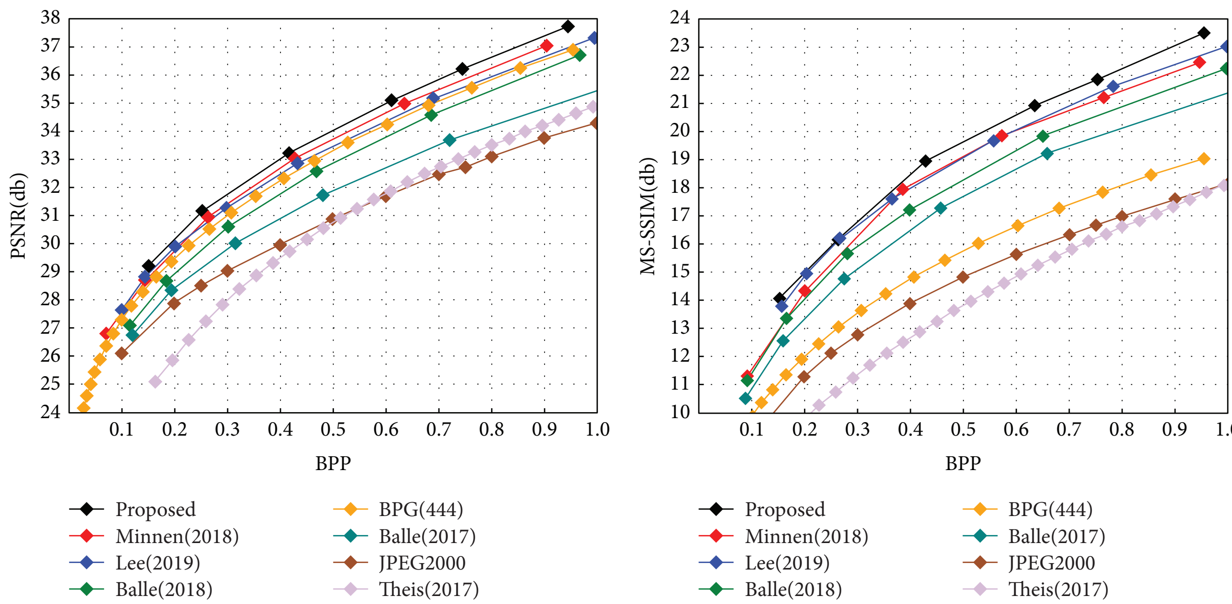

(a) (b)

Figure 6: Rate-distortion efficiency. (a) Rate-distortion plots for several methods on Kodak using the PSNR metric. (b) Rate-distortion plots for several methods on Kodak using the MS-SSIM metric.

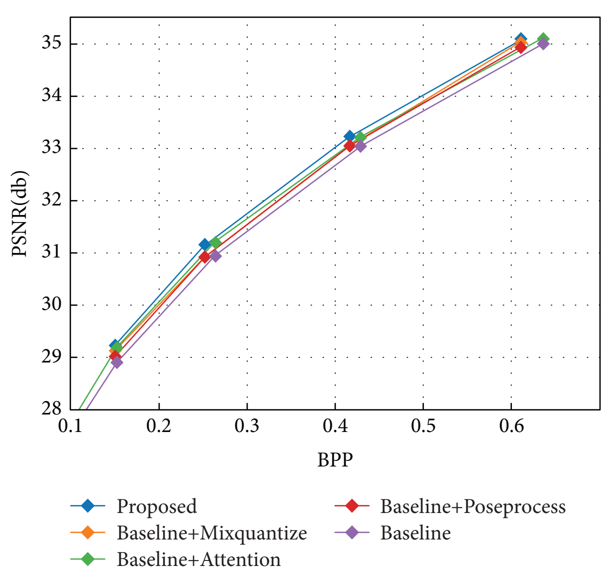

Figure 7: Effectiveness of each module in the proposed method.

important features (e.g., edge texture details), and allocates more bits to important features, and our framework also uses a hybrid quantization mechanism with the addition of an inverse quantization module and a postprocessing module, all of which can guide the network to use fewer bits to obtain higher reconstruction quality. Overall, the approach in this study is also superior in quality of visual comparison.

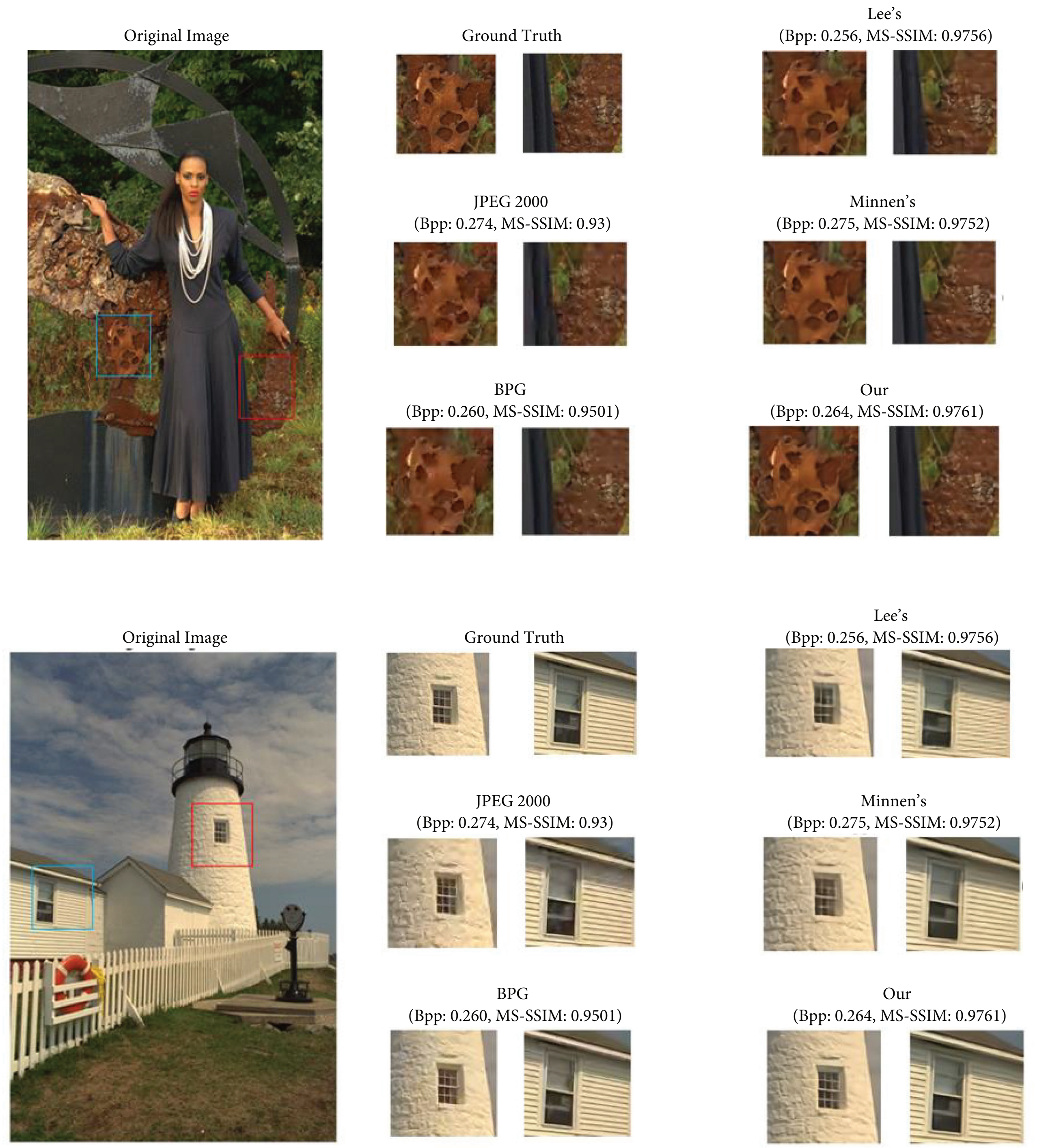

FIGURE 8: Image comparison with different compression methods under similar compression rates. The pictures are "Kodim18.png" and "Kodim19.png" in the test set Kodak Photo CD dataset [36], respectively.

5. Conclusions

We proposed an efficient trainable image compression method and achieve good performance. In particular, we add a hybrid domain attention module that not only improves the transforming capability of the encoder-decoder network but also generates more compact attention masks with hyperprior distribution, which facilitates more accurate probability estimates and thus improves entropy coding efficiency. In addition, our method combines the reuse of intermediate layer information to synthesize the final reconstructed image through a postprocessing enhancement module. We add a quantization adaptive adjustment module to repair quantization losses. This method reduces the total error by optimizing the network parameters through backward propagation. The results of experiments suggest that our method offers a substantial improvement over both traditional compression methods JPEG 2000 [2] and BPG

[3], and the learning-based method of Ballé et al. 2017 [6], compared to the advanced learning-based image compression methods of Minnen et al. [10]. This method also has a higher performance index and better visual effect. In the realm of learning-based image compression, extracting compact latent features is especially significant. Attention mechanisms can be still unable to completely eliminate data redundancy in latent features, and better capable attention mechanisms are still being explored. The addition of a postprocessing module on the decoder side and the inverse quantization module in hybrid quantization and the nonlocal block (NLB) [34] in the hybrid domain mechanism all add to the computational complexity, but the performance advantages are significant. We expect that more efficient and lightweight attention mechanisms for extracting latent features can be explored.

Data Availability

The data that support the findings of this study are available from the corresponding author, upon reasonable request.

Conflicts of Interest

The authors declare that they have no conflicts of interest.

Acknowledgments

This work was supported in part by the Science and Technology Demonstration Project of Social Development of Jiangsu Province under grant BE2019631.

References

[1] G. K. Wallace, "The JPEG still picture compression standard," *IEEE Transactions on Consumer Electronics*, vol. 38, no. 1, pp. xviii–xxxiv, 1992.

[2] M. Rabbani and R. Joshi, "An overview of the JPEG 2000 still image compression standard," *Signal Processing: Image Communication*, vol. 17, no. 1, pp. 3–48, 2002.

[3] G. J. Sullivan, J.-R. Ohm, W.-J. Han, and T. Wiegand, "Overview of the high efficiency video coding (HEVC) standard," *IEEE Transactions on Circuits and Systems for Video Technology*, vol. 22, no. 12, pp. 1649–1668, 2012.

[4] N. Ahmed, T. Natarajan, and K. R. Rao, "Discrete cosine transform," *IEEE Transactions on Computers*, vol. C-23, no. 1, pp. 90–93, 1974.

[5] J. Ballé, "Efficient nonlinear transforms for lossy image compression," in *Proceedings of the 2018 Picture Coding Symposium (PCS)*, pp. 248–252, IEEE, San Francisco, CA, USA, June 2018.

[6] J. Ballé, V. Laparra, and E. P. Simoncelli, "End-to-end optimized image compression," 2016, https://arxiv.org/abs/1611.01704.

[7] J. Ballé, D. Minnen, S. Singh, S. J. Hwang, and N. Johnston, "Variational image compression with a scale hyperprior," 2018, https://arxiv.org/abs/1802.01436.

[8] H. Liu, T. Chen, P. Guo et al., "Non-local attention optimized deep image compression," 2019, https://arxiv.org/abs/1904.09757.

[9] H. Ma, D. Liu, N. Yan, H. Li, and F. Wu, "End-to-end optimized versatile image compression with wavelet-like transform," in *Proceedings of the IEEE Transactions on Pattern Analysis and Machine Intelligence*, IEEE, 2020.

[10] D. Minnen, J. Ballé, and G. Toderici, "Joint autoregressive and hierarchical priors for learned image compression," 2018, https://arxiv.org/abs/1809.02736.

[11] J. Lee, S. Cho, and S. K. Beack, "Context-adaptive entropy model for end-to-end optimized image compression," 2018, https://arxiv.org/abs/1809.10452.

[12] D. He, Y. Zheng, B. Sun, Y. Wang, and H. Qin, "Checkerboard context model for efficient learned image compression," in *Proceedings of the IEEE/CVF Conference on Computer Vision and Pattern Recognition*, pp. 14771–14780, IEEE, New York, NY, USA, June 1993.

[13] L. Wu, K. Huang, and H. Shen, "A gan-based tunable image compression system," in *Proceedings of the IEEE/CVF Winter Conference on Applications of Computer Vision*, pp. 2334–2342, Waikola, HI, USA, January 2020.

[14] H. Akutsu, A. Suzuki, Z. Zhong, and K. Aizawa, "Ultra low bitrate learned image compression by selective detail decoding," in *Proceedings of the IEEE/CVF Conference on Computer Vision and Pattern Recognition Workshops*, pp. 118-119, IEEE, Los Alamitos, CA, USA, June 2020.

[15] Y. Bai, X. Liu, W. Zuo, Y. Wang, and X. Ji, "Learning scalable ly=-constrained near-lossless image compression via joint lossy image and residual compression," in *Proceedings of the IEEE/CVF Conference on Computer Vision and Pattern Recognition*, pp. 11946–11955, IEEE, Honolulu, HW, USA, July 2017.

[16] G. Toderici, D. Vincent, N. Johnston et al., "Full resolution image compression with recurrent neural networks," in *Proceedings of the IEEE Conference on Computer Vision and Pattern Recognition*, pp. 5306–5314, Honolulu, HW, USA, July 2017.

[17] N. Johnston, D. Vincent, D. Minnen et al., "Improved lossy image compression with priming and spatially adaptive bit rates for recurrent networks," in *Proceedings of the IEEE Conference on Computer Vision and Pattern Recognition*, pp. 4385–4393, Salt Lake City, Utah, July 2018.

[18] Z. Cheng, H. Sun, M. Takeuchi, and J. Katto, "Learned image compression with discretized Gaussian mixture likelihoods and attention modules," in *Proceedings of the IEEE/CVF Conference on Computer Vision and Pattern Recognition*, pp. 7939–7948, Seattle, WA, USA, June 2020.

[19] O. Rippel and L. Bourdev, "Real-time adaptive image compression," in *Proceedings of the International Conference on Machine Learning*, pp. 2922–2930, PMLR, Ho Chi Minh City, Vietnam, January 2017.

[20] M. Li, W. Zuo, S. Gu, D. Zhao, and D. Zhang, "Learning convolutional networks for content-weighted image compression," in *Proceedings of the IEEE Conference on Computer Vision and Pattern Recognition*, pp. 3214–3223, IEEE, Salt Lake City, Utah, June 2018.

[21] S. Jain and B. C. Wallace, "Attention is not explanation," 2019, https://arxiv.org/abs/1902.1018.

[22] Y. Cao, J. Xu, S. Lin, F. Wei, and H. Hu, "Gcnet: Non-local networks meet squeeze-excitation networks and beyond," in *Proceedings of the IEEE/CVF International Conference on Computer Vision Workshops*, October 2019.

[23] Y. Zhang, K. Li, K. Li, B. Zhong, and Y. Fu, "Residual non-local attention networks for image restoration," 2019, https://arxiv.org/abs/1903.10082.

[24] J. Sun and M. F. Tappen, "Learning non-local range Markov random field for image restoration," in *Proceedings of the*

CVPR 2011, pp. 2745–2752, IEEE, Colorado Springs, CO, USA, June 2011.
[25] M. Akbari, J. Liang, J. Han, and C. Tu, "Generalized octave convolutions for learned multi-frequency image compression," 2020, https://arxiv.org/abs/2002.10032.
[26] E. Agustsson, F. Mentzer, M. Tschannen et al., "Soft-to-hard vector quantization for end-to-end learning compressible representations," 2017, https://arxiv.org/abs/1704.00648.
[27] E. Agustsson, M. Tschannen, F. Mentzer, R. Timofte, and L. V. Gool, "Generative adversarial networks for extreme learned image compression," in *Proceedings of the IEEE/CVF International Conference on Computer Vision*, pp. 221–231, IEEE, Seoul, South Korea, October 2019.
[28] L. Zhou, Z. Sun, X. Wu, and J. Wu, "End-to-end optimized image compression with Attention Mechanism," in *Proceedings of the CVPR workshops*, Long Beach CA, USA, June 2019.
[29] H. Fu, F. Liang, J. Lin et al., "Learned image compression with discretized gaussian-laplacian-logistic mixture model and concatenated residual modules," 2021, https://arxiv.org/abs/2107.06463.
[30] G. J. Sullivan and T. Wiegand, "Rate-distortion optimization for video compression," *IEEE Signal Processing Magazine*, vol. 15, no. 6, pp. 74–90, 1998.
[31] Z. Wang, E. P. Simoncelli, and A. C. Bovik, "Multiscale structural similarity for image quality assessment,"vol. 2, pp. 1398–1402, in *Proceedings of the Thrity-Seventh Asilomar Conference on Signals, Systems & Computers*, vol. 2, pp. 1398–1402, Ieee, Pacific Grove, CA, USA, November 2003.
[32] Y. Qian, Z. Tan, X. Sun et al., "Learning accurate entropy model with global reference for image compression," 2020, https://arxiv.org/abs/2010.08321.
[33] S. Woo, J. Park, J.-Y. Lee, and I. S. Kweon, "Cbam: convolutional block attention module," in *Proceedings of the European conference on computer vision (ECCV)*, pp. 3–19, IEEE, Munich, Germany, September 2018.
[34] X. Wang, R. Girshick, A. Gupta, and K. He, "Non-local neural networks," in *Proceedings of the IEEE conference on computer vision and pattern recognition*, pp. 7794–7803, IEEE, Salt Lake City, Utah, June 2018.
[35] B. Lim, S. Son, H. Kim, S. Nah, and K. Mu Lee, "Enhanced deep residual networks for single image super-resolution," in *Proceedings of the IEEE conference on computer vision and pattern recognition workshops*, pp. 136–144, IEEE, Honolulu, HW, USA, July 2017.
[36] E. Kodak, "Kodak lossless true color image suite (PhotoCD PCD0992)," 1993, http://r0k.us/graphics/kodak/.
[37] UCL.JPEG, "Officials of softtware OpenJPEG[EB/OL," 2000, http://www.openjpeg.org/.
[38] D. P. Kingma and J. Ba, "Adam: A method for stochastic optimization," 2014, https://arxiv.org/abs/1412.6980.

Hindawi
Computational Intelligence and Neuroscience
Volume 2022, Article ID 3699647, 7 pages
https://doi.org/10.1155/2022/3699647

Research Article

Feature Extraction and Small-Sample Learning of Dexmedetomidine for Neurosurgery on Postoperative Agitation in Patients with Craniocerebral Injury

Chuan Ding,[1] Xiuhua Wang,[2] and Xiuqin Wang[1]

[1] *Department of Anesthesiology, Shandong Cancer Hospital and Institute, Shandong First Medical University and Shandong Academy of Medical Sciences, Jinan, Shandong 250117, China*
[2] *Department of Materials Chemistry, Anhui Normal University, Wuhu, Anhui 241002, China*

Correspondence should be addressed to Xiuqin Wang; wangxiuqin@sdfmu.edu.cn

Received 28 December 2021; Accepted 29 January 2022; Published 15 March 2022

Academic Editor: Xin Ning

Objective. To observe the controlled effect of dexmedetomidine for neurosurgery and the effect on postoperative cognitive function. The main task of this paper is to use data from a small sample. The proposed feature extraction algorithm based on the bilinear convolutional neurological network (BCNN) is based on a small sample of data. BCNN involves the simultaneous extraction of highly discriminative cross-sectional features from the input image using two parallel subnetworks. By optimizing the algorithm to minimize losses, the two subnetworks can be supervised by each other, improving the performance of the network and obtaining accurate recognition results without spending a lot of time adjusting parameters. The mean arterial pressure (MAP) and heart rate (HR) levels of cerebral oxygen metabolism were compared between the two groups before (T0), after (T1), immediately after (T2), and after intubation (T3). In the observation group, MAP and HR values at T3, arterial-internal jugular vein bulb oxygen difference $[D(a-jv)O_2]$ at T1, T2, and T3, cerebral oxygen uptake (CEO_2) levels, and postawakening agitation scores were lower than those of the control group during the same period ($P < 0.05$).

1. Introduction

Craniocerebral injury in surgery is more traumatic and patients suffer from nervousness and fear, which require appropriate anaesthetic hypnosis to reduce the occurrence of stress reactions and improve surgical safety. Postoperative extraction, aspiration, and postoperative pain stimulation can lead to excitation of the sympathetic-adrenergic system, increased blood pressure levels, increased heart rate, and even cardiovascular and cerebrovascular accidents [1]. Dexmedetomidine is highly selective for α_2 receptors, with an affinity more than 1,600 times that of α_1 receptors, inhibits norepinephrine release [2], reduces postsynaptic membrane excitability, has a low preoperative aerodynamic impact, has no respiratory depressant effect, effectively inhibits sympathetic excitation, lowers catechol levels, and reduces the stress response. When combined with opinions, it can prolong the duration of opiate analgesia and enhance the sedative effect with significant effect [3].

Craniocerebral injury is a difficult procedure as the vertebral body and the surrounding tissues are rich in blood vessels and the operation site is deep, making it difficult to stop bleeding [4]. Patients undergoing craniocerebral injury are mostly middle-aged and elderly, mostly combined with underlying diseases, so maintaining the hemodynamic stability of patients is of positive significance to improve the safety of surgery [5]. Dexmedetomidine is a new highly selective α_2-adrenergic agonist that can reduce the stress response during surgery and maintain aerodynamic stability [6]. This study will look at the effect of dexmedetomidine in controlled hypotension during craniocerebral injury and its effect on patients' postoperative cognitive function.

Under normal conditions, cerebral oxygen metabolic rate changes in synchrony with cerebral blood flow. When the cerebral oxygen metabolic rate increases, the cerebral vasculature also strengthens and automatically dilates, resulting in elevated cerebral blood flow, which can cause secondary brain damage to occur when the cerebral oxygen supply and demand are in an imbalance [7, 8]. In this study, we compared and analysed the differences in postoperative cognitive function between the two groups, and the results showed that cognitive function in the observation group was higher than that in the control group within a short period of time after surgery, which is consistent with the findings of Gunduz et al. [9], indicating that dexmedetomidine is beneficial to the recovery of cognitive function after anaesthesia. This may be due to the cerebral protective effect of dexmedetomidine, which reduces the cerebral oxygen metabolism rate, increases the superoxide dismutase content, and antagonises the brain damage caused by the anaesthetic.

In conclusion, dexmedetomidine is safe and effective for controlled hypotension in craniocerebral injury, effectively inhibiting cardiovascular responses during tracheal intubation, reducing the patient's preoperative cerebral metabolism level, and improving postoperative cognitive function.

2. Knowledge Background

2.1. Restlessness and Impact. Song et al. [10] define agitation as the hyperexcitability of the patient during the awakening period after the application of ether, cyclopropane, or ketamine anaesthesia, which is mainly manifested by unconscious movements of the limbs, uncontrollable crying, irrational speech, excitable agitation, and disorientation.

The causes of agitation are multiple and include surgical-related factors (postoperative incision pain and prolonged passive position), anaesthetic factors (partial anaesthetic drugs and residual effects of inotropic drugs), and various adverse stimuli (catheter and tracheal tube stimulation) [11]. However, it is still not possible to explain the exact mechanism by which all postoperative agitation occurs. Some scholars believe that it may be related to the different degrees of suppression of the central nervous system by anaesthetic drugs; such patients may have recovered consciousness during the awakening period of general anaesthesia, but due to the residual effects of some anaesthetic drugs, the patient's cerebral cortex is still suppressed, while their subcutaneous central functions have been restored. This inconsistent neurological state results in a lack of functional integrity of the brain, which ultimately leads to a state of central nervous system hyperexcitability [12]. This lack of functional integrity can take many forms, for example, after awakening from anaesthesia, the patient is generally quiet and drowsy, with a small number of patients having mild disorientation and a gradual normalisation of the functional brain response from blurred or sluggish, but a few of these susceptible patients can be agitated (reflexively antagonised) by any adverse stimulus (pain, distress, or discomfort) during the period of blurred or sluggish functional brain response [13].

2.2. Dexmedetomidine. a_2 adrenoceptor (a_2-AR) agonists are favoured by anaesthetists because of their unique mechanism of action in anaesthesia and the fact that they do not inhibit breathing. Dexmedetomidine (Dex) is a relatively recently discovered and used a_2 adrenoceptor agonist, which was first used in the USA in 1999 for short duration (<24 h) sedation of ICU patients; it has since been used in a wide range of clinical applications due to its unique pharmacological properties [14]. DEX inhibits the release of norepinephrine from neurons by making brainstem pontine, calms the brain, and resists anxiety. Its unique feature is to keep the brain awake in the case of hypoxia. This advantage makes Dex unique in the type of surgery that requires intraoperative patient cooperation [15].

In the perioperative period, many patients have an excessive stress response due to fear of anaesthesia and surgery, resulting in excitation of the sympathetic nervous system and increased release of catecholamines, which is reflected in circulatory fluctuations such as increased heart rate and blood pressure [16]. Dex significantly inhibits sympathetic hyperexcitability and the release of noradrenaline from neuronal endings, improving perioperative blood flow stability and thereby reducing the risk of perioperative myocardial ischemia [17].

3. Bilinear Convolutional Neural Network (BCNN)

The main task of this paper is to identify the craniocerebral injury of dextromethorphan. Our proposed BCNN structure is shown in Figure 1 [19]. Its innovation lies in (1) using two parallel subnetworks to simultaneously extract highly discriminative cross-sectional features from the input image; (2) fusing the extracted features to obtain fine features that help in recognition; and (3) minimizing losses through an optimization algorithm; the two subnetworks can supervise each other to improve the performance of the network and obtain accurate recognition results without spending a lot of time to adjust the parameters. The following will introduce the method of this paper in detail at network initialization, data acquisition and preprocessing, BCNN network design, etc.

3.1. Network Initialization. Network initialization has a significant impact on training, and poor initialization tends to trap the neural network in a gradient-depletion trap. Aryan et al. [7] pointed out that low-level CNNs learn features similar to the edge portion of the mask obtained by Gabor kernel filtering, and as depth grows, the CNN gradually learns distinctive features of the object; Therefore, many researchers have tried to fine-tune the parameters of the classification layer of the model to cope with different task scenarios using a migration learning-based training strategy. For the case of this study, which has a small sample of labelled dextromethorphan surgery data and is prone to overfitting in training, a migration learning strategy was adopted to initialize the subnetwork of the BCNN model using the ImageNet pretraining model, while the remaining parameters were initialized using Kaiming [21] initialization. The Kaiming initialization makes the output in training

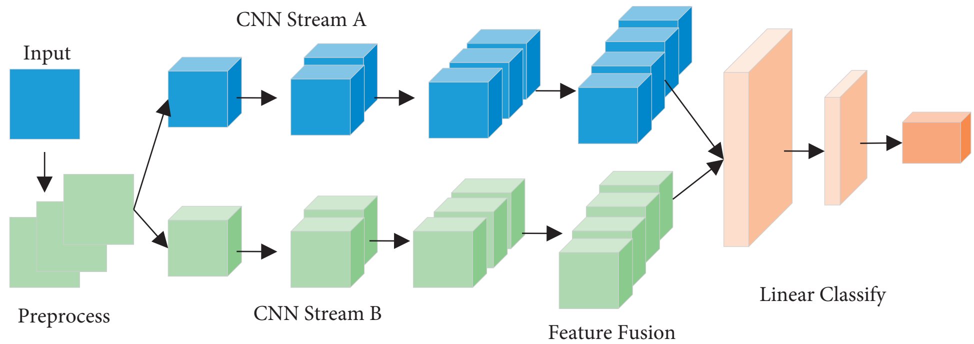

Figure 1: BCNN structure.

closer to the Gaussian distribution, which is conducive to the convergence of the network. The learning rate is set to 0.1 for the migration learning parameter layer and 1 for the Kaiming initialization parameter layer and decreases as the number of model iterations increases to provide a fine-tuning effect. This strategy allows the network model to maximize the learning of the distribution of the target data.

3.2. BCNNs. In the BCNN dextromethorphan surgery recognition algorithm constructed in this paper, the feature extraction part consists of two parallel CNN subnetworks, using ResNet and SqueezeNet as the backbone of the subnetworks, referred to as BCNN-R and BCNN-S in the following. $\beta = (F(A)F(B), P, C)$ represents the whole model, where F denotes the feature extraction layer of the network, F(A) and F(B) denote the features extracted from the two subnetworks, respectively, P denotes the outer product pooling function, and C is the classification function. The function of the feature extraction layer F is to map a point l on the input image L to a $J \times M$ dimensional feature, which is pooled by the P function given by equation (1), and the classification function C outputs the identified types using the softmax function in equation (2), where O_i is the output for class i.

$$(l, \mathrm{L}, \mathbf{F}(A), \mathbf{F}(B)) = \mathbf{F}(A)(l, L)^{\mathrm{T}}\mathbf{F}(B)(l, \mathrm{L}), \tag{1}$$

$$C_i = \frac{\exp(O_i)}{\sum_i^c \exp(O_i)}. \tag{2}$$

BCNN-S chose SqueezeNet [22] as the backbone network, mainly using the Fire module, which consists of two parts: compression and extension. The compression module fuses features of multiple dimensions into fewer dimensions, firstly convoy the input image using 3×3 convolution kernels to obtain a feature map with a higher number of channels and then convoying the feature map of the previous layer using fewer 1×1 convolution kernels to integrate features across channels to achieve the goal of reducing the number of feature dimensions. The extension module adopts a design similar to that of the Inception network [23], extending from the width of the network, using 1×1 and 3×3 convolution kernels to convolve the obtained feature maps in cascade, increasing the linear representation of the model, and improving the generalisation capability. The structure of the Fire module is shown in Figure 2.

In target recognition tasks, the only commonly used classification model is the single-branch network, consisting of a convolutional layer, a pooling layer, and a fully connected layer. The fusion of F(A) and F(B) yields a bilinear feature $X = \mathbf{F}(A)^{\mathrm{T}}\mathbf{F}(B)$ of size $M \times M$, transforming X into a bilinear vector of $M_2 \times 1$ for classification using linear layers. Intuitively, the bilinear form allows the features $F(A)$ and $F(B)$ to be constrained to each other and the outer product can be calculated for all forms of their combination, similar to the expansion of the perfect square formula. The feature fusion formula is shown in the following equation:

$$\mathbf{F}(A)^{\mathrm{T}}\mathbf{F}(B) = \begin{pmatrix} \mathbf{a}_1^{\mathrm{T}} \\ \vdots \\ \mathbf{a}_m^{\mathrm{T}} \end{pmatrix} \begin{pmatrix} \mathbf{b}_1 & \cdots & \mathbf{b}_m \end{pmatrix}. \tag{3}$$

As the convolutional neural network is end-to-end, i.e., the input is the original data and the output is the prediction, the training can be optimized using the backpropagation algorithm. Let $\mathrm{d}\ell/\mathrm{d}x$ be the gradient of the loss function with respect to the input x. Then, the gradient is chained to $F(A)$ and $F(B)$, respectively, and the gradient is shown in the following equation:

$$\begin{aligned} \frac{\mathrm{d}\ell}{\mathrm{d}A} &= \mathbf{F}(B)\left(\frac{\mathrm{d}\ell}{\mathrm{d}x}\right)^{\mathrm{T}}, \frac{\mathrm{d}\ell}{\mathrm{d}B} \\ &= \mathbf{F}(A)\frac{\mathrm{d}\ell}{\mathrm{d}x}. \end{aligned} \tag{4}$$

From equation (4), we can see that A and B influence each other's gradients, i.e., they play a supervisory role, so the model can fully learn the subtle differences between the different categories to avoid overfitting, and even without deliberately adjusting the model hypermastigote, we can get better recognition results [24, 25].

4. Case Studies

4.1. Materials. The study was approved by the hospital ethics committee. Patients undergoing craniocerebral injury in our hospital from August 2016 to October 2018 were selected.

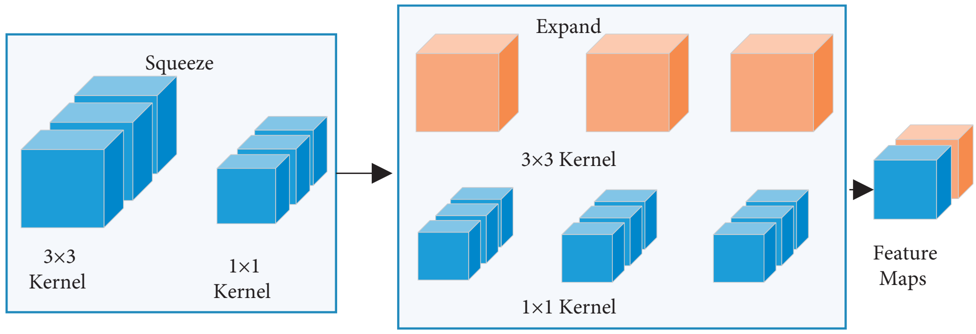

Figure 2: Structure of the Fire module.

Inclusion criteria were as follows: (1) patients with lumbar disc herniation or lumbar spine fracture who underwent elective surgical treatment in our hospital; (2) age 18–80 years; (3) American Society of Anesthesiologists (ASA) classification: grade I-II; (4) complete clinical data. Exclusion criteria were as follows: (1) combined with cranial trauma or severe central nervous system injury; (2) combined with hypertension, coronary artery disease, cardiac insufficiency, or severe cardiac arrhythmia; (3) combined with cardiac, hepatic, or renal dysfunction; (4) combined with coagulation or immune dysfunction; (5) presence of opium addiction, alcoholism, or drug abuse; (5) long-term use of immunosuppressive drugs; (6) combined with acid-base or electrolyte disorders; and (7) other internal endocrine disorders such as acid-base balance or electrolyte disorders. The 50 cases in the observation group were missing 2 cases due to follow-up, and a total of 48 cases were included, including 30 males and 28 females (age 35–77 years, mean (58.9 ± 5.9) years; body mass 47–81 kg, mean (61.9 ± 3.2) kg); 3 cases were illiterate, 8 cases were primary school students, and 37 cases were junior high school students or above; ASA classification: 29 cases of grade I and 19 cases of grade II. In the control group, there were 50 cases and 4 cases were missing from the follow-up, and a total of 46 cases were included, including 30 males and 16 females (age ranged from 37 to 78 years, mean (58.9 ± 5.8) years; body mass ranged from 48 to 80 kg, mean (61.8 ± 3.2) kg); 5 cases were illiterate, 9 cases were in primary school, and 32 cases were in junior high school or above; ASA classification: 25 cases in class I and 21 cases in class II. There was no statistically significant difference between the above general information of the two groups $(P > 0.05)$ [26].

5. Results

The differences in HR and MAP values at T0, T1, and T2 between the two groups were not statistically significant $(P > 0.05)$. The HR and MAP values at T3 in the observation group were lower than those in the control group $(P < 0.05)$ (see Table 1).

The differences in CE O_2 and $D(a - jv)O_2$ levels between the two groups at T0 were not statistically significant $(P > 0.05)$, while CE O_2 and $D(a - jv)O_2$ levels at T1 and T2 were higher than those at T0 in the same group $(P < 0.05)O_2$, $D(a - jv)O_2$ (see Table 2).

T4, T5, and T6 were higher in the observation group than those in the control group $(P < 0.05)$ (see Table 3).

The observation group had longer extubation and awakening times than the control group; the controlled hypotension time was shorter than that of the control group, and the postawakening agitation score was lower than that of the control group $(P < 0.05)$ (see Table 4).

The difference in the occurrence of adverse reactions between the two groups was not statistically significant $(P > 0.05)$ (see Table 5).

6. Postoperative Agitation Effect

There was no statistically significant difference in the time to recovery of breathing, time to awakening, and time to extubation between the two groups $(P > 0.05)$ (see Table 6).

The HR and MAP of group C were significantly higher than those of group D at all time points within 60 min after intubation, which was statistically different $(P < 0.05)$. The differences in HR and MAP at 120 min after intubation were not statistically significant between the two groups $(P > 0.05)$ (see Figures 3 and 4).

The Riker sedation and agitation scores at 60 min after extubation were statistically significantly higher in group C than in group D $(P < 0.05)$. There was no statistically significant difference in the Riker sedation agitation scores at 120 min after extubation $(P > 0.05)$ (see Figure 5).

The degree of agitation from the end of surgery to 120 min after extubation was higher in group C than in group D. The incidence of agitation was significantly higher in group D. There was a statistical difference $(P < 0.05)$ (see Table 7).

The Ramsay sedation scores of patients in group C were statistically significantly lower than those of group D at all points within 60 min after extubation $(P < 0.05)$. There was no statistically significant difference in Ramsay sedation scores between the two groups at 120 min after extubation $(P > 0.05)$ (see Figure 6).

The results should be related to the sedative effect of dexmedetomidine, and dexmedetomidine can also reduce patients' pain and relieve the negative emotion of nervousness and anxiety and fear to a certain extent while sedating them, thus reducing the occurrence of agitation [2].

Table 1: Comparison of mean arterial pressure and heart rate between the two groups at different time points.

Group	n	HR (times/min)				MAP (mmHg)			
		T0	T1	T2	T3	T0	T1	T2	T3
Observation group	48	74.1 ± 7.1	62.3 ± 6.9	65.6 ± 3.4	73.6 ± 9.3	93.9 ± 9.1	93.9 ± 9.1	93.9 ± 9.1	93.9 ± 9.1
Control group	46	74.7 ± 8.0	63.1 ± 7.9	66.4 ± 5.2	78.3 ± 9.8	94.3 ± 7.3	65.5 ± 7.4	66.9 ± 7.7	99.9 ± 7.5

Table 2: Comparison of cerebral oxygen metabolism levels between the 3 groups of patients at different time points ($\overline{x} \pm s$).

Group	n	CEO_2 (%)				$D(a-jv)O_2$ (Ml/dL)			
		T0	T1	T2	T3	T0	T1	T2	T3
Observation group	46	27.5 ± 6.5	31.3 ± 5.2	31.1 ± 3.9	28.1 ± 6.1	4.1 ± 0.8	4.0 ± 1.1	4.1 ± 1.1	4.4 ± 1.1
Control group	48	26.9 ± 6.3	39.5 ± 5.1	37.0 ± 5.2	35.4 ± 5.3	4.1 ± 1.5	6.4 ± 1.0	5.7 ± 0.9	5.9 ± 1.2

Table 3: Comparison of postoperative cognitive function between the two groups.

Group	n	T0	T4	T5	T6	T7
Observation group	48	28.7 ± 1.1	25.5 ± 0.9	26.5 ± 0.3	27.9 ± 0.8	28.8 ± 0.9
Control group	46	24.2 ± 0.8	25.5 ± 0.4	26.2 ± 0.8	28.8 ± 2.1	28.7 ± 0.8

Table 4: Comparison of the quality of awakening between the two groups.

Group	n	Controlled depressurization time (min)	Extubation time (min)	Waking time (min)	Agitation score (point)
Observation group	48	72.4 ± 9.8	18.1 ± 3.0	17.8 ± 2.2	1.6 ± 0.4
Control group	46	79.8 ± 9.1	15.1 ± 3.3	14.7 ± 2.1	2.3 ± 0.4

Table 5: Comparison of the occurrence of adverse reactions in the two groups (cases).

Group	n	Nausea	Vomit	Drowsiness	Total
Observation group	48	2	1	2	5
Control group	46	1	2	1	4

Table 6: Recovery of basic postoperative signs (min, $\overline{x} \pm s$).

Group	Number of cases	Respiratory recovery time	Wake up time	Extubation time
Group C	20	4.3 ± 2.3	5.5 ± 2.9	9.1 ± 3.2
Group D	20	4.2 ± 2.1	5.3 ± 3.1	9.2 ± 3.1

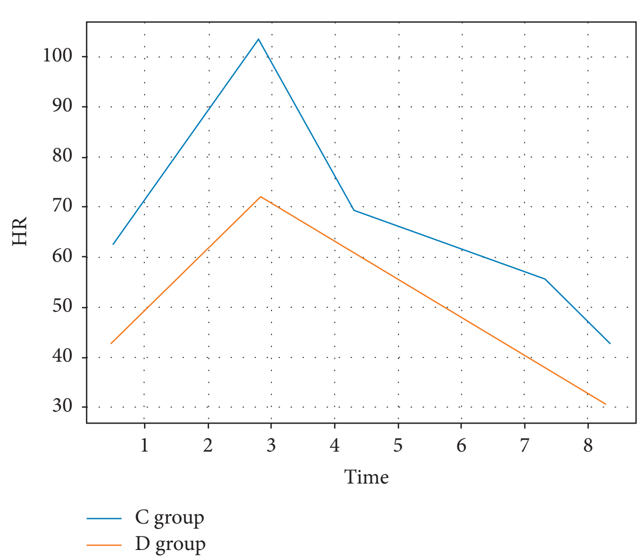

Figure 3: HR.

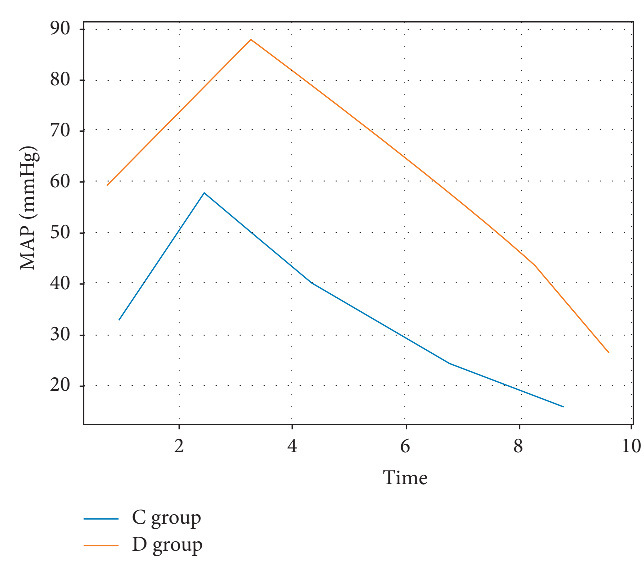

Figure 4: MAP.

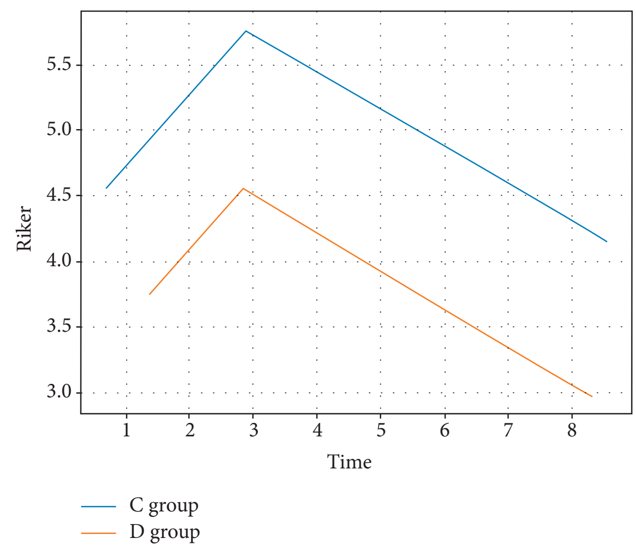

Figure 5: Riker score.

Table 7: Occurrence of postoperative agitation in both groups (cases; %, $\overline{x} \pm s$).

Group	Number of cases	Each agitation grade count					Incidence of agitation (%)
		3 points	4 points	5 points	6 points	7 points	
Group C	20	0	4	6	7	3	80
Group D	20	2	13	4	1	0	25

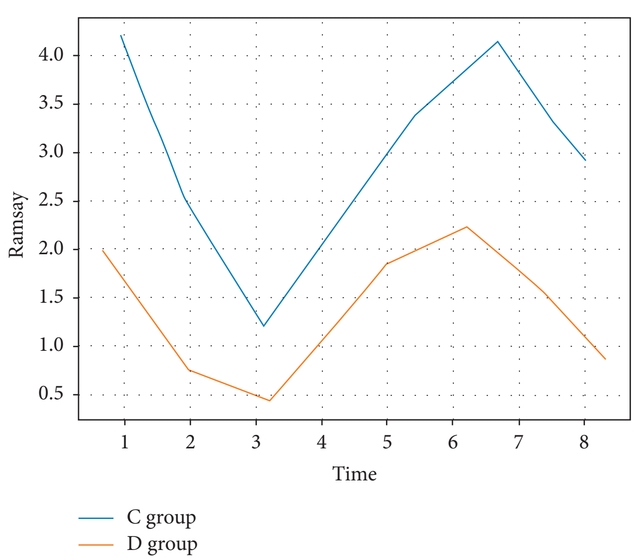

Figure 6: Ramsay score.

This study also showed the Ramsay sedation scores at the moment of awakening and the moment of exultation.

In addition, oversedation is a possible risk after dexmedetomidine application. Ramsay sedation score is commonly used by clinicians and anaesthetists to analyse the level of sedation of patients. In this study, the Ramsay sedation score of both groups was below 4, although the score of group D was higher than that of group C, suggesting that dexmedetomidine infusion had a good sedative effect and that no oversedation occurred in this study.

In conclusion, dexmedetomidine hydrochloride is an adjunct to general anaesthesia with certain advantages. The treatment protocol of a preinduction loading dose of 1 μg/kg (10 min) and a maintenance dose of 0.5 μg/kg-h continuous infusion is effective and safe to use, resulting in smoother hemodynamics during recovery from general anaesthesia after craniotomy in patients with, less postoperative agitation, and less interpretative anaesthetic. It is safe to use and results in more stable hemodynamics, less postoperative agitation, less introspective anaesthesia, and a lower incidence of postoperative chills and delirium.

7. Conclusions

The proposed feature extraction algorithm based on a bilinear convolutional neural network consists of simultaneous extraction of highly discriminative cross-sectional features from the input image using two parallel subnetworks. Dexmedetomidine can be safely used for controlled hypotension in craniocerebral injury to reduce preoperative cerebral metabolism and improve postoperative cognitive function.

Data Availability

The data underlying the results presented in the study are available within the article.

Conflicts of Interest

The authors declare that there are no conflicts of interest.

Acknowledgments

This study was supported by the Shandong Province Traditional Chinese Medicine Science and Technology Project (2021Z009) (Protective effect and mechanism of Xuesaitong combined with dexmedetomidine on cerebral ischemia-reperfusion in olderly rats through removing stasis and antioxidant).

References

[1] H. Higashi, S. Otsuka, K. Nishimoto, and Y. Andou, "Beneficial effects of dexmedetomidine for postoperative neurosurgical patients care(surgical techniques and perioperative management)," *Japanese Journal of Neurosurgery*, vol. 16, no. 8, pp. 646–651, 2007.

[2] Y. Günes, M. Türktan, T. Erman, and H. Özbek, "Anesthesia for craniotomy Comparison of sevoflurane, desflurane, or isoflurane anesthesia supplemented with an infusion of dexmedetomidine during supratentorial craniotomy," *Neurosurgery Quarterly*, vol. 19, no. 2, pp. 110–115, 2009.

[3] S. Su, C. Ren, H. Zhang, Z. Liu, and Z. Zhang, "The opioid-sparing effect of perioperative dexmedetomidine plus sufentanil infusion during neurosurgery: a retrospective study," *Frontiers in Pharmacology*, vol. 7, p. 407, 2016.

[4] W.-K. Kwon, J. H. Kim, J.-H. Lee et al., "Microelectrode recording (MER) findings during sleep-awake anesthesia using dexmedetomidine in deep brain stimulation surgery for Parkinson's disease," *Clinical Neurology and Neurosurgery*, vol. 143, pp. 27–33, 2016.

[5] I. Rozet, "Anesthesia for functional neurosurgery: the role of dexmedetomidine," *Current Opinion in Anaesthesiology*, vol. 21, no. 5, pp. 537–543, 2008.

[6] B. G. Kim and H. Kang, "The effect of preemptive perianal ropivacaine and ropivacaine with dexmedetomidine on pain after hemorrhoidectomy: a prospective, randomized, double-blind, placebo-controlled study," *Indian Journal of Surgery*, vol. 76, no. 1, pp. 49–55, 2014.

[7] H. E. Aryan, K. W. Box, D. Ibrahim, U. Desiraju, and C. P. Ames, "Safety and efficacy of dexmedetomidine in neurosurgical patients," *Brain Injury*, vol. 20, no. 8, pp. 791–798, 2006.

[8] J. D. Dreier, B. Williams, D. Mangar, and E. M. Camporesi, "Patients selection for awake neurosurgery," *HSR Proceedings in Intensive Care & Cardiovascular Anesthesia*, vol. 1, no. 4, pp. 19–27, 2009.

[9] M. Gunduz, Y. Gunes, H. Ozbek, D. Yilmaz, and G. Isik, "Comparison of dexmedetomidine or remifentanil infusion combined with sevoflurane anesthesia in craniotomy: hemodynamic variables and recovery," *Neurosurgery Quarterly*, vol. 19, no. 2, pp. 116–119, 2009.

[10] I.-K. Song, S. Yi, H.-S. Lim et al., "A population pharmacokinetic model of intravenous dexmedetomidine for mechanically ventilated children after neurosurgery," *Journal of Clinical Medicine*, vol. 8, no. 10, p. 1563, 2019.

[11] L. V. Havrylova, "Experience with the dexmedetomidine for sedation in pediatric neurosurgery in the early postoperative period," *Endovascular Neuroradiology*, vol. 33, no. 3, pp. 56–65, 2020.

[12] B. A. G. Herbert, P. M. G. Ramaciotti, F. Ferrari et al., "Uso de dexmedetomidina em neurocirurgia," *Revista Brasileira de Anestesiologia*, vol. 57, no. 2, pp. 223–231, 2007.

[13] J. Wan, J.-F. Fu, J.-F. Liu, J.-K. Shi, C.-G. Jin, and H.-P. Zhang, "Class imbalance problem in short-term solar flare prediction," *Research in Astronomy and Astrophysics*, vol. 21, no. 9, p. 6, 2021.

[14] V. K. Srivastava, S. Agrawal, S. Kumar, A. Mishra, S. Sharma, and R. Kumar, "Comparison of dexmedetomidine, propofol and midazolam for short-term sedation in postoperatively mechanically ventilated neurosurgical patients," *Journal of Neuroanaesthesiology and Critical Care*, vol. 02, no. 2, p. 164, 2015.

[15] T. Chowdhury, S. Kowalski, Y. Arabi, and H. Dash, "General intensive care for patients with traumatic brain injury: an update," *Saudi Journal of Anaesthesia*, vol. 8, no. 2, pp. 256–263, 2014.

[16] A. Wajekar, A. Shetty, S. Oak, and R. Jain, "Anaesthetic management for drainage of frontoparietal abscess in a patient of uncorrected Tetralogy of Fallot," *Indian Journal of Anaesthesia*, vol. 59, no. 4, p. 244, 2015.

[17] Y. Liu, F. Liang, X. Liu, X. Shao, N. Jiang, and X. Gan, "Dexmedetomidine reduces perioperative opioid consumption and postoperative pain intensity in neurosurgery: a meta-analysis," *Journal of Neurosurgical Anesthesiology*, vol. 30, pp. 146–155, 2017.

[18] V. Stambolija, M. Miklić Bublić, M. Lozić, Z. Gužvinec, and M. Vukić, "Analgosedation with dexmedetomidine in a patient with superior vena cava syndrome in neurosurgery," *Journal of Neurosurgical Anesthesiology*, vol. 30, no. 1, pp. 79-80, 2018.

[19] V. Stambolija, M. Miklić Bublić, M. Lozić, Z Gužvinec, and M Vukić, "Analgosedation with dexmedetomidine in a patient with superior vena cava syndrome in neurosurgery," *Journal of Neurosurgical Anesthesiology*, vol. 30, no. 1, pp. 79-80, 2018.

[20] H. Li, D. Zeng, L. Chen, Q. Chen, M. Wang, and C. Zhang, "Immune multipath reliable transmission with fault tolerance in wireless sensor networks," in *Proceedings of the International Conference on Bio-Inspired Computing: Theories and Applications*, pp. 513–517, Springer, Xi'an, China, October 2016.

[21] J. S. Jones, R. E. Cotugno, N. R. Singhal et al., "Evaluation of dexmedetomidine and postoperative pain management in patients with adolescent idiopathic scoliosis: conclusions based on a retrospective study at a tertiary pediatric hospital," *Pediatric Critical Care Medicine: A Journal of the Society of Critical Care Medicine and the World Federation of Pediatric Intensive and Critical Care Societies*, vol. 15, no. 6, pp. e247–52, 2014.

[22] A. Sharma, N. Kumar, M. Azharuddin, L. Mohan, and G. Ramachandran, "Evaluation of low-dose dexmedetomidine and neostigmine with bupivacaine for postoperative analgesia in orthopedic surgeries: a prospective randomized double-blind study," *Journal of Anaesthesiology Clinical Pharmacology*, vol. 32, no. 2, pp. 187–191, 2016.

[23] R. Stechow, I. Ivanova, M. Naveed, and S. Weiss, "Sample Preparation of Worn Surfaces for EBSD Analysis," *Practical Metallography*, vol. 53, no. 6, pp. 352–359, 2016.

[24] C. Cao, Y. Tang, D. Huang, W. Gan, and C. Zhang, "IIBE: an improved identity-based encryption algorithm for wsn security," *Security and Communication Networks*, vol. 2021, Article ID 8527068, 8 pages, 2021.

[25] B. W. Qualls, M. D. Bobry, and M. A. Feeney, "Certification circle: a peer support model to increase certification among medical-surgical inpatient nurses," *The Journal of Continuing Education in Nursing*, vol. 52, no. 10, pp. 468–470, 2021.

[26] X. Wang, J. Ji, L. Fen, and A. Wang, "Effects of dexmedetomidine on cerebral blood flow in critically ill patients with or without traumatic brain injury: a prospective controlled trial," *Brain Injury*, vol. 27, no. 13-14, pp. 1617–1622, 2013.

Hindawi
Computational Intelligence and Neuroscience
Volume 2022, Article ID 1465613, 10 pages
https://doi.org/10.1155/2022/1465613

Research Article

Application of the Flipped Classroom Mode under Few-Shot Learning in the Teaching of Health Physical Education in Colleges and Universities

Huimin Wang[1] and Min Chen[2]

[1]Southwest Minzu University, Chengdu, Sichuan 610041, China
[2]School of Physical Education, Yulin Normal University, Yulin, Guangxi 537000, China

Correspondence should be addressed to Min Chen; chenmin@ylu.edu.cn

Received 8 December 2021; Revised 25 December 2021; Accepted 27 December 2021; Published 11 March 2022

Academic Editor: Xin Ning

The flipped classroom is a revolutionary teaching method that reverses the traditional roles of teachers and students, as well as the traditional classroom and after-school schedules. The flipped classroom is currently the most popular English teaching reform, so the design and development must meet the practical needs of college physical education teaching. Subverting the classroom is a highly effective service for college physical education that promotes college physical education quality improvement. The research topic of this study is the application of the flipped classroom teaching model based on few-shot learning in public physical education in ordinary colleges and universities. It analyzes the conceptual advantages of the flipped classroom teaching model based on few-shot learning, combining its benefits with the current common college environment. There are issues in physical education, and a teaching model suitable for public physical education in ordinary colleges and universities is gradually being developed in order to improve students' enthusiasm for independent learning and classroom teaching quality. The flipped classroom teaching model has given rise to new ideas for the construction of a physical education model: first, students' physical learning is no longer limited to the physical education classroom, thanks to the use of network technology to change the learning environment. Teaching resources have been expanded to include many online sports resources, so students' physical learning is no longer limited to the physical education classroom. Students can learn anytime and anywhere, which allows them to continue their education throughout their lives; second, flipped classrooms increase teacher-student interaction and play an important role in re-establishing a harmonious teacher-student teaching relationship: third, online courses help students develop their skills. Autonomous learning's ability to shape students' personalized learning is better suited to the development of students' core literacy.

1. Introduction

The purpose, principles, and production process of the few-shot learning design for the general physical education major of college physical education are discussed in this article, which first outlines the general few-shot learning design and development. A typical case is taught in few-shot learning, a general physical education course [1]. The fifth section aims to develop the few-shot learning method, which is currently being used in general physical education teaching at colleges and universities, in conjunction with the flipped classroom teaching mode, in order to carry out actual teaching, strictly control the experiment process, and verify the few-shot learning teaching method. It is more beneficial to assist students in learning about sports technology [2].

Teachers and students use various methods in the teaching process to achieve common teaching goals and complete common teaching tasks, which is referred to as a teaching method. The teaching method chosen has a significant impact on the teaching effect, and different teaching methods have different teaching effects. The current physical education teaching method uses a class teaching system, which makes it difficult to respect student differences and even more difficult to provide personalized instruction [3].

The flipped classroom, on the other hand, is a new type of personalized teaching mode based on few-shot learning in the context of information technology. Students can learn anytime and anywhere using the teaching videos created by teachers, and they can track their progress based on their own understanding ability. Students can interact with one another if they have any doubts or incomprehension while self-studying [4]. Above all, teachers can gain a better understanding of each student's learning situation by receiving feedback from students prior to class. At the same time, teachers can group the students of different learning levels in class or group the students according to their mastery of a specific knowledge point and conduct hierarchical teaching according to the actual situation of each group in a targeted manner, taking into account each of them [5].

This article combines my own experience with few-shot learning, identifies flaws and areas that need to be addressed, and then presents my own insights and prospects for future research into few-shot learning. The traditional teaching method emphasizes the importance of continued training in order to improve technology quality. Excessive learning repetition will inevitably bore students and cause them to lose interest in learning. Few-shot learning, which became popular in the 1990s, helped to solve some of these issues [6]. Few-shot learning is being used in college physical education classes to reflect a more free and flexible teaching method, and the content of few-shot learning is being streamlined [7]. Physical education is a skill-based collective project, so it avoids students' resistance to a large amount of teaching content during the learning process, which reduces the classroom's teaching effect, reduces students' learning efficiency, and prevents students from mastering technical movements. A sense of learned helplessness is produced by weakness [8]. The use of the flipped classroom teaching model has improved the status and performance of physical education, facilitated the continued acquisition of physical skills at the university level, and improved the overall development of quality education. The flipped classroom teaching model promotes the advancement of sports reform, the achievement of student-centered physical education goals, the fulfillment of personal needs, and the development of students' interest in sports learning and practice. This study establishes a new practical physical education teaching model, changes the teaching model and organizational form simultaneously, and increases students' enthusiasm for learning and practice.

2. Related Work

In recent years, the research on the flipped classroom teaching model is relatively early, and various theoretical methods are relatively mature. Two high school teachers (Jonathan Berman and Aaron sans) from the United States were unable to use screen recording software to record courseware or lecture audio and upload these materials to the Internet, which made the absent students unable to enjoy the relevant course content. The essence of the flipped classroom is to "reverse" or "flip" the traditional teaching form, that is, to transform the traditional "teaching first and then learning" into "first learning and then teaching." It is subverting the traditional classroom form and forming new teachers and students. Relationship, this is not only a flip of the teaching form but more importantly, the change of teaching philosophy [9]. At the same time, flipping is just a means. Its real purpose is to leave more time in the classroom for teachers and students to fully communicate and interact, stimulate each other's intellectual potential, and free the teacher from the heavy work of repeated teaching. The time guides students to construct the correct knowledge framework and improve the efficiency of students' learning [10].

Literature [11] found through a large number of tests that human memory capacity is infinite in a sense, but people have limited access to learning and acquiring knowledge. There are too many things to learn, which is more than that from a psychological point of view. People's cognitive ability, in layman's terms, is that they are too greedy to chew. Few-shot learning focuses on its "micro" characteristics, the content is refined, the important and difficult points are prominent, and it is easy to quickly internalize the learned knowledge for personal use.

Few-shot learning, also known as few-shot learning process, is the abbreviation of microvideo network courses, according to literature [12]. It focuses on specific subject knowledge points using microteaching videos as the primary carrier, such as key points, difficult points, and doubts. Designed and developed a new type of contextualized and support for a variety of learning methods of online course resources, such as test sites or teaching links, such as learning activities, themes, experiments, and tasks. "Few-shot learning" is defined by literature [13] as "an online teaching video document aimed at explaining a certain point of knowledge, using short and succinct online videos as the form of expression, with the purpose of learning or teaching applications." Reference [14] considers "few-shot learning" to be beneficial. It is a type of situational and interesting development carefully designed and developed for a specific subject knowledge or teaching link in order to support a variety of learning methods such as flipped learning, blended learning, mobile learning, and fragmented learning, using short and succinct microteaching videos as the main carrier. The package of scientific and visual learning resources "few-shot learning" or "few-shot learning process" means that the time is less than 10 minutes and there is a clear teaching goal and content, according to literature [15]. A brief, small course aimed at explaining a problem. Microlearning is defined as a new type of learning based on microcontent and media that exist in the new media ecosystem, according to the literature [16]. Microlearning, according to the theory, can learn in a reasonable amount of fragmented time, with flexible learning time, no fixed learning location, and a variety of learning forms, including mobile phones, IPAD micromedia application terminals, and systematic learning microcontent to complete knowledge and skill learning tasks.

Literature [17] believes that few-shot learning is a kind of teaching aid resource, which is the basis for implementing flipped classrooms and the carrier of knowledge transfer. It needs a concise but complete teaching design, and an analysis of the learning situation and teaching purpose must be carried out first. Subject development and the actual needs of students choose the appropriate few-shot learning type, and then make a script recording, plus a series of exercises, tests, and other links, to produce short and concise teaching resources, which is a complete teaching system, and vice versa. The flipped classroom is the way to achieve the purpose of few-shot learning and teaching. Only by combining few-shot learning as a teaching resource, the flipped classroom can be effectively realized. Due to the accelerating pace of today's society, people's purpose of acquiring knowledge is stronger, most of them are to meet current needs. The learning time for a few-shot learning is basically between 5 and 15 minutes, and various fragmented ones can be used. Time to study, make full use of time reasonably, and the time requirement is not too high. The 60-second organic chemistry course proposed in the literature [18] was originally designed to allow more ordinary people to understand some basic chemistry knowledge in different situations and hope to apply it to other disciplines. This research has laid a good foundation for the future proposal of "few-shot learning."

Therefore, it is an urgent need to apply the theoretical results of previous studies to practical teaching in an efficient and reasonable manner, and it is also the greatest significance of this thesis. This article takes the application of few-shot learning in the teaching of general physical education courses of college physical education as the research object. Through the analysis of the disciplinary characteristics and teaching goals of the general physical education courses of physical education in colleges and universities, it uses the form of questionnaires to develop the general physical education The investigation of the current teaching situation of the course, and the measurement of the students' various sports indicators related to this research. Based on this, the design and development of few-shot learning and teaching resources are carried out. A comprehensive analysis of the influence of physical exercise attitude is carried out.

3. Few-Shot Learning and Flipped Classroom Related Theories

In the context of deep learning, each class requires at least thousands of training samples to saturate the performance of the CNN on the known classes [19, 20]. In addition, the generalization ability of neural networks is weak. When a novel class comes, it is difficult for the model to learn to recognize novel concepts through a small number of labeled samples. However, all of this is not a problem for humans. We humans have the ability to quickly learn from a small number of (single) samples. Even for a five- or six-year-old child, he has never seen a "panda." After his father showed him a picture of a panda, the child will recognize the dark circles when he arrives at the zoo. The fat animal is called "panda."

The following sentence "In Australia, humans have never seen a platypus. Humans will recognize a platypus if you show us a picture of one!" is considered as an illustration Ducks, civet cats, fish, and other animals we've seen in our lives represent prior knowledge of knowledge, while the platypus represents the unknown. This prior knowledge of knowledge is referred to as meta-knowledge, and our brain can quickly access it. A quick comparison of the platypus that has never been seen before and this meta-knowledge (there may be some other mental activities, such as visually extracting the features of objects) [21] leads to the conclusion that this one has the beak of a duck and can swim like a fish. The platypus is a new flat-bodied animal. The example in the preceding paragraph grossly undervalued the human brain. I'm just trying to demonstrate how novel concepts and established knowledge are inextricably linked. Of course, if we are completely unfamiliar with something, we need time to learn. Figure 1 depicts the general flow of the few-shot learning design.

There is a data set D, which we divide into two parts: Dbase and Dnovel, which do not overlap. Dbase is the basic training set that we used to train our model, while Dnovel is the test data. As an example, the 5-way 5-shot is considered. Each time Dnovel is tested, 5 classes (meaning 5-way) are collected. If each of these five classes has 100 samples, we will choose 100 samples at random. Among the 100 samples collected, 5 samples are used as the support set, and the remaining samples are used as the query set [22].

The traditional classroom model is to put the knowledge explanation part in the classroom, mainly to explain the teacher in the classroom, which is a complete teaching model; the flipped classroom model is to use Internet technology to liberate the knowledge of knowledge to the Internet. Students complete the teaching ahead of time through self-learning before class, which greatly reduces the teacher's teaching time in the classroom, allowing students more time to think independently, complete their homework, and communicate with each other in the classroom. The flipped classroom model greatly increases the students' "preparatory time," and teachers must do their best to achieve the high efficiency of "class time" [23]. The flipped classroom model is shown in Figure 2.

The role of the classroom has changed. In this mode, the teacher has changed from the former classroom teacher to the student's classroom coach. The change in the roles of teachers and students has greatly increased the students' interest in learning, making them more active, profound, interesting in their learning, and more proficient in sports training techniques and improving the quality of learning. In the traditional teaching model, the teacher is the center of the entire class. In the classroom, teachers mainly explain knowledge, while students passively accept knowledge [24]. Due to the lack of interaction and communication, students have lost interest in physical education. However, under the flipped classroom teaching model, the roles of teachers and students have undergone great changes, and students have gradually become the center of the entire class. This is the exchange and discussion of students in the classroom, and the teacher guides and answers questions. In the whole teaching process, teachers only need to control the learning process of students, and when appropriate, divide students into several study groups for communication, discussion,

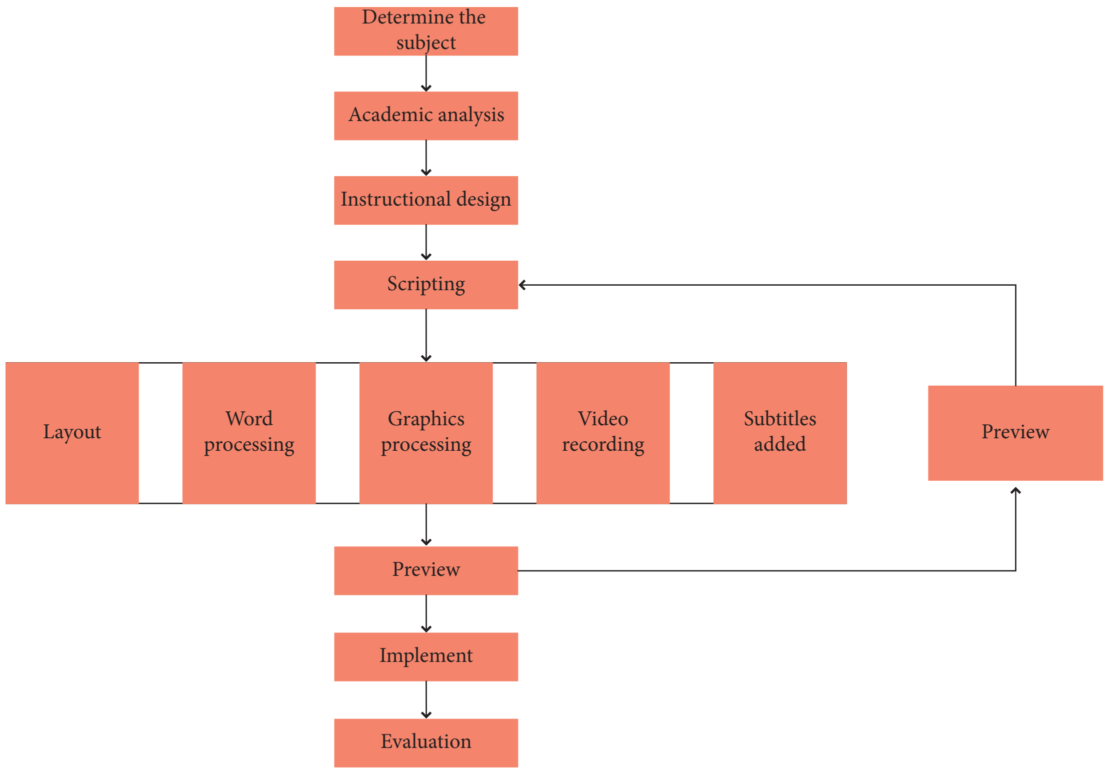

Figure 1: Few-shot learning design process.

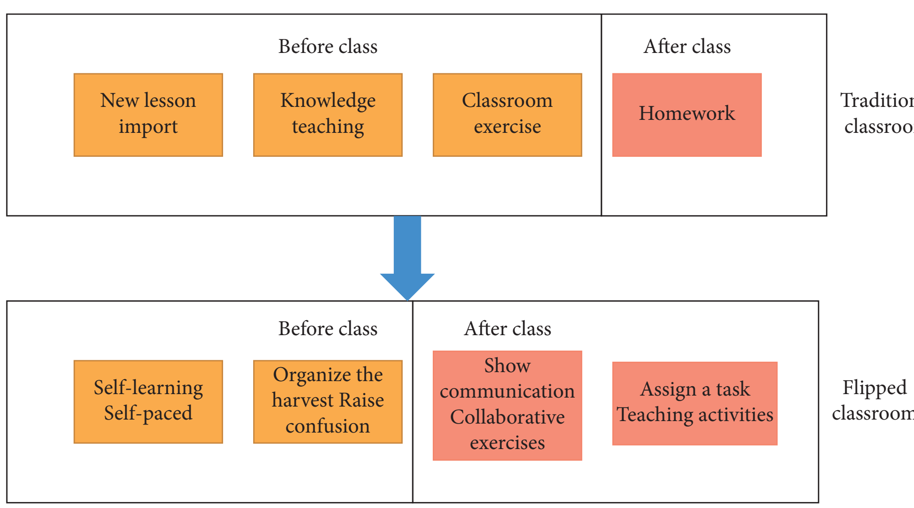

Figure 2: Flipped classroom mode.

and learning. Students not only learn knowledge but also improve their ability to operate sports techniques.

Few-shot learning is a type of educational resource. It serves as the foundation and knowledge transfer vehicle for flipped classroom implementation. It necessitates a concise but comprehensive teaching strategy. It must first assess the academic situation and teaching purpose in light of the subject's development and the students' current situation. To create short and concise teaching resources, you must first choose the appropriate few-shot type, then record a script, as well as a series of exercises, tests, and other activities, to create a complete teaching system. As a result, the flipped classroom is a one-shot deal. To effectively realize the flipped classroom, the method for achieving the teaching purpose must be combined with few-shot learning, a teaching resource. According to cognitive load theory, the human cognitive structure is made up of short-term and long-term memory. Working memory is another name for short-term memory. It has a very limited capacity. It can only store 5–9 pieces of basic data in most cases. The cognitive load will be exceeded if there is too much learning content. As a result, few-shot learning was born. It is based on small, refined learning content that follows the cognitive load theory and is gradually applied to various teaching methods.

4. Design and Practical Application of PE Teaching Model Based on Few-Shot Learning Flipped Classroom Model

The activities of teachers in the preclass stage are mainly the collection of teaching resources and the production of microvideos. Microvideos are mostly the key and difficult points in the teaching content. Therefore, teachers should formulate teaching goals and select teaching content according to the actual situation of students when making. At the same time, it is necessary to consider the individual differences of students, make multiple versions of videos, and explain the teaching content to different levels in a targeted manner. Detailed learning tasks are arranged, a variety of practice methods is provided, and students' problems in the learning process are collected. In the preclass stage, students mainly study independently on the teaching videos provided by the teacher and complete the tasks assigned by the teacher. First, a solution to the problems arising in the study is addressed or discussed and communicated between teachers and students, and between students and students through online platforms. The preclass stage mainly stimulates students' interest in learning and cultivates students' awareness and ability of independent learning, independent thinking, problem-solving ability, and innovative ability. The physical education teaching model design of the flipped classroom model based on few-shot learning is shown in Figure 3.

In the course of the class, the teacher mainly explains and demonstrates the problems that students have before class, organizes students to discuss and practice in groups, and corrects students' wrong actions in time during the tour guide. Students relearn what they have learned in the classroom to achieve knowledge internalization. In the middle of the class, the group discussion exercises mainly cultivate the students' unity and cooperation ability and language organization ability. The skill display link not only cultivates the students' sense of competition but also exercises the students' psychological quality. After class, teachers mainly reflect on the effect of classroom teaching and further improve and optimize the teaching plan. The main purpose is to improve teaching quality and improve student learning efficiency. Students' relearning after class is mainly to consolidate knowledge and further improve their technical level. The after-school period mainly cultivates students' good study habits and develops the consciousness of lifelong sports.

Teaching evaluation is the process of evaluating the process of teaching activities and results using certain standards and methods based on the teaching goals, that is, evaluating the process of teaching activities and results. Its purpose is to make course, teaching, and student training program decisions, with the most important aspect being to evaluate students' academic performance. Traditional teaching evaluation is primarily summative, that is, the assessment of students' learning outcomes at the end of each learning stage. This method focuses on assessing students' mastery of the curriculum, and while the generalization level is high, it may lead students to believe that they do not work hard in normal circumstances. During the exam, the "scallop effect" appears, which is not conducive to boosting students' learning motivation and forming a positive learning outlook.

When teaching evaluation is based on the few-shot teaching method, it uses a teaching evaluation method that is consistent with quality education, focusing on the developmental evaluation of students, and the overall development of student quality is used as the evaluation index. The fundamental principle is that each individual is responsible for his or her own actions. A student's development is based on the student's previous experiences, with a focus on the student's current situation and a greater emphasis on the student's future. The identification of learning levels and the description of student development characteristics are for the future development of students, with a focus on student evaluation in the learning process. Encouragement evaluation is carried out in the classroom, and students' classroom performance is factored into the evaluation of their academic performance. Among them, the timely, quality, and quantity completion of the after-school homework arranged by the teacher is also included in the student's score, that is, after each class, after the smashing skills are strengthened after the class, it is for everyone to communicate and evaluate and give extra points to active students. This evaluation method can not only provide timely feedback through teacher and student comments and help students improve their motor skills, but it can also promote students' subjective initiative and increase their motivation to learn.

5. Experimental Process and Design

5.1. Academic Analysis. Few-shot learning and instructional design is different from traditional instructional design. At the beginning of the design, it must take into account its short and powerful characteristics and highlight its original intention of explaining the important and difficult points. Compared with traditional teaching methods, few-shot learning with the help of videos, animations, and exquisite diagrams can attract the attention of students, increase their interest in learning, ignite their passion, stimulate their vitality in learning this sport, let them enjoy learning basic knowledge and skills and action methods in a happy atmosphere and learning by playing and playing while learning, constantly stimulate their potential, mobilize students' enthusiasm and subjective initiative in learning, and let them experience the joy of success through the learning of technical movements.

Before the teaching experiment, the subjects were surveyed with relevant questionnaires, and the survey results are shown in Figure 4.

It can be seen that the new teaching method is supported and welcomed by the students. At the same time, in the questionnaire survey, the learners' learning attitudes are analyzed, and when they have poor skills or technical actions that are not well understood in the learning process, which solutions students prefer, the results of the survey are shown in Figure 5:

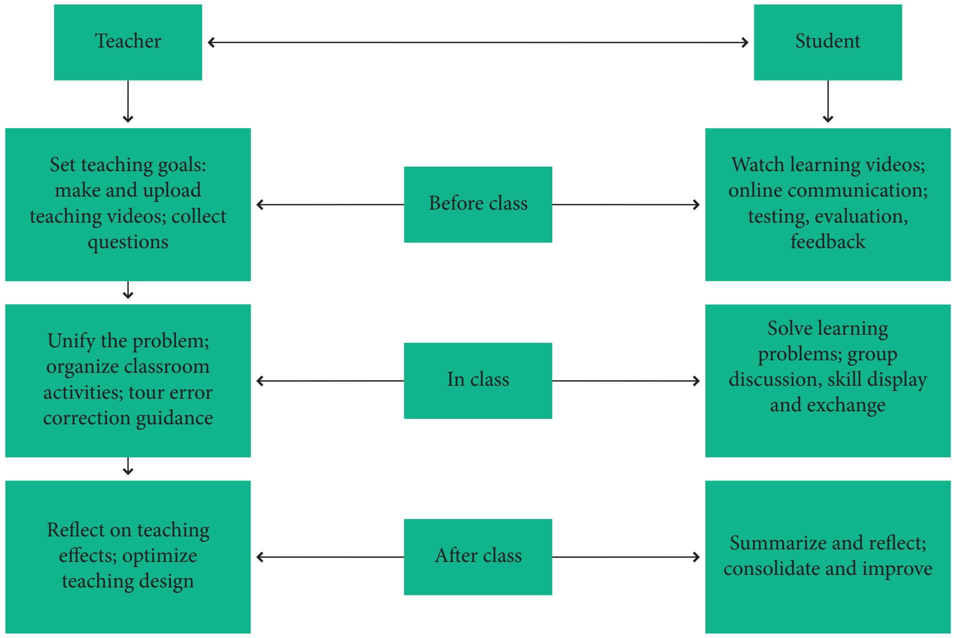

Figure 3: The design process of physical education model.

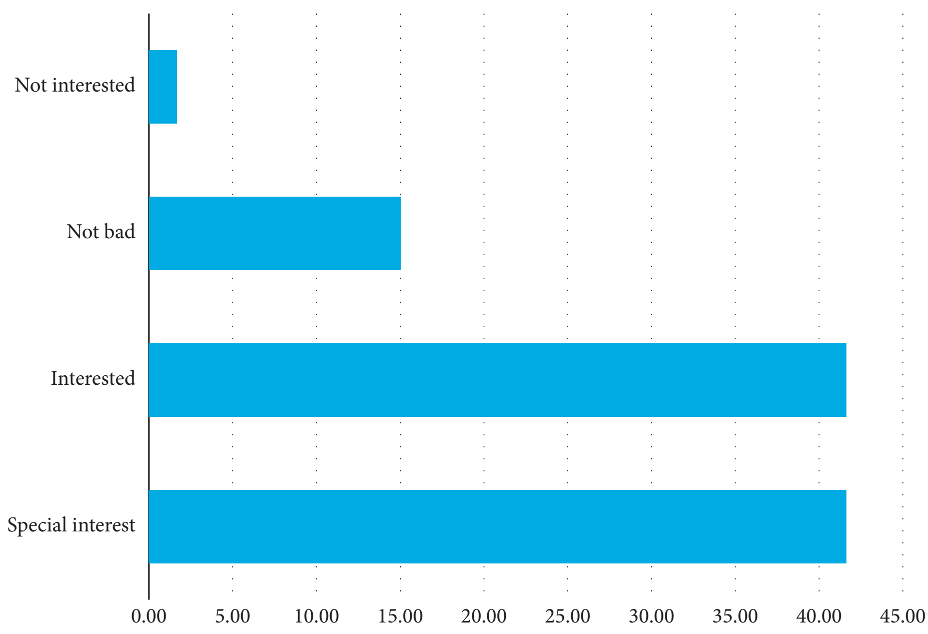

Figure 4: Attitudes toward physical education.

In the process of students learning in the past teaching methods, 83.33% of the students tend to ask the teacher and 11.67% of the students choose to watch the teaching video. Although these data are relatively small, it can be seen Although the number of samples we collected is relatively small, it can be seen from the results that the flipped classroom teaching model meets the requirements of current students' learning.

6. Instructional Design

This article randomly selects students from eight classes of the same grade. The body shape and physical fitness are used as the breakthrough test data to explain the problem, the four classes with no significant differences are chosen as the experimental class, and the other four classes are chosen as the control class. The experiment class adopts the new teaching mode of flipped

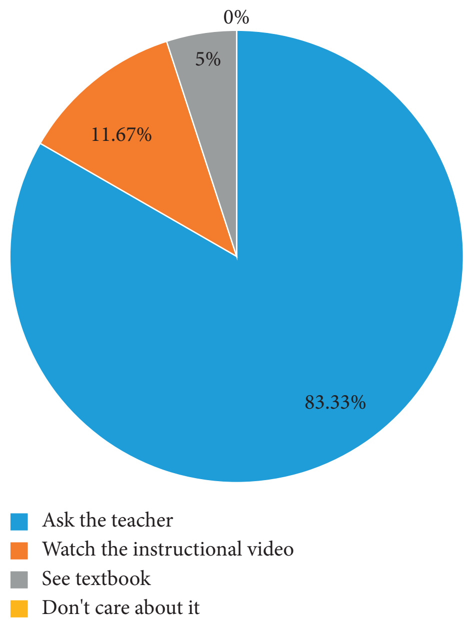

Figure 5: Students' problem-solving methods.

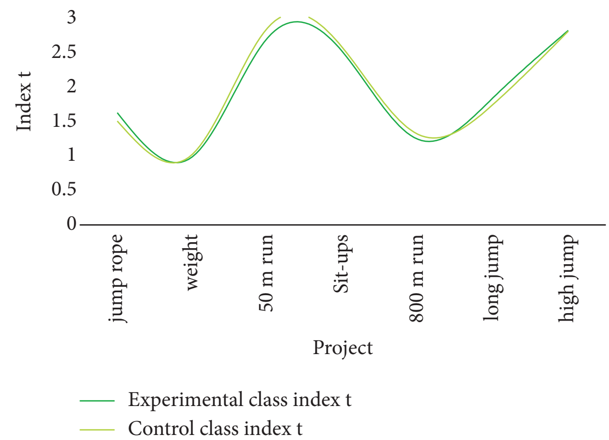

Figure 6: The physical condition of the students before the experiment.

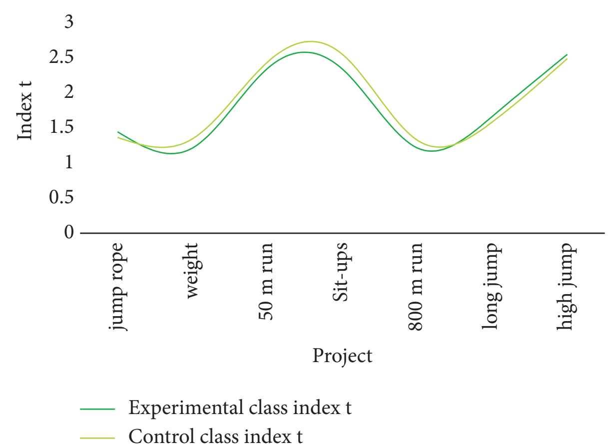

Figure 7: The physical fitness of students after training.

classroom, and the control class adopts the traditional teaching mode. Finally, the collected data were compared and the relevant data during the experiment was recorded.

Through the analysis of the pretest data of the experimental class and the control class, as shown in Figure 6.

The test data include height, weight, 50 m, and sit-ups (female) items. The data index t-test before the test showed that the P value was higher than 0.05, indicating that the experimental group and the control group had no significant differences in body shape and physical quality.

The data of students' physical fitness after training can be obtained from Figure 7.

The precheck items of human body shape and athletic ability were retested after the flipped classroom teaching model experiment. The P values are both large after t-testing, the height and weight test data are statistically obtained. The results revealed that there was no significant difference between the experimental and control groups' test results.

7. Significance Analysis of Attitudes toward Physical Training after Experimental Class and Control Class

After one semester of physical education, both classes have basically completed the smash and serve skills. At the same time, the physical exercise attitude of the two classes was investigated. The t-test was used to reflect the physical exercise attitude before and after the two semesters. Change, the difference in physical exercise attitude between the two classes, is shown in Tables 1 and 2. The corresponding results can be found in Figures 8–11.

Through analysis, it can be seen that the control class's attitude toward physical activity has slightly changed, whereas the experimental class's attitude toward physical activity has greatly improved, owing to the fact that the new teaching method is relatively new and the teaching method is relatively new. It is one of a kind and better suited to their learning styles. In conclusion, few-shot learning combined with a flipped classroom teaching mode has a greater impact on improving students' physical exercise attitudes than traditional teaching methods, resulting in increased physical activity behavior. This demonstrates that few-shot learning combined with the flipped classroom teaching mode can effectively improve students' basic level and their spiking skills. For middle-level students, both teaching methods have improved and the degree of improvement has increased. Few-shot learning combined with flipped classroom teaching mode is almost as good as traditional teaching methods in terms of improving students' high-level learning.

It was found that the physical fitness of the two classes had improved before and after the experiment. This was an inevitable result of one semester of sports training, and the improvement of the physical fitness of the two classes was roughly the same. This shows that this teaching method and traditional teaching methods are improving students There is no obvious advantage in physical fitness. The reason is that

Table 1: The analysis of the students' attitudes toward physical exercise before and after the experiment in the experimental class.

	Before the experiment		After the experiment	
	Mean	Standard deviation	Mean	Standard deviation
Action	27.58	4.37	28.78	5.42
Manner	41.89	6.05	45.95	7.39
Cognition	26.42	4.30	28.13	4.76
Habit	32.31	6.25	34.29	7.61
Emotion	31.72	4.81	23.81	5.40
Standard deviation	24.38	4.49	24.97	5.35
Intention	25.03	3.69	26.21	4.31
Subjective goal	20.03	3.32	20.11	3.61

Table 2: Analysis of students' attitudes toward physical exercise before and after the experiment in the control class.

	Before the experiment		After the experiment	
	Mean	Standard deviation	Mean	Standard deviation
Action	28.03	5.25	28.06	5.45
Manner	43.64	19.48	43.92	7.76
Cognition	26.02	4.13	26.67	5.21
Habit	33.54	8.61	32.56	7.61
Emotion	34.77	6.54	34.81	6.78
Standard deviation	24.21	3.71	23.84	5.72
Intention	25.31	4.39	24.89	4.67
Subjective goal	21.54	4.05	20.45	4.02

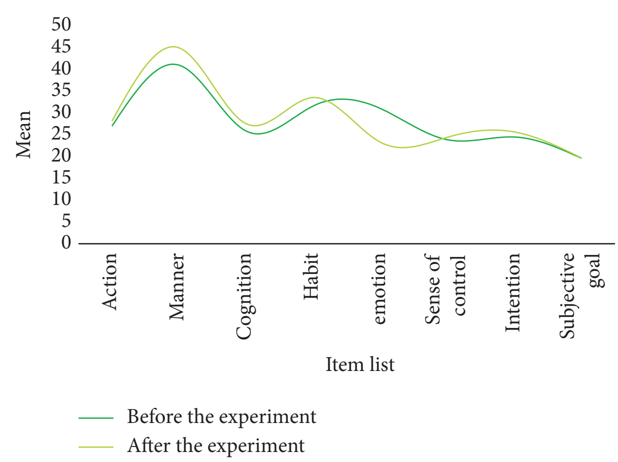

Figure 8: The average value of students' attitudes toward physical exercise before and after the experiment in the experimental class.

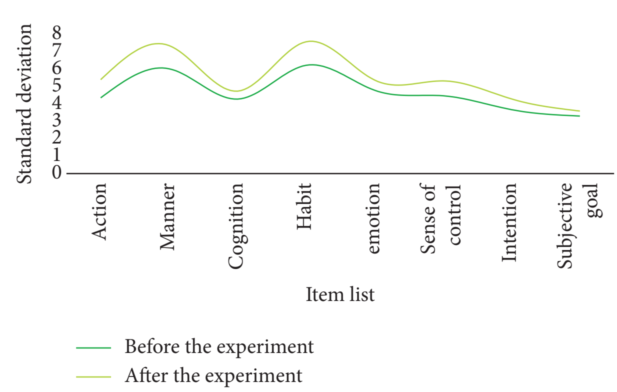

Figure 9: The standard deviation of students' physical exercise attitude before and after the experiment in the experimental class.

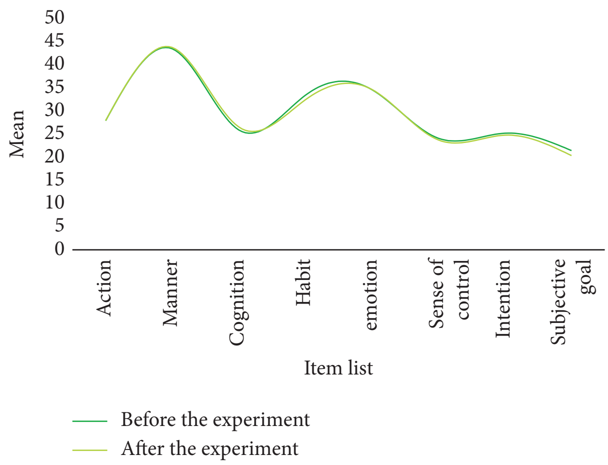

Figure 10: Mean values of students' physical exercise attitudes before and after the experiment in the control class.

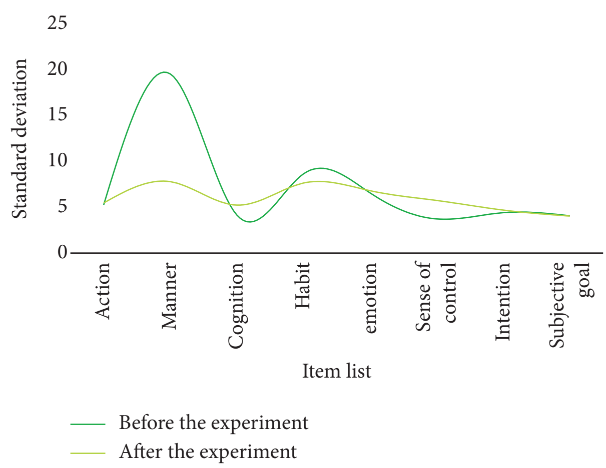

Figure 11: Standard deviation of students' physical exercise attitude before and after the experiment in the control class.

physical education has a lot of content and heavy tasks. In the teaching process, the teacher focuses more on skills and skills teaching and does not carry out special physical fitness exercises.

8. Conclusions

Both the school leaders and the teachers themselves must attach importance to the learning of few-shot learning and production technology and vigorously promote the use of few-shot learning and educational resources, but we should also pay attention to the effectiveness of the above methods in practical application. At the same time, the school should regularly invite few-shot learning and production experts to train all teachers, so that teachers can master the technology as soon as possible and complete the teaching tasks with quality and quantity.

When teaching evaluation is based on the few-shot learning and teaching method, it uses a teaching evaluation method that is consistent with quality education, focusing on the developmental evaluation of students and using the overall development of student quality as the evaluation index. The fundamental principle pertains to a student's development. Teachers who are quick to accept can help other teachers form a learning environment of mutual help and mutual assistance based on their own experience and expertise resource and encourage teachers to develop their own style of few-shot learning education based on their own experience and expertise resource. Furthermore, in order to more effectively share teaching resources, schools should create a few-shot learning and education resource information sharing platform as soon as possible to maximize information sharing. The traditional teaching method limits the assessment of students' learning to a review of their theoretical knowledge and skills. The evaluation method is relatively simple, which is detrimental to students' overall development. As a result, the content of future learning evaluations will be more diverse. The performance of students' affection and sense of cooperation should be given more attention. Similarly, evaluation methods should be varied, and a combination of methods can be used to make an objective and fair assessment of students' learning situations. It is based on the student's previous experiences, with a focus on the student's current situation and a greater emphasis on the student's future. The identification of learning levels and the description of student development characteristics are for the future development of students, with a focus on student evaluation in the learning process. Encouragement evaluation is carried out in the classroom, and students' classroom performance is factored into the evaluation of their academic performance. Students who are active will receive extra points for completing after-school homework on time, in a good quality and in a quantity that the teacher has assigned. This evaluation method can not only provide timely feedback through teacher and student comments and help students improve their motor skills, but it can also promote students' subjective initiative and increase their motivation to learn.

The teaching time for this experiment is relatively short for a variety of reasons, and there are some important and difficult points that students do not fully grasp. Simultaneously, the number of samples in the teaching experiment should be increased to make it more convincing. The use of this teaching method is encouraged.

Data Availability

The dataset used to support the findings of this study is available from the corresponding author upon request.

Conflicts of Interest

The authors declare that they have no conflicts of interest.

References

[1] S. Cai, "Thinking about the application of flipped classroom in college physical education[J]," p. 56, 2021 (2017-32).

[2] Party and government, "The application of flipped classroom in college physical education[J]," *China High-tech Zone*, vol. 000, no. 024, p. 283, 2018 82.

[3] D. Wang, "The application feasibility and application points of flipped classroom in college physical education[J]," p. 67, 2021 (2018-11).
[4] H. Ke, "On the application analysis of flipped classroom in college physical education[J]," pp. 210-211, 2021, (2018-19).
[5] S. Yang, "Application of MOOC - based flipped classroom in the teaching of basic computer application courses in physical education colleges [J]," *Modern Manufacturing Technology and Equipment*, vol. 000, no. 8, pp. 166–168, 2017.
[6] M. O. Faruk Khan, M. J. Deimling, and A. Philip, "Medicinal chemistry and the Pharmacy curriculum," *American Journal of Pharmaceutical Education*, vol. 75, no. 8, p. 161, 2011.
[7] P. G. O'Malley, K. Kroenke, J. Ritter, N. Dy, and L. Pangaro, "What learners and teachers value most in ambulatory educational encounters[J]," *Academic Medicine*, vol. 74, no. 2, pp. 186–191, 1999.
[8] C. Feenstra, B. Gordon, D. Hansen, and G. Zandee, "Managing community and Neighborhood Partnerships in a Community-based Nursing curriculum," *Journal of Professional Nursing*, vol. 22, no. 4, pp. 236–241, 2006.
[9] Y. Huang, "Research on flipped classroom teaching mode based on MOOC——taking physical education teaching in higher Vocational colleges as an example[J]," *Advances in Higher Education*, vol. 4, no. 10, 2020.
[10] T. Zhang, "Using the flipped classroom model to improve students' physical literacy——the application strategy of flipped classroom in junior high school physical education [J]," *New Curriculum (Part 2)*, vol. 498, no. 10, p. 420, 2019.
[11] Y. Ren, "The application of flipped classroom in college physical education," pp. 90-91, 2021, (2017-30).
[12] C. Zhang, "The application and strategy of flipped classroom in physical education[J]," *Heilongjiang Science*, vol. 9, no. 7, p. 2, 2018.
[13] Y. Dong, "Research on the application of flipped classroom teaching mode in physical education[J]," *Boxing and Fighting*, vol. 000, no. 10, pp. 15–64, 2016.
[14] Y. Wang and Y. Nie, "Analysis of the existing problems and countermeasures under the application of "flipped classroom" mode program in cheerleading teaching in colleges and universities[J]," *Sports Products (Academic Edition)*, vol. 35, no. 003, pp. 10-11, 2016.
[15] H. Wang, "The application of MOOC in PE flipped classroom teaching[J]," *Science and Fortune*, vol. 000, no. 034, p. 180, 2018.
[16] B. Hou, "Analysis on the construction of "flipped classroom" mode in college physical education[J]," *Contemporary Sports Science and Technology*, vol. 2018, no. 16, pp. 125-126, 2018.
[17] Di Zhang and X. Lingqiang, "The application of flipped classroom teaching mode in college yoga teaching[J]," *Family Life Guide*, vol. 2018, no. 09, p. 179, 2018.
[18] Z. Zhang, "Application research of flipped classroom in physical education [J]," *Contemporary Sports Science and Technology*, vol. 7, no. 36, p. 2, 2017.
[19] Z. Huang, Y. Liu, C. Zhan, C. Lin, W. Cai, and Y. Chen, "A novel group Recommendation model with two-stage deep learning," *IEEE Transactions on Systems, Man, and Cybernetics: Systems*, pp. 1–12, 2021.
[20] X. Li and J. Qiu, "A Multi-parameter video quality assessment model based on 3D Convolutional neural network on the Cloud," *ASP Transactions on Internet of Things*, vol. 1, no. 2, pp. 14–22, 2021.
[21] M. Zhang and Y. Chen, "The application and strategy of flipped classroom in school physical education," p. 138, 2021 (2018-33).
[22] R. Hui, "Research on the effective strategy of using the flipped classroom model in physical education[J]," *Sports Boutique*, vol. 40, no. 3, p. 2, 2021.
[23] L. Yuan, "The application value and strategy of flipped classroom in physical education[J]," *Quality Education in West China*, vol. 3, no. 12, p. 1, 2017.
[24] R. Chen, "Discussion on the application of flipped classroom in physical education teaching in secondary Vocational schools," pp. 138-139, 2021, (2017-8).

Hindawi
Computational Intelligence and Neuroscience
Volume 2022, Article ID 3422859, 8 pages
https://doi.org/10.1155/2022/3422859

Research Article

Visual Object Tracking Algorithm Based on Biological Visual Information Features and Few-Shot Learning

Dawei Zhang and Tingting Yang

School of Computer and Artificial Intelligence, Zhengzhou University, Zhengzhou, Henan 450001, China

Correspondence should be addressed to Dawei Zhang; iedwzhang@zzu.edu.cn

Received 14 January 2022; Revised 7 February 2022; Accepted 8 February 2022; Published 3 March 2022

Academic Editor: Xin Ning

Eye tracking is currently a research hotspot in the territory of service robotics. There is an urgent need for machine vision technique in the territory of video surveillance, and biological visual object following is one of the important basic research problems. By tracking the object of interest and recording the tracking trajectory, we can extract a structure from a video. It can also analyze the abnormal behavior of groups or individuals in the video or assist the public security organs in inquiring and searching for evidence of criminal suspects, etc. Moving object following has always been one of the frontier topics in the territory of machine vision, and it has very important appliances in mobile robot positioning and navigation, multirobot formation, lunar exploration, and intelligent monitoring. Moving object following has always been one of the frontier topics in the territory of machine vision, and it has very important appliances in mobile robot positioning and navigation, multirobot formation, lunar exploration, and intelligent monitoring. Moving object following in visual surveillance is easily affected by factors such as occlusion, rapid object movement, and appearance changes, and it is difficult to solve these problems effectively with single-layer features. This paper adopts a visual object following algorithm based on visual information features and few-shot learning, which effectively improves the accuracy and robustness of tracking.

1. Introduction

With the rapid expand of computer picture capabilities and technologies, and the improvement of the cost-effectiveness of a large number of digital picture equipment, vision systems have been widely adopted by mobile robots [1]. Computer vision is the most common method for humans to obtain environmental data via computers. Understanding the visual attention mechanism allows humans to process salient information in complex scenes quickly and efficiently, while masking and ignoring nonsalient regions autonomously. Machine learning is a century-old technology that is destined to thrive in the age of data. Machine learning's [2] advantage is that it can automatically analyze and process unknown data by mining and learning from existing data, reducing the need for human resources to the greatest extent possible. Scholars in the United States and abroad have conducted extensive and in-depth research on object recognition, object following, navigation, monitoring, and other technologies based on robot vision [3]. Machine vision's primary goal is to enable computers to mimic human thinking activities, obtain information from visual sensors to gain an understanding of the environment, and finally realize the computer's autonomous adaptation to the environment [4]. Researchers in the United States and abroad are using computers to create a visual attention model that simulates the human attention mechanism and incorporates it into the processes of object detection [5], object recognition, and moving object following, in order to bring the object processing process closer to the human cognitive mechanism and improve the algorithm's performance. This area of research has become one of the most active in the field of pattern recognition. Video image data contains the most information of all the data circulated or saved on the Internet, but extracting it is extremely difficult. According to the number of cameras mounted on the robot, monocular vision and stereo vision can be distinguished. Computer vision is a multidisciplinary field that includes computer science, physics, physiology, psychology, artificial intelligence [6, 7], semaphore processing, and applied mathematics.

The traditional mean-shift algorithm is based on the matching search process of the object color feature histogram, but the color features are not sensitive to noise and occlusion. So many surveillance cameras will generate massive amounts of surveillance video data every day, and these surveillance videos contain useful information that can be used to cardinaltain social stability, travel safety, and traffic guidance. Although the traffic police department has the right to use these surveillance cameras, there are many problems in analyzing these surveillance videos solely by the human eye. The cardinal difficulty in the research of moving object following algorithm in complex scene is the robustness and accuracy of the tracking algorithm. Monocular vision is inferior to stereo vision in terms of depth extraction, but it is comparable to stereo vision in terms of feature extraction and matching, and it avoids the problem of stereo vision binocular objecting, improves real-time performance, and has a simple structure. Machine vision technology has now penetrated many areas of the national economy, including aerospace, remote sensing and telemetry, medical aided diagnosis, map drawing, industrial security, multimedia communications, intelligent robots, and other areas. Simply relying on the human eye to analyze surveillance video will consume a significant amount of human resources, and the human eye has a blind spot and causes visual fatigue, making it impossible to maintain a long-term focus on the surveillance video [8]. This shows that there is an urgent need for machine vision technique in the territory of video surveillance [9]. With the expansion of machine vision, vision-based object following technique has become a hot spot in engineering and academia. Moving object tracking refers to the detection, identification and sports tracker objects in the video, and obtaining some motion parameters of the moving objects, such as speed, position, acceleration, and motion trajectory, so as to achieve higher-level processing and analysis [10]. The behavior of the object is understood and prepared to complete a specific task.

Object recognition is the foundation of tracking in an eye tracking system, and accurate object recognition is required for effective tracking [11]. This paper uses a visual object following algorithm based on visual information features to achieve accurate object following in complex backgrounds while overcoming partial occlusion and background fusion interference.

2. Related Work

The Harris affine detector was proposed in [12], which combines the Harris corner detector and the Laplace equation to ensure that the detected features are scale-invariant. Reference [13] proposes an edge-based area detector that constructs parallelograms around Harris corners using curved and straight edges. The most stable extremum region detector, which is a watershed-like approach, is proposed in [14]. To achieve effective multiview matching, [15] proposed using complex filters to generate kernel functions. Reference [16] proposes phase-based local features to improve lighting change robustness. Literature [17] proposed PCA-SIFT, which uses principal component analysis to simplify the SIFT descriptor, standardize the gradient region, and achieve fast matching and invariance under image distortion. Reference [18] proposes a rotation-invariant feature transformation, which divides each standard circle into a series of concentric circles, and each concentric circle is associated with a gradient orientation histogram. Reference [19] proposed that the gradient position and orientation histogram is an extension of the SIFT descriptor. Similar to PCA-SIFT, GLOH also reduces the dimensionality of descriptors through principal component analysis. Literature [20] proposed four color descriptors, namely, RGB histogram, hue histogram, vertex angle histogram, and spherical angle histogram. Reference [21] proposed a global positioning way for mobile robots based on monocular vision. Reference [22] proposes a hierarchical real-time localization and map creation way for mobile robots based on an active closed-loop strategy.

In this paper, a visual object following algorithm based on visual information features is adopted, which has good real-time performance, accuracy, and practicability. It combines sequential detection mechanism, binocular disparity information, and binocular vision calibration model to complete object recognition and localization and can achieve good tracking accuracy.

3. Research on Visual Object Tracking

3.1. Robot Vision. The identification and tracking module, the robot control module, and the robot platform make up the vision system [23]. Since their first appearance in the 1960s, robots have gone through three historical stages around the world. With the rapid growth of the robot industry at home and abroad, as well as significant progress in the field of artificial intelligence, the role of robots in human life has become increasingly important in recent years. Eye tracking is a hot topic in the field of machine vision as well as an important research direction in the field of intelligent mobile robots. With the advancement of science and technology in recent years, an increasing number of products have begun to use machine vision-related technologies, and an increasing number of scholars have devoted themselves to picture-related territories for research and expansion [24]. Algorithms started to evolve into useful devices. The advantages of visual semaphores include a wide range of semaphore detection and a large amount of data acquisition. Eye tracking has become one of the cardinal expansion orientations in the field of robotics, thanks to the rapid expansion of picture technique and computer processing capability in recent years. Robots currently perform the majority of their work by following preprogrammed instructions to perform repetitive and specific tasks [25]. The robot must be reprogrammed to adapt to the new operating environment if the operating environment changes.

Machine vision is booming, and it is providing a lot of technical support for robot technique improvement. Visual servosystems have recently emerged as a key research topic in the field of robot control. One of the key technologies of mobile robot vision is real-time sports tracker objects [26]. The basic principle block diagram of maneuvering object following is shown in Figure 1.

In order to achieve fast and effective tracking of the object, this paper proposes an improved eye tracking algorithm for mobile robots, which is based on the mean-shift algorithm, uses color features as the basis for eye tracking, and introduces Kalman filtering to predict the iterative window. The identification and tracking module adopts the improved Camshift algorithm and the way of Kalman filter [1] to identify and track the selected tracking object; the robot control module cardinally completes functions such as sending robot control instructions. With the continuous expansion of domestic and foreign scientific and technological level, computer technique, sensor technique, artificial intelligence, and robotics have developed rapidly, so that the application of robots is no longer limited to the industrial territory. Military territories such as territory, underwater, and space, as well as indoor environments such as hospitals and exhibition halls, have also been included in the application within the range [27]. At the same time, in recent years, the state has proposed the establishment of a smart city and a safe city where all things are perceived, connected, and intelligent, so that the domestic security industry can gain opportunities for rapid expansion, so that machine vision research continues to be hot, and robots can be obtained through the vision system and a large amount of information and then through the information processing and finally making a decision.

Eye tracking technique is an important research orientation in the territory of intelligent mobile robots, and it is also a hot issue in the territory of machine vision. Vision-based mobile robot tracking techniques have advanced rapidly in the last two decades. The robot's recognition and sports tracker objects require segmenting the image sequence obtained by the vision sensor into moving objects in the time do cardinal, as well as modeling, recognizing, and tracking these objects in the time do cardinal. The research on the robot with the object detection function can give the robot the ability to perceive the environment and perform servocontrol in response to changes in the environment. The visual servosystem completes the acquisition of visual image information through the camera during the robot control process, and the robot's function to obtain information from the outside world is realized. A mobile robot's intelligence is based on its ability to coordinate with external objects such as the environment and people. The vision system is crucial in this regard. A laptop and a control board comprise the robot platform. The eye tracking software is run on the laptop. The control board is in charge of driving the motor and gathering sensor data. The vision system can provide a wealth of information to the intelligent mobile robot, such as position and motion parameters, so that it can correctly perceive itself. Make the best decisions about your own behavior and the work environment in which you live.

3.2. Vision Based Object Tracking

3.2.1. Object Recognition Based on Local Features. Object recognition has been widely used in medical diagnosis, military technique, security detection, and other domains as an important research orientation in the field of picture and pattern recognition. Image understanding, automatic image segmentation, moving object following, and scene understanding are all built on this foundation. Traditional object detection and tracking algorithms typically only use the image's underlying visual features to construct object descriptors in order to obtain a description of the object's appearance for object detection and tracking and obtain the object's location information in order to realize the object's detection and tracking. Machine vision research's main goal is to use computers to simulate and realize visual functions similar to those performed by the human eye, such as object, scene, and motion detection, as well as three-dimensional reconstruction. The most important way for humans to obtain external information is through their vision system, and object recognition is a key topic in the field of machine vision and pattern recognition, which has a wide range of potential applications. Long-distance object recognition is difficult due to the image's complex background and the object's small number of pixels. Object detection is a hotspot of machine vision research, with applications in image retrieval, intelligent transportation, intelligent video surveillance, advanced human-computer interaction, and other areas. However, existing object detection methods have significant drawbacks, and a high-precision, high-efficiency, and high-robustness object detection algorithm in the field of machine vision is still urgently needed.

Common moving object detection ways can be divided into three categories: interframe difference way, optical flow way, and background subtraction way. Feature extraction is a key technique in object recognition, which plays a decisive role in the final result of recognition. Aiming at the problem of viewing angle, scale, and brightness condition changes in automatic object recognition, and the disadvantage of low recognition rate of local features is when the viewing angle and brightness change are large. The images generated in real scenes often have many complex situations such as changes in illumination intensity, object scale scaling, different imaging perspectives, object occlusion, and redundant background interference [28]. A problem in the actual process, in addition to the pose, scale, rotation, and translation changes of the object itself, is that there are also challenges such as illumination changes, complex backgrounds, and object occlusion. Recognition of objects/objects is one of the important orientations and can be divided into 3 categories according to the generality of the recognition objects: recognition of specific objects (the same thing), recognition of a series of objects (such as aircraft, ships, people, and face), and object recognition in general (and the ability to spot any object). In national defense construction, object recognition is a key technique in training, reconnaissance, and defense systems. For example, defense systems mostly use object recognition technique to track, identify, and guide missiles on mobile military objects. Robot is a multidisciplinary application technique that integrates machinery, computer, automatic control, etc.

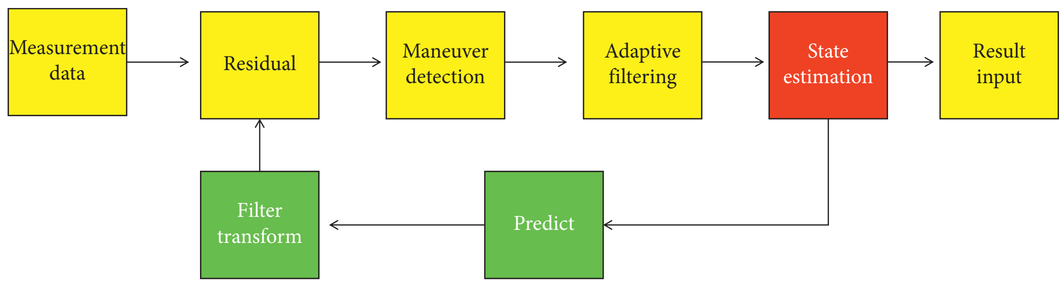

Figure 1: Basic principle block diagram of maneuvering object following.

At present, the research in this territory is active and the application is increasingly widespread. Object detection has become a challenging problem due to the uncertainty of the appearance shape of different objects, the complexity of the application scene, the mutual occlusion between objects and between objects and the background, etc. Neurophysiological studies have revealed in recent years that, in the primitive visual cortex of mammals, a sparse coding strategy is used. The human visual system can break down objects into a variety of small, meaningful pieces and use this information to identify the object robust to occlusion and pose changes, in addition other excellent properties. The object detection method based on local features has quickly become a research hotspot at home and abroad. The purpose of the local feature synthesis link is to combine a large number of local features into a single feature, resulting in more reliable features for the classifier design. The detection algorithm based on joint features is a new trend in current expansion because a single feature mode cannot accurately detect the object.

3.2.2. Object Description and Data Fusion in Visual Tracking. In recent years, with the rapid expansion of computer technique, computers no longer have simple data processing functions, but have become more and more intelligent. Target tracking is a research topic with extensive practical application significance in military and civilian territories. To realize the effective and accurate identification and tracking of the object under the difficult problem of tracking, the key is how to describe the tracking object adaptively and accurately model the tracking object. Since the expansion of object following technique in the middle of the last century, it has been widely used in various territories such as industrial robots, video surveillance, and missile interception. Intelligent video surveillance is a new type of video surveillance technique gradually developed by introducing relevant research results in machine vision into traditional video surveillance. Since the birth of the first robot in 1959, robot technique has made great progress and expansion and has become a comprehensive cutting-edge science that integrates machinery, electronics, computers, control, sensors, semaphore processing, and other disciplines. The role of robot object tracking in indoor environment is becoming more and more important.

Artificial intelligence technique subverts the traditional way of thinking of human beings, so that human beings have a new understanding of artificial intelligence. The key to effectively complete the corresponding tasks of the UAV lies in the various information provided by the external sensors mounted on it. The sensors usually used are mostly sonar, inertial navigation systems, barometers, magnetometers, etc., relying on Global Positioning System. The so-called machine vision is a simulation of biological vision using computers and related equipment. The origin of object following can be traced back to 1937, that is, on the eve of World War II, when a tracking radar named SCR-28 appeared for the first time, and its appearance marked that object following officially entered people's territory of vision. Intelligent video surveillance automatically comprehends image content without human intervention. When the individual or group behavior is abnormal, the alarm can be timely, so that the video surveillance can get rid of the dependence on the all-weather manual supervision. Intelligent robots can acquire, process, and recognize a variety of information and autonomously complete more complex tasks.

Continuous and stable sports tracker objects can not only obtain the position information of the current moving object, but also help to conduct a more in-depth analysis of the moving state of the object, so as to achieve precise positioning and intelligent control of moving objects. Guidance, vehicle navigation, human-computer interaction, and other territories have broad application prospects and great economic value. Detecting objects in videos solely using still image object detection methods is insufficient because they cannot handle useful information such as temporal and contextual information. Sensors commonly used are slightly insufficient for obtaining more accurate information about the surrounding environment or objects. When faced with this problem, applying machine vision techniques and visual sensors to UAVs, which have developed rapidly in recent decades, is an effective way to compensate for the shortcomings of traditional common sensors. Computer vision is the use of cameras or computers to simulate the capture of external objects instead of human eyes, and machine vision can process visual information according to the characteristics of computer systems through processing to enable people to understand intuitively. The technique of target tracking has grown in importance as a field of study. It has been widely concerned and applied, and it plays a pivotal and important role in industry, military affairs, and everyday life.

4. Visual Object Tracking Algorithm Based on Visual Information Features

4.1. Object Recognition Based on SIFT Features. Images have become a necessary means for humans to obtain information from the outside world as society has progressed and information technology has rapidly expanded, and the use of computers to process images to obtain information of interest to humans has become a hot research topic. Many vision appliances use image matching as a key technique. In this paper, the video stream monitored by the camera is used to control the specific object. Finally, key frame image matching is required, and the effect of matching has a direct impact on the effect of subsequent analysis and processing. Detecting and tracking moving objects has always been a challenge in video surveillance systems. Many scholars have conducted extensive research on this issue in recent years, but it remains a difficult subject. At the moment, the most common method of background modeling is to update the background statistics, with single Gaussian models, mixed Gaussian models, and their improved algorithms being the most commonly used methods. By modeling the surveillance area scene's mixed Gaussian background in the video stream, each pixel of the background image is modeled by a mixed Gaussian model made up of K Gaussian distributions:

$$\begin{aligned} P(X_i) &= \sum_{i=1}^{K} \omega_{i,t} \bullet \mu\left(X_t, \eta_{i,t}, \Sigma i, t\right), \\ X_t &= \left(x_t^r, x_t^g, x_t^b\right), \\ \eta_{i,t} &= \left(\mu_{i,t}^r, \mu_{i,t}^g, \mu_{i,t}^b\right). \end{aligned} \tag{1}$$

Before extreme point detection, the original image is preprocessed to remove noise. Then, an upscaled linear interpolation is performed on the image. Next, construct Gaussian pyramid and DOG pyramid to filter the image.

The scale space $L(x, y, \sigma)$ is established as follows:

$$L(x, y, \sigma) = G(x, y, \sigma)) * I(x, y). \tag{2}$$

Here $I(x, y)$ is the original image, σ is the standard mean square error, * is the convolution operation, and $G(x, y, \sigma)$ is the scale-variable Gaussian.

$$G(x, y, \sigma) = \frac{1}{2\pi\sigma^2} e^{-\left(x^2+y^2\right)/\left(2\sigma^2\right)}. \tag{3}$$

The DOG filter is defined as follows:

$$D(x, y, \sigma) = L(x, y, k\sigma) - L(x, y, \sigma). \tag{4}$$

Here k is a constant.

At the moment, most commercial object recognition systems use a template-matching approach. This method, however, places strict limitations on the object's position and brightness, and the matching effect is not ideal when the object's rotation, scaling, brightness, or 3D pose change. Many feature points are extracted by the traditional SIFT algorithm during the feature extraction stage, lengthening the recognition process and increasing the false matching rate. The camera is mostly stationary in most practical scenes, creating a "static background." However, as technology advances and the need to cut costs grows, the camera must move more and more to achieve continuous sports tracker objects and thus expand the monitoring range. The work-based object recognition technique is a type of pattern recognition that has both theoretical and practical applications. Despite the fact that significant progress has been made in this research, there are still numerous obstacles to overcome. Moving object detection and tracking has become commonplace in areas such as traffic management, image analysis and processing, video conferencing, and bank surveillance. The object position, including the object's pose change, can be accurately identified using the method described in this paper, and the recognition effect is good as shown in Figures 2, 3, and 4.

Because of its excellent matching performance, the matching algorithm based on multiscale space has attracted the attention of many researchers in recent years, and it has achieved great results by applying it to various appliances. A SIFT extreme value detection algorithm based on significant edge constraints is used to detect the bottom of the pyramid in the research on the identification of specific building areas in remote sense images, based on the characteristics of large territory of view remote sense images with large imaging range and complex scenes, combined with the geometric characteristics of the building area to be identified. To obtain binary images, adaptive threshold segmentation of images is used. To meet the requirements of object recognition, the SIFT feature matching algorithm needs to be improved according to the specific scene. Because image feature matching and object recognition have a lot in common, it is a good idea to use feature matching to achieve object recognition. The entire background changes as the camera moves, making it more difficult to detect moving objects against a static background. The flowchart of the background subtraction way is shown in Figure 5.

The identification of a specific object belongs to static image matching. The feature point extraction of the image and the calculation of the minimum distance are used as the cardinal ways to find the difference between the pixels of the same scene projected to the specific object image in the two images of the specific object and the given scene. Correspondence: in the past, object recognition technique based on image features has achieved good results in specific territories, and the emergence of feature extraction algorithms has brought a new idea and way to object recognition research. The detection of moving objects can obtain the relevant information of the object objects in the sequence images. By extracting the moving objects and their related information in the sequence images and segmenting and analyzing the objects, it lays the groundwork for the later part of the object following. In video surveillance system, moving object detection is the basis and premise of moving object tracking, which plays a very important role in many territories and is of great significance to video surveillance and so on.

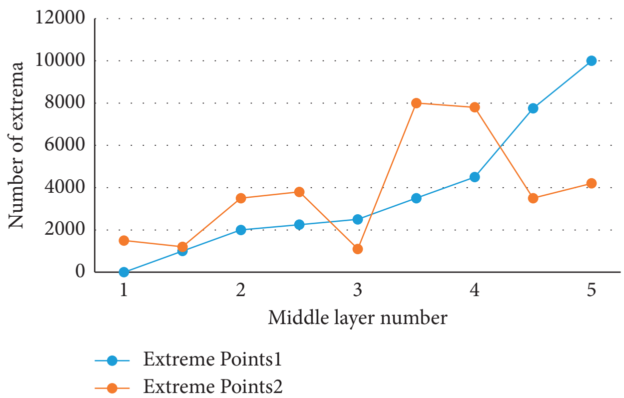

Figure 2: The relationship between the number of intermediate layers and the number of extreme points.

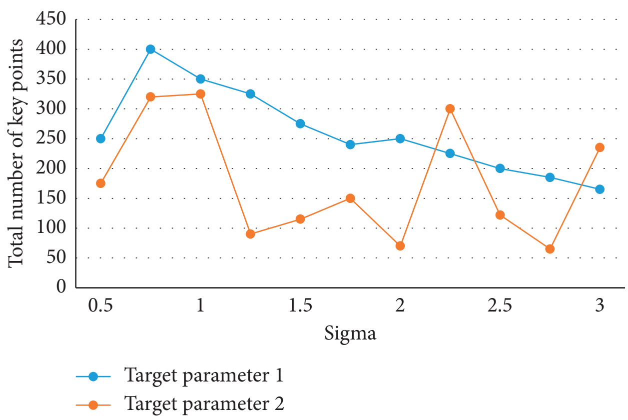

Figure 3: Relationship between the number of feature points and object parameters.

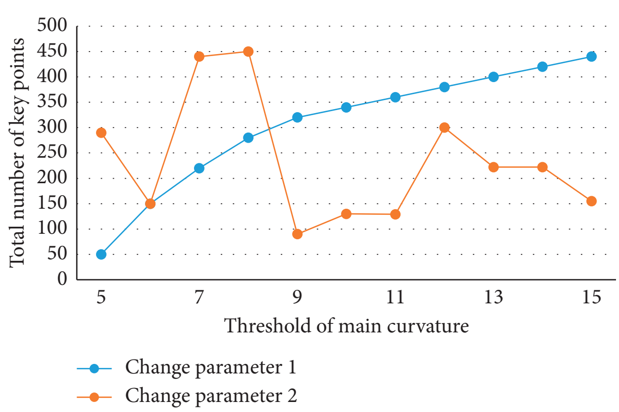

Figure 4: The relationship between the number of feature points and the changing parameters.

4.2. Tracking Algorithm Analysis. After decades of unremitting efforts of scholars, moving object detection and tracking technique has made great progress. However, due to the complexity of the application environment of the eye tracking system, such as illumination, occlusion, and other factors and the diversity of the object itself, it brings great difficulties to the object detection and tracking technique. In terms of accuracy, the appearance of the background and the object in the video image may change at any time, and it is difficult for the existing picture algorithms to accurately identify the object in the image sequence. Computer vision is a highly comprehensive subject with many interlaced disciplines. Its content involves many disciplines such as picture, artificial intelligence, pattern recognition, and neural network. The image is sent to the computer for related processing. Among the many research orientations of machine vision, eye tracking has always been one of the most important research hotspots at home and abroad and belongs to the middle-level processing part of machine vision. Its purpose is to process, detect, locate, and track objects of interest in the video sequence captured by the camera. Robotics is a combination of theoretical and scientific research achievements in various territories such as computer technique, automatic control, communication, machinery, and artificial intelligence. As robots play an increasingly important role in the current human economic expansion and technological progress, the application territories of robots continue to expand, the tasks faced by robots are becoming more and more complex, and the working environment is becoming more and more complex.

The research of machine vision has two meanings. One is to meet the requirements of artificial intelligence appliances, i.e., to use computers to realize the requirements of artificial vision systems. These findings can be installed on a variety of robots, giving them the ability to "see." Second, the machine vision model's research findings can help us better understand and study the human visual system's mechanism, as well as the human brain's mechanism, which is also important to know about. Picture algorithms generally model the appearance and background of the object in the image based on pixel points, which has the characteristics of a large amount of calculation, especially when faced with a large number of images to be processed, and the real-time performance of the object following algorithm can be solved significantly. Due to some flaws in human beings, they are unable to meet the current needs in terms of time and work intensity in such a big data era that today's society is experiencing. As the times demand, the intelligent video surveillance system emerges, successfully defeating traditional surveillance systems as well as human beings. The intelligent video surveillance system converts the traditional passive monitoring strategy of "forensics after the event" into an intelligent and active monitoring mode that incorporates "real-time monitoring and prior prevention." For incremental subspace learning in this paper, two eigenvectors are used. Figures 6 and 7 show how this works.

The trend of each monitored object and the interaction between the monitored objects can be obtained by tracking in the intelligent monitoring system, allowing for more in-depth analysis of the monitored object's behavior and the detection of specific events. In the realm of intelligent transportation, vehicle and pedestrian tracking can improve the degree of automation in traffic accident detection, as well as enabling judgment of vehicle driving states, which can then be used to understand road traffic conditions and

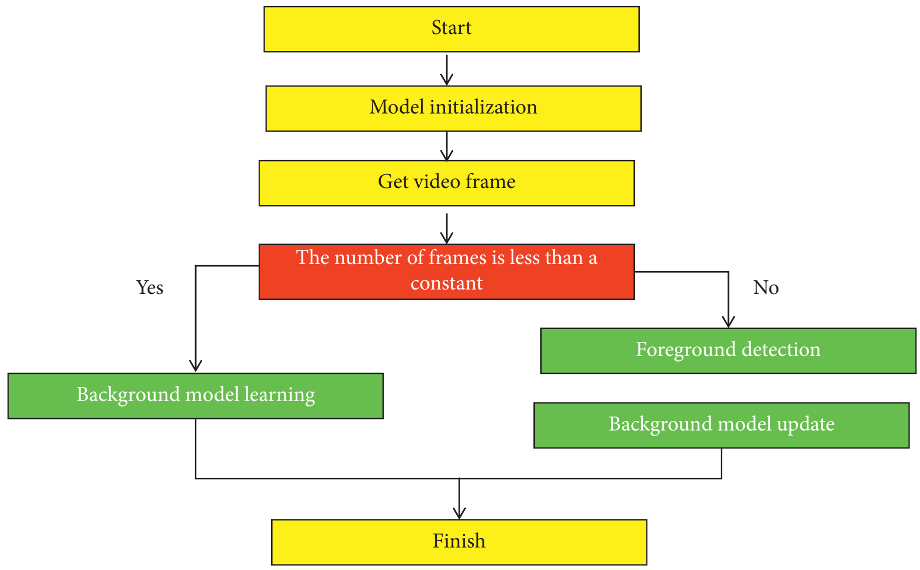

Figure 5: Flowchart of background subtraction way.

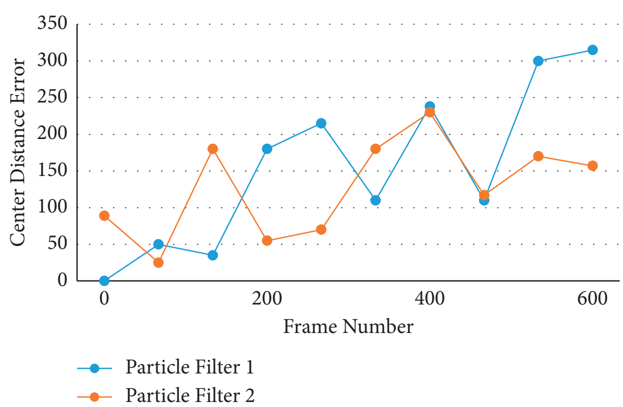

Figure 6: Center distance error 01.

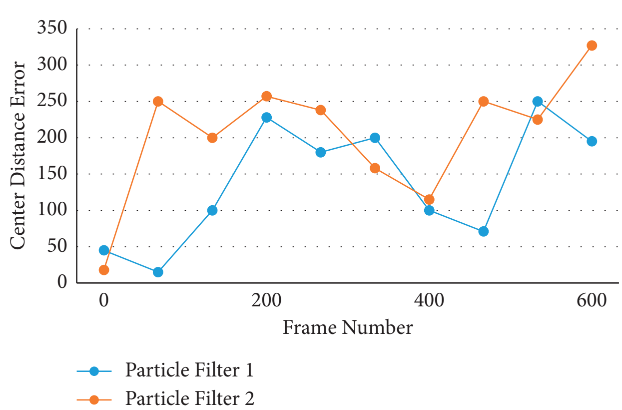

Figure 7: Center distance error 02.

provide intelligent traffic guidance. It is becoming increasingly difficult to meet the task requirements due to the limitations of a single robot's movement and perception abilities. The collaborative theory of heterogeneous robots was born out of this situation. People give multiple heterogeneous robots the ability to collaborate with one another, expand the robot's scope of action, and improve the robot's ability to complete complex tasks. Many researchers have conducted fruitful research on the eye tracking problem and proposed many tracking algorithms in order to achieve the goal of intelligent motion perception. They have proposed a number of solutions to the eye tracking issues. Through the collaboration and cooperation of multiple heterogeneous robots, the system can integrate all individual resources, and the entire system has parallelism in terms of space, time, information, and task execution. Improve the efficiency of processing tasks, thereby improving the completion rate of tasks and enhancing the robustness of the system.

5. Conclusions

Computer science, machine vision, picture, pattern recognition, artificial intelligence, automatic control, and other theories have come together to form mobile robot navigation and positioning. Through correlation filtering operations, the affine transformation information experienced by the object during motion can be extracted. A visual object following algorithm based on visual information features is proposed in this paper. The algorithm uses pixel-level object background segmentation to obtain a rough object distribution template and then uses that information to perform threshold-adaptive voting decision classification in the superpixel area to eliminate noise interference and obtain a more accurate object distribution. Video object tracking combines machine vision, image processing, pattern recognition, and artificial intelligence. It is a relatively new research approach. In recent years, it has attracted more and more researchers' interest. However, despite the extensive use of video tracking, there are still a number of issues that need to be investigated further.

Data Availability

The data used to support the findings of this study are included within the article.

Conflicts of Interest

The authors declare that they have no conflicts of interest.

Acknowledgments

The study was supported by the "Science and Technology Research Project of Henan Province of China (Grant No. 202102210133).

References

[1] H. Wu, Y. Chen, and H. Qin, "MPC based trajectory tracking for an automonous deep-sea tracked mining vehicle," *ASP Transactions on Internet of Things*, vol. 1, no. 2, pp. 1–13, 2021.
[2] Z. Huang, Y. Liu, C. Zhan, and L. Chen, "A novel group recommendation model with two-stage deep learning," *IEEE Transactions on Systems, Man, and Cybernetics: Systems*, 2020, In press.
[3] O. Akbarzadeh, M. R. Khosravi, and L. T. Alex, "Design and matlab simulation of Persian license plate recognition using neural network and image filtering for intelligent transportation systems," *ASP Transactions on Pattern Recognition and Intelligent Systems*, vol. 2, no. 1, pp. 1–14, 2022.
[4] H. Yang, D. Zhong, C. Liu, S. Chenyi, and Y. Kaiyou, "Robust eye tracking based on deep convolutional neural networks and kernelized correlation filters," *Journal of Electronic Imaging*, vol. 27, no. 2, p. 1, 2018.
[5] Y. Hu, J. Zhan, G. Zhou et al., *Fast forest Fire Smoke Detection Using MVMNet*, Knowledge-Based Systems, vol. 241, Article ID 108219, 2022.
[6] M. Zhao, A. Jha, Q. Liu et al., "Faster mean-shift: GPU-accelerated clustering for cosine embedding-based cell segmentation and tracking," *Medical Image Analysis*, vol. 71, Article ID 102048, 2021.
[7] J. Kong, H. Wang, X. Wang, X. Jin, X. Fang, and S. Lin, "Multi-stream hybrid architecture based on cross-level fusion strategy for fine-grained crop species recognition in precision agriculture," *Computers and Electronics in Agriculture*, vol. 185, Article ID 106134, 2021.
[8] L. Wang and C. Pan, "Visual object tracking via a manifold regularized discriminative dual dictionary model," *Pattern Recognition*, vol. 91, pp. 272–280, 2019.
[9] F. Li and S. Liu, "Object tracking via a cooperative appearance model," *Knowledge-Based Systems*, vol. 129, pp. 61–78, 2017.
[10] H. Yang, S. Qu, F. Zhu, and Z. Zheng, "Robust objectness tracking with weighted multiple instance learning algorithm," *Neurocomputing*, vol. 288, pp. 43–53, 2018.
[11] M. K. Rapuru, S. Kakanuru, P. M. Venugopal, D. Mishra, and G. R. K. S. Subrahmanyam, "Correlation-based tracker-level fusion for robust visual tracking," *IEEE Transactions on Image Processing*, vol. 26, no. 10, pp. 4832–4842, 2017.
[12] Y. Lu, Y. Yuan, and Q. Wang, *A Dense Connection Based Network for Real-Time Object Tracking*, Neurocomputing, vol. 410, pp. 229–236, 2020.
[13] K. Chen and W. Tao, "Learning linear regression via single convolutional layer for visual object tracking," *IEEE Transactions on Multimedia*, vol. 21, pp. 86–97, 2018.
[14] Y. Yin, D. Xu, X. Wang, and M. Bai, "Online state-based structured SVM combined with incremental PCA for robust visual tracking," *IEEE Transactions on Cybernetics*, vol. 45, no. 9, pp. 1988–2000, 2017.
[15] J. Shen, Z. Liang, J. Liu, H. Sun, L. Shao, and D. Tao, "Multiobject tracking by submodular optimization," *IEEE Transactions on Cybernetics*, vol. 49, pp. 1–12, 2018.
[16] P. Feng, C. Xu, Z. Zhao et al., "A deep features based generative model for visual tracking," *Neurocomputing*, vol. 308, pp. 245–254, 2018.
[17] C. Li, Q. Xing, Z. Ma, and K. Zang, "MFCFSiam: a correlation-filter-guided siamese network with multifeature for visual tracking," *Wireless Communications and Mobile Computing*, vol. 2020, no. 1, 19 pages, Article ID 6681391, 2020.
[18] Y. Kuai, G. Wen, and D. Li, "Masked and dynamic Siamese network for robust visual tracking," *Information Sciences*, vol. 503, pp. 169–182, 2019.
[19] D. E. Touil, N. Terki, and S. Medouakh, "Learning spatially correlation filters based on convolutional features via PSO algorithm and two combined color spaces for visual tracking," *Applied Intelligence*, vol. 48, no. 9, pp. 2837–2846, 2018.
[20] R. Duan, C. Fu, and E. Kayacan, "Tracking-recommendation-detection: a novel online target modeling for visual tracking," *Engineering Applications of Artificial Intelligence*, vol. 64, pp. 128–139, 2017.
[21] P. Chen, Y. Dang, R. Liang, and Z. Wei, "Real-time object tracking on a drone with multi-inertial sensing data," *IEEE Transactions on Intelligent Transportation Systems*, vol. 19, pp. 131–139, 2017.
[22] G. Jie, T. Xu, Z. Shen, and G. Shi, "Visual tracking via sparse representation with reliable structure constraint," *IEEE Signal Processing Letters*, vol. 24, no. 2, pp. 146–150, 2017.
[23] G. Wu and W. Kang, "Exploiting superpixel and hybrid hash for kernel-based visual tracking," *Pattern Recognition*, vol. 68, pp. 175–190, 2017.
[24] P. G. Bhat, B. N. Subudhi, T. Veerakumar, V. Laxmi, and M. S. Gaur, "Multi-feature fusion in particle filter framework for visual tracking," *IEEE Sensors Journal*, vol. 20, no. 5, pp. 2405–2415, 2020.
[25] K. Chen and W. Tao, "Learning linear regression via single-convolutional layer for visual object tracking," *IEEE Transactions on Multimedia*, vol. 21, no. 1, pp. 86–97, 2019.
[26] X. Gu, X. Huang, and A. Tokuta, "Multiscale spatially regularised correlation filters for visual tracking," *IET Computer Vision*, vol. 11, no. 3, pp. 220–225, 2017.
[27] H. Alzarok, S. Fletcher, and A. Longstaff, "3D visual tracking of an articulated robot in precision automated tasks," *Sensors*, vol. 17, no. 1, p. 104, 2017.
[28] C. Ma, Z. Miao, X.-P. Zhang, and M. Li, "A saliency prior context model for real-time object tracking," *IEEE Transactions on Multimedia*, vol. 19, no. 11, pp. 2415–2424, 2017.

Hindawi
Computational Intelligence and Neuroscience
Volume 2022, Article ID 2278416, 9 pages
https://doi.org/10.1155/2022/2278416

Research Article

Research on Optimization of Process Parameters of Traditional Chinese Medicine Based on Data Mining Technology

Xue Li,[1] Hao Yue ,[1] Jinlong Yin,[2] Yan Song,[3] Jinling Yin,[4] Xinlei Zhu,[4] and Bingchang Huang[4]

[1]*Jilin Ginseng Academy, Changchun University of Chinese Medicine, Jilin, Changchun 130117, China*
[2]*Department of Food Science and Engineering,Jilin Business and Technology College, Jilin, Changchun 130062, China*
[3]*Department of Clinical Medicine, Changchun University of Chinese Medicine, Jilin, Changchun 130117, China*
[4]*Jilin Haotai Health Industry Development Co., Ltd, Jilin, Changchun 130041, China*

Correspondence should be addressed to Hao Yue; songyan@ccucm.edu.cn

Received 15 December 2021; Revised 2 January 2022; Accepted 3 January 2022; Published 2 March 2022

Academic Editor: Xin Ning

Data mining technology and methods are used to effectively optimize manufacturing process parameters due to the complexity and uniqueness of the process parameters. The data-mining-based optimization method for traditional Chinese medicine (TCM) process parameters is presented, along with a list of process parameters that have shown to be effective in actual production. The influencing factors of process parameters are analyzed and modeled using an attribute weight analysis and classification analysis algorithm. The optimization scheme of process parameters that meet the requirements is selected, and an example is given for verification, by selecting data records that fall within a certain error range and incorporating the rules of association knowledge discovery. The support vector classification algorithm has a higher accuracy, despite the algorithm's results being understandable. The support vector regression algorithm developed a reliable process optimization model.

1. Introduction

Traditional Chinese medicine (TCM) is the treasure of the Chinese nation. TCM-manufacturing industry is a sunrise industry with international competitiveness and independent intellectual property rights in China's pharmaceutical industry [1]. The active ingredient extract of TCM has various uses and can be used in drugs, health products, and cosmetics. Therefore, the extraction of effective components of TCM has a wide range of practical scope and application prospects [2]. However, at present, the technical level of China's TCM-manufacturing industry has become increasingly backward compared with foreign countries. It is urgent to use modern science and tech to transform the traditional manufacturing mode of TCM products, promote the modern production of TCM, and then pave the way for TCM to rush out of the country and go to the world [3]. TCM production has moved from digitization to intelligence as a result of the rise of intelligent manufacturing technology around the world. It is necessary to continuously optimize the production process in the process of intelligent TCM production in order to gradually improve the product quality index [4]. One of the important contents of the modernization of TCM manufacturing is extracting stable active components from medicinal materials and ensuring the uniformity and stability of the drug dose-response relationship. As a result, TCM extraction is a critical step in the TCM-manufacturing process [5, 6]. It is the process of a solvent entering a medicinal material and transferring the active ingredients from the solid to the liquid phase. The choice of process parameters, such as extraction temperature, extraction time, and solvent volume, has a significant impact on the leaching of effective components in medicinal materials during the extraction process. Currently, orthogonal design is used to optimize the extraction process parameters [7].

With the promotion of advanced production technology, the manufacturing of TCM has gradually tended to be standardized. However, at present, the intelligent production of TCM has just started. It is a typical interdisciplinary subject, which needs the cooperation of control theory, pharmaceutical theory, and computer theory [8]. In the production of TCM, the selection of process parameters has an important impact on production efficiency and economic benefits. The selection of process parameters generally depends on workers' experience. These parameter values are only applicable to specific TCM products. When the production conditions change, the product quality is difficult to guarantee [9]. In the production of TCM, the production process needs to be continuously optimized to ensure the stability of the production process and the reliability of product quality. At present, the optimization of production process is still in the primary stage. The common method is to design comparative experiments in the laboratory environment to obtain the optimal production process scheme and then move the last to the production environment. In order to complete the comparative experiment, it often requires huge human and material resources [10]. TCM contains a variety of effective components, and different effective components have different effects. The extract can be used in medicine, health care products, and cosmetics. Therefore, the extraction of effective components of TCM has a wide range of practical value and application prospects. In this paper, data mining technology is applied to the optimization of process parameters of TCM, and the optimization model of process parameters of TCM is established.

Large-scale production data can be obtained as a result of the development of intelligent TCM manufacturing, and these actual production data have more practical significance than laboratory experimental data [11]. It contains the harsh conditions that occur during mass production. Using production data to create a production process model and optimize it through data mining rather than design and comparative experiment is not only a future trend but also a pressing problem to solve [12]. In the production of modern TCM, computers collect a large amount of data. Manually understanding, identifying, and optimizing these data and their relationships is typically difficult. There is no reference experience or manual for a new TCM product in the face of a new process, only accumulated data, especially for a new TCM product. At this time, it is necessary to quickly establish optimized process parameters according to traditional technologies and methods. The difficulty is great. As the manufacturing system of Chinese patent medicine is too complex and the front and rear sections interact with each other, at present, the TCM production still adopts the endpoint detection standard of production quality index for quality control, which means that the inspection of the effective components of finished drugs is the only standard to judge whether the drugs are qualified [13]. In the actual machining process of flexible manufacturing system, there are often many factors affecting the results. It is difficult to give an accurate mathematical model by using the traditional reasoning method. Through in-depth study of industrial process optimization, this paper puts forward an intelligent optimization scheme of TCM production process. Decision tree algorithm and support vector classification algorithm are used to construct the classifier of extraction times. Support vector regression algorithm is used to establish regression prediction models for extraction time and solvent amount, respectively. The experimental results show that the error of the optimal process parameters obtained by this algorithm is small, the results are accurate and reliable, and it has practical value, which can provide some reference for the industrialization of the extraction of effective components of TCM.

2. Related Work

Zhang et al. [14] used association rules to investigate the drug use law of ancient and modern asthma prescriptions, compare ancient and modern asthma drugs, and identify the core drugs for asthma treatment. Liu et al. [15] collected data from qualitative and quantitative angles to explore the syndrome differentiation of kidney yang deficiency syndrome based on the scale of kidney yang deficiency syndrome. A qualitative score was used to calculate the occurrence frequency of syndrome differentiation factors, and a quantitative score was used to perform hierarchical cluster analysis. Chen et al. [16] discussed the stroke cases of ancient famous doctors using data mining technology to analyze association rules, obtain the TCM commonly used by ancient famous doctors in the treatment of stroke, and identify common medicinal materials for stroke treatment. Data samples must be manually measured off-line in the research field of ultrasonic extraction of effective components of TCM, according to Hoogeveen et al.'s study [17]. This method of data collection has a long cycle and is extremely difficult. As a result, the amount of sample data available is limited, which is a small sample problem. Chaovalitwongse et al. [18] believe that although there are many medical record databases, the simple database has only query function and loses the core analysis function of the database. Bandaru et al. [19] emphasize the application of data mining technology in TCM medical case sorting and give the process of data mining technology in medical case information mining and the data mining method applied to medical case sorting. Lee et al. [20] propose to use data warehouse and data mining technology to save the clinical diagnosis and treatment data of old experts, analyze and mine the collected data using association rule analysis, factor analysis, discriminant analysis, and decision tree and form a knowledge base. Statistical analysis software is a data mining tool, which uses descriptive statistics analysis, frequency analysis, correlation analysis, discriminant analysis, decision tree, and neural network to analyze and mine the data related to syndrome differentiation in the database [21]. This paper explores the dialectical thinking mode of famous TCM in the diagnosis and treatment of vertigo and makes a preliminary summary of the law. Asadi et al. [22] proposed a set of relatively perfect time-series modeling theory and analysis method. In the process of optimizing the process parameters of coal plant sorting, Hyunjin and Eunok [23] designed a process-prediction real-time feedback system, which can detect the process parameters on the line in real time, predict the sorting index in real time, provide feedback and guide the production, and finally achieve the optimal sorting effect. Guo and Zhou [24] proposed data mining on medical records of threatened abortion, summarized the treatment characteristics and academic ideas of famous doctors in treating specific diseases, and played a guiding role in clinical diagnosis and treatment of diseases. When optimizing the high-pressure water jet cutting process, Angeli et al. [25] and Yd et al. established a polynomial regression model using the process parameters and cutting depth of the cutting process and optimized the parameters in the cutting process through the regression model. However, the ultrasonic extraction mechanism is complex, and the optimal process parameters are difficult to determine. Therefore, the information technology method can be combined with the ultrasonic extraction process. Introducing data mining technology into the study of modernization of TCM is another new attempt of applying computer technology to the study of modernization of TCM. This paper proposes an intelligent optimization solution of production process based on data mining, uses production data to establish an accurate quality index prediction model, screens key process parameters, and then optimizes key process parameters based on the above two steps. Thus, the intelligent optimization of process parameters using historical data is realized. The optimized process parameters are used for actual production, and the process parameters are monitored in real time. The results show that the model can optimize the process parameters and achieve good results in practical application.

3. Methodology

3.1. Data Mining. Data mining is a very dynamic research direction in the field of artificial intelligence [27, 28] and database, including classification, clustering, regression, association rule discovery, and other mining tasks. Data mining is a process of automatically searching for hidden and special relational information from a large amount of data. For massive and disorderly data, comprehensive analysis based on individual thinking will be limited by cognitive level, thinking mode, subjective factors, research methods, and research scope. It is an important part of the research on modernization of Chinese medicine to use data mining technology to acquire knowledge, remove the false and preserve the true, remove the rough and extract the fine from numerous Chinese medicine resources, so as to promote the development of Chinese medicine.

For complex and multidimensional systems, data mining technology is appropriate. We can find the rules using corresponding algorithms and break through the limitation of "information is jumbled and knowledge is scarce" in TCM with the help of a large amount of data. The primary function of data mining is discovery or prediction, and it encompasses a wide range of disciplines and methods. After "discovery," find out the hidden information patterns in a large amount of data, or find out the things or special cases in the designated area that deviate from the normal situation [29]. Prediction is the process of predicting the future based on patterns discovered. It is currently a very active research area in the fields of artificial intelligence and databases, with mining tasks such as classification, clustering, regression, and association rule discovery being included.

For the continuous storage and multilevel mining of TCM data, a high-quality and long-term updating of the data mining platform is essential. In the age of Big Data, creating a multimethod collaborative Chinese medicine mining model can help with TCM inheritance and development. Finding valuable hidden knowledge in large databases is the main problem that data mining must solve. We can create a systematic model and provide it to relevant departments for reference by analyzing and summarizing this valuable information. The medical field frequently employs drug frequency analysis, association rules, factor analysis, cluster analysis, and neural network analysis. Each of these algorithms has its own set of characteristics, and different algorithms can be used for different topics.

3.2. Application of Data Mining Technology in Optimizing Extraction Process of TCM. TCM prescription is the main means of TCM treatment. Through legislation based on differentiation of symptoms and signs, prescription is unified by law, and medicine is sent by prescription. In the prescription, there is an intricate correspondence among prescription, medicine, and syndrome [30]. As data mining technology can reflect the mutual mapping relationship between multidimensional data, it provides a very powerful research tool for the research of modern prescriptions. Under the premise of the trend of Big Data in the whole medical industry, at present, there is no system as a research system of TCM to be popularized and used in various famous doctor research systems. Only by accumulating data can we develop more knowledge to guide clinical or prescription research, which is more conducive to systematic experience inheritance of famous doctors. China's medical industry is currently in the primary stage of Big Data, which brings opportunities to the development of TCM. Through the platform of Big Data, there are more researches focusing on the origin of academic theory of TCM. A common problem is that the interpretation of data mining is not detailed enough. Using data mining to dig out potential and meaningful rules from the database can only be transformed into knowledge through high-quality data interpretation and analysis. The system established in this paper consists of four main modules: data preparation, data sorting, data analysis, and data analysis result visualization module. The main functional modules of the system are shown in Figure 1.

At present, in the field of TCM, data mining is most widely used in the research of TCM, and some progress has been made. In the process of extraction, the changes of temperature, density, pressure, liquid inlet, and other parameters have an impact on the quality of semifinished products. Using the data mining algorithm for scientific data analysis, the process parameters closest to the production results and the data interval of the process parameters that can produce qualified semifinished products can be obtained. Data mining can find the relationship between syndrome types and symptoms through a large number of

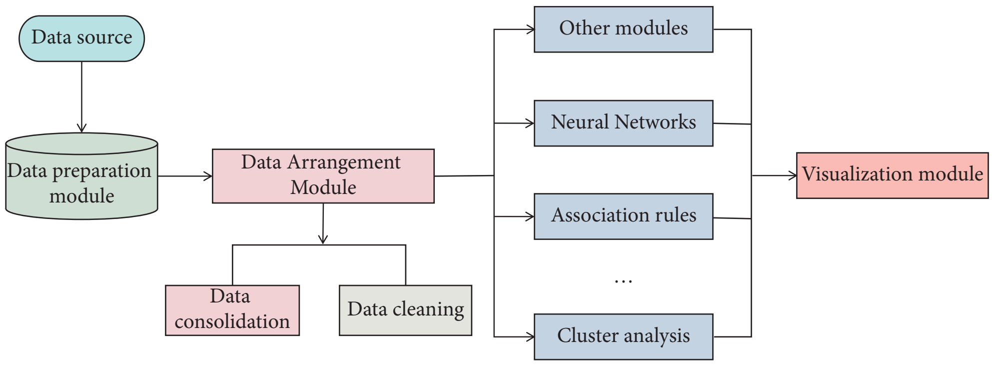

Figure 1: The functional structure diagram of the data mining system for Chinese medicine production.

clinical data, so as to assist clinical diagnosis. It has certain reference value for clinical treatment of diseases to obtain the commonly used drugs, pairs of drugs, and core prescriptions for the treatment of diseases through data mining, but it has the disadvantage of not ensuring the authenticity, accuracy, and universality of the data.

Medical records are complicated records of Chinese medicine diagnosis and treatment activities. We can master more and more objective syndrome rules if the factors are standardized first, and then data mining technology is used to analyze the contribution of qualitative variables to diseases and syndromes. The study should focus on the quality of screening documents, obtain first-hand case data from the original authors, further investigate the etiology and pathogenesis, improve clinical practice and observe the curative effect, or conduct animal experiments to further verify the effect and mechanism. The characteristics of data in TCM are discrete, continuous, mixed, and so on. The preprocessing of these data is extremely difficult, and the mining process necessitates frequent human-computer interaction, necessitating the use of professional technicians at every stage. We can only dig out truly valuable knowledge by choosing reasonable digging methods for different problems under the guidance of TCM theory and closely combined with clinical practice.

3.3. Optimization of Process Parameters of TCM Based on Data Mining. In the research of TCM, there are a lot of qualitative descriptions and a lot of vague concepts about the description of drugs, diagnosis and treatment process and disease symptoms. Especially for the description of drugs, the phenomenon that one drug has the same name as different drugs is also very common. The prescription of TCM takes the disease as the main body, adopts legislation based on syndrome differentiation, unifies prescription by law and sends medicine by prescription, and is determined by clinical practice. As data mining technology can reflect the mutual mapping relationship between multidimensional data, it provides a very powerful research tool for the research of modern prescriptions. In this paper, through the seamless integration of database and data mining algorithm, a process parameter optimization model based on data mining is constructed, which mainly uses data mining method to analyze and predict the extraction data of TCM. The data mining model of process parameter optimization is shown in Figure 2.

This system includes the function of adding multiple data files for analysis. Users do not need to combine multiple files into one by hand or third-party software to prepare data. The data related to the production of TCM are stored in different files according to the date. When importing these files, they are merged into a complete data set according to the records, and the data are cleaned to ensure that more accurate information can be mined.

The basic idea of support vector machines (SVMs) is dimension upgrading and linearization. Through the kernel function, the sample space is mapped to a high-dimensional or even infinite-dimensional feature space, the optimal linear hyperplane is found in the feature space, and the solution of the optimal hyperplane of the SVM is reduced to solving a convex optimization problem, so that the global optimal solution. SVM includes support vector classification (SVC) and support vector regression (SVR).

Let the sample set be AAA. For the linearly separable case, the sample set is separated by the hyperplane $wx + b = 0$. The problem of constructing the optimal hyperplane is transformed into

$$\begin{aligned} \min \varphi(w) &= \frac{1}{2}\|w\|^2 \\ &= \frac{1}{2}\left(w^T w\right), \\ s.t. \quad & y_i\left(x_i \cdot w + b\right) \geq 1, \quad i = 1, \ldots, n. \end{aligned} \tag{1}$$

Then, the original problem can be transformed into the dual problem of convex quadratic programming as follows:

$$\begin{aligned} &\max \sum_{i=1}^{n} a_i - \frac{1}{2}\sum_{i=1}^{n}\sum_{j=1}^{n} a_i a_j y_i y_j \left(x_i^T x_j\right), \\ &s.t. \sum_{i=1}^{n} a_i y_i = 0, \quad a_i \geq 0,\ i = 1, \ldots, n. \end{aligned} \tag{2}$$

According to the Kuhn–Tucker condition, this optimal solution must also satisfy:

$$a_i\left[y_i\left(w^T x_i + b\right) - 1\right] = 0. \tag{3}$$

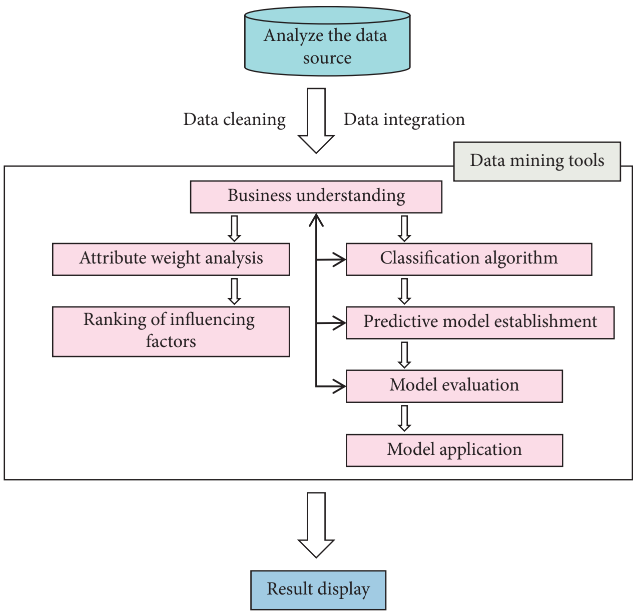

Figure 2: Data mining model for optimization of process parameters.

In the case of linear inseparability, non-negative relaxation variables can be introduced. The specific solution method is similar to the case of linear separability. Data mining analysis function includes three functional modules: cluster analysis, association rules, and neural network. By analyzing the characteristics of data that enterprises need to cluster, we know that all data attributes are continuous attributes, and the demand of enterprises is to try to divide the data with similar values into a group, so the best grouping method is to group the data with similar values according to the Manhattan distance between the data.

The multiobjective problem is transformed into a single-objective problem by linear fusion method, and then the single-objective problem is solved. Assuming that the number of process parameters to be optimized is N_v, the number of optimized objective functions is N_0, and the objective function is f, the problem can be described as follows:

$$\max F(x) = \max\left(f_1, f_2 \ldots, f_{N_o}\right). \tag{4}$$

Among them, the following constraints l and h, respectively, represent the threshold range in the parameter.

$$X = \left\{x_1, x_2 \ldots, x_{N_v} | l \leq x \leq h\right\}. \tag{5}$$

Usually, the optimal global objective function is constructed by multiobjective fusion, and the multiobjective problem is transformed into a single-objective problem. The general fusion methods include: (1) linear fusion. Linear fusion is the sum operation of each objective function according to a certain proportion, as shown in the following formula.

$$F(x) = \beta_0 + \beta_1 f_1 + \beta_2 f_2 + \ldots + \beta_n f_n. \tag{6}$$

(2) Logical integration: Logic fusion means that the output of the previous objective function is used as the input of another objective function as shown in the following formula.

$$F(x) = f_n(f_{n-1}(\ldots f_2(f_1))). \tag{7}$$

Regardless of which model fusion method is used, the goal is to reduce a multiobjective function to a single-objective function, which can then be solved using constraints. In the preparation process, there are many process parameter points to investigate, and each process parameter has a different unit of measurement. Even though some parameters have the same unit of measurement, their measured values vary widely, sometimes dramatically. If the collected data are directly analyzed and modeled based on their actual values, the role of some parameters with larger dimensions will be exaggerated, and the actual change relationship between the parameters will be obscured, resulting in the so-called false variation. As a result, the original data must be processed before being analyzed in order to eliminate the influence of dimensional effects of various variables on the model.

Many studies are unable to use randomized controlled trials due to the influence of traditional medical treatment modes and evaluation methods, and their clinical efficacy evaluation is limited to some extent, and the efficacy evaluation system is not perfect, making their research results difficult to be internationally recognized. The majority of data mining analyses are based on disease differentiation and syndrome differentiation laws, such as drug frequency analysis, association rule analysis, and cluster analysis and are combined with current disease understanding. Association rules can be used to analyze the patterns or rules of prescription compatibility. We can analyze the results of correlation data mining among different attributes such as drugs and symptoms, drugs and pathogenesis, and symptoms and pathogenesis using the frequent set method.

4. Results Analysis and Discussion

The neural network module uses the derived association rule module to integrate data, and its attributes include extracting the mean value of liquid inflow, extracting the variance of liquid inflow, extracting the mean value of temperature, extracting the variance of temperature and blending the liquid-solid content. When using attribute weight analysis algorithm and classification analysis algorithm to analyze the data, it is necessary to discretize the surface roughness in the sample data. The main technological parameters affecting the water content of TCM include the water content of extract, the temperature of feed liquid, the dripping humidity, the dripping time, the melting time, and so on. Their changes are shown in Figure 3.

From Figure 1, it can be seen that there are many uncertain factors in the process of dropping the preparation because the parameters affecting the water content change irregularly. Through the prediction of water content, the value range of each process parameter can be further determined, or the value range of some process parameters can be reduced, so that the production quality can be controlled.

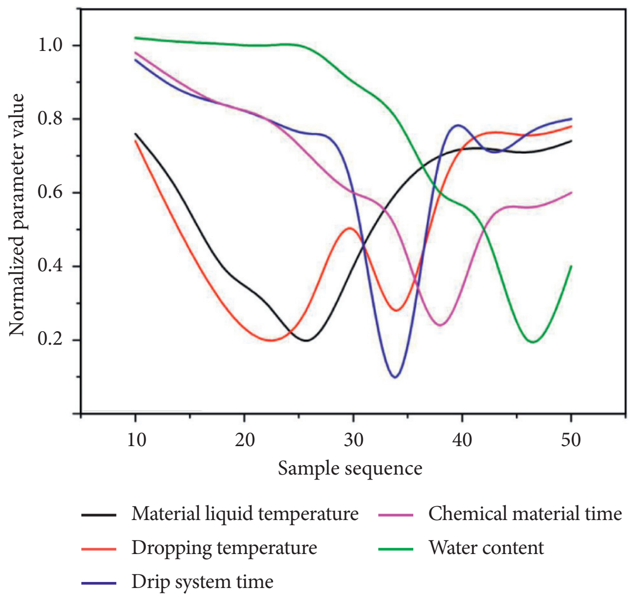

Figure 3: Changes in the main variables.

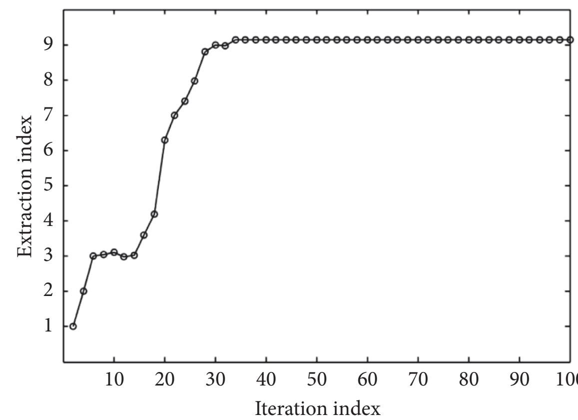

Figure 4: Forecast model optimization.

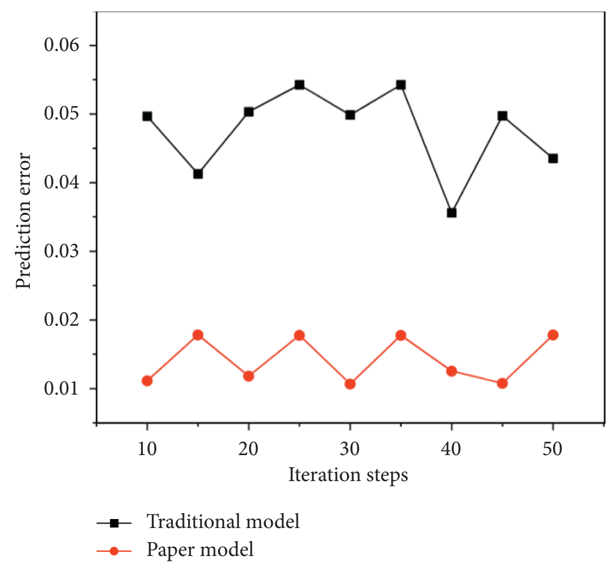

Figure 5: Forecast error analysis.

The optimization process of process parameters based on the prediction model in this paper is shown in Figure 4. To obtain the optimum conditions for ultrasonic extraction of Shaoyao Gancao Decoction.

The process parameters are modified, and the process parameters are tested in parallel for three times, with the average value taken, according to the aforementioned method, which takes into account the limitations of actual operation. The application of data mining in the field of TCM is dependent on the development of a data platform, and the continuous storage and multilevel mining of TCM data requires a high-quality and long-term updating of the data mining platform. To better serve the inheritance and development of Chinese medicine in the era of Big Data, a good data mining platform must have powerful data collection, management, and analysis functions, as well as the ability to establish a multimethod collaborative Chinese medicine mining model. The association rule module's data discretization system automatically discretizes data using a program that only requires the user to specify the number of divided intervals. When discretizing, it is necessary to keep track of the symbols for different attributes and intervals, as well as the attribute names and marks, which adds to the system's complexity but makes it easier to use.

Fingerprint of TCM is characterized by quantification, specificity, reproducibility and reproducibility, stability, integrity, and fuzziness of detail processing. Through data mining of TCM fingerprint, we can extract the hidden and potentially useful and ultimately understandable information. Taking the collected samples as the test set, the prediction model is simulated and analyzed, and the comparison results of prediction errors of different methods are shown in Figure 5.

Generally, neural network is a specific analysis of specific problems. There is no fixed model for all problems. The design of this system has a wide range of applications. It does not mean that a neural network structure is suitable for many practical problems, but users can set the network structure by themselves. Configure the input layer, output layer, and intermediate nodes according to different actual problems, so as to achieve the purpose of predicting results. In order to determine the relationship between process parameters and solid content, we select each attribute in the data except solid content as the input node, including: extracting the mean value of the liquid volume, extracting the variance of the liquid volume, extracting the average temperature, and extracting the four attributes of the temperature variance. The system predicts the solid content based on the information of these several production processes. The optimized input and output parameter values are converted into maximum and minimum inverse transformations, and the process parameter values of the preparation process can be obtained. Based on basic principles and training sample sets, a prediction model was established for the ultrasonic extraction of licorice and peony process parameters. The training result is shown in Figure 6, the test result is shown in Figure 7, and the test error is shown in Figure 8.

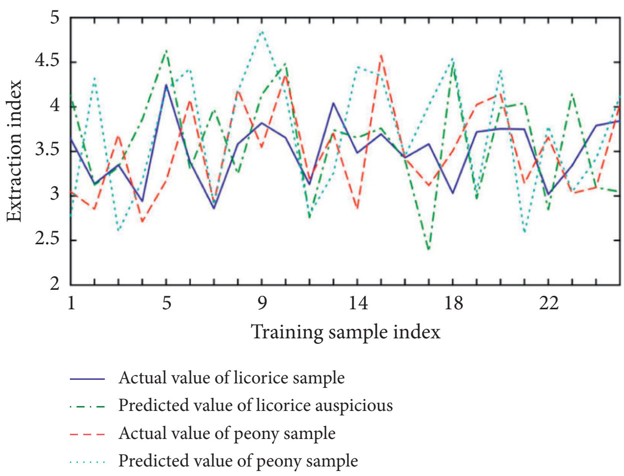

Figure 6: Predictive model training results.

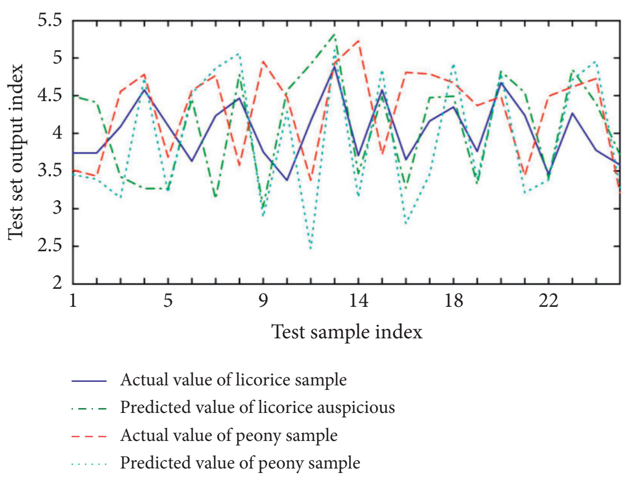

Figure 7: Predictive model test results.

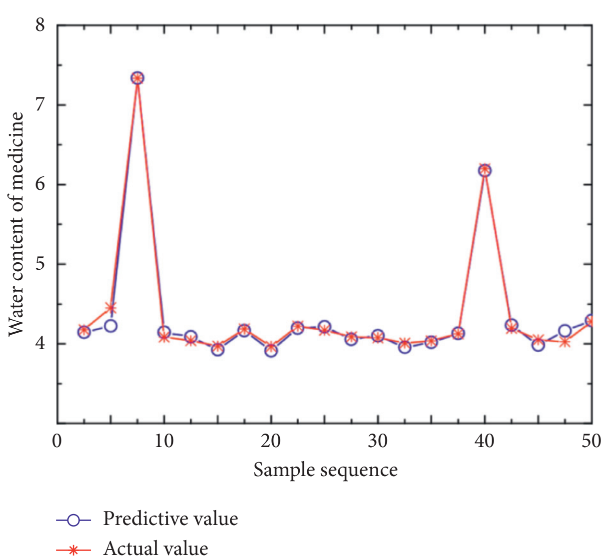

Figure 8: Comparison of predicted and true values.

Figure 6 shows that the prediction model's training effect is good. Figures 7 and 8 show that the difference between the predicted and actual values of the test sample obtained by the prediction model is generally small, indicating that this model's prediction accuracy is high. Process design knowledge is at the heart of all data in process parameter optimization. This model allows you to mine and analyze any type of continuous data. The importance of influencing factors is determined by establishing the association model of data mining and using attribute weight analysis, and the classification model of data mining is used to predict the cutting parameter scheme, and the scheme is optimized based on the predicted results. The system can analyze quality analysis data and TCM extraction data while also analyzing the data mining function of various data in various fields. It has the advantages of flexible deployment, free configuration, and expandability, and it better solves the problems of TCM extraction production data quality inspection standard optimization and process parameter optimization.

With the development of the times, the number of TCM information resources is increasing rapidly, but the characteristics of TCM information resources are complex and disorderly, which has formed a serious contradiction with the demand for information of professional and technical personnel. To solve this contradiction, an important way is to process all kinds of information and establish a relatively perfect information resource database. The algorithm of data mining part consists of attribute weight analysis algorithm and classification algorithm, and the classification model is built by data mining tools to predict the results. Show the results to users through visualization technology. In this paper, a data mining system platform is built to realize data mining of process parameter data and quality inspection data. Using data mining technology, the relationship between the extraction parameters and the description of the characteristics of TCM was discovered from the extraction data of TCM. The discovered knowledge can guide technologists to scientifically select the influencing factors of orthogonal test and the variation range of each factor level when determining the extraction process of a new drug, so as to ensure that the orthogonal test can obtain reliable optimized results.

5. Conclusion

In the research of modernization of TCM, the advanced information processing technology, represented by data mining, is used to study the knowledge acquirement of its implied essence. Systematizing and standardizing the documents left over from past dynasties can further extract and excavate the hidden essence. The research on knowledge acquisition with data mining technology has driven the improvement of the academic level of TCM. In this paper, an intelligent optimization scheme of TCM production process is proposed. From the historical data of TCM extraction process, the relevant knowledge of determining extraction parameters is mined, which is used to guide technologists to choose the influencing factors and the level of each factor in orthogonal test. Theoretical analysis and simulation research show that this method has fast learning speed, good tracking performance, strong generalization ability, low dependence on samples, and good popularization ability. In today's information explosion era, the combination of data mining technology and TCM is an inevitable trend. Data mining technology will further accelerate the pace of knowledge renewal of TCM, lay a solid foundation for the construction of modern TCM theory, and is the only way for the vigorous development of TCM.

Data Availability

The data used to support the findings of this study are available from the corresponding author upon request.

Conflicts of Interest

All the authors do not have any possible conflicts of interest.

References

[1] L. Li, L. Wang, W. Fan et al., "The application of fermentation technology in traditional Chinese medicine: a review," *The American Journal of Chinese Medicine*, vol. 48, no. 4, pp. 899–921, 2020.

[2] Z. Liu, Y. Yao, and H. Yu, "Based on data mining and analysis of traditional Chinese medicine in the treatment of diabetic neurogenic bladder medication," *China Medical Herald*, vol. 18, no. 12, p. 4, 2021.

[3] S. Hu, W. Dan, J. Liu et al., "The use of traditional Chinese medicine in relieving EGFR-TKI-associated diarrhea based on network pharmacology and data mining," *Evidence-based Complementary and Alternative Medicine*, vol. 2021, no. 2, pp. 1–16, 2021.

[4] M. Chen, "Optimization of the technical parameters of Magnolia officinalis, a traditional Chinese medicine feed additive," *Feed Research*, vol. 44, no. 12, p. 4, 2021.

[5] L. Dai, A. Lu, L. L. D. Zhong, G. Zheng, and Z. Bian, "Chinese herbal medicine for hyperlipidaemia: a review based on data mining from 1990 to 2016," *Current Vascular Pharmacology*, vol. 15, no. 3, pp. 520–531, 2017.

[6] Y. Su, Y. Yang, X. Yin, Y. Yang, and X. Chu, "Optimization of preparation process of traditional Chinese medicine compound aphrodisiac granules," *Chinese Journal of Veterinary Medicine*, vol. 54, no. 11, p. 6, 2020.

[7] S. Tian, E. Xu, and R. Sun, "Research on function evaluation of Chinese medicine compound health food based on data mining," *Chinese Journal of Chinese Materia Medica*, vol. 44, no. 5, p. 5, 2019.

[8] M. Zhao, A. Jha, Q. Liu et al., "Faster Mean-shift: GPU-accelerated clustering for cosine embedding-based cell segmentation and tracking," *Medical Image Analysis*, vol. 71, Article ID 102048, 2021.

[9] H. Wang, J. Cui, S. Zhao, Y. Cao, and J. Li, "Research on the prescription rule of traditional Chinese medicine for prevention and treatment of systemic lupus erythematosus based on data mining," *Chinese Journal of Basic Medicine in Traditional Chinese Medicine*, vol. 22, no. 7, p. 3, 2016.

[10] H. Lu, Q. Xiang, and Q. Xiao, "Based on data mining to study the medication rules of traditional Chinese medicine for lumbar spinal stenosis," *China Medical Herald*, vol. 014, no. 025, pp. 110–114, 2017.

[11] H. Zhou, H. Xiang, and H. Zhou, "A CNC machining process parameter optimization method based on instruction domain oscilloscope," *Machine Tool & Hydraulics*, vol. 46, no. 15, p. 6, 2018.

[12] Q. Yang, Y. Cheng, and J. Tong, "Data mining research on the clinical use of traditional Chinese medicine for bronchial asthma in the past 30 years," *Journal of Beijing University of Traditional Chinese Medicine*, vol. 42, no. 008, pp. 697–704, 2019.

[13] X. Xiao, H. Zhao, and K. Lu, "BDMOS: big data mining optimization system and its application in chemical process optimization," *Computers and Applied Chemistry*, vol. 35, no. 6, p. 7, 2018.

[14] S. Zhang, H. Wu, J. Liu, H. Gu, X. Li, and T. Zhang, "Medication regularity of pulmonary fibrosis treatment by contemporary traditional Chinese medicine experts based on data mining," *Journal of Thoracic Disease*, vol. 10, no. 3, pp. 1775–1787, 2018.

[15] L Liu, F Yang, Y Jing, and L Xin, "Data mining in Xu Runsan's Traditional Chinese Medicine practice: treatment of chronic pelvic pain caused by pelvic inflammatory disease," *Journal of traditional Chinese medicine = Chung i tsa chih ying wen pan*, vol. 39, no. 03, pp. 440–450, 2019.

[16] R. Chen, J. Chen, and F. Xiaochan, "Data mining based on the approval of domestic Chinese medicines from 2009 to 2014," *China Medical Guide*, vol. 20, no. 007, pp. 442–448, 2018.

[17] H. Hoogeveen, J. Tomczyk, and T. C. van der Zanden, "Flower power: finding optimal plant cutting strategies through a combination of optimization and data mining," *Computers & Industrial Engineering*, vol. 127, no. 1, pp. 39–44, 2019.

[18] W. A. Chaovalitwongse, C. A. Chou, Z. Liang, and S. Wang, "Applied optimization and data mining," *Annals of Operations Research*, vol. 249, no. 1-2, pp. 1–3, 2017.

[19] S. Bandaru, A. H. C. Ng, and K. Deb, "Data mining methods for knowledge discovery in multi-objective optimization: Part B-new developments and applications," *Expert Systems with Applications*, vol. 70, no. 3, pp. 119–138, 2016.

[20] E.-B. Lee, J. Kim, and S.-G. Lee, "Predicting customer churn in mobile industry using data mining technology," *Industrial Management & Data Systems*, vol. 117, no. 1, pp. 90–109, 2017.

[21] H. Zhang, L. Pang, and C. Liu, "Research on the use of traditional Chinese medicine compound prescriptions for the treatment of interstitial pulmonary diseases based on data mining," *Journal of Liaoning University of Traditional Chinese Medicine*, no. 7, pp. 109–113, 2018.

[22] A. Asadi, A. Verma, and Y. Kai, "Wastewater treatment aeration process optimization: a data mining approach," *Journal of Environmental Management*, vol. 203, no. 2, pp. 630–639, 2016.

[23] J. Hyunjin and P. Eunok, "Data-dependent scoring parameter optimization in MS-GF+ using spectrum quality filter," *Journal of Proteome Research*, vol. 2, 2018.

[24] Y. Guo and J. Zhou, "Data mining modeling technology integrating ontology and CBR and its application in process planning," *Mechanical Science and Technology*, vol. 36, no. 004, pp. 579–585, 2017.

[25] C. Angeli, S. K. Howard, J. Ma, J. Yang, and P. A. Kirschner, "Data mining in educational technology classroom research: can it make a contribution," *Computers & Education*, vol. 113, no. 10, pp. 226–242, 2017.

[26] A. Yd, A. Ww, and A. Pz, "Performance improvement of optimization solutions by POD-based data mining-ScienceDirect," *Chinese Journal of Aeronautics*, vol. 32, no. 4, pp. 826–838, 2019.

[27] Z. Huang, Y. Liu, C. Zhan, and C. Lin, W. Cai and Y. Chen, A novel group recommendation model with two-stage deep learning," *IEEE Transactions on Systems, Man, and Cybernetics: Systems*, pp. 1–12, 2021, In Press.

[28] Y. Tong, L. Yu, S. Li, J. Liu, H. Qin, and W. Li, "Polynomial fitting algorithm based on neural network," *ASP Transactions on Pattern Recognition and Intelligent Systems*, vol. 1, no. 1, pp. 32–39, 2021.

[29] M. Qin, L. Guo, P. Lin, P. He, and Y. Zhang, "Orthogonal test method to optimize the best fermentation process of traditional Chinese medicine waste residue," *Chinese Journal of Traditional Chinese Medicine*, vol. 38, no. 12, p. 4, 2020.

[30] J. Xu, J. Xia, and R. Di, "Application progress of data mining technology in traditional Chinese medicine research," *Medical Review*, vol. 25, no. 18, p. 6, 2019.

Hindawi
Computational Intelligence and Neuroscience
Volume 2022, Article ID 8247203, 9 pages
https://doi.org/10.1155/2022/8247203

Research Article

Online Small Sample Learner Modeling and Curriculum Recommendation with Healthy Emotional Factors of College Students

Xia Li, Ruibo Di, and Jun Cai

Zhejiang Gongshang University, Hangzhou College of Commerce, Hangzhou, Zhejiang 311599, China

Correspondence should be addressed to Ruibo Di; 1180086@zjhzcc.edu.cn

Received 21 December 2021; Revised 1 January 2022; Accepted 3 January 2022; Published 27 February 2022

Academic Editor: Xin Ning

Online education is a popular way for college students at present, and it is also a good compensation way to meet the special situation that traditional offline teaching cannot complete the teaching task. Traditional classroom teaching methods have been difficult to meet the learning requirements of contemporary college students, while online classroom has made up for the shortcomings of traditional classroom teaching to some extent because of its short class hours, prominent focus, and online mobile learning. First, this paper proposes an online SSL (small sample learner) model for college students to integrate healthy emotional factors. The characteristics of learners are divided into three categories: basic characteristics of learners, characteristics of behavioral factors, and characteristics of emotional factors, and the problem of solving mapping functions is transformed into the problem of solving kernel functions. Second, a novel curriculum recommendation model integrating healthy emotional factors is proposed, which fully considers the influence of user comments on similarity and transforms the similarity of users in the overall score of the project into the similarity of users in the emotional tendency of the special attributes of the project. Through the experimental evaluation, the accuracy and stability of the recommendation are greatly improved.

1. Introduction

With the continuous deep integration of big data, the Internet of Things, cloud computing, and other information technologies and education fields, the intelligent transformation of education has been promoted, and the advanced educational form in the era of educational informationization 2.0 represented by intelligent education has been achieved [1, 2]. At present, there are still some technical problems in intelligent education in the aspects of learning guidance, recommendation, answering questions, and evaluation, such as how to eliminate the semantic gap between learners and resources in resource recommendation; how to realize the large-scale online learners' answering guidance [3]; how to carry out refined teaching evaluation on learners, teachers, learning environment, and other objects.

Learning and communication through the online learning community provide people with a generalized learning method without the limitation of the number of participants and time and place [4]. Learning activities in such an environment can make everyone enjoy high-quality teaching resources and fair learning opportunities. Learning behavior data of learners in online learning communities can complete modeling and analysis of learners' behaviors, which can promote teachers and community managers to be more professional and meticulous in teaching management. A large amount of data has promoted the prosperity and development of artificial intelligence in recent years, especially the direction of DL (deep learning) [5, 6]. Due to its extremely nonlinear characteristics, DL can learn hidden patterns from a large amount of data. On the other hand, the rapid development of artificial intelligence in recent years largely depends on the development of data. Using learning data for modeling and analysis can help them to improve the quality of community content and various functions and inspire new ideas: from the perspective of teaching mode reform [7], by studying learners' learning behaviors, and can predict their learning trends, which can help them further in the rapid development of educational informationization.

Building a user portrait system can accurately depict each learner's personalized characteristics and then create a targeted study plan based on the subtle differences between different learners, which includes recommending currently suitable subjects based on learners' background knowledge structure, arranging course schedules based on learners' learning ability, recommending relevant counterpart courses based on learners' interests and hobbies, and predicting a learner's future success. Based on a review of the literature on learner models, this paper focuses on the recognition of learners' facial expressions and methods for obtaining emotional data and builds an online SSL (small sample learner) learner model that incorporates healthy emotional factors in an online classroom setting. Following that, a quantitative analysis method of curriculum recommendation model [8] suitable for integrating healthy emotional factors is discovered through an in-depth study of quantitative analysis technology of learners' characteristics.

2. Related Work

In the analysis and mining of educational big data, related universities have done a series of research and applications. For example, literature [9] developed an online learning assistant based on learner behavior analysis and intelligent dialogue. Taking the learning subject as the object, the key technologies such as the construction of an intelligent teaching environment, educational measurement, and evaluation are studied. Literature [10] constructs a learner behavior model by extracting the characteristics of learners' course completion rate and dropout rate and then predicts learners' learning behavior and judges whether learners can finally complete the course learning. Literature [11] studies the learning track and behavior data of college students learning Russian on an online education platform, extracts the data set of behavior characteristics for clustering analysis, and classifies learners according to the clustering results, so as to complete the special recommendation for learners. The literature [12] proposes a decision tree-based user performance prediction model. The end result reveals that the majority of students are in a passive learning mode. It also demonstrates how to use data mining technology to improve online teaching and learning, as well as making recommendations for students. Literature [13] proposes a comprehensive cognitive model for reconstruction analysis that integrates learners' comprehensive factors. A multimedia cognitive model has been proposed in the literature [14]. Literature [15] investigates the relationship between Facebook photos and users' personalities, primarily through Facebook's basic visual feature coding, which associates the activities associated with users' photos with the five-factor personality model. According to the literature [16], learners' utterances contain a great deal of information about their personalities, feelings, opinions, and habits in addition to semantic content.

FSL is an important goal of researchers in the process of exploring intelligent systems. Most researches on FSL are focused on neural networks [16, 17]. Literature [18] proposes to use a hierarchical nonparametric Bayesian model to realize FSL. In this model, categories are represented as tree-like hierarchical structures, such as sheep and horses for animals, cars and trucks for motor vehicles, and both animals and motor vehicles belong to a superclass. Each category is represented by two parameters, mean and variance, and knowledge transfer between different categories is realized by transfer parameters. Literature [19, 20] put forward the application of twin networks to small sample problems, which opened the prelude of neural networks to deal with small sample problems. Literature [21, 22] also proposed probability matrix decomposition and Bayesian probability matrix decomposition. Literature [23] puts forward a recommendation algorithm, which can push hot topics personalized for users to solve the problem of information overload faced by users. The content-based recommendation is simple and intuitive, but limited by the description degree of project content, and the recommendation effect is not good. Literature [24] combines and uses a variety of machine learning methods to complete the classification of a large number of movie commentary corpuses. Literature [25] introduces new feature words of semantic role tagging and discusses the application effect of multifeature word combination mode through experiments. This method has some shortcomings. The manual tagging process will take a lot of time and manpower, and it is not suitable for large-scale corpus analysis and research.

3. Research Method

3.1. Online SSL Modeling. The set of fluctuating emotions generated by learners in the learning environment that accompanies the entire learning process is referred to as learning emotion. Detailing learners' emotional characteristics, particularly the classification of basic emotional types and specific emotional characteristics, is crucial to developing an online SSL model that incorporates healthy emotional factors. In an online classroom setting, the basic learning emotions are divided into six categories: happiness, surprise, boredom, sadness, fear, and anger. Emotions can be expressed in a variety of ways, the most intuitive and quickly recognized being a change in facial expression.

The learner model, which incorporates healthy emotional factors, is the foundation and key to online classroom learners' learning analysis. This chapter focuses on the study of learners' emotional characteristics, referring to the norms of learners' models and various learners' personalized models, and divides learners' characteristic models into learners' basic characteristics, behavioral factor characteristics, and emotional factor characteristics, based on conceptual combing and theoretical analysis. A learner model incorporating healthy emotional factors is formed based on the above research. Most learners' models are currently built by analyzing and mixing learners' models from a single dimension, and most studies focus on the characteristics of learners with behavioral factors, with little attention paid to the study of learners' emotional factors. However, as intelligent teaching evolves, more educators must consider the impact of learners' emotional states on learning outcomes, and the analysis of learners' emotional states is becoming a common concern in learning analysis.

In this chapter, on the basis of summarizing the learner model specification and referring to the learner's personalized model, an online SSL model integrating healthy emotional factors is proposed, as shown in Figure 1.

Social network features include dot centrality, feature vector, and reciprocity. Emotion features include emotion data collection, expression recognition, and basic learning emotion, and the model mainly shows the basic learning emotion features. The learner model integrating healthy emotional factors is the basis and key to analyze the diverse characteristics of learners in an online classroom environment.

To analyze learners' dynamic cognitive level, first, the learning behavior of learners is indexed and then judged whether these behavior indicators obey normal distribution. It can be analyzed with corresponding correlation analysis methods, and the significant correlation detection results are obtained and judged whether to predict the model or abandon the indicators. First, a learning behavior index set is established, and the learning behavior index set is set as U, then

$$U = \{u_1, u_2, \ldots u_n\}. \tag{1}$$

Among them, u_n represents the learning behavior index, and n represents the number of learning behaviors. The goal of creating a learning behavior index set is to convert learners' specific learning behaviors into data and visual set elements, as well as to accurately present the cognitive level hidden behind learning behaviors so that learners' cognitive level can be accurately analyzed.

The data processed in SSL is often high-dimensional, and the distribution of data has no obvious structural information. Similarity w_{ij} between samples depends on the mapping function to map samples into a new space and then calculate w_{ij} in the new space. The specific calculation is as follows:

$$w_{ij} = \begin{cases} e^{\dfrac{\left\| f(x_i) - f(x_j) \right\|^2}{2\sigma^2}}, & i \neq j, \\ 0, & i = j. \end{cases} \tag{2}$$

where $f\colon R^D \longrightarrow R^M$ represents a mapping function. f map all samples to an M-dimensional space.

Let the optimal solution of the objective function be the kernel matrix K^*. The next task is to infer the category of query samples from K^*. The category to which query $\hat{x}$ belongs is obtained by the following type of weighted voting:

$$\hat{y} = \arg\max_i \sum_{x_j \in s_i} k_j^*, \tag{3}$$

where s_i represents the set of all support set samples of category i. In fact, the formula classifies the query samples into the category with the largest sum of kernel similarity, which is consistent with the classification idea in the matching network.

The frequency of course visits, the length of learning time, the degree of test completion, the number of data downloads, and other factors reflect the degree to which learners pay attention to education and reflect their behavior after accepting an online education platform. As a result, extracting and analyzing the characteristics of learners' learning behaviors are necessary in order to analyze learners' attitudes. To construct a learner's personalized model, relevant data from the database and behavior log data of an online education platform are extracted and mined. Personalized modeling, to put it simply, is the process of creating a detailed and personalized portrait of a learner.

The specific steps of the learner attitude analysis model are shown in Figure 2. In this paper, both the original data set and the feature set related to learners' behaviors are continuous data by default.

To analyze learners' attitude model, data collection is first needed. The click data, watching video data, discussion area data, and test data of learners are extracted from the online education platform, and the data related to learners' learning behaviors are extracted from them.

3.2. Curriculum Recommendation Integrating Health Emotional Factors. Generally, universities offer many elective courses, and students' elective courses are limited to some extent, so it is easy for students' scoring data to be extremely sparse. Due to the extreme sparseness of student rating data, the traditional similarity measurement method cannot effectively calculate the nearest neighbor of the target user, and the quality of CFR (collaborative filtering recommendation) system is also difficult to guarantee. The key to construct the student rating data matrix is to solve the sparseness of the data set.

Teaching quality evaluation, as an integral part of the teaching management system, aids teachers and schools in significantly improving teaching quality. Teaching quality evaluation is the process of systematically collecting data and assigning a value to teaching activities and outcomes in the classroom based on the requirements of teaching objectives and principles. The main source of teaching feedback information is the evaluation of teachers' classroom teaching quality, and it is also an important way to test teaching effect and evaluate teaching quality.

Research shows that in many recommendation methods, the most critical "emotional intelligence" factor in communication between recommendation system and people is often ignored. Especially for specific courses, such as music and movies, emotional factors often play a decisive role in recommendation, which requires the recommendation system to be able to actively meet the emotional needs of students.

The main idea is to pay attention to and mine the user comment data, mine the user's evaluation attitude towards each feature of the project, instead of calculating the user

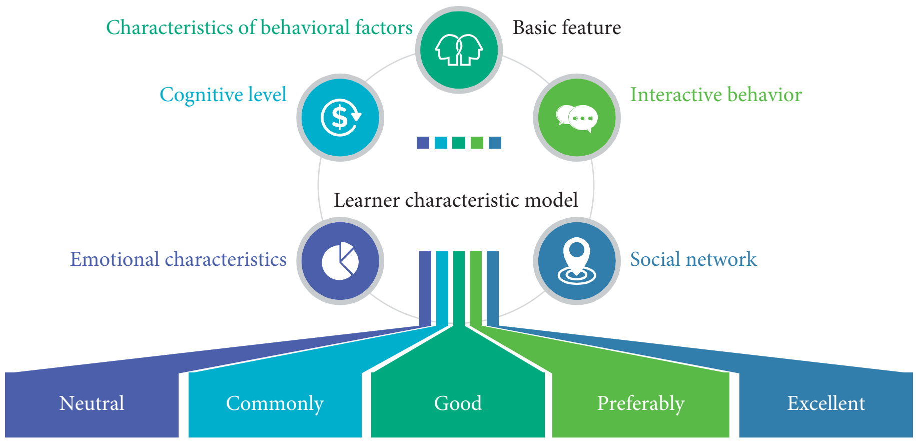

Figure 1: Online SSL model integrating health emotional factors.

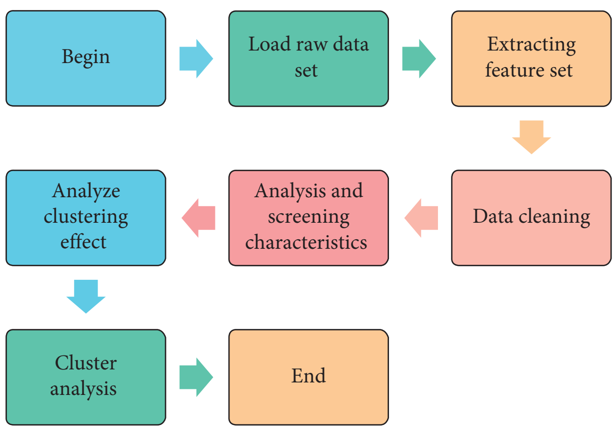

Figure 2: Generation flow chart of the multivariate cluster analysis model.

similarity based on the score information, measure the user's emotional similarity to the feature level of the project, and calculate the similarity and clustering by using the user's score of the feature of the project, so as to find the most similar N users for recommendation. The recommended framework is shown in Figure 3.

Content-based recommendation algorithm uses feature attributes to define course objects and makes recommendations based on students' evaluation of course objects. Therefore, the algorithm can be used to recommend courses in a sparse situation. First, the similarity between courses in the database and favorite courses is calculated, and formula (4)is used.

$$f(P, A) = \sum_{i=1}^{n} w_i \times \left(1 - \left|p_i - \alpha_i\right|\right), \tag{4}$$

where P represents a course in the database; A is a course that has been evaluated as a favorite by some students; n represents the number, of course, attributes corresponding to the category to which the course belongs; w_i represents the weight values of the above attributes; m_i represents the value of the i-th attribute of the course P; α_i represents the i-th attribute value of favorite course A.

By analyzing and calculating all the historical review data of a project, with the help of popular wisdom, it is possible to predict the scores of different attributes of the project.

$$\overline{R}_k = \frac{\sum_{i=1}^{N} s_{ik}}{N}, \tag{5}$$

where N represents N comments under a specific course, and $\overline{R}_k$ represents the average emotional score of the specific course on the k-th feature.

Using natural language processing technology to analyze the comment texts in the check-in history records, and further explore the emotional tendency of the texts, can accurately understand users' preferences and further improve the recommendation quality of POI (point-of-interest) [12].

Text is composed of words, and the polarity of emotional words in comments represents the tendency of text, so the tendency of comments can be obtained by calculating the polarity of emotional words. There are many ways to calculate emotion, and PMI (point mutual information) method is the simpler and more effective one.

Emotional polarity calculation usually assumes that when a word has a strong correlation with positive words, it has positive emotional polarity and vice versa. The polarity of emotion words is determined by calculating PMI between target emotion words and terms in emotion vocabulary. The PMI value between words w_i, w_j is defined as shown in formula (6).

$$PMI\left(w_i, w_j\right) = \log_2 \frac{p\left(w_i, w_j\right)}{p\left(w_i\right) * p\left(w_j\right)}, \tag{6}$$

where $p(w_i), p(w_j)$ is the probability of w_i, w_j in corpus, and $p(w_i, w_j)$ is the probability of w_i, w_j co-occurrence.

Friends often have similar behaviors and many common interests. Users usually refer to their opinions before visiting unknown POIs. Friends can influence users' choices of POIs more than ordinary users [14]. The distance between friends can be described by the number of the same friends among friends, and the similarity of interests among friends can be measured by the number of friends visiting the same POI.

Therefore, the strength of the social relationship between users and their friends can be calculated by equation.

$$sr_{ij} = \frac{\left|F_i \cap F_j\right|}{\left|F_i \cup F_j\right|} * \frac{\left|L_i \cap L_j\right|}{\left|L_i \cup L_j\right|}, \tag{7}$$

where F_i, F_j, respectively, represents the friend set of user u_i, u_j, and L_i, L_j, respectively, represents the sign-in POI set of user u_i, u_j.

Project recommendation generation is as follows:

$$R = \sum_{k=1}^{8} \overline{R}_k \times \lambda_k, \tag{8}$$

where λ_k is the attention of the target user to the k-th feature, and R is the predicted score of the candidate project, which can be regarded as the recommendation degree.

4. Results Analysis and Discussion

4.1. Emotional Feature Analysis. In this paper, emotional analysis refers to the process of gathering user feedback on a product, analyzing the content of the feedback, determining the polarity of the user's emotional tendency at the feature level of the project, that is, the favorable or unfavorable attitude and opinion toward the course or project, and then extracting more useful information.

According to the facial expression data of learners acquired by depth camera technology, the emotional state of learners is identified. The recognition result of the obtained layered RF (random forest) in the mixed expression database is shown in Figure 4.

Figure 4 shows that the hierarchical RF algorithm has a high recognition rate for learners' emotional state and can accurately judge learners' emotional state in the online classroom learning process.

It can be deduced from this that learners' emotional states changed during the stage of introducing the curriculum and teaching new lessons, and that learners always pay attention to the gradual progression of teaching content, and that learners' cognitive levels turn old and new, and that they actively construct meaningful knowledge. Features related to learners' learning behavior are extracted from all learners' features to form a feature set, which is used to analyze learners' learning attitude. Figure 5 shows the comparison of clustering results using SVS (single variable selection), RFE (recursive feature elimination), PCA (principal component analysis), and FSRF (feature selection based on the random forest).

It can be seen that when the clustering is 4 and the feature selection method is PCA, the contour coefficient reaches the maximum, and the classification effect is the best. Finally, the learner's feature data set is divided into four categories; that is, the learner's attitude model is divided into four categories.

In order to evaluate the performance of the algorithm, a small sample experiment was carried out on two data sets, namely, Omniglot [16] and miniImageNet [18]. On Omniglot data set, this paper tests the performance of the algorithm under 5-way 1-shot and 20-way 1-shot tasks. The experimental results are shown in Figure 6.

It can be seen from the figure that the performance of the SSL method based on graph regularity is slightly worse than that of prototype network with interval, because when there is only one sample in each class, the relationship between classes cannot be propagated, and it is a good strategy to simply take this sample as the representative of this class.

4.2. Course Recommendation Analysis. Here, the criteria for evaluating recommendation quality are set as MER (mean error rate) and SV (standard variance). MER is to determine the recommendation quality by predicting the deviation between the category and the actual category. The higher the MER value, the worse the recommendation quality. The calculation of SV follows the statistical method, which can directly measure the recommended quality. Here, the content-based recommendation algorithm and CFR algorithm are compared, and the three algorithms are repeatedly executed 80 times, respectively, and the recommendation quality is shown inFigures 7 and 8:

The hybrid algorithm has higher recommendation accuracy and better stability than the other two recommendation algorithms, as shown in the above figure, and clearly improves recommendation accuracy. This paper designs and compares four simplified models of curriculum recommendation model incorporating healthy emotional factors, namely, GP, CPP, SI, and ET, in order to analyze the importance of GP (geographical position), CPP (classification popularity preference), SI (social intensity), and ET (emotional tendency) factors in POI recommendation in the curriculum recommendation model incorporating healthy emotional factors.

As the evaluation indexes, AR (accuracy rate) and RR (recall rate) are chosen. The experimental results are shown in Figures 9 and 10.

Foreign countries have already integrated microcourses into daily teaching for students to preview and study independently, but domestic research on the application of microcourses is still relatively lagging behind, and the research on the process and effect analysis and evaluation of microcourses applied to teaching is not deep enough, and the research on the application of microcourses resources and learning experience tracking is almost blank. Because of the different teaching systems at home and abroad, the application of this model in China is still in the exploratory stage. Lessons from the successful experience of foreign applied microclass flipped classrooms are drawn, and the curriculum standards of various disciplines in our country are combined.

In this paper, the course features are clustered into 8 categories by analyzing the course evaluation set, and then, the attention of users to various attribute features is statistically obtained from the user's own comment set to form user preferences.

Traditional information literacy courses, like other courses, mostly use classroom teaching as the mainstay, supplemented by computer operation, and teachers as the

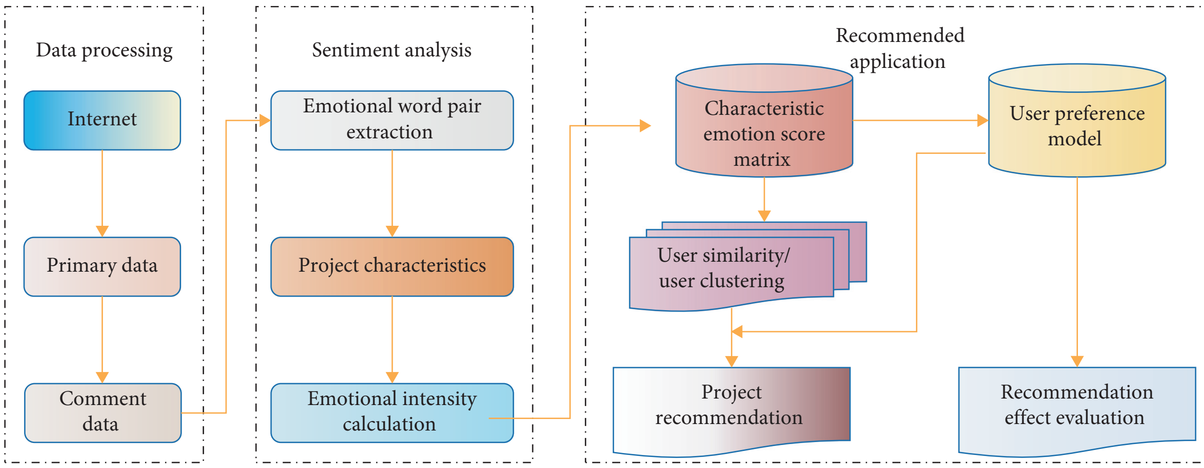

Figure 3: Personalized recommendation framework based on sentiment analysis.

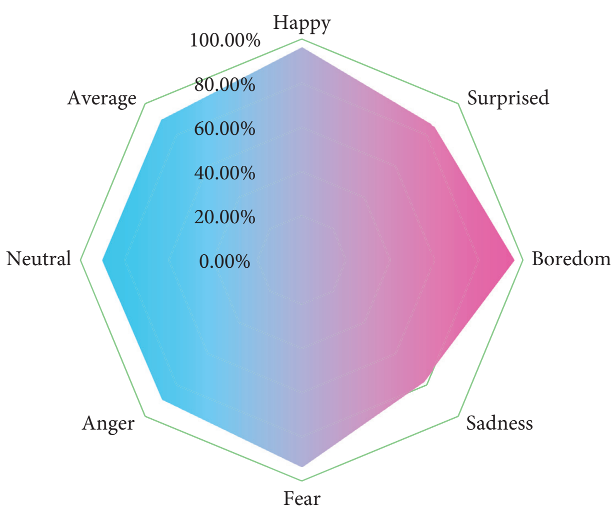

Figure 4: Recognition results of layered RF in mixed expression database.

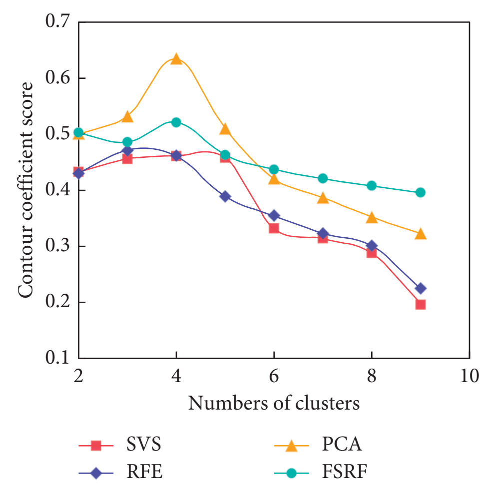

Figure 5: Influence of different feature selection methods on clustering effect.

mainstay and students as the supplement in the classroom, so it is difficult for students to reflect their personalized learning, and the teaching atmosphere can be imagined. Microcourses, on the other hand, have outstanding advantages, such as short time, abundant resources, and long online time, which meet the needs of students to flexibly choose learning time, learning place, and learning content to the maximum extent, and autonomous learning is relatively easy. At the same time, students can also reproduce the classroom teaching situation of a certain knowledge point at any time, which can well solve the problem of memorizing in class and forgetting after class, which is an important supplement and resource expansion of traditional classroom learning [7].

The key link in consolidating and digesting the curriculum's key and difficult problems is classroom teaching. Teachers break down teaching tasks and create various links to assist students in solving problems based on the syllabus. Teachers must periodically assess their students' knowledge and provide appropriate guidance and correction, as well as timely feedback. Teachers should be at the forefront of curriculum development, extracting a series of knowledge points from each class's teaching tasks based on the needs of class hours, and carefully designing and developing these knowledge points into special microcourses and series microcourses.

4.3. Teaching Suggestion. For starters, online education prevents students from interacting with teachers in real time, reduces teacher-student communication, fails to stimulate students' thinking, and causes them to lose their ability to think. Second, plagiarism in students' homework is a serious issue. Students are more likely to copy other people's learning achievements as the Internet has evolved, and they are unable to do so independently. Finally, the impact of paying attention in class has waned. After signing in before class, many students fall asleep and only watch the video, leaving the teacher to "perform" alone. To summarize, the quality of online education cannot be guaranteed at this time, and a good educational effect cannot be obtained in a

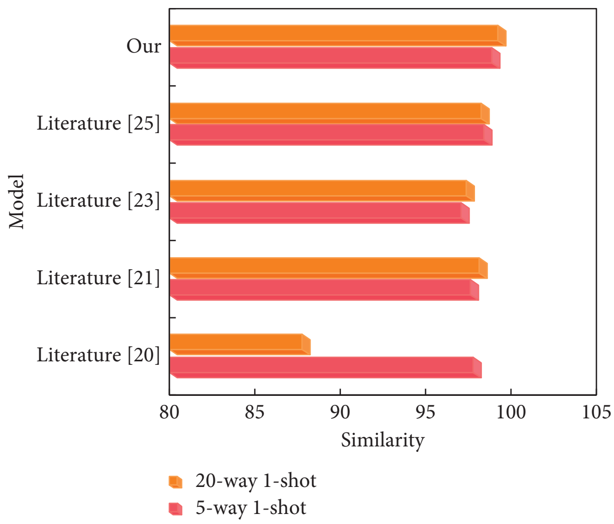

Figure 6: Small sample experimental results.

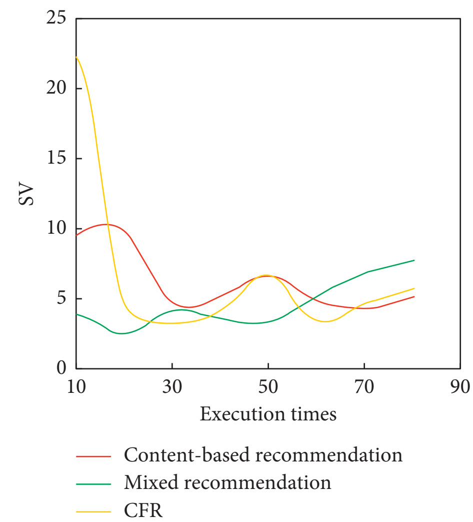

Figure 8: SV algorithm comparison.

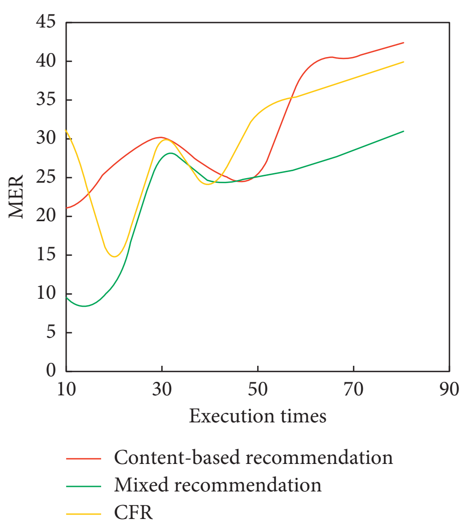

Figure 7: MER algorithm comparison.

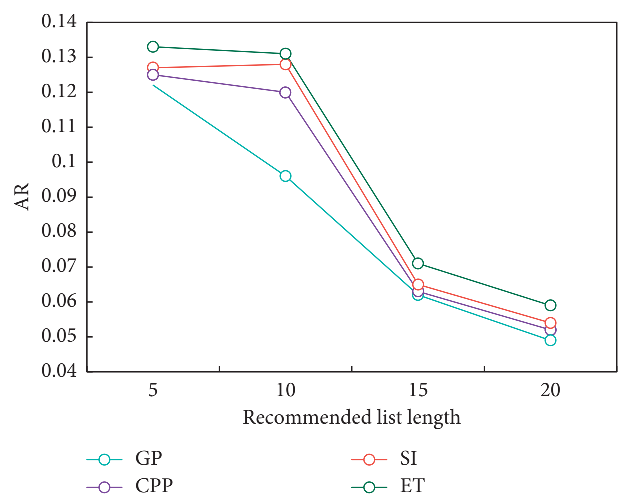

Figure 9: Comparison of different factors affecting recommended AR.

holistic manner. This development raises concerns about the future of online education.

To digitize teaching, the online classroom makes use of big data and cloud computing technologies. It comprehensively assesses students' learning quality and efficiency, starting with daily classroom study, daily assessment, semester assessment, and other aspects, making teachers' evaluation of students more objective, accurate, and fair, making teachers accurately assess students' growth, making teachers' teaching more targeted, and improving classroom teaching quality and efficiency. Students can interact with teachers more effectively in an online classroom environment. Interactive activities such as sign-in, selection of students, competition for answers, and the combination of online and offline interaction greatly improve the interaction efficiency between teachers and students, which is conducive to students' autonomous learning and teachers' accurate grasp of students' learning situations.

Teachers in the new era should change their roles in time, from the leader of the traditional classroom to the leader of the online classroom, guide, organize, and coordinate students' learning activities, and cultivate students' autonomous learning and cooperative learning ability. The ability to master and apply modern information technology is a new test for teachers, which not only requires teachers to skillfully use all kinds of learning tools and software but also requires teachers to establish data awareness, master relevant data processing technologies, and digitize and visualize the teaching process, so as to more efficiently and accurately analyze the learning situation. To improve the information-based teaching quality, an information technology mutual assistance group is established, intragroup exchange and discussion activities are organized, and teachers are helped with weak information technology to improve their information technology teaching ability.

In the aspect of educational content, a student-centered educational philosophy is established, pay attention to the combination of theory and practice, the material needs of

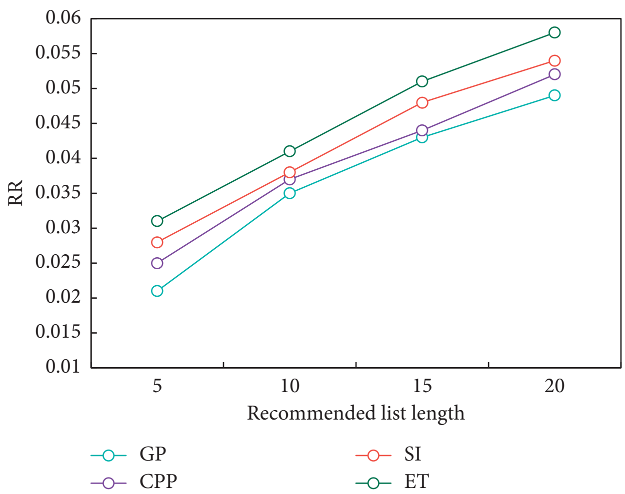

FIGURE 10: Comparison of recommended RR influenced by different factors.

students are met, and their spiritual needs are emphasized; that is, a balance among objective knowledge, value, and morality is sought.

In terms of teachers, teachers should change their teaching role orientation in time according to the changes of the times, change the traditional knowledge transmitter to become an interactive learner, and change the teaching controller to become an activity leader. Only when teachers take the lead in the initial change, students can make progress.

5. Conclusion

Personalized learning research is based on the construction of the learner model. This study integrates the above research emphases. In view of the current situation of insufficient research on the characteristics of learners' emotional factors in the study and analysis of learner model, combined with online classroom teaching environment, online SSL model research integrating healthy emotional factors is carried out. Based on the proposed learner model, this paper studies the learner feature analysis technology, focusing on the learner's emotional feature analysis technology. In the experimental part, experiments of multiple tasks are carried out on data sets, which proves that SSL based on graph regularity is effective. According to the social relationship, the social intensity among users is calculated, and the emotional tendency of users according to the comment text is analyzed and effectively combined them with collaborative filtering recommendation technology, so as to get the social-emotional score. Through experiments, even under extreme test conditions, the algorithm still shows good recommendation accuracy and timeliness, which greatly improves the recommendation quality.

In the future work, we will further explore the influence of time factors and content information such as photos and videos generated by users in POI on users' sign-in behavior, so as to further improve the recommendation quality.

Data Availability

The data used to support the findings of this study are included within the article.

Conflicts of Interest

All the authors do not have any possible conflicts of interest.

References

[1] C. Xu, Y. Sun, and G. Li, "Research on small sample commodity image classification based on deep metric learning," *Journal of Chongqing University of Technology: Natural Science*, vol. 34, no. 9, p. 8, 2020.

[2] L. Huang, "Preliminary study on the sample practice of routine and curriculum reform in the first grade of primary school," *Scientific Consultation*, vol. 31, no. 31, p. 1, 2017.

[3] L. Liu, Y. Chen, and L. Zhang, "Thirty years of quantitative sociology: taking "sociological research" as an example," *Journal of Jiangsu Administration Institute*, vol. 2, no. 2, p. 10, 2018.

[4] W. Gao, M. Yuan, and H. Zheng, "STEM curriculum construction from an integrated perspective: taking beijing primary and secondary schools as an example," *Elementary Education*, vol. 016, no. 004, pp. 13–23, 2019.

[5] J. Kong, C. Yang, J. Wang et al., "Deep-Stacking Network Approach by Multisource Data Mining for Hazardous Risk Identification in IoT-Based Intelligent Food Management Systems," *Computational Intelligence and Neuroscience*, vol. 2021, Article ID 1194565, 16 pages, 2021.

[6] M. Zhao, Q. Liu, A. Jha et al., "VoxelEmbed: 3D Instance Segmentation and Tracking with Voxel Embedding Based Deep Learning," 2021.

[7] T. Shi and W. Ge, "Research on the relationship between learning input, interactive behavior and academic performance in SPOC courses," *Chinese Medical Education Technology*, vol. 32, no. 3, p. 5, 2018.

[8] Z. Huang, Y. Liu, C. Zhan, C. Lin, W. Cai, and Y. Chen, "A novel group recommendation model with two-stage deep learning," *IEEE Transactions on Systems, Man, and Cybernetics: Systems*, vol. 3, 2021.

[9] Q. Xu, "Teaching design of "linear correlation and regression analysis mathematical modeling experiment course," *Middle School Mathematics Teaching Reference*, vol. 3, no. 3, p. 3, 2020.

[10] H. Wang, "Construction and practice of ERP training course learning process evaluation system," *Journal of Shanxi Normal University (Philosophy and Social Sciences edition): Natural Science Edition*, vol. 38, no. 5, p. 4, 2020.

[11] J. Zheng and Y. Tan, "Evaluation of the undergraduate course system of applied statistics based on SEM model——taking Hebei Normal University of Science and Technology as an example," *Journal of Hebei Normal University of Science&-Technology*, vol. 34, no. 4, p. 5, 2020.

[12] L. Gong, W. Zhao, and Y. Liu, "The latest progress and enlightenment of international K-12 robotics education research in the past ten years-based on systematic literature review," *China Distance Education*, vol. 3, no. 3, p. 10, 2020.

[13] X. Gao, Yu Chen, and S. Li, "Investigation and Research on the Learning Input of College Students," *Online General Courses——Taking Qingdao Agricultural University as an Example*, vol. 2020-5, pp. 38–45, 2021.

[14] Y. Chen, H. Hu, Bo Yang, X. Ren, C. Li, and G. Wang, "Online asynchronous teaching combined with UOOC platform and Tencent classroom," *University Chemistry*, vol. 35, no. 5, p. 6, 2020.

[15] C.-P. Chien and Li-J. Liang, "The impact of cognitive style and multiple intelligences on learning motivation and learning effectiveness-Taking the digital teaching of freshman Chinese courses in University of Science and Technology as an example," *Journal of Humanities and Social Sciences, National Taiwan University of Science and Technology*, vol. 13, no. 4, pp. 325–358, 2017.

[16] H. Yin, W. Wang, W. Hao, L. Chen, and X. Zhou, "Spatial-aware hierarchical collaborative deep learning for POI recommendation," *IEEE Transactions on Knowledge and Data Engineering*, vol. 29, no. 11, pp. 2537–2551, 2017.

[17] H. Liu, X. Kong, X. Bai, W. Wang, T. M. Bekele, and F. Xia, "Context-based collaborative filtering for citation recommendation," *IEEE Access*, vol. 3, pp. 1695–1703, 2017.

[18] X. Liu, "An improved clustering-based collaborative filtering recommendation algorithm," *Cluster Computing*, vol. 20, no. 2, pp. 1281–1288, 2017.

[19] D. Lian, Y. Ge, F. Zhang et al., "Scalable content-aware collaborative filtering for location recommendation," *IEEE Transactions on Knowledge and Data Engineering*, vol. 30, no. 6, pp. 1122–1135, 2018.

[20] T. Ha and S. Lee, "Item-network-based collaborative filtering: a personalized recommendation method based on a user's item network," *Information Processing & Management*, vol. 53, no. 5, pp. 1171–1184, 2017.

[21] G. Zheng, H. Yu, and W. Xu, "Collaborative filtering recommendation algorithm with item label features," *International Core Journal of Engineering*, vol. 6, no. 1, pp. 160–170, 2020.

[22] C. Gu, B. Liao, X. Li et al., "Network-based collaborative filtering recommendation model for inferring novel disease-related miRNAs," *RSC Advances*, vol. 7, no. 71, Article ID 44961, 2017.

[23] G. Biau, B. Cadre, and L. Rouvière, "Statistical analysis of k-nearest neighbor collaborative recommendation statistical analysis of k-nearest neighbor collaborative recommendation," *Annals of Statistics*, vol. 38, no. 3, pp. 1568–1592, 2019.

[24] X. Wu, B. Cheng, and J. L. Chen, "Collaborative filtering service recommendation based on a novel similarity computation method," *IEEE Transactions on Services Computing*, vol. 10, no. 99, p. 1, 2017.

[25] X. Yang, C. Liang, M. Zhao et al., "Collaborative filtering-based recommendation of online social voting," *IEEE Transactions on Computational Social Systems*, vol. 4, no. 1, pp. 1–13, 2017.

Hindawi
Computational Intelligence and Neuroscience
Volume 2022, Article ID 6993515, 9 pages
https://doi.org/10.1155/2022/6993515

Research Article

RNN Language Processing Model-Driven Spoken Dialogue System Modeling Method

Xia Zhu

Foreign Language Department, Guangzhou Huashang College, Guangdong 511300, China

Correspondence should be addressed to Xia Zhu; juliazhu@gdhsc.edu.cn

Received 7 January 2022; Revised 20 January 2022; Accepted 21 January 2022; Published 26 February 2022

Academic Editor: Xin Ning

Speech recognition and semantic understanding of spoken language are critical components in determining the dialogue system's performance in SDS. In the study of SDS, the improvement of SLU performance is critical. By influencing the factors before and after the input text sequence information, RNN predicts the next text information. The RNN language model's probability score is introduced, and the recognition's intermediate result is rescored. A method of combining cache RNN models to optimize the decoding process and improve the accuracy of word sequence probability calculation of language model on test data is proposed to address the problem of mismatch between test data and training data in recognition. The results of the experiments show that the method proposed in this paper can effectively improve the recognition system's performance on the test set. It has the potential to achieve a higher SLU score. It is useful for future research on spoken dialogue and SLU issues.

1. Introduction

Spoken Dialogue System (SDS) is composed of automatic speech recognition, spoken language understanding (SLU), dialogue management, language generation, speech synthesis, and so on. SLU performance is very important for SDS. The SLU system is a key component of SDS, which aims to help the computer "understand" the text recognized by the speech recognition module [1]. An important task in SLU is to automatically extract and classify semantic intentions or to fill in a set of parameters or slots embedded in the semantic framework so as to achieve the goal in man-machine dialogue [2]. Although related researchers have conducted research for many years, the task of slot filling and intention determination in SLU is still a challenging problem. The traditional methods to solve SLU are mainly conditional random fields, hidden Markov models, and other traditional methods based on statistics [3]. Natural language understanding is an important factor that determines the usability and naturalness of human-computer SDS. Its robustness directly affects the success rate of dialogue and the user-friendliness of the system [4]. However, due to the randomness of user sentences in spoken dialogue and the imperfection of speech recognition module, the traditional whole sentence analysis method cannot achieve a correct understanding of user sentences, but it is necessary to introduce a robust understanding mechanism to extract the key information in sentences. With the rise of deep learning, the application of Neural Networks (NN) training in the field of Nature Language Processing (NLP) has achieved great success. People began to explore different functions of NN.

With the rapid development of artificial intelligence, there are countless tasks in our society that need to process serialized data [5].The main goal of the early language calculation method is to automatically analyze the language structure and develop basic technologies like machine translation, speech recognition, and speech synthesis [6]. Researchers can use these technologies to create SDS and speech-to-speech translation engines in practical applications, mine social media content for health or financial data, and identify customers' feelings about products and services [7]. The goal of SLU is to automatically identify the fields, categories, and intentions of users' spoken language in order to express natural language and then extract related concepts in order to achieve the goal of system understanding of users' language. Through speech recognition, the computer converts it into corresponding text information, which is then processed by SLU. In recent years, the NN method has demonstrated remarkable performance in a variety of Natural Language Processing (NLP) tasks, particularly the method based on Recurrent Neural Networks (RNN), such as language model, language semantic understanding, and machine translation [8]. This paper employs RNN and its variants to improve the performance of SLU. On this foundation, an RNN-based SDS language understanding method is proposed.

An important task in SLU is to automatically extract and classify semantic intentions or to fill in a set of parameters or slots embedded in the semantic framework so as to achieve the goal in human-computer dialogue [9]. RNN has great advantages in extracting sequence information of natural language characters and using it to build mathematical models to solve corresponding problems [10, 11]. RNN has been verified to have a remarkable effect in solving the serialization problem. In this paper, an algorithm based on recurrent neural network is proposed, which stacks multiple nodes at one time node to deepen the complexity of nonlinear transformation. This method can store longer-term information with fewer parameters by adding storage history state information. According to more information obtained, feature information is extracted to increase the effectiveness of obtained information, improve the accuracy of SLU, and shorten the experimental time. The feature fusion network structure is applied to the data set for SLU experiment. Experimental results verify the effectiveness and reliability of the algorithm.

2. Related Work

A new framework for understanding probability was proposed in the literature [12]. A two-level search and comprehension algorithm is also used by the framework. The concept map is created at the second level using a rule-based tree expansion robust syntactic analysis algorithm in order to effectively obtain the overall structure information of the sentence. It solves the problem of a sentence's meaning being ambiguous and it being difficult to accurately extract the sentence's semantic information. To improve the robustness of language comprehension in SDS. Literature [13] proposed a two-level search understanding algorithm. Concept bundling is used to generate the concept map in the first level, and some interference components on the word map provided by the recognition module are removed. The improved robust syntactic analysis based on tree expansion is used to search for the best understanding result at the second level. The literature [14, 15] primarily investigates and implements the related technology of the SLU system's slot filling task. A joint model based on a two-way long- and short-term memory network and label splitting was proposed in the literature [16]. Furthermore, due to the ATIS data set's low-resource characteristics, an attempt was made to introduce external semantic information using foreign pretraining word vectors. An improved RNN language model based on context word vector features was proposed in the literature [17]. Enhance the RNN model's structure by adding a feature layer to the input layer. In response to the issue of language models' poor adaptability to different corpora, literature [18] proposed an adaptive method based on the CNN language model. Literature [19] proposes an RNN that uses external memory to improve memory ability. Literature [20] proposed a feature fusion-based RNN on the basis of RNN and introduced the application of the structural principle and method in SLU. Literature [21] proposed a feature fusion RNN structure based on the analysis of the basic RNN and its LSTM network and GRU network structure. Literature [22] uses adaptive data to adjust the parameters of the general background model and extracts topic features in the adaptive data to join the adaptive training of the RNN language model, enhances the model's ability to describe the adaptive corpus, and improves the language model's ability to adaptability under the corpus. Experimental results show that this method can improve the system's language recognition effect. Literature [23] mainly introduces the principle and performance index of SLU and the structural principle of basic RNN, mainly introduces two basic RNNs in detail, and analyzes its main methods. Literature [24] successfully trained a language model on a text corpus using feedforward NN. By mapping discrete words into continuous real number vectors, it successfully overcomes the impact of data sparseness on statistical modeling and at the same time solves the dimensionality disaster of model parameters' problem. Literature [25] compares the NN language model with other language models and finds that the NN model is compared with other models. For example, when the cache model or the part-of-speech-based model is combined, the resultant hybrid model has a better effect. The article summarizes the key and related research progress of the SLU task and compares the structure and principle of RNN with different structures. Propose an SDS language understanding algorithm based on RNN. The input is sent to the hidden layer for training to obtain a feature representation; then the feature information is sent to another hidden layer for training along with the source input and historical output information; finally, it is sent to the output layer to get the result. Select the data set and performance evaluation method widely used in this field and compare it with several other advanced models on the data set. The results show that the proposed RNN is effective for SLU tasks and has good accuracy and robustness.

3. Methodology

3.1. SDS. Oral English is the most direct and simple communication medium for people to communicate with each other in their daily lives. People can get information through language communication, which is one of the most important communication ways [26]. Based on this, whether people can communicate with computers directly is one of the research directions in the field of artificial intelligence, and spoken language is the natural language between people. In oral conversation, the speaker's psychological state inferred from various information can also be used to supplement the system's knowledge about the content of user statements [27].

The purpose of SLU module is to extract semantic information from the user's sentences, that is, to identify the intention of the input sentence and extract the corresponding semantic slot concept. The main function of SLU is to analyze sentences' input by users, extract semantic information, and obtain semantic representation. For the whole SDS, the key parts are SLU and dialogue management part [28]. Research shows that deep learning can extract high-level features from shallow features because of its special hierarchical structure. The problems of lack of information and excessive dimension in semantic representation of unified text have been well developed in the fields of image, pronunciation, and so on. At the same time, it has achieved some research results in the field of NLP and shows more potential application value.

SLU is an important component of the dialogue system, and its purpose is to allow the computer to "understand" the input language as if it were spoken by a human. As a result, SLU's performance is closely linked to that of the dialogue system. SLU research can help people apply SDS more accurately, which is more convenient for people's lives and work [29]. SLU's goal is to automatically identify the fields, categories, and intentions of users' oral natural language expressions and then extract related concepts in order to achieve a systematic understanding of the language they use. Domain detection, intention identification, and slot value filling are the three main components of SLU. Slot filling is a labeling task, while domain detection and intention identification are classification problems. The term "slot filling" refers to the practice of marking every word in a sentence [30]. Different semantic representations are used for different SLU tasks. We can use the semantic framework and semantic slot that conform to the semantic structure of the SLU task to model the input intuitively and clearly in the simple understanding task. This framework and semantic slot approach, on the other hand, are no longer suitable for more complex SLU tasks, such as tasks with long phrases.

The first step in a man-machine dialogue system is SLU. Its primary function is to analyze the user's conversation and collect other relevant data about conversation behavior and tasks. According to the information, the dialogue management part updates the current state of the dialogue and generates a dialogue strategy. The dialogue generation part outputs the natural language generated by the dialogue management strategy to the user. Three parts constitute a complete task-driven man-machine dialogue system, and each part has an important influence on the performance of the whole man-machine dialogue system, as shown in Figure 1 below.

Deep Neural Network (DNN) is a successful SLU model applied in NLP field. The biggest feature of DNN is that it can train massive data and then extract the feature information of these data by learning a lot of data. A remarkable feature of NLP applied deep learning is that the input comes from a large number of lexical symbols, which leads to the initial work of Neural Networks (NN) language modeling; that is, these lexical symbols are distributed through learning in the input or output layer, and these embedding and tasks are jointly trained and learned. Following this principle, various network architectures and training methods have been successfully applied.

The main difference between RNN language model and feedforward NN language model lies in the different representations of the historical information of words. In feedforward NN model, the representation method of historical information is similar to that of n-gram model, and the first $n-1$ words are still used. RNN model, on the other hand, obtains historical information through the constant circulation of hidden layer and learning from it. In RNN, the hidden layer can represent historical information, not just the first $n-1$ words. This model can theoretically represent longer context information.

RNN is an NN structure composed of an input layer, a circulation layer, and an output layer. Among them, the input layer reads each input word and the probability that the output layer generates the corresponding semantic tag. The most prominent feature of RNN is that the current predicted value can be obtained through the common information of the previously input words and the current input words. From the information processing ability of the network, the nodes in the network include input nodes, which are nodes that connect the outside world with the internal network structure of the network; implicit layer nodes and output nodes are nodes with processing capability. The RNN structure of feature fusion is shown in Figure 2.

SDS is like a communication tool for communication between human beings and machines. Through this communication tool, computers can communicate with human beings without obstacles, and computers can give correct answers to various demands of human beings. SDS will meet different users, and different users will have different speech habits. Moreover, dialogue systems usually have to face a lot of first-time users, and first-time users are generally not familiar with the "capabilities" of dialogue systems.

RNN can theoretically predict current word tags based on arbitrarily long historical data. However, because the weight parameters are updated using the random gradient descent method, there will be issues with gradient disappearance and explosion, resulting in the error information being unable to be transmitted far away in the back propagation. At the same time, it restricts RNN's storage and memory capabilities. The accuracy rate is the ratio of relevant labels to all labels trained by NN, which measures the experiment's accuracy rate; the recall rate is the ratio of trained related labels to all related labels, which measures the experiment's recall rate. To put it another way, the accuracy rate is the number of trained labels that are correct, while the recall rate is the ratio of trained correct labels to all correct labels.

3.2. SLU Algorithm Based on RNN. A careful analysis of the sentences of the participants in the oral conversation shows that the variability of sentence structure is mainly caused by two reasons: (1) flexibility of word order and (2) frequent use of nonkey components such as colloquial words, auxiliary words, and parenthesis. The key components in the field

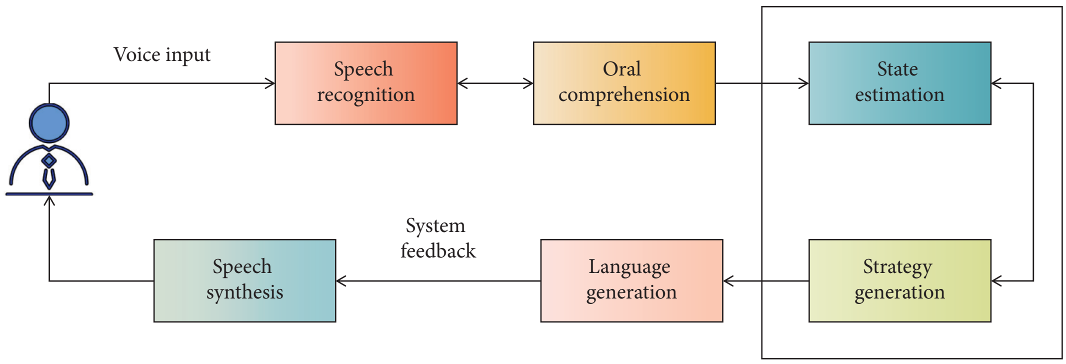

FIGURE 1: Man-machine dialogue system.

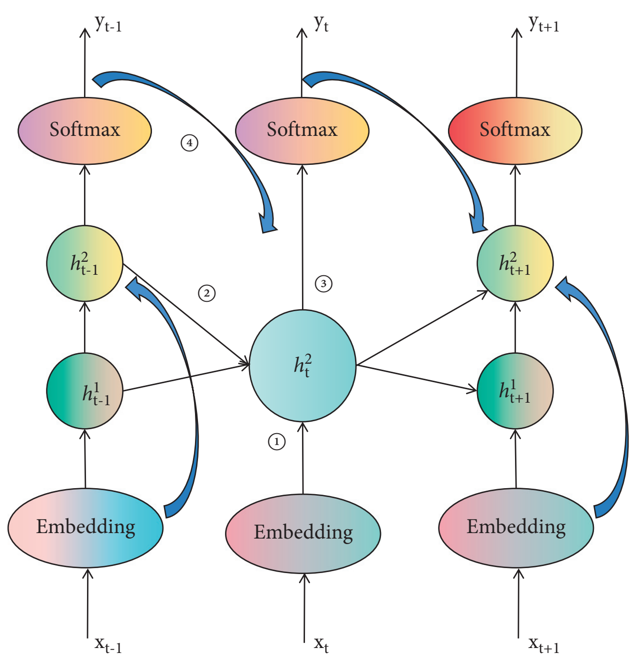

FIGURE 2: RNN structure of feature fusion.

often have relatively stable structures. Language understanding system is to process and output the input sentence and predict the tag of each word in the sentence. Generally, the input and output of these tasks are one-to-one correspondence, the input is a sequence of words, and the output is the corresponding tag sequence.

The function of nonlinear NN is more powerful than that of linear NN. The main reason is that nonlinear network can distinguish the nonlinear boundary between different data. With nonlinear NN structure, unlike linear NN, neurons with nonlinear activation function have strong learning ability, which can learn new representations through the nonlinearity of several hidden layers. This is because the input and output of the nonlinear activation function are mapped from one limited range to another.

The number of neurons and activation function in each layer of the NN, as well as between each layer, are mostly determined by the different task types. What kind of function can we use if it is a classification task? There will be different activation functions if it is a regression task. In general, only the best sentences generated by the recognition module are processed, but it is difficult to make use of the word graph's wealth of information. It is decided to use two-level processing. As the understanding result, the word graph is first transformed into a concept graph, and then an optimal path is searched on the concept graph using the concept binary grammar. The purpose of long-term dependence of information can be achieved by putting forward three gate units, the input gate, the forgotten gate, the output gate, and the corresponding cell state, and the gradient problem of RNN can be effectively solved by increasing the state of control unit.

The network structure of the model includes input layer, hidden layer, and output layer. The network does not calculate in the input layer and preprocesses the training corpus according to a certain representation; then, the calculation formula of the output of the input layer is

$$x(t) = w(t) + s(t-1). \tag{1}$$

The hidden layer of the RNN processes the information sent by input neurons, and the output layer is used to represent the network's output results. The neurons between layers in the network communicate via synapses, and the layers are linked by a weight matrix. The formula for the hidden layer and the output layer is as follows:

$$\begin{aligned} s_j(t) &= f\left(\sum_i w_i(t)u_{ji} + \sum_l s_l(t-1)w_{jl}\right), \\ y_k(t) &= g\left(\sum_i s_j(t)v_{kj}\right). \end{aligned} \tag{2}$$

In which $f(z)$ is sigmoid activation function $f(z) = 1/1 + e^{-z}$. $g(z)$ is sigmoid activation function $g(z_m) = e^{z_m}/\sum_k e^{z_m}$. i, j, and k represent the number of neurons in each layer. The output of the network is expressed in matrix form, and the above formula can be rewritten as

$$\begin{aligned} s(t) &= f(Uw(t) + Ws(t-1)), \\ y(t) &= g(Vs(t)). \end{aligned} \tag{3}$$

The output vector $y(t)$ represents the probability distribution $P(w(t+1)$ of the word to be predicted $w(t+1)$

given the current word $w(t)$ and historical information $s(t-1))|w(t)$, $s(t-1)$. The time complexity of each step during model training and testing is proportional to

$$O = H \times H \times H \times V = H \times (H + V), \tag{4}$$

where H is the size of the hidden layer and V is the size of the vocabulary.

At the first level, based on the word map given by the recognition module, the concept is bound according to the concept rules, and all possible concept candidates in the sentence are obtained, and the concept map is generated. In the second level, according to the sentence-level rule set, a robust syntax analysis algorithm based on tree expansion that can skip noncritical components is used to search for the optimal whole sentence comprehension result on the generated concept map. In RNN structure, the state of information is mainly nonlinear activation of input information. Except for nonlinear property, the state of information can only be updated through external input. Therefore, the storage state is added in the loop layer to store and update the historical information. While adding external information input sources, different nonlinear processing information flows are added so that long-term context storage information can be obtained. Long-term historical information can be stored and new information can be added through the added information flow. The current input information and the stored historical information are processed nonlinearly together, and more feature information that can express the input concept can be obtained through the processing and activation of nonlinear functions.

When the understanding module receives a new word graph, it first creates an empty concept graph; then, it uses the bottom-up chart syntax analysis method to analyze all of the arcs in the word graph according to the defined concept rule set and merges several word arcs that can be combined into a single concept into a concept arc. By weighting the input data, the perceptron activates the output vector, which contains information about the input data. The score is calculated and added to the concept map's corresponding nodes. The interaction between the unit that stores long-term historical information and the loop node can provide the most effective feature information.

The ability of a model trained on a given data set to run on previously unseen data that is similar to the training data is referred to as generalization. The following factors affect NN's generalization ability in order to make it more applicable: (1) NN's structural complexity, capacity, and scale. (2) Sample quality, NN's information content is the sum of all samples trained in the network. The stronger the generalization ability of NN, the more information content in the training samples. (3) The starting weight. (4) Hours of study time, the time it takes for a NN to learn is another factor that influences the network model's ability to generalize.

The learning part consists of the following adjustment parameters of RNN with n output layers.

$$\Theta = \left\{E, h^{(1)}(0), U^{(1)}, U^{'(1)}, \ldots, h^{(H)}(0), U^{(H)}, U'(H), V\right\}. \tag{5}$$

To be precise, the shape of the matrix is (4) and (5).

$$U^{(1)} \in M_{d_h \times d_e(2d+1)}(R) U^{'(1)}, \ldots, U^{(H)}, U^{'(H)} \in M_{d_h \times d_h}(R), \tag{6}$$

$$V \in M_{N \times d_h}(R). \tag{7}$$

For training, use random gradient descent. After calculating the gradient for each sentence in training set D, update the parameters to minimize the negative log likelihood. A sentence is considered as a word tuple and a slot tuple.

$$L(\Theta) = -\sum_{(S,W)\in D} \sum_{t=1}^{T} \log P_{\Theta}\left(s_t | l_0^{t+d}\right). \tag{8}$$

The length of each sentence may vary from one training sample to another, and the window size of context words is a superparameter.

Because the concept extraction and sentence comprehension are handled hierarchically, only 300 rules are used at the sentence level, which basically covers all kinds of user input situations in this field. After obtaining the concept map of the current user sentence, we do not simply search for an optimal path on the concept map according to the concept binary grammar as the final understanding result, but search the sentence space composed of the concept map by introducing sentence-level rules and adopting the improved robust syntax analysis method based on tree expansion. The information about context is mainly obtained by processing the input information and the saved context state together to obtain the feature information of context. These historical feature information are activated by nonlinear functions, and finally more detailed and specific feature information is obtained. Finally, the training results of the hidden layer are sent to the output layer for judgment and calculation.

The effect of network training can be influenced by data preprocessing in some cases. As a result, some data preprocessing decisions must be made. However, network training after preprocessing can sometimes achieve the same effect as training and learning the data directly, and data without preprocessing can sometimes achieve better results, making preprocessing redundant. In an RNN structure, the unit structure with the function of saving historical information primarily sends the current moment's input data and the previous moment's historical storage data to the storage unit for activation processing. The activation function is a nonlinear function in this case, and activation of the activation function yields feature information that has a strong correlation with the input historical data and current data.

4. Results Analysis and Discussion

In SDS, the meaning of the user's current statement has a strong correlation with the conversation history, so this information can be used to infer the meaning of the current statement. In order to bind concepts, which are the key components in the word map, we first need to define a group of concepts in current application fields and their corresponding composition rules. In order to prove the practicability of the RNN model proposed in this paper, this paper uses the data set widely used in experiments such as SLU, that is, the experiment of oral semantic understanding on the data set of Air Travel Information System (ATIS).

Check the analysis results of concept map. If there is a whole sentence analysis result, select the path with the highest score for semantic extraction; otherwise, search for an optimal path on the concept map and perform semantic extraction according to the context of dialogue management. The tuning parameters in the experiment include the number of units in the hidden layer. In this experiment, the number of units in the hidden layer is set to 200, the dimension of the word vector in the word embedding layer is set to 200, and the back calculation steps of the back propagation algorithm applied in this paper are set to 10. The weight matrix and offset of NN are updated by back propagation, respectively. In this section, the traditional Condition Random Fields (CRF) is compared with Convolution Neural Networks (CNN) and this model. In order to observe the process of network training and learning more intuitively, the performance index of the network is described by describing the change process of F1 value, and the line chart is drawn as shown in Figure 3.

Considering the guiding role of historical information in SDS and the structural characteristics of user sentences in the field of train information query, it is decided to use two aspects of information to bias the search space: user intention inference based on dialogue history and sentence feature phrases. At the same time, the relationship between entropy of training sets and iteration times of different models is compared to compare their convergence speed. The results are shown in Figure 4.

The training set entropy is expressed in logarithmic form. Compared with other models, the proposed model has lower training entropy and the best convergence speed. Experimental results show that this model has good accuracy and robustness and is suitable for SLU tasks. Defining the dialogue state based on the recent dialogue history greatly reduces the dimension of the state space, but it only uses limited local historical information, which reduces the accuracy of prediction. In order to give an efficient and accurate prediction of subrule set by using historical information as much as possible, a new prediction idea is proposed, which is not based on each specific historical state of conversation but based on the preconstructed user plan model to infer the user's intention.

CRF is the most commonly used method to deal with sequence tagging, and it has achieved good results in sequence processing. In this paper, CRF model, RNN, and CNN are used to perform feature fusion experiments on ATIS dataset. By changing the neurons in the network structure to process the data, the experimental results are shown in Figure 5.

The results of the above experiments show that the deep RNN feature fusion model outperforms CRF and CNN in SLU. When the optimal path analysis results are unavailable, this algorithm analyzes all concept maps, which saves time

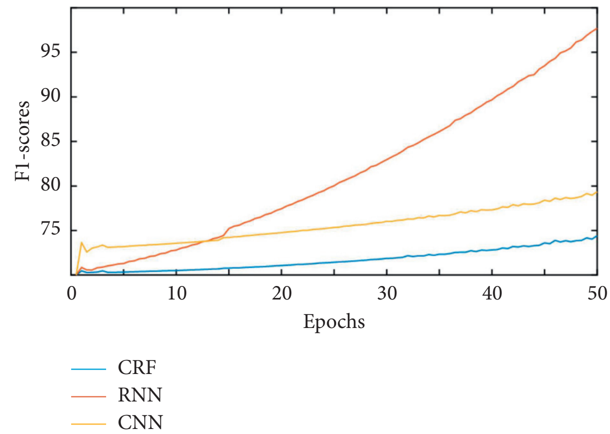

Figure 3: Comparison of training results of three models.

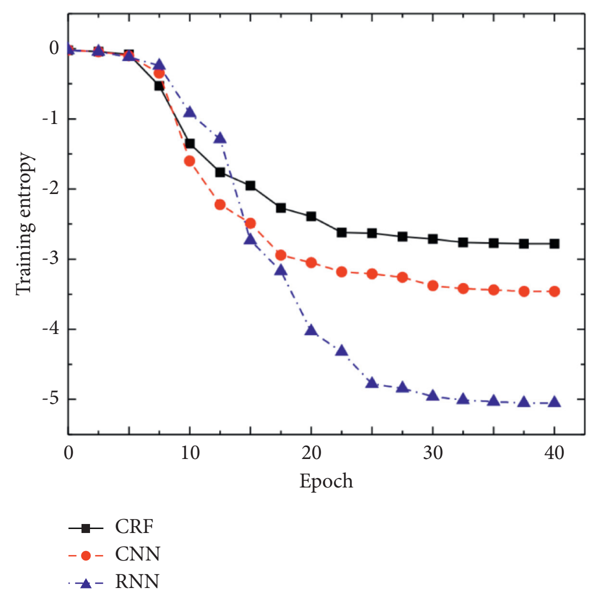

Figure 4: Comparison results of different models.

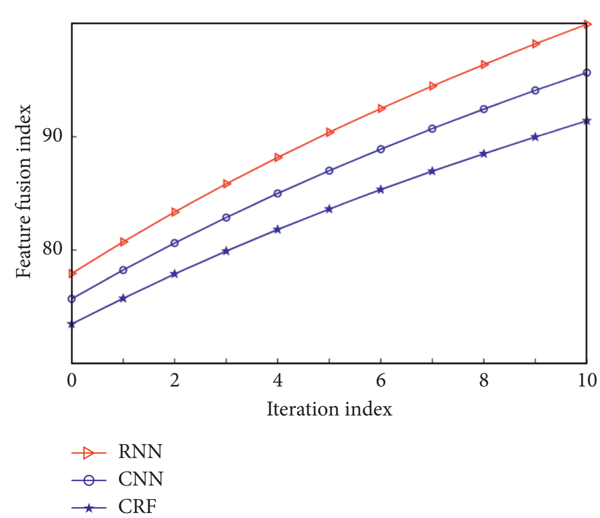

Figure 5: Model depth feature fusion.

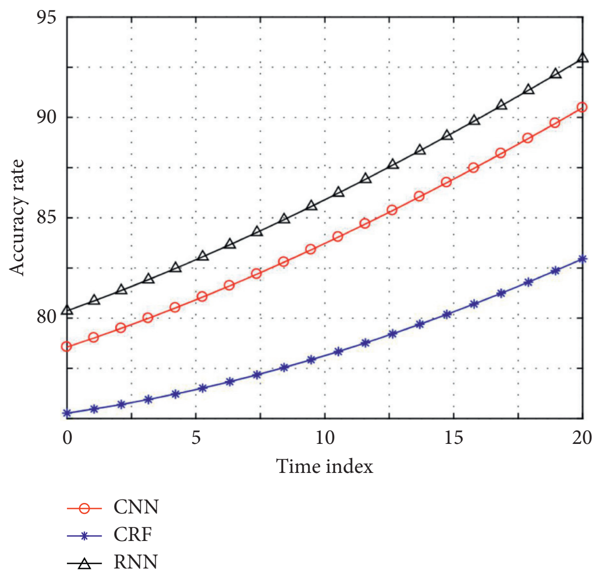

Figure 6: Accuracy comparison of different models.

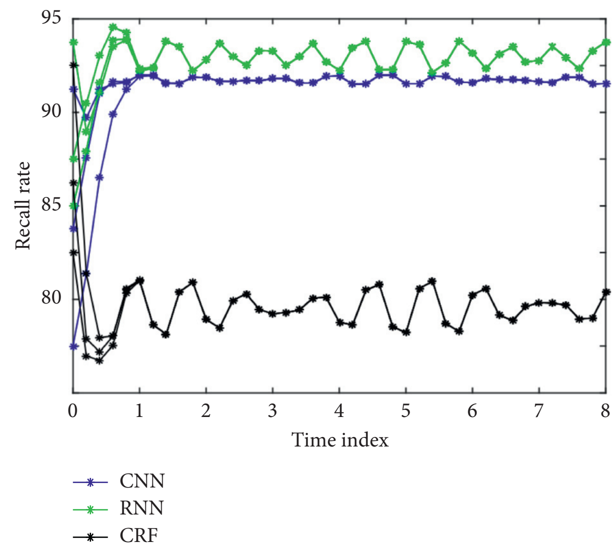

Figure 7: Comparison of recall rates of different models.

by not having to search all sentence spaces contained in concept maps. The pruning-while-expanding strategy can greatly reduce the scope of the search space during the analysis process. The precision, recall, and $F1$ performance indexes used in this experiment to assess oral semantic understanding are precision, recall, and $F1$. The proportion of correctly marked words to all correctly marked words is referred to as the accuracy rate, while the proportion of correctly marked words to all correctly marked words is referred to as the recall rate. In the labeling of evaluation data, the recall rate is the proportion of correct labels. The following is how $F1$ is written:

$$F_1 = \frac{2 \times \text{precision} \times \text{recall}}{\text{precision} + \text{recall}}. \tag{9}$$

In the process of dialogue, every time the user inputs a new sentence, the system reinfers and updates the user's intention according to the understanding result of the sentence and the historical information of the user's intention and then predicts the possible input of the next sentence by the user according to the inferred user's intention to determine the corresponding subrule set. Because the user's intention inference information and sentence feature phrase information based on dialogue history come from two independent information sources, the two kinds of information can be directly combined to restrict the search space. The three models are compared. Figure 6 shows the comparison of the accuracy of different models. Figure 7 shows the comparison of recall rates of different models. Figure 8 shows the $F1$ comparison of different models.

The SLU experiment on ATIS data set can be seen from the above results. The experimental results obtained by RNN model in this paper are always better than those obtained by CRF and CNN methods. The superiority of this method is verified. In this chapter, we propose the DNN structure of feature fusion through the NN structure described earlier and combine the features of DNN to concentrate multiple

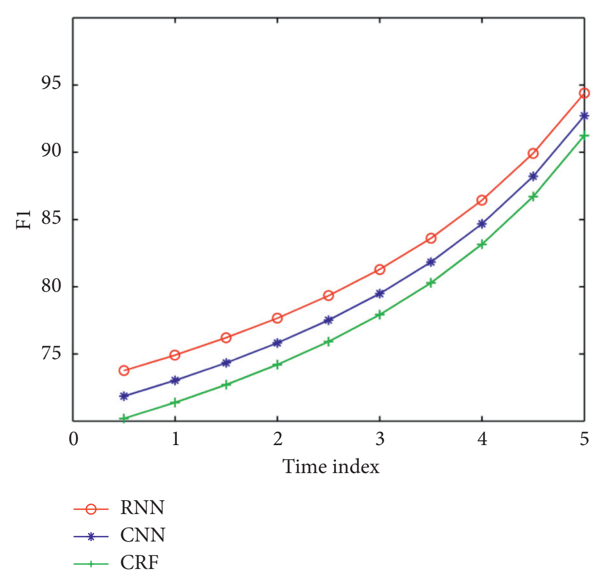

Figure 8: $F1$ comparison of different models.

features in a time node for calculation. This paper introduces the experiments of RNN, CNN, and CRF network structures on the database. The results show that the proposed RNN with external memory is effective for SLU tasks, has good accuracy and robustness, and has certain advantages in training error and convergence speed.

5. Conclusions

The basis of SLU is to represent words as symbols that can be read by machines, that is, the representation of words. In the task of SLU, it is mainly to label each word in the input text sentence with a corresponding label, and the most effective model algorithm to solve SLU is RNN. On this basis, this paper proposes an RNN that can store long-term historical information. The NN structure can solve the problem of gradient disappearance with fewer parameters. Based on the unified statistical framework of search, the information of user's intention inference and sentence feature phrases are introduced to constrain the search space, which further improves the robustness and real-time rate of understanding. At the same time, it achieves better results than CNN and GRU. In order to further improve the robustness and real-time rate of understanding, the information of user intention inference based on dialogue history and sentence feature phrases are introduced in the second level to restrict the scope of search space. The path is evaluated and pruned based on the statistical framework, which can ensure the real-time performance of the algorithm and obtain high understanding accuracy. The model in this paper is compared with other models on ATIS data set. Experimental results show that the SLU method based on RNN proposed in this paper is effective for SLU tasks and improves the robustness and accuracy of the original model. And the $F1$ value is significantly improved. The next task of this paper is to apply RNN to other NLP tasks in order to increase the universality of RNN network structure.

Data Availability

The data used to support the findings of this study are included within the article.

Conflicts of Interest

The author does not have any possible conflicts of interest.

Acknowledgments

This study was supported by the "Mentorship Program of Guangzhou Huashang College 2019, China (Grant no. 2019HSDS20), "Characteristic Innovation Program of Ordinary Colleges and Universities of Guangdong Province of China, 2019 (Grant no. 2018WTSCX232), and "Quality Program of Guangzhou Huashang College 2020, China (Grant no. HS2020ZLGC24).

References

[1] S. Järvelä, H. Järvenoja, and J. Malmberg, "Capturing the dynamic and cyclical nature of regulation: methodological progress in understanding socially shared regulation in learning," *International journal of computer-supported collaborative learning*, vol. 14, no. 4, pp. 425–441, 2019.

[2] L. Campillos-Llanos, C. Thomas, R. Bilinski, and Z. Pierre, "Designing a virtual patient dialogue system based on terminology-rich resources: challenges and evaluation," *Natural Language Engineering*, vol. 26, no. 2, pp. 1–38, 2019.

[3] Z. Grobelny, S. Golba, and J. Jurek-Suliga, "A new cyclic initiator system for the synthesis of novel star-shaped polyether-polyols (PEPOs) for fabrication of rigid cross-linked polyurethanes," *Iranian Polymer Journal (English Edition)*, vol. 27, no. 10, pp. 745–754, 2018.

[4] Á. Garab, "Absence of small solutions and existence of Morse decomposition for a cyclic system of delay differential equations," *Journal of Differential Equations*, vol. 269, no. 6, pp. 5463–5490, 2020.

[5] X.-B. Jin, W.-Z. Zheng, J.-L. Kong et al., "Deep-learning temporal predictor via bidirectional self-attentive encoder-decoder framework for IOT-based environmental sensing in intelligent greenhouse," *Agriculture*, vol. 11, no. 8, p. 802, 2021.

[6] H. Candice, C. Kut, and G. Haresh, "Managing a closed-loop supply system with random returns and a cyclic delivery schedule - sciencedirect," *European Journal of Operational Research*, vol. 255, no. 3, pp. 787–796, 2016.

[7] J. Cao and W. Xie, "Stability of a two-queue cyclic polling system with BMAPs under gated service and state-dependent time-limited service disciplines," *Queueing Systems*, vol. 85, no. 1, pp. 1–31, 2016.

[8] Y. Chuang, F.-B. Ueng, and Y.-S. Shen, "A cyclic prefix free multiple input multiple output generalized frequency division multiplexing system design," *Wireless Personal Communications*, vol. 117, no. 2, pp. 311–336, 2021.

[9] S. Guo, Y. Guan, H. Tan, R. Li, and X. Li, "Frame-based neural network for machine reading comprehension," *Knowledge-Based Systems*, vol. 219, no. 1, Article ID 106889, 2021.

[10] L.-R. Xing, Z. Lu, M. Li, J. Zheng, and D. Li, "Revealing high-lying intersystem crossing in brightly luminescent cyclic trinuclear CuI/AgI complexes," *Journal of Physical Chemistry Letters*, vol. 11, no. 6, pp. 2067–2073, 2020.

[11] C. Huynh, C. Kut, and G. Haresh, "Managing a closed-loop supply system with random returns and a cyclic delivery schedule," *European Journal of Operational Research*, vol. 255, no. 3, pp. 787–796, 2016.

[12] B. Zaa, C. Mae, D. Aae, H. Ye, and J. Zhang, "Forecasting gold price fluctuations using improved multilayer perceptron neural network and whale optimization algorithm," *Resources Policy*, vol. 61, pp. 250–260, 2019.

[13] W. A. Khan, S. H. Chung, M. U. Awan, and X. Wen, "Machine learning facilitated business intelligence (Part I)," *Industrial Management & Data Systems*, vol. 120, no. 1, pp. 164–195, 2019.

[14] E. Heyselaar, P. Hagoort, and K. Segaert, "In dialogue with an avatar, language behavior is identical to dialogue with a human partner," *Behavior Research Methods*, vol. 49, no. 1, pp. 46–60, 2017.

[15] J. Bavelas, J. Gerwing, and S. Healing, "Doing mutual understanding. Calibrating with micro-sequences in face-to-face dialogue," *Journal of Pragmatics*, vol. 121, pp. 91–112, 2017.

[16] C. Watanabe, K. Hiramatsu, and K. Kashino, "Understanding community structure in layered neural networks," *Neurocomputing*, vol. 367, no. 11, pp. 84–102, 2019.

[17] V.-K. Tran and L.-M. Nguyen, "Gating mechanism based natural language Generation for spoken dialogue systems," *Neurocomputing*, vol. 325, no. 1, pp. 48–58, 2019.

[18] S. Koike and A. Lee, "Spoken keyword detection using recurrent neural network language model," *Journal of the Acoustical Society of America*, vol. 140, no. 4, p. 3116, 2016.

[19] M. Kim and H. Kim, "Integrated neural network model for identifying speech acts, predicators, and sentiments of dialogue utterances," *Pattern Recognition Letters*, vol. 101, no. 1, pp. 1–5, 2017.

[20] L. Campillos-Llanos, C. Thomas, R. Bilinski, N. Antoine, R. Sophie, and Z. Pierre, "Lessons learned from the usability evaluation of a simulated patient dialogue system," *Journal of Medical Systems*, vol. 45, no. 7, pp. 1–20, 2021.

[21] Q. He, W. Liu, and Z. Cai, "B&Anet: combining bidirectional LSTM and self-attention for end-to-end learning of task-

oriented dialogue system," *Speech Communication*, vol. 125, no. 1, pp. 15–23, 2020.

[22] X. Liu, H. H. Chen, and S. Chen, "Symbol cyclic-shift equalization algorithm-A CP-Free OFDM/OFDMA system design," *IEEE Transactions on Vehicular Technology*, vol. 66, no. 1, pp. 282–294, 2017.

[23] J. Bastien, D. L. Scapin, and C. Leulier, "The ergonomic criteria and the ISO/DIS 9241-10 dialogue principles: a pilot comparison in an evaluation task," *Interacting with Computers*, vol. 3, pp. 299–322, 2018.

[24] F. Jiang, Y. Chiba, T. Nose, and A. Ito, "Automatic assessment of English proficiency for Japanese learners without reference sentences based on deep neural network acoustic models - ScienceDirect," *Speech Communication*, vol. 116, pp. 86–97, 2020.

[25] E. H. Middlebrooks, K. Yagmurlu, J. P. Szaflarski, M. Rahman, and B. Bozkurt, "A contemporary framework of language processing in the human brain in the context of preoperative and intraoperative language mapping," *Neuroradiology*, vol. 59, no. 1, pp. 69–87, 2017.

[26] F. F. d. Oliveira, S. d. M. C. Marin, and P. H. F. Bertolucci, "Neurological impressions on the organization of language networks in the human brain," *Brain Injury*, vol. 31, no. 2, pp. 140–150, 2016.

[27] C. Du, J. Wang, H. Sun, Q. Qi, and J. Liao, "Syntax-type-aware graph convolutional networks for natural language understanding," *Applied Soft Computing*, vol. 102, no. 2, Article ID 107080, 2021.

[28] Y. Xu, Y. Dai, C. Li, H Zhang, M Guo, and Y Yang, "PC software-based portable cyclic voltammetry system with PB-MCNT-GNPs-modified electrodes for *E. coli* detection," *Review of Scientific Instruments*, vol. 91, no. 1, Article ID 014103, 2020.

[29] S. Lee, H. Noh, and C. Lee, "A scaled cyclic delay diversity based precoding for coded MIMO-OFDM system," *IEEE Transactions on Vehicular Technology*, vol. 68, no. 6, pp. 5723–5731, 2019.

[30] L. Gong, C. Tian, and J. Li, "Quantum information processing quantum network dialogue protocol based on continuous-variable ghz states," *Quantum Information Processing*, vol. 17, no. 12, pp. 1–12, 2018.

Hindawi
Computational Intelligence and Neuroscience
Volume 2022, Article ID 1879483, 11 pages
https://doi.org/10.1155/2022/1879483

Research Article

An Entity Relation Extraction Method for Few-Shot Learning on the Food Health and Safety Domain

Min Zuo[1], **Baoyu Zhang**[1], **Qingchuan Zhang**[1], **Wenjing Yan**[1] **and Dongmei Ai**[2,3]

[1]*Beijing Technology and Business University, National Engineering Laboratory for Agri-product Quality Traceability, Beijing 100048, China*
[2]*Basic Experimental of Natural Science, University of Science and Technology Beijing, Beijing 100048, China*
[3]*School of Mathematics and Physics, University of Science and Technology Beijing, Beijing 100048, China*

Correspondence should be addressed to Qingchuan Zhang; zhangqingchuan@btbu.edu.cn

Received 5 January 2022; Accepted 27 January 2022; Published 21 February 2022

Academic Editor: Xin Ning

In recent years, entity relation extraction has been a critical technique to help people analyze complex structured text data. However, there is no advanced research in food health and safety to help people analyze the complex concepts between food and human health and their relationships. This paper proposes an entity relation extraction method FHER for the few-shot learning in the food health and safety domain. For few-shot learning in the food health and safety domain, we propose three methods that effectively improve the performance of entity relationship extraction. The three methods are applied to the self-built data sets FH and MHD. The experimental results show that the method can effectively extract domain-related entities and their relations in a small sample size environment.

1. Introduction

Food is inextricably linked to human health, particularly the nutritional components that can significantly improve health. For instance, increased spermidine intake protects against cancer, metabolic disease, heart disease, and neurodegeneration [1]. A higher intake of whole grains and dietary fiber is associated with a decreased risk of death from liver cancer and disease [2]. In addition, contaminants in food or an excessive amount of artificial additives have a detrimental effect on human health and even cause various diseases. For instance, interference with the intestinal microbiota's metabolites caused by food contaminants (polycyclic aromatic hydrocarbons, polychlorobiphenyls, brominated flame retardants, dioxins, pesticides, and heterocyclic amines) may promote the establishment of an inflammatory state in the intestine [3]. Food emulsifiers and thickeners influence the intestinal microbiota, mucosal barriers, and inflammatory pathways, and there are numerous possible pathogenic mechanisms [4].

With the proliferation of available human health data, humans use predictive or classification models to extract useful information, which helps people enjoy better health protection. Typical of this available human health data is the electronic health record (HER), the largest source of medical text data. One of the critical points in analyzing these unstructured textual data is to extract vital medical concepts, so many named entity recognition methods and entity relation extraction methods have emerged. Wan et al. proposed an ElMo-ET-CRF model approach for extracting medical named entities from Chinese electronic medical records (CEMR) using dynamic context-dependent ElMo character embedding to merge more lexical, syntactic, and semantic information that alleviate the long context-dependency problem [5]. Luo et al. proposed a novel tagging scheme considering overlapping relations to solve the overlapping problem in biomedical texts and then built the Att-BiLSTM-CRF model to extract the entities and their relations according to the rules [6]. Fei et al. proposed a new cross-graph neural model for joint extraction of overlapping entity relations in biomedical texts. They treat the entity relation extraction task as a relational triad prediction and construct entity graphs by enumerating possible candidate entity spans [7].

It is possible to help explicitly store the relationships between complex medical concepts for use in subsequent tasks by extracting them. Similarly, for the food health and safety domain, food regulators sample food products on the market and examine the ingredients and form structured data. However, in addition to structured data, more unstructured textual data goes beyond the act of food sampling and inspection to include announcements of food safety events, news reports, and knowledge about food and human health. Cenikj et al. proposed a method to detect the relationship between food and disease entities from text. They explored the feasibility of migration learning using a pretrained model based on BERT and achieved good results with few-shot learning [8]. Popovski et al. proposed a rule engine for extracting food concepts called FoodIE, a rule-based named entity recognition method with rule content describing food entities' computational linguistic and semantic information [9].

However, the food health and safety field does not have many available resources like the biomedical field, so few-shot learning becomes an effective method to improve information extraction. Qu et al. proposed a Bayesian meta-learning method for relation extraction in few-shot learning environment, applying graphical neural networks to global relation graphs to improve accuracy [10]. Sainz et al. reformulated relation extraction as an entailment task with good results for zero- or small-sample relation extraction tasks [11].

The essential technique for extracting valid information in the food health and safety domain is entity relation extraction. This task requires the model to identify entities and relations in a sentence correctly and combine them correctly. The complexity of the task and the small sample size together contribute to the difficulty of the entity relation extraction task with few-shot learning. For supervised deep learning models, small sample size can lead to an underfitting of the model. In other words, there is not enough information to train a valid model. In addition, the model tends to converge at a local optimum, leading to poorer practical results of the model.

To solve the underfitting problem, we propose two methods to enrich the semantic features of the input text. The first is to disassemble Chinese characters into radicals (https://en.wikipedia.org/wiki/Radical_(Chinese_characters)) and construct semantic input at the radical level. As pictographs, radicals are part of the structure of Chinese characters. The radicals have specific meanings; in other words, they represent part of the semantic information of the constituent characters. Therefore, constructing semantic input at the level of radicals can enrich the semantic information of the input text very well [12, 13]. The second approach to enrich semantic information is to fuse input text characters and word vectors. As units with independent meanings, characters are often given new meanings after forming words, and word information can significantly complement the interpretation of words within words [14]. For instance, the Chinese character "瘦 (lean)," "肉 (meat)," and "精 (essence)" form the word "瘦肉精," which stands for a drug that is banned from being added to animal feed. In their study, Chen and Hu also verified that Chinese words contain rich semantic information [15]. Tran et al. combined the advantages of character- and word-level translation and proposed a new method for translating Chinese into Vietnamese [16].

To solve the problem of the model falling into local optimality, we propose a text noise removal model to help the model converge quickly to the global optimum. As shown in Figure 1, for a given input text: "Enrofloxacin belongs to the third generation of quinolones, is a class of synthetic broad-spectrum antibacterial drugs, according to the "National Food Safety Standards Maximum Residue Limits for Veterinary Drugs in Food," the maximum residue limit of enrofloxacin in the skin and meat of fish is 100 μg/kg." There are four groups of entity relations combinations in the sentence.

We need to extract the two entity relation groups below the sentence in Figure 1 (index values 3 and 4 in Table 1). The two entity relation groups above the sentence (index values 1 and 2 in Table 1) are weakly related to food health and safety. In this paper, we believe that we need to accurately propose the entity relation groups that are food-health-related. The entity relation groups that are weakly related to food health and safety will become noise to affect the extraction effect.

To effectively extract entities and relations for texts in the food health and safety domain in a small-sample learning environment, this paper proposes a method for entity relation extraction in the food health and safety domain, FHER (food health entity relation extraction).

Our contribution can be summarized as follows:

(1) To reduce the influence of noise in the text, we propose a text denoising method for domain entity relation extraction to convert the text denoising task into a sequence prediction task, which effectively reduces the correct range of entity relation extraction.

(2) To address the lack of semantic information due to the small sample size under the few-shot learning, we propose constructing the input at the part-head level to enrich the semantic information.

(3) We propose the fused character and word method to improve the ambiguity problem caused by errors in Chinese word separation boundaries.

2. Related Works

There are two approaches in current research [17]. Traditionally, a pipeline approach is used to extract entity mentions using a named entity recognizer and then predict the relationship between each pair of extracted entity mentions [18, 19]. This approach inevitably brings the problem of error propagation. To alleviate the error propagation problem, Yu and Lam proposed a joint extraction approach that performs two subtasks simultaneously [20].

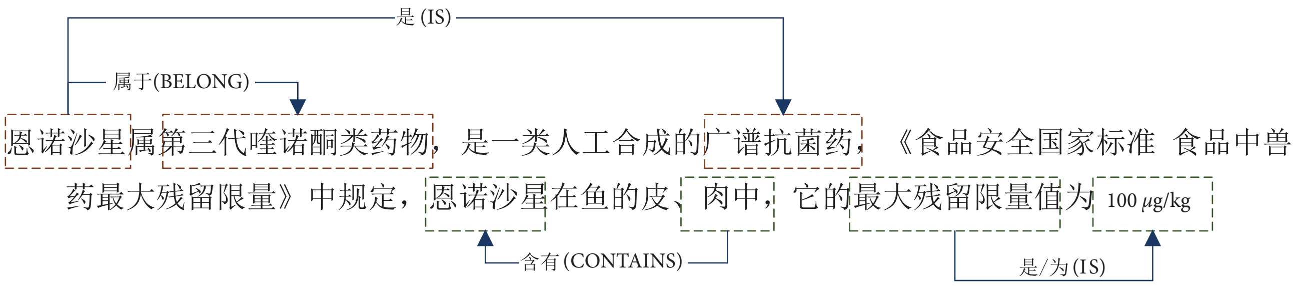

Figure 1: Examples of sentences in the field of food health and safety and the entity relations that exist within it.

Table 1: The combination of entity relations present in the text.

Index	Subject	Relation	Object	Definition
1	Enrofloxacin	Belong	The third generation of quinolones	Noise
2	Enrofloxacin	Is	Synthetic broad-spectrum antibacterial drugs	Noise
3	Skin and meat	Contain	Enrofloxacin	Useful
4	The maximum residue limit	Is	100 μg/kg	Useful

The joint extraction approach is gradually becoming mainstream in entity relation extraction tasks. Geng et al. proposed an end-to-end joint entity and relation extraction method based on a combined attention mechanism of convolutional and recurrent neural networks [21]. Wan et al. proposed a region-based hypergraph network (RHGN) for joint entity and relation extraction, introducing the concept of regional hyper nodes to enhance contextual connections [22]. Wei et al. proposed a cascading pointer labelling approach, which solves the problem of overlapping entity relations [23]. Qiao et al. proposed a joint entity relation extraction model BERT-BiLSTM-LSTM for agriculture and verified that the BERT model has better migration in agriculture [24].

Due to the scarcity of textual data in the food health and safety domain, few-shot learning can effectively improve the effectiveness of entity relation extraction. Most of the current research on small-sample learning has focused on relationship extraction tasks. For relation extraction in a few-shot learning environment, Qu et al. propose a Bayesian meta-learning method that applies graphical neural networks to global relation graphs to improve accuracy [10]. Sainz et al. reformulate relation extraction as an entailment task with good results for zero- or small-sample relation extraction tasks [11].

For the entity relation extraction task in food health and safety, we propose a joint entity relation extraction method FHER with noise removal and feature enhancement, which mainly addresses how to perform effective entity relation extraction in a few-shot learning environment with high noise and low data volume. Our model adopts a cascading pointer annotation approach [23] to mitigate the entity overlap problem in the entity relation extraction task.

3. Methodology

3.1. Overview. The FHER method divides the whole entity relation extraction task into five parts: the first is a text noise removal model, the second is the construction of a radical level input, the third is the fusion of character and word features, the fourth is the prediction of possible subjects in a sentence, and the last is the prediction of relations and corresponding objects.

Figure 2 shows the overall structure of the model. The input sentence In passes through the BERT Encoder layer to obtain vector H_c. The prediction sequence P_s is obtained after passing through the text noise removal model. The position vector E can be obtained through the binary function. Then, the input In_r of sentence In at the radical level is constructed, and the vector H_r is obtained after passing through the BERT encoder layer. The vectors H_c and H_r and the position vector E are fed into the fusion function to obtain the vector H_{cw} after fusing the characters and words. Using the position vector S and the fusion vector H_{cw}, we can obtain the possible object positions corresponding to each relation and thus the combination of entity relations present in the sentence.

We define the entity relation extraction task in the food health and safety domain: unstructured input text, output extracted human health-related concepts and their relationships, and further form food- and health-related knowledge triad. Formally, for a given sentence x, all possible triples $T\{s, r, o\}$ are extracted, with s representing the subject in sentence x, o representing the object in sentence x, and r representing the relationship between the subject and the object. For sentence x, the probability of all possible triples T that it contains is as follows:

$$\prod_{(s,r,o)\in T} p((s,r,o)|x) = \prod_{s\in T} p(s|x) \prod_{(r,o)\in T|s} p((r,o)|s,x), \tag{1}$$

where, according to the chain rule, $s \in T$ denotes the subject appearing in the triplet T, $T|s$ denotes the triplet T containing the subject, $(r, o) \in T|s$ denotes the combination of objects and relations appearing in the triplet containing the subject, and R is the set of relations. For a given training set D, the probability that all sentences may contain the triplet T is as follows:

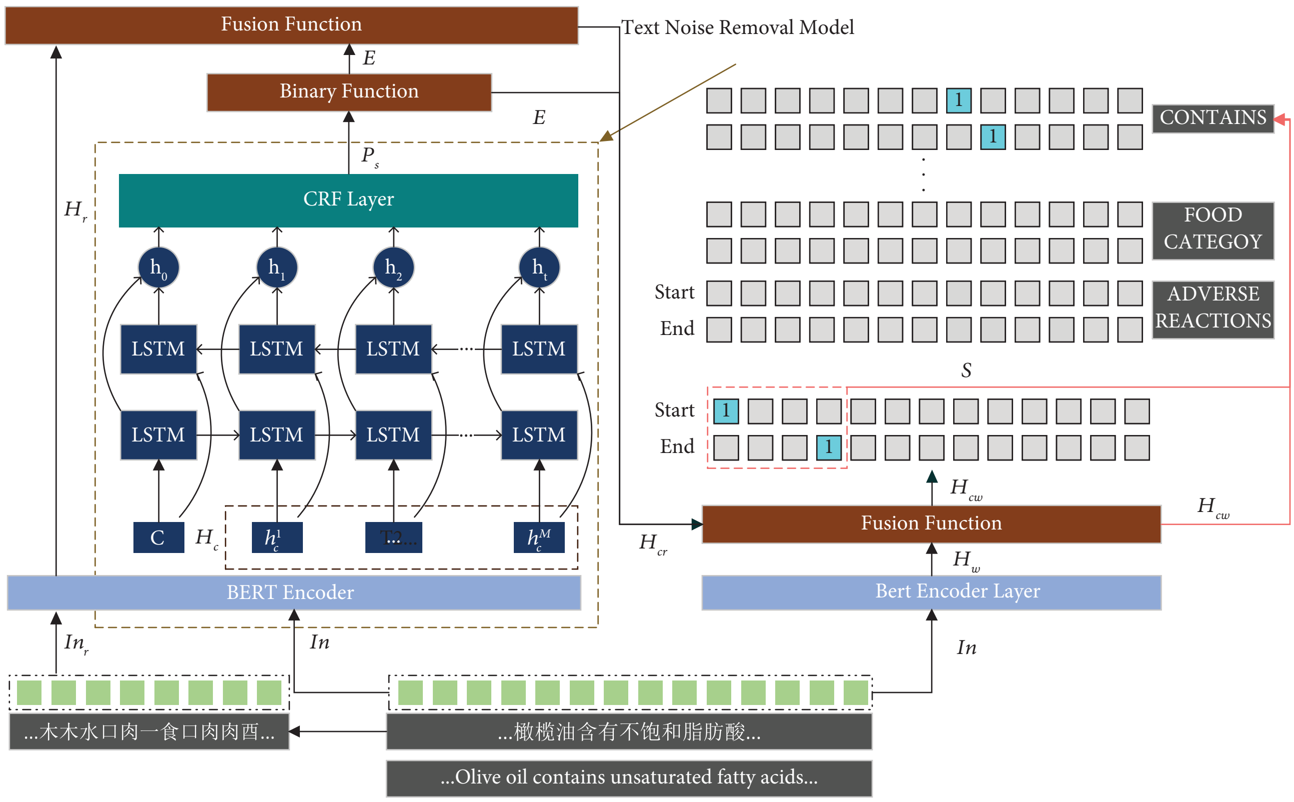

FIGURE 2: FHER model structure diagram.

$$T = \prod_{i=1}^{D} \left[\prod_{(s,r,o)\in T_i} p\left((s,r,o)|x_i\right) \right]. \tag{2}$$

The goal of the entity relation extraction task in the food health and safety domain is to find all possible triples (s, r, o) in the data set D.

3.2. BERT Encoder. The implementation of the language model basis of the model is the encoder layer (BERT encoder). The BERT model consists of a multilayer bidirectional transformer consisting of an encoder that learns the valid information in the context very well [25]. We use a pretrained BERT model using a Chinese corpus from the food domain to encode the context of the input sentence In. Formally, for a sentence of length M can be represented as $\mathrm{In} = [w_1, w_2, w_3, \ldots, w_M]$. We input these tokens into the same BERT encoder layer as the trained one to obtain a vector representation H_c of the input sentences as follows:

$$H_c = \left[h_c^1, h_c^2, h_c^3, \ldots, h_c^M\right] = \mathrm{BERTEncoder}(\mathrm{In}). \tag{3}$$

3.3. Text Noise Removal Model. We summarized the possible relationships between concepts related to food health and safety into 12 kinds by reading many food health and safety information. Table 2 lists the details of the relations since the text contains combinations of entity relations with low relevance to the domain; these irrelevant combinations of entity relations act as noise. It will interfere with identifying entity relation combinations in the food health and safety domain. To reduce the influence of noise in the text, we propose a text denoising method for domain entity relation extraction to convert the text denoising task into a sequence prediction task, which effectively reduces the correct range of entity relation extraction. Figure 3 shows the structure of the text noise removal model structure.

TABLE 2: Definition of relationships for the FH data set.

ID	Relation name (CH)	Relation name (EN)	Abbreviations
1	含有	Contains	CO
2	别名	Another name	AN
3	属于	Belong	BE
4	查处	Investigation	IN
5	功效	Efficacy	EF
6	不符合	Noncompliance	NC
7	是为	Is	IS
8	检出	Detection	DE
9	污染物	Contaminants	CT
10	食品类别	Food category	FC
11	不良反应	Adverse reactions	AR
12	无关	Other	O

We transformed the text noise removal task into a sequence prediction model. To capture the sentence context information, we used the BiLSTM layer for further feature extraction. Then, considering the dependencies between the labels, we use the undirected probabilistic statistical graphical model CRF layer to handle the exact sequence

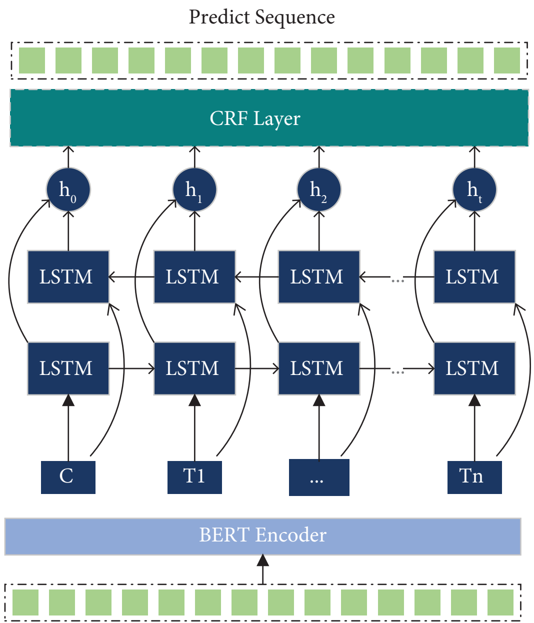

Figure 3: Text noise removal model structure.

labelling problem. Each character is assigned a BIO tag (B represents the beginning of an entity, I represents In an entity, and O represents Out of an entity). At the same time, we modified this tagging method to predict the possible types of entities (see Figure 4).

With the BERT encoder, we obtain the vector representation H_c of the sentence, which is then fed to the BiLSTM layer to obtain the intermediate vector representation H_{Bi} as follows:

$$H_{Bi} = \left[h_{Bi}^{1}, h_{Bi}^{2}, h_{Bi}^{3}, \ldots, h_{Bi}^{M}\right]. \tag{4}$$

For the input sequence In and the corresponding predicted label sequence Y, the model is trained to obtain the prediction sequence result P_s as follows:

$$P_s = \left[\hat{y}_1, \hat{y}_2, \hat{y}_3 \ldots, \hat{y}_M\right] = \mathrm{CRF}\left(H_{Bi}\right). \tag{5}$$

3.4. Construction of the Radical Feature. As the smallest semantic unit, radicals themselves have particular semantic meanings. Chinese characters are usually composed of smaller primary radicals, which are the most basic units that constitute the meaning of Chinese characters. In essence, this radical semantic information helps make characters with similar radical sequences (writing order) close to each other in the vector space, so it can be used to enrich the semantic information of the word vector and enhance the model effect. As shown in Figure 5, the sentence "Olive oil contains unsaturated fatty acids" can be represented at the radical level as "木木水口月一食口月月酉." The radical for the word fat is "月." When "月" is used as a radical, it can be interpreted as relating to the moon or meat. The radical of the character "酸" is "酉," and its meaning is related to alcohol and fermentation. The meaning of the decomposed radicals can enhance the semantic information of the word itself.

Formally, for the input sentence In, the corresponding radical input In_r is generated based on the radical decomposition, and for each character w_{ri} in In, the radical is added to In_r if there is a radical, or directly to In_r if it is a unique word. Finally, we get the input In_r at the radical level as follows:

$$\mathrm{In}_r = \left[w_{r1}, w_{r2}, w_{r3}, \ldots, w_{rM}\right]. \tag{6}$$

Similarly, the vector representation H_r corresponding to the input In_r can be obtained through the BERT encoder layer as follows:

$$H_r = \left[h_r^1, h_r^2, h_r^3, \ldots, h_r^M\right] = \mathrm{BERTEncoder}\left(In_r\right). \tag{7}$$

The sequence prediction result P_s obtained from the text noise removal model is converted into a position vector E by a binary function $I(\cdot)$. $I(\cdot)$ will mark the food health-related tag positions as 1 and the irrelevant tag positions as 0.

$$E = \left[e_1, e_2, \ldots, e_M\right] = I\left(P_s\right). \tag{8}$$

The input vectors H_c and H_r and the position vector E are input to the fusion function $G(\cdot)$. The function $G(\cdot)$ multiplies the position vectors E with the input vectors and concatenates them. At last, the vector H_{cr} is calculated as follows:

$$H_{er} = \mathrm{concatenates}\left(G\left(H_c, H_r, E\right)\right). \tag{9}$$

3.5. Character and Word Fusion. As in Section 3.1, we use the BERT encoder layer to get the vector representation of the input sentence H_w. The difference is that the BERT pretraining model used in the previous section is to segment the text into Chinese characters before training, while the BERT pretraining model used here is first to segment the text into Chinese words before training. The length of the input sentence after Chinese word separation is N.

$$H_w = \left[h_w^1, h_w^2, h_w^3, \ldots, h_w^N\right] = \mathrm{BERTEncoder}\left(\mathrm{In}\right). \tag{10}$$

Because of the difference between Chinese and English word construction methods, different characters will be combined into words in Chinese word construction. Then the generated words will generate new meanings. So, in the food health and safety domain, especially in few-shot learning, we need to use as much prior knowledge as possible to help us improve the recognition, so we fuse the character-based vector representation H_c and the word-based vector representation H_w.

We multiply the position vector E obtained from the text noise removal model with H_w to obtain the vector H_{we}. Then we concatenate H_{cr} to H_w according to the corresponding position to obtain the fused vector H_{cw} (see equation (11)), where the $K(\cdot)$ function expands the vector H_{cr} to the same length as H_w. For example, the vector for the word "食物" is A, and the vectors for the characters "食" and "物" are B and

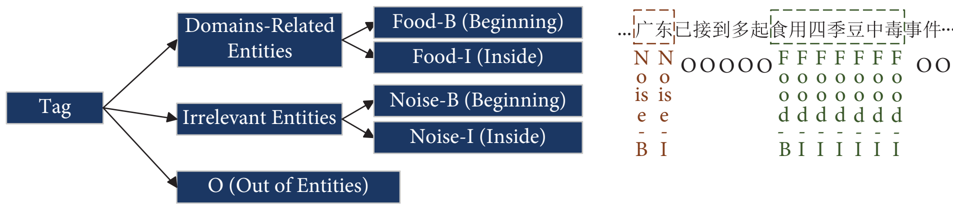

Figure 4: Modified BIO tagging method. The input text characters can be tagged as the beginning and middle positions of the entity and outside the entity. The "Food" prefix indicates that the entity is related to food health and safety, and the "Noise" prefix indicates that the entity is a noise that is not related to food health and safety.

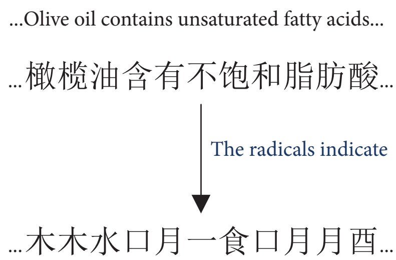

Figure 5: Representing sentences with radicals.

C, respectively. Then, concatenate vectors A and B, and concatenate vectors A and C.

$$H_{cw} = \text{concatenate}\left(G\left(H_{cr}\right)EH_{w}\right). \tag{11}$$

After combining characters and words, we can predict the location in the sentence where the subject may be. Because the entity relation extraction task itself suffers from the problem of overlapping entity relations, according to the view proposed by Wei et al. [23]: for a given subject s, any relation related to s (relations in T) corresponds to the corresponding object o in the sentence, while all other relations necessarily have no corresponding object in the sentence, that is, the set of corresponding objects is the empty set. So we first predict the possible positions of the subject in the sentence.

For a given input, we predict the location of potential subjects. Two binary classifiers form a subject marker, which marks potential subjects' starting and end positions. The subject marker is expressed as follows:

$$P_i^{\text{sub}_{\text{head}}} = \sigma\left(K_{\text{head}} H_{cw}^{i} + b_{\text{head}}\right), \tag{12}$$

$$P_i^{\text{sub}_{\text{tail}}} = \sigma\left(K_{\text{tail}} H_{cw}^{i} + b_{\text{tail}}\right), \tag{13}$$

where $P_i^{\text{sub}_{\text{head}}}$ denotes the probability that each position in the input vector may be the start position of the subject and $P_i^{\text{sub}_{\text{tail}}}$ in denotes the probability that each position in the input vector may be the end position of the subject. If this probability is greater than the threshold τ set in advance, it is for the position is a candidate for the start or end of the subject, marked as 1, and the rest is marked as 0. K_{head} and K_{tail} are learnable parameters, and b_{head} and b_{tail} are deviation parameters.

3.6. Relation Extraction. We obtain all possible sets of entity relations in the input sentence by object identification of each subject to all relations. After the subject tagger, we obtain the candidate subject position information, incorporated into the fusion vector as follows:

$$\widehat{H} = H_{cw}^{i} + \text{sub}. \tag{14}$$

Similarly, the object tagger predicts the potential object location, consisting of two binary classifiers. The object tagger is expressed as follows:

$$P_i^{\text{obj}_{\text{head}}} = \sigma\left(K_{\text{head}}^{r} \widehat{H} + b_{\text{head}}^{r}\right), \tag{15}$$

$$P_i^{\text{obj}_{\text{tail}}} = \sigma\left(K_{\text{tail}}^{r} \widehat{H} + b_{\text{tail}}^{r}\right). \tag{16}$$

The process of predicting the location of the object is similar to that of predicting the location of the subject. $P_i^{\text{obj}_{\text{head}}}$ in equation (15) denotes the probability that each position in the input vector may be the start position of the object, and $P_i^{\text{obj}_{\text{tail}}}$ in equation (16) denotes the probability that each position in the input vector may be the end position of the object. K_{head}^{r} and K_{tail}^{r} are learnable parameters, and b_{head}^{r} and b_{tail}^{r} are deviation parameters. All relations in the set R have an object tagger to mark the start and end positions of candidate objects.

4. Result Analysis and Discussion

4.1. Data Set and Evaluation Metrics. This paper uses an independently constructed food health-related data set FH (Food Health Dataset). Twelve types of food-health-related relationships are defined, and then "OTHER" relationship types are defined to represent less relevant relationships to food health in the sample data. Table 2 lists the 12 relationship types, the Chinese and English names of the included relationships, and their abbreviations. In addition, the paper constructs a small sample data set MHD (Medical Health Dataset) of medical-health-related data to measure the method's generalization performance. The data set MHD consists of 5 relationship types with 200 sentences. The training set contains 180 sentences, and the test set contains 20 sentences.

The total number of valid annotated sentences in the FH data set is 1,420. This paper divides the FH data set into a training set and a test set. Figure 6 shows the details of the data set.

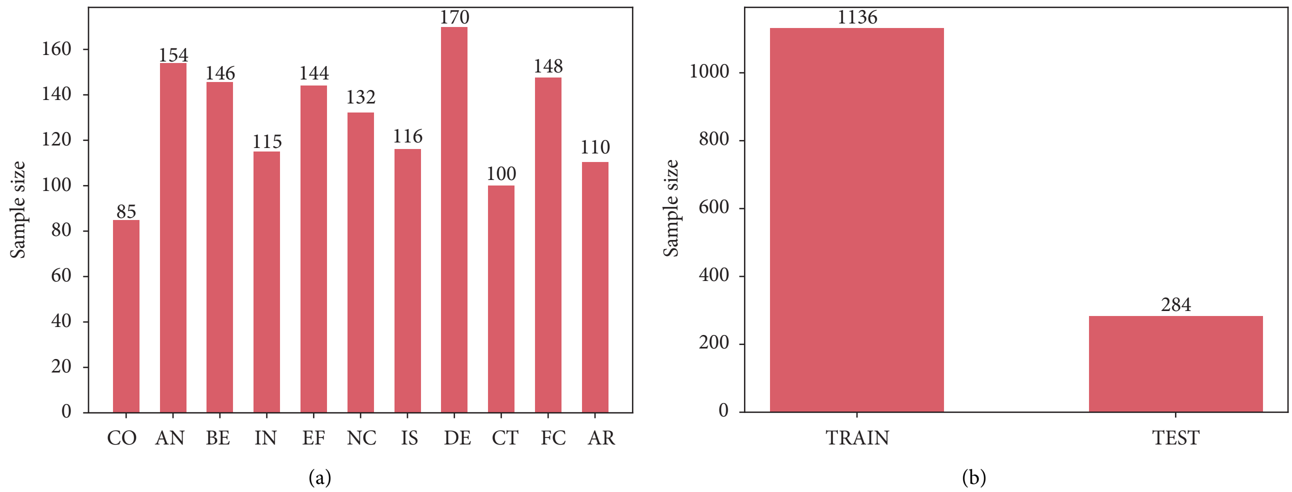

FIGURE 6: Details of the FH data set show: (a) the number of 11 food health and safety-related relationships and (b) the amount of data in the training and test sets.

To improve the performance of the model, we introduced more data samples from the public domain into the data set FH to form the incremental data set FH++, which is expanded from 1,420 sentences to 11,327 sentences to get better results in the text noise removal model. For the entity relation extraction task, we remove the "Other" relationships from the FH data set to form the FFH (filtered food health data) data set (http://39.96.33.199:9009/FFH_dataset.zip) used for entity relation extraction experiments.

For the evaluation metrics used in the experiments, we used three commonly used evaluation metrics, precision (P), recall (R), and $F1$ value, to measure the experimental results from different aspects. Their calculation criteria are as follows: in the formula, TP_i indicates that the model correctly predicts the number of relationships present in given sentence In_i, FP_i indicates that the model incorrectly predicts the number of relations that do not exist in given sentence In_i, and FN_i denotes the number of relations that the model failed to predict for given sentence In_i contained in the sentence.

$$
\begin{aligned}
P &= \frac{TP_i}{TP_i + FP_i} \\
R &= \frac{TP_i}{TP_i + FN_i} \\
F1 &= \frac{2 * P * R}{P + R}.
\end{aligned} \tag{17}
$$

For the text-to-noise model, we use the metric P to measure whether the model is predicting the location sequence correctly, the metric R to measure the model's ability to predict the location of entities in a complete way, and the metric $F1$ to measure model performance in aggregate. We focus more on metric P than on metrics R and $F1$, as it is more important to find the noise accurately.

For the entity relation extraction task, we use indicator P to measure how well the model extracts the correct combination of entity relationships in a sentence, indicator R to measure the model's ability to extract coverage in the face of sentences containing multiple relationships, and indicator $F1$ to measure the model's performance in aggregate.

4.2. Implementation Details. The pretrained BERT model we implemented in the deep learning framework PyTorch uses the Chinese pretrained BERT model (BERT-wmm) published by Cui et al. [26] with its default hyperparameter settings. The models in this research are implemented on a PC with the configuration of Intel(R) Xeon(R) CPU 3.50 GHz, 64 Gb RAM, and GTX3090 graphics. Table 3 records the other parameters used in the experiment.

The parameters used for the text noise removal model, construction of features at the part-head level, the fusion of character and word features, and entity relation extraction experiments are listed in Table 4.

4.3. Result of Text Noise Removal. The following are the experimental results of text noise removal, and the model is trained iteratively on the data set FH++. Figure 7 records the loss values and the final precision/recall curves during the training process, and it can be observed that the loss values gradually decrease, and the model gradually converges as the number of iterative training increases. The precision/recall curves indicate that the model has a good performance. Table 5 records the precision, recall, and $F1$ values for the text noise removal experiments on FH and the incremental data set FH++. The model can obtain better convergence and accuracy when training with the incremental data set. The positive and negative values in the experimental results shown in this paper are confidence intervals calculated by combining multiple results at a confidence level of 95%.

Table 6 records the experimental results obtained on the FH++ data set where we tried different structures to remove the noise, containing precision, recall, and $F1$ values. In Table 6, both the CNN and CNN-BiLSTM models use the softmax function as the activation function to transform the denoising task into a classification task. The results show that

Table 3: Hyperparameter setting.

Hyperparameter	Search space
Bert encoder	Base-uncased BERT-wmm
Bi-LSTM layer	Number of recurrent layers: [2–14, 16, 17]
Batch size	[128, 256, 512, 1024]
Learning rate	$[1\times e^{-3}, 1\times e^{-4}, 1\times e^{-5}]$
Epochs	[50, 100, 200]
Loss function	Binary cross-entropy Negative log-likelihood
Update strategy	[SGD, Adam]

Table 4: Detailed parameters of the experiment.

Model	Construction and output	Training hyperparameters
Text noise removal classifier	Input BERT character Bi-LSTM layer × 8 CRF	Batch size: 128 Learning rate: 0.001 Epochs: 100 Loss function: negative log-likelihood Update strategy: Adam
Feature enhancement	Input Convert function BERT character	—
Chars and words fusion	Input BERT words Combine function sigmoid × 2	Batch size: 128 Learning rate: 0.001 Epochs: 200 Loss function: binary cross-entropy

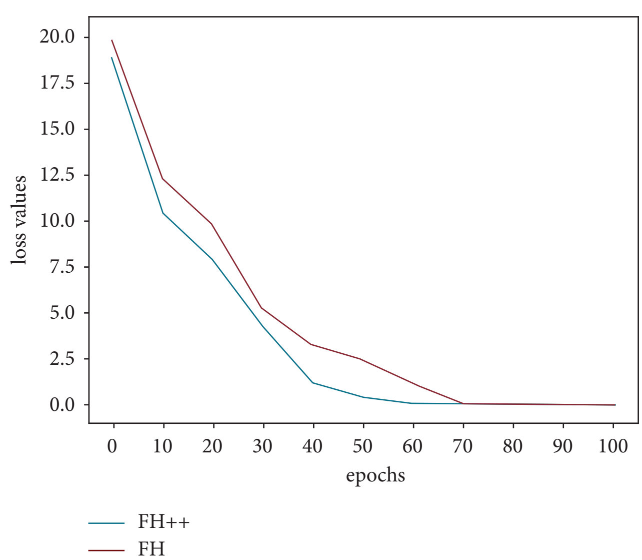

(a)

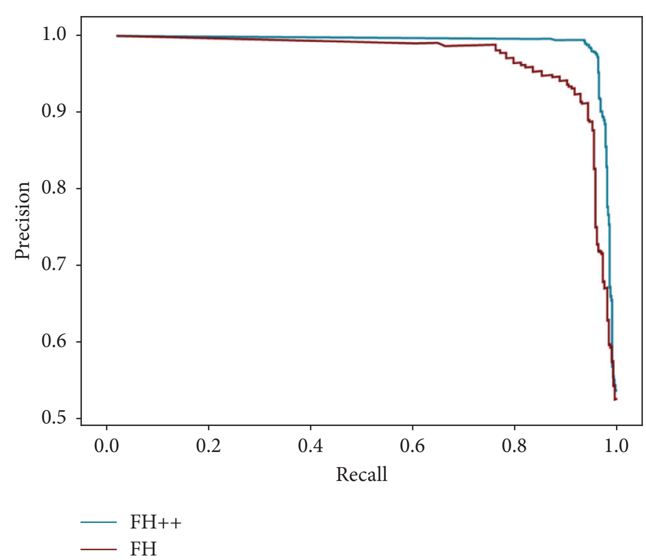

(b)

Figure 7: Loss values and PR curves. The blue curve represents the data set FH++, and the red curve represents the data set FH. (a) The curve represents the value of the loss function of the FHER method during the training phase. (b) Curve represents the PR curve based on the training results.

Table 5: Result of text noise removal experiments on data sets FH and FH++.

Data set	*P* (%)	*R* (%)	*F*1 (%)
FH	87.64 ± 0.47	70.12 ± 0.51	77.90 ± 0.53
FH++	**91.12** ± 0.33	**75.34** ± 0.21	**82.48** ± 0.51

Table 6: Comparison of noise removal models on data set FH++.

Model	P (%)	R (%)	$F1$ (%)
CNN	65.34 ± 0.47	33.21 ± 0.31	44.03 ± 0.23
CNN-BiLSTM	78.12 ± 0.33	75.21 ± 0.71	76.63 ± 0.51
BiLTSTM + CRF	**91.12** ± 0.33	**75.34** ± 0.21	**82.48** ± 0.51

Table 7: Experimental results for different number relations on data set FFH.

Number of relations	P (%)	R (%)	$F1$ (%)
$N = 1$	88.64 ± 0.27	63.13 ± 0.31	73.74 ± 0.53
$N = 2$	70.12 ± 0.13	61.24 ± 0.11	65.37 ± 0.31
$N = 3$	55.45 ± 0.42	53.81 ± 0.33	54.61 ± 0.31
$N = 4$	43.10 ± 0.12	50.01 ± 0.09	46.29 ± 1.21
$N = 5$	33.10 ± 0.12	42.01 ± 0.09	37.02 ± 2.21

Table 8: Text removal noise ablation experiment results.

Model	$N = 1$ (%)	$N = 2$ (%)	$N = 3$ (%)	$N = 4$ (%)	$N = 5$ (%)
FHER (noise)	85.31 ± 0.87	63.13 ± 0.31	42.74 ± 0.53	21.10 ± 0.32	12.21 ± 0.21
FHER	**88.64** ± 0.27	**70.12** ± 0.13	**55.45** ± 0.42	**43.10** ± 0.12	**33.10** ± 0.12

the sequence task using the BiLSTM + CRF model has a better denoising effect.

4.4. Result of Entity Relation Extraction. For the entity relation extraction task, Table 7 records the effect of the model on the data set FFH, which contains the values of precision, recall, and $F1$ for a given sentence containing one to five relationships. The experimental results show that the extraction effectiveness of the model decreases as the number of relations in the input sentences increases, which is related to the imbalance of the data itself, with most of the samples in the data set having less than three relations. However, the overall recognition effect is still good.

The FHER method achieves 91.32% accuracy, 82.21% recall, and 86.52% $F1$ value on the FFH data set and achieves good extraction results in few-shot learning.

We did ablation experiments on the proposed denoising model to verify the effectiveness of few-shot learning for denoising. In Table 8, N represents the number of relations in the sentence, and the value in the table is the precision values for the entity relation extraction task. The experimental results show a significant decrease in recognition precision after the denoising model for a sentence containing multiple relations because the model identifies group or entity relations that we do not want. Therefore, denoising the input samples in few-shot learning is an effective method.

Similarly, we conducted ablation experiments to add prefix features to enhance and fuse character and word features. Table 9 records the experimental results. According to the experimental results, richer semantic information can effectively improve the effect of entity relation extraction during few-shot learning. The NIC model represents no features at the constructive radical level in the model, and the NCW model indicates that there are no fused characters and words in the model, and the whole model uses a vector of characters as units.

Table 9: Comparison of different degrees of semantic information on data set FFH.

Model	P (%)	R (%)	$F1$ (%)
NIC	88.91 ± 0.25	81.34 ± 0.86	84.95 ± 0.53
NCW	91.12 ± 0.13	80.24 ± 0.21	85.33 ± 0.31
FHER	**92.32** ± 0.14	**82.21** ± 0.23	**86.97** ± 0.77

Table 10: Method generalisation performance experiments on data set MDH.

Model	P (%)	R (%)	$F1$ (%)
NIC	75.23 ± 0.75	64.14 ± 0.77	69.24 ± 0.81
NCW	73.03 ± 0.86	66.13 ± 0.92	69.40 ± 0.91
FHER	**79.32** ± 0.53	**74.21** ± 0.99	**76.67** ± 0.63

At last, we test the generalization performance of the method on the data set MDH. The experimental results show that constructing the input at the radical level and fusing characters and words can achieve good results even with smaller data set volumes. Table 10 records the results of the method FHER on the data set MDH.

4.5. Discussion. We discuss the degree of semantic information in the text after its transformation into a radical. There are as many as 3,500 commonly used Chinese characters (http://www.gov.cn/gzdt/att/att/site1/20130819/tygfhzb.pdf). These 3,500 characters can be combined in vast amounts of meaningful words, making the vector space generated after representation learning of Chinese through language models more complex. In contrast, the radicals, which are the main constituents of Chinese characters, can

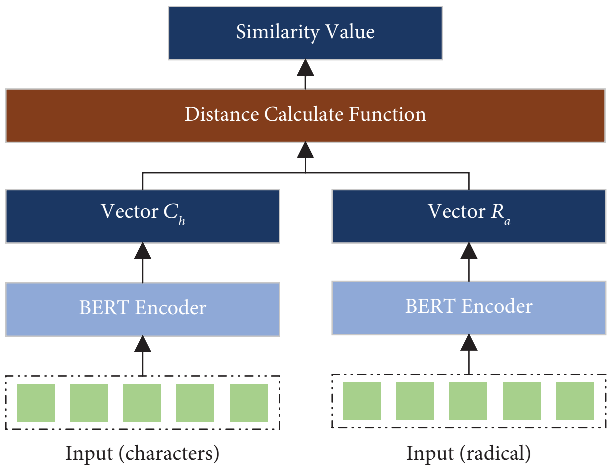

Figure 8: Text similarity calculation structure. The input at the character level and the input at the radical level are transformed by the pretrained model into vectors C_h and R_a. The text similarity is obtained by calculating the distance between the vectors C_h and R_a.

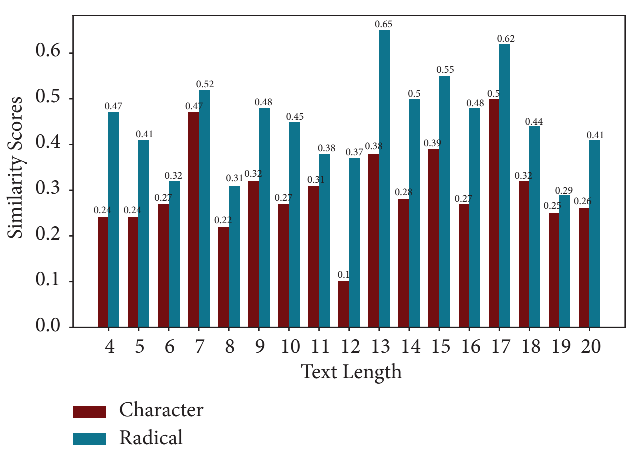

Figure 9: Results of text similarity calculations at the character level and the radical level. The horizontal coordinates represent the sum of the text lengths of the subject and object, while the vertical coordinates represent the similarity results. The blue bars represent radicals, and the red bars represent characters. The text similarity calculated at the radical level is higher than that at the character level.

be grouped into 201 radicals for 20,902 Chinese characters (http://www.moe.gov.cn/downloadvideo/yuxinsi/15hanzibushou.zip). Therefore, radicals reduce the complexity of the Chinese vector space.

For the entity groups "olive oil" and "unsaturated fatty acid" and their radical representations, we used the Chinese pretrained language model BERT-wmm to calculate their similarity based on the distance (see Figure 8). We collected subject-object combinations from the data set FFH. The sum of subject and object text lengths ranged from 4 to 20, so text similarity at the character level and the radical level was calculated between each pair of subjects and objects in them. Figure 9 shows the results of the text-similarity calculation. The experiment proves that the decomposition of Chinese characters into radical representations reduces the complexity of the text to a certain extent.

5. Conclusions

This paper proposes a method for entity relation extraction in food health and safety. Three methods are proposed for entity relation extraction under small sample learning to improve the entity relation extraction effect. Firstly, we propose removing text noise according to domain specialization. The experimental results show that removing entity relations in the text unrelated to the domain can significantly improve the effect of entity relation extraction. Then, we construct text features at the radical level by disassembling individual Chinese characters from the characters' structure. The experimental results show that the input at the radical level has low complexity and contains rich semantic features. Finally, we fuse the input text's character vectors and word vectors from the Chinese character constructions. The experimental results show that fusing characters and words can effectively enrich the semantic information in the input vectors. The above method has a good extraction effect in few-shot learning. In the method FHER, the effect of the entity relationship extraction task is subject to a threshold, which leads to an unstable performance of the model. In the future, we will further explore the influence of noise in the text on the degree of deep learning models, the semantic relationships, and differences between the three different levels of Chinese radicals, characters, and words. Moreover, we attempt to transfer the proposed method to other application fields such as agricultural image recognition, greenhouse environmental time-series prediction, and food safety risk assessment [27–31].

Data Availability

The FFH data sets used to support the findings of this study are included within the article.

Conflicts of Interest

The authors declare that they have no conflicts of interest.

Acknowledgments

This study was supported by Beijing Natural Science Foundation (No. 4202014), Natural Science Foundation of China (62006008 and 61873027), Humanity and Social Science Youth Foundation of Ministry of Education of China (No. 20YJCZH229), and Open Project Program of National Engineering Laboratory for Agri-Product Quality Traceability (AQT-2020-YB6).

References

[1] F. Madeo, T. Eisenberg, F. Pietrocola, and G. Kroemer, "Spermidine in health and disease," *Science (New York, N. Y.)*, vol. 359, no. 6374, p. 2788, 2018.

[2] X. Liu, W. Yang, J. L. Petrick, and L. M. Liao, "Higher intake of whole grains and dietary fiber are associated with lower risk of

liver cancer and chronic liver disease mortality," *Nature Communications*, vol. 12, no. 1, pp. 1–9, 2021.
[3] C. Defois, J. Ratel, G. Garrait et al., "Food chemicals disrupt human gut microbiota activity and impact intestinal homeostasis as revealed by in vitro systems," *Scientific Reports*, vol. 8, no. 1, Article ID 11006, 2018.
[4] E. P. Halmos, A. Mack, and P. R. Gibson, "Review article: emulsifiers in the food supply and implications for gastrointestinal disease," *Alimentary Pharmacology & Therapeutics*, vol. 49, no. 1, pp. 41–50, 2019.
[5] Q. Wan, J. Liu, J. Wei, and B. Ji, "A self-attention based neural architecture for Chinese medical named entity recognition," *Mathematical Biosciences and Engineering*, vol. 17, no. 4, pp. 3498–3511, 2020.
[6] L. Luo, Z. Yang, M. Cao, L. Wang, Y. Zhang, and H. Lin, "A neural network-based joint learning approach for biomedical entity and relation extraction from biomedical literature," *Journal of Biomedical Informatics*, vol. 103, Article ID 103384, 2020.
[7] H. Fei, Y. Zhang, Y. Ren, and D. Ji, "A span-graph neural model for overlapping entity relation extraction in biomedical texts," *Bioinformatics*, vol. 37, no. 11, pp. 1581–1589, 2021.
[8] G. Cenikj, T. Eftimov, and B. K. Seljak, "SAFFRON: tranSfer leArning for Food-disease RelatiOn extractioN," in *Proceedings of the 20th Workshop on Biomedical Language Processing*, pp. 30–40, online, Jun 2021.
[9] G. Popovski, S. Kochev, B. Korousic-Seljak, and T. Eftimov, "FoodIE: a rule-based named-entity recognition method for food information extraction," in *Proceedings of the ICPRAM 2019*, Prague, Czech Republic, February 2019.
[10] M. Qu, T. Gao, L. P. Xhonneux, and J. Tang, "Few-shot relation extraction via bayesian meta-learning on relation graphs," in *Proceedings of the 37th International Conference on Machine Learning*, vol. 199, pp. 7867–7876, PMLR), July, 2020.
[11] O. Sainz, O. L. de Lacalle, and G. Labaka, "Label verbalization and entailment for effective zero-and few-shot relation extraction," in *Proceedings of the 2021 Conference on Empirical Methods in Natural Language Processing*, Punta Cana, Dominican Republic, November 2021.
[12] Y. Wu, X. Wei, and Y. Qin, "A radical-based method for Chinese named entity recognition," in *Proceedings of the 2nd International Conference on Big Data Technologies*, Jinan, China, August 2019.
[13] C. Dong, J. Zhang, C. Zong, M. Hattori, and H. Di, "Character-based LSTM-CRF with radical-level features for Chinese named entity recognition," in *Proceedigs of the 5th CCF Conference on Natural Language Processing and Chinese Computing and 24th International Conference on Computer Processing of Oriental Languages*, Kunming, China, December 2016.
[14] F. Wu, P. P. Zhu, Z. Q. Wang, P. F. Li, and Q. M. Zhu, "Chinese event detection with joint representation of characters and words," *Computer Science*, vol. 48, no. 4, pp. 249–253, 2021.
[15] Z. Chen and K. Hu, "Radical enhanced Chinese word embedding," in *Chinese Computational Linguistics and Natural Language Processing Based on Naturally Annotated Big Data*Springer, Berlin, Germany, 2017.
[16] P. Tran, D. Dinh, and H. T. Nguyen, "A character level based and word level based approach for Chinese-Vietnamese machine translation," *Computational Intelligence and Neuroscience*, vol. 2016, Article ID 9821608, 11 pages, 2016.
[17] T. J. Fu, P. H. Li, and W. Y. Ma, "GraphRel: modeling text as relational graphs for joint entity and relation extraction," in *Proceedings of the 57th Annual Meeting of the Association for Computational Linguistics*, Florence, Italy, July 2019.
[18] G. Zhou, J. Su, J. Zhang, and M. Zhang, "Exploring various knowledge in relation extraction," in *Proceedings of the 43rd Annual Meeting of the Association for Computational Linguistics (Acl'05)*, Ann Arbor, Michigan, June 2005.
[19] Y. S. Chan and D. Roth, "Exploiting syntactico-semantic structures for relation extraction," in *Proceedings of the 49th Annual Meeting of the Association for Computational Linguistics: Human Language Technologies*, Portland, Oregon, USA, June 2011.
[20] X. Yu and W. Lam, "Jointly identifying entities and extracting relations in encyclopedia text via a graphical model approach," in *Proceedings of the Coling 2010*, Posters, Beijing, China, August 2010.
[21] Z. Geng, Y. Zhang, and Y. Han, "Joint entity and relation extraction model based on rich semantics," *Neurocomputing*, vol. 429, pp. 132–140, 2021.
[22] Q. Wan, L. Wei, X. Chen, and J. Liu, "A region-based hypergraph network for joint entity-relation extraction," *Knowledge-Based Systems*, vol. 228, Article ID 107298, 2021.
[23] Z. Wei, J. Su, Y. Wang, Y. Tian, and Y. Chang, "A novel cascade binary tagging framework for relational triple extraction," in *Proceedings of the 58th Annual Meeting of the Association for Computational Linguistics*, pp. 1476–1488, July 2020.
[24] B. Qiao, Z. Zou, Y. Huang, K. Fang, X. Zhu, and Y. Chen, "A joint model for entity and relation extraction based on BERT," *Neural Computing & Applications*, pp. 1–11, 2021.
[25] Y. Zhu, W. Zheng, and H. Tang, "Interactive dual attention network for text sentiment classification," *Computational Intelligence and Neuroscience*, vol. 2020, Article ID 8858717, 11 pages, 2020.
[26] Y. Cui, W. Che, T. Liu, B. Qin, and Z. Yang, "Pre-training with whole word masking for Chinese BERT," *IEEE/ACM Transactions on Audio, Speech, and Language Processing*, vol. 29, pp. 3504–3514, 2021.
[27] J. Kong, H. Wang, X. Wang, X. Jin, X. Fang, and S. Lin, "Multi-stream hybrid architecture based on cross-level fusion strategy for fine-grained crop species recognition in precision agriculture," *Computers and Electronics in Agriculture*, vol. 185, Article ID 106134, 2021.
[28] J. Kong, C. Yang, J. Wang et al., "Deep-stacking network approach by multisource data mining for hazardous risk identification in IoT-based intelligent food management systems," *Computational Intelligence and Neuroscience*, vol. 2021, Article ID 1194565, 16 pages, 2021.
[29] X. B. Jin, W. Z Zheng, J. L. Kong et al., "Deep-learning forecasting method for electric power load via attention-based encoder-decoder with Bayesian optimization," *Energies*, vol. 14, no. 6, p. 1596, 2021.
[30] X. B. Jin, W. Z. Zheng, J. L. Kong et al., "Deep-learning temporal predictor via Bi-directional self-attentive encoder-decoder framework for IOT-based environmental sensing in intelligent greenhouse," *Agriculture*, vol. 11, no. 8, p. 802, 2021.
[31] Y. Y. Zheng, J. L. Kong, X. B. Jin, X. Y. Wang, M. Zuo, and M. Zuo, "CropDeep: the crop vision dataset for deep-learning-based classification and detection in precision agriculture," *Sensors*, vol. 19, no. 5, p. 1058, 2019.

Hindawi
Computational Intelligence and Neuroscience
Volume 2022, Article ID 6168785, 11 pages
https://doi.org/10.1155/2022/6168785

Research Article

An Online Weighted Bayesian Fuzzy Clustering Method for Large Medical Data Sets

Cong Zhang[1], **Jing Xue**[2], **and Xiaoqing Gu**[3]

[1]*School of Computer and Information Engineering, Nantong Polytechnic College, Nantong 226001, Jiangsu, China*
[2]*Department of Nephrology, The Affiliated Wuxi People's Hospital of Nanjing Medical University, Wuxi 214023, Jiangsu, China*
[3]*School of Computer Science and Artificial Intelligence, Changzhou University, Changzhou, 213164, Jiangsu, China*

Correspondence should be addressed to Xiaoqing Gu; guxq@cczu.edu.cn

Received 31 December 2021; Revised 22 January 2022; Accepted 26 January 2022; Published 21 February 2022

Academic Editor: Xin Ning

With the rapid development of artificial intelligence, various medical devices and wearable devices have emerged, enabling people to collect various health data of themselves in hospitals or other places. This has led to a substantial increase in the scale of medical data, and it is impossible to import these data into memory at one time. As a result, the hardware requirements of the computer become higher and the time consumption increases. This paper introduces an online clustering framework, divides the large data set into several small data blocks, processes each data block by weighting clustering, and obtains the cluster center and corresponding weight of each data block. Finally, the final cluster center is obtained by processing these cluster centers and corresponding weights, so as to accelerate clustering processing and reduce memory consumption. Extensive experiments are performed on UCI standard database, real cancer data set, and brain CT image data set. The experimental results show that the proposed method is superior to previous methods in less time consumption and good clustering performance.

1. Introduction

In recent years, smart medical care has emerged with the vigorous development of artificial intelligence (AI) technology. At present, the application of AI technology in the medical field involves many aspects such as disease prediction, intervention and consultation, disease diagnosis and treatment, drug research and development, and health service management [1]. The fusion of AI and healthcare services can help clinicians reduce reading time, aid in early detection, and improve diagnostic accuracy. The technology of clustering plays a very wide role in the fields of medical data analysis.

As a typical unsupervised learning method, clustering mines the internal relationship between data samples and then puts the samples with the same or similar attributes in the same cluster, which avoids the dependence on the label data and saves a lot of manpower and material resources [2]. Fuzzy clustering is a typical representative of clustering methods, and the most classic fuzzy clustering is the fuzzy C-means algorithm (FCM). Fuzzy clustering improves the traditional hard clustering partition. There are a large number of derivative algorithms based on the FCM, including the probabilistic C-means algorithm (PCM), which uses probabilistic methods to express fuzzy membership to improve the limitation of fuzzy membership [3]. Recently, many researchers have improved the traditional FCM method from multiple perspectives and applied them in various scenes [4]. Hua et al. [5] developed a multiview fuzzy clustering based on the framework of FCM. Gu et al. [6] proposed a probabilistic FCM method to be used for antecedent parameter learning in Takagi-Sugeno-Kang fuzzy system. Zhou et al. [7] proposed a new membership scaling FCM method by selecting the unchanged clustering centers through triangular inequality, which solves the problems of slow convergence and a large amount of calculation when a FCM algorithm is dealing with large data sets. Mishro et al. [8] proposed a new type 2 adaptive weighted space FCM clustering algorithm to solve the problem of noise misclassification and inaccurate clustering center obtained by

FCM in the process of MR brain image segmentation. Wang et al. [9] proposed an FCM algorithm for irregular image segmentation, which has higher robustness and less computational effort compared to traditional segmentation algorithms. Based on hyperplane partitioning, Shen et al. [10] developed a feasible and efficient FCM algorithm to deal with large data sets. Jha et al. [11] designed and implemented a kernelized fuzzy clustering algorithm using its in-memory cluster computing technology. Liu et al. [12] proposed a FCM algorithm based on multiple surface approximate interval membership for processing artifacts in brain MRI images. Wang et al. [13] proposed a FCM algorithm based on wavelet frame, which can effectively remove image noise and preserve image details. This algorithm can provide a new way to segment images in an irregular domain. Li et al. [14] proposed a domain-qualified adaptive FCM method for processing MRI brain images with noise and uneven intensity. Zhang and Huang [15] studied the generalization error of a FCM algorithm from the perspective of theory and limited the generalization error from the perspective of convergence, which can provide guidance for the application of the sampling-based FCM method. Wu et al. [16] proposed an online clustering algorithm by combining FCM algorithm with an online framework set to solve the problem that batch learning cannot deal with large-scale data sets. Zhang et al. [17] combined FCM with a nonlinear genetic algorithm and proposed an apple defect detection method to improve fruit defect detection. Shen et al. [18] proposed a hyperplane partition method based on FCM to deal with big data clustering. Recently, the Bayesian fuzzy clustering (BFC) [19] algorithm is proposed to combine the fuzzy method into a probability model. BFC reinterprets the fuzzy method from the perspective of probability, expands the value range of the fuzzy index, and solves the problem that the fuzzy method is prone to local optimization. The many characteristics of the BFC algorithm make it very widely used in medical data processing. But due to the high complexity of the BFC method, its efficiency is not high, and it has received great limitations in practical applications.

Inspired by the above ideas, this paper proposes the online weighted Bayesian fuzzy clustering method (OWBFC) and uses an online clustering framework, which not only retains all the advantages of the Bayesian fuzzy clustering algorithm but also improves the efficiency of the Bayesian fuzzy clustering method through the online clustering framework. We verify the OWBFC method on a series of real-world data sets. Compared with the existed Bayesian fuzzy clustering algorithms, the contributions of our study are concluded as follows:

(1) OWBFC combines the probability method with the fuzzy method and realizes the fuzzy clustering through the probability method, which has the common advantages of the probability method and the fuzzy method.

(2) In the process of solving the parameters, the Markov chain Monte Carlo method (MCMC) is used for sampling instead of a closed solution, so the global optimal solution of the parameters can be obtained in OWBFC.

(3) The online clustering framework is used in OWBFC to deal with the problem that large data sets cannot be imported into memory, and the weighting mechanism is used to improve the clustering efficiency.

2. Related Work

The BFC algorithm combines the probabilistic method with the fuzzy method. From the perspective of prior knowledge and Bayesian theory, it expands the range of the fuzzy index of the traditional fuzzy method. The BFC algorithm uses the MCMC strategy [20] and particle filter method [21, 22] to solve the optimization problem. The maximum posterior probability (MAP) is used to process fuzzy clustering, and the normal distribution is further used to predict the number of clusters. Therefore, the BFC method is superior to the previous fuzzy or probabilistic methods in many aspects. However, the algorithm complexity of BFC is relatively high. This shortcoming makes the BFC method not suitable for large-scale data, and its application range is greatly limited, which does not meet the current actual needs. The BFC algorithm aims to solve fuzzy clustering from the perspective of probability. The probability model of BFC consists of three parts, namely fuzzy data likelihood (FDL), fuzzy membership prior (FCP), and cluster center prior, as follows. The fuzzy data likelihood is as follows:

$$p(\mathbf{X} \mid \mathbf{U}, \mathbf{C}) = \prod_{k=1}^{K} \mathrm{FDL}(\mathbf{x}_k \mid \mathbf{u}_k, \mathbf{C}) = \prod_{k=1}^{K} \frac{1}{Z(\mathbf{u}_k, m, \mathbf{C})} \prod_{n=1}^{N} \mathcal{N}(\mathbf{x}_k \mid \boldsymbol{\mu} = \mathbf{c}_n, \boldsymbol{\Lambda} = u_{kn}^{m}\mathbf{I}), \quad (1)$$

where $\boldsymbol{X}$, $\boldsymbol{U}$, and $\boldsymbol{C}$ are matrices of training data, fuzzy member, and cluster centers, respectively. K and N represent the numbers of samples and the numbers of clusters, respectively. u_{kn} is the membership of data point $\mathbf{x}_k$ in cluster n. The parameters m, $\mathbf{c}_n$, and $\boldsymbol{I}$ represent the fuzzy index, the cluster center, and the identity matrix, respectively. And, $Z(\mathbf{u}_k, m, \mathbf{C})$ is the normalization constant, and m is the fuzzy index. Since $Z(\mathbf{u}_k, m, \mathbf{C})$ will be eliminated by the following equation (2), it does not need to be calculated.

The prior of fuzzy membership is expressed as

$$p(\mathbf{U}|\mathbf{C}) = \prod_{k=1}^{K} \mathrm{FCP}(\mathbf{u}_n|\mathbf{C}) = \prod_{k=1}^{K} Z(\mathbf{u}_k, m, \mathbf{C}) \left(\prod_{n=1}^{N} u_{kn}^{-m\ D/2} \right) \mathrm{Dirichlet}(\mathbf{u}_k|\boldsymbol{\alpha}). \tag{2}$$

$p(\mathbf{U}|\mathbf{C})$ consists of three parts as follows: $F_1 = Z(\mathbf{u}_k, m, \mathbf{C})$, $F_2 = \prod_{n=1}^{N} u_{kn}^{-m\ D/2}$, and $F_3 = \mathrm{Dirichlet}(\mathbf{u}_k|\alpha)$. F_1 is to eliminate the normalizing constant in equation (1). F_3 is the Dirichlet distribution as follows:

$$\mathrm{Dirichlet}(\mathbf{x}|\boldsymbol{\alpha}) = \frac{\Gamma\left(\sum_{n=1}^{N}\alpha_n\right)}{\prod_{n=1}^{N}\Gamma(\alpha_n)} \prod_{n=1}^{N} x_n^{\alpha_n - 1}, \tag{3}$$

where $x_n \geq 0, n = 1, \ldots, N$ and $\sum_{n=1}^{N} x_n = 1$. The parameter α is the Dirichlet prior parameter, which controls the membership degree of the sample. Through Dirichlet distribution, the BFC algorithm breaks the constraint that the fuzzy index in the FCM algorithm must be greater than 1, so that the fuzzy index in the BFC algorithm can take any value.

Cluster center prior is defined as

$$p(\mathbf{C}) = \prod_{n=1}^{N} \mathcal{N}(\mathbf{c}_n|\boldsymbol{\mu}_c, \boldsymbol{\Sigma}_c). \tag{4}$$

It is noted that $p(\mathbf{C})$ is to match the high degree of membership produced by equation (4). μ_c and Σ_c are the mean and variance of all samples, as follows:

$$\begin{aligned} \boldsymbol{\mu}_c &= \frac{1}{K}\sum_{k=1}^{K}\mathbf{x}_k \\ \boldsymbol{\Sigma}_c &= \frac{\gamma}{K}\sum_{k=1}^{K}(\mathbf{x}_k - \boldsymbol{\mu}_c)(\mathbf{x}_k - \boldsymbol{\mu}_c)^T, \end{aligned} \tag{5}$$

where γ is a parameter that affects the strength of the prior, which is set by the user, and we use $\gamma = 3$ in our study. The joint likelihood of $\mathbf{X}$, $\mathbf{U}$, and $\mathbf{C}$ is obtained by multiplying equations (1), (2), and (4).

$$\begin{aligned} p(\mathbf{X}, \mathbf{U}, \mathbf{C}) &= p(\mathbf{X}|\mathbf{U}, \mathbf{C})p(\mathbf{U}|\mathbf{C})p(\mathbf{C}) \\ &\propto exp\left\{-\frac{1}{2}\sum_{k=1}^{K}\sum_{n=1}^{N}u_{kn}^{m}||\mathbf{x}_k - \mathbf{c}_n||^2\right\} \times \left[\prod_{k=1}^{K}\prod_{n=1}^{N}u_{kn}^{\alpha_n - 1} \times \exp\left\{-\frac{1}{2}\sum_{n=1}^{N}(\mathbf{c}_n - \boldsymbol{\mu}_c)^T\sum_{c}^{-1}(\mathbf{c}_n - \boldsymbol{\mu}_c)\right\}\right]. \end{aligned} \tag{6}$$

According to map theory, the joint likelihood form of equation (7) is its negative logarithm, and a factor of 2 can be multiplied to simplify. The joint likelihood form is as follows:

$$J(\mathbf{X}, \mathbf{U}, \mathbf{C}) = \sum_{k=1}^{K}\sum_{n=1}^{N}u_{kn}^{m}||\mathbf{x}_k - \mathbf{c}_n||^2 - 2\sum_{k=1}^{K}\sum_{n=1}^{N}(\alpha_n - 1)\log u_{kn} + \sum_{n=1}^{N}(\mathbf{c}_n - \boldsymbol{\mu}_c)^T\sum_{c}^{-1}(\mathbf{c}_n - \boldsymbol{\mu}_c). \tag{7}$$

Finally, BFC uses MAP inference and uses sampling to filter membership and cluster centers to obtain their optimal values.

From the above introduction, we can see that the BFC algorithm breaks through the constraints of the traditional fuzzy clustering fuzzy index and can obtain the global optimal solution, but its time complexity is too high to handle large data sets.

3. Online Weighted Bayesian Fuzzy Clustering

3.1. Weighted Bayesian Fuzzy Clustering. For large data sets, it is a difficult problem that the data cannot be imported into the computer at one time. In this paper, the online clustering framework is adopted. By dividing the large data set into several easy-to-handle small data blocks, the clustering center of each data block is defined as the representative point. In the process of processing the data blocks, the representative points of each data block and the corresponding weights of the representative points are combined into two new different sets, and then, the two new sets are processed to get the clustering center of the whole data and accelerate clustering. Since the OWBFC method uses a block and weighting mechanism to introduce weights for the clustering centers of each data block, the weighted Bayesian fuzzy clustering (WBFC) algorithm is introduced, and then, WBFC is extended to its online version.

To further judge the contribution of each sample point to the cluster in the process of clustering, this paper introduces the WBFC algorithm, which adaptively weights different sample points to select the representative sample points. The objective function of WBFC is defined as

$$p(\mathbf{X},\mathbf{U},\mathbf{C}) = p(\mathbf{X}|\mathbf{U},\mathbf{C})p(\mathbf{U}|\mathbf{C})p(\mathbf{C}) \propto exp\left\{-\frac{1}{2}\sum_{k=1}^{K}\sum_{n=1}^{N} w_n u_{kn}^m ||\mathbf{x}_k - \mathbf{c}_n||^2\right\} \times \left[\prod_{k=1}^{K}\prod_{n=1}^{N} u_{kn}^{\alpha_n - 1} \times \exp\left\{-\frac{1}{2}\sum_{n=1}^{N}(\mathbf{c}_n - \boldsymbol{\mu}_c)^T \sum_{c}^{-1}(\mathbf{c}_n - \boldsymbol{\mu}_c)\right\}\right], \tag{8}$$

where $w_k > 0$ represents the contribution of the nth sample to the final cluster division. How to set w_k will be described in detail in the next section. Following [19], the MCMC parameter optimization strategy is used in the WBFC algorithm. First, we initialize the parameter $\mathbf{u}_k$ and $\mathbf{c}_n$ by Dirichlet distribution and normal distribution. We sample the $\boldsymbol{U}$ matrix according to $\mathbf{U} \sim p(\mathbf{U}|\mathbf{X},\mathbf{C}) \propto p(\mathbf{X},\mathbf{U},\mathbf{C})$ using the Gibbs sampling. We judge whether the new membership sample is accepted. If it is accepted, then $\mathbf{u}_k$ is set as $\mathbf{u}_k = \mathbf{u}_k^{\Psi}$, $\mathbf{u}_k^{\Psi}$ as a new membership sample. The acceptation rate $A_{\mathbf{u}}$ is computed as

$$A_{\mathbf{u}} = \min\left\{1, \frac{p\left(\mathbf{x}_k, \mathbf{u}_k^{\Psi}|\mathbf{C}\right)}{p(\mathbf{x}_k, \mathbf{u}_k|\mathbf{C})}\right\}. \tag{9}$$

If $p(\mathbf{x}_k, \mathbf{u}_k^{\Psi}|\mathbf{C}^*) > p(\mathbf{x}_k, \mathbf{u}_k^*|\mathbf{C}^*)$, we set the current $\mathbf{u}_k^*$ as $\mathbf{u}_k^* = \mathbf{u}_k^{\Psi}$. The $p(\mathbf{x}_k, \mathbf{u}_k|\mathbf{C})$ is computed as

$$p(\mathbf{x}_k, \mathbf{u}_k|\mathbf{C}) = p(\mathbf{x}_k|\mathbf{u}_k,\mathbf{C})p(\mathbf{u}_k|\mathbf{C}) \propto \prod_{n=1}^{N} \exp\left(-\frac{1}{2}w_k u_{kn}^m \|\mathbf{x}_k - \mathbf{c}_n\|^2\right) u_{kn}^{\alpha_n - 1}. \tag{10}$$

Then, we sample $\boldsymbol{C}$ according to $\mathbf{C} \sim p(\mathbf{C}|\mathbf{X},\mathbf{U}) \propto p(\mathbf{X},\mathbf{U},\mathbf{C})$. We judge whether the new cluster center sample is accepted. If it is accepted, then $\mathbf{c}_n$ is set as $\mathbf{c}_n = \mathbf{c}_n^{\Psi}$. The acceptation rate $A_{\mathbf{c}}$ is computed as

$$A_{\mathbf{c}} = \min\left\{1, \frac{p\left(\mathbf{x}_k, \mathbf{c}_k^{\Psi}|\mathbf{C}\right)}{p(\mathbf{x}_k, \mathbf{c}_k|\mathbf{C})}\right\}. \tag{11}$$

If $p(\mathbf{X}, \mathbf{c}_n^{\Psi}|\mathbf{U}^*) > p(\mathbf{X}, \mathbf{c}_n^*|\mathbf{U}^*)$, we set the current $\mathbf{c}_n^*$ as $\mathbf{c}_n^* = \mathbf{c}_n^{\Psi}$, $\mathbf{c}_n^{\Psi}$ as a new cluster center. The $p(\mathbf{X}, \mathbf{c}_n|\mathbf{U})$ is computed as

$$p(\mathbf{X}, \mathbf{c}_n|\mathbf{U}) = p(\mathbf{X}|\mathbf{U}, \mathbf{c}_n)p(\mathbf{c}_n) \propto exp\left\{-\frac{1}{2}\sum_{k=1}^{K}\sum_{n=1}^{N} w_k u_{kn}^m ||\mathbf{x}_k - \mathbf{c}_n||^2\right\} \times \exp\left\{-\frac{1}{2}\sum_{n=1}^{N}(\mathbf{c}_n - \boldsymbol{\mu}_c)^T \sum_{c}^{-1}(\mathbf{c}_n - \boldsymbol{\mu}_c)\right\}. \tag{12}$$

Finally, we check the maximum likelihood of all samples using equation (9). The whole training process circulates several times until the model converges. The training procedure of WBFC is shown in Algorithm 1.

3.2. Online Weighted Bayesian Fuzzy Clustering. The WBFC algorithm aims to introduce object weights based on the BFC algorithm, so more representative sample points can be selected while clustering. Based on the characteristics of the WBFC algorithm, we further proposed the online version of WBFC algorithm called OWBFC algorithm. Inspired of the online algorithm advantage, the OWBFC algorithm can handle large data sets based on the WBFC algorithm. OWBFC divides the large-scale data into several easy-to-process data blocks. Then, OWBFC uses the WBFC algorithm to process each data block, merges the cluster center of each data block into a new set, calculates the weight of each cluster center, and merges the obtained weight. Finally, the new cluster center set and the corresponding weight set are processed to obtain the final cluster center. The weight factor w_n in OWBFC is computed as follows:

$$w_q = \sum_{k=1}^{K_l} u_{kq}, q = 1, \ldots, \mathrm{Q}, \tag{13}$$

where w_q represents the weight of representative points of each data block. Here, we give the training procedure of the OWBFC algorithm as shown in Algorithm 2. The parameter K_l represents the number of sample points in the lth block, u_{kq} is the membership of $\mathbf{x}_k$ in cluster q, and Q represents the number of clusters. First, we divide the training data $\boldsymbol{X}$ into d

blocks as $\mathbf{X} = \{\mathbf{X}_1, \ldots, \mathbf{X}_d\}$, and each block $\mathbf{X}_l$ has K_l sample points, $l = 1, 2, ..., d$. $\mathbf{U}_l$ and $\mathbf{C}_l$ are the fuzzy membership and clustering center matrices, respectively. We run the WBFC algorithm in the first block $\mathbf{X}_1$ and obtain the fuzzy membership and clustering center matrices in $\mathbf{X}_1$. Then, we run the WBFC algorithm in the rest blocks with the clustering center matrix $\boldsymbol{C}_{l-1}$.

4. Experiments

4.1. Data Sets and Experiment Settings. In the experiment, we use several medical data sets, including two cancer data sets, Armstrong-2002-v2 and Bhattacharjee-2001 [23], three medical data sets, and brain images in the UCI database [24]. Armstrong-2002-v2 is a data set to distinguish the expression of leukemia genes. It is divided into three categories, with a total of 72 samples. Bhattacharjee-2001 is a lung cancer classification data set, including five categories, a total of 203 samples. Because of the small sample size of these two data sets, they are not segmented here. The heart disease data set, diabetic retinopathy Debrecen (DRD) data set, and hepatitis C virus (HCV) for Egyptian patient data set are three UCI medical data sets. The heart disease data set contains 303 samples, and only 14 of them are used in this article. The DRD data set contains 1151 samples, and the HCV data set contains 1385 samples. To facilitate the division, this study takes 1000 samples for the diabetic retinopathy Debrecen data set. The HCV data set took 1,200 samples. A total of three brain CT images were selected as CT1, CT2, and CT3, with pixels of 275×273, 273×277, and 264×271. To facilitate segmentation, the pixels of the three pictures are reduced to 272×272, 272×272, and 264×264, respectively. The comparison algorithms include OFCM [25] and SPFCM [25], which can process large-scale data clustering. Among them, the two cancer data sets and one UCI medical data set are used to compare the clustering effects of OWBFC, OFCM, and SPFCM algorithms without segmentation. The remaining two UCI medical data sets are used to compare the clustering effects and time of OWBFC, OFCM, and SPFCM algorithms in different proportions of segmentation. The brain images are used to show the running time comparison of OWBFC and BFC. The OWBFC, OFCM, and SPFCM algorithms have two parameters: fuzzy index m and prior parameter α. In this study, we set $m = 1.7$ and $\boldsymbol{\alpha} = 1$. To visually display the clustering performance, we use four clustering performance indicators of accuracy, entropy, F-measure, and purity to show the clustering results. $R = \text{full}_t/\text{block}_t$ represents the ratio of the running time of the whole processing data set and the block processing data set of the algorithm, full_t represents the running time on the whole data set, and block_t represents the sum of the running time on each block. Although this part loads the data set into the memory at one time, this paper believes that R is similar to the data that cannot be loaded, because the total amount of data is the same, whether it is processed separately or at one time. Our experimental platform is AMD R5-5600X, six cores, 16G memory, Windows10 operating system, Matlab2016a.

4.2. Experimental Results on the Armstrong-2002-v2, Bhattacharjee-2001, and Heart Disease Data Set. To make SPFCM and OFCM algorithms run better, according to the suggestions of Havens et al. [25], we set the fuzzy index $m = 1.7$. For the Armstrong-2002-v2 data set, Bhattacharjee-2001 data set, and heart disease data set, the number of clusters is set to 3, 5, and 5, respectively. Because the sample size of these three data sets is small, they are not processed in blocks. Table 1 shows the experimental results of the OFCM, SPFCM, and OWBFC algorithms. We can see that the OFCM algorithm and the SPFCM algorithm have similar clustering performances on these three different data sets, and it is difficult to compare the advantages and disadvantages of the two algorithms. But comparing the OFCM algorithm, SPCM algorithm, and OWBFC algorithm, it is easy to see that the OWBFC algorithm has the best clustering results except for some special cases.

4.3. Clustering Performance on DRD and HCV Data Set. Like the parameter setting in Section 4.2, the DRD and HCV data sets are divided into 5%, 10%, and 50% of the whole data set, and the last column of the HCV data set is selected as the basis for the number of clusters, the fuzzy index $m = 1.7$, and the number of clusters is set to 4. The OFCM, SPFCM, and OWBFC algorithms run independently 10 times on the basis of random initialization to calculate the maximum, minimum, and average values of accuracy, entropy, F-measure, and purity. The clustering results of the two data sets are shown in Tables 2–5. From Table 2, it can be seen that the accuracy of the OFCM is slightly lower than that of the SPFCM algorithm when the number of data blocks is large, and the accuracy of the OFCM algorithm is higher than that of the SPFCM algorithm when the number of blocks is small. Overall, the accuracy of OFCM algorithm is similar to that of SPFCM algorithm, and the accuracy of OWBFC algorithm is the best. Tables 2–5 show the accuracy, entropy, F-measure, and purity of these two different data sets. For example, 74.78/74.90/74.66 represents the mean, max, and min accuracy values, respectively. Compared with the OFCM algorithm and SPFCM algorithm, the OWBFC algorithm has the best results whether it is entropy or F-measure or purity. Because the OWBFC algorithm uses the MCMC sampling method to solve the parameters, it can obtain the global optimization of the parameters. Therefore, the OWBFC algorithm can obtain better clustering performance. Only from Tables 3–5, the gap between the three algorithms is not obvious. Combining with Table 8, it can be clearly seen that the OWBFC algorithm has good clustering performance and also greatly reduces the time consumption of the algorithm. Table 8 shows the running time at different division ratios. Because the data set name is too long, the abbreviation is used in the experiment.

4.4. Brain Images. Three brain images are shown in Figure 1. We use them to verify the clustering performance of OWBFC for large-scale image segmentation. We compare the OWBFC and BFC algorithms in this subsection. According to the recommendations [19, 25], the parameters α set to 1, and the

Input:Training data $\boldsymbol{X}$, fuzzy index m, number of clusters N, number of sampling iteration N_{iter}, weight $\mathbf{w}$
Output:Fuzzy membership $\mathbf{U}^*$ and cluster prototypes $\mathbf{C}^*$
Step 1. Initialize parameters μ_c and Σ_c
Step 2. Initial $\mathbf{u}_k \sim \text{Dirichlet}(\alpha = \mathbf{1}_N), k = 1, \ldots, K$
Step 3. Initial $\mathbf{y}_c \sim \mathcal{N}(\mu_y, \Sigma_y), c = 1, \ldots, C$
Step 4. $\mathbf{u}_k^* = \mathbf{u}_k, \mathbf{c}_n^* = \mathbf{c}_n$,//assign map sample to current sample
Step 5. For $iter = 1, \ldots, N_{iter}$
//Sample $\boldsymbol{U}$ according to $\mathbf{U} \sim p(\mathbf{U}|\mathbf{X}, \mathbf{C}) \propto p(\mathbf{X}, \mathbf{U}, \mathbf{C})$
Step 7. for $k = 1, \ldots, K$
Step 8. Sample new membership $\mathbf{u}_k^\Psi$ by equation (3)
Step 9. Judge whether the new membership sample is accepted by equation (10). If it is accepted, then $\mathbf{u}_k = \mathbf{u}_k^\Psi$
Step 10. if $p(\mathbf{x}_k, \mathbf{u}_k^\Psi|\mathbf{C}^*) > p(\mathbf{x}_k, \mathbf{u}_k^*|\mathbf{C}^*)$ //Use Eq. (11)
Step 11. $\mathbf{u}_k^* = \mathbf{u}_k^\Psi$
Step 12. end
Step 13. end
//Sample $\boldsymbol{C}$ according to $\mathbf{C} \sim p(\mathbf{C}|\mathbf{X}, \mathbf{U}) \propto p(\mathbf{X}, \mathbf{U}, \mathbf{C})$
Step 14. for $n = 1, \ldots, N$
Step 15. Sample new cluster center $\mathbf{c}_n^\Psi$ from $\mathcal{N}(\mathbf{c}_n, \Sigma_c/\delta)$
Step 16. Judge whether the new cluster center sample is accepted by equation (12). If it is accepted, then $\mathbf{c}_n = \mathbf{c}_n^\Psi$
Step 17. if $p(\mathbf{X}, \mathbf{c}_n^\Psi|\mathbf{U}^*) > p(\mathbf{X}, \mathbf{c}_n^*|\mathbf{U}^*)$ //Use equation (13)
Step 18. $\mathbf{c}_n^* = \mathbf{c}_n^\Psi$
Step 19. end
Step 20. end
Step 21. //Check the maximum likelihood of all samples
Step 22. if $p(\mathbf{X}, \mathbf{U}, \mathbf{C}) > p(\mathbf{X}, \mathbf{U}^*, \mathbf{C}^*)$ //Use equation (9)
Step 23. $\mathbf{U}^* = \mathbf{U}$
$\mathbf{C}^* = \mathbf{C}$
Step 24. end
Step 25. end

Algorithm 1: Weighted Bayesian fuzzy clustering (WBFC) algorithm.

Input: Training data $\mathbf{X}$, fuzzy index m, number of clusters Q, number of sampling iteration N_{iter}, weight w_n, number of data blocks d
Output: Cluster prototypes $\mathbf{C}^*$
Step 1. Divide $\boldsymbol{X}$ into d blocks $\mathbf{X} = \{\mathbf{X}_1, \ldots, \mathbf{X}_d\}$//Each block has K_l sample points, $1 \le l \le d$
Step 2. Initialize $\mathbf{w} = \mathbf{1}_{K_l}$
Step 3. Use algorithm to obtain the $\mathbf{U}_1, \mathbf{C}_1 = \text{WBFC}(\mathbf{X}_1, Q_1, m)$ with $\mathbf{w}$
Step 4. for $l = 2$ to d
Step 5. Use algorithm to obtain the $\mathbf{U}_l$, $\mathbf{C}_l = \text{WBFC}(\boldsymbol{X}_l, Q_l, m)$ with $\boldsymbol{C}_{l-1}$
Step 6. end
Step 7. $\mathbf{C}^* = \mathbf{C}_1 \cup \mathbf{C}_2 \ldots \cup \mathbf{C}_d$
Step 8. $\mathbf{w}_q = \sum_{k=1}^{K_l} u_{kq}, q = 1, \ldots, Q$
Step 9. $\mathbf{C}^* = \text{WBFC}(\mathbf{C}^*, N, m, \{\mathbf{w}_1 \cup \ldots \cup \mathbf{w}_d\})$
Step 10. end

Algorithm 2: Online Weighted Bayesian Fuzzy Clustering (OWBFC) algorithm.

Table 1: Clustering performance on Armstrong-2002-v2, Bhattacharjee-2001, and Heart Disease data sets.

Data sets	Algorithms	Accuracy	Entropy	*F*-measure	Purity
	OFCM	0.7235	0.4728	0.7948	0.7331
Armstrong-2002-v2	SPFCM	0.7237	0.4697	**0.8011**	0.7372
	OWBFC	**0.7548**	**0.4632**	0.7964	**0.7489**
	OFCM	0.8213	0.2879	0.8637	0.8235
Bhattacharjee-2001	SPFCM	0.8635	0.2455	0.9294	0.8769
	OWBFC	**0.8792**	**0.2423**	**0.9328**	**0.8817**
	OFCM	0.7643	0.4675	0.7921	0.7039
Heart Disease	SPFCM	0.7659	0.4678	0.7914	0.7054
	OWBFC	**0.7768**	**0.4679**	**0.7932**	**0.7258**

The best average performances are shown in bold type in Tables 1–7.

Table 2: Accuracy (mean/max/min) on the DRD and HCV data sets (%).

DRD data set			
Block size	OFCM	SPFCM	OWBFC
5	73.16/73.32/72.95	73.26/73.37/73.18	**74.78/74.90/74.66**
10	73.34/74.44/73.12	73.37/73.54/73.15	**74.83/74.97/74.72**
50	73.53/73.64/73.31	73.51/73.62/73.43	**75.02/75.16/74.93**
HCV data set			
Block size	OFCM	SPFCM	OWBFC
5	74.16/74.41/74.11	74.17/74.31/74.09	**75.61/75.78/75.52**
10	74.29/74.44/74.16	74.24/74.42/74.13	**75.65/75.80/75.52**
50	74.37/74.48/74.31	74.33/74.47/74.25	**75.73/75.86/75.66**

Table 3: Entropy (mean/max/ min) on the DRD and HCV data sets (%).

DRD data set			
Block size	OFCM	SPFCM	OWBFC
5	47.72/47.88/47.65	47.77/47.92/47.61	**47.34/47.49/47.26**
10	47.75/47.89/47.67	47.77/47.91/47.63	**47.39/47.54/47.28**
50	47.81/47.95/47.76	47.82/47.97/47.74	**47.44/47.57/47.33**
HCV data set			
Block size	OFCM	SPFCM	OWBFC
5	46.65/46.78/46.52	46.79/46.87/46.68	**46.84/46.97/46.75**
10	46.69/46.78/46.53	46.81/46.89/46.72	**46.84/47.03/46.72**
50	46.71/46.82/46.66	46.88/46.96/46.75	**46.87/47.11/46.76**

Table 4: F-measure (mean/max/min) on the DRD and HCV data sets (%).

DRD data set			
Block size	OFCM	SPFCM	OWBFC
5	77.96/78.13/77.81	77.93/78.15/77.82	**78.42/78.57/78.30**
10	77.96/78.15/77.81	77.96/78.17/77.84	**78.47/78.60/78.33**
50	78.04/78.21/77.85	77.98/78.22/77.88	**78.51/78.63/78.38**
HCV data set			
Block size	OFCM	SPFCM	OWBFC
5	75.02/75.14/74.93	75.02/75.16/74.89	**75.96/76.13/75.84**
10	75.13/75.25/75.02	75.10/75.24/74.90	**76.03/76.17/75.91**
50	75.17/75.31/75.05	75.16/75.36/75.03	**76.15/76.31/76.02**

Table 5: Purity (mean/max/min) on the DRD and HCV data sets (%).

DRD data set			
Block size	OFCM	SPFCM	OWBFC
5	74.58/74.63/74.34	74.55/74.67/74.43	**75.27/75.43/75.16**
10	74.64/74.72/74.49	74.59/74.75/74.48	**75.31/75.46/75.24**
50	74.72/74.88/74.62	74.66/74.81/74.57	**75.37/75.50/75.26**
HCV data set			
Block size	OFCM	SPFCM	OWBFC
5	74.61/74.79/74.48	74.55/74.67/74.38	**75.25/75.37/75.18**
10	74.67/74.83/74.54	74.60/74.77/74.45	**75.29/75.43/75.16**
50	74.71/74.88/74.62	74.66/74.79/74.52	**75.33/75.46/75.19**

parameters m set to 1.7. We split brain images at a ratio of 25% and set all classes to 3. Figures 2 and 3 show the clustering results of three brain images by BFC and OWBFC algorithms, respectively. Table 6 shows the experimental results on three brain images. Table 7 shows the running time results of BFC and OWBFC on three brain images. We can see from Table 6 that the clustering performance of OWBFC is better than that of BFC. Meanwhile, from Table 7, we can clearly see that OWBFC has a shorter time consumption compared with BFC. In summary, compared with BFC, the OWBFC algorithm not only maintains a good clustering effect but also consumes less time.

Table 6: Clustering results of BFC and OWBFC on three brain images (%).

Data sets	Methods	Accuracy	Entropy	*F*-measure	Purity
Cta	BFC	87.54	23.64	91.26	87.43
	OWBFC	**88.01**	**21.98**	**91.32**	**88.15**
Ctb	BFC	88.65	21.38	91.97	88.76
	OWBFC	**89.23**	**21.05**	**92.28**	**89.61**
Ctc	BFC	86.91	24.33	90.65	87.15
	OWBFC	**87.06**	**23.96**	**91.43**	**87.34**

Table 7: Running time on three brain images (s).

Image	BFC	OWBFC
Cta	1224.23	**345.36**
Ctb	1231.14	**339.45**
Ctc	1219.56	**326.72**

Table 8: OWBFC running time on different block ratios (s).

Data sets	Block size				*R*		
	100%	50%	10%	5%	100%/50%	100%/10%	100%/5%
DRD	85.31	67.54	15.67	12.51	1.26	5.44	6.82
HCV	97.25	70.26	17.48	13.16	1.38	5.56	7.38

(a) (b) (c)

Figure 1: Three brain images used in the experiment. (a) cta, (b) ctb, and (c) ctc.

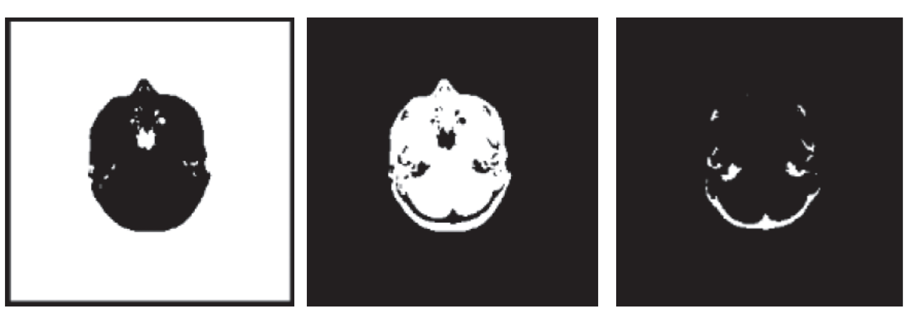

(a)

Figure 2: Continued.

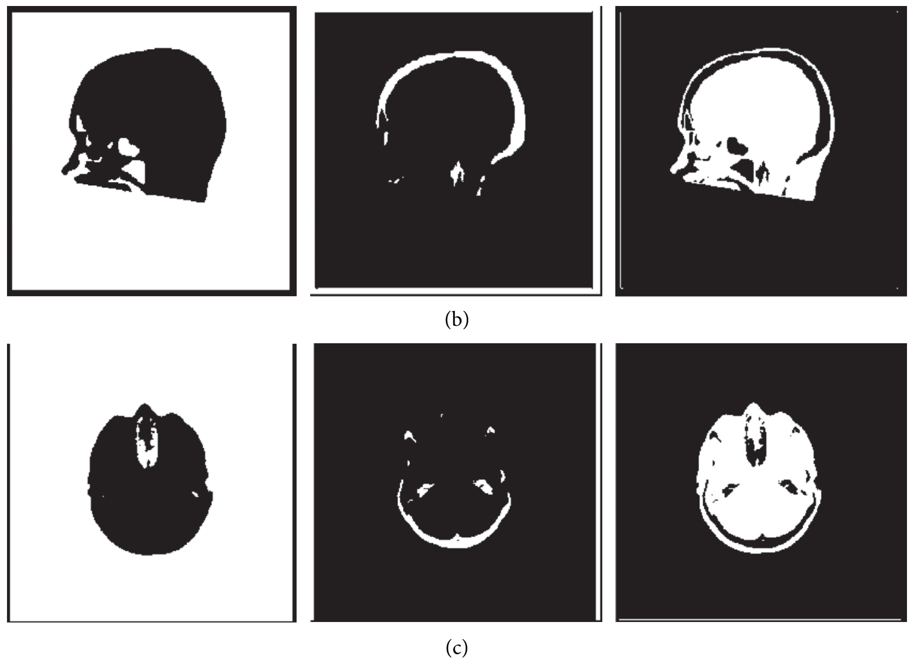

Figure 2: Clustering results of BFC on three brain images. (a) cta, (b) ctb, and (c) ctc.

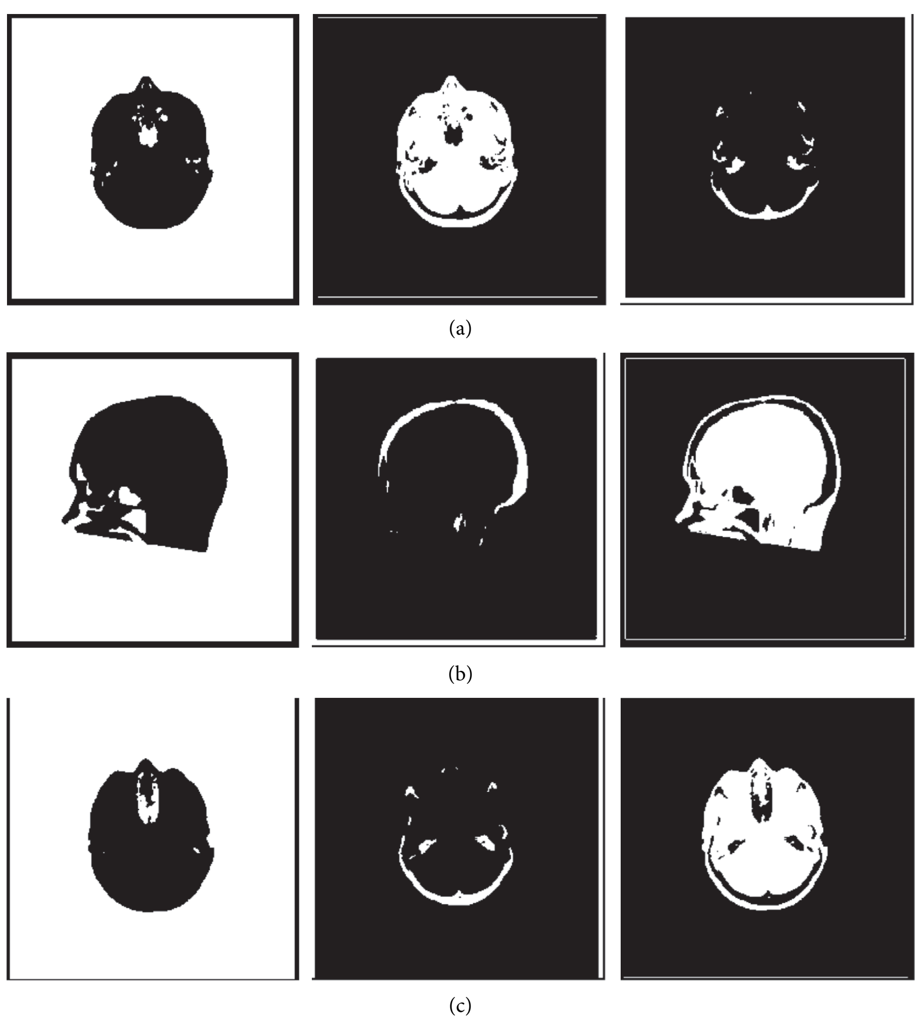

Figure 3: Clustering results of OWBFC on three brain images. (a) cta, (b) ctb, and (c) ctc.

5. Conclusion

With the advancement of science and technology, the collection of various medical data has become more frequent and easier, which makes the scale of medical data larger and larger, and it is impossible to import the data into the memory at one time, so the hardware requirements for processing these data become higher and the time consumption increases. This paper proposes an OWBFC method, which reduces the memory consumption of the computer and the time consumption of the algorithm by introducing an online clustering framework to process the data set in blocks. From the experimental results, the block processing can effectively reduce the time consumption of the algorithm. However, the online clustering framework adopted in this paper needs to merge and save the cluster centers of each data block in the process of processing data, which raises the space consumption of the algorithm. Therefore, how to avoid excessive space consumption while ensuring low time consumption is a problem worth thinking about.

Data Availability

Armstrong-2002-v2 and Bhattacharjee-2001 data sets can be downloaded from https://schlieplab.org/Static/Supplements/CompCancer/datasets.htm. The other data sets can be downloaded from http://archive.ics.uci.edu/ml/index.php.

Conflicts of Interest

The authors declare that they have no conflicts of interest.

Authors' Contributions

Cong Zhang and Jing Xue contributed equally to this work.

Acknowledgments

This work was supported in part by the National Natural Science Foundation of China (Grant 61806026), Future Network Scientific Research Fund Project (No. FNSRFP-2021-YB-36), and Science and Technology Project of Changzhou City (No. CE20215032).

References

[1] J. Jin and Y. Zhang, "The latest progress of research on the social risks and regulation of international artificial intelligent in medical treatment based on CiteSpace method," in *Proceedings of the 2020 IEEE Conference on Telecommunications, Optics and Computer Science (TOCS)*, pp. 55–59, Shenyang, China, December, 2020.

[2] Y. Jiang, X. Gu, D. Wu et al., "A novel negative-transfer-resistant fuzzy clustering model with a shared cross-domain transfer latent space and its application to brain CT image segmentation," *IEEE/ACM Transactions on Computational Biology and Bioinformatics*, vol. 18, no. 1, pp. 40–52, 2021.

[3] R. Krishnapuram and J. M. Keller, "A possibilistic approach to clustering," *IEEE Transactions on Fuzzy Systems*, vol. 1, no. 2, pp. 98–110, 1993.

[4] A. Gosain and S. Dahiya, "Performance analysis of various fuzzy clustering algorithms: a review," *Procedia Computer Science*, vol. 79, pp. 100–111, 2016.

[5] L. Hua, Y. Gu, X. Gu, J. Xue, and T. Ni, "A novel brain MRI image segmentation method using an improved multi-view fuzzy c-means clustering algorithm," *Frontiers in Neuroscience*, vol. 15, no. 3, Article ID 662674, 2021.

[6] X. Gu, F.-L. Chung, H. Ishibuchi, and S. Wang, "Imbalanced TSK fuzzy classifier by cross-class bayesian fuzzy clustering and imbalance learning," *IEEE Transactions on Systems, Man, and Cybernetics: Systems*, vol. 47, no. 8, pp. 2005–2020, 2017.

[7] S. Zhou, D. Li, Z. Zhang, and R. Ping, "A new membership scaling fuzzy C-means clustering algorithm," *IEEE Transactions on Fuzzy Systems*, vol. 29, no. 9, pp. 2810–2818, 2021.

[8] P. K. Mishro, S. Agrawal, R. Panda, and A. Abraham, "A novel type-2 fuzzy C-means clustering for brain MR image segmentation," *IEEE Transactions on Cybernetics*, vol. 51, no. 8, pp. 3901–3912, 2021.

[9] C. Wang, W. Pedrycz, Z. Li, M. Zhou, and S. S. Ge, "G-image segmentation: similarity-preserving fuzzy C-means with spatial information constraint in wavelet space," *IEEE Transactions on Fuzzy Systems*, vol. 29, no. 12, pp. 3887–3898, 2021.

[10] Y. Shen, W. Pedrycz, Y. Chen, X. Wang, and A. Gacek, "Hyperplane division in fuzzy C-means: clustering big data," *IEEE Transactions on Fuzzy Systems*, vol. 28, no. 11, pp. 3032–3046, 2020.

[11] P. Jha, A. Tiwari, N. Bharill, M. Ratnaparkhe, M. Mounika, and N. Nagendra, "A novel scalable kernelized fuzzy clustering algorithms based on in-memory computation for handling big data," *IEEE Transactions on Emerging Topics in Computational Intelligence*, vol. 5, no. 6, pp. 908–919, 2021.

[12] Z. Liu, X. Bai, H. Liu, and Y. Zhang, "Multiple-surface-approximation-based FCM with interval memberships for bias correction and segmentation of brain MRI," *IEEE Transactions on Fuzzy Systems*, vol. 28, no. 9, pp. 2093–2106, 2020.

[13] C. Wang, W. Pedrycz, J. Yang, M. Zhou, and Z. Li, "Wavelet frame-based fuzzy C-means clustering for segmenting images on graphs," *IEEE Transactions on Cybernetics*, vol. 50, no. 9, pp. 3938–3949, 2020.

[14] L. Li, P. Cao, J. Yang, D. Zhao, and O. Zaiane, "A robust fuzzy clustering algorithm using spatial information combined with local membership filtering for brain MR images," in *Proceedings of the 2020 IEEE International Conference on Bioinformatics and Biomedicine (BIBM)*, pp. 1987–1994, Seoul, Korea (South), December, 2020.

[15] Z. Zhang and J. Huang, "Theoretical analysis of the generalization error of the sampling-based fuzzy C-means," *IEEE Transactions on Fuzzy Systems*, vol. 29, no. 8, pp. 2432–2437, 2021.

[16] K. Wu, J. Liu, P. Liu, and F. Shen, "Online fuzzy cognitive map learning," *IEEE Transactions on Fuzzy Systems*, vol. 29, no. 7, pp. 1885–1898, 2021.

[17] W. Zhang, J. Hu, G. Zhou, and M. He, "Detection of apple defects based on the FCM-NPGA and a multivariate image analysis," *IEEE Access*, vol. 8, pp. 38833–38845, 2020.

[18] Y. Zhang, Z. Zhou, Y. Kang, C. Zhang, and B. Duan, "A quick screening approach based on fuzzy C-means algorithm for the second usage of retired lithium-ion batteries," *IEEE Transactions on Transportation Electrification*, vol. 7, no. 2, pp. 474–484, 2021.

[19] T. C. Glenn, A. Zare, and P. D. Gader, "Bayesian fuzzy clustering," *IEEE Transactions on Fuzzy Systems*, vol. 23, no. 5, pp. 1545–1561, 2015.

[20] C. Andrieu, N. Freitas, A. Doucet, and M. Jordan, "An introduction to MCMC for machine learning," *Machine Learning*, vol. 50, no. 1, pp. 5–43, 2003.
[21] N. Chopin, "A sequential particle filter method for static models," *Biometrika*, vol. 89, no. 3, pp. 539–552, 2002.
[22] V. Elvira, J. Djurie, and P. M. Djurić, "Adapting the number of particles in sequential Monte Carlo methods through an online scheme for convergence assessment," *IEEE Transactions on Signal Processing*, vol. 65, no. 7, pp. 1781–1794, 2017.
[23] U. Einav, Y. Tabach, G. Getz et al., "Gene expression analysis reveals a strong signature of an interferon-induced pathway in childhood lymphoblastic leukemia as well as in breast and ovarian cancer," *Oncogene*, vol. 24, no. 6, pp. 6367–6375, 2005.
[24] K. Bache and M. Lichman, "UCI machine learning repository," 2021, http://archive.ics.uci.edu/ml.
[25] T. C. Havens, J. C. Bezdek, C. Leckie, L. O. Hall, and M. Palaniswami, "Fuzzy c-means algorithms for very large data," *IEEE Transactions on Fuzzy Systems*, vol. 20, no. 6, pp. 1130–1146, 2012.

Hindawi
Computational Intelligence and Neuroscience
Volume 2022, Article ID 9016823, 17 pages
https://doi.org/10.1155/2022/9016823

Research Article

Modeling Soil Temperature for Different Days Using Novel Quadruplet Loss-Guided LSTM

Xuezhi Wang,[1,2] **Wenhui Li**,[1,2] **Qingliang Li**,[2,3] **and Xiaoning Li**[1,3]

[1] *College of Computer Science and Technology, Jilin University, Changchun 130012, China*
[2] *Symbol Computation and Knowledge Engineer of Ministry of Education, Jilin University, ChangChun, Jilin Province, China*
[3] *School of Computer Science and Technology, Changchun Normal University, Changchun 130032, China*

Correspondence should be addressed to Xiaoning Li; lixiaoning@ccsfu.edu.cn

Received 6 January 2022; Accepted 22 January 2022; Published 17 February 2022

Academic Editor: Xin Ning

Soil temperature (T_s), a key variable in geosciences study, has generated growing interest among researchers. There are many factors affecting the spatiotemporal variation of T_s, which poses immense challenges for the T_s estimation. To enrich processing information on loss function and achieve better performance in estimation, the paper designed a new long short-term memory model using quadruplet loss function as an intelligence tool for data processing (QL-LSTM). The model in this paper combined the traditional squared-error loss function with distance metric learning between the sample features. It can zoom analyze the samples accurately to optimize the estimation accuracy. We applied the meteorological data from Laegern and Fluehli stations at 5, 10, and 15 cm depth on the 1st, 5th, and 15th day separately to verify the performance of the proposed soil temperature estimation model. Meanwhile, this paper inputs the variables into the proposed model including radiation, air temperature, vapor pressure deficit, wind speed, air pressure, and past T_s data. The performance of the model was tested by several error evaluation indices, including root mean square error (RMSE), mean absolute error (MAE), Nash-Sutcliffe model efficiency coefficient (NS), Willmott Index of Agreement (WI), and Legates and McCabe index (LMI). As the test results at different soil depths show, our model generally outperformed the four existing advanced estimation models, namely, backpropagation neural networks, extreme learning machines, support vector regression, and LSTM. Furthermore, as experiments show, the proposed model achieved the best performance at the 15 cm depth of soil on the 1st day at Laegern station, which achieved higher WI (0.998), NS (0.995), and LMI (0.938) values, and got lower RMSE (0.312) and MAE (0.239) values. Consequently, the QL-LSTM model is recommended to estimate daily T_s profiles estimation on the 1st, 5th, and 15th days.

1. Introduction

Soil temperature (T_s) is a main physical variable of the land surface, which has a direct influence on the atmosphere [1]. Relevant fields including geoscience and forestry application aspects have drawn attention from researchers [2, 3]. In principle, all the interactions in terrestrial ecosystems are companied by T_s variations since they involve energy exchanges. T_s is an essential factor for growing crops that can facilitate the development of the root system by impacting microbial activity, soil decomposition, and fluidity of soil water [4]. In addition, the death of animals and plants produces plenty of carbon substrates and a high volume of greenhouse gases in the soil. Consequently, it results in an increase in T_s, thus expediting carbon dioxide emission to the atmosphere [5]. Therefore, accurate T_s monitoring is crucial for agricultural management and atmosphere environment forecast. However, T_s data in most areas is still measured by using traditional sensors, and the T_s data cannot be collected at different depths [6].

Therefore, it can be used to solve some problems in different fields for the study of T_s estimation. The essential environmental factors have a great influence on the accuracy of T_s estimation. At present, T_s is mainly predicted by methods based on physical models and data-driven methods. The physical method is based on the heat conduction model to estimate T_s [7]. Meanwhile, the method is greatly affected by related physical parameters and the scale problem [8].

The data-driven methods can explore the internal relationship between T_s and the surrounding environmental factors for T_s estimation. At present, several predictive models based on machine learning methods are used for estimating T_s [9–14]. For example, ANN is composed of a complex network structure that imitates the structure and function of the brain's neural network, and it has powerful data processing capabilities. Bilgili applied the multilayer perceptron (MLP) model to adequately describe T_s distribution at a monthly temporal scale from meteorological data [15]. Kisi et al. used three machine learning models to estimate monthly T_s at the soil depth of 5 cm and 10 cm, respectively, and verified the predictive performance of radial basis neural networks performed better than that of generalized regression neural networks and multilayer perceptron models [9]. But generalized regression neural networks had the better performance for deeper depth (50 cm and 100 cm). Kisi et al. applied ANN-based models to predict long-term T_s at a monthly temporal scale, and they found that genetic programming generated the best performance with the meteorological data [16]. Zeynoddin et al. applied a multilayer perceptron (MLP) model to describe daily T_s distribution at three soil depths (5, 10, and 20 cm) from past measurements of T_s [17]. Samadianfard et al. processed the meteorological data such as Ta, W, RH, Rs, Sunshine hours (Sh), and air pressure (Ap) and integrated ANN-based models separately to predict T_s at a monthly temporal scale [18]. Mehdizadeh et al. noted that machine learning models combined with time series models performed better performance than the predictive models based on the single machine learning method or single time series method for predicting T_s at a daily temporal scale [19]. Moazenzadeh et al. proposed SVR with krill herd algorithm (SVR-KHA) method in modeling T_s estimation at different depths (5, 10, 20, 30, 50, and 100 cm), which achieved the best performance, compared to SVR and SVR with firefly algorithm (SVR-FA) [11]. Delbari et al. proposed an SVR-based model to compute daily T_s at three depths (5, 30, and 100 cm) in Iran [12]. The ELM network featured by a single hidden layer could improve the learning speed and accuracy of the algorithm and can model the accurate T_s. Nahvi et al. used the improved ELM model on daily T_s estimation based on the self-adaptive evolutionary method and verified the improved predictive model can estimate the adequate T_s [20]. Sanikhani et al. tested the data from the Mersin station, and the results that show the performance of ELM has the best predictive performance than other predictive models. [14]. Feng et al. tested the loess plateau data with ELM and random forests (RF) and ANN-based models showed that ELM had the better performance for estimation T_s of half-hourly at different soil depths [13].

As a time loop neural network containing complex neural network modules, LSTM is used in this paper to solve long-term dependence problems, which can effectively alleviate gradient vanishing through the extraction of required features by the gate control unit. LSTM network [21] can learn long-term and short-term behaviors, and it has seen application in vast areas. By integrating LSTM and SVR, Guo et al. significantly improved the prediction accuracy of abnormal passenger flow fluctuations [22]. In hydrology, Zhang et al. designed a novel LSTM model with the dropout scheme to estimate the depth of the water table [23]. In the atmosphere field, Qing et al. estimated the solar irradiance based on the LSTM network [24]; the results showed the method could avoid the overfitting of the model. Li et al. designed a new GANs-LSTM model and noted that it could serve as an alternative method to estimate T_s [25].

This article focuses on the following issues. First, we select the environmental factors which will affect T_s estimation. T_s memory can help the predictive model "remember" a warm or cold condition when the anomaly is forgotten by the atmosphere forcing. In addition, recent literature reviews have revealed that the input for prediction models is either the past measurements of T_s or other meteorological information (Ta, W, RH, Rs, Sh, and Ap). Assume that the prediction models are constructed using input combinations of past T_s and other meteorological information; how does the prediction model performance? The second question is about the construction of loss function in LSTM. The predictive model for T_s estimation is a regression predictive modeling problem that involves predicting a real-valued quantity. The loss function is crucial for optimizing the predictive model which could express the degree of difference between predicted and observed T_s; meanwhile, it can optimize the predictive model by updating the weights. Recently, most previous studies in loss function of regression predictive model mainly focused on the distance metric learning between predicted values and real values [26–29]. However, the distance metric learning between the sample features (environmental factors) is usually ignored which has already been successfully applied to image processing [30–32]. To enrich information processing in loss function and further improve the estimation performance, how can we construct a novel loss function by combinations of distance metric learning? The last question is about timescale evaluating for T_s estimation. In previous studies, any evaluation at short-term T_s estimation (half-hourly, hourly, daily timescales) does not consider the timeliness of long-term T_s estimation. However, any evaluation at long-term T_s estimation (monthly timescale) does not include the information of T_s in a small timescale. An ideal decision-support tool for T_s estimation should provide a multifarious decision-making basis. How can we design a prediction scheme at the same timescale evaluation that provides not only the short-term decision-making basis but also the long-term decision-making basis?

This paper proposed a novel quadruplet loss function based on the LSTM network that combines traditional squared-error loss function with distance metric learning between the sample features, called QL-LSTM. The traditional squared-error loss function is usually applied to the predictive task with great accuracy. The current limitation of this loss function, however, involves the special variation on Ts based on different predictors. As shown in Figure 1, we have made labels according to T_s

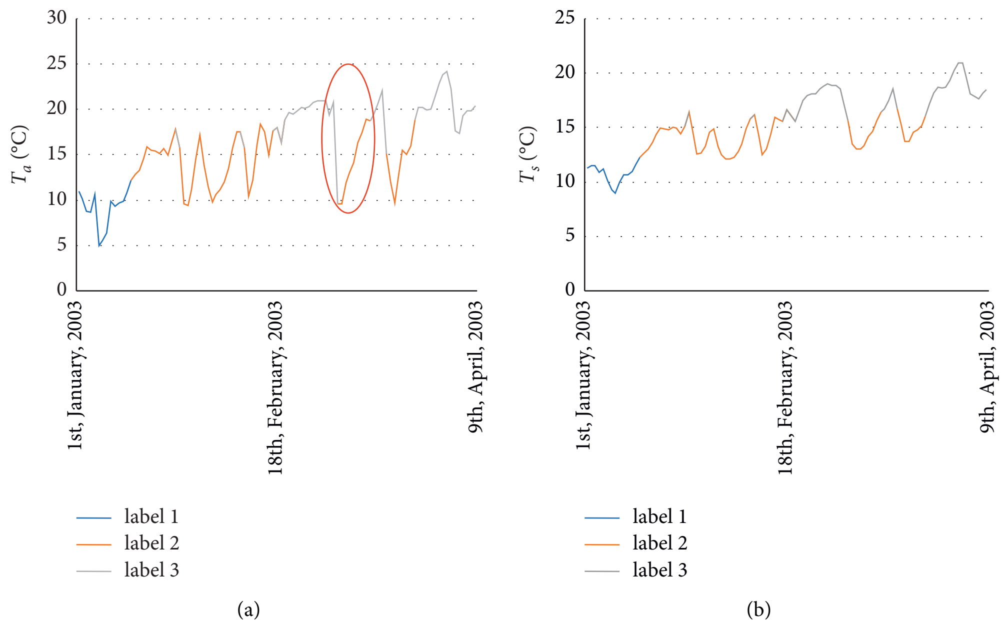

FIGURE 1: Variations of the daily air temperature (a) and soil temperature (b) at Laegern station (located in Switzerland) during 1st, January 2003–9th April 2003 (100 days).

values. The T_s data which are in the same range are made the same label (the T_s data which are in the range of 8–12°C are labeled as "1", the T_s data which are in the range of 12–16°C are labeled as "2", and the T_s data which are in the range of 16–22°C are labeled as "3"). Meanwhile, Ta data are labeled as the same as T_s data. In Figure 1(a), we noticed that the T_s data with the same label are almost within a stable range. However, in the red ellipse, Figure 1(b), we observed that similar Ta values may have different labels (T_s data with similar Ta values may vary considerably). The data with this feature will prevent predictive models from accurately exploring the internal relationship between T_s and the surrounding environmental factors discovering. To address this problem, the idea of triplet loss [33] is considered in this paper. Triplet loss optimization allows the anchor and positive points to accumulate and therefore prevent the negative points and realize the similarity calculation of samples. This approach can enrich processing information of loss function and overcome the disadvantage of the traditional squared-error loss function and further improve the estimation performance.

The main three contributions of this research paper are summarized as follows:

(1) As we know, the proposed method that combined traditional squared-error loss function with distance metric learning between the sample features is a new approach to be used for T_s estimation.

(2) Daily-scale prediction scheme was designed to provide the multifarious decision-making basis and was used to estimate the T_s on the next 1st, 5th, and 15th day. To achieve this end, we input the meteorological and past T_s data to the estimation model.

(3) Results showed that our QL-LSTM method outperformed the existing advanced methods in most cases.

2. Data and Methods

2.1. The Framework of Soil Temperature Estimation. The corresponding meteorological data T_s as the input of our QL-LSTM model are obtained from FLUXNET at first. In the meantime, several other advanced models based on data-driven technology (SVR, BPNN, ELM, and LSTM) were considered in T_s estimation. Traditional squared-error loss function and distance metric learning between the sample features were integrated into our model for accurate exploration of the internal relationship between T_s and the surrounding environmental factors. Finally, the comparison of model performance is reflected by five evaluating indicators (RMSE, MAE, NS, WI, and LMI). Figure 2 denoted the flow chart of soil temperature estimation.

2.2. Long Short-Term Memory (LSTM) Network. LSTM can process and learn long-term dependence problems. Due to the characteristics of the LSTM network, we use it to explore the internal relationship between T_s and the surrounding predictors. LSTM controls the transmission state through the gating state, remembers what needs to be remembered, and forgets unimportant information. Figure 3 shows the internal structure of an LSTM cell, and the calculation formula of the LSTM is as follows:

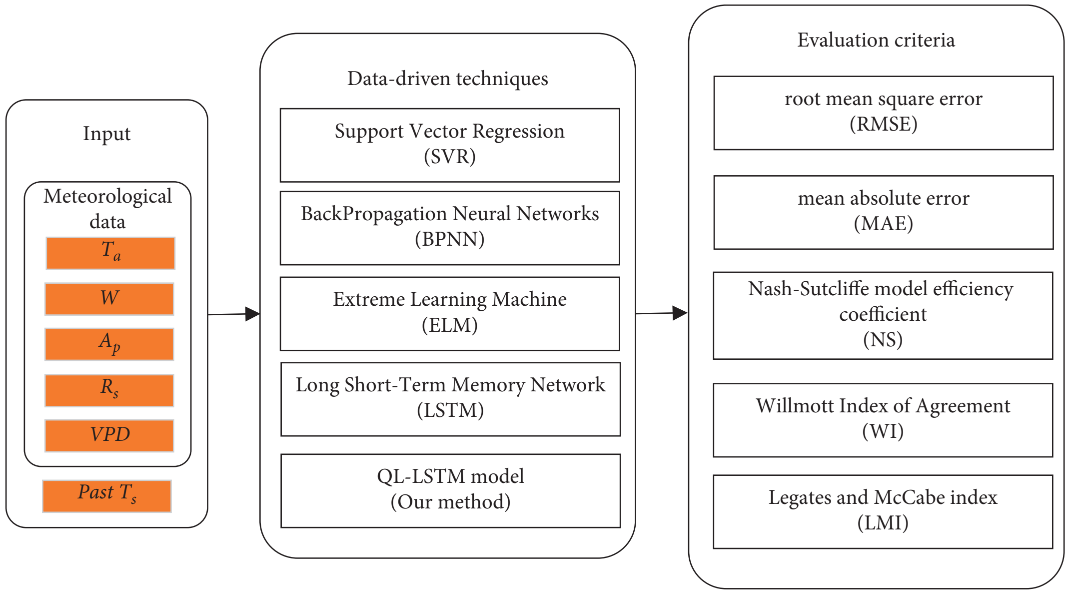

Figure 2: The flow chart of soil temperature estimation.

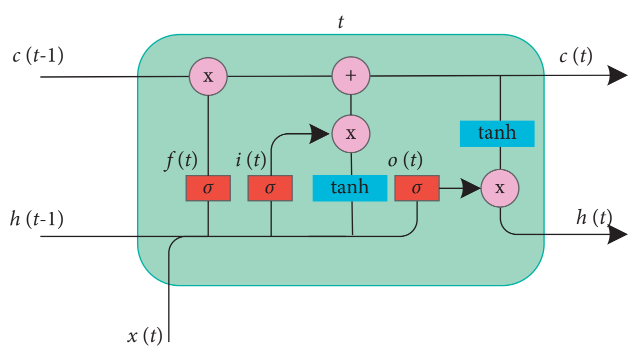

Figure 3: The internal structure of an LSTM cell.

$$
\begin{aligned}
i(t) &= \sigma\left(W_{ih}h(t-1) + W_{ix}x(t) + W_{ix}c(t-1) + b_i\right),\\
f(t) &= \sigma\left(W_{fh}h(t-1) + W_{fx}x(t) + W_{fx}c(t-1) + b_f\right),\\
c(t) &= f(t)\otimes c(t-1) + i(t)\otimes \tanh\left(W_{ch}h(t-1) + W_{cx}x(t) + b_c\right),\\
o(t) &= \sigma\left(W_{oh}h(t-1) + W_{ox}x(t) + W_{oc}c(t) + b_o\right),\\
h(t) &= o(t)\otimes \tanh(c(t)),\\
\hat{y}(t) &= W_{yh}h(t) + b_o,
\end{aligned}
\tag{1}
$$

where $x(t)$ is the input data, and $\hat{y}(t)$ is the output data; $i(t)$, $f(t)$, and $o(t)$ denote the input gate, forget gate, and output gate; $c(t)$ represents the unit status at the current moment; $h(t)$ is the current output value; $\sigma(\cdot)$ and $\tanh(\cdot)$ are the activation functions; W and b denote the weight matrix and bias term.

2.3. Triplet Loss. Triplet loss is a significant "learning criterion" for optimizing the predictive models, which is applied for adjusting the weight parameters of predictive models, including anchor (Anchor) example, positive (Positive) example, and negative (Negative) example. The similarity calculation of the samples is realized through triplet loss learning, which makes the anchor-to-positive distance smaller than the anchor-to-negative distance. And Figure 4 denoted the visual representation of triplet loss.

Equation (2) expresses the objective function of triplet loss as follows:

$$
\sum_{i}^{N}\left[\left\|f\left(x_i^a\right) - f\left(x_i^p\right)\right\|_2^2 - \left\|f\left(x_i^a\right) - f\left(x_i^n\right)\right\|_2^2 + \alpha\right]_+, \tag{2}
$$

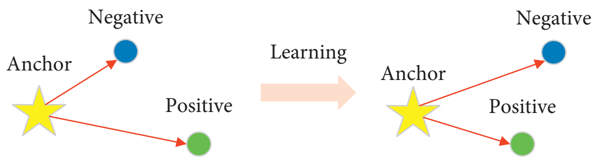

Figure 4: A visual representation of triplet loss.

where $f(x_i^a)$, $f(x_i^p)$, and $f(x_i^n)$ are the corresponding feature expression obtained by training a parameter in the triplet; α represents the minimum interval between the anchor-to-positive distance and the anchor-to-negative distance; the value of $[\cdot]_+$ defines the degree of loss.

2.4. QL-LSTM Model. Previous analysis shows that LSTM with traditional squared-error loss function could not accurately discover the special relationship between T_s and surrounding predictors. To address this problem, inspired by the study of triplet loss, we combined a predictive model with distance metric learning between the sample features. As far as we know, the method based on distance metric learning between the sample features has not been used to estimate T_s ever. It must be noted that the distance metric learning between the sample features is first proposed in the field of image processing. However, there is no description of the similarity of samples for T_s estimation. In this paper, the clustering method is used to label samples; thus, distance metric learning between the sample features could be further applied in T_s estimation.

The framework of our QL-LSTM is shown in Figure 5. Firstly, for its ability to cluster data efficiently and scalability, the T_s data were quantized by the clustering method (called Birch) [34]. In the quantization step, any T_s data quantized to the same label will be defined as similar samples (positive). In contrast, any T_s data quantized to different labels will be defined as the dissimilar samples (negative). It is worthwhile to observe that the number of labels should be neither too large nor too small [35]. Hence, the Calinski Harabasz Score (*CH*) and Y_Silhouette_score (*S*) are used to evaluate the quality of the cluster [36]. The larger value of CH or *S*, the better quality of the clustering results. Second, the labeled data are input into the predictive model (LSTM network). Finally, the weights of the predictive model are updated to reduce the loss based on our quadruplet loss function.

We set $X = \{(x_i, l_i)\}_{i=1}^{N}$ as the input data, where l_i represents T_s labeled as "i" and x_i represents the labeled environmental factors. Assume C is the total number of labels, where $l_i \in [1, 2, 3 \ldots, C]$. Then, we project an instance x_i onto the estimate T_s by $f_{\text{LSTM}}(.;\theta)$: $R^d \longrightarrow S^1$, where f_{LSTM} is an LSTM network parameterized by θ. Let $\{X_i^c\}_{i=1}^{N_c}$ be the environmental factors in the i -th labeled samples. N_c represents the total number of samples. We evaluate the similarity between samples through cluster analysis and expect the output of the model closer to the true value.

2.4.1. Hard Sample Mining. Hard sample mining generally refers to hard negative mining. Adding negative sample sets to participate in model training can improve the effectiveness of learning and training and mine hard negatives as much as possible [37, 38]. For each fixed picture, the farthest sample picture and the nearest negative sample picture in a training batch are applied to train the network to enhance the generalization ability of the network, so that the network can learn better representations.

Inspired by TriHard loss, we first define x_i^c as the test sample: $P_{c,i}\,(P_{c,i} = \{x_j^c | j \neq i\}, |P_{c,i}| = N_c - 1)$ is a collection, which includes the samples with the same label; $N_{c,i}\,(N_{c,i} = \{x_j^k | k \neq c\}, |N_{c,i}| = \sum_{k \neq c} N_k)$ represents the other samples' collection. $(x_i^c, y_i^c, P_{c,i}^*, N_{c,i}^*)$ is the quadruplet data set we defined. $P_{c,i}^*$ is the positive set; $N_{c,i}^*$ represents the negative set, $|P_{c,i}^*|$ and $|N_{c,i}^*|$ represent positive and negative sample pairs, and these tuples form the training sample pairs. The query sample is represented as x_i^c; when S_{ij}^+ satisfies the formula (3), $\{x_i, x_j\}$ is the pair that we need.

$$S_{ij}^+ > \min_{x_k \in P_{c,i}} S_{ik} + \mu, \tag{3}$$

where $S_{ij}^+ \langle f_{\text{LSTM}}(x_i;\theta), f_{\text{LSTM}}(x_j;\theta)\rangle$ represents the similarity between two samples, where $\langle \cdot, \cdot \rangle$ represents the calculation of an $n \times n$ similarity matrix. S_{ij} is the element in S at (x_i, x_j), and μ as a hyperparameter impacts the quadruplet that can control the number of hard positive samples. The condition for selecting a hard and negative pair is the same as above:

$$S_{ij}^- < \max_{x_k \in N_{c,i}} S_{ik} - \mu. \tag{4}$$

2.4.2. Optimization Objective. For each test sample x_i^c, we use the margin m to make it as close to the positive set $P_{c,i}$ as possible, and as far away from the negative set $N_{c,i}$ as possible. All the nontrivial positive points in $P_{c,i}$ are pulled together by minimizing:

$$L_P(x_i^c; f_{\text{LSTM}}) = \frac{1}{2} \sum_{x_i^c \in P_{c,i}^*} \left(\left[\left\| f_{\text{LSTM}}(x_i^c) - f_{\text{LSTM}}(x_j^c) \right\| - (r - m) \right]_+ \right)^2, \tag{5}$$

where $f_{LSTM}(x_i^c)$ and $f_{LSTM}(x_j^c)$ denote the estimated T_s of samples x_i^c and x_j^c, respectively, and $\| f_{LSTM}(x_i^c) - f_{LSTM}(x_j^c) \|$ is the Euclidean distance between $f_{LSTM}(x_i^c)$ and $f_{LSTM}(x_j^c)$. Similarly, all nontrivial negative points in $N_{c,i}$ need to push out of the boundary τ, by minimizing:

$$L_N(x_i^c; f_{\text{LSTM}}) = \frac{1}{2} \sum_{x_j^k \in N_{c,i}^*} \left(\left[\tau - \left\| f_{\text{LSTM}}(x_i^c) - f_{\text{LSTM}}(x_j^k) \right\| \right]_+ \right)^2. \tag{6}$$

Meanwhile, we applied the squared-error loss function to the LSTM model for T_s estimation, as follows:

$$L_{MSE}(x_i^c; f_{\text{LSTM}}) = \frac{1}{2} \sum_{x_i^c \in N_c} \left(f_{\text{LSTM}}(x_i^c) - y_i^c \right)^2. \tag{7}$$

In the QL-LSTM, three minimization objectives were put into the model, and they are optimized at the same time:

$$\begin{aligned} L_{\text{QL-LSTM}}(x_i^c; f_{\text{LSTM}}) = {} & L_P(x_i^c; f_{\text{LSTM}}) + L_N(x_i^c; f_{\text{LSTM}}) \\ & + L_{\text{MSE}}(x_i^c; f_{\text{LSTM}}), \end{aligned} \tag{8}$$

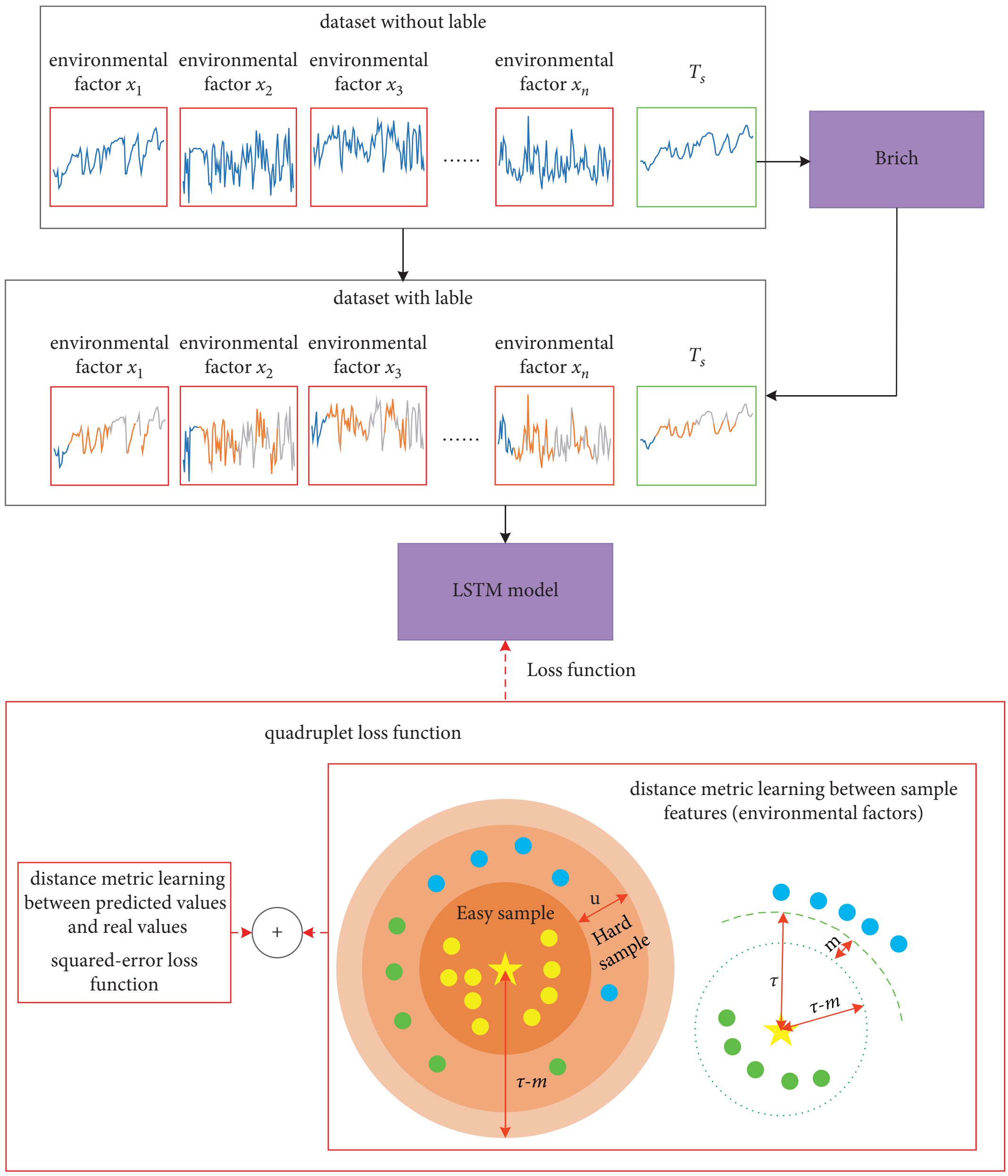

Figure 5: The framework of QL-LSTM.

We incorporate stochastic gradient descent and minibatch into the QL-LSTM to optimize the estimation model.

x_i^c is a sample of the minibatch, which is obtained by sampling the labels of the training samples randomly, and serves as an anchor. We represent the QL-LSTM of each minibatch as

$$L_{QL-LSTM}(X; f) = \frac{1}{N} \sum_{\forall_c \forall_i} L_{QL-LSTM}(x_i^c; f), \qquad (9)$$

where N denotes the batch size. Figure 6 represented the learning procedure of our QL-LSTM model.

2.5. Model Training and Testing. The input of our model is the corresponding meteorological data (T_a, W, A_p, R_s, VPD, and T_s) from Laegern and Fluehli stations in Switzerland. And we downloaded the data at https://fluxnet.fluxdata.org/ on FLUXNET with a total of 3,287 patterns from 2006 to 2014. Training datasets had 2465 patterns, and the rest as testing datasets.

Comparing our QL-LSTM model with the other advanced methods (SVR, BPNN, ELM, and LSTM), meanwhile, we calculate several evaluation criteria to analyze the model performance, including model fitting degree and the accuracy of the estimation model, as follows:

$$\mathrm{RMSE} = \sqrt{\frac{\sum_{n=1}^{N} \left(y_i - \hat{y}_i\right)^2}{N}},$$

$$\mathrm{WI} = 1 - \frac{\sum_{n=1}^{N} \left(y_i - \hat{y}_i\right)^2}{\sum_{n=1}^{N} \left(\left|\hat{y}_i - \overline{y}\right| + \left|y_i - \overline{y}\right|\right)^2},$$

$$\mathrm{NS} = 1 - \frac{\sum_{n=1}^{N} \left(y_i - \hat{y}_i\right)^2}{\sum_{n=1}^{N} \left(y_i - \overline{y}\right)^2}, \tag{10}$$

$$\mathrm{MAE} = \frac{\sum_{n=1}^{N}\left|y_i - \hat{y}_i\right|}{N},$$

$$\mathrm{LMI} = 1 - \frac{\sum_{n=1}^{N}\left|y_i - \hat{y}_i\right|}{\sum_{n=1}^{N}\left|y_i - \overline{y}\right|},$$

where N is the number of the whole data, y_i denotes the observed value, $\hat{y}_i$ is the predicted value, and $\overline{y}$ is the average of the true values.

2.6. Experiments. The data within half an hour is obtained from two meteorological stations in an ecological nature reserve, located in Switzerland, namely, Legern and Fluley. The corresponding meteorological data (T_a, W, A_p, R_s, VPD, and T_s) and past T_s data were input into the models. Meanwhile, the input variables are normalized to eliminate the dimensional influence between indicators. And the formula is as follows:

$$x_{\mathrm{norm}} = \frac{x - x_{\min}}{x_{\max} - x_{\min}}, \tag{11}$$

where the minimum value of the sample data is represented by $x_{\min}$, and the maximum value is represented by $x_{\max}$. Moreover, we have conducted research on the influence of the surrounding environmental factors on the model prediction. And we found the value of R_s in the data of the two stations is low, which is close to the normal distribution.

We conducted a statistical analysis of the data from the two stations. Table 1 listed the details of variables (minimum value ($x_{\min}$), maximum value ($x_{\max}$), average value (x_{mean}), standard deviation (z_{sd}), skewness (z_s), and variation coefficient (z_v)). We used the daily data to verify the performance of the model with every half an hour data. The results showed in Table 1 that A_p had the highest negative skewness and presents a normal distribution at 5 cm depth, which presented similar characteristics in both stations. Meanwhile, z_v showed the biggest difference between the two stations. T_s at the 5 cm, 10 cm, and 15 cm depths range −1.888–26.876°C, −0.181–22.193°C, and 0.16–20.826°C, respectively. In summary, results showed that the values of z_{sd}, z_s, and z_v change very slightly.

3. Results and Discussion

For testing the superiority of our QL-LSTM model performance for T_s estimation using scikit-learn, we compared our test results with those of other advanced models (SVR, BPNN, ELM, and LSTM).

We choose default parameters for the SVR model. For the BPNN model, the square error is used as the loss function, and the optimization is Adam. The number of samples selected for the model is 400, the iteration is set to 500, the learning rate is set to 5.0e-4, and the size of the nodes is set to 128. The elm function was used to model the ELM model, the sigmoid served to activate the function in the hidden layer, and we set the same size of the nodes to BPNN. Furthermore, we set the hyperparameters of the LSTM to be the same as that of QL-LSTM. As can be seen from Table 2 and 3, the different values of the hyperparameter can generate the different predictive results. When the number of samples selected for the model is set to 400, the iteration to 500, the $\mathrm{num}_{\mathrm{QL-LSTM}}$ to 128, and set the learning rate to 1.0e-3, the QL-LSTM model has the best performance.

3.1. Evaluation for the Hyperparameters in Quadruplet Loss Function. The quadruplet loss function has five main hyperparameters, which are the total number of labels C, hyperparameter μ in equations (3) and (4), and τ and m in equations (5) and (6). When we evaluate the above hyperparameters in the quadruplet loss function, we set the parameters $\mathrm{num}_{QL-\mathrm{LSTM}}$ to 128, the learning rate to 1.0e-3, the iteration time to 500, and the batch size to 400. We first select the best C based on the Calinski Harabasz Score and Y_Silhouette_score. Figure 7 denotes the Calinski Harabasz Score and Y_Silhouette_score with different numbers of labels. It is observed that both scores achieve the best result when C is 25. Then, we gradually tune the hyperparameters, τ and m. Figure 8 represented the results of the estimation model with different μ, τ, and m in Laegern meteorological station. We can see that when we set μ to be 5.0e-3, τ to be 1.0e-3, and m to be 5.0e-5, and our QL-LSTM model could achieve the best estimation performance (RMSE = 0.789, MAE = 0.605, NS = 0.977, WI = 0.994, and LMI = 0.865). It is probably because the smaller hyperparameters we set, the less hard samples would be computed. Meanwhile, when we set the larger hyperparameters, the more redundant samples would be computed.

3.2. The Impact of Different Inputs on the Performance of the Predictive Model. In this part, we analyzed the environmental factors that may affect our QL-LSTM model for T_s estimation. Considering that the interaction between different environmental factors would have an impact on the T_s estimation, we combine the meteorological variables accordingly and input them into the submodels we set as follows:

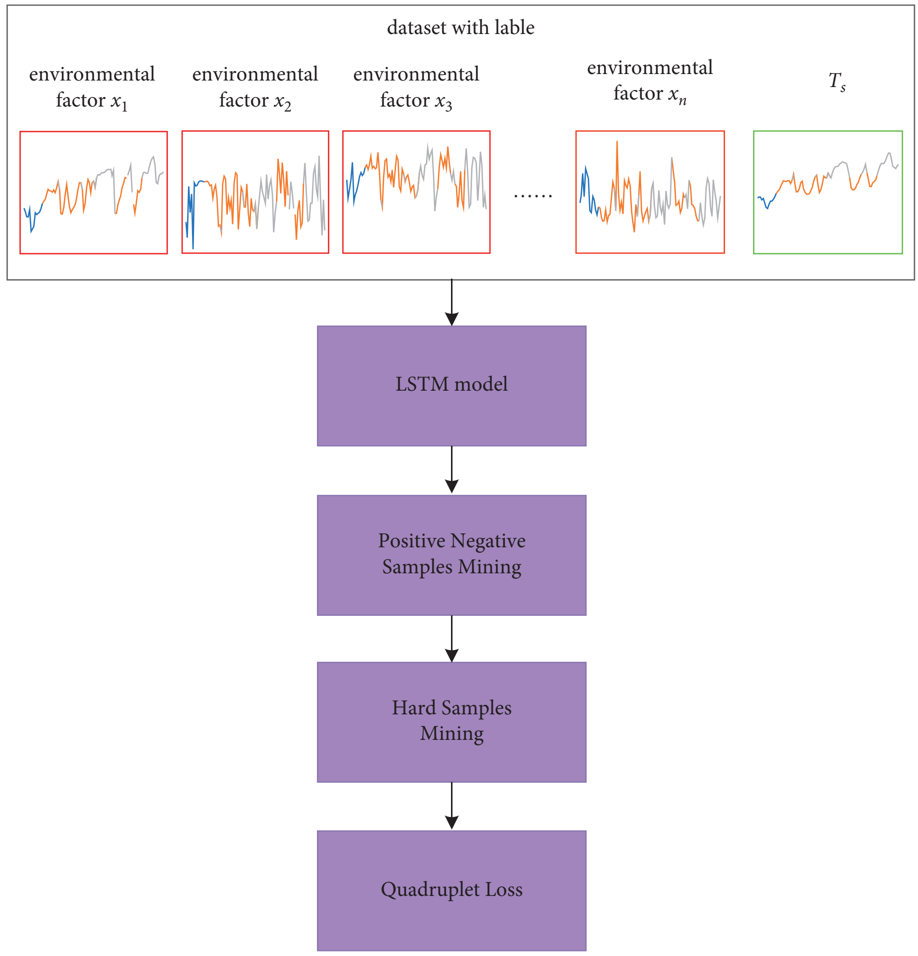

Figure 6: The learning procedure of QL-LSTM.

Table 1: Statistical results of the applied data for Laegern and Fluehli stations.

Station	Variable	$x_{\min}$	$x_{\max}$	x_{mean}	$z_{s\,d}$	z_s	z_v
Laegern	T_a (°C)	−14.509	23.646	7.857	7.084	−0.118	0.901
	R_s (W/m^2)	175.545	379.458	305.081	35.164	−0.418	0.115
	VPD (hpa)	0.54	15.937	3.271	2.334	1.424	0.713
	W (m/s)	0.668	8.025	2.237	1.005	1.411	0.449
	A_p (kpa)	89.876	95.163	93.237	0.714	-0.630	0.007
	T_s −5 cm (°C)	−1.888	26.876	10.104	6.061	0.103	0.599
	T_s −10 cm (°C)	−0.181	22.193	9.726	5.435	−0.031	0.558
	T_s −15 cm (°C)	0.16	19.394	9.010	5.025	−0.068	0.557
Fluehli	T_a (°C)	−14.448	22.877	7.708	6.906	−0.100	0.895
	R_s (W/m^2)	194.734	377.444	306.015	32.805	−0.327	0.107
	VPD (hpa)	0.416	9.662	2.129	1.543	1.410	0.724
	W (m/s)	0.342	4.636	1.476	0.619	0.894	0.419
	A_p (kpa)	82.308	87.164	85.493	0.711	−0.843	0.008
	T_s −5 cm (°C)	−0.35	21.822	8.729	6.338	0.075	0.726
	T_s −10 cm (°C)	−0.044	21.727	8.836	6.242	0.071	0.706
	T_s −15 cm (°C)	0.432	20.826	8.813	6.023	0.062	0.683

Table 2: Predictive performance with different $num_{QL-LSTM}$ and learning rates at Laegern station.

Learning rate	$num_{QL-LSTM}$	RMSE	MAE	NS	WI	LMI
1.0e-5	16	4.735	4.059	0.1799	0.325	0.093
	32	2.970	2.508	0.677	0.845	0.439
	64	1.346	1.061	0.933	0.980	0.763
	128	1.365	1.073	0.931	0.982	0.760
	256	1.341	1.049	0.934	0.983	0.765
	16	1.230	0.962	0.944	0.986	0.785
1.0e-4	32	1.175	0.915	0.949	0.987	0.795
	64	1.167	0.903	0.950	0.987	0.798
	128	1.159	0.884	0.950	0.987	0.802
	256	1.148	0.871	0.951	0.987	0.805
	16	1.129	0.855	0.953	0.988	0.808
5.0e-4	32	1.076	0.809	0.957	0.989	0.819
	64	1.001	0.757	0.963	0.990	0.830
	128	0.817	0.629	0.975	0.993	0.859
	256	0.852	0.657	0.973	0.993	0.853
	16	1.069	0.802	0.958	0.989	0.820
1.0e-3	32	0.950	0.716	0.966	0.991	0.839
	64	0.880	0.676	0.971	0.992	0.848
	128	**0.817**	**0.625**	**0.975**	**0.993**	**0.860**
	256	0.825	0.634	0.975	0.993	0.858
	16	0.871	0.675	0.972	0.993	0.849
5.0e-3	32	0.858	0.661	0.973	0.993	0.852
	64	0.868	0.661	0.972	0.993	0.852
	128	0.852	0.648	0.973	0.993	0.855
	256	0.854	0.649	0.973	0.993	0.855

Table 3: Predictive performance with different numbers of batch size and iterations at Laegern station.

Batch	Iteration	RMSE	MAE	NS	WI	LMI
100	100	0.860	0.666	0.972	0.993	0.851
	200	0.873	0.676	0.972	0.993	0.848
	500	0.880	0.667	0.971	0.992	0.850
	800	1.073	0.825	0.957	0.989	0.815
	100	0.849	0.654	0.973	0.993	0.853
200	200	0.817	0.625	0.975	0.993	0.860
	500	0.843	0.642	0.973	0.993	0.856
	800	0.916	0.692	0.969	0.992	0.845
	100	0.973	0.739	0.965	0.991	0.834
300	200	0.831	0.644	0.974	0.993	0.856
	500	0.817	0.626	0.975	0.993	0.860
	800	0.869	0.664	0.972	0.993	0.851
	100	1.038	0.784	0.960	0.990	0.824
400	200	0.851	0.654	0.973	0.993	0.853
	500	**0.809**	**0.622**	**0.976**	**0.993**	**0.860**
	800	0.817	0.628	0.975	0.993	0.859
	100	1.076	0.812	0.957	0.989	0.818
500	200	0.868	0.666	0.972	0.993	0.851
	500	0.809	0.623	0.976	0.993	0.860
	800	0.811	0.626	0.975	0.993	0.860

(i) Input I_1: T_a (d − 1)

(ii) Input I_2: T_a (d − 1) + R_s(d − 1)

(iii) Input I_3: T_a (d − 1) + R_s(d − 1) + VPD(d − 1)

(iv) Input I_4: T_a (d − 1) + R_s(d − 1) + VPD(d − 1) + W(d − 1)

(v) Input I_5: T_a (d − 1) + R_s(d − 1) + VPD(d − 1) + W(d − 1) + A_p(d − 1)

(vi) Output: T_s (d)

Then, we consider that the past T_s will continue to have an impact on the future T_s estimation, so we have carried out lag processing for the past T_s on different days, as follows:

(i) Input I_6: T_s (d − 1)

(ii) Input I_7: T_s (d − 1) + T_s (d − 2)

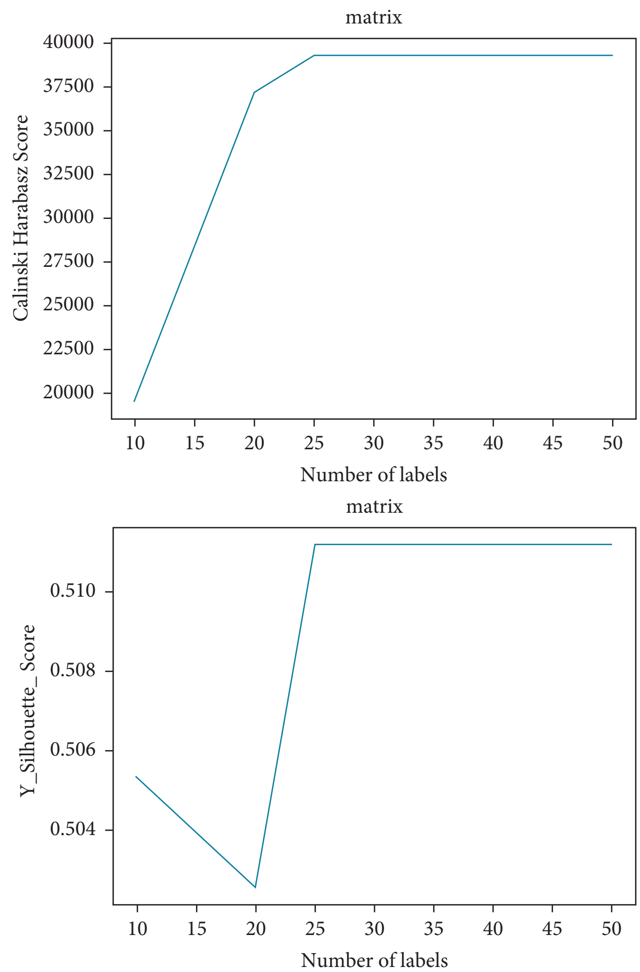

(a)

Figure 7: The Calinski Harabasz Score and Y_Silhouette_score with different numbers of labels.

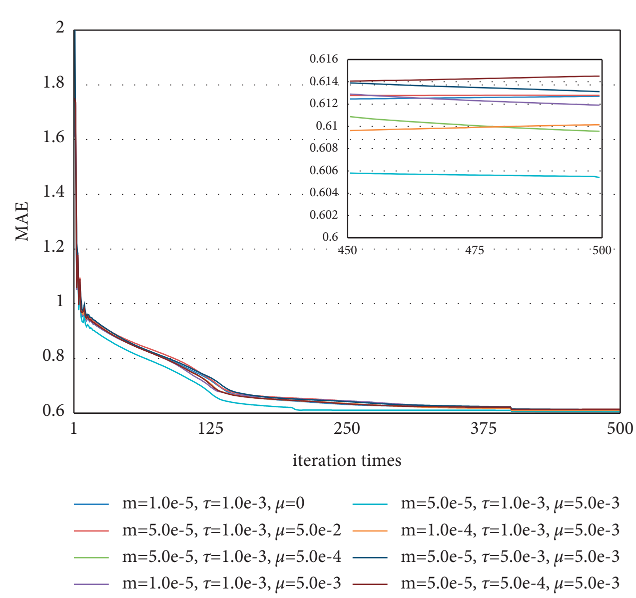

Figure 8: The estimation results with different μ, τ, and m at Laegern meteorological station.

Table 4: Predictive performance of QL-LSTM at 5 cm depth for the Laegern station.

Method	RMSE	MAE	NS	WI	LMI
QL-LSTM($_{I1}$)	1.469	1.143	0.921	0.980	0.744
QL-LSTM($_{I2}$)	1.444	1.113	0.923	0.981	0.751
QL-LSTM($_{I3}$)	**1.221**	**0.937**	**0.945**	**0.986**	**0.790**
QL-LSTM($_{I4}$)	1.396	1.078	0.928	0.982	0.759
QL-LSTM($_{I5}$)	1.454	1.143	0.922	0.980	0.744
QL-LSTM($_{I6}$)	1.143	0.866	0.952	0.987	0.806
QL-LSTM($_{I7}$)	1.095	0.823	0.956	0.988	0.815
QL-LSTM($_{I8}$)	**1.077**	**0.815**	**0.957**	**0.989**	**0.817**
QL-LSTM($_{I9}$)	1.096	0.834	0.956	0.988	0.813
QL-LSTM($_{I10}$)	1.115	0.842	0.954	0.988	0.811

(iii) Input I_8: T_s (d − 1) + T_s (d − 2) + T_s (d − 3)

(iv) Input I_9: T_s (d − 1) + T_s (d − 2) +T_s (d − 3) + T_s (d − 4)

(v) Input I_{10}: T_s (d − 1) + T_s (d − 2) +T_s (d − 3) + T_s (d − 4) + T_s (d − 5)

(vi) Output: T_s (d)

We input what we specified above into QL-LSTM to predict the T_s (d) at the 5 cm depth of the Laegern station. For our model, we first selected the hyperparameters μ as 5.0e-3, τ as 1.0e-3, m as 5.0e-5, C as 25, num$_{\text{QL-LSTM}}$ as 128, learning rate as 1.0e-3, iteration time as 500, and batch size as 400, and the results are presented in Table 4. Obviously, the methods of QL-LSTM(I_3) and QL-LSTM(I_8) are better than the others, respectively. Meanwhile, we could conclude that W (d − 1), A_p (d − 1), T_s (d − 4), and T_s (d − 5) all have an influence on the performance of the predictive model. In addition, by comparing the estimation results between meteorological variables input and past T_s input, we found that our model with past T_s could achieve greater accuracy in modeling than the one with meteorological variables. The reason may be that the predictive model with past T_s input has stronger memory for T_s variables. The estimation of the future T_s should make the best use of its continuity; in this way, we can make a reliable T_s estimation, which not only continues its historical tendency but also conforms to its actual performance. Hence, we construct the predictive model (QL-LSTM(I_{11})) by combining the environmental factors (T_a (d − 1), R_s(d − 1), VPD(d − 1)) with past T_s (T_s (d − 1), T_s (d − 2), T_s (d − 3)), which is also considered in estimating the T_s (d) at the 5 cm depth of the Laegern station. Experiment results prove that it could achieve the best estimation performance (RMSE = 0.789, LMI = 0.865, WI = 0.994, NS = 0.977, and MAE = 0.605). Hence, the final input for the predictive models is the environmental factors (T_a(d − 1), R_s(d − 1), VPD(d − 1)) and the past T_s (T_s (d − 1), T_s (d − 2), T_s (d − 3)).

The three methods (QL-LSTM(I_3), QL-LSTM(I_8), and QL-LSTM(I_{11})) are used to test the data of the Laegern station. Figure 9 shows the linear relationship between the predicted value and the observed value. The QL-LSTM(I_{11}) model gets the best predictive performance with $y = 0.9899x + 0.3022$ and the higher R^2 (0.9792) compared with the others. In the frequency diagram (Figure 10) of the models (QL-LSTM(I_3), QL-LSTM(I_8), and QL-LSTM(I_{11})), the QL-LSTM(I_{11}) also has a higher frequency (91%) compared to the others. Therefore, we can draw a conclusion that the predictive model (a combination of the environmental factors and the past T_s) normally outperformed the other two (by either past measurements of T_s or other meteorological information) in the T_s estimation.

3.3. Comparison with Different Models. In this part, our QL-LSTM model was compared with several advanced models, including SVR, BPNN, ELM, and LSTM. The data of T_a, R_s, and VPD on day "d − 1", and T_s data on different days were acted as input data to different predictive models, and the output was the predicted value of T_s on days "d", "d + 5", and "d + 15". Time steps were in days.

The testing results of five different models at 5, 10, and 15 cm depth on the 1st, 5th, and 15th days of the Laegern station were shown in Table 5. And we can see that our QL-LSTM model performs better than the existing advanced models at the 5 cm depth on the 1st day. Specifically, the value of RMSE is 0.789, which is reduced relative to 13% (LSTM), 22% (ELM), 28% (BPNN), and 22% (SVR), respectively. The MAE values amount to 0.605 (QL-LSTM), and the others are 0.813 (SVR), 0.872 (BPNN), 0.824 (ELM), and 0.821 (LSTM). Meanwhile, the QL-LSTM model achieved a higher value of NS, WI, and LMI. Hence, it is obvious that our model had the best performance in this case. For the results of 5 cm depth on the 15th day, the LSTM achieved a higher WI (0.892) than estimation from other models on the 15th day, but it is similar to the WI (0.891) of our model. For 10 and 15 cm depth results on the 1st, 5$^{\text{th}}$, and 15th days, the performance of our QL-LSTM model remains stable, although our QL-LSTM model has the lower values of WI (0.952 and 0.933) than the values of WI (0.954 and 0.934) on the LSTM model in individual cases. It can be found that the predictive performance will get better as the soil depth decreases (from 5 cm to 15 cm), but it will decrease as time goes on (from 1st to 15th days). The systematic errors caused this phenomenon for long-term estimation [39].

The same strategy was applied in the Fluehli station to further verify the performance of the models, with the results shown in Table 6. And our QL-LSTM model performs better compared with others. However, for 5 cm depth on the 15th day and 15 cm depth on the 5th day, the BPNN model performs better with the results of RMSE = 2.081, LMI = 0.584, WI = 0.937, NS = 0.769, and MAE = 2.099, and RMSE = 1.832, LMI = 0.726, WI = 0.973, NS = 0.897, and MAE = 1.352 and LMI = 0.726. Our method does not

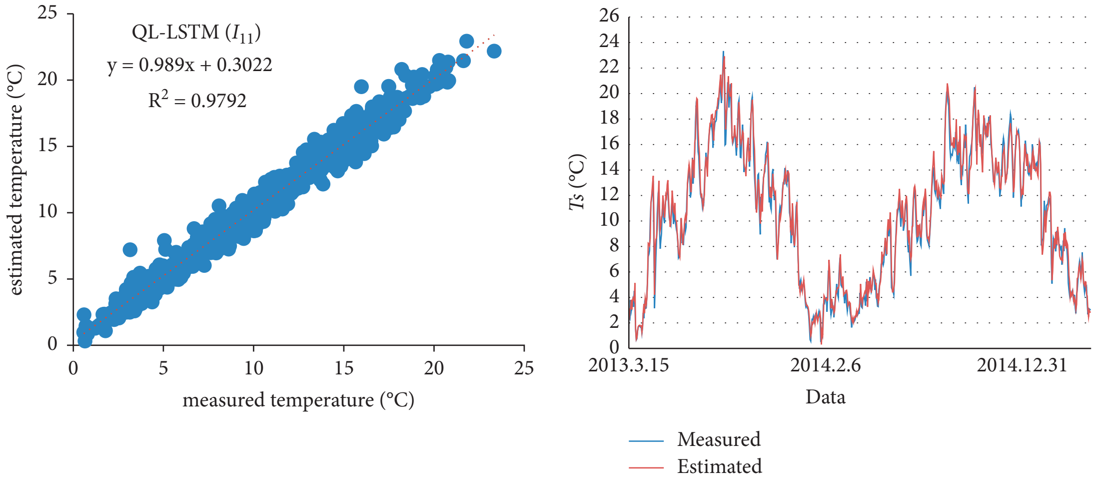

(a)

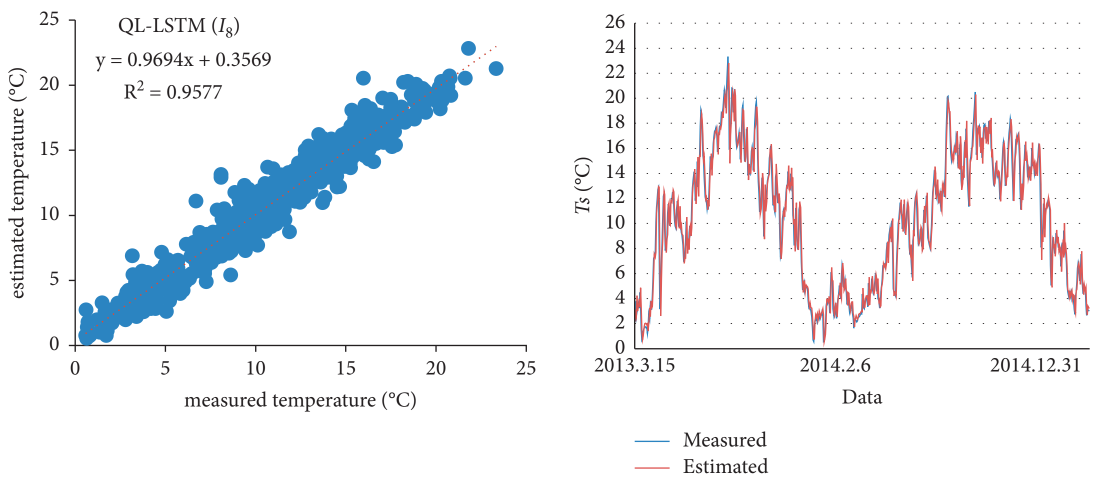

(b)

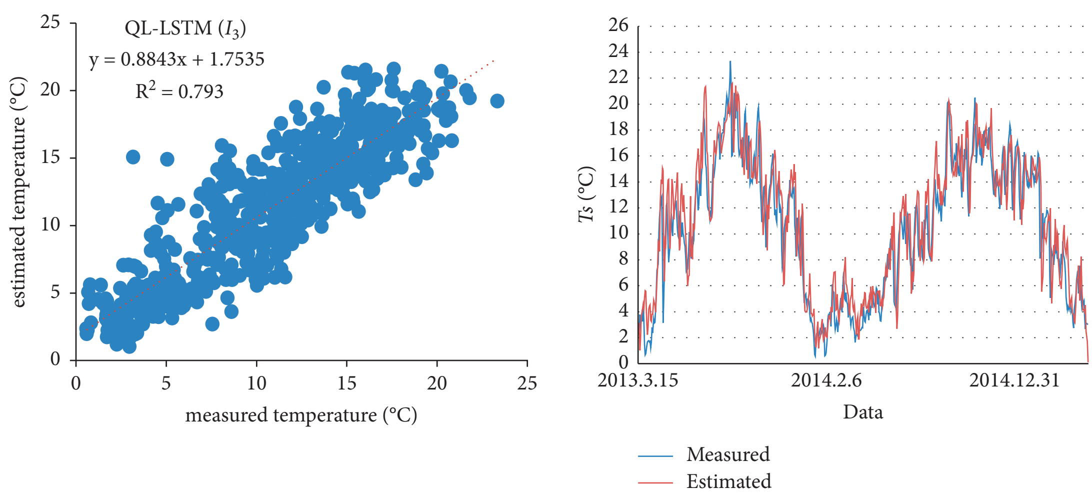

(c)

Figure 9: The scatterplots of the predictive model testing results (the values of estimated and observed) for the Laegern station. (a) QL-LSTM(I11), (b) QL-LSTM(I8) model, and (c) QL-LSTM(I3) model.

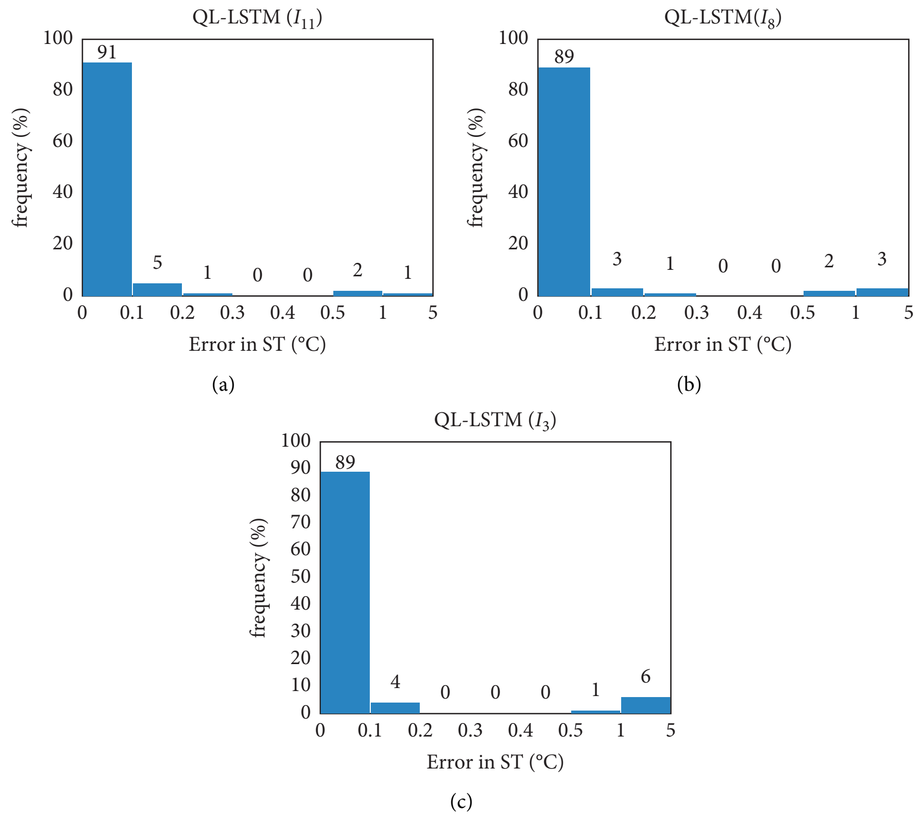

Figure 10: The frequency plot of the predictive models (absolute estimation error) for the Laegern station. (a) QL-LSTM(I11), (b) QL-LSTM(I8) model, and (c) QL-LSTM(I3) model.

Table 5: The predictive performance with different models at the Laegern station.

Depth (cm)	Day	Method	RMSE	MAE	NS	WI	LMI
		SVR	1.007	0.813	−1315.5	0.412	−882.6
		BPNN	1.101	0.872	0.930	0.982	0.838
	d	ELM	1.016	0.824	0.925	0.983	0.849
		LSTM	0.910	0.821	0.926	0.983	0.850
		QL-LSTM	**0.789**	**0.605**	**0.977**	**0.994**	**0.865**
		SVR	2.665	2.133	-1205.3	0.419	-845.1
		BPNN	2.812	2.230	0.700	0.919	0.535
5	d + 5	ELM	2.832	2.261	0.693	0.916	0.528
		LSTM	2.643	2.113	0.730	0.926	0.560
		QL-LSTM	**2.436**	**1.908**	**0.782**	**0.937**	**0.573**
		SVR	3.322	2.680	−1215.2	0.422	−846.9
		BPNN	3.271	2.657	0.601	0.886	0.438
	d + 15	ELM	3.403	2.723	0.572	0.881	0.424
		LSTM	3.278	2.652	0.601	**0.892**	0.439
		QL-LSTM	**3.078**	**2.428**	**0.651**	0.891	**0.455**

Table 5: Continued.

Depth (cm)	Day	Method	RMSE	MAE	NS	WI	LMI
10	d	SVR	1.011	0.850	−1291.5	0.414	−870.2
		BPNN	0.986	0.831	0.923	0.983	0.837
		ELM	1.090	0.862	0.916	0.981	0.830
		LSTM	0.980	0.824	0.923	0.983	0.839
		QL-LSTM	**0.761**	**0.605**	**0.975**	**0.993**	**0.854**
	d + 5	SVR	2.173	1.752	−1211.9	0.417	−842.1
		BPNN	2.188	1.751	0.774	0.935	0.608
		ELM	2.291	1.833	0.762	0.938	0.596
		LSTM	2.181	1.745	0.781	**0.954**	0.615
		QL-LSTM	**1.973**	**1.545**	**0.833**	0.952	**0.628**
	d + 15	SVR	2.794	2.220	−1244.5	0.431	−850.8
		BPNN	2.831	2.263	0.652	0.909	0.493
		ELM	2.920	2.300	0.632	0.899	0.484
		LSTM	2.763	2.131	0.667	0.907	0.509
		QL-LSTM	**2.538**	**1.975**	**0.724**	**0.917**	**0.524**
15	d	SVR	0.531	0.450	−1304.5	0.424	−873.5
		BPNN	0.525	0.442	0.942	0.987	0.921
		ELM	0.637	0.488	0.940	0.987	0.913
		LSTM	0.512	0.436	0.944	0.988	0.927
		QL-LSTM	**0.312**	**0.239**	**0.995**	**0.998**	**0.938**
	d + 5	SVR	1.761	1.400	−1262.3	0.426	−857.9
		BPNN	1.773	1.441	0.826	0.957	0.667
		ELM	1.921	1.532	0.800	0.950	0.643
		LSTM	1.742	1.408	0.831	0.958	0.675
		QL-LSTM	**1.533**	**1.203**	**0.882**	**0.968**	**0.687**
	d + 15	SVR	2.396	1.937	−1266.3	0.431	−857.4
		BPNN	2.406	1.926	0.707	0.933	0.537
		ELM	2.508	2.008	0.674	0.925	0.518
		LSTM	2.401	1.918	0.707	**0.934**	0.539
		QL-LSTM	**2.189**	**1.719**	**0.760**	**0.933**	**0.553**

Table 6: The predictive performance with different models at the Fluehli station.

Depth (cm)	Day	Method	RMSE	MAE	NS	WI	LMI
5	d	SVR	0.691	0.549	−1311.5	0.429	−868.5
		BPNN	0.718	0.550	0.942	0.918	0.916
		ELM	0.693	0.538	0.942	0.988	0.918
		LSTM	0.723	0.549	0.941	0.987	0.916
		QL-LSTM	**0.492**	**0.352**	**0.992**	**0.998**	**0.930**
	d + 5	SVR	2.316	1.745	−1266.6	0.431	−851.7
		BPNN	2.297	1.716	0.820	0.955	0.687
		ELM	2.463	1.880	0.799	0.949	0.654
		LSTM	2.291	1.718	0.821	0.956	0.686
		QL-LSTM	**2.084**	**1.526**	**0.872**	**0.966**	**0.698**
	d + 15	SVR	3.023	2.316	−1257.5	0.433	−847.4
		BPNN	**2.801**	**2.099**	**0.769**	**0.937**	**0.584**
		ELM	3.143	2.400	0.694	0.918	0.534
		LSTM	2.971	2.353	0.723	0.922	0.557
		QL-LSTM	2.815	2.165	0.766	0.933	0.570

Table 6: Continued.

Depth (cm)	Day	Method	RMSE	MAE	NS	WI	LMI
10	d	SVR	0.628	0.518	−1310.1	0.428	−870.4
		BPNN	0.635	0.508	0.944	0.988	0.926
		ELM	0.621	0.510	0.944	0.988	0.926
		LSTM	0.610	0.500	0.944	0.988	0.928
		QL-LSTM	**0.381**	**0.286**	**0.995**	**0.998**	**0.941**
	d + 5	SVR	2.043	1.529	−1274.5	0.430	−856.9
		BPNN	2.021	1.510	0.846	0.963	0.721
		ELM	2.153	1.600	0.830	0.958	0.697
		LSTM	**1.777**	1.506	**0.901**	**0.973**	**0.732**
		QL-LSTM	1.794	**1.307**	0.899	0.973	0.732
	d + 15	SVR	2.813	2.143	−1271.7	0.432	−854.43
		BPNN	2.792	2.112	0.738	0.933	0.594
		ELM	2.926	2.300	0.717	0.926	0.558
		LSTM	2.802	2.108	0.736	0.932	0.597
		QL-LSTM	**2.601**	**1.906**	**0.789**	**0.948**	**0.612**
15	d	SVR	0.631	0.506	−1291.9	0.430	−862.9
		BPNN	0.642	0.500	0.943	0.988	0.926
		ELM	**0.407**	0.468	0.944	0.988	0.930
		LSTM	0.618	0.465	0.944	0.988	0.931
		QL-LSTM	0.409	**0.290**	**0.994**	**0.998**	**0.941**
	d + 5	SVR	2.028	1.551	−1269.3	0.429	−853.7
		BPNN	**1.832**	**1.352**	**0.897**	**0.973**	**0.726**
		ELM	2.173	1.638	0.830	0.958	0.691
		LSTM	2.042	1.555	0.846	0.962	0.715
		QL-LSTM	1.835	1.354	0.896	0.972	0.725
	d + 15	SVR	2.771	2.156	−1257.7	0.433	−848.4
		BPNN	2.762	2.134	0.748	0.935	0.595
		ELM	2.802	2.200	0.741	0.931	0.579
		LSTM	2.795	2.112	0.742	0.933	0.597
		QL-LSTM	**2.552**	**1.931**	**0.805**	**0.949**	**0.608**

perform well in some cases probably because the weights of the LSTM model are randomly selected to generate the nonoptimal solution. Meanwhile, our novel loss function (quadruplet loss) is applied based on the LSTM model; it only improved estimation performance to a certain extent against the LSTM model. All in all, the results of our testing on the data of different regions show that the performance of our QL-LSTM model is usually better for T_s prediction with different depths and days.

4. Conclusions

Soil temperature (T_s) is a main physical variable of the land surface, which has an impact on many aspects, such as the growth and yield of crops. Therefore, how to predict T_s accurately is very important. This paper proposed the QL-LSTM model and compared it with the state-of-the-art predictive models to use the meteorological data and past T_s of the Laegern and Fluehli stations (Switzerland) for daily T_s estimation at 5, 10, and 15 cm depth on the 1st, 5th, and 15th days. The experiment results showed that the QL-LSTM model performed better than the existing advanced models for T_s estimation in multifarious cases.

In addition, to enrich processing information in loss function and further improve estimation performance, we attempt to design the novel quadruplet loss function that combines the traditional squared-error loss function with distance metric learning between the sample features. Similar samples can be zoomed and the dissimilar samples can be pushed.

The distance metric learning between the sample features is combined with the squared-error loss function, which could improve the estimation performance to a certain extent. However, the many hyperparameters in our method may cause sensitivity issues in estimation, which may lead to poor generalization ability of other estimations. In the future, the parametric adaptive method will be explored for a new loss function in the follow-up study.

Data Availability

The experimental data are available without any restriction.

Conflicts of Interest

The authors declare that there are no conflicts of interest.

Acknowledgments

This work was sponsored by the National Natural Science Foundation of China (NSFC) under Grant nos. 51805203, 42105144, and U1811464, the Science and Technology Development Plan of Jilin Province (20190201023JC), and the Development and Reform Commission of Jilin Province (2019C054-2).

References

[1] A. Keshavarzi, F. Sarmadian, E. S. E. Omran, and M. Iqbal, "A neural network model for estimating soil phosphorus using terrain analysis," *The Egyptian Journal of Remote Sensing and Space Science*, vol. 18, no. 2, pp. 127–135, 2015.

[2] L. Lai, X. Zhao, L. Jiang et al., "Soil respiration in different agricultural and natural ecosystems in an arid region," *PLoS One*, vol. 7, no. 10, Article ID e48011, 2012.

[3] H. Tabari, P. Hosseinzadeh Talaee, and P. Willems, "Short-term forecasting of soil temperature using artificial neural network," *Meteorological Applications*, vol. 22, no. 3, pp. 576–585, 2014.

[4] W. Wang, K. Akhtar, G. Ren, G. Yang, Y. Feng, and L. Yuan, "Impact of straw management on seasonal soil carbon dioxide emissions, soil water content, and temperature in a semi-arid region of China," *The Science of the Total Environment*, vol. 652, pp. 471–482, 2019.

[5] B. d. O. Silva, M. R. Moitinho, G. A. d. A. Santos, D. D. B. Teixeira, C. Fernandes, and N. La Scala, "Soil CO2 emission and short-term soil pore class distribution after tillage operations," *Soil and Tillage Research*, vol. 186, pp. 224–232, 2019.

[6] S. Mehdizadeh, J. Behmanesh, and K. Khalili, "Evaluating the performance of artificial intelligence methods for estimation of monthly mean soil temperature without using meteorological data," *Environmental Earth Sciences*, vol. 76, no. 8, p. 325, 2017.

[7] L. L. Liang, D. A. Riveros-Iregui, R. E. Emanuel, and B. L. McGlynn, "A simple framework to estimate distributed soil temperature from discrete air temperature measurements in data-scarce regions," *Journal of Geophysical Research: Atmospheres*, vol. 119, no. 2, pp. 407–417, 2014.

[8] Y. Liu, A. H. Weerts, M. Clark et al., "Advancing data assimilation in operational hydrologic forecasting: progresses, challenges, and emerging opportunities," *Hydrology and Earth System Sciences*, vol. 16, no. 10, pp. 3863–3887, 2012.

[9] O. Kisi, M. Tombul, and M. Z. Kermani, "Modeling soil temperatures at different depths by using three different neural computing techniques," *Theoretical and Applied Climatology*, vol. 121, no. 1-2, pp. 377–387, 2015.

[10] H. Tabari, A.-A. Sabziparvar, and M. Ahmadi, "Comparison of artificial neural network and multivariate linear regression methods for estimation of daily soil temperature in an arid region," *Meteorology and Atmospheric Physics*, vol. 110, no. 3-4, pp. 135–142, 2011.

[11] R. Moazenzadeh and B. Mohammadi, "Assessment of bio-inspired metaheuristic optimisation algorithms for estimating soil temperature," *Geoderma*, vol. 353, pp. 152–171, 2019.

[12] M. Delbari, S. Sharifazari, and E. Mohammadi, "Modeling daily soil temperature over diverse climate conditions in Iran—a comparison of multiple linear regression and support vector regression techniques," *Theoretical and Applied Climatology*, vol. 135, no. 3-4, pp. 991–1001, 2019.

[13] Y. Feng, N. Cui, W. Hao, L. Gao, and D. Gong, "Estimation of soil temperature from meteorological data using different machine learning models," *Geoderma*, vol. 338, pp. 67–77, 2019.

[14] H. Sanikhani, R. C. Deo, Z. M. Yaseen, O. Eray, and O. Kisi, "Non-tuned data intelligent model for soil temperature estimation: a new approach," *Geoderma*, vol. 330, pp. 52–64, 2018.

[15] M. Bilgili, "The use of artificial neural networks for forecasting the monthly mean soil temperatures in Adana, Turkey," *Turkish Journal of Agriculture and Forestry*, vol. 35, pp. 83–93, 2011.

[16] O. Kisi, H. Sanikhani, and M. Cobaner, "Soil temperature modeling at different depths using neuro-fuzzy, neural network, and genetic programming techniques," *Theoretical and Applied Climatology*, vol. 129, no. 3-4, pp. 833–848, 2017.

[17] M. Zeynoddin, H. Bonakdari, I. Ebtehaj, F. Esmaeilbeiki, B. Gharabaghi, and D. Zare Haghi, "A reliable linear stochastic daily soil temperature forecast model," *Soil and Tillage Research*, vol. 189, pp. 73–87, 2019.

[18] S. Samadianfard, E. Asadi, S. Jarhan et al., "Wavelet neural networks and gene expression programming models to predict short-term soil temperature at different depths," *Soil and Tillage Research*, vol. 175, pp. 37–50, 2018.

[19] S. Mehdizadeh, F. Fathian, M. J. S. Safari, and A. Khosravi, "Developing novel hybrid models for estimation of daily soil temperature at various depths," *Soil and Tillage Research*, vol. 197, Article ID 104513, 2020.

[20] B. Nahvi, J. Habibi, K. Mohammadi, S. Shamshirband, and O. S. Al Razgan, "Using self-adaptive evolutionary algorithm to improve the performance of an extreme learning machine for estimating soil temperature," *Computers and Electronics in Agriculture*, vol. 124, pp. 150–160, 2016.

[21] S. Hochreiter and J. Schmidhuber, "Long short-term memory," *Neural Computation*, vol. 9, no. 8, pp. 1735–1780, 1997.

[22] J. Guo, Z. Xie, Y. Qin, L. Jia, and Y. Wang, "Short-term abnormal passenger flow prediction based on the fusion of SVR and LSTM," *IEEE Access*, vol. 7, pp. 42946–42955, 2019.

[23] J. Zhang, Y. Zhu, X. Zhang, M. Ye, and J. Yang, "Developing a Long Short-Term Memory (LSTM) based model for predicting water table depth in agricultural areas," *Journal of Hydrology*, vol. 561, pp. 918–929, 2018.

[24] X. Qing and Y. Niu, "Hourly day-ahead solar irradiance prediction using weather forecasts by LSTM," *Energy*, vol. 148, pp. 461–468, 2018.

[25] Q. Li, H. Hao, Y. Zhao et al., "GANs-LSTM model for soil temperature estimation from meteorological: a new approach," *IEEE Access*, vol. 8, pp. 59427–59443, 2020.

[26] Y. Wang, D. Gan, M. Sun, N. Zhang, Z. Lu, and C. Kang, "Probabilistic individual load forecasting using pinball loss guided LSTM," *Applied Energy*, vol. 235, pp. 10–20, 2019.

[27] F. Kratzert, D. Klotz, M. Herrnegger, A. K. Sampson, S. Hochreiter, and G. S. Nearing, "Toward improved predictions in ungauged basins: exploiting the power of machine learning," *Water Resources Research*, vol. 55, no. 12, pp. 11344–11354, 2019.

[28] E. J. Ekpenyong and G. Sunday, "Bayes Estimator of the Shape Parameter of the Burr type XII with generalised squared error and Linex loss functions under some prior distributions," *International Journal of Statistics and Applied Mathematics*, vol. 3, no. 4, pp. 60–64, 2018.

[29] M. Han, "E-Bayesian estimation and its E-MSE under the scaled squared error loss function, for exponential distribution as example," *Communications in Statistics—Simulation and Computation*, vol. 48, no. 6, pp. 1880–1890, 2019.

[30] L. Fan, H. Zhao, and H. Zhao, "Distribution consistency loss for large-scale remote sensing image retrieval," *Remote Sensing*, vol. 12, no. 1, p. 175, 2020.

[31] Q. Li, R. Xu, H. Zhao, L. Xu, X. Shan, and P. Gong, "Computer-aided diagnosis of mammographic masses using local geometric constraint image retrieval," *Optik*, vol. 171, pp. 757–767, 2018.

[32] L. Fan, H. Zhao, H. Zhao, P. Liu, and H. Hu, "Image retrieval based on learning to rank and multiple loss," *ISPRS International Journal of Geo-Information*, vol. 8, no. 9, p. 393, 2019.

[33] A. Hermans, L. Beyer, and B. Leibe, "In Defense of the triplet loss for person Re-identification. Computer vision and pattern recognition (CVPR)," 2017, https://arxiv.org/abs/1703.07737.
[34] T. Zhang, R. Ramakrishnan, and M. Livny, "A new data clustering algorithm and its applications," *Data Mining and Knowledge Discovery*, vol. 1, no. 2, pp. 141–182, 1997.
[35] H. Zhao, Q. Li, and P. Liu, "Hierarchical geometry verification via maximum entropy saliency in image retrieval," *Entropy*, vol. 16, no. 7, pp. 3848–3865, 2014.
[36] R. Xu, J. Xu, and D. C. Wunsch, "A comparison study of validity indices on swarm-intelligence-based clustering," *IEEE Transactions on Systems Man & Cybernetics Part B*, vol. 42, no. 4, pp. 1243–1255, 2014.
[37] F. Schro, D. Kalenichenko, and J. Philbin, "A unified embedding for face recognition and clustering," in *Proceedings of the IEEE Conference on Computer Vision and Pattern Recognition (CVPR)*, pp. 815–823, Boston, MA, USA, June 2015.
[38] H. Liu, J. Cheng, and F. Wang, "Sequential subspace clustering via temporal smoothness for sequential data segmentation," *IEEE Transactions on Image Processing*, vol. 27, no. 2, pp. 866–878, 2018.
[39] K. Judd and M. Small, "Towards long-term prediction," *Physica D: Nonlinear Phenomena*, vol. 136, no. 1-2, pp. 31–44, 2000.

Hindawi
Computational Intelligence and Neuroscience
Volume 2023, Article ID 9756573, 1 page
https://doi.org/10.1155/2023/9756573

Retraction

Retracted: Sports Video Athlete Detection Based on Associative Memory Neural Network

Computational Intelligence and Neuroscience

Received 26 September 2023; Accepted 26 September 2023; Published 27 September 2023

This article has been retracted by Hindawi following an investigation undertaken by the publisher [1]. This investigation has uncovered evidence of one or more of the following indicators of systematic manipulation of the publication process:

(1) Discrepancies in scope
(2) Discrepancies in the description of the research reported
(3) Discrepancies between the availability of data and the research described
(4) Inappropriate citations
(5) Incoherent, meaningless and/or irrelevant content included in the article
(6) Peer-review manipulation

The presence of these indicators undermines our confidence in the integrity of the article's content and we cannot, therefore, vouch for its reliability. Please note that this notice is intended solely to alert readers that the content of this article is unreliable. We have not investigated whether authors were aware of or involved in the systematic manipulation of the publication process.

Wiley and Hindawi regrets that the usual quality checks did not identify these issues before publication and have since put additional measures in place to safeguard research integrity.

We wish to credit our own Research Integrity and Research Publishing teams and anonymous and named external researchers and research integrity experts for contributing to this investigation.

The corresponding author, as the representative of all authors, has been given the opportunity to register their agreement or disagreement to this retraction. We have kept a record of any response received.

References

[1] J. Yang, "Sports Video Athlete Detection Based on Associative Memory Neural Network," *Computational Intelligence and Neuroscience*, vol. 2022, Article ID 6986831, 9 pages, 2022.

Hindawi
Computational Intelligence and Neuroscience
Volume 2022, Article ID 6986831, 9 pages
https://doi.org/10.1155/2022/6986831

Research Article

Sports Video Athlete Detection Based on Associative Memory Neural Network

Jingwei Yang [1,2]

[1]*School of Physical Education, Xinyang Normal University, Xinyang 464000, China*
[2]*School of Physical Education, Central China Normal University, Wuhan 430079, China*

Correspondence should be addressed to Jingwei Yang; yjw@xynu.edu.cn

Received 30 December 2021; Revised 17 January 2022; Accepted 18 January 2022; Published 15 February 2022

Academic Editor: Xin Ning

Aiming at the detection of athletes in sports videos, an automatic detection method based on AMNN is proposed. The background image from the image sequence is obtained, the moving area is extracted, and the color information of pixels to extract the green stadium from the background image is used. In order to improve the accuracy of athletes' detection, the texture similarity measurement method is used to eliminate the shadow in the movement area, the morphological method is used to eliminate the cracks in the area, and the noise outside the stadium is removed according to the stadium information. Combined with the images of nonathletes, a training set is constructed to train the NN classifier. For the input image frames, image pyramids of different scales are constructed by subsampling and the positions of several candidate athletes are detected by NN. The center of gravity of candidate athletes is calculated, a representative candidate athlete is obtained, and then, the final athlete position through a local search process is determined. Experiments show that the system can accurately detect the motion shape of moving targets, can process images in real time, and has good real-time performance.

1. Introduction

Detecting and tracking athletes in sports videos can provide important information for high-level sports video processing, such as motion analysis, event detection, and 3D reconstruction [1, 2]. Attaching various sensors to athletes and then acquiring data through sensors are the traditional method of detecting and tracking athletes. These methods, on the other hand, place additional constraints on athletes and have a negative impact on their normal performance [3]. As a contactless method, the video-based athlete detection and tracking method developed in recent years have been widely studied and applied [4].

It is of great significance to detect and track athletes in sports videos, which is conducive to various higher-level processing of videos, such as adding automatic explanation function to videos, quick retrieval of important events in videos, and tactical analysis of videos [5, 6]. Moving target detection and tracking mainly involve the knowledge of image processing, pattern recognition, computer vision, artificial intelligence, and other disciplines, in many fields. For example, human-computer interaction, video surveillance, traffic management, and content-based video retrieval have wide application prospects and potential economic value [7]. Therefore, researchers have been inspired to do a lot of research on it, and many different methods have been put forward. Another important direction in sports video analysis is the detection of exciting events. Segmentation and tracking of sports videos can assist the detection of exciting events, as well as semantic and strategic analysis. We can judge the detection of some specific events through target detection and tracking analysis. In this paper, the neural network (NN) technology [8, 9] with associative memory (AM) function is studied. And, a sports video athlete detection model has been put forward based on associative memory neural network (AMNN).

Digital video technology has been developed and popularized in tandem with scientific and technological advancements. It is now possible to obtain various types of videos through various channels, thanks to increased network transmission bandwidth and lower costs of various hardware devices [10]. Computers can now execute various complex algorithms, thanks to increasing storage capacity and computing power [11]. These technological and equipment advancements lay the groundwork for future image processing and video analysis systems research and development. The focus of these people's attention to sports video also focuses on sports targets, balls, or players. Detecting athletes' areas in sports videos is the premise of tracking athletes [12]. The application based on AMNN can extract athletes' trajectory and other information from the game video, which can help coaches analyze players' behaviors and study opponents' strategies and weaknesses. Based on the analysis of the current main moving target detection and tracking algorithms, this paper focuses on the methods of detecting and tracking athletes in sports videos and improves the traditional moving target detection and tracking algorithms. Aiming at the characteristic that AMNN is easy to fall into local minimum, particle swarm optimization is introduced to optimize the network weights, and a network with high convergence performance is obtained. A prototype system is developed to verify the effectiveness of the algorithm.

2. Related Work

The athlete detection algorithm based on middle-level feature blocks and the athlete segmentation algorithm based on superpixel classification are realized in the literature [13, 14] based on a detailed analysis and summary of the characteristics of sports videos and related rules. The literature [15] proposed a method for detecting the stadium area by obtaining the stadium's adaptive color. A method to automatically extract the venue color in sports videos was proposed in the literature [16, 17]. It uses a Gaussian mixture model to calculate the parameters with an algorithm, which is different from previous studies, and the experiment is similar to the previous one. The Kalman filter models each pixel and tracks its change in the literature [18, 19]. This method can handle scene lighting changes, but it becomes invalid when new objects are added to the scene or the original objects are removed. For the detection of multiscale athletes in sports videos, literature [20] proposes an automatic detection method based on CNN. The literature [21] describes the function realization and concept of AM in detail, as well as the drawbacks of having to use a binary input signal in practice. By combining the advantages of strong nonlinear processing of BP networks with the advantages of fitting the network structure reasonably, the network structure can be widely used in practice. The dynamic method based on prediction is used to model the dynamic scene in literature [22, 23]. This method can deal better with light changes and subtle movements in the scene, such as water waves and branches swinging, but it requires a large number of images without moving objects to train the model. A key pose extraction system for weightlifting video was designed by literature [24]. A display module and a key frame extraction module are included in the system. The key frame extraction module includes feature extraction and key frame extraction of weightlifting video frames, while the display module includes video playback and key frame display. Literature [25] uses the Gaussian mixture model to model every pixel in the scene and updates the model in real time by the online approximation method, which can reliably deal with the situation of illumination change and disturbance of chaotic motion in the scene. At present, the commonly used tracking methods include model-based tracking, region-based tracking, and feature-based tracking. Literature [26] studied discrete Hopfield NN and discussed the structure and the theory of convergence stability in detail. The continuous adaptive mean shift algorithm proposed in literature [27] uses the color features of objects to track irregularly moving nonrigid objects in video frame sequence quickly and robustly. Literature [28] uses the combination of adaptive Gaussian mixture model and CamShift algorithm to detect and track players in badminton video. In this paper, a method of moving object detection in sports video based on the AMNN model is proposed. The experiment shows that the system can accurately detect the motion shape of moving targets, process images in real time, and has good real-time performance.

3. Methodology

3.1. AMNN. Artificial neural network (ANN) is an information processing system that simulates the structure and function of a simplified biological NN and abstractly utilizes some basic characteristic theories. This network receives external information through vision [29], smell, and taste, processes it in the brain, and then outputs signals through the executive organs, thereby forming a system with the characteristics of a closed-loop control system.

Humans can study ANN in the same way they can study the various functions of the human brain. Distributed storage and fault tolerance, large-scale parallel processing capabilities, self-learning, self-organization and adaptability, and the ability to handle complex systems are all features of ANN [30]. AM is a key component of NN theory, as well as a key function of NN in intelligent control, pattern recognition, and artificial intelligence. It primarily makes use of NN's high fault tolerance, which allows it to reconstruct incomplete, defaced, and distorted input samples into a complete prototype suitable for identification, classification, and other purposes.

The Hopfield network, also referred to as the AM network, is a type of computer network. Hopfield network is a typical single-layer feedback NN, with rich dynamic behavior, simple structure, and higher computing power when compared to other networks. A discrete-time system is a discrete Hopfield neural network (DHNN). A weighted undirected graph can be used to show it. Every node has a threshold, and each side of the graph has a weight. The graph's order corresponds to the network's order. As a standard network for classification tasks, NN will typically add a fully connected layer and a classifier to the final layer. During the training process, a dropout operation is added to the fully connected layer to prevent overfitting, and the output value of the node is randomly set to 0 to prevent overfitting. Although this slows down training, it effectively prevents overtraining. The basic structure of the Hopfield network is shown in Figure 1.

The network weakens the false state by adding an additional attractor to improve the fault tolerance of the network. Because one of the fundamental problems of Hopfield is that in addition to the existence of attractors with memory samples, there are also "redundant" stable states, that is, the existence of pseudo-states. The existence of pseudo-states affects Hopfield's fault tolerance. If the pseudo-states can be reduced or even eliminated, the attraction domain of the state can improve the fault tolerance of Hopfield and increase the memory capacity. Because the neurons in the Hopfield network are connected to each other, this fully interconnected way makes the output of each neuron in the network feedback to the input of other neurons at the same level, so the network has no other external input. Under these circumstances, it can also enter a stable state.

The learning process of DHNN, like that of other NNs, is the formation of a network connection weight matrix. Hopfield is a constantly changing system. Once the network's connection weight matrix is learned and formed, as long as a specific pattern sample is input, the network will continue to evolve until the system reaches the state space's steady state. This steady state is the network's output state, or the input vector's associative memory output. After the network has been trained, it can be run with an initial input X to determine the network's initial output state. This state is fed back to the input terminal and used as the input signal for the network processing stage's next iteration. Because the network takes a certain amount of time to transmit and process information, the two input signals may differ before and after the new input gives birth to the next output. The network's operation process, or the repeated feedback process, is an example of such a cycle. If the network is stable, the change in the output state of the network will decrease as the network runs with multiple feedbacks until it no longer changes and reaches a steady state.

3.2. Detection and Tracking of Moving Objects in Sports Videos. The so-called moving target tracking is to detect each independently moving target or region of interest to users in each frame of images and locate these targets or regions in subsequent frames. In practical application, tracking the moving target is very important. By tracking the moving target, we can get its motion parameters, such as position, velocity, and acceleration, which not only helps to calculate the motion trajectory of the moving target but also provides a reliable data source for the motion analysis and scene analysis of the target in the scene. Sports videos have different characteristics of different lens types, which can provide prior knowledge for video content analysis. The video is divided into shot sequences by shot boundary detection, and the types of shots are detected; that is, the shots are divided into short shots, medium shots, and long shots. This series of processing before athlete detection and segmentation is called video preprocessing. The athlete detection process is shown in Figure 2.

There are three commonly used algorithms in motion detection research: interframe difference, background subtraction, and optical flow. The difference between the current frame and the previous frame image is calculated using the interframe difference method, which is suitable for a dynamically changing environment. However, it only extracts the part of the logo that moves in relation to the background; it is not a fully moving object. The optical flow method is used to detect the application logo's changing optical flow characteristics over time. Its advantage is that it can detect moving objects independently without prior knowledge of the scene, and it can be used while the camera is moving. The disadvantage is that the calculation is time-consuming and difficult. Real-time detection is difficult to achieve without the necessary hardware support. Background subtraction is the most common technique for separating moving objects from a scene, particularly when the scene is relatively stable. The background subtraction method's main idea is to compare the current image to the background image by using a reference image that represents the background. If there are differences in pixel features, pixel area features, or other features in the same position, these are motion areas, which may correspond to actual moving targets.

Before detecting and identifying the image, it is necessary to preprocess the image, try to eliminate the noise, improve the image quality, protect the trade information, reduce the calculation amount of subsequent processing, and improve the accuracy of processing. There are strong rules in shooting and editing techniques in sports videos, and the characteristics of different shots and the differences between different shots are obvious. In the telephoto lens, the competition field occupies the largest proportion, and the athletes are also concentrated on the competition field, so the competition field area is detected first, and after the athletes are detected, more accurate athletes can be obtained by using the uniform color of the sports field and removing the color of the sports field. In the middle shot, the field color still occupies a certain proportion in the image, and if the telephoto scene has been processed, the stored ground color is used to remove the nonathlete area of the image of the middle shot that belongs to the competition field part.

In order to achieve an accurate positioning effect, a local search process is performed on the area around the center of each candidate athlete in the image scale space. In the image scale space, a small search space focused on the position of the candidate athlete is defined, which corresponds to a small pyramid focused on the center of the candidate athlete. The pyramid covers a scale from 0.8 to 1.5 times the size of the candidate athlete. For each scale, the candidate athlete is marked with a 16×16 pixel grid around the center of the candidate athlete. Mutual information can measure the similarity between two things. If two things are more similar, the mutual information between them will be smaller; otherwise, it will be larger. For shots, the frame images inside a shot are very similar, but the frame images between different shots are quite different. Therefore, mutual information is considered to measure the similarity between two frames.

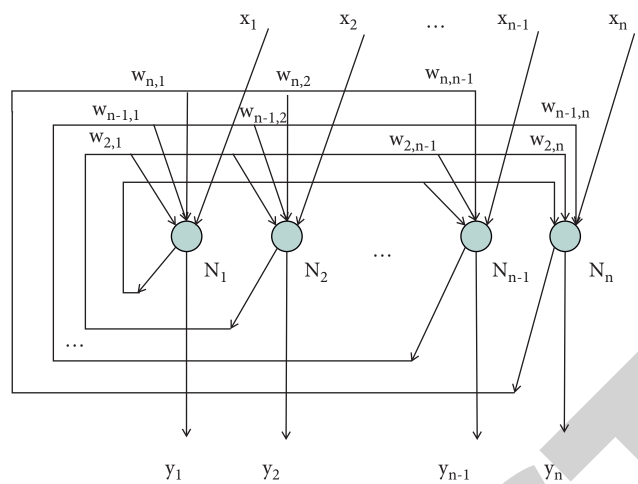

Figure 1: Basic structure of the Hopfield network.

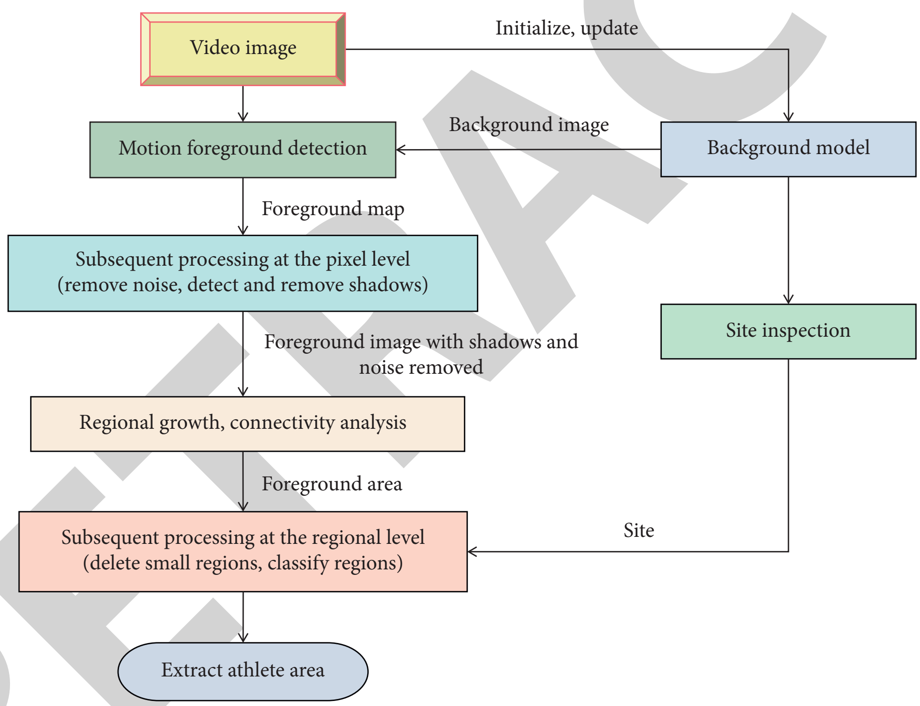

Figure 2: Athlete detection process.

3.3. Construction of the Detection Model Based on AMNN. The model-based tracking method models the shape characteristics of the target object and then tracks the model in the image sequence. The extraction of moving targets, that is, on the basis of existing images, extracts the required foreground targets through image segmentation.

Because an object is sometimes not a whole after image segmentation, it will be divided into several parts, or an object will be divided into several close independent areas. This paper makes a copy of the segmented image, expands it, and then assigns a number to it. If the areas after the expansion are connected to form a whole, they are identified as a whole, and the whole is marked as a region to be detected on the original image. The tracking accuracy of a model-based tracking method is dependent on the accuracy of the target object's geometric model. The main state transformations for a rigid moving target during movement are translation, rotation, and so on. When tracking a moving target, this method can produce better results.

Suppose a group composed of M particles flies at a certain speed in the n-dimensional search space, and the state attributes of particle i in the t-th iteration are set as follows:

Location:

$$\begin{aligned} X_i^t &= \left(x_{i1}^t, x_{i2}^t, \ldots, x_{in}^t\right), \\ x_{in}^t &\in \left[L_n, U_n\right]. \end{aligned} \tag{1}$$

L_n and U_n are the lower limit and upper limit of the search space, respectively.

Speed:

$$\begin{aligned} V_i^t &= \left(v_{i1}^t, v_{i2}^t, \ldots, v_{in}^t\right), \\ v_{in}^t &\in \left[v_{\min,n}, v_{\max,n}\right], \end{aligned} \tag{2}$$

where $v_{\min,n}$ and $v_{\max,n}$ are the minimum and maximum speeds, respectively.

Individual optimal position:

$$P_i^t = \left(p_{i1}^t, p_{i2}^t, \ldots, p_{in}^t\right). \tag{3}$$

Global optimal position:

$$P_g^t = \left(p_{g1}^t, p_{g2}^t, \ldots, p_{gn}^t\right). \tag{4}$$

Here, $1 \le i \le M$. With the above definition, the iterative formula of the algorithm can be described as follows:

$$\begin{aligned} v_{in}^{t+1} &= w v_{in}^t + c_1 r_1 \left(p_{in}^t - x_{in}^t\right) + c_2 r_2 \left(p_{gn}^t - x_{in}^t\right), \\ x_{in}^{t+1} &= x_{in}^t + v_{in}^{t+1}. \end{aligned} \tag{5}$$

Here, r_1, r_2 is a random number between (0, 1). c_1, c_2 is the acceleration factor. w is called the inertia weight, which determines how much the particle inherits to the current velocity. Appropriate value helps to balance search ability and development ability, and usually, a linear decrease method from 0.9 to 0.4 is used. The linear decreasing formula is

$$w = w_{\text{start}} - \frac{w_{\text{start}} - w_{\text{end}}}{t_{\max}} \times t, \tag{6}$$

where$t_{\max}$ is the maximum number of iterations; t is the current iteration number; w_{start} is the initial inertia weight; and w_{end} is the termination inertia weight.

Because the selection of threshold can't make all video frames have a better segmentation effect, when this paper intercepts the region of interest, more background information will be mistakenly regarded as foreground information. Mapping the detected pixel points of candidate athletes into the input image, the candidate athletes are grouped according to their distance in the image and scale space. Each group of candidate athletes is fused into a representative candidate athlete, whose center and size are the average of the center and size of each candidate athlete in this group. After the grouping algorithm is applied, a representative set of candidate athletes is obtained, which is used as the basis for accurately locating athletes and eliminating false positives in the next stage of the algorithm.

Occlusion between athletes and other objects is common in sports videos. In some videos, for example, athletes are blocked by the net, and there are various types of motion disturbances, as well as shadows. Because of the complexity of sports video, the detected motion foreground map frequently contains a lot of noise or has gaps in the motion area. To extract the athlete area more precisely in subsequent processing, the foreground image must be processed at the pixel level, removing noise, filling gaps, and eliminating shadows. Pixels are divided into boundary points and nonboundary points, with boundary points being classified as brighter or darker depending on the brightness of their surroundings. The gray level corresponding to the highest peak in the two histograms is used as the threshold, and the gray level corresponding to the highest peak in the two histograms is used as the histogram. This method is recursively applied to image system points whose gray levels are higher or lower than this threshold until a predetermined threshold number is obtained. In the iterative process, the centroid (x_c, y_c) of window w is as follows:

$$\begin{aligned} x_c &= \frac{\sum_{x\in w}\sum_{y\in w} xP(x, y)}{\sum_{x\in w}\sum_{y\in w} P(x, y)}, \\ y_c &= \frac{\sum_{x\in w}\sum_{y\in w} yP(x, y)}{\sum_{x\in w}\sum_{y\in w} P(x, y)}. \end{aligned} \tag{7}$$

Resize the window to

$$s = 2 \times \sqrt{\frac{\sum_{x\in w}\sum_{y\in w} P(x, y)}{256}}. \tag{8}$$

If only a fixed global threshold is used to segment the entire image when there are some situations in the image, such as shadows, uneven illumination, different contrasts in different places, sudden noise, and changes in background gray level, the segmentation effect will be affected because the situations in different parts of the image cannot be taken into account. To segment each part of the image separately, one option is to use a set of thresholds related to pixel positions. Athlete detection results based on middle-level feature blocks can provide polygonal areas of athletes in addition to rectangular box representation. To obtain more accurate segmentation results, the relationship between polygon domain representation and athlete contour is combined, using superpixels as the basic unit, marking the classification of superpixels according to the overlapping ratio of superpixels and polygon regions, and using the marking information and rectangular frames as interactive information.

4. Results Analysis and Discussion

In sports videos, athletes' movements are irregular, and their postures will change in various ways. The colors of athletes and scenes may be similar, and there is often mutual occlusion between athletes. In this paper, the obtained video is converted into a frame-by-frame video stream image as the system input. The system detects the input image, and if it is the first frame image, the image as the background is preprocessed and initialized the background model. Then, it is judged whether the input image is the second frame image, and if it is the second frame image, the image is preprocessed. The experimental results are shown in Figure 3.

Expansion is the process of merging the reasonable area in contact with the edge of an object into the object and expanding the boundary outward. If the number of expansions is too small, the lines forming the capture area are too thin to cover all possible ranges of soldiers, resulting in missing capture. If the expansion times are too large and the lines forming the capture area are too thick, the range of the capture area will be too large, which will increase the number of pixels searching for nonzero gray values and slow down the running speed of the algorithm. In further experiments, the detection speed of moving targets by different methods is compared, and the results shown in Figure 4 are obtained.

Noise and light sources often affect the sample points around the players, reducing their reliability. The farther away from the center of the athlete's area, the lower the pixel's reliability, and the greater the chance that the pixel is covered by other objects or belongs to the background. As a result, when calculating the histogram of the athlete area, it is reasonable to give different weights to pixels at different positions in the athlete area. The greater the weight corresponding to the pixel, the closer it is to the region's center, and vice versa. When the same video sequence is fast-forwarded at 4x speed under different quantization parameters, Figure 5 compares the number of transmission bits required by this method and the traditional method.

Even in the case of occlusion, the head of the human body still has obvious characteristics, so it is possible to divide multiple human bodies that are stuck or occluded into a single human body according to the characteristics of the head of the human body. Figure 6 is a comparison result of moving object segmentation results by different threshold processing methods.

There is a lot of foreground noise in the picture, which will have a great influence on the detection results. Because the moving target is blocky and has a moving rule, the foreground noise appears sporadically, and the position is random. In the following moving target tracking algorithm, the foreground noise can be removed according to these features to get the accurate moving target.

We can compare the textures of the corresponding areas in the foreground area and the background image and judge whether the foreground area is a shadow or a real moving target according to the similarity of the textures. The verification of the detection range is extracted from the position coordinates of the correct moving target in the detection result, as shown in Figure 7.

It can be seen that this method is superior to the other two methods in detecting athletes in sports video. The other two methods and this method are also used to detect athletes. The comparison results of interference handling capabilities of these three methods are shown in Figure 8.

As can be seen from the data in Figure 8, this method has the best interference handling ability. This method provides a better tracking effect while also achieving the desired result. To fully realize the detection of moving targets, a frame of the system's input image will first undergo image

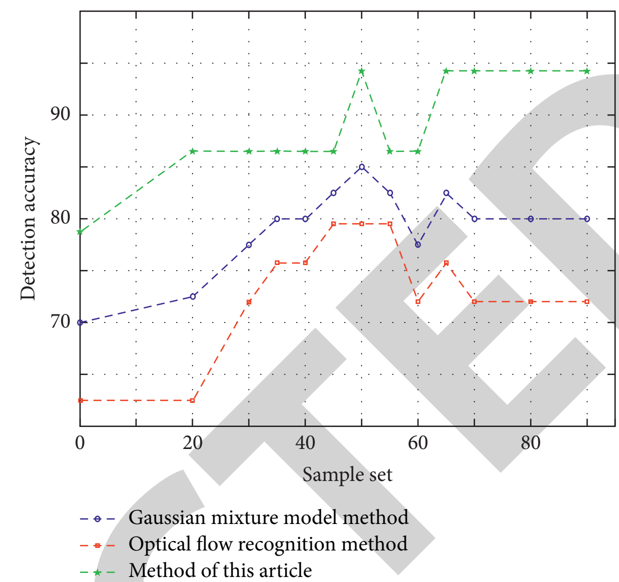

Figure 3: Comparison of detection accuracy of three methods.

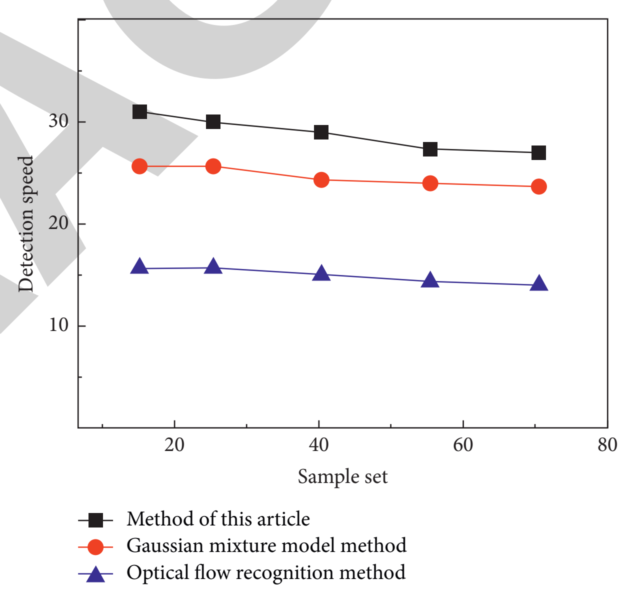

Figure 4: Comparison of detection speed of three methods.

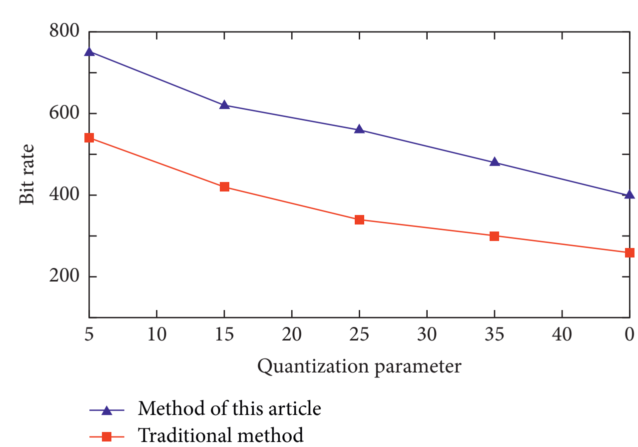

Figure 5: Comparison of the number of bits to be transmitted in double-speed fast forward.

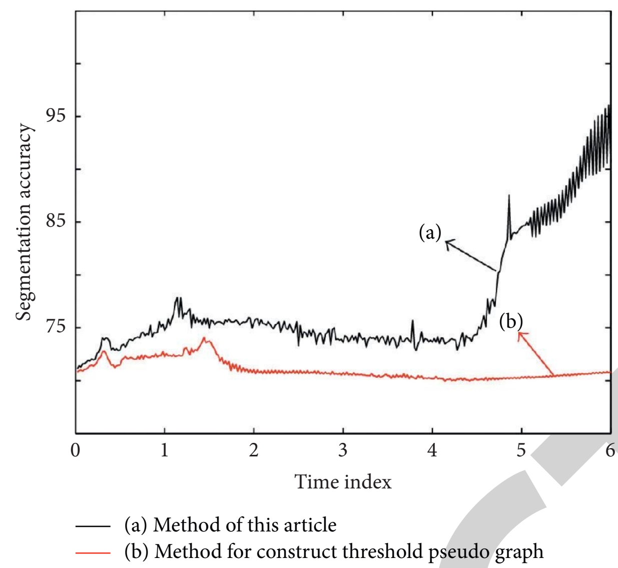

Figure 6: Comparison of segmentation results of moving objects by different threshold processing methods.

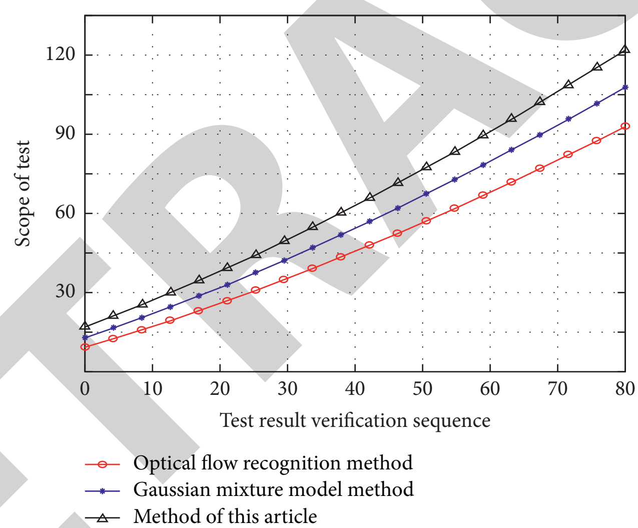

Figure 7: Verification results of the detection range of several methods.

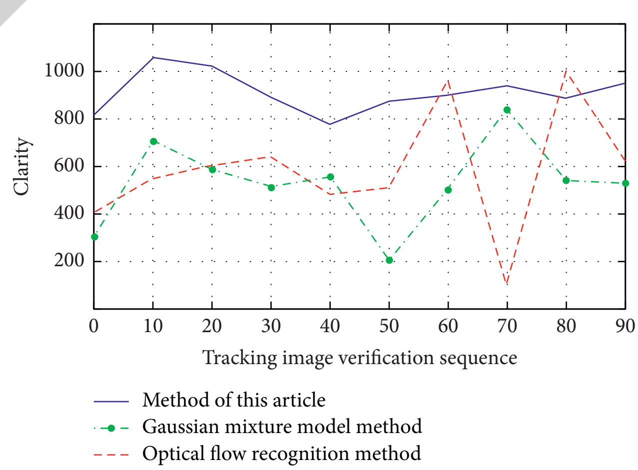

Figure 8: Interference handling ability verification result.

scale transformation, filtering, and denoising through image preprocessing and then undergo the steps of image binarization, morphological processing, target edge detection, and so on. Finally, the blocks in the tracking area are merged based on adjacency and similarity, and a unified gray value is assigned, revealing the moving target's detected shape. Experiments show that the system can detect the motion shape of moving targets with high accuracy, process images in real time, and perform well in real time.

5. Conclusions

Motion detection and tracking are difficult fields of study. In this field, researchers have done a lot of work and have made some breakthroughs in theory and application. The key step in analyzing and processing sports videos is detecting and tracking athletes. This paper focuses on the methods of detecting and tracking athletes in sports videos, based on an analysis of the current commonly used methods of detecting and tracking moving targets. This paper proposes an AMNN-based method for moving object detection in sports video that takes full advantage of various technologies and processing means and outperforms previous inspection models. To address the issue of the model's learning rate being too slow in the early stages, the model's updating method has been improved, and the learning rate has been accelerated. The detection method used in this paper is more capable of dealing with slow changes in illumination in a dynamic background. Furthermore, different lens types in sports videos have distinct characteristics, and athletes who use the same lens type compete under the same set of rules. This paper summarizes these traits and rules and employs a middle-level feature block classifier to distinguish between different lens types and train different athletes to detect athletes in the video. Simulation experiments back up the method presented in this paper. The results show that the method presented in this paper has a wide detection range and strong interference processing ability. This scheme has a high rate of detection.

Data Availability

The data used to support the findings of this study are included within the article.

Conflicts of Interest

The author declares no conflicts of interest.

References

[1] C. Aouiti, R. Sakthivel, and F. Touati, "Global dissipativity of high-order Hopfield bidirectional associative memory neural networks with mixed delays," *Neural Computing & Applications*, vol. 32, no. 14, pp. 10183–10197, 2020.

[2] M. S. M'Hamdi, "Pseudo almost automorphic solutions for multidirectional associative memory neural network with mixed delays," *Neural Processing Letters*, vol. 49, no. 3, pp. 1567–1592, 2019.

[3] K. Woosuk and K. Myunggyu, "On-line detection and segmentation of sports motions using a wearable sensor," *Sensors*, vol. 18, no. 3, p. 913, 2018.

[4] T. Guo, L. Wang, and M. Zhou, "A multi-layer memristive recurrent neural network for solving static and dynamic image associative memory," *Neurocomputing*, vol. 334, no. 3, pp. 35–43, 2019.

[5] H. Liang, "Evaluation of fitness state of sports training based on self-organizing neural network," *Neural Computing & Applications*, vol. 33, no. 9, pp. 3953–3965, 2021.

[6] C. Aouiti and E. A. Assali, "Stability analysis for a class of impulsive bidirectional associative memory (BAM) neural networks with distributed delays and leakage time-varying delays," *Neural Processing Letters*, vol. 50, no. 1, pp. 851–885, 2019.

[7] N. Abdo, "Video detection in remote desktop protocols," *Journal of Luminescence*, vol. 109, no. 3, pp. 155–162, 2016.

[8] W. Cai, Z. Wei, Y. Song, M. Li, and X. Yang, "Residual-capsule networks with threshold convolution for segmentation of wheat plantation rows in UAV images," *Multimedia Tools and Applications*, vol. 80, no. 21, pp. 32131–32147, 2021.

[9] Y. Tong, L. Yu, S. Li, J. Liu, H. Qin, and W. Li, "Polynomial fitting algorithm based on neural network," *ASP Transactions on Pattern Recognition and Intelligent Systems*, vol. 1, no. 1, pp. 32–39, 2021.

[10] C. Yuan, Y. Yang, and Y. Liu, "Sports decision-making model based on data mining and neural network," *Neural Computing & Applications*, vol. 33, no. 9, pp. 3911–3924, 2020.

[11] Y. Yuan, Z. Xiong, and Q. Wang, "An incremental framework for video-based traffic sign detection, tracking, and recognition," *IEEE Transactions on Intelligent Transportation Systems*, vol. 18, no. 7, pp. 1918–1929, 2017.

[12] R. Chi, Z. M. Lu, and Q. G. Ji, "Real-time multi-feature based fire flame detection in video," *IET Image Processing*, vol. 11, no. 1, pp. 31–37, 2017.

[13] X. Li, D. Ding, J. Feng, and S. Hu, "Existence and exponential stability of anti-periodic solutions for interval general bidirectional associative memory neural networks with multiple delays," *Advances in Difference Equations*, vol. 2016, no. 1, p. 190, 2016.

[14] L. Wu and H. Li, "Risk assessment of extreme rainfall climate change and sports stadium sports based on video summarization algorithm[J]," *Arabian Journal of Geosciences*, vol. 14, no. 16, p. 1661, 2021.

[15] W. He and L. Chu, "Exponential stability criteria for fuzzy bidirectional associative memory Cohen-Grossberg neural networks with mixed delays and impulses," *Advances in Difference Equations*, vol. 2017, no. 1, p. 61, 2017.

[16] P. Halén and K. M. Khan, "Finland's sports physiotherapy conference—athlete training and loading: helsinki 7–8 June 2019," *British Journal of Sports Medicine*, vol. 53, no. 3, pp. 137-138, 2019.

[17] E. A. Wilde, M. Newsome, S. D. Ott et al., "Persistent disruption of brain connectivity after sports-related concussion in a female athlete," *Journal of Neurotrauma*, vol. 36, no. 22, pp. 3164–3171, 2019.

[18] W. Wang, Y. Sun, M. Yuan et al., "Projective synchronization of memristive multidirectional associative memory neural networks via self-triggered impulsive control and its application to image protection," *Chaos, Solitons & Fractals*, vol. 150, no. 1, Article ID 111110, 2021.

[19] B. B. Forster, "Sports imaging: radiologists as team leaders in care of the athlete," *Radiology*, vol. 278, no. 2, pp. 313-314, 2016.

Hindawi
Computational Intelligence and Neuroscience
Volume 2022, Article ID 9274098, 9 pages
https://doi.org/10.1155/2022/9274098

Research Article

Music Choreography Algorithm Based on Feature Matching and Fragment Segmentation

Zhigang Wang

School of Music and Dance, Guangzhou University, Guangzhou 510006, Guangdong, China

Correspondence should be addressed to Zhigang Wang; ywwangzhigang@gzhu.edu.cn

Received 21 December 2021; Revised 17 January 2022; Accepted 18 January 2022; Published 12 February 2022

Academic Editor: Xin Ning

Choreography is an art form in and of itself. Because music and dance have always appeared at the same time throughout human history, music has had a significant influence on dance arrangement. It is important to arrange appropriate dance movements based on the music pieces chosen by users when creating choreography. This paper proposes a mixed density network-based music choreography algorithm in response to the current state of music choreography. The algorithm should be able to convert motion and music signals into a high-level semantic meaning that is compatible with human cognition, compare the degree of matching, and arrange the dance based on the music and motion segments that match. Furthermore, the consistency and authenticity of the movements in the dance created in this paper have been improved. Users' subjective feedback indicates that the choreography results in this paper are more closely aligned with the music. In the field of music choreography, it has some practical utility.

1. Introduction

Dance with music, as a form of artistic expression, enriches people's cultural lives and stimulates the public's creative enthusiasm [1]. It is the heart and soul of both music and dance. The most common variation is that the dance form changes as the music changes. The information of the music theme is conveyed through various forms of dance. Dance action matching technique in music choreography [2] is a type of dance work that is determined by the music style. People's matching effect of music and dance in modern music choreography requires strong synchronization between music changes and dance movements, as well as a deep understanding and strong grasp of music [3, 4]. In computer choreography, two major issues must be addressed. First, without using motion capture or manual production, how can you get real and unique dance moves? Second, how to improve the synchronization of music and dance by using appropriate music and motion features and matching algorithms.

As we all know, the element of music that appeals to individuals the most is "rhythm." We can see from the evolution of music in various countries that, even if the language is absurd, people in various countries will express their personal feelings through the rhythm of music [5]. As a result, it can be said that "music rhythm" has become a universal element. We pay more attention to rhythm than ever before, especially with the development of modern music [6]. Movement and rhythm are two essential core requirements in the process of music development, starting from the very beginning. In the fields of choreography and score, the matching of movements and music pieces is widely used [7]. It is necessary to arrange appropriate dance movements according to the music pieces chosen by users in choreography; it is also necessary to create appropriate background music for the dance actions chosen by users in score creation [8]. Action and music, on the other hand, are time series signals from two different perceptual channels. It is necessary to establish a reasonable action-music feature matching model [9] in order to properly evaluate the degree of matching between them. In light of this, this paper proposes a mixed density network-based music choreography model.

Dance is a form of performing art in which the main means of expression is rhythmic movements accompanied by music [10]. It necessitates a good sense of movement control and balance, accurate timing and rhythm, a rich imagination, and high aesthetic quality because it involves complex sensory and cognitive processes. In music and dance, the phenomenon of alternating strength and length is known as "rhythm" [11]. Humans can perceive human walking gait, strength, and action rhythm, as well as musical characteristics such as tone, pitch, timbre, and musical rhythm of note duration. The most easily perceived feature by the audience is rhythm, which is a common feature of dance and music, according to research. Animators manually establish the matching model of action and music in the traditional animation creation process. Animators must frequently create and listen to different music for the soundtrack and then manually select the music segment that best matches the given dance action segment. This is a time-consuming and tedious task. Based on the foregoing, this paper proposes a hybrid density network-based automatic music choreography algorithm. The algorithm uses a deep learning (DL) algorithm [12, 13] to train the model, which can automatically and intelligently generate dance actions that meet the expectations in combination with screening conditions, based on a large amount of existing music and dance data. Also, according to the established matching relationship, effectively store, retrieve, and edit the dance data. This algorithm can generate unique and imaginative dance movements, which is extremely useful.

2. Related Work

Based on genetic theory, literature [14] proposed an optimization method for matching dance technical movements to music. This method's correspondence can effectively show synchronization of music and dance movements, but it has some drawbacks, such as a time-consuming and tedious calculation process. Based on music emotion and sports style, literature [15] created a matching model of motion and music features. The choreography process is primarily driven by the rhythm of music and movements, as well as the correlation of density characteristics, according to literature [16]. By preconstructing an action graph to search for candidate actions, literature [17] improved the search efficiency of the choreography system. Literature [18] used an artificial neural network to create a motion-music matching model and to automate the creation of gesture animation based on music. A method of synthesizing dance movements was proposed and introduced in literature [19]. Manually marking the movement as a specific pattern synchronized with the beat is required during the training stage. First, beat detection is used to segment the audio, and then, the Mel frequency cepstral coefficient-recognized audio pattern is used to select the action pattern to be generated during the generation stage. Literature [20] used a dynamic programming algorithm to create a matching model between dance action and music feature points and then edited the music to match it, resulting in a semiautomatic score. Literature [21] suggests using machine learning to optimize the matching of dance technical movements and music in music choreography. First, by combining machine learning theory and historical sample data sets, the mapping relationship between dance movements and music is established, and the evaluation function of the dance movements-music matching relationship is obtained. As matched dance action feature sequences, we use constraint-based dynamic planning process matching and input music. Although this method has a high matching efficiency, the quality of the music and dance movements that it matches is poor. On the basis of greed theory, literature [22] proposed an optimization method for matching dance technical movements with music. This method produces a good match between dance movements and music rules, but it is time-consuming. Literature [23] introduces a sample-based matching model and uses it to test the feasibility and practicality of computer-generated choreography using the soundtrack score system of movies. Literature [24] sets scheduling rules based on aesthetic concepts, uses basic action segments to generate dance sequences unrelated to music, and then edits them properly when matching with music. The final result obtained is affirmed by dance professionals. Literature [25] puts forward the rhythm analysis method, which defines the rhythm of movements according to the vertical direction of feet and the change speed of hand displacement, takes the extreme point of joint angular velocity as the rhythm segmentation point, and then refits the movement characteristic curve. Literature [26, 27] added intensity features to the rhythm features and then used the rhythm and intensity features of music and movements as the matching basis to synthesize dance movements. The algorithm holds that the rhythm of music and the rhythm of action have a strong correlation, and the rhythm of action presented by "Stop Action" should be synchronized with the rhythm point of music. At the same time, the intensity of action has a strong correlation with the intensity of music and should also be synchronized. This paper proposes an automatic music choreography algorithm based on mixed density network. In addition, the entire process of computer music choreography is thoroughly examined, and a framework for computer music choreography is proposed. User control is introduced into the dance choreography module to improve the framework's practicability, and the user influences the choreography results by setting the thresholds of local bone speed and spatial characteristics. This framework can generate dance movements that are synchronized with the music. The results of the experiments show that this framework is very stable and generalizable.

3. Methodology

3.1. Automatic Music Choreography Technology. Automatic music choreography has a long history of study. The goal of the study is to use computer technology to reduce the amount of manual intervention in the music choreography process. People have gained a lot of valuable experience in the matching model of motion and music features [28] up until now. In terms of choreography, a matching model of motion and musical features is developed based on musical emotion and sporting style. To make the choreography process go more smoothly, research how to use the rhythm and density characteristics of music and movements. It is also possible to create action diagrams in advance for searching and selecting, which will improve the choreographer system's searching efficiency.

To create computer-assisted music choreography, dance action data must first be collected. Motion data are currently classified into two categories: motion capture data and key frame-based motion data. These two types of data, on the other hand, require a lot of manual processing, which is costly to obtain and difficult to edit. The DL algorithm has been applied to the field of motion generation as artificial intelligence technology [29] has progressed.

In music or dance, "rhythm" refers to the phenomenon of regular intensity and length appearing alternately. There are numerous types of perceptible human movements and musical characteristics. Rhythm is one of the most easily perceived features of an audience, according to research, and it is a common feature of dance movements and music. The action and rhythm sequences are both interdependent and independent in terms of the overall development of music. No matter how inventive the action sequences are, they are always bound by the rules of rhythm and melody. This is the rule that governs the progression of rhythmic sequences and movements. The introduction and widespread use of computers have resulted in a more precise system for dividing rhythm and the formulation of a set of standards. However, as computer technology advances and people's expectations for sound discrimination rise, the requirements for music rhythm measurement become more stringent [30]. The motion segments matching the target music are selected from the constructed motion database using the traditional artificially designed music and motion features and feature matching algorithm, synthesizing the dance. The motion database is usually composed of motion capture data. Figure 1 shows the framework of music choreography system.

In order to match the rhythm of computer action and music, it is necessary to turn the action and music signal into a sequence of feature points in rhythm semantics, that is, to express the rhythm information of music and action data abstractly in the form of functions. The collected music data are segmented, the action segments in the dance action database are connected and organized, the underlying features of historical music and dance actions are obtained, some feature pairs are extracted by correlation analysis, and the correlation coefficient between music and dance action features is calculated in order to establish the principle model of dance technical action system. It is more reasonable for all kinds of specifications required in the database to match the movements and music rhythms with computers. The function of information is required for its expression, and the final forms of expression are sequence and rhythm.

As computer animation and robotics advance, more and more applications require a large amount of real human motion data. In general, action diagrams and music diagrams are used to store and organize movement and music data, and automatic choreography and score are performed. That is, rhythm is used to segment motion and music data, and each segment is then turned into a node in the motion or music map. Data set construction, model training and action generation, dance choreography and synthesis, and dance visualization with 3D character animation are the four parts of the framework for music choreography system based on mixed density network proposed in this paper. Model training, action generation, and dance choreography based on music and action features are the main steps. Figure 2 shows the overall framework of the music choreography system based on mixed density network.

In comparison with traditional computer animation of a 3D model based on key frames, motion capture technology can more easily reconstruct complex motion and realistic physical interaction, and the obtained motion data are more realistic, as well as the workload of acquiring motion. Motion capture, on the other hand, necessitates specialized hardware and software to capture and process the data. The cost of required software, equipment, and personnel may be prohibitively expensive for small-scale production. Furthermore, editing the captured data twice is difficult. If there is a problem with the data, all you have to do is reshoot the scene. The path with the highest degree of matching will be chosen by the output result of automatic choreography or score. However, because the calculation process is time-consuming, it is necessary to create an action-music map based on rhythm to speed up the search for potential actions or music data.

When the action sequence is converted into the sequence value of action rhythm feature points and the music sequence is converted into the sequence value of music rhythm feature points, the matching degree between them needs to be calculated. The methods include using the classical Euclidean distance to solve the above problems, but the movement and music feature point sequences tend to have similar trends and they cannot be aligned on the time axis. In order to train the action generation model, it is necessary to construct the action data set and express the action data as vector as the input feature of the model.

3.2. Action Generation Algorithm Based on Mixed Density Network. The hybrid model is primarily used in computer vision for inverse or ambiguous problems. Instead of relying on manual production and motion capture data from users, it is necessary to solve the problem of motion generation in order to realize an effective computer choreography algorithm and ensure that the choreographed dance is real enough and novel. The mixed density network-based action generation algorithm is implemented in this chapter. The hybrid model has the capability of simulating the general distribution function in its entirety.

Extract the angular velocity curve of each joint point of the action data, and mark the extreme point of the curve as

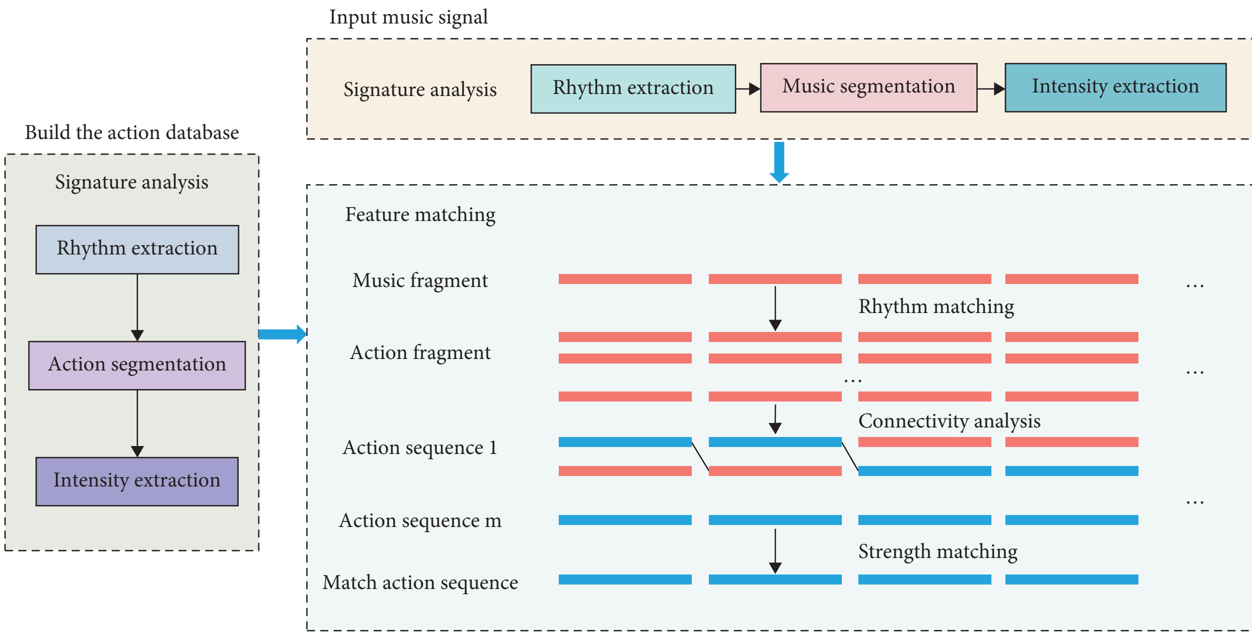

FIGURE 1: Music choreography system framework.

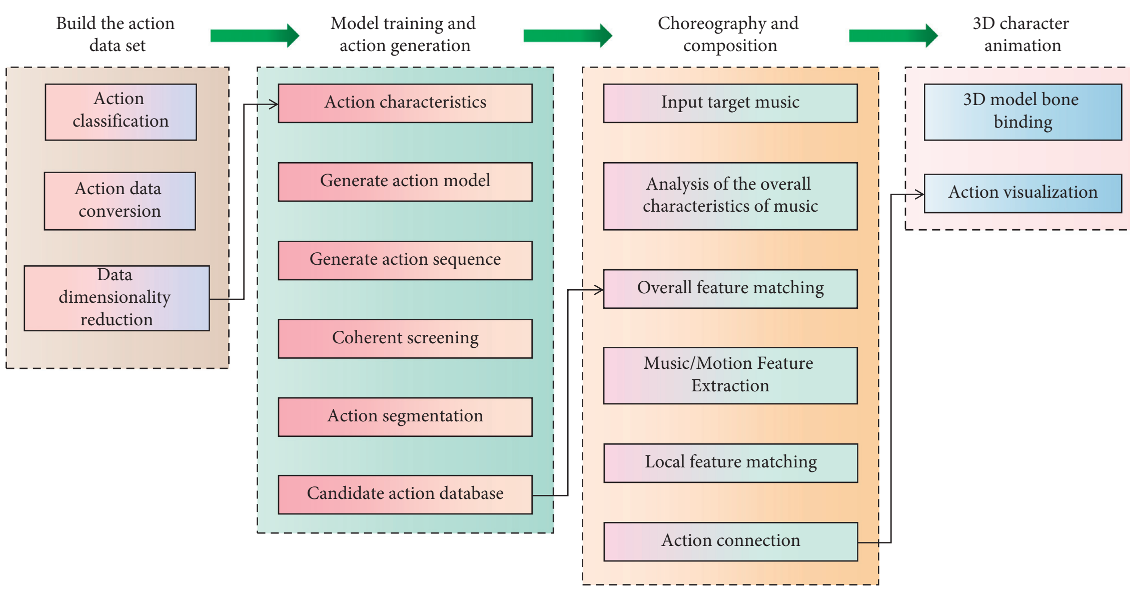

FIGURE 2: The overall framework of this system.

the rhythm reference point to form the time series $(t_0, t_1, \ldots, t_k, \ldots, t_n)$ of the reference point. Then, use the cosine curve to fit all the reference points, and the construction of the cosine function uses:

$$y_t = \begin{cases} \cos\left[2\pi\left[\dfrac{t - t_{k-1}}{t_k - t_{k-1}}\right]\right], t_{k-1} < t < t_k, \\ k = 2, \ldots, n, \\ 1, t = t_n. \end{cases} \tag{1}$$

Among them, y_t is the function value of the curve fitting at time t, and the extreme point of the angular velocity curve of the joint point is regarded as the rhythm candidate point of the joint point.

Convert the input music data file into discrete sampling points, and take 2N sampling points as a time window. There are N sampling points between different time windows, and the Fourier coefficient $X_0, \ldots, X_{N-1}$ is obtained after combining short-time Fourier analysis. $D_H(n)$ represents the mutation point function value of the nth time window, which is expressed by the following formula.

$$D_H(n) = \sum_{k=0}^{N} k\left|X_k[n]\right|, \tag{2}$$

where $X_k[n]$ represents the k-th coefficient of the nth time window.

It is necessary to transform movements and music signals into feature point sequences in rhythm semantics, that is, to abstract the rhythm information of music and movement data into one-dimensional feature point functions, in order to calculate the degree of rhythm matching between movements and music. When the action and music sequences are transformed into the sequence values of the action and music rhythm feature points, the matching degree between them must be calculated. The matching degree can be calculated in a variety of ways. In general, the classical Euclidean distance is adequate for solving the problems listed above. However, while the general trends of the action and music feature points are similar, their similar forms are not aligned on the time axis. This problem can be effectively solved by combining time planning and distance measurement, and the cumulative distance function it provides can be used as a criterion to calculate the degree of matching between actions and music pieces.

Assuming that the mutation point function value of the nth time window is $D_s(n)$, the extreme value detection is performed on the mutation point function of each time window, the obtained extreme point sequence is aligned according to the beat, and the final mutation point function is expressed by (3) value $D_{(n)}$.

$$D(n) = D_H(n) \times D_s(n). \tag{3}$$

Assuming the position of the music beat in the performance stage of the T_n generation, the position of the next music beat can be estimated through the music beat cycle:

$$T^{'}_{n+1} = T_n + \tau_{\max}. \tag{4}$$

Among them, $T^{'}_{n+1}$ represents the predicted value, and T_{n+1} represents the real beat position.

When a user inputs a music sequence, the system automatically outputs a dance action that matches the music sequence, which is called automatic choreography. Starting from the instructions of choreography, there are a large number of dance styles and types in the computer database. Different styles and types are the main body that is proficient in the early cutting and optimized to form music resources, and meet the basic requirements mentioned by users to a certain extent.

Based on the rate of change of velocity, the consistency of the motion sequence is screened. Firstly, the sum of absolute values of the first-order velocity difference of each joint in adjacent frames V(f) is calculated:

$$\begin{aligned} V(f) &= \sum_{k=1}^{c} |v(f+1,k) - v(f,k)|, \\ v(f,k) &= \left\| x_{f+1}^{(k)} - x_f^{(k)} \right\|. \end{aligned} \tag{5}$$

Among them, f is the sequence number of the frame in the action segment N_i, and x represents the action vector. $x_f^{(k)}$ represents the k-th dimensional motion data of the f-th frame, and c is the vector dimension of each frame of motion. v(f,k) represents the speed of the k-th dimension data in the f-th frame.

In computer music choreography, it is necessary to extract features that can reflect the common characteristics of music and actions in order to select dance actions that match the given target music. The complete action-music map is useful for automatic score and choreography, and its workflow can be broken down into two stages: pre-calculation and real-time operation. However, the candidate movements and music must still be processed in order to improve the rhythm matching between them and the music, as well as to meet the quality requirements of customers.

According to prior knowledge, the actual music beat position is usually the same as the extreme point of the mutation point function. The threshold ε is set in the vicinity of the estimated music beat position $T^{'}_{n+1}$, and all the extreme points within the interval $[T^{'}_{n+1} - \varepsilon, T^{'}_{n+1} + \varepsilon]$ are regarded as aligned candidate points. Define the extreme point function according to the obtained extreme point sequence, and use the following formula to express.

$$\text{Peak}(t) = \begin{cases} 1, & t \text{ is the extreme point}, \\ 0, & t \text{ is the nonextreme point}. \end{cases} \tag{6}$$

Suppose (M_j, A_i) represents an example of combined action-music segment training in music choreography. For each action feature p in M_j and music feature q in A_i, use the following formula to calculate the correlation coefficient between the two.

$$C_{(p,q)} = \frac{E(X-\mu_X)(Y-\mu_Y)}{\delta_X \delta_Y}. \tag{7}$$

Among them, $\mu_X, \mu_Y, \delta_X \delta_Y$ stands for mathematical expectation and standard deviation, respectively. X represents the characteristic sequence of dance movements $F_{j,l}^m(p), \ldots, F_{j,6}^m(p)$. Y represents the musical characteristic sequence $F_{i,l}^a(q), \ldots, F_{i,6}^a(q)$. $F_{j,k}^m(p)$ represents the k-th window of the j-th dance action segment M_j. $F_{i,k}^a(q)$ represents the qth window of the i-th music segment A_i.

After the motion generation model has been trained, the output of the model can be used to determine the spatial distribution probability of each bone joint point in the next frame, and the results obtained using various parameter control methods when estimating the position coordinates of each joint point are also different. The action and music data are usually stored and organized in the form of an action diagram and a music diagram, respectively, when performing automatic choreography and score. That is, rhythm is used to segment the action and music data, and each segment is then used as a node in the action and music graphs. The automatic choreography and score problem is thus transformed into a traversal problem on the action chart and music chart. That is, the rhythm matching model of actions and music calculates the degree of matching of all possible combinations of actions and music pieces, and then, the path with the highest degree of matching with the input actions or music data is chosen as the automatic choreography or score's output result.

4. Result Analysis and Discussion

Music features can be roughly divided into bottom features and top features. The bottom features include amplitude envelope, short-term energy, spectrum features, short-term power spectral density, etc. High-level features include the emotion and style of music. Because it is difficult to quantify and evaluate the high-level features of music, the current popular classification algorithm of music emotional style is to use machine learning algorithm to obtain the mapping relationship between the low-level features of music and emotional style. That is, the high-level features of music can be described by the low-level features.

Integration of movement and music has always been a difficult problem that needs to be improved and addressed more thoroughly. We should start by establishing the position of the action and music rhythm points and then segment the action and music data and the distance between nodes to establish their connectivity. It is divided into two categories: timbre distance and chord distance. The cubic spline interpolation function is used to fit the curve in this paper. To begin, the maximum value of continuous frame change data in video is obtained, and the upper envelope of the data sequence is fitted by a cubic spline function, followed by the minimum value of the lower envelope of the data sequence being fitted by a cubic spline function. Finally, as the final current data series fitting result, the mean value between the upper and lower envelopes is calculated as shown in Figure 3.

After obtaining the fitting results, we can observe the obvious segmentation points between various dance movements in a dance video. Two adjacent minima can determine a simple action sequence, and the minima position indicates the segmentation position of the action sequence frame.

When creating an action map or a music map, the action and music data must be segmented separately based on the positions of the action and music rhythm points. The connectivity between nodes is then analyzed and established based on the distance between nodes, making graph traversal easier. Each action sequence in the action database is divided into "action sections" based on the position of the action rhythm point. Each action bar has four action rhythm points, which are regarded as nodes in the action diagram and simulate the score structure of 4/4 beats. The action features are divided into two categories: bottom features and high-level features. The movement speed, acceleration, movement direction change, and action shape of each joint are the low-level features, while the emotion and style of action are the high-level features. With the help of a user score, analyze the synthesis effect of three different dance styles. To begin, analyze the music style in relation to the target music's overall characteristics, and then create choreography actions to match. Several target music pieces were analyzed in this experiment, and three target music pieces appropriate for street dance, classical dance, and modern dance were chosen and choreographed. The test participants scored the degree of matching between music and dance by judging the three segments' dance styles. The evaluation results are shown in Figure 4.

The choreography only considers the action connection between the segments, rather than the connection as a whole. To deal with the problem holistically, we can improve the agreement between some paragraphs by informing the connections between them, allowing the actions in the paragraphs to achieve complete overall coherence and matching. In music, on the other hand, in order to show the perfect melody completely between segments, the connection between segments can be obtained using the music cohesion rules of a computer database in this regard, resulting in the perfect integration of the entire melody.

Using this method and the method based on genetic theory and the method based on machine learning, the optimization experiment of dance action matching in music choreography is carried out, and the matching degree of dance action matching in music choreography is compared with the three methods. The comparison results are described in Figure 5.

It can be seen from the analysis that when using this method for music choreography, the matching degree of dance movements is better than that based on genetic theory and machine learning. The superiority of this algorithm is further verified. Using this method, the method based on genetic theory and the method based on machine learning, respectively, the optimization experiment of dance movement matching in music choreography is carried out. The three methods are compared for the synchronization of dance action matching in music choreography, and the comparison results are described in Figure 6.

The analysis shows that the synchronization of dance action matching is better than that of dance action matching based on genetic theory and machine learning. The simulation results show that the proposed method can fully reflect the synchronization of music and movement changes, and the music-dance matching quality matched by the improved dance movement matching method is higher.

Although qualitative experiments can verify the algorithm's effectiveness through visual effects, relying solely on this index makes it impossible to assess the experimental results quantitatively in all aspects. It is difficult to objectively and quantitatively evaluate the choreography effect in the field of computer-assisted music choreography. There is no universal objective and quantitative evaluation index available at the moment. As a result, subjective evaluation criteria are frequently used to assess the results of experiments. 200 students were asked to research the user experience using the user manual scoring method in this paper. In the training data set, show the participants two pieces of music and dance. One piece of music is paired with a dance, while the other is paired with mismatched dances to the same music. After the manual scoring, this paper counts the final scores of the experimental segments, and the results are shown in Figure 7.

In the process of matching and optimizing dance movements in music choreography, the synchronized dance movements and music data are divided by integrating the theory of music beat extraction, and a plurality of short movements-music fragment combinations are obtained. Detect the abrupt change point of the music segment, align

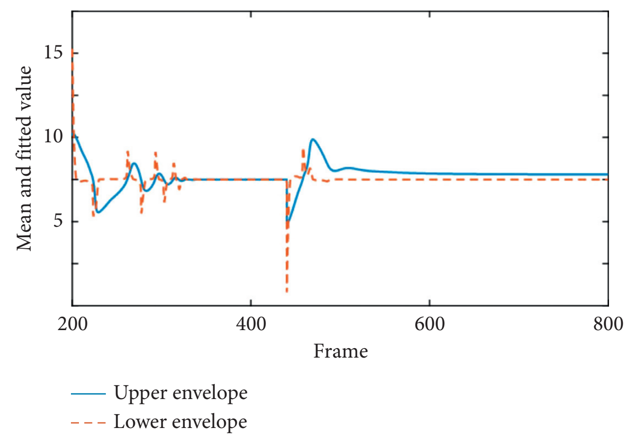

Figure 3: Final fitting result diagram.

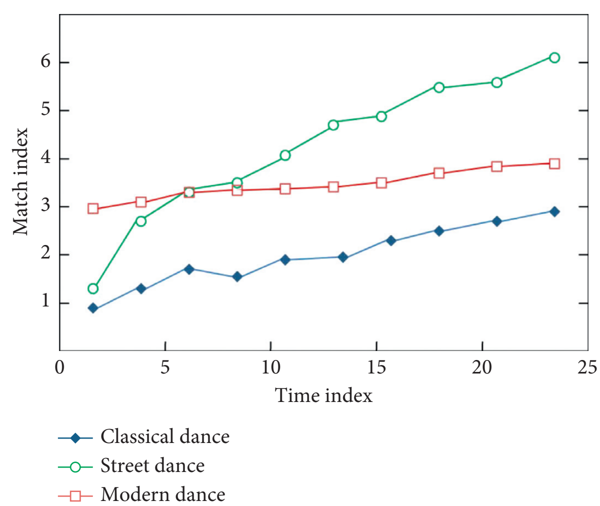

Figure 4: Matching degree test with music and dance.

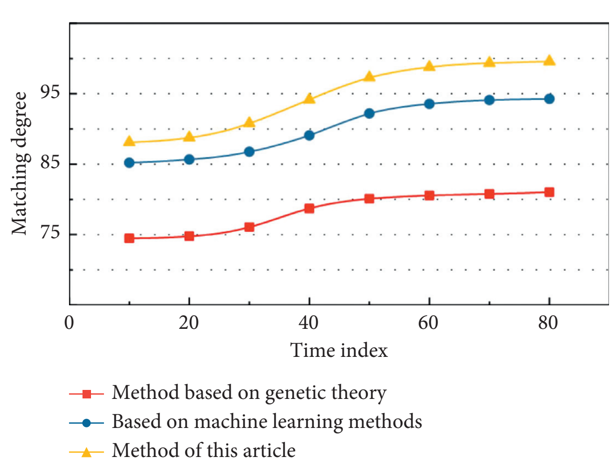

Figure 5: Comparison chart of matching degree of dance movements in different methods.

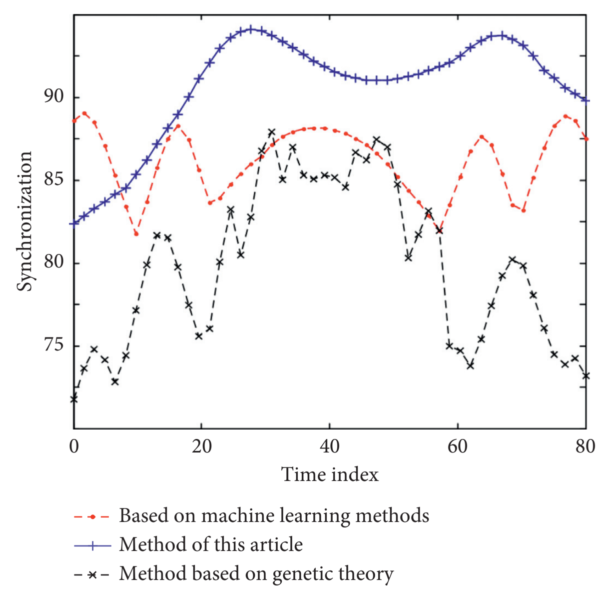

Figure 6: Method comparison chart of synchronization of different dance movement matching.

the beat predicted position obtained in each step, calculate the correlation coefficient between dance movements and music segments, and obtain the dance movement matching optimization objective function. The effectiveness of the hierarchical feature matching algorithm proposed in this paper is verified by comparing the users' scores of dances generated with or without music overall feature matching algorithm. The scoring situation is shown in Figure 8.

The results show that dance segments synthesized with the hierarchical feature matching algorithm proposed in this paper are better matched to music than dance segments synthesized with only the local feature matching algorithm. It demonstrates the effectiveness of the hierarchical feature matching algorithm proposed in this paper. The music-action data set is built in this chapter, as well as the data classification and feature representation of training data. Build an action generation model, complete the model's training and action generation, and control the parameters during the action generation process. The generated action is suitable for the subsequent dance arrangement in order to ensure the quality of the generated action. Both the local bone motion speed feature extraction algorithm and the dance spatial feature extraction algorithm proposed in this

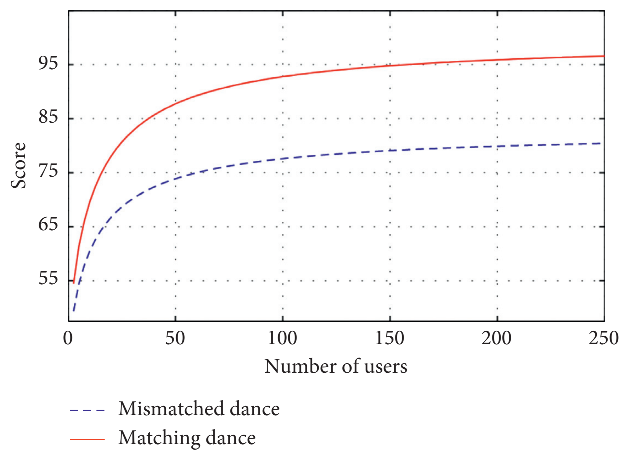

Figure 7: User experience rating.

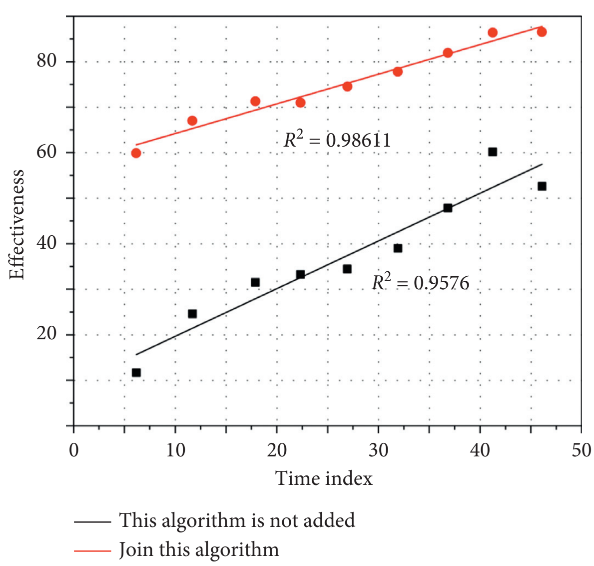

Figure 8: Effectiveness evaluation of matching algorithm.

paper can effectively reflect the corresponding dance features, according to the experimental results. Overall musical characteristics can accurately reflect musical style types and synthesize choreography actions of corresponding styles. The hierarchical feature matching algorithm outperforms the local rhythm and intensity feature matching algorithm, and the entire feature matching can be combined to create a dance that is better suited to the target music.

5. Conclusions

Dance with music enriches our cultural life as a form of artistic expression. The integration of technology and art is making a computer realize music-based automatic choreography. When artists use scientific and technological methods to create, this type of technology can act as a catalyst for inspiration and has a lot of potential. The data set created in this paper obtains enough dance data through motion capture devices, and downloading motion data corresponding to different music from the Internet is more cost-effective and convenient. The matching degree of all potential combinations of actions and music pieces in the database is precalculated with the rhythm feature matching model in the preprocessing stage, and an action-music map is created. In the real-time matching stage, the method of graph traversal is used to find the candidate actions or music that have the best rhythm match with the input, and then the rhythm feature points of these candidate actions or music data are further optimized and adjusted to form the automatic choreography result. Furthermore, the automatic music choreography algorithm proposed in this paper, which is based on a mixed density network, considers the coherence between adjacent motion segments as well as the naturalness of the entire dance motion. The experimental results show that this algorithm can generate a sufficient number of realistic and diverse dance movements, with the mean method producing the most stable movements. The human skeleton structure that generates movements becomes more and more real as training time goes on, and the relative relationship of joints becomes more and more stable. The coherence-based motion screening algorithm can also produce the desired results.

Data Availability

The data used to support the findings of this study are included within the article.

Conflicts of Interest

The author does not have any possible conflicts of interest.

References

[1] P. Zhou, X. Fang, Y. Fang, Y. Long, R. He, and X. Han, "Enhanced random access and beam training for mmWave wireless local networks with high user density[J]," *IEEE Transactions on Wireless Communications*, vol. 16, no. 99, pp. 7760–7773, 2017.

[2] M. Quinlan, "Gaga as metatechnique: negotiating choreography, improvisation, and technique in a neoliberal dance market[J]," *Dance Research Journal*, vol. 49, no. 02, pp. 26–43, 2017.

[3] C. Rosemary, "Choreographing American dance archives: artist-driven archival projects by eiko & koma, bebe miller company, and jennifer monson[J]," *Dance Research Journal*, vol. 50, no. 01, pp. 80–101, 2018.

[4] R. E. Estell and D. M. Anderson, D. K. James, D. M. Anderson, and D. K. James, Defoliation of Flourensia cernua (tarbush) with high-density mixed-species stocking," *Journal of Arid Environments*, vol. 130, no. 7, pp. 62–67, 2016.

[5] M. Templeton, "Walking with the self: zab Maboungou\\"s interventions against eurocentrism through contemporary african dance[J]," *Dance Research Journal*, vol. 49, no. 02, pp. 44–61, 2017.

[6] C. Bao, S. Tang, J. M. Horton et al., "Effect of overall grafting density on microphase separation of mixed homopolymer brushes synthesized from Y-Initiator-Functionalized silica particles[J]," *Macromolecules*, vol. 45, no. 19, pp. 8027–8036, 2016.

[7] C. Ó. Nuanáin, P. Herrera, and S. Jordá, "Rhythmic concatenative synthesis for electronic music: techniques,

implementation, and evaluation," *Computer Music Journal*, vol. 41, no. 2, pp. 21–37, 2017.

[8] C. Chang and L. Zhang, C. W. Hsu, L. Zhang, C.-W. Hsu, X.-F. Chuah, and S.-Y. Lu, Mixed NiO/NiCo2O4 nanocrystals grown from the skeleton of a 3D porous nickel network as efficient electrocatalysts for oxygen evolution reactions," *ACS Applied Materials & Interfaces*, vol. 10, no. 1, pp. 417–426, 2017.

[9] D. García-Meza, E. Andresen, L. Ríos-Casanova, and C. Martorell, "Seed density in monospecific and mixed patches affects individual and collective foraging in ants[J]," *Insectes Sociaux*, vol. 68, no. 1, pp. 81–92, 2021.

[10] L. Wang, S. Cai, T. Suekane, Gravitational fingering due to density increase by mixing at a vertical displacing front in porous media[J]," *Energy & Fuels*, vol. 32, no. 1, pp. 658–669, 2017.

[11] R. Chaleff, "Activating whiteness: racializing the ordinary in US American postmodern dance," *Dance Research Journal*, vol. 50, no. 3, pp. 71–84, 2018.

[12] Z. Huang, Y. Liu, C. Zhan, C. Lin, W. Cai, and Y. Chen, "A novel group recommendation model with two-stage deep learning," *IEEE Transactions on Systems, Man, and Cybernetics: Systems*, 2021, In Press.

[13] Y. Gu, A. Chen, X. Zhang, C. Fan, K. Li, and J. Shen, "Deep learning based cell classification in imaging flow cytometer," *ASP Transactions on Pattern Recognition and Intelligent Systems*, vol. 1, no. 2, pp. 18–27, 2021.

[14] J. Pons, T. Rode, J. Janer, T. Rode, and W. Nogueira, "Remixing music using source separation algorithms to improve the musical experience of cochlear implant users," *Journal of the Acoustical Society of America*, vol. 140, no. 6, pp. 4338–4349, 2016.

[15] H. Chen and X. Q. Zhao, Y. G. Xiao, X.-q. Zhao, Y.-g. Xiao, Y.-l. Liu, and Y. Liu, Radial mixing and segregation of granular bed bi-dispersed both in particle size and density within horizontal rotating drum," *Transactions of Nonferrous Metals Society of China*, vol. 26, no. 2, pp. 527–535, 2016.

[16] R. Shaughnessy, "Roger clegg and lucie skeaping, singing simpkin and other bawdy jigs: musical comedy on the shakespearean stage: scripts, music and context," *Dance Research*, vol. 34, no. 2, pp. 273-274, 2016.

[17] A. A. Kallio and H. Westerlund, "The ethics of survival: t," *International Journal of Music Education*, vol. 34, no. 1, pp. 90–103, 2016.

[18] F. R. Andreis, M. A. Favretto, S. Cossul, L. R. Nakamura, P. A. Barbetta, and J. L. B. Marques, "Linear mixed-effects models for the analysis of high-density electromyography with application to diabetic peripheral neuropathy[J]," *Medical, & Biological Engineering & Computing*, vol. 58, no. 7, pp. 1–12, 2020.

[19] K. H. Katrak, "Jay pather reimagining site-specific cartographies of belonging[J]," *Dance Research Journal*, vol. 50, no. 02, pp. 31–44, 2018.

[20] N. N. Kulov, A. V. Ochkin, and A. V. Ochkin, "Method for calculating the density of mixed solutions of strong electrolytes," *Theoretical Foundations of Chemical Engineering*, vol. 54, no. 6, pp. 1223–1228, 2020.

[21] J. C. O. Koh, M. Hayden, H. Daetwyler, and S. Kant, "Estimation of crop plant density at early mixed growth stages using UAV imagery[J]," *Plant Methods*, vol. 15, no. 1, pp. 1–9, 2019.

[22] R. Oriol, "'Embodied knowledge as revolutionary dance: representations of Cuban modern dance in alma guillermoprieto's dancing with Cuba," *Dance Research Journal*, vol. 51, no. 2, pp. 51–67, 2019.

[23] R. Pandharkar and M. R. Hermes, D. G. Truhlar, M. R. Hermes, D. G. Truhlar, and L. Gagliardi, A new mixing of nonlocal exchange and nonlocal correlation with multiconfiguration pair-density functional theory," *The Journal of Physical Chemistry Letters*, vol. 11, no. 23, pp. 10158–10163, 2020.

[24] A. Christmas, "When ballet became French: modern ballet and the cultural politics of France, 1909-1939. By ilyana karthas," *Journal of Social History*, vol. 50, no. 3, pp. 581–583, 2017.

[25] S. J. Schlecht and E. A. P. Habets, "The stability of multichannel sound systems with time-varying mixing matrices," *Journal of the Acoustical Society of America*, vol. 140, no. 1, pp. 601–609, 2016.

[26] J. I. Kai, "Battling in the bronx: social choreography and outlaw culture among early hip-hop streetdancers in New York city[J]," *Dance Research Journal*, vol. 50, no. 2, pp. 62–75, 2018.

[27] K. Vedel, "Migratory choreography and spaces of resistance," *Dance Research Journal*, vol. 52, no. 1, pp. 58–70, 2020.

[28] S. Kato Westby and R. Glynn, "Fabricating performance: reciprocal constructs of dance notation," *Nexus Network Journal*, vol. 20, no. 1, pp. 75–94, 2018.

[29] Y. Zhang, K. Xia, Y. Jiang et al., "Multi-modality fusion & inductive knowledge transfer underlying non-sparse multikernel learning and distribution adaption[J]," *IEEE/ACM Transactions on Computational Biology and Bioinformatics*, In Press, 2022.

[30] D. Goldman, R. J. Kowal, A. Lepecki, G. Morris, H. Buttimore, and H. Thomas, "Dance Research Journal," in *Proceedings of the 'Conference panel to honor mark franko's editorship of DRJ*, vol. 50, no. 1, pp. 6–22, The Ohio State University, columbus, Ohio, USA, 19 October 2018.

Hindawi
Computational Intelligence and Neuroscience
Volume 2022, Article ID 1756585, 8 pages
https://doi.org/10.1155/2022/1756585

Research Article

Intelligent Recommendation Model of Contemporary Pop Music Based on Knowledge Map

Yan Zhang

Department of Music, General Graduate School, Sejong University, Seoul 05006, Republic of Korea

Correspondence should be addressed to Yan Zhang; zymusic1987@163.com

Received 14 December 2021; Revised 1 January 2022; Accepted 3 January 2022; Published 9 February 2022

Academic Editor: Xin Ning

With the advent of the era of big data, the rise of Web2.0 completely subverts the traditional Internet model and becomes the trend of today's information age. Simultaneously, massive amounts of data and information have infiltrated various Internet companies, resulting in an increase in the problem of information overload. In the online world, learning how to quickly and accurately select the parts we are interested in from a variety of data has become a hot topic. Intelligent music recommendation has become a current research hotspot in music services as a viable solution to the problem of information overload in the digital music field. On the basis of precedents, this paper examines the characteristics of music in a comprehensive and detailed manner. A knowledge graph-based intelligent recommendation algorithm for contemporary popular music is proposed. User-defined tags are described as the free genes of music in this paper, making it easier to analyze user behavior and tap into user interests. It has been confirmed that this algorithm's recommendation quality is relatively high, and it offers a new development path for improving the speed of searching for health information services.

1. Introduction

Recommendation system is a smart software technology that can provide personalized recommendation services for users based on their interests, preferences, and characteristics [1]. The amount of music available is growing at an exponential rate, making it difficult for users to search for and find related music. As a result, researchers from all over the world are increasingly focusing on music retrieval research [2]. Intelligent music recommendation has become a research hotspot in current music services [3] as an effective way to solve the problem of information overload in the field of digital music. As the number of users has grown significantly, more and larger amounts of data have been generated. The recommendation system was created to address the issue of how to best use these data in order to provide more accurate services. To retrieve eligible music benefits, traditional music retrieval uses metadata. This retrieval method necessitates users remembering relevant information from the target track prior to retrieval, which is incompatible with users' fast-paced lives [4]. In modern life, what users need is to be able to play music that suits their interests continuously. However, how to provide different users with a list of songs that suit their interests or recommend interesting songs for them has become a problem that the current music recommendation system needs to solve. Intelligent music recommendation system is faced with the problems of accuracy, diversity, and novelty of recommendation, while its data set is sparse and information is missing.

In recent years, although the recommendation algorithms [5] in the fields of movies, news, and books have emerged one after another, there are not many recommendation systems in the field of music, mainly because the data in this field are often not made public, and unlike the ratings we usually use, there is basically no public data set that mentions the user's ratings [6]. Intelligent music recommendation system is an effective way to solve "information overload." The recommendation system mines users' potential interest preferences according to their historical behaviors, calculates the similarity between users and resources, and recommends music resources that users may be interested in [7]. At present, in the research of intelligent music resource recommendation methods, researchers focus on user feature modeling and resource attribute modeling and recommend by calculating the similarity between users and resources. In most cases, people background music and listen to music while studying, working, or exercising [8]. The emergence of music recommendation system enables users to quickly and continuously obtain music that suits their interests. The emergence and development of Web2.0 and social media allow users to act freely [9]. Users can define labels for music through their own understanding and feelings, and different labels can interpret users' understanding of music from different angles. Knowledge map is often used in intelligent search engines, recommendation systems, and other fields to improve its accuracy because of its strong organizational ability and relationship processing ability [10]. At present, the recommendation system based on a knowledge map is mainly divided into feature-based recommendation and path-based recommendation. Knowledge features are extracted through knowledge feature learning, and the ability of feature extraction, that is, the quality of knowledge representation, not only determines whether it can bring useful information for recommendation but also determines the quality of knowledge map construction. Therefore, this paper constructs a small-scale knowledge map in the field of machine learning and, on this basis, proposes a music resource recommendation algorithm based on a knowledge map, which integrates music connectivity and user interests.

In a broad sense, the recommendation system can be understood as recommending items that users may be interested in. The recommended items can be movies, music, books, short videos, and so on, depending on the specific field of application [11]. Today, with the continuous expansion of the Internet, the amount and types of information are increasing, and users put forward higher requirements for information retrieval and recommendation of related items [12]. Because different users have different interest preferences, the focus of attention, personal personality orientation, and so on, in order to meet the different recommendation needs of different users, an intelligent recommendation system featuring that everyone can get different recommendations from others came into being [13]. Traditional music recommendation algorithms based on "User-Item" usually only pay attention to the two-dimensional scoring relationship, ignoring the situation information of users when listening to music [14]. This paper proposes an improved algorithm based on a knowledge map, which is based on the traditional music recommendation algorithm and incorporates the users' situation information when listening to music. Simultaneously, this paper examines the existing music recommendation system in depth, combining it with some of the benefits provided by the recommendation algorithm. By analyzing the recommendation results, we can see that the system's overall performance is good and that it can effectively recommend results that users might be interested in to a degree, essentially achieving the system's intended goal.

2. Related Work

Literature [15] proposes to recommend music that meets users' needs and preferences by analyzing users' listening habits and the characteristics of the music itself. Literature [16] proposes that, in order to meet the personalized needs of different users for music, major well-known music recommendation systems are increasingly favored by consumers. Convolution matrix decomposition based on file additional information is proposed in literature [17]. Literature [18] introduces the information in the knowledge base such as structure information, text data, and image data into the recommendation system to improve the quality of the recommendation system. A session-based recurrent neural network recommendation model is proposed in literature [19]. A multirate depth learning model based on time recommendation is proposed in literature [20, 21]. Literature [22] introduces the concept of similarity based on meta path, in which meta path is a path composed of a series of relationships defined between different object types. A new similarity measure called PathSim is defined under the meta path framework, which can find objects in peer-to-peer networks. References [23,24] propose the method of using depth hierarchy model in film recommendation task. References [25, 26] propose a novel knowledge representation learning method named embodied type by using the naming of entity level type. Literature [27] introduces the potential features based on meta paths to represent the connectivity between users and projects on different types of paths and uses the relationship heterogeneity in the information network to provide high-quality intelligent recommendation results. Based on previous studies, this paper proposes an intelligent recommendation algorithm for contemporary pop music based on a knowledge map. The algorithm comprehensively analyzes user behavior by analyzing user interests and user preferences for different musical gene characteristics.

3. Methodology

3.1. Related Theories and Technologies. Music is an abstract art form that reflects people's real life and expresses their inner thoughts [28]. It is also a way to express their feelings and repose their feelings. With the rapid decline of the status of traditional records and the rapid promotion and spread of digital music, online audition and mobile music have become new ways for people to obtain music [29]. However, the keywords used by users do not correspond well with the item description tags, and converting audio information into digital information will lead to problems such as increased computation and prolonged response time. This content-based method also ignores the similar interests of different users, so it cannot adapt to the community-based network well.

Feature-based recommendation algorithms directly represent knowledge using a knowledge map, which fails to introduce multihop relationships and makes it difficult to use knowledge semantic network information. The path-based recommendation algorithm makes use of the knowledge map's multihop knowledge and effectively uses the knowledge map's semantic network information, but it usually relies on prior knowledge. As a result, studying the application of the knowledge map in the recommendation system is of great research value in addressing the problem of how to effectively use the semantic association information of knowledge in recommendation algorithms.

A web crawler is a program that requests websites and extracts information from them [30]. In the study of music recommendation systems, there are numerous data sets. However, it was discovered in this paper through the collection of various data sets that none of the existing data sets can contain weather information when users listen to music. This paper abandons existing public data sets in favor of using a web crawler to capture specific data sets in order to meet the research needs of intelligent music recommendation. The process of obtaining web page data by crawler is shown in Figure 1.

The construction of the knowledge map mainly includes three processes. They are information extraction, knowledge fusion, and knowledge processing. Through the above process, we can build a relatively complete and reliable knowledge map. According to the actual situation of users, this paper adopts a recommendation algorithm based on the knowledge map to form a recommendation list. Figure 2 shows the flowchart of intelligent recommendation of popular music based on the knowledge map.

Recommendation systems are intelligent software technologies that can provide personalized recommendations for users based on their interests, preferences, and characteristics. There are many definitions of recommendation systems available today, and different fields have different rules for defining them. The recommendation system is primarily used to estimate a user's preference for items that they have never seen before. It can be roughly divided into scoring prediction, ranking prediction, and classification prediction based on the output of the recommendation system. The scoring prediction is primarily aimed at the scoring matrix, with the goal of supplementing the matrix's vacancy scores. The ranking prediction is primarily intended to recommend items to a specific user who may be interested in them. Classification prediction is the process of categorizing items and recommending them to users who are interested in that category. Although the content-based recommendation is simple to calculate and understand and has been widely used in some fields, such as text recommendation, it is not without flaws that limit its development, as evidenced by the wide range of content feature extraction and recommendation results.

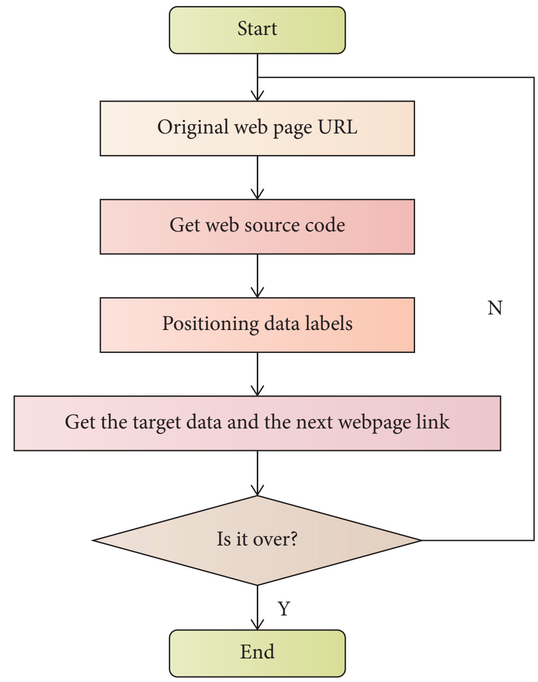

Figure 1: Process of obtaining web page data by crawler.

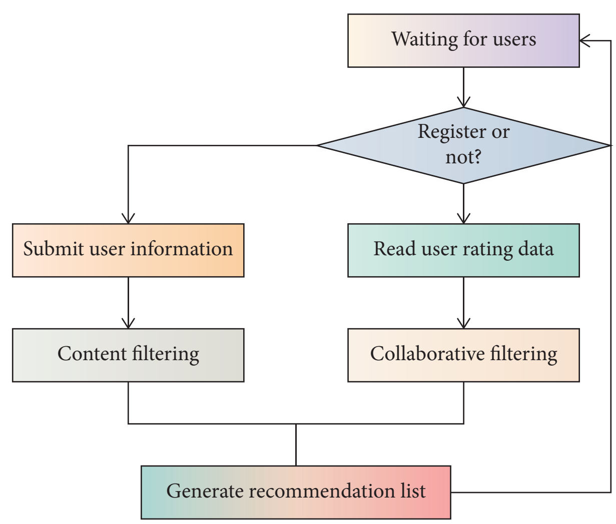

Figure 2: Technical framework of knowledge map.

3.2. Intelligent Music Recommendation System Based on Knowledge Map. The algorithm approaches the target user's score of an item according to the score of the target user's nearest neighbor. Define the target user a and the item i that has not been rated excessively, and then predict the score of a to i:

$$p_{a,i} = \overline{r}_a + \frac{\sum_{u=1}^{K}\left(r_{u,i} - \overline{r}_u\right)\omega_{a,u}}{\sum_{u=1}^{N}\omega_{a,u}}. \tag{1}$$

Among them, $r_{u,i}$ represents the score of user u on item i, r_u and $\overline{r}_a$ represent the average scores of user a and user u, respectively, and $\omega_{a,u}$ represents the similarity between user u and user a.

However, the collaborative filtering algorithm based on items thinks that users' scores of different items are similar. When users' scores of a certain item need to be estimated, users' scores of several similar items of the item can be used to estimate, as shown in the following formula:

$$p_{a,i} = \bar{r}_i + \frac{\sum_{k=1}^{M} \left(r_{a,k} - \bar{r}_k \right) \omega_{i,k}}{\sum_{k=1}^{M} \omega_{i,k}}. \quad (2)$$

Among them, $\bar{r}_i$ represents the average score of item i, and $\omega_{i,k}$ represents the similarity between item i and item k. In actual commercial applications, user-based collaborative filtering algorithms are more efficient than item-based. The number of songs in the corpus used in this paper is far greater than the number of users. In this paper, a user-based collaborative filtering algorithm is used as a comparative experiment to improve efficiency.

Knowledge map can filter data from the Internet and has multisource heterogeneous association information among entities. The filtered association information can fine-tune the feature information in users' projects, calculate the correlation between users and users, users and projects, and projects more precisely, and improve the recommendation system's interpretability, diversity, and accuracy.

If the current user's neighbors listen to a certain piece of music many times, it will greatly affect the recommendation effect. Therefore, in order to avoid this deviation, according to the characteristics of this corpus, the prediction score formula in collaborative filtering is treated as follows:

$$P_{a,i} = \frac{\sum_{u=1}^{K} \left(r_{u,i} - \bar{r}_a/\sigma_a - \bar{r}_u - \bar{r}_a/\sigma_a \right) * \omega_{a,u}}{\sum_{u=1}^{n} \omega_{a,u}}. \quad (3)$$

The threshold T_r of the number of times of listening to the same songs between two users is selected, and the number K of similar users of the current user is selected. After many experiments, it has been proved that these two parameters are $T_r = 20$ and $K = 15$, and the experimental effect is the best.

Knowledge features are extracted through knowledge feature learning, and the ability of feature extraction, that is, the quality of knowledge representation, not only determines whether it can bring useful information for recommendation but also determines the quality of knowledge map construction. When learning vectors, the knowledge model needs to construct negative triples to train the loss function. The usual method is to construct negative samples by randomly replacing the head entity or tail entity in the correct triples. The random method is effective at the beginning of training. However, with the continuous training, the scores of these randomly generated negative triples may exceed the sum of the correct triples scores and interval values, resulting in zero losses. As a result, the convergence speed gradually decreases, and the best result cannot be obtained.

For each relation r in the knowledge graph, two values are first counted. One is the average number of tail entities corresponding to each head entity, denoted as N_{tph}. The other is the average number of head entities corresponding to each tail entity, denoted as N_{hpt}. Then, defining the probability p, the calculation formula is as follows:

$$p = \frac{N_{tph}}{N_{tph} + N_{hpt}}. \quad (4)$$

Then, the replacement head entity and replacement tail entity obey the Bernoulli distribution with parameter P. Set

$$X = \begin{cases} 1, & \text{Replace head entity}, \\ 0, & \text{Replace tail entity}. \end{cases} \quad (5)$$

Then the distribution law of X is

$$P\{X = x\} = p^x (1 - p)^{1-x}, \quad x = 0 \cdot 1. \quad (6)$$

The purpose of a content-based recommendation algorithm is to make recommendations for users based on the similarity of their interests and project contents and to make recommendations independently for each user without taking into account the interests and hobbies of other users. For text information recommendation, this method is simple and effective. The goal of learning is to encode entities and relationships into a continuous low-dimensional vector space, according to the knowledge map. Many existing methods focus solely on learning representations of structured information from triples, ignoring the rich hierarchical type information of entity species available from most knowledge maps.

Assuming that the set that user u and user v have scored together is denoted by I_c and I_u, I_v are the set of items rated by user u and user v, respectively, the similarity sim (u, v) between user u and user v is

$$\mathrm{sim}(u, v) = \frac{\sum_{i \in I_c} \left(R_{u,i} - \bar{R}_u \right) \left(R_{v,i} - \bar{R}_v \right)}{\sqrt{\sum_{j \in I_u} \left(R_{u,j} - \bar{R}_u \right)^2} \sqrt{\sum_{j \in I_v} \left(R_{v,j} - \bar{R}_v \right)^2}}. \quad (7)$$

Among them, $R_{u,i}$ represents the rating of user u on item i, and $\bar{R}_u$ and $\bar{R}_v$, respectively, represent the average rating of user u and user v on the item. I_c represents the set of items scored by users u and v, I_u represents the set of items scored by user u, and I_v represents the set of items scored by user v.

Assuming that the set that user u and user v have evaluated at the same time is represented by I_c, the similarity sim(u, v) between user u and user v can be expressed by Pearson similarity as

$$\mathrm{sim}(u, v) = \frac{\sum_{k=1}^{K} \left(R_{u,k} - \bar{R}_u \right) \left(R_{v,k} - \bar{R}_j \right)}{\sqrt{\sum_{k=1}^{K} \left(R_{u,k} - \bar{R}_u \right)^2} \sqrt{\sum_{k=1}^{K} \left(R_{v,k} - \bar{R}_j \right)^2}}, \quad (8)$$

where $R_{u,k}$ and $R_{v,k}$, respectively, represent the ratings of user u and user v on item k, $\bar{R}_u$ and $\bar{R}_v$, respectively, represent the average ratings of user u and user v on a common rated item, and K is the number of repeated reviews of user u and user v.

Knowledge map is stored in triples composed of entities of entity relations, and entity relations will appear in multiple triples, presenting polysemy and complex relationship types.

In this section, several items with the highest analysis and forecast scores are presented to target users as recommended clearing units. User-based recommendation algorithm is more accurate when the data set is complete and the similarity algorithm is reliable, and it can avoid the differences in project content and make accurate recommendations and can implicitly and transparently explore the relationship between projects and user preferences.

4. Results Analysis and Discussion

The number of times users listen to a certain song to express the user's favorite degree of that song and the user's rating of the project according to his favorite degree is the data set used in this paper. When calculating the similarity between two documents in the context of data query, documents are frequently regarded as word frequency vectors, with the cosine value of the included angle between the two word frequency vectors used to express their similarity. The algorithm sort calculates the user-item relationship. A user query node in the algorithm is represented by a vector, with each dimension representing an item node in the association graph. Its value in this paper represents the number of times the user query node has listened to the music node or whether it has used the tag, indicating the degree to which users are interested in songs or tags.

The validity of the sequential user relationship model is the foundation of algorithm recommendation. To demonstrate the validity of the sequential user relationship model, the first step of the experiment is to compare the traditional nearest neighbor recommendation algorithm with the sequential nearest neighbor recommendation algorithm. The experimental results of the root mean square error comparison between them under different nearest neighbor numbers are shown in Figure 3.

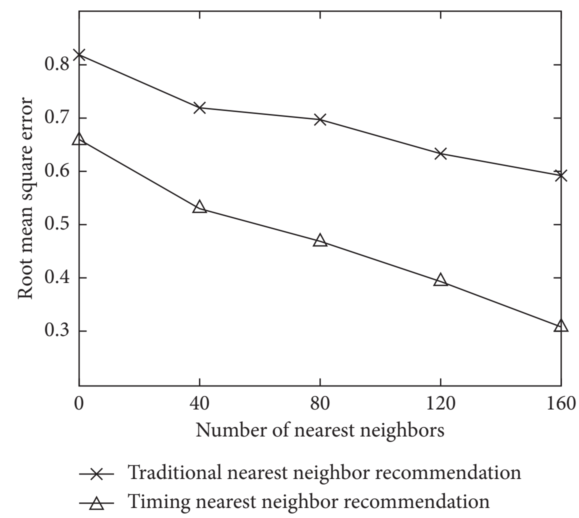

Figure 3: Comparison chart of root mean square error under different nearest neighbors.

From the graph, it can be seen that the effect of time-series nearest neighbor recommendation is always better than that of traditional nearest neighbor recommendation, whether the value of root mean square error is rising or falling, which proves the effectiveness of the time-series user relationship model. User preference extraction is the precondition of context awareness recommendation, and the purpose of contextual user preference extraction is to introduce contextual information into the user preference model. At present, there are two main types of situational user preference extraction technologies: quantitative analysis and qualitative analysis. The node type and relationship type in the knowledge map contain the design idea of the ontology library, and the entity information and semantic information between entities in the map show the extracted movie knowledge. The constructed knowledge map nodes and relationship types are reasonably designed, and the knowledge is accurate and comprehensive, which can be used for pop music retrieval.

In order to verify the effectiveness of the recommendation algorithm, the differences among traditional nearest neighbor recommendation, time-series nearest neighbor recommendation, and knowledge map recommendation are compared according to the different intervals in which users listen to music records. The root mean square error results of the three methods in different training set intervals are shown in Figure 4. The results fully prove the effectiveness of the recommendation.

The matrix decomposition model, also known as the hidden semantic model, assumes that several hidden factors influence a user's rating of a specific item. The matrix decomposition model decomposes the large problem scale "user-item" scoring matrix into the product of two small matrices, the user potential feature vector matrix and the item potential feature vector matrix, respectively, and the product of the two matrices maps the user and the item to a common hidden factor space. We ran 20 tests for each combination configuration and then averaged the test results to find the best parameter configuration based on the average ranking of the correct triples. Figure 5 shows the average ranking results under different embedded dimensions.

From the figure, we can see that, in all the dimensions of the experimental test, the improved negative sampling algorithm has a significant improvement in the average ranking compared to the original negative sampling algorithm. Figure 6 shows the top ten hit rate results in different dimensions.

The top ten hit rate results of negative sampling using the improved negative sampling algorithm are better than the original results in all dimensions, according to experimental results. The situational user preferences are converted into numerical scores in quantitative form using the quantitative analysis method, and mathematical calculations are performed using the corresponding preference extraction technology. In order to quantify situational user preferences, multidimensional vector scoring models and hierarchical models are commonly used. Heuristic and model-based technologies are two types of quantitative analysis methods. Similarity calculation, nearest neighbor algorithm, clustering, and other heuristic methods for extracting user preferences in scenarios are common. Users' playing records will

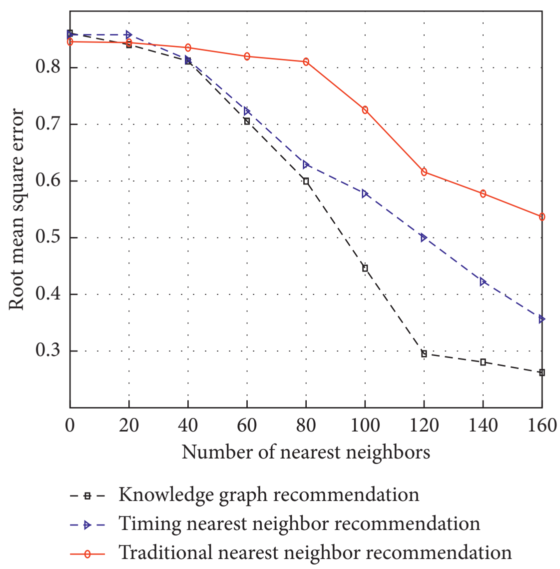

FIGURE 4: Comparison chart of root mean square error in different intervals.

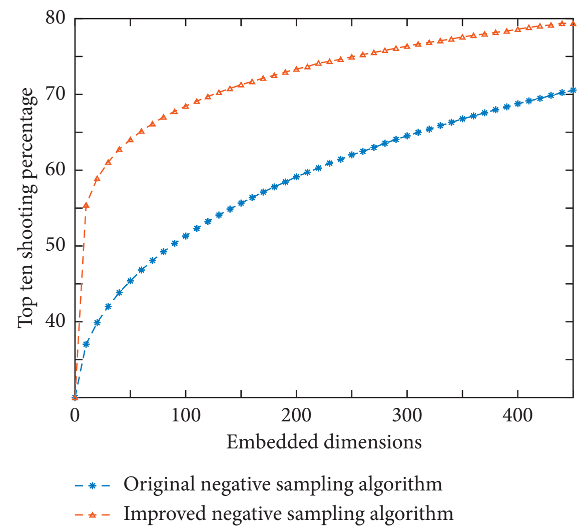

FIGURE 6: The top ten hit rates under different embedding dimensions.

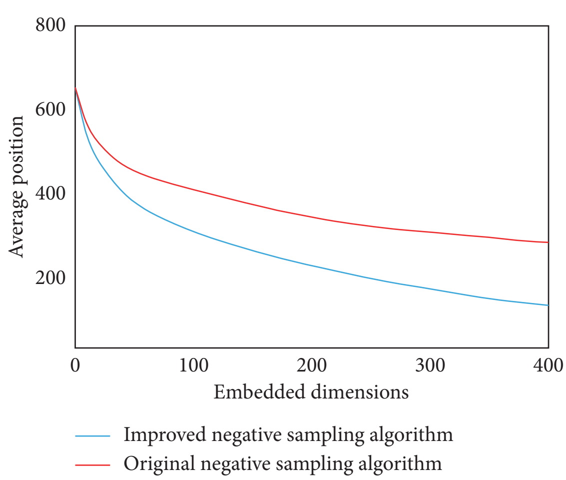

FIGURE 5: Average position under different embedding dimensions.

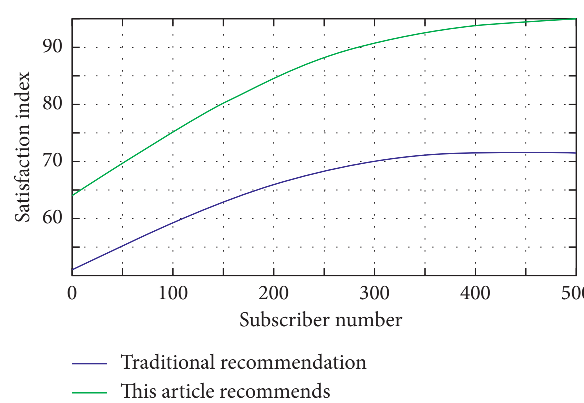

FIGURE 7: Comparison of user satisfaction evaluation.

be written into the database when they play music. All of the played music analyzed in this paper is recorded music for the sake of research. After existing users log in, the system will generate a list of recommendations based on the user's situation and then finish the prediction recommendation work. The user satisfaction of the music recommendation prototype system is assessed in this section, as well as the system's usability. The comparison of user satisfaction evaluation is shown in Figure 7.

By evaluating the recommendation results, we find that the overall performance of the system is good, and it can effectively recommend the results that users may be interested in to a certain extent, basically reaching the expected goal of the system design. Comparative experiments are carried out for different algorithms, in which each group of experiments is designed to compare the recommended algorithm with a simple model after adding tag information. The comparison results are shown in Figure 8.

It can be seen that, in the same data set, the recommendation effect of the recommendation algorithm proposed in this chapter is obviously better than the collaborative filtering algorithm based on users. The purpose of the algorithm is to get the music items that are most closely related to the user. The content-based recommendation method has the advantages of avoiding cold start and data sparseness because it does not need other users' related data. However, the premise of this method is to extract the project content into meaningful features, and the features require good structure, which is very restrictive in many recommendation systems. An important part of the recommendation algorithm experiment is to select and set reasonable experimental standards. If we want to detect the performance of the algorithm well, we must have a reliable evaluation standard. With the reliable evaluation standard, we can also detect the areas to be revised in the recommendation algorithm.

The recommendation system based on the knowledge map constructed in this paper realizes the function of recommending popular music for users and shows the actual

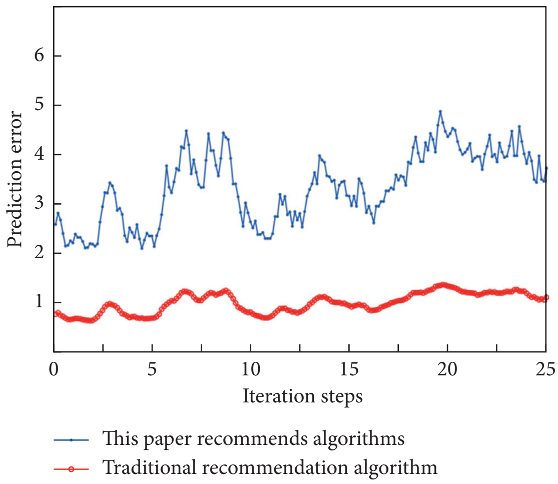

Figure 8: Comparison of two recommendation algorithms.

effect of the system. Experiments show that the algorithm can make full use of historical preferences and knowledge map relationship structure to deeply mine users' interests and hobbies. It has certain practicability.

5. Conclusions

With the advancement of the Internet and mobile networks, music has become an increasingly important form of entertainment in people's lives. Users, on the other hand, have higher standards for intelligent music recommendation. As a new application in the field of recommendation systems, intelligent music recommendation has a lot of research potential. Users' interest and loyalty to the system can be improved by using a knowledge map to analyze users' interests and accurately recommend personalized items that meet their interests, which is an inevitable trend in the development of commercial music systems and a hot field that scholars are scrambling to study. This paper builds a knowledge map-based recommendation system that is oriented to the application of music recommendation, realizes the function of recommending popular music to users, and shows the system's actual effect. A content recommendation algorithm with a unified embedding of behavior and knowledge features is proposed to solve the problem of knowledge map application in recommendation systems. To fully explore users' interests and hobbies, the algorithm makes extensive use of historical preferences and the knowledge map relationship structure. This paper uses the click prediction experiment to demonstrate the model's ability to dynamically learn related information and mine preferences deeply.

Data Availability

The data used to support the findings of this study are included within the article.

Conflicts of Interest

The author does not have any possible conflicts of interest.

References

[1] P.-J. Lu, A. Srivastav, T. A. Santibanez et al., "Knowledge of influenza vaccination recommendation and early vaccination uptake during the 2015-16 season among adults aged ≥18 years - United States," *Vaccine*, vol. 35, no. 34, pp. 4346–4354, 2017.

[2] Y. Huo, D. F. Wong, L. M. Ni, L. S. Chao, and J. Zhang, "Knowledge modeling via contextualized representations for LSTM-based personalized exercise recommendation," *Information Sciences*, vol. 523, pp. 266–278, 2020.

[3] W. Lv, L. Xu, and L. Jin, "A ten-year review of artificial intelligence research in China--based on the analysis of bibliometrics and knowledge graphs from 2008 to 2017," *Technoeconomics*, vol. 37, no. 10, p. 7, 2018.

[4] G. Zhu, B. Chenzhong, T. Gu, and C. Liang, "User preference neural modeling framework based on knowledge graph," *Pattern Recognition and Artificial Intelligence*, vol. 32, no. 7, p. 8, 2019.

[5] Z. Huang, Y. Liu, C. Zhan, C. Lin, W. Cai, and Y. Chen, "A novel group recommendation model with two-stage deep learning," *IEEE Transactions on Systems, Man, and Cybernetics: Systems*, vol. 5, 2021.

[6] M. C. Fowler, T. C. Clancy, and R. K. Williams, "Intelligent knowledge distribution: constrained-action POMDPs for resource-aware multiagent communication," *IEEE Transactions on Cybernetics*, no. 99, pp. 1–14, 2020.

[7] Z. Xu, Z. Yu, Y. Dong, and W. Yan, "Research on the construction of the knowledge graph of film review sentiment analysis," *Computer Simulation*, vol. 37, no. 8, p. 7, 2020.

[8] Y. Yasarni, "A new knowledge-based link recommendation approach using a non-parametric multilayer model of dynamic complex networks," *Knowledge-Based Systems*, vol. 143, no. 3, pp. 81–92, 2017.

[9] W. Hou, X. Zhang, K. Song, and Z. Hui, "Intelligent recommendation method combining knowledge graph and Bayesian network," *Journal of China Institute of Electronics*, vol. 15, no. 5, p. 7, 2020.

[10] H. Liu and P. S. MiaoFangyan, "Knowledge graph analysis of artificial intelligence ethics research," *Journal of Information*, vol. 038, no. 7, pp. 85–93, 2019.

[11] J. Sun, J. Wang, and G. Ding, "Spectrum knowledge graph: intelligent engine for future spectrum management," *Journal on Communications*, vol. 42, no. 5, p. 12, 2021.

[12] Y. Cui, "Intelligent recommendation system based on mathematical modeling in personalized data mining," *Mathematical Problems in Engineering*, vol. 2021, no. 3, 11 pages, Article ID 6672036, 2021.

[13] J. Lei, S. Li, and R. Zhao, "Research on the construction and application of knowledge graph for scientific research archives management," *Science and Technology Management Research*, vol. 40, no. 11, p. 8, 2020.

[14] H. Li, Y. Zhang, and Y. Kang, "Fusion of cyclic knowledge graph and collaborative filtering movie recommendation algorithm," *Computer Engineering and Applications*, vol. 56, no. 2, p. 9, 2020.

[15] L. ákos, F. András, L. Agnes et al., "Direct effect of contemporary health education programmes on the knowledge about hand hygiene and technique of hand washing in primary school age children," *Orvosi hetilap*, vol. 159, no. 12, pp. 485–490, 2018.

[16] X. Huang, "Research on big data intelligent question answering system of packaging industry based on knowledge

graph," *Modern Electronic Technology*, vol. 42, no. 14, p. 4, 2019.

[17] Y. Wu, X. Shen, and F. Xiao, "Design of intelligent question answering system in packaging field based on knowledge graph," *Packaging Engineering*, vol. 42, no. 15, p. 8, 2021.

[18] M. Shi, "Knowledge graph question and answer system for mechanical intelligent manufacturing based on deep learning," *Mathematical Problems in Engineering*, vol. 2021, no. 2, 8 pages, Article ID 6627114, 2021.

[19] D. Liu, R. Tong, and C. Zhang, "Intelligent diagnosis guidance algorithm based on multi-source knowledge graph fusion," *Chinese Journal of Information*, vol. 35, no. 1, p. 10, 2021.

[20] Z. Cheng and J. Shen, "On effective location-aware music recommendation," *ACM Transactions on Information Systems*, vol. 34, no. 2, pp. 1–32, 2016.

[21] A. Roy, S. Banerjee, M. Sarkar, A. Darwish, M. Elhoseny, and A. E. Hassanien, "Exploring New Vista of intelligent collaborative filtering: a restaurant recommendation paradigm," *Journal of Computational Science*, vol. 27, no. 7, pp. 168–182, 2018.

[22] Z. Jia, T. Gu, and B. Chenzhong, "Scenic spots recommendation based on feature learning of tourism knowledge graph," *Journal of Intelligent Systems*, vol. 14, no. 3, p. 8, 2019.

[23] L. Zhou, H. Liang, and Z. Gao, "Construction of tang poetry knowledge graph and its intelligent knowledge service design," *Library and Information Service*, vol. 63, no. 2, p. 10, 2019.

[24] Z. Xu, X. Zhao, and Y. Dong, "Video recommendation algorithm based on knowledge graph knowledge reasoning," *Computer Engineering and Design*, vol. 41, no. 3, p. 6, 2020.

[25] R. Kadaverugu, S. Dhyani, R. Dasgupta, P. Kumar, S. Hashimoto, and P. Pujari, "Multiple values of Bhitarkanika mangroves for human well-being: synthesis of contemporary scientific knowledge for mainstreaming ecosystem services in policy planning," *Journal of Coastal Conservation*, vol. 25, no. 2, pp. 1–15, 2021.

[26] Y. Li, X. Zhang, and Li Xin, "Construction and innovative application of disciplinary knowledge graph for smart education," *Audio-visual Education Research*, vol. 40, no. 8, p. 10, 2019.

[27] W. Zhao, N. Sun, and X. Yang, "Research and application of oriental music visualization education based on knowledge graph," *Computer Engineering and Science*, vol. 40, no. 1, p. 7, 2018.

[28] Y. Sun, K. Chang, and L. Zhu, "Large-scale knowledge graph and its application research," *Information Theory and Practice*, vol. 41, no. 11, p. 6, 2018.

[29] C. Jie, C. Zh, F. D. Hai, and Q. Meng, "Are providers' recommendation and knowledge associated with uptake of optional vaccinations among children? A multilevel analysis in three provinces of China," *Vaccine*, vol. 37, no. 30, pp. 4133–4139, 2019.

[30] R. Silva, C. K. Roy, M. M. Rahman et al., "CROKAGE: effective solution recommendation for programming tasks by leveraging crowd knowledge," *Empirical Software Engineering*, vol. 25, no. 10, pp. 1–52, 2020.

Hindawi
Computational Intelligence and Neuroscience
Volume 2022, Article ID 8202535, 10 pages
https://doi.org/10.1155/2022/8202535

Research Article

Vehicle Image Detection Method Using Deep Learning in UAV Video

Xiangqian Wang

School of Information on Engineering, Pingdingshan University, Pingdingshan, Henan, 467000, China

Correspondence should be addressed to Xiangqian Wang; 3431@pdsu.edu.cn

Received 29 December 2021; Revised 14 January 2022; Accepted 19 January 2022; Published 8 February 2022

Academic Editor: Xin Ning

Traditional machine learning algorithms are susceptible to objective factors such as video quality and weather environment in the vehicle detection of Unmanned Aerial Vehicle (UAV) videos, resulting in poor detection results. A vehicle image detection method using deep learning in UAV video is proposed. The algorithm in this paper treats surveillance video as many frames of images for vehicle detection in the image. First, perform HSV (Hue-Saturation-Value) spatial brightness translation operation on the original sample to increase the adaptability to different light conditions and sample diversity. Then, the Single Shot MultiBox Detector (SSD) model framework is used as the basis for vehicle detection. In order to obtain a better feature extraction effect, focus loss is added to the basic SSD for optimization. Finally, the trained network model is used to analyze the UAV video, and the detection performance is analyzed experimentally. The results show that the vehicle detection rate of this algorithm has reached 96.49%. It can ensure that the vehicle is accurately detected from the drone video.

1. Introduction

As the pace of urbanization in our country continues to accelerate, the number of roads and family cars in our cities is increasing, and road traffic pressure is increasing day by day. The research of intelligent transportation system is very important to ensure the smoothness and safety of roads [1, 2]. Intelligent transportation system uses information technology, such as image recognition, computer vision, etc. to realize more intelligent and automated road transportation system. It improves the throughput capacity of the road area and greatly facilitates the dispatch of the traffic management department. However, real-time acquisition of road traffic information is the basis for the realization of an intelligent transportation system. How to obtain high-quality road vehicle information has become an urgent problem to be solved.

At present, the collection methods of vehicle information mainly include loop coil detection, infrared detection and intelligent video surveillance detection [3–5]. Among them, the loop coil detection work is stable, the detection accuracy is high, and the traffic information can be counted. It is easy to install and set up, and is mostly used in areas such as traffic toll crossings and parking lots. Infrared detection mainly uses light-emitting diodes to detect vehicle speed, with high detection sensitivity. But it is easily affected by the environment, such as temperature, humidity, etc., resulting in low detection accuracy and low robustness. With the development of technologies such as image recognition and computer vision, intelligent video surveillance and detection has taken up an increasingly important position in traffic information collection. Intelligent video surveillance detection uses a camera set up at a traffic intersection to perform target analysis on the camera monitoring area to obtain unstructured information of the target in the video. The traffic monitoring video contains a wealth of information and is an important data source for intelligent traffic monitoring systems [6]. However, the data resources acquired by fixed cameras are limited. With the development of drone technology, it has begun to be widely used in traffic monitoring, with rich data types and efficient data acquisition. But how to detect the vehicle from the massive data is the difficulty of the research [7, 8].

At present, there have been many researches on vehicle identification in surveillance video. Reference [9] proposed an automatic detection method for smoke vehicles in traffic surveillance videos based on vehicle rear detection and multi-feature fusion. Using the Vibe background subtraction algorithm to detect foreground objects and remove non-vehicle objects according to the rules. An improved integral projection method is used to detect the rear of the vehicle to obtain the key area behind the rear of the vehicle. Effectively improve the accuracy of road safety early warning. Reference [10] proposed a smoke vehicle detection method by learning spatio-temporal representation from image sequences. The motion detection algorithm is used to obtain the tail of the vehicle that needs to be identified. And using time multi-layer perception or long short-term memory network to effectively train the smoke vehicle recognition model, which effectively improves the recognition accuracy. Reference [11] proposed a preprocessing framework with virtual single-layer sequences in traffic video surveillance. By fusing the effective element estimation module and the dynamic multi-stage parallel video image processing module, the robustness and effectiveness of vehicle detection in the video are improved.

With the rapid development of computer technology, machine learning algorithms have also been widely used in the field of image recognition. Reference [12] compares several commonly used video vehicle recognition methods including deep learning models and computer vision methods. The average accuracy, the semantics of recognizing vehicles, and the robustness of recognition when applied to data sets containing images with different lighting conditions are used to compare detection accuracy. The results show that the proposed deep learning method has better recognition performance. Reference [13] proposed a driver warning and collision avoidance system based on vehicle trajectory characteristics and long- and short-term memory neural network. By judging the video behavior of vehicles, road safety is effectively improved. However, the initial detection performance of the vehicle in the video still needs to be optimized. Reference [14] proposed a new type of hybrid artificial neural network and a mobile vehicle detection system based on the opposing gravity search optimization algorithm. Used to detect moving vehicles in traffic scenes to achieve effective traffic video surveillance. Optimizing the selection weights through the opposing gravity search optimization algorithm, effectively improving the recognition accuracy and speed of the artificial neural network. Reference [15] proposed a region-based Convolutional Neural Network (CNN) in vehicle detection algorithm. The rapid aggregation of road traffic data is effectively realized to improve traffic automation management. However, the above method is limited to the transmission image of the fixed camera for traffic video, and the flexibility is poor. Compared with ordinary video surveillance scenes, the video collected by drones has the advantages of wide surveillance range, less target occlusion, and more macroscopic traffic information provided. However, most existing machine learning methods are difficult to process real-time and massive drone video data. For this reason, a vehicle image detection method using deep learning in UAV video is proposed. The innovations of the proposed method are summarized as follows:

(1) Because a variety of different models, different appearances, and vehicle videos shot from different angles are collected from multiple video scenes. Light has a great influence on video recognition. The proposed method performs a spatial brightness translation operation on the original sample. To increase the adaptability of the classifier to different light conditions and sample diversity.

(2) In order to obtain a better feature extraction effect, the proposed method adds focus loss to the basic SSD for optimization to improve the detection accuracy.

2. UAV Video Characteristics Analysis

The video data used was hovered 50 meters directly above the road by the DJI phantom3 professional drone, and the camera lens was shot at -90°. The video resolution is 3840×2160. Video characteristics affect the choice of vehicle detection methods. Compared with ground-based fixed video, UAV video is mainly different in the following six aspects:

(1) Traffic information is more comprehensive, which is more valuable for application and research. From the UAV video, not only traffic information such as traffic flow and speed can be obtained, but also the traffic density of the road section and the accurate vehicle trajectory can be directly obtained [16]. It has important value in the study of traffic flow theory, driving behavior, car following (lane changing) and other traffic theories.

(2) There are more vehicles in the detection range, the smaller the vehicle size, and the greater the difficulty of detection. The UAV video image can contain hundreds of vehicles, so the vehicle size is small and the feature information is less.

(3) The video coverage is wider and the interference information is more. Under the premise of being able to detect vehicles, the UAV video range can reach up to several hundred meters. In addition to the concerned vehicle information in the image, there is also a large amount of invalid information. For example, buildings, street lights, signs and markings, motorcycles, etc.

(4) Different vehicle imaging has different vehicle detection methods. Usually, a fixed ground camera shoots the front or back of the vehicle. The drone shoots the top of the vehicle and uses the line characteristics to detect the vehicle in the fixed video. UAV video uses other methods.

(5) Video jitter is more obvious. Although the camera is installed on the drone's airborne gimbal, the drone is affected by the wind during the hovering flight, and the captured video image still exhibits irregular jitter. This increases the difficulty of accurately detecting vehicles [17].

(6) Due to the limitations of the drone's flight capability and endurance, it is usually only possible to obtain traffic videos in better weather conditions. The effective shooting time does not exceed 20 minutes.

The experimental data is a traffic video taken by a drone in a certain place in Zhengzhou in 2020. The video frame rate is 30 frames per second, and the video resolution is 1920 × 1080. Video 01 was shot at a straight intersection. Video 02 was shot at a T-junction. Video 03 was shot on an elevated section. The first frame of the experimental data is shown in Figure 1. And the detailed information of the experimental data is shown in Table 1.

3. Algorithm Design

3.1. Design Ideas of Vehicle Classifier. To achieve vehicle detection from the perspective of deep learning, use CNN method in deep learning to design a vehicle detector. The vehicle detector is realized by detecting whether the object in each detection frame is a vehicle. Therefore, it is necessary to design a vehicle classifier with improved CNN to realize the two-class classification of cars and non-cars. The process of training and testing the classifier model is shown in Figure 2.

First carry out a preprocessing operation on the training samples. Then put the training samples and corresponding labels into CNN for training, and get an improved CNN model. Then the test samples are also preprocessed, and the prediction results of the model are obtained by improving the CNN model. The prediction result is compared with the test sample label, and the final test result is obtained.

3.2. Dataset Preprocessing

3.2.1. Sample Collection. The size of 50 × 50 is selected as the input image size of the trained classifier, which is also the size of the vehicle detection frame in the actual video. For images whose sample size does not meet the requirements, the original samples that meet the requirements are obtained through cropping and scaling operations.

Because there is no vehicle sample set that includes different models and different angles. In multiple videos and many pictures, 2503 positive samples and 2,698 negative samples are collected to form a relatively complete vehicle classification data set. The pictures in the positive sample set include vehicles of different brands and types, and the angles at which they are taken are also different. The light conditions and background of each sample are also different, which fully guarantees the diversity of positive samples. If the classifier can identify these types of vehicles with different backgrounds, it is enough to show that the proposed classifier has strong adaptability [18, 19]. The negative sample set includes various background scenes without vehicles that may appear around the road. For example, there may be road signs, tree shades, pedestrians, trees, etc., which are also sufficiently diverse [20, 21].

3.2.2. Data Preprocessing. In order to enhance the adaptability of the classifier to different lighting environments and in the shade, the original data set is preprocessed in the HSV space. In the HSV color space, the V value represents the brightness, which is the brightness of the color, and it is also expressed as a percentage. Its value ranges from 0%, which means completely black, to 100%, which means completely bright. Therefore, the brightness can roughly indicate the brightness of the entire scene, and the brightness of the scene can be changed by the brightness shift operation. Shift the average V value of each original picture to 20%, 30%, 40%, 50%, 60% (because it is too dark at 20%, and the scene is too bright at 70%). While keeping the H value and S value unchanged, the new V value corresponding to each point is:

$$V_{\text{new}}(a,b) = \frac{V_{\text{old}}(a,b) \times \overline{V}_{\text{new}}}{\overline{V}_{\text{old}}}, \tag{1}$$

where $V_{\text{new}}(a,b)$, $V_{\text{old}}(a,b)$, $\overline{V}_{\text{new}}$, $\overline{V}_{\text{old}}$ represent the new lightness value, the old lightness value, the new lightness mean value and the old lightness mean value, respectively.

Through the above processing, a sample set covering multiple different brightness values is obtained. The number of positive and negative samples in the sample set has increased to 15,426 and 17,071 respectively. Before processing, first convert the image from RGB (Red-Green-Blue) to HSV space. After processing, all pictures need to be converted back to RGB space.

After that, all the samples processed above are grayed out. Using $R(a,b)$, $G(a,b)$ and $B(a,b)$ to denote the components of the R, G, and B channels of the pixel at position (a,b), respectively. Then the gray value of the corresponding point:

$$G(a,b) = 0.2989 \times R(a,b) + 0.5870 \times G(a,b) + 0.1140 \times B(a,b). \tag{2}$$

After grayscale, the grayscale value range of the grayscale image is [0, 255]. Finally, perform a simple normalization operation on the grayscale image data to obtain the input layer sample data:

$$I(a,b) = \frac{G(a,b)}{255}. \tag{3}$$

In summary, the preprocessing process of the original image is shown in Figure 3.

3.3. SSD Target Detection. The SSD network uses the classic network VGG as the basic network. Adding auxiliary structure after the basic network produces a detection with the following main characteristics.

The SSD network uses multi-scale feature map detection. The network adds the convolutional feature layer to the end of the extreme base. The size of these layers gradually decreases, and multiple scale detections are predicted values [22, 23]. The detected convolution model is different for each feature layer. Each feature layer (or optional existing feature layer of the base network) can use a set of convolution filters to generate a fixed set of predictions. For the feature layer of size $m \times n$ with d channels, use the $3 \times 3 \times d$ convolution kernel convolution operation to generate the score of category or the coordinate offset relative to the default box. At

(a) (b) (c)

Figure 1: First frame image of experimental data (a) Video 01 (b) Video 02 (c) Video 03.

Table 1: Details of experimental data.

No.	Length of time	Total frames
01	3 minutes and 35 seconds	5189
02	6 minutes and 12 seconds	12037
03	5 minutes and 49 seconds	10915

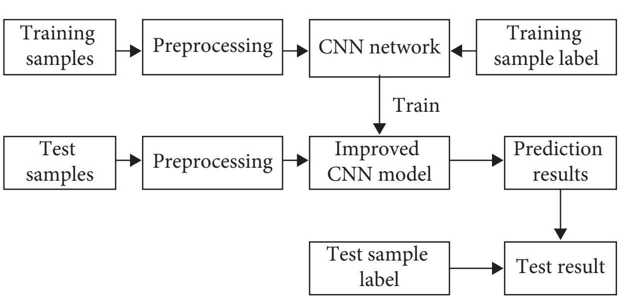

Figure 2: Process of training and testing CNN classifier.

each $m \times n$ size position where the convolution kernel operation is applied, an output value is generated. The output value of the bounding box offset is measured relative to the default box, and the default box position is relative to the feature map. The core of the SSD algorithm is to use both high-level feature maps and low-level feature maps for detection. The feature maps of different layers are used to imitate the detection of objects at different scales. The default candidate box refers to a series of fixed-size bounding boxes on each small grid of the feature map, as shown in Figure 4.

Assume that there are k default candidate boxes for each cell in each feature map. Each default candidate box needs to predict p category scores and 4 coordinate information. If the size of a feature map is $m \times n$, then each feature map has $m \times n \times k \times (p + 4)$ outputs. The meaning of these outputs is that a 3×3 convolution kernel is used, and the number of convolution kernels when convolving the feature map of this layer contains two parts. The first part of the quantity $m \times n \times k \times p$ is the output of confidence, which represents the confidence of each default candidate box, that is, the probability of the category. The second part $4 \times m \times n \times k$ is the output of the coordinate position, which represents the coordinate of each default candidate box after returning.

In training, another concept is a priori candidate box. Refers to the default alternative box selected in practice. During training, a complete picture is input to the network to obtain several feature maps [24]. For positive sample training, it is necessary to first match the prior candidate box with the correctly labeled candidate box. A successful match indicates that the a priori candidate box is the target to be

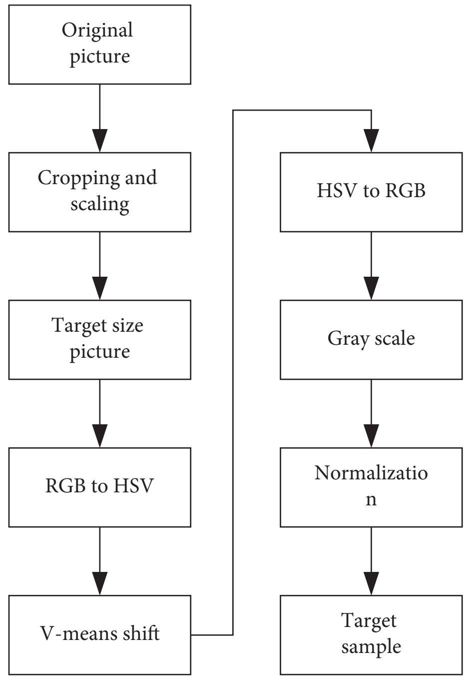

Figure 3: Preprocessing process of sample set.

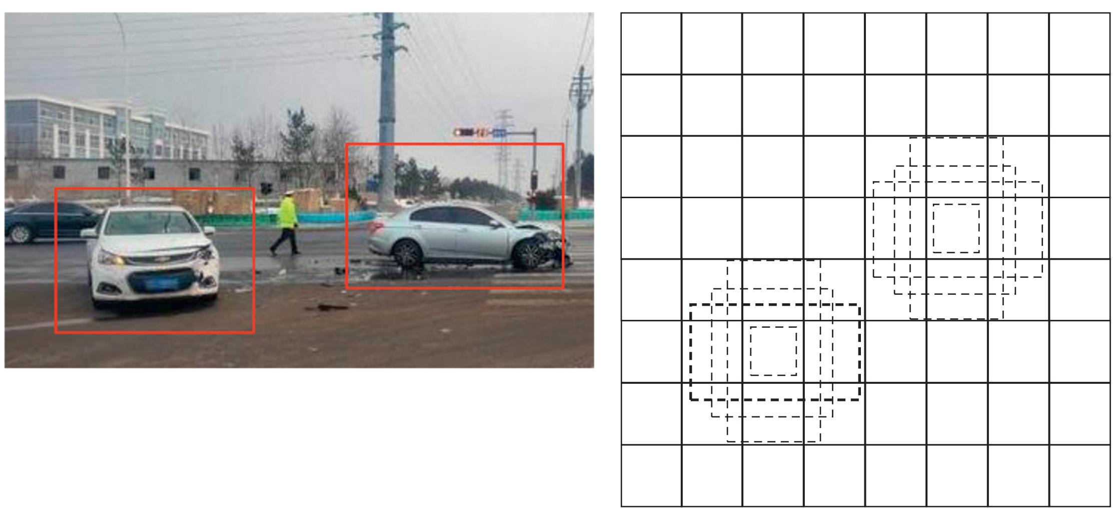

(a) (b)

Figure 4: Continued.

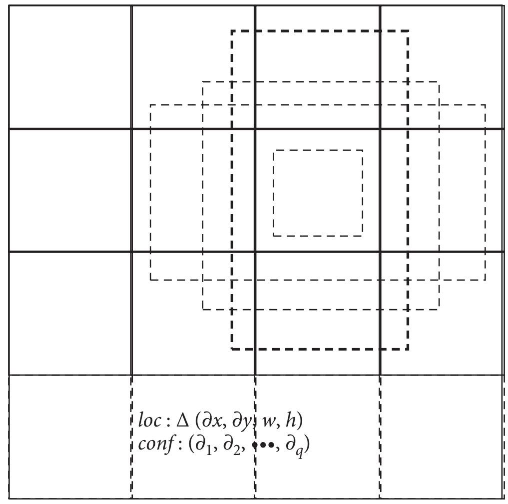

(c)

Figure 4: The generation of default candidate box (a) Image with GT boxes (b) 8 × 8 characteristic map (c) 4 × 4 characteristic map.

detected, but there is still a certain gap from the complete target. The purpose of training is to ensure the classification confidence of the default candidate box while returning the prior candidate box to the correctly labeled bounding box as much as possible. For example, suppose there are 2 correctly labeled bounding boxes in a training sample. There are totally 8732 default candidate frames obtained in all feature maps. Then there may be 10 and 20 a priori candidate boxes that can be matched with the two correctly labeled bounding boxes respectively. The training loss includes positioning loss and regression loss.

Experiments have shown that the greater the number of default candidate box shapes, the better the final effect. The default candidate box used here is the same as the candidate box in Faster R–CNN. The difference is that the candidate box in Faster R–CNN is only used in the last convolutional layer, but in SSD, the default candidate box is applied to multiple different feature maps. The size and aspect ratio of the default candidate box are determined by certain calculations. Assuming that g feature maps are used for prediction, the size of the default candidate box for each feature map is calculated as follows:

$$s_k = s_{\min} + \frac{s_{\max} - s_{\min}}{g-1}(k-1), \quad k \in [1, g], \tag{4}$$

where, $s_{\min} = 0.2$ indicates that the size of the bottom layer is 0.2. $s_{\max} = 0.9$ indicates that the size of the highest layer is 0.9.

For the aspect ratio, it is represented by β_r. There are five aspect ratios, namely $\beta_r = \{1, 2, 3, 1/2, 1/3\}$. Therefore, the width of each default candidate box is calculated as $w_k^\beta = s_k\sqrt{\beta_r}$. The calculation formula for height is $h_k^\beta = s_k\sqrt{\beta_r}$. In addition, when the aspect ratio is 1, specify the size as $s_k = \sqrt{s_k s_{k+1}}$ additionally. That is, there are a total of 6 different default candidate boxes.

The center position of each default candidate box on the feature map is set to $(a + 0.5/|f_k|, b + 0.5/|f_k|)$. Where $|f_k|$ represents the size of the k th feature map. The default frame coordinates captured by $a, b \in (0, |f_k|)$ make it always within [0, 1]. In fact, the distribution of default boxes can be designed to best fit a particular database.

By combining the predictions of all default boxes of different sizes and aspect ratios of many feature maps at all positions, a diversified set of predictions can be obtained, covering various input object sizes and shapes [25].

After the default candidate box is matched with the correctly labeled target box, it can be known that most of the default candidate boxes are negative samples, especially when the number of possible default selected boxes is large. This leads to a serious imbalance of positive and negative samples during training. The SSD algorithm is sorted according to the highest confidence of each default candidate box. And choosing those candidate boxes with high confidence so that the ratio between positive and negative samples is at most 3 : 1, instead of using all negative samples. After such processing, the optimization speed of the training process is faster and more stable.

In order to make the model more robust to the size and shape of various input objects, each training image is randomly sampled by one of three methods. (1) Using the entire original image as input. (2) Sampling a small fragment to make the object's smallest Intersection over Union (IoU) overlap of 0.1, 0.3, 0.5, 0.7, or 0.9. (3) Randomly sample a segment. The size of each sample segment is between 0.1 and 1 times the size of the original image, and the aspect ratio is between 0.5 and 2. If the correctly labeled target frame is in the sample segment, the overlapped part is retained. After the above sampling steps, the size of each sampling slice is adjusted to a fixed size and flipped horizontally with a probability of 0.5.

The commonly used objective loss function for multi-classification tasks is cross-entropy loss. Assuming that there are n samples in the task and the classification target has C class, the cross entropy CE is defined as follows:

$$\mathrm{CE} = \frac{1}{n}\sum_{i=1}^{n}\sum_{j=1}^{C} - y_j^{(i)} lb\Big(\widehat{f}\big(x^{(i)}\big)_j\Big), \tag{5}$$

where, $\widehat{f}(x)$ represents the predicted class probability. y is the one-hot vector of the actual category. The cross entropy function itself treats all types of objects equally. When encountering category imbalance phenomenon, it is easy to cause prediction deviation, and it is impossible to strengthen training on difficult-to-separate samples. In view of the category imbalance phenomenon, a weighting factor α can be introduced for different categories to weaken the influence of a large number of categories on the loss value:

$$\mathrm{CE} = \frac{1}{n}\sum_{i=1}^{n}\sum_{j=1}^{C} - \alpha_j y_j^{(i)} lb\Big(\widehat{f}\big(x^{(i)}\big)_j\Big). \tag{6}$$

Aiming at the problem of difficult samples, the higher the predicted probability of a sample, the stronger the model's ability to recognize the sample. This sample becomes an easy-to-separate sample, and vice versa, it is a difficult-to-separate sample. Based on the predicted probability, a weighting factor β can be introduced to weaken the influence of easily divided samples on the loss value. β is defined as follows:

$$\beta_j^{(i)} = \big(1 - y_j^{(i)}\big)^{\gamma}, \tag{7}$$

where γ is an adjustable hyper parameter. The focus loss FL is defined as:

$$\mathrm{FL} = \frac{1}{n}\sum_{i=1}^{n}\sum_{j=1}^{C} - \alpha_j \beta_j^{(i)} y_j^{(i)} lb\Big(\widehat{f}\big(x^{(i)}\big)_j\Big). \tag{8}$$

This paper applies the above-defined multi-category focus loss to the SSD model. The values of α and γ are both 0.75.

The SSD algorithm uses VGG16 as the basic network. First, perform pre-training on the data set, and convert Full Connection Layer (FC) 6 and FC7 into convolutional layers. The parameters are sampled from the FC6 and FC7 layers, and all dropout layers and FC8 layers are deleted. And using Stochastic gradient descent (SGD) to fine-tune the model. For each data set, the learning rate decay strategy is slightly different.

3.4. Network Training. Before training, perform image enhancement by performing operations such as horizontal flipping, contrast enhancement, saturation enhancement, and color transformation on all images. All models are implemented using the Tensorflow framework and trained for 400 cycles on the Nvidia1080 graphics card. For the Faster R–CNN model, the images are uniformly scaled to 1280×720 input network. The initial learning rate is 0.001. It drops to 1/10 of the previous value every 100 cycles. The gradient update method uses small batch stochastic gradient descent with momentum. The momentum factor is 0.99. For SSD models, the images are uniformly scaled to 500×500 input network. The initial learning rate is 0.001. Every 10 cycles it drops to 0.96 times the previous value. The gradient update uses RMSProp optimizer. The momentum factor is 0.99.

4. Experiment and Analysis

The hardware operating environment of the experiment is an Intel Core i5-6500 CPU, a notebook computer with a frequency of 3.20 GHz and a memory of 32 GB. The software environment mainly includes Windows 10 system, Visual Studio 2017 development environment and Open CV 3.2.0. Open CV is an open source computer vision library that provides various graphics processing functions. Open CV implements many general algorithms in graphics processing and computer vision. Among them, modules such as 2D features in Open CV, high-level interaction, video image reading and writing, image processing, and target tracking are mainly used. The proposed method is developed independently, and the development language is C++.

4.1. Evaluation Index. The goal of vehicle detection is to detect as many vehicles as possible. At the same time, as little as possible misdetection of vehicles occurs. In a real-world vehicle video stream, True Positive Rate (TPR), False Positive Rate (FPR), Average True Positive per Frame (ATP/Frame), Average False Positive per Frame (AFP/Frame), Average False Positive per Vehicle (AFP/Vehicle) and other indicators are evaluated. Among them, the last three index parameters are related to the actual video stream. Therefore, it is only used to evaluate the detection effect of the vehicle detection method in the real scene video stream. The first two parameters are not necessarily related to the video stream, and can also be applied to the training set and test set to evaluate the vehicle classification method.

TPR is the proportion of the number of vehicles Q_{TP} correctly detected as TP by the detector or classifier in a video stream segment or sample set to the actual total number of vehicles Q_{Total}:

$$\mathrm{TPR} = \frac{Q_{\mathrm{TP}}}{Q_{\mathrm{Total}}}. \tag{9}$$

FPR is the proportion of the number of targets Q_{FP} incorrectly determined as vehicles (FP) by the detector or classifier in all target Q_{P} determined as vehicles in a video stream segment or sample set:

$$\mathrm{FPR} = \frac{Q_{\mathrm{FP}}}{Q_{\mathrm{P}}}. \tag{10}$$

ATP/Frame is the average number of vehicles correctly detected per frame in a video stream segment:

$$\frac{\mathrm{ATP}}{\mathrm{Frame}} = \frac{Q_{\mathrm{TP}}}{z_{\mathrm{Frames}}}. \tag{11}$$

AFP/Frame is the number of vehicles that have been misdetected as non-vehicle targets in each frame in a video stream segment:

Table 2: Classification accuracy of different classifiers.

Classifier type	Number of correct tags/total tags	Accuracy rate (%)
LDM	2175/3068	70.89
SVM	2734/3068	89.11
Proposed method	2912/3068	94.92

$$\frac{\mathrm{AFP}}{\mathrm{Frame}} = \frac{Q_{\mathrm{FP}}}{z_{\mathrm{Frames}}}. \tag{12}$$

AFP/Vehicle is the ratio of the number of misdetected targets to the total number of vehicles $\Omega_{\mathrm{Vehicles}}$ in a traffic video stream segment:

$$\frac{\mathrm{AFP}}{\mathrm{Vehicle}} = \frac{Q_{\mathrm{FP}}}{\Omega_{\mathrm{Vehicles}}}. \tag{13}$$

By evaluating the above indicators of the video stream or sample set, the detection performance of a classifier or detector can be evaluated. Based on the above indicators, the higher the TRP, ATP/Frame, and the lower the FPR, AFP/Frame, AFP/Vehicle, the better the performance of vehicle detection method.

4.2. Compare the Classification Effects of Different Classifiers. First, compare the classification results of the proposed method with linear discriminant analysis (LDA), support vector machine (SVM) and other shallow classifiers on the test sample set.

It can be seen from Table 2 that among the shallow classifiers, the SVM classifier performs well in many sample sets. The same applies to the test sample set consisting of 3068 test samples. The classification accuracy rate using LDA is only 70.89%. Using the SVM classifier can increase the accuracy by about 19% to 89.11%. The proposed method has undergone 10-fold cross-validation, and finally obtained a relatively stable classification accuracy of 94.92%, which is 5 percentage points higher than the SVM method. This shows that the proposed method has a better classification effect than shallow classifiers in processing two-dimensional data sets. It is more suitable for vehicle detection.

Specifically, the entire test sample set is classified by the proposed method. The results are shown in Table 3.

According to the number of TP, TN, FP, and FN in Table 3, the sensitivity of the proposed method can be obtained: $S_n = \mathrm{TP}/\mathrm{TP} + \mathrm{FN} = 1399/1399 + 62 \times 100\% = 95.76\%$; The specificity is: $S_P = \mathrm{TN}/\mathrm{TN} + \mathrm{FP} = 1581/1581 + 26 \times 100\% = 98.38\%$; Therefore, the first type of error rate (false positive rate) of the classification model: $1 - S_p = 1.62\%$ indicates that 1.62% of the real non-vehicle samples were incorrectly judged as vehicle samples. The second type of error rate (false negative rate): $1 - S_n = 4.24\%$ indicates that among all the vehicle samples, 4.24% of the vehicles were not detected and were misjudged as vehicles.

The detailed classification results of the proposed method and LDA and SVM methods on the test set are shown in Table 4.

It can be seen from Table 4 that in the entire sample set, the TPR of the proposed method is 16.77% and 7.94% higher than that of the LDA and SVM classifiers, respectively. The FPR is 18.03% and 5.27% lower than LDA and SVM, respectively. It shows that under the comprehensive evaluation of these two performance indicators, the proposed method has better detection effect and fewer false detections.

The preprocessing of the original sample will have a greater impact on the later vehicle detection. Therefore, before and after preprocessing, the classification accuracy results of the three methods are shown in Table 5. The second column of data in the table is the classification accuracy of the three methods for the original samples without HSV spatial brightness translation. The third column of data corresponds to the training result after the original sample is subjected to a large brightness shift in the HSV color space.

It can be seen from Table 5 that the classification accuracy of LDA in the two cases is not much different, the difference is only 0.36%. However, the accuracy of SVM and the proposed method under the preprocessing of HSV data is about 5% higher than that of unprocessed data. It can be seen from this that sample training is required for vehicle detection. A richer sample set can significantly improve the classification performance of the classifier.

4.3. Performance Comparison of Different Models. In order to demonstrate the detection performance of the proposed model, compare it with reference [9, 11], and [15], and the results are shown in Table 6.

It can be seen from Table 6 that compared with other comparison models, the detection effect of the proposed model is better, and its TPR reaches 96.49%. Reference [9] realizes the automatic detection of smoke vehicles based on multi-feature fusion and improved integral projection method. It can accurately detect vehicles to a certain extent. However, the detection method is relatively traditional, and it is difficult to apply to UAV video data. Therefore, the detected TPR is only 81.92%. Reference [10] uses motion detection algorithms to acquire vehicle information, and uses temporal multi-layer perception or long- and short-term memory networks to train vehicle recognition models. Compared with reference [9], it can effectively improve the recognition accuracy, with a TPR of 88.61%. However, the UAV moves fast and has a lot of video data, so the recognition effect is limited to a certain extent. Reference [15] uses the regional CNN network to achieve vehicle detection, which can quickly aggregate road traffic data, thereby improving automated traffic management. However, it lacks data preprocessing, so the recognition accuracy rate of the proposed method is reduced by 3% to 6%. All the proposed models can achieve better vehicle detection. It uses HSV for data preprocessing, and both deep learning models can complete accurate learning of massive data.

Table 3: The classification effect of the proposed method in the test sample set.

Number	Judged as positive sample	Judged as negative sample	Total
Actual positive sample	1399 (TP)	62 (FN)	1461
Actual negative sample	26 (FP)	1581 (TN)	1607
Total	1425	1643	3068

Table 4: Detailed classification results of different methods in the test sample set.

Method	LDA	SVM	Proposed method
Number of positive samples	1461	1461	1461
Number of positive samples detected	1154	1283	1399
Number of negative samples	1607	1607	1607
Number of negative samples detected	1288	1493	1581
TPR (%)	78.99	87.82	95.76
FPR (%)	19.85	7.09	1.82

Table 5: Classification accuracy of different methods before and after pretreatment of original samples.

Method	Accuracy rate (%) (Raw data)	Accuracy rate (%) (HSV)
LDA	70.88	71.24
SVM	82.01	88.26
Proposed method	90.79	95.03

Table 6: Vehicle detection results of different models.

Model	TPR (%)
Ref. [9]	81.92
Ref. [11]	88.61
Ref. [15]	90.27
Proposed method	96.49

5. Conclusion

The accuracy and stability of UAV video vehicle detection is crucial to extracting traffic information. For this reason, a vehicle detection method using deep learning in UAV video is proposed. Based on the HSV spatial brightness translation operation of the original samples, two deep learning models, the improved Faster R–CNN and SSD, are used to detect vehicles in UAV videos. Based on the DJI UAV's shooting video data set for experimental analysis. The results show that the use of HSV for data transformation can enrich the sample set, thereby improving the detection accuracy. The accuracy before and after pretreatment is increased by about 5%. The SSD model of the proposed method processes the data after HSV transformation, and the powerful data learning ability of the model can improve the detection effect. Its vehicle detection rate reached 96.49%. And the SSD model can act on multiple feature maps, and its detection effect is better.

Deep learning technology has shown great potential in target detection, and it is more advantageous for rapid target detection in complex scenes. However, deep learning requires large samples for support, and speed is not an advantage. These two determine the limitations of deep learning in real-time target tracking applications. Therefore, in the future, we will focus on the application of deep learning under small sample training in video target detection, and focus on solving real-time problems.

Data Availability

The data used to support the findings of this study are included within the article.

Conflicts of Interest

The authors declare that there is no conflict of interest regarding the publication of this paper.

References

[1] Y. Yang, H. Song, S. Sun et al., "A fast and effective video vehicle detection method leveraging feature fusion and proposal temporal link," *Journal of Real-Time Image Processing*, vol. 18, no. 4, pp. 1–14, 2021.

[2] B. S. Kale, G. L. Gorale, U. K. Khalkar, and S. V. Patil, "Smart vehicle with automatic pneumatic bumper system and video surveillance," *International Journal of Electronics Engineering Research*, vol. 11, no. 1, pp. 1–8, 2019.

[3] Y. Zhang, D. Zhu, P. Wang, G. Zhang, and H. Leung, "Vision-based vehicle detection for VideoSAR surveillance using low-rank plus sparse three-term decomposition," *IEEE Transactions on Vehicular Technology*, vol. 69, no. 5, pp. 4711–4726, 2020.

[4] Z. Cui, H. M. Sun, R. N. Yin, G. Li, B. H. Sun, and R. S. Jia, "Real-time detection method of driver fatigue state based on deep learning of face video," *Multimedia Tools and Applications*, vol. 80, no. 17, Article ID 25515, 2021.

[5] T. Jiang, M. Cai, Y. Zhang, and X. Jia, "Fast video-based queue length detection approach for self-organising traffic control," *IET Intelligent Transport Systems*, vol. 13, no. 4, pp. 670–676, 2019.

[6] Z. Liu, D. Lu, W. Qian et al., "A method for restraining gyroscope drift using horizon detection in infrared video," *Infrared Physics & Technology*, vol. 101, no. 3, pp. 1–12, 2019.
[7] D. Sudha and J. Priyadarshini, "An intelligent multiple vehicle detection and tracking using modified vibe algorithm and deep learning algorithm," *Soft Computing*, vol. 24, no. 21, pp. 1–13, 2020.
[8] Q. Zhang, H. Sun, X. Wu, and H. Zhong, "Edge video analytics for public safety: a review," *Proceedings of the IEEE*, vol. 107, no. 8, pp. 1675–1696, 2019.
[9] H. Tao and X. Lu, "Automatic smoky vehicle detection from traffic surveillance video based on vehicle rear detection and multi-feature fusion," *IET Intelligent Transport Systems*, vol. 13, no. 2, pp. 252–259, 2019.
[10] Y. Cao and X. Lu, "Learning spatial-temporal representation for smoke vehicle detection," *Multimedia Tools and Applications*, vol. 78, no. 6, pp. 27871–27889, 2019.
[11] M. Sankaranarayanan, C. Mala, and S. Mathew, "Pre-processing framework with virtual mono-layer sequence of boxes for video based vehicle detection applications," *Multimedia Tools and Applications*, vol. 5, no. 6, pp. 1–28, 2020.
[12] M. Bugeja, A. Dingli, and M. Attard, "Comparison of vehicle detection techniques applied to IP camera video feeds for use in intelligent transport systems," *Transportation Research Procedia*, vol. 45, no. 5, pp. 971–978, 2020.
[13] X. Peng, Y. L. Murphey, and R. Liu, "Driving maneuver early detection via sequence learning from vehicle signals and video images," *Pattern Recognition*, vol. 103, no. 4, pp. 107276–107286, 2020.
[14] A. Appathurai, R. Sundarasekar, and C. Raja, "An efficient optimal neural network-based moving vehicle detection in traffic video surveillance system," *Circuits, Systems, and Signal Processing*, vol. 39, no. 2, pp. 734–756, 2020.
[15] P. Priyadharshini and P. Karthikeyan, "Vehicle data aggregation from highway video of madurai city using convolution neural network," *Procedia Computer Science*, vol. 171, no. 4, pp. 1642–1650, 2020.
[16] S. S. Esfahlani, "Mixed reality and remote sensing application of unmanned aerial vehicle in fire and smoke detection," *Journal of Industrial Information Integration*, vol. 15, no. 3, pp. 42–49, 2019.
[17] R. Feng, C. Fan, and Z. Li, "Mixed road user trajectory extraction from moving aerial videos based on convolution neural network detection," *IEEE Access*, vol. 8, no. 4, pp. 43508–43519, 2020.
[18] J. Athanesious, V. Srinivasan, and V. Vijayakumar, "Detecting abnormal events in traffic video surveillance using super-orientation optical flow feature," *IET Image Processing*, vol. 14, no. 9, pp. 1881–1891, 2020.
[19] P. Martinez and M. Barczyk, "Implementation and optimization of the cascade classifier algorithm for UAV detection and tracking," *Journal of Unmanned Vehicle Systems*, vol. 7, no. 4, pp. 296–311, 2019.
[20] M.-R. Lee and D.-T. Lin, "Vehicle counting based on a stereo vision depth maps for parking management," *Multimedia Tools and Applications*, vol. 78, no. 6, pp. 6827–6846, 2019.
[21] S. Houben, M. Neuhausen, and M. Michael, "Park marking-based vehicle self-localization with a fisheye topview system," *Journal of Real-Time Image Processing*, vol. 16, no. 2, pp. 289–304, 2019.
[22] B. Yca, B. Bm, and C. Hong, "Part alignment network for vehicle re-identification - ScienceDirect," *Neurocomputing*, vol. 418, no. 5, pp. 114–125, 2020.
[23] A. Alipour-Fanid, M. Dabaghchian, and N. Wang, "Machine learning-based delay-aware UAV detection and operation mode identification over encrypted wi-fi traffic," *IEEE Transactions on Information Forensics and Security*, vol. 15, no. 7, pp. 2346–2360, 2020.
[24] S. N. Hashmi, K. Kumar, and S. Khandelwal, "Real time license plate recognition from video streams using deep learning," *International Journal of Information Retrieval Research*, vol. 9, no. 1, pp. 65–87, 2019.
[25] M. Ali, "Real-time raindrop detection based on cellular neural networks for ADAS," *Journal of Real-Time Image Processing*, vol. 16, no. 4, pp. 931–943, 2019.

Hindawi
Computational Intelligence and Neuroscience
Volume 2022, Article ID 9082694, 10 pages
https://doi.org/10.1155/2022/9082694

Research Article

Automated Segmentation of Mass Regions in DBT Images Using a Dilated DCNN Approach

Jianming Ye,[1] Weiji Yang,[2] Jianqing Wang,[2] Xiaomei Xu,[2] Liuyi Li,[2] Chun Xie,[1] Gang Chen,[3] Xiangcai Wang,[1] and Xiaobo Lai[2]

[1]*First Affiliated Hospital, Gannan Medical University, Ganzhou, China*
[2]*School of Medical Technology and Information Engineering, Zhejiang Chinese Medical University, Hangzhou, China*
[3]*Department of Medical Engineering, The 73th Group Army Hospital of P.L.A, Xiamen, China*

Correspondence should be addressed to Gang Chen; cg174@sohu.com, Xiangcai Wang; wangxiangcai@csco.ac.cn, and Xiaobo Lai; dmia_lab@zcmu.edu.cn

Received 6 December 2021; Revised 2 January 2022; Accepted 15 January 2022; Published 2 February 2022

Academic Editor: Guangming Zhang

To overcome the limitations of conventional breast screening methods based on digital mammography, a quasi-3D imaging technique, digital breast tomosynthesis (DBT) has been developed in the field of breast cancer screening in recent years. In this work, a computer-aided architecture for mass regions segmentation in DBT images using a dilated deep convolutional neural network (DCNN) is developed. First, to improve the low contrast of breast tumour candidate regions and depress the background tissue noise in the DBT image effectively, the constraint matrix is established after top-hat transformation and multiplied with the DBT image. Second, input image patches are generated, and the data augmentation technique is performed to create the training data set for training a dilated DCNN architecture. Then the mass regions in DBT images are preliminarily segmented; each pixel is divided into two different kinds of labels. Finally, the postprocessing procedure removes all false-positives regions with less than 50 voxels. The final segmentation results are obtained by smoothing the boundaries of the mass regions with a median filter. The testing accuracy (ACC), sensitivity (SEN), and the area under the receiver operating curve (AUC) are adopted as the evaluation metrics, and the ACC, SEN, as well as AUC are 86.3%, 85.6%, and 0.852 for segmenting the mass regions in DBT images on the entire data set, respectively. The experimental results indicate that our proposed approach achieves promising results compared with other classical CAD-based frameworks.

1. Introduction

Breast cancer is one of the leading causes of diseases in women worldwide, and it is also the most common cause of cancer deaths in women. Since the late 70s of the last century, the incidence of breast cancer worldwide has been increasing. According to the report "The Status and Trends of Cancer in China 2017" released by the National Cancer Center, the incidence of breast cancer ranks first among female malignant tumours [1]. Early diagnosis and treatment can effectively reduce the mortality of breast cancer patients and improve their quality of life [2]. In developed countries, organized and opportunistic screening programs have significantly reduced breast cancer mortality. Although two-dimensional mammography uses a new detector, it is well known that it still has its limitations because the normal structures and pathological structures may overlap each other when obtaining the transmission X-ray image [3].

Digital breast tomosynthesis (DBT) is a quasi three-dimensional imaging technology. An X-ray tube rotates in a limited arc, and a digital detector obtains a series of low-dose projection images to reconstruct the tomographic images [4]. DBT can evaluate the dense breast tissues in detail by describing the breast tissues in three dimensions to overcome the limitation that standard mammography only displays a two-dimensional image. In addition, the reconstructed DBT slice images can partially reduce the often called "anatomical" or "structure" noise caused by tissue superimposition in conventional mammography [5]. It is crucial to segment the breast mass regions in DBT slice images to provide accurate radiologists' qualification. Although DBT has higher sensitivity and specificity in breast mass regions detection, it has dramatically increased the amount of data in the image, resulting in manually annotating breast mass regions in DBT images. It is not only tedious but also time consuming for radiologists [6]. Hence, it is significant to develop a computer-aided segmentation framework for DBT mass regions to aid radiology clinicians to reduce the workload of manual annotation for the radiologists.

Automatic segmentation of breast mass regions is challenging because the breast mass regions have low contrast differences among their neighboring tissues [7]. Although it is difficult to achieve accurately segment breast mass regions, many studies focus on designing various automatic or semi-automatic learning-based approaches for breast mass regions segmentation in recent years [8–10]. Whereas automatic segmentation of breast masses from two-dimensional (2D) mammography has been widely investigated, little has been reported on segmenting breast mass regions automatically for DBT slice images. For each mass region, eight shape parameters and ten enhancement texture features were extracted and then an artificial neural network was used to build the diagnostic model; the average area under the receiver operating curve (AUC) reported by the system was 0.76 [11]. Breast tissues detection results were obtained using the multivariate statistical analysis of mass spectrometer data with a sensitivity of 90.9% and specificity of 98.8% [12]. If two-dimensional projected slice images and three-dimensional reconstructed volume can be combined for analysis, a computer-aided diagnosis (CAD) system of DBT can produce a lower false-positive rate [13]. In addition to research on breast segmentation by maximizing the radial gradient index in three dimensions of Reiser et al. [14], some publications only used a single representative two-dimensional slice [15, 16] to quantitatively evaluate the accuracy of mass regions segmentation in DBT images. Chan et al. [17] presented an approach on automatic detecting for breast mass regions. van Schie et al. [18] proposed an automated segmentation approach of breast mass regions, which used the mammography image data set to train the models. Kim et al. [19] concentrated on the influence of the saliency of the reconstructed slices on DBT mass regions' detection performance and then presented an automated detection system of breast mass regions based on the saliency of DBT reconstructed slices. Palma et al. [20] built a CAD framework based on the antagonistic reasoning and fuzzy theory, which can detect breast mass regions in reconstructed DBT images.

In recent years, deep learning has been successfully utilized in various medical image recognition tasks, such as tumour boundary detection, region segmentation, and pattern classification, because it does not adopt various handcrafted features in supervised manners [21–23]. The ResNet-50 model pretrained with transfer learning and class activation map technique were employed in breast cancer classification and localization, resulting in an AUC of 0.96 [24]. Sampaio et al. [25] proposed a computational methodology, where the quality of mammography image was improved initially by preprocessing, and the external region of breast was removed to reduce noise and highlight the internal structure of breast; next, the region was segmented and shape descriptors (such as eccentricity, circular disproportion and density) were extracted by using cellular neural networks, followed by an SVM classifier; they reported a sensitivity of 80% and AUC of 0.87. Wichakam and Vateekul [26] used support vector machines (SVMs) with ConvNets to detect mass on mammograms, where the reported accuracy was 98.44%, which was superior to the baseline (ConvNets) by 8%.

In this study, we combine DBT, a breast cancer screening method, with the latest machine learning and deep learning technologies. We focus on the accurate segmentation of the mass regions in DBT images using a deep convolutional neural network (DCNN) architecture, which is a fully convolutional network with dilated filters (dilated DCNN) instead of pooling filters. Besides, instead of training the model with the whole image, we implement a patch-based training approach. To produce an end-to-end segmentation output, we apply a fully convolutional network approach. Our system is used to every slice in a volume separately.

The structure of the paper is as follows: In Section 2, the data sets used and dilated DCNN architecture are introduced in detail, and then the training and testing methods of the dilated DCNN model for the mass regions segmentation in DBT images are introduced; Section 3 provides the details and results of the experiments performed in this study; Section 4 introduces the discussion, and the paper ends with Section 5, in which the conclusions and future work are presented.

2. Methodology

In this section, we will describe the data set used, the sampling procedure for generating input image patches, the architecture of the dilated DCNN, and the strategy for training the dilated DCNN, followed by the approach applied to segment the mass regions in DBT images and the evaluation metrics used.

A fully automatic framework for mass regions segmentation in DBT images is developed, an overview of the proposed architecture is shown in Figure 1. We apply a fully convolutional network approach to produce an end-to-end segmentation output. Our system is used to every slice in a volume separately.

2.1. DBT Image Data sets. The benchmarking clinical DBT image data used in this study are obtained from the Zhejiang Chinese Medical University Affiliated Guangxing Hospital (DBT_gx) and Zhejiang Provincial Hospital of Traditional Chinese Medicine (DBT_tcm) with Institutional Review Board (IRB) approval. Each DBT volume is produced by low-dose exposure, and the total shot dose should be within the range of a regular mammogram dose. Each patient's DBT data is acquired in medio-lateral oblique and cranio-

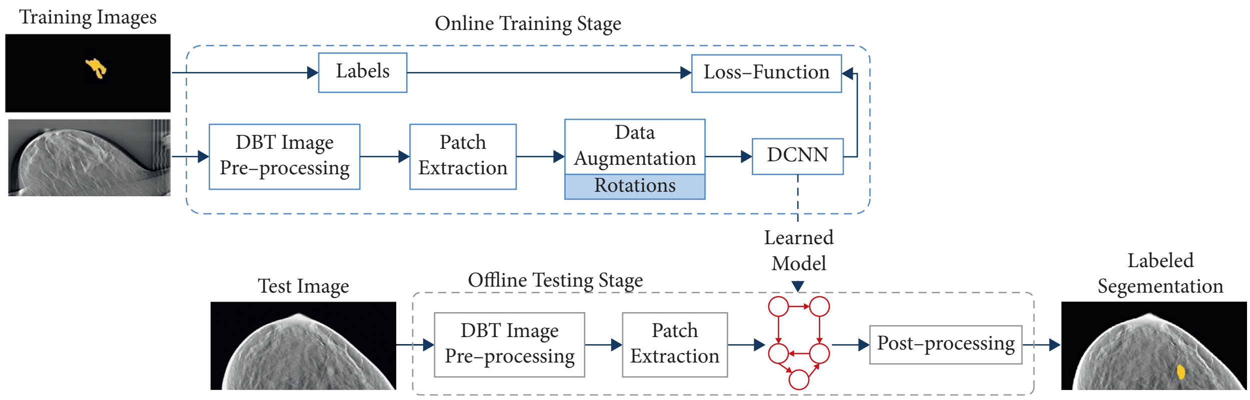

Figure 1: Overview of the proposed dilated DCNN approach.

caudal views (Siemens Mammomat Inspiration DBT system), using a total tomographic angular range of 60° with a 5° rotation increment and 12 projection views. Both sets of DBTs are reconstructed to 1 mm spacing slice with a resolution of 1200 × 901 pixels using the simultaneous algebraic reconstruction technique. We convert the images into TIFF stack/slices and used data in TIFF format to keep more details.

A total of 66 cases of breast cancer patients is included with a mean age of 53.65 years and an age range of 28–70 years. The entire DBT data set includes 146 views from 73 breasts with 97 masses, with size ranged from 4.7 to 37.8 mm (mean = 16.3 mm, median = 17.6 mm). Among them, 42 are benign lesions (absolutely healthy) and 55 were malignant lesions as determined by biopsy with subsequent histopathologic analysis. For each view (medio-lateral oblique or cranio-caudal), the number of slices ranged from 50 to 80 (mean = 69, median = 61). Two experienced radiologists manually annotate 97 masses and compared their annotations to reduce possible subjective errors. If there are any inconsistencies, the correct annotation of the mass regions in the image is determined by doctor consultation.

2.2. Slice Image Preprocessing. For a typical DBT screening system, radiation exposure is a vital factor to avoid the risk of radiation-induced cancer. Hence, the low radiation dose is usually used to generate the DBT images. However, the total radiation dose of DBT is slightly higher than that of standard mammography. Generally, DBT image generally contains Poisson distribution noise. Considering the top-hat transformation can not only preserve more local details and highlight the hidden information but also suppress noise amplification. DBT images are preprocessed before the input patch extraction step, including using the top-hat transformation to enhance the contrast between the candidate breast mass location regions and background tissues. Furthermore, to improve the low contrast of breast tumour candidate regions and depress the background tissue noise in the DBT image effectively, a constraint matrix generated by an isotropic radial basis function centered on the candidate breast mass location region with a variance δ^2 (δ is 5 mm) is established and multiplied with the DBT image. Figure 2 shows the DBT image preprocessing results before and after preprocessing procedure, where Figures 2(a), 2(b) are the DBT image before and after preprocessed, respectively.

2.3. Input Patch Extraction. In our research work, compared with other DCNN-based detection problems, the DBT data sets available have a small number of image samples, so using the whole image directly is likely to result in overfitting. We split the entire DBT images into patches to address this issue, which increases data set dimension and complexity. As shown in Figure 3, we apply the sliding window method to scan the entire DBT image data and extract all possible input patches. All the patches are then classified according to the ground truth provided in the data sets. If the central pixel of an input patch is in the breast mass region, the input image patch is marked as positive (breast mass region candidate); Otherwise, it is designated as a negative (no mass region) label. Because the no mass regions can also provide valuable information for breast mass regions segmentation in DBT images, we extract image patches from breast mass regions and no breast mass region to augment the training image data. In other words, we use the image patches extracted from the no breast mass regions as the additional negative sample of dilated DCNN architecture training to help the proposed model distinguish the confounding regions and breast mass regions in the DBT images.

2.4. Dilated DCNN Architecture. This part will briefly introduce the architecture of the proposed dilated DCNN model and its application to our DBT mass regions segmentation framework. One of the problems of traditional typical CNN architectures using the max-pooling technique is that they will down-sample the image, resulting in segmented output with a resolution smaller than the input size. As shown in Figure 4 and Table 1, we use a new convolution network architecture, using dilated convolutions specially designed to get dense segmented output. The purpose of this model is to combine the multiscale context information systematically without losing the resolution, which is based on the dilated convolution to support the exponential

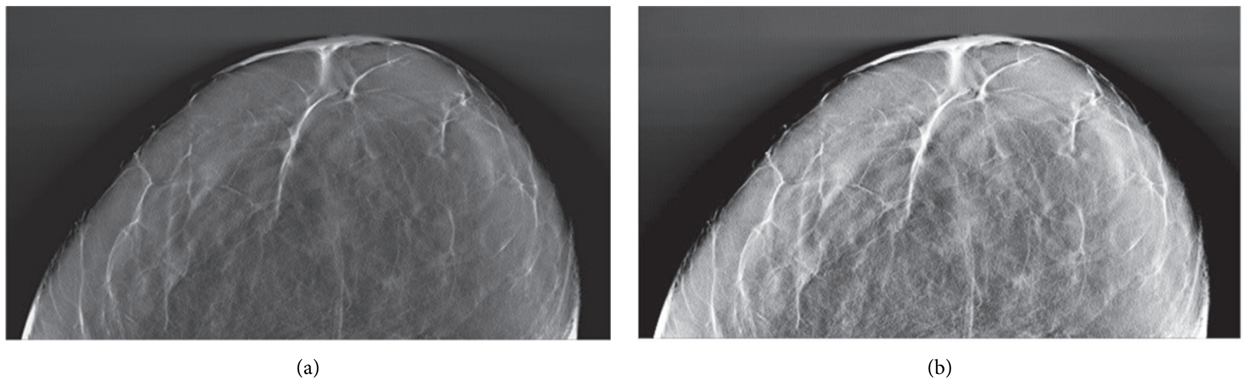

Figure 2: DBT image preprocessing results before and after preprocessing procedure. (a) DBT image before preprocessed. (b) DBT image after preprocessed.

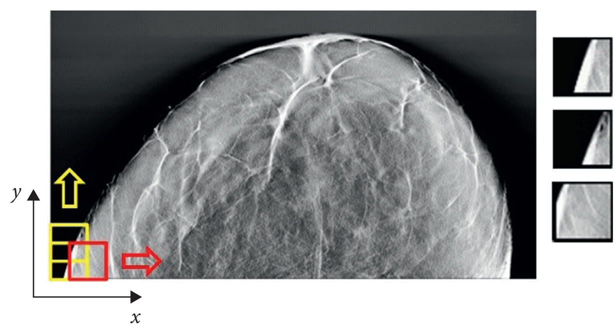

Figure 3: Sliding window method to scan the entire DBT image data and extract all possible input patches.

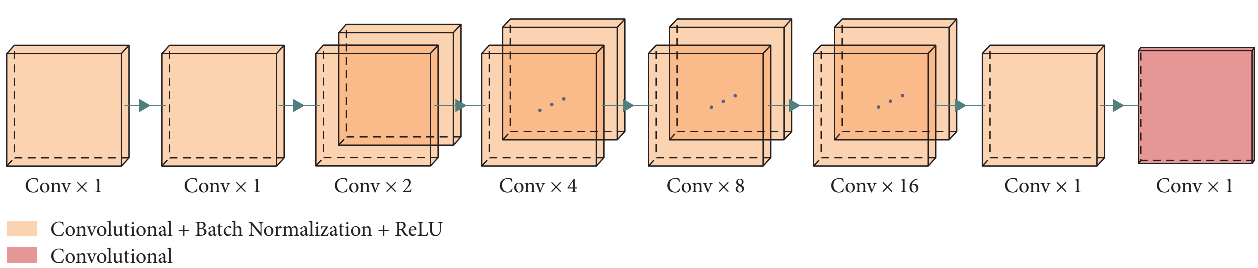

Figure 4: The proposed DCNN architecture.

expansion of the received field without losing the resolution or coverage.

Let f: Z^2 be a discrete function. Let $\Omega_k = [-k, k]^2 Z^2$, and let r: $\Omega_k \longrightarrow R$ be a discrete filter of size $(2k+1)^2$. The discrete convolution operator can be defined as

$$(f * r)(p) = \sum_{s+t=p} f(s) r(t). \tag{1}$$

We now generalize this operator. Let d be a dilation factor and let $*_d$ be defined as

$$(f *_d r)(p) = \sum_{s+dt=p} f(s) r(t). \tag{2}$$

We will refer $*_d$ as a dilated convolution or d-dilated convolution.

2.5. Patch-Based Training. The DBT image data sets used in our work exhibit serious class imbalance, i.e. the number of pixels in no breast mass regions is far more than that in breast mass regions. This brings a problem to the model's training because the pixels in the no breast mass regions influence the total loss function more than those in the breast mass regions. To settle this problem, we adopt an image patch-based training approach. In the training process, we balance the training image data by randomly resampling the same number of image patches of every class from all possible patches in each epoch. However, breast mass regions segmentation still has a similar problem of class imbalance. The number of positive samples is far less than the number of negative samples. Therefore, we adopt f_α-measure as cost function, which is also known as the Dice

Table 1: The proposed dilated DCNN configuration and parameters.

Layer	Type	Configuration	Dilation	Number of parameters
1	Convolutional Batch normalization ReLU	$3 \times 3 \times 1 \times 32$	1	2256
2	Convolutional Batch normalization ReLU	$3 \times 3 \times 32 \times 32$	1	18464
3	Convolutional Batch normalization ReLU	$3 \times 3 \times 32 \times 32$	2	36928
4	Convolutional Batch normalization ReLU	$3 \times 3 \times 32 \times 32$	4	73856
5	Convolutional Batch normalization ReLU	$3 \times 3 \times 32 \times 32$	8	147712
6	Convolutional Batch normalization ReLU	$3 \times 3 \times 32 \times 32$	16	295424
7	Convolutional Batch normalization ReLU	$3 \times 3 \times 32 \times 32$	1	295424
8	Convolutional	$1 \times 1 \times 32 \times 2$	1	16384

coefficient. Compared with conventional loss (e.g., mean square error), the f_α-measure enforces a better balance between performance on positive and negative regions, and thus is suitable for the task of mass regions in DBT images (having unbalanced samples in mass regions and nonmass regions).

Denote T and S as the ground truth heatmap and the predicted heatmap, respectively. Let M represent the number of elements (pixels) in T and S, and the f_α-measure-based loss function is defined in formula (3)

$$f_\alpha(S,T) = \frac{\left(1+\alpha^2\right)\sum_{i=1}^{M} s_i t_i}{\sum_{i=1}^{M} s_i + \sum_{i=1}^{M} t_i}, \tag{3}$$

where t_i is the ith element of the ground truth heatmap and s_i is the i-th element of the predicted heatmap. In this paper, we set $\alpha = 1$ based on the number of pixels in mass regions to the number of pixels in nonmass regions. If α is set to a higher value, the model loss mostly comes from the error of the mass regions, thus ignoring the error of the nonmass regions; otherwise, if setting to a smaller value, the model does not pay enough attention to the mass region because of the class imbalance, which reduces the segmentation accuracy.

2.6. DBT Image Data Augmentation. Extend the image data and generate more training data from the original image data to improve the performance of the proposed dilated DCNN model. Typical applications of the DCNN model for medical image analysis and computer vision tasks, rotations, and translations are often used to augment the data. In our work, the DBT image data consist entirely of 2D image patches. Hence, translation operation cannot augment the image data because it will cause a different image patch to have a possibly different class label. However, using rotation operations of the image patches might give some performance improvements. Therefore, we perform the rotation operation by using angles multiple of 90°.

2.7. Segmentation Postprocessing. In DBT images, some small clusters may be mistakenly classified as the breast mass regions. To deal with the problem, we impose a constraint by removing clusters in the segmentation output obtained by the proposed dilated DCNN-based system with less than 50 voxels in volumes.

2.8. Performance Analysis. To compare and analyze the performance with other classical CAD-based frameworks, the evaluation metrics used in this paper are (a) accuracy (ACC), sensitivity (SEN), and specificity (SPE) of the model; ACC refers to the ratio of the number of pixels correctly segmented to the number of total pixels in the image, SEN refers to the likelihood of a positive test among the subjects with the condition, and SPE refers to the probability of a negative test among the subjects without the condition. These three evaluation metrics are defined as follows:

$$\mathrm{ACC} = \frac{\mathrm{TP}+\mathrm{TN}}{\mathrm{TP}+\mathrm{TN}+\mathrm{FP}+\mathrm{FN}}, \tag{4}$$

$$\mathrm{SEN} = \frac{\mathrm{TP}}{\mathrm{TP}+\mathrm{FN}}, \tag{5}$$

$$\mathrm{SPE} = \frac{\mathrm{TN}}{\mathrm{TN} + \mathrm{FP}}. \quad (6)$$

TP, FP, TN, and FN denote true positive, false positive, true negative, and false negative, respectively, (b) free-response receiver operating characteristic curve (FROC), and (c) the area under the receiver operating curve (AUC). The FROC is used to evaluate the performance of the segmentation system on the DBT_gx and DBT_zcm data sets and is plotted between the fraction of correctly identified lesions as true-positive rate and the number of false-positive per volume (FPV) for all decision thresholds.

3. Results

3.1. Experimental Details. In this section, experiments with different training data sets are performed to evaluate the performance of the proposed dilated DCNN model. Note that in all cases, the original resolution of the processed DBT image is used. Patch-level data sets containing image patches of size 256×256 pixels are generated and used as the proposed dilated DCNN model inputs. In all experiments, a stride of 28×28 pixels is used to create the input image patches for training the dilated DCNN. The selection of the stride value is balanced according to the computational requirements and the number of training samples.

We apply the machine learning library Keras to implement the training and testing of the dilated DCNN model in Python 3.6. The training and testing experiments are performed on an NVIDIA Geforce Titan RTX 24G GPU with Intel Xeon Silver 4210 2.2 G GPU. The presented figures are generated using the plotting library matplotlib. To train the dilated DCNN, we used a batch size of 150 input image patches, 1000 batches per epoch, and 1000 epochs. We used an Adagrad optimizer [27] with a learning rate of 0.01.

3.2. Evaluation on Test Data sets. Given the limited data sets available in our study, mass regions segmentation in DBT images is performed using a ten-fold cross-validation strategy. Figure 5 presents FROC curves measuring the proposed dilated DCNN model trained on the DBT_gx and DBT_zcm data sets, respectively. Our dilated DCNN-based model's performance is substantially higher when the framework is tested on the DBT_gx data set with TPR = 0.971 ± 0.029 at 3.3 FPV, compared with that obtained on the DBT_zcm data set with TPR = 0.937 ± 0.008 at 4.0 FPV.

To further assess the mass regions segmentation performance in DBT images of our proposed method based on dilated DCNN, we evaluated the overlap between the proposed DBT mass labels and the ground truth maps. Figure 6 illustrates mass regions segmentation in DBT images on a few testing images using our proposed model. The 1st column shows individual segmentation results with our proposed dilated DCNN model for case #5, case #16, case #20, the 2nd column shows the corresponding ground truth maps, and a red arrow is used to indicate the lesion without obscuring the lesion in the 3rd column, respectively. The examples shown in Figure 5 indicate that the mass regions segmentation outputs predicted by our proposed dilated DCNN model are in high agreement with the manual annotations.

4. Discussion

In this study, a dilated DCNN architecture is specifically designed for the dense prediction of mass regions in DBT images, which systematically aggregates multiscale contextual information without losing resolution. Our proposed model adopts the f_{α}-measure as the cost function to suppress the influence of class imbalance. To generalize the applicability of the proposed dilated DCNN-based framework, we combine the two DBT image data sets into a larger data set, which is called the entire data set. In the experiments, we compare the performance of various typical automatic detection methods of breast mass regions in DBT images in terms of classifier used, DBT image data set size, SEN, ACC, and AUC. As can be seen in Table 2, our model based on dilated DCNN has achieved competitive results than some of them. Among these classic models, we will discuss the research work of Kim et al. [28], Fotin et al. [29], and Samara et al. [30] in detail. They applied deep learning to the detection and segmentation of breast mass regions in DBT images. Their research works evaluated the automated segmentation CAD frameworks for breast masses in DBT images using the hand-crafted feature- and DCNN-based models. The DCNN model proposed by Kim et al. [28] extracted low-level features from the regions of interest (ROIs) and corresponding ROIs, respectively, through the convolutional layers separately, which can recognize the latent bilateral feature representations of breast masses in the reconstructed DBT volumes. To represent the high-level bilateral features of breast masses in DBT images, they combined the low-level features into the fully connected layer. It was reported that the AUC of the latent bilateral feature representation model was 0.847. Fotin et al. [29] developed a DBT mass detection CAD framework using DCNN model. They trained the DCNN with the generated candidate ROIs, which included 1864 mammography breast lesions and 339 breast lesions from DBT images data. According to the report, 86.40% of ACC and 89% of SEN were obtained in their model. Samala et al. [30] proposed a DCNN framework composed of four convolutional layers and three fully connected layers. First, the DCNN model was trained on a large-scale two-dimensional mammography data set. The weights of the first three convolutional layers were frozen, and the rest weights continued to be trained and updated. Through the calculation results of the DCNN model, it can be seen that the AUC value was more than 0.8, and the SEN value was over 80%. As for the method proposed in our work, 87.1% ACC, 86.9% SEN, 88.2% SPE, and 0.859 AUC for the testing data set with 89 DBT volumes are obtained.

In other models not based on DCNN network, we select the studies of Chan et al. [17], van Schie et al. [16], Palma et al. [20], and Reiser et al. [31] for comparative analysis. Chan et al. [17] introduced three methods based on two-dimensional and three-dimensional, as well as the

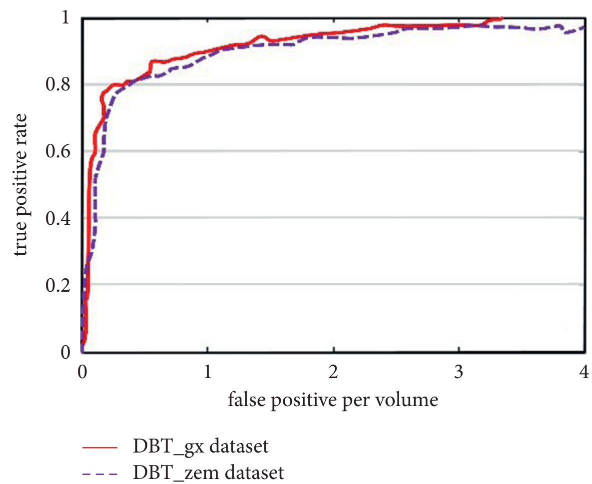

Figure 5: FROC curves for mass segmentation in DBT images on DBT_gx data set and DBT_zcm data set, respectively.

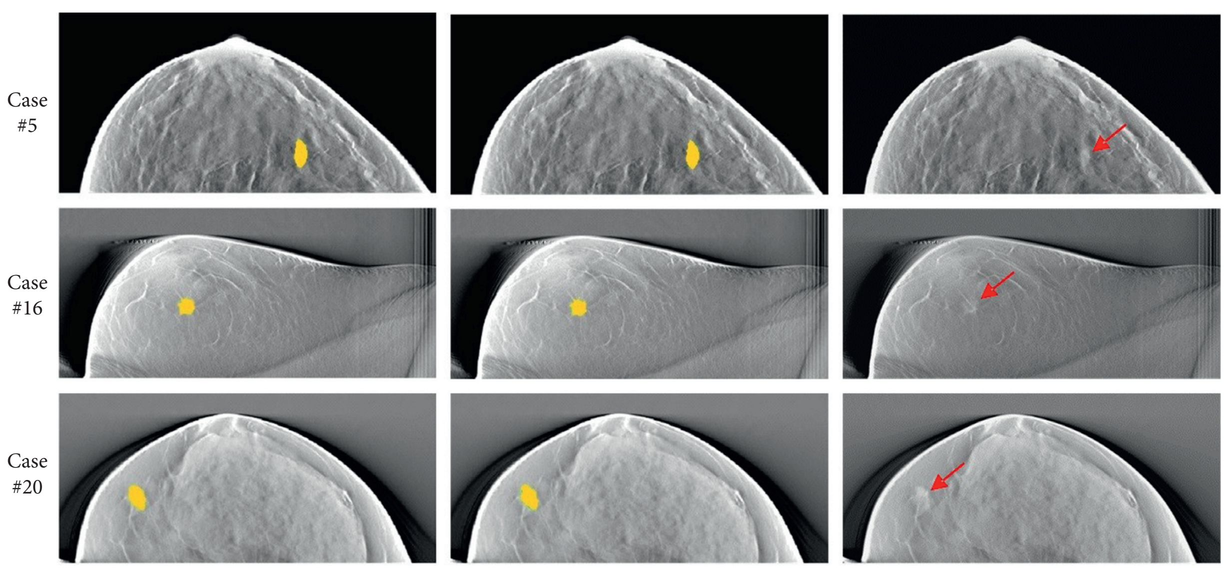

(a) Segmentation result (b) Ground truth map (c) Lesion location

Figure 6: Illustration of mass segmentation examples in DBT images using proposed model compared with manual labeled. (a) Segmentation result. (b) Ground truth map. (c) Lesion location.

combination of two-dimensional and three-dimensional methods. For the data set contained 100 DBT images from 69 patients with malignant patient cases, they obtained 80% SEN and 1.23 FPs/volume using the hybrid method. van Schie et al. [16] proposed a two-stage method, the first step was to locate ROIs in 2D slice images, and the second step was to locate 3D ROIs on DBT volumes combined with the extracted regions in 2D slice images. The results obtained from the DBT image data of 49 patients with one or more malignant tumours in 192 cases showed that 80% of the Sen was 3 FPs/volume. Palma et al. [20] developed a dual-channel DBT masses detection CAD framework in which each channel classified a type of DBT lesions. They combined discoveries and disjunction fusion methods from the channels. Their results showed that 90% SEN of the 101 DBT volumes contained 53 lesions. Reiser et al. [31] introduced a method of detecting DBT breast mass in two-dimensional projection views, and then reported 90% SEN for 36 DBT volumes using the visual angle range found in combination with detections.

Figure 7 shows examples of automatic segmentation of breast mass regions in DBT images by our dilated DCNN architecture and other typical CAD architectures, which is obtained by overlaying the breast mass regions in DBT images segmented by our proposed architecture and other typical CAD architectures to the original image, respectively. We carefully studied these methods presented by Kim et al. [28], Fontin et al. [29], Samala et al. [30], and Reiser et al. [31], then we configurated the frameworks and developed these models in Python 3.6 with the machine learning library Keras and applied the models to our own data set in our study. Otherwise, it is unfair to make a comparison of the

Table 2: Comparisons of typical studies in mass regions detection of the DBT images.

Method	Classifier	DBT image data set size	Sensitivity	Accuracy	AUC
Chan et al. [17]	LDA	100	80%	/	/
van Schie et al. [18]	NN	752	80%	/	/
Palma et al. [20]	SVM	101	90%	/	/
Kim et al. [28]	SVM	160	/	/	0.847
Fotin et al. [29]	DCNN	344	89%	86.4%	/
Samala et al. [30]	DCNN	324	80%	/	0.80
Reiser et al. [31]	LDA	36	90%	/	/
Proposed	Dilated DCNN	97	85.6%	86.3%	0.852

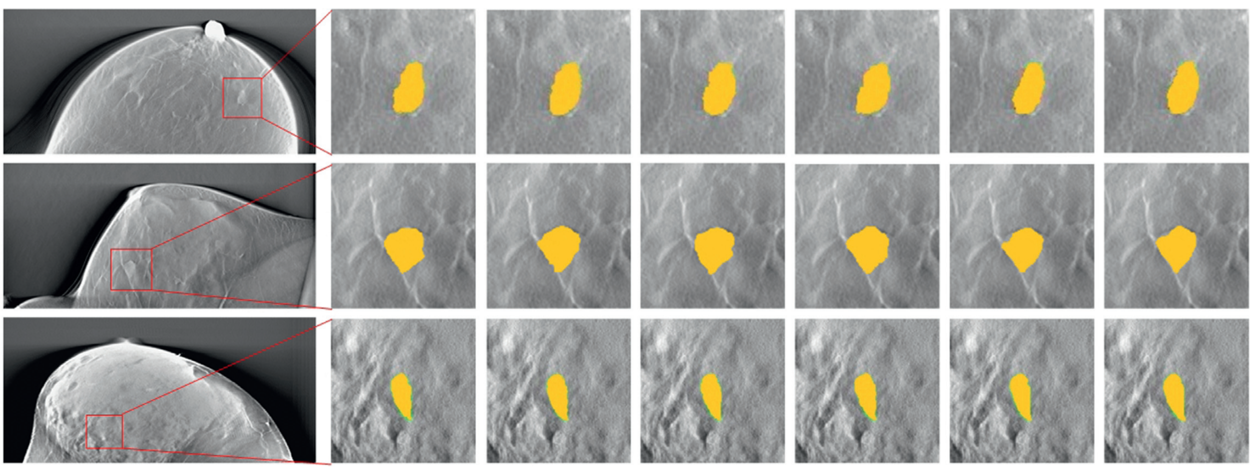

Figure 7: Examples of mass regions in DBT images segmented by our dilated DCNN framework and other typical CAD systems.

performance between our dilated DCNN model with other CAD models in automatic segmentation of breast masses in DBT images because other CAD models are trained and tested on different private data sets that are not available in public. Although the automatic segmentation model proposed in this paper cannot achieve the best overall DBT mass regions segmentation performance, our dilated DCNN framework achieves 86.3% ACC and 85.6% SEN with AUC of 0.852. The experimental results of this paper also indicate that our framework can get sound segmentation outputs on DBT image data set, and the dilated DCNN model is trained on the two-dimensional slice images of DBT volumes, not on the two-dimensional mammography data set. Although the proposed DCNN-based CAD framework has achieved promising results in automated segmentation of breast mass regions in DBT images, it can be further improved when there are more DBT image data. The main limitation of this study is the lack of sufficient DBT image data. To achieve satisfactory overall segmentation performance, our proposed automated segmentation framework for breast mass regions in DBT images needs more diverse data and structural distortion samples. Our proposed dilated DCNN-based approach can be applied to detect all early signs of breast tumour in DBT images, which is vital to decrease the review time for radiologists while maintaining or decreasing false positives.

5. Conclusions

This article presented a novel dilated DCNN-based architecture for mass regions segmentation in DBT images, performed experiments on an in-house collected DBT image data set, and obtained promising results. The constraint matrix is generated by using isotropic radial basis function and multiply with the DBT image to effectively improve the low contrast of candidate breast tumor regions and suppress the noise of background tissue regions. Our dilated DCNN architecture is specifically designed for dense prediction, systematically aggregating multiscale contextual information without losing resolution. Moreover, the proposed model adopts the f_α-measure as the cost function, further effectively suppresses the influence of class imbalance, and can improve the generalization ability of the segmentation. The average ACC, SEN, AUC obtained on the entire data set are promising and they are 86.3%, 85.6%, and 0.852, respectively. This study demonstrates that the presented dilated DCNN network has the potential to segment the mass regions in DBT Images accurately.

Data Availability

The raw/processed data required to reproduce these findings cannot be shared at this time as the data also forms part of an ongoing study.

Ethical Approval

The studies involving human participants were reviewed and approved by Institutional Review Board (IRB), Zhejiang Chinese Medical University. The patients/participants provided their written informed consent to participate in this study.

Disclosure

Jianming Ye and Weiji Yang are co-first authors.

Conflicts of Interest

No conflicts of interests, financial or otherwise, are declared by the authors.

Authors' Contributions

J. Ye, W. Yang, and X. Lai conceived and designed the study. J. Ye, W. Yang, J. Wang, X. Wang, and X. Lai contributed to the literature search. J. Ye, X. Xu, C. Xie, and X. Lai contributed to data analysis and data curation. J. Ye, L. Li, C. Xie, and X. Lai contributed to data visualization. J. Ye and G. Chen contributed for software implementation. J. Ye, W. Yang, J. Wang, C. Xie, X. Wang, and X. Lai contributed to the tables and figures. J. Ye, W. Yang, J. Wang, X. Xu, C. Xie, X. Wang, and X. Lai contributed to writing of the report. J. Ye, L. Li, G. Chen, and X. Lai contributed to review and editing. All the authors have read and approved the publication of this work. Jianming Ye and Weiji Yang contributed equally.

Acknowledgments

This work is funded in part by the Natural Science Foundation of Zhejiang Province of China (Grant no. LY16F010008) and also supported in part by the Medical and Health Science and Technology Plan of Zhejiang Province of China (Grant no. 2019RC224).

References

[1] X. Cheng, Z. Gu, X. Sun, and Z. Zhuang, "Study on the differences of opinions and choices of high-risk breast cancer populations in China before and after genetic testing," *Translational Cancer Research*, vol. 8, no. 8, pp. 2893–2905, 2019.

[2] S. P. Mihalco, S. B. Keeling, S. F. Murphy, and S. A. O'Keeffe, "Comparison of the utility of clinical breast examination and MRI in the surveillance of women with a high risk of breast cancer," *Clinical Radiology*, vol. 75, no. 3, pp. 194–199, 2020.

[3] S. Hong, S. Y. Song, B. Park et al., "Effect of digital mammography for breast cancer screening: a comparative study of more than 8 million Korean women," *Radiology*, vol. 294, no. 2, pp. 247–255, 2020.

[4] T. Hovda, A. S. Holen, K. Lång et al., "Interval and consecutive round breast cancer after digital breast tomosynthesis and synthetic 2D mammography versus standard 2D digital mammography in breastscreen Norway," *Radiology*, vol. 294, no. 2, pp. 256–264, 2020.

[5] A. E. Petropoulos, S. G. Skiadopoulos, A. N. Karahaliou, G. A. T. Messaris, N. S. Arikidis, and L. I. Costaridou, "Quantitative assessment of microcalcification cluster image quality in digital breast tomosynthesis, 2-dimensional and synthetic mammography," *Medical, & Biological Engineering & Computing*, vol. 58, no. 1, pp. 187–209, 2020.

[6] K. J. Geras, R. M. Mann, and L. Moy, "Artificial intelligence for mammography and digital breast tomosynthesis: current concepts and future perspectives," *Radiology*, vol. 293, no. 2, pp. 246–259, 2019.

[7] K. Mendel, H. Li, D. Sheth, and M. Giger, "Transfer learning from convolutional neural networks for computer-aided diagnosis: a comparison of digital breast tomosynthesis and full-field digital mammography," *Academic Radiology*, vol. 26, no. 6, pp. 735–743, 2019.

[8] C. A. Green, M. M. Goodsitt, K. K. Brock et al., "Deformable mapping technique to correlate lesions in digital breast tomosynthesis and automated breast ultrasound images," *Medical Physics*, vol. 45, no. 10, pp. 4402–4417, 2018.

[9] R. Girometti, L. Tomkova, L. Cereser, and C. Zuiani, "Breast cancer staging: combined digital breast tomosynthesis and automated breast ultrasound versus magnetic resonance imaging," *European Journal of Radiology*, vol. 107, pp. 188–195, 2018.

[10] R. A. Benedikt, J. E. Boatsman, C. A. Swann, A. D. Kirkpatrick, and A. Y. Toledano, "Concurrent computer-aided detection improves reading time of digital breast tomosynthesis and maintains interpretation performance in a multireader multicase study," *American Journal of Roentgenology*, vol. 210, no. 3, pp. 685–694, 2018.

[11] D. Newell, K. Nie, J. H. Chen et al., "Selection of diagnostic features on breast MRI to differentiate between malignant and benign lesions using computer-aided diagnosis: differences in lesions presenting as mass and non-mass-like enhancement," *European Radiology*, vol. 20, no. 4, pp. 771–781, 2010.

[12] E. R. St John, J. Balog, J. S. McKenzie et al., "Rapid evaporative ionisation mass spectrometry of electrosurgical vapours for the identification of breast pathology: towards an intelligent knife for breast cancer surgery," *Breast Cancer Research*, vol. 19, no. 1, p. 59, 2017.

[13] H. P. Chan, J. Wei, Y. Zhang et al., "Computer-aided detection of masses in digital tomosynthesis mammography: comparison of three approaches," *Medical Physics*, vol. 35, no. 9, pp. 4087–4095, 2008.

[14] I. Reiser, R. M. Nishikawa, M. L. Giger et al., "Computerized detection of mass lesions in digital breast tomosynthesis images using two- and three dimensional radial gradient index segmentation," *Technology in Cancer Research and Treatment*, vol. 3, no. 5, pp. 437–441, 2004.

[15] G. Peters, S. Muller, B. Grosjean, S. Bernard, and I. Bloch, "A hybrid active contour model for mass detection in digital breast tomosynthesis," *SPIE Proceedings of Medical Imaging*, vol. 6514, Article ID 65141V, 2007.

[16] L. Apffel, G. Palma, S. Muller, and I. Bloch, "Fuzzy segmentation of masses in digital breast tomosynthesis images based on dynamic programming," *Proceedings of the International Conference on Imaging Theory and Applications*, vol. 12, p. 7, 2010.

[17] H. P. Chan, J. Wei, B. Sahiner et al., "Computer-aided detection system for breast masses on digital tomosynthesis mammograms: preliminary experience," *Radiology*, vol. 237, no. 3, pp. 1075–1080, 2005.

[18] G. van Schie, M. G. Wallis, K. Leifland, M. Danielsson, and N. Karssemeijer, "Mass detection in reconstructed digital

breast tomosynthesis volumes with a computer-aided detection system trained on 2D mammograms," *Medical Physics*, vol. 40, p. 283, 2013.

[19] S. T. Kim, D. H. Kim, and Y. M. Ro, "Breast mass detection using slice conspicuity in 3D reconstructed digital breast volumes," *Physics in Medicine and Biology*, vol. 59, no. 17, pp. 5003–5023, 2014.

[20] G. Palma, I. Bloch, and S. Muller, "Detection of masses and architectural distortions in digital breast tomosynthesis images using fuzzy and a contrario approaches," *Pattern Recognition*, vol. 47, no. 7, pp. 2467–2480, 2014.

[21] M. Karimi, M. Majidi, H. MirSaeedi, M. M. Arefi, and M. Oskuoee, "A novel application of deep belief networks in learning partial discharge patterns for classifying corona, surface, and internal discharges," *IEEE Transactions on Industrial Electronics*, vol. 67, no. 4, pp. 3277–3287, 2020.

[22] C. Bai, L. Huang, X. Pan, J. Zheng, and S. Chen, "Optimization of deep convolutional neural network for large scale image retrieval," *Neurocomputing*, vol. 303, pp. 60–67, 2018.

[23] B. Wu, Y. Fang, and X. Lai, "Left ventricle automatic segmentation in cardiac MRI using a combined CNN and U-net approach," *Computerized Medical Imaging and Graphics*, vol. 82, Article ID 101719, 2020.

[24] W. E. Fathy and A. S. Ghoneim, "A deep learning approach for breast cancer mass detection," *International Journal of Advanced Computer Science and Applications*, vol. 10, p. 175, 2019.

[25] W. Borges Sampaio, E. Moraes Diniz, A. Corrêa Silva, A. Cardoso de Paiva, and M. Gattass, "Detection of masses in mammogram images using CNN, geostatistic functions and SVM," *Computers in Biology and Medicine*, vol. 41, no. 8, pp. 653–664, 2011.

[26] I. Wichakam and P. Vateekul, "Combining deep convolutional networks and svms for mass detection on digital mammograms," *International Conference on Knowledge and Smart Technology (KST)*, vol. 6, p. 239, 2016.

[27] S. Bera and V. K. Shrivastava, "Analysis of various optimizers on deep convolutional neural network model in the application of hyperspectral remote sensing image classification," *International Journal of Remote Sensing*, vol. 41, no. 7, pp. 2664–2683, 2020.

[28] D. H. Kim, S. T. Kim, and Y. M. Ro, "Latent feature representation with 3-D multi-view deep convolutional neural network for bilateral analysis in digital breast tomosynthesis," in *Proceedings of the IEEE International Conference on Acoustics, Speech and Signal Processing (ICASSP)*, p. 927, March 2016.

[29] S. V. Fotin, Y. Yin, H. Haldankar, J. W. Hoffmeister, and S. Periaswamy, "Detection of soft tissue densities from digital breast tomosynthesis: comparison of conventional and deep learning approaches," *Proceedings of the SPIE Medical Imaging*, vol. 9785, p. 495, 2016.

[30] R. K. Samala, H. P. Chan, L. Hadjiiski, M. A. Helvie, J. Wei, and K. Cha, "Mass detection in digital breast tomosynthesis: deep convolutional neural network with transfer learning from mammography," *Medical Physics*, vol. 43, no. 12, pp. 6654–6666, 2016.

[31] I. Reiser, R. M. Nishikawa, M. L. Giger et al., "Computerized mass detection for digital breast tomosynthesis directly from the projection images," *Medical Physics*, vol. 33, no. 2, pp. 482–491, 2006.

Hindawi
Computational Intelligence and Neuroscience
Volume 2022, Article ID 3698802, 9 pages
https://doi.org/10.1155/2022/3698802

Research Article

English Research Learning and Functional Research Based on Constructivism Theory and Few-Shot Learning

Chengyun Li

Zhengzhou ShengDa University, Zhengzhou, Henan 455000, China

Correspondence should be addressed to Chengyun Li; lichengyun0720@126.com

Received 18 December 2021; Revised 4 January 2022; Accepted 5 January 2022; Published 31 January 2022

Academic Editor: Xin Ning

Research-based learning is a comprehensive practical course that requires students to identify research topics from their study life and social life and acquires knowledge and applied knowledge through independent inquiry in a way similar to scientific research. Under the framework of CT (constructivism theory), through the study of English research-based learning and its functions, starting from few-shot learning, a college English teaching model based on the integration of network and research-based learning is constructed to explore the realization method of this model in the teaching process. UCSR-EW (user context-aware semantic-aware recommendation for English words) algorithm is used to generate English word recommendation, and the English word records are represented by the semantic model. Then, the acceptance of English words is measured according to the learning stage and English word records, and then, the similar users are matched, and finally, the intelligent recommendation of English words is realized. CC (confidence coefficient) is introduced into the pronunciation error correction algorithm to improve the traditional pronunciation error correction algorithm, so as to improve the error correction effect.

1. Introduction

Research-based learning is a concept opposite to receptive learning. It has many important functions, which are mainly manifested in helping to cultivate students' scientific inquiry ability, scientific spirit, independence and cooperation, social responsibility, innovative spirit, and innovative ability, helping to develop students' awareness and habits of exploration, helping to turn the learning process into a process of independent exploration, stimulating and enhancing learning motivation, and helping to cultivate students' sustainable development ability [1]. Therefore, as the inevitable trend of the current university curriculum reform, research-based learning has also become the focus of attention in the English teaching circle [2, 3]. More and more researchers are discussing the connotation of research-based learning and its application in English courses from theoretical and practical perspectives [4, 5].

CT (constructivism theory) is an important branch of cognitive learning theory, which is the result of psychologists' in-depth research on the cognitive law of the human learning process, and the further development of learning theory from behaviorism to cognitivism [6]. Because the learning environment required by CT is strongly supported by the latest information technology achievements, CT is increasingly combined with the teaching practice of teachers, thus becoming the guiding ideology of deepening teaching reform in schools at home and abroad [7, 8]. In order to meet the needs of modern quality education, middle school English curriculum standards have been revised several times, requiring middle school teachers to teach with brand-new teaching concepts, teaching methods, and means, take students as the center, pay attention to students' emotional factors, intelligence development, learning methods training and ability training, and teach them how to learn [9]. To achieve this goal, educators should provide a beneficial environment for students to help them create their own opinions independently or collectively [10]. The popularity of multimedia and network technology also makes the student-centered teaching structure have the material conditions for realization.

The importance of students' participation in research-based learning activities cannot be overstated. A multiperson activity is more likely to generate this type of participation. Building a learning society [11] necessitates multiperson activities, which are not only required by learning content. User information and English word learning records are collected and uploaded to the recommendation system, and a new recommendation method based on user similarity, as well as the recommendation system's model and process under the group intelligence perception mode, is explored and designed. Detection algorithms are created for various types of errors. Finally, various error detection algorithms detect the pronunciation to be processed separately, and corresponding corrective suggestions are provided for the incorrect pronunciation based on the results of the detection.

2. Related Work

The development of cognitive psychology and metacognition research provides rich theoretical knowledge for the study of learning strategies. Especially, cognitive psychology uses the viewpoint of information processing to explore the psychological mechanism within cognition, which makes it possible for human beings to explore their own implicit learning [12, 13]. Literature [14] divides learning strategies into macrostrategies and microstrategies. The former has a wider range of applications, involving more factors of emotion and motivation; the latter involves more special knowledge and skills, has a closer relationship with the cognitive execution process, and is easily influenced by education. In Literature [15], according to the theory of information processing and metacognition, it is proposed that learning strategies include cognitive strategies and metacognitive strategies. The former is the related method and technology for directly processing information, while the latter is the related method and technology for monitoring and mediating the information processing process. Literature [16] divides learning strategies into eight categories: retelling strategies of simple and complex learning tasks and finishing strategies for simple and complex learning tasks, simple and finishing organizational strategies, comprehensive adjustment strategies, and emotional strategies. Literature [17] puts forward the importance and necessity of learning strategy training in English learning. Literature [18] pointed out that research-based learning is a learning activity in which students, under the guidance of teachers, choose and determine topics for research from nature, society, and life, and actively acquire knowledge, apply knowledge, and solve problems during the research process. Literature [19] also gives two types of research-based learning: project research and project design. It is considered that objective knowledge structure is internalized into the cognitive structure through individual interaction with it. The interaction between learners and the environment involves two basic processes: "assimilation" and "hue".

A recommendation system is a software tool and technology that suggests items to users based on their preferences. These recommendations cover a wide range of decision-making processes, including purchasing goods, listening to music, and reading online news [20]. Cinema recommendations are made to a virtual community of movie aficionados via e-mail and the Internet bibliography [21]. Bibliography literature [22] introduces eight attack strategies, which are mainly divided into four categories: basic attack, weak cognitive attack, nuclear attack, and informed attack. The challenges of modeling the simulated human score at the process and result levels are listed in literature [23], and it is noted that in the field of speech features and speech recognition, it is currently impossible to model the evaluation process comprehensively. Literature [24] evaluates the speaker's speech at the phoneme level, which has the benefits of accurately locating the speaker's pronunciation errors, evaluating the similarity between the speaker's speech and the target speech, and detecting systematic differences by comparing with a standard speech database. The user's voice data should be scored in segments at the phoneme level, and the overall score of this voice should be calculated by combining the scores of each phoneme, according to literature [25].

3. Research Method

3.1. English Research Study Based on CT. The key to English research study is students' activities. It is a tool of language communication, and any tool has one characteristic activity. If people want to learn a language, they must master the language through activities, learn to communicate, and achieve the purpose of communication through restricted and purposeful language activities. The development of research-based learning is mainly manifested in two aspects:

(1) The model of research-based learning gives students full freedom, makes students truly become the main body of learning, fully demonstrates students' autonomy, and creates a good space for students' individual development

(2) The evaluation of research-based learning is not to compare students horizontally but to make every student have a successful psychological experience through positive evaluation, and have enough self-confidence, so as to motivate every student to make new progress and achieve new success on the basis of the original, thus inspiring the internal needs and motives for improvement and improvement, and starting internal vitality and subjective initiative [5]

The teaching effect is determined by the design of the teaching model. In essence, research-based learning is a type of resource-based learning. In order to fully embody the characteristics of resource utilization learning, self-discovery learning, negotiation and cooperation learning, and practical and creative learning, the construction of a college English research-based learning mode in a network environment should take full advantage of the network platform's advantages, such as diversity, sharing, expansibility, and interactivity, and fully utilize the advantages of the network platform, such as diversity, sharing, expansibility, and interactivity. CT learning is emphasized as a process in which students actively construct meaning. In order to cultivate their autonomous, research-oriented, and cooperative learning abilities, students should actively explore, analyze, and discover the essence of things and their interrelationships using various methods, resources, and tools that are beneficial to the construction of meaning, from mastering little knowledge to constructing a complicated knowledge network.

CT teaching thought includes the following aspects: knowledge view, learning view, student view, evaluation view, the orientation and role of teachers and students, and learning environment (Figure 1).

Learning is always associated with a certain social and cultural background, that is, the “situation”. Learning in the actual situation can enable learners to assimilate and lead out the new knowledge that they have learned so as to endow the new knowledge with a certain meaning. If the original experience cannot assimilates the new knowledge, it will cause the process of “adaptation”, that is, the original cognitive structure will be reformed and reorganized. In a word, only by “assimilation” and “adaptation” can the meaning of new knowledge be constructed.

Whether it is the study of language knowledge such as phonetics, vocabulary, and grammar or the cultivation of basic skills such as listening, speaking, reading and writing, student-centered, aiming at how to guide students to learn and teach them to learn. Teachers should be good at creating situations, stimulating students’ interest and motivation, setting appropriate learning tasks, creating lively and diverse activity environments, providing ample opportunities for practical language communication, allowing students to explore and solve problems by using their knowledge and original abilities, and also using language knowledge to communicate in activities to complete various tasks.

Combining the dominance and operability of classroom teaching, this study constructs a college English classroom teaching model based on the integration of network and research-based learning (Figure 2).

Research-based learning mode relying on network technology is subject-oriented, which changes the teaching process from traditional inheritance to inquiry. Students use the Internet to do a lot of online reading and online audio-visual, get “information input”, accumulate materials, and then refine their own views, transfer the perceived information to oral, form materials for oral expression, and provide “speaking” with the contents and ways of oral communication through logical transformation of thinking.

Teachers use the Internet to create real problem situations, guide students to discover and put forward problems that need to be explored, and generate a strong desire for research based on the teaching objectives, based on the content of teaching materials, and based on the principles of creativity, practicality, and novelty. Because the information on the computer network is linked by hypertext, it is easy for students to become disoriented, making teacher guidance crucial. The author primarily provides advice to students when they are debating a topic that is off-topic or disorderly.

Figure 1: Teaching thought of CT.

However, affirming students’ primary role in learning does not negate teachers’ hegemony in the classroom. The essence of teaching is guidance, and the shift in teachers’ roles is more focused on the promotion of educational concepts and the innovation of teaching strategies, which is to set new and higher standards for teaching and educating people in the new situation, rather than on the transfer of teaching and educating responsibilities and status. In essence, student-centered education requires teachers to create favorable conditions for students’ development and fully recognizes teachers’ dominant position.

Teachers should provide topic-related language materials, such as video or audio, while also supplementing literature materials with orientation and the appropriate degree to integrate language learning and consolidation into the application. The task’s input materials primarily come from English resources on the Internet, which are directly from the front lines of application and have authentic, rich, and practical characteristics. Through research-based learning, students find, sort, and use them, resulting in language acquisition.

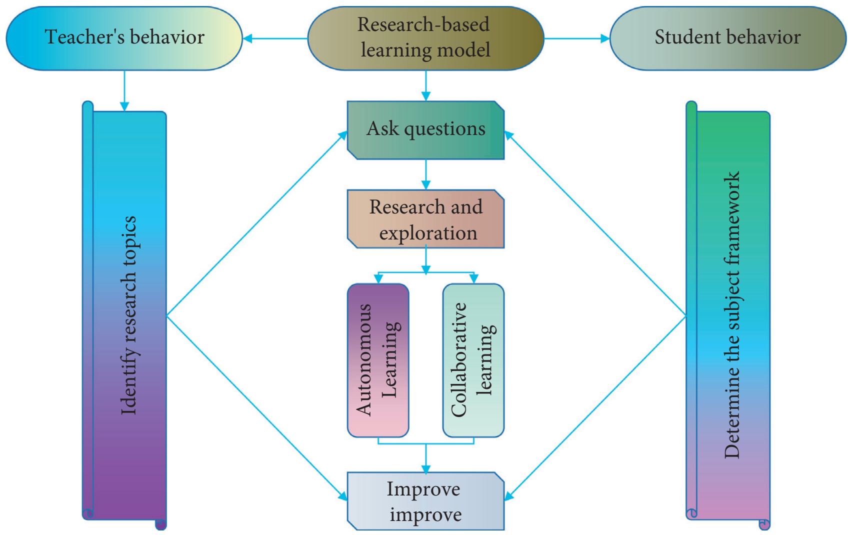

FIGURE 2: Web-based research-based learning model of college English.

3.2. UCSR-EW Algorithm. UCSR-EW (user context-aware semantic-aware recommendation for English words) algorithm uses word vectors to represent words, considers the relationship between English words from the semantic point of view, and, on this basis, introduces the context information of users, matches the words that users are interested in, and realizes intelligent recommendation of English words.

Word recommendation algorithm introduces the semantic model based on English word browsing records to calculate interest similarity among users. The context similarity between users is calculated by using the context information of users, and then, user similarity is calculated according to interest similarity and context similarity; the neighbor of the target user is selected according to the user similarity; neighbors generate neighbor recommendation lists according to their English word records; finally, all neighbor recommendation lists are merged to generate the final recommendation result. The specific algorithm framework is shown in Figure 3.

UCSR-EW algorithm first uses the trained semantic model to calculate the semantic similarity of words and then constructs the feature vector of English word browsing records.

Formula (1) is used to calculate the similarity between feature vector f_u and feature vector f_v, that is, the interest similarity of user u, v:

$$\mathrm{Sim}_{\mathrm{ic}}(u, v) = -\sqrt[2]{\frac{\sum_{i=1}^{k} (f_u)_i^2 - (f_v)_i^2}{k}}. \tag{1}$$

Feature vector f_v represents the semantic similarity of user v English word browsing records in user u word dimension, so the interest similarity of user u, v can be calculated by calculating the normalized Euclidean distance between feature vector f_u and feature vector f_v.

The age and geographical location of the user are used as context information, and the learning stage of the user is described by the context information of the user. The contextual similarity $\mathrm{Sim}_{\mathrm{sc}}$ of users will be calculated according to the age similarity $\mathrm{Sim}_{\mathrm{age}}$ and the regional similarity $\mathrm{Sim}_{\mathrm{location}}$, as shown in the following formula:

$$\mathrm{Sim}_{\mathrm{sc}} = \alpha \cdot \mathrm{Sim}_{\mathrm{age}} + \beta \cdot \mathrm{Sim}_{\mathrm{location}}. \tag{2}$$

Among them, α, β, respectively, represent the weight of age similarity $\mathrm{Sim}_{\mathrm{age}}$ and regional similarity $\mathrm{Sim}_{\mathrm{location}}$ in the calculation process of user context similarity $\mathrm{Sim}_{\mathrm{sc}}$, satisfying the condition $\alpha + \beta = 1$.

User-aware word semantic-aware recommendation algorithm is a recommendation method based on user similarity, which matches the neighborhood of the target user, and then generates recommendation results according to the neighbors of the target user (users in the neighborhood). User similarity $\mathrm{Sim}_{\mathrm{user}}$ can be calculated according to interest similarity and user context similarity, as shown in following formula:

$$\mathrm{Sim}_{\mathrm{user}} = W_{\mathrm{ic}} \cdot \mathrm{Sim}_{\mathrm{ic}} + W_{\mathrm{sc}} \cdot \mathrm{Sim}_{\mathrm{sc}}, \tag{3}$$

where $W_{\mathrm{ic}}, W_{\mathrm{sc}}$ represent the weights of interest similarity $\mathrm{Sim}_{\mathrm{ic}}$ and user context similarity $\mathrm{Sim}_{\mathrm{sc}}$, respectively.

After English words are duplicated and sorted, English words with large semantic similarity will always be ranked first, so that English words with small similarity but appearing in many neighbors' recommendation lists will never appear in the recommendation results. The word scoring model considering the frequency of English words is shown as follows:

$$\mathrm{score} = D_i \cdot \mathrm{Sim}_{\mathrm{word}}(w_i), \tag{4}$$

where D_i is the number of times the English word w_i appears in the neighbor recommendation list.

3.3. English Pronunciation Error Correction Algorithm. At present, the error correction evaluation of English pronunciation mainly focuses on the evaluation of acoustic characteristics, and the user's voice signal is cut into

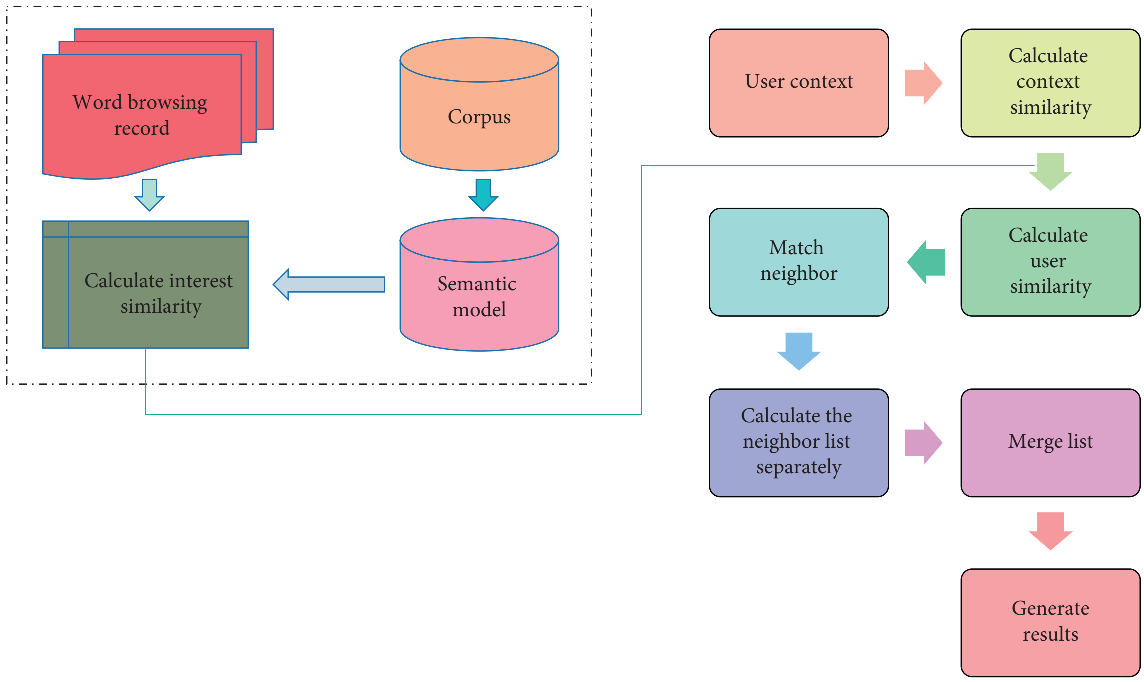

Figure 3: English word recommendation algorithm framework.

phoneme-level voice signals by forced alignment. Then, an evaluation score is obtained by calculating various similarities between the voice segments of each phoneme level and the standard phoneme acoustic model library.

This study develops a reasonable pronunciation error correction algorithm based on the above evaluation process and discusses and improves acoustic model training, phoneme segmentation, and similarity evaluation based on the characteristics of Chinese people speaking English. This study introduces the concept of CC (confidence coefficient), which calculates the confidence parameters such as likelihood ratio, likelihood ratio, and segment time to measure the similarity between this phoneme speech segment and the standard acoustic model, in order to correct users' pronunciation errors at the phoneme level and provide meaningful feedback information to users.

The pronunciation of this voice segment is the standard pronunciation. If the CC value of the observed sequence and the model of the standard phoneme is not within the range of the threshold value, the phoneme pronunciation of this speech segment is not standard, so as to further determine the wrong pronunciation of the user.

Assume that the phonetic sequence of word work is cut into three phoneme segments through a forced alignment network, corresponding to phoneme W, phoneme ER, and phoneme K, respectively. Let us take the phoneme ER as an example. First, let the observation sequence of the segmented ER be O_t, and the corresponding standard phoneme model be λ_{ER}.

The acoustic likelihood value of the frame corresponding to the standard phoneme model ER is defined as $l_i(o_t)$ where

$$l_i(o_t) = P(o_t|\lambda_{\mathrm{ER}}). \tag{5}$$

The likelihood of the inverse model corresponding to the phoneme ER is

$$l_i(o_t) = P\left(o_t|\lambda_{\overline{\mathrm{ER}}}\right), \tag{6}$$

where $\lambda_{\overline{\mathrm{ER}}}$ represents the inverse model of the phoneme ER.

Therefore, in the above formula, Ben multiplies the difference of ranking by the proportional difference of logarithmic probability, so that the reliability value of each phoneme will be influenced by ranking and logarithmic probability. The following is the set formula:

$$\mathrm{Confc} = \mathrm{PLLR}_{\mathrm{ER}}(o_t) * \mathrm{Confc}, \tag{7}$$

where Confc stands for the final CC.

The ratio of the number of phonemes whose error correction results are completely consistent with the expert labeling results to the total number of phonemes is known as the correct rate of phonemes. The algorithm's error correction rate is the ratio of the number of incorrect phonemes corrected by the algorithm to the total number of incorrect phonemes marked by all experts.

4. Results Analysis and Discussion

4.1. Analysis of English Word Recommendation Algorithm. In the process of research, using the method of group discussion, students are required to cooperate and help each other, which embodies the spirit of cooperation and mutual assistance among students. When the results are displayed between groups, they compete to show each other, hoping that their group is the best and the most perfect, which stimulates students' competitive consciousness. Pleasant cooperation and fair competition are two essential spirits for talent development today.

Students' ability to communicate correctly with pronunciation and intonation can only be cultivated in the real communication situation because changes in English stress, intonation, and rhythm are influenced by the actual communication environment and purpose. As a result, teachers should combine teaching materials to create language situations in which students can negotiate meanings and exchange emotions in communication and interaction, thereby assisting students in understanding the communicative function of pronunciation and intonation and forming an understanding of the English language. When speaking, students should be able to think clearly and express themselves using a variety of pronunciations and intonations.

The goal of the experiment of the word recommendation algorithm is to evaluate the word recommendation algorithm. The accuracy rate precision and recall are used to evaluate the effect of the recommendation algorithm. The higher the accuracy rate and recall rate, the better the recommendation effect.

The input of the UCSR-EW algorithm includes the user information file and English word record file. In addition, the algorithm also needs to input English word record length, English word number in the recommendation list, interest similarity weight W_{ic}, age similarity weight α, and user similarity threshold λ.

The key to learning a language is to imitate it. When students first learn how to pronounce vowels and consonants, it is critical that they imitate the pronunciation and practice it repeatedly in order to become proficient and accurate at it. Listening to the English pronunciations of many British and American people and imitating their pronunciation and intonation can help students to improve their English language skills.

The optimal value shown in Figure 4 is for the experimental data itself. When the experimental data change, the size of the optimal value and the value of the parameters may not be as shown in the experimental results.

In order to verify the performance of the English word recommendation algorithm proposed in this study, a comparative experiment was designed, and experiments of UCAR (user context-aware recommendation algorithm) algorithm and EWSAR (English word semantic awareness recommendation) algorithm were carried out on the same experimental data.

Without considering the browsing records of English words, the contextual similarity of users is the similarity of users, while the recommended English words will depend on the browsing records of other users with similar age and small city distance and have nothing to do with the English words browsed by the target users. Figure 5 shows the improved results of age similarity calculation, and Figure 6 shows the experimental results of the UCAR algorithm.

The communicative approach is helpful to improve students' communicative competence and enable them to learn to use correct and appropriate pronunciation and intonation. Teachers can provide students with various real communication situations and help students to correctly understand and choose the pronunciation and intonation suitable for the language environment, so as to achieve the purpose of communication.

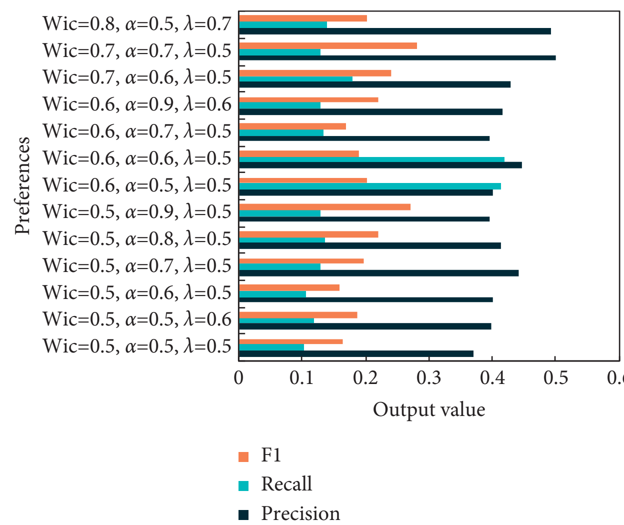

Figure 4: Experimental result.

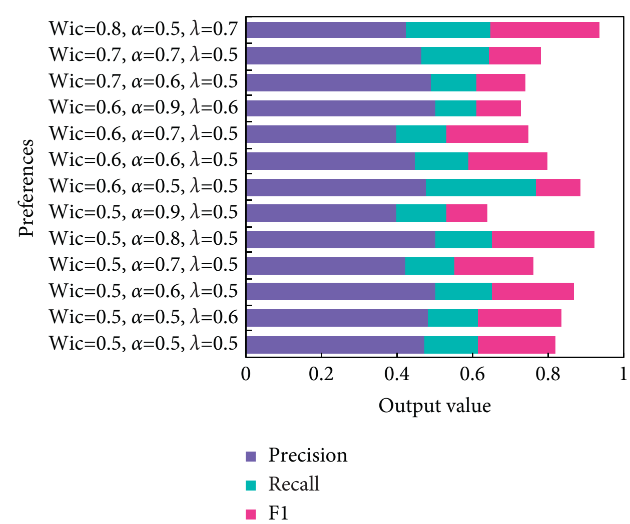

Figure 5: Improved results of age similarity calculation.

Comparison of performance between UCSR-EW algorithm, UCAR algorithm, and EWSAR algorithm is shown in Figure 7, and UCSR-EW algorithm is superior to UCAR algorithm and EWSAR algorithm in performance.

It replaced indoctrination with grammar instruction as the mainline of English instruction, and it transformed knowledge-imparting classroom instruction into ability-cultivating classroom instruction, improving students' interest in learning, assisting them in developing better learning strategies, improving their comprehensive English ability, cultivating their innovative spirit and practical ability, and improving teaching quality.

Of course, the single use of any kind of teaching method in teaching is not easy to get the best teaching effect. Teaching is an art in itself. Only by guiding teaching with advanced educational concepts, taking the best teaching

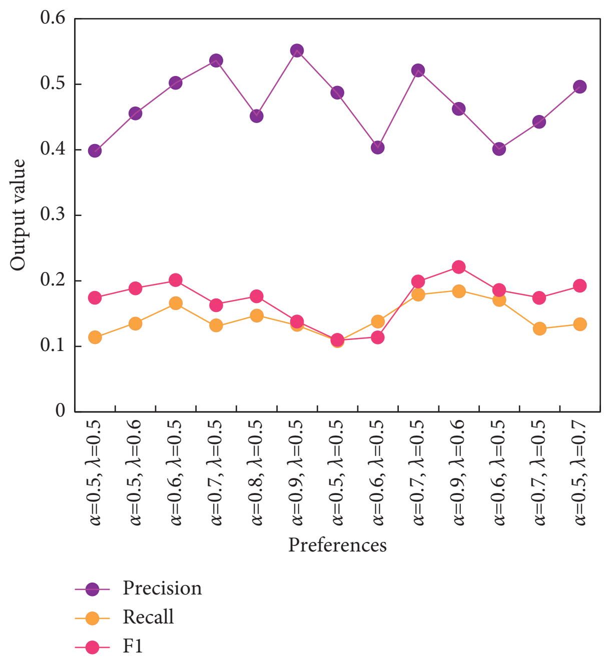

Figure 6: Experimental results of UCAR algorithm.

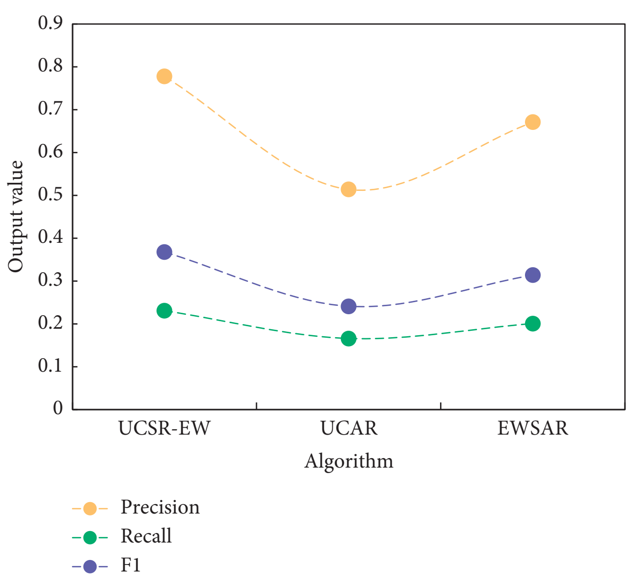

Figure 7: Algorithm performance comparison.

methods that meet the needs of the times, such as research-based learning as the leading factor, and combining all kinds of good teaching methods and creatively designing teaching can you get twice the result with half the effort.

The setting of learning objectives, the design of learning content, the provision of exercises, the transfer of adjacent knowledge, feedback, teaching assistance, learning evaluation, information organization, and other aspects should all well reflect the teaching nature. Teaching methods are not based on the learning content itself but attach importance to the creation of the learning environment. E-learning English does not just move the contents of English textbooks to the Internet intact but should combine learning theory and network characteristics to create a virtual learning environment for students and to pay attention to the organization of the teaching content, the richness, and the novelty of the content, so that students can find it worthwhile after browsing.

4.2. Analysis of Pronunciation Error Correction Algorithm. The main content of this section is to give the experimental results of adding the CC metric mentioned above to improve the traditional pronunciation error correction algorithm based on log likelihood. The experiment is designed and analyzed the experimental results in detail. The lower the threshold value, the more rigorous the algorithm is, the lower the phoneme accuracy rate, and the higher the threshold value, the looser the algorithm recognition, and the higher the phoneme accuracy rate. Figure 8 shows the phoneme accuracy of the traditional log-likelihood ratio and improved CC-based error correction algorithm.

The CC-based error correction algorithm outperforms the traditional log-likelihood algorithm in terms of phoneme accuracy, as shown in Figure 8. It is necessary to identify correctly pronounced phonemes in order to provide reliable feedback to users, but it is not sufficient to do so alone. The scale of phoneme recognition is relaxed as the ranking domain value increases, and the algorithm's error correction rate decreases. Although the user's pronunciation is assumed to be the same as the standard phoneme, experts have determined that the user's pronunciation is incorrect. At this time, the system missed a detection error, lowering the system's error correction rate.

The following experiment is designed to discuss the relationship between the correct rate of phonemes and the error correction rate of the algorithm. The experimental results are shown in Figure 9.

From the above experiments, it can be seen that with the increase of the threshold value, the limitation of the algorithm on phoneme ranking is relaxed, and the phoneme accuracy rate increases, but the phonemes that users send wrong may also be regarded as correct phonemes, so the error correction rate of the system will decrease accordingly.

In this way, by using the sigmoid function, the CC value relative to each phoneme model is limited between [0,1]. Figure 10 shows a discussion about the constant port and the relationship between CC value and rank when α takes different values.

English research-based learning evaluation is a type of evaluation that aims to fulfill the full scope of the evaluation. It emphasizes that the core of evaluation is students' absorption and mastery in the learning process, emphasizes the role of evaluation in students' development, and pays attention to positive encouragement and encouragement. It takes the promotion of students' development as the fundamental purpose, takes the promotion of students' development as the orientation, embodies the people-oriented thought, emphasizes that the core of evaluation is students' absorption and mastery in the learning process,

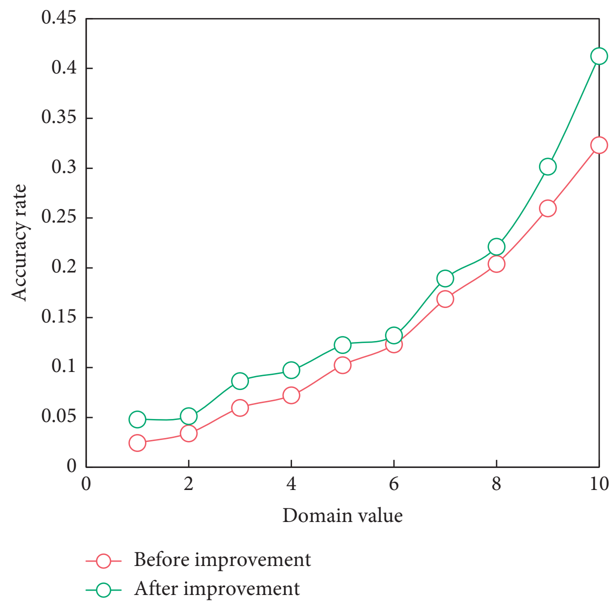

Figure 8: Comparison chart of phoneme accuracy before and after improvement.

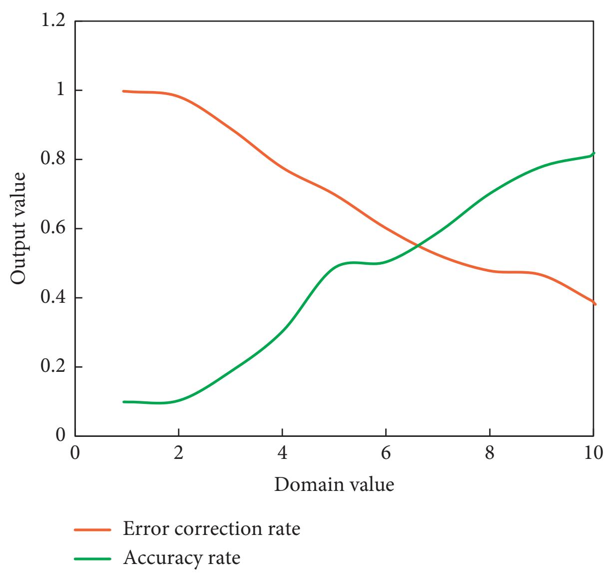

Figure 9: Relationship between error correction rate and phoneme accuracy rate of the algorithm.

emphasizes the role of evaluation in students' development, and pays attention to positive encouragement and to students' own interpretations of various phenomena, listen to their current perspectives, consider the origins of these ideas, and assist students in expanding or revising their own explanations, pay attention to students' personal development, and do not dismiss external guidance, such as teacher influence, pay attention to student inspiration and induction during teaching activities, and guide students through discussion activities and connection reasoning to explore and find problems, solve problems, and acquire knowledge.

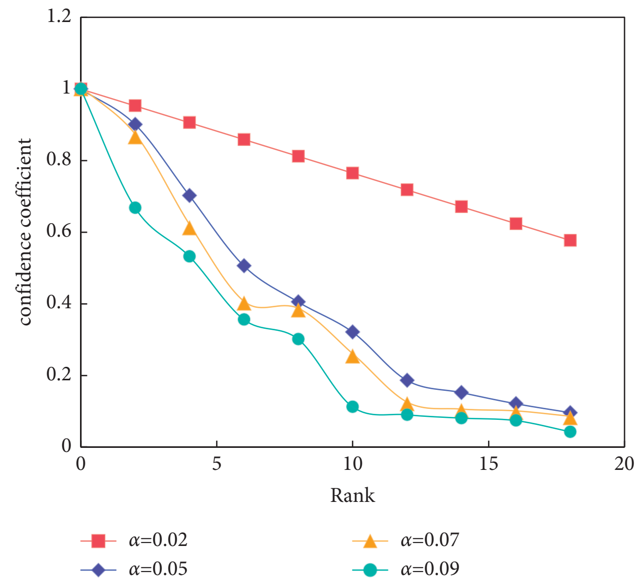

Figure 10: Relationship between α and rank rankings.

A colorful learning environment for students is created by creating situations that meet the requirements of teaching content and clues that suggest the relationship between old and new knowledge and help students to construct the meaning of what they are currently learning, to pay attention to the cultivation of cross-cultural awareness, method guidance, and strategy training, and to pay attention to guiding students to explore and discover the research-based learning style not only trains students' thinking but also cultivates their learning ability.

With the rapid development of multimedia computer and network education applications, CT is showing its strong vitality and expanding its influence in the world. Studying some learning theories of CT and carrying out teaching practice based on CT will carry out quality education with moral education as the core and cultivating students' spirit of exploration and innovation, active research and learning, cooperative learning, and practical ability as the focus, and promote the reform of teaching materials, which will have far-reaching influence and positive promotion.

5. Conclusion

Research-based learning is a teaching method in which subjects and objects are transformed and promoted by one another. This teaching model embodies the student-centered educational philosophy and emphasizes language acquisition and learning in the process and practice through the use of modern teaching methods. The central tenet of CT is that students are self-control knowledge builders. Teaching is primarily concerned with assisting students in improving their cognitive abilities. The UCSR-EW algorithm is proposed, which calculates an English word score based on semantic similarity and frequency of occurrence of English words and then recommends English words based on the score. In this study, we introduce CC into the phoneme error correction process and use it to calculate the CC rank of segmented phoneme segments and standard phoneme models to determine the accuracy of phoneme level in users' pronunciation. The results of the experiments show that including CC improves the correlation between system error correction and expert error correction significantly.

This study only looks at how phonemes are evaluated in spoken English, but there are many other aspects of spoken English that need to be highlighted for English learners, such as rhythm, and stress. Furthermore, the research and experiment in this study did not take into account the impact of regional dialects on English pronunciation. This will be the subject of more research in the future.

Data Availability

The data used to support the findings of this study are included within the article.

Conflicts of Interest

The author does not have any possible conflicts of interest.

References

[1] D. Yan, "Exploration and research on English linguistics teaching based on the perspective of constructivism[J]," *Journal of Educational Theory and Management*, vol. 3, no. 2, p. 5, 2019.

[2] Y. Liu, H. Liu, Y. Xu, and H. Lu, "Online English reading instruction in the ESL classroom based on constructivism," *International Journal of Technology-Enabled Student Support Services*, vol. 9, no. 2, pp. 39–49, 2019.

[3] L. Liang, Q. Yin, and C. Shi, "Exploring proper names online and its application in English teaching in university," *ASP Transactions on Computers*, vol. 1, no. 1, pp. 24–29, 2021.

[4] Heng, "Research on the English teaching platform based on the campus network multimedia[J]," *International English Education Research: English Version*, vol. 1, no. 3, p. 3, 2019.

[5] J. Chen, "The exploration of flipped classroom teaching mode in college English reading teaching R-based on the perspective of constructivism theory [J]," *Journal of Jiamusi Institute of Education*, vol. 000, no. 006, pp. 372–374, 2018.

[6] Y. Huang, "Research on the application of micro-courses of spoken English in higher vocational colleges based on constructivism learning theory [J]," *Journal of Guangdong Institute of Water Conservancy and Electric Power*, vol. 015, no. 001, pp. 67–70, 2017.

[7] H. Güner Berkant and S. Baysal, "Allosteric learning model in English lesson: teachers' views, the instructions of curriculum and course book, A sample of daily lesson plan," *Universal Journal of Educational Research*, vol. 5, no. 1, pp. 84–93, 2017.

[8] M. Yu, "Corpus English word detection and image recognition algorithm based on improved convolutional neural network[J]," *Microprocessors and Microsystems*, vol. 82, no. 2, Article ID 103920, 2021.

[9] C.-B. Yao, "Constructing a user-friendly and smart ubiquitous personalized learning environment by using a context-aware mechanism," *IEEE Transactions on Learning Technologies*, vol. 10, no. 1, pp. 104–114, 2017.

[10] W. Song, W. Ma, and Y. Qiao, "Particle swarm optimization algorithm with environmental factors for clustering analysis," *Soft Computing*, vol. 21, no. 2, pp. 283–293, 2017.

[11] Q. Wang, Y. Yu, H. Gao, and L. Zhang, "Network representation learning enhanced recommendation algorithm[J]," *IEEE Access*, vol. 1, no. 99, p. 1, 2019.

[12] J. C. ZhaoChen et al., "A recommendation algorithm based on Collaborative Filtering Technology in distance learning[J]," vol. 2017, no. -, pp. 2320–2323, 2017.

[13] G. Ou, H. Wang, Y. Jiang et al., "Hybrid recommendation algorithm based on deep learning [J]," *Sensors and Microsystems*, vol. 038, no. 007, pp. 131–134, 2019.

[14] A. Huang, "HELP: humor in English learning practices[J]," *Nephron Clinical Practice*, vol. 6, no. 6, pp. 295–310, 2018.

[15] J. Xiong, "Directed by zhaojie. The Importance of Learning English[J]," *Friends of junior high school students*, vol. 9, no. 9, p. 1, 2019.

[16] Shengmin, "Learning English or learning through English?——an analysis of lesson examples of learning other knowledge through English in school-based English teaching in junior middle school[J]," *English on campus*, vol. 3, no. 36, p. 2, 2018.

[17] P. Yin and L. Zhang, "Image recommendation algorithm based on deep learning[J]," *IEEE Access*, vol. 1, no. 99, p. 1, 2020.

[18] J. Jiao, X. Zhang, F. Li, and Y. Wang, "A novel learning rate function and its application on the SVD++ recommendation algorithm," *IEEE Access*, vol. 8, pp. 14112–14122, 2020.

[19] H. Xia, J. J. Li, and Y. Liu, "Collaborative filtering recommendation algorithm based on attention GRU and adversarial learning," *IEEE Access*, vol. 8, pp. 208149–208157, 2020.

[20] W. Lu and G. Altenbek, "A recommendation algorithm based on fine-grained feature analysis[J]," *Expert Systems with Applications*, vol. 163, Article ID 113759, 2020.

[21] X. Zhang, R. Li, B. Zhang, Y. Yang, J. Guo, and X. Ji, "An instance-based learning recommendation algorithm of imbalance handling methods," *Applied Mathematics and Computation*, vol. 351, pp. 204–218, 2019.

[22] M. Hopkins, M. Gluckman, and T. Vahdani, "Emergent change: a network analysis of elementary teachers' learning about English learner instruction," *American Educational Research Journal*, vol. 56, no. 6, pp. 2295–2332, 2019.

[23] jingyu Yang, "The evaluation of a MOOC——learning English for academic purpose from FutureLearn[J]," *Overseas English*, vol. 10, no. 10, p. 5, 2018.

[24] V. R. M. Garcia, "Learning English in the elderly: an analysis of motivational factors and language learning strategies," *BELT - Brazilian English Language Teaching Journal*, vol. 8, no. 2, p. 234, 2017.

[25] L. Lin, "An analysis of conceptions of learning English among college students in China[J]," *Sino-American English teaching: English version*, vol. 14, no. 4, p. 5, 2017.

Hindawi
Computational Intelligence and Neuroscience
Volume 2022, Article ID 3869087, 10 pages
https://doi.org/10.1155/2022/3869087

Research Article

Research on Quality Evaluation of Product Interactive Aging Design Based on Kano Model

Yin Liu[1] **and Weiwei Wang**[2]

[1]*Xi'an Eurasia University, EAAD School of Art and Design, Xi'an, Shaanxi 710000, China*
[2]*Shaanxi University of Science & Technology, College of Art and Design, Xi'an, Shaanxi 710000, China*

Correspondence should be addressed to Yin Liu; liuyin@eurasia.edu

Received 22 December 2021; Revised 6 January 2022; Accepted 7 January 2022; Published 31 January 2022

Academic Editor: Xin Ning

At present, China's population aging presents the characteristics of large base, fast aging process, and old age, but the research and development of product aging design in China is relatively late, which brings additional pressure to the daily life of the elderly. In such an environment, higher requirements are put forward for product aging design and service provision. Only products or services that timely meet the personalized and diversified needs of different customers can attract customers and improve customer satisfaction. How to design aging products with satisfactory appearance and humanized function is the focus of current research. Based on the product quality division of Kano model, this paper summarizes the domestic mainstream products and their functions. The designed questionnaire data are summarized; reliability and validity analysis, as well as descriptive statistical analysis, is performed on this basis for the constructed product service quality evaluation system. The service quality indicators are divided into three categories according to the Kano model: overall one-dimensional quality, charm quality, and necessary quality.

1. Introduction

With the refinement of management and the deepening of customer-centered management concept into enterprise management, the quality management of products and services has become a hot management issue [1]. Quality management methods and systems emerge one after another, and they have played an important role in different fields and contents. At the same time, with the deepening trend of aging in China, the number of elderly groups is increasing [1]. The educational needs of the elderly are also increasing. The popularity of smart phones and mobile Internet is affecting the daily life of the elderly. This paper collects and analyzes the relevant literature on product interactive aging design at home and abroad and finds that the current product interactive aging design in China is poor, and the product delivery design experience for the elderly needs to be improved [2]. Quality evaluation is a core part of quality management. Different quality management methods are permeated with corresponding quality evaluation methods. How to select scientific means to evaluate the service quality of enterprises in order to improve customer satisfaction and loyalty is a practical problem faced by enterprises [3]. At present, Kano model still has many limitations in practical application, and its quality evaluation method needs to be further supplemented and modified [4]. The Kano model is applied to the research of products for the elderly, mining the characteristics of products used by the elderly, and the corresponding design strategies are summarized, which is of great significance to guiding the aging design of products.

Today's environment faced by enterprises is not what it used to be. With the further interruption of monopoly industries, the market presents a strong competitive situation, which has played a significant role in promoting economic development, but at the same time, it poses severe challenges to competitive enterprises [5]. Population aging refers to the rising trend of the proportion of the elderly population in the total population under specific time and space conditions. With the increase of the number of the elderly in China, the educational needs of the elderly are becoming increasingly prominent [6]. In this environment, the interactive aging design of products is challenged. At present, many research contents focus on putting forward suggestions from the aspects of product interaction design and visual design, but there is lack of research on users' overall perception of product attributes. The overall perception research includes which attributes of the product are more important to users and which characteristics can better affect use satisfaction [7]. The introduction of Kano model into the design of aging interaction boundary of products can study the impact of different functions on user satisfaction and help designers reasonably allocate design resources. The service product itself has the characteristics of intangibility, which is more complex than the evaluation of physical products, which increases the risk in the process of consumer purchase [8]. Therefore, how to select scientific means to evaluate the service quality of enterprises in order to improve customer satisfaction and loyalty is a practical problem faced by enterprises. This paper constructs a service quality evaluation model of product interactive aging design, in order to help enterprises improve service quality and product interactive aging design.

The key to accelerating economic development is quality. There will be no real and tangible benefits unless quality is improved. Appropriate quality evaluation methods are essential for improving product quality and increasing enterprise international competitiveness [9]. To construct the nonlinear relationship between consumer satisfaction and product performance, a two-dimensional model can be used: on the one hand, it is the subjective feeling of consumers; on the other hand, it is the objective state of products. The Kano model converts specific attributes of products or services into customers' income, which is then divided into quality factors in order to analyze consumers' consumption intention and attitude [10]. As a result, the Kano model is widely used in quality control, new product development, and other areas. The rise in the number of elderly groups has heightened interest in their spiritual lives. Despite the fact that there are a lot of elderly products on the market, there are not many products specifically designed for them [11]. The current products are geared more toward teenagers, college students, and workers on the job. This paper examines the physiological and psychological characteristics, as well as the motivation and challenges of using a smartphone app by the elderly, and summarizes the pertinent information. This paper constructs a product interactive aging design quality evaluation model based on Kano model and uses Kano questionnaire to collect users' attitudes toward functions, so as to divide the functional attributes of products and rank the importance of each functional attribute. Combined with Kano model research results and interactive evaluation dimensions, the corresponding design strategies are obtained. The aging principle is verified by usability test and satisfaction evaluation, and the product interaction aging practice based on Kano model is completed.

2. Related Work

According to literature [12], quality means those characteristics in a product or service that can meet customer needs and make customers satisfied; it also means that a product or service is free of defects. According to literature [13], quality factors require not only a large category of judgment, but also a quantity that can effectively measure the category of quality factors in the Kano model's limitations. Only with this amount of data can a horizontal and comprehensive comparison of different products (or the same product) be made. Literature [14] proposed a Kano model-based system for evaluating personal online banking service quality and divided the service quality of personal online banking in China. According to the article, banks must improve the reliability and security of personal online banking; for one-dimensional quality, banks must improve the ease and speed of their operations and establish good communication with customers; and for charm quality, banks must improve innovation and market segmentation to improve service efficiency. According to the literature [15], customer satisfaction and perceived service quality have different relationships with expectations. A higher level of satisfaction does not imply a higher level of perceived quality. Expectations are divided into three categories: core attribute expectations, important attribute expectations, and other attribute expectations. Customers' perceived quality evaluation can be improved by meeting consumers' expectations of important attributes, and consumer satisfaction can be improved by meeting consumers' expectations of additional attributes. Customers' perceptions of service quality are multidimensional, according to literature [16], and service quality can be measured from five perspectives: reliability, responsiveness, assurance, empathy, and tangibility. Consumers' expected quality is determined by their personal needs and previous experience. A combination of four types of gaps can be used to express the gap between the quality of service and the quality expected by customers. Literature [17] believes that in the Kano model, a lot of information can be obtained by using sample data, which also plays an important supporting role for the dynamic changes of quality factors. Literature [18] proposed an I-Kano for customer satisfaction improvement decision-making, proposed Kano index and priority index, in order to use quantitative analysis methods, in the framework of the Kano model, combined with customer satisfaction, product, or service. The quality factors are judged and ranked by importance. Literature [19] applies the Kano model to engineering mechanics to determine the impact of various service qualities in the real estate industry on customer purchasing decisions. Literature [20] believes that perceived service quality includes two aspects: technical quality and functional quality. Literature [21] improved the calculation method of the Kano model and proposed a calculation method of the importance of the fuzzy Kano model. On the one hand, the fuzzy Kano questionnaire is used, and on the other hand, the demand importance adjustment function is introduced to calculate the importance of different quality attributes. This method is applied to the demand analysis of a company's combine harvester. Literature [22] proposed that customer expectation means the level expectation that customers can achieve for products or services, which is an exogenous variable. Perceived value is the perceived actual quality level, which is divided into two observation variables:

the price evaluation of relative quality and the quality evaluation of relative price. Literature [23] believes that the more sufficient the service quality is, the higher it is than consumers' expectations, the more satisfied consumers will be. Literature [24] proposed an analytical Kano model on the basis of analytical customer relationship management. The model realizes the objective classification of quality factors by constructing Kano satisfaction index and importance index. They integrate consumers' important perception of each product or attribute in the questionnaire design, and finally obtain the priority to improve the service quality attribute. Literature [25] holds that when incentive factors are available, they will increase people's job satisfaction, but when they are lacking, they will not lead to people's dissatisfaction. When health care factors are available, they will eliminate people's dissatisfaction, but will not increase people's satisfaction, while when they are lacking, they will cause people's dissatisfaction. Literature [26] uses the methods of fuzzy clustering and fuzzy transformation semantics to judge the quality attributes based on Kano model and puts forward a way to obtain product personalized requirements. In this paper, Kano model is used to explore the interactive aging design of products. And it explores the rules of consumers' judgment on the quality characteristics of products or services, find out the key quality factors such as charm quality, one-dimensional quality that affect consumers' satisfaction or attract consumers' attention, and explore the correlation degree between consumers' different personality characteristics and their judgment on quality factors, so as to provide suggestions for interactive aging design of products.

3. Methodology

3.1. The Design of Product Interaction Adaptive Aging Based on Kano Model. With the development of information age, China has entered a sub-deep aging society. In order to make the decline of old people's function and follow-up study of individual ability adapt to the rapid change of product interaction information, we should reconstruct the prototype of old people's interaction, optimize the interaction mechanism of old people's products, and build the design method system of product interaction suitable for aging [27]. Therefore, the interaction of products is more suitable for the physiological and psychological characteristics of the elderly group, the interaction of the elderly users is more accurate, natural, smooth, and relaxed, and the elderly products are safer, more comfortable, healthier, and more efficient.

Aging design is a design based on the physiological and psychological needs of the elderly and their experience, taking into account the security needs and belonging needs, and at the same time trying to realize the spiritual needs and self-realization needs of the elderly to improve their quality of life [28]. The research of product interaction aging design for aged care service with Chinese characteristics supports the scientific and reasonable generation of product aging interaction design system for social aged care service from the logical level. From the technical level, the interactive design of aging products for social pension services can be quickly and effectively transformed into an applied method system.

Product demand reflects the general requirements of users for enterprises and products and is the starting point of the whole life cycle of products. The process of product innovation and development largely depends on the understanding and analysis of product demand. Different personality consumers have different judgment results on quality factors [29]. Consumers with different personality types have different consumption preferences and habits, which makes it difficult to get satisfaction. According to the different influence modes of product attributes on consumer satisfaction, Kano model mainly classifies them into three different factors. They are charm factor, expectation factor, and necessary factor. Kano model divides users' demands into three categories: basic demands, normative demands, and interest demands. These three kinds of demands reflect the different levels of demands of users for products, and the demands will change with the changes of market and time. Interest will degenerate into normative demand, and normative demand will degenerate into basic demand. Aging products are designed and developed according to the needs of the elderly, so the products should reflect the needs of the elderly. The design elements of aging products include functional elements, aesthetic elements, safety elements, and ease of use elements. Figure 1 shows Kano model.

With the improvement of people's cultural level and living standard, the product system that carries the entertainment and life of the elderly has been popularized to some extent, which has also laid a certain foundation for aging products. Although the types of aged products on the market at present are very single, lacking in innovation and serious homogenization in design, they cannot bring rich product experience to the aged consumers. However, from the physiological characteristics, life and behavior of the elderly, the elderly products can be roughly divided into three categories:

(1) *Life Support Products*. Life support products are a common demand of the elderly. These products are designed by designers according to the specific life behavior needs of the elderly who need assistance. With these products and more professional medical care products, some elderly people can take care of themselves.

(2) *Fitness Products*. The improvement of the average life span of the elderly is closely related to the increase of leisure time, increasing attention to their healthy, happy, and full life. By participating in various ball games with friends, we can increase the fun of our later life, exercise our thinking system, and prevent inattention, memory decline, and slow response caused by aging and degeneration.

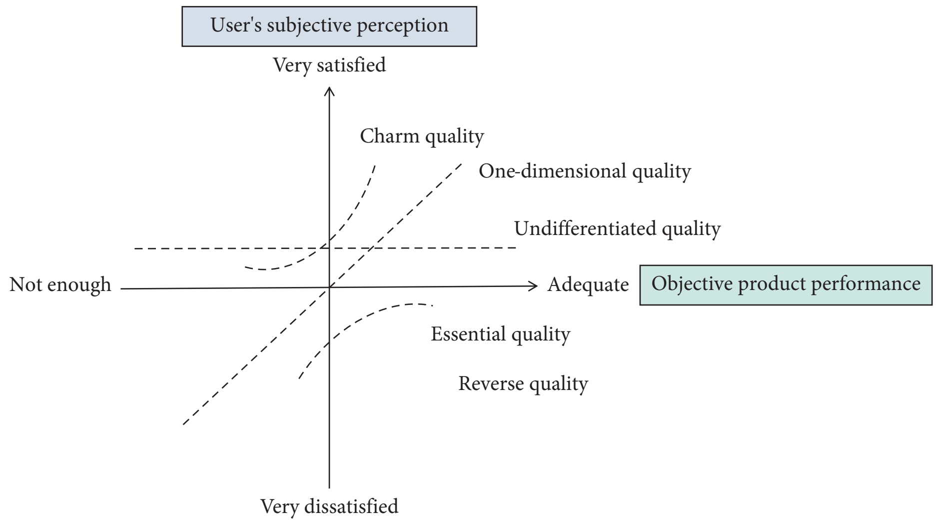

Figure 1: Kano model.

(3) *Leisure and Entertainment Products*. At ordinary times, the elderly will take part in some intellectual development projects because proper use of the brain can help to slow down brain degeneration and aging, prevent Alzheimer's disease, and maintain the vitality of thinking. These products are all aging products with the ultimate goal of developing the intelligence of the elderly, preventing brain degeneration by using the brain properly but not excessively, enhancing the interests and hobbies of the elderly, and increasing communication activities. To a certain extent, it can satisfy the spiritual needs of the elderly who are not satisfied with the old age, pursue health, hope to get attention and attention, and have their own hobbies.

There is a linear relationship between quality factors and customer satisfaction in the traditional quality model plough. To obtain the nonlinear relationship between customer satisfaction and product performance, the Kano model breaks through the previous one-dimensional model and uses the two-dimensional model of customer subjective feelings and objective performance of products and services. The Kano model can fully analyze product customized attributes and determine whether or not each customized attribute should be implemented and in what order. We should prioritize product customization attributes that can improve consumer satisfaction to a greater extent and make an appropriate trade-off between the manufacturer's production capacity and consumer satisfaction, in order to ensure that consumer satisfaction does not decline.

To implement the Kano model, the first step is to set up a questionnaire about product customization attributes. The results of the reliability analysis are not used to reflect the correctness of the results of the questionnaire, but to evaluate the reliability and stability of the questionnaire. Assuming that the result of the questionnaire is the algebraic sum of K items under investigation: $X = Y_1 + Y_2 + \cdots + Y_K$, then the Cronbach's a-reliability coefficient is defined as follows:

$$\alpha = \frac{K}{K-1}\left(1 - \frac{\sum_{i=1}^{K} \sigma_{Y_i}^2}{\sigma_Y^2}\right). \quad (1)$$

Among them, σ_Y^2 is the variance of the total score of the observed questionnaire test, and $\sigma_{Y_i}^2$ is the variance of all respondents' scores of the currently observed items.

Let domain $X = \{x_1, x_2, \ldots, x_k\}$, that is, the collection of all functional requirements. Fuzzy set $A = \{\mathrm{Br}, \mathrm{Pr}, \mathrm{Er}\}$, $A \in F(X)$.

There are n evaluation members, who are asked to independently give the estimated value $m_i\,(i = 1, 2, \ldots, n)$ of $\mu_A(x_0)$ and calculate its average $\overline{m}$ and deviation d:

$$\overline{m} = \frac{1}{n}\sum_{i=1}^{n} m_i,$$
$$d = \frac{1}{n}\sum_{i=1}^{n} \left|m_i - \overline{m}\right|. \quad (2)$$

For a given error $\varepsilon > 0$, $\mu_A(x_0)$ can be used as the approximate value of $\overline{m}$ if the deviation satisfies $d \leq \varepsilon$. If $d > \varepsilon$, repeat the above steps until satisfactory accuracy requirements are met.

When the evaluation experts estimate each membership degree, it is better to give the estimated value of $x_1, x_2, \ldots, x_k$ at a time than to estimate $a_i\,(i = 1, 2, \ldots, k)$ individually, because the overall estimation is carried out in comparison, which makes the decision easy to make and relatively reasonable.

3.2. Quality Evaluation Research. Intelligentization has become the Internet age's label, and the design of aging products is following suit, with many aging products already possessing some intelligence. As the elderly's functions deteriorate, they require more outside assistance. Intelligent aging products have a certain "wisdom" that can not only reduce the elderly's physical consumption, but also minimize the difficulty of use, and realize the operation and use of the products through systematic operation. Assume the elderly group is the research object, dynamically collect their living habits and behavior patterns, and build an elderly group behavior model. Data understanding, association reasoning, clustering analysis, and other algorithms are used to extract and deconstruct the typical behavior model of the elderly group, collect physiological signal information, and mine interactive information based on objects. The output interaction information is functionally reconstructed from the perspective of interaction mechanism, and the architecture forms are cognition, understanding, decision-making, implementation, and feedback, in order to construct the interaction prototype for observation and understanding, exploration and iterative design, and communication and evaluation, according to the interaction demand.

It is necessary for manufacturers to fully understand consumers' preferences and their information feedback on product satisfaction so as to formulate appropriate product optimization strategies and continuously improve product quality. The personality characteristics of consumers can be divided into three categories: introverted rational type, extroverted obedient type, and extroverted independent type. Among them, introverted rational consumers do not like to have too much interaction with others during the shopping process. Consumers with extroverted personality will show higher compliance with others. From the consumer's point of view, the quality of products is reflected in the degree of satisfaction of consumers. Figure 2 shows the structural model of customer satisfaction index.

Because consumers' own demand preferences are ambiguous and their cognitive process of demand preference is uncertain, it is often difficult for nonprofessional consumers to directly judge the quality of a product. However, from the standpoint of the product, the reasonable division of product attributes allows for the visualization of consumer demand, because consumer satisfaction with products can be measured by whether, how, and how these attributes are realized, and understanding the mapping relationship between consumer demand and product attributes is critical to the demand visualization process.

The attribution degree of quality elements is actually the problem of calculating the maximum leading degree of components in the distribution vector of quality elements. Therefore, the distribution vector is directly regarded as a set of numbers to calculate the maximum lead. The calculation method of the attribute degree of quality elements is as follows:

$$\eta\langle T\rangle = \eta\langle T(\mathrm{QE}, t)\rangle = (\eta' - \psi + 1)^{\arctan(N-1+\tan 1)}. \tag{3}$$

Among them, the determination of the value of ψ can use the half-number principle and can also be determined by means or other methods. The external advantage can be characterized by the discrete coefficient of a set of values other than the maximum value. The dispersion coefficient is a measure of the uniformity of the distribution between a group of numbers, which has the same points as the external advantages discussed in this article.

If we define a product attribute set $F = \{f_1, f_2, \ldots, f_i, \ldots, f_q\}$ that includes q product attributes, and a surveyed person set $E = \{e_1, e_2, \ldots, e_j, \ldots, e_p\}$ that includes p respondents, then, for each attribute, there are

$$\begin{aligned} &e_j \longrightarrow i = \left(a^+_{j\longrightarrow i}, a^-_{j\longrightarrow i}\right) \quad i = 1, 2, \ldots, q; \quad j = 1, 2, \ldots, p,\\ &a^+_{j\longrightarrow i}, a^-_{j\longrightarrow i} \in \{\text{"Like"}, \text{"Must} - \text{be"}, \text{"Neutral"}, \text{"Live with"}, \text{"Dislike"}\}. \end{aligned} \tag{4}$$

Among them, $a^+_{j\longrightarrow i}$ and $a^-_{j\longrightarrow i}$ are the answers to the positive and negative attribute questions, respectively.

Behavior mode is the foundation of product interaction mode, and product interaction mode is the result of behavior mode, which is interactive and interrelated. Different behavior mode information feedback determines different interaction modes, and different behavior mode information feedback determines different interaction modes. People-oriented user needs are prioritized in interactive design efforts to create and build meaningful relationships between people, products, and services. Interactive aging product design can improve elderly consumers' experiences with aging products, help them accept new things, and thus improve their quality of life. This paper investigates the relationship between elderly behavior patterns and product interaction based on a prototype of elderly interaction. The premise is that there is a mapping relationship between the physiological information of the elderly and product interactions, including the mapping content and structure. Its core is the old age behavior pattern's action mechanism on product interaction; its essence is the old age behavior pattern's support for product interaction and the reverse verification of old age behavior pattern by product interaction.

Define the transformation rule T and the frequency index $C_i(k)$:

$$\begin{aligned} &\mathrm{count}\left(T\left(e_{j\longrightarrow i}\right)\right) \equiv 1,\\ &C_i(k) = \sum_{j=1, T\left(e_{j\longrightarrow i}\right)=k}^{p} \mathrm{count}\left(T\left(e_{j\longrightarrow i}\right)\right),\\ &K(f_i) \in \left\{k' \mid C_i(k') = \max_{\forall k} C(k)\right\},\\ &T\left(e_{j\longrightarrow i}\right), k, k' \in \{A, O, M, I, R, Q\}. \end{aligned} \tag{5}$$

Among them, $K(f_i)$ is the Kano classification result of product attribute f_i. That is to say, by summing up the

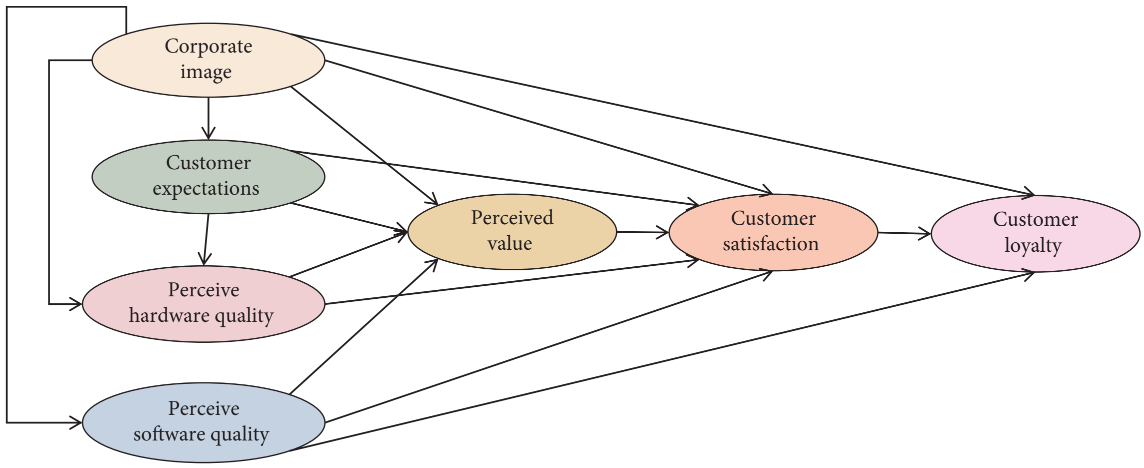

Figure 2: Customer satisfaction index structure model.

regional statistical percentages of each factor of a certain product attribute, the factor corresponding to the maximum value is the factor that the attribute is divided into.

The technology and environmental conditions provided by the mobile Internet make it possible to collect real-time and comprehensive data for the elderly. By using cloud processing and other means, it can not only reduce the functional burden of products, but also provide digital information services based on similar people. In the future, a big data information platform will be established for the elderly, which will provide conditions and entrances for the intervention of various comprehensive services. At the same time, the interactive experience based on communication will be realized through the construction of home or community networks, which will also provide the possibility for the optimization and upgrading of system services.

4. Results Analysis and Discussion

Kano model is based on customers' perceived quality. Kano model keeps approaching customers' expectations by developing charm quality characteristics, and its purpose is to maximize customers' potential needs. Kano model can be used to accurately find out the root causes of service quality problems, which is helpful for enterprises to prescribe the right medicine and formulate correct development strategies. Existing demand importance evaluation methods have obvious flaws when it comes to dealing with the importance issue. Because a large number of complicated and trivial needs of users are asked, it is easy to bore users and lead to incomplete and inaccurate inquiry results when using the user inquiry survey method. Although using the repetition frequency of users' requirements can avoid the drawbacks of the previous method, judging the importance solely on the basis of the repetition frequency of users' requirements is unreliable. Interest demand is a very rare occurrence in the Kano model's user demand acquisition process, but it is extremely important product demand information.

In the daily life of the elderly, cognitive ability is an important ability for the elderly to receive information about external things. The decline of cognitive ability of the elderly not only brings inconvenience to their own lives, but also troubles the lives of other family members. At the same time, the physiological function of the elderly is degraded due to the increase of age, as shown in Figure 3, it is physically and psychologically difficult to keep up with the fast-paced modern life.

The data of Kano questionnaire on product service quality are preliminarily summarized, and then the related quality characteristics are classified by Kano attributes. The priority order of attributes at the same level is determined by calculating the better-worse index. The value of better is usually positive, which means that if a certain attribute is provided, the user satisfaction will be improved. The larger the positive value, the stronger the effect of improving the user satisfaction, and the faster the increase. The value of worse is usually negative, which means that if a certain functional attribute is not provided, the user's satisfaction will decrease. The more negative the value is, the stronger the effect of decreasing the satisfaction will be and the faster it will decrease.

In this paper, the lowest threshold of hearing perception of elderly users is studied experimentally. The test mainly focuses on the sound threshold test of elderly users, and the sensitivity of elderly users to sound is found. When the elderly users are using the product, the sound prompt with appropriate volume can attract the attention of the elderly users so that the elderly users can grasp the state of the product. As shown in Figure 4, the sound threshold that the elderly users can distinguish is obtained, and the sound feelings that the elderly users hear are listed, which provides the data source for the research of product interactive hearing below.

The statistical data of sound threshold can be used to conclude that the elderly users' hearing loss is severe. The elderly users' auditory attention is hardly drawn to sound stimulation with a volume below 40 dB. The elderly users can only fully receive the sound stimulation and recognize the sound content when the volume is above 40 dB. As a result, in interactive aging product design, the sound feedback prompt of products must be above 40 dB in order for elderly users to recognize and master the product status.

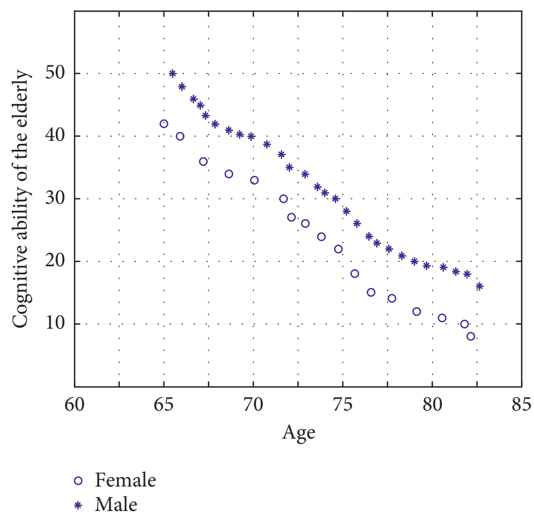

Figure 3: Trend of cognitive ability of the elderly with age.

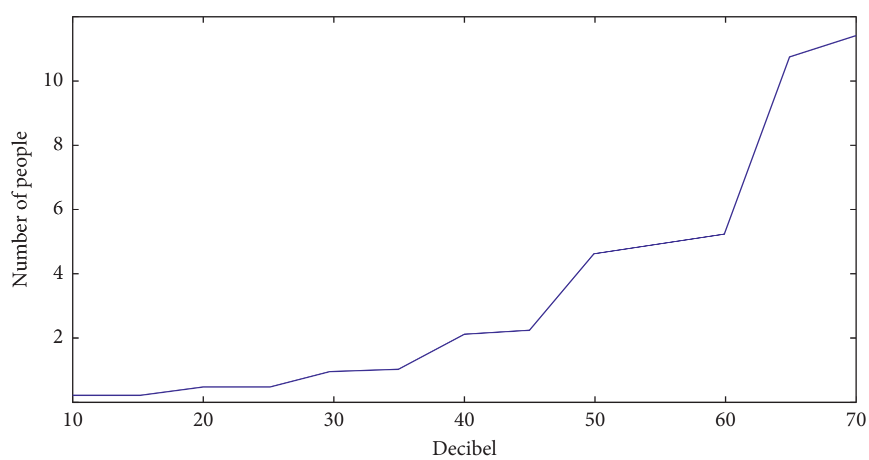

Figure 4: Minimum sound threshold statistical result.

On the one hand, the Kano model analysis results reflect the user's preference, which helps manufacturers gain a better understanding of their customers' individual needs and, ultimately, determine the customizable product attributes that must be entered into the aided design support system. On the other hand, it has the potential to improve the configuration process and efficiency. Consumers and manufacturers have formed a benign closed loop around their individual needs under this framework, from the perspective of consumers. Kano analysis, which improves the efficiency of product configuration in the CAD support system, fully reflects the collaborative value of consumer demand. He directly participates in the product configuration process as an individual consumer, efficiently obtains a personalized product design scheme through human-computer interaction, and fully satisfies his own preferences.

The visual effect and font size of the interface will affect the cognitive efficiency of the elderly users. In order to verify the feasibility of the operation interface of this scheme and whether it can meet the needs of the elderly users for easy identification and operation, the usability test of the operation interface is carried out. Using the software to make dynamic effects, key operation, feedback prompts, and so on, we simulate the operation mode of the old users' real use of the rice cooker and select an existing operation interface of the rice cooker in the market for comparative test. The experimental results are shown in Figure 5.

It can be seen from Figure 5 that the average time for the elderly users to operate the designed interface is less than that of the existing interface. The design scheme is obviously superior to the existing product scheme, benefiting from concise interface interaction, good human-machine dimension of parts, and appropriate feedback information. This also verifies the effectiveness of the aging design principle. The test of this design scheme relies on software to simulate the actual operation effect, and the final test result is convincing to a certain extent. The actual product interaction effect also needs real products as the evaluation object.

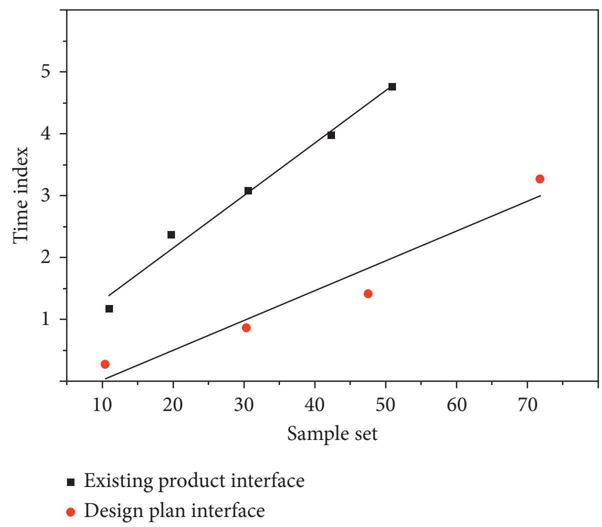

Figure 5: Average test time for two interfaces.

By refining the common factors that can represent the overall structure of the questionnaire, the cumulative explanatory quantity in the analysis results can explain to what extent the test questionnaire can reflect the true characteristics of the measured object; that is, it can test the structural validity of the questionnaire. Based on the two tests before and after the innovation activity, the transition matrix is constructed by analyzing the changes of a certain quality element among five categories of quality elements. Assuming that the innovation effect is stable, the stable state of Markov chain can indicate the degree of innovation. Figures 6 and 7 reflect the time taken by users to evaluate individual product design schemes in each generation population under the two methods.

According to the comparison results, the method proposed in this paper effectively reduces the user's operation time, and both the average time for evaluating each generation population and the total time for completing a product customization are less than the time required by traditional methods. Therefore, the method proposed in this paper can fully alleviate user fatigue in the process of product customization.

Although the importance analysis method for structural requirements is the same as for functional requirements, the distribution of weight values differs. Because of their complaints and dissatisfaction with the original product structure and behavior, users, for example, pay more attention to basic needs. If these factors are not adequately considered in the design of new products, user dissatisfaction will skyrocket, and the image of new products will suffer. As a result, businesses should adjust the criterion layer's weight set in accordance with their own product development strategies. Before the experiment, the data were set and recorded, and the behaviors and actions of the subjects using the products were coded to ensure the reliability and validity of the final data. The classification of behaviors should be complete and nonoverlapping, and behaviors should be clearly defined so that observation is not made more difficult or inconsistent. The behaviors in this experiment are grouped based on this requirement.

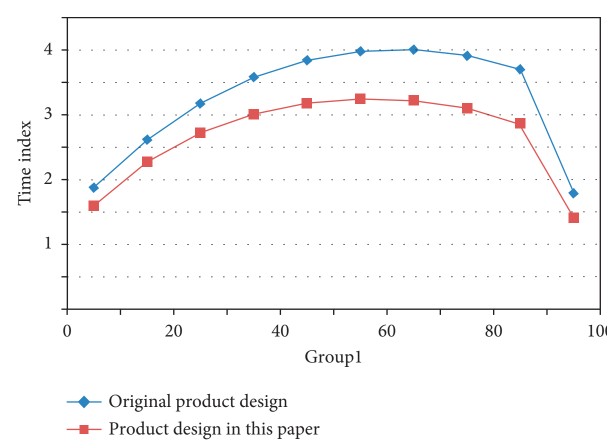

Figure 6: Time for single operation of the first group of users.

After the product design scheme is completed, in order to verify whether the design scheme can be accepted by the elderly users, the elderly users need to evaluate the product and obtain their satisfaction with the design scheme. This evaluation is mainly conducted from three aspects: product appearance, interface effect, and operation mode. Make Likert scale from the aspects of product appearance, usability, identifiability, interface layout, and operation mode. Figure 8 is a comparison of satisfaction evaluation between traditional product design and interactive aging product design for elderly users.

It can be seen from Figure 8 that typical elderly users are satisfied with the design scheme of this product. The average satisfaction of product appearance, usability, identifiability, interface layout, and operation mode is generally high. The scientific design of this paper is verified.

The characteristics of quality elements are examined in depth in this chapter. In terms of time characteristics, charm,

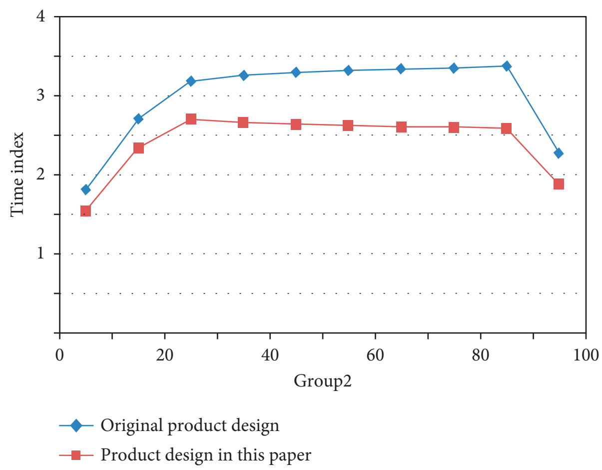

Figure 7: The second group of users' single operation time.

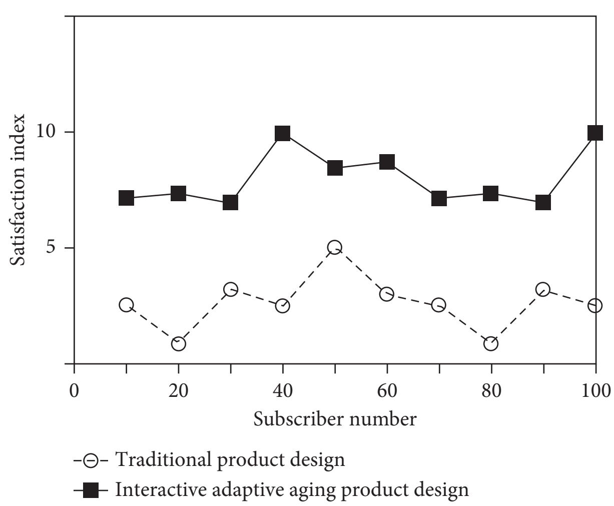

Figure 8: Comparison of product design satisfaction evaluation.

expected quality, and basic quality sink, from the perspective of enterprises, attractive quality is a pursuit goal, in which enterprises hope that the quality and physical characteristics of their products can become attractive quality to customers. The influencing factors of service quality are studied from the perspective of consumers' types, in combination with the characteristics of the elderly population and consumers' personality in the questionnaire survey results. To investigate the possible rules between different personality characteristics and Kano model quality judgment, summarize the consumers' Kano quality judgment results separately.

5. Conclusions

Fundamentally improving the interactive performance of the aged products, making the interaction between the aged users and the products more accurate and relaxed, and making the aged products safer, more comfortable, and more efficient, as well as improving the inclusiveness and interactivity of the hardware facilities for the aged groups under the aged care model with Chinese characteristics, and ensuring the level and quality of age care are of strategic and practical importance. The goal of designing products for the elderly is to provide a positive product experience based on barrier-free use so that product usage is more in line with the people-oriented concept and a high-quality user experience, promoting the stability and prosperity of a harmonious society. Product design, on the other hand, is an important aspect for businesses to remain evergreen. This paper develops a dynamic quality factor prediction model based on a thorough understanding of the characteristics of quality factors. It also introduces a brand-new method for assessing the impact of quality innovation activities. This paper proposes to evaluate the effect of interactive aging design of products using relevant Kano model theories from the perspective of the elderly. This method of assessment is more scientific and objective. At the same time, the evaluation model presented in this paper is straightforward and simple to implement.

Data Availability

The data used to support the findings of this study are included within the article.

Conflicts of Interest

All the authors do not have any conflicts of interest regarding the publication of this paper.

References

[1] Q. Wang, "Agricultural products processing characteristics and quality evaluation[J]," *Journal of Integrative Agriculture*, vol. 17, no. 05, pp. 15-16, 2018.

[2] Y. Shi and S. Han, "Research on medical service robot modeling design based on QFD and Kano model[J]," *Mechanical Design*, vol. 34, no. 12, p. 5, 2017.

[3] C. Li, J. Zeng, X. Jin, and W. Chu, "Quality index evaluation model of MPP sold under the E-commerce platform," *Mathematical Problems in Engineering*, vol. 2021, no. 12, pp. 1–9, 2021.

[4] J. Dou and R. Qi, "Research on voice user interface design strategy of age-appropriate smart home products based on context analysis[J]," *Packaging Engineering*, vol. 42, no. 16, p. 9, 2021.

[5] M. Tang, T. Wang, and D. Peng, "User-perceived hesitant and fuzzy Kano-Taguchi method of mobile library service quality evaluation[J]," *Information Theory and Practice*, vol. 43, no. 3, p. 7, 2020.

[6] M. Yun, J. Zhang, A. Wang, and B. Zhang, "Windbreaker product design research based on KJ method and Kano model [J]," *Wool Spinning Technology*, vol. 48, no. 5, p. 7, 2020.

[7] Y. Liu, L. Zhao, and J. Li, "Design and evaluation of ski wristbands based on Kano model and FAHP analysis[J]," *Packaging Engineering*, vol. 42, no. 4, p. 6, 2021.

[8] A. G. Galstyan, L. M. Aksyonova, A. B. Lisitsyn, L. A. Oganesyants, and A. N. Petrov, "Modern approaches to storage and effective processing of agricultural products for obtaining high quality food products[J]," *Herald of the Russian Academy of Sciences*, vol. 89, no. 2, pp. 211–213, 2019.

[9] H. Yu, Si Chenxi, and H. Wang, "Research on product iteration and service innovation based on fuzzy KANO model

[J]," *Science and Technology Management Research*, vol. 38, no. 9, p. 8, 2018.

[10] S. Smith, C. H. Lau, J. I. Mardel et al., "Physical aging in glassy mixed matrix membranes; tuning particle interaction for mechanically robust nanocomposite films[J]," *Journal of Materials Chemistry*, vol. 4, no. 27, pp. 10627–10634, 2016.

[11] S. Datta, "How does developer interaction relate to software quality? an examination of product development data[J]," *Empirical Software Engineering*, vol. 23, no. 3, pp. 1153–1187, 2018.

[12] C. Lu, Z. Xiao, and X. Fu, "User experience design of household integrated stove based on Kano model[J]," *Packaging Engineering*, vol. 41, no. 20, p. 6, 2020.

[13] G. Katz, U. Merin, D. Bezman, S. Lavie, L. Lemberskiy-Kuzin, and G. Leitner, "Real-time evaluation of individual cow milk for higher cheese-milk quality with increased cheese yield[J]," *Journal of Dairy Science*, vol. 99, no. 6, pp. 4178–4187, 2016.

[14] L. Zhang, L. Wang, and L. Yan, "Research on household washing machine design based on UCD-Kano model[J]," *Machine Design*, vol. 35, no. 12, p. 6, 2018.

[15] J. Barnes, J. L. Sheridan, C. Y. Dong, L. Harmark, S. Vohra, and M. Harrison-Woolrych, "Evaluation of a web-Based,'Purchase event' intensive monitoring method for pharmacovigilance of natural health products: lessons and insights from development work in New Zealand[J]," *Drug Safety*, vol. 43, no. 10, pp. 981–998, 2020.

[16] C. Guoqiang, H. Shi, and F. Zhang, "Innovative design of smart watches based on TRIZ and Kano models[J]," *Packaging Engineering*, vol. 37, no. 16, p. 4, 2016.

[17] Na Tang, "Research on the key factors of digital reference service quality based on Kano model[J]," *Library and Information Service*, vol. 60, no. 18, p. 8, 2016.

[18] E. R. Bornhorst, J. Tang, S. S. Sablani, G. V. Barbosa-Canovas, and F. Liu, "Green pea and garlic puree model food development for thermal pasteurization process quality evaluation [J]," *Journal of Food Science*, vol. 82, no. 9, pp. 1631–1639, 2017.

[19] J. Wei, Z. Li, L. Sun et al., "Evaluation and uncertainty estimate of next-generation geostationary meteorological Himawari-8/AHI aerosol products[J]," *The Science of the Total Environment*, vol. 692, no. 11, pp. 879–891, 2019.

[20] M. Y. Smith, A. Russell, P. Bahri et al., "The rimes statement: a checklist to assess the quality of studies evaluating risk minimization programs for medicinal products[J]," *Drug Safety*, vol. 41, no. 1, pp. 1–13, 2017.

[21] M. Yun, J. Zhang, A. Wang, and P. Mu, "UPLC-QTOF/MS-Based metabolomics applied for the quality evaluation of four processed panax ginseng products[J]," *Molecules*, vol. 23, no. 8, p. 2062, 2018.

[22] J. Judkins, J. Tay-Sontheimer, R. D. Boyce, and M. Brochhausen, "Extending the DIDEO ontology to include entities from the natural product drug interaction domain of discourse[J]," *Journal of Biomedical Semantics*, vol. 9, no. 1, 2018.

[23] M. Song, D. Tian, H. Xiao, and M. Qing Juan, "Research on user needs of Chinese RV design based on A-KANO model [J]," *Packaging Engineering*, vol. 41, no. 10, p. 6, 2020.

[24] T. Kano, K. Osuka, T. Kawakatsu, and A. Ishiguro, "Mathematical analysis for non-reciprocal-interaction-based model of collective behavior[J]," *Journal of the Physical Society of Japan*, vol. 86, no. 12, Article ID 124004, 2017.

[25] J. Song, X. Chen, Y. Jiang et al., "Association and interaction analysis of lipid accumulation product with impaired fasting glucose risk: a cross-sectional survey[J]," *Journal of Diabetes Research*, vol. 2019, no. 4, pp. 1–10, Article ID 9014698, 2019.

[26] P. A. Koval, A. V. Blakesley, T. C. Roberts, Y. Zick, and D. Leroith, "Interaction in vitro of the product of the c-Crk-II proto-oncogene with the insulin-like growth factor I receptor.[J]," *Biochemical Journal*, vol. 330, no. 1, pp. 923–932, 2019.

[27] H. B. Kim, J. G. Kim, T. Kim, and D. Alessi, "Interaction of biochar stability and abiotic aging: influences of pyrolysis reaction medium and temperature[J]," *Chemical Engineering Journal*, vol. 411, no. 7, Article ID 128441, 2021.

[28] M. Li and J. Zhang, "Integrating Kano model, AHP, and QFD methods for new product development based on text mining, intuitionistic fuzzy sets, and customers satisfaction[J]," *Mathematical Problems in Engineering*, vol. 2021, no. 5, pp. 1–17, 2021.

[29] V. Santos, S. Gomes, and M. Nogueira, "Sustainable packaging: does eating organic really make a difference on product-packaging interaction? [J]," *Journal of Cleaner Production*, vol. 304, no. 11, Article ID 127066, 2021.

Hindawi
Computational Intelligence and Neuroscience
Volume 2022, Article ID 3812055, 12 pages
https://doi.org/10.1155/2022/3812055

Research Article

Emotional Analysis Model for Social Hot Topics of Professional Migrant Workers

Gefeng Pang and Anze Bao

School of Economics and Business Administration, Chongqing University, Chongqing 400030, China

Correspondence should be addressed to Gefeng Pang; 20130483@cqu.edu.cn

Received 23 December 2021; Revised 6 January 2022; Accepted 7 January 2022; Published 31 January 2022

Academic Editor: Xin Ning

Text makes up a large portion of network data because it is the vehicle for people's direct expression of emotions and opinions. How to analyze and mine these emotional text data has become a hot topic of concern in academia and industry in recent years. The online LDA (Latent Dirichlet Allocation) model is used in this paper to train the social hot topic data of professional migrant workers on the same time slice, and the subtopic evolution and intensity are obtained. The topic development is divided into four categories, and the classification model is created using SVM (Support Vector Machine). Instead of decision makers, a virtual human with sensibility and rationality is built using a hierarchical emotional cognitive model to solve multiobjective optimization problems interactively. It analyzes human body structure and emotional signals, and then combines them with visual and physiological signals to create multimodal emotional data. An example is used to demonstrate the effectiveness of the proposed model.

1. Introduction

Entrepreneurship of professional migrant workers can effectively alleviate social employment pressure, narrow the income gap between urban and rural areas, and promote new urbanization. In recent years, professional migrant workers' entrepreneurship has been paid more and more attention by the government and academia. However, at present, most professional migrant workers' new ventures are in a development dilemma due to lack of competitive advantages in the fierce market competition [1]. With the rapid spread of the Internet, its social effects are also rapidly expanding. These energies are positive and negative, while events with negative energy are more likely to cause large-scale discussions. At this time, local problems may become public topics in the country, causing huge social panic, and sometimes even requiring government intervention [2, 3]. The process of urbanization and the innovation of social system have increased farmers' enthusiasm to move to cities. They are eager to gain economic benefits in cities, but they are also eager to integrate into urban life, but the reality is not as they wish.

To deal with public opinion of professional migrant workers' social hotspots, it is necessary to improve the predictability of hotspots, which necessitates the analysis of professional migrant workers' social hotspots and trend prediction. The monitoring of professional migrant workers' social hot-spot public opinion requires the use of Weibo's hot-spot detection. It is necessary to understand the development trend of hot-spot in order to make the right decision and ensure the development of Weibo platform in the direction of health, freedom, and vitality in order to correctly guide public opinion and curb online rumors [4]. Different emotional themes focus on different aspects of emotional content in a subjective text and are also related to different emotional words in the text. As a result, the distribution of text themes can reflect the text's overall semantic structure. However, because the emotional content of the text is treated equally to other content in the theme modeling process, and the semantic strength of the emotional theme is determined by the proportion of emotional words in the text, it is still insufficient in highlighting the emotional semantics [5, 6]. Furthermore, traditional theme modeling ignores semantic relationship patterns such as text sequence and word context, instead treating the text as a word bag and determining the theme solely based on the word co-occurrence relationship, which limits the text representation ability.

This topic focuses on emotional analysis and topic trend prediction of social hot topics for professional migrant workers, which refers to the trend prediction of topic state change, that is, to predict the change of topic state in the next period of time [7]. Through human-computer interaction and fuzzy cognitive evaluation, the quantitative relationship among personality characteristics, mood state, and emotional state is described. On this basis, a virtual human integrating sensibility and rationality is proposed, and then a multiobjective decision-making problem-solving method based on hierarchical emotional cognitive model [8] is given. The visual signals are linearly fused with four physiological signals to obtain four groups of multimodal information [9]. The principle based on feedback information and the recognition rate of multimodal information to emotional state is introduced to design the weight determination method. On this basis, decision-level weighted fusion is introduced, and an emotion recognition model based on multimodal signal decision-level weighted fusion is established.

The innovation of this paper: This topic focuses on the emotional analysis of social hot topics of professional migrant workers on the Weibo platform. Based on the existing historical data, this paper deeply analyzes the characteristics of users and texts, extracts a series of characteristics such as emotions and users from them, and constructs a regression model combining with the time series model to describe the development trend of hot topics in the near future, and finally predicts the development trend of hot topics, and helps to realize the early warning of the development of hot topics.

2. Related Work

A research hotspot is using emotion classification technology to solve practical problems in social hot topics of professional migrant workers. The method of statistical emotion words is used in literature [10] to calculate emotions under fixed topics, which can be applied to trend prediction and yields good results. Hong et al. [11] calculate the emotional time series using the ratio of Weibo number to positive and negative emotional words obtained from Twitter data every day, and then use a self-organizing fuzzy neural network to predict the Dow Jones Industrial Average. To predict the movie box office, the emotional ratio is calculated using emotional analysis of social hot topic data, which is then combined with the movie box office using the Pearson correlation coefficient [12]. This paper uses statistics to conduct an emotional analysis on the topics of these mobile phones on Twitter, and then uses classified methods to predict users' satisfaction [13–15]. Zhou et al. [16] looked at opinion leader fans on Twitter, classified their emotional comments, and discovered that followers are influenced by their emotions, and that the change in this influence is consistent with reality. This study confirms that a user's emotions have an impact on his followers, particularly opinion leaders' emotional changes, and uses this relationship to predict user emotional changes.

The research on emotional modeling and application has been paid extensive attention [17, 18]. Especially, literature [19, 20] puts forward the emotional cognitive learning and decision-making model by applying Boltzmann selection mechanism, which takes emotional factors as internal influences and external environment as external influences, and realizes emotional cognitive learning and decision-making by calculating the internal and external influence probabilities after decision-making; Sosa and Rodríguez [21] realized the coordinated control of robot behavior on the basis of emotional cognitive learning and decision-making model. However, the application of emotional model was limited because it adopted symbolic cognitive state and decision-making behavior. In literature [22], the author proposed an improved emotional interaction model, but it still did not take into account the influence of individual personality characteristics on the emotional model, so it was still limited when it was used to solve decision-making problems. Khare and Bajaj [23] put forward a multimodal emotion recognition model based on visual signals and physiological signals, which combines facial expression features and ECG features in series at feature level to form multimodal features. Experiments show that the recognition rate of multimodal features is higher than that of one modal feature. Schmidt et al. [24] put forward the multistream fusion hidden Markov model for emotion recognition. The multistream fusion hidden Markov model is the generalization of the two-stream fusion hidden Markov model, which is a general model-level modal fusion method. Mohammed and Karim [25] use the principle of equal weight to weight and fuse the classification results of audio, video, and text at the decision level, which is equivalent to unweighted fusion at this time. Tao [26] uses grid traversal (0,1) to get the optimal weight, and at the decision level, the classification results of facial expression signals and ECG (electrocardiogram) signals are weighted and fused to get the final recognition result.

Based on the above research, aiming at the characteristics of multimodal information, linear fusion is introduced at the feature level to obtain multimodal features, and the expressive force of multimodal features on emotional state is analyzed. Combining with the principle based on feedback information, the weight determination method is designed. Linear weighted fusion is introduced at the decision level, and an emotion recognition model based on multimodal information two-level fusion is established. Therefore, combining with the characteristics of human multimodal emotional information, it is of great significance to study the weighted fusion of feature level and decision level to improve the model recognition rate.

3. Research Method

3.1. Research on Long-Term Topic Prediction Based on Subtopic Separation. LDA (Latent Dirichlet Allocation) topic model belongs to the document generation model, which assumes that the document has multiple hidden topics, all of which can be composed of the word distribution in the fixed vocabulary [27]. After the topic was put forward, it was widely used, especially in the direction of text clustering and similarity calculation. Figure 1 is the LDA model diagram.

Assume that the rectangular square at the top of LDA graph model is the theme, and K is the number of themes. The letter M in the figure represents the number of all documents in the model, while N is the number of words in the documents and Z is the number of words in the word list.

The inner and outer boxes in the figure also have specific meanings, in which the outer box is a document, while the inner box represents the choice of topics and words in the document. The superparameter in the graph is defined as follows:

α represents document-topic distribution, and β represents topic-word distribution, both of which are fixed values, which are specified by users in advance. W in the graph is observable data, which is a $M \times N$-dimensional matrix, and W_{ij} represents the word j in document i; Document-topic distribution θ and topic-word distribution ϕ are both implicit variables.

The process of using LDA model to generate documents is as follows:

(1) Selecting word distribution $\phi_k, k \in \{1, \cdots, K\}$ of topic k from Dir (β) of parameter β

(2) Select the theme distribution θ_i of document i from Dir (α) of parameter α, $i \in \{1, \cdots, M\}$

(3) For the word at the j position in document i, $i \in \{1, \cdots, M\}$, $j \in \{1, \cdots, N\}$:

(1) Generating the theme Z_{ij} of the word j in the document i according to the polynomial distribution with the parameter θ_i

(2) According to the polynomial distribution with parameter $\phi_{Z_{ij}}$, the word W_{ij} of word j in document i is generated

A topic will inevitably change with time, but no matter how it changes, the new data will still carry the information of the old data, that is, the topic is persistent and stable. However, the training process of LDA model is to train all documents directly and generate various topics at the same time, which cannot deal with online new texts. Therefore, online LDA model should be born. In online LDA model, the distribution of topic words in time slice t obeys the following Dirichlet distribution:

$$\phi_k^t \sim \text{Dirichlet}\left(\beta_k^t\right) \sim \text{Dirichlet}\left(w\beta_k^{t-1}\right). \tag{1}$$

Among them, the matrix β_k^{t-1} retains the words of the previous time slice, and w is a weight vector indicating the proportion of historical words retained.

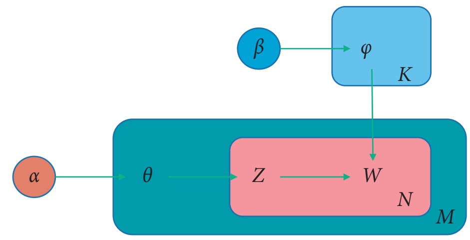

Figure 1: LDA model diagram.

Set the theme intensity of this article, that is, the document with clear theme tendency is regarded as high intensity, otherwise it is low. Calculate the intensity of each Weibo, finally get the total intensity of Weibo under the time slice, and calculate the theme intensity according to

$$T_S\left(Z_K\right) = \frac{\sum_{n=1}^{N} w_n^{\theta_{n,k}}}{\sum_{n=1}^{N} w_n}. \tag{2}$$

Among them, $\theta_{n,k}$ represents the estimated value of the distribution of the m-th Weibo on the k-th subtopic, and w_n represents the document weight. When the social hotspot is only related to this subtopic, the weight is set to 1. When social hotspots discuss multiple events at once, as shown in LDA, that is, when words with multiple topics appear in this social hot topic of professional migrant workers, and the weight is measured by the maximum value, the weight is measured by the maximum value.

When the theme evolves, the words change with it. The so-called variation is the dissimilarity. KL distance is generally used to measure the similarity. For the topics of $d-1$ time and d time, KL distance is

$$S_{\text{KL}} = \left(\phi_k^{d-1}, \phi_k^d\right) = \frac{1}{2}\left(\sum_{i=1}^{V} \phi_{k,i}^{d-1} \log \frac{\phi_{k,i}^{d-1}}{\phi_{k,i}^{d}}\right), \tag{3}$$

where ϕ_k^{d-1}, ϕ_k^d is the distribution of the same subtopic on the previous day and the next day, respectively, and the calculation result indicates the similarity between the two topics, then the topic variation rate is as shown in formula (4), which is

$$V = 1 - S_{\text{KL}}\left(\phi_k^{d-1}, \phi_k^d\right). \tag{4}$$

Considering that the ups and downs cannot reflect the overall change of the trend, according to the speed of topic trend change, the topic discussion degree is divided into four categories, and forecasts them separately. The specific division according to numerical values is shown in Figure 2.

These four categories are classified in this chapter based on subtopic intensity and subtopic variation rate, and the subtopic intensity and subtopic variation rate, as well as the classification results, are added as two features to each time slice, and the prediction is made using the GBDT method (gradient boosting decision tree).

3.2. Hierarchical Emotional Cognitive Model. Establish a hierarchical emotional cognitive model, which includes a personality characteristic layer, a mood state layer, an

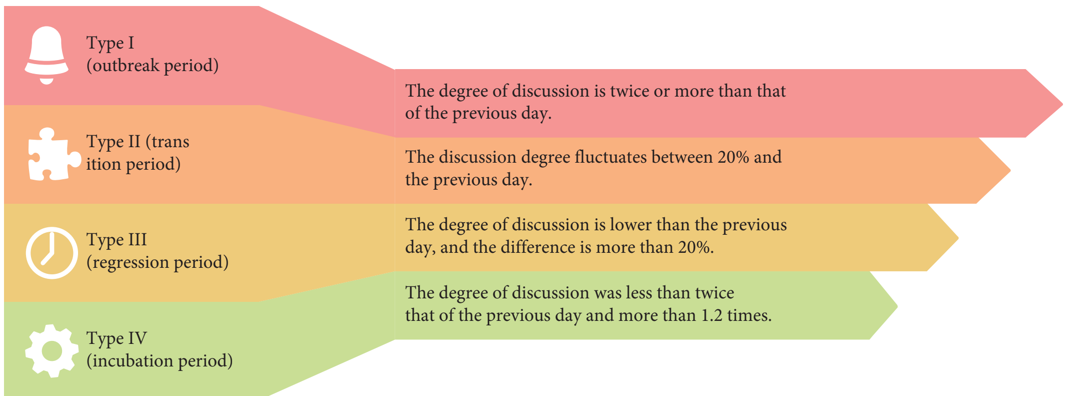

Figure 2: Classification table of long-term topic popularity value.

emotional state layer, and a cognitive evaluation module, as shown in Figure 3.

The personality layer realizes the acquisition of personality data through human-computer interaction, and influences the change process of the lower mood state through mapping and personality parameters; the cognitive module quantifies and evaluates the influence of external stimulus signals on the emotional model, and then transmits it to the mood layer of the emotional model.

In the process of emotion renewal, mood layer and emotion layer interact with each other, and the stability of personality layer, mood layer, and emotion layer decreases in turn, while personality layer is the most stable and emotion layer is the most prone to change.

Personality is a relatively stable parameter that can be used to describe a person's personality and is influenced by both heredity and acquired environment. Personality is an important parameter in the emotion model because it directly reflects the personality of the individual. Because personality has a direct impact on the size of each component of mood state and the speed with which states transition, emotion modeling requires accurate data on individual personalities.

The definite character characteristic vector is

$$\begin{aligned} &P_p = [P_N, P_E, P_O, P_C, P_A], \\ &P_X \in [0,1], \\ &X \in \{N, E, O, C, A\}. \end{aligned} \tag{5}$$

Among them, P_N, P_E, P_O, P_C, P_A represents neuroticism, extroversion, openness, conscientiousness, and agreeableness, respectively.

Mood level is used to represent people's mood state, which can be described by PAD (pleasure-arousal-dominance) model, where P represents the positive and negative characteristics of individual emotional state, A represents the individual's neurophysiological activation level, and D represents the individual's control over the situation and others. PAD model corresponds to a three-dimensional emotional space.

Define the mood state space as a three-dimensional PAD, and define the mood state vector as

$$M_{\text{ent}} = [m_P, m_A, m_D]. \tag{6}$$

Among them m_P, m_A, $m_D \in [-1,1]$, $M_{\text{ent}} = [0,0,0]$ corresponds to a calm state of mind.

In order to be suitable for multiobjective decision-making, two components, positive and negative characteristics of emotion and emotional intensity, are selected to represent the emotional state. The emotional state is defined as a two-dimensional vector:

$$E_e = [\chi, q], \chi\{-1, 0, 1\}, q \in (0, 1). \tag{7}$$

Among them χ represents the positive and negative characteristics of emotion, with a value of 1, 0, or 1, which respectively indicates that the current emotional state is negative, calm, and positive; q represents the current emotional intensity.

The cognitive evaluation of an emotion model for external stimulus signals should begin with the individual's intention and evaluation criteria for the evaluation subject, and then learn from the literature method [28]. Individuals' subjective wishes, preferences, and individual evaluation criteria determine their emotional expression, so the emotion model should pay attention to the design of wishes, preferences, and evaluation criteria for the cognition of stimulus signals.

The change of state of mind is influenced by personality characteristics and external stimuli, and at the same time, it will decay with time. Let M_t represent the state of mind corresponding to time t, then the updating process of state of mind space is as follows:

$$M_t = \varphi(M_{t-1}) + M_P + M(U) \tag{8}$$

Here, M_t, M_{t-1} is the state of mind of the current moment and the previous moment respectively; $\varphi(M_{t-1})$ is the mood state attenuation function; and $M(U)$ is the influence of external stimuli on mood, which is calculated by fuzzy cognitive evaluation module.

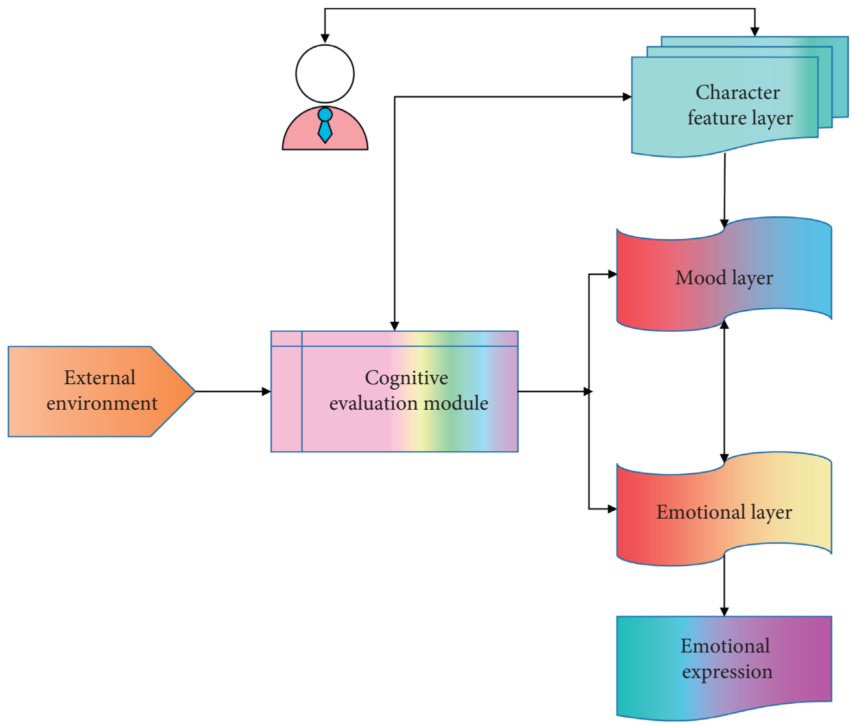

Figure 3: Hierarchical emotional cognitive model structure.

Normal multiobjective decision-making problem can be described as

$$\max M = \{f_1(x), f_2(x), \ldots, f_l(x)\}$$
$$s.t \begin{cases} g_i(x) \le 0, & i = 1, 2, \ldots, m, \\ X = (x_1, x_2, \ldots, x_n)^T, & x_* \in R, \end{cases} \quad (9)$$

where $g(x)$ is the constraint function.

Figure 4 shows an emotional interactive decision-making algorithm based on hierarchical emotional cognitive model. This algorithm takes goal achievement degree, priority of objective function and overall coordination degree as emotional cognitive evaluation factors, and combines rational decision-making with emotional decision-making to build a virtual human. After obtaining the cognitive model of decision-making experts through interaction, it can realize automatic emotional decision-making by computer.

Cognitive decision-making model consists of rational decision-making module and emotional decision-making module, which respectively give the adjustment range of goal attainment. The two parts of adjustment range of goal attainment represent external objective requirements and internal subjective desires, respectively.

3.3. Emotion Recognition Based on Multimodal Information Feature Level and Decision Level Fusion. Emotion can cause many changes such as external changes of facial expression and internal changes of human physiology at the same time, so it is imperative to study emotion recognition based on multimodal information [29]. Facial expression recognition based on visual signals, considering the dynamic feature information of facial expression changes, and using the temporal and spatial information of facial expression changes at the same time, can reflect the essence of facial expression changes more truly and has stronger practical applicability.

The process of expressing human emotions is a process in which various modal information complement each other comprehensively. Single-modal features can only show part of the attribute information of the object. In order to describe the target object more accurately, the integration of multimodal features is an inevitable trend. The emotional features involved in this chapter are visual signal features and four physiological signal features. After feature extraction [30–32], the visual signal features and four physiological signal features are combined in series to form four multimodal features.

SVM (Support Vector Machine) is a new learning algorithm developed on the basis of statistical learning theory. Support vector machine classifier has a good effect on small sample classification problem, and it is not necessary to take enough sample number as the theoretical condition. For the above reasons, this method has been widely used in pattern recognition.

This chapter chooses one-to-one method to solve the multiclassification problem of expressions based on support vector machine. For n expression categories, design a binary support vector machine classifier for every two expressions, that is, design $n(n-1)/2$ subsupport vector machine classifier, SVM_{ij}, $1 \le i < j \le k$. Among them, i, j is the expression category label.

In this chapter, the voting mechanism of multiple classifiers is adopted, and the complementary performance

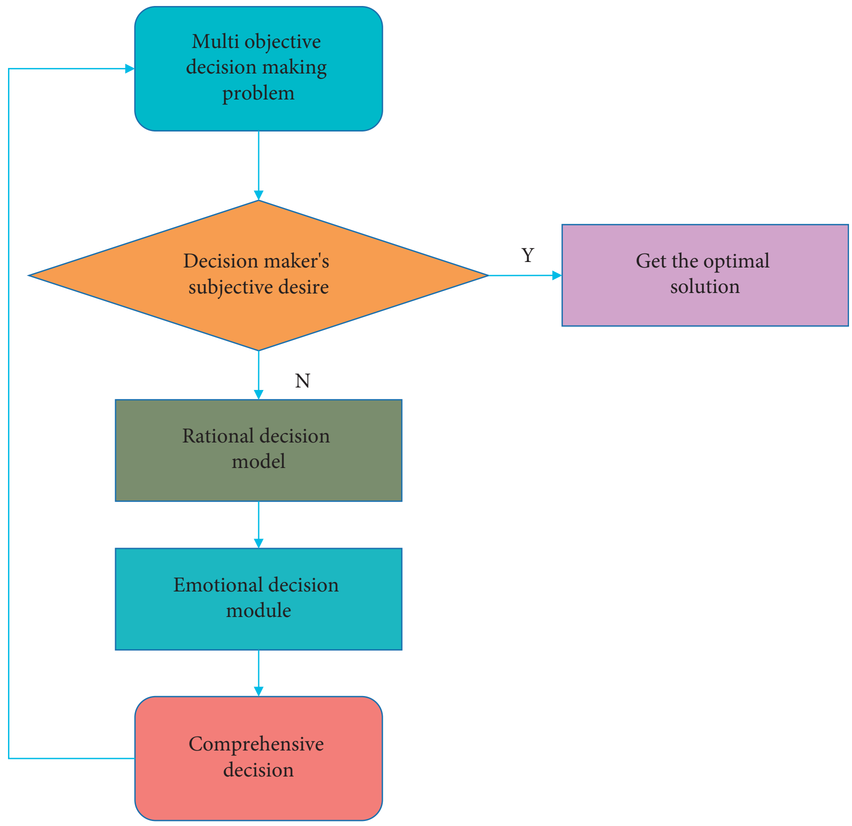

FIGURE 4: Cognitive decision-making process.

of multiple classifiers is used to improve the recognition effect. First, the recognition results of emotion state by emotion classifier based on multimodal signals are obtained. Then, for the experimental results of several subclassifiers, the final recognition results are obtained by weighted voting, and the specific calculation steps are as follows:

Get the weighting matrix of the multimodal signal, and then the weighting matrix $W_i\,(1 \le i \le 4)$ of the corresponding subclassifier is

$$W_i = \begin{bmatrix} p_{i1} & \cdots & 0 \\ \vdots & \ddots & \vdots \\ 0 & \cdots & p_{im} \end{bmatrix}. \tag{10}$$

Let $\overrightarrow{C}_i = (c_{i1}, c_{\mathrm{im}})^T\,(1 \le i \le 4)$ be the result of the subclassifier, where $|\overrightarrow{C}_i| = 1, c_{\mathrm{ij}} \in \{0, 1\}\,(1 \le i \le 4, 1 \le j \le m)$.

$$\overrightarrow{C} = \sum_{i=1}^{4} W_i \overrightarrow{C}_i = \sum_{i=1}^{4} \begin{bmatrix} p_{i1} & \cdots & 0 \\ \vdots & \ddots & \vdots \\ 0 & \cdots & p_{im} \end{bmatrix} \begin{bmatrix} c_{i1} \\ \vdots \\ c_{im} \end{bmatrix} = \begin{bmatrix} \sum\limits_{i=1}^{4} c_{i2} p_{i1} \\ \vdots \\ \sum\limits_{i=1}^{4} c_{im} p_{im} \end{bmatrix}. \tag{11}$$

Based on the maximum rule, the k-type emotional state with the highest score is the final recognition result, as shown below:

$$\mathrm{Max}_{j=1}^{m} \left\{ \sum_{i=1}^{4} c_{ij} p_{ij} \right\} = \sum_{i=1}^{4} c_{ik} p_{ik}. \tag{12}$$

For the emotion recognition model based on multimodal signals, because many modal signals are related to the emotional state, analyze the physiological structure of human body and the characteristics of emotion signals, and optimize the selection of visual signals (facial image signals) and four physiological signals (EEG (electroencephalogram) signals, ECG signals, respiratory signals and skin signals) that can be used for emotion recognition, as shown in Figure 5.

Four subclassifiers based on support vector machine are established, and four subclassifiers are trained and tested by using four multimodal emotion features, and the emotion recognition results are obtained. Finally, the model is trained and tested with four multimodal emotional features, and the final recognition result is obtained.

4. Analysis and Discussion

4.1. Long-Term Topic Prediction Analysis. Online LDA model trains data, using all data of the same topic every time, and dividing the data into different documents for each topic according to the daily time slice, and numbering the documents from 0 according to the date sequence. Compare the topic evolution and topic intensity with the topic discussion degree, as shown in Figure 6.

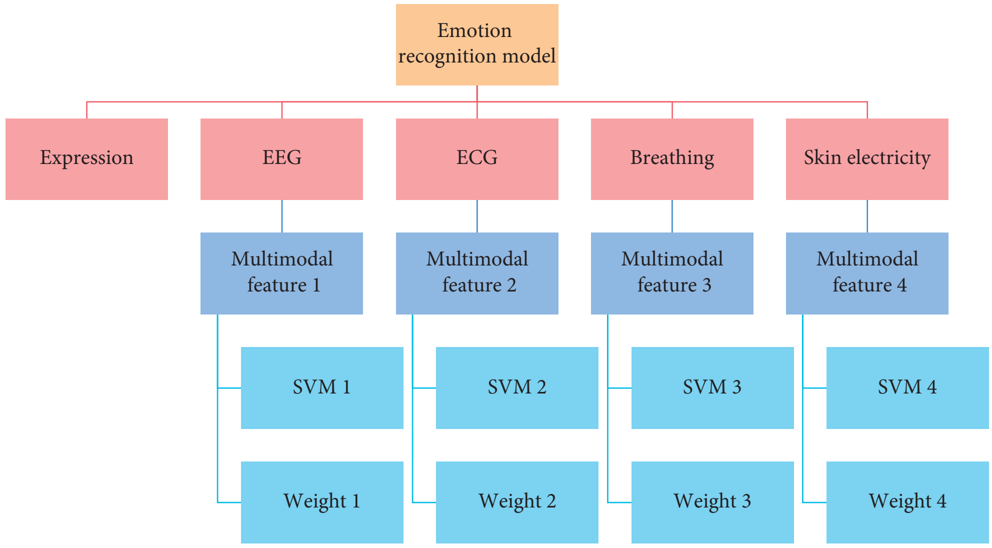

Figure 5: Emotion recognition model based on feature-level fusion and decision-level weighted fusion.

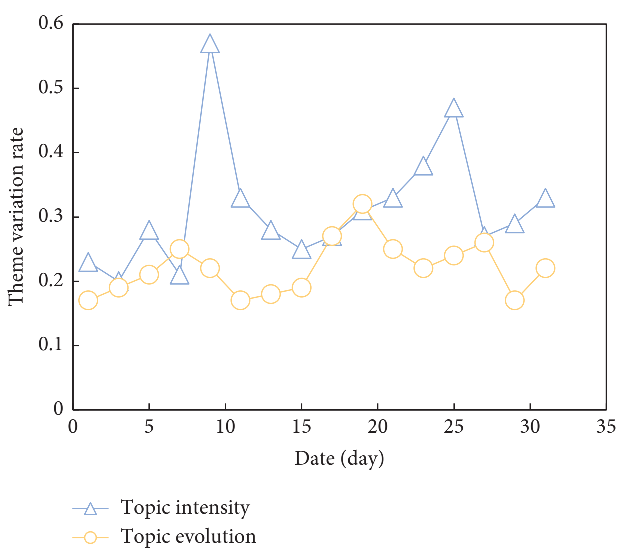

Figure 6: Topic intensity and topic evolution trend chart.

It can be found that when the topic variation rate and intensity are high, the topic discussion degree is also greatly improved, which shows that the topic discussion degree has a great relationship with the topic variation rate and the topic intensity. Careful observation shows that the trend chart between the topic variation rate and the topic intensity has the following relationship:

(1) The number of peaks is roughly the same, and they can all find the correspondence in the topic heat

(2) Theme enhancement lags behind the peak of theme evolution diagram

(3) The small peak of the topic is not closely related to the topic intensity and topic variation, but the big peak is closely related, and the peak of topic evolution is before the peak of the topic

SVM is widely used in classification and regression applications. In this section, SVM in sklearn Toolkit is used to classify forecast data into four categories, with the following characteristics:

(1) Subtopic intensity in the first four days

(2) Subtopic variation rate in the first four days

(3) The historical heat of the first four days

(4) Text features of the previous 4 days

After the features are normalized, SVM is used for training. SVM is very sensitive to the penalty factor c. gridsearchcv () in sklearn is used to automatically find the parameters by gridding. Figure 7 shows the subjective and objective classification error rates corresponding to four groups of feature combinations under several representative c values.

Theme evolution and theme intensity features are recorded as fea1, text content features as fea2 and data features as fea3.

After carefully adjusting the parameters again, the kernel function selects the linear kernel function, the parameter $c = 80$, $g = 0.03$. The final result is shown in Figure 8.

It can be found that the peak prediction rate is very high, which is very helpful for our future trend prediction, and the overall classification accuracy rate reaches 88%. In addition, it is found that these four stages usually occur in turn, so when the category is accurately predicted, this feature is added to the prediction feature to predict the data between two peaks.

In this section, four kinds of classification results are predicted in turn. Only the features of the previous day are used to predict the peak part, and all data before the arrival of the next peak are predicted by using the features of historical data of 4 days. If the calculation is less than 4 days from the peak, the previous features are filled with 0, and the GBDT regression method is used. Figure 9 shows the trend prediction results.

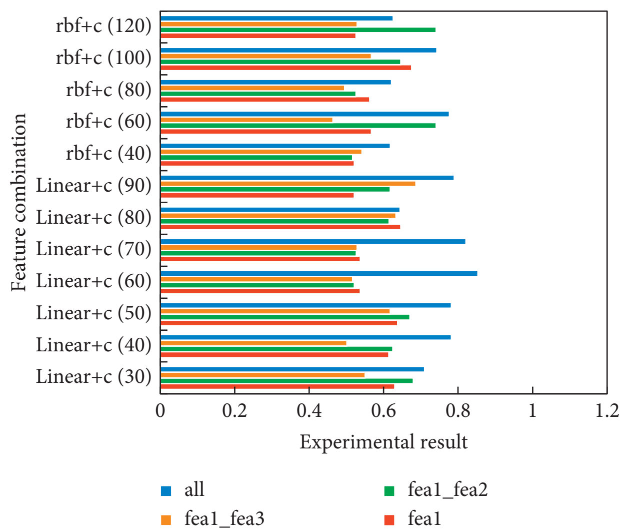

Figure 7: Comparison of experimental results with different characteristics.

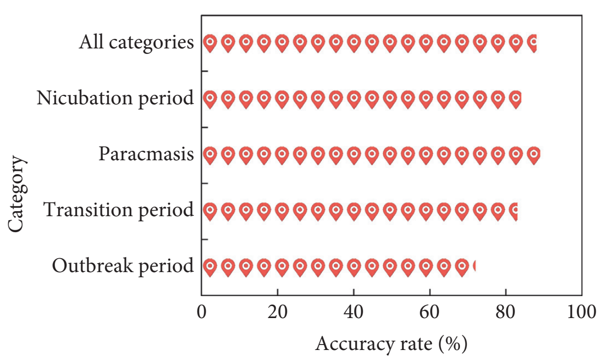

Figure 8: Four classification results.

From Figure 9, it can be seen that, after introducing online LDA model to separate subtopics, the mean square error dropped from 0.098 to 0.081, and the accuracy rate reached 0.77 from 0.74, both of which were better than the previous methods. Moreover, none of the previous forecast periods were accurate. After separation, most outbreak periods can be predicted accurately, but there is still a certain gap between the predicted values.

4.2. Cognitive Analysis. Firstly, the corresponding emotional cognitive model is established. By evaluating the decision makers' personality, the decision makers' personality parameters are $P_P = [\,0.33 \;\; 0.21 \;\; 0.56 \;\; 0.72 \;\; 0.83\,]$ and the influence component of mood is $M_P = [\,0.56 \;\; 0.12 \;\; 0.14\,]$.

When the optimal solution is $x^{*0} = (2.1, 3.1, 3.6)$, the goal achievement degree $\mu^0 = (0, 0, 0)$ and the overall coordination degree $\lambda^0 = 0.6$ are calculated. Then, the multi-objective decision-making is solved based on this emotional cognitive model.

On this basis, the third emotional cognitive decision was made, and the result obtained by the rational decision module was $\Delta\mu_1^3 = (0.233, -0.167, -0.332)$. The component transitions are shown in Figures 10–12.

Goal attainment: $\mu^3 = (0.778, 0.639, 0.507)$, overall achievement: $\lambda^3 = 0.778, s = \sqrt{\sum_{i=1}^{3} (\mu^3(i) - \mu^2(i))\wedge 2} = 0.063 < 0.1$, and satisfied $\mu(f_1(x^{*3})) > \mu(f_2(x^{*3})) > \mu(f_3(x^{*3}))$, Therefore, x^{*3} is the optimal solution to satisfy the subjective desire of decision makers.

4.3. Emotion Recognition. In this section, the experimental hardware devices are mostly desktop computers. The hardware configuration is as follows: inter (R) CORE (TM) i7-6700 CPU, 3.4 GHz, 4 GB memory, and 64 bit Windows 7 Ultimate operating system, which is primarily responsible for running various experimental tools and software, data processing, and result output. MATLAB and the EEG Lab toolbox are used to process a variety of physiological data, and the LibSVM software package is used to train and test the SVM classifier, with Python as the development environment.

The multimodal responses and self-emotional evaluations of 30 collected subjects were induced and recorded synchronously using 20 video clips from the database as stimuli. Emotional signals included peripheral/central nervous system physiological signals, image signals, audio signals, and eye tracking signals. The database's objects are of various ages, genders, races, cultures, and educational backgrounds, and the information coverage is extensive. Furthermore, the emotion-induced video is highly stimulating, the data collection environment is standard, and the emotion signals collected are of high quality.

First, the data set is divided into five types based on emotional tags using stratified random sampling. The training set is made up of a certain percentage of data samples extracted from each physiological signal's data set, while the test set is made up of the remaining data samples.

The emotion recognition model is trained and tested by using four kinds of multimodal signal emotion features, respectively, and the corresponding emotion recognition results are shown in Figure 13.

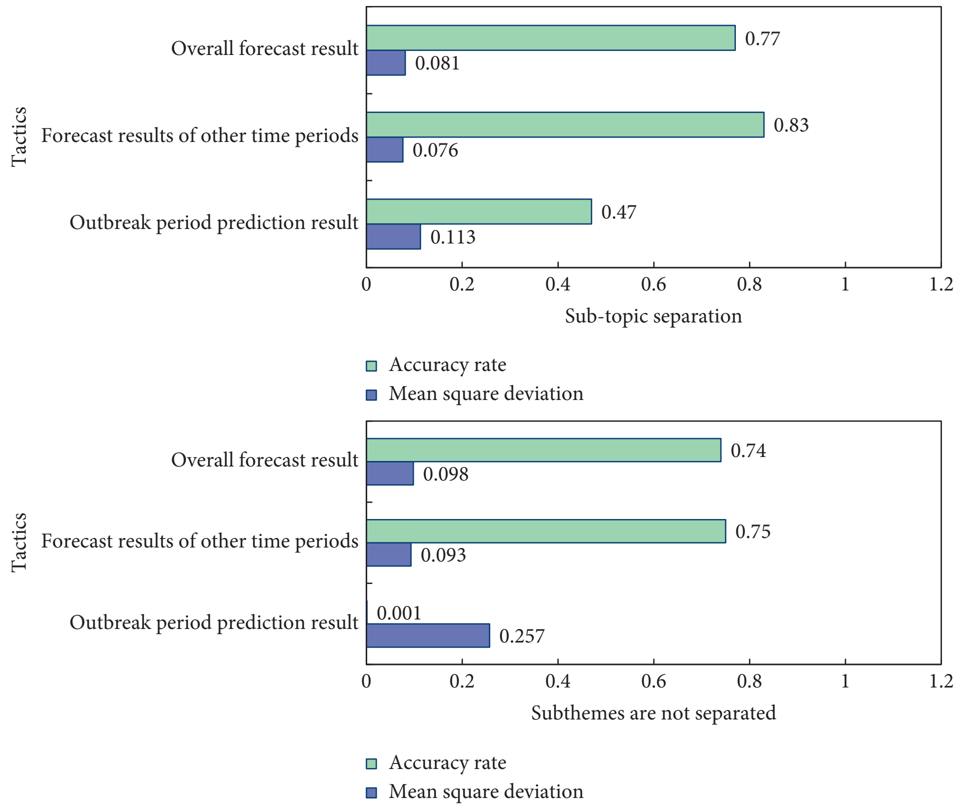

Figure 9: Trend prediction result.

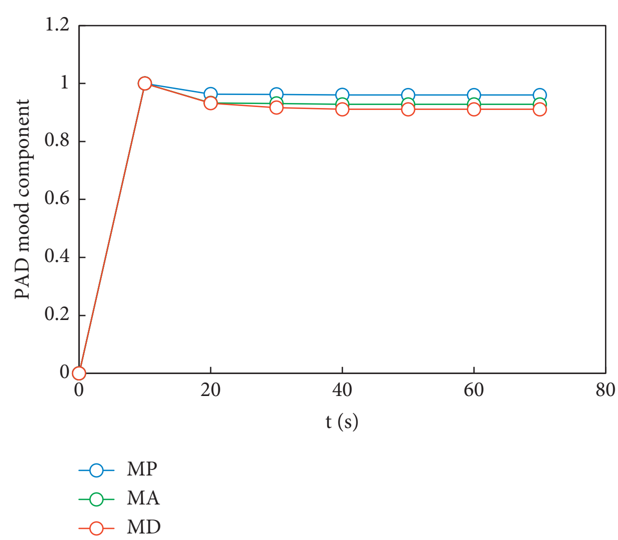

Figure 10: The transition process of each component of decision-making mood state of objective 1.

It can be found from Figure 13 that the local recognition rate of four emotional states is based on the multimodal signal 1 composed of visual signals and EEG signals, while the highest recognition rate of one emotional state "disgust" is based on the multimodal signal 2 composed of visual signals and ECG signals. In addition, the expressive power of four multimodal signals to five emotional states is different.

The types of emotional signals are analyzed in this chapter's research, and a feature-level fusion method is proposed that is universal and can be used for any multimodal emotional signal. This paper investigates the expressive power of multimodal emotional signals in identifying emotional states and proposes a universal weight determination method based on multimodal emotional signals for identifying emotional states. A universal decision-level weighted fusion modeling method is proposed, which can be applied to any multichannel emotional data. The modeling method based on two-level fusion can fully

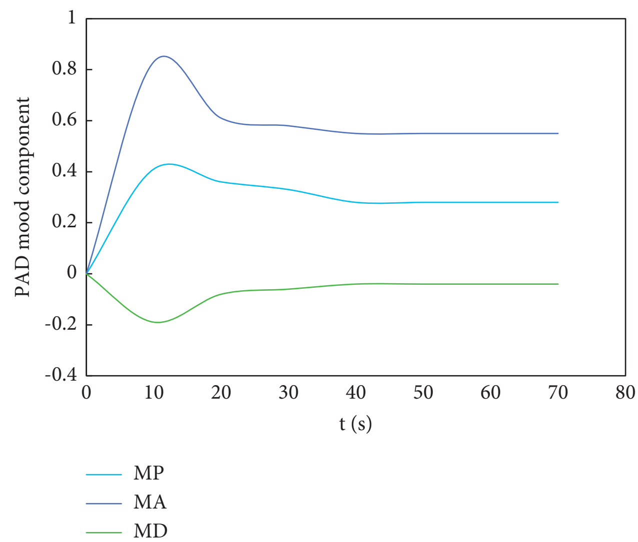

Figure 11: The transition process of each component of decision-making mood state of objective 2.

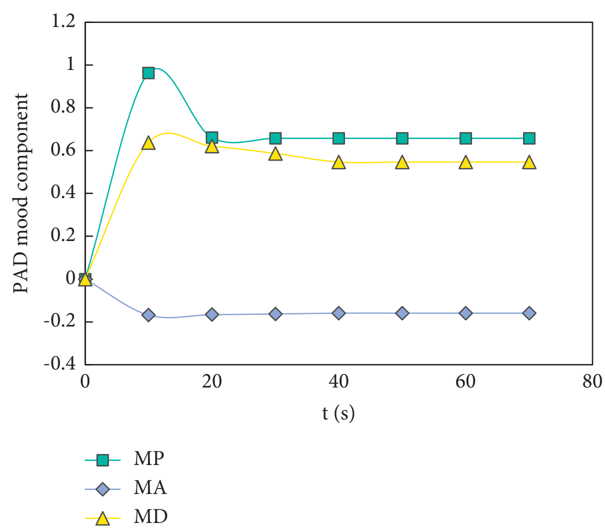

Figure 12: The transition process of each component of decision-making mood state of objective 3. At this point, $\Delta\mu^3 = (-0.186, 0.028, -0.034)$, the optimal solution of the third interactive decision is: $x^{*3} = (10.036, 8.875, 7.518)$, $f(x^{*3}) = (288.24, 241.28, 201.63)$.

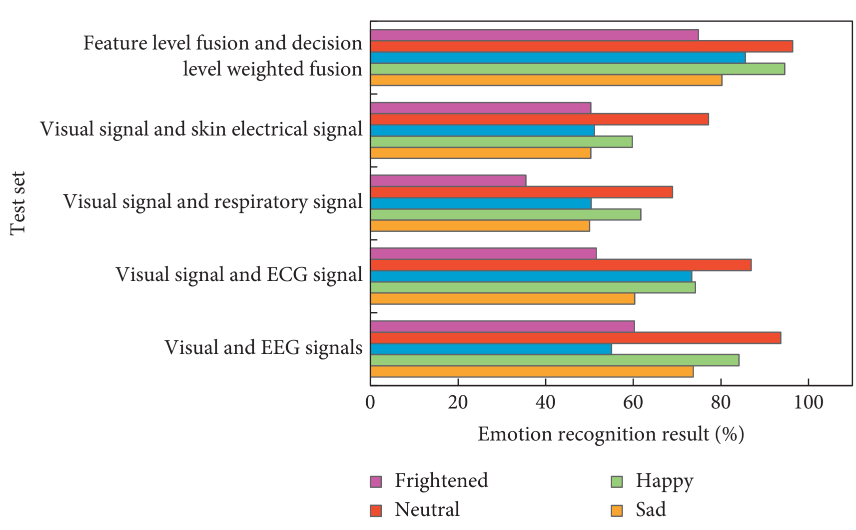

Figure 13: Emotion recognition results based on four multimodal emotion signals and two-level fusion.

exploit the benefits of each channel's emotional information, resulting in a higher model recognition rate.

5. Conclusion

Knowing the information trends of social events on the Weibo platform in real time, as well as tracking and predicting the social hot topics of professional migrant workers on a continuous basis, allows the government and enterprises to grasp public opinion trends in real time and guide public opinion, which is of great social importance to both the government and businesses. In this paper, the Weibo data is trained using an online LDA model on the same time slice, and the subtopic evolution and intensity are calculated. The development of the topic is divided into four categories. The classification model is built using SVM, and the data between two peaks is predicted using a short-term prediction model. The experimental results show that this method's topic popularity classification accuracy is 88 percent. A multiobjective emotional cognitive decision-making method is presented in this paper. This study lays the groundwork for implementing computer-assisted emotional decision-making in complex multiobjective problems. The classification results of four physiological signals are fused for decision-making according to the maximum rule, giving full play to the benefits of various physiological signals and thus improving the model recognition rate.

In this paper, an online LDA model is used to analyze the evolution of subtopics in long-term topics. However, due to the model's limitations, only the same number of subtopics can be fixed every day, which will need to be improved in future research. Various external factors, such as news media reports, public opinion climate, and so on, will influence the topic's trend.

Data Availability

The raw data supporting the conclusions of this article will be made available by the authors, without undue reservation.

Conflicts of Interest

The authors declare no conflicts of interest.

References

[1] Y. Y. Cao, X. H. Qin, J. J. Li, Q. Q. Long, and B. Hu, "Exploring seniors' continuance intention to use mobile social network sites in China: a cognitive-affective-conative model," *Universal Access in the Information Society*, vol. 7, no. 7, pp. 1–22, 2020.

[2] X. Qi, W. Wang, L. Guo, M. Li, X. Zhang, and R. Wei, "Building a plutchik's wheel inspired affective model for social robots," *Journal of Bionics Engineering*, vol. 16, no. 002, pp. 209–221, 2019.

[3] R. Xiang, J. Li, M. Wan et al., "Affective awareness in neural sentiment analysis," *Knowledge-Based Systems*, vol. 226, no. 2, Article ID 107137, 2021.

[4] M. Shi, "Research on parallelization of microblog emotional analysis algorithms using deep learning and attention model based on spark platform," *IEEE Access*, vol. 7, pp. 177211–177218, 2019.

[5] Y. Xu, Y. Chai, L. Wang, and F. Yuan, "Multilingual text emotional analysis model MF-CSEL," *Journal of Chinese Computer Systems*, vol. 040, no. 005, pp. 1026–1033, 2019.

[6] A. D. Marimpis, S. I. Dimitriadis, and R. Goebel, "A multiplex connectivity map of valence-arousal emotional model," *IEEE Access*, vol. 8, pp. 170928–170938, 2020.

[7] X. Zhai and W. Wei, "Emotional analysis of neural network text combined with attention mechanism," *International Core Journal of Engineering*, vol. 5, no. 10, pp. 123–128, 2019.

[8] W. Cai, M. Gao, R. Liu, and J. Mao, "MIFAD-net: multi-layer interactive feature fusion network with angular distance loss for face emotion recognition," *Frontiers in Psychology*, vol. 12, 2021.

[9] W. Cai, Y. Song, and Z. Wei, "Multimodal data guided spatial feature fusion and grouping strategy for E-commerce commodity demand forecasting," *Mobile Information Systems*, vol. 202114 pages, Article ID 5568208, 2021.

[10] J. Yang, F. Zeng, Y. Wang, and H. Yu, "Multiple music sentiment classification model based on convolutional neural network," *Proceedings of the International Conference on Computer Frontier*, vol. 3, no. 1, p. 3, 2019.

[11] I. Hong, Y. Ko, Y. Kim, and H. Shin, "A study on the emotional feature composed of the mel-frequency cepstral coefficient and the speech speed," *Journal of Computing Science and Engineering*, vol. 13, no. 4, pp. 131–140, 2019.

[12] C. X. Ma, J. C. Song, Q. Zhu, K. Maher, Z. Y. Huang, and H. A. Wang, "EmotionMap: visual analysis of video emotional content on a map," *Journal of Computer Science and Technology*, vol. 35, no. 3, pp. 576–591, 2020.

[13] M. Dahmane, J. Alam, P. L. St-Charles, M. Lalonde, K. Heffner, and S. Foucher, "A multimodal non-intrusive stress monitoring from the pleasure-arousal emotional dimensions," *IEEE Transactions on Affective Computing*, vol. 1, no. 99, p. 1, 2020.

[14] M. Gao, R. Liu, and J. Mao, "Noise robustness low-rank learning algorithm for EEG signal classification," *Frontiers in Neuroscience*, vol. 15, 2021.

[15] J. Kong, H. Wang, X. Wang, X. Jin, X. Fang, and S. Lin, "Multi-stream hybrid architecture based on cross-level fusion strategy for fine-grained crop species recognition in precision agriculture," *Computers and Electronics in Agriculture*, vol. 185, Article ID 106134, 2021.

[16] K. Zhou, R. Wei, Q. Zhang, and Z. Xu, "Learning System for air combat decision inspired by cognitive mechanisms of the brain," *IEEE Access*, vol. 8, no. 99, pp. 8129–8144, 2020.

[17] X. W. Jiang, T. H. Yan, J. J. Zhu et al., "Densely connected deep extreme learning machine algorithm," *Cognitive Computation*, vol. 12, no. 5, pp. 979–990, 2020.

[18] L. Yue, X. Gong, J. Li, H. Ji, M. Li, and A. K. Nandi, "Hierarchical feature extraction for early alzheimer's disease diagnosis," *IEEE Access*, no. 99, 7 pages, 2019.

[19] S. Panwar, P. Rad, K. K. R. Choo, and M. Roopaei, "Are you emotional or depressed? learning about your emotional state from your music using machine learning," *The Journal of Supercomputing*, vol. 75, no. 6, pp. 2986–3009, 2019.

[20] B. Wang, X. Hu, P. Li, and P. S. Yu, "Cognitive structure learning model for hierarchical multi-label text classification," *Knowledge-Based Systems*, vol. 218, no. 3, Article ID 106876, 2021.

[21] J. Sosa and A. Rodríguez, "A latent space model for cognitive social structures data," *Social Networks*, vol. 65, no. 1, pp. 85–97, 2021.

[22] A. Skrynnik, A. Staroverov, E. Aitygulov, K. Aksenov, V. Davydov, and A. I. Panov, "Hierarchical deep Q-network from imperfect demonstrations in minecraft," *Cognitive Systems Research*, vol. 65, no. 7676, pp. 74–78, 2021.

[23] S. K. Khare and V. Bajaj, "Time-Frequency representation and convolutional neural network-based emotion recognition," *IEEE Transactions on Neural Networks and Learning Systems*, vol. 32, no. 7, pp. 2901–2909, 2020.

[24] T. Schmidt, M. Schlindwein, K. Lichtner, and C. Wolff, "Investigating the relationship between emotion recognition software and usability metrics," *I-Com*, vol. 19, no. 2, pp. 139–151, 2020.

[25] S. N. Mohammed and A. Karim, "A novel facial emotion recognition scheme based on graph mining," *Defence Technology*, vol. 16, no. 5, pp. 1062–1072, 2020.

[26] J. Tao, "Emotion recognition for human-computer interaction," *Virtual Reality and Intelligent Hardware (Chinese and English)*, vol. 3, no. 1, p. 2, 2021.

[27] W. Jiaqi, H. Liu, and B. Wang, "Extreme learning machine for emotion recognition of tactile gestures," *Journal of Intelligent Systems*, vol. 014, no. 001, pp. 127–133, 2019.

[28] V. Sreenivas, V. Namdeo, and E. V. Kumar, "Group based emotion recognition from video sequence with hybrid optimization based recurrent fuzzy neural network," *Journal Of Big Data*, vol. 7, no. 1, p. 56, 2020.

[29] A. V. Haridas, R. Marimuthu, V. G. Sivakumar, and B. Chakraborty, "Correction to: emotion recognition of speech signal using Taylor series and deep belief network based classification," *Evolutionary Intelligence*, 2020.

[30] Z. Wu and W. Chu, "Sampling strategy analysis of machine learning models for energy consumption prediction," in *Proceedings of the 2021 IEEE 9th International Conference on Smart Energy Grid Engineering (SEGE)*, pp. 77–81, IEEE, Oshawa, ON, Canada, Auguest 2021.

[31] X. B. Jin, W. Z. Zheng, J. L. Kong et al., "Deep-learning forecasting method for electric power load via attention-based encoder-decoder with bayesian optimization," *Energies*, vol. 14, no. 6, p. 1596, 2021.

[32] M. Zhao, A. Jha, Q. Liu et al., "Faster mean-shift: GPU-accelerated clustering for cosine embedding-based cell segmentation and tracking," *Medical Image Analysis*, vol. 71, Article ID 102048, 2021.

Hindawi
Computational Intelligence and Neuroscience
Volume 2022, Article ID 3647549, 10 pages
https://doi.org/10.1155/2022/3647549

Research Article

An Analysis of the Motivation Mechanism of the Formation of Corporate Health Strategic Innovation Capability Based on the K-Means Algorithm

Tingting Shang

School of Information Management, Xinjiang University of Finance & Economics, Urumqi, Xinjiang 830000, China

Correspondence should be addressed to Tingting Shang; sting7111@163.com

Received 3 December 2021; Revised 24 December 2021; Accepted 27 December 2021; Published 29 January 2022

Academic Editor: Xin Ning

Improving enterprises' independent innovation capability is critical to improving their competitive strength, industries' independent innovation capability, industries' international competitiveness, and countries' independent innovation capability, as well as building an innovative country. It is now the era of strategic innovation. Many growing businesses are focused on strategic innovation, but they overlook the issue of ensuring that strategic innovation is implemented. Management and innovation are perennial themes in the long-term development of businesses. The most pressing issue in enterprises' strategic innovation activities is how to combine their strategic direction with their superior ability and choose a strategic innovation path that is appropriate for their development. This paper uses data mining theory to establish the K-means clustering algorithm to identify the best strategic orientation of enterprise innovation strategic direction selection based on the existing advantages and capabilities of enterprises based on the analysis of the direction of enterprise strategic innovation.

1. Introduction

Nowadays, society is developing rapidly and the competitive environment is fierce. The key to how enterprises can grow reversely in this environment lies in innovation. From the enterprise level, the creative ability of Chinese enterprises is not high, and the subject status is difficult to establish. The innovation power is insufficient, and the institutional foundation and social and cultural foundation are still relatively weak [1]. There is a shortage of external and internal investment resources for innovation, and a market-oriented enterprise's independent innovation mechanism has yet to be formed. In order to gradually solve these problems, we must form a linkage mechanism between the government, industry associations, and enterprises and establish an institutional system and a policy system to promote enterprises' independent innovation [2]. Management innovation is driven by the internal and external motivation of enterprises. A specific analysis of the motivation of management innovation can enable us to have a scientific understanding of the causes and laws of management innovation so as to provide guidance for future management innovation activities [3]. From the perspective of enterprise innovation ability, enterprises must have the ability to ensure that innovation activities are carried out in the established direction, and the ability is reflected by a series of ability elements [4].

In the face of intense market competition, businesses have been put to the test in terms of both survival and development. As a result, businesses must innovate [5]. The majority of entrepreneurs believe that technology is at the center of innovation. They believe that the only way for businesses to increase profits and gain competitive advantages is through technological reform and innovation. In fact, without a strategy, innovation will fail [6]. In this era of technological homogeneity, strategic innovation can help businesses create more value. Only strategic innovation can truly realize an enterprise's value creation. Breaking the original survival strategy, paying attention to operating enterprises with new strategic thinking, and constantly identifying and cultivating strategic innovation ability are all things that businesses must do. Only in this way will we be able to effectively implement strategic innovation and, as a result, create a continuous competitive advantage, allowing businesses to grow sustainably in the market [7]. When a company discovers that its strategy is no longer generating value for customers, it has the ability to reidentify, acquire, and integrate the industry's internal and external environmental resources. The current profit situation is changed using the strategic innovation method, completing the enterprise's strategic innovation goal. It is based on the accumulation of knowledge and is linked by organizational learning. Its goal is to continuously add value to businesses and customers in order to ensure that businesses have a long-term competitive advantage in the market. The K-means algorithm is used to build a clustering mining model in this paper. It has been successfully used in practice to evaluate mining results, form knowledge, and promote the development of a company's strategic innovation capability.

Innovation is the soul of a nation's progress and the inexhaustible motive force of a country's prosperity. Nowadays, innovation has increasingly become an important symbol of the liberation and development of social productive forces, which is related to the development process of a nation. Management and innovation are the eternal themes of the sustainable development of enterprises [8]. Management innovation mainly includes management idea innovation, organization innovation, management method innovation, system innovation, and cultural innovation. In the original sense of innovation, technological innovation is the commercial application of scientific and technological achievements, and this process should be mainly completed by enterprises. It is not only the main body of the market economy but also the main body of technological innovation [9]. The strength of a country's independent innovation capability is mainly determined by enterprises, and the key to improving the independent innovation capability is to improve the independent innovation capability of enterprises [10]. Based on the analysis of the dynamic mechanism of enterprise strategic innovation capability formation and the K-means algorithm, this paper constructs and designs a clustering mining model of enterprise strategic innovation capability based on the K-means algorithm. The K-means algorithm has high computational performance. It is verified that the algorithm is suitable for the research of this paper, which can better reflect the characteristics of the data in this paper, and the model is successfully applied to the analysis of strategic innovation capability of enterprises.

2. Related Work

According to literature [11], trust, integration, and collaboration are three-dimensional mechanisms for enterprises to realize integrated innovation. When conducting independent innovation, literature [12] suggests that businesses should invest heavily in technology research and development. Empirical evidence supports the positive relationship between R&D spending and independent innovation. From the perspective of absorptive capacity, literature [13] studies believe that good technical resources and a strong capability foundation are prerequisites for enterprises to engage in integrated innovation and achieve technological leapfrogging. Endogenous innovation, as opposed to imitation innovation, external introduction, and cracking, is a spontaneous behavior in the system, according to literature [14]. Literature [15] investigates the technology-driven formation mechanism of integrated innovation capability and develops a theoretical framework for the action mechanism of enterprise technology integration capability based on the three dimensions of technology integration. From various perspectives, literature [16] discusses and analyzes the application process and some application status of data mining in E-government. According to literature [17], technology integration is a process of innovation based on an enterprise's existing technological processes and capabilities. Literature [18] introduces four analytical frameworks: global technology framework, organizational framework, active learning, and technology transfer at the enterprise level. Literature [19] puts forward that independent innovation is the breakthrough of technology explored by enterprises through their own efforts or joint research. Literature [20] introduced the idea of ontology to build a government data warehouse. The successful construction of enterprises' basic information data warehouse verified the feasibility of the construction method of the government data warehouse. Literature [21] provides a possible attempt to explain the changes of endogenous technology. Literature [22] established a long-term economic growth model based on innovation. Literature [23] puts forward endogenous innovation and imitation innovation in parallel when analyzing economic growth. Reference [24, 25] designed an implementation scheme of the system based on multilevel architecture. When analyzing the change process of European science and technology policy, literature [26] proposed an integrated innovation policy integrating "scientific innovation policy" and "industrial innovation policy." This view is actually an extension of the concept of the regional innovation system and the national innovation system. Literature [27] puts forward that independent innovation is an activity for innovation subjects to achieve scientific and technological breakthroughs by relying on their own strength so as to support and lead economic and social development and ensure national security. Literature [28] first incorporated technological progress into the economic growth model, analyzed the internal factors, and internalized a part of the role of technological progress. In the enterprise strategic innovation model studied in this paper, enterprises innovate on the basis of their own inherent strategies. Through the K-means algorithm, enterprises can find the best way for enterprise innovation, and through repeated iterations, they can find out the strategic innovation points gradually clear in the process of clustering so as to determine the optimal direction of enterprise strategic innovation.

3. Methodology

3.1. The Formation Mechanism of the Enterprise's Integrated Innovation Capability. A new idea, a new discovery, a new organizational form, a policy system, and an institutional framework are all examples of innovation. Although this is a broad definition, innovation in the economic sense is very specific. It refers to a commercially motivated production process that aims to capture or maintain market share and maximize profits. With society's rapid development, competition has never been more fierce. It is critical for developing businesses to recognize that, in the face of fierce social competition, their strategies must be adjusted or recustomized [29].

What is the strategic innovation capability of enterprises? It is considered that with the goal of continuously creating enterprise and customer value, in the process of successfully completing the cognition, formulation, implementation, and control of enterprise innovation strategy, the existing resources inside and outside the enterprise can be discovered, acquired, utilized, and integrated to improve the utilization rate of existing resources or create new resources. In this way, the system composed of various elements of strategic innovation ability needed by enterprises to gain sustainable market competitive advantage can be ensured. The independent innovation capability system of enterprises is shown in Figure 1.

The research on integrated innovation capability mainly focuses on its formation mechanism. Integrated innovation is a process in which the innovation subject optimizes and reorganizes the elements to form an organic whole with multiple functions and adaptability to evolution. Any enterprise system is not isolated and static. They are closely related to the external environment and change with the changes of the external environment to maintain their own balance [30]. It includes integration dimensions such as technology, strategy, knowledge, and organization. Different dimensions do not exist in isolation, but are interconnected and interdependent. The nonlinear interaction between various elements within each enterprise system forms a balanced system and ensures the dynamic mechanism.

The key to establishing a management innovation mechanism is to understand the fundamental elements of management innovation. Understanding management innovation mechanisms requires a thorough understanding of the subject of innovation, as well as innovation motivation, ability, and behavior. Entrepreneurs, managers, and employees with knowledge reserves are among the subjects of innovation. Entrepreneurs are at the forefront of managerial innovation. Its primary responsibility is to coordinate, manage, and guide the innovation activities of the subject and object of innovation. The key to management innovation is managers. The source and foundation of management innovation are knowledge workers. Figure 2 depicts the relationship between enterprise innovation and other topics.

Only with certain ability can the subject of enterprise management innovation complete the process of management innovation. This necessary ability is a synthesis of various abilities, mainly including innovation ability, transformation ability, organization and coordination ability, and learning ability. Under the action of linearity, there will be no way for enterprises' strategic innovation capabilities to correlate with each other, which will lead to the failure of functional coupling of innovation subjects. What is more serious is that the strategic innovation capability system cannot update and evolve, and the capability cannot be improved, which will eventually lead to the collapse of enterprises.

3.2. Evaluation Index of Creative Ability of Enterprises. Enterprise strategic innovation capability is a capability system aiming at providing strategic innovation. After selecting, analyzing, and distinguishing the ability factors, it finally forms organic polymerization. In this way, we can help enterprises to have the competitiveness of sustained advantages. Among them, the degree of coordination among various factors will affect the efficiency of the overall strategic innovation capability system. Therefore, enterprises must find suitable strategic innovation capabilities and implement them to adapt to the market environment. The supervision, examination, and revision of management innovation are the last stages of the process of enterprise management innovation. It refers to a series of activities to evaluate and scientifically summarize innovation achievements after a period of relatively stable operation. And it is an important link to promote enterprises to carry out a new round of innovation and bring the innovation achievements of enterprise management into play. The general process of management innovation is shown in Figure 3.

The establishment of an evaluation index system for an enterprise's creative ability is critical both in the theoretical research of independent enterprise innovation and in the practice of promoting the formation and development of an enterprise's creative ability. From the standpoint of the strategic innovation process and strategic innovation obstacles, companies must use their innovation capabilities as a foundation to ensure that the strategic innovation process runs smoothly and that strategic innovation obstacles are overcome. Organizational structure innovation, business process innovation, functional management innovation, and strategic management innovation are the different levels of management innovation. Each level of innovation has a distinct focus and set of procedures to follow. The evaluation index system of enterprises' independent innovation capability includes 4 first-level indicators. The first is the index of potential technological innovation resources, the second is the evaluation index of technological innovation activities, the third is the index of technological innovation output capacity, and the fourth is the index of technological innovation environment. There are two media between the external environment and the system. One is the boundary between the system and environment, and the other is the boundary domain between the system and environment. System boundaries absorb and release capacity, substances, and information to hinder the filtering of these contents. In this process, the boundary domain plays a buffer role in the communication between the system and the environment.

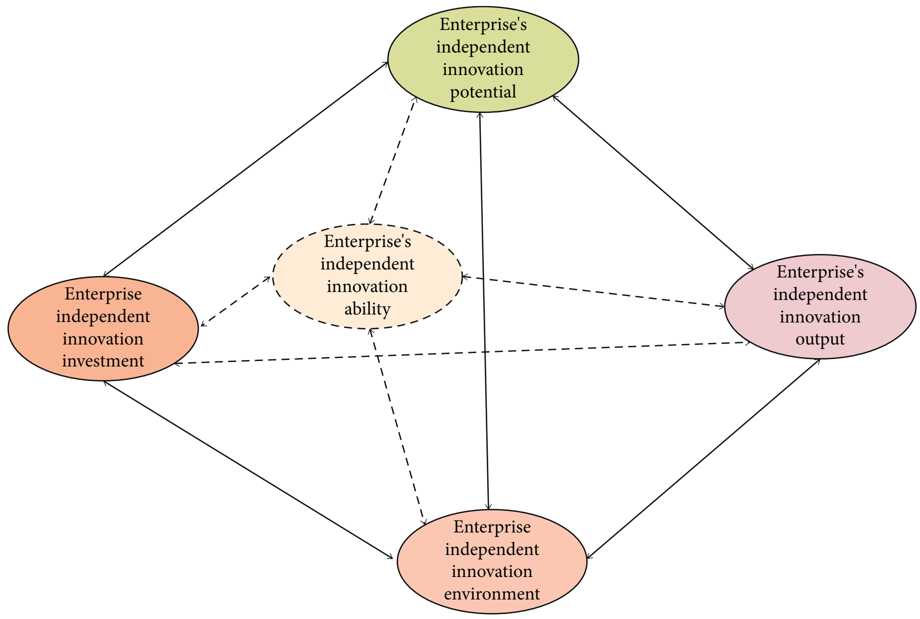

Figure 1: Enterprise's independent innovation capability system.

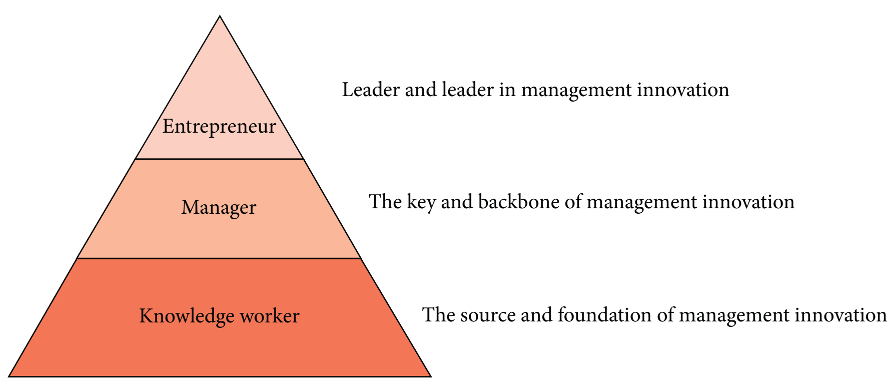

Figure 2: The relationship between innovation entities.

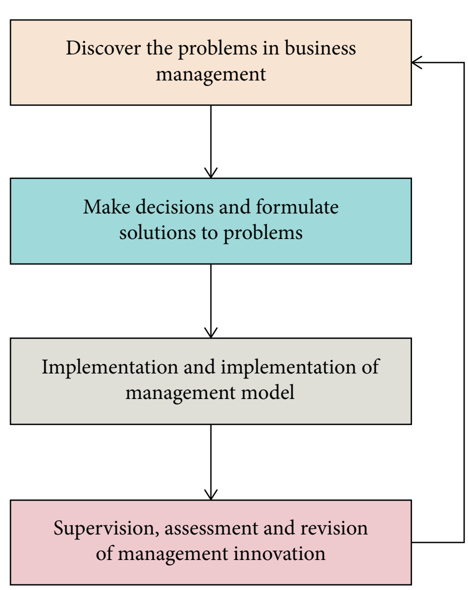

Figure 3: Process of management innovation.

With the emergence of information technology, the shortening of the product life cycle, product diversification, and the emergence of a large number of competitors, enterprises must timely adjust the organizational structure in order to seek survival and development in the market environment characterized by variability, uncertainty, and globalization. The evaluation of enterprises' creative ability should reflect the principles of scientificity, comprehensiveness and generality, feasibility and operability, representativeness and simplicity, and comparability and reliability. The enterprise strategic innovation ability itself is helping enterprises obtain a long-term competitive advantage. It explores what kind of ability enterprises should have from the perspective of enterprise strategic innovation so as to survive in a dynamic environment, seek long-term development, and form a sustainable competitive advantage.

The evaluation of the creative ability of enterprises is an important way for enterprises to know their own creative ability. The research on the evaluation of independent innovation capability of enterprises can not only discover the regular problems in the cultivation and improvement of independent innovation capability of enterprises but also provide reasonable evaluation tools for enterprises.

3.3. Enterprise Strategic Innovation Based on the K-Means Algorithm. K-means algorithm is one of the classical clustering algorithms, also known as K-means. The K-means clustering algorithm is the most traditional and classic clustering algorithm at present. By constantly adjusting and updating, it integrates the mean values of adjacent data from the central point and clusters the data. Its core idea is to find out a center point so as to minimize the deviation of each data point from its nearest center point, thus forming a "class." The algorithm has the advantages of high speed, good stability, and simple principle and is widely used in scientific research, industry and commerce, and other fields.

The K-means algorithm is based on the principle of minimizing the clustering performance index, and the commonly used clustering criterion function is the sum of the squares of the errors of each sample point in the dataset and minimizes it. The basic idea is that, firstly, k objects are randomly selected from n data objects as initial clustering centers; for that remaining other objects, according to their similarity with these cluster centers, they are, respectively, assigned to the cluster most similar to them; then, the cluster center of each new cluster is calculated; this process is repeated until the standard measure function begins to converge. The commonly used criterion function is the sum of the squared error (SSE). It is defined as follows:

$$\mathrm{SSE} = \sum_{i=1}^{k} \sum_{p \in c_j} \left\| p - m_i \right\|^2 . \tag{1}$$

Here, E is the sum of squared errors of all objects in the mining dataset, and p is a certain point in the space, which represents a given data object. m_i is the average value of cluster C. This criterion makes the generated clusters as compact as possible, and the clusters are separated as much as possible.

In the K-means algorithm, proximity, centroid, and objective function are the three key points of the algorithm. Usually, the proximity function is the squared Euclidean distance, the centroid is the mean, and the Euclidean distance calculation formula is as follows:

$$d_2^2 = \left| x_{i1} - x_{j1} \right|^2 + \left| x_{i2} - x_{j2} \right|^2 + \ldots + \left| x_{ip} - x_{jp} \right|^2 . \tag{2}$$

The selection of the initial cluster center has a greater impact on the clustering results. If the selection is not good, effective clustering results will not be obtained. We can compare the final calculation results by setting some different initial values. If the results have been stable, the selection is appropriate, but it is a waste of resources and time-consuming. Generally, the mean square error is used as the standard measurement function. The k clusters have the following characteristics: each cluster itself is as compact as possible, and each cluster is separated as much as possible.

The description object of cluster analysis can be expressed by a set of specific characteristics. The specific characteristic value can be a text, a numerical value, or a mixture of the two. For a given set of n objects, the possible ways to divide it into k clusters are

$$N(n,k) = \frac{1}{k!} \sum_{j=0}^{k} (-1)^j \binom{k}{j} (k-j)^n . \tag{3}$$

Therefore, n objects are divided into k clusters, and the number of possible cluster divisions is

$$\sum_{k=1}^{n} N(n,k). \tag{4}$$

The strategic convergence emphasizes that the strategic innovation capability of enterprises is a nonlinear organic aggregation through analyzing, selecting, and classifying various enterprise capability elements so as to help enterprises gain sustainable competitive advantages.

There are n objects to participate in the evaluation, and there are m quantitative evaluation indicators. The undetermined weight coefficient of each indicator is $b_j \, (j = 1, 2, 3, \ldots, m)$, the original data of each object on each indicator is $X_{ij} \, (i = 1, 2, 3, \ldots, n; \, j = 1, 2, 3, \ldots, m)$, and the standard data is $U_{ij} \, (i = 1, 2, 3, \ldots, n; \, j = 1, 2, 3, \ldots, m)$. Assuming that the data corresponding to the conversion of U_{ij} is Z_{ij}, the comprehensive evaluation index y_i for each object is

$$y_i = \sum_{j=1}^{m} b_j \cdot Z_{ij}, \quad i = 1, 2, 3, \ldots, n. \tag{5}$$

According to the size of y_i, the ranking of the comprehensive evaluation of each evaluation object can be given. The specific steps are as follows:

(1) Convert from standard data U_{ij} to Z_{ij}. The conversion formula is

$$Z_{ij} = \frac{x_{ij} - x_j}{S_j}. \tag{6}$$

Among them,

$$\begin{aligned} \overline{x_j} &= \sum_{i=1}^{n} x_{ij}, \\ S_j &= \sqrt{\frac{\sum_{i=1}^{n}\left(x_{ij} - \overline{x_j}\right)^2}{n}}. \end{aligned} \tag{7}$$

(2) Determination of index weight coefficient: the criterion for determining the weight coefficient b_j is to make y_i as dispersed as possible. Even if the sample variance σ^2 is the largest, the sum of squares of b_j is 1 at the same time. Such a set of weight coefficients is exactly the eigenvector corresponding to the largest eigenvalue of the matrix $W = ZT{\cdot}Z$. Iti is denoted as $B = [b_m]$. Among them,

$$\sigma^2 = \sum_{i=1}^{n} \frac{\left(y_i - \overline{y}\right)^2}{n} Z = \left[z_{ij}\right] = \begin{bmatrix} z_{11} \ldots z_{1m} \\ \ldots \\ z_{n1} \ldots z_{nm} \end{bmatrix}. \tag{8}$$

People are interested in using data mining methods to discover potential information and data patterns from large amounts of data, which have become a common demand. With the advancement of data mining, new mining methods emerge one after the other, the most basic of which is clustering. Among the clustering methods, the K-means algorithm is one of the most well-known and widely used partitioning methods. Cluster analysis is extremely useful in a wide range of situations. The K-means algorithm clustering result is better, and it can fully reflect the data's basic characteristics. Targeted management can be accomplished by analyzing system data. The algorithm played an important role in it and is very practical.

4. Result Analysis and Discussion

The level of enterprise management determines the survival of an enterprise to a certain extent. If an enterprise wants to survive and develop in a positive direction, it must strengthen management and improve its modernization level. Corporate strategic innovation capabilities are formed in the process of corporate strategic innovation, and the targeted discovery, acquisition, utilization, creation, and integration of their strategic innovation resources are emphasized. Fund management is the top priority of enterprise management. However, a considerable number of group companies have the problem of loose fund management due to the limitation of management modes and methods. The operating performance of a company from 2014 to 2020 is shown in Figure 4.

Enterprises' creative ability means that, over a period of time, in order to cultivate their own technical ability and market competitive advantage, they achieve major breakthroughs in key industrial technologies and cultivate their own brands by effectively integrating and applying internal and external resources, in order to master or affect the basic quality of the value distribution process. Some basic information about business development can be found in the enterprise's basic information base. The amount of information in an enterprise's basic information base is growing in tandem with the economy and the enterprise itself. The overall plan made by an enterprise for its long-term survival and development on the basis of analysis and research of the external environment and internal resource conditions is known as strategy. The process of an enterprise's independent innovation capability evolving from cultivation to promotion to a new level is referred to as the "evolution of independent innovation capability." Realize the improvement of the overall level of enterprises' creative ability and make enterprises' creative ability develop to a higher level on the basis of fully cultivating enterprises' creative ability. Figure 5 depicts the evolution of enterprise-wide innovation capability.

The study of management innovation mechanisms concentrates on the components of management innovation and their interactions. Enterprises that are arbitrarily closed and have no communication with external environmental resources are in the midst of a structural organization disintegration crisis and will eventually be isolated and destroyed. Cluster ecology is an important aspect of a company's ability to innovate strategically. This feature can help businesses transform and use resources more effectively, formulate new strategies more quickly, and take advantage of opportunities to implement enterprise strategic innovation. It is not only innovation essential for social and economic development, but it is also essential for business success. Figure 6 depicts the enterprise risk assessment.

For most of the risks, companies need to take certain actions to transfer or diversify the risks to reach an acceptable level for the company. The relationship between financial risk weight and sample evaluation is shown in Figure 7.

System evolution emphasizes that the strategic innovation capability of enterprises will go through a dynamic process from generation, cultivation, and promotion to maintenance with the passage of time so that enterprises can make better use of the environment to evolve their own capability systems and achieve their strategic goals. The preliminarily processed data are normalized. During this period, the three center points are constantly adjusted, and after three operations with the K-means algorithm, the customer value distribution map is obtained, as shown in Figure 8.

Promoting the development of enterprises with innovation is the latest topic that enterprises are facing today, and the key to the success of management innovation is to form an effective management innovation mechanism. Clustering is a common phenomenon in real society. Using the

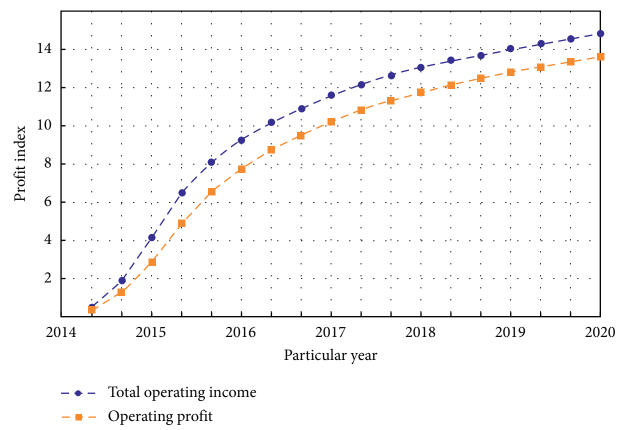

Figure 4: Operating performance.

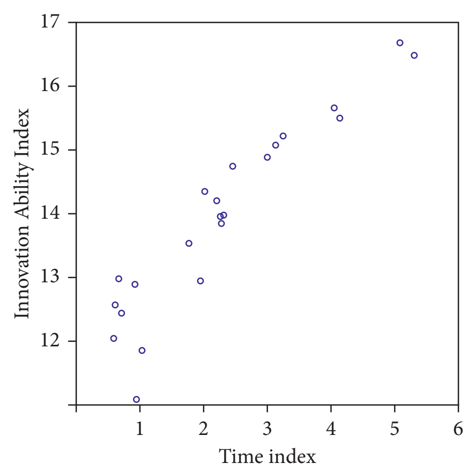

Figure 5: The evolution of independent innovation capabilities of enterprises.

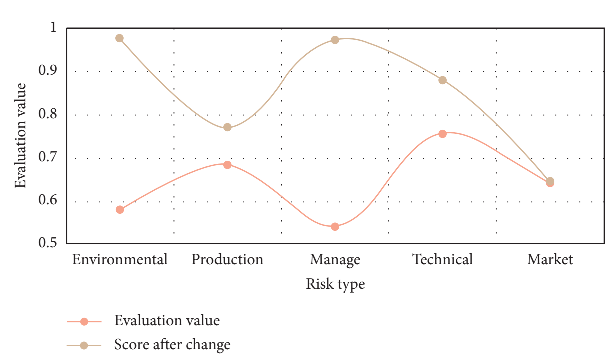

Figure 6: Enterprise risk evaluation.

optimized K-means algorithm, customers are divided into three parts. The red part is the most important customer, the blue part is the next most important customer, and the black part is the implied customer. From the graph, we can not only intuitively see the distribution of customer value but also get the number of customers in each value range, and the clustering effect is clear. The clustering effect diagram is shown in Figure 9.

Choosing an enterprise strategy is the primary choice of enterprise management innovation. Strategy is the soul of an enterprise. If an enterprise has no strategy, it will drift with the tide and always be in a passive position. The construction of the enterprise's creative ability evaluation index system includes the determination of element items and index items. It is inseparable from the definition of enterprise's creative ability. A correct understanding of the essence of

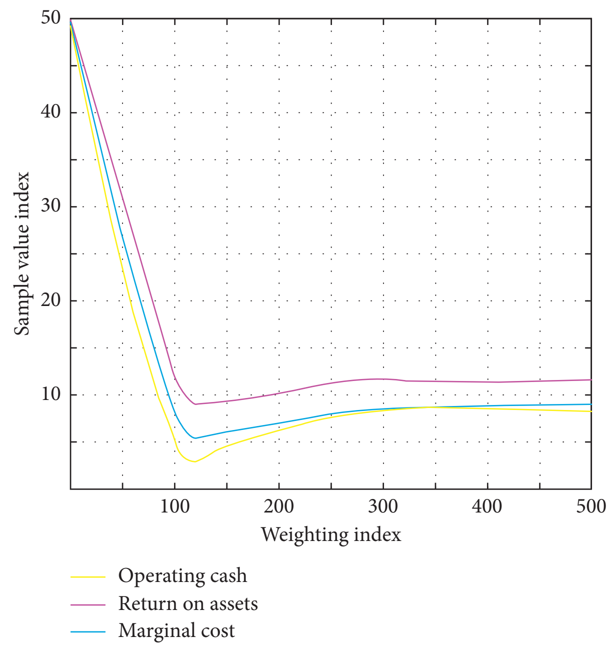

Figure 7: The relationship between financial risk weight and evaluation value.

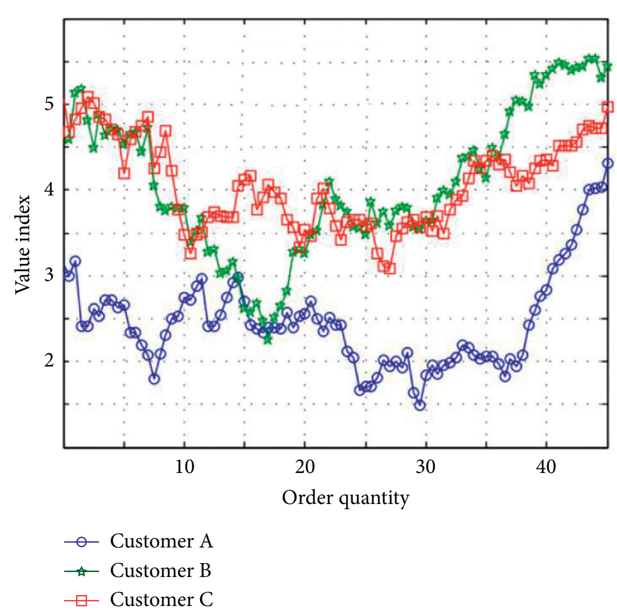

Figure 8: Distribution map of customer value.

enterprise's creative ability is the basic premise for the accurate evaluation of an enterprise's creative ability. Strategic innovation capability is a capability based on strategic innovation, which is a complex of strategic innovation and enterprise capability. Innovation guides the development direction, determines the development goal, and provides the development path for enterprise capabilities. Using the K-means algorithm in this paper, enterprises can find the best way for enterprise innovation, find out the strategic innovation points gradually clear in the process of clustering, and then determine the optimal direction of enterprise strategic innovation.

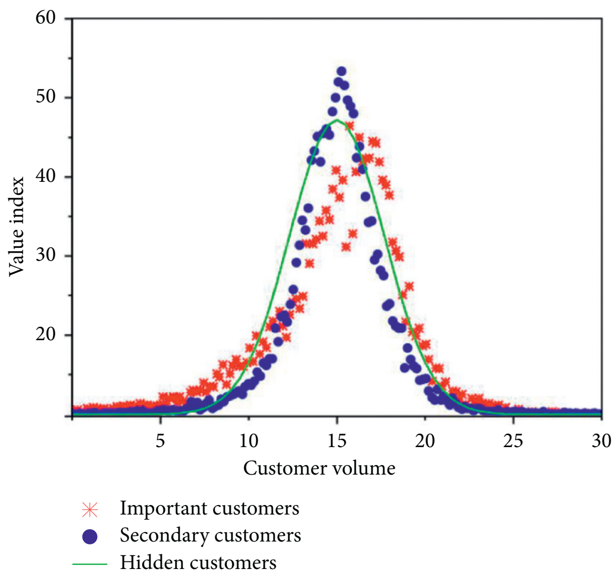

Figure 9: Clustering effect diagram based on K-means.

5. Conclusions

Enterprises must constantly carry out management innovation in order to survive and develop in the fierce market competition. Enterprises can only have flexibility and superiority in management mechanisms by implementing management innovation and thus remain invincible in the competition. All innovation must be strategic, and we must seize the strategic opportunity, highlighting the significance of strategic innovation. Strategic innovation underpins technological innovation. If a company has innovative technology but it does not fit into the company's overall innovation strategy, the company's technological innovation is pointless. The strategic innovation capability of a company cannot be created out of thin air, nor can it be born within a company. Through a dynamic mechanism, an enterprise's strategic innovation capability is formed during the process of strategic innovation. The openness, being far from equilibrium, nonlinear function, and fluctuation functions of the enterprise strategic innovation capability system cause the system information to self-replicate, stabilize, and generate a new order. The K-means algorithm studied in this paper can find the most suitable way for enterprise innovation, and through repeated iterations, find out the strategic innovation points gradually clear in the process of clustering. It can determine the optimal direction of enterprise strategic innovation.

Data Availability

The data used to support the findings of this study are included within the article.

Conflicts of Interest

The author declares that there are no conflicts of interest.

Acknowledgments

This study was supported by the Department of Water Resources of Xinjiang, "Forecast of future labor and water demand of general service industry in Southern Xinjiang" (NJSXM-2018-6).

References

[1] R. G. Negri, W. B. da Silva, and T. S. G. Mendes, "K-means algorithm based on stochastic distances for polarimetric synthetic aperture radar image classification," *Journal of Applied Remote Sensing*, vol. 10, no. 4, Article ID 045005, 2016.

[2] D. Zhu and H. Liu, "Research on UAV cooperative security based on the fusion of K-means and artificial fish school," *Aeronautical Computing Technology*, vol. 51, no. 5, p. 5, 2021.

[3] L. Qi, N. Zhang, and X. Qin, "Patent text clustering analysis based on K-means," *Computer Knowledge and Technology*, vol. 14, no. 22, pp. 206-207, 2018.

[4] Y. Huang, P. Wang, and Z. Fang, "K-means clustering algorithm for mixed data sets," *Journal of Electronic Commerce*, vol. 19, no. 1, pp. 1–28, 2017.

[5] S. Zhao, W. Li, and J. Cao, "A user-adaptive algorithm for activity recognition based on K-means clustering, local outlier factor, and multivariate Gaussian distribution," *Sensors*, vol. 18, no. 6, p. 1850, 2018.

[6] K. Kwon, J. W. Shin, and N. S. Kim, "Incremental basis estimation adopting global k-means algorithm for NMF-based noise reduction," *Applied Acoustics*, vol. 129, no. 1, pp. 277–283, 2018.

[7] X. Wang, Q. Zhang, X. Xin et al., "Robust weighted K-means clustering algorithm for a probabilistic-shaped 64QAM coherent optical communication system," *Optics Express*, vol. 27, no. 26, pp. 37601–37613, 2019.

[8] G. Wang, P. Wang, and Y. Han, "Coronary optical coherence tomography plaque segmentation based on K-means clustering and improved random walk algorithm," *Journal of Biomedical Engineering*, vol. 34, no. 6, p. 7, 2017.

[9] X. Cui, H. Wang, and S. Qian, "Application of improved K-means algorithm in customer classification," *Modern Computer (Professional Edition)*, no. 24, pp. 25–27, 2016.

[10] Z. Wang, Y. Xun, and J. Zhang, "A clustering algorithm for association rules based on K-means," *Journal of Taiyuan University of Science and Technology*, vol. 37, no. 6, pp. 429–437, 2016.

[11] Q. Zhao and Y. Li, "Optimization based on K-means algorithm and its application in aviation customer segmentation," *Modern Computer*, no. 4, pp. 5–10+15, 2018.

[12] N. Saha, T. Sáha, and P. Sáha, "Cluster strategies and smart specialisation strategy: do they really leverage on knowledge and innovation-driven territorial growth?" *Technology Analysis & Strategic Management*, vol. 30, no. 11, pp. 1256–1268, 2018.

[13] Y. Chong, W. Zhu, and T. Miao, "Credit decision model for maximizing bank effect based on K-means clustering," *Economics*, vol. 4, no. 3, pp. 30–32, 2021.

[14] H. Shi, "A heuristic algorithm for TSP problems based on K-means clustering and grouping strategy," *Journal of Liaoning University of Technology: Natural Science Edition*, vol. 41, no. 2, p. 4, 2021.

[15] J. Luo, "Implementation and improvement of K-means algorithm based on enterprise applications," *Computer Knowledge and Technology*, vol. 17, no. 18, p. 3, 2021.

[16] X. Gong, Z. Wang, and L. Wang, "Research on financial early warning model for papermaking enterprise based on particle swarm K-means algorithm," *Paper Asia*, vol. 34, no. 6, pp. 41–45, 2018.

[17] X. Huang, X. Liu, and Y. Ren, "Enterprise credit risk evaluation based on neural network algorithm," *Cognitive Systems Research*, vol. 52, no. 12, pp. 317–324, 2018.

[18] S. Gao, H. Zhu, Z. Liu, J. Zhao, and H. Bi, "Grouping method for echelon utilization of retired power batteries based on K-means clustering," *Power Technology*, vol. 44, no. 10, p. 5, 2020.

[19] V. N. Manju and A. Lenin Fred, "AC coefficient and K-means cuckoo optimisation algorithm-based segmentation and compression of compound images," *IET Image Processing*, vol. 12, no. 2, pp. 218–225, 2018.

[20] B. Sun and S. Tian, "Systematic thinking on the dynamic mechanism and evolution of the innovation diffusion of manufacturing enterprises," *East China Economic Management*, vol. 34, no. 11, p. 8, 2020.

[21] L. I. Taihao, N. Tuya, and J. Zhou, "An improved KMeans algorithm based on initial clustering center optimization," *ZTE Technology: English Edition*, vol. 15, no. 12, p. 4, 2017.

[22] X. Bao, Q. Qiao, and X. Yin, "A review of foreign research on the dynamic mechanism and influencing factors of enterprise continuous innovation," *East China Economic Management*, vol. 30, no. 7, p. 6, 2016.

[23] B. Zhao and W. Chen, "The dynamic mechanism and benefit conversion of Hunan's small and medium-sized enterprises' continuous innovation," *Journal of Hebei Energy Vocational and Technical College*, vol. 18, no. 1, p. 3, 2018.

[24] Yu Cao, G. He, and J. Tan, "Research on industry clustering based on factor analysis and K-means clustering algorithm," *Computer Science and Application*, vol. 10, no. 12, p. 10, 2020.

[25] Y. Lu and X. Yu, "Research on enterprise competitive intelligence based on improved K-means algorithm——based on social network analysis," *Information Science*, vol. 35, no. 12, p. 5, 2017.

[26] J. Liu, C. Cheng, and C. Zhuang, "Research on cloud data management model based on K-Means and grid clustering," *Journal of Chongqing University of Technology: Natural Science*, vol. 31, no. 9, p. 6, 2017.

[27] Z. Sun, "In search of complementarity in China's innovation strategy through outward strategic mergers and acquisitions policy: a behavioural additionality approach," *Science Technology & Society*, vol. 23, no. 1, pp. 107–136, 2018.

[28] H. Li, "Pricing scheme design of "photograph to make money" task under K-means cluster analysis," *Wireless Internet Technology*, vol. 16, no. 4, pp. 64-65, 2019.

[29] Y. Guan, X. Xu, and Y. Huang, "Location selection of emergency logistics center based on K-Means clustering algorithm," *Theoretical Mathematics*, vol. 9, no. 7, p. 4, 2019.

[30] J. Yang, Y. Ma, and X. Zhang, "An initialization method based on hybrid distance for k-means algorithm," *Neural Computation*, vol. 29, no. 11, pp. 1–24, 2017.

Hindawi
Computational Intelligence and Neuroscience
Volume 2022, Article ID 9051629, 9 pages
https://doi.org/10.1155/2022/9051629

Research Article

Financial Data Center Configuration Management System Based on Random Forest Algorithm and Few-Shot Learning

Xinxin Li [1] and Lina Wang [2]

[1] *Capital University of Economics and Business, Beijing 100070, China*
[2] *School of Financial Technology, Hebei Finance University, Baoding, Hebei 071051, China*

Correspondence should be addressed to Xinxin Li; 208088@cueb.edu.cn

Received 20 December 2021; Revised 8 January 2022; Accepted 10 January 2022; Published 28 January 2022

Academic Editor: Xin Ning

To form a unified configuration and information management platform, FCCMS (financial center configuration management system) will integrate and sort information based on various configuration data and relationships as well as integrate processes and permissions. However, the most serious issue that data centers are currently facing is how to effectively manage these infrastructures. For various infrastructures, the data center currently uses a decentralized operation and maintenance management model. When an infrastructure fails due to inexperienced configuration management, this mode is not conducive to quickly locating and resolving the problem. A detection method of RFCO (random forest algorithm based on clustering optimization) is proposed, and an appropriate tree is selected from RF to integrate, so as to achieve the best effect. In this paper, the target matching algorithm based on FSL (few-shot learning) is deeply studied, and the target detection model is applied to the target matching and positioning task by using the ML method. The performance of the algorithm is tested by experiments on relevant datasets to verify the effectiveness of the algorithm in various scenarios.

1. Introduction

In China, the business volume of major commercial banks has increased significantly year after year as banking business has become more integrated with local market demand and with the global financial environment. At the same time, the banking industry's reliance on IT systems is becoming increasingly apparent [1]. Due to the large number of application systems and servers, as well as the large scale of supporting network rooms, it is often difficult to quickly locate the causes of emergencies, analyze the true root causes of problems, and influence related modules due to poor consideration in upgrading and changing, making it difficult to ensure the high availability and work efficiency of data center systems [2, 3].

Many excellent algorithms have appeared in the field of computer vision, and these algorithms have made remarkable achievements in the fields of image classification, target location, target detection, etc. However, the establishment of many algorithms depends on a large amount of training data, but it is difficult to get rich data in practical application scenarios [4–6]. Usually, the change of financial data reflects this gradual process information; therefore, some algorithms can be used to analyze financial data and design a system that can scientifically reflect the company's financial status, so as to guide enterprise decision makers to formulate correct guidelines, improve business activities, and prevent such problems in time [7]. DL (deep learning) has begun to rise. The related algorithms based on this have found a breakthrough for FSL (few-shot learning) [8, 9]. We establish a data center configuration management system in line with this practice standard and finely manage various infrastructures, so as to establish a long-term mechanism of production and operation with safety production as the core and effectively improve the service level of the data center.

Currently, each department's configuration information is primarily managed by hand. Because there is no unified configuration information maintenance window, there will be unnecessary redundancy when the configuration information is maintained by different departments. Furthermore, the data center's massive IT resources will result in high manual maintenance costs [10]. Although the trading platform system has an automatic monitoring platform, analyzing the impact of events is difficult due to the lack of a systematic relationship between configurations and the corresponding relationship between levels of technical business configuration units. The FCCMS (financial center configuration management system) uses the RF (random forest) algorithm and FSL as the guiding framework to design, classify, and model various infrastructures, abstract them into various configuration items, give them appropriate attributes and names, and establish the relationship between configuration items.

2. Related Work

The univariate analysis model takes a single indicator variable, compares financial data from businesses in various stages of crisis, eliminates insignificant financial indicators, and determines the financial indicators with the best discrimination ability [11]. After the analysis, the conclusions are not completely consistent due to the different research samples selected by different researchers. According to the literature [12], the three financial indicator pairs of shareholders' equity/assets and liabilities, working capital/total capital, and current assets/current liabilities have the best ability to predict financial crises. The results of a study [13] comparing and analyzing four financial ratio indicators show that the current ratio and debt ratio have the best early warning effect. The improved fruit fly optimization algorithm is combined with the Z-score model to create a financial early warning model in literature [14], and the results show that the model has good forecasting ability. The neural network model is used in literature [15] to study enterprise financial crisis early warning and is compared to the multivariate discriminant analysis model. The results show that the neural network model's prediction effect is clearly greater than that of the multivariate discriminant analysis model. The financial crisis prediction model based on moderate financial indicators and a genetic algorithm is studied in the literature [16], and the results show that this type of model has a high prediction accuracy. Literature [17] compares an SVM-based early warning model to a neural network model and a multivariate discriminant analysis model. The results show that SVM outperforms other models in terms of prediction accuracy. In [18], bagging and boosting methods were used to create a financial crisis early warning model. In [19], the dimension of the index system is reduced through PCA (principal component analysis), and the top three financial indicators in order of importance are turnover per share, asset turnover rate, and current ratio.

In the financial data center, when the number of equipment systems in an IT environment increases to a certain scale, the system management team will definitely consider enabling appropriate tools to assist management. Mihelcic et al. [20] studied an online regression algorithm of nondistributed sampling. Lee and Moon [21] put forward the idea of nonindependent identical distribution in data analysis and processing and other related fields and formed a set of nonindependent identical distribution learning framework. Zhu et al. [22] proposed a corner extraction algorithm, which realized corner detection. Panigrahy et al. [23] obtained a model that can accurately match complex scenes through a large amount of data. By introducing DenseNet, the number of parameters is reduced and the training complexity of target detection network is optimized.

3. Research Method

3.1. Overall System Design

3.1.1. Basic Architecture Design of the System. All data centers are attempting to reduce operating and maintenance costs, and service integration has proven to be effective in practice. Reduced energy consumption and the implementation of virtualization are two strategies that can effectively reduce the cost of operation and maintenance. The specific implementation of these measures, on the other hand, must be based on a clear understanding of how many servers are running and which servers are deployed, that is, by establishing a system to share information and data, reflecting data relationships, and forming a unified data center with configuration information. System function modules are shown in Figure 1.

In the design of CMDB (configuration management database) configuration items, the query function should be considered, and the additional functions developed according to the outstanding query requirements of customers should be customized, including the following specific functions: query the configuration item list according to the configuration item type and attribute conditions and search the target configuration item list according to the specific relationship between the configuration items. You can filter the attribute conditions in the target configuration item list and import and export the query configuration for any related level configuration item query to facilitate repeated query requirements in the future.

From the perspective of the system administrator, combined with blocky information, users can quickly enter the system and use and complete system functions, such as server administrator, which is concerned with service configuration, which application services are attached to the server, which storage is attached to the server, and how the server is maintained, among other things. The database administrator is concerned with the database's character section, which applications receive database services, which databases each application corresponds to, and which application databases offer cluster services.

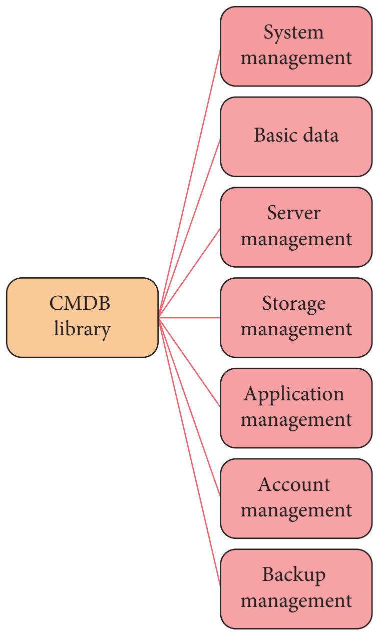

FIGURE 1: System function module diagram.

3.1.2. Hardware Architecture of the System. The configuration management system of the data center adopts the three-tier architecture of client, server, and NAS storage, in which the client is installed on the PC terminal that the operation and maintenance personnel use daily, and the operation and maintenance personnel of the data center can log in to the configuration management system by double-clicking the client, and the interface is intuitive and friendly and easy to operate.

As the core layer of the whole configuration management system, the web server is mainly responsible for responding to various requests submitted by clients, calling database services in the background by triggering events, and then the database server is responsible for data operation. All kinds of data information are finally stored in NAS storage. The hardware architecture of the configuration management system is shown in Figure 2.

The configuration management system uses 8 PC servers with high configuration of 48C96G as web servers, which are responsible for responding to requests from browsers, and 3 databases are installed with SQL Server 2005 database products. Client-server adopts B/S architecture which is widely used at present. The advantage of this architecture is that it is easy to operate and the client needs no maintenance.

3.1.3. System Security Architecture Design. Information security is the top priority for system construction. First of all, the most basic security measure is to establish an antivirus mechanism covering the whole network. In addition, a public four-tier security system model is proposed. In this four-layer model, the emphasis of each layer is different, as shown in Figure 3.

The first step of network security protection is planning. It is necessary to divide the trusted network and untrusted network from the business point of view, or the network area

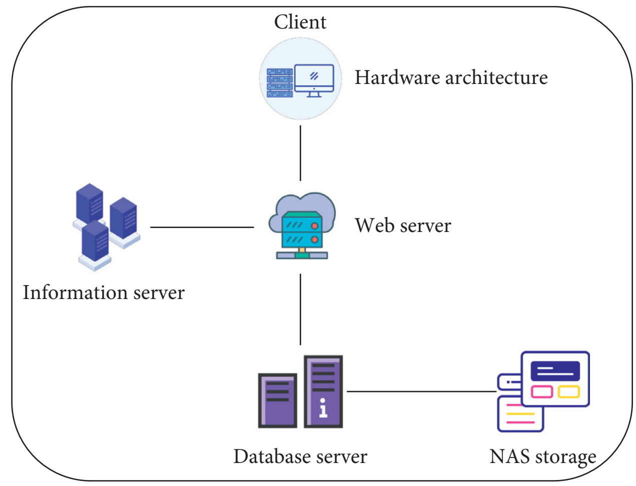

FIGURE 2: Configuration of the hardware architecture of the management system.

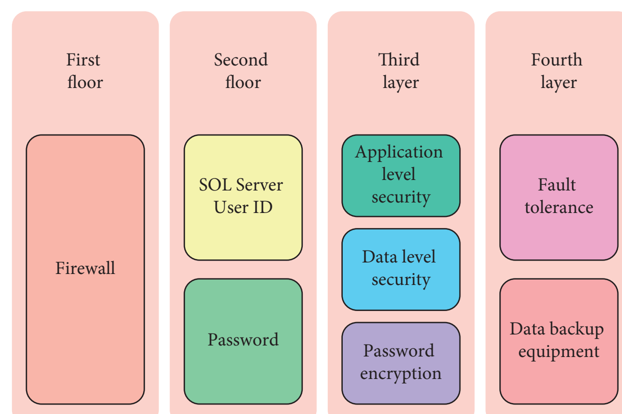

FIGURE 3: Deployment diagram of system architecture.

can be layered according to the distributed method, and each layer has different protection methods. Firewall devices are used to control or directly isolate users and services in different trust levels of network segments.

If users need access to the data center configuration library application system, they must first go through an identity authentication process. The most basic method is for the user to submit some identity authentication information to the application system in charge of identity authentication, and the application system compares that information to the correct data stored in the system. The user will be allowed to enter the configuration library application system if the verified information is legal and valid; otherwise, the user will be denied.

The creation, modification, deletion, and enabling and disabling of user accounts are all part of user management. Flexible operation and ease of use are required for user management. Grouping and authorizing user accounts, managing and maintaining permissions for user groups or roles, defining and maintaining permissions, and so on are all examples of permission management. Permission management necessitates a high level of security, accessibility, and hierarchical authorization.

3.2. Key Algorithm Design

3.2.1. Implementation of System Security Algorithm. The accuracy of member classifiers and the diversity of classifiers in classifier integration system are important issues that researchers have been paying attention to. Similarly, it is difficult to obtain satisfactory classification results by combining some classifiers with different distributions of classification errors but low performance.

RF algorithm is a classifier algorithm based on decision tree. RF has two kinds of important randomicity, the randomicity of training set extraction and the randomicity of node candidate segmentation feature set, which ensure the diversity of decision trees that make up RF. In addition, RF is a data-driven nonparametric classification method, which does not need prior knowledge, only needs to train and classify the given samples, and has a clear structure and is easy to understand.

The main idea of RF algorithm based on clustering optimization is to combine the two base classifiers with the highest correlation degree into a new cluster by using clustering algorithm based on correlation degree and then recalculate the correlation degree between the new clusters. By combining the base classifiers with high correlation, the RF model of aggregation based on correlation measure can be obtained. RFCO (random forest algorithm [25] based on clustering optimization) algorithm is mainly divided into three steps:

(1) Firstly, a large number of base classifiers are generated by RF algorithm, and these base classifiers are added to RF to prepare for the next clustering analysis.
(2) According to the similarity calculation rules between base classifiers, the similarity of base classifiers is calculated. Then, sort the similarity of all base classifiers to find out the two base classifiers with the greatest similarity.
(3) According to the results of clustering analysis, the algorithm will continue to merge the base classifiers, and when the predetermined termination condition is reached, the algorithm clustering will be terminated. Combining all cluster representatives, the RF model after cluster optimization is obtained.

According to the law of large numbers, when $m \longrightarrow \infty$, the function converges.

$$\frac{1}{m}\sum_{i=1}^{m}\alpha_i\left(H\left(x;\pi_i\right)=j\right),\quad j=1,2,\ldots,J. \tag{1}$$

Let the n-th base learning model not included in the m training sets be $H^n(x;\pi_i)$, $i = 1, 2, \ldots, m$; then, the strong learning model without included sample combination can be expressed as follows:

$$H_m^n(x)=\arg\max_j \frac{1}{M}\sum_{i=1}^{M}\alpha_i I\left(H^n\left(x;\pi_i\right)=j\right). \tag{2}$$

Therefore, the generalization error of RF algorithm based on clustering optimization can be estimated by test set. The generalization error of RF algorithm based on clustering optimization is constructed by training set as follows:

$$\frac{1}{N}\sum_{n=1}^{N}I\left(H_m^n\left(x_n\right)\neq y_n\right). \tag{3}$$

Therefore, network intrusion detection based on clustering optimized RF algorithm does not need to divide the collected network intrusion data into training set and test set. Furthermore, the optimized RF algorithm based on clustering and the optimal RF algorithm based on fruit fly are two separate algorithm implementation processes that do not clash, so they can be used together to improve the accuracy of network intrusion detection.

3.2.2. ML-Based Target Matching. With the development of machine learning, deep neural network is widely used. However, because deep neural network is easy to overfit in scenes with small sample size, some techniques to prevent overfitting in scenes with small sample size have been proposed. At present, among FSL methods in the field of computer vision, Bayesian learning, measurement network, ML (machine learning algorithm), and other methods are the mainstream methods.

For FSL problem, ML mainly uses the existing knowledge to solve the learning problem in the scene where there is only a small amount of data in the target field, and there have been many related technical achievements at present. For example, using self-learning technology, using a large number of unlabeled data in the source domain and samples in the target domain, and building an automatic sparse encoder to extract high-level features from samples, the task effect in the target domain is improved. According to the difference between the source domain and the target domain, the model structure is modified and different cost functions are set to get better results in the target domain. At present, the parameter migration method is widely used in image classification, target detection, and other tasks.

In this paper, a method of fast image transformation and solving the transformed target position is proposed. The specific affine matrix is generated according to the following formula:

$$M=M_{\text{scale}}M_{\text{rota}}M_{\text{shear}}M_{\text{trans}}=\begin{bmatrix}\theta_{11} & \theta_{12} & \theta_{13}\\ \theta_{21} & \theta_{22} & \theta_{23}\end{bmatrix}, \tag{4}$$

where M_{scale} is the scale transformation matrix, M_{rota} is the rotation matrix, M_{shear} is the staggered transformation matrix, and M_{trans} is the spatial translation matrix. By simulating the parameters of each matrix and then using the spatial transformation network transformation, the image can be simulated comprehensively by affine transformation.

At the same time, a row of $\begin{bmatrix}0 & 0 & 1\end{bmatrix}$ is filled under each spatial transformation matrix M, and the corresponding inverse matrix is generated for later calculation of the position of the transformed target, and the inverse matrix form is shown in the following formula:

$$M_{\text{inv}} = \begin{bmatrix} \theta'_{11} & \theta'_{12} & \theta'_{13} \\ \theta'_{21} & \theta'_{22} & \theta'_{23} \\ \theta'_{31} & \theta'_{32} & \theta'_{33} \end{bmatrix}. \tag{5}$$

When the input image is transformed by the spatial transformation network according to the matrix M, the target position in the new image will also change. The rectangular frame of the original target will become a parallelogram. The new target center position needs to be calculated. The calculation formula is shown in the following formula:

$$\begin{bmatrix} x_{gt'} \\ y_{gt'} \\ z_{gt'} \end{bmatrix} = \frac{\left(M_{\text{inv}} \begin{pmatrix} \left(x_{gt}/y_{gt}\right) \times 2 \\ 1 \end{pmatrix} + 1 \right)}{2}, \tag{6}$$

where $(x_{gt'}, y_{gt'})$ is the coordinate of the target center in the new image transformed by the spatial transformation network and $z_{gt'}$ represents irrelevant data. When calculating, first calculate the vector of diagonal vector after transformation, as shown in the following formula.

$$\begin{aligned} \begin{bmatrix} w^{tn}_{b1} \\ h^{tn}_{b1} \end{bmatrix} &= \begin{bmatrix} \theta'_{11} & \theta'_{12} \\ \theta'_{21} & \theta'_{22} \end{bmatrix} \begin{bmatrix} w_{gt} \\ -h_{gt} \end{bmatrix}, \\ \begin{bmatrix} w^{tn}_{b2} \\ h^{tn}_{b2} \end{bmatrix} &= \begin{bmatrix} \theta'_{11} & \theta'_{12} \\ \theta'_{21} & \theta'_{22} \end{bmatrix} \begin{bmatrix} w_{gt} \\ -h_{gt} \end{bmatrix}, \end{aligned} \tag{7}$$

where $(w^{tn}_{b1}, h^{tn}_{b1})$, $(w^{tn}_{b2}, h^{tn}_{b2})$ represents the vector of the diagonal vector of the target frame in the original image in the transformed image and $(\theta'_{11}, \theta'_{12}, \theta'_{21}, \theta'_{22})$ is the corresponding element in the inverse matrix M_{inv} of the affine matrix.

4. Result Analysis and Discussion

4.1. System Test Result Analysis. The configuration management system's main functions are data entry, data retrieval, and report generation. The developers will test the module's functionality after it has been developed. Submit the version control code after you have passed the test. Integrate and compile each branch code to form a complete system after all modules have been developed and tested. After the test is completed, the testers will create relevant reports based on the test cases formulated by the demanding personnel.

The configuration management system of an institution's interbank trading platform has been designed using the configuration management system design scheme. According to the actual test results of the system, the results fully show that the design and implementation scheme of the system can basically meet the requirements of configuration management and can significantly improve the work effect and efficiency in the financial data center, based on the measurement and comparison of the integrity of configuration information and timeliness of collecting configuration data, as well as the representativeness of configuration management requirements in the financial data center. The requirement compliance degree of the configuration management system is shown in Figure 4.

Managing related information of server hardware, configuration, maintenance, and so on is the core module of data center configuration library. All related software programs, services, applications, and so on are inseparable from servers, and the number of servers is often very large. One of the biggest features of the system, such as undeployed related services, supported specific applications, associated storage, change logs, maintenance support, and so on, can be quickly inquired through server links.

After the functional test, integration test, user test, and performance test are completed, and the related problems are solved, and they are finally reflected in the test report. After the test report is signed, it is regarded as an important document of system acceptance. The statistics of test results are shown in Figure 5.

After the configuration management system is put into use, in the quarterly assessment of key performance indicators, such as the variance rate of configuration management database audit, the variance rate of configuration information is always stable at around 1%, which is obviously improved compared with the variance rate of 25%–30% entered manually before.

Secondly, because the configuration management system integrates all kinds of basic information, the operation and maintenance personnel can query related configuration information in time, which saves a lot of precious time for solving incidents and problems and greatly improves the response and solving efficiency of emergencies.

The test results show that the system performs well in terms of scientific and automatic configuration management and IT service management, and the findings of this paper's research should be useful as a practical reference and application for similar data centers with a large number of application systems and infrastructures.

4.2. Algorithm Performance Analysis. This section mainly describes the intrusion detection capability of RFCO. The experimental results of SVM, MLP classifier algorithm, and RFCO in terms of accuracy are shown in Figure 6.

It can be seen from Figure 6 that the classification accuracy of network intrusion data by RFCO is higher than that of traditional MLP classifier and SVC model.

Storage management is the process of recording storage device configuration information, such as device number, model, supplier, basic configuration, current configuration, maintenance, and other configuration data, as well as the storage's division, use, server connection, and supported business systems. Storage device main table, storage device maintenance information table, storage device original configuration information table, and so on are some of the

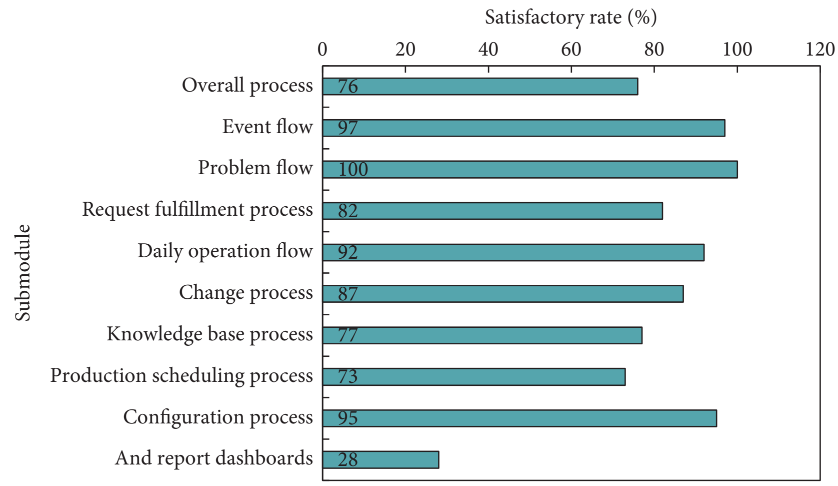

FIGURE 4: Management system requirements and configuration information integrity analysis table.

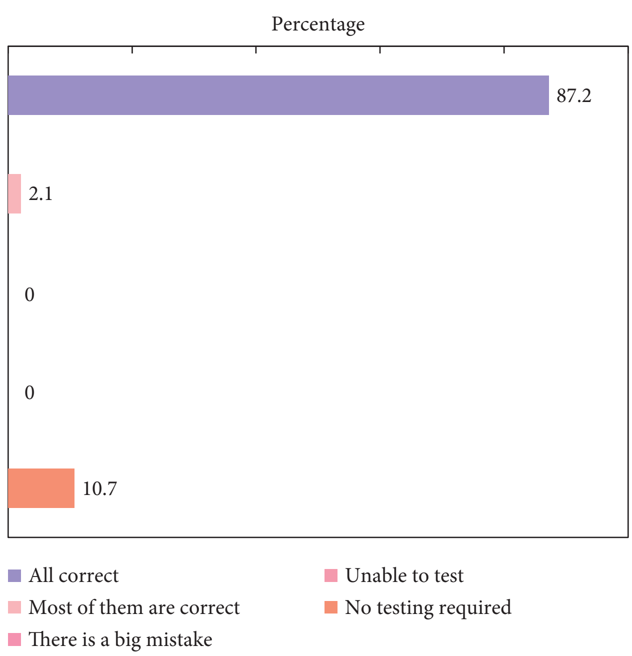

FIGURE 5: Test result statistics.

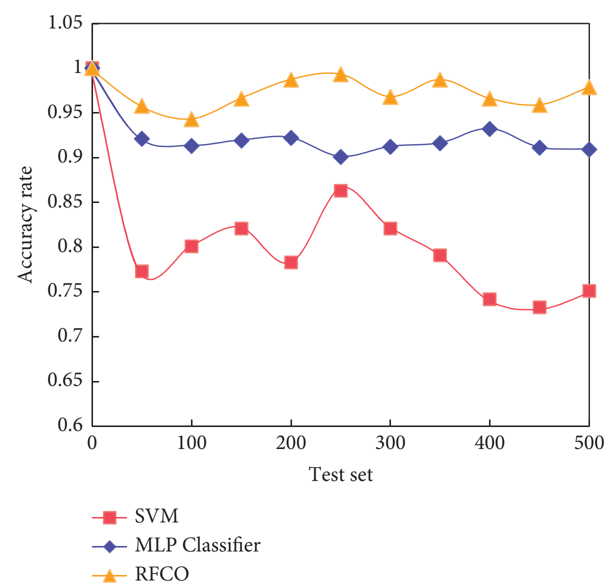

FIGURE 6: Accuracy comparison of algorithms.

main designed data tables. Storage device configuration information is kept in the main table, while storage device maintenance information is kept in the storage device maintenance information table.

Figure 7 compares MSE (mean square error) of three algorithms.

It can be seen from Figure 7 that the MSE value of RFCO for network intrusion detection model is very low. Therefore, the algorithm based on RFCO greatly reduces the MSE of network intrusion detection.

These evaluation parameters can reflect the accuracy, error, and various kinds of sample detection of various algorithms to a certain extent, but there are still some shortcomings in measuring the overall performance of the algorithms. Therefore, this section also uses F_1_score, precision, and recall parameters to measure the accuracy and robustness of the algorithms in combination with the relevant knowledge of machine learning algorithms. The experimental results are shown in Figure 8.

To sum up, compared with other algorithms, RFCO has a good classification effect, which can effectively solve the problem of various and complex features of network intrusion datasets. For other types of network intrusion data, RFCO also has a good detection effect.

Service management is the process of documenting the related service configuration information that is specifically supported by each application, such as software services, subservices, and the relationship configuration between a service and a specific application, among other things. Software service table, correspondence table between service and application, service relationship table, and so on are the main data tables involved in this module. The software service table primarily stores information about the service type, software name, patch configuration, and service type,

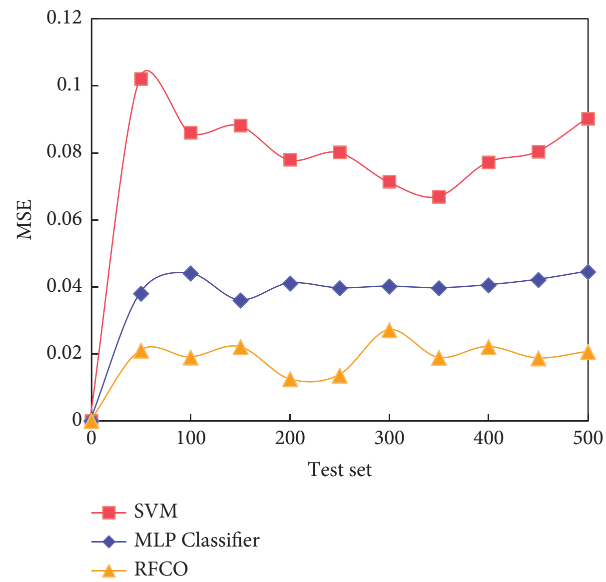

Figure 7: MSE comparison of three algorithms.

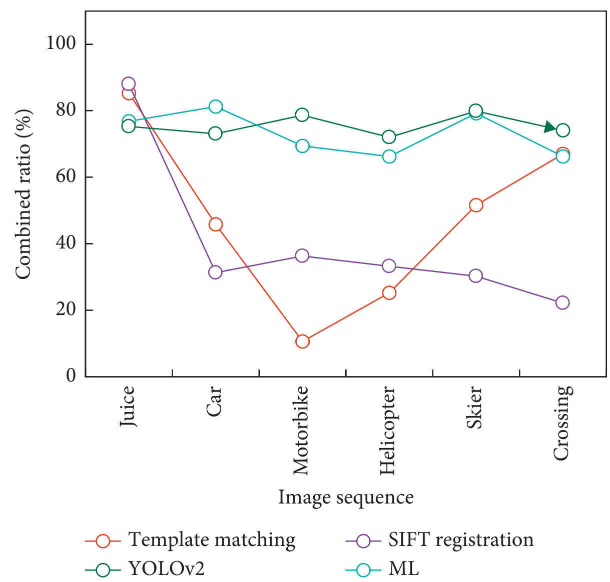

Figure 9: Cross-comparison experiment results.

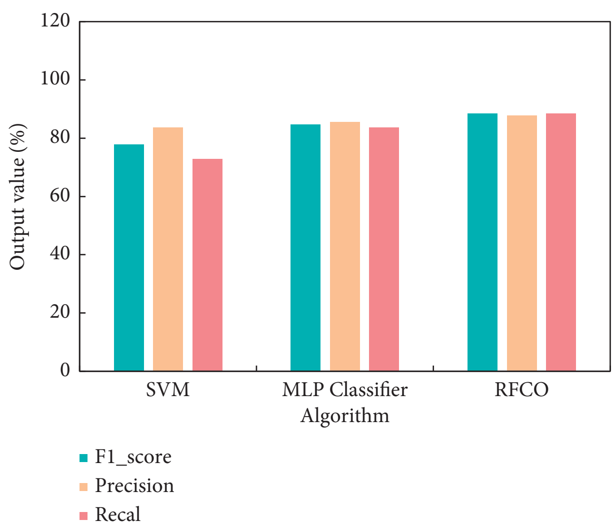

Figure 8: Experimental knot.

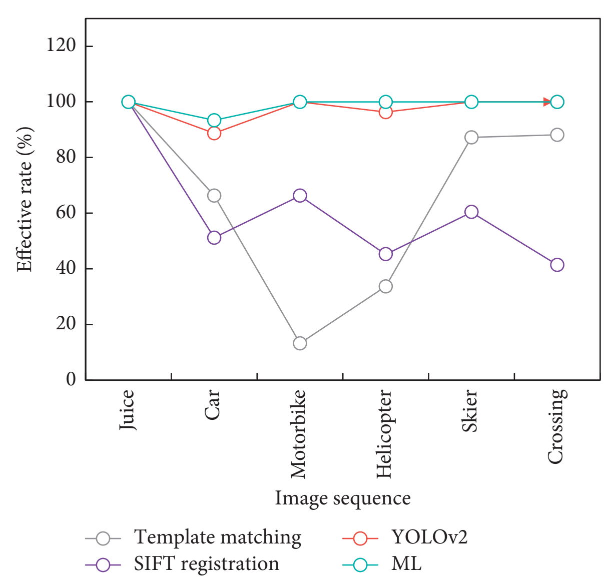

Figure 10: Effective experimental results.

among other things. The service and application correspondence table primarily records the relationship between the service and the corresponding application, as well as the service types that it supports, and the service relationship table is linked to related services.

Continue to verify image sequences using the VOT dataset and TempleColor128 dataset, including Juice, Car, and the other six groups. After manually removing the completely occluded and difficult-to-identify images from the above image sequences, about 10 images were chosen as training data and the remaining images were used as test data in the experiment. The intersection ratio results and the algorithm's efficiency results on six groups of image sequences are shown in Figures 9 and 10, respectively.

According to the above experimental data, it can be seen that the traditional algorithm has good effect only in some scenes, while the method based on DL has good generalization ability in all scenes.

In the daily operation of the data center, a series of changes, such as equipment replacement, system migration, project transformation, and so on, are often needed, and all these changes will cause the change of configuration information without exception, so it is necessary to maintain the configuration information to ensure that the currently recorded configuration information is consistent with the actual information in the production environment. Only when the configuration information is accurate can the normal operation of many processes such as service desk, event management, problem management, change management, and release management be supported.

If an existing configuration item template needs to be updated, the process loops back to the configuration item owner, who redesigns the template. The configuration management database administrator updates the configuration item template once the configuration process manager has approved it. The configuration information administrator is authorized to prepare relevant information in accordance with the modified new configuration item template in order to maintain the configuration item after the new configuration item template is established. The old value before the change and the new value after the change should be recorded in the maintenance record table. The name of the configuration item and all other configuration item names associated with the configuration item should be stored in the maintenance record table for a configuration item with the maintenance type "Delete."

The ML algorithm proposed in this paper maintains a high level of intersection ratio and efficiency. The ML-based target matching algorithm proposed in this paper keeps high efficiency in six scenes. At the same time, it is slightly worse than the previous twin network algorithm in the Car image sequence. The reason for analyzing similar scenes is that the target image and the target image with background are partially used in training, which affects the prediction results when the background changes drastically.

5. Conclusion

With the flourishing development of various businesses in the financial industry, particularly with the increasingly active transactions in the financial market and the increasing demand for regulatory statistics, the FCCMS design scheme in this paper has added new explorations and attempts, the theoretical basis and framework of the technical system have become clearer and more systematic, and the support for regulatory statistics has increased. Simultaneously, a large number of highly automated management software programs were chosen, enhancing IT management capability and level. RFCO synthesizes and optimizes the model's base classifiers, improving network intrusion detection accuracy. Finally, the target matching algorithm based on ML network proposed in this paper has significantly improved efficiency over traditional methods and has higher matching and positioning accuracy, according to the experimental results. The performance of small targets and scenes with spatial transformation has also been greatly improved when compared to the original YOLOv2 algorithm.

The FCCMS is currently unable to achieve full automation, and maintenance tasks such as establishing configuration item correlations and changing configuration item status and attributes still require manual intervention. We will strive to integrate the knowledge base, problem report, and other functions into the configuration management system in the future exploration so that the configuration management system can be more closely integrated with other processes and the data center's IT service quality can be improved further.

Data Availability

The data used to support the findings of this study are included within the article.

Conflicts of Interest

The authors declare that they have no conflicts of interest.

References

[1] T. I. Faiz and M. Noor-E-Alam, "Data center supply chain configuration design: a two-stage decision approach," *Socio-Economic Planning Sciences*, vol. 66, pp. 119–135, 2019.

[2] H. Cheung and S. Wang, "Optimal design of data center cooling systems concerning multi-chiller system configuration and component selection for energy-efficient operation and maximized free-cooling," *Renewable Energy*, vol. 143, pp. 1717–1731, 2019.

[3] G. Garnica, "Configuration management," *Naval Engineers Journal*, vol. 79, no. 4, pp. 555–562, 2018.

[4] L. Ambroise, I. Prim-Allaz, and C. Teyssier, "Financial performance of servitized manufacturing firms: a configuration issue between servitization strategies and customer-oriented organizational design," *Industrial Marketing Management*, vol. 71, pp. 54–68, 2018.

[5] H. Guo, S. Gao, and K. L. Tsui, "Simulation optimization for medical staff configuration at emergency department in Hong Kong," *IEEE Transactions on Automation Science and Engineering*, vol. 14, no. 4, pp. 1655–1665, 2017.

[6] B. Dai, G. Xu, B. Huang, P. Qin, and Y. Xu, "Enabling network innovation in data center networks with software defined networking: a survey," *Journal of Network and Computer Applications*, vol. 94, pp. 33–49, 2017.

[7] X. Y. Li, Y. Liu, and Y. H. Lin, "A generalized petri net-based modeling framework for service reliability evaluation and management of cloud data centers," *Reliability Engineering & System Safety*, vol. 207, no. 2, 2020.

[8] C. Huang, Q. Huang, and D. Wang, "Stochastic configuration networks based adaptive storage replica management for power big data processing," *IEEE Transactions on Industrial Informatics*, vol. 1, no. 99, p. 1, 2019.

[9] C. Nadjahi, H. Louahlia, and S. Lemasson, "A review of thermal management and innovative cooling strategies for data center," *Sustainable Computing: Informatics and Systems*, vol. 19, pp. 14–28, 2018.

[10] R. Trestian, K. Katrinis, and G. M. Muntean, "OFLoad: an OpenFlow-based dynamic load balancing strategy for datacenter networks," *IEEE Transactions on Network & Service Management*, vol. 14, no. 4, p. 1, 2017.

[11] Y. Cheng, X. Qiao, and X. Wang, "Random forest classifier for zero-shot learning based on relative attribute," *IEEE Transactions on Neural Networks and Learning Systems*, vol. 29, pp. 1662–1674, 2017.

[12] H. Xu, J. Wang, H. Li, D. Ouyang, and J. Shao, "Unsupervised meta-learning for few-shot learning," *Pattern Recognition*, vol. 116, no. 6, Article ID 107951, 2021.

[13] A. Trivedi, P. Bovornkeeratiroj, J. Breda, P. Shenoy, J. Taneja, and D. Irwin, "Phone-based ambient temperature sensing using opportunistic crowdsensing and machine learning," *Sustainable Computing: Informatics and Systems*, vol. 29, Article ID 100479, 2021.

[14] R. Feng, X. Zheng, and T. Gao, "Interactive few-shot learning: Limited supervision, better medical image segmentation,"

IEEE Transactions on Medical Imaging, vol. 40, no. 99, p. 1, 2021.

[15] Q. Sun-yuan, L. Da-jun, K. C. Chen, and C. Zeng, "QR code reconstruction algorithm based on binary random forest under non-uniform illumination," *Packaging Engineering*, vol. 40, no. 11, pp. 232–238, 2019.

[16] J. Park, S. Yi, Y. Choi, D. Y. Cho, and J. Kim, "Discriminative few-shot learning based on directional statistics," 2019, http://arxiv.org/abs/1906.01819.

[17] X. Li, Y. Rao, W. Wang, and C. Feng, "SLBCNN: a improved deep learning model for few-shot charge prediction," *Procedia Computer Science*, vol. 174, pp. 32–39, 2020.

[18] A. Paul, D. P. Mukherjee, P. Das, A. Gangopadhyay, A. R. Chintha, and S. Kundu, "Improved random forest for classification," *IEEE Transactions on Image Processing*, vol. 27, no. 8, pp. 4012–4024, 2018.

[19] G. A. Lujan-Moreno, P. R. Howard, O. G. Rojas, and D. C. Montgomery, "Design of experiments and response surface methodology to tune machine learning hyper-parameters, with a random forest case-study," *Expert Systems with Applications*, vol. 109, pp. 195–205, 2018.

[20] M. Mihelcic, S. Dzeroski, and N. Lavrac, "Redescription mining augmented with random forest of multi-target predictive clustering trees," *Journal of Intelligent Information Systems*, vol. 50, no. 1, pp. 1–34, 2018.

[21] S. Lee and N. Moon, "Location recognition system using random forest," *Journal of Ambient Intelligence and Humanized Computing*, vol. 9, no. 4, pp. 1–6, 2018.

[22] C. Zhu, J. Cui, and B. Zou, "Retinal vessel segmentation based on multiple feature fusion and random forest," *Journal of Computer-Aided Design & Computer Graphics*, vol. 29, no. 4, pp. 584–592, 2017.

[23] P. S. Panigrahy, D. Santra, and P. Chattopadhyay, "Decent fault classification of VFD fed induction motor using random forest algorithm," *Artificial Intelligence for Engineering Design Analysis and Manufacturing*, vol. 34, pp. 1–13, 2020.

[24] Y. Wang, H. Xia, X. Yuan, L. Li, and B. Sun, "Distributed defect recognition on steel surfaces using an improved random forest algorithm with optimal multi-feature-set fusion," *Multimedia Tools and Applications*, vol. 77, no. 13, pp. 16741–16770, 2018.

[25] D. Li, P. Zhang, Y. Zhang, and T. Xiao, "Application of random forest in the analysis of students' physical health test data," *ASP Transactions on Computers*, vol. 1, no. 2, pp. 7–11, 2021.

Hindawi
Computational Intelligence and Neuroscience
Volume 2022, Article ID 8464452, 11 pages
https://doi.org/10.1155/2022/8464452

Research Article

A Novel Molecular Representation Learning for Molecular Property Prediction with a Multiple SMILES-Based Augmentation

Chunyan Li,[1,2] Jihua Feng,[1] Shihu Liu,[1] and Junfeng Yao[2]

[1]*Yunnan Minzu University, Kunming, China*
[2]*School of Informatics, Xiamen University, Xiamen, China*

Correspondence should be addressed to Junfeng Yao; yao0010@xmu.edu.cn

Received 8 December 2021; Revised 15 December 2021; Accepted 27 December 2021; Published 28 January 2022

Academic Editor: Xin Ning

Deep learning has brought a rapid development in the aspect of molecular representation for various tasks, such as molecular property prediction. The prediction of molecular properties is a crucial task in the field of drug discovery for finding specific drugs with good pharmacological activity and pharmacokinetic properties. SMILES string is always used as a kind of character approach in deep neural network models, inspired by natural language processing techniques. However, the deep learning models are hindered by the nonunique nature of the SMILES string. To efficiently learn molecular features along all message paths, in this paper we encode multiple SMILES for every molecule as an automated data augmentation for the prediction of molecular properties, which alleviates the overfitting problem caused by the small amount of data in the datasets of molecular property prediction. As a result, by using the multiple SMILES-based augmentation, we obtained better molecular representation and showed superior performance in the tasks of predicting molecular properties.

1. Introduction

Traditionally, drug discovery is time-consuming and very expensive. For understanding the properties of a compound, many results of the simulations can be obtained via the experience of a chemist or pharmacist. The overall process is significantly complex, long, and always inefficient. Deep learning has brought a rapid development in the field of drug discovery and is expected to accelerate the process of drug discovery [1–8]. Nevertheless, deep learning methods still face some obstacles, such as small amount of data in molecular datasets, few label data [3], and label noise [5, 6], which leads to overfitting and poor model prediction performance.

Inspired by natural language processing techniques, many deep learning models use the simplified molecular input line entry system (SMILES) [9] as a line text representation of a molecule. SMILES string is in form of a 1D sequence of chemical structure that can be encoded using a one-hot vectorization form. A molecule may have multiple SMILES. Because SMILES are not unique, a molecule is often defined by canonical SMILES [10], which ensures that each molecule corresponds to a unique canonical SMILES. The SMILES-based methods [11–16] have shown great potential and have been widely used in the tasks of molecular property prediction [12–14] and molecular generation [15, 16]. The performances of the deep learning models are hindered by the nonunique nature of SMILES string, which affects the accuracy of molecular property prediction and the ability to explore the potential chemical space of molecules in molecular generation tasks [11]. Paul et al. proposed a mixed deep learning network architecture CheMixNet [12] to learn molecular representation by using several neural networks design (convolutional neural network (CNN), recurrent neural network (RNN), and multilayer perceptron (MLP)) for learning molecular SMILES sequences and molecular ACCess (MACCS) fingerprints, respectively. Then, concatenate the two parts of features and make the final prediction. Lin et al. learn molecular representation by using bidirectional gated recurrent unit (BiGRU) neural network architecture based on sequence manner [13], which is designed for solving the single- and multitask classification in the field of drug discovery. The methods input single SMILES sequence for a molecule to neural networks to learn representation. Therefore, the limited molecular representation affects the predictive performance of the neural network models. SMILES2vec [14] was proposed to train on SMILES for predicting chemical property using an RNN neural network via Bayesian optimization methods [17]. SMILES2vec was inspired by language translation using RNN in the field of natural language processing (NLP). SMILES2vec did not explicitly encode the grammar of SMILES specification. The LSTM-based [18] or GRU-based [19] recurrent neural network architecture is an effective neural network design for learning features from sequence or text data. The above neural network models based on SMILES have limitations because only the single SMILES of each molecule is considered, which cannot learn the grammatical features of SMILES well. Although SMILES enumeration [11] and all SMILES variational autoencoder [15] have considered multiple SMILES strings of single molecule to learn latent molecular representation. However, these methods are not used in the tasks of molecular property prediction. In this paper, we proposed a novel molecular representation method for molecular property prediction using multiple SMILES-based augmentation to alleviate the problem of a small amount of data and few labels in the molecular property prediction datasets , regardless of descriptors engineering and expert experience.

2. Related Work

A related method to this paper is the SMILES enumeration [11]. SMILES enumeration explored the fact that multiple SMILES represent the same molecule as a technique for data augmentation. The augmented dataset was bigger than the original. The neural network trained with the augmented dataset showed better performance on the test set than the original neural model trained with the unaugmented dataset. Another SMILES enumeration-based method is all SMILES variational autoencoder [15], which used multiple SMILES strings of single molecule to learn latent molecular representation for molecular generation. All SMILES variational autoencoder (VAE) encoded multiple SMILES by using several recurrent neural network layers and decoded them to molecular SMILES. All SMILES VAE learned a bijective mapping between molecules and the latent representations near the high-probability subspace of the prior. The result showed that all SMILES VAE obtained the state-of-the-art performance. However, these methods are not used in the tasks of molecular property prediction, recommended by MoleculeNet [8].

3. Methods

The key idea is that we focus on a multiple-SMILES representation learning as data augmentation for various downstream tasks. As we all know, the deep learning model must be fed with a large amount of data. Through learning a large amount of data, the model can find the law and obtain the potential knowledge of the data. Despite the presence of a large number of molecules, labeled datasets are scarce. In the task of molecular property prediction, the number of molecules in some datasets of property prediction is also very small. It leads to the problem of unstable prediction performance using the deep learning models due to overfitting and underfitting.

Inspired by the SMILES enumeration [11] and all SMILES VAE [15], we proposed a novel method of molecular property prediction using multiple SMILES-based augmentation to solve the overfitting and underfitting problem. The general framework is illustrated in Figure 1. Generally, before feeding the data into the deep neural network, the multiple SMILES-based augmentation must be completed (Figure 1(a)), which is related to whether the model can learn the potential knowledge in the datasets. It is a crucial step for the successful prediction of deep neural model. The process of data augmentation includes cleaning data and removing invalid molecules. Then multiple SMILES sequences are generated for each molecule, and further one-hot vectorization is carried out that can be fed to the neural network to learn molecular features. The deep neural network used in this paper is shown in Figure 1(b), which consists of stacked CNN and RNN. The "Gate" in Figure 1(b) is denoted as the gated recurrent unit (GRU) or long-short-term memory (LSTM). The final molecular representation can be used for a variety of downstream tasks, such as molecular property prediction.

In the following, we will describe technical details. We first give the mathematical definition of the problem (Section 3.1) and then propose a novel molecular representation method using multiple SMILES-based augmentation for molecular property prediction (Section 3.2).

3.1. Problem Definition. We define a feed-forward convolutional neural network as $\mathscr{CNN}_{(\text{kernel},\text{channel},\text{padding})}$, where kernel is the convolution kernel, channel denotes the convolution channel, and padding represents the type of padding. A recurrent neural network can be defined as $\mathscr{RNN}_{\text{gate}}$, where gate denotes the type of gate, such as LSTM and GRU. Let X_{os} be the original SMILES strings that have been cleaned and are valid molecules. Let mapping function of multiple SMILES be f_{ms}. X_{ms} is the multiple SMILES sequences. We define the vectorization function as f_{vect}. The problem is to learn the function f_{res} that maps the multiple SMILES vectors to molecular representation X_{mol}. The mapping relations are represented as follows:

$$\begin{aligned} X_{ms} &= f_{ms}(X_{os}), \\ &\left[f_{\text{vect}}(X_{ms}); \mathscr{CNN}_{(\text{kernel},\text{channel},\text{padding})}, \mathscr{RNN}_{\text{gate}}\right] \\ &\longrightarrow f_{\text{res}}\, X_{\text{mol}}. \end{aligned} \tag{1}$$

The whole process includes three mapping functions, namely, f_{ms}, f_{vect}, and f_{res}. The final molecular representation is what we want to get and can be further used in specific tasks such as molecular property prediction.

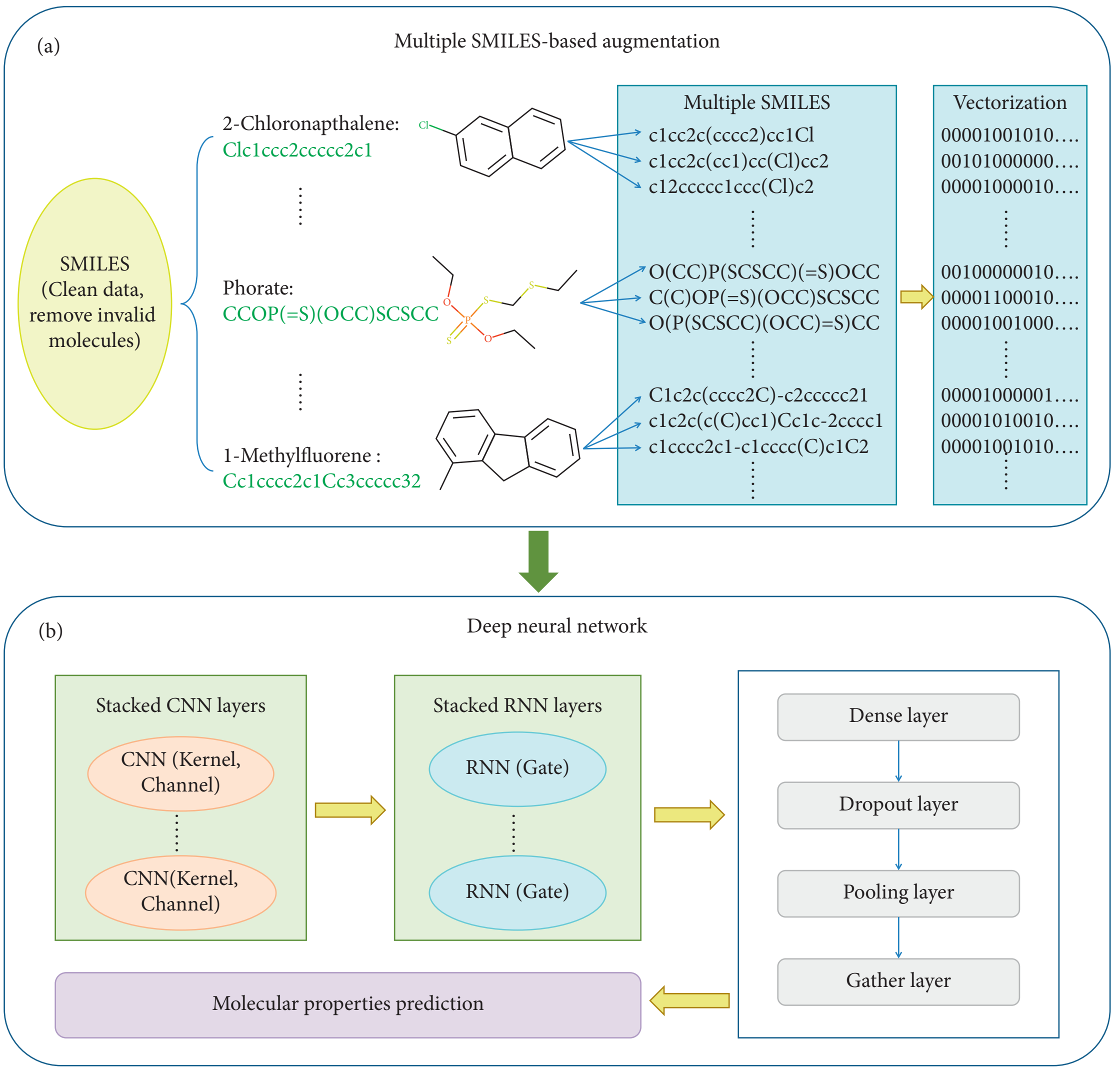

Figure 1: The architecture of molecular representation with a multiple SMILES-based augmentation for molecular property prediction. (a) The process of data augmentation using multiple SMILES. After cleaning and removing invalid molecules from the original datasets, multiple SMILES sequences are generated for each molecule, and further one-hot vectorization is carried out. (b) The stacked CNN and RNN neural networks. After passing through different layers (including dense layer, dropout layer, pooling layer, and gather layer), finally the characteristics such as molecular properties are predicted.

3.2. Multiple SMILES-Based Augmentation. The SMILES [9] is a popular specification for extracting the feature of molecular sequences that uses ASCII strings encoding molecular structures in the form of a line notation. The SMILES structure follows a certain grammar. The alphabets and numbers in SMILES denote atoms and rings, respectively. The special characters such as "=" and " ≡ " indicate the bond types, and the parentheses indicate side chains. The mapping function of multiple SMILES f_{ms} can be implemented using the method of renumbering atoms in RDKit [20] after performing randomization of a SMILES sequence and then regenerating a new SMILES sequence using the "MolToSmiles" method and setting canonical to be "False" in RDKit. Figure 2 takes estradiol as an example to randomly generate 10 multiple SMILES sequences. Estradiol is randomly selected from the ESOL dataset. Figure 3 demonstrates randomly generated 4 SMILES sequences with renumbered atoms in the molecular graph for estradiol. It is shown that atoms with different numbers in the molecule can generate different SMILES sequences. Therefore, the SMILES sequence of molecules is not unique, but canonical SMILES are unique for specific molecule.

The mapping function f_{vect} can be implemented using language translation technology in the field of natural language processing, which is an effective method for learning from text data. We need to construct a character set for all SMILES sequences in some datasets, which is similar to the corpus in natural language processing. Then randomization and vectorization to convert the SMILES array to a one-hot vector are performed. Figure 4 demonstrates the one-hot images of vectorization using multiple SMILES for estradiol. Each image of vectorization in Figure 4 highlights the one-hot vector for different SMILES sequences. The abscissa interval is [0, 9], and the 9 represents the number of

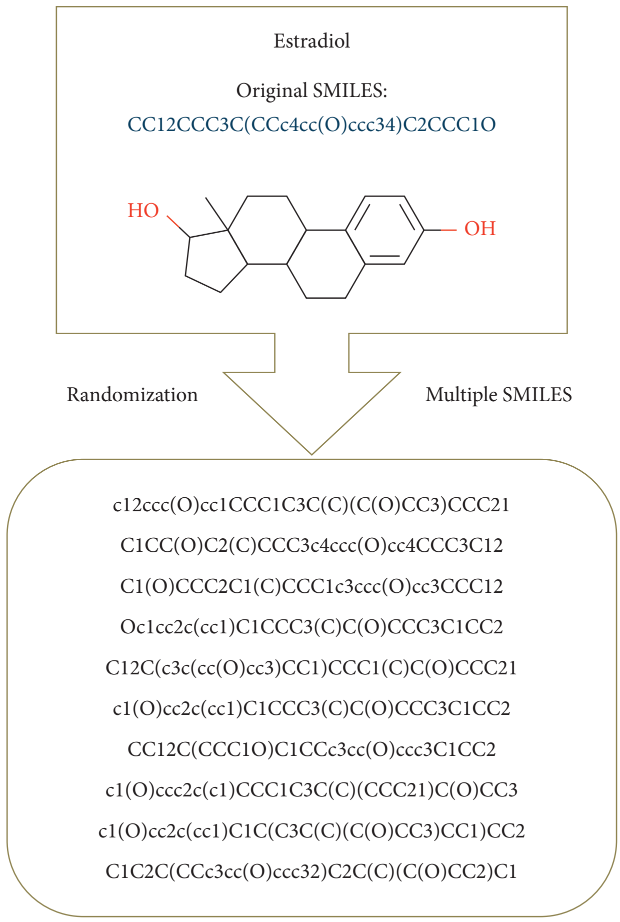

Figure 2: The generation of multiple SMILES for estradiol. The original SMILES is "CC12CCC3C(CCc4cc(O)ccc34)C2CCC1O" that is randomly selected from the ESOL dataset. Here, it is shown the randomly generated 10 SMILES sequences for estradiol molecule.

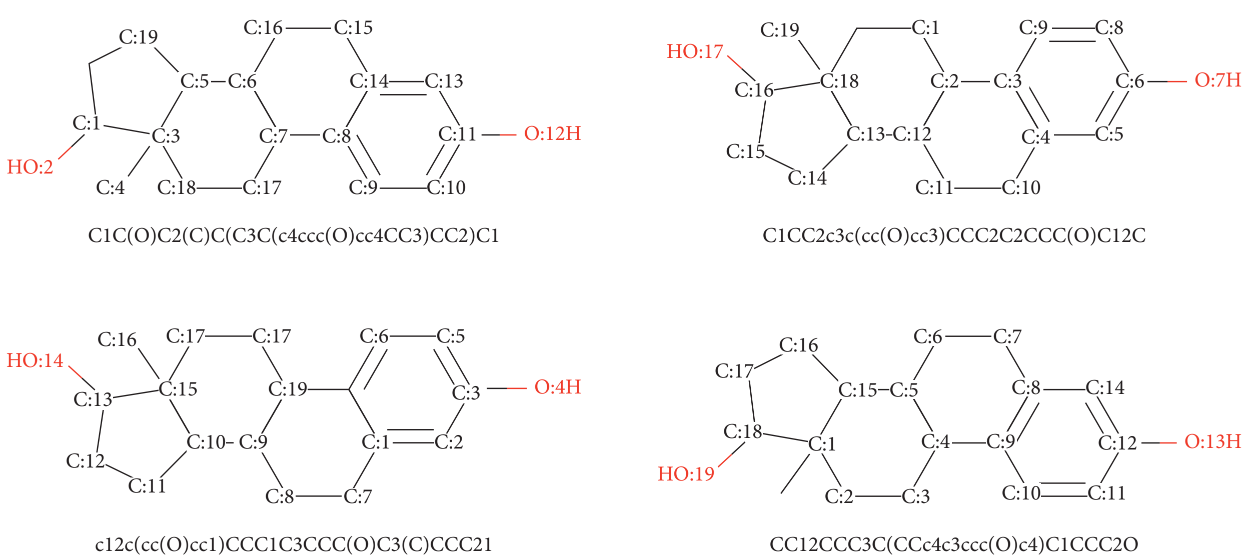

Figure 3: The randomly generated 4 SMILES sequences with renumbered atoms in the molecular graph for estradiol.

characters contained in the character set. The interval of the ordinate is [0, 37], and the 37 denotes the length of the SMILES string (including predefined extra padding).

The last mapping function f_{res} for obtaining molecular representation can be learned using stacked CNN and RNN mixed architecture. The RNN consists of an input layer, a

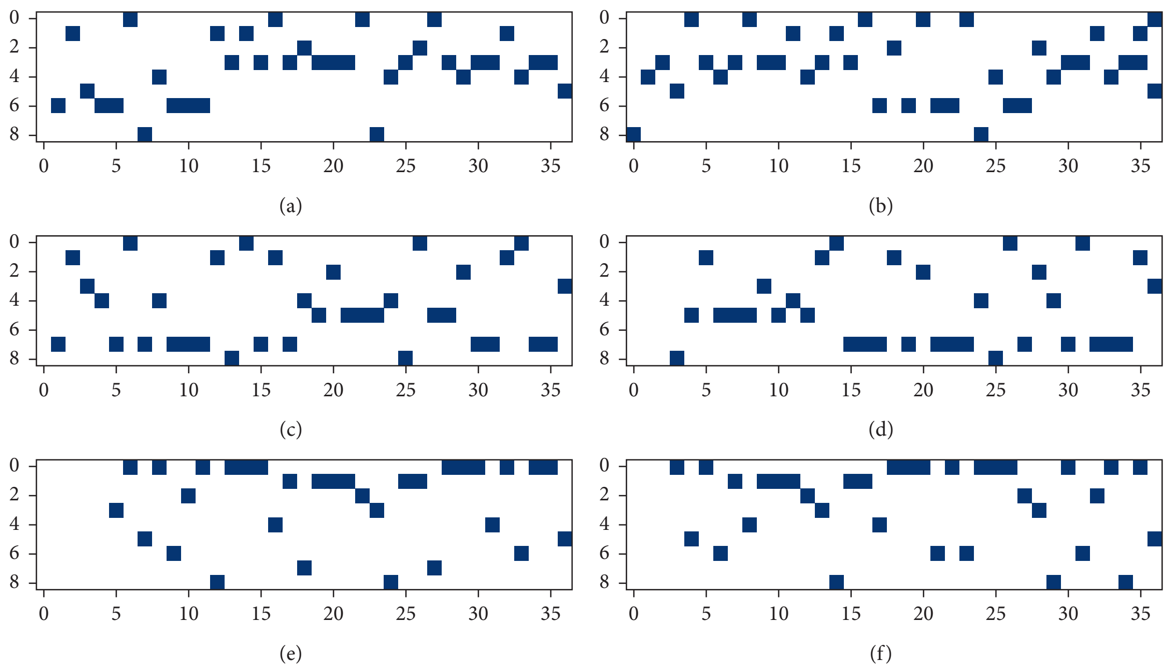

Figure 4: The images of one-hot vectorization using multiple SMILES for Estradiol molecule. It shows the vectorization of randomly generated 6 SMILES strings, using random order of the character set for Estradiol, which consists of 9 characters: "(", "3", "O", "c", "1", ")", "2", "4", "C". The length of padding is 37, that includes predefined extra padding. (a) c12cc(O)ccc1C1C(C3CCC(O)C3(C)CC1)CC2. (b) C1(O)C2(C)C(CC1)C1C(c3c(cc(O)cc3)CC1)CC2. (c) C12(C)C(CCC1O)C1C(c3ccc(O)cc3CC1)CC2. (d) Oc1ccc2c(c1)CCC1C3CCC(O)C3(C)CCC12. (e) OC1C2(C)CCC3c4ccc(O)cc4CCC3C2CC1. (f) C1C2c3ccc(O)cc3CCC2C2CCC(O)C2(C)C1.

hidden layer, and an output layer. Figure 5 shows the simple structure of RNN, where X is an input vector, H indicates the hidden vector of the hidden layer, O represents the output vector. W_{xh}, W_{ho}, and W_h denote the weight matrix from input layer to hidden layer from hidden layer to output layer, and hidden layer, respectively.

Figure 6 demonstrates the timeline structure of RNN. The output O_t of RNN at time t is related not only to the input x_t at time t but also to the hidden layer value h_{t-1} at time $t-1$. It is shown that RNN can better deal with sequence information, that is, the previous input is related to the subsequent input. SMILES string is precisely this sequence structure, which can extract features with designed RNN architecture.

The message passing process for stacked CNN and RNN mixed architecture can be found in Figure 7, which shows the message passing in the neural network at time t and time $t-1$. The result of the output layer at time t must be based on the input at time t and the result vector of the hidden layer at time $t-1$. The process can be summarized in the form of matrix as follows:

$$\begin{aligned} O_t &= \mathscr{P}\left(W_{\text{ho}} \cdot H_t\right), \\ H_t &= \mathscr{Q}\left(W_{xh} \cdot X_t + W_h \cdot H_{t-1}\right), \end{aligned} \tag{2}$$

where $\mathscr{P}$ and $\mathscr{Q}$ indicate some kind of neural network. Finally, the mapping function f_{res} for obtaining molecular representation can be represented using CNN and RNN as follows:

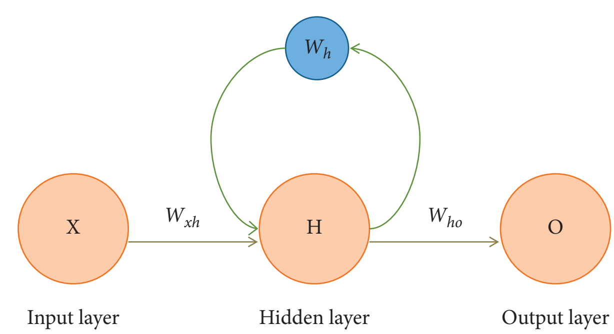

Figure 5: The structure of the recurrent neural network [21].

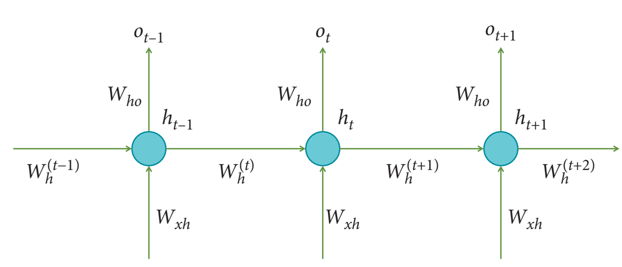

Figure 6: The timeline structure of the recurrent neural network [21].

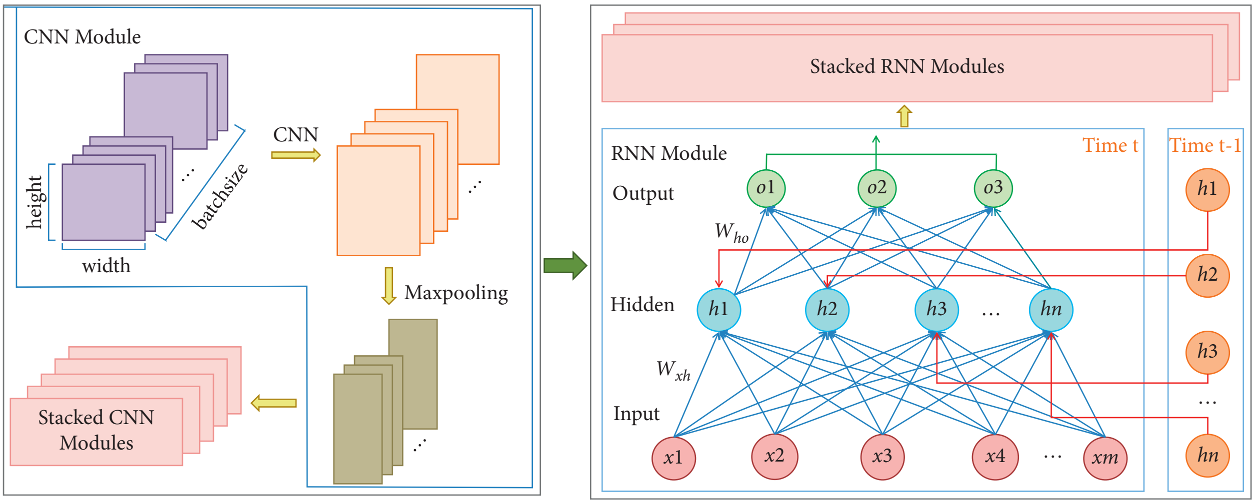

Figure 7: The message passing process for stacked CNN and RNN.

$$X_{cnn} = \mathscr{CNN}_{(\text{kernel,channel,padding})}\left(f_{\text{vect}}\left(X_{ms}\right)\right),$$
$$O_t = \mathscr{RNN}_{\text{gate}}\left(W_{ho}\cdot\left(\mathscr{Q}\left(W_{xh}\cdot X_{cnn}^{(t)} + W_h\cdot H^{(t-1)}\right)\right)\right),$$
$$X_{\text{mol}} = f_{(\text{Dense,Pooling,Gather})}\left(O_t\right), \tag{3}$$

where $f_{(\text{Dense,Pooling,Gather})}$ denotes the mapping of full-connection layer, pooling layer, and gather layer.

4. Experiments

Extensive experiments have been implemented to evaluate the performance of molecular representation using the multiple SMILES-based augmentation for the tasks of molecular property prediction. We will describe the datasets, baselines, and experimental results.

4.1. Dataset Description. We use five molecular property datasets recommended by MoleculeNet [8] for the experiments. Table 1 shows the information of five datasets.

The details of used datasets are shown as follows:

(i) ESOL: ESOL [22] contains the logarithmic aqueous solubility (mol/L) of 1,127 compounds, which is used as a regression task to predict water solubility in deep neural networks

(ii) Lipophilicity: lipophilicity [23] includes the octanol/water distribution coefficient (logD at pH 7.4) about 4,200 compounds, which is important in membrane permeability and solubility

(iii) FreeSolv: FreeSolv [24] provides the hydration free energy (kcal/mol) of 642 compounds in water

(iv) HIV: HIV [25] is used as a classification task in deep neural networks to predict the activity of inhibiting HIV replication, which contains 41,127 compounds

(v) BACE: BACE [26] is used as a classification task, which contains 1,513 molecules and provides quantitative and qualitative binding results for a set of inhibitors

The datasets must be cleaned before being input into the neural network. The cleaning and preprocessing process are shown in Figure 8. The original data are cleaned via five steps, namely, excluding invalid molecules, filtering organic molecules, removing salt and stereochemistry information, keeping the largest fragment, and converting to canonical SMILES. Then, we get the cleaned molecules that will be used to generate multiple SMILES sequences and vectorization. Finally, the feature of vectorization will be fed to the neural network to be trained.

4.2. Baselines. We compared our method with the following models:

(1) CheMixNet: CheMixNet [12] was proposed for predicting chemical properties using molecular SMILES sequences and fingerprints, which is a mixed deep neural network architecture. In this paper, we focus on the molecular SMILES sequence. Therefore, we do not consider computable characteristics, such as molecular fingerprints or physical descriptors. For a fair comparison with our method, we adopt the neural architecture of CNN and RNN in CheMixNet [12], which uses the SMILES as the sole input.

(2) Smi2Vec-BiGRU: Smi2Vec + BiGRU [13] was proposed for learning atoms and the single- and multitask classification tasks, which learns the low-dimensional representation for a molecule by transforming SMILES to vector based on bidirectional gated recurrent unit (GRU) [18] architectures.

(3) XGBoost: XGBoost [27] is an ensemble method to implement a gradient boosting decision tree (GBDT) for improving the speed and efficiency of the model.

Table 1: The description of public molecular datasets, including data type, task type, and the number of compounds before and after augmentation.

Dataset	Data type	Task type	Compound	Compound after augmentation
ESOL	SMILES	Regression	1127	6762
Lipophilicity	SMILES	Regression	4200	25200
FreeSolv	SMILES	Regression	642	3852
HIV	SMILES	Classification	41127	69987
BACE	SMILES	Classification	1513	9078

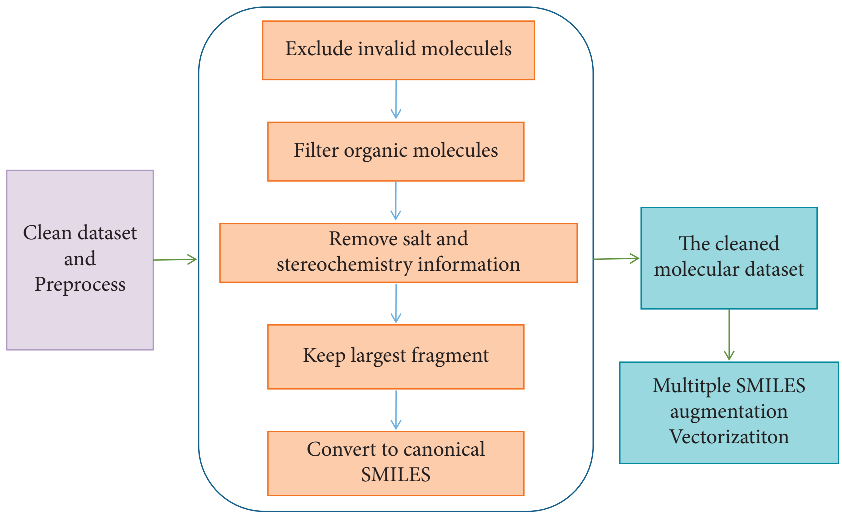

Figure 8: The process of data cleaning and preprocessing.

(4) Multitask: Multitask network [28] was proposed for sharing the processed input among all learning tasks in a dataset and then used separate linear classifiers or regressors for each different task.

(5) MPNN: Message Passing Neural Network (MPNN) is a generalized graph-based architecture [29], including the message passing phase and readout phase. The former phase is to learn the characteristics of the graph, and the latter phase is to obtain the full graph representation for predicting various tasks.

(6) GC: GC [30] is a standard feature extraction method for molecules based on circular fingerprints, which is a kind of graph convolutional model and operates directly on graphs with arbitrary size and shape.

(7) Weave: Weave [31] implemented graph convolutional operation on molecules using a simple encoding of the molecular graph including atoms, bonds, and distances.

(8) Pretraining GNN: pretraining GNN [32] proposed a new strategy and self-supervised methods for pretraining graph neural networks. In order to obtain useful local and global features, the strategy of pretraining GNN is to pretrain expressive graph neural networks by using individual nodes and entire graphs. Pretraining GNN achieved state-of-the-art performance on the tasks of molecular property prediction.

(9) Drug3D-Net: Drug3D-Net [2] is a grid-based 3D model for molecular representation using spatial-temporal gated attention, which uses the geometric information of molecules to extract the molecular characteristics.

(10) Multiple SMILES (RNN (one layer), RNN (two layers), CNN_RNN): this is the method presented in this article. The neural network architecture includes one layer RNN, two layers RNN, and the mixed networks of CNN and RNN.

4.3. Experimental Setup. In this experiment, we use root mean squared error (RMSE) and mean absolute error (MAE) to evaluate the performance of regression tasks. Similarly, we use the loss function of “binary_crossentropy” for classification datasets. We use the average area under the receiver operating characteristics curve (AUROC) and the area under the precision-recall curve (AUPRC) predicted from the test set to evaluate the performance of the model for classification tasks. Our experiment was trained based on the Keras framework and TensorFlow [33]. We used the Adam algorithm [34] for optimizing the parameters of the model. We set a total of 200 epochs, 64 batch sizes, and 5-fold cross-validation with checkpoint and early stopping. We set the learning rate as 0.001 with learning rate decay. We perform

Table 2: The RMSE and MAE values of various approaches in ESOL, lipophilicity, and FreeSolv datasets. The predictive values of the approaches are partly derived from the related references [2, 8].

Model		ESOL		Lipophilicity		FreeSolv	
		RMSE	MAE	RMSE	MAE	RMSE	MAE
CheMixNet	CNN_RNN	1.0419	0.8010	1.0513	0.8282	1.3553	1.0156
Conventional methods	XGBoost	0.9900	—	0.7990	—	1.7400	—
	Multitask	1.1200	—	0.8590	—	1.8700	—
Graph-based methods	MPNN	**0.5800**	—	0.7190	—	1.1500	—
	Weave	0.6100	—	0.7150	—	1.2200	—
3D-based models	Drug3D-Net	0.9683	0.7841	0.9930	0.8404	1.4709	1.1598
Our method (multiple SMILES)	RNN (one layer)	0.6585	0.5105	0.7929	0.6211	1.6051	1.2313
	RNN (two layers)	0.6394	0.4940	0.7960	0.6217	1.3575	1.0468
	CNN_RNN	0.5916	**0.4448**	**0.7054**	**0.5481**	**1.0033**	**0.7859**

The best results are highlighted in bold.

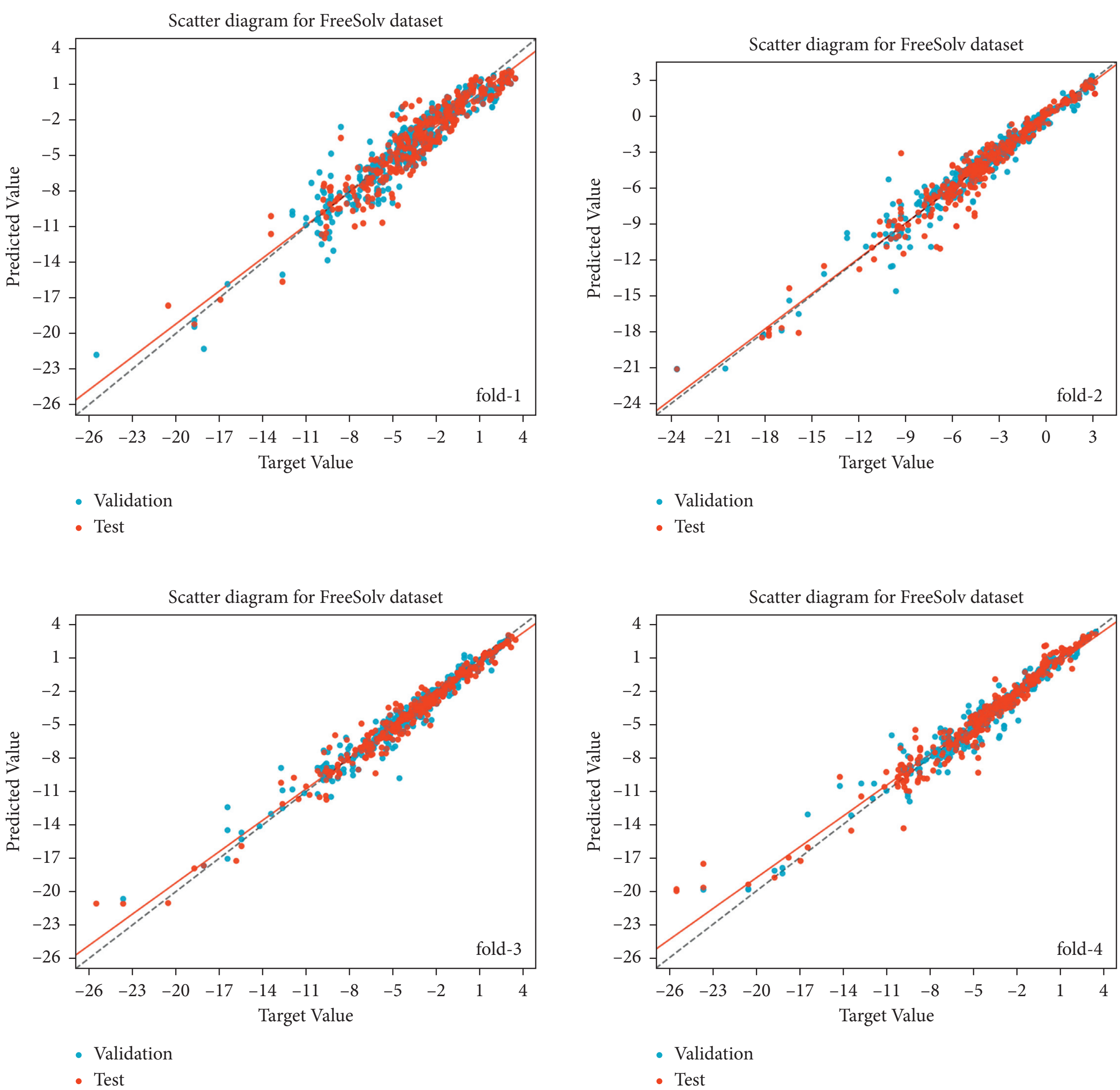

Figure 9: Scatter diagram of FreeSolv dataset for four training folds. The horizontal axis is the ground truth value, and the vertical axis is the predicted value by our model. The solid lines indicate the trend lines, and the dashed lines indicate the identity lines. The blue and red points represent the predicted values in the validation set and test set, respectively.

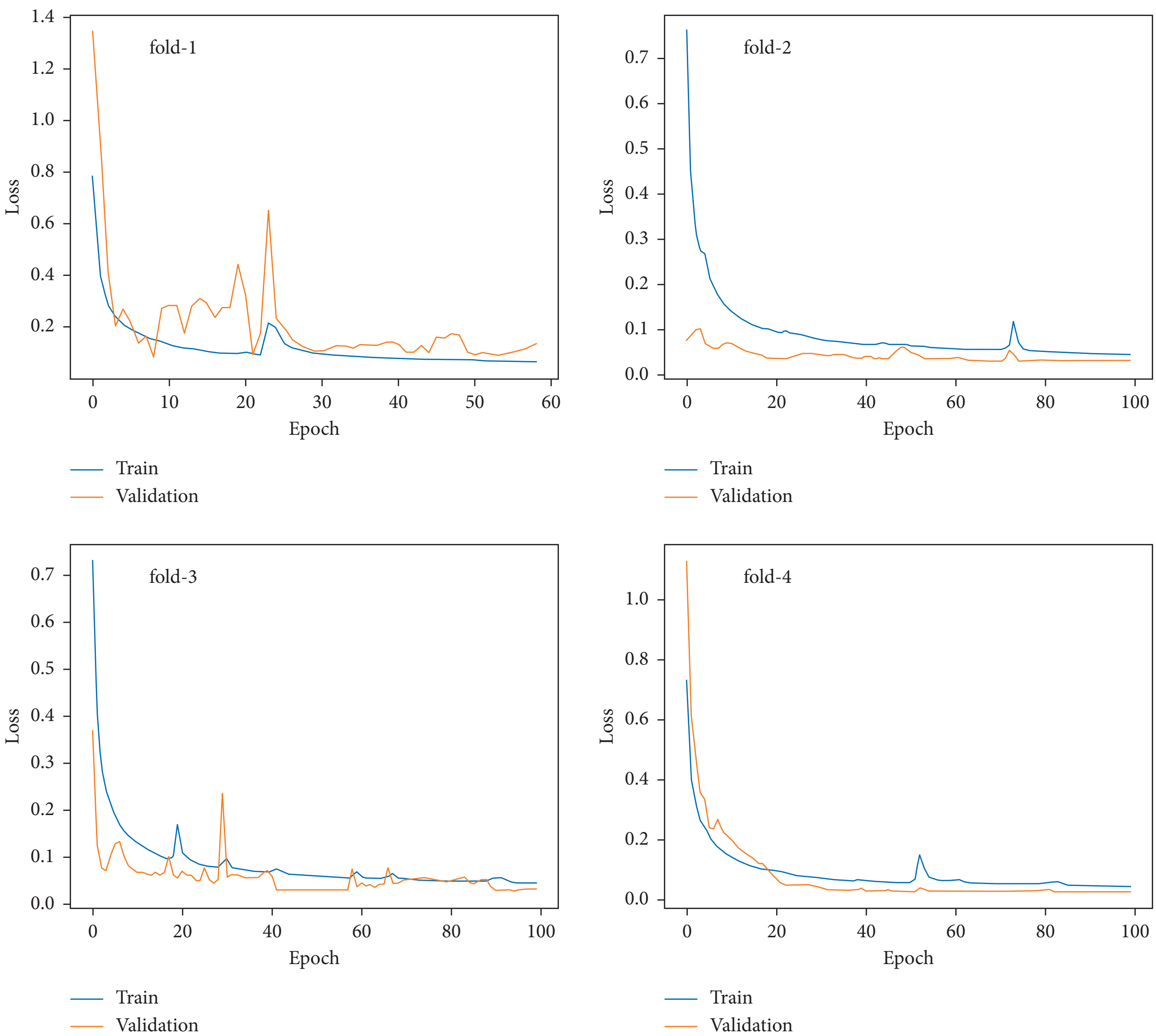

Figure 10: The loss curves during our model training for FreeSolv in the training set and validation set.

randomization of a SMILES string with the random number 5 for ESOL, lipophilicity, FreeSolv, and BACE datasets. As for the HIV dataset, we set random number 20 to implement multiple SMILES randomization only for positive samples so that we obtain a total of 30,303 positive examples compared with the original 39,684 negative samples.

4.4. Performance Comparison

4.4.1. Performance in Regressions. Solubility, lipophilicity, and free energy are very important physical chemistry properties, which are essential properties to understand molecular interaction with solvents. Table 2 demonstrates the predictive performances for water solubility (ESOL), octanol/water distribution coefficient (lipophilicity), and hydration free energy (FreeSolv). Our multiple SMILES-based model using mixed CNN and RNN architecture obtains the best performance. The smaller the value of RMSE and MAE, the better for ESOL, lipophilicity, and FreeSolv. As shown in Table 2, we obtain 0.4448 MAE and 0.5916 RMSE values for ESOL in the test set. The RMSE value of 0.5916 is slightly lower than the MPNN with the 0.5800 RMSE. However, as for lipophilicity and FreeSolv datasets, our method obtains superior performance on both RMSE and MAE values, which shows that the multiple SMILES-based data augmentation can alleviate the overfitting problem to a certain extent on a small amount of data, such as ESOL and FreeSolv datasets.

Figure 9 shows the scatter plots in the FreeSolv dataset for four training-folds, which indicates that the points on the test set closely surround the identity line, which shows that the prediction results in the test set are closer to the target value, although the trend lines deviate slightly from the identity lines in each training folds. In addition, Figure 10 shows the loss curves during our model training in the training set and validation set for the FreeSolv dataset. At the beginning of the training of the model, the loss on the training set and the validation set has a relatively large gap (training loss curve and validated loss curve are far away), indicating that the model is not stable. When the number of

Table 3: The AUROC and AUPRC scores of various approaches in HIV and BACE datasets. The predictive values of the approaches are partly derived from the related references [2, 8, 13, 32].

Model		HIV		BACE	
		AUROC	AUPRC	AUROC	AUPRC
CheMixNet	CNN_RNN	0.8204	0.8614	0.7429	0.7162
SMILES-based	Smi2Vec-BiGRU	0.9117	0.8963	0.8440	0.7872
Conventional methods	XGBoost	0.7560	—	0.8500	—
	Multitask	0.6980	—	0.8240	—
Graph-based methods	GC	0.7630	—	0.7830	—
	Weave	0.7030	—	0.8060	—
	Pretraining GNN	0.7990	0.7806	0.8450	0.7908
3D-based models	Drug3D-Net	0.9621	0.9617	0.7185	0.6397
Our method (multiple SMILES)	RNN (one layer)	0.9567	0.9525	0.7879	0.7577
	RNN (two layers)	0.9613	0.9636	0.8083	0.7665
	CNN_RNN	**0.9767**	**0.9798**	**0.8512**	**0.7919**

The best results are highlighted in bold.

training epochs increases, the loss curves on the training set and the validation set tends to be consistent and fit each other, indicating that the model tends to be stable and is slowly converging.

4.4.2. Performance in Classifications. Table 3 demonstrates the predictive performances for HIV activity (HIV) and inhibitors of human β-secretase 1 (BACE). The larger the AUROC and AUPRC score, the better for HIV and BACE. Our method based on mixed CNN and RNN architecture achieved the best performance on AUROC and AUPRC scores in the test set for HIV and BACE datasets. In HIV, we obtain 0.9767 AUROC and 0.9798 AUPRC scores compared with the 0.9621AUROC and 0.9617 AUPRC of the 3D-based method Drug3D-Net, although the Drug3D-Net considered the information of molecular geometry. In addition, the performance of our method exceeds that of the pretrained model pretraining GNN with a large margin.

In summary, our method shows superior performance in both regression datasets and classification datasets, which implies the good molecular representation ability of our proposed method.

4.5. Ablation Study. For different neural architectures of our multiple SMILES methods (shown in Tables 2 and 3), the mixed CNN_RNN architecture obtains the best performance among RNN (one layer), RNN (two layers), and CNN_RNN, which indicates that the CNN convolution in our model is essential and can improve the predictive performance for downstream tasks. Meanwhile, the performance of RNN (two layers) architecture is slightly better than that of RNN (one layer) architecture, which shows that the deeper neural networks can have better learning ability for extracting features. Therefore, it can show better performance in specific tasks, such as molecular property prediction.

5. Conclusion

In this study, we make full use of the nonunique nature of the SMILES string to perform randomization of a SMILES string multiple times for efficiently learning molecular features along all message paths. By encoding multiple SMILES for every molecule as an automated data augmentation, we obtain better molecular representation and the proposed method shows superior performance in the tasks of predicting molecular properties, which alleviates the overfitting problem caused by the small amount of data in the datasets of molecular property prediction.

Data Availability

All input data are publicly available and a detailed description for the same is mentioned in the Dataset Description.

Conflicts of Interest

The authors declare that they have no conflicts of interest.

Acknowledgments

This work was supported in part by the scientific research fund of Yunnan Provincial Department of Education (No. 2022J0450), the National Natural Science Foundation of China (Nos. 62072388 and 61966039), the Industry Guidance Project Foundation of Science Technology Bureau of Fujian Province in 2020 (No. 2020H0047), the Natural Science Foundation of the Science Technology Bureau of Fujian Province in 2019 (No. 2019J01601), and the Science Technology Bureau Project of Fujian Province in 2019 (No. 2019C0021).

References

[1] J. Shen and C. A. Nicolaou, "Molecular property prediction: recent trends in the era of artificial intelligence," *Drug Discovery Today: Technologies*, vol. 32–33, pp. 29–36, 2020.

[2] C. Li, J. Wang, Z. Niu, J. Yao, and X. Zeng, "A spatial-temporal gated attention module for molecular property prediction based on molecular geometry," *Briefings in Bioinformatics*, vol. 22, 2021.

[3] Z. Guo, C. Zhang, W. Yu et al., "Few-shot graph learning for molecular property," 2021, https://arxiv.org/abs/2102.07916.
[4] C. Li, W. Wei, J. Li, J. Yao, X. Zeng, and Z. Lv, "3DMol-net: learn 3D molecular representation using adaptive graph convolutional network based on rotation invariance," *IEEE Journal of Biomedical and Health Informatics*, 2021.
[5] A. Nigam, R. Pollice, M. F. D. Hurley et al., "Assigning confidence to molecular property prediction," 2021, https://arxiv.org/abs/2102.11439.
[6] S. Ryu, Y. Kwon, and W. Y. Kim, "A bayesian graph convolutional network for reliable prediction of molecular properties with uncertainty quantification," *Chemical Science*, vol. 10, no. 36, pp. 8438–8446, 2019.
[7] D. Chen, K. Gao, D. D. Nguyen et al., "Algebraic graph-assisted bidirectional transformers for molecular property prediction," *Nature Communications*, vol. 12, p. 3521, 2021.
[8] Z. Wu, B. Ramsundar, E. N. Feinberg et al., "MoleculeNet: a benchmark for molecular machine learning," 2018, https://arxiv.org/abs/1703.00564.
[9] D. Weininger, "SMILES, a chemical language and information system. 1. Introduction to methodology and encoding rules," *Journal of Chemical Information and Computer Sciences*, vol. 28, no. 1, pp. 31–36, 1988.
[10] N. M. O'Boyle, "Towards a universal smiles representation - a standard method to generate canonical smiles based on the inchi," *Journal of Cheminformatics*, vol. 4, p. 22, 2012.
[11] E. J. Bjerrum, "SMILES enumeration as data augmentation for neural network modeling of molecules," 2017, https://arxiv.org/abs/1703.07076.
[12] A. Paul, D. Jha, R. Al-Bahrani, W. Liao, A. Choudhary, and A. Agrawal, "CheMixNet: mixed DNN architectures for predicting chemical properties using multiple molecular representations," 2018, https://arxiv.org/abs/1811.08283.
[13] X. Lin, Z. Quan, Z. Wang, H. Huang, and X. Zeng, "A novel molecular representation with BiGRU neural networks for learning atom," *Briefings in Bioinformatics*, vol. 21, no. 6, pp. 2099–2111, 2020.
[14] G. B. Goh, N. O. Hodas, C. Siegel, and A. Vishnu, "SMILES2Vec: an interpretable general-purpose deep neural network for predicting chemical properties," 2017, https://arxiv.org/abs/1712.02034.
[15] Z. Alperstein, A. Cherkasov, and J. T. Rolfe, "All SMILES variational autoencoder," 2019, https://arxiv.org/abs/1905.13343.
[16] H. Dai, Y. Tian, B. Dai, S. Skiena, and L. Song, "Syntax-directed variational autoencoder for structured data," in *Proceedings of the Sixth International Conference on Learning Representations (ICLR'18)*, Vancouver, Canada, May 2018.
[17] I. Dewancker, M. McCourt, S. Clark, P. Hayes, A. Johnson, and G. Ke, "Evaluation system for a bayesian optimization service," 2016, https://arxiv.org/abs/1605.06170.
[18] S. Hochreiter and J. Schmidhuber, "Long short-term memory," *Neural Computation*, vol. 9, no. 8, pp. 1735–1780, 1997.
[19] J. Chung, C. Gulcehre, K. Cho, and Y. Bengio, "Gated feedback recurrent neural networks," in *Proceedings of the 32nd International Conference on Machine Learning (ICML)*, Lille, France, July 2015.
[20] G. Landrum, "RDKit: open-source cheminformatics software," 2016, https://www.rdkit.org/.
[21] Y. LeCun, Y. Bengio, and G. Hinton, "Deep learning," *Nature*, vol. 521, no. 7553, pp. 436–444, 2015.
[22] J. S. Delaney, "ESOL: estimating aqueous solubility directly from molecular structure," *Journal of Chemical Information and Computer Sciences*, vol. 44, no. 3, pp. 1000–1005, 2004.
[23] M. Wenlock and N. Tomkinson, "Experimental in vitro DMPK and physicochemical data on a set of publicly disclosed compounds," 2016.
[24] D. L. Mobley and J. P. Guthrie, "Freesolv: a database of experimental and calculated hydration free energies, with input files," *Journal of Computer-Aided Molecular Design*, vol. 28, no. 7, pp. 711–720, 2014.
[25] Zaharevd, "Aids antiviral screen data," 2004, https://wiki.nci.nih.gov/display/NCIDTPdata/AIDS+Antiviral+Screen+Data.
[26] G. Subramanian, B. Ramsundar, V. Pande, and R. A. Denny, "Computational modeling of β-secretase 1 (BACE-1) inhibitors using ligand based approaches," *Journal of Chemical Information and Modeling*, vol. 56, no. 10, pp. 1936–1949, 2016.
[27] T. Chen and C. Guestrin, "XGBoost: a scalable tree boosting system," in *Proceedings of the 22nd ACM SIGKDD International Conference on Knowledge Discovery and Data*, pp. 785–794, San Francisco, CA, USA, August 2016.
[28] B. Ramsundar, S. Kearnes, P. Riley, D. Webster, D. Konerding, and V. Pande, "Massively multitask networks for drug discovery," 2015, https://arxiv.org/abs/1502.02072.
[29] J. Gilmer, S. S. Schoenholz, P. F. Riley, O. Vinyals, and G. E. Dahl, "Neural message passing for quantum chemistry," in *Proceedings of the 34th International Conference on Machine Learning (ICML'17)*, vol. 70, pp. 1263–1272, Sydney,Australia, August 2017.
[30] D. Duvenaud, D. Maclaurin, J. Aguilera-Iparraguirre et al., "Convolutional networks on graphs for learning molecular fingerprints," in *Proceedings of the 28th International Conference on Neural Information Processing System (NIPS'15)*, vol. 2, pp. 2224–2232, Montreal Canada, December 2015.
[31] S. Kearnes, K. Mccloskey, M. Berndl, V. Pande, and P. Riley, "Molecular graph convolutions: moving beyond fingerprints," *Journal of Computer-Aided Molecular Design*, vol. 30, no. 8, pp. 595–608, 2016.
[32] W. Hu, B. Liu, J. Gomes et al., "Strategies for pre-training graph neural networks," in *Proceedings of the eighth International Conference on Learning Representations (ICLR'20)*, Addis Ababa, Ethiopia, April 2020.
[33] M. Abadi, P. Barham, J. Chen et al., "TensorFlow: a system for large-scale machine learning," in *Proceedings of the 12th USENIX Conference on Operating Systems Design and Implementation. ser. OSDI 2016*, pp. 265–283, USENIX Association, Savannah, GA, USA, November 2016.
[34] D. P. Kingma and J. Ba. Adam, "Adam: a method for stochastic optimization," in *Proceedings of the third International Conference on Learning Representations (ICLR'15)*, San Diego, CA, USA, May 2015.

Hindawi
Computational Intelligence and Neuroscience
Volume 2022, Article ID 8075708, 10 pages
https://doi.org/10.1155/2022/8075708

Research Article

"OBE" Concept for New Training Mode of Electronic Information Science and Technology Professionals under Big Data Analysis

Jifeng Liang

Xi'an Fanyi University Engineering & Technology College, Xi'an 710100, China

Correspondence should be addressed to Jifeng Liang; ljf348041879@163.com

Received 8 December 2021; Revised 26 December 2021; Accepted 28 December 2021; Published 27 January 2022

Academic Editor: Xin Ning

As an educational concept based on learning output, OBE (Outcome-Based Education) is student-centered and emphasizes students' personal progress and learning achievement. Based on BD (big data) analysis, this paper proposes a new talent training mode for the electronic information science and technology specialty. This model employs BD analysis technology to examine the correlation index between social demand and talent cultivation, based on the employment situation of students in the country in previous years. The teaching reform was carried out under the OBE concept, and a new training scheme was formed. Training objectives, graduation requirements, curriculum system, and continuous improvement mechanism were all determined. This paper proposes an algorithm for determining the degree of similarity between the knowledge required by the organization and the knowledge held by its employees. The person with the highest similarity is identified as the training candidate by the algorithm, and the training candidate is then trained according to the knowledge that the organization requires. Talent training in the field of electronic information science and technology has yielded positive results.

1. Introduction

The development of a talent training scheme is a crucial link in university talent training, as well as a vehicle for innovating talent training modes and improving talent training quality [1]. The key to developing a professional talent training plan is to establish talent training objectives, such as professional employment positions, professional skills and qualities that graduates should possess, etc., to create a talent training objective system with specific characteristics, and then to develop a professional talent training plan to enable graduates to acquire corresponding employment skills. Current teaching methods place an excessive amount of emphasis on book knowledge mastery, neglect practical application of knowledge, and are unable to guide students' creative thinking through engineering cases. Traditional examinations continue to dominate the assessment method, while process evaluation and formative evaluation are still in their infancy.

OBE (Outcome-Based Education) is a kind of educational concept oriented to students' learning outcomes, which emphasizes that engineering education must focus on students' achievement of expected learning outcomes. In the whole OBE teaching concept, students are always the center of education and highly involved, and all teaching links are carried out around students. Guiding the reform of engineering education with the concept of OBE education is conducive to solving the problem of mismatch between the current graduates' abilities and social needs and has practical significance [2]. Engineering talents, as the internal driving force of social development, have a profound impact on China's scientific and technological development level and people's quality of life [3, 4]. Engineering talents trained by local engineering colleges are of vital significance to local economic development and national engineering construction. At present, scholars' research on talent training quality evaluation mainly focuses on talent training quality standard, evaluation subject, evaluation index system, evaluation mechanism, evaluation system, and so on and has achieved certain research results [5]. However, there are still many problems, such as limited access to evaluation information and lack of in-depth analysis due to the single evaluation method, the lack of scientific evaluation index system, the inefficacy of fairness and authority of evaluation results in practice, and the lack of objectivity of evaluation, which leads to low reliability, insignificant validity, and the difficulty of practical results [6, 7].

The performance evaluation and information construction of education have become the driving force for the development of current university education as a result of the information age's impact. However, as university teaching levels improve, BD (big data) analysis is required to scientifically evaluate teaching performance in the practice of the training mode of talents majoring in electronic information science and technology, and how to improve the scientificity and effectiveness of performance evaluation through the digital network platform is the focus of this paper. A new talent training model for electronic information science and technology is proposed in this paper based on BD analysis. A more perfect talent training scheme is designed to provide a more scientific training mode for the training and output of national high-end technical talents by analyzing subjective and objective influencing factors.

The creative point of this research is as follows: this paper adopts the technical platform of big data analysis, based on the theory of constructing the evaluation index system of talent cultivation quality suitable for the collection and analysis of big data evaluation model, and then collects and analyzes data through the construction of functional modules, taking a university as an example to get the evaluation results. After repeated several times, a relatively perfect big data evaluation model can be formed, which is more widely used in the evaluation of talent cultivation quality in universities.

2. Related Work

Literature [8] discusses in detail the origin, essence, system, and principles of foreign OBE educational ideas and preliminarily realizes the advantages of OBE educational ideas in personnel training. Literature [9] pointed out that the results-oriented education should be reflected in the process of making clear the teaching purpose, making the teaching plan, implementing, and evaluating it. OBE, as a good belief, atmosphere, and method, is worth learning and learning from higher education in China. Literature [10] tries to learn from the American results-oriented education model, help you understand its theoretical composition, formation process, and manifestation, and promote the localization process of results-oriented education by analyzing the feasibility of learning from China. Literature [11] points out as follows: in the future, the development of a flexible, high-level, and sustainable OBE education concept should be promoted. Literature [12] focuses on the analysis of the problems existing in the training mode of applied talents and advocates the introduction of OBE education concept into the training process of applied talents from three aspects: students' expected learning outcomes, assessment system of learning outcomes, and practical teaching system of applied talents. Literature [13] emphasizes that local engineering colleges should take various forms to contribute to local development, train high-quality undergraduate students for local industrial development, and give full play to their advantages to run several influential disciplines in China. Literature [14] mainly discusses and studies how to define the training orientation in local engineering colleges. This paper defines the local engineering colleges from four aspects: the purpose of running a school, the type level, the scale of running a school, and the development goal. Literature [15] puts forward the idea of applying OBE concept to the curriculum system reform of local engineering colleges, but the particularity of this subject of local engineering colleges is not clear in the specific suggestions.

One of a university's main functions is talent cultivation, and the quality of talent cultivation is the focus of the university's overall quality. It does not exist in isolation at the university but is influenced by a variety of other factors. It has a lot of connotations and can react to the university's talent cultivation, so more research on the quality of talent cultivation is needed. According to literature [16], our universities have first experienced the quality concept of knowledge, then the quality concept of ability, and finally the diversified quality concept since the founding of the People's Republic of China. According to literature [17], the quality concept of university talent cultivation should be appropriate to meet students' continuous growth. According to the literature [18], talent training quality must be evaluated from a multidimensional and three-dimensional perspective. According to literature [19], in the evaluation process, the relationship between the university and society should be strengthened, and the appropriate evaluation mechanism and indicators should be established as a result. Literature [20] attaches importance to the use value of talents, and puts forward that evaluating the quality of talent training should meet the needs of the country and society, and should meet certain standards in the degree of conformity. According to literature [21], this paper evaluates the quality of talent training in universities from three aspects: training conditions, training process, and training effect, using analytic hierarchy process. According to literature [22], the fuzzy comprehensive evaluation method in the management model is used to analyze the quality of talent cultivation in universities. Literature [23] divides the evaluation modes of Chinese universities from the philosophical evaluation theory, the stakeholder theory of economics, and the diversified concept of evaluation subjects of pedagogy and puts forward the strategies of authentication mode, ranking mode, and evaluation mode for the construction of university evaluation modes.

3. Research Method

3.1. Design of a New Training Mode for Electronic Information Science and Technology Professionals Based on BD Analysis. OBE focuses on the training of professionals, which usually includes three stages (Figure 1).

The first step is to determine a graduate's professional postgraduation ability. To solve the problem of what kind of people the major trains, identify the target position of professional training, highlight professional characteristics, and analyze and refine the professional skills required by the

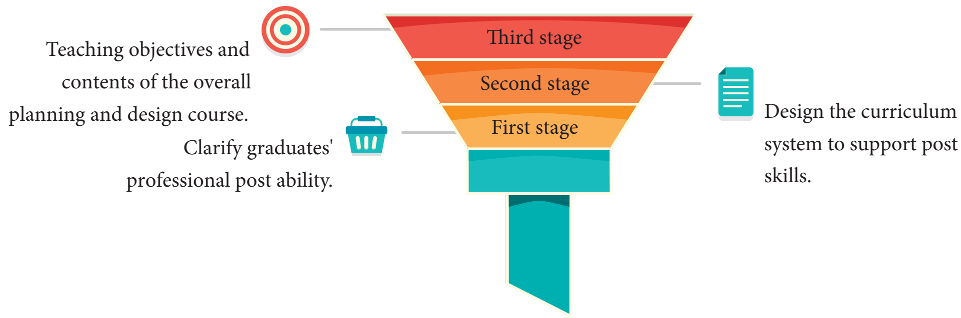

Figure 1: Three stages of personnel training of OBE concept.

major. The second step is to create a curriculum system that supports postsecondary skills. A reasonable curriculum system with ability expansion and extension is designed on the basis of clarifying job skills, guided by OBE education thought, focusing on the cultivation of students' ability literacy and quality literacy, in order to clarify the role of each course in achieving the training goal and solve problems such as why students should learn these contents. Third step is strong pertinence and adaptability in the overall planning and design of curriculum teaching objectives and teaching contents. The course teaching objectives are determined by the knowledge and skills needed to complete the work, in order to improve students' vocational skills and adaptability to the workplace, and to solve the problems of how to help students achieve these learning achievements, according to the needs of personnel training.

According to the training objectives and graduation requirements of computer electronic information science and technology specialty, combined with the general standard of engineering education certification and the supplementary standard of computer specialty, and according to the OBE education concept, the student-centered curriculum system is designed and constructed reversely.

Corresponding to the graduation requirements, build a modular curriculum system which is oriented by ability training, pays attention to knowledge application and quality training, and embodies interdisciplinary integration. The curriculum system consists of general education, professional education, quality development, and innovation and entrepreneurship [24], as shown in Figure 2.

In Figure 2, the general education module courses are set according to the relevant national requirements, general standards and supplementary standards of computer, and electronic information science and technology specialty of engineering education certification.

The module of engineering foundation and specialty foundation must conform to the "National Standard for the Teaching Quality of Computer Science and Technology in Ordinary Colleges and Universities" formulated by the Teaching Steering Committee of the Ministry of Education and cultivate students' professional basic abilities such as computational thinking, program design and implementation, algorithm analysis and design, system ability, etc., which can solve practical problems [25].

The major's optional module includes a number of hot technical courses as well as professional knowledge development courses. Students can choose a number of courses that satisfy the credit requirements based on their personal interests and development goals. Artificial intelligence, pattern recognition, Linux system operation and maintenance, information retrieval, digital image processing, and other topics are among the topics covered. To improve the integration between teaching and employment, talent education and training programs should be integrated with practical occupations, a "dual" education mechanism should be built, and new teaching and training programs should be set up according to actual occupational needs. Simultaneously, schools and businesses must improve their communication and collaborate to develop new education and training courses that meet the needs of talent development and businesses.

The essence of personnel training is to enable personnel to master new knowledge. Therefore, after analyzing the above problems from the perspective of knowledge, it is found that the content of personnel training should be the knowledge needed by the organization, and the identified candidates should be the personnel who are closest to the knowledge needed by the organization. Therefore, the process of organizing personnel training can be divided into as follows.

Firstly, the knowledge needed by the organization is determined, then the personnel closest to the knowledge needed by the organization are identified as training candidates, and then the training candidates are trained according to the determined knowledge needed by the organization. According to the relationship between the knowledge network and the personnel network, the knowledge easily lost by the organization can be determined by quantitative calculation. On this basis, the areas easily lost by the organization can be determined, and then the knowledge needed by the organization can be determined according to the actual situation of the organization.

Easy-to-lose knowledge refers to the knowledge owned by very few people in the organization. With the loss of people, this knowledge is easy to lose. The judgment formula of easy-to-lose knowledge is as follows:

$$L(ke) = \left\{ke_i \middle| \left|P(ke_i)\right| \leq \mathrm{thr}(\mathrm{elk})\right\}. \tag{1}$$

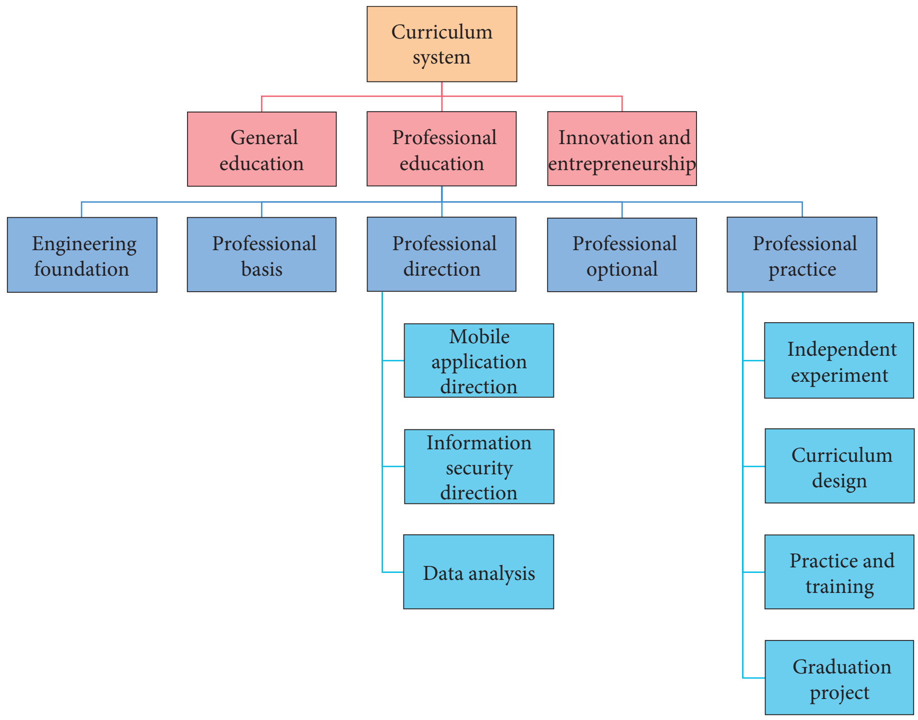

Figure 2: Curriculum system composition.

Among them, thr(elk) is the set threshold; when $|P(ke_i)| \leq \text{thr}(\text{elk})$, it is considered that ke_i is easy to lose knowledge. Ideally, $\text{thr}(\text{elk}) = 1$. Easy-to-lose knowledge needs to be repaired and stabilized in time, and its judgment is helpful to recognize the weak links of organizational knowledge.

After clustering $L(ke)$, a faction is formed, and the faction is regarded as a domain. Let $C_i(K)$ represent the set of knowledge elements that are easy to lose in domain C_i and judge whether C_i is a domain that is easy to lose according to the degree of domain knowledge loss.

The loss degree of domain knowledge is defined as follows: $C_i(L)/|C_i|$, where $|C_i(L)|, |C_i|$, respectively, represents the number of elements in their respective sets. Therefore, it means the proportion of the number of easily lost knowledge elements in C_i to the total number of knowledge elements. The judgment formula of easily lost domain can be expressed as follows:

$$Lc(C) = \left\{ C_i \middle| \frac{\|C_i(L)\|}{|C_i|} \geq \text{thr}(\text{eld}) \right\}. \tag{2}$$

Among them, thr(elk) is the set threshold, and when $|C_i(L)|/|C_i| \geq \text{thr}(\text{eld})$ is used, C_i is considered to be an easy-to-drain field, and ideally $\text{thr}(\text{eld}) = 100\%$.

To determine the knowledge that the organization requires, combine the knowledge that is easy to lose with the field that is easy to lose, and then combine the actual situation of the organization. Following the determination of the knowledge that the organization requires, the training candidates must be identified. The VSM (vector space model) is a traditional text-based calculation. The similarity between the organization needing knowledge and the personnel possessing knowledge represented by knowledge can be abstracted into the similarity between knowledge subjects if both the organization needing knowledge and the personnel possessing knowledge are regarded as knowledge subjects. Fields are formed after the knowledge network is clustered, and the similarity of knowledge subjects is investigated through the lens of fields.

In matrix T, rows represent knowledge subjects and columns represent fields, so the field vector of P_i is expressed as T_i, so the Sim calculation based on the similarity between P_i and P_j of the field vector is shown in formula (3).

$$\begin{aligned} \text{Sim}\left(P_i, P_j\right) &= \cos\left(\vec{T}_{\text{i}}, \vec{T}_{\text{j}}\right) \\ &= \frac{\vec{T}_{\text{i}} \cdot \vec{T}_{\text{j}}}{\left\|\vec{T}_{\text{i}}\right\| \cdot \left\|\vec{T}_{\text{j}}\right\|} \\ &= \frac{\sum_{k=1}^{m} c_{ik} \times c_{ji}}{\sqrt{\left[\left(\sum_{k=1}^{m} c_{ik}^2\right) \sum_{k=1}^{m} c_{jk}^2\right]}}. \end{aligned} \tag{3}$$

When calculating the similarity, it needs to be calculated first according to the similarity algorithm based on the domain, then calculate it according to the similarity algorithm based on the VSM, and then make a comprehensive judgment according to the results. The similarity algorithm based on the VSM is a classic algorithm, with guaranteed accuracy and recall rate.

3.2. BD Evaluation Model of Talent Cultivation. The BD evaluation model includes two aspects in the evaluation of talent training quality: one is the theoretical basis, that is, the index system and the second is the technical route, that is, the functional module. In the process of construction, it is necessary to write the theoretical basis, that is, the evaluation index system, into the background operation module of the model, which is reflected in the compilation of the underlying code.

From an intuitive point of view, the formation process of the evaluation model is a process of "conditional input, analysis tools, analysis methods, output results, result interpretation, model test, model correction and improvement."

In the process of building the concrete evaluation model, the main steps in the analysis mode are as follows: the first step, the acquisition scheme of evaluation data information, mainly through the crawler code to retrieve data and obtain evaluation information, and through the vertical search engine to trace the evaluation data layer by layer, obtain a certain amount of evaluation information and archive it to form the original database. The intuitive flow of BD model research is shown in Figure 3.

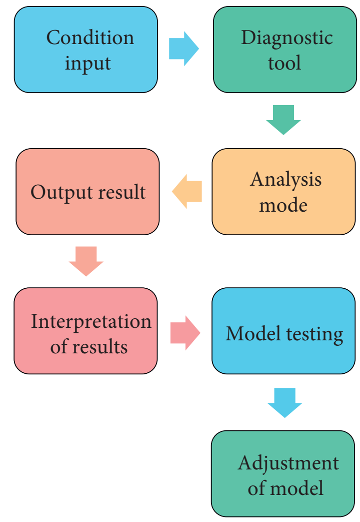

Figure 3: Flowchart of BD evaluation model construction.

To improve the integration between teaching and employment, talent education and training programs should be integrated with practical occupations, a "dual" education mechanism should be built, and new teaching and training programs should be set up according to actual occupational needs. Simultaneously, schools and businesses must improve their communication and collaborate to develop new education and training courses that meet the needs of talent development and businesses. Then, according to the training results, the school conducts secondary theoretical training for students' shortcomings to realize the cooperation between classroom and practice, and enterprises should provide training bases for students to enhance their practical operation ability; finally, the school conducts secondary theoretical training for students' shortcomings to realize the cooperation between classroom and practice.

According to the above-mentioned teaching mechanism, the calculation formula of students' training investment index under the new mechanism is as follows:

$$p = \frac{\lambda \cdot \mu f(p) - \Delta f}{\sqrt{m} \cdot (b_1 + b_2)}, \tag{4}$$

where p represents the investment index; λ represents the correlation index between social demand and talent cultivation; μ represents the deterioration index when learning engagement is low; F $f(p)$ represents a quantitative analysis function; Δf represents analysis error; m represents the index change value; b_1 said enterprise training investment parameters; and b_2 indicates the impact index of the improved educational mechanism.

Rebuild the talent cultivation teaching system based on the obtained indicators, which includes developing a modular curriculum system between schools and businesses; establish a task-based teaching and training procedure; and create training programs that are multichannel, multilevel, and multicategory. To achieve a diversified and systematic teaching system, create a centralized task-oriented training mode. Students' achievement is an important standard to measure students' mastery of knowledge in the process of cultivating talents in the electronic information science and technology specialty. Students with abnormal learning status are identified through outlier algorithm analysis of their scores, and managers provide personalized guidance to these students. At the same time, the neural network model is used to predict the scores of key subjects for these students with abnormal learning status, and targeted learning is carried out for the subjects with problems.

The Adagrad algorithm can obtain small learning updates for nonsparse features according to different learning rates for each parameter, and on the contrary, obtain large learning updates. So, this optimization algorithm is more suitable for dealing with sparse feature data. For the Adagrad algorithm, the update iteration method is as follows:

$$\theta_{t=1,i} = \theta_{t,i} - \frac{n}{\sqrt{G_t + \varepsilon}} \cdot g_{t,i}, \tag{5}$$

where $G_t \in R^{dd}$ is a diagonal matrix, where diagonal element e^{ii} represents the sum of squares of the gradient of the i-th parameter θ_i from the past to the present, and ε is the smoothing parameter.

Adam (Adaptive Moment Estimation) is also a method to determine the gradient descent at different rates according to different parameters. Its calculation is different from the historical gradient attenuation, and the historical square attenuation is not used. Its attenuation mode is similar to momentum, as follows:

$$\begin{aligned} m_t &= \beta_1 m_{t-1} + (1 - \beta_1) g_t, \\ v_t &= \beta_2 v_{t-1} + \left(1 - \beta_2 g_t^2\right), \end{aligned} \tag{6}$$

m_t, v_t is the weighted average and weighted deviation of gradient, respectively, and the initial value is 0 vector. Adam's researchers found that they are close to 0 vector, especially when the attenuation factor β_1, β_2 is close to 1. In order to solve this problem, the deviation of m_t, v_t is corrected:

$$\widehat{m}_t = \frac{m_t}{1-\beta_1^t},$$
$$\widehat{v}_t = \frac{v_t}{1-\beta_2^t}. \tag{7}$$

Finally, Adam's update equation is as follows:

$$\theta_{t+1} = \theta_t - \frac{\eta}{\sqrt{\widehat{v}_t + \varepsilon}}\widehat{m}_t. \tag{8}$$

In order to know the students' learning situation and find out the problems in the teaching process in time, some courses adopt the formative evaluation method of unit test. Teachers can get timely feedback in the teaching process, adjust teaching plans, and improve teaching methods at any time. Finally, at the end of each course, a questionnaire survey was conducted on the achievement of the course objectives of the course ε.

4. Results Analysis and Discussion

4.1. Evaluation Results of Talent Training Quality. The above contents of this paper have completed the theoretical and technical construction of BD evaluation model. Here, a case study of the actual utility of this evaluation model is made, that is, the application of BD evaluation model. By applying the evaluation model to practical cases, the corresponding evaluation results are obtained, and the availability of the evaluation model is evaluated reasonably by analyzing the evaluation results.

On the evaluation of personnel training quality by employers, the index scores are shown in Figure 4.

Through the analysis of Figure 4, it can be concluded that in terms of fairness, due to the lack of BD collection technology and scoring dictionary in this study, there may be some errors with the real situation, so the results presented in this figure are only a reference and partly reflect the objective truth of the talent training quality of this school. In the interpretation of the diagram, based on the knowledge and understanding of the major of electronic information science and technology, the specific interpretation conclusions are as follows.

The four subindicators have little difference in scores among the ideological and moral indicators, but the gap from the full score is still not a high score. The index design of this study played a role in the formation of this result. Because this study focuses on evaluating graduates' employability, social adaptability is primarily reflected in aspects of knowledge, ability, and other characteristics that are easy to examine and quantify, resulting in less evaluation information in ideological and moral aspects. This school's students excelled in terms of creativity and practical ability. As a student at this school, I can see election notices and good news about various innovation competitions on campus based on my knowledge of the school. This school has put in a lot of effort to develop innovative students. In terms of social practice, the school is the only university in the area with a bachelor's degree or higher, and it has a significant influence in the community. As a result, a variety of businesses, communities, and other institutions and organizations are willing to collaborate with the school to organize social practice activities that will enrich the lives of college students. In terms of social ability, this school's students' international ability was praised and scored highly. The social evaluation data show that the students in this school have a good work attitude, but there are some areas where employers criticize them. For example, despite students' short-term job-hopping behavior, their overall performance in this school is above average. On the one hand, this achievement is due to the balanced dilution of data in statistics; on the other hand, it also reflects students' lack of adaptability after work, or a lack of career education in this field in university talent development.

Specifically, in this study, because in the setting of the index system, in addition to the connotation of the index, there is also the consideration of the index weight; here, the product obtained by multiplying the scores of ten first-level indexes by their weights indicates the importance of the index in the whole evaluation system, as shown in Figure 5.

Through the analysis of Figure 5, it can be known that in the process of evaluating the quality of the training of electronic information science and technology professionals, the graduates of this school have received the most attention in terms of knowledge quality, social ability, and employment status, while the network evaluation has not paid much attention to students' entrepreneurship, students' source, further study, and ideological status. This result also enlightens us that in the evaluation of talent training quality, pay attention to the employability and employment status of talents, and explore the evaluation of talent training quality from the specific connotation of these indicators.

Take the employment statistics of students in the proposed talent training mode as the experimental group and the employment statistics of students in the traditional talent training mode as the control group. Figure 6 shows the test results.

By analyzing the above two groups of test results, it can be seen that under the application of the talent training model of BD analysis, students can improve their own technical level by strengthening practical training ability. At the same time, because this mode adjusts the teaching mode in time according to the market demand for talents, it makes the students' professional skills match with the social needs, thus increasing the number of employed people.

However, students who study under the traditional talent training mode are not fully trained in practical courses, and do not dig out the characteristics of correlation indexes between society and talent technology, which leads to the deviation between students' personal skills and social needs, which leads to poor matching effect, and then affects students' employment.

4.2. Neural Network Model Predicts the Scores of Outlier Students. Before designing the neural network model, the data need to be further preprocessed. Organize the course scores, classify the course scores according to students, and cut out unnecessary data fields and some courses in the

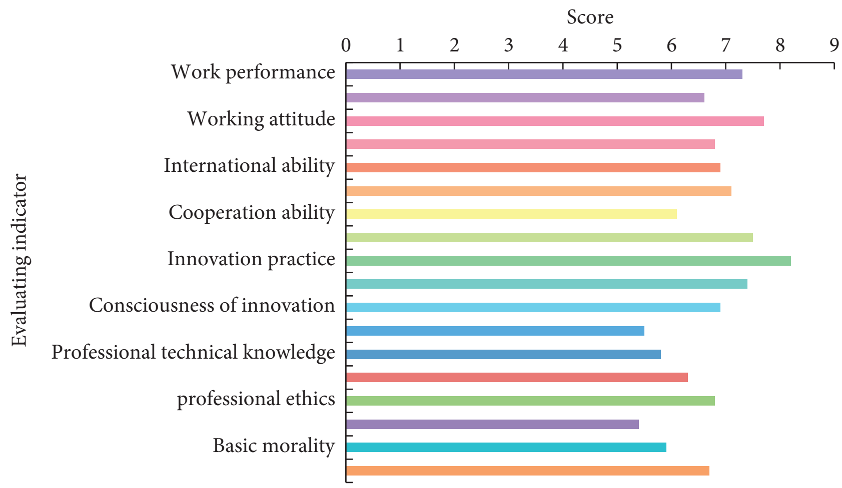

Figure 4: The evaluation index score of personnel training quality of employers.

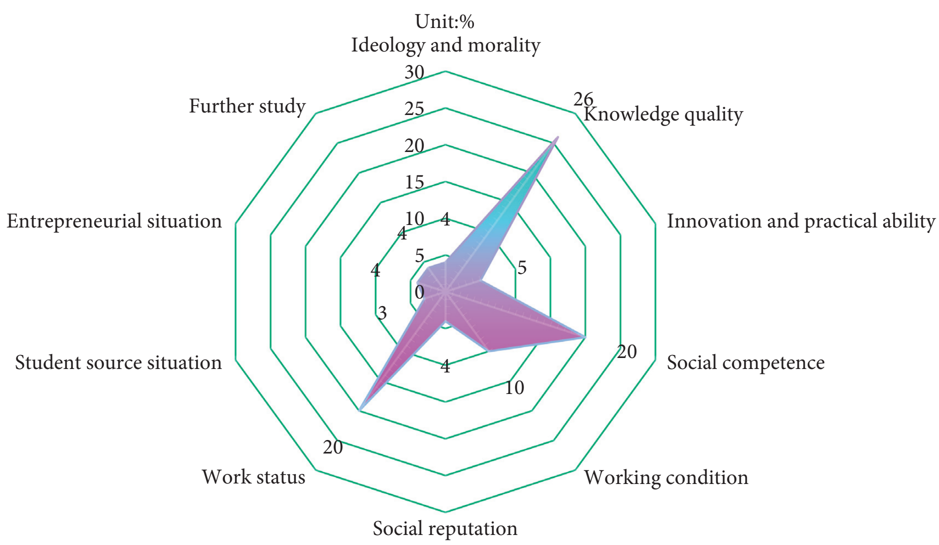

Figure 5: Proportion of indicators in importance.

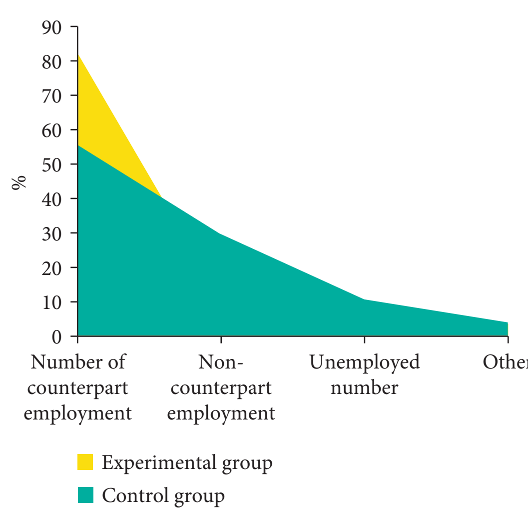

Figure 6: Test comparison results.

Table 1: Setting of neurons in each layer.

Number of experimental groups	First hidden layer	Second hidden layer	Third hidden layer
1	10	5	5
2	50	10	10
3	100	50	10

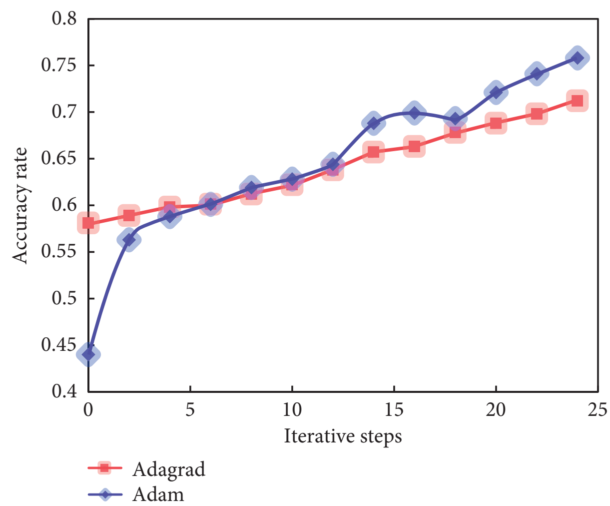

Figure 7: Algorithm comparison.

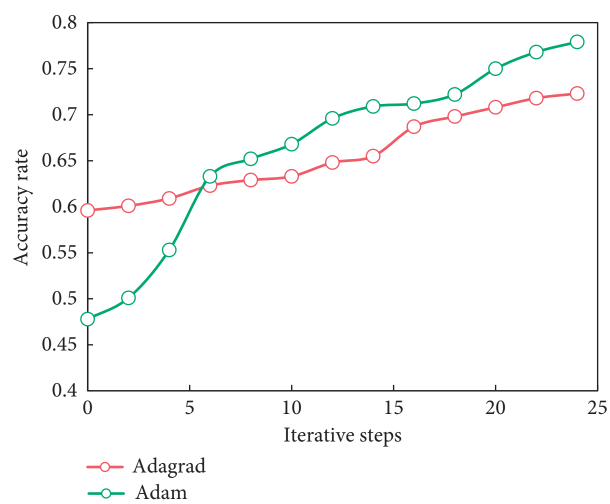

Figure 8: Algorithm comparison.

model design. Finally, the scores are processed, and the data are integrated according to three categories (the historical scores of the first five semesters of study courses, the name of target courses, and the category of target courses). When designing the neural network, the input layer inputs the scores of a certain student in the last semester, and the input dimension is 15. Finally, the probability of the category of the target course score is calculated through the Softmax layer. In the process of designing the neural network, three groups of experiments were designed. The number of neurons in each layer is shown in Table 1.

Through different optimizers, when the number of units in the first hidden layer is 10, the number of units in the second hidden layer is 5, and the number of units in the third hidden layer is 5, the accuracy of the classification results changes with the increase of iteration steps in the training process, as shown in Figure 7.

Similarly, when the number of the first hidden layer, the second hidden layer, and the third hidden layer are 50, 10, and 10, respectively, the change of the correct rate of the training set with the increase of the number of iterations is shown in Figure 8.

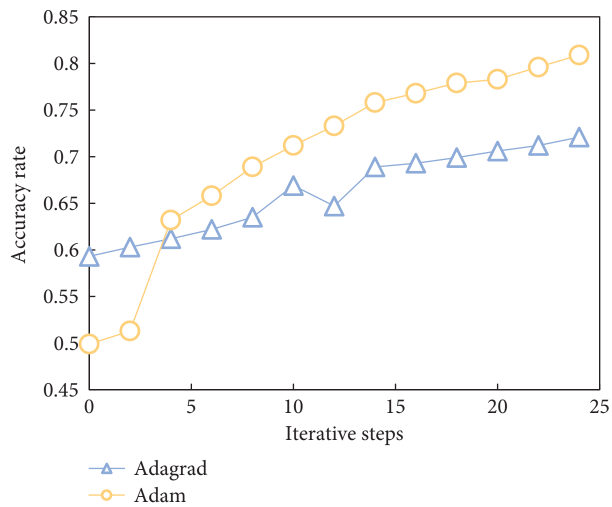

Figure 9: Algorithm comparison.

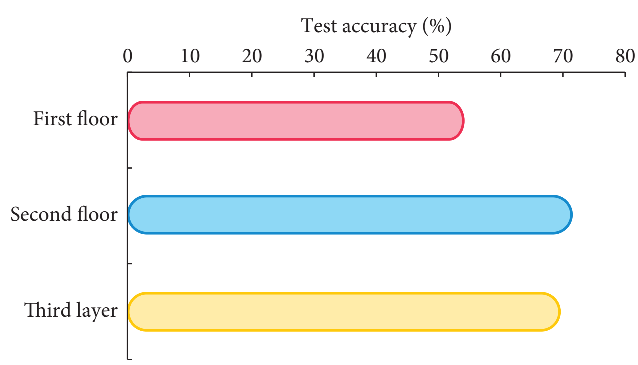

Figure 10: Test set accuracy rate.

Similarly, when the number of units in the first hidden layer, the second hidden layer, and the third hidden layer is 100, 50, and 10, the number of iterations increases, and the change of accuracy rate is shown in Figure 9.

It can be seen from these figures that with the increase of iteration times, the correct rate of training is constantly increasing, and the increasing trend is basically caused by different optimization algorithms. It is found that the Adam algorithm is better than the Adagrad algorithm in the training process.

When testing, the correct rate of Adam gradient update method is shown in Figure 10.

It is found that increasing the number of parameters will make the neural network model easier to over-fit, while too few parameters will make the model underfit. Finally, the Adam gradient updating method is used. The number of neurons in the first, second, and third hidden layers is 50, 10, and 10, respectively, as the final model.

5. Conclusion

The goal of OBE is to rebuild the curriculum system and update the curriculum training objectives to reflect changes in the industry, social needs, and the target orientation of skilled talent training. This paper examines the training model of electronic information science and technology professionals in universities with a BD background from various perspectives and performance evaluation frameworks, avoiding the blindness of university informatization decision-making, maximizing the scientific nature of large numbers, and laying a strong foundation for Chinese universities' modernization. In terms of data processing, the big data evaluation model is used to actively capture evaluation data on the network, and the importance of each index is scored using the emotion dictionary, after which the computer uses big data analysis technology to complete the comprehensive score of each index. Applying the OBE concept to BD technology and application talent training is a comprehensive reform of university talent training that also serves as a model for the training of professionals in electronic information science and technology.

The analysis of research status and specific application of OBE at home and abroad in this paper is not detailed enough, and some suggestions for improvement are too one-sided and general, and need to be further deepened and refined, due to the limited level of self-ability, which is limited by reference materials, number of articles, and writing time.

Data Availability

The data used to support the findings of this study are included within the article.

Conflicts of Interest

The author declares that there are no conflicts of interest.

Acknowledgments

This study was supported by Key Project of Education and Teaching Reform Research of Xi'an Fanyi University in 2020 Research on the New Training Mode of Electronic Information Science and Technology Specialty under the Background of New Engineering (J20A04) and 2021 Foundation Project of Xi'an Fanyi University "Artificial Intelligence Technology Application Research Team" (Project No. XFU21KYTDB02).

References

[1] C. Yang, L. Li, and H. Jia, "The construction of a tree-shaped talent training plan and goal based on the OBE concept and the way to achieve it," *Polymer Bulletin*, vol. 4, no. 4, p. 5, 2020.
[2] Z. Wang, "The reform and exploration of the training model for entrepreneurs and entrepreneurs based on the OBE concept: taking the Computer Application Technology Major of Huangshan Vocational and Technical College as an example," *Education Teaching Forum*, vol. 12, no. 12, p. 2, 2020.
[3] L. Zhang, Y. Chen, and C. Zhang, "The formulation and implementation of higher vocational talent training programs based on the OBE concept-taking e-commerce technology as an example," *Journal of Shijiazhuang Vocational and Technical College*, vol. 031, no. 2, pp. 22–24, 2019.
[4] J. Hu, B. Pan, and M. Zhang, "Research on the cultivation of engineering talents' leadership based on the OBE concept:

taking the course of engineering innovation design methodology as an example," *Education Teaching Forum*, vol. 45, no. 45, p. 3, 2017.

[5] Bo Wang, "Research on the quality evaluation system of talent cultivation in applied universities based on the OBE concept," *Journal of Science & Technology Economics Guide*, vol. 28, no. 30, pp. 195-196, 2020.

[6] Y. Wang, "Research on cross-border e-commerce talent training model based on OBE concept," *Education Modernization*, vol. 5, no. 48, pp. 32-33+40, 2018.

[7] S. Ma, "Research on the teaching reform of higher vocational statistics course based on OBE concept," *Modern Education Forum*, vol. 4, no. 8, pp. 48–50, 2021.

[8] C. Li, "Research on the design of animation talent training program based on OBE concept," *Journal of College Education*, vol. 8, pp. 168–171, 2021, In press.

[9] J. Peng and Q. Wu, "Innovative exploration of the practice teaching mode of legal talent cultivation based on the OBE concept," *Educational Observation*, vol. 10, no. 25, p. 4, 2021.

[10] B. Wang and W. Luo, "Exploration of the reform of the electric talent training system based on the OBE concept," *University Education*, vol. 8, no. 8, p. 3, 2021.

[11] X. Luo, "Innovation of talent training path in colleges and universities based on OBE concept," *Forum on Industry and Technology*, vol. 19, no. 20, p. 2, 2020.

[12] M. Li, D. Yueli, Z. Yunfei, and X. Yingdong, "Research on professional talent training mode on data science and big data technology in local application-oriented universities," in *Proceedings of the 2021 International Conference on Big Data Engineering and Education (BDEE)*, pp. 56–59, IEEE, Chengdu, China, August, 2021.

[13] F. Wang, "The construction and implementation of the evaluation mechanism of talent training goals based on the OBE concept: taking the secondary vocational tourism service major as an example," *Tomorrow Fashion*, vol. 16, no. 16, p. 2, 2019.

[14] X. Zhang and J. Hu, "Design of practical teaching system for human resource management based on OBE concept," *Laboratory Research and Exploration*, vol. 37, no. 6, p. 6, 2018.

[15] X. Han, Z. Yao, Y. Jin et al., "Thoughts on the reform of the biotechnology talent training model based on the OBE concept," *Contemporary Educational Practice and Teaching Research: Electronic Edition*, vol. 7, no. 7X, p. 1, 2017.

[16] H. Shen, "Research on the training mode of applied talents for drama major in local colleges based on OBE concept——taking guangxi university of arts as an example," *Art Education*, vol. 12, no. 12, p. 2, 2017.

[17] X. Sun and Y. Wu, "Civil engineering teaching reform and practice based on OBE teaching concept," *Shanxi Architecture*, vol. 43, no. 14, p. 3, 2017.

[18] Y. Cheng, Y. Wang, and B. Zhang, "Innovation and practice of clinical medical talent training model based on OBE concept," *Chinese Medical Ethics*, vol. 33, no. 5, p. 6, 2020.

[19] W. Weixian and J. Zhang, "Thoughts and explorations on the training mode of senior talents in the international financial market based on the OBE concept," *Finance*, vol. 21, no. 21, p. 2, 2018.

[20] J. Jing, L. Ma, and X. Liu, "Cultivation of civil engineering talents based on OBE concept and condensing of advantageous scientific research directions," *Education Modernization*, vol. 6, no. A0, pp. 7-8, 2019.

[21] Z. Zhang, B. Shen, and Z. Ren, "Construction of a talent training program for environmental protection equipment engineering professionals based on the OBE concept: taking Hebei University of Technology as an example," *Education Modernization*, vol. 7, no. 16, pp. 8-9, 2020.

[22] M. Liu, "The practice of training talents in Chinese education based on the OBE concept ——take the Chinese Language and Literature (Teacher) major of Lishui University as an example," *Journal of Lishui University*, vol. 40, no. 1, p. 6, 2018.

[23] L. Fan and Y. Sun, "Dual tutor system: a new mechanism for training law students based on the concept of OBE," *Legal System Expo*, vol. 28, no. 28, p. 2, 2017.

[24] K. A. Meerja, P. V. Naidu, and S. Kalva, "Price versus performance of big data analysis for cloud based internet of things networks," *Mobile Networks and Applications*, vol. 9, no. 9, pp. 1–17, 2019.

[25] R. G. Madhukar and R. Dharavath, "DSSAE-BBOA: deep learning-based weather big data analysis and visualization," *Multimedia Tools and Applications*, vol. 5, no. 5, pp. 1–23, 2021.

Hindawi
Computational Intelligence and Neuroscience
Volume 2022, Article ID 8241241, 10 pages
https://doi.org/10.1155/2022/8241241

Research Article

Research on Multifeature Intelligent Correction of Spoken English

Yanyan Luo

School of Foreign Languages, Hefei Normal University, Hefei 230601, China

Correspondence should be addressed to Yanyan Luo; luoyanyan0823@163.com

Received 14 December 2021; Revised 1 January 2022; Accepted 8 January 2022; Published 27 January 2022

Academic Editor: Xin Ning

For a long time, college English teaching in many Chinese universities has focused on cultivating students' reading abilities while ignoring the cultivation of students' speaking abilities, leaving many non-English majors unable to communicate in English even after years of English study. This paper outlines the entire design and development process for an intelligent correction system for spoken English, with a focus on the methods for implementing the functions of spoken English examination, question bank management, and marking. A multifeature fusion of SE (sample entropy) and MFCC (Mel frequency cepstrum coefficient) based speech emotion recognition method is proposed. It denotes the rate at which the SE nonlinear dynamic system generates new data. It can be used to describe the dynamic fluctuation of speech signals in response to various emotions. To process SE and its statistics, as well as MFCC, and calculate the probability that they belong to one of six emotions, the support vector machine is used. The spoken English recognition algorithm described in this paper has obvious performance improvements in many indicators, according to the experimental evaluation.

1. Introduction

At present, computer-aided evaluation system has gradually become one of the research hot spots [1]. Especially in large-scale examinations, it has begun to gradually replace teachers, which will become a major change in education. With the development of speech recognition technology, the speech evaluation system is also developing gradually. In spoken English recognition, the original phonetic training data is not accompanied by any language information. Therefore, the language information itself must be estimated during training [2, 3]. The method of discovering language categories is valuable for their potential application and theoretical insight. Therefore, spoken English has always been one of the main concerns in linguistics, rhetoric, discourse analysis, and corpus linguistics [4]. People study spoken English from many angles, including the description of the linguistic features of spoken English.

There are some features of pronunciation that Chinese English learners overlook, and there is no lack of neglect of some features in spoken English, which makes it the bottleneck for improving their spoken English level. It is uncommon to record the candidates' answers on the spot in a traditional oral exam [5, 6]. This makes it impossible to recreate the examinee's examination situation to other teachers or classmates at the time, as well as to comment on the examinee's answers at the time, and other candidates are unable to benefit from the examinee's experience and lessons [7]. For oral question-and-answer types, there are two methods of scoring: one is based on pronunciation, and the other is based on text. Pure speech scoring focuses on acoustic characteristics like pronunciation, frequency, and rhythm [8, 9]. This method, on the other hand, can be effective in limiting the types of speaking content. However, it is a little out of reach for open questions. The development of a multifeature fusion evaluation algorithm for spoken English based on speech recognition, natural language processing, and data fusion will pave the way for the development of an automatic spoken English evaluation system that can interact with users [10]. The learning efficiency of spoken English will be greatly improved by systematically imitating people's ways of thinking, evaluating users' spoken English, and providing suggestions.

This paper will look at audio processing, speech recognition, and intelligent English correction technology and design and implement a multifeature intelligent automatic correction model based on data from a college language training system. The automatic correction model aims to address the issue of automatic correction of open oral English questions, reduce teacher correction pressure, and provide effective oral English learning guidance for students.

2. Related Work

Spoken English is a language feature system that meets the needs of English users' oral communication. The immediacy, immediacy, and improvisation of oral communication determine that spoken English has its distinctive and unique linguistic features. In [11] through the research on the application of automatic speech recognition system to non-native language speech training, it is pointed out that if appropriate methods are used and mispronunciation detection is added, the evaluation system can provide the same evaluation results as human experts. In [12] pronunciation evaluation is divided into three parts: similarity of pronunciation content, similarity of pronunciation and intonation, and score adjustment based on nonlinear attenuation. Literature [13] proposed an algorithm to find similar speech sequences. This algorithm is also based on dynamic time planning algorithm. Compared with [14], the starting point and ending point are predefined, and then the similar phonetic sequences are found to be different in predefined areas. Literature [15] calculates all possible similarities and then determines the boundary of subsequences according to the similarity changes between adjacent elements. Literature [16] lists the challenges to be faced by modeling the simulated human score from the process and result levels and points out that it is impossible to model the evaluation process comprehensively in the field of speech features and speech recognition at present. In [17] evaluating what the interlocutor said at the phoneme level has the advantages that it can accurately locate where the speaker's pronunciation is wrong, evaluate the similarity between what the speaker said and the target pronunciation, and find the systematic difference by comparing it with the standard phonetic database.

Literature [18] divides pronunciation evaluation into three parts: similarity of pronunciation content, similarity of pronunciation and intonation, and score adjustment based on nonlinear attenuation. Based on the technology of speech recognition and accent adaptation based on hidden Markov model, this paper studies the accuracy and fluency of phoneme pronunciation, gives the pronunciation quality score at phoneme level, and further obtains the score result of the whole sentence. In [19] in the research of the same automatic composition correction system, it is pointed out that some composition correction systems have great deficiencies in content-based feedback and have certain limitations, such as being unable to identify whether students' compositions are irrelevant. Literature [20] studies an improved speech recognition method based on deep learning [21], which effectively improves the relevance of human-machine scoring in the spoken language scoring system based on speech recognition. Literature [22] discusses the significance of automatic correction system for online correction of English compositions, because automatic correction of compositions can not only reduce the burden of teachers, but also respond quickly, and the correction time is in seconds. Moreover, the automatic correction system has a profound influence on the role orientation of students and teachers and the teaching mode. Literature [23] expounds a working principle of automatic correction system. In [24] using the traditional machine learning model, Hidden Markov Model, to process audio files, directly extract sound features from audio, and then combine them with the rules of oral English scoring, an intelligent scoring system for oral English test was developed. Their research is very respectable. Not only is the model training of machine learning complicated, but the processing of audio files is extremely difficult. Voiceprint recognition has always been an important and difficult point for many scientists. Finding the rules of human voice has a very far-reaching impact on speech recognition and machine translation.

3. Research Method

3.1. Design of Intelligent Correction System for Spoken English. The connection mode of the campus LAN (local area network) is adopted between the student computer and the server. Because, after the exam, the student computer needs to upload a large number of audio data files to the server, it is required to get the maximum network transmission bandwidth between the student computer and the server as much as possible to reduce the delay caused by network transmission. Therefore, adopting the campus LAN can ensure the smooth progress of the examination process.

The application of this system will greatly improve the efficiency of oral examination, reduce the inequality caused by human factors in the course of oral examination, reproduce the candidates' answers at that time, improve students' oral English level, reduce the work intensity of teachers, and increase the safety and reliability of the examination.

The main function of the system is the learning and testing of spoken English. This requires the system administrator to set the learning mode or testing mode. The functional requirements of the system are shown in Figure 1.

In learning mode, the user first enters the system through a visual window, then selects the appropriate question bank, activates the demonstration voice, and follows and practices the instructions. The voice prompt and error correction functions are currently available. When a user enters the system in test mode, the system selects questions at random to ensure that the exam is fair. The voice prompt and error correction functions are currently disabled. The examinee's login, checking the examinee's information, auditioning before the exam, random selection of test questions, answering recording, and uploading the answering recording after the oral exam are the main functions of the oral exam. On the student test machine, the recording is completed, then packaged, and uploaded to the server. The server creates a corresponding folder based on the student's student ID and stores the received files in the folder for teachers to review and use after receiving the uploaded files.

The statistical subsystem is the feedback of candidates' achievements to teachers. Its main job is to help teachers make statistics after obtaining a large number of test scores.

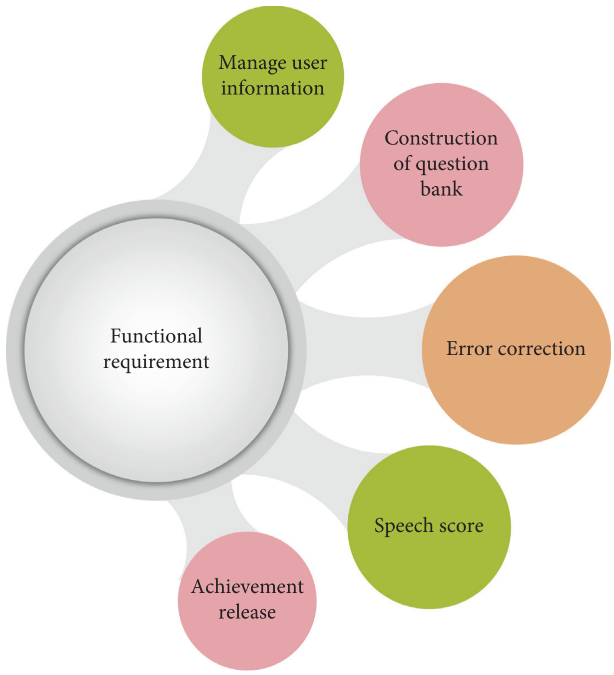

Figure 1: Functional requirements of the system.

Teachers will refer to the statistical results to better guide students to complete their studies and exams, so that they can achieve better results in future exams.

Computer-aided test system can help teachers or teaching administrators to design tests and generate test papers, implement tests under certain conditions, analyze tests, manage scores, and provide reports. Therefore, there are reasons to believe that we can design a computer-aided testing system specifically for spoken English testing.

A complete computer-aided test system not only has a question bank, but also has the functions of testing, evaluation, and analysis. The specific functional module structure is shown in Figure 2.

The computer can upload the results of students' answers to the server, and the server automatically judges objective questions such as multiple-choice and true-false questions, assigns scores based on whether they are correct or not, and records and saves the evaluation results of each student's test (generally including the question number, true or false information, waiting time for answers, and so on) for test analysis. For example, in the case of a balanced distribution of test difficulty, the majority of candidates can correctly answer the test's questions, while only those with poor academic performance can correctly answer fewer questions, indicating that this period of teaching was successful. For another example, if the candidates with excellent grades did not get it right but the candidates with poor grades did, this demonstrates that the topic cannot distinguish between excellent and poor students.

When the purpose of the test is to classify students and judge their level and ability, always hope that the test is fair and accurate. According to the requirements of educational evaluation, the test should have two necessary characteristics: evidence (validity) and reliability (reliability). Test paper analysis is the analysis of the reliability and validity of the test paper. The results of the analysis can reflect whether the test really checks the students' knowledge level and ability and whether the teaching process is successful or not. That is to say, it can be judged whether the test results can be used as the basis for evaluation.

3.2. Oral English Evaluation Algorithm Based on Multifeature Fusion

3.2.1. Feature Extraction. To evaluate the quality of a person's spoken English, usually give an overall evaluation first; for example, this person's spoken English is very good; then predict that the person's pronunciation is accurate and his intonation is well mastered, but his continuous reading is not good enough, and so on. The purpose of this study is to evaluate users' spoken English by computer and give the evaluation results. This requires a comprehensive evaluation algorithm, and an evaluation algorithm based on multifeature fusion is given in this paper.

This paper's proposed multifeature fusion evaluation algorithm is based on existing single-feature evaluation algorithms. At the very least, a multifeature comprehensive evaluation method should have the following characteristics: scalability, which means that the features chosen and the number of features chosen will have little impact on the system, and it should be simple to add and remove features. It has nothing to do with a single feature's evaluation algorithm; that is, changing the evaluation algorithm of a single feature has no effect on the system when the form of the evaluation result of a single feature remains unchanged.

As shown in Figure 3, the whole scoring system includes three parts: speech recognition, feature extraction, and linear regression.

The similarity features and syntactic features in feature extraction are extracted from the text after speech recognition, and the similarity features need to be compared with reference answers. Syntactic features are mainly used to measure the grammatical level of candidates' answers. The phonetic features, including pronunciation confidence and speaking fluency, are used to judge the accuracy of pronunciation and speaking fluency of candidates. These features are extracted from the preferred recognition results of speech recognition. Finally, score multiple features by using the trained linear regression model.

Firstly, multiple features are evaluated separately, and multiple evaluation results are obtained. Then quantify these evaluation results, the quantization standard is obtained through systematic training in advance, and the quantization result is $S_1, S_2, \ldots S_n$. Then, the weighted average of these quantized results is carried out to obtain the quantization result of comprehensive evaluation:

$$S = \sum_{i=1}^{n} a_i S_i, \tag{1}$$

where a_i is the weight of each feature, $\sum_{i=1}^{n} a_i = 1$; S_i is the quantified value of each evaluation result.

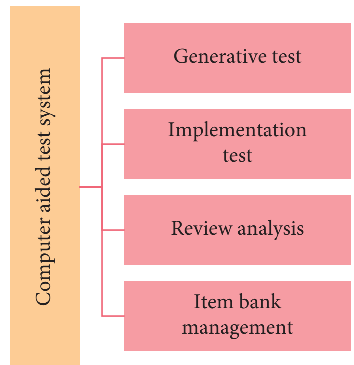

Figure 2: Functional module structure of computer-aided test system.

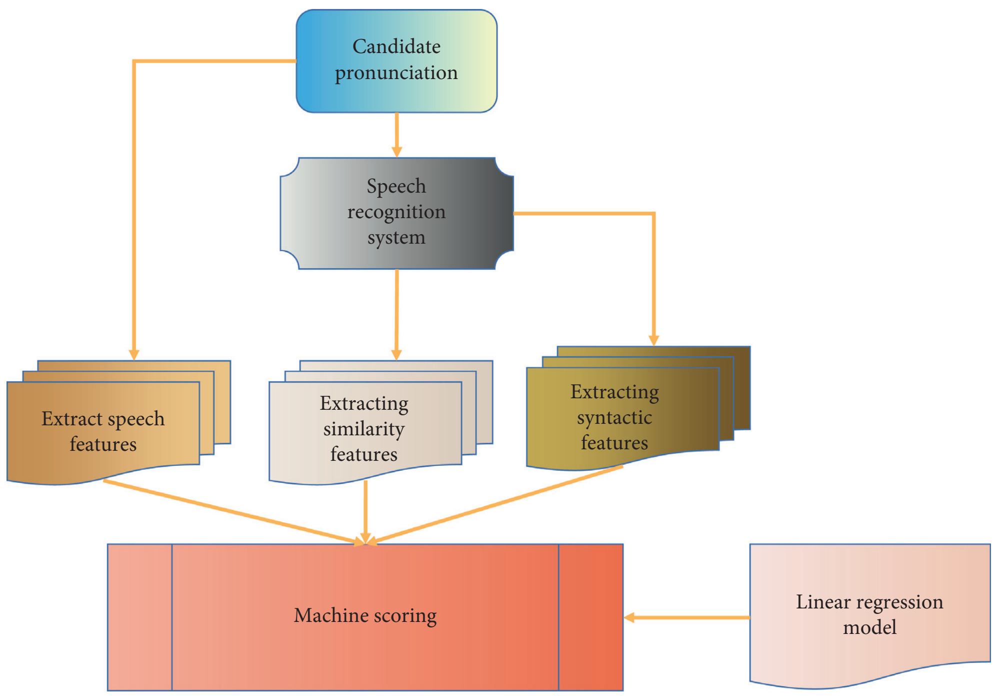

Figure 3: Scoring system framework.

Finally, based on the quantitative results, according to certain standards, the evaluation results are given. The evaluation results are divided into four grades, namely, "bad," "normal," "good," and "excellent".

SE (sample entropy) is a new method for measuring the complexity of time series, which is an improved statistic that does not count self-matching for the approximate algorithm.

It is defined as the conditional probability that the data vector will continue to maintain its similarity when it increases from m dimension to $m + 1$ dimension, and the SE of the original data with N points is expressed as

$$\begin{aligned} \mathrm{SampEn}(m, r, N) &= -\ln \frac{B^{m+1}(r)}{B^{m}(r)}, \\ SampEn(m, r, N) &= -\ln \frac{B^{m+1}(r)}{B^{m}(r)}. \end{aligned} \tag{2}$$

Traditional MFCC (Mel frequency cepstrum coefficient) only reflects the static features of speech signals, while SE can describe the dynamic changes of speech signals. The two features have different roles in distinguishing emotions. The two features of SE and MFCC are input into support vector machine, respectively, and the probabilities that they belong to six emotions are calculated. Then, the recognition results are obtained by combining addition rules and multiplication rules. This section concludes two kinds of fusion rules.

This paper uses two different fusion rules:

The addition rule is

$$F\left[P\left(\omega_i \mid f_1\right), \ldots, P\left(\omega_i \mid f_R\right)\right] = \sum_{j=1}^{R} P\left(\omega_i \mid f_j\right). \tag{3}$$

The multiplication rule is

$$F\left[P\left(\omega_i \mid f_1\right), \ldots, P\left(\omega_i \mid f_R\right)\right] = \prod_{j=1}^{R} P\left(\omega_i \mid f_j\right). \tag{4}$$

The algorithm steps of speech emotion recognition based on multifeature fusion of SE and MFCC are as follows:

Reading emotional speech signals and preemphasizing, framing, and windowing, with the frame length of 256 and the frame shift function of 128 as Hamming window;

Preprocessed speech signals of each frame are original data $x(1), x(2), \ldots, x(N)$, and this data is composed into a group of m-dimensional vectors in a continuous order:

$$x(i) = [x(i), x(i+1), x(i+m-1)], \quad i = 1 \sim N - m + 1. \tag{5}$$

Average $B_i^m(r)$:

$$B^m(r) = \frac{1}{N-m+1} \sum_{i=1}^{N-m+1} B_i^m(r). \tag{6}$$

According to the principle of addition and multiplication rules, the posterior probabilities of the two features are fused, and then the recognition rates of six emotions are calculated, respectively.

3.2.2. Semantic Discovery. When communicating in English, many Chinese college students rarely or never include nonverbal factors, such as lack of communicative competence in expression, body movements, and tone. Spoken English is the first step toward understanding a language and culture that is not one's own. When nonlanguage is combined with spoken English, one can gain a more comprehensive and in-depth understanding of the language, which will help students improve their practical ability to use English. Using dynamic programming technology, the semantic discovery algorithm detects the repeated parts of acoustic speech signals. In general, finding the shortest distance between sound input and a set of templates is used to recognize all duplicate parts. Local comparison [25] is used in this paper to reveal the repeated subparts of two acoustic signals using the cumulative quality scoring mechanism.

Input each spoken English as an acoustic feature vector U_m, and compare it with the stored feature vector V_n. The calculation method of cosine similarity is shown in formula (7).

$$D_{ij} = \frac{U_i \cdot V_j}{\left\|U_i\right\| \cdot \left\|V_j\right\|}. \tag{7}$$

For convenience of explanation, based on the above assumptions, in order to evaluate the reliability of system IP (indistinguishable phoneme) recognition, two relative measures are introduced, namely, the correct recognition rate $Q\ r$ and the false recognition rate e_i^j. The following are their exact definitions:

$$\begin{aligned} r &= \frac{N_{\text{right}}}{\left(N_{\text{right}} + N_{\text{error}}\right)}, \\ e_i^j &= \frac{N_c(i, j)}{n_t(i)}, \end{aligned} \tag{8}$$

where N_{right} is the number of phonemes correctly recognized by the system; N_{error} is the number of phonemes wrongly recognized by the system.

The normalization of input features refers to measuring the input feature values on the same standard. For example, the range of the output results of the grading network for vocabulary and grammar is [0.1]. The result of teacher's manual grading is 10 points. Therefore, it is necessary to normalize the teacher's manual score and the oral feature score mentioned earlier in this paper, so that the range of input features is uniform when training the multifeature correction model later. And after normalization, it can show candidates all the characteristics of spoken English. Namely:

$$x_i^{p^*} = \frac{x_i^p - x_i^{\min}}{x_i^{\max} - x_i^{\min}}. \tag{9}$$

In many spoken language scoring systems studied by predecessors, the scoring model is established by linear regression, which is a classic machine learning algorithm and can fit and predict data with linear characteristics. This paper will also use the method of linear regression to establish the scoring model. The definition of linear regression is as follows:

$$h_\theta(x) = \theta_0 + \theta_1 x_1 + \cdots + \theta_n x_n, \tag{10}$$

where n is the number of input features, and in this paper, $n = 5$. A linear regression model was also built using TensorFlow. Similarly, 80% of data sets are used as training sets and 20% as test sets.

4. Results Analysis and Discussion

4.1. Multifeature Recognition Results. In the simulation, all speech samples are divided into male, female, and mixed voice, and SE, fundamental frequency, energy, formant, and MFCC are extracted and their statistics are calculated. The mean and variance of SE are shown in Figure 4, and the average recognition rate of the three types of features and their statistics is shown in Figure 5.

Students have a strong desire for knowledge about the content of teachers' lectures, and their learning mentality is positive. Then, in the process of oral English practice, they

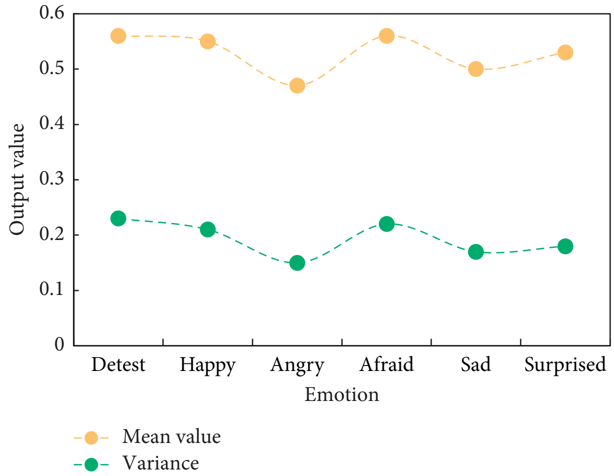

Figure 4: SE statistics of six kinds of emotions.

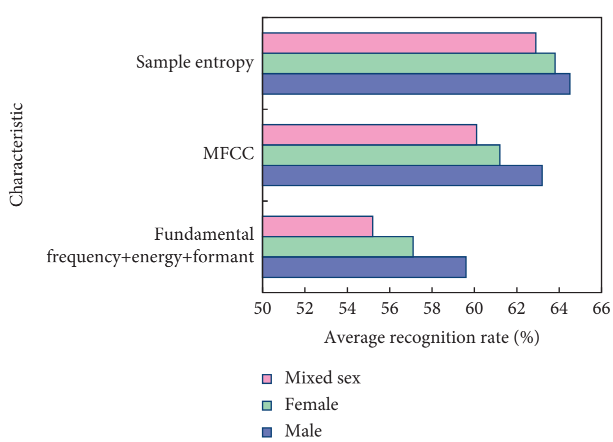

Figure 5: Average recognition rate of three kinds of features and their statistics.

need to be very careful and serious and will actively work to solve these problems and, at the same time, use a variety of oral English practice methods.

Their oral English ability is also different, but they are all studying hard, but their understanding of oral English can be summarized as repeated practice, and the content is mainly arranged by textbooks and teachers, while some English teachers are only teaching and emphasizing how students practice spoken English repeatedly; that is, they spend a lot of time repeatedly practicing reading every English word and sentence.

Figure 5 shows that the recognition rate of SE as a feature parameter is higher in male, female, and mixed voice samples than the other two feature parameters, with male voice samples having the highest recognition rate of 64.5 percent. Figure 6 shows the recognition results of six emotions of mixed male and female voice when SE is the feature parameter.

As can be seen from Figure 6, when SE and its statistics are used as feature parameters, the recognition rate of happy and surprised emotions is as high as 80%, the resolution of SE to happy and surprised emotions is high, and the emerging new information has a good distinction with other emotions.

Using the addition rule and multiplication rule in the previous section to fuse SE sum, respectively, the recognition result is shown in Figure 7.

From Figure 7, it can be seen that after SE and MFCC are merged, the recognition rate is obviously improved, and the highest recognition rate of multiplication rules is 68.8%. SE and MFCC have different emphasis on distinguishing emotions, and the recognition effect after fusion is ideal. The recognition rate of six emotions fused by multiplication rules is shown in Figure 8.

The recognition rate of happy emotions decreases after SE and MFCC are merged according to the multiplication rule, as the error rates of estimated probabilities of SE and MFCC accumulate, reducing the recognition rate of happy emotions. Fear and aversion emotion recognition rates improve dramatically after merging, and the average recognition rate of six emotions rises to 66.3 percent, up 3.9 percent from SE before merging. Various cultures found in the United States or English should be combined with a lot of oral English teaching. Because of the various users and environments, English will take on a variety of roles and meanings, particularly given the long-standing lifestyle differences between Westerners and Chinese. As a result, in the process of teaching oral English, teachers should not only pay attention to the pronunciation and grammatical accuracy of English words and phrases, but also teach students to understand the communication environment of characters and the relationships between characters in oral English, as well as analyzing the different meanings expressed by different words and phrases in different situations, because the change of tone directly affects the meanings expressed by different words and phrases in different situations.

4.2. Analysis of Intelligent Correction System for Spoken English. Creating a good atmosphere can help students get into the specific situation of the text faster and better and help students imagine abstract written words as concrete, vivid, and vivid pictures in their minds, so as to stimulate emotional resonance, enhance students' language perception ability, and finally let students enter the state of "reading aloud with affection." Reading forms can be arranged according to the classroom time, such as reading competitions among individuals, reading competitions among groups, reading by roles, etc. Individual reading forms are helpful for teachers to give targeted guidance and comment on students' reading effects, help students to correct shortcomings, and thus improve students' level of "emotional reading."

The training corpus C1 contains 1039 native natural oral recordings and scripts, while the test corpus C2 contains 128 IP clusters from native natural pronunciation recordings. Simultaneously, in order to complete the robustness testing, the author chose two students, one of whom graduated with a major in English and the other with a major in computer science. They have different levels of oral proficiency, so their recordings of the same corpus are labeled C3 and C4,

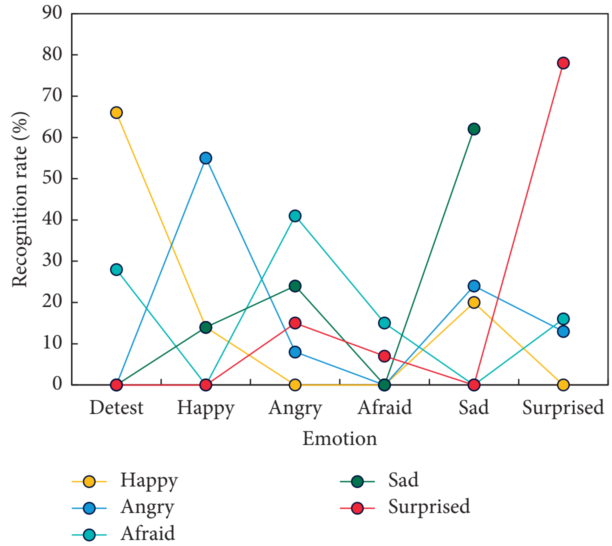

Figure 6: SE and its statistics on six kinds of emotion recognition rates.

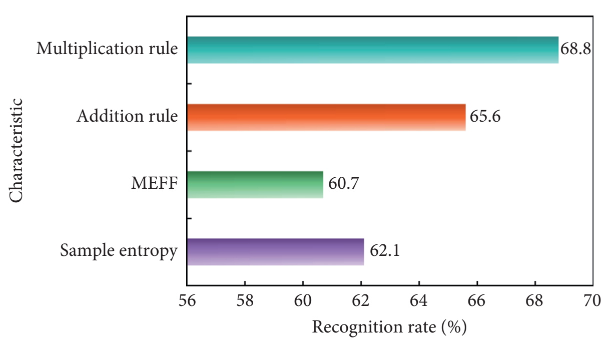

Figure 7: Average recognition rate of SE and MFCC and their fusion.

respectively. The results of voice evaluation for C2, C3, and C4 are shown in Figure 9.

These results show that our evaluation model can get reliable and robust evaluation results with the average phoneme recognition rate of the system.

In college, students are taught English orally. Schools have not paid much attention to English. Intensive reading and listening are two types of college English courses offered by many universities. While most listening courses are conducted in a centralized manner, which is limited by factors such as teachers, class size, and so on, the accuracy of the course accounts for nearly 3/4 of the total class hours. Furthermore, most universities do not include an oral exam in their English exams, resulting in students paying little attention to oral English learning.

The survey shows that 90% of teachers think that they mainly play the role of interpreter and demonstrator in English class, and 70% of teachers think that their role is mainly to guide students how to learn foreign languages and how to cultivate their foreign language learning ability. It can be seen that most English teachers can clearly understand how to effectively carry out teaching but rarely do this in actual teaching.

Figure 10 shows the size of training or test set; it reflects the performance of training or testing. The larger the performance, the better the performance.

From the above data, the integration method has the best stability, followed by the probability space distance method, and the probability mean method is the worst. In terms of performance, the method based on probability space distance is the best, followed by probability mean method, and the method based on Sugeno integral is the worst.

Teachers should create a positive learning environment for students, plan rich classroom activities, actively guide students to look at pictures and talk, intensify oral practice, and provide students with plenty of practical practice opportunities when teaching oral English. Their oral English level can only be improved to some extent through continued practice and practice. In order to improve one's language communication level, the process must be undertaken step by step, from easy to difficult, simple to tedious, and success cannot be rushed. Mechanical training can be done at the start of the training to gradually increase the level of fluent expression. Different ways of thinking exist in Chinese and foreign cultures, resulting in differences in language expression. The verbs in Chinese sentences are usually centered and spread horizontally, forming a flowing shape structure. The structure of Westerners' sentences is generally centered on subjects or predicates, and it is more complicated. As a result, students should use correct logical thinking to express themselves in the process of language expression, gain a deeper understanding of western culture, and improve the flexibility and smoothness of their oral expression.

Visual effects can make students more aware of the feelings attached to English that they have heard. In the practical use of English, when people communicate in English, they not only rely on their ears to listen, but also want to really understand what the other party wants to express, and they should combine their visual senses. In view of this, teachers can choose English movies that meet the

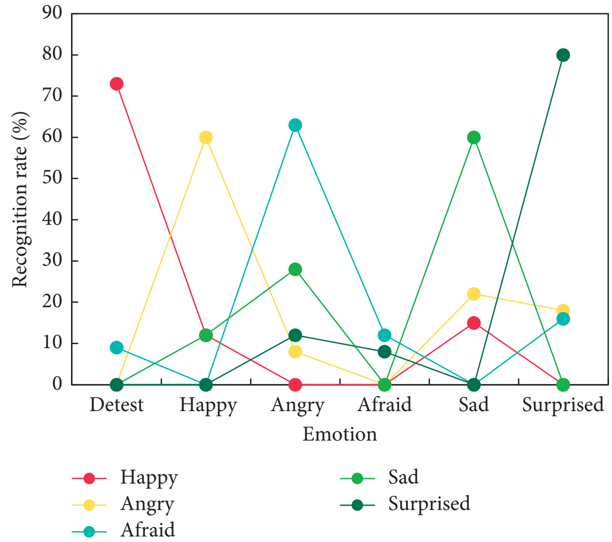

Figure 8: Six emotion recognition rates based on the fusion of SE and MFCC multiplication rules.

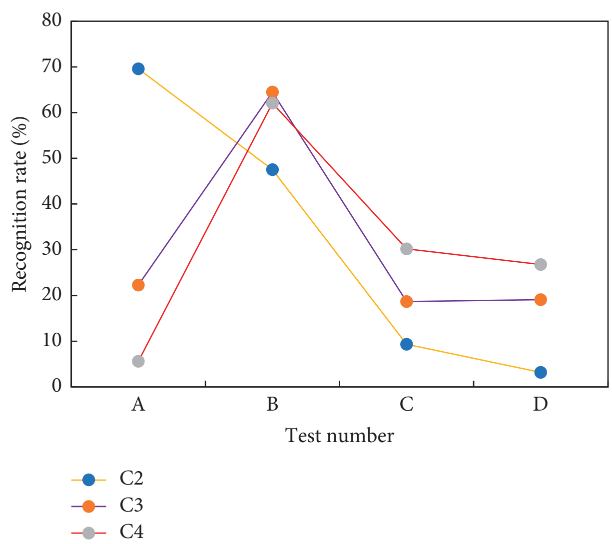

Figure 9: Comparison of open test results.

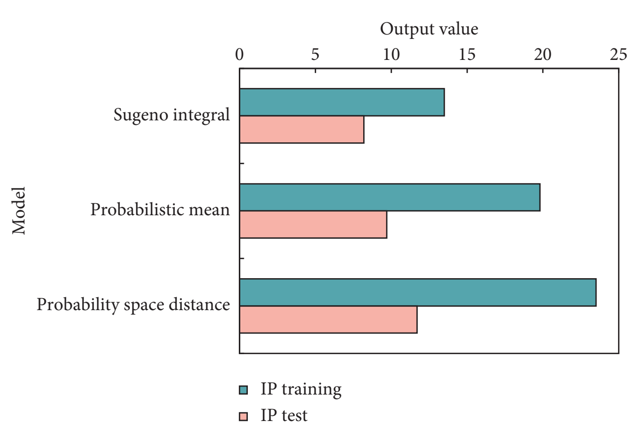

Figure 10: IP training and test results.

nonverbal communication factors for teaching. First, let students learn the nonverbal factors in the movies, because speaking English alone cannot effectively improve students' oral ability.

5. Conclusion

In college English classes, oral English instruction is a weak point. There are numerous issues that arise during the teaching process, such as a lack of a language environment, fewer class hours, and so on, and students' application ability is low. The analysis and design of the intelligent correction system for spoken English, as well as the specific implementation method, are detailed in this paper. The system greatly improves the efficiency of oral English tests while also reducing the difficulty of organizing them and teachers' workload. When SE is used alone as an emotion recognition feature, it outperforms MFCC and fundamental frequency. Finally, the MFCC and SE fusion recognition results are examined, and the fusion recognition rate is improved. Experiments show that the speech evaluation system presented in this paper is more in tune with people's subjective feelings and that the evaluation results can reflect the subjects' pronunciation level.

Due to the author's limited knowledge, there are still many flaws in the system's operation, and there are numerous areas for improvement and further research, such as expanding the question bank, improving system security, increasing system efficiency, and designing an analysis system for the data gathered during the examination process, among other things. In future research, the author will investigate and analyze the aforementioned issues in greater depth, with the goal of improving the system's functionality.

Data Availability

The data used to support the findings of this study are included within the article.

Conflicts of Interest

The author does not have any possible conflicts of interest.

Acknowledgments

This study was supported by the teaching reform project of the Education Department in Anhui Province, China (Grant no. 2021), Anhui educational science research project in Anhui Province, China (Grant no. JK21050), and Anhui philosophy and social sciences research project in Anhui Province, China (Grant no. 2021).

References

[1] L. Deng, "Design of an automatic evaluation system for the pronunciation quality of spoken English," *Automation and Instrumentation*, vol. 6, no. 6, 2019.

[2] X. Xu, D. Yao, and D. Huang, "Research on oral English test system based on SSM framework," *Microcomputer Applications*, vol. 36, no. 11, 2020.

[3] J. Hu, "The Status Quo of oral English teaching evaluation methods and development Countermeasures," *Comparative Research on Cultural Innovation*, vol. 9, no. 9, 2018.

[4] G. Luo and F. Zhao, "Design of automatic scoring system for spoken English test based on sequence matching," *Automation and Instrumentation*, vol. 6, no. 6, 2020.

[5] H. Sun and M. Zhang, "A comparative study of machine scoring and manual scoring in spoken English," *Foreign Language Research*, vol. 37, no. 4, 2020.

[6] H. Zhu, "Blended teaching practice and evaluation of college oral English courses," *Journal of Jiangxi Vocational and Technical College of Electric Power*, vol. 33, no. 6, 2020.

[7] C. Ren, "Application of formative assessment in college oral English teaching," *International Public Relations*, vol. 10, no. 10, 2019.

[8] H. Zhou, "The application of diversified evaluation system in college oral English teaching," *Good Parents*, vol. 33, no. 33, 2017.

[9] S. Lin, "An empirical study of college spoken English self-assessment based on Chinese-English language Transfer," *Overseas English*, vol. 2, no. 2, 2018.

[10] C. Ying, Y. Shuyu, L. Jing, D. Lin, and Q. Qi, "Errors of machine translation of terminology in the patent text from English into Chinese," *ASP Transactions on Computers*, vol. 1, no. 1, pp. 12–17, 2021.

[11] C. Zhou, "Why don't accumulate a lot of money?——on the training strategy of primary school English oral ability[J]," *Campus English*, vol. 45, no. 45, 2020.

[12] J. Zhuo, "Teaching material evaluation of "spoken English for practical Economics and Trade"——based on the textbook design model of Tom Hutchinson & alan waters," *Journal of Fuyang Vocational and Technical College*, vol. 28, no. 3, 2017.

[13] J. Liu, "A brief talk on oral English teaching Strategies in primary Schools," *Good Day*, vol. 7, no. 7, 2021.

[14] Y. Li and W. Geng, "Analysis of the chinese college students' oral english evaluation system," *College English*, vol. 1, no. 1, pp. 186–191, 2017.

[15] H. Sun, "A review of research on automatic scoring of spoken English at home and abroad," *Frontiers of Foreign Language Education Research*, vol. 4, no. 2, 2021.

[16] D. Wu, Q. Liang, and M. Wang, "Scoring of spoken English based on convolutional neural network," *Information & Technology*, vol. 44, no. 11, 2020.

[17] J. Hung, "Group peer assessment of oral English performance in a Taiwanese elementary school," *Studies In Educational Evaluation*, vol. 59, pp. 19–28, 2018.

[18] J. M. Goodrich and C. J. Lonigan, "Language-independent and language-specific aspects of early literacy: an evaluation of the common underlying proficiency model," *Journal of Educational Psychology*, vol. 109, no. 6, pp. 782–793, 2017.

[19] J. Yang, "The enlightenment of oral english skill competition to english teaching reform at vocational colleges," *English on campus*, vol. 26, no. 26, 2017.

[20] L. M. Bedore, E. D. Peña, and C. Fiestas, "language and literacy Together: Supporting grammatical development in dual language learners with risk for language and learning difficulties," *Language, Speech, and Hearing Services in Schools*, vol. 51, no. 2, pp. 282–297, 2020.

[21] Z. Huang, Y. Liu, C. Zhan, C. Lin, W. Cai, and Y. Chen, "A novel group recommendation model with two-stage deep learning," *IEEE Transactions on Systems, Man, and Cybernetics: Systems*, In press, 2021.

[22] K. Wang, N. An, B. N. Li, Y. Zhang, and L. Li, "Speech emotion recognition using Fourier parameters," *IEEE*

Transactions on Affective Computing, vol. 6, no. 1, pp. 69–75, 2017.

[23] B. W. Schuller, "Speech emotion recognition," *Communications of the ACM*, vol. 61, no. 5, pp. 90–99, 2018.

[24] L. Zhu, L. Chen, and D. Zhao, "Emotion recognition from chinese speech for smart affective services using a combination of svm and DBN," *Sensors*, vol. 17, no. 7, 2017.

[25] A. Jacob, "Modelling speech emotion recognition using logistic regression and decision trees," *International Journal of Speech Technology*, vol. 20, no. 4, pp. 1–9, 2017.

Hindawi
Computational Intelligence and Neuroscience
Volume 2022, Article ID 2700674, 10 pages
https://doi.org/10.1155/2022/2700674

Research Article

Development and Implementation Path of Kindergarten Stem Educational Activities Based on Data Mining

Liangfu Jiang [1,2]

[1]*College of Educational Science of Hunan Normal University, Changsha 410081, China*
[2]*Normal College of Hunan University of Arts and Sciences, Changde 41500, China*

Correspondence should be addressed to Liangfu Jiang; sfxyjlf@huas.edu.cn

Received 22 December 2021; Revised 6 January 2022; Accepted 7 January 2022; Published 25 January 2022

Academic Editor: Xin Ning

Early childhood education in China has given stem education constant attention and study. On the one hand, it has introduced many foreign research findings on stem education, such as curriculum practice, evaluation systems, teacher training, and so on; on the other hand, this paper investigates the localization implementation path of stem education based on the realities of kindergartens. This paper investigates the development and implementation path of kindergarten stem education activities using data mining, analyzes how the kindergarten stem education monitoring index system is developed and further improved using data mining algorithm, and determines the function path and mode of data mining algorithm in kindergarten stem education. It is expected to be used as a reference in the development and implementation of stem education and teaching activities. The development and implementation path of kindergarten stem educational activities based on data mining algorithm using data technology to realize continuous audit can not only improve the audit means and scope but also provide new research ideas for the expansion and innovation of audit work, which is useful in building a path model of kindergarten stem educational activities development and implementation.

1. Introduction

In recent years, China has seen a surge in stem education, which has piqued the interest and support of a growing number of people. Through the organic integration of science, technology, engineering, and mathematics, stem education is a project-based learning and problem-solving oriented curriculum organization that aims to cultivate the activity development innovation consciousness and innovation ability of kindergartens [1]. The application of the stem education concept in kindergarten teaching not only meets the needs of the kindergarten population and development, but it also meets the requirements of activity development of teaching reform. Early childhood education in China has paid close attention to and studied stem education. On the one hand, it has introduced many foreign research findings on stem education, such as curriculum practice, evaluation systems, teacher training, and so on; on the other hand, the localization implementation path of stem education has been explored based on the reality of kindergartens [2]. Children's education concept of stem focuses on cultivating students' comprehensive learning and practical ability. The application of tools in kindergarten classroom teaching can not only effectively improve the comprehensive quality and ability of kindergarten but also improve the teaching efficiency to a certain extent [3]. These explorations have accumulated rich resources, implementation paths, and experience for the current stem education in kindergartens [4, 5].

As a potential resource of STEM education in kindergartens, related research is still lacking. This paper takes this as a starting point to explore the development and implementation path of STEM education activities in kindergartens based on data mining [6]. Generally speaking, China's preschool children's science education has gone through the process of germination, stagnation, development, reference, localization, and scientific transformation, forming the curriculum system that emphasizes localization and local growth, the development goal of educational activities for the country, the curriculum content closely related to children's life, and the implementation path organization form that focuses on "doing". At present, there are many theoretical researches on STEM educational concept in kindergartens in China, but the practical research on STEM educational activity development in kindergartens is not very rich [7]. Therefore, based on the data mining algorithm, this paper attempts to explore the science course "Make a paper plane" which is integrated with STEM concept, in order to provide more thoughts on the implementation path for front-line kindergarten teachers [8, 9]. The development and implementation path of STEM education activities in kindergartens is to comprehensively apply the techniques and methods of mathematical statistics, machine learning, and data mining to process and analyze STEM education data in kindergartens. Through data modeling, the correlation between learners' learning results and variables such as learning content, learning resources, and teaching behavior can be found to predict learners' future learning trends [10].

Under the background of the new era, education should pay attention to the cultivation of top-notch innovative strategic talents with international competitiveness, which is an effective way from "science and education" to "rejuvenating the country" and even "strengthening the country". The development of stem educational activities in kindergartens, implementation of scientific educational activities in kindergartens' aims, and quality improvement [11]. Therefore, the research on the implementation path of the development of stem education activities in kindergartens is the objective demand to promote the development of stem education in preschool kindergartens. Ideal data mining algorithm for kindergarten stem education activity development and implementation path using data technology to realize continuous audit can not only enhance audit means and broaden audit scope but also provide new research ideas for the expansion and innovation of audit work, and help to build a kindergarten stem education activity development and implementation path model based on Data Mining [12, 13]. We can obtain valuable information in a variety of complex data using the data mining algorithm, which not only allows us to grasp problems that arise in the development of kindergarten stem education activities at any time, but also allows us to adjust current kindergarten stem education construction methods and objectives according to data technology [14, 15]. This paper analyzes how the kindergarten stem education monitoring index system is developed and further improved by using data mining algorithm, in order to obtain the role path and mode of data mining algorithm in kindergarten stem education. It is expected to be used as a reference in the development and implementation of kindergarten stem education activities.

2. Related Work

Bonneton-Botté et al. [16] suggest that teachers should adopt constructivism teaching strategies and refer to the precursor model of shadow formation, which has a positive effect on children's understanding and identification of physical phenomena of shadows. Through the method of big data analysis, in recent two years, more and more researchers have paid attention to STEM education in preschool stage, and most of them are foreign researchers, but the overall quantity is still small [17]. The research contents mainly focus on early childhood STEM education policies, kindergarten STEM courses, and kindergarten STEM teachers. Research shows that children can learn scientific concepts and vocabulary better by adopting reactive teaching or combining reactive teaching with explicit teaching [18]. Mcgoey et al. [19] point out that the practice of early science education is an effective strategy for science teaching and learning, and it is the foundation for the future development of kindergarten children's scientific literacy. Whiting et al. [20], through big data analysis [21], show that STEM education is very good at solving practical problems in real life. Therefore, teachers should observe their behaviors through daily contact with children, and then explore their interests and needs. Research shows that scaffolding instruction can help kindergarten and primary school teachers, as well as researchers, analyze the science education activities in kindergartens, and judge whether the adopted strategies are effective, which strategies need to be eliminated, and what other strategies may be needed [22]. Scannell et al. [23] point out that STEM education plays a significant role in improving national quality, stimulating employment and balanced income distribution, promoting ethnic equality and gender equality, strengthening national economic strength and driving innovation, etc., and it is a booster of American national competitiveness. Through the method of big data analysis, in children's daily life, although some contents are not initiated by young children, they are initiated by adults, but they play a great role in children's growth and habit formation, which requires teachers to pay more attention [24]. Research shows that experimental basic education has a positive impact on the ability of 5-year-old children to solve scientific problems [25]. Experiment-based science education projects include experiments aimed at improving children's scientific process skills, independent thinking, decision-making, and problem-solving process. Literature [1] pointed out that the poor status of STEM education at the present stage is mainly influenced by the high cost of university education, poor academic preparation, demographic factors, lack of local core staff, and so on.

This paper studies the development and implementation path of kindergarten stem education activities based on data mining, and finds that kindergarten stem activities and project-based learning fit well, and project-based learning provides a good platform and opportunity for stem education.

3. Principle and Model of Data Mining Algorithm

Data Mining is a new discipline of "developing methods and exploring unique types of data in the educational environment, so as to better understand students and their learning environment through these methods." Data mining

(DM) is a process of discovering interesting knowledge from a large amount of data stored in databases, data warehouses, or other information bases, and it is a marginal discipline involving database management, artificial intelligence, machine learning, pattern recognition, data visualization, and other disciplines. If we can dig out this hidden pattern from the development of STEM education activities in kindergartens, its significance is self-evident. We can describe the general process of kindergarten data implementation path as shown in Figure 1.

3.1. Establish Data Mining Database. Analyze the data characteristics of the existing kindergarten information system, and establish the mining database.

3.2. Data Preprocessing. For the activity development and implementation path-related data of the existing stem education information in the kindergarten, the sequence mining method is used for standardized processing to ensure the integrity and consistency of the data, smooth the noise data, identify and delete outliers, so as to improve the data quality, improve the mining accuracy and performance, and store the processed data in the mining database.

3.3. Design Mining Algorithm. A general mining algorithm for a single disease can be designed by combining clustering analysis and ant colony algorithm in bionic algorithm. Clusters of related diseases can be obtained by clustering, and ant colony algorithm can be used to optimize the formation of clusters, so as to form an optimized single path.

3.4. Establish the Implementation Path Database. According to the related concepts of stem education in kindergartens, the adult attributes and their constraints are explained, and the content database storing the extracted values is established. Through the corresponding expression, it will be transformed into the familiar implementation path.

To construct the development and implementation path of STEM education activities in kindergartens from the perspective of data mining, it is necessary to realize it with the help of information active push technology. The basic activities of education are often divided into three categories: teaching, management and scientific research, because there are some differences in business processes and objects of concern in various fields. Therefore, the application of data mining in education should also be divided into three areas, as shown in Figure 2.

In the application of information active push technology, it is usually through SMS notification and server client connection, which is not only conducive to better let the majority of teachers and students know the school related teaching information and management information, but also make use of personalized data mining technology and information customization technology to continuously improve the efficiency of information personalized service. The stem education research model is summarized as the “win-win” model of stem education research, as shown in Figure 3.

STEM education research model is not only conducive to obtaining more extensive and effective data, but also indirectly promotes STEM education concept and its culture. At the same time, this method is also helpful to strengthen inter-regional cooperation, improve the imbalance of inter-regional education development, and improve the quality of education in underdeveloped areas.

Path informatization is realized on the basis of the development of existing business system in kindergarten STEM education activities. The implementation of path system does not change the operation of existing system in kindergarten, but seamlessly links with it to realize the interaction and sharing of information. The operation scheme of the implementation path system is shown in Figure 4.

In this paper, K-means, a data mining algorithm based on partition, is used for text data mining. The advantage of K-means is simple and fast. The basic principle of K-means algorithm is as follows: assuming that the extracted original data set is $X_i = (X_1, X_2, \ldots, X_{N-1}, X_n)$, the purpose of K-means is to segment the original data set X into k categories under the condition of given clustering number k ($K \leq n$). The k-means algorithm is described below.

Assume that the data set to be classified is $X_i = \{X_1, X_2, \ldots X_{N-1}, X_n\}$, the output clusters are $C_j = \{C_1, C_2, \ldots, C_K\}$ $(1 \leq J \leq K,\ K \leq N)$, and the center value of cluster CJ is $M_J = \{M_1, M_2, \ldots M_K\}$.

$$Mj = \frac{1}{n_j} \sum_{X_i \in C_j} X_i, \tag{1}$$

where N_J represents the number of input data X_i contained in the output cluster C_J. Euclidean distance is used to calculate the distance between a word vector and the centroid. Since X_i and M_J are n-dimensional vectors, it is necessary to use Σ to calculate the Euclidean distance between two n-dimensional vectors

$$\text{distance} = \sqrt{\sum_{i,j=1}^{n} \left\| X_i - M_j \right\|^2}. \tag{2}$$

It is mainly used to extract keywords and abstracts for text, and its core ideas are as follows:

$$\text{WS}(V_i) = (1-d) + d * \sum_{V_j \in In(V_i)} \frac{w_{ji}}{\sum_{V_k \in \text{Out}(V_j)} w_{jk}} \text{WS}(V_j). \tag{3}$$

Assuming that data mining has been completed, there are n clusters, in which there are m points in cluster I, then the calculation process of Silhouette index is as follows

Step 1. calculate the intracluster distance $a(i, j)$ for the J-th point in cluster I, where $a\ (i,\ j)$ is the average distance between any data object J in cluster I and other data objects in the cluster

$$a(i, j) = \frac{1}{M-1} \sum_{k=1, k \neq j}^{M} \text{Distance}(j, k). \tag{4}$$

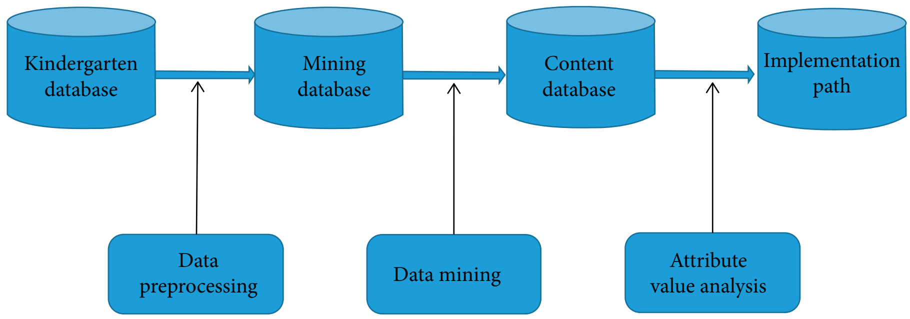

Figure 1: Data mining model.

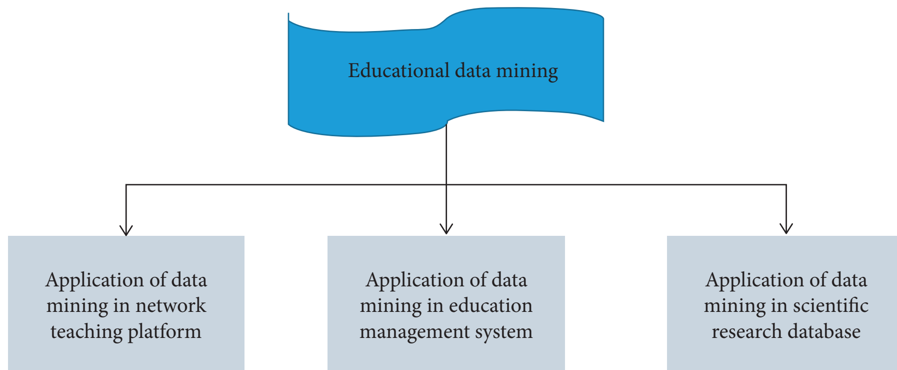

Figure 2: Distribution of educational data mining applications.

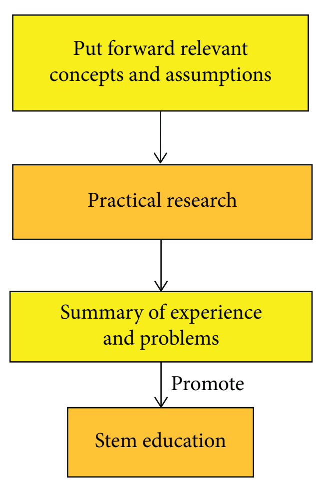

Figure 3: STEM educational research model.

Step 2. for the j-th point in cluster I, calculate the cluster spacing $b(i, j)$. $b(i, j)$ is the minimum of the average distance from any data object J in cluster I to any other data object in cluster I

$$b(i, j) = \min_{k=1 \longrightarrow N, k \neq i} (\text{Avg Distance}(j, k)). \tag{5}$$

Step 3. calculate the Silhouette index of point J in cluster I.

$$\text{Silhouette}(i, j) = \frac{b(i, j) - a(i, j)}{\max\{a(i, j), b(i, j)\}}. \tag{6}$$

Step 4. calculate the Silhouette index of cluster I.

$$avg\_\text{Silhouette}(i) = \frac{1}{M} \sum_{j=1}^{m} (\text{Silhouette}(i, j)). \tag{7}$$

Step 5. calculate the Silhouette index of the whole data set.

$$\text{avg\_SILHOUETTE} = \frac{1}{N} \sum_{i-1}^{N} (avg\_\text{Silhouette}(i)). \tag{8}$$

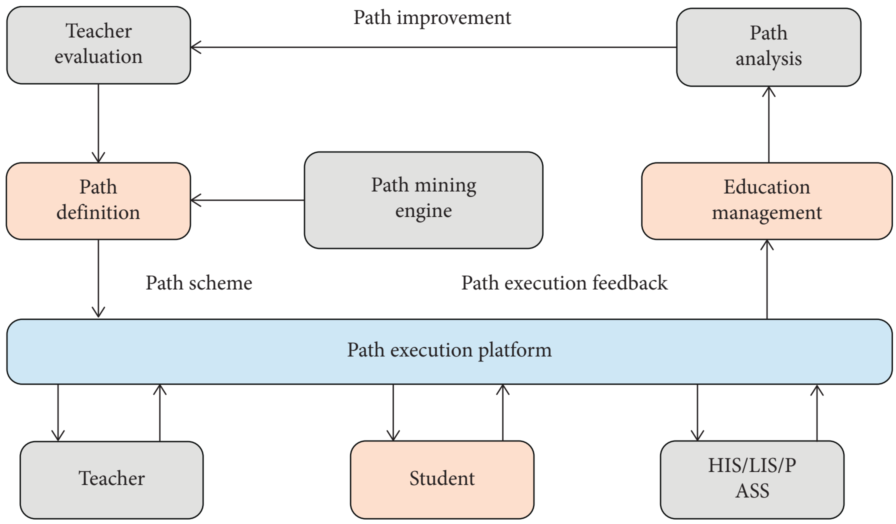

Figure 4: Implementation of route information system operation scheme.

The implementation path of the specified disease is excavated by the implementation path mining engine in this scheme, which is then put into teaching application after teacher evaluation and revision, resulting in a specific teaching scheme and teaching record. Then, to record the path's implementation, interact with the kindergarten systems. Finally, the feedback data is sent to the department in charge of handling abnormal alarms, abnormal monitoring, and statistics, as well as preparing for path analysis and optimization. The Data Mining Society defines educational data mining as "a new discipline that analyzes unique and growing large-scale data in the educational environment through development methods," which is similar to Baker's definition. Data mining is not only useful for improving the teaching and learning experiences of teachers and students, but it also has the potential to support scientific management decisions and strengthen school governance. In the data age, data mining meets the practical needs of mining the value of educational data and discovering the educational data implication law.

4. Development and Implementation Path of Stem Educational Activities in Kindergartens

4.1. Development and Implementation Path of Kindergarten Stem Education Activities Based on Data Mining. To carry out STEM education projects in kindergartens, first of all, teachers are required to have STEM concept and consciousness, and be able to guide their own specific practice by this, and to use STEM vision to discover the value contained in the projects, so as to effectively guide the activities. STEM education in kindergartens and educational research and practice activities are destined to be full of value, complexity, creativity, and uncertainty. In the research and practice of kindergarten STEM education, although data science or data mining can tell people what some phenomena and problems in kindergarten STEM education are, the present situation and state of kindergarten STEM education are, it cannot explain such valuable problems as "why is this so" and cannot put forward countermeasures and suggestions as "how to do" according to the characteristics and development rules of kindergarten STEM education activity development and kindergarten STEM education implementation path practice. The development and implementation path of STEM education activities in kindergartens has the characteristics of cross-domain, involving the study of science, technology, mathematics, and other fields of knowledge. Second, both of them pay attention to children's life experience. Based on the characteristics of children's thinking in concrete images, they emphasize the simplicity and interest of activities, and focus on exploration and operation, so that children can gain direct experience. Third, both of them often involve real problems in activities. Children need to communicate and discuss with peers and teachers in activities to form a small learning community, from which they can help each other to get useful experience and guidance, and then learn to solve real problems step by step.

Data mining is a novel situation and backdrop for the development and implementation of stem education activities in kindergartens, but it comes with its own set of challenges and shortcomings, including low data density, research ethics, personal privacy, and data security. While appreciating the value of data mining, we must also recognize its drawbacks and limitations. If children want to create a mental "primary school," they must first determine the construction project, then design and plan the school project in the form of painting, and finally construct the school. During the construction process, children must consider which materials to use, what to build first, what to build again, which method to use, how to solve balance and stability problems, and so on. All of these issues are related to engineering and technical education.

A series of practical researches on STEM project activities based on data mining algorithm were carried out. Under the guidance of the special research project "Research on STEM Education Practice in Kindergarten Based on Project Learning" of Shaanxi Academic Leaders Training

Plan, the exploration with project learning as the carrier was completed.

(1) Established the basis for the content selection of STEM education activities in kindergartens. Being close to children's life is a real problem that children are interested in and permeates all aspects of children's daily life.

(2) Summarize the implementation path of STEM education activities in kindergartens.

(3) Complete the compilation of Case Collection of STEM Education Activities, which contains 15 activity cases. The exploration at this stage helps us sort out the selection basis and implementation path of STEM education activities, and lays a solid foundation for the follow-up kindergarten STEM curriculum construction.

When screening children's interesting questions, teachers should be able to quickly judge whether the problem comes from children's life or impulse; judge whether the problem has the essence of science, mathematics, and technology; and judge whether the combination of children's teams can be used to solve problems. Stem education is a comprehensive science education based on constructivism, "learning by doing" and other theories. Developing stem education in early childhood has become a field of concern for researchers and early childhood educators at home and abroad. Integrating stem education concept into kindergarten education has become a new exploration direction. Generally speaking, data mining information collection is an organic combination of Official Statistical Organization database, daily management database of policy implementation department and field survey database. Therefore, through the data mining application path and method of developing and implementing the path monitoring index system in kindergarten stem education activities, China should strengthen the construction and analysis of data mining information in education monitoring, supervision, and evaluation; step up the construction of national education big data information center or database; and classify all kinds of Education data and information at all levels in China, improve the collection, analysis, and processing of relevant data of education monitoring index system at all levels, and build a data mining collection mechanism for kindergarten stem education activities in China. Real situations are often typical problem situations. After children experience complex and real problem situations, they will explore and understand knowledge and learn to transfer the understood knowledge to life. The development of stem educational activities in kindergartens often involves the real problems encountered by children. Children continue to push forward the process of activities through continuous problem exploration, solution, and implementation path.

The goal of the kindergarten STEM education activity based on data mining algorithm is to teach children how to effectively combine various disciplines to improve their problem-solving abilities. These various subject knowledge requirements are the foundation of STEM education activities in kindergartens and are required for solving problems. However, mathematics and science have distinct characteristics, and they can only be effectively integrated through engineering and design. As a result, we must focus on engineering and implementation path as the premise for STEM education activities in kindergartens. Garden A, with the support of the education administrative department and Shanghai Steiner Science Education Research Center, is implementing STEM project-based learning in kindergartens and, later, maker activities to broaden children's scientific and technological vision and cultivate their logical thinking, as part of the "Three-year Plan of Action for Preschool Education" and the second kindergarten curriculum reform. The development of kindergarten STEM education activities is a problem-solving activity, driven by the problems that children are most concerned about at the time, with a focus on the exploration and solution of practical problems in kindergarten STEM education, with an emphasis on children's understanding of knowledge and practical application on this basis.

4.2. Results and Analysis. Through the three-month investigation in kindergarten A, it is found that kindergarten A carries out activities in the form of themes, teaching around four theme activities in a semester, each theme lasts for two months, and each theme has about 50 collective activities, as shown in Figures 5–7.

The theme activity is "Visiting the Big Tree," as shown in Figures 5–7, with 11 collective activities accounting for about 24.5% of the total. The Kingdom of Paper has nine collective activities, which account for about 16% of all activities. Because the focus of teaching at the beginning of kindergarten is to guide children in adapting to their new environment and cultivating their basic life skills, the theme "Hello Friends" consists of ten collective activities, resulting in a lack of scientific education activities in the first theme. Color Kingdom has 20 collective activities, accounting for 18.5% of the total. The quantitative analysis of science education activities in kindergarten A reveals that the design of science education activities in kindergarten A is quantitatively balanced with the design of activities in other fields, taking into account the setting of courses in five fields, which is more beneficial to children's overall physical and mental development and also meets the Guide and Outline requirements. The key factor that determines the smooth progress of science education activities, as well as the effect of the entire activities and the direction of children's development, is whether the goal of science education activities is reasonable or not.

In this study, "overall observation situation" mainly refers to the main activity links of one-day life in kindergartens. The hypothesis of the study is: through action research, teachers' overall observation situations are becoming more and more diverse, and can infiltrate mathematics education and observation into all links of children's daily life. The following data shows the distribution of "overall observation situation" frequency of small class, middle class, and large class teachers, as shown in Figures 8–10.

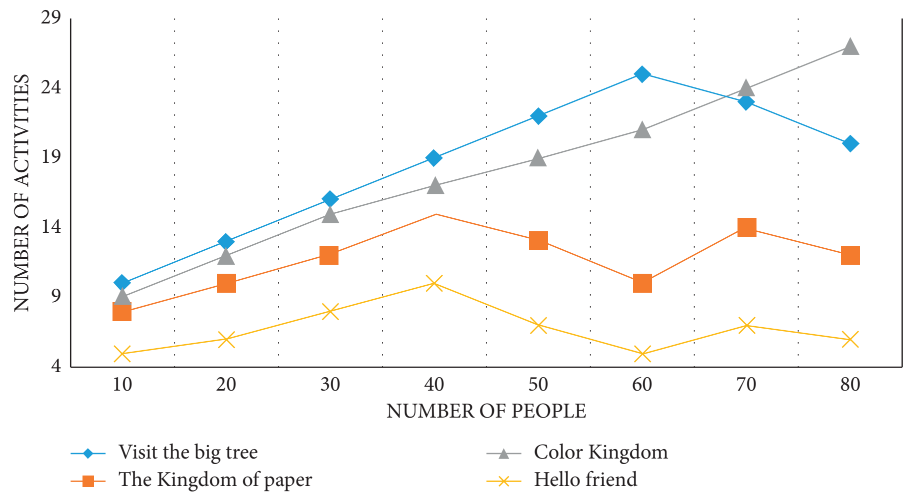

FIGURE 5: A number of theme activities in kindergarten during the first month.

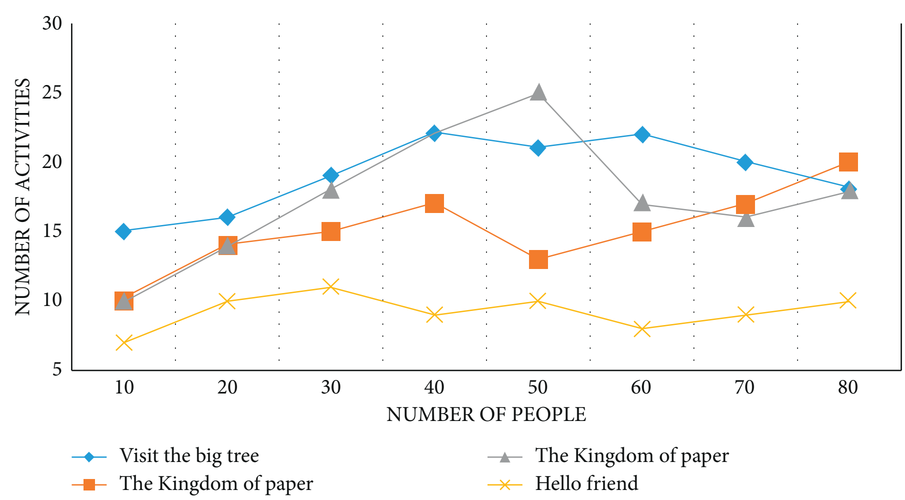

FIGURE 6: A number of theme activities in kindergarten for the second month.

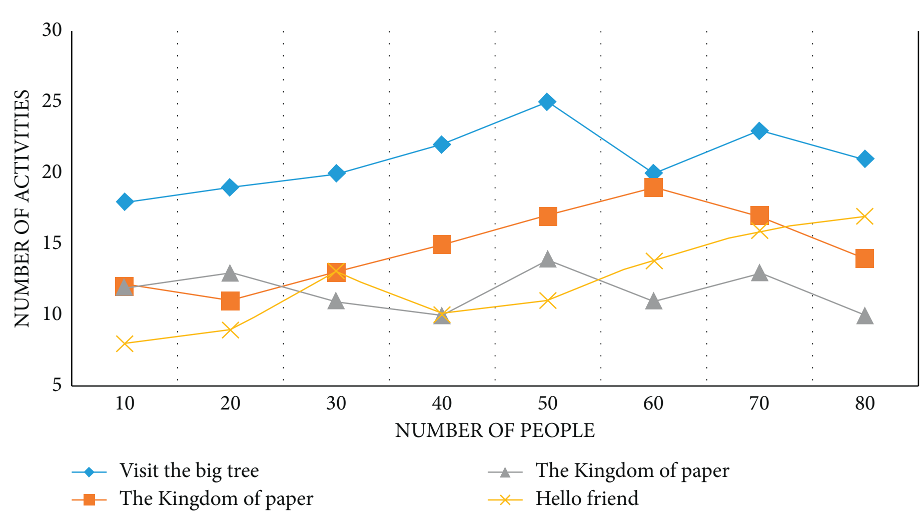

FIGURE 7: A number of theme activities in kindergarten for the third month.

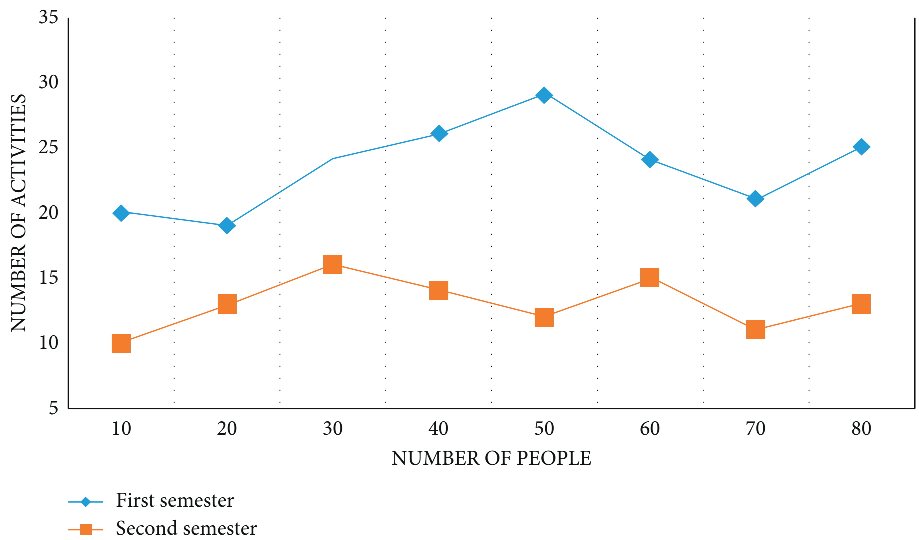

Figure 8: Distribution of “overall observation situation” frequency of small class teachers.

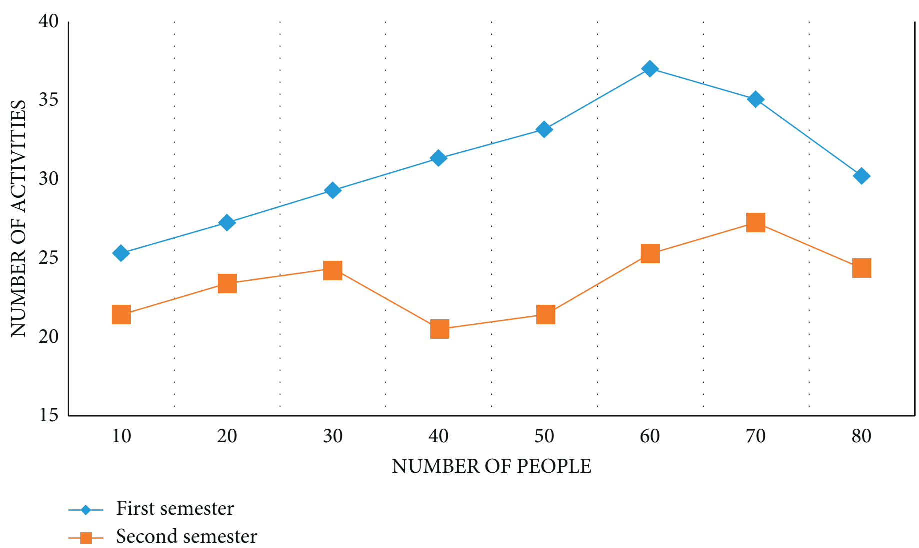

Figure 9: Distribution of “overall observation situation” frequency of middle-class teachers.

From the above data, it can be found that according to the chi-square test conditions, when comparing the composition ratio of two samples, this study needs to process the data and combine the frequencies in some columns to meet the test requirements. From the above data, we can see the main situations of observation in the first semester. The hypothesis of this study is that after action learning, teachers can naturally integrate the observation of children’s mathematics learning into various situations of daily life. In this study, observation situations are collectively referred to as “other situations,” and the data in these situations are combined to test whether the overall observation situation distribution of small class teachers has changed significantly.

According to the aforementioned data, the main situation observed by middle-class teachers in the first semester is “game activity.” The hypothesis of this study is that by incorporating observation of children’s mathematics learning into various situations in children’s day-to-day lives, preschool teachers can naturally integrate observation of children’s mathematics learning into various situations in children’s day-to-day lives. The observation situation is divided into “other situations” in this study, and the data from these situations are combined to see if the distribution of middle-class teachers’ observation situations has changed significantly. In other words, the composition ratio of middle school teachers’ “overall observation situation” did not change significantly from the first semester to the second semester. It is clear that, whether in the first or second semester, middle-class teachers’ observations are primarily focused on “game activities.”

From the above data, it can be found that from the first semester to the second semester, the “observation content” of large class teachers has changed significantly. Preschool teachers tend to “observe the learning results” in the first

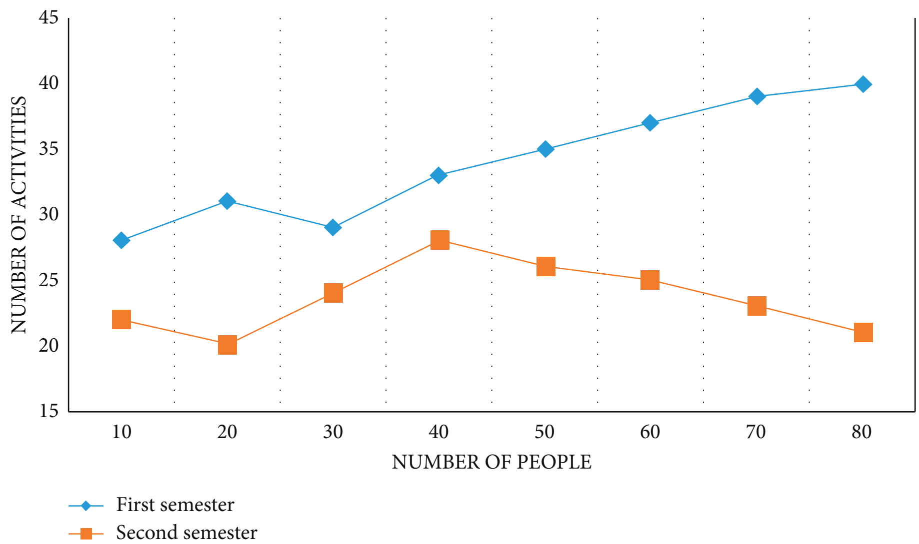

Figure 10: Distribution of “overall observation situation” frequency of large class teachers.

semester, which is related to observation habits developed over time; on the other hand, it is possible that the connotation of “evaluation of early childhood development” is not well understood, and there is no link between “evaluation” and “more effective early childhood learning support.” During the second semester, most teachers are able to observe the children’s mathematics learning process thoroughly and meticulously and record the important information learned. The details not only describe “what children learn” but also “how children learn,” according to the records. The research and implementation path for kindergarten STEM education is distinct. Data alone will not be able to solve all of the problems in kindergarten STEM education research and implementation. As a result, we should promote the reform and development of STEM education activities development and implementation path in kindergartens by using data mining as a new way of thinking and path, research paradigm and method, and practical tools and means based on STEM pedagogy.

5. Conclusions

To summarize, the article believes that correct ideas and reasonable methods are required for the actual implementation of stem education in kindergartens. Preschool teachers should also work on improving their professional quality in stem education. In the era of data mining, objectively analyzing the various paths and methods of data mining in the field of education is beneficial to our clearer and objective cognition of data mining, as well as thinking and using big data based on educational research and practice. As a result, China should strengthen the construction and analysis of data mining information in educational monitoring, supervision, and evaluation, as well as accelerate the construction of a national education big data information center or database, by developing stem educational activities in kindergartens and implementing data mining application paths and methods of path monitoring index system. The role and impact of data mining on education are discussed in this paper, which is based on data collection, acquisition, processing, and analysis. The stem education monitoring index system constructs the data hierarchy and category model of the index, analyzes the data collection mechanism of the index, and collects and obtains the data of each index of the index system, based on large-scale data investigation and database, using relevant ideas and methods of data mining. The development of stem educational activities in kindergartens frequently involves real-life issues that children face. Through a continuous problem exploration, solution, and implementation path, children continue to push the activity process forward.

Data Availability

The data used to support the findings of this study are included within the article.

Conflicts of Interest

The author does not have any possible conflicts of interest.

Acknowledgments

This study was supported by the Project of Hunan Social Science Achievement Evaluation Committee in 2022 “Casting rural Soul: A study on the Normal Path of Promoting rural revitalization in Hunan Local Universities” (XSP22YBC556); Education Reform Project of Hunan Province “Research on The Training Mode of Local Government-funded Directed Normal University Students under the Background of Rural Revitalization Strategy” (Xiangjiaotong [2019] nos. 291 and 699); Hunan Province Education Planning Base Platform Project “Research on the Transformation Path of Local Normal Education under Modern Governance Theory” (XJK19JGD002).

References

[1] K. Susanne, W. Olivia, W. Tamara et al., "Design, implementation, and study protocol of a kindergarten-based health promotion intervention," *BioMed Research International*, vol. 2017, pp. 1–9, Article ID 4347675, 2017.

[2] M. Heima, W. Lee, P. Milgrom, and S. Nelson, "e-caregivers education level and child's dental caries in African Americans: a path analytic study," *Caries Research*, vol. 49, no. 2, pp. 177–183, 2018.

[3] J. Yin, Y. Ding, and L. Fan, "Language ideologies, practices, and kindergarteners' narrative macrostructure development: crucial factors for sustainable development of early language education," *Sustainability*, vol. 6, pp. 13-14, 2021.

[4] J. Wyszyńska, P. Matosz, A. Szybisty, K. Dereń, A. Mazur, and J. Herbert, "The association of actigraphic sleep measures and physical activity with excess weight and adiposity in kindergarteners," *Scientific Reports*, vol. 11, no. 1, pp. 2298–2230, 2021.

[5] P. S. Macklin, N. Pillay, N. Pillay et al., "CM-Path Molecular Diagnostics Forum-consensus statement on the development and implementation of molecular diagnostic tests in the United Kingdom," *British Journal of Cancer*, vol. 121, no. 9, pp. 738–743, 2019.

[6] D. J. Adelstein, S. Koyfman, B. B. Burkey et al., "Successful development, implementation, and assessment of a clinical care path (CP) guide for the treatment of human papillomavirus (HPV)-Initiated oropharynx cancer," *International Journal of Radiation Oncology, Biology, Physics*, vol. 94, no. 4, pp. 895-896, 2016.

[7] A. Linden and P. R. Yarnold, "Maximizing predictive accuracy by P. R. Yarnold R. C. Soltysik. ODA books, chicago, IL, 2016, $98.00, 396 pp. ISBN 0 692 70092 7," *Journal of Evaluation in Clinical Practice*, vol. 22, no. 6, pp. 835–838, 2016.

[8] E. N. Souza, K. Boerder, S. Matwin, and W. Boris, "Improving fishing pattern detection from satellite AIS using data mining and machine learning," *PLoS One*, vol. 11, pp. 11-12, 2016.

[9] S. García, J. Luengo, and F. Herrera, "Tutorial on practical tips of the most influential data preprocessing algorithms in data mining," *Knowledge-Based Systems*, vol. 98, no. 15, pp. 1–29, 2016.

[10] H. Hong, H. R. Pourghasemi, and Z. S. Pourtaghi, "Landslide susceptibility assessment in Lianhua County (China): a comparison between a random forest data mining technique and bivariate and multivariate statistical models," *Geomorphology*, vol. 259, no. 15, pp. 105–118, 2016.

[11] T. Guo and J. V. Milanovic, "Online identification of power system dynamic signature using PMU measurements and data mining," *IEEE Transactions on Power Systems*, vol. 31, no. 3, pp. 1760–1768, 2016.

[12] D. T. Bui, T. C. Ho, B. Pradhan, P. Binh-Thai, N. Viet-Ha, and R. Inge, "GIS-based modeling of rainfall-induced landslides using data mining-based functional trees classifier with AdaBoost, Bagging, and MultiBoost ensemble frameworks," *Environmental Earth Sciences*, vol. 75, no. 14, pp. 1–22, 2016.

[13] M. Zhao, A. Jha, Q. Liu et al., "Faster Mean-shift: GPU-accelerated clustering for cosine embedding-based cell segmentation and tracking," *Medical Image Analysis*, vol. 71, Article ID 102048, 2021.

[14] Z. Huang, Y. Liu, C. Zhan, L. Chen, C. Weiwei, and C. Yunwen, "A novel group recommendation model with two-stage deep learning," *IEEE Transactions on Systems, Man, and Cybernetics: Systems*, 2021, In Press.

[15] T. Xiao, P. Zhang, Y. Zhang, D. Li, and J. Shen, "A research on the application of college students' physique data mining based on logistic regression algorithm," *ASP Transactions on Computers*, vol. 1, no. 2, pp. 12–18, 2021.

[16] N. Bonneton-Botté, S. Fleury, N. Girard et al., "Can tablet apps support the learning of handwriting? an investigation of learning outcomes in kindergarten classroom," *Computers & Education*, vol. 151, Article ID 103831, 2020.

[17] Y. Zeng, Z. Yuan, J. Yin, Y. Han, C.-I. Chu, and Y. Fang, "Factors affecting parental intention to vaccinate kindergarten children against influenza: a cross-sectional survey in China," *Vaccine*, vol. 37, no. 11, pp. 1449–1456, 2019.

[18] A. Gamoran, "Will latest U.S. law lead to successful schools in STEM?" *Science*, vol. 353, no. 6305, pp. 1209–1211, 2016.

[19] T. Mcgoey, Z. Root, M. W. Bruner, and B. Law, "Evaluation of physical activity interventions in children via the reach, efficacy/effectiveness, adoption, implementation, and maintenance (RE-AIM) framework: a systematic review of randomized and non-randomized trials," *Preventive Medicine*, vol. 82, no. 4, pp. 8–19, 2016.

[20] S. Whiting, R. Mendes, S. T. Morais et al., "Promoting health-enhancing physical activity in europe: surveillance, policy development and implementation 2015–2018," *Health Policy*, vol. 125, pp. 1023–1030, 2021.

[21] S. Ray and M. Saeed, "Applications of educational data mining and learning analytics tools in handling big data in higher education," *Applications of Big Data Analytics*, vol. 12, pp. 135–160, 2018.

[22] S. Belton, W. O'Brien, J. Mcgann, and I. Johann, "Bright spots physical activity investments that work: youth-Physical Activity towards Health (Y-PATH)," *British Journal of Sports Medicine*, vol. 53, pp. 53–55, 2019.

[23] B. P. Scannell, M. K. Wally, E. Flores, J. Levy, M. Waddell, and R. B. Seymour, "Development and implementation of a pediatric trauma survivors network program," *Journal of Trauma Nursing*, vol. 26, no. 2, pp. 71–75, 2019.

[24] C. House, G. Meades, and K. J. Linenberger, "Approaching a conceptual understanding of enzyme kinetics and inhibition: development of an active learning inquiry activity for pre-health and nonscience majors," *Journal of Chemical Education*, vol. 93, no. 8, pp. 1397–1400, 2016.

[25] J. M. Pavez, C. A. Vergara, D. Santibaez, and C. Hernán, "Using a professional development program for enhancing Chilean biology teachers' understanding of nature of science (NOS) and their perceptions about using history of science to teach NOS," *Science & Education*, vol. 25, no. 3, pp. 383–405, 2016.

Hindawi
Computational Intelligence and Neuroscience
Volume 2022, Article ID 8235308, 12 pages
https://doi.org/10.1155/2022/8235308

Research Article

A Study on Regional GDP Forecasting Analysis Based on Radial Basis Function Neural Network with Genetic Algorithm (RBFNN-GA) for Shandong Economy

Qing Zhang, Abdul Rashid Abdullah, Choo Wei Chong, and Mass Hareeza Ali

School of Business and Economics, Universiti Putra Malaysia, Seri Kembangan 43400, Malaysia

Correspondence should be addressed to Qing Zhang; gs57469@student.upm.edu.my

Received 6 December 2021; Revised 30 December 2021; Accepted 31 December 2021; Published 25 January 2022

Academic Editor: Xin Ning

Gross domestic product (GDP) is an important indicator for determining a country's or region's economic status and development level, and it is closely linked to inflation, unemployment, and economic growth rates. These basic indicators can comprehensively and effectively reflect a country's or region's future economic development. The center of radial basis function neural network and smoothing factor to take a uniform distribution of the random radial basis function artificial neural network will be the focus of this study. This stochastic learning method is a useful addition to the existing methods for determining the center and smoothing factors of radial basis function neural networks, and it can also help the network more efficiently train. GDP forecasting is aided by the genetic algorithm radial basis neural network, which allows the government to make timely and effective macrocontrol plans based on the forecast trend of GDP in the region. This study uses the genetic algorithm radial basis, neural network model, to make judgments on the relationships contained in this sequence and compare and analyze the prediction effect and generalization ability of the model to verify the applicability of the genetic algorithm radial basis, neural network model, based on the modeling of historical data, which may contain linear and nonlinear relationships by itself, so this study uses the genetic algorithm radial basis, neural network model, to make, compare, and analyze judgments on the relationships contained in this sequence.

1. Introduction

As economic policies become more relevant to people's lives, economic development has become a topic of discussion, and GDP, a measure of a country's or region's economic performance and level of development, has gradually become a national focus. The country's or region's future development trends are measured and evaluated. Shandong province's total GDP has ranked third among national economic provinces for many years, and according to the most recent data, its total GDP exceeded $7 trillion for the first time in 2017. Shandong province's economic development has a solid foundation. However, the gap between it and Guangdong and Jiangsu provinces, which are ranked first and second in terms of total GDP, is widening year by year [1]. Furthermore, Shandong province's total GDP ranking remains deficient when compared to its GDP per capita level; the level of GDP per capita indicates a region's level of development; for Shandong province, as a large population province, increasing GDP per capita is always a development goal. In terms of Shandong province's total GDP growth rate, it increased by 7.4 percent in 2020 compared to 2019, but the growth rate does not have an advantage over other provinces, and the economy of Shandong province still has a lot of room for development [2].

Based on the above background, it can be seen that the study of Shandong province's economic situation is very relevant and valuable, and the appropriate forecast of Shandong province's GDP can, to a certain extent, know the future economic development in advance, to be prepared in advance, and according to the forecast timely adjustment based on the existing situation. For the total economic volume of Shandong province, the situation of small per capita can explore the factors affecting the economic development of Shandong province and the interaction of Shandong province GDP and clarify the key to the economic development of Shandong province, based on the existing key transformation so that the economy of Shandong province attains healthy and stable development. Based on the development of the three major industries in Shandong province, there is still a lot of room for improvement, and the study and discussion of the GDP of each of the three major industries are conducive to further adjustment and optimization of the industrial structure and improvement of the economic development posture of Shandong province. Radial basis function (RBF) neural network is an efficient single-hidden layer forward network, which mimics the neural network structure of local regulation and mutual coverage of sensory domains in the human brain [3]. The gray forecasting model has unique advantages for forecasting with little data, missing data, or poor information, with low requirements for original data, high short-term forecasting accuracy, and ease of model testing; however, when data are scattered or the number of forecasting periods is long, the forecasting accuracy will significantly drop; the quadratic exponential smoothing method requires less historical data and has high short-term forecasting accuracy for forecasting with little data, missing data, or poor information; however, when the data are scattered or the number of RBF neural networks is a type of forward neural network that has global approximation capability and best approximation performance, it allows to approximate any nonlinear function. It differs from the BP (backpropagation) network in terms of network structure and learning algorithm, and it partially compensates for the BP network's shortcomings. In comparison to other types of forwarding neural networks, the RBF neural network has several advantages, including a simple network structure, a deep physiological foundation, fast learning ability, and good approximation performance [4]. The radial basis function combined with the genetic algorithm (RBFNN-GA) effectively avoids local minima and improves global retrieval ability by overcoming the overlearning phenomenon. The RBFNN-GA algorithm was used to conduct predictive analysis of the Shandong economic region, which provides useful information for future economic development strategy and policy.

2. Related Work

There are many research methods and empirical works on GDP forecasting in China and its provinces and cities, and the main methodological models are summarized as regression analysis, time series analysis, gray forecasting, artificial neural network, and a combination of these types of models. The literature [5] used five regression models to predict GDP and compared the prediction results and robustness; the literature [6] analyzed five influencing factors such as fiscal expenditure and residential consumption that affect China's GDP and built a linear regression model based on these five factors to predict China's GDP. The gray forecasting method has gained the attention of a huge amount of researchers with a smaller sample size to get higher prediction accuracy and is widely used in socioeconomic forecasting. The literature [7] used the time series data of the GDP of Jiangsu province from 1978 to 2009 and then used the GM model to forecast, and the test results showed that the model could provide accurate forecasts. Literature [8] established a gray GM model with different dimensions and an improved method of the gray model to forecast the GDP of Anhui province in 2015. Literature [9] used Lagrangian difference and segmented linear Newtonian difference methods and two orthogonalization methods to optimize the gray forecasting model to forecast the GDP growth of Xinjiang in 2018–2019. Due to their strong nonlinear fitting ability, artificial neural network models are frequently used to forecast GDP. The literature [10] used BP neural network models to forecast Guangxi GDP and found that BP networks are more informative. The literature [11] used the stepwise regression method to preprocess the data before applying the neural network method to predict the GDP of Jilin province, resulting in more accurate predictions. To build a GDP prediction model, the literature [12] combined the improved standard particle swarm algorithm with the dynamic Elman neural network with local memory function, which yielded GDP prediction values with higher accuracy. All of the above methods have produced positive results in predicting GDP, but as technology advances, the demand for accuracy and model stability grows. As a result, combined models for prediction are becoming more common, combining the benefits of each model to improve the model's applicability and prediction accuracy. To forecast GDP, literature [13] used the ARIMA model, exponential smoothing model, and a combined forecasting model with the residual inverse method, variance inverse method, and least-squares method. Literature [14] combined the time series model and regression analysis model to analyze and forecast the GDP of Anhui province. Literature [15] used gray forecasting GM and ARIMA models to separately forecast Chinese GDP and weighted average of the forecast values to get the final result to normalize. The literature [16] combined the ARIMA model with BP neural network method to form a new combined model to forecast the GDP of Shandong, studied its principle, and tested the generalization to derive the optimal forecasting model. The literature [17] empirically tests the impact of industrial structure on overall income and growth, and after discussing the detailed results of traditional shift-share analysis, it uses dynamic panel estimation to analyze a standard growth model extended by structural variables and, based on data from 28 OECD countries, concludes that industrial structure is a macroeconomic development and growth in the 1990s The conclusion that it is an important determinant of the literature [18], and others explored the link between public expenditure and economic growth, deriving conditions under which changes in the composition of expenditure lead to stable economic growth, and, using data from 43 developing countries, found that the current increase in the share of expenditure has a positive and significant growth effect, while in contrast, the relationship between the capital component of public expenditure and per capita growth is negative, with overuse of productive expenditures. There is no benefit to be derived from the excessive use of productive expenditures.

3. A Study on Regional GDP Forecasting Analysis of Shandong Economy in China Based on RBFNN-GA Algorithm

3.1. Radial Basis Function Neural Network Algorithm Combined with Genetic Algorithm. The basic idea of the RBFNN neural network is to transform the data from a low-dimensional space to a high-dimensional space so that the data can be linearly separated after the transformation. Both RBF and BP neural networks have a pretty nonlinear fitting ability. RBFNN contains only one hidden layer and computes the parameters by the idea of local approximation, which is computationally small and fast. RBF starts by choosing P basis functions, each of which will correspond to a training sample, and the individual basis functions are of the form $(\varphi\|X{-}X\|)$. Since the distances are radially identical, the radial basis functions get their name from this. Although both RBFNN and BP neural networks are universal approximators and belong to the same static feedforward neural network, they are always interchangeable in the same example. Figure 1 shows a radial basis function (RBF), whereas BP is a sigmoid function. Local minima in the parameter space, as shown in Figure 1, is a common problem with traditional neural network algorithms. Because any local minima is global minima if a function is convex, many models try to use convex optimization methods, such as the well-known support vector machine algorithm, which converts the problem into a dyadic problem using KKT conditions, and the dyadic problem is a convex optimization problem, allowing the global minima to be easily found. Because of their powerful nonlinear fitting ability, RBF neural networks can map a wide range of nonlinear relationships. In contrast, most loss functions, especially in deep learning, are nonconvex, and multiple local minima can be found [19]. In addition to the function's nonconvex nature, the spatial symmetry of the neural network's weights can result in a large number of local minima, emphasizing the importance of a good optimization algorithm. To find the existence of global minima, a genetic algorithm can be used to improve the traditional radial basis neural network algorithm.

The mathematical model of radial basis function neural network based on genetic algorithm (radial basis function neural network-genetic algorithm, RBFNN-GA) with three-layer network structure can be represented by the following:

$$T(i, j) = \frac{\overline{g}(i, j) + \overline{g}\max}{\overline{g}\max - \overline{g}\min} + |X - Y|^2, \tag{1}$$

where $X = (x_1, x_2, \ldots, x_n)$ is the input vector and $Y = (y_1, y_2, \ldots, y_n)$ denotes the center of the ith neuron node in the hidden layer; $|x{-}y|^2$ denotes the square of the Euclidean distance between the input vector and the centroid; g represents the activation function, which is usually Gaussian in radial basis function neural networks; σ denotes the smoothing factor of the activation function of the ith neural node, which is used to control the width of the activation function; A denotes the weight from the hidden layer to the output layer; and k and m denote the number of nodes of the hidden layer neurons and the dimension of the input vector, respectively. The structure of the three-layer radial basis function neural warp network in this study is shown in Figure 2.

A random radial basis function neural network differs from a general radial basis neural network, and in that the centers $y_i = (y_{i1}, y_{i2}, \ldots, y_{in})$ and the smoothing factor k of its hidden layer neuron nodes are generated in some way and need to be determined before the weights A of the output layer are derived by least squares. For any continuous function f and RBFNN-GA neural network, where $I \in [0, 1] \in R$, we define

$$Y = I_{nn} \cdot X_{nn} = \begin{pmatrix} I_{11} & \cdots & I_{1j} & \cdots & I_{1n} \\ \cdots & \cdots & \cdots & \cdots & \cdots \\ I_{i1} & \cdots & I_{ij} & \cdots & \cdots \\ \cdots & \cdots & \cdots & \cdots & \cdots \\ I_{in} & \cdots & \cdots & \cdots & I_{nn} \end{pmatrix} \cdot \begin{pmatrix} x_{11} & \cdots & x_{1j} & \cdots & I_{1n} \\ \cdots & \cdots & \cdots & \cdots & \cdots \\ x_{i1} & \cdots & x_{ij} & \cdots & \cdots \\ \cdots & \cdots & \cdots & \cdots & \cdots \\ x_{in} & \cdots & \cdots & \cdots & x_{nn} \end{pmatrix} = \begin{pmatrix} y_{11} & \cdots & y_{1j} & \cdots & y_{1n} \\ \cdots & \cdots & \cdots & \cdots & \cdots \\ y_{i1} & \cdots & y_{ij} & \cdots & \cdots \\ \cdots & \cdots & \cdots & \cdots & \cdots \\ y_{in} & \cdots & \cdots & \cdots & y_{nn} \end{pmatrix}. \tag{2}$$

The parameter b denotes the output threshold. Then, based on the predicted output O and the expected output T_k, the prediction error can be determined as

$$b = (O_k - T_k) \cdot g(k). \tag{3}$$

The update formula for the weights and thresholds is as follows:

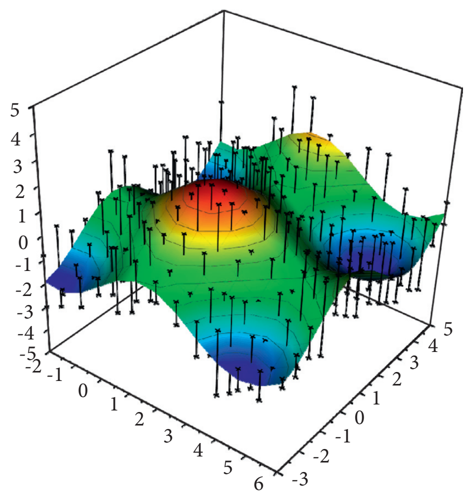

Figure 1: Schematic diagram of local minima.

$$\beta = \alpha_1 - \frac{(\alpha_2 + \alpha_1)\left(E_n^1 + \lambda_1\right)}{(\lambda_2 + \lambda_1)}. \tag{4}$$

When the input signal of the network is the kth training sample X_k, its output value of the jth neuron after the nonlinear transformation of the i-th hidden layer neuron is

$$X_k = T_k + b \sum_{i=1,j=1}^{n} X_{ij}^2, \tag{5}$$

where $j = 1,2, \ldots, J$. The basis function is generally chosen to be Green's function:

$$G(J) = j\frac{\partial \gamma}{\partial j} + \frac{1}{n}\sum_{i=1}^{n} X_i Y_i. \tag{6}$$

The core concept behind RBFNN networks is that the hidden layer transforms the input data, mapping the relatively low-dimensional input into a high-dimensional space, allowing the data to be transformed from indistinguishable in the low-dimensional space to divisible in the high-dimensional space. The division of the input space into several subspaces in hyperspherical form is the geometric core of RBFNN neural networks. Theoretically, it can be argued in this study that as long as there are enough hidden layer nodes, the RBF network can always achieve an infinite approximation to any arbitrary continuous function, regardless of how small the error is set. This study also shows that two-parameter weights in the formula and the center of the radial basis function have yet to be determined and will be determined through network training. The random selection of some parameters in radial basis function neural networks is a useful addition to the existing methods for determining the center and smoothing factor of these networks. The centers of radial basis functions are frequently calculated using clustering methods (K-means clustering, fuzzy C-means clustering, and principal component clustering methods) and other methods, similar to some fuzzy modeling technologies [20, 21]. The gradient descent method is frequently used to train the weights of the hidden layer to the output layer [22]. When the RBFNN-GA neural network has a very large number of hidden layers, it can be used to approximate any M-element continuous function with arbitrary accuracy, and the network can always be trained to find a corresponding set of weights to make the best approximation of the unknown nonlinear mapping relation $f(-)$ between the input and output. A regularized network is described in terms of the interpolation problem as complete interpolation, i.e., finding a hypersurface such that it passes through all sample points.

RBFNN-GA neural networks are nonlinear multilayer feedforward neural networks that have the same properties as multilayer perceptrons, with the exception that they are both general approximators, meaning that any multilayer perceptron can be replaced by an RBFNN-GA neural network, and any RBFNN-GA neural network can find a multilayer perceptron that performs the same function as it. However, there are some distinctions between the two networks.

(1) In terms of network structure, RBF neural networks have only one hidden layer, unlike multilayer perceptrons, which can have one or more hidden layers.

(2) In a multilayer perceptron, the implicit layer neuron model is identical to its output layer neuron model; in an RBFNN-GA neural network, the two models are quite different and the two models do not play the same role in the network.

(3) There can be linear or nonlinear implicit and output layers between multilayer perceptrons, and when they solve pattern classification problems, they generally choose nonlinear mapping relations, and if they are solving nonlinear regression problems, the output generally chooses linear relations, and it is different in RBFNN-GA neural networks, where the implicit layer is a nonlinear mapping relation while the output layer is a linear mapping relation.

(4) The excitation function of the RBFNN-GA neural network hidden layer neuron calculates the Euclidean distance between the input vector and the center, while the excitation function of the multilayer perceptron hidden layer neuron calculates the inner product between the input unit and its connection weights.

(5) The RBFNN-GA neural network uses a local exponentially decaying nonlinear function to make a local approximation of the nonlinear input-output mapping, while the multilayer perceptron is a global approximation of a nonlinear mapping. To put it another way, the multilayer perceptron requires many more parameters than the RBFNN-GA neural network in order to approximate the nonlinear input-output mapping with the same accuracy.

3.2. Application of RBFNN-GA Algorithm to GDP Forecasting and Analysis Studies. According to the literature and various theoretical proofs, the combined model's prediction effect can usually improve the single model to some extent.

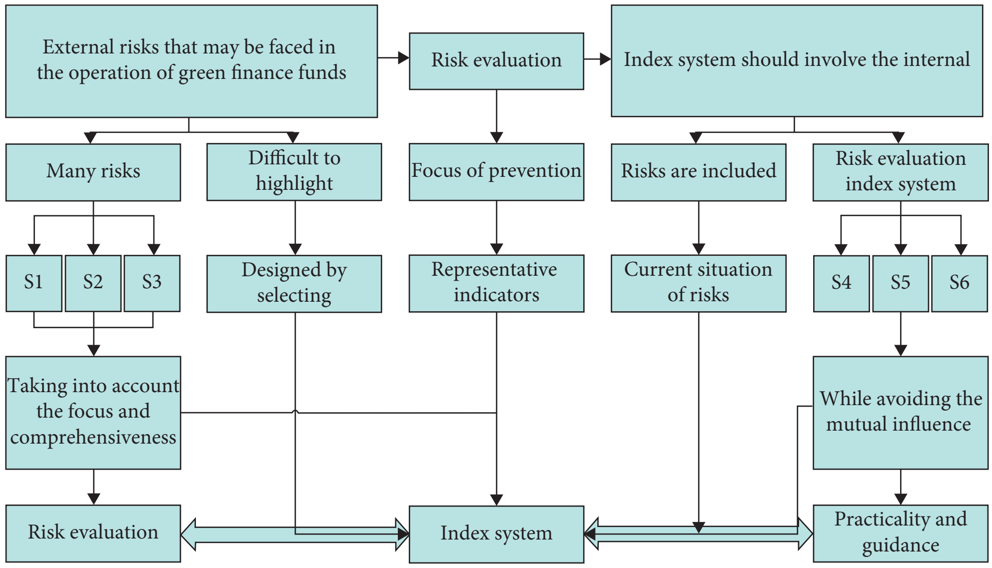

Figure 2: Structure of radial basis function neural network.

Because it is difficult to tell whether time series is linear or nonlinear in real-world applications based on time series modeling, a single model is often used for one of the mappings, whereas the combined forecasting method described in this study targets complex mapping relationships and can tap both linear and nonlinear features of the series. The rising trend of GDP in Shandong province is influenced by many factors and is a nonstationary series, so its series is judged to have both linear and nonlinear characteristics. The GA model is frequently used to model linear relationships, while the RBFNN neural network is used to mine the series' nonlinear relationships. Model compression techniques and scaling were combined with optimization goals to achieve an automatic selection of model compression techniques for various networks and task requirements. The combination of these two forecasting methods fully exploits their benefits and compensates for the single model's single mapping relationship flaw. Most of the data features of the GDP series in Shandong province can be mined using a combination of RBFNN and GA neural network, and the prediction accuracy of a single model can be improved.

The network structure of the RBFNN neural network algorithm is determined, and its training process is mainly divided into two parts: first is the forward propagation of information, which means that the information is input from the input layer, after the nonlinear mapping of neurons in the hidden layer, and passed into the output layer to output the result [23]. The second is error backward propagation, which refers to the error between the output result of the output layer and the true value by judging the error, and if it exceeds the range of the preset error, the error signal is gradually passed backward, while adjusting the weights and thresholds of each hidden layer passed through, so that the adjusted parameter model makes the output error decrease along the gradient direction. After repeatedly fixing the model after the parameters until the prediction error is controlled within the set range, the learning process of the network is ended and the weights and thresholds of each layer corresponding to the minimum mean square error are obtained, i.e., the nonlinear mapping relationship of the model is determined.

The compression algorithm is improved by studying three compression techniques, namely quantization, sparse, and cropping, to realize the compression of different models with different network structures at different scales of model compression. The experiments compare the models' load characteristics under various compression methods. The differences in performance between the various methods are tracked and analyzed. Finally, reasonable model compression and scaling techniques are demonstrated. By selecting a reasonable model compression technique and ratio, the model size, inference time, and energy consumption can be effectively reduced, and the performance of different compression methods in different network structures varies. The best compression method is determined by the target neural network's structure and the optimization constraints. The best compression method is determined by the target neural network's structure and the optimization constraints.

Combining the two algorithms of RBFNN and GA neural network, the main principles of the combined prediction model are as follows: (1) the GA model predicts the linear part of GDP in Shandong province; because the GA model builds a linear regression of the current data about its lagged data, so this study will apply the prediction result of the GA model as the linear part of the combined model prediction. The residual of the RBFNN model prediction, i.e., the white noise, as the part outside the linear part of the series, no longer has the value information of linear prediction, so it is hoped that the residual value of white noise can be extracted using nonlinear prediction. (2). RBFNN neural network model trains the white noise series and extracts the nonlinear features in the GDP series, mentions the residual series predicted by the GA model, and builds the RBFNN neural network model after the matrix transformation and normalization process. The predicted value of this model is used as the predicted value of the nonlinear part of the time series, i.e., the nonlinear information of the extracted time series. (3) The fitted value of the GA model is added to the predicted residual value of the RBFNN neural network and the obtained predicted value, which is the predicted value of the combined model proposed in this study. The specific steps are shown in Figure 3.

The variance of each variable in the model can be decomposed according to certain criteria, and the criterion of variance decomposition is to decompose the variance of the variable according to the proportional size of the influence of each random disturbance term on the variable, and the variance decomposition studies the proportion of the influence of the orthogonalized residuals on the mean squared error (MSE) of the prediction, so it can be seen that the variance decomposition studies the proportion of the influence of the orthogon. Because the variance decomposition yields the proportion of shocks' impact on variable change, the relative magnitude of each perturbation term's impact on the variables can be determined, and thus, the relative importance of each perturbation term on a variable can be determined. The sum of the percentage contributions of all orthogonalized disturbances to a variable's effect is 100 percent for its mean square error. The vast majority of time series in socioeconomic phenomena are nonstationary time series, as is well known. In order to convert the slowly varying trend terms, periodic seasonal terms, and smooth random noise terms in nonstationary time series into stationary time series, various data primitive transformations and more processing methods must be used in modeling. This can then be transformed into analysis modeling. As a result, transforming the time series into a smooth time series and ensuring that the trend information is extracted adequately become critical. When dealing with nonsmooth time series, a variety of treatments can be considered to smooth them out.

With the RBFNN algorithm, stochastic radial basis function neural networks have been shown to have fast learning ability and powerful function approximation capability, both in theory and practice. However, due to the random selection (uniform distribution) of the centers and smoothing factors of the radial basis functions in the network, it is easy to cause the output matrix of the hidden layer to be irreversible and even pathological. This leads to the instability of the solution when solving the output layer weights, which affects the stability of the RBFNN algorithm and the performance of the random radial basis function neural network. More importantly, the stochastic radial basis function neural network solving the output layer weights by the RBFNN algorithm does not avoid the overfitting phenomenon and usually performs very well in the training set but poorly in the test set. It is found that the above problem can be effectively avoided by model regularization, i.e., adding the l penalty term to the original model.

We need to preprocess the data before we can conduct the variable selection analysis, and the first step is to run a correlation test, as shown in Figure 4. The correlation coefficient between multiple sets of explanatory variables is above 0.8, and the multicollinearity between variables is serious, so it will lead to instability and difficulty in explaining the prediction model later, so in this step, we use the Lasso method to process for variable selection and solve the multicollinearity problem [24]. To free the model from the constraints of the explanatory variables' units and sizes, the data must be transformed into dimensionless, or normalized, form. Subsequently, we use the Glenmont package in R to implement the Lasso model for various X values. We can see how the model's coefficients change in the following diagram, and then, we use the cross-validation (CV) method to select the best parameter values and thus determine the variable selection results. Total energy supply and total disposable income per capita are the final economic explanatory variables we choose as the most relevant to Shandong province's GDP. This also demonstrates that Shandong province's GDP is highly correlated with agro-industry, indicating that the province's GDP is dominated by primary and secondary industries. Chemical, machinery, textile, metallurgy, and other energy-based industries account for the majority of Shandong province's main business income. Energy and raw material industries account for more than 40% of Shandong province's GDP, indicating that industrial agriculture remains the province's main contributor, and the development of tertiary industries, such as commerce, finance, and transportation and new industries such as the internet industry, is still in its infancy.

4. Experimental Verification and Conclusions

Figure 5 depicts the total economic volume of Shandong province over the next seven years, as predicted by the RBFNN-GA algorithm. It is expected that the total economic volume of Shandong province over the next seven years will continue to show an upward trend and grow at a high rate, with average annual growth rates of 3.98 percent, 5.63 percent, 6.39 percent, and 6.97 percent, respectively. GDP growth over the next five years is expected to be 7.63 percent on average, reaching 1,134.2 billion by 2025; GDP growth over the next five years is essentially the same as the growth rate in 2019–2020, is essentially consistent with the growth rate since 2015, and will remain at a higher level than in the previous 50 years. The average annual growth rate of total annual fixed-asset investment (FAI) over the next five years, 2022–2026, is forecasted to be 4.79 percent, reaching $801.95 billion in 2025; the growth rate of a total fixed-asset investment over the next five years is slightly higher than the growth rate in 2019–2020, but significantly lower than the growth rate since 2010, and will remain moderate and steady. Over the next five years, 2022–2026, the annual average growth rate of annual general public budget revenue (GBR) is expected to be 5.21 percent, reaching 947.8 billion by 2025. The general public budget revenue growth rate over the next five years is slightly higher than the rate in 2019–2020, which is largely consistent with the growth rate since 2010 and will annually increase. The initial individual's efficiency curve is the lowest, followed by the individual with the best head, and finally the individual with the best efficiency. The growth spokes of total fixed-asset investment

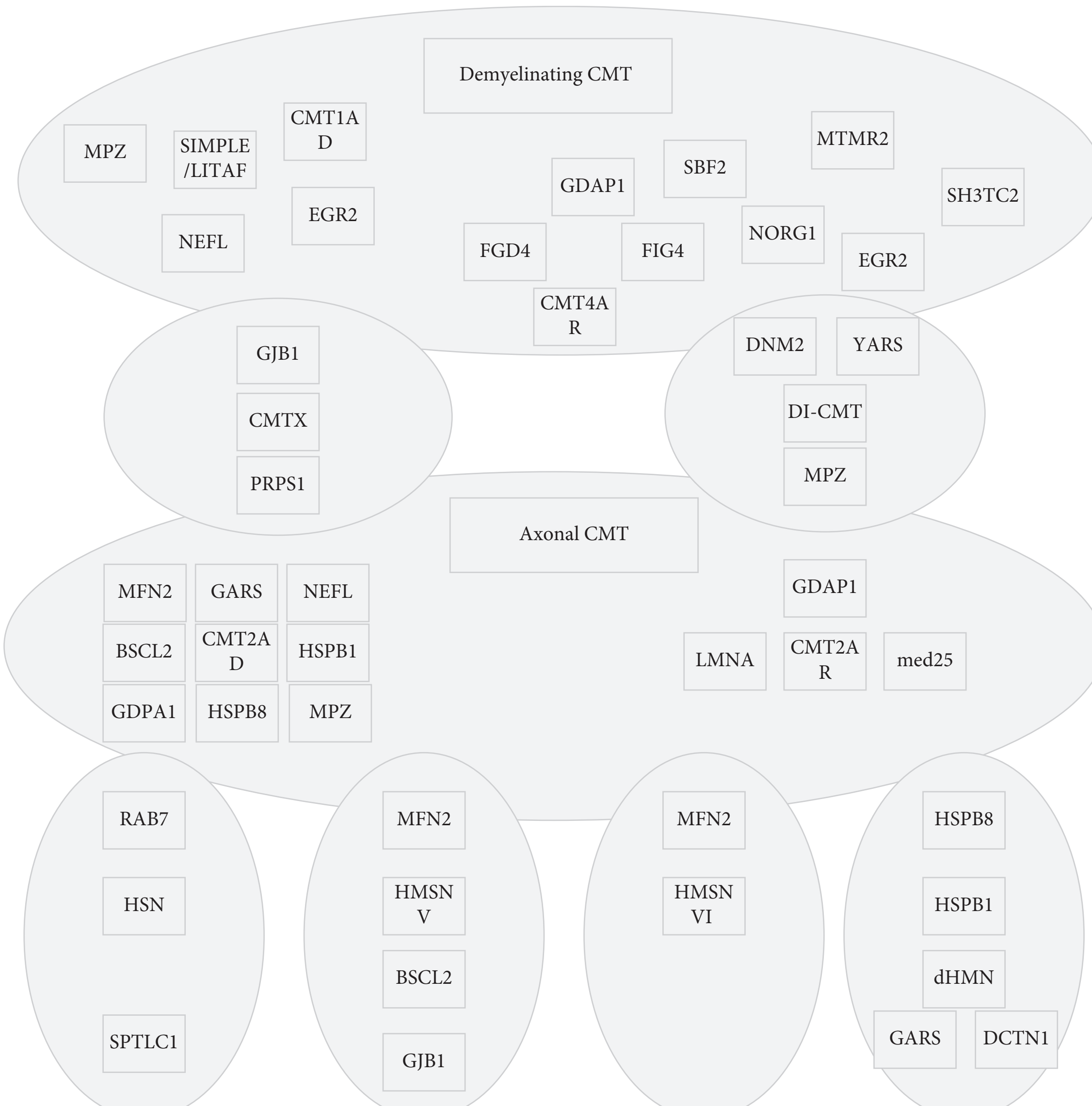

Figure 3: Flow chart of the combined model prediction.

and general public budget revenue are smaller when compared to GDP and total retail sales of consumer goods.

As shown in Figure 6, in the next five years, the regional GDP growth rate is expected to increase and then decrease, but the GDP growth rate does not change much, generally located in the range of 6.3%–6.8%. It can be seen that the economy of Shandong province has passed the stage of high growth, the growth rate has become slower and entered the stage of steady progress, the regional GDP will maintain moderate growth, at this time, the total regional production increased, not only the level of economic development but also the inflation rate is small, and this level of GDP growth rate is conducive to achieve high-quality economic development. Combined with the economic development history of Shandong province, Shandong province should implement a stable and progressive fiscal policy to improve the quality of economic development while stimulating the growth of economic aggregates.

Figure 7 shows the change in total energy production in Shandong province over the next five years as predicted by the RBFNN-GA model. The total energy production in Shandong province is expected to decline in the next five years, with an average annual growth rate of −3.98%. The average annual growth rate of total energy production in the five years of 2022–2026 is expected to be −3.25% and will drop to 103.52 million tons of standard coal by 2025; the growth rate of energy production in the next five years is slightly higher than that in 2019–2020, but it will remain negative. Insufficient energy supply will constrain the economy and reduce the rate of economic development.

The growth rate of disposable income per capita over the next five years in Figure 8 shows that urban disposable income per capita is increasing, with annual growth rates fluctuating between 5.7 and 6.5 percent, with an average annual growth rate of 6.13 percent; rural disposable income

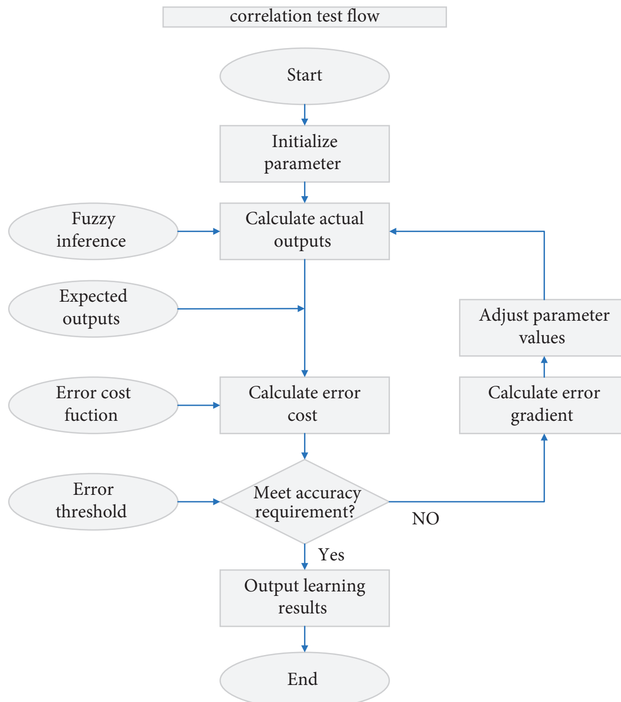

Figure 4: Flow chart of correlation test.

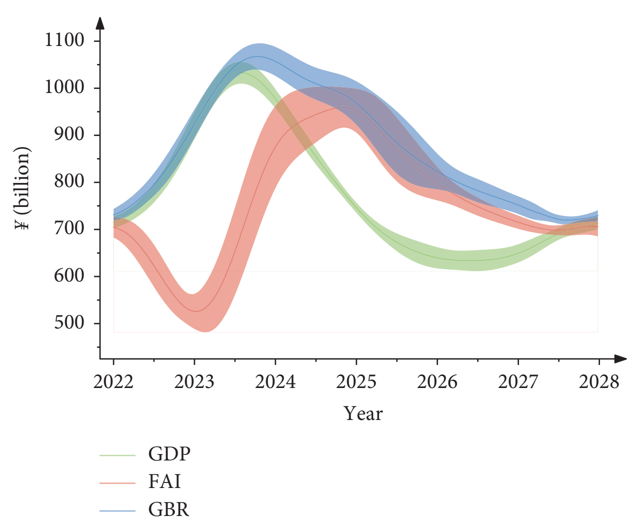

Figure 5: Economic aggregates projected by RBFNN-GA model for the next seven years in Shandong.

per capita is increasing, with annual growth rates fluctuating between 7.2 and 7.9 percent, with an average annual growth rate of 6.43 percent. Both growth rates are expected to be smaller than those seen since 2005, and the difference between the two is small and consistent. In terms of growth volume, although the difference between the growth rates of per capita disposable income of rural and urban residents is not large, or even slightly higher than that of urban areas, the average annual growth of per capita disposable income of urban residents is expected to be RMB 3,145 per person, while the average annual growth of per capita disposable income of rural residents is only RMB 1,403 per person, less than half of that of urban areas. The total economic volume of Shandong province is expected to continue to show an upward trend in the next seven years, maintaining steady growth at a high rate. In absolute terms, by 2025, the per capita disposable income of urban residents is expected to reach 63,146 yuan/person (a year), but only 27,893 yuan/person (a year) in rural areas, with the absolute difference in per capita disposable income increasing from 25,093 yuan/person to 35,253 yuan/person. In relative terms, the income ratio between urban and rural residents will decrease from 2.4873 in 2018 to 1.9758 in 2025, with a slight reduction in the relative gap.

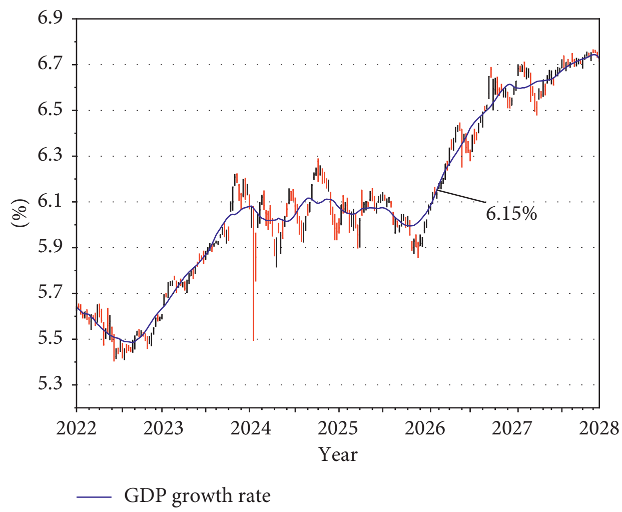

Figure 6: RBFNN-GA model forecasts the GDP growth rate in Shandong for the next five years.

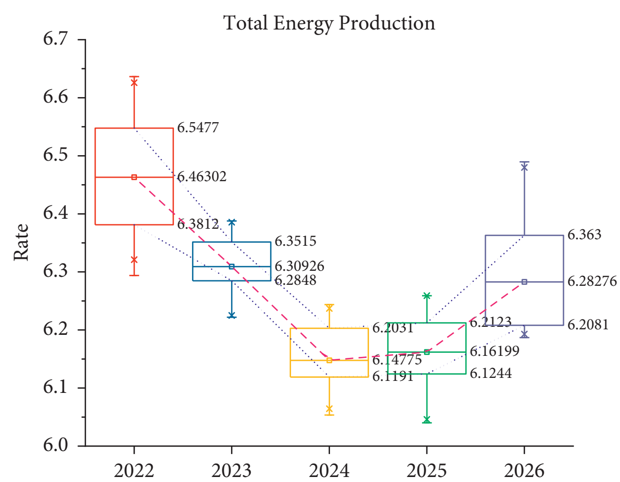

Figure 7: RBFNN-GA model projected changes in total energy production in Shandong over the next five years.

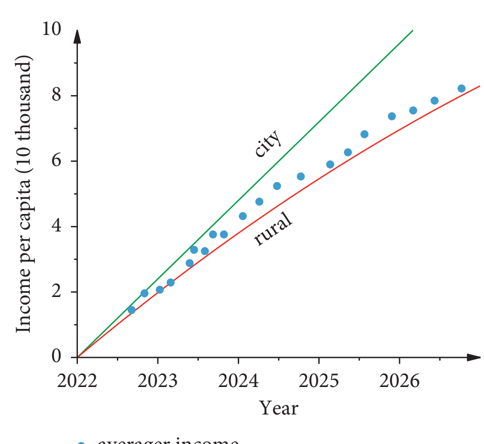

Figure 8: RBFNN-GA model forecasts disposable income per capita for the next five years in Shandong.

Currently, Shandong province's total economic output is at the forefront of the country, with total regional GDP in 2018 being the third highest in the country, GDP per capita the seventh highest in the country, and disposable income per capita in the first three quarters of 2019 ranked eighth in the country and will largely remain at this level over the next six years. In terms of growth, the projected GDP growth rate of 5.8% in Shandong province is not much different from the projected national GDP growth rate of about 4.7%, which is slightly lower in comparison; the per capita disposable income, especially the per capita disposable income of urban residents, will exceed the 50,000 yuan (/year) mark in 2022, and the per capita disposable income of rural residents will also exceed 20,000 yuan (/year) in the same year.

4.1. To Ensure Faster Economic Development and Improve the Quality of Economic Development. We should pursue progress while maintaining stability, improve the quality of economic development while stimulating economic output growth, and insist on promoting high-quality development as a general development strategy. To begin, we must vigorously develop high-tech industries and new industries, support the development of new services industries and promote development with "NEW," and take the early zone for the conversion of old and new dynamics and the pilot. We will also encourage the growth of innovation-driven digital intelligence, and new trade patterns, the development of marine industries, local economic cooperation between China, Japan, and Korea, and the rapid economic development of coastal cities. Second, sustained and steady growth should be ensured in total retail sales of consumer goods and fixed asset investment and growth should be promoted in line with demand by lowering fees and taxes and increasing government transfer payments. Finally, secondary energy conversion rates should be improved, new energy development should be accelerated, old kinetic energy should be replaced with new kinetic energy, and adequate energy supply should be ensured for industrial development.

4.2. Increase Agricultural Output and Promote Coordinated Urban and Rural Development. The data on per capita disposable income show that the gap between urban and rural residents' living standards is wide and unlikely to significantly narrow in the future. To begin, we should concentrate on the three rural areas, develop new agriculture, build new rural areas, and establish a model of rural revitalization in Qilu; second, we should promote village mergers and land transfers and develop large-scale agriculture and intensive agriculture; third, we should build high-standard farmland and develop green agriculture; fourth, we should establish agricultural science and technology companies, build high-tech agricultural demonstration parks, and accelerate the construction of high-tech agricultural demonstration parks. Second, in order to build beautiful villages, rural infrastructure should be strengthened, and the road hardening and toilet revolution should be accelerated. Finally, the urbanization of rural areas and the construction of small towns should be accelerated in two ways: first, the economic strength of counties, districts, and towns should be improved to close the gap between urban and rural areas in the province, and second, smart communities should be created and digital technology should be used to serve community management.

4.3. Pay Attention to the Spiritual Needs of the Masses and Enrich the Cultural Life of the Residents. The standard of living of the people has been greatly improved, and their concern for the world of design has been greatly increased. We should strengthen cultural construction, enrich cultural life, and improve the quality of life in the following ways: first, through building cultural communities, cultural squares, recreational clubs, and hosting cultural tours, to involve the masses and enrich the cultural life of the people; second, through activities such as culture in the community and culture in the countryside and through cultural storytelling and watching movies, etc., to promote local culture and positive mainstream culture to the masses, to improve the cultural literacy of the people, to promote the integration of culture and technology, to create a digital platform for cultural resources, a platform for the transformation of culture and technology, etc., to cultivate new cultural industries and enhance the people's sense of cultural access, to promote the development of culture and sports, such as hosting sports events, organizing national health games, sports, and cultural festivals, etc., and to find new ways to disseminate regional culture and popularize culture in daily exercise.

For future economic development, we recommend enhancing the development of the tertiary industry on the one hand and developing the service industry on the other hand. According to recent national economic data, the service industry's scale is growing, its quality and efficiency are greatly improved, and new industries and business models are emerging. Currently, the service industry in Shandong province requires further development. The service industry has the potential to bring a variety of new economic growth points, such as productive services, in the fine development of promising financial service industries of private fundraising, cultural tourism industry, internet economic industries such as big data, cloud computing, artificial intelligence, e-commerce, and so on. Simultaneously, the growth of the service sector can help to improve and support the current Shandong province economy, which is dominated by manufacturing and agriculture industries. In light of the new economic situation and the impact of the Sino-US trade war, it is more important than ever to fully tap domestic demand and to constantly activate the development of private enterprises, and small and microenterprises to generate new economic growth points. On the other hand, in light of the current economic situation and the escalation of difficulties, we cannot dismiss the importance of the state-owned economy, which has a significant impact on the economy of Shandong province. The Shandong economy state-owned system, which has a high starting point, high level, and high-quality state-owned enterprises, should be accelerated for further development. To stimulate market players and increase market-oriented reform, the upgrading and transformation of enterprises should be sped up that are not keeping up with market development. Simultaneously, increased support for scientific research undertakings is recommended; scientific and technological innovation can significantly improve productivity, more high speed, and high quality to enhance economic growth; not only the development of applied disciplines can be transformed into productivity, but also in the current situation, the development of basic disciplines is more important and can bring more critical core technological breakthroughs. It is suggested that spending on scientific research should be increased, that the construction of "double first-class" schools and disciplines should be strengthened, and that preferential policies for attracting talents, such as subsidies for settling talents and subsidies for high-end talents, should be increased.

5. Conclusions

This study completes the RBFNN-GA model's GDP prediction in Shandong province, and the results show that the RBFNN-GA model's prediction accuracy with input variables is higher than the univariate RBFNN model, and the RBFNN model's stability is also higher. To improve the accuracy of GDP prediction, this study combines the two algorithms of GA and RBFNN to create a combined model. Based on the assumption that the GA model mines the linear characteristics of the GDP series, the residual series predicted by the RBFNN model is taken as the part without linear information, and the RBFNN neural network model is built to extract the nonlinear information of this residual series. The linear part's predicted value is added to the nonlinear part's predicted value, and the resulting sum is the combined model's predicted value in this study. The way the residuals are predicted is the main difference between the improved combined model and the combinatorial model. By converting the genetic algorithm input information of both the fitted value sequence and the residual value sequence, the improved model predicts the residual value of the current period, and the value is added to the linear prediction result of the corresponding radial base model to obtain the prediction value of the improved model. After analyzing the experimental results, the improved combined model has the best prediction effect. The improved model predicts the current period's residual value by converting both the fitted and residual value sequences of the GA model into RBFNN neural network input information and then by adding the value to the linear prediction result of the corresponding RBFNN model to get the prediction value of the improved model. The improved combined model has the best forecasting effect, according to the experimental results. In this study, several more important economic indicators are chosen to provide reference opinions and strategies for Shandong's economic development policies in the next five years, including total economic volume and growth rate, energy supply, and people's living standards.

Data Availability

The data used to support the findings of this study are available from the corresponding author upon request.

Conflicts of Interest

The authors declare that there are no conflicts of interest.

Acknowledgments

This work in this paper was supported by the Universiti Putra Malaysia.

References

[1] H. Hassani, A. Rua, E. S. Silva, and D. Thomakos, "Monthly forecasting of GDP with mixed-frequency multivariate singular spectrum analysis," *International Journal of Forecasting*, vol. 35, no. 4, pp. 1263–1272, 2019.

[2] M. R. Abonazel and A. I. Abd-Elftah, "Forecasting Egyptian GDP using ARIMA models," *Reports on Economics and Finance*, vol. 5, no. 1, pp. 35–47, 2019.

[3] Z. Chen, F. Huang, W. Chen, J. Zhang, and W. Sun, "RBFNN-based adaptive sliding mode control design for delayed nonlinear multilateral telerobotic system with cooperative manipulation," *IEEE Transactions on Industrial Informatics*, vol. 16, no. 2, pp. 1236–1247, 2019.

[4] Q. Yu, Z. Hou, X. Bu, and Q. Yu, "RBFNN-based data-driven predictive iterative learning control for nonaffine nonlinear systems," *IEEE Transactions on Neural Networks and Learning Systems*, vol. 31, no. 4, pp. 1170–1182, 2019.

[5] Z. Chen, X. Yang, and X. Liu, "RBFNN-based nonsingular fast terminal sliding mode control for robotic manipulators including actuator dynamics," *Neurocomputing*, vol. 362, pp. 72–82, 2019.

[6] S. Ibrahim, C. E. Choong, and A. El-Shafie, "Sensitivity analysis of artificial neural networks for just-suspension speed prediction in solid-liquid mixing systems: performance comparison of MLPNN and RBFNN," *Advanced Engineering Informatics*, vol. 39, pp. 278–291, 2019.

[7] G. T. Reddy, M. P. K. Reddy, K. Lakshmanna, D. S. Rajput, R. Kaluri, and G. Srivastava, "Hybrid genetic algorithm and a fuzzy logic classifier for heart disease diagnosis," *Evolutionary Intelligence*, vol. 13, no. 2, pp. 185–196, 2020.

[8] R. Guha, M. Ghosh, S. Kapri et al., "Deluge based Genetic Algorithm for feature selection," *Evolutionary intelligence*, vol. 14, no. 2, pp. 357–367, 2021.

[9] S. Sayed, M. Nassef, A. Badr, and I. Farag, "A Nested Genetic Algorithm for feature selection in high-dimensional cancer Microarray datasets," *Expert Systems with Applications*, vol. 121, pp. 233–243, 2019.

[10] M. Nazarahari, E. Khanmirza, and S. Doostie, "Multi-objective multi-robot path planning in continuous environment using an enhanced genetic algorithm," *Expert Systems with Applications*, vol. 115, pp. 106–120, 2019.

[11] J. Luan, Z. Yao, F. Zhao, and X. Song, "A novel method to solve supplier selection problem: h," *Mathematics and Computers in Simulation*, vol. 156, pp. 294–309, 2019.

[12] Z. Jalali, E. Noorzai, and S. Heidari, "Design and optimization of form and facade of an office building using the genetic algorithm," *Science and Technology for the Built Environment*, vol. 26, no. 2, pp. 128–140, 2020.

[13] C. She, Z. Wang, F. Sun, P. Liu, and L. Zhang, “Battery aging assessment for real-world electric buses based on incremental capacity analysis and radial basis function neural network,” *IEEE Transactions on Industrial Informatics*, vol. 16, no. 5, pp. 3345–3354, 2019.

[14] M. Dua, R. Gupta, M. Khari, and R. G. Crespo, “Biometric iris recognition using radial basis function neural network,” *Soft Computing*, vol. 23, no. 22, pp. 11801–11815, 2019.

[15] Z. Zhao, Y. Lou, Y. Chen, H. Lin, R. Li, and G. Yu, “Prediction of interfacial interactions related with membrane fouling in a membrane bioreactor based on radial basis function artificial neural network (ANN),” *Bioresource Technology*, vol. 282, pp. 262–268, 2019.

[16] Z. Geng, D. Shang, Y. Han, and Y. Zhong, “Early warning modeling and analysis based on a deep radial basis function neural network integrating an analytic hierarchy process: a case study for food safety,” *Food Control*, vol. 96, pp. 329–342, 2019.

[17] N. M. Moawad, W. M. Elawady, and A. M. Sarhan, “Development of an adaptive radial basis function neural network estimator-based continuous sliding mode control for uncertain nonlinear systems,” *ISA Transactions*, vol. 87, pp. 200–216, 2019.

[18] D. Giveki and M. Karami, “Scene classification using a new radial basis function classifier and integrated SIFT-LBP features,” *Pattern Analysis & Applications*, vol. 23, no. 3, pp. 1071–1084, 2020.

[19] Z. Jin, Q. Han, K. Zhang, and Y. Zhang, “An intelligent fault diagnosis method of rolling bearings based on Welch power spectrum transformation with radial basis function neural network,” *Journal of Vibration and Control*, vol. 26, no. 9-10, pp. 629–642, 2020.

[20] Y. Jiang, X. Gu, D. Wu et al., “A novel negative-transfer-resistant fuzzy clustering model with a shared cross-domain transfer latent space and its application to brain CT image segmentation,” *IEEE/ACM Transactions on Computational Biology and Bioinformatics*, vol. 18, no. 1, pp. 40–52, 2021.

[21] Y. Jiang, Y. Zhang, C. Lin, D. Wu, and C.-T. Lin, “EEG-based driver drowsiness estimation using an online multi-view and transfer TSK fuzzy system,” *IEEE Transactions on Intelligent Transportation Systems*, vol. 22, no. 3, pp. 1752–1764, 2021.

[22] H. Wang, J. Gu, X. Di, D. Liu, J. Zhou, and X. Sui, “Research on classification and recognition of attacking factors based on radial basis function neural network,” *Cluster Computing*, vol. 22, no. 3, pp. 5573–5585, 2019.

[23] S.-B. Roh, S.-K. Oh, W. Pedrycz, K. Seo, and Z. Fu, “Design methodology for radial basis function neural networks classifier based on locally linear reconstruction and conditional fuzzy C-means clustering,” *International Journal of Approximate Reasoning*, vol. 106, pp. 228–243, 2019.

[24] L. Shi, B. Sun, and D. S. Ibrahim, “An active learning reliability method with multiple kernel functions based on radial basis function,” *Structural and Multidisciplinary Optimization*, vol. 60, no. 1, pp. 211–229, 2019.

Hindawi
Computational Intelligence and Neuroscience
Volume 2022, Article ID 8965622, 10 pages
https://doi.org/10.1155/2022/8965622

Research Article

Research on the Communication Strategy of History and Culture in Shaanxi Based on BP Neural Network Model

Dan Xie [1,2] and Chao Yin [3,4]

[1]General Department, Xi'an Traffic Engineering Institute, Xi'an 710300, Shaanxi, China
[2]University of Technology MARA, Shah Anam, Selangor 40450, Malaysia
[3]School of History and Culture, Shaanxi Normal University, Xi'an 710000, Shaanxi, China
[4]Xi'an Tie Yi Middle School, Xi'an 710000, Shaanxi, China

Correspondence should be addressed to Dan Xie; xiedan@xjy.edu.cn

Received 17 December 2021; Revised 5 January 2022; Accepted 6 January 2022; Published 24 January 2022

Academic Editor: Xin Ning

Shaanxi is one of China's most important cradles of civilization. The main vein of Chinese culture is rich history and culture, and brilliant red culture embodies the essence of socialist core values. It is still relatively weak to deeply analyze the related research of Shaanxi Province's cultural province construction on the basis of studying the achievements of cultural development in foreign countries and China and combining with the reality of Shaanxi Province. In this paper, a BPNN (BP neural network) model is selected to study the comprehensive evaluation of tourism competitiveness of smart tourism cities, and the software is used to realize the simulation of the comprehensive evaluation system of tourism competitiveness of smart tourism cities, which more comprehensively and objectively reflects the level of comprehensive competitiveness of each city. It is believed that there are some problems in Shaanxi regional cultural communication, such as insufficient exploration of content resources, insufficient communication channels, and low audience awareness, hoping to provide ideas and reference for further exploring the promotion of cultural communication power.

1. Introduction

Shaanxi is recognized as a province with rich cultural resources and is vigorously building Shaanxi as a province with rich historical culture, splendid revolutionary culture, distinctive folk culture, and modern culture with certain strength. How to develop Shaanxi's cultural undertakings with the help of rich cultural resources and develop a culturally rich province into a culturally strong province has become the direction of the joint efforts of provincial party committees and governments [1]. Although Shaanxi has made great achievements in the development of cultural undertakings and cultural industries in recent years, it is not commensurate with the requirements of being a big cultural province and building a strong cultural province. Compared with developed provinces, there is still a big gap, and the construction of a strong cultural province still faces some problems and difficulties [2, 3]. This is also the background of this topic.

Many cultural communication professionals began to actively study the internal relationship between the Internet and cultural communication content in the era of mobile Internet to better understand how to spread cultural content through the Internet. Cultural construction is an important aspect of socialist construction and a crucial component of the Chinese style socialist theoretical system. The classification and planning of historical and cultural cities, as well as the attention paid to implementation after the planning of famous city protection, are clearly inadequate. Protection planning should not be a one-size-fits-all approach [4, 5]. Protection planning should be evaluated in light of changes in implementation as protection work progresses, and this should be used as the basis for planning adjustments [6]. To enrich Shaanxi's cultural construction, it is critical to study the construction of Shaanxi Province as a strong cultural province. This paper examines the problems and reasons for the construction of a strong culture in Shaanxi Province, as well as the countermeasures and recommendations for the construction of a strong culture in Shaanxi Province, which is of reference value to the country's and other provinces' cultural construction.

Beginning with the scientific definition of culture, this paper examines the current state of Shaanxi's cultural province construction, highlighting the accomplishments and benefits of Shaanxi's cultural construction, and identifying the major issues that exist in Shaanxi's cultural construction. A transportation mode selection model based on the BPNN (back propagation neural network) algorithm is established after comprehensively considering the attribute variables and activity patterns of travelers, with a focus on the historical block, a special block. Using the protection of ancient cities as an example, it has been demonstrated that the BPNN evaluation model of the entire process of historic city protection planning can be used for historic city protection evaluation.

2. Related Work

The early research mainly focused on the background of cross-cultural generation, while the current research has already involved many disciplines of humanities and social sciences [7, 8]. Yang et al. [9] propose that some information is hidden in the context when people communicate with each other, and there are different levels of communication contexts among countries and ethnic groups. Countries such as Britain and the United States belong to the low-context society, while countries such as Japan and South Korea belong to the high-context society. By analyzing the current situation of foreign language education in China, Liu and Hu [10] pointed out that foreign language teaching in China attaches importance to language knowledge and language skills but neglects the cultivation of cultural factors, so that Chinese college students lack intercultural communication skills. Based on this, Hou [11] proposes to build a brand-new college English-teaching model based on intercultural communication. Wu and Ma et al. [12, 13] propose that to achieve effective communication across the gap of nationality, race, nationality, language, and culture, it is necessary to search for and think about the multidimensional interaction between self, people and society, people and culture, people and media, so as to find out the possible path of cross-cultural communication. Zhan [14] discusses smart tourism in depth and thinks that smart cities should have six dimensions: smart economy, smart environment, smart transportation space, smart people, smart families, and smart government. Through data analysis, it is found that innovation ability, attention to urban environmental quality, administrative management, and education level play an important role in the utilization of information technology and the intelligence of cities [15, 16].

The characteristics of artificial neural networks in terms of information processing are unique. It has been used successfully in a variety of fields. It has strong nonlinear mapping capabilities, as well as self-adaptation, self-learning, fault tolerance, and parallel processing capabilities. Neural networks have properties that make them ideal for studying chaotic sequence prediction. The use of neural networks [17] in multivariable time-series prediction and multivalue prediction has been studied in literature [18, 19], and Lu et al. [20] discuss the modeling mechanism and multivalue prediction of this method, as well as its application in stock price prediction. Tang and Yu [21] discuss the establishment mechanism of a time-series prediction model based on neural networks and then propose an adaptive time-series modeling and prediction by combining the time-difference method with BPNN. Sun and Lei [22] developed a radial basis function neural network model using cluster analysis, tested it using financial time series, and compared it to the radial basis function neural network model. Yuan et al. [23] established a time-delayed BPNN model and used the Bayesian regularization method to improve BPNN's generalization ability. Furthermore, many researchers used the search algorithm in optimization to improve the common BP learning method's convergence speed and network prediction performance.

3. Research Method

3.1. Communication Design of Shaanxi Regional History and Culture. The goal of Shaanxi Province as a strong cultural province is an indispensable part of the construction of "western province". Attaching great importance to cultural construction ideologically is an important prerequisite for building a strong cultural province. Shaanxi talents will have more sense of belonging and existence. Cultural construction is an important symbol of Shaanxi's comprehensive strength. A country pays attention to comprehensive national strength, and a province also pays attention to comprehensive labor saving, including not only material strength such as economic strength, scientific and technological strength, but also spiritual strength such as culture.

Culture, as a special component of comprehensive strength, is based on and backed by developed economy. Building a moderately prosperous society, to achieve the goal of building a culturally powerful province in the west also requires firm belief and guidance. Cultural construction provides intellectual support for the construction of a strong western province. China's modernization process, to a great extent, depends on the improvement of national quality and the development of human resources. Shaanxi should be highly aware of the importance of cultural construction ideologically, make full use of the advantages of efficient resources, train outstanding and high-quality talents, and provide backup forces for the construction of Shaanxi's strong cultural province.

As a kind of "soft power", culture is increasingly becoming an important factor of regional competitiveness and an important aspect of a region's comprehensive strength. Cultural background, cultural environment and atmosphere, and scientific and cultural quality of workers are increasingly becoming the important foundation and guarantee of economic development. The complex relationship between culture and economy is becoming more and more important. Therefore, the significance of cultural revival is not limited to simple economic development.

Thousands of years have passed since many cultural relics, historic sites, and cultural sites in historical and cultural cities were destroyed and rebuilt. They have remained tourist attractions for the time being, due to the cultural continuity and inheritance [24]. Aside from the continuation and inheritance of culture, the cultural sustainable development of famous historical and cultural cities is also very important for the innovation and development of culture, and it is an important index to measure the continuation of "context" of famous historical and cultural cities as well as the development of culture over time. It is a critical ally in the development of cultural tourism. Tourists are drawn to cultural relics and historic sites in well-known historical cities because they are diverse, have a long history, have a high taste, are valuable, and have a high ornamental value. At the same time, the material carriers of culture are the preservation of cultural relics and historic sites in well-known historical and cultural cities, the preservation of ancient architectural styles, and the preservation of cultural landscapes. The cultural evaluation index system of historical and cultural cities includes five major factors, which constitute an index system composed of three levels: target level, factor level, and index factor level, as shown in Figure 1.

The cultural industry in Shaanxi has more potential for economic growth. Shaanxi takes cultural tourism as a breaking point because of its diverse and colorful cultural resources, and labor drives many economic growth points throughout the industrial chain, including the cultural leisure industry, book publishing industry, and advertising exhibition industry. Culture is, at its core, a creative endeavor. Through the integration of various forms of cultural resources, various cultural products and services with fresh vitality can be continuously produced with the continuous input of creativity.

In the field investigation, the vast majority of tourists are in a positive and high emotional state, and a small number of tourists are mixed with negative emotions. In the specific tourism situation, this paper only selects tourists' positive tourism emotions as the focus of this paper. On the whole, the higher the tourists' positive tourism emotion, the stronger the tourists' sense of experience and identity to the tourist destination, and the greater the tourists' satisfaction. The structural model is shown in Figure 2.

Tourist satisfaction plays a part of intermediary role between positive tourism emotion and behavioral intention. As a senior creature, people's tourism emotion is complex in the process of tourism. The level of tourism emotion depends on tourists' experience and recognition of the tourism world, and its influence is far-reaching and extensive. On one hand, positive tourism emotion affects tourists' satisfaction with tourist destinations, on the other hand, it also has a direct effect on their behavior intention, but at the same time, tourists' positive tourism emotion also plays a role in behavior intention through overall satisfaction.

It is worth noting that while tourists' positive tourism emotion has a strong influence on behavior intention, the impact of positive tourism emotion on behavior intention is weakened when tourists' satisfaction factors are taken into account. As a result, the most important aspect of tourist destination management is to pay attention to tourist satisfaction. Xi'an tourists appreciate the ancient capital's incomparable charm because of its unique tourism resources and beautiful natural and cultural environment. As a result, Xi'an tourists' tourism emotion and satisfaction with tourism resources and culture, tourism environment, and facilities are related in the travel process, and there is a positive correlation. There is, however, no link between tourism emotion and tourism expectations, tourism service, or tourism price. The causal relationship between them cannot be determined using correlation analysis. The next step of regression analysis is required to investigate the relationship between tourists' tourism emotions and tourism resources and culture, tourism environment and facilities, and overall satisfaction.

3.2. BPNN Model Design

3.2.1. BPNN Structure. BPNN algorithm is a training algorithm based on the principle of error back propagation. It takes the minimum error mean square as the criterion and uses nonlinear differentiable function for weight training. BPNN is a multilayer forward anger network, which is composed of IL (Input layer), HL (hidden layer), and OL (Output layer). Usually, the number of layers of neural network does not include IL. Figure 3 is the BPNN structure diagram.

The HL transfer function of BPNN adopts the nonlinear function of continuously differentiable, usually Sigmoid function, while the transfer function of OL can adopt linear function or Sigmoid function, depending on the distribution range of OL vector.

Basic steps of algorithm: set the initial value of each weight or threshold: $w_{ji}(0), \theta_j(0)$ is a small random number.

Provide training samples: input vector $X_k, k = 1, 2, \ldots, P$; Expected output $d_k, k = 1, 2, \ldots, P$;

Calculate the actual output of the network and the state of HL unit:

$$o_{kj} = f_j\left(\sum_i w_{ji} o_{ki} - \theta_j\right). \quad (1)$$

Training error:

$$\begin{aligned} \delta_{kj} &= o_{kj}\left(1 - o_{kj}\right)\left(t_{kj} - o_{kj}\right), \\ \delta_{kj} &= o_{kj}\left(1 - o_{kj}\right)\sum_m o_{km} w_{mj}. \end{aligned} \quad (2)$$

Corrected weights and thresholds:

$$\begin{aligned} w_{ji}(t+1) &= w_{ji}(t) + \eta\delta_j o_{ki} + \alpha\left[w_{ji}(t) - w_{ji}(t-1)\right], \\ \theta_j(t+1) &= \theta_j(t) + \eta\delta_j + \alpha\left[\theta_j(t) - \theta_j(t-1)\right]. \end{aligned} \quad (3)$$

When k goes through 1 to P, judge whether the index meets the accuracy requirement.

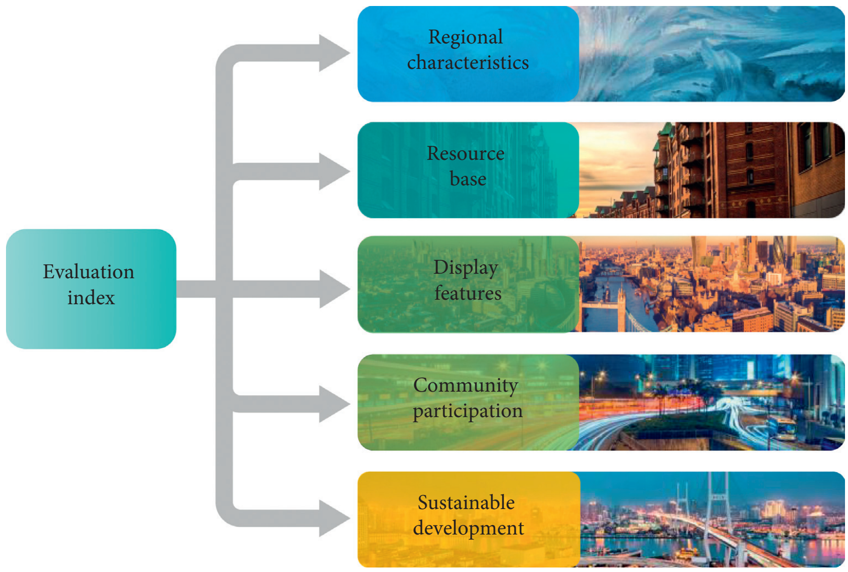

Figure 1: Cultural evaluation index system of famous historical cities.

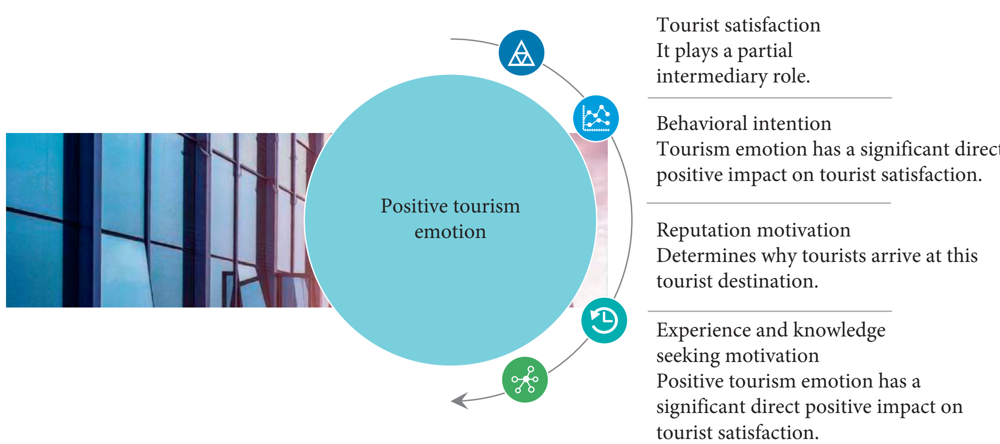

Figure 2: Structural equation model.

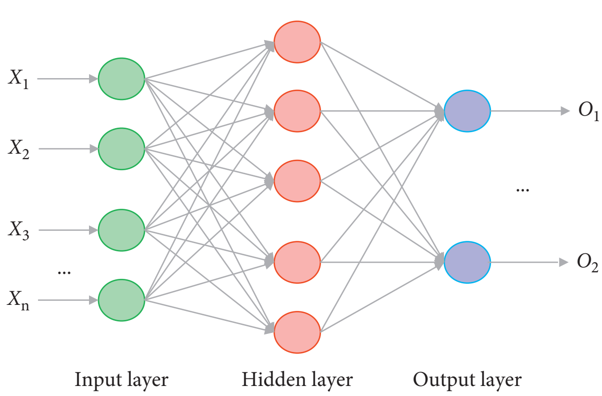

Figure 3: BPNN structure.

3.2.2. Establishment of the BPNN Evaluation Model. To meet the requirements of training error and prediction error, BPNN model training must include a series of constant comparisons between expected value and neural network output value, as well as repeated training and simulation operations. The comprehensive evaluation value of the implementation evaluation of historic city protection planning is obtained using the expert scoring method and is used as the expected value of BPNN model training samples.

The training samples come from 100 randomly generated sample evaluation values. According to the scores, the famous cities are evaluated and divided into five grades: (90–100) as good, (80–89) as good, (70–79) as good, (60–69) as fair and below 60 points as poor. The formula is as follows:

$$P = \sum C_i \times W_i, \tag{4}$$

where P is the comprehensive evaluation value for the protection planning of historic cities, C_i is the single score of evaluation index, and W_i is the weight of evaluation index.

3.2.3. Determination of the Number of HL Nodes. In the process of BPNN training, the weights and thresholds change randomly and change with the training times. The number of HL layers and the number of nodes in each layer will directly affect the training results. By setting the number of HL nodes, the training accuracy will be improved, and the error will be reduced. After debugging for many times, the number of HL nodes that reach the required accuracy and error is finally selected, and this number of HL nodes is the final required number of nodes.

There are many ways to determine the number of HL nodes, which are determined by empirical formula in this paper.

$$m = \sqrt{n + I} + a, \tag{5}$$

where n is the number of IL nodes, I is the number of OL nodes, and a is a constant from 1 to 10, so it is determined that the number of HL nodes is 13.

Each index has its own dimension. In the process of calculation, for the factors with different equivalent levels, dimensionless measures should be taken to make each factor in the same equivalent level. In this case, to make the input factors dimensionless, the actual travel time should be divided by 10 as the input of travel time, and the other seven factors should be converted into smaller values by stages, so as to avoid unnecessary errors caused by large data gaps and improve the training speed and accuracy.

3.2.4. Training Strategy. The sample data are usually divided into two parts when training the network: one part is used for training, and the other part is used to test the training effect. As BPNN is trained using the gradient descent method, the training set's error will decrease monotonically, while the average error on the test sample set will always be higher than the training sets, which will not decrease monotonically. The big trend is that after reaching a certain training level, the error on the training set decreases first, then increases again. As a result, rather than continuing to train until the error of the test set reaches the minimum point, the network usually stops training when the error of the test set reaches the minimum point.

4. Results Analysis and Discussion

4.1. Learning and Training Analysis of the BPNN Method. Shaanxi has a splendid red culture, in which the influence of Yan'an spirit radiates all over the country. Until now, the land of Sanqin has a large number of red cultural resources, including both material cultural resources and historical and cultural heritages, such as revolutionary documents, memorial sites, literary works, cultural relics, revolutionary war sites, and so on. In Shaanxi regional culture, there are many cultural resources rich in popular entertainment and expressive force, particularly some folk arts that are more suitable for media communication. These are priceless gems that must be thoroughly explored and exploited, and brands with distinct label value must be created to ensure strong and effective communication. Furthermore, the development of high-quality content in Shaanxi regional culture must be accelerated. There are some issues right now, such as a low level of innovation transformation, a lack of second creation, and a shallow interpretation.

In traffic mode division, the whole process of BPNN is divided into three steps. First, a suitable neural network must be established. Second, the network should be trained according to the existing input and output data to make the accuracy and error of the network as small as possible. Finally, the output prediction of other input data should be made according to the trained network. Train the network according to the nonlinear function, and get the output of the nonlinear function predicted by the trained network (Figure 4).

It can be seen from Figure 4 that on the basis of training, the remaining 15 pieces of data are used for prediction, and the predicted data basically accord with the expected data, which shows that BPNN algorithm has certain practicability in the research field of transportation mode selection.

Shaanxi's cultural market access conditions are constantly relaxed, but the cultural market order needs to be further standardized. A good cultural market environment is the foundation for the healthy development of the cultural industry. At present, the situation of fragmented, multihead management and fragmented cultural market in Shaanxi exists to a certain extent, which not only increases the difficulty of organizing capital operation but also causes waste and idleness of cultural resources. Cultural development is low and immature, and cultural products lack a standardized market trading environment and have not really formed a perfect market mechanism.

The above case proves that the BPNN algorithm is practical in the research field of transportation mode selection. The traffic sharing rates of Xi'an, Hanzhong, Luoyang and Baoji in Figure 1 are verified by BPNN method (Figures 5–7).

The verification results show that the predicted data of the traffic mode division model based on BPNN algorithm are basically consistent with the actual survey data.

The rich forms and contents of Shaanxi regional culture necessitate rich communication platforms or channels for all-around communication. In today's world, new media, in addition to traditional media, is a must-have communication channel. It is the audience's cultural communication's arrival terminal, so the effect of cultural communication power will eventually be reflected in the audience as the terminal. The investigation of the effect is primarily based on two levels of cultural awareness and recognition. It is necessary to divide the audience into groups, such as those who live in the province and those who live outside of it. Their understanding of Shaanxi regional culture differs, allowing them to communicate more effectively.

The cultural service system is sound. Public cultural facilities are scientifically planned, rationally laid out, and coordinated between urban and rural areas. Large and medium-sized cities have a number of modern symbolic cultural and entertainment facilities with high level, high standard, and unique style. Comprehensive cultural facilities and places for cultural activities at the grass-roots level are fully functional and basically can meet the needs of the masses to carry out regular cultural activities. The cultural service network is sound, with complete functions, wide coverage, and high service capacity and level.

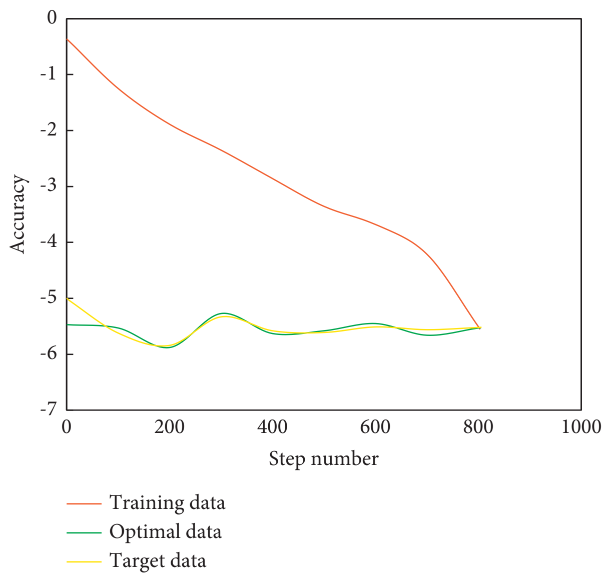

Figure 4: Schematic of BPNN training error.

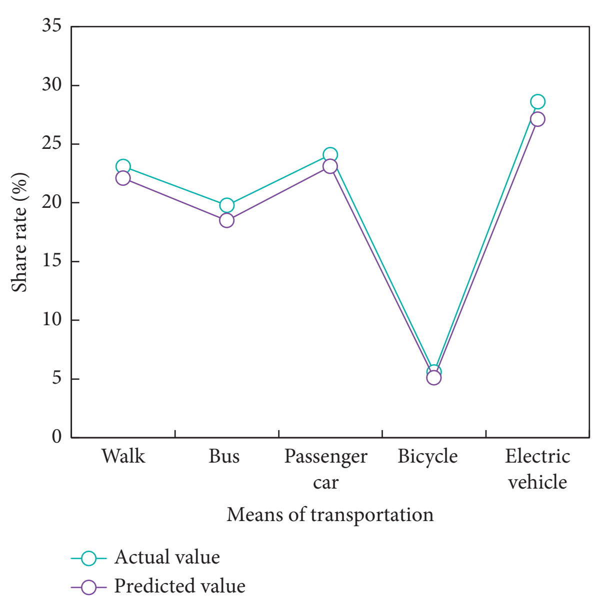

Figure 5: Comparison of Xi'an traffic mode sharing rate.

At present, the dissemination of Shaanxi regional culture is not accurate enough in audience segmentation, which leads to the loss of communication effect. Different audiences have uneven awareness of regional culture, and thus have different recognition of culture. In addition, the content, methods, channels, and skills of cultural communication all have an impact on the final communication effect, and these contents should be based on the accurate research of the audience.

4.2. Evaluation and Analysis of Shaanxi Regional Historical and Cultural Tourism. The research on the tourism competitiveness of smart tourism cities is a hot issue in the current tourism field. Under the development trend of modern tourism with the theme of science and technology and competition, the smart tourism city complex as a tourist destination has a comparative advantage with other smart tourism cities in the competition of tourism elements under the comprehensive action of tourism economic development, scientific and technological innovation, tourism resources, environmental support, geographical location, and other factors.

The tourism competitiveness of smart tourism cities is embodied in five aspects: economic development, scientific and technological innovation, potential competitiveness, environmental support, and development guarantee of smart tourism cities.

According to the established BPNN, relevant training comparison values can be obtained (as shown in Figure 8).

Figure 8 shows that the expected output value is very close to the value of neural network training output value. In other words, the BPNN model can accurately determine the general situation of tourism competitiveness of smart tourism cities according to various evaluation indexes. Therefore, the training of network model is over, and the evaluation model of tourism competitiveness of smart tourism cities based on BPNN has been constructed. When evaluating the tourism competitiveness of other smart tourism cities, only need to enter the normalized data of the evaluation sample index, and the required evaluation conclusion can be obtained.

Based on the results of BPNN evaluation on the competitiveness of smart tourism cities because the competitiveness of each city is different, by comparing other sample cities with those in an advantageous state, smart tourism cities can have an objective understanding of their own level of smart construction and the competitiveness of other cities, identify the gap and take corresponding measures to improve their competitiveness.

After BPNN training, the trained BPNN model is used for testing, and the index data of Xi'an and Shangluo test samples are input into the model, and the output results shown in Figure 9 are obtained.

The error of the test samples is close to the error of the training samples through the trained neural network, and it is assumed that the established network model can effectively approach the training samples based on the test samples in Figure 9. The relative and absolute error values of training and test samples in the BPNN model are also within acceptable bounds. As a result, the BPNN-based evaluation model of smart tourism city competitiveness developed in this paper is effective, and the directly trained neural network can be used to evaluate the competitiveness of other smart tourism cities.

Through the training results of BPNN, the evaluation results of 10 smart tourism city samples are compared and ranked, and the final competitiveness ranking is shown in Figure 10.

The core of culture is certain values and their concrete norms. Shaanxi is rich in cultural resources, but its influence is limited due to insufficient understanding and development. At the important stage of the transition period, it is necessary to fully understand and explore the spiritual

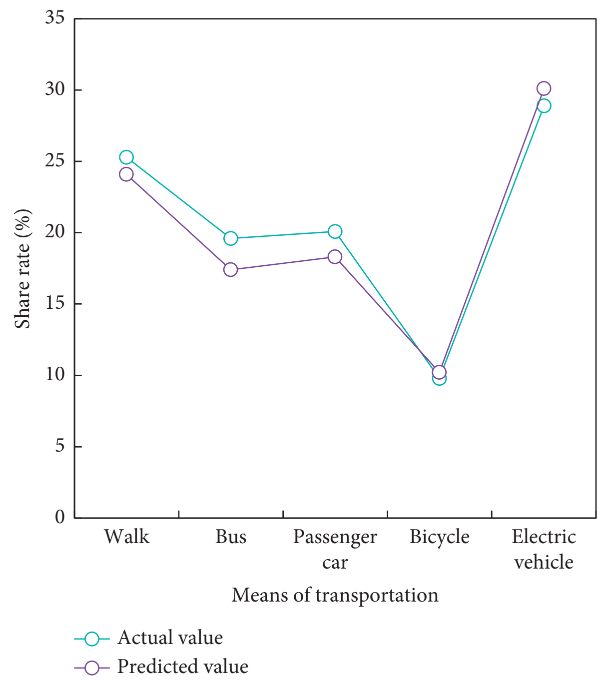

FIGURE 6: Comparison of traffic mode sharing rate in Hanzhong.

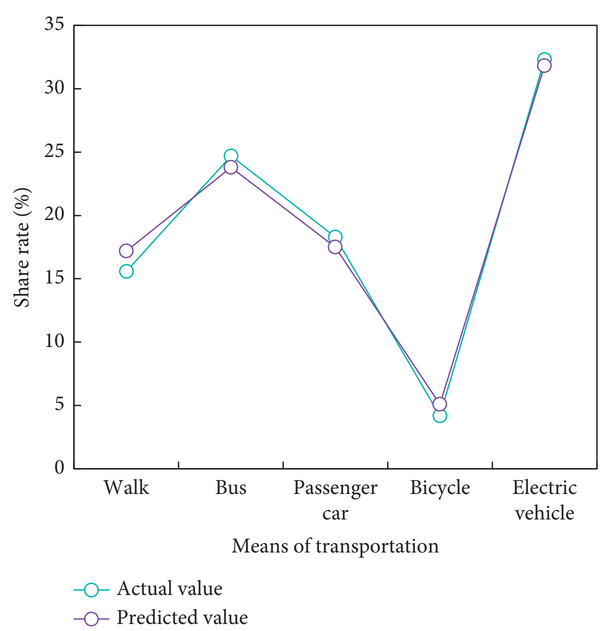

FIGURE 7: Comparison of traffic mode sharing rate in Baoji.

education value of Shaanxi's red cultural resources with Yan'an spirit and patriotism as the main connotation, so as to urge people to reflect on the spiritual emptiness and belief confusion that are prevalent now, draw positive energy from the values, outlook on life and spirit of life of revolutionary ancestors, establish correct value goals and value pursuits, shape social psychology of self-respect and self-improvement, and stimulate initiative and creativity.

Shaanxi is rich in science, education, and culture resources, and it is a big province of science and education, which provides intellectual support and powerful guarantee for the modernization of culture in terms of technology and manpower. The development of culture in the new period cannot be separated from scientific and technological innovation, such as animation industry, film, and television production industry, creative advertising industry and so on, which have highly accumulated scientific and technological content. Give full play to the advantages of Shaanxi education and the strength of science and technology, promote the integrated development of

Figure 8: Comparison chart of expected output and training output.

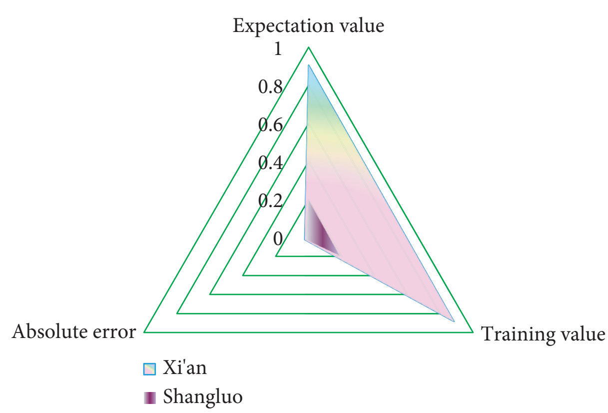

Figure 9: Comparison of output results of test sample expected value and training value.

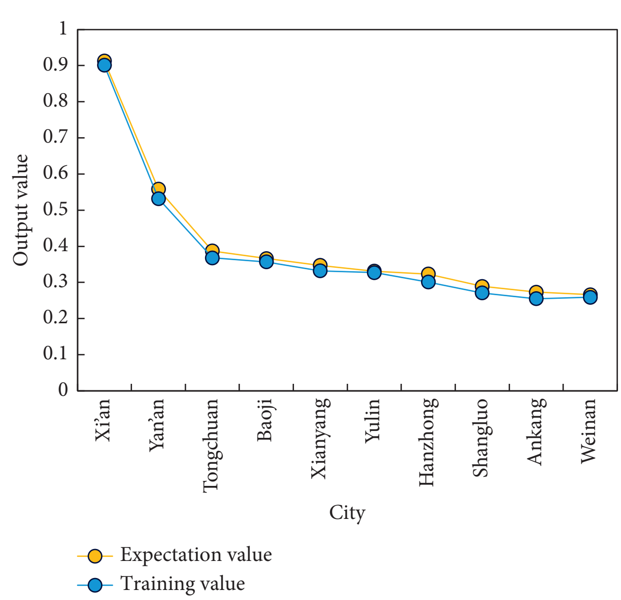

Figure 10: Ranking of evaluation results of tourism competitiveness of smart tourism cities.

enterprises in Industry-University-Research, realize the linkage between cultural industry capital and intellectual capital, and innovate and develop culture with high technology.

Culture and science and technology are the areas that need innovation most. If you plug in the wings of culture and technology, it will accelerate the transformation of culture and science and technology into real productive forces and maximize the cultural value. Shaanxi has both. As long as attach great importance to and develop reasonably, the resources of science and education will certainly promote the prosperity and development of Shaanxi culture.

5. Conclusion

At this new historical juncture, we must deeply comprehend the enormous significance and unavoidable requirements of building a socialist cultural power, adhere to a global and long-term vision, recognize the strategic importance of culture, strengthen the sense of mission and responsibility to promote cultural construction, and strive to realize the Chinese nation's cultural rejuvenation. As Shaanxi has unique and rich cultural resources, it is critical to explore and further revitalize these cultural resources as part of the province's overall economic and social development. The tourism competitiveness of smart tourism cities is evaluated using the BPNN model, and an empirical study is conducted in 10 smart tourism cities. The qualitative and quantitative index data are thoroughly investigated using the designed index system of tourism competitiveness of smart tourism cities. At the moment, audience segmentation for the dissemination of Shaanxi regional culture is insufficient, resulting in a loss of communication effect. Different audiences have varying levels of awareness of regional culture, and thus have varying levels of cultural recognition. Furthermore, cultural communication content, methods, channels, and skills all have an impact on the final communication effect, and these contents should be based on accurate audience research.

Although the BPNN model algorithm used in this paper is the most widely used algorithm in artificial neural networks, the samples chosen in this paper are somewhat fewer due to objective condition limitations, which reduces the accuracy and precision of BPNN model evaluation to some extent. It will be necessary to improve the sample data and the accuracy of data evaluation in future research.

Data Availability

The data used to support the findings of this study are included within the article.

Conflicts of Interest

The authors declare that they have no conflicts of interest.

Acknowledgments

This work was supported by Key Project of Scientific Research of Xi'an Traffic Engineering Institute (project no. 2021KY-10).

References

[1] Y. Zhang, "Shaanxi historical and cultural documentary and regional cultural communication," *News Knowledge*, vol. 4, no. 7, 2018.

[2] X. He and L. Nan, "Fusion and reconstruction: a study of animation art creation based on Shaanxi native cultural resources," *Northwest Art: Journal of 'Xi'an Academy of Fine Arts*, vol. 3, no. 4, 2018.

[3] Y. Li and Y. Liu, "The innovative research on Shaanxi cultural dissemination mode under the ""one belt one road"," *Journal of 'Xi'an University of Arts and Science: Social Science Edition*, vol. 24, no. 1, 4 pages, 2021.

[4] Y. Wang, D. Gao, and X. Wang, "Shortest path planning based on improved ant colony algorithm," *ASP Transactions on Computers*, vol. 1, no. 3, pp. 6–11, 2021.

[5] M. Liu and W. Guo, "The output strategy of Chinese traditional culture in English translation under the background of ""One Belt and One Road""——taking Shaanxi Province as an example," *Journal of Shaanxi Preschool Teachers College*, vol. 35, no. 12, 6 pages, 2019.

[6] Y. Hou, Y. Zhou, and L. Ma, "Research on the external dissemination strategy of Tibetan medicine culture in tibet under the vision of ""one belt and one road""," *Journal of Tibet Nationalities University: Philosophy and Social Sciences Edition*, vol. 41, no. 1, 4 pages, 2020.

[7] B. Yan and L. Cao, "The road and thinking of museum education and cultural innovation research and development——taking Shaanxi History Museum as an example," *Chinese Museum*, vol. 5, no. 3, 2020.

[8] Dragon Media, "The dissemination carrier of extending regional culture——a brief discussion on ""Shaanxi crosstalk and shenzhou Xing"," *Qu Yi*, vol. 2, no. 1, 2017.

[9] X. Yang, J. Liu, and Y. Wang, "Research on the problems and countermeasures of Shaanxi as a culturally powerful province," *Comparative Research on Cultural Innovation*, vol. 2, no. 6, 2020.

[10] X. Liu and W. Hu, "Research on Shaanxi"s image of foreign propaganda translation strategies——taking 'Shaanxi's excellent novel ""Bai Lu yuan"" as an example," *Shanxi Youth*, vol. 2, no. 20, 2018.

[11] N. Hou, "Research on the social function of museums under the new situation: taking Shaanxi History Museum as an example," *Museum*, vol. 5, no. 2, 2020.

[12] W. Wu, "Research on the development and design of cultural and creative products based on local historical and cultural archives resources--Taking Yanliang District of Xi"an as an example," *Shaanxi Archives*, vol. 2, no. 4, 2021.

[13] Y. Ma, C. Wang, and J. Zhao, "Research on the development strategy of Shaanxi local tea industry culture in the era of ""Internet +""," *Leisure*, vol. 1, no. 11, 2018.

[14] W. Zhan, "Research on the international dissemination path of Shaanxi's qin Opera culture under the cultural ""going out"" strategy," *Think Tank Times*, vol. 2, no. 44, 2019.

[15] Y. Wu and J. Wang, *Analysis of Shaanxi History Museum's Symbolic Expression of Regional Culture*, China Press, no. 14, Kuala Lumpur, Malaysia, 2021.

[16] Y. Zhang, "Research on Chinese costume culture translation strategy from the perspective of cultural communication," *Think Tank Times*, vol. 2, no. 6, 2018.

[17] M. Zhao, A. Jha, Q. Liu et al., "Faster Mean-shift: GPU-accelerated clustering for cosine embedding-based cell segmentation and tracking," *Medical Image Analysis*, vol. 71, Article ID 102048, 2021.

[18] S. Li and H. Yao, "Research on path optimization of cross-cultural transmission of Chinese traditional mythology," *Shaanxi Journal of Social Sciences*, vol. 8, no. 2, 4 pages, 2021.
[19] R. Zhang, "Research on the transmission channels of central plains culture," *Oriental Collection*, vol. 1, no. 3, 2017.
[20] X. Lu, X. Zhang, and Q. Zhang, "Research on Shaanxi's image external communication strategy in a new perspective," *News Research Guide*, vol. 12, no. 8, 2 pages, 2021.
[21] S. Tang and F. Yu, "Construction and verification of retinal vessel segmentation algorithm for color fundus image under BP neural network model," *The Journal of Supercomputing*, vol. 77, no. 1, pp. 1–15, 2021.
[22] X. Sun and Y. Lei, "Research on financial early warning of mining listed companies based on BP neural network model," *Resources Policy*, vol. 73, no. 2, Article ID 102223, 2021.
[23] S. Yuan, G. Wang, J. Chen et al., "Assessing the forecasting of comprehensive loss incurred by typhoons: a combined PCA and BP neural network model," *Artificial Intelligence Journal (English)*, vol. 1, no. 2, 20 pages, 2019.
[24] H. Li, "Spread Shaanxi silk road culture with digital technology innovation in the all-media era," *New Silk Road: Late*, vol. 2, no. 22, 2019.

Hindawi
Computational Intelligence and Neuroscience
Volume 2022, Article ID 2526821, 9 pages
https://doi.org/10.1155/2022/2526821

Research Article

ARIMA Model and Few-Shot Learning for Vehicle Speed Time Series Analysis and Prediction

Yingzi Wang ,[1,2] Ce Yu,[1] Jue Hou,[2] Sisi Chu,[2] Yongjia Zhang,[2] and Yue Zhu[2]

[1]*College of Intelligence and Computing, Tianjin University, Tianjin 300300, China*
[2]*Automotive Data of China (Tianjin) Co., Ltd., Tianjin 300300, China*

Correspondence should be addressed to Yingzi Wang; wangyingzi@tju.edu.cn

Received 3 December 2021; Revised 22 December 2021; Accepted 24 December 2021; Published 19 January 2022

Academic Editor: Xin Ning

In the fields of traffic management, traffic health, and vehicle safety, vehicle speed prediction is an important research topic. The greater the difference between vehicle speed and average vehicle speed, or the more discrete the vehicle speed distribution, the higher the accident rate. This paper proposes a vehicle speed prediction method based on adaptive KF (Kalman filtering) in the ARMA (Autoregressive Moving Average) environment to address the problem of high-speed moving vehicle speed prediction. The ARMA theory is used to model the prediction of speed time series. The contribution rate of each coefficient representing the original time series is different after fitting the original time series with the ARMA model, so each coefficient must be given a certain weight. Multisource traffic data fusion and interval speed prediction are carried out on the basis of few-shot data preprocessing and traffic state division, according to different traffic states. The speed prediction accuracy is very high, according to the algorithm verification results.

1. Introduction

According to statistics, intersections account for roughly 30% of all traffic accidents [1]. Even when traffic control lights are installed at intersections, deadly collisions caused by illegal activities such as speeding and running red lights still occur. At intersections, drivers must pay attention to influencing factors such as vehicles traveling in different directions, pedestrians, and nonmotor vehicles, as well as the relative positions of their own vehicles, and then make driving behavior decisions in a short amount of time [2, 3]. If the driver can be given some information about his own vehicle's operation ahead of time, it will greatly reduce the driver's driving difficulty at the intersection.

When driving on the road, drivers set their own speed based on the terrain and road conditions [4]. When the road's horizontal, vertical, and horizontal geometric elements exceed the minimum requirements for safe driving of automobiles on this grade of road, and external conditions such as traffic density, terrain, and climate are favorable, the actual driving speed of automobiles often approaches or exceeds the design speed [5, 6]. Entering the intersection and arranging them according to the time mark, according to existing research, can not only reflect the characteristics of drivers' individual driving behavior. Time series differ from ordinary series in that the data are organized in chronological order, and each numerical point has a corresponding time point [7]. These data are generated as part of the day-to-day operations of businesses, hospitals, schools, and other institutions, and they gradually accumulate into a large-scale time series database. The two types of data can be mutually supplemented and verified using data fusion. The accuracy of vehicle speed prediction across corresponding regions will be improved as well.

The above-mentioned contents are the focus of this paper. ARMA (Autoregressive Moving Average) predictive modeling was used [8]. The time series of vehicle speed generated when the object to be evaluated (own vehicle) and the vehicle in the direction of conflict (other vehicle) drive to the intersection at the same time serves as the evaluation basis and modeling data. The modeling data come from a real-world vehicle driving test. Multisource traffic data fusion and interval speed prediction are carried out according to different traffic states using data preprocessing and traffic state division.

2. Related Work

The purpose of travel time prediction is to use historical and real-time distance, speed, traffic flow, travel time, or some variables mathematically related to travel time to obtain the travel time of vehicles that will leave at a certain time in the future and whose starting and ending points are determined [9, 10]. These known variables can be obtained through equipment collection, estimation, or prediction [11]. In the process of predicting the travel time of expressway, combining the travel time of different sections in different time periods, the traffic operation conditions of different sections are obtained, and the results are extended to the whole section of expressway, and the final travel time prediction result is obtained, with a good result of about 10% error%. Literature [12] studies the daily travel time model and applies linear regression and tree model to travel time prediction. The input parameters include traffic flow information, occupancy data collected by single-loop detector, and historical travel time information (Literature [13]). Using the data collected by point traffic detectors, a short-term expressway travel time prediction method is mined. They took into account the spatial and temporal changes of traffic data and made use of the traffic measurement data collected from different places at the current moment and different places at the historical moment to do this [14]. Using the ARIMA model to determine the potential hot spots of taxis, in the process of research, they regard the demand of passengers for taxis as a simple linearly changing structure, so only linear models are used to predict. Literature [15] puts forward a model for forecasting service demand, which is suitable for a single taxi station. The use of traffic flow data in the forecasting process is a comprehensive place for them to consider, and the model can be used for real-time forecasting in online environment. However, according to their research ideas, different taxi stations in the same city must carry out different model training in order to achieve more accurate prediction results.

The speed information of vehicles before entering the intersection can be used as the basis of vehicle collision risk assessment at the intersection. Literature [16] studies the probability model between the speed of vehicles heading for the intersection and the occurrence of collision accidents, and there is a clear correlation between the speed and the acceptable gap in the workshop. Literature [17] puts forward a dynamic model and a communication model between vehicles after analyzing the characteristics and process of traffic conflicts at signalless intersections and sorts out a set of algorithms. Finally, the effectiveness of the algorithm is verified by computer programming simulation. Literature [18] developed a speed control device for vehicle turning left at intersection. Finally, the simulation results show that the device can really improve the safety of vehicle turning left at intersection. Literature [19] puts forward two strategies of setting left-turn phase and left-turn waiting area at intersections to improve the traffic quality at intersections. Literature [20] found that the intersection conflict simulated by software or model is very suitable for the actual intersection conflict research. Literature [21] holds that the occurrence of traffic accidents is mainly caused by the driver's mistakes, and the driver carries out a series of driving actions for a certain purpose, but the original driving intention cannot be realized due to the operation mistakes. Literature [22] establishes a hidden Markov model based on the pedal opening of the vehicle and the position information of the vehicle, so as to determine the intention that the driver really wants to achieve. Reference [23] establishes a hidden Markov model to infer the driver's intention when the vehicle deviates to different degrees. The final reasoning result is applied to the control device of the vehicle, which increases the safety of the vehicle when driving.

In order to determine the driver's driving intention, all types of state data must be collected, and an identification model must be established during the analysis of the driver's driving. The challenge is deciding what kind of data to collect, or choosing the feature vector for modeling. The difficulty of model building and the time it takes to identify a model can be reduced if the feature vector dimension is too small. However, the model's accuracy will deteriorate. Furthermore, collecting characteristic data in the actual driving environment of some vehicles is quite difficult. As a result, selecting the appropriate feature vector is critical in the study of predicting a driver's driving intention.

3. Research Method

3.1. Vehicle Speed Time Series Analysis. It is a critical variable in the field of speed traffic, and vehicle driving speed is a key index for reflecting traffic operations, and the driving state of floating vehicles can best reflect traffic operations over time. The traffic situation is constantly changing in real time, and the travel time of vehicles is directly influenced by the current traffic situation. As a result, understanding how to convert and correlate vehicle and traffic driving conditions, as well as how to display the short-term operation of traffic using appropriate variables, is critical. Under such conditions, road speed is generated.

In the research, this model is mainly used to calculate the traffic conditions before vehicles enter the expressway. When it is necessary to predict the travel time, the estimated travel time, the estimated starting point, and the expected ending point of the vehicle are all known. After getting the speed of the road section before the estimated travel time, then can know the traffic conditions during this period. At the same time, from the second 5 minutes to the first 5 minutes before the trip, one can get a general understanding of the changes in traffic operation. For the known estimated travel time, calculate the speed of each road segment within the first two 5 minutes of the trip, and arrange the speed of each road section according to the front and back position of the road section, so as to obtain the preliminary input characteristics.

In practical application, the complexity and unstructured degree of time series are very high, which forces the research to continuously improve the accuracy and applicability of time series mining algorithm. In reality, time series exists in all aspects. Finding the hidden rules and patterns from these complex data and finally serving for decision-making is the main purpose of data mining.

In the past research, the ARMA model was mostly used in forecasting. This paper mainly uses the ARMA model to extract features of time series. Determining the time series $\{X_t,\ t = 1, 2, \ldots, n\}$ can fit the ARMA model. We can find the basic model type judgment diagram in Figure 1.

If the accurate optimal value of (p, q) cannot be obtained by using autocorrelation function and partial autocorrelation function, AIC (Akaike information criterion) can be used to determine the order, which is a standard to measure the fitting effect of the model.

Increasing the parameter variables of the model will reduce the deviation between the estimated value of the model and the actual value, so that the model can better fit the original data. However, increasing the number of parameter variables will increase the complexity of the model, so the cost of increasing the variables should be punished.

The fitting ARMA model can be defined as follows:

$$\mathrm{AIC} = (p, q) = N \ln \sigma^2 (p, q) + 2 (p, q), \tag{1}$$

where N is the sample size, $k = p + q$ is the number of parameters in the ARMA model, and σ^2 is the estimation of noise variance.

BIC (Bayesian information criterion) is also a judgment criterion, which is expressed as follows:

$$\mathrm{BIC}(p, q) = N \ln \sigma^2 (p, q) + (p, q) \ln N. \tag{2}$$

The principle of this method is the same as that of AIC, but it increases the intensity of “punishment.” It can be seen that both of these criteria advocate the concise form of functions and use fewer variables to represent functions. When the number of samples is large, BIC principle is more effective, and AIC principle determines relatively many model parameters, so it is more suitable for small samples.

Check the autocorrelation and partial correlation between scattered data in time series data X_t. By observing the distribution of autocorrelation and partial correlation function values, if the distribution curve accords with the characteristics of “tailing” and “truncated,” it shows that the series is suitable for establishing the ARMA model. The calculation formulas of autocorrelation R_k and partial correlation function $\phi_{k,k}$ for correlation judgment are as follows:

$$\begin{cases} R_k = E\left[X_t, X_{t-k}\right], \\ \phi_{k,k} = \dfrac{E\left[X_t, X_{t-k}\right]}{\sqrt{E\left[X_t\right]^2, E\left[X_{t-1}\right]^2}}, \quad k = 1, 2, \ldots, n. \end{cases} \tag{3}$$

If the time series data do not meet the correlation requirements, it is necessary to perform differential, differential, or logarithmic operations on the data used for partial scatter points in X_t and then continue the subsequent steps when it becomes a stationary data series.

Select the appropriate p, q value to establish the analytical formula of ARMA model, and use the AIC rank criterion to determine the p, q value, even if the following formula is the minimum value:

$$\mathrm{AIC} = \min\left[N \cdot \ln \delta_k^2 + 2(p + q + 1)\right], \tag{4}$$

where N is the capacity of the selected speed sample and δ_k^2 is the residual variance of the model, that is,

$$\delta_k^2 = \sum_{k=1}^{N} \frac{\varepsilon_k^2}{N}. \tag{5}$$

If the absolute values of residual autocorrelation functions of the prediction results are less than $2/\sqrt{N}$, it indicates that the ARMA model meets the prediction requirements.

In general, data can be divided into numerical and nonnumerical types of characteristic attributes. These two types of filling are treated differently by the mean filling method. The missing values for numeric attributes will be filled using the average values of the attributes in other nonmissing samples. Fill in the values with the most frequent occurrences in the nonmissing samples, that is, the values with the highest frequency, for non-numeric attributes, according to the mode principle.

From the entire sample set, choose the road section speed that corresponds to the recorded road section and save it as the new adjacent road section sample set. Then, using a hierarchical clustering algorithm, this portion of the data is clustered, the centroid of each cluster is calculated, and the cluster centroid that is closest to the speed of the road section near the missing position is found. The values of data samples in the missing positions in the cluster are filled in the missing fields. This completes the missing item’s filling.

3.2. Vehicle Speed Prediction. At present, the prediction method generally uses the previous historical data, taking the day as the cycle, extracting the change rule of traffic parameters from it, and applying the extracted rule to the current time, thus obtaining the prediction result. According to the comprehensive evaluation of the previous traffic state dividing thresholds, the specific dividing standards are determined.

After dividing the continuous traffic data into traffic states, the traffic data belonging to different traffic states are classified. According to the historical traffic data of each traffic state, the state transition matrix required by the KF (Kalman filtering) method is trained by the artificial neural network, and then the interval speed prediction based on data fusion is carried out by the KF method.

In the ARMA environment, the dynamic performance of high-speed moving vehicles is very high. Therefore, when the parameters change little, we use a larger adaptive forgetting factor μ_k to increase the prediction strength. When the parameters change greatly, a small adaptive forgetting factor μ_k is used to enhance the identification accuracy. The

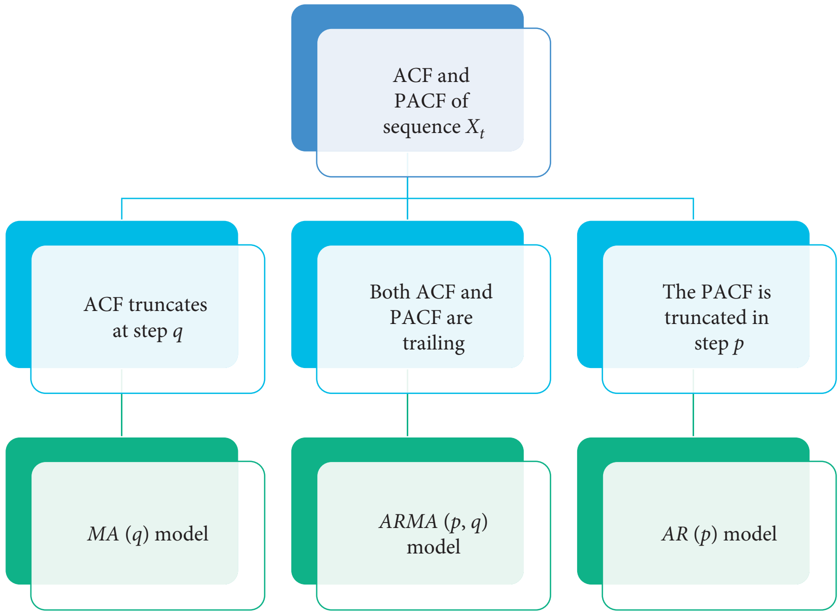

FIGURE 1: Basic model type judgment. ACF is autocorrelation function, PACF is partial autocorrelation function, MA is the moving average model, and AR is the autoregressive model.

formula of adaptive forgetting factor used in this paper is as follows:

$$\mu_k = \max\left\{1, \frac{tr(G_k)}{tr(H_k)}\right\}. \tag{6}$$

The core idea of memory decay is to apply a factor to the covariance matrix of prediction and increase the variance of prediction state vector, so as to make full use of the current measurement data.

$$G_k = M_k - CQC^T - R. \tag{7}$$

In equation (7), G_k and M_k represents the error variance at time k.

$$H_k = CAP_{k-1}A^T C^T. \tag{8}$$

In equation (8), H_k represents the error variance at time k, which ensures that the value of the error covariance matrix P_k is symmetric and positive, and improves the dynamic performance of the system.

In this paper, the flow of speed prediction operation of high-speed moving vehicles based on adaptive KF in ARMA environment is shown in Figure 2.

The contribution weight also plays a role in reducing dimension and simplifying operation to a certain extent. On this basis, this paper puts forward a new similarity measurement standard, and the process of clustering analysis becomes the following steps.

Using the ARMA model to fit the model, the time series will be represented by a set of coefficient vectors. Namely, the time series X, Y, and the parameter vectors of the fitting model are π_X, π_Y, respectively.

Find the contribution rate $(\alpha_1, \alpha_2, \ldots, \alpha_m)$ of the first m coefficients whose cumulative contribution rate reaches a certain percentage and then calculate the weight $\beta = (\beta_1, \beta_2, \ldots, \beta_m)$ of these m coefficients, where β is the weight vector and i represents the i th coefficient:

$$\beta_i = \frac{\alpha_i}{\sum_{i=1}^{m} \alpha_i}. \tag{9}$$

The newly obtained coefficient vectors are standardized, their Euclidean distance d_μ is used as similarity measure, and the corresponding clustering method is used to recluster, and finally the clustering result is obtained.

$$d_\mu = \sqrt{\sum_{k=1}^{m} (\mu_{Xk} - \mu_{Yk})^2}. \tag{10}$$

Due to the weekly similarity of traffic data, historical data with the same weather conditions in the same week as the forecast date in the last week were selected in the study. If the weather conditions are different, select the data of the same week last week. If the weather conditions are still different, select the data of the adjacent Sunday of last week.

Because the one-dimensional median filter is less affected by the contour of image samples, and the noise suppression effect of the two-dimensional median filter is obviously better than that of the one-dimensional median filter when the contour of image is not considered, one-dimensional and two-dimensional median filters can be used alternately when filtering. In addition, during filtering, the image can be iteratively filtered to get the optimal solution.

4. Results Analysis and Discussion

4.1. Modeling and Analysis of Time Series Prediction. Design the real vehicle driving data collection test according to the vehicle collision situation. The driving area is selected at the intersection of a newly built municipal road, and it is

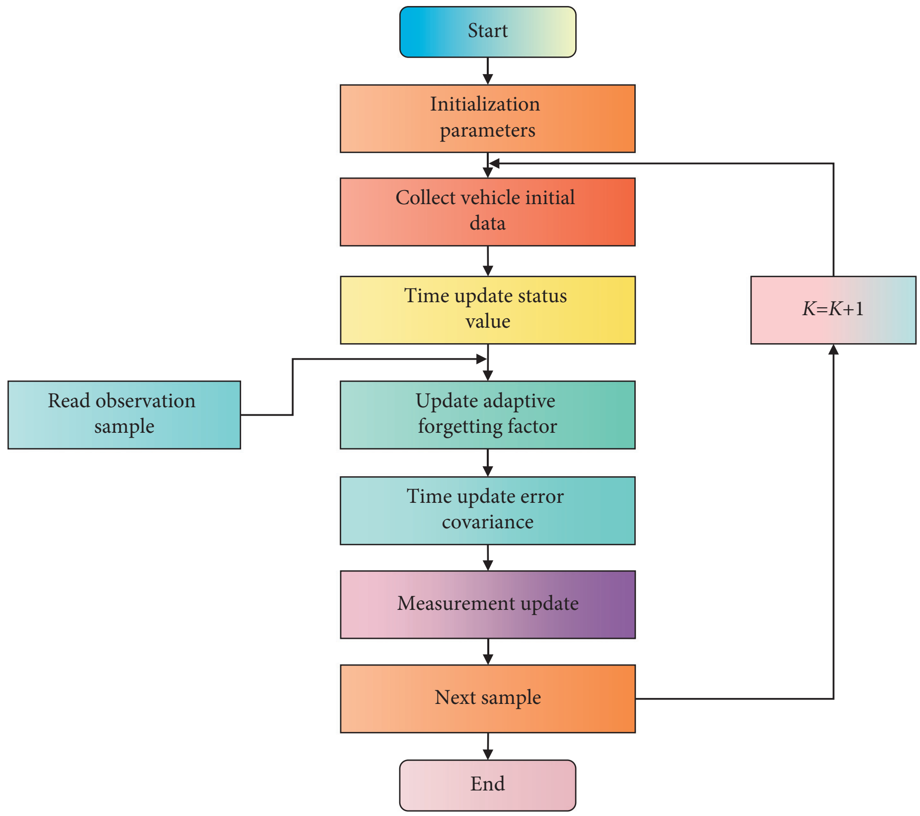

Figure 2: Adaptive KF speed prediction flow chart.

required that the road connecting the intersection should extend long enough, have a wide field of vision, and have small traffic flow. Motor vehicles 1 and 2 in the direction of conflict use the same type of small cars, and the vehicle speed is collected once every 1 s by the vehicle driving behavior test platform and stored in chronological order.

After the vehicle stops, determine the position of the collision point according to the traveling direction of the vehicle and measure the distance from the starting point to the collision point, as shown in Figure 3.

In straight-line sections, drivers will first choose between three types of traffic crossing options based on their destination and intersection design: straight, left, or right. The external information, such as traffic lights/signs, other vehicles, pedestrians, nonmotor vehicles, roads and obstacles at intersections, weather factors, and so on, is primarily received visually. The driver will adjust his speed to prepare for entering the intersection based on the above factors. The driver primarily uses the accelerator and brake pedals to adjust the speed of his own car on the straight road section.

The driving in the straight-line section and the driving in the intersection follow each other on the time axis. The purpose of driving on the straight road section is to prepare for driving in the intersection, so the speed fluctuation on the straight road section reflects the driver's turning preparations.

If you go straight through the intersection, the driver's main gaze targets are the vehicles and traffic lights ahead. Compared with the other two turning modes of crossing, the influencing factors of straight-through crossing are relatively simple. However, the change of traffic lights directly affects whether the vehicle stops or not. Therefore, the speed of straight-through traffic varies greatly.

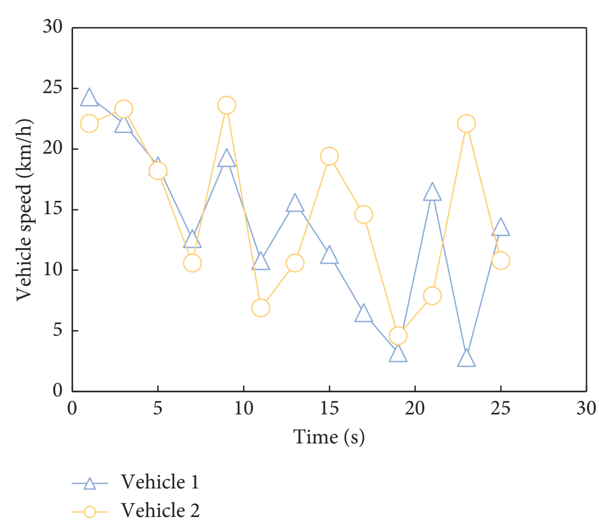

Figure 3: Time series of vehicle speeds 1 and 2 obtained from the real vehicle driving test.

Comparing the degree of difference between the curves in Figures 4 and 5, it can be seen that the prediction model [20] established by using the first 40 data in the vehicle speed series obtained from the experiment has a better prediction effect on the last 20 vehicle speeds.

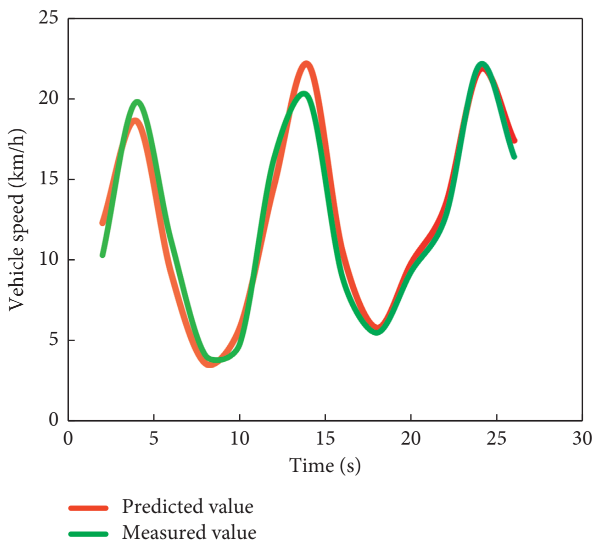

FIGURE 4: Comparison between predicted value and measured value of vehicle 1.

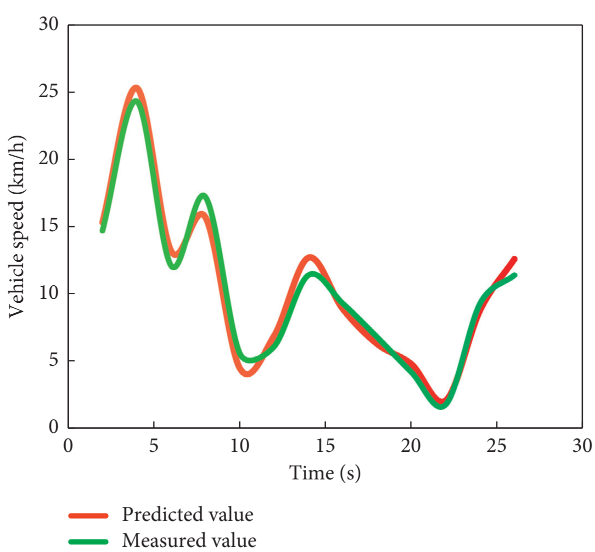

FIGURE 5: Comparison between vehicle 2 predicted value and measured value.

The vehicles run continuously in space, and the number and types of vehicles passing through different sections of each test section are basically the same in the same time period. However, for different observation points on the same section, the composition structure of vehicle types has spatial differences. In the process of driving on the expressway, certain drivers will frequently change lanes in order to choose the best route. This reflects the change of running speed in the direction.

By studying the speed change of different drivers when driving vehicles through the combination of curve and slope of the test section, the main influencing factors of drivers' driving behavior in the curve are found, so as to prepare for the later study of the running speed distribution characteristics of typical sections.

4.2. Verification and Analysis of Prediction Results. The vehicle will be acted on by centrifugal force pointing to the outside of the horizontal curve while driving on a curve. To improve the vehicle's lateral controllability, the driver typically slows down when entering the curve. The longitudinal stability of the vehicle is also involved in curve driving because the vehicle will decelerate when decelerating and the longitudinal stress will change. The safety of the entire route is largely determined by the quality of the curve's design, and curve speed characteristics have always been the focus of running speed research.

Because of the complexity and diversity of highway alignment composition, there are some differences in the running speed of entering the slope section, which affects the running speed of different sections on the slope section. Set at the longitudinal slope's beginning, middle, and end points, and increase the position section of the minimum sight distance point in the vertical curve section. You can track the vehicle to record the speed if the slope length is less than 800 meters. One person stands at the bottom of the slope or at the top of the slope, measuring the speed with a speed gun. Follow two people and keep track of their speed in two different directions. Because the speed measuring range of a radar speed measuring gun is limited when the slope is longer than 800 meters, more speed measuring personnel should be equipped. Record the relevant alignment and road surface parameters, roadside conditions, and road surface conditions of the point after the speed measurement test is completed, and take photos.

In the simulation experiment, three methods are used to predict the speed of high-speed vehicles. The predicted results of simulated vehicle speed are shown in Figures 6–8.

It can be seen from Figure 8 that during the whole iteration process, the maximum error between the actual running speed of the high-speed moving vehicle and the estimated speed based on the least square method is ±4 and fluctuates up and down here.

The original data obtained from the test include mileage, speed, and acceleration, which are continuously changing with the mileage. This paper mainly studies the distribution of running speed on curved slope sections, which are divided strictly according to the pile number. Therefore, the data obtained from the test should first be recalibrated according to the station number, so as to approximately get the continuous running state of vehicles on different sections.

The test shows that the mileage measured by the instrument is shorter than the actual pile number mileage. This is because the road pile number is based on the actual distance of the road centerline, and the instrument measures the actual mileage of the vehicle. However, when driving the vehicle, it is impossible for the driver to drive in strict accordance with the direction of the road centerline marking. Skilled drivers will often change lanes and choose shorter routes.

This kind of error caused by the driver's route selection is objective and inevitable in the test process, but the data can be recalibrated by setting special marking points, which are hereinafter referred to as "reference points." Data calibration is actually an artificial dispersion of experimental errors, and

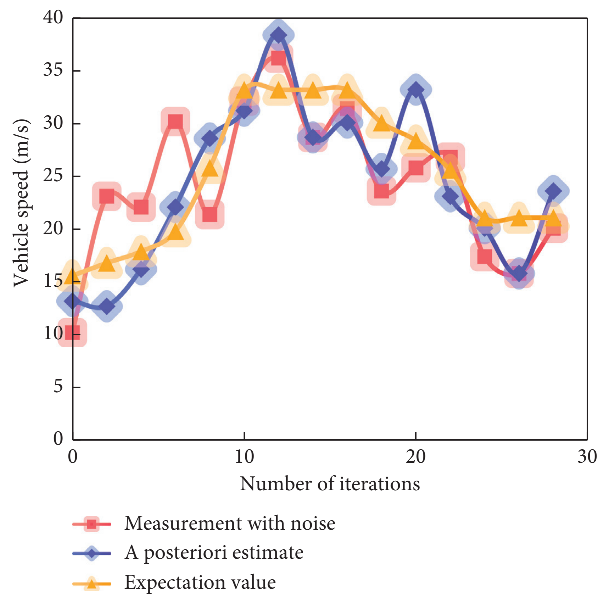

Figure 6: Speed prediction effect of the least square method.

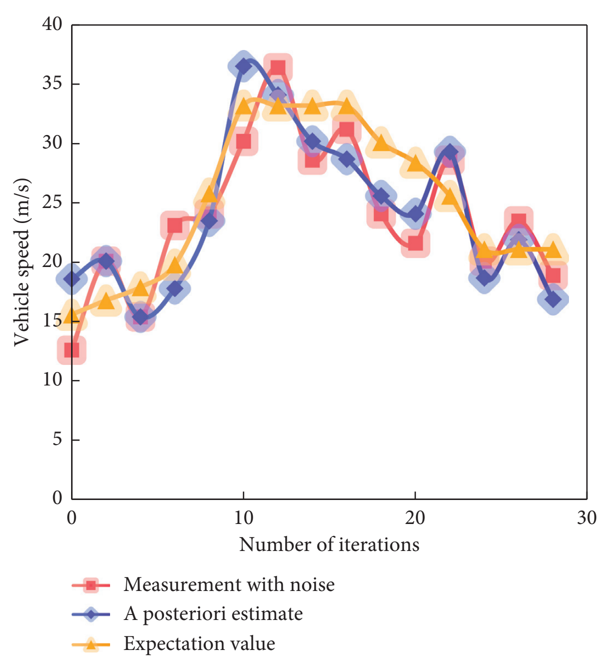

Figure 7: Speed prediction effect of KF.

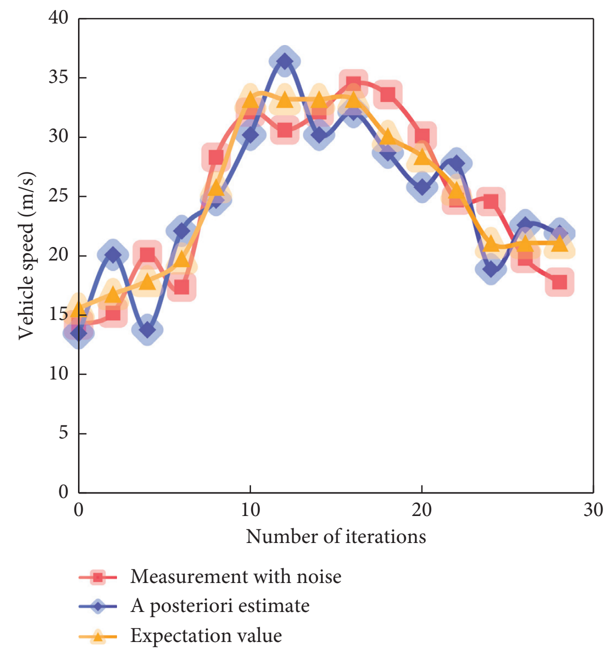

Figure 8: Speed prediction effect of adaptive KF.

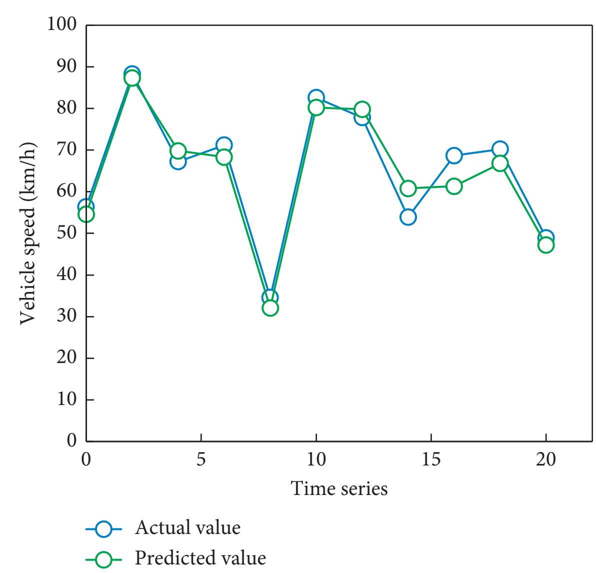

Figure 9: Comparison chart of data verification results.

the influence of this error can be reduced by increasing the number of "reference points" (Figures 9 and 10).

It can be seen from Figure 9 that the change trend of the predicted value is basically consistent with that of the real value. It can be seen from Figure 10 that the maximum relative error is 7.4, the error between the predicted result and the true value is small, and the predicted result is relatively accurate.

If you want to turn left through the intersection, the factors affecting the speed are more complicated than when you go straight through. Drivers should not only pay attention to the changes of traffic in intersections but also pay attention to the flow of people and nonmotor vehicles on crosswalks. According to the traffic rules, even if the traffic lights indicate that you can turn left, there are pedestrians and nonmotor vehicles crossing the street at the crosswalk.

The essence of the running speed method is to ensure the smooth and continuous running speed by controlling the gradual transition of the unit index values of adjacent road sections, thus improving the driving safety of the highway. In practice, the designer checks the consistency and coordination of technical indicators along the route direction through the running speed curve. If the vehicle speed curve under a certain set traffic volume is calculated, not only can you get the travel time between the start point and the end point, provide reference for road users' travel, but also

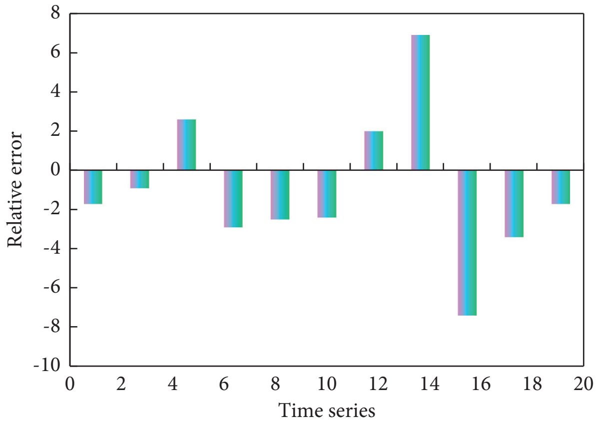

Figure 10: Relative error diagram of data.

measure the service level of the road, and then judge whether the design expectation is met and whether it is necessary to rebuild, expand, or build parallel lines.

5. Conclusion

This method improves KF's tracking ability by allowing it to record and predict the speed of high-speed moving vehicles in harsh environments, curves, uphill, and downhill. The predicted vehicle speed value is used to calculate vehicle displacement and distance between vehicles, which can be used to assess the risk of collisions in intersections between vehicles traveling in opposing directions. The research object is an ARMA model with a zero-mean random sequence. The simulation results show that the adaptive KF vehicle speed prediction method based on ARMA predicts values that are closer to reality, which improves the filter's convergence effect and reduces the fluctuation range, effectively overcomes the negative effects of process and measurement errors, and better reflects real-time effectiveness.

The vehicle speed prediction modeling and parameter tuning are done off-line, which is a flaw in this study. The ARMA modeling parameter self-tuning method and its implementation algorithm should be considered to help the prediction model adaptively adjust parameters to cope with changes in the driving environment, in order to improve the model's universality. The work described above will be continued in the follow-up study.

Data Availability

The data used to support the findings of this study are available from the corresponding author upon request.

Conflicts of Interest

The authors declare that they have no conflicts of interest.

Acknowledgments

This work was sponsored in part by Intelligent Manufacturing Project of Tianjin (20200213).

References

[1] H. Sabrina and H. Jan, "Analysis of CFSE time-series data using division-, age- and label-structured population models," *Bioinformatics*, vol. 32, no. 15, pp. 2321–2329, 2016.

[2] Z. Huang, Y. Liu, C. Zhan, C. Lin, W. Cai, and Y. Chen, "A novel group recommendation model with two-stage deep learning," *IEEE Transactions on Systems, Man, and Cybernetics: Systems*, 2021.

[3] B. Saka and B. Adra, "Nucleation and growth of cholesteric collagen tactoids: a time-series statistical analysis based on integration of direct numerical simulation (DNS) and long short-term memory recurrent neural network (LSTM-RNN)," *Journal of Colloid and Interface Science*, vol. 582, pp. 859–873, 2021.

[4] L.-H. Zhang, Y.-W. Wang, Y.-Q. Ni, and S.-K. Lai, "Online condition assessment of high-speed trains based on Bayesian forecasting approach and time series analysis," *Smart Structures and Systems*, vol. 21, no. 5, pp. 705–713, 2018.

[5] L. D. Condeixa, L. Bastos, F. Oliveira, and S. Barbosa, "Wind speed time series analysis using TBATS decomposition and moving blocks bootstrap," *International Journal of Energy & Stats*, vol. 05, no. 2, Article ID 1750010, 2017.

[6] M. Laib, L. Telesca, and M. Kanevski, "Long-range fluctuations and multifractality in connectivity density time series of a wind speed monitoring networ," *Chaos*, vol. 28, no. 3, Article ID 033108, 2018.

[7] C. Sarmiento, C. Valencia, and R. Akhavan-Tabatabaei, "Copula autoregressive methodology for the simulation of wind speed and direction time series," *Journal of Wind Engineering and Industrial Aerodynamics*, vol. 174, pp. 188–199, 2018.

[8] M. K. Khandani and W. B. Mikhael, "Effect of sparse representation of time series data on learning rate of time-delay neural networks," *Circuits, Systems, and Signal Processing*, vol. 40, no. 4, pp. 1–26, 2021.

[9] B. Cao, "Time sequence analysis and application research of highway tunnel on-site monitoring," *Architectural Engineering Technology and Design*, vol. 000, no. 17, pp. 2751-2752, 2018.

[10] P. Luo, Y. Jiang, Q. Xu, and B. Tang, "GPS landslide displacement monitoring time series analysis and combined modeling prediction," *Journal of the Institute of Disaster Prevention Science and Technology*, vol. 22, no. 4, p. 9, 2020.

[11] W. Jiang and X. Wang, "Xilinx FPGA timing analysis and optimization method," *China New Telecommunications*, vol. 2019, no. 9, p. 1, 2019.

[12] Y. Wang, K. Zhou, and M. Li, "Review of WCET analysis and prediction of real-time embedded systems," *Computer Science*, vol. 46, no. B06, p. 7, 2019.

[13] Y. Wang and J. Zhang, "Application of time series analysis related methods in information retrieval research," *Journal of Information Recording Materials*, vol. 009, no. 1, pp. 46–65, 2019.

[14] H. Xiao and H. Ge, "Research on structural damage warning of bridge crane based on time series analysis," *Journal of Wuhan University of Technology*, vol. 39, no. 1, p. 6, 2017.

[15] J. Liu and Z. Ouyang, "Research on short-term wind power prediction based on ARMA model," *Northwest Hydropower*, vol. 2017, no. 6, p. 5, 2017.

[16] H. Zhang, L. Zhao, and Z. Lei, "Research on compatibility terminal detection pipeline time prediction based on ARMA model," *Instrument Standardization and Metrology*, vol. 000, no. 1, pp. 39–42, 2017.

[17] M. She, "Research on the prediction model of vehicle running speed on continuous downhill sections based on cross-section observation method," *Highway Traffic Science and Technology: Applied Technology Edition*, vol. 2019, no. 7, p. 6, 2019.
[18] S. Zhang, Z. Guo, and L. Chen, "Long-range correlation analysis of vehicle speed on long downhill sections," *Comprehensive Transportation*, vol. 42, no. 2, p. 5, 2020.
[19] H. Lu, X. Nie, and K. Gu, "Research on intelligent vehicle tracking control based on adaptive model prediction," *Car Digest*, vol. 2021, no. 2, p. 6, 2021.
[20] W. Sun, P. Zhang, Z. Wang, and D. Li, "Prediction of cardiovascular diseases based on machine learning," *ASP Transactions on Internet of Things*, vol. 1, no. 1, pp. 30–35, 2021.
[21] F. Dietlein, D. Weghorn, A. Taylor-Weiner et al., "Identification of cancer driver genes based on nucleotide context," *Nature Genetics*, vol. 52, no. 2, pp. 208–218, 2020.
[22] J. Yan, S. Peng, and L. Zhang, "Urban road network traffic flow speed prediction considering large-scale vehicles," *Journal of Chongqing Jianzhu University: Natural Science Edition*, vol. 40, no. 1, p. 6, 2021.
[23] N. Zheng, W. Yang, and L. Ma, "VISSIM simulation analysis and prediction of the impact of traffic emergencies on mountain expressway traffic operation," *Safety and Environmental Engineering*, vol. 27, no. 4, p. 8, 2020.